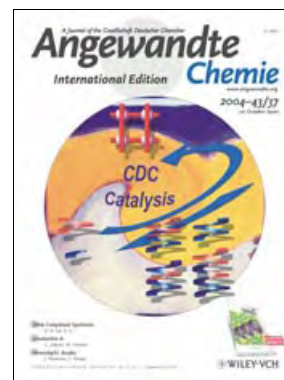


Cover Picture

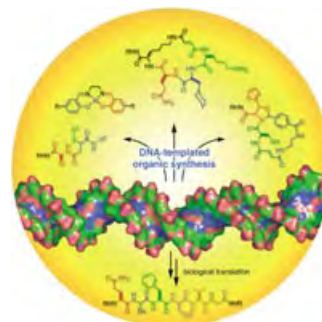
Nicolas Giuseppone, Jean-Louis Schmitt, and Jean-Marie Lehn*

Helices and grids two most fascinating architectures, which have been the subject of intense recent studies in view of their significance in chemistry, biology, and material science, are represented in the cover picture. They are interconnected in a thermodynamic equilibrium generated by a Lewis acid catalyzed pathway involving a constitutional dynamic reorganization, self-assembly, and control of helical folding. For further details see the Communication by J.-M. Lehn et al. on page 4902 ff.



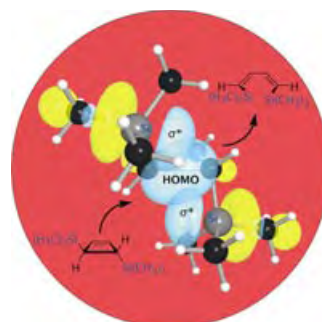
DNA-Templated Synthesis

In their Review on p. 4848 ff., X. Li and D. R. Liu present an approach to controlling chemical reactivity by modulating the effective molarity of highly dilute reactants through macromolecule-templated synthesis—an approach that mimics natural biosynthesis.



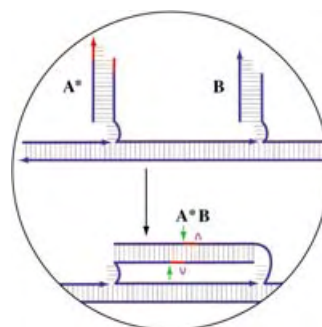
Electronic Effects

The powerful effect that electronic stabilization can have on the course of a reaction is described by M. Murakami and M. Hasegawa in their Communication on page 4873 ff with the ring opening of *trans*-3,4-disilylcyclobutene.



Nanorobotics

The progress of a six-nucleotide-long DNA fragment wandering along a self-assembled track with three anchor points is investigated by H. Yan, A. J. Turberfield, J. H. Reif et al. in their Communication on page 4906 ff.



Angewandte EarlyView®

The following Communications are available online (in Wiley InterScience). You can find them, as well as forthcoming Reviews, Highlights, and Essays, at www.angewandte.org, under Early View.

J. Du, Y. Chen*:
Organic-Inorganic Hybrid Nanoparticles with a Complex Hollow Structure
DOI: 10.1002/anie.200454244
Published online: September 3, 2004

K. C. Nicolaou,* B. S. Safina, M. Zak, A. A. Estrada, S. H. Lee:
Total Synthesis of Thiostrepton, Part 1: Construction of the Dehydropiperidine/Thiazoline-Containing Macrocyclic
DOI: 10.1002/anie.200461340
Published online: September 3, 2004

K. C. Nicolaou,* M. Zak, B. S. Safina, S. H. Lee, A. A. Estrada:
Total Synthesis of Thiostrepton, Part 2: Construction of the Quinaldic Acid Macrocyclic and Final Stages of the Synthesis
DOI: 10.1002/anie.200461341
Published online: September 3, 2004

Articles judged by the referees or the editor as being either very important or very urgent are immediately edited, proof-read, and electronically published once the manuscript has arrived in the editorial office in its final form. As long as there is no page number available these articles should be cited in the following manner:

Author(s), *Angew. Chem. Int. Ed.*, online publication date, DOI.

News

Materials Science:
Prize to M. Mayor _____ **4830**

Organometallic Chemistry:
Research Award to W. Tolman _____ **4830**

Solid-State Chemistry:
Prize to S. Alvarez _____ **4830**

Books

Gemini Surfactants

Raoul Zana, Jiding Xia

reviewed by I. Huc _____ **4831**

Organic Reaction Mechanisms

Mar Gómez Gallego, Miguel A. Sierra

reviewed by H. Zipse _____ **4832**

Highlights

Homoleptic Azides

C. Knapp, J. Passmore* _____ **4834–4836**

On the Way to “Solid Nitrogen” at Normal Temperature and Pressure? Binary Azides of Heavier Group 15 and 16 Elements

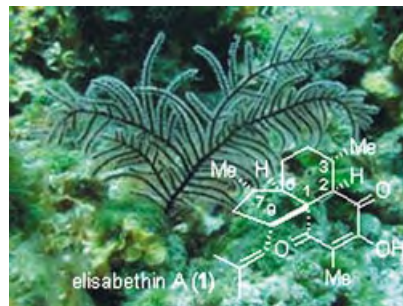


Caution explosive! Homoleptic azides are of great interest as polynitrogen compounds particularly because of their high energy content. A recent breakthrough is the first synthesis and characterization of the highly sensitive neutral tellurium azide $[\text{Te}(\text{N}_3)_4]$ and of ionic $(\text{N}_5)^+[\text{P}(\text{N}_3)_6]^-$ containing 23 nitrogen atoms.

Natural Product Synthesis

G. Zanoni,* M. Franzini _____ **4837–4841**

Elisabethin A: A Marine Diterpenoid Yet To Surrender to Total Synthesis



Mysterious and elusive, elisabethin A (1, pictured with the West Indian sea whip *Pseudopterogorgia elisabethae* from which it was isolated), has not yet succumbed to total synthesis—or has it? Two recent attempts at the synthesis of this challenging target are examined, but questions still remain as to the absolute configuration of the natural product and the synthetic material.

Essays

History of Science

P. Ball, M. Ruben* — 4842 – 4847

Color Theory in Science and Art: Ostwald and the Bauhaus



© VG Bild-Kunst, Bonn 2004

A historical confluence of the streams of science and art took place in Dessau, Germany, in 1927. The main participants were the artists of the Bauhaus School (represented by a painting by Kandinsky,

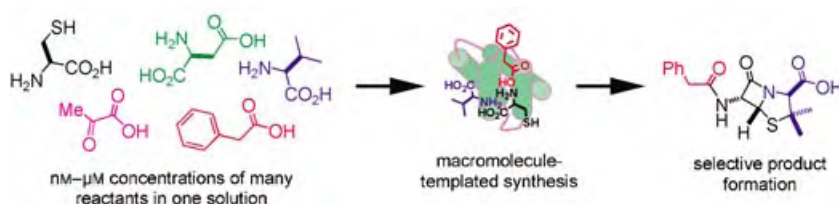
left) and the Nobel Laureate and avid painter Wilhelm Ostwald, who presented his theory of color (the basis for the etching on the right).

Reviews

Synthetic Methods

X. Li, D. R. Liu* — 4848 – 4870

DNA-Templated Organic Synthesis: Nature's Strategy for Controlling Chemical Reactivity Applied to Synthetic Molecules



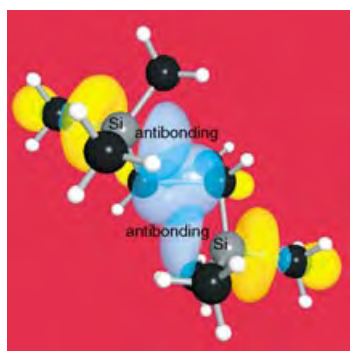
A surprisingly general way to control reactivity uses DNA base pairing to modulate the effective molarity of synthetic reactants. This approach mimics biosynthesis and enables complex mixtures

in a single solution to react with efficiencies and selectivities that cannot be achieved using conventional laboratory synthesis (see scheme).

Communications

Electronic Effects

M. Murakami,*
M. Hasegawa — 4874 – 4876

Synthesis and Thermal Ring Opening of *trans*-3,4-Disilylcyclobutene


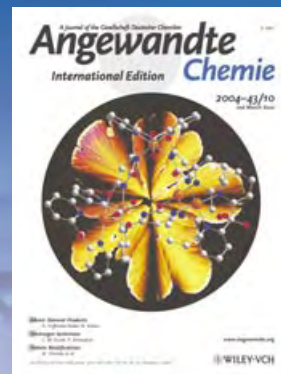
A true test of the power of electronic stabilization is provided by a ring-opening reaction of *trans*-3,4-bis(trimethylsilyl)cyclobutene. The two bulky silyl groups prefer inward rotation, despite the steric constraints. Electronic stabilization arising from the delocalization of the HOMO electron density into the two antibonding orbitals overcomes the steric congestion (see picture).

For the USA and Canada:
ANGEWANDTE CHEMIE International Edition (ISSN 1433-7851) is published weekly by Wiley-VCH PO Box 191161, D 69451 Weinheim, Germany. Air freight and mailing in the USA by Publications Expediting Inc. 200 Meacham Ave., Elmont, NY 11003. Periodicals

postage paid at Jamaica NY 11431. US POSTMASTER: send address changes to *Angewandte Chemie*, Wiley-VCH, 111 River Street, Hoboken, NJ 07030. Annual subscription price for institutions: Europe € 3430.00/3118.00; outside Europe US\$ 4499.00/4090.00 (valid for print and electronic/print or electronic delivery); for

individuals who are personal members of a national chemical society, or whose institution already subscribes, or who are retired or self-employed consultants, print only: Europe € 248.00/outside Europe US\$ 378.00. Postage and handling charges included. All Wiley-VCH prices are exclusive VAT.

The best in chemistry – for more than a hundred years



A Journal of the Gesellschaft Deutscher Chemiker
Angewandte
International Edition **Chemie**

www.angewandte.org

1888: The beginning
of a success story

Constant Innovations

- 1962:** First issue of the International Edition
- 1976:** Graphical abstracts
- 1979:** Cover pictures
- 1988:** Centenary of Angewandte
- 1989:** Routine use of color
- 1991:** New section: Highlights
- 1992:** Computerized editorial tracking system
- 1995:** Internet service for readers
- 1998:** Regular press service; full-text online
- 2000:** New section: Essays; EarlyView: Communications available online ahead of the printed version
- 2001:** New section: Minireviews
- 2002:** Online submission of manuscripts
- 2003:** Weekly publication; new section: News; new layout
- 2004:** Backfiles (1962-1997); ManuscriptXpress: Online system for authors and referees



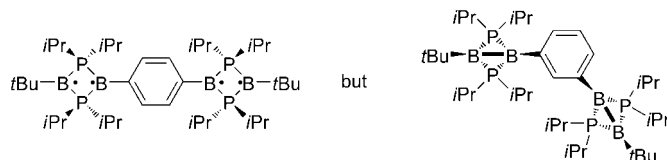
**Angewandte's
advisors...**

François Diederich
ETH Zürich

»» **Angewandte Chemie** has proven over the past two decades to be the most innovative of all chemical journals, taking leadership in both quality and presentation of the published material. Rapid, high visibility of important scientific work is readily ensured. It is a true privilege to serve on the Editorial Board.◀◀

Angewandte Chemie International Edition is
a journal of the German Chemical Society (GDCh)





Counting the calories: The coupling of two PBPB diradicals through an antiferromagnetic linker affords a singlet tetradical, whereas when they are coupled through a ferromagnetic linker, a bis(bicyclic) system is obtained (see picture).

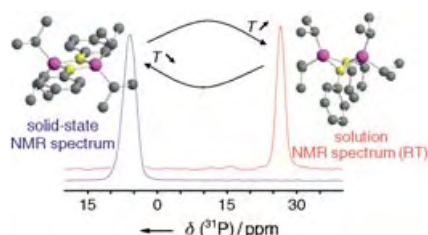
The energy difference between the planar form and the bicyclic isomer of substituted PBPB derivatives is only a matter of a few kcal mol⁻¹, thus a few kcal mol⁻¹ can make a tremendous difference.

Radicals

A. Rodriguez, F. S. Tham, W. W. Schoeller, G. Bertrand* 4876–4880

Catenation of Two Singlet Diradicals: Synthesis of a Stable Tetradical (Tetradicaloid)

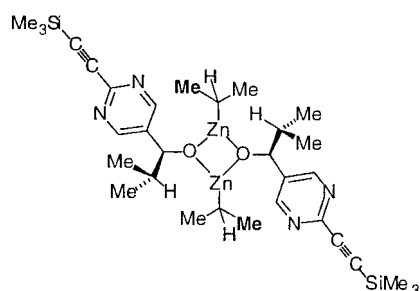
Lowering the temperature breaks the σ bond in the interconversion of 1,3-dibora-2,4-diphosphoniocyclobutane-1,3-diyl and its bicyclo[1.1.0]butane bond-stretch isomer (see picture). Variable-temperature NMR and UV/Vis experiments demonstrate for the first time the existence of two bond-stretch isomers that feature a transannular bonding π overlap, which allows for the thermal ring closure and opening processes.



Bond-Stretch Isomers

A. Rodriguez, R. A. Olsen, N. Ghaderi, D. Scheschkewitz, F. S. Tham, L. J. Mueller,* G. Bertrand* 4880–4883

Evidence for the Coexistence of Two Bond-Stretch Isomers in Solution

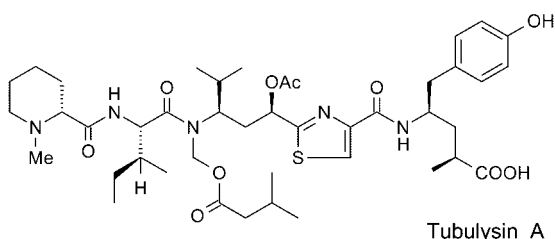


All square: A {ZnO}₂ square resting state in autocatalysis is revealed by NMR spectroscopy and endorsed by DFT calculations (see picture). Its dynamic behavior and reversible binding of excess *i*Pr₂Zn are defined.

Zinc Autocatalysts

I. D. Gridnev*, J. M. Serafimov, J. M. Brown* 4884–4887

Solution Structure and Reagent Binding of the Zinc Alkoxide Catalyst in the Soai Asymmetric Autocatalytic Reaction



Tubulysin A

Myxobacteria have it both ways: Whereas the epothilones stabilize the tubulin cytoskeleton and build microtubuli, tubulysins, which have now been isolated from *Archangium gephyra* and *Angiococcus disciformis*, have exactly the opposite effect.

They induce the disintegration of the microtubuli, and even picomolar concentrations can cause cell death by apoptosis. Their effect on cell cultures exceeds that of the most active epothilones by 50-fold.

Biosynthesis

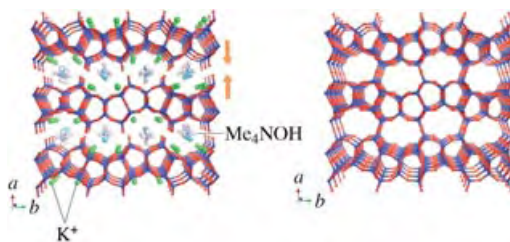
H. Steinmetz, N. Glaser, E. Herdtweck, F. Sasse, H. Reichenbach, G. Höfle* 4888–4892

Isolation, Crystal and Solution Structure Determination, and Biosynthesis of Tubulysins—Powerful Inhibitors of Tubulin Polymerization from Myxobacteria

Zeolites

T. Ikeda,* Y. Akiyama, Y. Oumi, A. Kawai,
F. Mizukami ————— **4892 – 4896**

The Topotactic Conversion of a Novel
Layered Silicate into a New Framework
Zeolite



High-density silicate sheets made up of five-membered rings with Me₄NOH molecules and K⁺ ions in the porelike interlayer space: This is the structure of the silicate PLS-1. When PLS-1 (left picture) was heated above 673 K under

vacuum, the novel zeolite CDS-1 (right picture) was obtained as the result of topotactic dehydration–condensation reactions. CDS-1 is a pure silicate and thermally stable, and should therefore find a range of industrial uses.

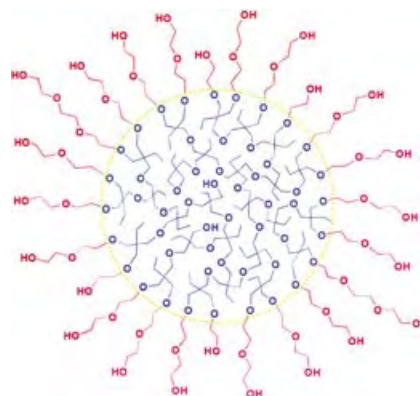


Polymer Vesicles

Y. Zhou, D. Yan* ————— **4896 – 4899**

Supramolecular Self-Assembly of Giant
Polymer Vesicles with Controlled Sizes

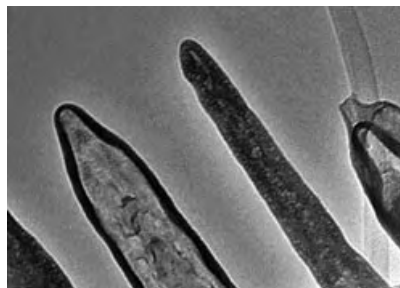
An ill-defined hyperbranched multiarm copolymer (see picture) with a high hydrophilic fraction (> 60%) self-assembles in water to form giant polymer vesicles (branched polymersomes). The size of the branched polymersomes can be easily controlled by adjusting the hydrophilic fraction of the copolymer, with the average diameter of the larger branched polymersomes exceeding 100 μm.



Nanostructures

A. R. Armstrong, J. Canales,
P. G. Bruce* ————— **4899 – 4902**

WO₂Cl₂ Nanotubes and Nanowires



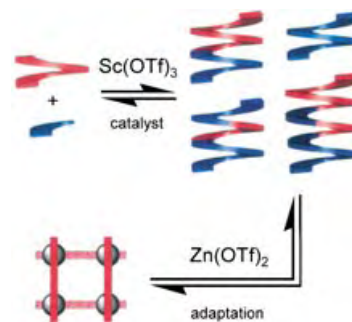
Mixed-anion nanotubes and nanowires have been synthesized, for the first time, by a simple process of exfoliation and restacking. The WO₂Cl₂ (oxyhalide) nanotubes and nanowires (see picture) may have some properties of both the halide and oxide anions.

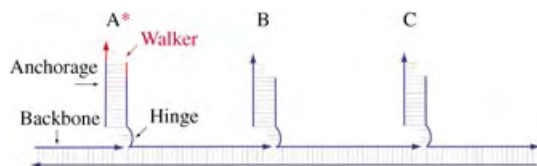
Constitutional Dynamics

N. Giuseppone, J.-L. Schmitt,
J.-M. Lehn* ————— **4902 – 4906**

Generation of Dynamic Constitutional
Diversity and Driven Evolution in Helical
Molecular Strands under Lewis Acid
Catalyzed Component Exchange

A stir in the library: The efficient Sc(OTf)₃-catalyzed transimination of helical oligo-hydrazone strands has been utilized to yield a highly diverse constitutional dynamic library through assembly, dissociation, and exchange of components. This library can subsequently undergo driven evolution in the presence of Zn^{II} ions to express preferentially [2 × 2] gridlike arrays by component recombination.





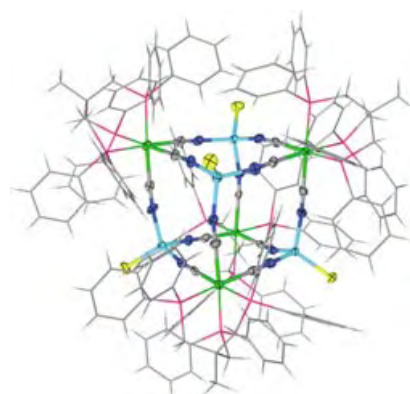
There's no turning back for an autonomous DNA walker that moves along a self-assembled track, driven by the hydrolysis of ATP. The track contains three anchorages (A, B, C) at which the walker (*), a six-nucleotide DNA fragment, can be bound

(see figure). The motion of the walker is unidirectional. At each step it is ligated to the next anchorage, then cut from the previous one by a restriction endonuclease.

Molecular Devices

P. Yin, H. Yan,* X. G. Daniell,
A. J. Turberfield,* J. H. Reif* **4906–4911**

A Unidirectional DNA Walker That Moves Autonomously along a Track



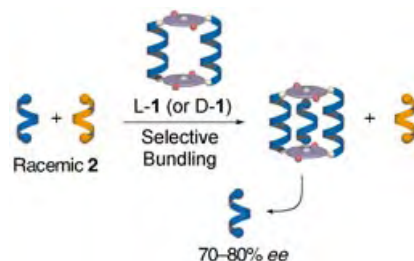
Two cyanide-bridged molecular cubes of general formula $[MCl]_4\{Re^{II}(\text{triphos})(CN)_3\}_4$, $M = Fe, Co$ (depicted), triphos = 1,1,1-tris(diphenylphosphanylmethyl)ethane, and their magnetic properties are reported. The cubes are prepared in good yields from the reaction of the Re^{II} complex $[Et_4N][Re^{II}(\text{triphos})(CN)_3]$ with the appropriate divalent metal halide and consist of octahedral Re^{II} and tetrahedral M corners bridged by cyanide ligands.

Single-Molecule Magnets

E. J. Schelter, A. V. Prosvirin, W. M. Reiff,
K. R. Dunbar* **4912–4915**

Unusual Magnetic Metal–Cyanide Cubes of Re^{II} with Alternating Octahedral and Tetrahedral Corners

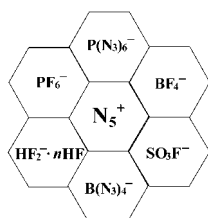
The helical sense of the peptidic parts of a cyclodimeric zinc porphyrin host with helical oligopeptide units (**1**) determines whether a right- or left-handed oligopeptide guest (**2**) is selectively bound (see picture). In contrast, enantiomers of nonhelical peptidic guests containing a point chirality are hardly discriminated.



Inclusion Compounds

Y.-M. Guo, H. Oike,* N. Saeki,
T. Aida* **4915–4918**

One-Pot Optical Resolution of Oligopeptide Helices through Artificial Peptide Bundling



23 nitrogens and only one phosphorus:
The N_5^+ ion is combined with energetic

anions in the form of $N_5^+[P(N_3)_6]^-$ and $N_5^+[B(N_3)_4]^-$ (see scheme), containing 91 and 96 wt %, respectively, of nitrogen. Also, the thermally unstable compound $N_5HF_2 \cdot nHF$ is prepared by metathesis from N_5SbF_6 and $CsHF_2$. Its usefulness as a reagent for the synthesis of new N_5^+ salts is demonstrated with the preparation of N_5PF_6 , N_5BF_4 , and N_5SO_3F .

Polynitrogen Chemistry

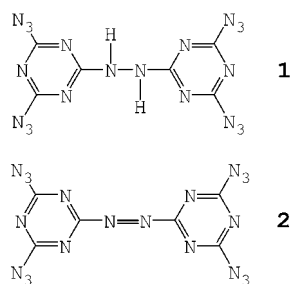
R. Haiges,* S. Schneider, T. Schroer,
K. O. Christe* **4919–4924**

High-Energy-Density Materials: Synthesis and Characterization of $N_5^+[P(N_3)_6]^-$, $N_5^+[B(N_3)_4]^-$, $N_5^+[HF_2]^- \cdot nHF$, $N_5^+[BF_4]^-$, $N_5^+[PF_6]^-$, and $N_5^+[SO_3F]^-$

High-Nitrogen Compounds

M.-H. V Huynh,* M. A. Hiskey,*
E. L. Hartline, D. P. Montoya,
R. Gilardi _____ 4924 – 4928

Polyazido High-Nitrogen Compounds:
Hydrazo- and Azo-1,3,5-triazine

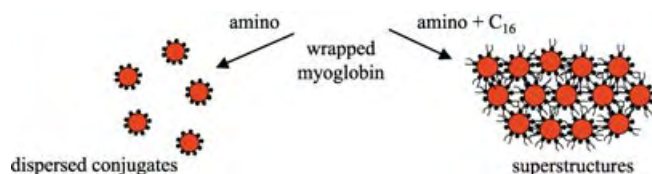


20 nitrogens and six carbons: The compounds **1** and **2**, demonstrate that hydrazo and azo linkages can be used to desensitize polyazido high-nitrogen compounds and also decrease their volatility. The compound **2** has the highest experimentally measured heat of formation reported for energetic organic compounds ($+2171 \text{ kJ mol}^{-1}$).

Protein-Inorganic Conjugates

A. J. Patil, E. Muthusamy,
S. Mann* _____ 4928 – 4933

Synthesis and Self-Assembly of Organo-
clay-Wrapped Biomolecules



Gift wrapped: Biomolecules can be enveloped within an ultrathin shell of an aminopropyl-functionalized magnesium (organo)phyllosilicate to produce aqueous dispersions of discrete protein-inorganic nanoparticles. Similar

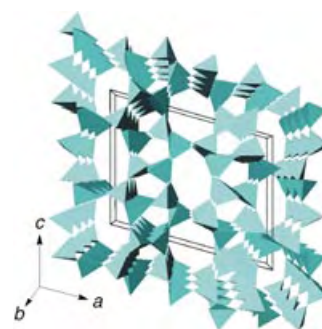
procedures but with organoclay oligomers that have pendent long-chain hydrophobic moieties result in self-assembly of the protein-inorganic nanoparticles into higher-order superstructures (see picture).

Zeolites

S. Zanardi,* A. Alberti, G. Cruciani,
A. Corma, V. Fornés,
M. Brunelli _____ 4933 – 4937

Crystal Structure Determination of
Zeolite Nu-6(2) and Its Layered
Precursor Nu-6(1)

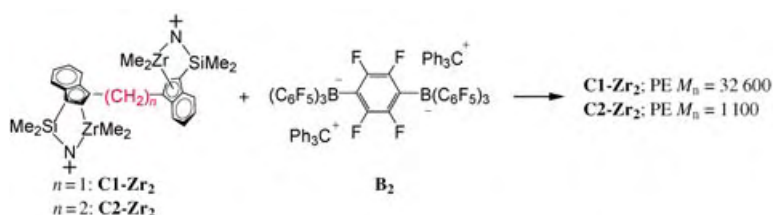
A small-pore pentasil zeolite (Nu-6(2)), which has a new topology, is obtained by thermal treatment of the 4,4'-bipyridyl silicate Nu-6(1). Crystal structure solution of the new zeolite and its layered precursor was achieved by combining high resolution X-ray powder pattern, direct methods, and model building. Nu-6(2) is characterized by a 1D channel system of two independent sets of eight-membered rings (see picture).



Polymerization

H. Li, L. Li, T. J. Marks* _____ 4937 – 4940

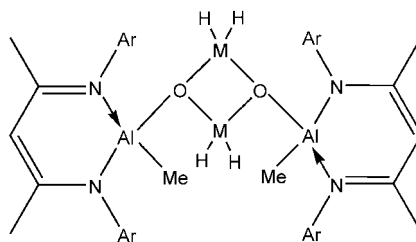
Polynuclear Olefin Polymerization Catalysis: Proximity and Cocatalyst Effects Lead to Significantly Increased Polyethylene Molecular Weight and Comonomer Enchainment Levels



Weight watching: In ethylene polymerization, approximately 70 fold increases in molecular weight are achieved with **C1-Zr₂** compared to ethylene-bridged **C2-Zr₂** (see scheme). With MAO as the cocatalyst, approximately 600 fold increases in polyethylene (PE) molecular weight are

achieved with **C2-Zr₂Cl₄** and **C1-Zr₂Cl₄** compared to a mononuclear analogue. These results support the argument that Zr-Zr proximity significantly influences chain-transfer rates, and such effects are highly cocatalyst-sensitive.

A core with corners: The first alumoxane containing an $\{Al_4O_2\}$ core as well as a gallium congener with an $\{Al_2Ga_2O_2\}$ core are prepared by the reaction of an organo-aluminum monohydroxide with $MH_3 \cdot NMe_3$ (see formula; $M = Al, Ga$; $Ar = 2,6\text{-}iPr_2C_6H_3$). These compounds contain reactive hydride groups on the central M_2O_2 rings and methyl groups on the terminal aluminum atoms.

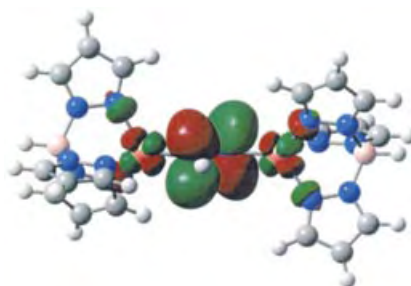


Al and Ga Compounds

S. Singh, S. S. Kumar, V. Chandrasekhar, H.-J. Ahn, M. Biadene, H. W. Roesky,* N. S. Hosmane, M. Noltemeyer, H.-G. Schmidt _____ **4940–4943**

Tetranuclear Homo- and Heteroalumoxanes Containing Reactive Functional Groups: Syntheses and X-ray Crystal Structures of $[\{[LAl(Me)](\mu-O)(MH_2)\}_2]$

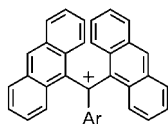
A strong antibonding π interaction has been shown by density functional calculations (see LUMO MO graph) to be a key characteristic of two new Cu^I -diazene complexes with hydrotris(pyrazolyl)borate ligands. The complexes have been further characterized by X-ray crystallography as well as 1H NMR, UV/Vis absorption, IR, far-IR, and resonance Raman spectroscopy.



Binuclear Complexes

K. Fujisawa,* N. Lehnert,* Y. Ishikawa, K.-i. Okamoto _____ **4944–4947**

Diazene Complexes of Copper: Synthesis, Spectroscopic Analysis, and Electronic Structure



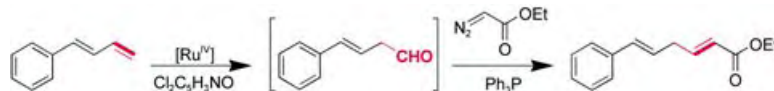
The highly crowded arylbis(9-anthryl)methyl cations (structure shown) have now been prepared. Their stability is due to the

doubly benzo-annelated structure of anthracene, which prevents Nazarov-type cyclization from taking place. The most remarkable feature of these cations is that they exhibit strong absorptions in the near-infrared region ($\lambda_{max} = 855\text{--}946\text{ nm}$) in trifluoroacetic acid. $Ar = p\text{-anisyl, 1-naphthyl, 2-naphthyl, phenyl, } p\text{-tolyl}$.

Hydrocarbon Cations

Y. Nishimae, H. Kurata, M. Oda* _____ **4947–4950**

Arylbis(9-anthryl)methyl Cations: Highly Crowded, Near Infrared Light Absorbing Hydrocarbon Cations



Aldehydes in excellent yields were obtained from the ruthenium-porphyrin-catalyzed oxidation of various terminal alkenes with 2,6-dichloropyridine *N*-oxide under mild conditions. The aldehydes generated from these ruthenium-cata-

lyzed alkene oxidations can be used in situ for olefination reactions with ethyl diazoacetate in the presence of PPh_3 in a one-pot diazoacetate olefination starting from alkenes (see example).

Alkene Oxidation

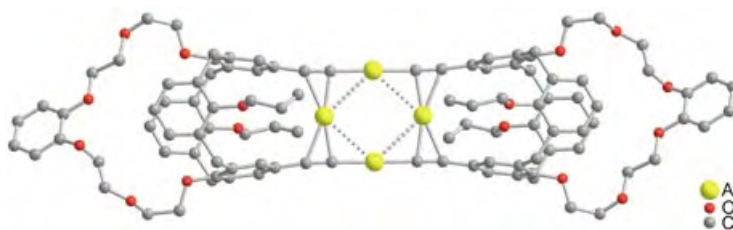
J. Chen, C.-M. Che* _____ **4950–4954**

A Practical and Mild Method for the Highly Selective Conversion of Terminal Alkenes into Aldehydes through Epoxidation–Isomerization with Ruthenium(IV)–Porphyrin Catalysts

Cluster Compounds

S.-K. Yip, E. C.-C. Cheng, L.-H. Yuan,
N. Zhu, V. W.-W. Yam* — 4954–4957

Supramolecular Assembly of Luminescent
Gold(I) Alkynylcalix[4]crown-6 Complexes
with Planar η^2, η^2 -Coordinated Gold(I)
Centers



Au...Au interactions between the gold(I)
centers arranged in a planar rhomboidal
array in a novel class of luminescent
tetranuclear gold(I) alkynylcalix[4]crown-6

complexes (see picture) give rise to rich
luminescence behavior, with long-lived
excited states and relatively high lumi-
nescence quantum yields.



Communications labeled with this symbol have been judged by two referees as being “very important papers”.

The issues for September 2004 appeared online on the following dates:
Issue 33: August 13 • Issue 34: August 25 • Issue 35: September 1 • Issue 36: September 7

Sources

Product and Company Directory

You can start the entry for your company in “Sources” in any issue of
Angewandte Chemie.

If you would like more information, please do not hesitate to contact us.

Wiley-VCH Verlag – Advertising Department

Tel.: ☎ 62 01 - 60 65 65

Fax: ☎ 62 01 - 60 65 50

E-Mail: MSchulz@wiley-vch.de

Service

Keywords 4958

Authors 4959

Angewandte's
Sister Journals 4960–4961

Sources A61

Preview 4963

Corrigendum

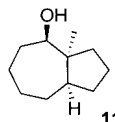
Pd^{II}- and Pt^{II}-Mediated Polycyclization Reactions of 1,5- and 1,6-Dienes: Evidence in Support of Carbocation Intermediates

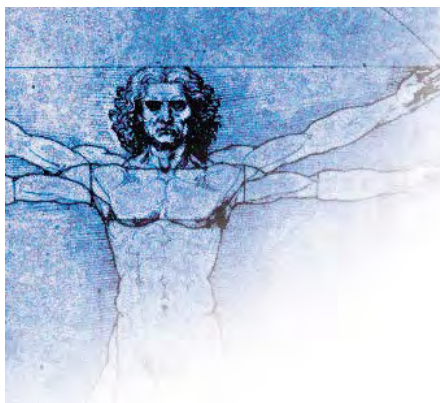
J. H. Koh, M. R. Gagné*

Angew. Chem. **2004**, 116, 3541–3543

DOI 10.1002/ange.200453913

The relative stereochemistry of compound **11** was drawn incorrectly in the published article. The correct structure (depicted) is epimeric at the carbinol center, an assignment that was supported by an NOE cross-signal between the carbinol hydrogen atom and the angular methyl group in the NOESY spectrum. The authors apologize for the oversight and any confusion it may have caused.





M. Mayor and Team Receive E. Schrödinger Prize



M. Mayor

The Erwin Schrödinger Prize is awarded annually in recognition of outstanding scientific or technically innovative achievements in interdisciplinary research. Members of the Helmholtz Association (made up of 15 major publicly funded research institutions in Germany) must be involved in the research. This year the prize goes to a team from the Institut für Nanotechnologie of the Forschungszentrum Karlsruhe (Germany): Marcel Mayor and Frank Hennrich (chemistry), as well as Ralph Krupke and Heiko Weber (physics).

Mayor completed his PhD in 1995 on vitamin B₁₂ derivatives at the Universität Bern (Switzerland) under the guidance of R. Scheffold and L. Walder. He then moved to the Université Louis Pasteur in Strasbourg, at first to undertake postdoctoral research with Jean-Marie Lehn on the design and synthesis of cryptatium compounds, and later to the Collège de France in Paris. Since 1998 he has led a research group at the Institut für Nanotechnologie in Karlsruhe. His research is focused on correlations between the chemical structure and electron-transport properties of molecules, supramolecular assemblies, and nanostructures, and on nanoscale objects with tailored physical properties. The prize was awarded in particular for interdisciplinary work on the separation of carbon nanotubes and electron transport through single molecules.^[1]

W. Tolman Receives Humboldt Prize



W. Tolman

William B. Tolman studied chemistry at Wesleyan University in Middletown, CT (USA) and completed his PhD in 1987 with K. P. C. Vollhardt at the University of California, Berkeley. He then undertook postdoctoral research with

S. J. Lippard at the Massachusetts Institute of Technology. His independent career, which began in 1990 at the University of Minnesota in Minneapolis, included a spell as a visiting professor in Berkeley in the research group of Judith Klinman. Now, as the recipient of an Alexander von Humboldt Prize, he will spend a year as a guest in the research group of W. A. Herrmann at the Technische Universität München.

Tolman's research, which encompasses synthetic bioinorganic chemistry, as well as organometallic and polymer chemistry, is focused on reaction mechanisms at active centers of metalloproteins and complexes of N-donor ligands that function as catalysts for the polymerization of cyclic esters. In München he intends to devote himself in particular to the development of catalysts for the synthesis of biodegradable polymers derived from renewable resources. In 2002 he co-authored a Review in *Angewandte Chemie* together with L. Que on biocatalytically relevant rhombic bis(μ -oxo)dimetal cores in copper and iron complexes.^[2]

Solvay Prize to S. Alvarez

Santiago Alvarez Reverter (University of Barcelona) received the 2003 Solvay Prize for Research in Chemical Sciences, awarded by a foundation of Spanish industrial companies, for "his contributions to the development of theoretical models for the study of a large number of chemical phenomena, in particular in molecular and nonmolecular solids". These quantum-chemical studies pertain

to the structure and symmetry of inorganic materials, in particular of molecular magnets. The award of this prize to Alvarez reflects the growing importance of quantum chemistry for industrial research.



S. Alvarez

Alvarez studied chemistry at the University of Barcelona and completed his PhD in 1980 on normal vibrations of sulfur oxyanions. He undertook postdoctoral research with R. Hoffmann at Cornell University (Ithaca, USA) and

has been a visiting scientist in the USA, France, Chile, and Israel. In 1989, he became professor at the University of Barcelona, where his research interests include molecular magnetism, electronic structure and bonding in solids and strained molecules, supramolecular inorganic chemistry, surfaces, metal-metal interactions, coordination chemistry, and bioinorganic chemistry. He recently reported on intermolecular Cu^I-Cu^I interactions^[3a] and on the stereochemistry of tetracoordinate transition-metal complexes^[3b] in *Chemistry—A European Journal*.

- [1] M. Mayor, H. B. Weber, J. Reichert, M. Elbing, C. von Hänisch, D. Beckmann, M. Fischer, *Angew. Chem.* **2003**, *115*, 6014; *Angew. Chem. Int. Ed.* **2003**, *42*, 5834.
- [2] a) L. Que, W. B. Tolman, *Angew. Chem.* **2002**, *114*, 1160; *Angew. Chem. Int. Ed.* **2002**, *41*, 1114; b) L. Que, W. B. Tolman, *Angew. Chem.* **2002**, *114*, 1900; *Angew. Chem. Int. Ed.* **2002**, *41*, 1821.
- [3] a) M. A. Carvajal, S. Alvarez, J. J. Novoa, *Chem. Eur. J.* **2004**, *10*, 2117; b) J. Cirera, P. Alemany, S. Alvarez, *Chem. Eur. J.* **2004**, *10*, 190.

On the Way to “Solid Nitrogen” at Normal Temperature and Pressure? Binary Azides of Heavier Group 15 and 16 Elements**

Carsten Knapp and Jack Passmore*

Keywords:

azides · Group 15 elements · hazardous materials · high-energy materials · polynitrogen compounds · selenium · tellurium

The first synthesis of a covalent azide HN_3 was reported by Curtius more than 100 years ago.^[1] However, the chemistry of coordinated azides received little attention until the early 1960s presumably because of their explosive nature and shock sensitivity. Today the high potential energy content of these compounds is the driving force to synthesize new and even more endothermic compounds that nevertheless have some kinetic stability. The relatively stable azide anion (**I**) contains two double bonds, but the covalent-bonded azides (**II**) are polarized towards structures containing a single and a triple bond, which facilitate the elimination of dinitrogen.^[2]



Every azido group adds about 70 kcal mol^{-1} to the energy content of the molecule, and so the synthesis of molecules with a high number of azido groups is a useful but challenging way to synthesize high-energy materials.

Azidometalates in salts containing large counter cations (e.g. $[\text{EPh}_4]^+$, $\text{E} = \text{P}, \text{As}$) and multiple azido groups can often be stabilized and safely handled.^[3d] The salt is stabilized by its crystal lattice enthalpy, and the dissociation energy into highly unstable covalent species by N_3^- transfer is minimized with large non-electrophilic counterions. In addition the activation energy barrier of the decomposition may be raised by separation of the azido groups with large counterions (dilution effect). Therefore the covalent azides incorporated into a salt containing large ions were often characterized prior to the corresponding neutral species. If there is an electronegativity difference between M and the azido group in the formally covalent $\text{M}-(\text{N}_3)$ bond, then the molecule will be stabilized by ionic resonance. However the $\text{M}-(\text{N}_3)$ bond will be particularly weak where M is large and the electronegativities are similar.^[4] Neutral covalent azides can be stabilized by adduct formation with a Lewis base (e. g. pyridine), which results in surprisingly thermally stable compounds, as was successfully shown for azides of Group 13^[3f] and 14.^[13a] Thus despite many difficulties, many fascinating inorganic azides have been prepared and structurally characterized over the last decades.^[3]

Klapötke and co-workers as well as Christe and co-workers have made some very significant advances in the field of highly energetic polynitrogen compounds. Christe's group discovered the novel N_5^+ ion,^[5] and Klapötke's group synthesized and characterized a number

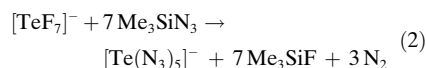
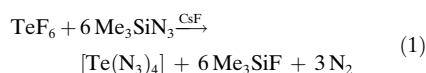
of main group azides.^[3b-e] One of last highlights in this race was the back-to-back publication of the syntheses and structure determinations of the first neutral and anionic binary tellurium azides.^[6]

This is remarkable, because binary tellurium–nitrogen compounds and homoleptic azides of Group 16 are rare. For many years the only structurally characterized binary tellurium azide was ionic lattice stabilized $[\text{Te}(\text{N}_3)_3][\text{SbF}_6]$ containing $[\text{Te}(\text{N}_3)_3]^+$,^[7] except for the few reports on extremely labile tellurium nitrides. The chemistry of tellurium azides commenced in 1972 with the synthesis of $\text{TeCl}_3(\text{N}_3)$ and $\text{TeCl}_2(\text{N}_3)_2$ by the reaction of TeCl_4 with Me_3SiN_3 by Wiberg and co-workers.^[8] Wiberg et al. predicted that TeF_4 would react with Me_3SiN_3 to give $[\text{Te}(\text{N}_3)_4]$ in a straightforward reaction, but at the same time warned of the likely potential explosive nature of the product.

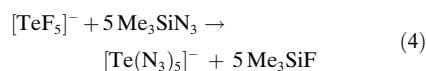
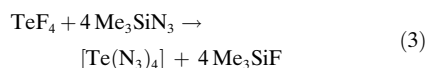
The first structurally characterized neutral azides containing tellurium were the organotellurium(IV) di- and triazides prepared by the reactions of organotellurium fluorides with Me_3SiN_3 .^[9] Ludman et al. investigated the system $\text{TeF}_6/\text{Me}_3\text{SiN}_3$ by ^{19}F NMR spectroscopy and found all members of the $\text{TeF}_n(\text{N}_3)_{6-n}$ ($n = 1-5$) series as well as partial reduction of Te^{VI} to Te^{IV} mediated by the azide ion.^[10] This fact was used by Christe et al. in their preparations of $[\text{Te}(\text{N}_3)_5]^-$ and $[\text{Te}(\text{N}_3)_4]$ starting from TeF_6 and $[\text{TeF}_7]^-$, respectively, and Me_3SiN_3 ; the fluoride–azide exchange and reduction occurred in one step [Eq. (1) and (2)].^[6b]

[*] Dr. C. Knapp, Prof. Dr. J. Passmore
Department of Chemistry
University of New Brunswick
Fredericton, NB, E3B 6E2 (Canada)
Fax: (+1) 506-453-4981
E-mail: passmore@unb.ca

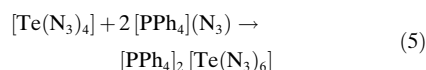
[**] Financial support by the Alexander von Humboldt foundation for a Feodor-Lynen fellowship (C.K.) is gratefully acknowledged.



Similar results were obtained by Klapötke et al. following the route suggested by Wiberg starting directly from the tellurium(IV) fluorides [Eq. (3) and (4)].^[6a]



The reaction of $[\text{Te}(\text{N}_3)_4]$ with $[\text{PPh}_4](\text{N}_3)$ led to the formation of the dianion $[\text{Te}(\text{N}_3)_6]^{2-}$ [Eq. (5)].^[6b]



The ionic, lattice-stabilized tellurium azides are relatively stable, whereas the neutral $[\text{Te}(\text{N}_3)_4]$ is very sensitive and can explode under various conditions.^[6]

These reactions appear to be very simple, however very special experimental knowledge and expertise is necessary to do chemistry of this kind.^[11] Potential safety hazards are reduced by preparing very small amounts of material and by the skilful use of various analytical tools (multinuclear NMR, Raman, and IR spectroscopy). The more stable ionic species were also characterized by single-crystal X-ray diffraction, whereas the complete structural determination of the neutral $[\text{Te}(\text{N}_3)_4]$ remains a challenge.

In all three known binary tellurium azide structures the free electron pair is sterically active. $[\text{Te}(\text{N}_3)_3]^+$ has a pseudo-tetrahedral AX_3E structure,^[7] and $[\text{Te}(\text{N}_3)_5]^-$ (Figure 1a), one of only two examples of a pentacoordinate azido species,^[12] has a pseudo-octahedral AX_5E geometry.^[6a] The free electron pair is sterically active (AX_6E) even in $[\text{Te}(\text{N}_3)_6]^{2-}$ (Figure 1b) and distorts the geometry from ideal S_6 symmetry,^[6b] which is found in the Group 14 azido AX_6 metalates $[\text{M}(\text{N}_3)_6]^{2-}$ ($\text{M} = \text{Si}, \text{Ge}$).^[13] Therefore all three tellurium

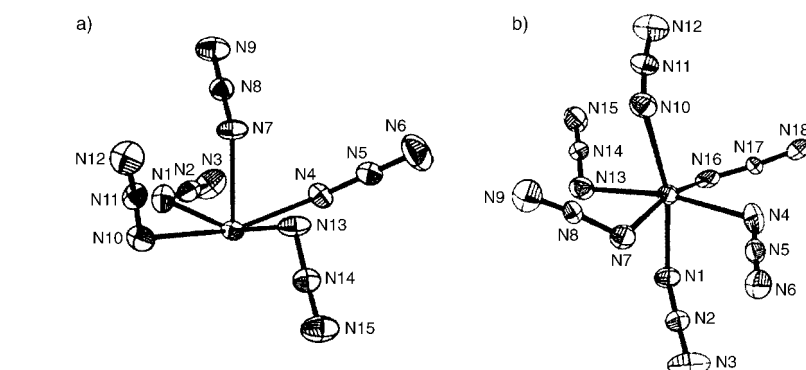


Figure 1. Structure of a) the $[\text{Te}(\text{N}_3)_5]^-$ (intermolecular Te–N interactions between $[\text{Te}(\text{N}_3)_5]^-$ are not shown) ion and b) the $[\text{Te}(\text{N}_3)_6]^{2-}$ ions.^[6]

ions have geometries in agreement with a simple VSEPR model. The as yet experimentally unknown structure of $[\text{Te}(\text{N}_3)_4]$, is predicted by theoretical calculations to have an AX_4E type structure like SF_4 , with two isomers having energies differing only by $1.8 \text{ kcal mol}^{-1}$ (Figure 2).^[6b]

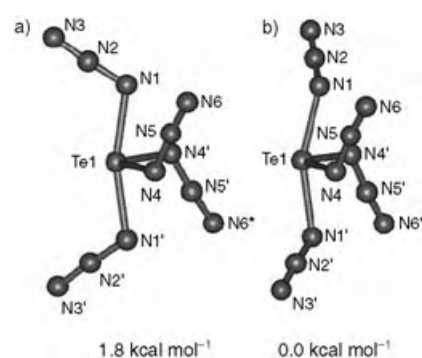


Figure 2. Calculated minimum-energy structures of $[\text{Te}(\text{N}_3)_4]$.^[6b]

Similar binary azides of the lighter homologues selenium and sulfur are still unknown. Over 30 years ago Wiberg et al. reacted SCl_4 and SeCl_4 with Me_3SiN_3 and observed the reduction of the chalcogen chlorides.^[8] Two years ago the first ionic selenonium azide $[\text{R}_3\text{Se}](\text{N}_3)$ ($\text{R} = \text{H}_3\text{C}, \text{C}_6\text{H}_5$) was prepared by the reaction of $[\text{R}_3\text{Se}]\text{I}$ with AgN_3 .^[14] Very recently the first covalent selenium azide 2- $\text{Me}_2\text{NCH}_2\text{C}_6\text{H}_4\text{Se}(\text{N}_3)$ was synthesized and structurally characterized.^[15] The latter compound is stabilized by an intramolecular dative bond formed by donation of the nitrogen lone pair into the σ^* orbital of the Se–N bond, which inhibits the elimination of dini-

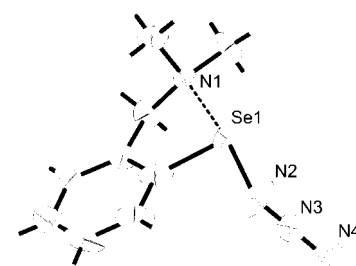


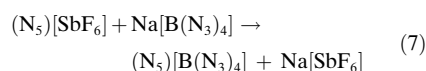
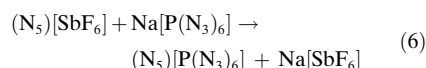
Figure 3. The structure of the azide 2- $\text{Me}_2\text{NCH}_2\text{C}_6\text{H}_4\text{Se}(\text{N}_3)$ stabilized by an intramolecular dative bond.^[15]

trogen and the formation of the corresponding stable diselenane (Figure 3).

In contrast, the binary azides of phosphorus ($[\text{P}(\text{N}_3)_3]$, $[\text{P}(\text{N}_3)_4]^+$, $[\text{P}(\text{N}_3)_5]$, $[\text{P}(\text{N}_3)_6]^-$) were prepared before the azides of the heavier homologues arsenic and antimony, although the crystal structures of the binary phosphorus azides are still to be determined.^[16] The ionic arsenic azide salts containing $[\text{As}(\text{N}_3)_4]^-$, $[\text{As}(\text{N}_3)_4]^+$, and $[\text{As}(\text{N}_3)_6]^-$ are stabilized by their corresponding lattice energies and the factors referred to in the introduction.^[17] The neutral arsenic and antimony azides are similar to the neutral tellurium azides but are much more explosive; however, they are stabilized by forming donor–acceptor adducts. This allows the isolation of the binary arsenic and antimony azides in the oxidation state +5 as Lewis base adducts $[\text{E}(\text{N}_3)_5]\text{LB}$ ($\text{E} = \text{As}, \text{Sb}$; $\text{LB} = \text{Lewis base}$, for example, py). The free azides $[\text{E}(\text{N}_3)_5]$ can be handled safely in solution, but could not be isolated even at -70°C .^[17b,18] Very recently the structures of the less explosive binary As^{III} and Sb^{III} azides have been determined.^[19] Both have AX_3E

geometries in which the free valence electron pair is sterically active and the structure of $[\text{Sb}(\text{N}_3)_3]$ (isoelectronic to $[\text{Te}(\text{N}_3)_3]^+$)^[7] presents an example of perfect C_3 symmetry.

Computational chemistry has become a valuable tool in evaluating the stability of compounds with high nitrogen content especially for neutral compounds where lattice enthalpies and solvation energies are not applicable or small.^[20] Recent theoretical (including estimates of lattice enthalpies) and experimental studies have shown that the very high energy density ionic forms of elemental nitrogen $(\text{N}_5)^+(\text{N}_3)^-(s)$ and $(\text{N}_5)^-(\text{N}_3)^+(s)$ will very likely never be prepared.^[21,22] However very recently Christe et al. were able to combine the N_5^+ ion with homoleptic azide anions by metathesis reactions according to Equations (6) and (7).^[23]



The phosphorus compound $(\text{N}_5)[\text{P}(\text{N}_3)_6]$ contains 23 nitrogen atoms and has a nitrogen content of 91 wt %. In the corresponding boron compound $(\text{N}_5)[\text{B}(\text{N}_3)_4]$ the nitrogen content is even higher (95.7 wt %). Both compounds are extremely sensitive and explode upon the slightest provocation.

These recent developments show that some of the most outrageous compounds imaginable can be prepared and characterized. We anticipate that in the next few years many other thermodynamically unstable and increasingly marginally kinetically unstable simple species with even greater nitrogen content will be isolated and characterized as real compounds that can be seen and weighed, and not just observed as images on a computer screen.

Published Online: August 20, 2004

- [1] T. Curtius, *Berichte* **1890**, 23, 3023–3033.
 [2] The increase in N–N bond energies (N–N: 40 kcal mol^{−1}; N=N: 100 kcal mol^{−1}; N≡N: 225 kcal mol^{−1}) with a higher bond order favors the disproportion and forming of multiple bonds (bond energies are

- taken from J. E. Huheey, E. A. Keiter, R. L. Keiter, *Inorganic Chemistry*, HarperCollins, New York, **1993**.)
 [3] a) Z. Dori, R. F. Ziolo, *Chem. Rev.* **1973**, 73, 247–254; b) I. C. Tornieporth-Oetting, T. M. Klapötke, *Angew. Chem.* **1995**, 107, 559–568; *Angew. Chem. Int. Ed. Engl.* **1995**, 34, 511–520; c) T. M. Klapötke, *Chem. Ber.* **1997**, 130, 443–451; d) A. Kornath, *Angew. Chem.* **2001**, 113, 3231–3232; *Angew. Chem. Int. Ed.* **2001**, 40, 3135–3136; e) W. Fraenk, T. M. Klapötke in *Inorganic Chemistry Highlights* (Eds.: G. Meyer, D. Naumann, L. Wesemann), Wiley-VCH, Weinheim, **2002**; f) J. Müller, *Coord. Chem. Rev.* **2002**, 235, 105–119.
 [4] The Pauling electronegativity of the azide group was estimated as $\chi_{(\text{N}_3)^-} = 2.95$ (A. F. Clifford, *J. Phys. Chem.* **1959**, 63, 1227–1231). The Pauling electronegativities of selected elements ($\chi_{\text{As}} = 2.18$, $\chi_{\text{Sb}} = 2.05$, $\chi_{\text{Se}} = 2.55$ and $\chi_{\text{Te}} = 2.1$) are taken from reference [2].
 [5] a) K. O. Christe, W. W. Wilson, J. A. Sheehy, J. A. Boatz, *Angew. Chem.* **1999**, 111, 2112–2118; *Angew. Chem. Int. Ed.* **1999**, 38, 2004–2009; b) A. Vij, J. W. W. Wilson, V. Vij, F. S. Tham, J. A. Sheehy, K. O. Christe, *J. Am. Chem. Soc.* **2001**, 123, 6308.
 [6] a) T. M. Klapötke, B. Krumm, P. Mayer, I. Schwab, *Angew. Chem.* **2003**, 115, 6024–6026; *Angew. Chem. Int. Ed.* **2003**, 42, 5843–5846; b) R. Haiges, J. A. Boatz, A. Vij, M. Gerken, S. Schneider, T. Schroer, K. O. Christe, *Angew. Chem.* **2003**, 115, 6027–6031; *Angew. Chem. Int. Ed.* **2003**, 42, 5847–5851.
 [7] J. P. Johnson, G. K. MacLean, J. Passmore, P. S. White, *Can. J. Chem.* **1989**, 67, 1687–1692.
 [8] N. Wiberg, G. Schwenk, K. H. Schmid, *Chem. Ber.* **1972**, 105, 1209–1215.
 [9] a) T. M. Klapötke, B. Krumm, P. Mayer, O. P. Ruscitti, *Inorg. Chem.* **2000**, 39, 5426–5427; b) T. M. Klapötke, B. Krumm, P. Mayer, H. Piotrowski, O. P. Ruscitti, A. Schiller, *Inorg. Chem.* **2002**, 41, 1184–1193.
 [10] I. B. Gorrell, C. J. Ludman, R. S. Matthews, *J. Chem. Soc. Dalton Trans.* **1992**, 2899–2903.
 [11] Covalent azides can decompose explosively and unexpectedly under various conditions. They should be handled only in very small scales and with appropriate safety equipment (thick leather or Kevlar gloves, face shield and protective clothing as leather jackets) and with methods and techniques appropriate to explosives.
 [12] J. Drummond, J. S. Wood, *J. Chem. Soc. Chem. Commun.* **1969**, 1373.
 [13] a) A. C. Filippou, P. Portius, D. U. Neumann, K.-D. Wehrstedt, *Angew. Chem.* **2000**, 112, 4524–4527; *Angew. Chem. Int. Ed.* **2000**, 39, 4333–4336; b) A. C. Filippou, P. Portius, G. Schnakenberg, *J. Am. Chem. Soc.* **2002**, 124, 12396–12397.
 [14] T. M. Klapötke, B. Krumm, P. Mayer, H. Piotrowski, K. Polborn, I. Schwab, *Z. Anorg. Allg. Chem.* **2002**, 628, 1831–1834.
 [15] T. M. Klapötke, B. Krumm, K. Polborn, *J. Am. Chem. Soc.* **2004**, 126, 710–711.
 [16] a) H. W. Roesky, *Angew. Chem.* **1967**, 79, 651; *Angew. Chem. Int. Ed. Engl.* **1967**, 6, 637; b) W. Buder, A. Schmidt, *Z. Anorg. Allg. Chem.* **1975**, 415, 263–267.
 [17] a) T. M. Klapötke, H. Nöth, T. Schütt, M. Warchhold, *Angew. Chem.* **2000**, 112, 2197–2199; *Angew. Chem. Int. Ed.* **2000**, 39, 2108–2109; b) K. Karaghiosoff, T. M. Klapötke, B. Krumm, H. Nöth, T. Schütt, M. Suter, *Inorg. Chem.* **2002**, 41, 170–179.
 [18] T. M. Klapötke, T. Schütt, *J. Fluorine Chem.* **2001**, 109, 151–162.
 [19] R. Haiges, A. Vij, J. A. Boatz, S. Schneider, T. Schroer, M. Gerken, K. O. Christe, *Chem. Eur. J.* **2004**, 10, 508–517.
 [20] For example, a theoretical study^[20a] predicted the homoleptic azides $[\text{M}(\text{N}_3)_4]$ (M = Ti, Zr, Hf) of Group 4 ($[\text{Ti}(\text{N}_3)_4]$ was prepared recently)^[20b] to be stable with respect to the formation of M and 6 N_2 , whereas the isomers with the formula $(\text{N}_3)[\text{MN}_7]$ will not be stable.^[20c] a) L. Gagliardi, P. Pyykkö, *Inorg. Chem.* **2003**, 42, 3074–3078; b) R. Haiges, J. A. Boatz, S. Schneider, T. Schroer, M. Yousufuddin, K. O. Christe, *Angew. Chem.* **2004**, 116, 3210–3214; *Angew. Chem. Int. Ed.* **2004**, 43, 3148–3152; c) L. Gagliardi, P. Pyykkö, *J. Phys. Chem. A* **2002**, 106, 4690–4694.
 [21] Evidence for N_5^- coordinated to Zn^{2+} in solution has been given based on ¹⁵N NMR spectroscopy,^[21a] and computational evidence implies that the gas-phase stability of some pentazolides were equal to or higher than the stability of the experimentally known phenylpentazole.^[21b] a) R. N. Butler, J. C. Stephens, L. A. Burke, *Chem. Commun.* **2003**, 1016–1017; b) M. Straka, P. Pyykkö, *Inorg. Chem.* **2003**, 42, 8241–8249.
 [22] D. A. Dixon, D. Feller, K. O. Christe, W. W. Wilson, A. Vij, V. Vij, H. D. B. Jenkins, R. M. Olson, M. S. Gordon, *J. Am. Chem. Soc.* **2004**, 126, 834–843.
 [23] R. Haiges, S. Schneider, T. Schroer, K. O. Christe, *Angew. Chem.* **2004**, 116, 5027; *Angew. Chem. Int. Ed.* **2004**, 43, 4919.

Elisabethin A: A Marine Diterpenoid Yet To Surrender to Total Synthesis**

Giuseppe Zanoni* and Maurizio Franzini

Keywords:

biomimetic synthesis · Diels–Alder reaction · secondary metabolites · terpenoids · total synthesis

Gorgonian corals have attracted considerable attention as a result of their wealth of bioactive secondary metabolites, such as acetogenins, sesquiterpenoids, diterpenoids, prostanoids, and steroids. Specifically, the West Indian sea whip *Pseudopterogorgia elisabethae*, collected in deep waters near San Andrés Island (Colombia), has been a goldmine for novel diterpenoids with rare carbon-skeleton architectures. Elisabethanes stand out among these diterpenoids for their interesting anti-inflammatory, antibacterial, analgesic, and cytotoxic activities. The intricate structure of elisabethin A (**1**), a representative member of this family whose biological properties have not been fully investigated,^[1] constitutes a formidable syn-

thetic challenge for organic chemists. Its structure was elucidated by exhaustive spectroscopic studies and X-ray diffraction analysis, which did not allow the establishment of the absolute configuration of the natural compound.^[1] The tricyclic *cis,trans*-fused 5,6,6 ring system of elisabethin A embodies a fully substituted enedione functionality and six contiguous stereogenic centers, of which one, at the junction of the three rings, is quaternary. To date, only two research groups, those led by Mulzer^[2] and Rawal,^[3] have tackled the task of the total synthesis of this unusual molecule. For the reader's convenience, the absolute configuration of the final product described in Mulzer's work is tentatively assumed to be that of the natural product.

In Mulzer's approach, two stereogenic centers were established in a convergent fashion through the condensation of two chiral units (Scheme 1). The first of these units, iodide **2**, was prepared in five steps and 55% overall yield from the known aldehyde **3**,^[4] which was obtained in turn from (*S*)-(+)-3-hydroxy-2-methylpropionic acid methyl ester, an expensive commercially available nonnatural chiral-pool compound.^[5]

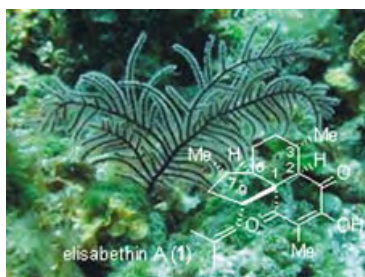
The dienyl system in iodide **2** was secured through a classical Horner–Wadsworth–Emmons reaction, followed by a salt-free Wittig ethenylation. The aromatic intermediate **4** was then assembled by means of a finicky diastereoselective alkylation of imide **5** (the second of the above-mentioned chiral units) with iodide **2**, followed by a straightforward four-step manipulation. Imide **5** was prepared from the com-

mercially available aldehyde **6** in 11 steps, the last of which consisted of a modified Evans oxazolidinone condensation with the mixed pivaloyl anhydride **7**. The product of the ensuing doubly stereodifferentiating alkylation was obtained with a satisfying 93:7 d.r. and in 69% yield after recycling of the starting material.

The other four contiguous stereogenic centers present in the natural product were installed by means of a unique Diels–Alder reaction performed on the quinoidal system **8**. After removal of the phenolic silyl ether protecting groups, an oxidation reaction promoted by aqueous ferric chloride afforded the desired cycloadduct via a transient quinonic intermediate. The surmised quinoidal system **8** was never isolated, but it was detected by TLC and by NMR spectroscopy. The subsequent intramolecular Diels–Alder (IMDA) reaction was monitored by TLC.

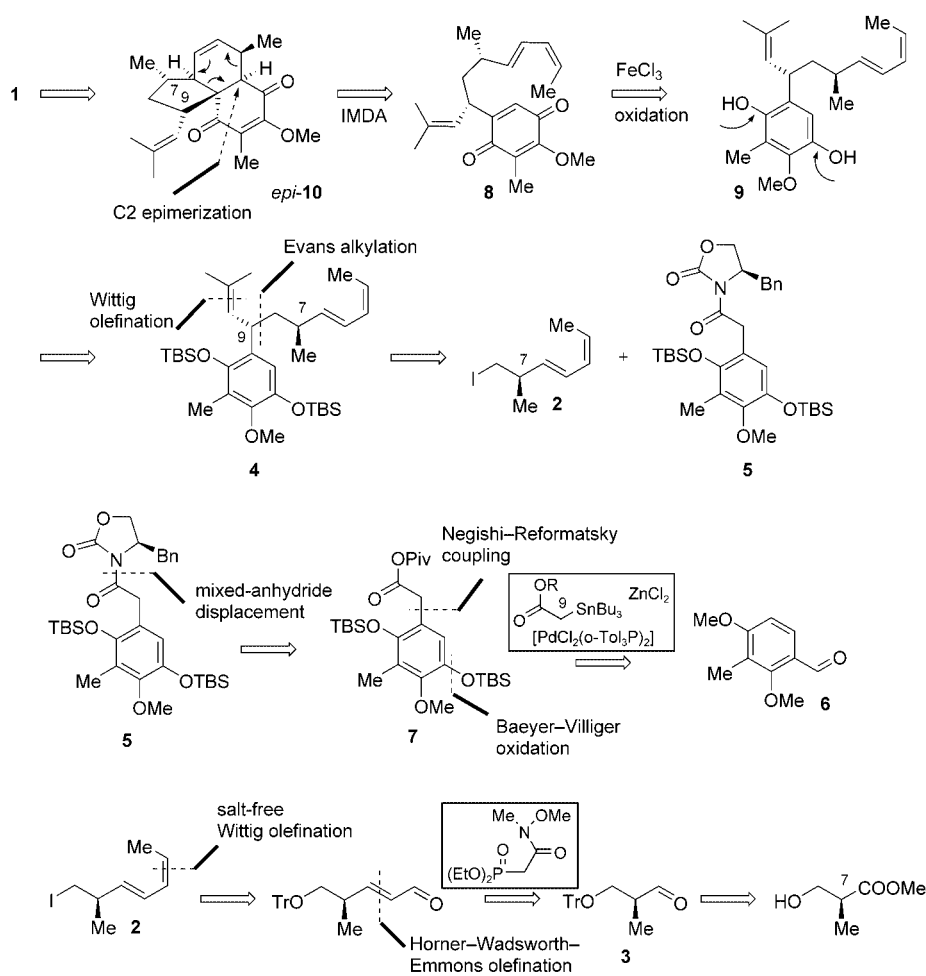
The comments of the authors about the IMDA reaction deserve additional mention. Although rare, there are indeed a few reported examples of the participation of acyclic terminal *Z* dienes in IMDA reactions.^[6] Because of their proclivity to preferentially undergo a thermally induced [1,5] H shift^[7] and/or thermal *Z* to *E* isomerization,^[8,6a] terminal *Z* dienes have been avoided in total synthesis. There are many more reports on failed attempts to carry out IMDA reactions with *E,Z* and *Z,Z* dienes than reports of successful cases.^[8a,9]

Secondly, the tenfold excess of iron chloride, employed as the oxidizing agent for hydroquinone **9**, might also act as a Lewis acid to catalyze the



[*] Dr. G. Zanoni
Dipartimento di Chimica Organica
Università di Pavia
Viale Taramelli, 10, 27100 Pavia (Italy)
Fax: (+39) 0382-507-323
E-mail: gzanoni@unipv.it
M. Franzini
Department of Chemistry
Stanford University
Stanford, CA 94305-5080 (USA)

[**] We thank Prof. Giovanni Vidari, Prof. Pierluigi Caramella, and Prof. Remo Gandolfi for helpful discussions.



Scheme 1. The Mulzer approach to elisabethin A. Bn = benzyl, TBS = *tert*-butyldimethylsilyl, Piv = pivaloyl, Tr = trityl.

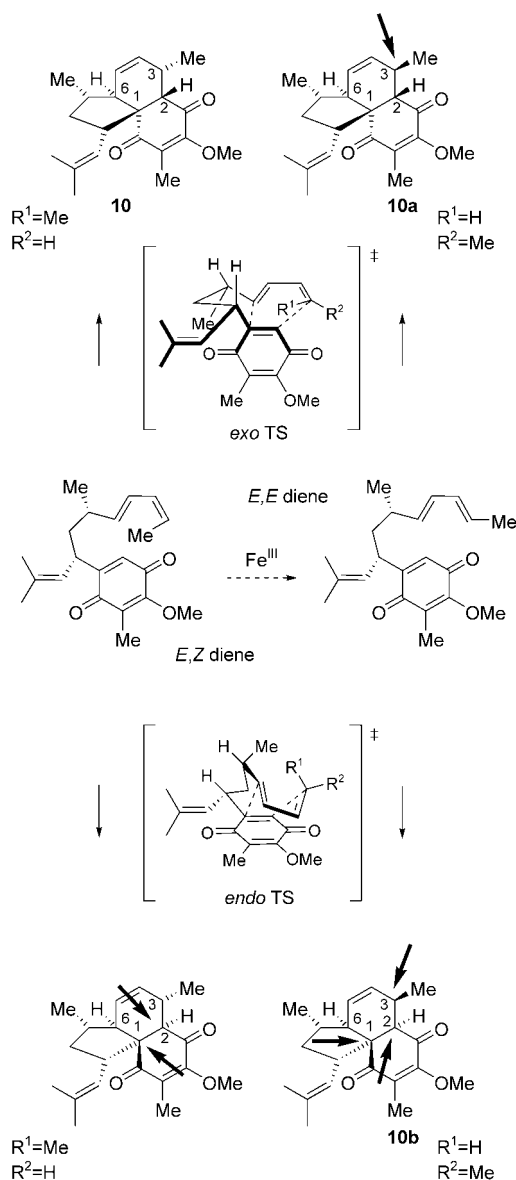
subsequent IMDA reaction through polarization of the carbonyl π bonds in the transient quinone.^[10] Moreover, the observed high substrate-dependent diastereoselectivity, as confirmed by the HPLC detection of less than 3% of an alleged minor epimer, would rule out the necessity for a Diels-Alderase in a hypothetical biosynthetic pathway to elisabethin A.^[11] Both of these points raise some reservations about the “virtually biomimetic” mode of this IMDA reaction, which was referred to in this way by the authors by virtue of the otherwise very mild reaction conditions (aqueous medium at room temperature).

The moot point in the synthesis described stems, however, from the proposed structure for the product of the cycloaddition, and therefore for the transition state leading to it. Although in principle an IMDA reaction can proceed through either an *exo* or an *endo* transition state (TS), the latter is known

to generally be highly preferred under conditions of Lewis acid catalysis, at low reaction temperatures, and in the presence of an electron-withdrawing group in close proximity to the dienophile.^[12,6b] Not only are these conditions met in this case, but minimization of the allylic strain between the isopropenyl group at C9 (elisabethin A numbering) and one of the quinone carbonyl groups would also favor an *endo* approach. Recent work on the IMDA reaction of masked *p*-benzoquinones generated in situ indeed showed that *endo* transition states largely prevail, almost independent of the substitution pattern of the dienyl unit.^[13]

Upon the realization that the initially proposed *endo* TS would give a different product from the obtained compound **10**, in a correction the authors proposed an *exo* TS ($R^1 = \text{Me}$, $R^2 = \text{H}$, Scheme 2) to account for the relative and absolute stereochemistry

assigned to compound **10**.^[14] Unfortunately, a cursory inspection of molecular models seems to hint at a lack of the required overlap and alignment of the HOMO/LUMO orbitals of the *E,Z* diene and quinoid dienophile, as a result of severe steric constraints. However, a *Z* to *E* isomerization of the terminal olefin could take place in the presence of the excess FeCl_3 ; Lewis acid mediated olefin isomerization reactions are well documented in the literature.^[15,12a] If such an isomerization was combined with an *exo* IMDA reaction ($R^1 = \text{H}$, $R^2 = \text{Me}$), the C3 epimer **10a** would clearly form (Scheme 2). Conversely, in a third, more plausible scenario, a *Z* to *E* isomerization in combination with an *endo* TS ($R^1 = \text{H}$, $R^2 = \text{Me}$) would lead to **10b**, with the opposite configuration at the three contiguous centers C1, C2, and C3 with respect to the purported cycloadduct (Scheme 2).

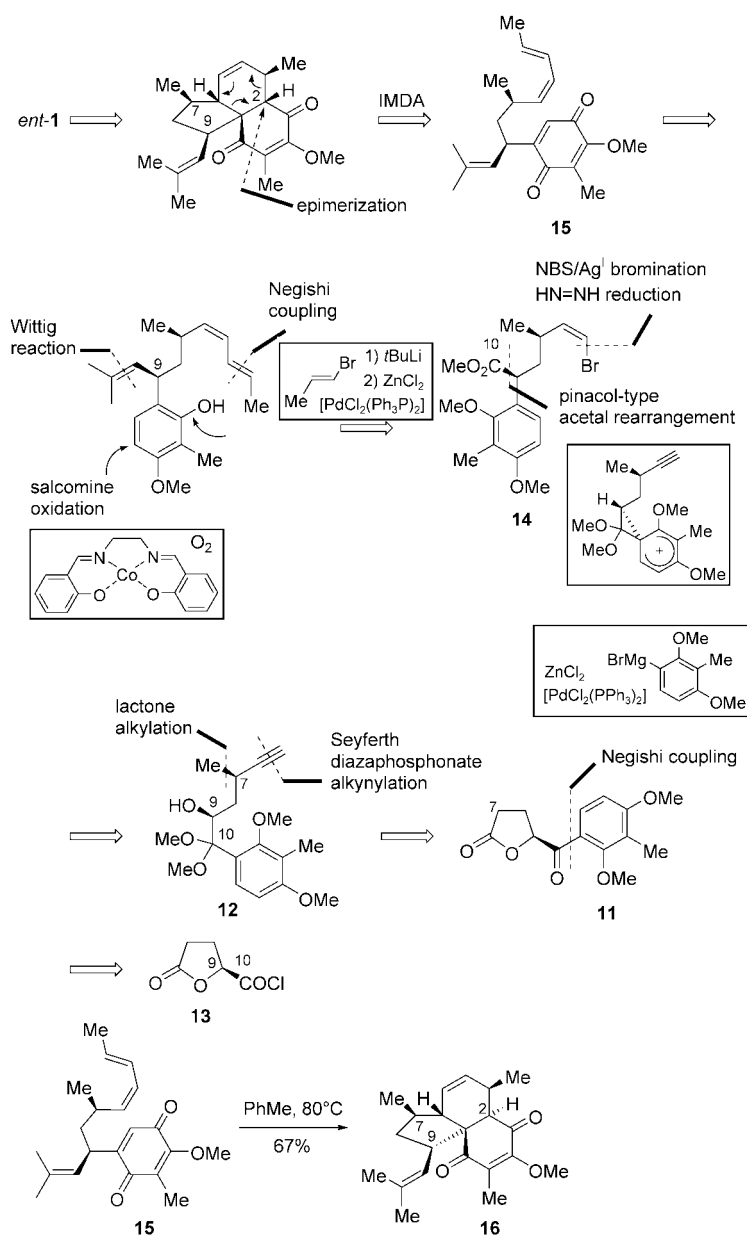


Despite the extensive NOESY spectroscopic studies reported, the correct structure for intermediate **10**, which was prepared in 16 linear steps and a remarkable 25% overall yield, can not be validated at this stage. Comparison of the ^{13}C NMR data of natural elisabethin A^[1] with those of the final synthetic product, obtained from **10** by hydrogenation of the C4–C5 endocyclic alkene, base-induced epimerization, and demethylation in modest overall yield, reveals several significant divergences in the chemical shifts (up to 0.5 ppm). Furthermore, the two ^1H NMR spectra are not completely superimposable. In light of the incongruities revealed by a

close examination of the work published by Rawal and discussed below in the spectroscopic and chemical characterization of the alleged common intermediate **10** (and its enantiomer), the identity of natural elisabethin A and of Mulzer's synthetic compound **1** can hardly be reaffirmed at this juncture.

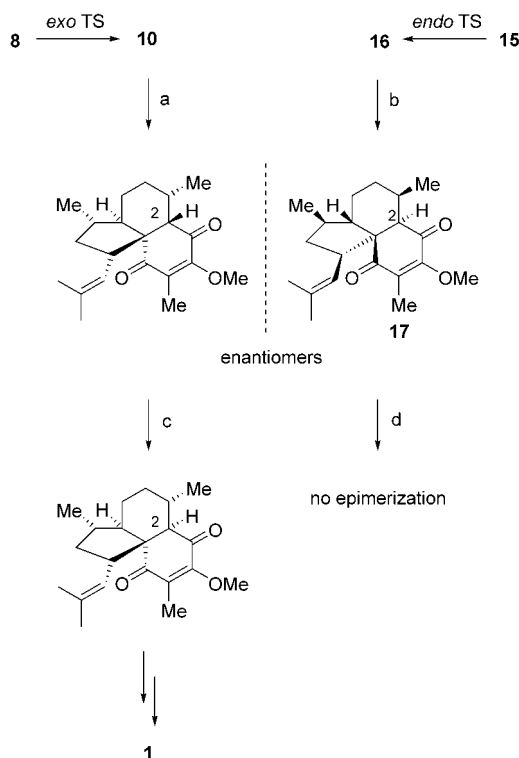
For the attempted total enantioselective synthesis of elisabethin A by Rawal and co-workers, L-pyrogutamic acid was selected from the

natural chiral pool as the initial source of chirality (Scheme 3). The construction of the other stereogenic centers was based on a sequence of internal asymmetric induction steps and a highly stereoselective chirality transfer step with quite a high degree of atom economy. The C7 stereogenic center was installed with a satisfying 8:1 d.r. by methylation of the enolate anion of lactone **11**, which was eventually converted into alkyne **12** through a one-carbon homologation. The configuration at C9 was established first through a Negishi coupling of acyl chloride **13**, followed later by a clever, underutilized



pinacol-like rearrangement to furnish the methyl ester intermediate **14**. The anchimeric assistance provided by the electron-rich aromatic counterpart in the migration dictates the overall retention of configuration observed at C9, which bears a methoxycarbonyl group in the product **14** as a precursor to the isopropenyl unit in the natural product. The *Z* bromovinyl group in **14** was readily elaborated from the terminal alkyne derived from alcohol **12**.

After constructing the *Z,E* dienyli moiety by means of a Negishi coupling of *Z*-bromoalkene **14** with (*E*)-1-bromopropene, Rawal and co-workers also relied on the high stereospecificity of an IMDA reaction to define the configuration of the remaining four stereogenic centers. The quinoidal functionality in **15**, the substrate for the IMDA addition, was formed in moderate yield by an O₂-induced oxidation catalyzed by salcomine. In the IMDA reaction, the *endo* TS, which avoids 1,3-allylic strain between the methyl group at C7 and the propenyl substituent on the *cis* double bond, delivered **16** as a single stereoisomer, whose carbon skeleton is epimeric at C2 with *ent*-elisabethin (*ent*-**1**).

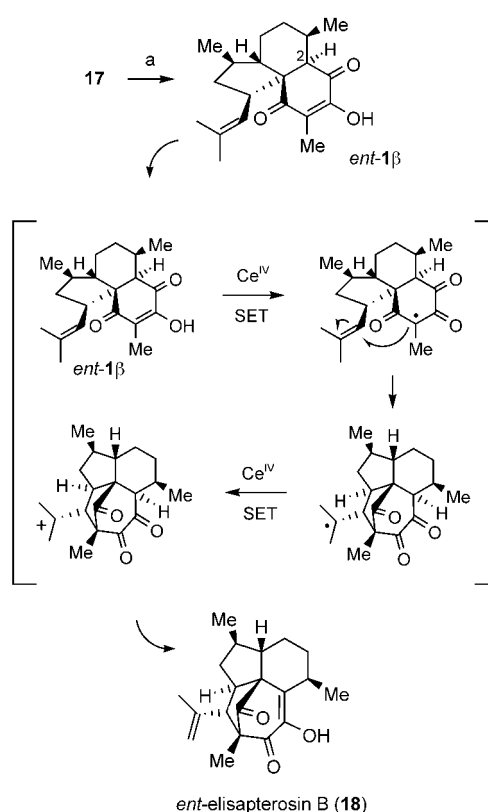


Scheme 4. a) Pd/C, H₂, EtOAc, room temperature, 1 h; b) Wilkinson catalyst, H₂; c) NaOH, MeOH/H₂O, 80°C, 5 h; d) NaOEt, EtOH, reflux.

Unfortunately, the synthesis of *ent*-elisabethin could not be completed. After the selective hydrogenation of **16** with the Wilkinson catalyst to form the tricyclic intermediate **17** (Scheme 4), which was obtained in a total of 16 linear steps and 1.7% overall yield, it was found that it was not possible to epimerize the C2 center under a variety of experimental conditions. Dreiding models seem to suggest that the C2–H bond is locked in an almost coplanar orientation with respect to the adjacent carbonyl group as a result of the rigidity of the polycyclic frame, in stereo-electronic misalignment for deprotonation.

The putative enantiomer of **17** prepared by Mulzer by the hydrogenation of **10**, however, underwent successful epimerization under basic aqueous conditions (Scheme 4). This discrepancy between the two alleged enantiomers can be attributed to inaccuracy in the stereochemical assignment of **10**, as alluded to above. The structure of the cycloadduct **16** was further confirmed by NOE studies reported by Rawal,^[3] and by chemical correlation after derivatization into *ent*-elisapterosin B,^[16] another natural diterpene of the same family, recently synthesized by Kim and Rychkovsky.^[17] The conversion of *ent*- β -elisabethin (*ent*-**1** β), formed by demethylation of **17**, into *ent*-elisapterosin **18** was inspired by a hypothetical biomimetic pathway. Thus, a Ce^{IV}-mediated oxidative cyclization was followed by base-induced tautomerization of the resulting diketone fragment. The former step probably proceeds by an oxidative single-electron transfer (SET) from *ent*-**1** β , which triggers the C–C bond formation (Scheme 5).^[18] Further oxidation by Ce^{IV} would generate the tertiary carbocation proposed by Rawal as an intermediate in his synthesis. Stereo-electronic constraints would favor deprotonation from one of the methyl groups, thus leading to the less substituted alkene as the product.

It would be premature to claim that a complete synthesis of elisabethin A has been achieved. Only X-ray diffrac-



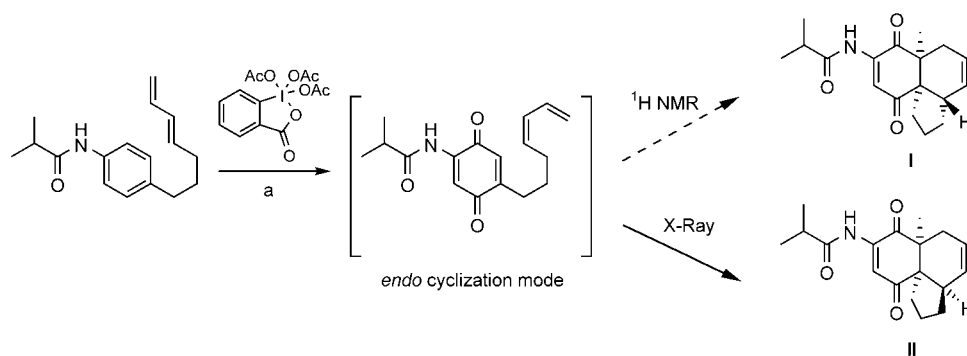
Scheme 5. a) 1. LiI, 2,6-lutidine, 80°C, 99%; 2. CAN, MeCN, 0°C, then pyridine, Et₃N, 50°C, 84%. CAN = (NH₄)₂Ce(NO₃)₆.

tion analysis of crystals of a key intermediate in Mulzer's route and the use of nonnatural D-pyrogutamic acid as chiral-pool source in Rawal's approach will defuse any remaining doubts about the structure of the synthetic elisabethin A and the absolute configuration of the natural product.

Cases of the incorrect assignment of the configuration of IMDA products are in fact known in the literature.^[19] For example, in a Communication on the preparation of the core carbon framework of elisabethin A by an IMDA reaction involving an *o*-imidoquinone,^[20] Nicolaou et al. initially assigned this unit the configuration **I** shown in Scheme 6. However, after the collection of crystallographic data, the same authors reassigned the configuration of this compound as **II** in a full paper a year later.^[13a]

In conclusion, further work is required before elisabethin A can be placed in the basket of natural products whose synthesis has been completed.

Published Online: September 3, 2004



Scheme 6. a) Dess–Martin periodinane (4.0 equiv), H₂O (2.0 equiv), CH₂Cl₂, 25 °C, 25 %.

- [1] A. D. Rodríguez, E. Gonzáles, S. D. Huang, *J. Org. Chem.* **1998**, *63*, 7083–7091.
- [2] T. J. Heckrodt, J. Mulzer, *J. Am. Chem. Soc.* **2003**, *125*, 4680–4681.
- [3] N. Waizumi, A. R. Stankovic, V. H. Rawal, *J. Am. Chem. Soc.* **2003**, *125*, 13022–13023.
- [4] J. Mulzer, S. Dupré, J. Buschmann, P. Luger, *Angew. Chem.* **1993**, *105*, 1538–1541; *Angew. Chem. Int. Ed. Engl.* **1993**, *32*, 1452–1454.
- [5] Available from Fluka, art. 55412.
- [6] a) J. Matikainen, S. Kaltia, M. Hamalainen, T. Hase, *Tetrahedron* **1997**, *53*, 4531–4538; b) S. Wattanasin, F. G. Kathawala, R. K. Boeckman, Jr., *J. Org. Chem.* **1985**, *50*, 3810–3815; c) R. K. Boeckman, Jr., T. R. Alessi, *J. Am. Chem. Soc.* **1982**, *104*, 3216–3217; d) J. Sauer, R. Sustmann, *Angew. Chem.* **1980**, *92*, 773–801; *Angew. Chem. Int. Ed. Engl.* **1980**, *19*, 779–807.
- [7] A well-studied example can be found in W. Oppolzer, C. Fehr, J. Warneke, *Helv. Chimica Acta* **1977**, *60*, 48–58.
- [8] a) T. A. Dineen, W. R. Roush, *Org. Lett.* **2003**, *5*, 4725–4728, and references therein; b) W. R. Roush, R. J. Sciotti, *J. Am. Chem. Soc.* **1998**, *120*, 7411–7419.
- [9] For an illustrative example, see: K. Fischer, S. Hünig, *Chem. Ber.* **1986**, *119*, 2590–2608.
- [10] D. B. Gorman, I. A. Tomlinson, *Chem. Commun.* **1998**, 25–27.
- [11] M. E. Layton, C. A. Morales, M. D. Shair, *J. Am. Chem. Soc.* **2002**, *124*, 773–775.
- [12] a) N. A. Yakelis, W. R. Roush, *Org. Lett.* **2001**, *3*, 957–960; b) D. Craig, *Chem. Soc. Rev.* **1987**, *16*, 187–238.
- [13] a) K. C. Nicolaou, P. S. Baran, Y.-L. Zhong, K. Sugita, *J. Am. Chem. Soc.* **2002**, *124*, 2221–2232; b) Y.-F. Tsai, R. K. Peddinti, C.-C. Liao, *Chem. Commun.* **2000**, 475–476.
- [14] T. J. Heckrodt, J. Mulzer, *J. Am. Chem. Soc.* **2003**, *125*, 9538.
- [15] W.-Q. Yang, L.-Y. Zhang, S.-Z. Chen, L. Huang, *Chin. Chem. Lett.* **1997**, *8*, 203–204.
- [16] A. D. Rodríguez, C. Ramírez, I. I. Rodríguez, C. L. Barnes, *J. Org. Chem.* **2000**, *65*, 1390–1398.
- [17] A. I. Kim, S. D. Rychnovsky, *Angew. Chem.* **2003**, *115*, 1305–1308; *Angew. Chem. Int. Ed.* **2003**, *42*, 1267–1270.
- [18] a) V. Nair, L. Balagopal, R. Rajan, J. Mathew, *Acc. Chem. Res.* **2004**, *37*, 21–30; b) T. Linker, *J. Organomet. Chem.* **2002**, *661*, 159–167.
- [19] G. Butora, A. G. Gum, T. Hudlicky, K. A. Abboud, *Synthesis* **1998**, 275–278.
- [20] K. C. Nicolaou, P. S. Baran, Y.-L. Zhong, K. Sugita, *Angew. Chem.* **2001**, *113*, 2203–2207; *Angew. Chem. Int. Ed.* **2001**, *40*, 2145–2149.

Color Theory in Science and Art: Ostwald and the Bauhaus**

Philip Ball and Mario Ruben*

Keywords:

art and science · biographies · history of science · Ostwald, Wilhelm

The outstanding but controversial position of Wilhelm Ostwald as a scientist and philosopher was highlighted exhaustively last year, in this journal among others, to mark the 150th anniversary of his birth.^[1] Yet among the many diverse activities Ostwald engaged in during his life, his artistic work and its impact on his philosophical ideas has generally been overlooked. During his scientific life, and especially after his formal retirement in 1906, he dedicated much time and energy to artistic endeavors. His favorite leisure activities were painting, playing the viola, and writing poetry. But Ostwald's interest in the arts was not incidental to his scientific and philosophical theories; rather, the two were interwoven. This is particularly evident in his work on color, which exerted a marked influence on the industry and fine art of his own period. Little has been said about the interac-

tion of Ostwald's ideas with fine art, and here we hope to close this gap somewhat by describing an historically rare mutual concordance between science and the arts, in which Ostwald and the personalities of the Bauhaus school of art, architecture, and design appear as the main actors.

The Bauhaus School

The Bauhaus School was founded in 1919 by the architect Walter Gropius under the utopian slogan "The building of the future". It sought to train a new type of artist, capable of reaching beyond the confines of academic specialization and of bridging the gulf between fine art and the traditional crafts. In essence, Gropius wanted to remove the long-standing distinction between the pure and the applied (something that surely resonates with scientists today). To achieve that, he recognized the necessity of establishing new teaching methods in his school. This was the goal he strove towards during the first period of the Bauhaus in Weimar; but after a somewhat anarchic beginning, the mission of practical training was reiterated when the school relocated, for political reasons, to Dessau in 1925. In the 1919 Bauhaus manifesto, Gropius wrote: "*Architects, painters, and sculptors must once again come to know and comprehend the composite character of a building, both as an entity and in terms of its various parts. Then their work will be filled with that true architectonic spirit which, as 'salon art', it has lost.*"^[2]

It soon became clear that this reconciliation of art and crafts could not be backward-looking (in the way that it had

been in the British Arts and Crafts movement), but needed to embrace the reality of a technical civilization, with its incipient methods of mass manufacturing. In short, the aesthetic of the artist had to be installed in the factory and workplace. In 1923, the Bauhaus acknowledged this with a new motto: "Art and technology—a new unity". The design standards promoted at the school would thenceforth recognize the demands of industry in both its functional and aesthetic aspects. The Bauhaus workshops produced prototype artifacts for mass production, ranging from individual household lamps to complete dwellings.^[2]

From 1921, every student of the Bauhaus was required to take a compulsory "preliminary course" (*Vorkurs*) before entering into a workshop of his choice, where he would be taught both practical and artistic skills in a unified manner. Ever since its foundation, the school was able to attract talented artists and craftsmen, acquiring an extraordinary collection of personalities that made the Bauhaus a thriving center of European art. Its illustrious gallery of teachers ("masters") and pupils favored late Expressionism and early Abstraction (Figure 1), and together they helped to define the course of artistic modernism. They included the painters Wassily Kandinsky, Paul Klee, Oskar Schlemmer, Johannes Itten, Lyonel Feininger, and Josef Albers, the architects Gropius himself and, in the late phase, Ludwig Mies van der Rohe and Marcel Breuer, and the photographers László Moholy-Nagy (also an accomplished painter) and Andreas Feininger. Students flocked to the school to study with these famous names, although Gropius

[*] Dr. M. Ruben
Institut für Nanotechnologie
Forschungszentrum Karlsruhe GmbH
Postfach 3640
76021 Karlsruhe (Germany)
Fax: (+49) 724-782-6434
E-mail: mario.ruben@int.fzk.de

Dr. P. Ball
Nature
4–6 Crinan Street
London N1 9XW (UK)

[**] We thank Ms. Gretel Brauer, the granddaughter of Wilhelm Ostwald, Großbothen, for her invaluable advice and help in locating the documents that provided the basis for this article. Furthermore, we would like to thank Prof. L. Beyer, University of Leipzig, Ms. Eckert from the Bauhaus-Archiv in Berlin, and Ms. Witzel from the Berlin-Brandenburgischen Akademie der Wissenschaften, Berlin, for their constructive help.



Figure 1. The masters on the roof of the Bauhaus building in Dessau. From the left: Josef Albers, Hinnerk Scheper, Georg Muche, László Moholy-Nagy, Herbert Bayer, Joost Schmidt, Director Walter Gropius, Marcel Breuer, Wassily Kandinsky, Paul Klee, Lyonel Feininger, Gunta Stölzl, and Oskar Schlemmer.^[2]

discovered that they tended to arrive with dreams of becoming fine artists rather than being content to turn out designs for factories.

Several masters of the Bauhaus were intensely interested in theories of color and its relation to form. Such “constructivist” work took place mainly in the courses directed by Itten, Kandinsky, and Klee, and to a lesser extent with Schlemmer, Moholy-Nagy, and Albers. There was a strong feeling that color composition could be pursued in an objective, “scientific” way. Itten, who was responsible for devising the preliminary course, believed that colors could be assigned definite and universal emotional values, an idea that he pursued with something akin to dogmatic mysticism (Figure 2, left). Klee made reference in his teachings to standard ideas about color taken from the theories of Goethe and the works of the

French painter Eugène Delacroix, which stressed the use of complementary pairs (red–green, blue–orange, yellow–violet). But he was always wary of too much theory: “Of course we may use it for a bit, but we hardly have any need for a theory of colors. All the infinite mixtures will never produce an emerald green, a Saturn red, a cobalt violet.”^[3] In other words, Klee felt that the characteristic hues of these materials engendered profound emotional effects that could not be dissected, laid out, and analyzed on color tables and charts.

But it was Kandinsky who was responsible for most of the color teaching at the Bauhaus. He experienced the condition of synesthesia, a neurological confusion of the senses in which two different sensations can be triggered by the same stimulus. This commonly results in an association of color with sound, so that certain timbres or pitches

create a sense of color. So it is not surprising that Kandinsky believed that “color directly influences the soul”—that a carefully chosen arrangement of colors could pluck the heartstrings of the emotions as deliberately as a pianist strikes chords on the keyboard. The task was then to identify the psychological meanings of different colors, which Kandinsky tried to establish by “scientific” tests. He issued a questionnaire^[4a] in which participants were asked to match the three primary colors (red, yellow, blue) to particular forms (circle, square, triangle)^[5]—with somewhat inconclusive results.

Thus the Bauhaus, standing at the intersection of art, design, and industry, turned out to be very receptive to all kinds of systematic approaches to art, including those that claimed to have a foundation in science.

Ostwald's Color System in Theory and Practice

Wilhelm Ostwald (Figure 3) was an enthusiastic amateur painter during most of his lifetime, especially after he retired from his academic career. He considered painting and drawing to be a form of “physical and psychic recovery”, and his first explicit reference to these activities was in 1884, when he painted during a journey.

After 1904, he undertook such painting excursions nearly every year (Figure 4). His artistic efforts, which were generally naturalistic and traditional (even, for their time, conservative), were, however, not simply a form of relaxation but an expression of his closely intertwined scientific and philosophical preoccupations, guided by his enormous intellectual curiosity. Since his childhood, Ostwald had used his interest in and knowledge of chemistry to synthesize pigments for use in art.

Around 1914, Ostwald began to develop a systematic theory of color as well as a quantitative color science, culminating in the publication of several books and publications on the topic between 1917 and 1922—most notably, *The Colour Primer* (original German version, 1917).^[9] Ostwald's most important contribution to color theory was the role he assigned to gray as a key

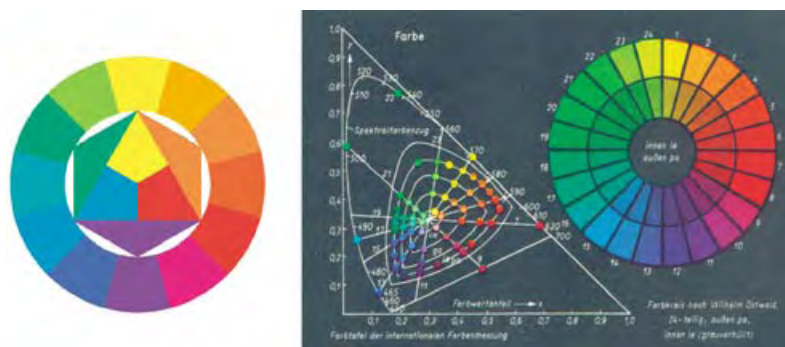


Figure 2. Two examples of color systems invented by Itten at the Bauhaus (left) and by Ostwald (right).^[6,7]



Figure 3. Portrait of Wilhelm Ostwald by A. Klamroth (pastel, 1904).^[8a]

coordinate of “color space” (Figure 2, right). His attempts to map this space were influenced by the work of the American artist and teacher Albert Munsell, whom Ostwald met in 1905. Munsell tried to quantify and standardize colors according to the parameters of hue (roughly speaking, the dominant wavelength), saturation (the intensity or “richness” of the color), and brightness (which can be crudely equated with the shade of gray the color gives in a black and white photo).^[4b] The last of these parameters was particularly important to Ostwald. He believed that a scale of perceptually equal steps in the brightness of a color could be achieved by adding black and white in ratios that followed a logarithmic progression. This, he said, provided a scheme for achieving perfect tonal balance and harmonious color composition in a painting. The idea of “harmony” in painting was one much discussed by Renaissance artists, and no doubt goes back even further. It alludes to the skill of combining colors so that no part of the composition stands out glaringly in relation to others. This is not necessarily a naturalistic device; even in their



Figure 4. One of the artistic products of Wilhelm Ostwald’s annual excursions: the painting *Clouds and Waves* from 1913.^[8a]

abstract works, painters like Klee and Kandinsky show an awareness of the need for harmony to lend unity to their pictures. Ostwald was, at face value, offering a foolproof set of rules for achieving such harmony (and he was quite prepared to criticize famous works of art which violated them).

Ostwald used his fame as a chemist and Nobel laureate to impress his color theory on the German paint industry. In 1912 he joined the Deutsche Werkbund, an organization dedicated to introducing standardization into industrial design, and in 1914 he arranged an exhibition of commercial paints and dyes at a Werkbund exhibition in Cologne. Eventually Ostwald established his own pigment factory near Leipzig, which operated from 1920 to 1923.

While at first Ostwald directed his artistic endeavors towards the “accurate” reproduction of nature, after 1915 his paintings reveal his experiments on

how his color theories should be put into practice (Figure 5). In other words, he was trying to create art from a scientific standpoint, which ultimately led him towards the notion of the “ideal” painting constructed according to principles of his color theory. He spoke about this idea in a lecture at a congress of the Werkbund in Stuttgart in 1919; but such a rigid program for art was rejected by most contemporary artists.^[10] In the same period Ostwald did little to endear himself to those of an artistic sensibility by announcing that Titian had once used a blue “two tones too high”.^[11]

Ostwald and the Bauhaus

Thus Ostwald was prepared to convert the artistic world to his ideas on color. Having encountered him on several previous occasions (for example, in the Werkbund), Walter Gropius seems

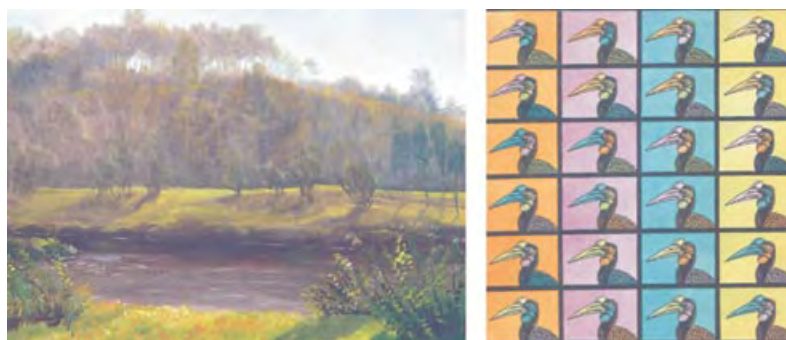


Figure 5. Two examples of Ostwald’s artistic work before (left) and after (right) being influenced by his own color theory.^[8a, 9]

to have approached him in late 1926 with a view to arranging a visit to the Bauhaus. In a letter to Ostwald on November 20, 1926, Gropius says “...enclosed you will find a small brochure describing how the teaching of form and color is organized within our institute... On November 4th we are going to inaugurate our new institute building. I send you an invitation and I would be very pleased to meet you again.”^[12] Ostwald’s reaction is recorded by his daughter Grete in her diary of December 1926: “He is so fascinated by a brochure written by Gropius that he even decided to visit it [the Bauhaus] on the occasion of the inauguration of its new buildings. Beauty = Law, this is what Gropius has also understood, and he [WO] is interested in how this can fit with Kandinsky and in particular with Klee. Indeed, it transpired that Gropius is the constructive head, but is indifferent to color. Unfortunately, it was only possible to exchange some brief words with him. On the other hand, he had a heated discussion and lunch together with a painter with a Polish name... , who is constructing paintings out of squares and rectangles.”^[13]

Beginning with the meeting on December 4, 1926, there was an intense exchange of letters and books between Ostwald on one side and Gropius, Moholy-Nagy, and the designer and typographer Herbert Bayer on the other. Grete’s diary mentions on February 28, 1927, that “he [WO] is looking forward to the promised Bauhaus week.”^[13] This week was first scheduled for the beginning of April 1927, but was later postponed so that it finally took place on June 10–15, 1927, in Dessau.

In a letter to his wife Helene written on June 10, 1927, Ostwald says that he arrived in Dessau in the morning and was invited to stay with Gropius in one of the recently erected school buildings in the famous Bauhaus style. After taking lunch with Gropius and his wife, the two men were clearly intent on entering into intense discussion: “...going a long distance together...”^[14] as Ostwald put it. This is confirmed by an entry in the diary of Gropius’s wife Ise concerning the same day: “Ostwald has arrived... he behaves very brightly and naturally here, and his intensity does not slow down for a moment.”^[15]

In the afternoon Ostwald gave his introductory talk and reported to his wife that 120 people attended, including “the professors, except for Klee ... it might be disconcerting for him to meet me”.^[14] Ise Gropius recorded on June 12, 1927, that Ostwald was giving daily talks which were well received by the Bauhaus pupils, and she praises Ostwald’s brio and vitality.^[15]

What kind of lectures did he give there? In her diary entry for the June 13, 1927, Ise mentions that “Ostwald gave his last lecture about his tenet of harmony. As big as the impact of his tenet of order has been, the opposition to his tenet of harmony is of comparable size. I too believe that it is wrong to apply his tenet of color to painters...”^[15] Later she refers to a “color organ” that Ostwald gave to the Bauhaus, which attracted interest from Bayer and Hinnerk Schepers, the designer who had devised the color scheme for the new building in Dessau.^[15,16] The connection between music and color has ancient origins, and it shaped Isaac Newton’s division of the visible spectrum into seven rainbow colors. The connection was particularly evident to the synesthetic Kandinsky (Figure 6), as well as to the Russian composer Alexander Scriabin, who had the same condition and composed in color for a “keyboard of light”. Ostwald explored these notions in a 1925 manuscript “Musical Art and the Art of Light”.^[16]

The tenets of color, order, and harmony to which Ise Gropius refers

might be related to Ostwald’s lecture manuscripts “The Euphonies of the World of Colors” (presumably 1927), “The General Order of Forms into Regular Networks—A Contribution to the Harmony of Forms” (presumably 1927), and “The Harmothek” (1926). All of these documents are still available in Ostwald’s written estate.^[16]

Ostwald’s Impact on the Artistic World

The reaction at the Bauhaus to Ostwald’s talks was mixed. He made a strong impression as a personality, but there was considerable skepticism towards his theories. It wasn’t the first time the artists had encountered them, of course—Ostwald’s ideas had been a topic of debate at least since the publication of *The Colour Primer*, and Gropius referred to them in the catalogue of the Bauhaus exhibition of 1923. Kandinsky had been initially ambivalent about Ostwald’s color theory, but had become more sympathetic to it by 1925; nonetheless, his color course after 1927 was not entirely uncritical of Ostwald’s framework. Klee, meanwhile, remained unwilling to be fettered by any scientific theory of color. He had come across Ostwald’s ideas as early as 1904, when he had read the chemist’s *Malerbriefe* (*Letters to a Painter*). He once commented on these theories in the most acerbic and dismissive terms: “That which most artists have in common, an

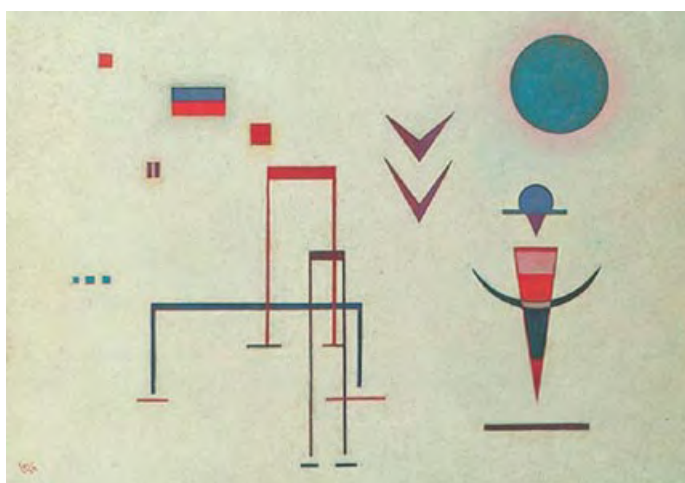


Figure 6. Wassily Kandinsky’s painting *Jocular Sounds* from the artist’s Bauhaus years (1929); virtually every element in the painting is adapted from music notation. (Copyright VG Bild-Kunst, Bonn, 2004).

aversion to color as a science, became understandable to me when a short time ago I read Ostwald's theory of colors. I gave myself a little time to see if I could succeed in getting something of value from it but instead was only able to get a few interesting thoughts... To hold that the possibility of creating harmony using a tone of equal value should become a general rule means renouncing the wealth of the soul. Thanks but no thanks."^[3]

Schlemmer, who must have been present in Dessau in 1927, echoed these sentiments: "Ostwald's color building is a typical scientific result; artistically it is nonsense."^[10] Ise Gropius likewise drew the conclusion that "he [WO] knows nothing whatsoever about the painters, although he is able to define 'the painter' in theory absolutely correctly. But if he stands next to him, he does not recognize him."^[15] Yet it must be said that Ostwald's color theory was rather positively received by Piet Mondrian and his colleagues in the "De Stijl" group in the early 1920s. *The Colour Primer* was enthusiastically reviewed in the group's journal in 1918, and Ostwald is said to have become something of a "cult figure" for them. Mondrian's work with simple primary colors bears some evidence of Ostwald's influence.^[4a,1b]

During the months after the visit, Gropius kept in close contact with Ostwald, who sent several of his pigments, binders, and books to Dessau. On June 28, 1927, Gropius asked Ostwald to join the advisory board of the Bauhaus, to which Ostwald replied two days later: "With thanks and joy I accept the honor of entering onto the board of trustees... I would like to add that I do not consider this membership a hollow formality, but I ask you to contact me whenever I can be useful to the Bauhaus..." (Figure 7).^[17]

Such a collaboration could have been as fruitful as it would have been controversial—but apparently it did not develop to Ostwald's own satisfaction. In August 1928, one year after the lectures, Gropius had to reassure Ostwald in a letter that "it is not true, as you believe, that your lectures have not left any trace at the Bauhaus. I know that Schepher has dealt with them intensively and is using your systems in his courses."^[18] Shortly after this assurance, Joost Schmidt contacted Ostwald to ask for

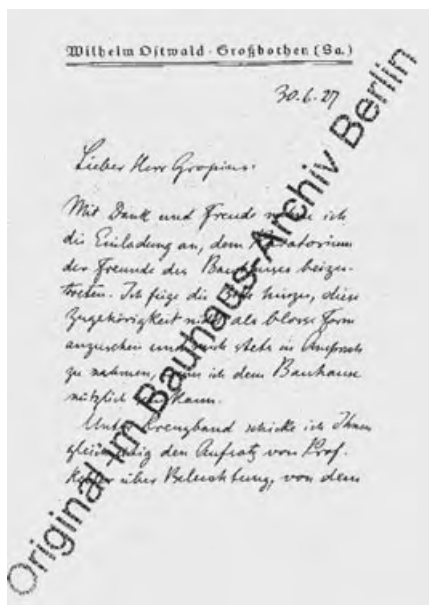


Figure 7. Facsimile of the first page of Ostwald's response to the invitation to join the Bauhaus board of trustees.^[17]

explanatory material, which he planned to use in the course of his classes dealing with advertising techniques, and he even seems to have visited Ostwald in Großbothen to that purpose.^[19] But there is no record of further visits by Ostwald after 1928, and he died in 1932, the year before the school, a center of "degenerate art", was closed by the Nazi regime. Its artistic stars were scattered across the world, several of them finding refuge in the USA. There, abstract expressionism was to establish color as the central constructive component of modern art, largely in isolation from any consensual theory about how color should be used or what it "meant". But at least the American artists' later engagement with the industrial materials championed by Ostwald was a matter of choice. After the closure of the Bauhaus, Oskar Schlemmer was forbidden to exhibit his work in Germany, and was reduced to making a living by testing materials for a paint company.

Published Online: August 4, 2004

- [1] a) R. Zott, *Angew. Chem.* **2003**, *115*, 4120–4126; *Angew. Chem. Int. Ed.* **2003**, *42*, 3990–3995; b) P. Ball, *Nature* **2003**, *425*, 904; c) P. Günther, *Angew. Chem.* **1932**, *45*, 489–496.

- [2] For comprehensive information concerning the history of the Bauhaus: www.bauhaus.de.
- [3] P. Cherchi, *Paul Klee teorico*, De Donato, Bari, **1978**, pp. 160–161.
- [4] a) J. Gage, *Kulturgeschichte der Farbe von der Antike bis zur Gegenwart*, Seemann, Leipzig, **2001**, chap. 14. [English: J. Gage, *Colour in Culture*, Thames & Hudson, London, **1993**].
- [5] W. Kandinsky, *Über das Geistige in der Kunst*, Benteli, Bern, **1952**; W. Kandinsky, *Punkt und Linie zu Fläche*, Benteli, Bern, **1955**.
- [6] J. Itten, *Kunst der Farbe*, Ravensburger Buchverlag, **1970**, p. 30. [English: J. Itten, *The Elements of Color*, Van Nostrand Reinhold, New York, **1970**].
- [7] *Meyers Neues Lexikon*, Brockhaus Verlag, Leipzig, **1978**, p. 326.
- [8] *Wilhelm Ostwald. Ostseebilder* (Ed.: R. Zimmermann), Baltic-Verlag Siegbert Bendt, Stralsund, **1992**; L. Beyer, R. Behrens, *De Artes Chemiae*, Passage, Leipzig, **2003**.
- [9] a) *Die Farbenfibel*, Unesma, Leipzig, **1917**; [English edition: *The Colour Primer*, Van Nostrand Reinhold, New York, **1969**]; b) *Der Farbenatlas*, Leipzig, **1918**; c) *Die Farbenlehre* in five volumes, Unesma, Leipzig, **1918–1922**; d) *Farb-normen-Atlas*, Unesma, Leipzig, **1920**.
- [10] *Oskar Schlemmer: Idealist der Form. Briefe, Tagebücher, Schriften* (Ed.: A. Hünecke), Reclam-Bibliothek, Leipzig, **1990**, Vol. 1312, p. 263.
- [11] M. Doerner, *Malmaterial und seine Verwendung im Bilde*, 18th ed, Ferdinand Enke, Stuttgart, **1994**, p. 267 [English: M. Doerner, *The Materials of the Artist*, Harcourt Brace, Orlando, FL, **1984**, pp. 169–170].
- [12] Letter of W. Gropius to W. Ostwald, November 20, 1926, Archive Berlin Brandenburgische Akademie der Wissenschaften, Berlin.
- [13] Diary of Grete Ostwald, Wilhelm-Ostwald-Archiv, Großbothen, www.wilhelm-ostwald.de.
- [14] Letter of W. Ostwald to his wife, June 10, 1927, Bauhaus-Archiv, Dessau.
- [15] Diary of Ise Gropius, Bauhaus-Archiv, Berlin.
- [16] Ostwald's estate, Archive of the Berlin-Brandenburgische Akademie der Wissenschaften, Berlin.
- [17] Letter from W. Ostwald to W. Gropius, June 30, 1927, Bauhaus-Archiv, Berlin.
- [18] Letter of W. Gropius to W. Ostwald, August 13, 1928, Archive of the Berlin Brandenburgische Akademie der Wissenschaften, Berlin.
- [19] Letters of J. Schmidt to W. Ostwald, October 3, 1928 and October 23, 1928, Archive of the Berlin Brandenburgische Akademie der Wissenschaften, Berlin.

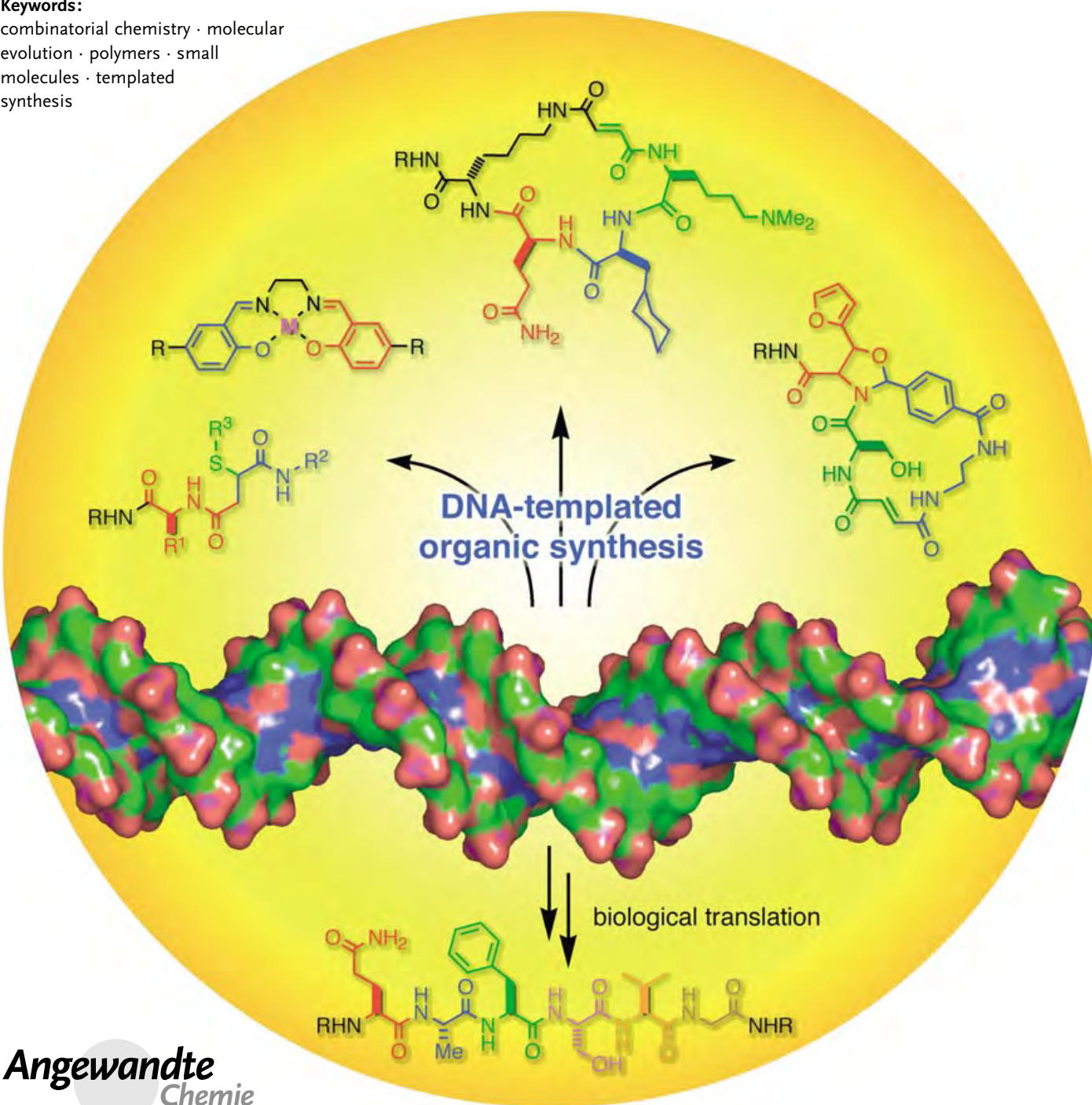
Synthetic Methods

DNA-Templated Organic Synthesis: Nature's Strategy for Controlling Chemical Reactivity Applied to Synthetic Molecules**

Xiaoyu Li and David R. Liu*

Keywords:

combinatorial chemistry · molecular evolution · polymers · small molecules · templated synthesis



Angewandte
Chemie

In contrast to the approach commonly taken by chemists, nature controls chemical reactivity by modulating the effective molarity of highly dilute reactants through macromolecule-templated synthesis. Nature's approach enables complex mixtures in a single solution to react with efficiencies and selectivities that cannot be achieved in conventional laboratory synthesis. DNA-templated organic synthesis (DTS) is emerging as a surprisingly general way to control the reactivity of synthetic molecules by using nature's effective-molarity-based approach. Recent developments have expanded the scope and capabilities of DTS from its origins as a model of prebiotic nucleic acid replication to its current ability to translate DNA sequences into complex small-molecule and polymer products of multistep organic synthesis. An understanding of fundamental principles underlying DTS has played an important role in these developments. Early applications of DTS include nucleic acid sensing, small-molecule discovery, and reaction discovery with the help of translation, selection, and amplification methods previously available only to biological molecules.

From the Contents

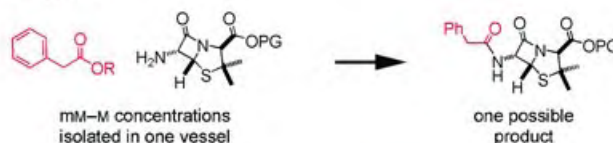
1. Introduction	4849
2. The Reaction Scope of DNA-Templated Synthesis	4850
3. Expanding the Synthetic Capabilities of DNA-Templated Synthesis	4854
4. DNA-Templated Polymerization	4858
5. Toward a Physical Organic Understanding of DNA-Templated Synthesis	4860
6. Applications of DNA-Templated Synthesis	4863
7. Summary and Outlook	4867
8. Abbreviations	4868

1. Introduction

The control of chemical reactivity is a ubiquitous and central challenge of the natural sciences. Chemists typically control reactivity by combining a specific set of reactants in one solution at high concentrations (typically mM to M). In contrast, nature controls chemical reactivity through a fundamentally different approach (Figure 1) in which thousands of reactants share a single solution but are present at concentrations too low (typically nM to μ M) to allow random intermolecular reactions. The reactivities of these molecules are directed by macromolecules that template the synthesis of necessary products by modulating the effective molarity of reactive groups and by providing catalytic functionality (Figure 2 shows several examples). Nature's use of effective molarity to direct chemical reactivity enables biological reactions to take place efficiently at absolute concentrations that are much lower than those required to promote efficient laboratory synthesis and with specificities that cannot be achieved with conventional synthetic methods.

Among nature's effective-molarity-based approaches to controlling reactivity, nucleic acid templated synthesis plays a central role in fundamental biological processes, including the replication of genetic information, the transcription of DNA into RNA, and the translation of RNA into proteins. During ribosomal protein biosynthesis, nucleic acid templated reactions effect the translation of a replicable information carrier into a structure that exhibits functional properties beyond that of the information carrier. This translation enables the expanded functional potential of proteins to be combined with the powerful and unique features of nucleic acids

Chemists' approach:



Nature's approach:

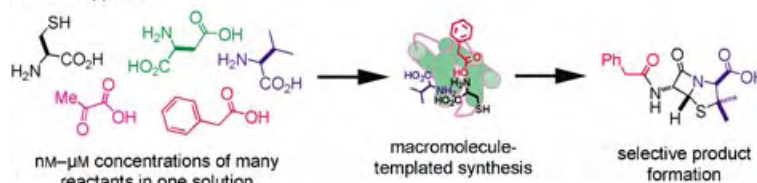


Figure 1. Two approaches to controlling chemical reactivity.

including amplifiability, inheritability, and the ability to be diversified. The extent to which primitive versions of these processes may have been present in a prebiotic era is widely debated,^[1–12] but most models of the precell world include some form of template-directed synthesis.^[1,2,13–26]

In addition to playing a prominent role in biology, nucleic acid templated synthesis has also captured the imagination of chemists. The earliest attempts to apply nucleic acid tem-

[*] Dr. X. Li, Prof. D. R. Liu
Harvard University
12 Oxford Street
Cambridge, Ma 02138 (USA)
Fax: (+1) 617-496-5688
E-mail: drliu@fas.harvard.edu

[**] Section 8 of this article contains a list of abbreviations.

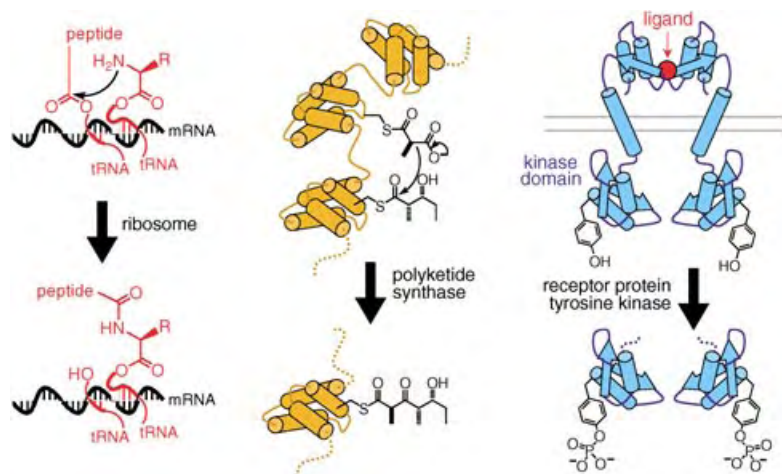


Figure 2. Examples of effective-molarity-based control of bond formation and bond breakage in biological systems.

plated synthesis to nonbiological reactants used DNA or RNA hybridization to accelerate the formation of phosphodiester bonds or other structural mimics of the nucleic acid backbone.^[1,14,24–41] More recently, researchers have discovered the ability of DNA-templated organic synthesis to direct the creation of structures unrelated to the nucleic acid backbone.^[42–48] A growing understanding of the simple but powerful principles underlying DTS has rapidly expanded its synthetic capabilities and has also led to emerging chemical and biological applications, including nucleic acid sensing,^[27–30,49–60] sequence-specific DNA modification,^[61–80] and the creation and evaluation of libraries of synthetic molecules.^[44,47,81,82]

Herein we describe representative early examples of nucleic acid templated synthesis and more recent developments that have enabled DNA templates to be translated into increasingly sophisticated and diverse synthetic molecules. We then analyze our current understanding of key aspects of DTS, describe applications that have emerged from this understanding, and highlight remaining challenges in using DTS to apply nature's strategy for controlling chemical reactivity to molecules that can only be accessed through laboratory synthesis.

2. The Reaction Scope of DNA-Templated Synthesis

A reactant for DTS consists of three components (Figure 3a): 1) a DNA oligonucleotide that modulates the effective molarity of the reactants but is otherwise a bystander, 2) a reactive group that participates in the DNA-templated chemical reaction, and 3) a linker connecting the first two components. When two DTS reactants with complementary oligonucleotides undergo DNA hybridization, their reactive groups are confined to the same region in space, increasing their effective concentration.

The extent to which the effective molarity of DNA-linked reactive groups increases upon DNA hybridization could depend in principle on several factors. First, the absolute concentration of the reactants is critical. For a DNA-templated reaction to proceed with a high ratio of templated to nontemplated product formation, reactants must be sufficiently dilute (typically nM to μ M) to preclude significant random intermolecular reactions, yet sufficiently concentrated to enable complementary

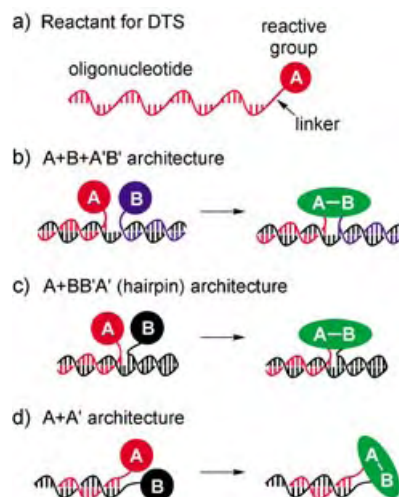


Figure 3. a) The three components of a reactant for DTS. b)–d) Template architectures for DTS. A/B and A'/B' refer to reactants containing complementary oligonucleotides, and + symbols indicate separate molecules.



David R. Liu was born in 1973 in Riverside, California. He received a BA in 1994 from Harvard University, where he performed research under the mentorship of Professor E. J. Corey. In 1999 he completed his PhD at the University of California Berkeley in the group of Professor P. G. Schultz. He returned to Harvard later that year as Assistant Professor of Chemistry and Chemical Biology and began a research program to study the organic chemistry and chemical biology of molecular evolution. He is currently

John L. Loeb Associate Professor of the Natural Sciences in the Department of Chemistry and Chemical Biology at Harvard University.



Xiaoyu Li was born in 1975 in Xining, China. He obtained a BSc in chemistry at Peking University and later completed his PhD at the University of Chicago with Professor D. G. Lynn in 2002. He is currently a postdoctoral fellow in Professor D. R. Liu's group.

oligonucleotides to hybridize efficiently. Second, the precision with which reactive groups are aligned into a DNA-like conformation could influence the increase in effective molarity upon DNA hybridization. It is conceivable, for example, that only those reactions that proceed through transition states consistent with the conformation of duplex DNA may be suitable for DTS. Recent studies have evaluated the importance of each of these factors and revealed the reaction scope of DTS. Additional factors influencing the effective molarity of reactive groups in DTS are analyzed in Section 3.

2.1. Nucleic Acid templated Synthesis of Nucleic Acids and Nucleic Acid Analogues

Nucleic acid templated syntheses prior to the current decade predominantly used DNA or RNA templates to mediate ligation reactions that generate oligomers of DNA, RNA, or structural analogues of nucleic acids (Figure 4).^[1,14,24–41,70,83,84] Since there are several excellent articles^[1,31,37,42,61] on the DTS of nucleic acids and their analogues, we summarize only a few key examples below. In these cases, the reactive groups were usually functionalities already present in the oligonucleotides or oligonucleotide analogues, and linkers were often absent. The template architecture used to support these DNA-templated reactions most frequently placed the site of reaction at the center of a nicked DNA duplex (Figure 3b). The reactive groups in these examples mimic the structure of the DNA backbone during product formation.

The first report of a nucleic acid templated nucleotide ligation was the observation of Naylor and Gilham in 1966^[13] that a poly(A) template could direct the formation of a native

phosphodiester bond between the carbodiimide-activated 5' phosphate of (pT)₆ and the 3' hydroxy group of a second (pT)₆ molecule (5% yield). Several examples of DNA- or RNA-templated oligonucleotide syntheses have since been reported (Figure 4), including Orgel's pioneering work on nucleic acid templated phosphodiester formation between 2-methylimidazole-activated nucleic acid monomers and oligomers (Figure 4a),^[1,85–87] Nielson's and Orgel's RNA-templated amide formation between PNA oligomers (Figure 4f),^[24] Joyce's DNA-templated peptide–DNA conjugation (Figure 4d),^[84] von Kiedrowski's carbodiimide-activated DNA coupling^[88] and amplification of phosphoramidate-containing DNA (Figure 4e),^[14] Lynn's DNA-templated reductive amination and amide formation between modified DNA oligomers (Figure 4b),^[31–39,83,84] Eschenmoser's nucleic acid templated TNA ligations,^[89–91] and Letsinger's and Kool's DNA- and RNA-templated phosphothioester and phosphoselenoester formation (Figure 4c).^[26–30,40,41] Oligonucleotide analogues have also served as templates for nucleotide ligation reactions. Orgel and co-workers used HNA, a non-natural nucleic acid containing a hexose sugar (see Figure 16), as a template for the ligation of RNA monomers through activated phosphate coupling,^[92] while Eschenmoser and co-workers have shown that nonnatural pyranosyl-RNA can template the coupling of complementary pyranosyl-RNA tetramers through phosphotransesterification with 2',3'-cyclic phosphates.^[93]

In addition to analogues of the phosphoribose backbone, products that mimic the structure of stacked nucleic acid aromatic bases have also been generated by DTS (Figure 5). Photoinduced [2+2] cycloaddition, typically involving the C5–C6 double bond of pyrimidines, has served as the most common reaction for the DTS of base analogues. One of the

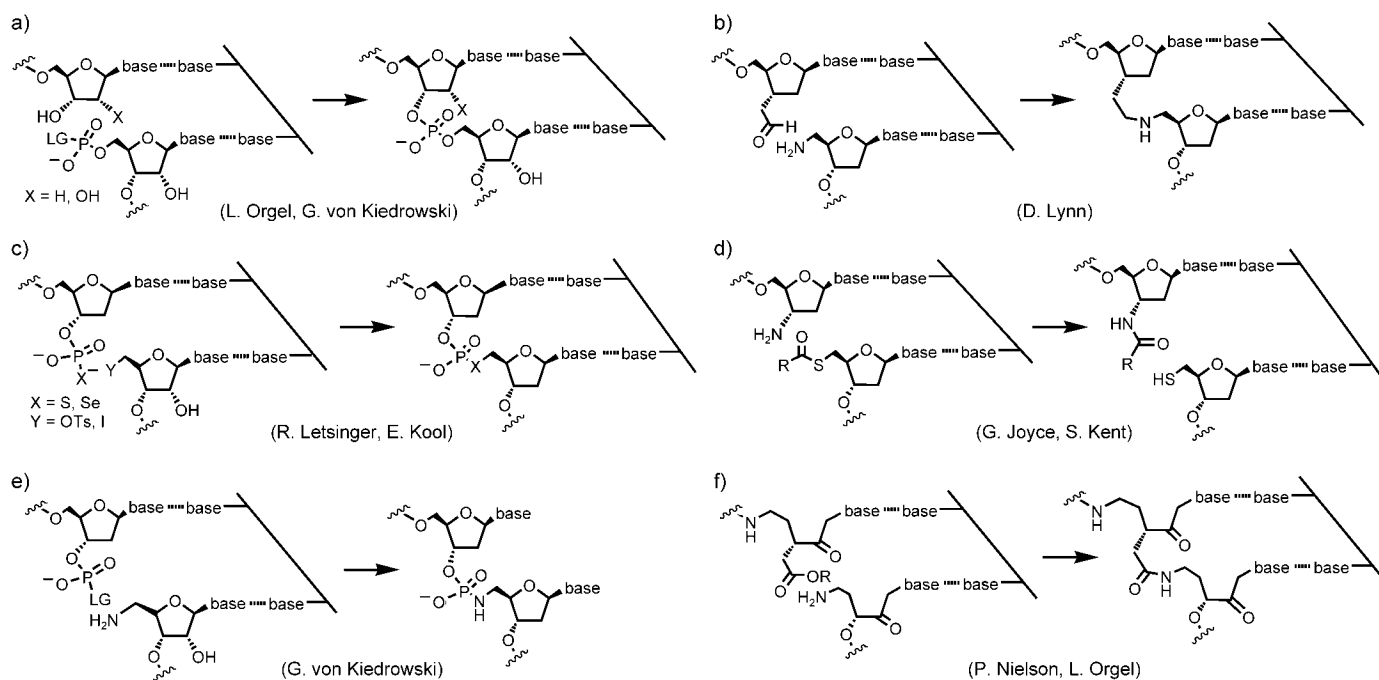


Figure 4. Representative DNA-templated syntheses of oligonucleotide analogues.^[1,14,24–41] LG: leaving group.

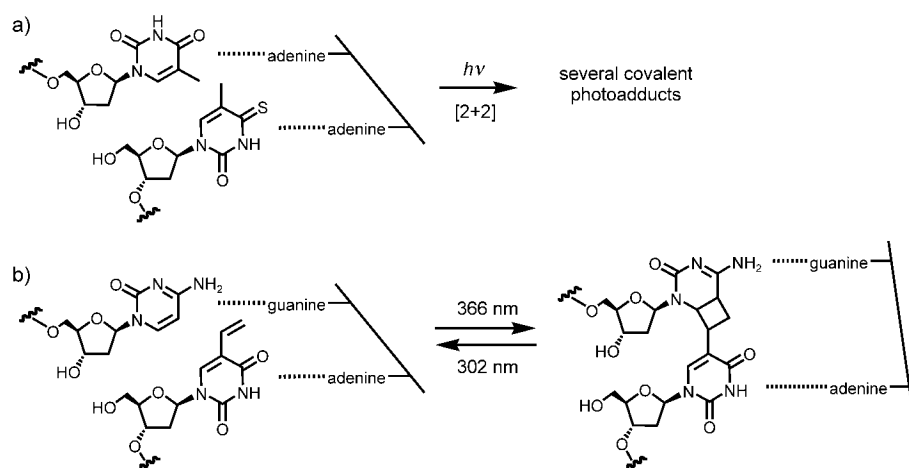


Figure 5. DNA-templated photoinduced [2+2] cycloaddition reactions.^[94–101]

first examples was the DNA-templated formation of a thymine dimer by irradiation at 290 nm described by Lewis and Hanawalt.^[94] DNA-templated photoligations between thymidine and 4-thiothymidine have also been reported (Figure 5 a).^[95] Other photoreactive groups used in DNA-templated [2+2] cycloaddition reactions include coumarins,^[96] psoralens,^[97] and stilbenes.^[98–100] Recently, Fujimoto, Saito, and co-workers described a reversible DNA-templated photoligation–photocleavage mediated by [2+2] cycloaddition between adjacent pyrimidine bases, one of them modified with a 5-vinyl group (Figure 5 b).^[101]

The products of the templated nucleotide ligation reactions described above are structurally similar to the nucleic acid backbone and typically preserve the six-bond spacing between nucleotide units or the relative disposition of adjacent aromatic bases. An implicit assumption underlying these studies is that a DNA-templated reaction proceeds efficiently when the DNA-linked reactive groups are positioned adjacently and the transition state of the reaction is similar to the structure of native DNA.

2.2. DNA-Templated Synthesis of Products Unrelated to the DNA Backbone

While structural mimicry of the DNA backbone may maximize the effective concentration of the template-organized reactants, it severely constrains the structural diversity and potential properties of products generated by nucleic acid templated reactions. The use of DTS to synthesize structures not necessarily resembling nucleic acids is therefore of special interest and has been a major focus of research in the field of template-directed synthesis since 2001.

Our group probed the structural requirements of DTS by studying DNA-templated reactions that generate products unrelated to the DNA backbone.^[44] A series of conjugate addition and substitution reactions

between a variety of nucleophilic and electrophilic groups (Figure 6) were found to proceed efficiently at absolute reactant concentrations of 60 nM.^[44] In contrast, products were not formed when the sequences of reactant oligonucleotides were mismatched (noncomplementary). These findings established that the effective molarity of two reactive groups linked to one DNA double helix can be sufficiently high that their alignment into a DNA-like conformation is not needed to achieve useful reaction rates.^[44] This conclusion is consistent with simple geometric models of effective molarity. For example, confining two reactive groups to 10 Å separation—achievable by conjugating them to the 5' and 3' ends of

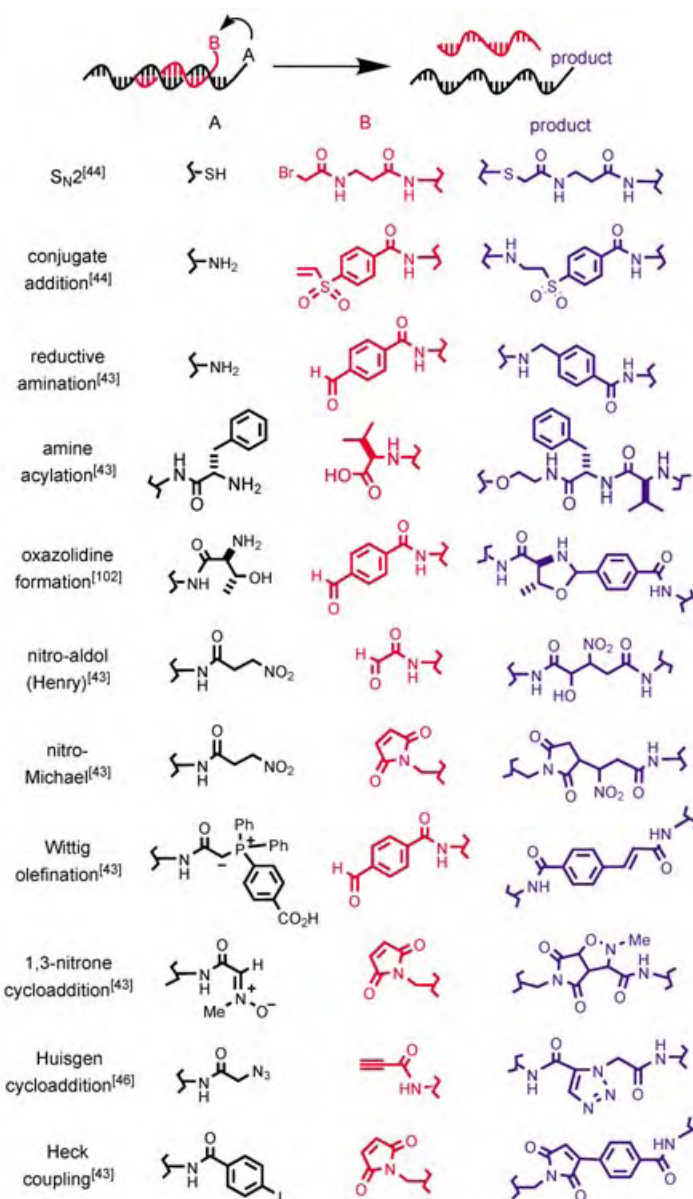


Figure 6. DNA-templated reactions that generate products not resembling nucleotides.^[43, 44, 46, 102]

hybridized oligonucleotides—can correspond to an effective molarity of 1 M.

We also compared the ability of two distinct DNA template architectures to mediate DTS. Both a hairpin template architecture (A+BB'A', a closed form of the A+B+A'B' architecture that enables products to remain covalently linked to templates, see Figure 3c) and a linear A+A' template architecture (Figure 3d) were found to mediate efficient product formation.^[44] The A+A' architecture is especially attractive because the corresponding reactants are the simplest to prepare. Furthermore, the oligonucleotide portion of the A+A' architecture is less likely to influence the outcome of a DTS beyond simple modulation of the effective molarity compared with a hairpin or A+B+A'B' arrangement in which the reaction site is flanked on both sides by DNA (see Section 5.3).

Following the discovery that DNA mimicry is not a requirement for efficient DTS, our group extended the reaction scope of DTS to include many types of reactions, the majority of which were not previously known to take place in a nucleic acid templated format.^[43,44] Conjugate additions of thiols and amines to maleimides and vinyl sulfones, S_N2 reactions, amine acylation, reductive amination,^[43,44] Cu^I-mediated Huisgen cycloaddition,^[46] and oxazolidine formation^[102] were found to proceed efficiently and sequence specifically with a DTS format using the A+A' template architecture (Figure 6).^[43] Several useful carbon–carbon bond formation reactions were also successfully transitioned into a DTS format, including the nitro-aldol addition (Henry reaction), nitro-Michael addition, Wittig olefination, Heck coupling, and 1,3-dipolar nitron cycloaddition (Figure 6).^[43,44] These transformations included the first carbon–carbon bond forming reactions other than photoinduced cycloaddition that are templated by a nucleic acid. The Pd-mediated Heck coupling was the first example of a DNA-templated organometallic reaction. Czapinski and Sheppard reported the DTS of metallosalens (Figure 7).^[45] Two salicylaldehyde-linked DNA strands were brought together by a complementary DNA template in the A+B+A'B' architecture. Metallosalen formation occurred in the presence of ethylenediamine and Ni²⁺ or Mn²⁺. Gothelf, Brown, and co-workers recently applied this reaction to the DNA-templated assembly of linear and branched conjugate structures (see Section 3.3).^[103]

Collectively, these studies have conclusively demonstrated that DTS can maintain sequence-specific control over the effective molarity even when the structures of

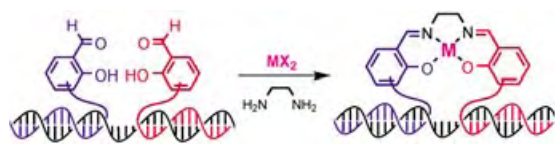


Figure 7. DNA-templated assembly of metallosalen–DNA conjugates (M = Ni²⁺ or Mn²⁺).

reactants and products are unrelated to that of nucleic acids. The array of reactions now known to be compatible with DTS, while modest compared with the compendium of conventional synthetic transformations developed over the past two centuries, is sufficiently broad to enable the synthesis of complex and diverse synthetic structures programmed entirely by a strand of DNA (see Sections 3.2 and 3.3).

2.3. DNA-Templated Functional Group Transformations

The examples described above used DNA hybridization to mediate the coupling of two DNA-linked reactive groups. While coupling reactions are especially useful for building complexity into synthetic molecules, functional group transformations are also important components of organic synthesis. A few DNA-templated functional group transformations have recently emerged.

Ma and Taylor used a 5'-imidazole-linked DNA oligonucleotide and the A+B+A'B' architecture for the DNA-templated hydrolysis of a 3'-*p*-nitrophenyl ester linked oligonucleotide (Figure 8a).^[49] The initial product of the templated reaction, an imidazolyl amide linked at both ends to DNA, undergoes rapid hydrolysis to generate the free

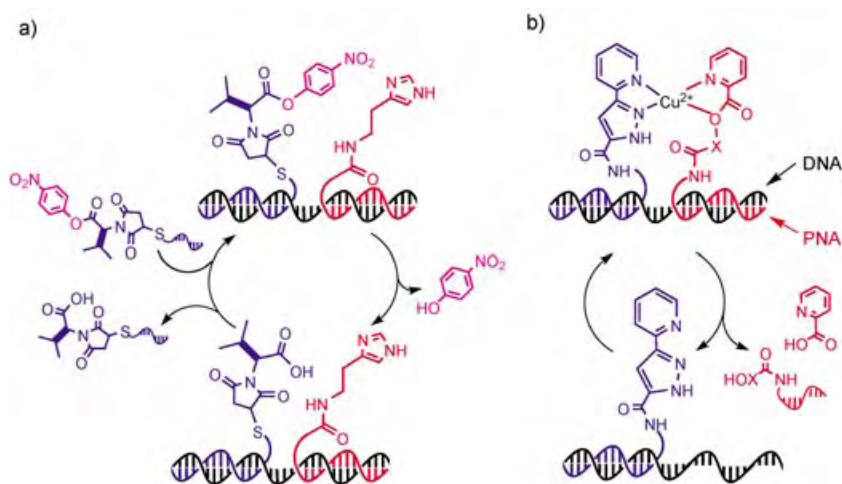


Figure 8. DNA-templated functional group transformations.^[49,104] X in (b): OCH₂CH₂.

carboxylic acid. The net outcome of this reaction is the DNA-templated functional group transformation of a *p*-nitrophenyl ester into a carboxylic acid. Ma and Taylor demonstrated that the template can dissociate from the product-linked DNA strand after ester hydrolysis and can participate in additional rounds of catalysis with other ester-linked oligonucleotides. Brunner, Kraemer, and co-workers recently developed a conceptually related DNA-templated functional group transformation that uses DNA templates to mediate a Cu²⁺-catalyzed aryl ester cleavage (Figure 8b).^[104] In this first example of templated catalysis involving DNA-linked metal complexes, DNA-linked aryl esters are transformed into alcohols.

3. Expanding the Synthetic Capabilities of DNA-Templated Synthesis

Together with the above efforts to broaden the reaction scope of nucleic acid templated synthesis, several recent insights and developments have significantly enhanced the synthetic capabilities of DTS. These findings include 1) DTS between reactive groups separated by long distances, 2) multistep DTS in which the product of a DNA-templated reaction is manipulated to serve as the starting material for a subsequent DNA-templated step, 3) the design of template architectures that increase the types of reactions which can be performed in a DNA-templated format, 4) synthesis templated by double-stranded DNA, and 5) new modes of controlling reactivity made possible by DTS that cannot be achieved with conventional synthetic methods.

3.1. Distance-Independent DNA-Templated Synthesis

The ability of DNA hybridization to direct the synthesis of molecules that do not mimic the DNA backbone suggests that functional group adjacency may not be necessary for efficient DTS. Our group evaluated the efficiency of simple DNA-templated conjugate addition and nucleophilic substitution reactions as a function of the number of intervening single-stranded template bases between hybridized reactive groups (Figure 9).^[44] Surprisingly, for both reactions tested, apparent second-order rate constants of product formation did not significantly change when the distance between hybridized reactive groups was varied from one to thirty bases (Figure 9). Reactions exhibiting this behavior were designated “distance-independent”. Replacement of the intervening single-stranded DNA bases with a variety of DNA analogues or with duplex DNA demonstrated that efficient long-distance templated synthesis requires a flexible intervening region, but

does not require a backbone structure specific to DNA. A significant fraction of the DNA-templated reactions studied by our group to date have demonstrated at least some distance independence.^[43,44]

Distance-independent DTS is initially puzzling in light of both the expected decrease in effective molarity as a function of distance and the notorious difficulty of forming macrocycles,^[105,106] but is in part explained by the ability of DNA hybridization to elevate the effective molarity to the point that bond formation for some reactions is no longer rate determining. Indeed, subsequent kinetic studies revealed that DNA hybridization, rather than covalent bond formation between reactive groups, is rate determining in distance-independent DTS.^[44] Additional factors contributing to efficient long-distance DTS are discussed in Section 5.1.

3.2. Multistep DNA-Templated Synthesis

Synthetic molecules of useful complexity typically must be generated through multistep synthesis. The discovery of distance-independent DTS was an important advance toward the DNA-templated construction of complex synthetic structures because it raised the possibility of using a single DNA template to direct multiple chemical reactions on progressively elaborated products.

Our group achieved this goal by developing a series of linker and purification strategies that enable the product of a DNA-templated reaction to undergo subsequent DNA-templated steps. The major challenges were to develop general solutions for separating the DNA portion of a DTS reagent from the synthetic product after DNA-templated coupling has taken place (Figure 10), and to develop methods appropriate for pmol-scale aqueous synthesis that enable the products of DNA-templated reactions to be purified away from unreacted templates and reagents.

Integrating the resulting developments, we used DNA templates containing three 10-base coding regions to direct three sequential steps of two different multistep DNA-templated synthetic sequences.^[47] Both a nonnatural tripeptide generated from three successive DNA-templated amine acylation reactions (Figure 11 a) and a branched thioether generated from an amine acylation–Wittig olefination–conjugate addition series of DNA-templated reactions (Figure 11 b) were prepared. These studies are the first examples of translating DNA through a multistep reaction sequence into synthetic small-molecule products.

Following these syntheses, the development of additional DNA-templated reactions, linker strategies, and template architectures (see Section 3.3) has enabled the multistep DTS of increasingly sophisticated structures. For example, we used recently developed DNA-templated oxazolidine formation, a new thioester-based linker, and the second-generation template architectures described in Section 3.3 to translate DNA templates into monocyclic and macro-bicyclic *N*-acyloxazolidines (see Figure 13).^[102] While the first products of multistep DTS are modest in complexity compared with many targets of conventional organic synthesis, these initial examples already suggest that sufficient complexity and structural diversity can

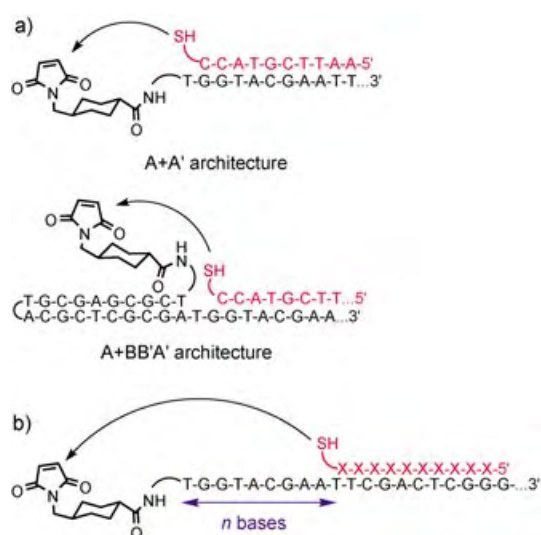


Figure 9. Distance-independent DNA-templated synthesis. a) Two distinct architectures that can support distance-independent DTS. b) A DTS reaction exhibits distance independence if the rates of product formation are comparable for a range of values of *n*.^[43,44]

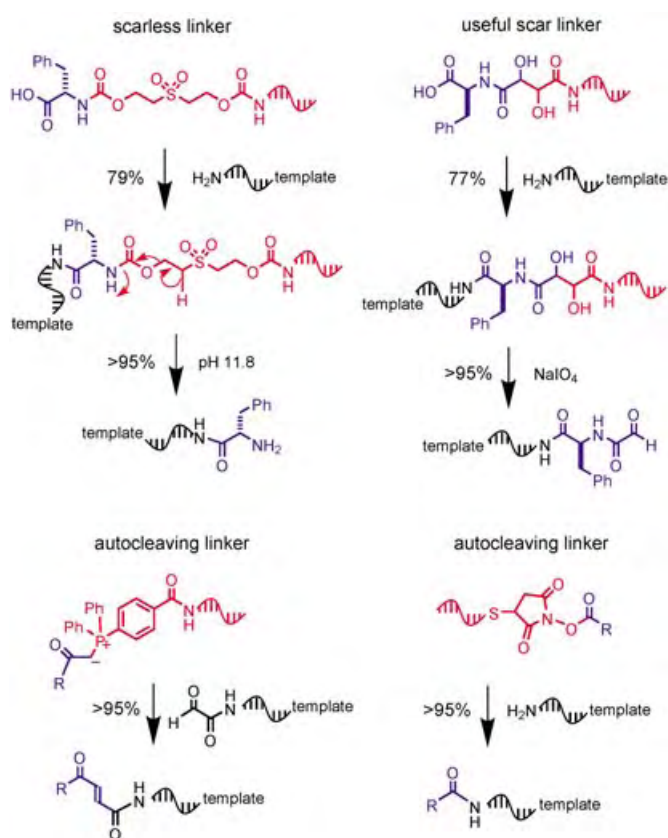


Figure 10. Three linker strategies for DNA-templated synthesis.^[47] Cleavage of a “useful scar linker” generates a functional group that serves as a substrate in subsequent steps. A “scarless linker” is cleaved without introducing additional unwanted functionality. An “autocleaving linker” is cleaved as a natural consequence of the reaction.

be generated to yield DNA-templated compounds with interesting biological or chemical properties.

3.3. New Template Architectures for DNA-Templated Synthesis

The DNA-templated reactions described above use one of three template architectures (Figure 3): A+A', A+B+A'B', or the hairpin form of the latter (A+BB'A'). The predictability of DNA secondary structures suggests the possibility of rationally designing additional template architectures that further expand the synthetic capabilities of DTS.

The distance dependence of some DNA-templated reactions (for example, nitron-olefin dipolar cycloaddition or reductive amination reactions) limits their use in multistep DTS because each of the three template architectures listed above can accommodate at most one distance-dependent reaction (by using the template bases closest to the reactive group). Our group developed a new template architecture that enables normally distance-dependent reactions to proceed efficiently when encoded by template regions far from the reactive group. Distance dependence was overcome by using three to five constant bases at the reactive end of the template to complement a small number of constant bases at

the reactive end of the DNA-linked reagent (Figure 12).^[46] This arrangement, the omega (Ω) architecture, made efficient distance-dependent reactions possible even when they were encoded by bases far from the reactive end of the template. Importantly, sequence specificity is preserved in the Ω architecture despite the presence of invariant complementary bases near the reactive groups because the favorable energetics of hybridizing the constant bases barely offset the entropic penalty of ordering the template bases separating the reactive groups (Figure 12a).^[46] In principle, any DNA-templated reaction can be encoded anywhere along a template of length comparable to those studied (up to ~40 bases) by using the Ω architecture.

A second template architecture developed in our group allows three reactive groups to undergo a DNA-templated reaction together in a single step.^[46] The efficient reaction of three groups in a single location on a DNA template is difficult in the A+A', A+B+A'B', or A+BB'A' template architectures because the rigidity of duplex DNA is known to inhibit DTS between reactive groups separated by double-stranded template–reagent complexes (Figure 12b).^[44] Relocating the reactive group from the end of the template to the non-Watson–Crick face of a nucleotide in the middle of the template enables two DNA-templated reactions involving three reactive groups to take place in a single DTS step (Figure 12a,c). This “T” architecture was used to generate a cinnamide in one step through DNA-templated substitution reaction and Wittig olefination of DNA-linked phosphane, α -iodoamide, and aldehyde groups. In a second example, we used the T architecture to synthesize a triazolylalanine from DNA-linked amine, alkyne, and azide groups through amine acylation and Cu^I-mediated Huisgen cycloaddition (Figure 12c).^[46] As some DNA polymerases used in PCR tolerate template appendages on the non-Watson–Crick face of nucleotides,^[107] the complete information within a T architecture template could be amplified by PCR.

These two second-generation template architectures were essential components of recent multistep DNA-templated syntheses of monocyclic and bicyclic *N*-acyloxazolidines (Figure 13).^[102] Beginning with an amine-linked T template, we used an Ω architecture-assisted long-distance DNA-templated amine acylation to generate T-linked amino alcohols. In the second step, DNA-templated oxazolidine formation was effected by recruiting DNA-linked aldehydes to the 3' arm of the amino alcohol linked T templates. The instability of the resulting oxazolidines required that the final reaction, the oxazolidine N acylation, takes place in the same step as the oxazolidine formation. The N acylation was therefore directed by the 5' arm of the T template. Linker and purification strategies, involving sulfone and thioester cleavage and biotin-based affinity capture and release, provided the DNA-linked *N*-acyloxazolidine in Figure 13a.^[102] A modified version of this synthesis was also implemented; it uses sulfone, phosphane, and diol linkers and ends with a Wittig macrocyclization, providing the bicyclic *N*-acyloxazolidine shown in Figure 13b.^[102]

Eckardt, von Kiedrowski, and co-workers recently achieved the DNA-templated formation of three hydrazone groups simultaneously by combining a branched Y-shaped

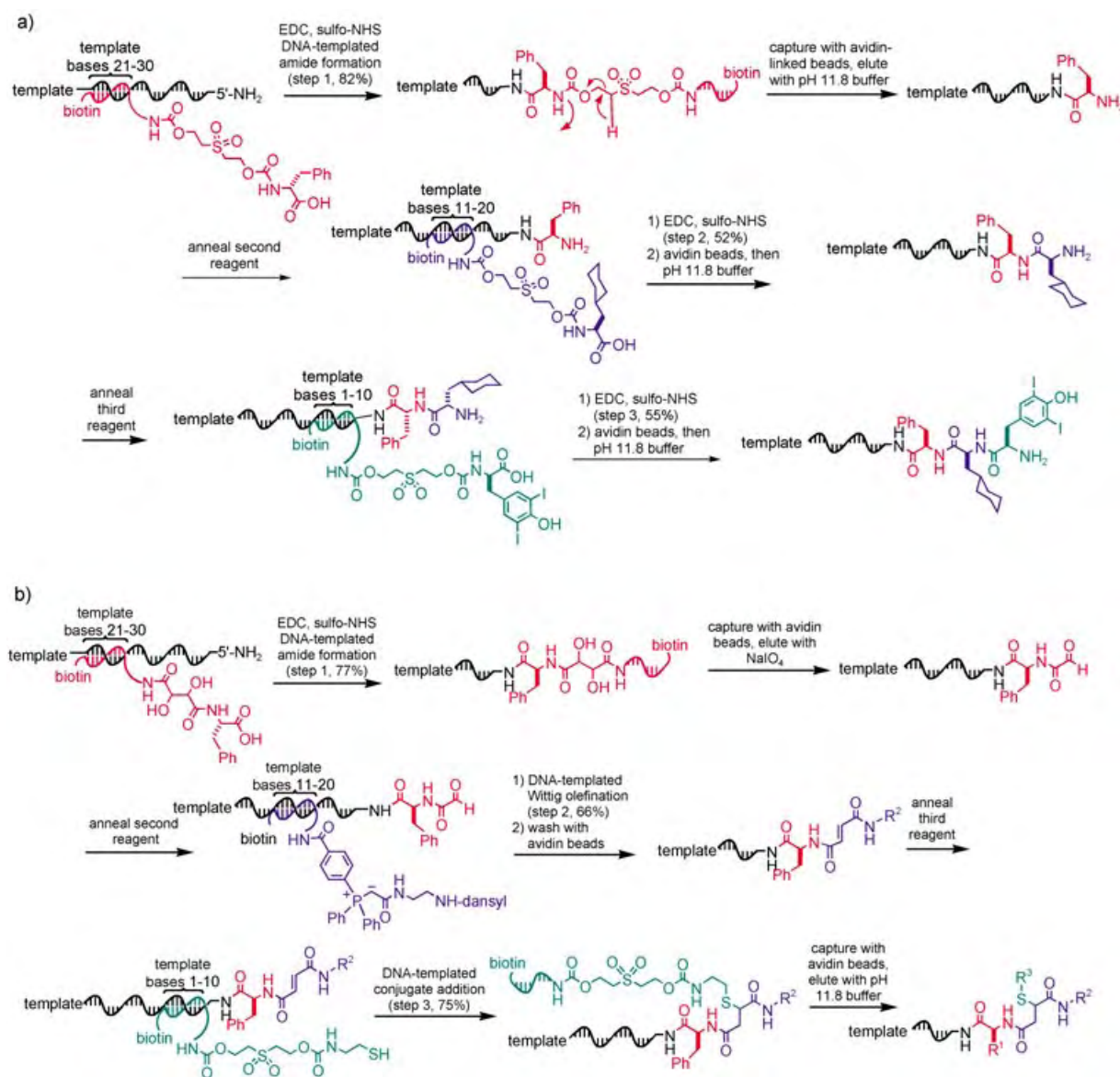


Figure 11. Multistep DNA-templated synthesis of a) a synthetic tripeptide and b) a branched thioether. Only one of the possible thiol addition regioisomers is shown in (b). R¹: CH₂Ph; R²: (CH₂)₂NH-dansyl; R³: (CH₂)₂NH₂; dansyl: 5-(dimethylamino)naphthalene-1-sulfonyl.^[47]

DNA template with three complementary hydrazide-linked oligonucleotides and free trimesaldehyde (Figure 12d).^[108] The branched nature of the template was copied into the Y-shaped product, demonstrating the nucleic acid templated replication of nonlinear connectivity. The complete sequence information and connectivity within a branched template, however, cannot easily be copied using polymerase-based reactions such as PCR and therefore such a template may be better suited for the replication of branched structures than for applications that require decoding of complete template information (see Section 6). The Y template architecture was also used by Gothelf, Brown, and co-workers to assemble branched conjugated polyenes linked by metallosalen groups.^[103]

The six template architectures described above (A+A', A+B+A'B', A+BB'A' (hairpin), Ω, T, and Y) are important developments in DTS because they expand the arrangements

of template sequences and reactive groups that can lead to efficient DNA-templated product formation. In some cases,^[102] the synthesis of a target molecule is only possible with a particular template architecture. The feasibility of generating novel DNA architectures in a predictable manner^[109–118] suggests that increasingly sophisticated template architectures will continue to expand the synthetic capabilities of DTS.

3.4. Synthesis Templated by Double-Stranded DNA

The examples described above all use single-stranded templates to bind complementary oligonucleotides linked to reactive groups by Watson–Crick pairing. Double-stranded DNA can also serve as a template for DTS by using either the major or the minor groove to bind reactants.^[119,120] Luebke

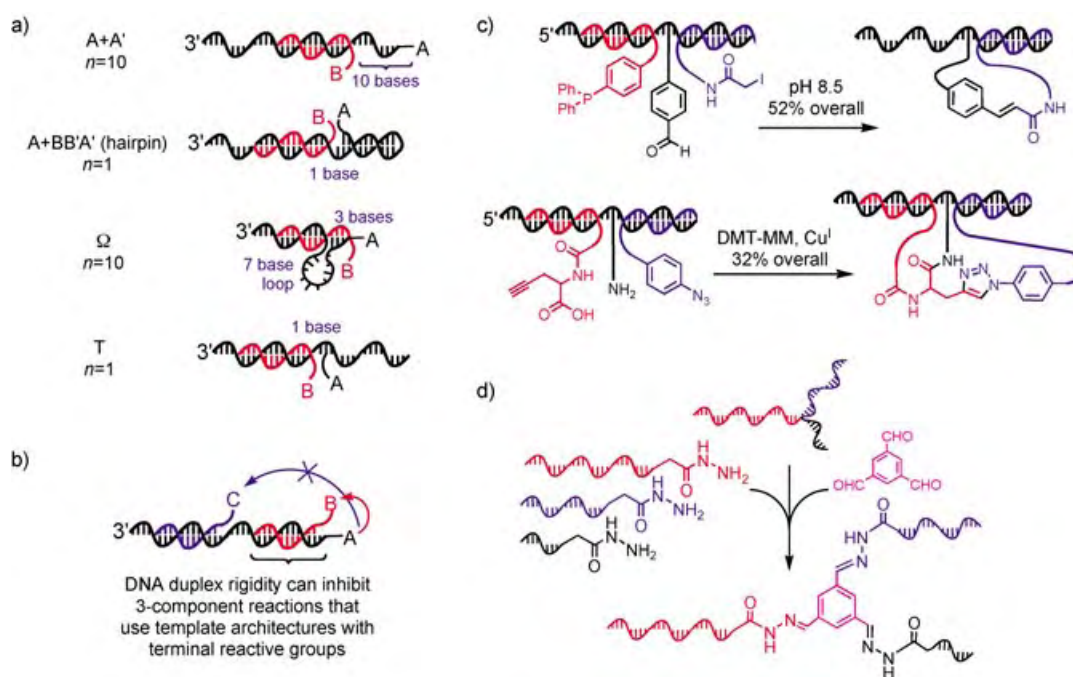


Figure 12. Architectures for DNA-templated synthesis. a) Representative examples of A+A', A+BB'A' (hairpin), Ω, and T architectures. b) Duplex template regions can preclude multiple DNA-templated reactions on a single template in one step. c) Two DNA-templated reactions on a single template in one solution mediated by the T architecture.^[46] d) A Y-shaped template mediates tris-hydrazone formation.^[108]

and Dervan reported duplex-DNA-templated 3',5'-phosphodiester formation between two DNA oligomers designed to bind adjacently in the major groove of a double-stranded template through Hoogsteen base pairing.^[119] The resulting triplex DNA product differs from the products of DNA-templated nucleic acid synthesis described in Section 2.1 in that the sequence of the third strand is neither identical to nor complementary (in a Watson–Crick sense) with that of the template.

Li and Nicolaou developed a self-replicating system that uses both double- and single-stranded DNA to template phosphodiester formation (Figure 14a).^[15] An A+A' double helix templated the synthesis of a third strand through triplex formation. Because A was a palindromic sequence, this third-strand product was identical to A. The newly synthesized A then dissociated from the A+A' duplex and templated the formation of its complement (A') from two smaller oligonucleotides to provide a second-generation A+A' duplex that is ready to enter the next round of replication.^[15] This cycle requires that replicating sequences be palindromic for the third-strand product to be identical to one of the two duplex strands. As with all triplex-based systems, these approaches are limited to homopurine:homopyrimidine templates.

A duplex-DNA-templated synthesis mediated by minor-groove rather than major-groove binding was recently reported by Poulin-Kerstien and Dervan.^[120] Hairpin polyamides containing *N*-methylpyrrole and *N*-methylimidazole groups are known to bind to duplex DNA in the minor groove sequence specifically.^[121] When conjugated to azide and alkyne functionalities, two adjacent hairpin polyamides undergo duplex-DNA-templated Huisgen cycloaddition^[122–126] to provide a branched polyamide that spans both

minor-groove binding sites and shows greater affinity than either of the polyamide reactants (Figure 14b). The reaction exhibits strong distance dependence, consistent with the rigidity of duplex templates^[44] compared with the flexibility of single-stranded DNA that can enable distance-independent DTS.^[44] This distance dependence may prove useful in the self-assembly of small molecules that target double-stranded DNA sequence specifically since both the spacing between binding sites and their sequences must be optimal for efficient coupling.

3.5. New Modes of Controlling Reactivity Enabled by DNA-Templated Synthesis

The use of effective molarity to direct chemical reactions enables nature to control reactivity in ways that are not possible in conventional laboratory synthesis. Primary amino groups, for example, undergo amine acylation during peptide biosynthesis, form imines during biosynthetic aldol reactions, and serve as leaving groups during ammonia lyase catalyzed eliminations—all in the same solution and in a substrate-specific manner. In contrast, under conventional synthetic conditions, amine acylation, imine formation, and amine elimination reactions cannot simultaneously take place in a controlled manner without the spatial separation of each set of reactants.

DTS enables synthetic molecules containing functional groups of similar reactivity to also undergo multiple, otherwise incompatible reactions in the same solution. We demonstrated this mode of controlling reactivity by performing (in one solution) three reactions of maleimides (amine

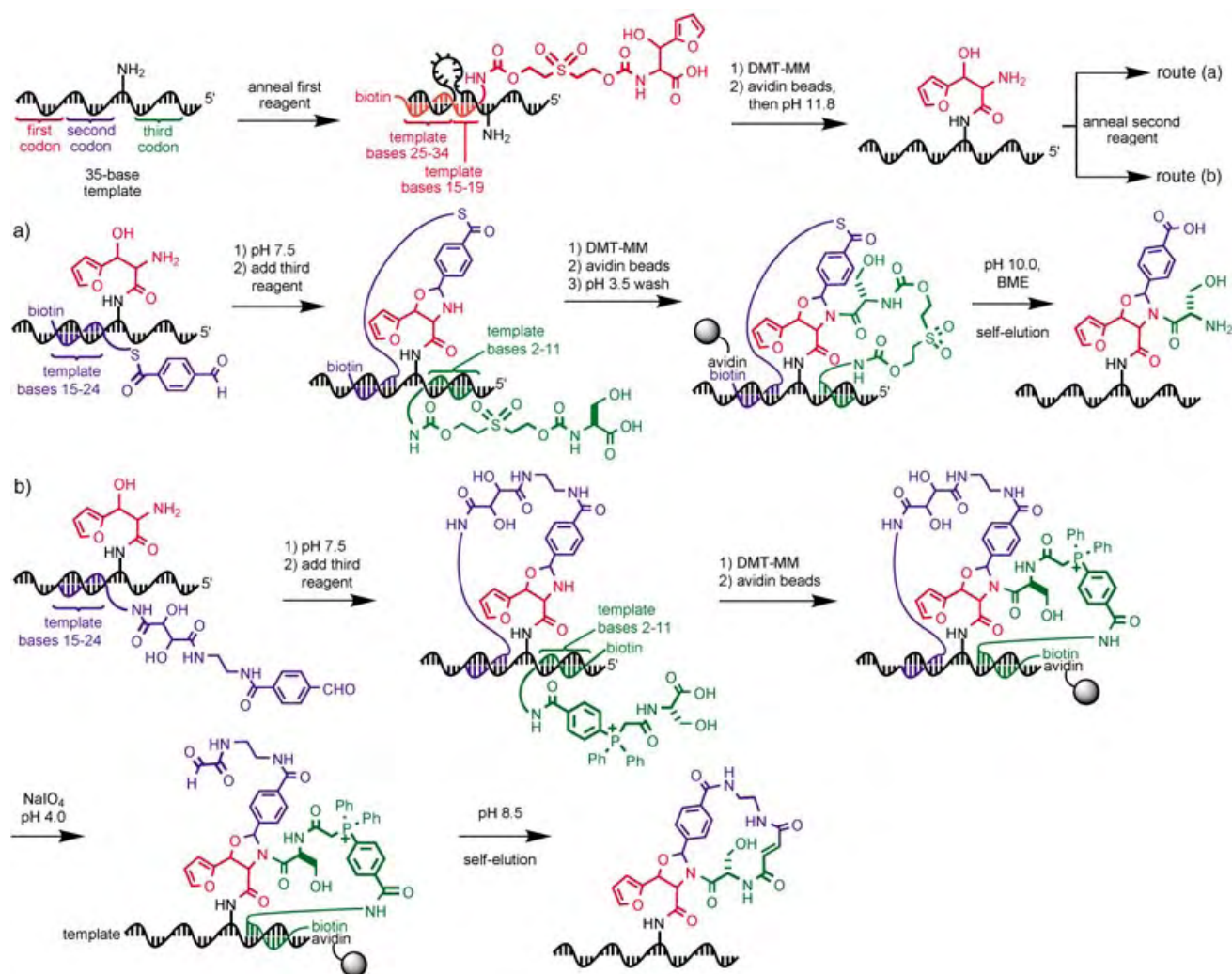


Figure 13. Translation of DNA into *N*-acyloxazolidines. Route (a): mutistep DNA-templated synthesis of a monocyclic *N*-acylated oxazolidine; route (b): multistep DNA-templated synthesis of a bicyclic *N*-acylated oxazolidine.^[102] BME: 2-sulfanyethanol.

addition, thiol addition, and nitro-Michael addition) which generated exclusively three sequence-programmed products out of nine possible products.^[126] Similarly, two aldehyde coupling reactions (reductive amination and Wittig olefination) were performed in one solution, and three amine reactions (amine acylation, reductive amination, and maleimide addition) were also performed in a separate single solution to afford only the desired DNA-templated products.^[126] Finally, all six of the above reactions were performed simultaneously by combining twelve DNA-linked reactive groups in a single solution (Figure 15). Even though the combination of these reactants in a conventional synthesis would lead to the formation of at least 28 possible products, the DNA-templated reactions exclusively generated the six sequence-programmed products shown in Figure 15.^[126]

These findings also suggest that DTS may enable the diversification of synthetic small-molecule libraries in a single solution by using different reaction types without the efforts or constraints associated with spatial separation. This strategy in principle can achieve some of the goals of recent diversity-oriented library syntheses (most notably, the work of

Schreiber and co-workers to introduce skeletal diversity into small-molecule libraries^[127]), but without the requirement of pre-encoding skeletal information within substrate groups. As with any DTS strategy, however, reactions used in this approach must be compatible with the mildly electrophilic and mildly nucleophilic groups present in DNA, and all non-DNA-linked reactants must be mutually compatible.

Finally, it has been recently shown (see the *Note Added in Proof* at the end of this article) that DTS enables heterocoupling reactions to take place between substrates that preferentially homocouple under conventional synthesis conditions. Exclusive heterocoupling is possible in a DNA-templated format because the effective molarity of the heterocoupling partners is much greater than the absolute concentration of any single homocoupling-prone substrate.

4. DNA-Templated Polymerization

DNA- and RNA-templated phosphodiester formation and amine acylation reactions are iterated in nature to

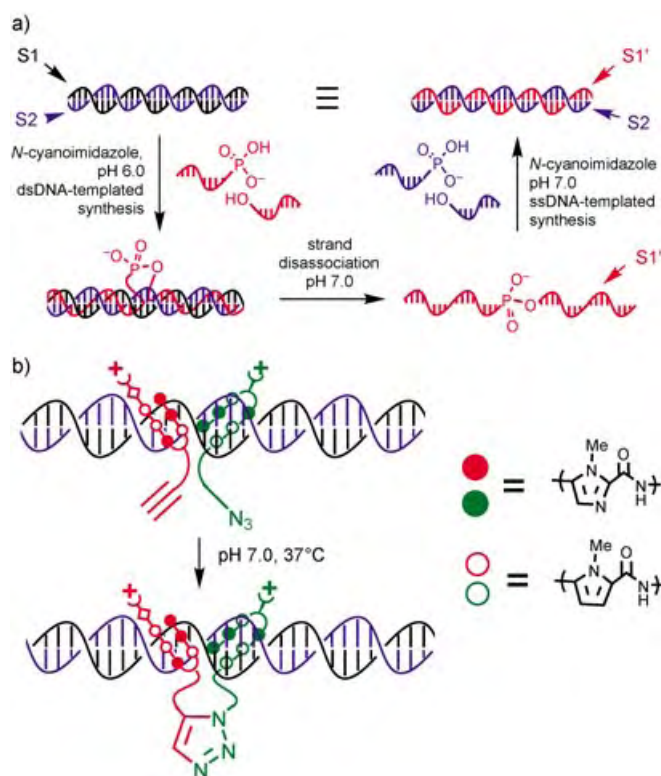


Figure 14. Duplex-DNA-templated synthesis. a) Replication of palindromic double-stranded DNA by using both single-stranded-DNA- and double-stranded-DNA-templated phosphodiester formation.^[15] b) Double-helical-DNA-templated dimerization of polyamides through sequence-specific minor-groove binding.^[120]

biosynthesize functional macromolecules. The efficient laboratory synthesis of sequence-defined synthetic heteropolymers of similar length to functional proteins and nucleic acids remains a daunting challenge. DNA polymerases,^[128–133] RNA polymerases,^[134–137] and the ribosomes^[138–142] are known to tolerate modified building blocks thus enabling the incorporation of modified nucleic acid bases and amino acids into nucleic acid and protein polymers, respectively. Natural enzymes for generating biopolymers, however, typically do not accept monomers containing nonnatural backbones, although as a notable exception, Chaput and Szostak recently

reported the ability of Deep Vent(exo-) DNA polymerase to extend a DNA primer by three α -L-TNA nucleotides.^[143] Nucleic acid templated polymerization has therefore attracted the interest of organic chemists because it may provide access to sequence-defined synthetic heteropolymers free from constraints imposed by polymerase or ribosome acceptance.

4.1. DNA-Templated Polymerization of DNA and RNA

Polymerization reactions are an especially challenging form of DTS because they require many successive reactions to take place efficiently and sequence specifically without the benefit of intermediate purification. A hypothetical DNA-templated coupling reaction that generates a product that is 80% sequence-specific in 80% yield only provides 1% overall yield of a final 10-mer product of correct sequence. The simplest (in retrospect, deceptively so) target for templated polymerization is the polymerization of activated DNA or RNA monomers (Figure 16). These studies, led by the pioneering work of Orgel and co-workers,^[1,85,92,144–150] demonstrated that monomers containing activated phosphate units could induce a small number of DNA-, RNA-, PNA-, HNA-, or ANA-templated phosphoesterification reactions between mono-, di-, tri-, or oligonucleotides to generate oligomeric DNA or RNA products with modest efficiency (generally ~50% yield per monomer coupling).

Acevedo and Orgel achieved the DNA-templated synthesis of an RNA 14-mer by using a DNA template and G and C 5'-phospho-2-methylimidazole monomers.^[147] The full-length polymer resulting from 13 DNA-templated coupling reactions was generated in $\leq 2\%$ overall yield. The sequence specificities of this oligomerization and other early DNA-templated polymerization reactions^[1,85,92,144,146,147,149,150] were not investigated in detail, however, and templates usually consisted of poly(G), poly(C), or mixed G/C bases. Subsequent studies by Stutz and Richert suggest that the error rates of related DNA-templated phosphoimidazole mononucleotide coupling reactions are as high as 30% for forming G:C pairs, and ~50% for forming A:T pairs,^[151] suggesting that these systems may not maintain sufficient sequence specificity to faithfully translate templates into sequence-defined synthetic polymers.

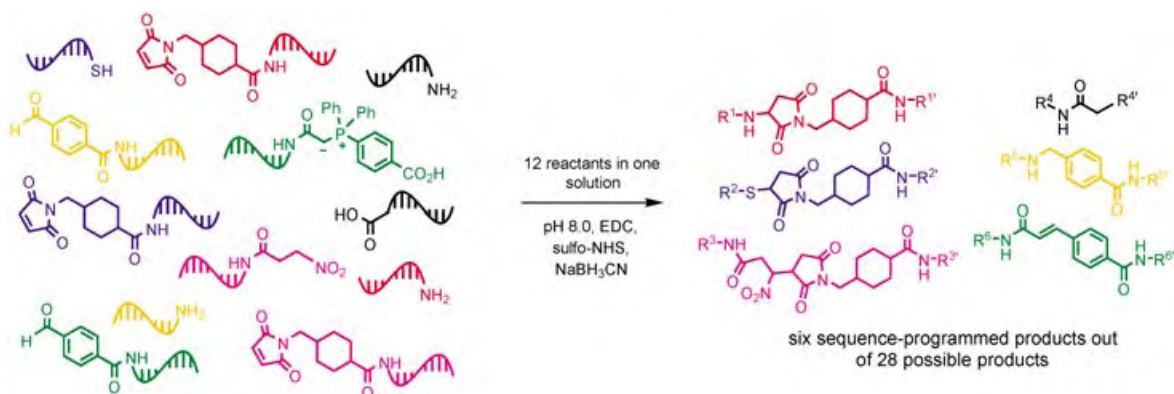


Figure 15. DTS can control multiple, otherwise incompatible reactions in a single solution. R', R'': linker or DNA oligonucleotide.^[126]

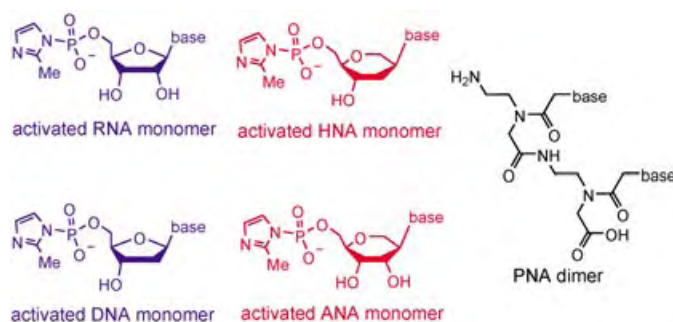


Figure 16. DNA and RNA monomers suitable for oligonucleotide-templated polymerization.^[24, 148–150]

4.2. Nonnatural Polymers Generated by DNA-Templated Polymerization

The DNA-templated oligomerization of non-DNA or non-RNA monomers has also been achieved. Nucleic acid analogues that have been oligomerized by DTS include peptide nucleic acids (PNAs)^[24, 149] and altritol nucleic acid (ANA, the hydroxylated analogue of HNA) (Figure 16).^[150] Bohler, Nielsen, and Orgel used DNA-templated amine acylation to oligomerize five PNA dimers gg on a dC₁₀ template.^[24] This 1995 study represents the first report of a nucleic acid templated synthesis of an oligomer containing a nonnatural backbone. Yields of full-length PNAs in this and subsequent studies,^[148] however, are modest (typically 25% relative to limiting template), and the sequence specificities of these DNA-templated PNA oligomerization reactions are unclear since some oligomeric products are observed even when PNA dimers complementary to portions of the template are excluded, or when the template itself is excluded.^[24, 148] In the case of the nucleic acid templated oligomerization of ANA, Kozlov, Orgel, and co-workers observed only isomeric mixtures of very short oligomers of four or fewer ANA nucleotides from phosphoimidazole transesterification reactions containing ANA or RNA C₁₀ templates.^[150] Chaput's and Szostak's findings that polymerases can catalyze the DNA-templated oligomerization of several TNA nucleotides^[143] raises the possibility that natural or laboratory-evolved polymerases may eventually enable DNA-templated polymerizations.

Reactions other than phosphodiester formation and amine acylation have also been used to effect DNA-templated oligomerization and polymerization, in some cases with remarkable results. In 2000, Fujimoto, Saito, and co-workers used an efficient and reversible DNA-templated photochemical [2+2] cycloaddition (Figure 5b) to oligomerize five DNA hexamers each containing a 5'-exocyclic vinyl group and a 3' pyrimidine on a complementary 30-mer DNA template. The full-length 30-mer product containing four cyclobutane linkages was generated in high yield upon irradiation at 366 nm and could be fragmented back to the monomers quantitatively by irradiation at 302 nm.^[101]

Li, Lynn, and co-workers significantly advanced the field of templated polymerization in 2002 by adapting their

previously described DNA-templated coupling of 5'-amino and 3'-formyl DNA analogues to address DNA-templated polymerization.^[31–35, 38, 39] In contrast with the DNA-templated DNA, RNA, PNA, and ANA oligomerization reactions described above (Figure 16) which generally proceed in low yields and with modest chain-length and sequence specificity, Li, Lynn, and co-workers found that reductive amination mediates the efficient coupling of eight 5'-amino-3'-formyl dT mononucleotides on a dA₈ template to generate the full-length octamer product in 80% yield (Figure 17). Importantly, products larger than eight nucleotides were not observed, oligomerization did not proceed in the absence of template, and studies using templates containing A and T bases showed that oligomerization does not occur when monomer and template sequences cannot form base pairs.^[34] These findings demonstrated that DTS can generate synthetic polymers efficiently with sequence and length specificity.

Our group studied the efficiency, regioselectivity, and sequence specificity of polymerization reactions of PNAs or formyl-PNAs by using amine acylation or reductive amination templated by 5'-amino-terminated hairpin DNA oligonucleotides.^[152] Consistent with the previous observation^[43, 126] of the distance independence of DNA-templated amine acylation, poor regioselectivity and poor yields of full-length products were observed when the polymerization was mediated by amine acylation. In contrast, polymerization mediated by the highly distance-dependent^[43, 46] reductive amination reaction proceeded very efficiently (90% yield of full-length products) and with excellent sequence specificity and regioselectivity (Figure 18),^[152] consistent with the findings of Lynn and co-workers.

We systematically examined the sequence specificity of DNA-templated formyl-PNA polymerization reactions with templates of mixed sequences containing all four bases,^[152] and found that tetrameric formyl-PNA of sequence gvvt (v = g, a, or c) were polymerized with excellent sequence specificity even in the presence of mixtures of all nine possible gvvt formyl-PNAs. In all cases, the polymerization terminated upon reaching the first template codon that did not complement any of the formyl-PNAs in solution. Integrating these findings, DNA-templated reductive amination was used to translate nine different DNA templates, each containing a 40-base coding region with approximately equal percentages of A, G, C, and T (ten consecutive four-base codons), into corresponding sequence-defined synthetic PNA heteropolymers (Figure 18).^[152] Full-length heteropolymeric products were generated in good yields only when the formyl-PNAs complementing all template codons were present. These studies established that synthetic polymers of length comparable to that of natural biopolymers with binding or catalytic properties^[153] can be generated efficiently and sequence specifically by nucleic acid templated synthesis.

5. Toward a Physical Organic Understanding of DNA-Templated Synthesis

Understanding key aspects of DNA-templated synthesis is valuable not only because it enhances the development of

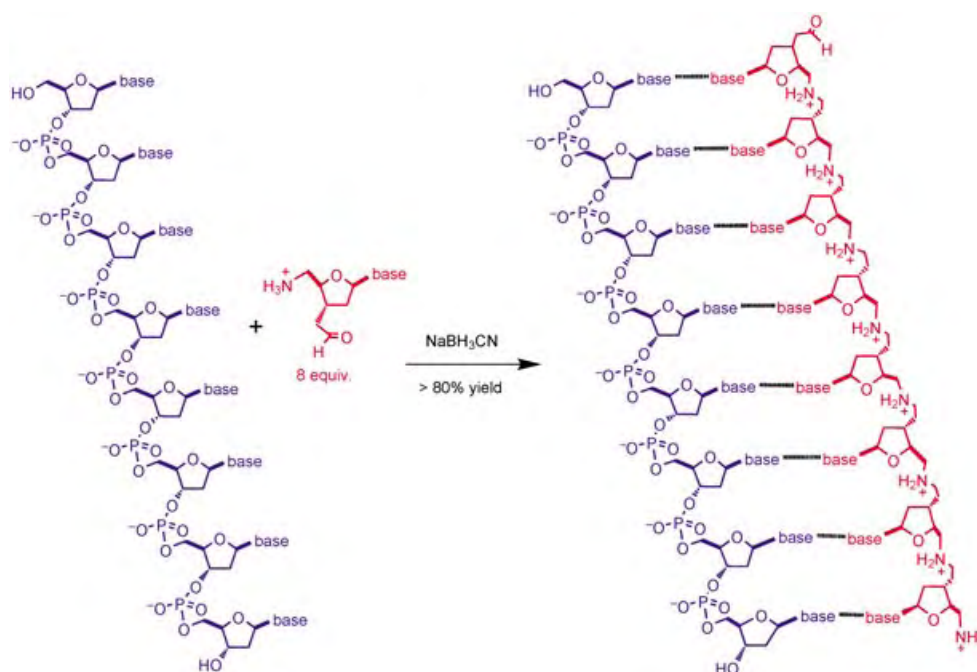


Figure 17. DNA-templated polymerization of 5'-amino-3'-formyl-modified dT monomers.^[34]

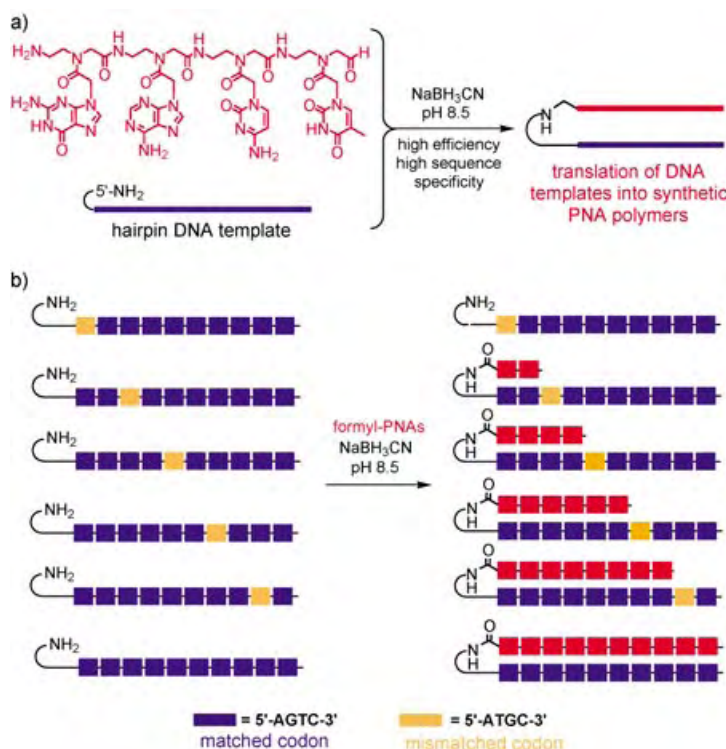


Figure 18. DNA-templated formyl-PNA polymerization. a) A 5'-amino-terminated DNA template (blue) directs the efficient oligomerization of modified formyl-PNAs (red) with high sequence specificity; b) mismatched codons (orange) in the templates halt the polymerization of formyl-PNAs and generate predominantly truncated products, demonstrating regioselectivity.^[132]

DTS but also because it reveals underlying principles that deepen our understanding of analogous biological and chemical systems. In this section we discuss three central

features of DTS for which an understanding of underlying principles is emerging.

5.1. Understanding Distance-Independent DNA-Templated Synthesis

One of the most unexpected and enabling properties of DTS is its ability to direct efficient reactions even when many intervening template nucleotides separate hybridized reactive groups (see Figure 9).^[44] This property raises two questions: 1) why is the rate of product formation for some, but not all, DTS reactions independent of the intervening distance between the hybridized reactive groups; and 2) why is long-distance DTS efficient at all, in contrast with the notorious difficulty^[105,106] of synthesizing macrocycles (which mimic the structure of long-distance DTS products)?

Our group began to address the first question by determining the role of the DNA backbone in mediating efficient long-distance DTS.^[43,44] The intervening nucleotides separating the reactive groups were systematically replaced with structural analogues of similar length but lacking the aromatic base, lacking the entire ribose ring, lacking the ribose and phosphate groups, or lacking nearly all heteroatoms (Figure 19 a). In all cases, efficient long-distance DTS was still observed.^[44] The efficiency of long-distance DTS was significantly reduced, however, when the intervening region was rigidified by hybridization with a complementary DNA oligonucleotide. These results established that structural elements of the DNA backbone are

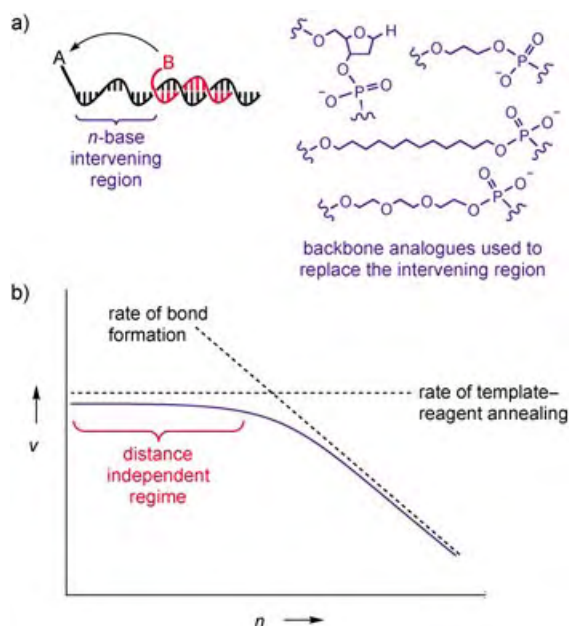


Figure 19. Understanding distance-independent DTS. a) The intervening region of a long-distance A+A' template was replaced with DNA backbone analogues. b) Conceptual model of distance-independent DTS.^[44, 47]

not responsible for distance independence, although flexibility in the intervening region is required.

Subsequent studies by our group^[43] demonstrated that product formation for distance-independent DNA-templated reactions exhibits second-order kinetics (first order in each of the two DNA-linked reactants). This simple finding began to unravel the mystery of distance-independent DTS because it indicated that bond formation between the reactive groups in the hybridized complex (a pseudo-unimolecular process) cannot be rate-determining for these reactions. Instead, the results suggested that hybridization of the two DNA-linked reactants (a bimolecular process) is rate-determining for these reactions. Distance independence therefore can occur when the effective molarity of the hybridized reactive groups is sufficiently high that bond formation occurs faster than DNA hybridization. Increasing the number of intervening nucleotides between the reactive groups in this situation does not decrease the observed rate of product formation until bond formation rates begin to approach or fall below rates of hybridization (Figure 19b).

This simple kinetic model for distance-independent DTS explains differences in behavior among different DNA-templated reactions such as the progressive loss of distance independence in the following series of reactions: Cu^I-mediated Huisgen cycloaddition (fastest rate of bond formation), amine acylation, Wittig olefination, and 1,3 dipolar nitron cycloaddition (slowest rate of bond formation).^[46] One DNA-templated reaction of particular importance (see Section 4.2), however, does not fit this model: reductive amination^[34, 35, 43] is highly distance-dependent,^[126] yet generates the product more rapidly than should be possible under the model in Figure 19b. The origins of this discrepancy are

not yet understood but could be explained if the rate of imine hydrolysis is enhanced by intervening single-stranded template bases, or if imine reduction is inhibited by intervening template nucleotides.

5.2. The Role of High Dilution and Aqueous Solvent

How can long-distance DTS be much more efficient than the equivalent non-templated (intermolecular) reaction considering that macrocyclizations are generally challenging synthetic reactions? There are at least two explanations. The first is the incongruity between reference states of DTS and conventional organic synthesis. Most of the DNA-templated small-molecule syntheses described above are performed at mid-nM reactant concentrations. At these concentrations, rates of nearly all intermolecular reactions including reactions between reactants linked to mismatched DNA are negligible. These intermolecular reaction pathways also include the dimerization and oligomerization of reactants and products—common sources of undesired products in traditional macrocyclization reactions even when performed under “dilute” (typically μM – mM) conditions. By eliminating the possibility of significant dimerization or oligomerization without impairing the formation of desired products, the extremely high dilution of DTS reactions contributes to their viability even in long-distance (pseudo-macrocyclic) format.

An additional key factor behind the efficiency of long-distance DTS compared with conventional synthetic macrocyclization reactions is the use of aqueous solvents in DTS reactions and predominantly nonaqueous solvents in the latter. Aqueous solvents can assist long-distance DTS in several ways. Water is a better solvent than nonaqueous alternatives for the wide range of reactions described above because the rate-determining transition states of these reactions (and indeed of most synthetic transformations) are generally more polar than the starting materials. For some DTS reactions, the aqueous environment enables bond formation rates to exceed the rate of DNA hybridization, resulting in distance independence. In addition, water is well-known to minimize the volume of organic reactants as a consequence of the entropic penalty incurred by ordered water molecules at the water–organic interface. This tendency is reflected in the unusually high cohesive energy density of water.^[154] The tendency of aqueous solvents to contract reactant volume makes water especially well-suited for macrocyclic joining reactions including long-distance DTS. Consistent with this analysis, previous comparisons of macrocyclization efficiencies in water and organic solvents^[105, 106, 154–158] highlight the benefits of aqueous media.

Both of the above proposed roles of aqueous solvents predict that DTS in organic solvents should be less efficient than DTS in water, and more distance-dependent. Early unpublished results by our group (Calderone and Liu) suggest that this is indeed the case. The use of long-chain tetraalkylammonium salts enable DNA-linked reactants to dissolve in organic solvents including dichloromethane, DMF, and methanol.^[159, 160] Remarkably, DTS can be sequence-specific in organic solvents, suggesting that base-pairing of some form

can still take place. However, DNA-templated amine acylation reactions, normally efficient and distance-independent in aqueous solvents, can be less efficient and more distance-dependent when performed in organic solvents.

While in some respects an aqueous solvent is a constraint that prevents the use of strongly basic or strongly acidic reactants, the above analysis suggests that water is also a key enabling aspect of DTS. The insolubility of organic reactants in aqueous solvents frequently precludes the use of water in conventional organic synthesis. In contrast, DNA-linked reactants for DTS, by virtue of their attached oligonucleotides and mM working concentrations, are not constrained by limited solubility in water.

5.3. Probing Template-Induced Effects by Using Stereoselectivity in DNA-Templated Synthesis

DTS is most general when the oligonucleotides modulate the effective molarities of reactants but do not perturb reaction outcomes. DNA-induced stereoselectivity during DTS is a sensitive probe of template-induced effects beyond elevating effective molarities. Moreover, stereoselective DTS serves as a model for how the chirality of an information carrier, in addition to its sequence, can be transferred to the products of a templated synthesis. In theory, stereoselective DTS could also be used to alter the distribution of stereoisomeric products arising from templated reactions to favor desired stereoisomers, although predicting and measuring the sense and magnitude of stereoselection on the minute molecular biology scale of DTS reactions are formidable challenges.

The earliest studies on stereoselectivity in nucleic acid templated synthesis were performed on systems that generated nucleic acid analogues. Joyce, Orgel, and co-workers showed in 1984 that the poly(C_{60})-templated oligomerization of D-guanosine 5'-phospho-2-methylimidazole (D-2-MeImpG) to generate oligo(G) was highly sensitive to inhibition by the enantiomeric monomer L-2-MeImpG.^[161] Interestingly, L-2-MeImpG is efficiently coupled by templated synthesis in response to the poly(C_{60}) template, but the resulting product is effectively capped and cannot undergo further extension. These findings introduced the importance of minimizing inhibition from enantiomeric monomers in prebiotic models of translation. Enantiomeric cross-inhibition was also observed in PNA-templated RNA oligomerization.^[162]

Bolli, Micura, and Eschenmoser demonstrated that stereoselectivity in nucleic acid templated synthesis extends beyond RNA synthesis and includes the synthesis of non-natural nucleic acid analogues.^[25] For example, the D-pyranosyl-RNA-templated oligomerization of complementary pyranosyl-RNA tetramers proceeds diastereoselectively, favoring the coupling of D-tetramers over tetramers with mixed pyranose chirality.^[25] In an elegant example of stereoselective DTS, Kozlov, Orgel, and Nielsen showed that as few as two D-DNA nucleotides when appended to an achiral PNA template could favor the enantioselective template-directed coupling of D-DNA dinucleotides in the A+B+A'B' archi-

ture (Figure 20).^[146] This enantioselectivity is striking because bond formation occurs far away from the inducing chiral groups, and on a different molecule.

We recently investigated stereoselectivity in the DTS of products unrelated to the nucleic acid backbone. The chirality

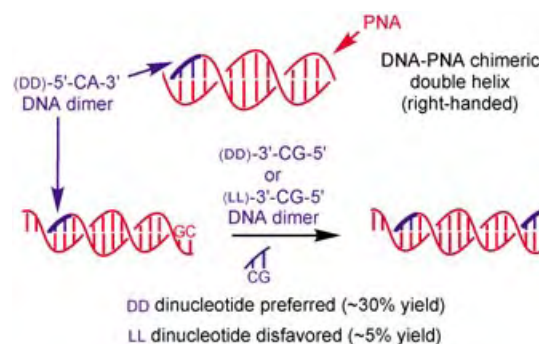


Figure 20. The chirality of a DNA dinucleotide (blue) terminally incorporated in a PNA template affects the stereoselectivity of a remote PNA-templated PNA–DNA coupling. As a result, the (DD)-3'-CG-5' DNA dinucleotide substrate is preferred over the (LL)-3'-CG-5' dimer.^[146]

of a DNA template was observed to induce modest stereoselectivity in DNA-templated thiol substitution reactions (Figure 21a).^[48] The observed stereoselectivity was surprisingly independent of the template architecture, favoring the reaction of the *S* substrate by a similar degree in either hairpin (A+BB'A') or long-distance A+A' architectures. Stereoselectivity was abolished, however, when flexible achiral linkers (three or more CH₂ or O groups) were introduced between the reactive groups and the DNA oligonucleotides (Figure 21b).^[48] These findings indicated that even short flexible linkers can remove template influences beyond modulation of the effective molarity of reactants, suggesting that the use of such linkers is important when DTS is to be performed in its most general form.

The observed stereoselectivity in small-molecule substitution reactions was traced to the macromolecular helical conformation of the single-stranded or double-stranded template, rather than to the chirality of any particular nucleotide group.^[48] This hypothesis was supported by the additional observation that stereoselectivity is inverted when the conformation of template hairpin DNA is transitioned from right-handed B-DNA to left-handed Z-DNA (Figure 21c). These findings also demonstrate how the chirality of information carriers can be transferred through their helicity to products unrelated to the structure of the template.

6. Applications of DNA-Templated Synthesis

DTS connects three broadly important components of chemical and biological systems: nucleic acid sequences, synthetic products, and reactions. This connection in principle allows mixtures of any one of the above three components to

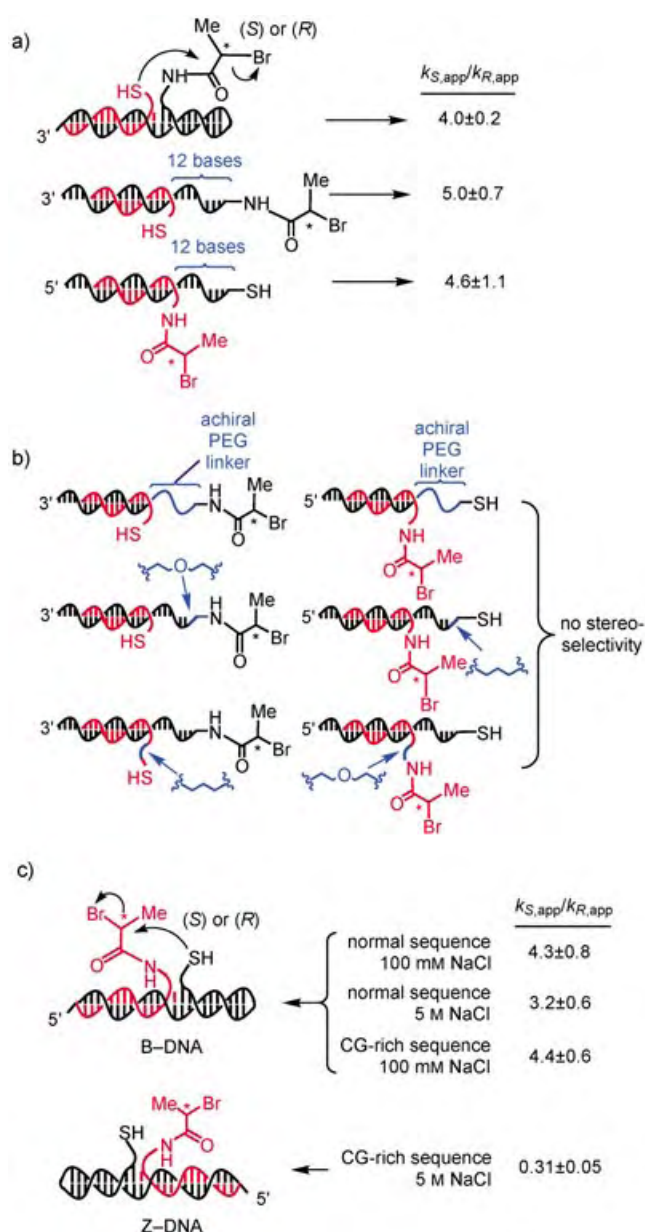


Figure 21. a) Stereoselective DNA-templated substitution reactions. b) Flexible achiral linkers abolish stereoselectivity during DNA-templated substitution reactions. c) Stereoselectivities are inverted when DNA undergoes a B-form (right-handed) to Z-form (left-handed) transition.^[48] k_{app} : apparent reaction rate.

be searched for a desired solution while the other two components are defined. This conceptual framework suggests three types of discovery-oriented applications for DTS: 1) detection of nucleic acid sequences for the DTS of a specific product (nucleic acid sensing), 2) identification of DNA-templated synthetic products with desired properties that arise from DTS (discovery from synthetic libraries), and 3) discovery of DNA-templated reaction schemes that enable template sequences to generate products (reaction discovery). Early studies have already begun to realize the potential of DTS-based approaches for each of these emerging

applications and are presented in the following sections (see the *Note Added in Proof* regarding the application of DTS to reaction discovery).

6.1. Nucleic Acid Sensing

The sequence specificity of DTS enables products to form exclusively in the presence of complementary templates. When the DNA-templated reactions and the product structures are chosen to facilitate the detection of DTS events, the resulting systems can be used to detect the presence of specific nucleic acid sequences.

Ma and Taylor described one of the earliest applications of DTS for nucleic acid detection (see Figure 8a).^[49] DNA templates brought together DNA-linked imidazole and DNA-linked *p*-nitrophenyl esters, inducing imidazole-catalyzed ester hydrolysis. Simple Michaelis–Menten kinetic behavior was observed with a k_{cat} of 0.018 min^{-1} when the ester-linked oligonucleotide was sufficiently short to allow dissociation from the template after hydrolysis. The authors proposed that this system might lead to the sequence-specific release of small-molecule drugs, although localizing DNA-linked reagents to target nucleic acids within living organisms is a significant challenge. This strategy might also be adapted to release a readily detected chromophore or fluorophore in response to a DNA or RNA analyte.

Mattes and Seitz used DNA-templated amine acylation to ligate two octamer PNA reagents for DNA detection.^[50] The formation of coupled PNA products, and therefore the inferred presence of complementary template sequences, was confirmed by MALDI-TOF mass spectrometry. Three template sequences could be detected simultaneously and independently by choosing PNA reagent sequences and lengths such that product masses are distinguishable. Increasing the sensitivity and number of templates that can be simultaneously detected may eventually enable efficient DNA single-nucleotide polymorphism (SNP) detection by this approach.

Kool and co-workers used DNA-templated substitution reactions between 3'-phosphorothioates and 5'-electrophilic groups in two distinct approaches to nucleic acid detection.^[27–30] In the first approach,^[28,29] DNA- or RNA-templated S_N2 reactions covalently link fluorescence resonance energy transfer (FRET) donor and acceptor fluorophores to the same oligonucleotide product (Figure 22a). The resulting proximity of the FRET donor and acceptor fluorophores generates a distinct signal. This approach was used to distinguish mixtures of complementary (matched) and mismatched RNA and DNA templates sequence specifically. In the second approach,^[30] Sando and Kool used DTS to induce the loss of a fluorescent quencher from a fluorescein-linked oligonucleotide probe conjugated to a dabsyl leaving group (Figure 22b). Using these reagents, the presence of complementary rRNA within fixed cells was detected by fluorescence unquenching.^[30]

DTS-based strategies for nucleic acid detection are attractive compared with existing enzyme-based approaches^[51–60] because the detection signal is transduced

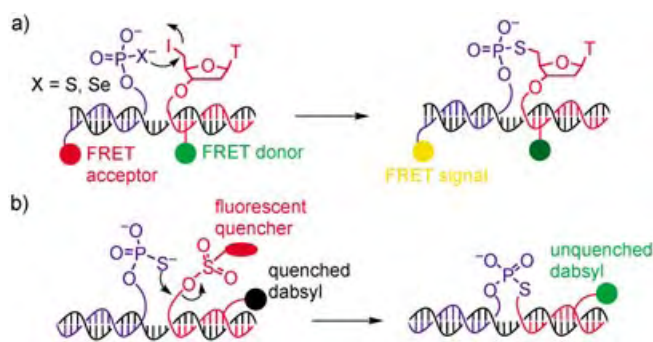


Figure 22. Nucleic acid sensing through DTS. a) A DNA- or RNA-templated substitution reaction enforces fluorophore proximity, creating a detectable FRET signal. b) RNA-templated ligation reactions can induce the unquenching of a tethered dabsyl group.^[27–30]

through chemistry chosen by the researcher rather than through the narrow range of ligation and polymerization reactions that can be mediated by enzymes. Indeed, the structures generated by the small number of early examples above have already significantly expanded the diversity of signals that can arise from nucleic acid sensing. Advances in sensitivity or turnover as well as more extensive use of the inherent ability of DTS to be multiplexed are still needed, however, before DTS-based nucleic acid sensing is likely to achieve widespread and general use.

6.2. Synthetic Small-Molecule and Polymer Evolution

The development of synthetic small molecules and polymers with desired properties is a persistent and widespread challenge in chemistry. Chemists most frequently address this challenge by synthesizing or isolating from nature candidate structures, then evaluating (screening) the candidates for desired compounds (Figure 23). Nature's approach

to functional biological molecules,^[163–169] in contrast, involves 1) the translation of nucleic acids into proteins in a manner that preserves their association, 2) the selection of proteins (and their associated encoding nucleic acids) with favorable properties, and 3) the amplification and occasional diversification of nucleic acids encoding functional proteins that survived selection (Figure 23). Compared with the chemists' approach, nature's evolutionary approach offers advantages including unparalleled sensitivity, efficiency, and throughput without the significant infrastructure requirements associated with conventional library synthesis, spatial separation, and screening.^[82,153,170–172]

Nature's evolution-based approach to discovery can only be applied to molecules that can be translated from amplifiable information carriers. The ribosomes and polymerases address this requirement for proteins, nucleic acids, and their close analogues, but cannot create general synthetic structures. Based on the properties of DTS described above, we hypothesized that DTS could be used to translate libraries of DNA templates sequence specifically into corresponding libraries of synthetic small molecules and polymers,^[44] addressing the major challenge involved in the evolution of synthetic molecules.

DTS products remain covalently associated with the encoding template if architectures such as A+A' or A+BB'A' (hairpin) are used, analogous to the association between nucleic acids and their encoded proteins that is required for protein evolution. Unlike natural translation, however, DTS is not limited to structures that are compatible with biological machinery. A scheme for the evolution of synthetic small molecules proposed by our group in 2001^[44] is shown in Figure 24. Multistep DTS was proposed as a means of translating a library of DNA templates into the corresponding complex synthetic small molecules. The resulting template-linked library could then be subjected to in vitro selections for desired properties. The templates conjugated to and encoding library members surviving selection could be

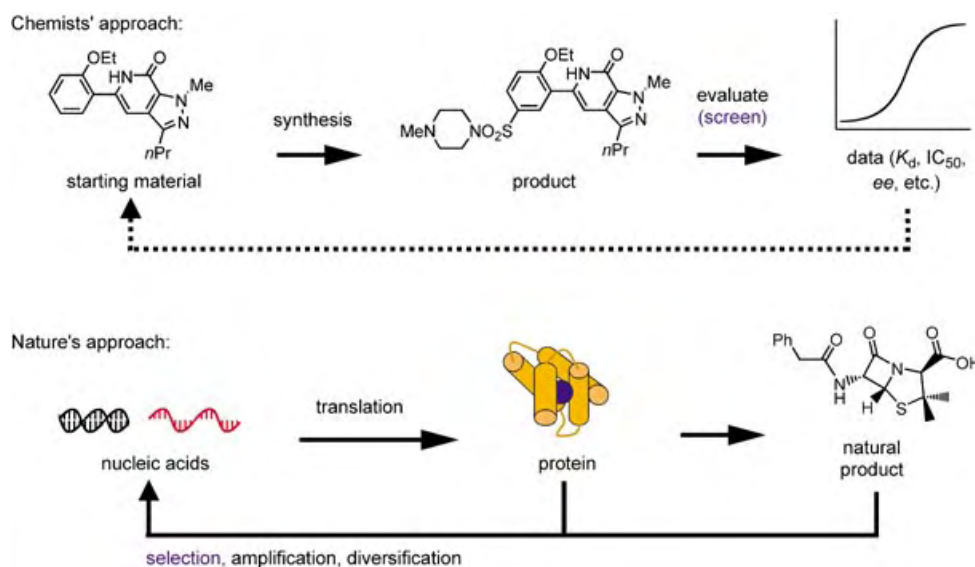


Figure 23. Two approaches to discovering functional molecules.

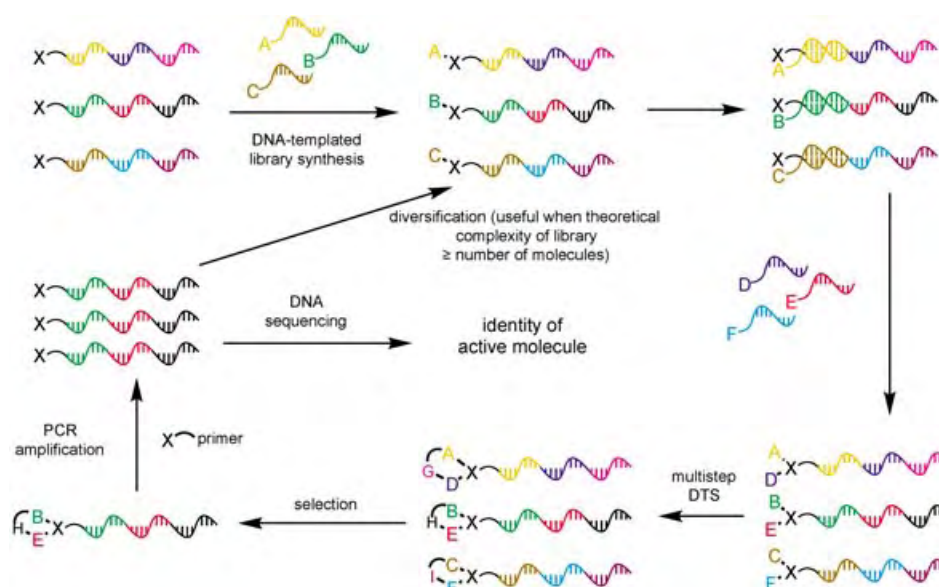


Figure 24. General scheme for the creation and evolution of libraries of synthetic molecules by using DNA-templated library synthesis, in vitro selection, PCR amplification, and DNA sequence diversification.^[44]

amplified by PCR and either sequenced to identify desired compounds, or diversified and subjected to additional cycles of DTS (translation), selection, and amplification.

The scheme in Figure 24 requires that DTS retains its efficiency and sequence specificity when performed in a library format, as opposed to a single-template format. To evaluate the sequence specificity of library-format DTS, we combined a library of 1025 maleimide-linked DNA templates with 1025 complementary thiol-linked reagents in a single solution (Figure 25).^[44] The templates that reacted with one of the 1025 thiol reagents (the only thiol reagent that was biotinylated) were isolated by in vitro selection, amplified by PCR, and characterized by restriction digestion and DNA sequencing. The predominant template was found to be the one complementary to the biotinylated thiol reagent.^[44] These results suggested that DTS can be sufficiently sequence-specific in a library format to enable templates to react with sequence-programmed reagents even in the presence of a large molar excess of mismatched, noncomplementary reagents.

The approach in Figure 24 also requires selections for DNA-linked synthetic molecules with desired properties. Our group developed highly sensitive and effective in vitro selections for DNA-linked synthetic small molecules with protein binding affinity or specificity.^[82] As few as 10^{-20} mol of DNA-linked protein-binding small molecules could be enriched and identified following affinity selections against six different proteins. Iteration of these selections enabled minute quantities of a DNA-linked protein ligand to be enriched starting from a mixture containing a 10^6 -fold excess of DNA-linked nonbinding control molecules.^[82]

Our group recently integrated the generality, sequence specificity, distance independence, and multistep synthetic capability of DTS to translate a library of DNA templates into a library of corresponding complex synthetic small molecules.^[81] Three successive DNA-templated reactions, each

encoded by a distinct 12-base region of a DNA template, followed by an efficient aqueous Wittig macrocyclization,

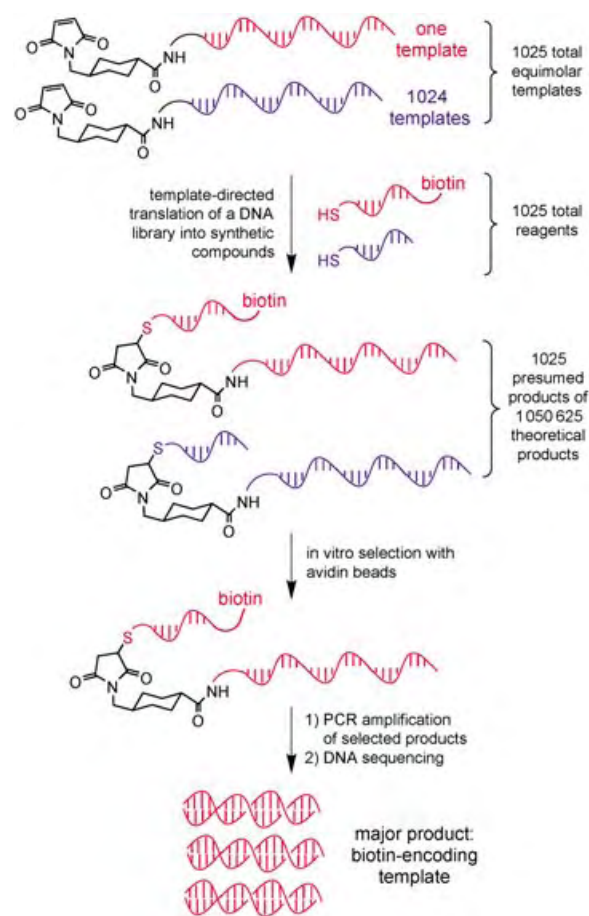


Figure 25. A model library-format DNA-templated synthesis, selection for protein binding, and PCR amplification.^[44]

were used to generate macrocyclic fumaramides conjugated to their encoding DNA templates. A pilot library of 65 macrocyclic fumaramides was translated sequence specifically in this manner from a single solution containing 65 DNA templates. The ability of libraries of DNA-templated synthetic small molecules to be selected for properties such as protein binding affinity was established by performing an *in vitro* selection on this 65-membered macrocyclic fumaramide pilot library. Two iterated rounds of selection for carbonic anhydrase affinity^[82] (without retranslation between rounds) enriched a single member of the 65-membered library. Sequence characterization of the PCR-amplified template emerging from this selection indicated that the selected macrocyclic fumaramide uniquely contained a phenyl sulfonamide group known to confer carbonic anhydrase affinity (Figure 26).^[81] These results collectively indicate that library-format DTS coupled with *in vitro* selection enables the translation, selection, and amplification of DNA sequences encoding not biological macromolecules but rather synthetic small molecules.

By analogy, recent successes in translating DNA templates sequence specifically into synthetic polymers even in the presence of several monomers of different sequence (see Figure 18, Section 4)^[152] suggest that it may be possible to evolve sequence-defined synthetic heteropolymers by analogous processes. Compared with the small-molecule discovery methods described above, DTS-driven synthetic-polymer discovery offers the additional attraction that the theoretical complexity of heteropolymers of even relatively modest length can easily exceed the total number of molecules present in a typical pmol-scale library (10^{12} molecules). Such an enormous sequence space can in principle be explored efficiently by iterated cycles of DTS-based translation, selection for desired binding or catalytic properties, template amplification by PCR, and template diversification by mutagenesis or recombination, representing a true evolutionary process. The possible structures of synthetic heteropolymers

evolved in this manner, however, are constrained to arise from monomers that can sequence specifically hybridize to a DNA template, or that can be cleaved from adapter molecules (analogous to natural tRNAs) that hybridize to DNA.

7. Summary and Outlook

DNA-templated synthesis has evolved dramatically over the past 40 years. DTS was first examined as a model system for prebiotic self-replication through phosphodiester formation. The recently discovered abilities of DTS to sequence specifically generate products unrelated to the phosphoribose backbone^[43–48] and to mediate sequence-programmed synthesis between groups separated by long distances on DNA templates^[47,102] have established DTS as a general method that enables the reactivity of synthetic molecules to be controlled by modulated effective molarities. These discoveries have also led to new developments that have rapidly expanded the synthetic capabilities of DTS, including multi-step DNA-templated small-molecule synthesis, new template architectures, synthesis templated by double-stranded DNA, efficient and sequence-specific DNA-templated polymerization, and DNA-templated library synthesis.

Controlling reactivity with DNA-programmed effective molarity rather than with conventional intermolecular reactions allows synthetic molecules to be manipulated in ways previously available only to the substrates of natural macromolecular templates. For example, otherwise incompatible reactions can take place in a single solution. Some reactions that cannot easily be performed by conventional synthetic methods, such as heterocoupling reactions between substrates that preferentially homocouple, can also take place in a DNA-templated format (see the *Note Added in Proof*). We anticipate that DTS may eventually enable ordered multistep syntheses in a single solution between reactants that would

normally generate uncontrolled mixtures of products. These unique features of effective-molarity-controlled reactivity may expand the accessibility and structural diversity of libraries of synthetic small molecules and heteropolymers beyond what is possible with current approaches.

The ability of DTS to translate amplifiable information into synthetic structures has also led to fundamentally new approaches to widespread discovery challenges that are faced by chemists. These challenges, including nucleic acid detection, synthetic small-molecule and polymer discovery, and reaction discovery, in principle can now be addressed

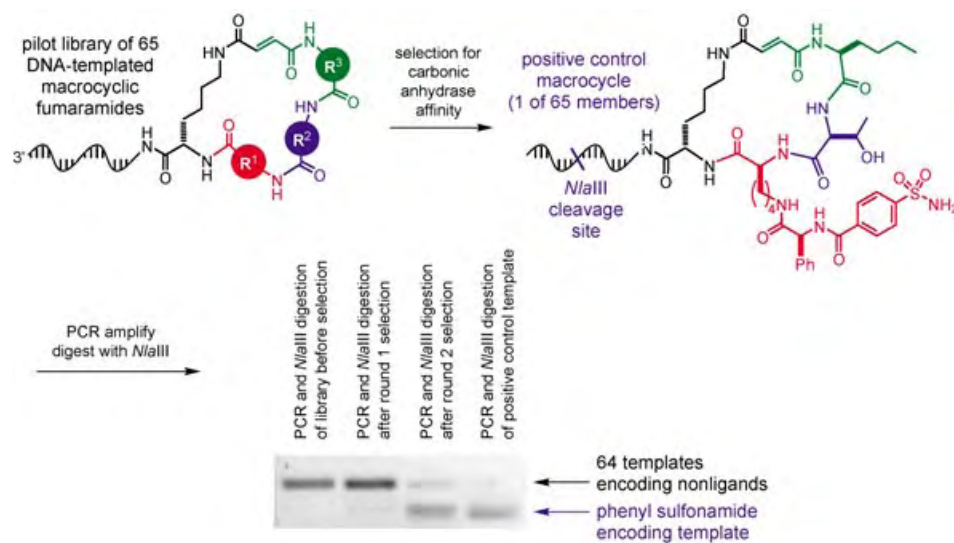


Figure 26. *In vitro* selection of a carbonic anhydrase ligand from a 65-membered library of DNA-templated macrocyclic fumaramides.^[81]

with the assistance of powerful translation, selection, amplification, and diversification strategies previously available only to biological macromolecules.

Several remaining goals must still be met for the vision presented herein to be fully realized. These goals include 1) continuing to expand the scope and synthetic capabilities of DTS beyond the modest fraction of synthetic organic chemistry represented above, 2) continuing to develop and apply new modes of controlling synthetic reactivity through DTS that cannot be realized by conventional synthetic methods, 3) discovering additional reactions that occur efficiently in a DTS format and that are not known to exist or that cannot take place in a nontemplated format, and 4) discovering functional synthetic small molecules and polymers that are difficult or impossible to find by other approaches. Leslie Orgel presciently wrote in 1995 that the development of chemical systems that incorporate fundamental and powerful features of biological molecules “will require a combination of the techniques of organic chemistry ... and the methods of molecular biology.”^[1] Less than a decade later, DNA-templated synthesis has transformed this prediction into a fertile frontier for organic chemistry.

Note Added in Proof (August 16, 2004): The third proposed application of DTS listed in section 6, reaction discovery, has now been realized and is reported in “Reaction Discovery Enabled by DNA-Templated Synthesis and In Vitro Selection”: M. W. Kanan, M. M. Rozenman, K. Sakurai, T. M. Snyder, D. R. Liu, *Nature* **2004**, in press.

8. Abbreviations

ANA	altritol nucleic acid
CDI	1-(3-dimethylaminopropyl)-3-ethylcarbodiimide
DMT-MM	4-(4,6-dimethoxy-1,3,5-triazin-2-yl)-4-methylmorpholinium chloride
Dabsyl	5-dimethylaminonaphthalene-1-sulfonyl
DTS	DNA-templated synthesis
EDC	3-(3-dimethylaminopropyl)-1-ethylcarbodiimide
FRET	fluorescence resonance energy transfer
HNA	hexitol nucleic acid
MALDI-TOF	matrix-assisted laser desorption ionization–time of flight
PCR	polymerase chain reaction
Sulfo-NHS	<i>N</i> -hydroxysulfosuccinimide sodium salt
TNA	threose nucleic acid

We thank Matt Kanan, Jeff Doyon, Allen Buskirk, Zev Gartner, Prof. Stuart Schreiber, and Prof. Matthew Shair for helpful discussions. X.L. is supported by NIH/NIGMS (R01 GM065865) and by the Office of Naval Research (N00014-03-1-0749).

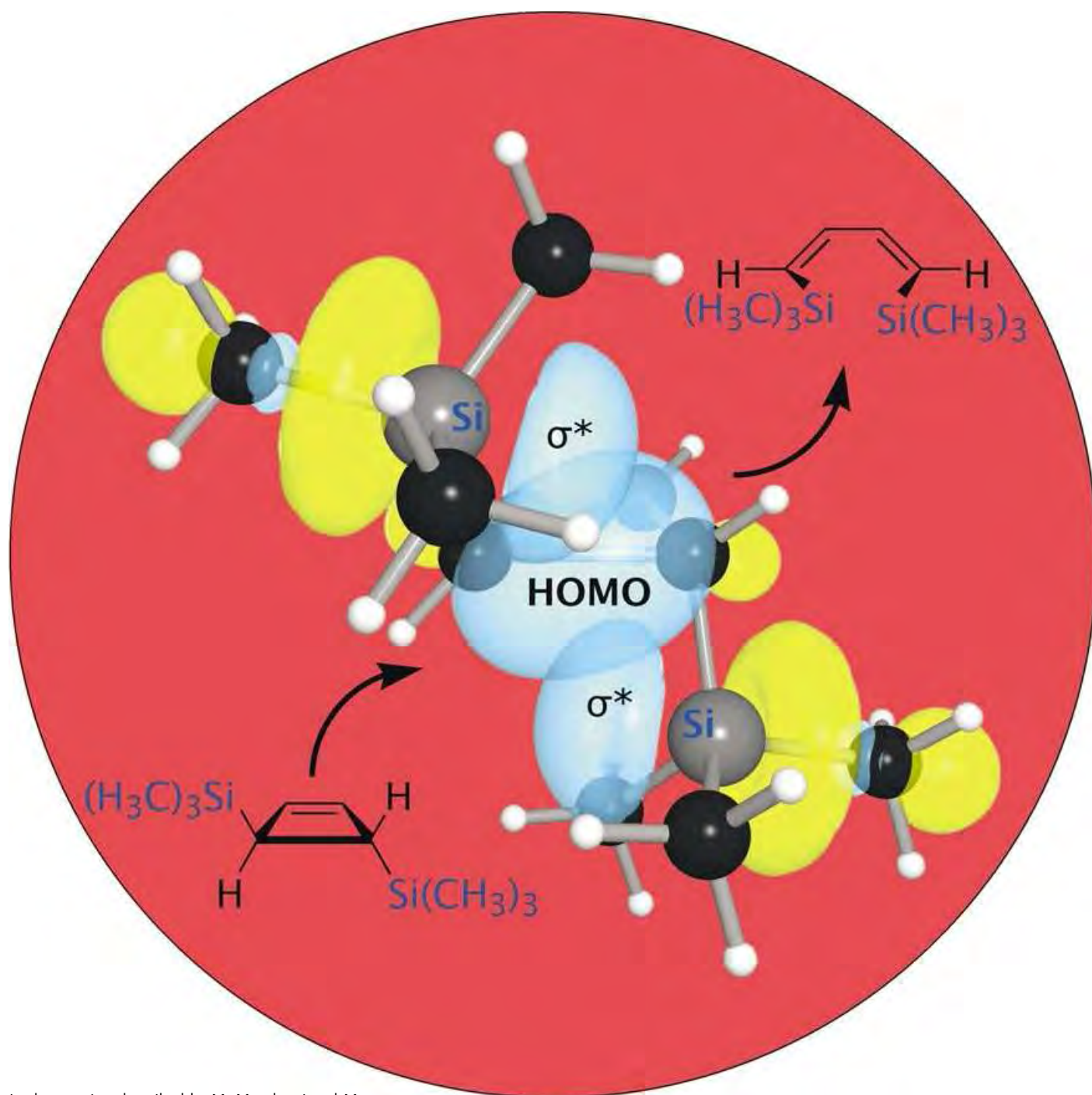
Received: February 13, 2004 [A656]

- [1] L. E. Orgel, *Acc. Chem. Res.* **1995**, 28, 109.
- [2] G. Ertem, J. P. Ferris, *Nature* **1996**, 379, 238.
- [3] L. E. Orgel, *Nature* **1992**, 358, 203.
- [4] J. P. Ferris, R. A. Sanchez, L. E. Orgel, *J. Mol. Biol.* **1968**, 33, 693.
- [5] M. P. Robertson, S. L. Miller, *Nature* **1995**, 375, 772.
- [6] R. Lohrmann, L. E. Orgel, *Science* **1968**, 161, 64.
- [7] W. D. Fuller, R. A. Sanchez, L. E. Orgel, *J. Mol. Biol.* **1972**, 67, 25.
- [8] G. Arrhenius, J. L. Bada, G. F. Joyce, A. Lazcano, S. Miller, L. E. Orgel, *Science* **1999**, 283, 792.
- [9] G. F. Joyce, *Nature* **2002**, 418, 214.
- [10] G. F. Joyce, *Nature* **1989**, 338, 217.
- [11] W. Gilbert, *Nature* **1986**, 319, 618.
- [12] J. P. Ferris, G. Ertem, *Science* **1992**, 257, 1387.
- [13] R. Naylor, P. T. Gilham, *Biochemistry* **1966**, 5, 2722.
- [14] A. Luther, R. Brandsch, G. von Kiedrowski, *Nature* **1998**, 396, 245.
- [15] T. Li, K. C. Nicolaou, *Nature* **1994**, 369, 218.
- [16] T. Inoue, L. E. Orgel, *J. Am. Chem. Soc.* **1981**, 103, 7666.
- [17] T. Inoue, L. E. Orgel, *Science* **1983**, 219, 859.
- [18] T. Inoue, G. F. Joyce, K. Grzeskowiak, L. E. Orgel, J. M. Brown, C. B. Reese, *J. Mol. Biol.* **1984**, 178, 669.
- [19] W. S. Zielinski, L. E. Orgel, *Nature* **1987**, 327, 346.
- [20] W. S. Zielinski, L. E. Orgel, *J. Mol. Evol.* **1989**, 29, 281.
- [21] H. Rembold, L. E. Orgel, *J. Mol. Evol.* **1994**, 38, 205.
- [22] L. Rodriguez, L. E. Orgel, *J. Mol. Evol.* **1991**, 33, 477.
- [23] C. B. Chen, T. Inoue, L. E. Orgel, *J. Mol. Biol.* **1985**, 181, 271.
- [24] C. Bohler, P. E. Nielsen, L. E. Orgel, *Nature* **1995**, 376, 578.
- [25] M. Bolli, R. Micura, A. Eschenmoser, *Chem. Biol.* **1997**, 4, 309.
- [26] M. K. Herrlein, J. S. Nelson, R. L. Letsinger, *J. Am. Chem. Soc.* **1995**, 117, 10151.
- [27] Y. Xu, E. T. Kool, *J. Am. Chem. Soc.* **2000**, 122, 9040.
- [28] Y. Xu, N. B. Karalkar, E. T. Kool, *Nat. Biotechnol.* **2001**, 19, 148.
- [29] Y. Xu, E. T. Kool, *Nucleic Acids Res.* **1999**, 27, 875.
- [30] S. Sando, E. T. Kool, *J. Am. Chem. Soc.* **2002**, 124, 9686.
- [31] Z.-Y. J. Zhan, J. Ye, X. Li, D. G. Lynn, *Curr. Org. Chem.* **2001**, 5, 885.
- [32] Z.-Y. J. Zhan, D. G. Lynn, *J. Am. Chem. Soc.* **1997**, 119, 12420.
- [33] P. Luo, J. C. Leitzel, Z.-Y. J. Zhan, D. G. Lynn, *J. Am. Chem. Soc.* **1998**, 120, 3019.
- [34] X. Li, Z.-Y. J. Zhan, R. Knipe, D. G. Lynn, *J. Am. Chem. Soc.* **2002**, 124, 746.
- [35] X. Li, D. G. Lynn, *Angew. Chem.* **2002**, 114, 4749; *Angew. Chem. Int. Ed.* **2002**, 41, 4567.
- [36] Y. Gat, D. G. Lynn, *Biopolymers* **1998**, 48, 19.
- [37] Y. Gat, D. G. Lynn in *Templated Organic Synthesis* (Eds.: P. J. Stang, F. Diederich), Wiley-VCH, Weinheim, **1999**, p. 133.
- [38] J. T. Goodwin, D. G. Lynn, *J. Am. Chem. Soc.* **1992**, 114, 9197.
- [39] J. C. Leitzel, D. G. Lynn, *Chem. Rec.* **2001**, 1, 53.
- [40] Y. Xu, E. T. Kool, *Tetrahedron Lett.* **1997**, 38, 5595.
- [41] Y. Xu, E. T. Kool, *Nucleic Acids Res.* **1998**, 26, 3159.
- [42] D. Summerer, A. Marx, *Angew. Chem.* **2002**, 114, 93; *Angew. Chem. Int. Ed.* **2002**, 41, 89.
- [43] Z. J. Gartner, M. W. Kanan, D. R. Liu, *Angew. Chem.* **2002**, 114, 1847; *Angew. Chem. Int. Ed.* **2002**, 41, 1796.
- [44] Z. J. Gartner, D. R. Liu, *J. Am. Chem. Soc.* **2001**, 123, 6961.
- [45] J. L. Czapinski, T. L. Sheppard, *J. Am. Chem. Soc.* **2001**, 123, 8618.
- [46] Z. J. Gartner, R. Grubina, C. T. Calderone, D. R. Liu, *Angew. Chem.* **2003**, 115, 1408; *Angew. Chem. Int. Ed.* **2003**, 42, 1370.
- [47] Z. J. Gartner, M. W. Kanan, D. R. Liu, *J. Am. Chem. Soc.* **2002**, 124, 10304.
- [48] X. Li, D. R. Liu, *J. Am. Chem. Soc.* **2003**, 125, 10188.
- [49] Z. Ma, J. S. Taylor, *Proc. Natl. Acad. Sci. USA* **2000**, 97, 11159.

- [50] A. Mattes, O. Seitz, *Angew. Chem.* **2001**, *113*, 3277; *Angew. Chem. Int. Ed.* **2001**, *40*, 3178.
- [51] U. Landegren, R. Kaiser, J. Sanders, L. Hood, *Science* **1988**, *241*, 1077.
- [52] K. J. Barringer, L. Orgel, G. Wahl, T. R. Gingeras, *Gene* **1990**, *89*, 117.
- [53] D. Y. Wu, R. B. Wallace, *Genomics* **1989**, *4*, 560.
- [54] D. A. Nickerson, R. Kaiser, S. Lappin, J. Stewart, L. Hood, U. Landegren, *Proc. Natl. Acad. Sci. USA* **1990**, *87*, 8923.
- [55] F. Barany, *Proc. Natl. Acad. Sci. USA* **1991**, *88*, 189.
- [56] M. Samiotaki, M. Kwiatkowski, J. Parik, U. Landegren, *Genomics* **1994**, *20*, 238.
- [57] J. Luo, D. E. Bergstrom, F. Barany, *Nucleic Acids Res.* **1996**, *24*, 3071.
- [58] R. Favis, J. P. Day, N. P. Gerry, C. Phelan, S. Narod, F. Barany, *Nat. Biotechnol.* **2000**, *18*, 561.
- [59] M. Nilsson, G. Barbany, D. O. Antson, K. Gertow, U. Landegren, *Nat. Biotechnol.* **2000**, *18*, 791.
- [60] C. E. Pritchard, E. M. Southern, *Nucleic Acids Res.* **1997**, *25*, 3403.
- [61] A. De Mesmaeker, R. Haner, P. Martin, H. E. Moser, *Acc. Chem. Res.* **1995**, *28*, 366.
- [62] D. G. Knorre, V. V. Vlassov, *Prog. Nucleic Acid Res. Mol. Biol.* **1985**, *25*, 291.
- [63] A. S. Boutorine, C. Boiziau, T. Le Doan, J. J. Toulme, C. Helene, *Biochimie* **1992**, *74*, 485.
- [64] A. S. Levina, M. V. Berezovskii, A. G. Venjaminova, M. I. Dobrikov, M. N. Repkova, V. F. Zarytova, *Biochimie* **1993**, *75*, 25.
- [65] J. F. Ortigao, A. Ruck, K. C. Gupta, R. Rosch, R. Steiner, H. Seliger, *Biochimie* **1993**, *75*, 29.
- [66] U. Piesles, B. S. Sproat, P. Neuner, F. Cramer, *Nucleic Acids Res.* **1989**, *17*, 8967.
- [67] J. M. Kean, A. Murakami, K. R. Blake, C. D. Cushman, P. S. Miller, *Biochemistry* **1988**, *27*, 9113.
- [68] D. S. Sigman, A. Mazumder, D. M. Perrin, *Chem. Rev.* **1993**, *93*, 2295.
- [69] J. Chin, *Acc. Chem. Res.* **1991**, *24*, 145.
- [70] C.-H. B. Chen, D. S. Sigman, *J. Am. Chem. Soc.* **1988**, *110*, 6570.
- [71] J. S. Sun, J. C. François, R. Lavery, T. Saison-Behmoaras, T. Montenay-Garestier, N. T. Thuong, C. Helène, *Biochemistry* **1988**, *27*, 6039.
- [72] T. Le Doan, L. Perrouault, C. Helène, M. Chassignol, N. T. Thuong, *Biochemistry* **1986**, *25*, 6736.
- [73] J. R. Morrow, L. A. Buttrey, V. M. Shelton, K. A. Berback, *J. Am. Chem. Soc.* **1992**, *114*, 1903.
- [74] D. Magda, R. A. Miller, J. L. Sessler, B. L. Iverson, *J. Am. Chem. Soc.* **1994**, *116*, 7439.
- [75] J. K. Bashkin, E. I. Frolova, U. S. Sampath, *J. Am. Chem. Soc.* **1994**, *116*, 5981.
- [76] J. Hall, D. Husken, U. Piesles, H. E. Moser, R. Haner, *Chem. Biol.* **1994**, *1*, 185.
- [77] D. R. Corey, D. Pei, P. G. Schultz, *Biochemistry* **1989**, *28*, 8277.
- [78] W. P. Ma, S. E. Hamilton, J. G. Stowell, S. R. Byrn, V. J. Davisson, *Bioorg. Med. Chem.* **1994**, *2*, 169.
- [79] S. Kanaya, C. Nakai, A. Konishi, H. Inoue, E. Ohtsuka, M. Ikehara, *J. Biol. Chem.* **1992**, *267*, 8492.
- [80] Q. Zhou, S. E. Rokita, *Proc. Natl. Acad. Sci. USA* **2003**, *100*, 15452.
- [81] Z. J. Gartner, B. N. Tse, R. Grubina, J. B. Doyon, T. M. Snyder, D. R. Liu, *Science* **2004**, in press.
- [82] J. B. Doyon, T. M. Snyder, D. R. Liu, *J. Am. Chem. Soc.* **2003**, *125*, 12372.
- [83] J. Ye, Y. Gat, D. G. Lynn, *Angew. Chem.* **2000**, *112*, 3787; *Angew. Chem. Int. Ed.* **2000**, *39*, 3641.
- [84] R. K. Bruick, P. E. Dawson, S. B. Kent, N. Usman, G. F. Joyce, *Chem. Biol.* **1996**, *3*, 49.
- [85] G. F. Joyce, *Cold Spring Harbor Symposia on Quantitative Biology, Vol. LII*, Cold Spring Harbor Press, Cold Spring Harbor, NY, **1987**, p. 41.
- [86] T. Wu, L. E. Orgel, *J. Am. Chem. Soc.* **1992**, *114*, 7963.
- [87] T. Wu, L. E. Orgel, *J. Am. Chem. Soc.* **1992**, *114*, 5496.
- [88] G. von Kiedrowski, *Angew. Chem.* **1986**, *98*, 932; *Angew. Chem. Int. Ed. Engl.* **1986**, *25*, 932.
- [89] K. Schoning, P. Scholz, S. Guntha, X. Wu, R. Krishnamurthy, A. Eschenmoser, *Science* **2000**, *290*, 1347.
- [90] X. Wu, G. Delgado, R. Krishnamurthy, A. Eschenmoser, *Org. Lett.* **2002**, *4*, 1283.
- [91] X. Wu, S. Guntha, M. Ferencic, R. Krishnamurthy, A. Eschenmoser, *Org. Lett.* **2002**, *4*, 1279.
- [92] I. A. Kozlov, B. De Bouvere, A. Van Aerschoot, P. Herdewijn, L. E. Orgel, *J. Am. Chem. Soc.* **1999**, *121*, 5856.
- [93] S. Pitsch, A. Eschenmoser, *Helv. Chim. Acta* **1995**, *78*, 1621.
- [94] R. J. Lewis, P. C. Hanawalt, *Nature* **1982**, *298*, 393.
- [95] J. Liu, J. S. Taylor, *Nucleic Acids Res.* **1998**, *26*, 3300.
- [96] G. P. Royer, K. A. Cruickshank, L. E. Morrison, EP 0214626A2, **1989**.
- [97] J. Woo, P. B. Hopkins, *J. Am. Chem. Soc.* **1991**, *113*, 5457.
- [98] R. L. Letsinger, T. Wu, R. Elghanian, *J. Am. Chem. Soc.* **1994**, *116*, 811.
- [99] R. L. Letsinger, T. Wu, R. Elghanian, *Nucleosides Nucleotides* **1997**, *15*, 643.
- [100] F. D. Lewis, T. Wu, E. L. Burch, D. M. Bassani, J.-S. Yang, S. Schneider, W. Jäger, R. L. Letsinger, *J. Am. Chem. Soc.* **1995**, *117*, 8785.
- [101] K. Fujimoto, S. Matsuda, N. Takahashi, I. Saito, *J. Am. Chem. Soc.* **2000**, *122*, 5646.
- [102] X. Li, Z. J. Gartner, B. N. Tse, D. R. Liu, *J. Am. Chem. Soc.* **2004**, in press.
- [103] K. V. Gothelf, A. Thomsen, M. Nielsen, E. Clo, R. S. Brown, *J. Am. Chem. Soc.* **2004**, *126*, 1044.
- [104] J. Brunner, A. Mokhir, R. Kraemer, *J. Am. Chem. Soc.* **2003**, *125*, 12410.
- [105] R. B. Woodward, E. Logusch, K. P. Nambiar, K. Sakan, D. E. Ward, B. W. Au-Yeung, P. Balaram, L. J. Browne, P. J. Card, C. H. Chen, *J. Am. Chem. Soc.* **1981**, *103*, 3210.
- [106] G. Illuminati, L. Mandolini, *Acc. Chem. Res.* **1981**, *14*, 95.
- [107] J. A. Bittker, K. J. Phillips, D. R. Liu, *Curr. Opin. Chem. Biol.* **2002**, *6*, 367.
- [108] L. H. Eckardt, K. Naumann, W. M. Pankau, M. Rein, M. Schweitzer, N. Windhab, G. von Kiedrowski, *Nature* **2002**, *420*, 286.
- [109] N. C. Seeman, *J. Theor. Biol.* **1982**, *99*, 237.
- [110] N. C. Seeman, *Angew. Chem.* **1998**, *110*, 3408; *Angew. Chem. Int. Ed.* **1998**, *37*, 3220.
- [111] N. C. Seeman, *Nature* **2003**, *421*, 427.
- [112] N. C. Seeman, *Trends Biotechnol.* **1999**, *17*, 437.
- [113] N. R. Kallenbach, R. I. Ma, N. C. Seeman, *Nature* **1983**, *305*, 829.
- [114] C. M. Niemeyer, *Curr. Opin. Chem. Biol.* **2000**, *4*, 609.
- [115] C. M. Niemeyer, *Angew. Chem.* **2001**, *113*, 4254; *Angew. Chem. Int. Ed.* **2001**, *40*, 4128.
- [116] C. M. Niemeyer, *Chem. Eur. J.* **2001**, *7*, 3189.
- [117] E. Winfree, F. Liu, L. A. Wenzler, N. C. Seeman, *Nature* **1998**, *394*, 539.
- [118] C. Mao, T. H. LaBean, J. H. Relf, N. C. Seeman, *Nature* **2000**, *407*, 493.
- [119] K. J. Luecke, P. B. Dervan, *J. Am. Chem. Soc.* **1989**, *111*, 8733.
- [120] A. T. Poulin-Kerstien, P. B. Dervan, *J. Am. Chem. Soc.* **2003**, *125*, 15811.
- [121] B. E. Edelson, P. B. Dervan, *Curr. Opin. Chem. Biol.* **2003**, *7*, 284.
- [122] H. C. Kolb, M. G. Finn, K. B. Sharpless, *Angew. Chem.* **2001**, *113*, 2056; *Angew. Chem. Int. Ed.* **2001**, *40*, 2004.

- [123] W. G. Lewis, L. G. Green, F. Grynszpan, Z. Radic, P. R. Carlier, P. Taylor, M. G. Finn, K. B. Sharpless, *Angew. Chem.* **2002**, *114*, 1095; *Angew. Chem. Int. Ed.* **2002**, *41*, 1053.
- [124] Q. Wang, T. R. Chan, R. Hilgraf, V. V. Fokin, K. B. Sharpless, M. G. Finn, *J. Am. Chem. Soc.* **2003**, *125*, 3192.
- [125] R. Huisgen in *1,3-Dipolar Cycloaddition Chemistry* (Ed.: A. Padiva), Wiley-Interscience, New York, **1984**.
- [126] C. T. Calderone, J. W. Puckett, Z. J. Gartner, D. R. Liu, *Angew. Chem.* **2002**, *114*, 4278; *Angew. Chem. Int. Ed.* **2002**, *41*, 4104.
- [127] G. C. Micalizio, S. L. Schreiber, *Angew. Chem.* **2002**, *114*, 160; *Angew. Chem. Int. Ed.* **2002**, *41*, 152.
- [128] D. M. Perrin, T. Garestier, C. Helène, *Nucleosides Nucleotides* **1999**, *18*, 377.
- [129] D. M. Perrin, T. Garestier, C. Helène, *J. Am. Chem. Soc.* **2001**, *123*, 1556.
- [130] J. A. Latham, R. Johnson, J. J. Toole, *Nucleic Acids Res.* **1994**, *22*, 2817.
- [131] T. Gurlain, A. Sidorov, N. Mignet, S. J. Thorpe, S. E. Lee, J. A. Grasby, D. M. Williams, *Nucleic Acids Res.* **2001**, *29*, 1898.
- [132] S. E. Lee, A. Sidorov, T. Gurlain, N. Mignet, S. J. Thorpe, J. A. Brazier, M. J. Dickman, D. P. Hornby, J. A. Grasby, D. M. Williams, *Nucleic Acids Res.* **2001**, *29*, 1565.
- [133] K. Sakthivel, C. F. I. Barbas, *Angew. Chem.* **1998**, *110*, 2998; *Angew. Chem. Int. Ed.* **1998**, *37*, 2872.
- [134] N. K. Vaish, A. W. Fraley, J. W. Szostak, L. W. McLaughlin, *Nucleic Acids Res.* **2000**, *28*, 3316.
- [135] J. Matulic-Adamic, A. T. Daniher, A. Karpeisky, P. Haeberli, D. Sweedler, L. Beigelman, *Bioorg. Med. Chem. Lett.* **2000**, *10*, 1299.
- [136] T. M. Dewey, A. A. Mundt, G. J. Crouch, M. C. Zyzniewski, B. E. Eaton, *J. Am. Chem. Soc.* **1995**, *117*, 8474.
- [137] T. M. Dewey, M. C. Zyzniewski, B. E. Eaton, *Nucleosides Nucleotides* **1996**, *15*, 1611.
- [138] A. C. Forster, Z. Tan, M. N. Nalam, H. Lin, H. Qu, V. W. Cornish, S. C. Blacklow, *Proc. Natl. Acad. Sci. USA* **2003**, *100*, 6353.
- [139] H. Tao, V. W. Cornish, *Curr. Opin. Chem. Biol.* **2002**, *6*, 858.
- [140] S. R. Starck, X. Qi, B. N. Olsen, R. W. Roberts, *J. Am. Chem. Soc.* **2003**, *125*, 8090.
- [141] A. Frankel, S. Li, S. R. Starck, R. W. Roberts, *Curr. Opin. Struct. Biol.* **2003**, *13*, 506.
- [142] A. Frankel, S. W. Millward, R. W. Roberts, *Chem. Biol.* **2003**, *10*, 1043.
- [143] J. C. Chaput, J. W. Szostak, *J. Am. Chem. Soc.* **2003**, *125*, 9274.
- [144] I. A. Kozlov, S. Pitsch, L. E. Orgel, *Proc. Natl. Acad. Sci. USA* **1998**, *95*, 13448.
- [145] I. A. Kozlov, P. K. Politis, A. Van Aerschot, R. Busson, P. Herdewijn, L. E. Orgel, *J. Am. Chem. Soc.* **1999**, *121*, 2653.
- [146] I. A. Kozlov, L. E. Orgel, P. E. Nielson, *Angew. Chem.* **2000**, *112*, 4462; *Angew. Chem. Int. Ed.* **2000**, *39*, 4292.
- [147] O. L. Acevedo, L. E. Orgel, *J. Mol. Biol.* **1987**, *197*, 187.
- [148] J. G. Schmidt, L. Christensen, P. E. Nielsen, L. E. Orgel, *Nucleic Acids Res.* **1997**, *25*, 4792.
- [149] J. G. Schmidt, P. E. Nielsen, L. E. Orgel, *Nucleic Acids Res.* **1997**, *25*, 4797.
- [150] I. A. Kozlov, M. Zielinski, B. Allart, L. Kerremans, A. Van Aerschot, R. Busson, P. Herdewijn, L. E. Orgel, *Chem. Eur. J.* **2000**, *6*, 151.
- [151] J. A. R. Stutz, C. Richert, *J. Am. Chem. Soc.* **2001**, *123*, 12718.
- [152] D. M. Rosenbaum, D. R. Liu, *J. Am. Chem. Soc.* **2003**, *125*, 13924.
- [153] D. S. Wilson, J. W. Szostak, *Annu. Rev. Biochem.* **1999**, *68*, 611.
- [154] C. J. Li, T. H. Chan, *Organic Reactions in Aqueous Media*, Wiley, New York, **1997**.
- [155] K. Eitner, F. Bartl, B. Brzezinski, G. Schroeder, *Supramol. Chem.* **2001**, *13*, 627.
- [156] B. Dietrich, P. Viout, J.-M. Lehn, *Macrocyclic Chemistry*, Wiley-VCH, Weinheim, **1993**.
- [157] D. Sinou in *Modern Solvent in Organic Synthesis* (Ed.: P. Knochel), Springer, Berlin, **1999**, p. 41.
- [158] H. Kinoshita, H. Shinokubo, K. Oshima, *J. Am. Chem. Soc.* **2003**, *125*, 7784.
- [159] J. P. Jost, J. Jiricny, H. Saluz, *Nucleic Acids Res.* **1989**, *17*, 2143.
- [160] S. M. Mel'nikov, B. Lindman, *Langmuir* **1999**, *15*, 1923.
- [161] G. F. Joyce, G. M. Visser, C. A. A. Boeckel, J. H. van Boom, L. E. Orgel, J. van Westrenen, *Nature* **1984**, *310*, 602.
- [162] J. G. Schmidt, P. E. Nielsen, L. E. Orgel, *J. Am. Chem. Soc.* **1997**, *119*, 1494.
- [163] J. Minshull, W. P. Stemmer, *Curr. Opin. Chem. Biol.* **1999**, *3*, 284.
- [164] F. Arnold, *Acc. Chem. Res.* **1998**, *31*, 125.
- [165] F. H. Arnold, L. Giver, A. Gershenson, H. Zhao, K. Miyazaki, *Ann. N. Y. Acad. Sci.* **1999**, *870*, 400.
- [166] M. B. Tobin, C. Gustafsson, G. W. Huisman, *Curr. Opin. Struct. Biol.* **2000**, *10*, 421.
- [167] U. T. Bornscheuer, M. Pohl, *Curr. Opin. Chem. Biol.* **2001**, *5*, 137.
- [168] M. Chartrain, P. M. Salmon, D. K. Robinson, B. C. Buckland, *Curr. Opin. Biotechnol.* **2000**, *11*, 209.
- [169] A. Jaschke, B. Seelig, *Curr. Opin. Chem. Biol.* **2000**, *4*, 257.
- [170] S. V. Taylor, P. Kast, D. Hilvert, *Angew. Chem.* **2001**, *113*, 3408; *Angew. Chem. Int. Ed.* **2001**, *40*, 3310.
- [171] H. Lin, V. W. Cornish, *Angew. Chem.* **2002**, *114*, 4580; *Angew. Chem. Int. Ed.* **2002**, *41*, 4402.
- [172] J. J. Bull, H. A. Wichman, *Annu. Rev. Ecol. Syst.* **2001**, *32*, 183.

Communications



In the reaction described by M. Murakami and M. Hasegawa on the following pages, the electronic effects are so dramatic that the sterically hindered substrate prefers to react by a more crowded pathway. This reaction will provide organic chemistry textbooks with a prime example of systems in which electronic effects are dominant over steric effects in determining the stereochemical outcome of a reaction.

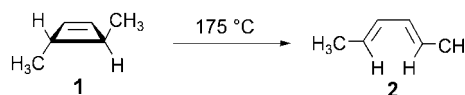
Electronic Effects

Synthesis and Thermal Ring Opening of *trans*-3,4-Disilylcyclobutene

Masahiro Murakami* and Munehiro Hasegawa

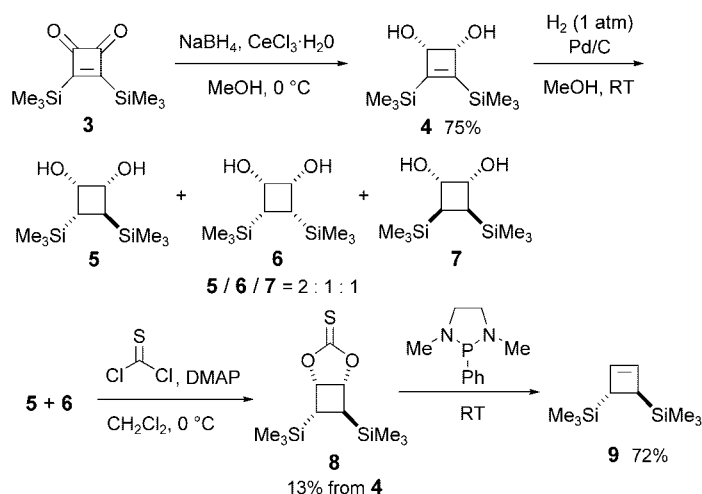
The electrocyclic ring opening of substituted cyclobutenes is a classical textbook example of concerted pericyclic reactions that obey the Woodward–Hoffmann rules.^[1] Substituents located at the 3- and 4-positions can move either toward the breaking bond (inward) or away from it (outward) during the thermal ring-opening reaction, provided that their movements are conrotatory. For example, (*E*)-penta-1,3-diene and the corresponding *Z* isomer can both arise from 3-methylcyclobutene without violating the Woodward–Hoffmann rules. However, experimentally, the *E* isomer is formed exclusively.^[2] The outward preference is intuitively reasonable, because significant steric congestion develops when the methyl substituent rotates inward during the ring-opening reaction. The inward transition state was calculated to be energetically higher than the outward transition state by 5.3 kcal mol⁻¹ (MP2/6-31G(d)//3-21G) in the case of 3-methylcyclobutene.^[3] On the other hand, theoretical studies predicted that an electron-accepting substituent would prefer to rotate inward.^[4] The delocalization of electron density from the highest occupied molecular orbital (HOMO) of the opening cyclobutene skeleton to the electron-accepting substituent stabilizes the inward transition state. This prediction has been verified experimentally with carbonyl-substituted cyclobutenes.^[5] We recently discovered the remarkable effects of a silyl substituent located at the 3-position.^[6,7] Although silicon is more electropositive than carbon, silyl substituents accelerate the reaction and promote inward rather than outward rotation, in spite of steric considerations. Stabilization of the inward transition state was explained by assuming that the energetically low-lying antibonding σ^* orbital of the silicon–carbon bond accepts electron density from the HOMO.^[6a,8,9]

In the case of *trans*-3,4-disubstituted cyclobutenes, the disadvantage of the inward transition state in which both substituents rotate in the sterically unfavorable direction would be enormous. For example, (*2E,4E*)-hexadiene (**2**) is exclusively formed during the ring-opening of *trans*-3,4-dimethylcyclobutene (**1**) (Scheme 1).^[10] The calculated energy difference of the inward and outward transition states amounts to 13.0 kcal mol⁻¹ (RHF/3-21G).^[4b] Organic chemistry textbooks present this reaction as a typical example of conrotatory ring opening.^[11]

Scheme 1. Ring-opening reaction of *trans*-3,4-dimethylcyclobutene **1**.

Previous studies on the effects of silyl substituents prompted us to examine the ring-opening reaction of *trans*-3,4-bis(trimethylsilyl)cyclobutene (**9**; Scheme 2), in which the two methyl substituents of **1** are replaced with two significantly bulkier trimethylsilyl substituents. The steric congestion arising from the inward rotation of two bulkier substituents may become insurmountable. Thus, we consider this a true test of the power of electronic stabilization.

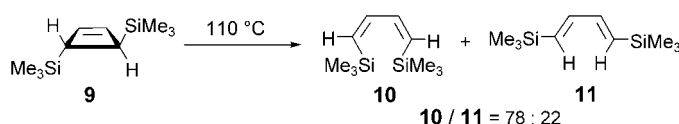
The synthesis of *trans*-3,4-bis(trimethylsilyl)cyclobutene (**9**) is shown in Scheme 2. Cyclobutenedione **3**, prepared according to a literature procedure,^[12] was reduced to the *cis*

Scheme 2. Synthesis of *trans*-3,4-bis(trimethylsilyl)cyclobutene (**9**). DMAP = 4-dimethylaminopyridine.

diol **4** with NaBH₄/CeCl₃.^[13] Hydrogenation over Pd/C in methanol afforded a diastereomeric mixture of diols **5**, **6**, and **7**.^[14] The diols **5** and **6** were separated from **7** by chromatography. The *cis* 1,2-diol unit was converted into a carbon–carbon double bond by using the Corey–Hopkins method.^[15] When a mixture of **5** and **6** was treated with thiophosgene, the diol **5** reacted much faster than **6**, probably as a result of steric reasons, permitting the isolation of the cyclic thiocarbonate **8**. The desired cyclobutene **9** was obtained by the reaction of **8** with 1,3-dimethyl-2-phenyl-1,3,2-diazaphospholidine.

The cyclobutene **9** thus obtained was heated in *n*-decane at 110 °C and underwent ring opening in a conrotatory fashion (*t*_{1/2} = 1.7 h) to afford a mixture of diene (1*Z*,3*Z*)-**10** and the corresponding *E,E* isomer **11** (both depicted in the *s-cis* conformation for convenience in Scheme 3). Remarkably, the *Z,Z* isomer **10** predominated over **11**, with a ratio of 78:22.^[16] The two trimethylsilyl substituents preferred inward rotation despite the significantly greater steric constraints on this reaction pathway.

[*] Prof. Dr. M. Murakami, M. Hasegawa
Department of Synthetic Chemistry and Biological Chemistry
Kyoto University
Katsura, Kyoto 615-8510 (Japan)
Fax: (+81) 75-383-2748
E-mail: murakami@sbchem.kyoto-u.ac.jp



Scheme 3. Ring-opening reaction of **9**.

Computational studies were carried out on the reaction of **9**. The energy diagram obtained by density functional calculations [B3LYP/6-31G(d)]^[17,18] is shown in Figure 1. The inward transition state is lower in energy than the outward transition state by 0.51 kcal mol⁻¹, whereas the product ratio experimentally obtained at 110 °C (78:22)

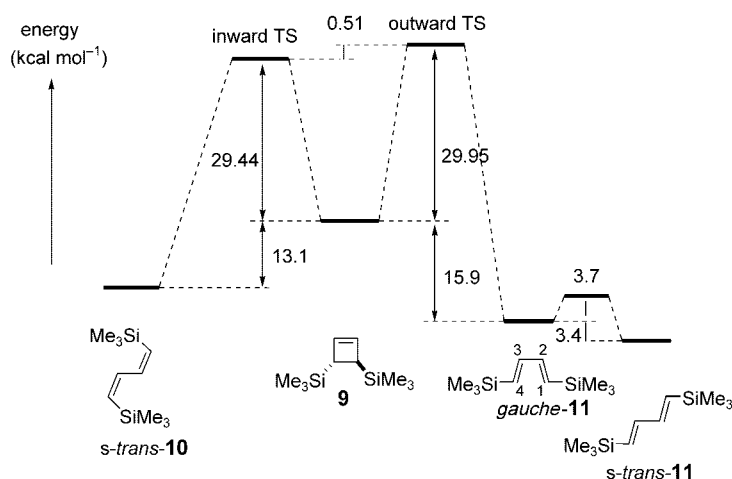


Figure 1. Potential energy diagram for the ring opening of **9** (383 K).

corresponds to an energy difference of 0.96 kcal mol⁻¹. Interestingly, the reaction through the inward pathway leads directly to **10** in the *s-trans* conformation, without the intervention of an energy minimum that corresponds to the *s-cis* (or *gauche*) conformation.^[19] In contrast, in the outward pathway the initial product **11** in the *gauche* conformation (the dihedral angle C₁-C₂-C₃-C₄ = 21°) exists as a local minimum before the final product *s-trans*-**11** is formed. The contrasting reaction profiles are another indication of the magnitude of steric congestion of the inward ring opening.

We attribute the counterintuitive rotational behavior of **9** to the electron-accepting nature of the two antibonding orbitals on the silicon atoms based on Houk's theory.^[4] The inward transition state is shown in Figure 2, in addition to the natural bond orbital (NBO) overlap image^[20] for the two antibonding orbitals of the Si5-C6 and Si9-C10 links, and the breaking C1-C4 σ bond, that is, the HOMO of the opening cyclobutene skeleton. This clearly shows the overlap of the antibonding orbitals with the HOMO. Electronic stabilization arising from the dual delocalization of the electron density of the HOMO into the two antibonding orbitals overcomes the steric congestion at the inward transition state, leading to the predominance of **10**.

Although steric arguments are commonly employed to understand the stereochemical outcomes of organic reactions,

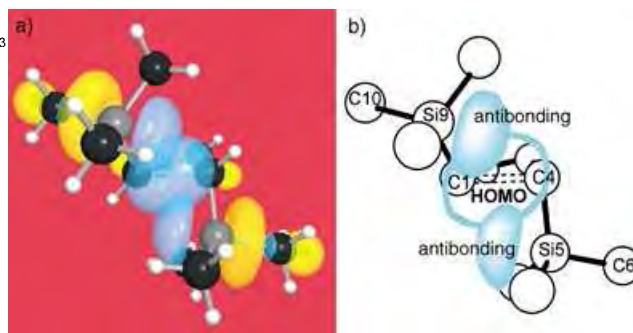


Figure 2. Overlap of the two antibonding orbitals on the silicon atoms with the HOMO in the inward transition state.

electronic effects may have a greater impact than generally supposed. In the system described herein, the effects are so dramatic that the more sterically hindered substrate prefers to react through a more crowded reaction pathway. This Communication will hopefully provide organic chemistry textbooks with a prime example of systems in which electronic effects are dominant over steric effects in determining the stereochemical outcome of a reaction. It is also remarkable that even though silicon is immediately below carbon in the periodic table, it exhibits a totally opposite rotational preference.

Experimental Section

Ring opening of 9: A solution of **9** (19.8 mg, 0.10 mmol) and galvinoxyl (2.0 mg, 4.7 μmol; added to prevent isomerization of the olefin geometries of the products)^[21] in *n*-decane (50 μL) was placed in a screw-capped vial under a nitrogen atmosphere. The mixture was then stirred at 110 °C in an oil bath. The ring-opening reaction to form **10** and **11** was monitored by ¹H NMR spectroscopy. **10**: ¹H NMR (300 MHz): δ = 6.98–7.06 (m, 2H), 5.74–5.82 (m, 2H), 0.17 ppm (s, 18H); ¹³C NMR (75 MHz): δ = 145.0, 135.1, 0.3 ppm. **11**: ¹H NMR (300 MHz): δ = 6.51–6.58 (m, 2H), 5.89–5.96 (m, 2H), 0.10 ppm (s, 18H); ¹³C NMR (75 MHz): δ = 146.6, 134.8, -1.3 ppm.^[22]

Received: March 29, 2004

Revised: June 14, 2004

Keywords: density functional calculations · electrocyclic reactions · ring-opening reactions · silicon · steric hindrance

- [1] R. B. Woodward, R. Hoffmann, *The Conservation of Orbital Symmetry*, Academic Press, New York, **1970**.
- [2] a) E. Gil-Av, J. Shabtai, *J. Org. Chem.* **1964**, *29*, 258; b) H. M. Frey, D. C. Marshall, *Trans. Faraday Soc.* **1965**, *61*, 1715.
- [3] S. Niwayama, E. A. Kallel, D. C. Spellmeyer, C. Sheu, K. N. Houk, *J. Org. Chem.* **1996**, *61*, 2813.
- [4] a) W. Kirmse, N. G. Rondan, K. N. Houk, *J. Am. Chem. Soc.* **1984**, *106*, 7989; b) N. G. Rondan, K. N. Houk, *J. Am. Chem. Soc.* **1985**, *107*, 2099.
- [5] a) K. Rudolf, D. C. Spellmeyer, K. N. Houk, *J. Org. Chem.* **1987**, *52*, 3708; b) E. Piers, Y.-F. Lu, *J. Org. Chem.* **1989**, *54*, 2267; c) C. W. Jefford, G. Bernardinelli, Y. Wang, D. C. Spellmeyer, A. Buda, K. N. Houk, *J. Am. Chem. Soc.* **1992**, *114*, 1157; d) S.

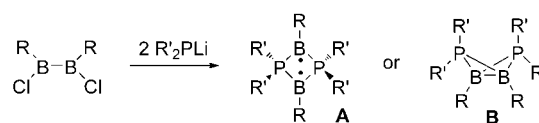
- Niwayama, K. N. Houk, *Tetrahedron Lett.* **1993**, 34, 1251, and references therein.
- [6] a) M. Murakami, Y. Miyamoto, Y. Ito, *Angew. Chem.*, **2001**, 113, 182; *Angew. Chem. Int. Ed.* **2001**, 40, 189; b) M. Murakami, Y. Miyamoto, Y. Ito, *J. Am. Chem. Soc.* **2001**, 123, 6441.
- [7] For an analogous effect in the ring opening of oxetene, see: M. Shindo, K. Matsumoto, S. Mori, K. Shishido, *J. Am. Chem. Soc.* **2002**, 124, 6840.
- [8] P. S. Lee, X. Zhang, K. N. Houk, *J. Am. Chem. Soc.* **2003**, 125, 5072.
- [9] For another explanation assuming geminal σ bond participation, see: H. Ikeda, T. Kato, S. Inagaki, *Chem. Lett.* **2001**, 270.
- [10] R. E. K. Winter, *Tetrahedron Lett.* **1965**, 6, 1207.
- [11] M. B. Smith, J. March, *March's Advanced Organic Chemistry*, 5th ed., Wiley, New York, **2001**, p. 1427.
- [12] D.-C. Zhao, A. D. Allen, T. T. Tidwell, *J. Am. Chem. Soc.* **1993**, 115, 10097.
- [13] J.-L. Luche, *J. Am. Chem. Soc.* **1978**, 100, 2226.
- [14] S. Nishimura, H. Sakamoto, T. Ozawa, *Chem. Lett.* **1973**, 855.
- [15] E. J. Corey, P. B. Hopkins, *Tetrahedron Lett.* **1982**, 23, 1979.
- [16] Kinetic studies showed the first-order nature, and the product ratio was constant to 80 % reaction.
- [17] Geometry optimization and energy calculations with thermal corrections were carried out with the GAUSSIAN 98 program (Revision A.11.4), M. J. Frisch, G. W. Trucks, H. B. Schlegel, G. E. Scuseria, M. A. Robb, J. R. Cheeseman, V. G. Zakrzewski, J. A. Montgomery, R. E. Stratmann, J. C. Burant, S. Dapprich, J. M. Millam, A. D. Daniels, K. N. Kudin, M. C. Strain, O. Farkas, J. Tomasi, V. Barone, M. Cossi, R. Cammi, B. Mennucci, C. Pomelli, C. Adamo, S. Clifford, J. Ochterski, G. A. Petersson, P. Y. Ayala, Q. Cui, K. Morokuma, D. K. Malick, A. D. Rabuck, K. Raghavachari, J. B. Foresman, J. Cioslowski, J. V. Ortiz, B. B. Stefanov, G. Liu, A. Liashenko, P. Piskorz, I. Komaromi, R. Gomperts, R. L. Martin, D. J. Fox, T. Keith, M. A. Al-Laham, C. Y. Peng, A. Nanayakkara, C. Gonzalez, M. Challacombe, P. M. W. Gill, B. G. Johnson, W. Chen, M. W. Wong, J. L. Andres, M. Head-Gordon, E. S. Replogle, J. A. Pople, Gaussian, Inc., Pittsburgh, PA, **1998**.
- [18] It has been demonstrated that B3LYP/6-31G(d) is a suitable method and basis set for many pericyclic reactions: O. Wiest, D. C. Montiel, K. N. Houk, *J. Phys. Chem. A.* **1997**, 101, 8378.
- [19] L. Deng, T. Ziegler, *J. Phys. Chem.* **1995**, 99, 612.
- [20] "Natural Bond Orbital Methods": F. Weinhold in *Encyclopedia of Computational Chemistry*, Vol. 3 (Eds.: P. von R. Schleyer, N. L. Allinger, T. Clark, J. Gasteiger, P. A. Kollman, H. F. Schaefer III, P. R. Schreiner), Wiley, Chichester, **1998**, pp. 1792–1811.
- [21] Isomerization of the *Z,Z* isomer **10** to the corresponding *E,Z* isomer occurred in the absence of galvinoxyl.
- [22] L. D. Field, M. G. Gardiner, C. H. L. Kennard, B. A. Messerle, C. L. Raston, *Organometallics* **1991**, 10, 3167.

Catenation of Two Singlet Diradicals: Synthesis of a Stable Tetraradical (Tetraradicaloid)**

Amor Rodriguez, Fook S. Tham, Wolfgang W. Schoeller, and Guy Bertrand*

Singlet and triplet diradicals are fascinating as they are even-electron molecules that have one bond less than the number permitted by the standard rules of valency.^[1] In localized singlet diradicals the partially filled orbitals reside on two different atoms that are connected by one or more saturated atoms.^[1b] These diradicals are also called “nonconjugated”. However, the partially filled atomic orbitals that are formally localized on the two radical centers can interact either through space or through the σ bonds of the atoms that connect them. Catenation of singlet diradicals, through appropriate linkers, are predicted to lead to antiferromagnetic low-spin polymers, in which the half-filled electron bands would confer the capability of metallic conduction without doping.^[1c,2] However, as noted by Berson,^[1c] a vast and largely unmapped terrain must still be explored before these practical objectives can be reached. Not only do we lack knowledge about the solid-state intermolecular interactions between chains, which can be decisive in the ultimate bulk conductivity of a polymer, but it is also necessary to understand the effects induced by the presence of a second diradical site on the first. For this purpose, several carbon-based tetraradical prototypes have already been prepared, but conclusions have been difficult to draw due to the instability of such species.^[3]

Similarly to its carbon congeners,^[4] 1,3-dibora-2,4-diphosphoniocyclobutane-1,3-diyls, **A**, feature a trans-annular bonding π -overlap^[5,6] that allows for the thermal ring closure to give 1,3-dibora-2,4-diphosphoniobicyclo[1.1.0]butanes, **B**^[7] (Scheme 1). However, we have shown that given the right set of substituents, strongly colored diradicals (or diradicaloids)^[8] of type **A** were indefinitely stable both in solution and in the solid state.^[9] This very unusual stability gave us the



Scheme 1. Synthesis of type **A** and **B** ring systems.

[*] Dr. A. Rodríguez, Dr. F. S. Tham, Prof. G. Bertrand
UCR-CNRS Joint Research Chemistry Laboratory (UMR 2282)
Department of Chemistry
University of California, Riverside, CA 92521-0403 (USA)
E-mail: gbertran@mail.ucr.edu

Prof. W. W. Schoeller
Fakultät für Chemie der Universität Bielefeld
Postfach 10 01 31, 33615 Bielefeld (Germany)

[**] We are grateful to the NSF (CHE 0213510), the DFG and RHODIA for financial support of this work.

opportunity to study whether strong spin coupling can be maintained in extended systems with more than two sites for unpaired electrons.

Herein we report the synthesis of the first stable singlet tetradical and our first results concerning the influence of the antiferromagnetic and ferromagnetic nature of the linkers^[10] on the relative stability of compounds **A/B**.

As shown in Scheme 1, the synthesis of derivatives of types **A** and **B** involved the addition of two equivalents of phosphide to the appropriate 1,2-halogenodiborane. Therefore the obvious precursors for derivatives *p*-**4** and *m*-**4** were tetrahalogenotetraboranes *p*-**3** and *m*-**3** (Scheme 2). The

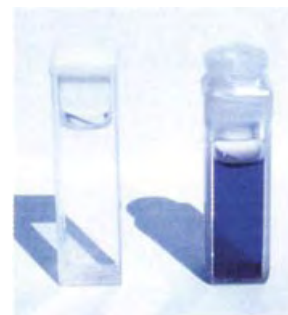
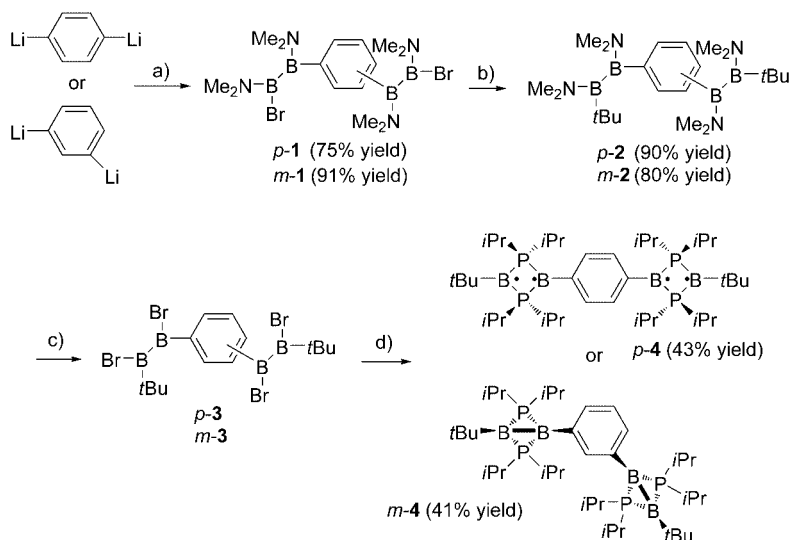


Figure 1. Hexane solutions of *p*-**4** (left) and *m*-**4** (right)



Scheme 2. Synthesis of *m*-**4** and *p*-**4**: a) $\text{Me}_2\text{N}(\text{Br})\text{BB}(\text{Br})\text{NMe}_2$ (2 equiv), hexane/diethyl ether, -78°C ; b) $t\text{BuLi}$ (2 equiv), hexane, -78°C ; c) BBr_3 (4 equiv), hexane, -78°C ; d) $i\text{Pr}_2\text{PLi}$ (4 equiv), hexane/diethyl ether, -78°C .

latter have been obtained in three steps. The addition of two equivalents of 1,2-bis(dimethylamino)-1,2-dibromodiborane to 1,4- and 1,3-dilithiobenzene afforded derivatives *p*-**1** (75% yield) and *m*-**1** (91% yield), respectively. Treatment of *p*-**1** and *p*-**1** with two equivalents of *tert*-butyllithium led to the tetrakis(dimethylamino)tetraboranes *p*-**2** and *m*-**2**, which were isolated in 90 and 80% yields. An exchange reaction with boron tribromide gave rise to the desired precursors *p*-**3** and *m*-**3** that can only be characterized by ^1H NMR spectroscopy due to their high instability.^[11] Then, addition of four equivalents of lithium diisopropylphosphide led to *p*-**4** and *m*-**4**, which were isolated in 43 and 41% yield, respectively, both as oxygen-sensitive but highly thermally stable crystals [m.p.: 261°C decomp (*p*-**4**); 246°C decomp (*m*-**4**)]. The similarities between the two isomeric derivatives *p*-**4** and *m*-**4** stop here. As can be seen in Figure 1, compound *p*-**4** is deep violet ($\lambda_{\text{max}} = 630\text{ nm}$, $\epsilon = 1374$), whereas *m*-**4** is colorless.^[12]

The X-ray diffraction analysis^[13] of *p*-**4** (Figure 2) revealed that the B atoms are in a planar environment, and the presence of two almost planar PBPB four-membered-ring moieties (interflap angle between the two PBB units 175°) linked by a phenyl ring that is coplanar to the two PBPB skeletons (torsion angle 2°). Another striking feature is the

B–B interatomic distance (2.568 \AA), which indicates that the B–B bonds have been cleaved. All these geometric parameters are very comparable to those found in the previously reported diradicals of type **A**.^[9,14]

In marked contrast, the PBPB cores of *m*-**4** strongly deviate from planarity (interflap angle between the two PBB units 120.7 and 123.6°), and the B–B interatomic distances (1.875 and 1.906 \AA) are shortened by more than 25% compared to *p*-**4** (Figure 3). Moreover, the phenyl ring is perpendicular to the PBPB skeletons. Clearly, the geometric parameters of *m*-**4** are very similar to those observed for bicyclic[1.1.0] derivatives of type **B**.^[7]

Antiferromagnetic coupling units such as that in *p*-**4** are known to be very effective and to lead to quinoid structures for which the singlet–triplet gap tends to reach zero.^[15] A close comparison of the x-ray data of *p*-**4** and *m*-**4**

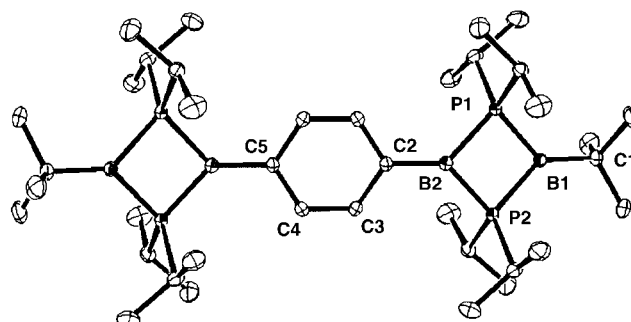


Figure 2. Molecular view of *p*-**4** in the solid state. Selected bond lengths [\AA] and angles [$^\circ$]: B1–B2, 2.568 ; B1–P1, 1.897 ± 2 ; P1–B2, 1.894 ± 2 ; B2–P2, 1.900 ± 2 ; P2–B1, 1.899 ± 2 ; B2–C2, 1.547 ± 3 ; C2–C3, 1.404 ± 3 ; C3–C4, 1.383 ± 3 ; C4–C5, 1.411 ± 3 ; C1–B1–P1, 132.46 ± 16 ; B1–P1–B2, 85.26 ± 10 ; P1–B2–C2, 132.50 ± 16 ; C2–B2–P2, 132.22 ± 17 ; P1–B2–P2, 94.76 ± 11 ; B2–P2–B1, 85.06 ± 10 ; P2–B1–C1, 132.86 ± 16 ; P2–B1–P1, 94.69 ± 11 .

shows that the quinoid character of *p*-**4** is very weak but not non-existent. In particular the B2–C2 bond length is a little shorter in *p*-**4** [$1.547(3)\text{ \AA}$] compared to *m*-**4** [$1.577(2)\text{ \AA}$], and there is an alternation between slightly shorter and longer

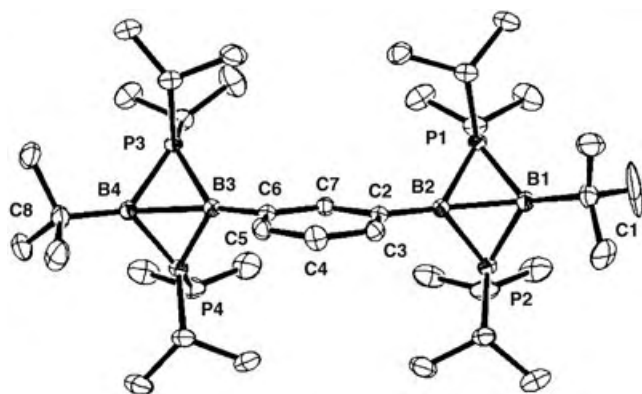


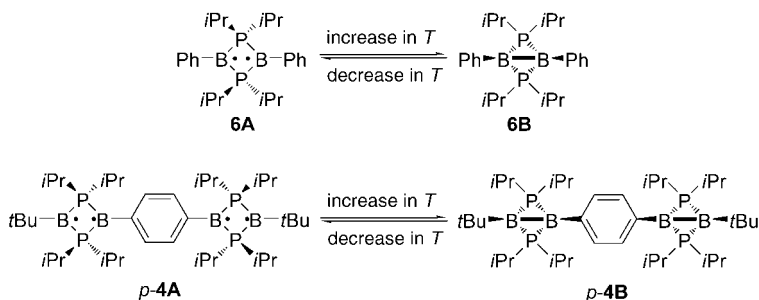
Figure 3. Molecular view of *m-4* in the solid state. Selected bond lengths [Å] and angles [°]: B1–B2, 1.909 ± 3; B1–P1, 1.8982 ± 19; P1–B2, 1.8769 ± 19; B2–P2, 1.875 ± 2; P2–B1, 1.898 ± 2; B2–C2, 1.577 ± 2; C2–C3, 1.396 ± 2 Å; C3–C4, 1.390 ± 3; C4–C5, 1.385 ± 2; C5–C6, 1.397 ± 2; C6–C7, 1.404 ± 2; C7–C2, 1.401 ± 2; C6–B3, 1.573 ± 2; B3–B4, 1.875 ± 3; B3–P3, 1.8751 ± 18; P3–B4, 1.905 ± 2; B4–P4, 1.903 ± 2; P4–B3, 1.8781 ± 19; C1–B1–P1, 131.99 ± 14; B1–P1–B2, 59.08 ± 8; P1–B2–C2, 132.97 ± 13; P1–B2–P2, 99.73 ± 9; C2–B2–P2, 126.61 ± 13; B2–P2–B1, 60.78 ± 8; P2–B1–C1, 129.01 ± 14; P2–B1–P1, 98.17 ± 9; C6–B3–P3, 130.92 ± 12; B3–P3–B4, 59.48 ± 8; P3–B4–C8, 130.38 ± 14; P3–B4–P4, 97.01 ± 9; C8–B4–P4, 131.65 ± 14; B4–P4–B3, 59.46 ± 8; P4–B3–P3, 98.90 ± 9; P4–B3–C6, 129.05 ± 12.

bonds in the phenyl ring of *p-4* [C2–C3: 1.404(3) and C4–C5: 1.411(3) versus C3–C4: 1.383(3) Å]. The coplanarity of the phenyl ring with the PBPB cores also suggests some delocalization between the 2p(B) orbitals and the π ring systems. Lastly, it is worth noting the absence of a signal in both the solution and solid-state electron paramagnetic resonance spectra from –80 °C to room temperature, which indicates that *p-4* has a singlet ground state.

To understand why *p-4* features a planar structure with long B–B bonds whereas *m-4* has a bis(bicyclic[1.1.0]) structure, ab initio calculations at the (U)B3LYP/6-31 g* level^[16] were performed for the parent compounds in the planar forms *p-5A* (D_{2h} symmetry) and *m-5A* (C_{2v} symmetry), and the

bis(bicyclic) forms *p-5B* and *m-5B* (Figure 4). Both open-form species have a singlet ground state, but interestingly the singlet–triplet gap (adiabatic, between two planar forms) for *p-5A* ($S^2=0.057$; 16.4 kcal mol^{–1}) is 3.9 kcal mol^{–1} smaller than for *m-5A* ($S^2=0.0$). In addition, *p-5A* is 2.2 kcal mol^{–1} more stable than *m-5A*, and the energy benefit for the ring closure of *p-5A* (16.8 kcal mol^{–1}) is smaller by 2.1 kcal mol^{–1} than for *m-5A*.

These small energy differences are in line with the X-ray data for *p-4* and *m-4* and corroborate the hypothesis that there is only a weak “communication” between both diradical sites of *p-4* through the antiferromagnetic linker. One possible reason for this communication is the weakness of B–C double bonds,^[17] which hampers the formation of the quinoid structure. However, despite the weakness of the phenomenon, the consequences are of importance since in the solid-state *p-4* has an open-form structure whereas *m-4* features a bis(bicyclic) structure. In fact, as shown in the preceding paper^[14] and in contrast with the parent compounds, the energy difference between the planar form and the bicyclic isomer of substituted PBPB derivatives is only a matter of a very few kcal mol^{–1}. Indeed, as in the case of the “monomeric” derivative **6**, the planar structure of *p-4* exists in the solid state but is in equilibrium in solution with the bicyclic structure *p-4B* (Scheme 3). Here also the open-structure *p-4A* predominates at low temperature ($\delta^{31}\text{P} = +1.0$ ppm at 173 K), whereas at room temperature, the bis(bicyclic) system *p-4B* is by far the major product ($\delta^{31}\text{P} =$



Scheme 3. Equilibrium between **6A** and **6B**, and between *p-4A* and *p-4B*.

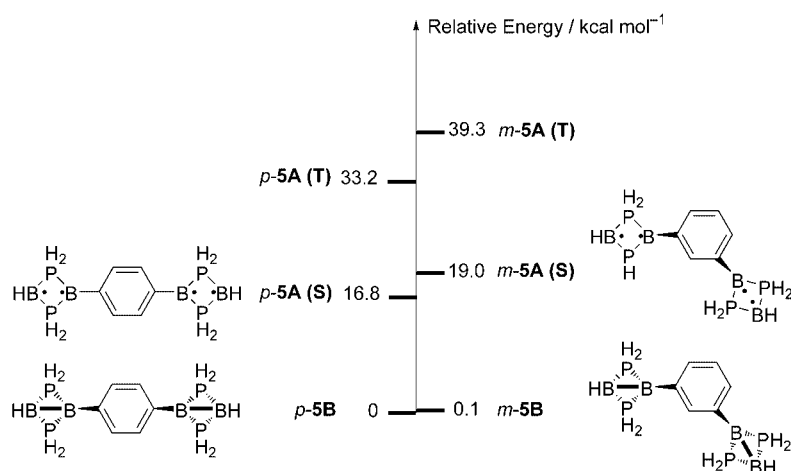


Figure 4. Relative energies of the bis(bicyclic) forms (*p-5B* and *m-5B*) and planar forms (*p-5A* and *m-5A*) in their singlet (S) and triplet (T) configurations.

–22.4 ppm); this has been confirmed by UV experiments, which show that the absorption considerably increases when the temperature decreases.^[18] In marked contrast, no dynamic behavior was observed for *m-4*: the ^{31}P chemical shift (–28.4 ppm) is not temperature dependent.

We are currently investigating the catenation of diradicals of type **A** with different antiferromagnetic linkers in the hope of quantifying to some extent their efficiency. Moreover, the synthesis of polymers featuring diradical units is underway.

Experimental Section

All reactions and manipulations were carried out under an atmosphere of dry argon by using standard Schlenk techniques.

p-1 and *m-1*: A solution of [BBr(NMe₂)₂] (2.70 g, 10 mmol) in hexane (20 mL) was added to a suspension of 1,4- or 1,3-

dilithiobenzene (1.24 g, 5 mmol) in ether (30 mL) at -78°C . The mixture was warmed to room temperature and stirred overnight. All the volatiles were removed in vacuo and the residue was extracted with toluene (40 mL). Yield: (*p*-**1**: 1.72 g, 75%; *m*-**1**: 2.08 g, 91%). *p*-**1**: ^1H NMR (300 MHz, CDCl_3): δ = 7.27 (s, 4H, CH_{aro}), 2.95, 2.91, 2.90 and 2.77 ppm (s, 6H, NMe_2); $^{13}\text{C}\{^1\text{H}\}$ NMR (75.5 MHz, CDCl_3): δ = 130.8 (s, CH_{aro}), (*Cipso* not observed), 44.6, 43.2, 40.4 and 29.5 ppm (s, NMe_2); $^{11}\text{B}\{^1\text{H}\}$ NMR (CDCl_3): δ = 44.88, 41.45. *m*-**1**: ^1H NMR (300 MHz, CDCl_3): δ = 7.21 (m, 4H, CH_{aro}), 2.89, 2.88, 2.85 and 2.71 ppm (s, 6H, NMe_2); $^{13}\text{C}\{^1\text{H}\}$ NMR (CDCl_3): δ = 134.5, 130.1 and 126.7 (s, CH_{aro}), (*Cipso* not observed), 44.8, 42.3, 40.2 and 37.8 ppm (s, NMe_2); $^{11}\text{B}\{^1\text{H}\}$ NMR (160.5 MHz, CDCl_3): δ = 40.3 ppm (br).

p-**2** and *m*-**2**: 5.01 mL of *t*BuLi (1.5M, pentane) were added dropwise to a solution of *p*-**1** or *m*-**1** (1.72 g, 3.76 mmol) in hexane (20 mL) at -78°C . The mixture was warmed to room temperature and stirred for 6 h. All the solvents were then removed in vacuo. Toluene was added and the salts were removed by filtration. Yield: (*p*-**2**: 1.39 g, 90%; *m*-**2**: 1.23 g, 80%). *p*-**2**: ^1H NMR (300 MHz, CDCl_3): δ = 7.25 (s, 4H, CH_{aro}), 2.97, 2.93, 2.85 and 2.84 (s, 6H, NMe_2), 0.93 ppm (s, 18H, *t*Bu); $^{13}\text{C}\{^1\text{H}\}$ NMR (75.5 MHz, CDCl_3): δ = 131.3 (s, CH_{aro}), (*Cipso* not observed), 46.8, 45.5, 40.3 and 39.9 (s, NMe_2), 29.6 ppm (s, *t*Bu); $^{11}\text{B}\{^1\text{H}\}$ NMR (160.5 MHz, CDCl_3): δ = 44 ppm (br). *m*-**2**: ^1H NMR (CDCl_3) δ = 7.10 (m, 4H, CH_{aro}), 2.87 and 2.85 (s, 3H, NMe_2), 2.84 (s, 6H, NMe_2), 2.79 and 2.78 (s, 3H, NMe_2), 2.73 (s, 6H, NMe_2), 0.80 (s, 9H, *t*Bu), 0.79 ppm (s, 9H, *t*Bu); $^{13}\text{C}\{^1\text{H}\}$ NMR (CDCl_3): δ = 136.5, 130.3 and 126.2 (s, CH_{aro}), (*Cipso* not observed), 46.7, 45.5, 40.3 and 39.8 (s, NMe_2), 29.5 ppm (s, *t*Bu); $^{11}\text{B}\{^1\text{H}\}$ NMR (160.5 MHz, CDCl_3): δ = 52 ppm (br).

p-**3** and *m*-**3**: A solution of BBR_3 (1.27 mL, 13.48 mmol) in hexane (20 mL) was added dropwise to a solution of *p*-**2** or *m*-**2** (1.39 g, 3.37 mmol) in hexane (40 mL) at -78°C . After the solution had been stirred for 30 min, all the volatiles were removed in vacuo and the residue was treated with hexane (20 mL), filtered and used for the next step without further purification. *p*-**3**: ^1H NMR (300 MHz, CDCl_3): δ = 7.8 (s, 4H, CH_{aro}), 1.1 ppm (s, 18H, *t*Bu). *m*-**3**: ^1H NMR (300 MHz, CDCl_3): δ = 8.4 (s, 1H, CH_{aro}), 8.2 (d, $J_{\text{HH}} = 7.2$, 2H, CH_{aro}), 7.6 (t, $J_{\text{HH}} = 7.2$, 1H, CH_{aro}), 1.20 ppm (s, 18H, *t*Bu).

p-**4** and *m*-**4**: A suspension of $i\text{Pr}_2\text{PLi}$ (prepared by adding *n*BuLi (4.80 mL, 2.5M, pentane) to $i\text{Pr}_2\text{PH}$ (12.04 mmol) in ether (20 mL) at -78°C and subsequent stirring at room temperature for 1 hour) was added to a solution of *p*-**4** or *m*-**4** (1.66 mL, 3.01 mmol) in hexane (20 mL) at -78°C . The reaction mixture was warmed to room temperature within 1 hour and the solvents were removed in vacuo. Toluene was added and the salts were filtered off. Violet crystals of *p*-**4** were obtained by cooling a saturated boiling toluene solution to room temperature. Yield: (0.96 g, 43%). Colorless crystals of *m*-**4** were obtained in THF at -30°C . Yield: (2.41, 41%). *p*-**4**: ^1H NMR (300 MHz, C_6D_6): δ = 7.67 (s, 4H, CH_{aro}), 2.06 (m, 8H, PCH), 1.36 (s, 18H, *t*Bu), 1.22 (dd, $J_{\text{HH}} = 16.5$ Hz, $J_{\text{HP}} = 7.2$ Hz, 24H, CHCH_3), 1.13 ppm (dd, $J_{\text{HH}} = 15.9$ Hz, $J_{\text{HP}} = 7.2$ Hz, 24H, CHCH_3); $^{13}\text{C}\{^1\text{H}\}$ NMR (75.5 MHz, C_6D_6): δ = 134.9 (s, CH_{aro}), (*Cipso* not observed), 34.5 (s, *t*Bu), 21.9 (t, $J_{\text{PC}} = 22.6$ Hz, PCH), 21.4 ppm (d, $J_{\text{PC}} = 14.3$ Hz, CHCH_3); $^{11}\text{B}\{^1\text{H}\}$ NMR (C_6D_6): δ = 2.67, -2.80 ppm; $^{31}\text{P}\{^1\text{H}\}$ NMR (C_6D_6): δ = -22.40 ppm. *m*-**4**: ^1H NMR (300 MHz, C_6D_6): δ = 7.88 (s, 1H, CH_{aro}), 7.51 (d, $J_{\text{HH}} = 7.5$, 2H, CH_{aro}), 7.30 (t, $J_{\text{HH}} = 7.5$, 1H, CH_{aro}), 2.01 (m, 8H, PCH), 1.41 (s, 18H, *t*Bu), 1.22 (dd, $J_{\text{HH}} = 16.2$ Hz, $J_{\text{HP}} = 6.9$ Hz, 24H, CHCH_3), 1.10 ppm (dd, $J_{\text{HH}} = 16.0$ Hz, $J_{\text{HP}} = 7.8$ Hz, 24H, CHCH_3); $^{13}\text{C}\{^1\text{H}\}$ NMR (75.5 MHz, C_6D_6): δ = 143.9, 133.3 and 127.0 (s, CH_{aro}), (*Cipso* not observed), 34.7 (s, *t*Bu), 28.8 (t, $J_{\text{PC}} = 21.9$ Hz, PCH), 21.4 ppm (d, $J_{\text{PC}} = 11.6$ Hz, CHCH_3); $^{11}\text{B}\{^1\text{H}\}$ NMR (160.5 MHz, C_6D_6): δ = -3.7 , -8.0 ppm; $^{31}\text{P}\{^1\text{H}\}$ NMR (C_6D_6): δ = -28.4 ppm.

Received: April 28, 2004

Keywords: boron · magnetic properties · phosphorus · radicals

- a) J. A. Berson in *Reactive Intermediate Chemistry* (Eds.: R. A. Moss, M. S. Platz, M. Jones, Jr.), Wiley-Interscience, Hoboken, NJ, **2004**, pp. 165–204; b) W. T. Borden in *Encyclopedia of Computational Chemistry* (Ed.: P. v. R. Schleyer), Wiley, New York, **1998**, pp. 708–722; c) J. A. Berson, *Acc. Chem. Res.* **1997**, *30*, 238; d) D. A. Dougherty, *Acc. Chem. Res.* **1991**, *24*, 88.
- Conjugated Polymers and Related Material* (Eds.: W. R. Salaneck, L. Lundstrom, B. Ranby), Oxford, New York, **1993**.
- H. S. M. Lu, J. A. Berson, *J. Am. Chem. Soc.* **1997**, *119*, 1428; H. S. M. Lu, J. A. Berson, *J. Am. Chem. Soc.* **1996**, *118*, 265.
- For recent work on carbon-based 1,3-diradicals: a) A. C. Goren, D. A. Hrovat, M. Seefeldter, H. Quast, W. T. Borden, *J. Am. Chem. Soc.* **2002**, *124*, 3469; b) M. Abe, W. Adam, T. Minamoto, Y. Ino, M. Nojima, *J. Org. Chem.* **2003**, *68*, 1796; c) M. Abe, W. Adam, W. T. Borden, M. Hattori, D. A. Hrovat, M. Nojima, K. Nozaki, J. Wirz, *J. Am. Chem. Soc.* **2004**, *126*, 574.
- Several heterocyclobutane-1,3-diyls that contain Group 14 and/or Group 15 elements confined by a trans-annular antibonding π -overlap, which makes the thermal ring closure forbidden have been isolated: a) E. Niecke, A. Fuchs, F. Baumeister, M. Nieger, W. W. Schoeller, *Angew. Chem.* **1995**, *107*, 640; *Angew. Chem. Int. Ed. Engl.* **1995**, *34*, 555; b) O. Schmidt, A. Fuchs, D. Gudat, M. Nieger, W. Hoffbauer, E. Niecke, W. W. Schoeller, *Angew. Chem.* **1998**, *110*, 995; *Angew. Chem. Int. Ed.* **1998**, *37*, 949; c) E. Niecke, A. Fuchs, M. Nieger, *Angew. Chem.* **1999**, *111*, 3213; *Angew. Chem. Int. Ed.* **1999**, *38*, 3028; d) W. W. Schoeller, C. Begemann, E. Niecke, D. Gudat, *J. Phys. Chem. A* **2001**, *105*, 10731; e) H. Sugiyama, S. Ito, M. Yoshifuji, *Angew. Chem.* **2003**, *115*, 3932; *Angew. Chem. Int. Ed.* **2003**, *42*, 3802; f) M. Sebastian, M. Nieger, D. Szieberth, L. Nyulaszi, E. Niecke, *Angew. Chem.* **2004**, *116*, 647; *Angew. Chem. Int. Ed.* **2004**, *43*, 637; g) C. Cui, P. P. Power, *Abstr. Am. Chem. Soc. Meet.* **2004**, 801; h) M. F. Lappert, *Abstr. Am. Chem. Soc. Meet.* **2004**, 427.
- For reviews on diradicals based on main group elements see: a) H. Grützmacher, F. Breher, *Angew. Chem.* **2002**, *114*, 4178; *Angew. Chem. Int. Ed.* **2002**, *41*, 4006; b) P. P. Power, *Chem. Rev.* **2003**, *103*, 789.
- D. Scheschkewitz, H. Amii, H. Gornitzka, W. W. Schoeller, D. Bourissou, G. Bertrand, *Angew. Chem.* **2004**, *116*, 595; *Angew. Chem. Int. Ed.* **2004**, *43*, 585.
- For discussions on the diradical character of derivatives of type **A**: a) M. Seierstad, C. R. Kinsinger, C. J. Cramer, *Angew. Chem.* **2002**, *114*, 4050; *Angew. Chem. Int. Ed.* **2002**, *41*, 3894; b) W. W. Schoeller, A. Rozhenko, D. Bourissou, G. Bertrand, *Chem. Eur. J.* **2003**, *9*, 3611; c) Y. Jung, M. Head-Gordon, *J. Phys. Chem. A* **2003**, *107*, 7475; d) M. J. Cheng, C. H. Hu, *Mol. Phys.* **2003**, *101*, 1319.
- a) D. Scheschkewitz, H. Amii, H. Gornitzka, W. W. Schoeller, D. Bourissou, G. Bertrand, *Science* **2002**, *295*, 1880; b) H. Amii, L. Vranicar, H. Gornitzka, D. Bourissou, G. Bertrand, *J. Am. Chem. Soc.* **2004**, *126*, 1344.
- a) A. Rajca, *Chem. Rev.* **1994**, *94*, 871; b) C. Rovira, D. Ruiz-Molina, O. Elsner, J. Vidal-Gancedo, J. Bonvoisin, J. P. Launay, J. Veciana, *Chem. Eur. J.* **2001**, *7*, 240.
- 1,2-diphenyl-1,2-dichloro-diborane is known to be highly unstable: H. Hommer, H. Nöth, J. Knizek, W. Ponikwar, H. Schwenk-Kircher, *Eur. J. Inorg. Chem.* **1998**, 1519.
- As observed for related carbon-based singlet 1,3-diradicals,^[4] derivatives of type **A** are strongly colored, whereas the bicyclic[1.1.0] isomers **B** are colorless.
- The Bruker SMART-1000^[19a] X-ray diffraction instrument with Mo-radiation was used for data collection of compounds *p*-**4** and *m*-**4**. All data frames were collected by using ω -scan mode (-0.3° ω -scan width, hemisphere of reflections) and integrated by using the Bruker SAINTPLUS program.^[19b] The intensity data were corrected for Lorentzian polarization and absorption corrections

were performed by using the SADABS program incorporated in the SAINTPLUS program. The Bruker SHELXTL program^[19c] was used for direct methods of phase determination and structure refinement. Atomic coordinates, isotropic and anisotropic displacement parameters of all the non-hydrogen atoms of the two compounds were refined by means of a full matrix least-squares procedure on F^2 . All H atoms were included in the refinement in calculated positions riding on the atoms to which they were attached. **p-4_{para}**: $C_{38}H_{78}B_4P_4$, $M_r = 702.12$, crystal size $0.35 \times 0.16 \times 0.01 \text{ mm}^3$, monoclinic, space group $P2_1/n$, $a = 8.2095(19)$, $b = 29.276(7)$, $c = 9.489(2) \text{ \AA}$, $\beta = 106.524(5)^\circ$, $V = 2186.4(9) \text{ \AA}^3$, $\rho_{\text{calcd}} = 1.067 \text{ g cm}^{-3}$, $2\theta_{\text{max}} = 52.74^\circ$, $\text{MoK}\alpha$ ($\lambda = 0.71073 \text{ \AA}$), low temperature = $223(2) \text{ K}$, total reflections collected = 12870, independent reflections = 4456 ($R_{\text{int}} = 0.0449$, $R_{\text{sig}} = 0.0554$), 3105 (69.7%) reflections were greater than $2\sigma(I)$, index ranges $-8 \leq h \leq 10$, $-36 \leq k \leq 31$, $-11 \leq l \leq 11$, absorption coefficient $\mu = 0.197 \text{ mm}^{-1}$; max/min transmission = $0.9980/0.9343$, 258 parameters were refined and converged at $R1 = 0.0442$, $wR2 = 0.1046$, with intensity $I > 2\sigma(I)$, the final difference map was $0.528/-0.204 \text{ e \AA}^{-3}$. **m-4**: Crystal size $0.46 \times 0.33 \times 0.19 \text{ mm}^3$, monoclinic, space group $P2_1/c$, $a = 15.197(2)$, $b = 14.183(2)$, $c = 22.454(3) \text{ \AA}$, $\beta = 107.369(3)^\circ$, $V = 4619.0(12) \text{ \AA}^3$, $\rho_{\text{calcd}} = 1.010 \text{ g cm}^{-3}$, $2\theta_{\text{max}} = 56.56^\circ$, $\text{MoK}\alpha$ ($\lambda = 0.71073 \text{ \AA}$), low temperature = $223(2) \text{ K}$, total reflections collected = 63660, independent reflections = 11453 ($R_{\text{int}} = 0.0540$, $R_{\text{sig}} = 0.0372$), 8073 (70.5%) reflections were greater than $2\sigma(I)$, index ranges $-20 \leq h \leq 20$, $-18 \leq k \leq 18$, $-29 \leq l \leq 29$, absorption coefficient $\mu = 0.186 \text{ mm}^{-1}$; max/min transmission = $0.9654/0.9192$, 569 parameters were refined and converged at $R1 = 0.0464$, $wR2 = 0.1150$, with intensity $I > 2\sigma(I)$, the final difference map was $0.522/-0.241 \text{ e \AA}^{-3}$. CCDC-236922 (**p-4**) and 236923 (**m-4**) contain the supplementary crystallographic data for this paper. These data can be obtained free of charge via www.ccdc.cam.ac.uk/conts/retrieving.html (or from the Cambridge Crystallographic Data Centre, 12, Union Road, Cambridge CB21EZ, UK; fax: (+44)1223-336-033; or deposit@ccdc.cam.ac.uk).

- [14] A. Rodriguez, R. A. Olsen, N. Ghaderi, D. Scheschke, F. S. Tham, L. J. Mueller, G. Bertrand, *Angew. Chem.* **2004**, *116*, DOI: 10.1002/ange.200460475; *Angew. Chem. Int. Ed.* **2004**, *43*, DOI: 10.1002/anie.200460475.
- [15] A fully quinoid structure, in which the unpaired electrons are located far to each other, is expected for the related parabiscyclobutanediylphenyl system. Consequently, CAS(4,4)/6-31g* calculations result in a singlet-triplet energy separation equal to zero.
- [16] Gaussian98 (Revision A.7), M. J. Frisch, G. W. Trucks, H. B. Schlegel, G. E. Scuseria, M. A. Robb, J. R. Cheeseman, V. G. Zakrzewski, J. A. Montgomery, R. E. Stratmann, J. C. Burant, S. Dapprich, J. M. Millam, A. D. Daniels, K. N. Kudin, M. C. Strain, O. Farkas, J. Tomasi, V. Barone, M. Cossi, R. Cammi, B. Mennucci, C. Pomelli, C. Adamo, S. Clifford, J. Ochterski, G. A. Petersson, P. Y. Ayala, Q. Cui, K. Morokuma, D. K. Malick, A. D. Rabuck, K. Raghavachari, J. B. Foresman, J. Cioslowski, J. V. Ortiz, B. B. Stefanov, G. Liu, A. Liashenko, P. Piskorz, I. Komaromi, R. Gomperts, R. L. Martin, D. J. Fox, T. Keith, M. A. Al-Laham, C. Y. Peng, A. Nanayakkara, C. Gonzalez, M. Challacombe, P. M. W. Gill, B. G. Johnson, W. Chen, M. W. Wong, J. L. Andres, M. Head-Gordon, E. S. Replogle, J. A. Pople, Gaussian, Inc., Pittsburgh, PA, **1998**.
- [17] a) A. Berndt, *Angew. Chem.* **1993**, *105*, 1034; *Angew. Chem. Int. Ed. Engl.* **1993**, *32*, 985; b) R. Boese, P. Paetzold, A. Tapper, R. Ziembinski, *Chem. Ber.* **1989**, *122*, 1057.
- [18] No evidence for the existence of the unsymmetrical compound featuring a bicyclic and a four-membered-ring unit has been found. Moreover, the equilibrium between **p-4A** and **p-4B** is not solvent dependent.

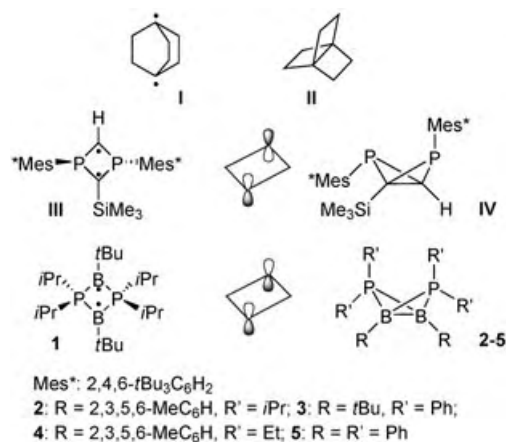
- [19] a) SMART Software Reference Manual, Version 5.054, Bruker Analytical X-ray System, Inc., Madison, WI **1997–1998**;
b) SAINTPLUS Software Reference Manual, Version 6.02A, Bruker Analytical X-ray System, Inc., Madison, WI **1997–1998**;
c) SHELXTL Software Reference Manual, Version 6.10, Dec. 5th, Bruker Analytical X-ray System, Inc., Madison, WI, **2000**.

Bond-Stretch Isomers

Evidence for the Coexistence of Two Bond-Stretch Isomers in Solution**

Amor Rodriguez, Ryan A. Olsen, Nima Ghaderi,
David Scheschkewitz, Fook S. Tham,
Leonard J. Mueller,* and Guy Bertrand*

The concept of “bond-stretch isomerism” has been introduced by Stohrer and Hoffmann by using strained tricyclic hydrocarbons (Scheme 1): “In the 2,2,2-system the optimum alignment for through-bond coupling of radical lobes creates the conditions for a new type of isomerism—two stable conformations related by a simple bond stretching. These are



Scheme 1. Some key compounds in the debate on bond-stretch isomerism.

[*] Dr. A. Rodriguez, R. A. Olsen, N. Ghaderi, Dr. D. Scheschkewitz, Dr. F. S. Tham, Prof. L. J. Mueller, Prof. G. Bertrand
 UCR-CNRS Joint Research Chemistry Laboratory (UMR 2282)
 Department of Chemistry
 University of California
 Riverside, CA 92521-0403 (USA)
 Fax: (+1) 909-787-2725
 E-mail: gbertran@mail.ucr.edu

[**] We are grateful to the NSF (CHE 0213510 and CHE 0349345) and RHODIA for financial support of this work.



Supporting information for this article is available on the WWW under <http://www.angewandte.org> or from the author.

the normal tricyclic form **II** and the stabilized diradical **I'**.^[1] The early attempts to characterize bond-stretch isomers either failed or were eventually rejected as crystallographic artifacts, and therefore the existence of bond-stretch isomers became questionable.^[2,3] According to the most recent review on this topic,^[4] the 1,3-diphosphacyclobutane-2,4-diyl **III** and 1,3-diphosphabicyclo[1.1.0]butane **IV** reported by Niecke et al.^[5] are the first and only known stretch isomers that have been isolated and independently characterized. It is important to note that because of a trans-annular antibonding π overlap, the thermal ring closure of **III** into **IV** is forbidden. Herein we report the first experimental evidence for the existence of two bond-stretch isomers that features a trans-annular bonding π -overlap, which allows for the thermal ring closure and opening processes.

We have recently reported the synthesis of a 1,3-dibora-2,4-diphosphoniocyclobutane-1,3-diyl **1**,^[6–8] as well as several 1,3-dibora-2,4-diphosphoniobicyclo[1.1.0]butanes **2–5**^[9] (Scheme 1); they differ by the nature of the boron and phosphorus substituents and therefore are not bond-stretch isomers. Derivatives **1** and **2–5** feature very different spectroscopic properties, which at first glance could be used as a fingerprint for the diradical versus the bicyclic structure. As observed for related carbon-based singlet 1,3-diradicals,^[10] compound **1** is strongly colored [λ_{max} (toluene) = 446 nm, ϵ = 2200], whereas all the derivatives **2–5** are colorless. Because the phosphorus is in a three-membered ring and the boron is tetracoordinated, the ^{31}P and ^{11}B NMR signals for **2–5** appeared at a much higher field than those for **1**.

In the course of a systematic study on the influence of the nature of the substituents on the ground state structure of the PBPB system, we have prepared a derivative that features *iso*-propyl at phosphorus and phenyl groups at boron. This compound has been isolated in 57% yield as very-air-sensitive, but thermally highly stable purple crystals (m.p.: 105 °C). In line with the strong coloration, X-ray diffraction analysis^[11] (Figure 1) revealed that in the solid state this compound adopts a very similar structure to that observed for **1**: a planar, almost square PBPB ring, with a very large B–B interatomic distance of 2.57 Å. Interestingly, the phenyl rings are almost coplanar to the PBPB skeleton (torsion angle

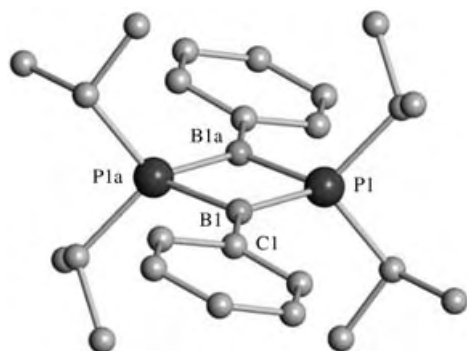


Figure 1. Molecular view of **6** in the solid state (H atoms are omitted). Selected bond lengths: P1–B1, 1.8943 ± 17 Å; P1–B1a, 1.8915 ± 16 Å; B1–C1, 1.557 ± 2 Å; B1–P1–B1a, 85.23 ± 7°; P1–B1–P1a, 94.77 ± 7°, P1–B1–C1, 129.47 ± 11°; P1a–B1–C1, 135.75 ± 12°.

13.5°), which suggests some delocalization between the 2p(B) orbitals and the π -ring systems.

The magic-angle-spinning solid-state NMR spectrum of the purple crystals shows a single ^{31}P signal at δ = 5.9 ppm, which is comparable to that observed for **1** both in solution and in the solid state, thus confirming the diradical structure in the solid state. However, the solution state NMR spectra of the same compound (Figure 2) at room temperature reveal a single ^{31}P signal at δ = –28 ppm and an ^{11}B resonance at δ = –9 ppm, which suggest a different structural preference. These chemical shifts are very comparable to those observed both in solution and in the solid state for the bicyclic derivative **2** (same substituents at the P atom and duryl instead of phenyl at the B atom). As the ^{31}P chemical shift was found to be temperature dependent and moves towards a lower field as the temperature decreased, these results as a whole suggest a fast interconversion between a diradical structure **6** and the corresponding bicyclic stretch isomer **7**, the latter being favored at higher temperatures. This hypothesis is consistent with the observed changes in the NMR line shape^[12] as the solution is cooled. But instead of two slow-exchange P signals, one for **6** and one for **7**, three resonances were observed at –145 °C. The signal at δ = 4.0 ppm can be easily assigned to the open form, **6**, whereas the signals at δ =

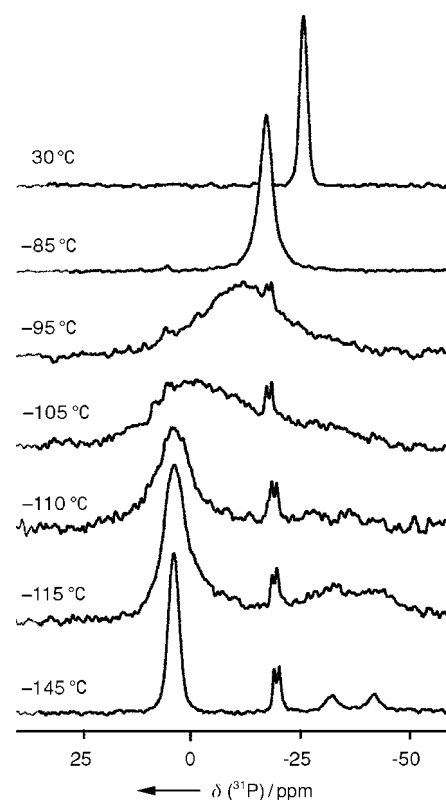


Figure 2. ^{31}P spectra of the interconverting singlet diradical **6** and bicyclic stretch isomers **7** as a function of temperature. Spectra were obtained on a 400 MHz (1 H) Bruker DMX spectrometer equipped with a 5 mm high-resolution double resonance probe and referenced through an external solution of 1% phosphoric acid at 30 °C. The temperature was measured by using an internal probe thermocouple calibrated versus a standard methanol chemical shift thermometer. The signals at –20 ppm are tentatively assigned to impurities.

–32.2 and –41.8 ppm could not be readily explained and prompted us to perform ab initio calculations.^[13]

For the planar structure, local minima that correspond to eight different arrangements of the isopropyl groups, including the crystallographically observed conformer **6**, were found. The calculated ³¹P NMR chemical shift (+6.0 ppm) agrees well with both the solid-state and the low-temperature liquid-state NMR data. For the bicyclic structures, ten local minima were found, among them **7a** and **7b** were the lowest and equivalent in energy (Figure 3). Due to the presence of

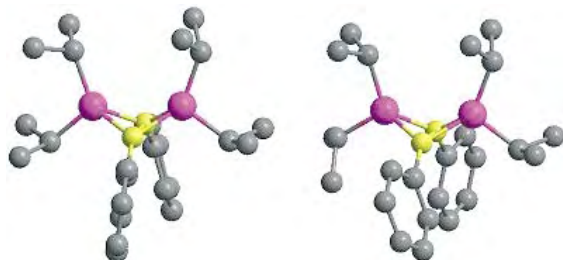


Figure 3. Optimized structures of the two most-stable bicyclic conformers **7a** and **7b**.

two inequivalent phosphorous nuclei, AX systems are calculated at $\delta = -36.3$ and -43.1 , and -31.9 and -40.3 ppm, for **7a** and **7b**, respectively. The observed signals of equal intensity and line width at $\delta = -32.2$ and -41.8 ppm fit well with a rapid low-temperature interconversion between **7a** and **7b**, although the participation of other conformers that preserves the AX system cannot be excluded.

As the temperature is raised above -145°C , the singlet diradical and bicyclic bond-stretch isomers exchange. Initially, the signals at high field broaden more rapidly due to the inequivalent exchange, which favors **6** over **7** by a 3:1 ratio at -145°C . Rates extracted from the line width of the diradical peak in the initial broadening regime (from -145 to -110°C) give a free energy of activation^[14] of 6.6 ± 1.8 kcal mol⁻¹ at -130°C for the pathway between **6** and **7**. The transition through intermediate exchange (-110 to -85°C) is somewhat convoluted as the equilibrium constant **6/7** also changes dramatically in this region with preference switching from **6** to the bicyclic forms **7** (1:2 at -85°C). Above -65°C , only a single fast-exchange resonance is observed with a temperature-dependent chemical shift that reflects the changing populations of the bond-stretch isomers, which reaches a **6/7** ratio of 1:7 at room temperature. We can extract a free-energy difference between the stretch isomers from these data by using a three-site exchange model, which gives $\Delta H = 1.4 \pm 0.2$ kcal mol⁻¹ (**6** being the most stable isomer) and $\Delta S = 7.2 \pm 1.6$ cal mol⁻¹ K. Although, ab initio calculations of the energy difference between the biradical and bicyclic forms favor the bicyclic isomer by 0.8 kcal mol⁻¹, this discrepancy is within the limit of error expected for such a comparison.

We note the excellent agreement of the limiting chemical shifts for the diradical **6** and bicyclic forms **7** with the related compounds **1** and **2**, respectively, as well as the agreement with the ab initio calculated shifts. These results give us confidence that the observed dynamic NMR behavior is not due to isopropyl group rotations^[15] within the planar bond-

stretch form **6**. This conclusion is confirmed by variable-temperature UV/Vis spectroscopy,^[16] which also tracks the population shift from the colorless bicyclic form **7** to the colored diradical species **6** as the temperature is decreased (Figure 4).

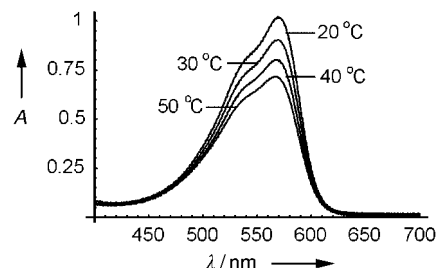


Figure 4. UV/Vis spectra showing the preference for the colored open form **6** over the colorless bicyclic form **7** as the temperature is lowered.

It can be concluded that the order of stability of the bond-stretch isomers **6** and **7** is strongly entropy driven. The diradical isomer with the coplanar phenyl group has fewer degrees of freedom than the bicyclic isomers in which free rotation of the phenyl groups and inversion at boron are both allowed. This is certainly a unique example of a reaction in which the breaking of a σ -bond is induced by decreasing the temperature and the bond formation is entropically favored. It is noteworthy that the B–B interatomic distance between **6** [257 (exp), 258 pm (calcd)] and **7** [186 pm (calcd)] varies by 40%. Combined with the phenomenon of temperature-dependent interconversion, these results open interesting perspectives for “molecular muscles”^[17] as well as electrical switch devices.^[18]

Experimental Section

All manipulations were performed under argon by using standard Schlenk techniques. Dry, oxygen-free solvents were employed.

Synthesis of [(iPr)₂PB(Cl)Ph]₂: (iPr)₂PSiMe₃ (3.05 g, 16.05 mmol) was added to a solution of commercially available PhBCl₂ (2.55 g, 16.05 mmol) in toluene (30 mL) at -80°C . The reaction mixture was heated overnight at 100°C . All the volatile products were removed under vacuum. Single crystals were obtained by cooling a saturated solution of product in toluene to -30°C . m.p.: 268°C , decomp; ¹³C{¹H} NMR (125.8 MHz, CDCl₃): $\delta = 132.9$, 127.7, 126.8 (s, C_{aro}), 24.4 (pseudo-t, $J_{\text{PC}} = 15.2$ Hz, PCH), 21.4 (s, CHCH₃), 20.3 ppm (s, CHCH₃), *ipso*-C atoms are not observed; ¹H NMR (300 MHz, CDCl₃): $\delta = 7.72$ (d, $^3J_{\text{HH}} = 6.0$ Hz, 4H, Ph-*o*-CH), 7.23 (m, 6H, Ph-*m,p*-CH), 3.02 (m, 4H, PCH), 1.28 (dd, $J_{\text{HP}} = 13.8$ Hz, $^3J_{\text{HH}} = 7.2$ Hz, 12H, CHCH₃), 0.75 ppm (dd, $J_{\text{HP}} = 13.8$ Hz, $^3J_{\text{HH}} = 7.2$ Hz, 12H, CHCH₃); ³¹P{¹H} (CDCl₃) $\delta = -5.2$ ppm; ¹¹B{¹H} (CDCl₃) $\delta = -1$ ppm.

Synthesis of derivative 6/7: A freshly prepared solution of Li-napthalene (6.4 mL, 0.8 M, thf) was added dropwise to a toluene solution (15 mL) of [(iPr)₂PB(Cl)Ph]₂ (2.5 mmol) at -80°C . The reaction mixture was warmed to room temperature and stirring was maintained for about 30 minutes. The solvents were immediately removed under vacuum and the residue was dissolved in pentane (30 mL). Salts were removed by filtration and pentane was removed under vacuum. Naphtalene was sublimed by heating to 80°C under vacuum for 30 minutes. Purple single crystals (57% yield) were obtained by cooling saturated solutions of product in pentane to -30°C . m.p.: 105°C ; ¹³C{¹H} NMR (125.8 MHz, C₇D₈): $\delta = 143.8$ (br,

i-C_{aro}), 136.3, 128.5, 126.3 (s, C_{aro}), 28.6 (pseudo-t, J_{PC} = 22 Hz, PCH), 21.4 ppm (s, CHCH₃); ¹H NMR (300 MHz, CDCl₃): δ = 7.48 (d, $^3J_{HH}$ = 7.2 Hz, 4H, Ph-*o*-CH), 7.01 (pseudo-t, $^3J_{HH}$ = 7.2 Hz, 4H, Ph-*m*-CH), 6.89 (t, $^3J_{HH}$ = 7.2 Hz, 2H, Ph-*p*-CH), 1.73 (d, sept., J_{HP} = 4.2 Hz, $^3J_{HH}$ = 7.2 Hz, 4H, PCH), 0.80 ppm (dd, J_{HP} = 16.5 Hz, $^3J_{HH}$ = 7.2 Hz, 24H, CHCH₃).

Received: April 28, 2004

Keywords: boron · NMR spectroscopy · phosphorus · radicals · UV/Vis spectroscopy

- [1] W. D. Stohrer, R. Hoffmann, *J. Am. Chem. Soc.* **1972**, *94*, 779.
- [2] a) G. Parkin, *Chem. Rev.* **1993**, *93*, 887; b) J. A. Labinger, *C. R. Chim.* **2002**, *5*, 235.
- [3] The question of bond-stretch isomerism has been considered theoretically with different combinations of heteroatoms. For examples, see: a) P. V. Sudhakar, O. F. Guner, K. Lammertsma, *J. Phys. Chem.* **1989**, *93*, 7289; b) J. A. Boatz, M. S. Gordon, *J. Phys. Chem.* **1989**, *93*, 2888; c) P. V. Sudhakar, K. Lammertsma, *J. Phys. Chem.* **1992**, *96*, 4830; d) T. Kudo, S. Nagase, *J. Phys. Chem.* **1992**, *96*, 9189.
- [4] M. M. Rohmer, M. Benard, *Chem. Soc. Rev.* **2001**, *30*, 340–354.
- [5] a) E. Niecke, A. Fuchs, M. Nieger, *Angew. Chem.* **1999**, *111*, 3213; *Angew. Chem. Int. Ed.* **1999**, *38*, 3028; b) E. Niecke, A. Fuchs, F. Baumeister, M. Nieger, W. W. Schoeller, *Angew. Chem.* **1995**, *107*, 640; *Angew. Chem. Int. Ed. Engl.* **1995**, *34*, 555; c) O. Schmidt, A. Fuchs, D. Gudat, M. Nieger, W. Hoffbauer, E. Niecke, W. W. Schoeller, W. W. *Angew. Chem.* **1998**, *110*, 995; *Angew. Chem. Int. Ed. Engl.* **1998**, *37*, 949; d) W. W. Schoeller, C. Begemann, E. Niecke, D. Gudat, *J. Phys. Chem.* **2001**, *105*, 10731; e) M. Sebastian, M. Nieger, D. Szieberth, L. Nyulaszi, E. Niecke, *Angew. Chem.* **2004**, *116*, 647; *Angew. Chem. Int. Ed.* **2004**, *43*, 637.
- [6] a) D. Scheschekewitz, H. Amii, H. Gornitzka, W. W. Schoeller, D. Bourissou, G. Bertrand, *Science* **2002**, *295*, 1880; b) H. Amii, L. Vranicar, H. Gornitzka, D. Bourissou, G. Bertrand, *J. Am. Chem. Soc.* **2004**, *126*, 1344.
- [7] For calculations see: a) M. Seierstad, C. R. Kinsinger, C. J. Cramer, *Angew. Chem.* **2002**, *114*, 4050; *Angew. Chem. Int. Ed.* **2002**, *41*, 3894; b) W. W. Schoeller, A. Rozhenko, D. Bourissou, G. Bertrand, *Chem. Eur. J.* **2003**, *9*, 3611; c) Y. Jung, M. Head-Gordon, *J. Phys. Chem. A* **2003**, *107*, 7475; d) M. J. Cheng, C. H. Hu, *Mol. Phys.* **2003**, *101*, 1319.
- [8] See also: a) H. Grützmaier, F. Breher, *Angew. Chem.* **2002**, *114*, 4178; *Angew. Chem. Int. Ed.* **2002**, *41*, 4006; b) P. P. Power, *Chem. Rev.* **2003**, *103*, 789.
- [9] D. Scheschekewitz, H. Amii, H. Gornitzka, W. W. Schoeller, D. Bourissou, G. Bertrand, *Angew. Chem.* **2004**, *116*, 595; *Angew. Chem. Int. Ed.* **2004**, *43*, 585.
- [10] a) W. Adam, W. T. Borden, C. Burda, H. Foster, T. Heidenfelder, M. Heubes, D. A. Hrovat, F. Kita, S. B. Lewis, D. Scheutzow, J. Wirz, *J. Am. Chem. Soc.* **1998**, *120*, 593; b) M. Abe, W. Adam, T. Heidenfelder, W. M. Nau, X. Zhang, *J. Am. Chem. Soc.* **2000**, *122*, 2019; c) M. Abe, W. Adam, M. Hara, M. Hattori, T. Majima, M. Nojima, K. Tachibana, S. Tojo, *J. Am. Chem. Soc.* **2002**, *124*, 6540; d) M. Abe, W. Adam, W. T. Borden, M. Hattori, D. A. Hrovat, M. Nojima, K. Nozaki, J. Wirz, *J. Am. Chem. Soc.* **2004**, *126*, 574.
- [11] The Bruker SMART-1000^[19a] X-ray diffraction instrument with Mo radiation was used for data collection of compound **6**. All data frames were collected by using ω -scan mode ($-0.3^\circ\omega$ -scan width, hemisphere of reflections) and integrated by using Bruker SAINTPLUS program.^[19b] The intensity data were corrected for Lorentzian polarization and absorption corrections were performed by using the SADABS program incorporated in the SAINTPLUS program. The Bruker SHELXTL program^[19c] was used for direct methods of phase determination and structure refinement. Atomic coordinates, isotropic and anisotropic displacement parameters of all the non-hydrogen atoms of the two compounds were refined by means of a full-matrix least-squares procedure on F^2 . All H atoms were included in the refinement in calculated positions riding on the atoms to which they were attached. C₂₄H₃₈B₂P₂, M_r = 410.10, crystal size $0.51 \times 0.30 \times 0.15$ mm³, monoclinic, space group $P2_1/c$, a = 8.8947(12) Å, b = 11.1419(15) Å, c = 12.6125(18) Å, β = 102.553(3)°, V = 1220.1(3) Å³, ρ_{calcd} = 1.116 g cm⁻³, $2\theta_{\text{max}}$ = 52.74°, MoK α (λ = 0.71073 Å), low temperature = 223(2) K, total reflections collected = 6967, independent reflections = 2474 (R_{int} = 0.0216, R_{sig} = 0.0239, redundancy = 2.8, completeness 100%) and 2151 (86.9%) reflections were greater than $2\sigma(I)$, index ranges $-10 \leq h \leq 11$, $-13 \leq k \leq 13$, $-15 \leq l \leq 9$, absorption coefficient μ = 0.186 mm⁻¹; max/min transmission = 0.9727/0.9112, 150 parameters were refined and converged at $R1$ = 0.0359, $wR2$ = 0.0954, with intensity $I > 2\sigma(I)$, the final difference map was 0.389/−0.143 e Å⁻³. CCDC-237053 contains the supplementary crystallographic data for this paper. These data can be obtained free of charge via www.ccdc.cam.ac.uk/conts/retrieving.html (or from the Cambridge Crystallographic Data Centre, 12, Union Road, Cambridge CB2 1EZ, UK; fax: (+44) 1223-336-033; or deposit@ccdc.cam.ac.uk).
- [12] a) *Dynamic Nuclear Magnetic Resonance Spectroscopy* (Eds.: L. M. Jackman, F. A. Cotton), Academic Press, New York, **1975**; b) *Dynamic NMR Spectroscopy* (Ed.: J. Sandstrom), Academic Press, London, **1982**.
- [13] Structures minimized (B3LYP/6-31G(d)) and chemical shifts calculated (B3LYP/6-311G(2d,p)) in the Gaussian98 (Revision A.7), M. J. Frisch, G. W. Trucks, H. B. Schlegel, G. E. Scuseria, M. A. Robb, J. R. Cheeseman, V. G. Zakrzewski, J. A. Montgomery, R. E. Stratmann, J. C. Burant, S. Dapprich, J. M. Millam, A. D. Daniels, K. N. Kudin, M. C. Strain, O. Farkas, J. Tomasi, V. Barone, M. Cossi, R. Cammi, B. Mennucci, C. Pomelli, C. Adamo, S. Clifford, J. Ochterski, G. A. Petersson, P. Y. Ayala, Q. Cui, K. Morokuma, D. K. Malick, A. D. Rabuck, K. Raghavachari, J. B. Foresman, J. Cioslowski, J. V. Ortiz, B. B. Stefanov, G. Liu, A. Liashenko, P. Piskorz, I. Komaromi, R. Gomperts, R. L. Martin, D. J. Fox, T. Keith, M. A. Al-Laham, C. Y. Peng, A. Nanayakkara, C. Gonzalez, M. Challacombe, P. M. W. Gill, B. G. Johnson, W. Chen, M. W. Wong, J. L. Andres, M. Head-Gordon, E. S. Replogle, J. A. Pople, Gaussian, Inc., Pittsburgh, PA, **1998**.
- [14] P. Pechukas, *Annu. Rev. Phys. Chem.* **1981**, *31*, 159.
- [15] Distinct conformers due to isopropyl rotations have been observed in slow exchange by NMR in unrelated systems. For a recent example: J. E. Anderson, A. de Meijere, S. I. Kozhushkov, L. Lunazzi, A. Mazzanti, *J. Am. Chem. Soc.* **2002**, *124*, 6706.
- [16] The same approach has been elegantly used to provide evidence for the existence of bishomoaromatic semibullvalene. a) H. Quast, M. Seefelder, *Angew. Chem.* **1999**, *111*, 1132; *Angew. Chem. Int. Ed.* **1999**, *38*, 1064; b) A. C. Goren, D. A. Hrovat, M. Seefelder, H. Quast, W. T. Borden, *J. Am. Chem. Soc.* **2002**, *124*, 3469.
- [17] M. J. Marsella, *Acc. Chem. Res.* **2002**, *35*, 944.
- [18] a) A. Rajca, *Chem. Rev.* **1994**, *94*, 871; b) J. A. Berson, *Acc. Chem. Res.* **1997**, *30*, 238.
- [19] a) SMART Software Reference Manual, Version 5.054, Bruker Analytical X-Ray System, Inc., Madison, WI, **1997–1998**; b) SAINTPLUS Software Reference Manual, Version 6.02A, Bruker Analytical X-Ray System, Inc., Madison, WI **1997–1998**; c) SHELXTL Software Reference Manual, Version 6.10, Bruker Analytical X-Ray System, Inc., Madison, WI, **2000**.

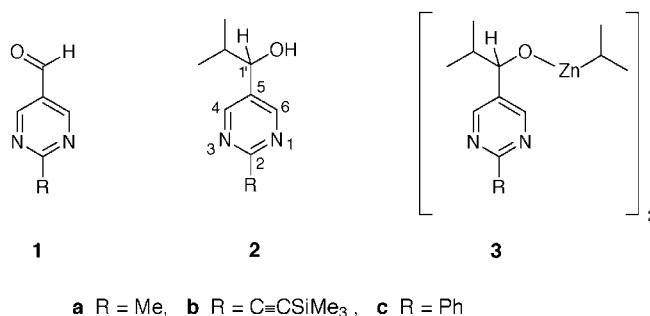
Zinc Autocatalysts

Solution Structure and Reagent Binding of the Zinc Alkoxide Catalyst in the Soai Asymmetric Autocatalytic Reaction**

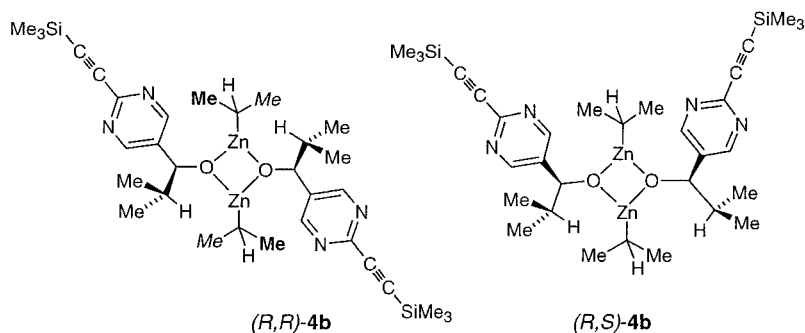
Ilya D. Gridnev,* Jörg M. Serafimov, and John M. Brown*

The remarkable zinc alkylation reactions discovered and developed by Soai and co-workers remain the sole example of amplifying asymmetric autocatalysis, even after more than seven years.^[1,2] The phenomenon is confined to rigid γ -aminoaldehydes, especially **1**, and uniquely limited to diisopropylzinc. An O-Zn-N monomeric chelate structure, common to all such structurally characterized catalysts for asymmetric zinc alkylation reactions, cannot operate in this case.^[3] The efficiency of the autocatalysis experiment is affected by substituents at the 2-position of the pyrimidine ring, with alkynyl groups being optimum.^[4] Understanding the structural and mechanistic principles of this reaction will permit the rational development of new examples of autocatalysis and a better understanding of spontaneous asymmetric synthesis in this system.^[5]

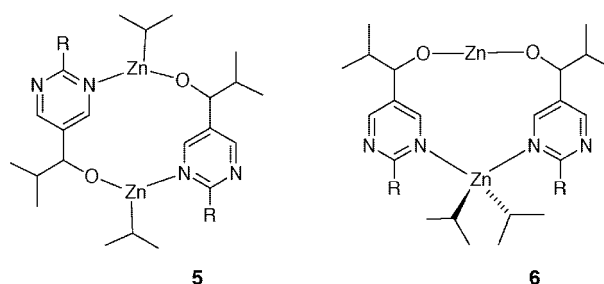
In earlier joint work we demonstrated that the resting state is a dimeric zinc alkoxide, which is active only in its homochiral form.^[6] Initial NMR spectroscopy experiments in C_7D_8 revealed the dynamic nature of the system. More easily interpretable spectra were obtained from **2a** and **2b** with iPr_2Zn in $[D_8]THF$ or $[D_7]DMF$, the solutions being more stable in $[D_8]THF$. In solution in THF, however, turnover is slow and amplifying autocatalysis does not occur, which is in keeping with the inhibiting effect of this strongly Lewis basic solvent.^[7] The statistical distribution between homo- and heterochiral associates of **3a** or **3b** was verified in $[D_8]THF$ (Figure 1). A further key observation made from the 1H NMR spectra defines the structure in solution. For enantiomerically pure **3b**, four distinct doublets are observed for the isopropyl methyl groups, indicating that both $ZnOCHCHMe_2$ and $ZnCHMe_2$ are diastereotopic (Figure 1a). For racemic **3b**, which contains equal proportions of the homo- and heterochiral dimers, three additional doublets arising from methyl



groups are seen (Figure 1b), with the $ZnCHMe_2$ pair now isochronous in all 1H and ^{13}C NMR spectra over a wide temperature range (Figure 1). This result demonstrates that the heterochiral form has a symmetry plane that encompasses $C-Zn \cdots Zn-C$. The results also fit uniquely with the structures of the homochiral and heterochiral dimers being (R,R) -**4b** and (R,S) -**4b**. These diastereomeric structures have been



verified by B3LYP DFT calculations on model compounds with a full 6-31G* basis set and shown to be comparable in enthalpy,^[8] whereas the previously postulated macrocyclic structure **5** has been shown to be significantly less favorable (Figure 2).^[9] A third possible dimeric structural type **6** of



permissible symmetry is ruled out by the 1H NMR spectra of a solution of (R) -**2b** in C_7D_8 treated with 0.5 equivalents of iPr_2Zn which indicate an equal mixture of (R,R) -**4b** and (R) -**2b**. There is good precedent for the postulated $\{ZnO\}_2$ square dimer form.^[10]

[*] Dr. I. D. Gridnev, J. M. Serafimov, Dr. J. M. Brown
Dyson Perrins Laboratory
University of Oxford
South Parks Road, Oxford OX1 3QY (U.K.)
Fax: (+44) 1865-275-642
E-mail: bjm@herald.ox.ac.uk

[**] We thank the Leverhulme Trust for support (to I.D.G.). Dr. T. D. W. Claridge and Dr. B. Odell were very helpful in obtaining the NMR spectra. We thank Mr. R. McLatchie for access to the Oxford Supercomputer facility OSWELL, and Prof. D. G. Blackmond for exchange of unpublished work.

Supporting information for this article is available on the WWW under <http://www.angewandte.org> or from the author.

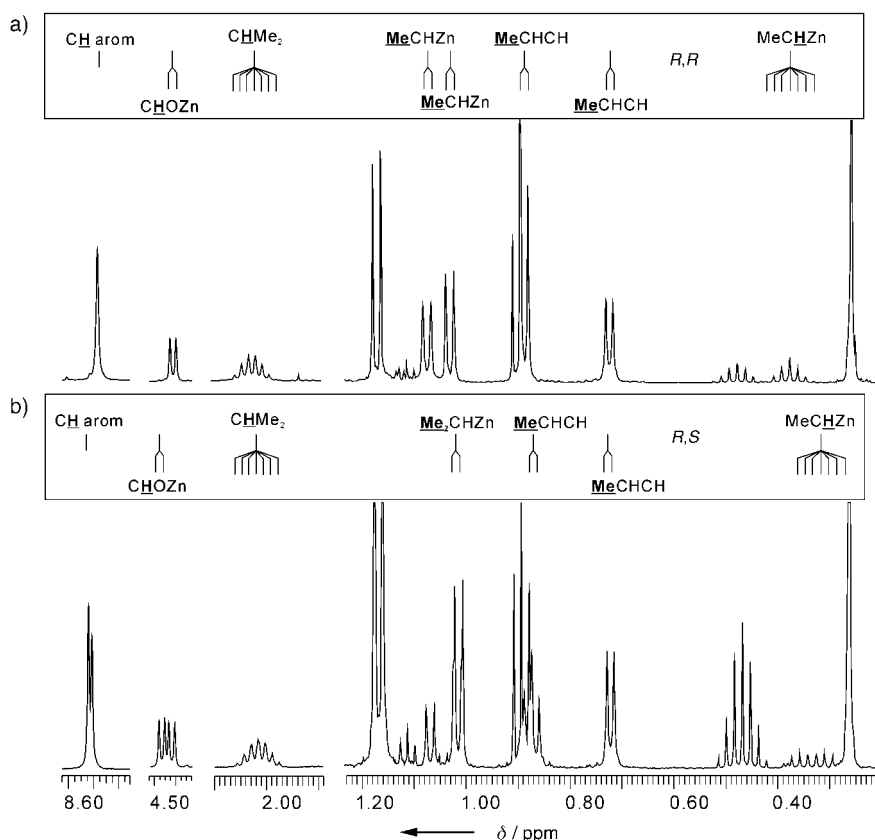


Figure 1. ^1H NMR spectra of a) (R,R) -**3b** and b) (R,S) -**3b** in $[\text{D}_8]\text{THF}$ at ambient temperature, 500 MHz. In the 1.5 to 0.5 ppm region, the upper trace of the homochiral dimer shows both pairs of magnetically inequivalent CHMe_2 groups. The lower trace (a 1:1 equilibrium mixture of homo- and heterochiral dimers) additionally shows the equivalent ZnCHMe_2 at 1.02 ppm (overlapping) and inequivalent CHCHMe_2 groups at $\delta = 0.88$ and 0.72 ppm (overlapping). Co-produced propane is at $\delta = 0.90$ ppm.

Encouraged by these results, we reverted to NMR analyses in toluene. Solutions of zinc alkoxides in C_7D_8 have a tendency to precipitate,^[11] which is alleviated by the addition of excess $i\text{Pr}_2\text{Zn}$. The general features of the NMR spectra in $[\text{D}_8]\text{THF}$ are reproduced in toluene, whilst reagent binding is more pronounced (see below). Specifically, the distinct resonance signals of the diastereotopic $i\text{PrCH}$ and $i\text{PrZn}$ methyl groups are observed in the homochiral form, and the signal for the $i\text{PrCH}$ methyl groups is also observed in the heterochiral form, whereas the signal for the $i\text{PrZn}$ methyl groups is broadened at ambient temperature. The proportions of homo- and heterochiral forms in the racemate are again quite comparable in C_7D_8 . The indicated structure is supported by numerous NOESY spectra; the absence of close contact between the 2-H atom of the phenyl substituent and the $i\text{PrCH}$ or $i\text{PrZn}$ moieties of **3c** in both C_7D_8 and $\text{C}_4\text{D}_8\text{O}$ is especially telling. For dimer **4a** prepared from aldehyde **1a** without added catalyst **2a**, two broadened singlets of similar intensity were observed at 298 K in the 8.5 ppm region, corresponding to the homo- and heterochiral forms (52:48). On increasing the temperature these broaden and then coalesce at 348 K. Line-shape analysis of the aryl protons over the range 313–353 K and extrapolation of the slope of $\ln k(\text{exchange})$ to ambient temperature indicates that the

half-life of an individual dimer molecule with respect to $R \leftrightarrow S$ exchange is in the region of 15 s at 293 K.^[12]

In a dilute solution (ca. 0.04 M) of (R,R) -**4b**, prepared from the alcohol by reaction with a modest excess of zinc reagent (0.08 M) in C_7D_8 , all the ^1H NMR signals associated with the pyrimidine entity broaden markedly on cooling. The oligomeric species formed at low temperature must have low symmetry, and distinct environments for the pyrimidine nitrogen atoms of individual rings, since 4-H and 6-H are inequivalent.^[13] The broad ^1H NMR signals observed for alkoxide **4b** in the ArH region under static conditions (that is, the probe is not spun) at 273 K is identical to that which develops when the autocatalytic reaction between aldehyde **1b** and $i\text{Pr}_2\text{Zn}$ is followed in situ.

The magnetic equivalence of the two aryl hydrogen atoms in the ambient-temperature ^1H NMR spectrum of all the mixtures of reactant **1** or alkoxide **4** with added $i\text{Pr}_2\text{Zn}$ requires that any N-association is dynamic. To investigate this further, the synthesis of ^{15}N -labeled pyrimidinal **1d** was carried out (Scheme 1).^[14] Association of reactant **1d** with varying $i\text{Pr}_2\text{Zn}$ concentration was conveniently studied at 213 K by ^{13}C , ^1H , and ^{15}N NMR spectroscopy, the latter by means of heteronuclear multiple-bond correlation (HMBC) spectra; at this temperature the aldehyde reacted only slowly with $i\text{Pr}_2\text{Zn}$. These spectra consistently demonstrate binding to $i\text{Pr}_2\text{Zn}$ by N coordination. The association constant of 5.8 M^{-1} derived from the ^1H NMR spectra is fully consistent with the value of 5.6 M^{-1} obtained by analysis of ^{15}N chemical shift data, in which shielding of up to 15.5 ppm is observed at high zinc concentration.^[15] The alkynyl ^{13}C NMR chemical shifts are also markedly affected by zinc binding; increased zinc alkyl concentration causes shielding of $\text{C1}'$, and deshielding of $\text{C2}'$ as well as deshielding of C4 . The results all demonstrate rapidly reversible association of $i\text{Pr}_2\text{Zn}$ with a pyrimidine nitrogen atom of **1d** without evident involvement of the carbonyl group.^[16]

Synthesis of labeled enantiomerically pure alcohol **2d** (Scheme 1) from aldehyde **1d** enabled further zinc-binding studies. Informative ^{15}N HMBC spectra were only obtained at 308 K in C_7D_8 for the zinc alkoxide dimer **4d**, and the progressive shielding of the ^{15}N signal with increasing $i\text{Pr}_2\text{Zn}$ concentration indicated association. A quantitative assay was obtained from the substantial ^{13}C chemical shift change of the alkynyl carbon atom signals of alkoxide **4b** on addition of $i\text{Pr}_2\text{Zn}$, and were interpreted as being the result of N coordination. The association constant is 4.6 M^{-1} . Similar

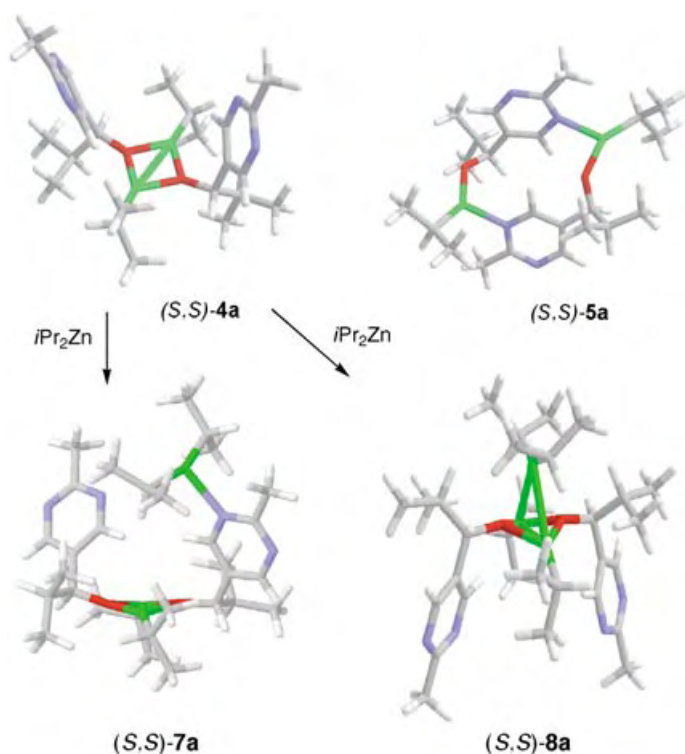
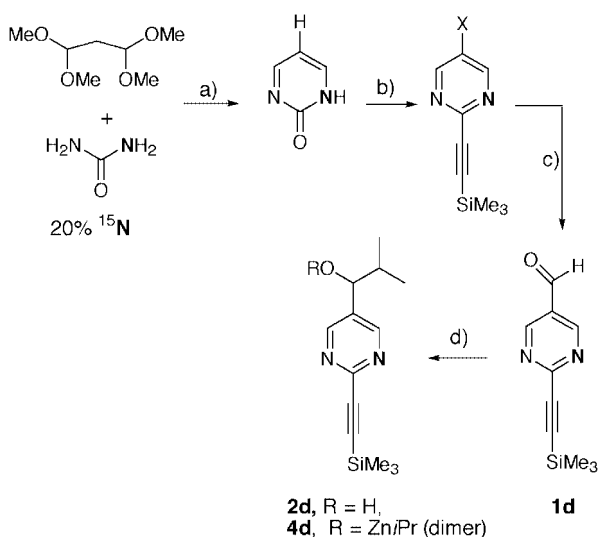


Figure 2. DFT minimized structures of square dimer **4a** and macrocyclic dimer **5a**. For formation of **4a** from monomer, $\Delta H_0 = -38.4 \text{ kcal mol}^{-1}$, and correspondingly for **5a**, $\Delta H_0 = -29.7 \text{ kcal mol}^{-1}$. $i\text{Pr}_2\text{Zn}$ -bound minimized structures **7a** and **8a**, respectively, have binding enthalpies of -10.2 (N-Zn) and $-6.5 \text{ kcal mol}^{-1} \text{ (O-Zn-O)}$.



Scheme 1. The synthesis of ^{15}N -labeled pyrimidines. a) reference [3a], b–d) references [3b, c].

changes were seen in $[\text{D}_8]\text{THF}$, but in this solvent the association constant is only 0.4 M^{-1} . THF does not function as a solvent for amplifying autocatalysis and the lower association constant probably reflects solvent coordination to zinc.^[17]

Allowing for the substantial temperature difference, these results indicate that the zinc alkoxide dimer **4** binds more strongly than the aldehyde **1** to $i\text{Pr}_2\text{Zn}$, and that both involve predominant N coordination. Both the CH and CH_3 resonance signals of the $i\text{Pr}_2\text{Zn}$ are shielded to an extent that depends on the degree of complexation. Under turnover conditions at 0°C , these resonance signals change in a manner that indicates increased zinc complexation ($\delta_{\text{CH}} = 0.670 \text{ ppm}$, $\delta_{\text{CH}_3} = 1.274 \text{ ppm}$ at 25 % reaction, $\delta_{\text{CH}} = 0.704 \text{ ppm}$, $\delta_{\text{CH}_3} = 1.294 \text{ ppm}$ at 80 %). More intriguingly, the alkoxide dimer acts as a chiral shift reagent towards $i\text{Pr}_2\text{Zn}$ with clear temperature-dependent separation of the diastereotopic $\text{ZnCHMeMe}'$ groups of the reagent (Figure 3).

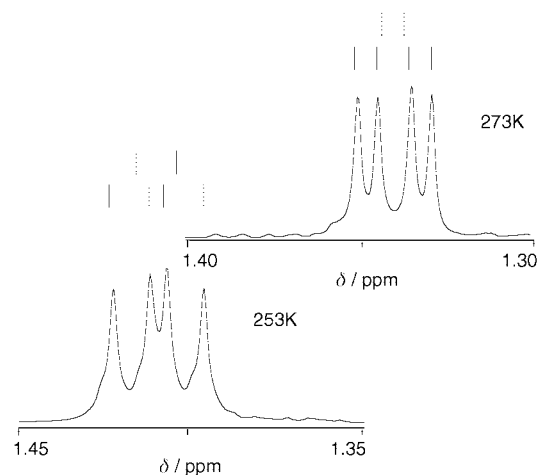


Figure 3. Detail of the ^1H NMR spectrum of zinc alkoxide **3b** (0.08 M) in C_7D_8 showing the CH_3 resonance signal of excess $i\text{Pr}_2\text{Zn}$ (0.04 M), shifted from its normal position of $\delta = 1.20 \text{ ppm}$ (at 273 K in the absence of **3b**).

In the presence of excess $i\text{Pr}_2\text{Zn}$ the EXSY spectrum of alkoxide dimer **4b** in both THF and toluene shows rapid exchange between zinc-bound isopropyl groups in the reagent and dimer. The reaction occurs for both racemic and homochiral dimers with comparable facility. In toluene the rate increases with increasing $i\text{Pr}_2\text{Zn}$ concentration, but in THF saturation occurs above 0.2 M reagent. This observation is consistent with the trigonal, coordinatively unsaturated zinc sites proposed in structure **4b**. In THF, desolvation may be necessary before the formally trigonally coordinated zinc site is exposed to the reagent.^[17] The proposed pathway is supported by computational studies on the $i\text{Pr}_2\text{Zn}$ complexes of **4a** (Figure 2). Of the two defined energy minima, the bridged $(\text{O-ZnR}_2\text{-O})$ structure **8a** is favorably disposed for alkyl exchange. The nitrogen-bonded isomer **7a** is somewhat more stable.

What is the relevance of these studies to autocatalysis? We postulate a $\{\text{Zn-O}\}_2$ square structure for the resting state, which has a significant affinity for the complexation of $i\text{Pr}_2\text{Zn}$. Under typical autocatalytic turnover conditions (0°C – 25°C , 0.05 – $0.2 \text{ M } i\text{Pr}_2\text{Zn}$),^[1b] both the dimer and its zinc-association complex are present. Any mechanism that seeks to explain the reaction is required to take this into account. The

aesthetically appealing possibility of a tetrameric transition state is encompassed by these studies, but the strong aldehyde–ZnR₂ binding postulated in the model proposed by Buono and Blackmond,^[18] remains unsupported by in situ observations.

Experimental Section

1d: The ¹⁵N labeled 2-hydroxypyrimidine hydrochloride was prepared in 77 % yield by condensation of ¹⁵N-urea (10 %, Aldrich) with 1,1,3,3-tetramethoxypropane.^[14] Further steps paralleled those for the unlabeled compound (see Scheme 1).

Received: December 18, 2003

Revised: June 1, 2004 [Z53572]

Keywords: alkylation · autocatalysis · NMR spectroscopy · O ligands · zinc

- [1] a) K. Soai, T. Shibata, H. Morioka, K. Choji, *Nature* **1995**, 378, 767–768; b) T. Shibata, T. Hayase, J. Yamamoto, K. Soai, *Tetrahedron: Asymmetry* **1997**, 8, 1717–1719; c) K. Soai, T. Shibata, I. Sato, *Acc. Chem. Res.* **2000**, 33, 382–390; d) K. Soai, I. Sato, *Chirality* **2002**, 14, 548–554, and intervening papers from this group.
- [2] a) F. B. Panosyan, J. Chin, *Org. Lett.* **2003**, 5, 3947–3949; b) for a recent review encompassing the principles and practice of autocatalysis, see: K. Mikami, M. Yamanaka, *Chem. Rev.* **2003**, 103, 3369–3400.
- [3] 5-Ring chelates: a) M. Kitamura, S. Okada, S. Suga, R. Noyori, *J. Am. Chem. Soc.* **1989**, 111, 4028; b) C. Bolm, G. Schlingloff, K. Harms, *Chem. Ber.* **1992**, 125, 1191–1203; c) M. Kitamura, S. Suga, M. Niwa, R. Noyori, *J. Am. Chem. Soc.* **1995**, 117, 4832–4842; d) D. Enders, J. Zhu, G. Raabe, *Angew. Chem.* **1996**, 108, 1827; *Angew. Chem. Int. Ed. Engl.* **1996**, 35, 1725; e) E. Hecht, *Z. Anorg. Allg. Chem.* **2000**, 626, 2223–2227; 6-ring chelates: C. Bolm, J. Mueller, G. Schlingloff, M. Zehnder, M. Neuburger, *Chem. Commun.* **1993**, 182–183.
- [4] T. Shibata, S. Yonekubo, K. Soai, *Angew. Chem.* **1999**, 111, 746–748; *Angew. Chem. Int. Ed.* **1999**, 38, 659–661.
- [5] a) D. A. Singleton, L. K. Vo, *J. Am. Chem. Soc.* **2002**, 124, 10010–10011; b) K. Soai, I. Sato, T. Shibata, S. Komiya, M. Hayashi, Y. Matsueda, H. Imamura, T. Hayase, H. Morioka, H. Tabira, J. Yamamoto, Y. Kowata, *Tetrahedron: Asymmetry* **2003**, 14, 185–188; c) K. Mislav, *Collect. Czech. Chem. Commun.* **2003**, 68, 849–864; d) I. D. Gridnev, J. M. Serafimov, H. Quiney, J. M. Brown, *Org. Biomol. Chem.* **2003**, 1, 3811–3819.
- [6] D. G. Blackmond, C. R. McMillan, S. Ramdeehul, A. Schorm, J. M. Brown, *J. Am. Chem. Soc.* **2001**, 123, 10103–10104.
- [7] a) Unpublished work of the authors, and D. G. Blackmond, personal communication; b) for the X-ray structure of a bisTHF complex of a Zn square see: D. J. Darensbourg, J. R. Wildeson, J. C. Yarbrough, J. H. Reibenspies, *J. Am. Chem. Soc.* **2000**, 122, 12487–12496; c) DFT calculations reveal that the mono- and bisTHF complexes of a closely related {Zn–O}₂ square dimer (addition of ZnMe₂ to **1a**) are stabilized by 12.2 and 21.1 Kcal·mol^{–1}, respectively, relative to the corresponding molecules without THF.
- [8] For recent high-level computation on Zn alkylation chemistry, see: a) J. Weston, *Organometallics* **2001**, 20, 713–720; b) M. Nakamura, A. Hirai, E. Nakamura, **2003**, 125, 2341–2350; c) M. Panda, P.-W. Phuan, M. C. Kozlowski, *J. Org. Chem.* **2003**, 68, 564–571; d) J. Rudolph, T. Rasmussen, C. Bolm, P.-O. Norrby, *Angew. Chem.* **2003**, 115, 3110–3013; *Angew. Chem. Int. Ed.* **2003**, 42, 3002–3005.
- [9] For X-ray structures of macrocyclic ZnX₂ nicotinamide dimers see: a) G. Davies, A. El-Toukhy, K. D. Onan, M. Veidis, *Inorg. Chim. Acta* **1984**, 84, 41; b) F. Bigoli, A. Braibanti, M. A. Pellinghelli, *Acta Cryst. B* **1973**, 29, 2708.
- [10] a) M. M. Olmstead, P. P. Power, S. C. Shoner, *J. Am. Chem. Soc.* **1991**, 113, 3379–3385; b) M. Parvez, G. L. Bergstresser, H. G. Richey Jr., *Acta Crystallogr. C* **1992**, 48, 641–644.
- [11] F. G. Buono, H. Iwamura, D. G. Blackmond, *Angew. Chem.* **2004**, 116, 2151–2155; *Angew. Chem. Int. Ed.* **2004**, 43, 2099–2103.
- [12] Amplifying autocatalysis functions as low as –45°C: I. Sato, D. Omiya, K. Tsukiyama, Y. Ogi, K. Soai, *Tetrahedron: Asymmetry* **2001**, 12, 1965–1969.
- [13] For crystallographically defined cubic tetramers (high symmetry) see: a) H. M. M. Shearer, C. B. Spencer, *Acta Crystallogr. B* **1980**, 36, 2046–2050; b) A. D. Bond, D. J. Linton, A. E. H. Wheatley, *Acta Crystallogr. E* **2001**, 57, 298–300; c) A. B. Charette, C. Molinaro, C. Brochu, *J. Am. Chem. Soc.* **2001**, 123, 12160–12167 and ref. [10a].
- [14] R. R. Covington, J. S. New, J. P. Yevich, D. L. Temple, *J. Labelled Compd. Radiopharm.* **1983**, 20, 1207–1211.
- [15] S. Berger, S. Braun, H.-O. Kalinowski, *NMR Spectroscopy of the Non-Metallic Elements*, Wiley, Chichester, **1999**, Chapter 4.2.8, p. 221; for reviews see: a) W. von Philipsborn, R. Müller, *Angew. Chem.* **1986**, 98, 381–412; *Angew. Chem. Int. Ed. Engl.* **1986**, 25, 383–413; b) J. Mason, *Chem. Rev.* **1981**, 81, 205–227.
- [16] The absence of aldehyde–ZnR₂ association reported in 1991 has not subsequently been refuted, although reversible aldehyde association with the Zn alkoxide monomer that is the true catalytic species in asymmetric alkylation is clearly detected by ¹H NMR spectroscopy: a) R. Noyori, M. Kitamura, *Angew. Chem.* **1991**, 103, 34–55; *Angew. Chem. Int. Ed. Engl.* **1991**, 30, 49–60; b) M. Kitamura, S. Suga, M. Niwa, R. Noyori, *J. Am. Chem. Soc.* **1995**, 117, 4832–4842.
- [17] For example: a) R. P. Davies, D. J. Linton, P. Schooler, R. Snaith, A. E. H. Wheatley, *Chem. Eur. J.* **2001**, 7, 3696–3704; b) A. D. Bond, D. J. Linton, P. Schooler, A. E. H. Wheatley, *J. Chem. Soc. Dalton Trans.* **2001**, 3173–3178; c) R. L. Geerts, J. C. Huffman, K. G. Caulton, *Inorg. Chem.* **1986**, 25, 1803–1805.
- [18] F. Buono, D. G. Blackmond, *J. Am. Chem. Soc.* **2003**, 125, 8978–8979. This recent publication from Buono and Blackmond raised the intriguing possibility that the limiting transition state for autocatalysis is tetrameric. To interpret the kinetics at high [Zn]/[A], (A = aldehyde) it was suggested that strong binding of *i*Pr₂Zn to the required aldehyde, 2-methylpyrimidine-5-aldehyde, might occur to produce a single coherent entity. NMR spectroscopic examination of the aldehyde/*i*Pr₂Zn system in C₇D₈ at 298 K does show minor upfield movement of ¹H and ¹³C resonances of the aldehyde in both the spectra at high zinc concentration. The association is weak, as exemplified by the ¹³C shift change for C4 in **1** (δ = –2.59 ppm at 0.33 M [Zn], 213 K) with that in 2-methylpyrimidine-5-aldehyde (δ = –0.34 ppm at 1.21 M [Zn], 298 K). Other changes are also in line with weak association.

Biosynthesis

Isolation, Crystal and Solution Structure Determination, and Biosynthesis of Tubulysins—Powerful Inhibitors of Tubulin Polymerization from Myxobacteria**

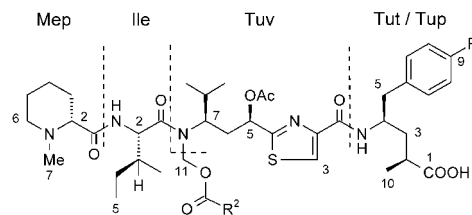
Heinrich Steinmetz, Nicole Glaser,
Eberhardt Herdtweck, Florenz Sasse,
Hans Reichenbach, and Gerhard Höfle*

The antifungal and cytotoxic myxobacterial metabolite epothilone^[1] was known for many years before Bollag et al.^[2] discovered in 1995 that its potent cytotoxicity is based on the induction of tubulin polymerization. In fact, epothilone was the first natural product after taxol to be found to have this mode of action, and, even more surprisingly, it was able to displace taxol from its binding site on microtubules. This and the fact that it retained its activity for taxol- and multidrug-resistant tumor cells initiated extensive worldwide chemical and biological research activity^[3,4] and clinical development.^[5] However, it also triggered the reinvestigation of other toxic natural products for which no mode of action was known. Very soon, this led to the discovery that discodermolide,^[6] eleutherobin/sarcodictyin,^[7] laulimalide,^[8] peloruside,^[9] dictyostatin-1,^[10] jatrophane,^[11] and hemiasterlin^[12] were also tubulin-polymerization inducers or inhibitors.

In our hands, the macrodiolide disorazol^[13] and a novel group of tetrapeptides named tubulysins^[14] from myxobacteria turned out to be, contrary to epothilone, inhibitors of tubulin polymerization, thereby mimicking the activity of the vinca alkaloids. Both disorazol and the tubulysins surpass epothilones, vinblastine, and taxol by a factor of 20–1000 with respect to growth inhibition potential; however, their therapeutic efficacy as anticancer drugs has still to be evaluated. Here we report on the isolation, structure elucidation, biosynthesis, and biological properties of tubulysins A–I (**1**–

9; Mep = *N*-methyl pipecolic acid, Ile = isoleucine, Tuv = tubuvaline, Tut/Tup = tubutyrosine/tubuphenylalanine).

Two different species of myxobacteria, *Archangium*



		R ¹	R ²
Tubulysin	A (1)	OH	CH ₂ CH(CH ₃) ₂
	B (2)	OH	CH ₂ CH ₂ CH ₃
	C (3)	OH	CH ₂ CH ₃
	D (4)	H	CH ₂ CH(CH ₃) ₂
	E (5)	H	CH ₂ CH ₂ CH ₃
	F (6)	H	CH ₂ CH ₃
	G (7)	OH	CH=C(CH ₃) ₂
	H (8)	H	CH ₃
	I (9)	OH	CH ₃

gephyra and *Angiococcus disciformis*, were identified to produce tubulysins, and the compounds were isolated by multistep chromatography from culture extracts. Whereas *A. gephyra* produces 2–4 mg L⁻¹ of tubulysin A and as minor components tubulysins B, C, G, and I, all of which are characterized by a *p*-hydroxyphenyl residue, *A. disciformis* produces 0.5 mg L⁻¹ of the phenyl analogues tubulysins D, E, F, and H.^[15] Structure elucidation of tubulysins by NMR spectroscopy was seriously complicated by signal broadening and even lack of signals for certain carbon and hydrogen atoms. At this stage an important clue came from a biosynthetic labeling study. Feeding with the ¹³C-enriched presumed polyketide precursors indicated incorporation of three acetate units and three methyl groups from methionine (see below). Thus, assignment of the ¹³C NMR spectra was facilitated, and, most importantly, the signal for the C11 atom of the Tuv building block became visible as a broad peak at around δ = 70 ppm. With this information, structure elucidation of tubulysin A (**1**; C₄₃H₆₅N₅O₁₀S) by 1D and 2D NMR spectroscopy was straightforward (Table 1).

Tubulysin A turned out to be a linear tetrapeptide of *N*-methyl pipecolic acid (Mep), isoleucine (Ile), a novel amino acid named tubuvaline (Tuv), and a novel chain-extended tyrosine analogue named tubutyrosine (Tut). In tubulysins D, E, F, and H the latter is replaced by tubuphenylalanine (Tup). Whereas the 5-acetoxy residue in Tuv is common to all tubulysins, the *N*-acyloxymethyl substituent varies in size from 3-methylbutyrate in tubulysins A (**1**) and D (**4**) to acetate in tubulysins H (**8**) and I (**9**). The *N*-acyloxymethyl substituent may also be regarded as a formaldehyde *N,O*-acetal, and formaldehyde was indeed liberated upon acidic hydrolysis. Remarkably, *N,O*-acetals of this type have been found only twice in nature, as the methyl ether^[16] or *O*-glycoside.^[17]

[*] Ing. H. Steinmetz, Dr. N. Glaser, Dr. F. Sasse, H. Reichenbach, Prof. Dr. G. Höfle
Bereich Naturstoffe
Gesellschaft für Biotechnologische Forschung mbH
Mascheroder Weg 1, 38124 Braunschweig (Germany)
Fax: (+49) 531-6181461
E-mail: gho@gbf.de

Dr. E. Herdtweck
Institut für Anorganische Chemie
Technische Universität München, München (Germany)

[**] Antibiotics from Gliding Bacteria, Part 100; for Part 99, see: B. Kunze, R. Jansen, G. Höfle, H. Reichenbach, *J. Antibiot.* **2004**, 57, 151–155. We thank I. Schleicher, K. Schober, S. Reinecke, A. Ritter, and B. Hinkelmann for technical assistance, Dr. A. Ross and colleagues at the bio-pilotplant of the GBF for help with fermentations, Dr. V. Wray and colleagues for recording NMR and mass spectra, and Dr. H.-J. Hecht for generating stereopictures. We also thank Prof. G. R. Pettit for a generous gift of dolastatin 10. This work was supported by Morphochem AG and the Fonds der Chemischen Industrie.

Supporting information for this article is available on the WWW under <http://www.angewandte.org> or from the author.

Table 1: ^{13}C and ^1H NMR (150 and 600 MHz) spectroscopic data of tubulysin A (**1**).^[a]

C atoms	δ [ppm]		H atoms	δ [ppm]	Multiplicity	J [Hz]	δ [ppm]	Multiplicity	J [Hz]
	in $[\text{D}_6]\text{DMSO}$	in CD_3OD			in $[\text{D}_6]\text{DMSO}$			in CD_3OD	
Mep:									
C1	172.8	173.3	2-H	2.46	dd	10.4, 3.1	3.05	brs	
C2	68.1	69.5	3a-H	1.37	m		1.66	m	
C3	24.8	31.1	3b-H	1.57	m		1.92	m	
C4	22.8	23.6	4a-H	1.16	qt	12.3, 3.6	1.41	qt	12.8, 3.7
C5	29.6	25.5	4b-H	1.63	m		1.83	m	
C6	54.7	56.4	5a-H	1.42	qt	12.5, 3.3	1.67	m	
C7	43.8	44.1	5b-H	1.55	m		1.76	m	
			6a-H	1.93	m		2.45	brs	
			6b-H	2.82	dt	11.5, 3.5	3.15	brd	11.8, 3.5
			7-H ₃	2.04	s		2.41	s	
Ile:									
C1	174.2	176.3	2-H	4.42	t	9.1	4.68	d	9.0
C2	52.6	55.3	2-NH	7.92	d	8.8	—		
C3	35.1	37.4	3-H	1.93	m		2.05	m	
C4	24.1	25.4	4a-H	1.09	m		1.25	ddq	13.7, 9.0, 7.4
C5	10.1	10.8	4b-H	1.48	ddd	13.4, 7.5, 2.8	1.67	m	
C6	15.3	16.4	5-H ₃	0.80	t	7.7	0.95	t	7.4
			6-H ₃	0.83	d	6.1	1.02	d	6.8
Tuv:									
C1	159.7	162.7	3-H	8.18	s		8.15	s	
C2	149.8	150.9	5-H	5.75	dd	11.3, 2.2	5.91	dd	11.1, 2.1
C3	124.2	125.4	6a-H	2.15	brs		2.38	brs	
C4	168.5	170.9	6b-H	2.40	m		2.51	brt	12.0
C5	68.9	70.9	7-H	4.38	brs		4.42	brs	
C6	34.3	35.9	8-H	1.83	brs		1.95	brs	
C7	55.8	58.7	9-H ₃	0.68	d	6.7	0.86	d	6.7
C8	30.0	32.2	10-H ₃	0.98	d	6.5	1.10	d	6.5
C9	19.3	20.4	11a-H	5.26	d	12.1	5.50	d	12.1
C10	20.2	20.7	11b-H	6.20	brd	12.1	6.12	brd	12.1
C11	68.9	70.5	5-OAc	2.11	s		2.20	s	
5-OAc	169.8	172.0	2'a-H	2.08	dd	14.9, 7.1	2.12	dd	15.0, 7.0
5-OAc	20.5	20.8	2'b-H	2.14	dd	14.9, 7.2	2.18	dd	15.0, 7.4
C1'	171.3	173.3	3'-H	1.90	m		2.04	m	
C2'	42.7	44.4	4'-H ₃	0.82	d	6.7	0.93	d	6.6
C3'	25.0	26.8	5'-H ₃	0.81	d	6.7	0.90	d	6.6
C4'	22.1	22.8							
C5'	22.0	22.8							
Tut:									
C1	177.1	180.7	2-H	2.38	m		2.58	ddq	9.3, 4.6, 7.0
C2	36.2	38.4	3a-H	1.52	ddd	13.6, 10.6, 4.9	1.65	m	
C3	37.6	39.3	3b-H	1.84	ddd	13.5, 9.1, 4.3	2.06	m	
C4	49.0	51.1	4-H	4.11	m		4.33	ddt	9.6, 5.4, 6.6
C5	39.5	41.1	4-NH	7.79	d	8.2	—		
C6	128.5	130.1	5a-H	2.67	dd	13.8, 6.3	2.85	dd	13.9, 7.0
C7	129.9	131.5	5b-H	2.73	dd	13.8, 7.3	2.87	dd	13.9, 6.3
C8	114.9	116.2	7-H	6.97	AA'	8.4	7.08	AA'	8.4
C9	155.5	157.0	8-H	6.62	BB'	8.4	6.70	BB'	8.4
C10	18.0	18.7	9-OH	9.1	brs		—		
			10-H ₃	1.06	d	7.0	1.21	d	7.0

[a] DMSO = dimethyl sulfoxide.

The absolute configuration of the seven stereocenters of the tubulysins, as depicted for compounds **1–9**, was first determined by acidic hydrolysis, degradation, and partial synthesis, coupled with GC analysis.^[18] However, some doubts remained with the assignment of the Tuv C5 and Tup C2 atoms, whose configuration may have been inverted during

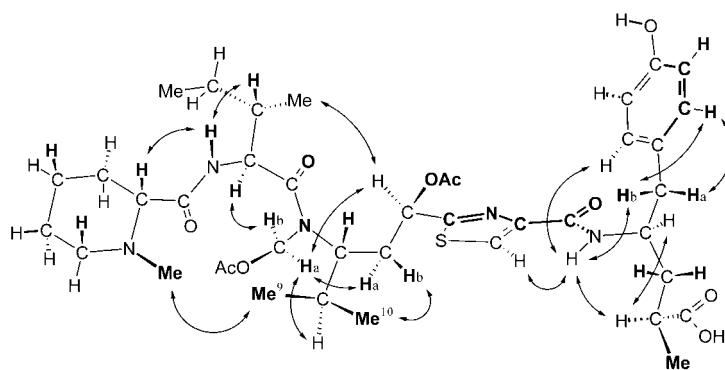
functional-group manipulation. Fortunately, tubulysin A crystallized spontaneously from a methanol/water solution, and an X-ray crystal structure analysis could be performed to confirm the structure and the proposed absolute configuration (Figure 1).^[19]

In the unit cell we find one tubulyisin A and five interstitial water molecules, but no methanol. Due to the limited resolution ($\leq 1.01 \text{ \AA}$) of the X-ray experiment, hydrogen atoms could not be located directly. Nevertheless, short interatomic distances and the geometry of the carboxyl group indicate that tubulyisin A crystallizes as a zwitterion. From the exterior angles the carboxyl group appears to be ionized (C7-C9-O2 $118(1)^\circ$ and C7-C9-O3 $120(1)^\circ$; crystal structure numbering differs from that shown in the structures above).^[20] On the other hand, the piperidine nitrogen atom shows one short intermolecular contact to the carbonyl oxygen atom (contact distance N5-O1 2.85 \AA). This is compatible only with a protonated piperidine nitrogen atom.

The protonation state of tubulysin A in methanol was investigated by observation of the chemical shifts of the Mep *N*-methyl and Tut 2H signals. After addition of ammonia and acetic acid the free and signals of the protonated *N*-methyl groups were observed at $\delta=2.19$ and 2.72 ppm, respectively, and the Tut 2H signals were observed at $\delta=2.42$ and 2.60 ppm. Based on these data, in free tubulysin A, with *N*-methyl and Tut 2H signals observed at $\delta=2.41$ and 2.58 ppm, respectively, the carboxyl group is only sparingly deprotonated, whereas the extent of protonation of the piperidine nitrogen atom is about 40%.

In tubulysins the Tuv *N*-acyloxymethyl substituent causes considerable crowding around the Ile–Tuv amide bond, and slow rotation in this tertiary amide is obviously responsible for the extensive line broadening of the Tuv C6 and C11 methylene signals and the C7 and C8 methine signals. Additionally, slow proton exchange at pH 7 causes line broadening in the vicinity of the Mep nitrogen atom and for the Tut 2H atom. Both ^1H and ^{13}C NMR signals sharpen up at elevated temperatures; however, even at 80°C the linewidth of these signals is still greater than that of other signals. As expected, this and the overlap of ^1H NMR signals complicated the solution-conformation analysis. Whereas ROESY spectra of tubulysin A in methanol showed a surplus of H–H contacts, NOE contacts in DMSO indicate the presence of one predominant conformer (Figure 2), which is very similar to that in the crystal structure. While no NOE contacts were observed across the thiazole ring, a strong NOE interaction between the Tuv 5H and Tut 4NH atoms indicates rotation of the thiazole ring by 180°, which brings these hydrogen atoms into close proximity. From vicinal coupling constants (Table 1) and NOE interactions, it is determined that the

Biosynthetic considerations suggested that the tubulysin backbone is formed by condensation of the common amino



acids pipecolic acid (lysine), isoleucine, valine, cysteine, and tyrosine or phenylalanine with two acetate units, followed by C- and N-methylation. Feeding with ^{13}C -labeled acetate and methionine indeed confirmed incorporation of these building blocks with high efficiency in the expected positions (Figure 3,

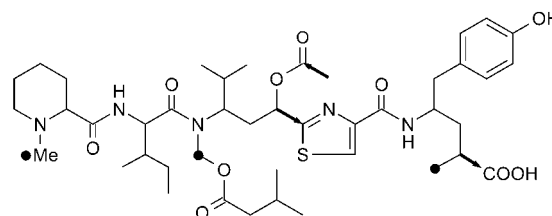


Figure 3. Biosynthesis of tubulysin A (**1**) from [$^{13}\text{C}_2$]acetate (\rightarrow) and [$^{13}\text{CH}_3$]methionine (\bullet).

Table 1 in the Supporting Information). The biosynthesis would be completed by P₄₅₀-mediated hydroxylation at the Tuv C5 atom and the Tuv *N*-methyl group, followed by acylation. Remarkably, the 5-hydroxy group is exclusively acetylated, whereas the *N*-hydroxymethyl group is acylated by a range of fatty acids. The fact that feeding the organism with specific fatty acids has no significant influence on the pattern of acyl groups indicates that these are specifically derived from a pool of fatty acid coenzyme A esters formed by amino acid degradation.^[21] Similarly, feeding with an excess of phenylalanine or tyrosine had no influence on the ratio of tubulysins formed. Whereas the tubulysin synthase complex of *A. gephyra* accepts exclusively tyrosine, that of

A. disciformis is only partially selective for phenylalanine (Phe/Tyr = 8:1). With the recent cloning of the tubulysin megasynthase complex from *A. disciformis*,^[22] the way is prepared for a detailed analysis and manipulation of the approximately 30 biosynthetic steps required to form tubulysin.

From a structural and biosynthetic point of view the tubulysins are related to dolastatin 10, which was isolated by Pettit et al. from the sea hare *Dolabella auricularia*.^[23] Both compounds are polypeptide–polyketide hybrids of similar size and amino acid composition. Although the sequence of building blocks is significantly different, both compounds target the tubulin system by inhibiting polymerization. Taken together, these similarities are a strong indication for a common ancestor of the dolastatin 10 and tubulysin biosynthesis genes in bacteria,^[24] an ancestor that during coevolution with eukaryotes has been optimized independently for the synthesis of two different molecules with high tubulin-binding affinity. It is a tempting idea to search now for “biosynthetic fossils” on the gene or product level.

The antiproliferative activity of tubulysins A–I correlates very well with their lipophilicity as indicated by the retention time on reversed-phase HPLC (Table 2). Regardless of the size of the Tuv 11-acyloxy residue, Tup-type tubulysins 4–6 and 8 are more lipophilic and more active than the Tut-type ones 1–3, 7, and 9, which have a phenolic hydroxy group. Within the two groups tubulysins D and A with a 3-methylbutyryl residue are the most active, and tubulysins H

Table 2: Biological activity, inhibition of tubulin polymerization, and lipophilicity of naturally occurring tubulysins A–I (1–9), dolastatin 10, and vinblastine.

Tubulysin	Lipophilicity $t_R^{[a]}$ [min]	L929 ^[b] IC ₅₀ [ng mL ⁻¹]	KB-V1 ^[c]	Tubulin-polymerization inhibition [%] ^[d]
D	17.5	0.011	0.25	47
E	16.4	0.013	0.25	48
F	15.3	0.015	0.35	50
H	13.9	0.031	1.3	36
A	13.6	0.070	1.4	46
G	13.0	0.093	2.9	39
B	12.6	0.091	2.3	57
C	11.6	0.30	4.0	57
I	10.4	0.68	6.8	34
dolastatin 10	17.4	0.10	1.5	–
vinblastine	17.7	23	93	20

[a] Retention time on RP-18 chromatography is used as a measure of the lipophilicity.^[25] [b] Mouse fibroblasts (DSMZ ACC 2). [c] Human cervix carcinoma, multidrug-resistant cell line (DSMZ ACC 149). [d] Determined at 10 μ M tubulin and 1 μ M tubulysin and vinblastine, respectively.^[26]

and I with an acetyl residue are the least active. Overall, the activity varies by a factor of 60 from 0.011–0.68 ng mL⁻¹. Contrary to the antiproliferative activity, the target activity, that is, inhibition of tubulin polymerization, is more or less the same for all tubulysins and is lower than cell culture activity by several orders of magnitude. These results can be explained, in part, by the preferential uptake of the lipophilic tubulysins from the culture medium. Indeed, incubation of L929 cells with a mixture of tubulysins A and D (50 ng mL⁻¹)

resulted in 25- and 100-fold enrichments, respectively, in the cells, according to HPLC/ESI-MS analysis. Whether this is the result of an active inward transport or of diffusion followed by binding to abundant tubulin in the cytoplasm is not known. Even with the multidrug-resistant cell line KB-V1, which has an active P-glycoprotein export system, the intracellular concentration of tubulysins remains high; this results in activity superior to that of dolastatin and vinblastine.

Ongoing work on the chemical modification of tubulysin A indicates that its inhibitory activity can be increased by a factor of 10. The tubulysins are therefore ideal candidates for immunoconjugation and tumor targeting. On the other hand, there is sufficient scope for reducing activity by derivatization while improving the therapeutic index. At first sight, total synthesis also seems an easy task; however, as we observed, clustering of space-demanding groups in the center of the structure poses an unexpected challenge.

Experimental Section

Isolation of tubulysins from *Archangium gephyra*: A fermentation batch (270 L) of strain Ar 315 was harvested and extracted as described previously.^[13a] The resulting crude extract (60 g) was partitioned between methanol and *n*-heptane to give a refined oily extract (52 g), which was separated by chromatography on Sephadex LH 20 with methanol as the eluent. The tubulysin-containing fraction (6.12 g) was further separated by MPLC (RP-18, methanol/50 mM ammonium acetate buffer (pH 6.5) 6:4) to give tubulysins A (856 mg), B (739 mg), and C (94 mg) as colorless amorphous solids. Tubulysins G (24 mg) and I (190 mg) were obtained from intermediate fractions by preparative HPLC (acetonitrile/50 mM ammonium acetate buffer (pH 6.5), 35:65).

Isolation of tubulysins from *Angiococcus disciformis*: A fermentation batch (300 L) of strain An d48 was harvested and extracted as described previously.^[13a] The resulting crude extract (36 g) was passed through a Sephadex LH 20 column (methanol) to give a tubulysin-enriched fraction (3.3 g), which was further separated by MPLC (Merck Prepbar, RP-18, methanol/75 mM ammonium acetate buffer (pH 6.5) 6:4) to give a polar fraction (209 mg) containing tubulysins A, B, F, and H and a more lipophilic fraction (308 mg) containing tubulysins D and E. Repeat MPLC chromatography of these fractions on RP-18 and subsequently on Sephadex LH 20 (CH₂Cl₂/MeOH 8:2) yielded tubulysins D (74 mg), E (11 mg), F (5 mg), and H (1 mg).

Tubulysin A (1): Colorless crystals from methanol/water, m.p. 106–108 °C; colorless crystals from 10 mM sodium phosphate buffer (pH 7), m.p. 107–110 °C; t_R = 13.6 min (Nucleosil C18, 125 \times 2 mm, 5 μ m, acetonitrile/10 mM ammonium acetate buffer (pH 5.5), gradient from 30:70 to 95:5 over 20 min, 0.3 mL min⁻¹); R_f = 0.42 (silica gel 60 on aluminium sheets, dichloromethane/acetone/methanol 70:20:10); $[\alpha]_D^{25}$ = 15.3 (c = 5, MeOH); UV (MeOH): λ_{max} (lg ϵ) = 205 (4.44), 225 (4.20), 250 sh (3.86), 276 (3.25), 287 nm (3.08); IR (KBr): $\tilde{\nu}_{max}$ = 3390, 2959, 2934, 2876, 1747, 1667, 1553, 1515, 1233 cm⁻¹; NMR: see Table 1; DCI MS: m/z (%): 844 (34) [M+H⁺], 742 (22), 504 (6), 239 (30), 120 (17), 103 (100); HR DCI MS: m/z calcd. for C₄₃H₆₆N₅O₁₀S [M+H⁺]: 844.4530; found: 844.4543.

Received: March 29, 2004

Keywords: antitumor agents · biosynthesis · natural products · peptides · structure elucidation

[1] G. Höfle, N. Bedorf, K. Gerth, H. Reichenbach (GBF), DE-4138042, 1993 [Chem. Abstr. 1993, 120, 52841].

- [2] D. M. Bollag, P. A. McQueney, J. Zhu, O. Hensens, L. Koupal, J. Liesch, M. Goetz, E. Lazarides, C. M. Woods, *Cancer Res.* **1995**, 55, 2325–2333.
- [3] G. Höfle, N. Bedorf, H. Steinmetz, D. Schomburg, K. Gerth, H. Reichenbach, *Angew. Chem.* **1996**, 108, 1671–1673; *Angew. Chem. Int. Ed. Engl.* **1996**, 35, 1567–1569; K. Gerth, N. Bedorf, G. Höfle, H. Irschik, H. Reichenbach, *J. Antibiot.* **1996**, 49, 560–563.
- [4] For reviews, see, for example, K. C. Nicolaou, F. Roschinger, D. Vourloumis, *Angew. Chem.* **1998**, 110, 2120–2153; *Angew. Chem. Int. Ed.* **1998**, 37, 2014–2045; K.-H. Altmann, *Mini-Rev. Med. Chem.* **2003**, 3, 149–158.
- [5] R. M. Borzilleri, G. D. Vite, *Drugs Future* **2003**, 27, 1149–1163.
- [6] E. ter Haar, R. J. Kowalski, E. Hamel, C. M. Lin, R. E. Longley, S. P. Gunasekera, H. S. Rosenkranz, B. W. Day, *Biochemistry* **1996**, 35, 243–250.
- [7] T. Lindel, P. R. Jensen, W. Fenical, B. H. Long, A. M. Casazza, J. Carboni, C. R. Fairchild, *J. Am. Chem. Soc.* **1997**, 119, 8744–8745.
- [8] S. L. Mooberry, G. Tien, A. H. Hernandez, A. Plubrukarn, B. S. Davidson, *Cancer Res.* **1999**, 59, 653–660.
- [9] K. A. Hood, L. M. West, B. Rouwé, P. T. Northcote, M. V. Berridge, S. J. Wakefield, J. H. Miller, *Cancer Res.* **2002**, 62, 3356–3360.
- [10] R. A. Isbrucker, J. Cumins, S. A. Pomponi, R. E. Longley, A. E. Wright, *Biochem. Pharmacol.* **2003**, 66, 75–82.
- [11] A. Miglietta, L. Gabriel, G. Appendino, C. Bocca, *Cancer Chemother. Pharmacol.* **2003**, 51, 67–74.
- [12] H. J. Anderson, J. E. Coleman, R. J. Andersen, M. Roberge, *Cancer Chemother. Pharmacol.* **1997**, 39, 223–226.
- [13] a) H. Irschik, R. Jansen, K. Gerth, G. Höfle, H. Reichenbach, *J. Antibiot.* **1995**, 48, 31–35; R. Jansen, H. Irschik, H. Reichenbach, V. Wray, G. Höfle, *Liebigs Ann. Chem.* **1994**, 759–773; b) Y. Elnakady, F. Sasse, H. Lünsdorf, H. Reichenbach, *Biochem. Pharmacol.* **2004**, 67, 927–935.
- [14] F. Sasse, H. Steinmetz, J. Heil, G. Höfle, H. Reichenbach, *J. Antibiot.* **2000**, 53, 879–885; M. W. Khalil, Doctoral Thesis, Technical University Braunschweig, **2002**.
- [15] In addition to **1–9**, the major tubulysins were also isolated in varying amounts as their Mep-*N*-oxides, characterized by the *N*-methyl ¹H and ¹³C NMR signals at $\delta = 3.10$ and 57.8 ppm, respectively. We found that these compounds were artefacts of the extraction with analytical grade ethyl acetate, which is commonly contaminated with peroxides. Unlike ether peroxides, the peroxide contaminants of ethyl acetate come from the (Tischtschenkow) production process. We found up to 3 mmolequiv L^{−1} of nonidentified peroxides in analytical grade ethyl acetate from several major distributors (analytical method: oxidation of triphenylphosphane). This observation should be a warning to all those who isolate *N*- or *S*-oxides from natural sources while using ethyl acetate as the solvent.
- [16] T. Iwagawa, M. Kaneko, H. Okamura, M. Nakatani, R. W. M. van Soest, *J. Nat. Prod.* **1998**, 61, 1310–1312.
- [17] B. H. Korsch, N. V. Riggs, *Tetrahedron Lett.* **1964**, 5, 523–525.
- [18] G. Höfle, N. Glaser, T. Leibold, U. Karama, F. Sasse, H. Steinmetz, *Pure Appl. Chem.* **2003**, 75, 167–178.
- [19] Experimental details of the crystal structure analysis of tubulysin A (**1**) can be found in the Supporting Information. CCDC-233087 (**1**) contains the supplementary crystallographic data for this paper. These data can be obtained free of charge via www.ccdc.cam.ac.uk/conts/retrieving.html (or from the Cambridge Crystallographic Data Centre, 12, Union Road, Cambridge CB2 1EZ, UK; fax: (+44)1223-336-033; or deposit@ccdc.cam.ac.uk).
- [20] For a typical example, see: Z. Ciunik, T. Glowiak, *Acta Crystallogr. Sect. C* **1983**, 39, 1271–1273.
- [21] T. Mahmud, H. B. Bode, B. Silakowski, R. M. Kroppenstedt, M. Xu, S. Nordhoff, G. Höfle, R. Müller, *J. Biol. Chem.* **2002**, 277, 32768–32771.
- [22] A. Sandmann, F. Sasse, R. Müller, *Chem. Biol.*, in print.
- [23] G. R. Pettit in *Progress in the Chemistry of Organic Natural Products, Vol. 70* (Eds.: W. Herz, G. W. Kirby, R. E. Moore, W. Steglich, C. Tamm), Springer, New York, **1997**, pp. 1–79.
- [24] H. Luesch, R. E. Moore, V. J. Paul, S. L. Mooberry, T. H. Corbett, *J. Nat. Prod.* **2001**, 64, 907–910.
- [25] H. Ellgehausen, C. D'Hondt, R. Fuerer, *Pestic. Sci.* **1981**, 12, 219–227.
- [26] For experimental conditions and calculation, see ref. [13b].

Zeolites

The Topotactic Conversion of a Novel Layered Silicate into a New Framework Zeolite**

Takuji Ikeda, Yoshikatsu Akiyama, Yasunori Oumi, Akiko Kawai, and Fujio Mizukami*

Zeolites have been widely used, among others, as catalysts, ion exchangers, detergents, and adsorbents, and their range of applications continues to grow. Thus, there is a large demand for new types of zeolites with high thermal and chemical stability. However, new zeolites are still mainly synthesized by trial and error, and molecular engineering in their synthesis has been underdeveloped. Here we report that a thermostable zeolite with a novel framework is obtained by molecular manipulation, that is, topotactic dehydration–

[*] Dr. T. Ikeda, Dr. A. Kawai, Dr. F. Mizukami
Laboratory for Membrane Chemistry
National Institute of Advanced Industrial Science and Technology, AIST
Tohoku, 4-2-4 Nigatake, Miyagino-ku, Sendai, 983-8551 (Japan)
Fax: (+81) 22-237-5226
E-mail: takuji-ikeda@aist.go.jp
Dr. Y. Akiyama
Ameraham Biosciences
K. K. Sanken Bldg. 3-25-1
Hyakunincho, Shinjuku-ku, Tokyo, 169-0073 (Japan)
Dr. Y. Oumi
School of Materials Science
Japan Advanced Institute of Science and Technology
Tatsunokuchi, Ishikawa 923-1292 (Japan)

[**] We thank Dr. T. Kodaira (AIST) for the use of his instruments and fruitful discussions. T.I. thanks Dr. F. Izumi of the National Institute for Materials Science for his advice on the structure analysis and for furnishing powerful powder diffraction data analysis software and put set spurs. T.I. also thanks YUASA-IONICS Co. LTD. for support of the Ar gas adsorption experiments. This work was supported by the New Energy and Industrial Technology Development Organization of Japan.



Supporting information for this article is available on the WWW under <http://www.angewandte.org> or from the author.

condensation between the layers of face-sharing pentagon cylinders in a new silicate.

Peculiar properties of zeolites arise as a result of the framework structure. This framework structure has been understood as the combination of ringed silicate building blocks,^[1–3] and some of the corresponding silicate oligomers have been detected and/or isolated.^[4,5] Therefore molecular engineering can be used to design zeolite frameworks by assembling block oligomers or appropriate precursors which dehydration–condensation. However, there has been no example for this kind of molecular manipulation in zeolite synthesis so far, although some syntheses were carried out with this intent.

For instance, we have investigated the transformation of the layered silicates kanemite and HLS (helix layered silicate) into the zeolites MFI (zeolite socony mobil five, ZSM-5) and SOD (sodalite), respectively.^[6–9] However, these conversions did not proceed with dehydration–condensation only, that is, they were not perfect block condensation polymerizations. In the case of kanemite→MFI a different type of bond breaking and recombination took place, and for HLS→SOD the presence of aluminum hydroxide or gallium hydroxide was essential. This means that the transformation to SOD is not a simple block condensation–polymerization, although the structures of HLS and SOD are very similar.

Schreyeck et al.^[10,11] have reported that the layered aluminosilicate PREFER was converted into an FER-type zeolite^[12] by dehydration–condensation. Since the crystal structure of PREFER has not been clearly determined, it is unknown if the conversion is a simple block condensation–polymerization. Furthermore, although not yet proven, such conversions were suggested for the transformation of EBR-1^[13] into MWW-type zeolites such as MCM-22 and ITQ-1 and the formation of RUB-24 from an intercalated layered material based on RUB-18.^[14] Here we show a concrete example of zeolite synthesis by complete block condensation–polymerization, which can be a guiding principle for the molecular engineering of zeolites.

A novel layered silicate was crystallized by the hydrothermal treatment of a mixture of SiO₂, H₂O, KOH, tetramethylammonium hydroxide (TMAOH), and 1,4-dioxane at 423 K. As observed in the X-ray crystal structure (see below), the silicate adopts a structure with shared faces of pentagon cylinders made up of five-membered silicon rings, or pentasil rings. Thus, it was named pentagonal cylinder-layered silicate (PLS-1). When PLS-1 was heated above 673 K under vacuum, a novel framework zeolite with a cylindrically double saw edged structure (CDS-1) was obtained as the result of dehydration–condensation between the pentasil layers. The as-synthesized PLS-1 contains TMAOH molecules between the layers (see below), and during the conversion into CDS-1 most of the TMAOH can be recovered by trapping the volatile components with liquid nitrogen.

Figure 1 shows the scanning electron microscope (SEM) images and ²⁹Si magic angle spinning (MAS) NMR spectra of powdered crystals of PLS-1 and CDS-1. In the SEM images, the two crystal morphologies are quite similar in the thin plate, suggesting that the conversion of PLS-1 into CDS-1 is a topotactic condensation–polymerization with simple dehy-

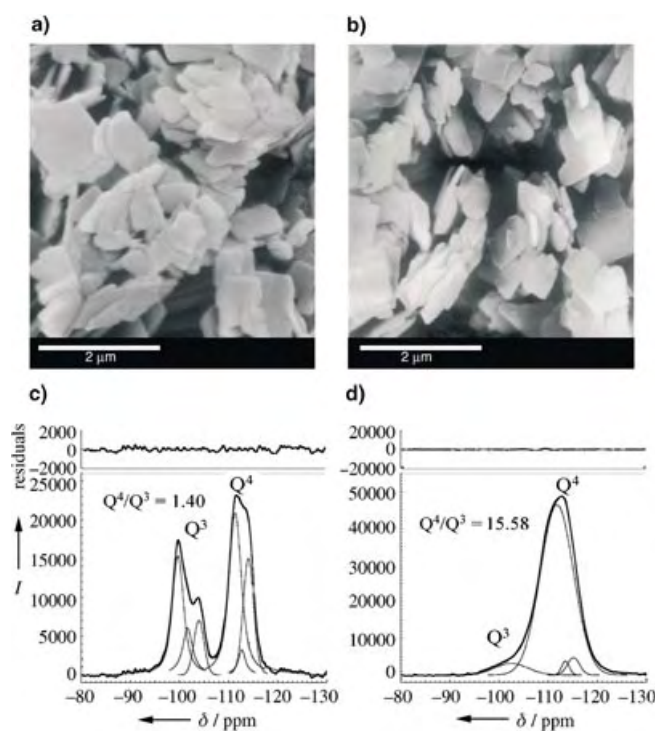


Figure 1. Top: SEM images of purified samples of PLS-1 (a) and CDS-1 (b) showing platelike microcrystals. Bottom: ²⁹Si-MAS NMR spectra of PLS-1 (c) showing three resonances and of CDS-1 (d) showing one broad resonance. The chemical shifts are given with respect to tetramethylsilane.

dration (strictly speaking, removal of H₂O and TMAOH). In the NMR spectra, PLS-1 exhibits resonances around $\delta = -102$ and -113 that are characteristic of $\text{HOSi}(\text{OSi})_3$ (Q³) and $\text{Si}(\text{OSi})_4$ (Q⁴) silicon sites, respectively. On the other hand, CDS-1 displays only a broad peak around $\delta = -112$ that is mostly due to Q⁴ structures and possibly contains a small amount of Q³. This indicates that during the conversion of PLS-1 into CDS-1, the Q³ sites lose their terminal silanol groups upon dehydration–condensation to become Q⁴ structures.

If layered silicates are converted into three-dimensional microporous crystals with pores large enough to accommodate gas molecules, the amount of gas adsorbed after the conversion should increase. Figure 2 shows the nitrogen

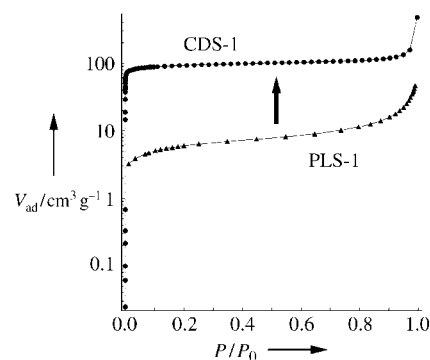


Figure 2. Nitrogen adsorption isotherm plots for PLS-1 and CDS-1.

adsorption isotherm curves for PLS-1 and CDS-1. Silicate CDS-1 adsorbs a much higher volume of nitrogen than PLS-1, and its curve exhibits the adsorption pattern characteristic of microporous crystals. The multipoint Brunauer–Emmett–Teller (BET) surface area and the Saito–Foley (SF) cumulative pore volume were calculated from the argon adsorption isotherm curve to be $301 \text{ m}^2 \text{ g}^{-1}$ and $0.13 \text{ cm}^3 \text{ g}^{-1}$, respectively, for CDS-1. These values are equal to or higher than those of typical zeolites such as FER and silicalite. The total pore volume was calculated to be $0.60 \text{ cm}^3 \text{ g}^{-1}$ at the maximum P/P_0 . In addition, the minimum of the pore size distribution calculated from the argon adsorption isotherm data with nonlocal density functional theory^[15] was 4.83 \AA . This is in good agreement with the pore diameter (ca. 4.8 \AA) of the main window of CDS-1 (a silicate eight-membered ring, 8MR), which was calculated on the basis of structural parameters, the ionic radius of an oxygen atom, and lattice constants obtained by the Rietveld refinement.

Figure 3 provides views of the crystal structures of PLS-1 and CDS-1. The structure of PLS-1 was elucidated from the preliminary X-ray structure determination (see the Supporting Information), and then the positions of the interlayer potassium ions and TMAOH molecules were estimated by the maximum entropy method (MEM).^[16,17] It was determined that PLS-1 is a three-dimensional layered silicate—the structure is similar to that proposed for PREFER and MCM-47^[18]—with different types of layer stacking. The X-ray

diffraction data for CDS-1 did not directly give the structure because the crystals were poor in crystallinity and contained various distortions and small domains of crystallites. Therefore, with molecular dynamics (MD) simulations, preliminary structural models for CDS-1 were derived from the layer structure of PLS-1, and then the most probable model was determined by structure analyses.^[19]

The crystal system of PLS-1 is a monoclinic phase with the space group $P2_1/m$ and lattice parameters $a = 10.5710(5)$, $b = 14.0064(3)$, $c = 7.4220(2) \text{ \AA}$, $\beta = 98.014(4)^\circ$, and $V = 1088.21(7) \text{ \AA}^3$. The framework contains a pair of high-density silicate sheets made up of five-membered rings, and the porelike interlayer space is occupied by TMAOH molecules and K^+ ions that are distributed with partial disorder (Figure 3a). The chemical composition was estimated to be $\text{Si}_{18}\text{O}_{34}(\text{OH})_4\text{K}_{1.3}\cdot 1.7(\text{CH}_3)_4\text{NOH}$ by the Rietveld refinement.

For CDS-1, indexing of the reflections gave an orthorhombic unit cell with $a = 18.355(3)$, $b = 13.779(2)$, $c = 7.3674(6) \text{ \AA}$, and $V = 1863.3(4) \text{ \AA}^3$; these values are very close to the corresponding values of zeolites FER. The reflection conditions afforded the space groups $Pnma$, $Pnnm$, and $Pbcm$ as well as $Cmcm$ on the assumption that CDS-1 has a centrosymmetric space group. Three preliminary models constructed on the basis of the MD calculation results^[20] were evaluated by the Rietveld method taking into account geometrical considerations. Finally, we adopted the highest symmetry model with space group $Pnma$. The framework obtained shows a novel type of topology, which has straight channels consisting of 8MRs along the $[010]$ and $[001]$ directions (Figure 3b). The chemical composition was calculated to be $\text{Si}_{36}\text{O}_{72}$, but the positions of the K^+ ions could not be determined because of insufficient resolution of the X-ray data. The comparison of the frameworks of PLS-1 to CDS-1 shows that the sheets of PLS-1 condense and polymerize along the $[100]$ direction by dehydration to form CDS-1. The TMAOH molecules are removed along the $[001]$ direction.

The X-ray diffraction patterns were then used for structure refinement by the MEM-based pattern fitting (MPF) technique at the electron density level.^[21] The MEM electron density distribution map of PLS-1 ($R_F = 0.0142$ after MPF refinement) shows that the TMAOH molecules and potassium ions exist in the interlayer (Figure 4a). Localized electron densities between TMA^+ and OH^- are clearly observed, and the chemical bonding is directed parallel to $[001]$. Small amounts of K^+ seem to be closely located to the silicate sheets; however, the ion sites could be replaced by water molecules. After a revision based on the electron density, the MPF refinement dramatically improved and the R_F of the final MPF became 0.0093.

On the other hand, the final electron densities of CDS-1 obtained by MEM ($R_F = 0.0267$) reveal the three-dimensional microporous structure composed of 5MRs and 8MRs (Figure 4b). No electron densities arising from water molecules and/or other adsorbed atoms or molecules are observed in the straight channels. Electron densities of oxygen atoms at the points connecting the sheets are anisotropically elongated, which means that the framework structure of CDS-1 has considerable lattice distortion and internal stress in comparison with other zeolite frameworks.

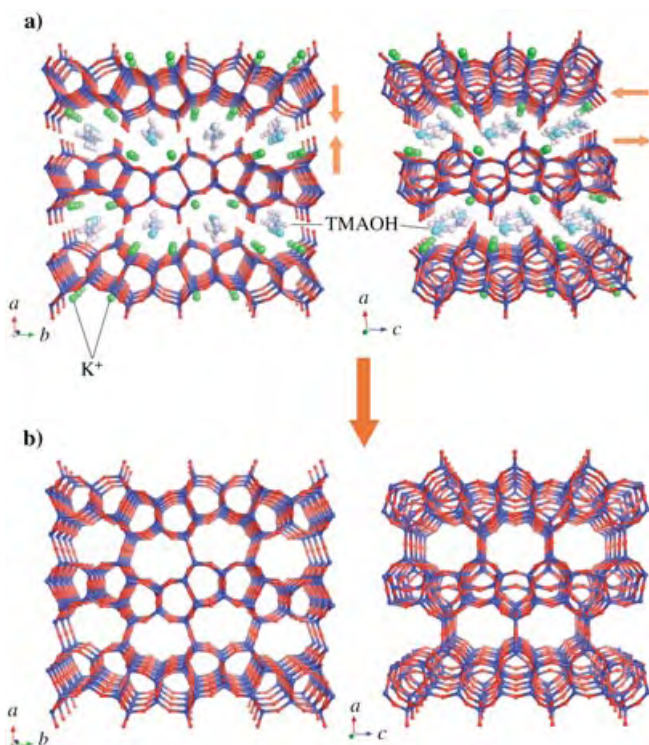


Figure 3. Perspective view of the crystal structure of a) PLS-1 along the $[001]$ (left) and $[010]$ directions (right) as well as b) CDS-1 along the $[001]$ (left) and $[010]$ directions (right). Color coding: blue = Si, red = O, green = K, white = C, cerulean = N, sky blue = OH. CDS-1 consists of silicates layers based on a framework of PLS-1 with 5MRs and forms 8MRs in the $[001]$ and $[010]$ directions.

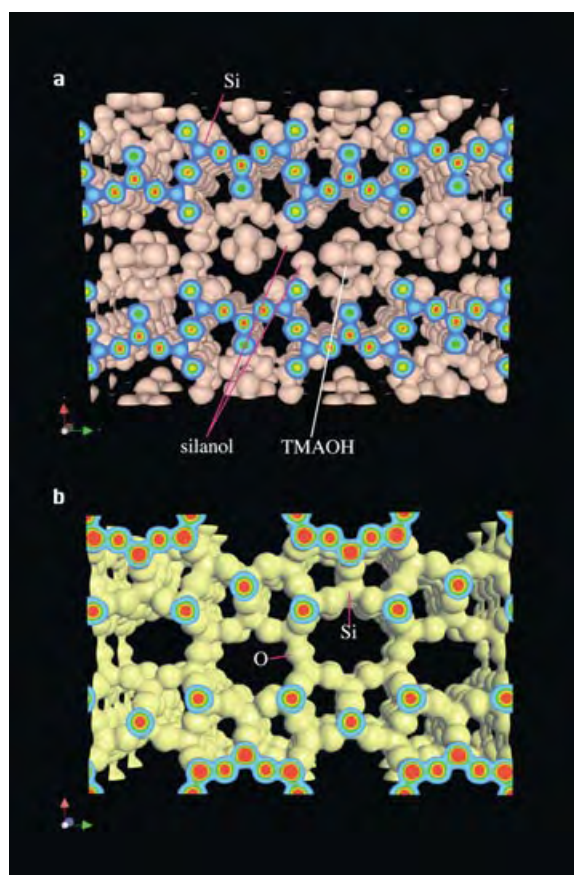


Figure 4. Electron-density images of PLS-1 (a) and CDS-1 (b) along the [001] direction. The equidensity level was set at $0.7 \text{ e}\text{\AA}^{-3}$ in both images.

Organic amines are effective for the formation of zeolite frameworks, and various types of zeolites have been synthesized so far.^[22] However, the amines are often difficult to synthesize and expensive to buy, and only several types of zeolites show sufficient thermal and chemical stability to be employed in industry. This stability generally increases with increasing silica content. Silicate CDS-1, with straight two-dimensional channels, is pure silicate and thermally stable. Furthermore, the TMAOH used in the synthesis of the CDS-1 precursor, PLS-1, is inexpensive and can be recovered. The Si atom defects, which are homogeneously distributed in the CDS-1 crystals, could be active sites for catalytic reactions or different metal ions could be incorporated to make new active sites. Thus, CDS-1 is expected to find wide application as a catalyst, adsorbent, separator, or ion exchanger for various industrial uses.

Experimental Section

PLS-1: Silica powder (Cab-O-Sil M5, 10.0 g), TMAOH (22.0 g, 15 wt %), 0.5 N KOH (5.0 g), and 1,4-dioxane (50.0 g) were consecutively suspended in distilled water (25.0 g). The sol mixture was vigorously stirred for 1 h at room temperature with a magnetic stirrer, and then heated at 423 K under autogenous pressure for 10 d in a stable PTFE-lined stainless-steel autoclave with an internal volume of 300 mL. The

crystalline product was filtered and washed with acetone and distilled water, then dried at 70 °C in a drying oven for 12 h.

CDS-1: Silicate PLS-1 was heated (range 673 to 1173 K) under vacuum (10^{-3} to 10^{-8} torr). Thus, the conversion was carried out reproducibly.

General: KOH and 1,4-dioxane were purchased from Wako chemical, and TMAOH was purchased from Tokyo Kasei Kogyo Co. Ltd. Cab-O-Sil M5 (CABOT Co.) was employed as a silica source. The SEM observations with a HITACHI S-800 microscope showed the samples to be thin microcrystals with a length of less than 1 μm and a thickness of about 0.1 μm . Solid-state ^{29}Si -MAS NMR spectra were obtained on a Bruker AMX-500 spectrometer. The recycle delay was 300 s for PLS-1 and 30 s for CDS-1 with the sample rotor spinning at 4 kHz. Nitrogen adsorption isotherm plots of all materials were obtained by using a Shimadzu ASAP-2010 instrument, and the argon adsorption isotherm plot of CDS-1 was measured with a Quantachrome Autosorb-1MP instrument. The X-ray diffraction data were collected at room temperature on a MAC Science MXP-3TA HR powder diffractometer in a Bragg–Brentano geometry for PLS-1 and a Debye–Scherrer geometry using a capillary specimen for CDS-1. The conditions of the diffraction experiments for both specimens were as follows: $\text{Cu}_{\text{K}\alpha 1}$ radiation using a Ge(111) primary monochromator, output 40 kV and 50 mA, scan range $6^\circ \leq 2\theta \leq 90^\circ$, step width 0.02° , counting time per step 120 s.

Received: March 31, 2004

Keywords: hydrothermal synthesis · polymerization · silicates · structure elucidation · zeolites

- [1] C. Baerlocher, W. M. Meier, D. H. Olson, *Atlas of zeolite structure types*, Structure Commission of the International Zeolite Association, 5th rev. ed., Elsevier, London, **2001**.
- [2] C. S. Cundy, P. A. Cox, *Chem. Rev.* **2003**, *103*, 663–701.
- [3] M. Ogura, Y. Kawazu, H. Takahashi, T. Okubo, *Chem. Mater.* **2003**, *15*, 2661–2667.
- [4] P. Bussian, F. Sobott, B. Brutschy, W. Schrader, F. Schüth, *Angew. Chem.* **2000**, *39*, 4065–4069; *Angew. Chem. Int. Ed.* **2000**, *39*, 3901–3905.
- [5] C. E. A. Kirschhock, S. P. B. Kremer, P. J. Grobet, P. A. Jacobs, J. A. Martens, *J. Phys. Chem. B* **2002**, *106*, 4897–4900.
- [6] S. Shimizu, Y. Kiyozumi, K. Maeda, F. Mizukami, G. Pál-Borbély, R. M. Mihályi, H. Beyer, *Adv. Mater.* **1996**, *8–9*, 759–762.
- [7] M. Salou, Y. Kiyozumi, F. Mizukami, P. Nair, K. Maeda, S. Niwa, *J. Mater. Chem.* **1998**, *8*, 2125–2132.
- [8] T. Ikeda, Y. Akiyama, F. Izumi, Y. Kiyozumi, F. Mizukami, T. Kodaira, *Chem. Mater.* **2001**, *13*, 1286–1295.
- [9] Y. Kiyozumi, F. Mizukami, A. Akiyama, T. Ikeda, T. Nishide, *Stud. Surf. Sci. Catal.* **2001**, *135H*, 191.
- [10] L. Schreyeck, P. Caullet, J. C. Mougénel, J. L. Guth, B. Marler, *Microporous Mater.* **1996**, *6*, 259–271.
- [11] L. Schreyeck, P. Caullet, J. C. Mougénel, J. L. Guth, B. Marler, *Stud. Surf. Sci. Catal.* **1997**, *105*, 1949–1956.
- [12] P. A. Vaughan, *Acta. Crystallogr.* **1966**, *17*, 983–990.
- [13] R. Millini, G. Perego, W. O. Parker, Jr., G. Bellussi, L. Carluccio, *Microporous Mater.* **1995**, *4*, 221–230.
- [14] B. Marler, N. Ströter, H. Gies, *Recent Research Reports of the 14th International Zeolite Conference*, **2004**, pp. 15–16.
- [15] R. Evans, *J. Phys. Condens. Matter* **1990**, *2*, 8989–9007.
- [16] D. M. Collins, *Nature* **1982**, *298*, 49–51.
- [17] M. Sakata, M. Sato, *Acta. Crystallogr. Sect. A* **1990**, *46*, 263–270.
- [18] A. Burton, R. J. Accardi, R. F. Lobo, M. Falcioni, M. W. Deem, *Chem. Mater.* **2000**, *12*, 2936–2942.
- [19] The structure was solved with the EXPO package,^[23] refined with the RIETAN-2000 package^[24] combined with the MEM

program PRIMA,^[25] and visualized with the VENUS package.^[25] The final number of structural parameters (fractional atomic coordinates, lattice, and isotropic atomic displacement parameters) was 68 for PLS-1 and 40 for CDS-1. Including the profile, scaling, and zero shift factors, the total number of refinable parameters was 155 for PLS-1 and 78 for CDS-1. The numbers of contributing *hkl* reflections are 929 (PLS-1) and 800 (CDS-1), the numbers of geometric restraints of type $d(\text{Si-O})$, $\phi(\text{O-Si-O})$, $d(\text{C-N})$, and $\phi(\text{C-N-C})$ are 21, 30, 3, and 4, respectively, for PLS-1; 24 and 36 restraints of $d(\text{Si-O})$ and $\phi(\text{O-Si-O})$ are adopted, respectively, for CDS-1. The MEM electron density distributions were calculated from “observed” structure factors based on the Rietveld refinement, using the program PRIMA and visualized by the program VEND built into the VENUS package.

- [20] Silicate CDS-1 was modeled by MD methods with the CRYSTAL Builder module in the Cerius2 program developed by Accelrys Inc., USA. The MD calculations were carried out with the MXDTRICL program developed by Kawamura et al.^[26] The Verlet algorithm was used to calculate the atomic motions, while the Ewald method was applied to calculate the electrostatic interactions.^[27,28] Temperature and pressure were controlled by means of scaling the atom velocities and unit cell parameters under three-dimensional periodic boundary conditions. The calculations were performed for 10000 steps with a time step of 2×10^{-15} s at 300 K.
- [21] F. Izumi, S. Kumazawa, T. Ikeda, T. Ida, *Powder Diffraction* (Ed.: S. P. Sen Gupta), Allied Publication, New Delhi, **1998**, pp. 24–36.
- [22] *Introduction to Zeolite Science and Practice* (Eds.: H. van Bekkum, E. M. Flanigen, P. A. Jacobs, J. C. Jansen), 2nd rev. ed., Elsevier, London, **2001**.
- [23] A. Altomare, M. C. Burla, M. Camalli, B. Carrozzini, G. L. Casciarano, C. Giacovazzo, A. Guagliardi, A. G. G. Moliterni, G. Polidori, R. Rizzi, *J. Appl. Crystallogr.* **1999**, 32, 339–340.
- [24] F. Izumi, T. Ikeda, *Mater. Sci. Forum* **2000**, 321–324, 198–203.
- [25] F. Izumi, R. A. Dilanian, *Recent Research Developments in Physics, Vol. 3, Part II*, Transworld Research Network, Trivandrum, **2002**, pp. 699–726.
- [26] K. Kawamura in *Molecular Dynamics Simulations* (Ed.: K. Kawamura), Springer, Berlin, **1990**.
- [27] L. Verlet, *Phys. Rev.* **1967**, 159, 98–103.
- [28] P. Ewald, *Ann. Phys.* **1921**, 64, 253–287.

Supramolecular Self-Assembly of Giant Polymer Vesicles with Controlled Sizes***Yongfeng Zhou and Deyue Yan**

Supramolecular self-assembled vesicles have attracted great attention for their potential applications in drug delivery, gene therapy, and model systems of biomembranes.^[1] Previous methods to make vesicles include the self-assembly of large copolymers and small amphiphiles such as lipids (liposomes);^[2–4] however, compared to liposomes, polymer vesicles possess unique properties such as good stability and permeability. Polymer vesicles have thus become attractive and promising research objects since the first observation of block copolymer vesicles by Eisenberg and co-workers,^[2] who called the aggregations of the block copolymer with small hydrophilic fractions (< 20 %) crew-cut micelles. Discher et al. reported another type of polymer vesicle formed from block copolymers having a similar hydrophilic fraction ($35 \pm 10\%$) to liposomes and these were termed polymersomes.^[3] Polymer vesicles have also been prepared from other materials, such as, polypeptides, rod-coil polymers, and dendrimers.^[5] The vesicle-forming systems based on small amphiphiles, dendrimers, or linear block copolymers have a well-defined molecular structure. The polymer vesicles resulting from the molecular self-assembly of ill-defined polymers such as hyperbranched copolymers have not yet been reported. Furthermore, giant polymer vesicles with diameters of 100 μm have not been observed to date, although Menger et al. have demonstrated in their research on liposomes that “giant vesicles” with diameters of 5–200 μm have many special advantages.^[4] We report here the preparation of new kind of polymer vesicle with a controlled size (the diameters of the larger polymer vesicles are above 100 μm) that are generated from the molecular self-assembly of ill-defined hyperbranched copolymers having a high hydrophilic fraction (> 60 %).

Recently, we reported^[6] macroscopic molecular self-assembly from a hyperbranched multiarm copolymer (HBPO-star-PEO) in acetone (HBPO = hyperbranched poly(3-ethyl-3-oxetanemethanol), PEO = poly(ethyleneglycol)), which gave rise to multiwalled tubes with diameters of the order of millimeters and lengths of the order of

[*] Dr. Y. Zhou, Prof. Dr. D. Yan
College of Chemistry and Chemical Engineering
State Key Laboratory of Metal Matrix Composites
Shanghai Jiao Tong University
800 Dongchuan Road, Shanghai 200240 (China)
Fax: (+ 86) 21-54741297
E-mail: dyyan@sjtu.edu.cn

[**] Financial support from the National Natural Science Foundation of China (Nos. 20274024, 50233030, and 20304007) and from the basic research foundation of the Shanghai Science and Technique Committee is acknowledged.



Supporting information for this article is available on the WWW under <http://www.angewandte.org> or from the author.

centimeters. It was found that the molecular structure of the HBPO-star-PEO copolymer greatly influenced the macroscopic self-assembly behavior. The work reported herein investigates the self-assembly of HBPO-star-PEO copolymers in water. Three HBPO-star-PEO copolymers with different hydrophilic fractions (PEO volume fraction) denoted HB1, HB2, and HB3 (Figure 1) were synthesized. The overall

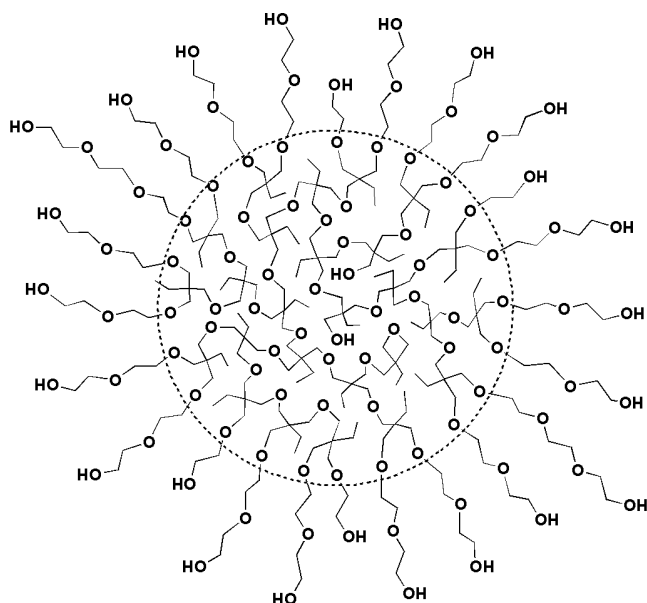


Figure 1. Schematic representation of the HBPO-star-PEO multiarm copolymer. The dashed circle shows the boundary between the HBPO core (inside) and the PEO arms.

structures of HB1–3 are different from those used in the macroscopic molecular self-assembly.^[6] The molecular self-assembly of HB1–3 involved directly placing the polymer into deionized water (polymer concentration: 10 mg mL^{−1}) under stirring at room temperature. The properties of HB1–3 and the aggregations are summarized in Table 1, while the synthesis, characterization, and self-assembly of HB1–3 are described in the Supporting Information.

Table 1: Details of vesicle-forming multiarm copolymers.^[a]

Sample	\bar{M}_n [g mol ^{−1}]	Polydispersity index	f_{EO}	Diameter [μm]	d [nm]
HB1	12200	1.5	0.69	112.8 ± 30	10 ± 2
HB2	16800	1.7	0.79	22.6 ± 4.2	5 ± 2
HB3	20800	1.9	0.86	4.0 ± 1.6	5 ± 2

[a] \bar{M}_n : the number-average molecular weight; Polydispersity index: weight-to-number average molecular weight; f_{EO} : the hydrophilic PEO volume fraction; d : the vesicle wall thickness. The HB1–3 samples have the same HBPO cores with a molecular weight of 6400 g mol^{−1}.

The optical and transmission electron microscopy (TEM) images of the resulting self-assembled objects are shown in Figure 2. It appears that HB1–3 directly self-assembled into a well-defined vesicular structure in water, and the vesicles increased in size from 1 to 200 μm as the hydrophilic fraction decreased. The HB2 and HB3 vesicles (polymer concentra-

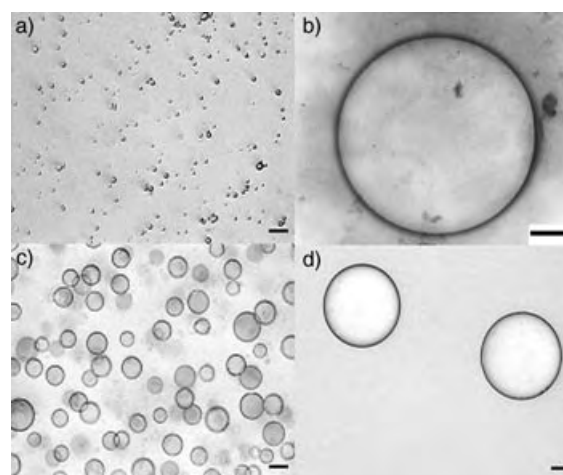


Figure 2. Optical micrographs (a, c, d) and TEM image (b) of HB1–3 vesicles. a), b) HB3 vesicles. c) HB2 vesicles. d) HB1 vesicles. The samples for TEM measurement were negatively stained with 2% aqueous uranyl acetate solution. The scale bars represent 25 μm in (a), (c), and (d), and 250 nm in (b).

tion less than 100 mg mL^{−1}, other morphologies were found for polymer solutions with concentrations higher than 100 mg mL^{−1}) could be stored for at least two months in water at around 20°C, but the HB1 vesicles settled under gravity at the bottom of the container underneath the medium. Compared with the polymer vesicles previously reported, the aggregation observed in this work has several unique characters: 1) the vesicles originate from an ill-defined hyperbranched amphiphilic multiarm copolymer; 2) the HB1–3 copolymers that can directly form vesicles in water have a higher hydrophilic fraction (> 60%) than those forming polymersomes and crew-cut micelles (block copolymers with a hydrophilic fraction higher than 40% often self-assemble into wormlike and spherical micelles); 3) the HB1–3 vesicles have giant sizes similar to those of giant liposomes,^[4] and to the best of our knowledge HB1 provides the largest known polymer vesicles, with diameters larger than 100 μm. In short, the aggregation of the giant vesicles reported herein is different from crew-cut micelles, polymersomes and other polymer vesicles, and results in a new sort of polymer vesicle. A new terminology, branched polymersome, is used to describe this new type of aggregation.

The size distributions of HB1–3 vesicles are displayed in Figure 3. The size of the vesicles was measured from the staff gauge in the microscopy studies, and the results were based on an analysis of 200 vesicles for HB2 and HB3 and 100 vesicles for HB1. The average diameters of the vesicles are 4.0 μm for HB3, 22.6 μm for HB2, and 112.8 μm for HB1 (Figure 3 and Table 1). Thus, the size of the generated vesicles increases and the size distribution becomes broader as the hydrophilic fraction of the HBPO-star-PEO molecules decreases from 0.86 to 0.69. However, the distribution of

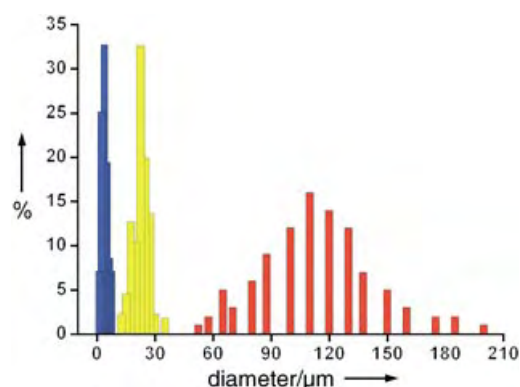


Figure 3. Size distribution of the giant polymer vesicles made from the HBPO-star-PEO multiarm copolymer. The blue, yellow, and red bars represent HB3, HB2, and HB1 vesicles, respectively.

the vesicle size is not directly related to the polydispersity index of the copolymer (Table 1). Discher and Eisenberg^[1a] also found that polydispersity is not a strict requirement for vesicle formation. Such a size dependence of the giant vesicles on the copolymer composition as shown in Figure 2 has not been observed before, and it presents an easy approach to the assembly of giant polymer vesicles with well-controlled sizes. In fact, submicroscopic vesicles (not shown) were also obtained through the self-assembly of HBPO-star-PEO with a much higher hydrophilic fraction in water, but they did not fall within the concept of “giant vesicles” discussed in this work. It is necessary to control the vesicle size in technological and scientific applications;^[2d] for example, giant vesicles are very good models for the simulation of the fluidization of cell membranes.^[4a]

The self-assembly mechanism of HBPO-star-PEO molecules in water includes two aspects: one is the self-assembly interaction, and the other is the molecule packing in the self-assembled vesicle wall. The hydrophobic interaction, which is attributed to the amphiphilic character of HBPO-star-PEO in water, and the formation of hydrogen bonds are responsible for driving the self-assembly. The importance of hydrogen bonds in the self-assembled HB1–3 vesicles has been confirmed by variable-temperature FTIR spectroscopy as well as by temperature- and concentration-dependent ¹H NMR spectroscopy. The molecule packing in the vesicle wall was investigated by solution-state ¹H NMR data. These studies show that the surface of the vesicle is covered by PEO arms and the HBPO cores are located inside the vesicle wall, thus resulting in the vesicle wall having a sandwich structure. A previous report^[6] on the macroscopic molecular self-assembly of HBPO-star-PEO molecules in acetone had shown that the tube walls possessed an alternate PEO and HBPO lamella structure, and thus suggested that the sandwich structure in the HB1–3 vesicle walls consisted of PEO-HBPO-PEO lamellae. In addition, small-angle X-ray scattering (SAXS) experiments further proved the lamellar structure in the HB1–3 vesicle wall. The lamellar thickness measured by SAXS experiments is 5.6 nm for HB3 vesicles, 5.3 nm for HB2 vesicles, and 11.1 nm for HB1 vesicles, which fits well with the wall thickness of the HB1–3 vesicles measured by TEM

studies (Table 1). Consideration of the HBPO-star-PEO molecule size, the lamella structure, the lamella thickness, and the vesicle wall thickness leads us to suggest that the HB2 and HB3 molecules pack into a monolayer structure in the related vesicle walls in the same way as a triblock copolymer,^[7,2g] and the HB1 molecules pack into a bilayer structure similar to that in diblock copolymer vesicles.^[2,3] For details of the experiments and analysis of the self-assembly mechanism see the Supporting Information.

A tentative molecular packing model for the walls of the HB1–3 vesicles is shown in Figure 4. In the monolayer model (Figure 4a) each HBPO-star-PEO molecule behaves as an

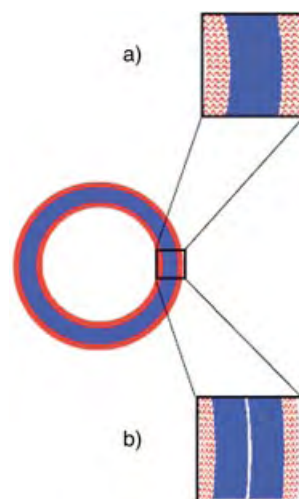


Figure 4. Proposed molecular packing models in the HB1–3 vesicle walls. The blue zones represent the condensed HBPO cores and the red wavy lines denote PEO arms. a) A monolayer structure. b) A bilayer structure. The illustrations are not drawn to scale.

amphiphilic triblock copolymer (ABA type) and spontaneously segregates into a molecular sandwich with an internal layer consisting of the HBPO core and outer shells of PEO arms as a result of the hydrophobic interaction, while the molecular sandwiches aggregate into giant vesicles. In the bilayer model (Figure 4b) each HBPO-star-PEO molecule segregates into a hydrophobic HBPO part and a hydrophilic PEO part similar to the amphiphilic structure of diblock copolymers, while the hydrophobic parts aggregate together to form the bilayer structure similar to that in vesicles formed by a diblock copolymer. The boundary between the two core layers in Figure 4b does not really exist, and the exaggerated boundary is only shown to illustrate the bilayer structure more clearly. Comparison of the HB1–3 molecules shows that HB1 has shorter hydrophilic PEO arms, which possibly could not stabilize the monolayer structure and resulted in HB1 forming a bilayer structure so as to keep the self-assembled objects stable.

In conclusion, we successfully obtained a new kind of giant polymer vesicle from an ill-defined hyperbranched multiarm copolymer having a high hydrophilic fraction (> 60%) through direct self-assembly in water. These polymer vesicles have been termed branched polymersomes. The

size of the branched polymersomes can be easily controlled by adjusting the hydrophilic fraction of the copolymer, with the average diameter of the larger branched polymersomes exceeding 100 μm . Two possible molecular packing models in the vesicle walls are proposed. The large size of the branched polymersomes suggests they will have applications for encapsulation and simulation of the biomembrane process. Further results of the morphology transition and membrane fluidity of these branched polymerases will be reported in the near future.

Received: April 14, 2004

Published Online: August 30, 2004

Keywords: block copolymers · self-assembly · supramolecular chemistry · vesicles

- [1] a) D. E. Discher, A. Eisenberg, *Science* **2002**, 297, 967; b) J.-M. Lehn, *Science* **2002**, 295, 2400; c) H. Ringsdorf, B. Schlarb, J. Venzmer, *Angew. Chem.* **1988**, 100, 117; *Angew. Chem. Int. Ed. Engl.* **1988**, 27, 113.
- [2] a) L. Zhang, A. Eisenberg, *Science* **1995**, 268, 1728; b) L. Zhang, A. Eisenberg, *Science* **1996**, 272, 1777; c) L. Zhang, A. Eisenberg, *Polym. Adv. Technol.* **1998**, 9, 677; d) H. Shen, A. Eisenberg, *Angew. Chem.* **2000**, 112, 13448; *Angew. Chem. Int. Ed.* **2000**, 39, 3310; e) L. Luo, A. Eisenberg, *J. Am. Chem. Soc.* **2001**, 123, 1012; f) L. Luo, A. Eisenberg, *Angew. Chem.* **2002**, 114, 1043; *Angew. Chem. Int. Ed.* **2002**, 41, 1001; g) F. Liu, A. Eisenberg, *J. Am. Chem. Soc.* **2003**, 125, 15059.
- [3] a) B. M. Discher, Y.-Y. Won, D. Ege, J. C.-M. Lee, F. S. Bates, D. E. Discher, D. A. Hammer, *Science* **1999**, 284, 1143; b) B. M. Discher, D. A. Hammer, F. S. Bates, D. E. Discher, *Curr. Opin. Colloid Interface Sci.* **2000**, 5, 125; c) J. C.-M. Lee, H. Bermudez, B. M. Discher, M. A. Sheehan, Y.-Y. Won, F. S. Bates, D. E. Discher, *Biotechnol. Bioeng.* **2001**, 73, 135; d) H. Bermudez, A. K. Brannan, D. A. Hammer, F. S. Bates, D. E. Discher, *Macromolecules* **2002**, 35, 8203; f) F. Ahmed, A. Hategan, D. E. Discher, B. M. Discher, *Langmuir* **2003**, 19, 6505.
- [4] a) F. M. Menger, K. D. Gabrielson, *Angew. Chem.* **1995**, 107, 2260; *Angew. Chem. Int. Ed. Engl.* **1995**, 34, 2091; b) F. M. Menger, J. S. Keiper, *Adv. Mater.* **1998**, 10, 888; c) F. M. Menger, J. S. Keiper, K. L. Caran, *J. Am. Chem. Soc.* **2002**, 124, 11842; d) F. M. Menger, V. A. Seredyuk, M. V. Kitaeva, A. A. Yaroslavov, N. S. Melik-Nubarov, *J. Am. Chem. Soc.* **2003**, 125, 2846; e) W. H. Binder, V. Barragan, F. M. Menger, *Angew. Chem.* **2003**, 115, 5980; *Angew. Chem. Int. Ed.* **2003**, 42, 5802.
- [5] a) H. Kukula, H. Schlaad, M. Antonietti, S. Förster, *J. Am. Chem. Soc.* **2002**, 124, 1658; b) M. Antonietti, S. Förster, *Adv. Mater.* **2003**, 15, 1323; c) F. Chécot, S. Lecommandoux, Y. Gnanou, H.-A. Klok, *Angew. Chem.* **2002**, 114, 1395; *Angew. Chem. Int. Ed.* **2002**, 41, 1340; d) S. I. Stupp, V. LeBonheur, K. Walker, L. S. Li, K. E. Huggins, M. Keser, A. Amstutz, *Science* **1997**, 276, 384; e) J. C. M. Vanhest, D. A. P. Delnoye, M. W. P. L. Baars, M. H. P. Van Genderen, E. W. Meijer, *Science* **1995**, 268, 1592.
- [6] D. Yan, Y. Zhou, J. Hou, *Science* **2004**, 303, 65.
- [7] a) H. Schuch, J. Klingler, P. Rossmanith, T. Frechen, M. Gerst, J. Feldthusen, A. H. E. Müller, *Macromolecules* **2000**, 33, 1734; b) H. Xu, R. Erhardt, V. Abetz, A. H. E. Müller, W. A. Goedel, *Langmuir* **2001**, 17, 6787; c) R. Erhardt, M. Zhang, A. Böker, H. Zettl, C. Abetz, P. Frederik, G. Krausch, V. Abetz, A. H. E. Müller, *J. Am. Chem. Soc.* **2003**, 125, 3260; d) K. Schillén, K. Bryskhe, Y. S. Mel'nikova, *Macromolecules* **1999**, 32, 6885.

WO₂Cl₂ Nanotubes and Nanowires**

A. Robert Armstrong, Jesus Canales, and
Peter G. Bruce*

Since the discovery of carbon nanotubes,^[1] there has been much interest in synthesizing nanotubes of greater chemical complexity such as, chalcogenides (e.g., MoS₂, WS₂),^[2] oxides (e.g., TiO₂, VO_x)^[3] and recently halides (e.g., NiCl₂).^[4] Complex nanotubes can exhibit fascinating new optical, electrical, and magnetic properties due to their dimensional confinement.^[5] In solid-state chemistry, the partial replacement of cations of one type by another is ubiquitous; yet partial replacement of the anions can often change the dimensionality of the compound. Partial replacement of O²⁻ ions in 3D oxides by the heavier halides can promote the formation of van der Waals bonded layered structures that in turn more readily form nanotubes and nanowires than the pure oxides do; yet such materials can maintain many properties of the oxides. Herein we report the synthesis of WO₂Cl₂ nanotubes and nanowires; this represents the first synthesis of a new class of nanotubes/nanowires based on mixed anion (oxyhalide) compounds.

It is no accident that, following the discovery of carbon nanotubes, the chalcogenides were one of the first classes of inorganic nanotubes to be synthesized. Their layered structures encourage the formation of nanotubes/nanowires (see for example reference [3a,b]). Similarly, it is not surprising that VO_x, TiO₂-B and other titanates have been prepared as nanotubes/nanowires. In the case of the titanium oxides, layered titanates form during the hydrothermal synthesis, which curve or scroll to form nanotubes/nanowires.^[5] However, the majority of oxides form 3D structures and other approaches have been adopted to promote 1D growth. For example, it is difficult to grow nanotubes/nanowires of WO₃, however, the reduced phases, such as W₁₈O₄₉, contain shear planes that limit growth thus forming wire shaped structures.^[6] Templates can also be used to promote crystal growth in certain directions.^[3b]

Partial replacement of O atoms by F atoms results in oxyfluorides, which generally adopt 3D structures. However if the O atoms are replaced in part by atoms of the heavier halides, Cl, Br, I then the resulting oxyhalides are often layered structures due to the propensity of the more electron-rich halides to exhibit van der Waals bonding between adjacent layers. Several compounds of this type are known

[*] Dr. A. R. Armstrong, Dr. J. Canales, Prof. P. G. Bruce
School of Chemistry
University of St. Andrews
Purdie Building
North Haugh, St. Andrews KY16 9St (UK)
Fax: (+44) 1334-463-808
E-mail: p.g.bruce@st-and.ac.uk

[**] P.G.B. is indebted to The Royal Society and the EPSRC (UK) for financial support.

for example, FeOCl , VOCl , WO_2Cl_2 , WO_2Br_2 , and MoO_2Cl_2 .^[7] They should form nanotubes/nanowires relatively easily and without the need to promote 1D growth. We have investigated the formation of nanotubes/nanowires based on WO_2Cl_2 .

WO_3 can adopt a number of distorted forms of the ReO_3 structure, Figure 1, in which WO_6 octahedra share common vertices, thus forming a 3D network. Replacing a layer of O^{2-} ions in WO_3 by two layers of Cl^- ions results in the formation of the van der Waals' bonded layered structure WO_2Cl_2 . The structure of this compound is shown in Figure 1b and is composed of layers containing W^{6+} coordinated by 4 O^{2-} ions to form a slightly distorted square in which each WO_4 units share common vertices. The W^{6+} ions are coordinated by a total of six anions, with the coordination being completed by two Cl^- ions, one immediately above and the other immediately below the $\text{W}-\text{O}$ plane. The complete structure of WO_2Cl_2 (orthorhombic space group $Immm$) consists of these trilayer blocks ($\text{Cl}-\text{WO}_2-\text{Cl}$) stacked in the c direction such that each trilayer block is displaced by a translation $x + \frac{1}{2}$,

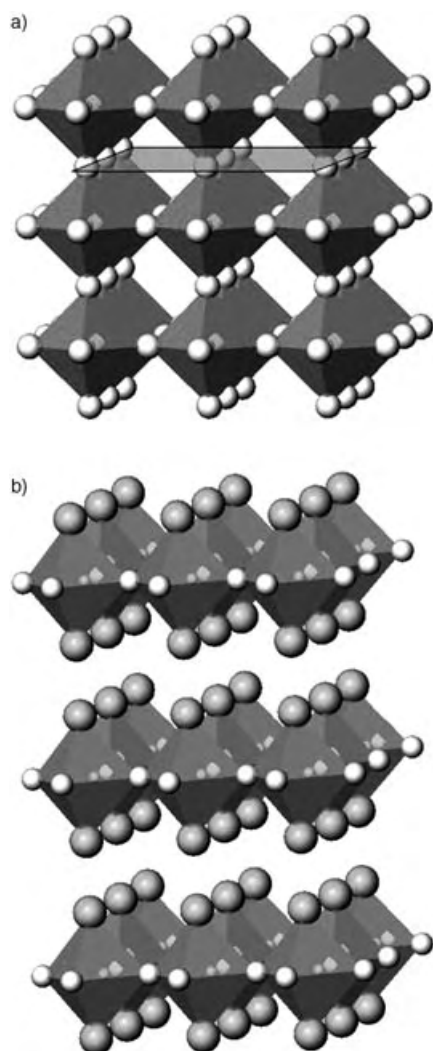


Figure 1. a) Ideal crystal structure of WO_3 showing vertex-sharing WO_6 octahedra. b) Crystal structure of WO_2Cl_2 showing the relationship to WO_3 .

$y + \frac{1}{2}$ with respect to its neighbor. Because the WO_2 layers in WO_3 (Figure 1) are preserved in WO_2Cl_2 , the band structure and electronic properties of WO_2Cl_2 are similar to WO_3 and may be derived from the latter, with a perturbation due to the presence of the Cl^- ions.^[8]

Nanotubes and nanowires of WO_2Cl_2 have been prepared by a simple process of exfoliation and restacking, the experimental details of which are described in the Experimental Section. Transmission electron micrographs of the resulting materials are shown in Figure 2. In general, the nanotubes/nanowires exhibit diameters in the range 30–80 nm and can be up to 5 μm in length.

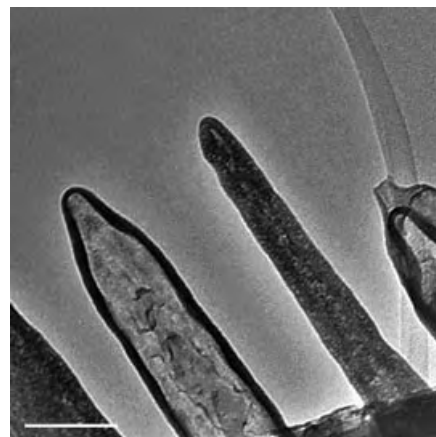


Figure 2. Transmission electron micrograph of WO_2Cl_2 nanotubes and nanowires. The bar on the image is 100 nm long.

There was no evidence of nanotubes/nanowires in the as-received WO_2Cl_2 , despite the fact that these materials are made by a solid/gas reaction ($\text{WO}_3 + \text{WCl}_6$) that is known to promote nanotube growth in other layered materials such as the chalcogenides.^[2,3a] Grinding the as-received WO_2Cl_2 , reduced the particle size to around 0.1 μm (as observed by scanning electron microscopy), but did not induce nanotube formation. Stirring a mixture of ground WO_2Cl_2 for two weeks in polar solvents such as propylene carbonate or a 1:1 (v/v) mixture of ethylene carbonate/dimethyl carbonate also provided no evidence of nanotube formation. We had noted in our previous studies of bulk WO_2Cl_2 that when in contact with non-aqueous Li electrolytes the latter developed a colloidal appearance. Following this earlier observation, the ground solid was stirred in a 1 M solution of LiPF_6 in a 1:1 (v/v) mixture of ethylene carbonate and dimethyl carbonate resulting in a colloidal solution which, when filtered then centrifuged, washed in dimethyl carbonate then dried, gave rise to a fine powder. The powder contained in excess of 90 % nanotubes/nanowires in equal proportions, based on TEM analysis. Figure 3 shows TEM images of nanotubes/nanowires taken from different regions of the sample from that of Figure 2, thus indicating the widespread nature of the nanotube and nanowire morphology. Although more detailed studies are necessary to elucidate the exact nature of the reaction, it seems clear that the electrolyte penetrates the van der Waals layers sufficiently to prize them apart and

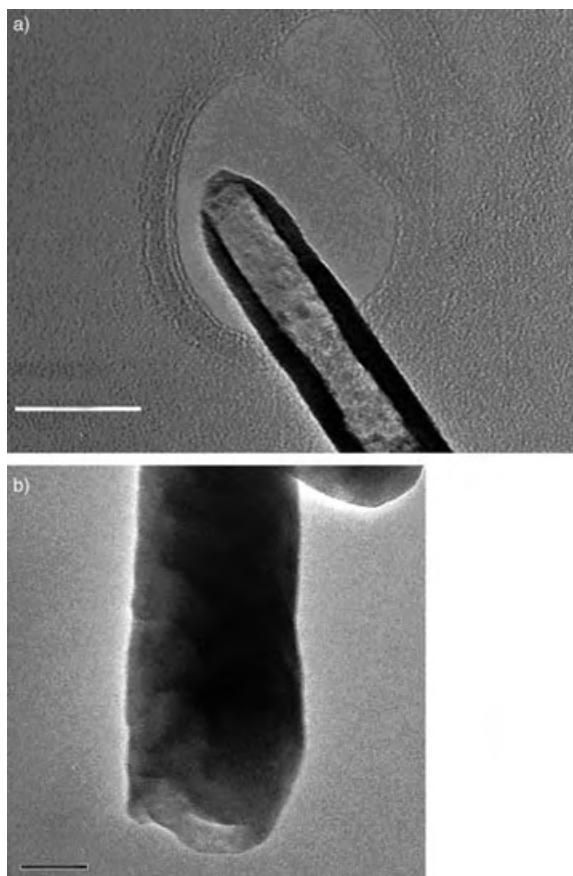


Figure 3. a) Transmission electron micrograph of a WO_2Cl_2 nanotube. b) Transmission electron micrograph of a WO_2Cl_2 nanowire. The bars are 50 nm long.

promote exfoliation. Subsequent repeated washing of the centrifuged material removes the electrolyte and restacks the layer but with the nanotube/nanowire morphology. This infers that while the layers are in solution they roll into tubes/wires. It is known from other studies that sheets in solution can roll into tubes or wires.^[9] The use of other electrolytes, such as those based on propylene carbonate or acetonitrile, did not yield significant quantities of nanotubes/nanowires.

Although most of the material is composed of approximately a 1:1 ratio of nanotubes to nanowires, we have observed some examples of particles that are both nanotubes and nanowires, Figure 4. High-resolution transmission electron microscopy (HRTEM) has allowed a more detailed investigation of the structure of the walls of the tubes and the wires, Figure 5, which are identical. The measurement of the lattice images and electron-diffraction patterns confirm that the structure is that of WO_2Cl_2 . The c -axis of the orthorhombic unit cell of WO_2Cl_2 , along which the layers are stacked, lies along the radius of the tubes/wires with the ab plane coinciding with the plane of curvature of the tube walls. The a and b lattice parameters extracted from the electron microscopy are $a \approx b \approx 3.75 \text{ \AA}$ (3.8414/3.8851 \AA), with values obtained from the previous X-ray diffraction study given in brackets.^[10] The HRTEM reveals that the tube walls consist of small domains, each of which adopts the WO_2Cl_2 structure with their c axis parallel to each other but with the structure of

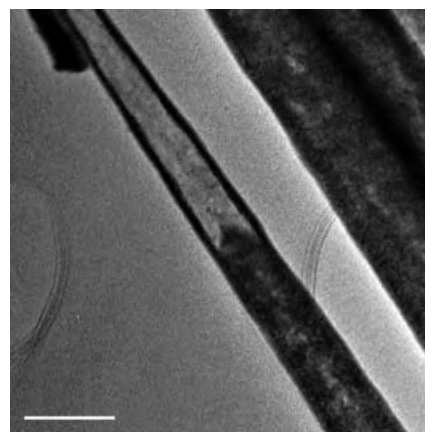


Figure 4. Transmission electron micrograph showing a combined tube and wire. The bar is 100 nm long.

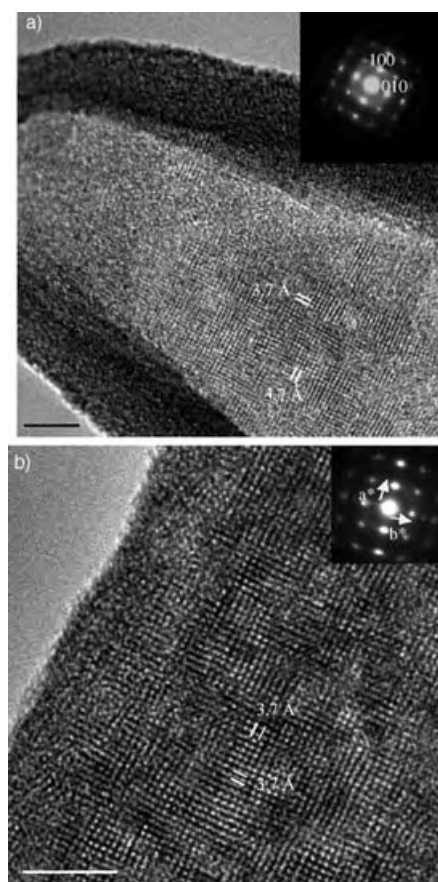


Figure 5. High-resolution transmission electron micrograph of a) a nanotube wall and b) a nanowire. In each case the lattice spacings are highlighted and selected area electron diffraction patterns down the [001] direction are shown as an inset. The bars are 5 nm long.

each domain being incoherent with its neighbors. It is interesting to note that the tubes are invariably capped as shown in Figure 2.

Layered structures in general favor the formation of nanotubes/wires. However the majority of examples are based on CdI_2 , CdCl_2 , or similar structure types, in which the MX_6 octahedra share common edges. In contrast, in WO_2Cl_2 the octahedra share common vertices. Although the

radius of curvature involved in bending a sheet into a scroll is relatively small compared with the average bond length, bending a sheet of edge-sharing octahedra is much more difficult than is the case of a sheet of corner-sharing octahedra; in the latter case this only requires a small deviation of the M-O-M angle from 180° in the direction of curvature of the tubes. Many oxides built from vertex-sharing polyhedra have M-O-M bond angles that are far from 180° .^[11] This demonstrates that the lattice energies are relatively insensitive to variations in the bond angles, in keeping with the nature of the metal-oxygen bonding in such materials. Therefore the vertex-sharing layered structures of materials such as WO_2Cl_2 are excellent candidates for nanotube formation. As a result, it is likely that other oxyhalides with similar structures for example, MoO_2Cl_2 , will also readily form nanotubes/wires.

WO_2Cl_2 is an intercalation host. Both Li and Na atoms have been intercalated up to a maximum of $\text{Li}_2\text{WO}_2\text{Cl}_2$ and $\text{Na}_{1.5}\text{WO}_2\text{Cl}_2$ respectively. Such intercalated materials are layered tungsten bronzes that exhibit a mixture of electronic and ionic conductivity and display an intense blue color. The ability to switch color on and off with intercalation/deintercalation is the basis of electrochromic displays. The tubes/wires have the same structure and hence the potential to act as intercalation hosts with attendant changes in the electronic, ionic and optical properties. However the confined dimensions of the tubes/wires can lead to rapid switching on intercalation/deintercalation. The intercalation of Li and Na atoms into WO_2Cl_2 nanotubes/wires is under investigation and will be reported subsequently.

In conclusion we have succeeded in preparing, for the first time, mixed anion (oxyhalide) nanotubes and nanowires. Doubtless, further examples of this new class of nanotubes/nanowires will be synthesized in the future.

Experimental Section

WO_2Cl_2 (Aldrich, 99%), was ballmilled for 1 to 1.5 h by using a SPEX Centri-Prep 8000M mixer/mill. All milling was carried out under an Ar atmosphere to prevent hydrolysis of the material. The milled solid was returned to the glove-box and stirred in a 1 M solution of LiPF_6 in a 1:1 (v/v) mixture of ethylene carbonate and dimethyl carbonate (Merck) for several days. The resulting colloidal solution was then centrifuged, washed in dimethyl carbonate and dried.

HRTEM imaging and selected-area electron diffraction (SAED) were carried out by using a JEOL-JEM 2011 electron microscope operating at 200 kV and equipped with a side-entry $\pm 20^\circ$ double-tilt specimen holder. The specimens were prepared by making a suspension of powdered samples in organic solvent and depositing one drop onto a holey carbon-coated Cu grid. This was carried out in the glovebox. The specimen holder was loaded so as to minimize the sample exposure to the atmosphere.

Received: April 15, 2004

Keywords: halides · nanostructures · nanotubes · tungsten

- [1] S. Iijima, *Nature* **1991**, 354, 56.
[2] a) R. Tenne, L. Margulis, M. Genut, M. Hodes, *Nature* **1992**, 360, 444; b) L. Margulis, G. Salitra, R. Tenne, M. Talianker, *Nature*

- 1993**, 365, 113; c) Y. Feldman, E. Wasserman, D. J. Srolovitz, R. Tenne, *Science* **1995**, 267, 222.
[3] a) C. N. R. Rao, M. Nath, *J. Chem. Soc. Dalton Trans.* **2003**, 1; b) G. R. Patzke, F. Krumeich, R. Nesper, *Angew. Chem.* **2002**, 114, 2554; *Angew. Chem. Int. Ed.* **2002**, 41, 2446; c) P. Hoyer, *Langmuir* **1996**, 12, 1411; d) X. Sun, Y. Li, *Chem. Eur. J.* **2003**, 9, 2229; e) A. R. Armstrong, G. Armstrong, J. Canales, P. G. Bruce, *Angew. Chem.* **2004**, 116, 2336; *Angew. Chem. Int. Ed.* **2004**, 43, 2286; f) M. E. Spahr, P. Bitterli, R. Nesper, M. Müller, F. Krumeich, H. U. Nissen, *Angew. Chem.* **1998**, 110, 1339; *Angew. Chem. Int. Ed.*, **1998**, 37, 1263.
[4] Y. R. Hachohen, E. Grunbaum, R. Tenne, J. Sloan, J. L. Hutchison, *Nature* **1998**, 395, 336.
[5] B. D. Yao, Y. F. Chan, X. Y. Zhang, W. F. Zhang, Z. Y. Yang, N. Wang, *Appl. Phys. Lett.* **2003**, 82, 281.
[6] a) X. W. Lou, H. C. Zeng, *Inorg. Chem.* **2003**, 42, 6169; b) A. Margolin, R. Rosentsveig, A. Albu-Yaron, R. Popovitz-Biro, R. Tenne, *J. Mater. Chem.* **2004**, 14, 617.
[7] a) M. S. Goldsztaub, *Bull. Soc. Fr. Mineral.* **1935**, 58, 49; b) P. Ehrlich, H. J. Seifert, *Z. Anorg. Allg. Chem.* **1959**, 301, 282; c) O. Jarchow, F. Schröder, H. Schulz, *Z. Anorg. Allg. Chem.* **1968**, 363, 58; d) G. A. Kokovin, N. K. Toropova, *Russ. J. Inorg. Chem.* **1965**, 10, 304; e) H. M. Neumann, N. C. Cook, *J. Am. Chem. Soc.* **1957**, 79, 3026.
[8] J. F. Ackermann, *Mater. Res. Bull.* **1988**, 23, 165.
[9] Q. Chen, W. Zhou, G. Du, L.-M. Peng, *Adv. Mater.* **2002**, 14, 1208.
[10] I. Abrahams, J. L. Nowinski, P. G. Bruce, V. C. Gibson, *J. Solid State Chem.* **1993**, 102, 140.
[11] a) A. Zemann, J. Zemann, *Acta Crystallogr.* **1961**, 14, 835; b) J. B. Goodenough, H. Y.-P. Hong, J. A. Kafalas, *Mater. Res. Bull.* **1976**, 11, 203.

Constitutional Dynamics

Generation of Dynamic Constitutional Diversity and Driven Evolution in Helical Molecular Strands under Lewis Acid Catalyzed Component Exchange**

*Nicolas Giuseppone, Jean-Louis Schmitt, and Jean-Marie Lehn**

Constitutional dynamic chemistry (CDC)^[1] rests on the implementation of dynamic features that act on the constitution of molecular^[2] as well as supramolecular^[3] entities

[*] Dr. N. Giuseppone, J.-L. Schmitt, Prof. Dr. J.-M. Lehn
Institut de Science et d'Ingénierie Supramoléculaires
8 Allée Gaspard-Monge, BP 70028
67083 Strasbourg cedex (France)
Fax: (+33) 3-9024-5140
E-mail: lehn@isis.u-strasbg.fr

[**] This work was supported by a predoctoral fellowship from the Ministère de la Jeunesse, de la Recherche et de la Technologie (J.-L.S.).

through reversible covalent bonds and noncovalent interactions, respectively. Dynamic constitutional diversity is generated by exchange and recombination of components, as expressed in particular by the recently developed dynamic combinatorial chemistry.^[4] CDC operates in the self-assembly^[5] of well-defined molecular or supramolecular species which is driven by molecular information and recognition processes.

Control of the folding of molecular strands has been the subject of intense recent activity^[6] in view of its significance in both chemistry and biology. In particular, the generation of helical species^[6–8] may be enforced through the implementation of specific helicity codons based on nonbonded interactions in polyheterocyclic strands^[7] or on hydrogen-bonding subunits.^[8] The self-assembly of helical strands by formation of reversible hydrazone-type bonds between suitably designed hydrazino and carbonyl components^[9,10] gives, in principle, access to dynamic libraries of molecular helices.

We report here a system that brings together the three major features mentioned above: constitutional dynamics, self-assembly, and control of helical folding.

The generation of dynamic constitutional diversity for both biological and materials science purposes depends on the availability of suitable chemical connections that are reversible in the desired conditions. The C=N unit, which is present in imines, hydrazones, and oximes, in principle offers highly attractive potentialities to CDC, provided that fast and efficient reversibility in organic solvents is achieved. Zinc(II) ions are known to catalyze transimination of Schiff bases^[11] and have been found in our research group to accelerate component exchange in polyimine materials.^[12] We now describe the efficient Lewis acid catalyzed exchange of hydrazones and apply the results to the generation of a constitutional dynamic library of helical strands incorporating hydrazone bonds that is capable of assembling, dissociating, and exchanging components. Moreover, we demonstrate that these libraries can undergo driven evolution in the presence of suitable metal ions to express $[2 \times 2]$ grid-type metal complexes preferentially from the mixture of helices. These processes are illustrated schematically in Figure 1.^[13]

The condensation of pyrimidine-derived difunctional hydrazine and carbaldehyde building blocks leads to helicity-encoded oligomeric^[9a] and polymeric^[9b] molecular strands. These strands have been found to resist many attempts to

perform component exchange,^[9b] thus indicating their high stability even at elevated temperature and/or in the presence of acid. As a model system for the exploration of potential exchange catalysts, cross-over experiments between the dihydrazone compound **A** and the dihydrazine **B** in chloroform at 60 °C were performed first (Figure 2). Only 7 % of **A**

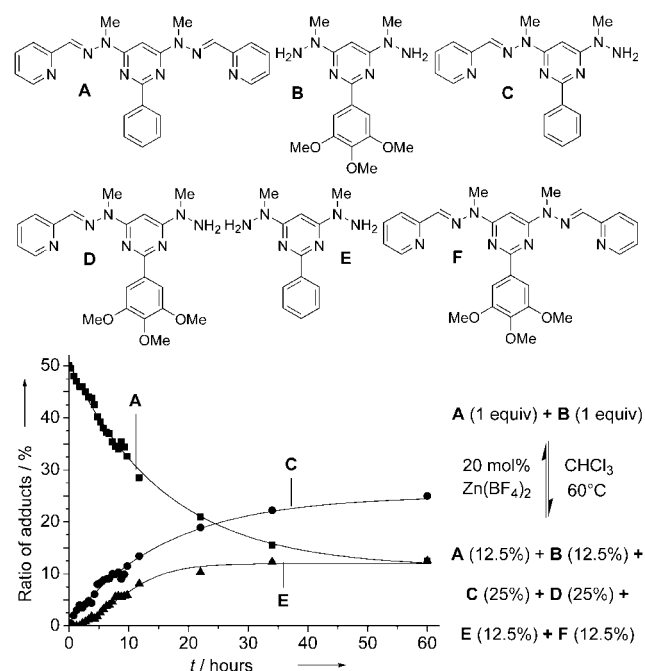


Figure 2. Evolution with time of the composition of a model hydrazone/hydrazine mixture **A** and **B** followed by ¹H NMR spectroscopy under Zn^{II} catalysis; *c*(**A**) = *c*(**B**) = 50 mM.^[13]

was consumed after 48 h in these conditions without catalyst and slow degradation of constituents of the mixture had taken place. Extensive decomposition into unidentified compounds other than **C–E** occurred under acid catalysis (20 mol% CF₃CO₂H). In contrast, addition of 20 mol% Zn(BF₄)₂·8H₂O led to complete exchange with a half-life of 10 h, without observable degradation. The statistical distribution of the products at equilibrium indicates the nonspecific interaction of the Zn^{II} ions with the different compounds and the isoenergetic nature of the library.^[4a] As in the case of

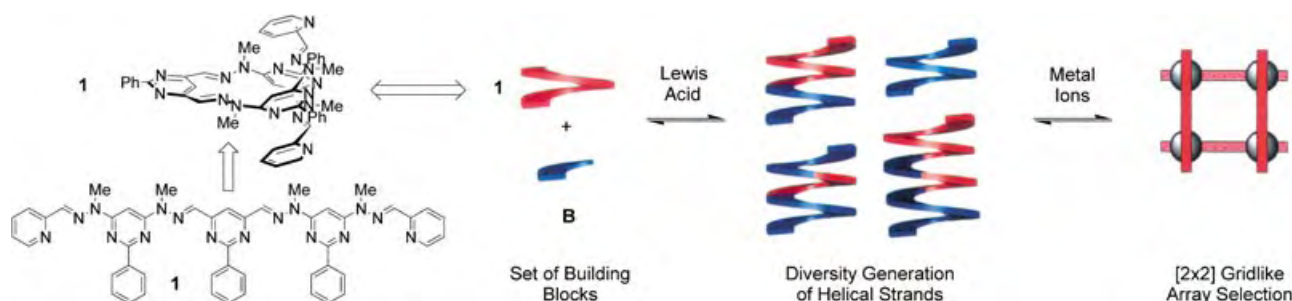


Figure 1. Schematic representation of the processes occurring in the present system. Left: Lewis acid catalyzed generation of dynamic constitutional diversity in helical molecular strands involving compounds **1** and **B** of Figure 3 (**1** is shown in both its extended and its preferred helical forms);^[9,13] right: evolution of the dynamic library towards formation of a $[2 \times 2]$ grid driven by suitable metal ions.

imines,^[11,12] the reaction proceeds through a transimination process; indeed, in similar conditions the pyrimidine 4,6-biscarboxaldehyde analogue of **B** and dihydrazone **A** did not show any detectable exchange after three days.

These promising results prompted us to explore the catalytic activity of other Lewis acids for the model exchange reaction depicted in Figure 3. The data indicated that the activity was directly correlated with the ionic radius of the trivalent metallic ions assayed, with scandium triflate being

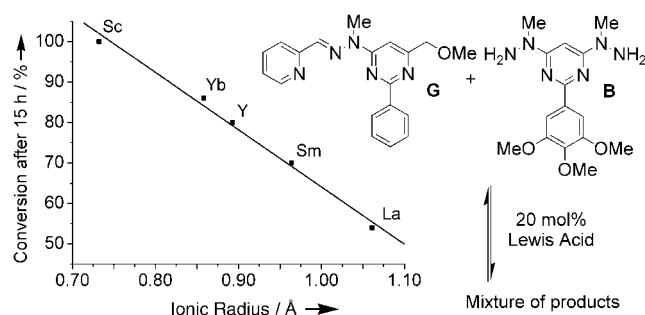


Figure 3. Comparative catalytic activity of different trivalent Lewis acids $M(OTf)_3$ for the exchange of hydrazones (right) as a function of ionic radius (left); $c(\mathbf{B}) = c(\mathbf{G}) = 5 \text{ mM}$ at 60°C in $CDCl_3$. The conversion is measured by following, through integration of the ^1H NMR signal, the decrease of compound **G** over 15 h, which was the time required for reaching equilibrium in the case of the most active catalyst, $Sc(OTf)_3$. In the same conditions, the conversions for the uncatalyzed and for the $Zn(OTf)_2$ - or $Zn(BF_4)_2$ -catalyzed reactions were 1% and 30%, respectively.^[13]

the most powerful Lewis acid catalyst for hydrazone scrambling. Moreover, utilization of scandium triflate in the exchange between compounds **A** and **B** (Figure 2) resulted in the half-reaction being reached after only 20 minutes, a 30-fold acceleration compared to the results obtained with $Zn(BF_4)_2 \cdot 8H_2O$.

To test the efficiency and generality of the system we turned to compound **1**,^[9a] a one-turn helical strand containing four hydrazone groups, which was expected to be much more reluctant to undergo component exchange (Figure 4, equilibrium (**a**)) than the shorter related structures (**A**, **C**, **D**, **F**, Figure 2), as a consequence of its folding and the resulting lower accessibility of its hydrazone sites. Compound **1** nevertheless underwent exchange of its two bishydrazone components with compound **B** in 48 h when mixed in a stoichiometric ratio in the presence of 20 mol % (namely, 5 mol % per hydrazone site of **1**) $Sc(OTf)_3$ in chloroform at 60°C . The equilibrium was reached after about 48 h as indicated by NMR spectroscopy and mass spectrometry. Extensive exchange had taken place after 48 h even with only 4% catalyst (that is, 1% per site), although the reaction was much slower. The constituents of the mixture could be separated and identified by HPLC/ESMS. The data analysis demonstrated that full recombination between **1** and **B** had taken place, with the generation of the set of compounds **1–28** containing expanded helices with up to ten hydrazone sites (more than three helical turns).^[9] Moreover, all the possible cross-combinations with phenyl and/or methoxyphenyl moieties were generated for each size of helical strand, thus highlighting the efficiency of the reorganization process. In

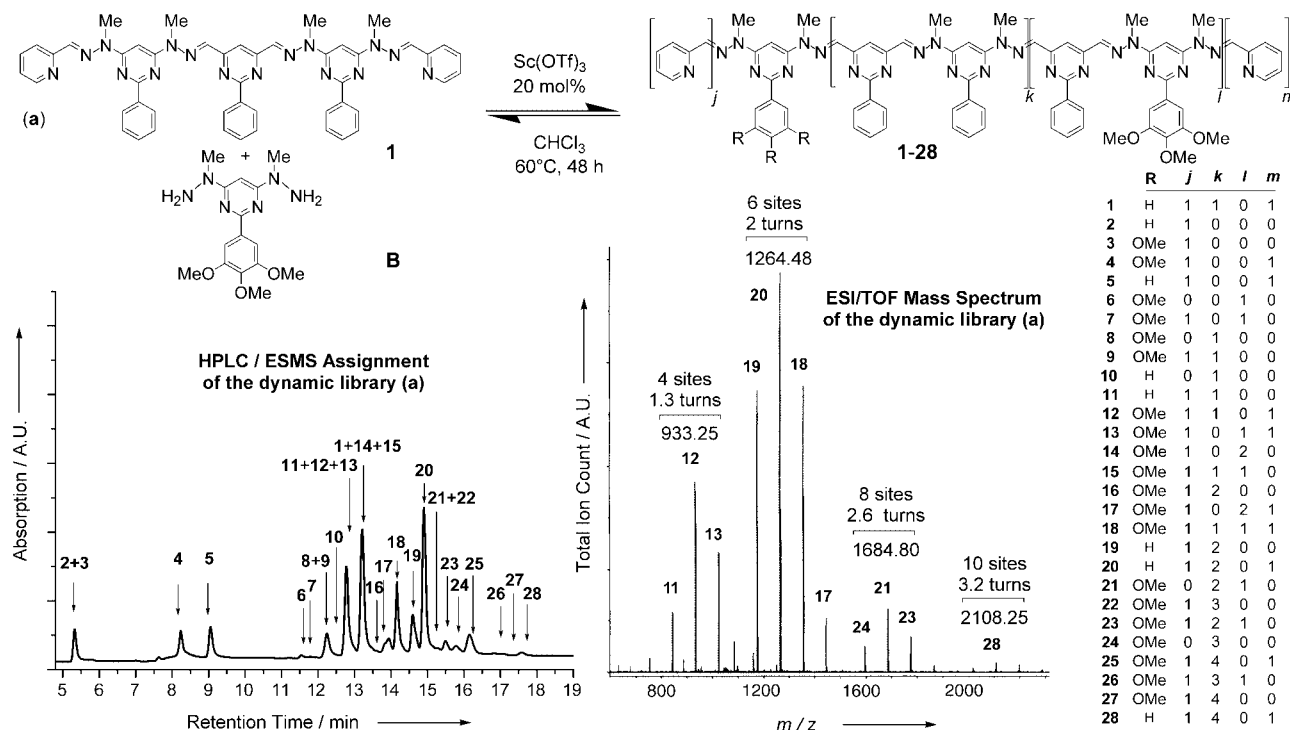


Figure 4. Generation of a highly diverse recombination library of helicity-encoded molecular strands from the one-turn/four-sites helical compound **1** ($c = 50 \text{ mM}$) and the dihydrazone **B** ($c = 50 \text{ mM}$) using $Sc(OTf)_3$ (20 mol%) as a catalyst in $CDCl_3$ at 60°C ; 28 constituents were identified by LC/MS (bottom left) and direct introduction ESI/TOF (bottom center) mass spectrometry, as indicated (bottom right).^[13]

the same conditions but under acid catalysis (20 mol % $\text{CF}_3\text{CO}_2\text{H}$) less than 5% of **1** was converted into compounds **11** and **3**; degradation of the dihydrazine **B** had also started (as shown by NMR analysis and LC/MS).^[14]

Finally, the dynamic library of helical structures under equilibrating conditions was treated with $\text{Zn}(\text{OTf})_2$ (1 equiv with respect to the initial amount of compound **1**), which is known to self-assemble with two-site ligands such as **5**, to yield $[2 \times 2]$ grid-type complexes in acetonitrile (Figure 5, equilibrium (b)).^[15] The formation of $[\text{Zn}_4\text{5}_4]$ as the major tetranuclear grid together with the $[\text{Zn}_4\text{5}_3\text{4}]$ and $[\text{Zn}_4\text{5}_2\text{4}_2]$ analogues was observed by ESI/TOF mass spectroscopy using direct injection. The HPLC trace (b) (displaying the ligands resulting from dissociation of the complexes on the column) and the ESMS data indicated a marked increase in the amount of **5**, which forms the $[2 \times 2]$ grid structure, accompanied by a decrease in the larger helical species compared to the initial equilibrium (a). Moreover, Zn^{II} ions favored formation of **5** over **4**, which contains a more bulky central group that hinders the formation of the homoleptic grid complex $[\text{Zn}_4\text{4}_4]$. These observations indicate that addition of Zn^{II} ions had driven the evolution of the dynamic set towards the expression of the ligand **5** under the pressure of the formation of the (less bulky) grid-type complex by dissociation and recombination of the subunits of the helical strands. The evolution was also found to depend on the concentration of Zn^{II} ions, as was demonstrated by using three equivalents of its triflate salt (Figure 5, equilibrium (c)). The HPLC trace

and direct introduction ESI/TOF mass spectroscopy showed that, in addition to an increase of **5** (and of **4** to a lesser extent), the main effect observed when three equivalents of $\text{Zn}(\text{OTf})_2$ were added to the mixture was the formation of mononuclear $[\text{Zn2}_2]$, $[\text{Zn(2)(3)}]$, and $[\text{Zn3}_2]$ complexes, thus leading to a huge amplification of the single site ligands **2** and **3** in the library compared to the equilibria (a) and (b). This observation may be explained as resulting from the adaptation of the system to generate the ligands providing the sites required for most complete zinc coordination.

The data reported here demonstrate the ability of Sc^{III} ions to efficiently catalyze the exchange of the components of hydrazones (and, by extension, of any $\text{C}=\text{N}$ functionality) in organic medium and to establish a library of equilibrating entities, a feature of crucial importance for CDC. The method provides a general and efficient procedure for establishing dynamic behavior in sets of discrete molecules (in particular bioactive ones) and in materials (such as polymers). It also allowed the generation of a highly diverse dynamic combinatorial library of oligomeric helical strands from two constituents undergoing assembly, dissociation, and exchange processes. Addition of Zn^{II} ions subsequently shifted this library towards the selective amplification of specific ligand constituents, driven by the formation of $[2 \times 2]$ gridlike complexes (Figure 1). From a broader perspective, the results described illustrate the ability of constitutional dynamic systems to respond to environmental parameters and to perform effector-driven evolution toward the fittest con-

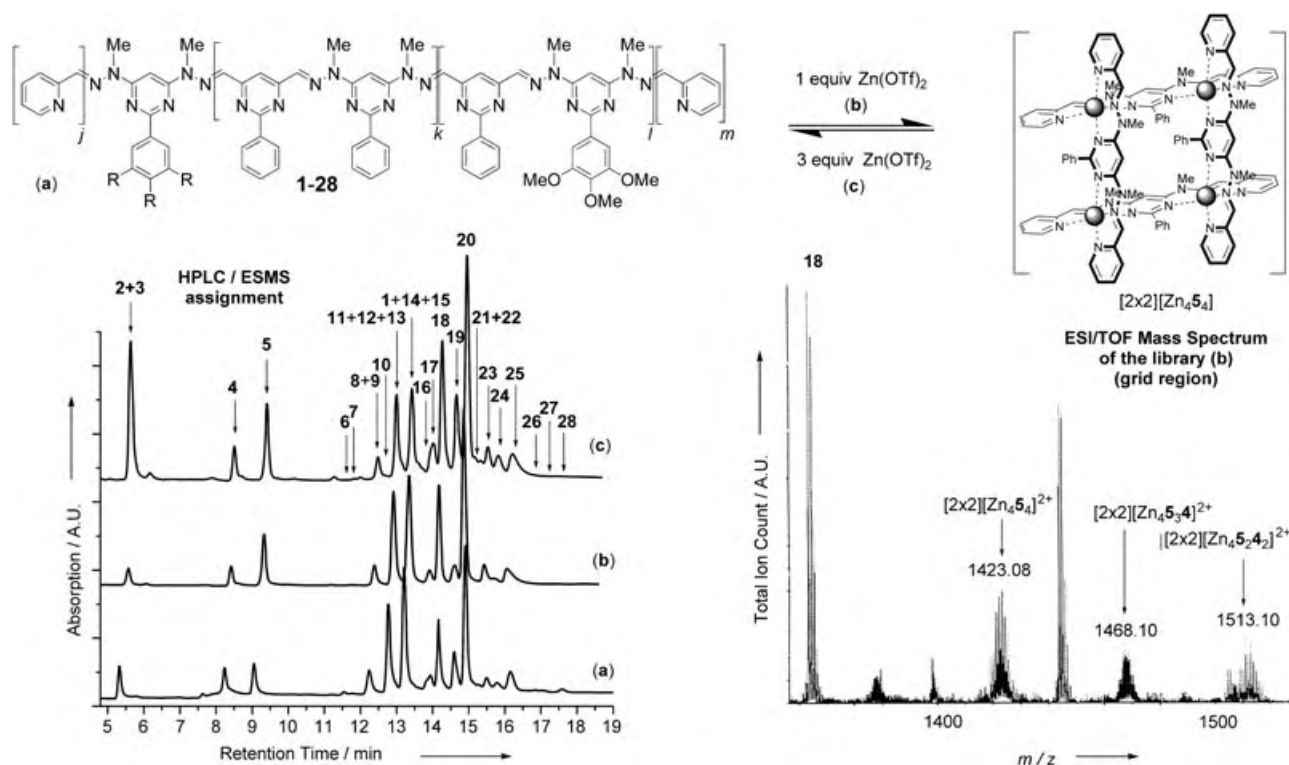


Figure 5. Driven evolution of the dynamic library (a) towards the generation of the $[2 \times 2]$ grid complex $[\text{Zn}_4\text{5}_4]$ (bottom left: HPLC traces; bottom right: ESMS direct injection) by addition of 1 (b) or 3 (c) equivalents of $\text{Zn}(\text{OTf})_2$ (CD_3CN ; 60°C ; 24 h) to the library (a), preequilibrated as in Figure 4 (20 mol % $\text{Sc}(\text{OTf})_3$; CDCl_3 ; 60°C ; 48 h), and then evaporated and redissolved in CD_3CN ; the equilibrium was not significantly affected by the change in solvent. The identification of compounds **1**–**28** is given in Figure 4. Compounds **4** and **5** are identical to **F** and **A**, respectively.^[13]

stituent, an essential feature characterizing the adaptive and evolutive nature of CDC under the pressure of external factors.

Received: April 16, 2004

Published Online: July 14, 2004

Keywords: combinatorial chemistry · Lewis acids · molecular evolution · scandium · self-assembly

- [1] a) J.-M. Lehn, *Proc. Natl. Acad. Sci. USA* **2002**, 99, 4763; b) J.-M. Lehn, *Science* **2002**, 295, 2400.
- [2] S. J. Rowan, S. J. Cantrill, G. R. L. Cousins, J. K. M. Sanders, J. F. Stoddart, *Angew. Chem.* **2002**, 114, 938; *Angew. Chem. Int. Ed.* **2002**, 41, 898.
- [3] J.-M. Lehn in *Supramolecular Science: Where It Is and Where It Is Going* (Eds.: R. Ungaro, E. Dalcaneale), Kluwer, Dordrecht, **1999**, p. 287.
- [4] a) J.-M. Lehn, *Chem. Eur. J.* **1999**, 5, 2455; b) R. L. Cousins, S. A. Poulsen, J. K. M. Sanders, *Curr. Opin. Chem. Biol.* **2000**, 4, 270.
- [5] a) J.-M. Lehn, *Supramolecular Chemistry—Concepts and Perspectives*, VCH, Weinheim, **1995**, chap. 9; b) D. Philp, J. F. Stoddart, *Angew. Chem.* **1996**, 108, 1242; *Angew. Chem. Int. Ed. Engl.* **1996**, 35, 1154; c) J. S. Lindsey, *New J. Chem.* **1991**, 15, 153.
- [6] a) A. E. Rowan, R. J. M. Nolte, *Angew. Chem.* **1998**, 110, 65; *Angew. Chem. Int. Ed.* **1998**, 37, 63; b) D. J. Hill, M. J. Mio, R. B. Prince, T. S. Hughes, J. S. Moore, *Chem. Rev.* **2001**, 101, 3893.
- [7] a) G. S. Hanan, J.-M. Lehn, N. Kyritsakas, J. Fisher, *J. Chem. Soc. Chem. Commun.* **1995**, 765; b) D. M. Bassani, J.-M. Lehn, G. Baum, D. Fenske, *Angew. Chem.* **1997**, 109, 2534; *Angew. Chem. Int. Ed. Engl.* **1997**, 36, 1845; c) M. Ohkita, J.-M. Lehn, G. Baum, D. Fenske, *Chem. Eur. J.* **1999**, 5, 3471.
- [8] a) V. Berl, I. Huc, R. G. Khoury, J.-M. Lehn, *Chem. Eur. J.* **2001**, 7, 2798; V. Berl, I. Huc, R. G. Khoury, J.-M. Lehn, *Chem. Eur. J.* **2001**, 7, 2810; b) B. Gong, *Chem. Eur. J.* **2001**, 7, 4337; c) X. Yang, L. Yuan, K. Yamato, A. L. Brown, W. Feng, M. Furukawa, X. C. Zeng, B. Gong, *J. Am. Chem. Soc.* **2004**, 126, 3148; d) I. Huc, *Eur. J. Org. Chem.* **2004**, 17.
- [9] a) J.-L. Schmitt, A.-M. Stadler, N. Kyritsakas, J.-M. Lehn, *Helv. Chim. Acta* **2003**, 86, 1598; b) J.-L. Schmitt, J.-M. Lehn, *Helv. Chim. Acta* **2003**, 86, 3417.
- [10] For the folding-driven synthesis of imine oligomers, see K. Oh, K.-S. Jeong, J. S. Moore, *Nature* **2001**, 414, 889; D. Zhao, J. S. Moore, *J. Am. Chem. Soc.* **2003**, 125, 16294.
- [11] a) B. E. Leach, D. L. Leussing, *J. Am. Chem. Soc.* **1971**, 93, 3377; for amine exchange in Schiff base complexes, see b) L. F. Lindoy, *Quat. Sci. Rev.* **1971**, 25, 379; c) E. J. Olszewski, D. F. Martin, *J. Inorg. Nucl. Chem.* **1965**, 27, 345; d) H. S. Verter, A. E. Frost, *J. Am. Chem. Soc.* **1960**, 82, 85; for lanthanide ion catalysis, see e) S. Kobayashi, M. Sugiura, H. Kitagawa, W. W.-L. Lam, *Chem. Rev.* **2002**, 102, 2227.
- [12] N. Giuseppone, J.-M. Lehn, unpublished results.
- [13] The molecules in all structural formulas in Figures 2–5 are shown, for clarity, in a linear, extended representation rather than in the correct helical form.^[9]
- [14] In all our attempts involving crossover reactions, the use of the metallic salts $\text{Zn}(\text{BF}_4)_2 \cdot 8\text{H}_2\text{O}$ or $\text{Sc}(\text{OTf})_3$ avoided the degradation of the library constituents, whereas uncatalyzed and, to a larger extent, proton-catalyzed reactions always underwent extensive side reactions.
- [15] M. Ruben, J.-M. Lehn, G. Vaughan, *Chem. Commun.* **2003**, 1338.

A Unidirectional DNA Walker That Moves Autonomously along a Track**

Peng Yin, Hao Yan,* Xiaoju G. Daniell,
Andrew J. Turberfield,* and John H. Reif*

A major challenge in nanotechnology is to precisely transport a nanoscale object from one location on a nanostructure to another location along a designated path. The successful construction of self-assembled DNA nanostructures provides a solid structural foundation to meet this challenge. DNA, with its immense information-encoding capacity and well-defined Watson–Crick complementarity, has been explored as an excellent building material for nanoconstruction.^[1,2] In particular, recent years have seen remarkable success in the construction of both self-assembled nanostructures and individual nanomechanical devices. For example, one- and two-dimensional DNA lattices have been constructed from a rich set of branched DNA molecules.^[3–7] These DNA lattices could provide a platform for embedded DNA nanomechanical devices to perform the desired transportation. A diverse group of DNA nanomechanical devices have also been demonstrated. These include DNA nanodevices that execute cycles of motions, such as opening/closing,^[8–11] extension/contraction,^[12–14] and reversible rotation.^[15,16] Such DNA-based nanodevices can be cycled between well-defined states by means of external intervention, for example, by the sequential addition of DNA “fuel strands”^[8–10,12–14,16] or by changing the ionic composition of the solution.^[11,15] However, these devices are unsuitable for the above challenge for two reasons: First, they demonstrate only local conformation changes, rather than progressive motion. Second, they do not move autonomously. Various schemes of autonomous DNA walker devices based on DNA cleavage and ligation have been explored theoretically but not experimentally;^[17] these schemes have been limited to random bidirectional movement. The use of DNA hybridization as an energy source for autonomous molecular motors has also been proposed.^[18] The

[*] P. Yin, Prof. H. Yan, X. G. Daniell, Prof. J. H. Reif
Department of Computer Science
Duke University
Durham, NC 27708 (USA)
Fax: (+1) 919-660-6519
E-mail: hy1@cs.duke.edu
reif@cs.duke.edu

Prof. A. J. Turberfield
Department of Physics, Clarendon Laboratory
University of Oxford
Parks Road, Oxford OX1 3PU (UK)
Fax: (+44) 1-865-272
E-mail: a.turberfield@physics.ox.ac.uk

[**] This work was supported by a grant from the NSF (EIA-0218359) to H.Y. and J.H.R., by NSF ITR grants EIA-0086015 and CCR-0326157, and by DARPA/AFSOR Contract F30602-01-2-0561.



Supporting information for this article is available on the WWW under <http://www.angewandte.org> or from the author.

construction of a non-autonomous DNA biped walker device^[19] and autonomous DNA tweezers^[20] have been reported recently. The production of a DNA motor capable of autonomous, unidirectional, progressive linear translational motion is an important next step in the development of DNA-based molecular devices.

Herein we report the design and construction of an autonomous, unidirectional DNA motor that moves along a DNA track. The self-assembled track contains three anchorages at which the walker, a six-nucleotide DNA fragment, can be bound. At each step the walker is ligated to the next anchorage, then cut from the previous one by a restriction endonuclease. Each cut destroys the previous restriction site, and each ligation creates a new site, in such a way that the walker can not move backwards. The motor is powered by the hydrolysis of adenosine triphosphate (ATP), a kinetically inert fuel whose breakdown may be accelerated by many orders of magnitude by protein catalysts.^[21] The operation of the motor was verified by tracking the radioactively labeled walker by gel electrophoresis.

The autonomous, unidirectional, along-the-track motion demonstrated by this prototype system represents a novel type of motion for DNA-based nanomechanical devices. The motion of the walker can be extended in principle beyond three anchorages. Embedding a walking device of this kind in a DNA lattice would result in a nanorobotics lattice that could meet the challenge stated above: a nanoscale “walker” that moves autonomously along a designated path over a microscopic structure, thereby serving as a carrier of information and possibly even physical cargo, such as nanoparticles.

The structural design of the device is shown in Figure 1a. (Base sequences for all components are given in the Supporting Information). The track consists of three evenly spaced DNA double-helical “anchorages” (A, B, and C), each tethered to another DNA duplex segment, which forms part of the backbone of the track, by means of a four-nucleotide “hinge”. Each anchorage consists of 13 base pairs, with a three-nucleotide single-strand overhang (“sticky end”). Each anchorage is positioned three helical turns (31 or 32 base pairs) away from its nearest neighbors. The duplex segments of the backbone of the track and of the three anchorages are expected to behave like rigid rods, since they are much shorter than the persistence length of duplex DNA (greater than 10 turns).^[22,23] In contrast, the four-nucleotide single-strand hinge is expected to be flexible, since the persistence length of the single DNA strand is three nucleotides.^[24] A six-nucleotide DNA “walker”, labeled * and colored red, moves sequentially along the track from anchorage A to B, then to C.

The device was constructed by mixing stoichiometric amounts of purified DNA oligonucleotides in hybridization buffer (see Experimental Section) and slowly cooling the system from 90 to 37°C. The solution was then supplemented with T4 ligase, endonuclease PflM I, and endonuclease BstAP I and incubated at 37°C. The autonomous motion of the walker was initiated by the addition of the energy source ATP.

The recognition sites and restriction patterns of PflM I and BstAP I are shown in Figure 1b. Figure 1c shows the sequence of structural changes that occur during the motion

of the walker; on the right-hand side the base sequence at the end of each anchorage at each stage is shown, as well as how these base sequences are transformed by the action of enzymes. The motion of the walker depends on alternate enzymatic ligation and restriction (cleavage). Before the motion starts, the walker, whose position is indicated by *, resides at anchorage A, as shown in panel 0 of Figure 1c. In this state anchorages A* and B have complementary sticky ends, which can hybridize with each other. T4 ligase can then seal the nicks at each end of the newly hybridized section, thus joining the two anchorages covalently ($A^*+B \rightarrow A^*B$); this is an irreversible step that consumes energy provided by the hydrolysis of ATP. The ligation of A*B creates a recognition site for endonuclease PflM I. In process II, PflM I cleaves A*B in such a way that the walker moves to anchorage B: $A^*B \rightarrow A+B^*$. The sticky end of anchorage B* can then hybridize with the complementary sticky end of anchorage C, and the two anchorages are ligated to form B*C in process III. The ligation product B*C contains a recognition site for the second endonuclease BstAP I. In process IV, B*C is cleaved by BstAP I to regenerate anchorage B and create C*. Thus, the walker moves from anchorage B to C to complete the autonomous, programmed motion of the walker.

The motion of the walker is unidirectional: the product of ligation between two neighboring anchorages can only be cleaved such that the walker moves onto the downstream anchorage (A*B and B*C can only be cut such that the walker is left attached to B and C, respectively). Two idling steps are possible: B* can be religated to A and regenerated by restriction by PflM I; similarly, C* can be religated to B and regenerated by BstAP I. However, these idling steps neither reverse nor block the overall unidirectional motion of the walker. Once B* has been ligated to C the walker can never return to A.

The autonomous and unidirectional motion of the walker was verified by using denaturing polyacrylamide gel electrophoresis (PAGE) to track the motion of the walker, which was radioactively labeled. The position reached by the walker in the presence of different combinations of enzymes can be determined by measuring the size of the labeled DNA fragment. Figure 2a is a schematic drawing of the experimental design. The 5' end of the walker (red) was labeled with $\gamma\text{-P}^{32}$, represented by a red dot in Figure 2a. Initially, the labeled strand (part of A*) is 52 nucleotides long. The completion of processes I, II, III, and IV can be detected by the appearance of bands corresponding to radioactively labeled DNA fragments of 68, 19, 57, and 41 nucleotides, respectively. The appearance of these bands corresponds to the transfer of the radioactively labeled fragment between the anchorages along the track. The system was incubated at 37°C in hybridization buffer supplemented with ATP and bovine serum albumin (BSA) in the presence of different combinations of enzymes, which were added to the system simultaneously. Figure 2b is an autoradiograph of a denaturing gel which shows the products formed during each reaction. The system in lane 1 is the control reaction without an enzyme or ATP. In lane 2 T4 ligase and ATP are present: The walker is expected to complete process I to produce a radiolabeled strand of 68 nucleotides, thus corresponding to the formation

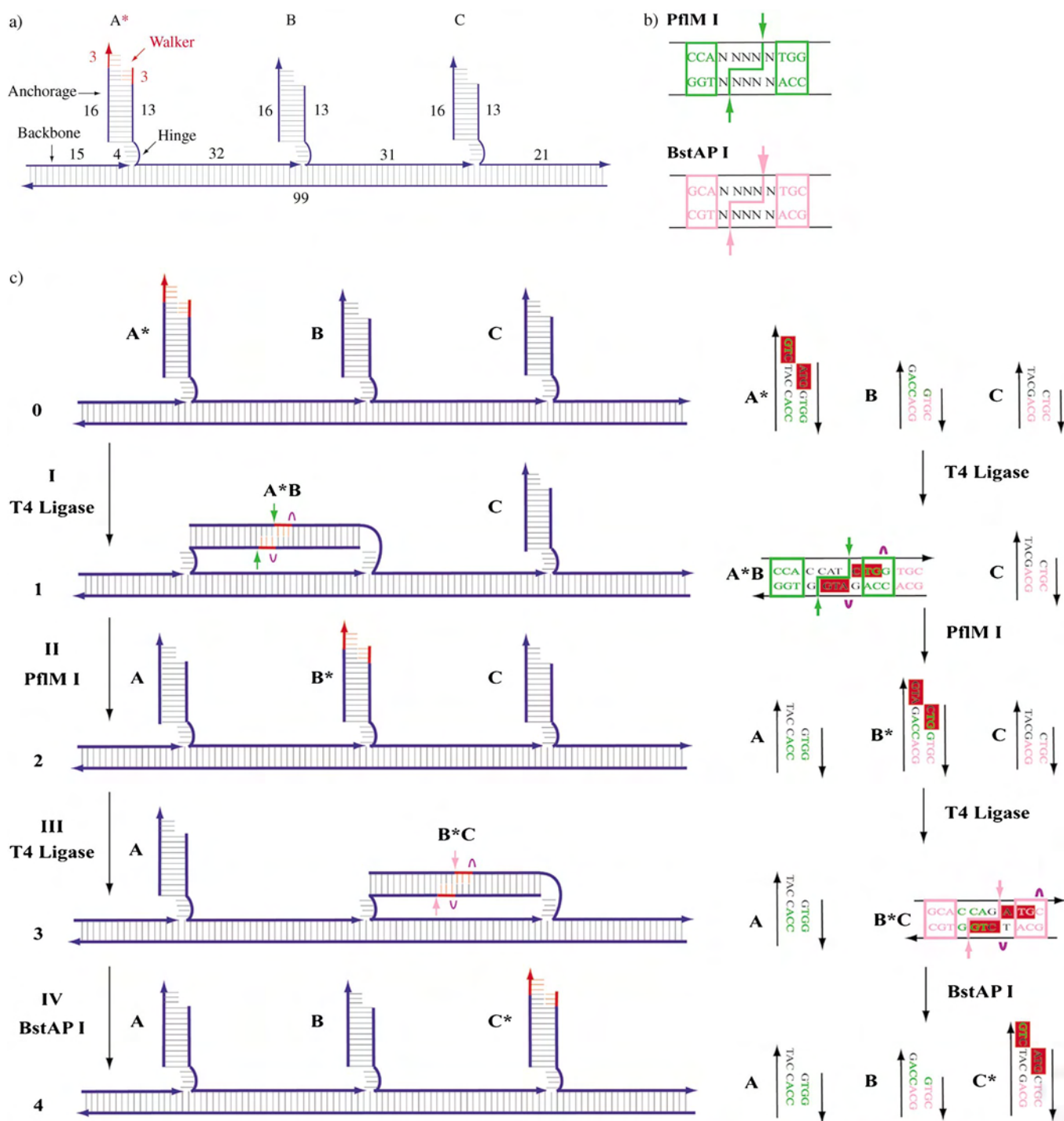


Figure 1. The structural design and operation of the autonomous unidirectional device. a) Structural design: The device contains two parts: the track and the walker. The track consists of three evenly spaced duplex-DNA anchorages, A, B, and C, each linked to the backbone by a hinge: a four-nucleotide flexible single-stranded DNA fragment. The walker is a six-nucleotide DNA fragment (colored red and indicated by *) initially positioned at anchorage A. The numbers give the lengths of DNA fragments in terms of the number of bases. b) Recognition sites and restriction patterns of PflM I and BstAP I: Green (pink) boxes indicate the recognition site of PflM I (BstAP I) and green (pink) arrows indicate their restriction sites. Bases that are important for PflM I (BstAP I) recognition are shown in bold green (pink) fonts. N indicates the position of a base that does not affect recognition. c) Operation of the device: The left-hand scheme shows the sequence of structural changes that occur during the operation of the device; the right-hand scheme describes the accompanying enzymatic reactions and shows how they affect the ends of the anchorages. Panel 0 depicts the device in its initial state. Process I is the ligation of anchorage A* and anchorage B, which have complementary sticky ends; purple curves indicate the ligation sites. Note that the ligation of A* with B creates a PflM I recognition site, which is indicated by green boxes in panel 1; the cuts made by this enzyme are indicated with two green arrows. In process II, the device is cleaved by PflM I, thus transferring the walker to anchorage B (panel 2). The new sticky end of B* is complementary to that of C. In process III, anchorage B* and anchorage C hybridize with each other, and are ligated by T4 ligase to create a recognition site for the endonuclease BstAP I. Purple curves in panel 3 indicate the ligation sites; pink boxes and arrows indicate the BstAP I recognition site and restriction pattern, respectively. In process IV, B*C is cleaved into B and C*, thus transferring the walker to anchorage C and completing the motion of the walker. The final product is shown in panel 4.

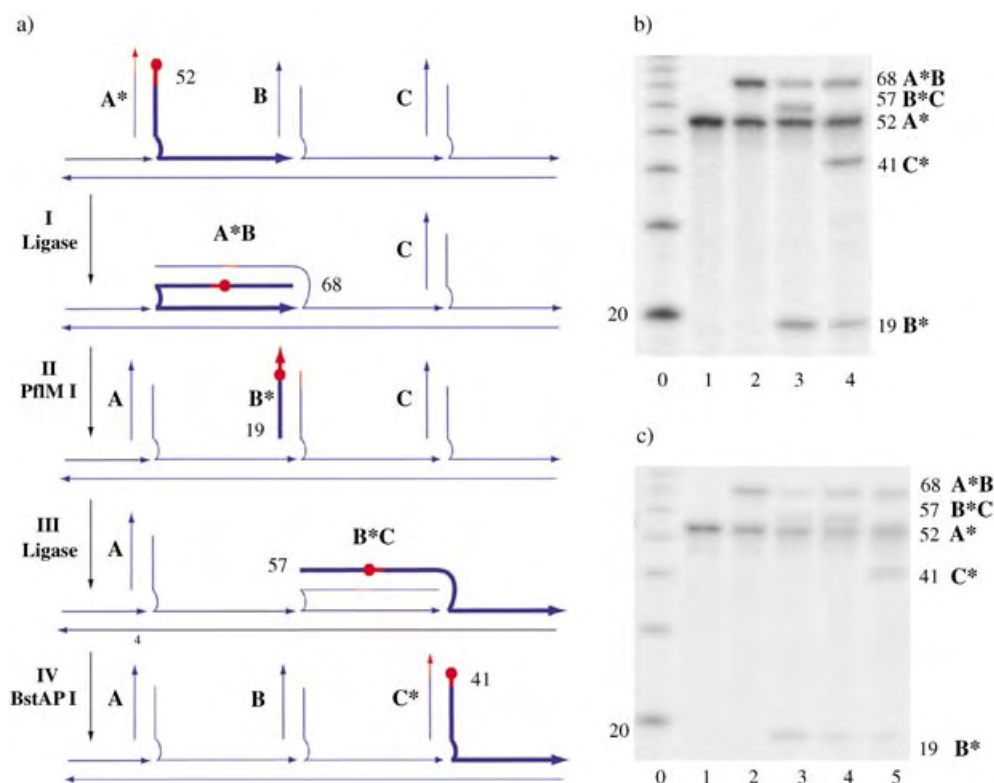


Figure 2. Evidence of the autonomous unidirectional motion of the walker. a) Experimental design: The six-nucleotide walker is colored red. The red dot indicates the radioactively labeled strand; at each stage the radioactively labeled strand is illustrated as a thickened line, with its length in terms of the number of bases shown near its 5' end. b) PAGE analysis of the autonomous motion of the walker. An autoradiograph of a 20% denaturing polyacrylamide gel identifies the position of the radioactively labeled walker. Lane 0: labeled 10-base-pair (bp) DNA ladder marker; lane 1: device with no enzyme (control); lanes 2–4: device with T4 ligase, ATP, and different combinations of the endonucleases PflM I and BstAP I (lane 2: no enzyme; lane 3: with PflM I; lane 4: with BstAP I and PflM I). c) PAGE analysis of the stepwise motion of the walker. Lane 0: labeled 10-bp DNA ladder marker; lane 1: device with no enzyme (control); lanes 2–5: samples corresponding to the stepwise completion of processes I, II, III, and IV in Figure 2a, respectively, as described in the text (lane 2: no enzyme; lane 3: with PflM I; lane 4: no enzyme; lane 5: with BstAP I). Oligonucleotide lengths (in numbers of bases) corresponding to DNA bands are indicated beside the gels.

of A*B. In lane 3 both T4 ligase and endonuclease PflM I are present: The walker is expected to be able to follow the reaction sequence shown in Figure 2a as far as the completion of process III. Upon the completion of process II, A*B is cut to produce A and B*, thus resulting in a labeled strand of 19 nucleotides. Subsequently, B* can be ligated to C to form B*C to give a strand of 57 nucleotides. (These stages in the motion of the walker were also observed in a time-course experiment; see the Supporting Information). In lane 4 all three enzymes are present: The walker is expected to be able to continue autonomously to the completion of process IV in which B*C is cleaved by BstAP I to generate C*, thus producing a labeled strand of 41 nucleotides. The radioactive bands in the gel shown in Figure 2b agree with all the above expectations and hence provide evidence for the designed autonomous, unidirectional motion of the walker.

To further test the operation of the system we forced the device to operate in a stepwise fashion (rather than autonomously) by adding and deactivating the enzymes sequentially. This experiment enabled us to inspect more closely the

products formed at the end of each process. The walker was radioactively labeled as described above. Figure 2c is an autoradiograph of a denaturing gel which shows the products after each step. The system was first supplemented with T4 ligase: The appearance of a band corresponding to a 68-nucleotide DNA fragment in lane 2 demonstrates the completion of process I and the formation of A*B. The solution was left at 37°C for one day to deactivate T4 ligase,^[a] then PflM I was added (lane 3). The band of 68 nucleotides, which corresponds to A*B, diminished, whereas a band of 19 nucleotides, which corresponds to B*, appeared, thus confirming the completion of process II. The system was then incubated at 37°C for two more days to deactivate PflM I,^[b] and was again supplemented with T4 ligase and ATP (lane 4). The intensity of the 19-nucleotide band corresponding to B* dramatically decreased, whereas the intensity of the 68-nucleotide band corresponding to A*B increased, and a 57-nucleotide band corre-

sponding to B*C also appeared. This is consistent with our expectation that B* can be ligated to both A and C. The formation of A*B is only an idling step in the motion of the walker. One more day later, after the enzymatic activity of T4 ligase had ceased, the addition of BstAP I resulted in the disappearance of the 57-nucleotide band and the appearance of a 41-nucleotide band, thus indicating the cleavage of B*C to B and C* (lane 5). The intensity of the 68-nucleotide band remained almost unchanged, which confirms that A*B is resistant to the restriction activity of BstAP I. These measurements provide further confirmation that the device operates as designed.

The unidirectional motion of the walker was also tested by the two control experiments depicted in Figure 3. In the first experiment, shown in Figure 3a,b, we intentionally con-

^[a] The half-life of T4 ligase at 37°C is approximately 4 h (New England Biolabs, unpublished observations).

^[b] The half-life of PflM I at 37°C is approximately 16 h (New England Biolabs, unpublished observations).

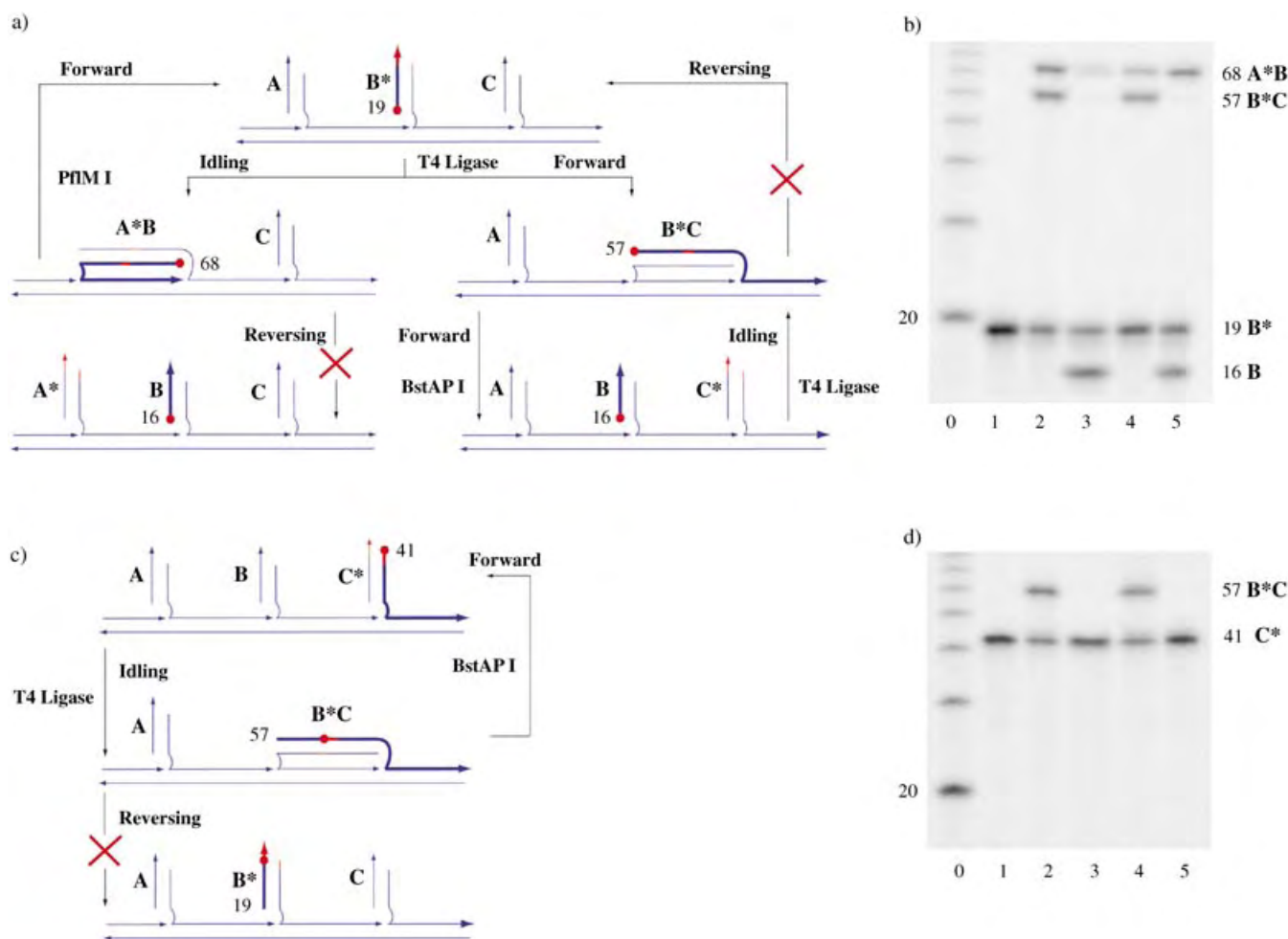


Figure 3. Control experiments. a) and c) show the design of control experiments in which the device is prepared with the walker (colored red) initially attached to anchorages B and C, respectively. Red dots indicate the γ -P³² label; the corresponding labeled strand is shown as a thickened line, with its length in number of bases shown near its 5' end. A red cross on a broken arrow means that the reaction indicated by that arrow is not expected to happen. b) and d) are autoradiographs of denaturing 20% PAGE gels that show the results of the experiments indicated in parts a) and c), respectively. b), d) Lane 0: labeled 10-bp DNA ladder marker; lane 1: device with no enzyme (control); lanes 2–5: device with T4 ligase, ATP, and different combinations of the endonucleases PflM I and BstAP I (lane 2: no enzyme; lane 3: with BstAP I and PflM I; lane 4: with PflM I; lane 5: with BstAP I). Oligonucleotide lengths (in numbers of bases) corresponding to DNA bands are indicated beside the gels.

structured the device such that the walker initially resides at anchorage B. Figure 3a shows the forward and idling processes that we expect to be allowed, and reverse processes that we expect to be forbidden. The 19-nucleotide strand B* was labeled with γ -P³² at its 5' end, as indicated by the red dot. Figure 3b shows the products generated upon the addition of different combinations of restriction enzymes and ligase. In the presence of T4 ligase (lane 2 of Figure 3b) the appearance of 68- and 57-nucleotide bands indicate the formation of A*B and B*C, respectively. The addition of BstAP I (lane 5), which is designed to cut B*C into B and C*, leads to a decrease in the intensity of the B*C band and to the generation of the 16-nucleotide fragment B, as expected. The addition of PflM I (lane 4), which is designed to cut A*B into A and B*, leads to a decrease in the intensity of the A*B band, but fragment B is not generated, again as expected. Lane 3 shows the case when all three enzymes are present.

In the second control experiment depicted in Figure 3c, the device was constructed with the walker initially at anchorage C. The 5' end of the 41-nucleotide strand of anchorage C* was labeled with γ -P³². In the presence of T4 ligase (lane 2 of Figure 3d), the appearance of a 57-nucleotide band indicated the formation of B*C as expected. Subsequent lanes, which correspond to different combinations of restriction enzymes and ligase, show that B*C can be restricted to B and C* by BstAP I as expected, but that no combination of enzymes leads to the reverse step B*C → B* + C (which would have been indicated by a 19-nucleotide labeled band corresponding to B*).

By measuring the intensities of the bands in Figure 2b we estimated the following yields for steps in the operation of the device: A* → A*B, 46%; A*B → B*C, 51%; B*C → C*, 97%. Both imprecise stoichiometry and low ligation/cleavage efficiency could cause low measured yields. Low enzymatic efficiencies might result from the steric constraints imposed

by the design of the motor; each substrate is created by hybridization of two anchorages, which are also linked by the backbone of the track. We are currently investigating design improvements, including structural modifications such as an increase in the length of the linkage between each anchorage and the backbone.

As the reactions described herein were carried out in solution, the possibility exists that the anchorages of two individual devices might interact with each other in such a way that the walker of one device might deviate from its designated track and move onto the track of another device. Through a control experiment described in the Supporting Information we have shown that under conditions corresponding to those under which the measurements described above were made, the linkage of two tracks is undetectable.

In summary, we have designed and constructed a nano-scale device in which an autonomous walker moves unidirectionally along a DNA track, driven by the hydrolysis of ATP. The motion of the walker can in principle be extended well beyond the three-anchorage system demonstrated herein.^[25] The discovery of new endonucleases with larger nonspecific spacing regions within their recognition sequences could lead to walkers of larger sizes. By encoding information into the walker and the anchorages, it should be possible to develop the device into a powerful autonomous computing device (and hence an “intelligent” robotics device).^[26]

Experimental Section

DNA sequences were designed and optimized with the SEQUIN software^[27] and are listed in the Supporting Information. DNA strands were synthesized commercially by Integrated DNA Technology, Inc. (www.idtdna.com) and purified by denaturing gel electrophoresis. The concentrations of DNA strands were determined by measurement of ultraviolet absorption at 260 nm. To assemble the track, the DNA strands were mixed stoichiometrically at 0.3 μM in hybridization buffer and incubated in a heating block from 90 to 37°C over a period of 3 h. NEB buffer purchased from New England Biolabs (www.neb.com) was used as the hybridization buffer: NEB 3 contains NaCl (100 mM), Tris-HCl (50 mM), MgCl_2 (10 mM), and dithiothreitol (1 mM, pH 7.7 at 37°C). Radioactive labeling: DNA strands were labeled with T4 polynucleotide kinase purchased from Invitrogen Inc. (www.invitrogen.com), by using the standard protocol recommended by the kinase kit. For the ligation experiments and cleavage by the endonucleases, a 30- μL solution containing 1 pmol of the assembled device was supplemented with BSA (100 $\mu\text{g mL}^{-1}$) and ATP (1 mM). 1 unit of T4 Ligase, 24 units of the endonuclease PflM I, and 5 units of the endonuclease BstAP I were added to the solution, followed by overnight incubation at 37°C. The endonucleases PflM I and BstAP I were purchased from New England Biolabs (www.neb.com). T4 ligase was purchased from Invitrogen Inc. (www.invitrogen.com). The reaction solution was NEB 3 buffer supplemented with BSA and ATP and containing NaCl (100 mM), Tris-HCl (50 mM), MgCl_2 (10 mM), dithiothreitol (1 mM, pH 7.7 at 37°C), BSA (100 $\mu\text{g mL}^{-1}$), and ATP (1 mM). The enzymatic reactions were carried out at 37°C. For denaturing gel electrophoresis, the mixture was heated at 90°C for 10 min, and applied to denaturing polyacrylamide gel. The positions of the radioactively labeled strands were detected by phosphor imaging. The relative concentrations of DNA

present in the bands were measured by using ImageQuant from Molecular Dynamics (www.mdyn.com).

Received: April 30, 2004

Published Online: August 30, 2004

Keywords: DNA · molecular devices · nanorobotics · nanostructures · self-assembly

- [1] N. C. Seeman, *Nature* **2003**, 421, 427–431.
- [2] C. M. Niemeyer, M. Adler, *Angew. Chem.* **2002**, 114, 3933–3937; *Angew. Chem. Int. Ed.* **2002**, 41, 3779–3783.
- [3] E. Winfree, F. Liu, L. A. Wenzler, N. C. Seeman, *Nature* **1998**, 394, 539–544.
- [4] C. Mao, W. Sun, N. C. Seeman, *J. Am. Chem. Soc.* **1999**, 121, 5437–5443.
- [5] T. H. LaBean, H. Yan, J. Kopatsch, F. Liu, E. Winfree, J. H. Reif, N. C. Seeman, *J. Am. Chem. Soc.* **2000**, 122, 1848–1860.
- [6] H. Yan, T. H. LaBean, L. Feng, J. H. Reif, *Proc. Natl. Acad. Sci. USA* **2003**, 100, 8103–8108.
- [7] H. Yan, S. H. Park, G. Finkelstein, J. H. Reif, T. H. LaBean, *Science* **2003**, 301, 1882–1884.
- [8] B. Yurke, A. J. Turberfield, A. P. Mills, Jr., F. C. Simmel, J. L. Neumann, *Nature* **2000**, 406, 605–608.
- [9] F. C. Simmel, B. Yurke, *Phys. Rev. E* **2001**, 63, 041913.
- [10] F. C. Simmel, B. Yurke, *Appl. Phys. Lett.* **2002**, 80, 883–885.
- [11] D. Liu, S. Balasubramanian, *Angew. Chem.* **2003**, 115, 5912–5914; *Angew. Chem. Int. Ed.* **2003**, 42, 5734–5736.
- [12] L. Feng, S. H. Park, J. H. Reif, H. Yan, *Angew. Chem.* **2003**, 115, 4478–4482; *Angew. Chem. Int. Ed.* **2003**, 42, 4342–4346.
- [13] P. Alberti, J.-L. Mergny, *Proc. Natl. Acad. Sci. USA* **2003**, 100, 1569–1573.
- [14] J. J. Li, W. Tan, *Nano Lett.* **2002**, 2, 315–318.
- [15] C. Mao, W. Sun, Z. Shen, N. C. Seeman, *Nature* **1999**, 397, 144–146.
- [16] H. Yan, X. Zhang, Z. Shen, N. C. Seeman, *Nature* **2002**, 415, 62–65.
- [17] J. H. Reif, *Lect. Notes Comput. Sci.* **2003**, 2568, 22–37.
- [18] A. J. Turberfield, J. C. Mitchell, B. Yurke, A. P. Mills, Jr., M. I. Blakey, F. C. Simmel, *Phys. Rev. Lett.* **2003**, 90, 118102.
- [19] W. B. Sherman, N. C. Seeman, *Nano Lett.* **2004**, in press.
- [20] Y. Chen, M. Wang, C. Mao, *Angew. Chem.* **2004**, 116, 3638–3641; *Angew. Chem. Int. Ed.* **2004**, 43, 3554–3557.
- [21] F. H. Westheimer, *Science* **1987**, 235, 1173–1178.
- [22] S. B. Smith, L. Finzi, C. Bustamante, *Science* **1992**, 258, 1122–1126.
- [23] G. S. Manning, *Biopolymers* **1981**, 20, 1751–1755.
- [24] S. B. Smith, Y. Cui, C. Bustamante, *Science* **1996**, 271, 795–799.
- [25] “Designs for Autonomous Unidirectional Walking DNA Devices”: P. Yin, A. J. Turberfield, J. H. Reif in *Tenth International Meeting on DNA Computing*, **2004**.
- [26] “Design for an Autonomous DNA Nanomechanical Device Capable of Universal Computation and Universal Translational Motion”: P. Yin, A. J. Turberfield, S. Sahu, J. H. Reif in *Tenth International Meeting on DNA Computing*, **2004**.
- [27] N. C. Seeman, *J. Biomol. Struct. Dyn.* **1990**, 8, 573–581.

Single-Molecule Magnets

Unusual Magnetic Metal–Cyanide Cubes of Re^{II} with Alternating Octahedral and Tetrahedral Corners**

Eric J. Schelter, Andrey V. Prosvirin, William M. Reiff, and Kim R. Dunbar*

The design of cyanide-bridged transition-metal clusters is one of the leading topics in the field of molecular magnetism.^[1] Two of the main reasons for this high interest are 1) cyanide chemistry easily lends itself to a building-block approach and 2) the nature (ferromagnetic versus antiferromagnetic) of magnetic exchange interactions through a linear cyanide ligand is largely predictable.^[2–4] These attributes have inspired numerous research groups to pursue the synthesis of high-spin, magnetically anisotropic metal cyanide molecules with the goal of engendering slow paramagnetic relaxation of the magnetization, a phenomenon that has been likened to the behavior of single-domain particles. This “superparamagnetic-like” magnetic behavior of molecules, commonly referred to as “single-molecule magnetism”,^[5–11] has been observed for paramagnetic clusters that exhibit a large spin ground state combined with an appreciable degree of anisotropy (i.e., a negative zero-field splitting parameter *D*).^[5,6,10,11] Single-molecule magnet (SMM) behavior was first noted over ten years ago for an {Mn₁₂} cluster of the oxide family,^[10,11] and many new examples of oxide-based SMMs have been prepared in the ensuing years.^[10,12] Progress in this area has been only incremental, however, in terms of raising the blocking temperature of the magnetization. One of the main reasons for this situation is that it is difficult to control the sign and magnitude of *D*. This limitation to realizing high-temperature SMMs is one of the focal points of research in the field.

One approach to increasing the magnetic anisotropy of paramagnetic clusters is to incorporate heavier transition elements, such as 5d metal ions, which exhibit strong spin-orbit coupling effects that can induce anisotropic magnetic-

exchange interactions.^[7,13–17] In this vein, we have been investigating the use of the paramagnetic Re^{II} anion complex [Re^{II}(triphos)(CN)₃][−] (triphos = 1,1,1-tris(diphenylphosphanyl)methyl)ethane) as a building block for high nuclearity clusters with unusual magnetic properties.^[18] As a backdrop for these studies, we undertook a full investigation of the magnetic behavior and theoretical modeling of [Et₄N][Re^{II}(triphos)(CN)₃][−], which revealed that the compound exhibits an unusually strong temperature-independent paramagnetism due to spin-orbit coupling of the *S* = 1/2 ground state and low-lying excited states.^[19–21] Given these intriguing findings, we proceeded to explore reactions of [Re^{II}(triphos)(CN)₃][−] with complementary building blocks including MCl₂ reagents (M = 3d metal ion). The results of these studies with Fe^{II} and Co^{II} chlorides are reported herein.

Single-crystal X-ray studies revealed the products to be distorted molecular cubes composed of both six- and four-coordinate vertices (Figure 1).^[22] The triphos ligands act as

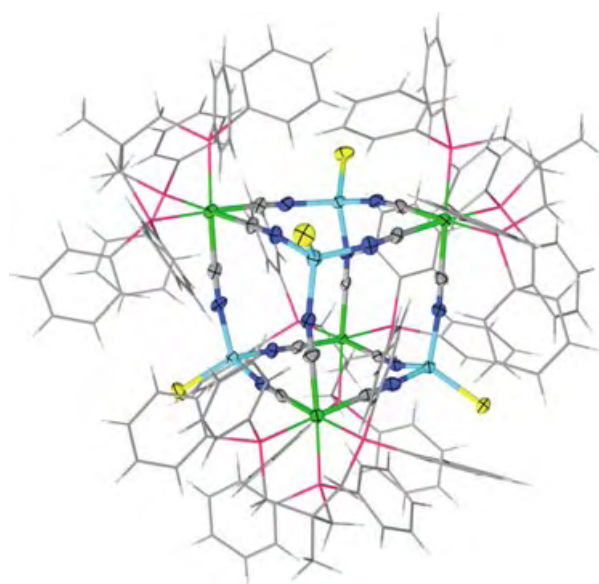


Figure 1. Thermal ellipsoid plot of [CoCl]₄[Re(triphos)(CN)₃]₄. Ellipsoids of the central core are drawn at the 50% probability level. The remaining atoms are depicted in stick mode for the sake of clarity.

facial-capping ligands for the Re^{II} centers, as expected, and a single chloride ligand completes the coordination spheres of the four 3d metal ions, which are in four-coordinate distorted tetrahedral environments. The steric demand of the triphos ligands, illustrated in the space filling diagrams in Figure 2, is clearly responsible for the lower coordination number of the Fe and Co centers in these compounds.^[23–25]

Relevant metal–ligand bond lengths and angles in [FeCl]₄[Re(triphos)(CN)₃]₄ (**1**) and [CoCl]₄[Re(triphos)(CN)₃]₄ (**2**) reveal subtle differences in the two molecular structures. The N–Fe–N angles in **1** range from 103.9(7)–108.2(8)° and the N–Fe–Cl angles range from 111.1(6)–113.9(7)°. The N–Co–N angles in **2** are slightly more acute than those in **1**, ranging from 101.9(3)–105.8(3)°; the N–Co–Cl angles are in the range 112.3(2)–

[*] E. J. Schelter, A. V. Prosvirin, K. R. Dunbar
Department of Chemistry
Texas A&M University
P.O. Box 30012, College Station, TX 77842-3012 (USA)
Fax: (+1) 979-845-7177
E-mail: dunbar@mail.chem.tamu.edu
W. M. Reiff
Department of Chemistry and Chemical Biology
Northeastern University
102 Hurtig Hall, 360 Huntington Ave., Boston, MA 02115 (USA)

[**] K. R. D. gratefully acknowledges the Department of Energy (DE-FG03-02ER45999), the National Science Foundation (NIRT-NSF DMR-0103455), the Welch Foundation A1449, and Texas A&M University (TITF) for funding of this research. The SMART CCD diffractometer and the SQUID magnetometer were purchased by funds provided by the National Science Foundation (Grants NSF-9807975 and NSF-9974899).

Supporting information for this article is available on the WWW under <http://www.angewandte.org> or from the author.

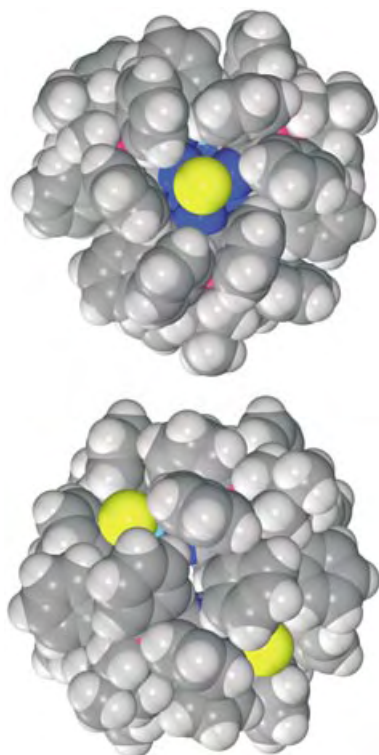


Figure 2. Space filling diagram for $[\{\text{CoCl}\}_4\{\text{Re}(\text{triphos})(\text{CN})_3\}_4]$ illustrating the high steric demand of the tripfos ligands. Top: View along Fe–Cl vector (pseudo- C_3 -axis of cube). Bottom: Side view of cube face.

116.1(2)°. In both structures, the fact that the N–M–N angles are $> 90^\circ$ is compensated by deviations of the CN^- ligands from linearity (Re–C≡N angles range from 169.3(18)–177(2)° and 175.0(8)–179.3(10)°; M–N≡C angles range from 163.3(18)–174.3(16)° and 165.4(8)–174.1(8)° in **1** and **2** respectively).

Infrared spectroscopy performed on polycrystalline samples of **1** and **2** as Nujol mulls revealed the presence of two sharp, intense $\nu_{(\text{C}\equiv\text{N})}$ stretches located at 2011 and 1992 cm^{-1} in **1** and 2111 and 2096 cm^{-1} in **2**. The $\nu_{(\text{C}\equiv\text{N})}$ modes in **1** are shifted by -49 and -78 cm^{-1} from the starting material (2060, 2070 cm^{-1}),^[18] whereas the $\nu_{(\text{C}\equiv\text{N})}$ stretching bands in **2** are shifted by $+51$ and $+26$ cm^{-1} respectively. Typically, CN stretches shift to higher energies in going from a terminal to bridging mode, so it was initially puzzling that compound **1** exhibited anomalous behavior. These differences can be explained, however, on the basis of different oxidation states for the Re ion in **1** and **2**. Far-infrared spectroscopy performed on **1** revealed a feature at 354 cm^{-1} that is consistent with a $\nu_{\text{Fe–Cl}}$ stretching mode for a ferric iron, and Mössbauer spectra at 4, 77, and 298 K indicate the presence of a single iron species, namely a high-spin Fe^{III} nucleus ($\delta = 0.43$ mm s^{-1} and $\Delta E = 0.53$ mm s^{-1} , Figure 3). These data indicate that the Fe^{II} ions have become oxidized in the course of the reaction, and, since there are no counterions in the crystals of **1**, one must assign the oxidation state of Re in the cluster as Re^{I} . This conclusion is substantiated by the electrochemical properties of $[\text{Et}_4\text{N}][\text{Re}(\text{triphos})(\text{CN})_3]$ which reveal an accessible, reversible $\text{Re}^{\text{II}} \rightarrow \text{Re}^{\text{I}}$ reduction process at $E_{1/2} = -0.74$ V

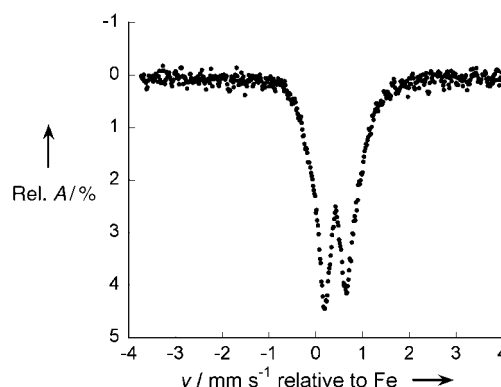


Figure 3. Mössbauer spectrum of $[\{\text{FeCl}\}_4\{\text{Re}(\text{triphos})(\text{CN})_3\}_4]$ at 77.5 K. The Quadrupole doublet indicates rapidly relaxing high-spin Fe^{III} center with $\delta = 0.43$ mm s^{-1} and $\Delta E = 0.53$ mm s^{-1} ; (Rel. A is the relative absorbance; v is velocity).

(dissolved in acetonitrile, versus Ag/AgCl).^[18] Moreover, there is a general contraction of Re–L bond lengths in **1** as compared to **2**, in accord with the presence of the Re^{I} ion, which can engage in stronger π -bonding interactions with the cyanide and phosphine ligands. The assignment of an $\text{Re}^{\text{I}}\text{–Fe}^{\text{III}}$ ground state is consistent with the shifted energies of the $\nu_{(\text{C}\equiv\text{N})}$ modes in the infrared spectra of the compounds, as it is well-known that these bands are sensitive to metal oxidation states.

Magnetization measurements were performed on **1** and **2** from $T = 2$ –300 K. The $\chi_m T$ versus T plot for **1** shows a room-temperature value of 14.72 emu K mol^{-1} (10.85 μ_B) and a low-temperature value of 1.45 emu K mol^{-1} (3.41 μ_B ; Figure 4).

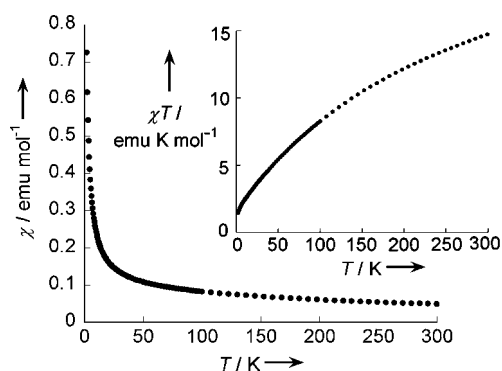


Figure 4. Temperature dependence of the magnetic susceptibility (χ_m) for $[\{\text{FeCl}\}_4\{\text{Re}(\text{triphos})(\text{CN})_3\}_4]$ (**1**). Inset shows $\chi_m T$ versus T .

The value of 14.72 emu K mol^{-1} is slightly low for four, non-interacting $S = 5/2$ Fe^{III} centers, (3.68 emu K mol^{-1} (5.43 μ_B) per Fe^{III} and low-spin, d^6 Re^{I} ions, which contribute only TIP).^[26] The calculated moment per Fe^{III} center continues to approach the spin-only value of 5.92 μ_B with increasing temperature, attaining a value of 5.60 μ_B at the limit of the experiment ≈ 350 K. Attempts to apply a simple model to the $\chi_m T$ versus T data that involved a combination of a small zero-field splitting parameter and weak next-nearest neighbor

interactions^[9] did not entirely reproduce the gradual slope of $\chi_m T$, but the data are reproducible for pure batches of crystals, thereby ruling out the presence of impurities. Further efforts are underway to develop a model for this system that accounts for the behavior of **1** over the entire temperature range.

In the case of compound **2**, the $\chi_m T$ versus T plot exhibits a high temperature product of 13.92 emu K mol⁻¹ (10.55 μ_B) and a low temperature product of 0.58 emu K mol⁻¹ (2.15 μ_B ; Figure 5). If the contribution of the Re^{II} centers at 300 K is

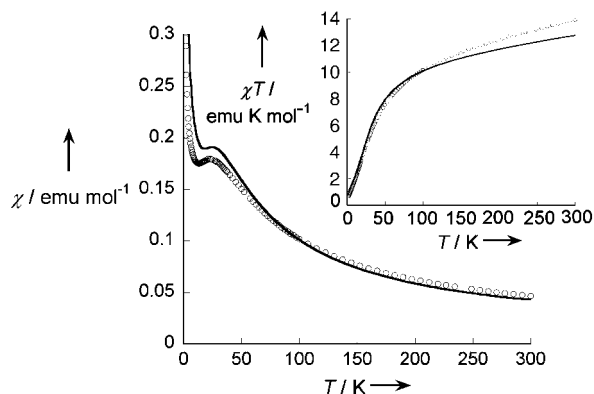


Figure 5. Temperature dependence of the magnetic susceptibility of $[\text{CoCl}_4][\text{Re}(\text{triphos})(\text{CN})_3]$ (**2**) and that of the model (solid line). Inset shows $\chi_m T$ vs T with that of the model (solid line). The model breaks down at higher temperatures due to the temperature dependence of the g value of the Co^{II} ions arising from zero-field splitting.

taken to be 0.63 emu K mol⁻¹ or 2.29 μ_B (the value of the parent compound $[\text{Et}_4\text{N}][\text{Re}(\text{triphos})(\text{CN})_3]$,^[18] one obtains a $\chi_m T$ value of 2.85 emu K mol⁻¹ (4.77 μ_B) for each Co^{II} ion, in accord with tetrahedral Co^{II} ($S=3/2$) and a typical orbital contribution.^[25] The χ_m versus T plot increases as the temperature is lowered until 21 K, after which temperature the value decreases before rapidly increasing again at 12 K. The $\chi_m T$ versus T data for **2** descends over the whole temperature range and approaches zero at low temperatures.

The magnetic data for **2** can be rationalized in terms of the well-described behavior of the 4A_2 ground state of the tetrahedral Co^{II} ion.^[27] Zero-field splitting of this ion ($\approx |7-15| \text{ cm}^{-1}$)^[27,28] leads to an effective spin $S'=1/2$ for the Co^{II} ion at low temperatures. The fact that both Re^{II} and Co^{II} ions in **2** are magnetically anisotropic poses a formidable challenge for the simulation of the magnetic behavior. A model for the magnetic susceptibility was developed by using MAGPACK (ANIMAG2),^[29] which accounts for the most influential factors on the susceptibility of **2**, namely, the zero-field splitting of the Co^{II} ions, the anisotropic g factors of the Co^{II} ions, and their anisotropic magnetic exchange. The data were reproduced by using an Ising exchange model and assumptions were made to limit the number of fitting parameters. The g values for the Re^{II} ion were set at $g_{\parallel}=2.4$ and $g_{\perp}=0.7$, values previously established by the $j-j$ coupling scheme developed for $[\text{Re}(\text{triphos})(\text{CN})_3]^-$.^[20] The best fit to the low-temperature data ($<40 \text{ K}$)^[30] was obtained for Co^{II} ion g values of $g'_{\parallel}=2.7$ and $g'_{\perp}=1.2$,^[31-34] $D_{\text{Co}}=-15 \text{ cm}^{-1}$ and $J_z=-5.5 \text{ cm}^{-1}$ (Figure 5).^[35] Most importantly, the model predicts

the maximum in χ_m vs T reasonably well. Additional work is currently underway to experimentally establish g and D values from EPR studies to further refine the model.

The results of this study demonstrate that the anion $[\text{Re}(\text{triphos})(\text{CN})_3]^-$ is a useful precursor for the high-yield self-assembly of unusual metal cyanide cubes in which four-coordinate pseudotetrahedral metal ions occupy four of the vertices of the cube along with the six-coordinate Re^{II} corners. The reaction with FeCl_2 led to a redox reaction to produce a cluster consisting of Re^I and high-spin Fe^{III} ions, a result that underscores the fact that choices of metal ions to combine with $[\text{Re}(\text{triphos})(\text{CN})_3]^-$ will need to be guided by a knowledge of their oxidation potentials. The combination of Re^{II} ($S=1/2$) and Co^{II} ($S=3/2$) in **2** leads to complex magnetic behavior dominated by the anisotropy of the ions as expected. In an effort to generalize this chemistry, we have also explored reactions of the divalent chlorides of Mn, Ni, Cu, Zn and crystallized analogous cubes in all cases. These preliminary results combined with the present studies constitute a family of homologous clusters whose comparative magnetic properties is expected to lend valuable insight into the parameters that affect the behavior, especially the large magnetic anisotropy of the Re^{II} ion.

Experimental Section

Synthesis of $[\text{FeCl}_4][\text{Re}(\text{triphos})(\text{CN})_3]$ (**1**): $[\text{Et}_4\text{N}][\text{Re}(\text{triphos})(\text{CN})_3]$ (0.080 g, 0.078 mmol) was dissolved in 5 mL of dry CH_3CN and treated with $\text{FeCl}_4(\text{thf})_6$ ^[36] (0.032 g, 0.034 mmol in 4 mL of CH_3CN and 1 mL of Et_2O) which produced a change from yellow to an intense blue. A crystalline blue sample was harvested after 18 h and washed with CH_3CN followed by Et_2O and air-dried. Yield: 0.053 g (63%). The synthesis of **2** (intense green) is identical to that of **1** except that the CH_3CN washings were minimized due to the higher solubility of **2** in CH_3CN . X-ray quality single crystals of **1** and **2** were obtained by layering CH_3CN solutions of the Re^{II} compound with $\text{CH}_3\text{CN}/\text{Et}_2\text{O}$ (9:1 v/v) solutions of MCl_2 . Elemental analysis calcd for **1**, $\text{C}_{176}\text{H}_{156}\text{N}_{12}\text{Cl}_4\text{P}_{12}\text{Fe}_4\text{Re}_4$: C 53.91, H 4.01, N 4.23, Cl 3.62; found: C 53.52, H 4.12, N 4.19, Cl 3.52. Elemental analysis calcd for **2**, $\text{C}_{176}\text{H}_{156}\text{N}_{12}\text{Cl}_4\text{P}_{12}\text{Co}_4\text{Re}_4$: C 53.74, H 4.00, N 4.27, Cl 3.61; found: C 53.89, H 4.16, N 4.12, Cl 3.58. IR (Nujol) for **1**: $\tilde{\nu}=2011, 1992 \text{ cm}^{-1}$ ($\text{C}\equiv\text{N}$); **2**: $\tilde{\nu}=2111, 2096 \text{ cm}^{-1}$ ($\text{C}\equiv\text{N}$). Mössbauer (77.5 K): **1**: $\delta=0.43 \text{ mms}^{-1}$ (relative to RT Fe), $\Delta E=0.53 \text{ mms}^{-1}$. DC magnetic susceptibility measurements were performed on microcrystalline samples of **1** and **2** with the use of a Quantum Design MPMS-2 SQUID magnetometer operating in the temperature range of 2–300 K at 0.1 T. Diamagnetic corrections were made with the use of Pascal's constants.

Received: May 10, 2004

Keywords: cage compounds · cluster compounds · cyanides · magnetic properties · rhenium

- [1] K. R. Dunbar, R. A. Heintz, *Prog. Inorg. Chem.* **1997**, 45, 283–391.
- [2] S. M. Holmes, G. S. Girolami, *J. Am. Chem. Soc.* **1999**, 121, 5593–5594.
- [3] W. R. Entley, G. S. Girolami, *Science* **1995**, 268, 397–400.
- [4] T. Mallah, S. Thiebaut, M. Verdaguer, P. Veillet, *Science* **1993**, 262, 1554–1557.

- [5] C. P. Berlinguette, D. Vaughn, C. Canada-Vilalta, J. R. Galan-Mascaros, K. R. Dunbar, *Angew. Chem.* **2003**, *115*, 1561–1564; *Angew. Chem. Int. Ed.* **2003**, *42*, 1523–1526.
- [6] J. J. Sokol, A. G. Hee, J. R. Long, *J. Am. Chem. Soc.* **2002**, *124*, 7656–7657.
- [7] F. Bonadio, M. Gross, H. Stoeckli-Evans, S. Decurtins, *Inorg. Chem.* **2002**, *41*, 5891–5896.
- [8] Z. J. Zhong, H. Seino, Y. Mizobe, M. Hidai, A. Fujishima, S. i. Ohkoshi, K. Hashimoto, *J. Am. Chem. Soc.* **2000**, *122*, 2952–2953.
- [9] V. Marvaud, C. Decroix, A. Scullier, F. Tuyeras, C. Guyard-Duhayon, J. Vaissermann, M. Marrot, F. Gonnet, M. Verdager, *Chem. Eur. J.* **2003**, *9*, 1692–1705.
- [10] D. Gatteschi, R. Sessoli, *Angew. Chem.* **2003**, *115*, 278–309; *Angew. Chem. Int. Ed.* **2003**, *42*, 268–297.
- [11] R. Sessoli, H. L. Tsai, A. R. Schake, S. Wang, J. B. Vincent, K. Folting, D. Gatteschi, G. Christou, D. N. Hendrickson, *J. Am. Chem. Soc.* **1993**, *115*, 1804–1816.
- [12] A. J. Tasiopoulos, A. Vinslava, W. Wernsdorfer, K. A. Abboud, G. Christou, *Angew. Chem.* **2004**, *116*, 2169–2173; *Angew. Chem. Int. Ed.* **2004**, *43*, 2117–2121.
- [13] O. Kahn, J. Larionova, L. Ouahab, *Chem. Commun.* **1999**, 945–952.
- [14] V. S. Mironov, L. F. Chibotaru, A. Ceulemans, *J. Am. Chem. Soc.* **2003**, *125*, 9750–9760.
- [15] S. Tanase, F. Tuna, P. Guionneau, T. Maris, G. Rombaut, C. Mathoniere, M. Andruh, O. Kahn, J. P. Sutter, *Inorg. Chem.* **2003**, *42*, 1625–1631.
- [16] R. Podgajny, C. Desplanches, B. Sieklucka, R. Sessoli, V. Villar, C. Paulsen, W. Wernsdorfer, Y. Dromzee, M. Verdager, *Inorg. Chem.* **2002**, *41*, 1323–1327.
- [17] J. Larionova, R. Clerac, B. Donnadieu, S. Willemin, C. Guerin, *Cryst. Growth Des.* **2003**, *3*, 267–272.
- [18] E. J. Schelter, J. K. Bera, J. Bacsá, J. R. Galan-Mascaros, K. R. Dunbar, *Inorg. Chem.* **2003**, *42*, 4256–4258.
- [19] K. R. Dunbar, E. J. Schelter, B. S. Tsukerblat, S. M. Ostrovsky, V. Y. Mirovitsky, A. V. Palii, *Polyhedron* **2003**, *22*, 2545–2556.
- [20] K. R. Dunbar, E. J. Schelter, A. V. Palii, S. M. Ostrovsky, V. Y. Mirovitskii, J. M. Hudson, M. A. Omary, S. I. Klokishner, B. S. Tsukerblat, *J. Phys. Chem. A* **2003**, *107*, 11102–11111.
- [21] K. R. Dunbar, E. J. Schelter, B. S. Tsukerblat, A. V. Palii, S. M. Ostrovsky, V. Y. Mirovitskii, S. I. Klokishner, *Adv. Quantum Chem.* **2003**, *44*, 413–428.
- [22] Crystal data for $[\text{FeCl}]_4[\text{Re}(\text{triphos})(\text{CN})_3]_4 \cdot 6.5 \text{CH}_3\text{CN}$ (**1**): $\text{C}_{189}\text{H}_{174.75}\text{Cl}_4\text{Fe}_4\text{N}_{18.50}\text{P}_{12}\text{Re}_4$, $M_r = 4186.86$, monoclinic, $C2/c$ (No. 15), $a = 66.829(19)$, $b = 18.811(5)$, $c = 32.575(9)$ Å, $\beta = 106.957(8)^\circ$, $V = 39170(19)$ Å³, $Z = 8$, $\rho_{\text{calc}} = 1.420 \text{ g cm}^{-3}$, $\mu = 2.954 \text{ mm}^{-1}$, 94524 reflections (33330 unique) to $2\theta = 49.42^\circ$, 1831 variables, $R = 0.1258$, $wR(F_o^2) = 0.2838$ [19686 data, $I > 2\sigma(I)$], $\text{GooF} = 1.108$. Crystal data for $[\text{CoCl}]_4[\text{Re}(\text{triphos})(\text{CN})_3]_4 \cdot 8.5 \text{CH}_3\text{CN} \cdot 0.5 \text{THF}$ (**2**): $\text{C}_{195}\text{H}_{184.75}\text{Cl}_4\text{Co}_4\text{N}_{20.50}\text{O}_{0.50}\text{P}_{12}\text{Re}_4$, $M_r = 4317.34$, monoclinic, $C2/c$ (No. 15), $a = 66.803(13)$, $b = 18.839(4)$, $c = 32.491(7)$ Å, $\beta = 106.62(3)^\circ$, $V = 39182(14)$ Å³, $Z = 8$, $\rho_{\text{calc}} = 1.464 \text{ g cm}^{-3}$, $\mu = 2.998 \text{ mm}^{-1}$, 141634 reflections (33382 unique) to $2\theta = 49.42^\circ$, 2089 variables, $R = 0.0648$, $wR(F_o^2) = 0.1520$ [27521 data, $I > 2\sigma(I)$], $\text{GooF} = 1.180$. X-ray data were measured at 110(2) K on a Siemens SMART CCD diffractometer with graphite monochromated $\text{MoK}\alpha$ ($\lambda_\alpha = 0.71073$ Å) radiation. Structures **1** and **2** were solved and refined using SHELX97 (G. M. Sheldrick, SHELXL97, Program for the Refinement of Crystal Structures, University of Göttingen, Germany, 1997) with the graphical interface X-SEED (L. J. Barbour, X-Seed, Graphical interface to SHELX-97 and POV-Ray, 1999). CCDC 241395 & 241396 (**1** and **2**) contain the supplementary crystallographic data for this paper. These data can be obtained free of charge via www.ccdc.cam.ac.uk/conts/retrieving.html (or from the Cambridge Crystallographic Data Centre, 12 Union Road, Cambridge CB2 1EZ, UK; fax: (+44) 1223-336-033; or deposit@ccdc.cam.ac.uk).
- [23] N. G. Connelly, O. M. Hicks, G. R. Lewis, A. G. Orpen, A. J. Wood, *Dalton* **2000**, 1637–1643.
- [24] V. Jacob, S. Mann, G. Huttner, O. Walter, L. Zsolnai, E. Kaifer, P. Rutsch, P. Kircher, E. Bill, *Eur. J. Inorg. Chem.* **2001**, 2625–2640.
- [25] M. Fritz, D. Rieger, E. Baer, G. Beck, J. Fuchs, G. Holzmann, W. P. Fehlhammer, *Inorg. Chim. Acta* **1992**, *198–200*, 513–526.
- [26] F. A. Cotton, G. Wilkinson, M. Bochmann, C. Murillo, *Advanced Inorganic Chemistry*, 6th ed., Wiley, New York **1998**.
- [27] R. L. Carlin, *Science* **1985**, *227*, 1291–1295.
- [28] J. Krzystek, S. A. Zvyagin, A. Ozarowski, A. T. Fiedler, T. C. Brunold, J. Telser, *J. Am. Chem. Soc.* **2004**, *126*, 2148–2155.
- [29] J. J. Borrás-Almenar, J. M. Clemente-Juan, E. Coronado, B. S. Tsukerblat, *J. Comput. Chem.* **2001**, *22*, 985–991.
- [30] At higher temperatures the system can no longer can be treated as an effective spin $S' = 1/2$, and the population of excited states is expected to lead to very different g values for the Co^{II} ion.
- [31] R. P. Stapele, H. G. Beljers, P. F. Bongers, H. Zijlstra, *J. Chem. Phys.* **1965**, *44*, 3719–3725.
- [32] H. G. Beljers, P. F. Bongers, R. P. van Stapele, H. Zijlstra, *Phys. Lett.* **1964**, *12*, 81–82.
- [33] N. Pelletier-Allard, *C. R. Hebd. Seances Acad. Sci.* **1964**, *258*, 1215–1218.
- [34] N. Pelletier-Allard, *C. R. Hebd. Seances Acad. Sci.* **1964**, *259*, 2999–3002.
- [35] Plots of the model of the temperature dependent anisotropic susceptibilities of **2** are provided as supporting information.
- [36] H. Zhao, R. Clerac, J. S. Sun, X. Ouyang, J. M. Clemente-Juan, C. J. Gomez-Garcia, E. Coronado, K. R. Dunbar, *J. Solid State Chem.* **2001**, *159*, 281–292.

Inclusion Compounds

One-Pot Optical Resolution of Oligopeptide Helices through Artificial Peptide Bundling

Yan-Ming Guo, Hideaki Oike, Naoko Saeki, and Takuzo Aida**

Molecular recognition through helix–helix interactions is an interesting subject in relation to biologically important peptide bundling.^[1] Although the design of peptide bundling

[*] Dr. Y.-M. Guo, Dr. H. Oike, N. Saeki, Prof. T. Aida
Aida Nanospace Project
Exploratory Research for Advanced Technology (ERATO)
Japan Science and Technology Agency (JST)
2-41 Aomi, Koto-ku, Tokyo 135-0064 (Japan)
Fax: (+81) 3-3570-9183
E-mail: oike@nanospace.miraikan.jst.go.jp

Prof. T. Aida
Department of Chemistry and Biotechnology
School of Engineering
The University of Tokyo
7-3-1 Hongo, Bunkyo-ku, Tokyo 113-8656 (Japan)
Fax: (+81) 3-5841-7310
E-mail: aida@macro.t.u-tokyo.ac.jp



Supporting information for this article is available on the WWW under <http://www.angewandte.org> or from the author.

(coiled-coil) based on natural peptide motifs has been studied extensively,^[2–4] secondary structure recognition between helical macromolecules has never been utilized in artificial host–guest chemistry for the one-pot separation of right- and left-handed helices in solution.^[5,6] Herein, we report the first example of one-pot optical resolution of helical oligopeptides (*rac*-**2** and *rac*-**3**) through stereoselective helix bundling by using a cyclodimeric zinc porphyrin host **1** bearing a guest-binding chiral cavity with two helical peptidic units (Figure 1).

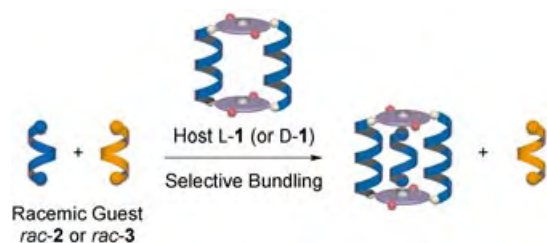
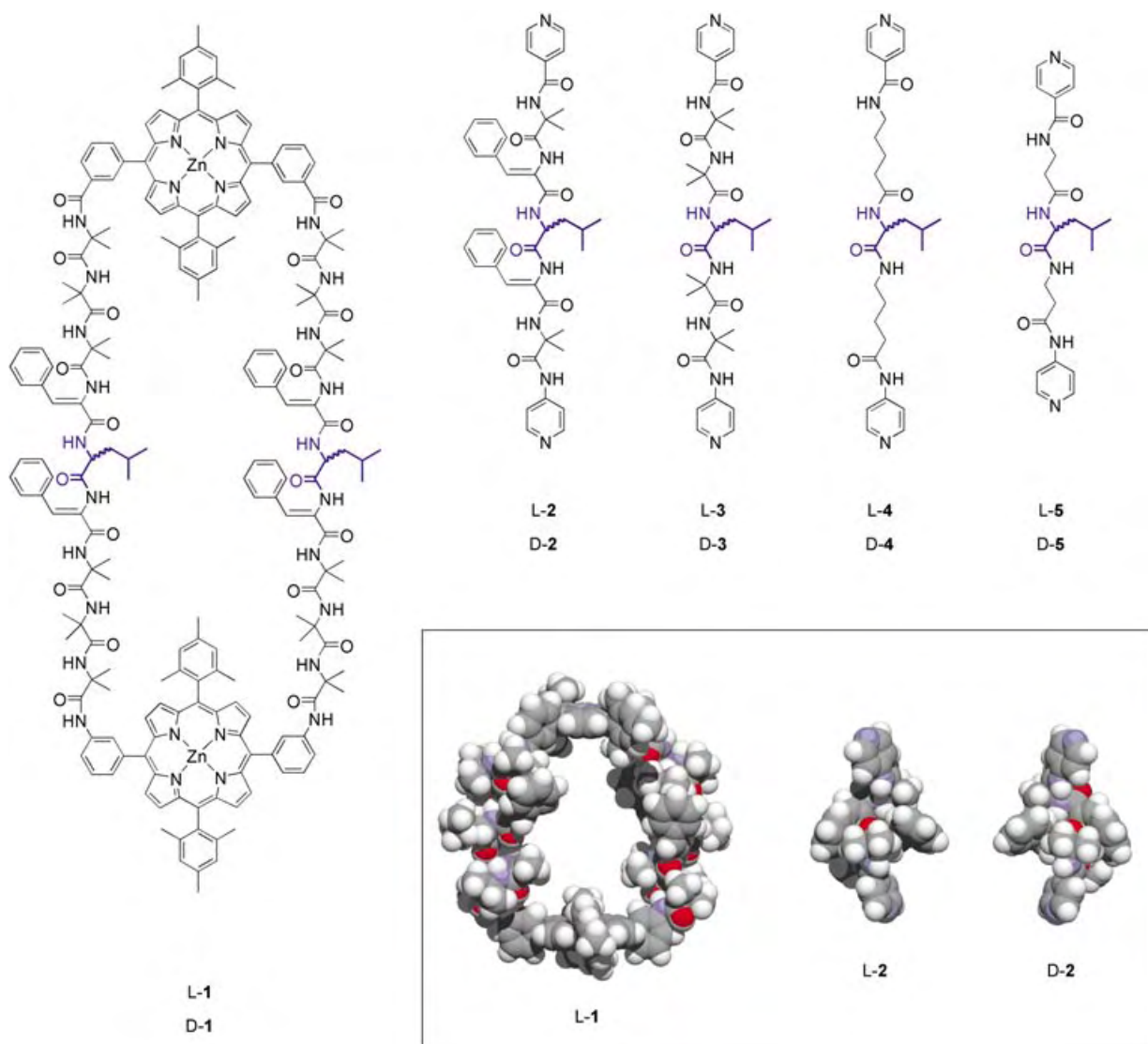


Figure 1. Schematic representation of helix-sense-selective host–guest complexation.

The oligopeptide parts in compounds **1–3** contain α -aminoisobutyric acid (Aib) units (Scheme 1).^[7] Poly(Aib) is known to adopt a dynamic helical structure, which switches back and forth between right- and left-handed conformations.^[8] Recently, we have found that a cyclodimeric zinc porphyrin with dynamic oligo(Aib) units can detect the helical sense of oligopeptides.^[9] Although this chiroptical sensor lacks a stereogenic center, it becomes optically active through stereochemical interactions with helical guests upon inclusion in its cavity. In contrast, host **1** and guests **2** and **3** (Scheme 1) possess leucine residues (Leu) as a chiral source, which can induce, depending on their configurations, either a right- or left-handed helicity in the oligopeptide chains. Therefore, the stabilities of the host–guest complexes may be affected by the conformational matching among the three single-handed oligopeptide helices. Compounds **1** and **2** also contain two dehydrophenylalanine (Δ Phe)^[10] units adjacent to the Leu residue whose benzylidene groups would have a steric influence on the host–guest interaction.



Scheme 1. Structures of helical oligopeptide host **1** and guests **2–5**, as well as molecular models of L-1, L-2, and D-2.

Cyclic host **1** was obtained by metalation with $\text{Zn}(\text{OAc})_2$ of a precursor free-base porphyrin cyclic dimer, synthesized by coupling of 5,15-bis(3-aminophenyl)-10,20-dimesitylporphyrin with a nonapeptide containing Leu and ΔPhe residues, followed by macrocyclization with 5,15-bis(3-carboxyphenyl)-10,20-dimesitylporphyrin.^[7] The CD spectrum (Figure 2a,

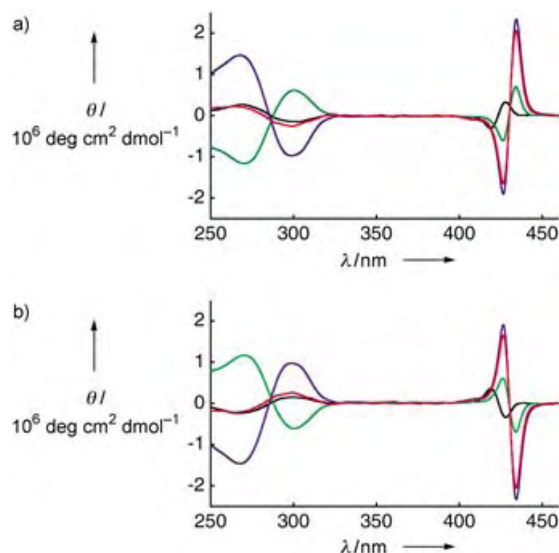


Figure 2. Complexation of **1** with **2** at $[\mathbf{2}]/[\mathbf{1}] = 10:1$ in CHCl_3 at 25°C . a) CD spectra of **L-1** in the absence (black curve) and presence of **L-2** (blue curve), **D-2** (green curve), and **rac-2** (red curve). b) CD spectra of **D-1** in the absence (black curve) and presence of **D-2** (blue curve), **L-2** (green curve), and **rac-2** (red curve).

black curve) of the L-leucine-containing host (**L-1**) in CHCl_3 displays an exciton-coupled CD band centered at 280 nm, as a result of the ΔPhe units. The oligopeptide units in **L-1** adopt a right-handed helical conformation, as evident by the sign of the split Cotton effect.^[10] A characteristic exciton-couplet is also observed at the Soret absorption band of the zinc porphyrin moieties (400–440 nm), which indicates a clockwise-twisted geometry of the two facing zinc porphyrin units.^[9,11] As expected, the CD spectrum of **D-1** bearing left-handed helical units (Figure 2b, black curve) is a perfect mirror-image of that of **L-1**.

Spectroscopic titration in CHCl_3 and Job plots^[7] suggest that **L-1** forms a stable 1:1 inclusion complex with **L-2**, a pyridine-anchored right-handed helical pentapeptide containing L-Leu, with an association constant $K_{\text{assoc}}(\text{L}\mathbf{1}\mathbf{L}\mathbf{2})$ of $14.2 \times 10^6 \text{ M}^{-1}$ (Table 1, entry 1). In contrast, the association constant for the complexation of left-handed helical guest **D-2** with **L-1**, is much smaller ($K_{\text{assoc}}(\text{L}\mathbf{1}\mathbf{D}\mathbf{2}) = 2.9 \times 10^6 \text{ M}^{-1}$, Table 1, entry 1). The large difference between these association constants ($K_{\text{assoc}}(\text{L}\mathbf{1}\mathbf{L}\mathbf{2})/K_{\text{assoc}}(\text{L}\mathbf{1}\mathbf{D}\mathbf{2}) = 4.9:1$) demonstrates that

right-handed **L-2** is favored over left-handed **D-2** in the complexation with **L-1**. Accordingly, host **D-1** (which has left-handed helical units) shows a much larger affinity toward left-handed **D-2** than right-handed **L-2** (Table 1, entry 5), and the observed $K_{\text{assoc}}(\text{D}\mathbf{1}\mathbf{D}\mathbf{2})/K_{\text{assoc}}(\text{D}\mathbf{1}\mathbf{L}\mathbf{2})$ ratio of 4.9:1 is identical to that observed for **L-1D2** (Table 1, entry 1).

Inclusion complexes **L-1D-2** and **L-1D-2** also display different CD spectral profiles (Figure 2a). Mixing **L-1** with the favorable guest **L-2** (10 equiv) results in the exciton-couplet at the Soret absorption band of the zinc porphyrin moieties being red-shifted from 424 to 431 nm (because of the coordination with the pyridyl terminus of **L-2**^[9]) and significantly enhanced (Figure 2a, black→blue curves), whereas mixing of **L-1** with the unfavorable left-handed **D-2** (10 equiv) results in a red-shifted but much less enhanced CD band (Figure 2a, black→green curves). When **D-1** is used as the host, an analogous CD enhancement is observed upon complexation with **D-2** (Figure 2b, blue curve) rather than with **L-2** (green curve). These observations indicate that the twisted geometry of the zinc porphyrin units in the host is likely stabilized by the inclusion of a favorable guest in its cavity to form a peptide bundle. Interestingly, mixing of **L-1** or **D-1** with racemic guest **rac-2** (10 equiv) also results in a large enhancement of the CD signal (Figure 2, black→red curves), the extent of which is 87% of those observed for the favorable host–guest combinations (Figure 2, blue curves). This result suggests the occurrence of optical resolution of **rac-2** in solution by selective binding with **1** under competitive conditions (Figure 1). To prove this^[7] inclusion complex **L-1D2**, formed upon mixing **L-1** with **rac-2** (10 equiv) in CHCl_3 , was isolated by size-exclusion chromatography (SEC) with

Table 1: Association constants (K_{assoc}) for the complexation of helical host **1** with guests **2–5** in CHCl_3 at 25°C , upon spectroscopic titration, and enantiomer ratios of **2** extracted from **1D2**, upon decomplexation.

Entry	Host	Guest	$K_{\text{assoc}}(\text{L}\mathbf{1}\mathbf{L}\mathbf{2}) [\text{M}^{-1}]$	$K_{\text{assoc}}(\text{L}\mathbf{1}\mathbf{D}\mathbf{2}) [\text{M}^{-1}]$	$K_{\text{large}}/K_{\text{small}}$	L-2/D-2 extracted from 1D2 ^[a]
1	L-1	2	14.2×10^6	2.9×10^6	4.9	86:14
2	L-1	3	4.0×10^6	1.2×10^6	3.3	–
3	L-1	4	2.1×10^5	2.7×10^5	1.3	–
4	D-1	5	3.2×10^5	3.6×10^5	1.1	–
5	D-1	2	$2.7 \times 10^6 [= K_{\text{assoc}}(\text{D}\mathbf{1}\mathbf{L}\mathbf{2})]$	$13.3 \times 10^6 [= K_{\text{assoc}}(\text{D}\mathbf{1}\mathbf{D}\mathbf{2})]$	4.9	10:90

[a] Determined by HPLC on a Daicel Chiralpak AD-H column.

CHCl_3 as eluent. Decomplexation of **L-1D2** in THF ^[12] followed by SEC with THF as eluent allowed isolation of guest **2** in 78% yield based on **L-1**. HPLC analysis on a chiral stationary phase (Daicel ChiralPak AD-H, Figure 3b) with **rac-2** as reference (Figure 3a) demonstrated that the **2** thus isolated was considerably enriched in the L isomer, with a **L-2/D-2** ratio of 86:14 (72% ee; Table 1, entry 1). However, the use of **D-1** in place of **L-1** for the competitive complexation with **rac-2**, followed by an analogous chromatographic analysis (Figure 3c), resulted in a **L-2b-2** ratio of 10:90 (80% ee; Table 1, entry 5).

To explore the origin of stereochemical guest selection we investigated the complexation of **L-1** with leucine-containing

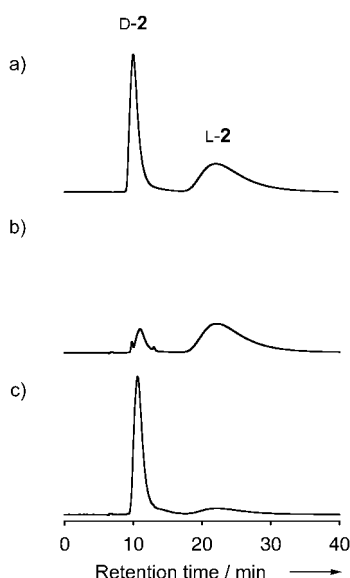


Figure 3. HPLC traces obtained on a chiral stationary phase of a) *rac*-**2** (reference) and b), c) **2** extracted from inclusion complexes with *L*-**1** and *D*-**1**, respectively (column: Daicel Chiralpak AD-H, eluent: hexane/2-propanol/ Et_2NH = 75:25:0.1).

guests **4** and shorter-chain **5** as nonhelical reference compounds (Scheme 1). Although the number of atoms along the main chain of **4** is identical to that of **2**, the molecular length of **5** is more likely to be similar to that of **2** adopting a helical conformation. Spectroscopic titration experiments showed that the association constants of these nonhelical guests with *L*-**1** are one order of magnitude smaller than those observed for helical **2**, and more importantly, their enantiomers were not discriminated stereochemically (Table 1, entries 3 and 4).^[7] From these observations we can conclude that a helix–helix (host–guest) interaction is responsible for the stereochemical guest selection in the complexation between **1** and **2**. Moreover, substituents on the helical chains play a role in the helix–helix interaction upon bundling.^[2–4,13] For example, smaller association constants are found for the complexation of *L*-**1** with the enantiomers of helical guest **3**, which does not contain benzylidene units, than those with **2** (Table 1, entry 2). In particular, the *L* enantiomer of **3** is preferentially selected by *L*-**1**, but the observed $K_{\text{assoc}}(\text{L} \supset \text{L})/K_{\text{assoc}}(\text{L} \supset \text{D})$ ratio of 3.3:1 is clearly smaller than that of *L*-**1** **2**.

In conclusion, we have demonstrated one-pot optical resolution of helical peptidic guests in solution by using a cyclodimeric zinc porphyrin host bearing single-handed oligopeptide units. In conjunction with control experiments on nonhelical chiral guests, the results clearly show that the host and guest molecules stereochemically recognize their helical structures, rather than the point chiralities (Leu) in their chains, upon bundling of the host molecule in the confined cavity. We believe that exploration of asymmetric transformations through artificial peptide bundling is worthy of further investigation.

Received: May 18, 2004

Keywords: amino acids · helical structures · optical resolution · peptides · porphyrinoids

- [1] a) A. Lupas, *Trends Biochem. Sci.* **1996**, *21*, 375–382; b) Y. Jiang, A. Lee, J. Chen, M. Cadene, B. T. Chait, R. Mackinnon, *Nature* **2002**, *417*, 523–526; c) R. B. Bass, P. Strop, M. Barclay, D. C. Rees, *Science* **2002**, *298*, 1582–1587.
- [2] a) R. B. Hill, D. P. Raleigh, A. Lombardi, W. F. DeGrado, *Acc. Chem. Res.* **2000**, *33*, 745–754; b) L. Baltzer, H. Nilsson, J. Nilsson, *Chem. Rev.* **2001**, *101*, 3153–3163; c) A. J. Doerr, M. A. Case, I. Pelczar, G. L. McLendon, *J. Am. Chem. Soc.* **2004**, *126*, 4192–4198.
- [3] a) K. Severin, D. H. Lee, A. J. Kennan, M. R. Ghadiri, *Nature* **1997**, *389*, 706–709; b) X. Li, J. Chmielewski, *J. Am. Chem. Soc.* **2003**, *125*, 11820–11821.
- [4] a) N. A. Schnarr, A. J. Kennan, *J. Am. Chem. Soc.* **2003**, *125*, 13046–13051; b) S. K. Sia, P. S. Kim, *Biochemistry* **2001**, *40*, 8981–8989.
- [5] For helix-sense-selective complexation between peptides and nonpeptidic chiral hosts, see: K. Konishi, S. Kimata, K. Yoshida, M. Tanaka, T. Aida, *Angew. Chem.* **1996**, *108*, 3001–3003; *Angew. Chem. Int. Ed. Engl.* **1996**, *35*, 2823–2825.
- [6] For binding of helical peptides with nonhelical oligomeric receptors, see: B. P. Orner, X. Salvatella, J. S. Quesada, J. de Mendoza, E. Giralt, A. D. Hamilton, *Angew. Chem.* **2002**, *114*, 125–127; *Angew. Chem. Int. Ed.* **2002**, *41*, 117–119.
- [7] See Supporting Information.
- [8] a) C. Toniolo, E. Benedetti, *Macromolecules* **1991**, *24*, 4004–4009; b) C. Toniolo, E. Benedetti, *Trends Biochem. Sci.* **1991**, *16*, 350–353; c) R. Geßmann, H. Brückner, M. Kokkinidis, *Acta Crystallogr. Sect. B* **1998**, *54*, 300–307.
- [9] Y.-M. Guo, H. Oike, T. Aida, *J. Am. Chem. Soc.* **2004**, *126*, 716–717.
- [10] a) Y. Inai, N. Ousaka, T. Okabe, *J. Am. Chem. Soc.* **2003**, *125*, 8151–8162; b) Y. Inai, Y. Ishida, K. Tagawa, A. Takasu, T. Hirabayashi, *J. Am. Chem. Soc.* **2002**, *124*, 2466–2473.
- [11] X. Huang, N. Fujioka, G. Pescitelli, F. E. Koehn, R. T. Williamson, K. Nakanishi, N. Berova, *J. Am. Chem. Soc.* **2002**, *124*, 10320–10335.
- [12] Host **1** did not show any changes in its absorption and CD spectra in the visible region upon mixing with guest **2** in THF.
- [13] a) A. Dehner, E. Planker, G. Gemmecker, Q. B. Broxterman, W. Bisson, F. Formaggio, M. Crisma, C. Toniolo, H. Kessler, *J. Am. Chem. Soc.* **2001**, *123*, 6678–6686; b) I. L. Karle, *Acta Crystallogr. Sect. B* **1992**, *48*, 341–356.

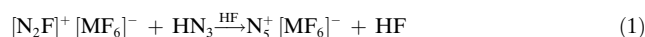
Polynitrogen Chemistry

High-Energy-Density Materials: Synthesis and Characterization of $N_5^+[P(N_3)_6]^-$, $N_5^+[B(N_3)_4]^-$, $N_5^+[HF_2] \cdot nHF$, $N_5^+[BF_4]^-$, $N_5^+[PF_6]^-$, and $N_5^+[SO_3F]^{-**}$

Ralf Haiges,* Stefan Schneider, Thorsten Schroer, and Karl O. Christe*

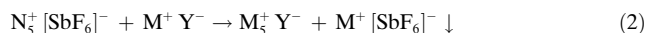
Dedicated to Professor Herbert Roesky on the occasion of his 70th birthday

During the past two decades, polynitrogen containing compounds have received increasing attention as promising candidates for high energy-density materials (HEDM).^[1–17] While most of the efforts were devoted to theoretical studies, the long-known existence of the stable azide anion (N_3^-)^[18] and the recent syntheses of stable salts of the pentanitrogen cation (N_5^+)^[1–3] have demonstrated the feasibility of experimentally pursuing polynitrogen-containing materials. The only known direct method for preparing N_5^+ compounds is their synthesis from an $[N_2F]^+$ salt with HN_3 in HF solution according to Equation (1).^[1,2]



This direct synthesis route is restricted by the small number of $[N_2F]^+$ salts available. Except for N_2FAsF_6 and N_2FSbF_6 and reports on unstable N_2FBF_4 ^[19] and N_2FPF_6 ^[20] salts, no other $[N_2F]^+$ compounds have been reported.

Other N_5^+ salts can be prepared by an indirect method using metathetical reactions^[3] [Eq. (2)].



For a successful metathetical reaction, each ion must be compatible with the solvent, and both starting materials and one of the products must be highly soluble, while the second reaction product must have low solubility. Because of its highly oxidizing nature, N_5SbF_6 is compatible with only a limited number of solvents, for example, HF, SO_2 and CHF_3 , thus severely restricting the general usefulness of the metathetical approach. Because SbF_5 is among the strongest

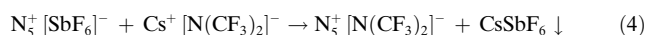
known Lewis acids,^[21] the displacement of SbF_5 in $N_5^+ [SbF_6]^-$ by a stronger Lewis acid is also rarely feasible. Therefore, the development of a more general method for the syntheses of N_5^+ compounds is desirable. Furthermore, in the interest of preparing N_5^+ salts of higher energy content, the combination of N_5^+ with highly energetic counterions was pursued. Previous attempts to combine N_5^+ with either N_3^- , $[ClO_4]^-$, $[NO_3]^-$, or $[N(NO_2)_2]^-$ had been unsuccessful.^[22]

While in theory, F^- abstraction from FN_5 by a strong Lewis acid, such as SbF_5 , could provide a general synthesis for N_5^+ salts [Eq. (3)], the required FN_5 precursor is unknown.



Theoretical studies^[23,24] identified at least six vibrationally stable isomers of FN_5 but, in accordance with experimental results, the predicted lifetimes of these species are only in the nanosecond range.^[23]

During attempts to prepare $N_5^+ [N(CF_3)_2]^-$ by metathesis from $N_5^+ [SbF_6]^-$ and $Cs^+ [N(CF_3)_2]^-$ in HF solution at $-78^\circ C$ [Eq. (4)], the expected $CsSbF_6$ precipitate was formed and removed by filtration.



However, after pumping off all volatile material from the filtrate at $-64^\circ C$, the low-temperature Raman spectrum of the resulting clear liquid residue exhibited only bands attributable to N_5^+ (Figure 1). This finding reminded us of a situation encountered 24 years ago with the metathetical reaction of NF_4SbF_6 and CsF in HF [Eq. (5)].

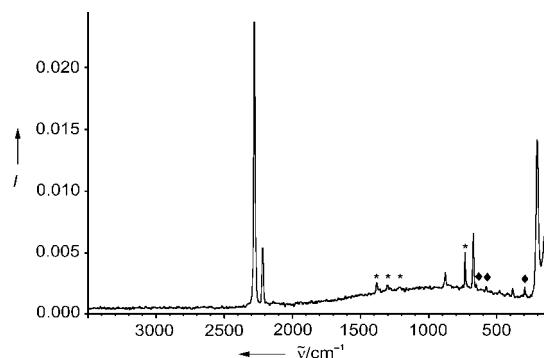
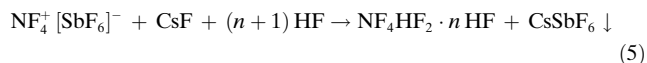


Figure 1. Low-temperature Raman spectrum of $N_5HF_2 \cdot nHF$. The bands marked by an asterisk (*) are due to the Teflon-FEP sample tube. Bands marked by ♦ arise from a trace of $[SbF_6]^-$ from the starting material. The intense, unlabeled bands are from N_5^+ .

This reaction resulted in the formation of thermally unstable, liquid $NF_4HF_2 \cdot nHF$,^[25] which exhibited characteristics very similar to those observed in the above N_5^+ reaction, that is, a failure to observe anion bands because a polybifluoride anion is an extremely weak Raman scatterer. The additional formation of $N_5HF_2 \cdot nHF$ in the reaction in

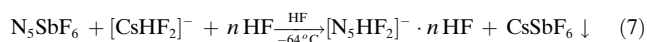
[*] Dr. R. Haiges, Dr. S. Schneider, Dr. T. Schroer, Prof. Dr. K. O. Christe
Loker Research Institute
University of Southern California
Los Angeles, CA 90089-1661 (USA)
Fax: (+1) 213-740-6679
E-mail: haiges@usc.edu
kchriste@usc.edu

[**] This work was funded by the Defense Advanced Research Projects Agency, the Air Force Office of Scientific Research and the National Science Foundation. R.H. thanks the Deutsche Forschungsgemeinschaft for a postdoctoral fellowship. We thank Prof. G. A. Olah, and Drs. A. Morrish, D. Woodbury, and M. Berman, for their steady support, and Dr. R. Wagner for his help and stimulating discussions.

Equation (4) can be explained if liquid HF is capable of displacing $\text{HN}(\text{CF}_3)_2$ from its $[\text{N}(\text{CF}_3)_2]^-$ salts according to Equation (6).

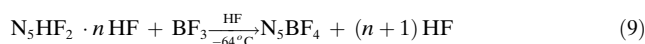
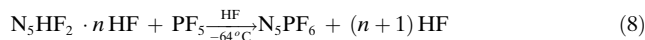


The above assumptions were confirmed by carrying out a reaction of N_5SbF_6 with CsF in anhydrous HF at -64°C which resulted in the expected precipitation of CsSbF_6 and the formation of a polybifluoride of N_5^+ [Eq. (7)].



$\text{N}_5\text{HF}_2 \cdot n \text{HF}$ was isolated as a clear, colorless liquid after filtering off the CsSbF_6 precipitate and removing all volatiles at -64°C from the filtrate. The observed low-temperature Raman spectrum was identical to that shown in Figure 1. It exhibits, in addition to some weak bands due to the Teflon-FEP sample container and a trace of $[\text{SbF}_6]^-$ from the starting material, only bands due to N_5^+ . The experimental Raman frequencies and assignments are listed in Table 1. On warming to room temperature, the $\text{N}_5\text{HF}_2 \cdot n \text{HF}$ salt decomposed under formation of *trans*- N_2F_2 , NF_3 , and N_2 , which were identified by checking for noncondensable gas at -196°C and FT-IR spectroscopy.

The usefulness of the $\text{N}_5\text{HF}_2 \cdot n \text{HF}$ salt as a reagent for the synthesis of other N_5^+ salts by displacement reactions with Lewis acids stronger than HF was explored by treating it with PF_5 , BF_3 , and HSO_3F ,^[26,27] resulting in the formation of N_5PF_6 , N_5BF_4 , and $\text{N}_5\text{SO}_3\text{F}$, respectively, according to Equations (8)–(10).



All these new salts are white, marginally stable solids that were characterized by NMR and vibrational spectroscopy. The ^{14}N NMR spectrum of N_5PF_6 was recorded in HF at -40°C . It showed a strong resonance at $\delta = -165.1$ ppm for the N_β atoms and a very broad line at about $\delta = -101$ ppm for the terminal N_α atoms, and is in good agreement with previously published values for N_5^+ salts.^[1–3] In the ^{14}N NMR spectra of N_5BF_4 and $\text{N}_5\text{SO}_3\text{F}$ in HF at -40°C , the resonances for the N_β atoms were observed at $\delta = -164.3$ ppm and $\delta = -164.7$ ppm, respectively. The experimental vibrational frequencies and assignments of the three salts and, for comparison, of N_5SbF_6 are listed in Table 1. The observed Raman and IR spectra of N_5PF_6 are shown in Figure 2, and the Raman spectra of N_5BF_4 and $\text{N}_5\text{SO}_3\text{F}$ are shown in Figure 3 and Figure 4, respectively. They establish beyond any doubt the composition of these salts^[1–3,28–30] and their ionic nature.

Whereas the N_5^+ ion is a highly energetic ion with a calculated endothermicity of $351.6 \text{ kcal mol}^{-1}$,^[22] all of its known salts contained non-energetic counterions.^[1–3] Although a significant advance in potential performance was achieved by successfully doubling the number of poly-

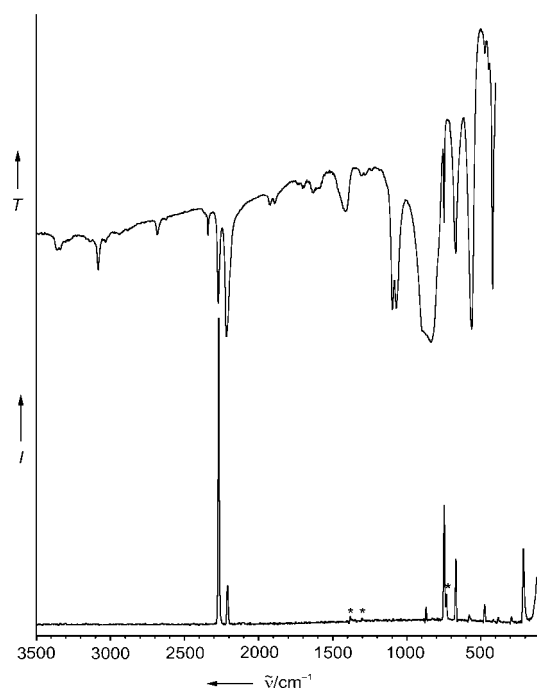


Figure 2. IR (upper trace) and Raman (lower trace) spectra of N_5PF_6 . The bands marked by an asterisk (*) are due to the Teflon-FEP sample tube.

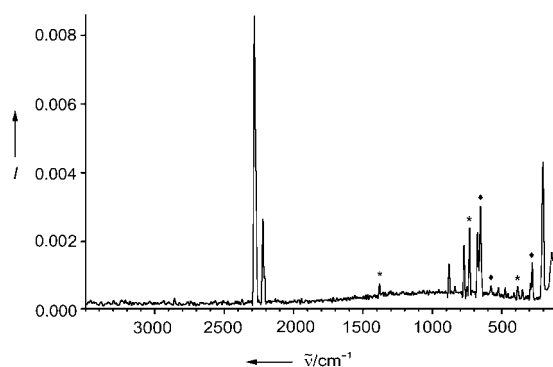


Figure 3. Low-temperature Raman spectrum of N_5BF_4 . The bands marked by an asterisk (*) are due to the Teflon-FEP sample tube. Bands marked by ♦ arise from a trace of $[\text{SbF}_6]^-$ from the starting material.

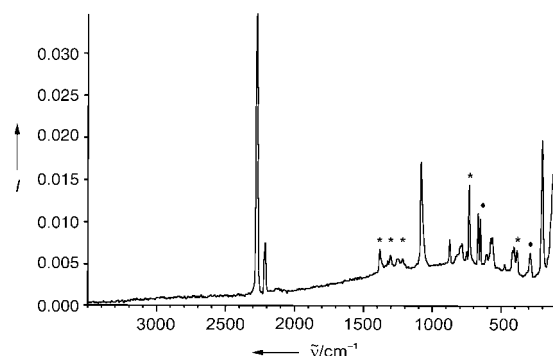


Figure 4. Low-temperature Raman spectrum of $\text{N}_5\text{SO}_3\text{F}$. The bands marked by an asterisk (*) are due to the Teflon-FEP sample tube. Bands marked by ♦ arise from a trace of $[\text{SbF}_6]^-$ from the starting material.

Table 1: Observed vibrational frequencies of $\text{N}_5\text{HF}_2 \cdot n\text{HF}$, N_5SbF_6 , N_5PF_6 , N_5BF_4 , and $\text{N}_5\text{SO}_3\text{F}$ and their assignments

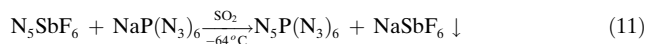
$\text{N}_5\text{HF}_2 \cdot n\text{HF}$ Raman	Observed frequency (cm^{-1}) and relative intensity						Assignments			
	$\text{N}_5\text{SbF}_6^{[2]}$ IR	Raman	IR	N_5PF_6 Raman	N_5BF_4 Raman	$\text{N}_5\text{SO}_3\text{F}$ Raman	$\text{N}_5^+ (\text{C}_{2v})$	$\text{MF}_6^- (\text{O}_h)$	$[\text{BF}_4]^- (\text{T}_d)$	$[\text{SO}_3\text{F}]^- (\text{T}_d)$
	3357 vw		3364 w				$(\nu_1 + \nu_3 + \nu_9)(\text{B}_2) = 3358$			
	3334 vw		3337 w				$(\nu_1 + \nu_8)(\text{B}_2) = 3323$			
	3079 vw		3082 mw				$(\nu_2 + \nu_7)(\text{B}_2) = 3077$			
	2681 vw		2685 w				$(\nu_1 + \nu_9)(\text{B}_2) = 2682$			
2279 (10)	2270 m	2268 (9.4)	2273 ms	2269 (10)	2283 (10)	2271 (10)	$\nu_1(\text{A}_1)$			
2218 (2.2)	2205 s	2205 (2.0)	2219 s	2209 (1.3)	2221 (3.0)	2210 (2.2)	$\nu_7(\text{B}_2)$			
	1921 vw		1926 w				$(\nu_3 + 3\nu_9)(\text{B}_2) = 1914$			
	1891 vw		1891 w				$(\nu_8 + 2\nu_9)(\text{B}_2) = 1883$			
	1240 vw					1303 (1.7)				$\nu_4(\text{E})$
	1092 ms		1099 s				$(\nu_3 + \nu_9)(\text{B}_2) = 1086^{[a]}$	comb. bands		
	1064 s		1072 s			1084 (5.3)	$\nu_8(\text{B}_2)$			$\nu_1(\text{A}_1)$
	902 vvw						$(\nu_5 + \nu_6)(\text{B}_2) = 903$			
877 (1.3)	871 w	872 (0.6)		869 (0.6)	880 (1.5)	871 (2.3)	$\nu_2(\text{A}_1)$			
840 (0.9)	835 vw	837 (0+)		826 (0+)	837 (0.7)	829 (1.7)	$(2\nu_9)(\text{A}_1) = 828^{[b]}$			
					771 (2.9)	785 (2.1)			$\nu_1(\text{A}_1)$	$\nu_2(\text{A}_1)$
672 (2.7)		672 (1)	672 s	668 (2.2)	674 (2.7)	669 (3.2)	$\nu_3(\text{A}_1)$			
	655 vs		881 s, 839 vs }					$\nu_3(\text{F}_{1u})$		
		652 (10)	750 m	747 (3.8)				$\nu_1(\text{A}_{1g})$		
						574 (2.4), 564 (2.4) }				$\nu_3(\text{A}_1)$
	582 w	571 (0.8)	563 vs	578 (0.3)				$\nu_2(\text{E}_g)$		
					525 (0.7)					$\nu_4(\text{F}_2)$
481 (0.7)		478 (0+)	473 w		476 (0.7)	477 (1.4)	$\nu_5(\text{A}_2)$			
	447 w		447 w				?			
422 (0.6)	425 ms				426 (0.4)	420 (1.9)	$\nu_6(\text{B}_1)$			
413 (0.6)	412 mw	416 (0+)		416 (0+)	412 (0.5)	407 (2.0)	$\nu_9(\text{B}_2)$			
	284 vs		563 vs					$\nu_4(\text{F}_{1u})$		
		282 (2.8)	473 w	474 (0.6)				$\nu_5(\text{F}_{2g})$		
					350 (0.6)					$\nu_2(\text{E})$
202 (5.8)		204 (5.0)		211 (2.5)	202 (4.8)	203 (5.7)	$\nu_4(\text{A}_1)$			
		107 (5.0)		120 (1.6)	113 (2.0)	111 (4.5)	lattice vibrations			

[a] In Fermi resonance with $\nu_8(\text{B}_2)$. [b] In Fermi resonance with $\nu_2(\text{A}_1)$.

nitrogen ions in a salt by formation of a 2:1 salt $[\text{N}_5^+]_2[\text{SnF}_6]^{2-}$,^[3] salts containing energetic counterions were still missing. Attempts to combine the N_5^+ ion with the energetic anions, $[\text{ClO}_4]^-$, $[\text{NO}_3]^-$ and N_3^- by metathetical reactions failed, and a recent theoretical analysis showed that,

after inclusion of entropy corrections, N_5^+N_3^- is unstable by 76 kcal mol⁻¹ with respect to spontaneous decomposition to N_3 and N_2 .^[22] In spite of these challenges, we have now successfully synthesized two highly energetic N_5^+ salts.

The metathetical reaction between N_5SbF_6 and $\text{NaP}(\text{N}_3)_6$ in SO_2 proceeded with the expected precipitation of NaSbF_6 and the combination of the N_5^+ ion with the energetic ion $\text{P}(\text{N}_3)_6^{3-}$ to form $\text{N}_5\text{P}(\text{N}_3)_6$ [Eq. (11)].

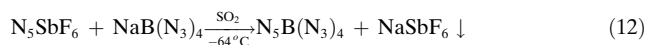


However, the compound is extremely shock sensitive and violently explodes upon the slightest provocation or warming towards room temperature (see Figure 5). In addition to its very high energy content, this salt is remarkable for its high nitrogen content of 91.2 wt %.



Figure 5. Single-ended 9-mm o.d. Teflon-FEP ampule, used for recording the Raman spectrum, after explosion of less than 500 mg of $\text{N}_5^+[\text{P}(\text{N}_3)_6]^-$.

In a similar fashion, $\text{N}_5\text{B}(\text{N}_3)_4$ was prepared from N_5SbF_6 and $\text{NaB}(\text{N}_3)_4$ [Eq. (12)].



Again, the salt is extremely shock-sensitive and explodes on warming towards room temperature. Its nitrogen content of 95.7 wt % significantly exceeds even that of $\text{N}_5\text{P}(\text{N}_3)_6$ and any other known, solid high-nitrogen compound. There are only five other compounds whose nitrogen content exceeds 90 wt %. These are: $[\text{NH}_4]^+\text{N}_3^-$ (93.3 %), $[\text{N}_2\text{H}_5]^+\text{N}_3^-$ (93.3 %), $[\text{N}_2\text{H}_5]^+\text{N}_3^-\cdot\text{N}_2\text{H}_4$ (91.6 %), 2H-tetrazolypentazole (90.6 %), and $\text{Li}^+[\text{B}(\text{N}_3)_4]^-$ (90.4 %).^[33] Attempts to carry out the above metathetical reactions with $\text{CsP}(\text{N}_3)_6$ and $\text{CsB}(\text{N}_3)_4$ in HF solution were unsuccessful because HF reacts with the polyazido anions to give $[\text{PF}_6]^-$ and $[\text{BF}_4]^-$, and lead to the isolation of N_5PF_6 and N_5BF_4 , respectively. Both polyazido salts were identified and characterized by low-temperature Raman spectroscopy.

The experimental vibrational frequencies and tentative assignments for $\text{N}_5\text{P}(\text{N}_3)_6$ and $\text{N}_5\text{B}(\text{N}_3)_4$ are given in the Experimental Section. The observed Raman spectra of $\text{N}_5\text{P}(\text{N}_3)_6$ and $\text{N}_5\text{B}(\text{N}_3)_4$ are shown in Figure 6 and Figure 7, respectively. In addition to high energy densities of about 2 kcalgram⁻¹ and extremely high sensitivities, these compounds exhibit the typical high detonation velocities of

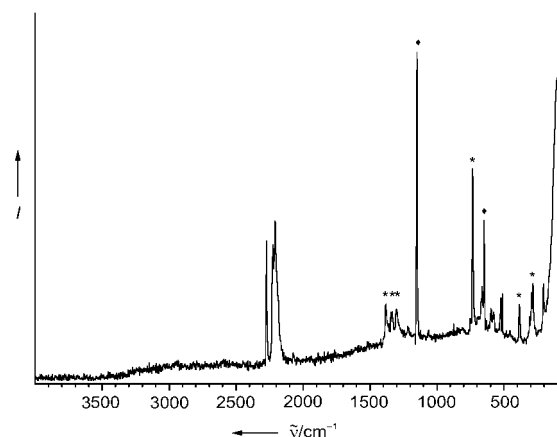


Figure 6. Low-temperature Raman spectrum of $\text{N}_5\text{P}(\text{N}_3)_6$. The bands marked by an asterisk (*) are due to the Teflon-FEP sample tube. The two bands marked with ♦ arise from the SO_2 solvent.

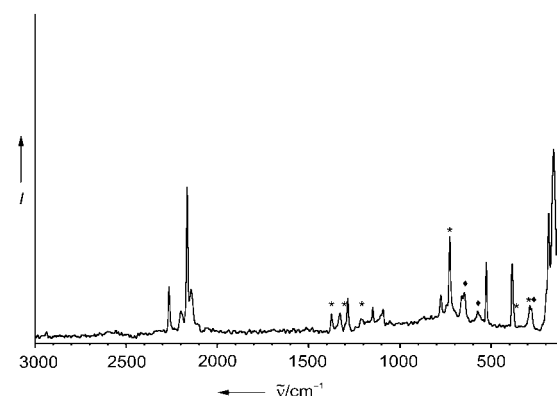


Figure 7. Low-temperature Raman spectrum of $\text{N}_5\text{B}(\text{N}_3)_4$. The bands marked by an asterisk (*) are due to the Teflon-FEP sample tube. Bands marked by ♦ arise from a trace of $[\text{SbF}_6]^-$ from the starting material.

covalent azides which render the handling and further characterization of these compounds particularly difficult.

Experimental Section

Caution! Azides and N_5^+ compounds are highly endothermic and can decompose explosively under various conditions! N_5^+ compounds are highly energetic oxidizers.^[1–3] Contact with potential fuels must be avoided. These materials should be handled only on a scale of less than 2 mmol. The polyazides in this work are extremely shock-sensitive. Because of the high energy content and high detonation velocities of these azides, their explosions are particularly violent and can cause, even on a one mmol scale, significant damage. The use of appropriate safety precautions, such as face shields, heavy leather welding suits, leather gloves, and ear plugs is mandatory.^[34] Teflon containers should be used, whenever possible, to avoid hazardous fragmentation. **Ignoring safety precautions can lead to serious injuries!**

All reactions were carried out in Teflon-FEP (FEP = perfluoroethylene-propylene polymer) ampules that were closed by stainless steel valves. Volatile materials were handled in stainless steel/Teflon-FEP or grease-free Pyrex-glass vacuum lines.^[35] Nonvolatile solids were handled in the dry argon atmosphere of a glove box. All reaction vessels and the stainless steel line were passivated with ClF_3 prior to use.

Infrared spectra were recorded in the range 4000–400 cm^{-1} on a Midac FT-IR model 1720 at a resolution of 1 cm^{-1} . Spectra of solids were obtained by using dry powders pressed between AgCl windows in an Econo press (Barnes Engineering Co.). Raman spectra were recorded in the range 4000–80 cm^{-1} on a Bruker Equinox 55 FT-RA spectrophotometer using a Nd:YAG laser at 1064 nm with power levels of 200 mW or less. Pyrex melting point tubes that were baked out at 300 °C for 48 h at 10 mTorr vacuum or 9-mm o.d. Teflon-FEP tubes with stainless steel valves that were passivated with ClF_3 were used as sample containers. ^{14}N NMR spectra were recorded unlocked at 36.13 MHz on a Bruker AMX 500 spectrometer using solutions of the compounds in DMSO in sealed standard glass tubes. Neat CH_3NO_2 (0.00 ppm) was used as the external reference.

The N_2FSbF_6 starting material was prepared from *cis*- N_2F_2 and SbF_5 in anhydrous HF solution.^[19,20,36–39] N_5SbF_6 was prepared from N_2FSbF_6 and HN_3 in HF .^[2] $\text{NaP}(\text{N}_3)_6$ was prepared from PCl_5 and NaN_3 ,^[31] and $\text{NaB}(\text{N}_3)_4$ from NaBH_4 and HN_3 .^[32] The HF (Matheson Co.) was dried by storage over BiF_5 (Ozark Mahoning).^[40] PCl_5 (Aldrich) was purified by sublimation in a dynamic vacuum. The CsF (KBI) was fused in a platinum crucible, transferred while hot to the dry box, and finely powdered. BF_3 (Matheson), PF_5 (Ozark Mahoning), NaN_3 (Aldrich), NaBH_4 (Aldrich), and HSO_3F (Aldrich) were used without further purification.

$\text{N}_5\text{HF}_2 \cdot n\text{HF}$: A solution of CsF (1.00 mmol) in HF (2 mL) was siphoned through a Teflon-FEP tube into a Teflon-FEP ampule containing a solution of N_5SbF_6 (1.00 mmol) in HF (3 mL) at -64°C . Immediately, a white precipitate was formed. The reaction mixture was stirred for 10 min to ensure complete reaction. The mixture was allowed to settle, and the supernatant liquid was siphoned into a second Teflon-FEP ampule kept at -64°C . The CsSbF_6 residue was washed twice with HF (about 1 mL each time). The HF was pumped off from the combined liquids at -64°C , leaving behind a colorless liquid (0.156 g; weight calculated for 1.00 mmol of $\text{N}_5\text{HF}_2 \cdot 2.5\text{HF}$: 0.159 g).

N_5PF_6 and N_5BF_4 : Excess PF_5 or BF_3 (2.0 mmol) was condensed at -196°C into an ampule containing a frozen solution of $\text{N}_5\text{HF}_2 \cdot n\text{HF}$ (1.00 mmol) in HF (1 mL). The temperature was raised to -64°C and the reaction mixture kept at this temperature for 1 h to ensure complete reaction. All volatile material was pumped off at -64°C , leaving behind a white solid (N_5PF_6 : 0.220 g, weight calculated for 1.00 mmol of N_5PF_6 : 0.215 g; N_5BF_4 : 0.167 g; weight calculated for 1.00 mmol of N_5BF_4 : 0.157 g).

$\text{N}_5\text{SO}_3\text{F}$: At -64°C , a solution of HSO_3F (1.00 mmol) in HF (2 mL) was added to a solution of $\text{N}_5\text{HF}_2 \cdot n\text{HF}$ (1.00 mmol) in HF (1 mL). The reaction mixture was stirred for 30 min at this temperature to ensure complete reaction. All volatiles were pumped off at -64°C leaving behind a white solid (0.175 g; weight calculated for 1.00 mmol of $\text{N}_5\text{SO}_3\text{F}$: 0.169 g).

$\text{N}_5\text{P}(\text{N}_3)_6$ and $\text{N}_5\text{B}(\text{N}_3)_4$: At -64°C , a solution of N_5SbF_6 (0.50 mmol) in SO_2 (3 mL) was added to a solution of $\text{NaB}(\text{N}_3)_4$ or $\text{NaP}(\text{N}_3)_6$ (0.50 mmol) in SO_2 (3 mL), respectively. After the mixture had settled, the liquid phase was transferred into another Teflon-FEP ampule that had been cooled to -64°C , and the remaining NaSbF_6 was washed twice with about SO_2 (1 mL). Pumping on the collected liquid phase at -64°C gave a white solid. $\text{N}_5\text{P}(\text{N}_3)_6$: 0.184 g, expected for 0.50 mmol: 0.177 g; Raman (50 mW, -80°C): $\tilde{\nu} = 2266(10.0)$ ($\text{N}_5^+ \nu_1$), 2203(7.5) ($\text{N}_5^+ \nu_7$), 2182(5.4)/2074(2.9) ($\text{P}(\text{N}_3)_6^- \nu_{\text{as}}\text{N}_3$), 1302(4.7) ($\text{P}(\text{N}_3)_6^- \nu_4\text{N}_3$), 873(3.9) ($\text{N}_5^+ \nu_2$), 730(7.4) ($\text{P}(\text{N}_3)_6^- \nu\text{PN}$), 666(8.0) ($\text{N}_5^+ \nu_3$), 522(5.0) ($\text{P}(\text{N}_3)_6^- \delta\text{N}_3$), 483(4.6) ($\text{N}_5^+ \nu_5$), 419(4.7) ($\text{N}_5^+ \nu_9$), 458(4.7) ($\text{P}(\text{N}_3)_6^- \delta\text{PNN}$), 327(4.9) ($\text{P}(\text{N}_3)_6^- \delta\text{PNN}$), 203(9.1) ($\text{N}_5^+ \nu_4$)

$\text{N}_5\text{B}(\text{N}_3)_4$: 0.137 g; expected for 0.50 mmol: 0.124 g; Raman (50 mW, -80°C): $\tilde{\nu} = 2269(1.9)$ ($\text{N}_5^+ \nu_1$), 2207(1.2) ($\text{N}_5^+ \nu_7$), 2172(5.4)/2148(2.0) ($\text{B}(\text{N}_3)_4^- \nu_{\text{as}}\text{N}_3$), 1334(2.9)/1292(3.7) ($\text{B}(\text{N}_3)_4^- \nu_4\text{N}_3$), 875(3.1) ($\text{N}_5^+ \nu_2$), 664(3.6) ($\text{N}_5^+ \nu_3$), 581(3.0)/532(4.7)

($\text{B}(\text{N}_3)_4^-$), 483(2.3) ($\text{N}_5^+ \nu_5$), 421(2.1) ($\text{N}_5^+ \nu_9$), 293(2.4) ($\text{B}(\text{N}_3)_4^-$), 203(2.6) ($\text{N}_5^+ \nu_4$), 189(5.0)/165(6.8)/123(10.0) ($\text{B}(\text{N}_3)_4^-$).

Received: March 11, 2004 [Z54242]

Keywords: azides · high energy-density materials (HEDM) · nitrogen · polynitrogen chemistry · vibrational spectroscopy

- [1] K. O. Christe, W. W. Wilson, J. A. Sheehy, J. A. Boatz, *Angew. Chem.* **1999**, *111*, 2112; *Angew. Chem. Int. Ed.* **1999**, *38*, 2004.
- [2] A. Vij, W. W. Wilson, V. Vij, F. S. Tham, J. A. Sheehy, K. O. Christe, *J. Am. Chem. Soc.* **2001**, *123*, 6308.
- [3] W. W. Wilson, A. Vij, V. Vij, E. Bernhardt, K. O. Christe, *Chem. Eur. J.* **2003**, *9*, 2840.
- [4] G. A. Olah, G. K. S. Prakash, G. Rasul, *J. Am. Chem. Soc.* **2001**, *123*, 3308.
- [5] M. T. Nguyen, T. K. Ha, *Chem. Phys. Lett.* **2001**, *335*, 311.
- [6] S. Fau, R. J. Bartlett, *J. Phys. Chem. A* **2001**, *105*, 4096.
- [7] R. J. Bartlett, *Chem. Ind.* **2000**, 140, and references therein; a compilation of data for N_2 to N_{10} can be found at <http://www.qtp.ufl.edu/~bartlett/downloads/polynitrogen.pdf>.
- [8] G. Chung, M. W. Schmidt, M. S. Gordon, *J. Phys. Chem. A* **2000**, *104*, 5647, and references therein.
- [9] M. N. Glukhovtsev, H. Jiao, P. von R. Schleyer, *Inorg. Chem.* **1996**, *35*, 7124, and references therein.
- [10] H. H. Michels, J. A. Montgomery Jr., K. O. Christe, D. A. Dixon, *J. Phys. Chem.* **1995**, *99*, 187.
- [11] G. Schatte, H. Willner, *Z. Naturforsch. B* **1991**, *46*, 483.
- [12] G. Rasul, G. K. S. Prakash, G. A. Olah, *J. Am. Chem. Soc.* **1994**, *116*, 8985.
- [13] W. E. Thompson, M. E. Jacox, *J. Chem. Phys.* **1990**, *93*, 3856.
- [14] J. P. Zheng, J. Waluk, J. Spanget-Larsen, D. M. Blake, J. G. Radziszewski, *Chem. Phys. Lett.* **2000**, *328*, 227.
- [15] T. Ruchti, T. Speck, J. P. Connelly, E. J. Bieske, H. Linnertz, J. P. Maier, *J. Chem. Phys.* **1996**, *105*, 2591.
- [16] F. Cacace, G. de Petris, A. Troiani, *Science* **2002**, *295*, 480.
- [17] M. I. Eremets, R. J. Hemley, H. Mao, E. Gregoryanz, *Nature* **2001**, *411*, 170.
- [18] T. Curtius, *Ber. Dtsch. Chem. Ges.* **1890**, *23*, 3023.
- [19] A. V. Pankratov, N. I. Savenkova, *Russ. J. Inorg. Chem.* **1968**, *13*, 1345.
- [20] K. O. Christe, R. D. Wilson, W. W. Wilson, R. Bau, S. Sukumar, D. A. Dixon, *J. Am. Chem. Soc.* **1991**, *113*, 3795.
- [21] K. O. Christe, D. A. Dixon, D. McLemore, W. W. Wilson, J. A. Sheehy, J. A. Boatz, *J. Fluorine Chem.* **2000**, *101*, 151.
- [22] D. A. Dixon, D. Feller, K. O. Christe, W. W. Wilson, A. Vij, V. Vij, H. D. B. Jenkins, R. M. Olsen, M. S. Gordon, *J. Am. Chem. Soc.* **2004**, *126*, 834.
- [23] H. M. Netzloff, M. S. Gordon, K. O. Christe, W. W. Wilson, A. Vij, V. Vij, J. A. Boatz, *J. Phys. Chem. A* **2003**, *107*, 6638.
- [24] A. Hammerl, T. M. Klapoetke, P. Schwerdtfeger, *Chem. Eur. J.* **2003**, *9*, 5511.
- [25] K. O. Christe, W. W. Wilson, R. D. Wilson, *Inorg. Chem.* **1980**, *19*, 1494.
- [26] W. W. Wilson, K. O. Christe, *J. Fluorine Chem.* **1982**, *19*, 253.
- [27] W. W. Wilson, K. O. Christe, *Inorg. Chem.* **1982**, *21*, 2091.
- [28] K. O. Christe, C. J. Schack, R. D. Wilson, *Inorg. Chem.* **1976**, *15*, 1275.
- [29] K. O. Christe, R. D. Wilson, C. J. Schack, *Inorg. Chem.* **1980**, *19*, 3046.
- [30] H. Siebert, *Anwendungen der Schwingungsspektroskopie in der Anorganischen Chemie, Anorganische und Allgemeine Chemie in Einzeldarstellungen, VII*, Springer, Heidelberg, **1996**.
- [31] a) H. W. Roesky, *Angew. Chem.* **1967**, *79*, 651; *Angew. Chem. Int. Ed. Engl.* **1967**, *6*, 637; b) P. Volgnandt, A. Schmidt, *Z. Anorg. Allg. Chem.* **1976**, *425*, 189.

- [32] a) E. Wiberg, H. Michaud, *Z. Naturforsch.* **1954**, *96*, 497; b) W. Freank, T. Haberer, A. Hammerl, T. M. Klapötke, B. Krumm, P. Mayer, H. Nöth, M. Warchhold, *Inorg. Chem.* **2001**, *40*, 1334; c) W. Fraenk, H. Nöth, T. M. Klapötke, M. Suter, *Z. Naturforsch. B* **2002**, *57*, 621.
- [33] A. Hammerl, T. M. Klapötke, *Inorg. Chem.* **2002**, *41*, 906, and references therein.
- [34] a) R. Haiges, A. Vij, J. A. Boatz, S. Schneider, T. Schroer, M. Gerken, K. O. Christe, *Chem. Eur. J.* **2004**, *10*, 508; b) R. Haiges, J. A. Boatz, A. Vij, M. Gerken, S. Schneider, T. Schroer, K. O. Christe, *Angew. Chem.* **2003**, *115*, 6027; *Angew. Chem. Int. Ed.* **2003**, *42*, 5847; c) R. Haiges, J. A. Boatz, S. Schneider, T. Schroer, M. Yousufuddin, K. O. Christe, *Angew. Chem.* **2004**, *116*, 3210; *Angew. Chem. Int. Ed.* **2004**, *43*, 3148.
- [35] K. O. Christe, W. W. Wilson, C. J. Schack, R. D. Wilson, *Inorg. Synth.* **1986**, *24*, 39.
- [36] D. Moy, A. R. Young, *J. Am. Chem. Soc.* **1965**, *87*, 1889.
- [37] J. K. Ruff, *Inorg. Chem.* **1966**, *5*, 1971.
- [38] H. W. Roesky, O. Glemser, D. Bormann, *Chem. Ber.* **1966**, *99*, 1589.
- [39] K. O. Christe, R. D. Wilson, W. Sawodny, *J. Mol. Struct.* **1971**, *8*, 245.
- [40] K. O. Christe, W. W. Wilson, C. J. Schack, *J. Fluorine Chem.* **1978**, *11*, 71.

High-Nitrogen Compounds

Polyazido High-Nitrogen Compounds: Hydrazo- and Azo-1,3,5-triazine**

My-Hang V. Huynh,* Michael A. Hiskey,*
Ernest L. Hartline, Dennis P. Montoya, and
Richard Gilardi

The performance of a high explosive is measured by its detonation velocity (v_D (kmsec⁻¹)) and detonation pres-

sure (P_{CI} (kbar)). These parameters are determined by the oxygen balance (OB_{CO}),^[1a] density (ρ), and heat of formation (ΔH_f),^[1b] the higher the oxygen balance, density, and heat of formation, the better the performance. The energy of traditional polynitro compounds (Scheme 1) is primarily derived from the combustion of the carbon backbone using the oxygen carried by the nitro group.^[2]

For modern polynitro compounds (Scheme 2), the performance is enhanced not only by an excellent oxygen balance but also by a ring/cage strain which improves both the heat of formation and density.^[4]

Recently, a new class of energetic compounds containing a large fraction of nitrogen has been investigated.^[5–8] These “high-nitrogen” compounds form a unique class of energetic materials^[5a,9] whose energy is derived from their very high positive heat of formation rather than from the combustion of the carbon backbone or the ring/cage strain (Scheme 3). The high heat of formation is directly attributable to the large number of inherently energetic N–N and C–N bonds.

High-nitrogen compounds containing polyazides possess even higher heats of formation because their energy content rapidly increases with the number of energetic azido groups in the molecule. However, they are notorious for their extreme sensitivity^[10a] to spark, friction, and impact (H_{50})^[10b] as well as poor thermal stability,^[10a,11,12] so their applications are very limited. Examples include 3,6-diazido-1,2,4,5-tetrazine^[13] and cyanuric azide (2,4,6-triazido-1,3,5-triazine;^[14] Scheme 4).

There is no literature precedence for high-nitrogen energetic materials containing hydrazo- and azo-1,3,5-triazine backbones. Although Loew and Weis reported the preparations of three inert compounds (4,4'-di(chloro)-6,6'-di(isopropylamino)azo-1,3,5-triazine, 4,4',6,6'-tetra(dimethylamino)azo-1,3,5-triazine, and 4,4',6,6'-tetra(chloro)azo-1,3,5-triazine) in 1976, few physical properties and no crystal structures were available.^[15]

We report herein the synthesis and properties of novel 4,4',6,6'-tetra(azido)hydrazo-1,3,5-triazine (**3**) and 4,4',6,6'-tetra(azido)azo-1,3,5-triazine (**4**), see Scheme 5. The hydrazo and azo linkages not only desensitize but also dramatically increase the melting point of the polyazido products. Remarkably, the heats of formation of these polyazido compounds (Scheme 5) are much higher than those of polynitro and high-nitrogen compounds (Scheme 1–3).

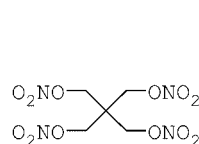
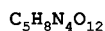
Rapid reaction occurs between 4,4',6,6'-tetra(chloro)hydrazo-1,3,5-triazine (**1**)^[15] and an excess of hydrazine monohydrate ($H_2NNH_2 \cdot H_2O$) in CH_3CN to give 4,4',6,6'-tetra(hydrazino)hydrazo-1,3,5-triazine (**2**) which underwent diazotization to yield **3** (Scheme 5). A suspension of **3** in 1:2 (v/v) $H_2O:CHCl_3$ solution was oxidized by chlorine gas at room temperature to **4**.

All products, **2–4**, were isolated and fully characterized by elemental analysis, differential scanning calorimetry (DSC), heat of formation, and IR and $^1H/^{13}C$ NMR spectroscopies.^[16] Compounds **3** and **4** were also characterized by X-ray crystallography, Figure 1–3.^[17] Compound **3** has only one polymorph ($\rho = 1.649 \text{ g cm}^{-3}$) in which two 1,3,5-triazine rings are not co-planar but have a central torsion angle of 105° (Figure 1). Compound **4** crystallized in α and β polymorphs, $\rho = 1.724 \text{ g cm}^{-3}$ and $\rho = 1.674 \text{ g cm}^{-3}$ (Figure 2). The β poly-

[*] Dr. M.-H. V. Huynh, Dr. M. A. Hiskey, E. L. Hartline, D. P. Montoya
Dynamic Experiment Division
DX-2: Materials Dynamics Group, MS C920
Los Alamos National Laboratory
Los Alamos, NM 87545 (USA)
Fax: (+1) 505-667-0500
E-mail: huynh@lanl.gov
hiskey@lanl.gov

Dr. R. Gilardi
Laboratory for the Structure of Matter
The Naval Research Laboratory
Washington, DC 20375 (USA)

[**] This work was supported by the Joint DOD/DOE Office of Munitions Program for the preparation and characterization of new energetic materials.

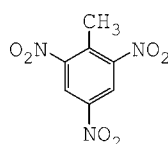

PETN


$$\text{OB}_{\text{CO}} = +15.18 \%$$

$$\rho = 1.78 \text{ g cm}^{-3}$$

$$\Delta H_f = -593 \text{ kJ mol}^{-1}$$

$$\text{N}(\Delta H_f) = -20.45 \text{ kJ atom}^{-1}$$

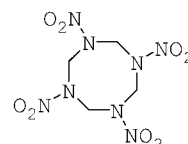
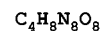

TNT


$$\text{OB}_{\text{CO}} = -17.17 \%$$

$$\rho = 1.65 \text{ g cm}^{-3}$$

$$\Delta H_f = -64 \text{ kJ mol}^{-1}$$

$$\text{N}(\Delta H_f) = -3.05 \text{ kJ atom}^{-1}$$

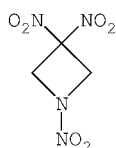

 β -HMX


$$\text{OB}_{\text{CO}} = 0.00 \%$$

$$\rho = 1.91 \text{ g cm}^{-3}$$

$$\Delta H_f = +75 \text{ kJ mol}^{-1}$$

$$\text{N}(\Delta H_f) = +2.68 \text{ kJ atom}^{-1}$$

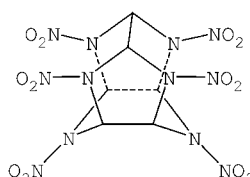
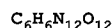
Scheme 1. Traditional energetic polynitro compounds.^[3a]

TNAZ


$$\text{OB}_{\text{CO}} = +8.33 \%$$

$$\rho = 1.86 \text{ g cm}^{-3}$$

$$\Delta H_f = +21 \text{ kJ mol}^{-1}$$

$$\text{N}(\Delta H_f) = +1.24 \text{ kJ atom}^{-1}$$

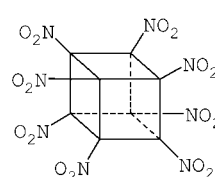

 ϵ -CL-20


$$\text{OB}_{\text{CO}} = +10.95 \%$$

$$\rho = 2.04 \text{ g cm}^{-3}$$

$$\Delta H_f = +377 \text{ kJ mol}^{-1}$$

$$\text{N}(\Delta H_f) = +10.47 \text{ kJ atom}^{-1}$$

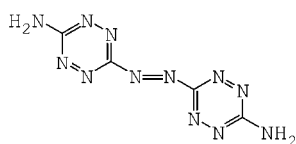

ONC


$$\text{OB}_{\text{CO}} = +27.58 \%$$

$$\rho = 1.979 \text{ g cm}^{-3}$$

$$\Delta H_f = +594 \text{ kJ mol}^{-1} \text{ (calc)}$$

$$\text{N}(\Delta H_f) = +18.56 \text{ kJ atom}^{-1}$$

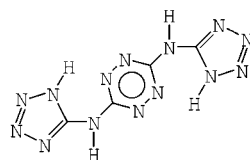
Scheme 2. Modern energetic polynitro compounds.^[3b]

DAAT


$$\text{OB}_{\text{CO}} = -43.60 \%$$

$$\rho = 1.78 \text{ g cm}^{-3}$$

$$\Delta H_f = +862 \text{ kJ mol}^{-1}$$

$$\text{N}(\Delta H_f) = +43.10 \text{ kJ atom}^{-1}$$

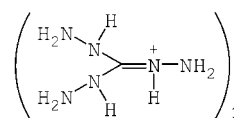

BTATz


$$\text{OB}_{\text{CO}} = -38.68 \%$$

$$\rho = 1.76 \text{ g cm}^{-3}$$

$$\Delta H_f = +883 \text{ kJ mol}^{-1}$$

$$\text{N}(\Delta H_f) = +40.14 \text{ kJ atom}^{-1}$$


TAG-AT


$$\text{OB}_{\text{CO}} = -55.56 \%$$

$$\rho = 1.60 \text{ g cm}^{-3}$$

$$\Delta H_f = +1075 \text{ kJ mol}^{-1}$$

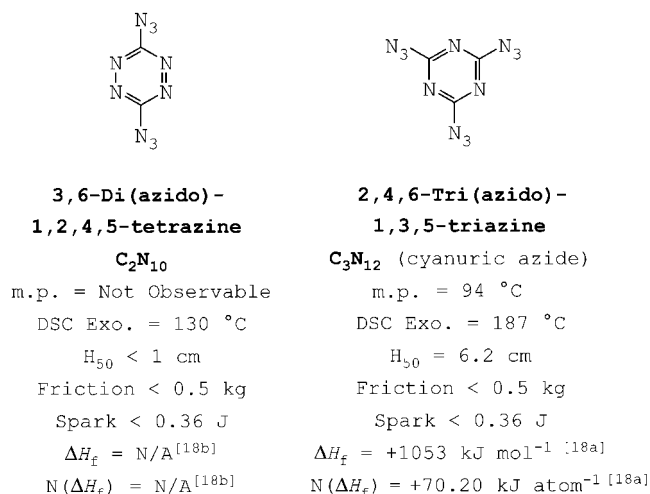
$$\text{N}(\Delta H_f) = +24.43 \text{ kJ atom}^{-1}$$

Scheme 3. High-nitrogen compounds.^[3c]

morph has two conformers whose azido substituents orient in different directions (Figure 3).

Reminiscent of 3,6-di(azido)1,2,4,5-tetrazine and cyanuric azide, none of the azido substituents of **3** and **4** tautomerize to form fused tetrazolo rings even though they were heated in polar solvents.

The hydrazo linkage in **3** and azo linkage in **4** result in a non-observable melting point up to their fast decomposition at 200 and 202 °C (DSC), respectively. Consequently, the azo and hydrazo linkages have significantly decreased volatility and increased melting point relative to cyanuric azide.



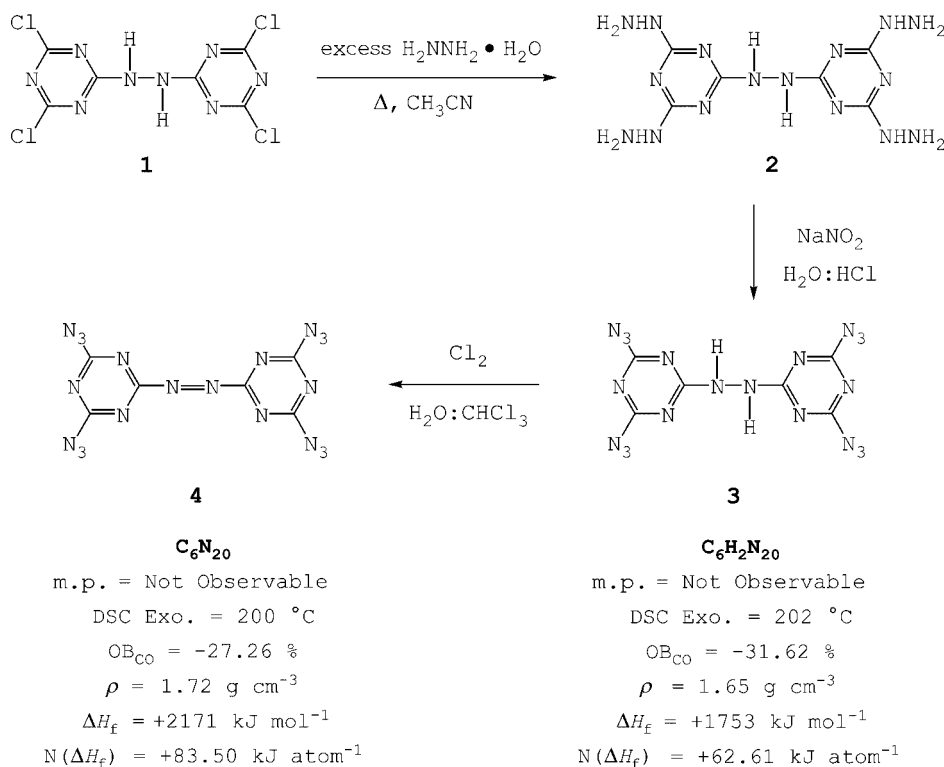
Scheme 4. Energetic materials containing azido groups. DSC Exo. = differential scanning calorimetry exotherm

Remarkably, the experimentally measured heat of formation for **4** (Scheme 5) is the highest reported for energetic materials.^[18] As shown by the ΔH_f data in ref. [16] and Scheme 5, the replacement of four hydrazino by four azido substituents in the hydrazo-1,3,5-triazine compound (**2**→**3**) increases the energy by 1347 kJ mol⁻¹, and 418 kJ mol⁻¹ is gained in the transformation from **3** into **4** (Scheme 6).

For comparison, the explosive properties and sensitivity of reference PETN, (Figure 1), cyanuric azide, **3**, and **4** are given in Table 1.^[10]

Cyanuric azide is extremely sensitive to friction and spark, and its impact is a half less than that of PETN. Compound **3** is spark sensitive, but its impact and friction are three and six times less sensitive than those of cyanuric azide, respectively (Table 1). The impact and spark sensitivity of **4** are comparable to cyanuric azide, but its friction sensitivity is at least five times less than that of cyanuric azide (Table 1).

The compounds in this study are novel and important in demonstrating that the hydrazo and azo linkages can be



Scheme 5. Preparation and properties of **3** and **4**.

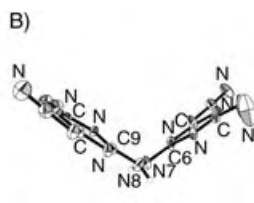
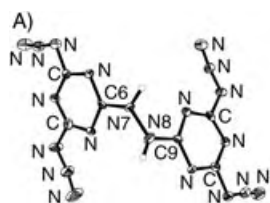


Figure 1. A) ORTEP diagram (thermal ellipsoids set at 25% probability) for **3**, B) end-on view: the central torsion angle C6-N7-N8-C9 is 105°, and the two halves of the molecule are fairly planar.

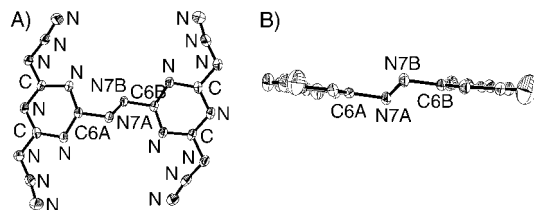


Figure 2. The α-polymorph of **4**: A) ORTEP diagram (thermal ellipsoids set at 25% probability) of **4**, B) an edge-on view of the molecule, showing the “step” in the azo chain that connects the two separate, essentially planar halves of the molecule.

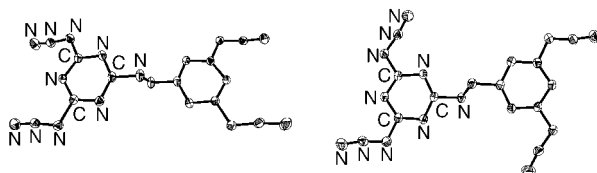
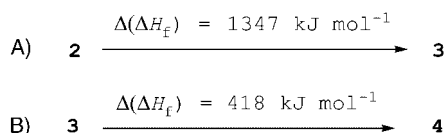


Figure 3. ORTEP diagrams (thermal ellipsoids set at 25% probability) and labeling scheme of the β polymorph crystallized in two conformers for **4**. Both molecules sit on a center of symmetry, and neither molecule is completely planar.



Scheme 6. A) $\Delta E_{\text{substitution}}$ from the hydrazino to azido substituent and B) $\Delta E_{\text{transformation}}$ from the hydrazo to azo linkage.

Table 1: Explosive properties and sensitivity.

Compound	DSC fast decomp [°C]	Impact H_{50} (Type 12) [cm]	Friction (BAM) [Kg]	Spark [J]
PETN	178	14.5	5.4	> 0.36
cyanuric azide	187	6.2	< 0.5	< 0.36
3	202	18.3	2.9	< 0.36
4	200	6.2	2.4	< 0.36

utilized to desensitize and to decrease volatility of polyazido compounds. The compound 4,4',6,6'-tetra(azido)azo-1,3,5-triazine (**4**) has the highest measured heat of formation.

Received: April 19, 2004

Keywords: azides · explosives · heat of formation · high energy-density materials (HEDM) · nitrogen

- [1] a) OB_{CO} is an index of the deficiency or excess of oxygen in a compound required to convert all C into CO and all H into H_2O . For a compound with the molecular formula of $C_aH_bN_cO_d$, $OB_{CO}(\%) = 1600[(d - a - 1/2b)FW^{-1}]$; b) A normalized heat of formation ($N(\Delta H_f)$ in kJ atom^{-1}) is calculated from the heat of formation divided by the number of atoms in a compound.
- [2] J. Köhler, R. Meyer, *Explosivstoffe*, 7th ed., Wiley-VCH, Weinheim, 1991.
- [3] a) PETN = pentaerythritol tetranitrate; TNT = 2,4,6-trinitrotoluene; β -HMX = octahydro-1,3,5,7-tetranitro-1,3,5,7-tetrazocine; b) TNAZ = 1,3,3-trinitroazetidine; ϵ -CL-20 = 2,4,6,8,10,12-hexanitro-2,4,6,8,10,12-hexaaza-tetracyclo[5.5.0.0.5,9.0.3,11]-dodecane; ONC = octanitrocubane; c) DAAT = diaminoazotetrazine or 3,3'-azobis(6-amino-1,2,4,5-tetrazine); BTATz = 3,6-bis(1H-1,2,3,4-tetrazol-5-ylamino)-1,2,4,5-tetrazine; TAG-AT = triaminoguanidinium-5,5'-azobis(1H-tetrazolate).
- [4] a) T. G. Archibald, R. Gilardi, K. Baum, C. George, *J. Org. Chem.* **1990**, 55, 2920–2924; b) A. T. Nielsen, A. P. Chafin, S. L. Christian, D. W. Moore, M. P. Nadler, R. A. Nissan, D. J. Vanderah, R. D. Gilardi, C. F. George, J. L. Flippen-Anderson,

- Tetrahedron* **1998**, 54, 11793–11812; c) R. L. Simpson, P. A. Urtiew, D. L. Ornellas, G. L. Moody, K. J. Scribner, D. M. Hoffman, *Propellants Explos. Pyrotech.* **1997**, 22, 249–255; d) M.-X. Zhang, P. E. Eaton, R. Gilardi, *Angew. Chem.* **2000**, 112, 422–426; *Angew. Chem. Int. Ed.* **2000**, 39, 401–404; e) P. E. Eaton, M.-X. Zhang, R. Gilardi, N. Gelber, S. Iyer, R. Surapaneni, *Propellants Explos. Pyrotech.* **2000**, 27, 1–6; f) A. M. Astakhov, R. S. Stepanov, A. Y. Babushkin, *Combust. Explos. Shock Waves* **1998**, 34, 85–87; g) J. Zhang, H. Xiao, X. Gong, *J. Phys. Org. Chem.* **2001**, 14, 583–588.
- [5] a) D. E. Chavez, M. A. Hiskey, R. D. Gilardi, *Angew. Chem.* **2000**, 112, 1861–1863; *Angew. Chem. Int. Ed.* **2000**, 39, 1791–1793, and references therein; b) M. A. Hiskey, N. Goldman, J. R. Stine, *J. Energ. Mater.* **1998**, 16, 119–127; c) D. E. Chavez, L. G. Hill, M. A. Hiskey, S. A. Kinkad, *J. Energ. Mater.* **2000**, 18, 219–236.
- [6] K. O. Christe, W. W. Wilson, J. A. Sheehy, J. A. Boatz, *Angew. Chem.* **1999**, 111, 2112–2118; *Angew. Chem. Int. Ed.* **1999**, 38, 2004–2009, and references therein.
- [7] A. Hammere, T. M. Klapötke, H. Nöth, M. Warchhold, *Propellants Explos. Pyrotech.* **2003**, 28, 165–173, and references therein.
- [8] J. Neutz, O. Grosshardt, S. Schäufele, H. Schuppler, W. Schweikert, *Propellants Explos. Pyrotech.* **2003**, 28, 181–188, and references therein.
- [9] a) D. E. Chavez, M. A. Hiskey, D. Naud, *Propellants Explos. Pyrotech.* **2004**, in press; b) A. Hammerl, T. M. Klapötke, H. Nöth, M. Warchhold, *Inorg. Chem.* **2001**, 40, 3570–3575.
- [10] a) For an explanation of methods for characterizing explosive sensitivity, see R. T. Paine, W. Koestle, T. T. Borek, E. Duesler, M. A. Hiskey, *Inorg. Chem.* **1999**, 38, 3738–3743; b) Definition of H_{50} : the height in centimeters at which the probability of an explosion is 50%—determined by a drop-weight machine or drop-hammer to evaluate impact sensitivity. In the test, a 2.5-kg weight is dropped from a set height onto a 40-mg sample of an explosive placed on 150-grit garnet sandpaper. A series of drops is made from different heights and an explosion or non-explosion is recorded; the test results are summarized as H_{50} .
- [11] a) R. Haiges, J. A. Boatz, A. Vij, M. Gerken, S. Schneider, T. Schroer, K. O. Christe, *Angew. Chem.* **2003**, 115, 6027–6031; *Angew. Chem. Int. Ed.* **2003**, 42, 5847–5851; b) R. Haiges, A. Vij, J. A. Boatz, S. Schneider, T. Schroer, M. Gerken, K. O. Christe, *Chem. Eur. J.* **2004**, 10, 508–517; c) K. O. Christe, J. A. Boatz, M. Gerken, R. Haiges, S. Schneider, T. Schroer, F. S. Tham, A. Vij, V. Vij, R. I. Wagner, W. W. Wilson, *Inorg. Chem.* **2001**, 41, 4275–4285.
- [12] a) T. M. Klapötke, B. Krumm, H. Piotrowski, K. Polborn, G. Holl *Chem. Eur. J.* **2003**, 9, 687–694; b) W. Fraenk, T. M. Klapötke, B. Krumm, H. Nöth, M. Suter, M. Warchhold, *J. Chem. Soc. Dalton Trans.* **2000**, 4635–4638; c) T. M. Klapötke, H. Nöth, T. Schütt, M. Warchhold, *Angew. Chem.* **2000**, 112, 2197–2199; *Angew. Chem. Int. Ed.* **2000**, 39, 2108–2109; d) W. Fraenk, T. Habereeder, A. Hammerl, T. M. Klapötke, B. Krumm, P. Mayer, H. Nöth, M. Warchhold, *Inorg. Chem.* **2001**, 40, 1334–1340; e) C. Aubauer, T. M. Klapötke, H. Nöth, A. Schulz, M. Suter, J. Weigand, *Chem. Commun.* **2000**, 2491–2492; f) T. M. Klapötke, B. Krumm, P. Mayer, I. Schwab, *Angew. Chem.* **2003**, 115, 6024–6026; *Angew. Chem. Int. Ed.* **2003**, 42, 5843–5846.
- [13] H. J. Marcus, A. Remanick, *J. Org. Chem.* **1963**, 28, 2372–2375.
- [14] E. Ott, E. Ohse, *Ber. Dtsch. Chem. Ges.* **1921**, 54, 179–186.
- [15] P. Loew, C. D. Weis, *J. Heterocycl. Chem.* **1976**, 13, 829–833.
- [16] Characterization: **2**: Elemental analysis (%) calcd for $C_6H_{14}N_{16}$: C 23.23, H 4.55, N 72.23; found: C 23.47, H 4.65, N 70.36, ΔH_f : $406(\pm 5) \text{ kJ mol}^{-1}$, IR (cm^{-1}): $\tilde{\nu}(\text{N-H})$ 3312 (s), 3269 (s); $\tilde{\nu}(\text{triazine})$ 1571 (vs), 1523 (vs), 1073 (vs), 941 (vs), 801 (vs), ^{13}C NMR (75 MHz, $[D_6]\text{DMSO}/\text{CDCl}_3/\text{D}_2\text{O}$, 25°C): $\delta = 164.9$, 165.4, 167.7 ppm. **3**: Elemental analysis (%) calcd for $C_6H_2N_{20}$: C

20.34, H 0.57, N 79.09; found: C 20.04, H 0.75, N 79.44, ΔH_f : 1753(± 3) kJ mol⁻¹, IR (cm⁻¹): $\tilde{\nu}(\text{N}_3)$ 2172 (vs), 2129 (vs), $\tilde{\nu}(\text{N-H})$ 3221 (s), 3091 (s); $\tilde{\nu}(\text{triazine})$ 1541 (vs), 1352 (vs), 1252 (vs), 972 (vs), 806 (vs), ¹H NMR (300 MHz, [D₆]DMSO, 25 °C): δ = 10.59 ppm, ¹³C NMR (75 MHz, [D₆]DMSO, 25 °C): δ = 168.3, 169.6, 170.2 ppm. **4**: Elemental analysis (%) calcd for C₆N₂₀: C 20.46, H 0.00, N 79.54; found: C 20.82, H 0.07, N 79.18, ΔH_f : 2171(± 10) kJ mol⁻¹, IR (cm⁻¹): $\tilde{\nu}(\text{N}_3)$ 2208 (vs), 2155 (vs), 2132 (vs); $\tilde{\nu}(\text{triazine})$ 1549 (vs), 1521 (vs), 1435 (vs), 1161 (vs), 1011 (vs), 823 (vs), ¹³C NMR (75 MHz, [D₆]DMSO, 25 °C): δ = 173.7, 176.4 ppm.

- [17] CCDC-235587 (**3**) and CCDC-235586 and CCDC-235588 (α and β polymorphs of **4**) contain the supplementary crystallographic data for this paper. These data can be obtained free of charge via www.ccdc.cam.ac.uk/conts/retrieving.html (or from the Cambridge Crystallographic Data Centre, 12 Union Road, Cambridge CB21EZ, UK; fax: (+44)1223-336-033; or deposit@ccdc.cam.ac.uk).
- [18] a) Cyanuric azide: $\Delta H_f = +1053$ kJ mol⁻¹ ($N(\Delta H_f) = 70.20$ kJ atom⁻¹) obtained from E. G. Gillan, *Chem. Mater.* **2000**, *12*, 3906–3912; b) Although the heat of formation for 3,6-di(azido)-1,2,4,5-tetrazine is the only one that is predicted to be higher than that for **4**, the material is too sensitive to work with. A detonation occurred even when 70 %:30 % (wt/wt) benzoic acid:3,6-di(azido)-1,2,4,5-tetrazine was gently mixed in water.

Protein-Inorganic Conjugates

Synthesis and Self-Assembly of Organoclay-Wrapped Biomolecules**

Avinash J. Patil, Eswaramoorthy Muthusamy, and Stephen Mann*

Protein-based nanostructures are expected to play a key role in the development of multifunctional materials and devices for bio-nanotechnological applications.^[1–3] Although proteins excel in functional specificity, their structural and chemical sensitivity to ambient conditions can seriously compromise the use and integration of such macromolecules in diverse

applications. Although there are numerous reports on the enhanced thermal and chemical stability of proteins by immobilization on surfaces^[4–8] or within matrices such as amorphous gels^[9–11] and layered solids,^[12,13] the wrapping of individual protein/enzyme molecules with inorganic materials to produce functionally isolated hybrid nanoparticles has not been reported. Herein we describe investigations that strongly suggest that individual molecules of met-myoglobin (Mb), haemoglobin (Hb) or glucose oxidase (GOx) can be wrapped with an ultrathin shell of an aminopropyl-functionalized magnesium (organo)phyllosilicate to produce aqueous dispersions of discrete protein–inorganic nanoparticles. Similar procedures but with organoclay oligomers that have pendent long-chain hydrophobic moieties result in self-assembly of the protein–inorganic nanoparticles into higher-order superstructures. In each case, the encapsulated proteins are structurally and functionally intact and show enhanced thermal stability up to temperatures of 85 °C.

In general, “armour-plated” protein/enzyme molecules were prepared by mixing solutions of Mb, Hb, or GOx with aqueous solutions containing oligomers of a positively charged exfoliated organoclay (Figure 1). The organoclay was prepared by chemical synthesis^[14,15] (see Experimental Section) and consisted of a highly disordered talclike 2:1 trioctahedral smectite structure with a central brucite sheet of octahedrally coordinated MgO/OH chains overlaid on both sides with an aminopropyl-functionalized silicate network to give an approximate unit cell composition of $[\text{H}_2\text{N}(\text{CH}_2)_3]_8\text{Si}_8\text{Mg}_6\text{O}_{16}(\text{OH})_4$. Protonation of the amino groups by dispersion of the clay in water resulted in exfoliation and partial disintegration of the organoclay layers into cationic oligomers that were fractionated by gel chromatography to produce stable transparent sols that were subsequently added to protein/enzyme solutions.

For each protein/enzyme investigated, TEM studies showed the presence of discrete electron-dense nanoparticles randomly arranged across the support film of the grid (Figure 2a–c). EDX analysis for samples prepared in the presence of Mb or Hb, confirmed that the nanoparticles comprised both protein (Fe, S) and organoclay (Si, Mg, Cl) species (Figure 2d). In general, the nanoparticles were spheroidal and monodisperse in size with mean dimensions of 4.0 nm ($\sigma = 0.6$ nm), 7.8 nm ($\sigma = 0.8$) and 6.4 ($\sigma = 0.9$ nm) for Mb, Hb and GOx samples, respectively. The variation in nanoparticle size showed a direct correlation with the respective molecular dimensions of the different proteins/enzyme (Mb, $4.5 \times 3.5 \times 2.5$ nm; Hb, $6.5 \times 5.4 \times 5.3$ nm; GOx, $6.0 \times 5.2 \times 3.7$ nm), which suggests that each nanoparticle consisted of a single biomolecule wrapped by a continuous sheet of condensed organoclay oligomers. Significantly, no organoclay nanoparticles were observed in the absence of the proteins or enzyme, suggesting that condensation of the magnesium (aminopropyl)phyllosilicate oligomers was specifically promoted by interactions with the biomolecule surface.

Analytical ultracentrifugation of the Mb–organoclay nanoparticles showed a single peak with a sedimentation coefficient (s^*) value of 1.5 S, thus indicating a narrow distribution in size and shape of the hybrid structures. The

[*] A. J. Patil, Dr. E. Muthusamy, Prof. S. Mann
School of Chemistry
University of Bristol
Bristol BS8 1TS (UK)
Fax: (+44) 117-929-0509
E-mail: s.mann@bristol.ac.uk

[**] We thank Dr. T. Ikoma (National Institute for Materials Science, Biomaterials Center, Tsukuba, Japan), Dr. D. Scott, Mrs G. Shaw and Dr. A. M. Seddon (University of Bristol) for help with CD spectroscopy, AUC, mass spectroscopy, and enzyme kinetics, respectively. The EPSRC (UK), Max Planck Society, and University of Bristol (ORS award to A.J.P.) are acknowledged for their financial support.

Supporting information for this article is available on the WWW under <http://www.angewandte.org> or from the author.

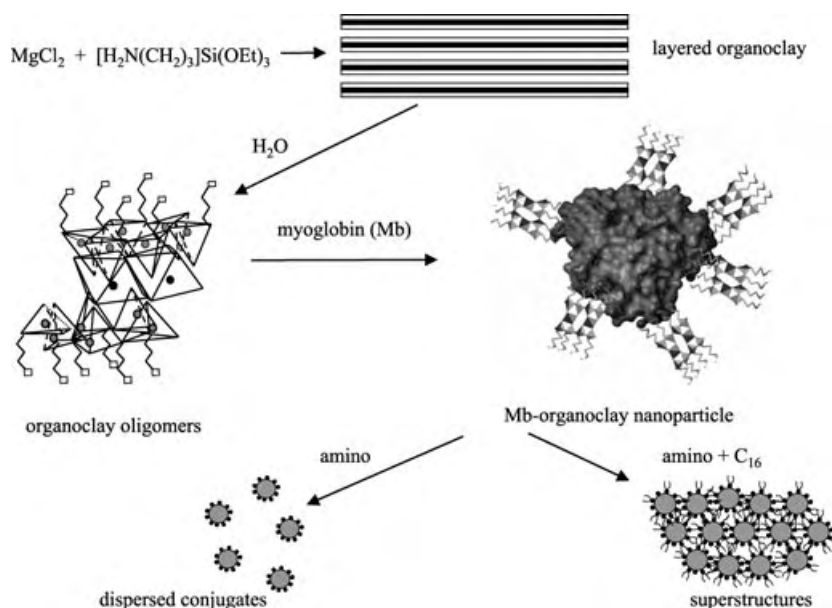


Figure 1. Scheme showing proposed molecular wrapping of Mb molecules by cationic organoclay oligomers with an about 1.6-nm-thick layer structure. Tessellation of the entire protein by binding of the organoclay sheet surface (*ab* face, $a = 0.53$ nm, $b = 0.91$ nm, $\chi = 90^\circ$) requires approximately 30 unit cells. Wrapping with aminopropyl-functionalized organoclay oligomers produces dispersed protein–organoclay nanoparticles, whereas hydrophobic interactions between the exposed C_{16} chains of the aminopropyl/hexadecyl-functionalized oligomers result in nanoparticle self-assembly into partially ordered superstructures.

sedimentation coefficient was reduced compared with native Mb ($s^* = 2.5$ S), which suggests a larger friction coefficient (viscous drag) due to an increase in surface roughness. This was consistent with the proposed core–shell structural model for the organoclay–protein nanoparticles. MALDI-TOF mass spectrometry showed primary peaks for intact Mb (16.9 k) as well as a distribution of organoclay oligomers principally in the mass/charge range of 400 to 700. Studies by using circular dichroism (CD) and FTIR spectroscopies indicated that the secondary structures of Mb, Hb, or GOx molecules were preserved within the organoclay–protein conjugates. For example, CD spectra of solutions of native met-Mb and Mb–organoclay nanoparticles showed characteristic bands^[10] for the π – π^* amide transitions at 192 nm and 209 nm, as well as an α -helical n – π^* amide transition at 220 nm (Figure 3a). Similarly, FTIR spectra of the nanoparticles obtained by solvent evaporation showed no changes in the protein amide I ($C=O$ str) and amide II ($N-H$ def, $C-N$ str) bands at 1653 cm^{-1} and at 1554 cm^{-1} , respectively. The spectra also showed absorption bands for CH_2 (2800 cm^{-1}), $Si-C$ (1150 cm^{-1}), $Si-O-Si$ (1025 cm^{-1}), and $Mg-O$, $Si-O$, $Si-O-Mg$ (564 – 482 cm^{-1}) vibrations, confirming that condensed magnesium (aminopropyl)phyllosilicate moieties were associated with the protein/enzyme molecules.

The functional integrity and accessibility of the nanoparticle conjugates to small molecules and ions were assessed by UV/Vis spectroscopy. Solutions of the Mb- or Hb-organoclay nanoparticles showed a distinct π – π^* solet band at 408 nm associated with an intact haem prosthetic group, which showed a characteristic shift to 433 nm on formation, for example, of deoxy-Mb by dithionite reduction (Figure 3b and Supporting Information). Reversible binding

of carbon monoxide under argon to the deoxy-Mb(Hb)–organoclay conjugate resulted in a shift in the solet band from 433 nm to 422 nm, which was further shifted after exposure to dioxygen to a value of 416 nm (Figure 3c and Supporting Information), consistent with the formation of oxy-Mb or oxy-Hb.^[10] Characteristic changes in the α and β absorption bands at around 580 and 545 nm were also observed. The enzymatic activities of native GOx and GOx–organoclay nanoparticles were monitored spectrophotometrically at 414 nm to determine the initial rates (V) for a range of substrate (S) concentrations (see Experimental Section). In both cases, plots of $1/V$ against $1/[S]$ showed characteristic linear plots consistent with Michaelis–Menton kinetics (Supporting Information). The corresponding values for V_{\max} were similar (free GOx, $2.7\text{ }\mu\text{mol}\cdot\text{min}^{-1}$; conjugated GOx, $2.95\text{ }\mu\text{mol}\cdot\text{min}^{-1}$), thus indicating that the turnover rate at substrate saturation was not significantly affected by interactions with the organoclay. In contrast, the K_m constant associated with the activity of the GOx–organoclay

nanoparticles was higher ($500\text{ }\mu\text{M}$) compared with free enzyme ($370\text{ }\mu\text{M}$), which suggests that glucose binding was partially inhibited at intermediate substrate concentrations possibly by restricted diffusion through the organoclay shell of the hybrid conjugate. Measurements of relative enzyme activities at different pH values showed a nonlinear dependence with a small (5–10%) enhancement for the GOx nanoparticles in acid or alkaline conditions compared with the free enzyme in solution (Figure 3d).

The thermal stabilities of organoclay-conjugated met-Mb or Hb molecules were assessed by temperature-dependent UV/Vis spectroscopy measurements of the intensity of the solet band.^[16] Compared with room-temperature values, native Mb and Hb showed, respectively, a 49% or 25% reduction in the intensity of the band at 408 nm after 5 min at 85°C , which is consistent with significant unfolding of the polypeptide chains.^[13] In contrast, a decrease of only 10% or 5% in the intensity of the solet band were observed over this temperature range for the met-Mb- or Hb–organoclay nanoparticles, respectively, (Figure 3e), thus indicating a marked increase in thermal stability of the encapsulated protein molecules. Similarly, an increased retention in the activity of GOx–organoclay nanoparticles compared with the native enzyme in solution was observed at elevated temperatures (Figure 3f). Although in both cases, the relative activities were compromised at temperatures above 60°C , the relative activity of the GOx nanoparticles was at least 10% higher even at 85°C .

The above results indicate that individual protein/enzyme molecules interact in solution with magnesium (aminopropyl)phyllosilicate oligomers to produce hybrid nanoparticles with preserved protein structure and function, and enhanced

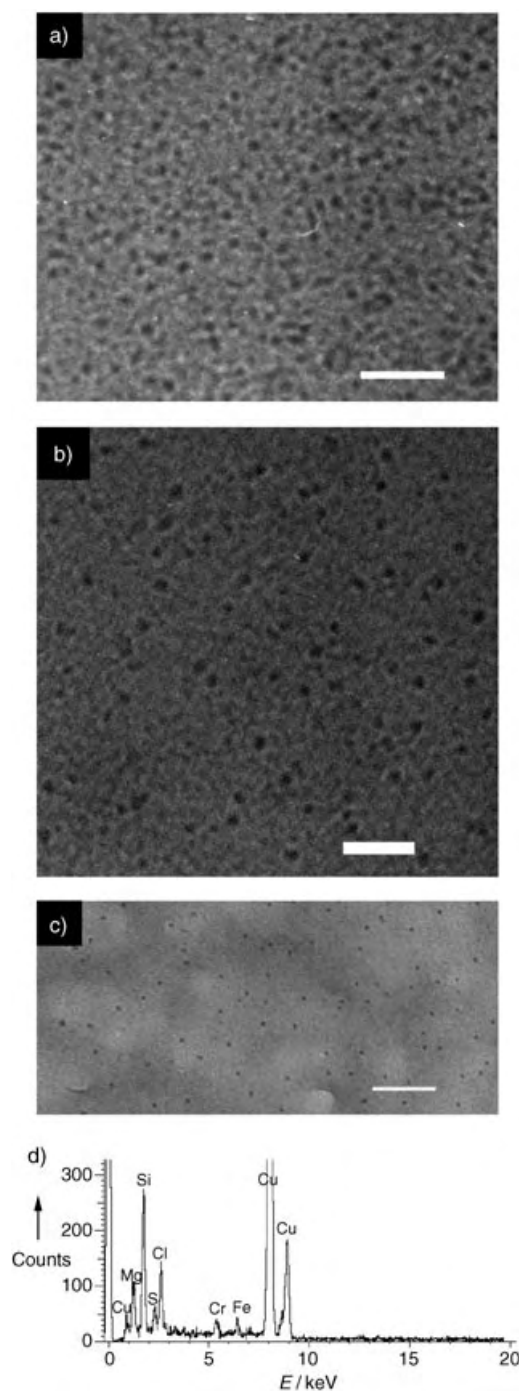


Figure 2. TEM images showing discrete protein-organoclay nanoparticles. a) Mb, b) Hb, and c) GOx.; scale bars = 50, 100, and 100 nm, respectively. d) corresponding EDX analysis for Mb-organoclay nanoparticles. Peaks for Cu and Cr in the EDX spectrum are from the sample holder.

thermal stability. Although further work is required to confirm the proposed structural model and putative wrapping mechanism, electrostatic interactions appear to be in part responsible for conjugation as hybrid nanoparticles were only produced when negatively charged native biomolecules [zeta potential measurements; Mb, -25 mV (pH 8.5); Hb, -26 mV (pH 8.5); GOx, -20 mV (pH 6)] were used in the presence of

the positively charged organoclay oligomers ($+12$ mV (pH 8.5). This mechanism was consistent with the observed absence of hybrid nanoparticles in the presence of cytochrome *c* (zeta potential = $+4$ mV at pH 8.5), as well as a reduction in the zeta potentials for Mb, Hb, and GOx-containing nanoparticles to values of -18 , -0.5 and $+1.8$ mV, respectively. A similar electrostatic model has recently been proposed to account for the wrapping of viologen polymer molecules within a sheath of partially condensed sodium silicate.^[17,18]

Finally, self-assembled superstructures of the Mb-organoclay nanoparticles were produced by replacing about 50% of the aminopropyl groups in the clay structure with covalently attached hydrophobic hexadecyl groups (see Experimental Section). Although the extent of exfoliation was reduced compared with the 100% aminopropyl-functionalized clay, TEM and EDX analysis showed the presence of self-organized protein-organoclay superstructures that consisted of close packed layers of discrete 4.5 nm-sized nanoparticles separated by an interparticle spacing of 4 to 5 nm (Figure 4). This spacing is commensurate with a bilayer of hexadecyl chains as shown from XRD studies of the aminopropyl/hexadecyl magnesium (organo)phyllosilicate clay that revealed an interlayer d_{001} spacing of 4.6 nm (data not shown). The results are consistent with the above structural model in which individual biomolecules are encapsulated by an organoclay shell with pendent organic functionalities, and indicate that macroscopic assemblies of protein-organoclay nanoparticles can be prepared by using interparticle hydrophobic interactions to drive the self-assembly process. Preservation of protein structure and function in these organized hybrid materials was confirmed by using the above experimental procedures (see the Supporting Information).

In conclusion, we have demonstrated that novel organoclay-protein conjugates can be prepared in the form of discrete electron-dense nanoparticles. On the basis of our results, we propose a core-shell structural model in which individual biomolecules are wrapped by an inorganic shell of condensed organoclay oligomers. The procedure is facile and could lead to new types of stabilized biomolecules that can be functionally isolated as discrete soluble units, or assembled and integrated into nanostructured materials. In particular, the use of “armour-plated” proteins should circumvent problems arising from the loss of functional isolation associated with adverse intermolecular interactions within interconnected networks of biomolecules. In addition, the enhanced thermal and chemical stability of inorganically wrapped proteins should markedly increase the scope for using protein-based nanostructures in areas such as tissue engineering and biomolecular sensing.

Experimental Section

Organoclay synthesis and exfoliation: Typically, an aminopropyl-functionalized magnesium (organo)phyllosilicate clay was prepared at room temperature by dropwise addition of 3-aminopropyltriethoxysilane (1.3 mL, 5.85 mmol) to an ethanolic solution of magnesium chloride (0.84 g, 3.62 mmol) in ethanol (20 g). The white slurry obtained after 5 min was stirred overnight and the precipitate isolated

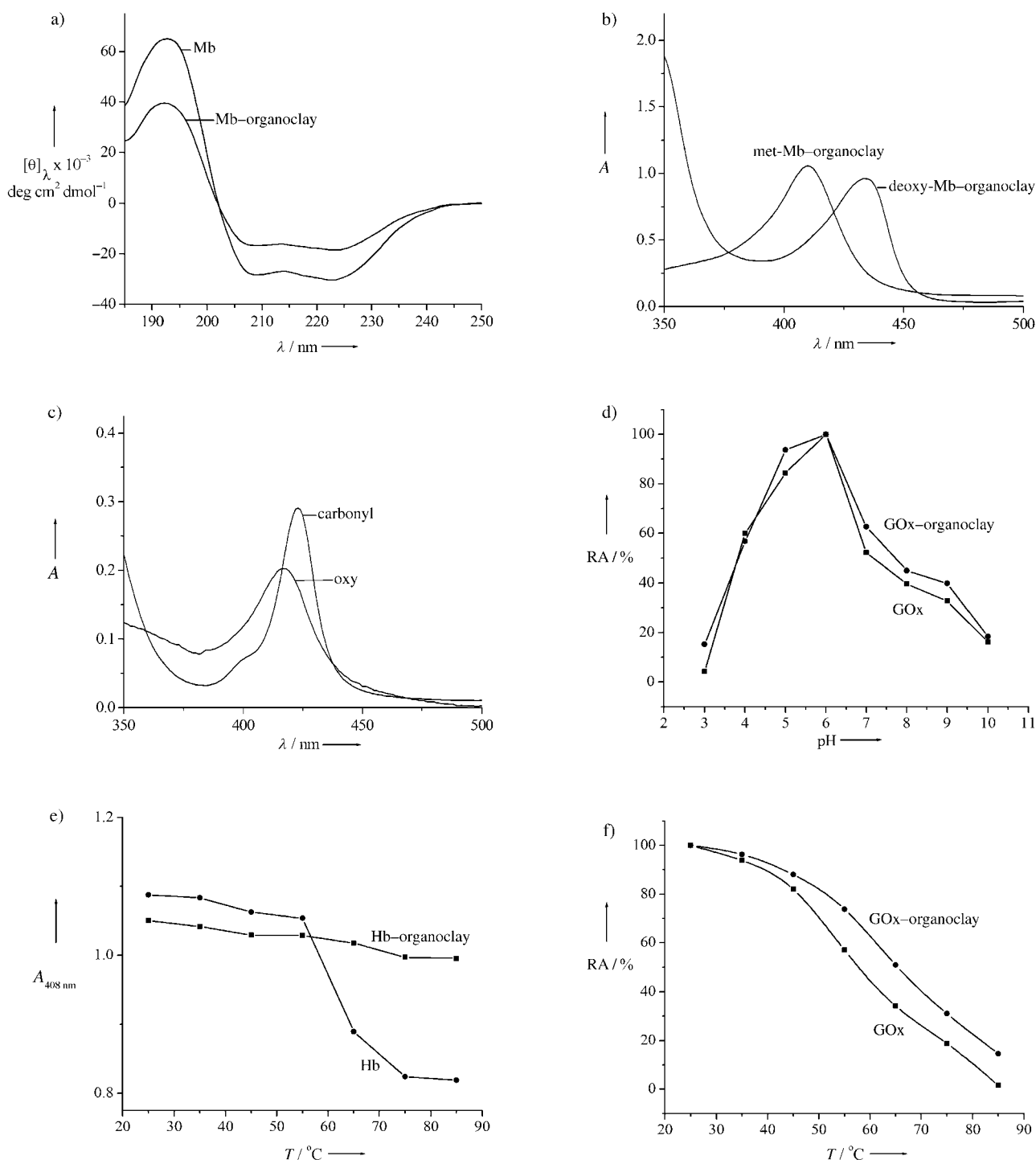


Figure 3. a) CD spectra of solutions of native Mb and Mb-organoclay nanoparticles that show π - π^* amide α -helical n - π^* amide transitions corresponding to intact secondary structures. b) UV/Vis spectra of met-Mb-organoclay conjugates that show Soret band absorptions for as-prepared nanoparticles and after dithionite reduction and formation of deoxy-Mb. c) UV/Vis spectra of Mb-organoclay nanoparticles after CO binding to the deoxy-protein and subsequent O_2 binding and formation of oxy-Mb. d) Plot of relative activity (RA, %) against pH for native GOx (■) and GOx-organoclay nanoparticles (●). e) Plots of absorbance intensity at 408 nm (A_{408}) with temperature for solutions of native Hb (●) and Hb-organoclay nanoparticles (■), showing increased thermal stability of the wrapped protein molecules. Samples were allowed to stand for 5 min at each temperature prior to analysis. f) Plot of relative activity (%) against temperature for native GOx (■) and GOx-organoclay nanoparticles.

by centrifugation, washed with ethanol (50 mL) and dried at 40°C . Exfoliation of the clay was undertaken by dispersing 10 mg of the dried clay in distilled water (10 mL) followed by ultrasonication for 5 mins. The resulting cloudy dispersion was passed through a

sephadex G-25/75 column (Aldrich), and the clear eluate collected and used for experiments with a range of biomolecules.

Organoclays consisting of covalently linked aminopropyl and long-chain hexadecyl groups were prepared by addition with constant

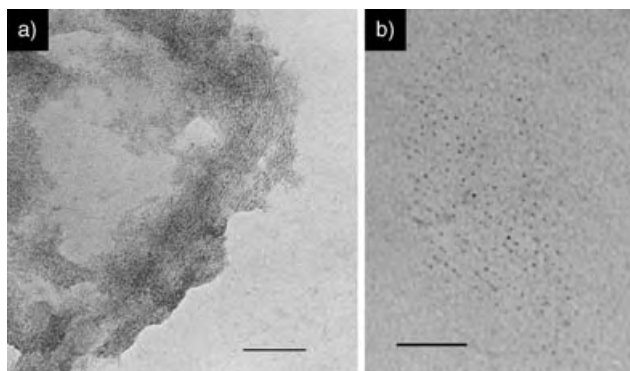


Figure 4. a) TEM image showing self-organized layers of Mb molecules wrapped by magnesium (aminopropyl/hexadecyl)phyllosilicate oligomers. The lamellar structure is viewed side-on such that the interlayer spacing of the superstructure is clearly revealed (arrow); scale bar = 100 nm. b) Corresponding image of a single layer viewed from above showing the presence of superstructural ordering of the protein-organoclay hydrophobic nanoparticles; scale bar = 50 nm.

stirring of a 1:1 molar ratio mixture of hexadecyltrimethoxysilane (1.80 mmol) and 3-aminopropyltriethoxysilane (1.80 mmol) in ethanol (10 g) to magnesium chloride (0.25 g, 1.08 mmol) dissolved in ethanol (10 g), followed by addition of aqueous sodium hydroxide (0.5 M, 20 mL). The reaction mixture was stirred for 24 h at room temperature, after which a finely divided white precipitate was collected by vacuum filtration and washed repeatedly with water and ethanol then dried at 40 °C in air for 24 h. Exfoliation of the bifunctional clay was undertaken by dispersion of 10 mg of a finely ground sample in a water/ethanol (15 mL/5 mL) mixture by ultrasonication for 2 min. (Exfoliation was not successful in pure water due to the highly hydrophobic character of the organoclay particles).

Protein-organoclay nanoparticles: A purified met-Mb aqueous solution (1 mL, 12.4 μ M, horse skeletal muscle (sigma), M_r = 16.9 k, sephadex G-25/75) was added dropwise to the amino-functionalized organoclay eluate (2 mL) to give a clear reddish-brown solution of pH \approx 8.5 of the clay-wrapped protein molecules, which became slightly turbid when left at room temperature for up to 24 h. Similar procedures were also undertaken with purified Hb (1 mL, 47 μ M, bovine (sigma), M_r = 64 k, sephadex G-25/75) and GOx (1 mL, 10 μ M, *Aspergillus niger*, type X-S, EC 1.1.3.4, M_r = 140 k, pH 6) aqueous solutions.

Alternatively, an Mb aqueous solution (1 mL, 10 mg mL⁻¹) was added to the exfoliated dispersion of an aminopropyl/hexadecyl-functionalized organoclay and stirred at room temperature for 5 days at pH \approx 8.5. The precipitate obtained was centrifuged, washed with water and dried at room temperature for two days.

Reduction of met-Mb (or met-Hb) to the deoxy form was undertaken by treating native Mb (10 mL, 0.10 mg mL⁻¹) or Mb-organoclay nanoparticles with sodium dithionite (1 mg) under an argon atmosphere. Binding of carbon monoxide to deoxy-Mb or deoxy-Mb-organoclay conjugate solutions prepared by dithionite reduction was undertaken by purging CO gas through the sample solutions for one hour at room temperature. Subsequent exchange of bound CO by dioxygen was undertaken by passing solutions of the carbonyl-Mb through a sephradex gel column in air.

The rates of oxidation of β -D-glucose to D-gluconolactone and H₂O₂ by native and organoclay-wrapped GOx were determined spectrophotometrically.^[19] Decomposition of H₂O₂ in the presence of horse radish peroxidase (HRP, type II, sigma) and an electron donor dye, 2,2'-azino-bis(3-ethylbenzethiazoline-6-sulfonic acid (ABTS, sigma) was monitored by increases in absorption at 414 nm (A_{414}) associated with formation of oxidized ABTS. Typically, reactions were carried out at 25 °C in 3 mL glass cuvettes at pH 6 by addition of

native GOx oxidase or GOx-organoclay nanoparticles (100 μ L, [GOx] = 10 μ M) to sodium phosphate buffered solutions (1.6 mL, 0.1 M) containing 100 μ L of ABTS (50 mM)/HRP (2.6 μ M, 25 units mL⁻¹) and β -D-Glucose (concentration range, 3.5 μ M to 50 μ M). Changes in A_{414} with time were converted to units of enzyme specific activity (μ mol min⁻¹ mg⁻¹) by using an extinction coefficient of 3.6×10^4 M⁻¹ cm⁻¹. Double reciprocal plots of 1/V (V = initial rate) against 1/[glucose] showed linear behavior consistent with Michaelis-Menton kinetics, and the Michaelis constant (K_M) and maximal rate (V_m) were determined directly from the plots. The above procedure was also carried out with native and organoclay-wrapped GOx under a range of pH values (3 to 10) and temperatures (25 and 85 °C). In each case, the specific activities of free GOx or GOx-organoclay nanoparticles were converted into percentage relative activities based on corresponding values obtained at pH 6 and 25 °C.

The thermal stabilities of native Mb/Hb and Mb/Hb-organoclay nanoparticles were determined by temperature-dependent UV/Vis spectroscopy (Perkin Elmer Lambda II) by using an attached Peltier temperature-control system and monitoring changes in the absorbance intensity of the 408 nm solet band of samples allowed to stand for 5 mins at temperatures between 35 and 85 °C. Temperature-dependent enzyme activities of free GOx and GOx-organoclay conjugates were also determined by using the Peltier control system. Samples were incubated for 5 mins at temperatures between 25 to 85 °C before measuring changes in absorbance changes at 414 nm.

Samples were characterized by TEM (JEOL 1200EX), EDX analysis (Oxford Instruments, ISIS300), and XRD (Bruker-Nonius D8 diffractometer, Cu α radiation, λ = 0.15405 nm). FTIR spectroscopy (Perkin Elmer Spectrum 1) was carried out by using KBr discs. CD spectra were measured at 298 K by using a JASCO model 725 spectrometer with a quartz cell and path length of 10 mm at a scan speed of 50 nm min⁻¹. Zeta potential measurements were undertaken by using a Zetaplus analyser. Analytical ultracentrifugation was carried out by using a Beckman Analytical Centrifuge at 40000 rpm. MALDI-TOF mass spectrometry (PE Biosystems Voyager-DE STR) was undertaken using a nitrogen laser operating at 337 nm. Samples and matrix (0.5 μ L each) were spotted onto a sample plate and calibrated against "Calmix 3" (PE, Biosystems) as external standard. The matrix solution was freshly prepared sinapinic acid (Fluka) at a concentration of 1 mg/100 μ L in a 50:50 mixture of acetonitrile/0.1 % TFA.

Received: January 27, 2004

Revised: April 26, 2004 [Z53868]

Keywords: biological activity · nanoparticles · organic-inorganic hybrid composites · self-assembly

- [1] T. O. Yeates, J. E. Padilla, *Curr. Opin. Struct. Biol.* **2002**, *12*, 464–470.
- [2] T. C. Holme, *Trends Biotechnol.* **2002**, *20*, 16–24.
- [3] J. D. Hartgerink, E. Beniash, S. I. Stupp, *Proc. Natl. Acad. Sci. USA* **2002**, *99*, 5133–5138.
- [4] M. Jiang, B. Nolting, P. S. Stayton, S. G. Sligar, *Langmuir* **1996**, *12*, 1278–1283.
- [5] Y. Zhou, N. Hu, Y. Zeng, J. F. Rusling, *Langmuir* **2002**, *18*, 211–219.
- [6] V. Panchagnula, C. V. Kumar, J. F. Rusling, *J. Am. Chem. Soc.* **2002**, *124*, 12515–12521.
- [7] M. Onda, A. Katsuhiko, T. Kunitake, *J. Biosci. Bioeng.* **1999**, *87*, 69–75.
- [8] F. Caruso, C. Schuler, *Langmuir* **2000**, *16*, 9595–9603.
- [9] I. Gill, A. Ballesteros, *Trends Biotechnol.* **2000**, *18*, 282–296.
- [10] L. M. Ellerby, C. R. Nishida, F. Nishida, A. Yamanaka, B. Dunn, J. S. Valentine, J. Zink, *Science* **1992**, *255*, 1113–1115.

- [11] Q. Gao, S. L. Suib, J. F. Rusling, *Chem. Commun.* **2002**, 2254–2254.
- [12] C. V. Kumar, A. Chaudhari, *J. Am. Chem. Soc.* **2000**, *122*, 830–837.
- [13] C. V. Kumar, A. Chaudhari, *Chem. Commun.* **2002**, 2382–2383.
- [14] S. L. Burkett, A. Press, S. Mann, *Chem. Mater.* **1997**, *9*, 1071–1073.
- [15] N. T. Whilton, S. L. Burkett, S. Mann, *J. Mater. Chem.* **1998**, *8*, 1927–1932.
- [16] G. Acampora, J. Hermans, *J. Am. Chem. Soc.* **1967**, *89*, 1543–1547.
- [17] I. Ichinose, T. Kunitake, *Chem. Rec.* **2002**, *2*, 339–351.
- [18] I. Ichinose, T. Kunitake, *Adv. Mater.* **2002**, *14*, 344–346.
- [19] R. C. Bateman, J. A. Evans, *J. Chem. Educ.* **1995**, *72*(12), A240–A241.

Zeolites

Crystal Structure Determination of Zeolite Nu-6(2) and Its Layered Precursor Nu-6(1)***Stefano Zanardi,* Alberto Alberti, Giuseppe Cruciani, Avelino Corma, Vicente Fornés, and Michela Brunelli*

It is widely known that the properties of a zeolite in catalytic or ion-exchange applications depend largely on the crystal structure of the zeolite. When a catalytic process takes place in a porous system with dimensions in the range 3–12 Å, the reaction pathway is strongly influenced by framework geometry and the steric constraints are fundamental for driving the reaction towards the desired products.^[1,2]

Even though a few extra-large pore zeolites (with channel delimited by more than twelve tetrahedra) have recently been reported, such as CIT-5,^[3] UTD-1,^[4] or ECR-34^[5] (charac-

terized by apertures of 18-membered rings), there are several possible applications that involve molecules larger than the pore dimensions of the available zeolites. To overcome this limitation, mesoporous molecular sieves MCM-41, MCM-48, and MCM-50, with pore dimensions larger (about 30–100 Å) than those of conventional zeolites have been developed.^[6] The alluminosilicates that belong to the mesoporous family M41S have a periodic pore structure (i.e., giving rise to coherent X-ray diffraction), whereas the silica walls are disordered and resemble more the structure of a glass. Unlike conventional zeolites, these materials are not strongly acidic,^[7] but they do show promise as supports in other types of catalysts, such as olefin polymerization.^[8]

Layered zeolitic materials represent another option for treating large molecules. These materials have an advantage in that they combine the good thermal stability of zeolites with active sites of zeolitic nature easily accessible to reactants. In fact, layered zeolitic materials can be pillared or delaminated to produce high-surface-area materials with a majority of their active sites exposed at the crystal surface.^[9–11] Nevertheless, so far, only a few structures of synthetic layered silicates have been reported, mainly for two reasons: 1) solution of the crystal structure by powder diffraction is a very challenging task and the small crystal size typically do not allow single-crystal X-ray diffraction experiments, piperazine silicate EU 19 being the only excellent exception;^[12] 2) as a consequence of the stacking disorder, which occurs between the layers, the powder-diffraction patterns of a layered material often suffer from severe peak broadening that precludes structure solution.

Notwithstanding the above difficulties, there has recently been an increased activity in the structure elucidation of layered materials.^[13–18] Among these materials, those composed by single zeolite sheets like PREFER are particularly interesting,^[16] which after calcination leads to the ordered 3D net of the FER-type zeolite. A very similar behavior was reported for the borosilicate named ERB-1,^[19] isostructural to MCM-22, the precursor of which is layered in 2D, and the 3D network is formed upon calcination through the condensation of the silanol groups located on the layer surface. Other examples of layered zeolite precursors are EU 19,^[12] precursor of the structurally unknown EU 20,^[20] its recently reported analogue MCM-69,^[17] and the hydrous layer silicate kanemite, a precursor of the industrial ion exchanger SKS-6.^[18]

In the early 1980s, Whittam reported the synthesis of new zeolite materials designated Nu-6(1) and Nu-6(2) by using 4,4'-bipyridyne as a structure-directing agent,^[21] at the temperatures of 200 °C Nu-6(1) can be converted to Nu-6(2). A wide range of hydrocarbon-conversion catalysts can be prepared from zeolite Nu-6(1) or Nu-6(2) by ion exchange or impregnation with cations.^[21] Such catalysts can find application in different process (e.g., catalytic dewaxing, disproportionation, isomerisation of alkanes and alkyl benzenes) in particular Nu-6(2) showed superior activity as catalyst for xylenes isomerization and the like.^[21,22] According to Corma et al., a new delaminated stable zeolite, referred to as ITQ-18, can be obtained after expansion and exfoliation of Nu-6(1).^[23] ITQ-18 shows a very-large external surface area,

[*] Dr. S. Zanardi, Prof. A. Alberti, Prof. G. Cruciani
Sez. di Mineralogia, Petrologia e Geofisica
Dip. Scienze della Terra
Università degli Studi di Ferrara
44100 Ferrara (Italy)
Fax: (+39) 053-221-0161
E-mail: zrs@unife.it

Prof. A. Corma, Dr. V. Fornés
Instituto de Tecnología Química, UPV-CSIC
Universidad Politécnica de Valencia
Avda. de los Naranjos s/n
46022 Valencia (Spain)

Dr. M. Brunelli
ID31, ESRF, 6 Rue Jules Horowitz
BP 220, 38043 Grenoble Cedex 9 (France)

[**] We thank the European Synchrotron Radiation Facility (ESRF) for providing beamtime. Special thanks to BM1 (the Swiss-Norwegian Beam Lines) staff for the kind assistance during data collections. Dr. A. Chica is acknowledged for performing catalytic tests. Dr. R. Rizzi (CNR-IC, Bari) and Dr. V. Ferretti (University of Ferrara) are gratefully thanked for the helpful discussions.

which is confirmed by its absorption of pyridine. This property of ITQ-18 is in contrast to that of Nu-6(2), which has a negligible amount of OH groups that can interact with the probe molecule. In the case of ITQ-18, all bridging OH groups are accessible to pyridine.^[23]

Although the catalytic performance of these materials has been intensively investigated, no crystal structures elucidations were reported so far.

Herein, we describe the crystal structure determination by using X-ray powder diffraction data and synchrotron radiation source of the layered 4,4'-bipyridyl silicate named Nu-6(1) and its calcined form Nu-6(2), which exhibits a new 3D framework topology.

Synchrotron X-ray powder pattern of the Nu-6(1) material was fully indexed by using the program ITO^[24] according to a monoclinic symmetry with the following unit cell parameters: $a = 27.741$, $b = 4.973$, $c = 13.936$ Å and $\beta = 103.72^\circ$ (see Table 1). A careful inspection of the systematic absences revealed that the possible space group was $P2_1/a$ (no. 14 International Tables of Crystallography). The integrated intensities of the as-synthesized compound were extracted by using the method of Le Bail et al.^[25] with the GSAS^[26] Rietveld program and then introduced in the direct methods program SIR97.^[27] Although relabeling of some atoms were necessary, a structural model, in which layers were formed by $[\text{SiO}_4]$ and $[\text{SiO}_3\text{OH}]$ tetrahedra, was readily found. Moreover, a careful examination of the interlayer atoms allowed us to localize fragments of the two crystallographically independent 4,4'-bipyridine molecules (44BPY-1 and 44BPY-2 in Figure 1). Analysis of the Fourier maps and extensive model building were necessary to complete the structural model. The Rietveld refinement was successfully completed in the $P2_1/a$ space group. Figure 2 shows the good agreement between calculated and observed X-ray diffraction

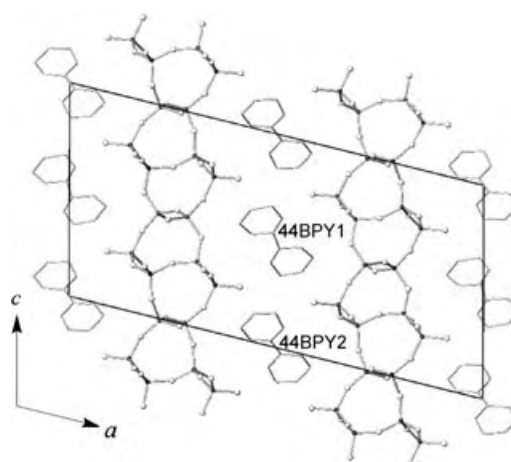


Figure 1. Ball and stick representation of the Nu-6(1) structure along the [010] direction.

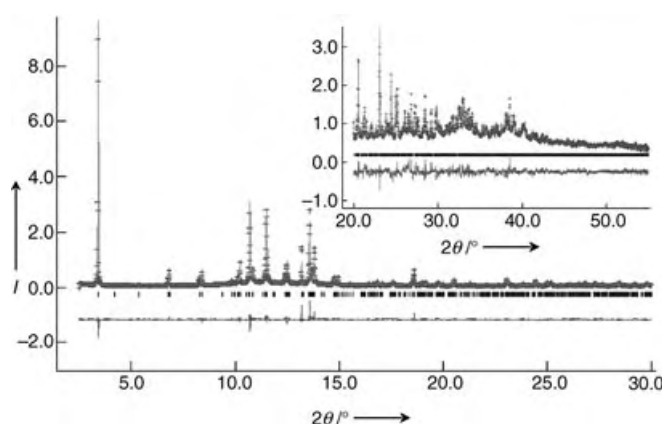


Figure 2. Observed (dotted upper line), calculated (solid upper line), and difference (solid lower line) synchrotron X-ray diffraction patterns of Nu-6(1) in $P2_1/a$.

Table 1: Crystallographic data and experimental conditions for the Rietveld refinement of Nu-6(1) and Nu-6(2).

Sample	Nu-6(1)	Nu-6(2)
chemical formula/unit cell	C40 N8 Si24 O52	Si24 O48
crystal system	monoclinic	
space group	$P2_1/a$	$P2_1/a$
a [Å]	27.7287(6)	17.257(2)
b [Å]	4.9731(1)	4.9881(4)
c [Å]	13.9350(2)	13.848(1)
β [°]	103.73(1)	106.09(1)
V [Å ³]	1866.6(1)	1145.3(2)
X-ray source	synchrotron—BM1B/ESRF	
λ [Å]	0.79982	
refined pattern 2θ range [°]	2.5–55	3.5–40
step size (° 2θ)	0.005	
no. of data points	10522	7361
no. of reflections	3714	1375
no. of parameters	137	62
R^2 [%]	11.9	7.1
R_p [%]	6.4	4.9
R_{wp} [%]	8.5	6.4
reduced χ^2	9.4	9.7
residual electron density (min/max eÅ ⁻³)	−0.682/0.915	−0.401/0.438
Durbin–Watson statistics	2.2	2.5

patterns. Details and parameters used during the X-ray powder-diffraction refinement are reported in the experimental section and in Table 1. Crystal structure of Nu-6(1) can be described by layers of $(\text{Si}_6\text{O}_{13})_n^{2n-}$ parallel to the (100) plane (see Figure 1), held together by hydrogen bonds to the organic molecule. The unit-cell content of the organic molecules from crystal structure refinement (4 per unit cell) is in satisfactory agreement with that inferred from thermogravimetric determination (about 22.8% wt) and elemental analysis (C 17.84%, H 1.59%, N 4.02%), which accounted for 3.5 organic molecules per unit cell.

Si–O bond lengths lie between 1.557(8) and 1.677(9) Å; O6 and O13 are the terminal oxygen ions, but their bond lengths do not differ significantly from the other Si–O bond lengths. Concerning the interaction between the silicate layer and the organic molecules, the distances calculated for 44BPY-2 (N1b–O13 = 2.56 Å) indicate a strong hydrogen bond, whereas distances refined for 44BPY-1 (N1–O6 = 2.85 Å) suggest a weaker interaction.

The structure of the silicate layer appears to be very similar to those of the layers previously reported for EU 19

and MCM-69.^[12,17] Two out of three cell parameters for Nu-6(1), EU 19, and MCM-69 have the same values (i.e., those of the base dimensions of the sheet); the larger size of the molecules with respect to those hosted in EU 19 and MCM-69 leads to a different stacking parameter, which explains the greater value of a found in Nu-6(1). Moreover the different shape of 4,4'-bipyridine is likely to induce a relative shift between the layers, which involves a different symmetry in Nu-6(1) with respect to EU 19 and MCM-69 ($P2_1/a$ instead of $C2/c$).

In the case of Nu-6(2), the quality of the XRD pattern is lower compared with that of the as-synthesized sample because of the concurrent presence of sharp and broad reflections, indicative of a partially disordered structure. Moreover, a pronounced background testifies that, to a certain extent, some layers undergo amorphization upon calcination (Figure 3). To obtain a structural model for Nu-

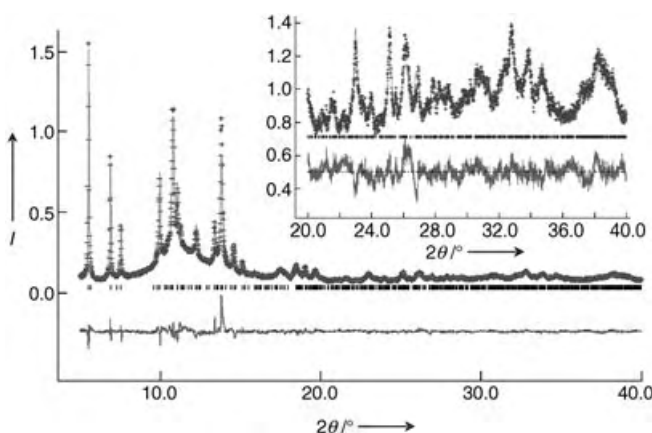


Figure 3. Observed (dotted upper line), calculated (solid upper line), and difference (solid lower line) synchrotron X-ray diffraction patterns of Nu-6(2) in $P2_1/a$.

6(2), an approach based on extensive model building was adopted: 1) the crystal structure of the as-synthesized form of Nu-6 was first transformed into a more flexible $P1$ structure; 2) the layers were condensed to form a fully connected 3D framework structure with cell parameters $a \sim 17.25$, $b \sim 4.98$, $c \sim 13.84$ Å and $\beta \sim 106^\circ$; 3) the atomic coordinates in $P1$ space group were introduced in the programme PLATON,^[28] which recognized a monoclinic symmetry with standard space group $P2_1/a$. The atomic coordinates were then successfully refined by the Rietveld method (see Figure 3).

Figure 4 shows that the framework structure of Nu-6(2) is characterized by the existence of 1D straight eight-membered-ring channels developing along the [010] direction; this feature places Nu-6(2) among the “small pore” zeolites. It must be noted that two non-equivalent sets of eight-ring channels, alternating along the crystallographic c direction, were found in the structure of Nu-6(2); these two sets of channels are referred to as A and B in Table 2, Figure 4 and Figure 5.

It is worth noting the close relationships between the cell parameters refined for Nu-6(2), given in Table 1, and those

Table 2: Selected distances (Å) across eight-ring channels (see also Figure 5).

Channel A			
O10–O10	O6–O6	O3–O3	O2–O2
3.6	4.3	4.0	3.2
Channel B			
O5–O5	O6–O6	O1–O1	O7–O7
2.4	4.8	3.5	3.0

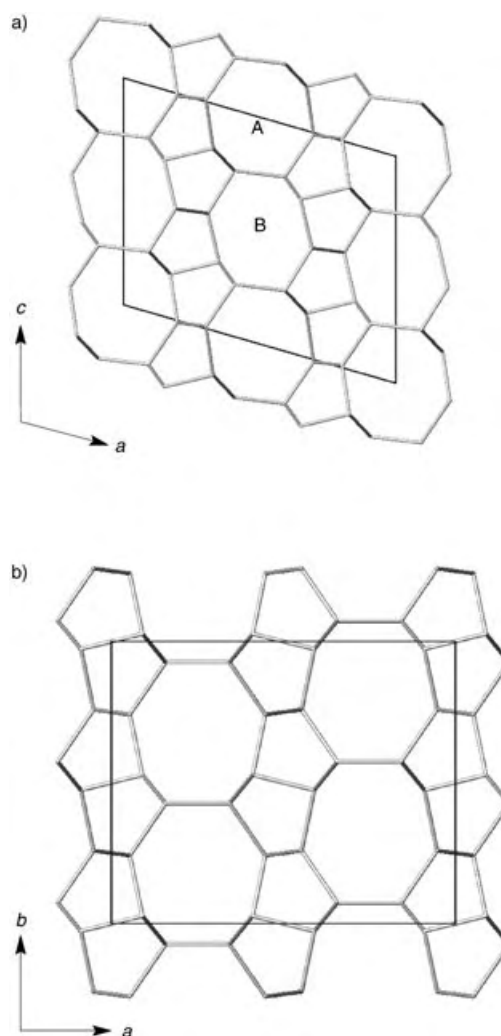


Figure 4. a) Stick representation of the framework structure of Nu-6(2); b) cesium aluminosilicate (IZA code CAS). The two nonequivalent channels, found in Nu-6(2), are labeled A and B.

reported for the orthorhombic cesium aluminosilicate^[29] (IZA code CAS) ($a = 13.828(5)$, $b = 16.776(5)$, $c = 5.021(1)$ Å). In fact, Nu-6(2) and CAS can be built by applying different symmetry operations to the same pentasil periodic building unit (the layer described above): inversion (i) in the case of Nu-6(2) and reflection (m) in the case of CAS (see Figure 4). However, the different crystal system and the significantly different XRD pattern confirm that the 3D framework topology found in Nu-6(2) has never been reported until now. By considering that the silicate layers

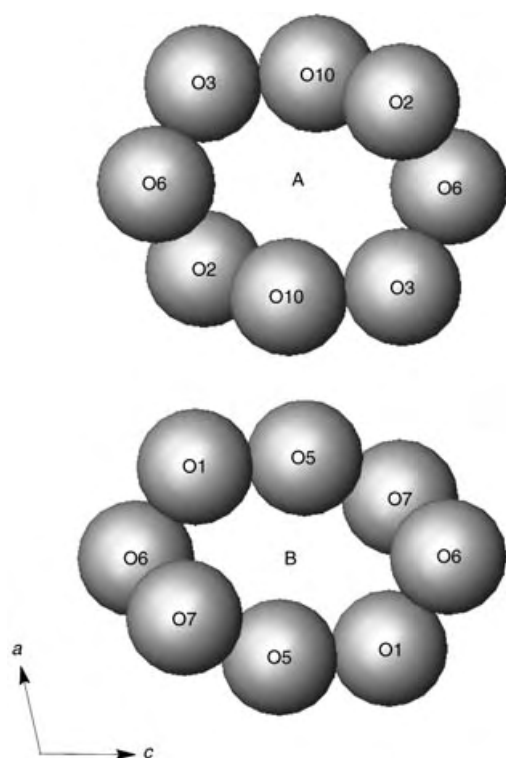


Figure 5. Sphere packing of oxygen atoms defining the A and B eight-ring channels of zeolite Nu-6(2). Please note that channel A and B are alternating along the *c* direction, as evidenced in Figure 4.

comprising EU 19 and Nu-6(1) are isostructural, we can suppose by extension that the structurally unknown EU 20 could have the same topology reported here for the Nu-6(2) structure.

The results of our catalytic tests on hydrocracking of *n*-decane show that Nu-6(2) is an active and selective dewaxing catalyst (see Table 3).

Table 3: Hydrocracking of *n*-decane of a Nu-6(2) zeolite with a Si/Al ratio of 45.

<i>T</i> [°C]	Conv. [%]	Isomerization [%]	Cracking [%]	MB [%] ^[a]	DB [%] ^[a]	NI [%] ^[b]
190	3.8	2.8	1.0	1.6	0.9	0.3
206	10.7	6.2	4.5	3.5	2.3	0.4
221	25.5	9.2	16.3	5.0	3.4	0.8
240	47.8	8.6	39.2	4.5	3.8	0.3
257	70.3	4.8	65.5	2.5	2.2	0.1
270	79.2	3.1	76.1	1.6	1.4	0.1

[a] MB and DB = monobranched and dibranched isomers respectively. [b] NI = non-identified products.

In light of this structural elucidation, we can fully explain the absorption data concerning the pyridine molecule on Nu-6(2);^[23] in fact the dimensions of the eight-ring channels are smaller than the pyridine molecule, thus access to the catalytic sites inside the channel is negligible, and the probe molecule can interact only with the bridging OH groups located on the crystal surface.

In conclusion the crystal structure of Nu-6(1) and Nu-6(2) has been determined by using an integrated approach based

on experiments and model building. We showed that the structure of precursor 4,4'-bipyridyl silicate is based on a pentasil layer previously recognized in EU 19 and MCM-69; however, the different structure-directing agent used in the synthesis gives rise to a different symmetry and stacking parameter. Moreover, we have demonstrated that upon calcination, silicate layers condense to form a 3D framework structure. The pore topology of this zeolite is unique, with straight eight-membered ring-channel systems along the *b* direction. Finally, *n*-decane hydrocracking catalytic test showed that Nu-6(2) is an active and selective dewaxing catalyst.

Experimental Section

The layered precursor Nu-6(1) was synthesized as follows: 4,4'-bipyridine (1.82 g, 12.3 mmol; Fluka, 98 %) were dissolved in ethanol (10.08 g; solution A) while sodium silicate (20.06 g, 0.18 mol; Merck, 24.92 % SiO₂) were diluted with water (13.38 g; solution B). Finally, aluminum sulfate (0.62 g, 1.8 mmol; Merck, 51.34 %) and of sulfuric acid (1.52 g, 98 %) were dissolved in water (22.78 g; solution C). The crystallization was carried out in tumbling teflon-lined autoclaves. After 3 days at 135 °C, the solids were isolated by filtration, washed with distilled water until the pH reached 7, then dried at 60 °C to produce the final Nu-6(1). The 3D Nu-6(2) zeolite was obtained from Nu-6(1) by calcination in air at 550 °C for 6 h.

Catalytic tests on hydrocracking of *n*-decane were performed with Nu-6(2) at atmosphere pressure, contact time of 0.52 h, and molar ration H₂/*n*-decane = 100. Reaction temperature was varied between 190 and 270 °C and the results are given in Table 3.

The high-resolution synchrotron X-ray powder diffraction patterns were collected on the as-synthesized and calcined Nu-6 samples at the beam line BM1B (the Swiss Norwegian Beam Lines), at the synchrotron radiation source ESRF in Grenoble. The beamline provides a robust diffractometer currently equipped with six counting chains, which allows six complete patterns to be collected simultaneously. An Si-111 analyzer crystal is mounted in front of each detector (Na-I scintillation counter). The beam line was set to deliver a wavelength of 0.79982 Å. The samples, placed in a borosilicate capillary 1.0 mm in diameter, were spun during data collection to minimize the preferred orientation.

Data were collected, at room temperature, in continuous mode over the range $1 \leq 2\theta \leq 55^\circ$, with accumulation times increasing with the scattering angle, and rebinned with a step size of $0.005^\circ 2\theta$.

X-ray powder-diffraction refinement was carried out by using the program GSAS;^[25] geometric soft constrain were applied to the Si–O, O–O, C–N and C–C bond length (1.62 ± 0.04 , 2.65 ± 0.1 , 1.40 ± 0.02 , 1.40 ± 0.02 Å, respectively). The weighting factor was gradually reduced as the refinement proceeded and reasonable bond lengths were finally obtained. Atoms of the same element type were constrained to have the same isotropic thermal displacement parameter and refined; only the displacement parameters of the atoms comprising the organic molecules were kept fixed. The occupancies of the organic molecules were refined during the early stage of the refinement; because they did not differ significantly from the unit, they were kept fixed to this value in the final stage of the refinement. Anisotropic broadening phenomena of the reflections were observed in the synchrotron X-ray powder diffraction (SXPDP) patterns, this phenomenon was accounted

for by including different terms in the pseudo-Voigt peak shape function during the refinements. Further details on the investigation of the crystal structure may be obtained from the Fachinformationszentrum Karlsruhe, 76344 Eggenstein-Leopoldshafen, Germany (fax: (+49)7247-808-666; e-mail: crysdata@fiz-karlsruhe.de), on quoting the depository numbers CSD-413852 and -413853.

Received: March 22, 2004

Keywords: layered compounds · structure elucidation · X-ray diffraction · zeolites

- [27] A. Altomare, M. C. Burla, M. Camalli, G. L. Cascarano, C. Giacovazzo, A. Guagliardi, A. G. G. Moliterni, G. Polidori, R. Spagna, *J. Appl. Crystallogr.* **1999**, 32, 115.
[28] A. L. Spek, *Acta Crystallogr. Sect. A* **1990**, 46, C34.
[29] T. Araki, *Z. Kristallogr.* **1980**, 152, 207.

- [1] A. Corma, M. J. Díaz-Cabañas, J. Martínez-Triguero, F. Rey, J. Rius, *Nature* **2002**, 418, 514.
[2] A. Corma, F. Rey, S. Valencia, J. L. Jorda, J. Rius, *Nat. Mater.* **2003**, 2, 493.
[3] M. Yoshikawa, P. Wagner, M. Lovallo, K. Tsuji, T. Takewaki, C. Chen, L. W. Beck, C. Jones, M. Tsapatsis, S. I. Zones, M. E. Davis, *J. Phys. Chem. B* **1998**, 102, 7139.
[4] C. C. Freyhardt, M. Tsapatsis, R. F. Lobo, K. J. Balkus, M. E. Davis, *Nature* **1996**, 381, 295.
[5] K. G. , Strohmaier, D. E. W. Vaughan, *J. Am. Chem. Soc.* **2003**, 125, 16035.
[6] J. S. Breck, J. C. Vartuli, W. J. Roth, M. E. Leonowicz, C. T. Kresge, K. D. Schmitt, C. T.-W. Chu, D. H. Olson, E. W. Sheppard, S. B. McCullen, J. B. Higgins, J. L. Schlenker, *J. Am. Chem. Soc.* **1992**, 114, 10834.
[7] A. Corma, M. S. Grande, V. Gonzalez-Alfaro, A. V. Orchilles, *J. Catal.* **1996**, 159, 375.
[8] T. Maschmeyer, F. Rey, G. Sankar, J. M. Thomas, *Nature* **1995**, 378, 159.
[9] A. Corma, V. Fornes, S. B. Pergher, *Nature* **1998**, 396, 353.
[10] A. Corma, V. Fornes, J. Martinez-Triguero, S. B. Pergher, *J. Catal.* **1999**, 186, 57.
[11] H. van Olphen, *An Introduction to Clay Colloid Chemistry*, Wiley, New York, **1963**.
[12] S. J. Andrews, M. Z. Papiz, R. McMeeking, A. J. Blake, B. M. Lowe, K. R. Franklin, J. R. Helliwell, M. M. Harding, *Acta Crystallogr. Sect. B* **1988**, 44, 73.
[13] A. Burton, R. J. Accardi, R. F. Lobo, M. Falcioni, M. W. Deem, *Chem. Mater.* **2000**, 12, 2936.
[14] U. Oberhagemann, P. Bayat, B. Marler, H. Gies, J. Rius, *Angew. Chem. Int. Ed. Engl.* **1996**, 35, 2869.
[15] S. , Vortman, J. Rius, S. Siegmann, H. Gies, *J. Phys. Chem. B* **1997**, 101, 1292.
[16] L. Schreyeck, P. Caullet, J. C. Mougénel, J. L. Guth, B. Marler, *Microporous Mater.* **1996**, 6, 259.
[17] L. D. Rollmann, J. L. Schlenker, S. L. Lawton, C. L. Cannedy, G. J. Kennedy, *Microporous Mesoporous Mater.* **2002**, 53, 179.
[18] S. Vortmann, J. Rius, B. Marler, H. Gies, *Eur. J. Mineral.* **1999**, 11, 125.
[19] R. Millini, G. Perego, W. O. Parker, Jr., G. Bellussi, L. Carluccio, *Microporous Mater.* **1995**, 4, 221.
[20] A. J. Blake, K. R. Franklin, B. M. Lowe, *J. Chem. Soc. Dalton Trans.* **1988**, 2513.
[21] T. V. Whittam, US Pat. 4 397 825, **1983**.
[22] I. J. S. Lake, T. V. Whittam, US Pat. 4 400 572, **1983**.
[23] A. Corma, V. Fornés, U. Diaz, *Chem. Commun.* **2001**, 2642.
[24] J. W. Visser, *J. Appl. Crystallogr.* **1969**, 2, 89.
[25] A. , Le Bail, H. Duroy, J. L. Fourquet, *Mater. Res. Bull.* **1988**, 23, 447–452.
[26] A. C. Larson, R. B. Von Dreele, GSAS Manual, Los Alamos Report No. LAUR-86-748, Los Alamos National Laboratory, USA, **1986**.

Polymerization

**Polynuclear Olefin Polymerization Catalysis:
Proximity and Cocatalyst Effects Lead to
Significantly Increased Polyethylene Molecular
Weight and Comonomer Enchainment Levels*****Hongbo Li, Liting Li, and Tobin J. Marks**

Abiotic attempts to mimic certain advantageous enzyme characteristics have recently focused on construction of multimetallic catalytic centers capable of achieving cooperative recognition/activation/reactivity effects between proximate transition-metal ions.^[1] Regarding such effects in single-site polymerization catalysis,^[2–4] we recently reported that a constrained geometry binuclear catalyst and binuclear cocatalyst combination (**C2-Zr₂** + **B₂**) affords, through the modification of chain-transfer pathways, significantly enhanced branching in ethylene homopolymerization and enhanced comonomer incorporation in ethylene and 1-hexene copolymerization versus a mononuclear combination of **Zr₁** + **B₁**.^[3c]

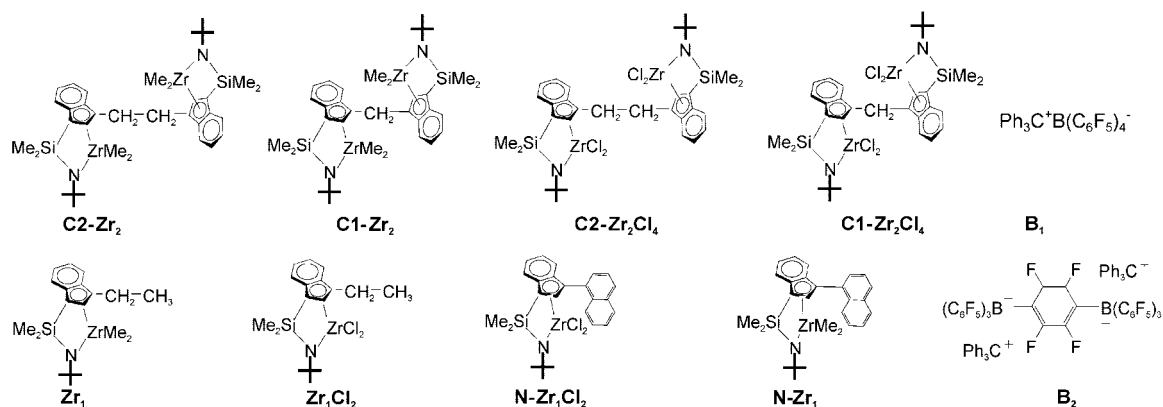
Nevertheless, constrained-geometry catalysts (CGC) of Zr typically produce unacceptably low- \bar{M}_w polyolefins,^[4c,d,5] (\bar{M}_w is the weight-average molar mass) raising the intriguing question of what effects closer metal-metal proximity and alternative cocatalysts might have. Here we communicate that in ethylene homopolymerizations under identical reaction conditions, methylene-bridged **C1-Zr₂** affords significantly higher molecular weight products than -CH₂CH₂-bridged **C2-Zr₂** ($\approx 70 \times \bar{M}_w$ increase) and mononuclear **Zr₁** ($\approx 130 \times \bar{M}_w$ increase). Furthermore, with MAO (methylaluminoxane) as cocatalyst, very large increases in polyethylene molecular weight are achieved with both **C2-Zr₂Cl₄** and **C1-**

[*] H. Li, L. Li, Prof. T. J. Marks
Department of Chemistry
Northwestern University
2145 Sheridan Road, Evanston, IL 60208-3113 (USA)
Fax: (+1) 847-491-2990
E-mail: t-marks@northwestern.edu

[**] This research was supported by grants from NSF (CHE-0415407) and DOE (86ER13511). We thank Dr. P. Nickias and K. Woodford of Dow Chemical for GPC measurements.



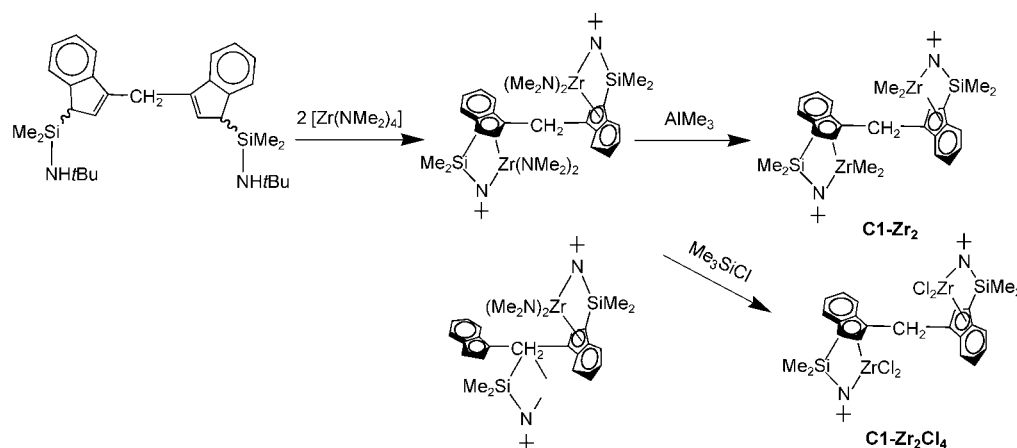
Supporting information for this article is available on the WWW under <http://www.angewandte.org> or from the author.



Zr₂Cl₄ versus mononuclear **Zr₁Cl₂** ($\approx 600 \times \bar{M}_w$ increase), while for ethylene + 1-hexene copolymerization, the shorter bridge enhances both product \bar{M}_w ($\approx 40 \times$ increase) and selectivity for α -olefin enchainment ($\approx 3 \times$ increase). Results from ligand-substituent and solvent experiments support the argument that the role of the proximate metal centers is not

to monomer^[7] is therefore the most probable source of branching in these polymerizations,^[3c] with the $\approx 8 \times$ greater ethyl branching per 1000 C atoms for **C2-Zr₂** versus **C1-Zr₂**, which correlates with the lower product \bar{M}_w arising from the former. For single-site polymerization, $\bar{M}_{n,w}$ (\bar{M}_n is the number-average molar mass) are typically proportional to

the net rate of chain propagation divided by the net rate of chain termination. Since **C1-Zr₂** polymerization activity is $\approx 20\%$ that of **C2-Zr₂** (Table 1), reasonably assuming comparable percentages of active catalytic centers^[8] (in situ ¹H NMR indicates rapid, quantitative Ph₃CCH₃ formation upon catalyst activation) infers that the net rate of **C1-Zr₂** propagation is $\approx 20\%$ that of **C2-Zr₂**, hence, the **C1-Zr₂** termination rate must be dra-



Scheme 1. Synthetic routes to complexes **C1-Zr₂** and **C1-Zr₂Cl₄**.

merely steric.

C1-Zr₂ was synthesized as shown in Scheme 1, while sterically encumbered naphthyl derivative **N-Zr₁**^[6] was prepared to probe ligand steric effects. New compounds were characterized by conventional methodologies, and polymerizations were carried out under rigorously anhydrous, anaerobic conditions with attention to exotherm and mass-transfer effects.^[3a,b] Ethylene homopolymerization results are summarized in Table 1. Entries 1–3 show that $70 \times$ and $130 \times$ increases in \bar{M}_w are achieved with **C1-Zr₂** versus **C2-Zr₂** and **Zr₁**, respectively, under identical polymerization conditions (**B₂** cocatalyst). As in the case of **C2-Zr₂**,^[3c] a combination of **C1-Zr₂** with **B₂** produces polyethylene with ethyl branching as a distinctive microstructural feature, and the \bar{M}_w is found to be essentially independent of ethylene pressure. Chain transfer

is dramatically depressed to obtain the large observed \bar{M}_w enhancement. These effects are likely to reflect differences in achievable Zr–Zr proximity^[9] and possible access to bridged structures (e.g., **1**). Note that the results with more sterically congested mononuclear **N-Zr₁** (Table 1, compare entries 1, 2, 4) support the argument that the effect of the proximate metal center is not simply steric in origin, while polymerization experiments in more polar, ion-pairing-weakening^[10] C₆H₅Cl

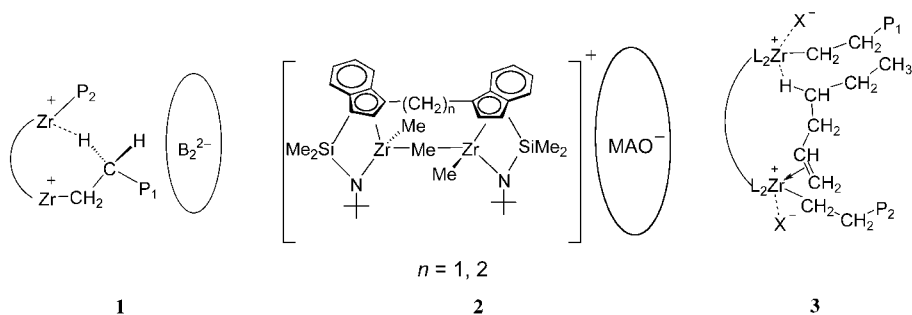


Table 1: Ethylene and ethylene + 1-hexene polymerization data for CGCZr catalysts with various nuclearities and cocatalysts.^[a]

Entry no	Catalyst	Monomer	μmol of catalyst	Reaction time [h]	Polymer yield [g]	Activity [$\times 10^3$] ^[b]	Ethyl branches per 1000C	<i>n</i> -Butyl branches per 1000 C	\bar{M}_n [$\times 10^2$] ^[c]	\bar{M}_w/\bar{M}_n ^[c]
1	Zr₁ + B₂ ^[d]	E	10	1.16	1.08	93 (11)	6.5	0.6	6.3	1.1
2	C1-Zr₂ + B₂	E	5.0	1.50	0.19	13 (3)	1.6	≈ 0	326	2.7
3	C2-Zr₂ + B₂ ^[d]	E	5.0	1.50	0.94	63 (7)	12	1.0	11	1.2
4	N-Zr₁ + B₂	E	10	1.50	0.51	34 (7)	≈ 0	≈ 0	25	2.3
5	Zr₁ + B₂ ^[e]	E	10	0.025	0.17	680 (20)	1.7	1.1	17	1.4
6	C1-Zr₂ + B₂ ^[e]	E	5.0	0.025	0.16	640 (20)	2.8	1.4	15	1.5
7	Zr₁Cl₂ + MAO ^[f]	E	10	1.50	0.37	25 (5)	≈ 0	≈ 0	9.5	1.3
8	C1-Zr₂Cl₄ + MAO ^[f]	E	5.0	1.50	0.38	25 (3)	≈ 0	≈ 0	2440	2.7
9	C2-Zr₂Cl₄ + MAO ^[f]	E	5.0	1.50	0.35	23 (5)	≈ 0	≈ 0	2680	2.8
10	N-Zr₁Cl₂ + MAO ^[f]	E	10	1.50	0.35	23 (5)	≈ 0	≈ 0	56	2.2
11	Zr₁ + B₂ ^[d]	E/H	10	0.75	1.00	133 (13)	6.0	3.2	7.3	1.1
12	C1-Zr₂ + B₂	E/H	5.0	1.50	0.13	8.6(5)	1.3	17.2	221	2.3
13	C2-Zr₂ + B₂ ^[d]	E/H	5.0	1.25	1.09	87 (9)	10	5.5	11	1.2
14	Zr₁Cl₂ + MAO ^[f]	E/H	10	1.50	0.46	15 (3)	≈ 0	5.4	3.4	1.3
15	C1-Zr₂Cl₄ + MAO ^[f]	E/H	5.0	1.50	0.33	11 (2)	≈ 0	22.8	1130	2.9
16	C2-Zr₂Cl₄ + MAO ^[f]	E/H	5.0	3.00	0.27	8.9 (6)	≈ 0	19.4	872	2.9

[a] Polymerizations carried out on high vacuum line at 24 °C in 100 mL of toluene under 1.0 atm ethylene pressure, [hexene] = 0.8 M. [b] (g polymer) (mol cationic metallocene)⁻¹ (atm)⁻¹ h⁻¹. [c] From GPC versus polystyrene standards. [d] from reference [3c] (other low- \bar{M}_w samples have a similarly low polydispersity pattern, reflecting imprecision in calibration). [e] Polymerizations carried out in chlorobenzene. [f] Al:Zr = 1000:1. MAO dried in vacuo for 48 h to remove excess Al₂Me₆.

In regard to cocatalyst effects, note that while the homopolymerization behavior of the combination of **Zr₁Cl₂** or **N-Zr₁Cl₂ + MAO** approximately parallels that of **Zr₁ + B₂** (Table 1, entries 1,7,10), the combinations of **C1-Zr₂Cl₄ + MAO** and **C2-Zr₂Cl₄ + MAO** both afford comparable polyethylenes of very high \bar{M}_w , with \bar{M}_w increased up to $\approx 600\times$ versus **Zr₁Cl₂ + MAO** (entries 8,9 versus 7).^[11,12] From Table 1, note that the activities **C1-Zr₂Cl₄ + MAO** and **C2-Zr₂Cl₄ + MAO** are similar to that of **Zr₁Cl₂ + MAO**, so by using the arguments outlined above, chain-transfer rates must be dramatically depressed in the binuclear catalysts. Comparing entries 8,9, and 2, we note that the MAO-activated species produce polyethylene with even higher molecular weight than **C1-Zr₂ + B₂**; the lower ethyl-branch content suggests a scenario in which the relative chain-termination rate is even slower for **Zr₂Cl₄ + MAO** than for **C1-Zr₂ + B₂** (assuming that ethyl branch formation requires chain transfer to monomer and subsequent α -olefin/polyolefin reinsertion^[3c]). For the MAO with **C1-Zr₂Cl₄** and **C2-Zr₂Cl₄** catalysts, we observe Zr(μ -CH₃)₂Zr species by in situ NMR, which confirms that the two Zr centers can approach closely,^[12,13] and the bulky^[14] MAO cocatalyst/counteranion may stabilize this structure, (for example, **2**; as encumbered H₃CB(perfluorobiphenyl)₃⁻ stabilizes cationic M(μ -CH₃)M⁺ species).^[13a] Note that bridge length plays, at most, a minor role when MAO is the cocatalyst (entries 8, 9).

Regarding cooperativity effects in copolymerization, experiments that involve a mixture of ethylene and 1-hexene indicate that a combination of **C1-Zr₂ + B₂** incorporates $\approx 3\times$ more 1-hexene than does **C2-Zr₂ + B₂** (Table 1 entries 11–13). The homopolymerization results are paralleled; the copolymer \bar{M}_w is $\approx 40\times$ greater for **C1-Zr₂ + B₂** than for **C2-Zr₂ + B₂**. Interestingly, ¹³C NMR data also reveal that the copolymer derived from **C1-Zr₂ + B₂** contains similar quantities of ethyl branches to those obtained in the above ethylene homopolymerizations, which suggests that the

same chain-transfer mechanism is again operative. With MAO as the copolymerization cocatalyst, **C1-Zr₂Cl₄** incorporates $4.2\times$ more, and **C2-Zr₂Cl₄** $3.5\times$ more, 1-hexene than does **Zr₁Cl₂** and with comparable polymerization activities. Paralleling the homopolymerizations, the copolymer \bar{M}_w from the **C1-Zr₂Cl₄**- and **C2-Zr₂Cl₄**-mediated polymerizations is again significantly greater ($\approx 600\times$) than in the **Zr₁Cl₂**-catalyzed process. These comonomer-enchainment-selectivity data implicate differences in achievable Zr–Zr proximity and structures likely to facilitate comonomer enchainment (e.g., **3**).

The present results significantly expand what is known about metal–metal proximity and cocatalyst/counteranion effects in binuclear CGC olefin polymerization catalysis. In ethylene homopolymerization, a large increase in product \bar{M}_w is achieved with **C1-Zr₂ + B₂** versus **C2-Zr₂ + B₂** and **Zr₁ + B₂**. In ethylene + 1-hexene copolymerizations, a combination of **C1-Zr₂ + B₂** incorporates significantly more 1-hexene than does **C2-Zr₂ + B₂**. When MAO is the cocatalyst, very large increases in \bar{M}_w occur with both **C1-Zr₂Cl₄** and **C2-Zr₂Cl₄** compared with **Zr₁Cl₂**, and in ethylene + 1-hexene copolymerization, both **C2-Zr₂Cl₄** and **C1-Zr₂Cl₄** enchain more 1-hexene than does **Zr₁Cl₂** to yield products with far higher molecular weights. These results support the argument that Zr–Zr cooperativity effects can decrease chain-transfer rates as well as increase selectivity for comonomer enchainment, and that such effects are highly sensitive to ion pairing. Ligand-substituent and solvent-control experiments reveal that the role of proximate metal centers is not merely steric.

Experimental Section

All manipulations were performed as described elsewhere with rigorous exclusion of O₂ and H₂O.^[3a] Ethylene polymerizations^[3c] were carried out on a high vacuum line in round-bottom three-neck Morton flasks. In typical experiments, dry toluene was vacuum-

were carried out on a high vacuum line in round-bottom three-neck Morton flasks. In typical experiments, dry toluene was vacuum-transferred into the reaction flask from Na/K and presaturated with 1.0 atm of ethylene. Catalytically active species were freshly generated by mixing measured amounts of precatalyst and cocatalyst in 1,2-difluorobenzene in septum-capped vials in the glove box (with MAO, the mixture was stirred vigorously for 30 min before use). The catalyst solution was then quickly injected into the rapidly stirred reaction flask. After a measured time interval, polymerization was quenched by the addition of 2% acidified methanol.

Received: April 10, 2004

Keywords: cooperative effects · copolymerization · homogeneous catalysis · zirconium

to a $\text{Zr}(\mu\text{-methyl})\text{Zr}$ moiety.^[13] Such a feature is not detectable in either $\text{Zr}_1\text{Cl}_2 + \text{MAO}$, $\text{C1-Zr}_2 + \text{B}_2$, or $\text{C2-Zr}_2 + \text{B}_2$ reaction mixtures, but can also be detected in $\text{C2-Zr}_2 + \text{tris(perfluorobiphenyl)borane (PBB)}$ reaction mixtures, a system known to readily form $\text{Zr}(\mu\text{-methyl})\text{Zr}$ moieties.^[13a] After the introduction of ethylene into the $\text{C2-Zr}_2\text{Cl}_4$ with MAO mixture, the intensity of the $\delta = -2.13$ ppm peak decreases dramatically, consistent with $\mu\text{-methyl}$ dissociation and subsequent activation of the Zr centers, analogous to previous observations on other MAO-activated $\mu\text{-methyl}$ systems.^[13c]

- [1] a) O. Iranzo, A. Y. Kovalevsky, J. R. Morrow, J. P. Richard, *J. Am. Chem. Soc.* **2003**, *125*, 1988–1993; b) B. M. Trost, T. Mino, *J. Am. Chem. Soc.* **2003**, *125*, 2410–2411; c) E. N. Jacobsen, *Acc. Chem. Res.* **2000**, *33*, 421–431; d) P. Molenveld, J. F. Engbersen, D. N. Reinhoudt, *Chem. Soc. Rev.* **2000**, *29*, 75–86.
- [2] For recent reviews of single site olefin polymerization, see: a) V. C. Gibson, S. K. Spitzmesser, *Chem. Rev.* **2003**, *103*, 283–316; b) J.-N. Pedetour, K. Radhakrishnan, H. Cramail, A. Deffieux, *Macromol. Rapid Commun.* **2001**, *22*, 1095–1123; c) special issue on “Frontiers in Metal-Catalyzed Polymerization” (Ed.: J. A. Gladysz): *Chem. Rev.* **2000**, *100*.
- [3] For studies of binuclear polymerization catalysis, see: a) H. Li, L. Li, T. J. Marks, L. Liable-Sands, A. L. Rheingold, *J. Am. Chem. Soc.* **2003**, *125*, 10788–10789; b) S. K. Noh, J. Lee, D. Lee, *J. Organomet. Chem.* **2003**, *667*, 53–60; c) L. Li, M. V. Metz, H. Li, M.-C. Chen, T. J. Marks, L. Liable-Sands, A. L. Rheingold, *J. Am. Chem. Soc.* **2002**, *124*, 12725–12741; d) M. L. H. Green, N. H. Popham, *J. Chem. Soc. Dalton Trans.* **1999**, 1049–1059, and references therein; e) W. Spaleck, F. Kuber, B. Bachmann, C. Fritze, A. Winter, *J. Mol. Catal. A* **1998**, *128*, 279–287; f) S. Jungling, R. Mülhaupt, H. Plenio, *J. Organomet. Chem.* **1993**, *460*, 191–195.
- [4] a) S. Arndt, J. Okuda, *Chem. Rev.* **2002**, *102*, 1953–1976; b) P. S. Chum, W. J. Kruper, M. J. Guest, *Adv. Mater.* **2000**, *12*, 1759–1767; c) A. L. McKnight, R. M. Waymouth, *Chem. Rev.* **1998**, *98*, 2587.
- [5] L. Jia, X. Yang, C. L. Stern, T. J. Marks, *Organometallics* **1997**, *16*, 842–857.
- [6] The syntheses of $\text{C2-Zr}_2\text{Cl}_4$ and Zr_1Cl_2 can be found in reference [3c]; syntheses of C1-Zr_2 , $\text{C1-Zr}_2\text{Cl}_4$, $\text{N-Zr}_1\text{Cl}_2$, and N-Zr_1 can be found in the Supporting Information.
- [7] a) L. Izzo, F. D. Riccardis, C. Alfano, L. Caporaso, L. Oliva, *Macromolecules* **2001**, *34*, 2–4; b) L. Wang, Y. Yuan, L. Feng, Y. Wang, J. Pan, C. Ge, B. Ji, *Eur. Polym. J.* **2000**, *36*, 851–855; c) L. Izzo, L. Caporaso, G. Senatore, L. Oliva, *Macromolecules* **1999**, *32*, 6913–6916.
- [8] a) Z. Liu, E. Somsook, C. R. Landis, *J. Am. Chem. Soc.* **2001**, *123*, 2915–2916; b) Z. Liu, E. Somsook, C. B. White, C. R. Landis, *J. Am. Chem. Soc.* **2001**, *123*, 11193–11207.
- [9] Approximate modeling at the Spartan level reveals that the minimum $\text{Zr}\cdots\text{Zr}$ approach distance in C1-Zr_2 with B_2 is ≈ 0.25 Å shorter than in C2-Zr_2 with B_2 .
- [10] a) M.-C. Chen, J. A. S. Roberts, T. J. Marks, *J. Am. Chem. Soc.* **2004**, *126*, 4605–4625; b) M.-C. Chen, T. J. Marks, *J. Am. Chem. Soc.* **2001**, *123*, 11803–11804.
- [11] A combination of $\text{C1-Zr}_2 + \text{MAO}$ exhibits polymerization behavior indistinguishable from that of $\text{C1-Zr}_2\text{Cl}_4 + \text{MAO}$, excluding artifacts due to Zr-Cl linkages.
- [12] In situ ^1H NMR of the reactions of $\text{C2-Zr}_2\text{Cl}_4$ with MAO and $\text{C1-Zr}_2\text{Cl}_4 + \text{MAO}$ reveals a $\delta = -2.13$ ppm resonance, assignable
- [13] a) Y.-X. Chen, M. V. Metz, L. Li, C. L. Stern, T. J. Marks, *J. Am. Chem. Soc.* **1998**, *120*, 6287–6305; b) S. Beck, M.-H. Prosenc, H.-H. Brintzinger, R. Goretzki, N. Herfert, G. Fink, *J. Mol. Catal.* **1996**, *111*, 67–79; c) I. Tritto, R. Donetti, M. C. Sacchi, P. Locatelli, G. Zannoni, *Macromolecules* **1999**, *32*, 264–269.
- [14] D. E. Babushkin, H.-H. Brintzinger, *J. Am. Chem. Soc.* **2002**, *124*, 12869–12873.

Al and Ga Compounds

**Tetranuclear Homo- and Heteroalumoxanes
Containing Reactive Functional Groups:
Syntheses and X-ray Crystal Structures of
[[[LAl(Me)](μ -O)(MH₂)]₂]****

*Sanjay Singh, S. Shravan Kumar,
Vadapalli Chandrasekhar, Hans-Jürgen Ahn,
Marianna Biadene, Herbert W. Roesky,*
Narayan S. Hosmane, Mathias Noltemeyer, and
Hans-Georg Schmidt*

There is considerable interest in organoaluminum compounds containing Al–O bonds. This is primarily due to the discovery of methylalumoxane (MAO) as an extremely potent cocata-

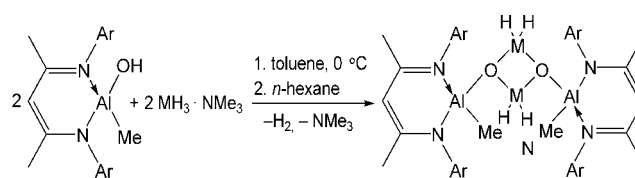
[*] Dipl.-Chem. S. Singh, Dipl.-Chem. S. S. Kumar,
Dipl.-Chem. H.-J. Ahn, Dipl.-Chem. M. Biadene,
Prof. Dr. H. W. Roesky, Dr. M. Noltemeyer, H.-G. Schmidt
Institut für Anorganische Chemie
Georg-August-Universität Göttingen
Tammannstrasse 4, 37077 Göttingen (Germany)
Fax: (+49) 551-393-373
E-mail: hroesky@gwdg.de
Prof. Dr. V. Chandrasekhar
Department of Chemistry
Indian Institute of Technology Kanpur
Kanpur-208016 (India)
Prof. Dr. N. S. Hosmane
Department of Chemistry and Biochemistry
Northern Illinois University, Dekalb, IL 60115-2862 (USA)

[**] This work was supported by the Deutsche Forschungsgemeinschaft and the Göttinger Akademie der Wissenschaften. S.S. thanks the Graduiertenkolleg 782 for a fellowship. V.C. thanks the Alexander von Humboldt foundation for the Friedrich Wilhelm Bessel Research Award. We thank the National Science Foundation for supporting this work and N.S.H acknowledges the senior award of the Alexander von Humboldt foundation. M = Al, Ga, L = 2,6-*i*Pr₂C₆H₃NC(CH₃)CHC(CH₃)NC₆H₃-2,6-*i*Pr₂=HC{(CMe)(2,6-*i*Pr₂C₆H₃N))₂.

lyst in the polymerization of ethylene and propylene by Group 4 metallocenes.^[1] There have been several attempts to prepare discrete molecular organoalumoxanes with well defined structures because the active site structure in MAO is not known. These efforts focussed on the controlled hydrolysis of aluminumtrialkyls or -triaryls where the substituent groups on aluminum are sterically encumbered.^[2] Although several interesting compounds have been isolated by the above approach and structurally characterized, none of these was as effective as MAO as a cocatalyst. The second problem of using controlled hydrolysis as a synthetic tool is the lack of predictability of the reaction in being able to assess the nature of the product. The task of assembling compounds with Ga–O–Ga bonds is similarly fraught with synthetic challenges although some trinuclear^[3] and a tetranuclear^[4] derivatives are known. To assemble soluble lipophilic organoalumoxanes in a predictable and rational manner a change in the synthetic approach is required. Thus, instead of taking the Al–C or Al–H bonds as the starting point for making Al–O–Al bonds it would be more convenient to use organoaluminum hydroxides containing Al–O linkages as the precursors. The recent isolation of a discrete aluminum dihydroxide [Al(OH)₂],^[5] prompted us to look for a suitable synthon that would allow a rational and facile assembly of structural units of alumoxanes as well as heteroalumoxanes. A second goal was to retain reactive groups on the metal centers in such compounds. This arrangement would allow a stepwise synthesis of cage structures. Herein, we describe the synthesis and structural characterization of [[LAl(Me)](μ-O)(AlH₂)₂]₂ (**2**) and [[LAl(Me)](μ-O)(GaH₂)₂]₂ (**3**; L = HC((CMe)(2,6-*i*Pr₂C₆H₃N))₂). The synthesis of **2** and **3** were possible by preparing an unprecedented terminal aluminum monohydroxide [LAlMe(OH)] (**1**).^[6] Compounds **2** and **3** are the first examples of a tetranuclear alumoxane^[7] and a gallium congener, respectively. Apart from being examples of simple building blocks (Al₂O₂ and Ga₂O₂) these compounds also contain a pair of reactive MH₂ (M = Al, Ga) groups in the central core and Al–Me groups as the terminal end groups, which should allow their rapid elaboration.

The reaction of [LAl(OH)Me] with a stoichiometric amount of MH₃·NMe₃ (M = Al, Ga) in toluene at 0 °C results in a vigorous evolution of hydrogen and the formation of **2** and **3** in good yields (Scheme 1). Thus, this synthetic method represents a viable and rational route for the preparation of novel compounds. While compound **2** is the first example of an alumoxane with an Al₄O₂ moiety which also carries reactive hydride groups on the aluminum centers, compound **3** is the first example of a Al–O–Ga unit bearing reactive hydride groups.

Compounds **2** and **3** have been unambiguously characterized by means of spectroscopic, spectrometric, and crystallographic techniques. Both **2** and **3** are colorless crystalline solids and are thermally quite stable. They decompose with melting at 260 and 234 °C, respectively. The EI mass spectrum of **2** revealed that the most intense peak appears at *m/z* 1007 and corresponds to the loss of one hydrogen atom from the molecular ion. Similarly a peak at *m/z* 1079 in **3** is due to [M⁺–CH₃]. The IR spectrum of **2** shows a sharp doublet (1833 and 1850 cm^{–1}) corresponding to the symmetric and antisym-



Scheme 1. Preparation of the tetranuclear alumoxane **2** (M = Al) and the gallium congener **3** (M = Ga); Ar = 2,6-*i*Pr₂C₆H₃.

metric stretch of the AlH₂ fragment. The corresponding stretching modes for **3** appear at 1901 and 1929 cm^{–1}. The ¹H NMR resonance signals for **2** and **3** are broad at room temperature. However, a variable temperature ¹H NMR spectroscopy study revealed that the room-temperature spectra of **2** and **3** are simplified by a dynamic process and upon cooling the broad signals become sharp and eventually resolve into different resonances for the two halves of the molecules as expected based on the solid-state structures for **2** and **3**. For **2** (–60 °C) and **3** (–70 °C) two sharp singlets were observed for the methyl groups which are located on the terminal aluminum atoms. This observation suggests that the local environment around the two aluminum centers is slightly different at least at lower temperatures. This feature is also reflected in the hydride resonances of the central Al₂O₂H₄ and Ga₂O₂H₄ units. Although the exact nature of the dynamic process involved has not been clearly established it is possible that this may be due to the restricted rotation of Al–O–Al(Ga) bond at lower temperatures.

Single crystals of **2** and **3** suitable for X-ray structural analysis were obtained from their *n*-hexane solutions (Figure 1 and Figure 2). Both the compounds crystallize with a molecule of *n*-hexane, compound **2** in the monoclinic space group *P*2₁/*c* and **3** in *P*2₁/*m*.^[11]

The X-ray crystal structure of **2** reveals that it is a dimer of the [LAl(Me)OAl(H)₂]₂ unit. The structure contains two terminal LAlMe units that are linked to a central {(H)₂AlO}₂ core. The terminal aluminum centers are part of the six-membered C₃N₂Al rings. Each aluminum center of the central {(H)₂AlO}₂ four-membered ring contains two reactive hydride groups. These are located above and below the plane of the Al₂O₂ ring. The two methyl groups on the terminal Al atoms are *cis* with respect to each other. The central four-membered ring is nearly planar. The terminal six-membered rings are displaced in an approximately perpendicular manner with respect to the central {(H)₂AlO}₂ ring. The metric parameters observed in **2** are not unusual. Thus, the Al–O bonds in the Al₂O₂ ring (1.824(14)–1.842(14), av 1.833 Å) are longer than the terminal Al–O bonds (1.748(14) Å and 1.772(13) Å, av 1.760 Å) and are similar to those found in aluminum alkoxides for example [(*t*Bu)₂(Me)COAlH₂]₂ (Al–O 1.841 Å)^[8] and [(*t*BuO)AlH₂]₂ (Al–O 1.815 Å).^[9] The average O–Al–O and Al–O–Al angles in the Al₂O₂ ring are 86.10 and 93.43°, respectively, while the average exocyclic Al–O–Al angles are 122.02 and 144.08°.

The molecular structure of **3** is analogous to that of **2**. Thus, compound **3** also exists as a dimer and contains reactive hydride groups on the central gallium atoms of the planar Ga₂O₂ ring. The terminal C₃N₂Al rings are arranged in an

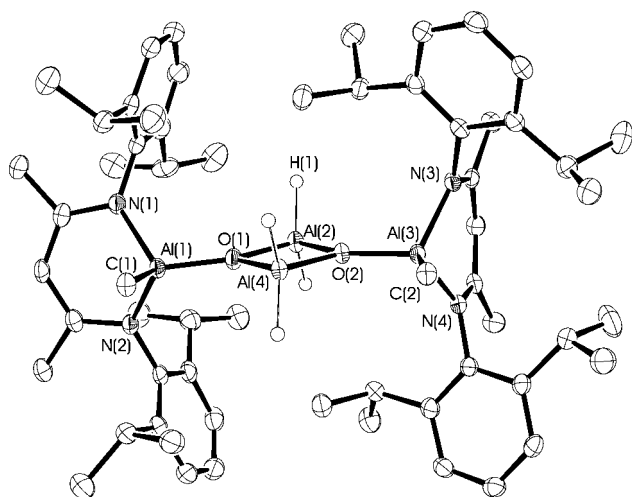


Figure 1. Molecular structure of **2**. The hydrogen atoms of the C–H bonds and hexane molecule are omitted for clarity. Selected interatomic distances [Å] and bond angles [°]: Al(1)–O(1) 1.748(14), Al(2)–O(1) 1.838(14), Al(2)–O(2) 1.828(14), Al(4)–O(2) 1.824(14), Al(4)–O(1) 1.842(14), Al(2)–Al(4) 2.679, Al(3)–O(2) 1.772(13), Al(1)–N(1) 1.913(16), Al(1)–C(1) 1.965(2); Al(1)–O(1)–Al(2) 145.44(8), Al(1)–O(1)–Al(4) 121.13(8), O(1)–Al(2)–O(2) 86.10(6), Al(2)–O(2)–Al(4) 94.36(6), Al(3)–O(2)–Al(2) 142.73(8), Al(3)–O(2)–Al(4) 122.91(8), N(1)–Al(1)–N(2) 96.51(7), N(1)–Al(1)–O(1) 113.52(7).

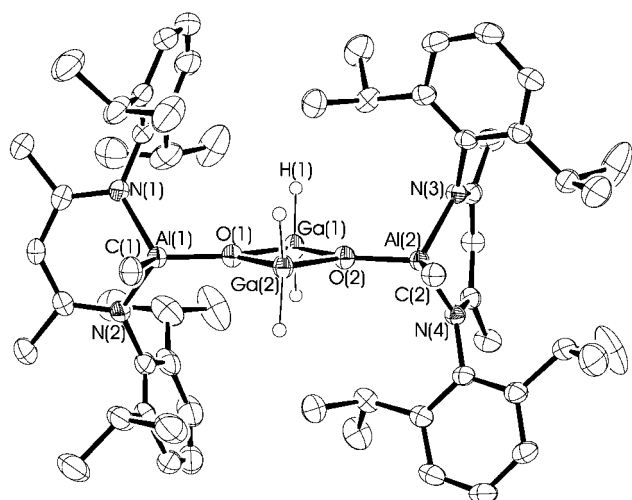


Figure 2. Molecular structure of **3**. The hydrogen atoms of the C–H bonds and hexane molecule are omitted for clarity. Selected interatomic distances [Å] and bond angles [°]: Al(1)–O(1) 1.733(2), Ga(1)–O(1) 1.933(2), Ga(1)–O(2) 1.924(2), Ga(2)–O(2) 1.917(2), Ga(2)–O(1) 1.939(2), Ga(1)–H(1) 1.516, Ga(1)–Ga(2) 2.849(7), Al(2)–O(2) 1.755(2), Al(1)–N(1) 1.920(19), Al(1)–C(1) 1.967(4); Al(1)–O(1)–Ga(1) 145.00(14), Al(1)–O(1)–Ga(2) 120.25(13), O(1)–Ga(1)–O(2) 84.73(9), Ga(1)–O(2)–Ga(2) 95.78(9), Ga(1)–O(2)–Al(2) 141.57(13), Ga(2)–O(2)–Al(2) 122.65(12), N(1)–Al(1)–N(2) 96.19(12), N(1)–Al(1)–O(1) 114.44(8).

approximately perpendicular manner with respect to the central Ga₂O₂ ring. Also, the methyl groups on the terminal aluminum centers are *cis* with respect to each other. The average O–Ga–O and Ga–O–Ga angles within the Ga₂O₂ ring are 84.73 and 95.27°, respectively. This may be compared with

those observed in [(*t*BuOGaH₂)₂] (101.4°).^[9] The slightly wider angle in the latter is perhaps due to the bulky *t*Bu group that elongates the O···O diagonal in the four-membered ring. The average exocyclic Al–O–Ga angles in **3** are 121.44 and 143.28°. The average terminal Al–O bond in **3** (1.744 Å) is similar to that found in **2**. The Ga–O bond within the Ga₂O₂ ring (1.917(2)–1.939(2) Å, av 1.928 Å) are similar to those found in gallium alkoxides for example [(*t*BuOGaH₂)₂] (Ga–O 1.908 Å)^[9] and in [(Me₂NCH₂CH₂OGaH₂)₂] (Ga–O 1.911 Å).^[10]

In conclusion we have demonstrated a new synthetic strategy for the preparation of an alumoxane and a corresponding gallium derivative. This procedure utilizes the reaction of an Al–OH motif and is a change in the standard synthetic protocols which rely on the use of Al–C or Al–H motifs. The resulting compounds [[{LAl(Me)}(μ-O)(AlH₂)₂]₂] and [[{LAl(Me)}(μ-O)(GaH₂)₂]₂] are novel tetranuclear building blocks. The reactive hydride and methyl groups present on the central and terminal metal atoms in these compounds should allow a further elaboration of these tetranuclear structures.

Experimental Section

All manipulations were performed under a dry and oxygen-free atmosphere (N₂ or Ar) using Schlenk line and glove box techniques.

2: [LAl(Me)OH] (0.95 g, 2.00 mmol) dissolved in toluene (20 mL) was added dropwise at 0°C to a stirred (1.0 M) solution of AlH₃·NMe₃ (2.10 mL, 2.10 mmol) in toluene (15 mL). The solution was allowed to warm to room temperature and stirred for 15 h. After removal of all the volatiles the residue was extracted with *n*-hexane (40 mL). Partial removal of the solvent and storage of the remaining solution at room temperature for 2 days afforded colorless crystals of **2**. Yield (0.75 g, 74% with respect to **1**). M.p. 258–260°C (decomp); elemental analysis (%) calcd for C₆₀H₉₂Al₄N₄O₂ (1008.65): C 71.40, H 9.19, N 5.55; found: C 71.75, H 9.55, N 5.14; EI-MS: *m/z* (%): 1007 (92) [*M*⁺–H], 993 (72) [*M*⁺–Me], 979 (60) [*M*⁺–Al–2H], 965 (100) [*M*⁺–Al–Me–3H], 951 (20) [*M*⁺–2Al–3H]; IR (Nujol): $\tilde{\nu}$ = 1850, 1833, 1552, 1527, 1318, 1260, 1177, 1101, 1055, 1023, 936, 874, 803, 726, 724, 656, 634 cm^{–1}; ¹H NMR (500 MHz, C₇D₈, –60°C): δ = 7.26–6.89 (m; Ar), 4.80 (s, 1H; γ -CH), 4.79 (s, 1H; γ -CH), 3.93 (br, 4H; AlH₂), 3.54 (sept, ³*J*_{H,H} = 6.3 Hz, 2H; CHMe₂), 3.40 (sept, ³*J*_{H,H} = 6.5 Hz, 2H; CHMe₂), 3.27 (sept, ³*J*_{H,H} = 6.5 Hz, 2H; CHMe₂), 2.97 (sept, ³*J*_{H,H} = 6.5 Hz, 2H; CHMe₂), 1.70–1.66 (m, 12H; CHMe₂), 1.46 (s, 6H; CMe), 1.39 (s, 6H; CMe), 1.34 (d, ³*J*_{H,H} = 6.3 Hz, 6H; CHMe₂), 1.20 (m, 12H; CHMe₂), 1.14 (d, ³*J*_{H,H} = 6.2 Hz, 6H; CHMe₂), 1.04 (d, ³*J*_{H,H} = 6.4 Hz, 6H; CHMe₂), 0.92 (d, ³*J*_{H,H} = 6.4 Hz, 6H; CHMe₂), 0.07 (s, 3H; AlMe), –0.81 ppm (s, 3H; AlMe); ¹H NMR (500 MHz, C₇D₈, 100°C): δ = 7.16–6.96 (m; Ar), 5.02 (s, 2H; γ -CH), 3.65 (br, 4H; AlH₂), 3.40 (sept, ³*J*_{H,H} = 6.7 Hz, 4H; CHMe₂), 3.14 (br, 4H; CHMe₂), 1.60 (s, 12H; CMe), 1.38–1.31 (br, 24H; CHMe₂ and CMe), 1.10 (m, 24H; CHMe₂), –0.56 ppm (s, 6H; AlMe).

3: The preparation of **3** was carried out by using a similar procedure as that for **2**. The quantities of the reactants used were [LAl(Me)OH] (1.43 g, 3.00 mmol), GaH₃·NMe₃ (0.40 g, 3.00 mmol). Yield (1.30 g, 79% with respect to **1**). M.p. 234°C (decomp); elemental analysis (%) calcd for C₆₀H₉₂Al₂Ga₂N₄O₂ (1094.81): C 65.82, H 8.47, N 5.12; found: C 65.67, H 8.33, N 5.29; EI-MS: *m/z* (%): 1094 (24) [*M*⁺], 1079 (100) [*M*⁺–Me], 1052 (16) [*M*⁺–Al–Me], 1022 (20) [*M*⁺–Ga–2H], 1007 (20) [*M*⁺–Me–Ga–2H]; IR (Nujol): $\tilde{\nu}$ = 1929, 1901, 1585, 1551, 1521, 1315, 1293, 1256, 1183, 1176, 1107, 1098, 938, 874, 797, 770, 755, 737, 709, 659, 642, 616, 531, 507 cm^{–1}; ¹H NMR (500 MHz, C₇D₈, –70°C): δ = 7.22–6.88 (m, Ar), 5.20 (s, 2H; GaH₂), 5.05 (s, 2H; GaH₂), 4.70 (s, 1H; γ -CH), 4.63 (s, 1H; γ -CH), 3.77 (m,

2H; CHMe_2), 3.45 (m, 2H; CHMe_2), 3.32 (m, 2H; CHMe_2), 2.96 (m, 2H; CHMe_2), 1.68 (d, $^3J_{\text{HH}} = 17.3$ Hz, 12H; CHMe_2), 1.49 (d, $^3J_{\text{HH}} = 5.8$ Hz, 12H; CHMe_2), 1.40 (s, 12H; CMe), 1.14 (dd, $^3J_{\text{HH}} = 17.3$ Hz, 18H; CHMe_2), 0.92 (d, $^3J_{\text{HH}} = 6.0$ Hz, 6H; CHMe_2), 0.04 (s, 3H; AlMe), -0.95 ppm (s, 3H; AlMe); ^1H NMR (500 MHz, C_7D_8 , 70°C): $\delta = 7.17$ – 6.96 (m; Ar), 4.91 [s, 6H (2H, γ -CH and 4H, GaH_2)], 3.48 (br, 4H; CHMe_2), 3.15 (br, 4H; CHMe_2), 1.56 (s, 12H; CMe), 1.43 (br, 12H; CHMe_2), 1.32 (br, 12H; CHMe_2), 1.17 (d, $^3J_{\text{HH}} = 6.5$ Hz, 12H; CHMe_2), 1.10 (d, $^3J_{\text{HH}} = 8.7$ Hz, 12H; CHMe_2), -0.65 ppm (s, 6H; AlMe).

Received: April 21, 2004

Keywords: aluminum · alumoxanes · gallium · hydrides · hydroxides

- [1] a) H. Sinn, W. Kaminsky, H.-J. Vollmer, R. Woldt, *Angew. Chem.* **1980**, 92, 396–402; *Angew. Chem. Int. Ed. Engl.* **1980**, 19, 390–392; b) E. Y.-X. Chen, T. J. Marks, *Chem. Rev.* **2000**, 100, 1391–1434; c) H. W. Roesky, M. G. Walawalkar, R. Murugavel, *Acc. Chem. Res.* **2001**, 34, 201–211.
- [2] a) T. L. Feng, P. L. Gurian, M. D. Healy, A. R. Barron, *Inorg. Chem.* **1990**, 29, 408–411; b) C. J. Harlan, M. R. Mason, A. R. Barron, *Organometallics* **1994**, 13, 2957–2969; c) R. J. Wehm-schulte, W. J. Grigsby, B. Schiemenz, R. A. Bartlett, P. P. Power, *Inorg. Chem.* **1996**, 35, 6694–6702; d) J. Storre, A. Klemp, H. W. Roesky, H.-G. Schmidt, M. Noltemeyer, R. Fleischer, D. Stalke, *J. Am. Chem. Soc.* **1996**, 118, 1380–1386; e) J. Storre, C. Schnitter, H. W. Roesky, H.-G. Schmidt, M. Noltemeyer, R. Fleischer, D. Stalke, *J. Am. Chem. Soc.* **1997**, 119, 7505–7513; f) Y. Koide, A. R. Barron, *Organometallics* **1995**, 14, 4026–4029; g) M. Veith, M. Jarczyk, V. Huch, *Angew. Chem.* **1998**, 110, 109–112; *Angew. Chem. Int. Ed.* **1998**, 37, 105–108; h) W. Schmitt, E. Baissa, A. Mandel, C. E. Anson, A. K. Powell, *Angew. Chem.* **2001**, 113, 3689–3693; *Angew. Chem. Int. Ed.* **2001**, 40, 3577–3581.
- [3] C. N. McMahon, S. J. Obrey, A. Keys, S. G. Bott, A. R. Barron, *J. Chem. Soc. Dalton Trans.* **2000**, 2151–2161.
- [4] D. A. Atwood, J. A. Jegier, S. Liu, D. Rutherford, P. Wie, R. C. Tucker, *Organometallics* **1999**, 18, 976–981.
- [5] a) G. Bai, Y. Peng, H. W. Roesky, J. Li, H.-G. Schmidt, M. Noltemeyer, *Angew. Chem.* **2003**, 115, 1164–1167; *Angew. Chem. Int. Ed.* **2003**, 42, 1132–1135; b) Y. Peng, G. Bai, H. Fan, D. Vidovic, H. W. Roesky, J. Magull, *Inorg. Chem.* **2004**, 43, 1217–1219; c) G. Bai, H. W. Roesky, J. Li, M. Noltemeyer, H.-G. Schmidt, *Angew. Chem.* **2003**, 115, 5660–5664; *Angew. Chem. Int. Ed.* **2003**, 42, 5502–5506; d) D. Neculai, H. W. Roesky, A. M. Neculai, J. Magull, B. Walford, D. Stalke, *Angew. Chem.* **2002**, 114, 4470–4472; *Angew. Chem. Int. Ed.* **2002**, 41, 4294–4296.
- [6] G. Bai, S. Singh, V. Jancik, H. W. Roesky, patent application pending.
- [7] a) W. Zheng, N. C. Mösch-Zanetti, H. W. Roesky, M. Noltemeyer, M. Hewitt, H.-G. Schmidt, *Angew. Chem.* **2000**, 112, 4446–4449; *Angew. Chem. Int. Ed.* **2000**, 39, 4276–4279; b) C. J. Carmalt, J. D. Mileham, A. J. P. White, D. J. Williams, *New J. Chem.* **2002**, 26, 902–905.
- [8] H. Nöth, A. Schlegel, J. Knizek, H. Schwenk, *Angew. Chem.* **1997**, 109, 2754–2758; *Angew. Chem. Int. Ed. Engl.* **1997**, 36, 2640–2643.
- [9] M. Veith, S. Faber, H. Wolfanger, V. Huch, *Chem. Ber.* **1996**, 129, 381–384.
- [10] S. J. Rittig, A. Storr, J. Trotter, *Can. J. Chem.* **1975**, 53, 58–66.
- [11] Crystallographic data for compound **2**: C_6H_{14} ($\text{C}_{66}\text{H}_{106}\text{Al}_4\text{N}_4\text{O}_2$): $M_r = 1095.47$, monoclinic, $P2_1/c$, $a = 20.420(2)$, $b = 17.760(10)$, $c = 18.850(10)$ Å, $\beta = 103.210^\circ(14)$, $V = 6655.2(8)$ Å³, $Z = 4$, crys-

tal size = $0.2 \times 0.1 \times 0.2$ mm³, $\rho_{\text{calcd}} = 1.093$ Mg m^{−3}, $2.22 \leq 2\theta \leq 58.93^\circ$, $T = 103(2)$ K, $\lambda = 1.54178$ Å, $\mu = 0.973$ mm^{−1}, $F(000) = 2392$, 61271 reflections collected, 9543 were independent and were used in the structure refinement of 786, $R1 = 0.0403$ ($I > 2\sigma(I)$), $wR2 = 0.1162$ (all data), min./max. residual electron density 0.411/−0.310 e Å^{−3}. Crystallographic data for compound **3**: C_6H_{14} ($\text{C}_{66}\text{H}_{106}\text{Al}_2\text{Ga}_2\text{N}_4\text{O}_2$): $M_r = 1180.95$, monoclinic, $P2_1/m$, $a = 9.4431(13)$, $b = 17.889(2)$, $c = 20.491(5)$ Å, $\beta = 103.117^\circ(14)$, $V = 3371.1(10)$ Å³, $Z = 2$, crystal size = $0.3 \times 0.2 \times 0.2$ mm³, $\rho_{\text{calcd}} = 1.163$ Mg m^{−3}, $3.06 \leq 2\theta \leq 49.60^\circ$, $T = 133(2)$ K, $\lambda = 0.71073$ Å, $\mu = 0.868$ mm^{−1}, $F(000) = 1268$, 20878 reflections collected, 5960 were independent and were used in the structure refinement of 388, $R1 = 0.0362$ ($I > 2\sigma(I)$), $wR2 = 0.09995$ (all data), min./max. residual electron density 0.719/−0.536 e Å^{−3}. CCDC-236234 (**3**) and CCDC-236235 (**2**) contain the supplementary crystallographic data. These data can be obtained free of charge via www.ccdc.cam.ac.uk/conts/retrieving.html (or from the Cambridge Crystallographic Data Centre, 12 Union Road, Cambridge CB2 1EZ, UK; fax: (+44)1223-336-033 or deposit@ccdc.cam.ac.uk). The structures were solved by direct methods using SHELXS-97 and refined against F^2 on all data by full-matrix least squares; G.M. Sheldrick programs for crystal structure refinement, Universität Göttingen, Göttingen (Germany), 1997. Hydrogen atoms were included at geometrically calculated positions and refined using a riding model.

Binuclear Complexes

Diazenes Complexes of Copper: Synthesis, Spectroscopic Analysis, and Electronic Structure**

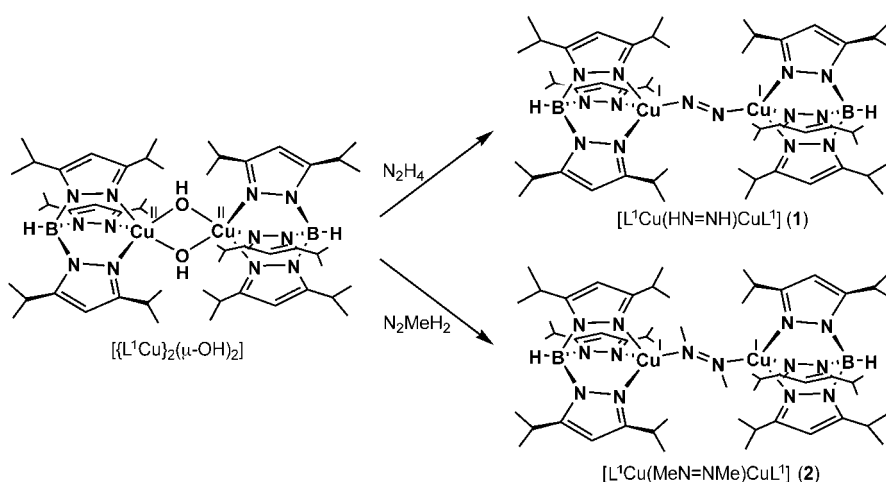
Kiyoshi Fujisawa,* Nicolai Lehnert,* Yoko Ishikawa, and Ken-ichi Okamoto

In memory of Dieter Sellmann

Diazenes are a very interesting molecule as a result of its ability to stereoselectively reduce some unsaturated organic substrates (probably via the *cis* isomer)^[1] as well as its relevance in biological nitrogen fixation. Evidence from X-ray analyses,^[2] spectroscopic studies,^[3] and density functional calculations^[4] suggests that HN=NH (1,2-diazenes) is a metal-bound intermediate in nitrogenase turnover. Diazenes are extremely unstable in their free state and undergo a bimolecular decomposition above -150°C to give N_2 and N_2H_4 .^[5] Its stability is greatly enhanced, however, when its lone pairs are coordinated to transition metals. The general importance of nitrogen fixation has resulted in many research groups having tried to make model complexes with coordinated diazenes, dinitrogen, or hydrazine ligands; the corresponding transition-metal-diazenes complexes have been synthesized by Sellmann^[6] amongst others.^[7,8] However, in the case of Cu, only three crystal structures—a complex of a 1,2-disubstituted diazenes ($[\text{Cu}_2\text{Cl}_2(\text{MeN}=\text{NMe})]_n$)^[9] and two hydrazine complexes ($[\text{CuCN}(\text{N}_2\text{H}_4)]_n$ ^[10a] and $[\text{CuCl}(\text{N}_2\text{H}_4)(\text{NaCl})]_n$ ^[10b])—have been published, and to the best of our knowledge no structural and spectroscopic data for Cu^{I} -

diazenes complexes have been reported so far. Herein we report the crystal structures and UV/Vis absorption and resonance-Raman spectra of two related Cu^{I} complexes with bridging *trans*-1,2-diazenes and *trans*-1,2-dimethyldiazenes ligands. The coordination sphere of the Cu^{I} centers is completed by a hydrotris(pyrazolyl)borate-type tripod ligand. The electronic structure of these systems has been evaluated with the help of density functional (DFT) calculations.

Addition of an excess of hydrazine monohydrate (2.5 equiv) to a solution of the precursor $[(\text{L}^{\text{I}}\text{Cu})_2(\mu\text{-OH})_2]$ (L^{I} = hydrotris(3,5-diisopropyl-1-pyrazolyl)borate anion)^[11] in CH_2Cl_2 /heptane (5:1) at -50°C caused a gradual color change from blue to dark purple. Filtration, concentration, and cooling of this solution afforded $[\text{L}^{\text{I}}\text{Cu}(\text{HN}=\text{NH})\text{CuL}^{\text{I}}]$ (**1**; yield: 60%) as a deep-purple, microcrystalline solid



Scheme 1. Synthesis of complexes **1** and **2**.

(Scheme 1).^[12–14] The oxidation of hydrazine to diazenes is mediated by the Cu^{II} centers, which are reduced to Cu^{I} -centers (similar hydrazine oxidations have been applied before to form diazenes complexes^[6,7]). The fact that a diazenes unit had formed from hydrazine was evident from: a) the appearance of a strong absorption band at 573 nm ($\epsilon = 3500 \text{ cm}^{-1} \text{ mol}^{-1} \text{ dm}^3$), whereas monomeric and dimeric Cu^{I} -hydrazine complexes are colorless;^[15] b) the appearance of a strong resonance-Raman band at 1358 cm^{-1} , which is the typical N–N stretching frequency of dimeric diazenes complexes (see below); c) the observation of a small signal in the ^1H NMR spectrum at $\delta = 4.90 \text{ ppm}$ which corresponds to the diazenes hydrogens; and d) the X-ray crystal structure shown in Figure 1, where a planar *trans*- N_2H_2 ligand bridges the two Cu^{I} ions.^[16] Together with the hydrotris(pyrazolyl)borate ligand, this leads to a distorted tetrahedral geometry at the Cu centers. Complex **1** has a crystallographic inversion center in the middle of the N=N bond. The N41–N41' bond length (1.13(1) Å) is slightly shorter than those of the N–N bonds of previously reported diazenes complexes (1.16–1.30 Å),^[6–9] and is clearly not in the range found for hydrazine complexes

[*] Prof. Dr. K. Fujisawa, Y. Ishikawa, Prof. Dr. K.-i. Okamoto
Department of Chemistry
University of Tsukuba
Tsukuba 305-8571 (Japan)
Fax: (+81) 29-853-6503
E-mail: kiyoshif@chem.tsukuba.ac.jp

Dr. N. Lehnert
Institut für Anorganische Chemie
Christian-Albrechts-Universität Kiel
Olshausenstrasse 40, 24098 Kiel (Germany)
Fax: (+49) 431-880-1520
E-mail: nlehnert@ac.uni-kiel.de

[**] This work was supported by Grants-in-Aid for Scientific Research (B) (nos. 13555257 and 14350471) from JSPS and by the 21st COE Program from MEXT (to KF).

Supporting information for this article is available on the WWW under <http://www.angewandte.org> or from the author.

IR spectrum of poly(2-vinylpyridine) showing relative intensity (rel. I) versus wavenumber ($\tilde{\nu}$ / cm^{-1}). The x-axis ranges from 400 to 2000 cm^{-1} . The y-axis ranges from 0 to 12000. Key peaks are labeled: (s) at ~700 cm^{-1} , (s) at ~720 cm^{-1} , 941, (s) at ~1180 cm^{-1} , 1198, 1365, (s) at ~1450 cm^{-1} , and 1474.

4945

Table 1: Raman assignments of complex **1**.

Mode	Symbol	Cu-N ₂ H ₂ -Cu (1)		[(Fe ^{II} N ₄ S ₄) ₂ (N ₂ H ₂)] exp. (ref. [19])
		exp. (Figure 2) ^[a]	calcd	
$\nu_s(\text{Cu-N})$	A	523 (513)	512	not observed
γ_s		not observed	603	667/659
	2 × A	1043 (1025)	—	—
$\nu(\text{N-N})$	B	1358 (1326/1310)	1421	1382
$\delta_s(\text{N-N-H})$		1547 (1536)	1573	1480
	A + B	1887 (1835)	—	—

[a] Band positions in the ¹⁵N-labeled material are given in brackets.

Table 2: Raman assignments of complex **2**.

Mode ^[a]	Cu-N ₂ Me ₂ -Cu (2)	
	exp. (Figure 3)	calcd
$\nu_s(\text{Cu-N})$	not observed	251/341
$\delta_s(\text{N-C-H}) + \nu_s(\text{C-N}) + \nu_s(\text{Cu-N})$	941	959
$\nu_s(\text{C-N}) + \delta_s(\text{N-C-H}) + \nu_s(\text{Cu-N})$	1198	1214
$\nu(\text{N-N}) + \delta_s(\text{H-C-H}) + \nu_s(\text{C-N})$	1365	1416
$\delta(\text{H-C-H}) + \nu(\text{N-N})$	1474	1491/1529

[a] The dominant contribution to a mode is given first in bold type.

N-C-H bends) complicates the interpretation. However, since the N-N stretch should show the strongest resonance enhancement in the Raman spectrum, its assignment to the peak at 1365 cm⁻¹ is straightforward, and is also in agreement with the calculations.

Previous work has shown that diazene is a σ -donor and π -acceptor ligand.^[19] However, the d¹⁰ electron configuration of the Cu^I ion means that no σ donation from the diazene into the d orbitals of copper is possible in **1** and **2**. Correspondingly, the interaction between the Cu^I center and the diazene corresponds to a pure back-bond. This bonding description is in agreement with the results of the DFT calculations for **1** and **2**. Figure 4 shows a schematic molecular orbital (MO) diagram for **1**. The LUMO corresponds to the antibonding combination of π_v^* —the π^* orbital of the diazene perpendicular to the Cu-N₂H₂-Cu plane—and the in-phase combination of the d_{xz} orbitals on the copper atoms. The corresponding out-of-phase combination of the d_{xz} orbitals is the HOMO, which is essentially nonbonding to the ligands. The bonding MO between d_{xz} and π_v^* is found at lower energy. This electronic structure is different from that obtained for the Fe^{II}-diazene complexes, where both a σ and a π bond between the metal and the diazene ligand are found.^[19]

Figure 5 shows the absorption spectrum of **1** together with resonance-Raman profiles of the peaks at 523, 1358, 1547, and 1887 cm⁻¹, which all show resonance enhancement with respect to the intense absorption of **1** at 573 nm. This band is therefore assigned as a d_{xz} → π_v^* (HOMO → LUMO) charge-transfer (CT) transition, as shown in Figure 4. This is similar to the Fe^{II}-diazene systems, where the corresponding CT transition is found at 580 and 620 nm for [(Fe^{II}N₄S₄)₂(N₂H₂)] and [(Fe^{II}S₄'(PPR₃))₂(N₂H₂)], respectively.^[6] In the case of **2**, the corresponding CT transition is at 484 nm (see Supporting Information).

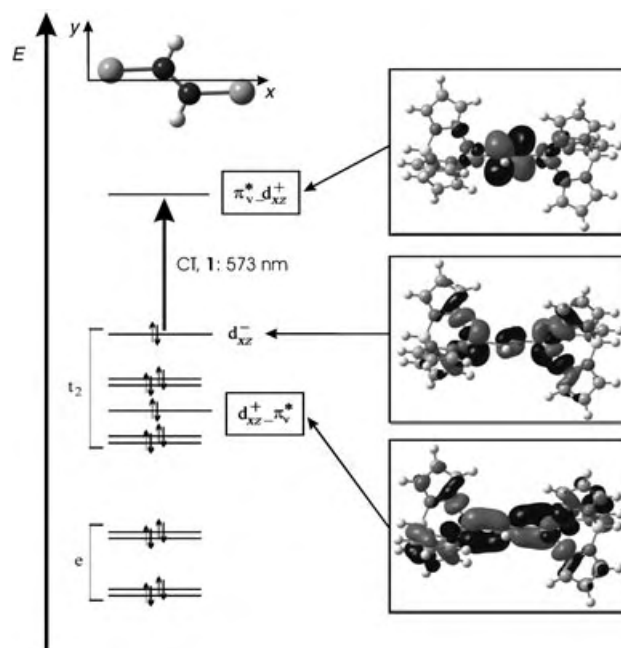


Figure 4. Schematic MO diagram of **1**. The insert in the top left corner shows the chosen coordinate system for the labeling of the orbitals. The orbital π_v^* (v = vertical) corresponds to the π^* function of diazene orthogonal to the Cu-N(H)=N(H)-Cu plane. The inserts on the right show important MO contours.

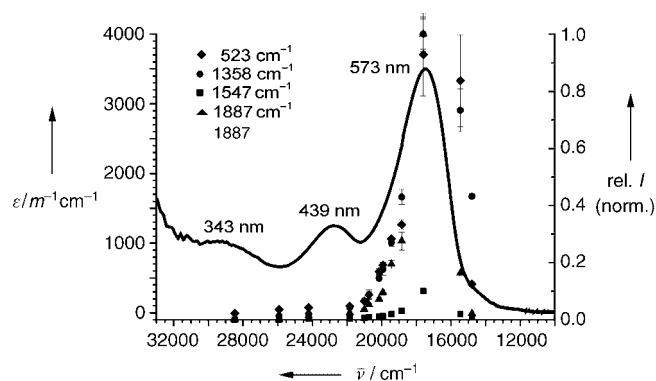


Figure 5. Resonance-Raman profiles of important vibrations of **1** plotted against the absorption spectrum.

We have described the preparation and characterization of novel Cu^I-diazene complexes. Spectroscopic results and crystal structures have been presented and related to known Fe^{II}-diazene complexes, thus proving the identity of the former compounds. In addition, the electronic structure of the Cu^I-diazene bond has been investigated with the help of density functional calculations.

Received: April 22, 2004

Keywords: copper · density functional calculations · N ligands · Raman spectroscopy · structure elucidation

- [1] a) E. J. Corey, D. J. Pasto, W. L. Mock, *J. Am. Chem. Soc.* **1961**, *83*, 2895; b) E. E. van Tamelen, R. S. Dewey, R. J. Timmons, *J. Am. Chem. Soc.* **1961**, *83*, 3725; c) E. E. van Tamelen, R. S. Dewey, R. J. Timmons, *J. Am. Chem. Soc.* **1961**, *83*, 3729; d) E. E. van Tamelen, R. J. Timmons, *J. Am. Chem. Soc.* **1962**, *84*, 1067.
- [2] a) J. Kim, D. C. Rees, *Science* **1992**, *257*, 1677; b) B. Schmid, M. W. Ribbe, O. Einsle, M. Yoshida, L. M. Thomas, D. R. Dean, D. C. Rees, B. K. Burgess, *Science* **2002**, *296*, 352; c) O. Einsle, F. A. Tezcan, S. L. A. Andrade, B. Schmid, M. Yoshida, J. B. Howard, D. C. Rees, *Science* **2002**, *297*, 1696.
- [3] a) B. E. Smith, *Adv. Inorg. Chem.* **1999**, *47*, 159; b) J. B. Howard, D. C. Rees, *Chem. Rev.* **1996**, *96*, 2965; c) B. K. Burgess, D. J. Lowe, *Chem. Rev.* **1996**, *96*, 2983; d) R. R. Eady, *Chem. Rev.* **1996**, *96*, 3013.
- [4] B. Hinnemann, J. K. Nørskov, *J. Am. Chem. Soc.* **2004**, *126*, 3920.
- [5] N. Wiberg, H. Bachhuber, G. Fischer, *Angew. Chem.* **1972**, *84*, 889; *Angew. Chem. Int. Ed. Engl.* **1972**, *11*, 829.
- [6] D. Sellmann, A. Hille, A. Rösler, E. W. Heinemann, M. Moll, G. Brehm, S. Schneider, M. Reiher, B. A. Hess, W. Bauer, *Chem. Eur. J.* **2004**, *10*, 819, and references therein.
- [7] a) T.-Y. Cheng, A. Ponce, A. L. Rheingold, G. L. Hillhouse, *Angew. Chem.* **1994**, *106*, 703; *Angew. Chem. Int. Ed. Engl.* **1994**, *33*, 657; b) J. P. Collman, J. E. Hutchison, M. S. Ennis, M. A. Lopez, R. Guilard, *J. Am. Chem. Soc.* **1992**, *114*, 8074; c) G. Huttner, W. Gartzke, K. Allinger, *J. Organomet. Chem.* **1975**, *91*, 47.
- [8] Recent reviews: a) B. A. Mackay, M. D. Fryzuk, *Chem. Rev.* **2004**, *104*, 385; b) M. Hidai, *Coord. Chem. Rev.* **1999**, *185–186*, 99; c) D. Sellmann, J. Sutter, *Acc. Chem. Res.* **1997**, *30*, 460.
- [9] I. D. Brown, J. D. Dunitz, *Acta. Crystallogr.* **1960**, *13*, 28.
- [10] a) D. T. Cromer, A. C. Larson, R. B. Roof, Jr., *Acta. Crystallogr.* **1966**, *20*, 279; b) D. Cheng, C. Feng, S. Xia, *Transition Met. Chem.* **2000**, *25*, 635.
- [11] N. Kitajima, K. Fujisawa, C. Fujimoto, Y. Moro-oka, S. Hashimoto, T. Kitagawa, K. Toriumi, K. Tatsumi, A. Nakamura, *J. Am. Chem. Soc.* **1992**, *114*, 1277.
- [12] The diazene complex **1** is unstable in the solid state at room temperature, even under an argon atmosphere, which is in accord with the observations made for the diazene complexes mentioned above. If a small amount of dioxygen is present in the solution at -50°C , **1** reacts immediately to form the bridging $\text{Cu}^{\text{II}} \mu\text{-}\eta^2\text{-}\eta^2$ peroxo complex, $[(\text{L}^1\text{Cu})_2(\mu\text{-O}_2)]^{[\text{II}]}$.
- [13] The new diazene complexes **1** and **2** exhibit satisfactory spectroscopic and analytical data (see Supporting Information).
- [14] When a solution of **1** or **2** was warmed to above -40°C under an argon atmosphere the color of the solution slowly changed to green. The nature of the decomposition products was unclear. For this reason, the characterization of these complexes in solution (NMR and electronic absorption spectroscopy) was performed on the reaction mixtures.
- [15] K. Fujisawa, N. Lehnert, unpublished results.
- [16] CCDC-235558 (**1**) and -235559 (**2**) contain the supplementary crystallographic data for this paper. These data can be obtained free of charge via www.ccdc.cam.ac.uk/conts/retrieving.html (or from the Cambridge Crystallographic Data Centre, 12 Union Road, Cambridge CB21EZ, UK; fax: (+44)1223-336-033; or deposit@ccdc.cam.ac.uk). Note that the Cu-N-N-Cu subunit in **1** and **2** is planar, which is a clear indication of bound diazene; in the case of bridging hydrazine the Cu-N-N-Cu core is strongly bent.^[15] The presence of Cu^{I} centers in **1** and **2** is evident from the fact that no counterions are found in either of the crystal structures.
- [17] Either aqueous NaOH solution or triethylamine was used to neutralize N,N' -dimethylhydrazine dihydrochloride. The ^1H NMR spectroscopic data and X-ray crystallographic analysis indicated that triethylamine reacted only as a neutralizing agent.
- [18] K. Fujisawa, Y. Moro-oka, N. Kitajima, *J. Chem. Soc. Chem. Commun.* **1994**, 623.
- [19] a) N. Lehnert, B. E. Wiesler, F. Tuzcek, A. Hennige, D. Sellmann, *J. Am. Chem. Soc.* **1997**, *119*, 8869; b) N. Lehnert, B. E. Wiesler, F. Tuzcek, A. Hennige, D. Sellmann, *J. Am. Chem. Soc.* **1997**, *119*, 8879.

Hydrocarbon Cations

Arylbis(9-anthryl)methyl Cations: Highly Crowded, Near Infrared Light Absorbing Hydrocarbon Cations**

Yuichi Nishimae, Hiroyuki Kurata, and Masaji Oda*

Triarylmethyl cations have been widely studied since the discovery of the triphenylmethyl cation in 1901,^[1,2] and highly crowded triarylmethyl cations in particular have been the subject of recent interest. Tris(1-naphthyl)methyl and tris(2-naphthyl)methyl cations (**1a** and **1b**) were synthesized as unstable species,^[3] whereas the tris(1-azulenyl)methyl cations **2** were reported to be stable.^[4] The arylbis(9-anthryl)methyl cations **3** should be even more highly crowded than **1** and **2**. In particular, the symmetric tris(9-anthryl)methyl cation **3f** would be a most fascinating molecule. However, none of the cations **3** have been reported.

The instability of **1a** and **1b** can be ascribed to their facile Nazarov-type cyclizations,^[5] that is, a kinetic instability rather than a thermodynamic instability. Cations **3** may be less prone to undergo this rearrangement because of the doubly benzo-annelated structure of anthracene. Therefore, they would be fairly stable once formed, though the conjugation between the aryl groups might be considerably reduced due to steric congestion.

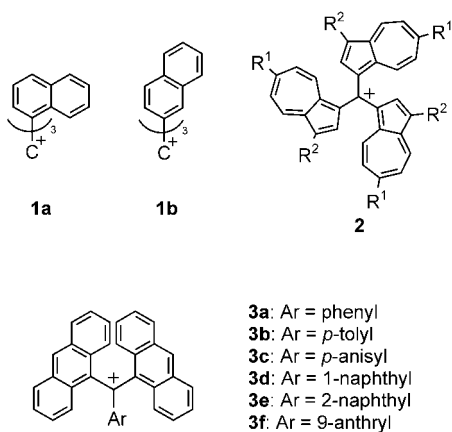
The reason for the total absence of cations **3** may be the difficulty of their synthesis. In principle, bis(9-anthryl) ketone (**4**, Scheme 1)^[6,7] should be a suitable starting material. However, we found that **4** is not reactive towards organo-

[*] Y. Nishimae, Dr. H. Kurata, Prof. M. Oda
Department of Chemistry
Graduate School of Science
Osaka University
Toyonaka, Osaka 560-0043 (Japan)
Fax: (+81) 6-6850-5384
E-mail: moda@chem.sci.osaka-u.ac.jp

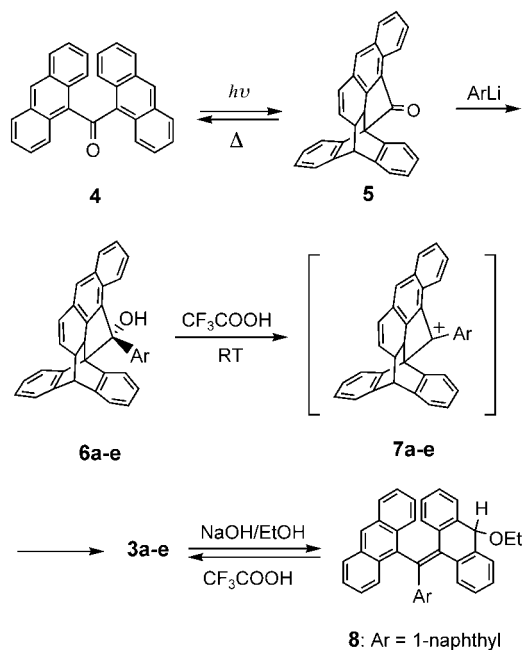
[**] This work was partially supported by the 21st Century COE Program, Japanese Government (Creation of Integrated EcoChemistry).



Supporting information for this article is available on the WWW under <http://www.angewandte.org> or from the author.



metallic reagents, probably due to steric hindrance or rapid electron transfer from the reagents.^[8] Thus, **4** does not afford the arylbis(9-anthryl)methyl alcohols that would be promising precursors to **3**.



Scheme 1. Synthesis of cations **3a–e** and further reaction of **3d** to **8**.

We discovered, however, that the photochemical intramolecular [4+2] cycloadduct of **4**, namely **5** (Scheme 1),^[6b,9] is susceptible to nucleophilic additions. The increased reactivity of **5** comes from the following structural and electronic features: 1) It has a rigid structure, 2) one face of the carbonyl group is less hindered than the other face (according to the PM3-optimized structure), 3) the carbonyl group is less conjugated than that of **4**, and 4) its electrochemical reduction potential is about 0.35 V higher than that of **4** (−1.94 V (half-wave potential) for **5**/CH₂Cl₂/*n*-Bu₄NClO₄ vs. −1.60 V (peak potential) for **4**). Compound **5** can cyclorevert to **4** fairly

easily upon heating ($E_a = 34.2 \pm 0.2$ kcal mol^{−1}; $t_{1/2} = 12.0$ h at 119 °C in [D₅]-bromobenzene).^[10] These findings have led to a novel synthesis of **3**, which we report here.

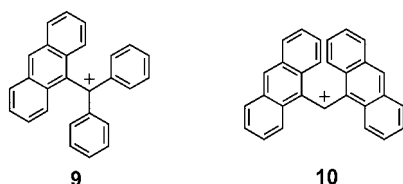
The reaction of ketone **5** with phenyllithium (3 equiv) in THF at room temperature afforded alcohol **6a** with high stereoselectivity in 82 % yield. Compound **6a** was determined to be an *exo* adduct by the observation of an NOE between the aromatic protons of the phenyl group and proton on C7 (the closest aliphatic methine proton on the bicyclo[2.2.2]octane framework, see Scheme 1). This is in agreement with the structural features of **5**. The reaction of **5** with *p*-tolyllithium, *p*-anisyllithium, 1-naphthyllithium, and 2-naphthyllithium furnished the corresponding addition products **6b** (80 %), **6c** (93 %), **6d** (51 %), and **6e** (64 %), respectively.

However, **5** still suffers from steric hindrance and attempted nucleophilic additions of the more bulky 9-anthryllithium or its Grignard reagent have been unsuccessful. The thermal cycloreversion also brought forth a problem for alcohols **6a–e**: Heating of **6a** resulted mostly in fragmentation rather than cycloreversion, probably initiated by homolytic carbon–carbon bond cleavage in the cyclopentanol moiety. The EI mass spectrum of **6a** agrees with this result, showing the molecular ion (m/z 474; 1 %) only weakly with strong fragment peaks at m/z 296 (100 %) and 178 (98 %) that correspond to the molecular weights of 9-anthryl *p*-tolyl ketone and anthracene. The considerable thermodynamic stability of the hydroxydiarylmethyl radical as well as the strain in the cyclopentanol moiety may be responsible for the preferential homolysis.

Despite the unsuccessful thermal cycloreversion of **6a**, it was found that addition of trifluoroacetic acid (TFA) to a colorless solution of **6a** in chloroform at room temperature affords the desired cation **3a** cleanly as a stable species in a deep green solution. Similarly, the tolyl, anisyl, and naphthyl compounds **6b–e** afforded the corresponding cations **3b–e** (see Scheme 1). Thus, it follows that the intermediate cations **7a–e** undergo a facile [4+2] cycloreversion at room temperature to yield the thermodynamically more stable triarylmethyl cations **3a–e** (stable for weeks in CDCl₃/TFA). To our knowledge, the 1-naphthyl compound **3d** is the most highly crowded triarylmethyl cation observed.

The ¹H and ¹³C NMR spectra of **3** are in agreement with the cation structures.^[11] For example, in the ¹H NMR spectrum of the *p*-tolyl compound **3b**, the signal for the proton on C10 ($\delta = 9.15$ ppm) of the anthryl groups is down-shifted by 0.75 ppm compared to the protons on C9,10 of anthracene, and the signal for the methyl protons ($\delta = 2.59$) of the *p*-tolyl group is down-shifted by 0.27 ppm compared to that of **6b** ($\delta = 2.32$). In the ¹³C NMR spectrum, the central cation center (C α) of **3a** is observed at $\delta = 190.97$ ($\delta = 191.84$, 187.66, 184.55, and 178.55 for **3b–e**, respectively). Thus, there is a trend of high-field shifts compared with the signal for C α of the 9-anthryldiphenylmethyl cation **9** ($\delta = 204.11$, see below)^[12,13] and the triphenylmethyl cation ($\delta = 211.56$).^[13]

When a solution of **3d** in CHCl₃/TFA is poured into NaOH/EtOH at 0 °C, the 10-ethoxy adduct **8** is formed in 52 % yield (Scheme 1). A similar alkoxy adduct has been described for **9**.^[12] When ether **8** is dissolved in CHCl₃/TFA, **3d** is cleanly regenerated.



The most remarkable feature of cations **3a–e** is a strong absorption in the near-infrared region ($\lambda_{\text{max}} = 855\text{--}946\text{ nm}$, band 3) in TFA (Figure 1, Table 1). There are two other absorptions in the visible region: $\lambda_{\text{max}} = 440\text{--}470\text{ nm}$ (band 1) and $666\text{--}748\text{ nm}$ (band 2). The appearance of two bands at wavelengths longer than 500 nm contrasts with the single band of **9** ($\lambda_{\text{max}} = 786\text{ nm}$ (780 nm in liquid SO_2 ^{[12])}) and the bis(9-anthryl)methyl cation **10** ($\lambda_{\text{max}} = 855\text{ nm}$).^[14]

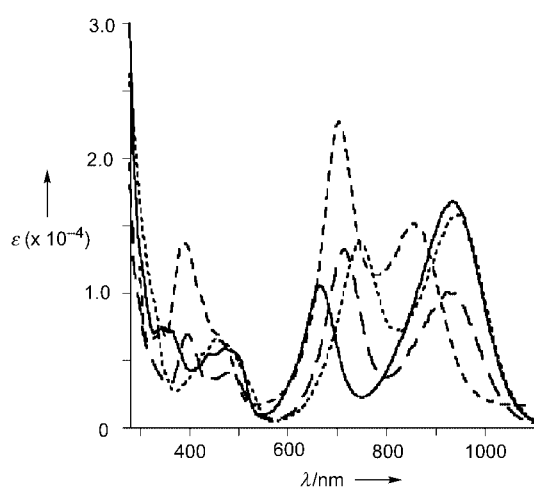


Figure 1. Absorption spectra of **3a** (solid line), **3c** (short broken line), **3d** (dotted line), and **3e** (long broken line) in CF_3COOH (ϵ in $\text{M}^{-1}\text{cm}^{-1}$). The absorption spectrum of **3b** is omitted for clarity (see Table 1).

Table 1: Absorption spectral data of **3a–e**, **9**, and **10** in CF_3COOH .

Compound	λ_{max} [nm^{-1}] ($\epsilon \times 10^{-4}$)
3a	936 (1.68), 666 (1.06), 498 sh (0.54), 472 (0.59), 441 (0.55)
3b	916 (1.37), 681 (1.20), 496 sh (0.43), 467 (0.51), 436 (0.50)
3c	855 (1.52), 704 (2.27), 461 (0.68), 390 (1.37), 343 (0.75)
3d	946 (1.59), 748 (1.37), 456 (0.66), 421 (0.51)
3e	926 (1.03), 713 (1.35), 478 (0.42), 443 sh (0.38), 395 (0.71)
9	786 (1.14), 443 (1.18), 400 (1.62)
10	855 (2.76), 539 sh (0.29), 473 (0.85)

In the case of cations **3**, with the exception of **3c**, band 3 is at longer wavelength than the absorption of **9**, where band 2 is at even shorter wavelength than the absorption of **8**. We think that bands 2 and 3 might be associated with orbital splitting by homoconjugation between the two 9-anthryl groups. Accord-

ing to a semi-empirical calculation (AM1), the optimized structure of **3a** (Figure 2) takes a deep propeller conformation and there are large coefficients for the HOMO orbitals at the 9-positions of the anthryl groups with small coefficients at $\text{C}\alpha$. In this situation, it seems possible that there is some interaction (homoconjugation) between the p orbitals at the 9-positions of the anthryl groups. The dianthrylmethyl cation



Figure 2. The HOMO orbitals of **3a** as obtained by the AM1 method. The orbital coefficients at $\text{C}\alpha$ and the phenyl group are small.

10 does not adopt a propeller conformation (AM1): One anthryl group is twisted against the plane of the 9-anthrylmethyl cation and the HOMO coefficients on the twisted anthryl group are small, disfavoring homoconjugation. The idea of orbital splitting due to homoconjugation is in agreement with the small difference in wavelength between bands 2 and 3 for the *p*-anisyl cation **3c** ($\Delta\lambda = 151\text{ nm}$, compared with $\Delta\lambda = 270\text{ nm}$ for **3a**) and the unusual blue shift of the longest wavelength absorption (855 nm for **3c** vs. 936 nm for **3a**). This blue shift contrasts with the appreciable red shift of the *p*-anisylidiphenylmethyl cation (476 nm) relative to the triphenylmethyl cation ($431, 404\text{ nm}$).^[15] The larger chemical shifts of the anthryl groups of **3c** ($\text{H}10: \delta = 9.03$; $\text{C}10: \delta = 187.66\text{ ppm}$) compared to those of **3a** indicate a considerable resonance contribution of the *para*-quinoid structure of the *p*-anisyl group as usually observed. This results in a slightly better coplanarity of the molecule (AM1), which is less favorable for homoconjugation.

In view of the stability of **3a–e**, the tris(9-anthryl)methyl cation **3f** should also be a stable species when once formed. Further studies on arylbis(9-anthryl)methyl cations including attempts to synthesize **3f** are under way. Transformation of **3a–e** to the corresponding methanes, carbanions, and radicals are also in progress.

Received: April 28, 2004

Keywords: cations · cycloaddition · nucleophilic addition · photochemistry · steric hindrance

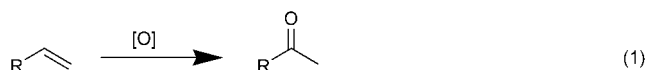
[1] Reviews: "Arylcarbonium Ions": H. H. Freedman, *Carbonium Ions*, Vol. IV (Eds.: G. A. Olah, P. von R. Schleyer), Wiley-Interscience, New York, 1972, pp. 1501–1578.

- [2] a) J. F. Norris, *Am. Chem. J.* **1901**, 25, 117; b) F. Kehrmann, F. Wentzel, *Ber. Dtsch. Chem. Ges.* **1901**, 34, 3815–3819; F. Kehrmann, F. Wentzel, *Ber. Dtsch. Chem. Ges.* **1902**, 35, 622.
- [3] G. A. Olah, Q. Liao, J. Casanova, R. Bau, G. Rasul, G. K. Surya Prakash, *J. Chem. Soc. Perkin Trans. 2* **1998**, 2239–2242.
- [4] a) S. Ito, N. Morita, T. Asao, *Bull. Chem. Soc. Jpn.* **1995**, 68, 1409–1436; b) S. Ito, S. Kikuchi, H. Kobayashi, M. Morita, T. Asao, *J. Org. Chem.* **1997**, 62, 2423–2431; c) S. Ito, S. Kikuchi, N. Morita, T. Asao, *J. Org. Chem.* **1999**, 64, 5815–5821.
- [5] Review: C. Santelli-Rouvier, M. Santelli, *Synthesis* **1983**, 429–442.
- [6] H. G. Latham, Jr., E. L. May, E. Mosettig, *J. Am. Chem. Soc.* **1948**, 70, 1079–1081; b) H.-D. Becker, L. Hansen, K. Andersson, *J. Org. Chem.* **1986**, 51, 2956–2961.
- [7] Compound **4** has been prepared by Friedel–Crafts acylation of anthracene with 9-anthracenecarbonyl chloride in rather poor yield (21 %).^[6b] We found that the oxidation of bis(9-anthryl)-methyl alcohol—readily obtainable by the reaction of 9-anthraldehyde with 9-anthryllithium—with 2,3-dichloro-5,6-dicyano-1,4-quinonediimine (DDQ) in THF at room temperature affords **4** in 95 % yield. Oxidation of the alcohol with pyridinium chlorochromate (PCC) resulted mostly in fragmentation to give 9-anthraldehyde and other compounds.
- [8] Upon addition of phenyllithium to a solution of **4** in THF at –70 °C, the mixture turned deep red; compound **4** was mostly recovered after quenching with water. The electrochemical reduction potential of **4** is about 0.45 V lower than that of benzophenone ($E_{1/2} = -2.06$ V, CH₂Cl₂), which indicates a considerably higher electron acceptor ability.
- [9] H.-D. Becker, V. Langer, B. W. Skelton, A. H. White, *Aust. J. Chem.* **1989**, 42, 603–610.
- [10] The activation energy was obtained by measurement of the decrease of signal intensity for the aliphatic protons of **5** by ¹H NMR spectroscopy at four different temperatures.
- [11] Cation **3a** showed broadening of the signals below 0 °C, which is suggestive of a dynamic process. However, the presence of TFA as the co-solvent has prevented detailed NMR measurements at low temperatures.
- [12] M. Nojima, M. Takagi, M. Morinaga, G. Nagao, N. Tokura, *J. Chem. Soc. Perkin Trans. 1* **1978**, 488–495.
- [13] Measured in our laboratory under similar conditions for **3a–e**.
- [14] Cation **10** was generated by dissolving bis(9-anthryl)methyl alcohol in TFA.
- [15] N. C. Deno, J. J. Jaruzelski, A. Schriesheim, *J. Am. Chem. Soc.* **1955**, 77, 3044–3051.

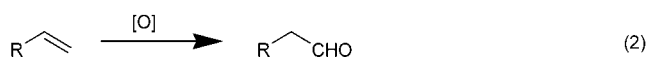
A Practical and Mild Method for the Highly Selective Conversion of Terminal Alkenes into Aldehydes through Epoxidation–Isomerization with Ruthenium(IV)–Porphyrin Catalysts**

Jian Chen and Chi-Ming Che*

The Wacker-type oxidation of alkenes to carbonyl compounds is one of the most important oxidation reactions in synthetic chemistry and the pharmaceutical industry.^[1] The conversion of alkenes RCH=CH_2 into acetaldehyde ($\text{R} = \text{H}$) or methyl ketones ($\text{R} \neq \text{H}$) through the Wacker process [Eq. (1)] has



been well documented;^[1] however, the highly selective formation of aldehydes through catalytic oxidation of RCH=CH_2 ($\text{R} \neq \text{H}$) without C=C bond cleavage [Eq. (2)]



remains a challenge. Previous work by Feringa,^[2a] Murahashi, and co-workers,^[2b] and Wenzel^[2c] showed that the oxidation of aliphatic alkenes (such as oct-1-ene and dec-1-ene), *N*-allyl amides/lactams, and allyl esters with O_2 or air in the presence of certain palladium or palladium/copper catalysts affords a mixture of aldehyde and methyl ketone products. Recently, Ho et al. reported the palladium/copper-catalyzed oxidation of several aliphatic 1,5-dienes with O_2 to form aldehydes in 60–99% yield.^[2d]

During our efforts to develop new oxidation technology based on ruthenium–porphyrin catalysts, we found that the oxidation of a wide variety of terminal alkenes with 2,6-

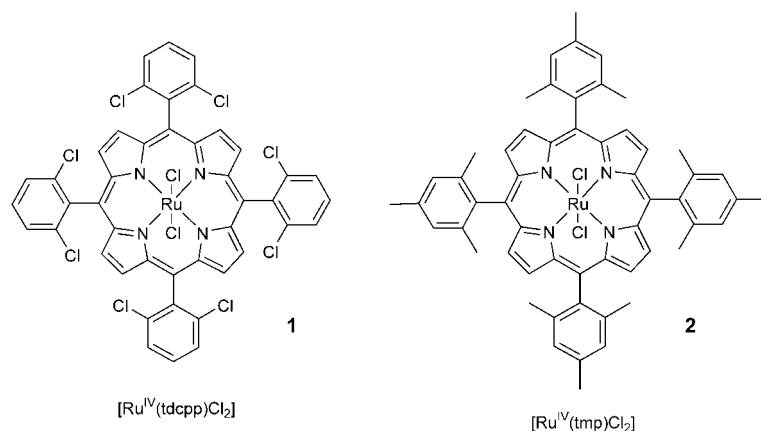
[*] J. Chen, Prof. Dr. C.-M. Che
Shanghai–Hong Kong Joint Laboratory in Chemical Synthesis
Shanghai Institute of Organic Chemistry
The Chinese Academy of Sciences
354 Feng Lin Road, Shanghai 200032 (China)
Prof. Dr. C.-M. Che
Department of Chemistry and
Open Laboratory of Chemical Biology of the
Institute of Molecular Technology for Drug Discovery and Synthesis
The University of Hong Kong, Pokfulam Road (Hong Kong)
Fax: (+852) 2857-1586
E-mail: cmche@hku.hk

[**] We are thankful for the financial support of The University of Hong Kong (Generic Drugs Research Program), the Area of Excellence Scheme (AoE 10/01P) administered by the University Grants Council (HKSAR), and the Hong Kong Research Grants Council (HKU7099/01P). J.C. thanks the Croucher Foundation of Hong Kong for a postgraduate studentship.



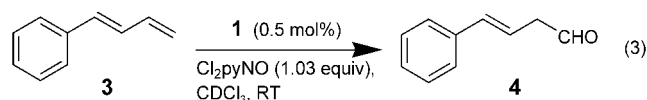
Supporting information for this article is available on the WWW under <http://www.angewandte.org> or from the author.

dichloropyridine *N*-oxide (Cl_2pyNO) in the presence of dichlororuthenium(IV)-porphyrin catalysts $[\text{Ru}^{\text{IV}}(\text{por})\text{Cl}_2]$ ($\text{por} = \text{tdcpp}$ **1**, tmp **2**)^[3] produced aldehydes in up to 99% yield with 100% substrate conversion without C=C bond cleavage. This unexpected ruthenium-catalyzed “Wacker-



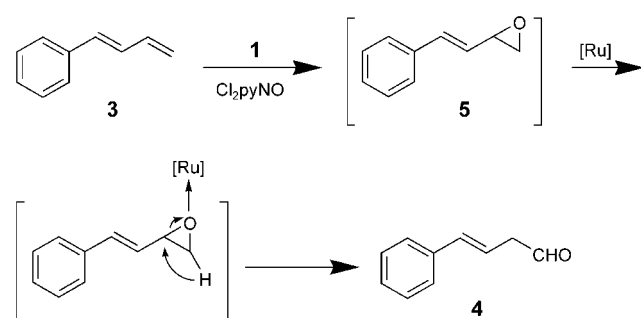
type oxidation” of terminal alkenes^[4,5] reported herein apparently proceeds by a different mechanism to those proposed for the palladium- or palladium/copper-catalyzed reactions.^[2] We also report herein a direct one-pot diazoacetate olefination of aldehyde substrates generated in situ by this ruthenium-porphyrin-catalyzed oxidation of alkenes.

When a solution of 1-phenyl-1,3-butadiene (**3**), Cl_2pyNO (1.03 equiv), and catalyst **1** (0.5 mol%) in CDCl_3 was stirred for 30 min at room temperature, the β,γ -unsaturated aldehyde 4-phenylbut-3-enal (**4**, styrylacetaldehyde) was formed in 99% yield [Eq. (3)]. No ketone products were detected in the reaction mixture. Similar results were obtained with CHCl_3 or



CH_2Cl_2 as the solvent. Other solvents, such as benzene, toluene, acetone, ether, and methanol, were inferior to CHCl_3 and CH_2Cl_2 for this catalytic process.

We propose that the 1,3-diene **3** is first oxidized by Cl_2pyNO to form epoxide **5** in the presence of catalyst **1** (Scheme 1). The same catalyst, or a derivative thereof,



Scheme 1. Proposed mechanism for the formation of aldehyde **4** by the Cl_2pyNO oxidation of **3** catalyzed by **1**.

induces subsequent isomerization of the epoxide to the β,γ -unsaturated aldehyde.^[6] We abbreviate the epoxidation of terminal alkenes followed by isomerization of the epoxide products as E–I reactions.

To provide support for the above mechanism, we examined the effect of Cl_2pyNO on the catalysis (Table 1). With excess Cl_2pyNO , the yield of aldehyde **4** decreased significantly from 99 to 51%, and epoxide **5** was obtained in 49% yield. This result could be rationalized by considering coordination of the epoxide to active ruthenium-porphyrin species for the isomerization reactions. Excess Cl_2pyNO would compete with the epoxide for coordination to ruthenium, thus decreasing the yield of the aldehyde. We found that the use of 1.01–1.03 equivalents of Cl_2pyNO gave the best results in terms of reaction time (30 min) and aldehyde yield (99%). Changing the temperature from room temperature to 10°C or 40°C did not affect the reaction appreciably.

Table 1: Oxidation of **3** catalyzed by **1** with varying amounts of Cl_2pyNO .^[a]

Entry	Cl_2pyNO [equiv]	Conversion of 3 [%]	Yield [%] ^[b]	
			5	4
1	2.0	100	49	51
2	1.03	100	0	99
3	0.9	90	0	> 99

[a] Reaction conditions: **3**: 0.1 mmol, **1**: 0.5 mol%, CDCl_3 : 0.5 mL; 25°C, open to air. [b] Determined by ^1H NMR spectroscopy (based on consumed substrate).

We also examined the effect of catalyst loading on the E–I reaction. When a lower loading of **1** (0.3 mol%) was used, with a molar ratio **3**/ Cl_2pyNO /**1** of 1:1.03:0.003, a mixture of **5**, **4**, and **3** was detected after the reaction. Figure 1 shows the

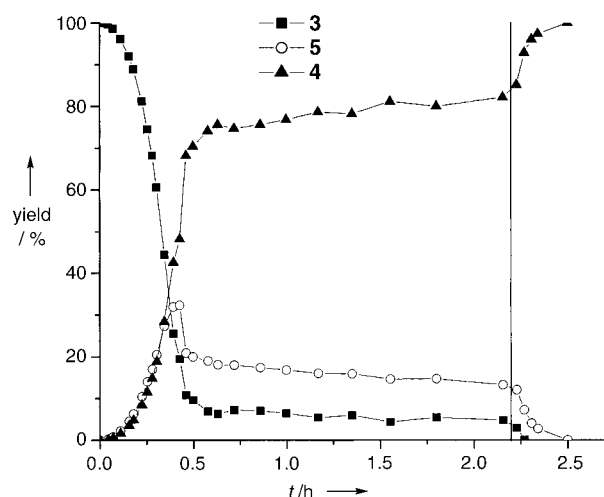


Figure 1. Time-course plot for the Cl_2pyNO oxidation of **3** catalyzed by **1**. Reaction conditions: **3**: 0.1 mmol, Cl_2pyNO : 1.03 equiv, **1**: 0.3 mol%, CDCl_3 : 0.5 mL; 17°C, open to air. The product yields were determined by ^1H NMR spectroscopy. More **1** (0.3 mol%) was added when the reaction had proceeded for about 2.2 h.

time course for this catalytic process. Evidently, after the reaction had proceeded for 2 h, **3** and **5** had not been completely converted into **4**. Analysis of the ruthenium–porphyrin species in the reaction mixture revealed that catalyst **1** had been converted into $[\text{Ru}^{\text{II}}(\text{tdcpp})(\text{CO})]$.^[7] Upon subsequent addition of a new batch of **1**, both **3** and **5** were completely converted into **4** in excellent yields within 15 min.

The E–I reaction of **3** with Cl_2pyNO was catalyzed equally efficiently by **2**, but less efficiently by $[\text{Ru}^{\text{VI}}(\text{tdcpp})\text{O}_2]$. The oxidation of **3** with Cl_2pyNO catalyzed by $[\text{Ru}^{\text{VI}}(\text{tdcpp})\text{O}_2]$ under similar conditions to those used with catalyst **1** (Cl_2pyNO : 1.03 equiv, catalyst loading: 1.7 mol %) afforded **4** in 41 % yield within 5 h. However, the complex $[\text{Ru}^{\text{II}}(\text{tdcpp})(\text{CO})]$ was a relatively inactive catalyst in the E–I reaction.

A series of other 1,3-dienes were treated with Cl_2pyNO (1.01–1.03 equiv) and **1** (0.5–1.0 mol %) at room temperature [Eq. (4), Table 2]. With dienes **6–10**, the corresponding β,γ -unsaturated aldehydes **13–17** were obtained in 81–99 % yield and were stable enough to be purified by flash chromatography on silica gel. However, the aldehyde product **18a**, formed in 90 % yield from the oxidation of diene **11**, was converted into **18b** upon flash chromatography on silica gel. The nonterminal diene **12** was oxidized more slowly to afford the β,γ -unsaturated ketone **19** in 99 % yield after a reaction time of 6 h at 60 °C (Table 2, entry 7).

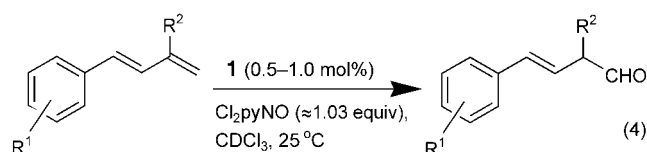


Table 2: Oxidation of 1,3-dienes **6–12** with Cl_2pyNO catalyzed by **1**.^[a]

R = OMe: **6**
 R = NO₂: **7**
 R = Me: **8**

R = H: **9**
 R = OMe: **10**

11

12

R = OMe: **13**
 R = NO₂: **14**
 R = Me: **15**

R = H: **16**
 R = OMe: **17**

18a

19

18b

Entry	Substrate	T [°C]	t [h]	Product	Yield [%] ^[b]
1	6	25	0.5	13	83
2	7	25	1	14	99
3	8	25	0.5	15	88
4	9	25	0.5	16	81
5 ^[c]	10	25	0.5	17	91 ^[d]
6	11	25	0.5	18a	90
7	12	60	6	19	99

[a] Reaction conditions: diene: 0.1 mmol, Cl_2pyNO : 1.03 equiv, **1**: 0.5–1.0 mol %, CDCl_3 : 0.5–1.0 mL; open to air. [b] Determined by GC or ^1H NMR spectroscopy. [c] Reaction conditions: diene: 0.65 mmol, Cl_2pyNO : 1.03 equivalents, **1**: 1.0 mol %, CHCl_3 : 10 mL; open to air. [d] Yield of isolated product.

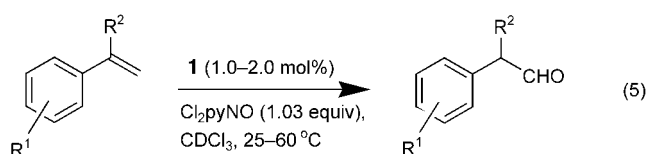


Table 3: Oxidation of terminal alkenes **20–26** with Cl_2pyNO catalyzed by **1**.^[a]

R = H: **20**, F: **21**,
 R = Me: **22**, MeO: **24**

23

25

26

R = H: **27**, F: **28**,
 R = Me: **29**, MeO: **31**

30

32

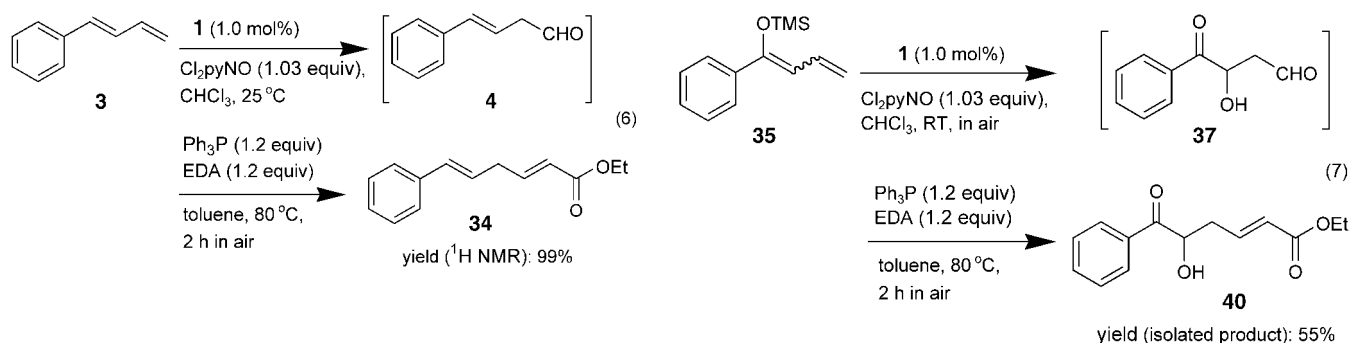
33

Entry	Substrate	T [°C]	t [h]	Product	Yield [%] ^[b]
1	20	60	12	27	99
2	21	60	12	28	99
3	22	60	2	29	96
4	22	25	60	29	99
5	23	25	0.5	30	91
6	24	25	0.5	31	99
7	25	25	0.5	32	92
8	26	60	24	33	0 ^[c]

[a] Reaction conditions: alkene: 0.1 mmol, Cl_2pyNO : 1.03 equiv, **1**: 1.0–2.0 mol %, CDCl_3 : 0.5–2.0 mL; open to air. [b] Determined by GC or ^1H NMR spectroscopy. [c] The corresponding epoxide was produced in 99 % yield (determined by ^1H NMR spectroscopy).

When styrene (**20**) was treated with Cl_2pyNO (1.03 equiv) and **1** (1.0 mol %) in CH_2Cl_2 at reflux for 5 h, styrene oxide and phenylacetaldehyde (**27**) were obtained as a mixture in 90 and 10 % yield, respectively.^[8] To our surprise, when more of catalyst **1** was added, and the reaction time was increased, the styrene oxide was completely converted into aldehyde **27**. For example, the reaction of styrene with Cl_2pyNO (1.03 equiv) in the presence of 2.0 mol % of **1** in CHCl_3 at 60 °C for 12 h afforded **27** in 99 % yield; no benzaldehyde was observed.^[5] Other styrene derivatives **21–25** could also be converted into the corresponding aryl acetaldehydes **28–32** in excellent yields [Eq. (5) and Table 3]. However, with the nonaromatic alkene **26**, only the epoxide product was obtained.

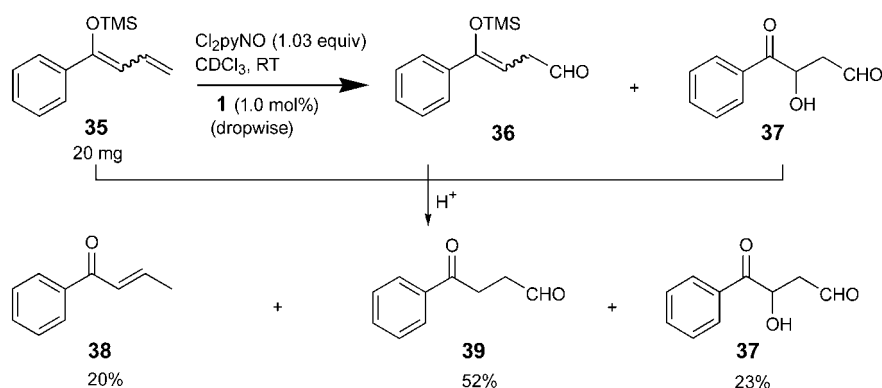
Recently, the research groups of Woo,^[9a] Aggarwal,^[9b] and Zhang^[9c] reported that the iron and ruthenium *meso*-tetraaryl porphyrins $[\text{Fe}^{\text{II}}(\text{ttp})]$ (H_2ttp = *meso*-tetrakis(*p*-tolyl)porphyrin), $[\text{Fe}^{\text{III}}(\text{ttp})\text{Cl}]$, and $[\text{Ru}^{\text{II}}(\text{ttp})(\text{CO})]$ catalyze the olefination of certain classes of aldehydes with ethyl diazoacetate (EDA) in the presence of triphenylphosphane. We observed that both **1** and



$[\text{Ru}^{\text{II}}(\text{tdcpp})(\text{CO})]$ also catalyze such olefination reactions. We recognized that the aldehyde products of the **1**-catalyzed E–I reactions could be used in situ as the substrates for olefination reactions and wanted to develop a practical one-pot E–I–olefination reaction, that is, a one-pot diazoacetate olefination starting directly from alkenes rather than from aldehydes.

By using the “**1**+ Cl_2pyNO ” protocol, **3** (0.1 mmol) was converted into aldehyde **4** in CHCl_3 within 30 min. Remarkably, upon removal of the solvent, followed by the addition of Ph_3P (1.2 equiv), toluene (1 mL), and EDA (1.2 equiv) and heating the reaction mixture at 80°C for 2 h, the olefination product **34** was obtained in 99% yield [Eq. (6)].

4-Oxo-4-aryl butanal derivatives are useful compounds in organic synthesis. For example, the preparation and application of 4-oxo-4-phenylbutanal (**39**) have been studied extensively.^[10] In this work, we found that **39** could be prepared in 52% yield (by ^1H NMR spectroscopy; isolated yield: 41%) through the E–I reaction of silyl enol ether **35** (Scheme 2).



Scheme 2. Oxidation of silyl enol ether **35** with Cl_2pyNO catalyzed by **1**. (The yields of **37–39** were determined by ^1H NMR spectroscopy).

The same reaction also afforded hydroxyketoaldehyde **37** in 23% yield. When 2.06 equivalents of Cl_2pyNO were used, **37** could be obtained in 88% yield (determined by ^1H NMR spectroscopy). From a one-pot E–I–olefination reaction of **35** similar to that of **3**, we isolated the olefination product **40** in 55% yield [Eq. (7)].

In summary, we have developed a mild and practical method with $[\text{Ru}^{\text{IV}}(\text{tdcpp})\text{Cl}_2]$ as a catalyst for the highly regioselective formation of aldehydes from terminal alkenes without C=C bond cleavage. This protocol supplements the Wacker process for the oxidation of terminal alkenes to

ketones or aldehydes. The catalytic reactions reported herein can be conducted in air at room temperature to afford a series of isolable β,γ -unsaturated aldehydes in good to excellent yields. The present work provides a new, practical, and convenient method for preparing multifunctionalized compounds. The application of this method to the synthesis of natural products is in progress.

Received: May 4, 2004

Keywords: homogeneous catalysis · metalloporphyrins · N ligands · oxidation · ruthenium

- [1] a) J. Smidt, W. Hafner, R. Jira, J. Sedlmeier, R. Sieber, R. Rüttinger, H. Kojer, *Angew. Chem.* **1959**, *71*, 176–182; b) J. Smidt, W. Hafner, R. Jira, R. Sieber, J. Sedlmeier, A. Sabel, *Angew. Chem.* **1962**, *74*, 93–102; *Angew. Chem. Int. Ed. Engl.* **1962**, *1*, 80–88; c) J. Tsuji, *Synthesis* **1984**, 369–384; d) J. Tsuji, *Palladium Reagents and Catalysts: Innovation in Organic Synthesis*, Wiley, New York, **1998**.
- [2] a) B. L. Feringa, *J. Chem. Soc. Chem. Commun.* **1986**, 909–910; b) T. Hosokawa, S. Aoki, M. Takano, T. Nakahira, Y. Yoshida, S.-I. Murahashi, *J. Chem. Soc. Chem. Commun.* **1991**, 1559–1560; c) T. T. Wenzel, *J. Chem. Soc. Chem. Commun.* **1993**, 862–864; d) T.-L. Ho, M. H. Chang, C. Chen, *Tetrahedron Lett.* **2003**, *44*, 6955–6957.
- [3] Porphyrin ligands: H_2tdcpp = *meso*-tetraakis(2,6-dichlorophenyl)porphyrin, H_2tmp = *meso*-tetramesitylporphyrin.
- [4] In previously reported alkene oxidations with Cl_2pyNO or air catalyzed by ruthenium porphyrins, only small or trace amounts of aldehydes, if any, were formed; see, for example: a) H. Ohtake, T. Higuchi, M. Hirobe, *Heterocycles* **1995**, *40*, 867–903; b) J. T. Groves, M. Bonchio, T. Carofiglio, K. Shalyaev, *J. Am. Chem. Soc.* **1996**, *118*, 8961–8962; c) A. Berkessel, M. Frauenkron, *J. Chem. Soc. Perkin Trans. 1* **1997**, 2265–2266; d) T.-S. Lai, R. Zhang, K.-K. Cheung, H.-L. Kwong, C.-M. Che, *Chem. Commun.* **1998**, 1583–1584; e) C.-J. Liu, W.-Y. Yu, S.-G. Li, C.-M. Che, *J. Org. Chem.* **1998**, *63*, 7364–7369; f) Z. Gross, S. Ini, *Org. Lett.* **1999**, *1*, 2077–2080; g) Z. Gross, S. Ini, *Inorg. Chem.* **1999**, *38*, 1446–1449; h) X.-Q. Yu, J.-S. Huang, W.-Y. Yu, C.-M. Che, *J. Am. Chem. Soc.* **2000**, *122*, 5337–5342; i) R. Zhang, W.-Y. Yu, K.-Y. Wong, C.-M. Che, *J. Org. Chem.* **2001**, *66*, 8145–8153; j) J.-L. Zhang, H.-B.

- Zhou, J.-S. Huang, C.-M. Che, *Chem. Eur. J.* **2002**, *8*, 1554–1562; k) J.-L. Zhang, C.-M. Che, *Org. Lett.* **2002**, *4*, 1911–1914; l) J.-L. Zhang, Y.-L. Liu, C.-M. Che, *Chem. Commun.* **2002**, 2906–2907; m) A. Berkessel, P. Kaiser, J. Lex, *Chem. Eur. J.* **2003**, *9*, 4746–4756; n) P. Le Maux, M. Lukas, G. Simonneaux, *J. Mol. Catal. A* **2003**, *206*, 95–103.
- [5] Note that the aerobic oxidation of styrene catalyzed by $[\text{Ru}^{\text{II}}(\text{Cl}_8\text{tpfpp})(\text{CO})]$ ($\text{H}_2\text{Cl}_8\text{tpfpp}$ = octachlorotetrakis(pentafluorophenyl)porphyrin) primarily affords benzaldehyde, a C=C bond-cleavage product; see: E. R. Birnbaum, J. A. Labinger, J. E. Bercaw, H. B. Gray, *Inorg. Chim. Acta* **1998**, *270*, 433–439.
- [6] Various Lewis acids and some metal complexes (including the iron–porphyrin complex $[\text{Fe}^{\text{III}}(\text{tpp})\text{OTf}]$; H_2tpp = *meso*-tetraphenylporphyrin) were previously reported to be good reagents or catalysts for the isomerization of epoxides to form aldehydes; see, for example: a) H. Alper, D. Des Roches, T. Durst, R. Legault, *J. Org. Chem.* **1976**, *41*, 3611–3613; b) R. Sudha, K. M. Narasimhan, V. G. Saraswathy, S. Sankararaman, *J. Org. Chem.* **1996**, *61*, 1877–1879; c) S. Kulasegaram, R. J. Kulawiec, *J. Org. Chem.* **1997**, *62*, 6547–6561; d) B. C. Ranu, U. Jana, *J. Org. Chem.* **1998**, *63*, 8212–8216; e) K. Suda, K. Baba, S. Nakajima, T. Takanami, *Tetrahedron Lett.* **1999**, *40*, 7243–7246; f) F. Martínez, C. del Campo, E. F. Llama, *J. Chem. Soc. Perkin Trans. 1* **2000**, 1749–1751.
- [7] This transformation of the catalyst might arise from the decarbonylation of the aldehyde by the ruthenium–porphyrin species. Previously, it was observed that the catalyst $[\text{Ru}^{\text{VI}}(\text{tmp})\text{O}_2]$ was converted into $[\text{Ru}^{\text{II}}(\text{tmp})(\text{CO})]$ during the epoxidation of alkenes: B. Scharbert, E. Zeisberger, E. Paulus, *J. Organomet. Chem.* **1995**, *493*, 143–147.
- [8] The oxidation of styrene with iodosylbenzenes or *tert*-butyl hydroperoxide catalyzed by metal complexes, including iron/manganese porphyrins or corroles, also affords a mixture of styrene oxide and **27**, with the former being the major product; see, for example: a) J. P. Collman, T. Kodadek, J. I. Brauman, *J. Am. Chem. Soc.* **1986**, *108*, 2588–2594; b) J. F. Kinneary, J. S. Albert, C. J. Burrows, *J. Am. Chem. Soc.* **1988**, *110*, 6124–6129; c) F. Minisci, F. Fontana, S. Araneo, F. Recupero, S. Banfi, S. Quici, *J. Am. Chem. Soc.* **1995**, *117*, 226–232; d) Z. Gross, G. Golubkov, L. Simkhovich, *Angew. Chem.* **2000**, *112*, 4211–4213; *Angew. Chem. Int. Ed.* **2000**, *39*, 4045–4047; e) G. Golubkov, J. Bendix, H. B. Gray, A. Mahammed, I. Goldberg, A. J. Dilibio, Z. Gross, *Angew. Chem.* **2001**, *113*, 2190–2192; *Angew. Chem. Int. Ed.* **2001**, *40*, 2132–2134.
- [9] a) G. A. Mirafzal, G. Cheng, L. K. Woo, *J. Am. Chem. Soc.* **2002**, *124*, 176–177; b) V. K. Aggarwal, J. R. Fulton, C. G. Sheldon, J. de Vicente, *J. Am. Chem. Soc.* **2003**, *125*, 6034–6035; c) Y. Chen, L. Huang, M. A. Ranade, X. P. Zhang, *J. Org. Chem.* **2003**, *68*, 3714–3717.
- [10] For selected examples, see: a) C. G. Kruse, J. P. Bouw, R. van Hes, A. van de Kuilen, J. A. J. den Hartog, *Heterocycles* **1987**, *26*, 3141–3151; b) G. A. Molander, S. W. Andrews, *Tetrahedron Lett.* **1989**, *30*, 2351–2354; c) G. A. Molander, K. O. Cameron, *J. Org. Chem.* **1991**, *56*, 2617–2619; d) G. A. Molander, K. O. Cameron, *J. Am. Chem. Soc.* **1993**, *115*, 830–846; e) F. Manescalchi, A. R. Nardi, D. Savoia, *Tetrahedron Lett.* **1994**, *35*, 2775–2778; f) K. Okada, K. Matsumoto, K. Oshima, K. Utimoto, *Tetrahedron Lett.* **1995**, *36*, 8067–8070.

Supramolecular Assembly of Luminescent Gold(I) Alkynylcalix[4]crown-6 Complexes with Planar η^2, η^2 -Coordinated Gold(I) Centers**

Sung-Kong Yip, Eddie Chung-Chin Cheng,
Li-Hua Yuan, Nianyong Zhu, and
Vivian Wing-Wah Yam*

During the last decade, supramolecular architecture in gold(I) chemistry has attracted growing attention owing to the aurophilic nature of gold and the rich luminescence properties that many gold(I) complexes exhibit.^[1,2] The majority of the work in this area has been focused on systems that involve phosphines as stabilizing ancillary ligands as well as carbon-, nitrogen-, and sulfur-donor ligands.^[1b,3] Examples without phosphine ligands are limited.^[1d-f,2d,4] Gold(I) alkynyl systems without phosphine ligands are usually polymeric or oligomeric in nature and their intractability usually prevents them from further study and development.^[5] Molecular complexes of this type are extremely scarce. Examples include the mononuclear homoleptic dialkynylaurate(I), $[\text{RC}\equiv\text{C}-\text{Au}-\text{C}\equiv\text{CR}]^-$, and the novel molecular gold(I) alkynyl complex in the form of two catenated hexanuclear rings recently reported by Mingos et al.^[6] As an extension of our recent interests on d^{10} metal-alkynyl complexes,^[2d,7-11] we believed that soluble polynuclear gold(I) alkynyls with interesting bonding and luminescence properties could be prepared through specially designed alkynyl ligands. Calixarenes, apart from their well-known ability as ion receptors, are one of the most important building blocks in supramolecular chemistry owing to their unique molecular structures, simple one-pot preparations, possible modifications on the lower and upper rims, and their “tunable” molecular shapes and conformations.^[12-14] Alkynylcalixarenes in predefined conformations and preorganized geometries may serve as versatile ligands for the construction of novel luminescent gold(I) alkynyl supramolecular assemblies. Herein, we report the synthesis, structural characterization, and photophysical properties of a series of novel tetranuclear gold(I)-alkynylcalix[4]crown-6 assemblies.

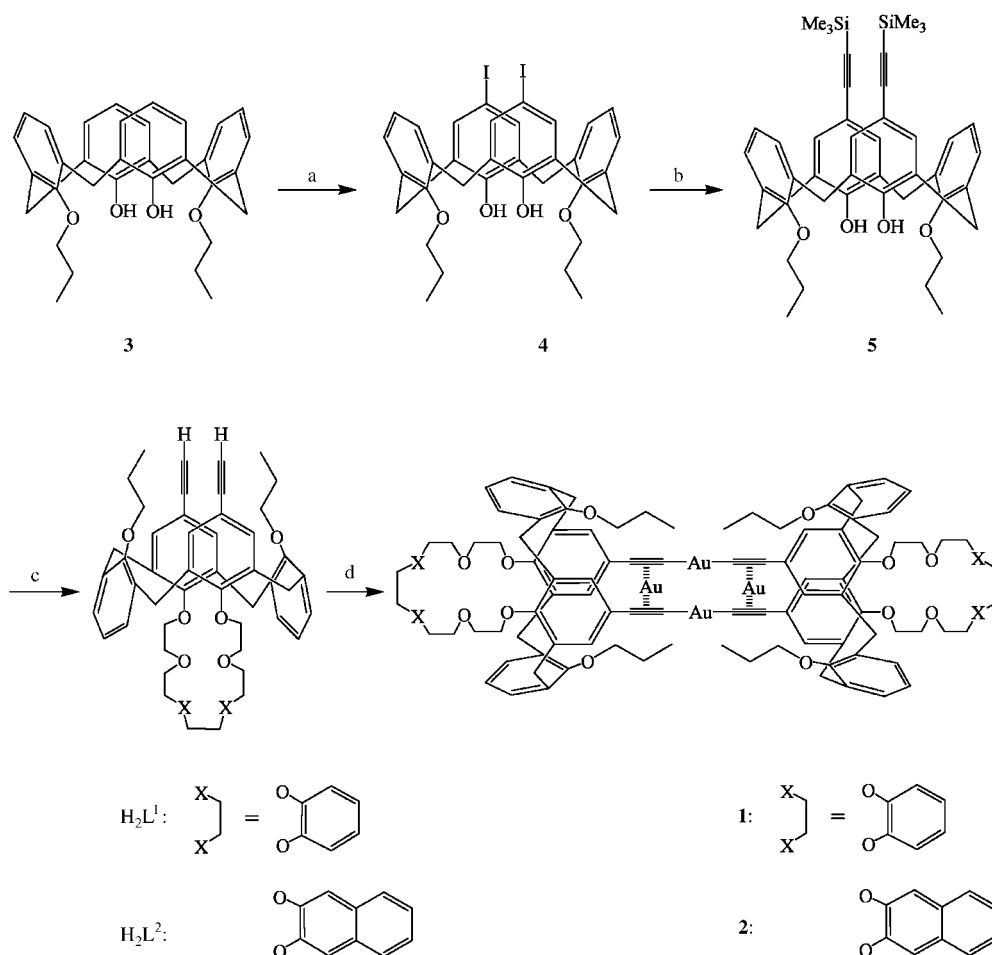
[*] S.-K. Yip, Dr. E. C.-C. Cheng, Dr. L.-H. Yuan, Dr. N. Zhu, Prof. Dr. V. W.-W. Yam
Centre for Carbon-Rich Molecular and
Nanoscale Metal-Based Materials Research
Department of Chemistry and HKU-CAS Joint Laboratory
on New Materials
The University of Hong Kong
Pokfulam Road, Hong Kong SAR (People's Republic of China)
Fax: (+852) 2857-1586
E-mail: wwyam@hku.hk

[**] V.W.-W.Y. acknowledges support from the University Development Fund of The University of Hong Kong and The University of Hong Kong Foundation for Education Development and Research Limited. This work has been supported by a grant from the Research Grants Council of the Hong Kong SAR, China (Project No. HKU 7097/01P). S.-K.Y. and E.C.-C.C. acknowledge the receipt of a postgraduate studentship and a postdoctoral fellowship, respectively, administered by The University of Hong Kong.

The syntheses of the alkynylcalix[4]crown-6

ligands and their tetranuclear gold(I) alkynylcalix[4]crown-6 complexes **1** and **2** are summarized in Scheme 1. Iodination of the dipropoxycalixarene **3** gave the diiodocalixarene **4**,^[10,15] which upon treatment with $\text{HC}\equiv\text{CSiMe}_3$ under Sonogashira cross-coupling reaction conditions^[16] gave the bis(trimethylsilyl)ethynyl)-substituted calixarene **5**. Subsequent reaction of **5** with the appropriate benzo- or naphtho-substituted pentaethylene glycol di-*p*-toluenesulfonate and Cs_2CO_3 to introduce the polyether linkages at the lower rim and to remove the trimethylsilyl (TMS) groups gave H_2L^1 and H_2L^2 , both in 1,3-alternate conformations, in moderate yields. Reaction of $\text{Au}(\text{tht})\text{Cl}$ (tht = tetrahydrothiophene) with H_2L^1 and H_2L^2 in the presence of Et_3N in CH_2Cl_2 afforded the respective desired complexes $\text{Au}_4(\text{L}^1)_2$ (**1**) and $\text{Au}_4(\text{L}^2)_2$ (**2**) as pale yellow crystals after subsequent recrystallization from dichloromethane-*n*-hexane and chloroform-*n*-hexane, respectively. The complexes **1** and **2** were characterized by elemental analysis, ^1H NMR and IR spectroscopy, and positive-ion FAB mass spectrometry. The crystal structure of **1** was also determined by X-ray crystallography.

The perspective drawing of **1** is depicted in Figure 1. It shows a double-cage structure, with the four gold(I) centers arranged in a rhomboidal array and capped by the two diethynylcalixcrown ligands on the two ends. Two of the gold(I) centers are each σ coordinated to two alkynyl units, whereas the other two Au centers are each π coordinated to two alkynyl units in a η^2, η^2 bonding fashion. The bridging gold atoms Au(2) and Au(2*) are two-coordinated with C–Au–C angles of $179.0(4)^\circ$: an almost ideal linear geometry. The C \equiv C bond lengths of 1.204(11) and 1.215(11) Å are comparatively longer than for typical terminal gold(I) alkynyl com-



Scheme 1. Synthetic route to complexes **1** and **2**: a) ICl , CH_2Cl_2 ; b) $\text{HC}\equiv\text{CSiMe}_3$, Et_3N , $[\text{Pd}(\text{PPh}_3)_2\text{Cl}_2]$, CuI , THF; c) $\text{Ar}\{(\text{OCH}_2\text{CH}_2)_2\text{OTs}\}_2$, Cs_2CO_3 , MeCN; d) Et_3N , $\text{Au}(\text{tht})\text{Cl}$, CH_2Cl_2 . Ar = C_6H_4 or C_{10}H_6 ; tht = tetrahydrothiophene.

plexes,^[11,17] in line with a weakening of the C \equiv C bond as a result of π coordination to Au(1) and Au(1*). The Au–C bond lengths for Au(1) and Au(1*) are in the range of 2.150(9)–2.359(8) Å. The torsion angle between the two C \equiv C units of each calixcrown is $1.5(10)^\circ$, which indicates that the two ethynyl groups are nearly parallel and are preorganized for π coordination to Au(1) and Au(1*) through an unusual planar η^2, η^2 coordination mode, which is the first of its kind for Au^{I} despite reported examples for other d^{10} metal centers.^[9,18,19] The two gold atoms Au(1) and Au(1*), sand-

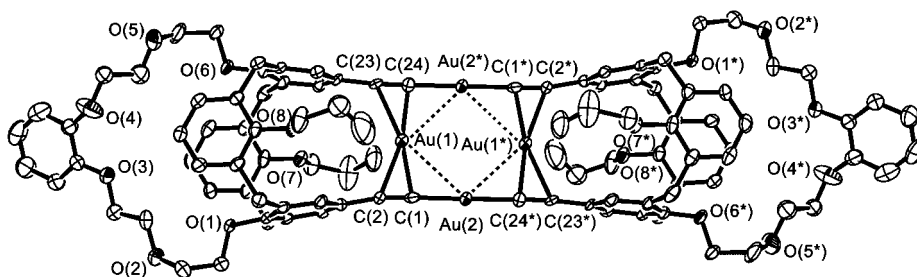


Figure 1. Perspective drawing of **1** with atomic numbering; thermal ellipsoids are shown at the 30% probability level.

wiched through π interactions between the alkynyl units, are also located on the same plane as the two $\text{C}\equiv\text{C}-\text{Au}-\text{C}\equiv\text{C}$ bridging units to form a rhomboidal array with an inversion center at the center of the Au_4 unit. The $\text{Au}\cdots\text{Au}$ distances between adjacent gold atoms are 3.1344(8) and 3.2048(8) Å, indicative of the presence of significant $\text{Au}-\text{Au}$ interactions.

To have a better understanding of the factors that govern the structures of these tetranuclear gold(I) complexes, attempts have been made to synthesize a related tetranuclear gold(I) complex with 5,17-diethynyl-25,27-dipropoxycalix[4]crown-6 (H_2L^3 , also in 1,3-alternate conformation) under similar conditions. Upon treatment of a solution of H_2L^3 in CH_2Cl_2 with $\text{Au}(\text{tht})\text{Cl}$ in the presence of Et_3N , the reaction mixture turned dark immediately, indicative of decomposition. The stability of **1** and **2** is believed to be associated with the crown ether unit. The presence of benzo- and naphtho- groups in the crown ether unit increases the rigidity of the calixcrown. Furthermore, the close proximity of the two ethynyl groups in the calixcrown ligand promotes the encapsulation of the two gold atoms through π coordination, with protection provided by the propoxy chains of the calixcrown ligands. All these factors would account for the much better stability of **1** and **2** relative to " $\text{Au}_4(\text{L}^3)_2$ ".

The electronic absorption spectra (not shown) of **1** and **2** as solutions in chloroform are dominated by very intense low-energy absorption bands at 344 nm which tail off towards ≈ 480 nm and a comparatively less intense high-energy band at $\approx 275\text{--}330$ nm. With reference to previous spectroscopic work on gold(I) ethynyl complexes^[2d,8,10,11] and the similarities of the absorption bands of the complexes with the corresponding free ligands, the high-energy absorption bands at $\approx 275\text{--}330$ nm are tentatively assigned to the intraligand transitions of the ethynylcalixcrown ligands. On the other hand, the low-energy absorption band, which is not observed in the free ligands, is likely to originate from metal-perturbed intraligand $\pi\rightarrow\pi^*(\text{C}\equiv\text{C})$ transitions probably with some mixing of metal-cluster-centered (ds/dp) states, characteristic of the polynuclear gold(I) ethynyl system.^[2d,8,10,11]

Both **1** and **2** show rich luminescence properties (see Table 1). Upon excitation at ≈ 370 nm, the solid-state emission spectra of complexes **1** and **2** show low-energy emission bands at $\approx 590\text{--}620$ nm at both 77 K and room temperature that are red-shifted with respect to the emission bands observed in solution (see Figure 2). In fact, the solid-state emissions of **1** and **2** were found to occur at a much lower energy than that for other dinuclear gold(I) calixcrown complexes, such as $[\text{Au}(\text{PR}_3)]_2\text{L}$ ($\text{R} = \text{Aryl}$; $\text{H}_2\text{L} = 5,17\text{-diethynyl-25,27-dimethoxycalix[4]crown-5}$) for which emission was observed at $\approx 450\text{--}480$ nm.^[10] Given the presence of short $\text{Au}\cdots\text{Au}$ distances as observed in the crystal structure of **1** and the likelihood of similarly short $\text{Au}\cdots\text{Au}$ distances in **2**, the relative red shift in the solid-state emission spectra is

Table 1: Photophysical data for **1** and **2**.

Complex	Absorption ^[a] λ_{abs} [nm] (ϵ_{max} [$\text{M}^{-1}\text{cm}^{-1}$])	medium (T [K])	Emission λ_{em} [nm] (τ [μs]) ^[d]	Φ_{lum} ^[f]
1	278 (48 820), 314 (40 900), 344 (83 260)	CHCl_3 (298)	588 (7.1)	0.22
		solid (298)	592 (0.8, 4.0) ^[e]	
		solid (77)	591 (1.1, 5.3) ^[e]	
		glass(77) ^[b]	586 (8.0)	
2	278 (48 840), 312 (37 950), 326 (40 680), 344 (69 550)	CHCl_3 (298)	587 (6.9)	0.21
		solid (298)	611 (0.4, 4.8) ^[e]	
		solid (77)	616 (0.9, 5.7) ^[e]	
		glass (77) ^[c]	587 (7.7)	

[a] In CHCl_3 at 298 K. [b] In $\text{CHCl}_3\text{--MeOH--EtOH}$ (2:1:3 v/v). [c] In $\text{CHCl}_3\text{--MeOH--EtOH}$ (4:1:2 v/v). [d] Emission lifetimes recorded with $\pm 10\%$ uncertainty. [e] Biexponential decay. [f] Luminescence quantum yield, measured at room temperature by using quinine sulfate in H_2SO_4 (1.0 N) as reference.

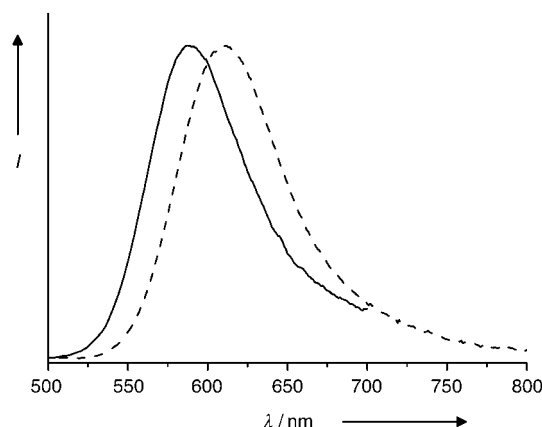


Figure 2. Normalized emission spectra of **2** as a solution in CHCl_3 (—, $\lambda_{\text{exc}} = 350$ nm) and in the solid state (----, $\lambda_{\text{exc}} = 370$ nm) at room temperature.

attributed to the presence of intramolecular $\text{Au}\cdots\text{Au}$ interactions in **1** and **2** in the solid state. Such intramolecular $\text{Au}\cdots\text{Au}$ interactions would give rise to a narrowing of the HOMO–LUMO energy gap, most probably as a result of $\text{d}\sigma\text{--d}\sigma^*$, $\text{d}\pi\text{--d}\pi^*$, $\text{d}\delta\text{--d}\delta^*$, $\text{s}\sigma\text{--s}\sigma^*$, and $\text{p}\sigma\text{--p}\sigma^*$ orbital splittings. It is likely that the low-energy emission is derived from states of metal-cluster-centered (ds/dp) character that are modified by $\text{Au}\cdots\text{Au}$ interactions and mixed with metal-perturbed intraligand $\pi\rightarrow\pi^*(\text{C}\equiv\text{C})$ states.

Upon excitation at ≈ 350 nm, the tetranuclear gold(I) calixcrown complexes **1** and **2** both gave intense emission bands at ≈ 587 nm at room temperature as solutions in chloroform and at 77 K as frozen matrices (glass). The luminescence quantum yields Φ_{lum} of complexes **1** and **2** in degassed chloroform are 0.22 and 0.21, respectively. Given the large Stokes shifts and the observed lifetimes, which are in the microsecond range, the emission is thought to have a triplet parentage. It is likely that the emission is derived from triplet states of a metal-cluster-centered (ds/dp) character with some mixing of metal-perturbed intraligand character.

In summary, we have demonstrated the importance and significance of strategic ligand designs on the structure and

bonding of d^{10} metal complexes. The successful isolation and discovery of the planar η^2, η^2 bonding mode in the gold(I) alkynyl systems should provide an understanding of the intriguing and unique photophysical properties of this class of compounds and should form the basis for the future design and isolation of luminescent molecular materials and supramolecular assemblies.

Experimental Section

$\text{Au}_4(\text{L}^1)_2$ (**1**): $\text{Au}(\text{tht})\text{Cl}$ (24 mg, 0.076 mmol) was added to a stirred solution of H_2L^1 (30 mg, 0.037 mmol) and Et_3N (5 mL) in CH_2Cl_2 (15 mL), and the reaction mixture was stirred under an inert atmosphere (N_2) for 30 mins. The solvent was then removed under reduced pressure, and the residue was washed with MeOH and Et_2O . Subsequent recrystallization by layering n -hexane onto a solution of the product in CH_2Cl_2 gave **1** as yellow crystals (22 mg, 50%). ^1H NMR (300 MHz, CDCl_3 , Me_4Si): δ = 1.22 (t, 12H, J = 7.5 Hz; CH_3), 2.06 (m, 8H; $\text{OCH}_2\text{CH}_2\text{CH}_3$), 3.40–3.77 (m, 24H; $\text{OCH}_2\text{CH}_2\text{O}$), 3.98 (s, 8H; Ar- CH_2 -Ar), 4.02 (s, 8H; Ar- CH_2 -Ar), 4.17 (t, 8H, J = 6.8 Hz; $\text{OCH}_2\text{CH}_2\text{CH}_3$), 4.32 (t, 8H, J = 7.0 Hz; Ar- $\text{OCH}_2\text{CH}_2\text{O}$), 6.62 (t, 4H, J = 7.5 Hz; Ar H *para* to OPr), 6.99 (m, 8H; 1,2-phenylene), 7.10 (d, 8H, J = 7.5 Hz; Ar H *meta* to OPr), 7.31 ppm (s, 8H; Ar H *meta* to crown linkage); IR (KBr disk): $\tilde{\nu}$ = 2011 cm^{-1} (w), $\nu(\text{C}\equiv\text{C})$; FAB MS (+ mode): m/z : 2435 [$M+K$] $^+$; elemental analysis: calcd for $\text{C}_{104}\text{H}_{104}\text{Au}_4\text{O}_{16}\cdot\text{CHCl}_3\cdot\frac{1}{2}\text{C}_6\text{H}_{14}$: C 50.67, H 4.40; found: C 50.65, H 4.34%.

$\text{Au}_4(\text{L}^2)_2$ (**2**): As for **1** but by using H_2L^2 (30 mg, 0.035 mmol). The product was recrystallized from chloroform- n -hexane to give **2** as yellow crystals (28 mg, 64%). ^1H NMR (300 MHz, CDCl_3 , Me_4Si): δ = 1.22 (t, 12H, J = 7.5 Hz; CH_3), 2.05 (m, 8H; $\text{OCH}_2\text{CH}_2\text{CH}_3$), 3.41–3.77 (m, 24H; $\text{OCH}_2\text{CH}_2\text{O}$), 4.00 (s, 8H; Ar- CH_2 -Ar), 4.04 (s, 8H; Ar- CH_2 -Ar), 4.25 (t, 8H, J = 6.7 Hz; $\text{OCH}_2\text{CH}_2\text{CH}_3$), 4.46 (t, 8H, J = 6.5 Hz; Ar- $\text{OCH}_2\text{CH}_2\text{O}$), 6.62 (t, 4H, J = 7.5 Hz; Ar H *para* to OPr), 7.10 (d, 8H, J = 7.5 Hz; Ar H *meta* to OPr), 7.22 (s, 4H; 1,2-naphthalene), 7.31 (s, 8H; Ar H *meta* to crown chain), 7.36 (q, 4H, J = 3.1 Hz; 1,2-naphthalene), 7.72 ppm (q, 4H, J = 3.1 Hz; 1,2-naphthalene); IR (KBr disk): $\tilde{\nu}$ = 2006 cm^{-1} (w), $\nu(\text{C}\equiv\text{C})$; FAB MS (+ mode): m/z : 2497 [$M+H$] $^+$, 2535 [$M+K$] $^+$; elemental analysis calcd for $\text{C}_{112}\text{H}_{108}\text{Au}_4\text{O}_{16}\cdot\text{CHCl}_3$: C 51.86, H 4.20; found: C 51.65, H 4.49%.

Crystal data for **1**: $[\text{C}_{104}\text{H}_{104}\text{Au}_4\text{O}_{16}]$; M_r = 2397.74, crystal dimensions $0.4 \times 0.3 \times 0.2 \text{ mm}^3$, monoclinic, space group $C2/c$, a = 36.517(7) Å, b = 12.551(3) Å, c = 24.041(5) Å, β = 123.90(3)°, V = 9146(3) Å 3 , Z = 4, ρ_{calcd} = 1.741 g cm^{-3} , $\mu(\text{MoK}\alpha)$ = 6.464 mm^{-1} , $F(000)$ = 4688, T = 253 K; R_1 = 0.0383, wR_2 = 0.0879 for 26699 reflections with $[I > 2\sigma(I)]$. MAR diffractometer, $\text{MoK}\alpha$ radiation (λ = 0.71073 Å); collection range $2\theta_{\text{max}}$ = 50.80° with 2°-oscillation step of φ , 480-seconds exposure time and scanner distance at 120 mm. 100 images were collected.

CCDC 238889 contains the supplementary crystallographic data for this paper. These data can be obtained free of charge via www.ccdc.cam.ac.uk/conts/retrieving.html (or from the Cambridge Crystallographic Data Centre, 12, Union Road, Cambridge CB2 1EZ, UK; fax: (+44) 1223-336-033; or deposit@ccdc.cam.ac.uk).

Received: May 21, 2004

Keywords: alkyne ligands · calixarenes · gold · luminescence · supramolecular chemistry

- [1] a) R. Y. Liao, A. Schier, H. Schmidbaur, *Organometallics* **2003**, 22, 3199; b) W. J. Hunks, M. C. Jennings, R. J. Puddephatt, *Inorg.*

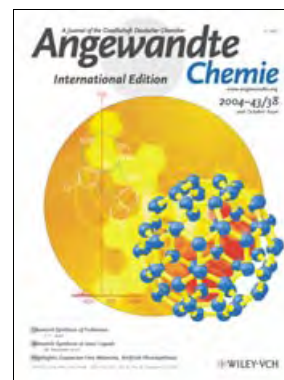
Chem. **2002**, 41, 4590; c) T. Mathieson, A. Schier, H. Schmidbaur, *J. Chem. Soc. Dalton Trans.* **2001**, 1196; d) M. A. Rawashdeh-Omary, M. A. Omary, J. P. Fackler, Jr., R. Galassi, B. R. Pietroni, A. Burini, *J. Am. Chem. Soc.* **2001**, 123, 9689; e) M. Stender, M. M. Olmstead, A. L. Balch, D. Rios, S. Attar, *Dalton Trans.* **2003**, 4282; f) M. M. Olmstead, F. Jiang, S. Attar, A. L. Balch, *J. Am. Chem. Soc.* **2001**, 123, 3260.

- [2] a) V. W.-W. Yam, E. C.-C. Cheng, K.-K. Cheung, *Angew. Chem.* **1999**, 111, 193; *Angew. Chem. Int. Ed.* **1999**, 38, 197; b) V. W.-W. Yam, E. C.-C. Cheng, Z.-Y. Zhou, *Angew. Chem.* **2000**, 112, 1749; *Angew. Chem. Int. Ed.* **2000**, 39, 1683; c) V. W.-W. Yam, E. C.-C. Cheng, N. Zhu, *Angew. Chem.* **2001**, 113, 1813; *Angew. Chem. Int. Ed.* **2001**, 40, 1763; d) V. W.-W. Yam, K.-L. Cheung, S.-K. Yip, K.-K. Cheung, *J. Organomet. Chem.* **2003**, 681, 196.
- [3] a) W. J. Hunks, M. A. MacDonald, M. C. Jennings, R. J. Puddephatt, *Organometallics* **2000**, 19, 5063; b) J. D. E. T. Wilton-Ely, A. Schier, N. W. Mitzel, S. Nogai, H. Schmidbaur, *J. Organomet. Chem.* **2002**, 643, 313.
- [4] a) R. L. White-Morris, M. Stender, D. S. Tinti, A. L. Balch, D. Rios, S. Attar, *Inorg. Chem.* **2003**, 42, 3237; b) R. L. White-Morris, M. M. Olmstead, A. L. Balch, *J. Am. Chem. Soc.* **2003**, 125, 1033.
- [5] G. H. Coates, C. Parkin, *J. Chem. Soc.* **1962**, 3220.
- [6] D. M. P. Mingos, J. Yau, S. Menzer, D. J. Williams, *Angew. Chem.* **1995**, 107, 2045; *Angew. Chem. Int. Ed. Engl.* **1995**, 34, 1894.
- [7] a) V. W.-W. Yam, W. K.-M. Fung, K.-K. Cheung, *Angew. Chem.* **1996**, 108, 1213; *Angew. Chem. Int. Ed. Engl.* **1996**, 35, 1100; b) W.-Y. Lo, C.-H. Lam, W. K.-M. Fung, H.-Z. Sun, V. W.-W. Yam, D. Balcells, F. Maseras, O. Eisenstein, *Chem. Commun.* **2003**, 1260.
- [8] V. W.-W. Yam, K. K.-W. Lo, *Chem. Soc. Rev.* **1999**, 28, 323.
- [9] V. W.-W. Yam, K.-L. Cheung, E. C.-C. Cheng, N. Zhu, K.-K. Cheung, *Dalton Trans.* **2003**, 1830.
- [10] a) V. W.-W. Yam, K.-L. Cheung, L.-H. Yuan, K. M.-C. Wong, K.-K. Cheung, *Chem. Commun.* **2000**, 1513; b) V. W.-W. Yam, S.-K. Yip, L.-H. Yuan, K.-L. Cheung, N. Zhu, K.-K. Cheung, *Organometallics* **2003**, 22, 2630.
- [11] a) V. W.-W. Yam, S. W.-K. Choi, *J. Chem. Soc. Dalton Trans.* **1996**, 4227; b) V. W.-W. Yam, S. W.-K. Choi, K.-K. Cheung, *Organometallics* **1996**, 15, 1734.
- [12] a) C. D. Gutsche, *Calixarenes: Monographs in Supramolecular Chemistry*, The Royal Society of Chemistry: Cambridge, **1989**; b) C. D. Gutsche, *Calixarenes Revisited*, The Royal Society of Chemistry: Cambridge, **1998**; c) Z. Asfari, *Calixarenes 2001*, Kluwer Academic Publishers, Dordrecht, **2001**.
- [13] C. D. Gutsche, M. Iqbal, *Org. Synth. Coll. Vol.* **1993**, 8, 75.
- [14] a) S. Shinkai, *Tetrahedron* **1993**, 49, 8933; b) V. Böhmer, *Angew. Chem.* **1995**, 107, 785; *Angew. Chem. Int. Ed. Engl.* **1995**, 34, 713.
- [15] B. Klenke, W. Friederichsen, *J. Chem. Soc. Perkin Trans. 1* **1998**, 3377.
- [16] S. Takahashi, Y. Kuroyama, K. Sonogashira, N. Hagihara, *Synthesis* **1980**, 627.
- [17] R. J. Cross, M. F. Davidson, *J. Chem. Soc. Dalton Trans.* **1986**, 411.
- [18] a) O. M. Abu-Salah, A. Razzak, A. Al-Ohaly, Z. F. Mutter, *J. Organomet. Chem.* **1990**, 391, 267; b) O. M. Abu-Salah, A. Al-Ohaly, A. Razzak, Z. F. Mutter, *J. Organomet. Chem.* **1990**, 389, 427; c) O. M. Abu-Salah, *J. Organomet. Chem.* **1990**, 387, 123; d) O. M. Abu-Salah, A. Al-Ohaly, A. Razzak, *J. Chem. Soc. Dalton Trans.* **1988**, 2297.
- [19] a) V. W.-W. Yam, K.-L. Yu, K. M.-C. Wong, K.-K. Cheung, *Organometallics* **2001**, 20, 721; b) K. M.-C. Wong, C.-K. Hui, K.-L. Yu, V. W.-W. Yam, *Coord. Chem. Rev.* **2002**, 229, 123.

Cover Picture

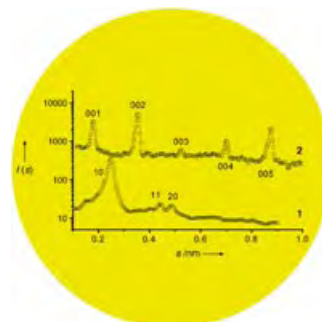
Lawrence T. Scott*

A high price in energy must be paid to impose curvature on the π system of a planar polycyclic aromatic hydrocarbon. This step was essential for the first chemical synthesis of C_{60} in isolable quantities, which stands as dramatic testimony to the power of the new synthetic methods devised for fullerene synthesis. In his Review on page 4994 ff., L. T. Scott describes the numerous syntheses of geodesic polyarenes reported, which serve to test the scope and limitations of the new methods.



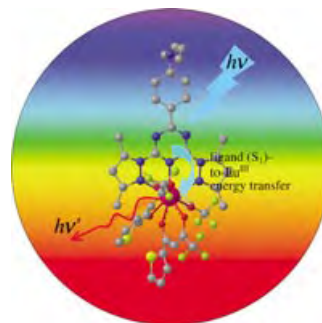
Nanomaterials

Their preorganized structure makes ionic liquids an ideal solvent for materials synthesis. M. Antonietti et al. explore the concept and perspectives of this strategy in their Minireview on page 4988 ff.



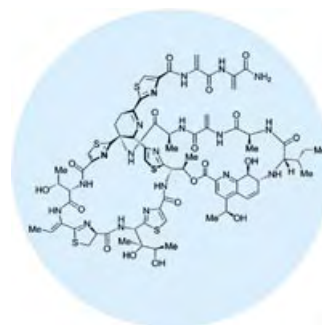
Luminescent Materials

Visible-light excitation of a europium complex leads to characteristic red emission as reported by Y. Wang, J.-P. Zhang, W.-T. Wong et al. in their Communication on page 5010 ff. Such excitation at longer wavelengths is required for many applications.



Natural Product Synthesis

The total synthesis of thiostrepton, a highly active antibiotic from *Streptomyces*, was completed by K. C. Nicolaou et al. The synthetic route can be followed in their Communications on pages 5087 ff and 5092 ff.



Angewandte EarlyView®

The following Communications are available online (in Wiley InterScience). You can find them, as well as forthcoming Reviews, Highlights, and Essays, at www.angewandte.org, under Early View.

C. Serre,* F. Millange, S. Surblé, G. Férey:
**A Route to the Synthesis of Trivalent
Transition-Metal Porous Carboxylates with
Trimeric Secondary Building Units**
DOI: 10.1002/anie.200454250
Published online: September 7, 2004

C. Mellõ-Draznieks,* J. Dutour, G. Férey:
**Hybrid Organic–Inorganic Frameworks:
Routes for Computational Design and
Structure Prediction**
DOI: 10.1002/anie.200454251
Published online: September 3, 2004

T. Shima, F. Hampel, J. A. Gladysz*:
**Molecular Gyroscopes: {Fe(CO)₃} and
{Fe(CO)₂(NO)} Rotators Encased in
Three-Spoke Stators; Facile Assembly by
Alkene Metatheses**
DOI: 10.1002/anie.200460534
Published online: August 27, 2004

Articles judged by the referees or the editor as being either very important or very urgent are immediately edited, proof-read, and electronically published once the manuscript has arrived in the editorial office in its final form. As long as there is no page number available these articles should be cited in the following manner:

Author(s), *Angew. Chem. Int. Ed.*, online publication date, DOI.

Obituary

Colin Eaborn (1923–2004): Organosilicon Compounds _____ 4978 J. D. Smith

Books

Basic Principles in Applied Catalysis

Manfred Baerns

reviewed by X. Nijhuis,
B. Weckhuysen _____ 4979

Computational Chemistry

Errol G. Lewars

reviewed by R. Berger _____ 4979

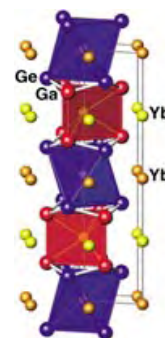
Highlights

Expansion-Free Materials

K. Stöwe* _____ 4982–4984

YbGaGe: Zero Thermal Expansion as a
Result of an Electronic Valence Transition?

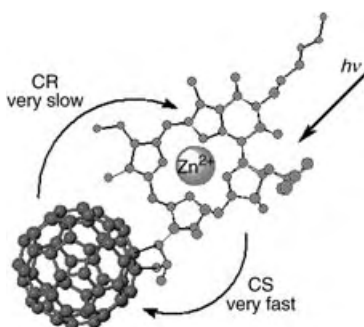
In contrast to classic ZTE materials (ZTE = zero thermal expansion), the ZTE effect in YbGaGe (see crystal structure) is caused by the change in the valency of the ytterbium ion from +2.6 to +2 with decreasing temperature. This change in the valence state compensates for the contraction of the net as the temperature decreases.



Electron Transfer

A. Harriman* _____ 4985–4987

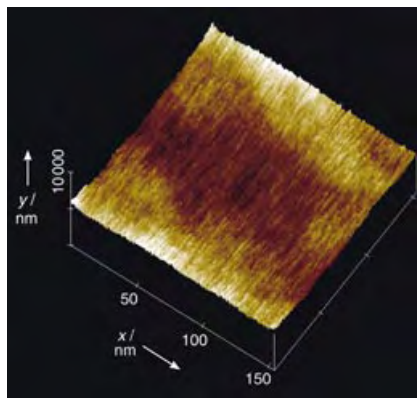
Unusually Slow Charge Recombination in
Molecular Dyads



Shedding new light on the matter: Rather than the conventional approach of utilizing the cascade effect, charge separation can be stabilized in artificial photosynthetic systems simply by the geometry. In these latter systems, light-induced charge separation (CS) in a closely spaced molecular dyad is followed by exceptionally slow charge recombination (CR, see picture) to give a charge-separated state with a lifetime of up to 120 s.

Minireviews

Crystalline nanoparticles can be prepared at ambient temperatures in ionic liquids—highly polar organic solvents with a preorganized solvent structure. The pronounced self-organization of the solvent is used in the synthesis of highly organized hybrid nanostructures like the lamellar silica shown in the picture.



Nanostructures

M. Antonietti,* D. Kuang, B. Smarsly,
Y. Zhou _____ 4988–4992

Ionic Liquids for the Convenient Synthesis
of Functional Nanoparticles and Other
Inorganic Nanostructures

From corannulene to C₆₀: Geodesic polyarenes can be synthesized in the laboratory by bending flat molecules and stitching them up into molecular bowls, baskets, and balls, using rational chemical methods.



Reviews

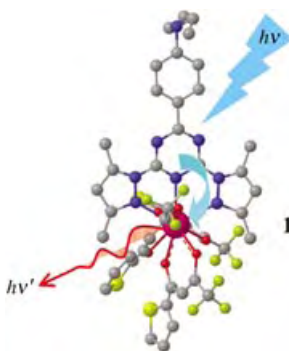
Polycyclic Arenes

L. T. Scott* _____ 4994–5007

Methods for the Chemical Synthesis of
Fullerenes

Red glow in daylight ... chemist's delight!

An efficient transfer of excitation energy from the ligand to the luminescent states of the coordinated Eu^{III} ion in **1** occurs from the singlet excited state of the ligand. The complex shows characteristic bright red Eu-centered emission with a quantum yield of 0.52 when sensitized with visible light.



Communications

Luminescence

C. Yang, L.-M. Fu, Y. Wang,* J.-P. Zhang,*
W.-T. Wong,* X.-C. Ai, Y.-F. Qiao, B.-S. Zou,
L.-L. Gui _____ 5010–5013

A Highly Luminescent Europium Complex
Showing Visible-Light-Sensitized Red
Emission: Direct Observation of the
Singlet Pathway

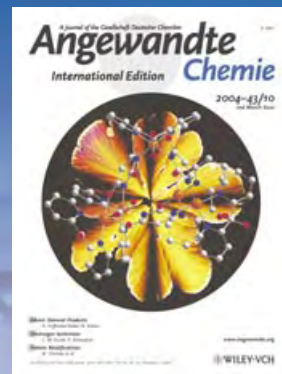
For the USA and Canada:

ANGEWANDTE CHEMIE International Edition (ISSN 1433-7851) is published weekly by Wiley-VCH PO Box 191161, D 69451 Weinheim, Germany. Air freight and mailing in the USA by Publications Expediting Inc. 200 Meacham Ave., Elmont, NY 11003. Periodicals

postage paid at Jamaica NY 11431. US POSTMASTER: send address changes to *Angewandte Chemie*, Wiley-VCH, 111 River Street, Hoboken, NJ 07030. Annual subscription price for institutions: Europe € 3760.00/3418.00; outside Europe US\$ 4948.00/4498.00 (valid for print and electronic/print or electronic delivery); for

individuals who are personal members of a national chemical society, or whose institution already subscribes, or who are retired or self-employed consultants, print only: Europe € 258.00/outside Europe US\$ 394.00. Postage and handling charges included. All Wiley-VCH prices are exclusive VAT.

The best in chemistry – for more than a hundred years



A Journal of the Gesellschaft Deutscher Chemiker
Angewandte Chemie
International Edition

www.angewandte.org

1888: The beginning
of a success story

Constant Innovations

- 1962:** First issue of the International Edition
- 1976:** Graphical abstracts
- 1979:** Cover pictures
- 1988:** Centenary of Angewandte
- 1989:** Routine use of color
- 1991:** New section: Highlights
- 1992:** Computerized editorial tracking system
- 1995:** Internet service for readers
- 1998:** Regular press service; full-text online
- 2000:** New section: Essays; EarlyView: Communications available online ahead of the printed version
- 2001:** New section: Minireviews
- 2002:** Online submission of manuscripts
- 2003:** Weekly publication; new section: News; new layout
- 2004:** Backfiles (1962-1997); ManuscriptXpress: Online system for authors and referees



Angewandte's advisors...

Robert Langer
Massachusetts Institute of
Technology

» **Angewandte Chemie** is one of the top chemistry journals in the world. As such, I try to publish there frequently and am honored to be a member of its International Advisory Board. «

Angewandte Chemie International Edition is
a journal of the German Chemical Society (GDCh)





Enantioselectivity Determination

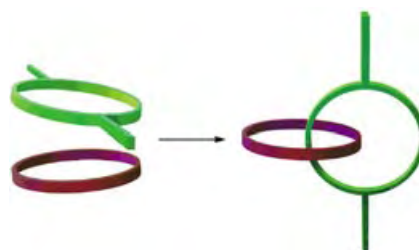
R. Eelkema, R. A. van Delden,
B. L. Feringa* _____ 5013–5016

Direct Visual Detection of the
Stereoselectivity of a Catalytic Reaction

Color vision: The enantiomeric excess of the products of an enantioselective catalytic reaction can be determined by a liquid-crystal-based color test. After a simple workup, doping of the reaction

product into a liquid crystal affords brightly colored LC phases, with colors depending on the enantiomeric excess of the product (see picture).

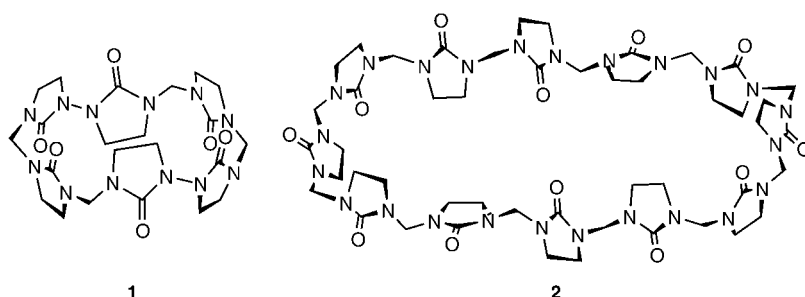
Magic rings: The trick of kinetically controlled cross-catenation of two different Pd^{II}-linked coordination rings (see picture) lies in the large difference in the catenation rate of the two rings as a result of steric hindrance of the ligands.



Self-Assembly

A. Hori, K. Yamashita,
M. Fujita* _____ 5016–5019

Kinetic Self-Assembly: Selective Cross-
Catenation of Two Sterically Differentiated
Pd^{II}-Coordination Rings



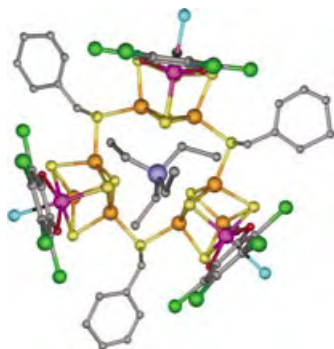
Inclusion Compounds

Y. Miyahara,* K. Goto, M. Oka,
T. Inazu _____ 5019–5022

Remarkably Facile Ring-Size Control in
Macrocyclization: Synthesis of Hemi-
cucurbit[6]uril and Hemicucurbit[12]uril

A question of concentration: The condensation of ethyleneurea and formaldehyde can be controlled perfectly by the HCl concentration to provide either a

hemicucurbit[6]uril **1**, which functions as a host, or hemicucurbit[12]uril **2**, which acts as a gelating agent, in yields of 94 and 93 %, respectively.



Three reversible reductions are observed for a new cyclic tricubane cluster. In the solid state, the cluster displays a large, electron-rich pocket containing an encapsulated Et₄N⁺ ion (see structure). These characteristics might allow the use of this cluster as a multielectron reducing agent.

Superclusters

M. Koutmos,
D. Coucouvanis* _____ 5023–5025

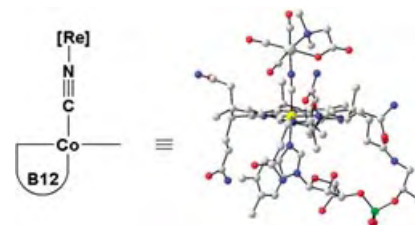
Superclusters: A Host–Guest Complex
with a Cyclic Array of Three Bridged
MoFe₃S₄ Clusters

Bioinorganic Chemistry

S. Kunze, F. Zobi, P. Kurz, B. Spingler,
R. Alberto* _____ **5025 – 5029**

Vitamin B12 as a Ligand for Technetium
and Rhenium Complexes

Robust complexes with a central {Co-CN-Re(Tc)} feature are formed when the cyanide ligand in vitamin B12 acts as bridging ligand between rhenium and technetium carbonyl complexes (see picture). This concept paves the way for radiolabeling of vitamin B12 or metal-mediated coupling of bioactive molecules.

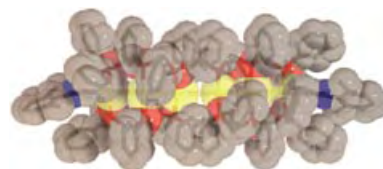


Cluster Compounds

E. Goto, R. A. Begum, S. Zhan, T. Tanase,*
K. Tanigaki, K. Sakai _____ **5029 – 5032**

Linear, Redox-Active Pt₆ and Pt₂Pd₂Pt₂
Clusters

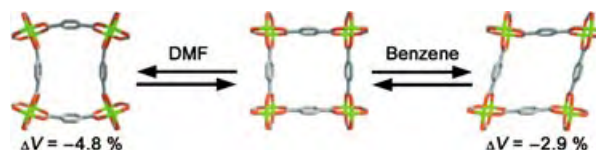
A piece of jewelry is the complex [Pt₄M₂(μ-H)(μ-dpmp)₄(XylINC)₂](PF₆)₃ (M = Pt, see structure), which contains the longest platinum chain characterized so far. This complex and the related compound with M = Pd are redox-active and can be readily oxidized to the electron-deficient clusters [Pt₄M₂(μ-dpmp)₄(XylINC)₂](PF₆)₄ (M = Pt, Pd) with dynamic structural changes in the metal strings. Xyl = 2,6-dimethylphenyl, dpmp = bis(diphenylphosphanyl-methyl)phenylphosphane.



Host–Guest Systems

D. N. Dybtsev, H. Chun,
K. Kim* _____ **5033 – 5036**

Rigid and Flexible: A Highly Porous
Metal–Organic Framework with Unusual
Guest-Dependent Dynamic Behavior



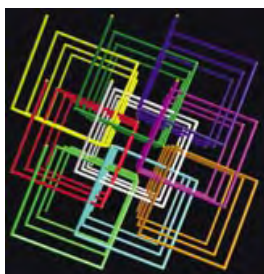
A large H₂ sorption capacity and high surface area are properties of the depicted metal–organic porous material, which is easily synthesized on a large scale from readily available chemicals. The rigid framework of [Zn₂(1,4-bdc)₂(dabco)]

(1,4-H₂bdc = 1,4-benzenedicarboxylic acid; dabco = diazabicyclo[2.2.2]octane) is also flexible enough to exhibit unusual guest-dependent dynamic behavior, as shown (DMF = *N,N*-dimethylformamide).

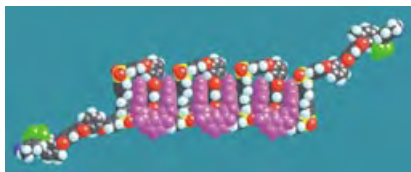
Self-assembly

X.-L. Wang, C. Qin, E.-B. Wang,* L. Xu,
Z.-M. Su,* C.-W. Hu _____ **5036 – 5040**

Interlocked and Interdigitated Architectures from Self-Assembly of Long Flexible Ligands and Cadmium Salts



Noninterpenetrating structures are formed by self-assembly of cadmium salts and long flexible ligands. In one case exceptional ninefold interlocked homochiral helices are built from achiral components (see picture). The helices are chemically independent but physically interwoven. This represents the highest degree of entanglement presently known for a noninterpenetrating system.



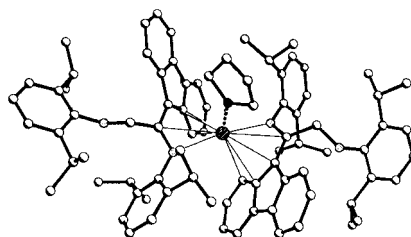
Specific monomer sequences in aromatic copolyimides are recognized through their π -stacking and hydrogen-bonding interactions with a sterically and electronically complementary molecular tweezer. These interactions enable the tweezer molecule to “read” monomer sequences comprising up to 27 aromatic rings by multiple adjacent binding to neighboring sites on the polymer chain (see picture).

Molecular Recognition

H. M. Colquhoun,* Z. Zhu – 5040 – 5045

Recognition of Polyimide Sequence Information by a Molecular Tweezer

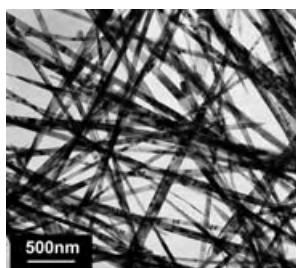
A couple of surprises: The reactions of $[(C_{13}H_9)_2Yb(thf)_2]$ with diazadienes $(2,6-iPr_2C_6H_3)N=CR-CR=N(2,6-iPr_2C_6H_3)$ ($R=H, Me$) result in unexpected Yb^{II} complexes, which arise either from the coupling of the fluorene and the diazadiene ligands (when $R=H$, see picture) or from C–H bond activation of the diazadiene ligand (when $R=Me$).



Diazadiene Ligands

A. A. Trifonov,* E. A. Fedorova, G. K. Fukin, N. O. Druzhkov, M. N. Bochkarev – 5045 – 5048

C–C Coupling and C–H Bond Activation—Unexpected Pathways in the Reactions of $[Yb(\eta^5-C_{13}H_9)_2(thf)_2]$ with Diazadienes



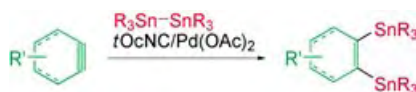
Made-to-measure nanobelts: Metastable vanadium dioxide single-crystal nanobelts (see picture) were prepared by a hydrothermal reduction method by treating an ammonium metavanadate solution with formic acid. The morphology of the belts could be adjusted by varying the reaction parameters, such as temperature, pH, and reaction time.

Nanostructures

J. Liu, Q. Li, T. Wang, D. Yu, Y. Li* – 5048 – 5052

Metastable Vanadium Dioxide Nanobelts: Hydrothermal Synthesis, Electrical Transport, and Magnetic Properties

Oxidative addition of a distannane to a palladium(0) complex occurs during the distannylation of in situ generated arynes with distannanes in the presence of a catalytic amount of a palladium/*tert*-octyl isocyanide (*t*OcNC) complex to give 1,2-distannylarenes in moderate to high yields (see scheme). Bisarynes and cyclohexynes can also be used as substrates for the reaction.



Homogeneous Catalysis

H. Yoshida,* K. Tanino, J. Ohshita, A. Kunai* – 5052 – 5055

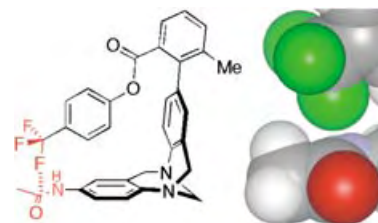
Distannylation of Strained C–C Triple Bonds Catalyzed by a Palladium Complex

Noncovalent Interactions

F. Hof, D. M. Scofield, W. B. Schweizer,
F. Diederich* ————— 5056 – 5059

A Weak Attractive Interaction between
Organic Fluorine and an Amide Group

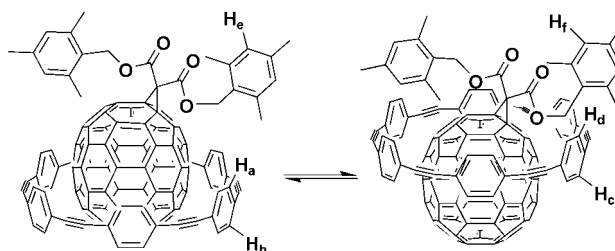
A **combination** of a chemical double-mutant cycle and a linear free energy relationship has demonstrated that a weak attractive interaction (-0.8 to -1.5 kJ mol $^{-1}$) exists between an organic fluorine substituent and the face of an amide functional group (see picture). This study supports recent results that have suggested that such an attraction may be operative in enzyme–inhibitor interactions.



Host–Guest Systems

T. Kawase,* N. Fujiwara, M. Tsutumi,
M. Oda,* Y. Maeda, T. Wakahara,
T. Akasaka* ————— 5060 – 5062

Supramolecular Dynamics of Cyclic
[6]Paraphenyleneacetylene Complexes
with [60]- and [70]Fullerene Derivatives:
Electronic and Structural Effects on
Complexation



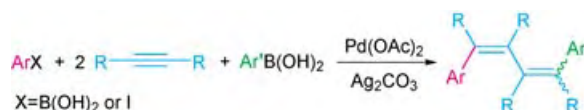
Stable inclusion complexes are formed between a carbon nanoring and C $_{70}$ as well as methano[70]fullerene derivatives. ^1H NMR spectroscopic studies show that at low temperatures the guest molecules are situated either above or below the center

of the cavity. The presence of the bulky ester groups results in the interconversion between the complexes (see scheme, $\Delta G^\ddagger \approx 11.0$ kcal mol $^{-1}$) being faster than decomplexation.

Multicomponent Coupling

T. Satoh, S. Ogino, M. Miura,*
M. Nomura ————— 5063 – 5065

Synthesis of Highly Substituted
1,3-Butadienes by Palladium-Catalyzed
Arylation of Internal Alkynes



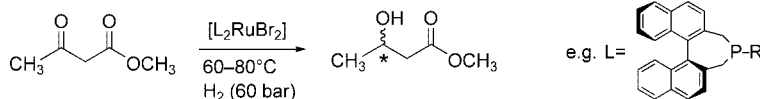
Four molecules are coupled together by the single treatment of aryl boronic acids with alkynes in the absence or presence of iodobenzene under palladium catalysis to afford 1,4-diaryl-1,3-butadienes as the

major product. Addition of a silver salt as oxidant and/or base effectively enables the selective catalytic production of the π -conjugated compounds.

Enantioselective Hydrogenation

K. Junge, B. Hagemann, S. Enthaler,
G. Oehme, M. Michalik, A. Monsees,
T. Riermeier, U. Dingerdisen,
M. Beller* ————— 5066 – 5069

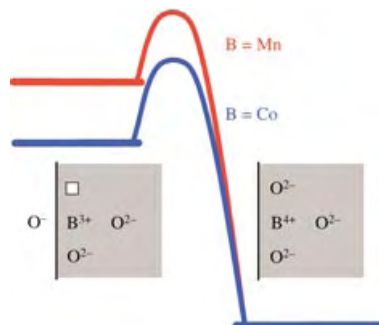
Enantioselective Hydrogenation of
 β -Ketoesters with Monodentate Ligands



Efficient and stable chiral monodentate phosphine ligands can be used in the ruthenium-catalyzed enantioselective hydrogenation of β -ketoesters (see scheme). The catalysts are remarkably

temperature-tolerant, and enantioselectivities of up to 95% *ee* are possible, even at 100–120°C. R = C $_6$ H $_5$, *p*-CH $_3$ OC $_6$ H $_4$, *p*-CF $_3$ OC $_6$ H $_4$, *i*Pr, Et, C $_6$ D $_5$.

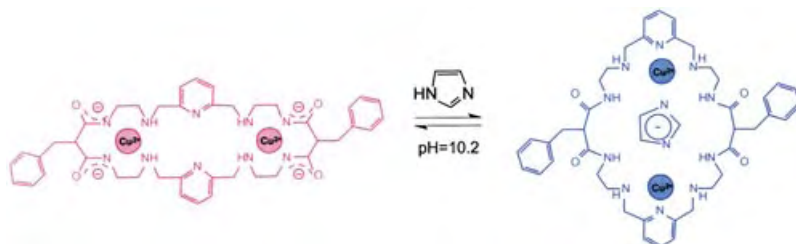
The variation of the activation enthalpy for surface oxygen exchange $\frac{1}{2}\text{O}_2 + \text{V}_\text{O}^{\bullet\bullet} \rightleftharpoons \text{O}_\text{O}^\times + 2\text{h}^\bullet$ with sample composition in $(\text{Ln}, \text{Sr})(\text{Mn}, \text{Fe}, \text{Co})\text{O}_{3-z}$ perovskites is rigidly coupled to the variation of the overall reaction enthalpy (see picture). This is the first mechanistically well-established example of a Hammett-like relationship for inorganic gas-solid reactions.



Reaction Kinetics

R. Merkle, J. Maier,*
H. J. M. Bouwmeester — 5069 – 5073

A Linear Free Energy Relationship for Gas-Solid Interactions: Correlation between Surface Rate Constant and Diffusion Coefficient of Oxygen Tracer Exchange for Electron-Rich Perovskites



pH-driven double Cu^{2+} ion translocation occurs inside an heteroditopic macrocycle. The movement opens and closes the system allowing or preventing it to function as receptor for bidentate anions. When imidazole is added to a solution

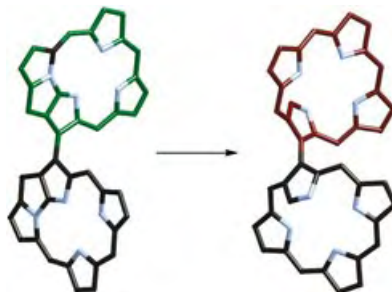
buffered at an appropriate pH value, opening of the system and substrate binding can be induced by the substrate itself, which results in a sharp color change (see picture).

Molecular Devices

L. Fabbrizzi,* F. Foti, S. Patroni,
P. Pallavicini,* A. Taglietti* — 5073 – 5077

A Sleeping Host Awoken by Its Guest: Recognition and Sensing of Imidazole-Containing Molecules Based on Double Cu^{2+} Translocation inside a Polyaza Macrocyclic

A covalently linked N-fused porphyrin dimer was synthesized by treatment of the monomer with $\text{Ag}(\text{OCOCF}_3)$. Subsequent reaction of this dimer with NaOMe led to a porphyrin dimer with two α, β -bound ("confused") pyrrole rings (see scheme) which adopt the inverted conformation. The dimer exhibits aromaticity in spite of its highly distorted structure.

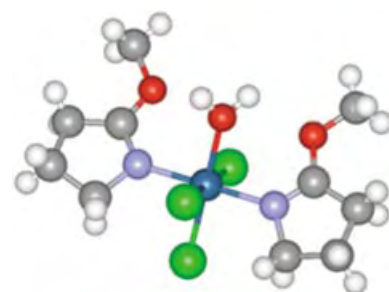


Porphyrinoids

T. Ishizuka, A. Osuka,
H. Furuta* — 5077 – 5081

Inverted N-Confused Porphyrin Dimer

The use of ancillary ligands resulted in the formation of $(\text{trans}-[\text{PtCl}_3(\text{OH}_2)-\{\text{N}=\text{C}(\text{OCH}_3)\text{CH}_2\text{CH}_2\text{CH}_2\}_2]^+)$ (see structure), the first intermediate aqua species in the oxidation of platinum(II) to platinum(IV) to be isolated and characterized. In chloroform this complex, but not the corresponding chloro species, reacts with excess Cl^- with O-demethylation of the ligands, indicating the importance of the coordinated water molecule.



Aqua Complexes

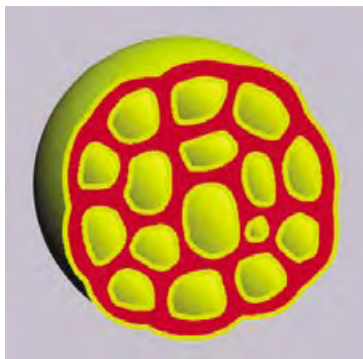
G. Tamasi, R. Cini, F. P. Intini, M. F. Sivo,
G. Natile* — 5081 – 5084

Unusual Reactivity at a Platinum Center Determined by the Ligands and the Solvent Environment

Self-Assembly

J. Du, Y. Chen* — 5084 – 5087

Organic–Inorganic Hybrid Nanoparticles with a Complex Hollow Structure



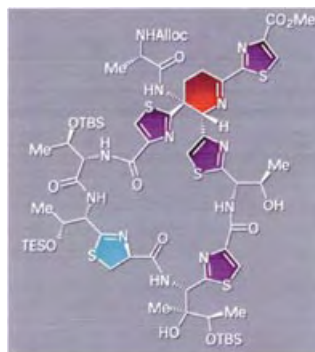
Secret chambers: Organic–inorganic hybrid nanoparticles (see picture) with a complex hollow structure were prepared by the self-assembly of a reactive block copolymer, poly(ethylene oxide)-*block*-poly[3-(trimethoxysilyl)propyl methacrylate], in DMF/water. Within these hybrid large-compound vesicles, several cavities are separated by crosslinked hybrid bilayers of uniform thickness.



Natural Products Synthesis

K. C. Nicolaou,* B. S. Safina, M. Zak, A. A. Estrada, S. H. Lee — 5087 – 5092

Total Synthesis of Thiostrepton, Part 1: Construction of the Dehydropiperidine/Thiazoline-Containing Macrocycle



A cornerstone of the RNA-binding antibiotic thiostrepton, namely the dehydropiperidine–thiazoline macrocyclic domain (see formula), was constructed through a hetero-Diels–Alder-type dimerization of an azadiene and selective elaboration of the resulting dehydropiperidine system.

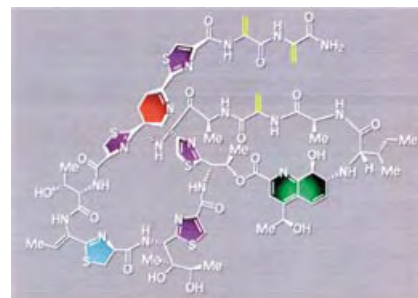


Natural Products Synthesis

K. C. Nicolaou,* M. Zak, B. S. Safina, S. H. Lee, A. A. Estrada — 5092 – 5097

Total Synthesis of Thiostrepton, Part 2: Construction of the Quinaldic Acid Macrocycle and Final Stages of the Synthesis

The flagship of the thiopeptide class of antibiotics, thiostrepton (see formula), was synthesized by fusion of the quinaldic acid moiety onto the dehydropiperidine–thiazoline macrocycle (see above) followed by demasking of its sensitive functionalities.



Communications labeled with this symbol have been judged by two referees as being “very important papers”.

Sources

Product and Company Directory

You can start the entry for your company in “Sources” in any issue of *Angewandte Chemie*.

If you would like more information, please do not hesitate to contact us.

Wiley-VCH Verlag – Advertising Department

Tel.: 0 62 01 - 60 65 65

Fax: 0 62 01 - 60 65 50

E-Mail: MSchulz@wiley-vch.de

Service

Keywords — 5098

Authors — 5099

Preview — 5101

Colin Eaborn (1923–2004): *Organosilicon Compounds*



Silicone waxes, sealants, and post-it slips are present in every home in the developed world. Millions of tonnes of silicones are manufactured each year. Conferences on organosilicon chemistry and

European Silicon Days are part of the chemistry scene. Yet in 1960, Colin Eaborn, who has died aged 80, was able to write a 500-page book entitled *Organosilicon Compounds*^[1] and cover all aspects of the subject as it was then known. Organosilicon chemistry developed so much during Eaborn's research career that it would be simply impossible for one person to undertake such a task today.

Eaborn was born in Cheshire (UK) in 1923 and completed his BSc degree in 1944 and PhD in 1947 at the University of Wales, Bangor. His research supervisor was the physical organic chemist E. D. Hughes, who gave him the task (which he thought would take a couple of years) of demonstrating the existence of the S_N1 , S_N2 , $E1$, and $E2$ mechanisms for reactions at silicon centers analogous to those recently discovered for reactions at carbon centers. This was a wholly unrealistic assignment, but it got Eaborn started on extraordinarily fruitful research on organosilicon compounds, electrophilic aromatic substitution (one of his first papers was on the cleavage of the aryl–silicon bond in p -MeOC₆H₄SiMe₃), and the use of bulky groups to stabilize species that would otherwise be too reactive to study.^[2]

He collaborated extensively with colleagues both in his own department and, more informally, throughout the world, and covered an astonishing range of topics in more than 550 research publications. Many of these topics were developed further as his co-workers became independent. Work with David Walton on poly(alkynyl)trimethylsilanes led to investigations on molecules in space and was one of the

factors that prompted Nobel Laureate Harry Kroto to look for C₆₀. Work with Roger Taylor on aromatic compounds led to a huge volume of further work also extended to cover fullerenes. Work with Richard Jackson, Andrew Hudson, and Iain Davidson led to extensive studies of radicals both in solution and in the gas phase. Work with Joseph Chatt and Alan Pidcock on compounds of Group 14 elements as ligands in transition-metal chemistry was followed by an extensive collaboration with David Smith resulting in over 100 publications on tris(trimethylsilyl)methyl (trisyl) and related compounds covering every group of the periodic table except the noble gases.^[3] There were also significant collaborations with colleagues in Germany, Poland, Italy, and New Zealand.

Eaborn's first appointment in 1947 was at University College Leicester (now the University of Leicester). He left there in 1961 to become the first professor of chemistry at the then new University of Sussex. As Head of Department, Dean, and Pro-Vice-Chancellor, Eaborn quickly built up a vibrant and internationally recognized research school, attracting other eminent chemists as colleagues, including six Fellows of the Royal Society and three Nobel Prize winners. He persuaded inorganic, organic, and physical chemists to talk to each other rather than compete for resources and urged his colleagues to make daring innovations in university teaching. The most notable of these new methods was the so-called "degree by thesis", in which a thesis and an oral presentation replaced the traditional written examinations of undergraduates in the UK. This initiative attracted original and highly motivated students, but it had to be phased out because of the legal implications of allowing technically unqualified undergraduates to work in research laboratories.

Eaborn received numerous honors and prizes. He was elected to the Fellowship of the Royal Society in 1970. He received the Frederick Stanley Kipping Award of the American Chemical Society in 1964: the first non-American to receive this prestigious prize. He received the Organometallic Award of the Royal Society of Chemistry in

1974, its Ingold Medal in 1976, and the Main Group Award in 1988. Although he was not a highly visible public figure, he had considerable influence on the development of chemistry at university level in the second half of the twentieth century. He chaired a committee (1966–1970) on the relationship between chemistry courses and the needs of industry, was honorary secretary of the Chemical Society (now the Royal Society of Chemistry) from 1965 to 1970, and served on the Council of the Royal Society from 1978 to 1980 and 1988 to 1989. He was instrumental in setting up regular meetings of the heads of chemistry departments to consider matters of mutual interest, and he corresponded with hundreds of chemists, especially in Europe, as a founding editor of the *Journal of Organometallic Chemistry*. Many are grateful for the care he gave to presentation, clarity, and good English in the manuscripts he received. He was the UK representative on the British–Italian Mixed Cultural Commission.

Colin Eaborn is survived by his wife Joyce, who provided support and companionship for more than 50 years. He leaves numerous students, co-workers, and colleagues who have been encouraged by his enthusiasm and generosity and cheered by his sense of humor.

J. David Smith

University of Sussex, Brighton (UK)

- [1] C. Eaborn, *Organosilicon Compounds*, Butterworth, London, **1960**.
- [2] C. Eaborn, *J. Chem. Soc. Dalton Trans.* **2001**, 3397.
- [3] C. Eaborn, J. D. Smith, *J. Chem. Soc. Dalton Trans.* **2001**, 1541.

YbGaGe: Zero Thermal Expansion as a Result of an Electronic Valence Transition?

Klaus Stöwe*

Keywords:

solid-state chemistry · functional materials · inter-metallic phases · thermal expansion

Usually materials expand upon heating: They have a positive coefficient of thermal expansion (PTE or positive CTE). Some compounds, however, show near-zero (NZTE), zero (ZTE) or even negative thermal expansion (NTE). The best-known NZTE material may be the ceran glass ceramics of the company Schott, from which main mirror supports for astronomical reflector telescopes and stove taps are produced. The oldest known NZTE material is invar, which was described by Guillaume^[1] as early as 1897 and can be formulated chemically as $\text{Fe}_{64}\text{Ni}_{36}$. Its expansion coefficient is about a tenth of that of steel. The CTE of invar is at its lowest when the alloy has been quenched from high temperatures or if it has been treated in a cold state. For superinvar—cobalt-doped invar of the composition $\text{Fe}_{63}\text{Ni}_{33}\text{Co}_4$ —even a negative thermal expansion coefficient (NTE) can be achieved this way. Recently it was also shown that invar can be inserted into carbon nanotubes at 800°C by pyrolysis of aerosols from $\text{Cp}_2\text{Fe}/\text{Cp}_2\text{Ni}$ mixtures in benzene. In this way flakes of filled and parallel-oriented nanotubes of $\leq 200\text{ }\mu\text{m}$ in length and $\leq 80\text{ nm}$ in diameter are created.^[2] The magnetic and mechanic properties of this material promise very interesting applications in the production of magnetic storage media and

nanoscale thermostates. Materials without thermal expansion that are also extremely light, thin, and very stable would be ideal raw materials for the thermal protection of reusable space shuttles. ZTE materials are much in demand as precision substrates for electronic components, as positioning devices that are ultraprecise on a nanometer scale for semiconductors, and as other highly precise machine components and circuits. Therefore, there have been numerous attempts to invent such materials or to develop them from systems with well-known thermal properties.

Only a few compounds show intrinsic NZTE, ZTE, or NTE behavior. These compounds include the minerals akaganeite (the β form of iron oxide hydroxide), β -cristobalite, and β -eukryptite. Through temperature-resolved X-ray powder-diffraction data the structural changes of akaganeite ($\text{Fe}_{7.6}^{3+}\text{Ni}_{0.4}^{2+}\text{O}_{6.35}(\text{OH})_{9.65}\text{Cl}_{1.25} \cdot n\text{H}_2\text{O}$) and its transformation into hematite in the temperature range of 26 to 800°C were investigated.^[3] Between room temperature and about 225°C, the unit cell of akaganeite shows NZTE behavior, above 225°C the cell volume slowly decreases, and at about 290°C the transformation into hematite starts. The structural mechanisms of the NZTE behavior of tetragonal β -eukryptite (LiAlSiO_4) were elucidated in detail through a Rietveld refinement of combined synchrotron and neutron diffraction data.^[4] The unusual thermal behavior of β -eukryptite can be explained as a result of several processes, including tetrahedral tilting, tetrahedral deformation, and shortening of the Si/Al–O bond. Furthermore, the thermal expansion

in ordered eukryptite differs from that in disordered eukryptite. In this context it is interesting that some silicates show an auxetic effect. Auxetic compounds have a negative Poisson ratio (defined as the quotient of lateral to longitudinal expansion) and differ from other compounds in that, unlike a rubber band, their diameter is not decreased but increased upon elongation. Besides “molecular” auxetic materials, such as α -cristobalite, lanthanum niobate, and some fcc (face-centered cubic) metals, there are also composites, polymers, and foams with a negative Poisson ratio known. Subtle structural differences can be decisive for the properties of a compound: α -Quartz is not auxetic, α -cristobalite is auxetic, and β -eukryptite is an NZTE material. All these phenomena depend on the existence of polyhedra with acute corners in the crystal structures of the compounds.

As an alternative to the development of materials with intrinsic ZTE behavior, one approach is to combine PTE and NTE substances to create ZTE composites. For example, the pore-free functional ceramic nexcera of the company Nippon Steel is a material with practically zero thermal expansion at room temperature.^[5] The company Matsushita Electric Industrial has applied for a European patent for another material.^[6] This ZTE material contains double oxides of the formula RQ_2O_8 ($\text{R} = \text{Zr}, \text{Hf}$ und $\text{Q} = \text{Mo}, \text{W}$) as an NTE component and MQX_4 ($\text{M} = \text{Mg}, \text{Ca}, \text{Sr}, \text{Ba}$ and $\text{X} = \text{O}, \text{S}$) as a PTE component. When the two components are mixed in a 1:1 ratio, the material that forms has a thermal expansion of nearly zero over a wide temperature range. The

[*] Priv.-Doz. Dr. K. Stöwe
Technische Chemie
Universität des Saarlandes
Postfach 151150
66041 Saarbrücken (Germany)
Fax: (+49) 681-302-2343
E-mail: k.stoeve@mx.uni-saarland.de

NTE component ZrW_2O_8 has already been used in mixtures with cement and sand to decrease the thermal expansion and to avoid cracks in paving stones.^[7]

Salvador et al. recently discovered a novel intrinsic ZTE material,^[8] the compound YbGaGe , which crystallizes like YbGaSn , CaGaGe , and SrGaSn in the YPtAs structure type with the space group $P6_3/mmc$. The YPtAs type can be derived as described by Hoffmann and Pöttgen^[9] from the AlB_2 structure type. It differs from the latter type in that the planar 6^3 boron nets in YPtAs are composed alternately of Pt and As atoms, and the nets are wavy. Because of the different atom types in the wavy 6^3 nets there are several possibilities for stacking along the c axis; in the YPtAs type the unit cell is quadrupled relative to the AlB_2 unit cell. LiGaGe with a doubled unit cell is also known. It contains three dimensionally linked units $^3[\text{GaGe}]^-$ analogous to hexagonal diamond. If two more electrons per $[\text{GaGe}]$ unit are formally added to this partial structure, puckered hexagonal layers $^2[\text{GaGe}]^{3-}$ analogous to black phosphorus are formed according to the $(8-N)$ rule. Thus, the two additional electrons effectively neutralize one of the four Ga–Ge bonds per atom by occupying antibonding states, and a free electron pair forms on each Ga and Ge atom. The compounds MGaT ($\text{M} = \text{Ca}, \text{Sr}, \text{Yb}$ and $\text{T} = \text{Ge}, \text{Sn}$) therefore bridge the two extremes mentioned above. Their $^2[\text{GaT}]^{2-}$ units are interconnected by Ga–Ga bonds to form double layers. The Ga–Ga distance in these compounds varies considerably: In CaGaGe it is the longest at 358 pm, followed by

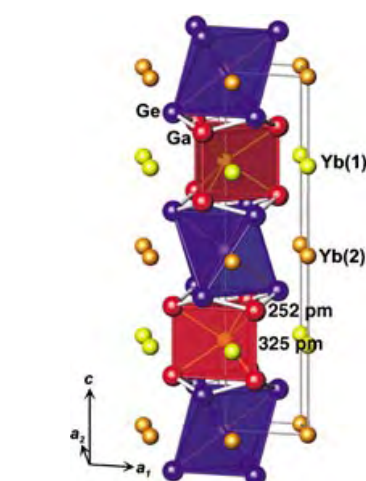


Figure 1. Crystal structure of YbGaGe .^[8]

330 pm in SrGaSn and 325 pm in YbGaGe (Figure 1). This distance is shortest in YbGaSn at 299 pm. These differences in the Ga–Ga bond lengths are the most apparent in the electron localization function (ELF) shown in Figure 2 for the compounds CaGaGe , YbGaGe , and YbGaSn in a section through the six-membered rings exactly in line with the Ga atoms. In Figure 2, the bond order decreases from right to left, and two free-electron pairs develop from the Ga–Ga bond. Furthermore, with a lengthening of the Ga–Ga bond, a shortening of the Ga–T bond within the six-membered rings of 2–3 pm results. The atoms M bridge the voids between the 6^3 rings, strung together lengthwise $[001]$ like pearls on a necklace. Two different crystallographic positions are occupied in the space group $P6_3/mmc$. M(1) is surrounded by six Ga atoms in a trigonal prism; M(2) is

surrounded octahedrally by six T atoms (see Figure 1). As a result of the different coordination surroundings two different valencies are possible for M, which is exactly what the authors suggest for the compounds YbGaGe and YbGaSn . The fact that the Ga–Ga bond is longer in YbGaGe than in YbGaSn means that more antibonding states must be occupied in the former compound; that is, the charge of the $[\text{GaGe}]$ unit must formally be a little higher than that of the $[\text{GaSn}]$ unit. In YbGaGe , this higher formal charge is balanced by the presence of two cations with different valencies, and the valencies of these cations also change with temperature, as shown by magnetic-susceptibility measurements on YbGaGe . As the valency of Yb changes with decreasing temperature from about +2.6 towards +2, the contraction of the whole lattice as a result of the decreasing temperature is compensated. Thus, two lattice parameters, a_1 and a_2 , increase with decreasing temperature, whereas the third parameter, c , decreases to the extent that the total volume remains constant. The CTE of the a axis in YbGaGe varies a little depending on the composition, as the phase exhibits a certain phase width. According to the authors, the CTE lies between $-1.3 \cdot 10^{-5}$ and $-1.8 \cdot 10^{-5} \text{ K}^{-1}$. For comparison, the corresponding value for YbGaSn is $+1.0 \cdot 10^{-4} \text{ K}^{-1}$.

This result shows that the ZTE effect in YbGaGe is based on a completely new mechanism. In contrast to classic ZTE materials, such as ZrW_2O_8 and related oxides, the ZTE behavior in YbGaGe is not of a geometric origin, nor caused by a cooperative rotation of

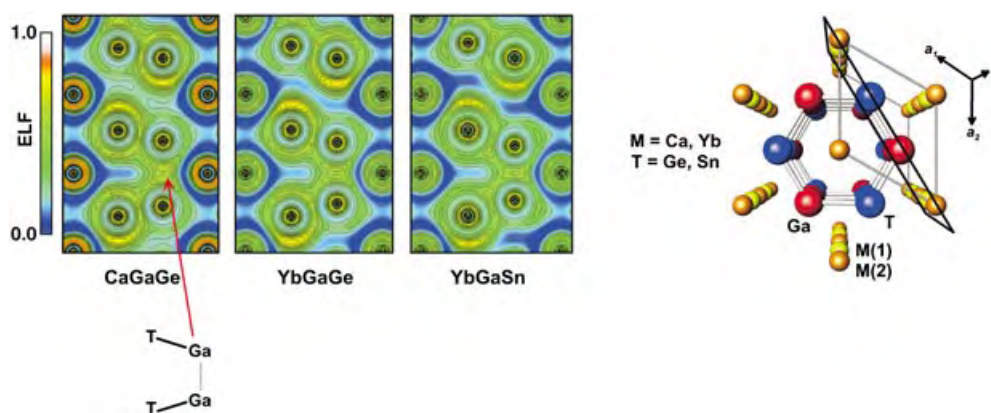


Figure 2. Total electron localization function (ELF) for CaGaGe , YbGaGe , and YbGaSn , calculated with LMTO-ASA. Section through the M atoms with the Ga–Ga bond, as indicated in the structural representation on the right.

oxide tetrahedra. No rotations of the polyhedra occur in YbGaGe, as the low-temperature X-ray diffraction investigations showed. Instead, an internal electron transfer between the Yb atoms and the anionic partial structure $[\text{GaGe}]^{2-}$ occurs. YbGaGe has the additional advantage over the oxides of being a metallic conductor. YbGaGe thus unites two interesting characteristics, which makes it a promising material for new applications.

Published Online: August 20, 2004

Note added after online publication on August 20, 2004: An article entitled "Thermal expansion in YbGaGe" (S. Bobev, D. J. Williams, J. D. Thompson, J. L. Sarrao, *Solid State Communications*

2004, 131, 431–433), has just appeared in which another two recent publications on this topic were cited. All three papers report that YbGaGe has a distinctly more positive thermal expansion coefficient than that reported by Salvador et al.^[8] The differences may be due to a deviation in the composition, that is, a variation in x in $\text{YbGa}_{(1+x)}\text{Ge}_{(1-x)}$. These newest results prompted the author of this Highlight to add a question mark to the title.

- [1] C. E. Guillaume, *C. R. Acad. Sci.* **1897**, 125, 235–238.
[2] N. Grobert, M. Mayne, M. Terrones, J. Sloan, R. E. Dunin-Borkowski, R. Kamalakaran, T. Seeger, H. Terrones, M.

- Rühle, D. R. M. Walton, H. W. Kroto, J. L. Hutchison, *Chem. Commun.* **2001**, 471–472.
[3] J. Post, P. J. Heaney, R. B. von Dreele, J. C. Hanson, *Am. Mineral.* **2003**, 88, 782–788.
[4] H. Xu, P. J. Heaney, D. M. Yates, R. B. von Dreele, M. A. Bourke, *J. Mater. Res.* **1999**, 14, 3138–3151.
[5] J. Sugawara, K. Abe, T. Mukai, *Tech. Dig. SPIE* **2003**, 93–95.
[6] T. Suzuki, A. Omote, J. Kuwata, Eur. Pat. 1277712 [*Eur. Pat. Appl.* **2002**, 11, 15224].
[7] M. Kofteros, S. Rodriguez, V. Tandon, L. E. Murr, *Scr. Mater.* **2001**, 45, 369–374.
[8] J. R. Salvador, F. Guo, T. Hogan, M. G. Kanatzidis, *Nature* **2003**, 425, 702–705.
[9] R. D. Hoffmann, R. Pöttgen, *Z. Kristallogr.* **2001**, 216, 127–145.

The definitive work in electrochemistry

Encyclopedia of Electrochemistry

Allen J. Bard, Department of Chemistry, University of Texas, USA
Martin Stratmann, Max Planck Institut für Eisenforschung, Düsseldorf, Germany
(Editors-in-Chief)

10 Volumes + Index

2004. Approx 6000 pages with 3000 figures and 1000 tables. Hardcover. ISBN 3-527-30250-6
€ 299.00* / £ 175.00 per volume.

*The €-Price is for Germany only

Available: Vols. I, II, III, IV, VI, IX

Forthcoming

Vol. VIII January 2004
Vol. V October 2004
Vol. X October 2004
Vol. VII December 2004

Stay up-to-date in electrochemistry

- ⊙ A total of 11 volumes makes this the first and only complete reference on electrochemistry
- ⊙ Covers all aspects, from fundamental research to applications in industry
- ⊙ Easy access to electrochemical topics

➔ www.wiley-vch.de/bard/eoe

John Wiley & Sons, Ltd., 1 Oldlands Way, Bognor Regis, West Sussex, PO22 9SA England · Fax: +44 (0) 1243-843-296
e-mail: cs-books@wiley.co.uk · www.wiley-europe.com



WILEY

WILEY-VCH · P.O. Box 10 11 61
69451 Weinheim, Germany · Fax: +49 (0) 62 01-60 61 84
e-mail: service@wiley-vch.de · www.wiley-vch.de



WILEY-VCH

Unusually Slow Charge Recombination in Molecular Dyads

Anthony Harriman*

Keywords:

donor–acceptor systems · electron transfer · photophysics · photosynthesis · reorganization energy

The photosynthetic reaction center complex operates as an elaborate device that uses visible light to separate electronic charge across a bilayer membrane. An essential feature of the natural process is the stepwise transfer of an electron over a series of redox-active cofactors until the membrane is spanned. Each step loses a fraction of the initial excitation energy and increases the distance between the positive and negative charges. The rates of successive electron-transfer steps become progressively slower as the need to compete with exergonic charge recombination become less important. By positioning the cofactors in a protein environment, where the total reorganization energy is kept modest, the initial electron-transfer events can be promoted at a high rate with a small driving force. As such, the activation energy for electron transfer is negligible and the reaction proceeds readily at low temperature. The elegance and sophistication of natural photosynthesis, especially when the ancillary light-harvesting features are taken into account, ensure that this process continues to receive intense investigation from biochemists, biophysicists, biologists, and chemists. A further motivation for studying natural photosynthesis stems from the urgent need to duplicate the essential features with laboratory models so that we might be

able to collect and store sunlight in the form of chemical potential. This latter area of research is known loosely as “artificial photosynthesis”.^[1]

Many different approaches have been taken in an effort to design molecular systems capable of effecting photo-induced charge separation under illumination with visible light. It is well known that the chromophore must be held in proximity to a redox-active partner so that electron transfer can compete with inherent deactivation of the initially formed excited state. Usually, the redox partners are assembled into a molecular dyad by covalent bonding that assures a constrained, if not rigid, geometry. Alternative forms of assembly, such as hydrogen bonding or electrostatic attraction, provide interesting diversions but have yet to challenge the supremacy of covalent bonding. Initially, these dyads comprised a porphyrin as both the chromophore and electron donor, and with a quinone as an electron acceptor.^[2] Other reagents have been proposed, and there now exists a multitude of light-active molecular dyads that undergo fast charge separation upon excitation. Until very recently, all such dyads underwent rapid charge recombination, which severely restricted the lifetime of the charge-separated state. Indeed, typical lifetimes for the charge-separated state in fluid solution are on the order of some hundreds of picoseconds to a few nanoseconds. This range is much too short to carry out useful chemistry with the intermediate radical ions.

Learning from nature, Gust et al.^[3] were the first to develop an effective strategy to overcome rapid charge re-

combination. Their approach was to attach secondary cofactors to the dyad so as to set up a cascade of electron-transfer steps leading to long-range charge separation. Since the rate of electron transfer decreases sharply with increasing separation, the significance of charge recombination is diminished with each successive transfer. In this way, molecular triads, tetrads, pentads, etc., have been synthesized and used to prolong the lifetime of the charge-separated species into the microsecond^[4] and even millisecond range.^[5] This is a tremendous achievement but it comes at a considerable price. The synthesis is time consuming, and therefore expensive, while the fraction of incident light “stored” upon charge separation is necessarily small. For a long time, however, it seemed that this cascade effect was the only way forward, but new research has confronted this conventional view and sought to stabilize charge separation in simple dyads by careful control of the geometry.^[6]

The molecular dyad introduced by Fukuzumi and co-workers^[7] (Figure 1 a) comprises a zinc chlorin, as the electron donor (D), and a fullerene, as the electron acceptor (A), separated by only 2.6 Å. Despite the proximity, the two subunits appear to be electronically isolated. Illumination of the chlorin results in charge separation occurring with a rate constant of $1.0 \times 10^{11} \text{ s}^{-1}$, although the yield of the charge-separated state is only about 12 %. There is a reasonable driving force ($\Delta G^0 = -0.5 \text{ eV}$) for charge separation and the resultant radical ion pair can be detected by transient absorption spectroscopy. A key feature of this system is that the

[*] Prof. A. Harriman
Molecular Photonics Laboratory
School of Natural Sciences (Chemistry)
Bedson Building, University of Newcastle
Newcastle upon Tyne, NE1 7RU (UK)
Fax: (+44) 191-222-8660
E-mail: anthony.harriman@ncl.ac.uk

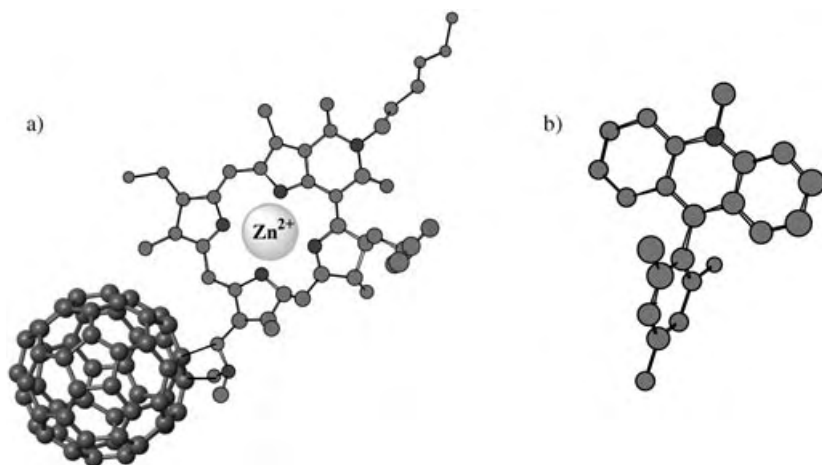


Figure 1. Structural representations of the lowest-energy conformations of molecular dyads described in this work. For details see references [7] (a) and [10] (b). Note, the hydrogen atoms have been omitted for clarity.

energy of the radical ion pair ($E_{\text{RIP}} = \text{ca. } 1.26 \text{ eV}$) is notably lower than that of the triplet excited states associated with either chlorin ($E_{\text{T}} = \text{ca. } 1.4 \text{ eV}$) or fullerene ($E_{\text{T}} = \text{ca. } 1.5 \text{ eV}$). This situation ensures that decay of the charge-separated state involves charge recombination to reform the ground state. Since the total reorganization energy accompanying charge recombination is significantly smaller than the thermodynamic driving force, charge recombination occurs well within the Marcus inverted region. The rate constant for this step is only $4.2 \times 10^3 \text{ s}^{-1}$, thereby corresponding to a lifetime of the charge-separated state of $230 \mu\text{s}$ in benzonitrile at 25°C . This is an exceptionally long-lived intermediate for such a simple molecular dyad. For example, related dyads based on tetrapyrrolic chromophores and characterized by closely coupled redox partners tend to form sub-nanosecond charge-separated states.^[8]

The difference between the dyad constructed by Fukuzumi and co-workers and related systems can be explained in terms of quantum mechanical tunneling from the charge-separated state. Normally, the full impact of the Marcus inverted region is not observed because nuclear tunneling^[9] lowers or removes the activation energy for charge recombination (Figure 2). As such, charge recombination is much faster than expected on the basis of classical Marcus theory. For this dyad, however, a very high activation energy for charge re-

combination ($E_{\text{A}} = \text{ca. } 0.23 \text{ eV}$) is observed. This situation leads to the exceptional lifetime for the charge-separated state of 120 s at -150°C ! Nuclear tunneling usually becomes more apparent at lower temperatures, where the activated rate is slow, but this seems not to be the case here. The Marcus inverted region is often characterized by a relatively narrow barrier to electron transfer and this realization greatly assists nuclear tunneling. The new dyads might possess broader charge-recombination

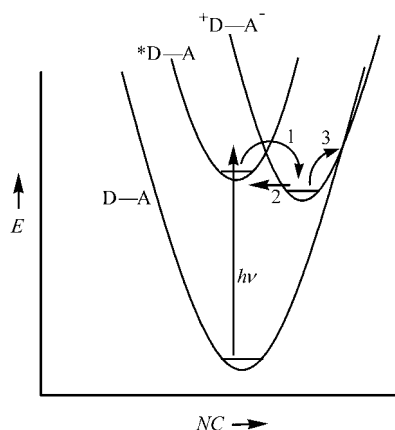


Figure 2. Potential energy diagram for charge separation and subsequent charge recombination in a molecular dyad (D-A). Light activation leads to formation of the local excited state (*D-A). Charge separation, in which the radical pair ($^+\text{D-A}^-$) is formed, is assumed to be activated and takes place by step 1. Charge recombination might involve nuclear tunneling (by step 2) or an activated process (by step 3) that corresponds to classical Marcus behavior in the inverted region.

barriers, because of their constrained geometries, which would be critical in minimizing nuclear tunneling.

There is ample experimental evidence to confirm the validity of the Marcus inverted region, but there are very few cases where quantum mechanical tunneling does not promote charge recombination. From the viewpoint of designing effective artificial photosynthetic systems it is important to identify if the above dyad is representative of a new class of compound or merely an isolated case. As such, it is interesting to note that Fukuzumi et al.^[10] have reported a second example of a closely coupled molecular dyad exhibiting very fast charge separation ($k_{\text{CS}} = 2.4 \times 10^{11} \text{ s}^{-1}$) at modest driving force ($\Delta G^0 = -0.31 \text{ eV}$), but with an unexpectedly slow rate of charge recombination at ambient temperature (Figure 1 b). In this latter case, the charge-separated state was formed in quantitative yield, but intramolecular charge recombination was much slower than the corresponding bimolecular process occurring in fluid solution. Charge recombination becomes intramolecular at higher temperatures, thus indicating that this process is strongly activated. Electronic coupling between the subunits is kept at a minimum by the perpendicular orientation and it seems likely that partial rotation around the connecting bond contributes towards the overall activation energy for charge recombination. Again, the question is raised as to why nuclear tunneling does not play an important role in promoting charge recombination in this system.

One advantage of having only a single bond between the donor and acceptor is that charge separation is likely to be very fast. In several cases it appears that charge separation proceeds from high vibrational levels of the excited state rather than from the thermally relaxed excited state (Figure 2). The unique linkage can also impose a highly constrained geometry and, indirectly, lead to a small solvent reorganization energy. However, related dyads^[8] display high rates of charge recombination and it is clear that the factors controlling the electron-transfer dynamics in such systems are not yet fully understood. It seems likely that the critical feature concerns the connecting

bond, but exactly how this translates to such a variable rate of charge recombination remains a mystery. In particular, it is necessary to consider very carefully the role of triplet states, either charge-transfer states or localized π, π^* triplets, in these systems. The use of magnetic field effects or an in-depth evaluation of the spin state of any EPR-active intermediates is essential if the detailed mechanism is to be uncovered.

The design of simple molecular dyads capable of fast charge separation but relatively slow charge recombination has clear advantages with regard to synthetic feasibility. In attempting to mimic natural photosynthesis with such dyads, even allowing for the contemporary preference to manufacture electricity rather than a chemical fuel, it is necessary to overcome at least two major obstacles. First, we must learn the design elements that will enable efficient systems to be engineered without too much of the tedious trial-and-error protocol. The recent work emerging from Fukuzumi's research group suggests that this is a strong possibility. The importance of this work lies with the realization that small molecular

dyads can replace the long multicomponent molecular-scale wires that dominate current thinking in the field of molecular photonics. Freed from the need to stabilize the charge-separated state against charge recombination, it might not be necessary to build long molecules. This could lead to a marked increase in charge density. Second, we must develop a methodology whereby individual dyads can be organized into a cooperative network where logical functions can be performed. The charge-separated state is now sufficiently long-lived and energetic to do something useful. This situation requires many thousands of molecules to align and work together. The next step is far from clear but the realization that light-activated charge separation in simple dyads can lead to unusually long-lived radical ion pairs compels us to think seriously about devices.

Published Online: July 26, 2004

- [1] A. Harriman, J.-P. Sauvage, *Chem. Soc. Rev.* **1996**, 25, 41.

- [2] M. R. Wasielewski, *Chem. Rev.* **1992**, 92, 435.
 [3] D. Gust, T. A. Moore, A. L. Moore, *Acc. Chem. Res.* **2001**, 34, 40.
 [4] D. Gust, T. A. Moore, A. L. Moore, A. N. Macpherson, A. Lopez, J. M. DeGraziano, I. Gouni, E. Bittersmann, G. R. Seely, F. Gao, R. A. Nieman, X. C. Ma, L. Demanche, D. K. Luttrell, S.-J. Lee, P. K. Perrigan, *J. Am. Chem. Soc.* **1993**, 115, 11 141.
 [5] H. Imahori, D. M. Guldi, K. Tamaki, Y. Yoshida, C. Luo, Y. Sakata, S. Fukuzumi, *J. Am. Chem. Soc.* **2001**, 123, 6617.
 [6] S. Fukuzumi, K. Ohkubo, E. Wenbo, Z. Ou, J. Shao, K. M. Kadish, J. A. Hutchison, K. P. Ghiggino, P. J. Sentic, M. J. Crossley, *J. Am. Chem. Soc.* **2003**, 125, 14984.
 [7] K. Ohkubo, H. Kotani, J. Shao, Z. Ou, K. M. Kadish, G. Li, R. K. Pandey, M. Fujitsuka, O. Ito, H. Imahori, S. Fukuzumi, *Angew. Chem.* **2004**, 116, 871; *Angew. Chem. Int. Ed.* **2004**, 43, 853.
 [8] I. V. Rubtsov, N. P. Redmore, R. M. Hochstrasser, M. J. Therien, *J. Am. Chem. Soc.* **2004**, 126, 2684.
 [9] J. Kroon, H. Oevering, J. W. Verhoeven, J. M. Warman, A. M. Oliver, M. N. Padon-Row, *J. Phys. Chem.* **1993**, 97, 5065.
 [10] S. Fukuzumi, H. Kotani, K. Ohkubo, S. Ogo, N. V. Tkachenko, H. Lemmetyinen, *J. Am. Chem. Soc.* **2004**, 126, 1600.

Nanostructures

Ionic Liquids for the Convenient Synthesis of Functional Nanoparticles and Other Inorganic Nanostructures

Markus Antonietti,* Daibin Kuang, Bernd Smarsly, and Yong Zhou

Keywords:

ionic liquids · mesophases · microporous materials · nanostructures · sol–gel processes

Ionic liquids are a new class of organic solvents with high polarity and a preorganized solvent structure. Very polar reactions can be carried out in these liquid in the absence of or with a controlled amount of water, and crystalline nanoparticles can be synthesized conveniently at ambient temperatures. The pronounced self-organization of the solvent is used in the synthesis of self-assembled, highly organized hybrid nanostructures with unparalleled quality. The extraordinary potential of ionic liquids in materials synthesis is described in this minireview and a physicochemical explanation is given.

Introduction

Ionic liquids (ILs) are organic salts with low melting points, sometimes as low as -96°C .^[1] ILs have received much attention in many areas of chemistry and industry due to their potential as a “green” recyclable alternative to traditional organic solvents.^[2] The ILs are liquid over a wide range of temperatures, in some cases in excess of 400°C . Because of their properties, such as high polarity, negligible vapor pressure, high ionic conductivity, and thermal stability, ILs can be used in catalysis,^[3,4] as inert solvents in electrochemistry,^[5] for polymer synthesis,^[6,7] and in the adaptation of enzymatic reactions to organic media.^[8] ILs can also be used to replace water in chemical or technical processes.

Although ionic liquids have found application only recently in chemistry, they are an old class of substances: the first description of an IL with a melting point of 12°C was published in 1914.^[9] The most extensively studied ILs are the 1-alkyl-3-methylimidazolium salts. Newer systems include species with additional functionality, for example, long-chain amphiphilic ILs with both lyotropic^[10] and thermotropic liquid crystallinity.^[11] Organic reactions can be conducted with increased selectivity in these ILs.^[12] Other liquid-

crystalline species with wide phase regions and a very high dipole moment and polarizability are described in ref. [13].

This review will not focus on the use of ILs in catalysis and organic/inorganic synthesis,^[14] as there are already excellent reviews and books^[15] available. Instead we will describe recent developments in which the advantages of ILs for materials chemistry and especially for the synthesis of novel nanostructures have been gradually realized.

Ionic Liquids for the Synthesis of Nanostructures

First, ILs were used in electrosynthesis: various metallic nanoparticles, such as palladium,^[16] iridium,^[17] and semiconductor nanoparticles such as stable Ge nanoclusters^[18] have been synthesized. The preparation of Ti nanowires onto graphite by electroreduction as described by Freyland et al.^[19] is exciting but still requires final proof. In all of these examples the large operation window for electrochemical reactions and the high polarity of ILs are exploited.

Very fine and stable noble-metal nanoparticles (Ir^0 and Ru^0 , 2.0–2.5 nm in diameter) can also be synthesized in ILs by chemical reduction.^[20] The colloidal system metal-nanoparticle/IL-stabilizer is extraordinarily stable and no ligands are required; extraordinarily high turnover numbers are achieved with this system in catalytic hydrogenation.

Besides the large electrochemical window, other advantages of ILs can be considered:

- Although polar, ILs can have low interface tensions which in addition seems to adapt to the other phase (e.g. for 1-butyl-3-methylimidazolium tetrafluoroborate the $\gamma \approx 38 \text{ mN m}^{-1}$ against air^[21]). Since low interface tensions result in high nucleation rates, very small particles can be generated which undergo Ostwald ripening only weakly.

[*] M. Antonietti, D. Kuang, B. Smarsly, Y. Zhou
Max Planck Institute of Colloids and Interfaces
Research Campus Golm
14424 Potsdam (Germany)
Fax: (+49) 331-567-9502
E-mail: pape@mpikg-golm.mpg.de

- Low interface energies for larger objects can be translated into good stabilization or solvation of molecular species. Obviously, the IL structures “adapt” to many species, as it provides hydrophobic regions and a high directional polarizability which be oriented parallel or perpendicular to the dissolved species. Put simply: reactions in ILs are like reactions in a pure “universal” ligand.
- Owing to the high thermal stability of ILs, reactions can be conducted at temperatures well beyond 100 °C in non-pressurized vessels.
- ILs facilitate inorganic synthesis from very polar starting materials under ambient conditions and under anhydrous or water-poor conditions. In this way, hydroxide or oxihydrate formation and the coupled generation of amorphous species can be suppressed, as low amounts of water drive the mass balance to completely condensed systems, which are usually directly crystalline.
- The most important advantage of ILs, however, is an unconventional and very rare property that cannot be emphasized sufficiently: ILs form extended hydrogen-bond systems in the liquid state^[22] and are therefore highly structured.^[23,24] ILs are therefore “supramolecular” solvents. Solvent structuration is the molecular basis of most molecular recognition and self-organization processes, with water being the most prominent and pronounced example.^[25] This special quality can be used as the “entropic driver” for spontaneous, well-defined, and extended ordering of nanoscale structures.

3. Sol–Gel Reactions in Water-Poor Ionic Liquids

First work on inorganic sol–gel reactions focussed on the formation of silica aerogels. It turned out that such aerogels can be dried without a supercritical drying procedure.^[26] This again speaks for a very low interface tension of the binary system and coupled low capillary forces. It is, however, even more interesting to make crystallizable species by sol–gel reactions in water-poor reaction media. Zhou et al. hydrolyzed titanium tetrachloride in 1-butyl-3-methylimidazolium tetrafluoroborate with some reaction water (water-poor conditions) in a low-temperature synthesis (at 80 °C).^[27] Anatase powders consisting of 2–3-nm-sized particles and with surface areas of 554 m² g^{−1} were obtained, which assembled to larger, spherical spongelike superstructures. These experiments look simple but they illustrate the multiple advantages of ILs. First, sol–gel reactions in water usually provide amorphous titania, which has to be calcined above 350 °C to result in the desired crystalline anatase. This usually prevents direct employment of anatase in organic/inorganic hybrid systems. Also, the nucleation rate of titania in the bulk is rather low (usually particles with diameters of ca. 20 nm are obtained). The IL solvent therefore not only facilitates direct synthesis of crystalline species under ambient conditions, it also increases the nucleation rate by more than a factor of 1000, owing to its low interface energy and adaptability. Only with this combination is the delicacy of the resulting structures possible.

The anatase obtained has a spongelike structure with high surface area and narrow pore-size distribution, and due to its increased volume it is easy to handle. This material is expected to have potential in solar energy conversion, catalysis, and optoelectronic devices, for example, for the



Markus Antonietti studied chemistry in Mainz, Germany, and received his PhD for research conducted under the direction of Prof. Hans Sillescu. He completed his habilitation on microgels in 1990 and joined the chemistry faculty at the University of Marburg in 1991. Since 1993 he has headed the Chemistry Department of the Max Planck Institute of Colloids and Interfaces in Golm. His research interests are complex, functional, and self-organizing soft-matter systems and hybrid materials.



Bernd Smarsly studied chemistry and physics at the University of Marburg, Germany, and received a Master degree of Natural Science in 1998. He completed his PhD studies in 2001 at the Max Planck Institute of Colloids and Interfaces, spent one year as a postdoc at the University of New Mexico at Albuquerque, USA, and returned in 2003 to become group leader for “Mesoporous Materials” at the Max Planck Institute of Colloids and Interfaces.



Daibin Kuang studied chemistry at the Normal University in Hunan, China, and received his B.S. in 1998. He then moved to Zhongshan University in Guangzhou, China, where he completed his M.S. studies in 2000 and his PhD thesis in 2003. Since September 2003, he has been a research scientist in the group led by Dr. Smarsly at the Max Planck Institute of Colloids and Interfaces.



Young Zhou studied chemistry and physics at the University of Science and Technology of China (USCT), received his Master degree in 1996, and finished his PhD thesis there in 2000. Afterwards he worked with Professor Chujo at the Kyoto University, Japan. He joined the group of Professor Antonietti at the Max Planck Institute of Colloids and Interfaces as an Alexander von Humboldt Fellow from 2001 to 2003. Currently he works with Dr. Takayoshi at the National Institute of Materials Science (NIMS) at Tsukuba, Japan, as a Japan Science and Technology Fellow.

potential one-step synthesis of dye-sensitized titania solar cells. IL-based quasi-solid-state electrolytes were just recently employed for such regenerative photoelectrochemical cells and yielded 7% energy efficiency, but nanostructure synthesis still took place by classical means.^[28] In another synthetic application Nakashima et al. reported the preparation of TiO₂ hollow microspheres in ionic liquids by means of a so-called interfacial sol-gel reaction.^[29]

The strong surface binding of ILs onto various nanoparticles was employed by Itoh et al., who showed that hydrophilic and hydrophobic properties of gold nanoparticles can be tuned by exchange of anions in the IL moiety.^[30] Backed by the same set of advantages of ILs as a reaction medium, microwave-assisted synthesis of single-crystalline tellurium nanorods and nanowires have been recently reported.^[31]

Solvent self-structuration and supramolecular effects become important when reactions are conducted with higher concentrations of inorganic reactant. Even standard ILs such as the 1-butyl-3-methylimidazolium tetrafluoroborate give nicely nanostructured gels. The reaction of silica^[32] gave a spongelike, bicontinuous phase with a characteristic length of 5 nm. NMR and Raman spectrometry indicated the IL molecules spontaneously form a double layer by binding to silica. This sounds unusual for such a small molecule but just reflects the very strong tendency of the ILs to form extended hydrogen-bonding networks, in this case an undulating two-dimensional structure. The liquid structure of ILs and their mixtures with other solvents are probably organized in a similar fashion.

The self-organization of ILs can be supported by using amphiphilic species with a longer hydrophobic tail. Again, due to a combination of hydrogen-bonding networks and polarity contrast (amphiphilicity), very well-organized lyotropic phases are obtained for both the pure RTILs as well as their mixtures with water, oils, and reactants. This tolerance of self-organization against loading is again very unusual, and even in water it is found only for some special surfactants that form microemulsions.

Following the reasoning given above, those phases always interact strongly with surfaces and usually align perpendicular (homeotropic) to the substrate surface. This is opposite to water systems where a parallel orientation is preferred, and can be explained by the very strong polarizability of the supramolecular IL structure along the aligned hydrogen-bonding networks. It can be assumed that similar orientation effects also exist in the nonamphiphilic ILs, which might be the reason that they have extraordinary lubrication properties,^[33] beyond that predicted from the molecular structure.

These oriented phases can be employed for material synthesis by using sol-gel synthesis with 1-hexadecyl-3-methylimidazolium chloride (**1**₁₆). Condensation products of these oriented phases give almost perfect textures as shown in Figure 1 for a silica made from a lamellar amphiphilic IL mesophase.^[34] The lamellae or sheets are exactly parallel over wide areas (see the Fourier transform inset), and even at the surface a perfect homeotropic organization prevails (see atomic force micrograph (AFM), Figure 1b). The real structure is presumably more complex and must contain pillars or bridges, as the described structure is stable

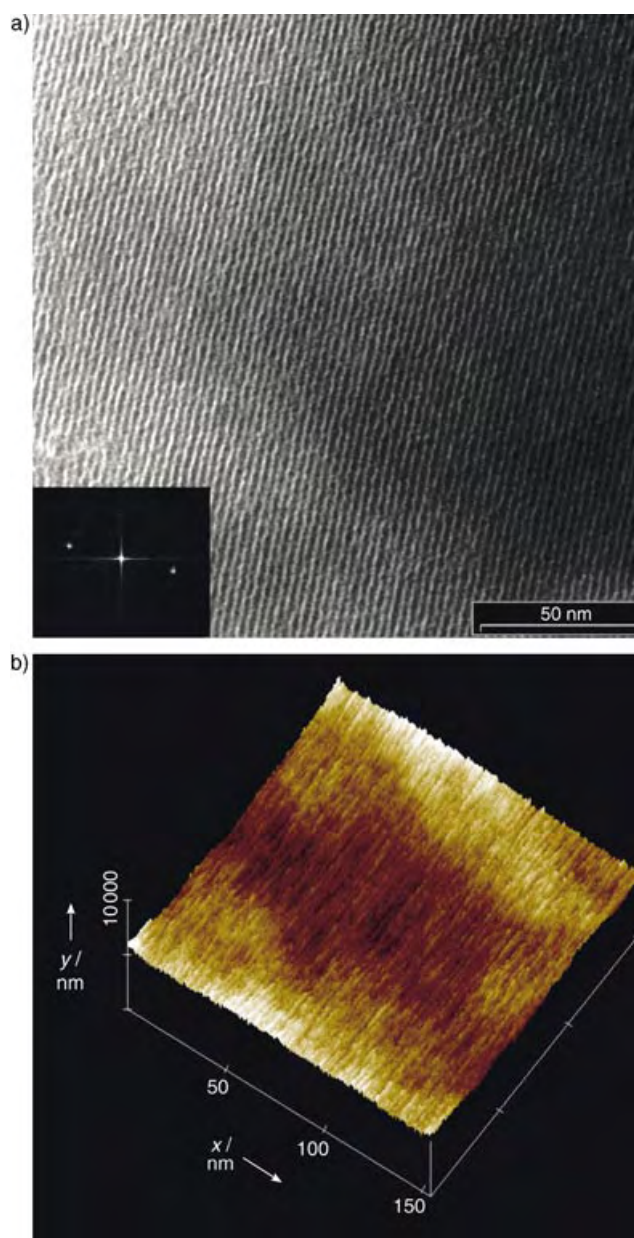


Figure 1. a) TEM image of **1**₁₆-templated porous silica prepared in a sol-gel reaction of 1 g of **1**₁₆ with effective 1 g of silica at a temperature of 40 °C. The scale bar is 50 nm. Inset: Corresponding 2D Fourier transform of the picture. b) Corresponding AFM picture of a surface of the same material.

throughout the removal of the IL and does not collapse. Such silicas have essentially the structural characteristics of clay minerals; however, the chemical composition can be adjusted freely to meet the requirements of the application at hand.

4. The Effect of Water

The role of extra water in ILs is complex and depends on the supramolecular structure of the ionic liquid. It seems to be safe to state that its structure and chemical reactivity is far

from that of bulk water, as it is tightly bound and activated in the H-bonding system of the IL.^[19] As a result reactions with water take place quite rapidly in these systems. On the other hand, water cannot function here as a solvating ligand since it is too involved in IL binding; this was deduced, for instance, from the absence of so-called solvent pores.^[30] This is a quite singular situation for colloid chemistry and material synthesis.

Water modifies the patterns of IL self-organization, and this is why the structural outcome of such reactions depends strongly on the water content. The peculiar self-aggregation behavior of the IL/water system is evident by comparing two sol-gel-derived IL-silica hybrid materials (with 1_{16}), prepared with varying amounts of water (Figure 2), but the same ratio

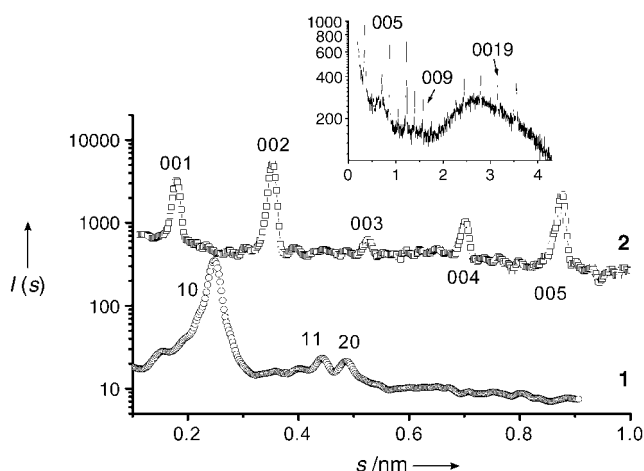


Figure 2. X-ray diffractograms for two mesostructured IL (1_{16})/silica materials prepared from precursors solutions with varying water content ($s=2/\lambda \sin \theta$); the ratio of IL to silica is about 1:1. Sample 1: 2D hexagonal mesostructure obtained with an excess of water. Sample 2: Lamellar mesostructure obtained with only stoichiometric amounts of water and keeping the natural H-bonding network intact. A TEM image of this structure is shown in Figure 1. The inset shows the higher order reflections of this species, which go up to the 23rd order.

of IL to silica. While sample 2 was obtained under water-poor conditions, sample 1 was made with a tenfold excess of water. The X-ray diffraction patterns indicate that this difference in the water content affects the self-organization behavior. Sample 1 represents a 2D hexagonal mesophase, while sample 2 corresponds to a lamellar structure with a long period of $d=5.6$ nm. The latter sample can be indexed up to the 23rd interference order, an exceptional perfection for self-organized mesostructures on the nanometer scale. Note that the sample is liquid, as indicated by the typical halo in the wide angle. This high order is also reflected in the reaction products made from such phases (see Figure 1) or seen in polarized optical microscopy image with textures spanning several millimeters.

These results demonstrate that ILs can also be applied in water-rich media. Here, they “only” play the role of a classical surfactant, however, with a very strong tendency towards self-organization with high order. The combination of polymer latexes and amphiphilic ILs in water-rich media as templates for porous silica indeed led to bimodal structures where both

typical textures coexisted.^[35] The resulting supermicroporous opals were discussed as optical sensor elements where reflection contrast depends critically on the absorption of trace amounts of organic molecules.

5. Conclusions and Outlook

We expect that ILs will find, in addition to organometallic synthesis, catalysis, and electrochemistry, a fourth area of application—the synthesis of nanostructured solids, either to make nanoobjects (e.g. particles and fibers) or for the design of nanopores and nanochannels in solids. The unique combination of adaptability towards other molecules and phases plus the strong H-bond-driven solvent structure makes ionic liquids potential key tools in the preparation of a new generation of chemical nanostructures.

Received: March 23, 2004

Published Online: August 27, 2004

- [1] K. R. Seddon, A. Stark, M. Torres, *Pure Appl. Chem.* **2000**, 72, 2275.
- [2] T. Welton, *Chem. Rev.* **1999**, 99, 2071.
- [3] J. Dupont, R. F. de Souza, P. A. Z. Suarez, *Chem. Rev.* **2002**, 102, 2667–3691.
- [4] R. Sheldon, *Chem. Commun.* **2001**, 23, 2399.
- [5] J. Fuller, R. T. Carkin, R. A. Osteryoung, *J. Electrochem. Soc.* **1997**, 144, 3881–3886.
- [6] Y. L. Zhao, J. M. Zhang, J. Jiang, C. F. Chen, F. Xi, *J. Polym. Sci., Part A* **2002**, 40, 3360–3366.
- [7] P. Kubisa, *Prog. Polym. Sci.* **2004**, 29, 3–12.
- [8] F. van Rantwijk, R. M. Lau, R. A. Sheldon, *Trends Biotechnol.* **2003**, 21, 131–138; S. V. Dzyuba, R. A. Bartsch, *Angew. Chem.* **2003**, 115, 158; *Angew. Chem. Int. Ed.* **2003**, 42, 148.
- [9] S. Sugden, H. Wilkins, *J. Chem. Soc.* **1929**, 1291.
- [10] T. A. Bleasdale, G. J. T. Tiddy, E. Wyn-Jones, *J. Phys. Chem.* **1991**, 95, 5385.
- [11] F. Neve, O. Francescangeli, A. Crispini, *Inorg. Chim. Acta* **2002**, 338, 51.
- [12] C. K. Lee, H. W. Huang, I. J. B. Lin, *Chem. Commun.* **2000**, 1911.
- [13] Y. Haramoto, M. Nanasawa, S. Ujiie, *Liquid Crystals* **2001**, 28, 557–560.
- [14] P. J. Dyson, *Transition Met. Chem.* **2002**, 27, 353.
- [15] *Ionic Liquids in Synthesis* (Eds.: P. Wasserscheid, T. Welton) Wiley-VCH, Weinheim, **2002**; P. Wasserscheid, W. Keim, *Angew. Chem.* **2000**, 112, 3926; *Angew. Chem. Int. Ed.* **2000**, 39, 3772.
- [16] R. R. Deshmukh, R. Rajagopal, K. V. Srinivasan, *Chem. Commun.* **2001**, 1544.
- [17] J. Dupont, G. S. Fonseca, A. P. Umpierre, P. F. P. Fichtner, S. R. Teixeira, *J. Am. Chem. Soc.* **2002**, 124, 4228.
- [18] F. Endres, S. Z. Abedin, *Chem. Commun.* **2002**, 8, 892–893.
- [19] I. Mukhopadhyay, W. Freyland, *Langmuir* **2003**, 19, 1951–1953.
- [20] G. S. Fonseca, A. P. Umpierre, P. F. P. Fichtner, S. R. Teixeira, J. Dupont, *Chem.-Eur. J.* **2003**, 9, 3263–3269.
- [21] As measured with a du Nuoy tensiometer (Krüss); this value seems to depend only weakly on water content.
- [22] A. Elaiwi, S. B. Hitchcock, K. R. Seddon, N. Srinivasan, Y. M. Tan, Y. M. T. Welton, J. A. Zora, *J. Chem. Soc. Dalton Trans.* **1995**, 21, 3467–3472.
- [23] A. Mele, C. D. Tran, S. H. D. Lacerda, *Angew. Chem.* **2003**, 115, 4500–4502; *Angew. Chem. Int. Ed.* **2003**, 42, 4364–4366.

- [24] S. Saha, S. Hayashi, A. Kobayashi, H. Hamaguchi, *Chem. Lett.* **2003**, 32, 740–741.
- [25] Much less pronounced, also formamide and water-free hydrazine are self-structured and allow, for instance, micelle formation.
- [26] S. Dai, Y. H. Ju, H. J. Gao, J. S. Lin, S. J. Pennycock, C. E. Barnes, *Chem. Commun.* **2000**, 3, 243–244.
- [27] Y. Zhou, M. Antonietti, *J. Am. Chem. Soc.* **2003**, 125, 14960–14961.
- [28] P. Wang, S. M. Zakeeruddin, P. Comte, I. Exnar, M. Gratzel, *J. Am. Chem. Soc.* **2003**, 125, 1166.
- [29] T. Nakashima, N. Kimizuka, *J. Am. Chem. Soc.* **2003**, 125, 6386.
- [30] H. Itoh, K. Naka, Y. Chujo, *J. Am. Chem. Soc.* **2004**, 126, 3026.
- [31] Y. J. Zhu, W. W. Wang, R. J. Qi, X. L. Hu, *Angew. Chem.* **2004**, 116, 1434; *Angew. Chem. Int. Ed.* **2004**, 43, 1410.
- [32] Y. Zhou, M. Antonietti, *NanoLett.* **2004**, 4, 477.
- [33] H. Z. Wang, Q. M. Lu, C. F. Ye, W. M. Liu, Z. J. Cui, *Wear* **2004**, 256, 44–48.
- [34] Y. Zhou, M. Antonietti, *Chem. Mater.* **2004**, 16, 544–550.
- [35] Y. Zhou, M. Antonietti, *Chem. Commun.* **2003**, 20, 2564–2565.

Quality counts...

The best of chemistry every week



Wiley-VCH

P.O. Box 10 11 61
69451 Weinheim
Germany

Phone +49 (0) 6201–606-400

Fax +49 (0) 6201–606-184

e-mail: angewandte@wiley-vch.de

www.angewandte.org

Angewandte Chemie International
Edition is a journal of the GDCh,
the German Chemical Society

GDCh

WILEY-VCH

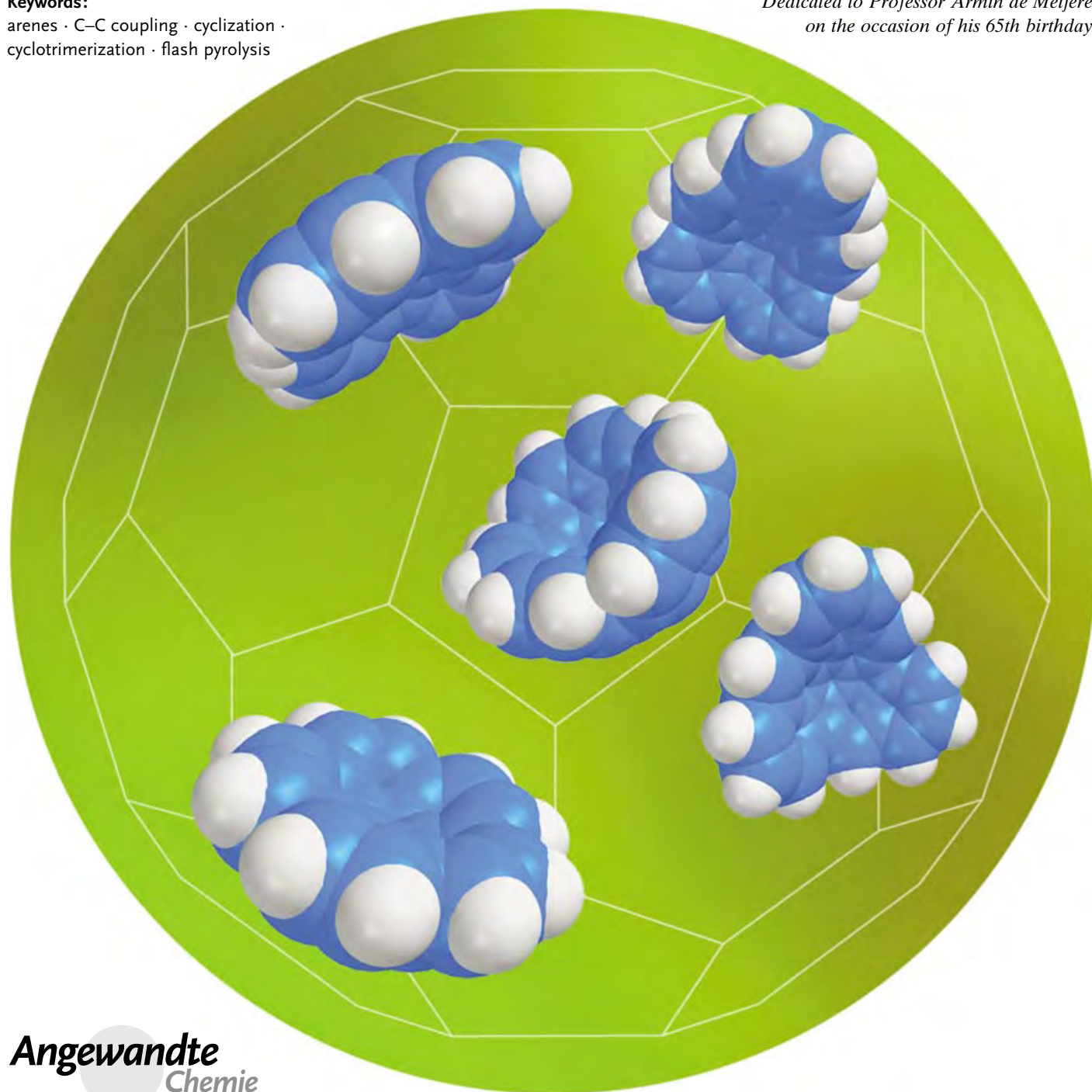
Polycyclic Arenes

Methods for the Chemical Synthesis of Fullerenes

Lawrence T. Scott*

Keywords:

arenes · C–C coupling · cyclization · cyclotrimerization · flash pyrolysis

*Dedicated to Professor Armin de Meijere
on the occasion of his 65th birthday*Angewandte
Chemie

C₆₀ has been synthesized by chemical methods in 12 steps. Lessons learned in the author's laboratory during a decade devoted to the synthesis and study of open geodesic polyarenes strongly influenced the strategy and methodology ultimately employed for preparing a suitable 60-carbon precursor and for closing it up to the fullerene ball. This review provides a personal account of how the new synthetic tools were developed and put to use.

1. Why Synthesize Fullerenes?

Fullerenes have been widely touted for their potential to fulfill dreams in the emerging realm of nanotechnology and across the broad span of materials science.^[1] An intrinsic scientific interest in their unusual curved networks of trigonal carbon atoms has also stimulated considerable research on the fundamental properties of other geodesic π systems.^[2,3] Despite intense scrutiny by scientists and engineers worldwide for more than a decade, however, these fascinating “Buckyballs” are still being made today by poorly understood empirical methods.^[1,4]

The vaporization of graphite by resistive heating under carefully defined conditions, for example, produces a soot from which fullerenes can be isolated by chromatography.^[4,5] Alternatively, the combustion of simple hydrocarbons in fuel-rich flames can produce fullerenes with even greater efficiency.^[6] A plant based on this latter technology was recently opened in Japan and already boasts a capacity to produce 40 metric tons of C₆₀ per year!^[7] A second plant opening in the U.S. advertises that their improved combustion process will further drop the price of C₆₀ to only \$200 per kg.^[6c]

Given such an abundant supply of C₆₀, made in one step from cheap starting materials, one might legitimately wonder: why would we ever need chemical methods to synthesize fullerenes? The answer to this question lies with the other fullerenes.

C₆₀ certainly exhibits some remarkable properties and novel chemical behavior,^[1,4] but surely it cannot be the “best” fullerene for every conceivable application. Most of the higher fullerenes have lower lying LUMOs than that of C₆₀, for instance, and most have higher lying HOMOs.^[8] Those differences translate to smaller HOMO–LUMO gaps than that of C₆₀ for most of the higher fullerenes, and some have HOMO–LUMO gaps close to zero.

Furthermore, all are less strained than C₆₀ and are thereby more stable thermodynamically. Will one of these higher fullerenes be the key to room-temperature superconducting materials or to some other great discovery?^[1,9] To find out, scientists need pure fullerenes with which to run experiments.

How many different fullerenes are there? For C₆₀, only one isomer is stable (i.e., obeys the “isolated pentagon rule”). The same is true for C₇₀, but two stable isomers are possible for C₇₆, and larger fullerenes are calculated to have even more stable isomers: 5 for C₇₈, 24 for C₈₄, 450 for C₁₀₀, and so on.^[8] More than 1000 different fullerenes that obey the isolated

From the Contents

1. Why Synthesize Fullerenes?	4995
2. Retrosynthetic Analysis of C ₆₀	4995
3. Bending Flat Molecules with Heat	4997
4. Intramolecular C(aryl)–C(aryl) Coupling Reactions	4999
5. Cyclodehydrogenations—What Makes Some Work?	5000
6. Hydrogen Atom 1,2-Shifts Can Circumvent Challenging Obstacles	5002
7. Applying these Methods to a Synthesis of C ₆₀	5003
8. Future Prospects	5005

pentagon rule can be assembled from 100 carbon atoms or fewer,^[8] and that number climbs into the millions rapidly as progressively larger fullerenes are considered. There is no limit, and each fullerene will have its own unique properties.

From fullerene soot, C₆₀ and C₇₀ are plentiful, and another dozen or so of the higher fullerenes can be isolated in small amounts.^[4,10] This small handful of molecules accounts for more than 99% of the fullerene material formed, yet it provides access to no more than 1–2% of the potentially valuable fullerenes in the range from C₆₀ to C₁₀₀.

How will scientists ever get their hands on the rest of these fullerenes to study their properties? Chemical synthesis is the logical long-range solution. This review describes work in our laboratory that has led to the first chemical synthesis of C₆₀ in isolable quantities.^[11] A milestone has been passed, but only the first stride has been taken in what likely will be a long journey.

2. Retrosynthetic Analysis of C₆₀

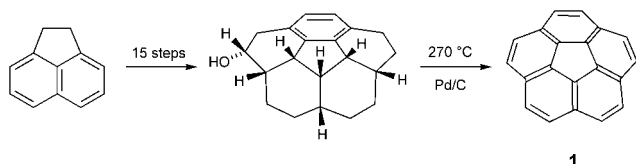
We chose C₆₀ as our first fullerene synthesis target for several reasons. Most importantly, it was anticipated that a successful synthesis would produce only small quantities of the target material, at least initially, and it was clear that success would be easiest to verify for a product whose properties were already well known. This “comparison with an authentic sample” has been the obligatory finale to syntheses of natural products throughout the history of organic chemistry, and the chemical synthesis of a fullerene

[*] Prof. Dr. L. T. Scott
Department of Chemistry
Merkert Chemistry Center
Boston College, Chestnut Hill, MA 02167-3860 (USA)
Fax: (+1) 617-552-6454
E-mail: lawrence.scott@bc.edu

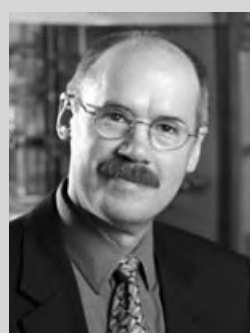
should meet the same rigorous standards. Additionally, since the strain energy of C_{60} exceeds that of all other stable fullerenes, any methods that work to synthesize C_{60} should be universally applicable to syntheses of higher fullerenes as well.

Before dissecting C_{60} , it is worth gauging the magnitude of the problem. Not counting π bonds, C_{60} has 90 C–C bonds, and that is more than one normally encounters in all but the largest natural products (cf. Taxol, for example, which has 47 C–C bonds). The strain energy of C_{60} is also enormous; heats of combustion measurements put the value somewhere in excess of $600 \text{ kcal mol}^{-1}$,^[12] and any synthesis must build in that strain. Finally, with only one exception other than fullerenes,^[13] polycyclic networks of trigonal carbon atoms pyramidalized all in the same direction were unknown when we began our work, so no general methods existed for their construction. The next few paragraphs weigh the pros and cons of four distinctly different approaches to solving this problem.^[14]

One strategy for synthesizing C_{60} and higher fullerenes that should work is to construct the complete carbon cage first with saturated atoms (sp^3 CH units) at a large number of the vertices and then dehydrogenate the ball in the last step. The Birch reduction product of C_{60} ($C_{60}H_{36}$) is known to revert easily to C_{60} ,^[15] so the last step would surely succeed, and a liberal sprinkling of tetrahedral carbon atoms throughout the polycyclic network (maybe 30–60%, but not 100%)^[16] would greatly reduce the strain energy of the penultimate synthetic intermediate. In fact, this strategy is precisely the one employed by Barth and Lawton in their classic synthesis of the first geodesic polyarene, corannulene (**1**, Scheme 1),^[13] a landmark achievement that predated the discovery of C_{60} by two decades. Quite recently, the same strategy has been



Scheme 1. The 1966 Barth and Lawton synthesis of the first geodesic polyarene.^[13]

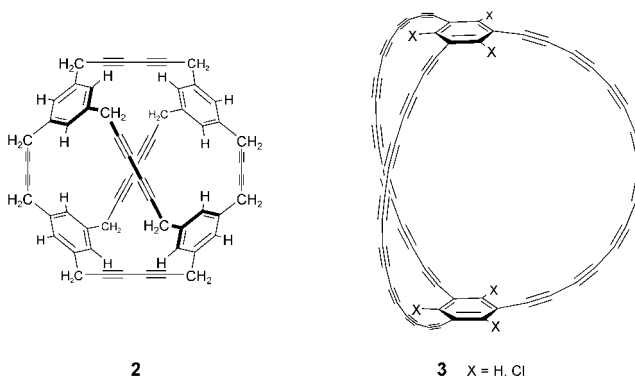


Lawrence T. Scott was born in 1944 and grew up in Urbana, Illinois. His lifelong passion for highly unsaturated polycyclic hydrocarbons arose from his undergraduate thesis project on bullvalene and related $(CH)_{10}$ compounds in the laboratory of Professor M. Jones Jr. at Princeton University (A.B. degree 1966) and intensified during his graduate research on larger hydrocarbons of theoretical interest under the direction of Professor R. B. Woodward at Harvard University. After completing his Ph.D. degree in 1970, he joined the chemistry faculty at UCLA as an

Assistant Professor. In 1975, he moved to the University of Nevada-Reno, and in 1993 he moved to his present position as professor of chemistry at Boston College.

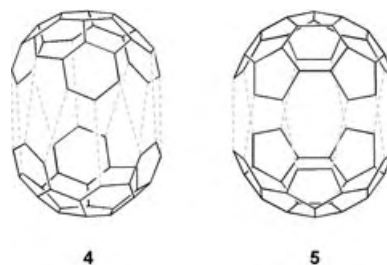
successfully applied also to the first synthesis of sumanene,^[17] another bowl-shaped polycyclic hydrocarbon whose ring system maps onto that of C_{60} .

Building a 60-carbon cage with 32 rings will be no trivial task, of course, even with the strain problem reduced, and we are unaware of anyone who has taken on the challenge. An alternative strategy is to assemble a highly-unsaturated 60-carbon cage with fewer than 32 rings and then collapse it to C_{60} through a series of transannular bond-forming reactions and dehydrogenations. Ten years ago, we tried to synthesize the strain free $C_{60}H_{36}$ cage **2**,^[18] but we ultimately abandoned that approach in favor of another.



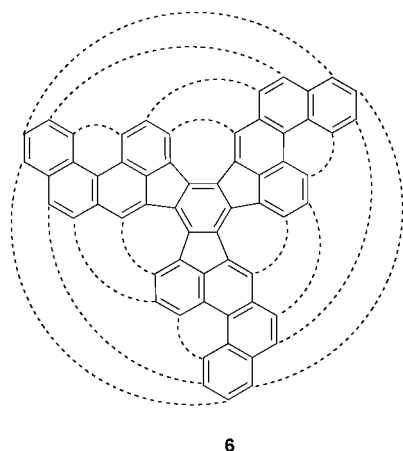
More recently, Rubin et al.^[19] and Tobe et al.^[20] have independently generated the highly strained cyclophane **3** by laser desorption of cleverly designed synthetic precursors, which do actually collapse to C_{60} under high energy conditions in the gas phase. Unfortunately, the final step has been achieved only in a mass spectrometer, and all attempts to isolate synthetic C_{60} generated from the same precursors have been unsuccessful.

One particularly seductive strategy for assembling an all-carbon ball is to join two identical hemispherical hydrocarbons (e.g., **4** or **5**, depicted schematically) and then stitch their rims together.^[21] We have actually synthesized hydrocarbon **4** on a preparatively useful scale^[22] (see Section 6), but methods for fusing two such molecules together do not currently exist.



To us, the most appealing strategy was the one derived from a retrosynthetic analysis that splits open the ball, peels back the sides, and leads to the relatively strain-free, threefold symmetric, polycyclic aromatic hydrocarbon **6**.^[23] This poten-

tial synthetic intermediate contains all 60 carbon atoms of the final target, 75 of the 90 C–C bonds, and 13 of the 20 benzene rings. Furthermore, the ring system of hydrocarbon **6** looks like one that should be accessible in reasonable quantities by classical synthetic methods.



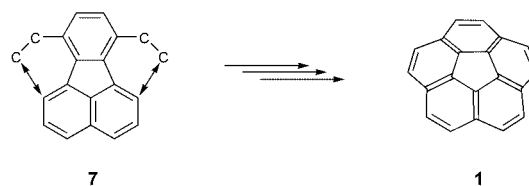
The looming question with this strategy, of course, is how to stitch up the seams between the arms to make the ball. Fifteen more C(aryl)–C(aryl) bonds still need to be established, and some provision must be made to bend the arms and build in the strain energy of the final target. We recognized early on that the solution to this aspect of the problem would require some fundamentally new synthetic methods. The “awesome power” of modern organic synthesis^[24] has made the laboratory preparation of complex natural products commonplace, but new tools are often required for the synthesis of new molecular targets that display unprecedented structural features. The following sections describe how we developed the methodology necessary to complete our synthesis of C₆₀^[11] from a simple derivative of **6**.

3. Bending Flat Molecules with Heat

To test new ideas on how planar polyarenes might be transformed into more highly strained curved π surfaces, we selected corannulene (**1**) as our initial practice target for several reasons. First of all, corannulene (C₂₀H₁₀) represents the smallest subunit of C₆₀ that retains a curved π surface. Second, corannulene was already known to be a stable compound,^[13] and a foreknowledge of its spectroscopic, chemical, and physical properties was anticipated to expedite product identification. Finally, the only previous synthesis of corannulene was so lengthy (Scheme 1)^[13] that for 25 years nobody had ever repeated it on a scale sufficient to explore the chemistry of this unique hydrocarbon. Thus, a new synthesis of corannulene would serve not only to test new synthetic methodology but also to make corannulene available for systematic chemical investigations.

A planar fluoranthene with two-carbon substituents attached at positions 7 and 10 (schematically represented by

structure **7**) contains all 20 carbon atoms and four of the six rings that make up corannulene and looks like an attractive synthetic precursor to corannulene (Scheme 2). Unfortunately, owing to the splayed out nature of the fluoranthene



Scheme 2. Strategy to build the bowl-shaped corannulene (**1**) from the planar 7,10-disubstituted fluoranthene **7**.

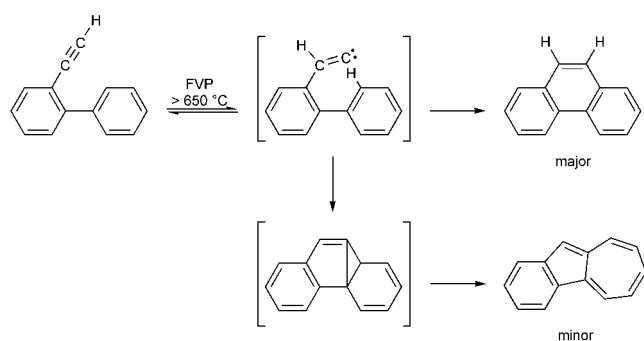
bay regions, the distances between the atoms that must be joined are too great to permit bond formation under ordinary laboratory conditions. Indeed, an early attempt to synthesize corannulene by exactly this strategy was thwarted by the failure of intramolecular Friedel–Crafts acylations to form the new six-membered rings.^[25]

Our plan was to bring together the carbon atoms that must be joined by taking advantage of the normal out-of-plane bending of the fluoranthene nucleus. Even at room temperature, fluoranthene experiences molecular vibrations that periodically distort it out-of-plane, like a closing book, with all five carbon atoms of the central ring temporarily pyramidalized in the same direction. We reasoned that the amplitude of these vibrations (and, consequently, the degree of pyramidalization) could be increased at high temperatures to a point at which bond formation would become feasible, and once the two new bonds were formed, the rim of the molecule would be too small to let the molecule relax back to a planar geometry—it would be trapped as a bowl. This was the thinking that prompted our first experiments.

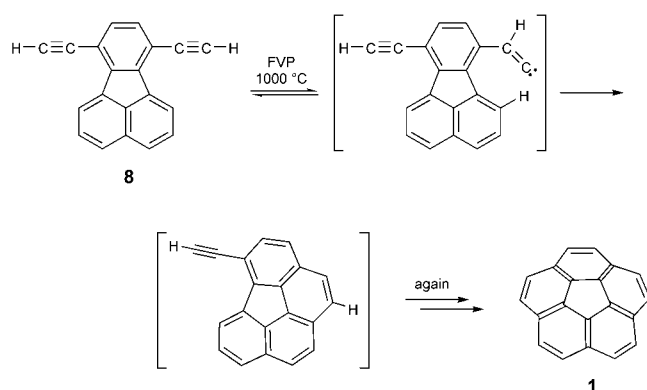
Flash vacuum pyrolysis (FVP) represents an exceptionally effective technique for introducing large amounts of thermal energy into organic molecules,^[26] and we were confident that the fluoranthene ring system would bend enough to permit the desired ring closures at temperatures of 1000 °C or more in the gas phase. Bond formation, however, requires not only that the requisite atoms approach each other but also that one atom be sufficiently reactive to “attack” the other and create the new bond. To fulfill this requirement, we exploited the “Roger Brown rearrangement” (Scheme 3),^[27] a novel method for generating carbenes reversibly at high temperatures that was already well known to those of us who used FVP on a daily basis.

Incorporating this chemistry into our generalized strategy (Scheme 2), we prepared 7,10-diethynylfluoranthene (**8**) in a few simple steps from commercially available starting materials and sublimed it under vacuum through a hot quartz tube (Scheme 4). Much to our delight, the crude product consisted of essentially pure corannulene!^[28]

The success of this reaction provided the very first validation of our hypothesis that heat can be used to bend totally flat molecules temporarily into highly distorted conformations, which can then be trapped to make bowl-shaped polyarenes by joining together formerly remote parts of the



Scheme 3. The Roger Brown rearrangement: an endothermic 1,2-shift of a hydrogen atom in a terminal alkyne at high temperatures.^[27a]



Scheme 4. The second synthesis of corannulene (**1**).^[28]

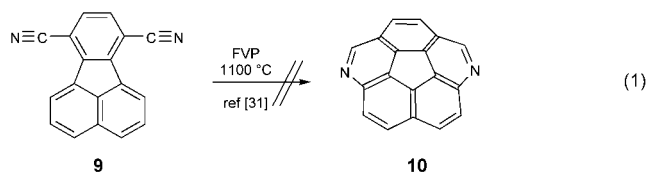
molecule. This principle became the cornerstone for our later synthesis of C_{60} and for syntheses of at least two dozen other geodesic polyarenes along the way. Presumably, the same principle operates also in the formation of fullerenes in fuel-rich flames and from graphite vaporization, both of which involve numerous intramolecular C–C bond-forming reactions within species that are born at high temperatures in the gas phase.

The failure of various transition-metal catalysts to effect the cyclization of **8** to **1** in solution^[29] underscores the importance of providing sufficient heat to bend the molecule out-of-plane.

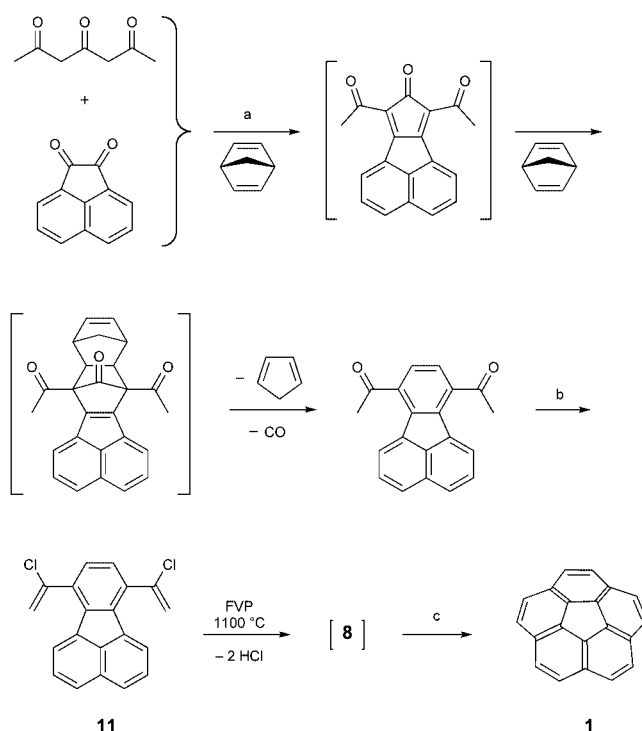
It is also important to stress one trivial point that could easily be overlooked. Isomerizations reactions, such as that of diyne **8** to corannulene (**1**), will give the desired product only if the overall reaction is exothermic. In the case at hand, the formation of two new σ bonds and two new benzene rings at the expense of two acetylenic π bonds provides more than enough thermodynamic driving force to favor the formation of corannulene, despite the rather large strain energy in the product.^[30a]

FVP of 7,10-dicyanofluoranthene (**9**) provides a good counter example. We prepared this dinitrile and subjected it to FVP at temperatures up to 1100 °C but could never detect even a trace of cyclization products [Eq. (1)].^[31] For this isomerization, molecular orbital calculations predict a lower heat of formation for the open dinitrile (**9**) than for the desired diazacorannulene (**10**).^[30b] Such thermodynamic con-

siderations have undoubtedly contributed to the fact that azacorannulenes remain completely unknown, although they ought to be stable if formed at ordinary temperatures.

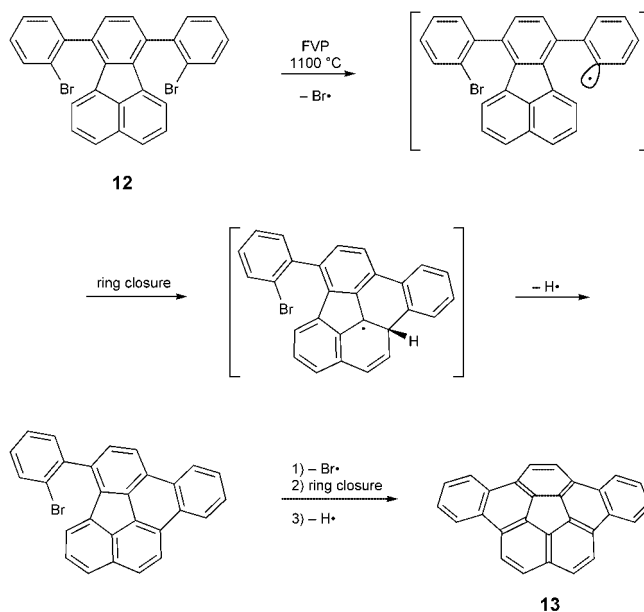
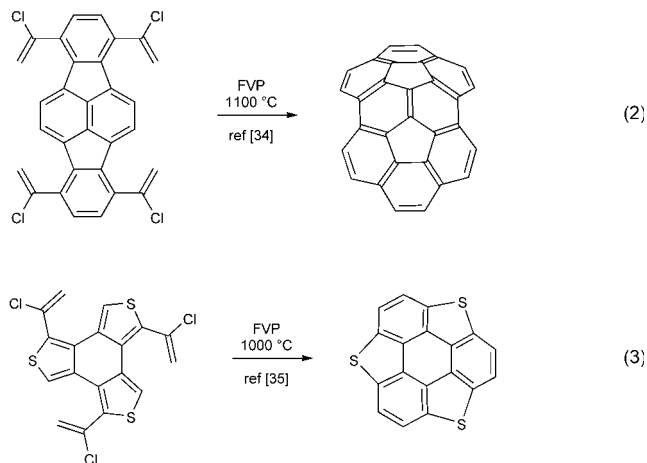


One shortcoming of the corannulene synthesis shown in Scheme 4 stems from the low volatility of the 20-carbon precursor (**8**). Even with a good vacuum, diyne **8** must be heated to cause it to sublime, and the heat promotes considerable polymerization of the starting material, thus lowering the yield of the reaction.^[28] We overcame this technical problem by devising a robust two-carbon side chain that shut down the polymerization, allowed clean sublimation, and then blossomed into an ethynyl group when it entered the high temperature zone of the FVP apparatus. As a “masked acetylene” side chain, the 1-chlorovinyl group performs magnificently,^[32] and this modification quickly resulted in a convenient three-step synthesis of corannulene (Scheme 5).^[32,33] A twisting of the 1-chlorovinyl groups out of conjugation with the aromatic ring in the crowded bay regions of 7,10-bis(1-chlorovinyl)fluoranthene (**11**) undoubtedly contributes to the resistance of this FVP precursor to polymerization.



Scheme 5. A convenient three-step synthesis of corannulene (**1**): a) glycine as catalyst, refluxing toluene, 72 h; b) PCl_5 , CH_2Cl_2 , 25 °C, 24 h; c) FVP, 1000 °C (see Scheme 4). The flash vacuum pyrolysis (FVP) step can be run routinely on a 1.0 g scale to produce 250–300 mg of **1**.^[33]

This strategy for synthesizing geodesic polyarenes by FVP, using 1-chlorovinyl groups as “masked acetylenes,” was adopted by Rabideau et al. for the first synthesis of a $C_{30}H_{12}$ semifullerene^[34] and by Aso et al. for the first synthesis of a geodesic polyarene that incorporates heterocyclic aromatic rings^[35] [Eq. (2) and (3)]. Many additional applications have also been reported.^[36]



Scheme 6. Building a geodesic polyarene by intramolecular trapping of aryl radicals.^[38]

As an historical point, it is worth noting that the recent quest for novel aromatic compounds has driven a dramatic expansion in the role of the FVP method, which had served since the 1800s primarily as a tool for mechanistic studies and as a means for transforming complex structures into simpler molecules through *destructive* reactions (e.g., retro-Diels–Alder reactions, acetate pyrolyses to produce olefins, etc.).^[26] Today, the FVP method also enjoys widespread use as a powerful *constructive* tool for synthesizing complex molecules from simpler structures.^[37]

4. Intramolecular C(aryl)–C(aryl) Coupling Reactions

Stitching up a C_{60} precursor such as **6** to create a fullerene ball requires the formation of many new C(aryl)–C(aryl) bonds. As we began thinking more about this aspect of the problem, our attention gradually shifted away from thermally generated carbenes toward possible uses of carbon centered radicals, the other major family of reactive intermediates at carbon that carry no charge and, hence, are suitable for gas phase reactions. Scheme 6 shows the first application of radical cyclizations to construct a geodesic polyarene.^[38] This transformation represents a free radical implementation of the same original strategy outlined in Scheme 2.

Bromine substituents serve as excellent precursors to radicals at the carbon atoms where new bonds are desired under FVP conditions, because aromatic C–Br bonds are weaker than all the C–C and C–H bonds in the molecule by at least 25–30 kcal mol^{−1}.^[39] The same starting material bearing chlorine atoms instead of bromine atoms also gives dibenzo[*a,g*]corannulene (**13**), although the yield drops from 38% to only 17%.^[31] In contrast to these results, FVP of the parent

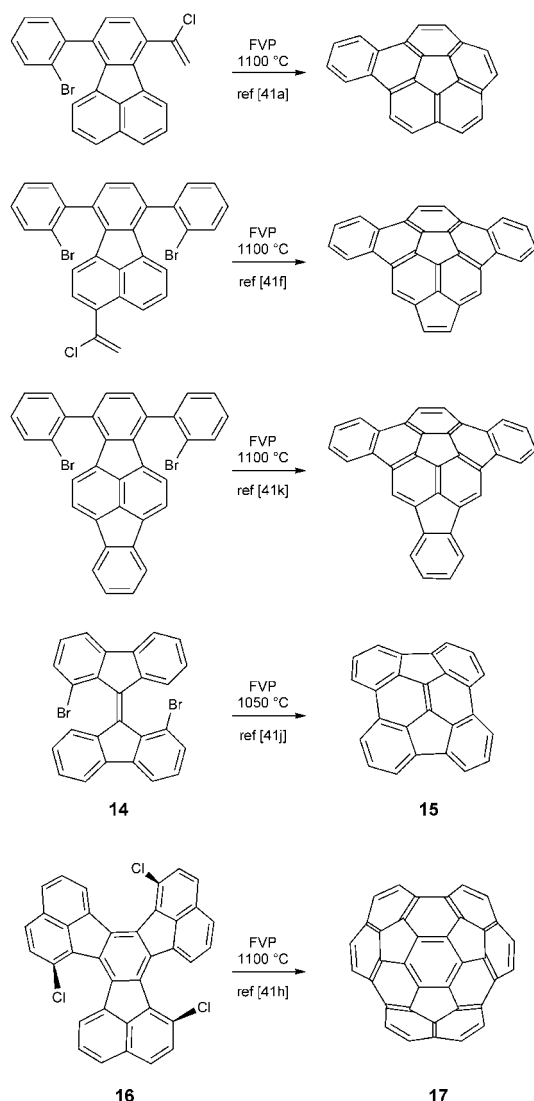
hydrocarbon (7,10-diphenylfluoranthene), which lacks halogen atoms completely, gives no dibenzo[*a,g*]corannulene (**13**) at all at 1100 °C.^[31] This control experiment provides dramatic testimony to the necessity for incorporating functionality that will generate a reactive center to trap the temporarily distorted molecule.

Radical generation alone, however, is not sufficient to promote the desired cyclization reactions. The radical, once formed, must be able to reach the π system of the ring across the wide bay of the fluoranthene nucleus. In this connection, we found that abstraction of the bromine atoms in **12** by tributyltin radicals in solution fails to produce dibenzo[*a,g*]corannulene (**13**), even at 150 °C in *tert*-butylbenzene.^[31] At 250 °C in *para*-di-*tert*-butylbenzene, abstraction of the bromine atoms in **12** by tributyltin radicals leads to one ring closure, but still no trace of dibenzo[*a,g*]corannulene (**13**) could be found.^[31] Under FVP conditions at 1100 °C, the much greater thermal energy available undoubtedly increases the rate of aryl radical attack on the π system across the bay region; however, the low pressures in the gas phase must surely play a significant role as well, by diminishing greatly the frequency of bimolecular encounters between the transient radical and potential hydrogen atom donors.

Irradiation with ultraviolet light has the potential to inject huge amounts of energy into an organic molecule, so it was only natural that we should explore the possibility of synthesizing dibenzo[*a,g*]corannulene (**13**) photochemically. From UV absorption spectroscopy, it is clear that the FVP precursor (**12**) and the parent hydrocarbon without the bromine substituents can both absorb high energy UV photons.^[31,40] In solution, however, the excess internal energy of the excited state species rapidly dissipates through internal rotations of the aryl groups and intermolecular collisions with the solvent. We were never able to promote

even the first cyclization reaction photochemically in solution.^[31,40]

Many examples of intramolecular C(aryl)–C(aryl) couplings to produce geodesic polyarenes by the high-temperature FVP of halogen-substituted aromatic hydrocarbons have now been recorded (Scheme 7).^[41] Unlike the carbene



Scheme 7. Representative examples of other geodesic polyarenes that have been successfully synthesized by intramolecular C(aryl)–C(aryl) coupling reactions (FVP yields typically 20–40%). Radical cyclizations of the sort depicted in Scheme 6 are presumed to operate in every case.

cyclizations in Section 3, these radical cyclizations are not isomerizations; bromine atoms and hydrogen atoms are permanently lost. The reactions are therefore effectively irreversible and not subject to the same thermodynamic constraints that limit the use of genuine isomerizations. At temperatures in the range of 1000–1100 °C, the entropic benefits of losing small fragments (halogens and hydrogens) from a molecule are enormous.

5. Cyclodehydrogenations—What Makes Some Work?

In our experience, intramolecular C(aryl)–C(aryl) coupling reactions under FVP conditions always work best when an aryl radical is deliberately generated at one of the two carbon atoms to be joined. Purely thermal “cyclodehydrogenations” (i.e., the joining of two unfunctionalized aromatic CH positions on proximal rings, with the expulsion of two hydrogen atoms) rarely work well. Exceptions are known, however, that may have valuable lessons to teach us.

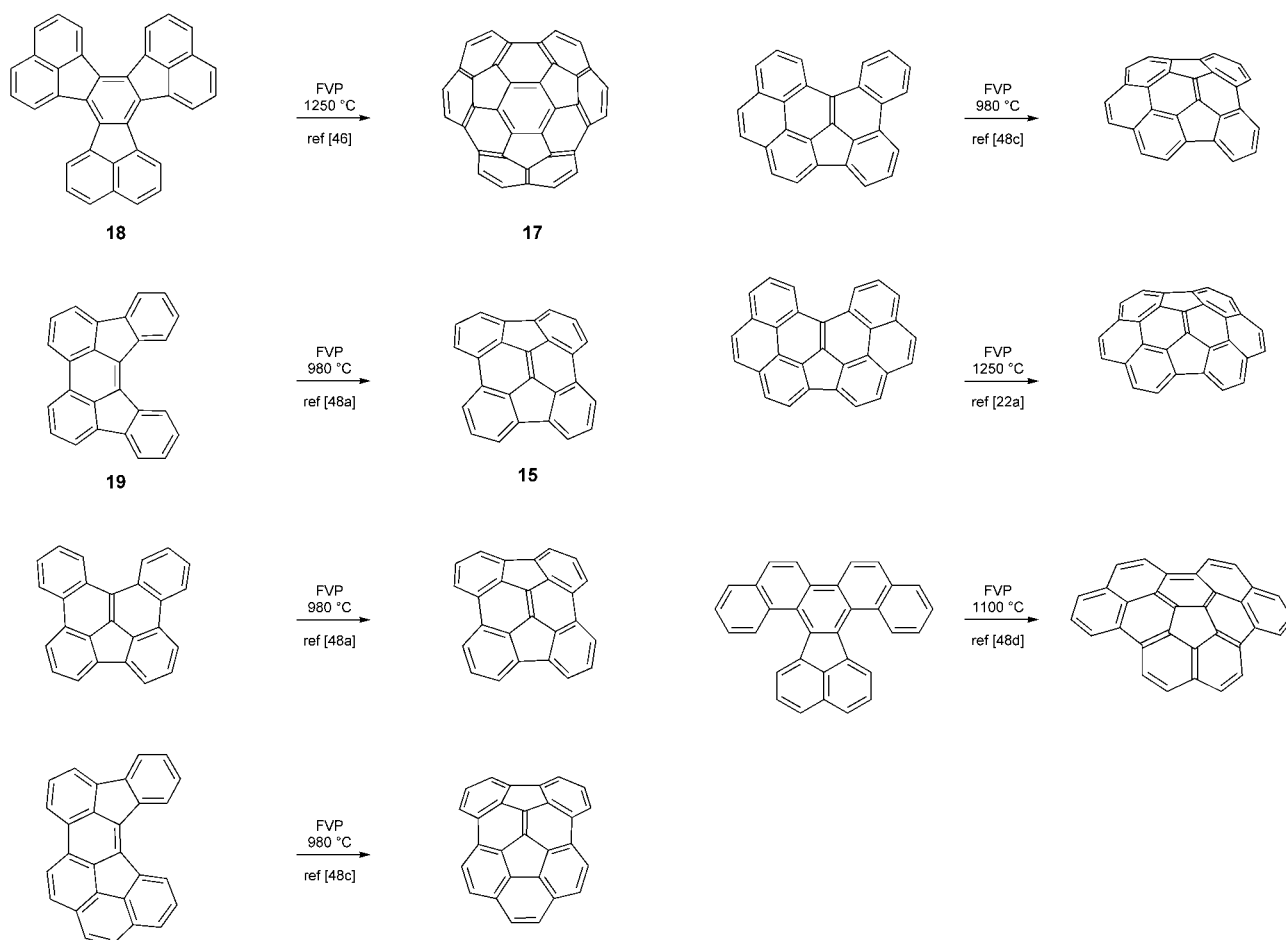
We were lured into testing the potential utility of thermal cyclodehydrogenations for synthetic purposes by the enticing resemblance of decacyclene (**18**, Scheme 8), a nearly planar polycyclic aromatic hydrocarbon,^[42] to circumtrindene (**17**), a geodesic dome that represents $\frac{3}{5}$ of C_{60} . Decacyclene (**18**) has been known since 1883^[43] and is commercially available,^[44] whereas **17** was still unknown in the early 1990s, and the prospect of making this spectacular hydrocarbon bowl in one step by cyclodehydrogenation of **18** was simply too tempting to pass up. We bought some **18**, but our first experiments failed completely.^[31] Eventually, we acquired a new FVP oven that allowed us to work at temperatures above 1100 °C,^[45] and, after many further experiments, we finally found that decacyclene (**18**) can indeed be stitched up to produce **17** under FVP conditions at 1200–1300 °C!^[46] Not surprisingly, the yield of **17** by this brute force method was abysmal (0.2 %^[46]); however, it was good enough to provide 10 mg samples of **17** from FVP of **18** in single runs of 5.0 g each.

Further tweaking of this reaction over the last eight years has raised the yield of circumtrindene (**17**) from FVP of decacyclene (**18**) to 0.6 %,^[47] but we no longer hold out hope of raising it any higher. Obviously, thermal cyclodehydrogenation of the unfunctionalized hydrocarbon is a hideously inefficient process in this case. By contrast, the incorporation of radical precursors in each fjord region of decacyclene (**16**, Scheme 7) allows the FVP to be run at lower temperature and improves the yield of circumtrindene by more than 50-fold!^[41h]

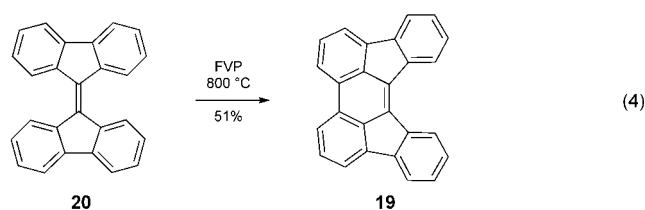
Scheme 8 shows several other thermal cyclodehydrogenations of unfunctionalized planar or nearly planar hydrocarbons that have been used to produce geodesic polyarenes. Without exception, the yields are terrible (always $\leq 3\%$),^[48] and such reactions more often fail completely. Little is known about the mechanistic details of these thermal cyclodehydrogenations,^[49] but they may be related to the primitive synthesis of biphenyl from thermal dimerization of benzene.^[50] Good mechanistic studies are sorely needed.

As alternatives to purely thermal cyclodehydrogenations for stitching up unfunctionalized aromatic hydrocarbons, catalytic methods in the gas phase and oxidative methods in solution have both proven effective for the synthesis of planar polyarenes.^[48,51] Unfortunately, no such methods have ever been successfully extended to the solution phase synthesis of geodesic polyarenes from unfunctionalized aromatic hydrocarbons.^[52]

In sharp contrast to the examples in Scheme 8, the thermal cyclodehydrogenation of bifluorenylidene (**20**) to **19** proceeds relatively efficiently [Eq. (4)].^[48a]



Scheme 8. Low-yield (0.6–3.0%) thermal cyclodehydrogenations of unfunctionalized planar or nearly planar polycyclic aromatic hydrocarbons to make geodesic polyarenes; most others fail completely.



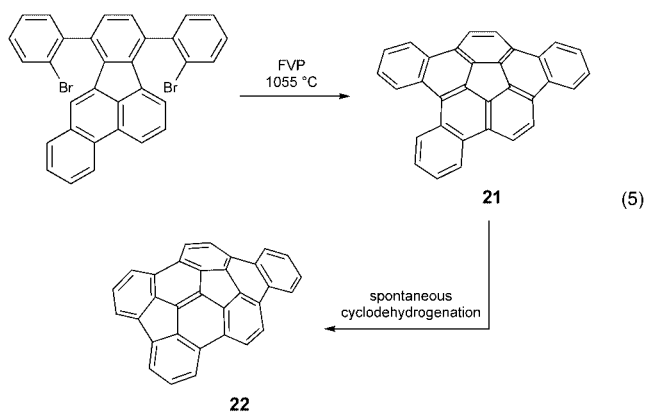
What makes this cyclization work so much better than the others? A close look at this case reveals that the starting material actually holds more strain than the product. Closing up the new ring to make **19** completely relieves the severe twisting at the central C–C double bond in bifluorenylidene (**20**). DFT calculations indicate that this C(aryl)–C(aryl) coupling is energetically more favorable by 19.0 kcal mol^{−1} than one in which unstrained starting materials give unstrained products.^[53] A second ring closure, to convert hydrocarbon **19** into the C₂₆H₁₂ geodesic polyarene **15**, on the other hand, is calculated to introduce an increase in strain energy of 36.1 kcal mol^{−1},^[53] and this thermal cyclodehydrogenation occurs in only 0.6% yield (Scheme 8).^[48a] The lesson here is that thermal cyclodehydrogenation may be useful as a synthetic method when the C(aryl)–C(aryl) coupling leads to

a decrease in strain energy but not when it leads to an increase in strain energy.

To synthesize the alkene-centered geodesic polyarene **15** from unfunctionalized bifluorenylidene (**20**) requires two successive FVP reactions, which give the product in an overall yield of only 0.3% (51% and 0.6% for the two steps, respectively).^[48a] As with the decacylene pyrolysis,^[46] however, the strategic incorporation of halogen atoms (see **14**) facilitates the C(aryl)–C(aryl) couplings and improves the overall yield by roughly two orders of magnitude.^[41]

Our first hint that cyclodehydrogenations might work better for the synthesis of a fullerene than they do for transforming flat molecules into geodesic polyarenes (Scheme 8) came from the discovery of an unexpected byproduct (**22**) in our synthesis of tribenzo[*a,d,j*]corannulene^[41c] [**21**, Eq. (5)].

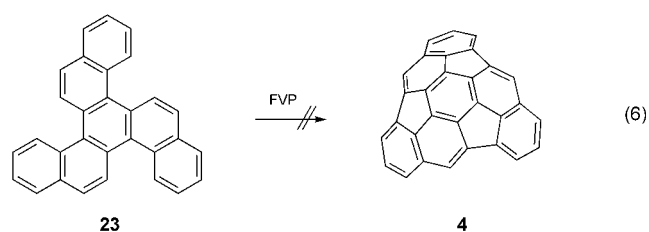
Clearly, the first two ring closures proceeded according to plan, producing **21** by the same sequence of steps that earlier had given us dibenzo[*a,g*]corannulene (Scheme 6). More importantly, however, once curvature had been imposed on the ring system through these initial cyclizations, some fraction of the molecules suffered an additional, unanticipated, cyclodehydrogenation, producing **22** and further curvature. Although the overall yield of **22** isolated from



this FVP was no more than 4–5 %, it gave hope that a cascade of cyclodehydrogenations might serve to stitch up the C_{60} ball from a molecular precursor such as **6**, provided that curvature were first introduced and locked in by aryl radical cyclizations of the sort that give circumtrindene (**17**, Scheme 7).^[41h] The amazingly high yield of C_{60} that has been achieved in hydrocarbon flames^[6] confirms the view that cyclodehydrogenations can proceed efficiently under the right conditions.

6. Hydrogen Atom 1,2-Shifts Can Circumvent Challenging Obstacles

Not long after we introduced the use of FVP as a method to distort flat molecules and turn them into geodesic polyarenes (Scheme 4), Faust and Vollhardt reported their attempt to synthesize the tantalizing $C_{30}H_{12}$ hemifullerene **4** (see Section 2) by FVP of hydrocarbon **23**.^[54] In light of what now is known about thermal cyclodehydrogenations, however (Section 5), one should not be surprised that this 3-fold cyclodehydrogenation failed, even when catalysts^[54] were used [Eq. (6)].

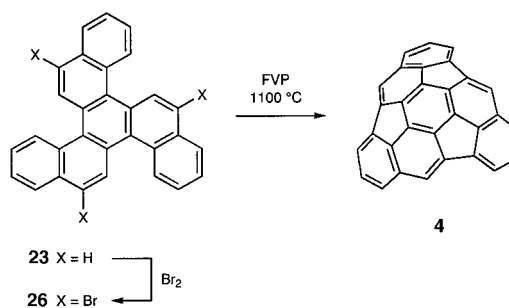
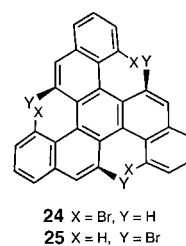


A straightforward solution to this problem, in principle, would be to incorporate a halogen atom or some other radical precursor at the mouth of each cove region in **23**. The challenge of synthesizing such a strained precursor for the FVP reaction (**24** or **25**), however, presented a major obstacle to the execution of this idea.

As predicted, direct bromination of **23** gives the less hindered isomer **26**. Optimization of the conditions even brings the yield up to nearly quantitative, but the product is **26** and not **24** or **25**.^[22a] We were enticed to explore this chemistry

by the prospect that FVP even of isomer **26** might yield **4**, and indeed it does (Scheme 9)!^[22a,55]

How do bromine atoms at the “wrong” positions promote these cyclizations? We speculated^[22a] that the only intra-molecular reaction available to the aryl radical generated by



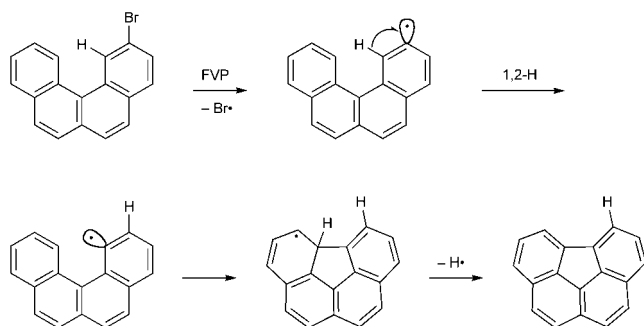
Scheme 9. A practical synthesis of the $C_{30}H_{12}$ hemifullerene **4** that involves three 1,2-shifts of hydrogen atoms.^[22,55]

homolytic loss of a bromine atom from **26** would be the 1,2-shift of a hydrogen atom out of the crowded cove region over to the radical center. This migration would create a new radical center at the mouth of the cove region, just as if we had started with isomer **25**, and cyclization of the new radical followed by rearomatization would close up the desired five-membered ring. Repeating the same sequence of steps on the other two arms would lead to **4**.

At the time when these experiments were run, nothing was known about 1,2-shifts of hydrogen atoms in aryl radicals, so we were gambling on the basis of our instincts. Subsequently, we devised and studied a simpler system that provided the first solid documentation of hydrogen atom 1,2-shifts in aryl radicals (Scheme 10); deuterium labeling was used to prove that the migrating hydrogen is not lost.^[56]

Our DFT calculations indicate that 1,2-shift of a hydrogen atom in phenyl radical has a barrier in the neighborhood of 60 kcal mol^{-1} ,^[56a] which is high enough to protect typical aryl radicals from such rearrangements in solution under ordinary laboratory conditions. Temperatures high enough to cleave C–Br bonds ($\text{BDE} = 82.7 \pm 1.1 \text{ kcal mol}^{-1}$)^[39] under FVP conditions, however, supply more than enough energy for the hydrogen atoms to scramble.

As the example in Scheme 9 nicely illustrates, the mobility of hydrogen atoms in aryl radicals under FVP conditions provides opportunities to replace challenging synthetic intermediates (e.g., **24** and **25**) with others that are far easier to prepare (e.g., **26**). Other investigators have begun putting this

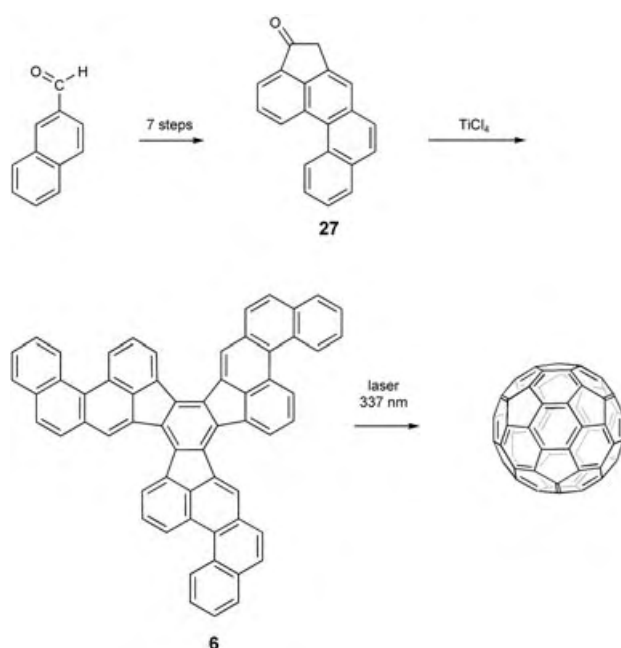


Scheme 10. The first well-documented 1,2-shift of a hydrogen atom in an aryl radical. Deuterium labeling confirms the non-dissociative, intramolecular pathway.^[56a]

trick to good use,^[41e,g] and it was the final tool we needed to complete our synthesis of C_{60} .

7. Applying these Methods to a Synthesis of C_{60}

Building up the 60-carbon ring system of **6** proved to be quite straightforward.^[57] The final acid-catalyzed aldol trimerization of ketone **27** gives the parent $C_{60}H_{30}$ (**6**) in 85 % yield on a gram scale (Scheme 11).^[11a] The head-to-tail nature of



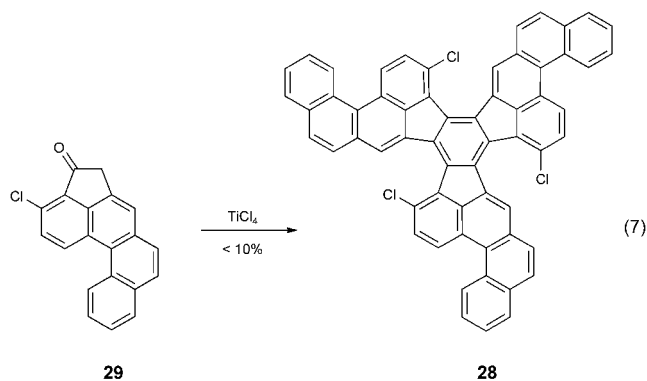
Scheme 11. Synthesis of the C_3 -symmetric $C_{60}H_{30}$ polyarene **6** by head-to-tail cyclotrimerization of **27** and laser-induced generation of C_{60} .^[11a]

this ancient but little-used method for assembling triply fused benzene rings^[58] guaranteed that the sickle-shaped arms of the product would all be oriented in the same sense, as required. Irradiation of **6** with a high intensity UV laser then converts it to C_{60} , which can be detected by mass spectrometry.^[11a]

We were gratified by the results of the laser irradiation experiments, of course, but this did not qualify as the completion of our synthesis. To a synthetic organic chemist, the job is finished only when the final product has been isolated, characterized, purified, and put in a bottle, at least in those cases where the target compound is stable. We were encouraged, however, by the results of further ^{13}C -labeling experiments, which verified that hydrocarbon **6** really does “zip up” to make C_{60} in the desired manner,^[11a] rather than decompose to smaller fragments that recombine randomly to give C_{60} by a process resembling that in the vaporization of graphite.

Our extensive experience with the synthesis of geodesic polyarenes (e.g., **13**, **15**, and **17**) taught us that the unfunctionalized hydrocarbon **6** probably would not perform well, if at all, as a precursor for the preparative scale synthesis of C_{60} by FVP; the incorporation of halogen atoms or other functionality that could generate radical intermediates at high temperatures in the gas phase would be essential to get curvature started in the π system. For the rest of the “zipping up” to form C_{60} , we were banking on a cascade of progressively easier cyclodehydrogenations, analogous to the one we had discovered earlier in a simpler system [Eq. (5)]. Thus, our focus all along was on derivatives of **6** bearing a halogen atom located deep in each fjord region (e.g., **28**).

Toward this objective, we repeated the synthesis of ketone **27**, starting from a compound that bore a chlorine atom in the appropriate position to yield ketone **29**.^[57] It was a dark day, however, when the chlorine atom we deemed so critical for the FVP step was found to ruin the aldol cyclotrimerization [Eq. (7)]. From the 85 % yield obtained in the unsubstituted system (Scheme 11), the yield dropped to no more than 5–10 % of **28**, despite extensive experimentation with other catalysts, solvents, temperatures, and conditions.^[57]



Were it not for our previous encounters with 1,2-shifts of hydrogen atoms in aryl radicals under FVP conditions (see previous section), such a serious setback might well have scuttled the entire campaign. To circumvent this obstacle, however, we merely modified our target by moving the chlorine atoms over to the unhindered neighboring positions (cf. **26** versus **24** and **25**), confident that the mobility of hydrogen atoms in the derived aryl radicals would provide viable pathways to ring closures, as in Scheme 9.^[59] Indeed,

the synthesis of ketone **30** proved no more difficult than that of **27** or **29**.^[57,11] The yield in the aldol trimerization returned to 85 %, and FVP of the $C_{60}H_{27}Cl_3$ intermediate **31** gave C_{60} , which we isolated, characterized, purified, and put in a bottle (Scheme 12).^[57,11]

The first indicators that our FVP had worked came from mass spectrometric and HPLC analysis of the crude product mixture, both of which corroborated the presence of C_{60} . For the mass spectrometric analysis, we intentionally avoided high energy methods, such as laser desorption-ionization and MALDI, which could conceivably generate C_{60} during the analysis, even if it were not already present in the product mixture.^[11a] Instead, we stirred a solution of the crude product with zinc metal to reduce any fullerenes in the mixture to their radical anions^[60] and then gently vaporized the resulting solution in an electrospray mass spectrometer. The spectrum (recorded in anionic mode) consisted of a single large peak at m/z 720, accompanied by the appropriate ^{13}C isotope peaks at $[M+1]^-$ and $[M+2]^-$ and a few minor peaks of much lower mass that we later traced to solvent impurities. No sign of any higher fullerenes (e.g., C_{70} , C_{76} , C_{84} , etc.) could be seen. Likewise, an HPLC of the crude product mixture gave a peak at the same retention time as authentic C_{60} and no peaks for any other fullerenes. The UV spectrum of the peak from the product mixture was recorded with a diode array detector and matched that of authentic C_{60} , so there could be no doubt about the success of our synthesis.

Finally, we collected the peak from the HPLC that matched the retention time of authentic C_{60} , removed the solvent, and isolated the synthetic C_{60} in pure form. Electrospray mass spectrometry of the purified C_{60} again confirmed its structure and the absence of other fullerenes.

The specificity of this synthesis, giving C_{60} to the exclusion of all other fullerenes, is unprecedented and bodes well for the

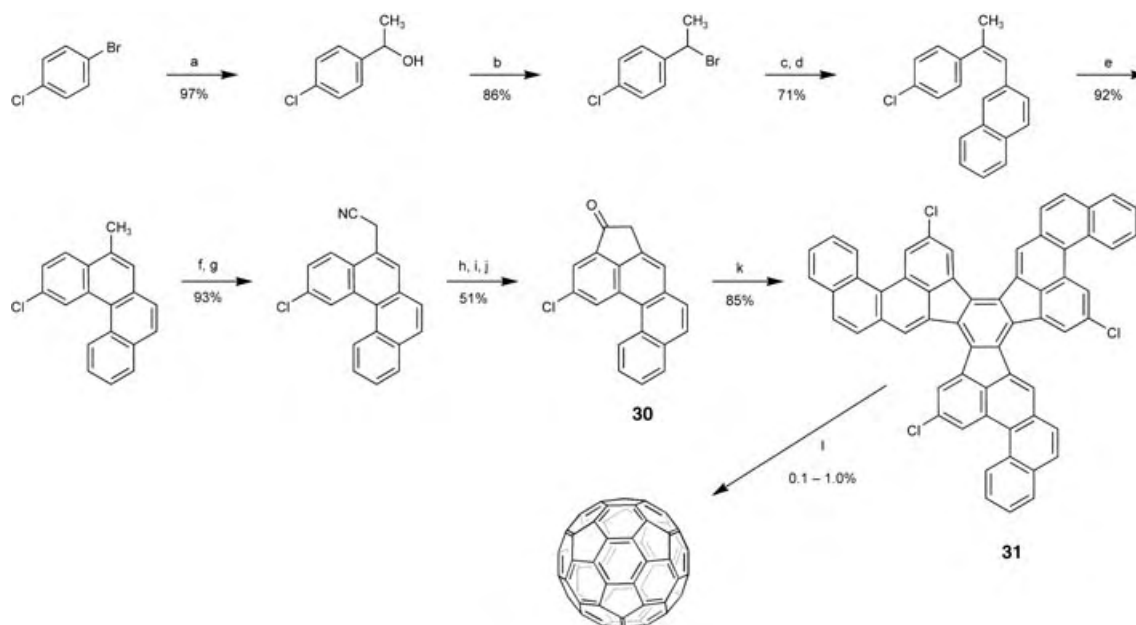
adaptation of this strategy and methodology to the chemical synthesis of other specific fullerenes by design, as discussed below.

First, however, some comments are in order about the yield of our C_{60} synthesis. We chromatographed and purified only a portion of our synthetic C_{60} , but the yield in the final step can be estimated to fall in the range of 0.1–1.0 %. This estimate is based on the total yield of soluble products obtained (ca. 25 %) and the integrated area of the C_{60} peak (4 %) in the HPLC of those products. Not knowing the structures of all the other components in the mixture, one cannot exclude the possibility that the UV detector on the HPLC instrument might respond with abnormally high sensitivity to C_{60} , so we conservatively include another factor of 10^{-1} in our estimate. Even a yield in the range of 0.1–1.0 %, however, means that the 15 new C–C bonds must have been formed with an average yield of greater than 60 % each $[(0.60)^{15} = 0.05 \text{ %}]$. Apparently, the cyclodehydrogenation cascade effect is real.

Four new principles made this synthesis possible:

1. Curvature can be temporarily induced in polyarenes by flash vacuum pyrolysis (FVP).
2. Radical-initiated C(aryl)–C(aryl) coupling reactions can be used to catch the distorted conformations.
3. Hydrogen atom 1,2-shifts can be exploited to circumvent onerous synthetic challenges.
4. Cyclodehydrogenation cascades can be relied on to stitch together adjacent arms of a π system, once curvature has already been introduced.

None of these four principles was known when we began working in this area. They all came to light during our work on the synthesis of smaller fullerene fragments, and, in that sense, the open geodesic polyarenes can all be viewed as having



Scheme 12. The first chemical synthesis of C_{60} in isolable quantities: a) Mg, diethyl ether, then acetaldehyde; b) PBr_3 , benzene; c) $P(C_6H_5)_3$, toluene; d) $LiOCH_2CH_3$, 2-naphthaldehyde, ethanol, dichloromethane; e) UV irradiation (254 nm), I_2 , propylene oxide, cyclohexane; f) *N*-bromosuccinimide, dibenzoylperoxide, carbon tetrachloride; g) KCN, tetrabutylammonium hydrogen sulfate, water, dichloromethane; h) KOH, ethylene glycol; i) $SOCl_2$; j) $AlCl_3$, dichloromethane; k) $TiCl_4$, *o*-dichlorobenzene; l) FVP, 1100 °C, 0.01 mm Hg.^[11,57]

served the role of “practice compounds” for the synthesis of fullerenes.

8. Future Prospects

At the dawn of the 21st century, the branch of materials science concerned with carbon-rich substances finds itself in a position not unlike that of the pharmaceutical industry in the middle of the last century. At that time, nearly all antibiotics, antimalarial drugs, steroids, vitamins, and other pharmaceutical agents were prepared either by fermentation or by enrichment from natural sources (e.g., penicillin, quinine, cortisone, vitamin A, etc.—notable exceptions being aspirin and the sulfa drugs). The ensuing decades, however, totally transformed the pharmaceutical industry into one that now relies absolutely on chemical synthesis, and it is inconceivable that organic chemists will be unable to develop increasingly powerful and versatile methods of chemical synthesis to transform the science of carbon-rich materials in a similar way. Our 12-step synthesis of C_{60} (Scheme 12)^[11] represents only one stride in the long journey toward that goal.

From a long-range perspective, even C_{60} must be viewed as just another “practice compound,” synthesized as a test for the new methodology. The ton quantities of C_{60} available today in one step from fuel-rich flames^[6,7] make it pointless to bother optimizing the FVP synthesis that is unlikely ever to produce more than mg quantities of pure C_{60} .

The real value of this work lies in the demonstration of new principles that should be adaptable to syntheses of other fullerenes and other carbon-rich targets. Moreover, we have established a benchmark that will stimulate other synthetic organic chemists to develop better strategies and more effective methods for achieving the same goals; there is vast room for improvement.

What other fullerenes are worth synthesizing? We see little point in synthesizing C_{70} by the FVP method, except perhaps as a means to determine whether or not the product will suffer sequential losses of C_2 units under the conditions of its formation and shrink down to C_{60} .^[61] More interesting would be the synthesis of higher fullerenes that have never been isolated before (e.g., some of the unknown isomers of C_{84}) to determine whether or not the products will survive as the intended isomers or rearrange to one (or more) of the more stable isomers under the conditions of their formation.^[62]

More exotic targets include ^{13}C -labeled C_{60} , azafullerenes, and other heterofullerenes. By synthesizing a multiply ^{13}C -labeled C_{60} , one could determine whether the product survives as a single isotopomer or if its carbon atoms become scrambled under the FVP conditions^[63,64] or upon subsequent irradiation.^[65] Azafullerenes with even numbers of nitrogen atoms can be closed-shell even-electron species (unlike $C_{59}N^{[66]}$), and the preference of amines for pyramidal geometries at the nitrogen atoms could relax the “isolated pentagon rule”, thus permitting the synthesis of polyazafullerenes with even fewer than 60 atoms total (e.g., $C_{52}N_4$). Many fullerenes with holes in them (atoms missing) might be easier to make “from the ground up” rather than by

degradation of an intact fullerene^[67] (e.g., $C_{54}H_6$, C_{60} with one hexagonal face missing).^[68] Trapping an atom or small molecule inside a fullerene as it zips up under FVP conditions, sadly, seems rather improbable, so the chemical synthesis of endohedral fullerene complexes still stands as an unmet challenge in this field.^[67,69] We are currently exploring possible extensions of the methods described here to the chemical synthesis of structurally uniform, single wall carbon nanotubes and other carbon-rich materials.

The author gratefully acknowledges not only the financial support for this work from the National Science Foundation and the Department of Energy, but also the enthusiasm and dedication of the hard working students and postdoctoral co-workers listed in the references cited.

Received: February 23, 2004

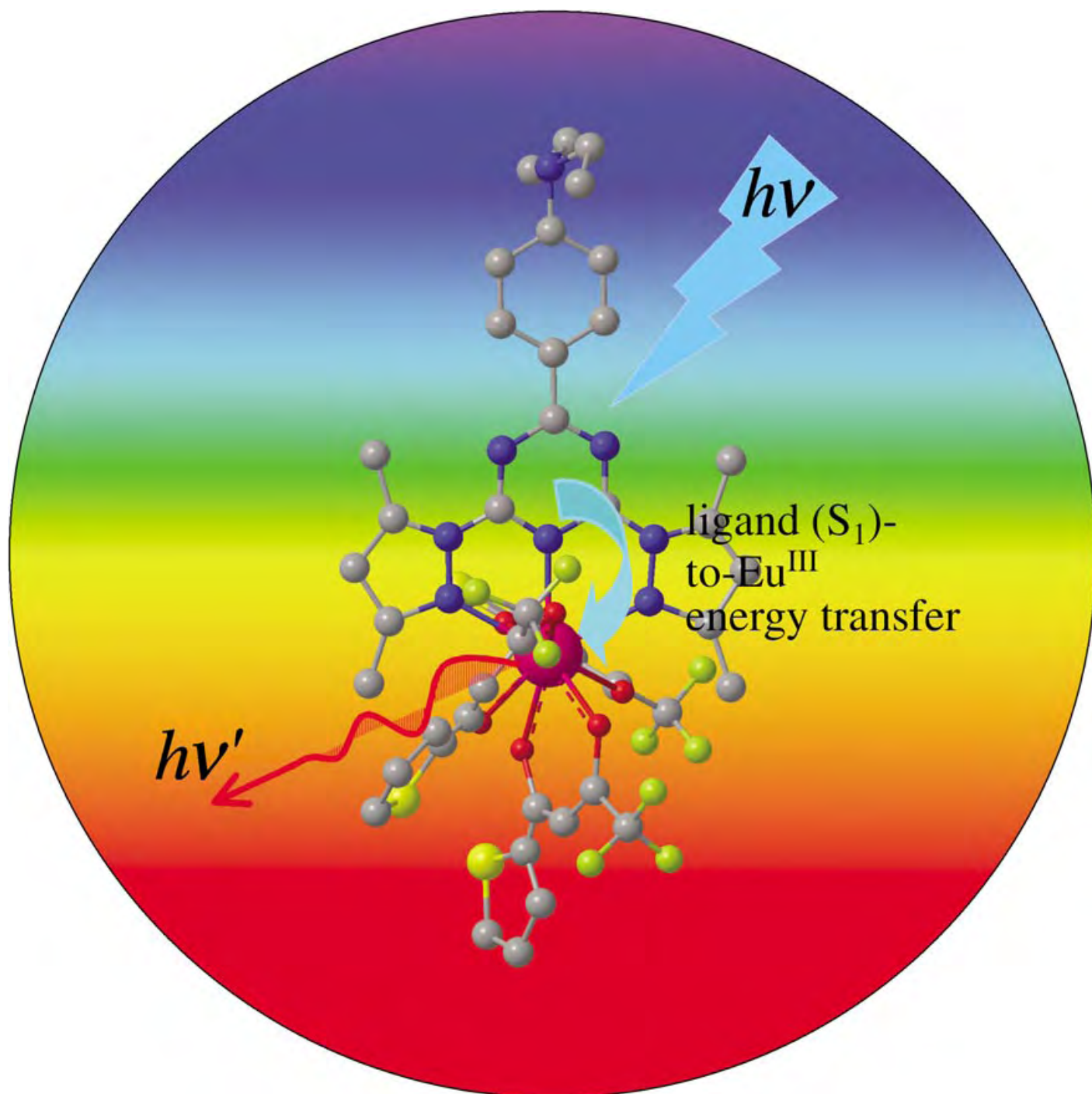
Published Online: September 9, 2004

- [1] a) *Fullerenes: Chemistry, Physics, and Technology* (Eds.: K. M. Kadish, R. S. Ruoff), Wiley, New York, **2000**; b) E. Osawa, *Perspectives of Fullerene Nanotechnology*, Kluwer, Dordrecht, **2002**; c) *Proceedings of the First International Symposium on Nanocarbons* (Eds.: E. Yasuda, M. Endo, T. Hayashi, M. Terrones, H. Terrones, T. Enoki, M. S. Dresselhaus) Taylor & Francis, London, **2002**; d) *Fullerenes and Nanotubes: The Building Blocks of Next Generation Nanodevices* (Eds.: P. V. Kamat, D. M. Guldi, F. D'Souza) Electrochemical Society, Pennington, **2003**.
- [2] a) L. T. Scott, *Pure Appl. Chem.* **1996**, 68, 291; b) L. T. Scott, H. E. Bronstein, D. V. Preda, R. B. M. Ansems, M. S. Bratcher, S. Hagen, *Pure Appl. Chem.* **1999**, 71, 209.
- [3] a) P. W. Rabideau, A. Sygula in *Advances in Theoretically Interesting Molecules, Vol. 3* (Ed.: R. P. Thummel), JAI, Greenwich, **1995**, p. 1; b) P. W. Rabideau, A. Sygula, *Acc. Chem. Res.* **1996**, 29, 235; c) G. Mehta, H. S. P. Rao, *Adv. Strain Org. Chem.* **1997**, 6, 139; d) G. Mehta, H. S. P. Rao, *Tetrahedron* **1998**, 54, 13325.
- [4] a) *Fullerenes and Related Structures: Topics in Current Chemistry* (Ed.: A. Hirsch), Vol. 199, Springer, Berlin, **1999**; b) R. Taylor, *Lecture Notes on Fullerene Chemistry: A Handbook for Chemists*, Imperial College, London, **1999**.
- [5] a) W. Krätschmer, L. D. Lamb, K. Fostiropoulos, D. R. Huffman, *Nature* **1990**, 347, 354; b) N. I. Alekseyev, G. A. Dyuzhev, *Carbon* **2003**, 41, 1343, and references therein.
- [6] a) J. B. Howard, J. T. McKinnon, Y. Makarovskiy, A. L. Lafleur, M. E. Johnson, *Nature* **1991**, 352, 139; b) A. Goel, J. B. Howard, *Carbon* **2003**, 41, 1949, and references therein; c) J. B. Howard, D. F. Kronholm, A. J. Modestino, H. Richter, (Nano-C, USA), US-A 2003021018, **2003**. See also www.nano-c.com.
- [7] a) J.-F. Tremblay, *Chem. Eng. News* **2003**, 81 (32), 13; b) H. Takehara, T. Yamamoto, (Mitsubishi Chemical Corp., Japan), JP 2003160317, **2003**; c) T. Yamamoto, H. Takehara, T. Takakura, (Mitsubishi Chemical Corp., Japan), JP 2003232505, **2003**. See also www.m-kagaku.co.jp/english/rel/2001/120301.htm.
- [8] P. W. Fowler, D. E. Manolopoulos, *Atlas of Fullerenes*, Oxford University, Oxford, **1995**.
- [9] S. Margadonna, K. Prassides, *J. Solid State Chem.* **2002**, 168, 639.
- [10] a) C. Thilgen, A. Herrmann, F. Diederich, *Angew. Chem.* **1997**, 109, 2362; *Angew. Chem. Int. Ed. Engl.* **1997**, 36, 2268; b) C. Thilgen, F. Diederich, *Top. Curr. Chem.* **1999**, 199, 135; c) Y. Achiba, H. Shiromaru, T. Wakabayashi, S. Suzuki, *Mesosc. Mater. Clusters* **1999**, 379.

- [11] a) M. M. Boorum, Y. V. Vasil'ev, T. Drewello, L. T. Scott, *Science* **2001**, 294, 828; b) L. T. Scott, M. M. Boorum, B. J. McMahon, S. Hagen, J. Mack, J. Blank, H. Wegner, A. de Meijere, *Science* **2002**, 295, 1500.
- [12] a) A. Rojas-Aguilar, *J. Chem. Thermodyn.* **2002**, 34, 1729; b) H. P. Diogo, M. E. M. Da Piedade, *Proc. Electrochem. Soc.* **1998**, 627, and references therein.
- [13] a) W. E. Barth, R. G. Lawton, *J. Am. Chem. Soc.* **1966**, 88, 380; b) R. G. Lawton, W. E. Barth, *J. Am. Chem. Soc.* **1971**, 93, 1730.
- [14] Many other strategies not discussed here are also possible. For examples, see: a) D. Loguercio Jr, Ph.D. dissertation, University of California, Los Angeles, **1988**; b) C. Fabre, A. Rassat, *C. R. Acad. Sci. Ser. II* **1989**, 308, 1223; c) D. Shen, Ph.D. dissertation, University of California, Los Angeles, (Los Angeles), **1990**; d) M. P. Barrow, J. K. Cammack, M. Goebel, I. M. Wasser, K. P. C. Vollhardt, T. Drewello, *J. Organomet. Chem.* **1999**, 572, 135; e) G. Mehta, P. V. V. S. Sarma, *Tetrahedron Lett.* **2002**, 43, 9343.
- [15] a) R. E. Haufler, J. Conceicao, L. P. F. Chibante, Y. Chai, N. E. Byrne, S. Flanagan, M. M. Haley, S. C. O'Brien, C. Pan, Z. Xiao, W. E. Billups, M. A. Ciufolini, R. H. Hauge, J. L. Margrave, L. J. Wilson, R. F. Curl, R. E. Smalley, *J. Phys. Chem.* **1990**, 94, 8634; b) Y. Vasil'ev, D. Wallis, T. Drewello, M. Nuchter, B. Ondruschka, A. Lobach, *Chem. Commun.* **2000**, 1233; c) J. Nossal, R. K. Saini, A. K. Sadana, H. F. Bettinger, L. B. Alemany, G. E. Scuseria, W. E. Billups, M. Saunders, A. Khong, R. Weisemann, *J. Am. Chem. Soc.* **2001**, 123, 8482.
- [16] a) S. M. Pimenova, S. V. Melkhanova, V. P. Kolesov, A. S. Lobach, *J. Phys. Chem. B* **2002**, 106, 2127; b) Y. Okamoto, *J. Phys. Chem. A* **2001**, 105, 7634, and references therein; c) B. W. Clare, D. L. Kepert, *Theochem* **2003**, 622, 185.
- [17] H. Sakurai, T. Daiko, T. Hirao, *Science* **2003**, 301, 1878.
- [18] T. M. Mitzel, Ph.D. dissertation, Boston College, Chestnut Hill, MA, **1994**.
- [19] Y. Rubin, T. C. Parker, S. J. Pastor, S. Jalisiatgi, C. Boulle, C. L. Wilkins, *Angew. Chem.* **1998**, 110, 1353; *Angew. Chem. Int. Ed.* **1998**, 37, 1226.
- [20] a) Y. Tobe, N. Nakagawa, K. Naemura, T. Wakabayashi, T. Shida, Y. Achiba, *J. Am. Chem. Soc.* **1998**, 120, 4544; b) Y. Tobe, H. Nakanishi, N. Nakagawa, R. Furukawa, *Proc. Electrochem. Soc.* **1999**, 99, 146; c) Y. Tobe, N. Nakagawa, J. Kishi, M. Sonoda, K. Naemura, T. Wakabayashi, T. Shida, Y. Achiba, *Tetrahedron* **2001**, 57, 3629.
- [21] The hypothetical synthesis of C₆₀ by dimerization of **5** bears a close resemblance to the hypothetical synthesis of dodecahedrane by dimerization of triquinacene, as originally proposed by: R. B. Woodward, T. Fukunaga, R. C. Kelly, *J. Am. Chem. Soc.* **1964**, 86, 3162. See also: a) G. N. Sastry, E. D. Jemmis, G. Mehta, S. R. Shah, *J. Chem. Soc. Perkin Trans. 2* **1993**, 1867; b) A. H. Abdourazak, Z. Marcinow, A. Sygula, R. Sygula, P. W. Rabideau, *J. Am. Chem. Soc.* **1995**, 117, 6410; c) F. Geneste, A. Moradpour, G. Dive, D. Peeters, J. Malthete, J.-F. Sadoc, *J. Org. Chem.* **2002**, 67, 605.
- [22] a) S. Hagen, M. S. Bratcher, M. S. Erickson, G. Zimmermann, L. T. Scott, *Angew. Chem.* **1997**, 109, 407; *Angew. Chem. Int. Ed. Engl.* **1997**, 36, 406; b) S. Hagen, L. T. Scott, *J. Org. Chem.* **1996**, 61, 7198.
- [23] Several research groups other than ours have independently conceived of this approach: a) L. Wang, P. B. Shevlin, *Abstracts of Papers, 212th National Meeting of the American Chemical Society*, Orlando, Florida, **1996**, abstract no. ORGN 345; b) M. Sarobe, R. H. Fokkens, T. J. Cleij, L. W. Jenneskens, N. M. M. Nibbering, W. Stas, C. Versluis, *Chem. Phys. Lett.* **1999**, 313, 31; c) B. Gomez-Lor, O. de Frutos, A. M. Echavarren, *Chem. Commun.* **1999**, 2431; d) B. Gomez-Lor, C. Koper, R. H. Fokkens, E. J. Vlietstra, T. J. Cleij, L. W. Jenneskens, N. M. M. Nibbering, A. M. Echavarren, *Chem. Commun.* **2002**, 370.
- [24] S. Danishefsky, *Abstracts of Papers, 224th National Meeting of the American Chemical Society*, Boston, MA, **2002**, abstract no. ORGN-045.
- [25] a) J. T. Craig, M. D. W. Robins, *Aust. J. Chem.* **1968**, 21, 2237; b) see also R. H. Jacobson, Ph.D. dissertation, University of California, Los Angeles, **1986**.
- [26] R. F. C. Brown, *Pyrolytic Methods in Organic Chemistry: Application of Flow and Flash Vacuum Pyrolytic Techniques*, Academic Press, New York, **1980**.
- [27] a) R. F. C. Brown, K. J. Harrington, G. L. McMullen, *J. Chem. Soc. Chem. Commun.* **1974**, 123; b) R. F. C. Brown, F. W. Eastwood, G. P. Jackman, *Aust. J. Chem.* **1977**, 30, 1757.
- [28] a) L. T. Scott, M. M. Hashemi, D. T. Meyer, H. B. Warren, *J. Am. Chem. Soc.* **1991**, 113, 7082; b) L. T. Scott, M. M. Hashemi, M. S. Bratcher, *J. Am. Chem. Soc.* **1992**, 114, 1920.
- [29] P. M. Donovan, L. T. Scott, *J. Am. Chem. Soc.* **2004**, 126, 3108.
- [30] Calculations at the B3LYP/6-31G(d) level of theory indicate that cyclization of diyne **8** to corannulene (Scheme 4) should be exothermic by 68.1 kcalol⁻¹, whereas cyclization of the corresponding dinitrile to 1,6-diazacorannulene [Eq. (1)] should be endothermic by 17.8 kcalmol⁻¹.
- [31] M. S. Bratcher, Ph.D. dissertation, Boston College, Chestnut Hill, MA, **1996**.
- [32] a) L. T. Scott, P.-C. Cheng, M. S. Bratcher, *Seventh International Symposium on Novel Aromatic Compounds*, Victoria, British Columbia, Canada, July 19–24, **1992**, abstract no. 64; b) P.-C. Cheng, M.S. thesis, University of Nevada, Reno (Reno, NV), **1992**.
- [33] a) L. T. Scott, P.-C. Cheng, M. M. Hashemi, M. S. Bratcher, D. T. Meyer, H. B. Warren, *J. Am. Chem. Soc.* **1997**, 119, 10963; b) further improvements: A. K. Rai, M.Sc. thesis, Boston College, Chestnut Hill, MA, **1997**.
- [34] P. W. Rabideau, A. H. Abdourazak, H. E. Folsom, Z. Marcinow, A. Sygula, R. Sygula, *J. Am. Chem. Soc.* **1994**, 116, 7891.
- [35] K. Imamura, K. Takimiya, T. Otsubo, Y. Aso, *Chem. Commun.* **1999**, 1859.
- [36] a) A. H. Abdourazak, A. Sygula, P. W. Rabideau, *J. Am. Chem. Soc.* **1993**, 115, 3010; b) M. Sarobe, J. W. Zwikker, J. D. Snoeijer, U. E. Wiersum, L. W. Jenneskens, *Chem. Commun.* **1994**, 89; c) M. Sarobe, J. W. Zwikker, J. D. Snoeijer, U. E. Wiersum, L. W. Jenneskens, *Chem. Commun.* **1994**, 1404; d) Z. Marcinow, F. R. Fronczek, Y.-H. Liu, P. W. Rabideau, *J. Org. Chem.* **1995**, 60, 7015; e) M. Sarobe, J. D. Snoeijer, L. W. Jenneskens, J. W. Zwikker, J. Wesseling, *Tetrahedron Lett.* **1995**, 36, 9565; f) M. Sarobe, S. Flink, L. W. Jenneskens, B. L. A. van Poecke, J. W. Zwikker, *Chem. Commun.* **1995**, 2415; g) P.-C. Cheng, Ph.D. dissertation, Boston College, Chestnut Hill, MA, **1996**; h) A. Necula, Ph.D. dissertation, Boston College (Chestnut Hill, MA), **1996**; i) L. W. Jenneskens, M. Sarobe, J. W. Zwikker, *Pure Appl. Chem.* **1996**, 68, 219; j) M. Sarobe, S. Flink, L. W. Jenneskens, J. W. Zwikker, J. Wesseling, *J. Chem. Soc. Perkin Trans. 2* **1996**, 2125; k) L. T. Scott, A. Necula, *J. Org. Chem.* **1996**, 61, 386; l) M. Sarobe, L. W. Jenneskens, *J. Org. Chem.* **1997**, 62, 8247; m) M. Sarobe, L. W. Jenneskens, J. Wesseling, U. E. Wiersum, *J. Chem. Soc. Perkin Trans. 2* **1997**, 703; n) L. T. Scott, A. Necula, *Tetrahedron Lett.* **1997**, 38, 1877; o) A. Weitz, E. Shabtai, M. Rabinovitz, M. S. Bratcher, C. C. McComas, M. D. Best, L. T. Scott, *Chem. -Eur. J.* **1998**, 4, 234; p) A. L. Lafleur, J. B. Howard, E. Plummer, K. Taghizadeh, A. Necula, L. T. Scott, K. C. Swallow, *Polycyclic Aromat. Compd.* **1998**, 12, 223; q) T. Visser, M. Sarobe, L. W. Jenneskens, J. W. Wesseling, *Fuel* **1998**, 77, 913; r) M. Sarobe, R. W. A. Havenith, L. W. Jenneskens, *Chem. Commun.* **1999**, 1021; s) M. Sarobe, H. C. Kwint, T. Fleer, R. W. A. Havenith, L. W. Jenneskens, E. J. Vlietstra, J. H. Van Lenthe, J. Wesseling, *Eur. J. Org. Chem.* **1999**, 1191; t) A. Necula, L. T. Scott, *J. Anal. Appl. Pyrolysis* **2000**, 22, 65; u) Z.

- Marcinow, P. W. Rabideau, *J. Org. Chem.* **2000**, *65*, 5063; v) See also ref [2a].
- [37] a) R. F. C. Brown, F. W. Eastwood, *Synlett* **1993**, 9; b) R. F. C. Brown, *Eur. J. Org. Chem.* **1999**, 3211, and references therein; c) see also refs. [2], [3], and [36].
- [38] a) M. S. Bratcher, L. T. Scott, *Abstracts of Papers, 207th National Meeting of the American Chemical Society*, San Diego, CA, **1994**, abstract no. ORGN 420; b) H. A. Reisch, M. S. Bratcher, L. T. Scott, *Org. Lett.* **2000**, *2*, 1427; c) see also ref [31].
- [39] a) G. E. Davico, V. M. Bierbaum, C. H. DePuy, G. B. Ellison, R. R. Squires, *J. Am. Chem. Soc.* **1995**, *117*, 2590; b) J. Berkowitz, G. B. Ellison, D. Gutman, *J. Phys. Chem.* **1994**, *98*, 2744.
- [40] D. T. Meyer, M.Sc. thesis, University of Nevada Reno, NV, **1991**.
- [41] a) C. C. McComas, L. T. Scott, *Abstracts of Papers, 211th National Meeting of the American Chemical Society*, New Orleans, LA, **1996**, abstract no. CHED-556; b) S. Hagen, M. S. Bratcher, M. S. Erickson, G. Zimmermann, L. T. Scott, *Angew. Chem.* **1997**, *109*, 407; *Angew. Chem. Int. Ed. Engl.* **1997**, *36*, 406; c) B. J. McMahon, B.S. thesis, Boston College (Chestnut Hill, MA), **1997**; d) M. D. Clayton, P. W. Rabideau, *Tetrahedron Lett.* **1997**, *38*, 741; e) G. Mehta, G. Panda, *Chem. Commun.* **1997**, 2081; f) C. C. McComas, M. D. Best, L. T. Scott, unpublished results; g) G. Mehta, G. Panda, P. V. V. S. Sarma, *Tetrahedron Lett.* **1998**, *39*, 5835; h) R. B. M. Ansems, L. T. Scott, *J. Am. Chem. Soc.* **2000**, *122*, 2719; i) Z. Marcinow, A. Sygula, A. Ellern, P. W. Rabideau, *Org. Lett.* **2001**, *3*, 3527; j) H. E. Bronstein, N. Choi, L. T. Scott, *J. Am. Chem. Soc.* **2002**, *124*, 8870; k) P. M. Andrusyszyn, M.S. thesis, Boston College, Chestnut Hill, MA, **2002**; l) Z. Marcinow, D. I. Grove, P. W. Rabideau, *J. Org. Chem.* **2002**, *67*, 3537.
- [42] D. M. Ho, R. A. Pascal Jr, *Chem. Mater.* **1993**, *5*, 1358.
- [43] P. Rehländer, Ph.D. dissertation, University of Berlin, **1883**, cited by P. Rehländer, *Chem. Ber.* **1903**, *36*, 1583.
- [44] Aldrich Chem. Co., Milwaukee, WI.
- [45] Quartz begins to soften at 1100°C, and tubes become brittle if heated for long periods of time above 1100°C, but they do not collapse under FVP conditions even at temperatures up to 1400°C.
- [46] L. T. Scott, M. S. Bratcher, S. Hagen, *J. Am. Chem. Soc.* **1996**, *118*, 8743.
- [47] R. B. M. Ansems, Ph.D. dissertation, Boston College, Chestnut Hill, MA, **2004**.
- [48] a) S. Hagen, U. Nuechter, M. Nuechter, G. Zimmermann, *Polycyclic Aromat. Compd.* **1995**, *4*, 209; b) S. Hagen, U. Nuechter, M. Nuechter, G. Zimmermann, *Tetrahedron Lett.* **1994**, *35*, 7013; c) S. Hagen, H. Christoph, G. Zimmermann, *Tetrahedron* **1995**, *51*, 6961; d) R. B. M. Ansems, D. A. Klumpp, L. T. Scott, unpublished results.
- [49] J. Cioslowski, P. Piskorz, D. Moncrieff, *J. Org. Chem.* **1998**, *63*, 4051.
- [50] M. Berthelot, *Z. Chemie* **1866**, 707 [Beilstein CNR 1668531].
- [51] a) N. S. Mills, J. L. Malandra, A. Hensen, J. A. Lowery, *Polycyclic Aromat. Compd.* **1998**, *12*, 239; b) M. D. Watson, A. Fechtenkötter, K. Müllen, *Chem. Rev.* **2001**, *101*, 1267, and references therein.
- [52] Solution-phase methods for imposing curvature on polycyclic aromatic hydrocarbons are being vigorously pursued; however, none yet work with unfunctionalized hydrocarbon precursors: a) T. J. Seiders, K. K. Baldrige, J. S. Siegel, *J. Am. Chem. Soc.* **1996**, *118*, 2754; b) A. Sygula, P. W. Rabideau, *J. Am. Chem. Soc.* **1998**, *120*, 12666; c) L. Wang, P. B. Shevlin, *Org. Lett.* **2000**, *2*, 3703; d) See also ref. [38b].
- [53] Calculations were performed at the pBP/DN** level of theory. Strain energy changes associated with the first and second thermal cyclizations of bifuorenylidene (**20**) were computed, respectively, according to the homodesmotic reactions: a) **20** + biphenyl → 2(benzene) + **19** b) **19** + biphenyl → 2(benzene) + **15**.
- [54] R. Faust, K. P. C. Vollhardt, *Seventh International Symposium on Novel Aromatic Compounds*, Victoria, British Columbia, Canada, July 19–24, **1992**, abstract no. 61.
- [55] The same C₃₀H₁₂ hemifullerene (**4**) has been synthesized in mg quantities by two other FVP routes.^[21b,41g]
- [56] a) M. A. Brooks, L. T. Scott, *J. Am. Chem. Soc.* **1999**, *121*, 5444; b) See also A. Necula, L. T. Scott, *J. Am. Chem. Soc.* **2000**, *122*, 1548.
- [57] M. M. Boorum, Ph.D. dissertation, Boston College, Chestnut Hill, MA, **2001**.
- [58] For a review on aldol cyclotrimerizations, see: M. M. Boorum, L. T. Scott in *Modern Arene Chemistry* (Ed.: D. Astruc), Wiley-VCH, Weinheim, Germany, **2002**, Ch. 1.
- [59] The 1,2-shifts of hydrogen atoms could come either from the fjord region, as proposed, or from the cove region on the other side. In either case, subsequent C(aryl)–C(aryl) coupling would introduce curvature into the polyarene π system.
- [60] M. Wu, X. Wei, L. Qi, Z. Xu, *Tetrahedron Lett.* **1996**, *37*, 7409.
- [61] D. Ben-Amotz, R. G. Cooks, L. DeJarme, J. C. Gunderson, S. H. Hoke, II, B. Kahr, G. L. Payne, J. M. Wood, *Chem. Phys. Lett.* **1991**, *183*, 149.
- [62] E. Osawa, H. Ueno, M. Yoshida, Z. Slanina, X. Zhao, M. Nishiyama, H. Saito, *J. Chem. Soc. Perkin Trans. 2* **1998**, 943.
- [63] a) Y. Kumeda, D. J. Wales, *Chem. Phys. Lett.* **2003**, *374*, 125; b) for ¹³C-labeling evidence on the thermal scrambling of atoms in planar aromatic hydrocarbons, see ref. [2a].
- [64] For experimental evidence against the occurrence of “Stone-Wales” rearrangements in planar aromatic hydrocarbons and in fullerenes under FVP conditions, see ref. [2a] and J. M. Hawkins, M. Nambu, A. Meyer, *J. Am. Chem. Soc.* **1994**, *116*, 7642.
- [65] C. Burda, A. C. S. Samia, D. J. Hathcock, H. Huang, S. Yang, *J. Am. Chem. Soc.* **2002**, *124*, 12400.
- [66] A. Hirsch, B. Nuber, *Acc. Chem. Res.* **1999**, *32*, 795.
- [67] a) Y. Rubin, *Top. Curr. Chem.* **1999**, *199*, 67; b) Y. Murata, M. Murata, K. Komatsu, *Chem. -Eur. J.* **2003**, *9*, 1600; c) S. Iwamatsu, T. Uozaki, K. Kobayashi, S. Re, S. Nagase, S. Murata, *J. Am. Chem. Soc.* **2004**, *126*, 2668.
- [68] For a short route to an attractive 54-carbon ring system, see: G. Mehta, P. V. V. S. Sarma, *Tetrahedron Lett.* **2002**, *43*, 6557.
- [69] a) *Endofullerenes: A New Family of Carbon Clusters* (Eds.: T. Akasaka, S. Nagase), Kluwer, Dordrecht, **2002**; b) N. Jux, K. Holczer, Y. Rubin, *Angew. Chem.* **1996**, *108*, 2116; *Angew. Chem. Int. Ed. Engl.* **1996**, *35*, 1986; c) Y. Rubin, *Chem. -Eur. J.* **1997**, *3*, 1009; d) Y. Murata, M. Murata, K. Komatsu, *J. Am. Chem. Soc.* **2003**, *125*, 7152.

Communications



Visible-light excitation of the europium complex shown leads to characteristic red emission from the Eu^{III} center. A spectroscopic study shows the nature of the sensitization process and accounts for why the complex can be excited at these longer wavelengths. For more information see the Communication by Y. Wang, J.-P. Zhang, W.-T. Wong et al. on the following pages.

A Highly Luminescent Europium Complex Showing Visible-Light-Sensitized Red Emission: Direct Observation of the Singlet Pathway**

Chi Yang, Li-Min Fu, Yuan Wang,* Jian-Ping Zhang,* Wing-Tak Wong,* Xi-Cheng Ai, Yi-Fang Qiao, Bing-Suo Zou, and Lin-Lin Gui

A challenge in the chemistry of the lanthanide ions is to develop luminescent Eu complexes that can be sensitized by visible light and to determine the energy-transfer mechanisms in these systems. Recently, this field has become much more important because of the demand for less-harmful labeling reagents in the life sciences and low-voltage-driven pure-red emitters in optoelectronic technology.^[1] The commonly

observed sensitization mechanism for luminescent europium complexes involves a triplet pathway, in which the transfer of the energy absorbed by the ligand to the Eu^{III} ion takes place from the ligand-centered triplet excited state (T₁). In this case, the optical excitation window for luminescent Eu complexes appears to be limited to <385 nm owing to the energetic constraints highlighted by Reinholdt and co-workers.^[2] With the use of 'antenna' chromophoric groups, which have a smaller energy gap between the lowest singlet excited state (S₁) and the T₁ state (e.g. acridone, diaryl ketones), it has been demonstrated by several research groups that the excitation wavelength for Eu complexes can be extended into the visible region through the usual triplet pathway.^[3–4] Another promising means of longer-wavelength sensitization of Eu^{III} emission is through the singlet pathway, in which the excited-state energy of a chromophore is directly transferred from its S₁ state to the luminescent states of the Eu^{III} center. In this way the energetic constraints from the T₁ state of the ligand can be avoided.

The singlet pathway for the sensitization of lanthanide luminescence was first proposed by Kleinerman in 1969.^[5] Horrocks and co-workers later examined the energy-transfer processes in lanthanide-ion-binding proteins and assumed that it was the singlet excited state of the chromophore that sensitized the lanthanide emission.^[6] However, owing to the lack of information regarding the emission from the excited states of the coordinated ligand and the difficulties in the determination of the ligand-localized triplet–triplet absorption spectra for lanthanide chelates, it has been very difficult to prove for certain which state is responsible for the energy-transfer process.^[7] All the experimental work conducted on the sensitization of lanthanide–chelate luminescence seems to support the triplet pathway, whereas the singlet pathway for the sensitization of the Eu complex has not been observed experimentally.^[7] Herein, we report the successful extension of the excitation window to the visible region for a Eu complex, which subsequently exhibits highly efficient Eu^{III}-centered luminescence. The sensitization mechanism is shown to take place through the singlet pathway by means of time-resolved luminescence spectroscopic studies.

We have previously demonstrated that dipyrzolyltriazine derivatives are good chromophores for the efficient sensitization of lanthanide ion luminescence.^[8] To achieve longer-wavelength sensitization of the Eu^{III} emission, we explored the effect of incorporating *N,N*-dialkyl aniline moieties into the dipyrzolyltriazine systems. The new ligand **3** was prepared by heating **2** and the potassium salt of 3,5-dimethylpyrazole in dry THF at reflux for 12 h (Scheme 1). The reaction of **3** and europium thenoyltrifluoroacetate [Eu(tta)₃·3H₂O] in THF yielded a yellow solution of the complex **4**, which showed a bright red emission under daylight illumination. After evaporation of the solvent, the residue was taken up in dry diethyl ether, and the solution was triturated with *n*-hexane; the complex Eu(tta)₃L (**4**) was obtained as a bright orange powder (Scheme 1).

The photophysical properties of a solution of complex **4** in toluene were investigated systematically. Upon the coordination of **3** to Eu^{III}, the ligand charge-transfer (CT) absorption band is shifted from 387 nm ($\epsilon = 38\,000\text{ cm}^2\text{ M}^{-1}$) to 406 nm

[*] Prof. Dr. Y. Wang, Prof. L.-L. Gui
State Key Laboratory for Structural Chemistry of Unstable and Stable Species
College of Chemistry and Molecular Engineering, Peking University
Beijing 100871 (China)
Fax: (+86) 10-6276-5769
E-mail: wangy@pku.edu.cn

Prof. Dr. J.-P. Zhang, Prof. Dr. X.-C. Ai
Institute of Chemistry, Chinese Academy of Sciences
Beijing 100080 (China)
Fax: (+86) 10-8261-6163
E-mail: jpzhang@iccas.ac.cn

Prof. Dr. W.-T. Wong
Department of Chemistry, The University of Hong Kong
Hong Kong (China)
Fax: (+85) 2-2547-2933
E-mail: wtwong@hkucc.hku.hk

Dr. C. Yang*
State Key Laboratory for Structural Chemistry of Unstable and Stable Species
College of Chemistry and Molecular Engineering, Peking University
Beijing 100871 (China)
and

Faculty of Chemical Engineering and Light Industry
Guangdong University of Technology, Guangzhou 510090 (China)

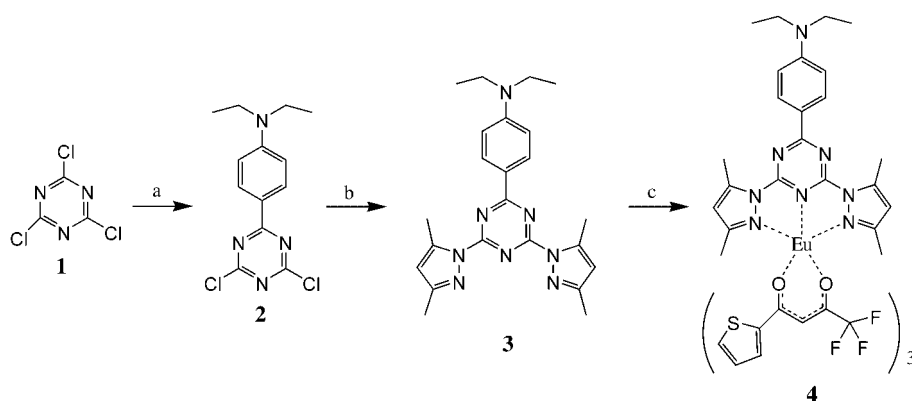
L.-M. Fu*
Institute of Chemistry, Chinese Academy of Sciences
Beijing 100080 (China)
and
Institute of Physics, Chinese Academy of Sciences
Beijing 100080 (China)

Y.-F. Qiao
Faculty of Chemical Engineering and Light Industry
Guangdong University of Technology
Guangzhou 510090 (China)

Prof. Dr. B.-S. Zou
Institute of Physics, Chinese Academy of Sciences
Beijing 100080 (China)

[†] These authors contributed equally to this work.

[**] We are grateful for the grants-in-aid from the NSFC (29925308, 20105003, 90206011, 20273077, 90101010), the Major State Basic Research Development Program (G2000077503), the Research Grant Council of Hong Kong, and the NSF of Guangdong (980128).



Scheme 1. Synthesis of the complex **4**. a) *N,N*-diethylaniline; b) potassium 3,5-dimethylpyrazolate; c) $[\text{Eu}(\text{tta})_3] \cdot 3 \text{H}_2\text{O}$.

($\epsilon = 55\,000 \text{ cm}^2 \text{ M}^{-1}$) owing to the stabilization of the very polar excited states (Figure 1). The excitation spectrum of complex **4** (emission monitored at 614 nm) is in agreement with its

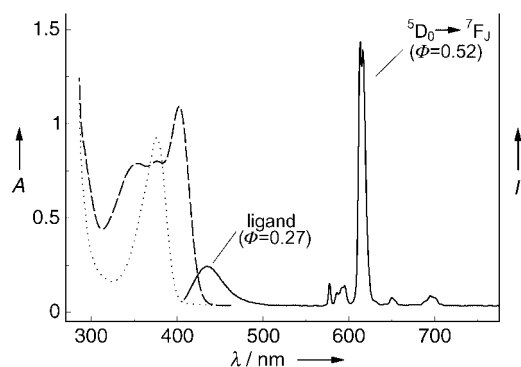


Figure 1. The room temperature UV/Vis absorption spectra of the Eu complex **4** (dashed line) and the ligand **3** (dotted line) as solutions in toluene, and the fluorescence emission spectrum of complex **4** (solid line, $\lambda_{\text{ex}} = 402 \text{ nm}$) at $\sim 1.0 \times 10^{-5} \text{ M}$. Luminescence quantum yields (ϕ) for **4** are given in parentheses.

ground-state absorption spectrum. The excitation window for complex **4** can be extended beyond 460 nm when the concentration is increased up to $1 \times 10^{-2} \text{ M}$. Upon selective excitation at the ligand CT band at room temperature, the emission spectrum of complex **4** displays a broad band centered at 430 nm, derived from the coordinated ligand, and the characteristic sharp peaks associated with the $^5\text{D}_0 \rightarrow ^7\text{F}_J$ transitions of the Eu^{III} ion (Figure 1). The five expected components of the $^5\text{D}_0 \rightarrow ^7\text{F}_{0-4}$ transitions are well resolved and the hypersensitive $^5\text{D}_0 \rightarrow ^7\text{F}_2$ transition is very intense, which reflects a low symmetry of the Eu^{III} site. The overall luminescence quantum yields for the emissions from the Eu^{III} ion and the coordinated ligand in **4** in toluene are 0.52 and 0.27, respectively ($\lambda_{\text{ex}} = 402 \text{ nm}$, room temperature). The observed quantum yield for the Eu^{III} emission is the highest reported value for such visible-light-sensitized Eu complexes. When the temperature was reduced to 77 K, the ligand

emission band at 430 nm vanished completely to leave only the intense $^5\text{D}_0 \rightarrow ^7\text{F}_{0-4}$ emission of Eu^{III} . This indicates that the Ligand-to- Eu^{III} energy transfer is more efficient at lower temperatures.

The kinetics and the time-resolved spectra of the luminescence from **4** were recorded on different timescales as shown in Figures 2a–d. On the nanosecond timescale (Figure 2a) and immediately following the pulsed excitation at 400 nm, broad spectra which extend up to 620 nm were observed (inset, 1–4 ns). These broad signals arise from the red edge of the $\text{S}_1 \rightarrow \text{S}_0$ fluorescent emission of the coordi-

nated ligand that is centered at $\approx 430 \text{ nm}$. Simultaneously, the emission from the $^5\text{D}_1 \rightarrow ^7\text{F}_3$ transition of the Eu^{III} ion at 585 nm is also clearly seen. The intensities of these signals vary upon increasing the delay time. The decay-time constant of the ligand S_1 -state emission exhibits a weak wavelength dependence, that is, 1.3 ns at 430 nm and 1.8 ns at 605 nm. On the other hand, the rise-time constant of the $^5\text{D}_1$ luminescence at 585 nm is found to be 1.8 ns. This decay-to-rise correlation strongly suggests direct energy transfer from the S_1 state of the coordinated ligand **3** to the $^5\text{D}_1$ state of Eu^{III} .

On the sub-microsecond timescale (Figure 2b), a tight correlation between the decay of the $^5\text{D}_1 \rightarrow ^7\text{F}_{1-3}$ luminescence signals at 535, 555, and 585 nm (decay constant, 387 ns) and the rise of the $^5\text{D}_0 \rightarrow ^7\text{F}_2$ luminescence at 614 nm (rise constant, 392 ns) can be established; this indicates the transfer of the excited-state population from the $^5\text{D}_1$ state to the $^5\text{D}_0$ state of the Eu^{III} ion. The kinetics of the $^5\text{D}_0 \rightarrow ^7\text{F}_2$ luminescence of Eu^{III} at 614 nm was examined on the millisecond timescale (Figure 2c). The lifetimes of the excited state are 0.48 and 0.65 ms at room temperature and 77 K, respectively.

To determine the energy of the T_1 state of the coordinated ligand **3**, we performed time-resolved phosphorescence measurements at 77 K (Figure 2d). The emission spectrum reveals an asymmetric broad phosphorescence band centered at $\approx 525 \text{ nm}$ ($19\,048 \text{ cm}^{-1}$) with a weak reminiscent $^5\text{D}_0 \rightarrow ^7\text{F}_2$ emission band at 614 nm. Most importantly, the lifetime of the T_1 -state of the coordinated ligand is determined to be 3.9 s, which is significantly longer than the lifetime of the $^5\text{D}_0$ state of the Eu^{III} metal center (0.65 ms). Therefore the excitation-energy transfer from the triplet state of the coordinated ligand **3** to the emissive states of the Eu^{III} ion ($^5\text{D}_1$ and $^5\text{D}_0$), if any, would have a very low probability ($< 10^{-3}$).^[9–10] On the basis of the above observations, we conclude that the sensitization of the Eu^{III} emission in complex **4** proceeds through the singlet pathway, whereas the triplet pathway is essentially inactive (Figure 3).

In conclusion, we have demonstrated the first observable case of excitation-energy transfer from the ligand to the luminescent states of Eu^{III} ion through the singlet pathway in a visible-light-sensitized europium complex. The excitation window for this complex has been extended up to 460 nm.

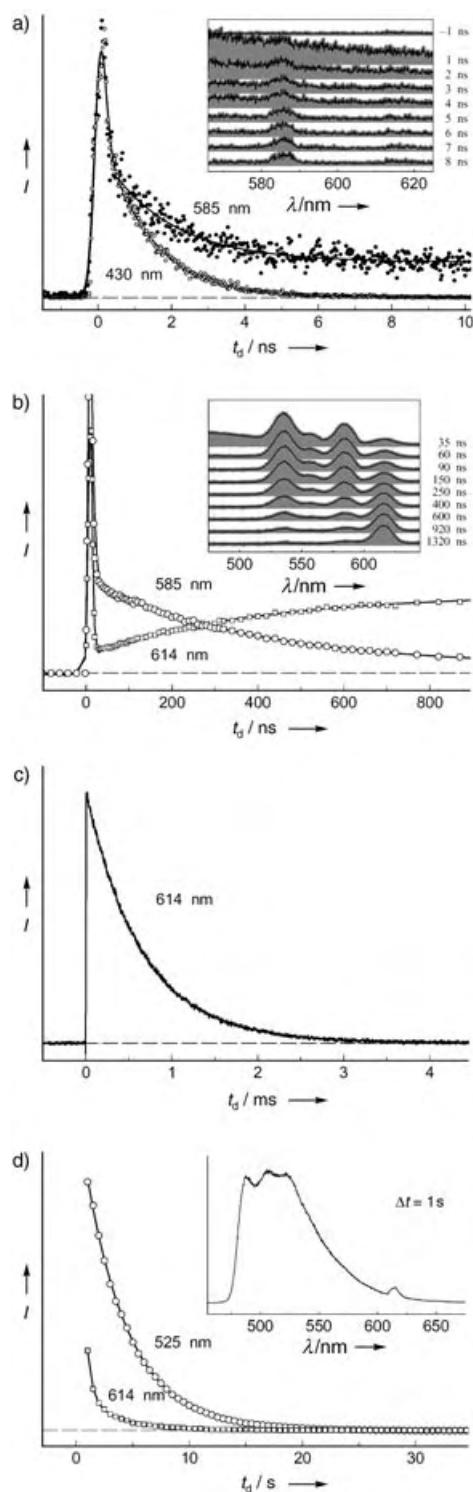


Figure 2. The time-resolved luminescence spectra of complex **4** in toluene on different timescales recorded at room temperature (a, b) and 77 K (c, d). a) Kinetics curves at 430 nm (○) and 585 nm (●) with an excitation pulse at 400 nm (130 fs); the inset shows the luminescence spectra at different delay times (t_d). b) Kinetics curves at 585 nm (○) and 614 nm (□) with an excitation pulse at 417 nm (5 ns); the inset shows the luminescence spectra at different delay times. c) Kinetics curves at 614 nm with an excitation pulse at 417 nm (5 ns). d) Kinetics curves at 525 nm (○) and 614 nm (□); the inset shows the phosphorescence spectrum of complex **4** after a delay time of 1 s.

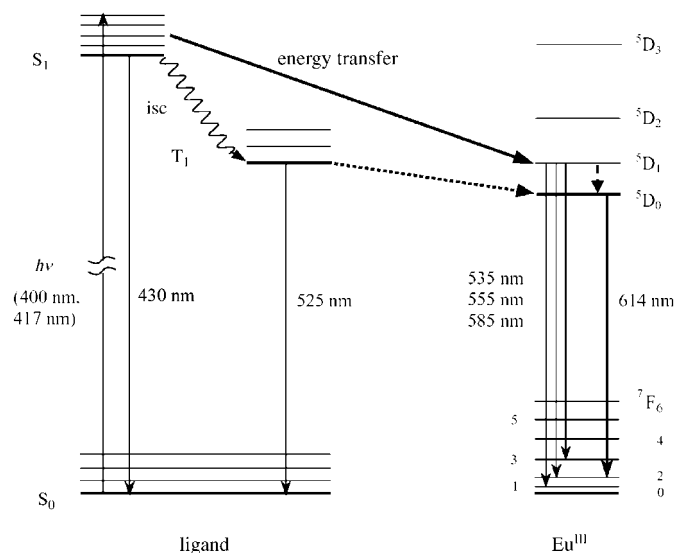


Figure 3. Energy-level diagram showing the energy-transfer pathways in complex **4**; isc denotes intersystem crossing.

Experimental Section

3: Potassium (0.08 g, 2.07 mmol) was added to a stirred solution of 3,5-dimethylpyrazole (0.288 g, 3.0 mmol) in dry THF (30 mL) under N_2 at 70 °C. After the metal dissolved, the colorless solution was cooled to $\approx 10^\circ C$ and **2** (0.297 g, 1.0 mmol) was added. The reaction mixture was stirred at room temperature for 0.5 h and then heated at reflux for 5 h. The solution was concentrated under reduced pressure, and the residue was purified by column chromatography on silica gel with a mixture of petroleum ether and benzene as eluent to afford **3** (0.36 g, 86 %). M.p. 235–236 °C; 1H NMR ($CDCl_3$, 300 MHz, 25 °C, TMS): δ = 8.39 (d, $^3J(H,H)$ = 9.2 Hz, 2H; Ph-H), 6.72 (d, $^3J(H,H)$ = 9.1 Hz, 2H; Ph-H), 6.08 (s, 2H; Pz-H), 3.46 (q, $^3J(H,H)$ = 7.0 Hz, 4H; NCH_2CH_3), 2.85 (s, 6H; Pz- CH_3), 2.35 (s, 6H; Pz- CH_3), 1.23 ppm (t, $^3J(H,H)$ = 6.9 Hz, 6H; NCH_2CH_3); ^{13}C NMR (300 MHz, $CDCl_3$, 25 °C, TMS): δ = 173.37, 163.98, 152.48, 151.59, 143.95, 131.57, 121.23, 111.35, 110.68, 44.64, 16.06, 14.06, 12.60 ppm; IR (KBr): $\tilde{\nu}$ = 2983, 2955, 2893, 2863 (C-H), 1587 (C=N), 1560 (C=N), 1537, 1509 (C=N), 1409 (C=N), 1389, 1355, 1338, 1268, 1184, 1067, 970, 803, 747 cm^{-1} ; FAB MS (nba): m/z : 417 [$M+1$]; elemental analysis: calcd for $C_{25}H_{28}N_8$: C 66.32, H 6.78, N 26.90; found: C 66.28, H 6.78, N 26.81 %.

4: A solution of $Eu(tta)_3 \cdot 3H_2O$ (87 mg, 0.1 mmol) in THF (10 mL) was added to a solution of **3** (41.6 mg, 0.1 mmol) in THF (10 mL) to give instantaneously a yellow solution with very bright red luminescence in daylight. After evaporation of the solvent, the residue was redissolved in a small amount of diethyl ether. Addition of *n*-hexane to the solution led to the precipitation of the ternary complex of $[Eu(tta)_3(\mathbf{3})]$ (**4**) as an orange powder ($\approx 86\%$). M.p. 138–139 °C; 1H NMR ($CDCl_3$, 300 MHz, 25 °C, TMS): δ = 25.54 (s, 3H; CH), 12.22 (s, 2H; Pz-H), 7.43 (d, $^3J(H,H)$ = 8.2 Hz, 2H; Ph-H), 6.91 (s, 3H; Th-H), 6.05 (s, 3H; Th-H), 5.90 (d, $^3J(H,H)$ = 8.2 Hz, 2H; Ph-H), 5.03 (s, 3H; Th-H), 4.82 (s, 6H; Pz- CH_3), 3.31 (q, $^3J(H,H)$ = 6.9 Hz, 4H; NCH_2CH_3), 0.95 (t, $^3J(H,H)$ = 6.6 Hz, 6H; NCH_2CH_3), –0.06 ppm (s, 6H; Pz- CH_3); IR (KBr): $\tilde{\nu}$ = 2978, 2931 (C-H), 1612, 1591, 1559 (C=N), 1538, 1502, 1415 (C=N), 1393, 1353, 1304, 1185, 1140, 1037, 808 (C=N), 783, 751, 716, 692, 641, 580 cm^{-1} ; FAB MS: m/z : 1232 [M^+]; elemental analysis: calcd for $EuC_{47}H_{40}N_8F_9O_6S_3$: C 45.82, H 3.27, N 9.10, S 7.81; found: C 45.35, H 3.28, N 9.03, S 7.59 %.

Steady-state UV/Vis absorption and photoluminescence (PL) measurements were carried out on an absorption spectrometer (U-

3310, Hitachi) and a fluorescence spectrophotometer (F-2500, Hitachi), respectively. Luminescence quantum yields were determined by the method described by Demas and Grosby,^[11] with 4-dicyanomethylene-2-methyl-6-*p*-dimethylaminostyryl-4*H*-pyran ($\Phi = 0.71$) as the reference.^[12]

Time-resolved PL spectroscopy on the nanosecond timescale was performed on a photon-counting type streak camera (C2909, Hamamatsu) combined with a polychromator (Chromex 250is, Chromex); the excitation pulses were provided by a regenerative amplifier (Spitfire, Spectra Physics), whose output wavelength was converted to 400 nm with the second-harmonic generation (≈ 200 nj, 120 fs, 1 KHz). The time-resolution was 30 ps. For the sub-microsecond PL measurements, a gated linear photodiode-array detector (1420, EG&G; gate width 5 ns) attached to a polychromator was employed; the excitation pulses (417 nm, 1 mj, 5 ns) were obtained with a hydrogen-charged Raman shifter (2 MPa) which was pumped by the third harmonics of a Nd:YAG laser (355 nm, 1 Hz, 40 mJ/pulse). The PL kinetics on a millisecond timescale were recorded on a PMT (R298, Hamamatsu) detector attached to a monochromator. The time-resolved phosphorescence measurements were carried out at 77 K. Excitation was realized with the aforementioned 400 nm laser beam, which was chopped by an electric shutter; phosphorescence emissions were sent to a polychromator (Spectropro 550i, Acton) equipped with a liquid-nitrogen cooled CCD detector (SPEC-10-400B/LN, Roper Scientific). A delay-pulse generator (DG535, Stanford Research System) was used to trigger the CCD detection (exposure time 0.1 s) at various delay times with intervals of 0.5 s.

Received: February 28, 2004

Revised: May 25, 2004 [Z54141]

Keywords: energy-transfer mechanisms · europium · luminescence · sensitizers · time-resolved spectroscopy

[10] As the T_1 level of the coordinated **3** (19048 cm^{-1}) in **1** seems suitably located for energy transfer to the 5D_1 (19000 cm^{-1}) and the 5D_0 (17500 cm^{-1}) states of the Eu^{III} ion, the unusually low probability of the ligand(T_1)-to- Eu^{III} ($^5D_{0-1}$) energy transfer is interesting and the reasons behind this are under current investigation.

[11] J. N. Demas, G. A. Crosby, *J. Phys. Chem.* **1971**, 75, 991–1024.

[12] P. R. Hammond, *Opt. Commun.* **1979**, 29, 331–334.

- [1] a) V. Vicinelli, P. Ceroni, M. Maestri, V. Balzani, M. Gorka, F. Vögtle, *J. Am. Chem. Soc.* **2002**, 124, 6461–6468; b) J. L. Bender, P. S. Corbin, C. L. Fraser, D. H. Metcalf, F. S. Richardson, E. L. Thomas, A. M. Urbas, *J. Am. Chem. Soc.* **2002**, 124, 8526–8527.
- [2] a) F. J. Steemers, W. Verboom, D. N. Reinhoudt, E. B. van der Tol, J. W. Verhoeven, *J. Am. Chem. Soc.* **1995**, 117, 9408–9414; b) M. Latva, H. Takalo, V. M. Mikkala, C. Matachescu, J.-C. Rodriguez-Ubis, J. Kankare, *J. Lumin.* **1997**, 75, 149–169.
- [3] M. H. V. Werts, M. A. Duin, J. W. Hofstraat, J. W. Verhoeven, *Chem. Commun.* **1999**, 799–800.
- [4] a) A. Dadabhoy, S. Faulkner, P. G. Sammes, *J. Chem. Soc. Perkin Trans. 2* **2000**, 2359–2360; b) A. Beeby, L. M. Bushby, D. Maffeo, J. A. G. Williams, *J. Chem. Soc. Perkin Trans. 2* **2000**, 1281–1283; c) Y. Bretonniere, M. J. Cann, D. Parker, R. Slater, *Chem. Commun.* **2002**, 1930–1931.
- [5] M. J. Kleinerman, *J. Chem. Phys.* **1969**, 51, 2370–2375.
- [6] a) W. D. Horrocks, Jr., W. E. Collier, *J. Am. Chem. Soc.* **1981**, 103, 2856–2862; b) J. Bruno, W. D. Horrocks, Jr., R. J. Zauhar, *Biochemistry* **1992**, 31, 7016–7026.
- [7] a) S. I. Klink, G. A. Hebbink, L. Grave, P. G. B. Oude Alink, F. C. J. M. van Veggel, M. H. V. Werts, *J. Phys. Chem. A* **2002**, 106, 3681–3689; b) G. F. de Sá, O. L. Malta, C. de Mello Donegá, A. M. Simas, R. L. Longo, P. A. Santa-Cruz, E. F. da Silva, Jr., *Coord. Chem. Rev.* **2000**, 196, 165–195.
- [8] a) C. Yang, W. T. Wong, *J. Mater. Chem.* **2001**, 11, 1298–1300; b) C. Yang, X. M. Chen, Y. S. Yang, *J. Chem. Soc. Dalton Trans.* **1996**, 1767–1768.
- [9] Nonparticipation of the first triplet state of the ligand in intramolecular energy transfer in Eu^{III} complexes with Ruhe-mann's purple has been observed: I. M. Alaoui, *J. Phys. Chem.* **1995**, 99, 13280–13282.

Enantioselectivity Determination

Direct Visual Detection of the Stereoselectivity of
a Catalytic Reaction***Rienk Eelkema, Richard A. van Delden, and
Ben L. Feringa**

The unique handedness of the essential molecules of life and the key role of homochirality in the development of new drugs^[1] is a source of inspiration for numerous efforts to design efficient catalytic procedures to prepare single enantiomers of biologically active compounds.^[2] The analysis of the enantioselectivity in the (high-throughput) screening of asymmetric catalysts^[3] is often the rate-determining step,^[3,4] despite the introduction of ingenious combinatorial methods^[4–6] and miniaturization.^[3,4] Thus, an instant read-out of the enantiomeric excess of a chiral product would be an important step forward.^[7] Herein we report a color test for the rapid determination of the stereoselectivity of a catalytic conversion, which offers a simple solution to the fundamental challenge of directly visualizing the molecular chirality of a reaction product. The incorporation of a mesogenic unit into a typical substrate used in the screening of chiral catalysts allows the immediate assessment of the enantiomeric excess of the product from the color induced in a liquid-crystalline matrix.

[*] R. Eelkema, Dr. R. A. van Delden, Prof. Dr. B. L. Feringa
Department of Organic and Molecular Inorganic Chemistry
Stratingh Institute
University of Groningen
Nijenborgh 4, 9747 AG Groningen (The Netherlands)
Fax: (+31) 50-363-4296
E-mail: feringa@chem.rug.nl

[**] This work was supported by the Chemical Sciences division of the Netherlands Organization for Scientific Research (NWO-CW). We would like to thank M. B. van Gelder and T. D. Tiemersma-Wegman for carrying out the HPLC separations, A. Duursma for providing (S)-1,3-diphenyl-1-pentanone (**2**), and Dr. H. Bernsmann for providing some of the ligands.



Supporting information for this article is available on the WWW under <http://www.angewandte.org> or from the author.

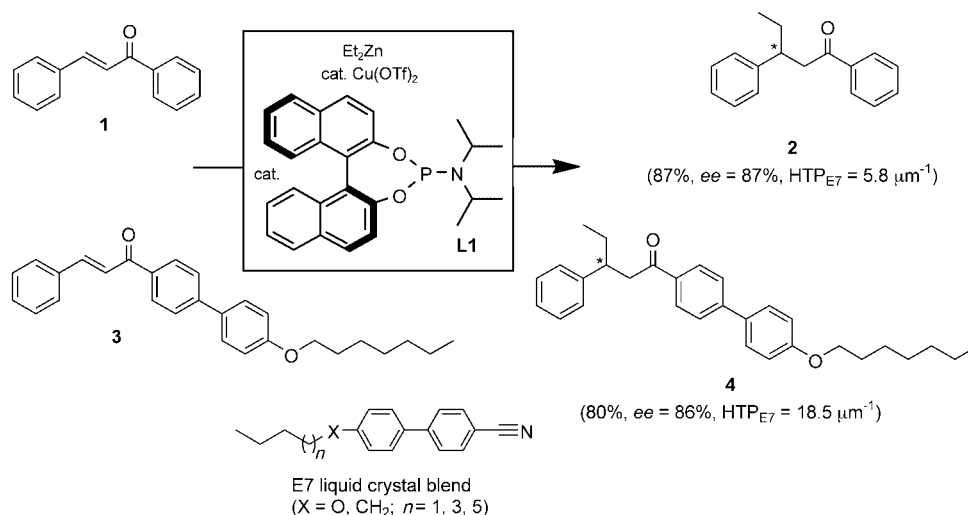
Our design is based on the principle of color generation in doped cholesteric liquid-crystalline (LC) films.^[8] Cholesteric or twisted nematic liquid-crystalline phases can be induced by doping an achiral nematic liquid-crystalline host compound with a suitable chiral nonracemic guest molecule (the dopant).^[9] Aligned films of these liquid-crystalline phases are known to reflect light of a particular wavelength. The wavelength can be tuned within the range of the visible spectrum (ca. 360–700 nm) by careful choice of the chiral dopant and leads to brightly colored liquid-crystalline films. The reflected wavelength is dependent on the pitch (p) and the refractive index (n) of the material as well as on the incident angle (α) of the light. The pitch, in turn, is inversely proportional to the concentration (c), the helical twisting power (β), and, most importantly for the present application, the enantiomeric excess (ee) of the chiral guest molecule. The wavelength of reflection is directly related to the enantiomeric excess according to Equation (1).^[9]

$$\lambda(\alpha) = np \cos[\sin^{-1}(\sin \alpha / n)] = n (\beta c ee)^{-1} \cos[\sin^{-1}(\sin \alpha / n)] \quad (1)$$

The helical twisting power, which is an intrinsic property of any chiral dopant, is a measure of the efficiency of the molecule to cause helical induction in a liquid-crystalline matrix. In general, the magnitude of the helical twisting power of typical products of enantioselective catalytic transformations is too small to obtain colored liquid-crystalline phases, since there is a limit to the dopant concentration in a liquid-crystalline host. To overcome this problem we envisioned that a reaction product with high structural resemblance to the liquid-crystalline host should give rise to both a higher helical twisting power and an improved compatibility. Recently, we reported a method based on this principle, which allowed the evaluation of the enantiomeric excess of chiral products by simple inspection of the color after a derivatization step.^[10,11] The major drawback of this method, particularly when performing multiple parallel reactions, is the essential, but time-consuming, derivatization step.

The common practice for initial screening of new effective catalysts involves conversion of benchmark reagents, thus we reasoned that a simple redesign of such substrates to incorporate a mesogenic unit would result in an immediate color test to assess the stereochemical outcome of a particular catalytic conversion. In other words, when the product of the enantioselective catalysis itself structurally resembles the liquid-crystalline host the enantiomeric excess can be deter-

mined directly after doping, without the need for any derivatization. To demonstrate this concept we chose the copper-catalyzed asymmetric conjugate addition of diethylzinc to chalcone as a model reaction, as this is a well-described and extensively studied C–C bond-formation reaction (Scheme 1).^[12–15]



Scheme 1. Copper-catalyzed asymmetric conjugate addition of diethylzinc to chalcone (**1**) and *para-n*-heptyloxyphenyl-substituted chalcone **3**. Tf = trifluoromethanesulfonyl.

The ethyl adduct **2** of the benchmark reagent chalcone **1** shows no structural resemblance to the liquid-crystalline host E7 and results in a low helical twisting power of $5.8 \mu\text{m}^{-1}$.^[16] It is, therefore, not possible to generate a colored liquid-crystalline film using E7 doped with **2**. To realize a structural resemblance between the asymmetric conjugate addition product and E7 we employed *para-n*-heptyloxyphenyl-substituted chalcone **3** (see Supporting Information) as a starting material instead of chalcone (**1**). A prominent structural motif both in the LC host material E7 and chiral product **4** is the *para*-alkoxy-substituted biphenyl mesogenic unit. This feature resulted in a significantly higher helical twisting power of $18.5 \mu\text{m}^{-1}$ for **4**, thus allowing color generation in liquid-crystalline films aligned on a polyimide-coated glass plate. In accordance with Equation (1), doping of achiral E7 with 21 wt % of enantiomerically pure **4** resulted in a violet-blue liquid-crystalline film. Samples of E7 doped with **4** with 100, 90, 80, 70, 60, and 50 % ee (prepared by mixing enantiomerically pure and racemic **4**) afforded liquid-crystalline phases with colors ranging from violet-blue (100 % ee) to deep red (50 % ee), thus allowing direct visual determination of the enantiomeric excess of the chiral dopant (Figure 1). The enantiomeric excess of the product can further be quantified by measuring the exact wavelength of reflection with high accuracy, since a change in the ee value of only 1 % results in a readily detectable shift of at least 4.0 nm in the wavelength of maximum reflection. A calibration curve for the determination of the enantiomeric excess was obtained during the spectroscopic measurement of the reflection wavelength of

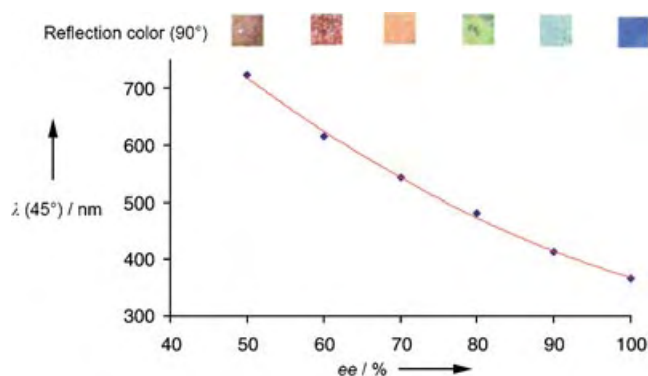


Figure 1. Color (90°) and wavelength ($\lambda(45^\circ)$) of the reflection of E7 doped with 21 wt% of **4** with different *ee* values. The depicted colors are photographs of the LC samples taken perpendicular (90°) to the surface of the film. The wavelengths of maximum reflection were measured at an incident light angle of 45°.

the colored phases described above (at an incident angle of 45°; Figure 1).

For compound **3** to be applicable as a benchmark reagent for enantioselective conjugate additions it is essential that yields and enantioselectivities are comparable to those of **1**, the typical substrate for these reactions. Compound **3** was tested as a substrate in the catalytic conjugate addition of diethylzinc using $\text{Cu}(\text{OTf})_2$ and ligand L1. It was rewarding to observe similar yields and enantioselectivities to those obtained for chalcone **1** (Scheme 1). The only difference was that compound **3** showed low solubility in toluene (the common solvent for these reactions) at -25°C ,^[13] and therefore the reactions on this substrate were performed in dichloromethane. However, the change in solvent had only a minor influence on the yield and the enantioselectivity of the reaction.

To examine whether it is possible to measure the enantioselectivity of a conjugate addition reaction directly by applying the method and substrate described above, six chiral phosphoramidite ligands were tested (Table 1). This class of ligands is widely applied in conjugate additions to effect C–C bond formation.^[13,15] The reactions were performed under standard conditions, and after quenching the reaction mixture and a simple filtration to remove the zinc and copper salts (as described in the Experimental Section) 21 wt% mixtures of the product and liquid-crystalline host E7 were applied to linearly rubbed, polyimide-coated glass plates to

generate colored liquid-crystalline films (Table 1). Comparison of the colors of these films to those of films of E7 doped with **4** with various known *ee* values allows quantification of the enantioselectivity of the reaction by visual inspection (Figure 1). It was possible to accurately assess the enantiomeric excess of product **4** by measuring the reflection wavelength and using the calibration curve depicted in Figure 1. To ascertain the accuracy of our new technique the *ee* values obtained from the color test were compared to those determined by HPLC on a chiral stationary phase. An excellent correlation was found in all cases, especially between the values obtained by reflection wavelength measurements and HPLC. The values obtained by visual inspection are less precise, although a difference in an *ee* value of $\leq 5\%$ can readily be detected by the naked eye. The possibility of visual inspection offers the advantage of instant read-out of the enantiomeric excess, which is ideal for screening purposes in combinatorial catalysis. Full conversion into the desired product was always achieved in these reactions; however, this color test can still be applied even if full conversion is not reached, since in this case the observed color can act as a measure of the combination of conversion and *ee* value [Eq. (1)].^[17]

These results clearly demonstrate that it is possible to determine the enantiomeric excess of the product of a catalytic asymmetric reaction by a liquid-crystalline-based color test, as illustrated for a key carbon–carbon bond-forming reaction. In the 1,4-addition of diethylzinc to **3**, product **4** was obtained with yields and enantioselectivities similar to the ethyl adduct of chalcone, which is a common

Table 1: Screening results of chiral catalysts,^[a] comparison of methods for the determination of *ee* values.

Ligand	Ligand structure	Color	<i>ee</i> (reflection wavelength) [%]	<i>ee</i> (HPLC) [%]
L1			86	86
L2			71	72
L3			60	59
L4			66	64
L5			60	58
L6			71	74

[a] Ligands were tested in the reaction with **3** in Scheme 1. See Experimental Section for details.

substrate in catalytic reactions leading to C–C bond formation. These results make substrate **3** a valuable benchmark reagent for these reactions. Enantioselectivities can be determined visually (by looking at the color of an aligned liquid-crystalline film doped with the product) or spectroscopically (by measuring the reflection wavelength and comparing it with a calibration curve). Both methods, although of different accuracy, give *ee* values comparable to results obtained by HPLC on a chiral stationary phase. This new procedure involves simple filtration and mixing, and does not require chiral auxiliaries or post-reaction derivatization. Furthermore, microgram quantities of product are sufficient. In conclusion, this methodology allows fast and accurate screening of enantioselectivities in asymmetric catalysis, and the development of simple color tests for a wide range of asymmetric transformations is envisioned based on this principle.

Experimental Section

General procedure: A chiral ligand (L1–L6, 15.0 μ mol, 10 mol %), Cu(OTf)₂ (2.7 mg, 7.5 μ mol, 5 mol %), and dichloromethane (4.2 mL) were added to a flame-dried Schlenk flask under argon. The mixture was stirred for 1 h at room temperature, and then substrate **3** (60.0 mg, 0.15 mmol) was added. This mixture was stirred for an additional 15 min and subsequently cooled to –25 °C. Et₂Zn (0.35 mL, 1.0 M solution in hexanes) was added and the mixture was stirred for 2 days at –25 °C. The reaction was then quenched by the addition of saturated aqueous NH₄Cl (1 mL). The resulting mixture was dissolved in dichloromethane (50 mL) and filtered through a 3-cm plug of SiO₂ and collected in a flask of known weight. After evaporation of the solvent, the flask was weighed to determine the yield of the product (typically around 54 mg). The product was dissolved in toluene (5.0 mL) and an appropriate amount of this solution containing 0.80 mg of product was mixed with 85.7 μ L of a stock solution of E7 in toluene (17.55 mg in 500 μ L). The solution was then poured onto a linearly rubbed, polyimide-coated glass plate. The color appeared immediately after evaporation of the toluene in the air at room temperature. These phases were stable for 1–3 days, depending on the cholesteric pitch. The colors of these phases could be detected by visual inspection or by measuring the reflection wavelength at a 45° angle by using a modified UV apparatus.

Received: May 28, 2004

Keywords: asymmetric catalysis · chirality · combinatorial chemistry · enantioselectivity · liquid crystals

- [8] D. Dunmur, K. Taniyama in *Handbook of liquid crystals, Vol. 1: Fundamentals* (Eds.: D. Demus, J. Goodby, G. W. Gray, H.-W. Spiess, V. Vill), Wiley-VCH, Weinheim, **1998**, pp. 215–239.
- [9] G. Solladié, R. G. Zimmermann, *Angew. Chem.* **1984**, *96*, 335–349; *Angew. Chem. Int. Ed. Engl.* **1984**, *23*, 348–362.
- [10] R. A. van Delden, B. L. Feringa, *Angew. Chem.* **2001**, *113*, 3298–3300; *Angew. Chem. Int. Ed.* **2001**, *40*, 3198–3200.
- [11] R. A. van Delden, B. L. Feringa, *Chem. Commun.* **2002**, 174–175.
- [12] Y. Chouan, Y. Yamamoto in *Modern Organocopper Chemistry* (Ed.: N. Krause), Wiley-VCH, Weinheim, **2002**, pp. 289–314.
- [13] B. L. Feringa, *Acc. Chem. Res.* **2000**, *33*, 346–353.
- [14] X. Hu, H. Chen, X. Zhang, *Angew. Chem.* **1999**, *111*, 3720–3723; *Angew. Chem. Int. Ed.* **1999**, *38*, 3518–3521.
- [15] N. Krause, A. Hoffmann-Röder, *Synthesis* **2001**, 171–196.
- [16] G. Heppke, F. Oestreicher, *Mol. Cryst. Liq. Cryst.* **1977**, *41*, 245–249.
- [17] A colored LC phase can be obtained, in theory, from any reaction mixture for **4** (% *ee* × % conversion) ≥ 5000 [Eq. (1)]. However, at this point no discrimination between the *ee* value and conversion can be made, but as a good chiral catalyst should give high conversion as well as high enantioselectivity this method can be applied in the screening of both quantities at the same time.

- [1] M. Breuer, K. Ditrich, T. Habicher, B. Hauer, M. Keßler, R. Stürmer, T. Zelinski, *Angew. Chem.* **2004**, *116*, 806–843; *Angew. Chem. Int. Ed.* **2004**, *43*, 788–824.
- [2] *Comprehensive asymmetric catalysis I–III* (Eds.: E. N. Jacobsen, A. Pfaltz, H. Yamamoto), Springer, Berlin, **1999**.
- [3] M. T. Reetz, *Angew. Chem.* **2002**, *114*, 1391–1394; *Angew. Chem. Int. Ed.* **2002**, *41*, 1335–1338.
- [4] M. T. Reetz, *Angew. Chem.* **2001**, *113*, 292–320; *Angew. Chem. Int. Ed.* **2001**, *40*, 284–310.
- [5] C. Markert, A. Pfaltz, *Angew. Chem.* **2001**, *113*, 2552–2554; *Angew. Chem. Int. Ed.* **2004**, *43*, 2498–2500.
- [6] P. Tielmann, M. Boese, M. Luft, M. T. Reetz, *Chem. Eur. J.* **2003**, *9*, 3882–3887.
- [7] Y. Kubo, S. Maeda, S. Tokita, M. Kubo, *Nature* **1996**, *382*, 522–524.

Self-Assembly

Kinetic Self-Assembly: Selective Cross-Catenation of Two Sterically Differentiated Pd^{II}-Coordination Rings***Akiko Hori, Ken-ichi Yamashita, and Makoto Fujita**

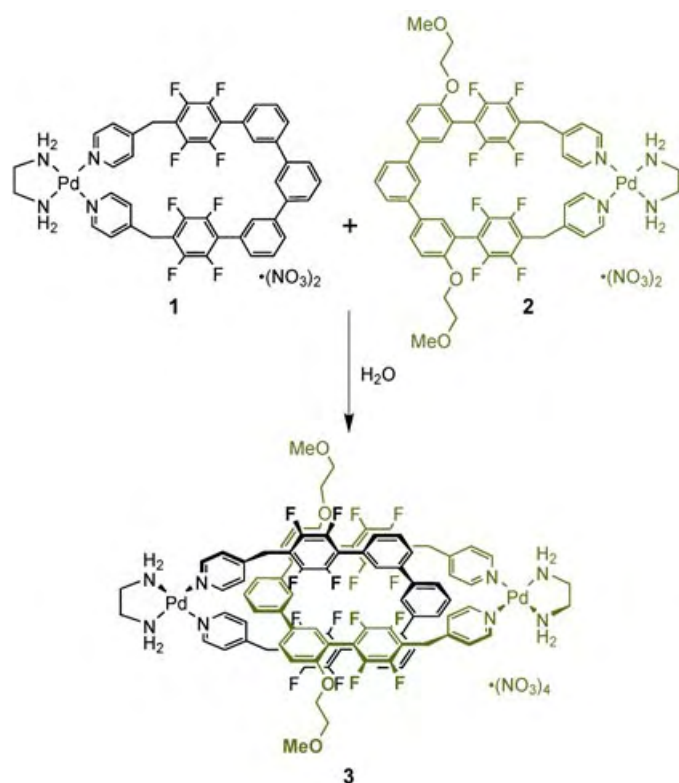
Like protein folding, self-assembly in biology is considered to be a kinetic process where the most favorable pathway to programmed structures is kinetically selected through meta-stable intermediary structures.^[1–3] Although numerous reports have appeared on thermodynamically controlled self-assembly,^[4–8] relatively few have discussed kinetic self-assembly in chemical systems.^[9–13] Here we deal with kinetic self-assembly based on the dynamic behavior of coordination rings. We emphasize that designing not only structures but also pathways is an important yet unexplored task for controlling molecular self-assembly.

The kinetic self-assembly discussed here is demonstrated by the cross-catenation^[14] of Pd^{II}-linked rings **1** and **2**, which

[*] Dr. A. Hori, K. Yamashita, Prof. Dr. M. Fujita
Department of Applied Chemistry, School of Engineering
The University of Tokyo
7-3-1 Hongo, Bunkyo-ku, Tokyo 113-8656 (Japan)
Fax: (+81) 3-5841-7257
E-mail: mfujita@appchem.t.u-tokyo.ac.jp

[**] This research was supported by the CREST project of the Japan Science and Technology Corporation (JST), for which M.F. is the principal investigator, and also, in part, by Genesis Research Institute, Inc., to which A.H. is thankful for a fellowship.

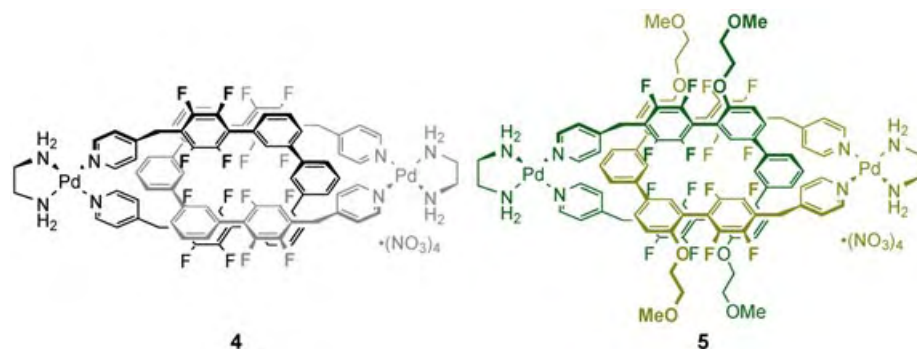
are differentiated by alkoxy side chains (Scheme 1). The homocatenation of **2** is kinetically unfavorable because of the steric demand of the alkoxy side chains.^[15] Accordingly, ring **2**



Scheme 1.

is only allowed to thread on less-hindered **1**, thus giving rise to the kinetic formation of cross-catenane **3**.

We first estimated the timescale of the homocatenation of **1** by 2D EXSY NMR spectroscopy.^[16] This sterically less hindered ring rapidly forms catenanes,^[17] and a clear correlation between **1** and its catenated dimer **4** was observed even after 30 ms mixing time, thus showing that the catenation takes place on a millisecond timescale. The rapid catenation should be retarded if a sterically demanding side chain is attached to the ligand of **1**. A bis(methoxyethoxy)-substituted ligand (the precursor of **2**) was synthesized and complexed



with $[\text{Pd}(\text{en})(\text{NO}_3)_2]$ (en = ethylenediamine) in DMSO to give **2** quantitatively. Since the catenation of Pd^{II} -linked rings is driven by aromatic-stacking interactions, which work efficiently in aqueous media,^[17] water was added to the solution of **2** in DMSO to transform it into homocatenane **5**. As expected, the catenation was significantly retarded, and took 4–5 h to be completed (Figure 1).

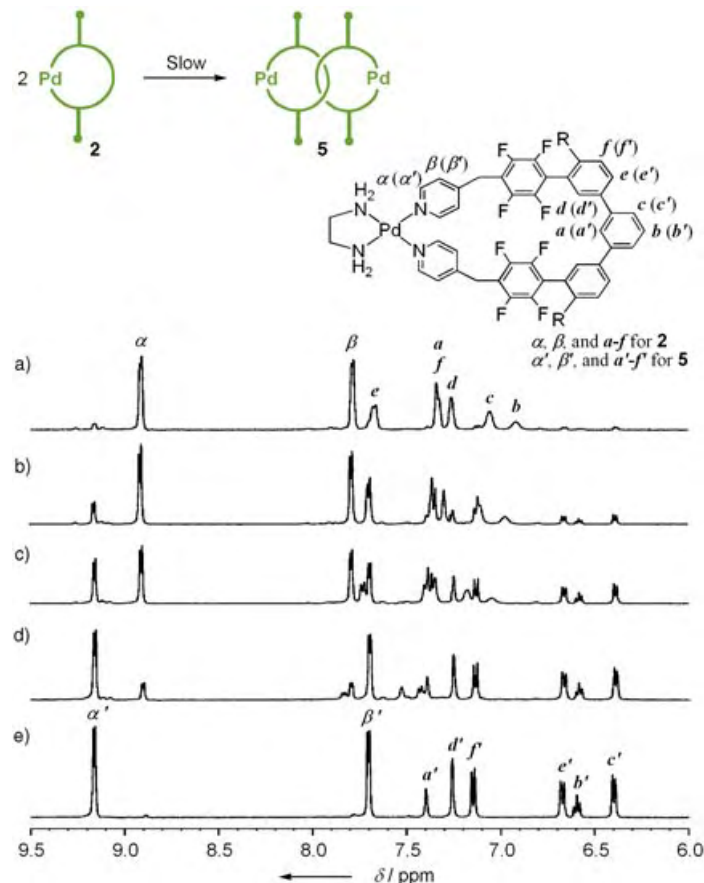


Figure 1. NMR spectra indicating the transformation of **2** into catenane **5** (aromatic region, 500 MHz, 300 K, $[\text{D}_6]\text{DMSO}/\text{D}_2\text{O}$ (1:1.5), TMS as an external standard); after a) 3 min, b) 10 min, c) 20 min, d) 60 min, e) 240 min.

Accordingly, we examined the cross-catenation of **1** and **2** by utilizing the large difference in the catenation rate of **1** and

2. Water (0.9 mL) was added to a solution of **1** (4.5 mg, 4.5 μmol) and **2** (5.2 mg, 4.5 μmol) in DMSO (0.6 mL) at ambient temperature. The two rings were immediately transformed into a single catenated product as indicated by NMR spectroscopic analysis (Figure 2). The large upfield shifts of the central aromatic protons are characteristic of interstrand stacking between the rings.^[18] Since this spectrum was different from those of homocatenated compounds **4** and **5**, the selec-

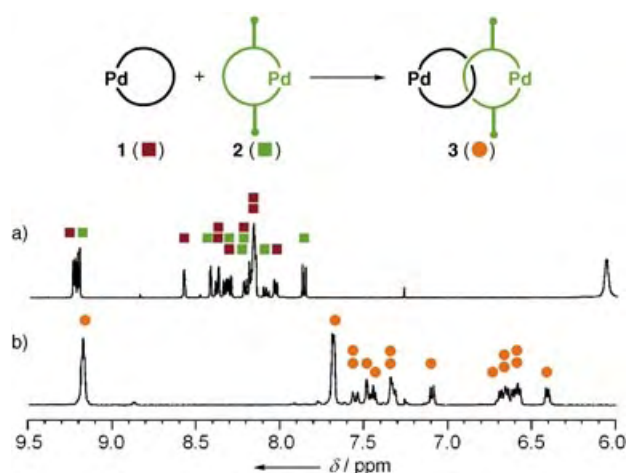


Figure 2. Observation of cross-catenation by NMR spectroscopy (aromatic region, 500 MHz, 300 K, TMS as an external standard): a) The spectrum of a mixture of **1** and **2** in $[D_6]DMSO$, b) the spectrum after the addition of D_2O .

tive formation of cross-catenane **3** was strongly suggested. A coldspray ionization mass spectrometry (CSI-MS)^[19] study confirmed the selective formation of cross-catenane **3** as evident from prominent signals that fully agreed with **3**: for example, m/z 572.0 $[3-(NO_3)_4+(DMSO)_5]^{4+}$ (Figure 3). Signals indicating the presence of **4** or **5** were barely visible.

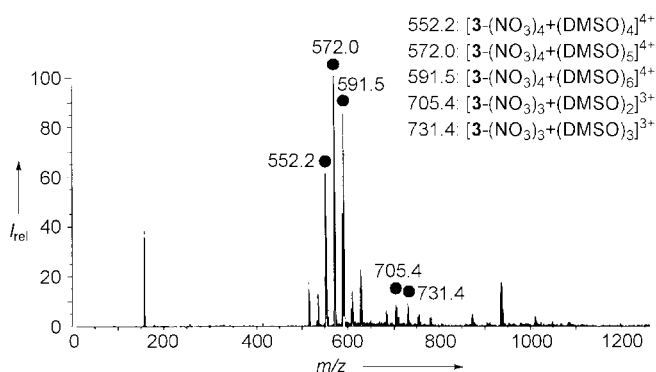


Figure 3. CSI mass spectrum of cross-catenane **3** in $DMSO/H_2O$ (1:1.5) solution.

The selective formation of **3** is explained by the energy diagram shown in Figure 4. Although three possible catenanes **3–5** have similar thermodynamic stability, the formation of **5** is kinetically inhibited because ring **2** must thread on the bulky ligand of **2** itself. Thus, the states [I] and [II] will rapidly equilibrate and favor the formation of cross-catenane **3**.

This speculation suggests that cross-catenane **3** (state [I]) will be equilibrated with **4** + **5** (state [III]) if the reaction time is long (or temperature is high) enough to promote the formation of **5**. In fact, when the solution of **3** was allowed to stand at 25 °C for a week, new signals assigned to homocatenanes appeared in the NMR spectrum. The ratio of **3**:**4**:**5** was estimated to be 4.3:1:1 and 2.8:1:1 after 1 day and 2 days, respectively. The ratio finally became statistical (2:1:1) after

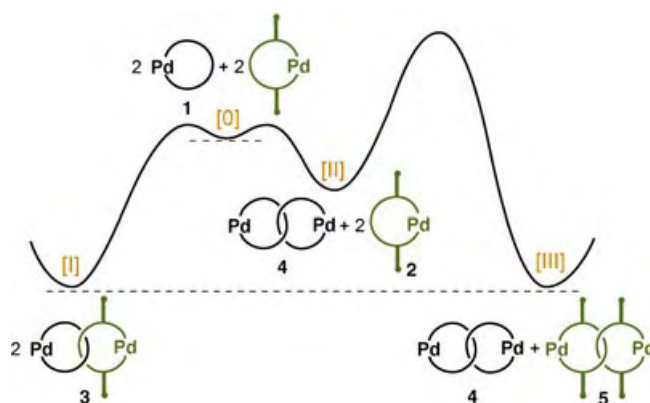


Figure 4. The energy diagram for the homo- and cross-catenation of **1** and **2**.

8 days. The same statistical mixture was also obtained when presynthesized catenanes **4** and **5** were combined in a mixture of H_2O and $DMSO$, and the solution was allowed to stand at 25 °C for 1 week. Clearly, the selective formation of cross-catenane over short times (minutes or hours) is kinetically controlled while the formation of a statistical mixture over longer times (days) is thermodynamically controlled. Of course, the equilibration became much slower at lower temperatures. The transformation of **3** into a statistical mixture took several months in a refrigerator (6 °C). Moreover, this transformation was completely suppressed in a freezer.

In summary, we have controlled the cross-catenation of two different rings by a kinetic method. Although still a preliminary study, the case detailed here demonstrates a new method of molecular self-assembly in which desired structures are generated by *programmed pathways*. Our results offer a good example of such kinetically controlled self-assembly and will, hopefully, be emulated by many other cases.

Received: May 15, 2004

Keywords: catenanes · molecular recognition · palladium · self-assembly

- [1] C. B. Anfinsen, *Science* **1973**, 181, 223.
- [2] P. A. Jennings, P. E. Wright, *Science* **1993**, 262, 892.
- [3] C. M. Dobson, A. Šali, M. Karplus, *Angew. Chem.* **1998**, 110, 908; *Angew. Chem. Int. Ed.* **1998**, 37, 868; A. R. Dinner, A. Šali, L. J. Smith, C. M. Dobson, M. Karplus, *Trends Biochem. Sci.* **2000**, 25, 331.
- [4] J.-M. Lehn, *Supramolecular Chemistry: Concepts and Perspectives*, VCH, Weinheim, **1995**.
- [5] J. L. Atwood, J. E. D. Davies, D. D. Macnicol, F. Vögtle, *Comprehensive Supramolecular Chemistry*, Vol. 9, Pergamon, Oxford, **1996**.
- [6] J.-M. Lehn, *Angew. Chem.* **1988**, 100, 91; *Angew. Chem. Int. Ed. Engl.* **1988**, 27, 89; J.-M. Lehn, *Angew. Chem.* **1990**, 102, 1347; *Angew. Chem. Int. Ed. Engl.* **1990**, 29, 1304.
- [7] J. S. Lindsey, *New J. Chem.* **1991**, 15, 153.
- [8] D. Philp, J. F. Stoddart, *Synlett* **1991**, 445.

- [9] M. Fujita, S. Nagao, K. Ogura, *J. Am. Chem. Soc.* **1995**, *117*, 1649; A. Hori, K. Kumazawa, T. Kusukawa, D. K. Chand, M. Fujita, S. Sakamoto, K. Yamaguchi, *Chem. Eur. J.* **2001**, *7*, 4142; S. Tashiro, M. Tominaga, T. Kusukawa, M. Kawano, S. Sakamoto, K. Yamaguchi, M. Fujita, *Angew. Chem.* **2003**, *115*, 3389; *Angew. Chem. Int. Ed.* **2003**, *42*, 3267.
- [10] B. Hasenknopf, J.-M. Lehn, N. Boumediene, E. Leize, A. V. Dorselaer, *Angew. Chem.* **1998**, *110*, 3458; *Angew. Chem. Int. Ed.* **1998**, *37*, 3265.
- [11] L. J. Prins, E. E. Neuteboom, V. Paraschiv, M. Crego-Calama, P. Timmerman, D. N. Reinhoudt, *J. Org. Chem.* **2002**, *67*, 4808; V. Paraschiv, M. Crego-Calama, T. Ishi-i, C. J. Padberg, P. Timmerman, D. N. Reinhoudt, *J. Am. Chem. Soc.* **2002**, *124*, 7638.
- [12] J. O. Jeppesen, J. Perkins, J. Becher, J. F. Stoddart, *Angew. Chem.* **2001**, *113*, 1256; *Angew. Chem. Int. Ed.* **2001**, *40*, 1216; J. O. Jeppesen, S. A. Vignon, J. F. Stoddart, *Chem. Eur. J.* **2003**, *9*, 4611; J. D. Badjie, S. J. Cantrill, J. F. Stoddart, *J. Am. Chem. Soc.* **2004**, *126*, 2288.
- [13] B. J. Holliday, Y.-M. Jeon, C. A. Mirkin, C. L. Stern, C. D. Incarvito, L. N. Zakharov, R. D. Sommer, A. L. Rheingold, *Organometallics* **2002**, *21*, 5713; B. J. Holliday, C. A. Mirkin, *Angew. Chem.* **2001**, *113*, 2076; *Angew. Chem. Int. Ed.* **2001**, *40*, 2022.
- [14] A. Hori, H. Kataoka, T. Okano, S. Sakamoto, K. Yamaguchi, M. Fujita, *Chem. Commun.* **2003**, 182; A. Hori, H. Kataoka, A. Akasaka, T. Okano, M. Fujita, *J. Polym. Sci. A* **2003**, *41*, 3478.
- [15] Molecular modeling studies clearly show that a Pd^{II}-linked ring cannot thread on the dissociated form of **2** because of the steric bulk of the side chain.
- [16] M. Fujita, F. Ibukuro, H. Seki, O. Kamo, M. Imanari, K. Ogura, *J. Am. Chem. Soc.* **1996**, *118*, 899.
- [17] A. Hori, A. Akasaka, K. Biradha, S. Sakamoto, K. Yamaguchi, M. Fujita, *Angew. Chem.* **2002**, *114*, 3403; *Angew. Chem. Int. Ed.* **2002**, *41*, 3269.
- [18] Selected data for **3**: ¹H NMR (500 MHz, [D₆]DMSO/D₂O = 1:1.5, 280 K, TMS as an external standard): δ = 9.23 (s, 8H, H_α and H_{α'}), 7.74 (s, 8H, H_β and H_{β'}), 7.61 (s, 1H, H_a), 7.59 (s, 1H, H_{a'}), 7.54 (s, 2H, H_d), 7.45 (t, *J* = 6.2 Hz, 2H, H_f), 7.39 (s, 2H, H_{f'}), 7.33 (d, *J* = 6.2 Hz, 2H, H_g), 7.11 (d, *J* = 8.0 Hz, 2H, H_f), 6.72 (t, *J* = 7.2 Hz, 1H, H_{g'}), 6.69 (d, *J* = 6.2 Hz, 2H, H_c), 6.64–6.58 (m, 5H, H_b, H_c, H_{c'}), 6.45 (d, *J* = 7.2 Hz, 2H, H_{c'}), 4.25 (s, 4H, CH₂), 4.17 (s, 8H, CH₂, CH_{2'}), 3.72 (s, 4H, CH₂), 3.32 (s, 6H, CH₃), 3.05 ppm (s, 8H, en, en'); ¹³C NMR (125 MHz, [D₆]DMSO/D₂O = 1:1.5, 280 K): δ = 155.4 (Cq), 152.1 (Cq), 152.0 (CH_a, CH_{a'}, Cq), 145.5–142.0 (4 × CF), 139.2 (Cq), 138.9 (Cq), 138.4 (Cq), 132.2 (Cq), 129.7 (CH_e), 129.6 (CH_f), 129.3, 129.2, 129.0 (CH_b, CH_{b'}, CH_{c'}), 128.1 (CH_β, CH_{β'}), 127.8 (CH_{d'}), 127.4 (Cq), 127.0 (CH_c), 126.4 (CH_d), 125.1 (CH_c), 124.2 (CH_{c'}), 123.3 (CH_a), 122.9 (CH_{a'}), 118.4 (Cq), 116.4 (Cq), 115.4–115.2 (3 × Cq), 113.9 (CH_f), 70.4 (CH_h), 68.5 (CH_g), 58.4 (CH_i), 46.9 (en, en'), 27.7 ppm (CH₂ and CH_{2'}).
- [19] S. Sakamoto, M. Fujita, K. Kim, K. Yamaguchi, *Tetrahedron* **2000**, *56*, 95.

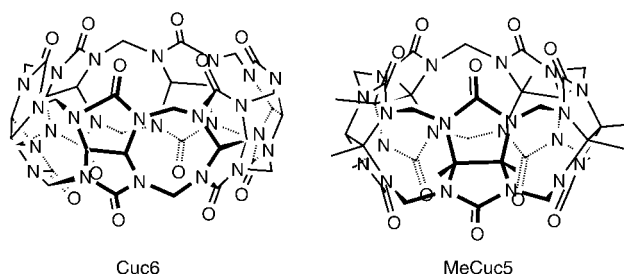
**Remarkably Facile Ring-Size Control in
Macrocyclization: Synthesis of
Hemicucurbit[6]uril and Hemicucurbit[12]uril****

Yuji Miyahara,* Kenta Goto, Masakazu Oka, and
Takahiko Inazu

*Dedicated to Professor Leo A. Paquette
on the occasion of his 70th birthday*

Recent developments in the chemistry of cucurbit[*n*]urils (Cuc N ; $n = 5-10$) reveal that their hydrophobic cavities are particularly useful for applications in supramolecular chemistry.^[1]

As previously reported, decamethylcucurbit[5]uril (MeCuc5) behaves as a “molecular” sieve if the portals, which are frilled by carbonyl oxygen atoms, are not stoppered



by cations.^[2] Since the polar interactions of the portals with cations are well known,^[3] we imagined that if the Cuc N molecules were cut in half along the equator, the resulting macrocycles, which we therefore call hemicucurbit[N]uril (hmCuc N), would capture a metal ion at the polar carbonyl side and an organic molecule at the hydrophobic ethylene side in the “cone” conformation.

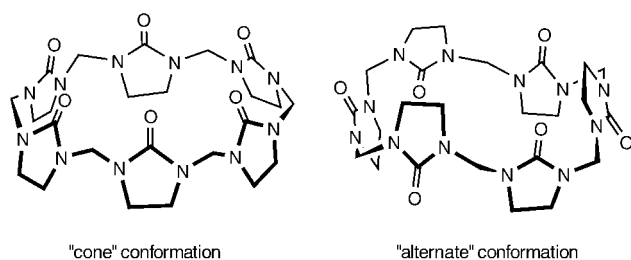
Since hmCuc N is simply a cyclic oligomer formed by condensation of ethyleneurea with formaldehyde we tried the reaction under the usual conditions used for synthesizing MeCuc5^[2] and Cuc N .^[4] However, the products of the reaction in concentrated acids at high temperatures were discolored syrups, from which no crystals could be isolated.

[*] Dr. Y. Miyahara, Dr. K. Goto, M. Oka, Emeritus Prof. T. Inazu
Department of Chemistry
Faculty of Sciences, Kyushu University
6-10-1 Hakozaki, Higashi-ku, Fukuoka 812-8581 (Japan)
Fax: (+81) 92-642-2607
E-mail: miyahscc@mbox.nc.kyushu-u.ac.jp

[**] The authors thank Prof. T. Shinmyozu of the Institute for Materials Chemistry and Engineering for use of a Rigaku RAPID X-ray instrument.



Supporting information for this article is available on the WWW under <http://www.angewandte.org> or from the author.



We found precedents for the condensation in the literature; for example, in 1955 Staudinger and Niessen reported linear oligomers with up to six ethyleneurea units.^[5] The higher polymers were prepared for practical applications.^[6] These studies indicate that the Mannich condensation itself proceeds even at pH 4 and suggest the possibility of forming hmCuc n under much milder conditions. This possibility is in sharp contrast to the synthesis of Cuc n , where the initially formed oligomers with random conformations must be transformed into the most stable cage structures by extensive bond scissions and recombinations under harsh conditions.^[7]

We therefore reinvestigated the condensation under a wide range of acidic conditions. The products were analyzed by means of gel permeation chromatography (GPC) by taking advantage of the fact that all the components of the products could be dissolved in chloroform after the residual water had been removed azeotropically.

The condensation of ethyleneurea and 37% formalin at pH 2 (72 h, 25 °C) provided a white powder which gave a GPC profile as shown in Figure 1. The product consists mainly of

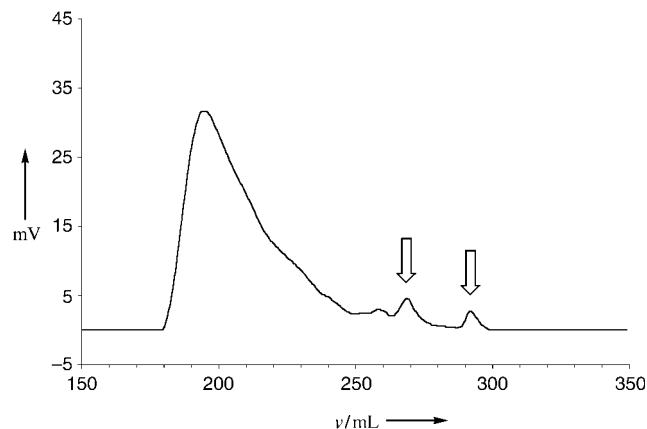
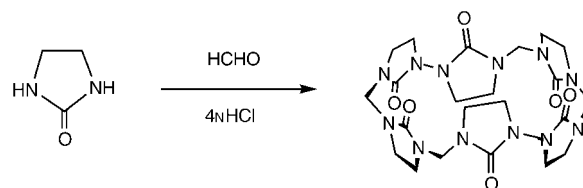


Figure 1. The GPC profile of the product after 72 h (RI detector response versus elution volumes).

polymers with number-averaged molecular weight (\bar{M}_n) of m/z 6345 which is higher than the reported value of m/z 4040 obtained by viscosity and osmometry measurements.^[3b] The two small but distinct peaks at the low-molecular-mass end were readily identified as a cyclic hexamer (hmCuc6) and an unexpectedly large cyclic dodecamer (hmCuc12) by ESI mass spectroscopy. We then varied the acid concentrations and temperatures to identify the best conditions for producing either of these compounds on a preparative scale and thus enable the structures of these compounds to be established.

The best conditions to form hmCuc6 could be reached fairly readily. Simply mixing equimolar amounts of ethyleneurea and 37% formalin in 4N HCl at RT (Scheme 1)



Scheme 1. Synthesis of hmCuc6.

resulted in turbidity after a few minutes and then deposition of granular crystals. The mild exothermic reaction was complete in less than 30 min. The crystals contained HCl and water (see below) but HCl-free hmCuc6 was obtained in 94% yield after drying in vacuo at 80 °C.^[8]

The X-ray crystal structure of the HCl adduct determined at -180 °C (Figure 2a) indicates that the Cl⁻ ion is located at

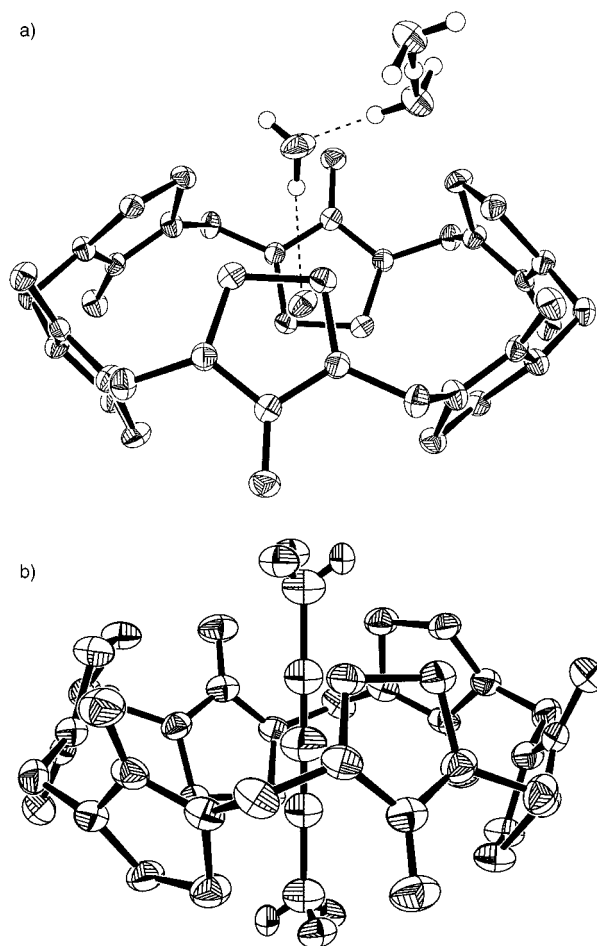


Figure 2. X-ray Structures of hmCuc6 including a) HCl and b) propargyl alcohol. Hydrogen atoms are omitted for clarity except for those attached to hydrogen-bonded water molecules. The propargyl alcohol is disordered over two symmetry related positions with further disorder of its oxygen atom.

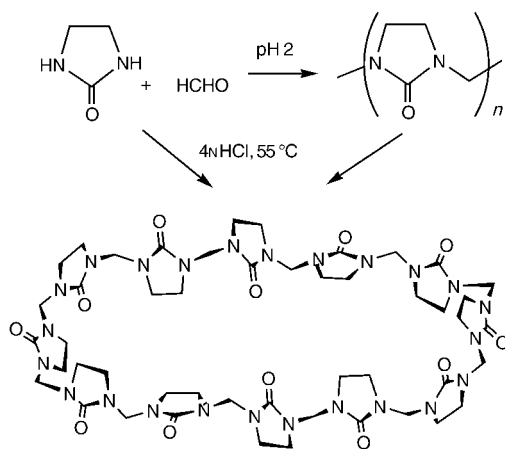
the center of the cavity in the “alternate” conformation of hmCuc6 and hydrogen bonded to a H₂O molecule, which in turn is hydrogen bonded to an external H₂O molecule. The H⁺ ion is shared by the H₂O and another H₂O molecule belonging to the other hmCuc6, thus making a rigid hydrogen-bonding network.^[8]

An acid concentration of 4 N, therefore, appears to be the optimum conditions under which the cyclization occurs around a Cl[−] ion template, and the resulting HCl adduct has the least solubility as a result of the hydrogen-bonding network.

Contrary to our expectations, hmCuc6 did not form complexes with common metal ions, possibly because of its “alternate” conformation. However, it can include an anion other than Cl[−], notably a thiocyanate. Although hmCuc6 is sparingly soluble in water (0.03 mg mL^{−1} at 25 °C), the solubility was dramatically increased when metal or ammonium thiocyanate was added (250 mg mL^{−1} if 150 mg of KNCS coexisted).^[8]

Other than an anion, hmCuc6 can include a small molecule, such as water and formamide. Of particular interest is that propargyl alcohol has a greater affinity for hmCuc6 relative to water and can be taken up from an aqueous solution and included in the cavity as shown by the X-ray crystal structure (Figure 2b).^[8,9] Further studies on its capability as a host molecule, along with its derivatization, are now in progress.

Finding the optimum conditions for the preparation of hmCuc12 met with considerable difficulty. However, once formation of a gel was found to be the key, the best procedure was readily found. Heating an equimolar mixture of ethyleneurea and 37% formalin in 1 N HCl at 55 °C for 3 h furnished a white uniform gel (Scheme 2). Neutralization turned the gel to fine, but readily filterable, particles. The product proved to be pure hmCuc12 by GPC. It contained two H₂O molecules even after drying in vacuo at 80 °C for 18 h, as determined by elemental analysis.^[8] The yield was as high as 93%. The same product was also obtained in 82% yield by depolymerization of the polymeric mixture described above under the same reaction conditions.



Scheme 2. Synthesis of hmCuc12.

The product was highly crystalline, as determined by powder X-ray diffraction studies, and sparingly soluble in common organic solvents except chloroform. Dissolving the powder in chloroform by rapid heating and cooling gave fine needles with a composition of hmCuc12·2 H₂O·2 CHCl₃.^[8] Further heating with azeotropic removal of water furnished colorless prisms suitable for X-ray analysis.^[8] As shown in Figure 3, the crystal contains three CHCl₃ molecules from

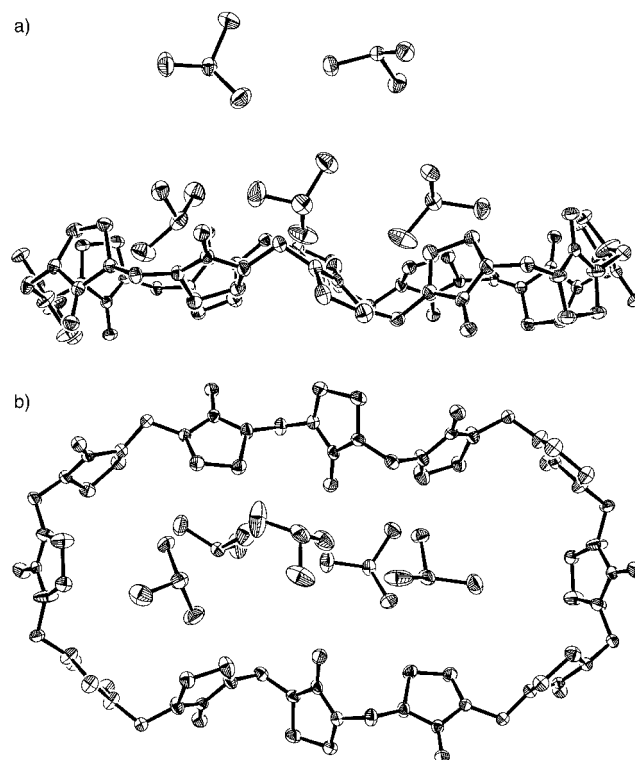


Figure 3. a) The side and b) top view of the X-ray structure of hmCuc12·10CHCl₃ (the H and disordered Cl atoms of minor occupancies are omitted for clarity).

above and three CHCl₃ molecules from below (not shown, symmetry-related) in the elongated cavity, and four CHCl₃ molecules in the lattice. The macro ring appears to be flattened out as a result of the inclusion of the CHCl₃ molecules and the packing forces in the solid state.

The CHCl₃ solvate, however, formed good crystals only by chance and mostly amorphous solid was obtained after standing for a long time. The reason for this was elucidated by NMR spectroscopic studies. When the chloroform solvate was made CHCl₃-free and dissolved in meticulously dried CDCl₃, the singlet peak for the NCH₂CH₂N protons at δ = 3.40 ppm was accompanied by a shoulder at δ = 3.38 ppm. The shoulder grew gradually larger with time and finally replaced the peak at δ = 3.40 ppm after 5 h (see the Supporting Information). This new peak may be attributable to conformers with dissymmetric structures. A twisted, figure-of-eight conformation, as obtained by Monte Carlo searches (SpartanPro) and ab initio calculations (Gaussian98, B3LYP/STO-3G; Figure 4), may be one of the possible conformations in such solutions.^[10]

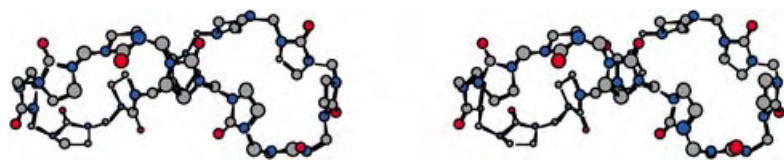


Figure 4. Stereoview of the B3LYP/STO-3G-optimized structure of hmCuc12.

In contrast, when hmCuc12 was dissolved in the usual CDCl_3 containing some water, the sharp singlet at $\delta = 3.40$ ppm did not change at all even when molecular sieves (3 \AA) were added (see the Supporting Information). Interestingly, as the amount of water decreased, the water peak at $\delta = 1.91$ ppm decreased and a new peak appeared at $\delta = 1.25$ ppm, which increased until its integral reached the amount corresponding to 4H. Therefore, the two H_2O molecules included in hmCuc12 maintain the conformational structure by hydrogen bonding.

The unprecedented efficiency in forming the large hmCuc12 molecule^[11] may not be explained solely by the stabilization of the macro ring by the intracavity H_2O molecules, but also by the formation of a stable gel by hydrogen-bonding interactions with intermolecular H_2O molecules. In fact, although the powder was insoluble in neutral H_2O , MeOH, or EtOH, it was dissolved in ethylene glycol by heating to $110\text{--}120^\circ\text{C}$ and formed a gel on cooling. Gel formation was observed over the concentration range of 0.5–5%. The gel was fibrous when viewed under a microscope (Figure 5). We envisage that the fibers are formed by linking the hmCuc12· $2\text{H}_2\text{O}$ units linearly by intervening ethylene



Figure 5. HmCuc12-ethylene glycol gel (0.5%) viewed under a phase-contrast microscope (20 \times).

glycol molecules. Gel formation was also observed with diols such as propylene glycol and diethylene glycol.

In summary, we have developed facile methods for synthesizing two new macrocyclic polyurea compounds,^[12] practical applications of which are currently under investigation.

Received: May 24, 2004

Keywords: cyclization · gels · host–guest systems · inclusion compounds · macrocycles

- [1] For the latest review, see J. W. Lee, S. Samal, N. Selvapalam, H.-J. Kim, K. Kim, *Acc. Chem. Res.* **2003**, *36*, 621–630.
- [2] Y. Miyahara, K. Abe, T. Inazu, *Angew. Chem.* **2002**, *114*, 3246–3249; *Angew. Chem. Int. Ed.* **2002**, *41*, 3020–3023.
- [3] The complexation of Cuc6 with a variety of metal salts was studied without knowing its structure, see R. Behrend, E. Meyer, F. Rusche, *Justus Liebigs Ann. Chem.* **1905**, 339, 1–37; for recent studies, see H.-J. Buschmann, E. Cleve, E. Schollmeyer, *Inorg. Chim. Acta* **1992**, *193*, 93–97 for Cuc6 and X. X. Zhang, K. E. Krakowiak, G. Xue, J. S. Bradshaw, R. M. Izatt, *Ind. Eng. Chem. Res.* **2000**, *39*, 3516–3520 for MeCuc5.
- [4] A. Day, A. P. Arnold, R. J. Blanch, B. Snushall, *J. Org. Chem.* **2001**, *66*, 8094–8100.
- [5] H. Staudinger, G. Niessen, *Makromol. Chem.* **1955**, *15*, 75–90.
- [6] a) O. Cicchetti, S. Fontani, G. Landoni, R. Locatelli, G. Bertelli, P. Roma, Eur. Pat. EP-A2-37,706 Chem. Abstr. **1982**, *96*, P20900d; b) G. Camino, M. P. Luda, L. Costa, M. Guaita, *Macromol. Chem. Phys.* **1996**, *197*, 41–60.
- [7] For the conditions and mechanisms of the Cucurbituril synthesis, see a) A. Day, A. P. Arnold, R. J. Blanch, B. Snushall, *J. Org. Chem.* **2001**, *66*, 8094–8100; b) A. Chakraborty, A. Wu, D. Witt, J. Lagona, J. C. Fetting, L. Isaacs, *J. Am. Chem. Soc.* **2002**, *124*, 8297–8306.
- [8] The properties and X-ray analyses of the compounds reported are given in the Supporting Information.
- [9] The solubility of hmCuc6 in water was appreciably increased by addition of propargyl alcohol. However, the changes in chemical shift were too small to determine the association constant. The addition of propargyl alcohol in the more soluble CDCl_3 led to precipitation of the complex.
- [10] The usual conformational search using molecular mechanics appears unreliable for polar urea derivatives. The B3LYP/STO-3G optimized structure is the best we could find so far, but the conformational problem in solution is apparently much more complex because of the flexibility and polar interactions. Internal thermal motion as found in supercoiled DNA may also be possible in this large macrocycle. For internal motion, see A. Stasiak in *Large Ring Molecules* (Ed.: J. A. Semlyen), Wiley, Chichester, UK, **1996**, pp. 43–97.
- [11] For a variety of natural and synthetic macrocycles, see, *Large Ring Molecules* (Ed.: J. A. Semlyen), Wiley, Chichester, UK, **1996**. There seems to be no prior examples for such an efficient control of macrocyclization.
- [12] Many macrocycles containing urea units have been synthesized by base-mediated $\text{S}_{\text{N}}2$ condensation, particularly when benzimidazol-2-one units are included; see J. Trepte, M. Czugler, K. Gloe, E. Weber, *Chem. Commun.* **1997**, 1461–1462; S. Kumar, D. Paul, G. Hundal, M. S. Hundal, H. Singh, *J. Chem. Soc. Perkin Trans. 1* **2000**, 1037–1043; Z. Shi, R. P. Thummel, *Tetrahedron Lett.* **1995**, *36*, 2741–2744; O. Meth-Cohn, Z. Yan, *J. Chem. Soc. Perkin Trans. 1* **1998**, 423–436. Benzimidazol-2-one proved to be much less reactive in its condensation with formaldehyde than ethyleneurea under acidic conditions. Trimethyleneurea units have also been utilized in macrocyclic hosts: J. A. Bryant, S. P. Ho, C. B. Knobler, D. J. Cram, *J. Am. Chem. Soc.* **1990**, *112*, 5837–5843, and references therein. Trimethyleneurea, though reactive with formaldehyde under acidic conditions, failed to give readily identifiable products.

Superclusters

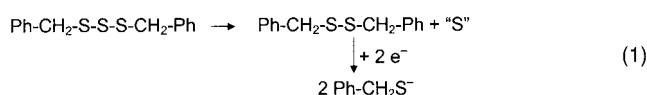
Superclusters: A Host–Guest Complex with a Cyclic Array of Three Bridged MoFe₃S₄ Clusters**

Markos Koutmos and Dimitri Coucouvanis*

Ongoing research in our laboratory has been directed towards the design and synthesis of high nuclearity Mo/Fe/S clusters as structural analogues of the FeMo cofactor of the nitrogenase protein. Even though recent X-ray structure determinations of the FeMo protein of nitrogenase^[1,2] have revealed in detail the structure of the FeMo cofactor, believed to be the site of nitrogen activation and reduction, the synthesis of exact analogues has not yet been accomplished.^[3] Nevertheless, partial analogues exist among the plethora of Fe/Mo/S clusters.^[4–6] Especially important among these are the [(Cl₄-cat)₂Mo₂Fe₆(PPr₃)₆] (**1**; Cl₄-cat = Cl₄-catecholate; R = Et, *n*Pr, *n*Bu) double cubane clusters containing the simple [MoFe₃S₄]²⁺ cores bridged in an edge-fused fashion.^[7] These are very useful starting reagents for the synthesis of novel Mo/Fe/S clusters and have enabled us to further investigate new approaches for the rational synthesis of large-core structures. Here we report the synthesis of the new cyclic tricubane cluster (Et₄N)₃[(Cl₄-cat)(PPr₃)MoFe₃S₄Cl]₃(μ-SCH₂Ph)₃ (**2**). This cluster is a potential three-electron reducing agent with interesting host–guest characteristics.

Cluster **2** is synthesized by the reaction of [(Cl₄-cat)₂Mo₂Fe₆(PPr₃)₆] with dibenzyltrisulfide (Bz₂S₃)^[8] and Et₄NCl at ambient conditions in THF (details are provided in the Supporting Information). The role of Bz₂S₃ in this reaction is dual [Eq. (1)]. It provides elemental “S”, which causes the oxidative removal of the trialkylphosphanes bound to the four Fe atoms and provides Bz₂S₃. The latter facilitates the oxidation of each [MoFe₃S₄]²⁺ subunit by one electron and promotes the breaking of the edge-shared fused arrangement, providing the bridging benzylthiolate ligands. The oxidation level of the subunits is supported by Mössbauer spectra consistent with the formulation [Mo³⁺Fe³⁺Fe²⁺S₄]³⁺ for each of the cubane units in the trimer.^[9]

Black crystals of **2** suitable for single crystal X-ray structure determination^[10] can be obtained upon recrystalli-



zation from THF/hexanes at room temperature. The molecular structure shows three [MoFe₃S₄]³⁺ cuboidal units linked by three μ₂-BzS[−] ligands (Figure 1). Each thiolate sulfur atom

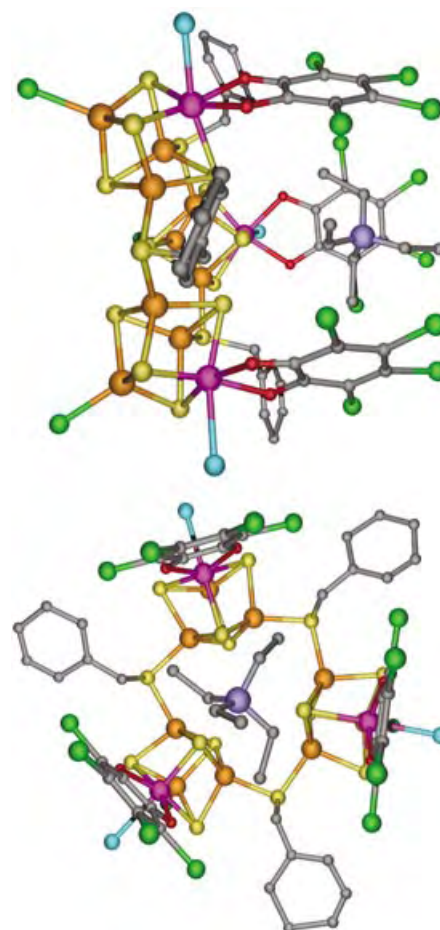


Figure 1. Two views of **2** showing the encapsulated Et₄N⁺ counterion. The two Et₄N⁺ ions outside the cavity and the alkyl groups of the phosphane ligands have been omitted for clarity.

bridges two Fe atoms from two different cubane clusters. The three bridging thiolate μ₂-sulfur atoms and the six Fe atoms that participate in bridging lie in the same plane. The coordination of the third Fe atom in each cubane core is completed by a Cl[−] ligand, whereas the Mo atom retains its original coordination environment (phosphane and Cl₄-cat). The Mo–Fe and Fe–Fe intracubane distances of the [MoFe₃S₄]³⁺ cores are not significantly different than those in the known single cubane clusters with the same core. The three Fe–Fe intercubane distances (3.515, 3.561, and 3.624 Å) show the deviation of **2** from an ideal three-fold symmetry and are too long to account for any direct metal–metal intercubane interactions.

[*] M. Koutmos, Prof. D. Coucouvanis
930 North University
Department Of Chemistry
The University Of Michigan
Ann Arbor, MI 48109-1055
Fax: (+1) 734-936-2916
E-mail: dcouc@umich.edu

[**] We thank Dr. Panagis Filippakopoulos for valuable assistance in the TOCSY NMR experiments and Dr. Yiannis Sanakis and Dr. A. Simopoulos at Demokritos Nuclear Research Center, Athens, Greece, for the Mössbauer spectra. Finally, the authors acknowledge the support of this work by a grant from the National Institutes of Health (GM33080).

Supporting information for this article is available on the WWW under <http://www.angewandte.org> or from the author.

An indication of intercubane electronic communication is apparent in the reduction properties as well as the EPR spectrum of **2**. The cyclic voltammogram (see the Supporting Information) reveals three reversible reduction waves at -0.47 , -0.63 , and 0.74 V, which correspond to the 3-/4-, 4-/5-, and 5-/6- couples, respectively. The single cubane clusters (with the $[\text{MoFe}_3\text{S}_4]^{3+}$ core) show a single reversible reduction wave with a potential that varies from 0.83 to 1.31 V.^[12] The EPR spectrum of **2** is rather complex and does not resemble the $S = 3/2$ signal of the single MoFe_3S_4 cubane clusters. This is probably due to intercubane coupling interactions.

In the solid state the three Et_4N^+ counterions of **2** are located in two sites. Two are found in general positions, whereas the third occupies a cavity formed by the three $\text{Cl}_4\text{-cat}$ ligands. The latter are bound to the Mo atoms of each cubane core and have a *syn* orientation, thus creating a large electron-rich "pocket" which is evident in the space-filling model (Figure 2).

A 2D-TOCSY ^1H NMR experiment^[13,14] was undertaken to determine whether the trapped Et_4N^+ ion is released in solution. The spectra revealed two sets of peaks that corresponded to Et_4N^+ ions in different environments (Figure 3). The resonances at $\delta = 3.683$ ($\text{CH}_3\text{CH}_2\text{N}$) and 1.822 ppm ($\text{CH}_3\text{CH}_2\text{N}$) and their crosspeaks correspond to one set of Et_4N^+ ions; the resonances at $\delta = 1.753$ ($\text{CH}_3\text{CH}_2\text{CH}_2\text{P}$), 1.603 ($\text{CH}_3\text{CH}_2\text{CH}_2\text{P}$), and 1.036 ppm ($\text{CH}_3\text{CH}_2\text{CH}_2\text{P}$) and their crosspeaks correspond to the phosphane ligands of the Mo atoms; and the resonances at $\delta = 1.822$ ($\text{CH}_3\text{CH}_2\text{N}$) and 0.886 ppm ($\text{CH}_3\text{CH}_2\text{N}$) and their crosspeaks correspond to a unique Et_4N^+ ion. If only one type of counterion was present, one set of peaks (at $\delta = 3.683$ and 1.822 ppm) would be observed for Et_4N^+ . The observation of two sets of resonances and the upfield shift of the second set provide direct evidence that, in solution, the trapped Et_4N^+ ion stays in the electron-rich cavity, and its protons experience the observed shielding.

The same motif of tricyclic arrangement of single cubane clusters exists in only one other example in the literature.^[15] In that case three $\text{Mo}_2\text{Fe}_2\text{S}_4$ cores are linked by three $\mu_2, \eta^2\text{-S}_4^{2-}$ ligands "η" that give rise to a neutral polycubane cluster. The

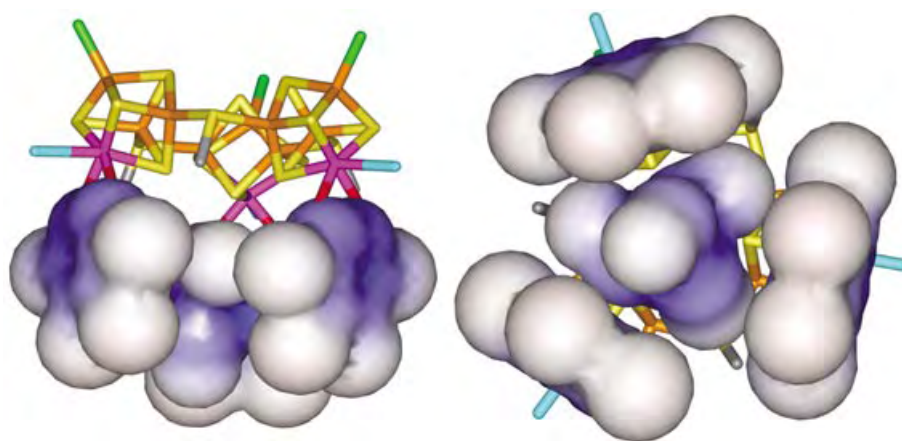


Figure 2. Space-filling model of the three $\text{Cl}_4\text{-cat}$ ligands (left) and the Et_4N^+ counterion inside the cavity (right).

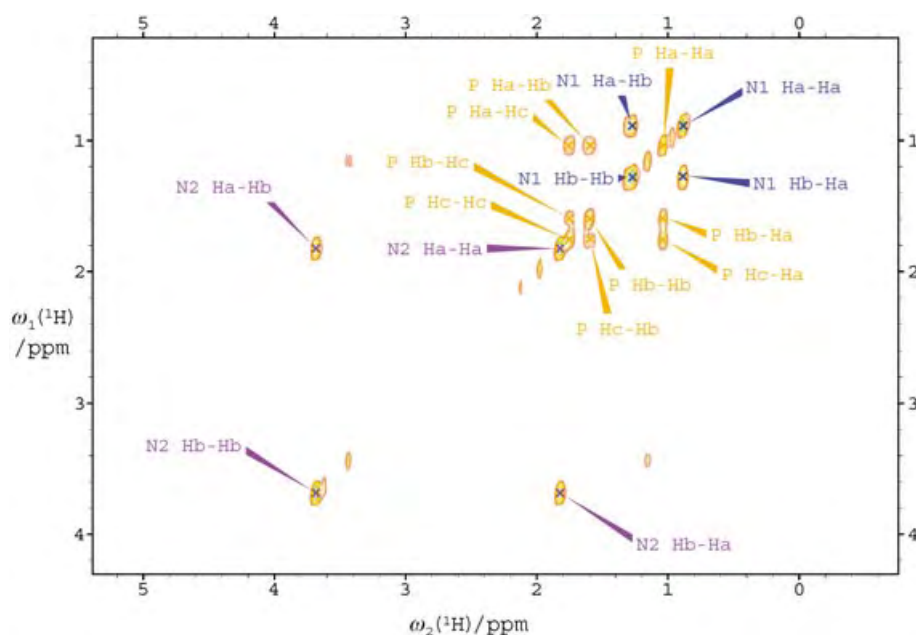


Figure 3. 2D-TOCSY ^1H NMR spectrum of **2**. The three sets of resonances and their crosspeaks have been depicted with different colors.

role of Et_4N^+ as a possible templating agent remains to be determined. It is unclear whether its presence is needed for an organization of the cubane cores prior to coupling. However, in experiments conducted with counterions other than Et_4N^+ , different products are obtained that do not exhibit this characteristic cyclic arrangement of cubane units.^[16] It should be emphasized that in the synthesis of the metastable Fe_6S_6 prismanes the role of Et_4N^+ is critical, as other counterions (Bu_4N^+ or Ph_4P^+) lead to the thermodynamically stable single cubane clusters.^[17]

In **2**, the trigonal arrangement of three $\mu_3\text{-S}$ ligands, from the three different cubane cores facing the interior of the cavity, defines a site that is well suited for coordination to metal ions such as Fe^{2+} or Cu^+ . At present, attempts are being made to replace the encapsulated Et_4N^+ ion in **2** with a

transition metal ion and generate a coordinatively unsaturated site that is potentially useful for the activation and multielectron reduction of small molecules.

Received: March 29, 2004

Keywords: cluster compounds · host–guest chemistry · nitrogenase · reduction · S ligands

- [1] O. Einsle, F. A. Tezcan, S. L. A. Andrade, B. Schmid, M. Yoshida, J. B. Howard, D. C. Rees, *Science* **2002**, 297, 1696–1700.
- [2] a) D. C. Rees, J. B. Howard, *Curr. Opin. Chem. Biol.* **2000**, 4, 559–566; b) J. B. Howard, D. C. Rees, *Chem. Rev.* **1996**, 96, 2965–2982; c) M. K. Chan, J. S. Kim, D. C. Rees, *Science* **1993**, 260, 792–794.
- [3] a) E. I. Stiefel, D. Coucouvanis, W. E. Newton in *Molybdenum Enzymes, Cofactors, and Model Systems*, American Chemical Society, Washington, DC, **1993**, Ch. 10–23 (ACS Symposium Series 535).
- [4] a) D. Coucouvanis, J. H. Han, N. Moon, *J. Am. Chem. Soc.* **2002**, 124, 216–224; b) J. H. Han, K. Beck, N. Ockwig, D. Coucouvanis, *J. Am. Chem. Soc.* **1999**, 121, 10448–10449.
- [5] S. M. Malinak, D. Coucouvanis, *Prog. Inorg. Chem.* **2001**, 49, 599–662.
- [6] a) Y. G. Zhang, R. H. Holm, *J. Am. Chem. Soc.* **2003**, 125, 3910–3920; b) Y. G. Zhang, J. L. Zuo, H. C. Zhou, R. H. Holm, *J. Am. Chem. Soc.* **2002**, 124, 14292–14293; c) F. Osterloh, Y. Sanakis, R. J. Staples, E. Münck, R. H. Holm, *Angew. Chem.* **1999**, 111, 2199–2203; *Angew. Chem. Int. Ed.* **1999**, 38, 2066–2070.
- [7] a) J. Han, M. Koutmos, S. Al Ahmad, D. Coucouvanis, *Inorg. Chem.* **2001**, 40, 5985–5999; b) K. D. Demadis, C. F. Campana, D. Coucouvanis, *J. Am. Chem. Soc.* **1995**, 117, 7832–7833; c) F. Osterloh, B. M. Segal, C. Achim, R. H. Holm, *Inorg. Chem.* **2000**, 39, 980–989; d) F. Osterloh, C. Achim, R. H. Holm, *Inorg. Chem.* **2001**, 40, 224–232.
- [8] M. G. Kanatzidis, M. Ryan, D. Coucouvanis, A. Simopoulos, A. Kostikas, *Inorg. Chem.* **1983**, 22, 179–181.
- [9] The Mössbauer spectrum is provided in the Supporting Information. Measurements in the presence of external magnetic fields in combination with EPR spectroscopy and magnetic susceptibility measurements are in progress to further characterize the magnetic and electronic properties of the complex.
- [10] Crystal structure determination of **2**: Crystal dimensions $0.08 \times 0.40 \times 0.028$ mm, triclinic space group $P\bar{1}$, $a = 17.622$, $b = 17.933$, $c = 26.2359$ Å, $\alpha = 104.664^\circ$, $\beta = 91.324^\circ$, $\gamma = 113.794^\circ$, $V = 7265.38$ Å³, $\rho_{\text{calc}} = 1.507$ mgm^{−3}. The full-matrix least-squares refinement based on F^2 converged to $R1$ ($I > 2\sigma$) = 0.0838 and $wR2 = 0.2126$, GooF = 0.936. The data were collected on a Bruker SMART CCD-based X-ray diffractometer, equipped with an LT-2 low-temperature device and normal focus Mo-target X-ray tube ($\lambda = 0.71073$ Å) operated at 158 K, at the University of Michigan X-Ray facility ($2\theta_{\text{max}} = 44.24^\circ$). The space group was determined based on systematic absences and intensity statistics. A successful direct-methods solution was calculated using the software package SHELXTL v.6.1^[11a] that revealed the locations of most non-hydrogen atoms. Several full-matrix least squares refinements followed by difference Fourier calculations were performed using SHELXTL, which located the remainder of the non-hydrogen atoms. All non-hydrogen atoms were refined with anisotropic thermal displacement parameters unless stated otherwise. All hydrogen atoms were placed in ideal positions and refined as riding atoms with individual isotropic thermal displacement parameters. From 43 589 collected reflections, 17 914 were independent; number of parameters 1324. The data were processed with SADABS for absorption correction.^[11b] CCDC-234743 contains the supplementary crystallographic data for this paper. These data can be obtained free of charge via www.ccdc.cam.ac.uk/conts/retrieving.html (or from the Cambridge Crystallographic Data Centre, 12, Union Road, Cambridge CB2 1EZ, UK; fax: (+44) 1223-336-033; or deposit@ccdc.cam.ac.uk).
- [11] a) SHELXTL, v.6.10., Siemens Industrial Automation Inc., Madison, WI(USA), **2000**; b) G. M. Sheldrick, SADABS, v.2.10. Program for Empirical Absorption Correction of Area Detector Data, University of Göttingen, Göttingen (Germany), **2003**.
- [12] a) T. E. Wolff, J. M. Berg, R. H. Holm, *Inorg. Chem.* **1981**, 20, 174–180; b) R. E. Palermo, R. H. Holm, *J. Am. Chem. Soc.* **1983**, 105, 4310; c) K. D. Demadis, D. Coucouvanis, *Inorg. Chem.* **1995**, 34, 436–448.
- [13] A homonuclear two-dimensional spectrum was collected in CD₂Cl₂ (no TMS) on a Bruker AMX 500 instrument (25°C). An optimized high power 90° pulse of 7.55 μs was used. Spinlock time for the TOCSY experiment was 75 ms with a 13 dB low-energy pulse. The data were processed with the software package nmrPipe, where they were zero filled, and after Fourier transformation and manual phasing baseline correction was applied using the built-in automated function. The processed FIDs were converted into the UCSF format and were analyzed and assigned using the software package SPARKY.
- [14] a) F. Delaglio, S. Grzesiek, G. W. Vuister, G. Zhu, J. Pfeifer, A. Bax, *J. Biomol. NMR* **1995**, 6, 277–293; b) T. D. Goddard, D. G. Kneller, SPARKY, v.3., *NMR Assignment and Integration*, University of California, San Francisco (USA), **1996–2002**.
- [15] H. Kawaguchi, K. Yamada, S. Ohnishi, K. Tatsumi, *J. Am. Chem. Soc.* **1997**, 119, 10871–10872.
- [16] Unpublished results.
- [17] M. G. Kanatzidis, W. R. Hagen, W. R. Dunham, R. K. Lester, D. Coucouvanis, *J. Am. Chem. Soc.* **1985**, 107, 953–961.

Bioinorganic Chemistry

Vitamin B12 as a Ligand for Technetium and Rhenium Complexes**

*Susanne Kunze, Fabio Zobi, Philipp Kurz, Bernhard Spingler, and Roger Alberto**

Vitamin B12 is a biomolecule that is fundamental for most living organisms despite being produced by only a few bacteria. It plays a key role in enzymatic processes in the

[*] S. Kunze, F. Zobi, P. Kurz, Dr. B. Spingler, Prof. Dr. R. Alberto
Institute of Inorganic Chemistry
University of Zürich, Winterthurerstrasse 190
8057 Zürich (Switzerland)
Fax: (+41) 1-635-6803
E-mail: ariel@aci.unizh.ch

[**] This work has been supported by Solidago AG, Bern, Switzerland, and Mallinckrodt Med. Inc., Petten, The Netherlands



Supporting information for this article is available on the WWW under <http://www.angewandte.org> or from the author.

mitochondria, cell nucleus, and cytoplasm. Its uptake in humans is very complex and requires at least three different transport proteins: intrinsic factor (IF), transcobalamin, and haptocorrin. The human organism uses vitamin B12 very efficiently: the daily requirement is only about 10 µg. Its chemistry, biochemistry, and biology has been comprehensively reviewed.^[1–4]

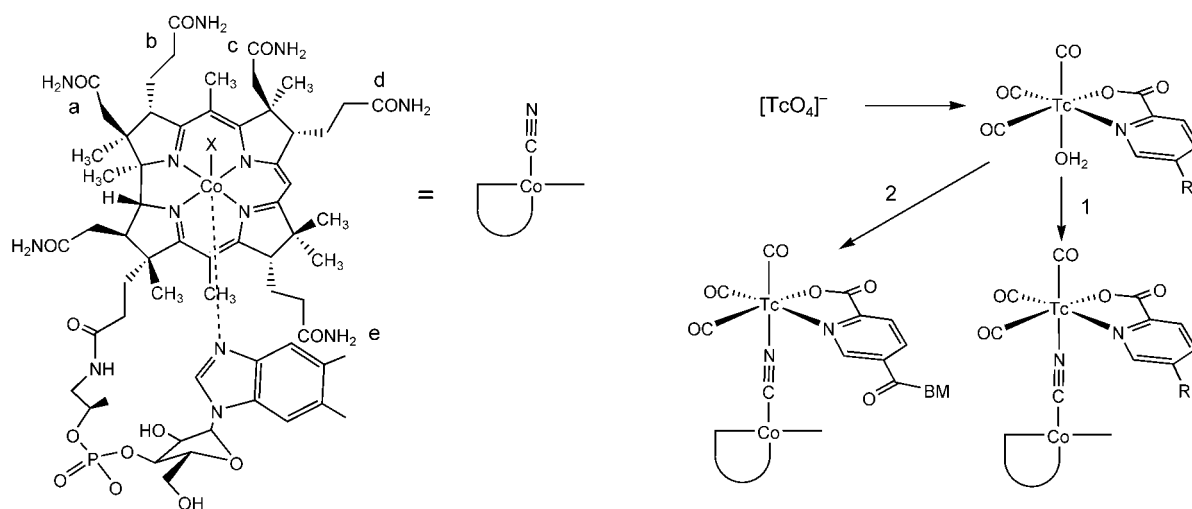
The demand for vitamin B12 (abbreviated as “B12”) is concentrated at sites of enhanced proliferation, in particular in cancer cells or at sites of bacterial infections. An organism’s need for B12 makes it an attractive targeting agent. Applications of B12 to the delivery of radioisotopes^[5,6] or as various cytotoxic agents to cancer cells, for which it can be used as a Trojan horse, have been the most actively studied areas of research.^[7–9] Both of these strategies require derivatization of B12, and so the introduction of ligands or receptor-binding molecules has been reported.^[5,6,9,10] Chelators for radiometals have been conjugated to peripheral acid groups (prepared by controlled amide hydrolysis) and coordinated to the 5′-OH group in the ribose ring of the backloop. Alternatively, a Co^{III} center can be reduced to Co^I and a molecule introduced by oxidative alkylation.^[8,11]

The only functionality in B12 that has not received much attention is the Co^{III}-coordinated cyanide group. It is well established that M–CN moieties tend to bridge two metal centers to form a M–C–N–M′ unit. Numerous examples have been published and reviewed to date,^[11] but examples with porphyrin-like systems are rare^[12–14] and, to the best of our knowledge, unknown for B12. The reverse situation in which [Fe(CN)₆]^{3–} or nitroprusside [Fe(NO)(CN)₅][–] are coordinated to Co^{III} or Co^{II} centers of aqua-cobalamin has been studied in detail.^[15–19]

It is intriguing to use the cyanide anion in B12 as a ligand and to introduce a metal complex either by direct coordination to B12 or by conjugation of an organic molecule through mediation by a metal complex (pathways 1 and 2 in Scheme 1). Since Co–CN–M′ is not very stable, M′ represents an inert complex fragment.

Our interest lies in radiopharmaceuticals containing the *fac*-[^{99m}Tc(CO)₃]⁺ moiety.^[20–22] The water ligands are readily exchanged in [^{99m}Tc(OH₂)₃(CO)₃]⁺, to yield complexes of high kinetic stability even with monodentate donors.^[23] The concept of our study involved B12 acting as a monodentate ligand while the other two sites of *fac*-[M(CO)₃]⁺ are bound to a bidentate ligand L². The complex [^{99m}Tc(OH₂)(L²)(CO)₃] is then coordinated to B12. The ligand L², introduced prior to B12 coordination, is variable and allows the biological authenticity of the final conjugate to be fine-tuned. The use of a bidentate and a monodentate ligand on the *fac*-[^{99m}Tc(CO)₃]⁺ moiety is consistent with a mixed ligand approach.^[24]

The reaction of [M(OH₂)₃(CO)₃]⁺ (M = ⁹⁹Tc, **1**; Re, **2**) in water with the monoanionic ligands (L²), imidazolecarboxylic acid (Himc), picolinic acid (Hpic), 2,4-dipicolinic acid (Hdipic) or serine (Hser), and *N,N*-dimethylglycine (Hdmg) yields [M(L²)(OH₂)(CO)₃]. The corresponding ^{99m}Tc complexes are prepared directly from [^{99m}TcO₄][–]. The bidentate ligand is tightly bound but the remaining water ligand can be replaced by the nitrogen atom from the cyanide anion in B12. [M(L²)(OH₂)(CO)₃] exhibits a strong affinity for imidazole-type ligands but coordination to intermediately released benzimidazole from B12 was not observed. The reaction of [Re(imc)(OH₂)(CO)₃] (**3**), [Re(dipic)(OH₂)(CO)₃] (**4**), [Re(ser)(OH₂)(CO)₃] (**5**), [Re(dmng)(OH₂)(CO)₃] (**6**), or their ^{99m}Tc analogues with B12 in methanol or water afforded [(**3**–B12)] (**7**), [(**4**–B12)] (**8**), [(**5**–B12)] (**9**), and [(**6**–B12)] (**10**). High-performance liquid chromatographic (HPLC) analysis after coordination of Re or ^{99m}Tc centers gave only two well-separated signals in a ratio of about 1:1. The comparable retention times from the UV/Vis analysis of, for example, **7** and the corresponding radioactivity trace of the ^{99m}Tc complex indicate the identity of the Re and Tc complexes (Figure 1). The signals can be understood by the two possible orientations adopted by the bidentate N,O ligand L² relative to the corrin ring ([M(L²)(OH₂)(CO)₃] complexes are racemic) and, thus, the presence of two diastereomers. The



Scheme 1. a) Structure of B12 with assignment of the side arms. b) Coordination of [^{99m}Tc(OH₂)(L²)(CO)₃] to B12: 1) for radiopharmaceuticals and 2) metal-mediated coupling of biomolecules (BM).

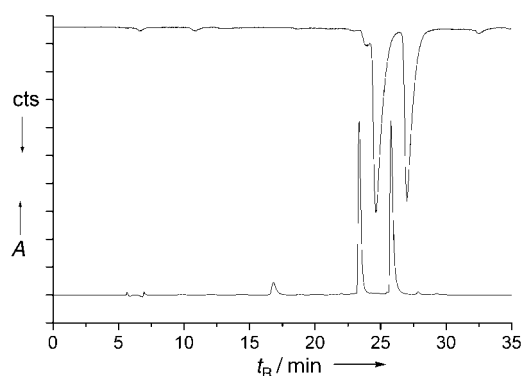


Figure 1. HPLC traces of the reaction between B12 and **3** showing the two diastereomers. Lower trace: UV/Vis spectrum at $\lambda = 360$ nm, upper trace: γ -detection of the ^{99m}Tc analogue of **7**.

two compounds could be separated by preparative HPLC and showed the same mass ($m/z = 869.1 [M^{2+}]$; $m/z = 1736.9 [M^+]$) in ESI-MS; ^1H , ^{13}C , and ^{31}P NMR spectroscopic analysis confirmed the proposed composition (see Supporting Information).

The orientation of B12 relative to the bidentate ligand was investigated by ROESY experiments, as recently performed for a (methoxycarbonyl)methyl derivative.^[25] The spectra did not show cross peaks even at low-temperature, thus indicating fast rotation of the complex. Since the equatorial planes of the complexes are relatively far away from the corrin framework, they are not locked in a fixed position. For all the complexes **7–10**, the two isomers could be readily separated by preparative HPLC. X-ray quality crystals for one of the isomers of both **7** and **10** could be grown, and so their structures could be elucidated (Figure 2).^[26]

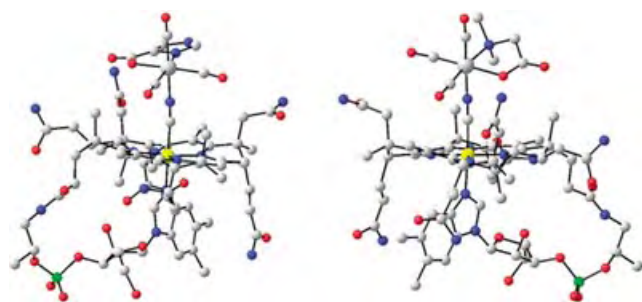


Figure 2. X-ray crystal analysis of **7** (left) and **10** (right). Important bond lengths [Å] and angles [°] are for **7**: Co–CN: 1.846(13), Co–N(benzimidazole): 2.010(8), C–N(cyanide): 1.113(14), CN–Re1A: 2.171(9), Co–C–N: 169(1), C–N–Re1A: 166(1); and for **10**: Co–CN: 1.90(1), Co–N(benzimidazole): 2.032(7), C–N(cyanide): 1.180(12), CN–Re: 2.14(1), Co–C–N: 167.7(9), C–N–Re: 169.2(9).

The relative orientation of the N,O ligands L^2 imc in **7** and dmg in **10** are reversed for the two structures. Both show a hydrogen bridge between the terminal carbonyl oxygen O74 in **7** and the coordinating O72 atom in **10** to the amide nitrogen atom of the a-side chain in B12 (Figure 3). The bridge is shorter in **7** than in **10** and probably determines the orientation of the Re complex in the solid state. We assume

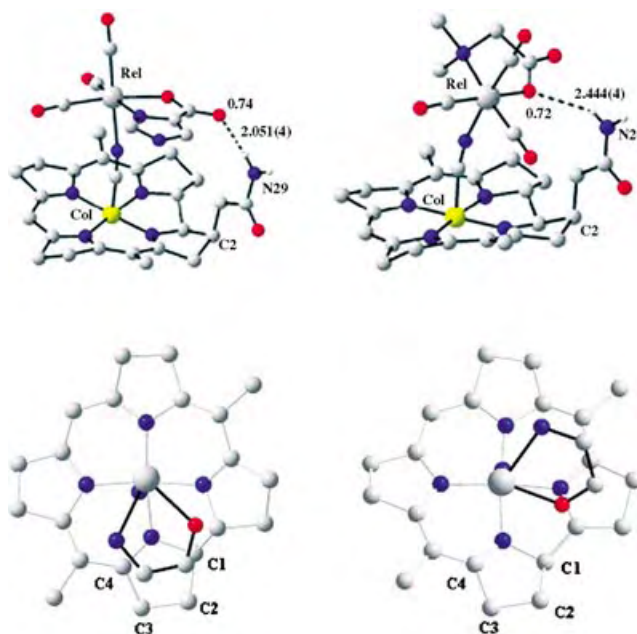


Figure 3. Hydrogen-bonding interactions in **7** and **10** (above) and orientation of the imc and dmg ligands relative to the corrin ring (below). C2 represents the carbon atom to which the a-side chain is attached.

that the respective diastereomer of each complex might be represented by the orientations as observed for **7** and **10**.

We observed that the diastereomerically pure complexes $[\text{M}(L^2)(L^1)(\text{CO})_3]$ with one labile ligand (for example, L-serine (L^2) and guanine L^1) always return to equilibrium in water within hours, probably through formation of a five-coordinate intermediate by dissociation of the monodentate ligand. The pure diastereomers of **7–10** do not interconvert into each other even after days in water at room temperature, which confirms the high kinetic stability of the monodentately bound B12. Acetonitrile is a strong ligand for complexes $[\text{Re}(L^2)(\text{OH}_2)(\text{CO})_3]$. Dissolving **7** or **9** in a water/acetonitrile mixture did not result in cleavage of **3** from B12 in **7** and only about a 10 % cleavage of **9** from **10**, which confirms again the stability of the Co–CN–Re(Te) bonds.

The electronic spectra of the two diastereomers of **10** both have essentially the shape of B12, but the shoulder at about 482 nm in the spectrum of B12 becomes a distinct peak at 475 nm (see Supporting Information). Furthermore, B12 and **7** behave different electrochemically. Whereas B12 exhibits a reduction wave ($E_{1/2} = -670$ mV versus Ag^+/AgCl) with about 60 % reversibility, the same process with **7** ($E_{1/2} = -625$ mV) is about 80 % reversible (Figure 4). The Co^{III} center in **7** is easier to reduce since coordination of the cyanide group through the nitrogen atom to the rhenium center reduces the electron density at the Co^{III} center. The increased ease of the reversibility can be understood by the more facile accommodation of the two additional electrons in the $\text{Co} \rightarrow \text{C}$ backbond. Complex **7** can be considered as an (inorganic) isocyanide complex of a Co^{III} center. Since isocyanides bind to low-oxidation states better than the cyanide anion, the Co^{I} center becomes stabilized.

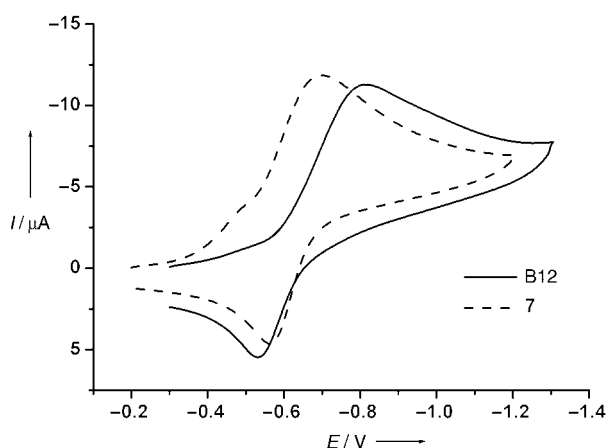


Figure 4. Cyclic voltammograms of complex **7** and B12. The shoulder results from the reduction of imc in **7**.

Biological applications of these compounds require them to be stable in serum and have an affinity for the various B12-binding proteins. It is known that haptocorrin recognizes derivatives of B12 whereas the transcobalamins are more sensitive towards structural changes.^[27–29] Derivatizations at the Co^{III} center are more readily tolerated by both proteins and direct labeling of B12 with [^{99m}Tc(L²)(OH₂)(CO)₃] is feasible. Complexes [^{99m}Tc(L²)(OH₂)(CO)₃] coordinated quantitatively to B12 between 10^{–2} and 10^{–3} M within 60 minutes at 37°C. Once formed and separated by HPLC, the isomers were stable for at least 24 hours at 37°C. Complex **10** was treated with human serum albumin at 37°C (1% in phosphate buffer) but no transmetalation to proteins could be observed. This opens a convenient way for studying the biological behavior of labeled native B12 by varying the nature of L². The intracellular B12-dependent enzymes might not recognize these derivatives anymore but then the radio-nuclide has already reached its target. We emphasize that the Re center is likely to mediate L²-coupled biologically active molecules and B12 (for example, through the free carboxylic acid functionality in dipic).

In conclusion, we have shown that CN[–] in B12 bridges to Re^I and Tc^I centers to yield robust complexes with the central structural feature {Co–CN–Re(Tc)}. This concept allows direct labeling of B12 with complexes [^{99m}Tc(OH₂)(L²)(CO)₃] for radiodiagnosis or with rhenium as a mediator between B12 and additional biomolecules. The observed kinetic stability implies that coordination of other fragments with the d⁶ or d⁸ configurations is also possible. The use of B12 as an enantiomerically pure and stereochemically demanding ligand provides water solubility, which could be useful for enantioselective synthesis with an appropriate catalyst. Binding studies with different B12 transporters and the coordination of other metal complexes are currently under investigation.

Received: June 9, 2004

Keywords: bridging ligands · cyanides · radiochemistry · technetium · vitamins

- [1] B. Kräutler, D. Arigoni, B. T. Golding, *Vitamin B12 and B12-Proteins*, Wiley-VCH, Weinheim, **1998**.
- [2] B. Kräutler in *Vitamin B12 and B12-Proteins*, Wiley-VCH, Weinheim, **1998**, pp. 3–43.
- [3] R. Banerjee, *Chemistry and Biochemistry of B12*, 1st Ed., Wiley-Interscience, New York, **1999**.
- [4] R. Banerjee, S. W. Ragsdale, *Annu. Rev. Biochem.* **2003**, *72*, 209.
- [5] D. A. Collins, H. P. C. Hogenkamp, M. W. Gebhard, *Mayo Clin. Proc.* **1999**, *74*, 687.
- [6] D. A. Collins, H. P. C. Hogenkamp, M. K. O'Connor, S. Naylor, L. M. Benson, T. J. Hardyman, L. M. Thorson, *Mayo Clin. Proc.* **2000**, *75*, 568.
- [7] M. J. Cannon, D. G. Myska, J. M. McGreevy, J. A. Holden, F. G. West, C. B. Grissom, *FASEB J.* **2001**, *15*, A556.
- [8] C. C. Smeltzer, M. J. Cannon, P. R. Pinson, J. D. Munger, F. G. West, C. B. Grissom, *Org. Lett.* **2001**, *3*, 799.
- [9] H. P. C. Hogenkamp, D. A. Collins, D. Live, L. M. Benson, S. Naylor, *Nucl. Med. Biol.* **2000**, *27*, 89.
- [10] D. S. Wilbur, D. K. Hamlin, P. M. Pathare, S. Heusser, R. L. Vessella, K. R. Buhler, J. E. Stray, J. Daniel, E. V. Quadros, P. McLoughlin, A. C. Morgan, *Bioconjugate Chem.* **1996**, *7*, 461.
- [11] T. G. Pagano, L. G. Marzilli, M. M. Flocco, C. Tsai, H. L. Carrell, J. P. Glusker, *J. Am. Chem. Soc.* **1991**, *113*, 531.
- [12] D. M. Corsi, N. N. Murthy, V. G. Young, K. D. Karlin, *Inorg. Chem.* **1999**, *38*, 848.
- [13] S. C. Lee, M. J. Scott, K. Kauffmann, E. Munck, R. H. Holm, *J. Am. Chem. Soc.* **1994**, *116*, 401.
- [14] S. Takano, T. Naito, T. Inabe, *J. Mater. Chem.* **1998**, *8*, 511.
- [15] G. Stochel, R. Vaneldik, H. Kunkely, A. Vogler, *Inorg. Chem.* **1989**, *28*, 4314.
- [16] H. Kunkely, A. Vogler, *Z. Naturforsch. B* **1996**, *51*, 245.
- [17] A. R. Butler, C. Glidewell, A. S. McIntosh, D. Reed, I. H. Sadler, *Inorg. Chem.* **1986**, *25*, 970.
- [18] A. R. Butler, C. Glidewell, *Chem. Soc. Rev.* **1987**, *16*, 361.
- [19] M. Wolak, G. Stochel, R. van Eldik, *J. Am. Chem. Soc.* **2003**, *125*, 1334.
- [20] R. Alberto, R. Schibli, A. Egli, U. Abram, T. A. Kaden, P. A. Schubiger, *J. Am. Chem. Soc.* **1998**, *120*, 7987.
- [21] R. Alberto, K. Ortner, N. Wheatley, R. Schibli, A. P. Schubiger, *J. Am. Chem. Soc.* **2001**, *123*, 3135.
- [22] J. Wald, R. Alberto, K. Ortner, L. Candraia, *Angew. Chem.* **2001**, *113*, 3152.
- [23] N. Aebischer, R. Schibli, R. Alberto, A. E. Merbach, *Angew. Chem.* **2000**, *112*, 260; *Angew. Chem. Int. Ed.* **2000**, *39*, 254.
- [24] S. Mundwiler, M. Kündig, K. Ortner, R. Alberto, *Dalton Trans.* **2004**, 1320.
- [25] M. Puchberger, R. Konrat, B. Kräutler, U. Wagner, C. Kratky, *Helv. Chim. Acta* **2003**, *86*, 1453.
- [26] Crystallographic analysis: **7** (C₇₀H₁₀₆CoN₁₆O₂₈PRe), red plates, 0.57 × 0.15 × 0.04 mm³, orthorhombic, space group P2₁2₁2₁, *a* = 15.958(1), *b* = 21.2328(12), *c* = 27.9776(13) Å, *V* = 9479.6(9) Å³, *Z* = 4, ρ_{calcd} = 1.328 g cm^{–3}, *R*₁(*I* ≥ 2σ(*I*)) = 0.0990, *wR*₂(*F*², *I* ≥ 2σ(*I*)) = 0.2370 for 16557 independent data (10604 observed), 1026 parameters, 40 restraints, numerical absorption correction, μ = 1.545 mm^{–1}, *T*_{min} = 0.5508, *T*_{max} = 0.9331, *Flack parameter* = –0.007(11). **10** (C₇₃H_{112.6}CoN₁₅O_{27.3}PRe), red needles, 0.46 × 0.08 × 0.07 mm³, orthorhombic, space group P2₁2₁2₁, *a* = 15.8758(7), *b* = 21.845(1), *c* = 26.3673(14) Å, *V* = 9144.4(8) Å³, *Z* = 4, ρ_{calcd} = 1.390 g cm^{–3}, *R*₁(*I* ≥ 2σ(*I*)) = 0.0662, *wR*₂(*F*², *I* ≥ 2σ(*I*)) = 0.1588 for 68628 collected data (17853 independent), 1071 parameters, 2 restraints, numerical absorption correction, μ = 1.601 mm^{–1}, *T*_{min} = 0.7060, *T*_{max} = 0.9257, *Flack parameter* = –0.014(8). CCDC-240399 (for **7**) and CCDC-240398 (for **10**) contain the supplementary crystallographic data for this paper. These data can be obtained free of charge from www.ccdc.cam.ac.uk/conts/retrieving.html (or from

the Cambridge Crystallographic Data Centre, 12 Union Road, Cambridge CB21EZ, UK; fax: (+44) 1223-336-033; or deposit@ccdc.cam.ac.uk).

- [27] E. Stupperich, E. Nexø, *Eur. J. Biochem.* **1991**, 199, 299.
- [28] P. M. Pathare, D. S. Wilbur, D. K. Hamlin, S. Heusser, E. V. Quadros, P. McLoughlin, A. C. Morgan, *Bioconjugate Chem.* **1997**, 8, 161.
- [29] P. M. Pathare, D. S. Wilbur, S. Heusser, E. V. Quadros, P. McLoughlin, A. C. Morgan, *Bioconjugate Chem.* **1996**, 7, 217.

Cluster Compounds

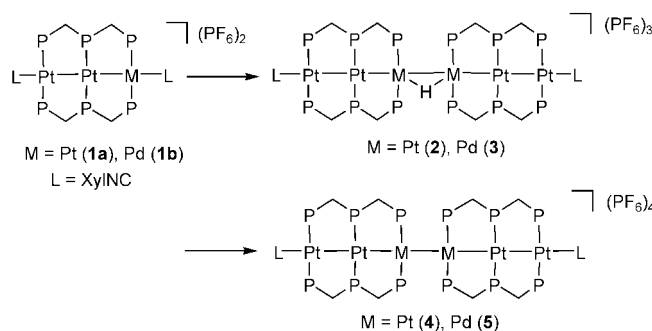
Linear, Redox-Active Pt₆ and Pt₂Pd₂Pt₂ Clusters**

Eri Goto, Rowshan A. Begum, Shuzhong Zhan,
Tomoaki Tanase,* Katsumi Tanigaki, and Ken Sakai

Transition metal clusters, which contain multinuclear metal sites connected by metal–metal bonds in a variety of geometrical structures, have attracted increasing attention due to their versatile chemical and physical properties as well as their potential to integrate multiple functions in a single molecule.^[1] In particular, clusters that show linear metal–metal bonding have been regarded as promising candidates in developing nanostructured materials including molecular electronic, optical, and chemical devices. However, synthetic methods using self-assembly of metal atoms often lead to polyhedral cluster cores, and thus routes to molecules with linear metal aggregations are limited.^[2–7] We have studied homo- and heterometallic dinuclear and trinuclear complexes supported by the tridentate phosphane ligand bis(diphenylphosphanylmethyl)phenylphosphane (dpmp).^[8] The linearly

ordered trinuclear complexes [Pt₂M(μ-dpmp)₂(XylNC)₂](PF₆)₂ (M = Pt (**1a**), Pd (**1b**); Xyl = 2,6-dimethylphenyl) were prepared by site-selective incorporation of a zero-valent Pt or Pd atom into the diplatinum complex [Pt₂(μ-dpmp)₂(XylNC)₂](PF₆)₂.^[8c] In the present study, we have examined a cluster core expansion of **1**, and have successfully synthesized linear hexametall clusters containing a redox-active Pt₂M₂Pt₂ metal string (M = Pt, Pd).

When the linear triplatinum complex **1a** was treated with excess NaBH₄ in ethanol, and the resultant brown precipitate was extracted and stirred in CH₂Cl₂, the dark blue, diamagnetic hexaplatinum cluster [Pt₆(μ-H)(μ-dpmp)₄(XylNC)₂](PF₆)₃ (**2**) was isolated in good yield (Scheme 1).



Scheme 1. Synthesis of **2–4**. PPP = dpmp

Compound **2** was also obtained in low yield from the reaction of **1** with NaOMe. Although the Pt₂Pd trinuclear complex **1b** failed to be expanded with NaBH₄, it readily reacted with NaOMe in CH₂Cl₂/MeOH to afford dark green crystals of [Pt₄Pd₂(μ-H)(μ-dpmp)₄(XylNC)₂](PF₆)₃ (**3**, Scheme 1). The changes in the ESI mass spectrum and the electronic absorption spectrum during the reaction to form **2** indicated that the initial brown compound, assigned as [Pt₃(H)₂(μ-dpmp)₂(XylNC)₂]²⁺ (**A**), was rapidly converted into [Pt₃(H)(μ-dpmp)₂(XylNC)]⁺ (**B**) in CH₂Cl₂. It is assumed that the monohydride intermediate **B** undergoes coupling and concomitant partial oxidation to generate complex **2**. However, the intervening species were not identified.^[9]

The crystal structure of **2** was determined by X-ray analysis.^[10] The cluster cation of **2** has a charge of +3 with a cluster valence electron count (CVE) of 86. It consists of six linearly ordered platinum atoms (Pt–Pt–Pt 174.87(2)–179.67(2)°) bridged by four dpmp ligands and terminated by two isocyanide molecules (Figure 1). The Pt₆ cluster core has a pseudo C₂ symmetry, and the average Pt–Pt distances are 2.7041 Å for the outer Pt1–Pt2 and Pt5–Pt6 bonds (*d*_{out}), 2.7329 Å for the inner Pt2–Pt3 and Pt4–Pt5 bonds (*d*_{inn}), and 3.3092(5) Å for the central Pt3–Pt4 bond (*d*_{cen}). The values for *d*_{out} and *d*_{inn} are comparable to those of the triplatinum complex **1**^[8] and indicate the presence of Pt–Pt σ bonds. Although the two central platinum atoms are not supported by any organic ligands and are sterically well protected by the four phenyl groups of the dpmp ligands, the remarkably long distance *d*_{cen} indicates the presence of a bridging hydride; this was unambiguously confirmed by ¹H NMR spectroscopy.

[*] Dr. E. Goto, Dr. R. A. Begum, Dr. S. Zhan, Prof. Dr. T. Tanase
Department of Chemistry
Faculty of Science
Nara Women's University
Kitaouya-higashi-machi, Nara 630-8285 (Japan)
Fax: (+81) 742-20-3399
E-mail: tanase@cc.nara-wu.ac.jp

Prof. Dr. K. Tanigaki
Department of Physics
Graduate School of Science
Tohoku University
Aoba-ku, Sendai 980-8578 and CREST, JST (Japan)
Prof. Dr. K. Sakai
Department of Applied Chemistry
Faculty of Science
Tokyo University of Science
Kagurazaka 1-3, Shinjuku-ku, Tokyo 162-8601 (Japan)

[**] This work was partly supported by Grants-in-Aid for Scientific Research from the Ministry of Education, Culture, Sports, Science and Technology, Japan.

Supporting information for this article is available on the WWW under <http://www.angewandte.org> or from the author.

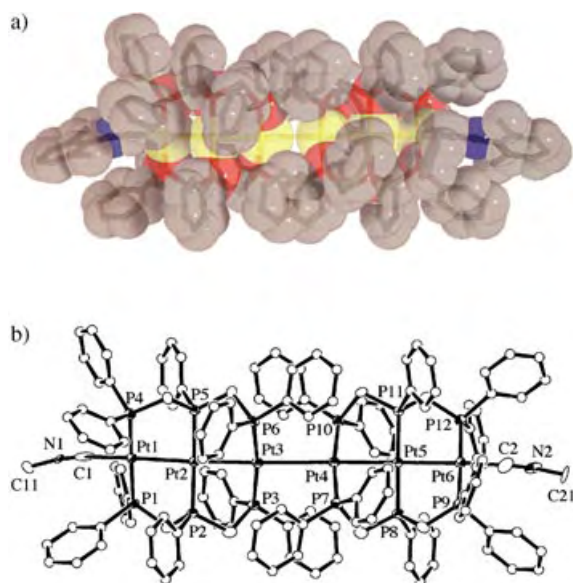
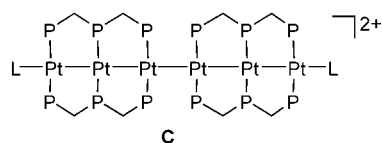


Figure 1. Crystal structure of **2**. a) A perspective plot with van der Waals radii superimposed on a wire-frame view; Pt yellow, P red, N blue, C gray. b) An ORTEP plot showing the linearly aligned coordinatively unsaturated metal sites; the xyllyl rings have been omitted for clarity. Selected bond distances [Å] and angles [°]: Pt1–Pt2 2.7073(5), Pt2–Pt3 2.7333(5), Pt3–Pt4 3.3092(5), Pt4–Pt5 2.7325(5), Pt5–Pt6 2.7008(5), Pt1–P1 2.300(3), Pt1–P4 2.299(3), Pt2–P2 2.254(2), Pt2–P5 2.255(2), Pt3–P3 2.268(3), Pt3–P6 2.264(3), Pt4–P7 2.266(2), Pt4–P10 2.269(2), Pt5–P8 2.248(2), Pt5–P11 2.256(2), Pt6–P9 2.291(2), Pt6–P12 2.303(2), Pt1–C1 2.02(1), Pt6–C2 1.94(1), N1–C1 1.12(1), N2–C2 1.19(1); Pt1–Pt2–Pt3 174.87(2), Pt2–Pt3–Pt4 178.47(2), Pt3–Pt4–Pt5 179.40(2), Pt4–Pt5–Pt6 179.67(2), Pt2–Pt1–C1 177.1(3), Pt5–Pt6–C2 177.0(3), Pt1–C1–N1 172.6(8), Pt6–C2–N2 176.3(9).

According to the X-ray crystal structure,^[11] the cluster cation of **3** is isomorphous to **2** (see the Supporting Information). It contains a Pt₂Pd₂Pt₂ hexametallc chain (M–M–M 175.10(2)–179.71(3)°) in which the central two metal positions are site-selectively occupied by Pd atoms and bridged by a hydride. The metal–metal distances are slightly longer than the corresponding values for **2** ($d_{\text{out}} = 2.7184$ Å (Pt–Pt), $d_{\text{inn}} = 2.7498$ Å (Pt–Pd), $d_{\text{cen}} = 3.355(1)$ Å (Pd–Pd)).

The ¹H NMR spectrum of **2** exhibited the resonance for the bridging hydride at $\delta = -8.6$ ppm, accompanied by a set of ¹⁹⁵Pt satellite peaks from two chemically equivalent Pt atoms ($J_{\text{PtH}} = 572$ Hz). The spectrum of **3** showed the corresponding peak at $\delta = -5.9$ ppm without any ¹⁹⁵Pt satellite peaks. This clearly indicated that the two central M atoms are symmetrically bridged by an acidic hydride, resulting in a MHM three-center two-electron (3c–2e) interaction.

To understand the electronic structure of these complexes, MO calculations were performed for **2** and [Pt₆(μ-dpmp)₄(XylNC)₂]²⁺ (**C**), a hypothetical hexaplutonium com-



plex that serves as a model contains a Pt^I–{Pt⁰}₄–Pt^I string with the precise CVE of 86.^[12] The HOMO of complex **C** lies at high energy and is mainly composed of a p_σ–p_σ bonding interaction of the two central Pt atoms. When a H⁺ ion is incorporated between the two central Pt atoms, the HOMO is significantly stabilized due to mixing with the low-lying d_σ–d_σ bonding orbital of the central Pt atoms and the s orbital of the H atom, resulting in a somewhat nonbonding character; this factor should be responsible for the stability of the isolated complex **2**.

In the UV/Vis spectra of complexes **2** and **3**, a very intense and broad absorption was observed around 580 nm (**2**) and 670 nm (**3**), which is characteristic of the MHM 3c–2e interaction. The ESI-TOF mass spectra of **2** and **3** in CH₂Cl₂ showed a trivalent parent peak for [Pt₄M₂(μ-H)(μ-dpmp)₄(XylNC)₂]³⁺ at $m/z = 1153.19$ (**2**, M = Pt) and 1094.19 (**3**, M = Pd). These results, along with the ³¹P{¹H} NMR spectra (see the Experimental Section), clearly demonstrated that complexes **2** and **3** are stable in solution and exist as linearly ordered hexanuclear molecules.

The cyclic voltammograms of **2** and **3** in CH₃CN showed irreversible multistep oxidation and reduction waves in a potential window of –2.0 to +0.8 V (vs. Ag/AgPF₆). Coulometric analyses of complex **2** suggested that the hexametallc core undergoes a two-step, one-electron oxidation at $E_{\text{pa}}^1 = -0.16$ V and $E_{\text{pa}}^2 = 0.01$ V, a two-electron oxidation at $E_{\text{pa}}^3 = 0.41$ V, and one- and two-electron reduction processes at $E_{\text{pc}}^1 = -1.23$ V and $E_{\text{pc}}^2 = -1.87$ V (Figure 2).^[13]

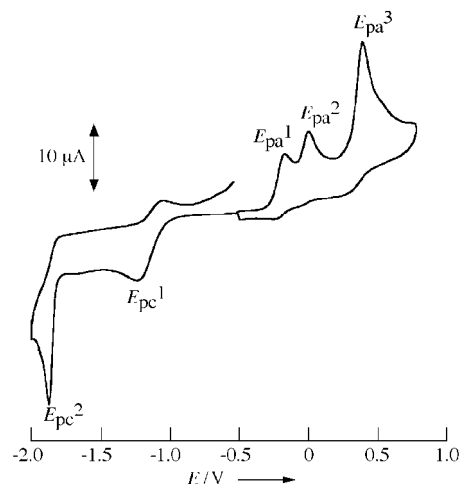


Figure 2. Cyclic voltammogram of **2** in acetonitrile containing 0.1 M (nBu₄N)(PF₆) at room temperature with a scan rate of 100 mV s^{–1}. E vs. Ag⁺/Ag.

The two-electron oxidized hexametallc clusters [Pt₄M₂(μ-dpmp)₄(XylNC)₂](PF₆)₄ (M = Pt (**4**), Pd (**5**)) were isolated by chemical oxidation of **2** and **3** with [Cp₂Fe][PF₆] or HPF₆ as well as by potentiostatic electrolyses (Scheme 1). In the electronic absorption spectra of **4** and **5**, the absorption around 580–670 nm characteristic of the bridging hydride is missing, and the ³¹P{¹H} NMR spectra suggested that the linear hexametallc cores remain intact, even in solution.

The structure of **5** was determined by X-ray crystallography (Figure 3).^[14] The cluster cation has a charge of +4 with a CVE of 84. Although the Pt₂Pd₂Pt₂ hexametallc core is

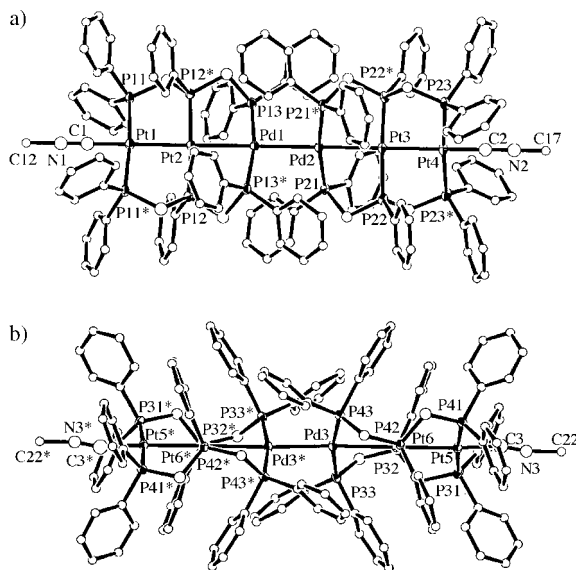


Figure 3. Crystal structure of **5**. The crystal contains two chemically equivalent, independent cluster cations; one cation has a crystallographically imposed C_2 axis along the hexametallc chain (a) and the other cation has a C_2 axis vertical to the metal axis (b). (ORTEP plots; the xyl rings have been omitted for clarity.) Selected bond distances [Å] and angles [°]: Pt1–Pt2 2.686(1), Pt2–Pd1 2.792(2), Pd1–Pd2 2.844(2), Pt3–Pd2 2.786(2), Pt3–Pt4 2.680(1), Pt5–Pt6 2.6854(9), Pt6–Pd3 2.789(1), Pd3–Pd3* 2.829(3), Pt1–Pt11 2.301(5), Pt2–Pt12 2.260(4), Pt3–Pt22 2.254(5), Pt4–Pt23 2.300(5), Pt5–Pt31 2.300(5), Pt5–Pt41 2.307(5), Pt6–Pt32 2.244(5), Pt6–Pt42 2.261(5), Pd1–Pd13 2.309(5), Pd2–Pd21 2.314(5), Pd3–Pd33 2.318(5), Pd3–Pd43 2.308(5), Pt1–C1 1.86(3), Pt4–C2 1.86(3), Pt5–C3 1.89(2), N1–C1 1.17(3), N2–C2 1.27(3), N3–C3 1.15(2); Pt1–Pt2–Pd1 (=Pt2–Pd1–Pd2 = Pd1–Pd2–Pt3 = Pd2–Pt3–Pt4) 180, Pt5–Pt6–Pd3 179.62(4), Pt6–Pd3–Pd3* 177.93(8), Pt2–Pt1–C1 (=Pt3–Pt4–C2) 180, Pt6–Pt5–C3 176.7(6).

retained, the metal–metal separations are different from those in **3**: $d_{\text{out}} = 2.684$ Å (Pt–Pt), $d_{\text{inn}} = 2.789$ Å (Pt–Pd), and $d_{\text{cen}} = 2.837$ Å (Pd–Pd). The central Pd–Pd distances are decreased by about 0.52 Å and the neighboring Pt–Pd bonds are elongated by about 0.04 Å upon two-electron oxidation or hydride elimination of **3**. The structure indicates the presence of metal–metal bonding between the central M atoms and delocalization of the metal–metal bonding electrons through the inner Pt–Pd–Pd–Pt unit. These results clearly demonstrated that hexametallc strings are redox-active without fragmentation of the cluster core. The bonding electrons in the adjacent M–Pt bonds migrate into the central M–M bond with a redox-coupled dynamic structural change upon two-electron oxidation of the hexametallc string.

In conclusion, the novel hexametallc clusters **2** and **3** were successfully synthesized and were demonstrated to be redox-active. They are readily oxidized to the electron-deficient clusters **4** and **5** with dynamic structural changes to the metal strings. Compounds **2** and **4** can be regarded as rigid-rod, discrete molecules (≈ 3 nm long) which contain the longest

platinum chain known so far.^[15] Furthermore, the present methodology could be applied to construct additional long metallic chains in a bottom-up strategy of molecular chemistry, and may lead to the development of molecular-based electronic devices.

Experimental Section

All procedures were performed under a dry nitrogen atmosphere using standard Schlenk techniques.

2: A mixture of **1a**·(CH₃)₂CO (215 mg, 97.2×10^{-3} mmol) and NaBH₄ (131 mg, 3.47 mmol) was dissolved in ethanol and stirred for 1 h to generate a brown precipitate. The solvent was removed under reduced pressure, and the brown residue was extracted with CH₂Cl₂. The color of the solution changed from dark green to dark blue within 1 h, and the solution was concentrated. After careful addition of Et₂O, the solution was allowed to stand at 2 °C to afford dark blue cubic crystals of **2**·3 CH₂Cl₂. Yield 88 mg, 44%; C, H, N analysis (%) calcd for C₁₄₉H₁₄₁Cl₆F₁₈N₂P₁₅Pt₆: C 43.13, H 3.42, N 0.68; found: C 42.92, H 3.45, N 0.64; IR (KBr): $\tilde{\nu} = 2131$ (N≡C), 839 cm^{−1} (PF₆); UV/Vis (CH₂Cl₂): λ_{max} (ϵ) = 583 (9.63×10^4), 402 (3.14×10^4), 379 nm (2.74×10^4); ¹H NMR (300 MHz, CD₂Cl₂, RT): δ = 8.7–6.2 (m, 106H, Ar), 5.1–4.7 (m, 8H, CH₂), 2.6 (brm, 4H, CH₂), 1.8 (brm, 4H, CH₂), 1.24 (s, 12H, *o*-CH₃), −8.61 ppm (brm, 1H, Pt–H, ¹J_{PtH} = 572 Hz); ³¹P{¹H} NMR (121 MHz, CD₂Cl₂, RT): δ = 6.5 (m, 4P, ¹J_{PtP} = 3395 Hz), −3.0 (m, 4P, ¹J_{PtP} = 2938 Hz), −15.3 ppm (m, 4P, ¹J_{PtP} = 3002 Hz); ESI-MS (CH₂Cl₂): m/z (z): 1153.194 (3) [Pt₆(H)(dmpm)₄(XylNC)₂]³⁺ (1153.179).

3: Complex **1b**·(CH₃)₂CO (189 mg, 89.2×10^{-3} mmol) and NaOMe (97 mg, 1.79 mmol) were dissolved in CH₂Cl₂/MeOH (1/1), and the mixture was stirred overnight. The color of the solution changed from orange to dark blue-green. The solvent was removed under reduced pressure, and the residue was extracted with CH₂Cl₂. The extract was concentrated, and careful addition of Et₂O afforded dark blue-green cubic crystals of **3**. Yield 84 mg, 51%; C, H, N analysis (%) calcd for C₁₄₆H₁₃₅F₁₈N₂P₁₅Pd₂Pt₄: C 47.17, H 3.66, N 0.75; found: C 46.97, H 3.65, N 0.81; IR (KBr): $\tilde{\nu} = 2135$ (N≡C), 841 cm^{−1} (PF₆); UV/Vis (CH₂Cl₂): λ_{max} (ϵ) = 674 (8.48×10^4), 438 (1.02×10^4), 395 (1.77×10^4), 346 nm (2.00×10^4); ¹H NMR (300 MHz, CD₂Cl₂, RT): δ = 8.7–6.2 (m, 106H, Ar), 5.2–4.3 (m, 8H, CH₂), 2.7 (brm, 4H, CH₂), 1.9 (brm, 4H, CH₂), 1.23 (s, 12H, *o*-CH₃), −5.90 ppm (m, 1H, Pd–H); ³¹P{¹H} NMR (121 MHz, CD₂Cl₂, RT): δ = 3.3 (m, 4P), −3.3 (m, 4P, ¹J_{PtP} = 2938 Hz), −11.0 ppm (m, 4P, ¹J_{PtP} = 2948 Hz); ESI-MS (CH₂Cl₂): m/z (z): 1094.194 (3) [Pt₄Pd₂(H)(dmpm)₄(XylNC)₂]³⁺ (1094.139).

4: [Cp₂Fe](PF₆) (5.7 mg, 17×10^{-3} mmol) was added to a solution of **2**·3 CH₂Cl₂ (35 mg, 8.4×10^{-3} mmol) in CH₂Cl₂, and the solution was stirred for 2 h. The solvent was removed under reduced pressure, and the black residue was washed with Et₂O and extracted with CH₂Cl₂. The extract was concentrated and addition of Et₂O afforded dark-green crystals of **4**·5 CH₂Cl₂. Yield 18 mg, 49%; C, H, N analysis (%) calcd for C_{149.5}H₁₄₁Cl₇F₂₄N₂P₁₆Pt₆: C 41.41, H 3.28, N 0.65; found: C 41.27, H 3.07, N 0.91; IR (KBr): $\tilde{\nu} = 2161$ (N≡C), 840 cm^{−1} (PF₆); UV/Vis (CH₂Cl₂): λ_{max} (ϵ) = 420 (2.16×10^4), 377 (7.11×10^4), 310 (sh, 4.06×10^4), 289 nm (sh, 5.06×10^4); ¹H NMR (300 MHz, [D₆]acetone, RT): δ = 8.3–6.7 (m, 106H, Ar), 5.0 (m, 8H, CH₂), 4.3 (brm, 4H, CH₂), 3.6 (brm, 4H, CH₂), 1.57 ppm (s, 12H, *o*-CH₃); ³¹P{¹H} NMR (121 MHz, [D₆]acetone, RT): δ = 20.8 (m, 4P, ¹J_{PtP} = 3413 Hz), −1.1 (m, 4P, ¹J_{PtP} = 2741 Hz), −6.9 ppm (m, 4P, ¹J_{PtP} = 2797 Hz).

5: A similar procedure to that for complex **4** using **3** as the starting material gave **5**·CH₂Cl₂. Yield 24 mg, 54%; C, H, N analysis (%) calcd for C₁₄₇H₁₃₆N₂P₁₆F₂₄Cl₂Pt₄Pd₂: C 44.74, H 3.47, N 0.71; found: C 44.27, H 3.86, N 0.71; IR (KBr): $\tilde{\nu} = 2162$ (N≡C), 839 cm^{−1} (PF₆); UV/Vis (CH₂Cl₂): λ_{max} (ϵ) = 461 (3.45×10^4), 370 (7.51×10^4), 343 (5.55×10^4), 310 nm (sh, 5.08×10^4); ¹H NMR (300 MHz, CD₃CN, RT): δ = 8.0–6.8 (m, 106H, Ar), 4.7 (m, 8H, CH₂), 4.1 (brm, 4H, CH₂), 3.8 (brm, 4H,

CH₂), 1.48 ppm (s, 12H, *o*-CH₃); ³¹P{¹H} NMR (121 MHz, CD₃CN, RT): δ = 5.9 (m, 4P), 0.4 (m, 4P, ¹J_{PP} = 2766 Hz), −11.1 ppm (m, 4P, ¹J_{PP} = 2887 Hz).

Received: May 18, 2004

Keywords: cluster compounds · oxidation · palladium · platinum · redox chemistry

- [1] a) *Metal–Metal Bonds and Clusters in Chemistry and Catalysis* (Ed.: J. P. Fackler), Plenum, New York, **1990**; b) D. A. Adams, F. A. Cotton, *Catalysis by Di- and Polynuclear Metal Cluster Complexes*, Wiley, New York, **1998**.
- [2] a) S.-Y. Lai, T.-W. Lin, Y.-H. Chen, C.-C. Wang, G.-H. Lee, M.-H. Yang, M.-K. Leung, S.-M. Peng, *J. Am. Chem. Soc.* **1999**, *121*, 250; b) Y.-H. Chen, C.-C. Lee, C.-C. Wang, G.-H. Lee, S.-Y. Lai, F.-Y. Li, C.-Y. Mou, S.-M. Peng, *Chem. Commun.* **1999**, 1667; c) C.-C. Wang, W.-C. Lo, C.-C. Chou, G.-H. Lee, J.-M. Chen, S.-M. Peng, *Inorg. Chem.* **1998**, *37*, 4059; d) S.-J. Shieh, C.-C. Chou, G.-H. Lee, C.-C. Wang, S.-M. Peng, *Angew. Chem.* **1997**, *109*, 57; *Angew. Chem. Int. Ed. Engl.* **1997**, *36*, 56.
- [3] a) R. Clérac, F. A. Cotton, K. R. Dunbar, T. Lu, C. A. Murillo, X. Wang, *J. Am. Chem. Soc.* **2000**, *122*, 2272; b) F. A. Cotton, L. M. Daniels, C. A. Murillo, X. Wang, *Chem. Commun.* **1999**, 2461.
- [4] a) T. Murahashi, T. Uemura, H. Kurosawa, *J. Am. Chem. Soc.* **2003**, *125*, 8436; b) T. Murahashi, Y. Higuchi, T. Katoh, H. Kurosawa, *J. Am. Chem. Soc.* **2002**, *124*, 14288; c) T. Murahashi, T. Nagai, T. Okuno, T. Matsutani, H. Kurosawa, *Chem. Commun.* **2000**, 1689; d) T. Murahashi, E. Mochizuki, Y. Kai, H. Kurosawa, *J. Am. Chem. Soc.* **1999**, *121*, 10660.
- [5] a) K. Mashima, H. Nakano, A. Nakamura, *J. Am. Chem. Soc.* **1996**, *118*, 9083; b) K. Mashima, M. Tanaka, K. Tani, A. Nakamura, S. Takeda, W. Mori, K. Yamaguchi, *J. Am. Chem. Soc.* **1997**, *119*, 4307; c) K. Mashima, A. Fukumoto, H. Nakano, Y. Kaneda, K. Tani, A. Nakamura, *J. Am. Chem. Soc.* **1998**, *120*, 12151.
- [6] C. Tejel, M. A. Ciriano, B. E. Villarroja, J. A. López, F. J. Lahoz, L. A. Oro, *Angew. Chem.* **2003**, *115*, 547; *Angew. Chem. Int. Ed.* **2003**, *42*, 530.
- [7] T. Zhang, M. Drouin, P. D. Harvey, *Inorg. Chem.* **1999**, *38*, 957.
- [8] a) T. Tanase, H. Ukaji, T. Igoshi, Y. Yamamoto, *Inorg. Chem.* **1996**, *35*, 4114; b) T. Tanase, H. Toda, Y. Yamamoto, *Inorg. Chem.* **1997**, *36*, 1571; c) T. Tanase, H. Ukaji, H. Takahata, H. Toda, T. Igoshi, Y. Yamamoto, *Organometallics* **1998**, *17*, 196; d) T. Tanase, R. A. Begum, *Organometallics* **2001**, *20*, 106; e) T. Tanase, R. A. Begum, H. Toda, Y. Yamamoto, *Organometallics* **2001**, *20*, 968.
- [9] Although the mechanism of formation for **3** was not clear and no intermediate species were monitored, experiments with ²H-labeled solvents suggested that the hydride H atom was derived from C–H cleavage of methanol or methoxide.
- [10] Crystal data for **2**: 4CH₂Cl₂·3H₂O (C₁₅₀H₁₄₈Cl₈F₁₈N₂P₁₅Pt₆O₃): *M*_r = 4287.57 (0.25 × 0.25 × 0.20 mm), triclinic, space group *P* $\bar{1}$ (no. 2), *a* = 20.6075(9), *b* = 21.874(1), *c* = 18.1441(8) Å, *α* = 91.065(3), *β* = 89.810(3), *γ* = 94.661(3)°, *V* = 8150.4(6) Å³, *Z* = 2, *ρ*_{calcd} = 1.747 g cm^{−3}, *F*(000) = 4154, 2*θ*_{max} = 52°, MoK α radiation (*λ* = 0.71070 Å, *μ* = 54.58 cm^{−1}), *T* = −120°C. A total of 27996 reflections were collected with a Rigaku/MSC Mercury CCD diffractometer (2*θ* = 6–55°, *ω* scans 0.25°). The crystal structure was solved by direct methods (SIR98) and refined with full-matrix least-squares techniques (teXsan). Non-hydrogen atoms were anisotropically refined, except for some atoms of the solvent molecules. The bridging H atom was not located, and the positions of carbon-bound H atoms were calculated and not refined. Final *R*₁ = 0.054 and *R*_w = 0.067 (19103 reflections, *I* > 2 σ (*I*), 6 < 2 θ < 52°) for 1811 variables. CCDC-238886 (**2**),
- CCDC-238887 (**3**), and CCDC-238888 (**5**) contain the supplementary crystallographic data for this paper. These data can be obtained free of charge via www.ccdc.cam.ac.uk/conts/retrieving.html (or from the Cambridge Crystallographic Data Centre, 12, Union Road, Cambridge CB21EZ, UK; fax: (+44)1223-336-033; or deposit@ccdc.ca.ac.uk). The ORTEP plot for complex **3** is available in the Supporting Information.
- [11] Crystal data for **3**: 5CH₂Cl₂·CH₃OH·4H₂O (C₁₅₂H₁₅₆Cl₁₀F₁₈N₂P₁₅Pd₂Pt₄O₅): *M*_r = 4245.18 (0.30 × 0.25 × 0.10 mm), triclinic, space group *P* $\bar{1}$ (no. 2), *a* = 18.290(1), *b* = 20.7102(5), *c* = 22.070(2) Å, *α* = 94.231(5), *β* = 90.730(1), *γ* = 90.1903(8)°, *V* = 8336.3(10) Å³, *Z* = 2, *ρ*_{calcd} = 1.691 g cm^{−3}, *F*(000) = 4166, 2*θ*_{max} = 54.7°, MoK α radiation (*λ* = 0.71070 Å, *μ* = 39.17 cm^{−1}), *T* = −120°C. Data were collected with a Rigaku/MSC Mercury CCD diffractometer (2*θ* = 6–52°, *ω* scans 0.25°). The crystal structure was solved by Patterson methods (Dirdif94 Patty) and refined with teXsan. Non-hydrogen atoms were anisotropically refined, except for some atoms of the solvent molecules. The bridging H atom was not located, and the positions of carbon-bound H atoms were calculated and not refined. Final *R*₁ = 0.064 and *R*_w = 0.081 for 1769 variables (18753 reflections, *I* > 3 σ (*I*), 6 < 2 θ < 52°).
- [12] The EHMO calculations were carried out on the model compound for **2**, and a simplified fragment MO interaction diagram is provided in the Supporting Information. Single point density functional calculations on the crystal structure of the complex cation of **2** were also carried out by the BECK3LYP method with the LANL2DZ basis set with the program Gaussian 98.
- [13] Cyclic voltammograms were measured with the following electrodes: glassy carbon (working), Pt coil (counter), Ag/AgPF₆ (reference). The cyclic voltammogram of **3** was similar to that of **2**, except that the first two-step oxidation waves at *E*_{pa}¹ = −0.16 V and *E*_{pa}² = 0.01 V in complex **2** were observed as a broad, one-step oxidation wave at *E*_{pa}¹ = −0.21 V. Under the experimental conditions, the ferrocene/ferrocenium redox couple was observed at 0.09 V.
- [14] Crystal data for **5**: 7CH₂Cl₂ (C₁₅₃H₁₄₈Cl₁₄F₂₄N₂P₁₆Pd₂Pt₄): *M*_r = 4455.91 (0.35 × 0.30 × 0.28 mm), orthorhombic, space group *C*22₁ (no. 20), *a* = 26.4070(9), *b* = 40.588(1), *c* = 41.353(1) Å, *V* = 44322(2) Å³, *Z* = 8, *ρ*_{calcd} = 1.335 g cm^{−3}, *F*(000) = 17424, 2*θ*_{max} = 55.0°, MoK α radiation (*λ* = 0.71070 Å, *μ* = 30.06 cm^{−1}), *T* = −120°C. Data were collected with Rigaku/MSC Mercury CCD diffractometer (2*θ* = 6–55°, *ω* scans 0.25°). The crystal structure was solved by Patterson methods (DIRDIF94 Patty) and refined with teXsan. The crystal contains two chemically equivalent, independent cluster cations; one cation (Figure 3a) has a crystallographically imposed *C*₂ axis along the hexametallic chain and the other cation (Figure 3b) has a *C*₂ axis vertical to the metal axis. The Pt, Pd, P, and F atoms were refined with anisotropic thermal parameters, and other non-hydrogen atoms were refined. Hydrogen atoms were calculated and not refined. Final *R*₁ = 0.069 and *R*_w = 0.086 for 1087 variables (15979 reflections, *I* > 3 σ (*I*), 6 < 2 θ < 55°).
- [15] Molecular compounds containing low-valent Pt chains are rare. The linear tetraplatinum complex reported in ref. [7] was the longest molecule thus far. In contrast, linearly assembled high-valent Pt compounds in the solid state have been well studied. See, for example, a) K. Matsumoto, K. Sakai, *Adv. Inorg. Chem.* **2000**, *49*, 375; b) K. Matsumoto, K. Sakai, K. Nishio, Y. Tokisue, R. Ito, T. Nishide, Y. Shichi, *J. Am. Chem. Soc.* **1992**, *114*, 8110.

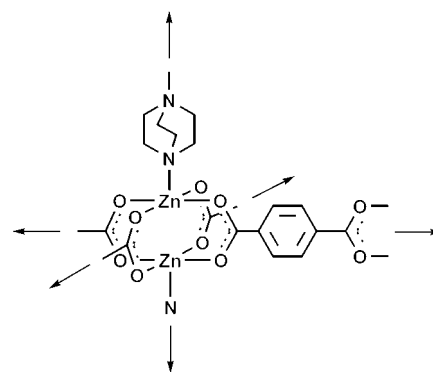
Rigid and Flexible: A Highly Porous Metal–Organic Framework with Unusual Guest-Dependent Dynamic Behavior**

Danil N. Dybtsev, Hyungphil Chun, and Kimoon Kim*

Porous metal–organic materials^[1] have attracted considerable attention in recent years because of their potential applications in many areas including gas storage,^[2] separation,^[3] and catalysis.^[4] Because high framework stability is essential for many practical applications, the quest for metal–organic materials with rigid frameworks has been a subject of intense research. Since the first reports of metal–organic frameworks with permanent porosity,^[5] many metal–organic frameworks have been reported to have stable porous structures; however, only a handful of these materials have a high surface area,^[6] which is another important virtue of this class of materials. There is also growing interest in metal–organic materials with flexible and dynamic frameworks,^[7] in particular, those that reversibly change their structures and properties in response to external stimuli as they may find applications, for example, in sensors.^[8] However, porous materials that have both high framework stability and framework flexibility are rare.^[9] Herein we report a novel metal–organic framework with permanent porosity and a high surface area, which also shows unusual guest-dependent dynamic behavior: the framework shrinks upon guest inclusion and expands upon guest release as proved unequivocally by single-crystal X-ray crystallography. These changes are fully reversible and depend on the nature of guests.

Heating a dimethylformamide (DMF) solution of $\text{Zn}(\text{NO}_3)_2$, terephthalic acid (or 1,4-benzenedicarboxylic acid, H_2bdc) and 1,4-diazabicyclo[2.2.2]octane (dabco) at 110 °C for 2 days gave the crystalline product $[\text{Zn}_2(1,4\text{-bdc})_2(\text{dabco})]\cdot 4\text{DMF}\cdot \frac{1}{2}\text{H}_2\text{O}$ ($1\cdot 4\text{DMF}\cdot \frac{1}{2}\text{H}_2\text{O}$) in over 80 % yield.^[10] The structure of $1\cdot 4\text{DMF}\cdot \frac{1}{2}\text{H}_2\text{O}$ was determined by single-crystal X-ray diffraction and the phase purity of the bulk material was independently confirmed by powder X-ray diffraction (XRD), thermal gravimetric analysis (TGA) and

elemental analysis. The framework in $1\cdot 4\text{DMF}\cdot \frac{1}{2}\text{H}_2\text{O}$ is composed of dinuclear Zn_2 units with a paddle wheel structure, which are bridged by 1,4-bdc dianions to form a distorted 2D square-grid $\{\text{Zn}_2(1,4\text{-bdc})_2\}$. The axial sites of the Zn_2 paddle wheels are occupied by dabco, which act as pillars to extend the 2D layers into a 3D structure (Scheme 1). The overall topology of the framework in $1\cdot 4\text{DMF}\cdot \frac{1}{2}\text{H}_2\text{O}$ is best described as a compressed primitive cubic (α -Po) net (Figure 1a). The dabco pillars are disordered along the



Scheme 1. The extension of the 2D square-grid of $\{\text{Zn}_2(1,4\text{-bdc})_2\}$ into a 3D structure by using dabco, which occupies the axial positions.

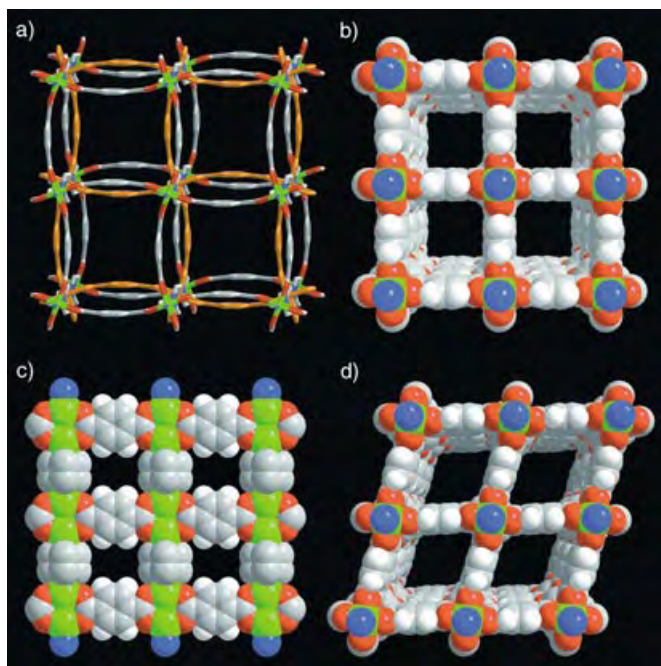


Figure 1. a) The view along fourfold axis of the metal–organic framework structure in $1\cdot 4\text{DMF}\cdot \frac{1}{2}\text{H}_2\text{O}$. One $\{\text{Zn}_2(1,4\text{-bdc})_2\}$ 2D Layer is colored orange to emphasize the alternation of stacking layer. Hydrogen atoms and guest molecules are omitted. b) Space-filling representation of evacuated framework **1**, which emphasizes the open square channels; view along fourfold axis. c) Side view of evacuated framework **1**, showing the windows interconnecting the channels. d) Space-filling representation of the metal–organic framework structure in $1\cdot 2\text{C}_6\text{H}_6$, showing rhombic-grid motif of $\{\text{Zn}_2(1,4\text{-bdc})_2\}$ layers. The guest molecules and dabco hydrogens are not shown. Legend: Zn green; N blue; O red; C grey; H white.

[*] Dr. D. N. Dybtsev,† Dr. H. Chun, Prof. Dr. K. Kim
National Creative Research Initiative Center for Smart Supramolecules, and
Department of Chemistry
Division of Molecular and Life Sciences
Pohang University of Science and Technology
San 31 Hyojadong, Pohang 790-784 (Republic of Korea)
Fax: (+82) 54-279-8129
E-mail: kkim@postech.ac.kr

[†] Permanent address:
Institute of Inorganic Chemistry
3, Lavrenteva st., Novosibirsk, 630090 (Russia)

[**] We gratefully acknowledge the Creative Research Initiative Program of the Korean Ministry of Science and Technology for support of this work.

Supporting information for this article is available on the WWW under <http://www.angewandte.org> or from the author.

crystallographic fourfold axis.^[11] Interestingly, the 1,4-bdc linker is unusually bent, which results in severe twisting of the Zn_2 paddle wheel from an ideal square grid. Due to this distortion $\mathbf{1} \cdot 4\text{DMF} \cdot \frac{1}{2}\text{H}_2\text{O}$ crystallizes in a body-centered unit cell ($I4/mcm$) instead of a primitive cell with $4/mmm$ symmetry. Such notable bending is unusual because 1,4-bdc is generally considered to be a linear and rigid linker. The TGA data indicate that $\mathbf{1} \cdot 4\text{DMF} \cdot \frac{1}{2}\text{H}_2\text{O}$ loses its guest molecules in the temperature range of 100–200 °C, and the resulting porous framework starts to decompose after 300 °C. The crystals of $\mathbf{1} \cdot 4\text{DMF} \cdot \frac{1}{2}\text{H}_2\text{O}$ maintain single crystallinity even after the guest has been removed completely by heating in a vacuum for 1 day, which allowed us to determine the guest-free structure by single-crystal X-ray crystallography.

The X-ray crystal structure of the guest-free framework **1** reveals the same connectivity, but the most striking change is that the 1,4-bdc ligands linking the Zn_2 paddle wheel units are now linear, which results in a perfect 2D square grid [$\text{Zn}_2(1,4\text{-bdc})_2$] (Figure 1b). The 2D layers are linked by disordered dabco pillars to form a 3D framework as in the parent structure. The guest-free framework **1** has large, three dimensionally interconnected voids. The wide open channels ($7.5 \times 7.5 \text{ \AA}^2$) running along the *c* axis are interlinked by smaller windows (ca. 4 \AA) along the *a* and *b* axes, which are still large enough for the passage of small gas molecules (Figure 1c). The guest-accessible volume for **1** is estimated to be 62 %.^[12] The structure of the guest-free framework **1** is similar to that proposed for $[\text{Cu}_2(1,4\text{-bdc})_2(\text{dabco})]$ based on powder XRD studies.^[2c] The linear geometry of the 1,4-bdc ligand in the guest-free framework **1** leads to a substantial increase in the distance between two neighboring Zn_2 paddle-wheel units in the layer (10.93 Å in **1** versus 10.65 Å in $\mathbf{1} \cdot 4\text{DMF} \cdot \frac{1}{2}\text{H}_2\text{O}$) as well as in the specific volume per Zn_2 unit (1147.6(3) Å³ versus 1091.8(4) Å³, respectively) upon the guest release. The structural changes can also be detected by powder XRD analysis (Figure 2). In the XRD pattern of the guest-free sample, all the peaks except for [00*l*] reflections shift to lower 2θ values, which is consistent with the expansion of the 2D square grid. The [00*l*] reflections remain unchanged as the distance between the 2D layers is primarily determined by the dabco pillars. The structural change associated with the guest removal is fully reversible. The powder XRD pattern of the

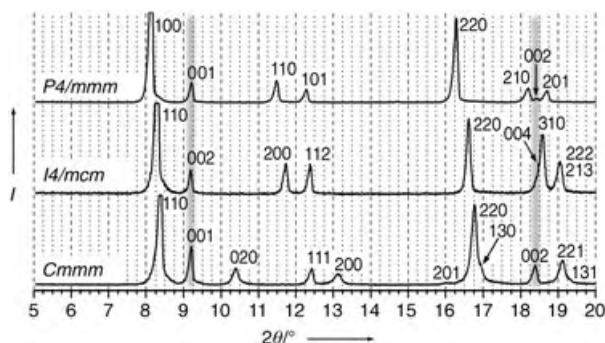


Figure 2. Powder X-ray diffractograms of evacuated framework **1** (top), as-synthesized $\mathbf{1} \cdot 4\text{DMF} \cdot \frac{1}{2}\text{H}_2\text{O}$ (middle) and benzene-exchanged $\mathbf{1} \cdot 2\text{C}_6\text{H}_6$ (bottom). The reflections, corresponding to the same [00*l*] interplanar distances are emphasized.

guest-free microcrystalline sample after soaking in DMF for 2 days is exactly the same as that for the as-synthesized material; therefore the host framework shrinks back upon guest inclusion. The whole cycle can be repeated several times without a significant loss of crystallinity of the material.

A different mode of the framework distortion leading to the shrinkage of pores was observed upon inclusion of benzene into the guest-free framework **1** as confirmed by power XRD studies (Figure 2). Once again, all the structural changes are reversible. The structure of the benzene-inclusion framework ($\mathbf{1} \cdot 2\text{C}_6\text{H}_6$) was also determined by single-crystal X-ray crystallography. The overall framework connectivity in $\mathbf{1} \cdot 2\text{C}_6\text{H}_6$ remains the same, but the Zn_2 paddle wheels and 1,4-bdc linkers now form a 2D rhombic grid (Figure 1d). Because the 1,4-bdc linkers in $\mathbf{1} \cdot 2\text{C}_6\text{H}_6$ adopt a linear geometry, the distance between two neighboring Zn_2 units is almost the same as that in the guest-free framework **1**, but due to the inclination of the 2D grid motif the specific volume per Zn_2 unit is smaller (1114.2(2) Å³) than that for the guest-free framework. Therefore, these data unambiguously prove that the porous metal–organic framework **1** responds to the guest inclusion in different ways depending on the nature of the guest. More interestingly, contrary to common host–guest materials, the framework shrinks upon guest inclusion and expands upon guest release. Prior to this work, to the best of our knowledge, there is only one example of similar guest-induced behavior based on powder XRD studies reported.^[6f,7a] Further work is in progress to understand the origin of the unusual structural changes associated with the guest inclusion and removal.

The permanent porosity of **1** has been confirmed by N_2 and H_2 gas sorption measurements at 78 K (Figure 3). The sorption of N_2 follows a type I isotherm with a BET surface

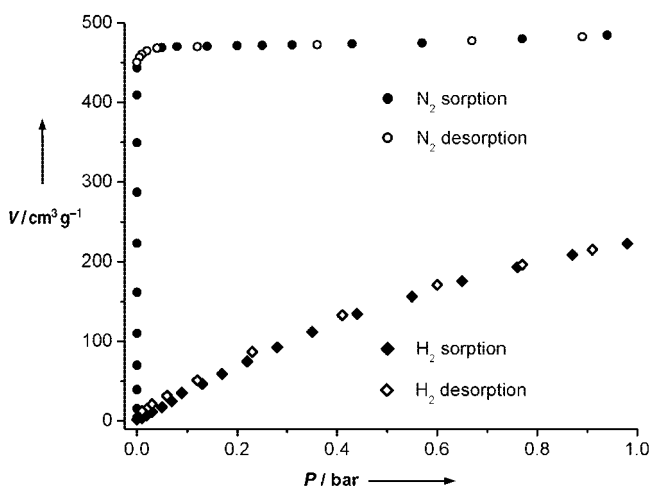


Figure 3. BET gas sorption isotherms of **1** at 78 K.

area of $1450 \text{ m}^2 \text{ g}^{-1}$.^[13] In contrast, the hydrogen sorption shows an unsaturated, almost linear isotherm with a maximum sorption capacity of $225 \text{ cm}^3 \text{ g}^{-1}$ (standard temperature and pressure) or 2.0 wt. % at 1 bar pressure, which is significantly higher than those of any zeolites or metal–

organic materials reported to date under the same conditions.^[14] Because of the incomplete saturation, an even higher H₂-sorption capacity is expected for **1** at elevated pressures.

In conclusion, we present a novel, highly porous metal-organic framework that has both rigidity and flexibility. This unusual combination leads to a stable framework with permanent porosity and guest-dependent dynamic behavior. It has an exceptionally high surface area and H₂ sorption capacity. Furthermore, the host framework shrinks upon inclusion of organic guest molecules and expands upon guest removal, a rare phenomenon in this class of materials. This material, which can be easily obtained in crystalline form in a one-pot, gram-scale synthesis starting from readily available chemicals, may thus find applications not only as a gas storage medium but also as a sensor. Further studies on the novel metal-organic framework and related materials are in progress.

Experimental Section

1·4DMF·½H₂O: A mixture of Zn(NO₃)₂·6H₂O (1.0 g, 3.36 mmol), H₂bdc (0.560 g, 3.37 mmol), and dabco (0.187 g, 1.67 mmol) was suspended in DMF (40 mL) and heated in a teflon-lined steel bomb at 120 °C for 2 days. The colorless crystalline precipitate formed was collected, washed with DMF, and dried under a reduced pressure at room temperature for 2 h (1.21 g, 83 %). Elemental analysis calcd for [Zn₂(C₈H₄O₄)₂(C₆H₁₂N₂)]₂·4DMF·½H₂O: C 46.80, H 5.66, N 9.63; found: C 46.60, H 5.56, N 9.71. TGA data: calcd weight loss for 4DMF + ½H₂O: 34.5%; found: 35.0%.

Single-crystal X-ray Crystallography: The full hemisphere data were collected on a Siemens SMART CCD diffractometer with Mo K_α radiation (λ = 0.71073 Å). After the data integration (SAINT) and semi-empirical absorption correction based on equivalent reflections (SADABS), the structure was solved by direct methods and subsequent difference Fourier techniques (SHELXL). Crystal data for [Zn₂(C₈H₄O₄)₂(C₆H₁₂N₂)]₂·4DMF·½H₂O (**1·4DMF·½H₂O**): tetragonal, *I4/mcm* (No. 140), *a* = 15.063(2), *c* = 19.247(5) Å, *V* = 4367.1(14) Å³, *Z* = 4, *T* = 243 K, *ρ*_{calcd} = 1.327 g cm⁻³, *μ* = 1.106 mm⁻¹, 2θ_{max} = 56.6°. Total number of reflections 1448 (*R*_{int} = 0.0353), *R*₁ = 0.0414 (1176 reflections with *I* > 2σ(*I*)), *wR*₂ = 0.1355 (all data), GOF = 1.073 and 94 parameters. **1:** A crystalline sample of **1·4DMF·½H₂O** was evacuated at 100 °C for 24 h to remove the guest molecules. Crystal data for [Zn₂(C₈H₄O₄)₂(C₆H₁₂N₂)] (**1**): tetragonal, *P4/mmm* (No. 123), *a* = 10.929(2), *c* = 9.608(1) Å, *V* = 1147.6(3) Å³, *Z* = 1, *T* = 223 K, *d*_{calcd} = 0.826 g cm⁻³, *μ* = 1.070 mm⁻¹, 2θ_{max} = 56.6°. Total number of reflections 880 (*R*_{int} = 0.0360), *R*₁ = 0.0277 (852 reflections with *I* > 2σ(*I*)), *wR*₂ = 0.0711 (all data), GOF = 1.170 and 49 parameters. **1·2C₆H₆:** Single-crystals of **1·4DMF·½H₂O** were soaked in benzene for 3 days. Crystal data for [Zn₂(C₈H₄O₄)₂(C₆H₁₂N₂)]₂·2C₆H₆ (**1·2C₆H₆**): orthorhombic, *Cmmm* (No. 65), *a* = 13.500(1), *b* = 17.066(1), *c* = 9.672(1) Å, *V* = 2228.3(3) Å³, *Z* = 2, *T* = 223 K, *ρ*_{calcd} = 1.672 g cm⁻³, *μ* = 2.219 mm⁻¹, 2θ_{max} = 52°. Total number of reflections 1262 (*R*_{int} = 0.0501), *R*₁ = 0.0619 (1129 reflections with *I* > 2σ(*I*)), *wR*₂ = 0.2039 (all data), GOF = 1.215 and 64 parameters. CCDC-238859–238861 contains the supplementary crystallographic data for this paper. These data can be obtained free of charge via www.ccdc.cam.ac.uk/conts/retrieving.html (or from the Cambridge Crystallographic Data Centre, 12 Union Road, Cambridge CB21EZ, UK; fax: (+44)1223-336-033; or deposit@ccdc.cam.ac.uk).

Received: May 19, 2004

Keywords: carboxylate ligands · coordination polymers · gas sorption · host-guest systems

- [1] a) C. N. R. Rao, S. Natarajan, R. Vaidyanathan, *Angew. Chem.* **2004**, *116*, 1490–1521; *Angew. Chem. Int. Ed.* **2004**, *43*, 1466–1496; b) S. Kitagawa, R. Kitaura, S. Noro, *Angew. Chem.* **2004**, *116*, 2388–2430; *Angew. Chem. Int. Ed.* **2004**, *43*, 2334–2375; c) O. M. Yaghi, M. O'Keeffe, N. W. Ockwing, H. K. Chae, M. Eddaoudi, J. Kim, *Nature* **2003**, *423*, 705–714; d) S. L. James, *Chem. Soc. Rev.* **2003**, *32*, 276–288; e) C. Janiak, *J. Chem. Soc. Dalton Trans.* **2003**, 2781–2804; f) M. E. Davis, *Nature* **2002**, *417*, 813–821; g) M. Eddaoudi, D. B. Moler, H. Li, B. Chen, T. Reineke, M. O'Keeffe, O. M. Yaghi, *Acc. Chem. Res.* **2001**, *34*, 319–330.
- [2] a) S. Noro, S. Kitagawa, M. Kondo, K. Seki, *Angew. Chem.* **2000**, *112*, 2161–2164; *Angew. Chem. Int. Ed.* **2000**, *39*, 2081–2084; b) M. Eddaoudi, J. Kim, N. Rosi, D. Vodak, J. Wachter, M. O'Keeffe, O. M. Yaghi, *Science* **2002**, *295*, 469–472; c) K. Seki, W. Mori, *J. Phys. Chem. B* **2002**, *106*, 1380–1385; d) N. L. Rosi, J. Eckert, M. Eddaoudi, D. T. Vodak, J. Kim, M. O'Keeffe, O. M. Yaghi, *Science* **2003**, *300*, 1127–1129; e) G. Férey, M. Latroche, C. Serre, F. Millange, T. Loiseau, A. Percheron-Guégan, *Chem. Commun.* **2003**, 2976–2977; f) J. L. C. Rowsell, A. R. Millward, K. S. Park, O. M. Yaghi, *J. Am. Chem. Soc.* **2004**, *126*, 5666–5667.
- [3] a) K. S. Min, M. P. Suh, *Chem. Eur. J.* **2001**, *7*, 303–313; b) K. Uemura, S. Kitagawa, M. Kondo, K. Fukui, R. Kitaura, H.-C. Chang, T. Mizutani, *Chem. Eur. J.* **2002**, *8*, 3587–3600; c) D. N. Dybtsev, H. Chun, S. H. Yoon, D. Kim, K. Kim, *J. Am. Chem. Soc.* **2004**, *126*, 32–33; d) D. Bradshaw, T. J. Prior, E. J. Cussen, J. B. Claridge, M. J. Rosseinsky, *J. Am. Chem. Soc.* **2004**, *126*, 6106–6114.
- [4] a) M. Fujita, Y.-J. Kwon, S. Washizu, K. Ogura, *J. Am. Chem. Soc.* **1994**, *116*, 1151–1152; b) J. S. Seo, D. Wand, H. Lee, S. I. Jun, J. Oh, Y. Jeon, K. Kim, *Nature* **2000**, *404*, 982–986.
- [5] a) H. Li, M. Eddaoudi, T. L. Groy, O. M. Yaghi, *J. Am. Chem. Soc.* **1998**, *120*, 8571–8572; b) S. S.-Y. Chui, S. M.-F. Lo, J. P. H. Charmant, A. Guy Orpen, I. D. Williams, *Science* **1999**, *283*, 1148–1150; c) H. Li, M. Eddaoudi, M. O'Keeffe, O. M. Yaghi, *Nature* **1999**, *402*, 276–279.
- [6] Metal-organic frameworks with a surface area higher than 1000 m² g⁻¹ (higher than those of any zeolites): see reference [2] and a) B. Chen, M. Eddaoudi, S. T. Hyde, M. O'Keeffe, O. M. Yaghi, *Science* **2001**, *291*, 1021–1023; b) F. Millange, C. Serre, G. Férey, *Chem. Commun.* **2002**, 882–883; c) K. Barthelet, J. Marrot, D. Riou, G. Férey, *Angew. Chem.* **2002**, *114*, 291–294; *Angew. Chem. Int. Ed.* **2002**, *41*, 281–284; d) S.-i. Noro, R. Kitaura, M. Kondo, S. Kitagawa, T. Ishii, H. Matsuzaka, M. Yamashita, *J. Am. Chem. Soc.* **2002**, *124*, 2568–2583; e) H. K. Chae, D. Y. Siberio-Perez, J. Kim, Y. Go, M. Eddaoudi, A. J. Matzger, M. O'Keeffe, O. M. Yaghi, *Nature* **2004**, *427*, 523–527; f) T. Loiseau, C. Serre, C. Huguenard, G. Fink, F. Taulelle, M. Henry, T. Bataille, G. Férey, *Chem. Eur. J.* **2004**, *10*, 1373–1382.
- [7] a) C. Serre, F. Millange, C. Thouvenot, M. Nogués, G. Marsolier, D. Louër, G. Férey, *J. Am. Chem. Soc.* **2002**, *124*, 13519–13526; b) M. P. Suh, J. W. Ko, H. J. Choi, *J. Am. Chem. Soc.* **2002**, *124*, 10976–10977; c) E. J. Cussen, J. B. Claridge, M. J. Rosseinsky, C. J. Keptert, *J. Am. Chem. Soc.* **2002**, *124*, 9574–9581; d) K. Biradha, M. Fujita, *Angew. Chem.* **2002**, *114*, 3542–3545; *Angew. Chem. Int. Ed.* **2002**, *41*, 3392–3395; e) D. V. Soldatov, I. L. Moudrakovski, C. I. Ratcliffe, R. Dutrisac, J. A. Ripmeester, *Chem. Mater.* **2003**, *15*, 4810–4818; f) O. Saied, T. Maris, J. D. Wuest, *J. Am. Chem. Soc.* **2003**, *125*, 14956–14957; g) K. Uemura, S. Kitagawa, K. Fukui, K. Saito, *J. Am. Chem. Soc.* **2004**, *126*, 3817–3828.

- [8] S. Kitagawa, M. Kondo, *Bull. Chem. Soc. Jpn.* **1998**, *71*, 1739–1753.
- [9] For metal–organic frameworks with permanent porosity and high framework flexibility see reference [6f, 7a] and a) K. Seki, *Phys. Chem. Chem. Phys.* **2002**, *4*, 1968–1971; b) R. Kitaura, K. Seki; G. Akiyama, S. Kitagawa, *Angew. Chem.* **2003**, *115*, 444–447; *Angew. Chem. Int. Ed.* **2003**, *42*, 428–431.
- [10] The synthesis is a part of our rational approach for the design of 2D and 3D frameworks, which will be published separately soon.
- [11] The metal–organic framework structure in $1.4\text{DMF}\cdot\frac{1}{2}\text{H}_2\text{O}$ solved in the space group *P*1 shows the same disorder of the dabco pillars proving that the high site symmetry is not the origin of the disorder.
- [12] A. L. Spek, PLATON, a multipurpose crystallographic tool, Utrecht University, Utrecht, The Netherlands, **2001**.
- [13] This value is similar to $1891\text{ m}^2\text{g}^{-1}$, obtained from the Ar sorption data of $[\text{Cu}_2(1,4\text{-bdc})_2(\text{dabco})]$.^[2c]
- [14] Previously reported^[2d] value of 4.5 % H_2 uptake was corrected recently to 1.3 %.^[2f] For other numbers for the H_2 sorption capacity in metal–organic frameworks see reference [2e, 2f, 3c] and E. Y. Lee, M. P. Suh, *Angew. Chem.* **2004**, *116*, 2858–2861; *Angew. Chem. Int. Ed.* **2004**, *43*, 2798–2801.

Self-assembly

Interlocked and Interdigitated Architectures from Self-Assembly of Long Flexible Ligands and Cadmium Salts**

Xin-Long Wang, Chao Qin, En-Bo Wang,* Lin Xu, Zhong-Min Su,* and Chang-Wen Hu

The current interest in the crystal engineering of coordination polymer frameworks not only stems from their potential applications in microelectronics, nonlinear optics, porous materials, and catalysis, but also from their intriguing variety of architectures and topologies.^[1,2] Up to now, a variety of

appealing interpenetrated nets, in which only internal connections are broken to separate individual nets, have been reported and reviewed by Batten and Robson.^[3] In contrast, other types of entangled architectures that have recently been described—such as infinite multiple helices,^[4] two-dimensional clothlike warp-and-weft sheet structures,^[5] interdigitated structures in a gearlike (or tongue-and-groove) fashion,^[6] and polythreaded structures with poly-pseudo-rotaxanes^[7]—can, in principle, be disentangled without breaking links. Moreover, these entangled nets can lead to synthetic supramolecular arrays with potential applications in asymmetric catalysis, drug-delivery vehicles, and sensor devices.

Unfortunately, these species are still rare, as evidenced in a recent review by Ciani and co-workers,^[8] and therefore the exploration of new synthetic routes to this class of supramolecular architectures is one of the most challenging issues in current synthetic chemistry. On the other hand, it is well-known that product topology can often be controlled and modulated by selecting the coordination geometry of the metal ions and the chemical nature of the organic ligands. Usually, long ligands will lead to larger voids that may result in interpenetrated structures,^[3] the most outstanding example of which is 1,2-bis(4-pyridyl)ethane (bpe). With this ligand, many beautiful interpenetrated networks of ingenious design have been constructed, ranging from interpenetrating 1D ladders to 3D nets.^[9]

However, these results do not mean that other types of entangled structures cannot be formed in the presence of long flexible ligands. If another configurational ligand is introduced, it may be possible to gain noninterpenetrating nets by combining different precursors. In this regard, for our synthetic strategy we choose an analogy of bpe, biphenylthene-4,4'-dicarboxylic acid (bpea), whose coordination chemistry, to the best of our knowledge, has not been previously investigated. Due to the replacement of two pyridyl groups by aromatic carboxy groups, bpea will be more flexible than bpe. Therefore, to avoid interpenetration the heterocyclic aromatic ligand 1,10-phenanthroline (phen) was introduced based on the following considerations: 1) The steric hindrance at the metal center will be increased when the bulky aromatic ligand binds to the metal ion; this reduces the dimension of the net formed. Lower dimensional nets are usually less likely to interpenetrate because there are more possible ways to maximize the packing efficiency.^[10] 2) Chelating bipyridyl-like ligands may provide recognition sites for π - π stacking interactions to form interesting supramolecular structures. 3) The conjugated π systems containing (hetero)-aromatic rings are currently of interest in the development of fluorescent materials and use as model compounds for electroluminescence and optical switching devices.^[11]

Due to the low solubility of the ligands, we adopted hydrothermal techniques and successfully synthesized three noninterpenetrating species. The first complex [Cd(bpea)(phen)₂] (**1**) exhibits a remarkable assembly of ninefold interlocked homochiral helices that are built from achiral components. [Cd₂(bpea)(pt)(phen)₂][Cd(pt)(phen)]·2H₂O (**2**, pt = phthalate) contains neutral 2D puckered sheets that are interdigitated by neutral 1D zigzag chains. The final compound [Cd₃(bpea)(phen)₃(OH)₃(H₂O)]·0.5bpea·4H₂O (**3**)

[*] Dr. X.-L. Wang, Dr. C. Qin, Prof. E.-B. Wang, Prof. L. Xu, Prof. C.-W. Hu
Institute of Polyoxometalate Chemistry
Department of Chemistry
Northeast Normal University
Changchun 130024 (China)
Fax: (+86) 431-5684009
E-mail: wangbenbo@public.cc.jl.cn

Prof. Z.-M. Su
Institute of Functional Materials
Department of Chemistry
Northeast Normal University
Changchun, Jilin, 130024 (China)
Fax: (+86) 431-5684009
E-mail: zmsu@nenu.edu.cn

[**] This work was financially supported by the National Natural Science Foundation of China (No. 20371011).

Supporting information for this article is available on the WWW under <http://www.angewandte.org> or from the author.

has unprecedented hexanuclear cadmium clusters that show a 3D supramolecular host–guest network.

X-ray crystallography^[12] shows that **1** has a 3D chiral framework assembled by nine interlocking nanotubes. Complex **1** crystallizes in the chiral space group $P4_1(3)$, with one Cd atom, one bpea ligand, and two phen ligands in the asymmetric unit. The Cd center is coordinated by four nitrogen atoms from two chelating phen ligands (mean Cd–N 2.477(3) Å) and two oxygen atoms from two monodentate carboxylate ends of two bpea ligands (mean Cd–O 2.259(3) Å) to furnish a distorted octahedral geometry. The $[\text{Cd}(\text{phen})_2]^{2+}$ molecular corners are bridged by long linear spacers to form an infinite helical chain running along the *c* axis (Figure 1a). The left-handed helix is generated around

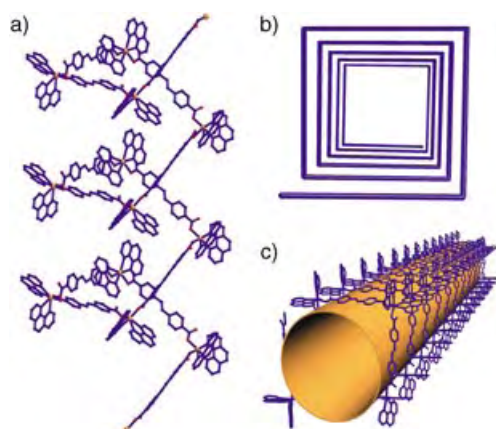


Figure 1. Crystal structure of **1**. a) View of the left-handed 4_1 helical chain. b) Schematic view of the helical chain. c) Perspective view of a chiral nanotube with an opening of about 1.8×1.8 nm.

the crystallographic 4_1 axis with a pitch of 24.46 Å. Notably, each pair of nearly perpendicular phen ligands bonded to the Cd atom point away from the helical axis; this steric orientation leads to the generation of a tetragonal nanotube with an opening of about 1.8×1.8 nm (Figure 1b,c).

The most fascinating structural feature of **1** is that each helical chain is chemically independent but physically interwoven with the same independent chains in all directions, whose unique entangled fashion can be described stepwise. First of all, four identical helices interweave the central one along the *a* and *b* axes with an extent of intercalation of about 0.72 nm. Another four helices further interlock the central one along the $[a,b]$, $[-a,-b]$, $[a,-b]$, and $[-a,b]$ directions with an extent of intercalation of about 0.24 nm. Thus, each helical chain is interlocked by eight equivalent polymeric units to give a periodically ordered interlocked architecture (Figure 2). The resulting 3D chiral network can therefore be described as an infinite interlocked array originating from ninefold interwoven homochiral helices. The framework is stabilized by strong π – π stacking interactions between the interwoven aryl groups: Parallel stacking with face-to-face distances of 3.350 Å between phen ligands and 3.400 Å between phen and bpea ligands. In contrast to the inter-

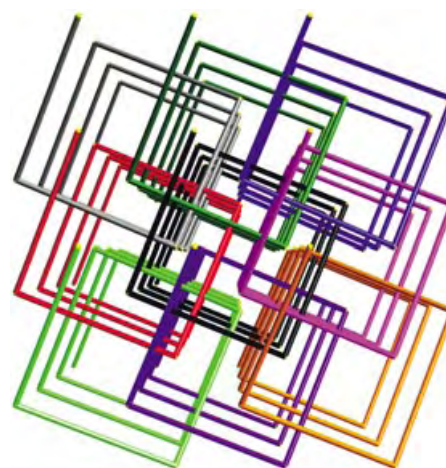


Figure 2. A schematic illustration of the ninefold interlocked homochiral helices of **1**.

penetrated network, the individual chains can “ideally” be separated without breaking links.

For typical interpenetrating systems, the world record is held by a tenfold interpenetrated diamondoid net exclusively based on coordinative bonds.^[13] Among the new structures showing entanglement, a rather remarkable example was reported by Lin and co-workers in which the 3D chiral framework results from the assembly of quintuple interwoven helices built from axially chiral bityridines.^[14] Therefore, to our knowledge, the ninefold interlocking homochiral helices constructed from achiral components in **1** represents the highest degree of entanglement known in a noninterpenetrating system.

The structure determination of **2** shows the presence of two crystallographically independent polymer motifs in the same crystal. One motif is a 1D zigzag chain constructed from mononuclear Cd atoms, pt, and phen (Figure 3a). The Cd center has a distorted octahedral coordination environment containing two nitrogen atoms of a chelating phen ligand (Cd–N 2.278(5) Å) and four oxygen atoms of two chelating carboxylate ends of two pt ligands (Cd–O 2.332(5) Å). The dangling phen groups are perpendicular to the propagation direction of the chain and bristle out in opposite directions. This arrangement paves the way for interdigitation.

The other polymer motif of **2** is a 2D puckered sheet of (4,4) topology built up from dinuclear Cd units with three types of ligands, that is, pt, bpea, and phen (Figure 3b). Although a few polymer frames with two kinds of aromatic ligands have been reported,^[15] there are no examples in which more than two different aromatic ligands are incorporated into a metal–organic polymer network. In contrast to the Cd atom in the first motif, the Cd center in the second motif adopts a seven-coordinate geometry made up of two nitrogen atoms of a chelating phen ligand (Cd–N 2.351(5) Å) and five oxygen atoms from one chelating bpea and two pt ligands (Cd–O 2.425(4) Å). Two crystallographically equivalent Cd atoms are bridged by two μ_3 -oxygen atoms to generate a dinuclear unit $[\text{Cd}\cdots\text{Cd}(\text{A})\ 3.693(9)\ \text{\AA}]$. Four such dinuclear

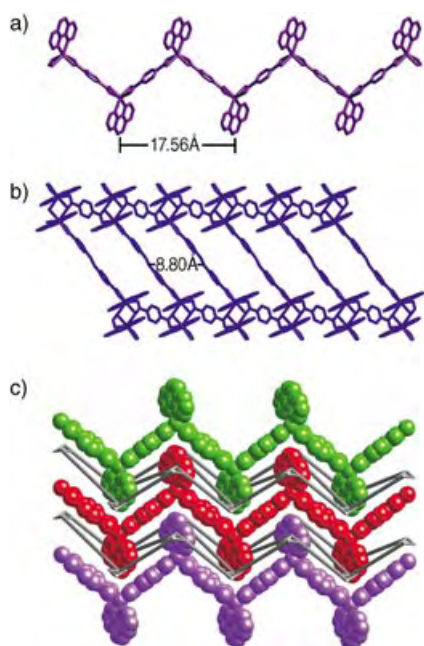


Figure 3. Crystal structure of **2**. a) View of the zigzag chain. b) View of the puckered sheet. c) View of the entanglement of the 1D chains and 2D sheets in the ABAB mode. The interdigitation of the phen groups is clearly visible.

units are alternately linked by pt and bpea ligands to form a long and narrow window, which provides a snug habitat for dangling phen groups of the 1D chain.

The unexpected aspect of **2** is how structurally divergent the two motifs are rationally combined together. The width of a window within a puckered sheet, dictated by the shortest carbon–carbon separation between two opposite bpea ligands, is about 8.80 Å, while the period of a zigzag chain is about 17.56 Å. This allows every other window of a sheet to be penetrated by one side of the phen groups of the 1D chains above the layer. The remaining windows are penetrated in the same way by the phen groups below the layer. Thus, each sheet is simultaneously interdigitated by chains located above and below. The two different structural motifs alternate in the crystals, stacking with a sequence ABAB to form a beautiful 3D array (Figure 3c).

The coexistence of different structural motifs in the same crystal is rather rare.^[16] Among the few examples of interdigitation—almost all with identical motifs, generally a 2D sheet^[6a–d]—only one involves two different polymer motifs, namely, $[\text{Zn}_{2.5}(\text{L})(\mu_3\text{-OH})](\text{H}_2\text{O})_5$ ($\text{L} = 3\text{-}[[4\text{-(4-pyridylethenyl)phenyl]ethenyl}]benzoate$).^[6e] In this structure the 1D and 2D motifs are both constructed from the L ligand. Therefore, compound **2**, in which the 1D and 2D motifs are constructed from different components (1D: pt and phen; 2D: pt, phen, and bpea) represents a new example of interdigitation: there has now been a progression from one motif with a single ligand, to different motifs with a single ligand, to finally different motifs with diverse ligands.

The structure of **3** consists of positive 1D pseudo-molecular ladders and negative bpea^{2-} ions. As shown in Figure 4a, the 1D ladder contains unprecedented hexanuclear

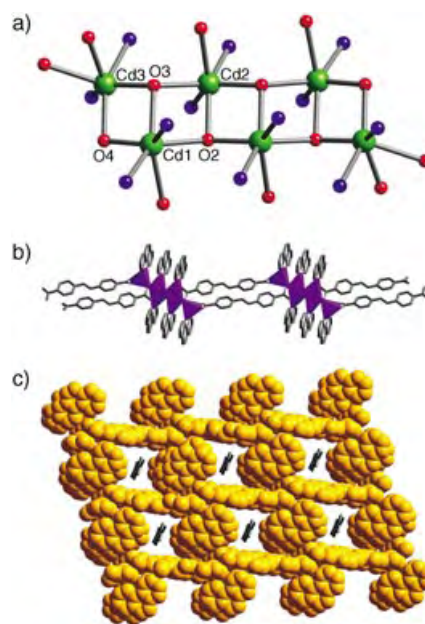


Figure 4. Crystal structure of **3**. a) View of the ladderlike hexanuclear cadmium cluster. b) View of the 1D ladder highlighting the hexanuclear metal clusters as rungs. c) View of the supramolecular host–guest network in which the location of the guest bpea^{2-} ions in the parallelogram channels is created by stacking of the ladders.

cadmium clusters in which three crystallographically independent cadmium(II) atoms exhibit three different coordination environments. In addition to a chelating phen ligand, Cd1 is coordinated by a monodentate bpea ligand and three $\mu_3\text{-OH}$ groups, Cd2 is coordinated by one aqua ligand and three $\mu_3\text{-OH}$ groups, and Cd3 is coordinated by a chelating bpea ligand and two $\mu_3\text{-OH}$ groups. Each $\mu_3\text{-OH}$ group interlinks three Cd atoms in a trigonal shape ($\text{Cd}\cdots\text{Cd}$ 3.511(6)–3.909(7) Å) to give an edge-sharing hexanuclear cadmium cluster. While a few $[\text{Cd}_3(\mu_3\text{-OH})]^{5+}$ cores^[17] and octanuclear cadmium clusters^[18] have been reported, such a hexanuclear ladderlike metal core featuring cadmium–hydroxy clusters has never been shown before. Neighboring hexanuclear cadmium clusters are linked by two linear bpea spacers, thus producing a new type of pseudo-molecular ladder in which the hexanuclear cadmium clusters act as inner rungs (Figure 4b). The phen ligands are orientated away from the ladder and play an important role in subsequent packing into a three-dimensional network.

Interestingly, adjacent ladders in **3** are interdigitated in a zipper fashion to form 2D layers with significant $\text{C}\cdots\text{H}\cdots\pi$ interactions between the aromatic rings of different ladders; the edge-to-face separation is about 3.70 Å. These layers are further packed into a 3D network featuring 1D parallelogram-shaped cationic channels (8.91×9.97 Å) under the direction of strong $\pi\cdots\pi$ stacking interactions between the phen groups; the face-to-face distance is about 3.414 Å. Completely deprotonated bpea guests reside in the channels and are hydrogen-bonded to the aqua ligands of the ladders ($\text{O}\cdots\text{O}$ 2.659(9) Å, Figure 4c). Therefore, the architecture of **3** can be best described as a 3D supramolecular host–guest network.

Compounds **1–3** have much in common: All are Cd(bpea)(phen) derivatives and contain 1D chain motifs in their crystal structures. This could be related to the fact that chelating ligands such as phen serve a “passive” role by occupying coordination sites on the metal centers and providing steric constraints, thus preventing spatial extension of the skeleton to higher dimensions. Similar behavior has been observed before.^[19] Despite the similarities among **1–3**, the three types of chains (helical, zigzag, and ladderlike) fulfill different functions in crystal packing. Although some possible factors have been discussed here, we are unable to propose definite reasons as to why each compound adopts a different strategy.

To examine the contribution of d¹⁰ metal polynuclear clusters to the photoluminescent properties of these systems, the luminescence of **3** was investigated. While the free H₂bpea ligand displays weak luminescence in the solid state at room temperature (see Figure S1 in the Supporting Information), compound **3** exhibits an intense blue radiation emission maximum at $\lambda \approx 489$ nm upon excitation at $\lambda = 386$ nm (Figure 5). The enhancement of luminescence may be attrib-

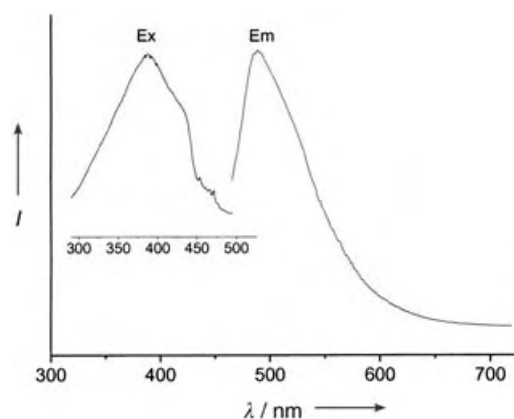


Figure 5. Photoluminescent spectra of **3** in the solid state at room temperature. Ex = excitation, Em = emission.

uted to ligand chelation to the metal center, which effectively increases the rigidity of the ligand and reduces the loss of energy by radiationless decay.^[20] As with other metal-hydroxy clusters,^[18b,21] the lifetime of **3** is about 14 ns, which is significantly longer than for systems without metal-hydroxy clusters. This fact may be ascribed to the presence of the metal clusters, since the μ_3 -OH ligand may tighten the whole skeleton, resulting in much weaker vibrations.

In conclusion, we have presented a rational synthetic strategy that successfully provided three coordination polymers by combining a long flexible ligand and a bulky heterocyclic aromatic ligand, which show different packing modes. Although the final polymeric architectures are impossible to predict with our present state of knowledge, the strategy represents a potential approach for the design of noninterpenetrating structures with long flexible ligands. In addition to the well-known interpenetrated frameworks, these new types of supramolecular entangled networks

represent another important branch in the realm of entanglement and open interesting perspectives in the study of these materials.

Experimental Section

1: A mixture of Cd(NO₃)₂·4H₂O (154 mg, 0.5 mmol), H₂bpea (134 mg, 0.5 mmol), phen (198 mg, 1 mmol), and water (10 mL) was placed in a 23-ml Teflon reactor and kept under autogenous pressure at 140 °C for 5 d. Then the mixture was cooled to room temperature at a rate of 10 °C h⁻¹, and colorless crystals of **1** were obtained (yield: 192 mg, 52% based on Cd). C, H, N analysis calcd (%) for C₄₀H₂₆CdN₄O₄: C 65.00, H 3.55, N 7.58; found: C 64.65, H 3.27, N, 7.81.

2: A mixture of Cd(NO₃)₂·4H₂O (460 mg, 1.5 mmol), H₂bpea (134 mg, 0.5 mmol), phen (300 mg, 1.5 mmol), H₂pt (250 mg, 1.5 mmol), and water (10 mL) was placed in a 23-ml Teflon reactor and kept under autogenous pressure at 160 °C for 5 d. Then the mixture was cooled to room temperature at a rate of 10 °C h⁻¹, and light-yellow crystals of **2** were obtained (yield: 140 mg, 56% based on Cd). C, H, N analysis calcd (%) for C₆₈H₄₆Cd₃N₆O₁₄: C 54.10, H 3.07, N 5.57; found: C 53.84, H 2.77, N, 5.75.

3: A mixture of Cd(NO₃)₂·4H₂O (308 mg, 1 mmol), H₂bpea (134 mg, 0.5 mmol), phen (300 mg, 1.5 mmol), and water (10 mL) was placed in a 23-ml Teflon reactor and kept under autogenous pressure at 180 °C for 3 d. Then the mixture was cooled to room temperature at a rate of 10 °C h⁻¹, and colorless crystals of **3** were obtained (yield: 302 mg, 64% based on Cd). C, H, N analysis calcd (%) for C₆₀H₅₂Cd₃N₆O₁₄: C 50.80, H 3.70, N 5.93; found: C 50.45, H 3.44, N, 6.38.

Received: May 24, 2004

Keywords: cadmium · hydrothermal synthesis · luminescence · polymers · supramolecular chemistry

- Reviews: a) P. J. Hagrman, D. Hagrman, J. Zubieta, *Angew. Chem.* **1999**, *111*, 2798; *Angew. Chem. Int. Ed.* **1999**, *38*, 2638; b) A. J. Blake, N. R. Champness, P. Hubberstey, W. S. Li, M. A. Withersby, M. Schröder, *Coord. Chem. Rev.* **1999**, *183*, 117; c) B. Moulton, M. J. Zaworotko, *Chem. Rev.* **2001**, *101*, 1629; d) O. R. Evans, W. Lin, *Acc. Chem. Res.* **2002**, *35*, 511; e) O. M. Yaghi, M. O’Keeffe, N. W. Ockwig, H. K. Chae, M. Eddaoudi, J. Kim, *Nature* **2003**, *423*, 705; f) A. Müller, S. K. Das, S. Talismanov, S. Roy, E. Beckmann, H. Bögge, M. Schmidtman, A. Merca, A. Berkle, L. Allouche, Y. Zhou, L. Zhang, *Angew. Chem.* **2003**, *115*, 5193; *Angew. Chem. Int. Ed.* **2003**, *42*, 5039; g) C. N. R. Rao, S. Natarajan, R. Vaidyanathan, *Angew. Chem.* **2004**, *116*, 1490; *Angew. Chem. Int. Ed.* **2004**, *43*, 1466; h) S. Kitagawa, R. Kitaura, S. I. Noro, *Angew. Chem.* **2004**, *116*, 2388; *Angew. Chem. Int. Ed.* **2004**, *43*, 2334.
- For recent examples, see a) E. Lee, J. Heo, K. Kim, *Angew. Chem.* **2000**, *112*, 2811; *Angew. Chem. Int. Ed.* **2000**, *39*, 2699; b) G. J. Halder, C. J. Kepert, B. Moubaraki, K. S. Murry, J. D. Cashion, *Science* **2002**, *298*, 1762; c) T. J. Prior, D. Bradshaw, S. J. Teat, M. J. Rosseinsky, *Chem. Commun.* **2003**, 500; d) A. Galet, M. C. Munoz, J. A. Real, *J. Am. Chem. Soc.* **2003**, *125*, 14224; e) B. Q. Ma, H. L. Sun, S. Gao, *Chem. Commun.* **2003**, 2164; f) L. Pan, H. Liu, X. Lei, X. Huang, D. H. Olson, N. J. Turro, J. Li, *Angew. Chem.* **2003**, *115*, 560; *Angew. Chem. Int. Ed.* **2003**, *42*, 542; g) X. L. Wang, C. Qin, E. B. Wang, Y. G. Li, C. W. Hu, L. Xu, *Chem. Commun.* **2004**, 378; h) X. H. Bu, M. L. Tong, H. C. Chang, S. Kitagawa, S. R. Batten, *Angew. Chem.* **2004**, *116*, 194; *Angew. Chem. Int. Ed.* **2004**, *43*, 192.

- [3] S. R. Batten, R. Robson, *Angew. Chem.* **1998**, *110*, 1558; *Angew. Chem. Int. Ed.* **1998**, *37*, 1460.
- [4] a) S. Sailaja, M. V. Rajasekharan, *Inorg. Chem.* **2000**, *39*, 4586; b) P. Grosshans, A. Jouaiti, V. Bulach, J. M. Planeix, M. W. Hosseini, J. F. Nicoud, *Chem. Commun.* **2003**, 1336; c) Y. Cui, H. L. Ngo, W. Lin, *Chem. Commun.* **2003**, 1388.
- [5] a) P. M. Van Calcar, M. M. Olmstead, A. L. Balch, *Inorg. Chem.* **1997**, *36*, 5231; b) L. Carlucci, G. Ciani, A. Gramaccioli, D. M. Proserpio, S. Rizzato, *CrystEngComm* **2000**, *29*; c) I. Ino, J. C. Zhong, M. Munakata, T. Kuroda-Sowa, M. Maekawa, Y. Suenaga, Y. Kitamori, *Inorg. Chem.* **2000**, *39*, 4273; d) Y. H. Li, C. Y. Su, A. M. Goforth, K. D. Shimizu, K. D. Gray, M. D. Smith, H. C. zur Loye, *Chem. Commun.* **2003**, 1630.
- [6] a) M. Kondo, T. Joshitomi, K. Seki, H. Matsuzaka, S. Kitagawa, *Angew. Chem.* **1997**, *109*, 1844; *Angew. Chem. Int. Ed. Engl.* **1997**, *36*, 1725; b) K. N. Power, T. L. Hennigar, M. J. Zaworotko, *New J. Chem.* **1998**, 177; c) L. Carlucci, G. Ciani, P. Macchi, D. M. Proserpio, S. Rizzato, *Chem. Eur. J.* **1999**, *5*, 237; d) S. R. Batten, B. F. Hoskins, R. Robson, *Chem. Eur. J.* **2000**, *6*, 156; e) P. Ayyappa, O. R. Evans, W. Lin, *Inorg. Chem.* **2002**, *41*, 3328.
- [7] a) C. V. K. Sharma, R. D. Rogers, *Chem. Commun.* **1999**, 83; b) L. Carlucci, G. Ciani, D. M. Proserpio, *Chem. Commun.* **1999**, 449; c) K. Biradha, M. Fujita, *Chem. Commun.* **2002**, 1866.
- [8] L. Carlucci, G. Ciani, D. M. Proserpio, *Coord. Chem. Rev.* **2003**, *246*, 247.
- [9] For example, see a) Y. B. Dong, R. C. Layland, N. G. Pschirer, M. D. Smith, U. H. F. Bunz, H. C. zur Loye, *Chem. Mater.* **1999**, *11*, 1413; b) L. Carlucci, G. Ciani, D. M. Proserpio, S. Rizzato, *CrystEngComm* **2003**, *5*, 190; c) J. Luo, M. Hong, R. Wang, R. Cao, L. Han, Z. Lin, *Eur. J. Inorg. Chem.* **2003**, 2705.
- [10] S. R. Batten, B. F. Hoskins, B. Moubaraki, K. S. Murray, R. Robson, *Chem. Commun.* **2000**, 1095.
- [11] U. W. Grummt, E. Birckner, E. Klemm, D. A. M. Egbe, B. Heise, *J. Phys. Org. Chem.* **2000**, *13*, 112.
- [12] Crystal data for **1** ($\text{C}_{40}\text{H}_{26}\text{CdN}_4\text{O}_4$): $M_r = 739.05$, tetragonal, space group $P4(3)$, $a = b = 11.1568(16)$, $c = 24.461(5)$ Å, $V = 3044.7(9)$ Å³, $Z = 4$, $\rho_{\text{calcd}} = 1.612$ mg m⁻³, Flack parameter = 0.028(16), final $R1 = 0.0267$ for 6819 independent reflections [$I > 2\sigma(I)$]. Crystal data for **2** ($\text{C}_{68}\text{H}_{46}\text{Cd}_3\text{N}_6\text{O}_{14}$): $M_r = 1508.31$, monoclinic, space group $P2_1/c$, $a = 16.776(3)$, $b = 10.141(2)$, $c = 17.559(4)$ Å, $\beta = 97.11(3)^\circ$, $V = 2964.2(10)$ Å³, $Z = 2$, $\rho_{\text{calcd}} = 1.690$ mg m⁻³, final $R1 = 0.0670$ for 6666 independent reflections [$I > 2\sigma(I)$]. Crystal data for **3** ($\text{C}_{60}\text{H}_{52}\text{Cd}_3\text{N}_6\text{O}_{14}$): $M_r = 1418.28$, triclinic, space group $P\bar{1}$, $a = 13.214(3)$, $b = 13.661(3)$, $c = 16.964(3)$ Å, $\alpha = 113.03(3)^\circ$, $\beta = 92.53(3)^\circ$, $\gamma = 90.27(3)^\circ$, $V = 2814.6(10)$ Å³, $Z = 2$, $\rho_{\text{calcd}} = 1.673$ mg m⁻³, final $R1 = 0.0613$ for 12603 independent reflections [$I > 2\sigma(I)$]. The data were collected at 298(2) K on a Rigaku R-Axis RAPID IP diffractometer with $\text{MoK}\alpha$ monochromated radiation ($\lambda = 0.71073$ Å). The structures were solved by direct methods using SHELXS-97 and refined using Fourier techniques. CCDC 239159–239161 contain the supplementary crystallographic data for this paper. These data can be obtained free of charge via www.ccdc.cam.ac.uk/conts/retrieving.html (or from the Cambridge Crystallographic Data Centre, 12, Union Road, Cambridge CB2 1EZ, UK; fax: (+44) 1223-336-033; or deposit@ccdc.cam.ac.uk).
- [13] L. Carlucci, G. Ciani, D. M. Proserpio, S. Rizzato, *Chem. Eur. J.* **2002**, *8*, 1519.
- [14] Y. Cui, S. J. Lee, W. Lin, *J. Am. Chem. Soc.* **2003**, *125*, 6014.
- [15] a) W. Chen, J. Y. Wang, C. Chen, Q. Yue, H. M. Yuan, J. S. Chen, S. N. Wang, *Inorg. Chem.* **2003**, *42*, 944; b) X. M. Chen, G. F. Liu, *Chem. Eur. J.* **2002**, *8*, 4811.
- [16] For example, see a) S. R. Batten, *CrystEngComm* **2001**, *18*; b) D. M. Ciurtin, M. D. Smith, H. C. zur Loye, *Chem. Commun.* **2002**, 74; L. Carlucci, G. Ciani, D. M. Proserpio, *Chem. Commun.* **2004**, 380.
- [17] a) W. Lin, Z. Wang, L. Ma, *J. Am. Chem. Soc.* **1999**, *121*, 11249; b) X. Xue, X. S. Wang, L. Z. Wang, R. G. Xiong, B. F. Abrahams, X. Z. You, Z. L. Xue, C. M. Che, *Inorg. Chem.* **2002**, *41*, 6544.
- [18] a) R. W. Saalfrank, N. Löw, S. Trummer, G. M. Sheldrick, M. Teichert, D. Stalke, *Eur. J. Inorg. Chem.* **1998**, 559; b) S. L. Zheng, J. H. Yang, X. L. Yu, X. M. Chen, W. T. Wong, *Inorg. Chem.* **2004**, *43*, 830.
- [19] P. J. Hargman, J. Zubietta, *Inorg. Chem.* **2000**, *39*, 5218.
- [20] a) *Photochemistry and Photophysics of Coordination Compounds* (Eds.: H. Yersin, A. Vogler), Springer, Berlin, **1987**; b) B. Valeur, *Molecular Fluorescence: Principles and Application*, Wiley-VCH, Weinheim, **2002**.
- [21] a) H. Kunkey, A. Vogler, *J. Chem. Soc. Chem. Commun.* **1990**, 1204; b) S. L. Zheng, J. P. Zhang, X. M. Chen, Z. L. Huang, Z. Y. Lin, W. T. Wong, *Chem. Eur. J.* **2003**, *9*, 3888.

Molecular Recognition

Recognition of Polyimide Sequence Information by a Molecular Tweezer**

Howard M. Colquhoun* and Zhixue Zhu

The recognition of sequence information in linear macromolecules underpins the whole of biology, most notably perhaps in protein synthesis through the operation of the genetic code,^[1] but also in the functioning of genetic regulatory proteins,^[2] of restriction enzymes,^[3] and of drug molecules that bind to specific nucleotide sequences in DNA.^[4] However, nucleic acids, when abstracted from their biological context, are simply random, four-monomer copolymers with no inherent order or information content. Their information-bearing function derives solely from the ability of other molecules to recognize specific monomer sequences through noncovalent interactions. The recognition of sequence information in high-molecular-weight copolymers by molecules of complementary structure is thus an essentially biological phenomenon.^[5] Sequence recognition in small (typically trimeric) peptides has, however, been achieved by using artificial “tweezer-type” peptides as receptors.^[6–11] Progress has also been made in the search for artificial enzymes by combinatorial attachment of amide side

[*] Prof. H. M. Colquhoun, Dr. Z. Zhu
School of Chemistry
University of Reading
Whiteknights, Reading, RG6 6AD (UK)
Fax: (+44) 118-378-8450
E-mail: h.m.colquhoun@rdg.ac.uk

[**] This work was supported by the University of Reading Research Endowment Trust and by the DuPont Corporation (European University Research Grant).

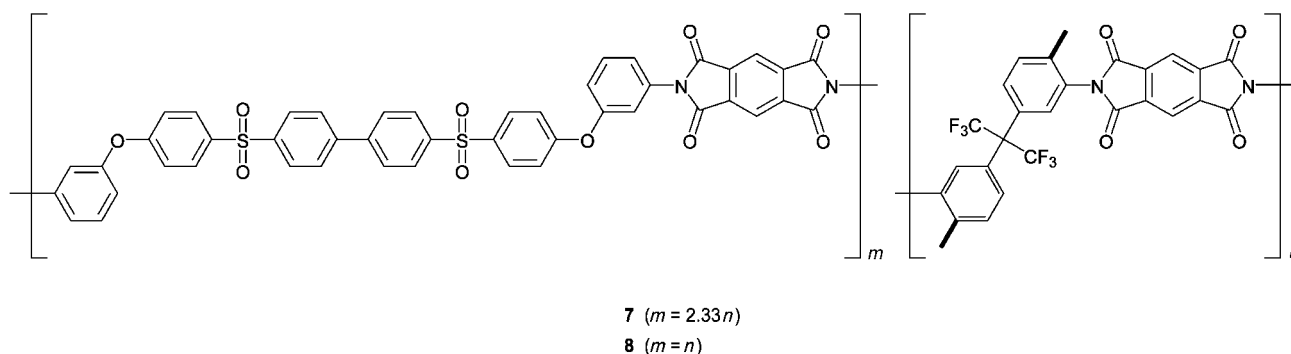
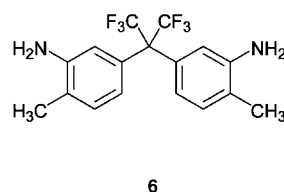
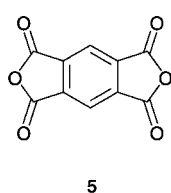
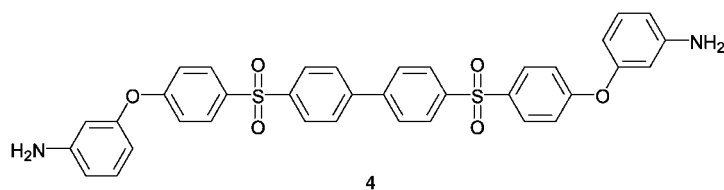
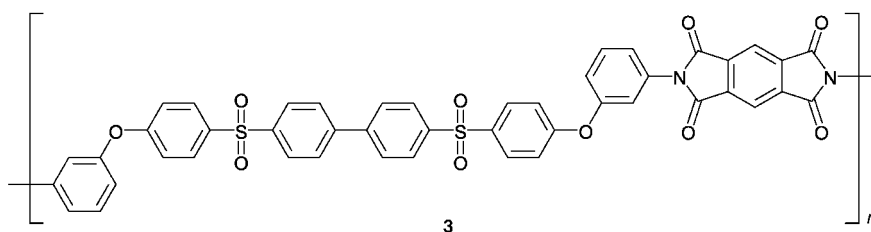
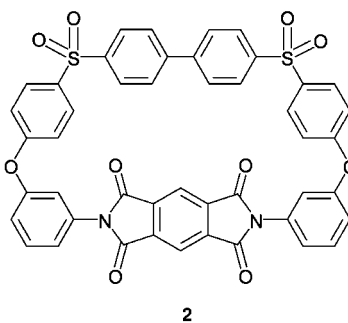
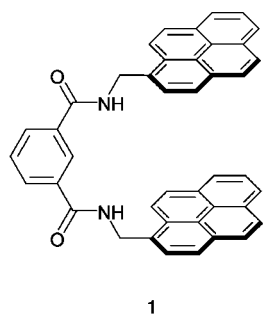


Supporting information for this article is available on the WWW under <http://www.angewandte.org> or from the author.

chains to polyamines, but the sequences responsible for catalytic activity in these latter systems are entirely unknown.^[12] Future technologies involving the storage and transcription of information on the molecular scale will certainly require materials with far greater stabilities than those of peptides and nucleic acids. Herein we investigate the possibility of supramolecular sequence recognition in high-molecular-weight aromatic polyimides, a class of materials

with outstanding resistance to thermochemical degradation.^[13] We have discovered that extended yet completely specific monomer sequences in copolyimides can be recognized through their interactions with a sterically and electronically complementary molecular tweezer.

We have shown previously that the molecular tweezer **1** binds strongly to pyromellitimide residues through complementary π - π stacking and hydrogen-bonding interactions and



that, in complexes with cyclic oligomers such as **2**, tweezer binding can be enhanced through further π -stacking with the adjacent 4,4'-biphenylenedisulfone unit.^[14] Extrapolation from the X-ray crystal structure of one such complex through computational modeling studies^[15] suggested that a set of analogous interactions should also occur between tweezer **1** and polymer **3** (the linear, high-molecular-weight homologue of macrocycle **2**). Specifically, these studies predicted that the binding of **1** to a pyromellitimide residue in the polymer chain would be promoted by chain folding of adjacent ether-sulfone units at the 3-aminophenoxy residue so bringing their 4,4'-biphenylenedisulfone residues into π -stacking contact with the pyrenyl arms of the tweezer (Figure 1a).

The molecular tweezer **1** was obtained by condensation of isophthaloyl chloride with 1-pyrenemethylamine,^[14] and high-molecular-weight polyimide **3** ($M_n \approx 160 \times 10^3$ Da by GPC)

was synthesized by polycondensation of diamine **4** with pyromellitic dianhydride (**5**) (see Supporting Information). Addition of tweezer **1** to a solution of polyimide **3** in chloroform/hexafluoropropan-2-ol gave an immediate deep-red solution, which was attributed to the charge-transfer absorption resulting from imide-tweezer π -stacking interactions. In keeping with computational predictions, ¹H NMR spectroscopy studies across a wide range of tweezer-to-imide molar ratios (from 1:80 to 4:1) confirmed that both imide and 4,4'-biphenylenedisulfone residues are involved in binding to tweezer **1**. In the presence of the tweezer, large aromatic ring-current shifts were observed for the pyromellitimide proton resonance ($\Delta\delta = 2.6$ ppm at 4:1 tweezer/imide mole ratio) and for the 4,4'-biphenylene resonances ($\Delta\delta = 0.8$ ppm for the protons *ortho* to the biaryl linkage; protons *meta* to this linkage lie close to the boundary between shielding and deshielding zones of the pyrene tweezer arm and are thus only slightly affected by complexation). However, no significant evidence for tweezer binding was found for non-imide-based polymers containing the 4,4'-biphenylenedisulfone residue, thus confirming that the pyromellitimide unit in polymer **3** represents the primary tweezer-binding site, and that neighboring 4,4'-biphenylenedisulfone units provide only secondary stabilizing interactions. Despite the high binding constant for the complexation of tweezer **1** with polymer **3** ($K_a = 8.6(\pm 0.9) \times 10^3 \text{ M}^{-1}$), which was determined from the charge-transfer absorption by a UV/Vis dilution technique,^[16] the pyromellitimide resonance remains as a sharp singlet in the presence of the tweezer, thus indicating fast exchange of the tweezer between binding sites at room temperature on the NMR timescale.

The monomer sequence that binds a single tweezer molecule contains 13 aromatic rings (Figure 1a and Scheme 1), but can be simply represented by the string SIS (I is the pyromellitimide binding site and S are the flanking diamine residues, each consisting of six aromatic rings, which upon chain-folding provide additional binding to the tweezer). If it were possible to introduce a diamine comonomer that inhibited, rather than promoted, π -stacking between the imide and the tweezer, then the polymer-sequence recognition and the sequence-specific binding might well be achieved. Computational modeling studies suggested that even a single *ortho* methyl group adjacent to the pyromellitimide unit could lead to significant steric inhibition of π -stacking between the polymer and the tweezer. For this reason, statistical copolymers **7** ($M_n \approx 60 \times 10^3$ Da) and **8** ($M_n \approx 100 \times 10^3$ Da) were synthesized by co-condensation of pyromellitic dianhydride with diamine **4** and with the *ortho*-methylated diamine **6** (chosen for its ability to maintain polymer solubility), in 70:30 and 50:50 mole ratios, respectively.^[17] Pyromellitimide resonances in the ¹H NMR spectra of copolymers **7** and **8** (Figure 2) are virtually superimposable,^[18] thus indicating that in the absence of external interactions the chemical shifts of these resonances are largely insensitive to sequence effects.

If the fluorinated comonomer **6** is defined as F, the possible imide-centered three-component sequences present in these copolymers can be represented by the strings FIF, SIF, FIS, and SIS (Scheme 1). As noted above, modeling

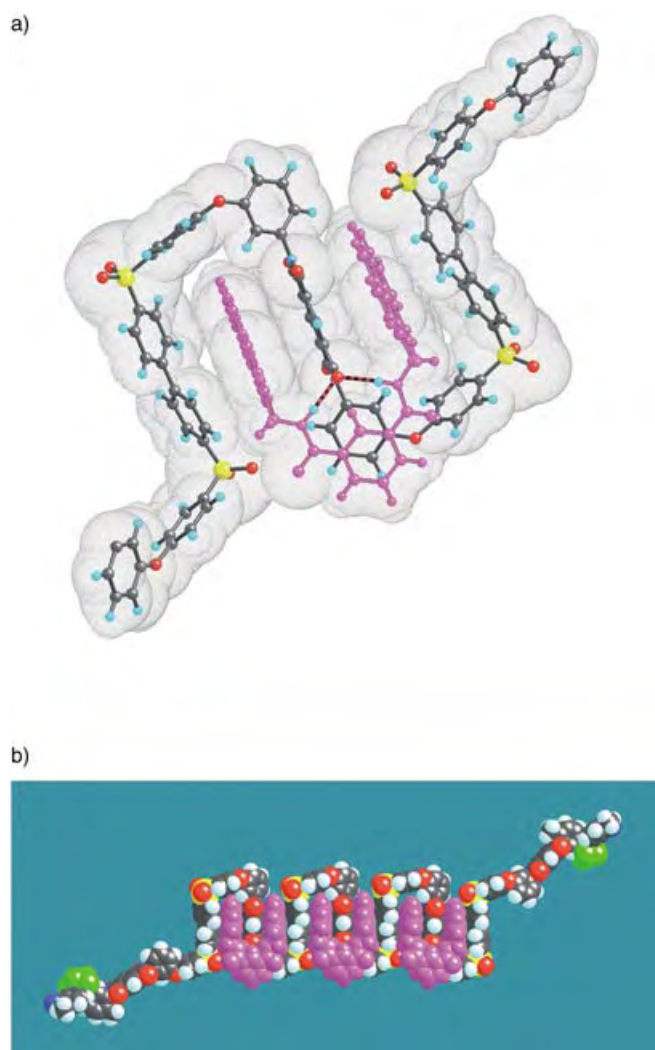
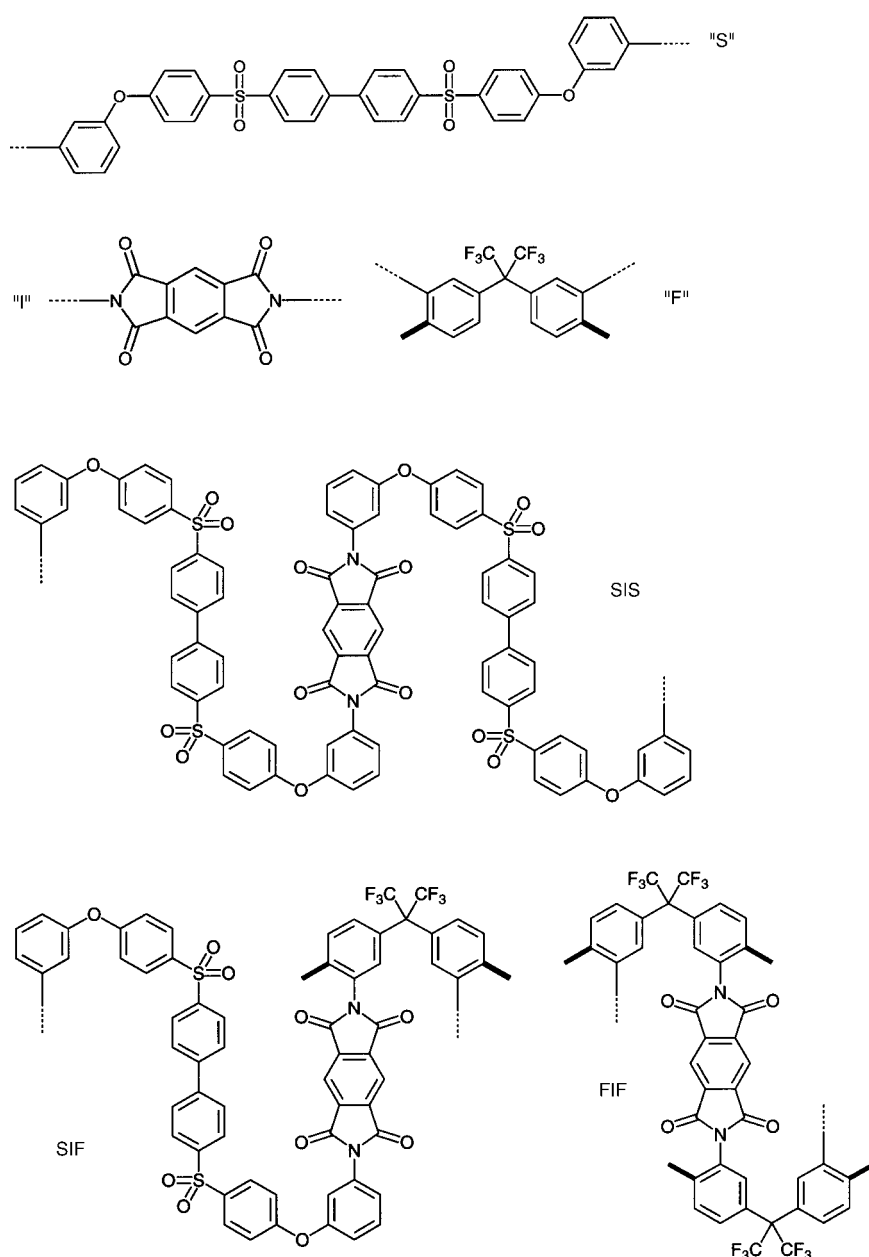


Figure 1. a) Energy-minimized model (re-parametrized Dreiding-II force field) for complexation of the molecular tweezer **1** with the polyimide chain-sequence SIS (see Scheme 1). Tweezer molecule **1** is shown in magenta; van der Waals surfaces are shown in gray; hydrogen bonds between an imide carbonyl oxygen atom and tweezer amide NH groups are shown in red and black. b) Energy-minimized space-filling model of a copolyimide chain showing triply adjacent binding of tweezer **1** (magenta) to the polymer chain-sequence FI-SISIS-IF.



Scheme 1. Imide-centered sequences in a statistical copolyimide based on diamines **4** and **6**. Methyl substituents are shown in bold; in the sequence FIF they can adopt non-interconverting *syn* and *anti* conformations relative to the imide unit. The sequence FIS (not shown) is degenerate with SIF in the present context.

studies indicated that imide groups in the sequences FIF, SIF, and FIS, where one or both aromatic rings adjacent to the imide carry *ortho* methyl groups, should bind only rather weakly to tweezer molecule **1**. However, the string SIS, as shown for homopolymer **3**, binds very strongly to **1** so that, even in a copolymer, the tweezer should induce a marked upfield shift of the imide resonance arising from this sequence. If sequence-recognition and specific binding did indeed occur in a copolyimide of diamines F and S, the imide resonance should separate into two peaks, one at higher field representing the strongly bound sequence SIS and one at

lower field representing the much more weakly bound sequences FIF, SIF, and FIS (the latter two sequences being degenerate in this context).

As shown in Figure 2, these predictions were confirmed by experimental data. To avoid possible intermolecular effects between polymer chains, ^1H NMR spectra were run at low polymer concentrations, typically 4 mM with respect to the pyromellitimide unit. Addition of tweezer **1** to solutions of copolymers **7** and **8** led to the imide resonance separating into “shifted” and “unshifted” peaks, with integrated intensities of about 1:1 and 3:1 for **7** and **8**, respectively (Figure 2, see column headed “1:80, tweezer/imide”). This peak separation is observed even at extremely low tweezer concentrations ($< 10^{-2}$ moles per mole of imide), where tweezer resonances themselves are scarcely detectable in the spectrum. The sequences FIF, SIF, FIS, and SIS should occur in proportions 0.09:0.21:0.21:0.49 for the 70:30 (S/F) copolymer **7**, and in proportions of 0.25:0.25:0.25:0.25 for the 50:50 copolymer **8**. Relative intensities for “unshifted” (FIF, SIF, and FIS) and “shifted” (SIS) imide resonances are thus predicted to be 0.51:0.49 (1.04:1) and 0.75:0.25 (3:1) for copolymers **7** and **8** respectively, which is in good agreement with the NMR data (Figure 2).

When the molar ratio of the tweezer to imide is increased, the SIS imide resonance in these copolymers moves progressively upfield ($\Delta\delta \approx 2.6$ ppm at a ratio of 4:1) and, astonishingly, separates into three clearly defined peaks (Figure 2, see column headed “4:1, tweezer/imide”). The only reasonable explanation for this is that the tweezer is detecting higher-order sequence information, since there are three dis-

tinguishable seven-component sequences of monomer residues which incorporate the key central string SIS. These are FISISIF, SISISIF, FISISIS, and SISISIS, with the second and third sequences being degenerate. Statistically, the relative proportions of these different SIS-centered sequences are 1:4.7:5.4 for random copolymer **7** and 1:2:1 for copolymer **8**. The relative intensities of SIS resonances shown in Figure 2 are fully consistent with these ratios, and comparisons of the spectra for **7** and **8** allow individual signals to be assigned to specific sequences on the basis of their positions and relative intensities. The resonance at highest field thus represents the

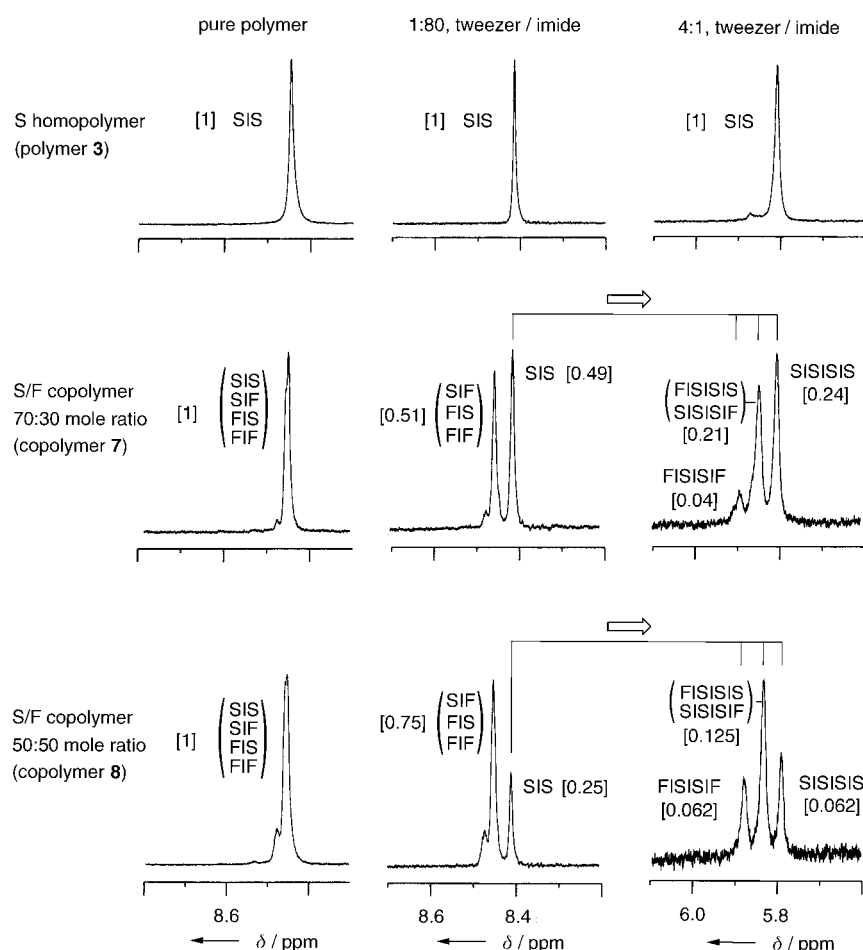


Figure 2. Imide resonances in the ^1H NMR spectra of homopolymer **3** and of copolymers **7** and **8** showing the response of imide-centered monomer sequences to the presence of molecular tweezer **1**. Relative integrals predicted from sequence-distribution probabilities are shown in square brackets. Spectra were recorded at 250 MHz in CDCl_3 /hexafluoropropan-2-ol (6:1 v/v), at a polymer concentration of 4 mM with respect to total pyromellitimide residues. See Supporting Information for full spectra.

central imide residue of the sequence SISISIS, the next highest-field signal corresponds to SISISIF and FISISIS, and that at lowest field to FISISIF.

It may seem remarkable that the tweezer is able to “read” sequence information over such extended stretches of the polymer chain (the string SISISIS for example represents no fewer than 27 aromatic rings) but it may be significant that FISISIF can bind only a single tweezer molecule, whereas SISISIF can bind two, and SISISIS three adjacent tweezers simultaneously, thus leading to the formation of chain-folded and multiply π -stacked clusters (Figure 1b). Multiple adjacent binding is only likely to be significant at high tweezer-to-imide ratios, where additional splitting of the SIS resonance is indeed observed. At high tweezer/imide ratios, even homopolymer **3** (Figure 2, top right) shows an additional, very weak, imide resonance (integral relative to the main imide peak about 0.02:1), which is tentatively assigned to tweezer-bound polymer end groups.

Short-range sequence information in aromatic copolyimides can thus be recognized through the binding of specific

monomer sequences to a sterically and electronically complementary molecular tweezer. More remarkably, long-range sequences may also be identified, through the sensitivity of imide ^1H NMR resonances to multiple adjacent binding of tweezer molecule **1**. While the issue of “writing” sequence information into the molecular structures of synthetic macromolecules remains to be addressed, it is perhaps worth noting that, in biology, copolymer sequence information is not in fact “written” at all—new DNA sequences arise simply by random mutation and are only ever copied or transcribed. The present work, however, clearly demonstrates that the “reading” of copolymer sequence information in synthetic macromolecules can be achieved through the binding of randomly generated monomer sequences to small molecules of complementary structure.

Received: April 20, 2004

Keywords: molecular recognition · molecular tweezers · π interactions · polyimides · sequence determination

- [1] M. Nirenberg, *Trends Biochem. Sci.* **2004**, 29, 46.
- [2] C. M. Falcon, K. S. Matthews, *Biochemistry* **2000**, 39, 11074.
- [3] J. M. Bujnicki, *Curr. Protein Pept. Sci.* **2003**, 4, 327.
- [4] T. G. Uil, H. J. Haisma, M. G. Rots, *Nucleic Acids Res.* **2003**, 31, 6064.
- [5] Site-specific, but not sequence-specific, binding of macrocyclic receptors to a number of synthetic polymers during polyrotaxane formation has previously been described.^[19–21] Polyrotaxanes involving the threading, chain-folding and π -stacking of various aromatic/aliphatic homopolymers with a bipyridinium-based macrocycle have also been reported.^[22,23] Polyrotaxane systems^[24,25] clearly have enormous potential for displaying sequence recognition, but this does not seem to have been realized in practice so far.
- [6] W. C. Still, *Acc. Chem. Res.* **1996**, 29, 155.
- [7] W. C. Still, C. T. Chen, H. Wagner, *Science* **1998**, 279, 851.
- [8] T. Fessmann, J. T. Kilburn, *Angew. Chem.* **1999**, 111, 2170; *Angew. Chem. Int. Ed.* **1999**, 38, 1993.
- [9] K. Ryan, L. J. Gershell, W. C. Still, *Tetrahedron* **2000**, 56, 3309.
- [10] R. Arenzio, J. D. Kilburn, *Tetrahedron* **2002**, 58, 711.
- [11] H. Wennemers, M. C. Nold, M. M. Conza, K. J. Kulicke, M. Neuburger, *Chem. Eur. J.* **2003**, 9, 442.
- [12] F. M. Menger, A. V. Eliseev, V. A. Migulin, *J. Org. Chem.* **1995**, 60, 6666.
- [13] *Polyimides* (Eds.: D. Wilson, H. D. Stenzenberger, P. M. Hergenrother), Blackie, London, **1990**.
- [14] H. M. Colquhoun, Z. X. Zhu, D. J. Williams, *Org. Lett.* **2003**, 5, 4353.
- [15] Computational modeling studies were carried out using Cerius² (version 3.5, Accelrys Inc., San Diego), with the Dreiding-II force field reparametrized for aromatic imide and sulfone-based structures.
- [16] M. B. Nielsen, J. O. Jeppesen, J. Lau, C. Lomholt, D. Damgaard, J. P. Jacobsen, J. Becher, J. F. Stoddart, *J. Org. Chem.* **2001**, 66, 3559.

- [17] The presence of methyl groups *ortho* to the nitrogen atoms in an aromatic diamine do not affect the reactivity of the amino groups towards imide formation, so that random-sequence copolymers can be obtained by co-condensation of *ortho*-methyl-substituted and unsubstituted diamines with aromatic dianhydrides.^[26]
- [18] The weak shoulder at lower field arises from an unresolved multiplet assigned to non-interconverting *syn* and *anti* arrangements of *ortho*-methyl substituents in FIF sequences.^[27]
- [19] C. G. Gong, T. E. Glass, H. W. Gibson, *Macromolecules* **1998**, *31*, 208.
- [20] S. Choi, J. W. Lee, Y. H. Ko, K. Kim, *Macromolecules* **2002**, *35*, 3526.
- [21] D. Tuncel, J. H. G. Steinke, *Macromolecules* **2004**, *37*, 288.
- [22] G. J. Owen, P. Hodge, *Chem. Commun.* **1997**, 11.
- [23] P. Hodge, P. Monvisade, G. J. Owen, F. Heatley, Y. Pang, *New J. Chem.* **2000**, *24*, 703.
- [24] S. A. Nepogodiev, J. F. Stoddart, *Chem. Rev.* **1998**, *98*, 1959.
- [25] K. Kim, *Chem. Soc. Rev.* **2002**, *31*, 96.
- [26] T. M. Wu, S. Chalun, J. Blackwell, S. Z. D. Cheng, Z. Q. Wu, F. W. Harris, *Polymer* **1995**, *36*, 2123.
- [27] K. D. Shimizu, T. M. Dewey, J. Rebek, *J. Am. Chem. Soc.* **1994**, *116*, 5145.

Diazadiene Ligands

C–C Coupling and C–H Bond Activation—Unexpected Pathways in the Reactions of $[\text{Yb}(\eta^5\text{-C}_{13}\text{H}_9)_2(\text{thf})_2]$ with Diazadienes**

Alexander A. Trifonov,* Elena A. Fedorova,
Georgy K. Fukin, Nikolai O. Druzhkov, and
Mikhail N. Bochkarev

The diversity of the coordination and redox properties of 1,4-disubstituted diazadienes (DAD) makes them advantageous ligands for transition-metal chemistry. The DAD molecule can coordinate to a metal atom as a neutral ligand. Possessing a quite pronounced electron affinity^[1] it can oxidize electro-positive lanthanide metals by accepting one or two electrons to form the radical anion^[2] or dianion,^[3] respectively. Owing to the low energy of the π^* orbital of the DAD ligands,^[1c] their complexes with ytterbium, which forms two stable

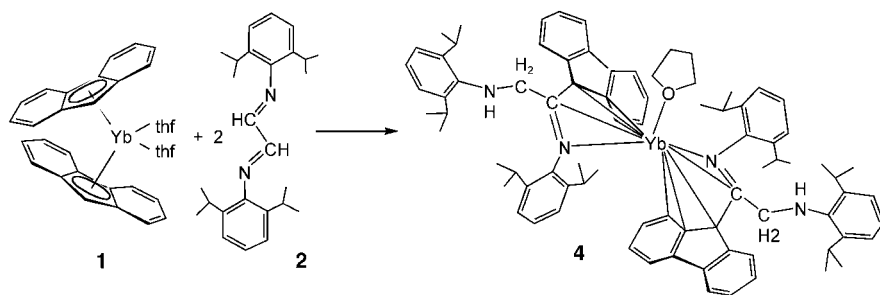
oxidation states and is characterized by a low potential of the $\text{Yb}^{\text{II}}/\text{Yb}^{\text{III}}$ transformation,^[4] are of particular interest as promising objects for investigating intramolecular metal–ligand electron transfer. In our previous studies the variable-temperature investigation of the magnetic properties of the complex $[(t\text{BuNCHCHN}t\text{Bu})_3\text{Yb}]^{[2b]}$ suggested to us the existence of temperature-induced valence tautomerism for this compound. Recently, for the complexes $[\text{YbR}_2(t\text{-BuNCHCHN}t\text{Bu})]$ ($\text{R} = \text{Cp} = \text{C}_5\text{H}_5$ or $\text{R} = \text{Cp}^* = \text{C}_5\text{Me}_5$) we demonstrated that the steric repulsion of DAD and Cp ligands as a result of their bulk might serve as a tool for tuning the Yb–N bond lengths and eventually determine the reversibility of the Yb–DAD electron transfer.^[2f,g] As part of our continuing studies on intramolecular redox processes in ytterbium complexes with redox-active ligands we attempted to synthesize novel mixed-ligand compounds with sterically demanding diazadienes. Herein we report the unexpected reactivity of $[\text{Yb}(\text{C}_{13}\text{H}_9)_2(\text{thf})_2]$ (**1**)^[5] towards diazadienes $[(2,6\text{-}i\text{Pr}_2\text{C}_6\text{H}_3)\text{-N=CR-CR=N-(2,6-}i\text{Pr}_2\text{C}_6\text{H}_3)]$ ($\text{R} = \text{H}$ (**2**), Me (**3**)) which results either in the coupling of the fluorenyl and DAD fragments or in proton abstraction from the DAD molecule, depending on the substituent R on the carbon atom of the imino group.

$t\text{BuN=CH-CH=N}t\text{Bu}$ readily oxidizes ytterbocenes $[\text{YbR}_2(\text{thf})_2]$ ($\text{R} = \text{Cp}, \text{Cp}^*$) to afford the trivalent ytterbium derivatives $[\text{YbR}_2(t\text{BuNCHCHN}t\text{Bu})]^{[2f,g]}$ which contain a DAD radical anion. Unexpectedly, the reactions of the bisfluorenyl analogue **1** with bulky diazadienes **2** and **3** under the same conditions do not lead to oxidation of the ytterbium atom but result in the formation of the Yb^{II} derivatives. Thus, the reaction of **1** with a twofold molar excess of **2** led to the isolation of the unexpected product $[\text{Yb}\{\eta^5\text{-C}_{13}\text{H}_8\text{C(=N[2,6-}i\text{Pr}_2\text{C}_6\text{H}_3])\text{CH}_2\text{NHC}_6\text{H}_3(2,6\text{-}i\text{Pr}_2\text{C}_6\text{H}_3)\}_2(\text{thf})]$ (**4**) in 80 % yield (Scheme 1).

Complex **4** is readily soluble in ethers and toluene, but sparingly soluble in hexane. The diamagnetic properties of **4** corroborate the divalent state of ytterbium.^[6] Crystallization of **4** by slow cooling of the solution in hexane resulted in single crystals of the hexane solvate **4**· C_6H_{14} that were suitable for crystal-structure analysis (Figure 1). The X-ray diffraction study revealed that the Yb^{II} cation is η^5 -coordinated by two novel multifunctional ligands $\{\text{C}_{13}\text{H}_8\text{C(=N[2,6-}i\text{Pr}_2\text{C}_6\text{H}_3])\text{CH}_2\text{NHC}_6\text{H}_3(2,6\text{-}i\text{Pr}_2\text{C}_6\text{H}_3)\}^-$, which arise from unprecedented coupling of the allylic carbon atom of the fluorenyl ligand with the imino carbon atom of the diazadiene **2**. The C–C bond (1.426(3), 1.434(3) Å) formation in **4** also implies that the two H atoms initially bonded to the coupled carbon atoms migrate to the second imino group, resulting in the hydrogenated $\text{CH}_2\text{-NH}$ fragment. Unlike the η^5 -bonding of the fluorenyl fragment to the Yb atom in the starting complex **1**,^[5] a rather unusual η^3 -type of coordination through one carbon atom of the five-membered ring and two carbon atoms of the six-membered ring occurs in **4**. The η^2 -coordination of the imino group to the Yb atom results in the formation of the planar (deviation from the plane is 0.11 Å) η^5 -bonded heteropentadienyl frame. The C–C bond lengths within this frame (1.398(3)–1.461(3) Å) fall within the range of values for aromatic C–C bonds,^[7] and the C–N bond lengths (1.324(3), 1.319(3) Å) are slightly longer than the

[*] Dr. A. A. Trifonov, Dr. E. A. Fedorova, Dr. G. K. Fukin,
Dr. N. O. Druzhkov, Prof. Dr. M. N. Bochkarev
G. A. Razuvaev Institute of Organometallic Chemistry
Russian Academy of Sciences
Tropinina 49, 603950 Nizhny Novgorod GSP-445 (Russia)
Fax: (+7) 8312-127-497
E-mail: trif@imoc.sinn.ru

[**] This work was supported by the Russian Foundation of Basic Research (Grant No 02-03-32112), Grant of President of RF supporting scientific schools (No.58.2003.3).



Scheme 1. Reaction of **1** and **2** to give **4**. Reagents and conditions: **1**, **2** (2 equiv), THF, 60 °C, 30 min; then toluene, 60 °C, 1 h; then toluene, 60 °C, 2 h.

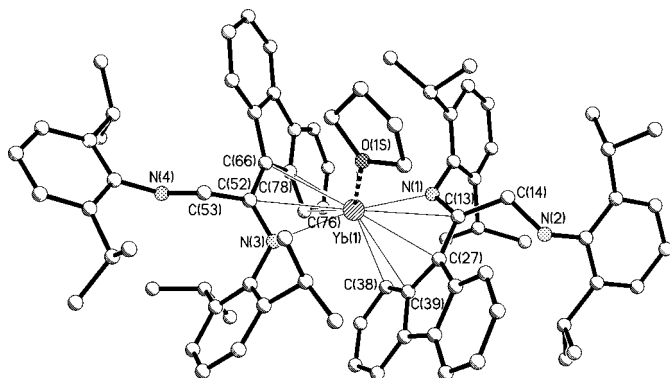


Figure 1. ORTEP representation of structure **4**. Selected bond lengths [Å] and angles [°]: Yb(1)–N(3) 2.445(2), Yb(1)–N(1) 2.466(2), Yb(1)–C(78) 2.759(2), Yb(1)–C(39) 2.768(2), Yb(1)–C(77) 2.786(2), Yb(1)–C(27) 2.795(2), Yb(1)–C(38) 2.798(2), Yb(1)–C(66) 2.868(2), Yb(1)–C(13) 2.933(2), Yb(1)–C(52) 2.952(2), N(1)–C(13) 1.324(3), N(1)–C(1) 1.443(3), C(13)–C(27) 1.426(3), C(13)–C(14) 1.521(3), C(27)–C(39) 1.459(3), C(38)–C(39) 1.398(3), N(2)–C(14) 1.447(3), N(3)–C(52) 1.319(3), N(4)–C(53) 1.464(3), C(52)–C(53) 1.514(3), C(52)–C(66) 1.434(3), C(66)–C(78) 1.461(3), C(77)–C(78) 1.403(3); N(3)–Yb(1)–C(77) 70.80(6), N(1)–Yb(1)–C(38) 70.21(6), O(1S)–Yb(1)–N(3) 97.56(5), O(1S)–Yb(1)–N(1) 96.31(5).

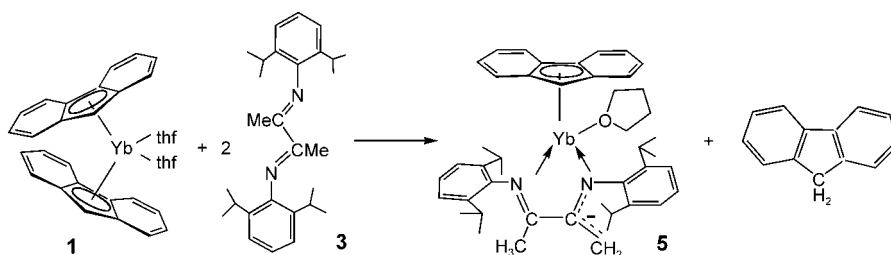
C=N bond in the parent diazadiene (1.266(3) Å).^[8] Such a bonding situation is evidence for a delocalized π system in the heteropentadienyl fragment. The dihedral angle between the N(3)–C(52)–C(66)–C(78)–C(77) and the N(1)–C(13)–C(27)–C(39)–C(38) planes is 64.4° and the angle Ct–Yb–Ct (Ct are the centroids of the N(3)–C(52)–C(66)–C(78)–C(77) and the N(1)–C(13)–C(27)–C(39)–C(38) rings) is 147.2° (reference: 136.3(3)° in [YbCp*₂(C₅H₅N)₂]).^[9] The Yb–C bond lengths in **4** (2.759(2)–2.952(2) Å) are somewhat longer than those in the starting complex **1** and are comparable to the distances reported for the Yb^{II}–bispentadienyl derivative [Yb{4,4'-(CH₂)₂-(2-C₆H₅)₂}(thf)₂] (2.709(9)–2.909(9) Å).^[10] The Yb–N bond lengths are very similar to those in Yb^{II}– β -diketiminates (2.418(9)–2.423(9) Å).^[11] The arrangement around the ytterbium atom in **4** determines the geometry of the hetero-

pentadienyl bent sandwich complex. Spectroscopic data consistent with this formulation were also obtained.

In an attempt to obtain insight into the mechanism of the observed ligand transformation, we investigated the reaction of **1** with the diazadiene **3** under the same conditions. We found that replacement of the imino hydrogen atoms by two methyl groups dramatically influences the reaction pathway and leads to the formation of different products. We followed the procedure described above and isolated the novel Yb^{II} derivative **5** (64%) and fluorene (81%). (Scheme 2)

Complex **5** was isolated as a deep green crystalline solid that is readily soluble in toluene but sparingly soluble in hexane. The compound is diamagnetic, which corresponds to the Yb^{II} oxidation state. Single crystals suitable for X-ray crystal-structure analysis (Figure 2) were obtained by recrystallization of **5** from toluene/hexane mixtures.

The crystal-structure analysis showed that the ytterbium atom in **5** is η^5 -coordinated by the sole fluorenyl ligand and by the two nitrogen atoms of the novel monoanionic ligand [(2,6-*i*Pr₂C₆H₃)N=C(CH₃)–C(CH₂)=N(2,6-*i*Pr₂C₆H₃)][–] (**6**), which results from proton abstraction from the methyl substituent of the imino group of **3**. The Yb–C bond lengths in **5** are in the range 2.655(2)–2.770(3) Å, slightly shorter than those in **1**. The Yb–N bonds in **5** are non-equivalent. The Yb(1)–N(2) bond length (2.315(2) Å) is similar to that of the Yb^{II}–N covalent bond in the complex [Yb{N(SiMe₃)}(thf)BPh₄] (2.314(2) Å)^[12a] and slightly longer than that in the complex [Yb{N(SiMe₃)₂}(Me₂P(CH₂)₂PMe₂)] (2.329(2) Å).^[12b] The Yb(1)–N(1) bond is essentially longer (2.388(2) Å), but nevertheless much shorter than the Yb^{II}–N coordination bonds (2.58(1)–2.65(1)).^[9,13] The N=C bonds of the NCCN fragment in **5** are longer than the corresponding bonds of the



Scheme 2. Reaction of **1** and **3** to give **5** and fluorene. Reagents and conditions: **1**, **3** (2 equiv), THF, 60 °C, 30 min; then toluene, 60 °C, 1 h; then toluene, 60 °C, 2 h.

parent diazadiene **3** (1.279(3), 1.280(3) Å)^[14] and differ significantly as well: N(1)–C(26) 1.318(3) Å and N(2)–C(28) 1.353(3) Å. The C–C bond length of the diazadiene fragment in **5** remains similar to that in **3** (1.498(3) Å).^[14] A short C(28)–C(29) bond length (1.398(4) Å) comparable to that of aromatic C–C bonds^[7] together with a flat geometry around the C(29) atom (the sum of the bond angles is 359.8°) provide evidence for sp² hybridization at this carbon atom.

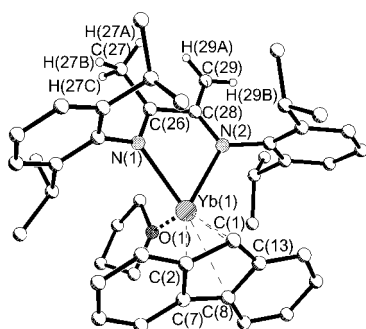


Figure 2. ORTEP representation of structure **5**. Selected bond lengths [Å] and angles [°]: Yb(1)–C(1) 2.649(3), Yb(1)–C(2) 2.655(2), Yb(1)–C(7) 2.727(2), Yb(1)–C(13) 2.744(3), Yb(1)–C(8) 2.770(3), Yb(1)–N(2) 2.315(2), Yb(1)–O(1) 2.352(2), Yb(1)–N(1) 2.388(2), N(1)–C(26) 1.318(3), N(1)–C(14) 1.439(3), N(2)–C(28) 1.353(3), N(2)–C(30) 1.435(3), C(26)–C(28) 1.499(4), C(26)–C(27) 1.471(4), C(28)–C(29) 1.398(4); N(2)–Yb(1)–O(1) 99.76(7), N(2)–Yb(1)–N(1) 9.37(7), O(1)–Yb(1)–N(1) 95.65(7), H(29A)–C(29)–H(29B) 119.5(2), C(28)–C(29)–H(29B) 119.3(2), C(28)–C(29)–H(29A) 121.0(2).

Unlike the geometry of the DAD radical anions in Yb^{III} complexes,^[2b,f,g] which exhibit redistribution of the bond distances (characteristic of delocalized NCCN π systems), the geometry of the monoanionic ligand **6** in **5** is indicative of a partial double bonding and delocalization of the negative charge only occurs in the N(2)–C(28)–C(29) fragment (Scheme 3).



Scheme 3. The geometry of the monoanionic ligand **6** is indicative of a partial double bond. Delocalization of the negative charge only occurs in the N(2)–C(28)–C(29) fragment.

The higher value of the effective negative charge on the N(2) atom results in the non-equivalence of the Yb–N bonds and in the shortening of the Yb(1)–N(2) bond. The ¹H and ¹³C NMR spectra of **5** are consistent with the structural data. The protons of the methyl radical by the imino group appear in the ¹H NMR spectrum as a singlet at δ = 1.67 ppm, whereas the two methylene protons become diastereotopic as a result of partial double bonding in the NCCCH₂ group, giving rise to two singlets of equal intensity at δ = 3.94 and 4.40 ppm.

Isolation of fluorene from the reaction in nearly quantitative yield proves that the fluorenyl anion is responsible for the abstraction of the proton from **3** and for the formation of the ligand **6**. Similar C–H bond activations in the ytterbium amido complexes were previously reported by Deacon and Forsyth^[12a] and by Dehnicke and co-workers.^[15]

Unfortunately, at the present stage of our investigation we are unable to rationalize definitely the formation of the complexes **4** and **5**. Undoubtedly, the first step is coordination of the diazadiene to the ytterbium atom and formation of the mixed-ligand derivatives [(C₁₃H₉)₂Yb(DAD)]. We presume

that oxidation of the ytterbium atom to Yb^{III} occurs in this step and we are currently attempting to prove of this hypothesis. Steric crowding of the coordination sphere of the ytterbium atom is most likely the factor that drives the transformation of the formed species into complexes **4** and **5**. Further work on this subject is being actively pursued at the moment.

Experimental Section

4: A solution of **2** (0.99 g, 2.65 mmol) in THF (10 mL) was added to a solution of **1** (0.86 g, 1.32 mmol) in THF (20 mL) and the reaction mixture was heated at 60 °C for 0.5 h. THF was evaporated in vacuo, toluene (20 mL) was added, and the reaction mixture was stirred at 60 °C for 1 h. The volatile material was evaporated in vacuo, and another portion of toluene (20 mL) was added. The mixture was stirred at 60 °C for an additional 2 h, after which time the solvent was evaporated in vacuo and the deep red solid residue was dissolved in hexane (35 mL). Slow concentration of the solution in hexane at –20 °C resulted in crystals of **4**. The mother liquor was decanted, and the crystals were washed with cold hexane and dried in vacuo at room temperature for 45 min to afford ruby-red crystals of **4** (1.41 g, 80 %). Elemental analysis: calcd (%) for C₈₂H₉₈N₄OYb: C 73.72, H 7.33, Yb 12.95; found: C 73.95, H 7.42, Yb 12.00; ¹H NMR (200 MHz, [D₆]benzene, 20 °C): δ = 0.76 (d, ³J_{HH} = 6.6 Hz, 18H; CH(CH₃)₂), 0.92 (d, ³J_{HH} = 6.6 Hz, 12H; CH(CH₃)₂), 1.05 (d, ³J_{HH} = 6.6 Hz, 12H; CH(CH₃)₂), 1.16 (m, 6H; CH(CH₃)₂), 1.20 (s, 4H; β -CH₂ (thf)), 1.42 (m, 4H; CH(CH₃)₂), 2.47 (sept, ³J_{HH} = 6.8 Hz, 4H; CH(CH₃)₂), 3.33 (br s, 4H; α -CH₂ (thf)), 3.56 (br s, 1H; NH), 4.01 (t, ³J_{HH} = 5.2 Hz, 1H; NH), 4.40 (d, ³J_{HH} = 4.4 Hz, 4H; CH₂), 6.94 (s, 6H; Ar-H), 7.10 (s, 6H; Ar-H), 7.15–7.46 (m, 8H; Ar-H), 7.92 (d, ³J_{HH} = 7.2 Hz, 4H; Ar-H), 8.16 ppm (d, ³J_{HH} = 7.6 Hz, 4H; Ar-H); ¹³C NMR (50 MHz, [D₆]benzene, 20 °C): δ = 23.6, 23.7, 25.0, 25.1 (CH(CH₃)₂), 25.4 (β -CH₂ (thf)), 27.5, 28.6 (CH(CH₃)₂), 52.6 (CH₂NH), 70.2 (α -CH₂ (thf)), 92.7 (Flu-C = NAr), 119.4, 121.5, 122.4, 123.5, 124.4, 125.5, 127.0, 128.1 (CH, Ar-C), 114.9, 131.9, 136.5, 139.8, 140.1, 144.0, 144.8, 172.8 ppm (quat. C, Ar-C); IR (Nujol, KBr): $\tilde{\nu}$ = 3400 (w), 3060 (w), 1640 (m), 1580 (m), 1300 (s), 1160 (m), 1080 (m), 950 (m), 860 (m), 780 (s), 750 (s), 730 cm^{–1} (s).

5: A solution of **3** (0.82 g, 2.03 mmol) in THF (10 mL) was added to a solution of **1** (0.65 g, 1.00 mmol) in THF (20 mL) and the reaction mixture was heated at 60 °C for 0.5 h. THF was evaporated in vacuo, toluene (20 mL) was added, and the reaction mixture was stirred at 60 °C for 1 h. The volatile material was evaporated in vacuo, and another portion of toluene (20 mL) was added. The mixture was stirred at 60 °C for an additional 2 h, after which time the solvent was evaporated in vacuo and the deep green solid residue was recrystallized from a mixture of toluene/hexane at –20 °C. The mother liquor was decanted and the crystals were washed with cold hexane dried in vacuo at room temperature for 45 min to afford deep green crystals of **5** (0.53 g, 64 %). The volatile material was removed from the mother liquor in vacuo, and fluorene (0.14 g, 81 %) was sublimed from the solid residue. Elemental analysis: calcd (%) for C₄₅H₅₆N₂OYb: C 66.44, H 6.88, Yb 21.26; found: C 66.64, H 6.70, Yb 21.20; ¹H NMR (200 MHz, [D₆]benzene, 20 °C): δ = 1.06–1.42 (m, 28H; CH(CH₃)₂ and β -CH₂ (thf)), 1.67 (s, 3H; N = CCH₃), 2.63 (br s, 2H; CH(CH₃)₂), 3.16 (br s, 2H; CH(CH₃)₂), 3.38 (br s, 4H; α -CH₂ (thf)), 3.94 (s, 1H; N = CCHH), 4.40 (s, 1H; N = CCHH), 6.63 (s, 1H; Flu-H), 6.97–7.02 (m, 4H; Ar-H), 7.24–7.42 (m, 8H; Ar-H), 7.99 ppm (m, 2H; Ar-H); ¹³C NMR (50 MHz, [D₆]benzene, 20 °C): δ 19.0 (N = CCH₃), 24.0, 24.3, 25.3, 25.6 (CH(CH₃)₂), 25.1 (β -CH₂ (thf)), 27.9, 28.1 (CH(CH₃)₂), 69.6 (α -CH₂ (thf)), 82.6 (C9 (Flu)), 90.5 (N = CCH₃), 114.9, 118.2, 119.6, 122.7, 123.4, 123.9, 125.7, 128.1 (CH, Ar-C), 119.3, 123.6, 127.6, 133.5, 138.0, 143.2, 143.7, 149.1, 156.6, 179.2 ppm (quat. C (Ar) and quat. C (N = CC)); IR (Nujol, KBr): $\tilde{\nu}$ = 3020 (w), 1525 (m),

1300 (s), 1230 (m), 1180 (m), 1080 (m), 1000 (m), 920 (m), 860 (s), 830 (m), 780 (s), 740 (s), 730 (s), 710 (s), 660 cm⁻¹ (m).

Crystal data for **4**: C₈₈H₁₁₂N₄OYb, *M*_r = 1414.86, triclinic, *P* $\bar{1}$ *P* $\bar{1}$, *a* = 13.0385(7), *b* = 13.8866(7), *c* = 21.9438(12) Å, α = 85.8100(10), β = 87.4260(10), γ = 69.0470(10)°, *V* = 3699.8(3) Å³, *Z* = 2, ρ_{calcd} = 1.270 Mg m⁻³, absorption coefficient 1.313⁻³, *F*(000) 1492, reflections collected 20549, independent reflections 12985, GOF 1.047, *R* = 0.0330, *wR*₂ = 0.0837.

Crystal data for **5**: C₄₅H₅₆N₂OYb, *M*_r = 813.96, orthorhombic, *Pbca*, *a* = 15.3796(10), *b* = 17.1883(12), *c* = 29.211(2) Å, α = 90.0, β = 90.0, γ = 90.0°, *V* = 7721.9(9) Å³, *Z* = 8, ρ_{calcd} = 1.400 Mg m⁻³, absorption coefficient 2.458⁻³, *F*(000) 3344, reflections collected 57402, independent reflections 6812, GOF 0.948, *R* = 0.0280, *wR*₂ = 0.0540. All crystallographic calculations were performed with the Bruker SHELXTL package.^[16] CCDC-241424 (**4**) and -241425 (**5**) contain the supplementary crystallographic data for this paper. These data can be obtained free of charge via www.ccdc.cam.ac.uk/conts/retrieving.html (or from the Cambridge Crystallographic Data Centre, 12, Union Road, Cambridge CB21EZ, UK; fax: (+44) 1223-336-033; or deposit@ccdc.cam.ac.uk).

Received: June 18, 2004

Keywords: C–C coupling · C–H activation · N ligands · ytterbium

- [1] a) H. tom Dieck, I. W. Renk, *Chem. Ber.* **1971**, *104*, 110–130; b) H. tom Dieck, K.-D. Franz, F. Hoffmann, *Chem. Ber.* **1975**, *108*, 163–173; c) J. Reinhold, R. Benedix, P. Birner, H. Hennig, *Inorg. Chim. Acta* **1979**, *33*, 209–213.
- [2] a) F. G. N. Cloke, H. C. de Lemos, A. A. Sameh, *Chem. Commun.* **1986**, 1344–1345; b) M. N. Bochkarev, A. A. Trifonov, F. G. N. Cloke, C. I. Dalby, P. T. Matsunaga, R. A. Andersen, H. Schumann, J. Loebel, H. Hemling, *J. Organomet. Chem.* **1995**, *486*, 177–182; c) A. Recknagel, M. Noltemeyer, F. T. Edelmann, *J. Organomet. Chem.* **1991**, *410*, 53–61; d) A. Scholz, K.-H. Thiele, J. Scholz, R. Weimann, *J. Organomet. Chem.* **1995**, *501*, 195–200; e) P. Poremba, F. T. Edelmann, *J. Organomet. Chem.* **1997**, *549*, 101–104; f) A. A. Trifonov, E. N. Kirillov, M. N. Bochkarev, H. Schumann, S. Muehle, *Russ. Chem. Bull.* **1999**, *48*, 382–384; g) A. A. Trifonov, Yu. A. Kurskii, M. N. Bochkarev, S. Muehle, S. Dechert, H. Schumann, *Russ. Chem. Bull.* **2003**, *52*, 601–606.
- [3] a) A. A. Trifonov, L. N. Zakharov, M. N. Bochkarev, Yu. T. Struchkov, *Izv. Akad. Nauk Ser. Khim.* **1994**, 148–151; b) H. Goerls, B. Neumueller, A. Scholz, J. Scholz, *Angew. Chem.* **1995**, *107*, 732–736; *Angew. Chem. Int. Ed. Engl.* **1995**, *34*, 673–676; c) J. Scholz, H. Goerls, H. Schumann, R. Weimann, *Organometallics* **2001**, *20*, 4394–4402.
- [4] a) R. G. Finke, S. R. Keenan, D. A. Shirardi, P. L. Watson, *Organometallics* **1986**, *5*, 598–601; b) L. R. Morss, *Chem. Rev.* **1976**, *76*, 827–841.
- [5] A. A. Trifonov, E. N. Kirillov, S. Dechert, H. Schumann, M. N. Bochkarev, *Eur. J. Inorg. Chem.* **2001**, 2509–2514.
- [6] W. J. Evans, M. A. Hozbor, *J. Organomet. Chem.* **1987**, *326*, 299–306.
- [7] F. A. Allen, O. Konnard, D. G. Watson, L. Brammer, G. Orpen, R. Taylor, *J. Chem. Soc. Perkin Trans. 1* **1987**, 1–19.
- [8] T. V. Laine, M. Klinga, E. Aitola, M. Leskela, *Acta Chem. Scand.* **1999**, *53*, 968–973.
- [9] T. Don Tilley, R. A. Andersen, B. Spencer, A. Zalkin, *Inorg. Chem.* **1982**, *21*, 2647–2649.
- [10] W. Weng, K. Kunze, A. M. Arif, R. D. Ernst, *Organometallics* **1991**, *10*, 3643–3647.
- [11] A. G. Avent, P. B. Hitchcock, A. V. Khvostov, M. F. Lappert, A. V. Protchenko, *J. Chem. Soc. Dalton Trans.* **2003**, 1070–1075.
- [12] a) G. B. Deacon, C. M. Forsyth, *J. Chem. Soc. Chem. Commun.* **2002**, 2522–2523; b) T. Don Tilley, R. A. Andersen, A. Zalkin, *J. Am. Chem. Soc.* **1982**, *104*, 3725–3727.
- [13] a) E. Sheng, S. Wang, G. Yang, S. Zhou, L. Cheng, K. Zhang, Z. Huang, *Organometallics* **2003**, *22*, 684–692; b) C. Qian, H. Li, J. Sun, W. Nie, *J. Organomet. Chem.* **1999**, *585*, 59–62.
- [14] For structure of **3** see: E. K. Cope-Eatough, F. S. Mair, R. G. Pitchard, J. E. Warren, R. J. Woods, *Polyhedron* **2003**, *22*, 1447–1454.
- [15] M. Karl, K. Harms, S. Seybert, W. Massa, S. Fau, G. Freking, K. Dehnicke, *Z. Anorg. Allg. Chem.* **1999**, *625*, 2055–2062.
- [16] G. M. Sheldrick, SHELXTL version 5.10, *Structure Determination Software Suite*, Bruker AXS, Madison, Wisconsin, USA, **1998**.

Nanostructures

Metastable Vanadium Dioxide Nanobelts: Hydrothermal Synthesis, Electrical Transport, and Magnetic Properties**

*Junfeng Liu, Qiuhong Li, Taihong Wang, Dapeng Yu, and Yadong Li**

One-dimensional (1D) nanostructures have attracted a great deal of attention as functional units for mediating the transport of electrons or optical excitations. Probing their intrinsic properties is critical to assess their possible roles in new types of nanoscale devices.^[1–3] Because of some critical limitations that are difficult to overcome in carbon nanotubes, many other 1D nanostructures have been developed.^[4–16]

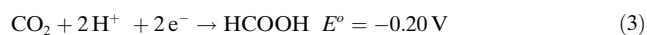
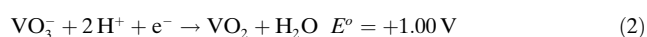
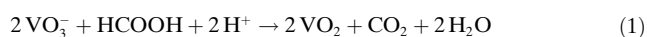
[*] J. Liu, Prof. Y. Li
Department of Chemistry and
the Key Laboratory of Atomic & Molecular Nanosciences
(Ministry of Education, China)
Tsinghua University
Beijing, 100084 (P.R. China)
and
National Center for Nanoscience and Nanotechnology
Beijing, 100084 (P.R. China)
Fax: (+86) 10-6278-8765
E-mail: ydli@tsinghua.edu.cn
Q. Li, Prof. T. Wang
Institute of Physics
Chinese Academy of Sciences
Beijing (P.R. China)
Prof. D. Yu
Department of Physics
Peking University
Beijing (P.R. China)

[**] This work was supported by NSFC (50372030, 20025102, 20151001), the Foundation for the Author of National Excellent Doctoral Dissertation of P.R. China, and the state key project of fundamental research in nanomaterials and nanostructures (2003CB716901).

VO₂(B), one of metastable phases of vanadium dioxide, is of great interest owing to its layered structure and promising properties in the nanometer regime.^[17–19] It is an attractive material for various applications especially as an electrode material for lithium batteries. VO₂(B) exhibits a maximum reversible capacity of about 320 mA h g^{−1} in the range 4 to 1 V in lithium cells.^[17,18] Huynh et al. reported that the operating properties of batteries depend not only on the structure, but also on the morphology of the electrode components.^[20] It was shown that 1D nanostructures are more prone to charge transport than the bulk crystalline structures. VO₂(B) can be prepared by traditional methods such as thermal reduction of V₂O₅ by H₂ or SO₂ gas, thermal decomposition of ammonium hexavanadate, and reduction of aqueous vanadate solution with potassium borohydride.^[21,22] However, most of the synthetic routes only lead to bulk VO₂(B), and the synthesis of VO₂(B) 1D nanostructures is still a challenge to material scientists. Herein, we report a convenient and controllable approach for the synthesis of metastable monoclinic vanadium dioxide single-crystal nanobelts, which requires neither sophisticated techniques nor catalysts. The electrical transport through individual nanobelts as well as the magnetic properties of these materials have also been investigated.

VO₂(B) consists of three-dimensional frameworks of VO₆ octahedra and adopts a structure derived from the structure of V₂O₅.^[21] Recently, we have obtained V₂O₅ nanobelts by hydrothermal synthesis by treating ammonium metavanadate with nitric acid. Thus, it was anticipated that the low-valent 1D vanadium oxides could be obtained by adding an appropriate mild reducing agent under similar hydrothermal conditions. Our experiments have revealed that formic acid can function both as the acidification and reducing agent and has enabled us to prepare the metastable phase of vanadium dioxide nanobelts on a large scale.

The basic reaction we employed for the synthesis of the VO₂ nanobelts can be formulated in Equation (1), which in turn comprises two half reactions [Eq. (2) and (3)].



On the basis of standard reduction potential (E°) values, the standard Gibbs free energy change ΔG_m° of the redox reaction [Eq. (1)] was estimated to be $-231.6\text{ kJ mol}^{-1}$, implying a very strong tendency for the reaction to progress toward the products.

By controlling the pH value and the temperature, the nanobelts could be conveniently prepared without the presence of template or catalyst. It is noteworthy that the as-synthesized nanobelts can be either prepared as stable colloidal solutions or self-assemble into the “paper form” only after suction filtration. Typical X-ray diffraction (XRD) patterns of the VO₂(B) nanobelts are given in Figure 1. Figure 1a shows a set of reflections at 14.4°, 29.0°, and 44.1° for the VO₂(B) nanobelts that assembled into the paper form, characteristic of (00 l) reflections for layered phases of

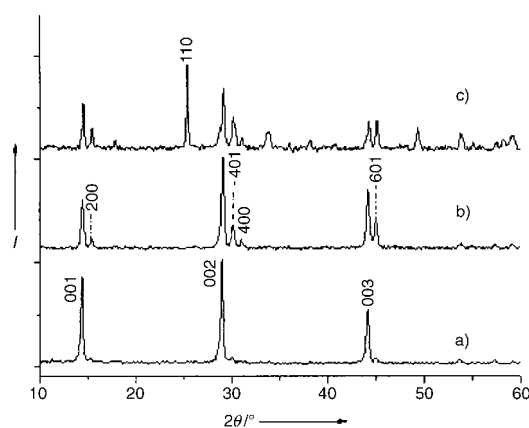


Figure 1. XRD patterns of VO₂(B). a) VO₂ film (the “paper-form” product obtained directly after filtering); b) the partly broken “paper-form” product; c) VO₂(B) powders ground from the “paper-form” product.

VO₂(B). The layer spacing of the phase is determined to be 6.15 Å from the (001) reflection. When the “paper-form” product was broken into pieces, peaks appeared in the XRD pattern at (200), (400), (−401), (−601) (Figure 1b). Finally, after the sample was thoroughly ground, all the peaks can be perfectly indexed to the monoclinic VO₂(B) phase (space group: *C2/m*) with lattice constants $a = 12.09$, $b = 3.702$, $c = 6.433$ Å, and $\beta = 106.6^\circ$ (JCPDS 81–2392) (Figure 1c). Interestingly, no peaks of any other phases or impurities were detected. In Figure 1c the more intense peaks are consistent with the JCPDS card, including the strongest peak at (110). But in the paper-form sample, most of these peaks are missing and only (00 l) peaks appeared. Considering these results with regard to the crystal structure of VO₂(B), it appears that most of the nanobelts packed along (001) in the paper-form sample, and the [010] direction was the growth axis of the belts.

The size and morphology of the products were also examined by scanning electron microscopy (SEM) and transmission electron microscopy (TEM). As shown in Figure 2, the VO₂ nanobelts are several micrometers long, typically 50–100 nm wide, and 10–20 nm thick. In addition, the TEM image and the selected area electron diffraction (SAED) pattern of an individual nanobelt are shown in Figure 2c. The [010] direction of the electron diffraction pattern is parallel to the belt axis, showing that growth occurs along the [010] direction, which is in agreement with the conclusion from the XRD pattern. A high-resolution TEM (HRTEM) image provides an insight into the prepared nanobelt structure. The HRTEM image (Figure 2d) of the end of an individual VO₂ nanobelt shows that it is a single crystal without the presence of dislocations and defects. The 17° orientation between the (010) and (110) lattice planes is consistent with the crystal structure. Energy-dispersive X-ray analysis (EDAX) spectra were also measured to determine the chemical composition of the as-prepared VO₂ nanobelts. Results from EDAX spectra show that the nanobelts only contain V and O; however, the atom ratio of V and O cannot be determined because one peak for the element V overlaps with the peak for the element O.

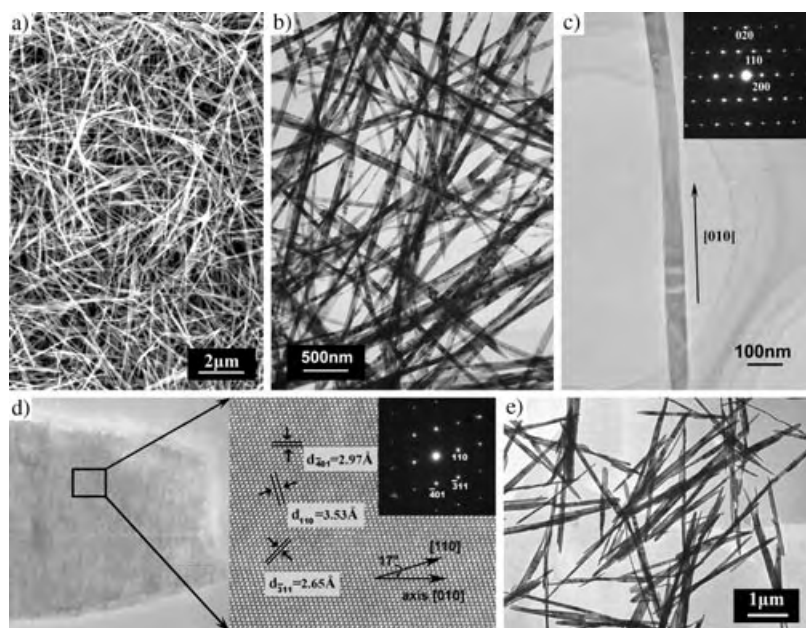


Figure 2. Typical field-emission SEM (a) and low-resolution TEM (b) images of the $\text{VO}_2(\text{B})$ nanobelts. c) Individual nanobelt on the [001] plane. d) HRTEM image of the end of VO_2 nanobelts showing that the nanobelt is single crystalline and free from dislocation and defects. The 17° orientation between [110] and long axis shows the growth direction to be [010]. e) $\text{VO}_2(\text{B})$ nanobelts synthesized in excess formic acid (pH 2).

The synthesis parameters, such as the pH value, temperature, and reaction time, play an important role in controlling the morphology. A series of experiments showed that using a lower temperature resulted in a V_2O_5 gel owing to the inefficient reduction, and shorter reaction times led to bad crystallization. Little product was generated at a pH > 3 owing to insufficient acidification, and only when the pH value was lower than 3 were large amounts of $\text{VO}_2(\text{B})$ nanobelts obtained. The average aspect ratio and width-to-thickness ratio of the nanobelts dropped as the pH value of the synthesis solution decreased from 3 to 2 on increasing the amount of formic acid. When the pH value was adjusted to 3, long belts were obtained for which the average aspect ratio was more than 100 and the width-to-thickness ratio was about 10 (Figure 2b). At a pH 2 the morphology of the vanadium dioxide changed from nanobelts to nanorods with a length of 2–3 μm and an aspect ratio of 20–30 (Figure 2e).

Further advancement of this approach for nanobelt synthesis requires a clear understanding of the growth mechanism. The growth axis of the nanobelt is related to its crystallographic characteristics. $\text{VO}_2(\text{B})$ is constructed from two different layers of VO_6 octahedra. When viewed down the c axis, $\text{VO}_2(\text{B})$ exhibits two edge-sharing octahedra to produce a layer of “steplike” octahedra. These layers are linked to each other at the protruding corners of each pair of octahedra to produce a three-dimensional framework (Figure 3).^[23]

The growth direction of the VO_2 crystal may be determined by the relative stacking rate of the octahedra at various crystal faces. As for the interface of VO_2 , the longest bond (V1–O3) is 2.677 Å (Figure 3), which makes [001] the slowest growth direction, and the average shortest bond along the

[010] direction indicates that the (010) plane has a relatively high stacking rate, which favors growth along the [010] axis. It is believed that detailed studies on the crystal structure and the symmetry will help to explain the results, and could also provide insight into how to control the morphology.

The transport properties of single-crystalline vanadium dioxide nanobelts have been investigated in vacuum by scanning the bias voltage. The 50-nm Au electrodes were deposited by e-beam deposition on a Si substrate covered with a 500-nm thick thermally grown SiO_2 layer. Then an individual vanadium dioxide nanobelt was deposited from an ethanol solution onto the top of the electrodes. A schematic illustration of our device and a typical SEM image recorded with it are given in Figure 4a. The distance between the two electrodes was about 500 nm. The measurements were performed in a vacuum of 3×10^{-5} mbar.

At room temperature, the samples exhibited non-linear, symmetric current/voltage (I/V) characteristics (Figure 4b). The curve is reproducible and no large fluctuations are observed even in the high bias region, indicating that the device is stable. The $I-V$ curve shows superlinear behavior, and closely follows the empirical formula: $I = a + bV + cV^2 + dV^3$, with experimental coefficients of $a \approx 0$, $b = 1.97$, $c = -0.01$, and

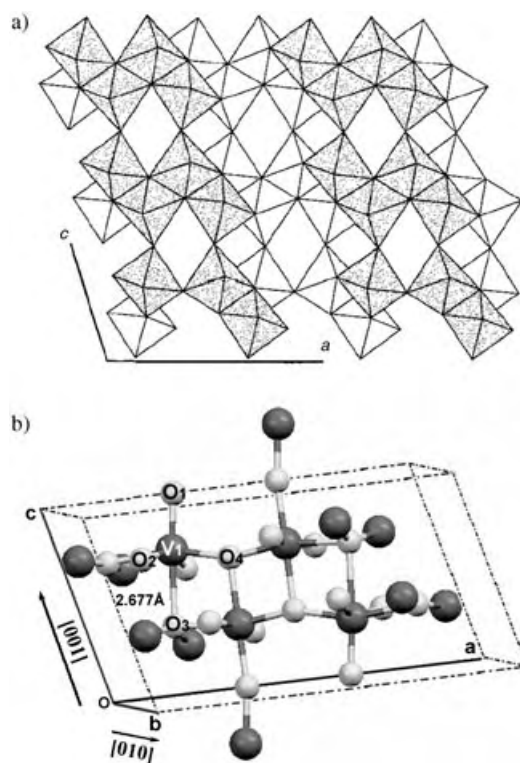


Figure 3. a) Projection of the $\text{VO}_2(\text{B})$ structure along [010]. b) Crystal structure of $\text{VO}_2(\text{B})$ nanobelts. The longest bond (V1–O3) is 2.677 Å, which makes [001] the smallest growth direction, and the average shortest bond along the [010] direction makes the (010) plane have the highest stacking rate.

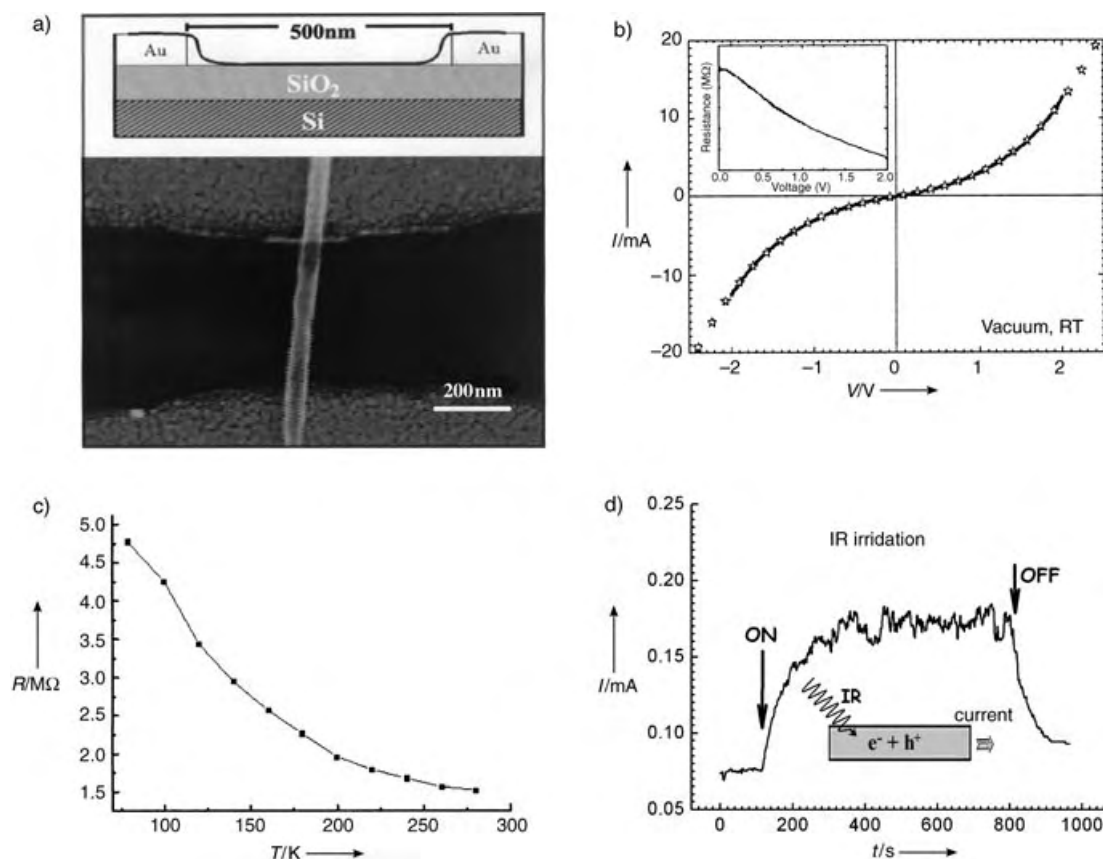


Figure 4. a) Schematic illustration of our device and a typical SEM image. b) I/V characteristics of the individual nanobelt at room temperature (solid line) and the empirical formula $I = a + bV + cV^2 + dV^3$ (starred line). The inset shows the plot of the resistance $R = V/I$ versus bias voltage V . c) Plot of the temperature dependence of the resistance R . d) IR response of a single nanobelt in vacuum. The inset is a schematic representation of the mechanism of the IR response.

$d = 1.05$. As shown in Figure 4b, the curves for the empirical formula and the current coincide with each other very well. The temperature dependence of the resistance is displayed in Figure 4c, which shows that the resistance increases as the temperature drops from 280 K to 50 K.

We analyzed the optoelectronic response of the device in vacuum. The behavior of a representative nanobelt is shown in Figure 4d. When exposed to IR light, the nanobelt conductance increased two- to threefold and stabilized within 1–2 min. The rise in conductance is due to the generation of photocurrent, which directly increases the number of free carriers within the device (inset pattern in Figure 4d). The effect was fully reversible when the light was turned off, with 90% decay of the photoresponse in 100–200 s. The photoswitching behavior was reproducible.

The magnetization of the as-prepared VO₂ nanobelts was measured with a superconducting quantum interference device (SQUID) magnetometer. The magnetization curves as a function of the applied field at 5 K under conditions of zero-field cooling (ZFC) and field cooling (FC) in a 100 Oe field are shown in Figure 5. The results indicate VO₂(B) nanobelts are paramagnetic materials.

In summary, we synthesized metastable monoclinic vanadium dioxide single-crystal nanobelts by a direct hydrothermal reduction method. The obtained nanobelts crystallize

well and allow dimensional control along the [010] direction. The single-crystalline VO₂ nanobelts can be prepared into stable colloidal solutions, or assembled into paper forms by tuning process parameters. The morphology of the samples can be adjusted by varying the parameters of the solution. The electrical transport through single nanobelts was investigated and the magnetic measurement showed VO₂(B) was a paramagnetic material. This hydrothermal method should be applicable for large-scale production of low-dimensional nanostructured vanadium dioxides.

Experimental Section

The vanadium dioxide nanobelts were synthesized under hydrothermal conditions. All chemicals were purchased from the Beijing Chemical Reagents Company and were used without further purification. In a typical synthesis, ammonium metavanadate (0.234 g) was dissolved in deionized water to form a light yellow clear solution. Formic acid was added dropwise to the ammonium metavanadate solution (0.1 M; 20 mL) until the final pH of the solution was about 2–3 under stirring. A clear orange solution was formed and the resultant solution was then transferred into a Teflon-lined autoclave with a stainless-steel shell. The autoclave was kept at 180 °C for two days and then allowed to cool to room temperature. The final product was washed with deionized water and pure alcohol

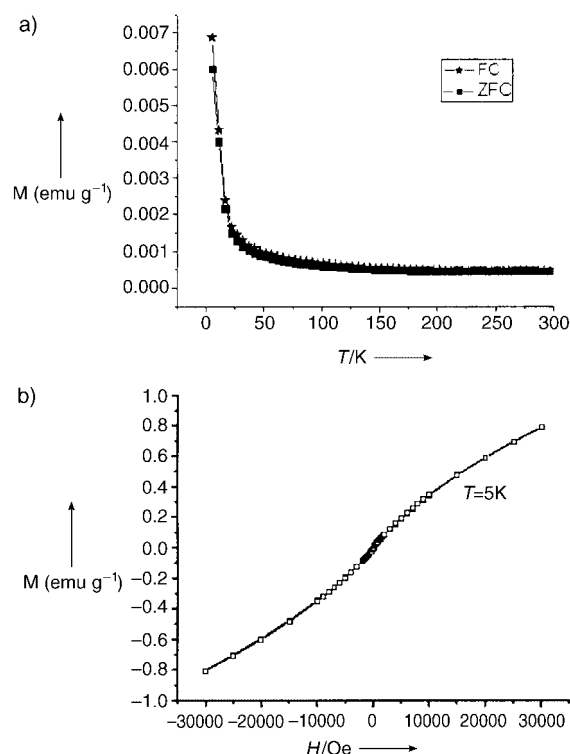


Figure 5. a) ZFC and FC curves of vanadium dioxide nanobelts measured with the field of 100 Oe. b) Magnetization of vanadium dioxide nanobelts plotted as a function of the applied field measured at 5 K.

several times to remove any other possible residues and then dried at 60 °C under vacuum for 6–8 h.

Powder X-ray diffraction (XRD) experiments on the products were conducted on a Bruker D-8 Avance X-ray diffractometer with $\text{Cu}_{\text{K}\alpha}$ radiation ($\lambda = 1.5418 \text{ \AA}$). The morphologies and structures of the vanadium dioxide nanobelts were observed at 200 kV by using a LEO-1530 field-emission scanning electron microscope (FE-SEM), a Hitachi H-800 transmission electron microscope (TEM), and a JEOL JEM-2010F high-resolution transmission electron microscope (HRTEM). Electron diffraction (ED) patterns were used to determine the growth orientation of the as-prepared 1D product.

Received: March 24, 2004

Keywords: electrical transport · hydrothermal synthesis · magnetic properties · nanostructures · vanadium

- [9] J. Q. Hu, Y. Bando, Z. W. Liu, J. H. Zhan, D. Golberg, T. Sekiguchi, *Angew. Chem.* **2004**, *116*, 65; *Angew. Chem. Int. Ed.* **2004**, *43*, 63.
- [10] D. Mann, A. Javey, J. Kong, Q. Wang, H. J. Dai, *Nano Lett.* **2003**, *3*, 1541.
- [11] C. N. R. Rao, A. K. Cheetham, *J. Mater. Chem.* **2001**, *11*, 2887.
- [12] C. N. R. Rao, G. U. Kulkarni, P. J. Thomas, P. P. Edwards, *Chem. Eur. J.* **2002**, *8*, 29.
- [13] Y. N. Xia, P. D. Yang, Y. G. Sun, Y. Y. Wu, B. Mayers, B. Gates, Y. D. Yin, F. Kim, Y. Q. Yan, *Adv. Mater.* **2003**, *15*, 353.
- [14] G. R. Patzke, F. Krumeich, R. Nesper, *Angew. Chem.* **2002**, *114*, 2554; *Angew. Chem. Int. Ed.* **2002**, *41*, 2446.
- [15] C. N. R. Rao, M. Nath, *Dalton Trans.* **2003**, 1.
- [16] C. N. R. Rao, F. L. Deepak, G. Gundiah, A. Govindaraj, *Prog. Solid State Chem.* **2003**, *31*, 5.
- [17] W. Li, J. R. Dahn, D. S. Wainwright, *Science* **1994**, *264*, 1115.
- [18] C. Tsang, A. Manthiram, *J. Electrochem. Soc.* **1997**, *144*, 520.
- [19] Z. Gui, R. Fan, W. Q. Mo, X. H. Chen, L. Yang, S. Y. Zhang, Y. Hu, Z. Z. Wang, W. C. Fan, *Chem. Mater.* **2002**, *14*, 5053.
- [20] W. U. Huynh, J. J. Dittmer, A. P. Alivisatos, *Science* **2002**, *295*, 2425.
- [21] F. Theobald, R. Cabala, J. Bernard, *J. Solid State Chem.* **1976**, *17*, 431.
- [22] A. M. Kannan, A. Manthiram, *Solid State Ionics* **2003**, *159*, 265.
- [23] C. Leroux, G. Nihoul, G. Van Tendeloo, *Phys. Rev. B* **1998**, *57*, 5111.

- [1] H. J. Dai, E. W. Wong, C. M. Lieber, *Science* **1996**, *272*, 523.
- [2] D. Bozovic, M. Bockrath, J. H. Hafner, C. M. Lieber, H. Park, M. Tinkham, *Appl. Phys. Lett.* **2001**, *78*, 3693.
- [3] H. J. Dai, *Acc. Chem. Res.* **2002**, *35*, 1035.
- [4] H. Kind, H. Q. Yan, B. Messer, M. Law, P. D. Yang, *Adv. Mater.* **2002**, *14*, 158.
- [5] J. Zhou, N. S. Xu, S. Z. Deng, J. Chen, J. C. She, Z. L. Wang, *Adv. Mater.* **2003**, *15*, 1835.
- [6] X. F. Duan, Y. Huang, R. Agarwal, C. M. Lieber, *Nature* **2003**, *421*, 241.
- [7] J. A. Zapien, Y. Jiang, X. M. Meng, W. Chen, F. C. K. Au, Y. Lifshitz, S. T. Lee, *Appl. Phys. Lett.* **2004**, *84*, 1189.
- [8] J. J. Urban, J. E. Spanier, O. Y. Lian, W. S. Yun, H. Park, *Adv. Mater.* **2003**, *15*, 423.

Homogeneous Catalysis**Distannylation of Strained Carbon–Carbon Triple Bonds Catalyzed by a Palladium Complex****

Hiroto Yoshida, Kenji Tanino, Joji Ohshita, and Atsutaka Kunai**

Transformations of arynes catalyzed by a transition-metal complex, although less common than stoichiometric reactions,^[1] have recently received considerable attention as a novel route for the synthesis of substituted arenes that are not accessible by conventional methods. Irrespective of the catalyst and reactant used, efforts have thus far been devoted mainly to developing cyclization reactions of arynes. The pioneering work on these transformations—palladium-catalyzed trimerization of arynes^[2] and cocyclization of arynes

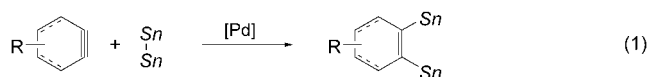
[*] Dr. H. Yoshida, K. Tanino, Prof. J. Ohshita, Prof. A. Kunai
Department of Applied Chemistry
Graduate School of Engineering
Hiroshima University
Higashi-Hiroshima 739-8527 (Japan)
Fax: (+81) 82-424-5494
E-mail: yhiroto@hiroshima-u.ac.jp
akunai@hiroshima-u.ac.jp

[**] We thank Central Glass Co Ltd. for a generous gift of trifluoromethanesulfonic anhydride.



Supporting information for this article is available on the WWW under <http://www.angewandte.org> or from the author.

with alkynes^[3]—was reported by Peña et al. Catalytic reactions of arynes with alkynes and/or allyl chlorides in the presence of a palladium complex have also been reported by Yamamoto and co-workers,^[4] while Murai and co-workers have developed cobalt-, rhodium-, and palladium-catalyzed carbonylative cycloadditions of arynes.^[5] Catalytic addition reactions of a σ bond^[6] to arynes have been limited to carbostannylation^[7a] and disilylation,^[7b] as reported previously. Herein we report that a tin–tin bond of a distannane readily adds to strained carbon–carbon unsaturated compounds, such as arynes or cyclohexynes, in the presence of a palladium complex [Eq. (1)]. This transition-metal-catalyzed element–element σ -bond addition reaction to cyclohexynes has no precedents, to the best of our knowledge.



We first examined the reaction of hexabutyldistannane (**1a**) and benzyne, prepared in situ from 2-(trimethylsilyl)phenyl triflate (**2a**),^[8] and a fluoride ion (KF/[18]crown-6) in the presence of a palladium/1,1,3,3-tetramethylbutyl isocyanide (*tert*-octyl isocyanide, *t*OcNC) complex,^[9] and found that the tin–tin bond of **1a** smoothly adds to benzyne to afford 1,2-bis(tributylstannyl)benzene (**3aa**) in 73% yield (entry 1, Table 1).^[10] The choice of catalyst and source of the fluoride ion are crucial: the reaction did not proceed in the presence of either [Pd(dba)₂] (dba = *trans,trans*-dibenzylideneacetone) or [Pd(PPh₃)₄], and the desired product was also not formed when CsF in MeCN^[11] was used as the source of the fluoride ion, even in the presence of the same palladium–isocyanide complex. The distannylation of various arynes was then investigated under the optimized reaction conditions. As in the case of benzyne itself, the 4-substituted benzynes formed in situ from precursors **2b–2d** react efficiently with **1a** to

provide the corresponding distannylation products **3ab–3ad**, respectively, in moderate to high yields (entries 2–4), whereas the reaction of 4-fluorobenzyne (formed from **2e**) gave only a low yield of the desired product (entry 5). The distannylation reaction was also applied to 4,5-disubstituted benzynes (formed from **2f** or **2g**) or sterically more congested arynes (formed from **2h–2j**) to afford good to high yields of products **3af–3aj**, respectively (entries 6–10). In addition to **1a**, hexamethyldistannane (**1b**) could also be used as the tin-containing starting material, and in this case the less-reactive 1,2-naphthalene (from **2k**), 3-phenylbenzyne (from **2l**), or 9,10-phenanthryne (from **2m**) were found to insert into the tin–tin bond (entries 11–14, respectively);^[12] in most cases a compound resulting from cyclotrimerization of the aryne (triphenylene) was formed as a by-product. The reaction with **1b** also produced a trace amount of 2,2'-distannybiaryl as well; for example, triphenylene and 2,2'-bis(trimethylstannyl)biphenyl were obtained in 9% and 3% yields in the reaction summarized in entry 11.

The reaction of an aryne containing two triple bonds is noteworthy: treatment of the bisaryne precursor **2n** with **1a** gave bis[3,4-bis(tributylstannyl)phenyl] ether **3an** in which four carbon–tin bonds are formed in one step [Eq. (2); Tf = trifluoromethanesulfonyl, TMS = trimethylsilyl].

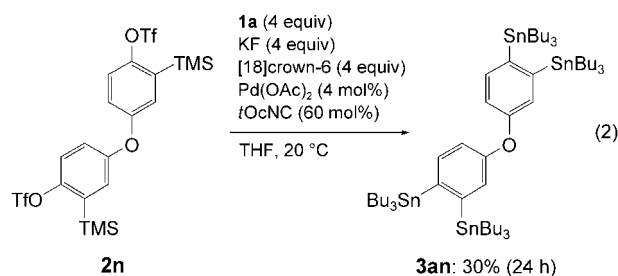


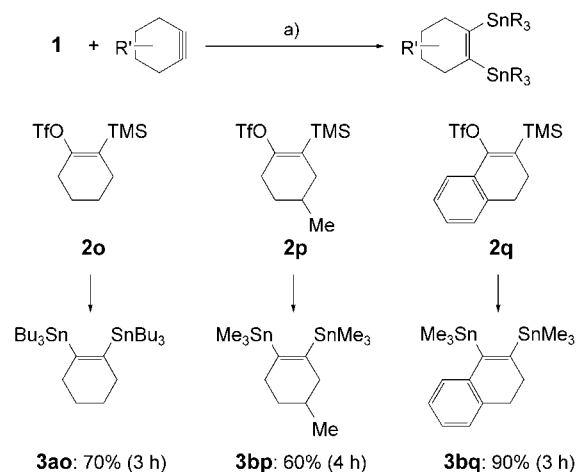
Table 1: Distannylation of arynes.

Entry	Distannane	R' in 2	Precursor	<i>t</i> [h]	Yield [%] ^[a]	Product
1	1a (R = Bu)	H	2a	3	73	3aa
2		4-Me	2b	3	71	3ab
3		4-MeO	2c	7	55	3ac
4		4-Ph	2d	4	40	3ad
5		4-F	2e	6.5	26	3ae
6		4,5-Me ₂	2f	3	73	3af
7		4,5-(CH ₂) ₃	2g	9	64	3ag
8		6-Me	2h	3.5	55	3ah
9		3-MeO	2i	6	59	3ai
10		3,6-(MeO) ₂	2j	5	63	3aj
11	1b (R = Me)	H	2a	4	56	3ba
12		3,4-(CH) ₄	2k	4.5	61	3bk
13		6-Ph	2l	5.5	39	3bl
14		dibenzo[c,e] ^[b]	2m	5	27	3bm

[a] Yield of isolated product based on distannane. [b] 9,10-Phenanthryne.

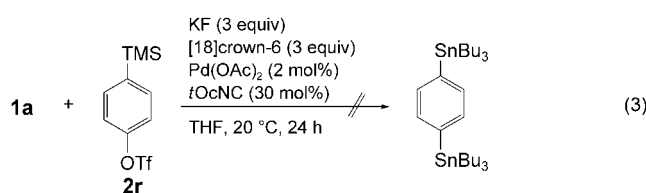
The distannylation reaction was also found to be suitable for cyclohexynes (Scheme 1). When in situ generated cyclohexyne (formed from **2o**) was treated with **1a** under the above-mentioned reaction conditions the insertion product 1,2-bis(tributylstannyl)cyclohexene (**3ao**) was obtained in 70% yield. Similarly, the reaction of substituted cyclohexynes (formed from **2p** or **2q**) with **1b** also took place successfully to provide the distannylation products (**3bp** or **3bq**) in 60 or 90% yield, respectively.

Since an aryl (or alkenyl) triflate readily undergoes a cross-coupling reaction with a distannane in the presence of a palladium catalyst,^[13] the distannylation might proceed by a pathway that does not

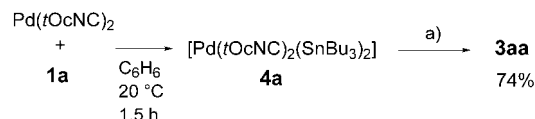


Scheme 1. Distannylation of cyclohexynes: a) KF (3 equiv), [18]crown-6 (3 equiv), Pd(OAc)₂ (2 mol%), tOcNC (30 mol%), THF, 20 °C.

involve an aryne (cyclohexyne) intermediate: cross-coupling of **2** at a C–OTf moiety with **1** followed by fluoride-ion-induced silicon–tin exchange between the resulting 2-(trialkylstannyl)arylsilane (2-(trialkylstannyl)cyclohexenylsilane) and R₃SnOTf.^[14] However, this pathway can be ruled out since the reaction of 4-(trimethylsilyl)phenyl triflate (**2r**) with **1a** did not give the respective distannylation product, thus confirming the intermediacy of an aryne (cyclohexyne) in the distannylation process [Eq. (3)].

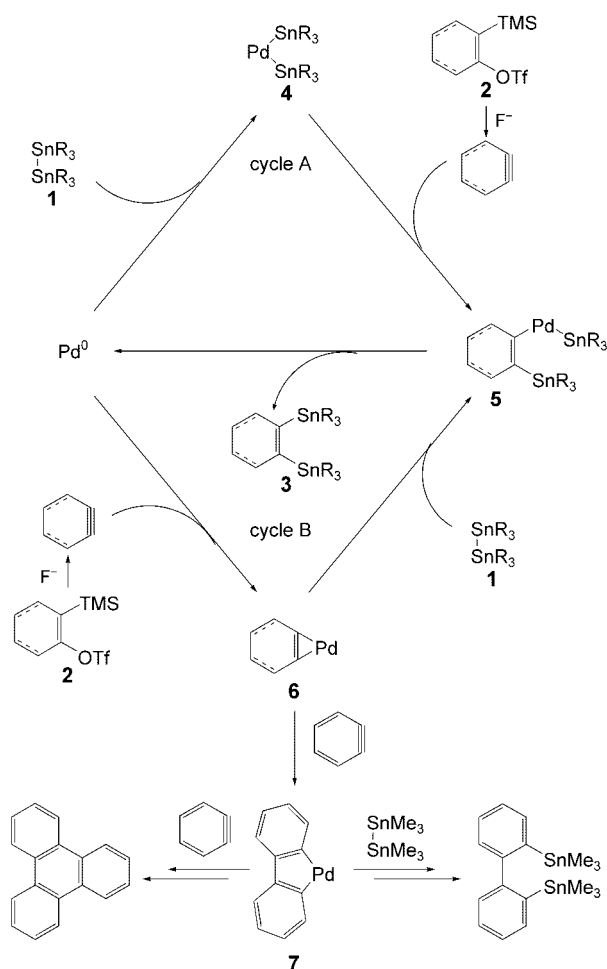


We assumed that this reaction is initiated by oxidative addition of an Sn–Sn bond of a distannane to a Pd⁰ complex^[15] and thus we examined the stoichiometric reaction shown in Scheme 2. Thus, treatment of the Pd⁰–isocyanide complex^[16]



Scheme 2. Elucidation of the mechanism by stoichiometric reactions: a) **2a** (1.5 equiv), KF (3 equiv), [18]crown-6 (3 equiv), THF, 20 °C, 1 h.

with an equimolar amount of **1a** led to the quantitative formation of the oxidative-addition product **4a**,^[17,18] which exhibits high reactivity for the insertion of benzyne to afford **3aa** in 74% yield. These results prompted us to propose cycle A depicted in Scheme 3. First, complex **4** is produced by oxidative addition of **1** to the Pd⁰ complex. Subsequent



Scheme 3. Catalytic cycles for the distannylation.

insertion of the triple bond of the aryne or cyclohexyne into an Sn–Pd bond of **4** to form palladium complex **5**, followed by reductive elimination, affords the product and regenerates the catalyst. However, formation of a triphenylene and distannybiaryl as by-products may suggest that another catalytic cycle is also operative. Thus, the Pd⁰ complex initially undergoes oxidative cyclization with the aryne to generate palladacycle **6**,^[19] which yields the product after reaction with **1** (cycle B).^[20,21] The by-products could also arise from **6**: the interaction of **6** with a second aryne instead of **1** gives a five-membered palladacycle **7**, which reacts further with a third aryne^[22] or **1**^[23] to afford a triphenylene or distannybiaryl, respectively.

In conclusion, distannylation of arynes or cyclohexynes has been accomplished in the presence of a catalytic amount of a palladium–*tert*-octyl isocyanide complex, and diverse 1,2-distannylarenes or 1,2-distannylcyclohexenes, which could have high synthetic utility as bis(anion) equivalents, have been readily synthesized. Moreover, the catalytic pathway, which includes oxidative addition of a distannane to a palladium(0) complex, has been confirmed by the stoichiometric reaction. Further studies on synthetic applications to other strained cycloalkynes and σ bonds are in progress.

Experimental Section

3aa: Compounds **1a** (0.13 g, 0.22 mmol) and **2a** (0.098 g, 0.33 mmol) were added to a solution (1.0 mL) of 1,1,3,3-tetramethylbutyl isocyanide (9.2 mg, 0.066 mmol), Pd(OAc)₂ (1.0 mg, 4.4 μmol), KF (0.038 g, 0.66 mmol) and [18]crown-6 (0.17 g, 0.66 mmol) in THF, and the resulting mixture was stirred at 20 °C for 3 h. The mixture was then diluted with ethyl acetate, filtered through celite, and concentrated. Column chromatography on alumina (hexane as eluent, activity IV) followed by gel-permeation chromatography (benzene as eluent) gave **3aa** as a colorless oil (0.11 g, 73 % yield); ¹H NMR (400 MHz, CDCl₃): δ = 0.88 (t, *J* = 7.1 Hz, 18H), 1.01–1.07 (m, 12H), 1.27–1.53 (m, 24H), 7.19–7.22 (m, 2H), 7.42–7.55 ppm (m, 2H); ¹³C NMR (99.5 MHz, CDCl₃): δ = 10.9, 13.6, 27.5, 29.2, 127.1, 137.5, 151.9 ppm; ¹¹⁹Sn NMR (147.5 MHz, CDCl₃): δ = –43.2 ppm. Elemental analysis calcd for C₃₀H₅₈Sn₂: C 54.91, H 8.91; found: C 55.18, H 8.97.

Received: April 1, 2004

Keywords: arynes · cycloalkynes · homogeneous catalysis · palladium · tin

- [1] Reviews: a) S. L. Buchwald, R. B. Nielsen, *Chem. Rev.* **1988**, 88, 1047; b) S. L. Buchwald, R. D. Broene, in *Comprehensive Organometallic Chemistry II*, Vol. 12 (Eds.: E. W. Able, F. G. A. Stone, G. Wilkinson), Pergamon, Oxford, **1995**, pp. 771–784; c) M. A. Bennett, H. P. Schwemlein, *Angew. Chem.* **1989**, 101, 1349; *Angew. Chem. Int. Ed. Engl.* **1989**, 28, 1296; d) M. A. Bennett, E. Wenger, *Chem. Ber./Recl.* **1997**, 130, 1029.
- [2] a) D. Peña, S. Escudero, D. Pérez, E. Guitián, L. Castedo, *Angew. Chem.* **1998**, 110, 2804; *Angew. Chem. Int. Ed.* **1998**, 37, 2659; b) D. Peña, D. Pérez, E. Guitián, L. Castedo, *Org. Lett.* **1999**, 1, 1555; c) D. Peña, A. Cobas, D. Pérez, E. Guitián, L. Castedo, *Org. Lett.* **2000**, 2, 1629.
- [3] a) D. Peña, D. Pérez, E. Guitián, L. Castedo, *J. Am. Chem. Soc.* **1999**, 121, 5827; b) D. Peña, D. Pérez, E. Guitián, L. Castedo, *Synlett* **2000**, 1061; c) D. Peña, D. Pérez, E. Guitián, L. Castedo, *J. Org. Chem.* **2000**, 65, 6944.
- [4] a) K. V. Radhakrishnan, E. Yoshikawa, Y. Yamamoto, *Tetrahedron Lett.* **1999**, 40, 7533; b) E. Yoshikawa, K. V. Radhakrishnan, Y. Yamamoto, *Tetrahedron Lett.* **2000**, 41, 729; c) E. Yoshikawa, Y. Yamamoto, *Angew. Chem.* **2000**, 112, 185; *Angew. Chem. Int. Ed.* **2000**, 39, 173; d) E. Yoshikawa, K. V. Radhakrishnan, Y. Yamamoto, *J. Am. Chem. Soc.* **2000**, 122, 7280.
- [5] N. Chatani, A. Kamitani, M. Oshita, Y. Fukumoto, S. Murai, *J. Am. Chem. Soc.* **2001**, 123, 12686.
- [6] Reviews on the addition of σ bonds to unsaturated organic compounds: a) I. Beletskaya, C. Moberg, *Chem. Rev.* **1999**, 99, 3435; b) M. Sugimoto, Y. Ito, *Chem. Rev.* **2000**, 100, 3221.
- [7] a) H. Yoshida, Y. Honda, E. Shirakawa, T. Hiyama, *Chem. Commun.* **2001**, 1880; b) H. Yoshida, J. Ikada, M. Shudo, J. Ohshita, A. Kunai, *J. Am. Chem. Soc.* **2003**, 125, 6638.
- [8] a) Y. Himeshima, T. Sonoda, H. Kobayashi, *Chem. Lett.* **1983**, 1211; b) D. Peña, A. Cobas, D. Pérez, E. Guitián, *Synthesis* **2002**, 1454.
- [9] A palladium–isocyanide complex has been shown by Ito and co-workers to be an efficient catalyst for disilylation, silylstannylation, or silylboration of unsaturated organic compounds such as alkynes and alkenes, see Ref. [6b].
- [10] For the palladium-catalyzed distannylation of alkynes, see a) T. N. Mitchel, A. Amamria, H. Killing, D. Rutschow, *J. Organomet. Chem.* **1983**, 241, C45; b) E. Piers, R. T. Skerlj, *J. Chem. Soc. Chem. Commun.* **1986**, 626; c) J. Mancuso, M. Lautens, *Org. Lett.* **2003**, 5, 1653.
- [11] The combination of CsF and MeCN has been employed frequently in the catalytic transformations of arynes, see Ref. [3–5] and [7a].
- [12] No trace of the distannylation products of these arynes was found in the reaction with **1a**.
- [13] a) S. A. Hitchcock, D. R. Mayhugh, G. S. Gregory, *Tetrahedron Lett.* **1995**, 36, 9085; b) G. Stork, R. C. A. Isaacs, *J. Am. Chem. Soc.* **1990**, 112, 7399.
- [14] B. P. Warner, S. L. Buchwald, *J. Org. Chem.* **1994**, 59, 5822.
- [15] Oxidative addition of a distannane to a palladium(0) complex has been proposed to be an initiation step in the distannylation of alkynes, see Ref. [6a].
- [16] a) S. Otsuka, A. Nakamura, Y. Tatsuno, *J. Am. Chem. Soc.* **1969**, 91, 6994; b) M. Sugimoto, H. Oike, S.-S. Park, Y. Ito, *Bull. Chem. Soc. Jpn.* **1996**, 69, 289.
- [17] The configuration of **4a** (*cis* or *trans*) could not be elucidated.
- [18] Oxidative addition of a distannane to a palladium(0)–phosphane complex: Y. Tsuji, K. Nishiyama, S. Hori, M. Ebihara, T. Kawamura, *Organometallics* **1998**, 17, 507.
- [19] M. Retbøll, A. J. Edwards, A. D. Rae, A. C. Willis, M. A. Bennett, E. Wenger, *J. Am. Chem. Soc.* **2002**, 124, 8348; see also Ref. [1c] and [1d].
- [20] The palladium-catalyzed carbostannylation of arynes has also been reported to proceed via palladacycle **6**: T. Matsubara, *Organometallics* **2003**, 22, 4297; see also Ref. [7a].
- [21] We could not substantiate cycle B by a stoichiometric reaction because an attempt to prepare palladacycle **6** by the reaction of [Pd(*r*OcNC)₂] with **2a** and KF/[18]crown-6 was unsuccessful.
- [22] The five-membered palladacycle **7** has been proposed to be a key intermediate in the palladium-catalyzed trimerization of arynes, see Ref. [2a].
- [23] The reaction of a five-membered palladacycle, derived from a Pd⁰ complex and 2 mol of an alkyne, with an organostannane has been demonstrated to be a key step in the palladium-catalyzed dimerization-carbostannylation of alkynes: a) E. Shirakawa, H. Yoshida, Y. Nakao, T. Hiyama, *J. Am. Chem. Soc.* **1999**, 121, 4290; b) H. Yoshida, E. Shirakawa, Y. Nakao, Y. Honda, T. Hiyama, *Bull. Chem. Soc. Jpn.* **2001**, 74, 637.

Noncovalent Interactions

A Weak Attractive Interaction between Organic Fluorine and an Amide Group**

Fraser Hof, Denise M. Scofield, W. Bernd Schweizer, and François Diederich*

Questions regarding the nature and strength of noncovalent interactions formed by organic fluorine atoms are increasingly being addressed and debated in the literature.^[1] We have been exploring noncovalent interactions of fluorine by carrying out a systematic fluorine scan^[2] at the active site of thrombin.^[3] While exploring the hydrophobic D pocket of this serine protease, we noticed that the potency of a closely related family of fluorinated inhibitors was strongly influenced by the position of the fluorine atom (Figure 1).^[3a] The 4-fluorobenzyl derivative (\pm)-**4** exhibits fivefold better inhibition than any other member of the family. The X-ray structure of the (+)-**4**-enzyme complex showed two close contacts between the fluorine atom and the C $_{\alpha}$ -H atom as well as the carbonyl C atom of Asn98 (Figure 1b). Subsequent searches in the Cambridge Structural Database and RCSB Protein Data Bank provided numerous examples of similar sub van der Waals contacts between organic fluorine atoms and carbonyl carbon atoms in chemical and biological samples. These interactions have a characteristic geometry: the fluorine atom tends to reside orthogonally above the pseudotrigonal axis of the carbonyl group, and the C-F bond

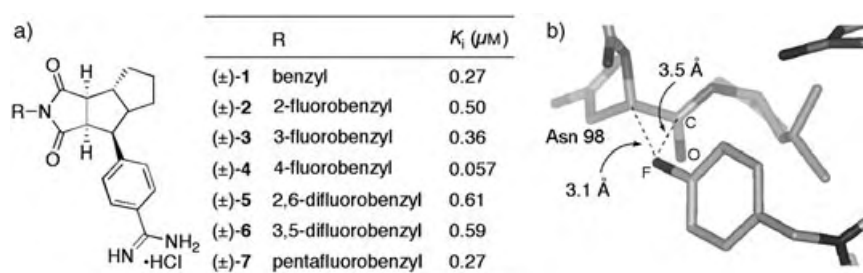


Figure 1. a) A family of inhibitors designed to probe the fluorophilicity of the D pocket at the thrombin active site. b) X-ray structure showing close contacts between the fluorine atom of inhibitor (+)-**4** and the protein backbone of thrombin.

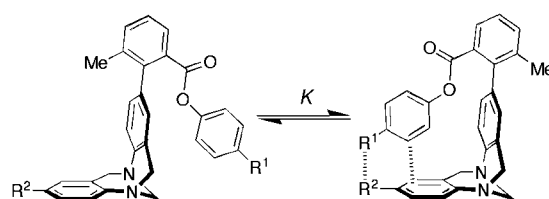
[*] Dr. F. Hof, D. M. Scofield, Dr. W. B. Schweizer, Prof. Dr. F. Diederich
Laboratorium für Organische Chemie
ETH-Hönggerberg, HCI
8093 Zürich (Switzerland)
Fax: (+41) 1-632-1109
E-mail: diederich@org.chem.ethz.ch

[**] F.H. thanks the Novartis Foundation and the Human Frontier Science Program for postdoctoral fellowship support. This research was supported by the ETH Research Council and F. Hoffmann-La Roche Ltd.

Supporting information for this article (synthesis and characterization of compounds (\pm)-**8**–(\pm)-**10** and (\pm)-**13** as well as complete error analysis of the physical data) is available on the WWW under <http://www.angewandte.org> or from the author.

approaches the plane of the carbonyl group from an angle between 100° and, at very short F...C distances, 140°.^[3a] Herein we report the first model system to evaluate the energetics of the proposed C-F...amide interactions.

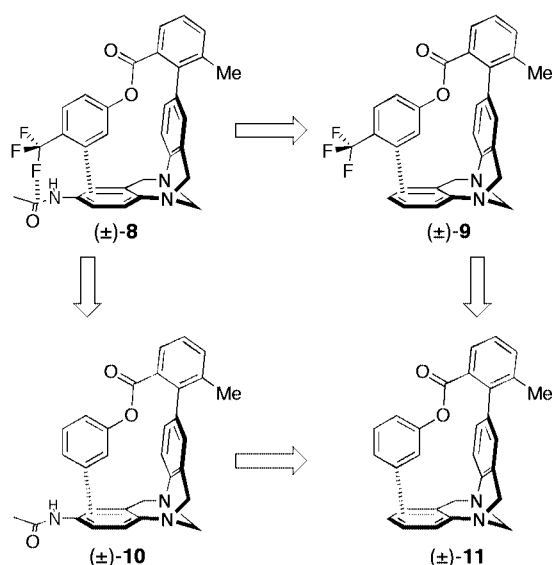
The distinct geometry of the orthogonal C-F...amide interaction presented an unusual challenge. We found an answer in the “molecular torsion balance” derived by Wilcox et al. from the Tröger base—a system designed for the accurate measurement of edge-to-face aromatic–aromatic interactions by the observation of a simple conformational equilibrium.^[4] We found through examination of existing crystal structures^[5] that appropriate substitution of the Tröger base skeleton would provide the perpendicular arrangement of functional groups required for our study (Scheme 1). The



Scheme 1. The torsion balance of Wilcox and co-workers. Modeling studies predict both edge-to-face aromatic–aromatic interactions and close contacts between substituents R¹ and R² for the folded state.

use of a trifluoromethyl group was required to approximate the optimal C-F...amide geometry. Based on the similarity of the results obtained from database searches for fluorine atoms attached to sp²- and sp³-hybridized carbon atoms, we anticipated that this substitution would have a negligible effect on the energetics of the proposed interaction.

The second challenge in characterizing fluorine–amide interactions is their expected weakness. The relative K_i values for compounds (\pm)-**1**–(\pm)-**7** suggest that the fluorine substitution provides approximately 4 kJ mol^{−1} of stabilizing energy. Hunter and co-workers have popularized chemical double-mutant cycles for the measurement of very small interaction energies in supramolecular systems, and have used this method to accurately measure various noncovalent interactions as weak as 1 kJ mol^{−1}.^[6] The application of this strategy to the Wilcox torsion balance is straightforward. The edge-to-face aromatic–aromatic interaction is the primary force behind the folding of the molecule, and the effect of each substitution on this primary force must be accounted for to determine the incremental folding free enthalpy provided by the two appended functional groups. A double-mutant cycle (Scheme 2) can be used to determine the influence of each appended group on the edge-to-face interaction independently from their interaction with each other. When the folding energies of all four molecules in the double-mutant cycle have

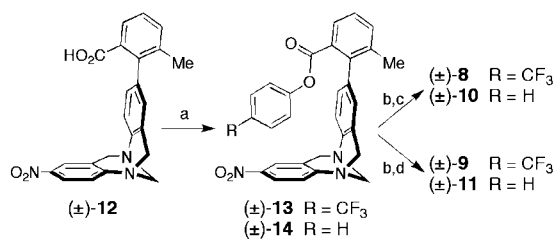


Scheme 2. Double-mutant cycle for determining the magnitude of the attraction between orthogonally oriented CF_3 and NHCOCH_3 groups.

been determined, the interaction energy of the two appended functional groups ($\Delta G_{\text{CF}_3 \cdots \text{NHCOCH}_3}$) is given by Equation (1).

$$\Delta G_{\text{CF}_3 \cdots \text{NHCOCH}_3} = \Delta G_{(\pm)\text{-}8} - \Delta G_{(\pm)\text{-}9} - \Delta G_{(\pm)\text{-}10} + \Delta G_{(\pm)\text{-}11} \quad (1)$$

The four molecules of interest were synthesized as shown in Scheme 3. The nitrocarboxylic acid intermediate (\pm)-**12**, prepared in thirteen steps using literature methods,^[7] was esterified with 4-(trifluoromethyl)phenol and phenol to give (\pm)-**13** and (\pm)-**14**, respectively.



Scheme 3. Synthesis of (\pm)-**8**–(\pm)-**11**. a) Et_3N , BOP, 4-(trifluoromethyl)phenol or phenol, CH_2Cl_2 , RT, 71–97%. b) H_2 (atm), RaNi , EtOAc /EtOH, RT, 90–100%. c) Ac_2O , CH_2Cl_2 , RT, 20–72%. d) 1. HCl , NaNO_2 , 5 °C; 2. H_3PO_2 , 5 °C, 25–63%. BOP = Benzotriazol-1-yloxy-tris(dimethylamino)phosphonium hexafluorophosphate, RaNi = Raney Nickel.

Reduction of the nitro group with H_2/RaNi gives the corresponding anilines. In divergent steps, each aniline is then acetylated to yield target compounds (\pm)-**8** and (\pm)-**10**, or converted into its corresponding diazonium salt, which is in turn reduced with H_3PO_2 to afford compounds (\pm)-**9** and (\pm)-**11**.

The interconversion between the two conformations of each molecule is slow on the NMR timescale ($E_a = 65$ – 75 kJ mol^{-1}).^[4a,8] Direct integration of the ^1H and/or ^{19}F resonances for each conformer allows the folding equilibrium to

be determined with well-defined estimations of error. The singlets corresponding to the methyl resonances of each folded state are resolved at 300 MHz, and the identity of each conformer is easily determined by analogy with related compounds (Figure 2).^[4] A summary of the folding energies

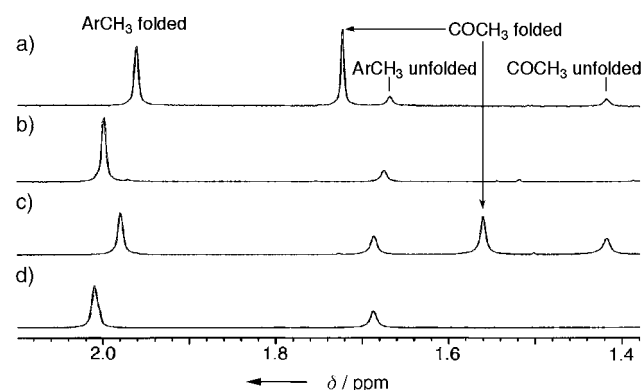


Figure 2. ^1H NMR spectra (methyl region, C_6D_6 , $c = 10 \text{ mM}$) of: a) (\pm)-**8**, b) (\pm)-**9**, c) (\pm)-**10**, d) (\pm)-**11**. The sensitivity of the acetamide COCH_3 resonance to the proximity of the trifluoromethyl group in the folded state is highlighted.

for compounds (\pm)-**8**–(\pm)-**11** in three different solvents is given in Table 1. The application of the double-mutant cycle in the form of Equation (1) provides the incremental free enthalpy for the interaction of the two appended functional groups. The interaction is weak, but measurable, in CDCl_3 ($-1.05 \pm 0.25 \text{ kJ mol}^{-1}$) and C_6D_6 ($-0.85 \pm 0.25 \text{ kJ mol}^{-1}$), while the value is essentially zero in CD_3OD ($-0.10 \pm 0.25 \text{ kJ mol}^{-1}$).

Table 1: Folding free enthalpies for compounds (\pm)-**8**–(\pm)-**11**.

Compound	$\Delta G [\pm 0.12 \text{ kJ mol}^{-1}]^{\text{[a]}}$		
	CDCl_3	C_6D_6	CD_3OD
(\pm)- 8	−2.46	−3.78	−2.88
(\pm)- 9	−1.95	−3.31	−2.37
(\pm)- 10	−0.45	−1.46	−1.72
(\pm)- 11	−1.00	−1.84	−1.31

[a] Determined by integration of signals in the NMR spectra of 10 mM solutions at 298 K. For a complete error analysis, see the Supporting Information.

Two main conditions must be satisfied for a double-mutant cycle to be valid. Firstly, the core must not undergo major structural rearrangements between different members of the cycle. With few degrees of freedom, the scaffold of Wilcox and co-workers derived from the Tröger base is exceptionally well organized. To determine the effect of trifluoromethyl substitution on the folded structure we solved the crystal structure of synthetic precursor (\pm)-**13** (Figure 3).^[9] Comparison with several existing crystal structures^[5] of related torsion-balance molecules shows there is little deviation in the folded edge-to-face geometry throughout the series. The crystal structure of precursor (\pm)-**13** also

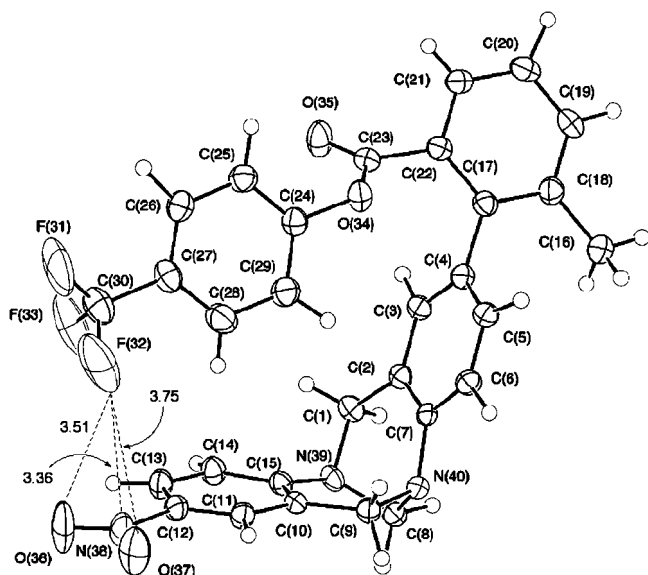


Figure 3. ORTEP plot with ellipsoids at 50% level showing the folded state of (±)-**13**. Distances between F(32) and the atoms of the nitro group are given in Å.

displays the desired perpendicular approach of the appended functional groups (in this case a trifluoromethyl and a nitro group). The trifluoromethyl group experiences no attraction to the adjacent nitro group (see below), and accordingly the close interatomic contacts involving F(32) are greater than the sum of van der Waals radii (Figure 3). Modeling studies on (±)-**8** suggest that the minute (<0.3 Å) vertical adjustment required to bring the fluorine atom close to the plane of the acetamide group can be accommodated, despite the rigidity of the scaffold. However, the modeling study also shows that for (±)-**8** the fluorine atom closest to the acetamide group may not reach its ideal position above the pseudotrigonal axis of the carbonyl unit. Instead, it may lie somewhere above the bond connecting the nitrogen atom to the carbonyl carbon atom, which suggests there is a geometric factor that can account for the slightly weaker than expected value measured for the fluorine–amide interaction.

In the absence of an X-ray structure of (±)-**8**, we turned to NMR studies to provide evidence for the proximity of the trifluoromethyl and acetamide groups in solution. The difference in the chemical shifts observed for the acetamide CH_3 group in the folded and unfolded states is larger for (±)-**8** ($\Delta\delta = 0.30$ ppm) than for control compound (±)-**10** ($\Delta\delta = 0.14$ ppm), which suggests that the acetamide residue experiences decreased shielding in the folded state of (±)-**8** because of the nearby fluorine atoms (Figure 2).

The validity of a double-mutant cycle also rests on the linear additivity of the secondary energy perturbations arising from each functional group mutation. A closer analysis of the data in Table 1 shows that the addition of an acetamide group to the “face” component of the primary edge-to-face interaction (from compound (±)-**11** to (±)-**10**) causes a small unfavorable change in the folding free enthalpy ($\Delta(\Delta G) = +0.4 \text{ kJ mol}^{-1}$ in C_6D_6). In comparison, the addition of a trifluoromethyl group to the “edge” component (from com-

pound (±)-**11** to (±)-**9**) causes a much larger favorable secondary effect ($\Delta(\Delta G) = -1.5 \text{ kJ mol}^{-1}$ in C_6D_6). This difference arises from the acidification of the neighboring *ortho* proton, which increases the strength of the $\text{CH}-\pi$ interaction at the heart of the folded conformation.

To get a better understanding of the effect of the trifluoromethyl group on the core edge-to-face interaction we synthesized a series of compounds in which the “face” component bears different substituents. The folding equilibrium constant of each was determined by using the same method as for compounds (±)-**8**–(±)-**11**, and the entire series was examined using a linear free energy relationship between the folding free enthalpy and the Hammett constants σ_{meta} (Figure 4).^[10] The correlation is excellent ($R^2 > 0.98$), thus

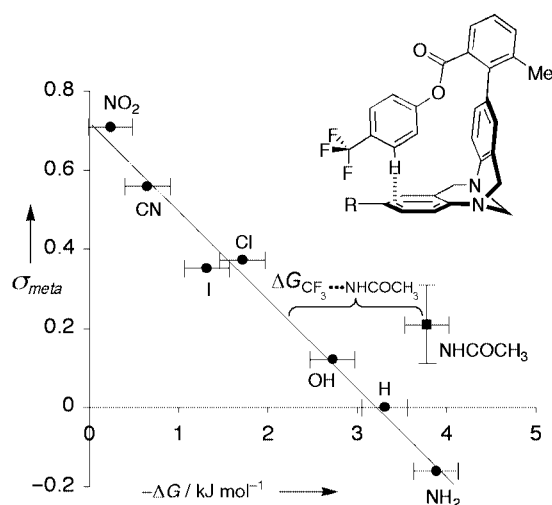


Figure 4. A linear free energy relationship showing substituent effects for edge-to-face interactions in a family of trifluoromethyl-substituted molecules.

showing that the primary $\text{CH}-\pi$ interaction follows a well-behaved continuum that depends on the electronic properties of the “face” component. The sole significant departure from this trend arises for the acetamide-substituted compound (±)-**8**.^[11] This compound is more folded by $1.5 \pm 0.7 \text{ kJ mol}^{-1}$ than substituent effects would predict—this value is similar to that obtained from the double-mutant cycle analysis.

What is the origin of the attraction between the appended trifluoromethyl and acetamide groups? It is unlikely that the amide NH group can be appropriately oriented to donate a hydrogen bond to the fluorine atoms, and the lack of any attraction for the more acidic phenol compound (Figure 4) confirms that this mode of weak hydrogen bonding does not stabilize the folded state.^[1a] It is possible that the model suggested by our previous database findings, in which the electronegative end of the carbon–fluorine dipole interacts favorably with the electropositive carbonyl carbon atom, is operative.^[3a] This dipolar electrostatic model accounts for the absence of any measurable attraction in the polar solvent CD_3OD . Alternatively, one can consider the approach of the unpolarizable, partially negative surface of the trifluoro-

methyl group^[12] close to the polarizable delocalized π cloud of the amide group. Attraction arises in this model from charge-induced dipole and dipole-induced dipole interactions. Arguments against such a model are indicated by a recent study in which a trifluoromethyl group is not attracted by the face of an aryl ring, regardless of the electrostatic potential of the ring.^[13] In the absence of structural information for compound (\pm)-**8**, it is impossible to conclude whether an atom-centered model or a functional-group-scale model of this attraction is more appropriate. We hope that further studies using different fluorine-containing functional groups and different carbonyl functional groups will shed light on this issue.

In summary, we have presented the first efforts to quantify the interactions of organic fluorine with the face of an amide functional group. A novel combination of the torsion balance developed by Wilcox and co-workers with two distinct physical methods—a double-mutant cycle and a linear free energy relationship—provided the initial measurement of an attractive interaction with a value of 0.8–1.5 kJ mol⁻¹ in nonpolar solvents. The effects of fluorination on the hydrophobicity, distribution, metabolism, and pharmacokinetics of potential drug molecules are increasingly well understood.^[14] Model studies such as those presented here help clarify the role played by fluorine atoms in altering the binding affinity and selectivity^[3,14d] of enzyme inhibitors.

Received: May 25, 2004

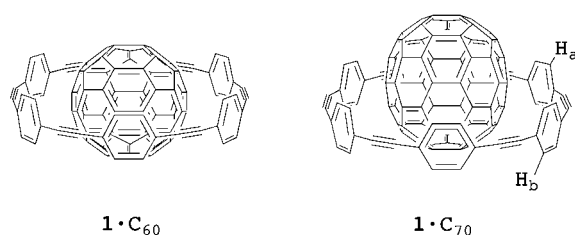
Keywords: amides · fluorine · molecular recognition · noncovalent interactions

- [1] a) J. D. Dunitz, R. Taylor, *Chem. Eur. J.* **1997**, *3*, 89–98; b) *ChemBioChem* **2004**, *5*, 557–726, Special Issue: Fluorine in the Life Sciences.
- [2] B. Kuhn, P. A. Kollman, *J. Am. Chem. Soc.* **2000**, *122*, 3909–3916.
- [3] a) J. A. Olsen, D. W. Banner, P. Seiler, U. Obst-Sander, A. D'Arcy, M. Stihle, K. Müller, F. Diederich, *Angew. Chem.* **2003**, *115*, 2611–2615; *Angew. Chem. Int. Ed.* **2003**, *42*, 2507–2511; b) J. Olsen, P. Seiler, B. Wagner, H. Fischer, T. Tschopp, U. Obst-Sander, D. W. Banner, M. Kansy, K. Müller, F. Diederich, *Org. Biomol. Chem.* **2004**, *2*, 1339–1352; c) J. A. Olsen, D. W. Banner, P. Seiler, B. Wagner, T. Tschopp, U. Obst-Sander, M. Kansy, K. Müller, F. Diederich, *ChemBioChem* **2004**, *5*, 666–675.
- [4] a) S. Paliwal, S. Geib, C. S. Wilcox, *J. Am. Chem. Soc.* **1994**, *116*, 4497–4498; b) E.-I. Kim, S. Paliwal, C. S. Wilcox, *J. Am. Chem. Soc.* **1998**, *120*, 11192–11193.
- [5] The X-ray structures of two related compounds can be found in the Cambridge Structural Database under record numbers PIWYAV and PIWYEZ. Four other related crystal structures are reported in references [7] and [8].
- [6] a) H. Adams, F. J. Carver, C. A. Hunter, J. C. Morales, E. M. Seward, *Angew. Chem.* **1996**, *108*, 1628–1631; *Angew. Chem. Int. Ed. Engl.* **1996**, *35*, 1542–1544; b) F. J. Carver, C. A. Hunter, E. M. Seward, *Chem. Commun.* **1998**, 775–776; c) H. Adams, C. A. Hunter, K. R. Lawson, J. Perkins, S. E. Spey, C. J. Urch, J. M. Sanderson, *Chem. Eur. J.* **2001**, *7*, 4863–4877; d) H. Adams, J.-L. J. Blanco, G. Chessari, C. A. Hunter, C. M. R. Low, J. M. Sanderson, J. G. Vinter, *Chem. Eur. J.* **2001**, *7*, 3494–3503; e) F. J. Carver, C. A. Hunter, P. S. Jones, D. J. Livingstone, J. F. McCabe, E. M. Seward, P. Tiger, S. E. Spey, *Chem. Eur. J.* **2001**, *7*, 4854–4862; f) C. A. Hunter, C. M. R. Low, C. Rotger, J. G. Vinter, C. Zonta, *Proc. Natl. Acad. Sci. USA* **2002**, *99*, 4873–4876; g) C. A. Hunter, C. M. R. Low, J. G. Vinter, C. Zonta, *J. Am. Chem. Soc.* **2003**, *125*, 9936–9937.
- [7] E.-I. Kim, PhD thesis, University of Pittsburgh (USA), **1996**.
- [8] S. Paliwal, PhD thesis, University of Pittsburgh (USA), **1996**.
- [9] Crystals of (\pm)-**13** were grown by vapor diffusion of pentane into a solution of (\pm)-**13** in EtOAc: yellow prism, 0.4 × 0.1 × 0.1 mm; orthorhombic, space group *F2dd*; *a* = 10.36, *b* = 25.37, *c* = 38.17 Å, *V* = 10030 Å³; ρ_{calc} = 1.445 Mg m⁻³; $2\theta_{\text{max}}$ = 60.06°; Mo_{K α} radiation, λ = 0.71073 Å; *T* = 152 K; 7164 independent of 7301 measured reflections *R*_{int} = 0.032, no absorption correction applied (μ = 0.113 mm⁻¹); structure solution using *SIR97* (A. Altomare, M. C. Burla, M. Camalli, G. L. Cascarano, C. Giacovazzo, A. Guagliardi, A. G. G. Moliterni, R. Spagna, *J. Appl. Crystallogr.* **1999**, *32*, 115–119); 5402 reflections with *I* > 3 σ (*I*) refined on $|F^2|$ using *SHELXL-97* (G. M. Sheldrick, *SHELXL97*, Program for the Refinement of Crystal Structures, University of Göttingen, Göttingen (Germany), **1997**); $\Delta/\sigma_{\text{max}}$ = 0.299, $\Delta\rho_{\text{max}}$ = 0.734 e Å⁻³, $\Delta\rho_{\text{min}}$ = -0.482 e Å⁻³; 449 parameters, all hydrogen atom parameters refined; *R*(all) = 0.0953, *R*(gt) = 0.0653, *wR*(ref) = 0.1920, *wR*(gt) = 0.1603. CCDC-239177 contains the supplementary crystallographic data for this paper and is available free of charge from the Cambridge Crystallographic Data Centre (CCDC, 12 Union Road, Cambridge CB2 1EZ (UK); Tel.: (+44) 1223-336-408, Fax: (+44) 1223-336-033, E-mail: deposit@ccdc.cam.ac.uk).
- [10] a) The linear free energy relationships of other edge-to-face systems have been previously reported: F. J. Carver, C. A. Hunter, D. J. Livingstone, J. F. McCabe, E. M. Seward, *Chem. Eur. J.* **2002**, *8*, 2847–2859; b) all values for the Hammett constants σ_{meta} were obtained from: D. H. McDaniel, H. C. Brown, *J. Org. Chem.* **1958**, *23*, 420–427.
- [11] The trifluoromethyl group should experience some repulsion when brought close to the large iodine atom. This effect is evident in the slightly under-folded state of the iodo compound.
- [12] J. C. Biffinger, H. W. Kim, S. G. DiMagno, *ChemBioChem* **2004**, *5*, 622–627.
- [13] H. Adams, S. L. Cockcroft, C. Guardigli, C. A. Hunter, K. R. Lawson, J. Perkins, S. E. Spey, C. J. Urch, R. Ford, *ChemBioChem* **2004**, *5*, 657–665.
- [14] a) D. O'Hagan, H. S. Rzepa, *Chem. Commun.* **1997**, 645–652; b) K. Park, N. R. Kitteringham, P. M. O'Neill, *Annu. Rev. Pharmacol. Toxicol.* **2001**, *41*, 443–470; c) B. E. Smart, *J. Fluorine Chem.* **2001**, *109*, 3–11; d) H.-J. Böhm, D. Banner, S. Bendels, M. Kansy, B. Kuhn, K. Müller, U. Obst-Sander, M. Stahl, *ChemBioChem* **2004**, *5*, 637–643, and references therein.

Supramolecular Dynamics of Cyclic [6]Paraphenyleneacetylene Complexes with [60]- and [70]Fullerene Derivatives: Electronic and Structural Effects on Complexation**

Takeshi Kawase,* Naoki Fujiwara, Masaki Tsutumi, Masaji Oda,* Yutaka Maeda, Takatsugu Wakahara, and Takeshi Akasaka*

Although a variety of host molecules have been studied extensively to elucidate the inclusion phenomena of buckminsterfullerene C₆₀, the supramolecular properties of other fullerenes, including fullerene derivatives, are not yet well understood.^[1–3] In contrast to I_h-symmetrical C₆₀, these other fullerenes are perturbed structurally and electronically. It has been known that the electronic properties of [60]fullerene derivatives correlate well with the electronegativity of the attached atoms.^[4] For example, the attachment of electron-positive silicon atoms considerably increase the electron density of the π systems of [60]fullerene derivatives.^[4,5] Recently we found that the carbon nanoring **1** (cyclic [6]paraphenyleneacetylene) forms stable inclusion complexes with the fullerenes C₆₀, C₇₀, and C₆₁(COOEt)₂ **2** in solution as



[*] Prof. Dr. T. Kawase, N. Fujiwara, M. Tsutumi, Prof. Dr. M. Oda
Department of Chemistry
Graduate School of Science
Osaka University
Toyonaka, Osaka 560-0043 (Japan)
Fax: (+81) 6-6850-5387
E-mail: tkawase@chem.sci.osaka-u.ac.jp
moda@chem.sci.osaka-u.ac.jp

Dr. Y. Maeda,† Dr. T. Wakahara, Prof. Dr. T. Akasaka
Center for Tsukuba Advanced Research Alliance
University of Tsukuba
Tsukuba, Ibaraki 305-8577 (Japan)
Fax: (+81) 29-853-6409
E-mail: akasaka@tara.tsukuba.ac.jp

[†] Present address: Department of Chemistry
Tokyo Gakugei University
Tokyo 184-8501 (Japan)

[**] This work was supported by a Grant-in-Aid for Scientific Research (No. 16655057 and 16350073) from the Ministry of Education, Culture, Sports, Science, and Technology (Japan). We thank Prof. Yoshito Tobe of Osaka University for measurement of FAB-MS spectra and the reviewers for their comments on the manuscript.

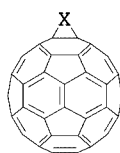
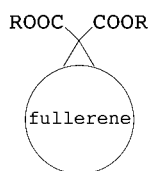
Supporting information for this article is available on the WWW under <http://www.angewandte.org> or from the author.

well as in the solid state.^[2b,6] Dynamic ¹H NMR spectra have revealed the interesting features of these complexes: 1) the Gibbs activation energies for dissociation ($\Delta G^\ddagger_{\text{dis}}$) provide a reliable measure for evaluating the stability of the fullerene complexes and 2) the center of each fullerene is not aligned with the center of **1**, and the activation energy for vibration of a C₇₀ molecule around the center of the cavity is higher than the value for dissociation of the complex, while that of C₆₀ is lower. These results can be attributed to the structural difference between C₆₀ and C₇₀. The inclusion phenomena of C₇₀ have been studied from the viewpoint of purification of fullerenes;^[2] however, the difference in the supramolecular properties of C₆₀ and C₇₀ has not been studied in detail so far. To explore the nature of the curved conjugated systems, and to construct new supramolecular structures based on fullerene derivatives,^[7] we have studied the dynamic behavior of the complexes of **1** with several fullerene derivatives (**3–10**) including the silylated fullerenes **6** and **7**.^[5]

New methanofullerene derivatives **3–5**, **9**, and **10**^[8] were prepared in moderate yields by treating the corresponding malonic esters with fullerenes under the conditions used by Camps and Hirsch.^[9] The formation and regiochemistry of these new compounds were confirmed by transesterification into the known derivatives **2** and **8**.^[10–12]

Fullerene derivatives **3–10** form stable inclusion complexes with **1** in CD₂Cl₂ solutions.^[13] Figure 1 shows the spectral changes of **1·7** and **1·9** as typical examples. Similar to the ¹H NMR spectra of **1·2**,^[6b] the spectrum of **1** shows two singlets of equal intensity at –100°C in the presence of an equal amount of **3–7**, but only one singlet at 30°C. However, one of the aromatic signals of **1** that appears as a singlet in the presence of an equal amount of **8–10** at 30°C begins to broaden at about –20°C, and two relatively small singlets of equal intensity first appear at about –50°C. The major signal finally splits into two singlets of equal intensity at –80°C (Figure 1b). The spectral changes indicate that the methano[70]fullerene complexes should exist in an equilibrium mixture of two diastereomers (A and B) as shown in Scheme 1. The ratio of the isomers varies with the substituents and temperatures (A:B for **1·8** = ca. 9:1, **1·9** = ca. 3:1 and **1·10** = ca. 9:1 at –80°C). The NOE experiments of **1·9** reveal that the major component is isomer A and the minor one is B. The chemical shifts of the inner protons (H_a and H_c) of both isomers resonate at about 0.4 ppm higher field than those of the outer protons (H_b and H_d) because of the anisotropy effect of the relatively flat midsection of C₇₀. Analysis of the NMR spectra provide one ΔG^\ddagger value for **1·3–7** and two ΔG^\ddagger values for **1·8–10** (Table 1).

The $\Delta G^\ddagger_{\text{dis}}$ values of C₆₀ derivatives are in the order **1** > **2–5** > **6** > **7**; the silylated fullerenes **6** and **7** exhibit considerably small values. Fullerenes **6** and **7** have bulky substituents on the silicon atoms, but they have little effect on the complexation, as shown by the ΔG^\ddagger values of **2–5** being almost identical to each other. The results also suggest that the dissociation of the host and guest should occur from the opposite side to the attached group of the fullerene derivatives. Thus, the order of $\Delta G^\ddagger_{\text{dis}}$ values would correspond to the electronic properties of fullerene π systems. It has been known that the silylated C₆₀ derivatives are electron rich,^[4,5]



[60]fullerene

2: R = Et

3: R = CH₂(2,4,6-trimethylphenyl)

4: R = CH₂(4-*t*-butylphenyl)

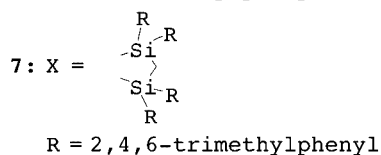
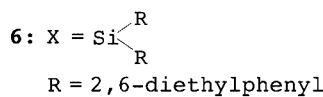
5: R = CH₂[3,5-di(*t*-butyl)phenyl]

[70]fullerene

8: R = Et

9: R = CH₂(2,4,6-trimethylphenyl)

10: R = CH₂[3,5-di(*t*-butyl)phenyl]



to the ΔG^\ddagger value for dissociation from complex A. The higher values are in the order **8** < **9** ~ **10**. Construction of CPK models revealed that the sizable ester groups of **9** and **10** should act as stoppers for **1**; therefore, the interconversion between complex A and B should occur faster than the dissociation of complex B. Thus, the values of about 11.0 kcal mol⁻¹ correspond to the activation energies for the vibration motion of the C₇₀ molecule in the cavity of **1**. On the other hand, the smaller value for **1**·**8** would arise from the simple dissociation of complex B.

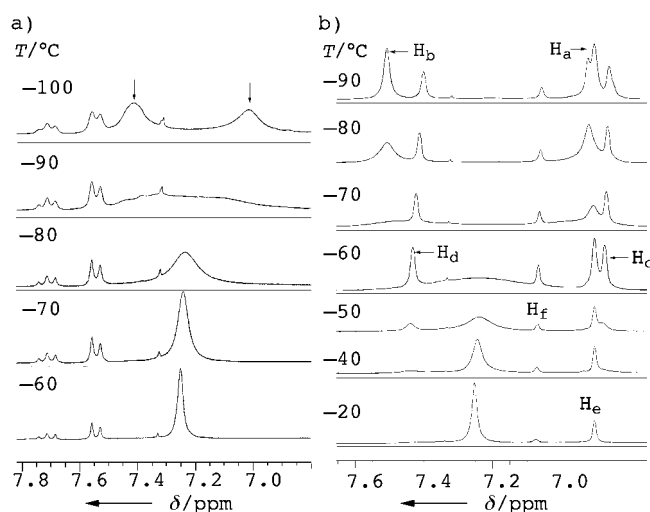


Figure 1. Temperature-variable NMR spectra of an equimolar solution of a) **1** and **7**, and b) **1** and **9**.

and therefore an electronic repulsion between **1** and **6** (or **7**) may play an important role in weak binding between the host and guest. The results are in good agreement with our previous conclusion.^[6b]

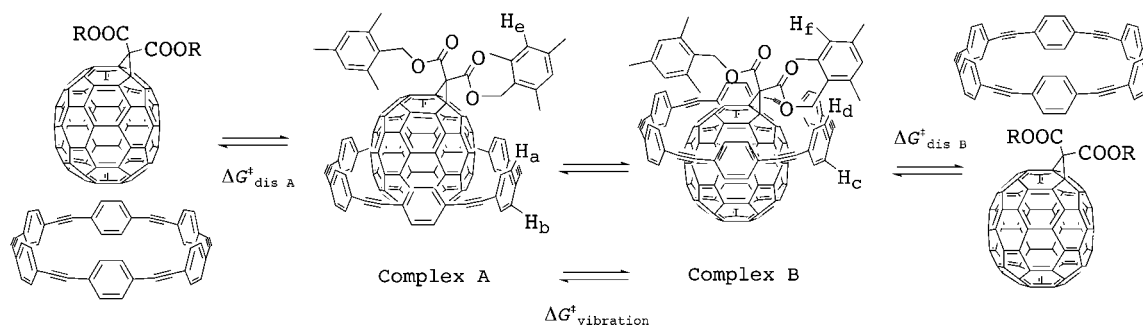
Table 1 also shows two ΔG^\ddagger values for the C₇₀ complexes. The lower values are similar to each other and can be assigned

Table 1: ΔG^\ddagger values of complexes with **1**.^[a]

Guest	ΔG^\ddagger	Guest	ΔG^\ddagger
C ₆₀	9.9 ± 0.2	C ₇₀	9.6 ± 0.2
2	9.4 ± 0.2	8	9.3 ± 0.1
3	9.2 ± 0.2	9	10.1 ± 0.1
4	9.3 ± 0.3	10	9.4 ± 0.1
5	9.3 ± 0.3		11.1 ± 0.2
6	8.8 ± 0.2		9.4 ± 0.1
7	8.5 ± 0.2		11.0 ± 0.2

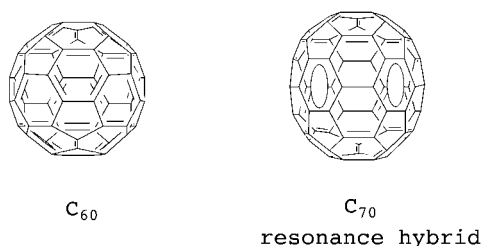
[a] These values were calculated from the observed coalescence temperatures and $\Delta\delta$ values of signals of **1** (kcal mol⁻¹).

The value for the vibration motion of C₇₀ is at least 2.5 kcal mol⁻¹ higher than that of C₆₀ (< 9.0 kcal mol⁻¹). The diameter of the midsection of C₇₀ seems identical to that of C₆₀. This fact means that there is some factor at work beyond just the “size” of the fullerene. This factor appears to be “friction” at the molecular level, since there is a greater surface area of contact between the nanoring and the fullerene in the transition state when the ring passes the equator of C₇₀ than when it passes the equator of C₆₀. A similar phenomenon was recently reported by Rubin et al. for squeezing helium and dihydrogen into and out of a fullerene through a narrow hole.^[14] The present discovery is thus a second example of “molecular friction” and is therefore particularly noteworthy. Moreover, the large barrier as well as



Scheme 1. Schematic representation of the complexation of **1** and methano[70]fullerene derivative, and the model structures of complexes A and B of **1**·**9**.

the relatively large anisotropy effect would also arise from the electronic properties of the relatively flat midsection of C_{70} . The structure of C_{70} can be illustrated as a combination of two corannulenes and [5]paraphenylene on the basis of the Kekulé resonance hybrid.^[15] Thus, C_{70} can be regarded as the smallest member of capped arm-chair [5.5]single-walled carbon nanotubes. The results suggest that there are substantial differences in the electronic properties between C_{60} and carbon nanotubes, and the convex surface of C_{60} would be considerably electron deficient.



Furthermore, complexes B can be regarded as fullerene-based pseudorotaxanes. The current results will open the way to the future construction of new supramolecular structures with novel machine characteristics.

Received: May 12, 2004

Keywords: fullerenes · host–guest systems · inclusion compounds · macrocycles · noncovalent interactions

- [1] a) F. Diederich, M. Gomez-Lopez, *Chem. Soc. Rev.* **1999**, 28, 263–277; b) M. J. Hardie, C. L. Raston, *J. Chem. Soc. Chem. Commun.* **1999**, 1153–1163; c) D. M. Guldi, and P. V. Kamat in *Fullerenes: Chemistry, Physics and Technology* (Ed.: K. M. Kadish and R. S. Ruoff), Wiley, New York, **2000**, and references cited therein.
- [2] For recent studies of host–guest chemistry of C_{70} , see: a) N. Komatsu, *Org. Biomol. Chem.* **2003**, 1, 204–209; b) T. Kawase, K. Tanaka, Y. Seirai, N. Shiono, M. Oda, *Angew. Chem.* **2003**, 115, 5755–5758; *Angew. Chem. Int. Ed.* **2003**, 42, 5597–5600; c) M.-X. Wang, X.-H. Zhang, Q.-Y. Zheng, *Angew. Chem.* **2004**, 116, 856–860; *Angew. Chem. Int. Ed.* **2004**, 43, 838–838.
- [3] For recent studies of the supramolecular chemistry of fullerene derivatives, see: A. Ikeda, S. Nobukuni, H. Udzu, Z. Zhong, S. Shinkai, *Eur. J. Org. Chem.* **2000**, 3287–3293; K. Tashiro, Y. Hirabayashi, T. Aida, K. Saigo, K. Fujiwara, K. Komatsu, S. Sakamoto, K. Yamaguchi, *J. Am. Chem. Soc.* **2002**, 124, 12086–12087; E. Nakamura, H. Isobe, *Acc. Chem. Res.* **2003**, 36, 807–815.
- [4] T. Suzuki, Y. Maruyama, T. Akasaka, W. Ando, K. Kobayashi, S. Nagase, *J. Am. Chem. Soc.* **1994**, 116, 1359–1363.
- [5] T. Akasaka, W. Ando, K. Kobayashi, S. Nagase, *J. Am. Chem. Soc.* **1993**, 115, 1605–1606; T. Akasaka, W. Ando, K. Kobayashi, S. Nagase, *J. Am. Chem. Soc.* **1993**, 115, 10366–10367.
- [6] a) T. Kawase, H. R. Darabi, Y. Seirai, M. Oda, Y. Sarakai, K. Tashiro, *Angew. Chem.* **2003**, 115, 1659–1662; *Angew. Chem. Int. Ed.* **2003**, 42, 1621–1624; b) T. Kawase, H. R. Darabi, K. Tanaka, M. Oda, *Angew. Chem.* **2003**, 115, 1662–1666; *Angew. Chem. Int. Ed.* **2003**, 42, 1624–1628; c) T. Kawase, K. Tanaka, N. Shiono, Y. Seirai, M. Oda, *Angew. Chem.* **2004**, 116, 1754–1756; *Angew. Chem. Int. Ed.* **2004**, 43, 1722–1724.
- [7] For recent examples of supramolecular systems based on fullerene derivatives, see: a) A. M. Cassell, C. C. Lee Asplund, J. M. Tour, *Angew. Chem.* **1999**, 111, 2565–2568; *Angew. Chem. Int. Ed.* **1999**, 38, 2403–2405; b) S. Zhou, C. Burger, B. Chu, M. Sawamura, N. Nagahama, M. Toganoh, U. E. Hackler, H. Isobe, E. Nakamura, *Science* **2001**, 291, 1944–1947; c) M. Sawamura, K. Kawai, Y. Matsuo, K. Kanie, T. Kato, E. Nakamura, *Nature* **2002**, 419, 702–705; d) N. Watanabe, N. Kihara, Y. Furusho, T. Tanaka, Y. Araki, O. Ito, *Angew. Chem.* **2003**, 115, 705–707; *Angew. Chem. Int. Ed.* **2003**, 42, 681–683; e) Y. Nakamura, S. Minami, K. Iizuka, J. Nishimura, *Angew. Chem.* **2003**, 115, 5755–5758; *Angew. Chem. Int. Ed.* **2003**, 42, 3158–3162.
- [8] Selected physical and spectral data: **3**: m.p. > 300 °C; MS (FAB): m/z 720 ($[C_{60}]^+$, 100); 1H NMR ($CDCl_3$, 270 MHz): δ = 2.28 (s, 6H), 2.33 (s, 12H), 5.51 (s, 4H), 6.86 ppm (s, 4H). **4**: m.p. 165–166 °C; MS (FAB): m/z 720 ($[C_{60}]^+$, 100); 1H NMR ($CDCl_3$, 270 MHz): δ = 1.31 (s, 18H), 5.43 (s, 4H), 7.35 (AA'BB', J_{AB} = 8.3 Hz, 4H), 7.39 ppm (AA'BB', J_{AB} = 8.3 Hz, 4H). **5**: m.p. 160–161 °C; MS (FAB): m/z 720 ($[C_{60}]^+$, 100); 1H NMR ($CDCl_3$, 270 MHz): δ = 1.24 (s, 36H), 5.41 (s, 4H), 7.21 (d, J = 1.8 Hz, 4H), 7.34 ppm (t, J = 1.8 Hz, 2H). **9**: black powder, m.p. 170–171 °C; MS (FAB): m/z 1207 ($[M+H]^+$, 43), 840 ($[C_{70}]^+$, 100); 1H NMR (400 MHz, $CDCl_3$): δ = 2.25 (s, 6H), 2.33 (s, 12H), 5.43 (s, 4H), 6.78 ppm (s, 4H). **10**: black powder, m.p. 158–159 °C; MS (FAB): m/z 1347 ($[M+H]^+$, 30), 840 ($[C_{70}]^+$, 100); 1H NMR (400 MHz, $CDCl_3$): δ = 1.30 (s, 36H), 5.42 (s, 4H), 7.27 (d, J = 1.8 Hz, 4H), 7.40 ppm (t, J = 1.8 Hz, 2H).
- [9] X. Camps, A. Hirsch, *J. Chem. Soc. Perkin Trans. I* **1997**, 1595.
- [10] C. Bingel, *Chem. Ber.* **1993**, 115, 9798.
- [11] A. Herrmann, M. Rüttimann, C. Thilgen, F. Diederich, *Helv. Chim. Acta* **1995**, 33, 43.
- [12] J.-P. Bourgeois, L. Echegoyen, M. fibbioli, E. Pretsch, F. Diederich, *Angew. Chem.* **1998**, 110, 2203–2207; *Angew. Chem. Int. Ed. Engl.* **1998**, 37, 2118–2121.
- [13] The absorption spectra of the methanofullerene derivatives showed some variation, but the changes were too small for the measurement of reliable association constants.
- [14] Y. Rubin, T. Jarroson, G.-W. Wang, M. D. Bartberger, K. N. Houk, G. Schick, M. Saunders, R. J. Cross, *Angew. Chem.* **2001**, 113, 1591–1594; *Angew. Chem. Int. Ed.* **2001**, 40, 1543–1546.
- [15] C. Thilgen, A. Herrmann, F. Diederich, *Angew. Chem.* **1997**, 109, 2362–2374; *Angew. Chem. Int. Ed. Engl.* **1997**, 36, 2268–2280; M. S. Meier, G.-W. Wang, R. C. Haddon, C. P. Brock, M. A. Lloyd, J. P. Selegue, *J. Am. Chem. Soc.* **1998**, 120, 2337–2342.

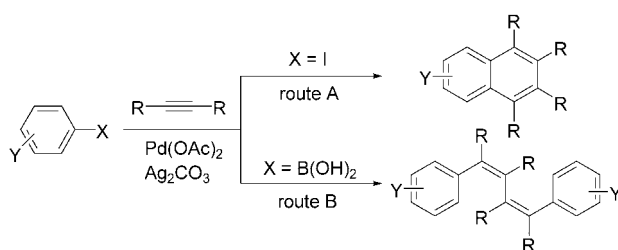
Multicomponent Coupling

Synthesis of Highly Substituted 1,3-Butadienes by Palladium-Catalyzed Arylation of Internal Alkynes**

Tetsuya Satoh, Shinji Ogino, Masahiro Miura,* and Masakatsu Nomura

The transition-metal-catalyzed arylation of alkynes by halogenated or metalated aromatic reagents through carbometallation is a powerful tool for constructing π -conjugated molecules.^[1] Some of these reactions are conducted in the presence of terminators such as hydrogen sources or organometallic reagents to give rise to three-component coupling products. In other cases, the reactions involve cyclometallation in the termination step to yield cyclic compounds.

As examples for the latter case, we reported rhodium-,^[2a] iridium-,^[2b] and palladium-catalyzed^[2c] coupling reactions of alkynes with aryl chlorides or aryl iodides to afford the corresponding indenones or naphthalenes. In the palladium-catalyzed reaction of aryl iodides, the use of silver(i) salts as base was essential for the effective sequential insertion of two alkyne molecules and the successive ring closure (Scheme 1, route A).^[2c,3]



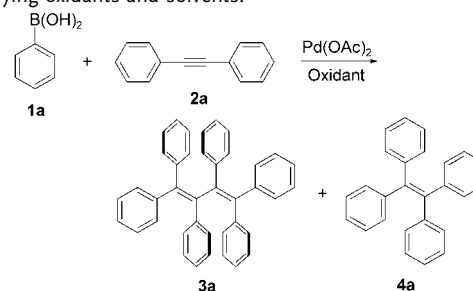
Scheme 1. Coupling of aryl iodides and aryl boronic acids with alkynes.

Silver(i) salts are known to act not only as base, but also as oxidant, in palladium-catalyzed coupling reactions.^[4] Consequently, we have undertaken alkyne arylation reactions with aryl boronic acids instead of aryl iodides under similar conditions to those employed in route A.^[2c] We found that the predominant products were not the expected naphthalenes, but rather 1,4-diaryl-1,3-butadienes by a 2:2 coupling reaction with the formation of three carbon–carbon bonds (Scheme 1, route B). Furthermore, it was revealed that the

addition of iodobenzene as the third component allows the construction of 1,3-dienes that bear two different aryl groups at C1 and C4. Among the related reactions reported to date^[5–12] are the palladium-catalyzed and -promoted arylations of alkynes with aryl tin^[5] and aryl magnesium^[6] reagents, respectively, in each of which 2:1 coupling occurs to give 1,2-diaryl ethenes selectively.^[7] Meanwhile, the palladium-catalyzed three-component coupling of aryl iodides, alkynes, and aryl boronic acids was also examined with KHCO_3 as base.^[11] In this case, 1:1:1 coupling takes place to give 1,2-diaryl ethenes effectively. This contrasts markedly with the present 1:2:1 coupling.^[12]

When phenylboronic acid (**1a**) was treated with diphenylacetylene (**2a**) (1 equiv) in the presence of $\text{Pd}(\text{OAc})_2$ (2.5 mol %) and Ag_2CO_3 (1 equiv) in 1-propanol/ H_2O (9:1) at 120 °C for 0.5 h, 1,1,2,3,4,4-hexaphenyl-1,3-butadiene (**3a**) was formed in 70 % yield along with a minor amount of 1,1,2,2-tetraphenylethene (**4a**) (Table 1, entry 1). The yield of **3a** was somewhat lower in the absence of H_2O , but the formation of **4a** was suppressed (Table 1, entry 2). The reaction also proceeded smoothly in 1,4-dioxane/ H_2O , whereas MeCN/ H_2O and DMF/ H_2O were not effective (Table 1, entries 3–5). Ag_2O and AgOAc could be used as oxidants instead of Ag_2CO_3 , albeit with lower efficiency (Table 1, entries 6 and 7). $\text{Cu}(\text{OAc})_2$ did not catalyze the reaction (Table 1, entry 8).

Table 1. Reaction of phenylboronic acid (**1a**) with diphenylacetylene (**2a**) with varying oxidants and solvents.^[a]



Entry	Oxidant (mmol)	Solvent	Yield [%] ^[b]	
			3a	4a
1	Ag_2CO_3 (2)	1-propanol/ H_2O (9:1)	70 (67)	6
2	Ag_2CO_3 (2)	1-propanol	63	2
3	Ag_2CO_3 (2)	1,4-dioxane/ H_2O (9:1)	65	3
4	Ag_2CO_3 (2)	MeCN/ H_2O (9:1)	14	27
5	Ag_2CO_3 (2)	DMF/ H_2O (9:1)	42	9
6	Ag_2O (2)	1-propanol	59	7
7	AgOAc (4)	1-propanol	40	2
8	$\text{Cu}(\text{OAc})_2$ (2)	1-propanol	6	trace

[a] The reaction of **1a** (2 mmol) with **2a** (2 mmol) was conducted with $\text{Pd}(\text{OAc})_2$ (0.05 mmol) in the solvent (5 cm^3) at 120 °C for 0.5 h. [b] Yield determined by GC. The value in parenthesis indicates the yield of the isolated product.

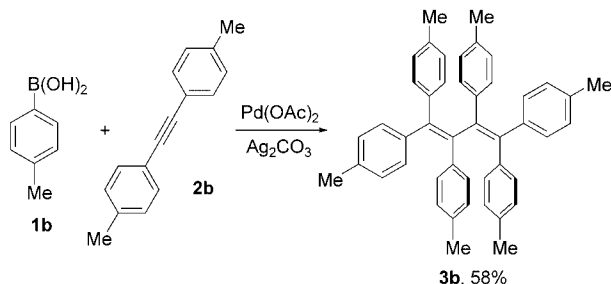
(4-Methylphenyl)boronic acid (**1b**) was treated with **2a** under the conditions used for the reaction in Table 1, entry 1. Although the coupling took place similarly to give 1,4-di(4-methylphenyl)-1,2,3,4-tetraphenyl-1,3-butadiene in 60 % yield, its NMR spectra indicated that it consists of at least

[*] Dr. T. Satoh, S. Ogino, Prof. Dr. M. Miura, Prof. Dr. M. Nomura
Department of Applied Chemistry
Faculty of Engineering, Osaka University
Suita, Osaka 565-0871 (Japan)
Fax: (+81) 6-6879-7362
E-mail: miura@chem.eng.osaka-u.ac.jp

[**] We thank Ms. E. Mochizuki, Osaka University, for X-ray crystal-structure analysis.

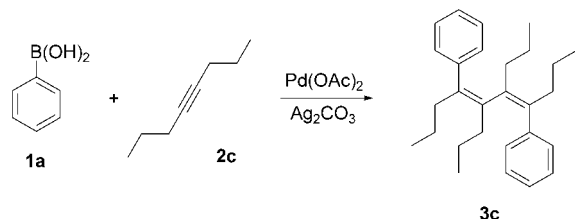
Supporting information for this article is available on the WWW under <http://www.angewandte.org> or from the author.

two geometrical isomers. As expected, the reaction of **1b** with di(4-methylphenyl)acetylene (**2b**) gave 1,1,2,3,4,4-hexa(4-methylphenyl)-1,3-butadiene (**3b**) in 58 % yield as the single major product (Scheme 2). Interestingly, the reaction of **1a**



Scheme 2. Reaction of **1b** with **2b**. Reaction conditions: **1b** (2 mmol), **2b** (2 mmol), Pd(OAc)₂ (0.05 mmol), Ag₂CO₃ (2 mmol), 1-propanol/H₂O (9:1), 120 °C, 0.5 h.

with 4-octyne (**2c**) afforded only (4*Z*,6*Z*)-4,7-diphenyl-5,6-dipropyl-4,6-decadiene (**3c**) without contamination with any other isomers (Scheme 3). The purity and structure of **3c** were

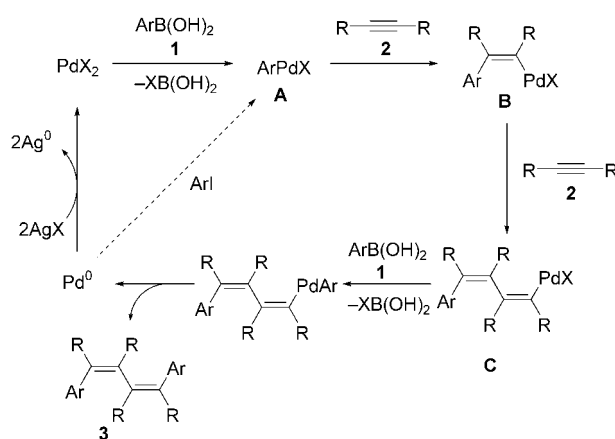


Scheme 3. Reaction of **1a** with **2c**. Reaction conditions: **1a** (2 mmol), **2c** (2 mmol), Pd(OAc)₂ (0.05 mmol), Ag₂CO₃ (2 mmol), 120 °C, 0.5 h. Yield of **3c**: 41 % in 1,4-dioxane/H₂O (9:1); 36 % in 1-propanol.

confirmed by NMR spectroscopic studies and X-ray^[13] crystal-structure analysis (see Supporting Information).^[14]

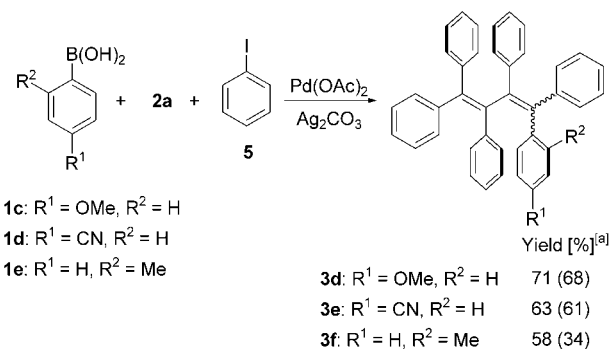
The first step of the present reaction may involve transmetalation to give an aryl palladium species **A** (Scheme 4).^[8,9b–d] Subsequently, the insertion of two alkyne molecules forms a dienylpalladium intermediate **C**. The successive second transmetalation and reductive elimination give 1,4-diarylated 1,3-diene **3**.^[15] The palladium(0) species generated in the last step may be reoxidized by the silver(I) species to close the catalytic cycle.^[16] The result of the reaction of **1b** with **2a** implies that *E/Z* isomerization in **B** and **C** may take place.^[17] However, the reason why it did not occur in the coupling of **1a** with **2c** is not clear.

The intermediate **A** may be generated directly through oxidative addition of aryl halides to a palladium(0) species (dotted arrow in Scheme 4). Thus, we next examined three-component reaction of aryl boronic acids, alkynes, and iodobenzene. When a mixture of (4-methoxyphenyl)boronic acid (**1c**; 1 mmol), **2a** (1 mmol), and iodobenzene (**5**; 1 mmol) was treated in the presence of Pd(OAc)₂ (0.05 mmol) and



Scheme 4. A plausible mechanism for the coupling of aryl boronic acids and aryl iodides with alkynes.

Ag₂CO₃ (1 mmol) in 1-propanol/H₂O at 120 °C for 0.5 h, 1-(4-methoxyphenyl)-1,2,3,4,4-pentaphenyl-1,3-butadiene (**3d**) was produced in 71 % yield (Scheme 5).^[18] Only a minor amount of 1,4-di(4-methoxyphenyl)-1,2,3,4-tetraphenyl-1,3-



Scheme 5. Reaction of **1** with **2a** and **5**. Reaction conditions: **1** (1 mmol), **2a** (1 mmol), **5** (1 mmol), Pd(OAc)₂ (0.05 mmol), Ag₂CO₃ (1 mmol), 1-propanol/H₂O (9:1), 120 °C, 0.5 h. [a] Yield determined by GC (The value in parenthesis indicates the yield of the isolated product).

butadiene (5 %), which may be the result of an oxidative 2:2 coupling of **1c** with **2a**, was detected by GC–MS. The use of the substrates in the ratio **1c/2a/5** = 1:2:1 resulted in a decrease in the yield of **3d** (45 %). (4-Cyanophenyl)- and (2-methylphenyl)boronic acids, **1d** and **1e** respectively, also reacted with **2a** and **5** to afford the corresponding dienes **3e** and **3f**. In these cases, the oxidative 2:2 coupling products were not detected. In each case, the major product **3** was found to consist of two possible isomers (≈ 2:1) by NMR spectroscopic analysis.

In summary, we have demonstrated that the coupling reactions of aryl boronic acids with alkynes in the absence and presence of iodobenzene can be performed with a palladium catalyst and a silver salt to give selectively 2:2 and 1:2:1 coupling products, respectively. These reactions offer a straightforward route to multiarylated butadienes, which are of interest for their photochemical, electrochemical, and biological properties.^[19]

Experimental Section

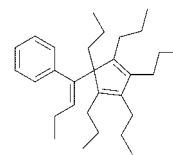
Typical procedure: A mixture of **1** (2 mmol), **2** (2 mmol), Pd(OAc)₂ (0.05 mmol, 11 mg), and Ag₂CO₃ (2 mmol, 550 mg) in 1-propanol/H₂O (9:1, 5 mL) was stirred under N₂ at 120 °C. After 0.5 h, the mixture was cooled to room temperature, Et₂O (100 mL) was added, and insoluble materials were removed by filtration through filter paper. The product was isolated by recrystallization from toluene/hexane and/or column chromatography on silica gel with hexane/EtOAc as eluent. Characterization data of products are summarized in the Supporting Information.

Received: April 22, 2004

Revised: July 26, 2004

Keywords: alkynes · arylation · C–C coupling · homogeneous catalysis · palladium

- [1] a) I. Marek, J. F. Normant in *Metal-catalyzed Cross-coupling Reactions* (Eds.: F. Diederich, P. J. Stang), Wiley-VCH, Weinheim, **1998**, p. 271; b) S. Bräse, A. de Meijere in *Handbook of Organopalladium Chemistry for Organic Synthesis* (Ed.: E. Negishi), Wiley-Interscience, New York, **2002**, p. 1369; c) K. Fagnou, M. Lautens, *Chem. Rev.* **2003**, *103*, 169.
- [2] a) K. Kokubo, K. Matsumasa, M. Miura, M. Nomura, *J. Org. Chem.* **1996**, *61*, 6941; b) T. Yasukawa, T. Satoh, M. Miura, M. Nomura, *J. Am. Chem. Soc.* **2002**, *124*, 12680; c) S. Kawasaki, T. Satoh, M. Miura, M. Nomura, *J. Org. Chem.* **2003**, *68*, 6836.
- [3] M. Kotora, H. Matsumura, G. Gao, T. Takahashi, *Org. Lett.* **2001**, *3*, 3467.
- [4] For examples, see: a) Y. Fujiwara, C. Jia in *Handbook of Organopalladium Chemistry for Organic Synthesis* (Ed.: E. Negishi), Wiley-Interscience, New York, **2002**, p. 2859; b) A. G. Myers, D. Tanaka, M. R. Mannion, *J. Am. Chem. Soc.* **2002**, *124*, 11250; c) L. M. Klingsmith, N. E. Leadbeater, *Tetrahedron Lett.* **2003**, *44*, 765.
- [5] H. Oda, M. Morishita, K. Fugami, H. Sano, M. Kosugi, *Chem. Lett.* **1996**, 811.
- [6] C. Broquet, H. Riviere, *J. Organomet. Chem.* **1982**, *226*, 1.
- [7] In contrast to the reactions with aryl metal reagents, the use of the corresponding methyl metal reagents results in 2:2 coupling to give 1,4-dimethyl-1,3-butadienes.^[5,6]
- [8] For the homocoupling of aryl boronic acids, see: a) K. A. Smith, E. M. Campi, W. R. Jackson, S. Marcuccio, C. G. M. Naeslund, G. B. Deacon, *Synlett* **1997**, 131; b) M. S. Wong, X. L. Zhang, *Tetrahedron Lett.* **2001**, *42*, 4087; c) G. W. Kabalka, L. Wang, *Tetrahedron Lett.* **2002**, *43*, 3067; d) J. P. Parrish, Y. C. Jung, R. J. Floyd, K. W. Jung, *Tetrahedron Lett.* **2002**, *43*, 7899; e) H. Yoshida, Y. Yamaryo, J. Ohshita, A. Kunai, *Tetrahedron Lett.* **2003**, *44*, 1541.
- [9] For Heck-type coupling of aryl boronic acids, see: a) C. S. Cho, S. Uemura, *J. Organomet. Chem.* **1994**, *465*, 85; b) X. Du, M. Suguro, K. Hirabayashi, A. Mori, T. Nishikata, N. Hagiwara, K. Kawata, T. Okada, H. F. Wang, K. Fugami, M. Kosugi, *Org. Lett.* **2001**, *3*, 3313; c) Y. C. Jung, R. K. Mishra, C. H. Yoon, K. W. Jung, *Org. Lett.* **2003**, *5*, 2231; d) M. M. S. Andappan, P. Nilsson, M. Larhed, *Chem. Commun.* **2004**, 218.
- [10] A 1:2 coupling of vinyl boronates with alkynes to give vinylidene cyclopentadienes has been reported.^[9b]
- [11] C. Zhou, D. E. Emrich, R. C. Larock, *Org. Lett.* **2003**, *5*, 1579.
- [12] The use of tetramethyltin, acetylene dicarboxylates, and aryl iodides affords 1:2:1 coupling products: a) R. van Belzen, H. Hoffmann, C. J. Elsevier, *Angew. Chem.* **1997**, *109*, 1833; *Angew. Chem. Int. Ed. Engl.* **1997**, *36*, 1743; b) R. van Belzen, R. A. Klein, H. Kooijman, N. Veldman, A. L. Spek, C. J. Elsevier, *Organometallics* **1998**, *17*, 1812.
- [13] CCDC-236664 contains the supplementary crystallographic data for this paper. These data can be obtained free of charge via www.ccdc.cam.ac.uk/conts/retrieving.html (or from the Cambridge Crystallographic Data Centre, 12, Union Road, Cambridge CB21EZ, UK; fax: (+44) 1223-336-033; or deposit@ccdc.cam.ac.uk).
- [14] In this case, the formation of a small amount of the 1:3 coupling product was observed (1% in dioxane/H₂O, 3% in 1-propanol). The structure of the by-product shown below was unambiguously determined by its 2D NMR spectra and NOE experiments. A similar product is formed by the reaction of iodobenzene with 3-hexyne: G. Wu, A. L. Rheingold, S. J. Gelb, R. F. Heck, *Organometallics* **1987**, *6*, 1941.
- [15] Although the reason why only two molecules of the alkynes are selectively incorporated into the products is not definitive at the present stage, it may be attributed to stabilization of the dienylpalladium intermediate (**C** in Scheme 4) by chelation; see: X. Zeng, Q. Hu, M. Qian, E.-I. Negishi, *J. Am. Chem. Soc.* **2003**, *125*, 13636.
- [16] The silver salts may also promote the transmetalation step: Y. Nishihara, H. Onodera, K. Osakada, *Chem. Commun.* **2004**, 192. A referee for this paper suggested an alternative pathway, in which the vinyl moiety of **B** migrates to Ag^I and thermal decomposition occurs to afford the diene: G. M. Whitesides, C. P. Casey, J. K. Krieger, *J. Am. Chem. Soc.* **1971**, *93*, 1379. It was confirmed that without addition of the silver salt, the stoichiometric reaction of **1a** (0.5 mmol) with **2a** (0.5 mmol) in the presence of Pd(OAc)₂ (0.25 mmol) in 1-propanol/H₂O at 120 °C for 0.5 h gave predominantly diene **3a** in 56% yield, along with a small amount of **4a** (2%). This result indicates that the diene formation can take place on Pd and that the participation of vinyl silver(I) species cannot be excluded.
- [17] G. Dyker, A. Kellner, *Tetrahedron Lett.* **1994**, *35*, 7633. Z,Z Butadienes are also known to undergo thermal isomerization to the corresponding E,E isomers via cyclobutenes: G. A. Doorakian, H. H. Freedman, *J. Am. Chem. Soc.* **1968**, *90*, 5310.
- [18] An alternative pathway initiated by the oxidative cyclization of Pd⁰ species with two alkyne molecules cannot be excluded. Both mechanisms via palladacycle^[12,18a] and acyclic intermediates^[18b] have been proposed for diene synthesis reactions: a) E. Shirakawa, H. Yoshida, Y. Nakao, T. Hiyama, *J. Am. Chem. Soc.* **1999**, *121*, 4290; b) H. Kinoshita, T. Nakamura, H. Kakiya, H. Shinokubo, S. Matsubara, K. Oshima, *Org. Lett.* **2001**, *3*, 2521.
- [19] For recent papers, see: a) S. Hünig, M. Kemmer, H. Wenner, F. Barbosa, G. Gescheidt, I. F. Perepichka, P. Bäuerle, A. Emge, K. Peters, *Chem. Eur. J.* **2000**, *6*, 2618; b) J.-H. Kim, S. Noh, K. Kim, S.-T. Lim, D.-M. Shin, *Synth. Met.* **2001**, *117*, 227; c) T. Suzuki, H. Higuchi, M. Ohkita, T. Tsuji, *Chem. Commun.* **2001**, 1574; d) R. Davis, V. A. Mallia, S. Das, *Chem. Mater.* **2003**, *15*, 1057; e) J. L. Gage, H. A. Kirst, D. O'Neil, B. A. David, C. K. Smith II, S. A. Naylor, *Bioorg. Med. Chem.* **2003**, *11*, 4083.

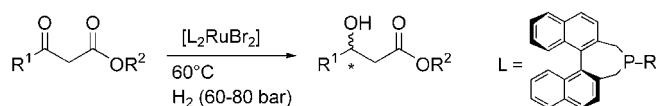


Enantioselective Hydrogenation

Enantioselective Hydrogenation of β -Ketoesters with Monodentate Ligands**

Kathrin Junge, Bernhard Hagemann, Stephan Enthaler, Günther Oehme, Manfred Michalik, Axel Monsees, Thomas Riermeier, Uwe Dingerdissen, and Matthias Beller*

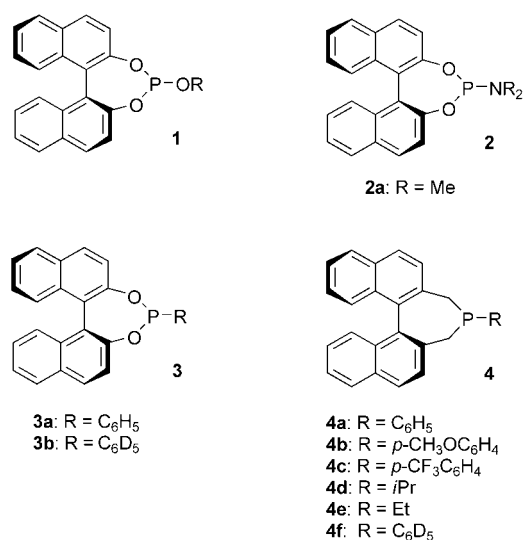
Transition-metal-catalyzed asymmetric reactions offer an efficient and elegant possibility for the synthesis of enantiomerically pure compounds.^[1] Among the different catalytic methods, enantioselective hydrogenations have been used extensively in the last two decades and are likely to provide the most important access to pharmaceutical intermediates.^[2] In this regard, the hydrogenation of β -ketoesters yields chiral β -hydroxyesters, which are useful building blocks for the synthesis of biologically active compounds and natural products (Scheme 1).^[3]



Scheme 1. Catalytic hydrogenation of β -ketoesters **5a–c**.

Pioneering work by Noyori and co-workers established the use of binap as a highly selective ligand for this transformation.^[4] More recent developments of chiral ligands were reported by the groups of Genet,^[5] Weissensteiner and Spindler,^[6] Imamoto,^[7] Knochel,^[8] Zhang,^[9] and others.^[10] Virtually all known ligands that induce significant enantioselectivity in the hydrogenation of β -ketoesters are optically active diphosphines.^[11]

Interestingly, monodentate ligands (Scheme 2) have recently become increasingly important for catalytic asymmetric hydrogenations of amino acid precursors.^[12] In this case, important contributions were made by Reetz et al. (phosphites **1**),^[13] de Vries, Feringa, and co-workers (phos-



Scheme 2. Selection of recently developed monodentate ligands.

phoramidites **2**),^[14] Pringle and co-workers (phosphonites **3**),^[15] and others.^[16] Parallel to the work of Zhang and Chi^[17] and Gladiali and co-workers,^[18] we have introduced new monodentate phosphines based on a 4,5-dihydro-3*H*-dinaphtho[2,1-*c*;1',2'-*e*]phosphepine structure **4**.^[19,20] Similar to phosphites and phosphoramidites, these ligands give high enantioselectivities (up to 95% *ee*) in the hydrogenation of α -dehydroamino acid methyl esters. Despite the more complicated synthesis, these ligands have advantages with regard to stability against water and other nucleophiles under typical reaction conditions. Herein we report the use of **2a**, **3a–b**, and **4a–f** in the hydrogenation of β -ketoesters. So far, these monodentate ligands have not been used for the synthesis of chiral β -hydroxyesters.

Initial studies of the influence of reaction conditions were carried out with methyl acetoacetate (**5a**) as substrate and our standard ligand 4-phenyl-4,5-dihydro-3*H*-dinaphtho[2,1-*c*;1',2'-*e*]phosphepine (**4a**). Typically the catalytic reactions were run in methanol as solvent in the presence of [Ru(cod)-(methallyl)₂] (1 mol %) and the ligand (2 mol %).

For full conversion within a reasonable time, the reactions had to be run under pressure (60 bar) at 60–80°C (Table 1, entries 4,6). We were pleased to find that under these conditions, good enantioselectivities (up to 84% *ee*) were achieved. Notably, the best result was obtained at a relatively high temperature (80°C; Table 1, entry 6), which is advantageous in terms of the increased rate and selectivity of the reaction.

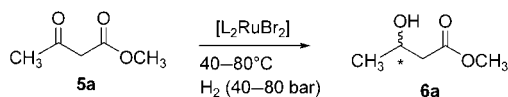
Next we focused our attention on the influence of different ligands in the hydrogenation of methyl acetoacetate (**5a**). Apart from the phenyl ligand **4a**, the *p*-methoxyphenyl derivative **4b**, the *p*-trifluoromethylphenyl derivative **4c**, the isopropyl derivative **4d**, the ethyl derivative **4e**, and the deuterated phenyl derivative **4f** were used (Table 2). All ligands **4a–f** were prepared in good yields by straightforward Grignard reaction of 1-chloro-4,5-dihydro-3*H*-dinaphtho[2,1-*c*;1',2'-*e*]phosphepine with the corresponding aryl and alkyl halides.^[21] Furthermore, monodentate state-of-the-art ligands

[*] Dr. K. Junge, Dipl.-Ing. B. Hagemann, S. Enthaler, Prof. Dr. G. Oehme, Prof. Dr. M. Michalik, Prof. Dr. M. Beller
Leibniz-Institut für Organische Katalyse
Universität Rostock e.V. (IfOK)
Buchbinderstrasse 5–6, 18055 Rostock (Germany)
Fax: (+49) 381-46693-24
E-mail: matthias.beller@ifok.uni-rostock.de

Dr. A. Monsees, Dr. T. Riermeier, Dr. U. Dingerdissen
Degussa AG, Rodenbacher Chaussee 4
63457 Hanau (Wolfgang) (Germany)

[**] The authors thank M. Heyken, H. Baudisch, Dr. W. Baumann, S. Buchholz, and Dr. C. Fischer (all IfOK) for analytical and technical support. Generous financial support for this project from the state Mecklenburg-Vorpommern (Landesforschungsschwerpunkt), the Fonds der Chemischen Industrie, and the Bundesministerium für Bildung und Forschung (BMBF) is gratefully acknowledged.

Table 1: Hydrogenation of **5a** in the presence of [Ru(cod)(methallyl)₂]/**4a**.^[a]



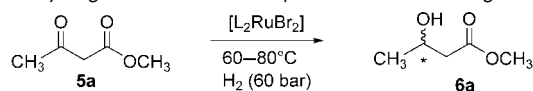
Entry	Solvent	<i>t</i> [h]	<i>p</i> [bar]	<i>T</i> [°C]	Conversion [%]	<i>ee</i> [%]
1	MeOH	16	20	60	25	53 (<i>R</i>)
2	MeOH	16	40	60	46	68 (<i>R</i>)
3	MeOH	16	60	60	51	74 (<i>R</i>)
4	MeOH	16	80	60	95	69 (<i>R</i>)
5	MeOH	16	60	40	28	34 (<i>R</i>)
6	MeOH	16	60	80	95	84 (<i>R</i>)
7	acetone	16	60	60	4	5 (<i>R</i>)
8	toluene	16	60	60	1	2 (<i>S</i>)
9	THF	16	60	60	< 1	8 (<i>R</i>)

[a] Conditions: solvent (20 mL), **5a** (3.8 mmol), [Ru(cod)(methallyl)₂] (38 μmol), **4a** (76 μmol).

from other groups such as (*R*)-monophos (**2a**) and the Pringle ligand **3a** were applied.^[22]

Importantly, in the presence of the monodentate phosphonate and phosphoramidite, only low enantioselectivity was observed (10–28% *ee*; Table 2, entries 1,2). More sur-

Table 2: Hydrogenation of **5a** in the presence of different ligands.^[a]



Entry	Ligand	<i>t</i> [h]	<i>T</i> [°C]	Conversion [%]	<i>ee</i> [%]
1	2a	16	80	85	10 (<i>S</i>)
2	3a	16	60	> 99	28 (<i>S</i>)
3	3b	16	60	> 99	56 (<i>S</i>)
4	4a	16	80	95	84 (<i>R</i>)
5	4b	48	80	98	93 (<i>R</i>)
6	4b	16	80	> 99	92 (<i>R</i>)
7	4c	16	80	> 99	51 (<i>R</i>)
8	4d	16	60	> 99	60 (<i>R</i>)
9	4e	16	60	96	10 (<i>R</i>)
10	4e	16	80	95	64 (<i>R</i>)
11	4f	16	80	95	59 (<i>R</i>)

[a] Conditions: methanol (20 mL), **5a** (3.8 mmol), [Ru(cod)(methallyl)₂] (38 μmol), **4a–f**, **2a**, or **3a, b** (76 μmol), 60 bar.

prisingly, the structurally analogous phosphonate **3a** gave a significantly lower enantioselectivity than **4a**. In this case, the formal exchange of two oxygen atoms by sterically similar CH₂ groups led to an increase in enantioselectivity from 28% (*S*) to 84% (*R*) (Table 2, entries 2,4). This clearly demonstrates the importance of electronic effects for achieving high selectivity in the test reaction. These findings inspired us to study the effect of variations of substituents on the phenyl group in **4a** more closely.

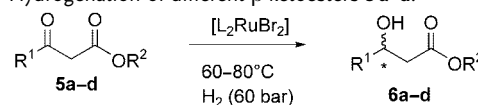
Among the different ligands, **4b** gave the highest enantioselectivity (up to 93% *ee*) (Table 2, entry 5). Only the introduction of electron-donating (*p*-methoxy) groups at C4 of the phenyl ring led to a slight increase in selectivity. One of the smallest structural variations possible within the ligand is

the exchange of hydrogen by deuterium atoms. We were curious to see if this minor change also influences the enantioselectivity. Thus, the pentadeuterated ligand **4f** was prepared in good yield by a similar method to that described above. A comparison of **4a** and **4f** under identical reaction conditions led to (*R*)-methyl 3-hydroxybutyrate in > 95% yield with 84 and 59% *ee*, respectively.

This is, to the best of our knowledge, the first example of an isotope influence on the stereoselectivity of catalytic asymmetric reactions. Because of this finding, we also compared the hydrogenation reaction in the presence of **3a** and its deuterated analogue **3b**. In this case, we noted even an increase in the selectivity upon substitution of the hydrogen atoms with deuterium atoms (28 versus 56% *ee*, respectively; Table 2, entries 2,3). As the mechanism for the ruthenium-catalyzed asymmetric hydrogenation of β-ketoesters is still vague,^[23] we do not have a clear rational explanation for the observed change in *ee* values. We believe that the phenyl ring also coordinates to the metal center during the catalytic cycle and therefore affects the outcome of the reaction. A comparison of catalytic reactions with the deuterated ligand **4f** in the presence of methanol (**5a**: 64% *ee*) and deuterated methanol (**5a**: 73% *ee*) demonstrates that deuteration of the solvent also influences the selectivity of the model reaction. Finally we applied ligands **4a, b, f** in the hydrogenation of different β-ketoesters (Table 3).

In general, all substrates were hydrogenated with excellent conversion and yield. The best selectivities were obtained

Table 3: Hydrogenation of different β-ketoesters **5a–d**.^[a]



Entry	4	5	R ¹	R ²	<i>t</i> [h]	<i>T</i> [°C]	Yield [%]	<i>ee</i> [%]
1	a	a	Me	Me	16	80	95	84 (<i>R</i>)
2	a	b	Et	Me	16	80	97	86 (<i>R</i>)
3	a	c	CH ₂ Cl	Et	24	80	81	13 (<i>S</i>)
4	a	d	C ₆ H ₅	Et	16	80	> 99	73 (<i>S</i>)
5	b	a	Me	Me	16	80	97	92 (<i>R</i>)
6	b	a	Me	Me	8	100	99	93 (<i>R</i>)
7	b	a	Me	Me	8	120	96	93 (<i>R</i>)
8	b	b	Et	Me	16	80	99	94 (<i>R</i>)
9	b	b	Et	Me	8	100	99	95 (<i>R</i>)
10	b	b	Et	Me	8	120	99	94 (<i>R</i>)
11	b	c	CH ₂ Cl	Et	16	80	98	6 (<i>S</i>) ^[b]
12	b	c	CH ₂ Cl	Et	8	100	73	23 (<i>S</i>) ^[b]
13	b	c	CH ₂ Cl	Et	8	120	77	38 (<i>S</i>) ^[b]
14	b	d	C ₆ H ₅	Et	16	80	> 99	94 (<i>S</i>) ^[b]
15	b	d	C ₆ H ₅	Et	8	100	99	95 (<i>S</i>) ^[b]
16	b	d	C ₆ H ₅	Et	8	120	99	91 (<i>S</i>) ^[b]
17	f	a	Me	Me	48	60	98	64 (<i>R</i>)
18	f	a	Me	Me	16	80	95	59 (<i>R</i>)
19	f	b	Et	Me	16	80	99	78 (<i>R</i>)
20	f	c	CH ₂ Cl	Et	16	80	97	9 (<i>S</i>) ^[b]
21	f	d	C ₆ H ₅	Et	16	80	> 99 ^[c]	64 (<i>S</i>) ^[b]

[a] Conditions: solvent (20 mL), **5** (3.8 mmol), [Ru(cod)(methallyl)₂] (38 μmol), **4a, b, f** (76 μmol) 60 bar; methanol was used as a solvent for methyl esters and ethanol for ethyl esters. [b] Owing to the change in priority of the substituents, the configuration of the stereocenter is changed. [c] Conversion; reaction run at 80 bar pressure of H₂.

by using the 4-methoxyphenyl-substituted dinaphthophosphine ligand **4b** at temperatures of 100–120 °C. Whereas 3-oxobutyrate and 3-oxopentanoate gave enantioselectivities of 93–95 % *ee*, the 4-chloro-3-oxobutyrate led only to 38 % *ee*.^[24] The phenyl-substituted β -ketoester gave up to 95 % *ee*. In agreement with the previous findings, the deuterated ligand **4f** showed a significantly different selectivity than that of ligand **4a** in every hydrogenation. Hence, the observed deuterium effect on the selectivity seems to be general for this type of reaction.

In conclusion, we have shown for the first time that monodentate phosphine ligands can be used efficiently for the ruthenium-catalyzed hydrogenation of β -ketoesters. The catalysts are remarkably temperature-tolerant: Enantioselectivities of up to 95 % *ee* were possible, even at 100–120 °C. A comparison of **4a** with structurally related **2a** and **3a** demonstrates the superiority of phosphines over phosphites, phosphonates, and phosphoramidites. Interestingly, the use of deuterated phenyl compounds **3b** and **4f** led to the observation of an isotope effect on the enantioselectivity of the reaction, which may be of interest to asymmetric reactions in general.

Experimental Section

Unless otherwise noted, all chemicals are commercially available and were used without further purification. The β -ketoesters **5a–d** were distilled under an argon atmosphere. Products were fully characterized (b.p., IR, MS, elemental analysis, NMR).

General procedure: in situ preparation of ruthenium catalyst:^[5] [Ru(cod)(methallyl)₂] (0.038 mmol) and ligand **2a**, **3**, or **4** (0.076 mmol) were placed in a dried 25-mL Schlenk tube under an argon atmosphere, and anhydrous and degassed acetone (5 mL) was added. After the dropwise addition of a solution of HBr in methanol (0.33 mL, 0.29 M) a brown precipitate was formed. Stirring was then continued over 30 min, the solvent was removed in vacuo, and methanol (20 mL) or ethanol (for substrates **5c** and **5d**) was added.

Asymmetric hydrogenation of β -ketoesters **5a–d**: Catalytic hydrogenation experiments were carried out in a Parr stainless-steel autoclave (100 mL). In a typical experiment, the autoclave was charged with a mixture of the catalyst [L₂RuBr₂] prepared in situ and **5a** (3.80 mmol) in methanol (20 mL) under a stream of argon. The autoclave was stirred under 40–80 bar pressure of hydrogen at 60–120 °C for 16–48 h. The autoclave was cooled to room temperature, and the hydrogen was released. The reaction mixture was filtered over silica gel, and the enantiomeric excess was determined by GC (Lipodex E) or HPLC (Chiracel OD-H). Most of the hydrogenation products have been described previously. Methyl 3-hydroxybutyrate (**6a**): GC (25 m Lipodex E, 95 °C isothermal): *t_r* = 4.9 (S), 5.7 min (R); methyl 3-hydroxyvalerate (**6b**): GC (25 m Lipodex E, 85 °C isothermal): *t_r* = 10.9 (S), 11.6 min (R); ethyl 3-hydroxy-4-chlorobutyrate (**6c**): GC (25 m Lipodex E, 95 °C isothermal): *t_r* = 20.4 (R), 20.6 min (S); ethyl 3-hydroxy-3-phenylpropionate (**6d**): HPLC (OD-H, hexane/ethanol 95:5, 0.5 mL min⁻¹), *t_r* = 10.1 (S), 11.5 min (R).

6a: B.p. 63–66 °C/10 Torr; IR (KBr): $\tilde{\nu}$ = 3439 br, 3140 w, 2974 w, 2967 m, 2937 m, 1737 br vs, 1439 vs, 1410 s, 1377 s, 1298 s, 1269 s, 1195 s, 1178 s, 1170 w, 1126 w, 1089 w, 1082 w, 946 s, 886 s, 862 m, 719 m, 598 m, 593 s, 475 cm⁻¹ w; MS (70 eV): *m/z* (%): 103 (16) [M–Me]⁺, 100 (3) [M–OH]⁺, 87 (16) [M–OMe]⁺, 85 (5), 74 (50), 71 (26), 61 (12), 59 (10) [COOCH₃]⁺, 45 (55) [CHOHCH₃]⁺, 43 (100), 42 (26), 31 (14) [CH₃O]⁺, 29 (17), 15 (21); ¹H NMR (400 MHz, CDCl₃): δ = 4.10–4.06 (m, 1 H; CH), 3.58 (s, 3 H; OCH₃), 3.30 (s, 1 H; OH), 2.34 (m, 2 H; CH₂), 1.11 ppm (d, *J* = 6.3 Hz, 3 H; CH₃); ¹³C NMR (100.6 MHz, CDCl₃): δ = 173.2 (CO), 64.2 (C–OH), 51.7 (CH₃O), 43.0 (CH₂),

22.7 ppm (CH₃); elemental analysis: calcd (%) for C₅H₁₀O₃ (118.17): C 59.15, H 8.54; found: C 59.01, H 8.59.

Received: April 1, 2004

Keywords: β -ketoesters · asymmetric catalysis · hydrogenation · ruthenium

- [1] a) R. Noyori, *Asymmetric Catalysis in Organic Synthesis*, Wiley, New York, **1994**; b) *Transition Metals for Organic Synthesis* (Eds.: M. Beller, C. Bolm), Wiley-VCH, Weinheim, **1998**; c) *Comprehensive Asymmetric Catalysis* (Eds.: E. N. Jacobsen, A. Pfaltz, H. Yamamoto), Springer, Berlin, **1999**.
- [2] Reviews: a) M. McCarthy, P. J. Guiry, *Tetrahedron* **2001**, *57*, 3809–3843; b) X. Zhang, *Enantiomer* **1999**, *4*, 541–555; c) S. Gladiali, D. Fabbri, *Chem. Ber.* **1997**, *130*, 543–554; d) F. Lagasse, H. B. Kagan, *Chem. Pharm. Bull.* **2000**, *48*, 315–324.
- [3] S. Servi, *Synthesis* **1990**, 1.
- [4] a) R. Noyori, T. Ohkuma, M. Kitamura, H. Takaya, N. Sayo, H. Kumobayashi, S. Akutagawa, *J. Am. Chem. Soc.* **1987**, *109*, 5856–5858; b) M. Kitamura, T. Ohkuma, S. Inoue, N. Sayo, H. Kumobayashi, S. Akutagawa, T. Ohta, H. Takaya, R. Noyori, *J. Am. Chem. Soc.* **1988**, *110*, 629–631.
- [5] a) O. Labeeuw, D. Blanc, P. Phansavath, V. Ratovelomanana-Vidal, J. P. Genet, *Eur. J. Org. Chem.* **2004**, 2352–2358; b) V. Ratovelomanana-Vidal, C. Girard, R. Touati, J. P. Tranchier, B. Ben Hasine, J. P. Genet, *Adv. Synth. Catal.* **2003**, *345*, 261–274; c) C. Girard, J. P. Genet, M. Bulliard, *Eur. J. Org. Chem.* **1999**, 2937–2942; d) P. Bertus, P. Phansavath, V. Ratovelomanana-Vidal, J. P. Genet, A. R. Touati, B. Ben Hasine, *Tetrahedron: Asymmetry* **1999**, *10*, 1369–1372; e) J. P. Genet, V. Ratovelomanana-Vidal, M. C. Cano De Andrade, X. Pfister, P. Guerreiro, J. Y. Lenoir, *Tetrahedron Lett.* **1995**, *36*, 4801–4804; f) J. P. Genet, C. Pinel, V. Ratovelomanana-Vidal, S. Mallart, X. Pfister, L. Bischoff, M. C. Cano De Andrade, S. Darses, C. Galopin, J. A. Laffitte, *Tetrahedron: Asymmetry* **1994**, *5*, 675–690.
- [6] T. Sturm, W. Weissensteiner, F. Spindler, *Adv. Synth. Catal.* **2003**, *345*, 160–164.
- [7] a) K. V. L. Crepy, T. Imamoto, *Adv. Synth. Catal.* **2003**, *345*, 79–101; b) T. Yamamoto, N. Taya, M. Kawada, T. Huang, T. Imamoto, *Tetrahedron Lett.* **1999**, *40*, 2577–2580.
- [8] T. Ireland, K. Tappe, G. Grossheimann, P. Knochel, *Chem. Eur. J.* **2002**, *8*, 843–852.
- [9] Y.-G. Zhou, W. Tang, W.-B. Wang, W. Li, X. Zhang, *J. Am. Chem. Soc.* **2002**, *124*, 4952–4953.
- [10] a) A. Hu, H. L. Ngo, W. Lin, *Angew. Chem.* **2004**, *116*, 2555–2558; *Angew. Chem. Int. Ed.* **2004**, *43*, 2501–2504; b) R. ter Halle, B. Colasson, E. Schulz, M. Spagnol, M. Lemaire, *Tetrahedron Lett.* **2000**, *41*, 643–646; c) V. Blandin, J.-F. Carpentier, A. Mortreux, *Tetrahedron: Asymmetry* **1998**, *9*, 2765–2768; d) P. J. Pye, K. Rossen, R. A. Reamer, R. P. Volante, P. J. Reider, *Tetrahedron Lett.* **1998**, *39*, 4441–4444; e) M. J. Burk, T. G. P. Harper, K. S. Kalberg, *J. Am. Chem. Soc.* **1995**, *117*, 4423–4424.
- [11] D. J. Ager, S. A. Laneman, *Tetrahedron: Asymmetry* **1997**, *8*, 3327–3355.
- [12] For a recent review on monophosphines, see: a) I. V. Komarov, A. Börner, *Angew. Chem.* **2001**, *113*, 1237–1240; *Angew. Chem. Int. Ed.* **2001**, *40*, 1197–1200; for some successful previous examples, see: b) F. Guillen, J.-F. Fiaud, *Tetrahedron Lett.* **1999**, *40*, 2939–2942; c) W. S. Knowles, M. J. Sabacky, B. D. Vineyard, *J. Chem. Soc. Chem. Commun.* **1972**, 10–11; d) J. D. Morrison, R. E. Burnett, A. M. Aguiar, C. J. Morrow, C. Phillips, *J. Am. Chem. Soc.* **1971**, *93*, 1301–1303; e) M. J. Burk, J. E. Feaster, R. L. Harlow, *Tetrahedron: Asymmetry* **1991**, *2*, 569–592; f) A.

- Marinetti, F. Mathey, I. Ricard, *Organometallics* **1993**, *12*, 1207–1212.
- [13] a) M. T. Reetz, T. Sell, *Tetrahedron Lett.* **2000**, *41*, 6333–6336; b) M. T. Reetz, G. Mehler, *Angew. Chem.* **2000**, *112*, 4047–4049; *Angew. Chem. Int. Ed.* **2000**, *39*, 3889–3891; c) M. T. Reetz, G. Mehler, G. Meiswinkel, T. Sell, *Tetrahedron Lett.* **2002**, *43*, 7941–7943; d) M. T. Reetz, G. Mehler, G. Meiswinkel, T. Sell, *Angew. Chem.* **2003**, *42*, 814–817; *Angew. Chem. Int. Ed.* **2003**, *42*, 790–793; e) M. T. Reetz, G. Mehler, *Tetrahedron Lett.* **2003**, *44*, 4593–4596.
- [14] a) L. A. Arnold, R. Imobos, A. Manoli, A. H. M. de Vries, R. Naasz, B. Feringa, *Tetrahedron* **2000**, *56*, 2865–2878; b) M. van den Berg, A. J. Minnaard, E. P. Schudde, J. van Esch, A. H. M. de Vries, J. G. de Vries, B. L. Feringa, *J. Am. Chem. Soc.* **2000**, *122*, 11539–11540; c) A. J. Minnaard, M. van den Berg, E. P. Schudde, J. van Esch, A. H. M. de Vries, J. G. de Vries, B. Feringa, *Chim. Oggi* **2001**, *19*, 12–13; d) D. Pena, A. J. Minnaard, J. G. de Vries, B. L. Feringa, *J. Am. Chem. Soc.* **2002**, *124*, 14552–14553; e) M. van den Berg, R. M. Haak, A. J. Minnaard, A. H. M. de Vries, J. G. de Vries, B. L. Feringa, *Adv. Synth. Catal.* **2002**, *344*, 1003–1007; f) M. van den Berg, A. J. Minnaard, R. M. Haak, M. Leeman, E. P. Schudde, A. Meetsma, B. L. Feringa, A. H. M. de Vries, C. E. P. Maljaars, C. E. Willans, D. Hyett, J. A. F. Boogers, H. J. W. Henderickx, J. G. de Vries, *Adv. Synth. Catal.* **2003**, *345*, 308–323; g) D. Pena, A. J. Minnaard, A. H. M. de Vries, J. G. de Vries, B. L. Feringa, *Org. Lett.* **2003**, *5*, 475–478.
- [15] a) C. Claver, E. Fernandez, A. Gillon, K. Heslop, D. J. Hyett, A. Martorell, A. G. Orpen, P. G. Pringle, *Chem. Commun.* **2000**, 961–962; b) A. Martorell, R. Naasz, B. L. Feringa, P. G. Pringle, *Tetrahedron: Asymmetry* **2001**, *12*, 2497–2499.
- [16] M. Ostermeier, J. Prieß, G. Helmchen, *Angew. Chem.* **2002**, *114*, 625–628; *Angew. Chem. Int. Ed.* **2002**, *41*, 612–617.
- [17] Y. Chi, X. Zhang, *Tetrahedron Lett.* **2002**, *43*, 4849–4852.
- [18] S. Gladiali and co-workers, unpublished results; see also: S. Gladiali, A. Dore, D. Fabbri, O. De Lucchi, M. Manassero, *Tetrahedron: Asymmetry* **1994**, *5*, 511–514.
- [19] a) K. Junge, G. Oehme, A. Monsees, T. Riermeier, U. Dingerdissen, M. Beller, *Tetrahedron Lett.* **2002**, *43*, 4977–4980; b) K. Junge, G. Oehme, A. Monsees, T. Riermeier, U. Dingerdissen, M. Beller, *J. Organomet. Chem.* **2003**, *675*, 91–96.
- [20] These ligands are commercially available from Degussa AG/Catalyst and Initiators.
- [21] Importantly, an alternative synthesis of ligand **4a** by double metallation of 2,2'-dimethylbinaphthyl with *n*-butyl lithium in the presence of tetramethylethylenediamine (TMEDA) and direct quenching with commercially available dichlorophenylphosphane gave the corresponding ligand with only 80–95% purity (impurities: lithium salts and organic by-products). This decreased purity led to a lower enantioselectivity in the reduction of **5a** and the product was obtained with opposite absolute configuration. We do not know currently which impurity is responsible for the different outcome. In this respect, it is also interesting that the addition of lithium and magnesium salts influences the enantioselectivity of the reduction of **5a** in the presence of **4a** by 5–10%.
- [22] We also tried phosphites similar to the Reetz ligand in β -ketoester hydrogenation, but these ligands did not prove to be stable under our conditions (80–120°C, methanol).
- [23] A. Wolfson, I. F. J. Vankelecom, S. Geresh, P. A. Jacobs, *J. Mol. Catal. A* **2003**, *198*, 39–45.
- [24] In the case of **5c**, dehydrochlorination was observed as a side reaction at higher temperature.

A Linear Free Energy Relationship for Gas-Solid Interactions: Correlation between Surface Rate Constant and Diffusion Coefficient of Oxygen Tracer Exchange for Electron-Rich Perovskites

Rotraut Merkle, Joachim Maier,* and
Henny J. M. Bouwmeester

Reactivity and transport properties can be traced back to materials parameters and control parameters. As far as the concentrations of electronic and ionic charge carriers are concerned, partial pressures P of the components, temperature T , and dopant content C are the most important control parameters. While their influence is often well-understood on a phenomenological level, the understanding of materials parameters such as enthalpies and entropies of reaction or activation usually requires an atomistic analysis. Phenomenological relationships connecting these parameters are very rare and, if established, extremely useful. The most prominent examples stem from organic solution chemistry, for example, the effect of substrate substitution on aromatic reactions (cf. the Hammett equation) or the Brønsted catalysis relation.^[1] These equations make use of a linear correlation between free activation enthalpy and free reaction enthalpy. Specifically, when enthalpies instead of free enthalpies are considered, this may be termed an Evans–Polanyi relationship.^[2] A few attempts to verify linear (free) energy relationships in solid-state chemistry have been reported,^[3] but without deeper insight into the mechanistic details or a conclusive correlation between data and model. Here we unambiguously demonstrate the validity of such a linear (free) energy relationship for inorganic solid-state reactions.

The interaction of gaseous O_2 with oxides is of technical relevance as well as of fundamental interest, and tracer experiments are an important tool for its investigation. The oxygen incorporation comprises the surface reaction from O_2 to oxide ions in the first bulk layer, and subsequent diffusion of oxide ions within the bulk. A surprising and strongly debated relationship between the experimentally determined effective surface rate constant \bar{k}^* and oxygen tracer diffusion coefficient D^* was found for the family of $(La_{1-x}Sr_x)(Mn_{1-y}Co_y)O_{3-z}$, $(La_{1-x}Sr_x)(Fe_{1-y}Co_y)O_{3-z}$, and $(Sm_{1-x}Sr_x)CoO_{3-z}$.

[*] Dr. R. Merkle, Prof. Dr. J. Maier
Max-Planck-Institut für Festkörperforschung
Heisenbergstrasse 1
70569 Stuttgart (Germany)
Fax: (+49) 711-689-1722
E-mail: sofia.weiglein@fkf.mpg.de

Prof. Dr. H. J. M. Bouwmeester
Department of Science and Technology &
MESA+ Research Institute for Nanomaterials
University of Twente (The Netherlands)



Supporting information for this article (containing details of the kinetic treatment: derivation of Eqs. (9) and (12) and discussion of alternative mechanisms) is available on the WWW under <http://www.angewandte.org> or from the author.

perovskites (Figure 1).^[4,5] To a good approximation, both quantities were reported to be related by the power law given in Equation (1). Assuming Arrhenius-type expressions for \bar{k}^*

$$\log \bar{k}^* \cong a + b \log D^* \quad (a \cong -1, b \cong 0.5) \quad (1)$$

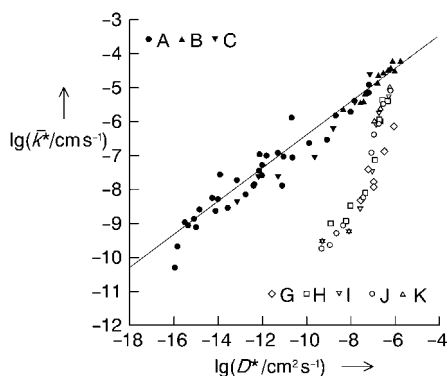


Figure 1. Correlation of the effective surface rate constant \bar{k}^* with the oxygen tracer diffusion coefficient D^* , reprinted from ref. [5] with permission from Elsevier, copyright 1999. A = (La,Sr)(Mn,Co)O_{3- δ} , B = (Sm,Sr)(Co)O_{3- δ} , C = (La,Sr)(Co,Fe)O_{3- δ} (electron-rich transition metal perovskites); G = La_{0.9}Sr_{0.1}Ga_{0.8}Mg_{0.2}O_{2.85}, H = Zr_{0.85}Y_{0.15}O_{1.925}, I = Ce_{0.90}Gd_{0.1}O_{1.95}, J = Zr_{0.81}Y_{0.19}O_{1.905} single crystal, K = Ce_{0.69}Gd_{0.31}O_{1.845} single crystal (electron-poor electrolyte materials). The line represents the \bar{k}^* – D^* correlation for samples A–C, as discussed in the text, and has a slope of $b = 0.5$.

and D^* , this implies an interrelation of the effective activation energies as well as the prefactors [Eqs. (2), (3)].

$$E_{k^*} = b E_{D^*} \quad (2)$$

$$\log k_0^* = a + b \log D_0^* \quad (3)$$

The data points in Figure 1 comprise variations in temperature, oxygen partial pressure, and composition of the perovskite phase. What makes Equation (1) so interesting and simultaneously so hard to understand is that its range of validity covers all materials within a given class and hence implies a variation of materials parameters such as reaction enthalpies. Figure 1 also shows data for electron-poor electrolyte materials (G–K): They deviate strongly from the line discussed below, indicating that these correlations hold only for families of materials with similar mechanistic parameters.

A detailed treatment of effective rate constants has previously been given that showed how \bar{k}^* ($\varepsilon = *$ (tracer), δ (chemical experiment), Q (electrical experiment)) can be obtained as a function of the control parameters P , C , and T .^[6] The temperature is essentially introduced through the microscopic rate constant of the rate determining step (rds) and through the mass action constants K_q of the fast reactions that have to be coupled in the kinetic scheme. Close to equilibrium and for a given parameter window, \bar{k}^* is given by Equation (4); \bar{A}_0^* is the equilibrium exchange rate, $\langle k \rangle$ denotes the geometric means of the forward and backward rate constants (subscript s indicates “surface”). The expression for D^* is,

$$\bar{k}^* \propto \bar{A}_0^*(\text{rds}) = \langle k \rangle_{\text{rds}}(T) \sum_q K_q^{\gamma_q}(T) C^M_s P^{N_s} \quad (4)$$

under Brouwer and Boltzmann conditions, determined with Equation (5), with σ and u being the conductivity and mobility of the mobile defect (the subscript ∞ refers to “bulk”).

$$D^* \propto \sigma_{\infty} = u(T) \sum_r K_r^{\gamma_r}(T) C^M_{\infty} P^{N_r} \quad (5)$$

For a given mechanistic scheme, these equations allow one to derive directly \bar{k}^* versus D^* upon variation of p , C , or T . For a given material, a linear $\log \bar{k}^*$ – $\log D^*$ relationship follows automatically if Arrhenius-type expressions hold for \bar{k}^* and D^* individually. If, however, the material is varied, as is the case here, the question becomes more delicate because then the enthalpy and entropy parameters in the above equations become variables themselves. A linear relationship as given in references [4,5] (see Figure 1) betrays the validity of further more subtle features of the materials. Since the mapping of $D^* \leftrightarrow \bar{k}^*$ involves various mass action “constants” and kinetic “constants”, a family relationship between reaction free enthalpies and activation free enthalpies may be anticipated.

Here we will show that the relationship given in Equation (6) correctly explains Figure 1 (δ denotes the compositional variation within the materials family). We also dem-

$$\delta \Delta H_{\text{rds}}^+ = -0.5 \delta \Delta H_{\text{ox}}^0 \quad (6)$$

onstrate that Equation (6) can be mechanistically corroborated and even tested by independent results. Since the entropies are mostly structurally determined and do not significantly change from material to material within the family under consideration, Equation (6) also represents a free energy relationship (owing to the small and constant mechanical work term, we do not differentiate between energy and enthalpy).

The tracer diffusion in the bulk follows a vacancy mechanism [Eq. (7), f = correlation factor = 0.69^[4]], where

$$D^* = f \frac{[V_{\text{O}}]}{c_{\text{O}}} D_{V_{\text{O}}} = 0.69 \frac{[V_{\text{O}}]}{c_{\text{O}}} D_{V_{\text{O}}} e^{-\Delta H_{V_{\text{O}}}^+ / k_B T} \quad (7)$$

the vacancy jump activation enthalpy $H_{V_{\text{O}}}^+$ of about 0.9 eV (= oxide ion jump activation enthalpy) and the prefactor D_{O} are approximately constant for all the samples within the materials family considered.^[7,8,4] The material- and temperature-dependent vacancy concentration $[V_{\text{O}}]$ can be calculated from the overall oxygen incorporation reaction [Eq. (8)]

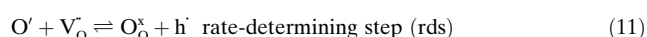
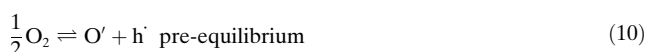


with a reaction enthalpy ΔH_{ox}^0 that is typically negative. Insertion of the mass action constant corresponding to the reaction in Equation (8) into Equation (7) shows that the overall D^* activation enthalpy includes contributions from vacancy formation and migration [Eq. (9), see the Supporting Information for details].

$$E_{D*} = -\Delta H_{\text{ox}}^0 + \Delta H_{\text{V}}^+ \quad (9)$$

Now let us select a reasonable mechanism for the surface reaction that operates for all the materials considered (it will be outlined later that within certain limits the details of the mechanism do not affect the validity of this rationale). Whereas for electron-poor materials the electron-transfer steps might be crucial for the overall rate, this is not likely to be the case for the electron-rich materials under regard. (The term “electron-rich” refers to the presence of excess electrons or to the presence of regular, but easily transferable electrons, and hence also includes the p-type conductors.^[9]) Although no direct evidence for the presence of adsorbed atomic oxygen species such as O^- exists for the materials considered here (largely due to experimental limitations), desorption measurements indicate their formation above 400 °C.^[10] On ZnO and SnO_2 the ratio of O^- to O_2^- increases with increasing temperature.^[11] Oxygen permeation measurements under surface limited conditions yield a reaction order of $\frac{1}{2}$ for O_2 (see e.g. $\text{SrCo}_{0.8}\text{Fe}_{0.2}\text{O}_{3-z}$ ^[12] and $\text{La}_{0.5}\text{Sr}_{0.5}\text{Ga}_{0.2}\text{Fe}_{0.8}\text{O}_{3-z}$ ^[13]), which indicates that only atomic oxygen species are involved in the rate determining step. The relationship in Equation (2) between the effective activation energies of \bar{k}^* and D^* and the mechanism of the diffusion process resulting in Equation (9) imply a significant contribution $b\Delta H_{\text{V}}^+$ to the effective activation energy E_{k^*} of the surface reaction, which stems from the V_{O} jump activation enthalpy. This may be seen as an indication that a V_{O} site exchange is involved in the rds, as already qualitatively concluded in ref. [5].

Hence, we assume that the reaction rate is determined by the ion transfer step, that is, by the incorporation of ionized atomic oxygen into the vacancy. The degree of ionization of surface oxygen is definitely less than two but more than zero, so that we adopt the mechanism given by Equations (10) and (11) (Kröger–Vink nomenclature, see the Supporting Information for other mechanisms). The resulting tracer exchange



rate is given by Equation (12) (see reference [6] for the

$$\bar{k}^* = \frac{1}{c_{\text{O}}} \sqrt{\bar{k}^+ \bar{k}^- [\text{O}'] [\text{V}_{\text{O}}] [\text{h}']} = \left(\frac{\bar{k}_0 [\text{h}']}{c_{\text{O}}} \right) e^{-\Delta \bar{H}^+ / k_{\text{B}} T} \quad (12)$$

method of derivation and the Supporting Information for details; all concentrations refer to equilibrium, $c_{\text{O}} = \text{oxide ion concentration} \approx \text{constant}$, \bar{k} and \bar{k}^- denote the forward and backward rate constants and may also include built-in electrical fields). The overall activation enthalpy approximately equals the activation enthalpy \bar{H}^+ of the backward reaction in reaction (11) [Eq. (13)].

$$E_{k^*} \approx \Delta \bar{H}^+ \quad (13)$$

As all data are measured in a limited $p\text{O}_2$ range (typically $10^{-3} \text{ bar} \leq p\text{O}_2 \leq 1 \text{ bar}$), the variation of \bar{k}^* and D^* with $p\text{O}_2$

can be neglected (typically $\bar{k}^*, D^* \propto (p\text{O}_2)^n$ where $|n| \leq 0.5$). Consequently, we are left with variations of temperature and sample composition. For Equation (1) to hold, the effective activation energies must fulfil the condition resulting from inserting Equations (9) and (13) into Equation (2) with $b \approx 0.5$ [Eq. (14), see the Supporting Information for the treatment of the prefactors k_0^*, D_0^*].

$$\Delta \bar{H}^+ = b(\Delta H_{\text{V}}^+ - \Delta H_{\text{ox}}^0) = 0.45 \text{ eV} - 0.5 \Delta H_{\text{ox}}^0 \quad (14)$$

This is indeed a linear relationship between an activation enthalpy and a reaction enthalpy. The importance of Equation (14) lies in the fact that $\delta \Delta \bar{H}^+ = -0.5 \delta \Delta H_{\text{ox}}^0$, that is, the slope (0.5) and the intercept (0.45 eV) do not perceptibly change when the material is varied within the family under concern. According to Equation (13), $\Delta \bar{H}^+$ is approximately identical to the effective activation energy of \bar{k}^* , and we arrive at the experimentally testable prediction that E_{k^*} varies linearly with the overall oxygen incorporation enthalpy ΔH_{ox}^0 when the sample composition varies. Figure 2 displays this

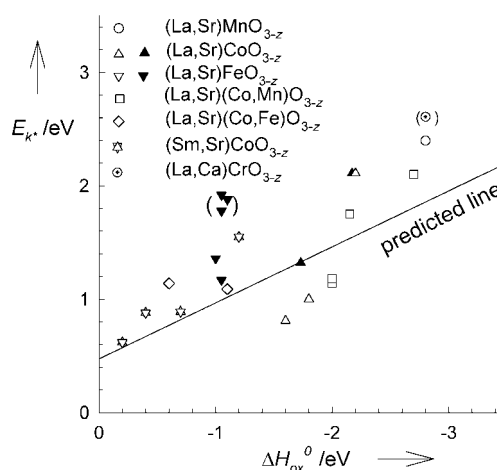


Figure 2. Correlation of the experimentally determined activation energy of surface exchange E_{k^*} and the overall oxygen incorporation enthalpy ΔH_{ox}^0 . Closed symbols: experimental ΔH_{ox}^0 data available, open symbols: ΔH_{ox}^0 estimated either from experimental D^* data and $\Delta H_{\text{V}}^+ = 0.9 \text{ eV}$ [see Eq. (9)] or from experimental data for materials with a slightly different composition. The line represents the predicted linear free energy relationship [Eq. (14)]. The data are from references [4, 5, 16] as well as [7, 17] ((La,Sr)CoO_{3-z}), [7, 18] ((La,Sr)FeO_{3-z}), [19] ((La,Sr)(Co,Fe)O_{3-z}), and [20, 21] ((La,Ca)CrO_{3-z}).

correlation (and includes materials of the same family that are not contained in Figure 1). The experimental E_{k^*} data tend to be slightly above the line predicted from Equation (14), which might be due to the small temperature dependence of the electronic charge carriers [see Eq. (12)]. Keeping in mind the experimental uncertainties (the typical error of E_{k^*} is 0.2 eV;^[5] for (La,Ca)FeO_{3-z} the data points in parentheses stem from similar sample compositions, but were measured by a different group^[7] as well as the approximations made in deriving Equation (14), the agreement is satisfactory (the deviation of (La,Ca)CrO_{3-z} might be due to the comparably strong d electron localization^[14]).

The main point is now the interpretation of Equation (14) on a mechanistic level. First, we have to emphasize again that such a relationship can only be valid for a class of materials for which the same mechanism is operative. The contributions of ΔH_{V}^0 and ΔH_{ox}^0 to $\Delta \bar{H}^{\ddagger}$ can be rationalized as follows: After the fast preequilibrium reaction (10), the activation energy of the rds has to be overcome (Figure 3); the rds is the transfer of

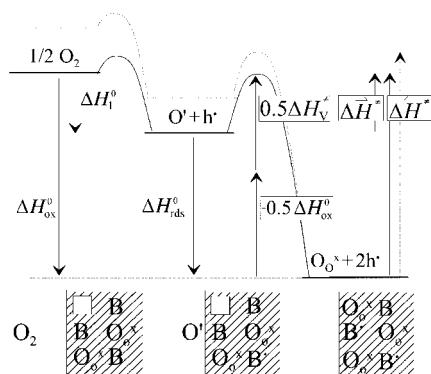


Figure 3. Top: Enthalpy diagram of oxygen incorporation according to reactions (10) and (11). The decomposition of $\Delta \bar{H}^{\ddagger}$ into contributions from ΔH_{V}^0 and ΔH_{ox}^0 is based on Equation (14). The dashed lines indicate the variation of the material, which results in a coupled increase of ΔH_{ox}^0 and $\Delta \bar{H}^{\ddagger}$ (for clarity the enthalpy profiles are normalized such that the final state exhibits the same energy level for both cases). Bottom: mechanistic picture of the reaction.

adsorbed O' into a vacancy with the simultaneous oxidation of the valence band ion (the B cation in Figure 3). Since the transferred atomic oxygen species is not a fully charged oxide ion, but has a charge between -1 and -2 (being approximately constant among the materials considered), and since the transfer occurs between the surface and the first bulk layer, we can assume that the threshold is reduced compared to bulk diffusion. Therefore, the contribution of the ionic motion to the overall activation enthalpy $\Delta \bar{H}^{\ddagger}$ is not $\Delta H_{\text{V}}^{\ddagger}$, but only a constant fraction $b \Delta H_{\text{V}}^{\ddagger}$. The actual numerical value $b \approx 0.5$ as given by the experimentally observed correlation is consistent with this picture. When passing through the rds, the reaction enthalpy of this step, ΔH_{rds}^0 , is released, and a fraction γ of it (the exact value depends on the precise location of the transition state on the reaction coordinate) is involved in the activation process (i.e., up to the transition state) and contributes to $\Delta \bar{H}^{\ddagger}$. Since for ΔH_{rds}^0 it can be estimated that $|\Delta H_{\text{rds}}^0| \leq |\Delta H_{\text{ox}}^0|$, the experimentally observed contribution of $-0.5 \Delta H_{\text{ox}}^0$ to $\Delta \bar{H}^{\ddagger}$ [Eq. (14)] implies a value of $\gamma \geq 0.5$ and thus a transition state closer to the intermediate state O' than to the final state O_O^{*}. The numerical prefactors that account for the ΔH_{V}^0 and the ΔH_{ox}^0 contributions to $\Delta \bar{H}^{\ddagger}$ are probably not completely identical, but the experimentally observed $\bar{k}^* - D^*$ correlation shows that $b \approx 0.5$ is indeed a good approximation.

Assuming as a first approximation that the oxygen site exchange is not influenced by the variation in composition (as

supported by the observed constancy of ΔH_{V}^0), the variation of $\Delta \bar{H}^{\ddagger}$ with composition refers to the partial electron transfer from the B cation to the oxygen in the transition state (the degree of intermediate charge is roughly independent of sample composition).^[15] Finally, the constancy of the parameter b reflects the validity of the same mechanism for all materials considered as well as the chemical and structural similarity of the family members. An important feature of the analysis is that the activation energy of vacancy migration also contributes to the surface reaction, which is attributed to the fact that the latter involves not only an electron transfer but also represents an ion site exchange. In the Supporting Information, two other hypothetical mechanisms are discussed which fulfil the prerequisites (atomic oxygen species as well as V_O^{*} in the rds). While one of these mechanisms is rather improbable, the other leads to similar conclusions. This demonstrates the validity of the given arguments irrespective of minor mechanistic details.

To summarize, we have shown that the astonishing $\bar{k}^* - D^*$ correlation for electron-rich perovskites can be understood on the basis of a linear free enthalpy relationship for gas–solid reactions. This relationship assumes a constant coupling between the \bar{k}^* activation enthalpy and the oxidation reaction enthalpy (constant with regard to variation among the materials family considered). This point was independently tested by referring to kinetic and thermodynamic data from the literature. The treatment demonstrates the usefulness of linear free energy relationships, which are state of the art for organic solution chemistry, for inorganic solid-state reactions.

Received: January 23, 2004

Revised: June 21, 2004

Keywords: charge transfer · defect chemistry · diffusion · kinetics · oxygen exchange

- [1] See textbooks of organic chemistry, for example, J. March, *Advanced Organic Chemistry*, Wiley, New York, **1992**, p. 258 and p. 278.
- [2] See, for example, B. P. Roberts, A. J. Steel, *J. Chem. Soc. Perkin Trans. 2* **1994**, 2155–2162.
- [3] a) R. Kapoor, S. T. Oyama, *J. Mater. Res.* **1997**, *12*, 474–479; b) D. A. Sverjensky, *Nature* **1992**, *358*, 310–313.
- [4] J. A. Kilner, R. A. De Souza, I. C. Fullarton, *Solid State Ionics* **1996**, *86*, 703–709.
- [5] R. A. De Souza, J. Kilner, *Solid State Ionics* **1999**, *126*, 153–161.
- [6] a) J. Maier, *Solid State Ionics* **1998**, *112*, 197–228; b) J. Maier, *Solid State Ionics* **2000**, *135*, 575–588.
- [7] T. Ishigaki, S. Yamauchi, K. Kishio, J. Mizusaki, K. Fueki, *J. Solid State Chem.* **1988**, *73*, 179–187.
- [8] J. Mizusaki, I. Yasuda, J. Shimoya, S. Yamauchi, F. Fueki, *J. Electrochem. Soc.* **1993**, *140*, 467–471.
- [9] T. Ohtani, K. Kuroda, K. Matsugami, D. Katoh, *J. Eur. Ceram. Soc.* **2000**, *20*, 2721–2726.
- [10] S. C. Chang, *J. Vac. Sci. Technol.* **1980**, *17*, 366–369.
- [11] M. Iwamoto, Y. Yoda, N. Yamazoe, T. Selyama, *J. Phys. Chem.* **1978**, *82*, 2564–2570.
- [12] H. J. M. Bouwmeester, H. Kruidhof, A. J. Burggraf, *Solid State Ionics* **1994**, *72*, 185–194.
- [13] S. Kim, S. Wang, X. Chen, Y. L. Wang, N. Wu, A. Ignatiev, A. J. Jacobson, B. Abeles, *J. Electrochem. Soc.* **2001**, *147*, 2398–2406.

- [14] D. P. Karim, A. T. Aldred, *Phys. Rev. B* **1979**, *20*, 2255–2263.
- [15] This fractional change in the rds activation energy with variation in the reagent–product energy difference bears some reminiscence to the Butler–Volmer equation even though the latter only makes a statement on the electrical field distribution.
- [16] R. A. De Souza, J. A. Kilner, *Solid State Ionics* **1998**, *106*, 175–187.
- [17] a) J. Mizusaki, Y. Mima, S. Yamauchi, K. Fueki, H. Tagawa, *J. Solid State Chem.* **1989**, *80*, 102–111; b) M. H. R. Lankhorst, H. J. M. Bouwmeester, H. Verweij, *J. Solid State Chem.* **1997**, *133*, 555–567; c) T. Ishigaki, S. Yamauchi, J. Mizusaki, K. Fueki, H. Tamura, *J. Solid State Chem.* **1984**, *54*, 100–107.
- [18] a) J. Mizusaki, M. Yoshihiro, S. Yamauchi, K. Fueki, *J. Solid State Chem.* **1985**, *58*, 257–266; b) J. E. ten Elshof, M. H. R. Lankhorst, H. J. M. Bouwmeester, *J. Electrochem. Soc.* **1997**, *144*, 1060–1066.
- [19] a) J. A. Lane, S. J. Benson, D. Waller, J. A. Kilner, *Solid State Ionics* **1999**, *121*, 201–208; b) S. Carter, A. Selcuk, R. J. Chater, J. Kajda, J. A. Kilner, B. C. H. Steele, *Solid State Ionics* **1992**, *53*, 597–605.
- [20] J. Mizusaki, S. Yamauchi, K. Fueki, A. Ishikawa, *Solid State Ionics* **1984**, *12*, 119–124.
- [21] I. Yasuda, K. Ogasawara, M. Hishinuma, *J. Am. Ceram. Soc.* **1997**, *80*, 3009–3012.

different use of this kind of molecule can be envisaged, which relies on one of their typical properties: when a molecular machine moves as a consequence of an external stimulus, an overall rearrangement of the molecular system takes place and its shape changes dramatically. According to the well-established lock-and-key concept, the shape of a molecule, and in particular the shape of a cavity inside a large molecule, is connected to its ability to act as a selective receptor, that is, its ability to recognize a complementary substrate. Provided that only one of the possible shapes assumed by a given molecular machine presents a cavity in which a chosen substrate can selectively fit, molecular machines could advantageously enter the field of molecular recognition by acting as receptors with a useful implemented function: to recognize and bind a given substrate only when the proper external stimulus is applied. Few examples have been published that consist of relatively simple photoisomerizable molecules, in which the stimulus required to make the system change towards the correct shape and recognize a substrate is provided by light.^[3]

Herein we report the first example of a new kind of molecular machine capable of molecular recognition. The stimulus required by the system for changing towards the correct shape for selective binding can be provided by the substrate itself. Accordingly, the molecular machine described in this paper behaves as a receptor, which merges the advantages of the lock-and-key principle (selectivity) with those of its adaptive behavior (activation in the presence of substrates). Moreover, the drastic color change associated with movement and recognition events turns this system in a very efficient colorimetric sensor.

Macrocyclic LH_4 ^[4] contains two couples of polydentate compartments capable of binding Cu^{2+} ions, and comprises two diamide–diamine (DADA) tetradentate and two pyridine–diamine (PDA) tridentate binding sets, which share the four secondary amino groups.

Potentiometric titrations carried out with standard base, first on a solution containing LH_4 and excess acid, then on a solution containing LH_4 , two equivalents of Cu^{2+} ions, and excess acid^[5] followed by nonlinear least-squares treatment of the obtained electrode potential versus added base data,^[6] allowed us to calculate the protonation constants of LH_4 and the formation constants of the copper-containing species present in solution in the pH range of 2–12 (see caption of Figure 1).^[7] From these data, a distribution diagram for the $\text{LH}_4/2\text{Cu}^{2+}$ system was drawn (Figure 1a). Subsequently, coupled pH-metric and spectrophotometric titrations were carried out. Two distinct colors and types of band are observed as a function of pH. A band centered at around 660 nm, responsible for the blue color of the solutions, starts to form at pH 3 and predominates without dramatic changes up to pH 9.5. At this pH, the intensity of the band at 660 nm decreases relative to the band centered at 515 nm then disappears leaving a purple–pink solution. The interpretation is straightforward: if the molar absorbance at 660 and 515 nm versus pH profiles are superimposed onto the distribution diagram (Figure 1a, filled and empty triangles, respectively): the relatively short wavelength band at 515 nm correlates with the $[\text{Cu}_2(\text{L})]$ neutral complex (form **a** in Scheme 1)^[8] and

Molecular Devices

A Sleeping Host Awoken by Its Guest: Recognition and Sensing of Imidazole-Containing Molecules Based on Double Cu^{2+} Translocation inside a Polyaza Macrocyclic**

Luigi Fabbrizzi,* Francesco Foti, Stefano Patroni, Piersandro Pallavicini,* and Angelo Taglietti*

Recently, a lot of attention has been focused on artificial molecular machines,^[1] in part for their potential to help understand and mimic natural biological systems but mainly from the perspective of developing molecular devices capable of information processing and data storage.^[2] However, a

[*] Prof. L. Fabbrizzi, Dr. F. Foti, Dr. S. Patroni, Dr. P. Pallavicini, Dr. A. Taglietti
Dipartimento di Chimica Generale
Università di Pavia
viale Taramelli 12, 27100 Pavia (Italy)
Fax: (+39) 0382-528-544
E-mail: luigi.fabbrizzi@unipv.it
psp@unipv.it
angelo.taglietti@unipv.it

[**] This work was financially supported by MIUR (Progetto “Dispositivi Supramolecolari”) and by EU (RT Network Molecular Level Devices and Machines, contract HPRN-CT-2000-00029).

Supporting information for this article is available on the WWW under <http://www.angewandte.org> or from the author.

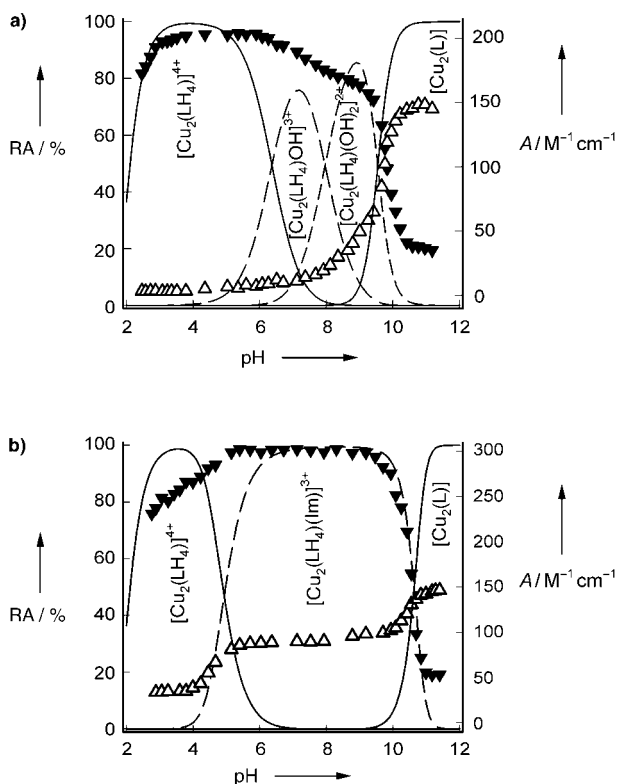
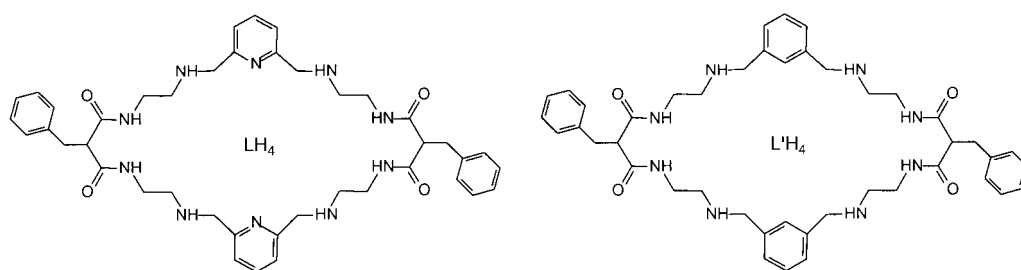


Figure 1. a) Distribution diagram (relative abundance% (RA), of species vs pH) for a system that contains $\text{Cu}(\text{CF}_3\text{SO}_3)_2$ at 10^{-3} M and LH_4 at 5×10^{-4} M. The calculated formation constants (expressed as $\log \beta$) for the species indicated (with uncertainties in parenthesis) are: $\text{LH}_5^+ = 7.66(0.01)$, $\text{LH}_6^{2+} = 14.80(0.01)$, $\text{LH}_7^{3+} = 21.55(0.01)$, $\text{LH}_8^{4+} = 27.73(0.01)$, $[\text{Cu}_2(\text{LH}_4)]^{4+} = 25.31(0.02)$, $[\text{Cu}_2(\text{LH}_4)(\text{OH})]^{3+} = 18.95(0.02)$, $[\text{Cu}_2(\text{LH}_4)(\text{OH})_2]^{2+} = 10.97(0.02)$, $[\text{Cu}_2(\text{L})] = -8.17(0.02)$. The full and empty triangles report the molar absorptivity of the complex at 660 and 515 nm vs pH, respectively, relative to $[\text{Cu}_2(\text{LH}_4)]^{4+}$ and to $[\text{Cu}_2(\text{L})]$; b) Distribution diagram (RA of species vs pH) for a system that contains $\text{Cu}(\text{CF}_3\text{SO}_3)_2$ at 10^{-3} M, and LH_4 and IMH at 5×10^{-4} M. The full and empty triangles report the molar absorptivity of the complex at 650 and 515 vs pH profiles, respectively, relative to $[\text{Cu}_2(\text{LH}_4)(\text{Im})]^{3+}$ and to $[\text{Cu}_2(\text{L})]$. The calculated formation constants are the same as in (a), to which these equilibria and constants have been added: $\text{LH}_4 + 2\text{Cu}^{2+} + \text{ImH} = [\text{Cu}_2(\text{LH}_4)(\text{Im})]^{3+} + \text{H}^+$, $\log K = 38.05(0.02)$; $\text{Im}^- + \text{H}^+ = \text{ImH}$, $\log K = 10.82(0.02)$; $\text{Im}^- + 2\text{H}^+ = \text{ImH}_2^+$, $\log K = 19.2(0.02)$.

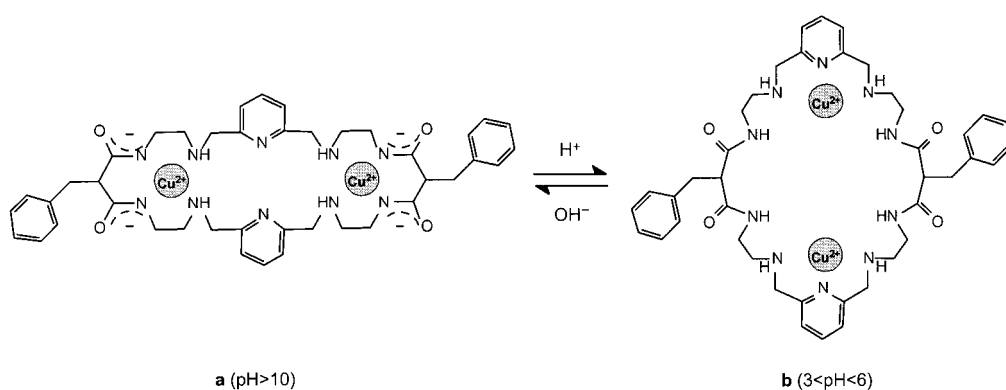
arises from the typical d–d transition for a tetra coordinated Cu^{2+} ion with square-planar geometry inside a bis-deprotonated DADA donor set.^[9]

On changing pH to lower values (3–6), the deprotonated amide groups are reprotonated, thus becoming noncoordi-

nating, and the two Cu^{2+} ions move to the two available separated tridentate PDA units. This form is the complex $[\text{Cu}_2(\text{LH}_4)]^{4+}$, form **b** in Scheme 1, in which each Cu^{2+} is tricoordinated by the ligand ($\lambda_{\text{max}} = 660$, deep blue), with the other coordination positions of the Cu^{2+} ion occupied by water molecules.^[10] On raising the pH

(6–9.5), two water molecules are deprotonated to give the blue species $[\text{Cu}_2(\text{LH}_4)(\text{OH})]^{3+}$ and $[\text{Cu}_2(\text{LH}_4)(\text{OH})_2]^{2+}$. According to these data, when a 1:2 molar ratio of $\text{LH}_4/\text{Cu}^{2+}$ is chosen, this system is capable of a pH-driven double cation translocation; in a solution with $4 < \text{pH} < 5$ the two Cu^{2+} ions are coordinated by the two PDA moieties to give $[\text{Cu}_2(\text{LH}_4)]^{4+}$ (form **b** in Scheme 1, 95% of the relative abundance, RA, in the distribution diagram), but if the pH is raised above 10.5 the four amide protons are released and each Cu^{2+} moves inside one of the two deprotonated DADA moieties to give the neutral complex $[\text{Cu}_2(\text{L})]$ (form **a** in Scheme 1, 99% in the distribution diagram). The movement is reversible and several translocation cycles have been carried out in various experiments, without significant variations (except those due to dilution) in the spectra of the **a** and **b** forms. To check the correctness of the interpretation of spectral and potentiometric data, we carried out the same measurement set on the reference compound $\text{L}'\text{H}_4$, which lacks the pyridine nitrogen atoms and should not give rise to the same behavior. Infact, no blue was seen in the whole pH range, and only a very weak shoulder in the spectra between 600–700 nm was observed at low pH, which completely disappeared before pH 7. On the other hand, pink, pertinent to the band centered at 510 nm, started to appear at a pH of around 5 and the intensity of this band reached a plateau at pH 7 (see the Supporting Information), which did not change with an increase in pH, thus showing that: 1) no blue dicopper complex is formed; 2) a pink complex $[\text{Cu}_2(\text{L}')]^{2+}$ is completely formed (> 95%) at pH 7, which is more than two pH units below the pH at which the analogous complex with LH_4 exists. These results clearly show that the nitrogen atom of the pyridine moiety is essential to the formation of the blue complex, giving rise to two binding cavities in which the two copper ions can be positioned in a wide pH range. These cavities have such a good affinity for Cu^{2+} ions that they prevent them from entering the DADA ligand sets before pH 9.

$[\text{Cu}_2(\text{L})]$ is a neutral, quite-rigid molecule in which each Cu^{2+} centre is four-coordinated and square-planar. Moreover, it is well-established that inside a similar donor set the Cu^{2+} ion is coordinatively saturated, that is, it does not interact with any ligand added to the solution.^[11] $[\text{Cu}_2(\text{L})]$ can be considered the “closed” form of the system. On the other hand, in the $[\text{Cu}_2(\text{LH}_4)]^{4+}$ form, each Cu^{2+} is only three-coordinated by the ligand and the water molecules that complete the coordination sphere can be easily substituted by stronger ligands. Thus, the system is in its “open” form and resembles a whole category of dicopper complexes inside ditopic macro-



Scheme 1. pH dependent intramolecular dislocation of the Cu^{2+} ions.

cyclic ligands,^[12] which are able to bind in cascade several bidentate ligands in a bridging fashion. Consequently, we investigated the behavior of the system in the presence of typical copper-coordinating bridging substrates.

A solution of the complex, buffered at pH 7 with HEPES (4-(2-hydroxyethyl)-1-piperazineethanesulfonic acid) (0.05 M) was titrated with several anions such as dicarboxylates (oxalate and malonate), phosphates (phosphate and pyrophosphate), azide and imidazolate. At the chosen pH the $[\text{Cu}_2(\text{LH}_4)(\text{OH})]^{3+}$ species is predominant (> 70 %). In all cases, (except azide) the formation of 1:1 adduct was observed. Following our interests on imidazole (ImH) and histidine detection,^[13] we decided to further investigate the behavior of the complex in the presence of imidazole.

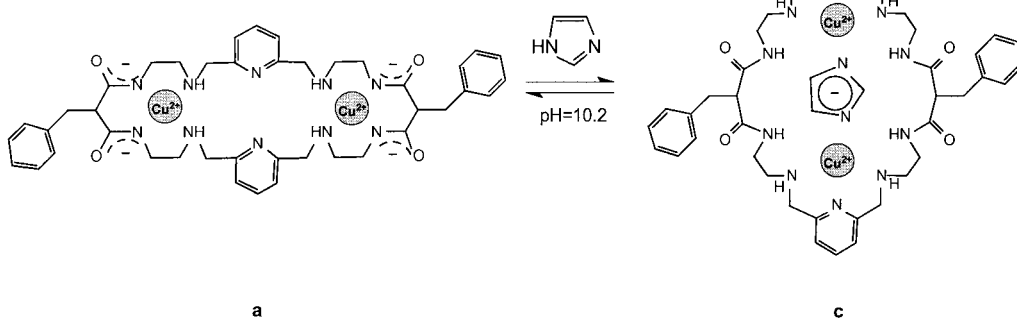
Potentiometric titrations were carried out with standard base on solutions containing LH_4 , Cu^{2+} , and ImH in a 1:2:1 molar ratio with excess acid. The formation constants of the species in solution for this system have been calculated and the relative distribution diagram drawn (Figure 1b, see caption for additional equilibrium and the relative constants).^[14] In the range of $3 < \text{pH} < 4.5$ $[\text{Cu}_2(\text{LH}_4)]^{4+}$ is predominant, as it is in the absence of ImH, whereas an increase in pH above 4.5 result in the gradual formation of $[\text{Cu}_2(\text{LH}_4)(\text{Im})]^{3+}$ (form **c** in Scheme 2), which predominates in the pH range of 6.0 to 10.0. This latter species contains a bridging imidazolate anion (Im^-), which forms thanks to the particularly stable^[15,13c] $\{\text{Cu}^{2+}-(\text{Im}^-)-\text{Cu}^{2+}\}$ disposition. Cou-

pled pH-spectrophotometric titrations evidence the formation of the blue complex $[\text{Cu}_2(\text{LH}_4)]^{4+}$ ($\lambda_{\text{max}} = 660 \text{ nm}$, $A = 204 \text{ M}^{-1} \text{ cm}^{-1}$) in the expected range of $3 < \text{pH} < 4.5$, while a rise in the pH up to 6 induces the shift of the maximum to 646 nm and an increase in the intensity of this band ($A = 302 \text{ M}^{-1} \text{ cm}^{-1}$), which displays λ and A values consistent with a $\{\text{Cu}^{2+}-(\text{Im}^-)-\text{Cu}^{2+}\}$ moiety.^[16]

This band persists in the pH range in which $[\text{Cu}_2(\text{LH}_4)(\text{Im})]^{3+}$ is prevalent (Figure 1b, full triangles). On further increasing the pH over 10.0, the blue disappears, leaving the pink of the $[\text{Cu}_2(\text{L})]$ species, which displays a band with the same λ and ϵ values found when no ImH is present. It has to be stressed that in the presence of imidazole no OH-containing species are found in the 2–12 pH range and that $[\text{Cu}_2(\text{LH}_4)(\text{Im})]^{3+}$ is so stable that it exists in a very large pH range (< 90 % in the 5.8–10.2 pH range), thus pushing the formation of $[\text{Cu}_2(\text{L})]$ to a pH value one unit higher than in the absence of imidazole. Double cationic translocation also occurs in the presence of imidazole, as the correct and reversible spectral changes are observed on changing pH from, for example, 11.0 to 7.0 and back again. Moreover, it has to be pointed out that at pH 11.0 ImH is free in solution and does not interact with $[\text{Cu}_2(\text{L})]$ (form **a**, closed), while at pH 7.0 the two Cu^{2+} ions translocate, the system is in its open form and it is able to bind bridging anions such as Im^- , thus representing an example of controllable binding action obtained inside a molecular machine after a chemical (ΔpH) stimulus.

A comparison of the distribution diagrams in the absence and presence of imidazole (Figure 1a and b) shows that in a sharp pH range ($10.0 < \text{pH} < 10.4$) in the absence of imidazole the $[\text{Cu}_2(\text{L})]$ species is at 95 %, whereas in the presence of imidazole, it is at 10 % and the $[\text{Cu}_2(\text{LH}_4)(\text{Im})]^{3+}$ species is around 90 %. Thus, we can expect that when a pink solution

buffered at pH 10.2 is treated with one equivalent of imidazole, translocation takes place with imidazolate binding, according to the equilibrium described in Scheme 2. Although it is somewhat slow, this process is indeed observed, as can be seen by the series of spectra obtained from a solution of $[\text{Cu}_2(\text{L})]$ buffered at pH 10.2 after addition of 1 equivalent of ImH.



Scheme 2. The imidazole-induced translocation equilibrium at pH 10.2.

Figure 2 shows the formation of the band typical of $[\text{Cu}_2(\text{LH}_4)(\text{Im})]^{3+}$ with time. The absorbance versus time profile corresponds to a first-order kinetic, with $k =$

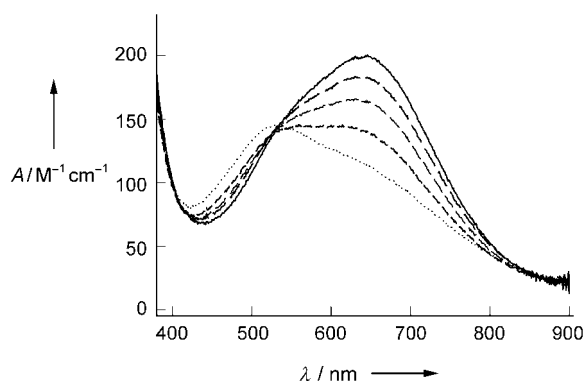


Figure 2. The effects on absorption spectra of addition of one equivalent of imidazole to a solution (7.5×10^{-4} M) of the complex buffered at pH 10.2 with CAPS (3-cyclohexylamino-1-propanesulfonic acid) (0.05 M). Sample spectra showed are taken at $t=0$ (dotted line), 20, 50, 90, 150 min (solid line).

0.00037 s^{-1} ($\tau=45$ min). According to this result, in this system it is the substrate itself that makes the cations translocate and causes the system to open, thus allowing binding to take place. A high degree of selectivity is found: when pH is fixed at 10.2 the system is in its closed form (form **a**), and the addition of potentially bridging anions (N_3^- , PO_4^{3-} , $\text{P}_2\text{O}_7^{4-}$, $\text{C}_2\text{O}_4^{2-}$) give no spectral change even after the addition of up to fivefold excess of anions. The same behavior is observed when several equivalents of representative aminoacids and other biologically relevant substrates are added to the solution: no color change is observed upon addition of several equivalents of glycine, arginine, proline, glutamate, ADP, ATP. On the other hand, as expected, the addition of histidine or histamine gives the same effect already observed with imidazole. The same response (switch from pink to blue) is observed when titrations with imidazole, histidine, and histamine are repeated in the presence of a fivefold excess of the potential interferents. Only histidine and histamine are recognized and sensed colorimetrically. The receptor is a sleeping host that is closed to all guests we have tried so far, except imidazole-containing molecules, which have the key (the imidazole fragment itself) to switch the host cavity to the open, binding form. This recognition is associated to a neat color change, thus providing a signal of the selective inclusion. The peculiar, extreme case of selectivity relies on the unique energy gain obtained from the particularly stable $[\text{Cu}^{2+}(\text{Im})-\text{Cu}^{2+}]$ moiety, which more than compensates the energy barrier necessary for the movement of the molecular machine, that is, double Cu^{2+} translocation. The design and synthesis of devices based on this approach are being performed in our laboratory. This peculiar kind of selectivity can be exploited by simply changing the groups appended between the two amide functions for a broader range of applications such as fluorimetric sensing (appending fluorogenic fragments),

transport across apolar membranes (by using lipophilic tails), histamine removal from biological fluids or its controllable release from nanodevices.

The Supporting Information for this article (distribution diagram for ligand LH_4 and pH-spectrophotometric titration of the reference compound L'H_4 in presence of two equivalents of Cu^{II} ions) is available on the WWW under <http://www.angewandte.org> or from the author.

Received: May 6, 2004

Keywords: copper · molecular devices · molecular recognition · receptors · sensors

- [1] V. Amendola, L. Fabbrizzi, C. Mangano, P. Pallavicini, *Acc. Chem. Res.* **2001**, *34*, 488–493.
- [2] V. Balzani, A. Credi, M. Venturi, *Molecular Devices and Machines—A Journey into the Nanoworld*, Wiley-VCH, Weinheim, **2003**.
- [3] S. Shinkai in *Molecular Switches* (Ed.: B. L. Feringa), Wiley-VCH, Weinheim, **2001**, pp. 281–307.
- [4] Macrocyclic ligand LH_4 and L'H_4 were synthesized through a 2+2 condensation via Schiff base formation of 6-benzyl-1,4,8,11-tetraazaundecane-5,7-dione and, respectively, 2,6-pyridine dicarboxyaldehyde (for LH_4) and isophthalaldehyde (for L'H_4). A solution of 6-benzyl-1,4,8,11-tetraazaundecane-5,7-dione (0.8 mmol) in acetonitrile (30 mL) was added dropwise to a solution of the corresponding dialdehyde (0.8 mmol) in the same solvent (60 mL) at room temperature under a nitrogen atmosphere over a period of 30 min. The reaction mixture was stirred overnight, then was reduced in situ with an excess of NaBH_4 (0.6 g). The solvent was removed from the reaction mixture on a rotary evaporator and the solid residue was treated with water (50 mL). Extraction with CH_2Cl_2 , drying with MgSO_4 , and removal of the solvent under vacuum gave the desired product as a solid in 72% yield (LH_4) and 73% (L'H_4). Elemental analysis calcd (%) for LH_4 $\text{C}_{42}\text{H}_{54}\text{N}_{10}\text{O}_4$: C 66.12, H 7.13, N 18.36; found C 66.48, H 7.06, N 18.15; for L'H_4 $\text{C}_{44}\text{H}_{56}\text{N}_8\text{O}_4$: C 69.45, H 7.42, N 14.72; found C 69.32, H 7.16, N 14.11. MS(ESI): m/z : 764 $[\text{LH}_4+\text{H}^+]$, 762 $[\text{L'H}_4+\text{H}^+]$.
- [5] Measurements were carried out in a solution of NaClO_4 (0.05 M) in 1:4 v/v water/ethanol. The water/ethanol mixture was chosen instead of pure water for the low water solubility of the less protonated or neutral forms of the ligand. All the presented experiments and data were obtained in the aforementioned solvent mixture. However, it has to be stressed that both the $[\text{Cu}_2(\text{L})]$ and the $[\text{Cu}_2(\text{LH}_4)]^{4+}$ complexes are fairly soluble also in pure water (up to 5×10^{-3} M).
- [6] P. Gans, A. Sabatini, A. Vacca, *Talanta* **1996**, *43*, 1739.
- [7] The distribution diagram for protonated species (i.e., in the absence of Cu^{2+}) is available in the Supporting Information.
- [8] The two metal/one ligand nature of the complexes responsible of the 515 and 660 nm bands, that is, $[\text{Cu}_2(\text{L})]$ and $[\text{Cu}_2(\text{LH}_4)]^{4+}$, has been checked also by means of spectrophotometric titrations: A solution of KOH (0.01 M; i.e., at $\text{pH} \approx 12$) in water/ethanol (1:4 v/v) that contained 5×10^{-4} M LH_4 were titrated with standard aqueous $\text{Cu}(\text{CF}_3\text{SO}_3)_2$; a linear increase of the 515 nm band and a clear end point at 1:2 ligand/metal molar ratio was observed; on the other hand, solutions buffered at pH 4.5 (acetic/acetate buffer) that contained 5×10^{-4} M LH_4 were titrated with standard aqueous $\text{Cu}(\text{CF}_3\text{SO}_3)_2$; a linear increase of the 660 nm band with a sharp end point at 1:2 ligand/metal molar ratio was observed. Solid samples of $[\text{Cu}_2(\text{L})]$ and $[\text{Cu}_2(\text{LH}_4)(\text{OH})](\text{CF}_3\text{SO}_3)_3 \cdot 5 \text{H}_2\text{O}$, which gave satisfactory CHN analysis, were obtained by slow

- evaporation of solutions at pH 11.5 and 7.0, respectively. Mass spectra (ESI) carried out for $[\text{Cu}_2(\text{L})]$ gave the expected m/z peak m/z : 887 $[[\text{Cu}_2(\text{L})] + \text{H}^+]$.
- [9] V. Amendola, L. Fabbri, C. Mangano, H. Miller, P. Pallavicini, A. Perotti, A. Taglietti, *Angew. Chem.* **2002**, *114*, 2665–2668; *Angew. Chem. Int. Ed.* **2002**, *41*, 2553–2556.
- [10] K. D. Karlin, J. C. Hayes, S. Juen, J. P. Hutchinson, J. Zubietta, *Inorg. Chem.* **1982**, *21*, 4108–4109.
- [11] V. Amendola, C. Brusoni, L. Fabbri, C. Mangano, H. Miller, P. Pallavicini, A. Perotti, A. Taglietti, *J. Chem. Soc. Dalton Trans.* **2001**, 3528.
- [12] a) M. G. B. Drew, J. Hunter, D. J. Marrs, J. Nelson, C. Harding, *J. Chem. Soc. Dalton Trans.* **1992**, 3235–3242; b) R. Menif, J. Reibebispies, A. E. Martell, *Inorg. Chem.* **1991**, *30*, 3446.
- [13] a) M. A. Hortalà, L. Fabbri, N. Marcotte, F. Stomeo, A. Taglietti, *J. Am. Chem. Soc.* **2003**, *125*, 20; b) L. Fabbri, G. Francese, M. Licchelli, A. Perotti, A. Taglietti, *Chem. Commun.* **1997**, 581; c) L. Fabbri, P. Pallavicini, L. Parodi, A. Perotti, A. Taglietti, *J. Chem. Soc. Chem. Commun.* **1995**, 2439.
- [14] Formation constants for the protonation equilibria involving imidazole have been recalculated, as the titration experiments were carried out in 1:4 water/ethanol mixture and not in water. The formation constants for the species that do not contain imidazole have been maintained at a constant, with the same values determined in the previous experiments.
- [15] a) P. K. Coughlin, S. J. Lippard, A. E. Martin, J. E. Bulkowski, *J. Am. Chem. Soc.* **1980**, *102*, 7616–7617; b) C. A. Salata, M.-T. Youinou, C. J. Burrows, *J. Am. Chem. Soc.* **1989**, *111*, 9278–9279.
- [16] a) S. Kawabata, T. Soma, K. Ichikawa, *Chem. Lett.* **1997**, 1199; b) Q.-Y. Chen, Z.-Q. Pan, Q.-H. Luo, L.-M. Zhen, X.-L. Hu, Z.-H. Wang, Z.-Y. Zhou, C.-H. Yeung, *J. Chem. Soc. Dalton Trans.* **2002**, 1315–1318.

core is considered to be planar because of the resonance stabilization resulting from the 18- π electron aromatic system.^[1] By contrast, porphyrin analogues display versatile structures, especially in the expanded porphyrin families where an inverted arrangement of the pyrrole rings is frequently observed.^[2] The inversion of the tellurophene ring in the heteroporphyrin analogue ditelluraporphyrin (**2**) was demonstrated by Latos-Grażyński and co-workers;^[3] however, such ring inversion has been rarely observed and remains unproven for the tetrapyrrolic framework (Scheme 1).

Previously, we reported the formation of the N-fused porphyrin (NFP) **4**^[4] from an N-confused porphyrin (NCP) **3**,^[5] which should proceed by ring inversion within the confused pyrrole and bond formation. In addition to this, we suggested the involvement of the inverted conformation of the confused pyrrole ring during the NH tautomerism of NCP.^[6] Furthermore, density functional theory (DFT) calculations indicate that the energy difference between the inverted and normal conformations is much smaller than that of porphyrin.^[7] The tilted angles were increased by the introduction of substituents at the inner carbon atom of the confused pyrrole. This observation led to the question of what would happen if a larger substituent, such as porphyrin, was introduced into the core. Would it induce pyrrole inversion and stabilize the inverted conformation of the confused pyrrole ring? To examine this possibility, we planned to synthesize an NCP dimer where the two NCP molecules are connected at both of the inner-carbon atoms. The synthetic strategy involved the initial preparation of an NFP dimer followed by the nucleophilic, bond-cleavage reaction necessary to generate a covalently bonded NCP dimer. Both the structures have been elucidated by X-ray diffraction analysis. The confused pyrrole rings in the NCP dimer keep the inverted conformation and each NCP ring exhibits aromaticity, despite the highly distorted structure.

The NFP dimer was synthesized in a similar method to that used for the *meso-meso* porphyrin dimer,^[8] in which a Ag(I)-promoted, oxidative-coupling reaction is employed. Briefly, N-fused tetrakis-(*p*-tolyl)porphyrin (NFTTP, **4a**) was treated with silver(I) trifluoroacetate in CHCl₃ at reflux for 24 hours to afford the NFP dimer **5**, in which the NFP units were covalently bonded to each other at the C2 carbon atoms of the fused rings, in a yield of 61 % (Scheme 2).

The structure of **5** was elucidated by X-ray diffraction analysis (Figure 1).^[9a] The asymmetric nature of NFP and the axial chirality of dimer **5** results in the unit cell, as determined from the crystallography data, contains an enantiomeric pair of molecules of **5**. The bridging bond (1.476(9) Å) was formed between C2 and C2'. Each of the NFP units was almost planar and the mean deviations from the porphyrin plane, which consists of the core 24 atoms, were 0.072(7) and 0.083(7) Å, respectively. The NFP units were in a nearly rectangular arrangement with respect to each other and the dihedral angle between the NFP units of 75.72(5)°. The bond lengths and angles of the NFP moieties were comparable to those of **4a**.^[4b] The inner NH atoms were positioned at N4 and N4', as judged by the C α -N-C α angles. The three inner nitrogen atoms were located close together and form hydrogen bonds that shared

Porphyrinoids

Inverted N-Confused Porphyrin Dimer

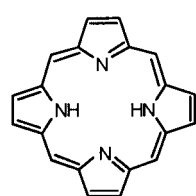
Tomoya Ishizuka, Atsuhiko Osuka, and
Hiroyuki Furuta*

Porphyrin (**1**) is a well-known tetrapyrrolic macrocycle that has four nitrogen atoms arranged inside the core that are able to co-ordinate a variety of metal ions. Normally, the porphyrin

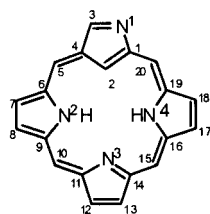
[*] T. Ishizuka, Prof. Dr. H. Furuta*
Department of Chemistry and Biochemistry
Graduate School of Engineering
Kyushu University, Fukuoka 812-8581 (Japan)
Fax: (+81) 92-651-5606
E-mail: hfuruta@cstf.kyushu-u.ac.jp
Prof. Dr. A. Osuka
Department of Chemistry
Graduate School of Science
Kyoto University, Kyoto 606-8502 (Japan)
Fax: (+81) 75-753-3970

[†] PRESTO, JST

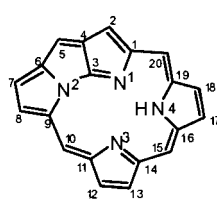
Supporting information for this article is available on the WWW under <http://www.angewandte.org> or from the author.



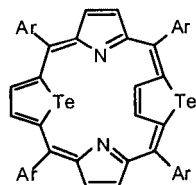
Porphyrin (1)



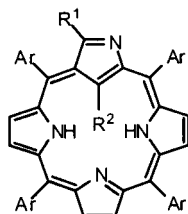
N-Confused Porphyrin (NCP)



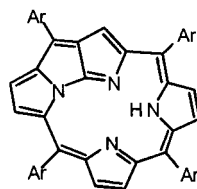
N-Fused Porphyrin (NFP)



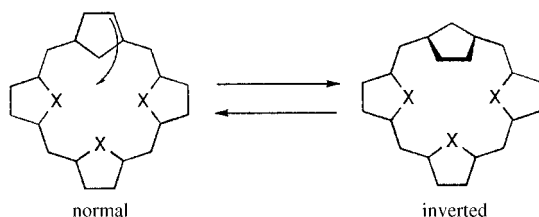
Ditetelluraporphyrin (2)



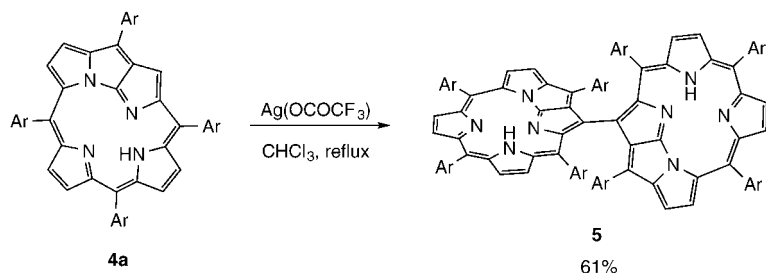
3a Ar = *p*-Tol, R¹ = H, R² = H
3b Ar = Ph, R¹ = H, R² = H
7 Ar = *p*-Tol, R¹ = H, R² = NO₂
8 Ar = Ph, R¹ = OMe, R² = H



4a Ar = *p*-Tol
4b Ar = Ph



Scheme 1. Normal and inverted conformation of porphyrinoids.



Scheme 2. Synthesis of N-fused porphyrin dimer 5.

the inner NH hydrogen atom. Steric crowding meant that the coplanarity between the NFP core and the *meso*-aryl group at the C5 position (Ph1) found in 4^[4b] was slightly lost, as shown by with dihedral angles of 29.8(2) and 35.4(2)°, and the bond lengths of the C_{meso}–C_{ipso} bonds were relatively long (1.48(1) and 1.46(1) Å). In addition, the *meso*-aryl groups at C20 and C20' (Ph4 and Ph4') participate in π – π stacking with the NFP moieties that are separated by distances of 3.27(1) and 3.25(1) Å, respectively.

The ¹H NMR spectrum of 5 at room temperature in CDCl₃ shows that the proton resonance signals were rela-

tively broad but each was distinctive and strong aromaticity was inferred from the β -proton signals of 5 appearing in the same region as those of 4a. The four methyl signals were observed at δ = 2.73, 2.58, 1.96, and 0.22 ppm, respectively, thus reflecting the symmetry of the molecule. The latter two signals are assignable to the *meso*-aryl groups (Ph1 and Ph4) that are located on the other NFP ring in the X-ray crystal structure. Similarly, the phenyl protons of Ph4 exhibited upfield shifts and four distinctive proton signals were observed at δ = 4.41 and 4.72 ppm for the *ortho* protons and at δ = 6.17 and 6.55 ppm for the *meta* protons, which indicates that the rotation of the benzene ring is completely disturbed by the π – π interactions with the other NFP ring, as shown in the structure determined by X-ray crystallography.

The aromaticity of the system is further demonstrated by the electronic absorption spectrum of dimer 5 which displays a similar profile in the 300–1000 nm region to that observed for 4a (Figure 2a). The absorption band at the longest wavelength appeared at 977 nm, which is a bathochromic shift of 36 nm relative to 4a.

Next, cleavage of the bridging C–N bond at the fused ring to generate the NCP ring was attempted.^[4] When NFP dimer 5 was treated with sodium methoxide in THF for one hour, a diastereoisomeric mixture of covalently bonded NCP dimers 6 was produced quantitatively (Scheme 3). The signal at *m/z* 1400 in the mass spectrum suggested the introduction of two methoxy groups at the α -carbon atom of the confused pyrrole. The ratio of each diastereomer was determined from the ¹H NMR spectrum recorded in CDCl₃ to be 9:1.^[10] The preferential formation of one of the diastereomers suggests that the second methoxide attack occurred mainly from one direction, probably because of steric hinderance in the intermediate NFP–NCP dyad. Isolation of the major diastereomer was achieved by repeated purification by column chromatography on silica gel, and, fortunately, single crystals suitable for X-ray diffraction analysis were afforded.^[9b]

The ORTEP diagram of 6 is shown in Figure 3. The NCP units are linked by a covalent bond between C2 and C2' with a length of 1.480(7) Å. The two methoxy groups are attached at the α -carbon atoms of the confused pyrroles and the inner NH hydrogen atoms are located at the N2 and N4 positions. Surprisingly, the confused pyrroles are still inverted, namely, the β -carbon atom points outward, whereas the N–C _{α} bond is directed to the inside of the ring. As a result, the NCP core planes are highly distorted and the mean deviations from the plane, which consist of 24 core atoms, are 0.338(5) and 0.365(5) Å. The dihedral angles between the least-squares plane of the four *meso*-carbon atoms and the pyrrole rings are 130.8(2) and 131.1(1)° for Py1 and Py1',

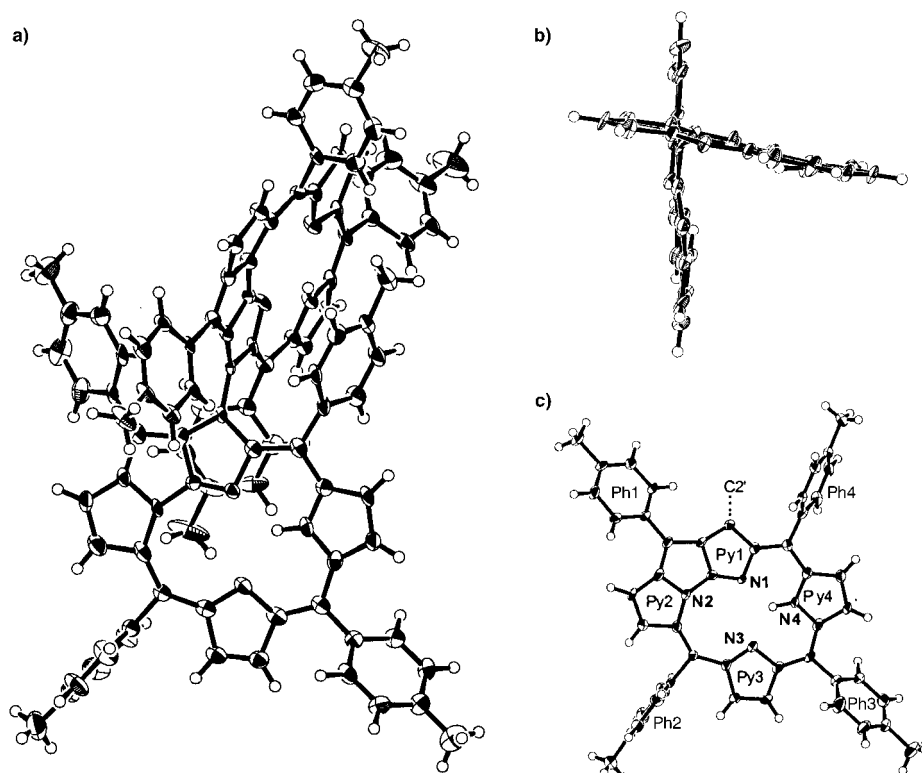


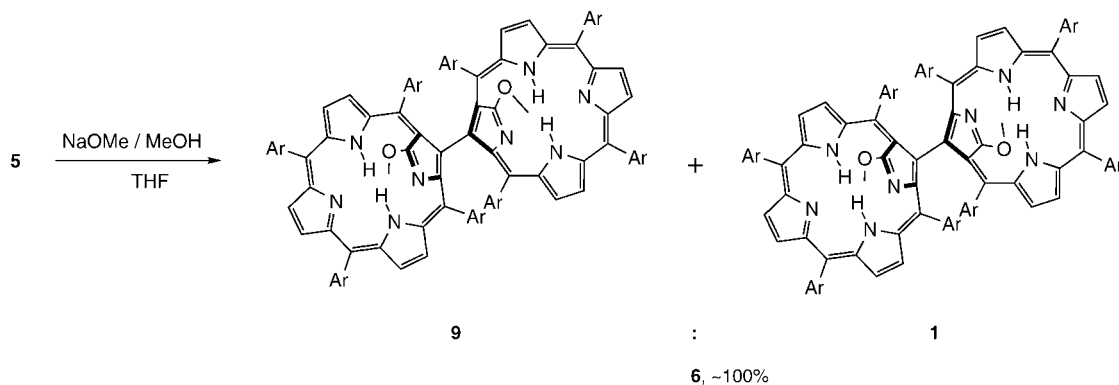
Figure 1. X-ray crystal structure of **5**. a) Top view, b) side view, and c) monomer unit. *Meso*-tolyl groups are omitted for clarity in (b).

9.2(2) and 10.5(2)° for Py2 and Py2', 9.2(2) and 11.3(2)° for Py3 and Py3', and 13.9(2) and 15.8(2)° for Py4 and Py4', respectively. The confused pyrroles (Py1 and Py1') are, thus, highly tilted relative to **3b** (24.6(1)°)^[5a] and the nitro-substituted NCP **7** (41.3(2)°).^[4b] The hydrogen-bonding interaction between N1 and N4-H probably helps to retain the inverted conformation, as judged by the short atom distances between N1 (N1') and N4 (N4') of 2.673(6) (2.687(6)) Å, and the larger tilting angles of Py4 than those of Py2 and Py3. The two NCP molecules were crossed diagonally and the dihedral angle between them was 52.36(4)°. Furthermore, the *meso*-aryl groups at C20 and C20' (Ph4 and Ph4') form π - π stacking pairs with other NCP

rings, with mean distances of 3.264(6) and 3.248(6) Å. The bond lengths and angles of the NCP units in **6** were very similar to **3b** except that the bond angles of the adjacent *meso*-carbon atoms of the confused pyrrole and the interior angles of the *meso*-carbon atoms were relatively narrow: 116.8(4) and 115.4(5)° for C4-C5-C6 and C4'-C5'-C6', and 117.2(4) and 117.1(4)° for C1-C20-C19 and C1'-C20'-C19', respectively. The similarity of the bond lengths and angles suggests that the NCP rings maintain their aromaticity despite their distorted structures.

The ¹H NMR spectrum of the major diastereomer of **6** in CDCl₃ at room temperature shows that the proton resonance signals were degenerate and reflects the molecule's twofold symmetry. The methoxy groups located on the NCP ring were observed at δ = -0.40 ppm because of the diamagnetic ring current effect, which causes a δ = 4.4 ppm upfield shift relative to the outer

α -methoxy NCP **8**.^[4b] Similar π - π stacking was observed in **6** to that seen in the NFP dimer **5**. For example, the methyl signals of the *meso*-tolyl groups at the C5 and C20 positions (Ph1 and Ph4) also exhibited upfield shifts and resonated at δ = 2.03 and 0.18 ppm, respectively. The benzene protons of Ph4 produced broad signals at δ = 3.23 (*o*), 4.32 (*o*), 5.35 (*m*), and 5.78 (*m*) ppm. The signals of the inner NH atoms appeared distinctively at δ = -3.31 and -2.76 ppm, and the sharpness of these signals indicates that the hydrogen atoms are localized on the NMR timescale. The fact that the signals of the β protons of Py2 and Py4 were observed as double doublets because they couple with the inner NH protons supports this observation. In addition, the chemical shifts of



Scheme 3. Synthesis of N-confused porphyrin dimer **6**.

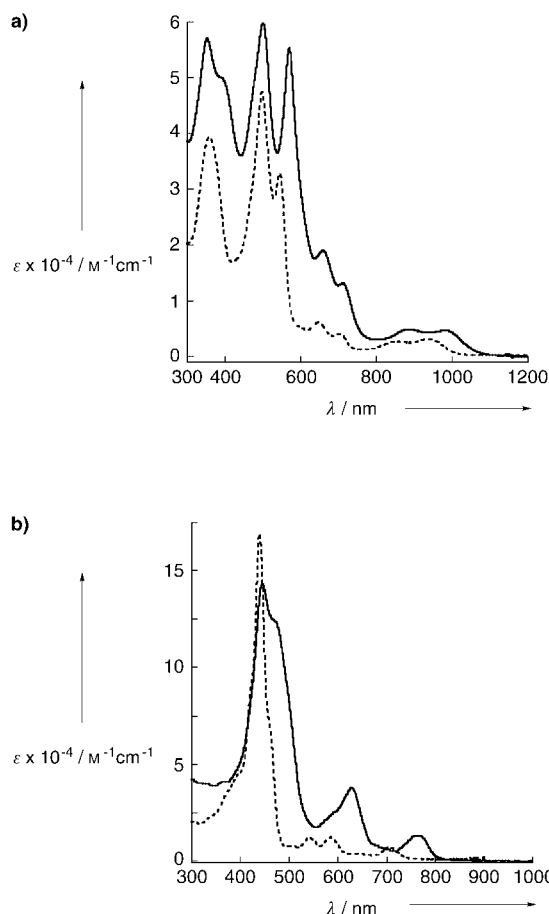


Figure 2. Optical absorption spectra of a) **4a** (.....) and **5** (—) and b) **6** (—) and **8** (.....) in CH_2Cl_2 .

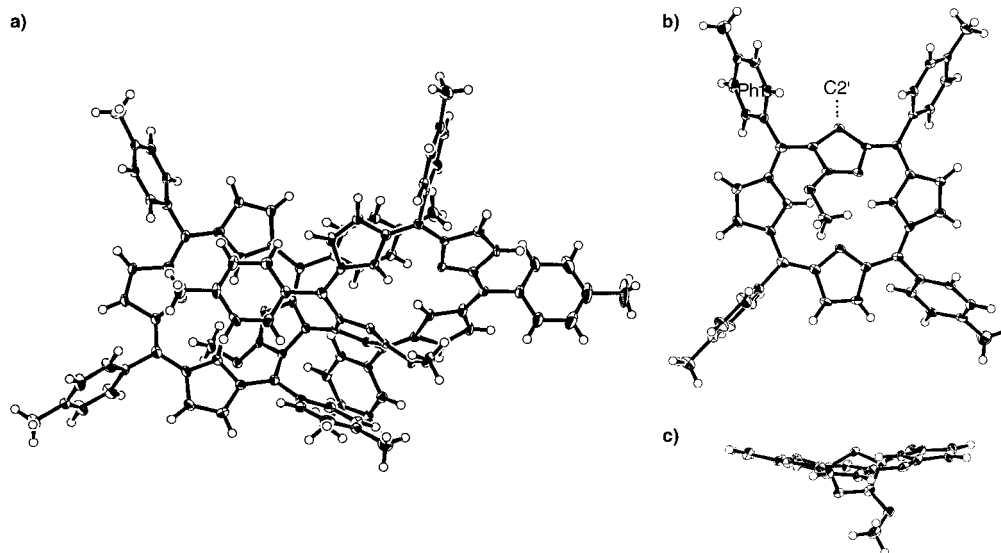


Figure 3. X-ray crystal structure of **6**. a) Top view, b) the monomer unit, and c) side view. *Meso*-tolyl groups are omitted for clarity in (c).

the inner NH protons and the β -H signals are comparable to those of **3a**^[5a] and **8**^[4b] which also indicates the aromatic nature of **6**.

The UV/Vis spectrum of the major diastereomer of **6** in CH_2Cl_2 displayed a clear Soret band at 446.5 nm and two Q-bands at 629 and 765 nm, respectively (Figure 2b). The Soret band had a shoulder at 470 nm, which is possibly derived from exciton coupling between the two chromophores.^[11]

In conclusion, covalently linked NFP and NCP dimers **5** and **6** were synthesized and their structures characterized by X-ray diffraction analysis. NCP dimer **6** possesses an inverted confused pyrrole ring in its macrocyclic framework and exhibits aromaticity and intense optical absorption despite its highly distorted structure. Hence, structural flexibility and pyrrole inversion are intrinsic to the nature of NCP, and the control of such properties is considered to be important to the development of NCP-based functional molecules.

Experimental Section

5: Silver trifluoroacetate (44.34 mg, 0.201 mmol) was added to a solution of **4a** (12.97 mg, 0.0194 mmol) in CHCl_3 (30 mL), and the reaction mixture was heated to reflux for 24 h. After removing the solvent, the residue was purified by column chromatography on silica gel with 5% $\text{MeOH}/\text{CH}_2\text{Cl}_2$. The purple fraction was collected and the product was recrystallized from CH_2Cl_2 /hexane. Violet crystals of **5** (7.9 mg) were obtained in a yield of 61%. ^1H NMR (CDCl_3): δ = 9.15 (brs, 2H), 8.74 (brs, 2H), 8.39 (d, J = 6.0 Hz, 4H), 8.10 (brs, 4H), 7.94 (m, 6H), 7.80 (brs, 2H), 7.70 (brs, 2H), 7.54 (m, 8H), 7.35 (brs, 2H), 6.66 (d, J = 8.4 Hz, 4H), 6.55 (d, J = 6.6 Hz, 2H), 6.17 (brs, 2H), 4.72 (d, J = 7.2 Hz, 2H), 4.41 (brs, 2H), 2.73 (s, 6H), 2.58 (s, 6H), 1.96 (s, 6H), 0.22 ppm (s, 6H); UV/Vis (CH_2Cl_2): λ_{max} (nm) ($\log \epsilon$ [$\text{mol}^{-1} \text{dm}^3 \text{cm}^{-1}$]) = 977 (3.68), 887 (3.73), 713 (4.12), 659 (4.27), 571 (4.74), 501 (4.78), 354 (4.77); MALDI-TOF-MS: m/z 1335 (calcd for $[M^+]$ 1334.6).

6: Sodium methoxide (25% solution in MeOH , 0.5 mL) was added to a solution of **5** (3.88 mg, 2.9 μmol) in dry THF (5 mL). The reaction mixture was poured into aqueous NH_4Cl after stirring for 1 h. The product was extracted with CH_2Cl_2 (20 mL) and the organic phase was separated and dried over Na_2SO_4 . After removing the solvent, the residue was purified by column chromatography on silica gel with 2% $\text{MeOH}/\text{CH}_2\text{Cl}_2$. The green fraction was collected and the product was recrystallized from CH_2Cl_2 /MeOH. Green crystals of **6** (3.96 mg) were obtained quantitatively as a mixture of diastereomeric pairs. Further purification by repeated flash column chromatography afforded the major diastereomer of **6**. Major diastereomer of **6**: ^1H NMR (CDCl_3): δ = 8.99 (dd, J = 4.8, 2.1 Hz, 2H), 8.55 (dd, J = 4.8, 2.0 Hz, 2H), 8.40 (d, J = 4.5 Hz, 2H), 8.33 (d, J = 5.1 Hz, 4H), 8.19 (dd, J = 7.7, 1.7 Hz, 2H), 7.94 (m, 4H), 7.88 (dd, J = 4.8, 2.1 Hz, 2H), 7.78 (d, J = 7.5 Hz, 2H), 7.61 (d, J = 7.5 Hz, 2H), 7.54 (d, J = 8.1 Hz, 2H), 7.41 (m, 6H), 7.14 (d, J = 7.8 Hz, 4H), 5.78 (brs, 2H), 5.35 (brs, 2H), 4.32

(brs, 2H), 3.23 (brs, 2H), 2.72 (s, 6H), 2.60 (s, 6H), 2.03 (s, 6H), 0.18 (s, 6H), -0.40 (s, 6H), -2.76 (s, 2H), -3.31 ppm (s, 2H); UV/Vis (CH₂Cl₂): λ_{max} (nm) (log ϵ [mol⁻¹ dm³ cm⁻¹]) 766 (4.14), 629 (4.59), 447 (5.16); MALDI-TOF-MS: m/z 1400 (calcd for [M+H⁺] 1399.6).

Received: March 16, 2004

Keywords: aromaticity · macrocyclic ligands · N ligands · N-confused porphyrins · porphyrinoids

- [1] Nonplanar porphyrins are also known. J. A. Shelnutt, X.-Z. Song, J.-G. Ma, S.-L. Jia, W. Jentzen, C. J. Medforth, *Chem. Soc. Rev.* **1998**, 27, 31–41.
- [2] a) J. L. Sessler, S. J. Waghorn, *Expanded, Contracted & Isomeric Porphyrins*, Pergamon, New York, **1997**; b) *The Porphyrin Handbook*, Vol. 2 (Eds.: K. M. Kadish, K. M. Smith, R. Guilard), Academic Press, San Diego, **2000**; c) A. Jasat, D. Dolphin, *Chem. Rev.* **1997**, 97, 2267–2340; d) T. D. Lash, *Angew. Chem.* **2000**, 112, 1833–1837; *Angew. Chem. Int. Ed.* **2000**, 39, 1763–1767; e) J. L. Sessler, D. Seidel, *Angew. Chem.* **2003**, 115, 5292–5333; *Angew. Chem. Int. Ed.* **2003**, 42, 5134–5175.
- [3] E. Pacholska, L. Latos-Grażyński, Z. Ciunik, *Angew. Chem.* **2001**, 113, 4598–4601; *Angew. Chem. Int. Ed.* **2001**, 40, 4466–4469.
- [4] a) H. Furuta, T. Ishizuka, A. Osuka, T. Ogawa, *J. Am. Chem. Soc.* **1999**, 121, 2945–2946; b) H. Furuta, T. Ishizuka, A. Osuka, T. Ogawa, *J. Am. Chem. Soc.* **2000**, 122, 5748–5757.
- [5] a) H. Furuta, T. Asano, T. Ogawa, *J. Am. Chem. Soc.* **1994**, 116, 767–768; b) P. J. Chmielewski, L. Latos-Grażyński, K. Rachlewicz, T. Głowiak, *Angew. Chem.* **1994**, 106, 805–808; *Angew. Chem. Int. Ed. Engl.* **1994**, 33, 779–781; c) L. Latos-Grażyński in *The Porphyrin Handbook*, Vol. 2 (Eds.: K. M. Kadish, K. M. Smith, R. Guilard), Academic Press, San Diego, **1999**, chap. 14; d) H. Furuta, H. Maeda, A. Osuka, *Chem. Commun.* **2002**, 1795–1804; e) J. D. Harvey, C. J. Ziegler, *Coord. Chem. Rev.* **2003**, 247, 1–19.
- [6] H. Furuta, T. Ishizuka, A. Osuka, H. Dejima, H. Nakagawa, Y. Ishikawa, *J. Am. Chem. Soc.* **2001**, 123, 6207–6208.
- [7] L. Sztterenber, L. Latos-Grażyński, *J. Porphyrins Phthalocyanines* **2001**, 5, 474–480.
- [8] a) A. Osuka, H. Shimidzu, *Angew. Chem.* **1997**, 109, 93–95; *Angew. Chem. Int. Ed. Engl.* **1997**, 36, 135–137; b) N. Aratani, A. Osuka, Y.-H. Kim, D.-H. Jeong, D. Kim, *Angew. Chem.* **2000**, 112, 1517–1521; *Angew. Chem. Int. Ed.* **2000**, 39, 1458–1462.
- [9] a) Crystal data for **5**: C₉₆H₇₀N₈, M_r = 1279.64, triclinic, space group $P\bar{1}$ (no. 2), a = 12.328(2), b = 15.263(2), c = 19.177(3) Å, α = 92.526(3), β = 96.507(3), γ = 103.889(3)°, V = 3471.0(9) Å³, T = -173.0°C, Z = 2, 53358 measured reflections, 18522 unique reflections, 5745 with $I \geq 3\sigma(I)$ used in refinement, R = 0.081, R_w = 0.083, GOF = 0.957; b) crystal data for **6**: C₉₈H₇₈N₈O₂·CH₂Cl₂·2H₂O, M_r = 1520.71, triclinic, space group $P\bar{1}$ (no. 2), a = 12.8732(9), b = 14.891(1), c = 21.011(1) Å, α = 87.385(2), β = 86.629(1), γ = 76.697(1)°, V = 3910.7(5) Å³, T = -173.0°C, Z = 2, 24876 measured reflections, 24876 unique reflections, 13668 with $I \geq 3\sigma(I)$ used in refinement, R = 0.099, R_w = 0.129, GOF = 0.999. CCDC-233747 (**5**) and 233748 (**6**) contains the supplementary crystallographic data for this paper. These data can be obtained free of charge via www.ccdc.cam.ac.uk/contents/retrieving.html (or from the Cambridge Crystallographic Data Centre, 12, Union Road, Cambridge CB21EZ, UK; fax: (+44) 1223-336-033; or deposit@ccdc.cam.ac.uk).
- [10] See the Supporting Information.
- [11] M. Kasha, H. R. Rawls, M. A. El-Bayoumi, *Pure Appl. Chem.* **1965**, 11, 371–92.

Oxidation

Unusual Reactivity at a Platinum Center
Determined by the Ligands and the Solvent
Environment**

Gabriella Tamasi, Renzo Cini, Francesco P. Intini,
Maria F. Sivo, and Giovanni Natile*

The oxidation of platinum(II) to platinum(IV) by dihalides (X_2) has been widely investigated in the past years.^[1] In this process, two consecutive reactions occur in aqueous solution: 1) Rapid oxidation, assisted by solvent participation, that leads to the formation of a *trans*-haloaquaplatinum(IV) intermediate and a free halide ion, and 2) attack by the halide ion upon the platinum(IV) intermediate to yield the *trans*-dihaloplatinum(IV) end product.^[2–4]

The intermediate aqua species formed by this procedure have generally been characterized in solution, but, to the best of our knowledge, they were never isolated as pure solids. We have found that ancillary ligands can stabilize the aqua species to such an extent that it becomes the stable end product. Here we report, for the first time, the X-ray structure of such a species: (*trans*-[PtCl₃(OH₂)]{N=C(OCH₃)CH₂CH₂CH₂})⁺ (**2**, see Scheme 1). Furthermore, in chlorinated solvents and in the presence of excess chloride, **2** undergoes O-demethylation of the ancillary ligands with release of methyl chloride. The X-ray structure of the demethylation product (*trans*-[PtCl₃(OH)]{N=C(OH)CH₂CH₂CH₂}{N=C(O)CH₂CH₂CH₂})[–] (**4**, see Scheme 1) is also presented.

The platinum(II) complex *trans*-[PtCl₂{N=C(OCH₃)CH₂CH₂CH₂}] (**1**) reacts with Cl₂ in water to form *trans*-[PtCl₃(OH₂)]{N=C(OCH₃)CH₂CH₂CH₂}]Cl (**2**Cl, Scheme 1). This species is stable for days in water in the presence of 5×10^{-2} M HCl and 10^{-3} M **1** (platinum(II) catalyzes the anation reaction, that is, replacement of the coordinated solvent molecule by an entering anion, in platinum(IV) complexes). Other aqua species, under similar reaction conditions, undergo complete anation within minutes.^[3] Because of the low solubility of **1** in water, the reaction was repeated by

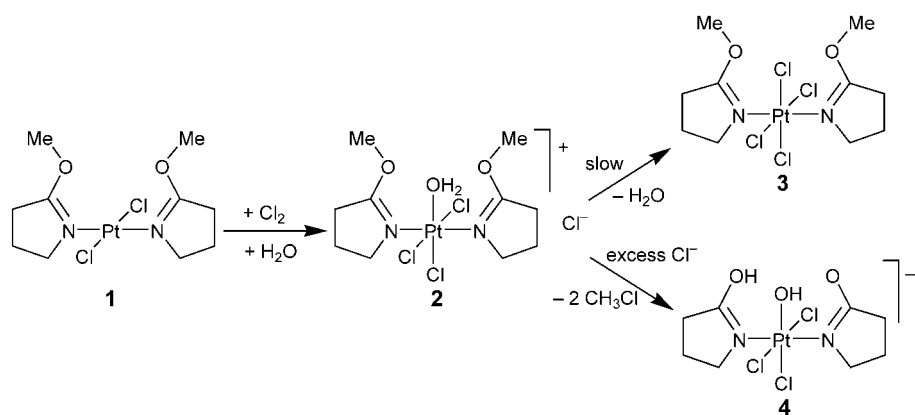
[*] Dr. F. P. Intini, Dr. M. F. Sivo, Prof. G. Natile
Dipartimento Farmaco-Chimico
Università degli Studi di Bari
Via E. Orabona 4, 70125 Bari (Italy)
Fax: (+39) 080-544-2230
E-mail: natile@farmchim.uniba.it

Dr. G. Tamasi, Prof. R. Cini
Dipartimento di Scienze e Tecnologie Chimiche e dei Biosistemi
Università degli Studi di Siena
Via A. Moro 2, 53100 Siena (Italy)

[**] The authors are grateful to the University of Bari (Contribution ex 60%), the Ministero per Istruzione Università e Ricerca (MIUR, Cofin. N° 2001053898), and the EC (COST Chemistry Action D20) for support. Dr. Francesco Cannito is gratefully acknowledged for his assistance in the preparation of the manuscript.



Supporting information for this article is available on the WWW under <http://www.angewandte.org> or from the author.



Scheme 1. Synthesis of **2Cl** and further reaction to form **3** or **4**. See text for details.

treating a solution of **1** in chloroform with a solution of Cl_2 in CCl_4 (undried solvents). Again, the only reaction product was the aqua species **2** (see the Supporting Information, Figure S1).

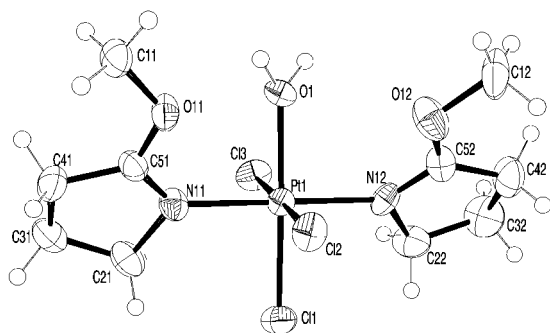


Figure 1. Drawing of complex **2** in the crystalline state. The ellipsoids enclose 50% probability. Selected bond distances [Å] and angles [°]: Pt1–Cl1 2.283(3), Pt1–Cl2 2.308(3), Pt1–Cl3 2.310(3), Pt1–O1 2.035(7), Pt1–N11 2.021(9), Pt1–N12 2.023(9), N11–C51 1.281(15), C51–O11 1.333(14), N12–C52 1.331(15), C52–O12 1.311(15); O1–Pt1–Cl2 94.6(2), O1–Pt1–Cl3 85.1(2), Cl1–Pt1–Cl2 88.8(1), Cl1–Pt1–Cl3 91.5(1), Pt1–N11–C51 129.6(8), Pt1–N12–C52 129.8(8), N11–C51–O11 120(1), N12–C52–O12 118(1).

The X-ray structure of **2** is shown in Figure 1.^[5–7] The bond distances agree well with those previously reported for Pt^{IV} complexes (Pt–N 2.022(9), Pt–O 2.035(7), Pt–Cl 2.309(3) Å for mutually *trans* chloride ligands and 2.283(3) Å for chloride *trans* to oxygen).^[8] The bond angles between the *cis* ligands are in the range of 88.7–91.5°, except for H_2O –Pt–Cl2 (94.6(2)°) and H_2O –Pt–Cl3 (85.1(2)°). In the organic ligands there is extensive electron delocalization over the oxygen atom and the C=N π system, as already observed in related systems (av C–O 1.32(1), av C–N 1.30(3) Å).^[9,10] The methyl groups of the 5-methoxy substituents are directed away from the metal center, thus allowing the methoxy oxygen atoms to be close to the coordinated water molecule (O1...O11 2.68(1), O1...O12 2.87(1) Å).

Under analogous conditions, the related dihydro oxazole complex *trans*-[PtCl₂{N=C(CH₃)OCH₂CH₂}₂] (in which a

methyl group has taken the place of the methoxy substituent) reacts with Cl_2 to give the tetrachloro platinum(IV) species *trans*-[PtCl₄{N=C(CH₃)OCH₂CH₂}₂] (see the Supporting Information, Figure S2).^[11] Therefore, the presence of two methoxy oxygen atoms is essential for the stabilization of the aqua species **2**.

In chloroform **2Cl** slowly reacts to the tetrachloro species *trans*-[PtCl₄{N=C(OCH₃)CH₂CH₂CH₂}₂] (**3**; $t_{1/2} \approx 12$ h, see Scheme 1 and the Supporting Information, Figure S3). The reaction appears to be catalyzed by a small amount of the platinum(II) compound **1**, which is formed by disproportionation of **2Cl** into **1** and Cl_2 .^[2]

Addition of excess Cl^- does not help in the conversion of **2** into **3**, but instead promotes the demethylation of **2** with formation of *trans*-[PtCl₃(OH){N=C(OH)CH₂CH₂CH₂}₂]{N=C(O)CH₂CH₂CH₂}[–] (**4**) according to Equation (1) (see Scheme 1 and the Supporting Information, Figure S4).



Compound **4** is stable in chloroform, even in the presence of excess chloride ion, and represents the first mononuclear platinum complex with 5-hydroxy-3,4-dihydro-2H-pyrrole ligands to be isolated and fully characterized. In contrast, a large number of platinum complexes with bridging 5-oxy-3,4-dihydro-2H-pyrrole ligands (α -pyrrolidonato) have been reported.^[12]

The X-ray structure of **4** is shown in Figure 2. The coordination sphere of **4** is similar to that of **2** (Pt–N 2.050(5), Pt–O 2.025(4), Pt–Cl 2.318(5) Å for mutually *trans* chloride atoms and 2.312(1) Å for chloride *trans* to oxygen; the bond angles between the *cis* ligands are in the range 87.5–91.6°). The Pt–O bond distance is 0.01 Å shorter in **4** than in **2**,

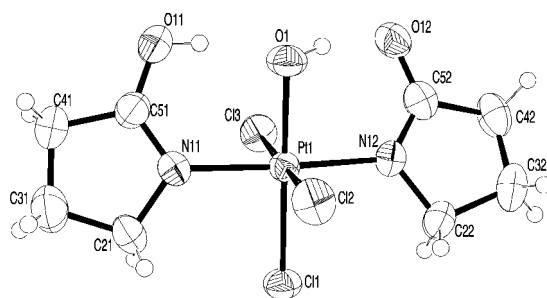


Figure 2. Drawing of complex **4** in the crystalline state. The ellipsoids enclose 50% probability. Selected bond distances [Å] and angles [°]: Pt1–Cl1 2.312(1), Pt1–Cl2 2.313(1), Pt1–Cl3 2.322(1), Pt1–O1 2.025(4), Pt1–N11 2.055(5), Pt1–N12 2.045(4), N11–C51 1.310(7), C51–O11 1.273(7), N12–C52 1.311(7), C52–O12 1.258(7); O1–Pt1–Cl2 87.5(1), O1–Pt1–Cl3 91.1(1), Cl1–Pt1–Cl2 91.1(1), Cl1–Pt1–Cl3 90.4(1), Pt1–N11–C51 124.1(4), Pt1–N12–C52 124.5(4), N11–C51–O11 125.8(5), N12–C52–O12 126.3(5).

while the Pt–Cl distance *trans* to Pt–O is 0.03 Å longer in **4** than in **2**; this reflects the different nature of the O donor (OH[−] and OH₂, respectively). The hydroxo ligand, while donating a hydrogen bond to the 5-oxy-dihydropyrrole ligand, accepts a hydrogen bond from the 5-hydroxy-dihydropyrrole ligand (O1...O12 2.551(7) Å, O1–H...O12 165(1)°; O1...O11 2.426(7) Å, O1...H–O11 167(1)°). Furthermore, there is extensive electron delocalization over the oxygen atom and the C=N π system of the dihydropyrrole ligands (av C–O 1.27(1), av C–N 1.31(1) Å).

The demethylation reaction does not take place in the case of compound **3**. Therefore, the coordinated water molecule in **2** appears to play an important role in the nucleophilic substitution of the nearby methoxy group by an external chloride ion. The coordinated water molecule can help in capturing this chloride ion. Furthermore, **2** is positively charged while **3** is neutral, and therefore in chloroform **2** can form an ionic couple with Cl[−]. The inertness of **2** in water, even in the presence of 5 × 10^{−2} M HCl and 10^{−3} M platinum(II) catalyst—as compared to its slow reactivity in chloroform, where it affords **3** or, in the presence of excess Cl[−], **4**—must be connected with the greater ability of water to solvate ionic species.

The O-demethylation is an important reaction in biological systems^[13] as well as in organic chemistry.^[14] Metal-mediated O-demethylation of coordinated ligands is also described in the literature.^[15,16] However, in the case of platinum substrates there are only very few reports. These include Arbuzov-like dealkylation of coordinated phosphites promoted by Cl[−],^[17] demethylation of a coordinated O⁶-methyldeoxyguanosine with thiophenol,^[18] and dealkylation of 2-alkoxyphenylphosphanes to form O-metalated chelates.^[19] All these reactions generally require high temperatures and long reaction times.

In conclusion, it appears that concepts that usually apply to complex natural substrates—such as intramolecular hydrophobic–hydrophilic interactions and organization of a reactive site—can also apply to simple coordination compounds with interesting and unexpected changes in their behavior. Therefore, compound **2**, in which the coordinated water molecule is surrounded by the oxygen atoms of two 5-methoxy-dihydropyrrole ligands, is favored over the fully chlorinated species **3** and represents the end product in aqueous solution. Moreover, the hydrophilic site of the complex, with a coordinated water molecule and nearby methoxy oxygen atoms, is suited to host the Cl[−] anion, which promotes demethylation in a hydrophobic solvent.

Experimental Section

All reagent-grade chemicals were purchased from Aldrich and used without further purification.

Compound **1** was synthesized by ligand cyclization of *trans*-[PtCl₂{HN=C(OCH₃)CH₂CH₂CH₂Cl}], which was prepared according to the procedure described in reference [9] for analogous compounds. The cyclization reaction was performed in acetone with powdered KOH and is complete in 1 h at 25°C, leading to the quantitative formation of **1**.

The treatment of **1** in chloroform with a solution of Cl₂ in CCl₄ (undried solvents) leads to the instantaneous and quantitative

formation of **2**Cl. A solution of **2** in chloroform, left standing at room temperature, undergoes slow transformation with formation of **3** (t_{1/2} ≈ 12 h at 25°C). Treatment of a solution of **2**Cl in chloroform with excess (PPh₄)Cl leads to ligand demethylation with formation of (PPh₄)**4** and release of CH₃Cl (t_{1/2} ≈ 5 h in 2 × 10^{−3} M (PPh₄)Cl at 25°C).

Further details of the synthesis and elemental analysis of **1–4** are given in the Supporting Information. The ¹H NMR spectra of **1–4** were recorded at 25°C on a Bruker DMX 300 spectrometer. The spectral changes for the oxidation of **1** to **2**Cl by Cl₂, for the spontaneous transformation of **2**Cl into **3**, and for the reaction of **2**Cl with excess (PPh₄)Cl to give (PPh₄)**4** and CH₃Cl are given in the Supporting Information (Figures S1, S3, and S4, respectively). Because of fast proton exchange between residual water in the solvent and coordinated water molecule (**2**) or hydroxyl groups (**4**), only a broad signal is observed below 2 ppm. This is clearly shown in Figure S3 of the Supporting Information, where the very broad signal at ca. 1.6 ppm in the initial spectrum becomes sharp and shifts to 1.5 ppm as the coordinated water molecule of **2** is replaced by Cl[−].

Received: February 26, 2004

Revised: July 5, 2004 [Z54111]

Keywords: demethylation · O ligands · oxidation · platinum · solvent effects

- a) L. M. Rendina, R. J. Puddephatt, *Chem. Rev.* **1997**, 97, 1735–1754; b) R. A. Gossage, A. D. Ryabov, A. L. Spek, D. J. Stufkens, J. A. M. van Beek, R. van Eldik, G. van Koten, *J. Am. Chem. Soc.* **1999**, 121, 2488–2497, and references therein.
- Y. N. Kukushkin, *Russ. J. Inorg. Chem.* **1963**, 8, 417–420.
- K. A. Morgan, M. M. Jones, *J. Inorg. Nucl. Chem.* **1972**, 34, 259–274; K. A. Morgan, M. M. Jones, *J. Inorg. Nucl. Chem.* **1972**, 34, 275–296.
- M. Crespo, R. Puddephatt, *Organometallics* **1987**, 6, 2548–2550.
- Crystal data for **2**Cl·2H₂O (C₁₀H₂₄Cl₄N₂O₅Pt): *M*_w = 589.2, colorless parallelepiped crystal, monoclinic space group *P*2₁/*c*, *a* = 16.246(2), *b* = 7.865(1), *c* = 15.055(1) Å, β = 94.46(1)°, *V* = 1917.8(4) Å³, *Z* = 4, ρ_{calcd} = 2.041 g cm^{−3}, Siemens P4 diffractometer, 2θ_{max} = 50°, radiation MoKα, λ = 0.71073 Å, scan mode ω, *T* = 293 ± 2 K; of 4351 measured reflections, 3350 were independent and 2859 were included in the refinement (*I* > 2σ(*I*)). Lorentz and polarization corrections were performed, absorption corrections were made through the ψ-scan technique, μ = 7.893 mm^{−1}. The structure was solved by direct methods and refined with Fourier methods (SHELX97-WINGX),^[6,7] no. of parameters 223, hydrogen atoms were included in calculated positions (HFIX-SHELX97),^[6,7] *R*1 = 0.0450 and *wR*2 = 0.1494 for the observed reflections, *R*1 = 0.0592 and *wR*2 = 0.1785 for all reflections, refinement residual electron density 1.813 e Å^{−3}. Crystal data for (PPh₄)**4** (C₃₂H₃₄Cl₃N₂O₃Pt): *M*_w = 827.06, pale yellow prism, monoclinic space group *P*2₁/*n*, *a* = 11.596(2), *b* = 11.040(2), *c* = 25.058(5) Å, β = 99.55(1)°, *V* = 3163.5(10) Å³, *Z* = 4, ρ_{calcd} = 1.736 g cm^{−3}, 2θ_{max} = 50°, radiation MoKα, λ = 0.71073 Å, scan mode ω, *T* = 293 ± 2 K; of 7186 measured reflections, 5574 were independent and 5574 were included in the refinement (*I* > 2σ(*I*)). Lorentz and polarization corrections were performed, absorption corrections were made through the ψ-scan technique, μ = 4.776 mm^{−1}. The structure was solved by direct methods and refined with Fourier methods; no. of parameters 383, *R*1 = 0.0323 and *wR*2 = 0.0699 for the observed reflections, *R*1 = 0.0463 and *wR*2 = 0.0749 for all reflections, refinement residual electron density 0.602 e Å^{−3}. Methods for treatment of hydrogen atoms, instruments, computers and software as for **2**. CCDC-231767 (**2**Cl·2H₂O) and CCDC-231768 ((PPh₄)**4**) contain the supplementary crystallographic

data for this paper. These data can be obtained free of charge via www.ccdc.cam.ac.uk/conts/retrieving.html (or from the Cambridge Crystallographic Data Centre, 12, Union Road, Cambridge CB21EZ, UK; fax: (+44)1223-336-033; or deposit@ccdc.cam.ac.uk).

- [6] G. M. Sheldrick, SHELXS 97, Program for the Solution of Crystal Structures, University of Göttingen, Germany, **1997**.
- [7] G. M. Sheldrick, SHELXL 97, Program for the Refinement of Crystal Structures, University of Göttingen, Germany, **1997**.
- [8] a) H. Junicke, K. Schenzel, F. W. Heinemann, K. Pelz, H. Bogel, D. Steinborn, *Z. Anorg. Allg. Chem.* **1997**, 623, 603–607; b) J. Müller, F. Glahe, E. Freisinger, B. Lippert, *Inorg. Chem.* **1999**, 38, 3160–3166; c) H. Schollhorn, R. Beyerle-Pfnur, U. Thewalt, B. Lippert, *J. Am. Chem. Soc.* **1986**, 108, 3680–3688; d) I. Dieter, B. Lippert, H. Schollhorn, U. Thewalt, *Z. Naturforsch. B* **1990**, 45, 731–740; e) F. P. Intini, M. Lanfranchi, G. Natile, C. Pacifico, A. Tiripicchio, *Inorg. Chem.* **1996**, 35, 1715–1717.
- [9] R. Cini, P. A. Caputo, F. P. Intini, G. Natile, *Inorg. Chem.* **1995**, 34, 1130–1134.
- [10] A. M. Gonzales, R. Cini, F. P. Intini, C. Pacifico, G. Natile, *Inorg. Chem.* **2002**, 41, 470–478.
- [11] $\text{trans-[PtCl}_2\{\text{N}=\text{C}(\text{CH}_3)\text{OCH}_2\text{CH}_2\}_2]$ was prepared according to the method reported by R. A. Michelin, R. Bertani, M. Mozzon, G. Bombieri, F. Benetollo, R. J. Angelici, *Organometallics* **1991**, 10, 1751–1757. The oxidation reaction was performed as reported for compound **1**.
- [12] a) B. Lippert in *Cisplatin; Chemistry and Biochemistry of a Leading Anticancer Drug* (Ed.: B. Lippert) Verlag Helvetica Chimica Acta, Zürich, **1999**, pp. 379–403; b) K. Matsumoto in *Cisplatin; Chemistry and Biochemistry of a Leading Anticancer Drug* (Ed.: B. Lippert) Verlag Helvetica Chimica Acta, Zürich, **1999**, pp. 455–475; c) J. K. Barton, H. N. Rabinowitz, D. J. Szalda, S. J. Lippard, *J. Am. Chem. Soc.* **1977**, 99, 2827–2829; d) T. V. Halloran, P. K. Mascharak, I. D. Williams, M. M. Roberts, S. J. Lippard, *Inorg. Chem.* **1987**, 26, 1261–1270; e) K. Sakai, Y. Tanaka, Y. Tsuchiya, K. Hirata, T. Tsubomura, S. Iijima, A. Bhattacharjee, *J. Am. Chem. Soc.* **1998**, 120, 8366–8379; f) K. Matsumoto, K. Fuwa, *Inorg. Chem.* **1983**, 22, 4086–4090; g) K. Matsumoto, H. Takahashi, K. Fuwa, *J. Am. Chem. Soc.* **1984**, 106, 2049–2054; h) K. Ito, R. Somazawa, J. Matsunami, K. Matsumoto, *Inorg. Chim. Acta* **2002**, 339, 292–296.
- [13] D. W. Nebert, F. J. Gonzales, *Annu. Rev. Biochem.* **1987**, 56, 945–993.
- [14] a) J. R. Hwu, S.-C. Tsay, *Chem. Commun.* **1998**, 161–168; b) A. Maercker, *Angew. Chem.* **1987**, 99, 1002–1019; *Angew. Chem. Int. Ed. Engl.* **1987**, 26, 972–989.
- [15] T. B. Brill, S. J. Landon, *Chem. Rev.* **1984**, 84, 577–585.
- [16] a) R. D. Simpson, *Organometallics* **1997**, 16, 1797–1799; b) C. W. Rogers, B. O. Patrick, J. Rettig, M. O. Wolf, *J. Chem. Soc. Dalton Trans.* **2001**, 1278–1283; c) T. Ren, V. De Silva, G. Zou, C. Lin, L. M. Daniels, C. F. Campana, J. C. Alvarez, *Inorg. Chem. Commun.* **1999**, 2, 301–303.
- [17] a) T. Miyamoto, *J. Organomet. Chem.* **1977**, 134, 335–362; b) J. M. Solar, R. D. Rogers, W. R. Mason, *Inorg. Chem.* **1984**, 23, 373–377.
- [18] K. Kohda, I. Terashima, N. Sawada, I. Nozaki, M. Yasuda, Y. Kawazoe, *Chem. Res. Toxicol.* **1992**, 5, 8–91.
- [19] a) J. S. Sun, C. E. Uzelmeier, D. L. Ward, K. R. Dunbar, *Polyhedron* **1998**, 17, 2049–2063; b) C. E. Jones, B. L. Shaw, B. L. Turtle, *J. Chem. Soc. Dalton Trans.* **1974**, 992–999.

Organic–Inorganic Hybrid Nanoparticles with a Complex Hollow Structure***Jianzhong Du and Yongming Chen**

Block copolymers spontaneously self-organize into nanometer-scale structures and are therefore of great interest for emerging nanomaterials and nanotechnologies.^[1] Well-defined polymer aggregates, such as spheres, vesicles, rods, tubules, and lamellae, form in selective solvents.^[1–11] Vesicles, which contain a cavity, are particularly interesting owing to their potential applications in encapsulation, drug release, and catalyst supports.^[2,3b,c,4,7] However, copolymer-derived nanoparticles with complex internal structure are less common. Eisenberg and co-workers discovered so-called large-compound vesicles (LCVs) in their family of crew-cut aggregates formed by self-assembly of asymmetric polystyrene-*b*-poly(acrylic acid) and polystyrene-*b*-poly(ethylene oxide) block copolymers in solution.^[8] LCVs, which were supposed to be the fusion of many vesicles, consist of many small compartments separated by a copolymer matrix. Furthermore, meso-sized crystallike aggregates with internal hexagonally packed hollow hoops (HHHs) in the matrix have been reported.^[9] These are the only examples of polymer aggregates with complex hollow structures as far as we know.^[10] Moreover, if one segment of block copolymers bears reactive groups, the resulting aggregates can be fixed by chemical crosslinking. Such nanoparticles are shape-persistent, even with changes in the environment. Thus far, a few successful crosslinking reactions within the vesicle wall have been reported, such as photodimerization and polymerization.^[3b,c,4,11]

Herein, we report a simple approach to prepare novel organic–inorganic hybrid nanoparticles with a complex hollow structure. The method is based on the self-assembly of a reactive amphiphilic block copolymer, poly(ethylene

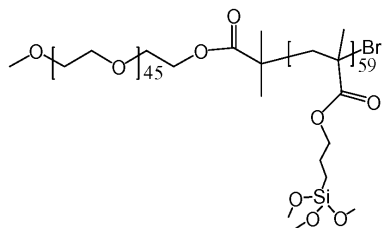
[*] Dr. J. Du, Prof. Dr. Y. Chen
State Key Laboratory of Polymer Physics and Chemistry
Joint Laboratory of Polymer Sciences and Materials
Institute of Chemistry, The Chinese Academy of Sciences
Beiyijie No. 2, Zhongguancun, Haidian, Beijing 100080 (People's Republic of China)
Fax: (+86) 10-62559373
E-mail: ymchen@iccas.ac.cn
Dr. J. Du
Graduate School of The Chinese Academy of Sciences
Yuquanlu No. 19 (Jin). Shijingshan, Beijing 100039 (People's Republic of China)

[**] Financial supports from BAIREN Project and the Directional Innovation Project (KJCX2-SW-H07) of the CAS are greatly acknowledged. Authors thank Professor Charles C. Han in Institute of Chemistry the CAS, Professor Anchang Shi in McMaster University, Professor Manfred Schmidt in Mainz University and Professor Dale Schaefer in University of Cincinnati for valuable discussions.



Supporting information for this article is available on the WWW under <http://www.angewandte.org> or from the author.

oxide)-*block*-poly[3-(trimethoxysilyl)propyl methacrylate] (PEO-*b*-PTMSPMA, Scheme 1) in *N,N*-dimethylformamide (DMF)/water solution, followed by a sol-gel process cata-



Scheme 1. The structure of poly(ethylene oxide)-*block*-poly[3-(trimethoxysilyl)propyl methacrylate] (PEO-*b*-PTMSPMA).

lyzed by triethylamine (TEA).^[11] Owing to the crosslinking in preformed polymer aggregates, the particles are very stable and shape-persistent. PEO₄₅-*b*-PTMSPMA₅₉ diblock copolymer was first dissolved in DMF, and then water, a selective solvent for PEO, was added dropwise.^[12] A pale, blue solution formed spontaneously, indicating micelle formation.^[12] Finally, a small amount of TEA (1.5 wt %) was added to fix the morphology by hydrolysis and polycondensation of the -Si(OCH₃)₃ groups. Several days later, a drop of this solution was spread on a carbon-coated copper grid for transmission electron microscopy (TEM) analysis.

A TEM image of the gelated mesoporous particles obtained at an initial polymer concentration (*c*_i) of 0.1 mg mL⁻¹ is shown in Figure 1A. The majority of the material consists of particles with a well-defined and uniform internal structure. Since the polysilsesquioxane absorbs more of the electron beam relative to PEO, the white area corresponds to the cavities, which are separated by the crosslinked walls. The size of these interior compartments ranges from 5 to 20 nm, and the compartment wall thickness is around 15 nm. In addition, a few simple vesicles were also found. Exclusive complex particles with many small cavities were found as the *c*_i was increased to 1.0, 2.0, 6.0, and 8.0 mg mL⁻¹.^[12] A typical TEM image (*c*_i = 2.0 mg mL⁻¹) is shown in Figure 1B. The size of the particles increased, and the amount of the cavities increased while the cavity size remains essentially constant. The morphology is quite similar to that of the LCVs^[8] reported in the literature, but the particle size is much smaller and shows low polydispersity (see Supporting Information). Such hollow particles were produced at *c*_i = 2.0 mg mL⁻¹, and the proportion of water ranged from 40 to 94 wt %. A typical TEM image for a sample prepared in 94 wt % water is shown in Figure 1C.

In particular, flowerlike particles appeared when *c*_i was increased to 10 or 20 mg mL⁻¹. The corresponding TEM images are shown in Figure 1D and in the Supporting Information. A scanning electron microscopy (SEM) image of the flower (Figure 1E) shows a clear three-dimensional morphology consistent with a robust particle that does not collapse when the water is removed.^[13] Interestingly, there are some vesicle-like mastoids protruding from the multicavity core. The core of the flowers did not collapse in the dry state,

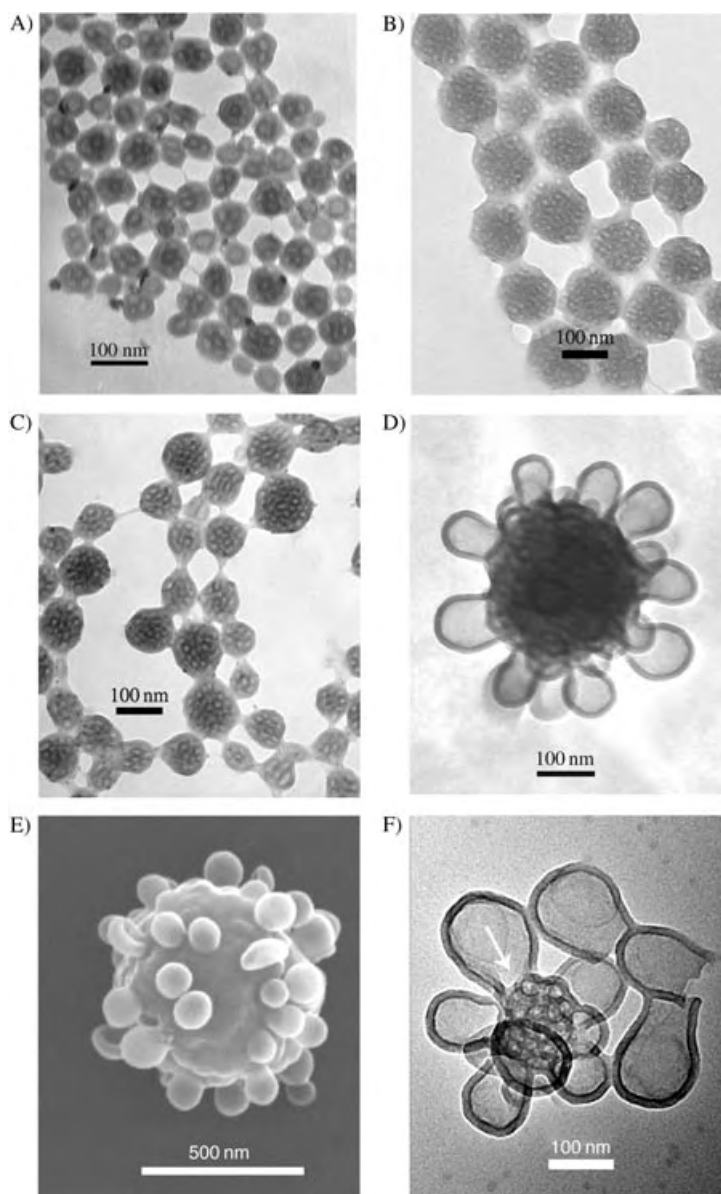


Figure 1. Typical TEM (A, B, C, D, and F) and (E) SEM images of complex hollow particles. The initial polymer concentration in DMF (*c*_i) is 0.1 (A), 2.0 (B, C), and 20.0 mg mL⁻¹ (D, E, F). Water content is 51.4 wt %, except for C (94 wt %). F: TEM image of a smaller flower and fallen petals.

although the diameter reached 500 nm.^[14] Thus, an internal polymer skeleton must be present to support the particle. The “wavy skin” between the petals reflects the complicated inner structure beneath the skin. From the smaller particles in Figure 1F (see also Supporting Information) which contain fewer cavities, we observe that the cavities are separated by uniform walls whose thickness (≈ 15 nm) is the same as that of the petals. There are few individual vesicles with an opening like that in Figure 1F. Accordingly, some holes are observed from the surface of some flower cores (see Supporting Information). The holes result from stripping the petals, possibly during stirring or sample preparation.

To confirm further the multihollow structure, a powder sample was embedded in epoxy resin, and sections ≈ 50–

80 nm thick were obtained by microtoming. As indicated by the white spots in Figure 2A, the particles formed at lower c_i have a multicavity hollow structure with polydispersed cavity sizes. This observation agrees with the TEM results in Figure 1B. More cavities form with increasing particle size, as a result of increasing c_i . The size of the honeycombl-like cavities ranges from 19 to 26 nm, which is more uniform than that of particles prepared at lower c_i (Figure 2B).

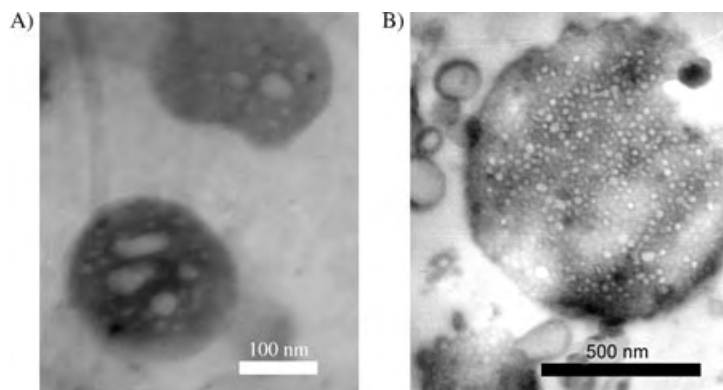


Figure 2. TEM images of particles embedded in epoxy resin showing the internal morphology of the hollow particles. In this case, A and B correspond to the samples of Figure 1B and D, respectively.

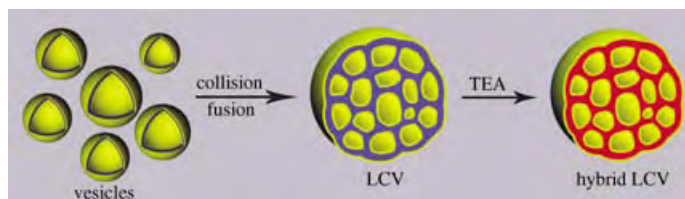
The novel particles with the complex hollow structure described herein are striking. However, it is still difficult to know the actual morphology before gelation, as the particles are too soft to retain their fine inner structure in the dry state. After addition of the TEA catalyst, however, we believe that the gelation fixes the aggregates without altering the hollow structure. This conclusion works with simple vesicle formation.^[11] This is because the hydrolysis reaction catalyzed by the base is slower than polycondensation. Once partial hydrolysis occurs in the PTMSPMA domain, the polycondensation proceeds simultaneously. As a result, the morphology is retained. Furthermore, the wall thickness of the hollow particles is very uniform and is consistent with a bilayer structure^[15]

that results from the self-assembly of a block copolymer in solution. In addition, similar hollow structures were also found with the self-assembly of other block copolymers.^[8,9]

The diblock copolymer PEO-*b*-PTMSPMA self-assembles into LCVs, which are possibly fused vesicles, in DMF/water. This result is very different from the simple vesicles in the methanol/water mixture described in our previous work.^[11] Actually, the bilayer which consists of PTMSPMA aggregated phase and PEO corona at two sides, is still the basic structure of LCVs, just like the simple vesicles. The morphological difference is related to the nature of common solvents. The vesicles in methanol/water solution are stabilized by the repulsive interaction of the PEO corona. However, such interactions are not strong enough to stabilize the individual vesicles in the DMF/water system owing to the high interfacial potential. The vesicles tend to undergo adhesion and fusion to decrease the interfacial potential,

thus leading to the formation of LCVs. Therefore, the thickness of the wall of the outermost particle and that of the membrane between the cavities inside the core are uniform, that is, a bilayer structure. At low c_i , the amount of vesicles in solution is lower, and therefore correspondingly fewer vesicles are fused to produce smaller LCVs with fewer cavities (Figure 1A). As c_i increases, the number of vesicles increases, and more vesicles are fused to give larger particles with more cavities (Figure 1B). Therefore, like simple vesicles, the hydrophilic PEO corona covers the two sides of a bilayer; but many solvent pools are encapsulated by the copolymer matrix inside one particle (Scheme 2). When the gelation catalyst was introduced, the crosslinking reaction occurred immediately, and the morphologies were fixed (Scheme 2). However, the formation of flowerlike particles at high c_i is still puzzling. We speculate that different sizes of simple vesicles were formed at high c_i . The interfacial potential is high for smaller particles and relatively low for larger particles. Therefore, adhesion and fusion occur preferentially with smaller rather than with larger vesicles. After the smaller vesicles are consumed, the larger vesicles adhere to the surface of the compound vesicles and fuse with them.

In conclusion, organic–inorganic hybrid particles with complex hollow structures were prepared very simply by the gelation of trimethoxysilyl groups in the preformed self-assembly of PEO-*b*-PTMSPMA in DMF/water solution.



Scheme 2. Possible mechanism for the formation of hybrid large-compound vesicles (LCVs): Simple vesicles collide each other and then fuse into LCVs. The triethylamine (TEA) catalyzes the hydrolysis and polycondensation reactions. Yellow: PEO, blue: PTMSPMA, red: polyorganosiloxane from the sol-gel processes of PTMSPMA.

Inside the resulting particle, there are many cavities insulated by crosslinked hybrid bilayers of uniform thickness. Owing to gelation, the morphology of particles is stable against drastic changes in conditions.^[16] The potential application of such novel nanomaterials in encapsulation is very promising. For example, as there are many cavities inside the particles, it may be possible to encapsulate functional species into different cavities of a particle for stepwise-release.

Experimental Section

The block copolymer, PEO₄₅-*b*-PTMSPMA₅₉ (composition determined from ¹H NMR spectrum (CDCl₃), $M_w/M_n = 1.34$ by SEC calibrated by PS standard), which was synthesized by atom-transfer radical polymerization.^[11a,17] To prepare micelles, copolymer (0.1–20 mg) was dissolved in DMF (1.0 mL), and water was then added dropwise over 10 min by syringe with vigorous stirring. A pale blue

solution forms spontaneously, indicating the formation of polymeric micelles. After five hours, TEA (20 μL) was added to induce the hydrolysis and crosslinking of micelles. TEM images were obtained on a JEM 100 instrument. To prepare TEM samples, 5 μL of micelle solution was dropped on a carbon-coated copper grid and dried at ambient temperature for 2 or more days. For the observation of internal morphologies of the particles, a powder sample was embedded in a mixture of epoxy resin and diethylenetriamine (100:11, w/w), and then placed in an oven at 60°C for 12 h. Sections (50–80 nm) were obtained by microtoming. To obtain an SEM image, a drop of solution was spread on a silica wafer and left to dry. Samples were coated with platinum and viewed on an Hitachi S-4300 electron microscope operated at 15 kV. The images were recorded with a digital camera. Particle size and size distribution were determined from the TEM image.

Received: March 12, 2004

Revised: June 21, 2004 [Z54244]

Keywords: block copolymers · micelles · self-assembly · sol-gel processes · vesicles

- [13] A low-magnification view of the flowers is shown in the Supporting Information.
 - [14] Simple vesicles larger than 100 nm obtained from a methanol/water mixture may collapse upon dryness for analysis; unpublished results.
 - [15] The wall thickness by TEM is ~ 15 nm, and the contour length of PTMSPMA₅₀ is 14.8 nm.
 - [16] The shape of the flowers did not change when the particle solution was sonicated for 30 min, and no clear change was found when the sample was calcined at 450°C for 7 h.
 - [17] J. Z. Du, Y. M. Chen, *Macromolecules* **2004**, *37*, 6322–6328.
-
- [1] a) I. W. Hamley, *Angew. Chem.* **2003**, *115*, 1730–1752; *Angew. Chem. Int. Ed.* **2003**, *42*, 1692–1712; b) S. Förster, M. Konrad, *J. Mater. Chem.* **2003**, *13*, 2671–2688.
 - [2] a) L. Zhang, A. Eisenberg, *Science* **1995**, *268*, 1728–1731; b) N. S. Cameron, M. K. Corbierre, A. Eisenberg, *Can. J. Chem.* **1999**, *77*, 1311–1326.
 - [3] a) Y. Y. Won, H. T. Davis, F. S. Bates, *Science* **1999**, *283*, 960–963; b) B. M. Discher, Y.-Y. Won, D. S. Ege, J. C.-M. Lee, F. S. Bates, D. E. Discher, D. A. Hammer, *Science* **1999**, *284*, 1143–1145; c) B. M. Discher, H. Bermudez, D. A. Hammer, D. E. Discher, Y. Y. Won, F. S. Bates, *J. Phys. Chem. B* **2002**, *106*, 2848–2854.
 - [4] a) F. Henselwood, G. J. Liu, *Macromolecules* **1998**, *31*, 4213–4217; b) J. Ding, G. J. Liu, *J. Phys. Chem. B* **1998**, *102*, 6107–6113.
 - [5] K. B. Thurmond, T. Kowalewski, K. L. Wooley, *J. Am. Chem. Soc.* **1996**, *118*, 7239–7240.
 - [6] a) J. Ruez, I. Manners, M. A. Winnik, *Langmuir* **2002**, *18*, 7229–7239; b) J. Ruez, I. Manners, M. A. Winnik, *J. Am. Chem. Soc.* **2002**, *124*, 10381–10395.
 - [7] a) S. A. Jenekhe, X. L. Chen, *Science* **1998**, *279*, 1903–1907; b) S. A. Jenekhe, X. L. Chen, *Science* **1999**, *283*, 372–375.
 - [8] a) K. Yu, L. F. Zhang, A. Eisenberg, *Langmuir* **1996**, *12*, 5980–5984; b) L. F. Zhang, A. Eisenberg, *Macromolecules* **1996**, *29*, 8805–8815; c) K. Yu, A. Eisenberg, *Macromolecules* **1998**, *31*, 3509–3518.
 - [9] a) L. F. Zhang, C. Bartels, Y. S. Yu, H. W. Shen, A. Eisenberg, *Phys. Rev. Lett.* **1997**, *79*, 5034–5037; b) K. Yu, C. Bartels, A. Eisenberg, *Langmuir* **1999**, *15*, 7157–7167.
 - [10] A microsphere with a complex hollow loop structure was produced by microphase separation in a droplet of emulsion. Z. H. Lu, G. J. Liu, F. T. Liu, *Macromolecules* **2001**, *34*, 8814–8817.
 - [11] Simple vesicles were found by similar strategy in a methanol/water mixture: a) J. Z. Du, Y. M. Chen, Y. H. Zhang, C. C. Han, K. Fischer, M. Schmidt, *J. Am. Chem. Soc.* **2003**, *125*, 14710–14711; b) J. Z. Du, Y. M. Chen, *Macromolecules* **2004**, *37*, 5710–5716.
 - [12] The initial concentration (c_i) of the block copolymer was 0.1, 1.0, 2.0, 6.0, 8.0, 10, 20 mg mL^{-1} . The proportion of water was 51.4 wt %. If c_i is higher than 10 mg mL^{-1} , the solution becomes turbid, but no precipitation occurs for several months. The corresponding final particle diameter is 63 ± 10 , 125 ± 24 , 100 ± 12 , 148 ± 23 , 172 ± 19 , 278 ± 60 , 530 ± 113 nm, respectively.

Natural Products Synthesis

**Total Synthesis of Thiostrepton, Part 1:
Construction of the Dehydropiperidine/
Thiazoline-Containing Macrocycle****

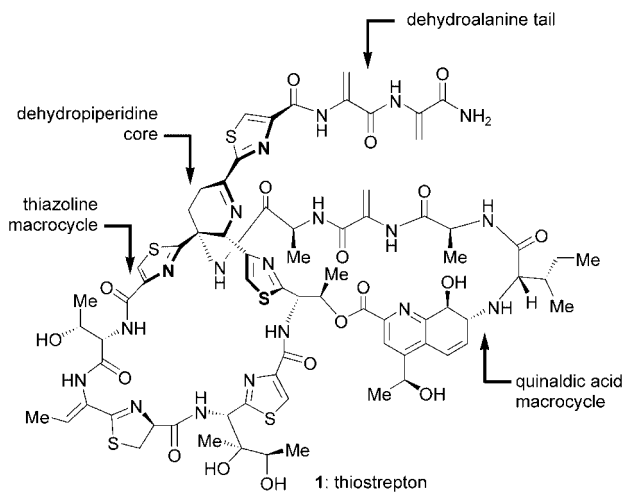
K. C. Nicolaou,* Brian S. Safina, Mark Zak,
Anthony A. Estrada, and Sang Hyup Lee

In memory of Murray Goodman

Thiostrepton (**1**), a powerful antibiotic isolated from *Streptomyces azureus* ATCC 14921, *Streptomyces hawaiiensis* ATCC 12236, and *Streptomyces laurentii* ATCC 31255,^[1] exhibits a remarkable biological profile and an imposing molecular architecture. Recognized as the flagship member of the growing class of thiopeptide antibiotics, this naturally occurring substance is extensively used in animal health care.^[2] In addition, thiostrepton (**1**) exhibits impressive antimalarial activity and is effective against *Plasmodium falciparum*, the parasite responsible for the majority of human malaria.^[3] Furthermore, selective cytotoxicity against cancer cells has been recently attributed to preparations that contain thiostrepton (**1**).^[4] The antibiotic activity of **1** against Gram-positive bacteria has been traced to its binding to the 23S

[*] Prof. Dr. K. C. Nicolaou, B. S. Safina, M. Zak, A. A. Estrada,
Dr. S. H. Lee
Department of Chemistry and The Skaggs Institute for Chemical
Biology
The Scripps Research Institute
10550 North Torrey Pines Road, La Jolla, California 92037 (USA)
Fax: (+1) 858-784-2469
and
Department of Chemistry and Biochemistry
University of California, San Diego
9500 Gilman Drive, La Jolla, California 92093 (USA)
E-mail: kcn@scripps.edu

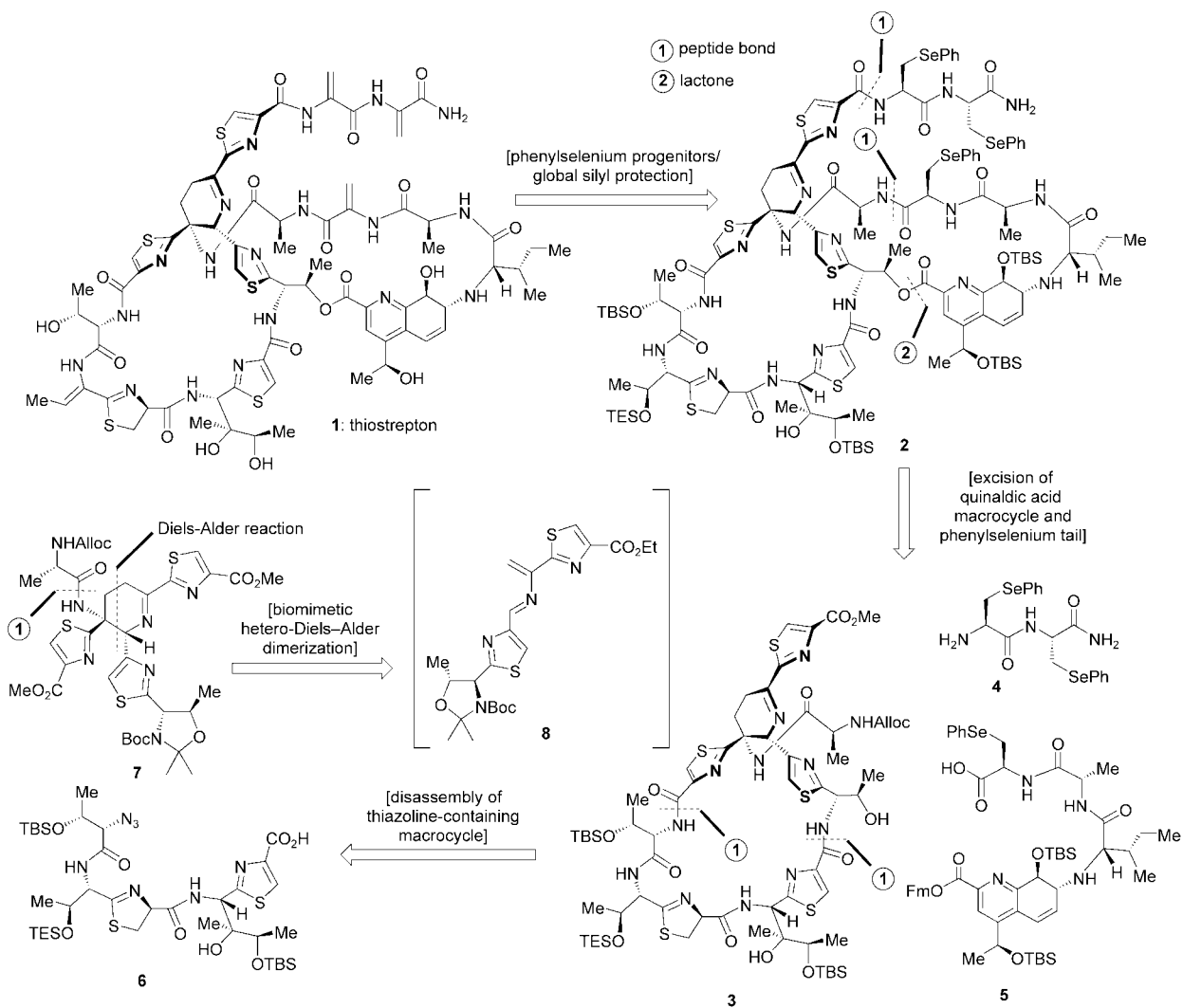
[**] We thank Dr. D. H. Huang and Dr. G. Siuzdak for NMR spectroscopic and mass spectrometric assistance, respectively. Financial support for this work was provided by grants from the National Institutes of Health (USA) and the Skaggs Institute for Chemical Biology, and fellowships from the National Institutes of Health (USA) (to A.A.E.) and The Skaggs Institute for Research (to M.Z.).



region of ribosomal RNA and protein L11, an event that blocks the GTPase-dependent activities of the 50S ribosomal subunit.^[5] The molecular architecture of **1** is both stunningly complex and highly sensitive. At its heart lies a dehydropi-

peridine core which serves as a lynchpin holding the bisdehydroalanine tail and the two macrocyclic domains, the 26-membered thiazoline-containing ring and the 27-membered quinaldic acid ring system. This acid- and base-sensitive structure contains 10 rings, 11 peptide bonds, an imine functionality, a secondary amine, numerous sites of unsaturation, and 17 stereogenic centers, all of which make the task of its total synthesis all the more daunting, as already recognized by several potential suitors.^[6] Herein and in the following Communication in this issue^[7] we report the total synthesis of thiostrepton (**1**) in its naturally occurring form by a highly convergent strategy.

After several aborted attempts to synthesize **1**, we finally settled on the general strategy depicted retrosynthetically in Scheme 1. Because of the sensitive nature of the three dehydroalanine units of **1**, it was decided to protect them as phenylseleno surrogate groups; the equally sensitive *Z* double bond conjugated to the thiazoline moiety was also masked as a TES-protected hydroxy group, thereby leading (with further protection) to advanced intermediate **2** as a potential progenitor to **1**. It was anticipated that these delicate

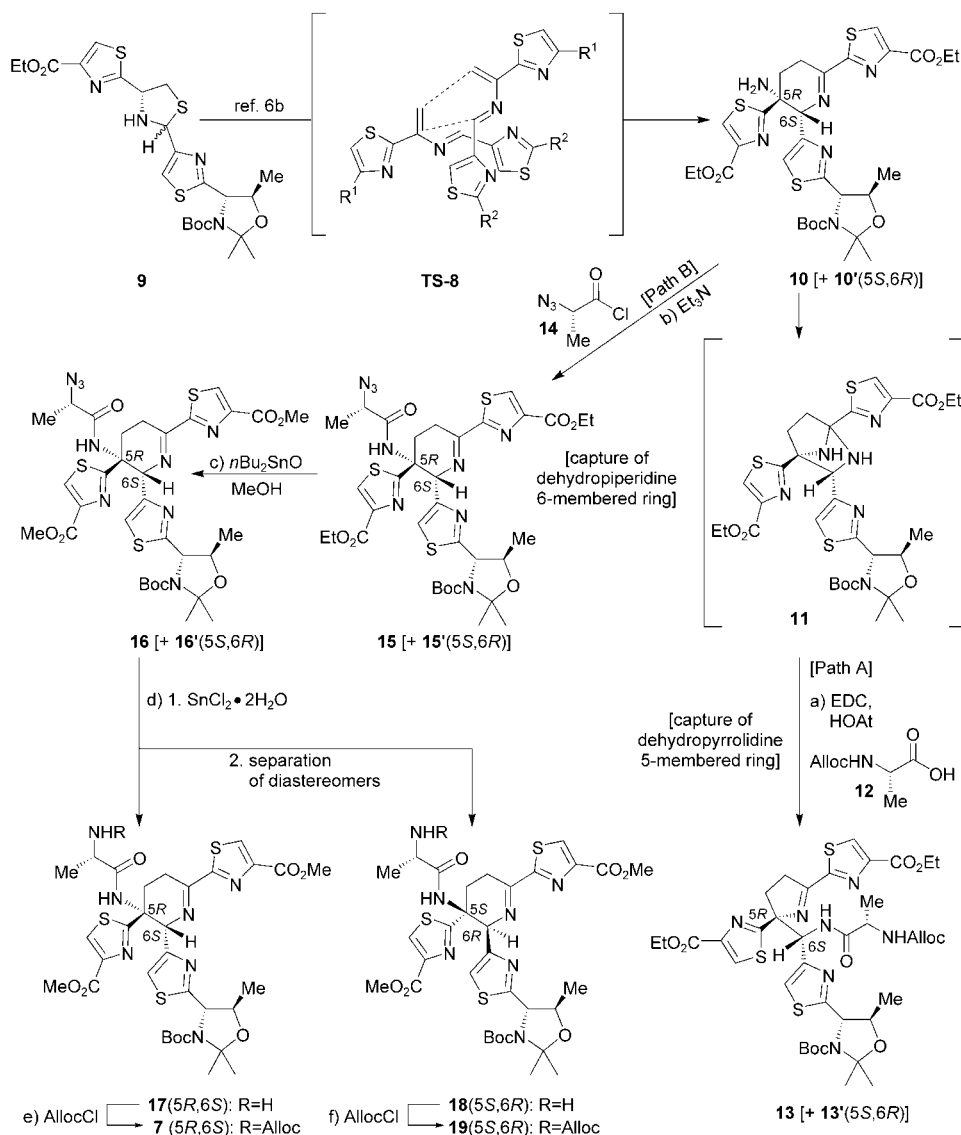


Scheme 1. Retrosynthetic analysis of thiostrepton (**1**). Alloc = allyloxy carbonyl; Boc = *tert*-butoxycarbonyl; TBS = *tert*-butyl dimethylsilyl; TES = triethylsilyl; FM = 9-fluorenylmethyl.

functionalities would be released, the latter in its proper geometrical form, under suitably mild conditions at the end of the synthesis to generate the desired target without risking its feared destruction. The retrosynthetic transformation of **2** led to macrocycle **3**, truncated by the excision of the bisphenyl-selenium derivative **4** and the quinaldic acid intermediate **5**. Retrosynthetic cleavage of macrocycle **3** at the two indicated peptide bonds (note the flexibility of macrolactamization site) led to azido thiazoline derivative **6** and dehydropiperidine core **7** (Scheme 1). Finally, disassembly of **7** through a hetero-Diels–Alder-type dimerization led to heterodiene **8**, which was previously demonstrated in our laboratories^[6b] to be a fleeting but viable precursor to the desired dehydropiperidine scaffold in a manner not so dissimilar to that proposed to be preferred by nature.^[8]

The first task was to prepare the dehydropiperidine building block **7**, an objective that turned out to be a considerable challenge, despite our early success in securing the free primary amine of the dehydropiperidine core **10**.^[6b] Scheme 2 outlines the chemical steps by which subtarget **7** was reached. Thus, as previously reported,^[6b] treatment of thiazolidine **9** with silver carbonate in the presence of DBU (1,8-diazabicyclo[5.4.0]undec-7-ene) and benzylamine generated fleeting azadiene **8**, whose spontaneous hetero-Diels–Alder dimerization (see **TS-8**) afforded, upon aminolysis, the dehydropiperidine core primary amine **10** as a 1:1 mixture with its chromatographically inseparable 5*S*,6*R* diastereomer **10'**.^[6b] Capturing the free amino group of these dehydropiperidine intermediates as amides with carboxy-activated alanine derivatives proved to be a thorny synthetic problem, as these substrates were susceptible to an apparent imine contraction facilitated by the neighboring amine function (see **11**, Scheme 2). The failed attempts to couple **10** (+ **10'**) with alanine derivatives under several conditions are exemplified by the reaction of *N*-Alloc alanine (**12**) in the presence of EDC–HOAt which led to the five-membered ring imine **13** (+ **13'**), presumably via the indicated amination **11** (path A), as previously reported.^[6c] It was only after extensive experimentation that precise conditions were found to capture the six-membered imine in its tracks by engaging its amino group before it had a chance to instigate the troublesome imine contraction. These conditions

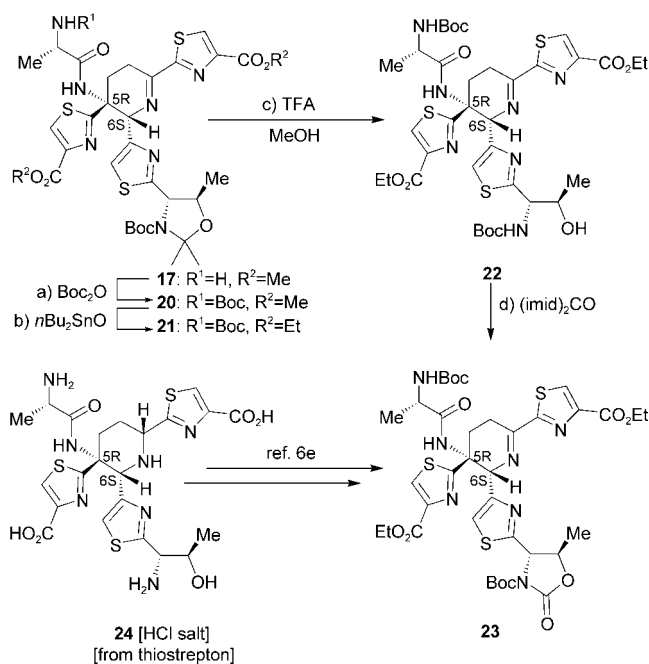
involved the use of the smaller, more-reactive electrophile **14**, the acyl chloride of the azide equivalent of alanine.^[9] Thus, treatment of the dehydropiperidine amine **10** (+ **10'**) with excess **14** and triethylamine in THF at 0 °C for 12 h (path B) produced, exclusively and in 68 % yield, amide **15** (+ **15'**) in which the six-membered imine ring was intact. The diastereomeric alanine-coupled dehydropiperidine derivatives continued to behave as inseparable mixtures until their ethyl esters were exchanged for the methyl esters (*n*Bu₂SnO, MeOH, 76 % yield, **16** (+ **16'**)) and the azide groups were reduced to primary amines (SnCl₂·2H₂O, 79 % total yield **17** (+ **18**)), at which stage they were separated by silica-gel flash-column chromatography. The individual primary amines were



Scheme 2. Construction of dehydropiperidine core **7**. Reagents and conditions: a) **12** (2.0 equiv), EDC (1.2 equiv), HOAt (1.3 equiv), DMF, 25 °C, 12 h, 84 %; b) **14** (2.0 equiv), Et₃N (4.0 equiv), THF, 0 °C, 12 h, 68 %; c) *n*Bu₂SnO (2.0 equiv), MeOH, 75 °C, 6 h, 76 %; d) 1. SnCl₂·2H₂O (3.0 equiv), MeOH, H₂O, 25 °C, 2 h; 2. silica gel, 100 % EtOAc; then 5 % MeOH/EtOAc, (5*R*,6*S*)-**17** 44 %, (5*S*,6*R*)-**18** 35 %; e) AllocCl (5.0 equiv), *i*Pr₂EtN (10.0 equiv), 4-DMAP (0.1 equiv), THF, 25 °C, 92 %; f) AllocCl (5.0 equiv), *i*Pr₂EtN (10.0 equiv), 4-DMAP (0.1 equiv), THF, 25 °C, 89 %. **TS-8**, R¹ = CO₂Et, R² = Boc acetonide threonine side chain. EDC = 1-ethyl-3-(dimethylaminopropyl)carbodiimide hydrochloride; HOAt = 1-hydroxy-7-azabenzotriazole; DMF = *N,N*-dimethylformamide; 4-DMAP = 4-(dimethylamino)pyridine.

then protected as their *N*-Alloc derivatives **7** (Table 1) and **19** (AllocCl, *i*Pr₂NEt, 4-DMAP (cat.), 92 % yield **7**, 89 % yield **19**).

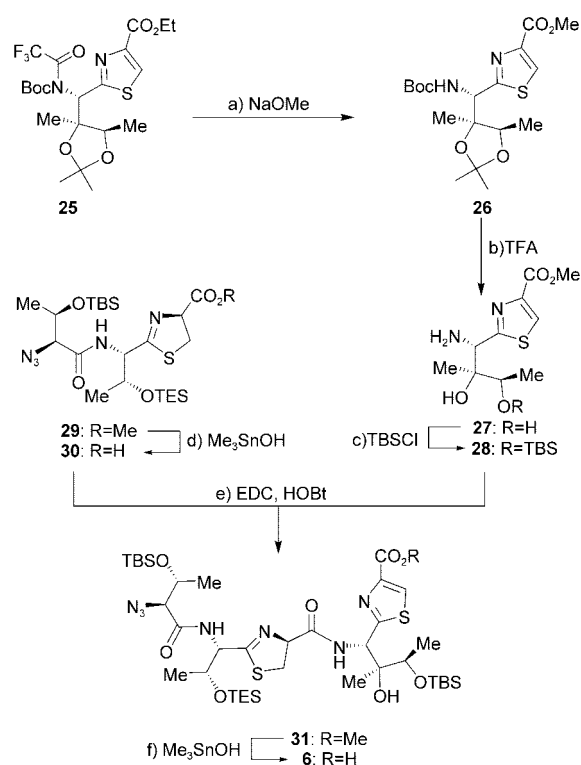
To distinguish between the 5*R*,6*S* and 5*S*,6*R* diastereomeric amines **17** and **18**, respectively, it was necessary to convert one of them into the known degradation product **23**^[6c] for spectroscopic comparison (Scheme 3). Thus, the less polar of the two diastereomers (which turned out to be **17**) was converted into compound **23** by the route shown in Scheme 3.



Scheme 3. Determination of C5, C6 stereochemistry of dehydropiperidine **17**. Reagents and conditions: a) Boc₂O (5.0 equiv), *i*Pr₂EtN (10.0 equiv), 4-DMAP (0.1 equiv), THF, 25 °C, 1 h, 61 %; b) *n*Bu₂SnO (2.0 equiv), EtOH, 65 °C, 5 h, 79 %; c) TFA, MeOH, 0 °C, 30 min, 54 % plus 40 % recovered starting material; d) (imid)₂CO (3.0 equiv), 4-DMAP (0.1 equiv), DMF, 25 °C, 24 h, 81 %. Boc = *tert*-butoxycarbonyl; imid = imidazole; TFA = trifluoroacetic acid.

The ¹H and ¹³C NMR spectra of synthetic **23** were identical to those previously reported^[6c] for the 5*R*,6*S* diastereomer, thereby confirming the correct stereochemistry for our less-polar synthetic intermediate **17**. With this stereochemical ambiguity clarified, we turned our attention to the required thiazoline building block **6**.

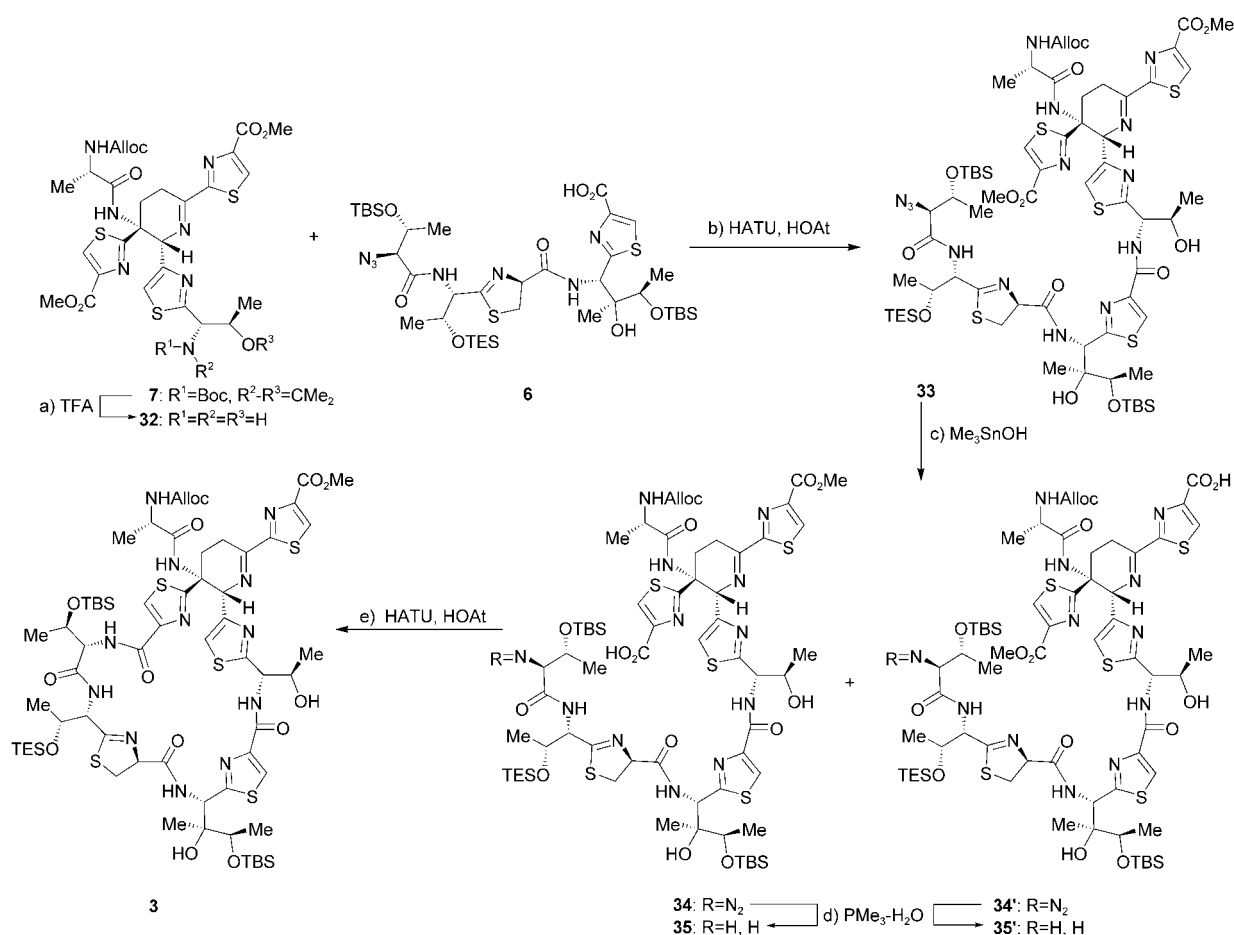
Scheme 4 summarizes the construction of the thiazoline–thiazole-containing fragment **6** from the previously synthesized building blocks, thiazole **25**^[6c] and thiazoline **29**^[6c]. In our attempts to liberate the carboxylic acid group within thiazoline **29** we faced the expected epimerization and elimination problems, both of which were solved through a remarkably mild and efficient protocol in which trimethyltin hydroxide was used. Thus, exposure of methyl ester **29** to Me₃SnOH^[10] in 1,2-dichloroethane at 80 °C led to carboxylic acid **30** in quantitative yield. In parallel, protected thiazole derivative **25** was converted into its amino methyl ester derivative **28** by: a) ester exchange and concomitant cleavage



Scheme 4. Construction of thiazoline–thiazole subunit **6**. Reagents and conditions: a) NaOMe (3.2 equiv), MeOH, 0 °C, 4 h, 91 %; b) TFA/CH₂Cl₂/MeOH (1.1:1.0:1), 0 °C, 1 h, 99 %; c) TBSCl (2.2 equiv), Et₃N (3.3 equiv), CH₂Cl₂, 0 °C, 3 h, 87 %; d) Me₃SnOH (3.0 equiv), 1,2-dichloroethane, 80 °C, 1 h, 100 %; e) EDC (1.2 equiv), HOBt (1.2 equiv), DMF, 0 °C, 1.5 h, 73 %; f) Me₃SnOH (3.0 equiv), 1,2-dichloroethane, 80 °C, 1 h, 100 %. HOBt = hydroxybenzotriazole.

of the *N*-trifluoroacetate (to give **26** in 91 % yield), b) cleavage of the *N*-Boc and acetonide protecting groups (to afford **27** in 99 % yield), and finally c) protection of the more reactive secondary alcohol as a TBS ether to provide **28** in 87 % yield. The two fragments **28** and **30** were then coupled through the action of EDC–HOBt to furnish dipeptide **31** (Table 1) in 73 % yield. The methyl ester of **31** was hydrolyzed under mild conditions to afford the target carboxylic acid **6** in quantitative yield and without epimerization or elimination around the sensitive thiazoline site.

The elaboration of the two advanced building blocks **7** and **6** into the thiazoline-containing macrocycle **3** is outlined in Scheme 5. Thus, in preparation for coupling with the thiazoline-containing carboxylic acid **6**, the dehydropiperidine derivative **7** was subjected to the action of TFA in CH₂Cl₂ at 0 °C to furnish amino alcohol **32** in good yield. The union of the latter compound with **6** was facilitated by HATU–HOAt and led to coupled product **33** in 73 % overall yield from **7**. The mild action of Me₃SnOH in 1,2-dichloroethane at 50 °C resulted in the formation of monoacids **34** and **34'** (54 % total yield) together with considerable amounts of the corresponding diacid (28 % yield) and starting diester (14 %). (Both the diacid and starting diester could be recovered and recycled—the diacid after methylation with EDC–MeOH.) Finally, the mixture of azido compounds **34** and **34'** was reduced with PMe₃–H₂O^[9] to afford the corresponding mixture of primary



Scheme 5. Construction of advanced thiazoline-containing macrocycle **3**. Reagents and conditions: a) TFA/ CH_2Cl_2 (1:1), 0°C, 2 h; b) **6** (1.0 equiv), HATU (1.2 equiv), HOAt (1.2 equiv), iPr_2NEt (3.0 equiv), DMF, 0°C, 30 min, 73% (two steps); c) Me_3SnOH (8.0 equiv), 1,2-dichloroethane, 50°C, 5 h, 54% (28% diacid, 14% recovered starting material); d) Me_3P (6.0 equiv), THF/ H_2O (10:1), 0°C, 1 h; e) HATU (5.0 equiv), HOAt (5.0 equiv), iPr_2NEt (6.0 equiv), DMF (2.0 mm), 65 h, 32% (from mixture of monoacids **34** and **34'**). HATU = *O*-(7-azabenzotriazol-1-yl)-*N,N,N',N'*-tetramethyluronium hexafluorophosphate.

Table 1: Selected physical properties for compounds **31**, **7**, and **3**.

31: $R_f=0.32$ (silica gel, EtOAc/hexanes 1:3); $[\alpha]_D^{25}=-22.9$ ($CHCl_3$, $c=1.0$); IR (film): $\tilde{\nu}_{max}=3392, 2959, 2881, 2115, 1725, 1680, 1497, 1247, 1103, 836, 775\text{ cm}^{-1}$; 1H NMR (600 MHz, CD_3OD): $\delta=8.37$ (s, 1 H), 5.45 (s, 1 H), 5.01 (dt, $J=9.7, 1.3$ Hz, 1 H), 4.7 (m, 1 H), 4.48 (dq, $J=6.6, 3.0$ Hz, 1 H), 4.36 (dq, $J=6.1, 2.2$ Hz, 1 H), 4.03 (q, $J=6.1$ Hz, 1 H), 3.93 (d, $J=4.0$ Hz, 1 H), 3.91 (s, 3 H), 3.62 (dd, $J=11.4, 1.7$ Hz, 1 H), 3.38 (dd, $J=11.4, 1.7$ Hz, 1 H), 1.35 (d, $J=6.2$ Hz, 3 H), 1.27 (d, $J=6.2$ Hz, 3 H), 1.23 (d, $J=6.2$ Hz, 3 H), 1.01 (s, 3 H), 0.99 (t, $J=14.5$ Hz, 9 H), 0.95 (s, 9 H), 0.90 (s, 9 H), 0.64 (dq, $J=7.9, 2.6$ Hz, 6 H), 0.12 (s, 6 H), 0.09 (s, 3 H), 0.08 ppm (s, 3 H); ^{13}C NMR (150 MHz, CD_3OD): $\delta=175.8, 173.5, 127.8, 170.9, 163.3, 146.5, 130.0, 79.3, 76.3, 71.4, 71.1, 70.3, 70.3, 59.7, 57.9, 52.8, 36.8, 26.6, 26.4, 21.6, 21.5, 18.9, 18.9, 18.3, 17.9$ ppm; HRMS (ESI-TOF): calcd for $C_{39}H_{73}N_7O_8S_2Si_3H^+$ [$M+H^+$]: 916.4342; found: 916.4343

7: $R_f=0.43$ (silica gel, EtOAc/hexanes 8:2); $[\alpha]_D^{25}=+14.2$ (solvent $CHCl_3$, $c=1.0$); IR (film) $\tilde{\nu}_{max}=3318, 3096, 2966, 2919, 1719, 1701, 1502, 1478, 1367, 1237, 1214, 1132, 1096, 991, 773\text{ cm}^{-1}$; 1H NMR (500 MHz, CD_3CN , 66°C): $\delta=8.27$ (s, 1 H), 8.04 (s, 1 H), 7.13 (s, 1 H), 5.84–5.75 (m, 1 H), 5.68 (br s, 1 H), 5.35 (br s, 1 H), 5.20 (dq, $J=17.3, 1.8$ Hz, 1 H), 5.11 (dq, $J=11.6, 1.8$ Hz, 1 H), 4.75 (d, $J=5.8$ Hz, 1 H), 4.30 (dd, $J=13.2, 6.3$ Hz, 1 H), 4.24–4.17 (br, 1 H), 4.02 (dt, $J=20.6, 7.0$ Hz, 1 H), 3.90 (s, 3 H), 3.85 (s, 3 H), 3.41 (ddd, $J=13.9, 7.0, 2.2$ Hz, 1 H), 3.14 (ddt, $J=19.8, 6.3, 2.2$ Hz, 1 H), 2.97–2.86 (m, 1 H), 2.72–2.63 (m, 1 H), 1.64 (s, 3 H), 1.59 (s, 3 H), 1.39 (d, $J=6.3$ Hz, 3 H), 1.33, (br, 9 H), 1.31 ppm (d, $J=6.9$ Hz, 3 H); ^{13}C NMR (125 MHz, CD_3CN , 66°C): $\delta=176.7, 174.3, 173.9, 170.7, 164.7, 162.7, 157.0, 153.5, 148.8, 147.8, 134.4, 131.9, 129.1, 120.3, 96.1, 81.8, 78.7, 67.7, 67.2, 66.5, 61.1, 53.4, 52.9, 52.8, 28.9, 28.4, 26.0, 19.1, 18.5$ ppm; HRMS (ESI-TOF): calcd for $C_{36}H_{45}N_7O_{10}S_3H^+$ [$M+H^+$]: 832.2463; found: 832.2459

3: $R_f=0.37$ (silica gel, EtOAc/hexanes 7:3); $[\alpha]_D^{25}=+16.9$ ($CHCl_3$, $c=1.0$); IR (film) $\tilde{\nu}_{max}=3394, 2927, 1670, 1528, 1483, 1256, 1101\text{ cm}^{-1}$; 1H NMR (500 MHz, CD_3CN , 66°C): $\delta=8.30$ (s, 1 H), 8.16 (s, 1 H), 7.87 (br d, $J=10.0$ Hz, 1 H), 7.77 (br d, $J=8.4$ Hz, 1 H), 7.37 (s, 2 H), 5.95–5.90 (br, 1 H), 5.80–5.71 (m, 1 H), 5.57 (d, $J=8.8$ Hz, 1 H), 5.37–5.33 (m, 1 H), 5.27–5.22 (m, 1 H), 5.18 (dq, $J=17.3, 1.5$ Hz, 1 H), 5.08 (dq, $J=10.7, 1.5$ Hz, 1 H), 4.98 (dt, $J=9.2, 1.9$ Hz, 1 H), 4.83 (br d, $J=8.8$ Hz, 1 H), 4.73–4.69 (br, 1 H), 4.64–4.59 (br, 1 H), 4.30–4.23 (br, 3 H), 4.10 (q, $J=6.3$ Hz, 1 H), 3.95 (quint, $J=7.0$ Hz, 1 H), 3.64 (dd, $J=13.2, 7.4$ Hz, 1 H), 3.57 (d, $J=9.2$ Hz, 2 H), 3.24 (br d, $J=16.5$ Hz, 1 H), 2.92–2.83 (m, 1 H), 2.49–2.42 (m, 1 H), 1.32 (d, $J=6.2$ Hz, 3 H), 1.24 (d, $J=6.3$ Hz, 3 H), 1.23 (d, $J=7.0$ Hz, 3 H), 1.21 (d, $J=6.6$ Hz, 3 H), 1.10 (d, $J=6.3$ Hz, 3 H), 1.05 (s, 3 H), 0.98 (s, 9 H), 0.96 (t, $J=8.1$ Hz, 9 H), 0.95 (s, 9 H), 0.64 (q, $J=7.7$ Hz, 6 H), 0.20 (s, 3 H), 0.19 (s, 3 H), 0.12 (s, 3 H), 0.09 (s, 3 H); HRMS (ESI-TOF): calcd for $C_{65}H_{100}N_{12}O_{14}S_5Si_3H^+$ [$M+H^+$]: 1517.5466; found: 1517.5432

amines **35** and **35'**, which upon ring closure in the presence of HATU–HOAt–*i*Pr₂NEt gave the desired macrocycle **3** in 32% overall yield from mono acids **34** and **34'** as the only identifiable cyclic product. The formation of only one macro-lactam in this reaction is remarkable, and was noted with a measure of considerable trepidation, as the product, in principle, could have had the wrong connectivity (i.e. that arising from **35'**). Only the eventual conversion of **3** (Table 1) into thiostrepton (**1**) could confirm its proper structure, a wish that came true as we describe in the following Communication in this issue.^[7]

Received: July 16, 2004

Published Online: September 3, 2004

Keywords: antibiotics · azadienes · cycloaddition · natural products · total synthesis

q) T. R. Kelly, C. T. Jagoe, Z. Gu, *Tetrahedron Lett.* **1991**, 32, 4263–4266.

- [7] K. C. Nicolaou, M. Zak, B. S. Safina, S. H. Lee, A. A. Estrada, *Angew. Chem.* **2004**, 116, 5202–5207; *Angew. Chem. Int. Ed.* **2004**, 43, 5092–5097; see following Communication in this issue.
- [8] U. Mocek, Z. Zeng, D. O'Hagan, P. Zhou, L.-D. G. Fan, J. M. Beale, H. G. Floss, *J. Am. Chem. Soc.* **1993**, 115, 7992–8001.
- [9] Prepared from the corresponding azide carboxylic acid by exposure to (COCl)₂ (1.0 equiv) in THF at 0°C in the presence of catalytic amounts of DMF; for azide preparation from L-alanine and reduction of azides with PMe₃–H₂O, see: P. T. Nyffeler, C.-H. Liang, K. M. Koeller, C.-H. Wong, *J. Am. Chem. Soc.* **2002**, 124, 10773–10778.
- [10] R. L. E. Furlan, E. G. Mata, O. A. Mascaretti, *J. Chem. Soc. Perkin Trans. 1* **1998**, 355–358.

- [1] Isolation: a) J. F. Pagano, M. J. Weinstein, H. A. Stout, R. Donovan, *Antibiot. Annu.* **1955–1956**, 554–559; b) J. Vandeputte, J. D. Dutcher, *Antibiot. Annu.* **1955–1956**, 560–561; c) B. A. Steinberg, W. P. Jambor, L. O. Suydam, *Antibiot. Annu.* **1955–1956**, 562–565; structure determination: d) C. S. Bond, M. P. Shaw, M. S. Alphey, W. N. Hunter, *Acta Crystallogr. Sect. D* **2001**, 57, 755–758; e) B. Anderson, D. C. Hodgkin, M. A. Viswamitra, *Nature* **1970**, 225, 233–235.
- [2] S. M. Dennis, T. G. Nagaraja, A. D. Dayton, *Res. Vet. Sci.* **1986**, 41, 251–256.
- [3] a) G. A. McConkey, M. J. Rogers, T. F. McCutchan, *J. Biol. Chem.* **1997**, 272, 2046–2049; b) J. G. Hardman, L. E. Limbird, P. B. Molinoff, R. W. A. Ruddon, G. Gilman, *Goodman & Gilman's The Pharmacological Basis of Therapeutics*, 9th ed., McGraw-Hill, New York, **1996**, pp. 965–985.
- [4] K. Jonghee, PCT Int. Appl. WO 2002066046, **2002**.
- [5] Y. Xing, D. E. Draper, *Biochemistry* **1996**, 35, 1581–1588.
- [6] For synthesis studies from these laboratories, see: a) K. C. Nicolaou, B. S. Safina, C. Funke, M. Zak, F. J. Zécri, *Angew. Chem.* **2002**, 114, 2017–2020; *Angew. Chem. Int. Ed.* **2002**, 41, 1937–1940; b) K. C. Nicolaou, M. Nevalainen, B. S. Safina, M. Zak, S. Bulat, *Angew. Chem.* **2002**, 114, 2021–2025; *Angew. Chem. Int. Ed.* **2002**, 41, 1941–1945; c) K. C. Nicolaou, M. Nevalainen, M. Zak, S. Bulat, M. Bella, B. S. Safina, *Angew. Chem.* **2003**, 115, 3540–3546; *Angew. Chem. Int. Ed.* **2003**, 42, 3418–3424; for synthesis studies from other laboratories, see: d) S. Higashibayashi, M. Kohno, T. Goto, K. Suzuki, T. Mori, K. Hashimoto, M. Nakata, *Tetrahedron Lett.* **2004**, 45, 3707–3712; e) S. Higashibayashi, K. Hashimoto, M. Nakata, *Tetrahedron Lett.* **2002**, 43, 105–110; for the total syntheses of simpler members of the thiopeptide class of antibiotics, see: f) R. A. Hughes, S. P. Thompson, L. Alcaraz, C. J. Moody, *Chem. Commun.* **2004**, 946–948; g) S. Higashibayashi, T. Mori, K. Shinko, K. Hashimoto, M. Nakata, *Heterocycles* **2002**, 57, 111–122; h) M. C. Bagley, K. E. Bashford, C. L. Hesketh, C. J. Moody, *J. Am. Chem. Soc.* **2000**, 122, 3301–3313; i) M. A. Ciufolini, Y.-C. Shen, *Org. Lett.* **1999**, 1, 1843–1846; j) K. Okumura, T. Suzuki, Y. Nakamura, C.-g. Shin, *Bull. Chem. Soc. Jpn.* **1999**, 72, 1561–1569; k) K. Okumura, A. Ito, D. Yoshioka, C.-g. Shin, *Heterocycles* **1998**, 48, 1319–1324; l) C. J. Moody, M. C. Bagley, *Chem. Commun.* **1998**, 2049–2050; m) C.-g. Shin, K. Okumura, M. Shigekuni, Y. Nakamura, *Chem. Lett.* **1998**, 139–140; n) M. A. Ciufolini, Y. C. Shen, *J. Org. Chem.* **1997**, 62, 3804–3805; o) K. Okumura, M. Shigekuni, Y. Nakamura, C.-g. Shin, *Chem. Lett.* **1996**, 1025–1026; p) Y. Nakamura, C.-g. Shin, K. Umemura, J. Yoshimura, *Chem. Lett.* **1992**, 1005–1008;

Natural Products Synthesis

**Total Synthesis of Thiostrepton, Part 2:
Construction of the Quinaldic Acid Macrocycle
and Final Stages of the Synthesis****

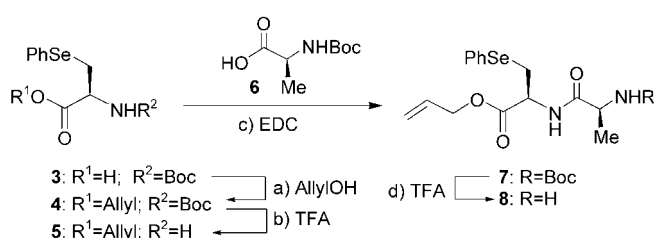
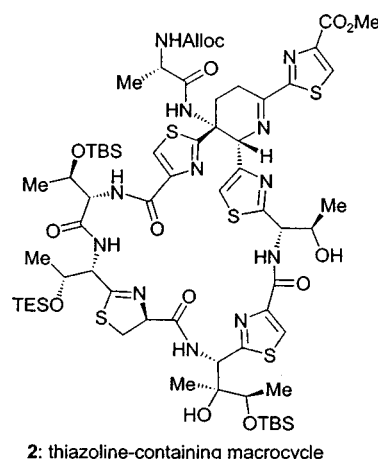
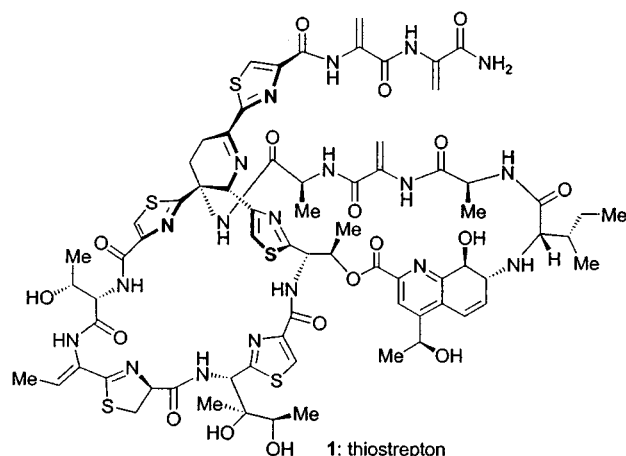
K. C. Nicolaou, Mark Zak, Brian S. Safina,
Sang Hyup Lee, and Anthony A. Estrada*

In the preceding Communication in this issue^[1] we described the construction of the thiazoline-containing macrocycle **2** as an advanced intermediate toward the total synthesis of thiostrepton (**1**). Herein we report the construction of suitable dipeptide (**8**, Scheme 1) and quinaldic acid (**22**, Scheme 2) fragments, their union with **2**, and the final stages of the total synthesis of **1**.

Scheme 1 outlines the synthesis of the required dipeptide derivative **8** from **3**, a known phenylseleno-substituted derivative of alanine.^[2] Thus, **3** was converted into allyl ester **4**, which was treated with TFA to effect its conversion into the amino derivative **5**. Coupling of amine **5** with Boc-L-alanine

[*] Prof. Dr. K. C. Nicolaou, M. Zak, B. S. Safina, Dr. S. H. Lee,
A. A. Estrada
Department of Chemistry and The Skaggs Institute for Chemical
Biology
The Scripps Research Institute
10550 North Torrey Pines Road, La Jolla, California 92037 (USA)
Fax: (+1) 858-784-2469
and
Department of Chemistry and Biochemistry
University of California, San Diego
9500 Gilman Drive, La Jolla, California 92093 (USA)
E-mail: kcn@scripps.edu

[**] We thank Dr. D. H. Huang and Dr. G. Siuzdak for NMR spectroscopic and mass spectrometric assistance, respectively. Financial support for this work was provided by grants from the National Institutes of Health (USA) and the Skaggs Institute for Chemical Biology, and fellowships from the National Institutes of Health (USA) (to A.A.E.) and The Skaggs Institute for Research (to M.Z.).



Scheme 1. Construction of dipeptide **8**. Reagents and conditions: a) AllylOH (2.0 equiv), EDC (1.1 equiv), 4-DMAP (0.1 equiv), CH_2Cl_2 , 25 °C, 3 h, 70%; b) TFA/ CH_2Cl_2 (1:1), 0 °C, 1 h; c) Boc-L-Ala-OH (1.1 equiv), HOAt (1.1 equiv), EDC (1.1 equiv), DMF, 25 °C, 2 h, 60% (two steps); d) TFA/ CH_2Cl_2 (1:1), 0 °C, 30 min, 99%. EDC=1-ethyl-(3-dimethylaminopropyl)carbodiimide hydrochloride, 4-DMAP=4-dimethylamino pyridine; TFA=trifluoroacetic acid; Boc=*tert*-butoxycarbonyl; HOAt=1-hydroxy-7-azabenzotriazole; DMF=*N,N*-dimethylformamide.

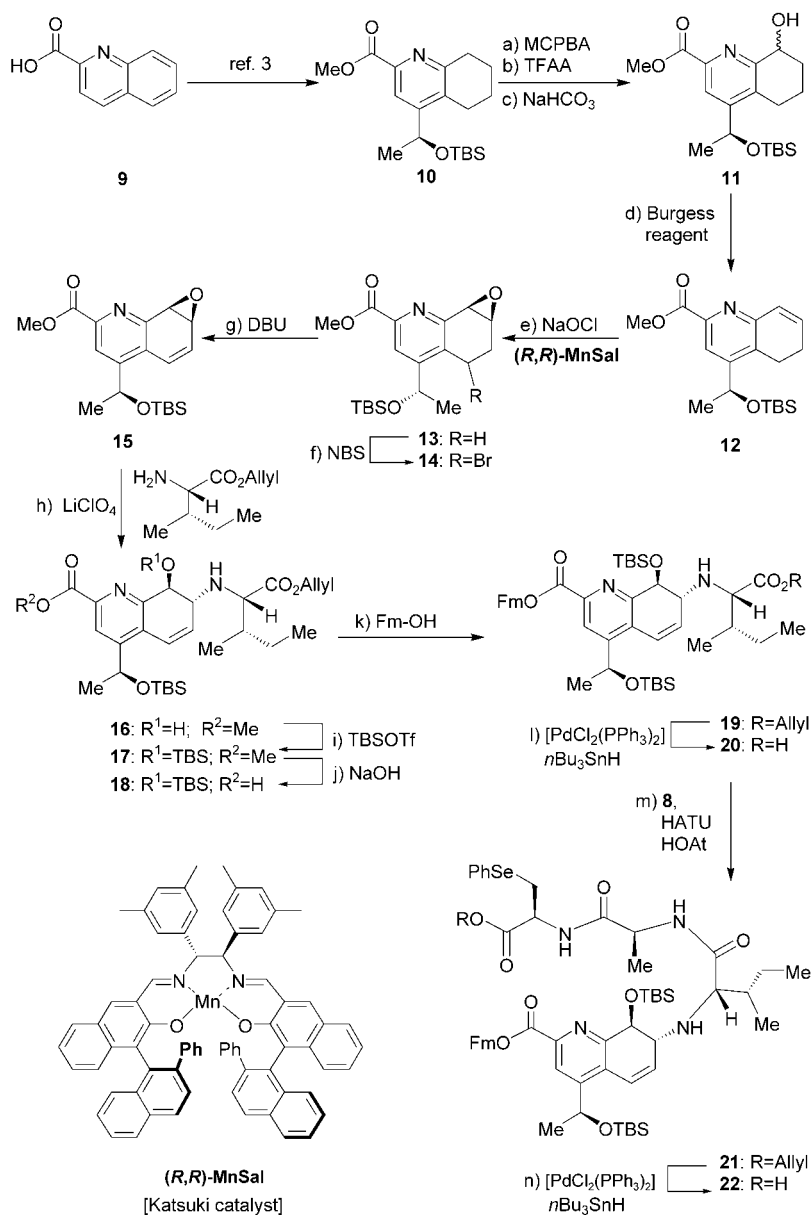
(6) proceeded under the influence of EDC–HOAt to afford dipeptide **7** (60% overall yield from **4**), whose TFA-mediated deprotection liberated primary amine **8**, ready for coupling with the appropriate quinaldic acid moiety.

Scheme 2 delineates the synthesis of the entire quinaldic acid chain **22** which commenced from 2-quinoline carboxylic acid (**9**) and proceeded through asymmetric epoxidation of olefin **12** and sequential attachment to the resulting epoxide of an isoleucine residue and of dipeptide **8**. Thus, **9** was converted in five steps and good overall yield as previously described^[3] into functionalized methyl ester **10**. The latter compound was then oxygenated to afford **11** in 65% overall yield through a Boekelheide-type sequence^[4] involving a) MCPBA-mediated *N*-oxide formation; b) TFAA-induced acylation of the generated *N*-oxide; and c) $NaHCO_3$ -facilitated rearrangement–hydrolysis of the resulting trifluoroacetate. Alcohol **11** was then dehydrated by treatment with Burgess reagent to afford olefin **12** in 68% yield. The product **12** served well as the precursor to the desired compound **13** in a diastereoselective epoxidation reaction brought about by NaOCl in the presence of the Katsuki manganese–salen catalyst (*R,R*)-MnSal and 4-phenyl-pyridine *N*-oxide.^[5]

Under these conditions, epoxide **13** was obtained as a mixture of diastereomers with the desired one predominating in $\approx 87:13$ ratio and 82% combined yield. Chromatographic separation of **13** followed by radical bromination led to a mixture of diastereomeric bromides **14** (40% yield plus 26% recovered starting material) which were eliminated by exposure to DBU to afford epoxyolefin **15** in 96% yield. The epoxide moiety within **15**

was then regio- and stereoselectively opened by the free amine of L-isoleucine allyl ester in the presence of lithium perchlorate to afford aminoalcohol **16** in 69% yield. Presumably, the observed regioselectivity in this reaction is due to coordination of the lithium ion with the quinaldic acid nitrogen atom which simultaneously activates the epoxide moiety and deactivates the benzylic site through destabilization of the incipient carbocation at that position.^[6] The hydroxy group of **16** was then protected as a TBS ether by treatment with TBSOTf in the presence of *i*Pr₂NEt to furnish bis(silyl ether) **17** (96% yield), whose methyl ester was selectively hydrolyzed by exposure to NaOH to afford carboxylic acid **18** (89% yield). This maneuver was necessary to install a protecting group on the pyridine-bound carboxy group suitable for the subsequent and rather delicate elaboration of the growing chain of the molecule. As such a moiety, the fluorenylmethyl (Fm) group was then introduced at this position by esterification with FmOH and through the Yamaguchi^[7] protocol, leading to ester **19** in 64% yield. The allyl ester group was then removed from the isoleucine residue by palladium-catalyzed reductive cleavage,^[8] which gave rise to the corresponding carboxylic acid **20** in good yield. Coupling of **20** with dipeptide **8** (Scheme 1) under established conditions generated quinaldic acid derivative **21** (Table 1) in 66% yield from **19**. Finally, treatment of **21** with $[PdCl_2(PPh_3)_2]$ –*n*Bu₃SnH liberated the targeted carboxylic acid **22** in 87% yield, ready for incorporation into the growing frame of **1**.

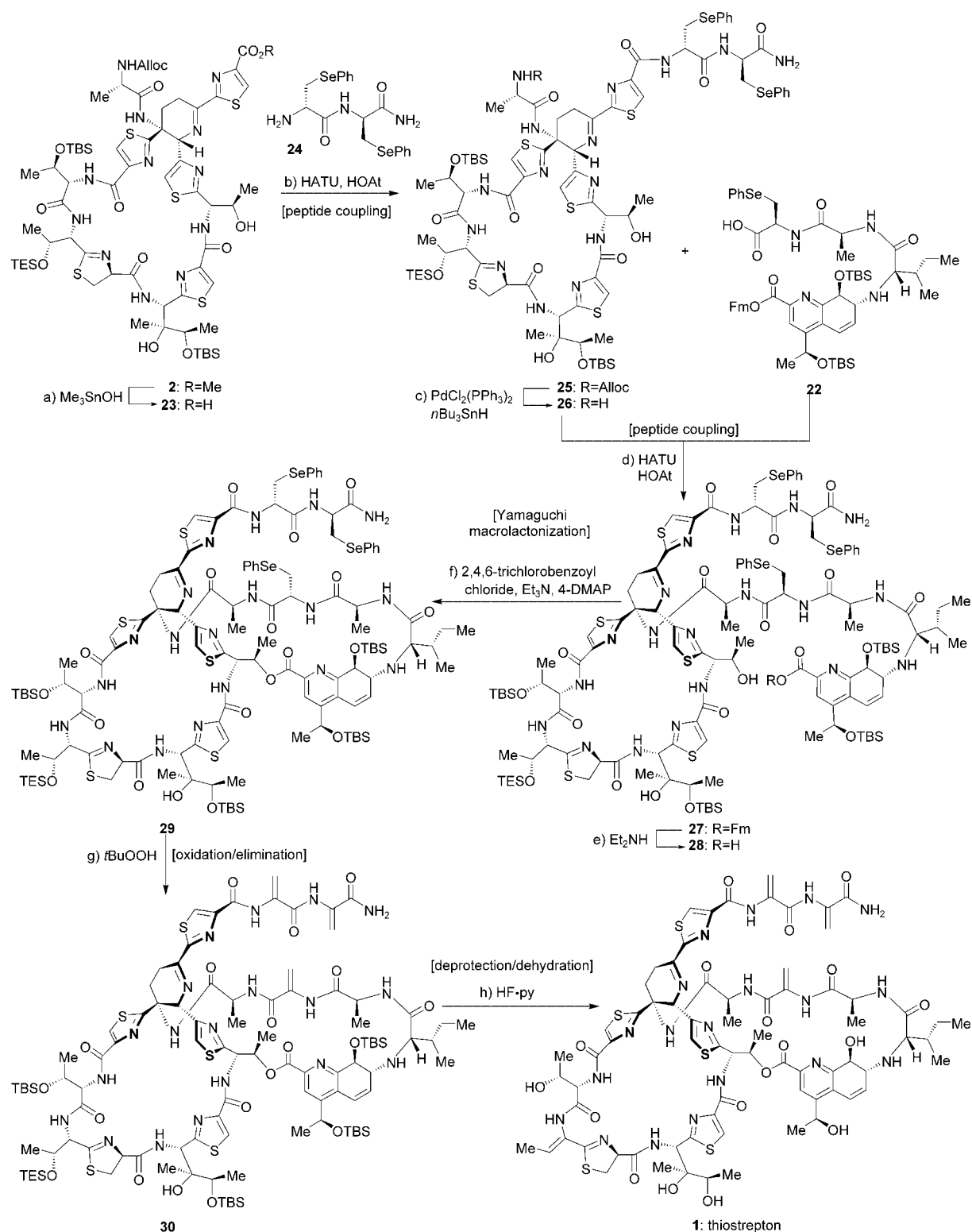
The completion of the total synthesis of thioestrepton (**1**) is depicted in Scheme 3. Advanced thiazoline macrocycle **2**^[1] was treated with Me_3SnOH ^[9] in 1,2-dichloroethane at 65 °C to liberate carboxylic acid **23**, which was coupled with the bisphenylselenium tail derivative **24** (prepared as previously described)^[10] under the influence of HATU–HOAt to afford intermediate **25** (Table 1) in 83% overall yield from **2**. Exposure of **25** to $[PdCl_2(PPh_3)_2]$ –*n*Bu₃SnH^[8] cleaved its Alloc group and furnished primary amine **26** in 86% yield in preparation for the incorporation of **22**. Indeed, coupling of amino compound **26** with carboxylic acid **22** was effected once again with HATU–HOAt, leading to polypeptide **27** (Table 1) in 64% yield. It was now time to consider the final macro-



Scheme 2. Synthesis of quinaldic acid subunit **22**. Reagents and conditions: a) MCPBA (1.0 equiv), CH₂Cl₂, 25 °C, 12 h; b) TFAA (3.0 equiv), CH₂Cl₂, 25 °C, 12 h; c) NaHCO₃ (2 M), CH₂Cl₂, 8 h, 65 % (three steps); d) Burgess reagent (1.2 equiv), THF/benzene (1:1), reflux, 3.5 h, 68%; e) (*R,R*)-**MnSal** (0.01 equiv), 4-Ph-py-*N*-oxide (0.1 equiv), NaOCl (0.79 M), phosphate buffer adjusted to pH 11.5 with NaOH (2.0 M), CH₂Cl₂, 25 °C, 1 h, 82%, ≈87:13 ratio of products; f) NBS (1.1 equiv), AIBN (0.1 equiv), CCl₄, 80 °C, 40 min, 40% (and 26% recovered starting material); g) DBU (1.1 equiv), THF, 25 °C, 2 h, 96%; h) H-L-Ile-OAlllyl (3.0 equiv), LiClO₄ (5.0 equiv), MeCN, 60 °C, 22 h, 69%; i) TBSTf (3.0 equiv), *i*Pr₂NEt (5.0 equiv), THF, 25 °C, 3 h, 96%; j) NaOH, MeOH, THF, 25 °C, 6 h, 89%; k) 2,4,6-trichlorobenzoyl chloride (2.0 equiv), Et₃N (6.0 equiv), toluene, 25 °C, 12 h; then FmOH (3.0 equiv), 4-DMAP (0.1 equiv), 25 °C, 12 h, 64%; l) [PdCl₂(PPh₃)₂] (0.1 equiv), *n*Bu₃SnH (1.1 equiv), CH₂Cl₂, 0 °C, 1 h; m) **8** (1.1 equiv), HATU (1.1 equiv), HOAt (1.1 equiv), DMF, 25 °C, 3 h, 66% (two steps); n) [PdCl₂(PPh₃)₂] (0.1 equiv), *n*Bu₃SnH (1.1 equiv), CH₂Cl₂, 0 °C, 30 min, 87%. MCPBA = *m*-chloroperoxybenzoic acid; TFAA = trifluoroacetic anhydride; NBS = *N*-bromosuccinimide; AIBN = 2,2'-azobisisobutyronitrile; DBU = 1,8-diazabicyclo[5.4.0]undec-7-ene; TBS = *tert*-butyldimethylsilyl; OTf = trifluoromethanesulfonate; Fm = 9-fluorenylmethyl; HATU = *O*-(7-azabenzotriazol-1-yl)-*N,N,N',N'*-tetramethyluronium hexafluorophosphate.

cyclization to the thiostrepton skeleton from this long-sought precursor. To this end, the Fm group was ejected from **27** by exposure to Et₂NH, and the resulting hydroxy acid **28** (87% yield) was subjected to macrolactonization under the Yamaguchi^[7] conditions to afford polycycle **29** (42% yield). All that now remained before reaching the coveted target, thiostrepton (**1**), was the unmasking of all its functionalities. First, all

three phenylseleno groups within **29** were expelled by *t*BuOOH-mediated oxidation, followed by spontaneous *syn* elimination of the resulting selenoxides, to furnish **30** (68% yield) with all three dehydroalanine subunits in place. Finally, the TES and four TBS groups were removed by exposure to excess HF·py in THF at ambient temperature, conditions which also caused the desired elimination of the oxygen



Scheme 3. Completion of the total synthesis of thiostrepton (**1**). Reagents and conditions: a) Me_3SnOH (10.0 equiv), 1,2-dichloroethane, 65°C , 2.5 h; b) **24** (2.0 equiv), HATU (1.2 equiv), HOAt (1.2 equiv), $i\text{Pr}_2\text{NEt}$ (3.0 equiv), DMF, 0°C , 2 h, 83% (two steps); c) $[\text{PdCl}_2(\text{PPh}_3)_2]$ (0.1 equiv), $n\text{Bu}_3\text{SnH}$ (50.0 equiv), 0°C , 1 h, 86%; d) **22** (1.1 equiv), HATU (1.1 equiv), HOAt (1.1 equiv), $i\text{Pr}_2\text{NEt}$ (3.0 equiv), DMF, 0°C , 1.5 h, 64%; e) $\text{Et}_2\text{NH}/\text{CH}_2\text{Cl}_2$ (1:6.5), 25°C , 2.5 h, 87%; f) 1. 2,4,6-trichlorobenzoyl chloride (30 equiv), Et_3N (40 equiv), concentrated in toluene, 25°C , 24 h; 2. 4-DMAP (30 equiv), toluene (0.5 mm), 24 h, 25°C , 42%; g) $t\text{BuOOH}$ (6.0 M in decane)/ CH_2Cl_2 (1:10), 25°C , 3 h, 68%; h) $\text{HF}\cdot\text{py}$ /THF (1:5), 25°C , 24 h, 52%. Alloc = allyloxycarbonyl; TBS = *tert*-butyldimethylsilyl; TES = triethylsilyl.

Table 1: Selected physical properties for compounds **21**, **25**, **27**, and **1**.

21: $R_f = 0.3$ (silica gel, EtOAc/hexanes 1:5); $[\alpha]_D^{25} = +44$ (CHCl₃, $c = 0.045$); IR (film): $\tilde{\nu}_{\max} = 3302, 2954, 2857, 1739, 1647, 1517, 1458, 1249, 1211, 1124, 1090$ cm⁻¹; ¹H NMR (600 MHz, CD₃CN, 70 °C): $\delta = 8.10$ (s, 1 H), 7.85–7.75 (m, 4 H), 7.54–7.52 (m, 2 H), 7.44–7.41 (m, 2 H), 7.39–7.34 (m, 2 H), 7.28–7.26 (m, 4 H), 6.99 (br d, $J = 3.0$ Hz, 1 H), 6.89 (d, $J = 10.0$ Hz, 1 H), 6.40 (dd, $J = 10.1, 5.3$ Hz, 1 H), 5.89–5.82 (m, 1 H), 5.29–5.18 (m, 4 H), 4.80 (d, $J = 3.5$ Hz, 1 H), 4.75–4.63 (m, 4 H), 4.51–4.48 (m, 1 H), 4.46–4.40 (m, 2 H), 4.35–4.32 (quint, $J = 7.3, 7.0$ Hz, 1 H), 3.49–3.46 (m, 1 H), 3.35–3.23 (m, 4 H), 3.07 (d, $J = 5.3$ Hz, 1 H), 1.70–1.60 (br s, 1 H), 1.38 (d, $J = 6.6$ Hz, 3 H), 1.30 (d, $J = 7.0$ Hz, 3 H), 0.94 (t, $J = 5.1$ Hz, 3 H), 0.90 (s, 9 H), 0.86 (d, $J = 7.1$ Hz, 1 H), 0.14 (s, 3 H), 0.10 (s, 3 H), –0.015 (s, 3 H), –0.098 ppm (s, 3 H); ¹³C NMR (150 MHz, CD₃CN, 70 °C): $\delta = 174.8, 173.5, 171.3, 166.5, 157.5, 152.6, 147.3, 145.5, 145.5, 144.4, 143.7, 142.7, 134.6, 134.5, 134.5, 133.8, 133.5, 130.8, 130.6, 129.2, 128.8, 128.6, 128.3, 126.8, 126.6, 123.3, 123.1, 121.4, 119.0, 76.1, 68.2, 68.1, 67.0, 65.7, 65.6, 58.8, 54.2, 50.0, 48.5, 39.9, 30.3, 29.1, 27.8, 26.7, 26.6, 26.5, 19.5, 19.3, 19.2, 19.2, 19.1, 18.9, 16.7, 14.2, 12.2, –3.5, –3.8, –4.0, –4.2$ ppm; HRMS (ESI-TOF): calcd for C₅₉H₈₀N₄O₈SeSi₃ [M+Na⁺]: 1131.4572; found: 1131.4598.

25: $R_f = 0.40$ (silica gel, 7% MeOH/CH₂Cl₂); ¹H NMR (600 MHz, CD₃CN, 70 °C): $\delta = 8.16$ (s, 1 H), 8.03 (d, $J = 7.0$ Hz, 1 H), 7.90 (d, $J = 9.2$ Hz, 1 H), 7.80–7.57 (m, 2 H), 7.56–7.52 (m, 1 H), 7.50–7.49 (m, 2 H), 7.39 (s, 1 H), 7.28–7.27 (m, 4 H), 7.24–7.23 (m, 3 H), 5.93 (br s, 1 H), 5.79–5.75 (m, 1 H), 5.58 (d, $J = 9.2$ Hz, 1 H), 5.39–5.38 (m, 1 H), 5.24 (br s, 1 H), 5.20 (dd, $J = 17.1, 1.3$ Hz, 1 H), 5.09 (dd, $J = 10.6, 1.1$ Hz, 1 H), 5.00 (dt, $J = 9.2, 1.4$ Hz, 1 H), 4.86–4.84 (m, 1 H), 4.72–4.65 (m, 2 H), 4.6 (br s, 1 H), 4.52–4.48 (m, 2 H), 4.32–4.25 (m, 4 H), 4.12 (q, $J = 6.1, 2.4$ Hz, 1 H), 4.00 (quint, $J = 6.6, 2.5$ Hz, 1 H), 3.69–3.64 (m, 1 H), 3.58 (d, $J = 9.2$ Hz, 2 H), 3.44–3.19 (m, 6 H), 2.89 (br s, 1 H), 2.46 (br s, 1 H), 1.33 (d, $J = 6.1$ Hz, 3 H), 1.25 (d, $J = 4.0$ Hz, 3 H), 1.24 (d, $J = 3.0$ Hz, 3 H), 1.22 (d, $J = 6.6$ Hz, 3 H), 1.10 (d, $J = 6.1$ Hz, 3 H), 0.98 (s, 9 H), 0.97–0.94 (m, 9 H), 0.95 (s, 9 H), 0.66 (q, $J = 7.9$ Hz, 6 H), 0.20 (s, 3 H), 0.19 (s, 3 H), 0.12 (s, 3 H), 0.09 ppm (s, 3 H); HRMS (ESI-TOF): calcd for C₈₂H₁₁₇N₁₅O₁₅Se₂Si₃ [M+Na⁺]: 1978.4987; found: 1978.4973.

27: $R_f = 0.55$ (silica gel, 7% MeOH/CH₂Cl₂); ¹H NMR (600 MHz, CD₃CN, 70 °C): $\delta = 8.15$ (s, 1 H), 8.09 (s, 1 H), 8.02 (d, $J = 7.9$ Hz, 1 H), 7.87 (d, $J = 8.3$ Hz, 1 H), 7.84–7.82 (m, 2 H), 7.76 (d, $J = 7.9$ Hz, 1 H), 7.73 (d, $J = 7.0$ Hz, 1 H), 7.57–7.56 (m, 2 H), 7.50–7.48 (m, 2 H), 7.46 (br s, 1 H), 7.41–7.38 (m, 2 H), 7.32 (t, $J = 7.4$ Hz, 2 H), 7.26–7.15 (m, 9 H), 7.14 (d, $J = 4.0$ Hz, 1 H), 6.87 (s, 1 H), 6.86 (d, $J = 10.1$ Hz, 1 H), 6.36 (dd, $J = 10.1$ Hz, 1 H), 5.56 (d, $J = 9.7$ Hz, 1 H), 5.37 (s, 1 H), 5.25–5.23 (m, 2 H), 4.97 (m, 1 H), 4.84–4.82 (m, 1 H), 4.77 (d, $J = 3.5$ Hz, 1 H), 4.72–4.60 (m, 5 H), 4.52–4.49 (m, 2 H), 4.41 (t, $J = 6.0$ Hz, 1 H), 4.38–4.31 (m, 2 H), 4.28–4.24 (m, 2 H), 4.19 (t, $J = 8.2$ Hz, 1 H), 4.10–4.05 (m, 2 H), 3.63–3.55 (m, 4 H), 3.48–3.45 (m, 1 H), 3.44–3.32 (m, 4 H), 3.30–3.10 (m, 2 H), 2.96–2.86 (m, 1 H), 2.45 (br s, 1 H), 1.35 (d, $J = 7.0$ Hz, 3 H), 1.32 (d, $J = 6.1$ Hz, 3 H), 1.24–1.21 (m, 9 H), 1.16–1.15 (d, $J = 6.1$ Hz, 3 H), 1.09 (d, $J = 6.1$ Hz, 3 H), 1.03 (s, 3 H), 0.97–0.90 (m, 27 H), 0.88 (s, 9 H), 0.82 (d, $J = 6.6$ Hz, 3 H), 0.75 (s, 9 H), 0.66 (q, $J = 8.3$ Hz, 6 H), 0.17 (s, 3 H), 0.16 (s, 3 H), 0.11 (s, 3 H), 0.10 (s, 3 H), 0.09 (s, 3 H), 0.08 (s, 3 H), –0.03 (s, 3 H), –0.11 ppm (s, 3 H); HRMS (ESI-TOF): calcd for C₁₃₄H₁₈₇N₁₉O₂₀S₅Se₃Si₅ [M+H⁺]: 2922.9217; found: 2922.9215.

1 (thiostrepton, synthetic and natural): ¹H NMR (600 MHz, [D₈]THF, thiostrepton is more soluble and stable in this solvent than in CDCl₃; for proton numbering and abbreviations, see: ref. 11): $\delta = 10.03$ (s, 1 H; CONH), 9.69 (s, 1 H; CONH), 9.30 (s, 1 H; CONH), 8.65 (s, 1 H; CONH), 8.39 (s, 1 H; Ar-H), 8.31 (br s, 1 H; OH or NH), 8.29 (s, 1 H; Ar-H), 8.20 (s, 1 H; Ar-H), 8.03 (br s, 1 H; CONH), 7.62 (d, $J = 5.6$ Hz, 1 H; CONH), 7.58 (d, $J = 10.3$ Hz, 1 H; CONH), 7.54 (br s, 1 H; Thstn 3-OH), 7.53 (s, 1 H; Ar-H), 7.48 (br s, 1 H; OH or NH), 7.42 (d, $J = 7.7$ Hz, 1 H; CONH), 7.32 (s, 1 H; Ar-H), 7.07 (d, $J = 7.7$ Hz, 1 H; Q 8-OH), 6.99 (br s, 1 H; OH or NH), 6.92 (d, $J = 9.7$ Hz; Q 5-H), 6.75 (d, $J = 2.0$ Hz, 1 H; Deala-H), 6.58 (d, $J = 7.5$ Hz, 1 H; CONH), 6.56 (s, 1 H; Deala-H), 6.45 (q, $J = 6.1$ Hz, 1 H; Thr(2) 3-H), 6.32 (dd, $J = 9.7, 5.6$ Hz; Q 6-H), 6.13 (q, $J = 7.1$ Hz, 1 H; But 3-H), 5.89 (d, $J = 9.8$ Hz, 1 H; Thr(2) 2-H), 5.84 (d, $J = 9.2$ Hz, 1 H; Thstn 2-H), 5.77 (s, 1 H; Deala-H), 5.55 (s, 1 H; Deala-H), 5.49 (s, 1 H; OH or NH), 5.47–5.46 (m, 1 H, Pip 6-H β), 5.30 (q, $J = 6.1$ Hz, 1 H; Q 11-H), 5.20 (s, 1 H; Deala-H), 5.04 (dd, $J = 8.7, 4.1$ Hz, 1 H; Cys 4-H β), 4.84 (t, $J = 7.7$ Hz, 1 H; Ala(2) 2-H), 4.73 (d, $J = 7.1$ Hz, 1 H; Q 8-H), 4.35 (dd, $J = 7.9, 3.5$ Hz, 1 H; Thr(1) 2-H), 4.29 (d, $J = 4.6$ Hz, 1 H; Q 7-H β), 4.20–4.15 (m, 2 H; Pip 4-H α , Thstn 4-OH), 3.90 (quint, $J = 6.5$ Hz, 1 H; Ala(1) 2-H), 3.85 (quint, $J = 5.7$ Hz, 1 H; Thstn 4-H), 3.24 (t, $J = 12.3$ Hz, 1 H; Cys 5-H α), 3.00–2.93 (m, 2 H; Ile 2-H, Pip 3-H α), 2.39–2.35 (m, 1 H; Pip 4-H β), 1.60 (d, $J = 7.2$ Hz, 3 H; CH₃), 1.33 (d, $J = 3.5$ Hz, 3 H; CH₃), 1.32 (d, $J = 3.1$ Hz, 3 H; CH₃), 1.27 (d, $J = 6.6$ Hz, 3 H; CH₃), 1.16 (s, 3 H; CH₃), 1.14 (s, 3 H; CH₃), 1.06 (d, $J = 6.1$ Hz, 3 H; CH₃), 0.96 (t, $J = 7.0$ Hz, 3 H; CH₃), 0.88 ppm (d, $J = 6.6$ Hz, 3 H; CH₃).

marked with the TES group to form the required thiazoline-conjugated double bond in its proper *Z* geometry, leading directly to thiostrepton (**1**). Synthetic **1** exhibited identical physical properties (R_f , HPLC, optical rotation, ¹H NMR, mixed ¹H NMR, ¹³C NMR, and MS) to an authentic sample of **1** (Table 1).^[11]

The chemistry described herein and in the preceding Communication in this issue^[1] constitutes a highly convergent and stereoselective synthesis of the most complex member of the thiopeptide class of antibiotics, thiostrepton (**1**). With the impressive range of biological effects exhibited by members of this proliferating family of natural products, these studies may facilitate chemical biology and drug-discovery efforts in diverse areas of current interest.

Received: July 16, 2004

Published Online: September 3, 2004

Keywords: antibiotics · natural products · peptide coupling · protecting groups · total synthesis

- [1] K. C. Nicolaou, B. S. Safina, M. Zak, A. A. Estrada, S. H. Lee, *Angew. Chem.* **2004**, *116*, 5197–5202; *Angew. Chem. Int. Ed.* **2004**, *43*, 5087–5092; see preceding Communication in this issue.
- [2] N. M. Okeley, Y. Zhu, W. A. van der Donk, *Org. Lett.* **2000**, *2*, 3603–3606.
- [3] K. C. Nicolaou, B. S. Safina, C. Funke, M. Zak, F. J. Zécri, *Angew. Chem.* **2002**, *114*, 2017–2020; *Angew. Chem. Int. Ed.* **2002**, *41*, 1937–1940.
- [4] C. Fontenas, E. Bejan, H. A. Haddou, G. A. Galavoine, *Synth. Commun.* **1995**, *25*, 629–633.
- [5] a) K. Ito, M. Yoshitake, T. Katsuki, *Tetrahedron* **1996**, *52*, 3905–3920; b) H. Sasaki, R. Irie, T. Hamada, K. Suzuki, T. Katsuki, *Tetrahedron* **1994**, *50*, 11827–11838; c) for a pertinent review in this area, see: T. Katsuki, *Curr. Org. Chem.* **2001**, *5*, 663–678.
- [6] a) D. R. Boyd, R. J. H. Davies, L. Hamilton, J. J. McCullough, J. F. Malone, H. P. Porter, A. Smith, *J. Org. Chem.* **1994**, *59*, 984–990; b) D. R. Bushman, J. M. Sayer, D. R. Boyd, D. M. Jerina, *J. Am. Chem. Soc.* **1989**, *111*, 2688–2691.
- [7] a) J. Inanaga, K. Hirata, H. Saeki, T. Katsuki, M. Yamaguchi, *Bull. Chem. Soc. Jpn.* **1979**, *52*, 1989–1993; b) K. C. Nicolaou, A. P. Patron, K. Ajito, P. K. Richter, H. Khatuya, P. Bertinato, R. A. Miller, M. J. Tomaszewski, *Chem. Eur. J.* **1996**, *2*, 847–868.

- [8] B. G. de la Torre, J. L. Torres, E. Bardají, P. Clapés, N. Xaus, X. Jorba, S. Calvet, F. Albericio, G. Valencia, *J. Chem. Soc. Chem. Commun.* **1990**, 965–967.
- [9] R. L. E. Furlan, E. G. Mata, O. A. Mascaretti, *J. Chem. Soc. Perkin Trans. 1* **1998**, 355–358.
- [10] K. C. Nicolaou, M. Nevalainen, M. Zak, S. Bulat, M. Bella, B. S. Safina, *Angew. Chem.* **2003**, *115*, 3540–3546; *Angew. Chem. Int. Ed.* **2003**, *42*, 3418–3424.
- [11] a) O. D. Hensens, G. Albers-Schönberg *J. Antibiot.* **1983**, *36*, 799–813; b) O. D. Hensens, G. Albers-Schönberg, *J. Antibiot.* **1983**, *36*, 814–831; c) O. D. Hensens, G. Albers-Schönberg, *J. Antibiot.* **1983**, *36*, 832–845.

Life's Simple Pleasures!



No need to waste precious time looking for the right information – Register now for the free **Wiley-VCH Alerting Service**.

It's simple – and it's fast.

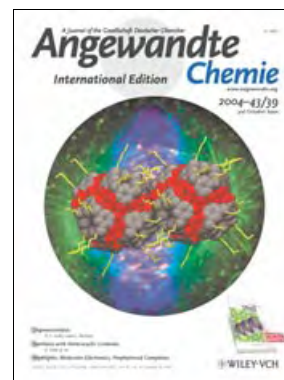
To receive regular news per e-mail tailored precisely to your needs and interests, just fill in the registration form at www.wiley-vch.de/home/pas/



Cover Picture

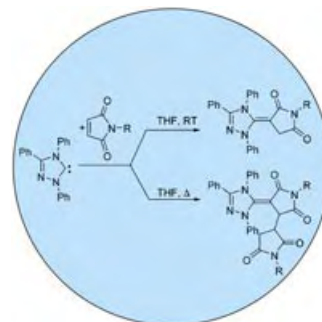
Gareth W. V. Cave, Jochen Antesberger, Leonard J. Barbour, Robert M. McKinlay, and Jerry L. Atwood*

Nanoscale molecular capsules are assembled by means of noncovalent interactions and enclose over 1300 Å³ of molecular space. The supramolecular interactions between two independent nanocapsules lead to changes in the dynamic structure of the capsule walls. This dramatically alters the packing and fluidity of the guest matrix within the host. In their Communication on page 5263 ff., J. L. Atwood and co-workers provide valuable insight into the interactions and fluidity of the so-called “new phase of matter”.



Carbenes in Synthesis

Nucleophilic heterocyclic carbenes, well known as ligands in organometallic chemistry, are also being used increasingly as reagents and catalysts in organic synthesis. V. Nair et al. give an overview on page 5130 ff.



Organocatalysts

Are organometallic compounds really unavoidable in organic synthesis? P. I. Dalko and L. Moisan show the scope of alternative methods with purely organic catalysts in their Review on page 5138 ff.



Dendrimers

M. B. Steffensen and E. E. Simanek describe a one-pot multistep procedure for the synthesis of dendrimers with up to six different functionalities in their Communication on page 5178 ff.



Angewandte EarlyView®

The following Communications are available online (in Wiley InterScience). You can find them, as well as forthcoming Reviews, Highlights, and Essays, at www.angewandte.org, under Early View.

E. Hevia, G. W. Honeyman, A. R. Kennedy, R. E. Mulvey,*
D. C. Sherrington:

Synergic Monodeprotonation of Bis(benzene)chromium by Using Mixed Alkali Metal–Magnesium Amide Bases and Structural Characterization of the Heterotrimetallic Products

DOI: 10.1002/anie.200460637

Published online: September 7, 2004

J. M. Herrera, V. Marvaud,* M. Verdaguer, J. Marrot, M. Kalisz,
C. Mathonière*:

Reversible Photoinduced Magnetic Properties in the Heptanuclear Complex $[\text{Mo}^{\text{IV}}(\text{CN})_2(\text{CN}-\text{CuL})_6]^{8-}$: A Photomagnetic High-Spin Molecule

DOI: 10.1002/anie.200460387

Published online: September 3, 2004

Articles judged by the referees or the editor as being either very important or very urgent are immediately edited, proof-read, and electronically published once the manuscript has arrived in the editorial office in its final form. As long as there is no page number available these articles should be cited in the following manner:

Author(s), *Angew. Chem. Int. Ed.*, online publication date, DOI.

News

Organic Synthesis:

K. C. Nicolaou Receives

Arthur C. Cope Award _____ 5116

Hydrocarbon Chemistry:

G. A. Olah Awarded

Priestley Medal _____ 5116

Books

Handbook of Size Exclusion

Chromatography and Related Techniques

Chi-San Wu

reviewed by B. Trathnigg _____ 5117

Basic Atomic and Molecular Spectroscopy

J. Michael Hollas

reviewed by D. Smith _____ 5117

Highlights

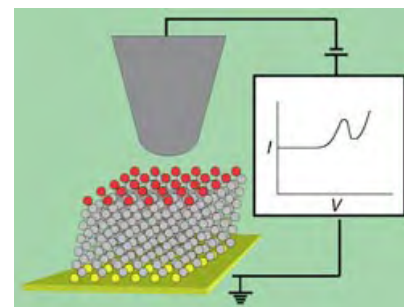
Molecular Electronics

R. A. Wassel,

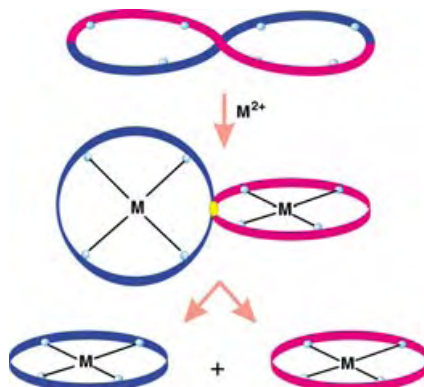
C. B. Gorman* _____ 5120–5123

Establishing the Molecular Basis for
Molecular Electronics

Molecular structure–property relationships for molecular electronics are beginning to emerge. Recent experiments lend credibility to the single-molecule nature of transport measurements and illustrate the molecular features that give rise to various interesting conductance behaviors (see picture).



Molecular mitosis: Figure-eight octaphyrins form binuclear metal complexes that can split into two covalently spiro-linked corrolates. In a unique case binuclear Cu^{II} [36]octaphyrin divides thermally into two Cu^{II} [18]porphyrins presumably with participation of a transient spirocyclobutane species (see schematic representation).



Porphyrinoid Complexes

L. Latos-Grażyński* — 5124–5128

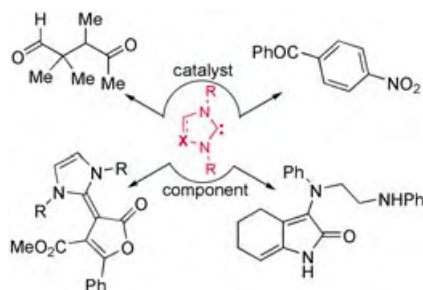
Bimetallic Figure-Eight Octaphyrins Split into Four-Pyrrolic Macrocycles

Minireviews

Carbene Reagents

V. Nair,* S. Bindu,
V. Sreekumar — 5130–5135

N-Heterocyclic Carbenes: Reagents, Not Just Ligands!



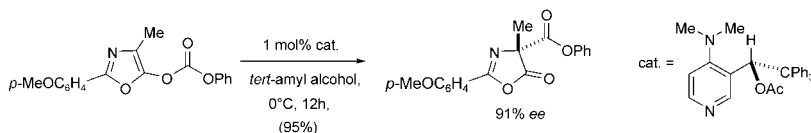
Species of curiosity for a long time and more recently ligands for metals, nucleophilic heterocyclic carbenes deserve renewed attention as reagents and catalysts in organic synthesis. Their known chemistry (see scheme) foretells an impressive future.

Reviews

Asymmetric Catalysis

P. I. Dalko,* L. Moisan — 5138–5175

In the Golden Age of Organocatalysis



Metal-free synthesis: An increasing number of asymmetric organic reactions can be catalyzed by a chiral organic molecule. Although substrate dependency remains an important issue in many

cases, a large number of organocatalytic transformations are as efficient as current standards in asymmetric synthesis demand (see example).

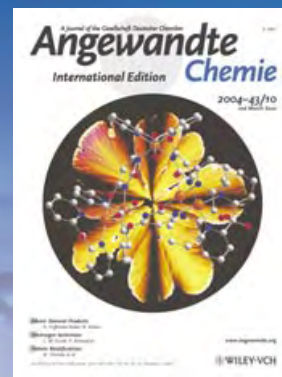
For the USA and Canada:

ANGEWANDTE CHEMIE International Edition (ISSN 1433-7851) is published weekly by Wiley-VCH PO Box 191161, D 69451 Weinheim, Germany. Air freight and mailing in the USA by Publications Expediting Inc. 200 Meacham Ave., Elmont, NY 11003. Periodicals

postage paid at Jamaica NY 11431. US POSTMASTER: send address changes to *Angewandte Chemie*, Wiley-VCH, 111 River Street, Hoboken, NJ 07030. Annual subscription price for institutions: Europe € 3430.00/3118.00; outside Europe US\$ 4499.00/4090.00 (valid for print and electronic/print or electronic delivery); for

individuals who are personal members of a national chemical society, or whose institution already subscribes, or who are retired or self-employed consultants, print only: Europe € 248.00/outside Europe US\$ 378.00. Postage and handling charges included. All Wiley-VCH prices are exclusive VAT.

The best in chemistry – for more than a hundred years



A Journal of the Gesellschaft Deutscher Chemiker
Angewandte
International Edition **Chemie**

www.angewandte.org

1888: The beginning
of a success story

Constant Innovations

- 1962:** First issue of the International Edition
- 1976:** Graphical abstracts
- 1979:** Cover pictures
- 1988:** Centenary of Angewandte
- 1989:** Routine use of color
- 1991:** New section: Highlights
- 1992:** Computerized editorial tracking system
- 1995:** Internet service for readers
- 1998:** Regular press service; full-text online
- 2000:** New section: Essays; EarlyView: Communications available online ahead of the printed version
- 2001:** New section: Minireviews
- 2002:** Online submission of manuscripts
- 2003:** Weekly publication; new section: News; new layout
- 2004:** Backfiles (1962-1997); ManuscriptXpress: Online system for authors and referees



Angewandte's advisors...

Jean-Marie Lehn
Université Strasbourg
Collège de France

» **Angewandte Chemie** provides timely reviews of great depth and wide interest together with short reports of top quality frontier research. Creative work remains creative wherever it is published! However, **Angewandte Chemie** brings high visibility while keeping restraint and rigor. Finally, it is also supranational, as science is. «

Angewandte Chemie International Edition is
a journal of the German Chemical Society (GDCh)

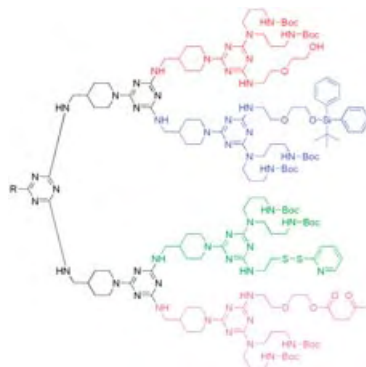


Communications

Dendrimer Synthesis

M. B. Steffensen,
E. E. Simanek* ————— 5178–5180

Synthesis and Manipulation of
Orthogonally Protected Dendrimers:
Building Blocks for Library Synthesis

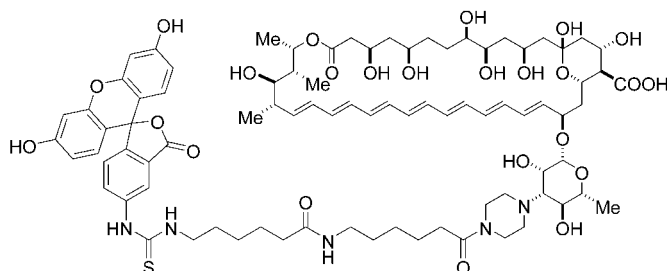


Fruits of the laboratory: Dendrimers containing up to six different functional groups can be prepared in multistep one-pot reactions by using a selective manipulation and deprotection strategy (see example). The authors call these multifunctional dendrimers molecular fruit-salad trees; they could function as useful building blocks for drug-delivery systems and novel materials.

Bioorganic Chemistry

A. Zumbuehl, D. Jeannerat, S. E. Martin,
M. Sohrmann, P. Stano, T. Vigassy,
D. D. Clark, S. L. Hussey, M. Peter,
B. R. Peterson, E. Pretsch, P. Walde,
E. M. Carreira* ————— 5181–5185

An Amphotericin B–Fluorescein
Conjugate as a Powerful Probe for
Biochemical Studies of the Membrane



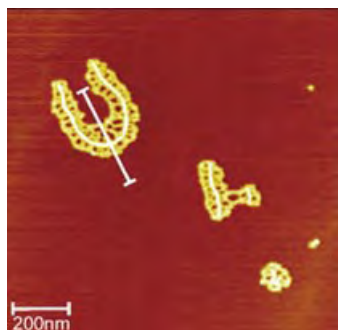
Not only skin deep: A fluorescein–amphotericin B conjugate with a new piperazine linker (see structure) was prepared and used as a probe of the bio-membrane and the mechanism of action

of amphotericin B both in vivo and in liposomal experiments. The amphotericin B analogue localizes at the membrane of yeast cells but is internalized by mammalian cells.

Radical Polymerization

A. Zhang, J. Barner, I. Göessl, J. P. Rabe,*
A. D. Schlüter* ————— 5185–5188

A Covalent-chemistry Approach to Giant
Macromolecules and Their Wetting
Behavior on Solid Substrates

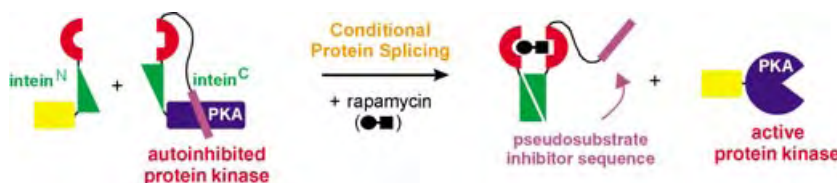


Hair raising! Poly(methyl methacrylate) chains grown on a dendronized polymer (denpol) having repeat units with terminal 2-bromoisobutyramide groups produce a hairy surface. When adsorbed on mica, MoS₂, and highly oriented pyrolytic graphite, the hairy denpol molecules have a quasi two dimensional backbone conformation. The 50-nm-long hairs bend back on the MoS₂ (see image) and graphite substrates.

Enzyme Activity

H. D. Mootz, E. S. Blum,
T. W. Muir* ————— 5189–5192

Activation of an Autoregulated Protein
Kinase by Conditional Protein Splicing



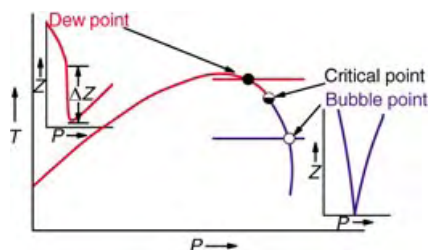
A protein rheostat: A strategy for controlling enzyme activity by cleavage of a low-affinity “pseudosubstrate” inhibitor from an autoregulated version of the enzyme (see figure) is described. Peptide-bond

cleavage was mediated by conditional protein splicing. The small molecule rapamycin was used to induce intein *trans*-splicing of the catalytic subunit of cAMP-dependent protein kinase A (PKA).

Supercritical Fluids

J. Ke,* R. M. Oag, P. J. King, M. W. George,
M. Poliakoff* ————— 5192–5195

Sensing the Critical Point of High-
Pressure Mixtures

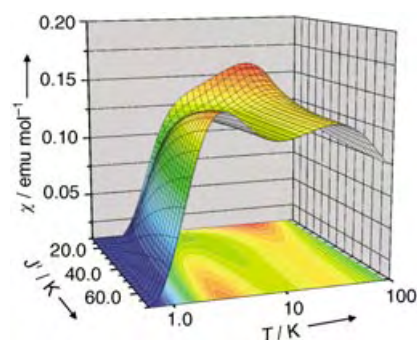


A new, general and objective approach to locating critical points of fluid mixtures is described (see picture). It is new because it exploits the fact that the liquid phase forms preferentially on the surface of the sensor. It is general because it can be used with any type of surface-sensitive sensor, and it is objective because it is based on the numerical output of a sensor rather than the visual image normally used for phase equilibrium studies.

Magnetic Properties

O. Cador, D. Gatteschi, R. Sessoli,*
F. K. Larsen, J. Overgaard, A.-L. Barra,
S. J. Teat, G. A. Timco,*
R. E. P. Winpenny* ————— 5196–5200

The Magnetic Möbius Strip: Synthesis,
Structure, and Magnetic Studies of
Odd-Numbered Antiferromagnetically
Coupled Wheels

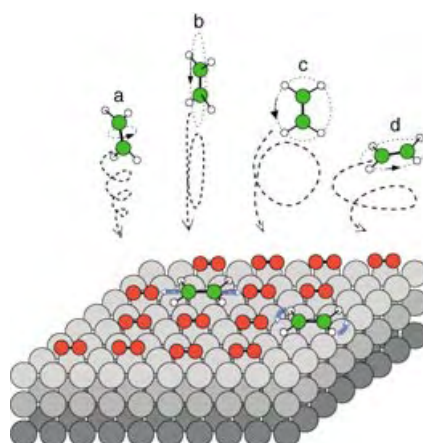


Understanding frustration: The control of structure through the choice of the template has allowed the synthesis of non-nuclear metal wheels that contain {Cr₈Ni} or {Cr₇(VO)₂} cores. Magnetic studies (see picture) of one of these wheels shows that it behaves as a magnetic Möbius strip. These are the first detailed magnetic studies of an odd-numbered ring larger than trinuclear and should help in the understanding of spin-frustrated systems.

Gas–Surface Interactions

L. Vattuone,* A. Gerbi, M. Rocca,
U. Valbusa, F. Pirani, F. Vecchiocattivi,
D. Cappelletti ————— 5200–5203

Stereodynamic Effects in the Adsorption
of Ethylene onto a Metal Surface

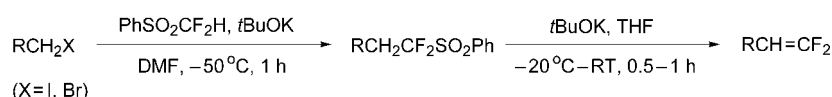


Molecular gymnastics: Ethylene molecules (C atoms in green) rotating along the principal axes impinge perpendicularly on an Ag (001) metal surface precovered with O₂ (O atoms in red) and may stick in some favorable cases. The sticking probability *S* depends on the approach of the C=C bond to the surface: “helicopters” (d) stick better than “cartwheels” (b and c) or “cigars” (a).

Fluorinated Alkenes

G. K. S. Prakash,* J. Hu, Y. Wang,
G. A. Olah ————— 5203–5206

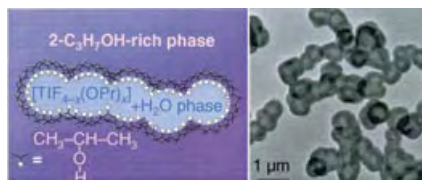
Difluoromethyl Phenyl Sulfone, a Difluoromethylidene Equivalent: Use in the Synthesis of 1,1-Difluoro-1-alkenes



A nucleophilic substitution–elimination reaction strategy in which difluoromethyl phenyl sulfone is used as a selective

difluoromethylidene equivalent allows the facile synthesis of 1,1-difluoro-1-alkenes from primary alkyl halides (see scheme).

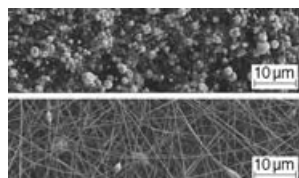
Gutsy chemistry: A solvothermal process has been developed for the controlled creation of interior space in TiO_2 intestines (either hollow (see TEM image) or partially filled) or spheres in the anatase polymorph. A morphological transformation from intestine to sphere is observed when the water content of the water/2-propanol mixture is decreased.



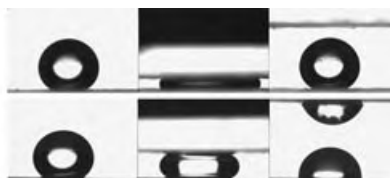
Materials Science

H. G. Yang, H. C. Zeng* — 5206–5209

Creation of Intestine-like Interior Space for Metal-Oxide Nanostructures with a Quasi-Reverse Emulsion



Dry films: An electrospinning process was used to form films with high water contact angles (166.7°) and low sliding-angles (4.3°). The electrospun films exhibit



excellent superhydrophobic Cassie-regime stability: The figure shows a nonwetting water droplet, even after 400 Pa of uniaxial loading.

Superhydrophobic Films

K. Acatay, E. Simsek, C. Ow-Yang, Y. Z. Menceloglu* — 5210–5213

Tunable, Superhydrophobically Stable Polymeric Surfaces by Electrospinning



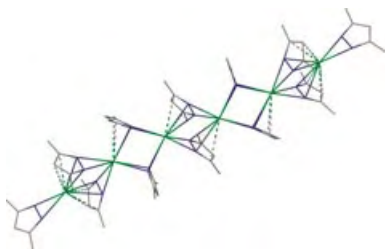
Stable! The first stable salts containing a simple, inorganic cation with an N–Cl bond are prepared (see picture). They are

$[\text{NH}_3\text{Cl}]^+[\text{BF}_4]^-$, $[\text{NH}_3\text{Cl}]^+[\text{AsF}_6]^-$, and $[\text{NH}_3\text{Cl}]^+[\text{SbF}_6]^-$ and can be safely prepared from $(\text{Me}_3\text{Si})_2\text{NCl}$ in mixtures of HF and the corresponding Lewis acids and could be used as storable generators for monochloramine gas.

Inorganic Cations

S. Schneider,* R. Haiges, T. Schroer, J. Boatz, K. O. Christe* — 5213–5217

The $[\text{NH}_3\text{Cl}]^+$ Ion

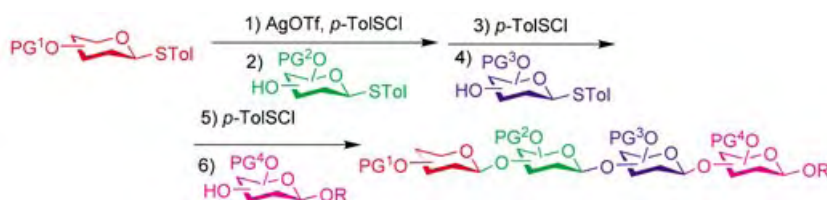


The bigger the better: Increasing metal size seems to be the determining factor in the formation of an unprecedented series of homoleptic linear pyrazolates of the heavy alkaline-earth metals (Ca, Sr, Ba, see picture, Ba = green, N = blue, C = black), with the formation of trinuclear calcium, tetranuclear strontium, and hexanuclear barium derivatives. The linear oligomers display a noteworthy array of metal–ligand bonds.

Alkaline-Earth-Metal Complexes

J. Hitzbleck, G. B. Deacon,* K. Ruhlandt-Senge* — 5218–5220

Linear Finite “Mers”—Homoleptic Polynuclear Heavy Alkaline Earth Metal Pyrazolates



Straight to the point! Preactivation of a *p*-tolyl thioglycoside donor, followed by sequential addition of *p*-tolyl thioglycosyl acceptors in *one* reaction flask allowed rapid syntheses of oligosaccharides

independent of anomeric reactivities of donors and acceptors (see scheme). This strategy greatly streamlines the assembly of oligosaccharides.

Carbohydrates

X. Huang,* L. Huang, H. Wang, X.-S. Ye* — 5221–5224

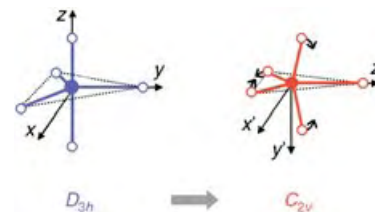
Iterative One-Pot Synthesis of Oligosaccharides

Titanium Complexes

P. J. Alonso, L. R. Falvello, J. Forniés,
M. A. García-Monforte,
B. Menjón* — 5225 – 5228

A Five-Coordinate Homoleptic
Organotitanium(III) Compound

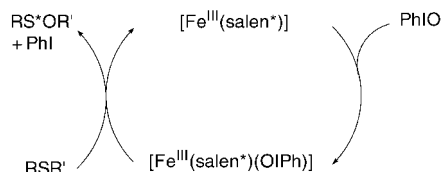
Reversed Berry pseudorotation (see picture) results in a severely distorted trigonal-bipyramidal geometry with C_{2v} symmetry in the paramagnetic (d^1) anion $[\text{Ti}(\text{C}_6\text{F}_5)_5]^{2-}$, which was obtained by the low-temperature reaction of $\text{TiCl}_4 \cdot x\text{Et}_2\text{O}$ and LiC_6F_5 and is the first homoleptic organometallic compound containing a $[\text{TiR}_5]^{2-}$ unit.



Asymmetric Catalysis

K. P. Bryliakov,* E. P. Talsi — 5228 – 5230

Evidence for the Formation of an Iodosylbenzene(salen)iron Active Intermediate in a (Salen)iron(III)-Catalyzed Asymmetric Sulfide Oxidation



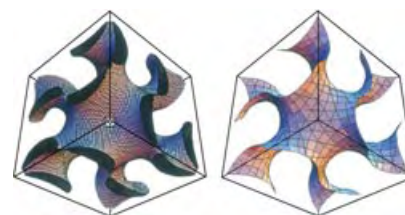
Catalytic converter: A (salen)iron(III) complex (salen* = asymmetric bis(salicylidene)ethylenediamine ligand) can be used as a catalyst system for the asymmetric oxidation of aryl sulfides by iodosylbenzene (see scheme). An iodosylbenzene(salen)iron(III) species has been identified as the active intermediate by EPR and NMR spectroscopy. R = aryl, R' = alkyl.

Mesoporous Materials

Y. Sakamoto, T.-W. Kim, R. Ryoo,
O. Terasaki* — 5231 – 5234

Three-Dimensional Structure of Large-Pore Mesoporous Cubic $la\bar{3}d$ Silica with Complementary Pores and Its Carbon Replica by Electron Crystallography

A bicontinuous cubic structure was revealed by electron crystallography on a large-pore mesoporous silica with a cubic $la\bar{3}d$ symmetry synthesized by using a triblock copolymer as a structure-directing agent. Its reconstructed structure (picture, left) is composed of an enantiomeric pair of interwoven three-dimensional mesoporous networks. Ordered complementary pores form interconnections



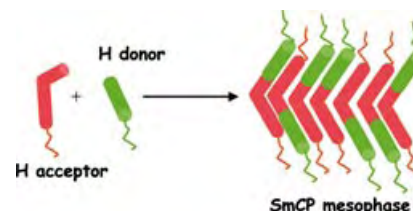
between the two main channel systems at a special flat point of the G-surface (right).

Liquid Crystals

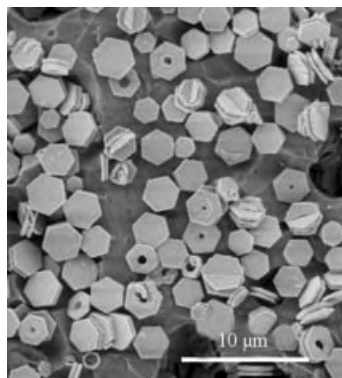
N. Gimeno, M. B. Ros,* J. L. Serrano,*
M. R. de la Fuente — 5235 – 5238

Hydrogen-Bonded Banana Liquid Crystals

Top banana! Hydrogen-bonded bent complexes of benzoic acids (H donor) and nonmesomorphic V-shaped 4'-stilbazoles (H acceptor) give rise to polar smectic C (SmCP, see graphic) mesophases. The multifunctional character of these noncovalent materials is confirmed through their electrooptical, dielectric, and luminescent responses.



Solution-phase synthesis of single-crystal ZnO disks and rings was achieved in high yield at low temperature (70–90 °C) by using an anionic surfactant as a template. The reaction can be controlled by means of the growth temperature and the molar ratio of reagents to favor formation of disks or rings. A growth mechanism is proposed on the basis of structural information provided by SEM and TEM.

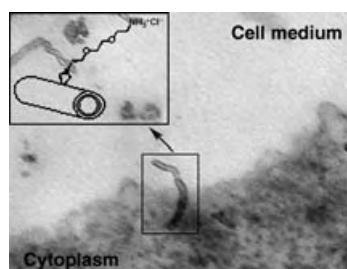


ZnO Nanostructures

F. Li,* Y. Ding, P. Gao, X. Xin,
Z. L. Wang* — 5238 – 5242

Single-Crystal Hexagonal Disks and Rings of ZnO: Low-Temperature, Large-Scale Synthesis and Growth Mechanism

Genetic vaccination and gene therapy research could benefit from the application of carbon nanotubes. Functionalized, positively charged, water-soluble carbon nanotubes are able to penetrate into cells (see figure) and can transport plasmid DNA by formation of noncovalent DNA–nanotube complexes. Such nanotubes can be used as novel nonviral delivery systems for gene transfer.

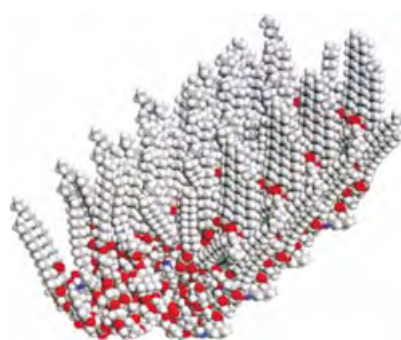


Gene Technology

D. Pantarotto, R. Singh, D. McCarthy,
M. Erhardt, J.-P. Briand, M. Prato,*
K. Kostarelos,* A. Bianco* — 5242 – 5246

Functionalized Carbon Nanotubes for Plasmid DNA Gene Delivery

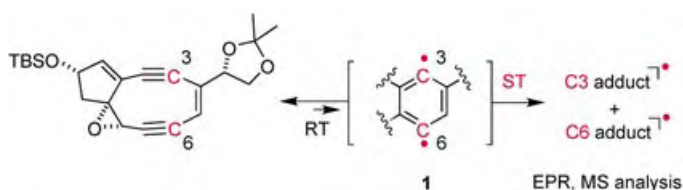
One-dimensional supramolecular assembly of dendrimers (see picture) has been achieved by multiple weak interactions between highly branched molecules with irregular structures. This finding contradicts the widely accepted assumption that precise matching of directional interactions and steric constraints is required to facilitate long-range one-dimensional supramolecular assembly.



Self-Assembly of Dendrimers

M. Ornatska, K. N. Bergman, B. Rybak,
S. Peleshanko,
V. V. Tsukruk* — 5246 – 5249

Nanofibers from Functionalized Dendritic Molecules



A new spin on things? Spin trapping of ^{13}C -labeled bicyclic mimics of natural nine-membered enediynes provided persuasive evidence for the spontaneous

thermal generation of biradicals **1** and the differential reactivity of the resulting C3 and C6 radical centers (see scheme; ST spin trap; TBS *tert*-butyldimethylsilyl).

Radical Chemistry

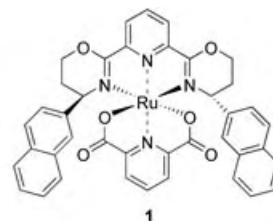
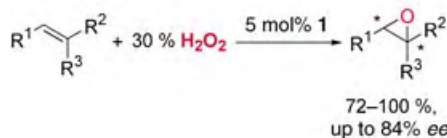
T. Usuki, T. Mita, M. J. Lear,* P. Das,
F. Yoshimura, M. Inoue, M. Hirama,*
K. Akiyama,* S. Tero-Kubota — 5249 – 5253

Spin Trapping of ^{13}C -Labeled *p*-Benzynes Generated by Masamune–Bergman Cyclization of Bicyclic Nine-Membered Enediynes

Homogeneous Catalysis

M. K. Tse, C. Döbler, S. Bhor, M. Klawonn,
W. Mägerlein, H. Hugl,
M. Beller* _____ **5255 – 5260**

Development of a Ruthenium-Catalyzed
Asymmetric Epoxidation Procedure with
Hydrogen Peroxide as the Oxidant



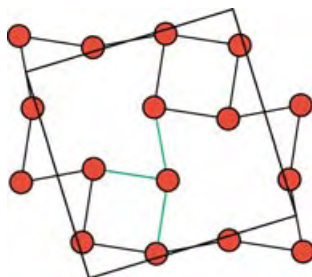
Novel pyboxazines and the known pybox ligands are used in the ruthenium-catalyzed asymmetric epoxidation of olefins with H_2O_2 (see scheme). This new cata-

lytic system is successful in the conversion of differently substituted aromatic olefins and gives ee values of up to 84 %.

Solid-State Structures

A. Assoud, K. M. Kleinke, N. Soheilnia,
H. Kleinke* _____ **5260 – 5262**

T-Shaped Nets of Antimony Atoms in the
Binary Antimonide Hf_5Sb_9

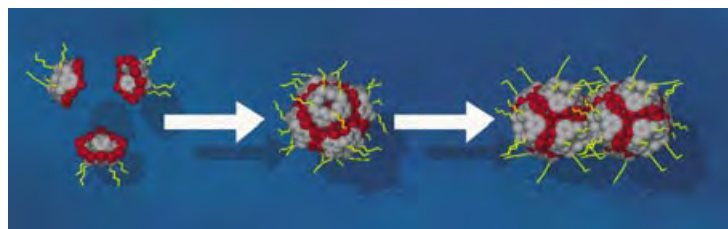


T time: The new binary antimonide Hf_5Sb_9 forms a unique variant of a square-planar net, namely an unprecedented yet simple T-shaped net (see picture, green) formed by antimony atoms (red). The electronic structure and bonding in the solid state are analyzed by theoretical methods.

Host–Guest Chemistry

G. W. V. Cave, J. Antesberger, L. J. Barbour,
R. M. McKinlay,
J. L. Atwood* _____ **5263 – 5266**

Inner Core Structure Responds to
Communication between Nanocapsule
Walls



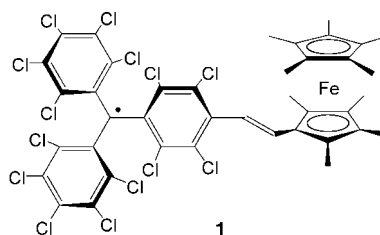
The facile self-assembly of six pyrogallol[4]arene molecules leads to a globular truncated octahedron, which encapsulates a guest cluster consisting of ethyl

acetate and water molecules (see scheme). The interactions between host capsules can be controlled by derivatization of the exterior surface of the capsule.

Molecular Switches

C. Sporer, I. Ratera, D. Ruiz-Molina,
Y. Zhao, J. Vidal-Gancedo, K. Wurst,
P. Jaitner, K. Clays, A. Persoons, C. Rovira,
J. Veciana* _____ **5266 – 5268**

A Molecular Multiproperty Switching
Array Based on the Redox Behavior of a
Ferrocenyl Polychlorotriphenylmethyl
Radical



All change: Three different output signals, chromic, nonlinear optical, and magnetic, can be altered simultaneously with the molecular switch based on radical **1**. The electrochemical reduction and oxidation of **1** is completely reversible. These redox cycles can be repeated several times, and the corresponding changes in the optical properties can be monitored by visible spectroscopy.



Communications labeled with this symbol have been judged by two referees as being “very important papers”.

Looking for outstanding employees?

Do you need another expert for your excellent team?

... Chemists, PhD Students, Managers, Professors, Sales Representatives...

Place an advert in the printed version and have it made available online for 1 month, free of charge!

Angewandte Chemie International Edition

Advertising Sales Department: Marion Schulz

Phone: 0 62 01 - 60 65 65

Fax: 0 62 01 - 60 65 50

E-Mail: MSchulz@wiley-vch.de

Service

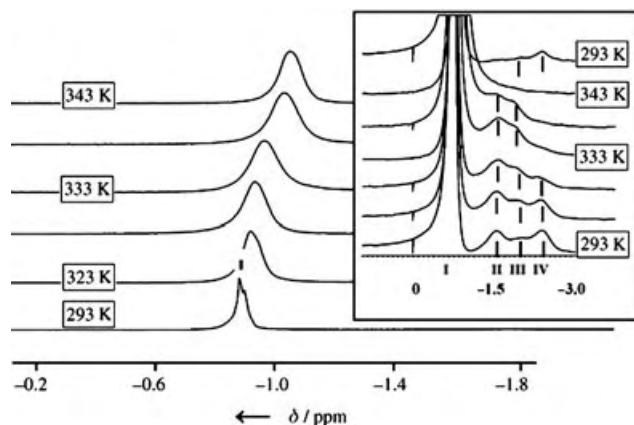
Keywords 5270

Authors 5271

Preview 5273

Corrigendum

In this Communication, the temperature assignments on the right-hand side of Figure 4 were incorrect. The Editorial Office apologises for this error. The correct figure is shown.



Artificial Cells: Temperature-Dependent, Reversible Li⁺-Ion Uptake/Release Equilibrium at Metal Oxide Nanocontainer Pores**

A. Müller,* D. Rehder,* E. T. K. Haupt,
A. Merca, H. Bögge, M. Schmidtman,
G. Heinze-Brückner 4466–4470

Angew. Chem. Int. Ed. **2004**, 43

DOI 10.1002/anie.200453762



K. C. Nicolaou Receives Arthur C. Cope Award

K. C. Nicolaou's outstanding achievements in the total synthesis of architecturally novel and biologically important natural products have earned him widespread recognition in the chemical community as well as numerous prestigious awards, now to be complemented by the Arthur C. Cope Award 2005, administered by the American Chemical Society. The award is endowed with \$25000 and an unrestricted grant-in-aid of \$150000 for research in organic chemistry.

New synthetic strategies and methods are developed by Nicolaou and his research group to meet the challenges presented by the enormous structural complexity of the target compounds. One of his most recent synthetic accomplishments was the revision of the structure of the mussel toxin azaspiracid-1 and its total synthesis, as highlighted on the cover of issue 33/2004 of *Angewandte Chemie*.^[1] The total synthesis of the antibiotic thiostrepton was also described recently.^[2] A sequel to his very popular book *Classics in Total Synthesis* (co-authored by Erik J. Sorensen, Wiley-VCH, 1996) appeared last year, with Scott A. Snyder as co-author (Wiley-VCH, 2003).



K. C. Nicolaou

Born in Cyprus in 1946, Nicolaou moved to the UK at the age of 18. He received a BSc in 1969 from the University of London (Bedford College) and completed his PhD in 1972 at University College (with F. Sondheimer and P. J. Garratt). After postdoctoral studies with T. J. Katz (Columbia University) and E. J. Corey (Harvard University) he remained in the USA to begin his independent career at the University of Pennsylvania. Since 1989 he has held joint positions at the University of California, San Diego and at The Scripps Research Institute, where he is Skaggs Professor of Chemical Biology and holds the Darlene Shiley Chair in Chemistry. He is a member of the International Advisory Board of *Angewandte Chemie*.

G. A. Olah Awarded Priestley Medal

The Priestley Medal is awarded annually by the ACS in recognition of distinguished services to chemistry. The recipient for 2005, George A. Olah, won the Nobel Prize in Chemistry in 1994 for his contribution to carbocation chemistry.^[3] Olah's research in hydrocarbon chemistry comprises a broad range of topics, including the preparation of superacids, their use in the direct conversion of methane



G. A. Olah

into higher hydrocarbons and derived products, the development of reagents and methods for synthesis, and nitration.

Born in Budapest (Hungary) in 1927, Olah completed his undergraduate studies and PhD (1949) at the Technical University of Budapest with Geza Zemplén, a student of Emil Fischer. In 1954, Olah joined the newly established

Central Chemistry Research Institute of the Hungarian Academy of Sciences. He and his family fled Hungary in December 1956 via London to Canada, where he joined the company Dow Chemical. In 1965 he returned to academic life as a professor at Western Reserve University (OH, USA), and in 1977 became director of the new Loker Hydrocarbon Research Institute at the University of Southern California, Los Angeles, where he is Donald P. and Katherine B. Loker Distinguished Professor of Organic Chemistry. Co-author of the reference *Hydrocarbon Chemistry* (2nd ed., Wiley Interscience, 2003) with Á. Molnár, and co-editor of *Carbocation Chemistry* (Wiley Interscience, 2004) with G. K. Prakash, Olah has also described his remarkable career in his autobiography *A Life of Magic Chemistry* (Wiley Interscience, 2000). For his most recent publication in *Angewandte Chemie*, with deals with the use of difluoromethyl phenyl sulfone as a difluoromethylidene equivalent in the synthesis of 1,1-difluoro-1-alkenes, see page 5203 ff. of this issue.^[4]

- [1] K. C. Nicolaou, S. Vyskocil, T. V. Koftis, Y. M. A. Yamada, T. Ling, D. Y.-K. Chen, W. Tang, G. Petrovic, M. O. Frederick, Y. Li, M. Satake, *Angew. Chem.* **2004**, *116*, 4412; *Angew. Chem. Int. Ed.* **2004**, *43*, 4312; K. C. Nicolaou, T. V. Koftis, S. Vyskocil, G. Petrovic, T. Ling, Y. M. A. Yamada, W. Tang, M. O. Frederick, *Angew. Chem.* **2004**, *116*, 4418; *Angew. Chem. Int. Ed.* **2004**, *43*, 4318.
- [2] K. C. Nicolaou, B. S. Safina, M. Zak, A. A. Estrada, S. H. Lee, *Angew. Chem.* **2004**, *116*, 5197; *Angew. Chem. Int. Ed.* **2004**, *43*, 5087; K. C. Nicolaou, M. Zak, B. S. Safina, S. H. Lee, A. A. Estrada, *Angew. Chem.* **2004**, *116*, 5202; *Angew. Chem. Int. Ed.* **2004**, *43*, 5092.
- [3] G. A. Olah, *Angew. Chem.* **1995**, *107*, 1519; *Angew. Chem. Int. Ed. Engl.* **1995**, *34*, 1393.
- [4] G. K. S. Prakash, J. Hu, Y. Wang, G. A. Olah, *Angew. Chem.* **2004**, *116*, 5315; *Angew. Chem. Int. Ed.* **2004**, *43*, 5203.

Establishing the Molecular Basis for Molecular Electronics

Ronald A. Wassel and Christopher B. Gorman*

Keywords:

electron transport · molecular devices · molecular electronics · single-molecule studies · structure–activity relationships

Performing logic and memory operations with one or a very small collection of molecules would be the ultimate in electronic-device miniaturization. For this reason, the field of molecular electronics has received attention that ranges from scientific curiosity to the generation of intellectual property and venture capital. While new paradigms and financial rewards in nanotechnology will probably come (although perhaps not as fast as an investor would like), answers to several key questions are a necessary first step in this evolution. In this regard, chemists (who might be regarded as molecular engineers) have an exciting task ahead of them—sorting out the fundamental precepts that will govern this field. A number of central questions have emerged. Some loom large and will probably require substantial shifts in our approaches for working with molecules. For example, what mix of lithography (top-down engineering) and self-assembly (bottom-up manufacturing) will be required to achieve the dense integration of components that allow us to truly exploit the size scale of single-molecule devices? How will nanotubes be used in these regards?^[1] To date, no realistic approach has addressed this issue. Other questions have proven to be more manageable and are equally important. They require us to question fundamentally how molecular science will work in nanometer-scale

collections. For example, how does one make contact with a molecule? What is the electronic structure of a molecule when it is in contact with “wires”? Can molecular structure–property relationships be derived that relate the structure of a molecule to nonlinear current–voltage behaviors, switching, and, ultimately, gating? These latter questions have been addressed with some recent, plausible approaches. Such work is highlighted herein.

In performing nanoscale electronic measurements, the issue at hand, first and foremost, is how to make electrical contact to these elements. In doing so, one must confront the issue that this contact is going to perturb the molecules under study. The first strategies for contact to small collections of molecules began with the mechanical break junction.^[2] A break junction is formed by attaching a metal wire onto a flexible substrate and then bending the substrate just until the wire has broken. The gap produced is then exposed to molecules designed to bind across it. Resistances are measured that are determined to be consistent with the resistance of a single molecule.^[3]

A second top contact can be made to a collection of molecules (e.g., a self-assembled monolayer (SAM) or Langmuir–Blodgett (LB) film) by metal evaporation. In a nanopore configuration^[4] the area of the nanopore is designed to be smaller than the domain size of the SAM and the evaporated metal accumulates only on the top of the SAM. By using nanopores, Reed, Tour, et al. showed current–voltage measurements in molecules containing a nitroamine redox center that exhibited negative differential resistance.

As these metal–molecule–metal assemblies must be made one at a time, it can be difficult to get a sense of how variable their behavior is. Furthermore, although evaporating a top contact makes a metal–molecule–metal sandwich that most naturally resembles a device, metals are strong reducing agents. Reduced molecules are typically quite chemically reactive. Thus, the molecule that is placed into the sandwich may not be the structure that is ultimately measured. This concern is exacerbated by the fact that the geometry of the sandwich precludes any spectroscopic characterization of the molecules in that device.

To address this issue, a number of investigators have employed the tip of a scanning tunneling microscope (STM, or conducting atomic force microscope, AFM) as a second contact to a molecule (often organized into a self-assembled monolayer).^[5–21] Several examples are noted. Hipsps and co-workers reported orbital-mediated tunneling through phthalocyanines and porphyrins that contain metal centers.^[5–8] Tour, Bard, and co-workers displayed peak shaped *I*–*V* curves in phenylene ethynylene oligomers (OPEs) by using a tuning-fork STM.^[9,10] We have studied negative differential resistance in patterned, electroactive SAMs by using STM.^[16] Weiss and co-workers inserted individual OPEs into an insulating *n*-alkanethiolate SAM background and determined that these molecules were more conducting than the background.^[11–14] By visualizing individual molecules over time, they observed changes in conductance. These variations in conductance (stochastic switching) were attributed to

[*] R. A. Wassel, Prof. C. B. Gorman
Department of Chemistry
North Carolina State University
Raleigh, NC 27695-8204 (USA)
Fax: (+1) 919-515-8920
E-mail: chris_gorman@ncsu.edu

conformational variations in the molecules rather than the electrostatic effects of charge transfer. Similar stochastic switching has been observed by Lindsay and co-workers on carotenoid molecules with a gold nanoparticle on top^[20,21] and by our group on ferrocenyl-terminated alkanethiols inserted into an *n*-alkane-thiolate SAM.^[17]

Although these approaches that make use of scanning probe microscopy address several key aspects of molecular contacts, they still leave an important issue largely open. How do metallic contacts influence the electronic structure of the molecule between them? A recent report by Nazin et al. has elegantly illustrated how the electronic structure of a molecule evolves as it is contacted with larger and larger metal bridges.^[22] Specifically, a low-temperature ultrahigh-vacuum (UHV) STM was used to make nanostructures composed of a copper phthalocyanine (CuPc) molecule bonded to chains of various numbers of gold atoms. These nanostructures were assembled on a NiAl(110) surface by thermally evaporating single Au atoms and CuPc molecules onto the surface (Figure 1).

When the STM tip was close enough to the surface, it could be employed to pull the Au atoms along the direction of the moving tip. In this way, chains of gold atoms were built along Ni troughs. The authors made two chains of gold

atoms separated by 5 Ni–Ni lattice constants and then moved a CuPc molecule into the space between them. When the CuPc molecule was contacted to two Au atoms, peaks in the dI/dV curves that were ascribed to the CuPc were shifted and split. When more Au atoms were added on to each chain, the molecular peaks did not shift further when compared to the peaks with just two Au atoms. The Au atoms in contact with the molecule can now be considered to be part of an extended CuPc molecule. Peaks in the dI/dV curves taken over the last Au atom in the chain, shifted to higher energies when compared to Au chains that are not in contact with a CuPc molecule. The Au atoms that were in direct contact with the molecule shifted out of resonance with the rest of the Au chain. From these data, it was illustrated to what extent the degree of coupling between the CuPc and the various Au chains could vary. This significant variation will have an important role on the conductivity that will be measured across these junctions. Thus, from a chemist's perspective, metal–molecule–metal junctions should be regarded as extended molecular systems, and the nature and type of contact is going to be a dominant factor in the rational design of molecular-scale devices.

The effects of contact to a molecule have also been illustrated by Kubatkin et al., in which electronic transport was measured at 4 K through a single *para*-phenylene vinylene oligomer deposited into a small (2 nm) gap on a semiconducting substrate that acts as a gate electrode.^[23] The gate voltage (V_g) of the single-electron transistor (SET) with a single molecule in the nanogap changed in small steps from -4.3 V to $+4.3$ V. Source–drain I – V measurements were taken at each step. Eight different open states in the molecule were probed, which is consistent with a molecule of this type having a large number of discrete states. However, the energies of these electronic states obtained from the data on this SET were strongly perturbed compared to those obtained from measurements on the molecule in solution. It was suggested that image charges in the source and drain electrodes could account for this perturbation. Again, contact between a molecule and

a metal is not just a simple connection. There are many other factors involved when electronic behavior is investigated.

A second key issue in molecular electronics is to relate electronic behavior to the structure of the molecule(s) being probed. Chemists have always sought to systematically vary properties with structure to illustrate an optimal molecular structure for a given behavior. However, in a still very-young field, establishing structure–property relationships has an even more important role. This variation can help support the hypothesis that the behavior under observation is influenced by the structure of the molecule and thus, the behavior is attributable to the molecule.

A number of papers have reported the systematic study of the conductance of molecules of various lengths. These studies almost always took place on simple *n*-alkanethiolate SAMs^[11,19] or on SAMs composed of various conjugated or aromatic molecules.^[2,10,12,14,18,21,24–34] These studies established that the conductance varies with molecular length when scaled with the relative rate of a discrete electron transfer through a similar molecular bridge (e.g., the electron-transfer coefficient (β) value for a given molecular architecture in which $-\ln k_{et} = \beta r$ and r is the distance between a donor and acceptor group).

The phenomenon of Kondo resonance has been exploited in two key papers that credibly relate a unique structural feature of a given molecule to an electronic behavior that relies on that feature. In the Kondo effect, the spin state of an “impurity” (in this case, a molecule) in a wire affects its conductance. Liang et al. demonstrated Kondo resonance in a single-molecule transistor by using a single divanadium complex (“ V_2 ”) that could be tuned by changing the gate voltage to alter the spin and charge state of the molecule.^[35] A sharp dI/dV peak was observed when the gate voltage was modulated to set the V_2^+ molecules to an $S=1/2$ spin state. The peak was not observed when the molecules were set to an $S=0$ spin state. Another feature of Kondo resonance is the splitting of dI/dV peaks by an applied magnetic field when $S=1/2$. Park et al. reported Kondo resonance by

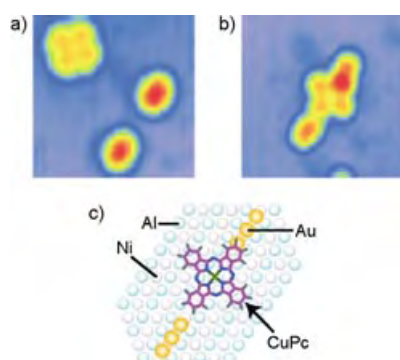


Figure 1. CuPc@2Au₃ hybrid structures
a) Bare 2Au₃ junctions before the molecules were added (imaging conditions: $V_{bias}=1$ V, $I=1$ nA; image size is 47 Å by 47 Å).
b) Assembled hybrid structures ($V_{bias}=0.5$ V, $I=1$ nA; these imaging conditions emphasize the molecular adsorption configuration).
c) Representation of Au–CuPc–Au (metal–molecule–metal) assembled on a NiAl(110) surface. Adapted from reference^[22].

changing the degree of coupling of a $\text{Co}^{2+/3+}$ ion to the electrodes.^[36] The $\text{Co}^{2+/3+}$ ion is bonded in an octahedral environment to two terpyridinyl linker molecules with thiol end groups, which are placed between gold electrodes in a break junction. A peak in the dI/dV curves was observed in the Co^{2+} complex, which was also split by applying a magnetic field. Thus, by selecting molecules that could exist in different spin states under the influence of different gate voltages, a link between a molecular property and an electronic property of those molecules in a junction could be established.

Most recently, Mayor et al. have documented how electronic transport through a molecule is affected by its structure.^[37–40] Mechanical break junctions that contain two 9,10-bis(phenylethynyl)anthracene molecules were compared; the position of the thiol anchor group was varied from *para* to *meta* (Figure 2).

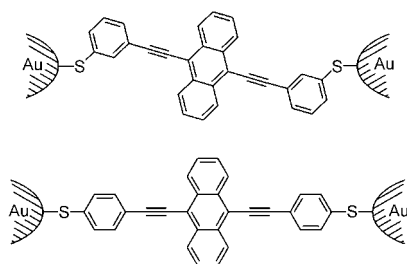


Figure 2. Representation of molecules containing a bis-9,10-phenyl-ethynylantracene core with a thiol linker in the *meta* (top) and *para* (bottom) position inserted into a break junction.

The lack of a fully conjugated pathway in the *meta*-linked molecule significantly reduces the electronic communication between the metal electrodes and the molecule when compared to analogous data obtained with the molecule linked by *para*-thiol groups. Specifically, the immobilization of the molecule with the thiol linker in the *meta* position afforded I - V curves with currents that were almost two orders of magnitude smaller than the values measured for the molecule in the *para* position. In addition, I - V curves measured on the *meta*-linked molecule at 30 K showed steps in the current curves, which were attributed to resonant tunneling through the HOMO of the molecule.

There are many challenges that need to be addressed before a viable molecular device can be fabricated. While this task may seem daunting, the work presented herein is revealing as to how the structure of a molecule relates to its electronic properties and how the binding of molecules to bulk metal electrodes influences their electronic properties. These results provide an intriguing step in the evolution of this field.

Published Online: September 16, 2004

- [1] P. Avouris, J. Appenzeller, R. Martel, S. J. Wind, *Proc. IEEE* **2003**, 91, 1772.
- [2] M. A. Reed, C. Zhou, C. J. Muller, T. P. Burgin, J. M. Tour, *Science* **1997**, 278, 252.
- [3] M. Mayor, H. B. Weber, *Chimia* **2002**, 56, 494.
- [4] J. Chen, M. A. Reed, A. M. Rawlett, J. M. Tour, *Science* **1999**, 286, 1550.
- [5] W. L. Deng, K. W. Hipps, *J. Phys. Chem. B* **2003**, 107, 10736.
- [6] K. W. Hipps, D. E. Barlow, U. Mazur, *J. Phys. Chem. B* **2000**, 104, 2444.
- [7] X. Lu, K. W. Hipps, X. D. Wang, U. Mazur, *J. Am. Chem. Soc.* **1996**, 118, 7197.
- [8] X. Lu, K. W. Hipps, *J. Phys. Chem. B* **1997**, 101, 5391.
- [9] F.-R. F. Fan, J. Yang, S. M. Dirk, D. W. Price, D. Kosynkin, J. M. Tour, A. J. Bard, *J. Am. Chem. Soc.* **2001**, 123, 2454.
- [10] F.-R. F. Fan, J. P. Yang, L. T. Cai, D. W. Price, S. M. Dirk, D. V. Kosynkin, Y. X. Yao, A. M. Rawlett, J. M. Tour, A. J. Bard, *J. Am. Chem. Soc.* **2002**, 124, 5550.
- [11] L. A. Bumm, J. J. Arnold, T. D. Dunbar, D. L. Allara, P. S. Weiss, *J. Phys. Chem. B* **1999**, 103, 8122.
- [12] M. T. Cygan, T. D. Dunbar, J. J. Arnold, L. A. Bumm, N. F. Shedlock, T. P. Burgin, L. Jones, D. L. Allara, J. M. Tour, P. S. Weiss, *J. Am. Chem. Soc.* **1998**, 120, 2721.
- [13] Z. J. Donhauser, B. A. Mantooth, K. F. Kelly, L. A. Bumm, J. D. Monnell, J. J. Stapleton, D. W. Price, A. M. Rawlett, D. L. Allara, J. M. Tour, P. S. Weiss, *Science* **2001**, 292, 2303.
- [14] L. A. Bumm, J. J. Arnold, M. T. Cygan, T. D. Dunbar, T. P. Burgin, L. Jones, D. L. Allara, J. M. Tour, P. S. Weiss, *Science* **1996**, 271, 1705.
- [15] C. B. Gorman, R. L. Carroll, Y. He, F. Tian, R. Fuijrer, *Langmuir* **2000**, 16, 6312.
- [16] C. B. Gorman, R. L. Carroll, R. R. Fuijrer, *Langmuir* **2001**, 17, 6923.
- [17] R. A. Wassel, R. R. Fuijrer, N. Kim, C. B. Gorman, *Nano Lett.* **2003**, 3, 1617.
- [18] G. Leatherman, E. N. Durantini, D. Gust, T. A. Moore, A. L. Moore, S. Stone, Z. Zhou, P. Rez, Y. Z. Liu, S. M. Lindsay, *J. Phys. Chem. B* **1999**, 103, 4006.
- [19] X. D. Cui, X. Zarate, J. Tomfohr, O. F. Sankey, A. Primak, A. L. Moore, T. A. Moore, D. Gust, G. Harris, S. M. Lindsay, *Nanotechnology* **2002**, 13, 5.
- [20] G. K. Ramachandran, T. J. Hopson, A. M. Rawlett, L. A. Nagahara, A. Primak, S. M. Lindsay, *Science* **2003**, 300, 1413.
- [21] G. K. Ramachandran, J. K. Tomfohr, J. Li, O. F. Sankey, X. Zarate, A. Primak, Y. Terazono, T. A. Moore, A. L. Moore, D. Gust, L. A. Nagahara, S. M. Lindsay, *J. Phys. Chem. B* **2003**, 107, 6162.
- [22] G. V. Nazin, X. H. Qiu, W. Ho, *Science* **2003**, 302, 77.
- [23] S. Kubatkin, A. Danilov, M. Hjort, J. Cornil, J. L. Bredas, N. Stuhr-Hansen, P. Hedegard, T. Bjornholm, *Nature* **2003**, 425, 698.
- [24] M. P. Samanta, W. Tian, S. Datta, J. I. Henderson, C. P. Kubiak, *Phys. Rev. B* **1996**, 53, R7626.
- [25] M. Magoga, C. Joachim, *Phys. Rev. B* **1997**, 56, 4722.
- [26] V. J. Langlais, R. R. Schlittler, H. Tang, A. Gourdon, C. Joachim, J. K. Gimzewski, *Phys. Rev. Lett.* **1999**, 83, 2809.
- [27] C. Zhou, M. R. Deshpande, M. A. Reed, L. Jones, J. M. Tour, *Appl. Phys. Lett.* **1997**, 71, 611.
- [28] T. Ishida, W. Mizutani, U. Akiba, K. Umemura, A. Inoue, N. Choi, M. Fujihira, H. Tokumoto, *J. Phys. Chem. B* **1999**, 103, 1686.
- [29] T. Ishida, W. Mizutani, N. Choi, U. Akiba, M. Fujihira, H. Tokumoto, *J. Phys. Chem. B* **2000**, 104, 11680.
- [30] S. Howell, D. Kuila, B. Kasibhatla, C. P. Kubiak, D. Janes, R. Reifengerger, *Langmuir* **2002**, 18, 5120.
- [31] T. Ishida, W. Mizutani, Y. Aya, H. Ogiso, S. Sasaki, H. Tokumoto, *J. Phys. Chem. B* **2002**, 106, 5886.
- [32] J. G. Kushmerick, D. B. Holt, S. K. Pollack, M. A. Ratner, J. C. Yang, T. L. Schull, J. Naciri, M. H. Moore, R. Shashidhar, *J. Am. Chem. Soc.* **2002**, 124, 10654.
- [33] J. Reichert, H. B. Weber, M. Mayor, H. von Löhneysen, *Appl. Phys. Lett.* **2003**, 82, 4137.
- [34] J. J. Stapleton, P. Harder, T. A. Daniel, M. D. Reinard, Y. X. Yao, D. W. Price, J. M. Tour, D. L. Allara, *Langmuir* **2003**, 19, 8245.
- [35] W. J. Liang, M. P. Shores, M. Bockrath, J. R. Long, H. Park, *Nature* **2002**, 417, 725.
- [36] J. Park, A. N. Pasupathy, J. L. Goldsmith, C. Chang, Y. Yaish, J. R. Petta, M. Rinkoski, J. P. Sethna, H. D. Abruña, P. L. McEuen, D. C. Ralph, *Nature* **2002**, 417, 722.

- [37] M. Mayor, H. B. Weber, J. Reichert, M. Elbing, C. von Hanisch, D. Beckmann, M. Fischer, *Angew. Chem.* **2003**, *115*, 6014; *Angew. Chem. Int. Ed.* **2003**, *42*, 5834.
- [38] J. Reichert, H. B. Weber, M. Mayor, H. von Lohneysen, *Appl. Phys. Lett.* **2003**, *82*, 4137.
- [39] H. B. Weber, J. Reichert, F. Weigend, R. Ochs, D. Beckmann, M. Mayor, R. Ahlrichs, H. von Lohneysen, *Chem. Phys.* **2002**, *281*, 113.
- [40] H. B. Weber, J. Reichert, R. Ochs, D. Beckmann, M. Mayor, H. von Lohneysen, *Phys. E* **2003**, *18*, 231.

E. Heilbronner / F. A. Miller

A Philatelic Ramble through Chemistry

278 pages with 1025 color reproductions.

Softcover. € 79.00/ sFr 116.00.

ISBN 3-906390-31-4

A Philatelic Ramble through Chemistry is a light-hearted, historically based survey of chemistry and some related topics in physics. It is illustrated with more than 1000 beautiful color reproductions of postage stamps and covers. Many stories and anecdotes have been included. The book provides delightful personal reading and may be useful for courses on the history of chemistry. It is a source of numerous anecdotes which instructors can use to enliven their lectures.

€ -price is available only for Germany.

Wiley-VCH, Postfach 10 11 61, 69451 Weinheim, Germany
Fax: +49 (0) 6201 606-184, e-Mail: service@wiley-vch.de,
www.wiley-vch.de



Softcover edition!

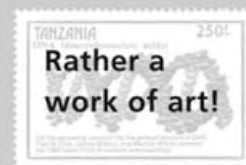
Praise for the Hardcover Edition

'This is a gem of a book. [...] I recommend it to all those to whom chemistry means more than an academic discipline, but a multi-faceted part of human culture, as Heilbronner and Miller so beautifully demonstrated.'

Interdisciplinary Science Reviews

'The creation of an exceptional book must be driven not only by knowledge but also by passion. This book by two chemists, Heilbronner and Miller, is clearly the product of a love for the world of postage stamps as well for chemistry in its widest sense.'

Advanced Materials



14170409_vo



WILEY-VCH

Bimetallic Figure-Eight Octaphyrins Split into Four-Pyrrolic Macrocycles

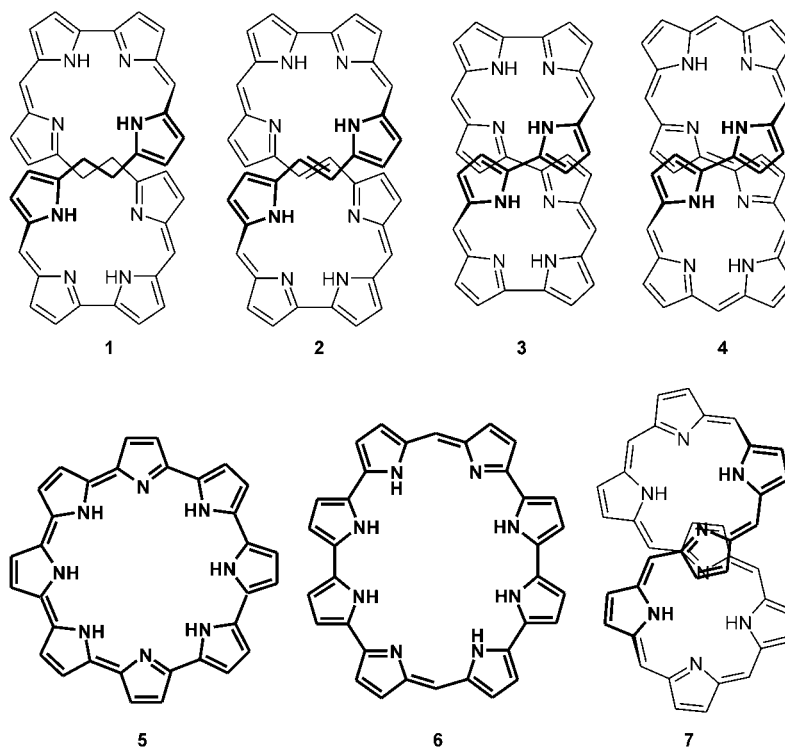
Lechosław Latos-Grażyński*

Keywords:

macrocyclic ligands · octaphyrins · porphyrinoids · rearrangement · spiro compounds

Expanded porphyrins can be considered as suitable and adjustable macrocyclic frameworks for the construction of binuclear or polynuclear coordination compounds.^[1] It can be expected that a multifunctional expanded porphyrin structure will enforce structurally unique coordination motifs and provide models for bimetallic metalloenzymes. Significantly, two adjacent, possibly co-operating, metal ions are in a position to prefer some unknown reaction routes that could be exploited in catalytic processes. Representative examples of such coordination chemistry have been demonstrated by amethyrins,^[2] accordion porphyrins,^[3] N-confused hexaphyrins,^[4] calix[4]pyrrole Schiff base macrocycles,^[5] rubyrins,^[6] structural analogues of Pac-Man porphyrins,^[7] and other macrocycles containing a pyrrolic unit.^[8] Bimetallic complexes were also obtained for octaphyrins,^[9] and these are the primary topic of this Highlight.^[10–14]

Vogel and co-workers demonstrated that an acid-catalyzed MacDonald condensation of a bipyrrrole derivative and a complementary, suitably functionalized bipyrrrole component resulted in the formation of octapyrrole **1** or the octaphyrins [36]octaphyrin(2.1.0.1.2.1.0.1) (**2**),^[9,15] [32]octaphyrin(1.0.1.0.1.0.1.0) (**3**),^[16] and [34]octaphyrin(1.1.1.0.1.1.1.0) (**4**; Scheme 1).^[15] The syntheses of [30]octaphyrin(0.0.0.0.0.0.0.0) (**5**)^[17] and [32]octaphyrin(1.0.0.0.1.0.0.0) (**6**)^[18] were re-



Scheme 1. Tetrahydrooctaphyrin **1** and octaphyrins **2–7** (the β and *meso* substituents are omitted for clarity).

ported by Sessler and co-workers. These expanded porphyrins contain eight pyrrolic fragments linked directly by $C_\alpha-C_\alpha$ bonds or by unsubstituted *meso*-methine $(CH)_n$ units ($n = 1, 2$).

A modification of the Rothmund-type synthesis resulted in the formation of expanded porphyrins, which contain more than six pyrrole moieties. Acid-catalyzed condensation of tetraalkylbipyrrrole and *ortho*-substituted benzaldehydes yielded a series of giant porphyrins, including *meso*-substituted [32]octaphyrin(1.0.1.0.1.0.1.0) (**3**).^[19] [36]Octaphyrin(1.1.1.1.1.1.1.1) (**7**), the fundamental macrocycle used in octaphyrin splitting studies, is obtained by straight-

forward condensation of pyrrole and pentafluorobenzaldehyde as reported by Osuka, Furuta, and co-workers.^[20] The fact that these expanded porphyrins are synthesized from commonly accessible substrates by a relatively simple methodology creates a foundation for extensive studies, including of their coordination chemistry and anion-binding properties.

This Highlight focuses on octaphyrins **2–4** and **7**, which have skeletons with a helical figure-eight arrangement.^[9,11,14–16,20] Such octaphyrin molecules exist in a chiral figure-eight conformation of two equidirectional helices. The crossing points in the octaphyrins

* Prof. Dr. L. Latos-Grażyński
Department of Chemistry
University of Wrocław
14 F. Joliot-Curie Street
Wrocław 50 383 (Poland)
Fax: (+48) 713-282-348
E-mail: llg@wchuwr.chem.uni.wroc.pl

discussed consist of chemically different moieties which belong to the upper and bottom part of the macrocyclic frame. The nitrogen atoms of the pyrrole rings adjacent to the crossing location are oriented in opposite directions, thus creating a “zigzag” turn.

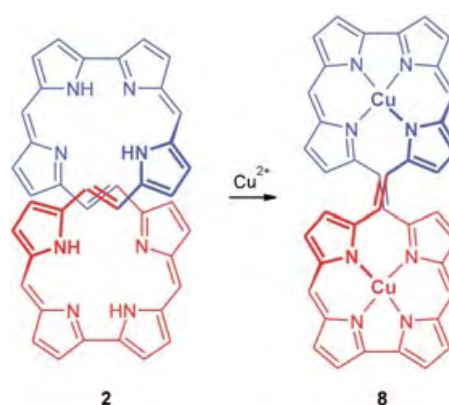
The figure-eight molecules reveal specific intramolecular mobility and two mechanisms were considered to account for the dynamic behavior of octaphyrins.^[21–23] The first mechanism involves an equilibrium between two enantiomeric forms of the double helical, figure-eight macrocycle and includes inversion of the helix. In selected cases the restriction of the intramolecular mobility allowed the separation of two enantiomers.^[9] The second mechanism which seems to be operating for the figure-eight molecules cyclooctapyrroles,^[11,15,22] 41,43,45,47-tetrathia-[36]octaphyrin(1.1.1.1.1.1.1.1),^[23] and turcasarin^[21] involves a conveyor-belt-like movement of the whole ring, but excludes, however, racemization. Rearrangement of the whole figure-eight ring of the molecule eventually takes place to reconstruct the geometry around “zigzag” spacers.

Figure-eight octaphyrins can contain either $4n+2$ or $4n$ π electrons, thus corresponding to the classical Hückel formulation for aromatic and antiaromatic rings, respectively. Consequently the ^1H NMR spectra of these molecules exhibit the presence of either residual diatropic or paratropic ring currents.^[21,23] As regards to this effect, one has to be aware of the figure-eight geometry compared to prototypical planar conjugated porphyrins or extended porphyrins. The marked influence of the size of the main conjugation pathway, which involves either $4n$ π electrons for **2** and **3** or $(4n+2)$ π electrons for **4**, was demonstrated by the electronic spectra: a correlation between the wavelength of the most intense band versus the number of conjugated π electrons was observed for a series of species formed in the course of redox processes.^[10] The spectra of the $(4n+2)$ π -electron species in particular exhibit an intense and sharp absorption band which reflects an intense conjugation in the ligand.

The cyclooctapyrroles **1–4** and **7** appear to be suitably prearranged to form binuclear metal complexes since

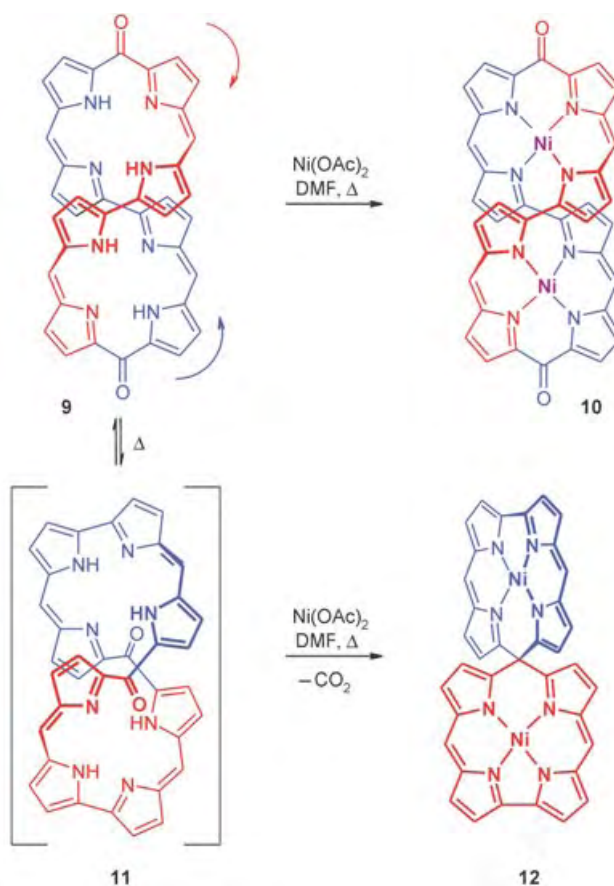
the remarkable conformation of these macrocycles creates two structurally identical, helical N_4 pockets distinctly separated by the figure-eight twist. For example, the X-ray structure of **2** shows the four dipyrin units are almost planar in each case, thus the helical conformation of the two tetrapyrrole subunits is mainly attributable to the torsions of the single bonds between the bipyrrole units.^[9] Significantly, the molecular symmetry remains unaffected after insertion of two Pd^{II} or Cu^{II} ions into the two N_4 pockets of **2**. There are marked conformational changes which are reflected by mutual orientation of the bridging $(\text{CH})_2$ units. The $\text{CH}=\text{CH}$ bonds are orthogonal in the free base **2** (Scheme 1), but they are parallel in complex **8** (Scheme 2).

The ring skeleton of [32]octaphyrin(1.1.1.0.1.1.1.0) (**3**) was functionalized to yield the dioxoderivative **9**.^[11] The macrocycle binds two Ni^{II} ions with preservation of the macrocyclic skeleton. Each Ni^{II} ion of **10** is coordinated by two practically planar dipyrin units.



Scheme 2. Conformation changes on insertion of Cu^{2+} ions into **2**.

Remarkably, the binuclear Ni^{II} spirodicorrole **12** was obtained in addition to the expected insertion product **10** (Scheme 3). In compound **12** two orthogonally oriented corrolates (both as isoforms) are linked through a common spiro carbon atom without any spacer. Directly linked porphyrins (*meso-meso*, $\beta\text{-}\beta$, or *meso-}\beta*) are, at present, the subject of extensive investigation.^[24,25]



Scheme 3. Transformation of **9** during the insertion of Ni^{II} ions.^[11]

Significantly, the spirodicorrole unit in **12** and the still to be synthesized spiro-diporphyrin provide a unique mode of covalently linking two porphyrin units.

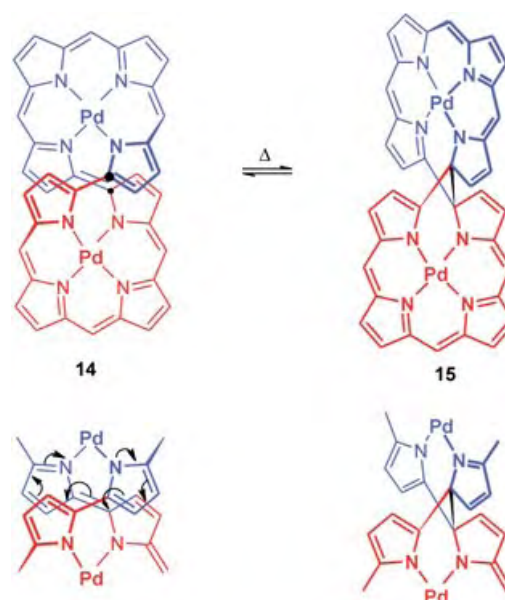
The electronic spectra and electrochemically measured redox potentials of **12** reflect the spiro effect.^[12] The homoconjugative interaction across the spiro center (spiroconjugation), that is, a homoconjugative interaction between the π systems of the two halves of the molecule separated by the tetragonal spiro center, is feasible because of the structural constraints of **12**.

The considered mechanism which explains the formation of **12** includes the conveyor-belt movement of **9** (marked by arrows in Scheme 3) which causes the carbonyl groups to meet at the crossing center of conformer **11**. The suggested skeletal rearrangement is presented in Scheme 4 (bottom) and involves an electrophilic attack of the Ni^{II} ion (or of a proton) on one of the carbonyl groups followed by its conversion into a carbenium ion and consecutive formation of the oxygen bridge.^[11] The carbenium ion thus generated undergoes a Wagner–Meerwein-type rearrangement to give the lactone **13**, which is expected to undergo a radical or ionic cleavage of the $\text{C}_{\text{spiro}}\text{--O}$ bond followed by subsequent loss of CO_2 from the diradical/zwitterionic species.

To date only two other octaphyrins, namely **4** and **7**, revealed intramolecular reactivity which led to their eventual

splitting into two cyclotetrapyrroles. Insertion of Pd^{II} ions into **4** yielded, apart from the expected binuclear Pd^{II} octaphyrin **14**, its constitutional isomer **15** (Scheme 5).^[11] Complex **15** contains a transannular C–C linkage between two pyrrolic $\alpha\text{--}\alpha'$ positions. The ligand consists of two identical tetrapyrrolic ring systems linked by the newly formed C–C bond. Remarkably the binuclear Pd^{II} octaphyrin **14** and its spiro isomer **15** remain in reversible thermal equilibrium, with **15** predominating at room temperature. The equilibrium can be displaced photochemically towards **14**. The thermal isomerization requires the presence of coordinated metal ions, since the free ligand does not reveal this type of rearrangement. The incorporation of palladium substantially reduces the distance between the reaction centers C_α and $\text{C}_{\alpha'}$ from 4.10 to 2.99 Å (as established by PM3 calculations) and induces strain between the reaction centers C_α and $\text{C}_{\alpha'}$ bond.

The transannular ring closure can be interpreted as a type of intramolecular Michael addition in which the electrophilic azafulvene unit serves as the acceptor and a nucleophilic pyrrole anion functions as a donor. Thermal



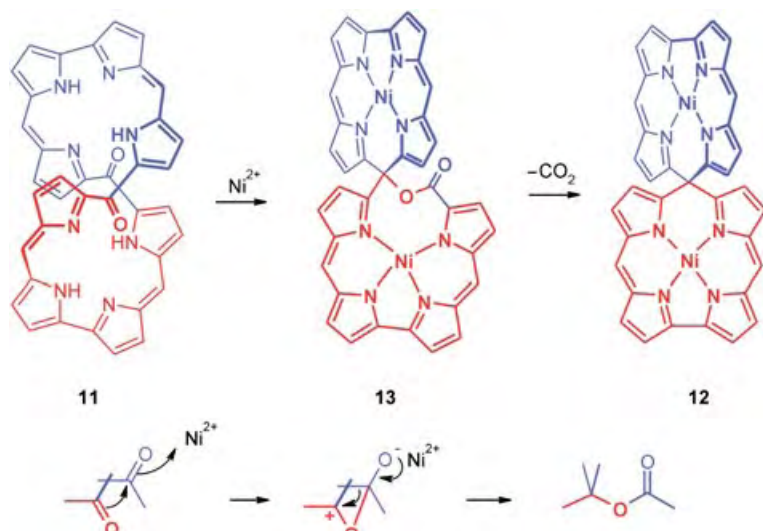
Scheme 5. Thermal equilibrium between binuclear Pd^{II} complex **14** and its bis-spirodiporphin isomer **15**. The black dots in structure **14** mark the C_α and $\text{C}_{\alpha'}$ reaction centers. Bottom: the postulated mechanism.^[11]

18- π -electron electrocyclization for each subunit was considered as an alternative mechanism.

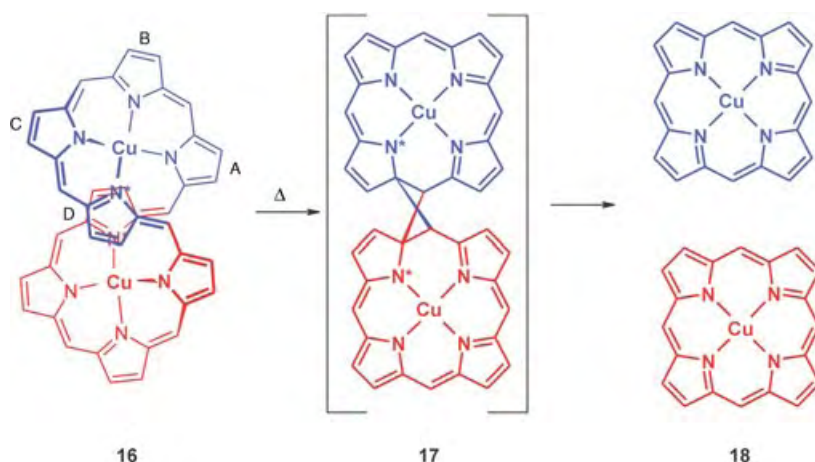
The collaborating research groups of Vogel and Houk observed unprecedented behaviors of bimetallic octaphyrins. The common feature is that the macrocycles split into two cyclic, four-pyrrolic compartments which remain covalently linked by a spiro carbon atom.^[11]

Recently, Osuka and co-workers discovered a logical termination of the sequence of the events observed in intramolecular octaphyrin reactivity, that is, a total cleavage of octaphyrin.^[14] Thus, their important contribution reveals an ultimate step in the sequence of figure-eight octaphyrin transformations, namely thermal splitting of a single binuclear Cu^{II} [36]octaphyrin-(1.1.1.1.1.1.1.1) complex (**16**) into two molecules of Cu^{II} [18]porphyrin(1.1.1.1) (**18**, Scheme 6).^[14] As discussed previously, [36]octaphyrin(1.1.1.1.1.1.1.1) (**7**) acquires a figure-eight geometry in the solid-state, with two identical porphyrin-like tetrapyrrolic ligands which are available for step-wise metalation by one or two Cu^{II} ions.

X-ray diffraction analysis of **16** revealed its effective C_2 symmetry and the presence of two copper ions centrally bound within the core of a severely



Scheme 4. Rearrangement of **9** into the binuclear Ni^{II} spirodicorrole **12** via **11** and the binuclear Ni^{II} lactone complex **13**. Bottom: the postulated mechanism.^[11]



Scheme 6. Thermal transformation of the binuclear Cu^{II} complex **16**.^[14]

distorted octaphyrin macrocycle. A tri-pyrrolic unit consisting of B–D pyrrole rings is relatively flat while the plane of pyrrole A is tilted by 63°. The structure of **16** reveals a severe distortion of the coordination geometry compared to the practically planar structure of **18**. These features suggest that the relief of strain in **16** may be a main driving force for this thermal splitting reaction. The splitting reaction of **16** was found to be a unimolecular process with an enthalpy for the formation of **18** of -135 kJ mol^{-1} . One possible mechanism may be a [2+2] cycloaddition to give the spirocyclobutane intermediate **17**, which divides into two molecules of **18** by a cycloreversion reaction. Significantly, a similar cleavage of octaphyrin **7** was detected for the binuclear Pd^{II}, Co^{II}, and Ni^{II} complexes of **7** but in rather small yields.^[14]

As demonstrated above, the Cu^{II}-metalation of [36]octaphyrin-(1.1.1.1.1.1.1.1) (**7**) gave rise to a facile splitting which provided a rare example of “molecular mitosis” for expanded porphyrins.^[14] In these terms, the molecular rearrangements, which result in the formation of binuclear Ni^{II} spirodiporphyrin **12** and binuclear Pd^{II} bis-spirodiporphyrin **15** from appropriate bimetallic octaphyrins, illustrate some imaginable snapshots of intermediates preceding the final phase of the “octaphyrin mitosis”.

The intriguing reaction which splits octaphyrin **9** into two covalently spiro-linked corrolates **12** seems to be facilitated by the proximity effect at the figure-eight crossing center,^[11] which is in fact a common structural feature of

figure-eight bimetallic octaphyrins. Theoretically, this peculiar transannular reactivity is feasible for any figure-eight metalloctaphyrin providing that a pre-organization step (the metal-ion coordination) creates a geometry at the crossing center which resembles the transition state for splitting.

The feasible routes for further exploration can be directed toward molecular electronics and catalysis. The noteworthy reversibility of the binuclear Pd^{II} [34]octaphyrin–spirodiporphyrin (**14–15**) isomerization (Scheme 5) leads to the conclusion that such a system behaves as a molecular switch containing two nondegenerate quasi-stable molecular states that are clearly distinguishable by electronic spectroscopy. Evidently the internal structural transformations, highlighted here for metalloctaphyrins, drastically modify the coordination cores surrounding two metal ions and consequently may create reversibly or irreversibly different chemical properties of metallic centers.

The coordination chemistry of expanded porphyrins is still in its infancy. The transformation detected for figure-eight octaphyrins revealed unusual coordination and transformation modes. It remains to be seen how the most fundamental factors, that is, the nature of the ribbon crossing motifs or the choice of the metal ions influence the stability of the transient species and eventually favor the splitting into two porphyrinic units over formation of a spirodiporphyrin.

Published Online: September 15, 2004

- [1] J. L. Sessler, D. Seidel, *Angew. Chem.* **2003**, *115*, 5292; *Angew. Chem. Int. Ed.* **2003**, *42*, 5134.
- [2] S. J. Weghorn, J. L. Sessler, V. Lynch, T. F. Baumann, J. W. Sibert, *Inorg. Chem.* **1996**, *35*, 1089.
- [3] W. A. Reiter, A. Gerges, S. Lee, T. Deffo, T. Clifford, A. Danby, J. Bowman-James, *Coord. Chem. Rev.* **1998**, *174*, 343.
- [4] A. Srinivasan, T. Ishizuka, A. Osuka, H. Furuta, *J. Am. Chem. Soc.* **2003**, *125*, 878.
- [5] J. M. Veauthier, W.-S. Cho, V. M. Lynch, J. L. Sessler, *Inorg. Chem.* **2004**, *43*, 1220.
- [6] S. J. Narayanan, B. Sridevi, T. K. Chandrashekar, U. Englich, K. Ruhlandt-Senge, *Inorg. Chem.* **2001**, *40*, 1637.
- [7] G. Givaja, A. J. Blake, C. Wilson, M. Schröder, J. B. Love, *Chem. Commun.* **2003**, 2508.
- [8] H. Adams, M. R. J. Elsegood, D. E. Fenton, S. L. Heath, S. J. Ryan, *J. Chem. Soc. Dalton Trans.* **1999**, 2031.
- [9] A. Werner, M. Michels, L. Zander, J. Lex, E. Vogel, *Angew. Chem.* **1999**, *111*, 3866; *Angew. Chem. Int. Ed.* **1999**, *38*, 3650.
- [10] J. Bley-Eschrich, J. P. Gisselbrecht, E. Vogel, M. Gross, *Eur. J. Inorg. Chem.* **2002**, 2829.
- [11] E. Vogel, M. Michels, L. Zander, J. Lex, N. S. Tuzun, K. N. Houk, *Angew. Chem.* **2003**, *115*, 2964; *Angew. Chem. Int. Ed.* **2003**, *42*, 2857.
- [12] G. Hohlneicher, D. Bremm, J. Wytke, J. Bley-Eschrich, J.-P. Gisselbert, M. Gross, M. Michels, J. Lex, E. Vogel, *Chem. Eur. J.* **2003**, *9*, 5636.
- [13] J. Bley-Eschrich, J.-P. Gisselbert, M. Michels, L. Zander, E. Vogel, M. Gross, *Eur. J. Inorg. Chem.* **2004**, 492.
- [14] Y. Tanaka, W. Hoshino, S. Shimizu, K. Youfu, N. Aratani, N. Maruyama, S. Fujita, A. Osuka, *J. Am. Chem. Soc.* **2004**, *126*, 3046.
- [15] E. Vogel, M. Bröring, J. Fink, D. Rosen, H. Schmickler, J. Lex, K. W. K. Chan, Y.-D. Wu, D. A. Plattner, M. Nendel, K. N. Houk, *Angew. Chem.* **1995**, *107*, 2705; *Angew. Chem. Int. Ed. Engl.* **1995**, *34*, 2511.
- [16] M. Bröring, J. Jendry, L. Zander, H. Schmickler, J. Lex, Y.-D. Wu, M. Nendel, J. G. Cheng, D. A. Plattner, K. N. Houk, E. Vogel, *Angew. Chem.* **1995**, *107*, 2709; *Angew. Chem. Int. Ed. Engl.* **1995**, *34*, 2515.
- [17] D. Seidel, V. Lynch, J. L. Sessler, *Angew. Chem.* **2002**, *114*, 1480; *Angew. Chem. Int. Ed.* **2002**, *41*, 1422.
- [18] J. L. Sessler, D. Seidel, V. Lynch, *J. Am. Chem. Soc.* **1999**, *121*, 11257.
- [19] J. Setsune, S. Maeda, *J. Am. Chem. Soc.* **2000**, *122*, 12405.

- [20] J.-Y. Shin, H. Furuta, K. Yoza, S. Igarashi, A. Osuka, *J. Am. Chem. Soc.* **2001**, *123*, 7190.
- [21] J. L. Sessler, S. J. Weghorn, V. Lynch, M. R. Johnson, *Angew. Chem.* **1994**, *106*, 1572; *Angew. Chem. Int. Ed. Engl.* **1994**, *33*, 1509.
- [22] J. A. Wytko, M. Michels, L. Zander, J. Lex, H. Schmickler, E. Vogel, *J. Org. Chem.* **2000**, *65*, 8709.
- [23] N. Sprutta, L. Latos-Grażyński, *Chem. Eur. J.* **2001**, *7*, 5099.
- [24] A. Tsuda, H. Furuta, A. Osuka, *J. Am. Chem. Soc.* **2001**, *123*, 10304.
- [25] X. Peng, N. Aratani, A. Tagaki, T. Matsumoto, T. Kawai, I.-W. Hwang, T. K. Ahn, D. Kim, A. Osuka, *J. Am. Chem. Soc.* **2004**, *126*, 4468.

Life's Simple Pleasures!



No need to waste precious time looking for the right information – Register now for the free **Wiley-VCH Alerting Service**.

It's simple – and it's fast.

To receive regular news per e-mail tailored precisely to your needs and interests, just fill in the registration form at www.wiley-vch.de/home/pas/

 **WILEY-VCH**

Carbene Reagents

N-Heterocyclic Carbenes: Reagents, Not Just Ligands!

Vijay Nair,* Santhamma Bindu, and Vellalath Sreekumar

Keywords:

carbenes · cycloadditions · Michael–Stetter reaction · multicomponent reactions · transesterification

Dedicated to Professor Gilbert Stork

The unique properties of N-heterocyclic carbenes (NHCs) have attracted much attention, mainly from theorists and organometallic chemists, the latter using them impressively as ligands for metals. Less well known, however, has been their suitability as excellent catalysts and nucleophilic reagents. Transesterification, nucleophilic aromatic substitution, and cycloaddition reactions are examples in which NHCs can play an important role. Asymmetric reactions using catalytic amounts of chiral NHCs are an efficient approach to optically active compounds. This minireview focuses on this aspect of the chemistry of NHCs.

1. Introduction

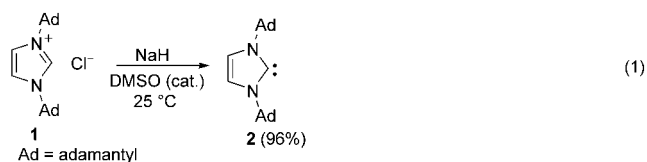
In recent years N-heterocyclic carbenes (NHCs) have evoked considerable interest, and this is attributed in large measure to the isolation of a stable imidazol-2-ylidene by Arduengo et al. in 1991.^[1] The close analogy of NHCs to trialkylphosphanes and their excellent σ -donating properties make them ligands of choice for transition metals, thus leading to the preparation of organometallic catalysts of enormous utility in organic synthesis.^[2] NHC-containing organometallic catalysts are found to be much more effective than conventional catalysts in a number of reactions, for example, the Heck reaction and olefin metathesis. Although the use of NHCs in coordination chemistry and organometallic reactions has been studied extensively, very little is known about the fundamental chemistry of these species. The purpose of this review is to cast some light on the chemistry of NHCs and to underscore the fact that, apart from being excellent ligands for palladium^[16] and related metals, they have a place of their own as reagents in organic synthesis. Our objective is to inspire organic chemists to explore the seemingly vast and untapped potential of NHCs. As a prelude to this, a brief history of N-heterocyclic carbenes is also included. By design, this review is primarily focused on the

carbenes derived from five-membered heterocycles in which the carbene center is flanked by two nitrogen atoms. The choice is based on the stability and versatility of these species

relative to that of the carbenes derived from other nitrogen heterocycles.

2. History of N-Heterocyclic Carbenes

Studies on NHCs date back to the work of Wanzlick in the 1960s.^[3] Although Wanzlick was unsuccessful in isolating any carbenes at that time, his recognition that a carbene center at the 2-position of the imidazole ring would be stable due to the electron-donating effects of adjacent nitrogen atoms provided the conceptual framework for the development of the chemistry of these species. As mentioned earlier, the current growth in the chemistry of NHCs is mainly ascribed to the pioneering work of Arduengo and co-workers, who isolated a stable crystalline N-heterocyclic carbene by the deprotonation of bis(1-adamantyl)imidazolium chloride with sodium hydride in tetrahydrofuran in the presence of a catalytic amount of dimethyl sulfoxide [Eq. (1)].^[1]

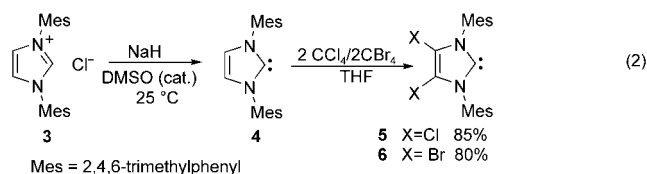


[*] Dr. V. Nair, Dr. S. Bindu, V. Sreekumar
Organic Chemistry Division
Regional Research Laboratory (CSIR)
Trivandrum 695 019 (India)
Fax: (+91) 471-249-1712
E-mail: vijaynair_2001@yahoo.com

The carbene isolated was found to be a thermally stable crystalline compound whose structure was unequivocally established by single-crystal X-ray analysis. The unusual

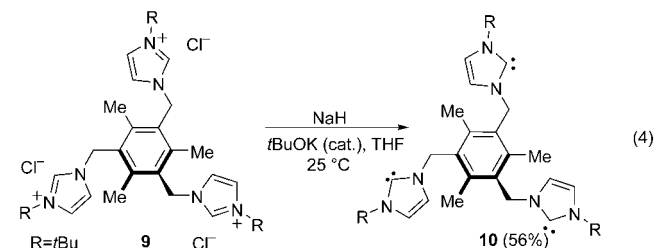
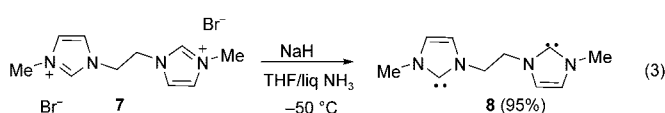
stability of **2** was explained by a number of factors, for example, the large singlet–triplet energy gap in imidazol-2-ylidene ($\sim 336 \text{ kJ mol}^{-1}$), π interactions in the imidazole ring, and the electronegativity of the nitrogen atoms. In addition to electronic factors, steric effects were also believed initially to play a major role in stabilizing the carbene **2**. Later Arduengo et al. demonstrated that stable carbenes can be prepared by the deprotonation of imidazolium salts bearing less bulky substituents in the 1- and 3-positions.^[4]

Since then, a wide variety of aminocarbenes have been synthesized, including the first air-stable carbene in 1997 [Eq. (2)]. A solid sample of the stable carbene **5** exposed to

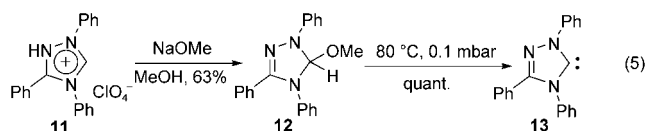


air did not show any decomposition even after two days.^[5] The remarkable stability of **5** was explained on the basis of the electronegative effect of the chlorine atoms, which reduce the reactivity and make the carbene air stable. Very recently, Cole and co-workers have reported the synthesis of bromo analogue of **5** from **4** by treatment with carbon tetrabromide. The carbene **6** thus generated was characterized by single-crystal X-ray analysis and found to be indefinitely stable in air.^[6]

The commonly used Arduengo prescription for the generation of N-heterocyclic carbenes involves the deprotonation of azolium salts with NaH, KH, or KOtBu^[4] in THF. Enhanced rates of deprotonation with NaH or KH have been observed with the addition of catalytic amounts of DMSO or KOtBu.^[1,7] More recently, Herrmann and co-workers have developed a more general and efficient route. NaH or KH in liquid ammonia was used to rapidly convert the azolium salts to their corresponding carbenes in a homogeneous phase.^[8] An illustration of this strategy is the synthesis of the stable biscarbene **8** [Eq. (3)] and the triscarbene **10** [Eq. (4)].^[9] Stable N-functionalized “pincer” biscarbenes have also been reported and used in the synthesis of various organometallic catalysts.^[10]

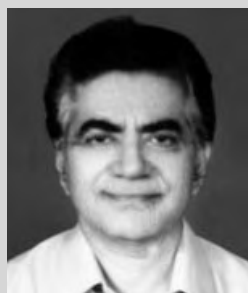
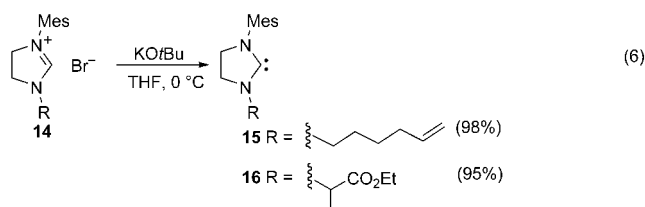


Enders and co-workers reported the first synthesis of the crystalline triazole-derived carbene **13** by the thermal decomposition of the 5-methoxytriazole **12** [Eq. (5)].^[11] Mention



may also be made of an earlier method for the synthesis of alkyl-substituted N-heterocyclic carbenes by the reaction of potassium with cyclic thiones in THF.^[12]

Fürstner and co-workers reported the synthesis and isolation of N-heterocyclic carbenes consisting of pendant alkenes and C–H acidic sites; the structures of these have been established by single-crystal X-ray analysis [Eq. (6)].^[13]

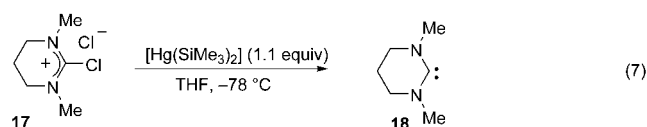


Vijay Nair has PhD degrees from the Banaras Hindu University (1967, with Professor R. H. Sahasrabudhey) and the University of British Columbia (1969, with Jim Kutney), and he was a postdoctoral fellow with Gilbert Stork at Columbia University. After a 16-year career (Outstanding Scientist Award, 1981) with Lederle Laboratories (American Cyanamid Company) in Pearl River, NY, he returned to India and joined the Regional Research Laboratory (CSIR) in 1990. From 1997 to 2001 he was the Director of the Institute. Presently he is continuing as a Director-Grade Scientist. In addition, he is an Honorary Professor in the Cochin University of Science and Technology.



Santhamma Bindu obtained her MSc degree in chemistry (first rank) from Mahatma Gandhi University. She completed her PhD thesis (2003) under the supervision of Dr. Vijay Nair at the Regional Research Laboratory (CSIR). Subsequently she joined the group of Professor Robert Coates at the University of Illinois in Urbana-Champaign as a postdoctoral fellow.

Very recently Bertrand reported a novel procedure using bis(trimethylsilyl)mercury for generating diaminocarbenes, and it has been applied to the synthesis of the stable six-membered NHC **18** [Eq. (7)].^[14] The generality of this reaction remains to be established.

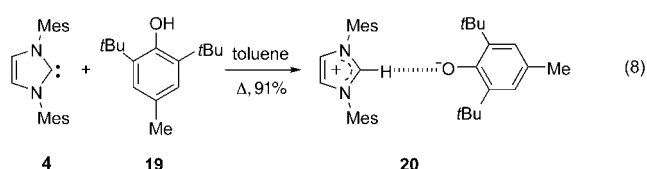


3. Reactivity of N-Heterocyclic Carbenes

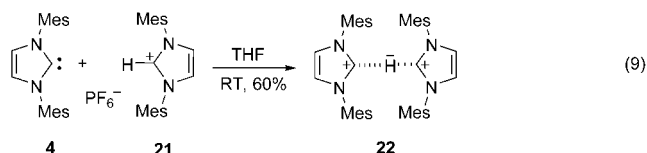
By virtue of their strong σ -donating ability, N-heterocyclic carbenes have found impressive use as ligands in the preparation of catalysts in organometallic chemistry. It is worthy of note that the aminocarbene-incorporated ruthenium alkylidene catalysts were found to be more versatile than the conventional Grubbs catalyst in olefin metathesis reactions.^[15d] Although we will not address the application of NHCs in organometallic chemistry here, since it is not directly relevant to the present account, we note that important contributions to this area have been made by the groups led by Herrmann,^[2c, 15a] Grubbs,^[15b,c] Cavell,^[16] and Nolan.^[2d,c] Excellent reviews on the subject are available in the literature.^[2a,b]

Alder and co-workers determined the nucleophilicity and basicity of various aminocarbenes based on the Brønsted–Lowry concept. They reported the $\text{p}K_a$ of 1,3-diisopropyl-4,5-dimethyl-imidazol-2-ylidene as **24** in $[\text{D}_6]\text{DMSO}$ and found that it is a much stronger base than 1,5-diazabicyclo[3.4.0]non-5-ene (DBN), 1,8-diazabicyclo[5.4.0]undec-7-ene (DBU), and proton sponge (1,8-bis(dimethylamino)naphthalene) but weaker than phosphazene bases.^[17] Recently Streitwieser and Kim calculated the $\text{p}K_a$ of 1,3-di(*tert*-butyl)imidazol-2-ylidene in THF as 20, which is much less than that of the dimesityl derivative reported by Alder.^[18] The pronounced basicity of the N-heterocyclic carbene **4** is attested by the isolation of crystalline compounds with organic acids such as phenols [Eq. (8)].^[19]

Similarly, Arduengo et al. reported the isolation of stable hydrogen-bonded bis(carbene) complex **22** by the interaction



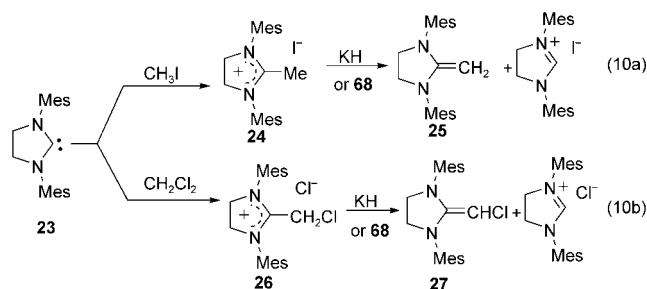
of carbene **4** with its azolium salt [Eq. (9)].^[20a] Stable carbene **4** also forms C–H \cdots C (π) complexes with hydrocarbons such as indene and fluorene.^[20b]



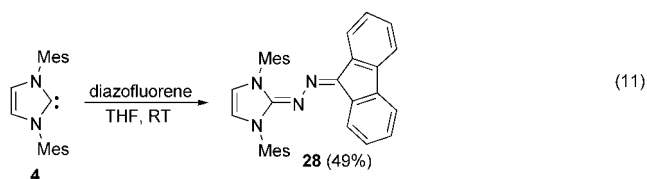
The reactivity of stable diaminocarbenes towards water, oxygen, and hydrogen has also been investigated. Imidazolin-2-ylidenes underwent instant hydrolysis on exposure to moist THF, whereas hydrolysis of the aromatic congeners such as 1,3-di(*tert*-butyl)imidazol-2-ylidene to the corresponding aldehydes took days.^[21] These carbenes were found to be inert towards oxygen and hydrogen, but in the presence of hydrogen and a platinum or palladium catalyst, they underwent slow hydrogenation.

Aminocarbenes such as triazolylidene have been shown to insert into strongly polar X–H bonds ($\text{X} = \text{OR}^1, \text{NR}_2$) to afford the corresponding 1,1-addition product. The insertion of such species into unpolarized C–H bonds, however, has not been reported so far.^[11]

Imidazolin-2-ylidene **23** was shown to react with methyl iodide and dichloromethane to afford the olefins **25** and **27** along with the corresponding imidazolium salts [Eq. (10)].^[5] Similar addition products were obtained from the reaction of imidazol-2-ylidenes with trimethylsilyl iodide.^[22]



The reaction of 1,3-dimesitylimidazol-2-ylidene with diazo compounds such as diazofluorene and diphenyldiazomethane afforded the corresponding azines as the addition products [Eq. (11)], whereas the reaction of the carbene with



Vellalath Sreekumar obtained his MSc degree in chemistry from the University of Calicut (2001). Currently he is a research fellow working towards his PhD in the group of Dr. Vijay Nair at the Regional Research Laboratory (CSIR).

azidotrimethylsilane furnished the imine by Staudinger ligation of the azide mediated by phosphanes.^[23]

As early as 1958, Breslow recognized the role of N-heterocyclic carbenes as nucleophilic catalysts in enzymatic reactions. His seminal work showed that the vitamin B₁ enzyme cofactor thiamine (**29**), a naturally occurring thiazolium salt, plays a crucial role in biochemical transformations (Figure 1).^[24] As thiamine diphosphate, it catalyzes the

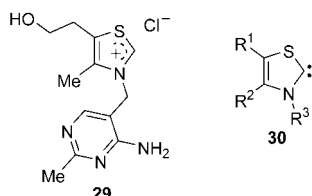
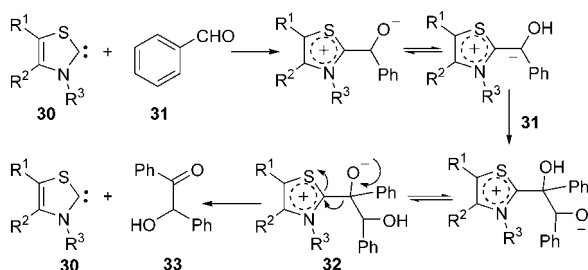


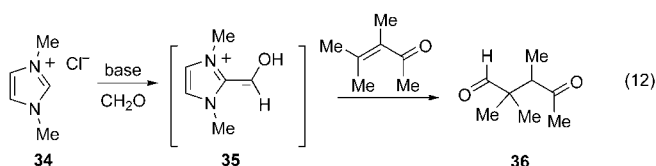
Figure 1. Thiamine (**29**) and the derived carbene **30**.

decarboxylation of pyruvic acid to active acetaldehyde as well as the benzoin condensation of aromatic aldehydes. The active species involved in this reaction was found to be the thiazolylidene **30** (Scheme 1).



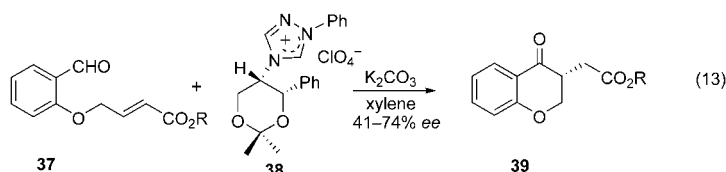
Scheme 1. Mechanism of the benzoin condensation catalyzed by thiamine.

Aliphatic aldehydes are also reported to undergo benzoin-type condensation called the Stetter reaction under ylide catalysis. Several azolium salts such as imidazolium, thiazolium, and triazolium salts were found to be effective as catalysts for this transformation. When α,β -unsaturated ketones are employed, the reaction is called the Michael–Stetter reaction; a typical reaction involving an imidazolium salt, an α,β -unsaturated ketone, and an aldehyde is shown in Equation (12).^[25]

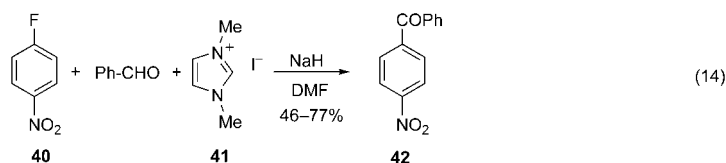


The polycondensation of formaldehyde under ylide catalysis leads to the formation of carbohydrylates.^[26] An asymmetric version of the Michael–Stetter reaction employing a chiral azolium salt for the synthesis of the benzopyran derivative **39** was first reported

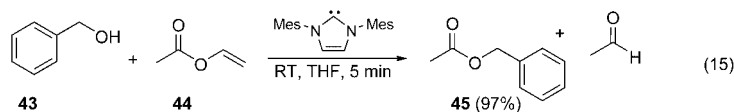
by Enders et al. [Eq. (13)].^[27a,b] Independently, Kerr and Alaniz showed that the use of a fused chiral triazolium salt leads to the product in higher yield and enantioselectivity.^[27c]



The potential utility of NHCs as catalysts in nucleophilic aromatic substitution reactions was demonstrated by Miyashita et al. in their report on the acylation of aryl fluorides catalyzed by imidazol-2-ylidene [Eq. (14)].^[28]

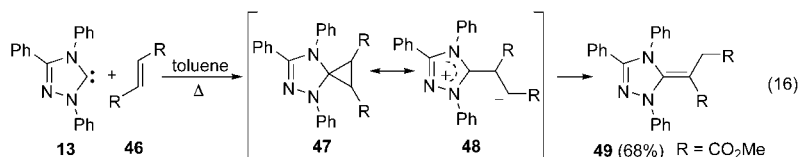


Stable NHCs have been found to be very efficient catalysts for transesterification and acylation reactions [Eq. (15)].^[29]



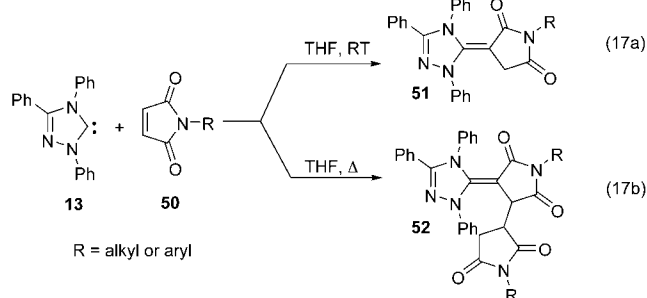
A number of imidazolium salts have found widespread use as ionic liquids. Afonso and co-workers reported on the beneficial properties of imidazolium salts as ionic liquids in the Baylis–Hillman reaction.^[30] However, in a more recent study, it was shown that the use of imidazolium salts as ionic liquids in the Baylis–Hillman reaction results in low yields of products due to side reactions of the carbene generated with aldehydes.^[31] Importantly, the study demonstrated that the deprotonation of imidazolium salts requires only mild bases such as 1,4-diazabicyclo[2.2.2]octane (DABCO) and 3-hydroxyquinuclidine.

The reactivity of stable diaminocarbenes towards C–C multiple bonds has been studied by Enders and co-workers, who showed that unlike other singlet carbenes, the triazolylidene **13** does not furnish any cyclopropane derivative with dimethyl fumarate; instead it affords the methylene triazoline derivative **49** [Eq. (16)]. According to them, the initial event

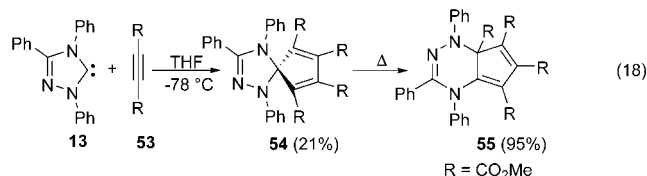


in this reaction is the [2+1] cycloaddition of the carbene with the alkene to form the cyclopropane derivative **47**, which undergoes rapid ring opening to afford the zwitterionic intermediate **48**. Subsequent [1,2]-hydrogen shift affords the methylene triazoline derivative **49**.^[11]

Similarly, the reaction of **13** with *N*-alkyl or *N*-aryl maleimides afforded the corresponding 1:1 and 1:2 adducts depending on the conditions employed [Eqs. (17a) and (17b)].^[32]

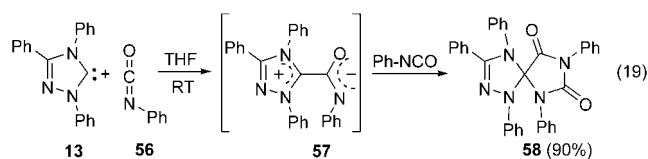


A similar reaction of triazolyliene **13** with dimethyl acetylenedicarboxylate (DMAD) afforded the spiro compound **54**, which rearranged to the more stable bicyclic compound **55** on heating [Eq. (18)].^[33] Presumably, **54** arises



by the addition of a second molecule of DMAD to the initially formed zwitterion.

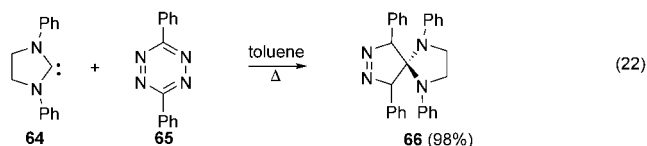
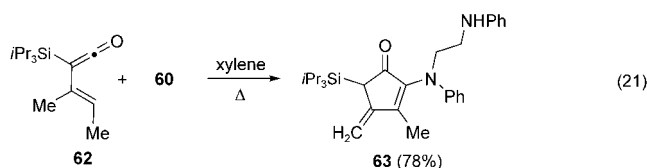
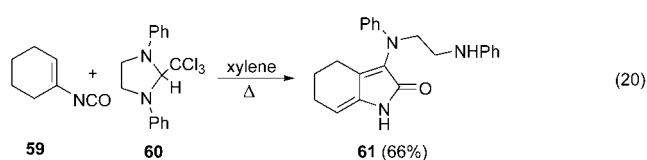
A mechanistically related reaction involving **13** and excess phenyl isocyanate led to the formation of the spiro compound **58**, presumably by means of a [3+2] cycloaddition with the intermediate betaine **57** [Eq. (19)].^[33]



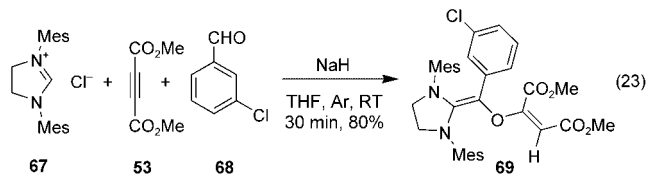
In a recent report, Rigby and Wang have shown that the [4+1] cycloaddition of *N*-heterocyclic carbenes with vinyl isocyanates and vinyl ketenes leads to functionalized hydroindolone [Eq. (20)]^[34a] and cyclopentenone derivatives [Eq. (21)].^[34b]

The [4+1] cycloaddition of **64** with diphenyl tetrazine has been shown to afford the spiro compound **66** [Eq. (22)].^[35]

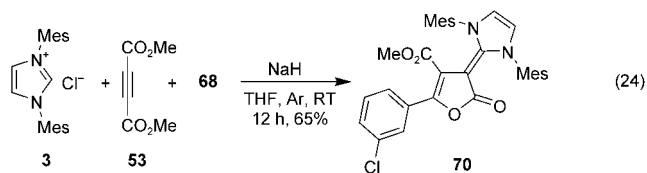
As a part of our continued interest in devising novel multicomponent reactions based on nucleophilic carbenes,^[36]



we embarked on a systematic investigation of the reactivity of various *N*-heterocyclic carbenes towards activated acetylenes and aldehydes. Our studies started with the reaction of an aminocarbene, which was generated in situ from **67**, with DMAD and aldehyde; the corresponding 2-oxymaleate derivative **69** was obtained in good yield [Eq. (23)].^[37]



The reaction was found to be sensitive to the nature of the carbene employed. When the less nucleophilic 1,3-dimesitylimidazol-2-ylidene was employed, the reaction followed a different but interesting pathway leading to the furanone derivative **70** in good yield [Eq. (24)]. Although the mechanistic underpinnings are yet to be investigated, these reactions point to a rich and fascinating area of research that lies ahead.



4. Conclusion

In conclusion, the chemistry of NHCs reviewed in this article underlines the enormous potential of these species in effecting a wide range of synthetic applications. In particular, the close analogy of NHCs to phosphanes makes them valuable as powerful nucleophiles in many synthetically

useful reactions. Beyond this, the ability of NHCs to participate as reactants towards a variety of electrophilic species, leading to novel molecular frameworks offers promise for their use in organic synthesis. It is conceivable that the exploration of NHCs will uncover much fascinating and useful chemistry.

Received: September 26, 2003

Revised: March 9, 2004

Published Online: August 19, 2004

- [1] A. J. Arduengo III, R. L. Harlow, M. K. Kline, *J. Am. Chem. Soc.* **1991**, *113*, 361.
- [2] a) W. A. Herrmann, *Angew. Chem.* **2002**, *114*, 1342; *Angew. Chem. Int. Ed.* **2002**, *41*, 1290; b) W. A. Herrmann, C. Köcher, *Angew. Chem.* **1997**, *109*, 2257; *Angew. Chem. Int. Ed. Engl.* **1997**, *36*, 2162; c) T. Weskamp, W. C. Schattenmann, M. Spiegler, W. A. Herrmann, *Angew. Chem.* **1998**, *110*, 2631; *Angew. Chem. Int. Ed.* **1998**, *37*, 2490; d) S. P. Nolan, R. A. Kelly III, O. Navarro, *J. Am. Chem. Soc.* **2003**, *125*, 16194.
- [3] a) H.-W. Wanzlick, *Angew. Chem.* **1962**, *74*, 129; *Angew. Chem. Int. Ed. Engl.* **1962**, *1*, 75; b) H.-W. Wanzlick, H.-J. Schönherr, *Justus Liebigs Ann. Chem.* **1970**, 731, 176.
- [4] A. J. Arduengo III, H. V. R. Dias, R. L. Harlow, M. K. Kline, *J. Am. Chem. Soc.* **1992**, *114*, 5530.
- [5] A. J. Arduengo III, F. Davidson, H. V. R. Dias, J. R. Goerlich, D. Khasnis, W. J. Marshall, T. K. Prakasha, *J. Am. Chem. Soc.* **1997**, *119*, 12742.
- [6] M. L. Cole, C. Jones, P. C. Junk, *New J. Chem.* **2002**, *26*, 1296.
- [7] A. J. Arduengo III, R. Krafczyk, R. Schmutzler, *Tetrahedron* **1999**, *55*, 14523.
- [8] W. A. Herrmann, C. Köcher, L. Goossen, G. R. Artus, *Chem. Eur. J.* **1996**, *2*, 1627.
- [9] a) W. A. Herrmann, M. Elison, J. Fischer, C. Köcher, G. R. Artus, *Chem. Eur. J.* **1996**, *2*, 772; b) H. V. R. Dias, W. Jin, *Tetrahedron Lett.* **1994**, *35*, 1365.
- [10] A. A. Danopoulos, S. Winston, T. Gelbrich, M. B. Hursthouse, P. R. Toose, *Chem. Commun.* **2002**, 482.
- [11] D. Enders, K. Breuer, J. Raabe, J. Runsink, J. H. Teles, J.-P. Melder, S. Brode, *Angew. Chem.* **1995**, *107*, 1119; *Angew. Chem. Int. Ed. Engl.* **1995**, *34*, 1021.
- [12] N. Kuhn, T. Kratz, *Synthesis* **1993**, 561.
- [13] A. Fürstner, H. Krause, L. Ackermann, C. W. Lehmann, *Chem. Commun.* **2001**, 2240.
- [14] M. Otto, S. Conejero, Y. Canac, V. D. Romanenko, V. Rudzhevitch, G. Bertrand, *J. Am. Chem. Soc.* **2004**, *126*, 1016.
- [15] a) W. A. Herrmann, M. Elison, J. Fischer, C. Köcher, G. R. J. Artus, *Angew. Chem.* **1995**, *107*, 2602; *Angew. Chem. Int. Ed. Engl.* **1995**, *34*, 2371; b) M. Scholl, T. M. Trnka, J. P. Morgan, R. H. Grubbs, *Tetrahedron Lett.* **1999**, *40*, 2247; c) T.-L. Choi, R. H. Grubbs, *Chem. Commun.* **2001**, 2648; d) A. Fürstner, L. Ackermann, B. Gabor, R. Goddard, C. W. Lehmann, F. Mynott, F. Stelzer, O. R. Thiel, *Chem. Eur. J.* **2001**, *7*, 3236.
- [16] a) M. J. Green, K. J. Cavell, B. W. Skelton, A. H. White, *J. Organomet. Chem.* **1998**, *554*, 175; b) D. S. McGuinness, M. J. Green, K. J. Cavell, B. W. Skelton, A. H. White, *J. Organomet. Chem.* **1998**, *565*, 165; c) D. S. McGuinness, K. J. Cavell, B. W. Skelton, A. H. White, *Organometallics* **1999**, *18*, 1596; d) D. S. McGuinness, K. J. Cavell, *Organometallics* **2000**, *19*, 4918; e) D. S. McGuinness, K. J. Cavell, *Organometallics* **2000**, *19*, 741; f) M. A. Duin, N. D. Clement, K. J. Cavell, C. J. Elsevier, *Chem. Commun.* **2003**, 400.
- [17] R. W. Alder, P. R. Allen, S. J. Williams, *Chem. Commun.* **1995**, 1267.
- [18] Y.-J. Kim, A. Streitwieser, *J. Am. Chem. Soc.* **2002**, *124*, 5757.
- [19] J. A. Cowan, J. A. C. Clyburne, M. G. Davidson, R. L. W. Harris, J. A. K. Howard, P. Küpper, M. A. Leech, S. P. Richards, *Angew. Chem.* **2002**, *114*, 1490; *Angew. Chem. Int. Ed.* **2002**, *41*, 1432.
- [20] a) A. J. Arduengo III, S. F. Gamper, M. Tamm, J. C. Calabrese, S. Davidson, H. A. Craig, *J. Am. Chem. Soc.* **1995**, *117*, 572; b) S. Filippini, J. N. Jones, J. A. Johnson, A. H. Cowley, F. Grepioni, D. Braga, *Chem. Commun.* **2003**, 2716.
- [21] M. K. Denk, M. J. Rodezno, S. Gupta, A. L. Lough, *J. Organomet. Chem.* **2001**, 617–618, 242.
- [22] N. Kuhn, T. Kratz, D. Bläser, R. Boese, *Chem. Ber.* **1995**, *128*, 245.
- [23] J. M. Hopkins, M. Bowdridge, K. N. Robertson, S. Cameron, H. A. Jenkins, J. A. Clyburne, *J. Org. Chem.* **2001**, *66*, 5713.
- [24] R. Breslow, *J. Am. Chem. Soc.* **1958**, *80*, 3719.
- [25] J. H. Teles, J. P. Melder, K. Ebel, R. Schneider, E. Gehrler, W. Harder, S. Brode, D. Enders, K. Breuer, G. Rabbe, *Helv. Chim. Acta* **1996**, *79*, 1271.
- [26] J. H. Davis, Jr., K. Forrester, *Tetrahedron Lett.* **1999**, *40*, 1621.
- [27] a) D. Enders, K. Breuer, J. Runsink, J. H. Teles, *Helv. Chim. Acta* **1996**, *79*, 1899; b) D. Enders, U. Kallfass, *Angew. Chem.* **2002**, *114*, 1812; *Angew. Chem. Int. Ed.* **2002**, *41*, 1743; c) M. S. Kerr, J. R. D. Alaniz, *J. Am. Chem. Soc.* **2002**, *124*, 10298.
- [28] a) Y. Suzuki, T. Toyota, F. Imada, M. Sato, A. Miyashita, *Chem. Commun.* **2003**, 1314; b) A. Miyashita, K. Suzuki, E. O. Iwamoto, T. Higashino, *Heterocycles* **1998**, *49*, 405; c) A. Miyashita, A. Suzuki, E. O. Iwamoto, T. Higashino, *Chem. Pharm. Bull.* **1998**, *46*, 390.
- [29] a) G. A. Grasa, R. M. Kissling, S. P. Nolan, *Org. Lett.* **2002**, *4*, 3583; b) G. A. Grasa, T. Güveli, R. Singh, S. P. Nolan, *J. Org. Chem.* **2003**, *68*, 2812; c) G. W. Nyce, J. A. Lamboy, E. F. Connor, R. M. Waymouth, J. L. Hedrick, *Org. Lett.* **2002**, *4*, 3587; d) R. Singh, R. M. Kissling, M.-A. Letellier, S. P. Nolan, *J. Org. Chem.* **2004**, *69*, 209.
- [30] J. N. Rosa, C. A. M. Afonso, A. G. Santos, *Tetrahedron* **2001**, *57*, 4189.
- [31] V. K. Aggarwal, I. Emme, A. Mereu, *Chem. Commun.* **2002**, 1612.
- [32] D. Enders, K. Breuer, J. Raabe, J. Runsink, J. H. Teles, *Liebigs Ann.* **1996**, 2019.
- [33] a) N. Kuhn, M. Steimann, G. Z. Weyers, *Z. Naturforsch. B* **1994**, *49*, 427; b) N. Kuhn, C. Maichle-Mossmeyer, G. Z. Weyers, *Z. Anorg. Allg. Chem.* **1999**, 625, 851; c) N. Kuhn, M. Steimann, G. Weyers, G. Z. Henkel, *Z. Naturforsch. B* **1999**, *54*, 434; d) N. Kuhn, H. Bohnen, G. Z. Henkel, *Z. Naturforsch. B* **1994**, *49*, 1473; e) N. Kuhn, G. Weyers, G. Henkel, *Chem. Commun.* **1997**, 627.
- [34] a) J. H. Rigby, Z. Wang, *Org. Lett.* **2002**, *4*, 4289; b) J. H. Rigby, Z. Wang, *Org. Lett.* **2003**, *5*, 263.
- [35] H. Mohrle, H. Dwuletzi, *Chem.-Ztg.* **1987**, *111*, 9.
- [36] V. Nair, S. Bindu, V. Sreekumar, L. Balagopal, *Synthesis* **2003**, *10*, 1446.
- [37] V. Nair, S. Bindu, V. Sreekumar, N. P. Rath, *Org. Lett.* **2003**, *5*, 665.

Asymmetric Catalysis

In the Golden Age of Organocatalysis**

Peter I. Dalko* and Lionel Moisan

Keywords:

asymmetric catalysis · chiral auxiliaries · organocatalysis · synthetic methods



The term “organocatalysis” describes the acceleration of chemical reactions through the addition of a substoichiometric quantity of an organic compound. The interest in this field has increased spectacularly in the last few years as result of both the novelty of the concept and, more importantly, the fact that the efficiency and selectivity of many organocatalytic reactions meet the standards of established organic reactions. Organocatalytic reactions are becoming powerful tools in the construction of complex molecular skeletons. The diverse examples show that in recent years organocatalysis has developed within organic chemistry into its own subdiscipline, whose “Golden Age” has already dawned.

From the Contents

1. Introduction	5139
2. Reactions via Covalent Transition Complexes	5140
3. Reactions via Noncovalent Activation Complexes	5158
4. Enantioselective Phase-Transfer Reactions	5164
5. Asymmetric Transformations in a Chiral Cavity	5168
6. Summary and Outlook	5169

1. Introduction

Organocatalysis is the acceleration of chemical reactions with a substoichiometric amount of an organic compound which does not contain a metal atom.^[1]

Despite the very recent introduction of this type of catalysis to synthetic chemistry, organocatalytic reactions look back on a venerable history. Evidence has been found that this type of catalysis played a determinant role in the formation of prebiotic key building blocks, such as sugars, and thus allowed the introduction and spread of homochirality in living organisms.^[2] According to this hypothesis, enantiomerically enriched amino acids, such as L-alanine and L-isovaline, which may be present with up to 15% *ee* in carbonaceous meteorites, catalyze the dimerization of glycol and an aldol-type reaction between glycol and formaldehyde to afford sugar derivatives with significant enantiomeric excess.

Although organic molecules have also been used since the beginnings of chemistry as catalysts, their application in enantioselective catalysis has only emerged as a major concept in organic chemistry in the last few years.^[3,4] As a result of both determined scientific interest, such as usually accompanies emerging fields, and the recognition of the huge potential of this new area, organocatalysis has received considerable attention.^[3,4]

The goal of this Review is to update and extend our previous account on enantioselective organocatalysis.^[3a] Thus, we focus herein on enantioselective reactions that have appeared in the last three years. We attempt to offer a comprehensive overview of the field with emphasis on practical aspects. When available, mechanistic models are presented for the rationalization of the reaction process.

Which are the newest and conceptually most challenging ideas in organocatalysis? The pinpointing of “privileged” catalyst classes showing general superiority for many reaction types is undoubtedly one of the most intriguing aspects and may have a considerable impact on the development of new catalytic systems.^[5] Some organic and organometallic molecules have the extraordinary capacity to mediate efficiently a variety of mechanistically distinct reactions.^[6] In closely

related reactions, such as aldol and Mannich reactions, the similarities in the reaction profiles can be understood and exploited. When a catalyst, such as L-proline, performs well in one reaction, it can be expected to mediate all similar reactions under optimized reaction conditions. However, less closely related reactions may also be promoted by catalysts of the same class. For example, chiral thiourea derivatives and their analogues catalyze the hydrocyanation of imines (Strecker reaction) as well as asymmetric Mannich reactions. This finding is surprising, when one considers that the Strecker and Mannich reactions have quite different reactivity and stereoselection profiles. Likewise, short-chain oligopeptides, which are established catalysts for asymmetric acylation, can also mediate selective 1,4-addition reactions. Cinchona alkaloids are another example of a privileged catalyst class.^[7] Their ability to mediate an astonishingly wide variety of enantioselective transformations is discussed in this Review.

Important progress has been made in the development of site-selective reactions with organic catalysts. These results have far-reaching consequences: From a philosophical point of view, the boundaries between enzyme- and small-molecule-mediated reactions are becoming blurred. From a practical

[*] Dr. P. I. Dalko
Laboratoire de Recherches Organiques associé au CNRS
ESPCI, 10 rue Vauquelin, 75231 Paris Cedex 05 (France)
Fax: (+33) 1-4079-4660
E-mail: peter.dalko@espci.fr

L. Moisan
CEA-SACLAY, Service de Marquage Moléculaire
et de Chimie Bioorganique
Bât 547, 91191 Gif-sur-Yvette Cedex (France)

[**] The illustration on the frontispiece is taken from the codex *The Book of Chess, Dice, and Board Games*, completed around 1280 by Alfonso X of Castille. Alfonso's heritage represents above all a great cultural bridge between the Christian West and the Muslim East. In a similar way, organocatalysis represents a link between two major forms of catalysis: metal-complex-mediated and enzymatic catalysis, and thus between synthetic and bioorganic chemistry.

point of view, this type of reaction may allow the use of nonprotected substrates in synthesis.^[8,9]

Our understanding of the mechanistic details of individual reaction pathways is improving. Organocatalytic reactions proceed either by a much “tighter” or a much “looser” transition state than those mediated by chiral metal complexes. The former class of organocatalysts includes compounds that act as covalently bonded reagents. The latter class induces a high level of enantioselectivity mainly through such interactions as hydrogen bonding or ion pairing. The enormous potential of hydrogen bonding as an activating interaction has been recognized only recently.^[10,11]

The scope of organocatalytic reactions has been expanded considerably. Typical transition-metal-mediated coupling reactions, such as Suzuki,^[12] Sonogashira,^[13] Ullmann,^[14] and Heck-type coupling reactions,^[15] as well as the Tsuji–Trost reaction,^[16] can now be performed under metal-free conditions. The development of catalysts with a higher molecular weight and increased complexity often leads to a sharp improvement not only in the selectivity of the catalyst, but also in its kinetic profile. In an increasing number of asymmetric reactions these catalysts can meet the high standards of modern synthetic methods.

Whereas many metal centers are good Lewis acids, organic catalysts tend to react as heteroatom-centered (mainly N(O)-, P(O)-, and S(O)-centered) Lewis bases. However, novel, previously unexplored catalyst classes are emerging. For example, asymmetric catalysis by Brønsted acids is a recent addition to the field of organic catalysis. Moreover, the design and use of synergic systems and bifunctional catalysts, which have two distinct functionalities (e.g. a Lewis base and a Brønsted acid) within the same molecule, is becoming more and more common.^[17]

Organocatalytic methods have great practical potential in devising multicomponent and tandem sequences. In the future all these reactions will also find use outside the academic environment for the synthesis of complex molecular structures.

2. Reactions via Covalent Transition Complexes

2.1. Nucleophilic Catalysis: Activation of the Donor

Most organocatalysts used currently are bifunctional, commonly with a Brønsted acid and a Lewis base center.^[4e]

These compounds activate both the donor and the acceptor, thus resulting in a considerable acceleration of the reaction rate.

The vast majority of organocatalytic reactions are amine-based reactions.^[18] In this asymmetric aminocatalysis amino acids, peptides, alkaloids, and synthetic nitrogen-containing molecules are used as chiral catalysts. Most of these reactions proceed by the generalized enamine cycle or as charge-accelerated reactions through the formation of imonium intermediates. These two types of activation are often complementary and can therefore sometimes be used as alternatives in the same transformation. The donor molecule can be activated through the formation of an enamine, which leads to an increase in the electron density at the reactive center or centers; the acceptor molecule can be activated through the formation of an onium salt, which leads to a decrease in the electron density at the reactive center or centers (Figure 1).

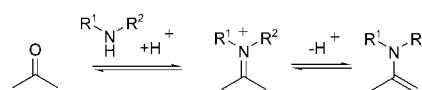


Figure 1. Electrophilic or nucleophilic activation of a carbonyl group by a secondary amine.

2.1.1. The Generalized Enamine Catalytic Cycle^[19]

Chiral secondary amine catalysts can form imonium ions with ketones or aldehydes. These intermediates react by imine–enamine tautomerism or a related mechanism to form a nucleophilic enamine species, which can be trapped conveniently by an activated π electrophile, for example, an aldehyde, ketone, or azodicarboxylate.

Until now the most successful catalyst for enamine-type reactions has undoubtedly been L-proline. Although the natural L form is usually used, both enantiomers of proline are available,^[20] which is an advantage over enzymatic methods.^[21] It is remarkable the variety of reactions that may be mediated with this simple amino acid, whose simplicity contrasts with the complex machinery of the natural enzymes (class I aldolases) capable of performing similar transformations (Figure 2).^[19]

What are the main features that make proline such a good catalyst? Proline is the only natural amino acid with a



Peter I. Dalko was born in 1960 in Budapest (Hungary). He studied chemistry at the Budapest Technical University (Hungary) and obtained his doctorate with Dr. S. D. Géro in Gif-sur-Yvette (France). After undertaking postdoctoral research with Sir Derek H. Barton at Texas A&M University (USA) and Prof. Yoshito Kishi at Harvard University he joined Prof. Janine Cossy's research group at the ESPCI in Paris. His current main research interest is the development of novel asymmetric reactions.



Lionel Moisan was born in Annemasse (France) in 1975. He studied chemistry at the Ecole Supérieure de Physique et de Chimie Industrielles (ESPCI, Paris) and obtained his Diplôme d'Etudes Approfondies in organic and bioorganic chemistry at the Pierre et Marie Curie University (Paris) in 2000. He is currently carrying out research towards his PhD in organic chemistry at the Commissariat à l'Energie Atomique (Saclay), in the research group of Dr. C. Mioskowski under the supervision of Dr. B. Rousseau.

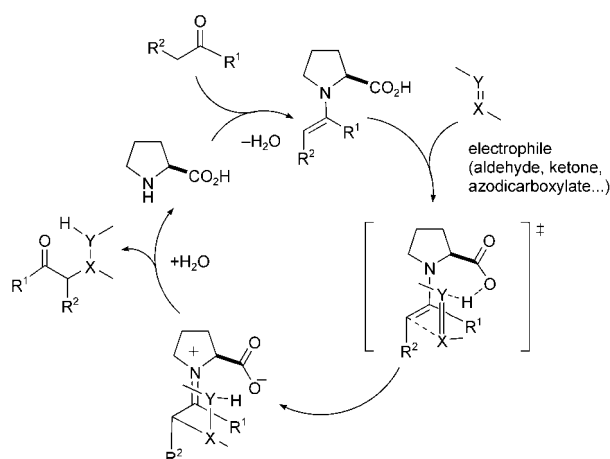


Figure 2. The L-proline-mediated enamine catalytic cycle.

secondary amine functionality and thus has a higher pK_a value and enhanced nucleophilicity relative to other amino acids. Proline can therefore react as a nucleophile with carbonyl groups or Michael acceptors to form iminium ions or enamines. As the carboxylic acid functionality of the amino acid acts as a Brønsted acid in these reactions, proline can be regarded as a bifunctional catalyst.

The high, often exceptional enantioselectivity of proline-mediated reactions can be rationalized by the capacity of this molecule to promote the formation of highly organized transition states with extensive hydrogen-bonding networks. In all proline-mediated reactions the proton transfer from the amine or the carboxylic acid group of proline to the forming alkoxide or imide is essential for charge stabilization and C–C bond formation in the transition state.^[22] Although most, if not all, partial steps in amine-catalyzed reactions are equilibrium reactions, enhanced nucleophilicity of the catalyst can lead to a number of equilibrated reactions with electrophiles present in the medium, resulting in a low turnover number. This drawback can be remedied by using a higher catalyst loading if the catalyst is inexpensive.

Proline is not the only organic molecule able to promote enamine reactions, and not all enamine reactions can be mediated by L-proline.^[23,24] Furthermore, synthetic shortcomings persist; for example, in the dimerization or oligomerization of α -unbranched aldehydes it is difficult to avoid competing reactions. Reactions with acetaldehyde or acetophenone generally lead to low yields and low selectivity. Although proline continues to play a central role in aminocatalysis, its supremacy is being challenged by new synthetic analogues and by more-complex oligopeptides. Chiral imidazolidinone catalysts also offer better rates and selectivity in a number of reactions (Figure 3).

2.1.1.1. Aldol Condensations^[25]

In the last 25 years the L-proline-mediated Robinson annulation has not attracted particular interest, although it offers a practical and enantioselective route to the Wieland–Miescher ketone, which is an important building block for total synthesis.^[26] Applications in total synthesis, such as in the

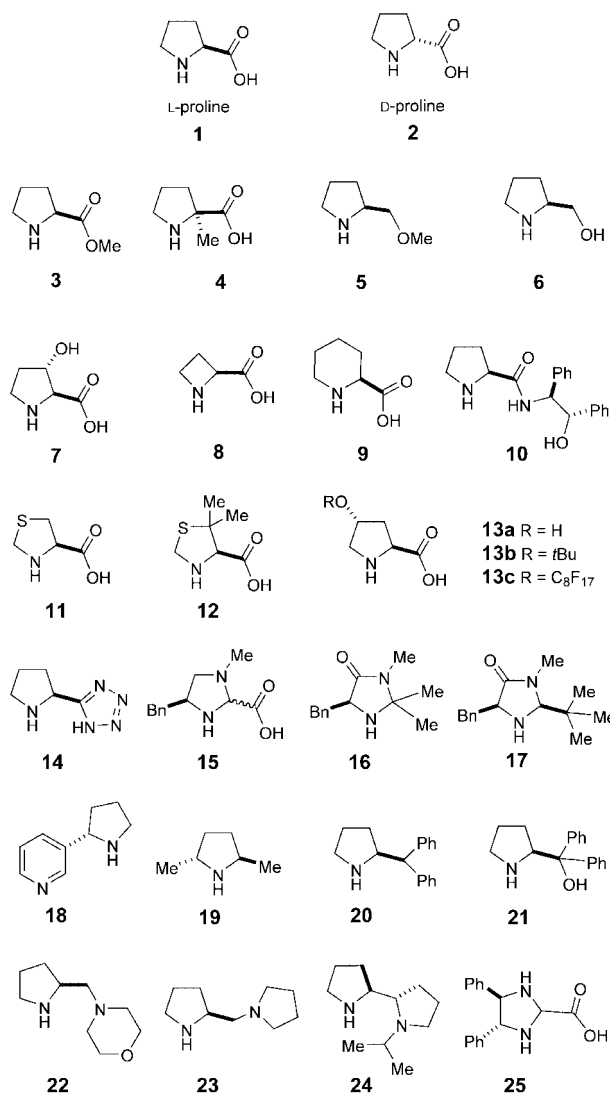
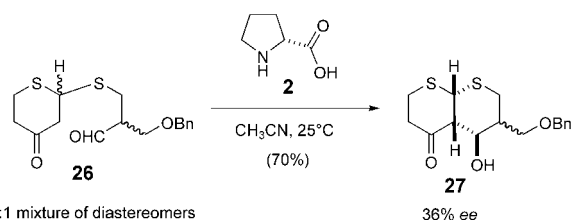


Figure 3. Some proline analogues used as organocatalysts.

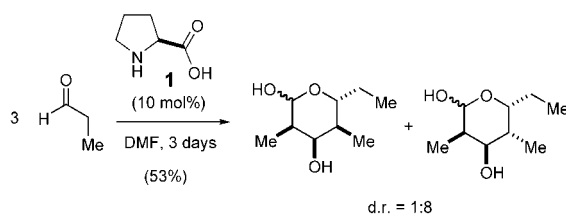
synthesis of erythromycin by Woodward et al.,^[27] appeared as isolated examples. Remarkably, in this synthesis the racemic keto aldehyde **26** could be used in an aldol reaction in the presence of D-proline (**2**) as the catalyst. All of the asymmetric centers of the erythronolide backbone were derived directly or indirectly from this rather poor reaction, which gave the product **27** with only 36% *ee*. However, enantiomerically pure **27** could be obtained by simple recrystallization, which made the process eminently practical (Scheme 1).



Scheme 1. The proline-mediated epimerization and intramolecular aldol reaction in the synthesis of erythromycin by Woodward and co-workers. Bn = benzyl.

Renewed interest in this reaction was awakened by the observation that proline is able to catalyze not only intramolecular^[28] but also intermolecular reactions with high selectivity and in high yield (Scheme 2).^[29] Early cross-aldol reactions were developed in which acetone derivatives reacted as donors with aromatic aldehydes or α -hydroxyaldehydes in the presence of a high concentration of the catalyst ($\geq 20\%$). To increase the relative concentration of the reagents and thus accelerate the reaction, an aqueous micellar version of the aldol reaction (of ketones) was also developed.^[29b] Usually a polar solvent is employed for this transformation, such as dimethyl sulfoxide (DMSO), *N,N*-dimethylformamide (DMF), water, or an ionic liquid;^[30] it has been shown that the use of high pressure may increase the efficiency of the transformation.^[31]

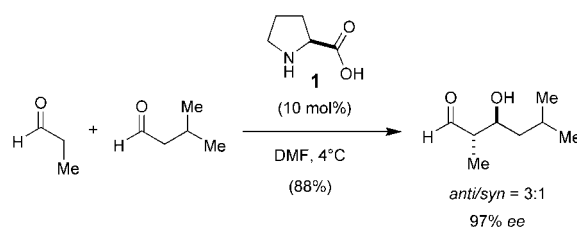
The development of intermolecular aldol reactions has been hindered by the self-condensation of the aldehyde or ketone donors in the presence of acceptors that react slowly. However, these self-condensations can be exploited for the synthesis of cyclic dimers and trimers (Scheme 2).^[33]



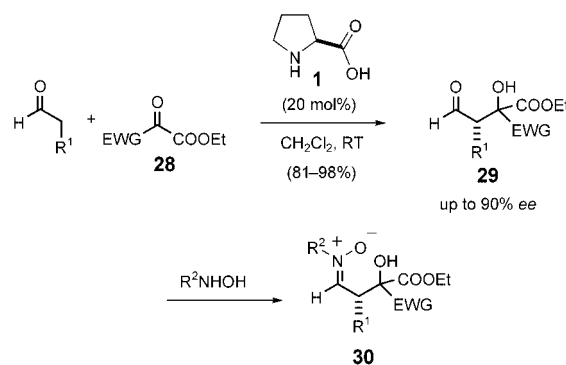
Scheme 2. The proline-catalyzed aldol reaction of propionaldehyde.

The first intermolecular cross-aldol reactions were developed between aldehydes as acceptors and ketones as donors, and this research area remains active.^[32] As the enamine intermediates generated from aldehydes are less reactive than those generated from ketones, intermolecular cross-coupling reactions between unmodified aldehydes are troublesome. Until now, aldehydes could only be used as nucleophiles in their unmodified form for catalytic asymmetric synthesis through organocatalysis.^[34] Both the reaction conditions and the nature of the acceptor are crucial to the success of the reaction: To avoid the self-condensation reaction, the temperature of the reaction should be kept at 4°C. The small differences in reactivity of the aldehyde components with the catalyst can be amplified by the slow addition of the most reactive (nucleophilic) component.^[35] Remarkably, under these conditions only a single regioisomer of the cross-aldol product is obtained when both the aldol donor and acceptor contain enolizable α -methylene hydrogen atoms (Scheme 3). Lower catalyst loadings (10 mol %) can be used without a decrease in the efficiency of the reaction.

The cross-aldol reaction of aldehydes can also be facilitated by the use of activated, non-enolizable acceptors, such as diethyl ketomalonate (**28**, EWG = CO₂Et; Scheme 4).^[36] When hydroxylamines are added to the mixture at the end of the reaction, β -hydroxynitrones, which are otherwise difficult to access, can be obtained.^[37]



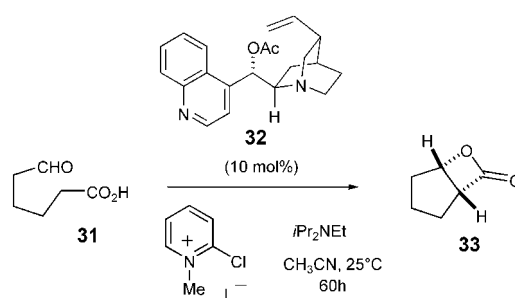
Scheme 3. Intermolecular proline-catalyzed cross-aldol reaction.



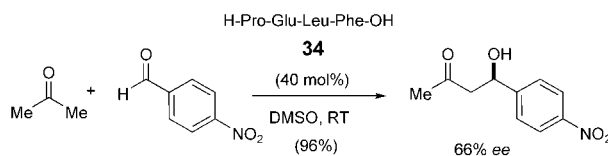
Scheme 4. Aldol reaction of aldehydes with activated carbonyl compounds. EWG = electron-withdrawing group.

Although proline has been used extensively in nucleophilic organocatalytic aldol reactions, systems based on cinchona alkaloids and oligopeptides were also developed in parallel. The asymmetric intramolecular aldol reaction of **31** was catalyzed by the *O*-acylated cinchona alkaloid **32**; the aldol product underwent cyclization in situ to form the bicyclic β -lactone **33** (Scheme 5).^[38] A variety of esters, carbamates, and carbonates of the parent cinchona alkaloid lead to similar enantioselectivities.

Oligopeptides such as **34** with *N*-terminal proline residues have been used instead of L-proline as catalysts (Scheme 6).^[39] The advantage of this catalyst system is its



Scheme 5. Cinchona-alkaloid-catalyzed intramolecular aldol reaction with lactone formation.



Scheme 6. Oligopeptide-catalyzed asymmetric aldol reaction.

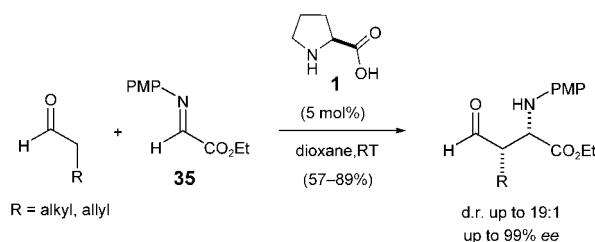
modular structure: The catalyst can be optimized for the substrate and reaction conditions.

2.1.1.2. Mannich Reactions^[40]

The proper choice of reaction conditions and reaction partners is key to the success of organocatalytic Mannich reactions. Nevertheless, the reaction tolerates a wide range of acceptors, donors, and amine reagents, and can be carried out in a large variety of polar solvents. The reaction also tolerates a certain amount of water, although the presence of water may result in diminished reaction rates.

Organocatalytic Mannich reactions can be carried out either as three-component one-pot reactions or as reactions of preformed (protected) imines with aldol donors. Proline was found to catalyze both reaction variants, usually in good yield and with high selectivity. In the former case the highest *ee* values were observed with aromatic aldehydes.

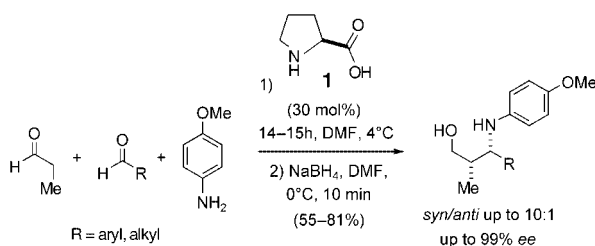
The one-pot three-component Mannich reaction of a ketone, an aldehyde, and *p*-anisidine offers practical access in the presence of L-proline to a number of enantiomerically enriched β -amino carbonyl compounds.^[41] The use of preformed imines, such as *N*-PMP-protected α -imino ethyl glyoxylate (**35**), is a more recent development (Scheme 7).



Scheme 7. Proline-catalyzed Mannich reaction of aldehydes with *N*-PMP-protected α -imino ethyl glyoxylate. PMP = *p*-methoxyphenyl.

The advantage of this modification is that potential side reactions are minimized under these conditions, and both ketones and aldehydes can be used as aldol donors.^[34]

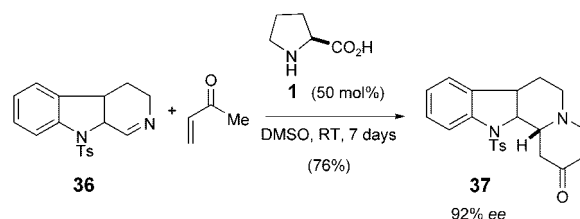
Surprisingly, when unmodified aldehydes are used as donors, the cross-Mannich reaction can proceed faster than the competing cross-aldol reaction (Scheme 8).^[42–44] The three-component cross-Mannich reaction exhibits higher stereo- and chemoselectivity ($k_{\text{Mannich}} > k_{\text{aldol}}$) at temperatures below 0°C. With electron-rich aromatic acceptor aldehydes



Scheme 8. Proline-catalyzed asymmetric Mannich reaction with aldehydes as a three-component one-pot reaction.

the use of a syringe pump was not necessary and a lower catalyst loading was possible.

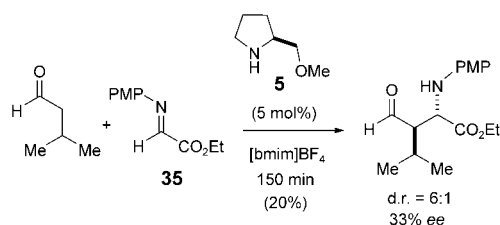
The reaction is ideally suited for tandem processes, and an astonishing variety and complexity of transformations have been devised. Scheme 9 shows a tandem Mannich–Michael



Scheme 9. Asymmetric tandem Mannich–Michael reaction catalyzed by L-proline. Ts = *p*-toluenesulfonyl.

reaction. The L-proline-catalyzed asymmetric addition of methyl vinyl ketone to the β -carboline **36** gave the tetracyclic precursor **37** to yohimbine and deserpidine.^[45] In some cases, the addition of a small amount of water (50–100 equiv) improved the selectivity of the reaction. However, the addition of more water resulted in a decrease in the reaction rate.

Interestingly, the proline-catalyzed Mannich reaction occurs with the opposite diastereo- and enantioselectivity to the related aldol reactions.^[22a] The *syn* adducts are usually obtained as the major isomers. In contrast, *anti* addition was observed in reactions of *N*-PMP-protected α -imino ethyl glyoxylate (**35**) with aldehydes in the presence of the catalyst (*S*)-2-(methoxymethyl)pyrrolidine (SMP, **5**; Scheme 10).^[46]



Scheme 10. Synthesis of the *anti* product in an SMP-catalyzed Mannich reaction in the ionic liquid [bmim]BF₄. bmim = 1-butyl-3-methylimidazolium.

Aldol and Mannich reactions have similar reaction profiles. Several models have been proposed to explain the stereoselectivity of these transformations. According to kinetic and stereochemical evidence, for both intra- and intermolecular aldol reactions only one proline molecule participates in the transition state.^[22c] Although early models focused principally on the formation of a Zimmerman–Traxler six-membered-ring chairlike transition state, it has since been found that this six-membered-ring conformation is not an absolute criterion: In the preferred transition state for the aldol reaction the carboxylic acid group should be *anti* to the forming C–C bond, whereas a pseudoequatorial orientation of the substituent on the aldehyde should facilitate the

stereodetermining proton transfer from the carboxylic acid of proline to the forming alkoxide (Figures 2 and 4).^[22] In the aldol reaction the aldehyde substituent occupies a pseudo-equatorial position, whereas in the Mannich reaction the substituent is forced into a pseudoaxial orientation, since the

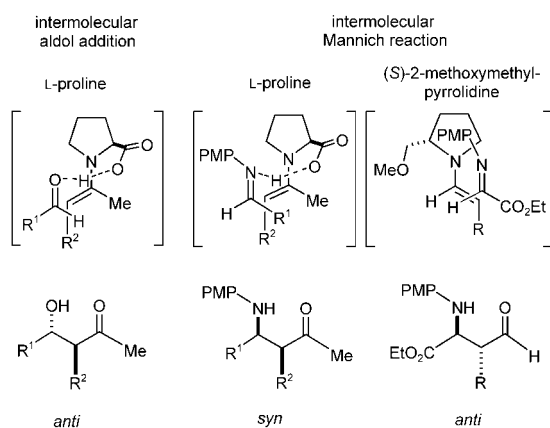


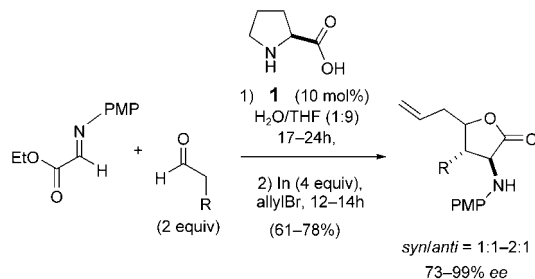
Figure 4. Proposed transition states (top) and products (bottom) for the intermolecular aldol and Mannich reactions.

E imine is more stable than the *Z* imine. These differences explain the opposite stereoselectivities observed for the proline-catalyzed Mannich and aldol reactions.

A detailed study demonstrated that proline-derived catalysts containing heteroatoms or lacking the carboxylic acid functionality are less efficient in this transformation than proline itself.^[47]

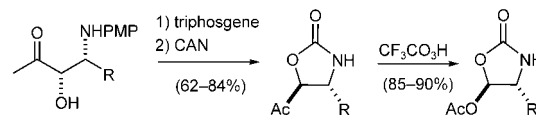
The lengthy reaction times, which are a disadvantage of both proline- and SMP-catalyzed Mannich reactions, can be considerably decreased (by a factor of 4 to 50) by replacing standard organic solvents by ionic liquids, such as [bmim]BF₄ or [bmim]PF₆.^[48,49] With this modification as little as 1 mol % of the catalyst may be used with reasonable reaction times (approximately 2 h). The products are usually formed in higher yields than in organic solvents, and similar enantioselectivities are observed. The enhanced reaction rates may result from activation of the imine electrophile by the ionic liquid.

A number of domino reactions were developed in which the Mannich reaction was combined with hydrocyanation,^[50] allylation,^[51] or conjugate addition,^[52] allowing access to complex structures with defined stereogenic centers from simple starting materials (Scheme 11).



Scheme 11. One-pot Mannich reaction/allylation in the asymmetric synthesis of substituted amino acids.

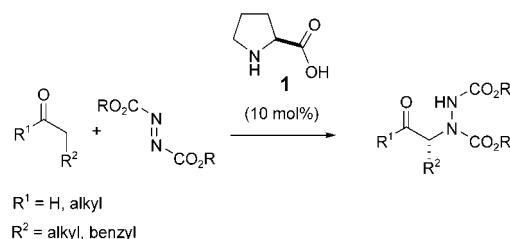
Efforts have also been made to convert Mannich products into synthetically more useful intermediates. Scheme 12 shows a short sequence with a Baeyer–Villiger oxidation, during which essentially no racemization occurs. The polyfunctional acyloxy oxazolidinone products are formed with high optical purity and can be converted readily into 4-alkyl 2-oxazolidinones or protected β -amino alcohols.^[53]



Scheme 12. Transformation of Mannich adducts into 5-acetoxoxazolidin-2-ones.

2.1.1.3. α Amination^[54]

The electrophilic addition of substituted azodicarboxylates to reactive enamines, generated in situ from aldehydes^[55a,b] or ketones^[55c] and a catalytic amount of a chiral secondary amine, yields chiral α -hydrazino carbonyl compounds (Scheme 13).^[55] This reaction offers access to α -amino acids and α -amino alcohols. Unsymmetrical ketones react regioselectively to afford the products of amination at the more substituted α position.

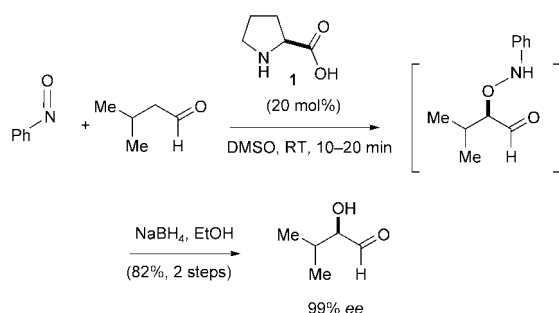


Scheme 13. L-Proline-catalyzed α amination of aldehydes and ketones.

The reaction can be extended to the preparation of enantiomerically enriched tertiary amines when α -substituted aldehydes are used as donors.^[56] Both L-proline (**1**) and structurally similar L-azetidinecarboxylic acid (**8**) catalyze this transformation, although the use of the former catalyst led to higher enantioselectivities.

2.1.1.4. α -Aminooxylation of Aldehydes and Ketones

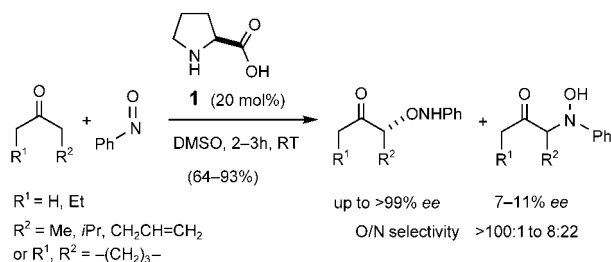
As discussed in Section 2.1.1.1, aldehydes are usually unsuitable donors in enamine reactions because they undergo competing self-condensation. In α hydroxylations this undesired reaction can be minimized when nitrosobenzene is used as the acceptor (Scheme 14).^[57] The superior reactivity of nitrosobenzene causes a dramatic decrease in self-aldolization and enables the use of a nearly equimolar amount of the aldehyde. These reactions are anomalously rapid relative to other proline-catalyzed reactions. Another interesting facet of the transformation is the O-selective attack of the enamine; in



Scheme 14. L-Proline-catalyzed α aminooxylation of aldehydes.

contrast, nitroso-aldol reactions proceed through selective attack at the N atom.^[58] The nitrosoaldehyde can be trapped in a domino sequence through an indium-promoted allylation to afford *syn* or *anti* 1,2-diols in high yields and with excellent enantioselectivities.^[59]

Excellent chemo-, regio-, and enantioselectivities (> 99% *ee*) were observed in the direct α aminooxylation of cyclic and acyclic ketones.^[60] Although double aminooxylation can take place with ketones that have two enol forms, the double attack could be circumvented by the slow addition of the nitroso electrophile (Scheme 15). Improved yields and



Scheme 15. L-Proline-catalyzed α aminooxylation of ketones.

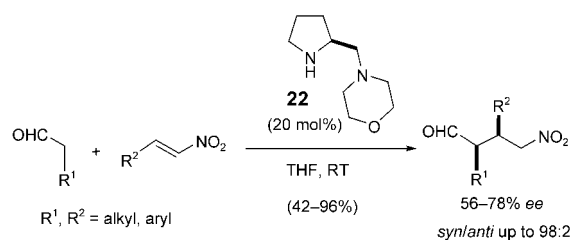
selectivities were observed upon the slow addition of the nitrosobenzene to a solution of the ketone in DMF.^[61] In this way the homodimerization of PhNO and the double aminooxylation of the ketone reagent could be avoided, and the desired product was formed with up to > 99% *ee* in nearly quantitative yield.

A similar enamine mechanism to that for aldol and Mannich reactions (see Section 2.1.1.2) provides an ideal model to rationalize the stereoselectivity of the reaction.^[22,64d]

2.1.1.5. Asymmetric Conjugate Addition^[62,63]

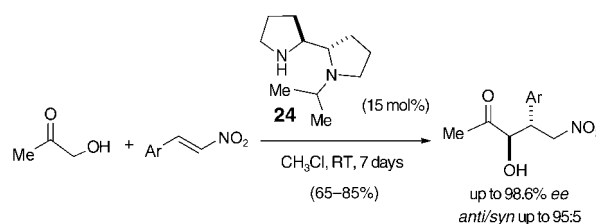
In contrast to aldol-type reactions, the proline-mediated conjugate addition of various enolizable carbonyl compounds to activated olefins occurs with only modest enantioselectivity.^[64] Higher enantioselectivity was observed with structurally similar (*S*)-2-(morpholinomethyl)pyrrolidine (**22**), which was tested in the *syn*-selective addition of ketones and aldehydes to *trans*- β -nitrostyrene (Scheme 16).^[65]

Interestingly, *N*-isopropyl-2,2'-bipyrrolidine (iPBP, **24**) mediates an *anti*-selective Michael addition. The reversal of



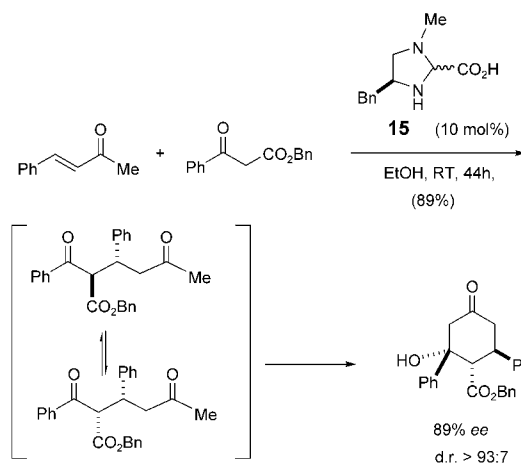
Scheme 16. (*S*)-2-(morpholinomethyl)pyrrolidine-catalyzed Michael addition of aldehydes to nitroalkenes.

the diastereoselectivity with α -hydroxyacetone can be ascribed to the putative formation of a *Z* enamine intermediate, which is favored through the formation of hydrogen bonds between the OH group of α -hydroxyacetone and the tertiary nitrogen atom of the catalyst (Scheme 17).^[66]



Scheme 17. Asymmetric addition of a hydroxyketone to nitrostyrenes catalyzed by (*S,S*)-*N*-(2-propyl)-2,2'-bipyrrolidine (iPBP).

For comparative purposes Scheme 18 shows conjugate addition involving electrophilic activation with the structurally related imidazolidine-2-carboxylic acid **15** (see Section 2.2.1.1). With suitable substrates an intramolecular



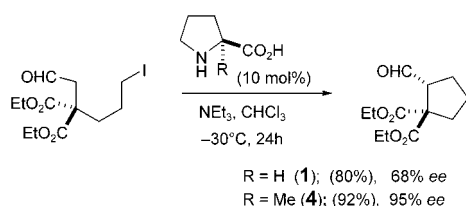
Scheme 18. Domino Michael–aldol reaction of β -ketoesters with α,β -unsaturated ketones.

aldol reaction mediated by the same catalyst (with nucleophilic activation) may follow the Michael addition step.^[67] This domino reaction sequence affords cyclohexanones with three or four contiguous stereogenic centers with high

enantio- and diastereoselectivities. The transformation can also be applied to β -aroyl and β -heteroaroyl β -ketoesters, which can be converted readily upon treatment with α,β -unsaturated ketones into valuable building blocks for the synthesis of complex molecules.

2.1.1.6. S_N2 Alkylation

An efficient intramolecular alkylation of iodoaldehydes catalyzed by proline derivatives was described recently.^[68] Best results were obtained with (*S*)- α -methylproline (**4**), which led to both a higher reaction rate and higher enantioselectivity than observed with L-proline (Scheme 19). Although the mechanism of the enantiodiffer-

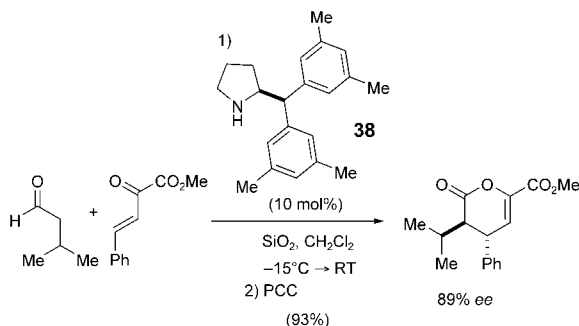


Scheme 19. Direct asymmetric intramolecular α alkylation of aldehydes: effect of β -geminal substitution.

entiation step has not been fully elucidated, the selectivity of the most effective catalyst was rationalized as an effect of α disubstitution, whereby the equilibrium is shifted toward the *anti* form of the enamine to minimize 1,3-allylic strain.

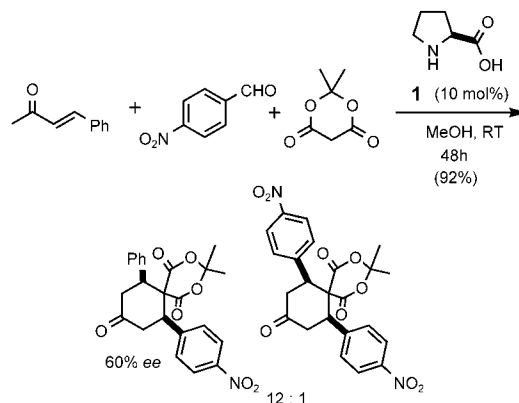
2.1.1.7. [4+2] Addition

Asymmetric organocatalytic [4+2] addition reactions with inverse electron demand have a similar reaction profile to conjugate addition reactions mediated by chiral organocatalysts. However, although the latter reactions proceed with low selectivity, both the yields and enantioselectivities of [4+2] additions are usually high (up to 94% *ee*). Chiral secondary amines react with aldehydes to form electron-rich enamines, which then react as dienophiles with enones (Scheme 20).^[69] To make a catalytic cycle possible, a small amount of silica is required to transform the hemiaminal into an acetal and thus release the catalyst.



Scheme 20. Hetero-Diels–Alder reaction with inverse electron demand. PCC = pyridinium chlorochromate.

Similarly, enamine catalysis can be used to generate the diene component in situ from α,β -unsaturated ketones for reaction with nitroalkenes^[70] or as one of three components in a Knoevenagel/Diels–Alder sequence (Scheme 21).^[71] This domino reaction affords highly substituted spiro[5.5]undecane-1,5,9-triones with high enantio- and diastereoselectivity.



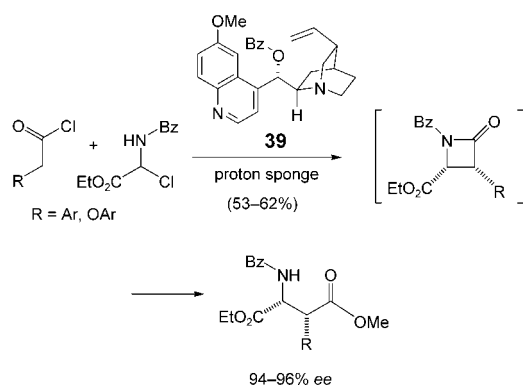
Scheme 21. Asymmetric three-component domino Knoevenagel/Diels–Alder reaction.

2.1.2. [2+2] Cycloaddition

The mechanism of [2+2] cycloaddition reactions catalyzed by chiral tertiary amines is similar to that of ammonium ylide reactions (Section 2.1.5).^[3a]

The most efficient chiral catalysts for the dimerization of ketenes and related cycloadditions between ketenes and compounds with a C=O or C=N bond are cinchona alkaloids. For the formation of ketenes from acyl chlorides not only are homogeneous bases, such as a proton sponge and 2-*tert*-butylimino-2-diethylamino-1,3-dimethylperhydro-1,3,2-diazaphosphorine (BEMP), available, but also heterogeneous bases, such as K_2CO_3 ,^[72] NaH,^[73] $NaHCO_3$,^[74] and a resin-bound variant of BEMP.^[75] However, side reactions that do not involve [2+2] cycloaddition may predominate, in particular when a stoichiometric amount of a proton sponge or the Hünig base is used.^[76] The dimerization reaction can be performed without epimerization of the newly formed stereocenters when nonpyrolytic methods are used for the preparation of the ketene reagent, or when *O*-functionalized quinine or quinidine derivatives, such as *O*-Bz, *O*-*n*Pr, and *O*-TMS (trimethylsilyl) analogues, are used (Scheme 22).^[77]

Aldehydes react with ketenes to form the corresponding β -lactones with high selectivity and in high yield.^[78] This reaction was also extended to the addition of ketenes to imines to afford β -lactams,^[78c] and applied in a one-pot preparation of β -substituted aspartic acid derivatives through a [2+2] enantioselective cycloaddition catalyzed by a cinchona alkaloid (Scheme 22). In this procedure the chiral nucleophilic catalyst benzoylquinine plays four distinct roles: 1) catalytic dehydrohalogenation of the acid chloride to form the ketene, 2) dehydrohalogenation of the α -chloroamine to form the corresponding imine, 3) catalyzation of the cyclo-



Scheme 22. Benzoylquinine-catalyzed one-pot asymmetric synthesis of β -amino acids. Bz = benzoyl.

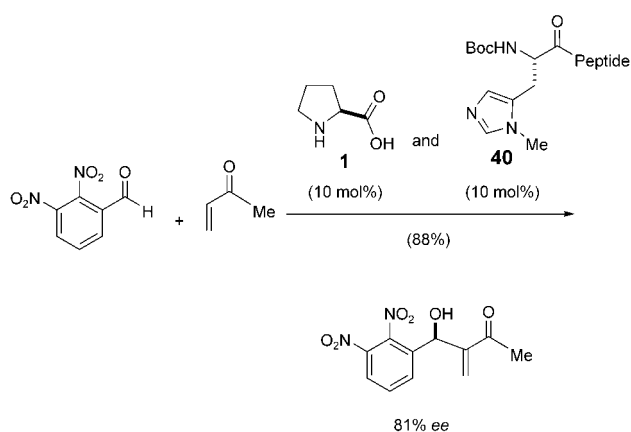
addition to produce the β -lactam intermediate, and finally 4) ring opening to form the aspartic acid derivative. All of these steps rely on the exchange of protons between the nucleophilic catalyst and a nonnucleophilic proton sponge, and of course on the nucleophilicity of the quinine derivatives.

A reactor system was developed for a continuous-flow variant of the β -lactam synthesis.^[79] Each of a sequence of columns contains the solid-phase-bound reagents for one step of the synthesis. Thus, the formation of the reactive ketene, the formation of the imine, and the cycloaddition were linked in sequence and followed by the removal of unwanted by-products to afford the pure β -lactam.

2.1.3. The Morita–Baylis–Hillman Reaction^[80]

Nucleophilic amines or phosphines are known to catalyze the addition of aldehydes to electron-deficient alkenes.^[81] The functionalized allylic alcohol products are valuable building blocks for synthesis. Organocatalytic variants of the reaction are often considered to be less efficient in terms of enantioselectivity and reaction rate than the metal-complex-mediated alternatives. With few exceptions, the products are obtained with less than 50 % ee, thus leaving plenty of room for improvement.^[82] Cinchona alkaloids are the chiral organocatalysts that have been used the most. A direct correlation has been found between the pK_a value and the activity of the quinuclidine-based catalysts: the higher the pK_a value, the faster the rate.^[83] The presence of proton donors as additives, such as methanol, triethanolamine, formamide, and water, led to additional rate acceleration.

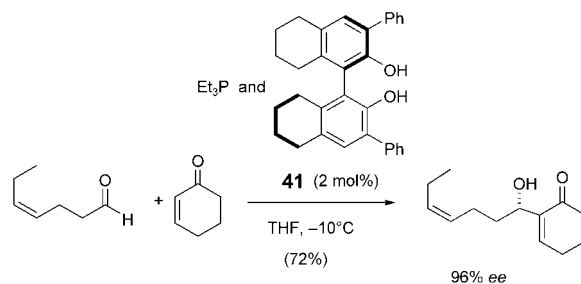
Although cinchona alkaloids continue to play a major role as catalysts in the asymmetric Morita–Baylis–Hillman reaction, peptide-based catalysts are emerging as alternatives. One exciting advance is the use of a nucleophilic catalyst (cinchona alkaloid or peptide **40**) in combination with a suitable acid as a cocatalyst, such as proline or a proline-containing oligopeptide, in a Morita–Baylis–Hillman reaction with methyl vinyl ketone (Scheme 23).^[84,85] Although the cocatalyst accelerates the reaction and improves the enantioselectivity, the influence of the configuration of the additive is minimal.^[84b,85] Noncovalent interactions between the nucleo-



Scheme 23. Synergistic effect of a peptide-based catalyst and L-proline in the enantioselective Baylis–Hillman reaction.

philic catalyst and the cocatalyst were evoked to explain the synergistic effect.

Alternatively, chiral Brønsted acids, such as **41**, can be used with achiral trialkyl phosphines to catalyze the enantioselective addition of aldehydes to cyclic enones (Scheme 24).^[86] The Brønsted acid may serve to promote

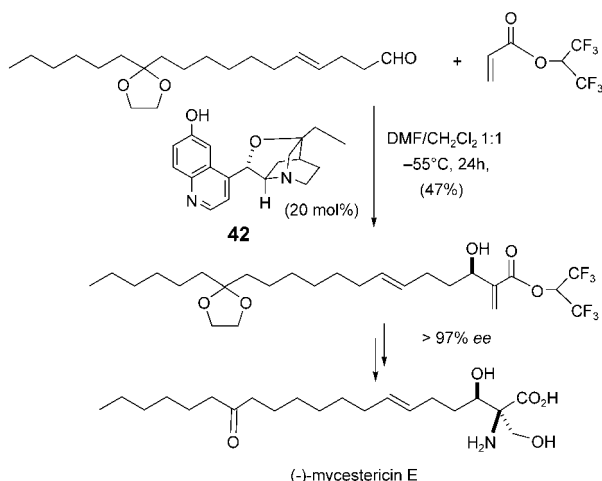


Scheme 24. In the presence of a chiral Brønsted acid the asymmetric Morita–Baylis–Hillman reaction with achiral phosphine catalysts leads to a chiral product.

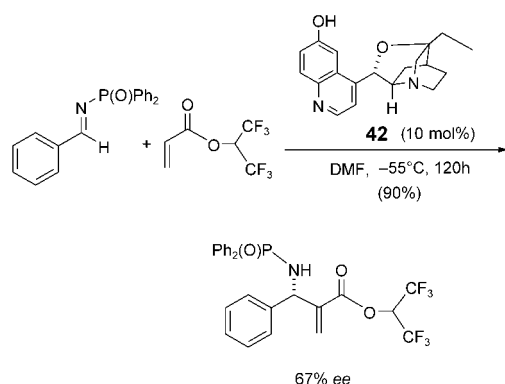
the conjugate addition step of the reaction and remains hydrogen bonded to the resulting enolate in the enantioselectivity-determining addition of the enolate to the aldehyde.

The asymmetric Morita–Baylis–Hillman reaction was used in the synthesis of (–)-mycestericin,^[87] a potent immunosuppressor, and epopromycin B,^[88] an inhibitor of cell-wall synthesis in plants (Scheme 25). Both syntheses rely on the same β -isocupreidine organocatalyst **42**, as well as the use of hexafluoroacrylate, which had proved considerably more reactive than the corresponding methyl ester in previous studies.

Activated amines can also be used as acceptors in the Morita–Baylis–Hillman reaction catalyzed by β -isocupreidine (**42**; Scheme 26).^[89] β -Isocupreidine was shown to be a much more efficient catalyst than the related quinidine derivative. In the reaction described the major product is the *S* adduct; with aldehydes the *R* product is formed.^[89a]



Scheme 25. Asymmetric synthesis of (–)-mycestericin E.



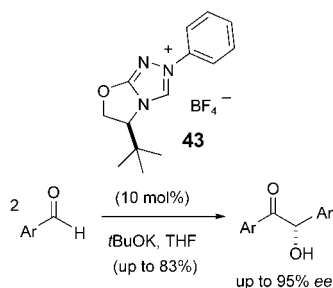
Scheme 26. The β -isocupreidine-catalyzed Morita–Baylis–Hillman reaction of an activated imine with an acrylate.

2.1.4. Asymmetric Synthesis with Carbene Catalysts

2.1.4.1. The Benzoin Condensation^[90]

Heteroazolium salts in the presence of a base are the most frequently used nucleophiles for the umpolung of an aldehyde for an asymmetric addition to another aldehyde or an imine.

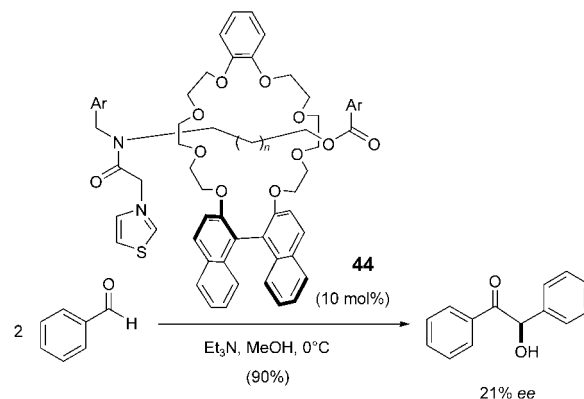
The asymmetric benzoin condensation of various aryl aldehydes was carried out with the Wanzlick carbene catalyst derived from **43** (Scheme 27).^[91] The rigidity of the bicyclic



Scheme 27. Benzoin condensation catalyzed by the chiral triazolium salt **43**.

structure of the catalyst and the presence of a sterically demanding *tert*-butyl group account for the high enantioselectivity of the reaction (53–95% *ee*).

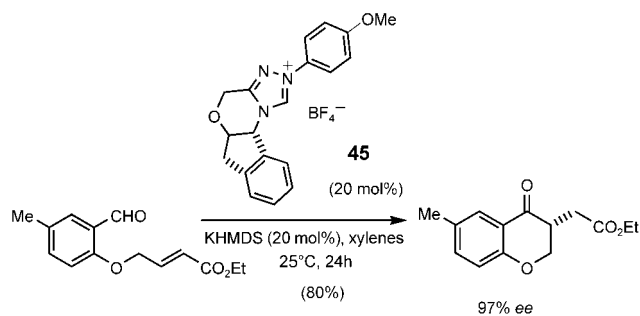
The asymmetric benzoin condensation can also be mediated by the rotaxane-based catalyst **44** (Scheme 28).^[92] The distinctive characteristic of this system is the cooperation of the “axle”, which contains the catalytic site, and the “wheel”, a ring on which the chiral template is located. Although this cooperation is relatively inefficient, the originality of the system may inspire further studies.



Scheme 28. Asymmetric benzoin condensation with a rotaxane catalyst. Ar = 3,5-di-*tert*-butylphenyl.

2.1.4.2. The Stetter Reaction

The intramolecular 1,4-addition of an aldehyde-derived nucleophile to a conventional Michael acceptor (the Stetter reaction) could be catalyzed by the structurally similar chiral triazolium salt **45** (Scheme 29).^[93] The indanoyl moiety of the most efficient catalyst is reminiscent of the aminoindanol recently developed by Merck for chiral derivatization and resolution, and as a ligand in asymmetric reactions. The reaction was applied to the synthesis of chromanes (up to 97% *ee*).^[93] The electronic properties of the catalyst were optimized by functionalization of the *N*-phenyl substituent. KHMDS was found to be the most suitable base and xylene the most suitable solvent for the reaction.



Scheme 29. Asymmetric Stetter reaction with the tetrazolium compound **45** as the catalyst. HMDS = hexamethyldisilazide.

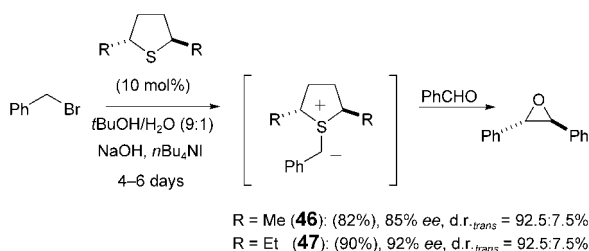
2.1.5. Asymmetric Reactions with Ylide Intermediates

Ylides can be prepared either by the alkylation of chiral dialkyl sulfides or trialkyl amines by using reactive organic halides, such as benzyl bromide, or by carbene-transfer reactions. To ensure efficient catalytic turnover phase-transfer conditions can be used, in which case the chiral catalyst is not the phase-transfer agent.

2.1.5.1. Epoxidation

Sulfur ylides react with aldehydes to form epoxides, predominantly as the *trans* isomer. Although the stoichiometric asymmetric sulfur ylide mediated epoxidation reactions have become useful tools in organic chemistry,^[94] the catalytic version presents difficulties: Not only is substrate incompatibility a problem, but also the control of the relative and absolute configuration, which show opposite trends in these systems. These trends can be explained by the stability of the ylide intermediate.^[95] High *trans* diastereoselectivity but low enantioselectivity were observed in reactions in which the betaine intermediates were formed reversibly. In contrast, nonreversible betaine formation resulted in low diastereoselectivity and high enantioselectivity. The solvent and counterion have an important effect on the stereoselectivity of the reactions: An increase in enantioselectivity was observed when protic solvent mixtures and lithium salts were used. This observation is explained by the nonreversible formation of the *anti* betaine, whose charge is better stabilized in a protic medium through solvation. Conversely, diastereoselectivity can be improved through the use of an aprotic solvent and the avoidance of species capable of solvating an alkoxide.

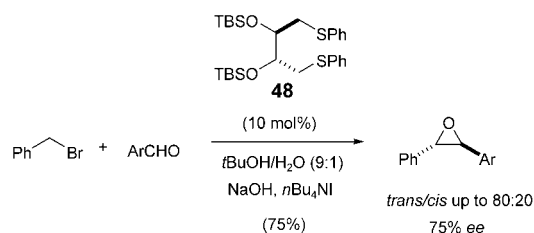
With a chiral sulfonium ion derived from a C_2 -symmetric thiolane, such as **46** or **47**, and benzyl bromide, aryl aldehydes can be converted into oxiranes (Scheme 30).^[96] The reaction



Scheme 30. Asymmetric epoxidation of aryl aldehydes with the C_2 -symmetric sulfonium catalyst.

at room temperature under optimized conditions with 10 mol% of the chiral sulfide **46** and an aldehyde concentration of 0.5 M was complete within 4 days in 82% yield, with 85% ee and d.r. 92:8. The use of the diethyl thiolane catalyst **47** led to higher selectivities but slower reaction rates.

The C_2 -symmetric chiral sulfide **48** (Scheme 31) can be synthesized on a large scale from tartaric acid.^[97] The TBS-protected catalyst with aryl substituents was the most effective, and the best result was obtained with *trans*-cinnamaldehyde (75% yield, 75% ee, d.r. 80:20).

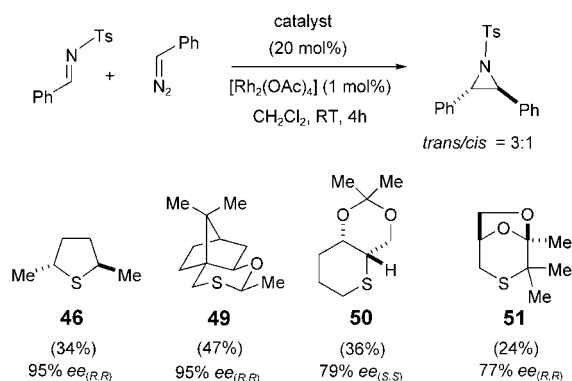


Scheme 31. Asymmetric epoxidation of aldehydes catalyzed by the tartrate-derived C_2 -symmetric phenylsulfanyl-substituted catalyst **48**. TBS = *tert*-butyldimethylsilyl.

Although the main features of the epoxidation process are known (addition of the ylide to the carbonyl group followed by elimination of the sulfide yields the epoxide), details of this reaction remain unclear. Computational studies have been carried out on the formation of the betaine.^[98]

2.1.5.2. Aziridination

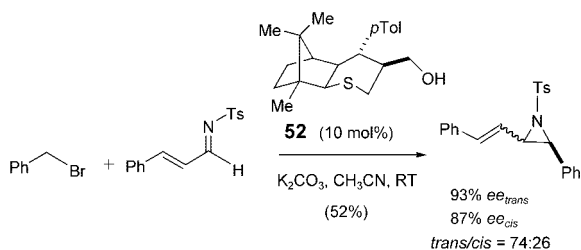
Phenyldiazomethane as well as the more stable diazoesters and diazoacetamides were tested as aziridinating agents for activated aryl aldimines in the presence of different sulfide catalysts (**46**, **49–51**; Scheme 32).^[99] An inversion of diastereoselectivity was observed: Diazoesters gave predominantly the *cis* aziridine, whereas phenyldiazomethane gave the *trans* isomer as the major product.



Scheme 32. Sulfide catalysts in the aziridination of activated benzaldimines with phenyldiazomethane.

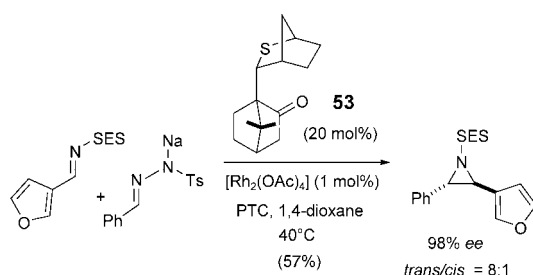
A catalytic amount of the camphor-derived sulfide **52** mediates the asymmetric aziridination of cinnamylidene-*N*-tosylamine and benzyl bromide with K_2CO_3 as a solid base.^[100] Heating at reflux in acetonitrile does not lead to a significant loss of enantioselectivity (Scheme 33).

The sulfur ylide catalyzed asymmetric synthesis of *trans* aziridines from imines and tosylhydrazines^[101] was applied to the synthesis of the side chain of taxol.^[102] The reaction sequence is based on the regio- and stereoselective conversion of a *trans* aziridine into a *trans* oxazoline, the ring opening of which then gives the side chain. *N*-Trimethylsilyl-ethylsulfonyl (SES) imines, which were more stable under the conditions of the catalytic aziridination than *N*-carbonyl



Scheme 33. Enantioselective aziridination of cinnamylidene-N-tosylamine with benzyl bromide. The chiral sulfide catalyst is derived from camphor.

imines, were treated with the tosylhydrazone salt in the presence of a phase-transfer catalyst, $[Rh_2(OAc)_4]$, and the chiral sulfide **53** (20 mol%). In the example shown in Scheme 34 the aziridine was obtained in 57% yield in a

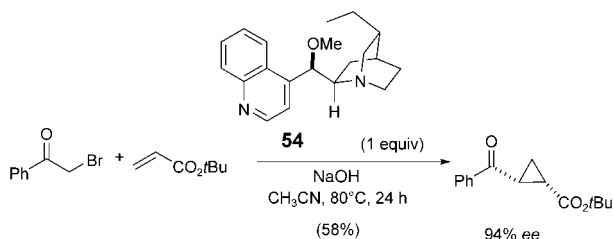


Scheme 34. Asymmetric aziridination with a sulfur ylide as the catalyst in the synthesis of the side chain of taxol. SES = 2-(trimethylsilyl)ethanesulfonyl.

$trans/cis$ diastereomeric ratio of 8:1 (with 98% ee for the $trans$ isomer). The high selectivity of the aziridination is probably a consequence of the favorable combination of several key factors: the formation of a single diastereomer of the sulfonium ylide, the high level of control of both the ylide conformation and the facial selectivity of the reaction, and the irreversible formation of the betaine intermediate.

2.1.5.3. Cyclopropanation

A further application of organocatalysts is an asymmetric cyclopropanation via an ammonium ylide.^[103] With the cinchona-alkaloid catalyst **54** the $trans$ product is obtained diastereoselectively (Scheme 35). In the intermolecular reac-



Scheme 35. Asymmetric intermolecular cyclopropanation with an intermediate ammonium ylide formed from the catalyst **54** and the alkyl bromide.

tion the catalytic cycle is inefficient, and a stoichiometric amount of the catalyst is required for the cyclopropanation of *tert*-butyl acrylate with phenacyl bromide. The reaction is truly catalytic, however, under intramolecular conditions.

2.1.6. Acyl-Transfer Reactions: Desymmetrization and Kinetic Resolution^[104]

The nature of the interaction (covalent bond or ion pair) between the catalyst and the transferring acyl group in the activated complex remains a subject of controversy. It is possible that the type of interaction depends on the individual system.^[104a]

Both the desymmetrization of cyclic anhydrides by selective ring opening with alcohols, amines, or other nucleophiles and the kinetic resolution of secondary alcohols have been at the center of much interest. Although there may be differences in the mechanistic details of these transformations, high-performing catalysts mediate both types of reaction efficiently.

A number of chiral nucleophilic catalysts derived from 4-dimethylaminopyridine (DMAP), proline, oligopeptides, and phosphines have been designed both for kinetic resolution through acylation and asymmetric desymmetrization (Figures 5 and 6 and Scheme 43). In these transformations organic catalysts have advantages over chiral metal-derived Lewis acid catalysts, which may promote racemization.^[105]

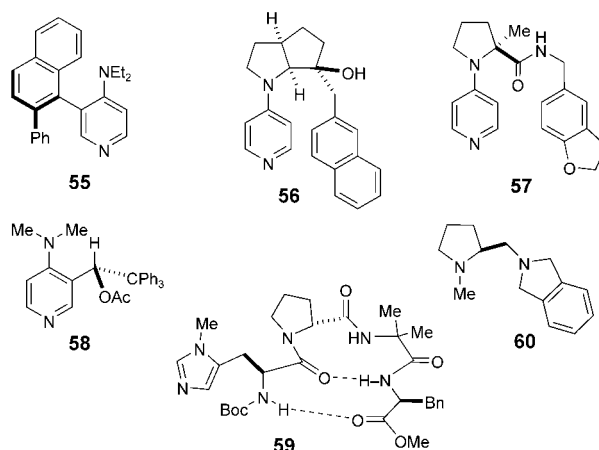


Figure 5. Selected nitrogen-containing chiral acyl-transfer catalysts. Boc = *tert*-butoxycarbonyl.

2.1.6.1. Cinchona-Alkaloid Catalysts

The first systems for catalytic asymmetric acylation were based on naturally occurring cinchona alkaloids, which allow a remarkably high degree of desymmetrization of *meso* anhydrides. More complex catalysts with two cinchona-alkaloid units, such as $(DHQD)_2AQN$ (**61b**) and $(DHQ)_2AQN$ (**62b**; Figure 6), which were developed originally as ligands for asymmetric dihydroxylation, exhibit high activity and selectivity in desymmetrization reactions (Figure 6).^[106] In contrast to reactions with other catalysts, a

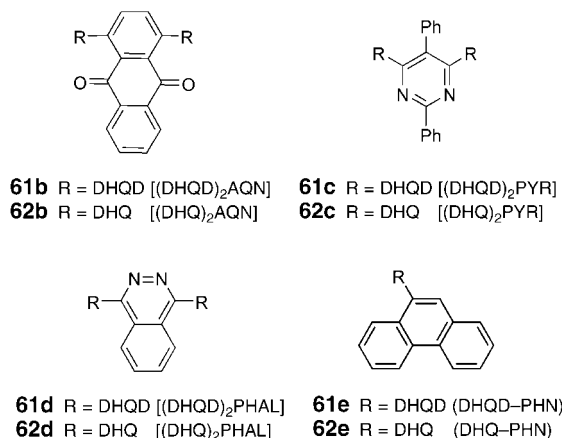
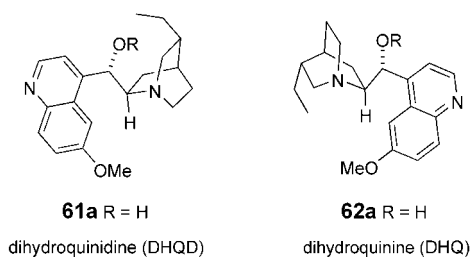
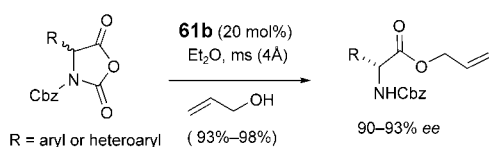


Figure 6. C₂-Symmetric cinchona-alkaloid derivatives as acyl-transfer catalysts.

stoichiometric amount of a base is not required, thus suggesting that the protonated form of the catalyst is equally active in the acyl-transfer reaction.

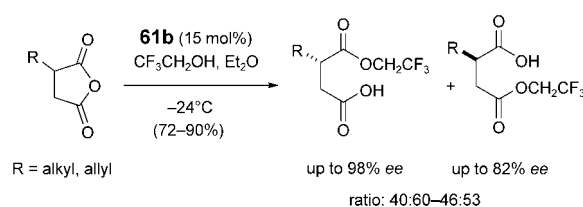
The highly enantioselective dynamic kinetic resolution of dioxolanediones,^[106b] succinic anhydride derivatives,^[106d] and *N*-protected cyclic anhydrides of α -amino acids^[106a,c] by **61b** has been reported. (DHQD)₂AQN (**61b**, 10–20 mol %) mediates the alcoholysis of the cyclic anhydride in diethyl ether at 10 °C (Scheme 36). The catalyst plays a dual role by



Scheme 36. Dynamic kinetic resolution of Cbz-protected α -amino acid *N*-carboxyanhydrides. Cbz = benzyloxycarbonyl.

catalyzing both the racemization and the enantioselective alcoholytic ring opening.^[106a,b] Yields are greater than 50 % if the racemization is faster than the alcoholysis step: $k_{\text{racemization}} \gg k_{\text{alcoholysis}}$.

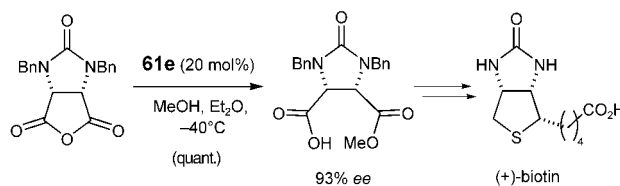
Cinchona alkaloids were known previously to catalyze the desymmetrization of cyclic anhydrides into chiral hemiesters with moderate enantioselectivity (up to 76 % ee). Biscinchona alkaloids, such as **61b**, were more efficient in this transformation.^[106c] With this catalyst hemiesters were obtained in yields ranging from 72 to 90 % and with up to 98 % ee (Scheme 37).^[106d] Ab initio calculations suggest that the



Scheme 37. Parallel kinetic resolution of 2-alkyl succinic anhydrides.

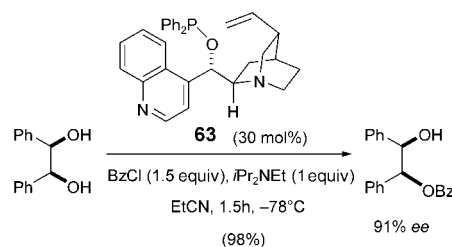
dipole moment rather than hydrogen-bonding interactions account for the selectivity of the catalyst.

In the synthesis of (+)-biotin a catalytic enantioselective desymmetrization of a *meso* cyclic anhydride served as a key step (Scheme 38).^[107] The best result for this transformation was obtained with DHQD-PHN (**61e**).



Scheme 38. Asymmetric synthesis of (+)-biotin through the desymmetrization of a *meso* anhydride with the cinchona-alkaloid catalyst DHQD-PHN (**61e**).

The different functional groups of the chiral phosphinite **63** derived from a cinchona alkaloid act cooperatively in the acylation reaction to activate the acylating reagent and trap a proton (Scheme 39).^[108] The catalyst mediates the asymmetric desymmetrization of diols: With benzoyl chloride as the acylating agent, the monoacylated hydrobenzoin was obtained in almost quantitative yield and with 91 % ee.



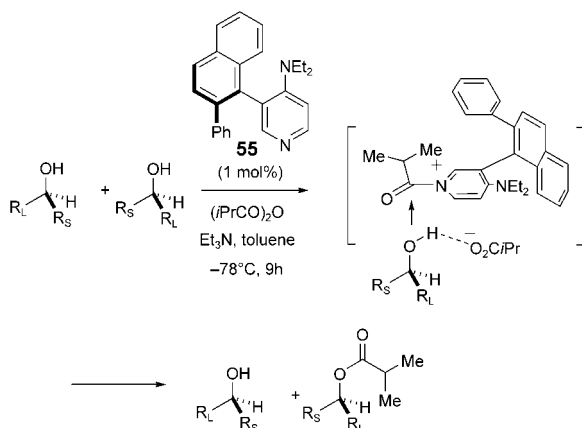
Scheme 39. Asymmetric desymmetrization of a *meso* 1,2-diol by the chiral phosphinite catalyst **63** derived from a cinchona alkaloid.

2.1.6.2. DMAP Derivatives^[109]

The substitution pattern of the chiral DMAP (4-dimethylaminopyridine) derivative is a key factor in both the stereo-selectivity and the reactivity of the catalyst.^[110–115] Although 2-substituted DMAP derivatives enable remarkable stereochemical induction, the presence of a substituent at the 2-position inhibits catalytic turnover. Chiral atropisomeric biaryl DMAP derivatives^[110] and variously substituted

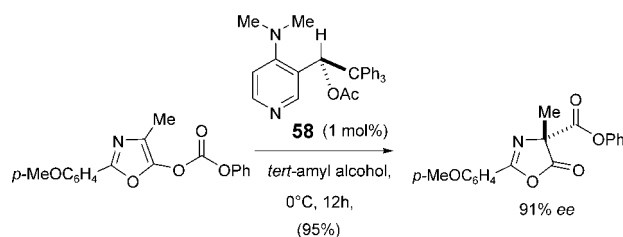
DMAP analogues containing chiral amino or acyloxy groups have been developed as catalytically active analogues.^[110–115]

The preparation and resolution of these catalysts generally requires multistep synthesis. A notable exception is the axially chiral, atropisomeric biaryl 4-aminopyridine **55**, which can be prepared in three steps by synthesis and resolution.^[110a] The chirality transfer from the acyl pyridinium species derived from the catalyst to the substrate is ascribed to steric and π - π interactions between the substrate and the catalyst (Scheme 40).



Scheme 40. Kinetic resolution of secondary alcohols mediated by an atropisomeric pyridine catalyst. R_S = smaller substituent, R_L = larger substituent.

In the case of a new class of chiral pyridine derivatives (e.g. **58**), the reactive acyl pyridinium intermediate has restricted conformational freedom.^[115] In the presence of the catalyst **58** the Steglich rearrangement of enol carbonates leads to the corresponding azlactones with quaternary carbon atoms in excellent yields and with high *ee* values (Scheme 41).



Scheme 41. Asymmetric Steglich rearrangement with the nucleophilic pyridine catalyst **58**.

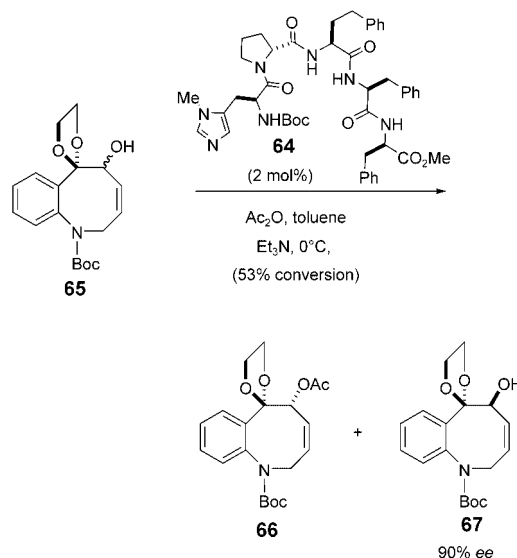
2.1.6.3. Proline Derivatives

In contrast to most pyridine-based catalysts, the preparation of proline-derived catalysts is straightforward.^[113,114] During the last steps of the synthesis of these catalysts a wide range of substituents can be introduced. This class of catalysts seems, however, to have limited substrate generality. With *N*-4-aminopyridyl- α -methylproline derivatives, such as

57 (Figure 5), the efficient kinetic resolution of ethanolamine derivatives is possible,^[113] whereas proline-derived diamines, such as **60**, only catalyze benzoylation reactions.

2.1.6.4. Oligopeptides^[116]

Oligopeptides such as **64** with *N*-terminal histidine residues were shown early on to catalyze asymmetric acyl-transfer reactions. A recent application of this class of catalysts in the synthesis of a mitosane core structure illustrates the scope and the power of these catalysts in kinetic resolution (Scheme 42).^[116f]



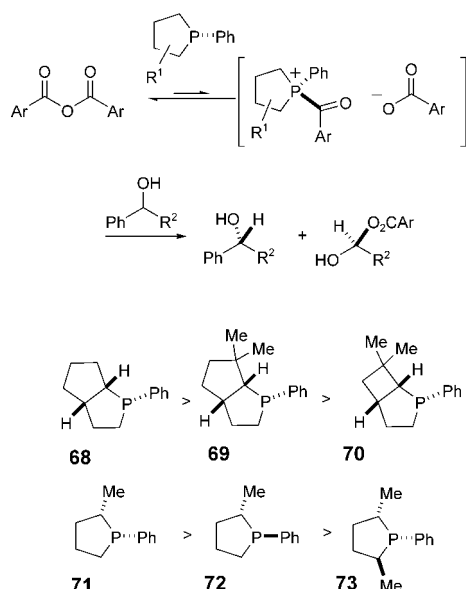
Scheme 42. Kinetic resolution of a mitosane core structure.

2.1.6.5. Phosphorus-Based Catalysts^[117]

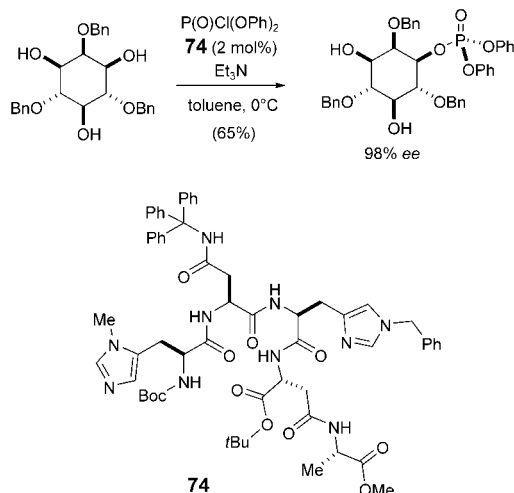
Phosphane catalysts are efficient enzyme substitutes in acyl-transfer reactions of benzylic and allylic alcohols.^[118] A study showed that the bicyclic phospholanes **68–70** were more reactive as acyl-transfer catalysts than the monocyclic analogues **71–73** by about two orders of magnitude (Scheme 43).^[118c,f] This increased reactivity can be attributed to destabilization of the ground state of the bicyclic compounds by the *P*-phenyl group, which also forces these compounds to adopt a conformation that is closer to that of the transition state.

2.1.6.6. Asymmetric Phosphorylation^[119]

Asymmetric phosphorylation with the catalyst **74** derived from a short-chain peptide not only allowed the kinetic differentiation of two enantiotopic stereocenters of a myo-inositol derivative, but also the regioselective transformation of the substrate (Scheme 44).^[120] Such “artificial kinase” catalysts were obtained through the screening of a library of 39 synthetic peptides. Depending on the peptide structure, either stereoisomer of inositol could be prepared selectively. This result underlines the fact that peptides that are not



Scheme 43. A comparison of monocyclic and bicyclic phospholanes as acyl-transfer catalysts.



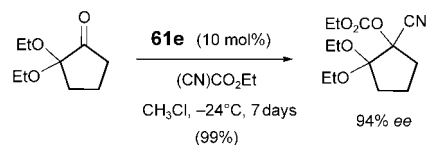
Scheme 44. Asymmetric phosphorylation with the short-chain oligopeptide **74** as the catalyst. The absolute configuration of the product was not established.

enantiomerically pure may afford a high degree of enantioselectivity in the sense of enantiodivergence.^[21] The incorporation of histidine derivatives with restrictions in the dihedral angle was important for the optimization of the catalyst. As little as 2 mol% of the peptide effects the asymmetric phosphorylation of one of the hydroxy groups of myoinositol to give myoinositol-1-phosphate with > 98% *ee* and in 65% yield in a very direct manner (Scheme 44).

2.1.6.7. Cyanation: Lewis Base Activation

Modified cinchona alkaloids, such as DHQD-PHN (**61e**) and (DHQD)₂AQN (**61b**, Figure 6), catalyze the addition of ethyl cyanoformate to carbonyl groups to form tertiary

cyanohydrin carbonates (Scheme 45).^[121] The enantioselectivity of these transformations is particularly noteworthy: With some cyclic ketones the products were formed with greater than 90% *ee*.



Scheme 45. Asymmetric cyanation of ketones with the modified cinchona alkaloid **61e** as the catalyst.

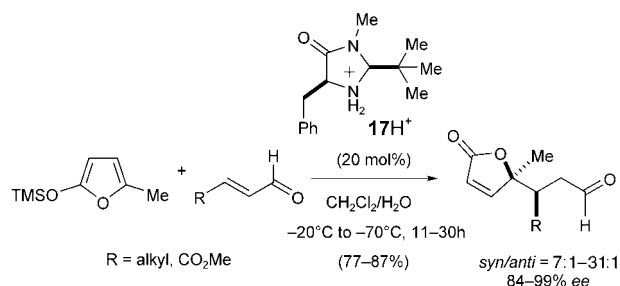
2.2. Electrophilic Catalysis: Activation of the Acceptor

Lewis acid activation in organocatalytic reactions is possible through the formation of either an iminium ion or ion pairs (see below). In the former case the condensation of a carbonyl compound with a secondary amine leads to the formation of an iminium ion, whose LUMO is lowered in energy through conjugation with a π system, such as an alkene or an aromatic ring. This activation effect is similar to that typically associated with reactions involving metal-derived Lewis acids and may be exploited in a number of transformations, such as cycloaddition or alkylation reactions in the presence of electron-rich aromatic rings or stabilized carbanions of malonates or nitro compounds. As the chiral amine catalyst is often used in these reactions in the form of a salt, asymmetric catalysis through proton transfer, whereby the chiral amine acts as a ligand, can not be excluded as an alternative mechanism.

2.2.1. 1,4-Addition

2.2.1.1. Reactions with Enolates or Enolate Equivalents

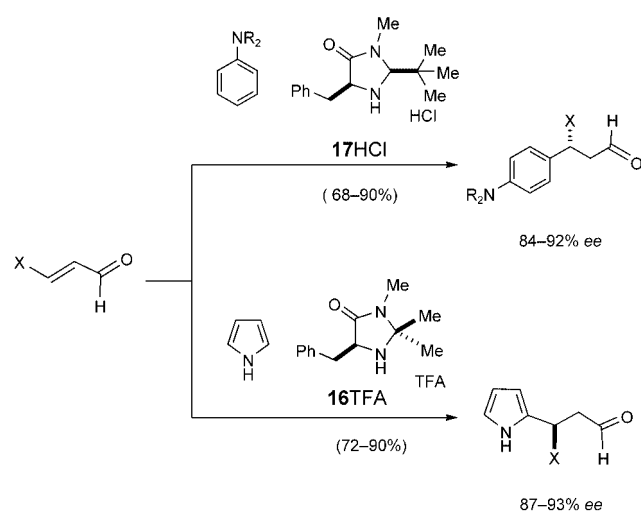
Chiral imidazolidinone salts, such as **17H⁺** formed from **17** and a stoichiometric amount of 2,4-dinitrobenzoic acid, catalyze the addition of silyl enol ethers to α,β -unsaturated aldehydes (Scheme 46).^[146] The chemoselectivity of the transformation is remarkable: The products of 1,4-addition are formed, whereas metal-containing Lewis acid catalysts mediate 1,2-addition preferentially. This reaction can be used to prepare enantiomerically enriched butenolides under catalytic conditions. The treatment of a 2-silyloxy furan with unsaturated aldehydes afforded the desired adducts with



Scheme 46. Addition of silyl enol ethers to α,β -unsaturated aldehydes in the presence of chiral imidazolidinone catalysts.

good *syn* selectivity and 84–99% *ee* (Scheme 46). The *anti* isomer can be obtained simply by changing the solvent and the acid cocatalyst. High yields were only observed when a protic cosolvent, such as water or an alcohol, was added to the reaction mixture. The effect of the additive on the yield was attributed to its ability to quench the putative silyl cation formed, which inhibits the catalytic cycle through the formation of $(\text{TMS})_2\text{O}$. This transformation was used in the synthesis of spiculiporic acid.^[146]

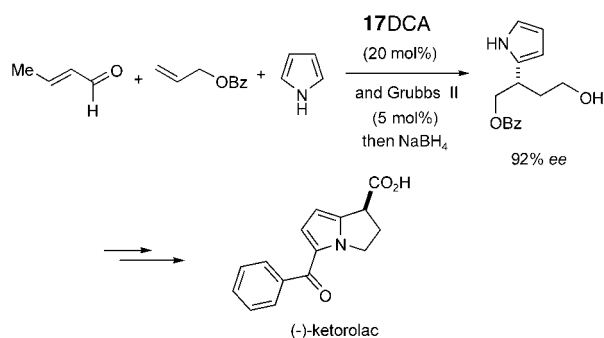
The lowering of the energy of the LUMO through the formation of an onium ion conjugated with a double bond can be exploited for the alkylation of α,β -unsaturated aldehydes with electron-rich nucleophiles, such as pyrroles, indoles, and benzene derivatives (Scheme 47).^[147] Formally, the reaction is



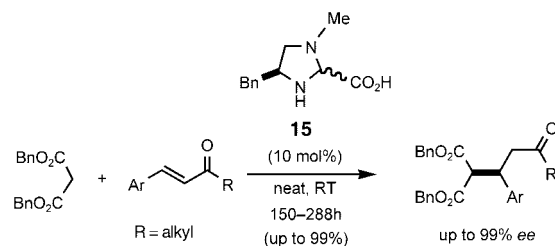
Scheme 47. Enantioselective 1,4-addition of electron-rich nucleophiles to α,β -unsaturated aldehydes in the presence of chiral imidazolidinone catalysts.

a conjugate 1,4-addition of the aromatic or heteroaromatic ring to the α,β -unsaturated aldehyde. This strategy was used in tandem with a ruthenium-catalyzed cross-metathesis reaction in the synthesis of (–)-ketorolac (99% *ee*), a non-steroidal anti-inflammatory drug (Scheme 48).^[148]

The 1,4-addition of malonates to α,β -unsaturated carbonyl compounds was performed with the imidazolidine catalyst **15**, which has a carboxylic acid functionality (Scheme 49).^[149]



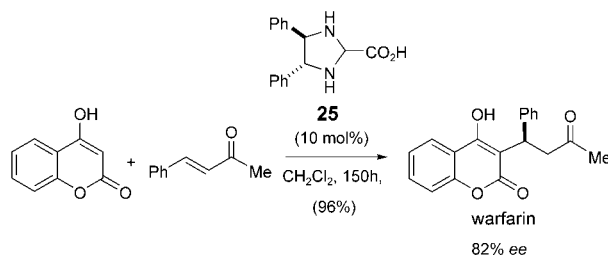
Scheme 48. Tandem olefin metathesis/asymmetric Michael addition in the synthesis of (–)-ketorolac. DCA = dichloroacetic acid.



Scheme 49. Enantioselective Michael addition of malonates to enones in the presence of chiral imidazolidine catalysts.

To ensure optimum reaction rates, solvent-free conditions were used (reaction times ranged from 150 to 288 h). The substitution pattern of the malonate ester significantly influences both the yield and the selectivity of the reaction. Best results were obtained with dibenzyl malonate, which was then used to screen a wide range of unsaturated cyclic and acyclic ketones. The best yields and enantioselectivities (up to 99% *ee*) were observed with enones that were not sterically hindered. The conjugate addition of nitroalkanes to unsaturated enones follows a similar reaction course.^[150]

The chiral imidazolidine **25** derived from diphenylethylenediamine was also shown to be efficient in catalyzing the Michael addition of cyclic 1,3-dicarbonyl compounds to α,β -unsaturated ketones. One elegant application is the synthesis of the anticoagulant warfarin (coumadin) and analogues (Scheme 50).^[151] This reaction also proceeds on a kilogram



Scheme 50. Enantioselective one-step synthesis of warfarin.

scale without a decrease in yield or enantioselectivity. Although the reaction affords the product with just 82% *ee*, a single recrystallization from a water/acetone mixture provides the enantiomerically pure product (>99.9% *ee*). Remarkably, the use of L-proline as the catalyst in this reaction leads to a racemic mixture of the product.

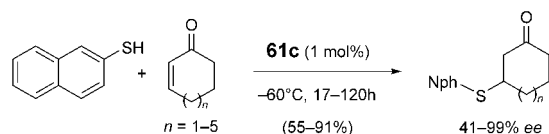
The reaction may proceed either via the previously discussed iminium intermediates (Section 2.1.1.1), or alternatively via aminal intermediates. Although no intermediates have been structurally characterized, the results of computational studies suggest the latter pathway is more likely because this structure accounts for better shielding of the substrate.

2.2.1.2. Heteroatom-Centered 1,4-Addition

The asymmetric addition of 2-thionaphthol to a wide range of cyclic enones is catalyzed by just 1 mol % of

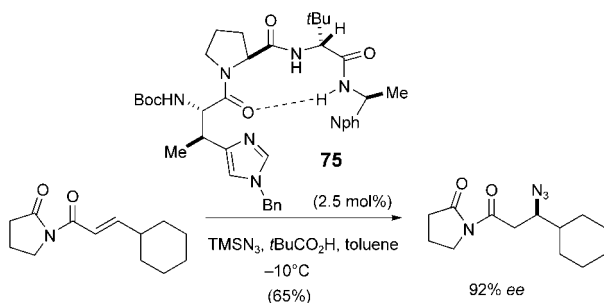
(DHQD)₂PYRE (**61c**) to afford the desired products with greater than 90 % *ee* (Scheme 51).^[152]

Short-chain peptides such as **75**, with a His or modified His residue and a well-defined β -turn structure, catalyze with a L-Pro-D-*tert*-Leu sequence (proline contribution) the con-



Scheme 51. Asymmetric 1,4-addition of 2-thionaphthol to cyclic enones under the catalysis of the bisquinoline alkaloid (DHQD)₂PYR (**61c**). Nph = β -naphthyl.

jugate addition of an azide ion to α,β -unsaturated carbonyl compounds.^[153] These oligopeptides were tested earlier in asymmetric acylation reactions.^[154] Both the secondary structure and the amine base are necessary for the activity of the catalyst, whose imidazole ring acts as the catalytic center. Conformational restriction through functionalization of the β position of the His residue (restriction of the dihedral angle) resulted in improved selectivity in the azidation (Scheme 52).



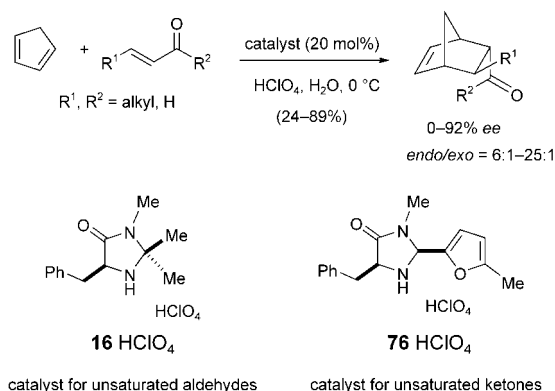
Scheme 52. Asymmetric 1,4-addition of azide to an enone catalyzed by the short-chain oligopeptide **75**. Nph = α -naphthyl.

2.2.2. Cycloaddition

2.2.2.1. [4+2] Cycloaddition

Chiral secondary amines also catalyze [4+2] cycloadditions through the reversible formation of iminium intermediates from an unsaturated aldehyde and the catalyst. The acceleration of the rate of the cycloaddition is a consequence of the lowering of the energy of the HOMO of the iminium ion through conjugation with the double bond.^[155] The most efficient catalysts for this transformation are usually the ammonium salts of chiral imidazolidines and pyrrolidines.

The previously described [4+2] cycloaddition of α,β -unsaturated aldehydes was extended recently to α,β -unsaturated ketones.^[156,157] The chiral salt derived from the amine **16** led to poor yields and no enantioselectivity in these cases. A structural analogue, **76**, however, mediated the cycloaddition reaction of a wide range of cyclic or acyclic enones to give the products in yields between 24 and 89 % and with up to 92 % *ee* (Scheme 53).

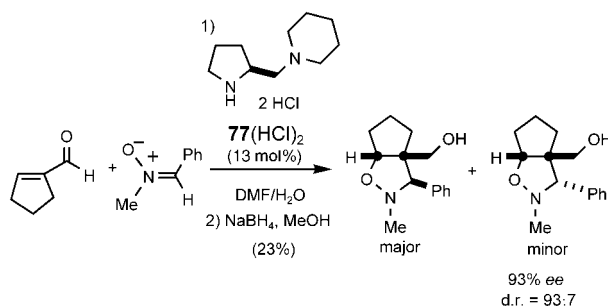


Scheme 53. Asymmetric [4+2] cycloaddition of α,β -unsaturated aldehydes and ketones with cyclopentanone in the presence of chiral imidazolidinone catalysts.

Polymer-^[158a] and silica-supported^[158b] catalysts were also developed as alternatives for use in the asymmetric [4+2] cycloaddition. A tyrosine-derived imidazolidin-4-one was immobilized on a modified poly(ethylene glycol) matrix and converted in situ into a soluble catalyst. This polymer was shown to be an efficient catalyst for the asymmetric [4+2] cycloaddition of acrolein to 1,3-cyclohexadiene and 2,3-dimethyl-1,3-butadiene.^[158a] Catalyst recycling (up to four cycles) led to only a small decrease in chemical efficiency and enantioselectivity.

2.2.2.2. [3+2] Cycloaddition

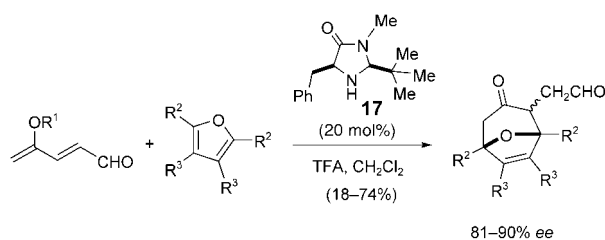
The scope of the chiral organocatalyst **77** in 1,3-dipolar cycloadditions was extended to the condensation of acyclic nitrones with cyclic aldehydes (Scheme 54).^[159] Maximum yields were between 70 and 80 % (d.r. up to 97:3 and up to 93 % *ee*).



Scheme 54. 1,3-Dipolar cycloaddition of an acyclic nitrone with an aldehyde in the presence of a chiral organocatalyst.

2.2.2.3. [4+3] Cycloaddition

The chiral imidazolidine **17** catalyzes the addition of silyloxy pentadienals to substituted furans (Scheme 55). A seven-membered-ring cycloadduct forms as the product of the reaction with *endo* selectivity (up to 90 % *ee*).^[160] Although the finer details of the reaction mechanism have not yet been



Scheme 55. The asymmetric [4+3] cycloaddition of silyloxypentadienals with substituted furans. $R^1 = \text{SiR}_3$, $R^2 = \text{alkyl}$, $R^3 = \text{H}$, TFA = trifluoroacetic acid.

elucidated, it is conceivable that an iminium ion is formed that is in resonance with an allylic cation, thus leading to charge acceleration.

2.2.3 Oxidation

2.2.3.1. Epoxidation

2.2.3.1.1. Chiral Dioxiranes^[161, 162]

Dioxiranes generated in situ from chiral ketones through oxidation with oxone have been shown to be highly enantioselective for the asymmetric epoxidation of a variety of olefins (Figure 7).

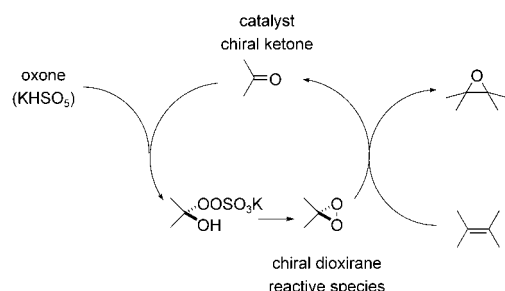


Figure 7. The catalytic cycle of oxidation with oxone in the presence of a ketone.

The fructose-derived ketones **78–80** have emerged as particularly effective catalysts for the epoxidization of *E*-configured and trisubstituted olefins (Figure 8).^[163] If the epoxidation is slow, however, the decomposition of the catalyst, presumably by Baeyer–Villiger oxidation, is often a competing process. The stability and reactivity of the catalyst can be increased by decreasing the electron density in the proximity of the carbonyl group; for example, by replacing

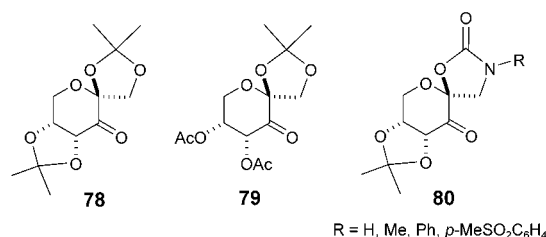
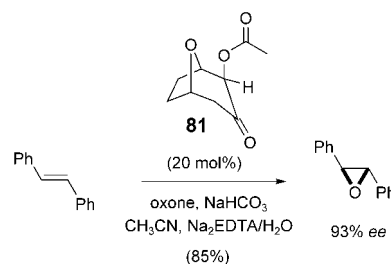


Figure 8. Sugar-derived ketones for the asymmetric epoxidation of alkenes.

the fused ketal of **78** by more strongly electron withdrawing groups, such as the acetate groups in **79** (Figure 8).^[163] This modification allows the epoxidation of *E* cinnamates, although **79** is unsuitable as a catalyst for the oxidation of *E* aliphatic α,β -unsaturated esters.^[164]

Further improvement resulted from the replacement of the spiroketal appendage of **78** with *N*-aryl substituted oxazolidinones.^[165] The use of the catalyst **80** for the epoxidation of *Z* olefins and styrenes leads to encouragingly high enantioselectivities.^[166] The substituents on the nitrogen atom of the ketone catalyst have a significant effect on the enantioselectivity of the epoxidation reaction.^[166] This influence is believed to be electronic rather than steric in nature when styrene is used as the substrate. The attractive interaction between the aryl group of the substrate and the *N*-aryl group of the catalyst can be enhanced by introducing electron-withdrawing groups on the *N*-aryl group.

A variety of ketones of natural and fully synthetic origin were tested as alternative catalysts to the fructose derivatives for asymmetric epoxidation. Binaphthyl ketones, tropinone derivatives,^[167] dehydrocholic acid, and the synthetic bicyclic ketone **81** were also shown to react with high enantioselectivity and high conversion rates (Scheme 56).^[167–169]



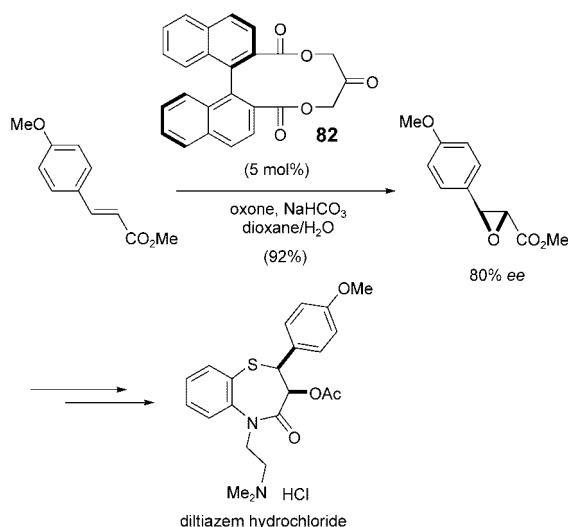
Scheme 56. Asymmetric epoxidation of stilbene with the chiral organocatalyst **81**.

The synthesis of diltiazem, a potent calcium antagonist, illustrates the scope of the reaction.^[170] A key intermediate was prepared in high yield, although with moderate enantioselectivity, by using the binaphthyl catalyst **82**, which was found to be the most efficient catalyst for the asymmetric epoxidation (Scheme 57). Recrystallization provided the key intermediate in enantiomerically pure form.

Chiral fluoroketones, such as **83** and **84**, were investigated as catalysts for asymmetric epoxidation with oxone as the bulk oxidant (Figure 9).^[171] The presence of α -fluoro substituents considerably increases the reactivity of the carbonyl group. The tropinone derivative **83** showed excellent reactivity but only modest enantioselectivity. The biphenyl ketone **84** exhibited modest reactivity, but higher enantioselectivity relative to **83** in most cases. Better results were obtained with the chiral fluoro-substituted binaphthyl ketone **85** (Scheme 58).^[172]

2.2.3.1.2. Chiral Oxaziridines

Oxaziridinium salts have been utilized in oxidation reactions far less than chiral ketones. The intermediate



Scheme 57. Asymmetric epoxidation of an α,β -unsaturated ester with the chiral organocatalyst **82** in the synthesis of diltiazem.

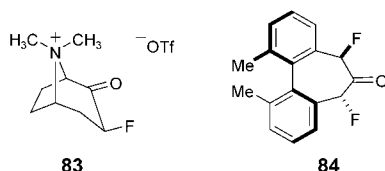
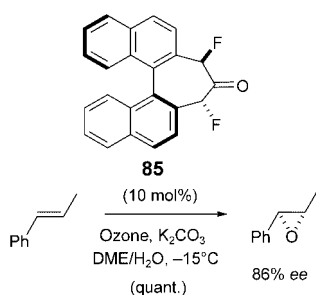


Figure 9. α -Fluoroketone catalysts for the asymmetric epoxidation of alkenes. Tf = trifluoromethanesulfonyl.



Scheme 58. Asymmetric epoxidation of *trans*- β -methylstyrene mediated by the chiral fluorinated binaphthyl ketone catalyst **85**.

oxaziridines, which are formed from the iminium salt upon reaction with oxone, typically in aqueous acetonitrile, are efficient oxygen-transfer reagents. They generally enable the epoxides to be obtained in 60–70 % yield, but not with higher than 60 % *ee*. In the most effective catalysts **86–89** (Figure 10) the asymmetric centers are located close to the reaction site.^[173] A complicating feature of this process is the potential for the formation of diastereomeric oxaziridinium salts from the iminium species. Each diastereomer can transfer the oxygen atom to one of the prochiral faces of the alkene substrate with a different degree of enantioselectivity.

The iminium salts can also be generated in situ through the condensation of a chiral amine with an aldehyde.^[174] This

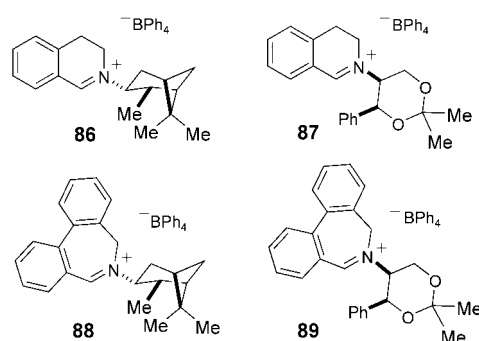
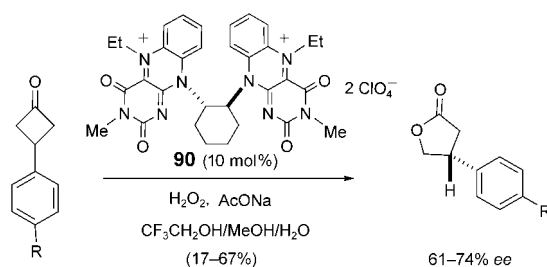


Figure 10. Iminium catalysts for the asymmetric epoxidation of alkenes.

method allows greater flexibility in modulating the structure of the catalyst.

2.2.3.2. Asymmetric Baeyer–Villiger Reaction

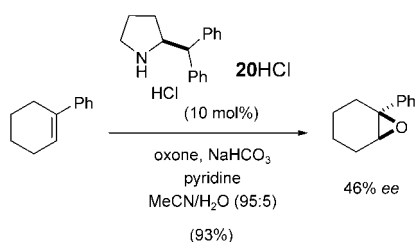
Chiral ketones are not suitable catalysts for the asymmetric Baeyer–Villiger oxidation as a result of competing decomposition under the reaction conditions. As an alternative, the planar-chiral bisflavin catalyst **90** was developed. This compound catalyzes the oxidation of cyclobutanones to the corresponding lactones in 17–67 % yield and with up to 74 % *ee* (Scheme 59).^[175] The solvent has a considerable influence on the enantioselectivity: Best results were obtained with protic solvents.



Scheme 59. Asymmetric Baeyer–Villiger oxidation of 3-aryl cyclobutanones with a flavin catalyst.

2.2.3.2.1. Amine Catalysts

Alkenes can be epoxidized under phase-transfer conditions with a chiral amine catalyst and oxone in a pyridine–acetonitrile/water–sodium bicarbonate biphasic system.^[176] The oxidation of 1-phenyl cyclohexene gave the corresponding epoxide with 46 % *ee* with the catalyst (*S*)-2-(diphenylmethyl)pyrrolidine (**20**; Scheme 60). Although the reaction mechanism has not been fully elucidated, the finding that secondary ammonium salts are considerably more active than tertiary, which in turn are more active than quaternary ammonium salts, shows that the protonated amine does not only act as a phase-transfer catalyst. The active oxidant is believed to be the peroxysulfate of the chiral amine: The ammonium ion activates the peroxymonosulfate through hydrogen bonding, thus generating a more electrophilic



Scheme 60. Amine-catalyzed epoxidation of 1-phenylcyclohexene with oxone under PTC conditions.

species. The problems with reproducibility encountered previously were solved when the protonated amine catalyst **20**-HCl was used. In this way the catalyst is protected from oxidation under the reaction conditions.

2.2.3.2.2. Peptides^[177]

The mechanism of the oxidation of enones with free or supported polyamino acids as catalysts (the so-called Julià-Colonna reaction) is not yet well understood. The group nearest to the N terminus seems to play an important role in the stereoselectivity of the reaction. Polypeptides derived from β -amino acids (instead of α -amino acids) were also tested, and it was found that poly- β -leucines are effective catalysts for the epoxidation of chalcones and their analogues (up to 70 % ee).

3. Reactions via Noncovalent Activation Complexes

A growing number of asymmetric organocatalytic reactions are accelerated by weak Lewis acid/Lewis base interactions. These weak interactions were seldom exploited to promote chemical reactions in the past. The rationalization of the mechanism of these reactions is often difficult, and our current understanding of the key structural elements that determine the selectivity of the reactions is poor.

3.1. Asymmetric Proton Catalysis

The proton is arguably the most common Lewis acid found in nature. It forms hydrogen bonds, which can be divided into two classes according to the nature of the interaction: polar covalent ($\text{RX}-\text{H}$) and polar ionic ($\text{RX}^+\text{H}\cdots\text{Y}^-$). In the former case the conjugate base carries the chiral information, whereas in the latter case the anion is achiral and the proton is complexed with a chiral ligand (usually an amine base). Polar covalent proton catalysis is developing rapidly as an important method in asymmetric synthesis. Polar ionic catalysis is a more recent and also a more elusive strategy. Until recently, it seemed to make no chemical sense to design an asymmetric catalytic reaction with an ionic hydrogen bond as the catalyst, for at least two main reasons: Because of the spherical symmetry of the empty 1s orbital of the proton, no stereoisomerically discrete coordination complexes should exist. Furthermore, the non-

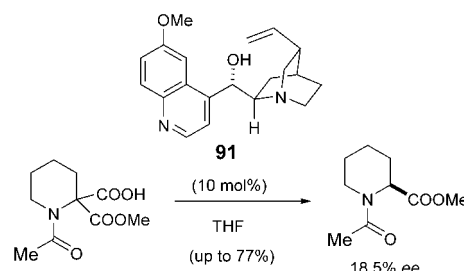
selective nature of proton catalysis relative to that of other Lewis acids suggested that any possible catalysis by a chiral proton complex would be suppressed by competing achiral catalysis by a protonated solvent molecule.

Although the approach to the design of each of these types of chiral proton catalyst is quite different, the reactions of both types of catalyst proceed via noncovalently activated complexes and will therefore be discussed together in this section.

3.1.1. Catalytic Enantioselective Protonation^[178]

Despite the apparently simple concept behind the enantioselective protonation of a prostereogenic enol derivative, the mechanism of this transformation is not fully understood. We believe, however, that the majority of the catalytic processes are more like organometallic reactions in which the chiral organic molecule serves as a ligand. Therefore, they are out of the scope of this Review.

The enantioselective decarboxylation and reprotonation of a malonate precursor is a further example of a metal-free asymmetric protonation. This transformation in the presence of enzymes or microorganisms has been known for some time; however, it has received little attention in synthetic chemistry.^[179] Although a stoichiometric variant with cinchona alkaloids, such as **91**, as chiral protonating agents gave good results, the catalytic reaction proceeded with only modest enantioselectivity (Scheme 61).^[180]



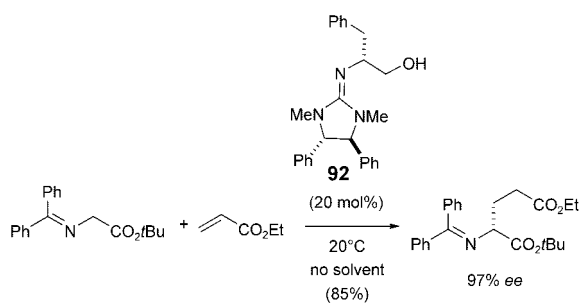
Scheme 61. Enantioselective decarboxylation-reprotonation of α -aminomalonnate derivatives.

3.1.2. Catalytic Enantioselective Deprotonation^[181]

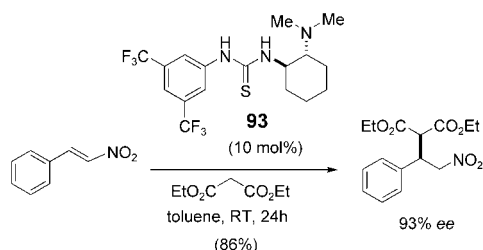
Chiral Brønsted bases used as catalysts in asymmetric synthesis are mainly metal-containing compounds, such as chiral lithium amides and magnesium bisamides. Metal-free superbases were recently developed as alternatives. In the presence of a catalytic amount of the modified guanidine **92** (20 mol %) asymmetric Michael reactions proceed with high enantioselectivity (Scheme 62).^[182]

3.1.3. 1,4-Addition to Activated Alkenes

The bifunctional thiourea-derived catalyst **93** mediates the enantioselective Michael addition of malonates to nitroalkenes (Scheme 63).^[183] The basic, nucleophilic tertiary amine activating group in the catalyst and the thiourea



Scheme 62. Asymmetric Michael reaction of a glycine imine with an acrylate in the presence of a modified guanidine catalyst.

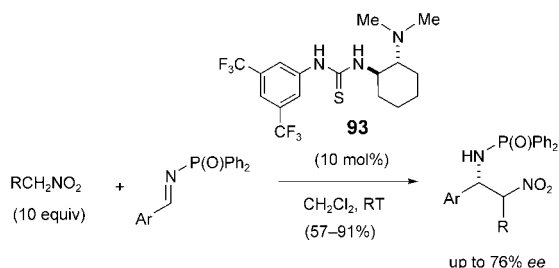


Scheme 63. Enantioselective 1,4-addition of diethyl malonate to β -nitrostyrene mediated by the bifunctional thiourea catalyst **93**.

reaction center act in a synergistic manner. The tertiary amine functionality has a significant effect on the reaction rate, but only a slight effect on the enantioselectivity. Its precise mechanistic role is not clear.

3.1.4. The Aza-Henry Reaction

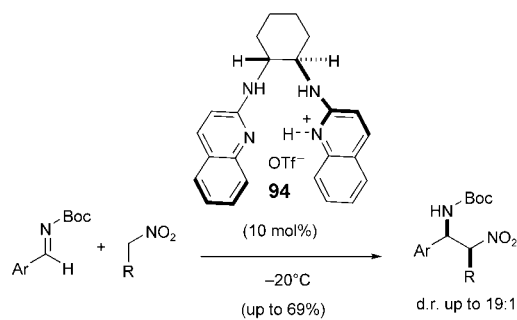
The bifunctional thiourea derivative **93** also catalyzes the reaction of nitroalkanes with activated imines to afford the corresponding β -nitroamines (Scheme 64).^[184] Noteworthy is



Scheme 64. Aza-Henry reaction with the bifunctional organocatalyst **93**.

that the thiourea and amine only have a synergistic effect in this reaction if they are tethered.

The chiral Brønsted acid **94**, formed from a 1:1 mixture of the quinoline bisamidinium ligand and HOTf, accelerates considerably the addition of nitroalkanes to Boc-activated aldimines at -20°C (Scheme 65).^[185] The enantioselectivity and yield of the transformation are best for EWG-activated aldimine derivatives. High diastereoselectivities were

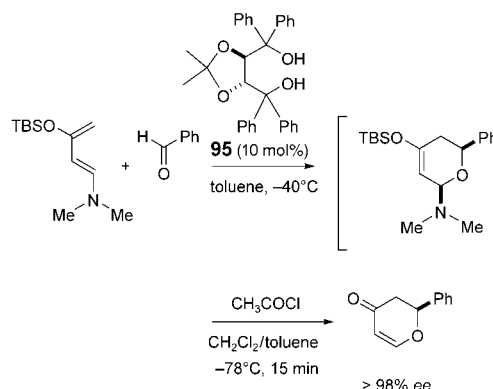


Scheme 65. Asymmetric proton-catalyzed aza-Henry reaction.

observed when substituted nitromethane derivatives were used as nucleophiles.

3.1.5. [4+2] Cycloaddition

A catalytic amount of taddol (**95**; 10 mol %) promotes the hetero-Diels–Alder reaction of a variety of aldehydes and dienes (Scheme 66).^[186] The cycloadduct is formed as a single diastereoisomer in $>98\%$ ee. Aryl aldehydes are particularly effective dienophiles in this hetero-Diels–Alder reaction.



Scheme 66. Taddol-catalyzed asymmetric hetero-Diels–Alder reaction.

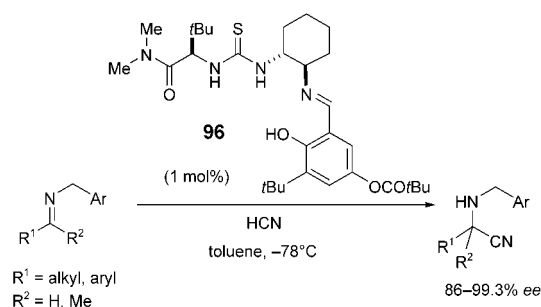
3.1.6. Hydrocyanation

3.1.6.1. The Asymmetric Strecker Reaction

Chiral peptidic urea catalysts have been studied in considerable detail.^[187] Surprisingly, the same class of catalyst can be used both in asymmetric cyanation reactions of aldimines and methyl ketimines and in asymmetric Mannich reactions of *N*-Boc aldimines with silyl ketene acetals.^[188]

Oligopeptide-like catalysts were prepared and tested in the hydrocyanation of *N*-benzyl and *N*-allyl aldimines and ketimines by a parallel-library approach.^[189] Optimization of the structure of the catalyst led to the derivative **96** with a single amino acid unit (Scheme 67). This catalyst promotes the asymmetric addition of a silyl ketene acetal to *N*-Boc benzaldehyde with 94% ee.^[188b]

The reaction has remarkably broad generality: the same catalyst afforded the products in greater than 95% ee for all aldimines examined, including substrates with aromatic sub-



Scheme 67. The oligopeptide-like thiourea catalyst **96** for the asymmetric Strecker reaction. The absolute configuration of the product was not determined.

stituents and those with bulky (e.g. *tert*-butyl) or small (e.g. *n*-pentyl) aliphatic substituents. Ketimines can also be used. This degree of generality is still unusual in asymmetric catalysis.

The mode of action of the catalysts in the Strecker reaction has been investigated.^[189a] A mechanism was proposed based on the results of screening a library of catalysts prepared by parallel synthesis. According to this model, an imine–catalyst complex forms reversibly through the formation of a hydrogen bond between the nitrogen atom of the *Z*-configured imine and the acidic protons of the urea. This hypothesis is supported by the Michaelis–Menten kinetics of the transformation, with a first order dependence on both the catalyst and HCN, and saturation kinetics with respect to the imine substrate. The interaction between the imine and the catalyst in the complex was found to be stronger than the classical hydrogen bond in catalyst–product complexes, thus explaining the efficient catalyst turnover. An investigation of the structure of the transition state showed which factors were responsible for the high enantioselectivity of the reaction: The steric demands of the substituents flanking the imine group should be markedly different, the substituent on the nitrogen atom should favor the formation of the *Z* isomer of the imine, and the addition of HCN should take place from the diaminocyclohexane side of the catalyst.

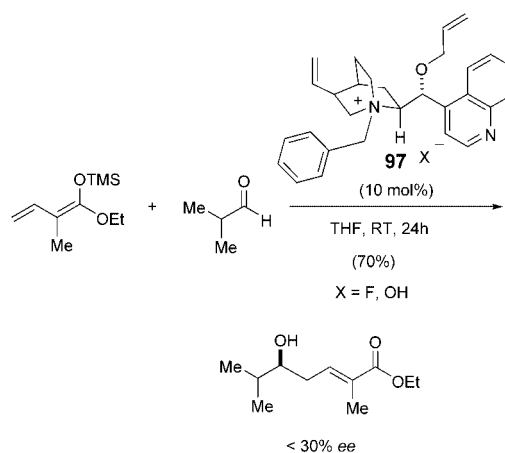
3.2. Ammonium Ions as Chiral Templates in Homogeneous Catalytic Reactions

3.2.1. The Mukaiyama Aldol Reaction

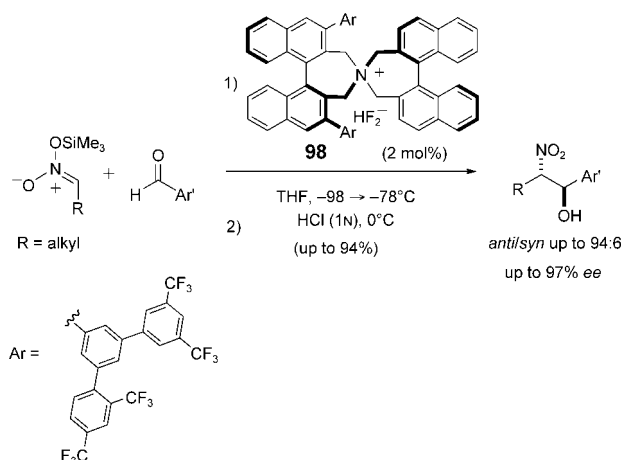
Chiral ammonium fluorides, such as **97** ($X = \text{F}$), catalyze the asymmetric vinylogous Mukaiyama aldol reaction with modest efficiency (Scheme 68).^[190] Surprisingly, the ammonium hydroxide **97** ($X = \text{OH}$) was also found to mediate the reaction in quantitative yield, albeit with less than 30% ee.

3.2.2. Nitroaldol Reaction of Silyl Nitronates

The chiral ammonium fluoride salt **98** was engineered for the asymmetric nitroaldol reaction of silyl nitronates with aryl aldehydes.^[191] High enantioselectivity and *anti* diastereoselectivity were observed when a 3,3'-substituted catalyst with bulky aryl substituents was used (Scheme 69).



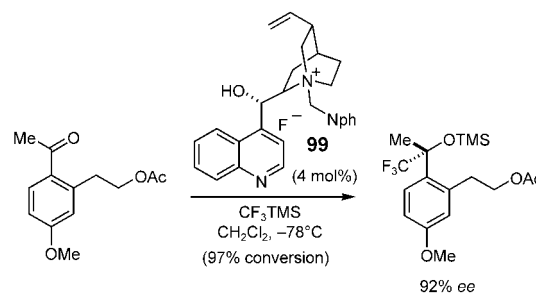
Scheme 68. The asymmetric vinylogous Mukaiyama aldol reaction.



Scheme 69. Asymmetric nitroaldol reaction of silyl nitronates with aromatic aldehydes.

3.2.3. Trifluoromethylation of Ketones

The cinchonine catalyst **99** was used in the enantioselective addition of a trifluoromethyl anion to aryl ketones (Scheme 70).^[192] Although the reaction parameters are reminiscent of those of a phase-transfer reaction, the reaction takes place under homogeneous conditions. The trifluoro-

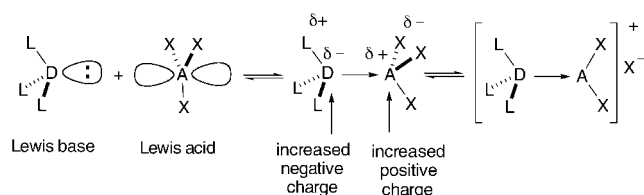


Scheme 70. Enantioselective nucleophilic addition of a trifluoromethyl anion to a ketone mediated by the cinchonine catalyst **99**.

methyl anion is formed from CF_3TMS by activation by the fluoride counter ion of the catalyst. Catalysts such as **99** with a free hydroxy function afford products in near-quantitative yield in the reaction shown in Scheme 70. The protection of the free OH group of the cinchonine catalyst resulted in a drastic decrease in reactivity.

3.3. Activation of Lewis Acids by Lewis Bases^[122]

The concept of the activation of a Lewis acid by a Lewis base may appear to contradict general chemical intuition, as the reaction between a donor and an acceptor entity is expected to lead to the averaged rather than the polarized electron density of the molecule. There are, however, well-defined circumstances under which charge separation may operate and lead to decreased electron density at a particular central atom. In these cases, electron transfer does not take place towards the central atom of the Lewis acid, but towards its peripheral ligands. Once the ligand is ionized the positive charge can be assigned to the central atom, thus translating into enhanced Lewis acidity at this center. This phenomenon can also be considered as ligand-accelerated catalysis, whereby the acidity of the active center is considerably enhanced after complexation with the Lewis base.^[123]



This principle operates during activation by silicon halides in the presence of catalytic amounts of chiral bases, such as hexamethyl phosphoramide (HMPA) or pyridine *N*-oxide derivatives, trialkylamines, and sulfoxides. Weak Lewis acids, such as SiCl_4 and RSiCl_3 , coordinate to these bases to give hypervalent silyl cations, which act as strong Lewis acids in a chiral environment. An important advantage of this process is that the use of an excess of the weak, achiral Lewis acid does not compromise the enantioselectivity of the transformation by participating in competing nonstereoselective background reactions. This dual activation (the binding of the Lewis base to the nucleophile and the formation of a reactive hypercoordinate silicon center, which coordinates to the electrophile) leads to high reaction rates and excellent transfer of stereochemical information, because of the tight transition-state structure. The catalytic cycle is made possible through the noncovalent interactions between the chiral Lewis base and the chlorosilane substrate.

3.3.1. Allylation and Propargylation Reactions

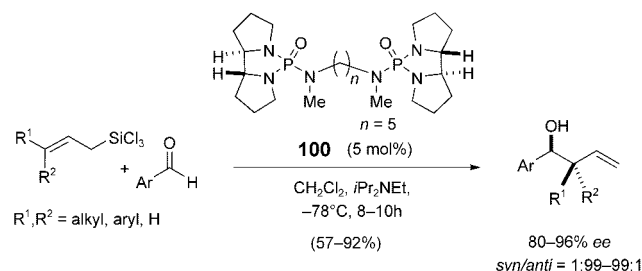
The allylation of aldehydes with allyltrialkyl silanes in the presence of a chiral Lewis acid (the Sakurai–Hosomi reaction) has had a considerable impact on asymmetric syn-

thesis.^[124] The complementary activation with chiral Lewis bases is less common. The substrates in this reaction are halosilane derivatives; enantiomerically pure phosphoramides, tartrates, 2-pyridinyloxazolines, formamides, urea derivatives, and axially chiral bis(heteroallyl) *N,N'*-dioxides act as catalysts.

3.3.1.1. Chiral Phosphoramides

Whereas chiral HMPA derivatives can activate allyl or propargyl tin compounds,^[125] allyltrimethylsilane is unreactive. Allyltrichlorosilane, however, can be used for the allylation of aromatic and heteroaromatic aldehydes. Recent efforts have been directed towards the extension of the reaction to aliphatic aldehydes. In these reactions chiral bidentate phosphoramides gave variable results; among them, imidodiphosphoric tetramides were found to be suitable catalysts for the allylation of aryl aldehydes.^[126]

A systematic investigation of bisphosphoramides revealed that the catalysts with a pentamethylene bridge between the two phosphoramide units were the most enantioselective.^[127] The optimization of the catalyst led to the bis(phosphoramide) **100**, with two 2,2'-bispyrrolidine substituents, which catalyzes the addition of allyltrichlorosilane, as well as (*E*)- and (*Z*)-2-butenyltrichlorosilane, to unsaturated aldehydes with excellent diastereo- and enantioselectivities (Scheme 71).^[128] This method was also applied to the synthesis



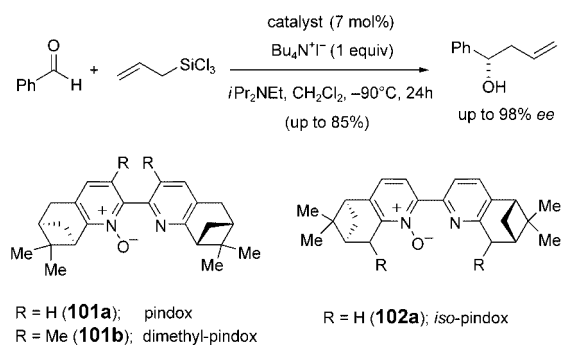
Scheme 71. Asymmetric allylation of aryl aldehydes with the tethered phosphoramide catalyst **100**.

of compounds with quaternary stereocenters ($R_1, R_2 = \text{alkyl, aryl}$).^[128, 129] To illustrate its preparative value, it was also used in the synthesis of the serotonin antagonist LY426965.^[129]

3.3.1.2. Chiral Pyridine *N*-Oxides

Amine *N*-oxides are good electron-pair donors, and this property has been exploited in organocatalytic reactions in a chiral environment. In particular, chiral 2,2'-bipyridine *N*-oxides and *N,N'*-dioxides catalyze a broad range of asymmetric reactions.

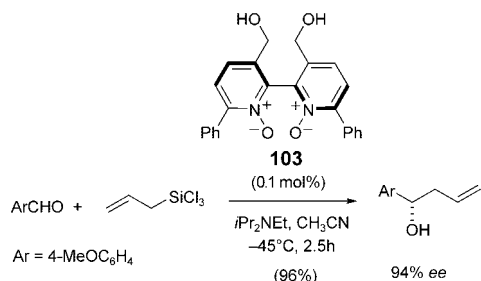
The high degree of enantioselectivity observed in allylations with allyl silanes can be attributed to steric and π – π interactions between the substrate and the bipyridine *N*-oxide catalyst **101** or **102**.^[130] The best results were obtained with pyridine *N*-oxide catalysts derived from (–)- β -pinene (pindox, dimethylpindox) or (–)-pinocarbonyl (*iso*-pindox; Scheme 72).^[131] The products were obtained in 10–85% yield



Scheme 72. Asymmetric allylation of aromatic aldehydes with chiral 2,2'-bipyridine-*N*-monoxide catalysts.

and with up to 98% *ee*. With both types of catalyst good diastereo- and enantioselectivities were observed in crotylation reactions with (*E*)- and (*Z*)-crotyltrimethylsilane, although the use of *iso*-pindox led to better yields. Mechanistic analysis suggests that the *N*-oxide activates the trichlorosilyl functionality and the other nitrogen atom stabilizes the complex by chelation, thus leading to a closed, chair-like transition state.^[130a,d] Depending on the structure of the catalyst and the substrate, π - π or C-H- π interactions were also used to explain stabilization effects and the formation of the compact transition state. The solvent has a major effect on the reaction rate.

The symmetrical bidentate 2,2'-bipyridine *N,N'*-dioxide **103** has also been reported in the catalytic asymmetric allylation of various activated electron-rich aromatic aldehydes (up to 98% *ee*; Scheme 73).^[132,133] The selectivity of the



Scheme 73. Asymmetric allylation of aromatic aldehydes with the chiral 2,2'-bipyridine *N,N'*-dioxide **103** as the catalyst.

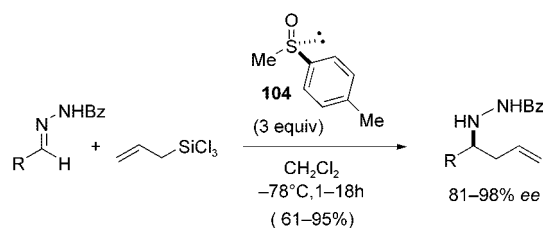
catalyst can be tuned by varying the substitution pattern of the pyridyl group. The best selectivity was observed with the phenyl-substituted derivative **103**. This result was explained by a π -stacking interaction between the substrate and the catalyst in the transition state of the stereodiscriminating step.

3.3.1.3. Chiral Sulfoxides

Unlike P(O) or N(O) Lewis bases, which are excellent catalysts in a number of reactions, chiral sulfoxides have seldom been used. The catalytic turnover is generally low: Synthetically useful yields were only observed when excess sulfoxide was used. High diastereo- and enantioselectivities

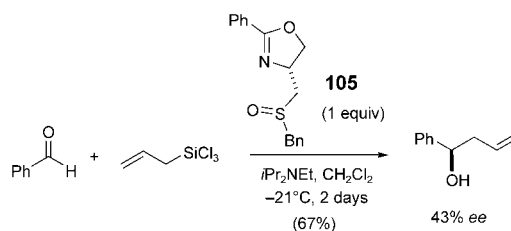
were observed in the allylation of *N*-acyl hydrazones when the chiral sulfoxide catalyst **104** was used with allyltrimethylsilane (Scheme 74).^[134,135]

Sulfoxides of oxazolines, such as **105**, have been used as bidentate ligands for metal catalysts in enantioselective



Scheme 74. Allylation of hydrazones in the presence of a chiral sulfoxide catalyst.

cyanohydrin synthesis.^[136] In the absence of a metal, these molecules are also able to mediate the enantioselective allylation of aldehydes with allyltrimethylsilane with moderate enantioselectivity (Scheme 75).^[137] However, the catalytic turnover is low, and a stoichiometric amount of the catalyst is required.



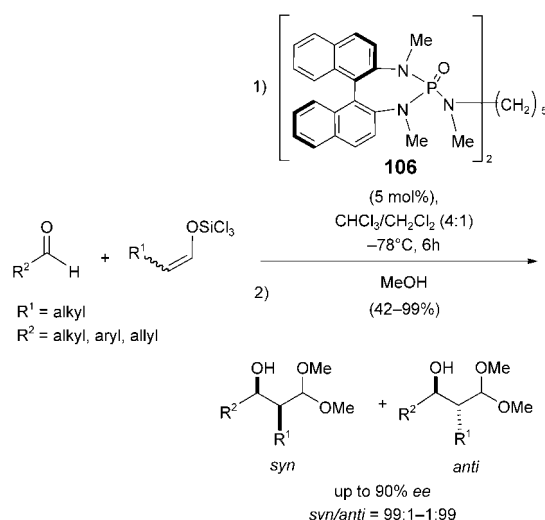
Scheme 75. Enantioselective allylation of benzaldehyde with allyltrimethylsilane in the presence of the chiral sulfoxide catalyst **105**.

3.3.2. Aldol Reactions^[25]

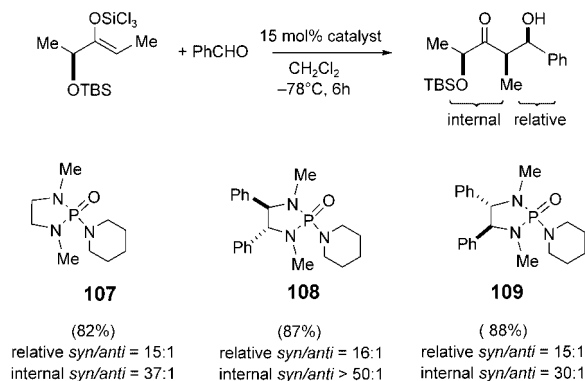
Bisphosphoramides also mediate the selective cross-aldolization of aldehydes.^[138] The geometrically defined trichlorosilyl enolates of aldehydes undergo reaction with a variety of aromatic or α,β -unsaturated aldehydes to afford the cross-aldol products with high diastereo- and enantioselectivities. The mechanism of the transformation is similar to that for allylation with the formation of a closed, chairlike transition state centered around a hexacoordinated silicon atom (Scheme 76).

With chiral phosphoramides as catalysts, α -oxygenated chiral ketone enolates react to give the 1,4-*syn* products in a highly diastereoselective manner.^[139] The selectivity is dictated by the substrate: Both internal and relative stereocontrol is high even with the achiral HMPA analogue **107**. The diastereoselectivity can be only slightly improved by using the matched chiral catalyst **108** (Scheme 77).

The effect of the stereogenic center bearing the silyloxy substituent fades with increasing distance from the reaction center. In the case of substrates with a β -silyloxy substituent, the chiral catalyst governs the diastereoselectivity in the



Scheme 76. Enantioselective aldol reaction of silyl enolates catalyzed by the chiral bisphosphoramidate **106**.

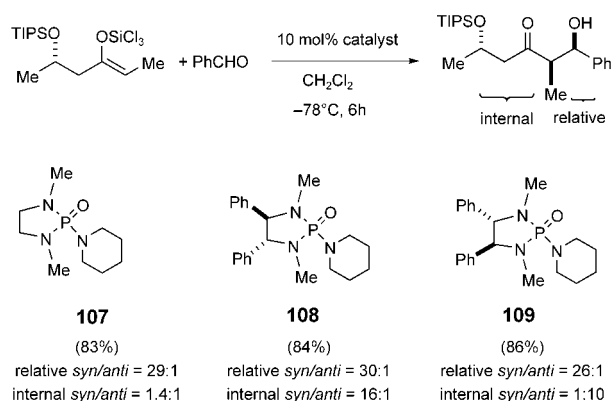


Scheme 77. The effect of the structure of the substrate on the diastereoselectivity of the phosphoramidate-catalyzed asymmetric aldol reaction of silyl enolates.

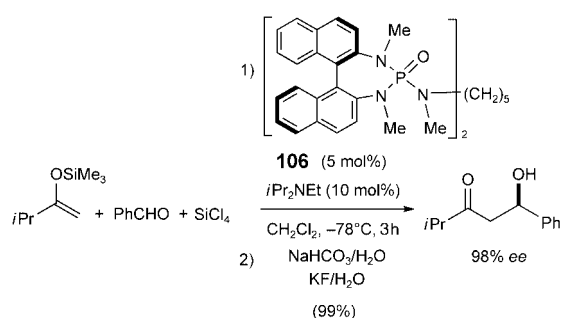
addition of a chiral enolate to an aldehyde (Scheme 78).^[140] In these reactions the effect of the remote stereogenic center is low, and the internal diastereoselectivity is mainly controlled by the catalyst. This result can be compared to aldol reactions of boron enolates in which 1,5-*anti* stereoinduction is observed.

Complementary studies on substrates with a small, non-chelating substituent, such as a methyl group, in the proximity of the reacting silyl enol ether showed that the configuration of the newly formed stereogenic is determined principally by the catalyst.^[141]

High selectivities were observed in the addition of various *exo* trimethylsilyl enolates to aromatic aldehydes in the presence of the bisphosphoramidate catalyst **106** (Scheme 79).^[142] The protonolysis of the TMS enol ether, which results in diminished conversion, was suppressed by the addition of a small amount (10%) of an amine base. Under these conditions the reaction affords the desired β -hydroxyketones in nearly quantitative yield with remarkable selectivity. Aliphatic aldehydes are unreactive under these conditions.

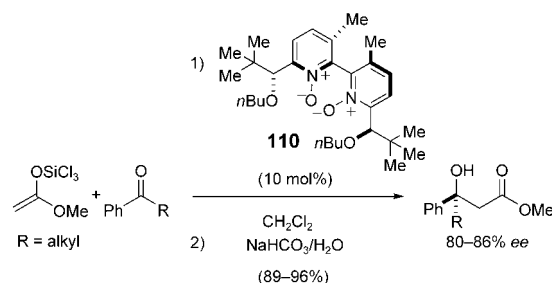


Scheme 78. The effect of a remote substituent on the diastereoselectivity of the phosphoramidate-catalyzed asymmetric aldol reaction of silyl enolates.



Scheme 79. Enantioselective aldol reaction of benzaldehyde with an *exo* TMS enolate in the presence of a chiral bis(phosphoramidate) catalyst.

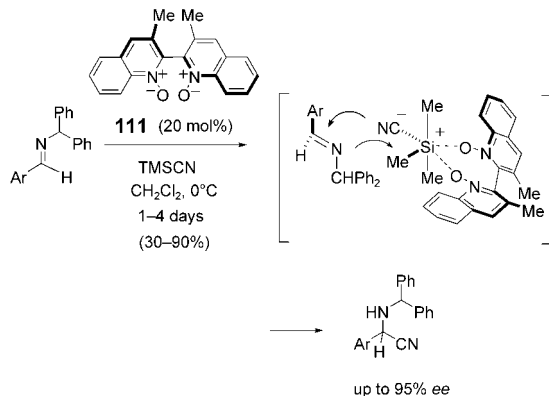
As in aminocatalysis, the enantioselective aldol addition of preformed enolates to ketone acceptors with phosphoramidate catalysts remains elusive. The difficulty in devising such a reaction arises both from the attenuated reactivity of the ketone and the smaller differences between the flanking substituents, making stereodifferentiation more difficult. The addition of trichlorosilyl acetals of ketenes to ketones in the presence of the chiral bis-*N*-oxide catalyst **110** was described recently (Scheme 80).^[143] Good enantioselectivities were observed with aromatic ketones (80–86% ee), but the products were only obtained with 20–41% ee from aliphatic ketones.



Scheme 80. Asymmetric addition of a trichlorosilyl methyl ketene acetal to aryl ketones in the presence of the chiral 2,2'-bipyridine *N,N'*-dioxide derivative **110**.

3.3.3. Nucleophilic Catalysts for the Hydrocyanation of Imines

The axially chiral biquinoline *N,N'*-dioxide **111** was used to promote the asymmetric Strecker reaction between aryl or heteroaryl aldimines and trimethylsilyl cyanide (Scheme 81).^[144] The presence of electron-withdrawing sub-



Scheme 81. Enantioselective Strecker reaction between aldimines and trimethylsilyl cyanide mediated by the chiral 2,2'-bipyridine *N,N'*-dioxide catalyst **111**.

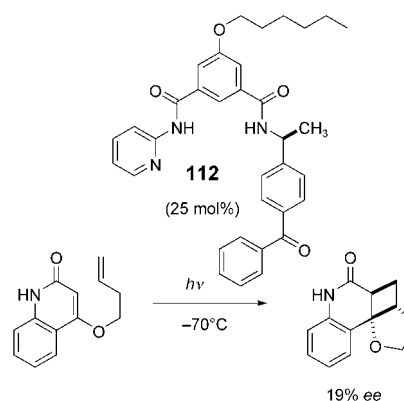
stituents on the aryl ring resulted in an increase in both the yield and the enantioselectivity of the reaction. According to the proposed transition-state model, a hypervalent silicon center forms through coordination of the biquinoline *N,N'*-dioxide catalyst to TMSCN. The hexacoordination at silicon results in enhanced nucleophilicity of the cyano group, which reacts with the aldimine in such way that the nitrogen atom of the aldimine coordinates simultaneously to the silicon atom.

3.4. Chiral Sensitizing Receptors as Catalysts

Until now preparative applications of enantioselective transformations in photochemistry have been restricted to photoreactions in which the chirality transfer is assured by a stoichiometric amount of a chiral auxiliary or host,^[193] such as a clathrate or chirally modified zeolite. Recently, it was shown that even a substoichiometric amount (up to 25 mol %) of the photosensitizing receptor **112** mediated a photocycloaddition in quantitative yield and with 19% *ee* (Scheme 82).^[194] In this system the synthetic receptor both assures a well-defined chiral environment upon binding to the template and offers a highly selective energy transfer to the substrate via a triplet exciplex. This transfer is efficient when the lifetime of the exciplex is comparable to the rate of cyclization.

4. Enantioselective Phase-Transfer Reactions^[195]

Phase-transfer catalysis (PTC) is an attractive alternative for organic reactions in which charged intermediates are involved. Reactions are usually carried out in two- or three-



Scheme 82. Intramolecular [2+2] photocycloaddition of an enone-alkene catalyzed by the chiral molecular receptor **112**.

phase systems, most commonly in vigorously stirred aqueous/apolar solvent mixtures. An inorganic base, such as K_2CO_3 or Cs_2CO_3 , is used to form the reactive enolate. The role of the catalyst is primarily that of an ion shuttle. Chiral nonracemic catalysts also act as templates to direct the approach of the reagent.

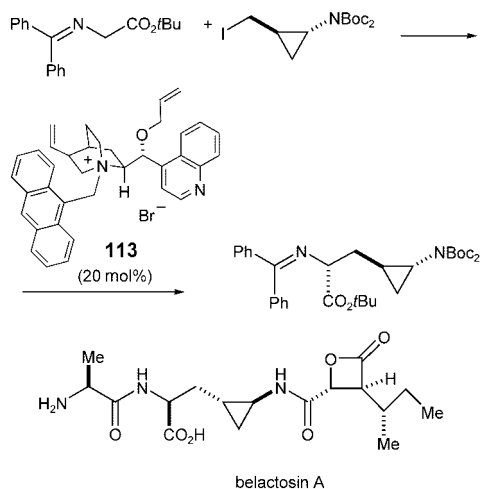
Phase-transfer reactions were initially carried out with cinchona alkaloids. Recently, the enantioselectivities were improved significantly by optimizing the catalyst structures, the reagent types, and the reaction conditions. Despite significant progress, however, low reactivity, in particular at low temperatures, as well as substrate incompatibility, are commonly encountered problems. These disadvantages continue to motivate the search for new efficient catalysts. Other catalysts (usually C_2 symmetric), both derived from natural products and fully synthetic, are being developed. The ready accessibility of phase-transfer catalysts and the mild experimental conditions make asymmetric phase-transfer reactions appealing both for academic research and for industrial applications.

4.1. Cinchona Alkaloids as Phase-Transfer Catalysts

Cinchona alkaloids were the first efficient phase-transfer catalysts for asymmetric catalysis, and the majority of the most recent work is also dedicated to this class of catalysts. Somewhat surprisingly, neither the electronic nor the steric factors that determine the enantioselectivity of this class of catalysts are yet fully understood. Although the elucidation of the structure of some salts of cinchona alkaloids in solution was an important step toward the rational design of such catalysts,^[196] the development of the catalysts has been based mainly on empirical observations. It was recognized early that the substituents on both the oxygen and the nitrogen atom of the quinuclidine moiety of the cinchona alkaloids play a key role in the enantioselectivity.^[197,198] Whereas the influence of the substitution pattern of the secondary alcohol is a matter of controversy, it is clearly established that a bulky substituent at the quaternary nitrogen atom increases the enantioselectivity of the catalyst.

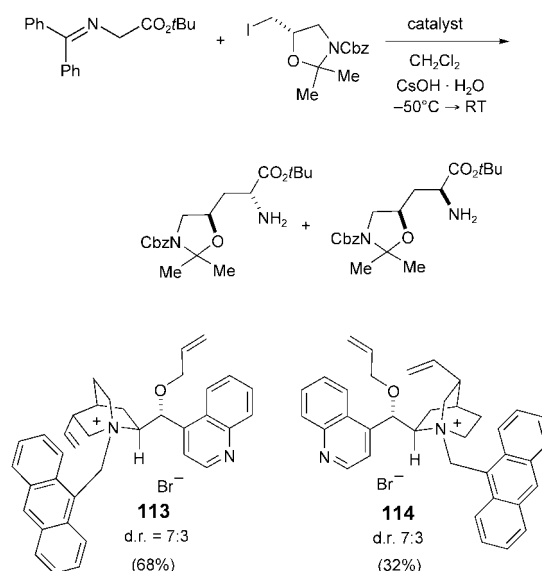
This observation initiated the synthesis of a number of *N*-benzyl and *N*-antracenylnmethyl derivatives, referred to generally as second- and third-generation catalysts. In alkylation reactions *O*-allyl-*N*-antracenylnmethyl (third-generation) catalysts are usually the most efficient cinchona-alkaloid catalysts.^[199,200] These molecules can be prepared either by multistep synthesis or, more conveniently, in situ.^[201] The one-pot procedure is particularly suitable for automated catalyst screening. The catalysts perform well in alkylation reactions with glycine-derived Schiff bases as substrates and in conjugate addition reactions with nitroalkanes and malonates.^[201] The selectivity of the catalyst can be improved by replacing the vinyl side chain with an ethyl group. The substitution pattern of the glycine derivative also has a major impact on the stereoselectivity of the alkylation. Recent studies demonstrated that the *tert*-butyl ester of the glycine reagent can be advantageously replaced by a diphenylmethyl ester when the catalyst **126** (Figure 14) is used.^[202]

Phase-transfer alkylations are being used increasingly in multistep synthesis. A key intermediate in the synthesis of the *ent*-fragment of the potential antitumor agent belactosin A was prepared through asymmetric phase-transfer catalysis.^[203] Whereas the (aminocyclopropyl)alanine enantiomer shown was prepared by using the cinchonidinium bromide catalyst **113** (66% yield, d.r. 97:3; Scheme 83). A similar strategy was devised to prepare the caprolactam subunit of the antitumor agent bengamide.^[204]



Scheme 83. Synthesis of belactosin A through the asymmetric alkylation of a glycine derivative under phase-transfer conditions.

It is often difficult to control the selectivity of the alkylation when one of the reagents possesses a stereocenter. For example, in the synthesis of a protected hydroxyornithine derivative the selectivity of the alkylation was dictated by the substrate rather than by the chiral catalyst, regardless of the structure and the configuration of the latter (Scheme 84).^[205] When achiral tetrabutylammonium bromide was used as the catalyst, roughly the same diastereoselectivity was observed as with the cinchonidine and cinchonine catalysts **113** and **114**, respectively. To enhance the catalyst activity, bis-^[206] and



Scheme 84. Asymmetric synthesis of protected hydroxyornithine as an example of a substrate-controlled stereoselective alkylation.

triscinchona^[207] derivatives were prepared and tested (Figure 11).^[7b,208]

The deprotonation of compounds with acidic hydrogen atoms followed by an asymmetric transformation in the presence of a cinchona alkaloid under phase-transfer con-

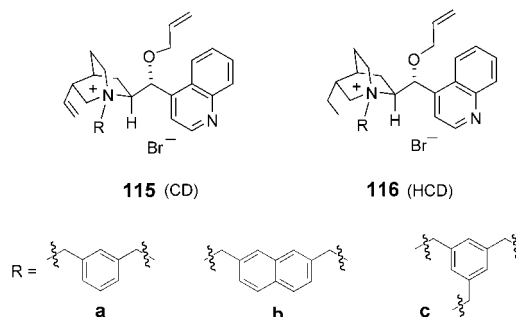
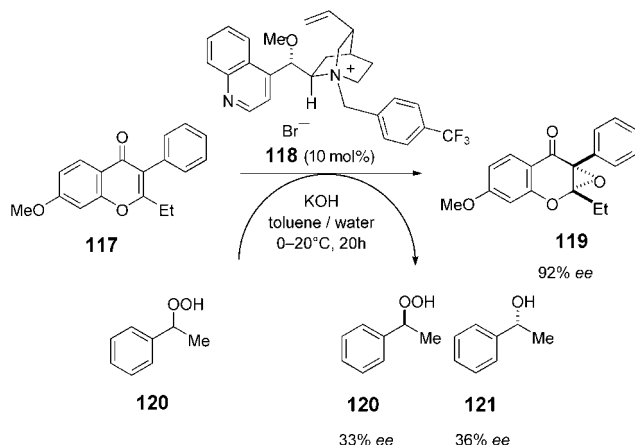


Figure 11. Bis- and triscinchonine derivatives as phase-transfer catalysts. CD = cinchonidinium, HCD = hydrocinchonidinium.

ditions has been used in a number of related reactions, such as asymmetric deuteration, hydroxylation,^[209] electrophilic fluorination,^[210] isomerization of alkynes to chiral allenes,^[212] and the Darzens reaction,^[211] to afford products with moderate to good *ee* values. Asymmetric alkylation reactions in micelles^[213] and on a solid support have also been reported.^[214] The rate of alkylation reactions, Michael additions, and the epoxidation of enones under phase-transfer conditions could be increased by ultrasonic irradiation.^[215]

Ammonium salts of cinchona alkaloids catalyze the asymmetric epoxidation of activated olefins in the so-called Weitz–Scheffer reaction. A range of enones were transformed into oxiranes under these conditions with either inorganic oxidants, such as H₂O₂,^[216] hypochlorite salts,^[217] trichloroisocyanuric acid,^[218] or chlorates,^[219] or with organic perox-

ides.^[220] When the 1-phenyl hydroperoxide **120** was used as the oxidant in the asymmetric epoxidation of the isoflavon **117**, the reaction also allowed the kinetic resolution of the oxidizing agent, albeit with modest enantioselectivity (Scheme 85).^[220] This relatively inefficient enantiodifferentiation is probably the consequence of a weak interaction between the phase-transfer catalyst **118** and the hydroperoxide.



Scheme 85. Asymmetric epoxidation of the isoflavon **117** with a parallel kinetic resolution of the hydroperoxide oxidizing agent **120**.

4.2. C₂-Symmetric Phase-Transfer Catalysts

A considerable amount of work has been devoted to the development of ammonium catalysts from either natural compounds, such as tartaric acid, or purely synthetic compounds, such as 1,1'-(2,2'-binaphthol), for use in asymmetric phase-transfer reactions.^[221–228] Among these catalysts, *N*-spiro biaryl derivatives, such as **122** and **123**, lead to remarkable selectivity and reactivity in a variety of reactions (Figure 12).^[222] A considerable advantage of this class of compounds over other synthetic phase-transfer catalysts is

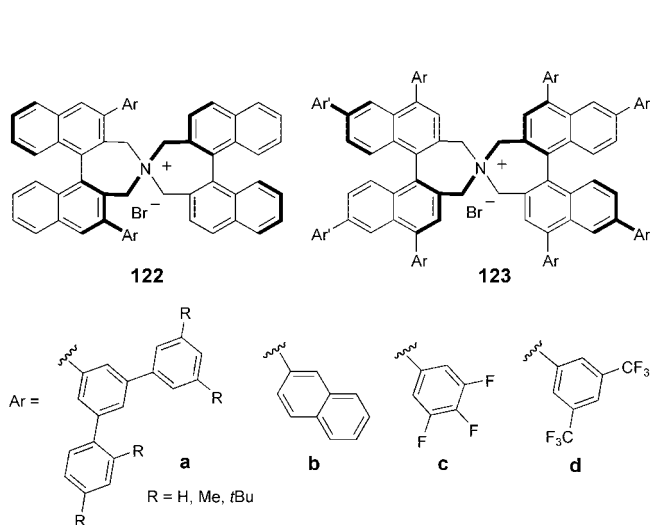


Figure 12. Some *N*-spiro biaryl ammonium phase-transfer catalysts.

that their structure can be modified easily, thus allowing rapid access to a variety of analogues.

The *N*-spiro biaryl catalysts are more active and often more selective than cinchona alkaloids in the alkylation of glycine-derived Schiff bases; the fluorinated derivatives **122c** and **122d** afforded excellent results (up to 99% *ee*) (Figure 12).^[223] Good to excellent results were also obtained with the symmetrical 4,4',6,6'-binaphthyl-substituted catalyst **123** (up to 97% *ee*).^[224] Interestingly, not only glycine-derived Schiff bases but also *N*-terminal oligopeptides can be alkylated in a highly selective manner.^[225]

Simplified catalysts, such as **124**, with one of the two chiral binaphthyl units replaced by a flexible achiral biphenyl moiety, were also prepared (Figure 13). The catalyst design

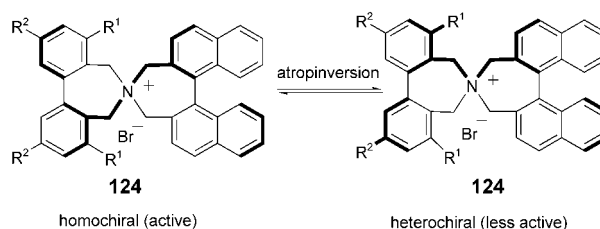
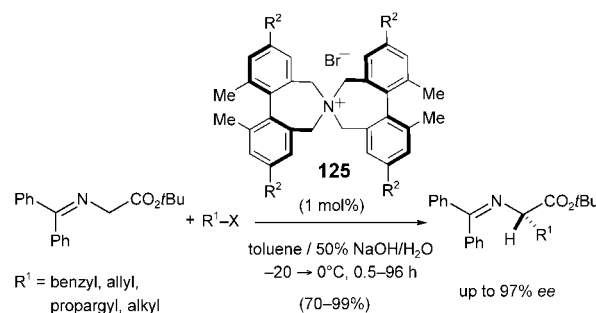


Figure 13. The hetero- and homochiral conformations of *N*-spiroammonium catalysts are in equilibrium.

relies on the concept of “induced atropisomerism”:^[226] The chirality of the binaphthyl group is magnified by the fact that the biphenyl group can adopt two interconverting conformations, which are either homo- or heterochiral relative to the conformation of the catalyst. The enantioselectivity of the catalyst can be improved by increasing the steric hinderance in the achiral biphenyl moiety near the quaternary nitrogen atom.

As an extension to this work, symmetrically 4,6-disubstituted atropisomeric *N*-spiro catalysts, such as **125**, were also prepared (Scheme 86).^[227] These catalysts mediate the alkylation of glycine-derived Schiff bases with sterically less



Scheme 86. Enantioselective alkylation of the Schiff base of tert-butyl glycinate and benzophenone with the *N*-spiro biphenyl phase-transfer catalyst **125**. R² = 1,1-dimethylbenzyl.

demanding electrophiles, such as allylic and propargylic bromides, with high enantioselectivity (up to 97% *ee*).

The non-atropisomeric biaryl catalyst **126** was also prepared and tested in the alkylation of the glycine Schiff

base with alkyl halides (up to 97% *ee*; Figure 14).^[228] In this system the additional chiral centers may enhance the selectivity of the catalyst and can be modified for optimal efficiency.

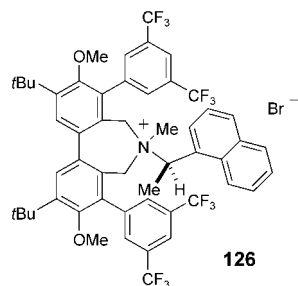


Figure 14. An asymmetric phase-transfer catalyst with a methylnaphthylammonium unit.

Tartrate-derived catalysts were also shown to be efficient in mediating phase-transfer reactions. A series of phase-transfer catalysts, such as **127** and **128**, with two reactive quaternary nitrogen centers were prepared and tested in asymmetric alkylation and Michael addition reactions (Figure 15).^[229] The best results for the asymmetric alkylation

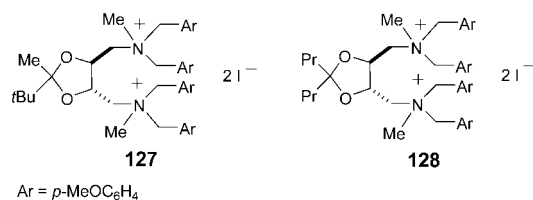
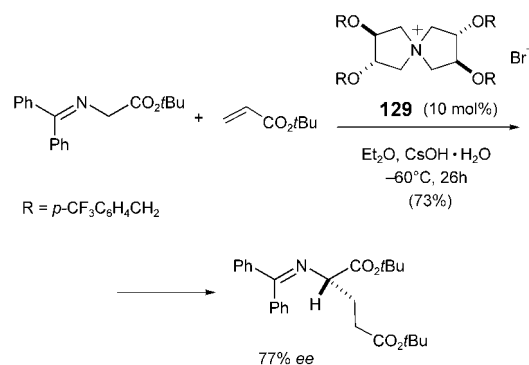


Figure 15. Tartrate-derived diammonium phase-transfer catalysts.

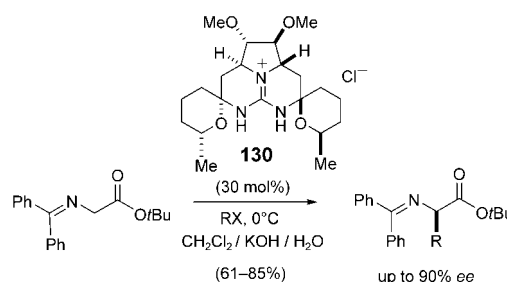
of the glycine Schiff base were obtained with the unsymmetrical catalyst **127**, whereas a C_2 -symmetric catalyst **128** was found to be more efficient in mediating Michael-type additions. Surprisingly, the opposite stereoselectivity was observed in the asymmetric alkylation to that observed in the Michael addition. It was suggested that the catalyst functions as a bifunctional catalyst and activates both the nucleophile and the electrophile in the Michael addition. The catalyst **127** was used in the synthesis of the serine protease inhibitor aeruginosin 298-A.^[230]

The spiroammonium catalyst **129** derived from L-tartrate was tested in the Michael addition of a glycine Schiff base and *tert*-butyl acrylate under phase-transfer conditions (Scheme 87).^[231] Diethyl ether and *tert*-butyl methyl ether were found to be the best solvents for this reaction. The product was formed in 73% yield and with 77% *ee* with the trifluoromethylbenzyl-substituted catalyst (Scheme 87).

The structure of the C_2 -symmetric chiral pentacyclic guanidine catalyst **130** was inspired by the marine natural product ptilomycin A (Scheme 88). The compound mediates efficiently the enantioselective 1,4-addition of anions derived from glycine esters to acrylates. The same catalyst can



Scheme 87. Asymmetric Michael reaction catalyzed by the L-tartrate-derived *N*-spiroammonium catalyst **129**.

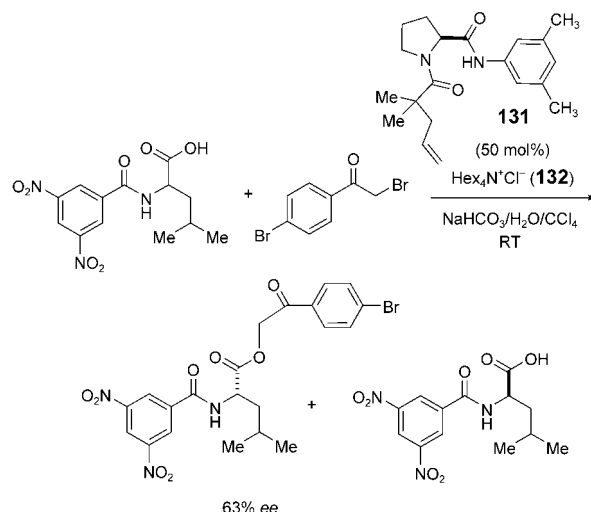


Scheme 88. Asymmetric alkylation with the guanidine derivative **130** as a phase-transfer catalyst.

also be used for asymmetric PTC alkylation with a variety of electrophiles (yields between 61 and 85%, up to 90% *ee*).^[232]

4.3. Chiral Selectors and Phase-Transfer Agents

The design of chiral selectors is a novel concept for the kinetic resolution of racemic molecules.^[233] The phase-transfer catalyst tetrahexylammonium bromide (THAB, **132**)



Scheme 89. Enantioselective esterification of an *N*-acyl amino acid. The phase-transfer catalyst is a system comprising the two components **131** and **132**.

transports both enantiomers of a polar molecule (for example, a carboxylate anion) into the apolar phase, where it is converted in the presence of a chiral selector (typically a proline derivative, such as the *N*-acylated L-proline anilide **131**) in an asymmetric transformation (such as esterification) into an enantiomerically enriched product (Scheme 89). In contrast to traditional phase-transfer catalysis the chiral information is not present in the phase-transfer agent, but in a separate compound, the chiral selector.

The concept has been used for acylation, nucleophilic aromatic substitution, and the enantioselective hydrolysis of esters. In the last two cases the basic principle is the same: The chiral selector shields one of the two enantiomers from the reaction through noncovalent interactions.

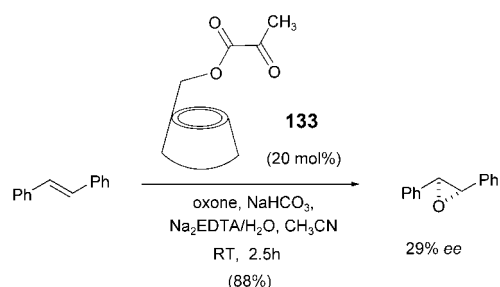
5. Asymmetric Transformations in a Chiral Cavity

The selective recognition of substrates based on their molecular structure by using engineered molecular cavities in which a chemical transformation then takes place is a technique modeled on the principle of enzyme catalysis. The developing understanding of the mechanisms of enzyme catalysis, in particular the theory of transition-state stabilization, has also served as a major source of inspiration for devising new structures and functions. This concept, however, emulates enzyme functions only partially. We now know that other factors are also important for the acceleration of reactions by enzymes: Electrostatic effects, quantum-mechanical tunneling, coupled protein motion, low-barrier hydrogen bonds, and near attack conformations enable enzymes to enhance reaction rates by a factor of up to 10^{20} .^[234] On the other hand, the mimicking of enzymes by catalytically active polymers has a number of disadvantages related to the microstructure of the catalyst, such as accessibility, local solvation, and homogeneity of the catalytic centers, and to the rigidity of the structure. When the structure of the starting material is similar to that of the product the host–guest complex formed is often too stable, thus resulting in product inhibition. Whereas enzyme catalysts are capable of undergoing conformational changes to release the product, the rigidity of artificial catalysts does not allow efficient catalytic turnover. The development of systems for the dynamic release of products after the reaction is therefore a promising area of further research.

5.1. Cyclodextrins and Calixarenes in Catalytic Asymmetric Synthesis

Cyclodextrins and calixarenes can form inclusion complexes with a variety of guests, depending on size, structure, and polarity. Nevertheless, little is known about the enzyme-like catalytic activity of these substrates.^[235]

Scheme 90 shows, as an example, the asymmetric epoxidation of alkenes with the cyclodextrin-substituted ketoester **133**.^[236] Convalently modified cyclodextrins mimic cytochrome P450 in catalytic oxidations.^[237] In the enantioselective epoxidation of styrene derivatives with 20–100 mol % of



Scheme 90. Asymmetric epoxidation of *trans*-stilbene with oxone catalyzed by the cyclodextrin ketoester **133**.

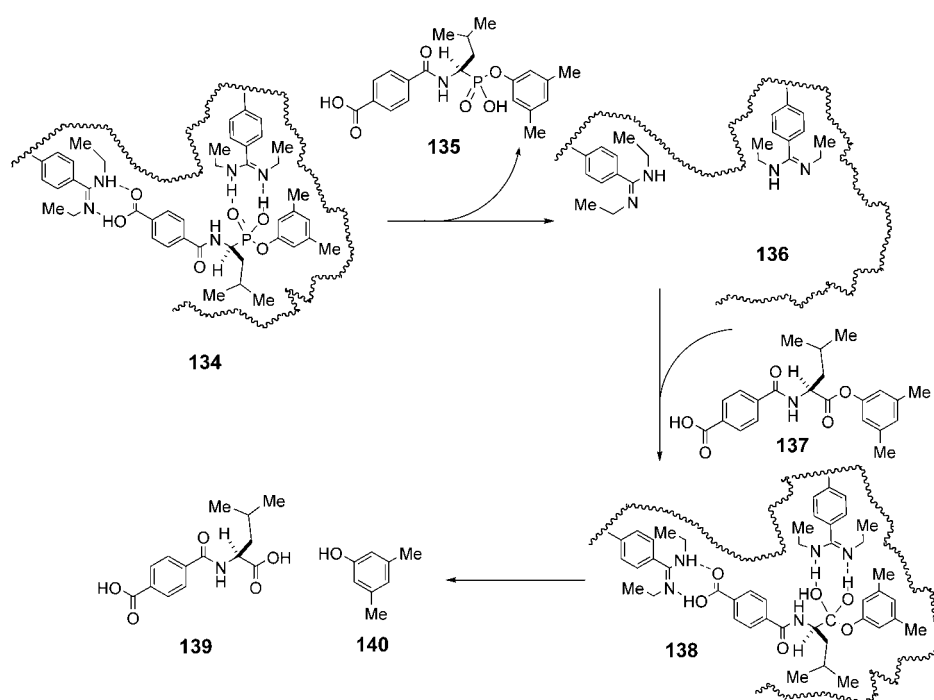
133 up to 40 % *ee* was observed. It was demonstrated by NMR spectroscopic studies that the reaction proceeds via inclusion complexes, at least for the substrates investigated.^[236]

5.2. Molecular Imprinting^[238, 239]

Molecular imprinting involves the formation of a structure, most often a polymer, around a molecular template. When the template is removed by extraction a catalytic cavity remains, which is characterized by both its shape and the arrangement of functional groups. This site can have a variety of properties engineered into it, ranging from the selective binding of specific molecules (molecular recognition) to enzymelike catalysis. In addition to traditional applications in chromatography, new applications in sensors and catalysis are emerging.

Early efforts led to successful catalytic ester hydrolysis, and this area is still significant. By analogy with proteolytic biopolymers, the “catalytic triad” motif of serine, histidine, and aspartic acid (as the carboxylate anion) present in the serine protease enzyme family served as a model for catalyst design. L-Arginine with a guanidinium group also plays an important role in catalyzing the basic hydrolysis of esters. Recently, a wider range of reactions have been addressed, including C–C bond-forming reactions. This progress was made possible by new and improved techniques, which have enhanced the quality of molecularly imprinted substances. In parallel, innovative approaches to the design of receptors based on dynamic combinatorial libraries are emerging.^[240] Although shape-selective transformation also infers enantio-discrimination, truly asymmetric transformations with imprinted polymers remain scarce.^[241]

To mimic the catalytic triad of the active site of chymotrypsin, imidazole rings, phenolic hydroxy groups, and carboxy groups were used as catalytically active groups. Enantiomerically pure phosphonic acid monoesters, such as **135**, were prepared as stable transition-state analogues and used as templates (Scheme 91).^[242] They were connected by defined noncovalent interactions with the amidinium unit of the binding site. After polymerization and removal of the template, the polymer **136** obtained mediated the hydrolysis of the nonactivated phenyl amino acid ester **137** with remarkable enantio- and substrate selectivity. The hydrolysis proceeded 80 times faster than with a control polymer



Scheme 91. Substrate-selective and enantioselective hydrolysis of a phenyl amino acid ester mediated by a molecularly imprinted catalyst.

containing the same functionalities but prepared without the template. Even more interesting was the relatively high enantioselectivity (a consequence of both selective binding and selective formation of the transition state) observed in the comparison of L and D substrates (catalytic efficiency = 1.65).

6. Summary and Outlook

An increasing number of asymmetric organic reactions can be accelerated by a catalytic amount of a chiral organic molecule. This novel type of catalysis has emerged as a major concept in organic chemistry in the last few years and is currently experiencing its golden age. Although substrate dependence remains an important issue in many of the reactions discussed, more and more transformations now meet the standards of established asymmetric reactions. Despite the considerable progress that has been made in the elucidation of transition states, we are only beginning to understand the basic factors that control reactivity and selectivity in these reactions, and the rational design of catalysts remains in most cases a dream. The number of organocatalytic (non-asymmetric) reactions is steadily increasing, which provides a solid basis for the development of novel enantioselective reactions.^[243] New asymmetric reactions are constantly being reported.^[244–251] Although creativity and persistence will certainly remain the major factors in the success of this research, the increasing use of automatization and computational techniques may facilitate both the discovery of novel catalyst structures and the screening of reactions for catalysts of the next generations.

We thank Prof. Carlos F. Barbas III, Prof. Eric N. Jacobsen, Prof. Pavel Kočovský, Prof. Ben List, Prof. Keiji Maruoka, Prof. Scott Miller, and Prof. Alan C. Spivey for the critical reading of the manuscript and Dr. Michael Gray for his help in the editing.

Received: January 19, 2004

- [1] a) In many cases it is difficult to define the boundary between organometallic and purely organic asymmetric catalysis. Organometallic reactions, in which a catalytic amount of an organic ligand participates, are not considered as organocatalytic reactions. The elements that can be contained in “organic” compounds can also be decided arbitrarily, in particular for metalloid elements. For example, according to general consensus, silicon is not considered to be a metal, but boron is. On the other hand, the absence of a metal is not an

absolute criterion: Thus, in phase-transfer reactions a metal ion (e.g. Na⁺, K⁺, Cs⁺) may play an indirect role through association with the base. For this reason, in organocatalytic reactions the “absence of metals” is more correctly considered within the context of the postulated “primary” catalytic cycle. b) This overview covers enantioselective reactions that were described since our preceding account,^[3a] between 2001 and 2004.

- [2] S. Pizzarello, A. L. Weber, *Science* **2004**, *303*, 1151.
 [3] a) P. I. Dalko, L. Moisan, *Angew. Chem.* **2001**, *113*, 3840–3864; *Angew. Chem. Int. Ed.* **2001**, *40*, 3726–3748; b) A. Berkessel, H. Gröger, *Metal-Free Organic Catalysts in Asymmetric Synthesis*, Wiley-VCH, Weinheim, **2004**; c) M. Benaglia, A. Puglisi, F. Cozzi, *Chem. Rev.* **2003**, *103*, 3401–3430; d) “Special issue: Asymmetric Organocatalysis”, *Acc. Chem. Res.* **2004**, *37*, 487–631.
 [4] For reviews on enantioselective catalysis dealing partly with organocatalytic reactions, see: a) H. Tye, P. J. Comina, *J. Chem. Soc. Perkin Trans. 1* **2001**, 1729–1747; b) S. Bräse, F. Lauterwasser, R. E. Zieger, *Adv. Synth. Catal.* **2003**, *345*, 869–929; c) P. McMorn, G. J. Hutchings, *Chem. Soc. Rev.* **2004**, *33*, 108–122; d) *Organic Synthesis Highlights V* (Eds.: H.-G. Schmalz, T. Wirth) Wiley-VCH, Weinheim, **2003**; e) J.-A. Ma, D. Cahard, *Angew. Chem.* **2004**, *116*, 4666–4683; *Angew. Chem. Int. Ed.* **2004**, *43*, 4566–4583; f) “Special Feature: Asymmetric Catalysis”, *Proc. Natl. Acad. Sci. USA*, **2004**, *101*, 5311–5696 (issue 15).
 [5] T. P. Yoon, E. N. Jacobsen, *Science* **2003**, *299*, 1691–1693.
 [6] The term was coined in analogy with pharmaceutical compound classes that are active against a number of different biological targets.
 [7] a) K. Kacprzak, J. Gawronsky, *Synthesis* **2001**, 961–998; b) S.-K. Tian, Y. Chen, J. Hang, L. Tang, P. McDaid, L. Deng, *Acc. Chem. Res.* **2004**, *37*, 621–631.
 [8] a) For the concept of “ideal synthesis”, see: P. A. Wender, S. T. Handy, D. L. Wright, *Chem. Ind.* **1997**, *19*, 765–769.

- [9] D. Gani, *Nature* **2001**, *414*, 703–705.
- [10] For a review, see: P. R. Schreiner, *Chem. Soc. Rev.* **2003**, *32*, 289–296.
- [11] See also: a) T. Schustere, M. Kurz, M. W. Göbel, *J. Org. Chem.* **2000**, *65*, 1697–1701; b) Y. Huang, V. H. Rawal, *J. Am. Chem. Soc.* **2002**, *124*, 9662–9663; c) L. R. Dominge, J. Andrés, *J. Org. Chem.* **2003**, *68*, 8662–8668.
- [12] a) N. E. Leadbeater, M. Marco, *Angew. Chem.* **2003**, *115*, 1445–1447; *Angew. Chem. Int. Ed.* **2003**, *42*, 1407–1409; b) N. E. Leadbeater, M. Marco, *J. Org. Chem.* **2003**, *68*, 5660–5667.
- [13] a) N. E. Leadbeater, M. Marco, B. J. Tominack, *Org. Lett.* **2003**, *5*, 3919–3922; b) P. Appukkuttan, W. Dehaen, E. Van der Eycken, *Eur. J. Org. Chem.* **2003**, 4713–4716.
- [14] D. Ma, Q. Cai, *Synthesis* **2004**, 128–130.
- [15] R. Zhang, F. Zhao, M. Sato, Y. Ikushima, *Chem. Commun.* **2003**, 1548–1549.
- [16] C. Chevrin, J. Le Bras, F. Hénin, J. Muzart, *Tetrahedron Lett.* **2003**, *44*, 8099–8102.
- [17] a) H. Gröger, *Chem. Eur. J.* **2001**, *7*, 5246–5251; b) M. Shibasaki, H. Sasaki, T. Arai, *Angew. Chem.* **1997**, *109*, 1290–1311; *Angew. Chem. Int. Ed. Engl.* **1997**, *36*, 1236–1256.
- [18] B. Westermann, *Angew. Chem.* **2003**, *115*, 161–163; *Angew. Chem. Int. Ed.* **2003**, *42*, 151–153.
- [19] a) B. List, *Synlett* **2001**, *11*, 1675–1686; b) H. Gröger, J. Wilken, *Angew. Chem.* **2001**, *113*, 545–548; *Angew. Chem. Int. Ed.* **2001**, *40*, 529–532; c) B. List, *Tetrahedron* **2002**, *58*, 5573–5590; d) E. R. Jarvo, S. J. Miller, *Tetrahedron* **2002**, *58*, 2481–2495; e) M. Movassaghi, E. N. Jacobsen, *Science* **2002**, *298*, 1904–1905; f) N. Gathergood, *Aust. J. Chem.* **2003**, *55*, 615; g) W. Notz, F. Tanaka, C. F. Barbas III, *Acc. Chem. Res.* **2004**, *37*, 580–591.
- [20] The natural compound is mostly extracted from chicken feathers; for more details, see reference [28] and the cover picture of *Angew. Chem.* **2003**, *115*; *Angew. Chem.* **2003**, *42*, issue 2.
- [21] For a recent review on enantiodivergence, see: M. P. Sibi, M. Liu, *Curr. Org. Chem.* **2001**, *5*, 719–755.
- [22] a) S. Bahmanyar, K. N. Houk, *Org. Lett.* **2003**, *5*, 1249–1251; b) S. Bahmanyar, K. N. Houk, H. J. Martin, B. List, *J. Am. Chem. Soc.* **2003**, *125*, 2475–2479; c) L. Hoang, S. Bahmanyar, K. N. Houk, B. List, *J. Am. Chem. Soc.* **2003**, *125*, 16–17; d) S. Bahmanyar, K. N. Houk, *J. Am. Chem. Soc.* **2001**, *123*, 12911–12912; e) S. Bahmanyar, K. N. Houk, *J. Am. Chem. Soc.* **2001**, *123*, 11273–11283; f) C. Allemann, R. Gordillo, F. R. Clemente, P. H.-Y. Cheong, K. N. Houk, *Acc. Chem. Res.* **2004**, *37*, 558–569; see also: g) J. Kofoed, J. Nielsen, J. L. Reymond, *Bioorg. Med. Chem. Lett.* **2003**, *13*, 2445–2447.
- [23] T. P. Brady, S. H. Kim, K. Wen, E. A. Theodorakis, *Angew. Chem.* **2004**, *116*, 757–760; *Angew. Chem. Int. Ed.* **2004**, *43*, 739–742.
- [24] For related derivatives, see: a) M. Nakadaï, S. Saito, H. Yamamoto, *Tetrahedron* **2002**, *58*, 8167–8177; b) Z. Tang, F. Jiang, L.-T. Yu, X. Cui, L.-Z. Gong, A.-Q. Mi, Y.-Z. Jiang, Y.-D. Wu, *J. Am. Chem. Soc.* **2003**, *125*, 5262–5263; c) F. Fache, O. Piva, *Tetrahedron: Asymmetry* **2003**, *14*, 139–143; d) T. J. Dickerson, K. D. Janda, *J. Am. Chem. Soc.* **2002**, *124*, 3220–3221; e) A. J. A. Cobb, D. M. Shaw, S. V. Ley, *Synlett* **2004**, 558–560.
- [25] a) B. Alcaide, P. Almendros, *Eur. J. Org. Chem.* **2002**, 1595–1601; b) B. Alcaide, P. Almendros, *Angew. Chem.* **2003**, *115*, 884–886; *Angew. Chem. Int. Ed.* **2003**, *42*, 858–860; c) C. Palomo, M. Oiarbide, J. M. García, *Chem. Eur. J.* **2002**, *8*, 36–44; d) C. Palomo, M. Oiarbide, J. M. García, *Chem. Soc. Rev.* **2004**, *33*, 65–75; e) S. Saito, H. Yamamoto, *Acc. Chem. Res.* **2004**, *37*, 570–579.
- [26] See, for example: S. J. Danishefsky, J. J. Masters, W. B. Young, J. T. Link, L. B. Snyder, T. V. Magee, D. K. Jung, R. C. A. Isaacs, W. G. Bornmann, C. A. Alaimo, C. A. Coburn, M. J. Di Grandi, *J. Am. Chem. Soc.* **1996**, *118*, 2843–2859.
- [27] R. B. Woodward, E. Logusch, K. P. Nambiar, K. Sakan, D. E. Ward, B.-W. Au-Yeung, P. Balaram, L. J. Browne, P. J. Card, C. H. Chen, R. B. Chênevert, A. Fliri, K. Frobel, H.-J. Gais, D. G. Garratt, K. Hayakawa, W. Heggie, D. P. Hesson, D. Hoppe, I. Hoppe, J. A. Hyatt, D. Ikeda, P. A. Jacobi, K. S. Kim, Y. Kobuke, K. Kojima, K. Krowicki, V. J. Lee, T. Leutert, S. Malchenko, J. Martens, R. S. Matthews, B. S. Ong, J. B. Press, T. V. RajanBabu, G. Rousseau, H. M. Sauter, M. Suzuki, K. Tatsuta, L. M. Tolbert, E. A. Truesdale, I. Uchida, Y. Ueda, T. Ueyhara, A. T. Vasella, W. C. Vladuchick, P. A. Wade, R. M. Williams, H. N.-C. Wong, *J. Am. Chem. Soc.* **1981**, *103*, 3210–3213. We thank Prof. T. V. RajanBabu for drawing our attention to this work.
- [28] See, for example: C. Pidathala, L. Hoang, N. Vignola, B. List, *Angew. Chem.* **2003**, *115*, 2891–2894; *Angew. Chem. Int. Ed.* **2003**, *42*, 2785–2788.
- [29] a) A. Córdova, W. Notz, C. F. Barbas III, *Chem. Commun.* **2002**, 3024–3025; b) Y.-Y. Peng, Q.-P. Ding, Z. Li, P. G. Wang, J.-P. Cheng, *Tetrahedron Lett.* **2003**, *44*, 3871–3875; for a PEG-supported catalyst, see: c) M. Benaglia, M. Cinquini, F. Cozzi, A. Puglisi, G. Celentano, *Adv. Synth. Catal.* **2002**, *344*, 533–542; d) M. Benaglia, G. Celentano, F. Cozzi, *Adv. Synth. Catal.* **2001**, *343*, 171–173.
- [30] a) T.-P. Loh, L.-C. Feng, H.-Y. Yang, J.-Y. Yang, *Tetrahedron Lett.* **2002**, *43*, 8741–8743; b) P. Kotrusz, I. Kmentová, B. Gotov, S. Toma, E. Solcániová, *Chem. Commun.* **2002**, 2510–2511. c) For a temperature-dependent dynamic solvent effect, see: G. Cainelli, P. Galetti, D. Giacomini, A. Gualandi, A. Quintavalla, *Helv. Chim. Acta* **2003**, *86*, 3548–3559.
- [31] a) Y. Sekiguchi, A. Sasaoka, A. Shimomoto, S. Fujioka, H. Kotsuki, *Synlett* **2003**, 1655–1658; see also: b) Y. Hayashi, W. Tsuboi, M. Shoji, N. Suzuki, *J. Am. Chem. Soc.* **2003**, *125*, 11208–11209.
- [32] a) Q. Pan, B. Zou, Y. Wang, D. Ma, *Org. Lett.* **2004**, *6*, 1009–1012; see also: b) Z. Tang, F. Jiang, L.-T. Yu, X. Cui, L.-Z. Gong, A.-Q. Mi, Y.-Z. Jiang, Y.-D. Wu, *J. Am. Chem. Soc.* **2003**, *125*, 5262–5263; c) Gy. Szöllösi, G. London, L. Balásipiri, Cs. Somlai, M. Bartók, *Chirality* **2003**, *15*, S90–S96; d) H. Torii, M. Nakadaï, K. Ishihara, S. Saito, H. Yamamoto, *Angew. Chem.* **2004**, *116*, 2017–2020; *Angew. Chem. Int. Ed.* **2004**, *43*, 1983–1986; e) T. D. Dickerson, K. D. Janda, *J. Am. Chem. Soc.* **2002**, *124*, 3220–3221; f) Y.-Y. Peng, Q.-P. Ding, Z. Li, P. G. Wang, J.-P. Cheng, *Tetrahedron Lett.* **2003**, *44*, 3871–3875; g) S. P. Mathew, H. Iwamura, D. G. Blackmond, *Angew. Chem.* **2004**, *116*, 3379–3383; *Angew. Chem. Int. Ed.* **2004**, *43*, 3317–3321.
- [33] a) A. Córdova, W. Notz, C. F. Barbas III, *J. Org. Chem.* **2002**, *67*, 301–303; b) N. S. Chowdari, D. B. Ramachary, A. Córdova, C. F. Barbas III, *Tetrahedron Lett.* **2002**, *43*, 9591–9595; c) A. E. Asato, C. Watanabe, X.-Y. Li, R. S. H. Liu, *Tetrahedron Lett.* **1992**, *33*, 3105–3108.
- [34] a) W. Notz, K. Sakthivel, T. Bui, G. Zhong, C. F. Barbas III, *Tetrahedron Lett.* **2001**, *42*, 199–201; b) A. Córdova, W. Notz, G. Zhong, J. M. Betancort, C. F. Barbas III, *J. Am. Chem. Soc.* **2002**, *124*, 1842–1843; c) A. Córdova, S.-i. Watanabe, F. Tanaka, W. Notz, C. F. Barbas III, *J. Am. Chem. Soc.* **2002**, *124*, 1866–1867; see also: d) N. Mase, F. Tanaka, C. F. Barbas III, *Org. Lett.* **2004**, *5*, 4369–4372; e) N. Mase, F. Tanaka, C. F. Barbas III, *Angew. Chem.* **2004**, *116*, 2474–2477; *Angew. Chem. Int. Ed.* **2004**, *43*, 2420–2423; f) R. Thayumanavan, F. Tanaka, C. F. Barbas III, *Org. Lett.* **2004**, *6*, ASAP, DOI: 10.1021/ol0485417..
- [35] A. Northrup, D. W. C. MacMillan, *J. Am. Chem. Soc.* **2002**, *124*, 6798–6799.
- [36] A. Bøgevig, N. Kumaragurubaran, K. A. Jørgensen, *Chem. Commun.* **2002**, 620–621.

- [37] A. Bøgevig, T. B. Poulsen, W. Zhuang, K. A. Jørgensen, *Synlett* **2003**, 1915–1918.
- [38] G. S. Cortez, R. L. Tennyson, D. Romo, *J. Am. Chem. Soc.* **2001**, *123*, 7945–7946; G. S. Cortez, S. H. Oh, D. Romo, *Synthesis* **2001**, 1731–1736.
- [39] a) H. J. Martin, B. List, *Synlett* **2003**, 1901–1902; b) J. Kofoed, J. Nielsen, J.-L. Reymond, *Bioorg. Med. Chem. Lett.* **2003**, *13*, 2445–2447.
- [40] A. Córdova, *Acc. Chem. Res.* **2004**, *37*, 102–112.
- [41] a) B. List, *J. Am. Chem. Soc.* **2000**, *122*, 9336–9337; b) B. List, P. Pojarliev, W. T. Biller, H. J. Martin, *J. Am. Chem. Soc.* **2002**, *124*, 827–833.
- [42] a) A. Córdova, *Synlett* **2003**, 1651–1654; b) A. Córdova, *Chem. Eur. J.* **2004**, ASAP.
- [43] Y. Hayashi, W. Tsuboi, I. Ashimine, T. Uroshima, M. Shoji, K. Sakai, *Angew. Chem.* **2003**, *115*, 3805–3808; *Angew. Chem. Int. Ed.* **2003**, *42*, 3677–3680.
- [44] a) W. Notz, F. Tanaka, S.-i. Watanabe, N. S. Chowdari, J. M. Turner, R. Thayumanavan, C. F. Barbas III, *J. Org. Chem.* **2003**, *68*, 9624–9634; see also: b) N. S. Chowdari, J. T. Suri, C. F. Barbas III, *Org. Lett.* **2004**, *6*, 2507–2510; c) W. Zhuang, S. Saaby, K. A. Jørgensen, *Angew. Chem.* **2004**, *116*, 4576–4578; *Angew. Chem. Int. Ed.* **2004**, *43*, 4476–4478.
- [45] T. Itoh, M. Yokoya, K. Miyauchi, K. Nagata, A. Ohsawa, *Org. Lett.* **2003**, *5*, 4301–4304.
- [46] A. Córdova, C. F. Barbas III, *Tetrahedron Lett.* **2002**, *43*, 7749–7752.
- [47] W. Notz, F. Tanaka, S.-i. Watanabe, N. S. Chowdari, J. M. Turner, R. Thayumanavan, C. F. Barbas III, *J. Org. Chem.* **2003**, *68*, 9624–9634.
- [48] N. S. Chowdari, D. B. Ramachary, C. F. Barbas III, *Synlett* **2003**, 1906–1909.
- [49] Y. R. Jorapur, *Synlett* **2004**, 746–747.
- [50] S.-i. Watanabe, A. Córdova, F. Tanaka, C. F. Barbas III, *Org. Lett.* **2002**, *4*, 4519–4522.
- [51] A. Córdova, C. F. Barbas III, *Tetrahedron Lett.* **2003**, *44*, 1923–1926.
- [52] B. List, C. Castello, *Synlett* **2001**, 1687–1689.
- [53] P. Pojarliev, W. T. Biller, H. J. Martin, B. List, *Synlett* **2003**, 1903–1905.
- [54] For a recent Review, see: R. O. Duthaler, *Angew. Chem.* **2003**, *115*, 1005–1008; *Angew. Chem. Int. Ed.* **2003**, *42*, 975–978.
- [55] a) B. List, *J. Am. Chem. Soc.* **2002**, *124*, 5656–5657; b) A. Bøgevig, K. Juhl, N. Kumaragurubaran, W. Zhuang, K. A. Jørgensen, *Angew. Chem.* **2002**, *114*, 1868–1871; *Angew. Chem. Int. Ed.* **2002**, *41*, 1790–1793; c) N. Kumaragurubaran, K. Juhl, W. Zhuang, A. Bøgevig, K. A. Jørgensen, *J. Am. Chem. Soc.* **2002**, *124*, 6254–6255; see also: d) H. Iwamura, S. P. Mathew, D. G. Blackmond, *J. Am. Chem. Soc.* **2004**, *126*, ASAP, DOI: 10.1021/ja046258x; for a Review, see: e) P. Merino, T. Tèjero, *Angew. Chem.* **2004**, *116*, 3055–3058; *Angew. Chem. Int. Ed.* **2004**, *43*, 2995–2997.
- [56] H. Vogt, S. Vanderheiden, S. Bräse, *Chem. Commun.* **2003**, 2448–2449.
- [57] a) G. Zhong, *Angew. Chem.* **2003**, *115*, 4379–4382; *Angew. Chem. Int. Ed.* **2003**, *42*, 4247–4250; b) Y. Hayashi, J. Yamaguchi, K. Hibino, M. Shoji, *Tetrahedron Lett.* **2003**, *44*, 8293–8296; c) S. P. Brown, M. P. Brochu, C. J. Sinz, D. W. C. Mac-Millan, *J. Am. Chem. Soc.* **2003**, *125*, 10808–10809.
- [58] a) H. Momiyama, H. Yamamoto, *Org. Lett.* **2002**, *4*, 3579–3582; b) N. Momiyama, H. Yamamoto, *J. Am. Chem. Soc.* **2004**, *126*, 6498.
- [59] G. Zhong, *Chem. Commun.* **2004**, 606–607.
- [60] A. Bøgevig, H. Sunden, A. Córdova, *Angew. Chem.* **2004**, *116*, 1129–1132; *Angew. Chem. Int. Ed.* **2004**, *43*, 1109–1112.
- [61] Y. Hayashi, J. Yamaguchi, T. Sumiya, M. Shoji, *Angew. Chem.* **2004**, *116*, 1132–1135; *Angew. Chem. Int. Ed.* **2004**, *43*, 1112–1115.
- [62] For reviews, see: a) O. M. Berner, L. Tedeschi, D. Enders, *Eur. J. Org. Chem.* **2002**, 1877–1894; b) N. Krause, A. Hoffmann-Röder, *Synthesis* **2001**, 171–196; c) M. P. Sibi, S. Manyem, *Tetrahedron* **2000**, *56*, 8033–8061.
- [63] For related metal-complex-catalyzed asymmetric conjugate additions, see, for example: a) C. A. Luchaco-Cullis, A. H. Hoveyda, *J. Am. Chem. Soc.* **2002**, *124*, 8192–8193; b) T. Hayashi, *Synlett* **2001**, 879–887; c) A. Duursma, A. J. Minnaard, B. L. Feringa, *Tetrahedron* **2002**, *58*, 5773–5778; d) A. Alexakis, C. Benhaim, S. Rosset, M. Humam, *J. Am. Chem. Soc.* **2002**, *124*, 5262–5263; e) A. Rimkus, N. Sewald, *Org. Lett.* **2003**, *5*, 79–80; f) D. M. Barnes, J. Ji, M. G. Fickes, M. A. Fitzgerald, S. A. King, H. E. Morton, F. A. Plagge, M. Preskill, S. H. Wagaw, S. J. Wittenberger, J. Zhang, *J. Am. Chem. Soc.* **2002**, *124*, 13097–13105.
- [64] a) O. Andrey, A. Alexakis, G. Bernardinelli, *Org. Lett.* **2003**, *5*, 2559–2561; b) D. Enders, A. Seki, *Synlett* **2002**, 26–28; c) B. List, P. Pojarliev, H. J. Martin, *Org. Lett.* **2001**, *3*, 2423–2425; d) K. Sakthivel, W. Notz, T. Bui, C. F. Barbas III, *J. Am. Chem. Soc.* **2001**, *123*, 5260–5267; for intramolecular addition, see: e) M. T. Hechavarria Fronseca, B. List, *Angew. Chem.* **2004**, *116*, 4048–4050; *Angew. Chem. Int. Ed.* **2004**, *43*, 3958–3960.
- [65] a) J. M. Betancort, K. Sakthivel, R. Thayumanavan, C. F. Barbas III, *Tetrahedron Lett.* **2001**, *42*, 4441–4444; b) J. M. Betancort, C. F. Barbas III, *Org. Lett.* **2001**, *3*, 3737–3740; see also: c) T. Ishii, S. Fujioka, Y. Sekiguchi, H. Kotsuki, *J. Am. Chem. Soc.* **2004**, *126*, 9558–9559; d) N. Mase, R. Thayumanavan, F. Tanaka, C. F. Barbas III, *Org. Lett.* **2004**, *6*, 2527–2530.
- [66] a) A. Alexakis, O. Andrey, *Org. Lett.* **2002**, *4*, 3611–3614; b) D. Enders, A. Seki, *Synlett* **2002**, 26–28; c) O. Andrey, A. Alexakis, G. Bernardinelli, *Org. Lett.* **2003**, *5*, 2559–2561.
- [67] N. Halland, P. S. Aburel, K. A. Jørgensen, *Angew. Chem.* **2004**, *116*, 1292–1297; *Angew. Chem. Int. Ed.* **2004**, *43*, 1272–1277.
- [68] N. Vignola, B. List, *J. Am. Chem. Soc.* **2003**, *125*, 450–451.
- [69] K. Juhl, K. A. Jørgensen, *Angew. Chem.* **2003**, *115*, 1536–1539; *Angew. Chem. Int. Ed.* **2003**, *42*, 1498–1501.
- [70] R. Thayumanavan, B. Dhevalapally, K. Sakthivel, F. Tanaka, C. F. Barbas III, *Tetrahedron Lett.* **2002**, *43*, 3817–3820.
- [71] D. B. Ramchary, N. S. Chowdari, C. F. Barbas III, *Angew. Chem.* **2003**, *115*, 4365–4369; *Angew. Chem. Int. Ed.* **2003**, *42*, 4233–4237.
- [72] A. M. Hafez, A. E. Taggi, H. Wack, J. Esterbrook, T. Lectka, *Org. Lett.* **2001**, *3*, 2049–2051.
- [73] A. E. Taggi, H. Wack, A. M. Hafez, S. France, T. Lectka, *Org. Lett.* **2002**, *4*, 627–629.
- [74] M. H. Shah, S. France, T. Lectka, *Synlett* **2003**, 1937–1939.
- [75] a) A. M. Hafez, A. E. Taggi, T. Lectka, *Chem. Eur. J.* **2002**, *8*, 4114–4119; b) A. M. Hafez, A. E. Taggi, T. Dudding, T. Lectka, *J. Am. Chem. Soc.* **2001**, *123*, 10853–10859; c) H. Wack, A. E. Taggi, A. M. Hafez, J. J. Drury III, T. Lectka, *J. Am. Chem. Soc.* **2001**, *123*, 1531–1532.
- [76] For a review on asymmetric reactions with ketenes, see: R. K. Orr, M. A. Calter, *Tetrahedron* **2003**, *59*, 3545–3565.
- [77] a) M. A. Calter, W. Liao, *J. Am. Chem. Soc.* **2002**, *124*, 13127–13129; b) M. A. Calter, R. K. Orr, W. Song, *Org. Lett.* **2003**, *5*, 4745–4748.
- [78] a) A. E. Taggi, A. M. Hafez, T. Dudding, T. Lectka, *Tetrahedron* **2002**, *58*, 8351–8356; b) T. Dudding, A. M. Hafez, A. E. Taggi, T. R. Wagerle, T. Lectka, *Org. Lett.* **2002**, *4*, 387–390; c) A. E. Taggi, A. M. Hafez, H. Wack, B. Young, D. Ferraris, T. Lectka, *J. Am. Chem. Soc.* **2002**, *124*, 6626–6635; d) A. M. Hafez, A. E. Taggi, T. Dudding, T. Lectka, *J. Am. Chem. Soc.* **2001**, *123*, 10853–10859; e) H. Wack, S. France, A. M. Hafez, W. J. Drury III, A. Weatherwax, T. Lectka, *J. Org. Chem.* **2004**,

- 69, 4531–4533; for a review, see: f) S. France, A. E. Taggi, T. Lectka, *Acc. Chem. Res.* **2004**, *37*, 592–600.
- [79] a) A. E. Taggi, A. M. Hafez, T. Lectka, *Acc. Chem. Res.* **2003**, *36*, 10–19; b) A. M. Hafez, T. Dudding, T. R. Wagerle, M. H. Shah, A. E. Taggi, T. Lectka, *J. Org. Chem.* **2003**, *68*, 5819–5825.
- [80] For recent reviews, see: a) D. Basavaiah, A. J. Rao, *Chem. Rev.* **2003**, *103*, 811–891; b) P. Langer, *Angew. Chem.* **2000**, *112*, 3177–3180; *Angew. Chem. Int. Ed.* **2000**, *39*, 3049–3052.
- [81] a) K. Morita, Z. Suzuki, H. Hirose, *Bull. Chem. Soc. Jpn.* **1968**, *41*, 2815; b) A. B. Baylis, M. E. D. Hillman, German Patent 2155113, **1972**; A. B. Baylis, M. E. D. Hillman, US-A 3743669, **1972**; [*Chem. Abstr.* **1972**, *77*, 34174q].
- [82] L. M. Walsh, C. L. Winn, J. M. Goodman, *Tetrahedron Lett.* **2002**, *43*, 8219–8222.
- [83] V. K. Aggarwal, I. Emme, S. Y. Fulford, *J. Org. Chem.* **2003**, *68*, 692–700.
- [84] a) M. Shi, J.-K. Jiang, *Tetrahedron: Asymmetry* **2002**, *13*, 1941–1947; b) M. Shi, J.-K. Jiang, C.-Q. Li, *Tetrahedron Lett.* **2002**, *43*, 127–130.
- [85] J. E. Imbriglio, M. M. Vasbinder, S. J. Miller, *Org. Lett.* **2003**, *5*, 3741–3743.
- [86] N. T. McDougal, S. E. Schaus, *J. Am. Chem. Soc.* **2003**, *125*, 12094–12095.
- [87] Y. Iwabuchi, M. Furukawa, T. Esumi, S. Hatakeyama, *Chem. Commun.* **2001**, 2030–2031.
- [88] Y. Iwabuchi, M. Sugihara, T. Esumi, S. Hatakeyama, *Tetrahedron Lett.* **2001**, *42*, 7867–7871.
- [89] a) S. Kawahara, A. Nakano, T. Esumi, Y. Iwabuchi, S. Hatakeyama, *Org. Lett.* **2003**, *5*, 3103–3105; b) D. Balan, H. Adolfsson, *Tetrahedron Lett.* **2003**, *44*, 2521–2524; c) M. Shi, Y.-M. Xu, *Angew. Chem.* **2002**, *114*, 4689–4692; *Angew. Chem. Int. Ed.* **2002**, *41*, 4507–4510.
- [90] J. S. Johnson, *Angew. Chem.* **2004**, *116*, 1348–1350; *Angew. Chem. Int. Ed.* **2004**, *43*, 1326–1328.
- [91] D. Enders, U. Kallfass, *Angew. Chem.* **2002**, *114*, 1822–1824; *Angew. Chem. Int. Ed.* **2002**, *41*, 1743–1745.
- [92] Y. Tachibana, N. Kihara, T. Takata, *J. Am. Chem. Soc.* **2004**, *126*, 3438–3439.
- [93] a) M. S. Kerr, J. R. de Alaniz, T. Rovis, *J. Am. Chem. Soc.* **2002**, *124*, 10298–10299; b) M. S. Kerr, T. Rovis, *J. Am. Chem. Soc.* **2004**, *126*, 8876–8877.
- [94] A. Solladié-Cavallo, M. Roje, T. Isarno, V. Sunjic, V. Vinkovic, *Eur. J. Org. Chem.* **2000**, 1077–1080, and references therein; for a theoretical study on asymmetric sulfur-ylide epoxidation, see: b) M. A. Silva, B. R. Bellenie, J. M. Goodman, *Org. Lett.* **2004**, *6*, 2559–2562.
- [95] V. K. Aggarwal, J. Richardson, *Chem. Commun.* **2003**, 2644–2651.
- [96] J. Zanardi, C. Leriverend, D. Aubert, K. Julienne, P. Metzner, *J. Org. Chem.* **2001**, *66*, 5620–5623.
- [97] M. Ishizaki, O. Hoshino, *Heterocycles* **2002**, *57*, 1399–1402.
- [98] V. K. Aggarwal, J. N. Harvey, J. Richardson, *J. Am. Chem. Soc.* **2002**, *124*, 5747–5756.
- [99] V. K. Aggarwal, M. Ferrara, C. J. O'Brien, A. Thompson, R. V. H. Jones, R. Fieldhouse, *J. Chem. Soc. Perkin Trans. 1* **2001**, 1635–1643.
- [100] T. Saito, M. Sakairi, D. Akiba, *Tetrahedron Lett.* **2001**, *42*, 5451–5454.
- [101] V. K. Aggarwal, E. Alonso, G. Fang, M. Ferrara, G. Hynd, M. Porcelloni, *Angew. Chem.* **2001**, *113*, 1482–1485; *Angew. Chem. Int. Ed.* **2001**, *40*, 1433–1436.
- [102] V. K. Aggarwal, J.-L. Vasse, *Org. Lett.* **2003**, *5*, 3987–3990.
- [103] a) C. D. Papageorgiou, S. V. Ley, M. J. Gaunt, *Angew. Chem.* **2003**, *115*, 852–855; *Angew. Chem. Int. Ed.* **2003**, *42*, 828–831; b) N. Bremeyer, S. C. Smith, S. V. Ley, M. J. Gaunt, *Angew. Chem.* **2004**, *116*, 2735–2738; *Angew. Chem. Int. Ed.* **2004**, *43*, 2681–2684; see also: c) C. D. Papageorgiou, M. A. Cubillo de Dios, S. V. Ley, M. J. Gaunt, *Angew. Chem.* **2004**, *116*, 4741–4744; *Angew. Chem. Int. Ed.* **2004**, *43*, 4641–4644.
- [104] a) For a review of asymmetric acyl-transfer reactions, see: A. C. Spivey, A. Maddaford, A. Redgrave, *Org. Prep. Proced. Int.* **2000**, *32*, 3131–3134.
- [105] B. M. Trost, T. Mino, *J. Am. Chem. Soc.* **2003**, *125*, 2410–2411.
- [106] a) J. Hang, H. Li, L. Deng, *Org. Lett.* **2002**, *4*, 3321–3324; b) L. Tang, L. Deng, *J. Am. Chem. Soc.* **2002**, *124*, 2870–2871; c) J. Hang, S.-K. Tian, L. Tang, L. Deng, *J. Am. Chem. Soc.* **2001**, *123*, 12696–12697; d) Y. Chen, L. Deng, *J. Am. Chem. Soc.* **2001**, *123*, 11302–11303; e) Y. Chen, S.-K. Tian, L. Deng, *J. Am. Chem. Soc.* **2000**, *122*, 9542–9543.
- [107] C. Choi, S.-K. Tian, L. Deng, *Synthesis* **2001**, 1737–1741.
- [108] S. Mizuta, M. Sadamori, T. Fujimoto, I. Yamamoto, *Angew. Chem.* **2003**, *115*, 3505–3507; *Angew. Chem. Int. Ed.* **2003**, *42*, 3383–3385.
- [109] For a review on DMAP catalysts, see: R. Murugan, E. F. V. Scriven, *Aldrichimica Acta* **2003**, *36*, 21–27.
- [110] a) A. C. Spivey, F. Zhu, M. B. Mitchell, S. G. Davey, R. L. Jarvest, *J. Org. Chem.* **2003**, *68*, 7379–7385; b) C. Malardier-Jugroot, A. C. Spivey, M. A. Whitehead, *J. Mol. Struct.* **2003**, *623*, 263–276; c) A. C. Spivey, P. Charbonneau, T. Fekner, D. H. Hochmuth, A. Maddaford, C. Malardier-Jugroot, A. J. Redgrave, M. A. Whitehead, *J. Org. Chem.* **2001**, *66*, 7394–7401; d) A. C. Spivey, A. Maddaford, D. Leese, A. J. Redgrave, *J. Chem. Soc. Perkin Trans. 1* **2001**, 1785–1794.
- [111] K.-S. Jeung, S.-H. Kim, H.-J. Park, K.-J. Chang, K. S. Kim, *Chem. Lett.* **2002**, 1114–1115.
- [112] a) A. Córdova, M. R. Tremblay, B. Clapham, K. D. Janda, *J. Org. Chem.* **2001**, *66*, 5645–5648; b) B. Clapham, C.-W. Cho, K. D. Janda, *J. Org. Chem.* **2001**, *66*, 868–873.
- [113] a) G. Priem, B. Pelotier, S. J. F. Macdonald, M. S. Anson, I. B. Campbell, *J. Org. Chem.* **2003**, *68*, 3844–3848; b) G. Priem, B. Pelotier, I. B. Campbell, S. J. F. Macdonald, M. S. Anson, *Synlett* **2003**, 679–683; c) G. Priem, M. S. Anson, S. J. F. Macdonald, B. Pelotier, I. B. Campbell, *Tetrahedron Lett.* **2002**, *43*, 6001–6003.
- [114] a) T. Kawabata, R. Stragies, T. Fukaya, Y. Nagaoka, H. Schedel, K. Fuji, *Tetrahedron Lett.* **2003**, *44*, 1545–1548; b) T. Kawabata, R. Stragies, T. Fukaya, K. Fuji, *Chirality* **2003**, *15*, 71–76; c) T. Kawabata, K. Yamamoto, Y. Momose, H. Yoshida, Y. Nagaoka, K. Fuji, *Chem. Commun.* **2001**, 2700–2701.
- [115] S. A. Shaw, P. Aleman, E. Vedejs, *J. Am. Chem. Soc.* **2003**, *125*, 13368–13369.
- [116] a) N. Papaioannou, J. T. Blank, S. J. Miller, *J. Org. Chem.* **2003**, *68*, 2728–2734; b) B. R. Sculimbrene, A. J. Morgan, S. J. Miller, *J. Am. Chem. Soc.* **2002**, *124*, 11653–11656; c) E. R. Jarvo, S. J. Miller, *Tetrahedron* **2002**, *58*, 2481–2495; d) B. R. Sculimbrene, S. J. Miller, *J. Am. Chem. Soc.* **2001**, *123*, 10125–10126; e) M. M. Vasbinder, E. R. Jarvo, S. J. Miller, *Angew. Chem.* **2001**, *113*, 2824–2827; *Angew. Chem. Int. Ed.* **2001**, *40*, 2824–2827; f) N. Papaioannou, C. A. Evans, J. T. Blank, S. J. Miller, *Org. Lett.* **2001**, *3*, 2879–2882; g) E. R. Jarvo, C. A. Evans, G. T. Copeland, S. J. Miller, *J. Org. Chem.* **2001**, *66*, 5522–5527; h) G. T. Copeland, S. J. Miller, *J. Am. Chem. Soc.* **2001**, *123*, 6496–6502; i) M. B. Fierman, D. J. O'Leary, W. E. Steinmetz, S. J. Miller, *J. Am. Chem. Soc.* **2004**, *126*, 6967–6971.
- [117] For recent reviews, see: a) E. Vedejs, O. Daugulis, J. A. MacKay, E. Rozners, *Synlett* **2001**, 4166–4205; b) O. Molt, T. Schrader, *Synthesis* **2002**, 2633–2670; c) D. H. Valentine, Jr., J. H. Hillhouse, *Synthesis* **2003**, 2437–2460; d) D. H. Valentine, Jr., J. H. Hillhouse, *Synthesis* **2003**, 317–334.
- [118] a) E. Vedejs, O. Daugulis, J. A. MacKay, E. Rozners, *Synlett* **2001**, 1499–1505; c) For a three-phase system, see: E. Vedejs, E. Rozners, *J. Am. Chem. Soc.* **2001**, *123*, 2428–2429;

- d) E. Vedejs, J. A. MacKay, *Org. Lett.* **2001**, 3, 535–536; e) E. Vedejs, O. Daugulis, L. A. Harper, J. A. MacKay, D. R. Powell, *J. Org. Chem.* **2003**, 68, 5020–5027; f) E. Vedejs, O. Daugulis, N. Tuttle, *J. Org. Chem.* **2004**, 69, 1389–1392.
- [119] For a review, see: B. R. Sculimbrene, A. J. Morgan, S. J. Miller, *Chem. Commun.* **2003**, 1781–1785.
- [120] a) B. R. Sculimbrene, S. J. Miller, *J. Am. Chem. Soc.* **2001**, 123, 10125–10126; c) B. R. Sculimbrene, A. J. Morgan, S. J. Miller, *J. Am. Chem. Soc.* **2002**, 124, 11653–11656.
- [121] S.-K. Tian, L. Deng, *J. Am. Chem. Soc.* **2001**, 123, 6195–6196.
- [122] For reviews, see: a) S. E. Denmark, J. Fu, *Chem. Rev.* **2003**, 103, 2763–2794; b) S. E. Denmark, J. Fu, *Chem. Commun.* **2003**, 167–170.
- [123] a) V. Gutmann, *The Donor-Acceptor Approach to Molecular Interactions*, Plenum, New York, **1978**; b) W. B. Jensen, *The Lewis Acid-Base Concepts*, Wiley, New York, **1980**, Chap. 4, pp. 136–137.
- [124] A. Hosomi, *Acc. Chem. Res.* **1988**, 21, 200–206.
- [125] a) S. E. Denmark, T. Wynn, *J. Am. Chem. Soc.* **2001**, 123, 6199–6200; b) S. E. Denmark, T. Wynn, *J. Am. Chem. Soc.* **2002**, 124, 13405–13407.
- [126] J. Hellwig, T. Belser, J. F. K. Miller, *Tetrahedron Lett.* **2001**, 42, 5417–5419.
- [127] S. E. Denmark, J. Fu, *J. Am. Chem. Soc.* **2003**, 125, 2208–2216.
- [128] S. E. Denmark, J. Fu, *J. Am. Chem. Soc.* **2001**, 123, 9488–9489.
- [129] S. E. Denmark, J. Fu, *Org. Lett.* **2002**, 4, 1951–1953.
- [130] a) A. V. Malkov, M. Orsini, D. Pernazza, K. W. Muir, V. Langer, P. Meghani, P. Kočovský, *Org. Lett.* **2002**, 4, 1047–1049; b) A. V. Malkov, M. Bell, M. Orsini, D. Pernazza, A. Massa, P. Herrmann, P. Meghani, P. Kočovský, *J. Org. Chem.* **2003**, 68, 9659–9668.
- [131] A. V. Malkov, L. Dufkova, L. Farrugia, P. Kočovský, *Angew. Chem.* **2003**, 115, 3802–3805; *Angew. Chem. Int. Ed.* **2003**, 42, 3674–3677.
- [132] T. Shimada, A. Kina, S. Ikeda, T. Hayashi, *Org. Lett.* **2002**, 4, 2799–2801; b) T. Shimada, A. Kina, T. Hayashi, *J. Org. Chem.* **2003**, 68, 6329–6337.
- [133] See also: M. Nakajima, M. Saito, M. Uemura, S. Hashimoto, *Tetrahedron Lett.* **2002**, 43, 8827–8829, and references therein.
- [134] S. Kobayashi, C. Ogawa, H. Konishi, M. Sugiura, *J. Am. Chem. Soc.* **2003**, 125, 6610–6611.
- [135] For related allylation reactions, see: a) A. Massa, A. V. Malkov, P. Kočovský, A. Scettri, *Tetrahedron Lett.* **2003**, 44, 7179–7181; b) A. Massa, A. V. Malkov, P. Kočovský, A. Scettri, *Tetrahedron Lett.* **2003**, 44, 9067.
- [136] G. J. Rowlands, *Synlett* **2003**, 236–290.
- [137] G. J. Rowlands, W. K. Barnes, *Chem. Commun.* **2003**, 2712–2713.
- [138] S. E. Denmark, S. Ghosh, *Angew. Chem.* **2001**, 113, 4895–4898; *Angew. Chem. Int. Ed.* **2001**, 40, 4759–4762.
- [139] S. E. Denmark, S. M. Pham, *Org. Lett.* **2001**, 3, 2201–2204.
- [140] S. E. Denmark, S. Fujimori, *Org. Lett.* **2002**, 4, 3477–3480.
- [141] S. E. Denmark, S. Fujimori, *Org. Lett.* **2002**, 4, 3473–3476.
- [142] S. E. Denmark, J. R. Heemstra, *Org. Lett.* **2003**, 5, 2303–2306.
- [143] S. E. Denmark, Y. Fan, *J. Am. Chem. Soc.* **2002**, 124, 4233–4235.
- [144] a) B. Liu, X. Feng, F. Chen, G. Zhang, X. Chui, Y. Jiang, *Synlett* **2001**, 1551–1554; b) Z. Jiao, X. Feng, B. Liu, F. Chen, G. Zhang, Y. Jiang, *Eur. J. Org. Chem.* **2003**, 3818–3826.
- [145] S. Kobayashi, C. Ogawa, H. Konishi, M. Sugiura, *J. Am. Chem. Soc.* **2003**, 125, 6610–6611.
- [146] S. P. Brown, N. C. Goodwin, D. W. C. MacMillan, *J. Am. Chem. Soc.* **2003**, 125, 1192–1194.
- [147] a) N. A. Paras, D. W. C. MacMillan, *J. Am. Chem. Soc.* **2001**, 123, 4370–4371; b) J. F. Austin, D. W. C. MacMillan, *J. Am. Chem. Soc.* **2002**, 124, 1172–1173; c) N. A. Paras, D. W. C. MacMillan, *J. Am. Chem. Soc.* **2002**, 124, 7894–7895.
- [148] R. L. Pederson, I. M. Fellows, T. A. Ung, H. Ishihara, S. P. Hajela, *Adv. Synth. Catal.* **2002**, 344, 728–735.
- [149] N. Halland, P. S. Aburel, K. A. Jørgensen, *Angew. Chem.* **2003**, 115, 685–689; *Angew. Chem. Int. Ed.* **2003**, 42, 661–665.
- [150] N. Halland, R. G. Hazell, K. A. Jørgensen, *J. Org. Chem.* **2002**, 67, 8331–8338.
- [151] N. Halland, T. Hansen, K. A. Jørgensen, *Angew. Chem.* **2003**, 115, 5105–5107; *Angew. Chem. Int. Ed.* **2003**, 42, 4955–4957.
- [152] P. McDaid, Y. Chen, L. Deng, *Angew. Chem.* **2002**, 114, 348–350; *Angew. Chem. Int. Ed.* **2002**, 41, 338–340.
- [153] D. J. Guerin, S. J. Miller, *J. Am. Chem. Soc.* **2002**, 124, 2134–2136, and references therein.
- [154] T. E. Horstmann, D. J. Guerin, S. J. Miller, *Angew. Chem.* **2000**, 112, 3781–3784; *Angew. Chem. Int. Ed.* **2000**, 39, 3635–3638.
- [155] M. C. Kozłowski, M. Panda, *J. Org. Chem.* **2003**, 68, 2061–2076.
- [156] A. B. Northrup, D. W. C. MacMillan, *J. Am. Chem. Soc.* **2002**, 124, 2458–2460.
- [157] A literature summary on the MacMillan organocatalysts is provided at www.sigmaaldrich.com.
- [158] a) M. Benaglia, G. Celentano, M. Cinquini, A. Puglisi, F. Cozzi, *Adv. Synth. Catal.* **2002**, 344, 149–152; b) S. A. Selkälä, J. Tois, P. M. Pihko, A. M. P. Koskinen, *Adv. Synth. Catal.* **2002**, 344, 941–945.
- [159] S. Karlsson, H. E. Högberg, *Tetrahedron: Asymmetry*, **2002**, 13, 923–926.
- [160] M. Harmata, S. K. Ghosh, X. Hong, S. Wacharasindhu, P. Kirchhoefer, *J. Am. Chem. Soc.* **2003**, 125, 2058–2059.
- [161] For reviews, see: a) S. E. Denmark, Z. Wu, *Synlett* **1999**, 847–859; b) M. Frohn, Y. Shi, *Synthesis* **2000**, 1979–2000; c) Y. Shi, *Acc. Chem. Res.* **2004**, 37, 488–496; d) D. Yang, *Acc. Chem. Res.* **2004**, 37, 497–505.
- [162] For related organometallic systems, see: T. Nemoto, T. Ohshima, M. Shibasaki, *J. Am. Chem. Soc.* **2001**, 123, 9474–9475.
- [163] H. Tian, X. She, Y. Shi, *Org. Lett.* **2001**, 3, 715–718, and references therein.
- [164] X.-Y. Wu, X. She, Y. Shi, *J. Am. Chem. Soc.* **2002**, 124, 8792–8793.
- [165] L. Shu, P. Wang, Y. Gan, Y. Shi, *Org. Lett.* **2003**, 5, 293–296.
- [166] a) H. Tian, X. She, H. Yu, L. Shu, Y. Shi, *J. Org. Chem.* **2002**, 67, 2435–2446; b) H. Tian, X. She, J. Xu, Y. Shi, *Org. Lett.* **2001**, 3, 1929–1931.
- [167] a) A. Armstrong, W. O. Moss, J. R. Reeves, *Tetrahedron: Asymmetry* **2001**, 12, 2779–2781; b) A. Armstrong, G. Ahmed, B. Dominguez-Fernandez, B. R. Hayter, J. S. Wailes, *J. Org. Chem.* **2002**, 67, 8610–8617.
- [168] O. Bortolini, M. Fogagnolo, G. Fantin, S. Maietti, A. Medici, *Tetrahedron: Asymmetry* **2001**, 12, 1113–1115.
- [169] K. Matsumoto, K. Tomioka, *Tetrahedron Lett.* **2002**, 43, 631–633.
- [170] M. Seki, T. Furutani, R. Imashiro, T. Kuroda, T. Yamanaka, N. Harada, H. Arakawa, M. Kusama, T. Hashiyama, *Tetrahedron Lett.* **2001**, 42, 8201–8205.
- [171] S. E. Denmark, H. Matsuhashi, *J. Org. Chem.* **2002**, 67, 3479–3486.
- [172] C. J. Stearman, V. Behar, *Tetrahedron Lett.* **2002**, 43, 1943–1946.
- [173] a) P. C. Bulman Page, G. A. Rassias, D. Barros, D. Bethell, M. B. Schilling, *J. Chem. Soc. Perkin Trans. 1* **2000**, 3325–3334; b) P. C. Bulman Page, G. A. Rassias, D. Barros, A. Ardakani, B. Buckley, D. Bethell, T. A. D. Smith, M. Z. Slawin, *J. Org. Chem.* **2001**, 66, 6926–6931; c) P. C. Bulman Page, G. A. Rassias, D. Barros, A. Ardakani, D. Bethell, E. Merifield, *Synlett* **2002**, 4, 580–582; d) P. C. Bulman Page, D. Barros, B. R. Buckley, A. Ardakani, B. A. Marples, *J. Org. Chem.* **2004**, 69, 3595–3597; e) P. C. Bulman Page, B. R. Buckley, A. J. Blacker, *Org. Lett.* **2004**, 6, 1543–1546.

- [174] M.-K. Wong, L.-M. Ho, Y.-S. Zheng, C.-Y. Ho, D. Yang, *Org. Lett.* **2001**, 3, 2587–2590.
- [175] S.-i. Murahashi, S. Ono, Y. Imada, *Angew. Chem.* **2002**, 114, 2472–2474; *Angew. Chem. Int. Ed.* **2002**, 41, 2366–2368.
- [176] V. K. Aggarwal, C. Lopin, F. Sandrinelli, *J. Am. Chem. Soc.* **2003**, 125, 7596–7601.
- [177] For recent reviews, see: a) C. Lauret, S. M. Roberts, *Aldrichimica Acta* **2003**, 36, 47–51; b) S. Baars, K.-H. Drauz, H.-P. Krimmer, S. M. Roberts, J. Sander, J. Skidmore, G. Zanardi, *Org. Process Res. Dev.* **2003**, 7, 509–513; see also: c) P. A. Bentley, R. W. Flood, S. M. Roberts, J. Skidmore, C. B. Smith, J. A. Smith, *Chem. Commun.* **2001**, 1616–1617; d) P. E. Coffey, K.-H. Drauz, S. M. Roberts, J. Skidmore, J. A. Smith, *Chem. Commun.* **2001**, 2330–2331.
- [178] a) J. Eames, N. Weerasooriya, *Tetrahedron: Asymmetry* **2001**, 12, 1–24; for a related reaction, see also: b) Y. Hamashima, H. Somei, Y. Shimura, T. Tamura, M. Sodeoka, *Org. Lett.* **2004**, 6, 1861–1864.
- [179] For selected examples, see: a) O. Roy, M. Diekmann, A. Riahi, F. Hénin, J. Muzart, *Chem. Commun.* **2001**, 533–534; b) O. Roy, A. Riahi, F. Hénin, J. Muzart, *Eur. J. Org. Chem.* **2002**, 3986–3994; c) M. Baur, A. Riahi, F. Hénin, J. Muzart, *Tetrahedron: Asymmetry* **2003**, 14, 2755–2761; see also in: d) K. Nishimura, M. Ono, Y. Nagaoka, K. Tomioka, *Angew. Chem.* **2001**, 113, 454–456; *Angew. Chem. Int. Ed.* **2001**, 40, 440–442.
- [180] a) H. Brunner, P. Schmidt, *Eur. J. Org. Chem.* **2000**, 2119–2133; b) L. M.-A. Rogers, J. Rouden, L. Lecomte, M.-C. Lasne, *Tetrahedron Lett.* **2003**, 44, 3047–3050.
- [181] For recent reviews, see: a) J. Eames, *Eur. J. Org. Chem.* **2002**, 393–401; b) J.-C. Plaquevent, T. Perrard, D. Cahard, *Chem. Eur. J.* **2002**, 8, 3301–3307; c) T. Ishikawa, T. Isobe, *Chem. Eur. J.* **2002**, 8, 553–557.
- [182] T. Ishikawa, Y. Araki, T. Kumamoto, H. Seki, K. Fukuda, T. Isobe, *Chem. Commun.* **2001**, 245–246.
- [183] T. Okino, Y. Hoashi, Y. Takemoto, *J. Am. Chem. Soc.* **2003**, 125, 12672–12673.
- [184] T. Okino, S. Nakamura, T. Furukawa, Y. Takemoto, *Org. Lett.* **2004**, 6, 625–627.
- [185] B. M. Nugent, R. A. Yoder, J. N. Johnston, *J. Am. Chem. Soc.* **2004**, 126, 3418–3419.
- [186] Y. Huang, A. K. Unni, A. N. Thadani, V. H. Rawal, *Nature* **2003**, 424, 146.
- [187] For related thiourea-mediated reactions, see: a) T. Okino, Y. Hoashi, Y. Takemoto, *Tetrahedron Lett.* **2003**, 44, 2817–2821; b) P. R. Schreiner, A. Wittkopp, *Org. Lett.* **2002**, 4, 217–220; c) A. Wittkopp, P. R. Schreiner, *Chem. Eur. J.* **2003**, 9, 407–414; for a Review, see: d) C. Spino, *Angew. Chem.* **2004**, 116, 1796–1798; *Angew. Chem. Int. Ed.* **2004**, 43, 1764–1766.
- [188] a) A. G. Wenzel, E. N. Jacobsen, *J. Am. Chem. Soc.* **2002**, 124, 12964–12965; b) A. G. Wenzel, M. P. Lalonde, E. N. Jacobsen, *Synlett* **2003**, 1919–1922.
- [189] a) P. Vachal, E. N. Jacobsen, *J. Am. Chem. Soc.* **2002**, 124, 10012–10014; b) J. T. Su, P. Vachal, E. N. Jacobsen, *Adv. Synth. Catal.* **2001**, 343, 197–200; c) P. Vachal, E. N. Jacobsen, *Org. Lett.* **2000**, 2, 867–870.
- [190] G. Bluet, J.-M. Campagne, *J. Org. Chem.* **2001**, 66, 4293–4298.
- [191] T. Ooi, K. Doda, K. Maruoka, *J. Am. Chem. Soc.* **2003**, 125, 2054–2055.
- [192] S. Caron, Nga M. Do, P. Arpin, A. Larivée, *Synthesis* **2003**, 1693–1698.
- [193] See, for example: T. Bach, B. Grosch, T. Strassner, E. Herdtweck, *J. Org. Chem.* **2003**, 68, 1107–1116, and references therein.
- [194] D. F. Cauble, V. Lynch, M. J. Krische, *J. Org. Chem.* **2003**, 68, 15–21.
- [195] For recent reviews, see: a) K. Maruoka, T. Ooi, *Chem. Rev.* **2003**, 103, 3013–3028; b) C. Nájera, *Synlett* **2002**, 1388–1403; c) M. J. O'Donnell, *Aldrichimica Acta* **2001**, 34, 3–15; d) B. Lygo, B. I. Andrews, *Acc. Chem. Res.* **2004**, 37, 518–525; e) for related metal-containing phase-transfer systems, see: Y. N. Belokon, N. B. Bespalova, T. D. Churkina, I. Císařová, M. G. Ezernitskaya, S. R. Harutyunyan, R. Hrdina, H. B. Kagan, P. Kočovský, K. A. Kochetkov, O. V. Larionov, K. A. Lyssenko, M. North, M. Polášek, A. S. Peregodov, V. V. Prisyazhnyuk, Š. Vyskočil, *J. Am. Chem. Soc.* **2003**, 125, 12860–12871; f) see also: S. Vyskočil, L. Meca, I. Tišlerova, I. Císařová, M. Polášek, S. R. Harutyunyan, Y. N. Belokon, R. M. J. Stead, L. Farrugia, S. C. Lockhart, W. L. Mitchell, P. Kočovský, *Chem. Eur. J.* **2002**, 8, 4633–4648.
- [196] C. Hofstetter, P. S. Wilkinson, T. C. Pochapsky, *J. Org. Chem.* **1999**, 64, 8794–8800.
- [197] For recent studies on this topic, see: S.-s. Jew, M.-S. Yoo, B.-S. Jeong II, I. Y. Park, H.-g. Park, *Org. Lett.* **2002**, 4, 4245–4248.
- [198] See also: B. Lygo, B. I. Andrews, J. Crosby, J. A. Peterson, *Tetrahedron Lett.* **2002**, 43, 8015–8018.
- [199] a) B. Lygo, J. Crosby, J. A. Peterson, *Tetrahedron* **2001**, 57, 6447–6453; b) B. Lygo, L. D. Humphreys, *Tetrahedron Lett.* **2002**, 43, 6677–6679.
- [200] See also: L. Ducry, F. Diederich, *Helv. Chim. Acta* **1999**, 82, 981–1004.
- [201] a) D. Y. Kim, S. C. Huh, S. M. Kim, *Tetrahedron Lett.* **2001**, 42, 6299–6301; b) D. Y. Kim, S. C. Huh, *Tetrahedron* **2001**, 57, 8933–8938.
- [202] B. Lygo, B. Allbutt, *Synlett* **2004**, 326–328.
- [203] A. Armstrong, J. N. Scutt, *Org. Lett.* **2003**, 5, 2331–2334.
- [204] a) R. K. Boeckman, Jr., T. J. Clark, B. C. Shook, *Org. Lett.* **2002**, 4, 2109–2112; b) R. K. Boeckman Jr., T. J. Clark, B. C. Shook, *Helv. Chim. Acta* **2002**, 85, 4532–4560.
- [205] R. Lépine, A.-C. Carbonnelle, J. Zhu, *Synlett* **2003**, 1455–1458.
- [206] a) S.-s. Jew, B.-S. Jeong, M.-S. Yoo, H. Huh, H.-g. Park, *Chem. Commun.* **2001**, 1244–1245; b) H.-g. Park, B.-S. Jeong, M.-S. Yoo, J.-H. Lee, M.-k. Park, Y.-J. Lee, M.-J. Kim, S.-s. Jew, *Angew. Chem.* **2002**, 114, 3162–3164; *Angew. Chem. Int. Ed.* **2002**, 41, 3036–3038; c) H.-g. Park, B.-S. Jeong, M.-S. Yoo, J.-H. Lee, B.-s. Park, M.-J. Kim, S.-s. Jew, *Tetrahedron Lett.* **2003**, 44, 3497–3500.
- [207] H.-g. Park, B.-s. Jeong, M.-s. Yoo, M.-k. Park, H. Huh, S.-s. Jew, *Tetrahedron Lett.* **2001**, 42, 4645–4648.
- [208] S. Kim, J. Lee, T. Lee, H.-g. Park, D. Kim, *Org. Lett.* **2003**, 5, 2703–2706.
- [209] M. Masui, A. Ando, T. Shioiri, *Tetrahedron Lett.* **1988**, 29, 2835–2838.
- [210] D. Y. Kim, E. J. Park, *Org. Lett.* **2002**, 4, 545–547.
- [211] S. Arai, T. Shioiri, *Tetrahedron* **2002**, 58, 1407–1413.
- [212] M. Oku, S. Arai, K. Katayama, T. Shioiri, *Synlett* **2000**, 493–494.
- [213] T. Okino, Y. Takemoto, *Org. Lett.* **2001**, 3, 1515–1517.
- [214] H. Yu, H. Koshima, *Tetrahedron Lett.* **2003**, 44, 9209–9211.
- [215] a) T. Ooi, E. Tayama, K. Doda, M. Takeuchi, K. Maruoka, *Synlett* **2000**, 1500–1502; b) B. Török, K. Balazsik, K. Felföldi, M. Bartok, *Ultrason. Sonochem.* **2001**, 8, 191–200.
- [216] a) S. Arai, H. Tsuge, M. Oku, M. Miura, T. Shioiri, *Tetrahedron* **2002**, 58, 1623–1630.
- [217] D. Y. Kim, Y. J. Choi, H. Y. Park, C. U. Joung, K. O. Koh, J. Y. Mang, K.-Y. Jung, *Synth. Commun.* **2003**, 33, 435–443.
- [218] J. Ye, Y. Wang, R. Liu, G. Zhang, Q. Zhang, J. Chen, X. Liang, *Chem. Commun.* **2003**, 2714–2715.
- [219] B. Lygo, D. C. M. To, *Chem. Commun.* **2002**, 2360–2361.
- [220] a) W. Adam, P. B. Rao, H.-G. Degen, C. R. Saha-Möller, *Tetrahedron: Asymmetry* **2001**, 12, 121–125; b) W. Adam, P. B. Rao, H.-G. Degen, A. Levai, T. Patonay, C. R. Saha-Möller, *J. Org. Chem.* **2002**, 67, 259–264.

- [221] See, for example: N. Mase, T. Ohno, N. Hoshikawa, K. Ohishi, H. Morimoto, H. Yoda, K. Takabe, *Tetrahedron Lett.* **2003**, *44*, 4073–4075.
- [222] a) T. Ooi, M. Kameda, K. Maruoka, *J. Am. Chem. Soc.* **1999**, *121*, 6519–6520; b) T. Ooi, M. Takeuchi, M. Kameda, K. Maruoka, *J. Am. Chem. Soc.* **2000**, *122*, 5228–5229; c) T. Ooi, M. Taniguchi, M. Kameda, K. Maruoka, *Angew. Chem.* **2002**, *114*, 4724–4726; *Angew. Chem. Int. Ed.* **2002**, *41*, 4542–4544; d) T. Ooi, M. Takahashi, K. Doda, K. Maruoka, *J. Am. Chem. Soc.* **2002**, *124*, 7640–7641; e) T. Ooi, M. Kameda, K. Maruoka, *J. Am. Chem. Soc.* **2003**, *125*, 5139–5151; f) T. Ooi, D. Sakai, M. Takeuchi, E. Tayama, K. Maruoka, *Angew. Chem.* **2003**, *115*, 6048–6050; *Angew. Chem. Int. Ed.* **2003**, *42*, 5868–5870; g) T. Ooi, T. Miki, M. Taniguchi, M. Shiraishi, M. Takeuchi, K. Maruoka, *Angew. Chem.* **2003**, *115*, 4111–4113; *Angew. Chem. Int. Ed.* **2003**, *42*, 3796–3798.
- [223] a) K. Maruoka, *J. Fluorine Chem.* **2001**, *112*, 95–99; for a review, see: b) T. Ooi, K. Maruoka, *Acc. Chem. Res.* **2004**, *37*, 526–533.
- [224] a) T. Hashimoto, Y. Tanaka, K. Maruoka, *Tetrahedron: Asymmetry* **2003**, *14*, 1599–1602; b) T. Hashimoto, K. Maruoka, *Tetrahedron Lett.* **2003**, *44*, 3313–3316.
- [225] T. Ooi, E. Tayama, K. Maruoka, *Angew. Chem.* **2003**, *115*, 599–602; *Angew. Chem. Int. Ed.* **2003**, *42*, 579–582.
- [226] T. Ooi, Y. Uematsu, M. Kameda, K. Maruoka, *Angew. Chem.* **2002**, *114*, 1621–1624; *Angew. Chem. Int. Ed.* **2002**, *41*, 1551–1554.
- [227] T. Ooi, Y. Kubota, K. Maruoka, *Synlett* **2003**, 1931–1933.
- [228] B. Lygo, B. Allbutt, S. R. James, *Tetrahedron Lett.* **2003**, *44*, 5629–5632.
- [229] a) T. Shibuguchi, Y. Fukuta, Y. Akachi, A. Sekine, T. Ohshima, M. Shibasaki, *Tetrahedron Lett.* **2002**, *43*, 9539–9543.
- [230] T. Ohshima, V. Gnanadesikan, T. Shibuguchi, Y. Fukuta, T. Nemoto, M. Shibasaki, *J. Am. Chem. Soc.* **2003**, *125*, 11206–11207.
- [231] S. Arai, R. Tsuji, A. Nishida, *Tetrahedron Lett.* **2002**, *43*, 9535–9537.
- [232] T. Kita, A. Georgieva, Y. Hashimoto, T. Nakata, K. Nagasawa, *Angew. Chem.* **2002**, *114*, 2956–2958; *Angew. Chem. Int. Ed.* **2002**, *41*, 2832–2834.
- [233] a) S. E. Snyder, A. B. Shvets, W. H. Pirkle, *Helv. Chim. Acta* **2002**, *85*, 3605–3615; b) S. E. Snyder, W. H. Pirkle, *Org. Lett.* **2002**, *4*, 3283–3286; c) W. H. Pirkle, S. E. Snyder, *Org. Lett.* **2001**, *3*, 1821–1823.
- [234] a) M. Garcia-Viloca, J. Gao, M. Karplus, D. G. Truhlar, *Science* **2004**, *303*, 186–195; b) see also: S. J. Benkovic, S. Hammes-Schiffer, *Science* **2003**, *301*, 1196–1202.
- [235] For a recent review on cyclodextrins, see: E. Engeldinger, D. Armspach, D. Matt, *Chem. Rev.* **2003**, *103*, 4147–4174; for calixarenes, see: K. Goto, Y. Yano, E. Okada, C.-W. Liu, K. Yamamoto, R. Ueoka, *J. Org. Chem.* **2003**, *68*, 865–870, and references therein.
- [236] W.-K. Chan, W.-Y. Yu, C.-M. Che, M.-K. Wong, *J. Org. Chem.* **2003**, *68*, 6576–6582.
- [237] For recent results, see: a) R. Breslow, J. Yang, J. Yan, *Tetrahedron* **2002**, *58*, 653–659; b) J. Yang, B. Gabriele, S. Belvedere, Y. Huang, R. Breslow, *J. Org. Chem.* **2002**, *67*, 5057–5067, and references therein.
- [238] a) *Molecular and Ionic Recognition with Imprinted Polymers* (Eds.: R. A. Bartsch, M. Maeda), American Chemical Society, **1998**; b) *Molecularly Imprinted Polymers: Man-Made Mimics of Antibodies and their Application in Analytical Chemistry* (Ed.: B. Sellergren), Elsevier, Amsterdam, **2001**; c) *Molecularly Imprinted Materials—Sensors and Other Devices* (Eds.: K. J. Shea, M. Yan, M. J. Roberts, P. S. Cremer, R. M. Crooks), *Materials Res. Soc. Proc.* **2002**, *723*, *Materials Research Society*, **2002** (Symposia Held in San Francisco California, April 2–5, 2002); d) M. Komiyama, T. Takeuchi, T. Mukawa, H. Asanuma, *Molecular Imprinting: From Fundamentals to Applications*, Wiley-VCH, Weinheim, **2003**; e) M. Sibrian-Vazquez, D. A. Spivak, *J. Am. Chem. Soc.* **2004**, *126*, 7827–7833.
- [239] For recent reviews, see: a) C. Alexander, L. Davidson, W. Hayes, *Tetrahedron* **2003**, *59*, 2025–2056; b) G. Wulff, *Chem. Rev.* **2002**, *102*, 1–28; c) W. B. Motherwell, M. J. Bingham, *Tetrahedron* **2001**, *57*, 4663–4686; d) B. Clapham, T. S. Reger, K. D. Janda, *Tetrahedron* **2001**, *57*, 4637–4662.
- [240] a) S. Otto, R. L. E. Furlan, J. K. M. Sanders, *Curr. Opin. Chem. Biol.* **2002**, *6*, 321–327; b) R. L. E. Furlan, S. Otto, J. K. M. Sanders, *Proc. Natl. Acad. Sci. USA* **2002**, *99*, 4801–4804; c) S. Otto, R. L. E. Furlan, J. K. M. Sanders, *Science* **2002**, *297*, 590–593; d) S. Otto, R. L. E. Furlan, J. K. M. Sanders, *Drug Discovery Today* **2002**, *7*, 117–125; e) S. J. Rowan, S. J. Cantrill, G. R. L. Cousins, J. K. M. Sanders, J. F. Stoddart, *Angew. Chem.* **2002**, *114*, 938–993; *Angew. Chem. Int. Ed.* **2002**, *41*, 898–952; f) G. R. L. Cousins, S. A. Poulsen, J. K. M. Sanders, *Curr. Opin. Chem. Biol.* **2000**, *4*, 270–279.
- [241] See, for example: a) A. Biffis, G. Wulff, *New J. Chem.* **2001**, *25*, 1537–1540; b) J. M. Kim, K. D. Ahn, G. Wulff, *Macromol. Chem. Phys.* **2001**, *202*, 1105–1108; c) A. G. Strikovsky, D. Kasper, M. Grun, B. S. Green, J. Hradil, G. Wulff, *J. Am. Chem. Soc.* **2000**, *122*, 6295–6296, and references therein.
- [242] M. Emgenbroich, G. Wulff, *Chem. Eur. J.* **2003**, *9*, 4106–4117.
- [243] For some recent examples, see: a) J.-C. Wang, M. J. Krische, *Angew. Chem.* **2003**, *115*, 6035–6037; *Angew. Chem. Int. Ed.* **2003**, *42*, 5855–5857; b) A. L. Williams, J. N. Johnston, *J. Am. Chem. Soc.* **2003**, *125*, 1612–1613; c) W. Zhou, L. Liu, R. Breslow, *Helv. Chim. Acta* **2003**, *86*, 3560–3567; d) H. Kuroda, I. Tomita, T. Endo, *Org. Lett.* **2003**, *5*, 129–131; e) C. A. Evans, S. J. Miller, *J. Am. Chem. Soc.* **2003**, *125*, 12394–12395; f) X.-F. Zhu, J. Lan, O. Kwon, *J. Am. Chem. Soc.* **2003**, *125*, 4716–4717.
- [244] For the dynamic kinetic resolution of Morita–Baylis–Hillman acetates, see: C.-W. Cho, J.-R. Kong, M. J. Krische, *Org. Lett.* **2004**, *6*, 1337–1339.
- [245] For halogenation, see: a) M. P. Brochu, S. P. Brown, D. W. C. MacMillan, *J. Am. Chem. Soc.* **2004**, *126*, 4108–4109; b) M. Marigo, N. Kumaragurubaran, K. A. Jørgensen, *Eur. J. Org. Chem.* **2004**, 2133–2137; c) N. Halland, A. Brautun, S. Bachmann, M. Marigo, K. A. Jørgensen, *J. Am. Chem. Soc.* **2004**, *126*, 4790–4791.
- [246] For selenylation, see: W. Wang, J. Wang, H. Li, *Org. Lett.* **2004**, *6*, 2817–2820.
- [247] For aza-Friedel–Crafts alkylation, see: D. Uraguchi, K. Sorimachi, M. Terada, *J. Am. Chem. Soc.* **2004**, *126*, ASAP, DOI: 10.1021/ja046185h.
- [248] For a Mannich-type reaction catalyzed by a chiral Brønsted acid, see: T. Akiyama, J. Itoh, K. Yokota, K. Fuchibe, *Angew. Chem.* **2004**, *116*, 1592–1594; *Angew. Chem. Int. Ed.* **2004**, *43*, 1566–1568.
- [249] For the synthesis of sulfinate esters through dynamic resolution, see: J. W. Evans, M. B. Fierman, S. J. Miller, J. Ellman, *J. Am. Chem. Soc.* **2004**, *126*, 8134–8135.
- [250] For oxidation, see: A. Córdova, H. Sundén, M. Engqvist, I. Ibrahim, J. Casas, *J. Am. Chem. Soc.* **2004**, *126*, 8914–8915.
- [251] For the reduction of ketimines, see: a) A. V. Malkov, A. Mariani, K. N. MacDougall, P. Kočovský, *Org. Lett.* **2004**, *6*, 2253–2256; b) F. Iwasaki, O. Omonura, K. Mishima, T. Maki, Y. Matsumura, *Tetrahedron Lett.* **2001**, *42*, 2525–2528.

Communications



The synthesis of dendrimers containing up to six different functional groups by multistep one-pot reactions involving a selective manipulation and deprotection strategy is described by E. E. Simanek and M. B. Steffensen in their Communication on the following pages.

Dendrimer Synthesis

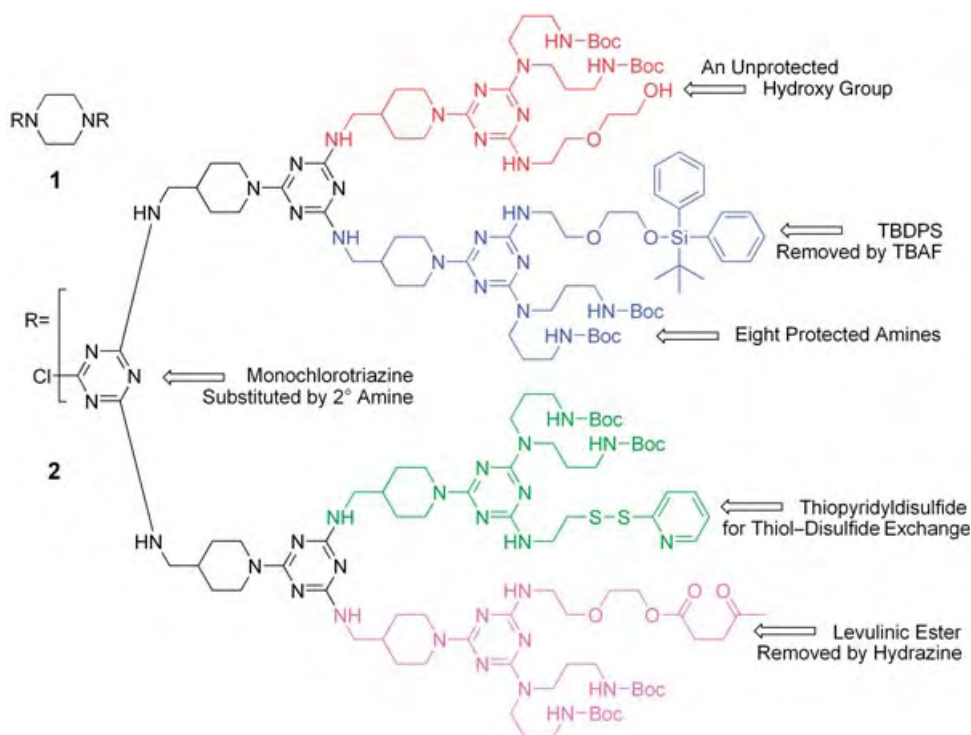
Synthesis and Manipulation of Orthogonally Protected Dendrimers: Building Blocks for Library Synthesis**

Mackay B. Steffensen and Eric E. Simanek*

Even when reduced to trivial manipulations, the synthesis of dendrimers still remains laborious^[1] with few exceptions—notably, one-pot syntheses.^[2] As applications are pursued for these architectures, the need to execute structure–property relationships only further increases the burden of synthesis. Not surprisingly, the number of reports of libraries of dendrimers are exceedingly few, and in many cases these libraries are the result of substoichiometric (with respect to the number of reactive surface groups) and statistical reactions at the periphery to yield cocktails of molecules as opposed to single-molecule chemical entities.^[3] We and others interested in these architectures have continued to pursue the preparations of versatile targets that are amenable to post-synthetic substoichiometric manipulation.^[4] In our hands, the targets reported here (**1** and **2**) are the building blocks of drug-delivery vehicles,^[5] while in other hands they may be the basis for novel materials such as poly(block) polymers or other novel materials.^[6] Here, we describe the synthesis of these molecules and their manipulation upon selective removal of protecting groups.

Dendrimers **1** and **2** have five and six groups for manipulation, respectively:^[7] the free hydroxy group(s) are readily acylated; the levulinic acid ester (Lev) can be unmasked using hydrazine;^[8] the *tert*-butyldiphenylsilyl

(TBDPS, $C_4H_9SiPh_2$) ether can be removed using tetrabutylammonium fluoride;^[9] the thiopyridyl group (PyrS) can participate in thiol–disulfide exchange reactions with free thiols or be removed with dithiothreitol and subsequently alkylated or acylated;^[10] the *tert*-butoxycarbonate groups (Boc: C_4H_9OCO) can be removed with trifluoroacetic acid or formic acid;^[11] and the monochlorotriazine of **2** can be treated with a variety of amine nucleophiles.^[12] Here, we describe the



synthesis of these targets and establish that selective deprotection and subsequent reaction can be effected.

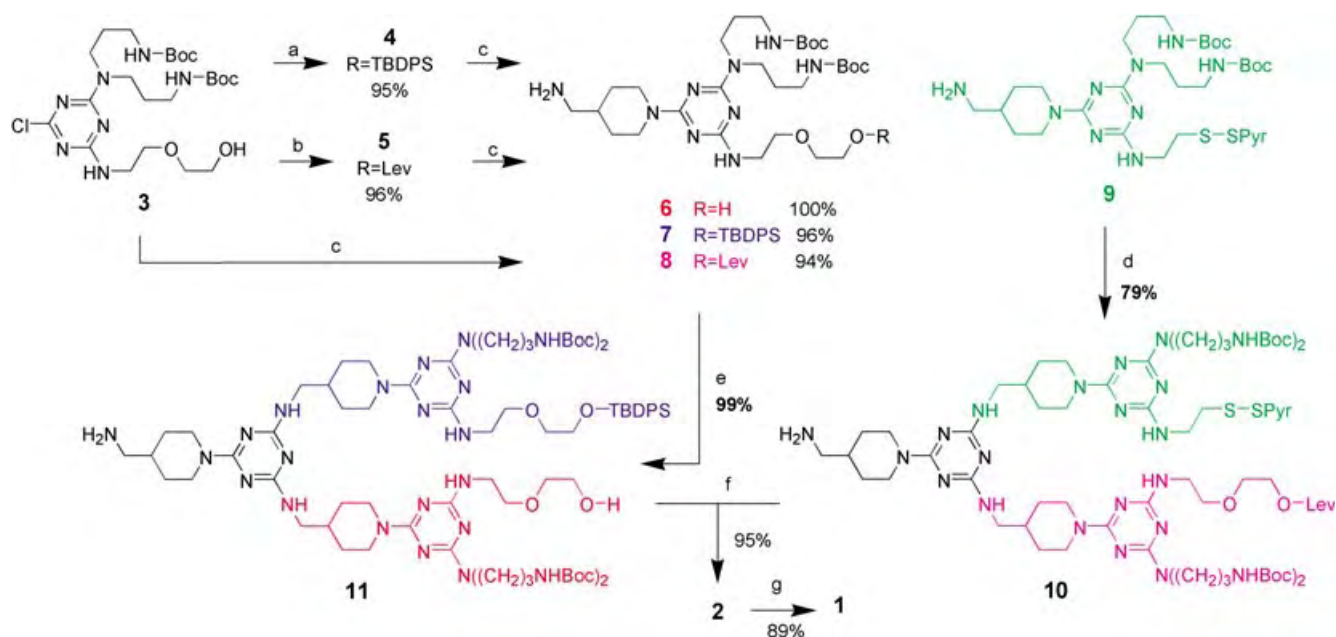
The convergent synthesis of these molecules proceeds in a highly efficient manner. Of the four building blocks used (**4–7**, Scheme 1; each indicated with a different color), three (**4–6**) originate from a common intermediate (**3**) and are available in yields exceeding 90%. The selective substitution of the triazine ring reduces the synthesis of these dendrimers to a trivial procedure. The use of diamines that react chemoselectively with monochlorotriazines obviates the need for protecting groups or great excesses of reagents.^[12]

Intermediate **3** is obtained in quantitative yields by treating the bisprotected triamine^[11] with cyanuric chloride followed by the addition of 2-(2-aminoethoxy)ethanol in the same pot. This protocol is commonly executed on a 10-gram scale. The synthesis of **6–8** from the common intermediate **3** proceeds cleanly, starting with protection of the alcohol using TBDPSCl to yield **4** or esterification using levulinic acid and DCC to yield **5**. These reactions are routinely run on a 5-g scale and the products are easily purified by chromatography on silica gel. The secondary amine of 4-aminomethylpiperidine (4-AMP) reacts more than 20 times faster than the primary amine to provide the building blocks **6–8** in greater than 90% overall yield.^[12]

[*] M. B. Steffensen, Dr. E. E. Simanek
Texas A&M University
Department of Chemistry
College Station, TX 77843-3255 (USA)
Fax: (+1) 979-845-9452
E-mail: simanek@tamu.edu

[**] This work was supported by a grant from the N.I.H. (NIGMS 64650). M.B.S. received a predoctoral fellowship from the Chemistry-Biology Training Grant (NIH TM GM08523).

Supporting information for this article is available on the WWW under <http://www.angewandte.org> or from the author.



Scheme 1. Synthesis of **1** and **2**. Reagents and conditions: a) TBDPSCl, imidazole, THF, RT, 8 h; b) levulinic acid, DCC, DMAP, THF, RT, 8 h; c) 4-AMP, THF, RT, 8 h; d) **7**+C₃N₃Cl₃, DIEA, THF, 0°C, 2 h; then **6**, RT, 24 h; then 4-AMP, RT, 18 h; e) C₃N₃Cl₃, DIEA, THF, 0°C, 2 h; then **8**, RT, 18 h; then 4-AMP, RT, 18 h; f) **11**+C₃N₃Cl₃, DIEA, THF, 0°C, 2 h; then **6**, RT, 18 h; g) piperazine, THF, 0°C, 20 h, extraction, then **2**, RT, 10 days. DIEA = diisopropylethylamine, DCC = dicyclohexylcarbodiimide, DMAP = 4-dimethylaminopyridine, 4-AMP = 4-aminomethylpiperidine.

The preparation of the fourth building block (**9**) occurs in a single-pot reaction that commences with monosubstitution of cyanuric chloride with 2-pyridyldithioethylamine (PDA), followed by addition of the bisprotected triamine, and concluding with the addition of 4-AMP. The overall yield for this reaction sequence is 93%, with the final product isolated by chromatography. Synthesis of **10** occurs in a single-pot procedure that relies on first treating **9** with cyanuric chloride, then **8**, and concluding with addition of 4-AMP. This series of manipulations provides **10** in only 79% yield. The uncharacteristically low yield for this series of reactions is presumably a consequence of the condensation of the keto group of the levulinic ester with the free primary amine upon workup. Signals corresponding to the dimerization of **10** minus the loss of water appear in the mass spectra.

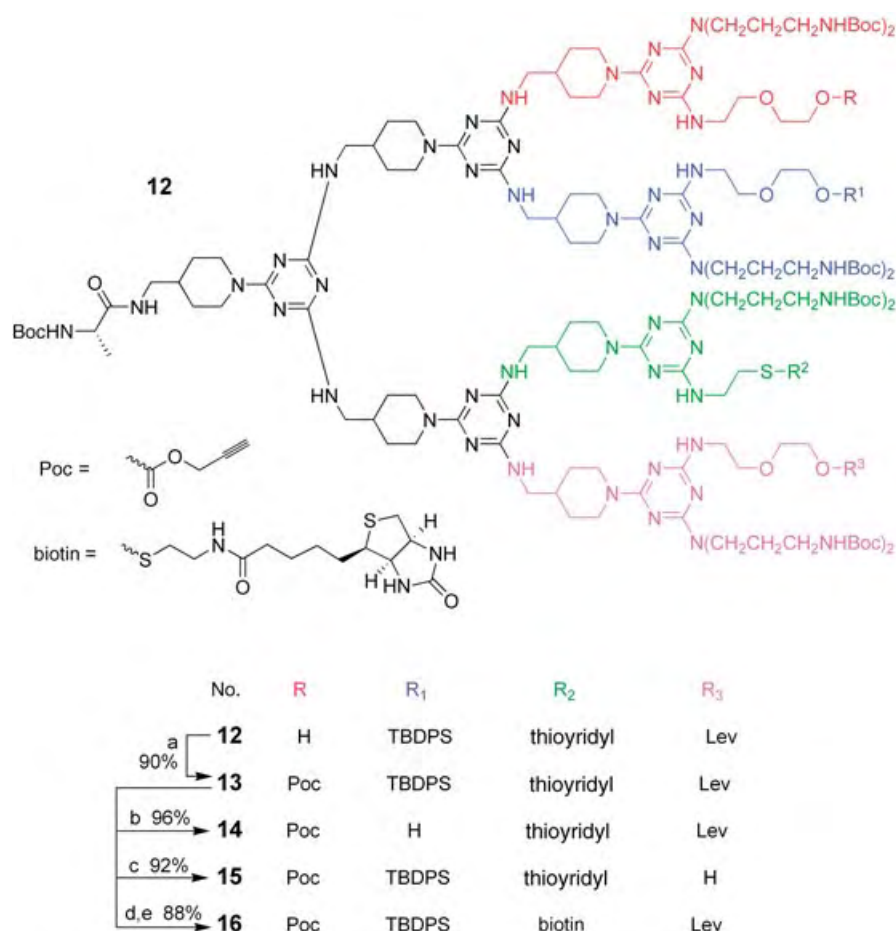
The synthesis of **11** proceeds in a manner similar to that of **10**. This reaction is illustrative of the ease at which these multistep, one-pot reactions can be monitored by thin-layer chromatography (TLC). Addition of cyanuric chloride to a solution of **7** ($R_f = 0.3$ in 9:1 CH₂Cl₂:CH₃OH) at 0°C results in the dichlorotriazine intermediate forming rapidly to give a single new spot by TLC ($R_f = 0.6$ in 9:1 CH₂Cl₂:CH₃OH). After addition of **6** and consumption of the dichlorotriazine, a single spot is again visible by TLC ($R_f = 0.4$ in 9:1 CH₂Cl₂:CH₃OH) which corresponds to the monochlorotriazine. The final reaction with 4-AMP gives **11**, a material that has an R_f value of 0.25 (9:1 CH₂Cl₂:CH₃OH) because of the presence of a free primary amine. Intermediate **11** is obtained in 99% yield.

To obtain **2**, intermediate **11** is treated sequentially with cyanuric chloride and then **10**. Overall, a total of 18 reactions are involved in the synthesis. The longest continuous reaction sequence is only five reactions and provides **2** in 80% overall

yield. This route has been executed to produce more than 10 g of **2**. (The route with the lowest yield commences with **9** and produces **2** in three steps and 70% overall yield.) Dendrimer **1** could be obtained by dimerizing **2** with piperazine, but to avoid errors that could arise in the stoichiometry of the reactants as a result of the substantial differences in the molecular weight of **2** and piperazine, we adopt a two-step procedure.^[13] Initially, **2** is treated with an excess of piperazine. The excess piperazine is then removed and the remaining material is treated with **1**. The process proceeds in 89% overall yield and the product is purified by chromatography on silica gel.

We evaluated the selective manipulation and deprotection of these scaffolds using **2** (Scheme 2). In short, nucleophilic aromatic substitution with amino acid derivatives can be executed to yield **12**. The free hydroxy group of **12** is amenable to modification with a chloroformate group to yield carbonate **13**. The propargyloxycarbonyl (Poc) group can serve as either a protecting group^[13] or a reagent for click chemistry.^[14] Selective deprotection of the silyl ether is achieved with tetrabutylammonium fluoride to yield **14**. Cleavage of the levulinic acid ester is facilitated with hydrazine to yield **15**. The pyridyl disulfide group on **1** was cleaved with dithiothreitol before coupling with the commercially available biotin-PDA (an activated biotin–disulfide conjugate) to form disulfide **16**. Triscarboxylethylphosphane reduced the disulfide with concomitant removal of the Poc group. The generality of this reaction is unclear as previous methods for removal of the Poc group typically required heterogeneous solutions of tetrathiomolybdate.^[13c] Excess hydrazine can also lead to loss of the Poc group.

Targets **1** and **2** represent useful building blocks for the preparation of dendrimer libraries for diverse purposes.



Scheme 2. Manipulation of the core. Reagents and conditions: a) propargylchloroformate, pyridine, THF, RT, 2 h; b) TBAF, THF, RT, 4 h; c) hydrazine, THF, RT, 2 h; d) DTT, CH₂Cl₂, RT, 2 h; e) biotin-PDA, DMF, RT, 2 h. Boc-Ala-4-Amp: see Supporting Information for preparation, TBAF = tetrabutylammonium fluoride, DTT = dithiothreitol, biotin-PDA = biotin-pyridyldithioethylamine.

These molecules suffer the limitation that the deprotection steps occur in yields of about 90 % and release the protecting group as a by-product into solution, thus necessitating purification. The incorporation of these groups onto a solid support, a current aim of our research, addresses these limitations. We refer to these dendrimers as molecular fruit-salad trees, the nanoscale variant of a tree produced by grafting branches that yield different fruits on a common trunk.^[15] Further studies on these architectures will be reported in due course.

Received: March 17, 2004
Published Online: August 12, 2004

Keywords: amines · dendrimers · protecting groups · synthesis design

- [1] a) S. M. Grayson, J. M. J. Fréchet, *Chem. Rev.* **2001**, *101*, 3819–3867; b) G. R. Newkome, F. Vögtle, C. N. Moorefield, *Dendrimers and Dendrons: Concepts, Syntheses, Applications*, VCH, New York, **2001**; c) J. M. J. Fréchet, D. A. Tomalia, *Dendrimers and Other Dendritic Polymers*, Wiley, New York, **2002**.

- [2] a) M. Okaniwa, K. Takeuchi, M. Asai, M. Ueda, *Macromolecules* **2002**, *35*, 6232–6238; b) S. P. Rannard, N. J. Davis, *J. Am. Chem. Soc.* **2000**, *122*, 11729–11770.
- [3] a) P. Singh, *Bioconjugate Chem.* **1998**, *9*, 54–63; b) G. R. Newkome, C. D. Weis, C. N. Moorefield, G. R. Baker, B. J. Childs, J. Epperson, *Angew. Chem.* **1998**, *110*, 318–321; *Angew. Chem. Int. Ed.* **1998**, *37*, 307–310; c) G. R. Newkome, B. J. Childs, M. J. Rourke, G. R. Baker, C. N. Moorefield, *Biotechnol. Bioeng.* **1999**, *61*, 243–253; d) J. R. Baker, A. Quintana, L. Piehler, M. Banazak-Holl, D. Tomalia, E. Raczka, *Biomed. Microdevices* **2001**, *3*, 61–69.
- [4] a) W. Zhang, D. T. Nowlan III, L. M. Thomson, W. M. Lackowski, E. E. Simanek, *J. Am. Chem. Soc.* **2001**, *123*, 8914–8922; b) Z. Bo, A. Schäfer, P. Franke, A. D. Schlüter, *Org. Lett.* **2000**, *2*, 1645–1648; c) H.-F. Chow, C.-F. Leung, K.-W. Wong, L. Xi, *Angew. Chem.* **2003**, *115*, 5069–5073; *Angew. Chem. Int. Ed.* **2003**, *42*, 4919–4923; d) S. Li, M. L. Szalai, R. M. Kevitch, D. V. McGrath, *J. Am. Chem. Soc.* **2003**, *125*, 10516–10517; e) K. L. Wooley, C. J. Hawker, J. M. J. Fréchet, *J. Chem. Soc. Perkin Trans. 1* **1991**, 1059–1076; f) W. Zhang, S. E. Tichy, L. M. Pérez, G. Maria, P. A. Lindahl, E. E. Simanek, *J. Am. Chem. Soc.* **2003**, *125*, 5086–5094.
- [5] a) S.-E. Stiriba, H. Frey, R. Haag, *Angew. Chem.* **2002**, *114*, 1385–1390; *Angew. Chem. Int. Ed.* **2002**, *41*, 1329–1334; b) F. Aulenta, W. Hayes, S. Rannard, *Eur. Polym. J.* **2003**, *39*, 1741–1771; c) M. J. Cloninger, *Curr. Opin. Chem. Biol.* **2002**, *6*, 742–748; d) R. Esfand, D. A. Tomalia, *Drug Discovery Today* **2001**, *6*, 427–436; e) A. K. Patri, I. J. Majoros, J. R. Baker, Jr., *Curr. Opin. Chem. Biol.* **2002**, *6*, 466–471.
- [6] Materials are available in limited supply to other investigators by contacting Professor Simanek.
- [7] Inspiration from: C.-H. Wong, X.-S. Ye, Z. Zhang, *J. Am. Chem. Soc.* **1998**, *120*, 7137–7138.
- [8] a) J. H. van Boom, P. M. J. Burgers, *Tetrahedron Lett.* **1976**, *17*, 4875–4878; b) N. Jeker, C. Tamm, *Helv. Chim. Acta* **1984**, *67*, 190.
- [9] S. Hanessian, P. Lavalley, *Can. J. Chem.* **1977**, *55*, 562–565.
- [10] J. Connor, A. J. Schroit, *Biochemistry* **1988**, *27*, 848–851.
- [11] D. A. Westerberg, P. L. Carney, P. E. Rogers, S. J. Kline, D. K. Johnson, *J. Med. Chem.* **1989**, *32*, 236–243.
- [12] M. B. Steffensen, E. E. Simanek, *Org. Lett.* **2003**, *5*, 2359–2361.
- [13] a) S. Sinha, P. Ilankumaran, S. Chandrasekaran, *Tetrahedron Lett.* **1999**, *40*, 771–774; b) R. G. Bhat, S. Sinha, S. Chandrasekaran, *Chem. Commun.* **2002**, 812–813; c) P. R. Sridhar, S. Chandrasekaran, *Org. Lett.* **2002**, *4*, 4731–4733.
- [14] H. C. Kolb, M. G. Finn, K. B. Sharpless, *Angew. Chem.* **2001**, *113*, 2056–2075; *Angew. Chem. Int. Ed.* **2001**, *40*, 2004–2021.
- [15] Fruit-salad trees are commercially available: <http://www.fruitsaladtrees.com/>.

An Amphotericin B–Fluorescein Conjugate as a Powerful Probe for Biochemical Studies of the Membrane**

Andreas Zumbuehl, Damien Jeannerat, Scott E. Martin, Marc Sohrmann, Pasquale Stano, Tamas Vigassy, Daniel D. Clark, Stephen L. Hussey, Mathias Peter, Blake R. Peterson, Ernő Pretsch, Peter Walde, and Erick M. Carreira*

Dedicated to Professor Peter B. Dervan

Amphotericin B is an antimycotic agent extracted and isolated from a soil streptomycete^[1] and is currently in clinical use against chronic fungal infections. An enormous amount of data on the biological activity of this polyketide has been accumulated, which underlines the potency and effectiveness of the medicament, as well as its importance in membrane research.^[2] Even so, after five decades of intensive research the details of the mechanism of action of amphotericin B remain far from completely elucidated.^[3] It is generally accepted that amphotericin B induces leakage of electrolytes and small molecules from exposed cells. However, a definitive answer to the question of whether such electrolyte efflux is

the primary cause of amphotericin-B-induced cell death remains elusive.^[4] Recent attempts at mechanistic inquiry have involved use of the tools of synthesis^[5] and metabolic engineering.^[6] There is a need for the design and synthesis of amphotericin B probes with which to test the various existing hypotheses.^[7] Herein, we describe the use of a readily accessible piperazine linker as a synthetic anchor for the introduction of reporter groups such as fluorescein to amphotericin B. We used the resulting probe to conduct several *in vivo* and *in vitro* comparative studies involving mammalian and fungal cells, as well as vesicles (Liposomes). Several of the observations documented herein are of particular significance: 1) the amphotericin–fluorescein conjugate is rapidly internalized in mammalian cells, but no such uptake occurs in fungal cells; 2) in contrast, the conjugate is localized in the fungal membrane, as observed by epifluorescence microscopy; 3) despite the fact that liposome studies show the amphotericin conjugate to lead to rapid K⁺ efflux, the compound is not lethal to yeast over a wide range of concentrations; 4) the conjugate was found to be uniformly distributed throughout the membrane in exponentially growing and budding yeast. The various intriguing properties of this probe may facilitate further studies aimed at gaining an understanding of the difference between the behavior of amphotericin towards mammalian cells and that towards fungal cells, and may already provide an insight into the origins of the severe side-effects of the drug.

Despite the density of functionality of amphotericin B, it only has two addressable reactive centers that allow selective conjugation: the primary amine function found in the pendant mycosamine moiety and the carboxylic acid group in the amphoteronolide fragment (Scheme 1). Analysis of prior work in this area^[8] suggests that conjugates anchored through the mycosamine moiety must contain a linker that preserves a protonatable amine function to allow observation of the fast kinetics of K⁺ release in liposomes. Murata and co-workers^[5c] recently published a study in which a linker was introduced

[*] A. Zumbuehl, Prof. Dr. E. M. Carreira
Laboratorium für Organische Chemie
ETH Hönggerberg, HCI H335
8093 Zürich (Switzerland)
Fax: (+41) 1-632-1328
E-mail: carreira@org.chem.ethz.ch

Dr. D. Jeannerat
Département de Chimie Organique
Université de Genève
1211 Genève 4 (Switzerland)

Dr. S. E. Martin, D. D. Clark, Dr. S. L. Hussey, Prof. Dr. B. R. Peterson
Departement Materialwissenschaft
ETH Hönggerberg
8093 Zürich (Switzerland)

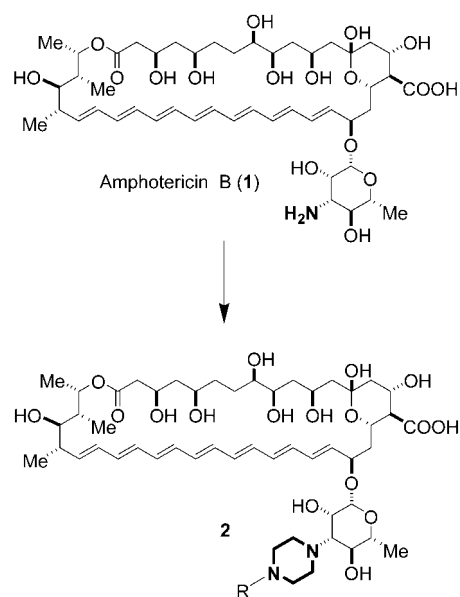
Dr. M. Sohrmann, Prof. Dr. M. Peter
Institut für Biochemie
ETH Hönggerberg
8093 Zürich (Switzerland)

P. Stano, Prof. Dr. P. Walde
Department of Chemistry
The Pennsylvania State University
Pennsylvania 16802 (USA)

Dr. T. Vigassy, Prof. Dr. E. Pretsch
Laboratorium für Organische Chemie
ETH-Hönggerberg
8093 Zürich (Switzerland)

[**] We would like to thank Prof. Dr. Josef Brunner for helpful discussions. E.M.C. is grateful for generous support from the Eidgenössische Technische Hochschule (ETH), Zürich (TH-Gesuch) and from F. Hoffmann LaRoche. B.R.P. acknowledges support from the National Institutes of Health, USA (Grant no. RO1-CA83831).

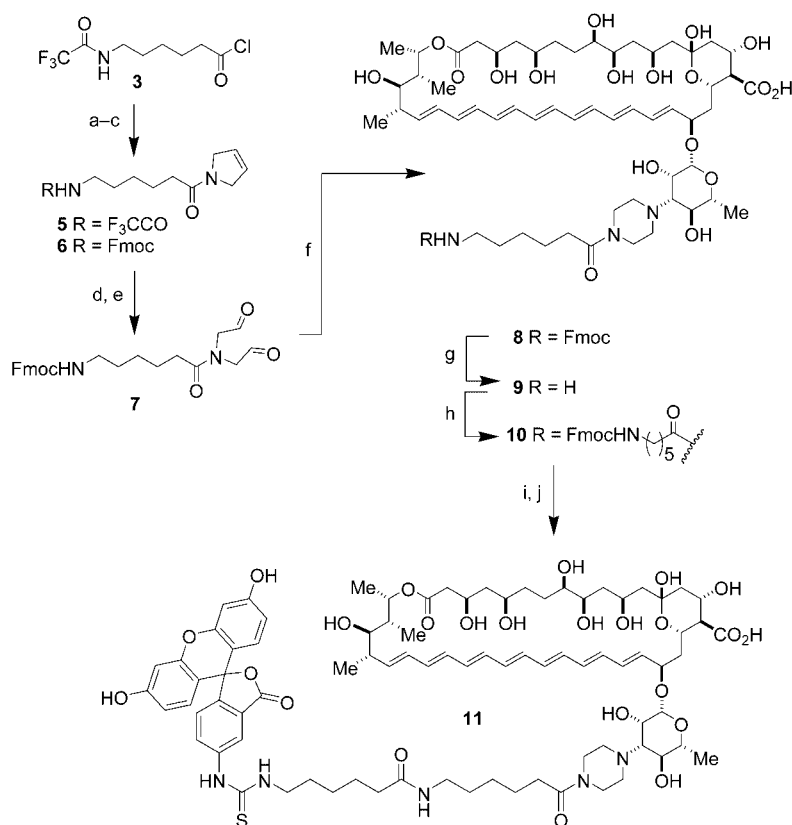
Supporting information for this article is available on the WWW under <http://www.angewandte.org> or from the author.



Scheme 1.

onto amphotericin B (**1**) through reductive amination of an aldehyde. Such a strategy suffers from the disadvantage that a second reductive alkylation can ensue, a process that can be difficult to control.^[9] Our attempts to carry out reductive monoalkylation at the amphotericin B mycosamine function proved the process to be capricious; production of a mixture of secondary and tertiary amines could not be avoided, and separation of these compounds was far from simple. We sought a novel alternative conjugation strategy and reasoned that a linker programmed to undergo double reductive alkylation would completely obviate the problems outlined above. Moreover, the tertiary amines **2** so produced would retain their basicity and could be protonated under physiological conditions.^[8]

There is no precedence for the use of such a linker with amphotericin B, or any other biomolecule. We developed an easy, straightforward synthetic route to attach a piperazine linker to amphotericin B, which allowed subsequent conjugation (Scheme 2). Coupling of 6-*N*-trifluoroacetamide-hexanoyl chloride (**3**)^[10] with 3-pyrroline (**4**)^[11] gave **5**, which was converted into the corresponding Fmoc-protected amide **6**. Oxidative cleavage of **6** afforded dialdehyde **7**^[12]. This aldehyde readily underwent double reductive amination with the primary amine group of amphotericin B to form **8** in 63% yield.



Scheme 2. a) 3-pyrroline (**4**), pyr, CH₂Cl₂, 3 h, 69%; b) K₂CO₃, MeOH, H₂O, 13 h, 82%; c) FmocOSu, DMF, pyr, 12 h, 77%; d) K₂O₃·2 H₂O, acetone, H₂O, tBuOH, 16 h, 66%; e) NaIO₄, Si gel, CHCl₃, H₂O, 0.5 h; f) amphotericin B, DMF, NaCNBH₃, HCl, 13 h, 63% over 2 steps; g) piperidine, DMSO, quantitative; h) *N*-Fmoc-6-NH-(CH₂)₅CO₂Su, iPr₂NEt, DMF, 38%; i) piperidine, DMSO, quantitative; j) fluorescein isothiocyanate, iPr₂NEt, DMF, 66%. Pyr, pyridine. DMF = dimethylformamide, DMSO = dimethyl sulfoxide, Fmoc = 9-fluorenylmethoxycarbonyl, Su = succinimide.

Quantitative deprotection (piperidine/DMSO) of **8** to form the free amine **9** prepared the compound for conjugation.^[13] Treatment of **9** with the Fmoc-protected 6-amino-hexanoic acid *N*-hydroxysuccinimide ester gave **10**, which was deprotected (piperidine, DMSO, quantitative yield) then allowed to react with fluorescein isothiocyanate (Hünig's base, DMF, 66% yield) to form the amphotericin B-fluorescein conjugate **11**.^[14–16]

To evaluate the new linker system, the free amine **9** and the amphotericin B-fluorescein conjugate **11** were examined thoroughly in both liposomal and cellular assays. For each of the two compounds we determined the minimal inhibitory concentration (MIC) required to inhibit growth of *Saccharomyces cerevisiae*. Native amphotericin B (**1**; MIC = 1 μM) and the aminohexanoyl piperazinyl conjugate **9** (MIC = 1.6 μM) are equally active, which indicates the usefulness of the new linker system. The fluorescein-amphtotericin B conjugate **11** is not toxic in the measured range of up to 500 μM.

We adapted a vesicle assay to our purposes.^[17,18] Large unilamellar vesicles (LUVs) made from POPC (1-palmitoyl-2-oleoyl-*sn*-glycero-3-phosphocholine) or from POPC admixed with sterols (mimicking conditions in natural biomembranes^[19]) were prepared from a thin film of the lipid(s) in a mixture containing KCl (150 mM) and 2-[4-(2-hydroxyethyl)-1-piperazinyl]ethanesulfonic acid (HEPES) buffer (5 mM) at pH 7.4.^[20] The unilamellar vesicles were dialyzed against NaCl to create an ion gradient (K⁺ inside, Na⁺ outside). The amphotericin B conjugates were added to the vesicle suspension to form ion channels leading to K⁺ efflux, which was measured with freshly prepared valinomycin-based K⁺-selective electrodes.^[21,22]

Native amphotericin B (**1**), the conjugate with the piperazine linker **9**, and the fluorescein conjugate **11** all induced immediate total release of trapped K⁺ from ergosterol-containing vesicles (Figure 1). Treatment of cholesterol-containing vesicles with the new conjugates **9** and **11** resulted in a slower release of ions than treatment with amphotericin B (**1**), which indicates that the piperazine-linked conjugates have a preference for ergosterol-containing rather than cholesterol-containing vesicles.^[23] K⁺ release from sterol-free vesicles was slow, as we expected based on literature data for amphotericin B.^[2] The fluorescein-amphtotericin B conjugate **11** induced rapid K⁺ release from vesicles while having no toxic effect on yeast cell growth. This observation is consistent with previous proposals that channel formation is not sufficient to induce cell death.^[4]

We tested fluorescein-amphtotericin B conjugate **11** in a variety of other in vivo experiments. A cholesterol-derived synthetic membrane anchor has recently been developed that allows the uptake of antifluorescein antibodies and the associated Protein A into mammalian cells.^[24] Since amphotericin B is known to insert into membranes,^[1] we tested the fluorescein-amphtotericin B conjugate **11** in the same assay.

To investigate the recruitment of **11** both by *Saccharomyces cerevisiae* FY250 and by Jurkat human T cells, the cells were incubated with **11** for 1 h at 37°C

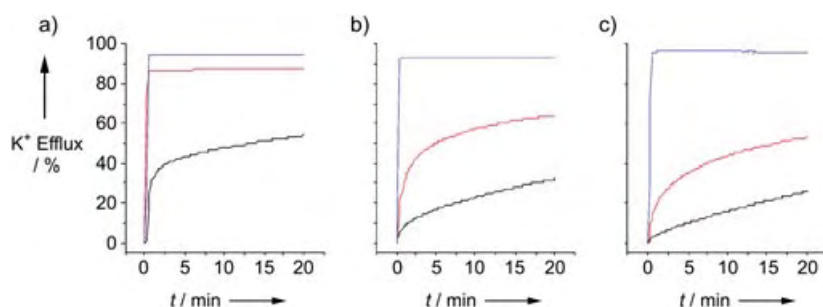


Figure 1. K^+ efflux from vesicles prepared from pure POPC (black), POPC admixed with 30 mol% cholesterol (red), and POPC admixed with 13 mol% ergosterol (blue). The concentration of amphotericin B (**1**, a) and its conjugates **9** (b) or **11** (c) after addition (as a DMSO solution) to the stirred vesicle suspension was 5 μ M. The total concentration of lipids (POPC + sterol) was 1 mM in 5 mM HEPES buffer at pH 7.4.

(Jurkat cells) or 30 °C (*S. cerevisiae*) and the cultures were washed with media (Phosphate-buffered saline (PBS) for the yeast cells and RPMI media for the Jurkat cells, see Supporting Information) and resuspended. Subsequent analysis by flow cytometry revealed that both yeast and Jurkat lymphocytes recruit **11**, but the compound has a slight preference for the mammalian cell line.^[25]

We next conducted experiments aimed at establishing the avidity of anti fluorescein IgG for cellular plasma membranes incubated with **11**. We employed nonfluorescent rabbit IgG complexed with red fluorescent conjugates of commercially available Protein A (PrA) from *Staphylococcus aureus* in a previously described assay.^[26,27] Flow cytometry allowed quantification of the recruitment of anti fluorescein IgG bound to Alexa Fluor 633-conjugated PrA by Jurkat lymphocytes and yeast.^[25] Jurkat cells were treated with **11** for 1 h and then with IgG for 4 h at 37 °C. The cells were washed with 5-aminofluorescein prior to measurement to ensure that all the noninternalized IgG was removed. Yeast cells were treated similarly but were not washed with 5-aminofluorescein. The results of these experiments lead to the conclusion that **11** associates with both yeast and Jurkat human T cells in a dose-dependent manner, which is in line with the results of the studies described above. More importantly, treatment with the amphotericin conjugate leads to a significant increase in the uptake of IgG by Jurkat lymphocytes. No internalization of **11** or its complex with anti fluorescein IgG by yeast cells was observed.

To investigate the nature of the interaction of **11** with the cellular targets in the presence of IgG in greater detail, cells incubated with **11** were examined by epifluorescence microscopy (see Figure 2). Uptake into Jurkat lymphocytes and IgG recruitment by yeast were assayed as described above, except that Alexa Fluor 594-conjugated Protein A was substituted for Alexa Fluor 633-conjugated Protein A. Both cell lines showed red and green fluorescence. It is particularly interesting that the amphotericin B-conjugate **11** is localized at the membrane in yeast, while the micrograph of the mammalian cell lines reveals that the amphotericin conjugate has been taken up by the cells. The fact that the fluorescein-amphotericin B conjugate **11** is taken up into mammalian cells leads us to hypothesize about the mechanism of action of amphotericin B with reference to its reported side-effects on

mammalian cells. The generally held view is that, despite the inherent preference of amphotericin B for channel formation in yeast membranes as a result of ergosterol stabilization, the compound retains the ability to form channels competitively in mammalian membranes. Model studies with vesicles have shown that approximately 16 amphotericin B molecules are required for channel formation.^[28] In the light of the observations described above for Jurkat cells, we propose that transport of the molecules across mammalian cell membranes into the interior depletes amphotericin B at the membrane and thus diminishes channel formation. Oxidative (free radical)

activity inside the cell may be the source of the observed side-effects of the drug.^[2e,f]

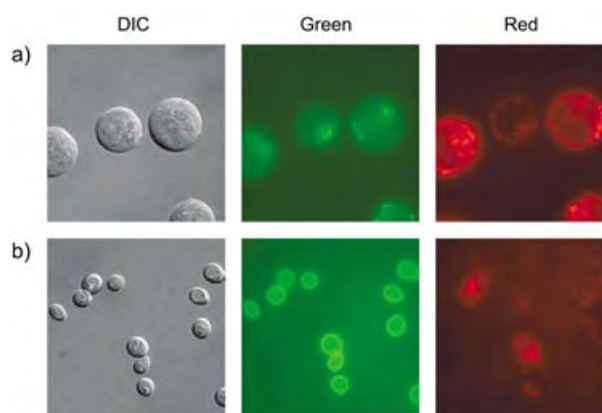


Figure 2. Epifluorescence and differential interference contrast (DIC) microscopy of compound-treated Jurkat lymphocytes (a) and *Saccharomyces cerevisiae* (b) 30 min after IgG addition. Green fluorescence: $\lambda_{\text{ex}} = 480$ nm, $\lambda_{\text{em}} = 535$ nm; red fluorescence: $\lambda_{\text{ex}} = 560$ nm, $\lambda_{\text{em}} = 645$ nm.

We carried out additional in vivo experiments on yeast cells to demonstrate the utility of conjugate **11** as a probe for investigation of biological phenomena at the membrane. Previous work has suggested that ergosterol-rich plasma membrane domains localize in areas of cell polarization. Polyene macrolide filipin was used as a probe because it is known to associate with ergosterol.^[29,30] Localized fluorescence regions were observed in *S. cerevisiae* at the tip of mating projections formed in response to pheromones.^[31] In previous studies with the fission yeast *S. pombe*, ergosterol appeared to accumulate at cell-division-associated regions and at the growing poles.^[32] We therefore wanted to investigate whether **11** distributes uniformly throughout the plasma membrane of *S. cerevisiae* or accumulates specifically in polarized regions of the cells. We analyzed cells during exponential growth, when the cells polarize towards the newly forming daughter bud (Figure 3a and c), and in the course of the formation of mating projections in response to pheromones (Figure 3b and d). In both cases, fluorescein-amphotericin conjugate **11** appeared to be distributed uniformly throughout the plasma membrane of each yeast cell. Ampho-

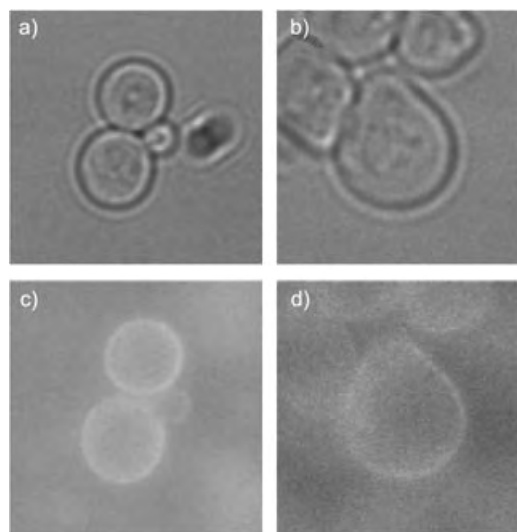


Figure 3. Localization of **11** in the plasma membrane of yeast cells. The cell outlines were observed by phase contrast microscopy (a, b), and the localization of **11** by fluorescence microscopy (c, d). The figure shows exponentially growing cells (a, c) and cells forming mating projections after exposure to mating pheromone (b, d).

tericin B is expected to undergo pronounced complex formation with ergosterol^[33] so these observations suggest that ergosterol-rich domains might not accumulate significantly in distinct regions of the plasma membrane. In support of this hypothesis, recent data suggests that filipin itself might perturb the local composition of cellular membranes.^[34] Further work is required to determine whether filipin and amphotericin B bind to the same molecular structures in vivo, and to answer the question of whether ergosterol-rich membrane domains are polarized during yeast cell growth.

In conclusion, we have established a new piperazine linker system for bioconjugation through amines that allows the synthesis of amphotericin B conjugates on a multigram scale. This linking strategy is suitable for bioconjugation in a number of other biologically important systems for which functionalization through a primary amine is required and may be used to obtain molecules with interesting new properties. A fluorescein conjugate was prepared as a benchmark case. This conjugate displayed preserved K⁺ efflux-inducing properties in an LUV assay but completely lacks toxic effects on yeast cell growth. These results imply that ion-channel formation in artificial vesicles and the lethal effect induced by amphotericin B are separate phenomena. We also demonstrated that amphotericin B–fluorescein conjugate **11** can function as a useful probe of biological activity. Our studies revealed that **11** associates with both yeast (*Saccharomyces cerevisiae* FY250) and Jurkat human T cells in a dose-dependent manner but that it is taken up by mammalian cells whilst it remains localized in the yeast membrane. Additional investigations with this probe in yeast cells revealed a uniform distribution of the compound throughout the plasma membrane, which opens up the possibility that ergosterol might not accumulate in polarized regions of the cells as suggested previously. Additional applications can be envisioned for this new fluorescein–amphotericin B conjugate, for example, it could be used as a means for studying

transmembrane transport or as an anchor for selective mediation of the delivery of toxins to fungal cells.

Received: April 28, 2004

Revised: June 24, 2004

Keywords: antifungal agents · bioorganic chemistry · biophysics · fluorescent probes · synthetic methods

- [1] a) T. H. Sternberg, E. T. Wright, M. Oura, *Antibiot. Annu.* **1955–1956**, 566–573; b) B. A. Steinberg, W. P. Jambor, L. O. Suydam, *Antibiot. Annu.* **1955–1956**, 574–578; c) W. Gold, H. A. Stout, J. F. Pagano, R. Donovan, *Antibiot. Annu.* **1955–1956**, 579–586; d) J. Vandeputte, J. L. Wachtel, E. T. Stiller, *Antibiot. Annu.* **1955–1956**, 587–591.
- [2] a) G. Medoff, J. Brajtburg, G. S. Kobayashi, *Annu. Rev. Pharmacol. Toxicol.* **1983**, 23, 303–330; b) J. Bolard, *Biochim. Biophys. Acta* **1986**, 864, 257–304; c) J. Brajtburg, W. G. Powderly, G. S. Kobayashi, G. Medoff, *Antimicrob. Agents Chemother.* **1990**, 34, 183–188; d) F. C. Szoka, Jr., M. Tang, *J. Liposome Res.* **1993**, 3, 363–375; e) S. C. Hartsel, C. Hatch, W. Ayenew, *J. Liposome Res.* **1993**, 3, 377–408; f) J. Bolard, V. Joly, P. Yeni, *J. Liposome Res.* **1993**, 3, 409–427; g) S. C. Hartsel, J. Bolard, *Trends Polym. Sci.* **1996**, 17, 445–449; h) I. Al-Mohsen, W. T. Hughes, *Ann. Saudi Med.* **1998**, 18, 28–38; i) B. E. Cohen, *Int. J. Pharm.* **1998**, 162, 95–106; j) I. M. Hann, H. G. Prentice, *Int. J. Antimicrob. Agents* **2001**, 17, 161–169; k) S. B. Zotchev, *Curr. Med. Chem.* **2003**, 10, 211–223.
- [3] a) W. Huang, Z. Zhang, X. Han, J. Tang, J. Wang, S. Wang, S. Dong, E. Wang, *Biophys. J.* **2002**, 83, 3245–3255; b) B. V. Cotero, S. Rebolledo-Antunez, I. Ortega-Blake, *Biochim. Biophys. Acta* **1998**, 1375, 43–51; c) G. Fujii, J.-E. Chang, T. Coley, B. Steere, *Biochemistry* **1997**, 36, 4959–4968; d) M. Baginski, E. Borowski, *J. Mol. Struct. (Theochem)* **1997**, 389, 139.
- [4] a) C. C. Hsu-Chen, D. S. Feingold, *Nature* **1974**, 251, 656–659; b) M. L. Sokol-Anderson, J. Brajtburg, G. Medoff, *J. Infect. Dis.* **1986**, 154, 76–83; c) W. H. Beggs, *Antimicrob. Agents Chemother.* **1994**, 38, 363–364.
- [5] a) S. D. Rychnovsky, *Chem. Rev.* **1995**, 95, 2021–2040; b) B. N. Rogers, M. E. Selsted, S. D. Rychnovsky, *Bioorg. Med. Chem. Lett.* **1997**, 7(24), 3177–3182; c) N. Matsumori, N. Yamaji, S. Matsuoka, T. Oishi, M. Murata, *J. Am. Chem. Soc.* **2002**, 124, 4180–4181; d) N. Yamaji, N. Matsumori, S. Matsuoka, R. Oishi, M. Murata, *Org. Lett.* **2002**, 4, 2087–2089; e) S. Matsuoka, N. Matsumori, M. Murata, *Org. Biomol. Chem.* **2003**, 1, 3882–3884; f) N. Matsumori, R. Masuda, M. Murata, *Chem. Biodiversity* **2004**, 1, 346–352.
- [6] a) P. Caffrey, S. Lynch, E. Flood, S. Finnan, M. Oliynyk, *Chem. Biol.* **2001**, 8, 713–723; b) B. Byrne, M. Carmody, E. Gibson, B. Rawlings, P. Caffrey, *Chem. Biol.* **2003**, 10, 1215–1224; c) J. F. Aparicio, P. Caffrey, J. A. Gil, S. B. Zotchev, *Appl. Microbiol. Biotechnol.* **2003**, 61, 179–188.
- [7] a) J. Krüger, E. M. Carreira, *Tetrahedron Lett.* **1998**, 39, 7013–7076; b) J. Tholander, E. M. Carreira, *Helv. Chim. Acta* **2001**, 84, 613–622.
- [8] M. Chéron, B. Cybulska, J. Mazerski, J. Grzybowski, A. Czerwinski, E. Borowski, *Biochem. Pharmacol.* **1988**, 37, 827–836.
- [9] J.-P. Salvi, N. Walchshofer, J. Paris, *Tetrahedron Lett.* **1994**, 35, 1181–1184.
- [10] J. S. Clark, P. A. Hodgson, M. D. Goldsmith, L. J. Street, *J. Chem. Soc. Perkin Trans. 1* **2001**, 24, 3312–3324.
- [11] J. S. Warmus, G. J. Dilley, A. I. Meyers, *J. Org. Chem.* **1993**, 58, 270–271.
- [12] M. Daumas, Y. Vo-Quang, L. Vo-Quang, F. Le Goffic, *Synthesis* **1989**, 64–65.

- [13] The importance of structural assignment for any subsequent mechanistic investigation led us to confirm the success of the conjugation reaction by using a spectral aliasing technique to acquire high-resolution HSQC and HMBC spectra (see refs. [15, 16]). All but a few signals in the double-bond regions of such ^1H , ^{13}C , DEPT, COSY, HSQC, and HMBC spectra were unambiguously assigned to **8**.
- [14] For the synthesis of an NBD (7-Nitro-2-oxa-1,3-diazol-4-yl)-amphotericin conjugate with an amide linker, see: N. O. Petersen *Spectrosc. Int. J.* **1983**, *2*, 408–414. No characterization data were given for this conjugate; to the best of our knowledge it has not been used for biological studies.
- [15] a) D. Jeannerat, *Magn. Reson. Chem.* **2002**, *41*, 3; b) D. Jeannerat, D. Ronan, Y. Baudry, A. Pinto, J.-P. Saulnier, S. Matile, *Helv. Chim. Acta*, in press; c) D. Jeannerat, D. Ronan, Y. Baudry, A. Pinto, J.-P. Saulnier, S. Matile, *Helv. Chim. Acta*, in press; d) D. Ronan, Y. Baudry, D. Jeannerat, S. Matile, *Org. Lett.* **2004**, *6*, 885–887; e) <http://rmn.unige.ch/simplealias>. We applied the most practical implementation (see ref. [15c]), which allows the acquisition conditions of heteronuclear experiments (HSQC and HMBC) to be optimized by copying and pasting a list of carbon chemical shifts into an internet base program (see ref. [15e]). See the Supporting Information for further details.
- [16] a) A. Aszalos, A. Bax, N. Burlinson, P. Roller, C. McNeal, *J. Antibiot.* **1985**, *38*, 1699–1713; b) P. Sowinski, J. K. Pawlak, E. Borowski, P. Gariboldi, *Magn. Reson. Chem.* **1992**, *30*, 275–279; c) P. Sowinski, J. K. Pawlak, E. Borowski, T. Iwashita, *J. Antibiot.* **1985**, *38*, 175–180; d) J. M. Brown, P. J. Sidebottom, *Tetrahedron* **1981**, *37*, 1421–1428.
- [17] a) P. van Hoogevest, B. de Kruijff, *Biochim. Biophys. Acta* **1978**, *511*, 397–407; b) D. S. Orlov, T. Nguyen, R. I. Lehrer, *J. Microbiol. Methods* **2002**, *49*, 325–328.
- [18] The use of external Ca^{2+} instead of Na^+ ions (as reported previously) seemed to block the pores and yielded no results.
- [19] J. Barwicz, P. Tancrède, *Chem. Phys. Lipids* **1997**, *85*, 145–155.
- [20] V. Dorovska-Taran, R. Wick, P. Walde, *Anal. Biochem.* **1996**, *240*, 37–47.
- [21] L. A. R. Pioda, V. Stankova, W. Simon, *Anal. Lett.* **1969**, *2*, 665–674. For improved ruggedness, ion-selective membranes were used that had a higher than usual (see ref. [22]) content of PVC and a lipophilic salt was added to compensate for the increased resistance.
- [22] E. Bakker, P. Bühlmann, E. Pretsch, *Chem. Rev.* **1997**, *97*, 3083–3132.
- [23] This result may imply a beneficial increase in the therapeutic effect of amphotericin B.
- [24] S. L. Hussey, E. He, B. R. Peterson, *J. Am. Chem. Soc.* **2001**, *123*, 12712–12713.
- [25] For flow cytometry data, see the Supporting Information.
- [26] PrA is a 57-kDa protein that binds to the invariant Fc fragment of rabbit-derived IgG proteins with a dissociation constant of approximately 60 nM. See ref [24].
- [27] L. Cedergren, R. Andersson, B. Jansson, M. Uhlen, B. Nilsson, *Protein Eng.* **1993**, *6*, 441–448.
- [28] G. Fujii, J.-E. Chang, T. Coley, B. Steere, *Biochemistry* **1997**, *36*, 4959–4968.
- [29] K. Takeo, *J. Gen. Microb.* **1985**, *131*, 309–316.
- [30] W. Drabikowski, E. Lagwinska, M. G. Sarzala, *Biochim. Biophys. Acta* **1973**, *291*, 61–70.
- [31] M. Bagnat, K. Simons, *Proc. Natl. Acad. Sci. USA* **2002**, *99*, 14183–14188.
- [32] V. Wachtler, S. Rajagopalan, M. K. Balasubramanian, *J. Cell Sci.* **2003**, *116*, 867–874.
- [33] I. Gruda, P. Nadeau, J. Brajtburg, G. Medoff, *Biochim. Biophys. Acta* **1980**, *602*, 260–268.
- [34] J. Valdez-Taubas, H. R. B. Pelham, *Curr. Biol.* **2003**, *13*, 1636–1640.

A Covalent-Chemistry Approach to Giant Macromolecules and Their Wetting Behavior on Solid Substrates**

Afang Zhang, Jörg Barner, Ildiko Göessl,
Jürgen P. Rabe,* and A. Dieter Schlüter*

Synthetic polymers commonly lack any sizable extension into the second dimension (thickness) and are best described as more or less flexible threads. Recently there have been two synthetic approaches to address the problem of how to make macromolecules “thick”: one is referred to as molecular brushes,^[1,2] the other as dendromized polymers.^[3] Dendromized polymers (denpols) differ from molecular brushes in that their side chains are not linear but highly and regularly branched (dendrons), which results in a considerable density of molecular segments in the direct neighborhood of the central backbone. Denpols, especially those of higher generation, have the built-in character of a cylindrical object, a feature which found application in basic experiments in nanoscience in which the bottom-up approach was investigated.^[4] These objects can reach lengths of several hundred nanometers and widths of 5–7 nm depending on their chemical structure and generation number and, in this regard, are amongst the largest molecules ever prepared. It seems difficult, for both synthetic and space reasons, to extend the denpol concept to a degree such that the dimensions of biologically relevant cylindrical objects such as the tobacco mosaic virus (TMV envelope: diameter 18 nm, length ca. 300 nm) can be mimicked. Therefore, we set out to merge the brush and denpol concepts. Herein, we report a joint synthetic and scanning force microscopy (SFM) inves-

[*] Dipl.-Phys. J. Barner, Dr. I. Göessl, Prof. Dr. J. P. Rabe
Institut für Physik, Humboldt Universität zu Berlin
Newtonstrasse 15, 12489 Berlin (Germany)
Fax: (+49) 30-2093-7632
E-mail: rabe@physik.hu-berlin.de
Prof. Dr. A. Zhang,⁺ Prof. Dr. A. D. Schlüter⁺⁺
Institut für Chemie, Freie Universität Berlin
Takustrasse 3, 14195 Berlin (Germany)
Fax: (+49) 30-838-53357
E-mail: adschlue@chemie.fu-berlin.de
dieter.schluter@mat.ethz.ch

[†] New address:
College of Materials Engineering, Zhengzhou University
Daxue 75, Zhengzhou 450052 (China)

[++] New address:
Department of Materials, Swiss Federal Institute of Technology
Institute of Polymers ETH Zürich-Hönggerberg
Wolfgang-Pauli-Strasse 10, HCI J 541
8093 Zürich (Switzerland)

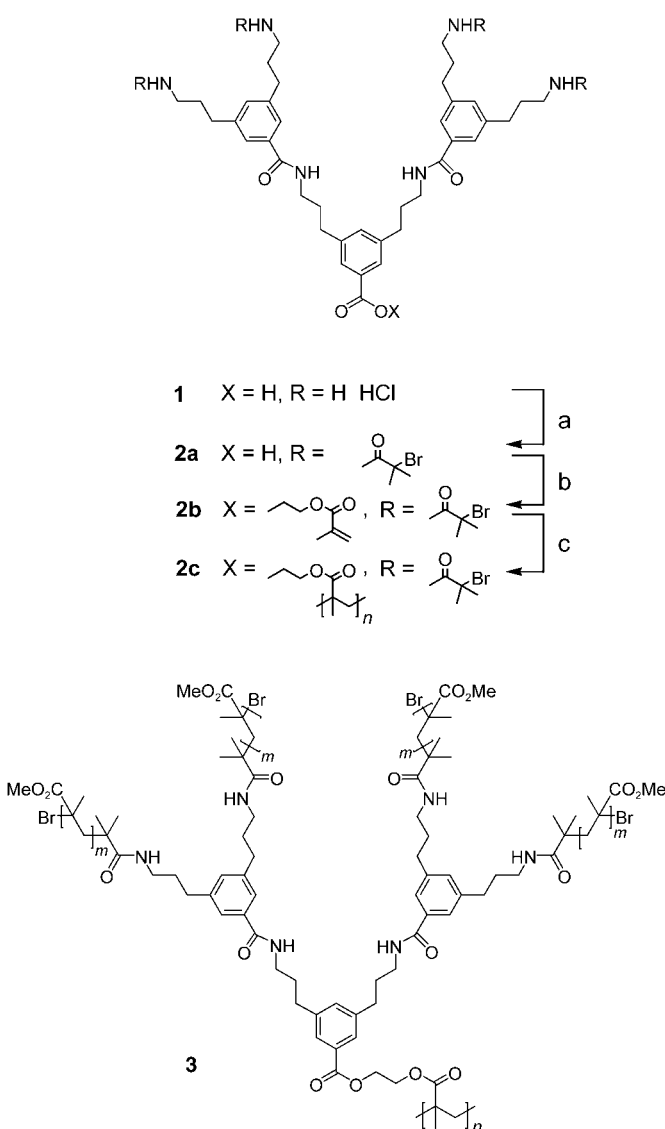
[**] We thank the German Science Foundation (Sfb 448, TPs A1 and A11) for financial support. We cordially thank C. Ecker, HU Berlin, for helpful discussions on aspects of persistence lengths.



Supporting information for this article is available on the WWW under <http://www.angewandte.org> or from the author.

tigation of our attempts to further increase the diameter of denpols. The synthetic issues comprise: a) synthesis of a denpol macroinitiator whose number of initiator sites per repeat unit (four) is inherently fixed; b) growth of poly(methyl methacrylate) (PMMA) chains off this denpol's "surface"^[5] by using atom-transfer radical polymerization (ATRP);^[2a,6] c) determination of polymer hair length; and d) estimation of the initiation efficiency. Since the starting material already has a molar mass easily in the range of 1×10^6 Daltons, it was clear that a complete characterization of the product according to organic chemistry standards would not be feasible. We therefore carried out a detailed characterization of the starting material, restricted ourselves at this initial stage to second-generation (G2) denpols, and performed model reactions for the growing process. SFM was used to investigate the interaction of the hairy denpols with solid substrate surfaces and served not only to further characterize these huge molecules but also, and more importantly, to study the response of hairy denpols to the nature of the surface on which they are adsorbed. These investigations specifically included: a) the imaging of spin-coated samples on three different substrates, namely mica, MoS₂, and highly oriented pyrolytic graphite (HOPG); b) characterization of the denpol backbone contour as well as the structure of the hairy shell; and c) observation of whether there is a systematic tendency of the hairs to fold back as their interaction with the substrate becomes increasingly less favorable. This latter aspect is considered important for a distant goal of this research, which is to force the hairs to completely fold back and produce cylindrical molecular entities with unprecedented dimensions, for example, by subsequent photochemical cross-linking.

The present study was carried out with the G2 denpol **2c**, which has four terminal 2-bromoisobutyrate groups in each repeat unit. They serve as initiator sites for the ATRP of methyl methacrylate. The synthesis starts from the known G2 dendron **1**, whose amine functions are completely converted by reaction with the succinidyl active ester of 2-bromoisobutyrate, and then the resultant **2a** is converted into the methacrylate G2 macromonomer **2b** (Scheme 1). Compounds **2a** and **2b** were fully characterized (see Supporting Information). As has already been discovered for similar dendronized macromonomers, simple heating of **2b** to 55 °C for a few hours in an extremely highly concentrated solution (0.6 g of **2b** in 0.4 mL of benzene) resulted in its polymerization to the high-molecular weight polymer **2c**. Notably, polymer **2c** automatically has four initiator sites per repeat unit in this mode of synthesis.^[7] Standard workup and lyophilization from dioxane^[8] afforded a colorless foam (yields: 82–86%) which, despite its hygroscopic character, gave correct data from combustion analysis (see Supporting Information). Additionally, the ¹H (500 MHz) and ¹³C NMR spectra could be fully assigned, although the signals were relatively broad as a result of the high molecular weight. Gel permeation chromatography (GPC) in DMF calibrated with G1 denpol standards^[9] furnished number-average molar masses between 900 000 and 1 500 000 g mol⁻¹ and polydispersity indices (PDI) of 3.4–4.0. The GPC elution curves were basically monomodal (see Supporting Information). For the



Scheme 1. Reagents and conditions: a) **1**, 2,5-dioxopyrrolidin-1-yl 2-bromoisobutyrate, TEA, CH₂Cl₂, MeOH, -30 °C, 15 h (86%); b) **2a**, DCC, HEMA, DMAP, CH₂Cl₂, RT, 15 h (68%); c) **2b**, DCM, 55 °C, 8 h (85%). TEA = triethylamine, DCC = *N,N'*-dicyclohexylcarbodiimide, HEMA = hydroxyethylmethacrylic acid, DMAP = 4-dimethylaminopyridine.

following experiments the highest molecular weight sample with PDI = 3.4 was used.

Molecular brushes were prepared by grafting polymeric chains from the backbone,^[1c,f,2a] in which the most critical aspect is cross-linking. ATRP is a so-called controlled radical polymerization (CRP) procedure, which means that the lifetime of a free radical chain end is reduced by the action of a transition metal (Cu^I in the case of ATRP). Thus, chain termination by radical recombination (and disproportionation), which would lead to intra- and intermolecular cross-linking, is reduced. A rough estimation of the number of initiator sites shows that polymer **2c** can initiate 6000 PMMA chains per individual **2c** chain in the optimum case.^[10] Although not many of the chain ends will be active at the same time, from this simple estimation it suggests that the experimental conditions should be better designed such that

cross-linking is reduced as far as possible. Approximately 30 independent experiments to grow hairs off the denpols were performed, each using 58 mg of **2c** and 5 g of methyl methacrylate (MMA). Cu^IBr and pentamethyldiethylenetriamine (PMDETA) were always employed in a constant molar ratio to **2c**; the reaction time, however, was varied from 0.5 to 2 hours to change the lengths of the hairs (for a detailed synthetic procedure, see the Supporting Information). The volume of the solvent DMF was critical.^[11] In a number of cases where 58 mg of polyinitiator **2c** and 5 g of monomer were dissolved in 5 mL of DMF cross-linking could instantaneously be visually recognized and no soluble product could be isolated. Cross-linking still occurred if 10 mL of DMF was used but some hairy denpols, specifically those with “short hair” at low conversion and short reaction times (10 min), could be isolated. The optimum results were finally obtained with 20 mL of DMF, where only small amounts of insoluble product were obtained (ca. 5 mass%). For both reaction times all other material was fully soluble and was purified by passing it through a short column of silica gel (100–200 mesh, eluent: dichloromethane), which left the Cu salts behind as a blue layer on the top of the column. This process was associated with a considerable loss of material, which stayed on the column and could not be eluted despite the fact that it was fully soluble before.^[12] Removal of solvent furnished 1 g (0.5 h) and 1.2 g (2 h) of a colorless, transparent film (20 and 25 % conversion, respectively, based on MMA). The apparent number-average molar masses of **3** obtained by GPC were 2000000 (0.5 h) and 3500000 (2 h) (apparent PDIs: 2.5 and 1.4, respectively). These values need to be considered with care because there is no appropriate standard available for such complex molecular structures. The actual molar masses will most probably be higher.^[9] The hair lengths were roughly estimated by hydrolyzation experiments with denpol **3** and a model compound to be on the order of 20000–25000 g mol⁻¹ (PDIs ca. 1.3; see Supporting Information). These figures were used to derive the number of initiator sites per repeat unit of **2c** that had actually been active. Assuming the above

hair molecular weights are correct and doing a simple mass consideration, an initiator efficiency of roughly 50 % (two out of four) was obtained (see Supporting Information).

Denpol **3**, which had been purified from nonbound PMMA chains,^[13] was spin-coated from diluted chloroform solution onto mica, MoS₂, and highly oriented pyrolytic graphite (HOPG) and investigated by SFM in the tapping mode (Figure 1a–c). In all cases the adsorbed denpol molecules exhibit a backbone conformation in quasi two dimensions.^[14] Single denpol molecules are found on mica and MoS₂ on atomically flat terraces, whereas on HOPG they are predominantly in islands and at step edges because of a high mobility on the HOPG terraces. The image on mica (Figure 1a) reveals single denpol molecules with a central backbone and a frayed-out corona, with a total width of about 122 nm (average value from 64 cross-sectional profiles) and a thickness between 0.5 and 1 nm, which decreases gradually from the backbone toward the edge. In addition, there are small islands with the same apparent thickness as the corona and no backbone. We attribute the corona to extended flat-lying PMMA chains covalently linked to the denpol backbone and the islands to free PMMA chains, which obviously had not been removed during purification. Given a number-average molar mass of $M_n = 20000 \text{ g mol}^{-1}$, a fully extended chain (hair) would on average be 50 nm long, which is in good agreement with half of the corona width (61 nm). The backbone conformation was analyzed by plotting $\langle \cos \Theta \rangle$ versus ℓ , where Θ is the change in orientation between two segments at a distance ℓ apart along the backbone contour. A fit to the wormlike chain model in 2D^[15] would result in a persistence length of 65 nm (see Supporting Information). The corona exhibits holes and a sharp edge on MoS₂. Moreover, it is narrower (90 nm, average value from 114 cross-sectional profiles) and thicker (between 1 and 2 nm), and the apparent persistence length of the backbone amounts to 164 nm. The corona width is not so well defined on HOPG since, because of their high mobility, free PMMA molecules diffuse across the surface and into the corona of the denpol,

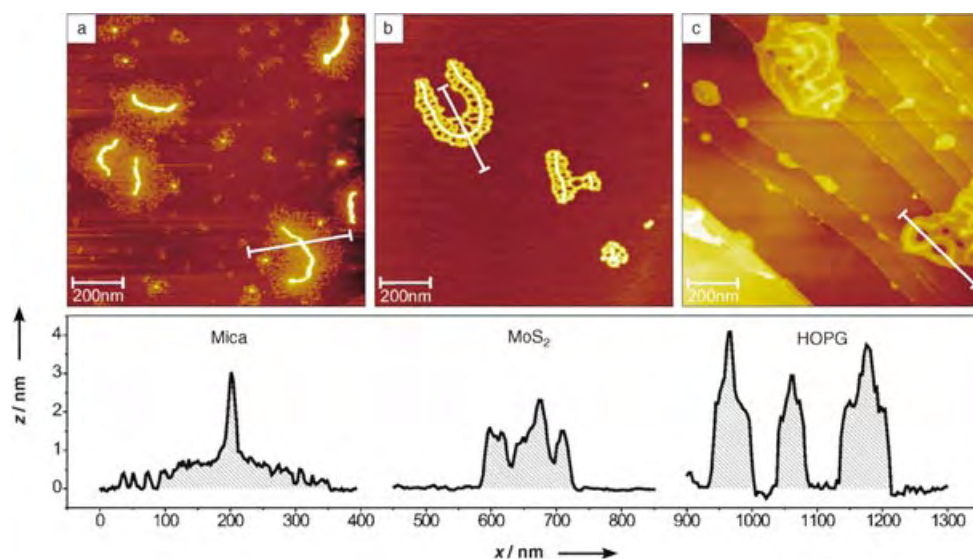


Figure 1. SFM images and cross-sectional profiles of **3** with PMMA hairs of $M_n = 20000\text{--}25000 \text{ g mol}^{-1}$ on a) mica, b) MoS₂, and c) HOPG.

thereby increasing its thickness. A typical distance between the backbones on the order of 50 nm is observed in the islands, which is attributed to a corona width. The height profile indicates a homogeneous layer of roughly constant height of about 2 nm, which decreases sharply at the edge.

The determined hair lengths of approximately 50 nm correspond well with half of the corona width on mica, which indicates that the PMMA chains are more or less stretched out perpendicular to the backbone direction. The fraying reflects the polydispersity of the hairs. The narrower corona on MoS₂ shows that the hairs now deviate from an all-stretched conformation by bending back. They dewet into bundles that form a sharp corona edge, thus indicating a less favorable interaction of the PMMA chains with MoS₂ as compared to mica. The relatively small distance of 50 nm between the backbones on HOPG indicates that the PMMA chains also bend back on this substrate. There is no indication of the above kind of dewetting. The continuous increase in apparent corona height on going from mica to MoS₂ and HOPG (Figure 1, bottom) suggests that the hair/substrate interaction on HOPG is the least favorable.

The results show that the hair/substrate interaction has a considerable effect on hair conformation. The hairs behave quite differently on MoS₂ and HOPG, but in either case the all-stretched conformation perpendicular to the backbone direction is avoided, which results in a much narrower corona than on mica. The hairy denpols, with their sensitive response to solid substrates, open the possibility of controlling the persistence of a single polymer at a surface. This could potentially be exploited for polymers having hairs of different natures and lengths on the same substrate or, alternatively, for the same polymer on different substrates. SFM studies of hairy denpols clearly also allows the independent investigation of hairs and backbone. This can lead to a better understanding of the mutual hair/backbone interaction.

The next steps include increasing the interaction of the hairs with the denpol backbone and decreasing their interaction with the substrate. Also, it seems likely that the use of a "thicker" backbone (e.g., G4), where the hairs near to the backbone "see" only other hairs, may also have a positive effect.

Received: April 21, 2004

Keywords: chain structures · dendrimers · polymers · scanning probe microscopy

- [1] a) Y. Tsukahara, K. Mizuno, A. Segawa, Y. Yamashita, *Macromolecules* **1989**, *22*, 1546–1550; b) M. Wintermantel, M. Schmidt, Y. Tsukahara, K. Kajiura, S. Kohjiya, *Macromol. Rapid Commun.* **1994**, *15*, 279–284; c) P. Dziezok, S. S. Sheiko, K. Fischer, M. Schmidt, M. Möller, *Angew. Chem.* **1997**, *109*, 2894–2897; *Angew. Chem. Int. Ed. Engl.* **1997**, *36*, 2812–2815; d) S. Qin, K. Matyjaszewski, H. Xu, S. S. Sheiko, *Macromolecules* **2003**, *36*, 605–612; e) M. Zhang, T. Breiner, H. Mori, A. H. E. Müller, *Polymer* **2003**, *44*, 1449–1458; f) C. Li, N. Gunari, K. Fischer, A. Janshoff, M. Schmidt, *Angew. Chem.* **2004**, *116*, 1121–1124; *Angew. Chem. Int. Ed.* **2004**, *43*, 1101–1104.

- [2] For recent reviews, see: a) K. Matyjaszewski, J. Xia, *Chem. Rev.* **2001**, *101*, 2921–2990; b) N. Hadjichristidis, M. Pitsikalis, H. Iatrou, S. Pispas, *Macromol. Rapid Commun.* **2003**, *24*, 979–1013.
- [3] A. D. Schlüter, J. P. Rabe, *Angew. Chem.* **2000**, *112*, 860–880; *Angew. Chem. Int. Ed.* **2000**, *39*, 864–883; A. Zhang, L. Shu, Z. Bo, A. D. Schlüter, *Macromol. Chem. Phys.* **2003**, *204*, 328–339; A. D. Schlüter, *Top. Curr. Chem.* **2004**, in press.
- [4] L. Shu, A. D. Schlüter, C. Ecker, N. Severin, J. P. Rabe, *Angew. Chem.* **2001**, *113*, 4802–4805; *Angew. Chem. Int. Ed.* **2001**, *40*, 4666–4669; J. Barner, F. Mallwitz, L. Shu, A. D. Schlüter, J. P. Rabe, *Angew. Chem.* **2003**, *115*, 1976–1979; *Angew. Chem. Int. Ed.* **2003**, *42*, 1932–1935.
- [5] A. Zhang, A. D. Schlüter, *Polym. Prepr. Am. Chem. Soc. Div. Polym. Chem.* **2003**, *44*, 524–525.
- [6] M. Kamigaito, T. Ando, M. Sawamoto, *Chem. Rev.* **2001**, *101*, 3689–3746.
- [7] In brush synthesis the polymeric initiators are normally prepared by attaching initiator sites to a precursor polymer in an independent synthesis step, which may lead to complications and incompleteness. Structural proof of the resulting macro-initiators does not always meet accepted standards.
- [8] If the lyophilization was done in DMF or benzene, the polymer was obtained in a morphology which did not dissolve or molecularly disperse in DMF, the medium for the following ATRP step, but instead formed a gel.
- [9] A. Zhang, B. Zhang, E. Wächtersbach, M. Schmidt, A. D. Schlüter, *Chem. Eur. J.* **2003**, *9*, 6083–6092; A. Zhang, L. Okrasa, T. Pakula, A. D. Schlüter, *J. Am. Chem. Soc.* **2004**, *126*, 6658–6666.
- [10] Given an average molecular weight of 1500000 and 1000 for polymer **2c** and its repeat unit, respectively, an individual chain has $1500 \times 4 = 6000$ initiator sites. Of course, one has to consider that not all the initiator sites will actually act as such for steric reasons.
- [11] Several experiments were also tried in toluene but cross-linking could not be prevented. Presumably toluene does not dissolve or disperse **2c**. In a recent report on cross-linking reactions in ATRP, Cu^{II} salts were proposed to deactivate the reactivity of the chain end: K. Matyjaszewski, S. Qin, J. R. Boyce, D. Shiravanyants, S. S. Sheiko, *Macromolecules* **2003**, *36*, 1843–1849.
- [12] In three independent experiments these losses amounted to 59% (100 mesh), 50% (100 mesh), and 76% (300–400 mesh). It is assumed that it is the high-molecular weight hairy denpols which strongly adhere to the silica surface. Tests confirmed that nonconnected PMMA easily passed through the column.
- [13] The denpols were purified by preparative GPC such that no PMMA was detectable. Nevertheless, all samples still contained some nonbound PMMA hairs, as observed in the SFM images.
- [14] There must have been a process which converts the 3D structures into the 2D structures in solution.
- [15] C. Rivetti, M. Guthold, C. Bustamante, *J. Mol. Biol.* **1996**, *264*, 919–932.

Enzyme Activity

Activation of an Autoregulated Protein Kinase by Conditional Protein Splicing**

Henning D. Mootz, Elyse S. Blum, and Tom W. Muir*

The temporal and spatial control of protein function is of fundamental importance in biology. Most cellular processes require that a small subset of the proteome be active at a particular time and place, and that this activity have a defined duration. To probe the role of a protein in a biological system, one must be able to control these parameters as precisely as possible.^[1,2] We recently developed a new tool, termed conditional protein splicing (CPS), to control the primary structure, and hence function, potentially of any protein by using a small molecule.^[3,4] The basic principle of CPS is illustrated in Figure 1a. Exploitation of a split intein that is only active in the presence of the small molecule rapamycin allows proteins or polypeptides to be linked by a peptide bond through protein splicing. The sequences of interest are expressed as recombinant fusions to the N- and C-terminal halves of the intein, which are themselves linked to FKBP and FRB domains. These domains form a high-affinity ternary complex with rapamycin.^[5] The induced proximity of the intein halves in this complex mediates the reconstitution of the active intein. Since CPS acts at the posttranslational level, it has the advantage of a short response time (as little as 10 min), which allows high temporal resolution.

There are many conceivable strategies for specifically altering the function of a protein by CPS. The most obvious method is to reassemble the protein from two inactive pieces and thereby switch on its activity. This strategy exploits the bond-making feature of CPS and requires that the newly spliced polypeptide spontaneously adopts an active structure. We decided to take advantage of another feature of the CPS reaction, the peptide-bond-breaking steps. The CPS system depicted in Figure 1a can be regarded not only as a conditional protein ligase that forms the peptide bond between the two extein sequences, but also as a conditional protease that breaks the peptide bonds between the intein and extein sequences. We conceived a strategy in which the protein of

interest and a peptide sequence that acts as an inhibitor are fused to opposite ends of one of the CPS constructs such that they are cleaved from one another in the course of the protein splicing reaction. This cleavage should result in a relative increase in the activity of the protein because the inhibitor should display a lower potency when free than while fused to the protein as a result of its higher local concentration in the intramolecular arrangement. This design borrows from the principles often used by nature to control the activity of enzymes. So-called active-site-directed intrasteric autoregulation^[6] has been observed for many proteins, for example, zymogens are kept in an autoinhibited state until posttranslational processing reveals the active protease.

Protein kinases are key players in a myriad of important processes in the cell and are thus attractive targets upon which to test our idea. We chose the cAMP-dependent protein kinase (PKA) for our investigations because it is probably one of the best-understood kinases in terms of its structure, regulation, and function.^[7] PKA is the major mediator of cAMP responses in mammalian cells. The PKA holoenzyme is an inactive tetramer composed of two catalytic subunits and two regulatory subunits. The regulatory subunits each contain a pseudosubstrate sequence that competitively inhibits the catalytic subunit by binding to the substrate recognition pocket. Binding of cAMP to the regulatory subunit results in release of the active catalytic subunit, which is then able to phosphorylate Ser/Thr-containing consensus sequences in substrate proteins such as the cyclic AMP response element binding protein. Peptide inhibitors of the catalytic subunit with inhibition constants (K_i) ranging from low nanomolar to micromolar values have been described.^[8,9] These peptides are derived from the heat-stable protein kinase inhibitor (PKI), a 75-residue protein that, like the regulatory subunit of PKA, contains a pseudosubstrate sequence. Biochemical^[8,9] and structural^[10] studies have allowed the key residues in PKI that interact with the kinase to be defined. The 20-mer peptide PKI(5–24) has the sequence TTYAD-FIASGRTGRRNAIHD (key residues underlined) and a K_i value of 2.3 nM.^[8] Lawrence and co-workers exploited these structure–activity data to design and prepare a caged version of the catalytic subunit of PKA in which a low-affinity peptide inhibitor is chemically linked to an active-site Cys residue.^[11] The caged kinase was found to be autoinhibited until the peptide was released by photolysis, which led to kinase activation. This important study suggests that it should be feasible to design an autoinhibited PKA by using the general CPS-based strategy outlined in Figure 1b.

We designed a protein construct (**2**) in which a pseudo-substrate peptide sequence, TGRRNAI ($K_i \approx 1 \mu\text{M}$, extrapolated from data given in ref. [8]; key residues underlined), and the PKA catalytic subunit were genetically fused to the N and C termini, respectively, of the FRB-intein^C (FRB-I^C) component of the CPS system (Figure 1b, see the Supporting Information for full experimental protocols). In this arrangement, the catalytic subunit represents the C-terminal extein, which following the protein splicing reaction ends up on a different protein fragment from the peptide inhibitor. The catalytic subunit was incorporated as the C-terminal, rather than the N-terminal, extein because the N terminus of the

[*] Dr. H. D. Mootz,† E. S. Blum, Prof. Dr. T. W. Muir
Laboratory of Synthetic Protein Chemistry
Rockefeller University
1230 York Avenue, New York, NY 10021 (USA)
Fax: (+1) 212-327-7358
E-mail: muir@rockefeller.edu

[†] Current address:
Philipps-Universität Marburg
Fachbereich Chemie/Biochemie
Hans-Meerwein-Strasse, 35032 Marburg (Germany)

[**] We would like to thank the members of the Muir laboratory and Jörn Lausen for technical and scientific advice during the course of this work. This work was supported by a National Institutes of Health grant awarded to T.W.M. (Grant no. R01-GM59908).

Supporting information for this article is available on the WWW under <http://www.angewandte.org> or from the author.

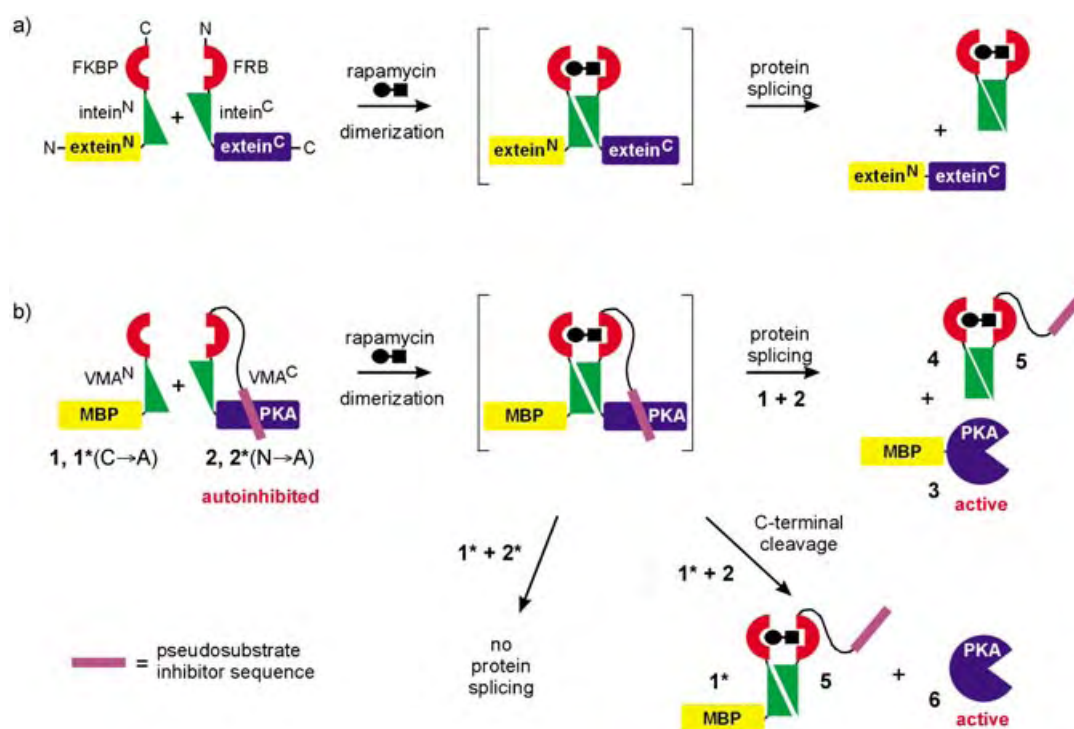


Figure 1. Activation of an enzyme by conditional protein splicing. a) The principle of CPS. The complementary halves of the *PI-Sce* vacuolar ATPase (VMA) intein (ATP, adenosine triphosphate) are marked intein^N and intein^C.^[3,21,22] FKBP and FRB are the rapamycin interaction domains. b) Scheme for controlling the kinase activity of the catalytic subunit of cAMP-dependent protein kinase (PKA; AMP, adenosine monophosphate) by CPS. Constructs 1* and 2* contain inactivating mutations within intein^N and intein^C, respectively. The His tags present at the N and C termini of constructs 2 and 1, respectively, are not shown. MBP maltose-binding protein.

protein is less structured than the C terminus.^[12] The complementary construct **1** contains the FKBP domain with the counterpart intein^N and carries a maltose-binding protein as the N-terminal extein (Figure 1b). This construct was described previously.^[4]

Constructs **1** and **2** were overexpressed separately in *Escherichia coli* and purified from the soluble fractions after cell lysis. Protein splicing reactions were initiated by mixing the purified proteins together, either with or without rapamycin. After incubation at 25°C for 2 h, product formation was analyzed by SDS-PAGE and Western blotting with anti-MBP and anti-PKA antibodies. Formation of the expected splicing product, MBP–PKA (**3**), was observed in the presence of rapamycin but not in its absence (Figure 2a, lanes denoted **1+2**). The cleaved intein fragments **4** and **5** were also observed in the reaction mixture containing rapamycin (data not shown). We investigated the kinase activity of the catalytic subunit in these splicing reactions by measuring enzyme-catalyzed phosphoryl group transfer from γ -[³²P]-ATP to the serine residue of the short “Kemptide” peptide substrate LRRASLG.^[8] As shown in Figure 2b, a 4- to 5-fold increase in kinase activity was observed for the reaction mixture containing both protein constructs and rapamycin compared to the reaction without the small molecule inducer. A control sample containing only construct **2** displayed even lower kinase activity than the mixture containing **1** and **2** (about 7-fold lower than that of the rapamycin-induced sample). The increased kinase activity of **2** in the presence of **1** is possibly the result of a small amount

of background splicing that occurs in the absence of rapamycin. This phenomenon has been observed previously for in vitro reactions with similar intein constructs containing model extein sequences.^[4] Other control reactions in which either construct **2** or the substrate was omitted from the mixture resulted in background levels of activity (Figure 2b). Addition of a PKI-derived peptide inhibitor, the 18-mer “Wiptide” peptide (TTYADFIASGRTGRRNAI), which has a reported *K*_i value of 3.1 nM for the catalytic subunit,^[8] reduced the kinase activity of the autoinhibited construct **2** to background levels. This result suggests that autoinhibition with the TGRRNAI sequence is not as efficient as inhibition with the native inhibitor PKI.

We conducted a series of control experiments to verify that the observed rapamycin-dependent induction of PKA activity indeed occurs by the proposed mechanism, that is, cleavage of the inhibitor sequence during protein splicing. To rule out the effects of possible conformational changes or steric clashes caused by the simple dimerization of constructs **1** and **2**, we sought to uncouple the rapamycin-induced protein dimerization from the protein splicing event. Mutations were introduced at key intein residues to abrogate protein splicing without affecting the dimerization domains FKBP and FRB (Figure 1b).

We prepared a mutant version of construct **1** in which the catalytic cysteine residue in the I^N fragment was changed to an alanine residue (construct 1*). Incubation of the mutant with construct **2** resulted in rapamycin-dependent peptide bond cleavage at the intein–C-extein junction, that is, between PKA

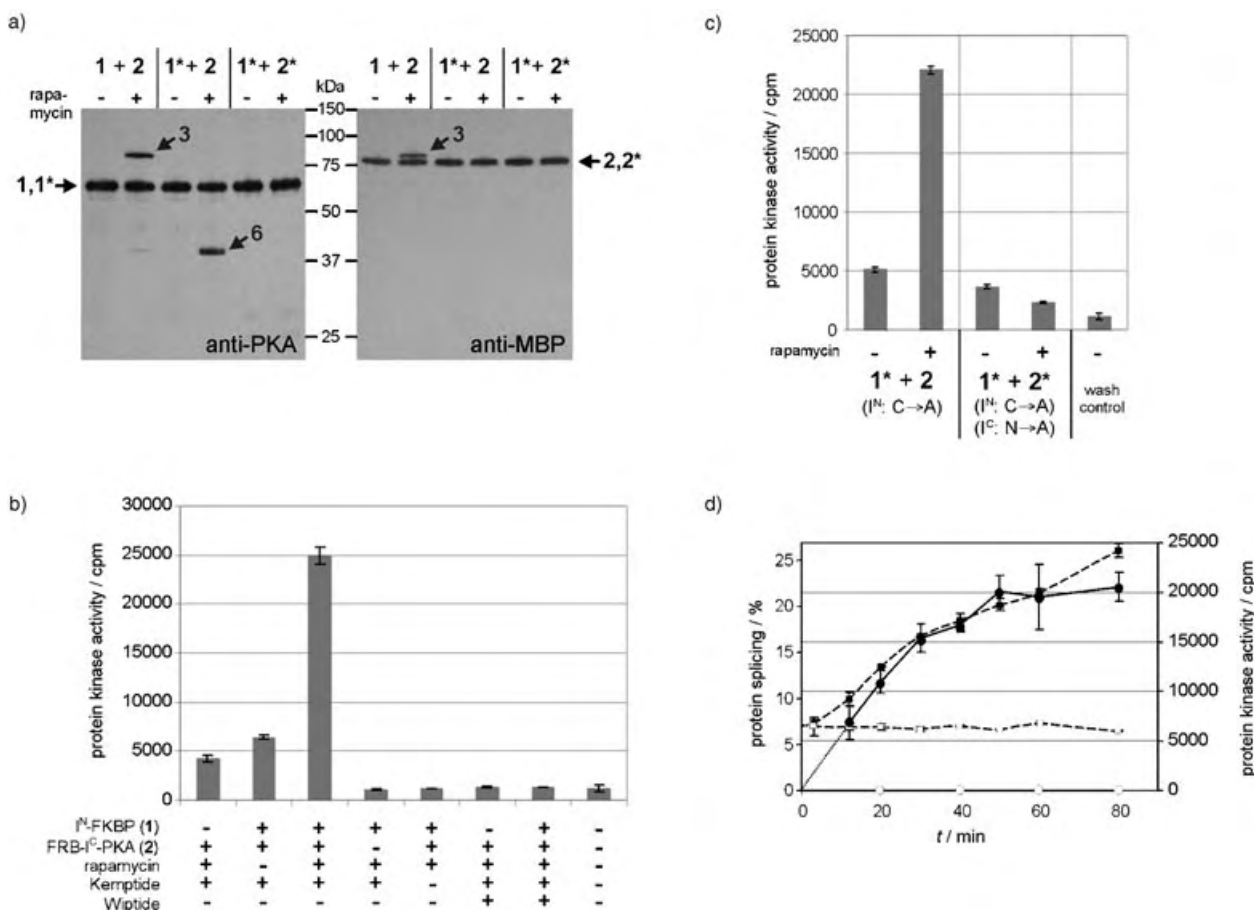


Figure 2. In vitro CPS and kinase activities. a) Western blot of CPS reaction products treated either with anti-PKA or with anti-MBP antibodies. Splicing reactions were carried out by mixing complementary proteins (1 μM each) in assay buffer (50 mM tris(hydroxymethyl)aminomethane/HCl, 300 mM NaCl, 1 mM ethylenediaminetetraacetate, 5 mM 1,4-dithiothreitol, pH 8.0) and adding rapamycin from a stock solution (1 mM) in dimethylsulfoxide (DMSO) to a final concentration of 10 μM . For reactions without rapamycin, the equivalent volume of DMSO was added. The reactions were allowed to run for 2 h at 25 $^{\circ}\text{C}$. b, c) In vitro phosphorylation of the Kemptide substrate peptide by the indicated CPS mixtures. CPS reaction mixtures were incubated for 2 h and the kinase activity was measured by using a radioactive filter-binding assay (see the Supporting Information for details). Each bar represents the average result of three experiments \pm standard deviation (SD). d) Time courses of protein splicing (solid lines) and kinase activity (dashed lines). Rapamycin addition was carried out at $t=0$ (filled circles and squares) and was omitted in negative controls (empty circles and squares). Splicing efficiency was determined by quantification of the bands in the Western blots and kinase activity was monitored as described in (B). Each data point is the average result of two experiments \pm SD.

and the I^{C} fragment (Figure 2a, lanes $1^* + 2$). Mutant inteins that support cleavage at the intein-C-extein junction have been reported previously^[13,14] but this is the first example of a pH/temperature-independent inducible cleavage system. This mutant CPS system acts as a specific conditional protease and could thus be of general utility. As illustrated in Figure 1b, this cleavage process also unleashed the protein kinase from its fused inhibitory peptide, which explains the observed induction of kinase activity at similar levels to those observed with **1** and **2** (Figure 2c).

To block the C-terminal cleavage reaction, the catalytic asparagine residue in the intein^C fragment of **2** was mutated to alanine to give construct **2***. No protein splicing or C-terminal cleavage was observed when mutated constructs **1*** and **2*** were mixed with rapamycin (Figure 2a, lanes $1^* + 2^*$) and we observed no increase in kinase activity during incubation with the small molecule (Figure 2c). These results show that formation of the dimeric complex does not induce PKA

activation. We also performed a time-course experiment with constructs **1** and **2**, which revealed that the level of PKA activation is correlated with the degree of protein splicing (Figure 2d). These data suggest that kinase activity would increase by around 25-fold at 100% splicing efficiency. Together, our results demonstrate that the kinase is switched from an autoinhibited to an active state by the proposed mechanism, which involves unleashing the enzyme from its inhibitor.

Optimization of kinase autoinhibition and activity induction was achieved by replacing the TGRRNAI sequence with a series of peptide sequences exhibiting gradually increasing affinities for the active site of PKA (see the Supporting Information for details). Insertion of the entire high-affinity “Wiptide” sequence (see above) or the sequence TGAANAI in which the key recognition arginine residues were mutated provided further controls. In these systems, the kinase was either fully inhibited irrespective of the progress of protein

splicing, or almost completely lacked autoinhibition (see the Supporting Information).

In conclusion, we have prepared an autoregulated version of a protein kinase that is activated by cleavage of a specific peptide bond, much like a zymogen. Protein design principles have previously been used to generate artificially autoregulated enzymes^[11,15–17] but our design is the first in which allosteric ligand binding and concomitant processing are integrated into the same autoregulation system. Our studies also demonstrate that kinase activation depends upon the extent of protein splicing and the nature of the autoinhibitor (Figure 2 and Supporting Information). Both these parameters can be controlled; the level of protein splicing depends on the amount of rapamycin added to the system and the duration of the reaction,^[3,4] whilst the autoinhibitor sequence is defined at the genetic level. In effect, the system acts like a protein rheostat that can be adjusted in one of several ways. It should be possible to translate the autoregulation scheme described herein to other protein kinases, and perhaps other classes of enzymes for which peptidic inhibitors are available.

We demonstrated in previous studies that CPS works in mammalian cells.^[4] Therefore, the autoregulation strategy described herein should work in an appropriate cellular context (e.g. where the endogenous enzyme has been knocked out or knocked down) and could allow the timing and level of enzyme activity to be controlled. Our system is also one of the few examples^[18,19] of activation of an enzyme by the addition of a small molecule; most chemical genetic studies result in the design or discovery of small-molecule inhibitors.^[2] In principle, it should be possible to switch an enzyme on with rapamycin and then turn it off again with a second specific small molecule, for example with an allele-specific inhibitor.^[20] Thus, the use of CPS to control the activation of an autoregulated enzyme therefore holds great potential as a way to probe the function of proteins.

Received: June 11, 2004

Keywords: enzymes · inhibitors · protein kinase · protein splicing

- [1] S. L. Schreiber, *Bioorg. Med. Chem.* **1998**, 6, 1127.
- [2] M. A. Shogren-Knaak, P. J. Alaimo, K. M. Shokat, *Annu. Rev. Cell Dev. Biol.* **2001**, 17, 405.
- [3] H. D. Mootz, T. W. Muir, *J. Am. Chem. Soc.* **2002**, 124, 9044.
- [4] H. D. Mootz, E. S. Blum, A. B. Tyszkiewicz, T. W. Muir, *J. Am. Chem. Soc.* **2003**, 125, 10561.
- [5] J. Choi, J. Chen, S. L. Schreiber, J. Clardy, *Science* **1996**, 273, 239.
- [6] B. Kobe, B. E. Kemp, *Nature* **1999**, 402, 373.
- [7] D. A. Johnson, P. Akamine, E. Radzio-Andzelm, M. Madhusudan, S. S. Taylor, *Chem. Rev.* **2001**, 101, 2243.
- [8] D. B. Glass, H. C. Cheng, L. Mende-Mueller, J. Reed, D. A. Walsh, *J. Biol. Chem.* **1989**, 264, 8802.
- [9] J. D. Scott, M. B. Glaccum, E. H. Fischer, E. G. Krebs, *Proc. Natl. Acad. Sci. USA* **1986**, 83, 1613.
- [10] D. R. Knighton, J. H. Zheng, L. F. Ten Eyck, N. H. Xuong, S. S. Taylor, J. M. Sowadski, *Science* **1991**, 253, 414.
- [11] K. Curley, D. S. Lawrence, *J. Am. Chem. Soc.* **1998**, 120, 8573.
- [12] M. Batkin, I. Schvartz, S. Shaltiel, *Biochemistry* **2000**, 39, 5366.

- [13] S. Chong, Y. Shao, H. Paulus, J. Benner, F. B. Perler, M. Q. Xu, *J. Biol. Chem.* **1996**, 271, 22159.
- [14] D. W. Wood, W. Wu, G. Belfort, V. Derbyshire, M. Belfort, *Nat. Biotechnol.* **1999**, 17, 889.
- [15] C.-Y. Chang, T. Fernandez, R. Panchal, H. Bayley, *J. Am. Chem. Soc.* **1998**, 120, 7661.
- [16] A. Saghatelian, K. M. Guckian, D. A. Thayer, M. R. Ghadiri, *J. Am. Chem. Soc.* **2003**, 125, 344.
- [17] P. Plankum, S. M. Fuchs, S. Wiyakrutta, R. T. Raines, *Nat. Struct. Biol.* **2003**, 10, 115.
- [18] F. R. Papa, C. Zhang, K. Shokat, P. Walter, *Science* **2003**, 302, 1533.
- [19] B. R. Stockwell, S. L. Schreiber, *Curr. Biol.* **1998**, 8, 761.
- [20] C. M. Niswender, R. W. Ishihara, L. M. Judge, C. Zhang, K. M. Shokat, G. S. McKnight, *J. Biol. Chem.* **2002**, 277, 28916.
- [21] S. Chong, M. Q. Xu, *J. Biol. Chem.* **1997**, 272, 15587.
- [22] X. Duan, F. S. Gimble, F. A. Quirocho, *Cell* **1997**, 89, 555.

Supercritical Fluids

Sensing the Critical Point of High-Pressure Mixtures**

Jie Ke,* Robert M. Oag, P. J. King, Michael W. George, and Martyn Poliakoff*

Supercritical fluids are becoming increasingly attractive as solvents for chemical reactions and processes.^[1–3] This development is creating a greater need for critical-point data for the multicomponent mixtures used in these applications. Critical-point data are important for the rigorous testing of computer models of the vapour–liquid equilibria, which are required to realize these chemical processes in practice. Surprisingly, most of the techniques available for locating critical points have hardly changed for more than a century and are time-consuming and often subjective.^[4] Herein we describe a completely new approach, which is far more objective. Our strategy is to use a single, simple sensor in an unusual manner so as to distinguish between the dew point

[*] Dr. J. Ke, Prof. M. W. George, Prof. M. Poliakoff
School of Chemistry
University of Nottingham
University Park, Nottingham NG7 2RD (UK)
Fax: (+44) 115-951-3058
E-mail: pcxjk2@unix.ccc.nottingham.ac.uk
martyn.poliakoff@nottingham.ac.uk

Dr. R. M. Oag, Dr. P. J. King
School of Physics and Astronomy
University of Nottingham
University Park, Nottingham NG7 2RD (UK)

[**] This work was supported by EU FP5 project CPFCO2 and the Paul Instrument Fund of the Royal Society of London. We are grateful to Profs. J. S. Rowlinson and S. Palmer for valuable comments. We thank Drs. M. V. Avdeev, S. K. Ross and C. J. Mellor for help and M. Guyler, K. Stanley, R. Wilson, P. Fields for technical support.

and bubble point curves of the mixture and hence to locate the point at which the two curves meet, the critical point.

In principle, the critical point of any pure, single-component substance can be found by simply observing the fluid as it is heated in a closed cell fitted with suitably pressure-resistant windows. The critical temperature and pressure, T_c and P_c , are the maximum values, for which gas and liquid can coexist. The problem becomes inherently more complicated with binary or multicomponent mixtures since additional components introduce extra degrees of freedom into the phase diagram. In particular, the critical point becomes just one of many points along the phase boundary and neither T_c nor P_c is necessarily the maximum value for coexistence. The critical point is now defined as the point at which all intensive properties are identical for the two coalescing phases; in particular the composition and density are the same for both phases. The critical point can therefore be recognized by the disappearance of the meniscus exactly halfway up the view cell when a liquid mixture is heated under a fixed volume. However, in practice, judging this condition is fraught with uncertainty. Our method relies on an alternative property of the critical point, namely, that it occurs at the intersection of the bubble point and dew point curves of the mixture.

Trying to monitor phase separation with a single sensor might seem to be a fruitless exercise because sensors tend to measure average properties of the phases. However we have overcome this problem by using a sensor that only responds to a density-dependent property of the fluid layer in immediate contact with the surface of the sensor. Hence, it gives substantially different signals for liquids and gases. The sensor is mounted near the bottom of a variable-volume cell fitted with a powerful stirrer.^[5] Unlike traditional apparatus for phase measurements, there is no need for any window through which to observe the fluid.

Our method is based on the so-called “synthetic” approach in which one finds the temperature and pressure of the phase transition of a mixture of fixed composition in a sealed vessel. The experiment normally begins with the cell at high pressure and low volume, conditions under which the fluid mixture is in a single homogeneous phase. The volume of the cell is increased, the pressure drops and the density decreases smoothly until phase separation occurs. This separation registers as a discontinuity in the signal from the sensor. The key to our method is that this discontinuity is qualitatively different in form on the bubble and dew point curves of the fluid.

On the bubble point curve, phase separation involves the nucleation of small bubbles, which rise to the top of the cell, far removed from the sensor. Therefore, the sensor registers a modest increase in the density in the bulk of the fluid, Figure 1 a. In contrast, on the dew point curve, a thin film of liquid is formed on the walls of the cell and the surface of the sensor. This liquid is continually thrown around by the stirrer so that a liquid film is maintained on the surface of the sensor, which registers a sudden jump ($\Delta|Z|_{\min}$) from gas-like to liquid-like densities, Figure 1 b. The further the system is from the critical point, the greater the difference in density between the gas and liquid densities and the greater the

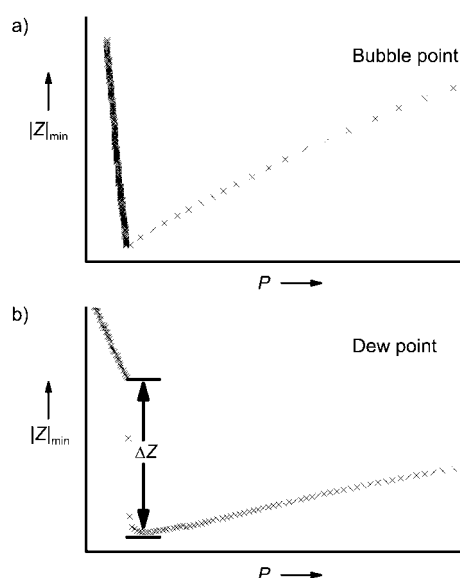


Figure 1. Shear-mode sensor responses ($|Z|_{\min}$) as a function of pressure along two isotherms showing the difference in the discontinuity caused by phase transitions on a) the bubble point and b) the dew point. In b) a new liquid phase appears from the gas phase after the phase separation, which results in a sudden jump ($\Delta|Z|_{\min}$) that is related to the difference in density between the two coexisting phases.

jump. The procedure is repeated at a series of different temperatures and the critical point is located by extrapolating to the temperature at which $\Delta|Z|_{\min}$ tends zero.

We have used two different types of sensor to validate this method. The first is a quartz “shear-mode” sensor,^[6] which is set up to register its equivalent resistance, $|Z|_{\min}$, an indication of the acoustic coupling between the sensor and the fluid. $|Z|_{\min}$ is proportional to “ γ ”, the square root of the product of density and viscosity of the fluid. The sensor gives a high value of $|Z|_{\min}$ in a liquid-like environment and a low value in a gas-like fluid. Similar sensors are used in quartz microbalances for monitoring volatile organic compounds^[7] and as shear-mode sensors for chiral discrimination.^[8] The second sensor is a fiber-optic reflectometer,^[9] in which U , the ratio of the intensity of the light entering the fiber to that back-reflected by the end of the fiber, depends on the difference in the refractive index between the fiber and the fluid, and hence on the density of the fluid. Its response is the inverse of that of the shear-mode sensor, high for gas and low for liquid-like densities. For the first study, $\text{CO}_2 + \text{MeOH}$, both sensors were mounted simultaneously in the same cell.

$\text{CO}_2 + \text{MeOH}$ is an extremely well studied mixture,^[10–14] particularly because of the widespread use of MeOH as a cosolvent to enhance the rather low solvent power of pure CO_2 . Even so, there are considerable differences in the value of T_c reported by different studies on mixtures of apparently similar composition.^[10–14] Figures 2 a and b show the traces recorded from the two sensors over the section of the phase boundary, which includes the critical point. As expected, for each temperature the two sensors agree within experimental error on the pressure at which phase separation occurs and the data agree well with literature values.^[11] The traces recorded by both sensors at higher temperatures display the

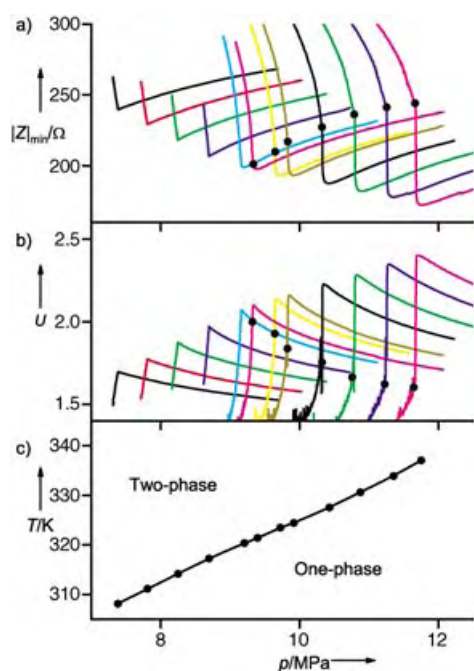


Figure 2. The binary mixture of MeOH + CO₂ with $x_{\text{MeOH}} = 0.139$. a) Plot of the shear-mode sensor response ($|Z|_{\min}$) to pressure along 12 isotherms, with temperature increasing from left to right. The minimum on each isotherm indicates the phase transition. For those isotherms on the right-hand side, a “jump” can be seen after the phase transition, as indicated by (●). b) Optic-fiber reflectometer response measured simultaneously with the data shown in a). The signal U is normalized with respect to the response in air. The maximum on each of these isotherms indicates the phase transition, and the sudden decreases in U are marked as (●). c) The P - T phase boundary (●, indicates measured points); note that there is no obvious indication of precisely where the critical point is located on this featureless curve.

characteristic “jump” indicative of the dew point curve (Figure 2). The optic fiber sensor, which has an extremely small active area compared to the shear-mode sensor, sometimes gave a “noisier” signal at the dew point because of the comparable dimension of the fiber tip and the liquid droplets. Extrapolation of these jumps back to the phase boundary locates the critical temperature, T_c , of the mixture. Figure 3 shows that the two sensors yield very similar values of T_c , 320.9 ± 0.2 K (shear-mode) and 320.8 ± 0.3 K (optic fiber). The critical pressure, P_c (9.30 MPa and 9.29 MPa respectively) can be found from the phase boundary in Figure 2c. In this way, the critical point can be identified in a relatively objective manner on a phase boundary that is essentially featureless.

The second mixture N₂(0.14) + CO₂(0.86) is of great historical interest. It was studied by Thomas Andrews^[15] in 1871–2, the first binary gas mixture ever to be studied in this way. His experiments involved compressing the mixture with a mercury “piston” in a vertical glass capillary tube sealed at the upper end. Andrews was concerned that the mixture might not be properly mixed in the narrow tube and he was unable to explain the mysterious evaporation of liquid on increasing the pressure. This was subsequently recognized as retrograde condensation.^[15] Therefore, until 2003, Andrews’s

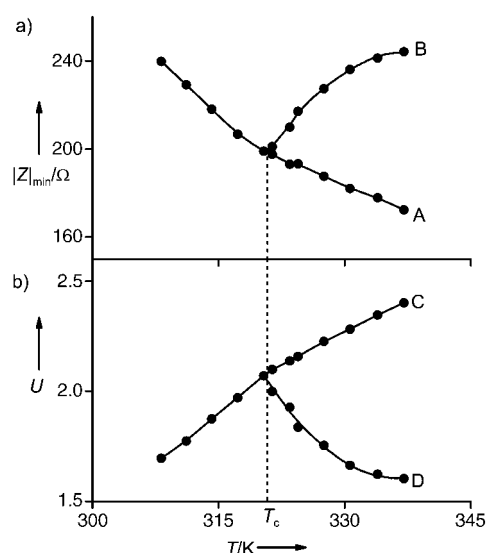


Figure 3. Locating the critical temperature (T_c) by using a) the shear-mode sensor, and b) the optic fiber sensor. Curves A and C correspond to the phase-transition curves, and Curves B and D are the sensor responses from the new liquid phase after the phase transition, marked as (●) in Figure 2a, b, respectively. Curve A was fitted with a cubic spline and B was fit with a cubic polynomial; the point at which the curves A and B intersect is the critical point. Similar treatments were made on curves C and D in Figure 3b. The dashed line indicates the critical temperature.

work remained unpublished^[15] and, surprisingly, no one had studied this mixture in the intervening 132 years.^[16–19]

Figure 4 shows the results of studying Andrews’s mixture with the shear-mode sensor. The traces look more complicated than for CO₂ + MeOH because of the curvature of the phase boundary. Figure 4b compares the experimental T , P phase envelope with the line derived from Andrews’s notebook.^[15] Excitingly, this shows that Andrews’s value of the maximum temperature of the phase envelope 21°C (294 K), is extremely close to our measured value, 293.6 ± 0.2 K, although the true error could be marginally greater because the composition of our mixture and Andrews’s might be slightly different. Interestingly, we also agree on the temperature at which the maximum pressure is observed, 282 K, but the maximum pressure itself, 9.8 MPa, is about 1.0 MPa lower than estimated^[15] from his results.

Just as with CO₂ + MeOH, the sensor registers a jump at the points along the dew-point curve. However, the curvature of the lines, shown in Figure 5a makes locating the intersection of the curves less certain than in Figure 3a. Therefore, we have tried a different approach by finding the temperature at which $\Delta|Z|_{\min}$ extrapolates to zero (Figure 5b). $\Delta|Z|_{\min}$ is defined as the difference in $|Z|_{\min}$ between liquid and gas at the dew point. This gives 290.9 ± 0.2 K for T_c and 9.42 MPa for P_c . Thus, T_c is 2.7 K lower than the maximum temperature, thereby explaining why Andrews could not understand the nature of the effect, which he observed over a narrow temperature range close to T_{\max} . This contrasts with the predictions of the Peng–Robinson equation of state (EOS), one of the most common EOS for supercritical mixtures, which predicts 293.4 K for T_c only 0.2 K below T_{\max} . By a

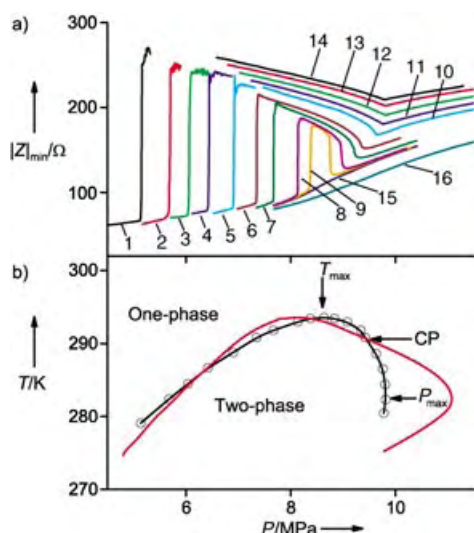


Figure 4. The binary mixture of N_2 and CO_2 with $x_{N_2}=0.14$, the same composition^[15] as used by Andrews in 1871–72. a) Plot of the variation of $|Z|_{\min}$ with pressure at various temperatures in the critical region. Isotherms 1–9 (279.1–293.4 K) display a dew point “jump” in $|Z|_{\min}$ after the phase transition; some isotherms (e.g., 9) have two jumps for a given temperature, thus indicating that there are two dew points along that isotherm, at which the retrograde condensation occurs. Isotherms 10–14 (280.5–288.6 K) show the “tick-shape” discontinuity characteristic the bubble-point on the phase boundary. Isotherms 15–16 (293.9 K and 297.0 K, respectively) have no discontinuities because they are above the maximum temperature of two-phase coexisting region. b) The points (○) indicate the experimental P – T phase boundary derived from a), together with the phase boundary (—) deduced from Andrews’s notebook;^[15] CP indicates the critical point.

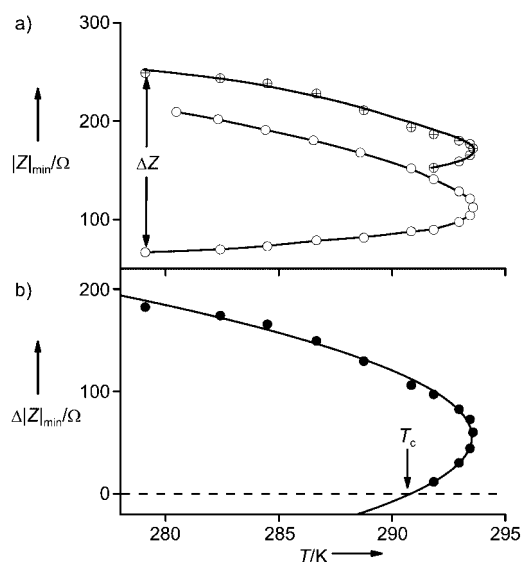


Figure 5. a) $|Z|_{\min}$, T projection: (○) from bulk phase at the phase boundary (⊕) from the new liquid phase after the phase separation. b) $\Delta|Z|_{\min}$ – T curve. This curve was fitted with a cubic polynomial and extrapolated to $\Delta|Z|_{\min}=0$ to find T_c . At the dew point, $\Delta|Z|_{\min}$ represents the difference in $|Z|_{\min}$ between liquid and gas which is indicated by the arrows in a).

strange quirk of fate, Figure 4b shows that Andrews’s phase boundary and ours intersect almost exactly at the critical point!

We have described a new, general and objective approach to locating critical points of fluid mixtures. It is new because it exploits the fact that the liquid phase forms preferentially on the surface of the sensor. It is general because it can be used with any type of surface-sensitive sensor and it is objective because it is based on the numerical output of a sensor rather than the visual image normally used for phase equilibrium studies.

Received: May 11, 2004

Keywords: phase diagrams · phase transitions · sensors · supercritical fluids

- [1] J. D. DeSimone, *Science* **2002**, 297, 799–803.
- [2] M. Poliakov, P. J. King, *Nature* **2001**, 412, 125.
- [3] E. J. Beckman, *J. Supercrit. Fluids* **2004**, 28, 121–191.
- [4] M. A. McHugh, V. J. Krukonis, *Supercritical fluid extraction: principles and practice*, 2nd Ed., Butterworth-Heinemann, Boston, **1994**.
- [5] R. M. Oag, P. J. King, C. J. Mellor, M. W. George, J. Ke, M. Poliakov, V. K. Popov, V. N. Bagratashvili, *J. Supercrit. Fluids* **2004**, DOI 10.1016/j.supflu.2003.09.021.
- [6] R. M. Oag, J. Ke, M. W. George, P. J. King, C. J. Mellor, M. Poliakov, *Anal. Chem.* **2003**, 75, 479–485.
- [7] M. Schlupp, T. Weil, A. J. Berresheim, U. M. Wiesler, J. Bargon, K. Mullen, *Angew. Chem.* **2001**, 113, 4124–4129; *Angew. Chem. Int. Ed.* **2001**, 40, 4011–4015.
- [8] K. Bodenhofer, A. Hierlemann, J. Seemann, G. Gauglitz, B. Koppenhoefer, W. Gopel, *Nature* **1997**, 387, 577–580.
- [9] M. V. Avdeev, A. N. Konovalov, V. N. Bagratashvili, V. K. Popov, S. I. Tsykina, M. Sokolova, J. Ke, M. Poliakov, *Phys. Chem. Chem. Phys.* **2004**, 6, 1258–1263.
- [10] P. S. Wells, S. Zhou, J. F. Parcher, *Anal. Chem.* **2003**, 75, 18A–24A.
- [11] S.-D. Yeo, S.-J. Park, J.-W. Kim, J.-C. Kim, *J. Chem. Eng. Data* **2000**, 45, 932–935.
- [12] A. D. Leu, S. Y. K. Chung, D. B. Robinson, *J. Chem. Thermodyn.* **1991**, 23, 979–985.
- [13] E. Brunner, W. Hueltenschmidt, G. Schlichthaerle, *J. Chem. Thermodyn.* **1987**, 19, 273–291.
- [14] E. Brunner, *J. Chem. Thermodyn.* **1985**, 17, 671–679.
- [15] J. S. Rowlinson, *Notes Rec. R. Soc. Lond.* **2003**, 57, 143–159.
- [16] B. Yucelen, A. J. Kidnay, *J. Chem. Eng. Data* **1999**, 44, 926–931.
- [17] N. Xu, J. Dong, Y. Wang, J. Shi, *Fluid Phase Equilib.* **1992**, 81, 175–186.
- [18] Y. Arai, G. Kaminishi, S. Saito, *J. Chem. Eng. Jpn.* **1971**, 4, 113–122.
- [19] N. K. Muirbrook, J. M. Prausnitz, *AIChE J.* **1965**, 11, 1092–1096.

The Magnetic Möbius Strip: Synthesis, Structure, and Magnetic Studies of Odd-Numbered Antiferromagnetically Coupled Wheels**

Olivier Cador, Dante Gatteschi, Roberta Sessoli,*
Finn K. Larsen, Jacob Overgaard, Anne-Laure Barra,
Simon J. Teat, Grigore A. Timco,* and
Richard E. P. Winpenny*

The previously reported cyclic 3d-metal structures, from the first—the ferric wheel of Lippard and co-workers^[1]—to the largest all contain an even number of metal centres.^[2] There are very few odd-numbered cyclic structures larger than three; all are pentametallic and feature polydentate inflexible ligands.^[3] Raptis and co-workers have very recently reported a nine-membered ring but only as part of higher nuclearity structures.^[4] It is difficult to rationalize the absence of odd-numbered wheels, especially as odd-numbered metallocrowns, that is, wheels centered with a further metal cation, are known.^[5] This is particularly frustrating because the magnetic properties of such wheels should be of great interest to physicists interested in magnetic frustration.^[6] Spin frustration is, in turn, important in areas as diverse as high temperature superconductors^[7] and CMR materials.^[8] Herein we report the first detailed magnetic characterization of an odd-numbered wheel larger than a triangle. The new molecular species synthesized allows us to study frustration at a mesoscopic scale at which quantum calculations are still

possible; hopefully the understanding gained here can later be applied more generally to other frustrated systems.

In a preceding paper^[9] we have shown how the chemistry of $[\text{Cr}_8\text{F}_8(\text{O}_2\text{CCMe}_3)_{16}]$ can be exploited to produce a series of heterometallic analogues $[\text{R}_2\text{NH}_2][\text{Cr}_7\text{MF}_8(\text{O}_2\text{CCMe}_3)_{16}]$, in which $\text{M} = \text{Ni}^{\text{II}}$ **1**, Co^{II} , Mn^{II} , or Fe^{II} and R can be a range of alkyl groups from methyl to *n*-octyl. The secondary ammonium cation is found encapsulated within the metal wheel, and this suggested that if we varied the size of the cation we might be able to vary the size of the wheel.

The reaction of hydrated chromium(III) fluoride with basic nickel carbonate in pivalic acid in the presence of dicyclohexylamine, followed by crystallization from THF/toluene produced well-shaped hexagonal crystals. Elemental analysis and electrospray mass spectroscopy (ESMS) provide convincing evidence for the formation of $[(\text{C}_6\text{H}_{11})_2\text{NH}_2][\text{Cr}_8\text{NiF}_9(\text{O}_2\text{CCMe}_3)_{18}]$ **2**. The ESMS spectrum of **2** contains a peak for the anionic wheel in the negative-ion spectrum and two significant peaks in the positive-ion spectrum for the molecular ion plus one sodium as well as for the ring plus two sodium ions. These are the only significant high-mass peaks.

The crystals of **2** appear to be single, but the X-ray diffraction pattern has an extraordinary distribution. Proper Bragg diffraction spots are found within a rather flat spheroidal shaped volume of reciprocal space and with pronounced diffuse scattering in the reciprocal planes perpendicular to the apparent sixfold crystal axis of rotation. This makes it difficult to integrate the Bragg intensities for determining structure factors and thus also creates a problem in assigning the space group. The structure can either be described in some hexagonal space groups or in the orthorhombic *Pbna* space group, which gives the lower internal *R* value of integrated reflections. Solving the structure in *Pbna* reveals a nona-metallic core, bridged by single atoms. Atoms of the nearest-neighbor octahedral coordination sphere can be located but the atomic structure does not develop further by subsequent least-squares refinement and difference Fourier methods. Undoubtedly there is much disorder of the outer parts of the pivalate ligands. The combined information of Bragg intensities and distribution of diffuse scattering supports the following model of the structure: The molecules that have a nine-membered ring form layers, and these molecules are stacked to form columns that are close-packed. The distribution of diffuse scattering over the reciprocal plane perpendicular to the stacking direction indicates disorder between the stacks of molecules. Little information concerning the identity of ligands attached to the metal core could be discerned, but existence of the nine-membered ring with indication of an ordered Ni position could be substantiated from the analysis of the Bragg intensities. The equivalent $\{\text{Cr}_8\text{Co}\}$ wheel compound was synthesized; it showed very similar cell constants and intensity distribution but had even more pronounced diffuse scattering, and full structural characterization remained elusive.

In an attempt to improve the knowledge of the nona-nuclear wheel structure we decided to investigate a system in which the metal sites are more likely to be ordered. Whereas in **1** the nickel site is disordered over the eight metal positions, if vanadyl is used the octanuclear wheel that results, $[\text{Et}_2\text{NH}_2]$

[*] Dr. O. Cador, Prof. D. Gatteschi, Prof. R. Sessoli
Laboratorio di Magnetismo Molecolare
Dipartimento di Chimica & INSTM
Università degli Studi di Firenze
Polo Scientifico Universitario
Via Lastruccia n. 3, 50019 Sesto Fiorentino (Italy)
Fax: (+39) 055-4573372
E-mail: roberta.sessoli@unifi.it

Dr. G. A. Timco, Prof. R. E. P. Winpenny
Department of Chemistry
The University of Manchester
Oxford Road, Manchester, M13 9PL (UK)
Fax: (+44) 161-275-4616
E-mail: grigire.timco@man.ac.uk
richard.winpenny@man.ac.uk

Prof. F. K. Larsen, Dr. J. Overgaard
Department of Chemistry
University of Aarhus
Aarhus (Denmark)

Dr. A.-L. Barra
Laboratoire des Champs Magnetiques Intenses-CNRS
38042 Grenoble Cedex 9 (France)

Dr. S. J. Teat
CCLRC Daresbury Laboratory
Warrington, Cheshire, WA4 4AD (UK)

[**] This work was supported by the EPSRC (UK), the EC-TMR Networks "MolNanoMag" (HPRN-CT-1999-00012) and "QuEMolNa" (MRTN-CT-2003-504880), the German DFG (SPP 1137) and INTAS (00-00172).

$[\text{Cr}_6(\text{VO})_2\text{F}_8(\text{O}_2\text{CCMe}_3)_{15}]$ **3**, has ordered metal sites, with the two VO^{2+} units next to each other within the wheel.^[12] Therefore we treated chromium trifluoride with pivalic acid and dicyclohexylamine in the presence of vanadyl acetate. The product that formed was isolated as $[(\text{C}_6\text{H}_{11})_2\text{NH}_2][\text{Cr}_7(\text{VO})_2\text{F}_9(\text{O}_2\text{CCMe}_3)_{17}]$ **4** (Figure 1). X-ray characteriza-

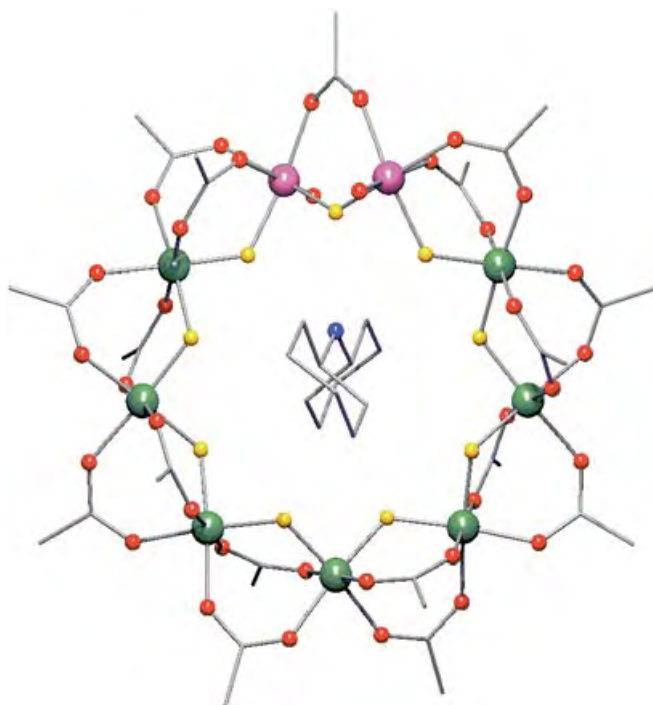


Figure 1. The structure of **4** in the crystal. The hydrogen atoms have been omitted for clarity. Bond length ranges [Å]: Cr–F 1.9098–1.9338, Cr–O 1.915–1.968, V–F 1.9494–2.0114, V–O(oxide) 1.580, V–O(pivalate) 1.989–2.185 (av esd 0.002). Cr dark green; V purple; F yellow; O red; N blue; C grey.

tion demonstrates,^[10] beyond doubt, that we have made nonanuclear metal wheels. Each $\text{Cr}\cdots\text{Cr}$ and $\text{Cr}\cdots\text{V}$ edge is bridged by one fluoride and two pivalate ions while the $\text{V}\cdots\text{V}$ edge is bridged by one fluoride ion and one pivalate ion.

The magnetic behavior of these nonanuclear wheels is fascinating. Compound **2** contains an even number of unpaired electrons due to the presence of a Ni^{II} ion, with $S=1$, and eight Cr^{III} ions with $S=3/2$ spins; this allows a diamagnetic ground state, and therefore **2** is not a typical example of a frustrated system: for example, the doubly degenerate $S=1/2$ ground states predicted to occur in odd-membered rings of half-integer spins. Nevertheless in **2** not all the antiferromagnetic interactions can be simultaneously satisfied and therefore it can be regarded as frustrated.^[13] A way to visualize the problem is its analogy with the Möbius strip, which better reflects the finite size of this system, compared to standard soliton or domain-wall pictures. The odd number of spins makes it impossible for all spins to align antiparallel to their nearest neighbor—as preferred where the exchange is antiferromagnetic. We can think of the region where the neighboring spins are alternately “up and down” as the flat region of the Möbius strip, while a “knot” occurs

between the nearest neighbors where the spins cannot be arranged antiparallel. More interesting and much less obvious is how the presence of this knot in the ring manifests itself in the magnetic properties.

The temperature dependence of the magnetic molar susceptibility, χ_M , is shown in Figure 2. At room temperature

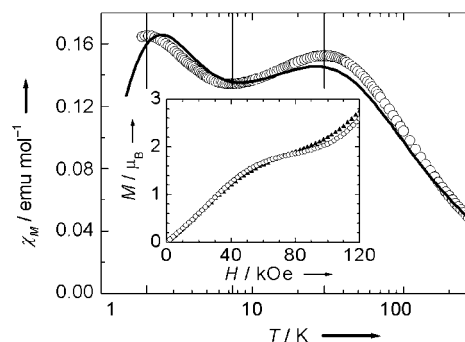


Figure 2. Variation of χ_M with temperature for **2**. The solid line corresponds to the calculated values with $J=16$ K, $J'=70$ K, and $\langle g \rangle=2$. In the inset the magnetization versus field measured at 1.6 K (\circ) and 2.0 K (\blacktriangle) is shown.

the $\chi_M T$ value is equal to $13.2 \text{ emu K mol}^{-1}$, lower than expected ($16 \text{ emu K mol}^{-1}$) for eight Cr^{III} and one Ni^{II} isolated spins with $g=2.00$. This may indicate that strong antiferromagnetic interactions are already operative at room temperature. χ_M increases when the temperature is lowered down to $T_{\text{max}1}=30$ K, at which it passes through a broad maximum, and then decreases when the temperature is lowered further. At $T_{\text{min}}=7.4$ K it passes through a minimum then increases again, and finally reaches a second maximum at $T_{\text{max}2}=2$ K. This behavior is unusual and to our knowledge has never been observed before. What is common, and expected, is the presence of one maximum in a χ_M vs. T curve as observed for antiferromagnetic homometallic even-membered wheels, for example, **1**.

The magnetic properties of the system are determined by Heisenberg-type superexchange interactions between the magnetic centers. The simplest Hamiltonian describing the system is the following:

$$\mathcal{H} = J'(\mathbf{S}_{\text{Cr}_1} \mathbf{S}_{\text{Ni}} + \mathbf{S}_{\text{Cr}_8} \mathbf{S}_{\text{Ni}}) + J \sum_{i=1}^7 \mathbf{S}_{\text{Cr}_i} \mathbf{S}_{\text{Cr}_{i+1}} \quad (1)$$

in which J' and J are the superexchange coupling parameters between the nickel spin and its two chromium neighbors and between the nearest neighbor chromium ions, respectively. The \mathbf{S}_i values are the spin quantum operators associated with spin values $S_{\text{Ni}}=1$ and $S_{\text{Cr}}=3/2$ of nickel and chromium ions, respectively. The presence of two maxima strongly indicates an $S=0$ ground state. The first step was to simulate the χ_M versus T curves for several sets of parameters J and J' . Based on previous work on Cr_8 wheels, we set J/k_B to 16 K. J'/k_B was varied between zero and 70 K. Only when $J'/k_B > 36$ K are two maxima in the susceptibility observed (Figure 3).

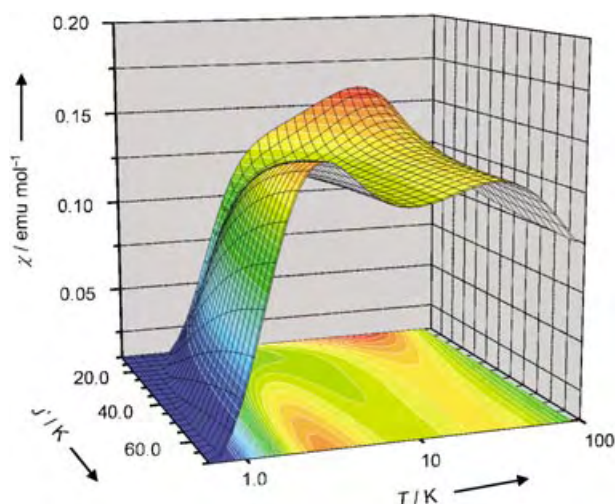


Figure 3. Simulation of the variation of χ_M as a function of both T (log scale) and J'/J . J has been set equal to 16 K.

Qualitatively the observation of two maxima in the χ versus T curve can be explained by the presence of several states with low total spin values (S_T) that are very close in energy to the ground $S_T=0$ state. If $J'=0$ the ground state is $S_T=1$ because the spin of the nickel is not correlated to the antiferromagnetic chain of chromic spins. Inclusion of an antiferromagnetic J' rapidly stabilizes a diamagnetic ground state, with the first three excited states being characterized by $S_T=1$. A ferromagnetic J' , even if does not remove spin frustration, stabilizes an $S=2$ ground state with disappearance of the maxima in the χ versus T curve. An antiferromagnetic $\text{Cr}^{\text{III}}\text{--Ni}^{\text{II}}$ interaction has been unambiguously observed in a similar $\{\text{Cr}_7\text{Ni}\}$ ring.^[9]

To discuss the “knot” of the Möbius strip, that is, the point at which the spins on nearest neighbors are not antiparallel, the eigen vectors of the low lying states are needed. In this particular case it is very convenient to use for the basis set the representation in which we couple the chromic spins on odd sites to give an intermediate spin S_{odd} and analogously for the spins on the even sites, S_{even} . These two intermediate spins are coupled together, to give the total spin for the chromium chain, S_{TCr} , and this last is coupled to the spin of the nickel to give the total spin, S_T . There are 2764 different ways of obtaining an $S_T=1$ state, therefore the wave functions of Hamiltonian (1), are linear combinations $\psi = \sum_{2764} c_i \varphi_i$. However, for the states lowest in energy only a few c_i 's are significantly different from zero. The composition of the first excited $S_T=1$ state strongly depend on the J'/J ratio. If $J' < J$ ψ_1 is mainly given by $S_{\text{even}}=6$, $S_{\text{odd}}=6$, with $S_{\text{TCr}}=0$ and can be seen as mainly given by the uncorrelated spin of the nickel ion. The knot is then localized on the nickel site, as shown in Figure 4b. On the contrary when $J' \gg J$ the largest contribution comes from $S_{\text{TCr}}=2$ antiferromagnetically coupled with the nickel spin to give $S_T=1$. In this case the “up–down” orientation of spins is more rigid at the nickel site and the knot is instead delocalized on the chromium chain as shown in Figure 4a.

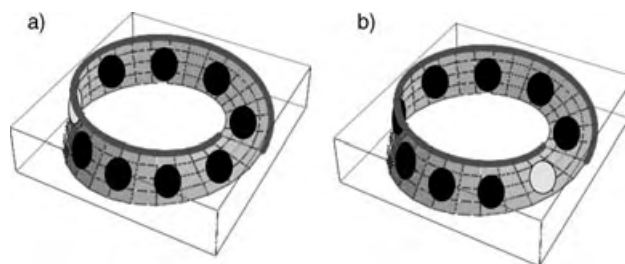


Figure 4. Representation of the spin frustration in **2** as a Möbius strip, with the white circle as the Ni site, and black circles as Cr. The knot is the point at which the thick grey line is discontinuous: a) with $J' \gg J$ and the knot on the chromium chain; b) with $J' < J$ and the knot is at nickel.

A measurement of the magnetization does not usually provide information on the wave function composition and more sophisticated techniques must be used. As Ni^{II} and Cr^{III} ions have significantly different g values, 2.2 versus 1.98, respectively, an accurate measurement of the g values of the lowest excited state will directly reflect the composition of the wave function. By using the spin projection techniques it is relatively easy to calculate the g factor of the different φ_i states starting from the values of the single ions. For the $S_{\text{TCr}}=0$ $S_T=1 >$ state $g = g_{\text{Ni}} = 2.2$, whereas for $S_{\text{TCr}}=2$ $S_T=1 > g = \frac{3}{2}g_{\text{Cr}} - \frac{1}{2}g_{\text{Ni}} = 1.86$. In intermediate cases the calculation of g requires us to consider the contribution of all φ_i states which appear in ψ_1 with a $c_i \neq 0$. The same procedure can be applied to any state ψ .

A true fitting procedure of the χ versus T curve is hampered by the strong g dependence on the spin state that has a stronger effect on the value of χ than J' . To take into account the wavefunction composition of the excited states is an unmanageable task, given the dimension of the S subspaces in the spin Hamiltonian matrix. In Figure 2 we report the χ versus T curve calculated for $J=16$ K and $J'=70$ K. The spectrum of low-lying energy states shows the first and second $S=1$ states at ≈ 3.7 and ≈ 10.7 K from the $S=0$ ground state, respectively. The first $S=2$ is calculated to occur at ≈ 22 K above the ground state. This energy scheme is not significantly varied if J' is reduced by a factor of two, as is usual in the presence of spin frustration. The M versus H curve shows a first plateau at about $1.8 \mu_B$, which is in agreement with the predicted $g < 2$ value. Interestingly a maximum in the dM/dH curve at 1.6 K is observed around 28 kOe (not shown). This observation suggests a gap between the ground and the first excited $S=1$ state of about 3 K, which is in agreement with the calculated energy spectrum. The further increase of M above 100 kOe, without reaching the plateau at about $4 \mu_B$ expected for an $S=2$ state, suggests that the first $S=2$ state starts to be populated at these fields, but that it is at least 15 K above the first $S=1$ state, as calculated.

To confirm our interpretation, we have used electron paramagnetic resonance (EPR) spectroscopy. In Figure 5 we report the polycrystalline powder high field EPR spectra recorded at a frequency of 285 GHz; an unconventionally high frequency has been used to better resolve the difference in the g value. At 20 K a single isotropic line is observed centered at $g \approx 2$, as a result of many populated spin states. On

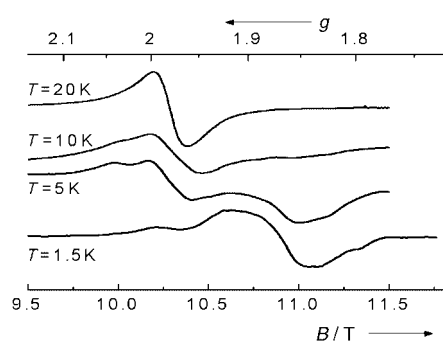


Figure 5. Variable-temperature EPR spectra of **2** recorded at 285 GHz by using a laboratory built spectrometer based on a Gunn diode source of far-infrared radiation.

lowering the temperature, a line centered at $g = 1.86$ increases in intensity at the expense of the line at $g \approx 2$, confirming that the lowest magnetic state has a g factor significantly smaller than 2. Similar results are obtained at 190 GHz. The lines have a nonresolved fine structure, probably due to the magnetic anisotropy (the so called zero-field splitting) of the states, but the observed shift to low g values on lowering the temperature unambiguously confirms that $J' \gg J$ as suggested also by the presence of two maxima in the magnetic susceptibility. The spin frustration is therefore delocalized on the chromium chain, as represented by the Möbius strip of Figure 4a.

This heterometallic odd-membered ring provides a fascinating example of how the supramolecular approach can be used to observe new magnetic phenomena. It is possible to tune the delocalization of the frustrated bonds in the ring and to detect it in a very simple way, thus providing a textbook example of spin frustration. Similar phenomena are observed in **4** and detailed studies will be reported later.

Experimental Section

2: $\text{CrF}_3 \cdot 4\text{H}_2\text{O}$ (5.0 g, 28 mmol), $(\text{cy-C}_6\text{H}_{11})_2\text{NH}$ (2.1 g, 12 mmol), basic nickel carbonate ($2\text{NiCO}_3 \cdot 3\text{Ni}(\text{OH})_2 \cdot 4\text{H}_2\text{O}$; 0.5 g, 0.9 mmol) and $\text{Me}_3\text{CCO}_2\text{H}$ (15.0 g, 147 mmol) were heated at 140°C for 7.0 h, then allowed to cool to room temperature. Acetone (50 mL) was added and the resulting mixture was stirred for 15 mins. The microcrystalline product was filtered, washed with a large quantity of acetone, dried in air, dissolved in hot THF (75 mL), filtered, and the filtrate was diluted with toluene (40 mL). The solution was concentrated by evaporation at approx. 40°C to 30 mL and then very slowly cooled to room temperature. The solution was left to stand for 24 h to yield green hexagonal crystals, which were isolated by filtration and washed with toluene; yield 1.7 g (17%, calculated from $\text{CrF}_3 \cdot 4\text{H}_2\text{O}$). Elemental analysis calcd (%) for $\text{C}_{116}\text{H}_{202}\text{Cr}_8\text{F}_9\text{NNiO}_{36}$: Cr 14.69, Ni 2.07, C 49.19, H 7.19, N 0.49, F 6.04; found: Cr 14.51, Ni 1.83, C 49.64, H 7.25, N 0.48, F 5.85. ESMS m/z (%): -2465 (100) $[\text{Cr}_8\text{NiF}_9(\text{O}_2\text{CCMe}_3)_{18}]^-$; $+2671$ (100) $[\text{M}+\text{Na}]^+$; $+2511$ (50) $[\text{Cr}_8\text{NiF}_9(\text{O}_2\text{CCMe}_3)_{18}]^+$.

4: $\text{CrF}_3 \cdot 4\text{H}_2\text{O}$ (5.0 g, 28 mmol), $(\text{C}_6\text{H}_{11})_2\text{NH}$ (2.40 g, 13.2 mmol) and $\text{Me}_3\text{CCO}_2\text{H}$ (14.0 g, 137 mmol) were heated with stirring at 140°C for 2.0 h. $[\text{VO}(\text{O}_2\text{CCMe}_3)_2]^{[14]}$ (1.5 g, 5.6 mmol when $n=1$) was added, and the mixture then heated for 4.0 h. The reaction mixture was cooled to room temperature, acetone (30 mL) was added, and the solution was stirred for a further 15 mins. A green solid was collected by filtration, washed with acetone (3×15 mL) and dried

in air. The product was separated by column chromatography on silica gel by using toluene as eluent. It was eluted as the first band from the column. The solution was then evaporated to dryness under reduced pressure and the residue was redissolved in warm hexane (150 mL). Slow evaporation of the solvent at ambient temperature produced X-ray quality green crystals of **4** after two weeks. Crystals were collected by filtration washed with cold hexane and dried on air at room temperature; yield 2.15 g (30%; calculated from $[\text{VO}(\text{O}_2\text{CCMe}_3)_2]_n$). Elemental analysis calcd (%) for $\text{C}_{97}\text{H}_{177}\text{Cr}_7\text{F}_9\text{NiO}_{36}\text{V}_2$: Cr 14.16, V 3.96, C 45.33, H 6.94, N 0.54, F 6.65; found: Cr 14.08, V 4.10, C 45.49, H 6.62, N 0.48, F 6.37. ESMS m/z (%): -2387 (100%) $[\text{Cr}_7(\text{VO})_2\text{F}_9(\text{O}_2\text{CCMe}_3)_{17}]^-$.

Magnetic measurements: magnetic measurements were recorded on a polycrystalline powder samples with an Oxford Instruments Vibrating Sample Magnetometer (VSM) operating in the temperature range 1.5–300 K with magnetic fields up to 120 kOe. It has been checked that the magnetic susceptibility was independent of the amplitude of the applied field by recording the magnetization with two different magnetic fields, 1 and 10 kOe.

Received: April 2, 2004

Revised: July 8, 2004

Keywords: cage compounds · chromium · heterometallic complexes · magnetic properties · spin frustration

- [1] K. L. Taft, C. D. Delfs, G. C. Papaefthymiou, S. Foner, D. Gatteschi, S. J. Lippard, *J. Am. Chem. Soc.* **1994**, *116*, 823–832.
- [2] R. E. P. Winpenny, *Comprehensive Coordination Chemistry II*, Vol. 7 (J. A. McCleverty, T. J. Thomas), Elsevier, Oxford, **2004**, pp. 125–176, and references therein.
- [3] a) B. Hasenknopf, J.-M. Lehn, B. O. Kneisel, G. Baum, D. Fenske, *Angew. Chem.* **1996**, *108*, 1987–1990; *Angew. Chem. Int. Ed. Engl.* **1996**, *35*, 1838; b) C. S. Campos-Fernández, R. Clérac, J. M. Koomen, D. H. Russell, K. R. Dunbar, *J. Am. Chem. Soc.* **2001**, *123*, 773–774.
- [4] G. Mezei, P. Baran, R. G. Raptis, *Angew. Chem.* **2004**, *116*, 584–587; *Angew. Chem. Int. Ed.* **2004**, *43*, 574–577.
- [5] V. L. Pecoraro, A. J. Stemmler, B. R. Gibney, J. J. Bodwin, H. Wang, J. W. Kampf, A. Barwinski, *Prog. Inorg. Chem.* **1997**, *45*, 83–117.
- [6] G. Toulouse, *G. Comm. Phys.* **1977**, *2*, 115–119.
- [7] F. Nori, E. Gagliano, S. Bacci, *S. Phys. Rev. Lett.* **1992**, *68*, 240–243.
- [8] V. Caignaert, E. Suard, A. Maignan, Ch. Simon, B. Raveau, *J. Magn. Magn. Mater.* **1996**, *153*, L260–L264.
- [9] F. K. Larsen, E. J. L. McInnes, J. Overgaard, S. Piligkos, G. Rajaraman, E. Rentschler, A. A. Smith, G. M. Smith, G. A. Timco, R. E. P. Winpenny, *Angew. Chem.* **2003**, *115*, 105–109; *Angew. Chem. Int. Ed.* **2003**, *42*, 101–105.
- [10] Crystal data for **2**: $(\text{C}_{102}\text{H}_{186}\text{Cr}_8\text{F}_9\text{NNiO}_{36})$; $M_r = 2648.41 \text{ g mol}^{-1}$; dark green hexagonal shaped blocks, orthorhombic, space group possibly *Pbna*, $a = 19.587(5)$, $b = 24.818(6)$, $c = 33.925(9) \text{ \AA}$, $V = 16490(7) \text{ \AA}^3$, $Z = 4$, $T = 200(2) \text{ K}$, $\rho = 1.067 \text{ g cm}^{-3}$, $F(000) = 5576$, $\mu(\text{MoK}\alpha) = 0.683 \text{ mm}^{-1}$. Crystal data for **4** $\text{C}_{101.5}\text{H}_{187.5}\text{Cr}_7\text{F}_9\text{NO}_{36}\text{V}_2$; $M_r = 2634.9 \text{ g mol}^{-1}$; green prism, orthorhombic, space group *Pbcn*, $a = 23.9765(13)$, $b = 31.2265(18)$, $c = 19.3562(11) \text{ \AA}$, $V = 14492(1) \text{ \AA}^3$, $Z = 4$, $T = 150(2) \text{ K}$, $\rho = 1.208 \text{ g cm}^{-3}$, $F(000) = 5546$, $\mu(\text{MoK}\alpha) = 0.701 \text{ mm}^{-1}$. Data were collected on Bruker SMART CCD diffractometers ($\text{MoK}\alpha$, $\lambda = 0.71069 \text{ \AA}$ for **2** and 0.6898 \AA for **4**). Selected crystals were mounted on the tip of a glass pin by using Paratone-N oil and placed in the cold flow produced with an Oxford Cryocooling device. Complete hemispheres of data were collected using ω -scans (steps of 0.6° for **2** and 0.3° for **4**, 30 s frame $^{-1}$). Integrated intensities were obtained with

SAINT+^[11] and they were corrected for absorption by using SADABS.^[11] Structure solution and refinement was performed with the SHELX program.^[11] The structures were solved by direct methods and **3** was completed by iterative cycles of ΔF syntheses and full-matrix least-squares refinement against F^2 to give, for **4** by using 705 parameters and 418 restraints, $wR_2 = 0.2241$ (19676 unique reflections), $R_1 = 0.0681$ (14946 reflections with $I > 2\sigma(I)$). For **2** the structure did not develop past the localization of the atomic structure of the nona-metallic wheel and the octahedral first coordination sphere of the metals. CCDC-231873 (**4**) contains the supplementary crystallographic data for this paper. These data can be obtained free of charge via www.ccdc.cam.ac.uk/conts/retrieving.html (or from the Cambridge Crystallographic Data Centre, 12 Union Road, Cambridge CB21EZ, UK; fax: (+44)1223-336-033; or deposit@ccdc.cam.ac.uk).

- [11] G. M. Sheldrick, Programs for Crystal Structure Analysis, University of Göttingen, **1998**.
- [12] F. K. Larsen, J. Overgaard, S. Parsons, E. Rentschler, G. A. Timco, A. A. Smith and R. E. P. Winpenny, *Angew. Chem.* **2003**, *115*, 6160–6163; *Angew. Chem. Int. Ed.* **2003**, *42*, 5978–5981.
- [13] O. Kahn, *Chem. Phys. Lett.* **1997**, *265*, 109–114.
- [14] R. C. Paul, A. Rumar, *J. Inorg. Nucl. Chem.* **1965**, *27*, 2537–2547.

tal investigations. We have employed a novel technique to prepare highly aligned supersonic beams and we show that ethylene molecules that impinge on silver surfaces precovered with molecular oxygen as “helicopters” have a higher sticking probability than “cartwheels” (Figure 1). The sticking prob-

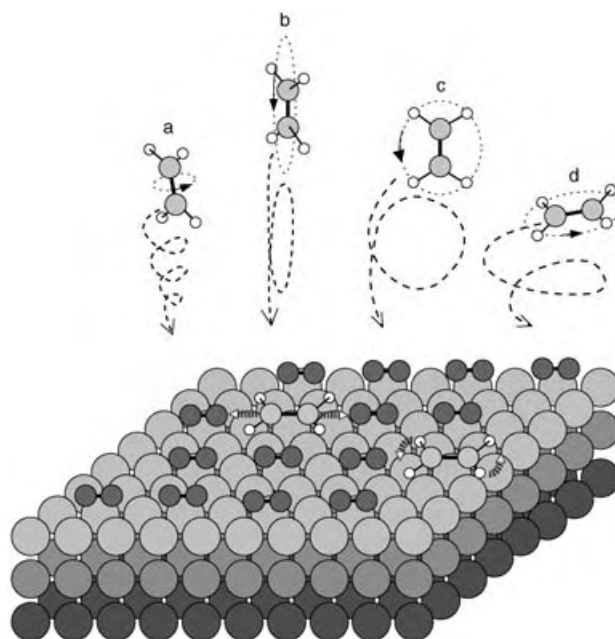


Figure 1. Ethylene molecules rotating along the principal axes impinge perpendicularly on Ag (001) metal surface precovered with O₂ and may stick in some favorable cases. A net variation of the coverage dependence of the sticking probability *S* when changing the geometry of approach of the C=C bond to the surface is observed: “helicopters” (d) stick better than “cartwheels” (b and c) or “cigars” (a).

Gas–Surface Interactions

Stereodynamic Effects in the Adsorption of Ethylene onto a Metal Surface^{*,**}

Luca Vattuone,^{*} Andrea Gerbi, Mario Rocca, Ugo Valbusa, Fernando Pirani, Franco Vecchiocattivi, and David Cappelletti

The role of molecular alignment of nonpolar molecules in gas–surface interactions has so far escaped direct experimen-

tal investigations. Herein we report the dependence of *S* on molecular alignment for ethylene, an apolar molecule, interacting with a metallic surface, specifically O-recovered Ag (001). The observed steric effect is large, thus strongly influencing adsorption. The study of such a prototype system is very important to clarify the dynamics in the entrance channels of the potential energy surfaces controlling the catalytic epoxidation of unsaturated hydrocarbons.

Measuring *S* for a molecule in a well-defined quantum state represents a major goal of physical chemistry.^[1] The extensive use of molecular beams in conjunction with the well-known retarded reflector method^[2] allowed the determination of the dependence of *S* on translational energy and angle of incidence and on surface temperature and coverage for a wide set of gas–surface adsorption systems already in the first years of surface science.

However, the characterization of the dependence of *S* on the molecular internal state became accessible only recently, mainly as a result of the availability of high-power lasers, which allowed the preparation of molecules in well-defined

[*] Dr. L. Vattuone, A. Gerbi, Prof. M. Rocca
INFN Unità di Genova, Dipartimento di Fisica
Università di Genova
and
IMEM-CNR Sezione di Genova
Via Dodecaneso 33, Genoa (Italy)
Fax: (+39) 010-314218
E-mail: vattuone@fisica.unige.it

Prof. U. Valbusa
INFN Unità di Genova, Dipartimento di Fisica
Università di Genova
Via Dodecaneso 33, Genoa (Italy)
Prof. F. Pirani
INFN Unità di Perugia, Dipartimento di Chimica
Università di Perugia, Perugia (Italy)
Prof. F. Vecchiocattivi, Dr. D. Cappelletti
Dipartimento di Ingegneria Civile ed Ambientale
Università di Perugia, Perugia (Italy)

[**] We acknowledge funding by INFN-PURS 1VA-2002 and PRIN 2003023939.

rotational^[3] and vibrational states.^[4] Relevant information has been obtained by measuring the quantum state of molecules scattered off the surface and by applying detailed balance arguments.^[5] The role of the spatial orientation of molecules impinging on a surface, or more specifically of the polarization of their rotational angular momentum J , has thus far not been investigated in much detail, even though the steric factor has often been addressed as a topic of fundamental interest.^[6] The first investigations, performed by using electrostatic devices suitable to select which end of a polar symmetric top (A species showing two identical moments along two of the three principal inertia axes, one of which coincides with the molecular symmetry axis) molecule hits the surface, shed light on the behavior of a symmetric NO-like species^[7] and subsequently on polar polyatomic projectiles such as CH_3F ^[8] and ND_3 .^[9] Other methods to generate molecular orientation or alignment have been developed and include high electric or magnetic fields,^[10a,b] polarized laser light,^[10c] and intense nonresonant laser fields.^[10d] Unfortunately, they work only for molecules that exhibit particular features, for example, large dipole moments or large polarizability anisotropies.

An alternative approach is based on the use of seeded molecular beams, for which the alignment of J is naturally generated by collisions during a supersonic expansion^[11] and exploits the dependence of the resulting alignment degree on the final molecular speed.^[12] This is a general phenomenon, as demonstrated by the study of a variety of molecules such as O_2 (paramagnetic),^[12] N_2 (diamagnetic),^[13] C_6H_6 (aromatic),^[14] and very recently C_2H_2 and C_2H_4 (unsaturated aliphatic hydrocarbons).^[15] For the lighter molecules, the experiments described above^[12,13,15] suggest that: 1) When the nozzle source is operating at room temperature they are basically relaxed in the lowest rotational levels (essentially $J=1$ and 2). 2) The slow speed tail (ST) of the molecular beam velocity distribution (corresponding to velocities lower than 0.95 times the peak velocity) is essentially composed of molecules with an isotropic spatial distribution of J . In the language of angular momentum physics, such zero-alignment situations correspond to equally populated helicity states in which the helicity defines the projection of J , and indirectly also the orientation of the molecular rotational plane with respect to the molecular beam velocity direction. 3) The fast speed tail (FT) of the same velocity distribution (involving velocities larger than 1.05 times the peak velocity) consists of molecules with a high J alignment degree, that is, with marked nonstatistical helicity state population. Specifically, $85 \pm 10\%$ of molecules in the FT populate particular helicity states (zero helicity in the case of O_2 , N_2 , and C_2H_2).^[16] The cited studies^[12,13,15] also suggest that it is often sufficient to perform a proper velocity selection to control molecular speed and molecular alignment simultaneously, as also proved by recent gas-phase scattering experiments.^[17]

Therefore, when the molecular beam impinges at normal incidence on the surface, as in the case of the present experiments with C_2H_4 (an asymmetric top molecule), FT essentially provides “cartwheels”, molecules with their C=C bond rotating parallel to the molecular beam axis, whereas ST supplies about two thirds of “helicopters”, that is, molecules

with the C=C bond rotating perpendicularly to the beam direction.

In work described herein, the choice of the C_2H_4 -Ag(001) system is motivated by a previous observation of a strong rotational dependence of the physisorption probability^[18] and, even more importantly, by the fact that the ethylene-silver interaction is sufficiently weak so that steering effects are expected to play only a minor role. The well-known role of O_2 precoverage is to promote a measurable ethylene adsorption.^[19,20] Chemisorption occurs in the π -bonded state, with an adsorption energy of ≈ 0.4 eV/molecule^[21] and with the molecule lying flat on the surface.^[20]

The Ag (001) single crystal was cleaned by following the usual procedure,^[18] which consists of sputtering and annealing cycles to 700 K. The base pressure in the chamber reads 2×10^{-10} mbar and increases to 3×10^{-10} mbar when the supersonic beam is introduced. The uptake from the background is thus negligible during the timescale of the experiment. Aligned molecules in the FT, are separated from those statistically distributed, flying in the ST, by using a novel mechanical velocity selector (described in detail elsewhere^[22]) positioned along the supersonic molecular-beam path, in the second stage of its collimation.^[23] The beam flux is calibrated by a spinning rotor gauge and is corrected for the transmission of the velocity selector, which is measured by comparing the increase in the partial pressure caused by the unselected beam with that observed when selecting ST and FT. Notably, the angular divergence of the supersonic beam entering the ultrahigh-vacuum chamber is determined by the diameter of the collimators inserted along the beam path and reads 0.2° , thus ensuring the same beam intensity profile across the sample for ST and FT. Moreover, ST and FT experiments were performed with nearly identical fluxes. The diameter of the spot illuminated by the molecular beam is smaller than the sample diameter (10 mm), as determined by examining the ordered LEED (Low Energy Electron Diffraction) structures which form after exposing a clean Pd (100) sample to a supersonic O_2 beam seeded in He.

The upper panel of Figure 2 reports the backscattered C_2H_4 flux Φ versus time, measured by exposing the sample, at normal incidence, to a molecular beam of ethylene seeded in He (incident energy $E = 0.36$ eV). The corresponding dependence of S on ethylene coverage (Θ_{Et}) which was obtained by integrating S over time and multiplying by flux, is shown in the lower panel. Uptake experiments were performed at $T = 110$ K. The Ag (100) sample is precovered with a defined amount of O_2 prior to each ethylene uptake by dosing O_2 with a supersonic beam seeded in He. The O_2 coverage (Θ_{Ox}) can thus be accurately controlled and reproduced. The data reported in Figure 2 were obtained with $\Theta_{\text{Ox}} = 0.03$ ML. The data obtained without the oxygen precoverage ($\Theta_{\text{Ox}} = 0$ ML) are also reported in Figure 2 for comparison (shifted).

It is apparent from Figure 2 that: a) for the bare Ag (001) surface ($\Theta_{\text{Ox}} = 0$ ML) there is no difference between molecules in FT and ST; b) for the O_2 -precovered surface ($\Theta_{\text{Ox}} = 0.03$ ML) the initial sticking probability increases, but does not depend on molecular alignment; c) with increasing C_2H_4 coverage, S increases for molecules in the ST but decreases for

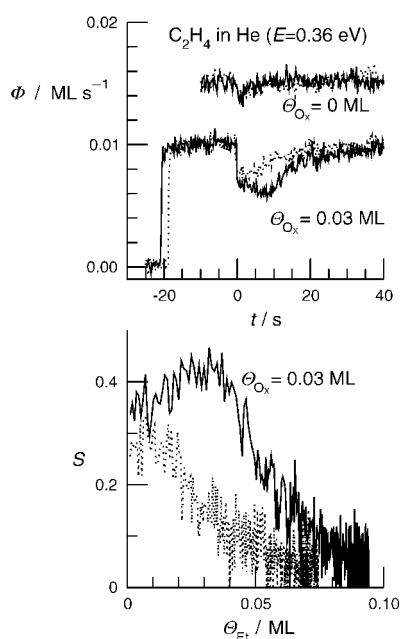


Figure 2. Scattered C_2H_4 flux Φ versus time (upper panel) and sticking coefficient S of C_2H_4 versus coverage θ_{Et} (lower panel) on an Ag (001) surface precovered with oxygen ($\theta_{\text{Ox}}=0.03$ ML). Data are reported for the interaction of ST (continuous) and FT (dotted) of an ethylene beam seeded in He. The initial increase in the C_2H_4 flux corresponds to the introduction of the molecular beam into the ultrahigh-vacuum chamber, where an inert flag intercepts the beam to prevent it from hitting against the surface. When the flag is removed ($t=0$), the scattered flux decreases owing to the gettering action of the surface of the crystal. The upper traces (shifted) in the upper panel show the results for the bare Ag surface ($\theta_{\text{Ox}}=0$).

the FT. A large difference in S is already measured when selecting molecules in ST and FT with the ethylene coverage at only a few percent of a monolayer.

The difference in S between the two sets of velocity-selected molecules from the same molecular beam cannot be due to the small difference in translational energy, as demonstrated by performing the measurements at the same O_2 precoverage with ethylene seeded in Ne, for which the translational energy differs by a factor of three (Figure 3). The lower panels of Figures 2 and 3 shows that a qualitatively similar steric effect is found for the two very different incident energies. Moreover, the effect cannot be due to a possible change in the J distribution between ST and FT which would yield a lower average J , and hence a higher S , for FT molecules,^[18] contrary to experimental evidence. We are therefore confident that the different behavior of ST and FT can only arise from the different degree of rotational alignment of the selected molecules. Points a) and b) clearly indicate that the interaction of incoming ethylene with bare silver atoms and with chemisorbed O_2 molecules is independent of the initial alignment of the incoming C_2H_4 .

Point c) can only be accounted for if 1) ethylene molecules that are not scattered immediately after the first hit with the surface are temporarily trapped as a mobile and non-thermalized precursor with a memory of their initial alignment, and 2) “cartwheel” molecules in such a precursor state

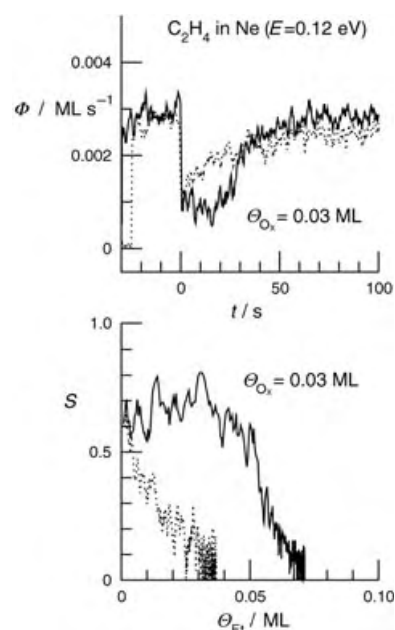


Figure 3. As in Figure 2, but for a molecular beam of ethylene seeded in Ne.

have a higher chance of being scattered back into the gas phase than “helicopters”, when colliding with already chemisorbed flat-lying C_2H_4 molecules. The role of the mobile precursor is introduced to explain the strong dependence of S both with θ_{Et} as well as with θ_{Ox} . Because the ST and FT sticking curves already deviate at $\theta_{\text{Et}}=0.01$ ML, we deduce that the molecules in the precursor state “memorize” their initial rotational alignment for the time needed to explore a radius of some ten lattice spacings around the initial point of impact. When an ethylene in such a precursor state collides with a chemisorbed C_2H_4 , it may be scattered off the surface with different probability, depending on the specific rotational mode involved.

In conclusion we have shown herein that a novel technique can be successfully applied to determine the role of molecular alignment in gas–surface interactions. We demonstrated that the steric effects can be quite large when interactions between transiently trapped and already chemisorbed molecules come into play, as is the case for the ethylene–Ag system reported herein. As hydrocarbon adsorption on metal surfaces often occurs through a precursor mechanism,^[24] the present result may also be relevant for other adsorption systems. In fact, we have already observed similar alignment effects for propylene interactions with bare Ag (001), whereas no effect was observed for the more strongly bound O_2 –Ag (100) and C_2H_4 –Pd (100) systems in which σ bonding occurs.

Received: July 14, 2004

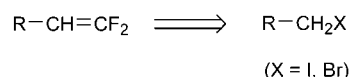
Keywords: heterogeneous catalysis · hydrocarbons · molecular beams · silver · surface chemistry

- [1] a) R. N. Zare, *Z. Phys. D* **1988**, *10*, 377–382; b) G. O. Sitz, *Rep. Prog. Phys.* **2002**, *65*, 1165–1193.
- [2] D. A. King, M. G. Wells, *Surf. Sci.* **1972**, *29*, 454.
- [3] M. Gostein, G. O. Sitz, *J. Chem. Phys.* **1997**, *106*, 7378–7390.
- [4] a) R. D. Beck, P. Maroni, D. C. Papageorgopoulos, T. T. Dang, M. P. Schmid, T. R. Rizzo, *Science* **2003**, *302*, 98–100; b) R. R. Smith, D. R. Killelea, D. F. DelSesto, A. L. Utz R, *Science* **2004**, *304*, 992–995.
- [5] a) M. J. Weida, J. M. Sperhac, D. J. Nesbitt, *J. Chem. Phys.* **1996**, *105*, 749–766; b) A. Hodgson, *Prog. Surf. Sci.* **2000**, *30*, 1.
- [6] a) U. Heinzmann, S. Holloway, A. W. Kleyn, R. E. Palmer, K. J. Snowdon, *J. Phys. Condens. Matter* **1996**, *8*, 3245–3269; b) H. Hou, S. J. Goulding, C. T. Rettner, A. M. Wodtke, D. J. Auerbach, *Science* **1997**, *277*, 80–82.
- [7] E. W. Kuipers, M. G. Tenner, A. W. Kleyn, S. Stolte, *Nature* **1988**, *334*, 420–422.
- [8] T. J. Curtiss, R. B. Bernstein, *Chem. Phys. Lett.* **1989**, *161*, 212–218.
- [9] M. E. La Villa, S. I. Ionov, *Phys. Rev. Lett.* **1992**, *68*, 129–132.
- [10] a) B. Friedrich, D. R. Herschbach, *Nature* **1991**, *353*, 412–414; b) H. J. Loesch, J. Moller, *J. Chem. Phys.* **1992**, *97*, 9016–9030; c) Z. Karny, R. C. Estler, R. N. Zare, *J. Chem. Phys.* **1978**, *69*, 5199–5201; d) H. Stapelfeldt, T. Seideman, *Rev. Mod. Phys.* **2003**, *75*, 543–557.
- [11] a) M. P. Sinha, C. D. Caldwell, R. N. Zare, *J. Chem. Phys.* **1975**, *61*, 491–503; b) D. P. Pullman, B. Friedrich, D. R. Herschbach, *J. Chem. Phys.* **1990**, *93*, 3224–3236.
- [12] V. Aquilanti, D. Ascenzi, D. Cappelletti, F. Pirani, *Nature* **1994**, *371*, 399–402.
- [13] V. Aquilanti, D. Ascenzi, D. Cappelletti, R. Fedeli, F. Pirani, *J. Phys. Chem. A* **1997**, *101*, 7648–7656.
- [14] F. Pirani, D. Cappelletti, M. Bartolomei, V. Aquilanti, M. Scotoni, M. Vescovi, D. Ascenzi, D. Bassi, *Phys. Rev. Lett.* **2001**, *86*, 5035–5038.
- [15] M. Bartolomei, PhD thesis, Università di Perugia (Italy), **2002**, available online at <http://leo.tech.ing.unipg.it/TESE/tesimax.pdf>.
- [16] The alignment degree of ethylene has been determined in a scattering experiment carried out in Perugia.^[15] Ethylene is a planar polyatomic asymmetric top species. The analysis of scattering results^[15] indicates that, despite such peculiarities in the molecular structure, ethylene molecules behave like diatomic species of similar mass (O₂, N₂) and reach a comparable degree of collision-induced alignment. To maintain the same qualitative alignment degree in the present surface-scattering study, we operated the supersonic molecular beam source under the same conditions as those used in the Perugia experiment.
- [17] a) V. Aquilanti, D. Ascenzi, D. Cappelletti, S. Franceschini, F. Pirani, *Phys. Rev. Lett.* **1995**, *74*, 2929–2932; b) V. Aquilanti, D. Ascenzi, M. Bartolomei, D. Cappelletti, S. Cavalli, M. DeCastro Vitores, F. Pirani, *Phys. Rev. Lett.* **1999**, *82*, 69–72;
- [18] L. Vattuone, U. Valbusa, M. Rocca, *Phys. Rev. Lett.* **1999**, *82*, 4878–4881.
- [19] L. Vattuone, L. Savio, M. Rocca, *Int. J. Mod. Phys. B* **2003**, *17*, 2497–2526.
- [20] S. Gao, J. R. Hahn, W. Ho, *J. Chem. Phys.* **2003**, *119*, 6232–6236.
- [21] L. Vattuone, L. Savio, M. Rocca, L. Rumiz, A. Baraldi, S. Lizzit, G. Cornelli, *Phys. Rev. B* **2002**, *66*, 85403(1)–85403(5).
- [22] F. Pirani, D. Cappelletti, F. Vecchiocattivi, L. Vattuone, A. Gerbi, M. Rocca, U. Valbusa, *Rev. Sci. Instrum.* **2004**, *75*, 349–354.
- [23] M. Rocca, U. Valbusa, A. Gussoni, M. Maloberti, L. Racca, *Rev. Sci. Instrum.* **1991**, *62*, 2172–2176.
- [24] J. A. Stinnett, R. J. Madix, J. C. Tully, *J. Chem. Phys.* **1996**, *104*, 3134–3142.

Difluoromethyl Phenyl Sulfone, a Difluoromethylidene Equivalent: Use in the Synthesis of 1,1-Difluoro-1-alkenes**

G. K. Surya Prakash,* Jinbo Hu, Ying Wang, and George A. Olah

1,1-Difluoro-1-alkenes are unique compounds with unusually high electrophilicity from the *gem*-difluorovinyl group, and recently have drawn many synthetic and theoretical endeavors.^[1] *gem*-Difluorovinyl functionality has been known to act as a bioisostere for aldehydes and ketones,^[2] and it is critical to many biologically active molecules such as enzyme inhibitors^[1,3] and pesticides.^[4] 1,1-Difluoro-1-alkenes are also useful synthetic precursors for the preparation of other fluorinated compounds and polymers.^[5] Although several different methods for the preparation of 1,1-difluoro-1-alkenes have been disclosed in the literature including the Wittig reaction using difluoromethylene ylides,^[6] we now report an efficient method for the transformation of readily available primary alkyl halides into 1,1-difluoro-1-alkenes (Scheme 1).



Scheme 1. Preparation of 1,1-difluoro-1-alkenes from primary alkyl halides.

One can envision a nucleophilic substitution–elimination strategy for this transformation, that is, a fluorine-bearing nucleophile (such as CF_3^-) substitutes the halogen atom of the alkyl halide followed by an α,β -elimination ($-\text{HF}$ or others). However, while alkyl halides can readily react with various carbon nucleophiles (mostly by $\text{S}_{\text{N}}2$ reactions) to form carbon–carbon bonds, their nucleophilic substitution reactions with fluorine-bearing carbon nucleophiles are generally difficult due to their unmatched hard–soft nature.^[7] In addition, although fluorinated organocopper reagents (R_fCu) can be used to couple with aryl, vinyl, benzyl, and allyl halides, their reactions with simple alkyl halides are not effective.^[8]

[*] Prof. Dr. G. K. S. Prakash, Dr. J. Hu, Y. Wang, Prof. Dr. G. A. Olah
Loker Hydrocarbon Research Institute and
Department of Chemistry
University of Southern California
University Park, Los Angeles, CA 90089-1661 (USA)
Fax: (+1) 213-740-6270
E-mail: gprakash@usc.edu

[**] Support of our work by Loker Hydrocarbon Research Institute is gratefully acknowledged.



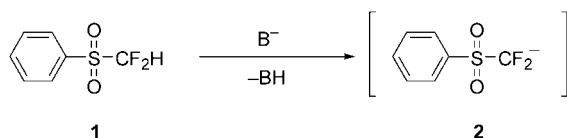
Supporting information for this article is available on the WWW under <http://www.angewandte.org> or from the author.

The possible solution to this problem is to introduce a proper auxiliary functional group connecting to the fluorinated carbon nucleophile to increase its softness, since the alkyl halide is a soft electrophile. Furthermore, the proper auxiliary group should be easily removed or transformed into other functional groups afterwards. The benzenesulfonyl group (PhSO₂) is one of the choices, for its softness and its varying chemical reactivities (so-called “chemical chameleon”).^[9] Difluoromethyl phenyl sulfone (**1**) is the ideal compound for this purpose, due to its easy generation of the (benzenesulfonyl)difluoromethyl anion **2** after the deprotonation of its CF₂H group (Scheme 2).^[10] Difluoromethyl phenyl sulfone can be read-

Table 1: Optimization of the reaction conditions for the nucleophilic substitution of **1** with alkyl halides and triflates.

		PhSO ₂ CF ₂ H + RX		base solvent		PhSO ₂ CF ₂ R	
		1	3			4	
Run	1 (equiv)	3 (equiv)	Base (equiv)	Solvent	T [°C]	t [h]	Yield of 4 [%] ^[a]
1	1.0	<i>n</i> -C ₅ H ₁₁ Br (2.1)	<i>t</i> BuOK (1.0)	DMF	−50–25	1.0	34
2	1.0	<i>n</i> -C ₅ H ₁₁ Br (2.1)	<i>t</i> BuOK (1.0)	DMF	−50–25	16.0	29
3	1.0	<i>n</i> -C ₅ H ₁₁ Br (2.1)	<i>t</i> BuOK (2.0)	DMF	−50–25	1.0	52
4	1.0	<i>n</i> -C ₅ H ₁₁ Br (4.0)	<i>t</i> BuOK (2.0)	DMF	−50	1.0	61
5	1.0	<i>n</i> -C ₅ H ₁₁ I (4.0)	<i>t</i> BuOK (2.0)	DMF	−50	1.0	85
6	1.0	<i>n</i> -C ₅ H ₁₁ Br (10.0)	NaOH (25.0) ^[b]	CH ₂ Cl ₂	25	20.0	0 ^[c]
7	1.0	<i>n</i> -C ₂ H ₅ I (4.0)	<i>t</i> BuOK (2.0)	DMF	−50	1.0	65
8	1.0	<i>n</i> -C ₂ H ₅ I (4.0)	<i>t</i> BuOK (2.0)	THF	−50	1.0	0 ^[d]
9	1.0	2-iodobutane (4.0)	<i>t</i> BuOK (2.0)	DMF	−50	1.0	0 ^[d]
10	1.0	CF ₃ SO ₂ CH ₃ (4.0)	<i>t</i> BuOK (2.0)	DMF	−50	1.0	0 ^[e]
11	1.0	CF ₃ SO ₂ CH ₃ (4.0)	<i>t</i> BuOK (2.0)	THF	−50	1.0	0 ^[e]

[a] Yields were determined by ¹⁹F NMR spectroscopy using PhOCF₃ as an internal standard. [b] 50 wt% aqueous NaOH solution was used, with the catalytic amount of phase-transfer agent Aliquat 336. [c] Unreacted **1** and a small amount of the by-product PhSO₂CF₂SPh were observed. [d] A messy product mixture was observed. [e] Starting material **1** was recovered.



Scheme 2. Generation of (benzenesulfonyl)difluoromethide from difluoromethyl phenyl sulfone and a base.

ily prepared from sodium thiophenoxide and chlorodifluoromethane followed by oxidation.^[10,11] The nucleophilic addition of **1** with carbonyl compounds in the presence of a base has been demonstrated.^[10b,c] Recently, we have reported the synthetic application of **1** as a difluoromethyl anion equivalent (“CF₂H[−]”)^[12] as well as a selective difluoromethylene dianion equivalent (“CF₂^{2−}”).^[10c] Herein, we disclose another significant synthetic application of **1** as a difluoromethylidene equivalent (“=CF₂”), which enables a novel synthesis of 1,1-difluoro-1-alkenes from primary alkyl halides using an unprecedented nucleophilic substitution–elimination approach.

The nucleophilic substitution of difluoromethyl phenyl sulfone **1** with alkyl bromides, alkyl iodides, and alkyl triflates were examined, to produce alkylated difluoromethyl sulfone **3**, with careful modifications of the reaction conditions (Table 1). The reactions were typically performed under an argon atmosphere, and a base was added to a mixture of **1** and **3**. The best product yield was obtained when one equivalent of **1** was treated with four equivalents of primary alkyl iodide and two equivalents of *t*BuOK as a base in DMF at −50 °C for 1 h (Table 1, run 5). Primary alkyl bromides are also suitable for the reaction but with somewhat lower yields (Table 1, runs 1–4). A secondary alkyl halide, however, did not give the anticipated product (Table 1, run 9), indicating that the reaction proceeds by a typical S_N2 pathway. Methyl triflate did not react with **1** either to give the expected product

(Table 1, runs 10, 11), which may be due to the fast reaction between DMF, alkyl triflate, and *t*BuOK to form the dialkyl acetal of DMF.^[13]

Following optimization of the reaction conditions, a variety of alkyl-substituted *gem*-difluoromethyl phenyl sulfones **4** were prepared in good yields (Table 2). Various primary alkyl iodides with different chain lengths were able to be substituted with (benzenesulfonyl)difluoromethide (in situ generated from **1**) and *t*BuOK (Table 2, entries 1–6). Substituted alkyl iodides also behave in the similar way, which leads to the formation of structurally diverse *gem*-difluorinated sulfones (Table 2, entries 7–12). Alkyl-substituted difluoromethyl sulfones themselves are a group of useful compounds used as nonlinear optical materials.^[14] The known available method for their preparation is by the α-fluorination of sulfoxides bearing α-hydrogen atoms by elemental fluorine

Table 2: Preparation of substituted difluoromethyl sulfones **4** from **1** (1 equiv), alkyl iodides (4 equiv), and *t*BuOK (2 equiv) in DMF at −50 °C for 1 h.

Entry	RCH ₂ I	RCH ₂ CF ₂ SO ₂ Ph (4)	Yield [%] ^[a]
1	CH ₃ (CH ₂) ₆ I	CH ₃ (CH ₂) ₆ CF ₂ SO ₂ Ph (4a)	79
2	CH ₃ (CH ₂) ₄ I	CH ₃ (CH ₂) ₄ CF ₂ SO ₂ Ph (4b)	80
3	CH ₃ (CH ₂) ₃ I	CH ₃ (CH ₂) ₃ CF ₂ SO ₂ Ph (4c)	84
4	CH ₃ (CH ₂) ₂ I	CH ₃ (CH ₂) ₂ CF ₂ SO ₂ Ph (4d)	73
5	CH ₃ CH ₂ I	CH ₃ CH ₂ CF ₂ SO ₂ Ph (4e)	62
6	CH ₃ I	CH ₃ CF ₂ SO ₂ Ph (4f)	42
7	Ph(CH ₂) ₃ I	Ph(CH ₂) ₃ CF ₂ SO ₂ Ph (4g)	71
8	Ph(CH ₂) ₄ I	Ph(CH ₂) ₄ CF ₂ SO ₂ Ph (4h)	52
9	Ph(CH ₂) ₅ I	Ph(CH ₂) ₅ CF ₂ SO ₂ Ph (4i)	59
10	Ph(CH ₂) ₆ I	Ph(CH ₂) ₆ CF ₂ SO ₂ Ph (4j)	50
11	Ph ₂ CH(CH ₂) ₂ I	Ph ₂ CH(CH ₂) ₂ CF ₂ SO ₂ Ph (4k)	37
12	PhO(CH ₂) ₃ I	PhO(CH ₂) ₃ CF ₂ SO ₂ Ph (4l)	71
13	PhO(CH ₂) ₄ I	PhO(CH ₂) ₄ CF ₂ SO ₂ Ph (4m)	60

[a] Yield of isolated product.

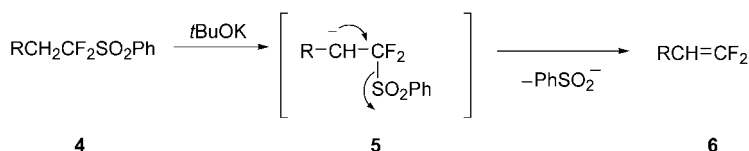
with low yields (10~20 %).^[15] Our current methodology possesses many advantages such as convenience, safety, cost, and efficiency.

During the preparation of alkyl-substituted difluoromethyl sulfones **4**, the formation of a small amount of 1,1-difluoro-1-alkenes as by-products was observed. This is due to the high acidity of the α -hydrogen atom of the difluoromethylene group, which allows the easy deprotonation by *t*BuOK to generate a new carbanion species **5** (Scheme 3). Intermediates **5** readily undergo β -elimination to eliminate the benzenesulfonyl group (rather than a fluorine atom) to afford 1,1-difluoro-1-alkenes **6**. The benzenesulfonyl group is

substituted difluoromethyl sulfones are highly efficient in their facile transformations into 1,1-difluoro-1-alkenes by base-induced eliminations. Difluoromethyl phenyl sulfone acts as a difluoromethylidene equivalent. This new methodology promises to be a highly useful synthetic tool for many other potential applications.

Received: May 27, 2004

Keywords: alkenes · fluorination · elimination · fluorine · nucleophilic substitution



Scheme 3. The formation of 1,1-difluoro-1-alkenes.

known to be a better leaving group than a fluoride.^[9a] Hence, we readily prepared 1,1-difluoro-1-alkenes **6** from the isolated substitution product **4** with *t*BuOK in THF at -20°C to ambient temperature. The deprotonation/ β -elimination reactions proceeded rapidly (within 1 h). Various 1,1-difluoro-1-alkenes were prepared in good to excellent yields by this method using the previously prepared sulfone compounds **4** (Table 3). Thus, the primary alkyl iodides were transformed

Table 3: Preparation of 1,1-difluoro-1-alkenes **6** by deprotonation–elimination reactions using **4** and *t*BuOK in THF at temperatures ranging from -20°C to room temperature.

Entry	RCH ₂ CF ₂ SO ₂ Ph (4)	RCH=CF ₂ (6)	Yield [%] ^[a]
1	Ph(CH ₂) ₃ CF ₂ SO ₂ Ph	Ph(CH ₂) ₂ CH=CF ₂ (6a)	85
2	Ph(CH ₂) ₄ CF ₂ SO ₂ Ph	Ph(CH ₂) ₃ CH=CF ₂ (6b)	71
3	Ph(CH ₂) ₅ CF ₂ SO ₂ Ph	Ph(CH ₂) ₄ CH=CF ₂ (6c)	82
4	Ph(CH ₂) ₆ CF ₂ SO ₂ Ph	Ph(CH ₂) ₅ CH=CF ₂ (6d)	80
5	Ph ₂ CH(CH ₂) ₂ CF ₂ SO ₂ Ph	Ph ₂ CHCH ₂ CH=CF ₂ (6e)	84
6	<i>p</i> -MeO-C ₆ H ₄ - (CH ₂) ₄ CF ₂ SO ₂ Ph	<i>p</i> -MeO-C ₆ H ₄ -(CH ₂) ₃ CH= CF ₂ (6f)	55
7	PhO(CH ₂) ₃ CF ₂ SO ₂ Ph	PhO(CH ₂) ₂ CH=CF ₂ (6g)	88
8	PhO(CH ₂) ₄ CF ₂ SO ₂ Ph	PhO(CH ₂) ₃ CH=CF ₂ (6h)	87

[a] Yield of isolated product.

into 1,1-difluoro-1-alkenes in two steps by a substitution–elimination sequence. The advantage of this method is that the reactions are facile and straightforward, and necessitate only safe and inexpensive reagents and simple experimental procedures.

In conclusion, the unprecedented nucleophilic substitution reactions (S_N2) of (benzenesulfonyl)difluoromethide (generated in situ from difluoromethyl phenyl sulfone and a base) with primary alkyl halides (preferentially primary alkyl iodides) have been developed, which demonstrates the efficient carbon–carbon bond formation between a fluorinated carbanion and primary alkyl halides. The new alkyl-

- H=CF₂
- 6
- [1] a) K. Ando, *J. Org. Chem.* **2004**, 69, 4203; b) J. Ichikawa, H. Fukui, Y. Ishibashi, *J. Org. Chem.* **2003**, 68, 7800; c) J. R. McCarthy, *Utility of Fluorine in Biologically Active Molecules*, ACS Fluorine Division Tutorial, 219th National ACS Meeting, San Francisco, March 26, **2000**; d) *Selective Fluorination in Organic and Bioorganic Chemistry*, ACS Symposium Series 456 (Ed.: J. T. Welch), American Chemical Society, Washington, DC, **1991**.
- [2] W. B. Motherwell, Jr., M. J. Tozer, B. C. Ross, *J. Chem. Soc. Chem. Commun.* **1989**, 1437.
- [3] W. R. Moor, G. L. Schatzman, E. T. Jarvi, R. S. Gross, J. R. McCarthy, *J. Am. Chem. Soc.* **1992**, 114, 360.
- [4] a) T. Abe, R. Tamai, M. Tamaru, H. Yano, S. Takahashi, N. Muramatsu, WO 2003042153, **2003** [*Chem. Abstr.* **2003**, 138, 401741]; b) T. Abe, R. Tamai, M. Ito, M. Tamaru, H. Yano, S. Takahashi, N. Muramatsu, WO 2003029211, **2003** [*Chem. Abstr.* **2003**, 138, 304304]; c) K. Fuji, Y. Hatano, K. Tsutsumiuchi, Y. Nakahon, JP 2000086636, **2000** [*Chem. Abstr.* **2000**, 132, 222532].
- [5] a) J. M. Percy, *Contemp. Org. Synth.* **1995**, 2, 251; b) J. Ichikawa, H. Miyazaki, K. Sakoda, Y. Wada, *J. Fluorine Chem.* **2004**, 125, 585; c) M. J. Tozer, T. F. Herpin, *Tetrahedron* **1996**, 52, 8619.
- [6] a) D. J. Burton, D. G. Naeae, *J. Fluorine Chem.* **1971**, 1, 123; b) D. J. Burton, D. G. Naeae, *Synth. Commun.* **1973**, 3, 197; c) J. Ichikawa, *J. Fluorine Chem.* **2000**, 105, 257; d) D. P. Matthews, S. C. Miller, E. T. Jarvi, J. S. Sabol, J. R. McCarthy, *Tetrahedron Lett.* **1993**, 34, 3057; e) A. J. Bennett, J. M. Percy, M. H. Rock, *Synlett* **1992**, 483; f) J. M. Percy, *Tetrahedron Lett.* **1990**, 31, 3931; g) T. Tsukamoto, T. Kitazume, *Synlett*, **1992**, 977; h) J.-P. Begue, D. Bonnet-Delpon, M. H. Rock, *Tetrahedron Lett.* **1995**, 36, 5003; i) G. Shi, X. Huang, F.-J. Zhang, *Tetrahedron Lett.* **1995**, 36, 6305; j) J.-P. Begue, D. Bonnet-Delpon, M. H. Rock, *Tetrahedron Lett.* **1994**, 35, 6097; k) K. -I. Kim, J. R. McCarthy, *Tetrahedron Lett.* **1996**, 37, 3223; l) A. K. Brisdon, K. K. Banger, *J. Fluorine Chem.* **1999**, 100, 35; m) P. L. Coe, *J. Fluorine Chem.* **1999**, 100, 45.
- [7] The nucleophilic substitution reaction of CF₃⁻ (generated in situ from TMS-CF₃ and fluoride) with alkyl halides has been attempted by us with no success. However, the nucleophilic trifluoromethylation of primary alkyl triflates was successful using TMS-CF₃ and fluoride. See: D. V. Sevenard, P. Kirsch, G.-V. Roschenthaler, V. N. Movchun, A. A. Kolomeitsev, *Synlett* **2001**, 379.
- [8] a) *Synthetic Fluorine Chemistry* (Eds: G. A. Olah, R. D. Chambers, G. K. S. Prakash), Wiley, New York, **1992**; b) H. Urata, T. Fuchikami, *Tetrahedron Lett.* **1991**, 32, 91; c) D. J. Burton, G. A. Hartgraves, J. Hsu, *Tetrahedron Lett.* **1990**, 31, 3699; d) Y. Kobayashi, K. Yamamoto, I. Kumadaki, *Tetrahedron Lett.* **1979**, 42, 4071; e) G. E. Carr, R. D. Chambers, T. F. Holmes, *J. Chem. Soc. Perkin Trans. I* **1988**, 921; f) Q.-Y. Chen, J.-X. Duan, *Tetrahedron Lett.* **1993**, 34, 4241.

- [9] a) *Sulfones in Organic Synthesis, Tetrahedron Organic Chemistry Series, Vol. 10* (Eds.: J. E. Baldwin, P. D. Magnus), Pergamon, New York, **1993**; b) B. M. Trost, M. R. Chadiri, *J. Am. Chem. Soc.* **1984**, *106*, 7260; c) B. M. Trost, *Bull. Chem. Soc. Jpn.* **1988**, *61*, 107.
- [10] a) J. Hine, J. J. Porter, *J. Am. Chem. Soc.* **1960**, *82*, 6178; b) G. P. Stahly, *J. Fluorine Chem.* **1989**, *43*, 53; c) G. K. S. Prakash, J. Hu, T. Mathew, G. A. Olah, *Angew. Chem.* **2003**, *115*, 5374; *Angew. Chem. Int. Ed.* **2003**, *42*, 5216.
- [11] B. R. Langlois, *J. Fluorine Chem.* **1988**, *41*, 247.
- [12] G. K. S. Prakash, J. Hu, G. A. Olah, *J. Org. Chem.* **2003**, *68*, 4457.
- [13] D. Mesnard, L. Miginiac, *J. Organomet. Chem.* **1989**, *373*, 1.
- [14] W. M. Wijekoon, S. K. Wijaya, J. D. Bhawalkar, P. N. Prasad, T. L. Penner, N. J. Armstrong, M. C. Ezenyilimba, D. J. Williams, *J. Am. Chem. Soc.* **1996**, *118*, 4480.
- [15] a) A. Toyota, Y. Ono, J. Chiba, T. Sugihara, C. Kaneko, *Chem. Pharm. Bull.* **1996**, *44*, 703; b) J. Chiba, T. Sugihara, C. Kaneko, *Chem. Lett.* **1995**, 581.

Materials Science

Creation of Intestine-like Interior Space for Metal-Oxide Nanostructures with a Quasi-Reverse Emulsion**

Hua Gui Yang and Hua Chun Zeng*

Hollow inorganic micro- and nanostructures have attracted great attention in recent years because of their promising properties for scale-dependent applications such as photonic devices, drug delivery, active-material encapsulation, ionic intercalation, surface functionalization, robust catalysts/carriers, and size-selective reactions.^[1–5] Until now there have been two basic templating methods, with either hard or soft templates, for synthesizing these hollow structures. For example, colloid particles, fibers, organogelators, anodic alumina membranes, or sacrificial cores are commonly utilized in the hard-templating method, and the inorganic layers are coated onto the inner or outer surfaces by layer-by-layer, sol-gel casting, redox replacement, or nanoparticle adsorption methods;^[1–9] the desired hollow interiors are generated upon removal of the templates by calcination or dissolution. In the soft-templating method ionic organic surfactants, such as sodium dodecyl sulfate (SDS, in non-

aqueous emulsions),^[10] or nonionic polymeric surfactants, such as alkyl poly(ethylene oxide),^[11,12] have been widely used; even gas bubbles generated in situ can be used to form microscale hollow spheres.^[13] To overcome the complexity associated with templating methods a number of template-free methods for hollow inorganic microspheres have been developed very recently, in which large quantities of an inorganic additive such as $(\text{NH}_4)_2\text{SO}_4$, NH_4OH , KCl , or an ionic liquid, are involved,^[14–17] including the Ostwald ripening and Kirkendall effect for solid-hollowing in solution.^[18,19] Nonetheless, the reported syntheses are not perfect either, because it is hard to avoid inclusion of additive impurities and is difficult to achieve size control in the sub-micrometer regime or other morphological tuning.^[14,17]

In searching for other synthetic methods it seemed possible that existing solution inhomogeneity (that is, microheterogeneity) in common cosolvent systems could be utilized. For example, it has recently been confirmed by Raman spectroscopy, small-angle X-ray scattering, and molecular dynamics simulations that alcohols such as *n*-propanol and 2-propanol tend to self-assemble in dilute aqueous solution and result in solution microheterogeneities (that is, local compositions which differ from the average ones).^[20–22] It is now known that, despite the fact that these alcohols and water are infinitely miscible, the solution is far from homogeneous.^[22] We report here a novel “quasi-reverse-emulsion” solvothermal method to generate hollow nanostructures for metal oxides with monodisperse morphologies in a mixture of water and 2-propanol. In particular, intestine-like or spherical hollow interiors have been created for phase-pure anatase TiO_2 nanostructures with 100% morphological yield. The success of this method can be attributed to the presence of microheterogeneities in the solvent mixture.

Figure 1 shows the results of our transmission electron microscopy and selected-area electron diffraction (TEM/SAED) investigations. The wall thickness of intestine-like TiO_2 can be controlled precisely in the present template-free synthesis by varying the reactant concentrations. As an illustration, a uniform wall thickness of about 125–150 nm (Figure 1 A) can be prepared with a higher concentration of TiF_4 in the starting solution, while the wall thickness can be reduced to as little as 20–30 nm by reducing the amount of TiF_4 present (Figure 1 B and C). A similar concentration dependency is also observed for the outer diameters (500–550 nm in Figure 1 A can be reduced to 400–450 nm in Figure 1 B). A further reduction in diameter to about 250–300 nm can be achieved with an even lower concentration of TiF_4 (see Supporting Information). The inner cavities of the nanostructures were clearly identified by TEM contrast images as well as the corresponding scanning electron microscopy (SEM) and field-emission SEM (FESEM) images. Interestingly, either a hollow interior or a partially filled interior (with a solid core) can be selected (compare Figure 1 A with 1 B and see the Supporting Information). SAED patterns from the as-prepared TiO_2 intestines show diffraction rings typical of the anatase phase (Figure 1),^[23,24] which is consistent with the X-ray diffraction (XRD) finding of the same polymorph (see the Supporting Information; phase-pure anatase TiO_2 , space group: $I4_1/amd$; JCPDS file

[*] H. G. Yang, Prof. Dr. H. C. Zeng
Department of Chemical and Biomolecular Engineering
Faculty of Engineering
National University of Singapore
10 Kent Ridge Crescent, Singapore 119260 (Singapore)
Fax: (+65) 6779-1936
E-mail: chezhc@nus.edu.sg

[**] The authors gratefully acknowledge financial support from the Ministry of Education, Singapore.

Supporting information for this article is available on the WWW under <http://www.angewandte.org> or from the author.

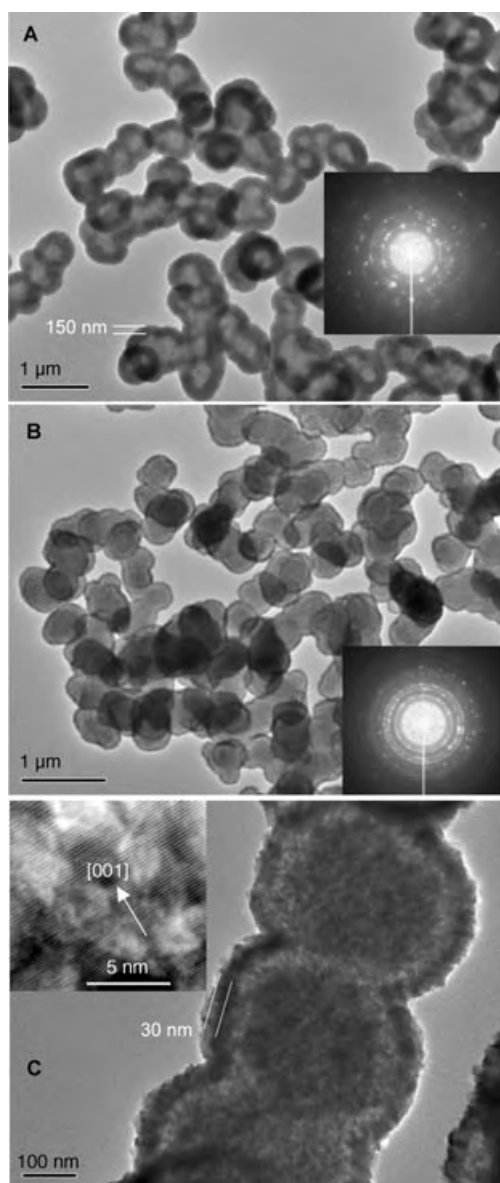


Figure 1. TEM images and SAED patterns (inset) of intestine-like TiO_2 hollow structures synthesized at 180°C (water/alcohol = 20:80 w/w): A) 5.0 mL of 0.040 M TiF_4 + 20.0 g of 2-propanol, 20 h; B) 2.0 mL of 0.040 M TiF_4 + 3.0 mL of H_2O + 20.0 g of 2-propanol, 22 h; C) high magnification image of (B), together with an HRTEM image of the shell (inset).

No. 21-1272) and energy-dispersive X-ray (EDX) analysis of the solid composition (atomic ratio $\text{Ti}/\text{O} = 1/2$; see the Supporting Information). The crystallite size is about 10–20 nm (high-resolution TEM (HRTEM); see Figure 1 C and the Supporting Information); within a set of growth parameters, the crystallinity increases with aging time (see the Supporting Information). In particular, the lattice fringes of d_{004} ($2.3 \pm 0.2 \text{ \AA}$) can be easily identified and indicate a preferred $\langle 001 \rangle$ alignment of the TiO_2 nanocrystallites along the shells of the intestines. The specific surface areas of these samples are in the range $50\text{--}60 \text{ m}^2 \text{ g}^{-1}$, and depend on the synthetic conditions employed (see Experimental Section).

As shown in Figure 2, smaller and less interconnected TiO_2 intestines with diameters ranging from 300 to 450 nm can also be tailored with a shorter reaction time (for example,

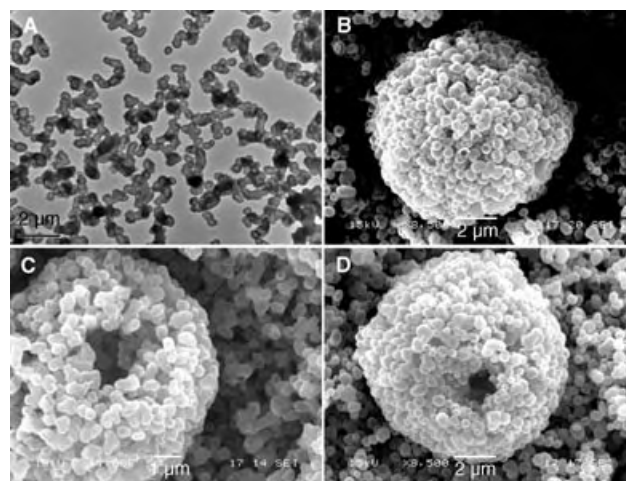


Figure 2. Primary short intestine-like TiO_2 hollow nanostructures (A: TEM image) and their microscale-assembled colloidosomes (B–D: SEM images). Synthetic conditions: 2.0 mL of 0.040 M TiF_4 + 3.0 mL of H_2O + 20.0 g of 2-propanol, at 180°C for 5 h (water/alcohol = 20:80 w/w).

5 h versus the 22 h of Figure 1 B). More interestingly, these short TiO_2 hollow structures can self-aggregate into microscale hollow spheres, or “colloidosomes” (Figure 2 B–D). Compared to the colloidosomes fabricated recently with polymeric beads in water/oil emulsions,^[5] the present mesostructures possess more-complex hierarchical pores, with an interior space within the short TiO_2 intestines, an inter-intestine space created by the intestines, and a large central cavity within the colloidosomes. In addition to the above thick-shelled colloidosomes, thinner spherical organizations or curved platelets assembled from the primary TiO_2 intestines can also be prepared by microemulsion methods (see the Supporting Information).

The formation of the intestine morphology is sensitive to the composition of the solvent mixture: isolated discrete TiO_2 hollow nanospheres can be fabricated with a diameter of 250–450 nm and a wall thickness of about 40 nm if the water content is reduced (Figure 3). Both the sphere diameter and crystallite size in the shells can be tuned by varying the aging time (Figure 3 B) and starting TiF_4 concentration. For example, freestanding TiO_2 hollow spheres with a diameter ranging from 100 to 450 nm can be synthesized when the reaction time is as short as 1.5 or 3 h (see the Supporting Information; the size of the nanocrystallites is around 20–30 nm). In addition to the SAED result shown in Figure 3 A, an XRD investigation (see the Supporting Information) further confirmed the same anatase phase for the hollow spheres.

On the basis of the above results, a growth mechanism is proposed (Figure 4). It is noted that alcohols such as 2-propanol possess self-hydrophobic interactions even though they are miscible with water.^[20–22] The water molecules in the aqueous phase interact preferentially amongst themselves

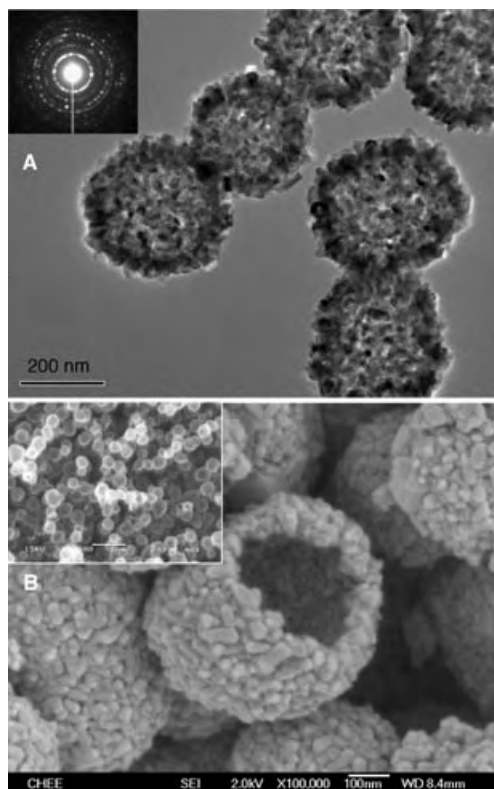


Figure 3. Isolated, discrete TiO_2 hollow nanospheres: A) TEM image and SAED pattern, and B) FESEM image of the wall crystallites and inner cavity; the insert (SEM image) shows an overview of the nanospheres. Synthetic conditions: 1.0 mL of 0.040 M TiF_4 + 3.0 mL of H_2O + 21.0 g of 2-propanol, at 180 °C for 42 h (water/alcohol = 16:84 w/w).

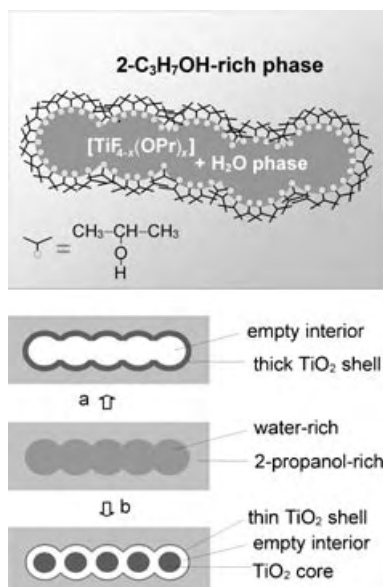


Figure 4. Proposed formation mechanism of intestine-like TiO_2 in a “quasi-reverse-emulsion” (water is the minor phase): a) formation of thick-walled TiO_2 nanostructures, and b) formation of smaller thin-walled TiO_2 nanostructures with some internal cores.

through strong hydrogen-bonding interactions, which result in microheterogeneities, since 2-propanol has only a small disrupting effect on the hydrogen bond between water molecules.^[20–22] Considering the electronegativity sequence $\text{F} > \text{O} \gg \text{C}$ and the hydrophobic interactions between the 2-propanol molecules, it is expected that TiF_4 and its other forms of complexes^[25],^[26] will exist primarily in the water-rich regions (that is, emulsified spherical droplets, Figure 4) because of various hydrogen-bonding interactions (for example, $\text{H}-\text{O}\cdots\text{H}$ and $\text{O}-\text{H}\cdots\text{F}$). In other words, TiF_4 can also help water to stabilize aqueous droplets, and this means that the dimensions of the resultant TiO_2 intestines are indeed proportional to the starting concentration of TiF_4 (see Figure 1 and the Supporting Information). The water-rich region, in which a series of aqueous droplets are linked together, is then surrounded by a self-assembled 2-propanol-rich phase and vice versa. In good agreement with this model, the aqueous droplets become more isolated when the water to alcohol ratio is decreased, thus resulting in the formation of isolated nanospheres (see Figure 3 and the Supporting Information). Figure 5 displays three UV/Vis spectra mea-

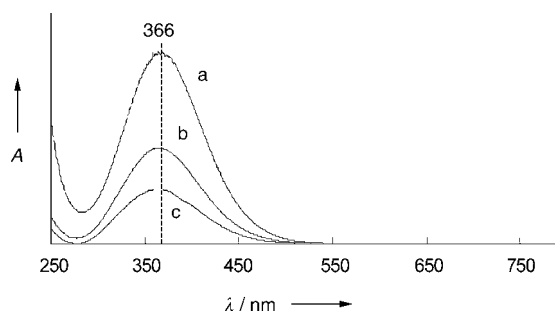


Figure 5. UV/Vis spectra of various solution phases at room temperature: a) 5.0 mL of 0.040 M TiF_4 + 20.0 g of 2-propanol, b) 2.0 mL of 0.040 M TiF_4 + 3.0 mL of H_2O + 20.0 g of 2-propanol, and c) 1.0 mL of 0.040 M TiF_4 + 3.0 mL of H_2O + 21.0 g of 2-propanol.

sured for different starting solutions. It is apparent that in acidic aqueous phase TiF_4 is first stabilized as complex fluoro ions, predominantly in the form of stable TiF_6^{2-} ions (which is colorless).^[25] After the addition of 2-propanol an alkoxylation reaction takes place to give alkoxy-substituted Ti^{IV} complexes such as $[\text{TiF}_{4-x}(\text{OPr})_x]$ (for example, $x=2$).^[26] The peak at 366 nm is assigned to the absorption of this type of complex; the absorbance increases linearly with the initial concentration of TiF_4 . Addition of a small amount of HF caused the yellowish solution to become colorless again, thus indicating that the TiF_6^{2-} ion had been regenerated. Under these conditions, TiO_2 would nucleate and grow at the interface (shell) as well as in the bulk aqueous phase (core) by hydrolysis and adopt the shape of the aqueous phase (See Figure 4). To a certain extent, therefore, the water/2-propanol system used is analogous to a “quasi-reverse-emulsion”, albeit with a weaker hydrophobic effect of 2-propanol than the oil hydrocarbons used in standard reverse-emulsion methods.^[27] Indeed, a series of syntheses using ethanol, *n*-propanol, 2-propanol, and 2-methyl-2-propanol indicated that larger TiO_2 hollow structures can be generated when the

hydrophobicity of the aliphatic alcohols is increased; the structure of the shell wall is sensitive to the alcohol used, which confirms the tendency to form larger “micelles” with an increase in the hydrophobic interaction of the aliphatic alcohols (see the Supporting Information). These results confirm the generality of this synthetic approach using water–alcohol mixtures. As a final remark, the present solvent system has also been applied to our preliminary work on the fabrication of other metal-oxide hollow nanostructures; generally it works well.^[28]

In summary, we have developed a solvothermal process for the controlled creation of interior space in metal-oxide nanostructures. In particular, anatase TiO₂ with either an intestine-like or spherical morphology can be selected by varying the starting chemical composition and reaction time. Apart from the size control, an entirely empty or partially filled interior can be further tailored with this one-step approach. The self-aggregation of micrometer-scale TiO₂ colloidosomes indicates the possibility of constructing even more complex hierarchical hollow structures. The method has also been shown to be general for other metal oxides; the formation of hollow structures can be ascribed to the existence of microheterogeneities in the mixed-solvent system.

Experimental Section

Hydrochloric acid (1.5 M) was used to adjust the pH of deionized water (1.0 L) to around 2. Titanium tetrafluoride (Aldrich Chemical) was then dissolved in this solution to a concentration of 0.040 M, during which the pH value changed to 1.8. The water/2-propanol mixture used was prepared by weight. In a typical synthesis, the aqueous TiF₄ solution (1–5 mL, 0.040 M) and H₂O (0–3 mL) were first added to a teflon-lined autoclave, then 20–21 g of 2-propanol added; the mixture was kept at 180 °C for 1.5–42 h in an electric oven. When mixed with TiF₄, the colorless 2-propanol became clear yellowish. After completion of the reaction the solution became colorless again (since Ti⁴⁺ complexes were consumed) and a white precipitate (TiO₂ product) formed on the bottom of the teflon reactor. Organization of the as-prepared TiO₂ intestines into spherical or curved assemblies was conducted in oil–water emulsions. In addition to 2-propanol, similar syntheses using ethanol, *n*-propanol, and 2-methyl-2-propanol were also carried out to verify some of the conclusions drawn from this work. The solid products obtained were washed three times with deionized water (10 mL each time) and then dried in vacuum for further characterization.

The crystallographic phase of the hollow TiO₂ structures was determined by powder X-ray diffraction (XRD, Shimadzu XRD-6000, CuK_α radiation) and selected-area electron diffraction (SAED).^[23,24] The particle size, crystal morphology, and chemical composition of the TiO₂ products were determined by scanning electron microscopy (SEM/EDX, JSM-5600 LV; FESEM/EDX, JSM-6700F), transmission electron microscopy, and energy dispersive X-ray diffractometry (TEM/SAED, JEM 2010, 200 kV; HRTEM/EDX, JEM 3010, 300 kV).^[29] The specific surface areas of the TiO₂ samples were also measured by the BET method (NOVA-3000). A UV/Vis scanning spectrophotometer (UV-3101PC, Shimadzu)^[30] was also used to investigate the formation of Ti⁴⁺ complexes in water/2-propanol mixtures at room temperature.

Received: May 25, 2004

Keywords: materials science · nanostructures · polymorphism · solvent effects · titanium

- [1] F. Caruso, R. A. Caruso, H. Möhwald, *Science* **1998**, 282, 1111.
- [2] C. G. Göltner, *Angew. Chem.* **1999**, 111, 3347; *Angew. Chem. Int. Ed.* **1999**, 38, 3155.
- [3] Y. Sun, Y. Xia, *Science* **2002**, 298, 2716.
- [4] Y. Sun, B. Mayers, Y. Xia, *Adv. Mater.* **2003**, 15, 641.
- [5] A. D. Dinsmore, M. F. Hsu, M. G. Nikolaides, M. Marquez, A. R. Bausch, D. A. Weitz, *Science* **2002**, 298, 1006.
- [6] R. A. Caruso, J. H. Schattka, A. Greiner, *Adv. Mater.* **2001**, 13, 1577.
- [7] Z. Yang, Z. Niu, Y. Lu, Z. Hu, C. C. Han, *Angew. Chem.* **2003**, 115, 1987; *Angew. Chem. Int. Ed.* **2003**, 42, 1943.
- [8] J. J. Zhu, S. Xu, H. Wang, J. M. Zhu, H. Y. Chen, *Adv. Mater.* **2003**, 15, 156.
- [9] S. Kobayashi, N. Hamasaki, M. Suzuki, M. Kimura, H. Shirai, K. Hanabusa, *J. Am. Chem. Soc.* **2002**, 124, 6550.
- [10] A. M. Collins, C. Spickermann, S. Mann, *J. Mater. Chem.* **2003**, 13, 1112.
- [11] J. L. Blin, A. Léonard, Z. Y. Yuan, L. Gigot, A. Vantomme, A. K. Cheetham, B. L. Su, *Angew. Chem.* **2003**, 115, 2978; *Angew. Chem. Int. Ed.* **2003**, 42, 2872.
- [12] Z. Y. Yuan, T. Z. Ren, B. L. Su, *Adv. Mater.* **2003**, 15, 1462.
- [13] Q. Peng, Y. Dong, Y. Li, *Angew. Chem.* **2003**, 115, 3135; *Angew. Chem. Int. Ed.* **2003**, 42, 3027.
- [14] C. W. Guo, Y. Cao, S. H. Xie, W. L. Dai, K. N. Fan, *Chem. Commun.* **2003**, 700.
- [15] H. J. Hah, J. S. Kim, B. J. Jeon, S. M. Koo, Y. E. Lee, *Chem. Commun.* **2003**, 1712.
- [16] P. Afanasiev, I. Bezverkhy, *J. Phys. Chem. B* **2003**, 107, 2678.
- [17] T. Nakashima, N. Kimizuka, *J. Am. Chem. Soc.* **2003**, 125, 6386.
- [18] H. G. Yang, H. C. Zeng, *J. Phys. Chem. B* **2004**, 108, 3492.
- [19] Y. Yin, R. M. Rioux, C. K. Erdonmez, S. Hughes, G. A. Somorjai, A. P. Alivisatos, *Science* **2004**, 304, 711.
- [20] A. Idrissi, S. Longelin, *J. Mol. Struct.* **2003**, 651–653, 271.
- [21] E. Ruckenstein, I. Shulgin, *Chem. Eng. Sci.* **2001**, 56, 5675.
- [22] A. B. Roney, B. Space, E. W. Castner, R. L. Napoleon, P. B. Moore, *J. Phys. Chem. B* **2004**, 108, 7389.
- [23] H. G. Yang, H. C. Zeng, *Chem. Mater.* **2003**, 15, 3113.
- [24] H. G. Yang, H. C. Zeng, *J. Phys. Chem. B* **2003**, 107, 12244.
- [25] F. A. Cotton, G. Wilkinson, *Advanced Inorganic Chemistry*, 6th ed, Wiley, New York, **1999**, chap. 17.
- [26] H. Weingarten, J. R. Van Wazer, *J. Am. Chem. Soc.* **1965**, 87, 724.
- [27] M.-P. Pileni, *Nat. Mater.* **2003**, 2, 145.
- [28] H. G. Yang, H. C. Zeng, unpublished results.
- [29] X. W. Lou, H. C. Zeng, *J. Am. Chem. Soc.* **2003**, 125, 2697.
- [30] J. T. Sampanthar, H. C. Zeng, *J. Am. Chem. Soc.* **2002**, 124, 6668.

Superhydrophobic Films

Tunable, Superhydrophobically Stable Polymeric Surfaces by Electrospinning**

Kazim Acatay, Eren Simsek, Cleve Ow-Yang, and Yusuf Z. Menceloglu*

The high water repellence of superhydrophobic surfaces is attributed to the limited contact area between the solid and water which is manifested by a high static water contact angle (WCA) and a low sliding angle. The solid-liquid interfacial energy can be minimized by engineering not only the chemistry but also the topography of the solid surface.^[1,2] For example, epicuticular wax on the lotus leaf is an intrinsically hydrophobic material.^[3] However, when nano-sized crystals of wax cover a micron-level rough surface, as is the case on the lotus leaf, the WCA is further enhanced to 160°, which is defined as superhydrophobic.^[4–8] In this case, the water droplet forms a three-dimensional, discontinuous, triphasic (water–air–solid) contact line^[9] that is relatively longer and less stable than such a line on a macroscopically smooth surface. Moreover, a nonhydrophobic material can also be rendered hydrophobic with a WCA well above 150° by chemical modification, for example, through the incorporation of fluorine or silicone, as well as by increasing the roughness.^[9–14] Such an extreme water repellence is highly attractive for novel industrial and practical applications: continuously clean buildings, windows, and outdoor decorations, stain-resistant fabrics, antifouling marine structures, and oxidation-resistant surfaces.^[2,8,10] Currently, the production of superhydrophobic surfaces is based on time-consuming, expensive, and/or nonversatile processes, such as controlled crystallization, lithography, etching, and templating.^[9–13,15]

To mimic the topography of the lotus leaf and to achieve a high WCA, we fabricated a polymeric film surface with a high degree of roughness through a simple and practical electrospinning process.^[16] Electrospun films consist of a continuous, nonwoven web of fibers (with diameters in the order of 1–1000 nm) and, depending on processing conditions, with polymer droplets either as isolated spheres (> 1 µm in diameter) or strung along a fiber.^[17–22] The electrospun film is produced by applying an electrical bias from the tip of a polymer solution-filled syringe to a grounded collection plate. Along the trajectory of the extruded polymer fiber, most of the solvent evaporates, such that a mat of randomly aligned fibers collects and form a thin film. In addition to surface roughness, the film properties were optimized by chemical

modification, such as the addition of fluorine to enhance and stabilize WCA values and the incorporation of crosslinking for solvent resistance. Our ability to engineer both the physical and chemical properties of the electrospun films enables flexibility in tuning the degree of hydrophobicity.

A thermoset polymer was synthesized by first reacting acrylonitrile (AN) and α,α -dimethyl *meta*-isopropenylbenzyl isocyanate (TMI) in *N,N*-dimethylformamide (DMF), and then mixing the resultant poly(AN-co-TMI) with a perfluorinated linear diol (fluorolink-D) and tin(II) ethyl hexanoate (T2EH) in DMF. The solution was mixed and immediately electrospun onto an aluminum foil substrate covering the electrically grounded screen. The processing parameters used throughout this study were fixed for the 30-min electrospinning periods: tip-to-ground distance 10 cm, flow rate of the polymeric mixture 12.5 µL min⁻¹, spinning voltage 16 kV. The remaining mixture was subsequently cast onto microscope slides for wetting comparison. The electrospun samples and the corresponding cast films were subsequently annealed at 70 °C for at least 8 h, which enabled the reorientation of the perfluorinated groups to the solid–air interface.^[22] A comparison of the measured static WCA between an electrospun film and a cast version of the same composition reveals an enhancement of up to 60° (Figure 1 a and b).

One parameter that allowed the topography of the electrospun film to be tuned was the viscosity, which we investigated by mixing poly(AN-co-TMI) with fluorolink-D (50 wt %) in various quantities of DMF to create a range of viscosities (31–350 mPa s). As the viscosity increased, the morphology of the micro-textured films changed from one containing predominantly beads to another of only fibers, as

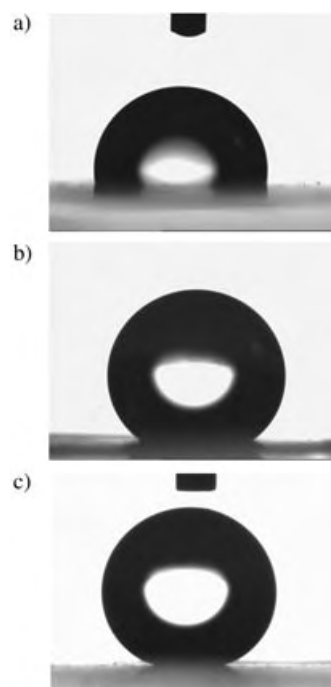


Figure 1. Photographs taken during WCA measurements: a) cast film of 31 mPa s mixture (WCA = 96°), b) electrospun film of 31 mPa s mixture (WCA = 156°), and c) electrospun low-molecular-weight (LMW) copolymer (WCA ≈ 167°).

[*] Dr. K. Acatay, E. Simsek, Dr. C. Ow-Yang, Prof. Y. Z. Menceloglu
Materials Science and Engineering Program
Faculty of Engineering and Natural Sciences
Sabanci University
Orhanli 34956 Tuzla-Istanbul (Turkey)
Fax: (+90) 216-483-9550
E-mail: yusufm@sabanciuniv.edu

[**] We thank Cytec and Ausimont for their kind donations of TMI and fluorolink-D, respectively.

revealed by scanning electron microscope (SEM) imaging (Figure 2a,b,c). A surface consisting of mostly 2–3- μm diameter beads can be rougher than a surface covered with 200–400-nm thick fibers. Moreover, the bead-rich topography

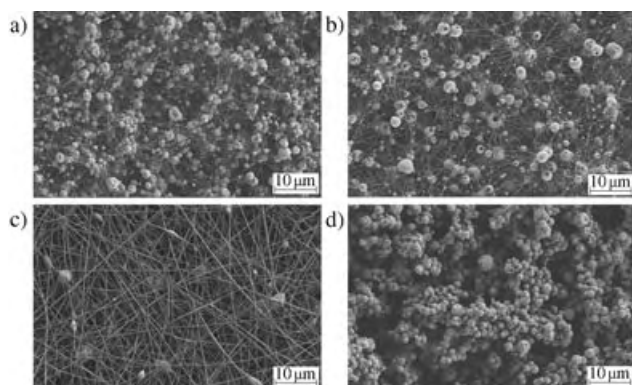


Figure 2. Scanning electron microscope images of electrospun films of copolymers with viscosities: a) 31 mPa s, b) 102 mPa s, and c) 348 mPa s (HMW copolymer), and d) 51 mPa s (LMW copolymer). The measurements were carried out at 1 keV and 5000 \times magnification.

increases the discontinuities in the triphasic contact line^[11] much more than does the fiber-rich surface. The measured static WCA of the films ranged from 156° (for a solution viscosity of 31 mPa s) to 148° (350 mPa s), with a maximum standard deviation of $\pm 2^\circ$. In contrast, cast films of corresponding compositions yielded WCAs in the range 96–99°.

Because the tilt angle of a superhydrophobic surface indicates the water–solid interface energy that immobilizes a water droplet, the self-cleaning ability of a surface can effectively be characterized by the threshold sliding angle. We determined the sliding angle of a water drop on an electrospun sample by placing a 10-mg drop of water on the textured film surface, which was then inclined at increasing angles until the drop started to roll. As the fiber content increased on our micro-textured surfaces, we observed a concurrent increase in sliding angle: Figure 2a, tilt angle = $20.7 \pm 7.5^\circ$; Figure 2b, tilt angle = $52.6 \pm 5.6^\circ$; Figure 2c, no rolling at 90° tilt.

The viscosity study suggested that the WCA on our micro-textured surfaces increased as the bead ratio increased, implying that a surface morphology containing solely beads may generate even larger WCAs. However, the use of a polymer solution with a viscosity lower than 31 mPa s for electrospinning produced surfaces with low roughness, because the non-evaporated solution also reached the grounded plate. In the electrospinning of low-molecular-weight polymer solutions, extensive droplet formation was observed^[23] which was attributed to Rayleigh instability in the fluid flow. In fact, more beads form as the molecular weight of the polymer decreases. Thus as expected, we observed a direct relationship between the molecular weight of poly(AN-co-TMI) and the WCA on the electrospun film. A poly(AN-co-TMI) substance of low molecular weight was synthesized by changing the polymerization reaction solvent from *N,N*-

dimethylformamide (DMF) to tetrahydrofuran (THF), while using the same reactant ratio, temperature, and time. When the viscosity average molecular weight of the polymers was measured, we found that the copolymer synthesized in DMF has a higher molecular weight ($\sim 20000 \text{ g mol}^{-1}$, the HMW copolymer), whereas the copolymer synthesized in THF has a lower molecular weight ($\sim 4000 \text{ g mol}^{-1}$, the LMW copolymer). When the LMW copolymer was mixed with fluorolink-D and electrospun (51 mPa s), the electrospun film consisted of only clustered polymeric beads ranging from 1 to 3 μm in diameter (Figure 2d). In contrast, when the HMW copolymer with a similar viscosity was electrospun under the same processing conditions, the result was a fibrous morphology also containing beads (Figure 2a). The static WCA of $166.7 \pm 2.2^\circ$ measured on the electrospun LMW copolymer (Figure 1c), was the maximum average WCA that we have obtained for the electrospun films. Also, the relatively low tilt angle of $4.3 \pm 0.8^\circ$ indicated that this film is more suitable for self-cleaning applications than the fiber-containing, electrospun films. Evidently, the presence of fibers decreases the variation in roughness amplitude, so that a film morphology of predominantly beads enhances water immobilization owing to a long and discontinuous interface at the bottom of the droplet. In contrast, a mat of fibers creates a nano-textured surface that is relatively smooth at the micron level.

Recently, there has been much discussion in the literature about the stability of the superhydrophobic state of micro-textured surfaces, which effectively determines the potential for the self-cleaning behavior of these surfaces.^[1,7] Two different equilibrium states defined in the literature for rough superhydrophobic surfaces are the Cassie^[24] and Wenzel^[25] states. The Wenzel state exhibits a high WCA owing to an increase in surface area, whereas the Cassie state describes a high WCA owing to trapped air pockets in the rough surface. The Cassie regime offers a lower hysteresis between advancing and receding WCAs, because the water droplet is mostly in contact with the trapped air, and the hydrophobic surface has a lower sliding (roll-off) angle. On the other hand, because the Wenzel regime is a consequence of a larger water–solid interface energy pinning that fixes the droplet to the film surface, the hysteresis is larger, and the droplet cannot slide as easily.

However, the type of superhydrophobic state is not always clearly either Cassie or Wenzel in nature, and can be misleadingly designated as a metastable Cassie state.^[7] To understand how such a metastable Cassie state can simultaneously exist with a Wenzel state, consider a water drop sitting on a surface of the metastable Cassie-type. If this drop is uniaxially loaded above a material-specific threshold level, the trapped air in the pockets is irreversibly pushed out and replaced with water, and the increase in surface contact area is accompanied by a sudden decrease in the postpressing WCA values. Thus, the water drop is immobilized, the Cassie state is irreversibly transformed into the Wenzel state, and the self-cleaning ability of the surface is lost. Moreover, owing to the increased adhesion to both pressing plates, upon release of the load, the drop can split into two hemispheres, with one half adhering to the top plate, and the other half to the bottom plate.

To determine the hydrophobic state of our textured films, water droplets were placed between two plates covered with HMW copolymer electrospun films (Figure 2a,b), and uniaxially loaded (Figure 3). We were able to load the water

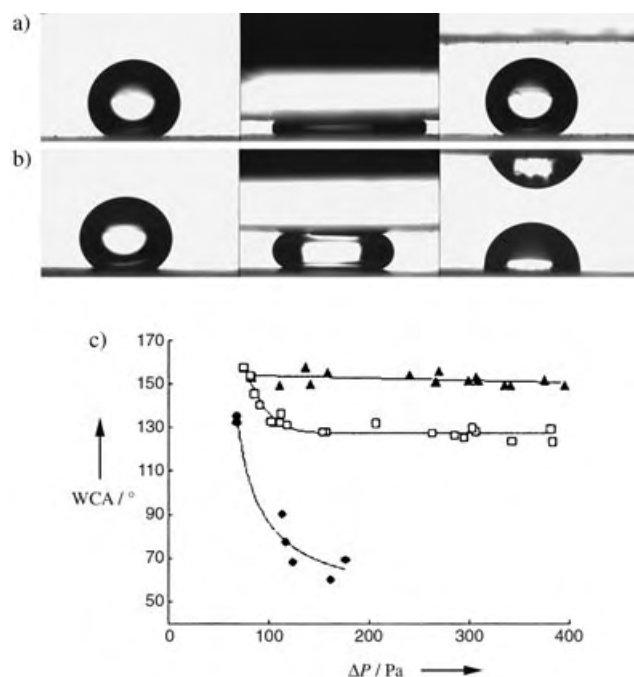


Figure 3. Water droplet pressing between two identical surfaces of: a) 31 mPa s electrospun at Figure 2a. b) 348 mPa s electrospun at Figure 2c. Photos were taken before, during, and after pressing of the droplet. c) Plot showing the variation in measured postpressing WCA of droplets versus applied pressure (ΔP) for fluorinated HMW copolymer surfaces (\blacktriangle 31 mPa s, \square 102 mPa s, \bullet 348 mPa s).

droplets up to 350–400 Pa (calculated by using the Laplace equation^[7]) and to measure the static postpressing WCAs (Figure 3c). As the fiber ratio increases, the postpressing WCA of the textured surfaces decreases, following trends observed in the static WCA and sliding angle analyses. The static WCA of the electrospun film at Figure 2a does not change even at 400 Pa (Figure 3a), which is consistent with a very stable Cassie state of superhydrophobic behavior and the two-level roughness condition stipulated by Lafuma and Quéré.^[7] However, for films electrospun from the solution with a viscosity of 102 mPa s (Figure 2b), the postpressing WCAs stabilized at 125° at roughly 400 Pa ($\approx 30^\circ$ decrease in WCA). Figure 3b shows that the water droplet had split into two hemispheres under a load of ≈ 80 Pa for the film described in Figure 2c. Although this experiment was not performed on the sample with the bead-only morphology owing to the insufficient mechanical integrity of the film, we can still conclude from the trend in our observations that as the fiber ratio of the fluorinated samples increases, the textured surface begins to exhibit an unstable, Wenzel-type superhydrophobicity.

To achieve a stable (Cassie) superhydrophobic state, a material must have a surface topography of at least bilevel roughness in addition to being chemically hydrophobic. In

fact, there are actually three levels of roughness on our samples with the higher WCAs. To see this third level, consider the uniform height of lithographically patterned, superhydrophobic surfaces. Our samples showed an even broader distribution in roughness amplitude, creating yet another macroscopic level of roughness. Because this gave rise to a much longer triphasic contact line with more discontinuities, the water–solid interface energy was consequently lowered, and the water drop moved more readily on the stable superhydrophobic surface, consistent with the Cassie model.^[12] We speculate that the irregular, micron-level fluctuations in amplitude enabled our films to achieve a stable superhydrophobic state with a WCA exceeding that of the lotus leaf. Manipulation of the water–solid interface energy enabled us to produce extremely water-repellent, potentially self-cleaning, stable coatings by a simple electrospinning process.

Experimental Section

The acrylonitrile (AN, Merck) was used after purification by double distillation over CaH_2 under nitrogen. DMF (Aldrich), THF (Aldrich), AIBN (Fluka), TMI (Cytec), and fluorolink-D (Ausimont) were all used as received.

The viscosity average molecular weight of poly(AN-co-TMI) (AN:TMI $\approx 10:1$) was measured on a Cannon Ubbelohde Viscometer (Size 1B). During calculations, the constants of polyacrylonitrile (PAN) in DMF at 25°C ($K = 39.2 \times 10^{-5}$ and $a = 0.75$) were used. Viscosities of the polymer solutions were measured on a DV-III Rheometer (Brookfield) coupled with a Wells-Brookfield Cone/Plate. SEM imaging of the electrospun films was performed on a LEO Supra VP35 FE-SEM, after sputter deposition of a thin conductive gold coating onto the films. The CAs were measured on a Krüss GmbH DSA 10 Mk 2 goniometer with DSA 1.8 software. At least ten droplets of 5 mg freshly distilled ultrapure water were averaged. For sliding-angle measurements, at least ten 10-mg water droplets were placed onto the films, and slowly inclined by a simple system.

Received: June 26, 2004

Keywords: electrospinning · hydrophobic effects · nanostructures · polymers · surface chemistry

- [1] D. Quere, A. Lafuma, J. Bico, *Nanotechnology* **2003**, *14*, 1109.
- [2] A. Nakajima, K. Hashimoto, T. Watanabe, *Monatsh. Chem.* **2001**, *132*, 31.
- [3] S. Herminghaus, *Europhys. Lett.* **2000**, *52*, 165.
- [4] R. Blossey, *Nat. Mater.* **2003**, *2*, 301.
- [5] W. Barthlott, C. Neinhuis, *Planta* **1997**, *202*, 1.
- [6] C. Neinhuis, W. Barthlott, *Ann. Bot.* **1997**, *79*, 667.
- [7] A. Lafuma, D. Quéré, *Nat. Mater.* **2003**, *2*, 457.
- [8] P. Gould, *Mater. Today* **2003**, *6*, 44.
- [9] D. Oner, T. J. McCarthy, *Langmuir* **2000**, *16*, 7777.
- [10] H. Y. Erbil, A. L. Demirel, Y. Avcı, O. Mert, *Science* **2003**, *299*, 1377.
- [11] W. Chen, A. Y. Fadeev, M. C. Hsieh, D. Öner, J. Youngblood, T. J. McCarthy, *Langmuir* **1999**, *15*, 3395.
- [12] M. Miwa, A. Nakajima, A. Fujishima, K. Hashimoto, T. Watanabe, *Langmuir* **2000**, *16*, 5754.
- [13] S. R. Coulson, I. Woodward, J. P. S. Badyal, S. A. Brewer, C. Willis, *J. Phys. Chem. B* **2000**, *104*, 8836.
- [14] L. Feng, S. Li, H. Li, L. Zhang, J. Zhai, Y. Song, B. Liu, L. Jiang, D. Zhu, *Adv. Mater.* **2002**, *14*, 1857.

- [15] a) L. Feng, S. Li, H. Li, L. Zhang, J. Zhai, Y. Song, B. Liu, L. Jiang, D. Zhu, *Angew. Chem.* **2002**, *114*, 1269; *Angew. Chem. Int. Ed.* **2002**, *41*, 1221; b) Y. Zhao, J. Zhai, L. Jiang, *Angew. Chem.* **2004**, *116*, 4438; *Angew. Chem. Int. Ed.* **2004**, *43*, 4338.
- [16] K. Acatay, Y. Z. Menciloglu, M. A. Gulgun, PCT/TR03/0067, **2003**.
- [17] Z.-M. Huang, Y.-Z. Zhang, M. Kotaki, S. Ramakrishna, *Compos. Sci. Technol.* **2003**, *63*, 2223.
- [18] J. Doshi, D. H. Reneker, *J. Electrostat.* **1995**, *35*, 151.
- [19] M. M. Demir, M. A. Gulgun, Y. Z. Menciloglu, B. Erman, S. S. Abramchuk, E. E. Makhaeva, A. R. Khokhlov, V. G. Matveeva, M. G. Sulman, *Macromolecules* **2004**, *37*, 1787.
- [20] Y. M. Shin, M. M. Hohman, M. P. Brenner, G. C. Rutledge, *Polymer* **2001**, *42*, 9955.
- [21] H. Fong, I. Chun, D. H. Reneker, *Polymer* **1999**, *40*, 4585.
- [22] J. M. Deitzel, W. Kosik, S. H. McKnight, N. C. BeckTan, J. M. DeSimone, S. Crette, *Polymer* **2002**, *43*, 1025.
- [23] A. Koski, K. Yim, S. Shivkumar, *Mater. Lett.* **2004**, *58*, 493.
- [24] A. B. D. Cassie, S. Baxter, *Trans. Faraday Soc.* **1944**, *40*, 546.
- [25] R. N. Wenzel, *Ind. Eng. Chem.* **1936**, *28*, 988.

Inorganic Cations

The $[\text{NH}_3\text{Cl}]^+$ Ion**

Stefan Schneider,* Ralf Haiges, Thorsten Schroer,
Jerry Boatz, and Karl O. Christe*

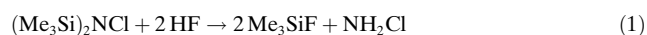
Dedicated to Professor George Olah

Whereas at least seven simple inorganic cations, $[\text{NH}_3\text{F}]^+$,^[1,2] $[\text{NH}_2\text{F}_2]^+$,^[3] $[\text{NF}_4]^+$,^[4] $[\text{N}_2\text{F}]^+$,^[5] $[\text{N}_2\text{F}_3]^+$,^[6] $[\text{ONF}_2]^+$,^[7] and $[\text{N}_3\text{NOF}]^+$,^[8] which contain N–F bonds, have been prepared and well characterized, the existence of corresponding N–Cl bond containing cations is not well established. Thus, only two N–Cl containing cations, $[\text{NCl}_4]^+$ ^[9] and $[\text{ONCl}_2]^+$,^[10,11] have been reported, however, our repeated attempts to duplicate their syntheses were unsuccessful, and the crystal structure,

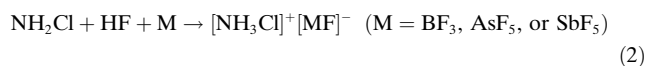
published for $[\text{ONCl}_2]^+[\text{SbCl}_6]^-$,^[10] has been challenged on theoretical grounds.^[12] The paucity of data on simple inorganic N–Cl containing cations can be attributed to the general explosiveness and instability of nitrogen chlorides.^[13–15] Herein, the synthesis and characterization of $[\text{NH}_3\text{Cl}]^+\text{M}^-$ salts ($\text{M} = \text{BF}_4$, AsF_6 , or SbF_6), the first examples of compounds containing a stable, simple inorganic cation with an N–Cl bond, are reported. To our knowledge, the formation of the $[\text{NH}_3\text{Cl}]^+$ ion has only been postulated based on investigations of aqueous solutions,^[16] by theoretical calculations,^[17] and by mass spectrometric studies.^[17,18]

Without doubt, the most important member of the family of halogenamines is monochloramine, NH_2Cl . It is the crucial intermediate in the industrial synthesis of hydrazine.^[13] Furthermore it is a very powerful disinfectant and germ killer.^[14,19,20] Dilute aqueous solutions of NH_2Cl can conveniently be prepared by the chlorination of aqueous ammonia with hypochlorite.^[13,14] However, the highest practical NH_2Cl concentration of these solutions is 97%, and purer compounds decompose extremely fast. At -110°C , NH_2Cl begins to melt with partial decomposition and, at -40°C , it decomposes continuously and often explosively, owing to the formation of ammonium chloride and more highly chlorinated products, such as NCl_3 .^[13] Therefore, the use of pure NH_2Cl is not feasible for the preparation of $[\text{NH}_3\text{Cl}]^+$ salts.

The handling problem of pure monochloramine was overcome by generating it at low temperature from $(\text{Me}_3\text{Si})_2\text{NCl}$ and HF [Eq. (1)].



The conversion of a $(\text{R}_3\text{Si})_2\text{N}$ group into an H_2N group using a strong acid, such as CF_3COOH , has previously been demonstrated by Wiberg and co-workers for the syntheses of substituted tetrazenes.^[21] When the reaction in Equation (1) is carried out in the presence of a strong Lewis acid, the $[\text{NH}_3\text{Cl}]^+$ salts are immediately formed, thus avoiding significant decomposition of NH_2Cl [Eq. (2)].



The $[\text{NH}_3\text{Cl}]^+$ salts are formed in high yields, with small amounts of the corresponding $[\text{NH}_4]^+$ salts being the only impurities, which can be detected by vibrational or NMR spectroscopy. In one of our $[\text{NH}_3\text{Cl}]^+[\text{BF}_4]^-$ preparations, the formation of $[\text{NH}_4]^+[\text{BF}_4]^-$ as a by-product was also confirmed by its X-ray crystal structure. All attempts to obtain single crystals of the $[\text{NH}_3\text{Cl}]^+$ salts, suitable for a crystal-structure determination, failed. The formation of some $[\text{NH}_4]^+$ ions as a by-product is difficult to avoid because the acid-catalyzed decomposition of NH_2Cl starts already at -110°C . This observation is in accord with the report by Allenstein and Goubeau that neat solid NH_2Cl explodes on contact with BF_3 even at -120°C .^[15]

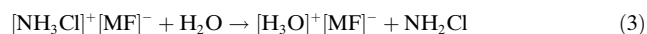
All the $[\text{NH}_3\text{Cl}]^+$ salts, prepared in this study, are stable above room temperature. Unfortunately, reliable melting points could not be determined because of the $[\text{NH}_4]^+$ impurities. The salts readily dissolve in water with the

[*] Dr. S. Schneider, Dr. R. Haiges, Dr. T. Schroer, Prof. Dr. K. O. Christe
Loker Research Institute
University of Southern California
Los Angeles, CA 90089-1661 (USA)
Fax: (+1) 213-740-6679
E-mail: stefan.schneider@edwards.af.mil
kchriste@usc.edu

Dr. J. Boatz
Space and Missile Propulsion Division
Air Force Research Laboratory (AFRL/PRSP)
10 East Saturn Boulevard
Bldg 8451, Edwards Air Force Base, CA 93524 (USA)

[**] This work was funded by the Defense Advanced Research Projects Agency, with additional support from the Air Force Office of Scientific Research and the National Science Foundation. We thank Drs. A. Morrish, D. Woodbury, and M. Berman, for their steady support, and Dr. R. Wagner for his help and stimulating discussions. Dedicated to Professor George Olah on the occasion of winning the Priestley Award.

formation of the corresponding oxonium salts and monochloramine. The monochloramine was identified by gas-phase IR spectroscopy and its characteristic intense smell [Eq. (3)].



The reaction in Equation (3) is in accord with the observation by Muench that even $(\text{CH}_3)_2\text{NCl}$, which is considerably more basic than NH_2Cl ,^[22] can be displaced from $[(\text{CH}_3)_2\text{NCIH}]^+[\text{CF}_3\text{SO}_3]^-$ by water.^[23] These displacement reactions are somewhat surprising because NH_2Cl possesses a higher gas-phase basicity ($\text{GB} = 761 \pm 5 \text{ kJ mol}^{-1}$)^[17b] than H_2O ($\text{GB} = 691 \text{ kJ mol}^{-1}$)^[22] and, therefore, H_2O should not displace NH_2Cl from its $[\text{NH}_3\text{Cl}]^+$ salts. However, in aqueous solution or in solid-gas reactions, the relative basicities might be different. Unfortunately, the basicity of NH_2Cl in water is difficult to measure and, as yet, has not been reliably determined because of its instability in acidic solutions. Arguments have been presented that NH_2Cl should be either slightly more basic^[17b,22,23] or more acidic than water.^[23,24] That even in the case of the stronger base $(\text{CH}_3)_2\text{NCl}$, the displacement reactions with water proceed could be explained by the reaction in Equation (3) being an equilibrium which is shifted to the right by an excess of water and continuous removal of NH_2Cl owing to either its volatility or rapid decomposition. Equation (3) might also explain why, in the presence of water, protonation of NH_2Cl and formation of $[\text{NH}_3\text{Cl}]^+$ salts have not been observed. Although knowing the pK_a value of $[\text{NH}_3\text{Cl}]^+$ would be desirable, its experimental measurement would be very difficult because of the above problems and the unavoidable presence of $[\text{NH}_4]^+$ impurities.

The stability of the $[\text{NH}_3\text{Cl}]^+$ salts and their ability to generate NH_2Cl , when exposed to atmospheric moisture, make them ideally suited for NH_2Cl gas generation. This property could be exploited for a convenient gas-phase method of deactivating spores, such as anthrax.^[25] Furthermore, previous work by Snyder and Margerum has indicated that the $[\text{NH}_3\text{Cl}]^+$ ion is a very reactive chlorinating agent for the transfer of chlorine to other amines, such as methylamine, amino acids, and peptides, while being a less reactive oxidant than Cl_2 or HOCl .^[16c]

Conclusive evidence for the $[\text{NH}_3\text{Cl}]^+$ ion comes from the observed IR, Raman and NMR spectra and their comparison with theoretical calculations. To assess the accuracy of these calculations, we have tested these methods for isoelectronic

CH_3Cl which is experimentally well characterized.^[26] As can be seen from Table 1, the MP2 and CCSD(T) geometries deviate by less than 0.01 Å and 0.3° from the experimental values, while the B3LYP distances are, as expected, slightly longer. Therefore, we expect the geometry, predicted for $[\text{NH}_3\text{Cl}]^+$ (Table 1), to be also a good approximation of the

Table 1: Calculated geometries of $[\text{NH}_3\text{Cl}]^+$, compared to observed^[a] and calculated geometries of isoelectronic CH_3Cl .

	$[\text{NH}_3\text{Cl}]^+$				CH_3Cl			
	$r(\text{N-Cl})$ [Å]	$r(\text{N-H})$ [Å]	$\angle \text{H-N-Cl}$ [°]	$\angle \text{H-N-H}$ [°]	$r(\text{C-Cl})$ [Å]	$r(\text{C-H})$ [Å]	$\angle \text{H-C-Cl}$ [°]	$\angle \text{H-C-H}$ [°]
MP2/aug-cc-pvtz	1.735	1.025	109.2	109.8	1.780	1.084	108.4	110.6
CCSD(T)/aug-cc-pvtz	1.743	1.023	109.1	109.8	1.784	1.084	108.3	110.6
CCSD(T)/6-311++G(3df,3pd) ^[b]	1.747	1.026	109.3	109.7	—	—	—	—
B3LYP/aug-cc-pvtz	1.755	1.025	109.1	109.8	1.802	1.085	108.2	110.7
observed	—	—	—	—	1.776	1.085	108.6	110.4

[a] Data from ref. [26]. [b] Data from ref. [17b].

true geometry of the free gaseous ion. Similarly, a comparison of the observed and calculated vibrational frequencies of CH_3Cl shows very good agreement (Table 2). Note, however, that the calculated frequencies are harmonic values for the free gas at 0 K, and that the experimentally observed frequencies require large anharmonicity corrections, partic-

Table 2: Calculated harmonic and experimental anharmonic and harmonic vibrational frequencies and calculated IR and Raman intensities of CH_3Cl .^[a]

Band		Calculated harmonic frequency			Experimental frequency	
		MP2	B3LYP	CCSD(T)	anharmonic	harmonic
A_1	ν_1	3111.2 (22) [150]	3071.0 (23) [155]	3098.5 (23)	2953.9	3088.4
	ν_2	1401.1 (11) [0.04]	1375.6 (12) [0.004]	1394.7 (12)	1354.9	1396.3
	ν_3	764.2 (24) [17]	707.3 (27) [17]	749.1 (22)	732.8	751.2
E	ν_4	3222.5 (4.6) [95]	3165.7 (7.9) [107]	3176.4 (7.8)	3039.3	3183.3
	ν_5	1511.0 (11) [7.5]	1482.8 (12) [7.7]	1510.2 (11)	1452.2	1496.2
	ν_6	1050.0 (4.0) [0.98]	1027.3 (4.1) [1.1]	1039.4 (3.5)	1018.1	1036.8

[a] For all calculations, the aug-cc-pvtz basis set was used; frequencies in cm^{-1} , IR and Raman intensities in km mol^{-1} and $\text{\AA}^4 \text{ amol}^{-1}$, respectively.

ularly for the vibrations involving hydrogen atoms. Therefore, most of the differences between the observed and calculated frequencies can be attributed to anharmonicity effects, and the agreement between the harmonic values is much better.

A comparison between the observed (Table 3 and Figure 1) and calculated vibrational frequencies of $[\text{NH}_3\text{Cl}]^+$ is given in Table 4. The differences between the observed anharmonic and the calculated harmonic frequencies are comparable to those in CH_3Cl and establish the new species as the $[\text{NH}_3\text{Cl}]^+$ ion. The slight variation in the observed vibrational frequencies of the $[\text{NH}_3\text{Cl}]^+$ ion in the different salts is attributed to solid-state effects, such as various degrees of anion-cation interactions and hydrogen bonding. Further support for the presence of the $[\text{NH}_3\text{Cl}]^+$ ion comes from the ^{35}Cl - ^{37}Cl isotopic shift of the N-Cl stretching vibration. The N-Cl stretching vibration (Figure 1) shows a splitting of approximately 6 cm^{-1} , in accord with the calculated harmonic

Table 3: Observed vibrational spectra^[a] of solid $[\text{NH}_3\text{Cl}]^+ \text{M}^-$ ($\text{M} = \text{BF}_4^-, \text{AsF}_6^-, \text{SbF}_6^-$) and their assignments.

$[\text{NH}_3\text{Cl}]^+[\text{BF}_4]^-$		$[\text{NH}_3\text{Cl}]^+[\text{AsF}_6]^-$		$[\text{NH}_3\text{Cl}]^+[\text{SbF}_6]^-$		$[\text{NH}_3\text{Cl}]^+ (\text{C}_{3v})$	M^-
Raman	IR	Raman	IR	Raman	IR	$[\text{BF}_4]^- (\text{T}_d)$ $[\text{AsF}_6]^-$ $[\text{SbF}_6]^- (\text{O}_h)$	
3247.6(18)	3221vw	3241.2(16)	3209w	3229.6(8)	3217vw	$\nu_4 (\text{E})$	
3188.6(9)		3167.7(3)	3172w	3168.0(4)	3112vw	$\nu_1 (\text{A}_1)$	
1552.2(1)	1570w	1566.7(0+)	1564w	1557.0(0+)	1569w	$\nu_5 (\text{E})$	
1454.8(0+)	1458m	1447.0(0+)	1435s	1433.5(0+)	1435s	$\nu_2 (\text{A}_1)$	
n.o.	n.o.	1071.0(0+)	1071w	1068.8(0+)	1072m	$\nu_6 (\text{E})$	
759.0(82)	763w	766.4(15)	^[b]	766.2(49)	767w	$\nu_3^{35}\text{Cl} (\text{A}_1)$	
753.8(50)		761.2(9)	^[b]	761.2(30)	762w	$\nu_3^{37}\text{Cl} (\text{A}_1)$	
1079.0(0+)	1035vs,vb					$\tilde{\nu}_3 (\text{F}_2)$	
772.0(100)	769w		703vs,b		659vs	$\tilde{\nu}_1 (\text{A}_1)$	
		688.6(100)		654.4(100)			$\tilde{\nu}_3 (\text{F}_{1u})$
		573.8(22)		570.1(28)			$\tilde{\nu}_1 (\text{A}_{1g})$
							$\tilde{\nu}_2 (\text{E}_g)$
528.8(14)	530/524m					$\tilde{\nu}_4 (\text{F}_2)$	
354.5(18)						$\tilde{\nu}_2 (\text{E})$	
		373.0(43)		281.6(38)			$\tilde{\nu}_5 (\text{F}_{2g})$

[a] Frequencies in cm^{-1} and uncorrected relative intensities. [b] Observed as shoulders on the very intense 703 cm^{-1} band; n.o. = not observed.

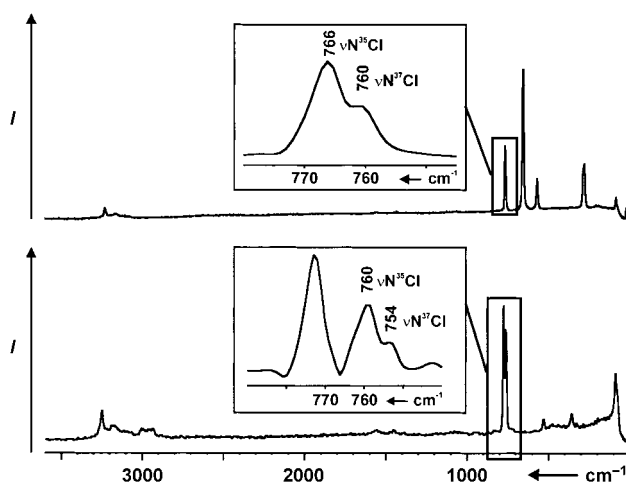

Figure 1. Raman spectra of $[\text{NH}_3\text{Cl}]^+[\text{SbF}_6]^-$ (upper) and $[\text{NH}_3\text{Cl}]^+[\text{BF}_4]^-$ (lower). The enlarged sections of the spectra show a 35/37 chlorine isotopic splitting in the N–Cl vibration.

Table 4: Calculated harmonic and experimental anharmonic vibrational frequencies and calculated IR and Raman intensities of $[\text{NH}_3\text{Cl}]^+.$ ^[a]

Band		Calculated harmonic frequency				Range of experimental anharmonic frequency
		MP2	B3LYP	CCSD(T)		
				aug-cc-pvtz	6-31++G(3df,3pd) ^[b]	
A ₁	ν_1	3374.7 (85) [87]	3357.1 (79) [91]	3404.1 (78)	3355.1	3112–3188
	ν_2	1475.9 (59) [0.48]	1466.5 (57) [0.45]	1474.0 (56)	1467.9	1435–1458
	ν_3	785.0 (2.6) [12]	737.5 (2.4) [13]	762.9 (2.1)	741.5	759–767
E	ν_4	3480.6 (386) [42]	3445.0 (356) [47]	3484.1 (349)	3441.9	3209–3247
	ν_5	1642.1 (101) [6.1]	1628.9 (105) [6.5]	1646.7 (100)	1628.8	1552–1570
	ν_6	1054.8 (37) [1.35]	1037.0 (36) [1.69]	1045.8 (35)	1039.2	1069–1072

[a] For the MP2 and B3LYP calculations, the aug-cc-pvtz basis set was used; frequencies in cm^{-1} , intensities (infrared) and [Raman] in km mol^{-1} and $\text{Å}^4 \text{amu}^{-1}$, respectively. [b] Data from ref. [17b].

splittings, ranging from 6.6 (B3LYP) to 7.1 (MP2) cm^{-1} . If the observed isotopic shifts were corrected for anharmonicity, the agreement would be even better. In CH_3Cl , anharmonicity corrections increase the observed ^{35}Cl – ^{37}Cl isotopic shift by 0.29 cm^{-1} from the anharmonic value, $\Delta\nu = 5.83$, to the harmonic value, $\Delta\omega = 6.12 \text{ cm}^{-1}$.^[26] The complexity of the Raman bands of $[\text{NH}_3\text{Cl}]^+[\text{BF}_4]^-$ in the region of the N–H stretching modes (Figure 1) can be explained by Fermi resonance between $\nu_1(\text{A}_1)$ and $2\nu_5(\text{A}_1)$ and the possible presence of some $[\text{NH}_4]^+$ impurity.

Additional support for the $[\text{NH}_3\text{Cl}]^+$ ion comes from the results of a normal coordinate analysis (Table 5). The general harmonic force field, calculated for the $[\text{NH}_3\text{Cl}]^+$ ion at the CCSD(T) level, corresponds very closely to that of isoelectronic CH_3Cl .^[25] All vibrations are highly characteristic, and only the N–Cl stretching vibration mixes, as expected, to a small extent with the NH_3 umbrella deformation mode.

The ^{14}N and ^1H NMR spectra of $[\text{NH}_3\text{Cl}]^+[\text{SbF}_6]^-$ in HF and DF solutions (Table 6) exhibit single resonances at $\delta = -364$ and 7.91 ppm, respectively. The observed chemical shifts are in good agreement with our expectations for the

$[\text{NH}_3\text{Cl}]^+$ ion: the nitrogen atom in the $[\text{NH}_3\text{Cl}]^+$ ion is slightly deshielded compared with that in $[\text{NH}_4]^+$ ($\delta = -367$ ppm), but significantly more shielded than that in $[\text{NH}_3\text{F}]^+$ ($\delta = -252.1$ ppm).^[27] The proton shift ($\delta = 7.91$ ppm) falls in between those of the $[\text{NH}_4]^+$ ($\delta = 5.71$ ppm) and $[\text{NH}_3\text{F}]^+$ ($\delta = 10.4$ ppm) ions.^[2] The similarity of the ^{14}N shifts of the $[\text{NH}_3\text{Cl}]^+$ and $[\text{NH}_4]^+$ ions cannot be attributed to signal averaging between the $[\text{NH}_3\text{Cl}]^+$ ion and either the $[\text{NH}_3\text{Cl}]^+$ ion or the solvents, because in all spectra separate signals were observed for the $[\text{NH}_3\text{Cl}]^+$ and

Table 5: General harmonic force field^[a] of C_{3v} [NH₃Cl]⁺ and potential energy distribution^[b] calculated at the CCSD(T)/aug-cc-pvtz level of theory.

Band	Approximate mode description	Frequency [cm ⁻¹]	Symmetry	Force constants	PED
A ₁	ν_1 ν sym NH ₃	3404.1	F ₁₁	F ₂₂ 6.746	F ₃₃ 0.138 0.100 99.6 (1)
	ν_2 δ sym NH ₃	1474.0	F ₂₂		0.619 -0.454 99.7 (2)
	ν_3 ν N-Cl	762.9	F ₃₃		3.997 86.3 (3) + 13.7 (2)
E	ν_4 ν asym NH ₃	3484.1	F ₄₄	F ₅₅ 6.591	F ₆₆ -0.136 0.000 98.3 (4)
	ν_5 δ asym NH ₃	1646.7	F ₅₅		0.610 -0.011 95.3 (5)
	ν_6 δ wag NH ₃	1045.8	F ₆₆		0.668 95.2 (6)

[a] Stretching constants in mdyÅ⁻¹, deformation constants in mdyÅ/rad², and stretch-bend interaction constants in mdy/rad. [b] PED in percent. Symmetry coordinates contributing less than 5% are omitted. Symmetry coordinates, taken from ref.^[26], are defined as follows: S₁ = ν sym (N-H), S₂ = δ sym (H-N-H-H-N-Cl), S₃ = ν (N-Cl), S₄ = ν asym (N-H), S₅ = δ asym (H-N-H), S₆ = δ asym (Cl-N-H).

Table 6: Observed NMR spectra of HF/DF solutions of [NH₃Cl]⁺[SbF₆]⁻.^[a]

Solvent, T	Chemical shift [ppm] (line width [Hz])
	$\delta^{14}\text{N}$ $\delta^1\text{H}$
HF, 20°C	-363 (188) [b]
DF, 20°C	-364 (125) 7.91 (3.8)

[a] In addition to the resonances arising from the [NH₃Cl]⁺ ion, $\delta^{14}\text{N}$ resonance signals arising from the [NH₄]⁺ ion were observed at -368 (q, 54.7 Hz) in HF and at -367 (q, 54.8 Hz) ppm in DF; the $\delta^1\text{H}$ resonance signals from the [NH₄]⁺ ion were observed at 5.65 (tr, 54.6 Hz) in HF and at 5.71 (tr, 54.4 Hz) ppm in DF. [b] Resonance obscured by the HF solvent signal.

[NH₄]⁺ ions which were always separated by the same amount, and the [NH₄]⁺ ion proton resonance consisted of very narrow triplets of equal intensity arising from ¹⁴N-¹H spin-spin coupling. The similarity of the ¹⁴N shifts in the [NH₄]⁺ and [NH₃Cl]⁺ ions is attributed to nitrogen and chlorine having very similar electronegativities, resulting in a low polarity of the N-Cl bond and a weak electron-withdrawing effect of chlorine. In contrast, substitution of one hydrogen atom by a highly electronegative fluorine atom results in strong deshielding of the nitrogen atom. A similar trend is also reflected, although to a lesser degree, in the ¹³C shifts of CH₄ (δ = -2.1 ppm), CH₃Cl (δ = 25.6 ppm), and CH₃F (δ = 71.6 ppm).^[28]

In summary, this study provides [NH₃Cl]⁺, the first stable, simple, inorganic cation containing an N-Cl bond. For the syntheses of the [NH₃Cl]⁺ salts, the explosiveness and thermal instability of the parent molecule NH₂Cl was circumvented by using a safe organosilicon derivative, (R₃Si)₂NCl, as a precursor. Conclusive evidence for the existence of the [NH₃Cl]⁺ ion is given by its vibrational and NMR spectra and theoretical calculations.

Experimental Section

Caution! Neat chloramines are highly unstable and often can decompose explosively. They should be handled on a small scale with appropriate safety precautions.

All reactions were carried out in Teflon-FEP (FEP = perfluoro ethylene propylene polymer) ampules that contained Teflon-coated magnetic stirring bars and were closed by stainless steel valves. Volatile materials were handled on a stainless steel vacuum line. Nonvolatile solids were handled in the dry nitrogen atmosphere of a glove box. IR spectra were recorded on a Midac, M Series, FT-IR spectrometer using AgCl pellets. The pellets were prepared inside the glove box using an Econo press (Barnes Engineering Co.). Raman spectra were recorded in the range 4000–80 cm⁻¹ on a Bruker Equinox 55 FT-RA spectrometer using a Nd-YAG laser at 1064 nm with power levels of 800 mW or less. Pyrex melting point capillaries, glass NMR or 9 mm Teflon-FEP tubes were used as sample containers. NMR spectra were recorded unlocked on a Bruker AMX 500 NMR spectrometer at room temperature. The ¹⁴N and ¹H NMR spectra were referred to external samples of neat nitromethane and tetramethylsilane in CDCl₃, respectively.

The (Me₃Si)₂NCl starting material was prepared from (Me₃Si)₂NH and *t*BuOCl using a literature method.^[29] The HF/DF solvents (Matheson Co./Ozark Mahoning) were dried^[30] by storage over BiF₅ (Ozark Mahoning). SbF₅ (Ozark Mahoning) was purified by distillation prior to use. BF₃ (Matheson) and AsF₅ (Ozark Mahoning) were used as received.

[NH₃Cl]⁺M⁻ [M = BF₄, AsF₆, SbF₆]: In a typical experiment, anhydrous HF (2 mL of liquid) and BF₃, AsF₅, or SbF₅ (1.44 to 3.176 mmol) were combined at -196°C in a 9 mm Teflon-FEP ampule closed by a stainless steel valve. The mixture was warmed to 25°C and then recooled to -196°C. A stoichiometric amount of (Me₃Si)₂NCl was added to the ampule at -196°C, and additional HF was condensed on top of it at a very slow rate to avoid contact of the frozen silyl compound with liquid HF during the condensation process. The frozen mixture was warmed first to -78°C and then slowly to 25°C. During warm-up, a colorless precipitate was formed, which was only partially soluble in the HF. The ampule was immediately recooled to -64°C and all volatiles were pumped off at this temperature. Colorless stable solids of [NH₃Cl]⁺[BF₄]⁻, [NH₃Cl]⁺[AsF₆]⁻, or [NH₃Cl]⁺[SbF₆]⁻ were left behind which contained small amounts of the corresponding [NH₄]⁺ salts as the only impurities, detectable by vibrational spectroscopy.

Theoretical calculations were performed using the GAMESS,^[31] Gaussian98,^[32] and ACES II^[33] program systems, and the augmented correlation-consistent polarized valence triple-zeta basis set (aug-cc-pvtz) of Dunning et al.^[34] Computational methods included density functional theory with the hybrid B3LYP functional,^[35] second order perturbation theory (MP2, also known as MBPD(2))^[36] and coupled-cluster singles and doubles^[37] with perturbative estimates of triple excitations (CCSD(T)).^[38]

Received: May 4, 2004

Revised: June 26, 2004

Keywords: cations · nitrogen chlorides · NMR spectroscopy · theoretical chemistry · vibrational spectroscopy

- [1] a) V. Grakauskas, A. H. Remanick, K. Baum, *J. Am. Chem. Soc.* **1968**, *90*, 3839; b) V. Grakauskas, *J. Inorg. Nucl. Chem.* **1973**, *35*, 3034.
- [2] a) R. Minkwitz, R. Nass, *Z. Naturforsch. B* **1982**, *37*, 1558; b) R. Minkwitz, A. Liedtke, R. Nass, *J. Fluorine Chem.* **1987**, *35*, 307.
- [3] K. O. Christe, *Inorg. Chem.* **1975**, *14*, 2821.

- [4] a) K. O. Christe, J. P. Guertin, A. E. Pavlath, *Inorg. Nucl. Chem. Lett.* **1966**, 2, 83; b) I. V. Nikitin, V. Ya. Rosolovskii, *Russ. Chem. Rev.* **1985**, 54, 426.
- [5] a) D. Moy, A. R. Young, *J. Am. Chem. Soc.* **1965**, 87, 1889; b) J. K. Ruff, *Inorg. Chem.* **1966**, 5, 1791; c) H. W. Roesky, O. Glemser, D. Bormann, *Chem. Ber.* **1966**, 99, 1589; d) A. V. Pankratov, N. I. Savenkova, *Russ. J. Inorg. Chem.* **1968**, 13, 1345; e) J. Shamir, J. Binenboym, *J. Mol. Struct.* **1969**, 4, 100; e) K. O. Christe, R. D. Wilson, W. Sawodny, *J. Mol. Struct.* **1971**, 8, 245; f) K. O. Christe, R. D. Wilson, W. W. Wilson, R. Bau, S. Sukumar, D. A. Dixon, *J. Am. Chem. Soc.* **1991**, 113, 3795.
- [6] a) J. K. Ruff, *J. Am. Chem. Soc.* **1965**, 87, 1140; J. K. Ruff, *Inorg. Chem.* **1966**, 5, 1791; c) A. R. Young, D. Moy, *Inorg. Chem.* **1967**, 6, 178; d) E. W. Lawless, *Anal. Lett.* **1967**, 1, 153; A. M. Qureshi, F. Aubke, *Can. J. Chem.* **1970**, 48, 3117; K. O. Christe, C. J. Schack, *Inorg. Chem.* **1978**, 17, 2749.
- [7] a) W. B. Fox, J. S. MacKenzie, N. Vanderkooi, B. Sukornik, C. A. Wamser, J. R. Holmes, R. E. Eibeck, B. B. Stewart, *J. Am. Chem. Soc.* **1966**, 88, 2604; b) K. O. Christe, W. Maya, *Inorg. Chem.* **1969**, 8, 1253; c) C. A. Wamser, W. B. Fox, B. Sukornik, J. R. Holmes, B. B. Stewart, R. Juurick, N. Vanderkooi, D. Gould, *Inorg. Chem.* **1969**, 8, 1249; d) K. O. Christe, J. F. Hon, D. Pilipovich, *Inorg. Chem.* **1973**, 12, 84; e) J. Mason, K. O. Christe, *Inorg. Chem.* **1983**, 22, 1849; f) F. Cacace, F. Pepi, *J. Phys. Chem.* **1994**, 98, 8009; f) R. J. Gillespie, E. A. Robinson, G. L. Heard, *Inorg. Chem.* **1998**, 37, 6884; g) A. Vij, X. Zhang, K. O. Christe, *Inorg. Chem.* **2001**, 40, 416.
- [8] W. W. Wilson, K. O. Christe, H. Willner, J. A. Boatz, A. Vij, V. Vij, 225th National ACS Meeting (New Orleans, LA, March 24), **2003**, paper 449.
- [9] R. Minkwitz, D. Bernstein, W. Sawodny, *Angew. Chem.* **1990**, 102, 185; *Angew. Chem. Int. Ed. Engl.* **1990**, 29, 181.
- [10] K. Dehnicke, H. Aeissen, M. Koelmel, J. Straehle, *Angew. Chem.* **1977**, 89, 569.
- [11] R. Minkwitz, D. Bernstein, W. Sawodny, H. Haertner, *Z. Anorg. Allg. Chem.* **1990**, 580, 109.
- [12] a) M. Brumm, G. Frenking, W. Koch, *Chem. Phys. Lett.* **1991**, 182, 310; b) M. Brumm, G. Frenking, J. Breidung, W. Thiel, *Chem. Phys. Lett.* **1992**, 197, 330.
- [13] J. Jander, U. Engelhardt in *Developments in Inorganic Nitrogen Chemistry* (Ed.: C. B. Colburn), Elsevier Scientific Publishing Company, Amsterdam, **1973**, p. 70.
- [14] A. F. Holleman, N. Wiberg, *Lehrbuch der Anorganischen Chemie*, Walter de Gruyter, Berlin, **1995**, p. 678.
- [15] E. Allenstein, J. Goubeau, *Z. Anorg. Allg. Chem.* **1963**, 322, 145.
- [16] See for example: a) P. K. Wrona, *J. Electroanal. Chem.* **1998**, 453, 197; b) M. Elkhathib, A. Marchand, L. Peyrot, J. J. Counioux, H. Delalu, *Int. J. Chem. Kinet.* **1997**, 29, 89; c) M. P. Snyder, D. W. Margerum, *Inorg. Chem.* **1982**, 21, 2545; d) E. T. Gray, Jr., D. W. Margerum, R. P. Huffman in *Organometals and Organometaloids, Occurrence and Fate in the Environment* (Eds.: F. E. Brinkmann, J. M. Bellama), American Chemical Society, Washington DC, **1978**; *ACS Symp. Ser.* **1978**, 82, 264.
- [17] a) R. K. Millburn, C. F. Rodriguez, A. C. Hopkinson, *J. Phys. Chem. B* **1997**, 101, 1837; b) A. Ricci, M. Rosi, *J. Phys. Chem. A* **1998**, 102, 10189.
- [18] T. Kotiaho, B. J. Shay, R. G. Cooks, M. N. Eberlin, *J. Am. Chem. Soc.* **1993**, 115, 1004; and references therein.
- [19] *Ullmann's Encyclopedia of Industrial Chemistry*, Vol. A6, 5th ed. (Ed.: W. Gerhartz), VCH Verlagsgesellschaft mbH Weinheim, **1985**, p. 533.
- [20] N. N. Greenwood, A. Earnshaw, *Chemistry of the Elements*, Pergamon, Oxford, **1984**.
- [21] N. Wiberg, *Adv. Organomet. Chem.* **1985**, 24, 179, and references therein.
- [22] I. Weil, J. C. Morris, *J. Am. Chem. Soc.* **1949**, 71, 3123.
- [23] V. Muench, *Z. Anorg. Allg. Chem.* **1981**, 477, 217.
- [24] W. L. Jolly, *J. Phys. Chem.* **1956**, 60, 507.
- [25] a) S. W. Chensue, *Am. J. Pathol.* **2003**, 163, 1699; b) M. J. Rosowitz, S. H. Leppla, *Nature* **2002**, 418, 825; c) K. Brown, *Science* **2001**, 294, 1813.
- [26] G. M. Black, M. M. Law, *J. Mol. Spectrosc.* **2001**, 205, 280, and references therein.
- [27] J. Mason, K. O. Christe, *Inorg. Chem.* **1983**, 22, 1849.
- [28] S. Berger, S. Braun, H.-O. Kalinowski, *NMR Spectroscopy of the Non-Metallic Elements*, Wiley, Chichester, **1997**, p. 169.
- [29] N. Wiberg, F. Raschig, *J. Organomet. Chem.* **1967**, 10, 15.
- [30] K. O. Christe, W. W. Wilson, C. J. Schack, *J. Fluorine Chem.* **1978**, 11, 71.
- [31] M. W. Schmidt, K. K. Baldridge, J. A. Boatz, S. T. Elbert, M. S. Gordon, J. H. Jensen, S. Koseki, N. Matsunaga, K. A. Nguyen, S. J. Su, T. L. Windus, M. Dupuis, J. A. Montgomery, *J. Comput. Chem.* **1993**, 14, 1347.
- [32] Gaussian 98 (Revision A.7), M. J. Frisch, G. W. Trucks, H. B. Schlegel, G. E. Scuseria, M. A. Robb, J. R. Cheeseman, V. G. Zakrzewski, J. A. Montgomery, R. E. Stratmann, J. C. Burant, S. Dapprich, J. M. Millam, A. D. Daniels, K. N. Kudin, M. C. Strain, O. Farkas, J. Tomasi, V. Barone, M. Cossi, R. Cammi, B. Mennucci, C. Pomelli, C. Adamo, S. Clifford, J. Ochterski, G. A. Petersson, P. Y. Ayala, Q. Cui, K. Morokuma, D. K. Malick, A. D. Rabuck, K. Raghavachari, J. B. Foresman, J. Cioslowski, J. V. Ortiz, B. B. Stefanov, G. Liu, A. Liashenko, P. Piskorz, I. Komaromi, R. Gomperts, R. L. Martin, D. J. Fox, T. Keith, M. A. Al-Laham, C. Y. Peng, A. Nanayakkara, C. Gonzalez, M. Challacombe, P. M. W. Gill, B. G. Johnson, W. Chen, M. W. Wong, J. L. Andres, M. Head-Gordon, E. S. Replogle, J. A. Pople, Gaussian, Inc., Pittsburgh, PA, **1998**.
- [33] J. F. Stanton, J. Gauss, J. D. Watts, M. Nooijen, N. Oliphant, S. A. Perera, P. G. Szalay, W. J. Lauderdale, S. R. Gwaltney, S. Beck, A. Balkova, D. E. Bernholdt, K. K. Baek, P. Rozyczko, H. Sekino, C. Hober, R. J. Bartlett, *ACES II, Quantum Theory Project*, University of Florida: Integral packages included are VMOL (J. Almlöf, P. R. Taylor), BPROPS (P. R. Taylor), and ABACUS (T. Helgaker, H. J. Aa. Jensen, P. Jorgensen, J. Olsen, P. R. Taylor).
- [34] a) T. H. Dunning, Jr., *J. Chem. Phys.* **1989**, 90, 1007; b) R. A. Kendall, T. H. Dunning, Jr., R. J. Harrison, *J. Chem. Phys.* **1992**, 96, 6796; c) D. E. Woon, T. H. Dunning, Jr., *J. Chem. Phys.* **1993**, 98, 1358.
- [35] The B3LYP functional uses a three-parameter exchange functional of Becke (B3) [A. D. Becke, *J. Chem. Phys.* **1993**, 98, 5648; P. J. Stephens, C. F. Devlin, C. F. Chabalowski, M. J. Frisch, *J. Phys. Chem.* **1994**, 98, 11623] and the Lee, Yang, and Parr (LYP) correlation gradient-corrected functional [C. Lee, W. Yang, R. G. Parr, *Phys. Rev. B* **1988**, 37, 785].
- [36] a) J. A. Pople, J. S. Binkley, R. Seeger, *Int. J. Quantum Chem.* **1976**, 10, 1; b) R. J. Bartlett, D. M. Silver, *Int. J. Quantum Chem.* **1975**, 9, 183; c) M. Dupuis, S. Chin, A. Marquez in *Relativistic and Electron Correlation Effects in Molecules* (Ed.: G. Malli), Plenum, New York, **1994**; d) M. J. Frisch, M. Head-Gordon, J. A. Pople, *Chem. Phys. Lett.* **1990**, 166, 275; e) "Applications of post-Hartree-Fock methods: A Tutorial": R. J. Bartlett, R. J. Stanton in *Reviews of Computational Chemistry*, Vol. V (Ed.: D. B. Boyd, K. B. Lipkowitz), VCH, New York, **1994**.
- [37] G. D. Purvis III, R. J. Bartlett, *J. Chem. Phys.* **1982**, 76, 1910.
- [38] K. Raghavachari, G. W. Trucks, J. A. Pople, M. Head-Gordon, *Chem. Phys. Lett.* **1989**, 157, 479.

Linear Finite “Mers”—Homoleptic Polynuclear Heavy Alkaline Earth Metal Pyrazolates**

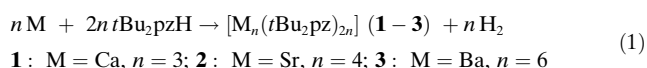
Julia Hitzbleck, Glen B. Deacon,* and Karin Ruhlandt-Senge*

The increased demand for highly volatile precursor molecules for the production of Group 2 solid-state materials sparked our interest in alkaline earth metal pyrazolate (pz) chemistry. Well explored for di- and trivalent rare earth metal derivatives,^[1,2] the pyrazolate ligand system is uniquely capable to induce a multitude of metal–ligand binding modes.^[2,3] This structural flexibility, when used in conjunction with donor molecules, enabled the isolation of several families of monomeric alkaline earth metal pyrazolates.^[4,5] Studies probing the utility of the pyrazolates as precursor molecules showed that not all compounds sublime intact,^[5,6] and frequently loss of donors and consequent reduction in volatility is observed. As an example, Winter and co-workers reported that $[\text{Ca}(\text{tBu}_2\text{pz})_2(\text{thf})_2]$ (tBu_2pz = 3,5-di-*tert*-butylpyrazolate; thf = tetrahydrofuran) sublimates with partial decomposition (200 °C, 0.1 mm Hg) into a white solid of the composition $[\text{Ca}(\text{tBu}_2\text{pz})_2]_n$ but with an unknown structure.^[5]

Herein we present a family of coligand-free, heavy alkaline earth metal pyrazolates, rare examples of homoleptic linear oligomers with a noteworthy array of metal–ligand binding modes. These feature a metal-size dependent degree of association, namely, the trimeric $[\text{Ca}_3(\text{tBu}_2\text{pz})_6]$ **1**, the tetrameric $[\text{Sr}_4(\text{tBu}_2\text{pz})_8]$ **2** and the unprecedented hexameric $[\text{Ba}_6(\text{tBu}_2\text{pz})_{12}]$ **3**. The only other structurally characterized homoleptic alkaline earth metal pyrazolate is the dimeric $[\text{Mg}_2(\text{tBu}_2\text{pz})_4]$ **4**,^[3g] which is now shown to be the junior member of the series.

Compounds **1–3** were prepared by the direct treatment of 3,5-di-*tert*-butylpyrazole (tBu_2pzH) with the appropriate metal at 250 °C [Eq(1)]. X-ray quality crystals were obtained

by recrystallization from a nondonating high-boiling solvent or sublimation.



The solid-state structures of **1–3** were established by low temperature X-ray crystallography.^[7] The structures of compounds **1–3** are presented in Figures 1–3, showing linear chains held together by diverse types of bridging pyrazolates.

Plausibly, $[\text{Ca}_3(\text{tBu}_2\text{pz})_6]$ **1** corresponds to the product of thermal decomposition of $[\text{Ca}(\text{tBu}_2\text{pz})_2(\text{thf})_2]$,^[5] as mentioned above. Thus, important information is obtained on the fate of the monomeric solid-state precursors upon solvent loss as frequently experienced in a CVD reactor. Complex **1** displays

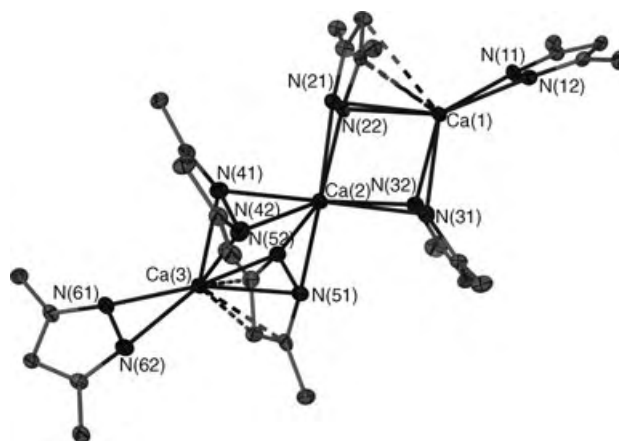


Figure 1. Structure of $[\text{Ca}_3(\text{tBu}_2\text{pz})_6]$ **1**; *tert*-butyl groups have been omitted for clarity. (Ca(1)–N(11,12,21,22,31,32) 2.303(3), 2.318(3), 2.577(3), 2.583(3), 2.447(4), 2.450(4), Ca(1)–C(23, 24, 25) 2.816(5)–2.960(4) Å; Ca(2)–N(21,22,31,32,41,42,51,52) 2.446(3), 2.418(3), 2.557(4), 2.597(4), 2.517(4), 2.618(4), 2.455(4), 2.415(4) Å; Ca(3)–N(41,42,51,52,61,62) 2.481(4) Å, 2.438(4), 2.560(4), 2.610(3), 2.292(3), 2.327(3) Å; Ca(3)–C(53,54,55) 2.804(4)–2.995(4) Å).

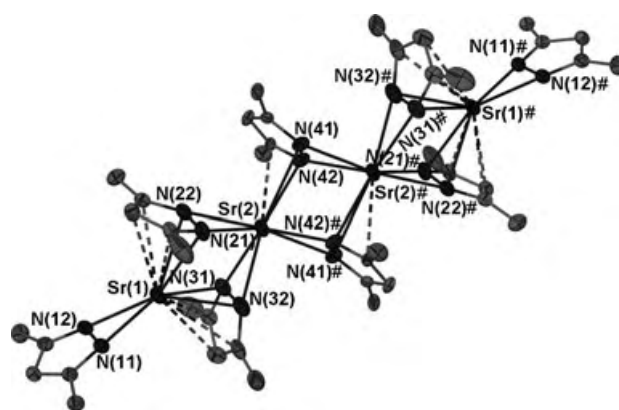


Figure 2. Structure of $[\text{Sr}_4(\text{tBu}_2\text{pz})_8]$ **2**; *tert*-butyl groups and the disordered components pzX, pzY, pzZ have been omitted for clarity. (Sr(1)–N(11,12,21,22,31,32) 2.485(5), 2.455(5), 2.758(7), 2.730(6), 2.779(6), 2.741(7) Å; Sr(1)–C(23,24,25,33,34,35) 3.029(7)–3.381(9) Å; Sr(2)–N(21,22,31,32,41,42,51,52) 2.586(7), 2.575(7), 2.648(6), 2.580(8), 2.913(9), 2.734(9), 2.453(9), 2.523(9) Å; Sr(2)–C(43) 3.22(1) Å).

[*] J. Hitzbleck, Prof. Dr. G. B. Deacon, Prof. Dr. K. Ruhlandt-Senge
School of Chemistry
Monash University
Clayton, Victoria 3168 (Australia)
Fax: (+61) 3-9905-4597
E-mail: glen.deacon@sci.monash.edu.au
kruhlandt@sydney.edu

J. Hitzbleck, Prof. Dr. K. Ruhlandt-Senge
Department of Chemistry
1-014 Center for Science and Technology
Syracuse University
Syracuse, NY 13244-4100 (USA)
Fax: (+1) 315-443-4070

[**] This work was supported by the Monash University Small Grant Scheme and the National Science Foundation under grant No. CHE-9702246 and CHE-0108098 including a supplement making possible the collaboration between SU and Monash U.

Supporting information for this article is available on the WWW under <http://www.angewandte.org> or from the author.

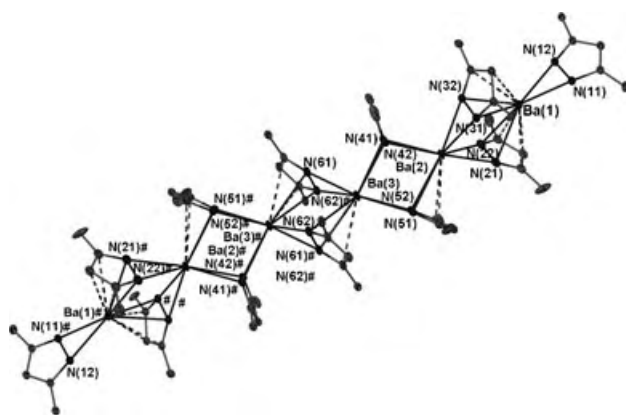


Figure 3. Structure of $[\text{Ba}_6(\text{tBu}_2\text{pz})_{12}]$ **3**; *tert*-butyl groups and the disordered components pz2', pz3', pz4', pz5' and pz6' have been omitted for clarity. (Ba(1)–N(11,12,21,22,31,32) 2.610(7), 2.651(7), 2.96(1), 2.96(1), 2.90(1), 2.89(1), Ba(1)–C(23,24,25,33,34,35) 3.10(1)–3.39(1) Å; Ba(2)–N(21,22,31,32,41,42,51,52) 2.84(1), 2.83(1), 2.72(1), 2.79(1), 2.79(1), 2.77(1), 2.98(1), 3.06(1) Å, Ba(2)–C(53,55) 3.38(2), 3.28(2) Å; Ba(3)–N(41,42,51,52,61,62) 2.92(1), 2.85(1), 2.69(1), 2.78(1), 2.67(1), 2.59(1) Å; Ba(3)–N(61,62) 3.06(1), 3.08(1) Å; Ba(3)–C(63,65) 3.36(1), 3.33(1) Å).

a linear array of calcium atoms, linked by pyrazolate bridges, and framed by two terminally bonded symmetrical ($\text{Ca}–\text{N}_{\text{ter}}$ 2.292(3)–2.327(3) Å) η^2 -pyrazolates, which are in line (pz1 165.2(1)°, pz6 167.0(1)°) with the Ca(1)–Ca(3) axis. There are two classes of bridging pyrazolates: pz3 and pz4 that display $\mu-\eta^2:\eta^2$ coordination with ligand planes perpendicular to the Ca₃-axis (pz3 85.7(1)°, pz4 86.1(1)°), while pz2 and pz5 are inclined towards the outer calcium atoms (pz2 36.4(1)°, pz5 41.9(1)°). The resulting close proximity of calcium to the carbon atoms of the pyrazolate rings pz2 and pz5 (Ca–C 2.804(4)–2.995(4) Å) reveals distances that lie well within the sum (3.7 Å) of the metallic radius of Ca (1.97 Å)^[8] and the van der Waals radius of an aromatic ring (1.73 Å),^[9] thus suggesting $\mu-\eta^2:\eta^5$ ligation of calcium. Both bonding modes contrast the more common $\mu-\eta^1:\eta^1$ bridging observed in $[\text{Mg}_2(\text{tBu}_2\text{pz})_4]$.^[3g] When the overall coordination number is taken into account, these distances compare well with the Ca π -arene interactions in sandwich complexes such as $[\text{Ca}(\text{Cp})_2]_n$ or $[\text{Ca}(\text{Cp}^*)_2]$.^[10] Surprisingly, there is a higher formal coordination number (8) for the central metal than for the outer metals (7) but the points of attachment ($\Sigma\eta^n = 9$) for Ca(1,3) exceed that (8) for Ca(2). The pairs of $\mu-\eta^2:\eta^2$ and $\mu-\eta^2:\eta^5$ bridges resemble the structures of $[\text{Ln}_3(\text{Ph}_2\text{pz})_9]$ (Ln = La, Nd; Ph₂pz = 3,5-diphenylpyrazolate).^[11]

The tetranuclear complex **2** is a dimer of dinuclear units. The terminal pyrazolates bind fairly symmetrically ($\text{Sr}–\text{N}_{\text{ter}}$ 2.455(5), 2.485(5) Å) and are parallel to the Sr₄ axis (pz1 172.3(2)°); but in contrast to the calcium analogue all bridging pyrazolates are now inclined. Nevertheless, the degree of tilting varies leaving only the outer pyrazolates at an almost ideal angle for π -bonding (pz2 43.5(3)°, pz3 41.1(4)°; Sr(1)–N_{br} 2.730(6)–2.779(6) Å) and $\mu-\eta^2:\eta^5$ -bridging. The larger inclination angle of the central pz4 ring towards Sr(2) (48.4(3)°) allows close contacts only for C(43) (Sr–C 3.22(1) Å), hence displaying a $\mu-\eta^2:\eta^3$ metal coordination,

previously known only in lanthanoid coordination.^[3c,d] The corresponding europium complex $[\text{Eu}_4(\text{tBu}_2\text{pz})_8]$ **5**^[2c] is isomorphous with **2**, the only minor structural difference consisting of a slightly smaller inclination angle (46.6(7)°) towards the central metals.

The hexanuclear barium complex **3** is a dimer of trinuclear units with three different types of barium centers. Analogous to **1** and **2**, the terminal metals are sandwiched between two $\mu-\eta^2:\eta^5$ -pyrazolates (pz2 45.6(6)°, pz3 47.2(5)°) and a terminal η^2 -pyrazolate (Figure 3). While Ba(1) and Ba(2) are bridged by two $\mu-\eta^2:\eta^5$ -pyrazolates, Ba(2) and Ba(3) are connected by a $\mu-\eta^2:\eta^2$ - (pz4 87.8(9)°) and an inclined (towards Ba(2)) $\mu-\eta^2:\eta^4$ -pyrazolate (pz5 44.8(8)°). The central bridging pyrazolate pz6/pz6' (' indicates disordered components) between Ba(3) and Ba(3)# is tilted 44.7(9)° towards the symmetry generated metal (Ba(3)–N_{br} 2.421(9)–2.67(1) Å; Ba(3)–N_{br} 3.054(9)–3.203(9) Å). Surprisingly, pz6' shows the most unsymmetrical bridging with even shorter (0.18 Å) Ba(3)–N contacts than the terminal η^2 -pyrazolate pz1 and even more elongated Ba(3)–N(61') (3.203(9) Å) bonds than the other $\mu-\eta^2:\eta^4$ -pyrazolates. Overall, the barium–pyrazolate interactions (Figure 3) compare well with those of $[\text{Ba}_6(\text{Me}_2\text{pz})_8(\text{thf})_6(\text{OSiMe}_2)_2\text{O}]$ **6**,^[12] which has terminal η^2 -Ba–N 2.665(9), 2.694(8) Å; $\mu-\eta^2:\eta^2$ -Ba–N 2.792(7)–3.007(8) Å; and $\mu-\eta^2:\eta^5$ -Ba–N 2.755(7)–2.984(8) Å.

A low-temperature ¹H NMR spectrum in $[\text{D}_8]\text{toluene}$ of **2** shows the separation of the pz(C4–H) signal into three well defined peaks with a ratio of 2:2:4 upon cooling to –60°C, which correspond to the three different ligand-binding types, thus confirming the geometrical arrangement observed in the solid state. The corresponding spectrum of **1** shows the same trend but incomplete separation of the three signals negates integration. The broad *tert*-butyl signal at room temperature changed into overlapping singlets at low temperature for both compounds. Insufficient solubility of **3** precluded analogous studies. Instead, the ¹H- and ¹³C{¹H}-NMR spectra of **3** in $[\text{D}_8]\text{THF}$ revealed sharp peaks that correspond to a single magnetic environment consistent with the formation of a solvated, monomeric complex. However, extraction of crude **1–3** with THF and crystallization yield dimeric $[\text{M}(\text{tBu}_2\text{pz})_2(\text{thf})_n]_2$, which are being structurally characterized.^[13]

Isolation of **1–3** together with the earlier **4** shows that in the series $[\text{M}(\text{tBu}_2\text{pz})_2]_n$, the degree of association increases with the ionic radius of the metal with $n = 2$ (Mg),^[3g] **3** (Ca), **4** (Sr), **6** (Ba). Although this is not associated with a major change in formal coordination number, except from Mg (CN = 4) to Ca (CN = 7,8), the points of attachment increase on descending the group, from **1** ($\Sigma\eta^n = 9$ Ca(1,3), 8 Ca(2)) to **2** ($\Sigma\eta^n = 12$ Sr(1), 9 Sr(2)) and **3** ($\Sigma\eta^n = 12$ Ba(1), 10 Ba(2,3)), thus supporting the lengthening of the chain.

The stable trinuclear **1** is in striking contrast to the behavior of ytterbium (ionic radii of Yb²⁺ and Ca²⁺ are comparable)^[14] for which direct metallation between *t*Bu₂pzH and excess metal affords the mixed oxidation state species $[\text{Yb}_2^{\text{II,III}}(\text{tBu}_2\text{pz})_5]$.^[15] On the other hand, with **2** being isomorphous with **5**, the close relationship between alkaline earth and rare earth metals (in this case Sr²⁺/Eu²⁺) is reinforced. There are even similarities between calcium and

trivalent rare earth derivatives, shown by a comparison of **1** with $[\text{Ln}_3(\text{Ph}_2\text{pz})_9]$ ($\text{Ln} = \text{La}, \text{Nd}$).^[11] They both have $\mu\text{-}\eta^2\text{:}\eta^2$ and $\mu\text{-}\eta^2\text{:}\eta^5$ bridging and a lower formal coordination number for the terminal metal, despite the difference in the metal framework (**1** linear/ $[\text{Ln}_3(\text{Ph}_2\text{pz})_9]$ bent).

Experimental Section

The compounds described herein are extremely air- and moisture-sensitive and so require all manipulations to be carried out under an inert-gas atmosphere. 3,5-Di-*tert*-butylpyrazole^[16] (0.72 g, 4.0 mmol), excess alkaline earth metal pieces (Ca, 0.41 g; Sr, 0.88 g; Ba, 1.37 g; 10 mmol), and 1,2,4,5-tetramethylbenzene (≈ 0.5 g) were heated in a sealed, evacuated Carius tube at 250 °C for 48 h. After sublimation of the solvent, the excess metal pieces were removed and the crude product washed with hexane (30 mL) leaving a white solid of good purity. Crystals suitable for X-ray diffraction were obtained by recrystallisation of small amounts of product from 1,2,4,5-tetramethylbenzene for **1** and **2** and 1,3,5-tri-*tert*-butylbenzene for **3**. Pure material was also obtained by sublimation, but the mechanical stress on the crystals upon removal from the walls of the reactor decreased crystal quality. Crystallographic analyses for compounds **1–3** were conducted as described.^[4a] The bridging pyrazolates in **2** and **3** are disordered over two sites (**2**: occupancy pz2,pz3/pzX,pzY 0.82/0.18; pz4/pz5 0.56/0.44; **3**: pz2/pz2' 0.65/0.35; pz3/pz3' 0.63/0.37; pz4/pz4' 0.52/0.48; pz5/pz5' 0.55/0.45; pz6/pz6' 0.61/0.39) in addition to disorder due to the rotation of the *tert*-butyl groups. IR data for **2** and **3** and ¹³C NMR for **1–3** are listed in the Supporting Information.

1: $[\text{Ca}_3(\text{tBu}_2\text{pz})_6]$ (0.76 g, 95 %). M.p. (sealed tube/N₂): 168–173 °C; IR (Nujol): $\tilde{\nu}$ = 3108 (m), 2713 (m), 2196 (w), 2031 (w), 1723 (w), 1622 (w), 1595 (w), 1556 (w), 1503 (s), 1405 (s), 1315 (m), 1250 (s), 1218 (s), 1098 (w), 981 (s), 930 (m), 867 (w), 812 (s), 779 (s) cm^{−1}; ¹H NMR (300 MHz, [D₆]benzene, 25 °C): δ = 6.12 (s, 6H; C4-H(pz)), 1.38 ppm (bs, 108H; *t*Bu-H); ¹H NMR (300 MHz, [D₈]toluene, −55 °C): δ = 6.20 (s, C4-H(pz)), 6.05 (s), overlapping with 6.00 (bs, combined integration 6H; C4-H(pz)), 1.37 (bs; *t*Bu-H), overlapping with 1.18 ppm (s, combined integration 108H; *t*Bu-H); elemental analysis calcd (%) for C₆₆H₁₁₄Ca₃N₁₂ (1195.93): C 66.28, H 9.61, N 14.06; found C 64.85, H 9.56, N 13.58.

2: $[\text{Sr}_4(\text{tBu}_2\text{pz})_8]$ (0.85 g, 95 %). M.p. (sealed tube/N₂): 348–353 °C; IR (Nujol): similar to **1**. ¹H NMR (300 MHz, [D₆]benzene, 25 °C): δ = 6.00 (bs, 8H; C4-H(pz)), 1.33 ppm (bd, 144H; *t*Bu-H); ¹H NMR (300 MHz, [D₈]toluene, −60 °C): δ = 6.31 (s, 2H; C4-H(pz)), 6.16 (s, 2H; C4-H(pz)), 6.08 (s, 4H; C4-H(pz)), 1.48 ppm (s; *t*Bu-H), overlapped by 1.85–0.97 ppm (bm, 144 H combined integration; *t*Bu-H); elemental analysis calcd (%) for C₈₈H₁₅₂N₁₆Sr₄ (1784.74): C 59.22, H 8.58, N 12.57; found C 58.19, H 8.49, N 12.41.

3: $[\text{Ba}_6(\text{tBu}_2\text{pz})_{12}]$ (0.95 g, 96 %). M.p. (sealed tube/N₂): > 350 °C; IR (Nujol): similar to **1**. ¹H NMR (300 MHz, [D₈]THF, 25 °C): δ = 5.81 (s, 12H; C4-H(pz)), 1.26 ppm (s, 272H; *t*Bu-H); elemental analysis calcd (%) for C₁₃₂H₂₈₈Ba₆N₂₄ (2975.35): C 53.29, H 7.72, N 11.30; found C 52.70, H 7.67, N 11.15.

Received: May 11, 2004

Keywords: alkaline-earth metals · coordination modes · N ligands · solvolysis · structure elucidation

C. M. Forsyth, A. Gitlits, R. Harika, P. C. Junk, B. W. Skelton, A. H. White, *Angew. Chem.* **2002**, *114*, 3383–3385; *Angew. Chem. Int. Ed.* **2002**, *41*, 3249–3251; c) G. B. Deacon, A. Gitlits, P. W. Roesky, M. R. Bürgstein, K. C. Lim, B. W. Skelton, A. H. White, *Chem. Eur. J.* **2001**, *7*, 127–138.

[3] a) C. Yelamos, M. J. Heeg, C. H. Winter, *Inorg. Chem.* **1998**, *37*, 3892–3894; b) G. B. Deacon, E. E. Delbridge, B. W. Skelton, A. H. White, *Angew. Chem.* **1998**, *110*, 2372–2373; *Angew. Chem. Int. Ed.* **1998**, *37*, 2251–2252; c) G. B. Deacon, E. E. Delbridge, D. J. Evans, R. Harika, P. C. Junk, B. W. Skelton, A. H. White, *Chem. Eur. J.* **2004**, *5*, 1193–1204, and references herein; d) G. B. Deacon, E. E. Delbridge, C. M. Forsyth, *Angew. Chem.* **1999**, *111*, 1880–1882; *Angew. Chem. Int. Ed.* **1999**, *38*, 1766–1767; e) R. Falvello, J. Fornies, A. Martin, R. Navarro, V. Sicilia, P. Villarroya, *Chem. Commun.* **1998**, 2429–2430; f) J. R. Perera, M. J. Heeg, H. B. Schlegel, C. H. Winter, *J. Am. Chem. Soc.* **1999**, *121*, 4536–4537; g) D. Pfeiffer, M. J. Heeg, C. H. Winter, *Angew. Chem.* **1998**, *110*, 2674–2676; *Angew. Chem. Int. Ed.* **1998**, *37*, 2517–2519.

[4] a) J. Hitzbleck, G. B. Deacon, A. Y. O'Brien, K. Ruhlandt-Senge, *Chem. Eur. J.* **2004**, *10*, 3315–3323; b) J. Hitzbleck, G. B. Deacon, A. Y. O'Brien, K. Ruhlandt-Senge, provisional patent application, **2003**.

[5] D. Pfeiffer, M. J. Heeg, C. H. Winter, *Inorg. Chem.* **2000**, *39*, 2377–2384.

[6] A. Y. O'Brien, J. Hitzbleck, K. Ruhlandt-Senge, unpublished results.

[7] **1**: C₆₆H₁₁₄Ca₃N₁₂; *Mr* = 1195.94. Triclinic *P*-1, *a* = 13.8474(2), *b* = 14.0132(2), *c* = 20.2472(4) Å, α = 75.185(1)°, β = 77.698(1)°, γ = 75.725(1)°, *V* = 3633.5(1) Å³, ρ_{calcd} (*Z* = 2) = 1.093 g cm^{−3}; *N*_t = 49616, *N* = 12763 unique (*R*_{int} = 0.0672), *N*_o = 8489 (*2* θ_{max} = 50°); *R* = 0.0728, *R*_w = 0.1705. **2**: C₈₈H₁₅₂N₁₆Sr₄; *Mr* = 1784.74. Triclinic *P*-1, *a* = 13.149(1), *b* = 13.508(1), *c* = 15.701(1) Å, α = 77.652(2)°, β = 73.123(2)°, γ = 66.040(2)°, *V* = 2424.0(4) Å³, ρ_{calcd} (*Z* = 1) = 1.217 g cm^{−3}; *N*_t = 19969, *N* = 8542 (*R*_{int} = 0.0358), *N*_o = 5885 (*2* θ_{max} = 50°); *R* = 0.0707, *R*_w = 0.1831. **3**: C₁₃₂H₂₈₈Ba₆N₂₄; *Mr* = 2975.35. Triclinic *P*-1, *a* = 13.1215(2), *b* = 13.5635(2), *c* = 23.4625(4) Å, α = 74.172(1)°, β = 81.333(1)°, γ = 66.707(1)°, *V* = 3685.61(11) Å³, ρ_{calcd} (*Z* = 1) = 1.309 g cm^{−3}; *N*_t = 54705, *N* = 12948 (*R*_{int} = 0.0468), *N*_o = 9220 (*2* θ_{max} = 50°); *R* = 0.0922, *R*_w = 0.1749. CCDC 222108–222110 (**1–3**) contain the supplementary crystallographic data for this paper. These data can be obtained free of charge via www.ccdc.cam.ac.uk/conts/retrieving.html (or from the Cambridge Crystallographic Data Centre, 12 Union Road, Cambridge CB21EZ, UK; Fax; (+44)1223-336-033; or e-mail: deposit@ccdc.cam.ac.uk).

[8] A. F. Wells, *Structural Inorganic Chemistry*, 5th Ed., Clarendon, Oxford, **1984**.

[9] L. Pauling, *The Nature of the Chemical Bond*, 3rd Ed., Cornell University Press, Ithaca, **1960**.

[10] a) R. Zenger, G. Stucky, *J. Organomet. Chem.* **1974**, *80*, 7–17; b) R. A. Williams, T. P. Hanusa, J. C. Huffman, *Organometallics* **1990**, *9*, 1128–1134.

[11] G. B. Deacon, C. M. Forsyth, A. Gitlits, B. W. Skelton, A. H. White, *Dalton Trans.* **2004**, *8*, 1239–1247.

[12] A. Steiner, G. T. Lawson, B. Walfort, D. Leusser, D. Stalke, *Dalton Trans.* **2001**, *3*, 219–221.

[13] J. Hitzbleck, K. Ruhlandt-Senge, G. B. Deacon, in preparation.

[14] a) R. D. Shannon, *Acta Crystallogr. Sect. A* **1976**, *32*, 751–767; b) S. Harder, *Angew. Chem.* **2004**, *116*, 2768–2773; *Angew. Chem. Int. Ed.* **2004**, *43*, 2714–2718.

[15] G. B. Deacon, A. Gitlits, B. W. Skelton, A. H. White, *Chem. Commun.* **1999**, 1213–1214.

[16] J. Elguero, E. Gonzalez, R. Jacquier, *Bull. Soc. Chim. Fr.* **1968**, 707–713.

[1] a) J. E. Cosgriff, G. B. Deacon, *Angew. Chem.* **1998**, *110*, 298–299; *Angew. Chem. Int. Ed.* **1998**, *37*, 286–287; b) F. Nief, *Eur. J. Inorg. Chem.* **2001**, 891–904.

[2] a) D. Pfeiffer, B. J. Ximba, L. M. Liable-Sands, A. L. Rheingold, M. J. Heeg, D. M. Coleman, H. B. Schlegel, T. F. Kuech, C. H. Winter, *Inorg. Chem.* **1999**, *38*, 4539–4548; b) G. B. Deacon,

Iterative One-Pot Synthesis of Oligosaccharides**

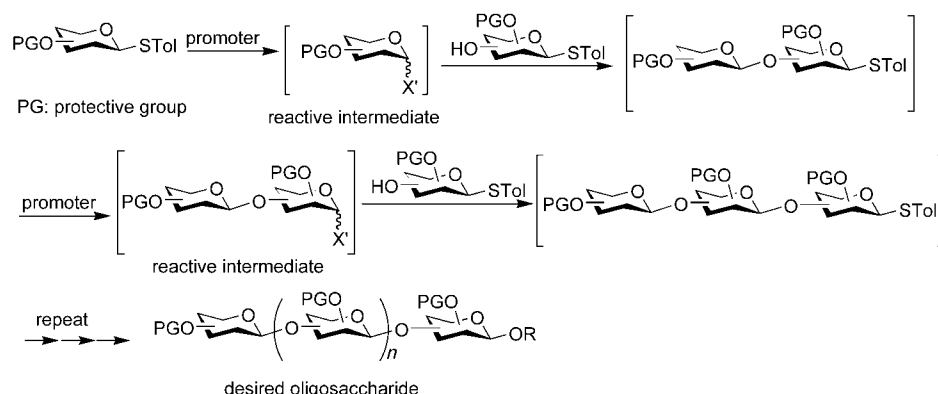
Xuefei Huang,* Lijun Huang, Haisheng Wang, and
Xin-Shan Ye*

Traditional oligosaccharide synthesis is a time-consuming process, primarily due to tedious protective group manipulation and intermediate separation. To reduce the number of synthetic and purification steps, many innovative methodologies have been developed, such as automated solid-phase synthesis,^[1] orthogonal glycosylation,^[2] iterative glycosylation,^[3] and chemoselective glycosylation,^[4] among which the reactivity-based one-pot method is particularly noteworthy.^[5] The reactivity-based one-pot method refers to one in which glycosyl donors with decreasing anomeric reactivities are allowed to react sequentially in a single reaction flask. Large oligosaccharides can be assembled in this fashion without tedious purification of intermediates or adjustment of anomeric leaving groups, as witnessed by total syntheses of complex oligosaccharides such as fucosyl GM1,^[5a] Le^Y,^[5c] and Globo H,^[5d] as well as assembly of oligosaccharide libraries.^[5b,e] However, to obtain building blocks with suitable

anomeric reactivities, extensive protective group manipulations and/or aglycon adjustments must be carried out.^[5] This excessive synthetic manipulation on building blocks complicates the synthetic process and decreases overall efficiency.

To overcome limitations of existing approaches, we have investigated the possibility of designing a general one-pot method independent of differential glycosyl donor reactivities. This can be achieved by pre-activating the donor,^[6] which generates a reactive intermediate in the absence of the acceptor (Scheme 1). Upon addition of the second building block to the pre-activated donor, a disaccharide will be formed with an identical activatable aglycon at the reducing end. This process can be repeated *in the same reaction vessel* allowing rapid assembly of oligosaccharides. Several prerequisites, however, must be satisfied for a successful iterative one-pot synthesis: 1) the promoter utilized must be stoichiometric in activation of a wide range of glycosyl donors and be completely consumed by the donor to prevent activation of following building blocks; 2) the intermediate generated after pre-activation must be stable till addition of acceptor, yet reactive for rapid high-yielding glycosylations; and 3) side products formed from activation must not interfere with glycosylations.

After much experimentation examining the effects of various promoters,^[7] aglycon leaving groups,^[8] and additives,^[9]



Scheme 1. Iterative one-pot synthesis of oligosaccharides.

[*] Prof. X. Huang, Dr. L. Huang
Department of Chemistry
University of Toledo
2801 W. Bancroft St. MS 602, Toledo, OH 43606 (USA)
Fax: (+1) 419-530-4033
E-mail: xuefei.huang@utoledo.edu

H. Wang, Prof. X.-S. Ye
The State Key Laboratory of Natural and Biomimetic Drugs
School of Pharmaceutical Sciences
Peking University
Xue Yuan Road 38, Beijing, 100083 (China)
Fax: (+86) 10-62014949
E-mail: xinshan@mail.bjmu.edu.cn

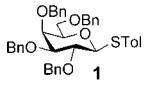
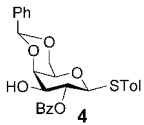
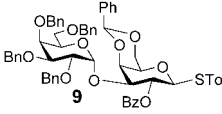
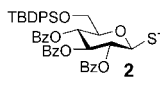
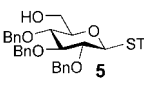
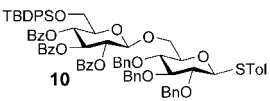
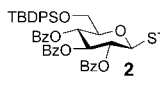
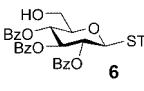
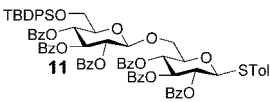
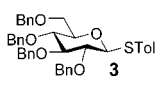
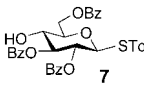
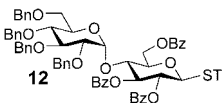
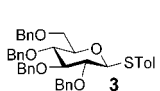
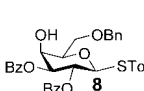
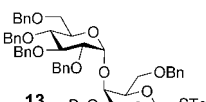
[**] This work was supported by the University of Toledo (X.H.), the National Natural Science Foundation of China, and Peking University (X.Y.).

Supporting information for this article is available on the WWW under <http://www.angewandte.org> or from the author.

general reaction conditions were established by using *p*-tolyl thioglycosides as building blocks, *p*-toluenesulfonyl triflate (*p*-TolSOTf),^[10] formed in situ from *p*-toluenesulfonyl chloride (*p*-TolSCl) and silver triflate (AgOTf), as the stoichiometric promoter, in the presence of the dehydrating reagent MS-AW300. Chemoselective glycosylation of donors was observed independent of the reactivities of donors and acceptors, producing disaccharides bearing an anomeric *p*-thiotolyl moiety in satisfactory yields (Table 1).

Introduction of one equivalent of *p*-TolSCl to a mixture of armed donor **1**, AgOTf, and MS-AW300 in diethyl ether at -60°C led to instantaneous complete activation of the glycosyl donor.^[11] Addition of the acceptor **4** to the pre-activated donor rapidly formed disaccharide **9** in just a few minutes, which was isolated in 87% yield as the α anomer due to the anomeric effect (Table 1, entry 1). The *p*-tolyl disulfide generated from activation did not perturb the glycosylation.

Table 1: Results of chemoselective glycosylations of thioglycoside donors.

Donor + AgOTf (2 equiv)		p -TolSCI (1 equiv), MS-AW300	Acceptor	Product	Yield [%]
		Et_2O , -60°C			
Entry	Donor + Acceptor	Product			Yield [%]
1	 + 				87
2	 + 				69
3	 + 				72
4	 + 				67
5	 + 				65

p -TolSOTf is a powerful promoter capable of stoichiometrically activating highly disarmed donors as well. Disarmed donor **2** with the participating benzoyl moiety at C-2 reacted smoothly with the more reactive armed acceptor **5** to give disaccharide **10** in 69% as the β anomer (Table 1; entry 2). No products due to the self-coupling of acceptor **5** were isolated. This reversal of reactivity, that is, the less reactive donor is

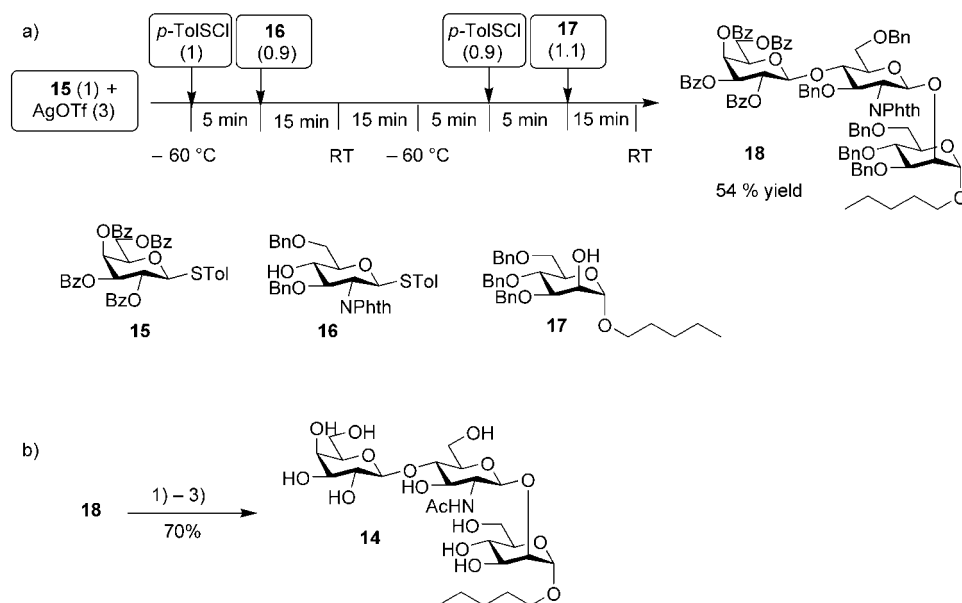
selectively glycosylated with the more reactive acceptor, is not possible with the traditional reactivity-based approach.

To explore the scope of the current method, glycosylations with poorly nucleophilic acceptors are examined, which are known to be challenging due to reduced glycosylation rates and/or competition of other more nucleophilic compounds in the reaction mixture.^[5f,12] With our protocol, donor **2** reacted readily with a disarmed acceptor **6** to give disaccharide **11** in a few minutes in 72% yield (Table 1, entry 3). Two poorly nucleophilic acceptors **7** and **8**^[12c] were also glycosylated smoothly by pre-activated donor **3** in 67% and 65% yields, respectively (Table 1, entries 4 and 5).^[13]

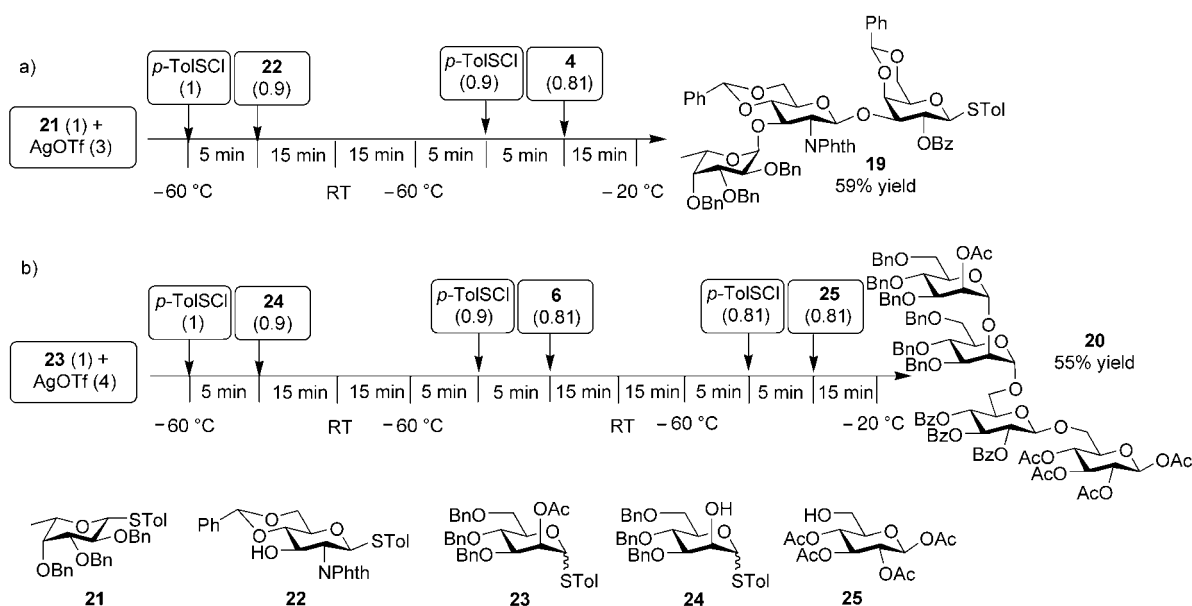
We next focused on applying this strategy to the one-pot synthesis of oligosaccharides. A sub-stoichiometric amount (0.9 equiv) of acceptor was utilized for each coupling to ensure complete consumption of the acceptor. The

reaction mixture was warmed up to room temperature after each glycosylation to decompose the slight excess of activated donor that had been present to prevent the formation of deletion sequences.

The trisaccharide motif **14** occurs in complex *N*-glycoprotein structures containing the demanding Gal- β 1,4-GlcNAc and GlcNAc- β 1,2-Man linkages. Because our strat-



Scheme 2. One-pot synthesis and deprotection of trisaccharide **18**. The values given in parentheses denote the number of equivalents of each reagent. Reagents and conditions: 1) ethylenediamine, EtOH, reflux; 2) Ac_2O , MeOH; 3) H_2 , Pd/C.



Scheme 3. One-pot syntheses of oligosaccharides **19** and **20**. The values given in parentheses denote the number of equivalents of each reagent.

egy does not require tuning of reactivities, this allowed us to select the readily available building blocks **15–17** (Scheme 2). Pre-activation of the disarmed thiogalactoside **15** (1 equiv) by *p*-TolSOTf (1 equiv) at -60°C was followed by addition of the more reactive armed glucosamine building block **16** (0.9 equiv) (Scheme 2a). The reaction mixture was warmed up to room temperature for 15 min, and then cooled down back to -60°C . Activation of the newly formed disaccharide with *p*-TolSOTf followed by addition of acceptor **17** produced the trisaccharide **18**^[14] within one hour in 54% yield. The progress of the reaction was readily monitored by TLC. The trisaccharide **18** was then deprotected in 70% yield by using a three-step sequence to give **14** (Scheme 2b). Trisaccharide **14** has also been synthesized by employing automated solid-phase methodology using an excess of each glycosyl donor (12 equiv) in 37.2% overall yield for assembly and deprotection.^[1a] Our iterative one-pot method has the advantages of using a near-stoichiometric amount of building blocks, ease in reaction monitoring, and simplicity of operation while achieving similar overall synthetic efficiencies in the syntheses of medium-sized oligosaccharides.

To illustrate the generality of our methodology, trisaccharide **19**^[14] and tetrasaccharide **20**^[14] which contain biologically relevant glycosidic linkages such as Fuc- α 1,3-GlcNAc, GlcNAc- β 1,3-Gal, Man- α 1,2-Man, Man- α 1,6-Glc, and Glc- β 1,6-Glc, were assembled as outlined in Scheme 3. One-pot sequential coupling of fucosyl thioglycoside **21**, glucosamine **22** and thiogalactoside **4** produced trisaccharide **19** in 59% yield in only one hour (Scheme 3a). With its anomeric *p*-thiotolyl moiety, the trisaccharide **19** can be immediately utilized as a donor in the synthesis of Le^x oligosaccharides without any aglycon modifications. Consecutive condensation of building blocks **23**, **24**, **6**, and **25** promoted by *p*-TolSOTf led to formation of tetrasaccharide **20** in 55% yield in less than two hours (Scheme 3b). It should be noted that both α and β linkages were constructed in one

pot within the same oligosaccharide with excellent stereo-selectivities.

In summary, a new iterative one-pot glycosylation approach is developed for the efficient assembly of oligosaccharides, which is based upon pre-activation of a *p*-tolyl thioglycoside donor, followed by sequential addition of building blocks in a single reaction flask. This strategy obviates the need for the extensive adjustment of protective groups required for traditional reactivity-based one-pot synthesis, significantly reducing the amount of time needed for preparing building blocks. Furthermore, a single glycosylation protocol was found applicable for the assembly of a wide range of oligosaccharides. This will be particularly advantageous for designing oligosaccharide libraries. Studies are ongoing to further explore the scope of this method and apply it to syntheses of complex oligosaccharides as well as carbohydrate libraries.

Received: March 31, 2004

Keywords: carbohydrates · glycosylation · iterative synthesis · synthetic methods

- [1] a) O. J. Plante, E. R. Palmacci, P. H. Seeberger, *Science* **2001**, 291, 1523; b) P. H. Seeberger, *Chem. Commun.* **2003**, 1115; c) O. J. Plante, E. R. Palmacci, P. H. Seeberger, *Adv. Carbohydr. Chem. Biochem.* **2003**, 58, 35.
- [2] a) O. Kanie in *Carbohydrates in Chemistry and Biology*, Vol. 1 (Eds.: B. Ernst, G. W. Hart, P. Sinay), Wiley-VCH, Weinheim, **2000**, p. 407; b) A. V. Demchenko, C. De Meo, *Tetrahedron Lett.* **2002**, 43, 8819; c) G. X. Chang, T. L. Lowary, *Org. Lett.* **2000**, 2, 1505; d) H. Paulsen, *Angew. Chem.* **1995**, 107, 1562; *Angew. Chem. Int. Ed. Engl.* **1995**, 34, 1432.
- [3] a) S. Yamago, T. Yamada, T. Maruyama, J.-I. Yoshida, *Angew. Chem.* **2004**, 116, 2197; *Angew. Chem. Int. Ed.* **2004**, 43, 2145; b) S. Yamago, T. Yamada, O. Hara, H. Ito, Y. Mino, J.-I. Yoshida, *Org. Lett.* **2001**, 3, 3867; c) H. M. Nguyen, J. L. Poole, D. Y. Gin,

- Angew. Chem.* **2001**, *113*, 428; *Angew. Chem. Int. Ed.* **2001**, *40*, 414; d) R. W. Friesen, S. J. Danishefsky, *J. Am. Chem. Soc.* **1989**, *111*, 6656.
- [4] a) J. D. C. Codee, L. J. van den Bos, R. E. J. N. Litjens, H. S. Overkleeft, C. A. A. van Boeckel, J. H. van Boom, G. A. van der Marel, *Tetrahedron* **2004**, *60*, 1057; b) M. Lahmann, S. Oscarson, *Can. J. Chem.* **2002**, *80*, 889; c) T. Zhu, G.-J. Boons, *Org. Lett.* **2001**, *3*, 4201.
- [5] a) T. K.-K. Mong, H.-K. Lee, S. G. Duron, C.-H. Wong, *Proc. Natl. Acad. Sci. USA* **2003**, *100*, 797; b) T. K. Ritter, K.-K. T. Mong, H. Liu, T. Nakatani, C.-H. Wong, *Angew. Chem.* **2003**, *115*, 4805; *Angew. Chem. Int. Ed.* **2003**, *42*, 4657; c) K.-K. T. Mong, C.-H. Wong, *Angew. Chem.* **2002**, *114*, 4261; *Angew. Chem. Int. Ed.* **2002**, *41*, 4087; d) F. Burkhardt, Z. Zhang, S. Wacowich-Sgarbi, C.-H. Wong, *Angew. Chem.* **2001**, *113*, 1314; *Angew. Chem. Int. Ed.* **2001**, *40*, 1274; e) X.-S. Ye, C.-H. Wong, *J. Org. Chem.* **2000**, *65*, 2410; f) Z. Zhang, I. R. Ollman, X.-S. Ye, R. Wischnat, T. Baasov, C.-H. Wong, *J. Am. Chem. Soc.* **1999**, *121*, 734; g) M. Fridman, D. Solomon, S. Yogeve, T. Baasov, *Org. Lett.* **2002**, *4*, 281; h) H. Tanaka, M. Adachi, H. Tsukamoto, T. Ikeda, H. Yamada, T. Takahashi, *Org. Lett.* **2002**, *4*, 4213; i) N. L. Douglas, S. V. Ley, U. Lucking, S. L. Warriner, *J. Chem. Soc. Perkin Trans. 1* **1998**, 51; j) S. Raghavan, D. Kahne, *J. Am. Chem. Soc.* **1993**, *115*, 1580.
- [6] While pre-activation of donors in the absence of an acceptor has been reported before (for several examples see ref. [3a,c, 4a, and 10a,b]), the conditions utilized are not applicable to iterative one-pot synthesis due to the need for excess promoter, excess acceptor, extra rearrangement steps, additional quenching reagent, or intermediate aglycon adjustments.
- [7] Other promoters such as N-iodosuccinimide (NIS)/TMSOTf, dimethyl (methylthio) sulfonium triflate (DMTST), *p*-nitrophenylsulfenyl chloride/AgOTf, phenylselenenyl bromide/AgOTf, and the newly developed 1-benzenesulfinyl piperidine/Tf₂O, were also examined. None of them gave desired oligosaccharides consistently in satisfactory yields.
- [8] Thioglycosyl donors of varying electron-withdrawing power and steric sizes, such as *p*-methoxyphenyl, *p*-nitrophenyl, *p*-trifluoromethylphenyl, *o*-fluorophenyl, 2,6-dimethylphenyl, *i*Pr, and *t*Bu have been examined, and have been found to give lower yields compared with those obtained by using *p*-tolyl thioglycoside donors. Other excellent donors such as glycosyl sulfoxide, *n*-pentenyl glycoside, glycosyl fluoride, and glycosyl iodide may be potentially utilized in iterative one-pot synthesis as well.
- [9] Additives such as tetrabutylammonium triflate, lithium perchlorate, and 2,6-di-*tert*-butyl 4-methylpyridine did not lead to higher yields.
- [10] a) D. Crich, S. Sun, *Tetrahedron* **1998**, *54*, 8321; b) D. Crich, W. Cai, *J. Org. Chem.* **1999**, *64*, 4926; c) V. Martichonok, G. M. Whitesides, *J. Org. Chem.* **1996**, *61*, 1702; d) F. Dasgupta, P. J. Garegg, *Carbohydr. Res.* **1988**, *177*, c13.
- [11] Although Crich and co-workers have convincingly demonstrated the presence of α -glycosyl triflate as the dominant intermediate after pre-activation of several thioglycosides through a series of outstanding low-temperature NMR experiments, the identity of kinetically reactive species remained to be illustrated. For references regarding the reactive intermediate, see: ref. [10a,b], and A. A. H. Abdel-Rahman, S. Jonke, E. S. H. El Ashry, R. R. Schmidt, *Angew. Chem.* **2002**, *114*, 3100; *Angew. Chem. Int. Ed.* **2002**, *41*, 2972.
- [12] a) F. Belot, J.-C. Jacquinot, *Carbohydr. Res.* **1996**, *290*, 79; b) H. Yu, B. Yu, X. Wu, Y. Hui, X. Han, *J. Chem. Soc. Perkin Trans. 1* **2000**, 1445; c) Y. Du, M. Zhang, F. Yang, G. Gu, *J. Chem. Soc. Perkin Trans. 1* **2001**, 3122.
- [13] Pre-activated donor **2** did not react with acceptors **7** or **8**, and we are currently investigating the reasons for this.
- [14] Compound **18**: ¹H NMR (599.87 MHz, CDCl₃): δ = 0.80 (t, *J* = 7.2 Hz, 3H), 1.10–1.26 (m, 4H), 1.36 (quin, *J* = 7.2 Hz, 2H), 2.94 (dd, *J* = 6.6, 10.8 Hz, 1H), 3.11 (dt, *J* = 7.2, 9.0 Hz, 1H), 3.38–3.52 (m, 5H), 3.55 (d, *J* = 10.2 Hz, 1H), 3.70–3.76 (m, 2H), 4.08 (m, 4H), 4.22–4.43 (m, 8H), 4.65 (d, *J* = 12.0 Hz, 1H), 4.72 (d, *J* = 12.0 Hz, 1H), 4.73 (d, *J* = 12.0 Hz, 1H), 4.74 (d, *J* = 10.8 Hz, 1H), 4.98–5.02 (m, 2H), 5.17 (d, *J* = 7.8 Hz, 1H), 5.43 (dd, *J* = 3.6, 10.8 Hz, 1H), 5.79 (dd, *J* = 7.8, 10.8 Hz, 1H), 5.85 (d, *J* = 3.6 Hz), 6.78–6.82 (m, 2H), 7.06–7.68 (m, 39H), 7.74–7.78 (m, 2H), 7.89–7.94 (m, 4H), 8.06–8.42 ppm (m, 2H); ¹³C NMR (100.5 MHz, CDCl₃): δ = 14.20, 22.62, 28.41, 29.21, 55.77, 60.64, 61.97, 67.89, 68.32, 68.43, 70.24, 70.62, 70.83, 71.40, 71.92, 71.97, 73.08, 73.75, 73.87, 74.49, 74.94, 75.07, 76.80, 77.25, 78.03, 78.37, 97.16, 100.82, 123.32, 127.28, 127.49, 127.56, 127.64, 127.74, 127.98, 128.06, 128.12, 128.38, 128.45, 128.48, 128.52, 128.55, 128.61, 128.68, 129.17, 129.32, 129.71, 129.98, 130.06, 132.02, 133.47, 133.51, 133.68, 138.25, 138.69, 138.76, 138.81, 165.22, 165.53, 165.69, 166.26 ppm; HRMS C₉₄H₉₁NNaO₂₁ [*M*+Na⁺] calcd 1952.5981 found 1952.5961. Compound **19**: ¹H NMR (599.87 MHz, CDCl₃): δ = 0.81 (d, *J* = 6.6 Hz, 3H), 2.27 (s, 3H), 3.38 (d, *J* = 1.8 Hz, 1H), 3.52–3.65 (m, 6H), 3.79 (d, *J* = 9.6 Hz, 1H), 3.93 (q, *J* = 6.6 Hz, 1H), 4.01–4.08 (m, 3H), 4.23 (d, *J* = 11.4 Hz, 1H), 4.28–4.38 (m, 4H), 4.42–4.47 (m, 2H), 4.66 (d, *J* = 3.0 Hz, 1H), 4.68 (d, *J* = 9.6 Hz, 1H), 4.73 (d, *J* = 11.4 Hz, 1H), 5.31 (t, *J* = 9.6 Hz, 1H), 5.48 (s, 1H), 5.51 (s, 1H), 5.55 (d, *J* = 9.6 Hz, 1H), 6.88–6.92 (m, 2H), 6.93–6.96 (m, 2H), 7.08–7.50 (m, 32H), 7.62–7.66 ppm (m, 2H); ¹³C NMR (100.5 MHz, CDCl₃): δ = 16.67, 21.46, 55.50, 66.27, 67.45, 68.77, 68.99, 69.37, 70.25, 72.62, 73.32, 74.88, 75.61, 76.28, 76.33, 78.13, 79.68, 80.06, 82.08, 86.02, 99.77, 100.16, 101.19, 101.33, 122.92, 126.19, 126.80, 127.49, 127.58, 127.66, 127.67, 127.71, 127.89, 128.01, 128.27, 128.38, 128.43, 128.49, 128.72, 129.68, 129.84, 129.86, 132.81, 133.45, 134.19, 137.21, 137.94, 138.26, 138.54, 138.71, 139.10, 164.55 ppm; HRMS C₇₅H₇₁NNaO₁₆S [*M*+Na⁺] calcd 1296.4391 found 1296.4384. Compound **20**: ¹H NMR (599.87 MHz, CDCl₃): δ = 1.91 (s, 3H), 1.92 (s, 3H), 1.97 (s, 3H), 1.98 (s, 3H), 2.10 (s, 3H), 3.46–3.92 (m, 17H), 4.32–4.53 (m, 8H), 4.60 (d, *J* = 10.8 Hz, 1H), 4.68 (d, *J* = 12.0 Hz, 1H), 4.78–4.85 (m, 4H), 4.87 (t, *J* = 9.0 Hz, 1H), 4.93 (dd, *J* = 8.4, 9.6 Hz, 1H), 4.99 (d, *J* = 1.8 Hz, 1H), 5.10 (t, *J* = 9.6 Hz, 1H), 5.44 (dd, *J* = 7.8, 9.6 Hz, 1H), 5.46–5.49 (m, 1H), 5.50 (d, *J* = 9.6 Hz, 1H), 5.57 (d, *J* = 8.4 Hz, 1H), 5.80 (t, *J* = 9.6 Hz, 1H), 7.08–7.42 (m, 42H), 7.48–7.52 (m, 1H), 7.78–7.82 (m, 2H), 7.87–7.90 (m, 2H), 7.96–8.02 ppm (m, 2H); ¹³C NMR (100.5 MHz, CDCl₃): δ = 20.76, 20.91, 21.38, 66.93, 67.46, 68.80, 68.92, 69.05, 69.27, 70.40, 70.59, 71.83, 72.05, 72.08, 72.88, 73.16, 73.35, 73.57, 74.27, 74.47, 74.50, 74.89, 75.18, 75.24, 77.44, 78.33, 79.69, 91.80, 99.22, 99.76, 101.06, 127.56, 127.63, 127.70, 127.74, 127.77, 127.83, 127.99, 128.09, 128.30, 128.38, 128.45, 128.48, 128.52, 128.55, 128.64, 129.17, 129.26, 129.59, 129.98, 130.17, 133.33, 133.35, 133.49, 138.25, 138.55, 138.64, 138.71, 138.77, 138.87, 165.22, 165.36, 166.01, 168.94, 169.38, 169.61, 170.22, 170.32 ppm; ¹J(¹³C,¹H): 166.4 Hz (δ = 91.80 ppm, β linkage), 171.8 Hz (δ = 99.22 ppm, α linkage), 172.3 Hz (δ = 99.76 ppm, α linkage), 163.9 Hz (δ = 101.06 ppm, β linkage); HRMS C₉₇H₁₀₀NNaO₂₉ [*M*+Na⁺] calcd 1751.6248 found 1751.6301.

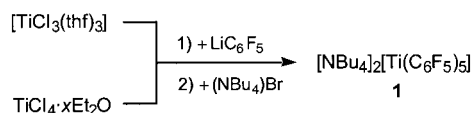
Titanium Complexes

A Five-Coordinate Homoleptic Organotitanium(III) Compound**

Pablo J. Alonso, Larry R. Falvello, Juan Forniés,
M. Angeles García-Monforte, and Babil Menjón*

The term “homoleptic”, as coined by Lappert for $[\{MR_x\}_n]^{q-}$ species ($q = 0, \pm 1, \pm 2, \dots$), is a logical extension of the classical concept of “binary” compounds E_nX_m , used in traditional chemistry.^[1] Both kinds of compounds are of fundamental importance: They are simple species whose stability, structure, and chemical properties are determined by a minimum number of factors: 1) the electronic and steric properties of a single type of atom X or group R, and 2) the electron configuration, charge, and size of the atom E or metal M. The latter set of factors is inextricably related to the oxidation state of a given element (E or M). In the realm of organotitanium chemistry, the five-coordinate species $[Ti^{IV}Me_5]^-$ has been isolated^[2] and structurally characterized.^[3] To the best of our knowledge, however, no related $[TiR_5]^{2-}$ species has yet been described containing titanium(III), a much less studied oxidation state for this metal. In fact, the only well-established homoleptic organotitanium(III) compounds conform to the $[TiR_2]^+$ ($R = C_5Me_5$),^[4] $[TiR_3]$ ($R = C_5H_5$,^[5] $CH(SiMe_3)_2$),^[6] and $[TiR_4]^-$ ($R = C_6Cl_5$)^[7] stoichiometries. We now report the synthesis and characterization of $[NBu_4]_2[Ti(C_6F_5)_5]$ (d^1 , paramagnetic), containing discrete $[Ti^{III}(C_6F_5)_5]^{2-}$ units, which is an unprecedented formula for homoleptic organotitanium compounds.

The low-temperature reaction of a suspension of $TiCl_4 \cdot xEt_2O$ in Et_2O with LiC_6F_5 in the presence of $[NBu_4]Br$ proceeds with metal reduction and affords $[NBu_4]_2[Ti^{III}(C_6F_5)_5]$ (**1**) as an orange-red solid in moderate yield (Scheme 1). Compound **1** can alternatively be prepared under similar conditions from the titanium(III) complex $[TiCl_3(thf)_3]$. Note that the reaction of $[TiCl_3(thf)_3]$ with LiC_6Cl_5 has been reported to afford the four-coordinate compound $[Li(thf)_4][Ti^{III}(C_6Cl_5)_4]$.^[7] Compound **1** is



Scheme 1.

extremely air sensitive, both in solution and in the solid state. Solid **1** easily explodes under slight mechanical stress, for example, from percussion or a sharp temperature change. The IR spectrum shows only a weak absorption assignable to the X-sensitive vibration mode^[8] of the C_6F_5 group at 801 cm^{-1} .

The crystal and molecular structures of **1** were established by X-ray diffraction. Two crystallographically independent $[Ti(C_6F_5)_5]^{2-}$ anions were found in the asymmetric unit of the crystal but, because of their similarity, we refer to only one of them (Figure 1). The Ti center is located in a heavily distorted

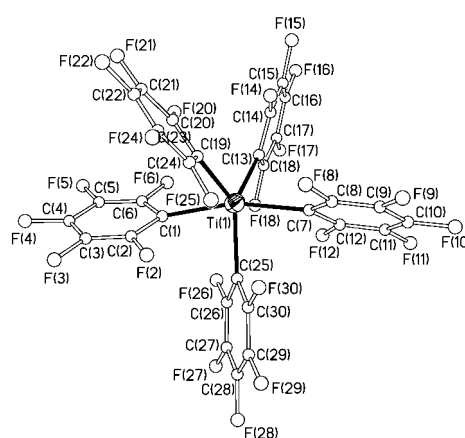


Figure 1. Thermal ellipsoid diagram (50% probability) of one of the two crystallographically independent $[Ti(C_6F_5)_5]^{2-}$ anions in **1**. Selected bond lengths [pm] and angles $^\circ$: Ti(1)–C(1) 226.2(8), Ti(1)–C(7) 225.7(8), Ti(1)–C(13) 222.1(7), Ti(1)–C(19) 223.8(7), Ti(1)–C(25) 223.5(6); C(1)–Ti(1)–C(7) 164.6(2), C(1)–Ti(1)–C(13) 105.2(3), C(1)–Ti(1)–C(19) 79.4(3), C(1)–Ti(1)–C(25) 81.5(2), C(7)–Ti(1)–C(13) 86.5(3), C(7)–Ti(1)–C(19) 108.3(3), C(7)–Ti(1)–C(25) 83.4(3), C(13)–Ti(1)–C(19) 101.7(2), C(13)–Ti(1)–C(25) 129.6(3), C(19)–Ti(1)–C(25) 128.3(2).

trigonal-bipyramidal ($TBPY-5$) environment formed by five terminal, σ -bonded C_6F_5 ligands. The axial positions are defined by the C_6F_5 groups with the widest interligand angle ($C(1)-Ti(1)-C(7)$ $164.6(2)^\circ$). The sum of the interligand $C_{eq}-Ti-C_{eq}$ angles is $359.3(3)^\circ$, that is, the equatorial plane shows no pyramidalization at the Ti atom. Although weaker $M-L_{ax}$ bonds would be expected for a d^n ($TBPY-5$)- ML_5 species with $n < 5$,^[9] no significant difference between the average values of $Ti-C_{ax}$ (226.2(8) pm) and $Ti-C_{eq}$ (223.1(7) pm) bond lengths can be observed in **1**. The mean $Ti-C$ bond length (224.4(8) pm) is slightly longer than that observed in the homoleptic, tetrahedral anion $[Ti^{III}(C_6Cl_5)_4]^-$ ($Ti-C$ 220.7(5) pm),^[7] a fact that can be ascribed to the different coordination numbers in the two anionic species, as well as to their different global charges. Important angular deviations from ideal $TBPY-5$ geometry are observed in the Ti coordi-

[*] Prof. Dr. P. J. Alonso, Prof. Dr. L. R. Falvello, Prof. Dr. J. Forniés, Dipl.-Chem. M. A. García-Monforte, Dr. B. Menjón
Instituto de Ciencia de Materiales de Aragón
Facultad de Ciencias
Universidad de Zaragoza-C.S.I.C.
C/Pedro Cerbuna 12, 50009 Zaragoza (Spain)
Fax: (+34) 976-761-187
E-mail: menjon@unizar.es

[**] This work was supported by the Spanish MCYT (DGI)/FEDER (Projects BQU2002-03997-CO2-02 and BQU2002-00554) and the Gobierno de Aragón (Grupo Consolidado: Química Inorgánica y de los Compuestos Organometálicos). The Gobierno de Aragón is also acknowledged for a grant to M.A.G.-M. We thank Dr. I. Ara for collecting the X-ray diffraction data.

Supporting information for this article (PDB files of the crystallographically independent anions and variable-temperature EPR spectrum of **1**) is available on the WWW under <http://www.angewandte.org> or from the author.

nation sphere. The equatorial C_6F_5 groups are tilted from the equatorial plane by between 28.5° and 47.3° , but they fail to arrange helically around the ideal axial direction, in contrast to the disposition adopted by the C_6Cl_5 groups in the related anions ($TBPY-5-11$)-[$M(C_6Cl_5)_3Cl_2$] $^-$ ($M = Zr, Hf$).^[7a] Since the $C_{eq}-Ti-C_{eq}$ angle between the two like-rotated C_6F_5 rings ($C(13)-Ti-C(19)$ $101.7(2)^\circ$) is significantly more acute than those between counterrotated rings (ca. 130°), an equatorial Y distortion occurs.^[10] The axial C_6F_5 groups depart by about 17° from the normal to the equatorial plane: Axial C(1) leans toward the $C(19)-Ti(1)-C(25)$ bisector, while axial C(7) leans to the bisector of $C(13)-Ti(1)-C(25)$, resulting in acute $C_{ax}-Ti(1)-C(25)$ angles of about 82° (reversed Berry distortion towards a so-called edge-bridged tetrahedron, with a precession angle of $\beta \approx 17^\circ$).^[10,11] The angular distortions in the $[Ti(C_6F_5)_5]^{2-}$ anion yield an approximate C_{2v} local symmetry and can be jointly described as a “totally reversed Berry distortion” in which C(25) acts as the pivot substituent (Figure 2).

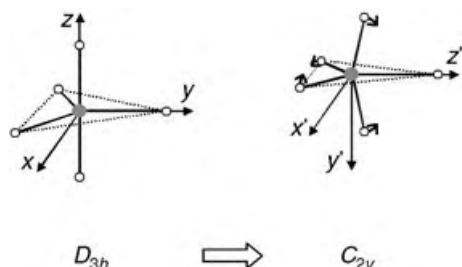


Figure 2. Schematic representation of the Ti^{III} environment in **1** as a distortion of an ideal $TBPY-5$ geometry with the appropriate choice of reference frame in each case.

The stereochemistry of five-coordinate compounds has always been a difficult and controversial issue.^[12] When purely electrostatic factors are considered, the $TBPY-5$ geometry is generally found to be more stable than the $SPY-5$ alternative.^[13] However, in our case an idealized $TBPY-5$ geometry would lead to the orbitally degenerate electronic state $e''(xy, xz)^1$ (Figure 3),^[14] which, according to the Jahn–Teller theorem, should be unstable.^[15] On the other hand, detailed calculations at different levels of theory on homoleptic $[MR_5]^{q-}$ systems bearing purely σ -donor ligands (e.g., H or

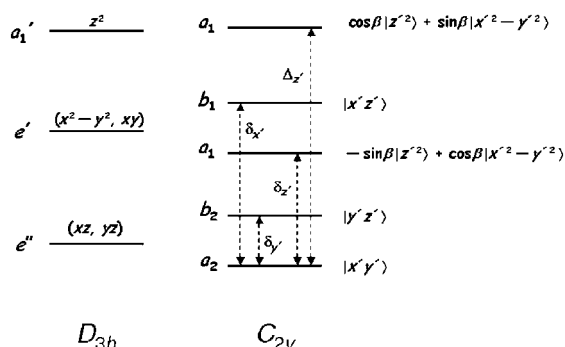


Figure 3. Energy level diagrams corresponding to a $[MR_5]^{q-}$ ($q = 0, \pm 1, \pm 2, \dots$) species with ideal $TBPY-5$ geometry (D_{3h}) and with the lowering of symmetry experimentally observed in **1** (C_{2v}). The labels identify the primary character of the orbitals.

Me) point to the “non-VSEPR”^[16] $SPY-5$ geometry as the most energetically favored.^[3,11,16–18] These theoretical predictions were experimentally confirmed in a number of d^0 and d^1 species, such as $[Ta(CH_2C_6H_4)]$ (d^0),^[19] $[TaMe_5]$ (d^0),^[20] and $[MoMe_5]$ (d^1).^[18] These results departing from simple VSEPR models apply for covalent, essentially nonpolar species.^[16,21] The fact that $[Ti(C_6F_5)_5]^{2-}$ in **1** with a distorted $TBPY-5$ structure more closely resembles a transition state calculated^[11] for the anion $[TiH_5]^-$ than the ground-state structure of this and the aforementioned organometallic compounds could be related to the polarity of the $Ti-C$ bonds caused by the strongly electron withdrawing character of the C_6F_5 group.^[22] It can be concluded that, on a simple VSEPR basis, both the high polarity of the $Ti-C$ bond and the bulkiness of the C_6F_5 ligand would be expected to favor the $TBPY-5$ geometry. The significant deviations observed in the solid-state structure of **1** could be attributed to the Jahn–Teller effect, as well as to steric problems possibly encountered in arranging five highly anisotropic C_6F_5 ligands around the Ti^{III} centre.

Variable-temperature EPR spectra (77.3 to 250 K) were measured on polycrystalline samples of **1**. The results obtained (Figure 4; see also Supporting Information) can be

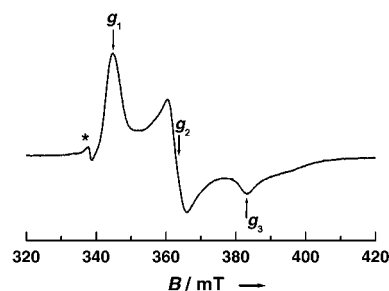


Figure 4. EPR spectrum of **1** at 77.3 K (X-band, polycrystalline sample). The asterisked signal at $g \approx 2.00$ is assigned to some spurious radical species.

assigned to an $S = 1/2$ species with the following principal values of the \tilde{g} tensor: $g_1 = 1.971(1)$, $g_2 = 1.871(1)$, and $g_3 = 1.771(1)$. These values denote a more markedly orthorhombic character than in the related^[7] four-coordinate species $[Ti(C_6Cl_5)_4]^-$ and are also appreciably more shifted from the free-electron g factor ($g_e = 2.0023$). The two crystallographically independent Ti^{III} sites in **1** are sufficiently similar to give a single type of EPR signal (within its resolution limit). According to the molecular structure of the $[Ti(C_6F_5)_5]^{2-}$ anion and following the energy-level diagram given in Figure 3 for the C_{2v} distortion of $TBPY-5$ geometry depicted in Figure 2, it is reasonable to assign the $a_2(x'y')^1$ configuration as the (orbitally nondegenerate) ground state.^[23] The principal values of the \tilde{g} tensor would be given, in this case, by Equation (1).

$$g_{x'} = g_e - \frac{2\lambda}{\delta_{x'}}, g_{y'} = g_e - \frac{2\lambda}{\delta_{y'}}, g_{z'} = g_e - \left(\frac{\cos^2 \beta}{\delta_{z'}} + \frac{\sin^2 \beta}{\Delta z'} \right) \quad (1)$$

The energy differences are defined in Figure 3, λ is the spin-orbit coupling parameter, and β accounts for mixing

between the a_1 orbitals. Starting from an ideal *TBPY*-5 geometry and considering the C_{2v} distortion as a perturbation in a first order approximation ($\beta = \pi/3$), Equation (2) applies.

$$g_{z'} = g_e - \frac{2\lambda}{\delta z'} - \frac{6\lambda}{\Delta z'} \quad (2)$$

In line with this reasoning, the assignments in Equation (3) can be made.

$$g_1 = g_{x'}, g_3 = g_{y'}, g_2 = g_{z'} \quad (3)$$

In summary, $[\text{NBu}_4]_2[\text{Ti}(\text{C}_6\text{F}_5)_5]$ (**1**) is the first example of a $[\text{TiR}_5]^{2-}$ unit in organometallic chemistry. Precedents for this stoichiometry in coordination chemistry are also very rare, namely, $[\text{TiX}_5]^{2-}$ ($\text{X} = \text{F}, \text{Cl}$). No structural data are known for $\text{K}_2[\text{TiCl}_5]$,^[24] and the salt $[\text{NH}_4]_2[\text{TiF}_5]$ was found to contain infinite chains of octahedral $[\text{TiF}_6]^{3-}$ units sharing fluoro ligands in *trans*-disposed vertices.^[25] Compound **1** occupies a unique position not only in the organometallic but also in the coordination chemistry of titanium. Experimental work aiming to extend these results to the heavier Group 4 metals, Zr and Hf, is underway.

Experimental Section

General working techniques are described in ref. [7]. **CAUTION:** **1** has been found to explode by percussion, and sometimes for no obvious reason.

1: Method A: $[\text{TiCl}_3(\text{thf})_3]$ ^[27] (1.60 g, 4.31 mmol) suspended in Et_2O (15 cm^3) was added to a solution of LiC_6F_5 ^[26] (ca. 26 mmol) in Et_2O (50 cm^3) at -78°C . The mixture was allowed to warm to -30°C and, after addition of $[\text{NBu}_4]\text{Br}$ (1.40 g, 4.31 mmol), the temperature was allowed to rise to 0°C . After 3 h of stirring at this temperature, an orange-red solid had precipitated, which was collected by filtration, washed with Et_2O ($3 \times 3 \text{ cm}^3$), dried under vacuum, and extracted with CH_2Cl_2 (60 cm^3) at 0°C . The extract was concentrated to about 15 cm^3 , and slow diffusion of a Et_2O layer (50 cm^3) at -30°C yielded **1** as an orange-red microcrystalline solid (2.30 g, 1.68 mmol; 39 % yield based on the titanium precursor). Satisfactory elemental analysis. IR (KBr): $\tilde{\nu} = 1629$ (m), 1533 (m), 1493 (s, C_6F_5), 1436 (vs), 1382 (w), 1369 (w), 1320 (w), 1237 (w), 1179 (w), 1108 (w), 1060 (m), 1041 (s), 979 (w), 946 (vs, C_6F_5 : C–F),^[8] 882 (w, NBu_4^+), 801 (w, C_6F_5 : X-sensitive vibr.),^[8] 741 (w, NBu_4^+), 713 (w), 593 (w), 480 cm^{-1} (w).

Method B: A suspension of yellow $\text{TiCl}_4 \cdot x\text{Et}_2\text{O}$ in Et_2O (prepared by mixing TiCl_4 (0.5 cm^3 , 4.6 mmol) and Et_2O (25 cm^3), both precooled at -78°C) was added to a solution of LiC_6F_5 ^[26] (ca. 30 mmol) in Et_2O (60 cm^3) at -78°C . Following the procedure described in Method A, including the addition of $[\text{NBu}_4]\text{Br}$ (1.47 g, 4.60 mmol) where appropriate, gave **1** in 34 % yield (2.13 g, 1.55 mmol).

Crystal data for **1**: $\text{C}_{62}\text{H}_{72}\text{F}_{25}\text{N}_2\text{Ti}$; monoclinic; space group $P2_1/c$; $a = 1876.0(2)$, $b = 2095.1(2)$, $c = 3225.3(4)$ pm, $\beta = 89.893(2)^\circ$, $V = 12.677(3) \text{ nm}^3$; $Z = 8$; $T = 100(2) \text{ K}$; $\lambda = 71.073 \text{ pm}$; abs. coeff. 0.249 mm^{-1} ; range for data collection $1.09 < \theta < 25.05^\circ$; reflns collected/unique: 69322/22367 ($R_{\text{int}} = 0.1417$); Bruker Smart CCD diffractometer. The crystallographic data were corrected for absorption with SADABS.^[28] The structure was solved by direct methods, and refinement against F^2 with SHELXL-97^[29] converged to final residual indices of $R_1 = 0.0668$, $wR_2 = 0.1325$ [$I > 2\sigma(I)$] and $R_1 = 0.1840$, $wR_2 = 0.1773$ (all data). GoF = 1.011. CCDC-233902 contains the supplementary crystallographic data for this paper. These data can be obtained free of charge via www.ccdc.cam.ac.uk/contents/retrieving.html (or from the Cambridge Crystallographic Data

Centre, 12, Union Road, Cambridge CB21EZ, UK; fax: (+44) 1223-336-033; or deposit@ccdc.cam.ac.uk).

EPR spectra were recorded on a Bruker ESP380E spectrometer working in the X-band. Measurements at liquid-nitrogen temperature (77.3 K) were made in a quartz immersion Dewar vessel. A Bruker ERV4111T device was used for variable-temperature measurements. The microwave frequency was determined with a Hewlett-Packard HP5350B frequency counter, and the magnetic field strength with a Bruker ER035M gaussmeter.

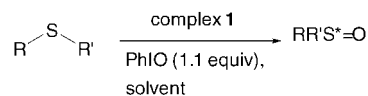
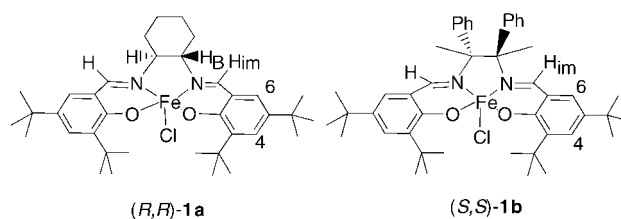
Received: March 24, 2004

Revised: June 16, 2004

Keywords: EPR spectroscopy · fluorinated ligands · homoleptic compounds · metal–carbon bonds · titanium

- [1] P. J. Davidson, M. F. Lappert, R. Pearce, *Chem. Rev.* **1976**, 76, 219.
- [2] H. Rau, J. Müller, *Z. Anorg. Allg. Chem.* **1975**, 415, 225; J. Müller, H. Rau, P. Zdzunneck, K.-H. Thiele, *Z. Anorg. Allg. Chem.* **1973**, 401, 113; K.-H. Thiele, K. Milowski, P. Zdzunneck, J. Müller, H. Rau, *Z. Chem.* **1972**, 12, 186.
- [3] S. Kleinhenz, K. Seppelt, *Chem. Eur. J.* **1999**, 5, 3573.
- [4] M. W. Bouwkamp, J. de Wolf, I. del Hierro Morales, J. Gercama, A. Meetsma, S. I. Troyanov, B. Hessen, J. H. Teuben, *J. Am. Chem. Soc.* **2002**, 124, 12956.
- [5] R. A. Forder, K. Prout, *Acta Crystallogr. Sect. B* **1974**, 30, 491; F. W. Siegert, H. J. de Liefde Meijer, *J. Organomet. Chem.* **1969**, 20, 141; E. O. Fischer, A. Löchner, *Z. Naturforsch. B* **1960**, 15, 266.
- [6] G. K. Barker, M. F. Lappert, J. A. K. Howard, *J. Chem. Soc. Dalton Trans.* **1978**, 734; G. K. Barker, M. F. Lappert, *J. Organomet. Chem.* **1974**, 76, C45.
- [7] a) I. Ara, J. Fornies, M. A. Garcia-Monforte, A. Martín, B. Menjón, *Chem. Eur. J.* **2004**, 10, 4186; b) P. J. Alonso, J. Fornies, M. A. Garcia-Monforte, A. Martín, B. Menjón, *Chem. Commun.* **2002**, 728.
- [8] R. Usón, J. Fornies, *Adv. Organomet. Chem.* **1988**, 28, 219; E. Maslowsky, Jr., *Vibrational Spectra of Organometallic Compounds*, Wiley, New York, **1977**, pp. 437–442.
- [9] A. R. Rossi, R. Hoffmann, *Inorg. Chem.* **1975**, 14, 365.
- [10] S. Alvarez, M. Llunell, *J. Chem. Soc. Dalton Trans.* **2000**, 3288.
- [11] T. R. Ward, H.-B. Bürgi, F. Gilardoni, J. Weber, *J. Am. Chem. Soc.* **1997**, 119, 11974.
- [12] R. R. Holmes, *Prog. Inorg. Chem.* **1984**, 32, 119; see also ref. [10].
- [13] J. Zemann, *Z. Anorg. Allg. Chem.* **1963**, 324, 241; see also H. K. McDowell, H. L. Chiu, J. F. Geldard, *Inorg. Chem.* **1988**, 27, 1674.
- [14] R. R. Holmes, *J. Am. Chem. Soc.* **1984**, 106, 3745; see also ref. [9].
- [15] H. A. Jahn, E. Teller, *Proc. R. Soc. London Ser. A* **1937**, 161, 220.
- [16] M. Kaupp, *Angew. Chem.* **2001**, 113, 3642; *Angew. Chem. Int. Ed.* **2001**, 40, 3535.
- [17] S. K. Kang, H. Tang, T. A. Albright, *J. Am. Chem. Soc.* **1993**, 115, 1971; T. A. Albright, H. Tang, *Angew. Chem.* **1992**, 104, 1532; *Angew. Chem. Int. Ed. Engl.* **1992**, 31, 1462.
- [18] B. Roessler, S. Kleinhenz, K. Seppelt, *Chem. Commun.* **2000**, 1039.
- [19] C. J. Piersol, R. D. Profilet, P. E. Fanwick, I. P. Rothwell, *Polyhedron* **1993**, 12, 1779.
- [20] Gas-phase electron diffraction: C. Pulham, A. Haaland, A. Hammel, K. Rypdal, H. P. Verne, H. V. Volden, *Angew. Chem.* **1992**, 104, 1534; *Angew. Chem. Int. Ed. Engl.* **1992**, 31, 1464; for solid-state X-ray diffraction, see ref. [18].
- [21] C. R. Landis, T. Cleveland, T. K. Firman, *J. Am. Chem. Soc.* **1998**, 120, 2641; C. R. Landis, T. K. Firman, D. M. Root, T. Cleveland, *J. Am. Chem. Soc.* **1998**, 120, 1842.

- [22] W. A. Sheppard, *J. Am. Chem. Soc.* **1970**, 92, 5419; C. A. Tolman, *J. Am. Chem. Soc.* **1970**, 92, 2953.
- [23] C. Furlani, *Coord. Chem. Rev.* **1968**, 3, 141.
- [24] P. Ehrlich, G. Kupa, K. Blankenstein, *Z. Anorg. Allg. Chem.* **1959**, 299, 213.
- [25] M. Dadachov, L. Eriksson, *Acta Crystallogr. Sect. C* **1999**, 55, 1739.
- [26] R. Usón, A. Laguna, *Inorg. Synth.* **1982**, 21, 71.
- [27] L. E. Manzer, *Inorg. Synth.* **1982**, 21, 135.
- [28] G. M. Sheldrick, SADABS, program for correction of systematic errors in diffraction data, version 2.03, University of Göttingen, Göttingen, Germany, **1996**.
- [29] G. M. Sheldrick, SHELXL-97, Program for the refinement of crystal structures from diffraction data, University of Göttingen, Göttingen, Germany, **1997**.



Scheme 1. Iron-catalyzed asymmetric oxidation of sulfides.

Asymmetric Catalysis

Evidence for the Formation of an Iodosylbenzene(salen)iron Active Intermediate in a (Salen)iron(III)-Catalyzed Asymmetric Sulfide Oxidation**

Konstantin P. Bryliakov* and Evgenii P. Talsi

Asymmetric sulfoxides are finding increasing use in the pharmaceutical industry.^[1] Most methodologies for catalytic asymmetric sulfide oxygenation involve a transition metal (titanium, vanadium, or manganese) and a chiral ligand, such as bidentate diethyl tartrate,^[2a] diols,^[2b] binaphthol (binol),^[2c,d] tridentate Schiff base ligands,^[2e-h] or tetradentate salen-type ligands (salen = (salicylidene)ethylenediamine).^[2i-l] Recently, inexpensive active systems based on hydrogen peroxide as the oxidant and nontoxic chiral iron(III) complexes as catalysts were reported.^[3] Rajagopal and co-workers published a mechanistic study of the nonenantioselective [Fe^{III}Cl(salen)]-catalyzed oxidation of sulfides with iodosylbenzene.^[4,5] Herein, we present asymmetric [Fe^{III}Cl(salen*)] catalytic systems (complexes **1a** and **1b**, where salen* = the corresponding chiral Schiff base ligand; Scheme 1) and report the NMR spectroscopic investigation of the [Fe^{III}(salen*)(OIPh)] active intermediates.

Complexes **1a** and **1b** were synthesized either according to the known procedure^[6] or an original one (see Supporting Information). The electron paramagnetic resonance (EPR)

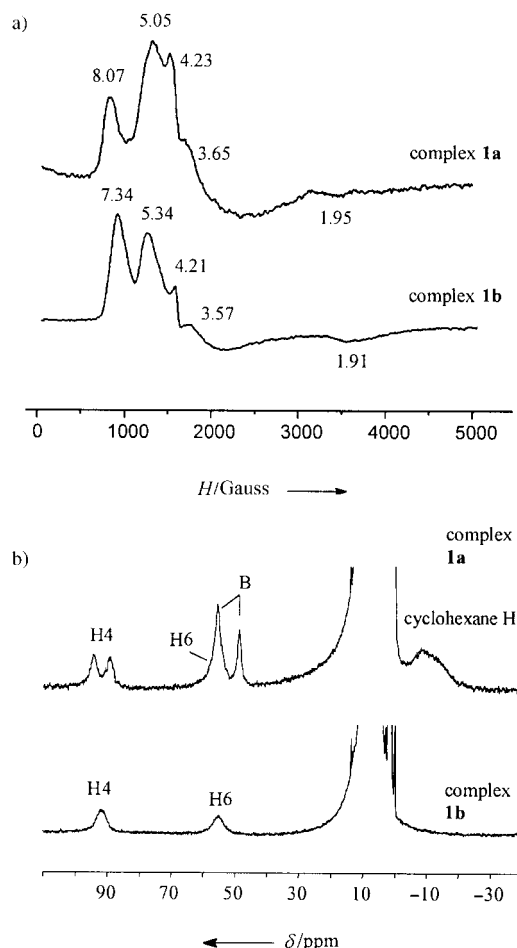


Figure 1. a) EPR spectra (−196°C) of 0.015 M solutions of complexes **1a** and **1b** in CH₂Cl₂. b) ¹H NMR spectra (0.02 M in CDCl₃, +20°C) of complexes **1a** and **1b**. Admixtures at $g = 4.2$ were observed in the EPR spectra.

[*] Dr. K. P. Bryliakov, Prof. E. P. Talsi
Boreskov Institute of Catalysis
Siberian Branch of the Russian Academy of Sciences
630090, Pr. Lavrentieva 5, Novosibirsk (Russian Federation)
Fax: (+7) 3832-34-3766
E-mail: bryliako@catalysis.nsk.su

[**] The authors are grateful to the Russian Foundation for Basic Research (grant 03-03-32009) for financial support. Salen = bis-(salicylidene)ethylenediamine.

Supporting information for this article is available on the WWW under <http://www.angewandte.org> or from the author.

The asymmetric sulfide oxidation results are summarized in Table 1. Typically, the reaction was complete in 2 hours at 0°C, with the catalyst performing 100–200 turnovers. How-

Oxoferryl π -cation radicals are expected to have typical $S=3/2$ spectra with resonances at $g^{\text{eff}} \approx 4$ and $g^{\text{eff}} \approx 2$.^[8] However, treatment of complexes **1a** and **1b** with PhIO and *m*-chloroperoxybenzoic acid (*m*-CPBA, which was reported to generate (oxoferryl)porphyrin π -cation radicals^[8,9a]) did not lead to formation of $S=3/2$ -type spectra, only a sharp peak at $g=4.2$ belonging to an unidentified $S=5/2$ species (see Supporting Information). The latter species would not contribute to the catalytic cycle, as it is stable for hours even in the presence of the substrate, and its concentration estimated by EPR spectroscopy does not exceed 10% of the total Fe concentration.^[10] Thus, this species must be interpreted as a minor inactive high-spin Fe^{III} admixture.

The ¹H NMR spectra (−20°C) showed the formation of a new Fe^{III} complex after interaction of **1a** with PhIO (Figure 2a). This new species has a *t*Bu peak at $\delta=4.75$ ppm (the *t*Bu peak of **1a** is at $\delta=5.44$ ppm) and its concentration is up to 40% of the total observable Fe^{III} concentration. We particularly emphasize that at this stage no PhI signals are observed in the spectrum (Figure 2a). Thus, it is natural to conclude that this new species is **1a**(PhIO), similar to the iodosylbenzene–iron(III) porphyrin intermediates recently discussed in the literature.^[9a–c] Indeed, after addition of an excess of the substrate (*p*-BrPhSMe) and warming the sample to 0°C, the PhI ¹H NMR signal appeared at $\delta=7.71$ ppm and the *p*-BrPhSOCH₃ signal at $\delta=2.73$ ppm (Figure 2c). At the same time, the intensity of the **1a**(PhIO) signal decreased. After consumption of the **1a**(PhIO) intermediate, shaking with additional PhIO (Figure 2d,e) restored its concentration. Thus, the reaction cycle for the reported catalytic system could be represented as given in Scheme 2, which includes the Lewis acid activation of iodosylbenzene,^[9d] the oxygen-transfer step proceeding probably by precoordination of the sulfide to the **1a**(PhIO) active species.^[4]

In summary, we have proposed a new catalytic system for the asymmetric oxidation of sulfides by PhIO, based on an asymmetric (salen)iron(III) complex, and performed the catalytic oxidation of several aryl sulfides. The active species

Table 1: Catalytic enantioselective oxidation of sulfides with PhIO catalyzed by iron complexes **1a** and **1b**.

Entry	Sulfide 2	Catalyst	Solvent	Conversion [%]	Selectivity [%] ^[a]	<i>ee</i> [%] ^[b]	Config. ^[c]
1	PhSMe	1a	CH ₂ Cl ₂	74	99	20	(S)-(-)
2	PhSMe	1a	CH ₃ CN	96	83	22	(S)-(-)
3	<i>p</i> -BrPhSMe	1a	CH ₂ Cl ₂	95	96	41	(S)-(-)
4	PhCH ₂ SPh	1a	CH ₂ Cl ₂	94	92	58	(S)-(-)
5	PhCH ₂ SPh	1a	C ₆ H ₆ ^[d]	90	69	57	(S)-(-)
6	PhCH ₂ SPh	1a	C ₆ H ₅ CN	no reaction	–	–	–
7	PhCH ₂ SPh	1a	CH ₂ Cl ₂ ^[e]	96	89	55	(S)-(-)
8	PhCH ₂ SPh	1a	CH ₂ Cl ₂ ^[f]	96	86	55	(S)-(-)
9	PhCH ₂ SPh	1a	CH ₃ CN	95	91	62	(S)-(-)
10	PhCH ₂ SPh	1a	CH ₃ CN ^[d]	92	91	55	(S)-(-)
11	PhCH ₂ SPh	1a	CH ₃ CN ^[d,g]	96	72	55	(S)-(-)
12	<i>p</i> -BrPhSMe	1b	CH ₃ CN	90	90	43	(R)-(-)
13	PhCH ₂ SPh	1b	CH ₃ CN	91	85	62	(R)-(-)

Reaction conditions (unless otherwise stated): Fe complex (0.001 mmol), solvent (1 mL), sulfide (0.1 mmol), PhIO (0.11 mmol), 0°C, 150 rpm stirring for 2 h. [a] Selectivity=[RSOR]/([RSOR]+[RSO₂R]). [b] Determined by ¹H NMR spectroscopy with a [Eu(hfc)₃] chiral shift reagent in CCl₄ (Hfc = 3-(heptafluoropropylhydroxymethylene)-D-camphorate). [c] Determined by comparing [Eu(hfc)₃]-shifted NMR patterns of sulfoxides with those of the sulfoxides with known absolute configuration. [d] At room temperature. [e] DMF was added, [DMF]:[Fe]=5:1. [f] *N*-methylmorpholine-*N*-oxide was added, [NMO]:[Fe]=10:1. [g] Fe (0.0001 mmol), solvent (0.4 mL), substrate (0.05 mmol), thus substrate/catalyst ratio of 500; reaction time 7 h.

ever, at least 500 turnovers can be made without loss of enantioselectivity (Table 1, entries 10 and 11; in these cases, the reaction was carried out at room temperature to shorten the reaction time). The corresponding sulfoxides, sulfones, and residual sulfides were found in the reaction mixtures. Both complexes demonstrated similar enantioselectivities, (*R,R*)-**1a** and (*S,S*)-**2a** affording *S* and *R* sulfoxides, respectively. The highest *ee* values were achieved in acetonitrile as solvent (see entries 4–6 and 9); donor additives did not lead to an increase in enantioselectivity (entries 7 and 8). Increasing the temperature led to lower enantioselectivity (entry 10). Further ligand adjustment seems to be possible to improve the *ee* value.

Interestingly, catalysts **1** can oxidize sulfides using terminal oxidants other than PhIO with remarkable chemical selectivity (Table 2). However, in all these cases the reaction gave racemic products, which implies that it is PhIO that is responsible for the formation of the specific active sites of oxidation. Recently, the active sites were proposed to be [Fe^{IV}=O(salen)]⁺ species;^[4] however, the characterization was unreliable. Our spectroscopic observations provide evidence in favor of other active species.

Table 2: Catalytic oxidation of sulfides catalyzed by iron complexes **1a** and **1b**.

Entry	Sulfide 2	Complex (mol %)	Solvent	Oxidant	Conversion [%] (after)	Selectivity [%]	<i>ee</i> [%]
1	PhSMe	1a (4)	CH ₃ CN	H ₂ O ₂ (2.5 equiv)	71 (16 h)	75	0
2	PhSMe	1a (3)	CH ₃ CN	TBHP (1.4 equiv)	59 (40 h)	98	0
3	PhCH ₂ SPh	1b (2)	CH ₂ Cl ₂	NaOCl (1.0 equiv)	no reaction	–	–
4	PhCH ₂ SPh	1b (1)	CH ₂ Cl ₂	H ₂ O ₂ (2.0 equiv)	4 (36 h)	not measured	0
5	PhCH ₂ SPh	1b (1)	CH ₃ CN	<i>m</i> -CPBA (1.2 equiv)	100 (2 h)	78	0

Reaction conditions (unless otherwise stated): Fe complex, solvent (1 mL), sulfide (0.1 mmol), room temperature, 150 rpm stirring. TBHP = *tert*-butylhydroperoxide.

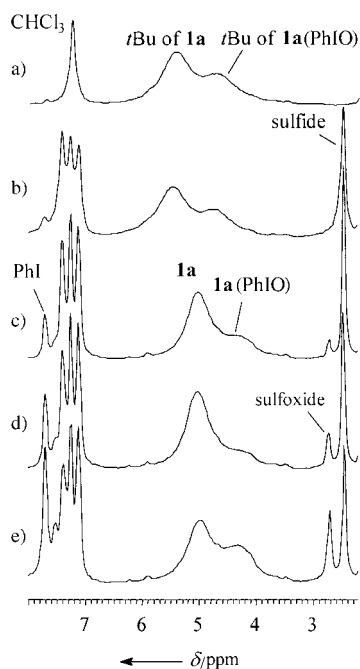
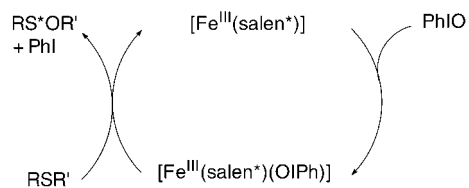


Figure 2. ^1H NMR spectra (in the range 8 to 2 ppm) of a) complex **1a** (0.02 M in CDCl_3) shaken for 5 min with PhIO (2 equiv) on cooling, -20°C ; b) after addition of *p*-BrPhSMe (5 equiv); c) after warming to 0°C ; d) after storing for 5 min at 0°C ; e) after shaking with additional PhIO (1 equiv) without cooling, recorded at 0°C .



Scheme 2. Proposed catalytic cycle for iron-catalyzed asymmetric oxidation of sulfides.

was detected and shown to be an iodosylbenzene(salen)-iron(III) complex. We hope this new knowledge will be of interest to those scientists who deal with metal-salen catalytic systems and asymmetric oxidation of sulfides, and foresee further ligand designs to improve the enantioselectivity.

Received: March 24, 2004

Keywords: asymmetric catalysis · enantioselectivity · iron · oxidation · sulfides

- [1] a) S. Morita, J. Matsubara, K. Otsubo, K. Kitano, T. Ohtani, Y. Kawano, M. Uchida, *Tetrahedron: Asymmetry* **1997**, *8*, 3707–3710; b) E. Carlsson, P. Lindberg, S. V. Unge, *Chem. Br.* **2002**, *38*, 42–45; c) M. Matsugi, N. Fukudo, Y. Muguruma, T. Yamaguchi, J. Minamikawa, S. Otsuka, *Tetrahedron* **2001**, *57*, 2739–2744; d) S. Naito, M. Nishimura, *Yakugaku Zasshi* **2001**, *121*, 989–994; e) H. Cotton, T. Elebring, M. Larsson, L. Li, H. Sørensen, S. V. Unge, *Tetrahedron: Asymmetry* **2000**, *11*, 3819–3825; f) S. Padmanabhan, R. C. Lavin, G. J. Durranat, *Tetrahedron: Asym-*

- metry* **2000**, *11*, 3455–3457; g) A. M. Rouhi, *Chem. Eng. News* **2003**, *81*(19), 56–61.
- [2] a) H. B. Kagan in *Catalytic Asymmetric Synthesis* (Ed.: I. Ojima), 2nd ed., Wiley-VCH, Weinheim, **2000**; b) K. Yamamoto, H. Ando, T. Shuetake, H. Chikamatsu, *J. Chem. Soc. Chem. Commun.* **1989**, 754–755; c) K. Komatsu, Y. Nishibayashi, T. Sugata, S. Unemura, *Tetrahedron Lett.* **1986**, *27*, 5394–5397; d) C. Bolm, F. Bienewald, *Synlett* **1998**, 1327–1328; e) S. Colonna, A. Manfredi, M. Spadoni, L. Casella, M. Gullotti, *J. Chem. Soc. Perkin Trans. 1* **1987**, 71–73; f) C. Bolm, F. Bienewald, *Angew. Chem.* **1995**, *107*, 2883–2885; *Angew. Chem. Int. Ed. Engl.* **1995**, *34*, 2640–2642; g) J. Skarzewski, E. Ostrycharz, R. Siedlecka, *Tetrahedron: Asymmetry* **1999**, *10*, 3457–3461; h) K. P. Bryliakov, N. N. Karpyshev, A. G. Tolstikov, S. A. Fominsky, E. P. Talsi, *J. Mol. Catal. A* **2001**, *171*, 73–80; i) A. Colombo, G. Marturano, A. Pasini, *Gazz. Chim. Ital.* **1986**, *116*, 35–40; j) K. Nakajima, C. Sasaki, M. Kojima, T. Aoyama, S. Ohba, Y. Saito, J. Fujita, *Chem. Lett.* **1987**, 2189–2192; k) K. Noda, N. Hosoya, R. Irie, Y. Yamashita, T. Katsuki, *Tetrahedron* **1994**, *50*, 9609–9618; l) C. Kokubo, T. Katsuki, *Tetrahedron* **1996**, *52*, 13895–13900.
- [3] a) C. Duboc-Toia, S. Menage, C. Lambeaux, M. Fontecave, *Tetrahedron Lett.* **1997**, *38*, 3727–3730; b) Y. Mekmouche, H. Hummel, R. Y. N. Ho, L. Que, V. Schünemann, F. Thomas, A. X. Trautwein, C. Lebrun, K. Gorgy, J.-C. Leprêtre, M.-N. Collomb, A. Deronzier, M. Fontecave, S. Ménage, *Chem. Eur. J.* **2002**, *8*, 1196–1204; c) J. Legros, C. Bolm, *Angew. Chem.* **2003**, *115*, 5645–5647; *Angew. Chem. Int. Ed.* **2003**, *42*, 5487–5489.
- [4] V. K. Sivasubramanian, M. Ganesan, S. Rajagopal, R. Ramaraj, *J. Org. Chem.* **2002**, *67*, 1506–1514.
- [5] For the use of PhIO as a terminal oxidant in oxidation reactions see: B. Meunier, A. Robert, G. Pratiel, J. Bernardou in *The Porphyrin Handbook*, Vol. 4 (Eds.: K. M. Kadish, K. M. Smith, R. Guilard), Academic Press, New York, **2000**, chap. 31, pp. 119–187.
- [6] T. Liu, Q.-X. Liu, W.-J. Ruan, Z.-A. Zhu, Y.-T. Chen, A. S. C. Chan, *Chin. J. Chem.* **2001**, *19*, 352–355.
- [7] For recent examples of EPR and NMR spectroscopic analysis of Fe complexes with multidentate ligands see for example: a) J. Simaan, S. Poussereau, G. Blondin, J. Girerd, D. Defaye, C. Philouze, J. Guilhem, L. Tshertanov, *Inorg. Chim. Acta* **2000**, *299*, 221–230; b) F. A. Walker, *Inorg. Chem.* **2003**, *42*, 4526–4544; c) S. Yoon, H.-J. Lee, K.-B. Lee, H. J. Jang, *Bull. Korean Chem. Soc.* **2000**, *21*, 923–928; d) Y. Zang, J. Kim, Y. Dong, E. C. Wilkinson, E. H. Appelmann, L. Que, *J. Am. Chem. Soc.* **1997**, *119*, 4197–4205. Spectra of Fe^{III} complexes were modeled by: H. Weihe, SIM program for EPR spectra simulations, University of Copenhagen, Denmark, **2002**.
- [8] a) A. X. Trautwein, E. Bill, E. L. Bominaar, H. Winkler, *Struct. Bonding (Berlin)* **1998**, *78*, 1–95; b) K. Jayaraj, J. Terner, A. Gold, D. A. Roberts, R. N. Austin, D. Mandon, R. Weiss, E. Bill, M. Muther, A. X. Trautwein, *Inorg. Chem.* **1996**, *35*, 1632–1640; c) D. Mandon, P. Ochsenbein, J. Fischer, R. Weiss, K. Jayaraj, R. N. Austin, A. Gold, P. S. White, O. Brigaud, P. Battioni, D. Mansuy, *Inorg. Chem.* **1992**, *31*, 4404–4409.
- [9] a) W. Nam, S. K. Choi, M. H. Lim, J.-U. Rohde, I. Kim, J. Kim, C. Kim, L. Que, *Angew. Chem.* **2003**, *115*, 113–115; *Angew. Chem. Int. Ed.* **2003**, *42*, 109–111; b) J. P. Collman, A. S. Chien, T. A. Eberspacher, J. I. Brauman, *J. Am. Chem. Soc.* **2000**, *122*, 11098–11100; c) J. P. Collman, L. Zeng, R. A. Decréau, *Chem. Commun.* **2003**, 2974–2975; d) Y. Yang, F. Diederich, J. S. Valentine, *J. Am. Chem. Soc.* **1990**, *112*, 7826–7828.
- [10] The concentration of this paramagnetic admixture was estimated to be 5–10% of the original concentration of complexes **1a** and **1b** (see Supporting Information).

Three-Dimensional Structure of Large-Pore Mesoporous Cubic $Ia\bar{3}d$ Silica with Complementary Pores and Its Carbon Replica by Electron Crystallography**

Yasuhiro Sakamoto, Tae-Wan Kim, Ryong Ryoo, and Osamu Terasaki*

Large-pore three-dimensional (3D) mesoporous silicas are among the most interesting mesoporous materials discovered in recent years, and they have attracted much attention for potential applications requiring easily accessible, uniform, large pores. Examples of these are SBA-15 ($p6mm$) and SBA-16 ($Im\bar{3}m$), which have cylindrical- and cage-type structures, respectively. It has been reported that hexagonally ordered large-pore mesoporous SBA-15 silica made by using a block copolymer contains complementary pores, while such pores were not found in MCM-41 with the same 2D hexagonal $p6mm$ symmetry.^[1] These complementary pores are arranged in a disordered way between the hexagonally ordered large-pore channels.

Recently, large-pore mesoporous silicas with a cubic $Ia\bar{3}d$ structure were synthesized by using triblock copolymers as structure-directing agent under various synthesis conditions.^[2] The mesoporous silica with a bicontinuous cubic structure of $Ia\bar{3}d$ symmetry is composed of an enantiomeric pair of 3D mesoporous networks that are interwoven, as observed in the MCM-48 structure.

The structures of these highly ordered mesoporous materials can hardly be determined from powder XRD patterns alone, because the few reflections that are observed at low scattering angles are especially broad and overlap. Electron microscopy is the main tool for characterization of such structures. The advantage over XRD is the stronger interaction of electrons with matter, which enables us to obtain structural information from a single crystal with only a few hundred unit cells. In electron crystallography (EC) the phases and amplitudes of the structure factors are obtained by Fourier transformation of high-resolution TEM (HRTEM)

images. By calculating the inverse Fourier transform of the structure factors, a 3D electrostatic potential distribution of the structure can be obtained. This is another advantage compared to traditional single-crystal XRD. Based on the 3D electrostatic potential distribution of the structure, direct information on the detailed structures inside the mesoporous crystals such as diameter, shape, and connectivity of the pores can be obtained.^[3]

Herein we report on the structure of the large-pore mesoporous silica with cubic $Ia\bar{3}d$ symmetry after removal of the surfactant by calcination and, in particular, on its ordered complementary pores between two independent channel systems, determined by using EC methods. Furthermore, the structure of its carbon replica, made by using this large-pore mesoporous silica as a hard template and then removing the template, is reported.

Figure 1 shows HRTEM images of mesoporous silica with $Ia\bar{3}d$ symmetry taken with the incident beam parallel to the

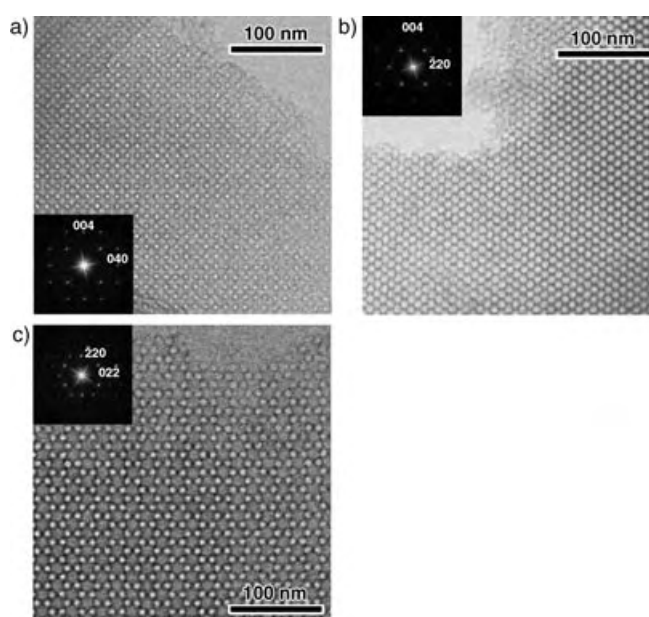


Figure 1. HRTEM images of the large-pore mesoporous silica taken with the incident beam parallel to the [100] (a), [110] (b), and [111] (c) directions; corresponding Fourier diffractograms are inset in each image.

[100] (a), [110] (b), and [111] (c) directions. Corresponding Fourier diffractograms (FDs) are inset in each image. The FDs of these images clearly show the reflection conditions: hkl , $h+k+l=2n$; $0kl$, k and $l=2n$; hhl , $2h+l=4n$ and $l=2n$; $00l$, $l=4n$. From these observations, the space group symmetry was uniquely determined to be $Ia\bar{3}d$. The lattice constant derived from the 211 spot of the electron diffraction (ED) pattern with [111] incidence is 2.3×10^2 Å. Figure 2a shows the XRD pattern of the specimen; the lattice constant obtained from the 211 peak position is 2.38×10^2 Å.

These images taken with three different axes, [100], [110], and [111] were used for the reconstruction process. The resolution of the reconstructed distribution was limited to 26.2 Å, although some images showed a few higher resolution

[*] Dr. Y. Sakamoto, Prof. Dr. O. Terasaki

Structural Chemistry
Arrhenius Laboratory
Stockholm University
10691 Stockholm (Sweden)
Fax: (+46) 8-162-379
E-mail: terasaki@struc.su.se

T.-W. Kim, Prof. Dr. R. Ryoo
National Creative Research Initiative Center for
Functional Nanomaterials and
Department of Chemistry (School of Molecular Science-BK21)
Korea Advanced Institute of Science and Technology
Daejeon, 305-701 (Korea)

[**] This work was supported by the Swedish Natural Science Council (VR) and the Japan Science and Technology Agency (JST).

Supporting information for this article is available on the WWW under <http://www.angewandte.org> or from the author.

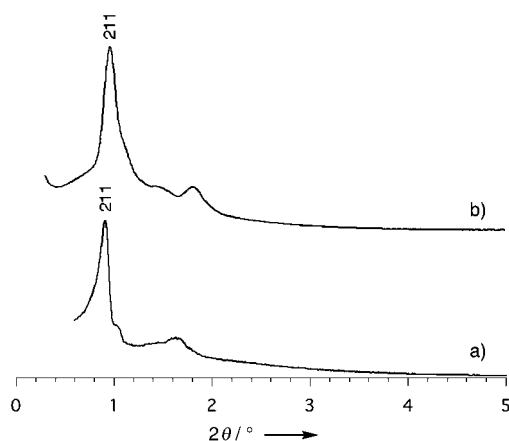


Figure 2. XRD of the large-pore mesoporous silica (a) and the carbon replica (b).

spots. Those for 25 reflections were determined in 33 unique reflections within the resolution limit, that is, $h^2 + k^2 + l^2 = 78$. A summary of observed 3D crystal structure factors after normalization by common reflections and correction of the contrast transfer function (CTF) is given in Table 1. The 512, 631, 543, 721, 732, 741, 653, and 813 reflections cannot be obtained from [100], [110], and [111] incidences. However, it was confirmed in ED studies by tilting the crystal that the intensities of all of these reflections were very weak. The values of other vacant cells in Table 1 were ignored (i.e., $S/N < 3$). From the structure factors, the 3D electrostatic potential map (arbitrary scale) was uniquely obtained by calculating the inverse Fourier transform of the structure factors. Figure 3

shows the 3D electrostatic potential maps of the mesoporous silica. The bright parts correspond to the pore, and dark parts to the silica wall. The sections are parallel to the (010) plane at $y = 0$ (a) and 0.125 (b) and the (111) plane through the origin, $x = y = z = 0$ (c).

A threshold value that defines the boundary between the silica wall and the pore must be determined in order to obtain the 3D pore structure of the mesoporous silica from 3D electrostatic potential maps. This value corresponds to the potential density constant, where 1 represents the pore and 0 the silica wall. The total pore volume of mesoporous silica as determined from N_2 adsorption/desorption measurements is $1.149 \text{ cm}^3 \text{ g}^{-1}$, calculated from the amount adsorbed at a relative pressure of 0.99. Assuming a density of the silica wall of 2.20 g cm^{-3} , the pore volume fraction corresponds to 71.7% and a threshold value of 0.218 (see Supporting Information 1). Figure 4a shows the 3D pore structure of the mesoporous

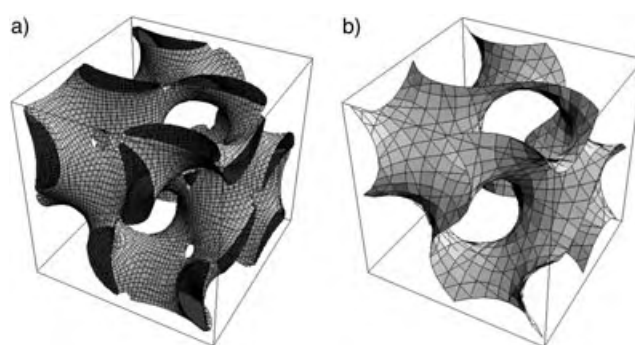


Figure 4. Schematic drawing of 3D arrangement of pores for a pore fraction of 71.7% and a threshold value of 0.218 (a) and G-surface (b).

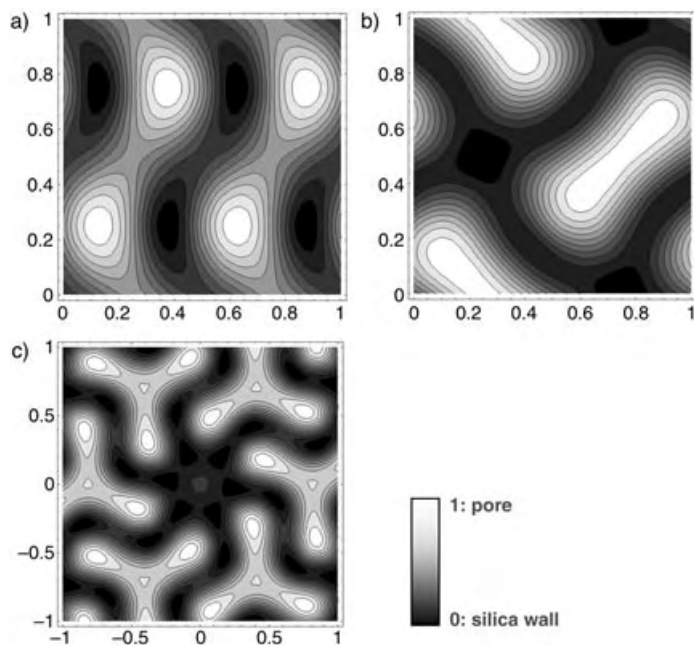


Figure 3. Electrostatic potential maps of the large-pore mesoporous silica. Sections parallel to the (010) plane at $y = 0$ (a) and 0.125 (b), and the (111) plane through the origin (c). Bright parts correspond to the pores, and dark parts to the silica wall. One unit cell is shown for each orientation, where $a = 2.3 \times 10^2 \text{ Å}$.

silica with this threshold value. It is clear that the silica wall exactly follows the G-surface (Figure 4b). The pore diameter and wall thickness of the silica estimated from the 3D pore structure are 83 and 35 Å, respectively. Complementary pores of 17 Å were found to form interconnections between the two main channel systems at a special flat point of the G-surface, that is, $\bar{3}$ position on the 3-fold axis, $16a$ site (Wyckoff notation) of the space group $Ia\bar{3}d$ (see Supporting Information 2). In contrast to SBA-15, these complementary pores are ordered.

Figure 5 shows N_2 adsorption/desorption isotherm data. The isotherm is of type IV, which is typical for mesoporous materials, and it is similar to those observed for cylindrical-type mesoporous structures.^[2] The isotherm is characterized by a sharp capillary condensation step in the adsorption branch at high relative pressures ($p/p_0 = 0.75\text{--}0.8$), and an H1 hysteresis loop in the desorption branch of the isotherm. The pore diameter calculated by the BJH method is 78 Å. On the other hand, the DFT model assuming a cylindrical pore geometry^[4] gives diameters of 18 Å for the complementary pores and 124 Å for the main pores. The t-plot analysis reveals the presence of complementary pores with a micropore surface area of $69.0 \text{ m}^2 \text{ g}^{-1}$ (see Supporting Information 3). The BJH model is known to underestimate pore size,^[4] and this explains the difference in main pore diameter between the BJH and DFT methods of pore size analysis. The

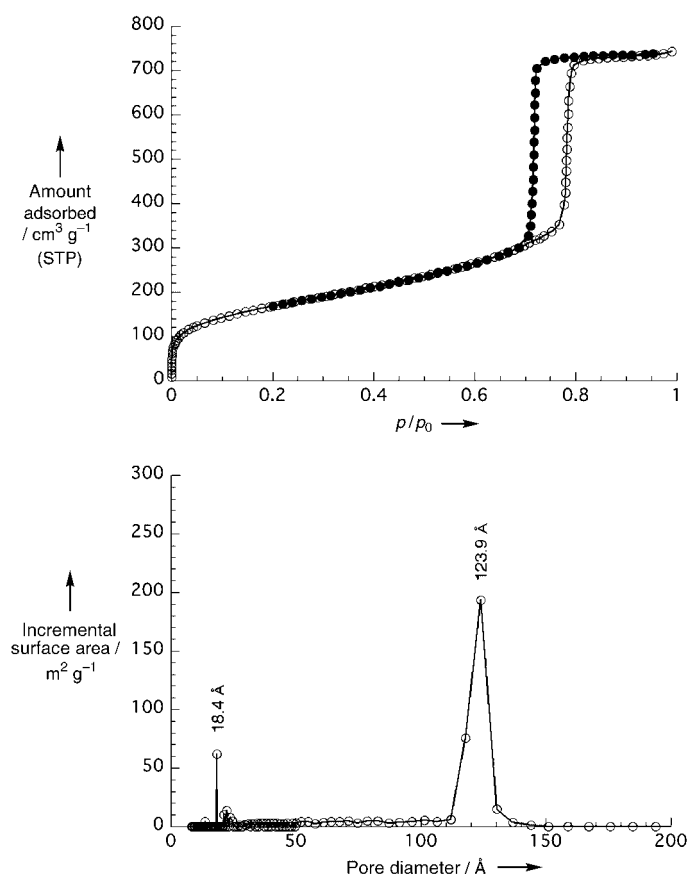


Figure 5. N₂ adsorption(●)/desorption(○) isotherm (a) and pore size distribution (b).

complementary-pore size derived from the DFT model is in good agreement with that from the 3D reconstructed structure. The BET surface area S_{BET} is about $600 \text{ m}^2 \text{ g}^{-1}$.

Figure 6 shows HRTEM images along the [100], [110], and [111] directions of the carbon replica made by using the mesoporous silica as template. Corresponding FDs are inset in each image. The FDs clearly show the extinction rule. From these observations, the space-group symmetry was uniquely determined to be $1a\bar{3}d$, which is the same as that of the mesoporous silica template. These images show well-ordered carbon structures and inverse contrasts with respect to those of the mesoporous silica. The lattice constant obtained from the 211 spot of the ED pattern with [111] incidence is $2.2 \times 10^2 \text{ Å}$. Figure 2b shows the XRD pattern of the carbon replica, and the lattice constant obtained from the 211 peak position is $2.26 \times 10^2 \text{ Å}$. The 3D structure of the carbon replica was determined from these three images by EC in the same way as the 3D reconstruction of the mesoporous silica. The 3D structure factors were collected in the range of 23.5 Å , and those for 27 reflections were determined as shown in Table 1. Note that the phases of the first ten structure factors are exactly opposite to those of the mesoporous silica. The pores of the hard template, both right- and left-handed channel systems, are filled uniformly by carbon, and therefore Babinet's principle applies. Deviation from Babinet's principle for reflections with larger scattering vectors may be

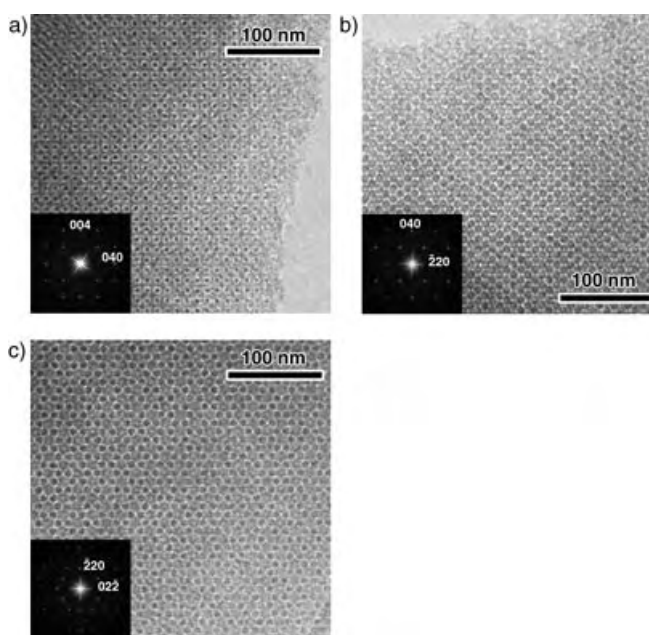


Figure 6. HRTEM images of the carbon replica taken with the incident beam parallel to the [100] (a), [110] (b), and [111] directions; corresponding Fourier diffractograms are inset in each image.

attributed to the minor changes together with lattice contraction after dissolution of silica.

The electrostatic potential map of the carbon replica was uniquely obtained by calculating the inverse Fourier transform of the structure factors. To obtain the structure of the carbon, the threshold value of the boundary between carbon and space was chosen by taking account of carbon without overlapping the silica wall of the large-pore mesoporous silica, which is defined by a threshold value of 0.218. In this case, the carbon has the threshold value of 0.648 (see Supporting Information 1), whereby the boundary between the silica wall and the pores of the large-pore mesoporous silica is same as that between carbon and the space of the carbon replica. Hence, the carbon replica is continuously formed in the space of the mesoporous silica (see Supporting Information 4).

The 3D structure of large-pore mesoporous silica was obtained by the Fourier transform of the structure factors, which were extracted from the HRTEM images. Complementary pores through the silica wall at the special flat point of the G-surface between two channel systems on the threefold axis (16a site) was found. The size of the complementary pore is sensitive to the threshold value, which defines the boundary between the silica wall and the spaces, and also dependent on silica density. The diameter is 17 Å for an assumed silica wall density of 2.20 g cm^{-3} . With decreasing silica density, the size of complementary pore becomes smaller, and at a silica wall density of 2.05 g cm^{-3} , which corresponds to a pore volume fraction of 70.2% and a threshold value of 0.227, the complementary pore is closed.

The 3D structure of the carbon replica was also reconstructed. The carbon replica follows the pore space of the mesoporous silica continuously and retains the $1a\bar{3}d$ symme-

Table 1: Crystal structure factors obtained by electron crystallography.

hkl	$h^2 + k^2 + l^2$	Large-pore mesoporous silica ^[a]			Carbon replica ^[b]		
		d [Å]	$ F_{hkl} / F_{211} $	phase	d [Å]	$ F_{hkl} / F_{211} $	phase
211	6	94.4	100.00	π	90.0	100.00	0
220	8	81.7	34.69	π	78.0	47.92	0
321	14	61.8	6.33	0	58.9	11.04	π
400	16	57.8	6.61	0	55.1	27.52	π
420	20	51.7	4.63	0	49.3	13.58	π
332	22	49.3	3.89	π	47.0	18.97	0
422	24	47.2	1.48	π	45.0	9.73	0
431	26	45.3	0.70	π	43.2	6.52	0
521	30	42.2			40.3		
440	32	40.9	0.46	0	39.0	0.95	π
532	38	37.5	0.19	0	35.8	0.57	π
611	38	37.5	0.51	π	35.8	1.82	π
620	40	36.6	0.31	π	34.9	1.04	π
541	42	35.7	0.34	0	34.0	0.20	π
631	46	34.1			32.5		
444	48	33.4	0.32	0	31.8	1.85	0
543	50	32.7			31.2		
640	52	32.1	0.27	π	30.6	0.69	π
552	54	31.5	0.16	0	30.0	0.30	0
633	54	31.5	0.20	0	30.0	0.52	0
721	54	31.5			30.0		
642	56	30.9	0.20	0	29.5	0.69	0
651	62	29.4	0.02	π	28.0	0.26	0
732	62	29.4			28.0		
800	64	28.9	0.13	0	27.6	0.24	0
741	66	28.5			27.1		
820	68	28.0	0.14	0	26.7	0.13	0
653	70	27.6			26.4		
660	72	27.2	0.11	π	26.0	0.17	π
822	72	27.2	0.04	π	26.0	0.17	π
743	74	26.9	0.06	π	25.6		
831	74	26.9			25.6		
752	78	26.2	0.14	π	25.0	0.11	0
840	80	25.8			24.7		
842	84	25.2			24.1		
655	86	24.9			23.8	0.15	0
761	86	24.9			23.8	0.21	0
921	86	24.9			23.8		
664	88	25.6			23.5	0.16	0

[a] $a = 2.3 \times 10^2$ Å. [b] $a = 2.2 \times 10^2$ Å.

try of the template. This is responsible for the complete replication by carbon with the same symmetry, which is a notable difference from the previously synthesized CMK-1 carbon.^[5]

Experimental Section

The large-pore mesoporous silica with cubic $Ia\bar{3}d$ symmetry was prepared by following the procedure using the triblock ethylene oxide (EO)-propylene oxide (PO)-EO copolymer Pluronic P123 ($\text{EO}_{20}\text{PO}_{70}\text{EO}_{20}$, $M_{\text{av}} = 5800$), butanol, and tetraethyl orthosilicate (TEOS).^[2] Replication of the silica was performed by following a known synthesis procedure, with the modification of using furfuryl alcohol instead of sucrose as the carbon source.^[6]

Powder XRD patterns were recorded with $\text{CuK}\alpha$ radiation ($\lambda = 1.5406$ Å) at 50 kV and 30 mA (1.5 kW) in step-scan mode (fixed time) with a small divergent slit.

Transmission electron microscopy (TEM) was conducted with a JEOL-3010 microscope operating at 300 kV ($C_s = 0.6$ mm, resolution 1.7 Å). Images were recorded with a CCD camera (model Keen View, SIS analysis, size 1024×1024 pixels, pixel size 23.5×23.5 μm) at $30000\text{--}50000\times$ magnification under low-dose conditions.

The N_2 adsorption/desorption measurements were performed at 77 K on an ASAP2020 Micromeritics Instrument. The sample was degassed for 6 h at 423 K and 0.3 kPa. The BET specific surface area S_{BET} was calculated from adsorption branches in the relative pressure range from 0.05 to 0.3. The total pore volume was estimated from the amount adsorbed at a relative pressure of 0.99. Pore size distribution curves were derived by DFT, as developed recently by Ravikovitch et al.,^[4] by assuming a cylindrical pore geometry.

Received: April 26, 2004

Keywords: carbon · electron crystallography · mesoporous materials · silica

- [1] a) R. Ryoo, C. H. Ko, M. Kruk, V. Antochshuk, M. Jaroniec, *J. Phys. Chem. B* **2000**, *104*, 11465; b) Z. Liu, O. Terasaki, T. Ohsuna, K. Hiraga, H. J. Shin, R. Ryoo, *ChemPhysChem* **2001**, *2*, 229; c) S. H. Joo, S. J. Choi, I. Oh, J. Kwak, Z. Liu, O. Terasaki, R. Ryoo, *Nature* **2001**, *412*, 169; d) O. Terasaki, Z. Liu, T. Ohsuna, H. J. Shin, R. Ryoo, *Microsc. Microanal.* **2002**, *8*, 35.
- [2] a) X. Liu, B. Tian, C. Yu, F. Gao, S. Xie, B. Tu, R. Che, L. Peng, D. Zhao, *Angew. Chem.* **2002**, *114*, 4032; *Angew. Chem. Int. Ed.* **2002**, *41*, 3876; b) Y. T. Chan, H. P. Lin, C. Y. Mou, S. T. Liu, *Chem. Commun.* **2002**, 2878; c) H. Yang, Q. Shi, X. Liu, S. Xie, D. Jiang, F. Zhang, C. Yu, B. Tu, D. Zhao, *Chem. Commun.* **2002**, 2842; d) K. Flodström, V. Alfreðsson, N. Källrot, *J. Am. Chem. Soc.* **2003**, *125*, 4402; e) S. Che, A. E. Garcia-Bennett, X. Liu, R. P. Hodgkins, P. A. Wright, D. Zhao, O. Terasaki, T. Tatsumi, *Angew. Chem.* **2003**, *115*, 4060; *Angew. Chem. Int. Ed.* **2003**, *42*, 3930; f) F. Kleitz, S. H. Choi, R. Ryoo, *Chem. Commun.* **2003**, 2136.
- [3] a) A. Carlsson, M. Kaneda, Y. Sakamoto, O. Terasaki, R. Ryoo, S. H. Joo, *J. Electron Microsc.* **1999**, *48*, 795; b) Y. Sakamoto, M. Kaneda, O. Terasaki, D. Zhao, J. M. Kim, G. D. Stucky, H. J. Shin, R. Ryoo, *Nature* **2000**, *408*, 449; c) M. Kaneda, T. Tsubakiyama, A. Carlsson, Y. Sakamoto, T. Ohsuna, O. Terasaki, S. H. Joo, R. Ryoo, *J. Phys. Chem. B* **2002**, *106*, 1256; d) Y. Sakamoto, I. Diaz, O. Terasaki, D. Zhao, J. P. Pariente, J. M. Kim, G. D. Stucky, *J. Phys. Chem. B* **2002**, *106*, 3118.
- [4] a) P. I. Ravikovitch, G. L. Haller, A. V. Neimark, *Adv. Colloid Interface Sci.* **1998**, *76–77*, 203; b) P. I. Ravikovitch, A. V. Neimark, *Langmuir* **2000**, *16*, 2419.
- [5] R. Ryoo, S. H. Joo, S. Jun, *J. Phys. Chem. B* **1999**, *103*, 7743.
- [6] S. Jun, S. H. Joo, R. Ryoo, M. Kruk, M. Jaroniec, Z. Liu, T. Ohsuna, O. Terasaki, *J. Am. Chem. Soc.* **2000**, *122*, 10712.

Liquid Crystals

Hydrogen-Bonded Banana Liquid Crystals**

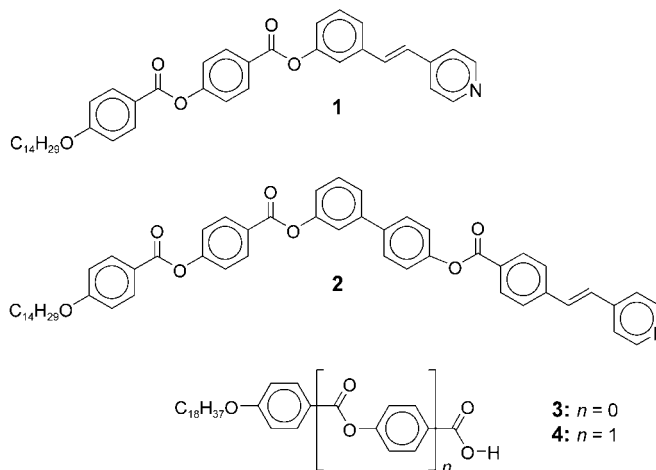
Nélida Gimeno, Maria Blanca Ros,* José Luis Serrano,*
and Maria Rosario de la Fuente

There are numerous examples in nature that demonstrate the crucial role of hydrogen bonds. Through imitation of this phenomenon, hydrogen bonds have been used to good effect by researchers to achieve specific synthetic targets.^[1] Fields such as supramolecular chemistry and materials science are indebted to this strategy,^[2] and important breakthroughs have been achieved by exploiting these inter- or intramolecular “strong and directional, and... lovely”^[3] interactions. Liquid crystals, which are related to both of the aforementioned fields, are another example of the attractive possibilities of this interaction.^[4] Mesomorphic properties result from a suitable combination of the shape of a molecule and the magnitude and direction of interactions between the molecules. Hydrogen bonding, through self-assembly, has been used to order thermotropic and lyotropic liquid crystals in which the magnitude and the direction of the interactions have been appropriate to maintain order within the fluid state. Calamitic and columnar mesophases of low or high molecular-weight materials have been stabilized with this approach. Such systems have also been obtained by the use of either mesogenic or non-liquid-crystalline moieties.

In 1996, a new type of mesogenic material appeared in the field of liquid crystals: the so-called “banana-compounds”.^[5] These mesomorphic materials are of interest from both an academic and a practical point of view.^[6] These systems form a distinct class of liquid-crystalline compounds as they give rise to new types of mesophases that do not have analogues among classical calamitic phases. Interestingly, some of these compounds exhibit the unique feature of forming polar ordered mesophases with achiral molecules to provide anti-ferroelectric, ferroelectric or nonlinear optical responses—often with exceptional values for the relevant parameters.^[7] Herein, we report a study that addresses a pertinent question that has not successfully been answered to date: is it possible to stabilize this type of mesophase through hydrogen bonding

interactions? On the basis of the following results, the answer to this question is a resounding yes!

Having taken into account the structural molecular requirements that 1) govern these new macroscopic liquid-crystal phase arrangements^[5] and 2) allow appropriate H bonded complexation, we focused our interests on the V-shaped H acceptor structures **1** and **2** shown in Scheme 1 and



Scheme 1. General structures of the H acceptors (**1** and **2**) and H donors (**3** and **4**).

two benzoic acid derivatives of varying lengths as the H donor moieties **3** and **4**. The V-shaped 4'-stilbazoles (**1** and **2**) were prepared according to the synthetic route outlined in Scheme 2 (see also Supporting Information), and the acids (**3** and **4**) were prepared according to literature methods.^[8] The synthesis of the desired bent complexes required the two components (H donor and H acceptor) to be mixed in precise equimolecular proportions in a common solvent (THF) followed by removal of the solvent. The formation of the complex was easily confirmed through polarizing optical microscopy measurements; the solid samples melted cleanly without the appearance of biphasic regions, which would otherwise have indicated the presence of nonstoichiometric complexes.

Despite the nonmesomorphic nature of both of the H acceptor compounds studied, all of the complexes were liquid crystalline over temperature ranges that were different to the ranges at which the carboxylic acids displayed calamitic phases (Table 1). More interestingly, the complexes exhibit textural features which are identical to those reported^[8,9] and observed by us for SmCP (smectic C polar) mesophases. A schlieren texture and highly birefringent domains were observed upon cooling the sample from the isotropic liquid (Figure 1 a). From a structure–activity point of view, the larger the number of aromatic rings, the broader and more stable the mesophases are. Furthermore, hysteresis of the solidification processes of around 20 degrees was also observed.

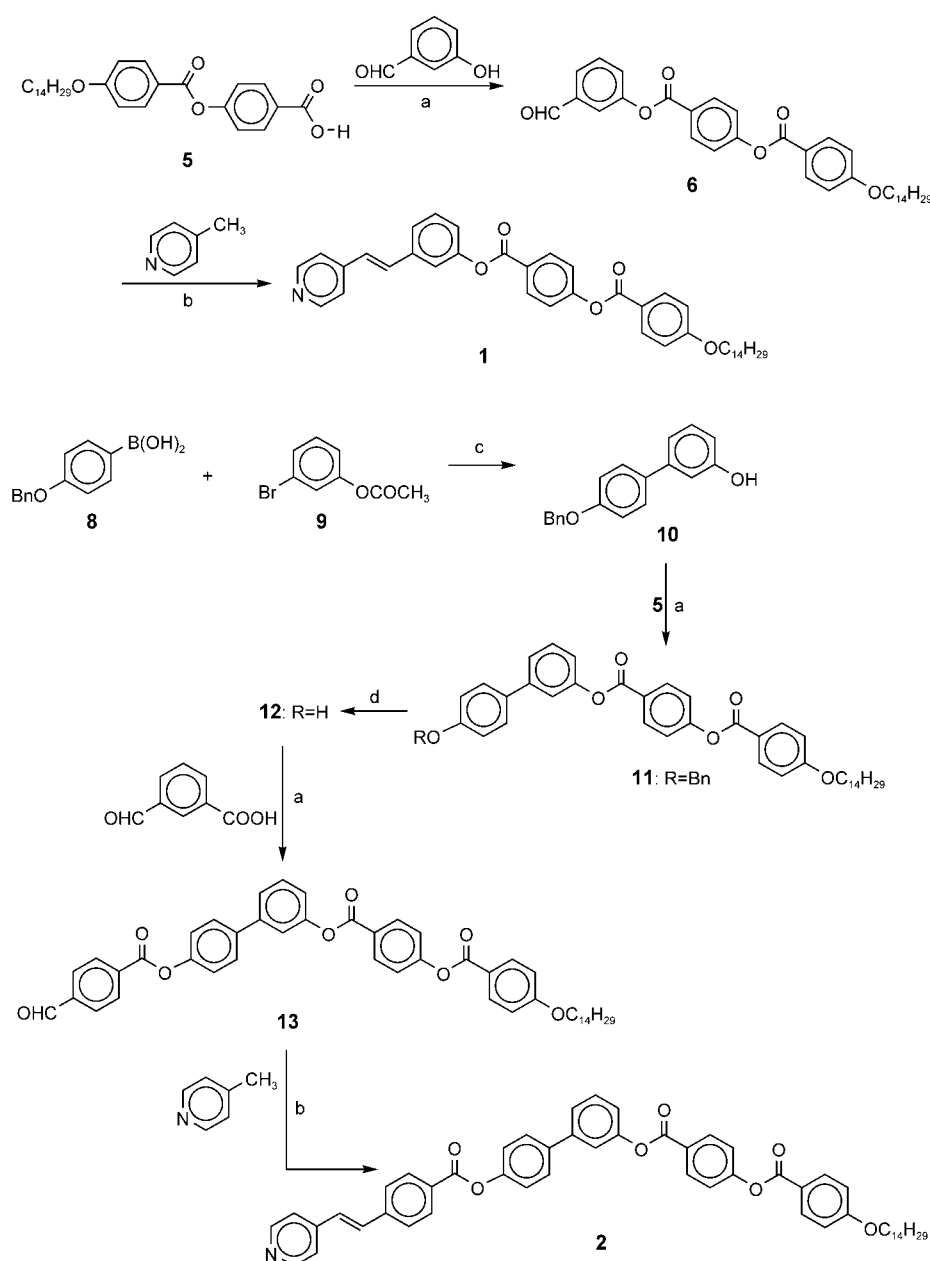
The stability of the hydrogen bonding that leads to these banana complexes was also examined. The IR spectra of these materials (KBr pellets) show features that are characteristic of pyridine–carboxylic acid complexes.^[4b,10] Thus, the forma-

[*] N. Gimeno, Dr. M. B. Ros, Prof. J. L. Serrano
Dpto. Química Orgánica, Facultad de Ciencias–ICMA
Universidad de Zaragoza–CSIC, 50009-Zaragoza (Spain)
Fax: (+34) 976-761209
E-mail: bros@unizar.es
joseluis@unizar.es

Prof. M. R. de la Fuente
Dpto. Física Aplicada II, Facultad de Ciencias
Universidad del País Vasco, 48080-Bilbao (Spain)
Fax: (+34) 94-664-8500

[**] This work was supported by the Spanish Government (project CICYT MAT2003-07806-C02), the European Union (FEDER), and the Government of Aragón.

Supporting information for this article is available on the WWW under <http://www.angewandte.org> or from the author.



Scheme 2. Synthetic routes to the H acceptors **1** and **2**. a) DCC, DMAP, CH_2Cl_2 ; b) $(\text{CH}_3\text{CO})_2\text{O}$; c) $\text{Pd}[\text{P}(\text{Ph})_3]_4$, NaHCO_3 , DME; d) $\text{Pd}(\text{OH})_2/\text{C}$, cyclohexene, EtOH. DCC = Dicyclohexyl carbodiimide, DMAP = dimethylaminopyridine, DME = 1,2-dimethoxyethane.

Table 1: Thermal properties of the H donors, H acceptors and the complexes studied.

Compounds	Phase transition ^[a,b] [°C] (ΔH [kJ mol ⁻¹])
1	K 108.2 (56.2) I
2	K 168.9 (37.0) I
3	K 104.6 (53.5) SmC 125.0 (7.9) I
4	K 101.6 (30.7) SmC 206.5 (13.8) I
1:3	K 98.2 (58.6) SmCP 118.8 (29.6) I
1:4	K 82.9 (59.3) SmCP 142.6 (26.1) I
2:3	K 117.9 (19.0) SmCP 173.8 (28.7) I

[a] Data determined by DSC at a scanning rate of $10^\circ\text{C min}^{-1}$. [b] K: crystalline; SmC: smectic C mesophase; SmCP: smectic C polar mesophase; I: isotropic liquid phase.

tion of the H bond is detected through the modification of the O–H stretching band of the acid. The complexes exhibit two absorptions at ≈ 2500 and 1950 cm^{-1} which correspond to the O–H $\cdots\text{N}(\text{Py})$ interaction, whereas carboxylic acid dimers exhibit a band (O–H) at $\approx 2650\text{ cm}^{-1}$. On the other hand, an absorption band at 1683 cm^{-1} which also corresponds to the acid dimers was not detected for the bent complexes. Furthermore, variable-temperature IR spectra were recorded for all of the complexes and these reveal that a carbonyl band, which arises from the dissociation of the hydrogen bonding, is not observed in either the crystalline phase or the mesophase.

The X-ray diffraction patterns of the three complexes in their mesophases are very similar. In the wide-angle region there is diffuse scattering, whereas in the small-angle regions there are sharp layer reflections up to third order (Table 2 and Figure 2). This indicates well-defined layer structures for the liquid-crystalline phase in all cases; that is, the complexes arrange themselves in smectic phases without in-plane order. The estimated length of the “molecules” ($67\text{--}76\text{ \AA}$) is larger than the interlayer distances measured and indicates tilted arrangements of the complexes in the liquid-crystalline phase with angles of around $39\text{--}45^\circ$.

An attractive feature of the SmCP mesophase is its switching response under electric fields.^[5b,6,7a,9] This behavior was investigated for our H bonded materials: $5\text{-}\mu\text{m}$ ITO (indium tin oxide)-coated cells were filled with the samples and their switching behavior was studied. On slow cooling from the isotropic liquid, a texture with focal-conics containing fringe patterns and some circular domains was perfectly visible. The direction of the extinction brushes coincides with the polarizer and the analyzer (see Figure 1 b).

Application of direct current (d.c.) fields causes the brushes to rotate (see Figures 1 c and d). The higher the field, the larger the tilt of the extinction brushes (with a saturation value around 45°). All these facts are consistent with a SmCP mesophase in which molecules are organized in layers and tilted. The tilt alternates from layer to layer to give rise to an anticlinic and antiferroelectric SmC_AP_A structure. Under a high enough d.c. field, the structure becomes a synclinic ferroelectric SmC_SP_F structure.^[6,9] Moreover, upon application of triangular-wave fields, all these complexes show a tri-stable switching process typical of an antiferroelectric response. Figure 3 shows a typical plot of the inversion of

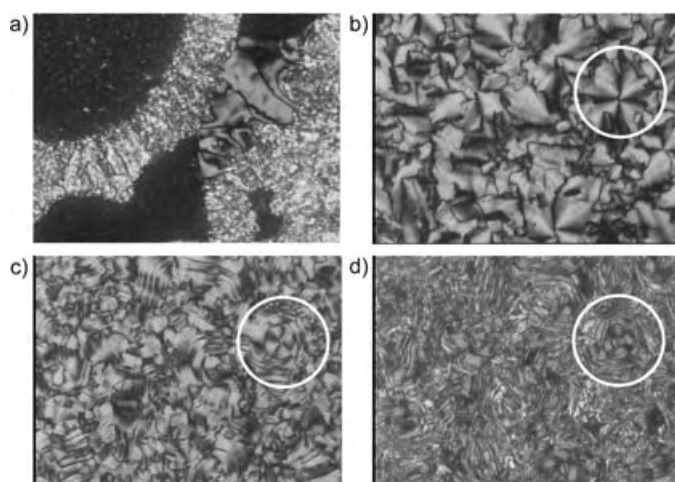


Figure 1. Textures of the mesophase SmCP: a) Complex **2-3** at 144 °C, uncoated cell; b) complex **1-3** at 100 °C, $V=0$, coated cell; c) complex **1-3** at 100 °C, $V=70$ (d.c.), coated cell; d) complex **1-3** at 100 °C, $V=100$ (d.c.), coated cell. The orientation of the extinction brushes is seen clearly in the circles indicated.

Table 2: X-ray data for the complexes studied.

Complex	Measured spacings [Å]	Miller index	Layer thickness [Å]
1-3	52.2 (vs) ^[a]	001	d : 52.05
	26.3 (w)	002	
	17.25 (m)	003	
1-4	50.5 (vs)	001	d : 51.04
	25.7 (m)	002	
	17.1 (m)	003	
2-3	61.6 (vs)	001	d : 61.6
	30.8 (m)	002	

[a] Intensity of the reflection: vs: very strong; w: weak; m: medium.

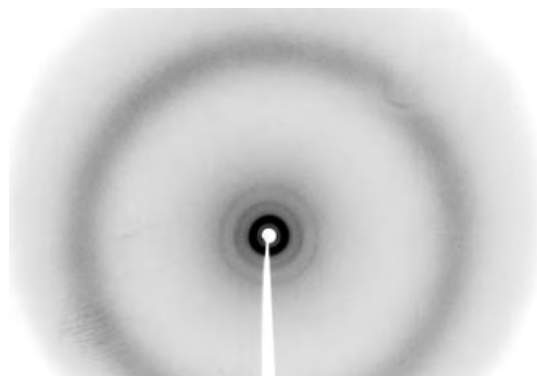


Figure 2. X-ray diffraction pattern of complex **1-4** at 120 °C in the SmCP mesophase.

the polarization current. Two peaks for each half-period are clearly visible. The integration of these peaks^[11] gives a value around 200 nC cm⁻² for the dielectric polarization for all of the complexes.

The presence of stilbazole structures in these materials also led us to assess their luminescent response, which, if present, would increase the multifunctional character of these

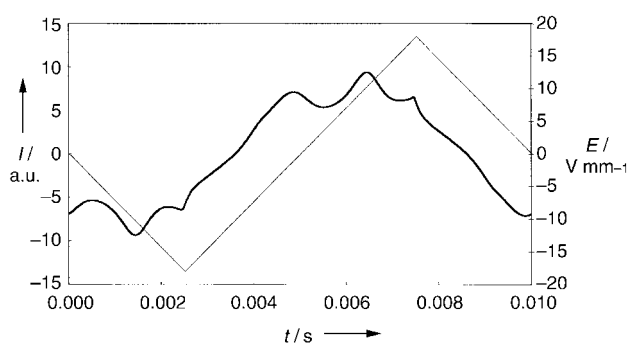


Figure 3. Polarization switching current of complex **1-3** under a triangular-wave electric field: 100 Hz, 36 Vpp μm⁻¹ (5 μm-Linkam cell).

novel systems. As an initial study, the one-photon-excited fluorescence emissions of these complexes were determined in solution (10⁻⁶ M in THF); representative results from these

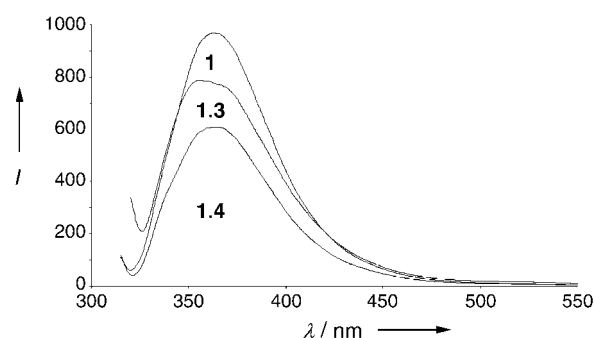
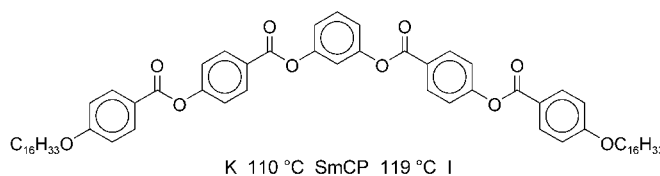


Figure 4. Fluorescence spectra of compound **1** and complexes **1-3** and **1-4** at room temperature in THF. Excitation wavelength 310 nm, emission wavelength 355 nm.

studies are shown in Figure 4. The H donor compounds or the H bonded complexes absorb at 310 nm (**1** and its complexes) or 320 nm (**2** and its complex) and they exhibit fluorescence emissions around 355 nm and 365 nm, respectively. A decrease in the absorptivity of the H donors is observed upon complexation. To determine the potential of the complexes as fluorescent materials, more in-depth studies of their luminescent behavior will be undertaken in a future project—particularly with respect to the novel SmCP mesophase as, to our knowledge, there is no precedence in the literature for this property in ‘banana’ liquid crystals.

Although we were unable to find an example of a compound in the literature that could be considered as a covalent analogue of our bent complexes, we compared the mesomorphic properties of **1-3** with the longest related



Scheme 3. ‘Banana’ ester compound for comparison with **1-3**.

'banana' ester reported by Pelzl's group^[12] (Scheme 3). From the data obtained, we tentatively conclude that despite the slight difference in length in the two materials, the similarity in their thermal behavior is sufficiently close to acknowledge the formation of H bonded complexes as a useful strategy to design and, more interestingly, to identify new 'banana' liquid crystals. In an attempt to obtain new mesophases, as well as to approach different V-shaped structures by H bonding, the complexation of some pyridine structures with different carboxylic acids is currently in progress.

In summary, further evidence of the versatility of hydrogen bonding for the anisotropic self-organization of functional materials has been obtained. A successful method to obtain novel mesophases, namely the most studied SmCP liquid-crystalline phase, through H bonding interactions has been developed. More interestingly, the attractive electro-optical and dielectric responses of this polar phase were also determined for these noncovalent systems. Furthermore, these results indicate that these V-shaped H bonded structures are an easily obtained and attractive "testing bank", not only for the induction of different mesophases but also as a potential way to obtain different multifunctional 'banana' liquid crystals.

Received: May 4, 2004

Keywords: fluorescence · hydrogen bonds · liquid crystals · mesophases · supramolecular chemistry

- [1] a) M. C. Etter, *Acc. Chem. Res.* **1990**, 23, 120; b) M. C. Etter, *J. Phys. Chem.* **1991**, 95, 4601; c) G. A. Jeffrey, *An Introduction to Hydrogen Bonding*, Oxford University Press, New York, **1997**.
- [2] For reviews, see: a) J.-M. Lehn, *Supramolecular Chemistry—Concepts and Perspectives*, VCH, Weinheim, **1995**; b) D. S. Lawrence, T. Jiang, M. Levett, *Chem. Rev.* **1995**, 95, 2229; c) C. Schmuck, W. Wienand, *Angew. Chem.* **2001**, 113, 4493; *Angew. Chem. Int. Ed.* **2001**, 40, 4363; d) T. Steiner, *Angew. Chem.* **2002**, 114, 50; *Angew. Chem. Int. Ed.* **2002**, 41, 48.
- [3] "A hydrogen bond is like the attraction of a hummingbird to a flower ... strong and directional, and also, lovely" by M. C. Etter in M. C. Etter, *Chem. Mater.* **1994**, 6, Cover page.
- [4] For reviews, see: a) C. M. Paleos, D. Tsiourvas, *Angew. Chem.* **1995**, 107, 1839; *Angew. Chem. Int. Ed. Engl.* **1995**, 34, 1696; b) T. Kato in *Handbook of Liquid Crystals* (Eds.: D. Demus, J. Goodby, G. W. Gray, H. W. Spiess, V. Vill), Weinheim, Wiley-VCH, **1998**, p. 969; c) T. Kato, *Struct. Bonding (Berlin)* **2000**, 96, 95; d) L. Brunsfeld, B. J. B. Folmer, E. W. Meijer, R. P. Sijbesma, *Chem. Rev.* **2001**, 101, 4071; e) U. Beginn, *Prog. Polym. Sci.* **2003**, 28, 1049.
- [5] a) T. Niori, T. Sekine, J. Watanabe, F. Fukurawa, H. Takezoe, *J. Mater. Chem.* **1996**, 6, 1231; b) G. Pelzl, S. Diele, W. Weissflog, *Adv. Mater.* **1999**, 11, 707, and references therein; c) "Anisotropic Organic Materials—Approaches to Polar Order" D. M. Walba, E. Körblova, R. Shao, J. E. MacLennan, D. E. Link, M. A. Glaser, N. A. Clark, *ACS Symp. Ser.* **2001**, 789, 281.
- [6] a) D. M. Walba, E. Körblova, R. Shao, J. E. MacLennan, D. R. Link, M. A. Glaser, N. A. Clark, *Science* **2000**, 288, 2181; b) D. A. Coleman, J. Fernsler, N. Chattham, M. Nakata, Y. Takanishi, E. Körblova, D. R. Link, R. F. Shao, W. G. Jang, J. E. MacLennan, O. Mondainn-Monval, C. Boyer, W. Weissflog, G. Pelzl, L. C. Chien, J. Zasadzinski, J. Watanabe, D. M. Walba, N. Takezoe, N. A. Clark, *Science* **2003**, 301, 1204; c) A. Jákli, D. Krüerke, G. G. Nair, *Phys. Rev. E* **2003**, 67, 051702.
- [7] a) M. Nakata, D. R. Link, F. Araoka, J. Thisayukta, Y. Takanishi, K. Ishikawa, J. Watanabe, H. Takezoe, *Liq. Cryst.* **2001**, 28, 1301; b) J. Etchebarria, C. L. Folcia, J. Ortega, M. B. Ros, *Phys. Rev. E* **2003**, 67, 042702; c) J. Ortega, J. A. Gallastegui, C. L. Folcia, J. Etchebarria, N. Gimeno, M. B. Ros, *Liq. Cryst.* **2004**, 31, 579.
- [8] a) M. Ikeda, T. Hatakeyama, *Mol. Cryst. Liq. Cryst.* **1976**, 33, 201; b) D. Shen, A. Pegenau, S. Diele, I. Wirth, C. Tschierske, *J. Am. Chem. Soc.* **2000**, 122, 1593.
- [9] D. R. Link, G. Natale, R. Shao, J. E. MacLennan, N. A. Clark, E. Körblova, D. M. Walba, *Science* **1997**, 278, 1924.
- [10] a) S. L. Johnson, K. A. Rumon, *J. Phys. Chem.* **1965**, 69, 74; b) T. Kato, J. M. J. Fréchet, *Macromolecules* **1989**, 22, 3818; c) C. G. Bazuin, F. A. Brandys, *Chem. Mater.* **1992**, 4, 970; d) T. Kato, J. M. J. Fréchet, P. G. Wilson, T. Saito, T. Uryu, A. Fujishima, C. Jin, K. Kanenedi, *Chem. Mater.* **1993**, 5, 1094; e) M. Plass, *Z. Phys. Chem.* **1996**, 194, 223; f) S. Valiyavechil, K. Müllen, *New J. Chem.* **1998**, 89, 95.
- [11] M. R. De la Fuente, A. Ezcurra, M. A. Pérez-Jubindo, J. Zubia, *Liq. Cryst.* **1990**, 7, 51.
- [12] M. W. Schröder, S. Diele, G. Pelzl, W. Weissflog, *ChemPhys-Chem* **2004**, 5, 99.

ZnO Nanostructures

Single-Crystal Hexagonal Disks and Rings of ZnO: Low-Temperature, Large-Scale Synthesis and Growth Mechanism**

Feng Li, Yong Ding, Puxian Gao, Xinquan Xin, and Zhong L. Wang**

The optical response of a particle depends on its particular size, shape, and local dielectric environment.^[1] Synthesis of size- and shape-controlled nanostructures is important in controlling their chemical and physical properties.^[2,3] ZnO, with a wide band gap of 3.37 eV, is a candidate for

[*] Dr. F. Li

Department of Chemistry
University of New Orleans
New Orleans, LA 70148 (USA)
Fax: (+1) 504-280-6860
E-mail: fli@uno.edu

Dr. Y. Ding, P. Gao, Prof. Dr. Z. L. Wang
School of Materials Science and Engineering
Georgia Institute of Technology
Atlanta, GA 30332-0245 (USA)
Fax: (+1) 404-894-9140
E-mail: zhong.wang@mse.gatech.edu

Prof. X. Xin
Department of Chemistry
Nanjing University
Nanjing 20093 (P. R. China)

[**] The authors gratefully acknowledge the financial support of the National Science Foundation of China (No.90101028) and the National Science Foundation.

applications in electronics, photoelectronics, and sensors.^[4–9] Among the developed approaches, solid–vapor phase growth (SVG) at high temperature is favored for its simplicity and high-quality in producing ZnO nanowires, nanobelts, nanocantilevers, and nanonails.^[6–17] In addition to fabrication of rings by lithography^[1,18–20] and self-assembly^[21,22], our recent significant progress based on the SVG approach is the synthesis of single-crystal ZnO rings from self-assembled polar nanobelts.^[23,24] The SVG approach has been used for discovering a diversity of nanostructures,^[25] but its major limitation is low yield.

Solution phase synthesis (SPS), including microemulsion and hydrothermal growth, has also proved effective and convenient in preparing ZnO nanowires, nanorods, and helical rods at low temperature on a large scale.^[4,5,26–32] In this approach, it is believed that the shape of micelles plays a key role in the controlled growth of one-dimensional (1D) nanostructures in solution.^[26] Since surfactants can be made to form micelles with diverse shapes from spheres to rods to ellipsoids to disks, and even much more complex shapes, by adjusting experimental parameters,^[33] we can further control the nanostructures by means of the SPS approach. Here we report a rational synthesis of single-crystal hexagonal ZnO nanodisks and rings on a large scale by the SPS approach, and demonstrate its potential for low-temperature, large-scale, controlled synthesis of single-crystal ZnO nanostructures. The approach may be extendible to the synthesis of a wide range of nanomaterials. The hexagonal disks and rings are new members in the family of ZnO nanostructures. On the basis of structural information provided by electron microscopy, a growth mechanism is proposed for the formation of disks and rings.

The ZnO rings and disks were synthesized by a solution-phase approach. The procedure involves 1) preparation of an oil-in-water microemulsion with surfactant, namely, sodium bis(2-ethylhexyl) sulfosuccinate (NaAOT), in a water/1-butanol/Zn(NO₃)₂ system, and 2) subsequent growth of ZnO rings and disks in microreactors. Figure 1a shows a typical low-magnification SEM image of ZnO nanostructures grown at 70 °C. The as-synthesized product is pure and uniform, and is dominated by hexagonal-based thin disks with uniform size and well-defined shape. The disks are 2–3 μm in diameter and 50–200 nm thick. An enlarged image shows the back-to-back paired stacking of the disks (Figure 1b), with one side of the disk surface smoother, and the other rougher. The two adjacent contacting surfaces are rather smooth. Some of the disks have a hole at the middle, and are thus hexagonal rings (Figure 1c).

The morphology of the disks can be modified by adjusting the growth temperature. Increasing the growth temperature from 70 to 90 °C dramatically increases the yield of hexagonal rings (Figure 2a). Most of the rings have a hexagonal base and their morphology is fairly uniform. The size of the inner holes varies from ring to ring, and they are mostly hexagonal (Figure 2b, c). In some cases, the shape of the hole is irregular (Figure 2d).

Detailed examination revealed that the top and bottom surfaces of the hexagonal rings and disks are quite different; one side is smooth, and the other rough (Figure 3a). The

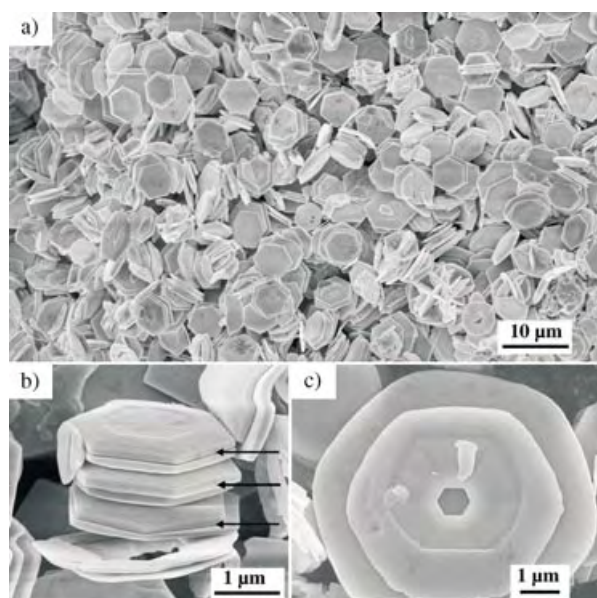


Figure 1. a) Low-magnification SEM image recorded from the as-synthesized ZnO sample prepared at 70 °C, demonstrating the predominance of hexagonal disks. b), c) Enlarged SEM images displaying detailed structures of the hexagonal disks.

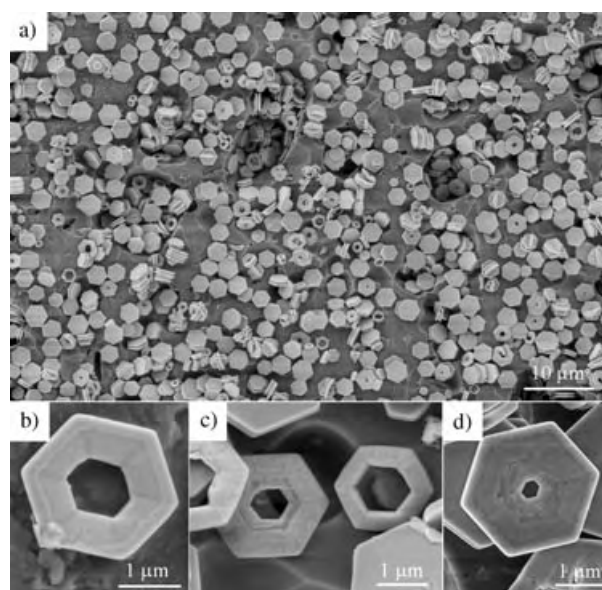


Figure 2. a) Low-magnification SEM image recorded from the as-synthesized ZnO sample prepared at 90 °C; the higher yield of hexagonal rings is evident. b)–d) Enlarged SEM images displaying detailed structures of the hexagonal rings.

rough side had a higher “etching” rate (see below), so that the surface is nonuniform, and there is a small hole at the middle (Figure 3b). The nonuniform morphology of the top surface can be best seen by tilting the disk (Figure 3c), which reveals the grooved surface structure associated with the crystal symmetry on one side (Figure 3d). In contrast, the backside of the ring is rather flat. The hole appeared to have been created from the rougher side and extends half way through the thickness (Figure 3e). For a small hole that passes throughout

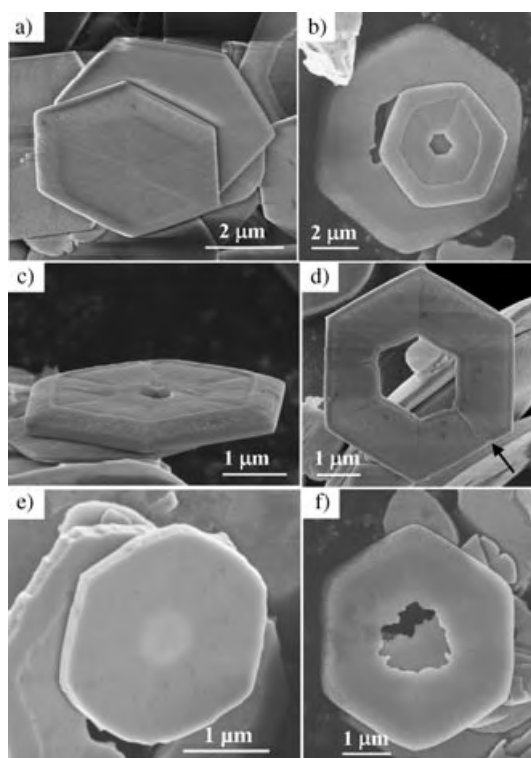


Figure 3. SEM images recorded from ZnO hexagonal disks showing the structural features on the rougher and smoother surfaces of the disks.

the thickness, a rough edge at the inner surface is apparent (Figure 3 f).

The TEM analysis of the hexagonal disk showed a single-crystal structure, with (0001) top/bottom surfaces, and $\{1\bar{1}00\}$ side facets (Figure 4 a). The dark-field image of the disk shows defects, which are distributed radially with a higher concentration at the center. The defects are most likely low-angle grain boundaries (Figure 4 b). Some thickness fringes are observed, which correspond to the reduced thickness towards the center.

The hexagonal ring also shows a single-crystal structure, with (0001) top/bottom surfaces and $\{1\bar{1}00\}$ side surfaces (Figure 4 c, d). An important feature observed in the TEM image is the presence of defects closely parallel to $\langle 2\bar{1}\bar{1}0 \rangle$ in the ring. The disk has a wedge shape that becomes thinner towards the center. A high-resolution TEM image recorded from the inner edge of the ring (Figure 4 e) shows surface steps, atomically sharp and free of contamination. The TEM image also reveals the decrease in disk thickness towards the center.

Several experiments were carried out to determine the parameters other than temperature that are important for the formation of disks and rings: 1) No hexagonal ZnO disks were produced in the absence of NaAOT or when NaAOT was replaced with sodium dodecyl sulfate (SDS). 2) The use of *n*-butanol is also crucial to the formation of shape-controlled ZnO disks. No hexagonal ZnO disks are produced in the reaction if only water is used as solvent to dissolve NaAOT, or *n*-butanol is replaced with octane. 3) Zn^{2+} cations can react

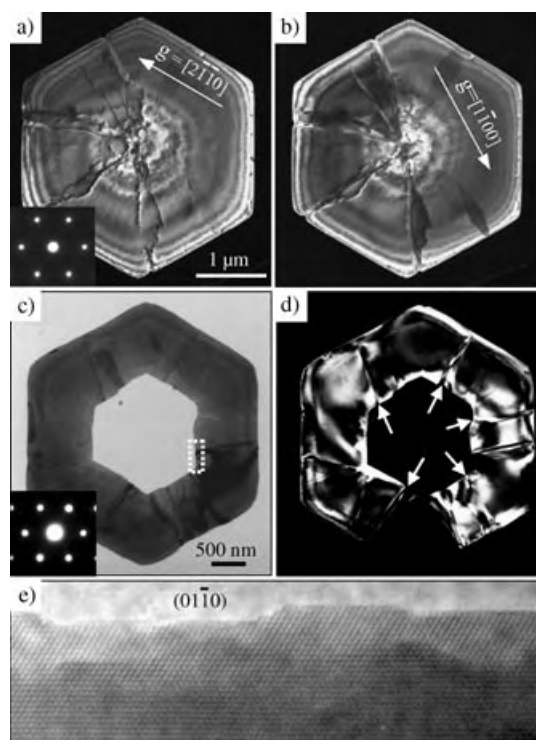
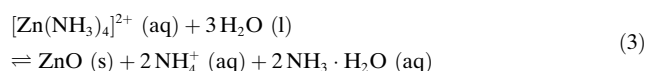
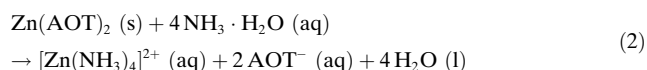
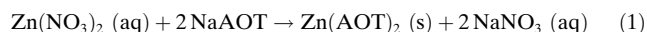


Figure 4. a), b) Dark-field TEM images and corresponding diffraction pattern of a hexagonal disk, showing planar defects in the disk, which are likely to be low-angle grain boundaries induced during crystal growth. c) Bright-field TEM image of a hexagonal ring and its corresponding diffraction pattern, showing that the ring has a top/bottom (0001) surfaces and inner/outer $\{1\bar{1}00\}$ surfaces. d) Dark-field TEM image of the ring, displaying defects closely parallel to $\{2\bar{1}\bar{1}0\}$. e) High-resolution TEM image recorded from the inner edge marked in c), showing clean and sharp surfaces.

with AOT^- directly to form white precipitates in water. 4) Further investigations revealed that the molar ratio of Zn^{2+} to $\text{NH}_3 \cdot \text{H}_2\text{O}$ is one of the dominant parameters for the formation of well-structured disks and rings. Hexagonal disks and rings are produced at $\text{Zn}^{2+}/\text{NH}_3 \cdot \text{H}_2\text{O}$ molar ratios of $1/3$, $1/4$, $1/5$, and $1/6$, but no ZnO particles were observed in a reaction carried out at a molar ratio of $1/2$. Thus, in the oil-in-water microemulsion system, the reaction temperature and the concentration of $\text{NH}_3 \cdot \text{H}_2\text{O}$ are the dominant parameters in the formation of hexagonal rings and disks.

On the basis of the information we have gathered, a growth process of the hexagonal disks and rings can be proposed. From the crystal structure, ZnO can be described as a number of alternating planes composed of tetrahedrally coordinated O^{2-} and Zn^{2+} ions, stacked alternately along the *c* axis. The oppositely charged ions produce positively charged Zn^{2+} (0001) and negatively charged O^{2-} ($000\bar{1}$) polar surfaces. Therefore, the positively charged Zn^{2+} (0001) and the negatively charged O^{2-} ($000\bar{1}$) surfaces can have very different self-catalysis properties,^[11] and the spontaneous polarization along the *c* axis leads to the formation of nanospirals,^[24] rings,^[23] and nanobows^[26] due to electrostatic interaction. The large polar surface is generally energetically unfavorable unless the surface charge is compensated by a passivation agent. On the other hand, it was reported that the

anionic surfactant NaAOT can be made to form micelles with diverse shapes by adjusting experimental parameters.^[33–36] The self-assembled AOT[−] layers at the interface of water and oil could act as template for growing ZnO. The hydrophilic head of AOT[−] can form an anionic surface exposed to water, and thus Zn²⁺ cations can directly attach to the negatively charged AOT[−] template to initiate the first layer of crystal growth [Eq. (1)]. The produced Zn(AOT)₂ then can be transformed into [Zn(NH₃)₄]²⁺ by reaction with NH₃·H₂O [Eq. (2)], so that the positively charged Zn²⁺ (0001) surface of ZnO tends to directly interface with the anionic surface of the AOT[−] template in the subsequent hydration of [Zn(NH₃)₄]²⁺ at higher temperature [Eq. (3)].^[29]



Fast growth along $\langle 2\bar{1}\bar{1}0 \rangle$ results in the formation of a hexagonal disk (Figure 5a). Slight bending of the self-assembled AOT[−] monolayer makes it possible to accommodate local strain in the disk by formation of small-angle grain

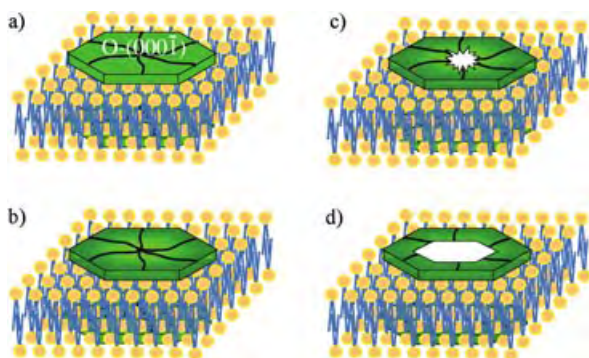


Figure 5. Proposed formation process of the ZnO hexagonal disks and rings, as well as their back-to-back stacking.

boundaries closely parallel to $\{2\bar{1}\bar{1}0\}$. Therefore, some of the grown disks may have this defect.

The Zn²⁺ (0001) surface bonds strongly to AOT[−] due to charge interaction, and the densely packed AOT[−] will protect the surface from further “etching” or reaction, resulting in the formation of the flat side of the disks (see Figures 1 and 3). The AOT[−] template stabilizes the surface charge and the structure.

The exposed negatively charged O^{2−} (000 $\bar{1}$) surface of the disk may be reactive towards NH₄⁺ and NH₃·H₂O, as shown in Equation (3). The equilibrium will move in the reverse direction on adding excess NH₃·H₂O. The rate toward the reverse direction of Equation (3) also increases drastically with increasing temperature; thus, etching of the O^{2−} (000 $\bar{1}$) surface by NH₄⁺ and excess NH₃ results in the rougher surface (see Figure 3a).

From the TEM image presented in Figure 4b, the density of defects is highest at the center of the disk. A higher etching/reaction rate is possible at the defect sites. Therefore, a high density of planar defects at the center may result in a higher local etching rate and eventually lead to the formation of a hole at the center. The hole is initiated from the O^{2−} (000 $\bar{1}$) surface and it may not penetrate the entire thickness if the reaction time is insufficient (see Figure 3e), as presented in Figure 5b. As the reaction proceeds, the etching can create a hole through the disk (Figure 5c). As the hole becomes larger, its side surfaces eventually take on the lower energy $\{1\bar{1}00\}$ facets of ZnO, and the disk becomes a hexagonal ring (Figure 5d). The grooved feature on the surface of the ring along $\langle 2\bar{1}\bar{1}0 \rangle$ may be due to the dependence of the local etching rate on the crystal orientation. On the other hand, the etching rate is sensitive to the growth temperature and the molar ratio of reactants; thus rings were not formed at 70 °C, but at 90 °C or higher.

The formation of paired disks, as seen in Figure 1b, may be due to the fact that AOT[−] usually forms self-assembled double layers and multilayers in lamellar micelles. The growth of ZnO disks and rings can take place simultaneously on both sides of the template and thus result in back-to-back growth of paired disks or rings. After removing the oil phase from the system, a close attachment of the two disks at the smoother surfaces is energetically favorable because of the van der Waals interaction between the long tails of the self-assembled AOT[−] monolayer on the surfaces.

In summary, using NaAOT as template, we have demonstrated a solution-based synthesis of ZnO rings and disks at low temperature and on a large scale. The as-synthesized materials are structurally uniform and pure. By controlling growth temperature and molar ratio of reactants, the disks could be converted into rings. The growth mechanism of the hexagonal disks is suggested to be due to charge compensation of the anionic AOT[−] template at the Zn²⁺ (0001) surface of ZnO; fast growth along $\langle 2\bar{1}\bar{1}0 \rangle$ forms hexagonal disks enclosed by $\{10\bar{1}0\}$ facets. A higher density of defects at the center of the disk results in a higher local reaction/etching rate by NH₄⁺ and NH₃. A through-thickness hole, as defined by the $\{10\bar{1}0\}$ facets at the center, leads to the formation of a hexagonal ring. The technique demonstrated here could be extended for synthesizing a wide range of nanomaterials. Using such well-structured materials as building blocks, one could design a diverse range of nanodevices, from nanoscale lasers to sensors and photonic crystals.

Experimental Section

For the preparation of ZnO discs and rings, a NaAOT microemulsion was first prepared by adding an aqueous solution of Zn(NO₃)₂·6H₂O (0.025 M) to a solution of NaAOT (0.10 M) in 1-butanol and vigorously stirring for 2 h. The volume ratio of the aqueous phase to the organic phase was 10:1. Then a concentrated aqueous solution of NH₃·H₂O (17.65 M) with 4:1 molar ratio to Zn(NO₃)₂·6H₂O was added dropwise to the well-stirred microemulsion. After addition was complete, stirring was continued for 3 h at room temperature. The resulting milky white mixture was subsequently kept at 70 or 90 °C for 5 days. A white suspension was obtained and centrifuged to separate the precipitate, which was washed several times with distilled water and

absolute ethanol. Finally, a white powder was obtained by drying at 70 °C in vacuum. The as-synthesized samples were first analyzed with a LEO 1530 field-emission scanning electron microscope (FE-SEM). Transmission electron microscopy was carried out at 400 kV with a JEOL 4000EX.

Received: May 25, 2004

Keywords: crystal growth · nanostructures · oxides · zinc

- [1] J. Aizpurua, P. Hanarp, D. S. Sutherland, M. Käll, G. W. Bryant, F. J. García de Abajo, *Phys. Rev. Lett.* **2003**, *90*, 57401.
- [2] F. Li, J. He, W. Zhou, J. B. Wiley, *J. Am. Chem. Soc.* **2003**, *125*, 16166.
- [3] F. Li, L. Xu, W. L. Zhou, J. He, R. H. Baughman, A. A. Zakhidov, J. B. Wiley, *Adv. Mater.* **2002**, *14*, 1528.
- [4] K.-S. Choi, H. C. Lichtenegger, G. D. Stucky, E. W. McFarland, *J. Am. Chem. Soc.* **2002**, *124*, 12402.
- [5] J. Zhang, L. Sun, J. Yin, H. Su, C. Liao, C. Yan, *Chem. Mater.* **2002**, *14*, 4172.
- [6] P. X. Gao, Z. L. Wang, *J. Am. Chem. Soc.* **2003**, *125*, 11299.
- [7] X. D. Wang, C. J. Summers, Z. L. Wang, *Nano Lett.* **2004**, *4*, 423.
- [8] J. Q. Hu, Y. Bando, J. H. Zhan, Y. B. Li, T. Sekiguchi, *Appl. Phys. Lett.* **2003**, *83*, 4414.
- [9] J. Y. Lao, J. G. Wen, Z. F. Ren, *Nano Lett.* **2002**, *2*, 1287.
- [10] M. H. Huang, S. Mao, H. Feick, H. Yan, Y. Wu, H. Kind, E. Weber, R. Russo, P. Yang, *Science* **2001**, *292*, 1897.
- [11] Z. L. Wang, X. Y. Kong, J. M. Zuo, *Phys. Rev. Lett.* **2003**, *91*, 185502.
- [12] H. Yan, R. He, J. Johnson, M. Law, R. J. Saykally, P. Yang, *J. Am. Chem. Soc.* **2003**, *125*, 4728.
- [13] W. I. Park, G.-C. Yi, M. Kim, S. J. Pennycook, *Adv. Mater.* **2002**, *14*, 1841.
- [14] Z. W. Pan, Z. R. Dai, Z. L. Wang, *Science* **2001**, *291*, 1947.
- [15] P. X. Gao, Z. L. Wang, *J. Phys. Chem.* **2002**, *106*, 12653.
- [16] J.-J. Wu, S.-C. Liu, *Adv. Mater.* **2002**, *14*, 215.
- [17] P. Hu, Y. Liu, X. Wang, L. Fu, D. Zhu, *Chem. Commun.* **2003**, 1304.
- [18] N. Jiang, G. G. Hembree, J. C. H. Spence, J. Qin, F. J. García de Abajo, J. Silcox, *Appl. Phys. Lett.* **2003**, *83*, 551.
- [19] M. Mayer, M. Korkusinski, P. Hawrylak, T. Gutbrod, M. Michel, A. Forchel, *Phys. Rev. Lett.* **2003**, *90*, 186801.
- [20] H. Xu, W. A. Goedel, *Angew. Chem.* **2003**, *42*, 4845; *Angew. Chem. Int. Ed.* **2003**, *42*, 4696.
- [21] K. T. Nam, B. R. Peelle, S.-W. Lee, A. M. Belecher, *Nano Lett.* **2004**, *4*, 23.
- [22] W. L. Zhou, J. He, J. Fang, T.-A. Huynh, T. J. Kennedy, K. L. Stokes, C. J. O'Connor, *J. Appl. Phys.* **2003**, *93*, 7340.
- [23] X. Y. Kong, Y. Ding, R. Yang, Z. L. Wang, *Science* **2004**, *303*, 1348.
- [24] X. Y. Kong, Z. L. Wang, *Nano Lett.* **2003**, *3*, 1625.
- [25] Z. L. Wang, *Mater. Today* **2004**, *7*(6), 26.
- [26] W. Hughes, Z. L. Wang, *J. Am. Chem. Soc.* **2004**, *126*, 6703.
- [27] L. Guo, Y. L. Ji, H. Xu, P. Simon, Z. Wu, *J. Am. Chem. Soc.* **2002**, *124*, 14864.
- [28] Z. R. Tian, J. A. Voigt, J. Liu, B. McKenzie, M. J. Mcdermott, M. A. Rodriguez, H. Konishi, H. Xu, *Nat. Mater.* **2003**, *2*, 821.
- [29] C. Pacholski, A. Kornowski, H. Weller, *Angew. Chem.* **2002**, *114*, 1234–1237; *Angew. Chem. Int. Ed.* **2002**, *41*, 1188–1191.
- [30] Z. Li, Y. Xie, Y. Xiong, R. Zhang, W. He, *Chem. Lett.* **2003**, *32*, 760.
- [31] Z. R. Tian, J. A. Voigt, J. Liu, B. McKenzie, M. J. Mcdermott, *J. Am. Chem. Soc.* **2002**, *124*, 12954.
- [32] B. Liu, H. C. Zeng, *J. Am. Chem. Soc.* **2003**, *125*, 4430.
- [33] L. E. Greene, M. Law, J. Goldberger, F. Kim, J. C. Johnson, Y. Zhang, R. J. Saykally, P. Yang, *Angew. Chem.* **2003**, *115*, 3139; *Angew. Chem. Int. Ed.* **2003**, *42*, 3031.
- [34] M. Magalhães, D. Pusiol, M. E. Rania, A. M. Figueiredo Nedo, *J. Chem. Phys.* **1998**, *108*, 3835.
- [35] A. I. Bulavchenko, A. F. Batishchev, E. K. Batishcheva, V. G. Torgov, *J. Phys. Chem.* **2002**, *106*, 6381.
- [36] R. Köhling, J. Woenckhaus, N. L. Klyachko, R. Winter, *Langmuir* **2002**, *18*, 8626.

Gene Technology

Functionalized Carbon Nanotubes for Plasmid DNA Gene Delivery**

Davide Pantarotto, Ravi Singh, David McCarthy, Mathieu Erhardt, Jean-Paul Briand, Maurizio Prato, Kostas Kostarelos,* and Alberto Bianco**

Dedicated to Professor Giorgio Modena on the occasion of his 80th birthday

Exploration of the biological and medical applications of carbon nanotubes (CNTs) is a rapidly expanding field of

[*] Dipl.-Chem. D. Pantarotto, Prof. M. Prato

Dipartimento di Scienze Farmaceutiche

Università di Trieste

34127 Trieste (Italy)

Fax: (+39) 040-5272

E-mail: prato@univ.trieste.it

Dipl.-Chem. R. Singh, Dipl.-Chem. D. McCarthy, Dr. K. Kostarelos

Centre for Drug Delivery Research and

Electron Microscopy Unit

The School of Pharmacy

University of London

London WC1N 1AX (United Kingdom)

Fax: (+39) 207-7535942

E-mail: kostas.kostarelos@ulsop.ac.uk

Dipl.-Chem. D. Pantarotto, Dr. J.-P. Briand, Dr. A. Bianco

Institut de Biologie Moléculaire et Cellulaire

UPR9021 CNRS

Immunologie et Chimie Thérapeutiques

67084 Strasbourg (France)

Fax: (+33) 388-610-680

E-mail: A.Bianco@ibmc.u-strasbg.fr

Dr. M. Erhardt

Institut de Biologie Moléculaire des Plantes

67084 Strasbourg (France)

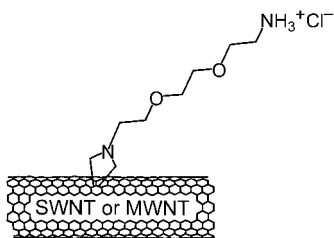
[**] This work was supported by the Centre National de la Recherche Scientifique (CNRS), Università di Trieste, and Ministero dell'Istruzione, dell'Università e della Ricerca (MIUR; cofin 2002, prot. 2002032171). Transmission electron microscopy (TEM) analysis was performed at the microscopy facility of the Institute of Biomedical Problems and was cofinanced by CNRS, Région Alsace, Louis Pasteur University, and the Association de la Recherche pour le Cancer. The authors wish to acknowledge C. D. Partidos for helpful and stimulating discussions. We thank Mr. Claudio Gamboz (Centro Servizi Polivalenti di Ateneo (CSPA), Università di Trieste) for his great help with the TEM measurements.



Supporting information for this article is available on the WWW under <http://www.angewandte.org> or from the author.

research.^[1–11] In particular, the use of CNTs as carriers of biologically active molecules holds great promise.^[6,11] Functionalized carbon nanotubes are interesting as material for engineering a novel gene delivery system.^[12] Herein, we show that ammonium-functionalized CNTs (*f*-CNTs) are able to associate with plasmid DNA through electrostatic interactions. Upon interaction with mammalian cells, these *f*-CNTs penetrate the cell membranes and are taken up into the cells. The nanotubes exhibit low cytotoxicity and *f*-CNT-associated plasmid DNA is delivered to cells efficiently; gene expression levels up to 10 times higher than those achieved with DNA alone were observed. These findings reveal a novel combination of properties attributable to soluble carbon nanotubes and establish the potential of these structures as components of advanced delivery systems for a variety of therapeutics.

Carbon nanotubes were covalently modified by using a method based on the 1,3-dipolar cycloaddition of azomethine ylides.^[13,14] Both single-walled and multi-walled carbon nanotubes (SWNTs and MWNTs) were functionalized with a pyrrolidine ring bearing a free amino-terminal oligoethylene glycol moiety attached to the nitrogen atom. The presence of



this functional group increases the solubility of carbon nanotubes remarkably, particularly in aqueous solutions.^[14] The concentration of functional groups on the carbon nanotubes was calculated as about 0.55 and 0.90 mmol g^{−1} for *f*-SWNTs and *f*-MWNTs, respectively.^[15]

The electrostatic interactions of the positively charged ammonium *f*-CNTs with the phosphate groups of plasmid DNA were studied by TEM. Figure 1 A shows a bundle of *f*-SWNTs deposited from an aqueous solution onto a carbon-coated TEM grid. Although one might expect repulsion between the positive charges of the ammonium salts, which could lead to bundle disruption, nanotube association patterns such as those shown in Figure 1 A were observed throughout. These bundles are less tightly bound than pristine CNTs, probably because of the presence of the functionalization chains. When a solution of *f*-SWNTs (720 μg mL^{−1}) in water was mixed with plasmid DNA (5 μg mL^{−1}) in a 6:1 (+/−) charge ratio, globular and supercoiled structures were observed in different regions of the nanotube surface (see black arrows in Figure 1 B and C).

Spherical, toroidal, or supercoiled structures between 15 and 300 nm in diameter are typically obtained when plasmid DNA is allowed to interact with positively charged groups or cations. Such interaction leads to varying degrees of plasmid condensation depending on the charge density, the hydrophobic character of the interaction, and the number of plasmid DNA molecules in the condensate.^[16] We observed

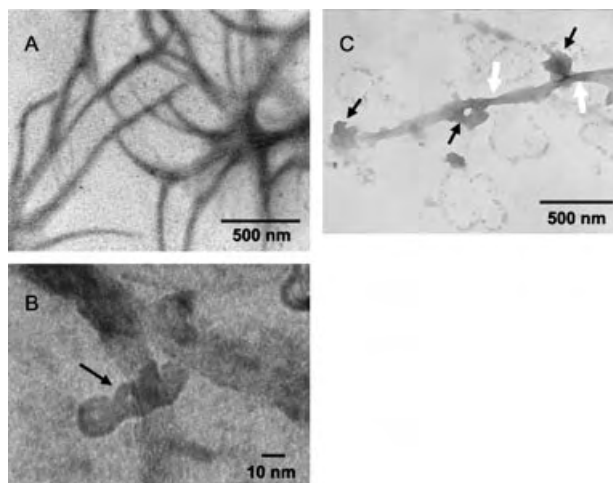


Figure 1. TEM images of *f*-SWNTs (A) and *f*-SWNT:DNA complexes (B and C).

tighter packing of the *f*-SWNTs (see white arrows in Figure 1 C) within regions where condensation of plasmids onto the carbon nanotube bundles took place.

To determine whether it is possible to use these *f*-SWNTs for intracellular delivery applications we studied their interaction with mammalian HeLa cells. We recently reported that CNTs functionalized with a fluorescent group (fluorescein isothiocyanate) and a fluorescent peptide are able to traverse cell membranes.^[6] We did not necessarily expect to observe this property for the positively charged *f*-CNTs used in this study since the high number of charged ammonium groups could interfere with the mechanism of cell binding and uptake. Fluorescence detection is not possible for the ammonium-CNTs described herein because of the lack of an appropriate chromophore. The interaction of the *f*-CNTs with cells was therefore studied by TEM. HeLa cells were incubated with ammonium *f*-SWNTs and *f*-MWNTs at a concentration of 2.5 mg mL^{−1}. The nanotubes were allowed to interact with the cells for 1 h and were then embedded in an epoxy resin. Ultrathin sections of the polymer (about 90 nm thick) were cut on an ultramicrotome with a diamond knife and examined by TEM. Figure 2 shows HeLa cells incubated with *f*-MWNTs. The various cellular compartments are indicated by white arrows in Figure 2 A. Many nanotubes are clearly visible inside the cell. Subsequent magnifications (Figure 2 B and C) provide a higher-resolution view of the intracellular localization of the *f*-MWNTs. Interestingly, a degree of nuclear localization of the nanotubes was observed consistently throughout the samples. Careful analysis of the cell sections also permitted observation of nanotubes in the process of crossing the plasma membrane barrier.

Figure 2 D shows an *f*-MWNT during interaction with the cell membrane and uptake into the cell. The observed nanotube has a diameter of about 20 nm and an apparent length of around 200 nm. Although the mechanism of cellular uptake is still unclear, the semirigid and elongated form of the tube rules out an endocytosis process.^[17] This deduction was confirmed by preincubation of the cells with sodium azide or 2,4-dinitrophenol, typical inhibitors of energy-dependent cell

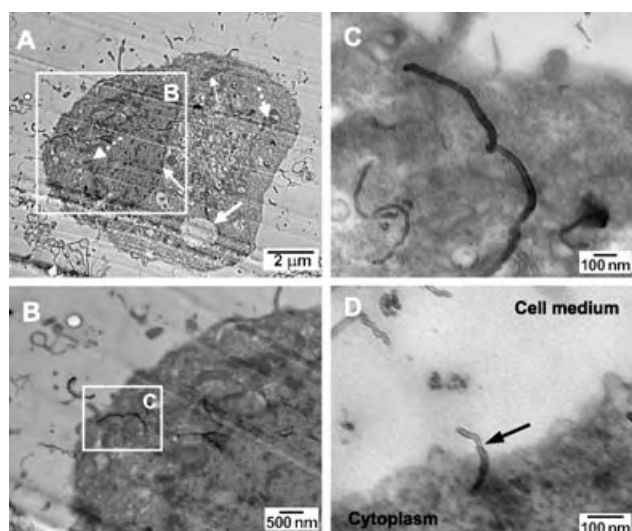


Figure 2. Ultrathin transverse section of HeLa cells treated with *f*-MWNTs. After incubation, the cells were fixed, stained, dehydrated, and embedded in Epon 812 resin. Ultrathin layers (90 nm thick) were cut with an ultramicrotome. A) The entire cell; B) and C) two subsequent magnifications. D) A multi-walled carbon nanotube crossing the cell membrane. Dotted white arrow, chromatin; dashed white arrow, a mitochondrion; thin white arrow, Golgi complex; medium white arrow, nuclear membrane; thick white arrow, a vacuolium.

processes such as endocytosis. The carbon nanotubes used in this study probably enter the cell by a spontaneous mechanism in which they behave like nanoneedles and pass through the cell membrane without causing cell death.^[18] Very recently published molecular dynamics simulation data suggest that hydrophobic nanotubes with hydrophilic functional groups can spontaneously insert into a lipid bilayer.^[19]

Such mechanistic modeling results correlate well with our experimental observations on the interaction between *f*-CNTs and plasma membranes (Figure 2D). We believe that the cationic functional groups bind the nanotubes to the cell membrane, then a spontaneous insertion mechanism allows the nanotubes to pass through the biomembrane as predicted by theoretical studies. Subsequent translocation of the *f*-CNTs within the intracellular region could follow this non-endocytotic process.

The ability of the ammonium-functionalized carbon nanotubes to enter cells and potentially reach their nuclei was further exploited for the delivery of plasmid DNA to the cell. Figure 3 shows the levels of marker gene (β -galactosidase; β -gal) expression in CHO cells after exposure to nanotubes connected to plasmid DNA encoding the gene.

As with other nonviral gene delivery vectors,^[20–22] the charge ratio between the ammonium groups at the SWNT surface and the phosphate groups of the DNA backbone seems to be a determinant factor in the level of gene expression. *f*-SWNT/DNA charge ratios between 2:1 and 6:1 (+/–) led to 5–10 times higher levels of gene expression than treatment of the cells with DNA alone. No cytotoxicity was observed in this study (the highest nanotube concentration used in our gene delivery experiments was 1.2 mg mL^{-1}),^[18] even when the *f*-SWNT:DNA complexes were incubated with the CHO cells for 3 h. We observed an increase in gene expression with increasing incubation times for *f*-SWNT:DNA complexes with charge ratios that resulted in optimum gene delivery capacity (i.e. between 2:1 and 6:1); the three-hour incubation period led to peak gene delivery for these complexes. The functionalized carbon nanotubes used in this study offer considerable advantages over other nanomaterials recently explored as components of systems for the delivery of DNA to mammalian cells.^[23–25] The nanotubes

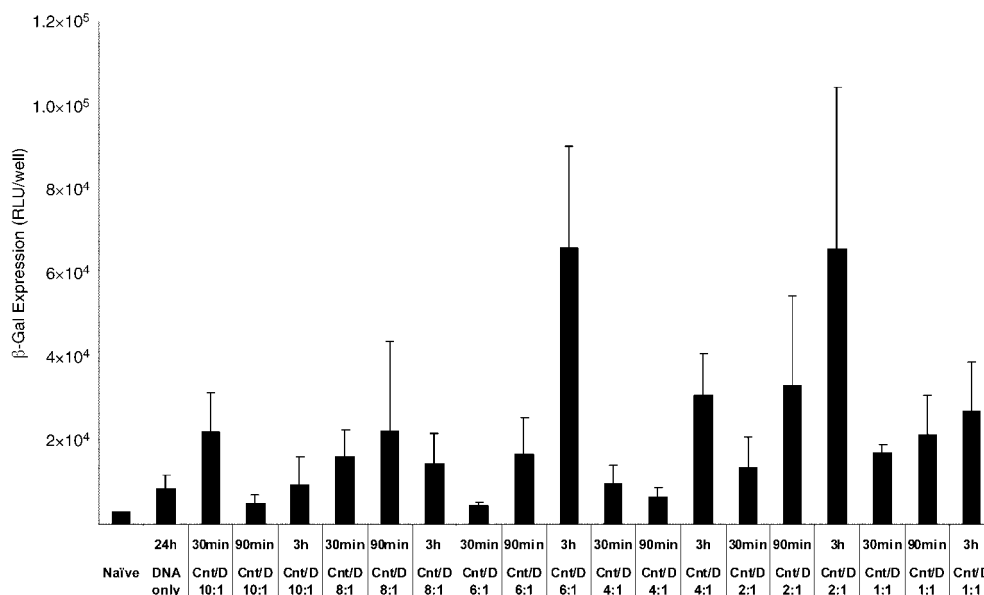


Figure 3. Delivery of plasmid DNA by *f*-SWNTs and expression in cells. Levels of marker gene (β -gal) expression in CHO cells in relative light units (RLU) per mg total protein. Various *f*-SWNT/DNA charge ratios were tested with three different incubation time periods. Toxicity manifested as cell detachment and death was not observed at any point during this study. *f*-SWNT and DNA are denoted in the figure as Cnt and D, respectively.

described herein allow relatively facile further functionalization of their surface and are therefore chemically versatile, they are capable of penetrating the cell membrane, and they have a lower cytotoxicity than other nanomaterials. Other cationic macromolecules, such as peptides, dendrimers, and liposomes generally achieve effective delivery of DNA by causing destabilization of the cell membrane, which leads to pronounced cytotoxicity.^[26–29] Preliminary comparative gene expression data for lipid:DNA and *f*-CNT:DNA delivery systems show that our first generation of functionalized carbon nanotubes is less effective for transfection in vitro than lipid:DNA systems.

The study reported herein constitutes the first example of the utilization of carbon nanotubes as components for engineering a novel nanotube-based gene delivery vector system. The functionalized nanotubes formed supramolecular complexes with plasmid DNA through ionic interactions. These complexes are able to bind to, and penetrate within cells by what seems to be an endosome-independent mechanism. *f*-SWNTs complexed with plasmid DNA were able to facilitate higher DNA uptake and gene expression in vitro than could be achieved with DNA alone. In view of these interesting properties, the delivery of other types of therapeutic agents by *f*-CNTs through noncovalent interactions of the nanotubes with the agent can be envisaged.

Experimental Section

***f*-SWNT:DNA complexes:** *f*-SWNTs were hydrated in deionized water at a concentration of 6 mg mL^{−1}. Plasmid DNA (pBgal, Clontech) was hydrated in deionized water at a concentration of 1 mg mL^{−1}. Aliquots were stored frozen at −20 °C until needed. The appropriate volume of nanotubes was diluted to a total volume of 300 µL in Optimem. pBgal (3 µg) was added to a separate sample of Optimem (300 µL). The diluted nanotubes were added dropwise to the DNA and the mixture was pipetted briefly. Complexes were allowed to form for 10 min prior to use. This process was repeated for each charge ratio tested. For the electron microscopy investigations, the nanotubes and DNA were always allowed to interact in water. An aqueous sample containing *f*-SWNT:DNA complexes was deposited onto a 300-mesh copper grid coated with a Formvar/carbon support film (Taab Labs Ltd.). Prior to preparation, the grids were “glow discharged” in an Emitech K350G system (Emitech Ltd) for 3 min at 30 mA (negative polarity). Imaging was carried out with a FEI/Philips CM120 BioTwin transmission electron microscope (Eindhoven) at an accelerating voltage of 120 kV, and with a Philips TEM 208 instrument at an accelerating voltage of 100 kV.

Preparation of cell sections for TEM analysis: SWNTs and MWNTs were purchased from Carbon Nanotechnology, Inc. and Nanostructured & Amorphous Materials, Inc., respectively, and were functionalized as described in the literature.^[14] HeLa cells (1.25 × 10⁵) were cultured in Dulbecco's minimal essential medium in a 16-well plate at 37 °C in the presence of 5% CO₂ until 75% confluency was reached. The cells were then incubated with a solution of *f*-SWNT and *f*-MWNT (2.5 mg mL^{−1} each) in phosphate-buffered saline (PBS) for 1 h, washed twice with PBS, and fixed by treatment with 2.5% glutaraldehyde in a cacodilate buffer (0.075 M sodium cacodilate, 1 mM MgCl₂, 1 mM CaCl₂, 4.5% sucrose, pH 7.3) for 2 h at room temperature. An aliquot (10% v/v) of a saturated solution of picric acid in cacodilate buffer (1/10) was added to each well and the cells were incubated overnight at 4 °C. The specimen was washed three times with distilled water (15 min each wash) then treated with a 1% OsO₄ solution in cacodilate buffer for 2 h at room temperature. Cells

were carefully rinsed with distilled water and post-fixed with a 2% solution of uranyl acetate in water overnight at 4 °C. After several washes, the cells were dried by treatment with 70% and 90% ethanol for 10 min each, and twice with absolute ethanol for 20 min. A fresh sample of Epon 812 resin was prepared as suggested by Electron Microscopy Sciences and distributed through the cells in each well. The plate was stored in an oven at 65 °C for three days. Each resin block was then removed from the plastic support and cut. A Reichert-Jung Ultracut-E ultramicrotome with a diamond knife (Ultramicrotomy 45°) was used to cut the resin containing the cells into 90-nm thick slices. Three consecutive slices were deposited on a formvar grid and observed through a Hitachi 600 electronic transmission microscope at 75 kV. Images were taken with an AMT high-sensitivity camera at various levels of magnification.

Gene delivery studies: CHO cells (ATCC) were grown to 90% confluency in F12K medium containing 10% fetal bovine serum and 1% penicillin/streptomycin (all from Gibco) in 96-well tissue culture dishes (Corning-Costar). CHO cells are one of the most popular cell lines used for gene transfer studies since they exhibit adequate levels of gene expression after treatment with various nonviral transfection agents; these cells are also commonly used for genetic screening purposes.^[30] The culture medium was removed, *f*-SWNT:DNA complexes (50 µL) were added, and the cells were analyzed in triplicate under each set of test conditions. After 30, 90, or 180 min, the transfection medium was removed and replaced with fresh culture medium. As a control, three wells were transfected with DNA (0.25 µg) in Optimem (50 µL). Cells were incubated for 48 h then harvested. β-galactosidase activity was measured by using the Tropic Galactolight Plus kit and a Berthold 9507 luminometer according to the manufacturers' instructions.

Received: April 25, 2004

Revised: June 24, 2004

Keywords: carbon nanotubes · gene delivery · plasmid DNA · supramolecular chemistry

- [1] J. Bradbury, *Lancet* **2003**, 362, 1984–1985.
- [2] A. Bianco, M. Prato, *Adv. Mater.* **2003**, 15, 1765–1768.
- [3] K. H. Park, M. Chhowalla, Z. Iqbal, F. Sesti, *J. Biol. Chem.* **2003**, 278, 50212–50216.
- [4] K. A. Williams, P. T. M. Veenhuizen, B. G. de la Torre, R. Eritjia, C. Dekker, *Nature* **2002**, 420, 761.
- [5] R. J. Chen, S. Bangsaruntip, K. A. Drouvalakis, N. W. Kam, M. Shim, Y. Li, W. Kim, P. J. Utz, H. Dai, *Proc. Natl. Acad. Sci. USA* **2003**, 100, 4984–4989.
- [6] D. Pantarotto, J.-P. Briand, M. Prato, A. Bianco, *Chem. Commun.* **2004**, 16–17.
- [7] M. Zheng, A. Jagota, E. D. Semke, B. A. Diner, R. S. McLean, S. R. Lustig, R. E. Richardson, N. G. Tassi, *Nat. Mater.* **2003**, 2, 338–342.
- [8] M. Zheng, A. Jagota, M. S. Strano, A. P. Santos, P. Barone, S. G. Chou, B. A. Diner, M. S. Dresselhaus, R. S. McLean, G. B. Onoa, G. G. Samsonidze, E. D. Semke, M. Usrey, D. J. Walls, *Science* **2003**, 302, 1545–1548.
- [9] C. Richard, F. Balavoine, P. Schultz, T. W. Ebbesen, C. Mioskowski, *Science* **2003**, 300, 775–778.
- [10] C. R. Martin, P. Kohli, *Nat. Rev. Drug Discovery* **2003**, 2, 29–37.
- [11] N. W. Shi Kam, T. C. Jessop, P. A. Wender, H. Dai, *J. Am. Chem. Soc.* **2004**, 126, 6850–6851.
- [12] K. Kostarelos, *Adv. Colloid Interface Sci.* **2003**, 106, 147–168.
- [13] V. Georgakilas, K. Kordatos, M. Prato, D. M. Guldi, M. Holzinger, A. Hirsch, *J. Am. Chem. Soc.* **2002**, 124, 760–761.
- [14] V. Georgakilas, N. Tagmatarchis, D. Pantarotto, A. Bianco, J.-P. Briand, M. Prato, *Chem. Commun.* **2002**, 3050–3051.

- [15] D. Pantarotto, C. D. Partidos, R. Graff, J. Hoebeke, J.-P. Briand, M. Prato, A. Bianco, *J. Am. Chem. Soc.* **2003**, *125*, 6160–6164.
- [16] R. W. Wilson, V. A. Bloomfield, *Biochemistry* **1979**, *18*, 2192–2196.
- [17] L. A. Kuelto, C. R. Middaugh, *J. Pharm. Sci.* **2003**, *92*, 1754–1772.
- [18] The cytotoxicity of the *f*-CNTs was assessed by flow cytometry. The behavior of cells was tested at *f*-CNT concentrations of 0.01–10 mgmL^{−1} after incubation for 6 h. Up to an *f*-CNT concentration of 1 mgmL^{−1}, more than 80 % of the cells remained alive; only at the very high concentration of 10 mgmL^{−1} did cell survival drop to 50 % (see the Supporting Information). For toxicity studies of pristine carbon nanotubes, see: A. A. Shvedova, V. Castranova, E. R. Kisin, D. Schwegler-Berry, A. R. Murray, V. Z. Gandelsman, A. Maynard, P. Baron, *J. Toxicol. Environ. Health Part A* **2003**, *66*, 1909–1926; D. B. Warheit, B. R. Laurence, K. L. Reed, D. H. Roach, G. A. Reynolds, T. W. Webb, *Toxicol. Sci.* **2004**, *47*, 117–125; C. W. Lam, J. T. James, R. McCluskey, R. L. Hunter, *Toxicol. Sci.* **2004**, *47*, 126–134.
- [19] C. F. Lopez, S. O. Nielsen, P. B. Moore, M. L. Klein, *Proc. Natl. Acad. Sci. USA* **2004**, *101*, 4431–4434.
- [20] D. Joubert, J. van Zyl, A. Hawtrey, M. Ariatti, *Drug Delivery* **2003**, *10*, 209–211.
- [21] H. Eliyahu, N. Serval, A. J. Domb, Y. Barenholz, *Gene Ther.* **2002**, *9*, 850–858.
- [22] J. H. Lee, Y. Lim, J. S. Choi, Y. Lee, T. Kim, H. J. Kim, J. K. Yoon, K. Kim, J. Park, *Bioconjugate Chem.* **2003**, *14*, 1214–1221.
- [23] A. K. Salem, P. Searson, K. W. Leong, *Nat. Mater.* **2003**, *2*, 668–671.
- [24] T. Paunesku, T. Rajh, G. Wiederrecht, J. Maser, S. Vogt, N. Stojicevic, M. Protic, B. Lai, J. Oryhon, M. Thurnauer, G. Woloschak, *Nat. Mater.* **2003**, *2*, 343–346.
- [25] T. E. McKnight, A. V. Melechko, G. D. Griffin, M. A. Guillorn, V. I. Merkulov, F. Serna, D. K. Hensley, M. J. Doktycz, D. H. Lowndes, M. L. Simpson, *Nanotechnology* **2003**, *14*, 551–556.
- [26] K. Rittner, A. Benavente, A. Bompard-Sorlet, F. Heitz, G. Divita, R. Brasseur, E. Jacobs, *Mol. Ther.* **2003**, *5*, 104–114.
- [27] U. Boas, P. M. H. Heegaard, *Chem. Soc. Rev.* **2004**, *33*, 43–63.
- [28] K. Keifer, J. Clement, P. Garidel, R. Peschka-Süss, *Pharm. Res.* **2004**, *21*, 1009–1017.
- [29] C. R. Dass, *J. Pharm. Pharmacol.* **2002**, *54*, 593–601.
- [30] S. Grimm, *Nat. Rev. Genet.* **2004**, *5*, 179–89.

Nanofibers from Functionalized Dendritic Molecules**

Maryna Ornatska, Kathy N. Bergman, Beth Rybak, Sergiy Peleshanko, and Vladimir V. Tsukruk*

Because of their architectural symmetry, the vast majority of dendritic molecules have globular or nearly globular shapes and can form uniform molecular layers on solid surfaces.^[1–3] Only dendritic molecules with peculiar architectures were shown to be capable of forming self-assembled one-dimensional supramolecular structures such as rods, fibers, ribbons, and helices, which are of special interest for nanotechnology. These architectures include shape-persistent planar dendrimers, hairy rod and discotic polymers, rod-coils, rod-dendrons, and tapered molecules.^[4–10] A proper combination of steric constraints, stacking interactions, and hydrogen bonding is postulated to be critical for precise assembly of these molecules. In contrast, there are very few reports on organized structures from hyperbranched molecules,^[11] which, because of their irregular architecture and higher polydispersity, are not expected to form regular structures.^[12–15]

It is widely accepted that a precise matching of directional interactions and steric constraints is required to facilitate long-range one-dimensional supramolecular assembly. On the contrary, here we demonstrate that multiple weak interactions among irregular, branched molecules with relatively high molecular weight and high polydispersity can facilitate their assembly into well-ordered one-dimensional supramolecular structures such as long and uniform micro- and nanofibers. To the best of our knowledge, this is the first example of one-dimensional supramolecular structures assembled from irregular, highly branched, dendritic molecules.

Synthesis and comprehensive chemical characterization are described elsewhere.^[16] The theoretical chemical structure of the highly branched amphiphilic compound studied here (fourth-generation hyperbranched polyester) with a degree of branching of 40% and chemical composition determined by NMR spectroscopy is presented in Figure 1. Note that these and other data, as well as the chemical structure, of irregular hyperbranched architectures should be considered only as averages.^[17,18] The shell of the modified core after fractiona-

[*] M. Ornatska, K. N. Bergman, B. Rybak, S. Peleshanko, Prof. V. V. Tsukruk
Department of Materials Science and Engineering
Iowa State University
3053 Gilman Hall, Ames, IA 50011 (USA)
Fax: (+1)515-294-7202
E-mail: vladimir@iastate.edu

[**] The authors thank K. Genson, R. Gunawidjaja and D. Vaknin for technical assistance. This work is supported by NSF-DMR-0308982 and AFOSR F496200210205 Grants.



Supporting information for this article is available on the WWW under <http://www.angewandte.org> or from the author.

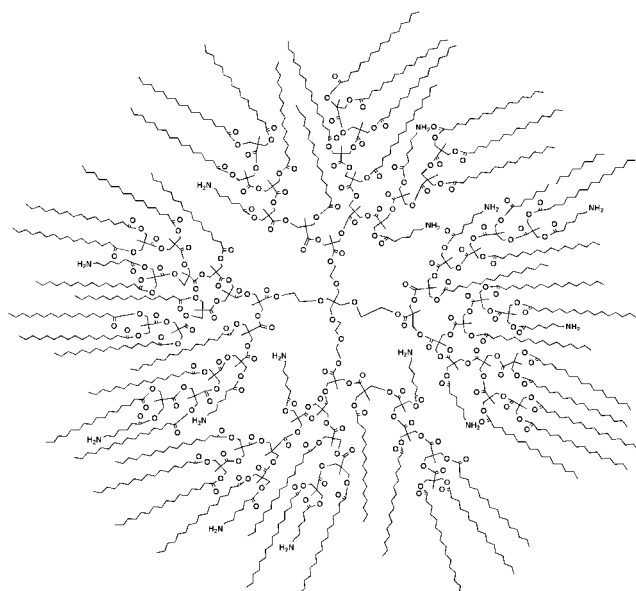


Figure 1. Structural formula of the amphiphilic hyperbranched polyester with a degree of branching of 40%, modified with terminal alkyl and amino groups.

tion was composed of about 50 hydrophobic C_{16} alkyl tails, about 14 amino-terminated groups, and 1–2 hydroxy-terminated branches.

The modified hyperbranched polymer, deposited at an air/water interface, exhibited stable amphiphilic surface behavior with increasing surface pressure during compression to an area per molecule (APM) of less than 12 nm^2 .^[16] This is in sharp contrast to the “naked” hyperbranched cores, which desorbed in the water subphase during compression.

Remarkably, uniform, stable one-dimensional surface morphologies were formed by these molecules on a silicon surface. At very low surface pressures ($\text{APM} > 15 \text{ nm}^2$), isolated individual nanofibers became evident all over the surface (Figure 2a). They had an overall height of about 2 nm, lengths of less than 500 nm, and uniform but punctured shapes. The individual nanofibers became more uniform, better defined, and more clearly visible at slightly higher surface pressure (Figure 2b). These longer nanofibers (ca. $1 \mu\text{m}$ long) were curved and had a low degree of branching with occasional splitting.

At even higher surface pressure, the uniform nanofibers formed densely packed bundles weaving across large surface areas with overall lengths exceeding several micrometers (Figure 2c,d). At higher pressures the height of these structures increased slightly to 3–4 nm. In this condensed state they formed a dense interwoven network with a texture typical of nematic liquid-crystalline phases with characteristic topological defects.^[19] Remarkably, the nanofibers preserved their identity without merging into thicker fibers, even at high packing density. These surface structures were exceptionally stable under normal scanning conditions and resisted higher shear forces even in the hard tapping mode.

High-resolution imaging in the tapping mode at low forces revealed a dilated shape of the nanofibers, which is a typical artifact produced by the AFM tip (Figure 2). We carefully

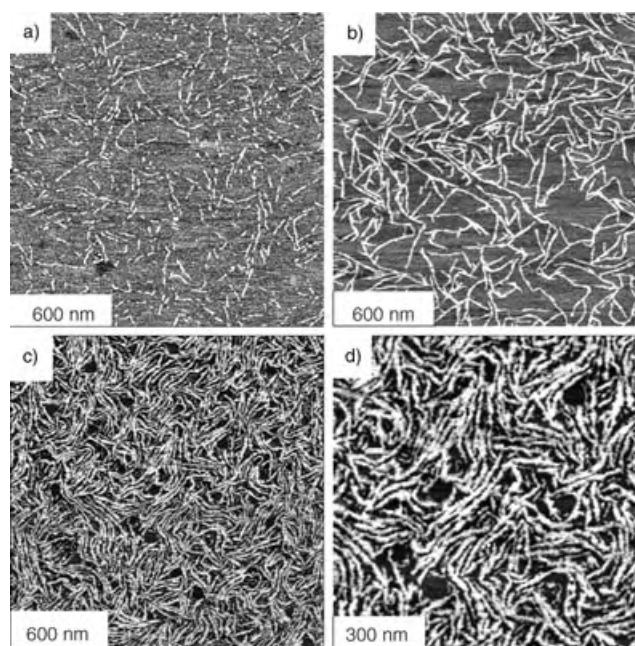


Figure 2. AFM phase images of nanofibrillar structures formed from dendritic molecules at different surface pressures. a) 0.2 mN m^{-1} ; b) 5 mN m^{-1} ; c, d) 30 mN m^{-1} , different scales.

analyzed the shape of these nanostructures with a very sharp carbon nanotube tip with a calibrated radius of less than 8 nm to deconvolute the tip shape and estimate the true lateral dimensions. We used a hemispherical approximation to account for tip dilation, in accordance with a known approach.^[20] Considering the very small height of the one-dimensional structures of 2–4 nm (analysis of 30 randomly selected cross sections), tip dilation generally contributed less than 50 % of the apparent width, which makes this correction quite reliable. These results led us to the conclusion that the observed one-dimensional structures are indeed nanofibers with a height of 3–4 nm and lateral dimensions of 4–8 nm, that is, close to molecular dimensions estimated from molecular models.

We considered possible molecular conformations of amphiphilic hyperbranched molecules on a hydrophilic surface, including edge-on packing and flattened cores.^[21] However, X-ray reflectivity studies on the molecules at the air/water interface demonstrated that the alkyl tails are predominantly oriented upwards with a certain tilt and a total monolayer thickness of about 3 nm.^[18] From the analysis of the combined AFM and X-ray data on nanofiber dimensions, Langmuir isotherm data of molecular areas, X-ray data on tail orientation, and molecular dimensions from minimized molecular models, we suggest asymmetric molecular packing of these nanofibers (Figure 3). In this model, the molecules adopt a hemispherical conformation in which hydrophilic cores are squashed against the solid surface, as was suggested for amphiphilic dendrimers.^[13] A number of important observations support this model. First, the proposed conformation maximizes interactions between terminal amino groups and surface silanol groups and thus makes this structure energetically favorable.^[22] Second, this conforma-

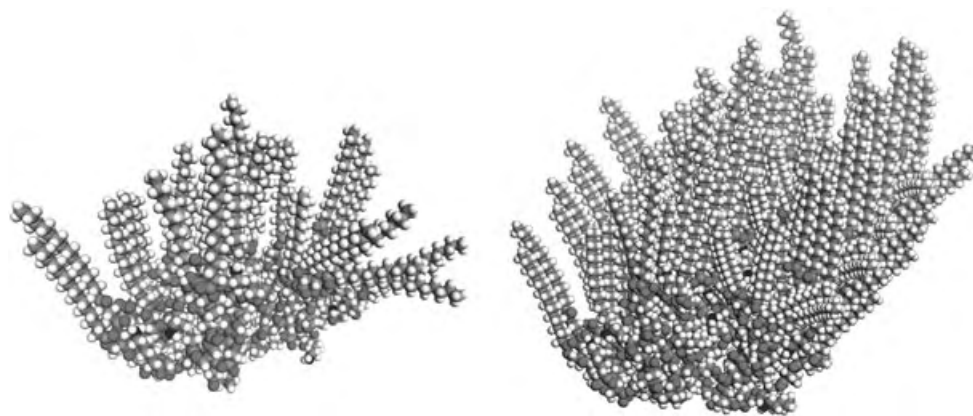


Figure 3. Molecular graphics representation of the suggested conformation of a single amphiphilic hyperbranched molecule on a solid hydrophilic surface (left) and their aggregation in the one-dimensional supramolecular structure (right).

tion results in the the overall height of the molecules of 2–4 nm and the lateral dimensions of 4–8 nm, depending upon the degree of tail orientation and core conformation, and closely corresponds to both X-ray and AFM data. Third, the hydrophobic alkyl tails that dominate in the shell are oriented upwards, tilted, cover most of the core, and thus define the surface APM of about 11 nm², which is close to the results of Langmuir isotherms of condensed monolayers. Finally, the proposed molecular arrangement should result in a modestly hydrophobic surface, which was confirmed by measurement of the contact angle (60–80°). All other known conformations that were examined (edge-on, face-on, and face-on flattened orientations) could not satisfy the whole set of experimental data.

Dense lateral stacking is suggested as a way of assembling these branched molecules in one-dimensional continuous rows resembling hemicylindrical micelles. Although the nature of the driving forces behind this one-dimensional assembly is not clear, we suggest that directional crystallization of alkyl tails could play a significant role. The less disturbed alkyl tails oriented vertically in the central portion of the molecules could be involved in local ordering, while more distorted, tilted alkyl tails along the edges could prevent crystallization in the lateral direction. X-ray scattering showed highly disturbed (paracrystalline) packing of alkyl chains in this material.^[23] On the other hand, the proposed stacking provides the best chance for the amino, hydroxy, ester, and carboxy groups of the cores and inner shells of neighboring molecules to form a saturated network of hydrogen bonds and polar interactions without significant interference with the packed alkyl tails.^[24] This would be impossible in a symmetrical face-on conformation. The critical role of these interactions is supported by the fact that similar molecules without amino groups do not form nanofibrillar structures.^[16]

Cylindrical and hemicylindrical micellar structures similar to those reported here were observed for conventional ionic surfactants.^[25,26] A fine balance of weak intermolecular interactions was considered to be crucial for the formation of these surface micellar structures. However, the core-shell architecture of the amphiphilic hyperbranched molecules

studied here makes these one-dimensional nanofibrillar supramolecular structures unique. The multiple intermolecular hydrogen bonding and polar interactions between flexible cores stabilize these nanofibers and make them robust but flexible, unlike unstable hemicylindrical micelles from conventional surfactants, which are easily disrupted by drying and rarely form microscopically continuous fibers.

The peculiar internal organization of these nanofibrils with hydrophilic inner core and hydrophobic shell makes them an intriguing candidate for templating inorganic wired nanostructures, as already demonstrated for rigid molecules.^[4] However, we believe that these flexible branched molecules could be much more versatile because of their straightforward one-pot synthesis.^[27] Moreover, our findings question the current paradigm calling for well-defined, shape-persistent, and rigid molecules with precisely placed functional groups as building blocks for one-dimensional supramolecular nanostructures, and extend the known concept of steric balance and intermolecular interactions beyond well-defined shape-persistent (e.g., rod-dendron) architectures. Our results show the critical role of a highly branched chemical structure with multiple specific intermolecular interactions in the assembly of organized supramolecular structures. The amplification of weak, directional interactions facilitated by the presence of multiple peripheral branches of irregular, flexible molecules can lead to their efficient self-assembly into stable nanofibrillar structures. This example demonstrates that one-dimensional supramolecular assembly can be achieved without tedious multistep synthesis of shape-persistent molecules.

Received: April 13, 2004

Revised: May 25, 2004

Keywords: dendrimers · nanostructures · self-assembly

- [1] *Dendrimers and Other Dendritic Polymers* (Eds.: J. M. J. Fréchet, D. A. Tomalia), Wiley, London, **2002**.
- [2] V. V. Tsukruk, *Adv. Mater.* **1998**, *10*, 253–255.
- [3] V. Tsukruk, *Prog. Polym. Sci.* **1997**, *22*, 247–311.
- [4] E. R. Zubarev, M. U. Pralle, E. D. Sone, S. I. Stupp, *J. Am. Chem. Soc.* **2001**, *123*, 4105–4106.

- [5] S. Loi, H. Butt, U. Wiesler, K. Müllen, *Chem. Commun.* **2000**, 13, 1169–1170.
- [6] D. Liu, H. Zhang, P. C. Grim, S. De Feyter, U. Wiesler, A. Berresheim, K. Müllen, F. C. De Schryver, *Langmuir* **2002**, 18, 2385–2391.
- [7] M. Menger, S. Lee, X. Tao, *Adv. Mater.* **1995**, 7, 669–671.
- [8] S. Lecommandoux, H. A. Klok, M. Sayar, S. I. Stupp, *J. Polym. Sci. Part A* **2003**, 41, 3501–3518.
- [9] M. Lee, J.-W. Kim, S. Peleshanko, K. Larson, Y.-S. Yoo, D. Vaknin, S. Markutsya, V. V. Tsukruk, *J. Am. Chem. Soc.* **2002**, 124, 9121–9128.
- [10] V. V. Tsukruk, K. L. Genson, S. Peleshanko, S. Markutsya, A. Greco, M. Lee, Y. Yoo, *Langmuir* **2003**, 19, 495–499.
- [11] J. M. J. Frechet, C. J. Hawker, I. Gitsov, J. W. Leon, *J. Macromol. Sci. Part A* **1996**, 33, 1399–1425.
- [12] A. Sunder, M.-F. Quincy, R. Mülhaupt, H. Frey, *Angew. Chem.* **1999**, 111, 3107–3110; *Angew. Chem. Int. Ed.* **1999**, 38, 2928–2930.
- [13] B. Voit, *J. Polym. Sci. Part A* **2000**, 38, 2505–2525.
- [14] X. Zhai, S. Peleshanko, N. S. Klimenko, K. L. Genson, M. Ya. Vortman, V. V. Shevchenko, D. Vaknin, V. V. Tsukruk, *Macromolecules* **2003**, 36, 3101–3110.
- [15] S. E. Stiriba, H. Kautz, H. Frey, *J. Am. Chem. Soc.* **2002**, 124, 9698–9699.
- [16] M. Ornatska, S. Peleshanko, K. L. Genson, B. Rybak, K. N. Bergman, V. V. Tsukruk, *J. Am. Chem. Soc.* **2004**, ASAP, DOI:10.1021/ja 0498944..
- [17] H. Magnusson, E. Malmstrom, A. Hult, *Macromolecules* **2000**, 33, 3099–3104; A. Burgath, A. Sunder, H. Frey, *Macromol. Chem. Phys.* **2000**, 201, 782–791; E. Zagar, M. Zigon, *Macromolecules* **2002**, 35, 9913–9925.
- [18] F. Chu, C. J. Hawker, P. J. Pomery, D. J. Hill, *J. Polym. Sci. Part A* **1997**, 35, 1627–1633; R. Hanselman, D. Holter, H. Frey, *Macromolecules* **1998**, 31, 3790–3801.
- [19] V. V. Tsukruk, V. V. Shilov, *Structure of Polymeric Liquid Crystals*, Science, Kiev, **1990**.
- [20] V. V. Tsukruk, *Rubber Chem. Technol.* **1997**, 70, 430–467.
- [21] H. Engelkamp, S. Middelbeek, R. J. Nolte, *Science* **1999**, 284, 785–788.
- [22] V. V. Tsukruk, V. N. Bliznyuk, *Langmuir* **1998**, 14, 446–455.
- [23] M. Ornatska, S. Peleshanko, B. Rybak, K. N. Bergman, G. Holzmüller, V. V. Tsukruk, *Adv. Mater.*, in press.
- [24] S. Schneider, *Hydrogen Bonding*, Oxford University Press, **1997**.
- [25] H. E. Gaub, S. Manne, *Science* **1995**, 270, 1480–1482.
- [26] W. A. Ducker, E. J. Wanless, *Langmuir* **1999**, 15, 160–168.
- [27] C. Nguyen, C. J. Hawker, R. D. Miller, E. Huang, J. L. Hedrick, R. Gauderon, J. G. Hilborn, *Macromolecules* **2000**, 33, 4281–4284; I. Sendijarevic, A. J. McHugh, L. J. Markoski, J. S. Moore, *Macromolecules* **2001**, 34, 8811–8813.

Spin Trapping of ^{13}C -Labeled *p*-Benzynes Generated by Masamune–Bergman Cyclization of Bicyclic Nine-Membered Eneidyne**

Toyonobu Usuki, Takashi Mita, Martin J. Lear,*
Parthasarathi Das, Fumihiko Yoshimura,
Masayuki Inoue, Masahiro Hiramata,* Kimio Akiyama,*
and Shozo Tero-Kubota

In memory of Satoru Masamune

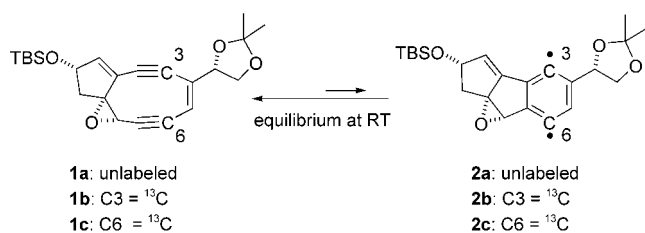
Our understanding of the chemistry and biology of the enediyne class of antitumor antibiotics is still developing and faces further challenges.^[1] The cleavage of double-stranded DNA through hydrogen abstraction by enediyne-derived radicals is a generally well-accepted mechanism.^[1b,e] However, the mechanisms of several unexpected and complex cytotoxic effects of enediynes, such as RNA^[2] and protein^[3] damage or the generation of *p*-quinone species,^[4] have yet to be fully elucidated. Despite several carefully crafted experimental^[5] and theoretical^[6] studies on simplified systems, the behavior of the major chemical perpetrators of such cytotoxicity, namely the biradical intermediates formed by natural enediynes, remains more a matter of conjecture than a point of fact.^[7]

There is clearly a need to study and accurately represent the presumed thermal behavior of the reactive bicyclic cores of natural enediynes, especially those featuring nine-membered rings.^[7,8] We first recognized this need in 1995 after observing the paramagnetic activity of the bicyclic epoxyenediyne core **1a** of the kedarcidin chromophore (Scheme 1).^[7a] We speculated that a spontaneous equilibration similar to that likely to take place between **1** and the *p*-

[*] T. Usuki, Dr. T. Mita, Dr. M. J. Lear, Dr. P. Das, Dr. F. Yoshimura,
Dr. M. Inoue, Prof. Dr. M. Hiramata
Department of Chemistry
Graduate School of Science
Tohoku University
Sendai 980-8578 (Japan)
Fax: (+81) 22-217-6566
E-mail: martin@ykbsc.chem.tohoku.ac.jp
hiramata@ykbsc.chem.tohoku.ac.jp

Prof. Dr. K. Akiyama, Prof. Dr. S. Tero-Kubota
Institute of Multidisciplinary Research
for Advanced Materials
Tohoku University
Sendai 980-8577 (Japan)
Fax: (+81) 22-217-5612
E-mail: akiyama@tagen.tohoku.ac.jp

[**] This work was supported by CREST (Core Research for Evolutional Science and Technology), the Japan Science and Technology Agency (postdoctoral fellowship to P.D.), and the Ministry of Education, Culture, Sports, Science and Technology. We are grateful for three Research Fellowships for Young Scientists (T.U., T.M., and F.Y.) from the Japanese Society for the Promotion of Science. We thank Dr. Jonathan Hobley, Tohoku University, for many insightful comments and fruitful discussions.



Scheme 1. Spontaneous thermal Masamune–Bergman cyclization of the nine-membered ring of enediyne **1** to form *p*-benzyne biradical **2**. TBS, *tert*-butyldimethylsilyl.

benzyne biradical **2** at ambient temperatures would occur within other natural chromophores that contain a nine-membered ring.^[7b,c] In the study described herein, we expanded and reinforced these earlier speculations by using isotopomers of **1** with ¹³C labels at the supposed radical-forming positions 3 and 6. To tackle the daunting task of obtaining a continuous supply of the unstable compounds **1** in sufficient quantities, we remodeled our previous synthesis of **1a**^[7a] and recently devised efficient and reproducible routes to the ¹³C isotopomers **1b** and **1c**.^[9] Through a combination of EPR spin trapping^[10] and MS experiments we have now obtained new spectroscopic evidence for the spontaneous thermal generation of the *p*-benzyne biradical **2** as an intermediate in the Masamune–Bergman cyclization^[11] of **1**.^[1a]

To derive the optimum amount of evidence for the existence of the highly transient biradical **2**^[7a] and to obtain stable adducts for MS analysis, we studied the spin-trapping reaction of **1** with both 2-methyl-2-nitrosopropane (MNP) and 5,5-dimethyl-1-pyrrolidine *N*-oxide (DMPO).^[12,13] Figure 1a shows the continuous wave (CW) EPR spectrum of the

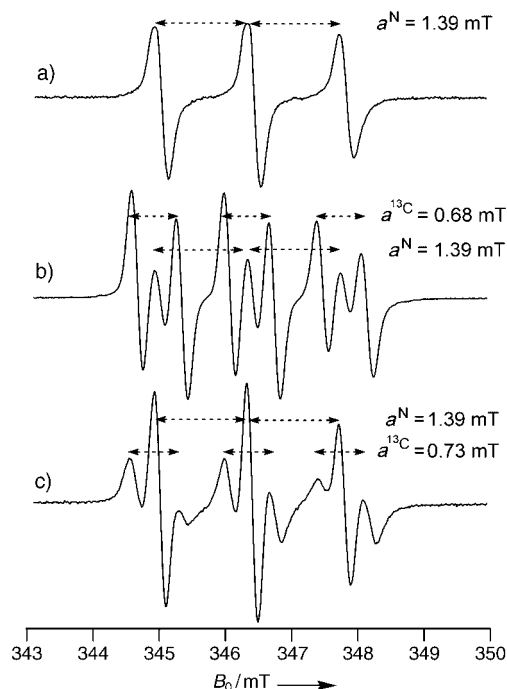
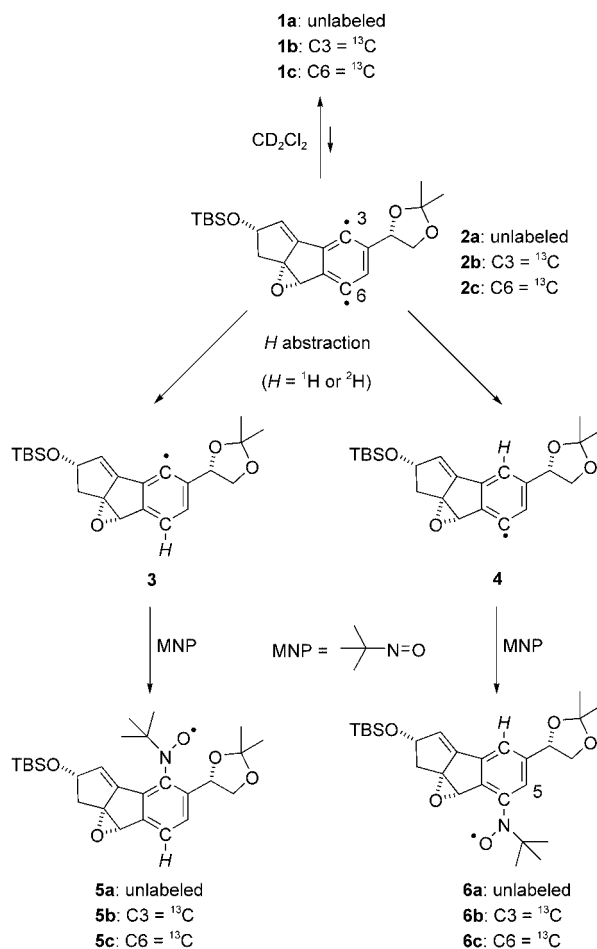


Figure 1. CW EPR (X-band) spectra of spin-trapped MNP adducts of **1** in CD₂Cl₂. a) Unlabeled enediyne **1a**; b) ¹³C3-labeled enediyne **1b**; c) ¹³C6-labeled enediyne **1c**.

unlabeled enediyne **1a**, measured upon addition of MNP to a solution of **1a** in CD₂Cl₂ at RT. The observed three-line spectrum (with $a^N = 1.390$ mT, $g = 2.006$) is attributable to the phenyl radical adducts **5a** and **6a** (Scheme 2) and is in good



Scheme 2. Proposed pathway from **1** to the observed MNP adducts **5** and **6**, through the *p*-benzyne biradical **2** and phenyl radicals **3** and **4**.

agreement with data reported in the literature for the phenyl radical–MNP adduct in CH₂Cl₂ ($a^N = 1.335$, $a^{Ho} = 0.170$, $a^{Hp} = 0.170$, $a^{Hm} = 0.085$ mT).^[14] The spectra of the ¹³C-labeled compounds **1b** and **1c** exhibit two distinct splitting patterns (cf. Figure 1b and 1c) different from that shown in Figure 1a.^[15] One of the three observed patterns agrees well with that of the unlabeled compound **1a**, whilst the other two show additional ¹³C splittings of 0.680 mT (Figure 1b) and 0.730 mT (Figure 1c). These latter values are in good agreement with the hyperfine splitting (HFS) constants described for ¹³C-centered radicals and the spectra are as expected for the ¹³C-labeled phenyl radical adducts **5b/6b** and **5c/6c**, respectively (Scheme 2).^[16] Integration of the spectra led to an estimated C3/C6 adduct ratio of around 2:1. This signal ratio remains constant throughout the time period of the EPR experiment (30–60 min).

First and foremost, the spectra of Figure 1 demonstrate that MNP attaches to both the C3 and C6 radical-forming positions. The spectra in Figure 1b and 1c complement each

other. Each shows two coexisting signal components, one of which undergoes additional splitting by ^{13}C .^[15b] The spectra demonstrate that a difference exists between the relative kinetics of spin trapping and quenching at the C3 and C6 positions. Although the quenching event could conceivably involve the substrate **1** as part of a dimerization or oligomerization process, the MS data described herein lead us to favor the intervention of a hydrogen isotope from, for example, the solvent, a substrate molecule, the spin-trapping agent or residual water. All our data support the conclusion that the *p*-benzyl biradical intermediate **2** is a viable precursor of the species responsible for the observed EPR spectra.

To account for the observed EPR signals and the ratios of the spin-trapped monoadducts **5** and **6** produced, we propose a single hydrogen abstraction as the predominant event (among other possibilities) before spin trapping, and the phenyl radicals **3** and **4** as plausible precursors of **5** and **6** (Scheme 2). This hypothesis does not discount the possibility that the spin trap might intercept the biradical **2**.^[15b] We favor the hypothesis that the radical centre at the more exposed C6 position is more reactive than that at the sterically shielded C3 position^[17] and C6 more readily undergoes hydrogen abstraction before intervention of the bulky MNP spin trap. We used the signal intensities of the paramagnetic species **1** (Figure 1) that steadily accumulated during the EPR experiment (30–60 min) to estimate the yield of observable^[15b] spin-trapped adducts. We calculated a yield of around 3–6% relative to 2,2,6,6-tetramethylpiperidine-*N*-oxyl (TEMPO, used as a standard), which we consider reasonable in view of the low estimated equilibrium constant of the process supplying **2**.^[7a] Unfortunately, the MNP adducts could not be detected by soft-ionization MALDI or ESI TOF mass spectrometry, presumably because of the inherent instability of the adducts formed during the EPR experiments to mass analysis (see the Experimental Section). Clear mass spectra would validate our hypothesis that quenching by an ^1H or a ^2H source takes place, rather than oligomerization of the substrate. No high-molecular weight signals assignable to dimeric or trimeric products were detected under a variety of mass detection conditions, which suggests that oligomerization does not occur.^[13]

The behavior of **1** was also studied with DMPO as the spin-trapping reagent. The CW EPR spectrum of a mixture of **1a** and DMPO in CD_2Cl_2 at RT under steady-state conditions is shown in Figure 2a. The HFS values $a^{\text{N}} = 1.450$ and $a^{\text{H}} = 2.140$ mT ($g = 2.006$, cf. simulated spectrum, Figure 2b) were determined from this spectrum. The reported hyperfine constants of DMPO adducts of the phenyl radical ($a^{\text{N}} = 1.440$, $a^{\text{H}} = 2.020$ mT in MeCN; $a^{\text{N}} = 1.390$, $a^{\text{H}} = 1.940$ mT in benzene)^[18] suggest that the observed values are attributable to the monoadducts **7** (Scheme 3).^[15b] The EPR spectra derived from the ^{13}C -labeled systems **1b** and **1c** with DMPO could not be resolved with confidence because of the presence of contaminants in the EPR mixture.^[13] However, additional spectra recorded for DMPO, combined with the spectrum of unlabeled compound **1a** with DMPO (Figure 2), suggest not only the presence of two paramagnetic components, but also the predominance of a C3-trapped component

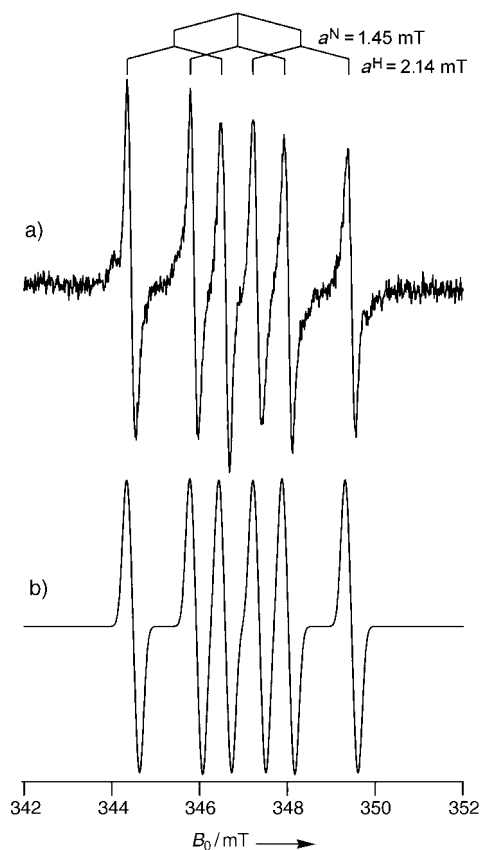
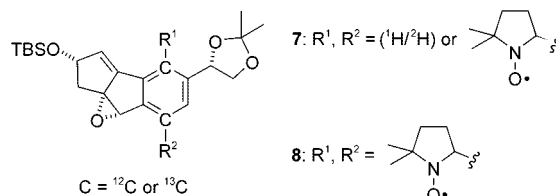


Figure 2. CW EPR (X-band) spectra of DMPO adducts in CD_2Cl_2 . a) Observed upon addition of DMPO to **1a** at RT; b) simulated spectrum.



Scheme 3. DMPO monoadducts **7** and bis adducts **8**, detected by MALDI-TOF MS.

experiencing extra ^{13}C splitting, rather than a C6-trapped component. Direct MALDI-TOF mass spectrometry of these and other EPR mixtures of **1** with DMPO gave clean spectroscopic evidence for the presence of both the monoadducts **7** and the bis adducts **8** (Scheme 3; monoadduct **7a**, calcd for $\text{C}_{29}\text{H}_{42}\text{NO}_5\text{Si}$: 512.28 $[M]^+$; found: 512.29; bis adduct **8a**, calcd for $\text{C}_{35}\text{H}_{53}\text{N}_2\text{O}_6\text{Si}$: 625.37 $[M+H]^+$; found: 625.39; monoadducts **7b/c**, calcd for $\text{C}_{28}^{13}\text{CH}_{42}\text{NO}_5\text{Si}$: 513.29 $[M]^+$; found: 513.28; bis adducts **8b/c**, calcd for $\text{C}_{34}^{13}\text{CH}_{53}\text{N}_2\text{O}_6\text{Si}$: 626.37 $[M+H]^+$; found: 626.37).^[13] No signs of dimeric or oligomeric adducts were observed. The intensities of the signaling patterns of the monoadducts **7** indicated a 4:1 ratio of ^1H to ^2H incorporation, which supports our proposal of the quenching event shown in Scheme 2.

We have disclosed new EPR and mass spectroscopic evidence for the existence of both mono and bis spin-trapped

adducts derived from **1**. This evidence was obtained by effectively increasing the extremely low equilibrium concentrations^[7a] of the elusive biradical **2** through spin trapping with MNP and DMPO. The ¹³C-labeled models **1b** and **1c** were shown to generate reactive unpaired radicals at both the C3 and C6 positions, as demonstrated by the observed characteristic hyperfine splittings of ¹³C-centered nitroxyl radical adducts (Figure 1). This work not only provides persuasive, albeit indirect, evidence for the spontaneous Masamune–Bergman cyclization^[11] of **1** to form the *p*-benzyl biradical **2**, but also points to the differential reactivity of the C3 and C6 radical positions for the first time. The close structural similarity of our compounds to the reactive bicyclic enediyne core of the nine-membered-ring chromophores, and the thermal activation mechanism of **1**^[7] make the observed difference in reactivity between C3 and C6 interesting for researchers aiming to detail the initial events in hydrogen abstraction of DNA by naturally derived *p*-benzynes.

Experimental Section

X-band (9.6 GHz) EPR spectra were recorded on a Bruker ESP 380E spectrometer at RT.

MNP (4 μmol) or DMPO (2 μmol) in CD₂Cl₂ (110 μL) was introduced to a solution of enediyne **1** (4 μmol) in CD₂Cl₂ (125 μL) in a quartz tube (Ø 5 mm) at RT under atmospheric pressure. After the EPR experiments, the same samples of **1** containing the spin trap (MNP or DMPO) were used for mass analysis. The MALDI-TOF mass spectra of the DMPO-containing samples were measured in positive ion mode on an Applied Biosystems Voyager DE STR SI-3 instrument by adding aliquots of the CD₂Cl₂ solutions to THF solutions of the matrix (α-cyano-4-hydroxy cinnamic acid). ESI-TOF mass analyses were found ineffective for mass detection under a variety of conditions. The spin-trapping reagents MNP and DMPO were purchased from Kanto Chemical Co. Ltd. and were used without further purification. The degree of deuteration of the solvent CD₂Cl₂ was 99.8% (Merck Co. Ltd.).

Received: February 27, 2004

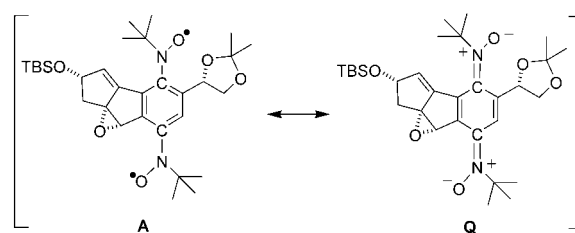
Revised: May 24, 2004 [Z54133]

Keywords: cyclization · enediynes · isotopic labeling · radicals · spin trapping

- [1] Enediyne reviews: a) H. H. Wenk, M. Winkler, W. Sander, *Angew. Chem.* **2003**, *115*, 518; *Angew. Chem. Int. Ed.* **2003**, *42*, 502; b) Z. Xi, I. H. Goldberg in *Comprehensive Natural Products Chemistry*, Vol. 7 (Eds.: D. H. R. Barton, K. Nakanishi), Elsevier, Dordrecht, **1999**, p. 553; c) J. W. Grissom, G. U. Gunawardena, D. Klingberg, D. Huang, *Tetrahedron* **1996**, *52*, 6453; d) M. E. Maier, *Synlett* **1995**, 13; e) A. L. Smith, K. C. Nicolaou, *J. Med. Chem.* **1996**, *39*, 2103; K. C. Nicolaou, W.-M. Dai, *Angew. Chem.* **1991**, *103*, 1453; *Angew. Chem. Int. Ed. Engl.* **1991**, *30*, 1387.
- [2] J.-M. A. Battigello, M. Cui, S. Roshong, B. J. Carter, *Bioorg. Med. Chem.* **1995**, *3*, 839.
- [3] a) J. B. Biggins, K. C. Onwuene, J. S. Thorson, *Science* **2003**, *301*, 1537; b) G. B. Jones, G. Hynd, J. M. Wright, A. Purohit, G. W. Plourde II, R. S. Huber, J. E. Mathews, A. Li, M. W. Kilgore, G. J. Bubley, M. Yancisin, M. A. Brown, *J. Org. Chem.* **2001**, *66*, 3688 and references cited therein; c) M. Hashimoto, M. M. Greenberg, Y. W. Kow, J.-T. Hwang, R. P. Cunningham, *J. Am. Chem. Soc.* **2001**, *123*, 3161; d) N. Zein, W. Solomon, K. L. Colson, D. R. Schroeder, *Biochemistry* **1995**, *34*, 11591.
- [4] a) L. H. Jones, C. W. Harwig, P. Wentworth, Jr., A. Simeonov, A. D. Wentworth, S. Py, J. A. Ashley, R. A. Lerner, K. D. Janda, *J. Am. Chem. Soc.* **2001**, *123*, 3607; b) G. B. Jones, P. M. Warner, *J. Org. Chem.* **2001**, *66*, 8669.
- [5] a) P. G. Wenthold, R. R. Squires, W. C. Lineberger, *J. Am. Chem. Soc.* **1998**, *120*, 5279; b) M. J. Schottelius, P. Chen, *J. Am. Chem. Soc.* **1996**, *118*, 4896; c) R. Marquardt, A. Balster, W. Sander, E. Kraka, D. Cremer, J. G. Radziszewski, *Angew. Chem.* **1998**, *110*, 1001; *Angew. Chem. Int. Ed.* **1998**, *37*, 955; d) B. A. Hess, *Eur. J. Org. Chem.* **2001**, 2185; e) W. Sander, *Acc. Chem. Res.* **1999**, *32*, 669; f) H. H. Wenk, A. Balster, W. Sander, D. A. Hrovat, W. T. Borden, *Angew. Chem.* **2001**, *113*, 2356; *Angew. Chem. Int. Ed.* **2001**, *40*, 2295.
- [6] a) P. R. Schreiner, *J. Am. Chem. Soc.* **1998**, *120*, 4184; b) C. J. Cramer, *J. Am. Chem. Soc.* **1998**, *120*, 6261; c) F. S. Amegayibor, J. J. Nash, A. S. Lee, J. Thoen, C. J. Petzold, H. I. Kenttamaa, *J. Am. Chem. Soc.* **2002**, *124*, 12066; d) C. F. Logan, P. Chen, *J. Am. Chem. Soc.* **1996**, *118*, 2113; e) A. E. Clark, E. R. Davidson, *J. Am. Chem. Soc.* **2001**, *123*, 10691; f) S. Koseki, Y. Fujimura, M. Hiramata, *J. Phys. Chem. A* **1999**, *103*, 7672.
- [7] a) For our first synthesis of **1a** and our report of its thermal equilibration with **2a**, see: K. Iida, M. Hiramata, *J. Am. Chem. Soc.* **1995**, *117*, 8875; b) for direct evidence that C-1027 and kedarcidin form paramagnetic radical species within their protective carrier apoproteins, as well as the design of a supra-C-1027 kinetically stabilized by deuteration of its apoprotein, see: M. Hiramata, K. Akiyama, T. Tanaka, T. Noda, K. Iida, I. Sato, R. Hanaishi, S. Fukuda-Ishisaka, M. Ishiguro, T. Otani, J. E. Leet, *J. Am. Chem. Soc.* **2000**, *122*, 720; T. Usuki, M. Inoue, M. Hiramata, T. Tanaka, *J. Am. Chem. Soc.* **2004**, *126*, 3022; c) for recent evidence that the kedarcidin chromophore undergoes spontaneous cyclization and is unlikely to require initial nucleophilic activation in vivo, see: A. G. Myers, A. R. Hurd, P. C. Hogan, *J. Am. Chem. Soc.* **2002**, *124*, 4583; d) for our earlier studies on enediynes, see: K. Yoshida, Y. Minami, T. Otani, Y. Tada, M. Hiramata, *Tetrahedron Lett.* **1994**, *35*, 5253; T. Mita, S. Kawata, M. Hiramata, *Chem. Lett.* **1998**, 959; T. Kaneko, M. Takahashi, M. Hiramata, *Angew. Chem.* **1999**, *111*, 1347; *Angew. Chem. Int. Ed.* **1999**, *38*, 1267; T. Kaneko, M. Takahashi, M. Hiramata, *Tetrahedron Lett.* **1999**, *40*, 2015.
- [8] For thermally-activated, 10-membered cyclic enediynes and theoretical studies, see: G. B. Jones, J. M. Wright, G. Hynd, J. K. Wyatt, P. M. Warner, R. S. Huber, A. Li, M. W. Kilgore, R. P. Sticca, R. S. Pollenz, *J. Org. Chem.* **2002**, *67*, 5727 and references cited therein.
- [9] P. Das, T. Mita, M. J. Lear, M. Hiramata, *Chem. Commun.* **2002**, 2624.
- [10] For a review of the spin-trapping method, see: E. G. Janzen, *Acc. Chem. Res.* **1971**, *4*, 31.
- [11] a) N. Darby, C. U. Kim, J. A. Salaüm, K. W. Shelton, S. Takada, S. Masamune, *Chem. Commun.* **1971**, 1516; S. Masamune, N. Darby, *Acc. Chem. Res.* **1972**, *5*, 272; b) R. M. Jones, R. G. Bergman, *J. Am. Chem. Soc.* **1972**, *94*, 660; R. G. Bergman, *Acc. Chem. Res.* **1973**, *6*, 25.
- [12] a) For the different spin-trapping behaviors of MNP and DMPO in biological EPR studies on C-1027, see: T. Usuki, M. Inoue, K. Akiyama, M. Hiramata, *Chem. Lett.* **2002**, 1148; b) for related spin trapping and EPR studies, see: C. Hazlewood, M. J. Davies, B. C. Gilbert, J. E. Packer, *J. Chem. Soc. Perkin Trans. 2* **1995**, 2167; W. F. Ho, B. C. Gilbert, M. J. Davies, *J. Chem. Soc. Perkin Trans. 2* **1997**, 2525; B. C. Gilbert, S. Silvester, P. H. Walton, A. C. Whitwood, *J. Chem. Soc. Perkin Trans. 2* **1999**, 1891.
- [13] Various spin-trapping behaviors and adduct stabilities are to be expected: a) MNP is known to have a higher reactivity than DMPO, H. Taniguchi, K. P. Madden, *J. Am. Chem. Soc.* **1999**,

121, 11857; b) MNP is specific for carbon-centered radicals, whereas DMPO can also trap oxygen-centered radicals; c) the extra HFS constants of ^{13}C -labeled MNP adducts are typically clear enough to assign the position of the pre-existing free radical, which is centered on or α to the carbon-13 atom. See also refs. [16] and [18].

- [14] G. Chapelet-Letourneux, H. Lemaire, A. Rassat, *Bull. Soc. Chim. Fr.* **1965**, 11, 3283.
- [15] a) Our analysis of the EPR spectra shown in Figure 1 suggests that line-broadening (anisotropy) is due to a small, four-bond a^{H} splitting caused by the *ortho*-C5 β -proton (see **6a**, Scheme 2); b) bis-nitroxyl spin-trapped biradicals **A** (if present in the EPR mixtures, Figure 1) are likely to exist in a self-quenched, quinoidal state **Q**: S. Nakazono, S. Karasawa, N. Koga, H. Iwamura, *Angew. Chem.* **1998**, 110, 1645; *Angew. Chem. Int. Ed.* **1998**, 37, 1550.
- [16] The MNP adduct of the ^{13}C -labeled phenyl radical has the HFS values $a^{\text{N}} = 1.550$, $a^{13\text{C}} = 0.710$ mT: S. Y. Qian, Y.-R. Chen, L. J. Deterding, Y. C. Fann, C. F. Chignell, K. B. Tomer, R. P. Mason, *Biochem. J.* **2002**, 363, 281.



- [17] It is well known that the lifetimes of free radicals are highly influenced by steric factors, for example, bulky substituents surrounding phenyl radical centers: D. Griller, K. U. Ingold, *Acc. Chem. Res.* **1976**, 9, 13; G. Brunton, D. Griller, L. R. C. Barclay, K. U. Ingold, *J. Am. Chem. Soc.* **1976**, 98, 6803; G. Brunton, J. A. Gray, D. Griller, L. R. C. Barclay, K. U. Ingold, *J. Am. Chem. Soc.* **1978**, 100, 4197.
- [18] P. Barker, A. L. J. Beckwith, W. R. Cherry, R. Huie, *J. Chem. Soc. Perkin Trans. 2* **1985**, 1147.

Homogeneous Catalysis

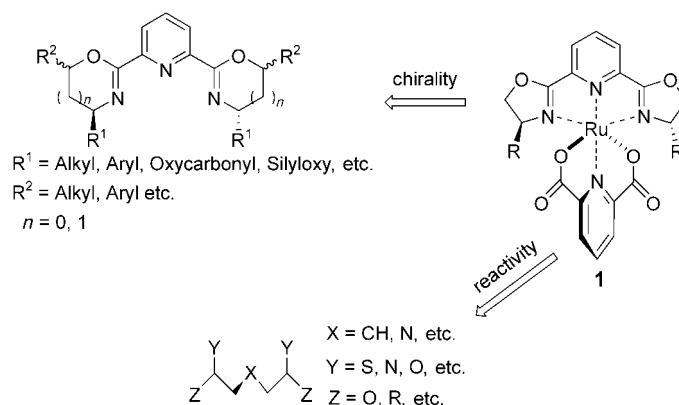
Development of a Ruthenium-Catalyzed Asymmetric Epoxidation Procedure with Hydrogen Peroxide as the Oxidant**

Man Kin Tse, Christian Döbler, Santosh Bhor, Markus Klawonn, Wolfgang Mägerlein, Herbert Hugl, and Matthias Beller*

The need of environmentally benign and clean oxidation reactions remains an important goal of chemical research. Although oxidation reactions constitute core technologies for converting bulk chemicals into useful higher-value products,^[1] they are among the more problematic processes with regard to general usage. Even today most of the known textbook oxidation methods^[2] lead to a significant amount of waste and therefore should be avoided. Criteria for state-of-the-art oxidation technologies should include high atom economy and selectivity, broad substrate scope, usage of environmentally benign oxidation reagents, and sufficient catalyst stability and productivity. By comparing different oxidation methods, it is apparent that the oxidant used in the respective transformation defines the quality and applicability of the method. Clearly, molecular oxygen is the most ideal oxidant for a number of oxidation reactions.^[3] However, mostly only one oxygen atom of an oxygen molecule is used productively for oxidation (50 % atom efficiency),^[4,5] thus at least stoichiometric amounts of unwanted by-products are generated during the reactions. One of the few examples in which both oxygen atoms are used efficiently is the aerobic dihydroxylation of olefins, which we developed some time ago.^[6,7] Apart from molecular oxygen, hydrogen peroxide is an environmentally benign oxidant, which theoretically generates only water as a by-product.^[8] Also it is advantageous compared to other oxidants because of the availability and low price (<0.6 € kg⁻¹ of 100 % H₂O₂).^[9] Owing to its characteristic physical properties H₂O₂ is particularly useful for liquid-phase oxidations for the synthesis of fine chemicals, pharmaceuticals, agrochemicals, and electronic materials. Hence, the discovery of new catalysts using H₂O₂ is an important goal in oxidation chemistry.^[10,11]

For the enantioselective epoxidations of olefins to date transition-metal complexes based on titanium (Sharpless epoxidation)^[12] and manganese (Jacobsen–Katsuki epoxidation)^[13] have been the most successful catalysts. In addition, significant progress using organic catalysts based on chiral ketones (ketone catalysts from Shi, Yang, and co-workers)^[14,15] was reported recently. However, in spite of extensive research efforts, the development of a general and catalytic asymmetric-epoxidation method using H₂O₂ has not been achieved.^[16] Herein we report the development of a new catalytic asymmetric-oxidation method that uses H₂O₂ in the presence of ruthenium complexes, allows for general epoxidation of olefins in high yield with *ee* values up to 84 %, and is simple to employ. In addition a novel class of chiral tridentate ligands (pyboxazines) is presented.

We looked for ruthenium complexes^[17] with a combination of two meridional ligands which should provide the ability to tune both the activity and the asymmetric induction of the catalyst separately. Therefore, we chose the ruthenium (R₂pybox)(pyridinedicarboxylate) complex **1** (pybox = 2,6-di-4,5-dihydro-1,3-oxazol-2-yl pyridine) which has been reported by Nishiyama et al. to catalyze the epoxidation of *trans*-stilbene in the presence of PhI(OAc)₂ as the stoichiometric oxidant.^[18] Although transition-metal complexes rapidly decompose H₂O₂,^[19] we thought after initial tests with RuCl₃/2,6-pyridinedicarboxylic acid^[20] that it should be possible to tune complex **1** to a more general asymmetric epoxidation catalyst with H₂O₂ (Scheme 1).



Scheme 1. Strategy of catalyst design.

Clearly, the enantioselective induction could be controlled by the readily accessible pybox or new pyboxazine type ligands (pyboxazine = 2,2'-pyridine-2,6-diyl bis(5,6-dihydro-4*H*-1,3-oxazine)), which can be synthesized from commercially available α - or β -amino acids.^[21] Changing the donating atoms (S, C, N, or O) in the pyridinedicarboxylate ligand should influence the reactivity and the selectivity of the catalyst.

The epoxidation of styrene using hydrogen peroxide is amongst the more challenging asymmetric epoxidation reactions both with regard to chemo- and enantioselectivity. We used our recently developed *in situ* catalyst system^[17d,e] and investigated the influence of different ligands and reaction conditions (Table 1).

[*] Dr. M. K. Tse, Dr. C. Döbler, Dipl.-Chem. S. Bhor, Dipl.-Chem. M. Klawonn, Prof. Dr. M. Beller
 Leibniz-Institut für Organische Katalyse (IfOK)
 Universität Rostock e.V.
 Buchbinderstrasse 5–6, 18055 Rostock (Germany)
 Fax: (+49) 381-466-9324
 E-mail: matthias.beller@ifok.uni-rostock.de
 Dr. W. Mägerlein, Dr. H. Hugl
 Bayer AG
 51368 Leverkusen (Germany)

[**] This work has been financed by the State of Mecklenburg-Western Pomerania, the Bundesministerium für Bildung und Forschung (BMBF), and the Deutsche Forschungsgemeinschaft. M.K.T. thanks the Alexander von Humboldt Stiftung for granting him an AvH-fellowship.

Supporting information for this article is available on the WWW under <http://www.angewandte.org> or from the author.

Table 1: Effects of ligands on ruthenium catalyzed asymmetric epoxidation of styrene.^[a]

$\text{Ph-CH=CH}_2 + 30\% \text{ H}_2\text{O}_2 \xrightarrow[\text{L}^1, \text{L}^2]{[\text{Ru}(p\text{-cymol})\text{Cl}_2]_2} \text{Ph-CH(O)}_2\text{CH}_2$ <div style="text-align: center;"> $\text{L}^1 =$ $\text{L}^2 =$ </div>						
Entry	L ²	t [h]	Conv. [%] ^[b]	Yield [%] ^[b]	Sele. [%] ^[c]	ee [%] ^[d]
1	–	–	12	20	0	0
2		12	80	49	61	24 ^[e]
3 ^[f]		12	> 99	70	70	31 ^[e]
4		12	20	8	40	n.d. ^[g]
5		12	20	10	50	n.d. ^[g]
6		12	40	22	55	9 ^[e]
7	–	12	31	14	45	13 ^[e]
8 ^[h]		12	22	6	27	–

[a] Reaction conditions: In a 25-mL Schlenk tube, $[\text{Ru}(p\text{-cymene})\text{Cl}_2]_2$ (0.0125 mmol) and L¹ (0.025 mmol) were stirred at room temperature in 2-methylbutan-2-ol (2 mL) under Ar for 10 min. A solution of L² (0.025 mmol) and Et₃N (1.2 equiv per acid group) in 2-methylbutan-2-ol (2 mL) was added by cannular. The whole reaction mixture was heated at 65 °C for 1 h. After cooling to room temperature, the catalyst solution was diluted with 2-methylbutan-2-ol (5 mL), followed by the addition of styrene (0.5 mmol) and dodecane (GC internal standard, 100 µL). To this reaction mixture, a solution of 30% H₂O₂ (170 µL, 1.5 mmol) in 2-methylbutan-2-ol (830 µL) was added over 12 h by a syringe pump. [b] Determined by comparing with authentic sample on GC-FID. [c] Chemoselectivity for epoxide formation. [d] Determined by HPLC. [e] (R)-(+)-styrene oxide was the major enantiomer. [f] The defined complex **1a** was used. [g] Not determined. [h] Performed without L¹.

The reactions were run at room temperature in the presence of 2.5 mol% of $[\text{Ru}(p\text{-cymene})\text{Cl}_2]_2$ and 5 mol% of each ligand. In general all experiments were performed with three equivalents of H₂O₂ (30% in water), which was slowly dosed into the reaction mixture over 12 h. With $[\text{Ru}(p\text{-cymene})\text{Cl}_2]_2$ alone (Table 1, entry 1), no epoxide was detected, only unspecific decomposition of H₂O₂ and styrene. To our delight, a combination of (S,S)-Ph₂-pybox and H₂pydic (pydic = pyridine dicarboxylate) led to a remarkable increase in activity and chemoselectivity (61%) with a moderate enantioselectivity (Table 1, entry 2). Using the pre-made complex **1a** gave better yield (70%) as well as a higher enantioselectivity (31% ee) presumably owing to the higher concentration of the well-defined catalyst (Table 1, entry 3). Modification of the pydic ligand resulted in a significant loss of reactivity (Table 1, entries 2–6). In the presence of only one of the ligands (pybox or pydic) only a small amount of epoxide is formed (Table 1, entries 7 and 8). This result suggests that the combination of these meridional ligands, pybox and pydic, plays a crucial role in the reactivity and enantioselectivity and offers the opportunity to epoxidize olefins with 30% H₂O₂.

Different ruthenium complexes were tested in the epoxidation of styrene (Table 2). All ruthenium catalysts were directly prepared from the corresponding pybox ligand, Na₂pydic, and $[\text{Ru}(p\text{-cymene})\text{Cl}_2]_2$.^[18] Apart from the

known complexes, $[\text{Ru}((S,S)\text{-Ph}_2\text{pybox})(\text{pydic})]$ (**1a**) and $[\text{Ru}((S,S)\text{-}i\text{Pr}_2\text{pybox})(\text{pydic})]$ (**1e**) new complexes, $[\text{Ru}(\text{H}_2\text{-(}S,S\text{)-Ph}_2\text{pybox})(\text{pydic})]$ (**1b**), $[\text{Ru}((S,S)\text{-indanol}_2\text{pybox})(\text{pydic})]$ (**1c**), and $[\text{Ru}((R,R)\text{-Ph}_2\text{-(}S,S\text{)-Ph}_2\text{pybox})(\text{pydic})]$ (**1d**), which derived from known pybox ligands, were also synthesized.^[21]

All the $[\text{Ru}(\text{pybox})(\text{pydic})]$ complexes catalyzed the epoxidation of styrene with 30% H₂O₂ in good yield (Table 2, entries 1–5). All reactions were run with 5 mol% of Ru catalyst. However, a similar level of efficiency is reached with 0.5 mol% of catalyst (Table 3, entry 12). Moreover, the catalytic system had a 67% efficiency with respect to H₂O₂ (Table 3, entry 13). Substituents on the 4-position of the 4,5-dihydrooxazol ring positively influence the enantioselectivity of the reaction more than those on the 5-position since the 4-position is closer to the metal center (Table 2, entries 1 and 2). Moreover, a flexible aryl ring in the substituent seems to be essential (Table 2, entries 1 and 3) for high enantioselectivity. The presence of the comparatively sterically bulky *iso*-propyl group gave a system that was not as reactive and showed lower enantioselectivity (Table 2, entries 1 and 5). The epoxidation of 1-methylcyclohexene in the standard conditions with 5 mol% **1a** led to 100% conversion with 86% yield, however, with

less than 5% ee. This result suggests that a π - π interaction between the ligand and the substrate may be present.^[22]

For the first time we employed pyboxazine ligands, which are structurally related to pybox, and can be synthesized easily from β -amino acid derivatives. The β -amino acid was reduced by LiAlH₄ directly or its methyl ester was reduced by NaBH₄ in the presence of acid to the corresponding β -amino alcohol.^[21b] Cyclization of the β -amino alcohol with dimethyl pyridine-2,6-dicarboximidate in anhydrous CH₂Cl₂ gave the pyboxazine ligand, which can be used directly for complex formation.^[21c,e] The metal complex, $[\text{Ru}((S,S)\text{-Ph}_2\text{pyboxazine})(\text{pydic})]$ (**2a**), was obtained accordingly. Enlargement of the five-membered ring to a six-membered ring resulted in a system that increased the ee value to 48% (Table 2, entry 6).

These results show some important factors which can rationalize the development of a new H₂O₂ catalyst: 1) the combination of pybox and pydic ligands at a ruthenium center provides the reactivity and enantioselectivity, 2) an aryl group on the 4-position of the dihydrooxazole ring results in good ee values with aromatic olefins, 3) a sterically bulky aryl substituent may further improve the enantioselective induction, 4) the newly developed six-membered “pyboxazine” is better than the five-membered “pybox” with respect to enantioselectivity. Following these principles, we designed and synthesized $[\text{Ru}((R,R)\text{-1-naphthyl}_2\text{pyboxazine})(\text{pydic})]$ (**2b**) and $[\text{Ru}((R,R)\text{-2-naphthyl}_2\text{pyboxazine})(\text{pydic})]$ (**2c**;

Table 2: [Ru(pybox)(pydic)]- and [Ru(pyboxazine)(pydic)]-catalyzed epoxidation of styrene.^[a]

$\text{Ph-CH=CH}_2 + 30\% \text{ H}_2\text{O}_2 \xrightarrow{[\text{Ru}(\text{pybox})(\text{pydic})]} \text{Ph-CH(O)-CH}_2\text{O}$						
Entry	Catalyst	t [h]	Conv. [%] ^[b]	Yield [%] ^[b]	Selec. [%] ^[c]	ee [%] ^[d]
1		12	> 99	70	70	31 ^[e]
2		12	100	66	66	3 ^[f]
3		20	91	59	65	18 ^[e]
4		12	100	78	78	18 ^[f]
5		20	72	45	63	19 ^[e]
6		12	81	56	69	48 ^[e]
7		12	100	65	65	38 ^[e]
8		12	82	59	72	48 ^[e]

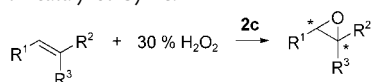
[a] In a 25-mL Schlenk tube, the catalyst (0.025 mmol) was stirred at room temperature in 2-methylbutan-2-ol (9 mL) for 10 min. Styrene (0.5 mmol) and dodecane (GC internal standard, 100 μL) were added. To this reaction mixture, a solution of 30% H_2O_2 (170 μL , 1.5 mmol) in 2-methylbutan-2-ol (830 μL) was added over 12 h by a syringe pump. [b] Determined by comparing with authentic samples on GC-FID. [c] Chemoselectivity for epoxide formation. [d] Determined by HPLC. [e] (R)-(+)-styrene oxide was the major enantiomer. [f] (S)-(-)-styrene oxide was the major enantiomer.

Table 2, entries 7 and 8). In the epoxidation, **2b** give a lower enantioselectivity while **2c** gave the same *ee* value as **2a** under non-optimized conditions. However, after optimization **2c** was the best catalyst.

Different aromatic olefins were oxidized in the presence of catalyst **2c** in good to excellent yield with good *ee* values under mild conditions (Table 3). With styrene, in the presence of acetic acid (HOAc) as cocatalyst (20 mol %), it was found that the yield increased to 85% and the *ee* value increased to 59% with **2c** as the catalyst (Table 3, entries 1 and 2). To our knowledge, this is the highest *ee* value for asymmetric epoxidation of styrene using H_2O_2 as the oxidant. Mechanistic studies indicated that HOAc accelerates the reaction, possibly by stabilizing the active intermediates against self-degradation. The water content increases with the addition of H_2O_2 as the oxidant, this means that the faster the reaction is, the higher the enantioselectivity. We have also demonstrated that over-dosage of H_2O in the epoxidation of *trans*-stilbene catalyzed by **1a** using $\text{PhI}(\text{OAc})_2$ as the oxidant decreased the *ee* value.^[17d] So this additive effect is most prominent with less reactive substrates and is diminished when electron-rich olefins are employed. The highest *ee* value (84%) was obtained with 2-methyl-1-phenyl-1-propene at 0°C with 20 mol% HOAc and 1.5 equivalents of 50% H_2O_2 (Table 3, entry 16). To date the new catalytic system has been applied successfully to mono-, di-, and trisubstituted olefins (Table 3). The best results are obtained with *trans* disubstituted olefins and trisubstituted olefins. Hence, the new procedure complements the known manganese-catalyzed asymmetric epoxidations. Apart from differently substituted aromatic olefins, allylic acetates and even allylic chloride could be epoxidized in high yield (Table 3, entries 15 and 16).

Preliminary mechanistic studies of the active species indicate

Table 3: Asymmetric epoxidation catalyzed by **2c**.^[a]



Entry	R ¹	Substrate R ²	R ³	t [h]	Conv. [%] ^[b]	Yield [%] ^[b]	Selec. [%]	ee [%] ^[c]
1	Ph	H	H	12	82	59	72	48 ^[d]
2	Ph	H	H	12	100	85	85	59 ^{[d], [e]}
3	<i>p</i> -Cl-C ₆ H ₄	H	H	12	100	76	76	54 ^[e]
4	<i>p</i> -F-C ₆ H ₄	H	H	12	100	82	82	60 ^[e]
5	<i>p</i> -CF ₃ -C ₆ H ₄	H	H	12	65	57	88	55 ^[e]
6	<i>p</i> -CH ₃ -C ₆ H ₄	H	H	12	100	80	80	58 ^[e]
7	<i>o</i> -CH ₃ -C ₆ H ₄	H	H	12	100	> 99	> 99	64 ^[e]
8	<i>o</i> -Cl-C ₆ H ₄	H	H	12	86	78	91	58 ^[e]
9	Ph	Ph	H	12	100	100	100	54 ^[f]
10	Ph	CH ₃	H	12	100	95	95	72 ^{[d], [g]}
11 ^[h]	Ph	CH ₃	H	12	93	90	97	70 ^{[d], [g]}
12 ^[i]	Ph	CH ₃	H	12	100	67 ^[j]	67	74 ^{[d], [g]}
13	<i>p</i> -CH ₃ O-C ₆ H ₄	CH ₃	H	12	100	> 99	> 99	53
14	Ph	1,1-cyclohexyl	H	12	100	> 99	> 99	79
15	Ph	CH ₃	CH ₃	12	100	93	93	80
16	Ph	CH ₃	CH ₃	26	94	91	97	84 ^{[e], [k]}
17	Ph	CH ₂ OAc	H	12	84	83	99	48 ^[e]
18	Ph	CH ₂ Cl	H	12	79	68	86	28 ^[e]

[a] In a 25-mL Schlenk tube, the catalyst (0.025 mmol) was stirred at room temperature in 2-methylbutan-2-ol (9 mL) for 10 min. Olefin (0.5 mmol) and dodecane (GC internal standard, 100 µL) were added. To this reaction mixture, a solution of 30% H₂O₂ (170 µL, 1.5 mmol) in 2-methylbutan-2-ol (830 µL) was added over 12 h by a syringe pump. [b] Determined by comparing with authentic samples on GC-FID. [c] Determined by HPLC, absolute configurations were not determined unless mentioned. [d] (*R*)-(+)-styrene oxide was the major enantiomer. [e] 20 mol% of HOAc was added. [f] (*S,S*)-(-)-stilbene oxide was the major enantiomer. [g] (*R,R*)-(+)-1-Phenyl-1-propene oxide was the major enantiomer. [h] In a 25-mL Schlenk tube, **2a** (0.0025 mmol) was stirred at room temperature in 2-methylbutan-2-ol (9 mL) for 10 min. *trans*-1-Phenyl-1-propene (0.5 mmol), HOAc (5.7 µL, 0.10 mmol) and dodecane (GC internal standard, 100 µL) were added. Cooled to 0°C, a solution of 50% H₂O₂ (102 µL, 1.5 mmol) in 2-methylbutan-2-ol (898 µL) was added over 12 h by a syringe pump. [i] In a 25-mL Schlenk tube, **2a** (0.025 mmol) was stirred at room temperature in 2-methylbutan-2-ol (9 mL) for 10 min. *trans*-1-Phenyl-1-propene (0.6 mmol), HOAc (5.7 µL, 0.10 mmol), and dodecane (GC internal standard, 100 µL) were added. To this reaction mixture, a solution of 50% H₂O₂ (34 µL, 0.5 mmol) in 2-methylbutan-2-ol (966 µL) was added 12 h by a syringe pump. [j] Yield based on H₂O₂. [k] 0°C, a solution of 50% H₂O₂ (51 µL, 0.75 mmol) in 2-methylbutan-2-ol (949 µL) was added by syringe pump.

that the corresponding ruthenium dioxo complex is the active catalyst. In stoichiometric reactions of **1a** with PhI(OAc)₂, *t*BuOOH, and H₂O₂, UV/Vis spectroscopy showed that the same active species are formed. Electrospray ionization mass spectrometry of the reaction mixture showed molecular ion peaks corresponding to [Ru((*S,S*)-Ph₂pybox)pydic](O) (**3a**) and [Ru((*S,S*)-Ph₂pybox)(pydic)(O)₂] (**3b**), regardless of whether or not HOAc was present. While **3b** seems to be quite unstable, **3a** could be independently synthesized by treating **1a** with two equivalents of 30% H₂O₂ in 2-methylbutan-2-ol. Even when using a stoichiometric amount of **3a**, no oxo-transfer from **3a** to *trans*-1-phenyl-1-propene occurred. Hence, we postulate that **3b** is the real active catalyst in solution.

In summary, a general ruthenium-catalyzed asymmetric epoxidation procedure of olefins using H₂O₂ has been developed. For the first time high yield and chemoselectivity have been obtained using H₂O₂ as the oxidant. Enantioselectivities (typically in between 50–80%) up to 84% were observed for different aromatic olefins. An important factor for the success was the introduction of a new class of ligands,

the so-called pyboxazines. It is expected that these ligands will complement nicely the catalytic behavior of the well-known pybox derivatives.^[23] The use of two different ligands significantly simplifies structural variations on the catalyst thus allowing easy tuning of the catalytic properties. This situation is an important advantage compared to most catalysts and ligands used in asymmetric oxidation catalysis. Full experimental detail can be found in the Supporting Information.

Received: April 30, 2004

Keywords: asymmetric catalysis · epoxidations · homogeneous catalysis · ruthenium

- [1] K. Weissmehl, H.-J. Arpe, *Industrial Organic Chemistry*, 4th ed., Wiley-VCH, Weinheim, 2003.
- [2] For example, epoxides can be produced by cyclization of halohydrins or 1,2-glycols, epoxidation of olefins by peracids, reaction of carbonyl compounds with *gem*-dihalides and Li or *n*BuLi, condensation between aldehydes and α-halo esters, -ketones, or -amides, addition of sulfur ylides or diazomethane to aldehydes or ketones, and bimolecular reduction of aldehydes or ketones. See: J. March, *Advanced Organic Chemistry*, 3rd ed., Wiley, New Delhi, 1992.
- [3] R. A. Sheldon, J. K. Kochi, *Metal-Catalyzed Oxidations of Organic Compounds*, Academic Press, New York, 1981.
- [4] For recent examples see: a) I. E. Markó, P. R. Giles, M. Tsukazaki, S. M. Brown, C. J. Urch, *Science* 1996, 274, 2044–2046; b) G.-J. ten Brink, I. W. C. E. Arends, R. A. Sheldon, *Science* 2000, 287, 1636–1639; c) B. Betzemeier, M. Cavazzini, S. Quici, P. Knochel, *Tetrahedron Lett.* 2000, 41, 4343–4346; d) Y. Ishii, S. Sakaguchi, T. Iwahama, *Adv. Synth. Catal.* 2001, 343, 393–427; e) Y. Nishiyama, Y. Nakagawa, N. Mizuno, *Angew. Chem.* 2001, 113, 3751–3753; *Angew. Chem. Int. Ed.* 2001, 40, 3639–3641; f) Y. Nishiyama, T. Hayashi, Y. Nakagawa, N. Mizuno, *Stud. Surf. Sci. Catal.* 2003, 145, 255–258; g) A. M. Khenkin, L. J. W. Shimon, R. Neumann, *Inorg. Chem.* 2003, 42, 3331–3339; h) T. Nishimura, S. Uemura, *Synlett* 2004, 201–216; i) R. Irie, T. Katsuki, *Chem. Rec.* 2004, 4, 96–109.
- [5] a) L. I. Simándi, *Catalytic Activation of Dioxygen by Metal Complexes*, Kluwer Academic, Dordrecht, 1992; b) *The Activation of Dioxygen and Homogeneous Catalytic Oxidation* (Eds.: D. H. R. Barton, A. E. Bartell, D. T. Sawyer), Plenum, New York, 1993; c) *Advances in Catalytic Activation of Dioxygen by Metal Complexes* (Ed.: L. I. Simándi), Kluwer Academic, Dordrecht, 2003.
- [6] a) C. Döbler, G. Mehlretter, M. Beller, *Angew. Chem.* 1999, 111, 3211–3212; *Angew. Chem. Int. Ed.* 1999, 38, 3026–3028; b) C. Döbler, G. Mehlretter, U. Sundermeier, M. Beller, *J. Am. Chem. Soc.* 2000, 122, 10289–10297; c) G. M. Mehlretter, C. Döbler, U. Sundermeier, M. Beller, *Tetrahedron Lett.* 2000, 41, 8083–8087; d) C. Döbler, G. M. Mehlretter, U. Sundermeier,

- M. Beller, *J. Organomet. Chem.* **2001**, 621, 70–76; e) U. Sundermeier, C. Döbler, G. M. Mehlretter, W. Baumann, M. Beller, *Chirality* **2003**, 15, 127–134.
- [7] For other examples of using oxygen or air, see: a) J. T. Groves, R. Quinn, *J. Am. Chem. Soc.* **1985**, 107, 5790–5792; b) I. R. Paeng, K. Nakamoto, *J. Am. Chem. Soc.* **1990**, 112, 3289–3297; c) *Metalloporphyrins Catalyzed Oxidations* (Eds.: F. Montanari, L. Casella), Kluwer, Dordrecht, **1994**; d) I. E. Markó, P. R. Giles, M. Tsukazaki, I. Chellé-Regnant, C. J. Urch, S. M. Brown, *J. Am. Chem. Soc.* **1997**, 119, 12661–12662; e) K. P. Peterson, R. C. Larock, *J. Org. Chem.* **1998**, 63, 3185–3189; f) K. S. Coleman, C. Y. Lorber, J. A. Osborn, *Eur. J. Inorg. Chem.* **1998**, 1673–1675; g) J. Christoffers, *J. Org. Chem.* **1999**, 64, 7668–7669.
- [8] a) *Catalytic Oxidations with Hydrogen Peroxide as Oxidant* (Ed.: G. Strukul), Kluwer Academic, Dordrecht, **1992**; b) C. W. Jones, *Applications of Hydrogen Peroxide and Derivatives*, Royal Society of Chemistry, Cambridge, **1999**.
- [9] a) *Ullmann's Encyclopedia of Industrial Chemistry*, 5th Ed., Vol. A13 (Eds.: B. Elvers, S. Hawkins, M. Ravenscroft, G. Schulz), VCH, New York, **1989**, p. 443; b) *Kirk-Othmer Encyclopedia of Chemical Technology*, 4th ed., Vol. 13 (Eds.: J. I. Kroschwitz, M. Howe-Grant), Wiley, New York, **1995**, p. 961.
- [10] Selected recent examples using H₂O₂ as oxidant: a) J. Rudolph, K. L. Reddy, J. P. Chiang, K. B. Sharpless, *J. Am. Chem. Soc.* **1997**, 119, 6189–6190; b) L. Shu, Y. Shi, *J. Org. Chem.* **2000**, 65, 8807–8810; c) M. C. White, A. G. Doyle, E. N. Jacobsen, *J. Am. Chem. Soc.* **2001**, 123, 7194–7195; d) Y. Shi, *J. Synth. Org. Chem. Jpn.* **2002**, 60, 342–349; e) K. A. Srinivas, A. Kumar, S. M. S. Chauhan, *Chem. Commun.* **2002**, 2456–2457; f) M. K. Carter, *J. Mol. Catal. A* **2003**, 200, 191–203; g) D. E. De Vos, B. F. Sels, P. A. Jacobs, *Adv. Synth. Catal.* **2003**, 345, 457–473; h) R. Noyori, M. Aoki, K. Sato, *Chem. Commun.* **2003**, 1977–1986; i) S. Y. Jonsson, H. Adolfsson, J.-E. Bäckvall, *Chem. Eur. J.* **2003**, 9, 2783–2788; j) G. Maayan, R. H. Fish, R. Neumann, *Org. Lett.* **2003**, 5, 3547–3550; k) S. Velusamy, T. Punniyamurthy, *Tetrahedron Lett.* **2003**, 44, 8955–8957; l) M. V. Vasylyev, R. Neumann, *J. Am. Chem. Soc.* **2004**, 126, 884–890.
- [11] For reviews of H₂O₂ as epoxidation oxidant see: a) G. Grigoropoulou, J. H. Clark, J. A. Elings, *Green Chem.* **2003**, 5, 1–7; b) B. S. Lane, K. Burgess, *Chem. Rev.* **2003**, 103, 2457–2473; for a commentary see: c) M. Beller, *Adv. Synth. Catal.* **2004**, 346, 107–108; for other asymmetric oxidations using H₂O₂ see: d) N. Komatsu, T. Murakami, Y. Nishibayashi, T. Sugita, S. Uemura, *J. Org. Chem.* **1993**, 58, 3697–3702; e) A. Gusso, C. Baccin, F. Pinna, G. Strukul, *Organometallics* **1994**, 13, 3442–3451; f) C. Bolm, F. Bienewald, *Angew. Chem.* **1995**, 107, 2883–2885; *Angew. Chem. Int. Ed. Engl.* **1995**, 34, 2640–2642; g) M. Costas, A. K. Tipton, K. Chen, D. H. Jo, L. Que, Jr., *J. Am. Chem. Soc.* **2001**, 123, 6722–6723; h) S.-I. Murahashi, S. Ono, Y. Imada, *Angew. Chem.* **2002**, 114, 2472–2474; *Angew. Chem. Int. Ed.* **2002**, 41, 2366–2368; i) S. A. Blum, R. G. Bergman, J. A. Ellman, *J. Org. Chem.* **2003**, 68, 150–155; j) J. Legros, C. Bolm, *Angew. Chem.* **2003**, 115, 5645–4657; *Angew. Chem. Int. Ed.* **2003**, 42, 5487–5489.
- [12] Reviews for Ti: a) R. A. Johnson, K. B. Sharpless in *Catalytic Asymmetric Synthesis* (Ed.: I. Ojima), VCH, New York, **1993**, Chapter 4.1; b) T. Katsuki, V. S. Martin, *Org. React.* **1996**, 48, 1–299.
- [13] Reviews for Mn: a) E. N. Jacobsen in *Catalytic Asymmetric Synthesis* (Ed.: I. Ojima), VCH, New York, **1993**, Chapter 4.2; b) T. Katsuki in *Catalytic Asymmetric Synthesis*, 2nd ed. (Ed.: I. Ojima), Wiley-VCH, New York, **2000**, pp. 287–325; c) T. Katsuki, *Adv. Synth. Catal.* **2002**, 344, 131–147.
- [14] For examples of asymmetric epoxidation mediated by chiral ketones see: a) D. Yang, Y.-C. Yip, M.-W. Tang, M.-K. Wong, J.-H. Zheng, K.-K. Cheung, *J. Am. Chem. Soc.* **1996**, 118, 491–492; b) Y. Tu, Z.-X. Wang, Y. Shi, *J. Am. Chem. Soc.* **1996**, 118, 9806–9807; c) Z.-X. Wang, Y. Tu, M. Frohn, J.-R. Zhang, Y. Shi, *J. Am. Chem. Soc.* **1997**, 119, 11224–11235; d) D. Yang, M.-K. Wong, Y.-C. Yip, X.-C. Wang, M.-W. Tang, J.-H. Zheng, K.-K. Cheung, *J. Am. Chem. Soc.* **1998**, 120, 5943–5952, and references therein.
- [15] For reviews of asymmetric epoxidation mediated by organic compounds see: a) P. I. Dalko, L. Moisan, *Angew. Chem.* **2001**, 113, 3840–3864; *Angew. Chem. Int. Ed.* **2001**, 40, 3726–3748; b) W. Adam, C. R. Saha-Möller, P. A. Ganeshpure, *Chem. Rev.* **2001**, 101, 3499–3548, and references therein.
- [16] Selected examples of asymmetric epoxidation using H₂O₂ as oxidant: a) R. Sinigalia, R. A. Michelin, F. Pinna, G. Strukul, *Organometallics* **1987**, 6, 728–734; b) T. Schwenkreis, A. Berkessel, *Tetrahedron Lett.* **1993**, 34, 4785–4788; c) R. Irie, N. Hosoya, T. Katsuki, *Synlett* **1994**, 255–256; d) P. Pietikäinen, *Tetrahedron Lett.* **1994**, 35, 941–944; e) A. Berkessel, M. Fraenkron, T. Schwenkreis, A. Steinmetz, *J. Mol. Catal. A* **1997**, 117, 339–346; f) C. Bolm, D. Kadereit, M. Valacchi, *Synlett* **1997**, 687–688; g) M. B. Francis, E. N. Jacobsen, *Angew. Chem.* **1999**, 111, 987–991; *Angew. Chem. Int. Ed.* **1999**, 38, 937–941; h) R. M. Stoop, A. Mezzetti, *Green Chem.* **1999**, 1, 39–41; i) R. M. Stoop, C. Bauer, P. Setz, M. Wörle, T. Y. H. Wong, A. Mezzetti, *Organometallics* **1999**, 18, 5691–5700; j) R. M. Stoop, S. Bachmann, M. Valentini, A. Mezzetti, *Organometallics* **2000**, 19, 4117–4126; k) C. Bolm, N. Meyer, G. Raabe, T. Weyhermüller, E. Bothe, *Chem. Commun.* **2000**, 2435–2436; l) P. Pietikäinen, *J. Mol. Catal. A* **2001**, 165, 73–79; m) L. Shu, Y. Shi, *Tetrahedron* **2001**, 57, 5213–5218; n) R. I. Kureshy, N.-u. H. Khan, S. H. R. Abdi, S. T. Patel, R. V. Jasra, *Tetrahedron: Asymmetry* **2001**, 12, 433–437.
- [17] For an excellent review using Ru complexes for epoxidation reactions, see: a) G. A. Barf, R. A. Sheldon, *J. Mol. Catal. A* **1995**, 102, 23–39; for achievements in Ru-based epoxidations with different oxidants, see: b) N. End, A. Pfaltz, *Chem. Commun.* **1998**, 589–590; c) Z. Gross, S. Ini, *Org. Lett.* **1999**, 1, 2077–2080; d) M. K. Tse, S. Bhor, M. Klawonn, C. Döbler, M. Beller, *Tetrahedron Lett.* **2003**, 44, 7479–7483; e) S. Bhor, M. K. Tse, M. Klawonn, C. Döbler, W. Mägerlein, M. Beller, *Adv. Synth. Catal.* **2004**, 346, 263–267; recent using Ru salen complexes see: f) T. Takeda, R. Irie, Y. Shinoda, T. Katsuki, *Synlett* **1999**, 1157–1159; g) K. Nakata, T. Takeda, J. Mihara, T. Hamada, R. Irie, T. Katsuki, *Chem. Eur. J.* **2001**, 7, 3776–3782; h) A. Berkessel, P. Kaiser, J. Lex, *Chem. Eur. J.* **2003**, 9, 4746–4756.
- [18] H. Nishiyama, T. Shimada, H. Itoh, H. Sugiyama, Y. Motoyama, *Chem. Commun.* **1997**, 1863–1864.
- [19] a) P. R. Ortiz de Montellano, *Acc. Chem. Res.* **1987**, 20, 289–294; b) M. Yagi, M. Kaneko, *Chem. Rev.* **2001**, 101, 21–35; c) A. J. Wu, J. E. Penner-Hahn, V. L. Pecoraro, *Chem. Rev.* **2004**, 104, 903–938.
- [20] M. Klawonn, M. K. Tse, S. Bhor, C. Döbler, M. Beller, *J. Mol. Catal. A* **2004**, 218, 13–19.
- [21] a) H. Nishiyama, *Enantiomer* **1999**, 4, 569–574; b) S. Liu, J. F. K. Müller, M. Neuburger, S. Schaffner, M. Zehnder, *Helv. Chim. Acta* **2000**, 83, 1256–1267; c) G. Desimoni, G. Faita, M. Guala, C. Pratelli, *Tetrahedron: Asymmetry* **2002**, 13, 1651–1654; d) G. Desimoni, G. Faita, P. Quadrelli, *Chem. Rev.* **2003**, 103, 3119–3154; e) a close related bisoxazine ligand was reported recently: C. Mazet, L. H. Gade, *Inorg. Chem.* **2003**, 42, 210–215.
- [22] a) K. B. Sharpless, S. S. Woodard, M. G. Finn, *Pure Appl. Chem.* **1983**, 55, 1823–1836; b) E. J. Corey, Y. Matsumura, *Tetrahedron Lett.* **1991**, 32, 6289–6292; c) A. Loupy, A. Zaparucha, *Tetrahedron Lett.* **1993**, 34, 473–476; d) T. Hamada, R. Irie, T. Katsuki, *Synlett* **1994**, 479–481; e) L. Cai, Y. Han, H. Mahmoud, B. M. Segal, *J. Organomet. Chem.* **1998**, 568, 77–86; f) R. Noyori, M. Yamakawa, S. Hashiguchi, *J. Org. Chem.* **2001**, 66, 7931–7944; g) K. Jitsukawa, A. Katoh, K. Funato, N. Ohata, Y. Funahashi, T. Ozawa, H. Masuda, *Inorg. Chem.* **2003**, 42, 6163–6165; h) H.

Ait-Haddou, O. Hoarau, D. Cramailere, F. Pezet, J.-C. Daran, G. G. A. Balavoine, *Chem. Eur. J.* **2004**, *10*, 699–707; i) T. C. Wabnitz, J.-Q. Yu, J. B. Spencer, *Chem. Eur. J.* **2004**, *10*, 484–493.

- [23] For examples of catalysis with pybox derivatives, see: a) A. Pfaltz, *Acc. Chem. Res.* **1993**, *26*, 339–345; b) H. Nishiyama, Y. Itoh, H. Matsumoto, S.-B. Park, K. Itoh, *J. Am. Chem. Soc.* **1994**, *116*, 2223–2224; c) A. K. Ghosh, P. Mathivanan, J. Cappiello, *Tetrahedron: Asymmetry* **1998**, *9*, 1–45; d) G. Sekar, A. Datta-Gupta, V. K. Singh, *J. Org. Chem.* **1998**, *63*, 2961–2967; e) J. S. Johnson, D. A. Evans, *Acc. Chem. Res.* **2000**, *33*, 325–335; f) C.-X. Zhao, M. O. Duffey, S. J. Taylor, J. P. Morken, *Org. Lett.* **2001**, *3*, 1829–1831; g) J. Zhou, G. C. Fu, *J. Am. Chem. Soc.* **2004**, *126*, 1340–1341; h) D. Cuervo, M. P. Gamasa, J. Gimeno, *Chem. Eur. J.* **2004**, *10*, 425–432, and references in [21a] and [21d].

Solid-State Structures

T-Shaped Nets of Antimony Atoms in the Binary Antimonide Hf_5Sb_9 **

Abdeljalil Assoud, Katja M. Kleinke, Navid Soheilnia, and Holger Kleinke*

Regular planar square nets of antimony atoms occur in many antimonides, for example, in the HfCuSi_2 ^[1–6] and SmSb_2 types.^[7] Less common types with antimony square nets include LnGaSb_2 (Ln = rare-earth element),^[8] $\text{LnIn}_{1-x}\text{Sb}_2$ ^[9] and LaMSb_3 (M = transition metal).^[10,11] Such square nets of main-group elements have an ideal valence-electron count of six, for example, formal Sb^- atoms, with four so-called half (“hypervalent” one-electron) bonds per atom of roughly 300–310 pm.^[12,13] These nets are prone to undergo Peierls distortions, for example to *cis-trans* chains (found in GdPS with two single bonds per P atom^[14]) or zigzag chains (in CeAsS with two As–As single bonds^[15] and in CeSbTe with two Sb–Sb bonds^[16]). Several defect variants of the ZrSiS type (isopointal (pseudoisosstructural) with PbFCl) are known, including large commensurately modified superstructures, for example, $\text{Gd}_8\text{Se}_{15}$, a 24-fold superstructure of the ZrSiS type,^[17] and GdS_{2-x} , a 144-fold superstructure.^[18] Furthermore, incommensurately modified superstructures may form as well, for example, in tellurides (recently reviewed by Kanatzidis et al.^[19]).

Our interest in nonclassical Sb–Sb bonding of Group 4 antimonides dates back to 1998, when we found linear chains of Sb atom in a metal-rich antimonide.^[20] Our recent

discovery, that the so-called “ $\beta\text{-ZrSb}_2$ ” with planar “Sb” ribbons is actually a ternary silicide–antimonide,^[46] motivated us to turn our attention to orthorhombic HfSb_2 ^[21] and its tetragonal high-temperature form, for which to date only the lattice dimensions are known.^[22] In Pearson’s handbook,^[23] the tetragonal high-temperature form is assigned to the Cu_2Sb type, isopointal with $\text{ZrSiS}/\text{PbFCl}$. If this is the case then the Sb atoms would form an undistorted planar square net with interatomic distances of 277 pm. This is unreasonably short for Sb–Sb half (“hypervalent”) bonds, which are typically between 300 and 310 pm, as found in USb_2 (302 pm)^[24] and ThSb_2 (307 pm),^[25] both forming the ZrSiS type. Moreover, the density of the high-temperature hafnium–antimonide would be about 6% higher than that of the low-temperature form of HfSb_2 , if the stoichiometry were indeed HfSb_2 . Therefore we decided to study its crystal structure, expecting both deficiencies and deviations from the ideal geometry.

We prepared orthorhombic HfSb_2 by annealing elemental hafnium and antimony in the stoichiometric 1:2 ratio at 650 °C as described elsewhere.^[26] Next, we performed a temperature-dependent combined differential scanning calorimetry (DSC) and thermogravimetric (TG) measurement between room temperature and 1080 °C.^[27] An endothermic reaction was observed during the heating process at 1020 °C. No reaction was visible during the cooling process. Assuming that the observed weight loss came exclusively from evaporation of antimony, we calculated that 5.5% of the antimony was lost in the process. A powder diffraction diagram of the product (INEL powder diffractometer) showed no trace of the orthorhombic HfSb_2 ; the experimentally obtained diagram strongly resembled the postulated one of HfSb_2 in the ZrSiS type, accompanied by traces of elemental antimony.

To obtain single crystals of our target compound, we placed the elements in the Hf:Sb ratio of 1:4 (using Sb as a reactive flux) into a small ceramic crucible, placed it in a fused silica tube, and sealed the tube under dynamic vacuum of 10^{-3} mbar. The tube was heated in a resistance furnace under dynamic vacuum at 1075 °C for 32 h, and then cooled to 500 °C at a rate of 5 °C min^{−1}, that is, within two hours. Thereafter, the furnace was switched off to maximize the cooling rate. Small beads of excess antimony were found at the top of the tube, while the ceramic crucible at the bottom of the tube contained the majority of the sample, mostly small black platelike crystals. A powder diffraction diagram of these crystals showed almost exclusively reflections belonging to tetragonal “ HfSb_2 ”. Hence, the cooling rate was fast enough to prevent the formation of orthorhombic HfSb_2 , which is thermodynamically preferred below 1020 °C in the presence of excess antimony. Qualitatively the same results, albeit with worse crystal quality, are obtained by arc-melting HfSb_2 under Argon. Energy dispersive spectroscopy (EDS)^[28] analyses on selected crystals of the tube reaction using orthorhombic HfSb_2 as a standard gave an Hf:Sb ratio of 37(1):63 atomic percent (at %).

The single-crystal structure study performed on a plate-like crystal revealed that the so-called high-temperature “ HfSb_2 ” is actually Hf_5Sb_9 , which is a $\sqrt{5} \times \sqrt{5} \times \sqrt{1}$ superstructure of the originally reported cell,^[29] hence a new structure type. The Hf:Sb ratio (36:64 in at %) concurs well

[*] Dr. A. Assoud, K. M. Kleinke, N. Soheilnia, Prof. H. Kleinke
Department for Chemistry
University of Waterloo
Waterloo, Ontario, N2L 3G1 (Canada)
Fax: (+1) 519-746-0435
E-mail: kleinke@uwaterloo.ca

[**] We are indebted to the Natural Sciences and Engineering Research Council of Canada for financial support.

with the EDS results, and is quite similar to the Zr:Sb ratio in $\text{Zr}_{11}\text{Sb}_{18}$ (38:62) which contains a 3D antimony network.^[30] The projection of the crystal structure along [100] confirms that the Hf_5Sb_9 structure is a distorted (deficient) superstructure variant of the ZrSiS type (Figure 1).

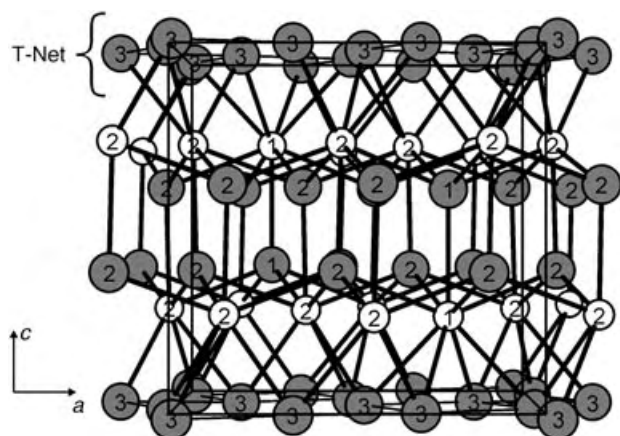


Figure 1. Projection of the Hf_5Sb_9 structure along [010]. Small, white circles = Hf; large, gray circles = Sb. The numbers indicate the atomic labels (Figure 2).

Of the two symmetry-independent hafnium sites, one (Hf1) is coordinated by nine antimony atoms, and the second (Hf2) by eight (noting that the multiplicities of Hf1 and Hf2 are two and eight, respectively), whereas the coordination number of the M atoms in the ZrSiS type is nine. Both coordination polyhedra are best described as distorted mono-capped square antiprisms, in the case of Hf2 one corner is unoccupied (Figure 2). All these Hf–Sb bonds of Hf_5Sb_9 (289–

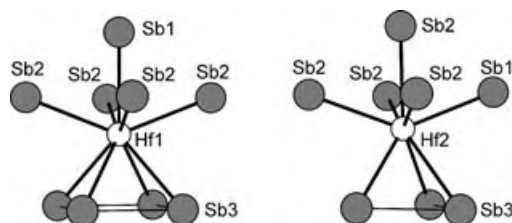


Figure 2. Hf1 Sb_9 (left) and Hf2 Sb_8 (right) polyhedra.

319 pm) are comparable to those of HfSb_2 (293–339 pm), in which the coordination numbers of the Hf atoms are eight and nine as well.

The most interesting structural feature is the unique T-shaped net formed by the Sb3 atoms, in which each atom has the T-shaped coordination environment found in the molecular interhalides BrF_3 and ClF_3 . A significant deviation from the orthogonal T geometry is apparent, with angles of 70.5°, 90°, and 160.5° (instead of $2 \times 90^\circ$ and 180°). As pointed out in a recent overview of T nets given by Hoffmann et al., this net, albeit the simplest 2D net of this family, was not realized before.^[31] Figure 3 shows how the observed Sb3 net is related to the undistorted square net: after removing every fifth atom, the four atoms closest to the resulting hole are shifted

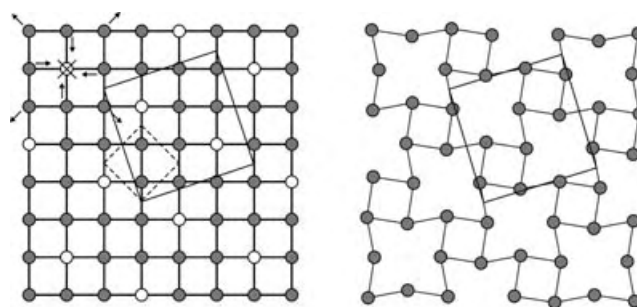


Figure 3. Antimony nets of Hf_5Sb_9 projected along [001] formed exclusively by the Sb3 atoms (large square: unit cell). Left: hypothetical undistorted square net (dashed square = ZrSiS unit cell); right: experimentally observed T-shaped net. Every fifth Sb positions is unoccupied (open circles in the left part, arrows indicate change in atom positions required to generate the observed net from the hypothetical net).

slightly towards each other, and the four next-nearest shifted away from each other. This results in three Sb–Sb contacts of 299 and 2×303 pm per Sb3 atom, instead of four times 277 pm in the hypothetical undistorted fully occupied net.

Overall this net is composed of undistorted square $(\text{Sb}_3)_4$ planes of ideal D_{4h} symmetry, which are interconnected by four Sb3–Sb3 bonds per square to the neighboring squares. The neighboring squares are shifted by 3.6 pm relative to each other, so that the Sb3 layer is slightly puckered. To date, antimony atoms in a T-coordination environment were only found in 1D substructures, that is, ladders as in FeSb_2 ,^[32] MoSb_2S ,^[33] and $(\text{Zr,Ti})\text{Sb}$.^[34] A 2D net with Te atoms in a T-coordination environment is found in $\text{Cs}_3\text{Te}_{22}$ ^[35] (and $\text{Cs}_4\text{Te}_{28}$ ^[36]) in which the Te_4 squares are interconnected by an additional bridging, linearly coordinated Te atom. This arrangement results in the formation of Te_{12} squares, each with one Cs atom in its center. The Te–Te bonds in $\text{Cs}_3\text{Te}_{22}$ of 300–308 pm are comparable to the Sb–Sb bonds in Hf_5Sb_9 (Sb and Te atoms have almost the same covalent radii (139 pm vs. 137 pm)).^[37] Because of the unique nature of the CsTe_6 net, its electronic structure was studied in detail both by Extended Hückel^[38] and by LMTO^[39,40] calculations.

Our LMTO studies on Hf_5Sb_9 and its hypothetical undistorted variant with the vacancies as indicated in Figure 3 (left), showed that the experimentally detected distortion leads to a lower total energy of 2.1 eV per unit cell. The densities of states (DOS, Figure 4, left) indicate

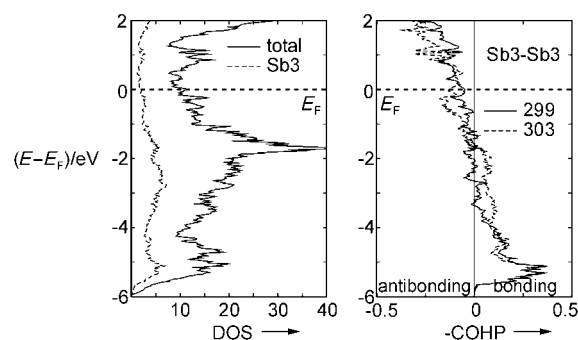


Figure 4. Densities of states (left) and Sb3–Sb3 COHP curves (right) of Hf_5Sb_9 .

metallic properties, with the Fermi level (E_F) lying close to a local nonzero minimum. The area below E_F is dominated by the antimony contributions.

The crystal orbital Hamilton population curves (COHP)^[41] of the two different Sb3–Sb3 interactions are shown in Figure 4(right). The integrated COHP values (ICOHPs) of –0.72 and –0.71 eV per bond reveal overall bonding character, significantly weaker than expected for an Sb–Sb single 2-electron 2-center bond. The shortest Sb–Sb bond in $Zr_{11}Sb_{18}$ (311 pm in an anchorlike Sb_6 unit) has an ICOHP of –0.41 eV, and the shortest Sb–Sb bond in $ZrSb_2$ (289 pm, in a 2D strip), which is classified as a regular single bond,^[42,43] has an ICOHP of –1.21 eV.^[30] The fact that antibonding Sb3–Sb3 states start to become filled at –1.5 eV below E_F indicates that the Sb3 net comprises more than the ideal number of valence electrons. Both curves show a striking qualitative resemblance to the corresponding curves for the Te–Te bonds of Cs_3Te_{22} .^[39]

A detailed electronic structure investigation of the T net of Sb3 atoms of Hf_5Sb_9 , accompanied by temperature-dependent physical property measurements, will show whether this unique net of main-group elements undergoes a Peierls distortion at lower temperatures. Moreover, what is to be expected upon changing the valence-electron concentration? Thus far, three different binary Group 4 antimonides with M:Sb ratios between 1:1 and 1:2 are known, namely Ti_5Sb_8 ,^[44] $Zr_{11}Sb_{18}$, and Hf_5Sb_9 . Ti_5Sb_8 can accommodate the other Group 4 elements (both Zr and Hf to large extents),^[45] while V atoms can be incorporated in $Zr_{11}Sb_{18}$.^[30] We will therefore study the possibilities (and consequences) of replacing part of Hf with M = Ti, Zr, V, Nb, Mo, as well as Sb with Se and Te, in Hf_5Sb_9 .

Received: April 28, 2004

Keywords: antimony · electronic structure · hafnium · solid-state structures

- [1] G. Cordier, H. Schäfer, P. Woll, *Z. Kristallogr.* **1985**, *40B*, 1097–1099.
- [2] A. Leithe-Jasper, P. Rogl, *J. Alloys Compd.* **1994**, *203*, 133–136.
- [3] O. Sologub, K. Hiebl, P. Rogl, H. Noël, O. Bodak, *J. Alloys Compd.* **1994**, *210*, 153–157.
- [4] P. Wollesen, W. Jeitschko, M. Brylak, L. Dietrich, *J. Alloys Compd.* **1996**, *245*, L5–L8.
- [5] J. H. Albering, W. Jeitschko, *Z. Naturforsch. B* **1996**, *51*, 257–262.
- [6] K. D. Myers, S. L. Bud'ko, I. R. Fisher, Z. Islam, H. Kleinke, A. H. Lacerda, P. C. Canfield, *J. Magn. Magn. Mater.* **1999**, *205*, 27–52.
- [7] R. Wang, H. Steinfink, *Inorg. Chem.* **1967**, *6*, 1685–1692.
- [8] A. M. Mills, A. Mar, *J. Am. Chem. Soc.* **2001**, *123*, 1151–1158.
- [9] M. J. Ferguson, R. E. Ellenwood, A. Mar, *Inorg. Chem.* **1999**, *38*, 4503–4509.
- [10] M. Brylak, W. Jeitschko, *Z. Naturforsch. B* **1995**, *50*, 899–904.
- [11] M. J. Ferguson, R. W. Hushagen, A. Mar, *J. Alloys Compd.* **1997**, *249*, 191–198.
- [12] W. Tremel, R. Hoffmann, *J. Am. Chem. Soc.* **1987**, *109*, 124–140.
- [13] G. A. Papoian, R. Hoffmann, *Angew. Chem.* **2000**, *112*, 2500–2544; *Angew. Chem. Int. Ed.* **2000**, *39*, 2408–2448.

- [14] F. Hulliger, R. Schmelzer, D. Schwarzenbach, *J. Solid State Chem.* **1977**, *21*, 371–374.
- [15] R. Ceolin, N. Rodier, P. Khodadad, *J. Less-Common Met.* **1977**, *53*, 137–140.
- [16] Y. C. Wang, K. M. Poduska, R. Hoffmann, F. J. DiSalvo, *J. Alloys Compd.* **2001**, *314*, 132–139.
- [17] E. Dashjav, O. Oeckler, T. Doert, H. Mattausch, P. Böttcher, *Angew. Chem.* **2000**, *112*, 2089–2091; *Angew. Chem. Int. Ed.* **2000**, *39*, 1987–1988.
- [18] R. Tamazyan, S. van Smaalen, I. G. Vasilyeva, H. Arnold, *Acta Crystallogr. B* **2003**, *59*, 709–719.
- [19] R. Patschke, M. G. Kanatzidis, *Phys. Chem. Chem. Phys.* **2002**, *4*, 3266–3281.
- [20] H. Kleinke, *Chem. Commun.* **1998**, 2219–2220.
- [21] A. Kjekshus, *Acta Chem. Scand.* **1972**, *26*, 1633–1639.
- [22] W. Rossteutscher, K. Schubert, *Z. Metallkd.* **1965**, *56*, 813–822.
- [23] P. Villars, *Pearson's Handbook, Desk Edition*, American Society for Metals, Materials Park, OH, **1997**.
- [24] R. Ferro, *Accad. Med. Accad. Lincei* **1952**, *13*, 151–157.
- [25] R. Ferro, *Acta Crystallogr.* **1956**, *9*, 817–818.
- [26] H. Kleinke, *Inorg. Chem.* **1999**, *38*, 2931–2935.
- [27] Apparatus: NETZSCH STA 409PC Luxx. The measurement was performed under a constant flow of argon, with heating and cooling rates of 20 °C min^{–1}. The sample started to lose weight above 780 °C, with a total weight loss of 3.2 %.
- [28] Electron microscope: LEO 1530, with an additional EDS device (EDAX Pegasus 1200). No impurities, for example, stemming from the reaction container, were found.
- [29] The single-crystal structure study was performed using a Smart APEX CCD diffractometer (Bruker), utilizing $Mo_{K\alpha}$ radiation, up to $2\theta = 70^\circ$. Hf_5Sb_9 crystallizes in the tetragonal space group $P4/n$, with lattice dimensions of $a = 874.83(3)$, $c = 866.46(6)$ pm ($Z = 2$). Final residual factors are $R1 = 0.0355$, $wR2 = 0.0899$, $GOF = 1.246$ (all data, 1330 independent reflections, 35 parameters). Further details on the crystal-structure investigation may be obtained from the Fachinformationszentrum Karlsruhe, 76344 Eggenstein-Leopoldshafen, Germany (fax: (+49) 7247-808-666; e-mail: crysdata@fiz-karlsruhe.de), on quoting the depository number CSD-413979.
- [30] I. Elder, C.-S. Lee, H. Kleinke, *Inorg. Chem.* **2002**, *41*, 538–545.
- [31] A. Ienco, D. M. Proserpio, R. Hoffmann, *Inorg. Chem.* **2004**, *43*, 2526–2540.
- [32] H. Holseth, A. Kjekshus, *Acta Chem. Scand.* **1968**, *22*, 3284–3292.
- [33] C.-S. Lee, H. Kleinke, *Eur. J. Inorg. Chem.* **2002**, 591–596.
- [34] H. Kleinke, *J. Am. Chem. Soc.* **2000**, *122*, 853–860.
- [35] W. S. Sheldrick, M. Wachhold, *Angew. Chem.* **1995**, *107*, 490–491; *Angew. Chem. Int. Ed. Engl.* **1995**, *34*, 450–451.
- [36] W. S. Sheldrick, M. Wachhold, *Chem. Commun.* **1996**, 607–608.
- [37] L. Pauling, *The Nature of the Chemical Bond, 3rd Ed.*, Cornell University Press, Ithaca, NY, **1948**.
- [38] Q. Liu, N. Goldberg, R. Hoffmann, *Chem. Eur. J.* **1996**, *2*, 390–397.
- [39] F. Boucher, R. Rousseau, *Inorg. Chem.* **1998**, *37*, 2351–2357.
- [40] O. K. Andersen, *Phys. Rev. B* **1975**, *12*, 3060–3083.
- [41] R. Dronskowski, P. E. Blöchl, *J. Phys. Chem.* **1993**, *97*, 8617–8624.
- [42] E. Garcia, J. D. Corbett, *J. Solid State Chem.* **1988**, *73*, 452–467.
- [43] G. Papoian, R. Hoffmann, *J. Am. Chem. Soc.* **2001**, *123*, 6600–6608.
- [44] Y. Zhu, H. Kleinke, *Z. Anorg. Allg. Chem.* **2002**, *628*, 2233.
- [45] H. Kleinke, *Inorg. Chem.* **2001**, *40*, 95–100.
- [46] N. Soheilnia, A. Assoud, H. Kleinke, *Inorg. Chem.* **2003**, *42*, 7319–7325.

Inner Core Structure Responds to Communication between Nanocapsule Walls**

Gareth W. V. Cave, Jochen Antesberger, Leonard J. Barbour, Robert M. McKinlay, and Jerry L. Atwood*

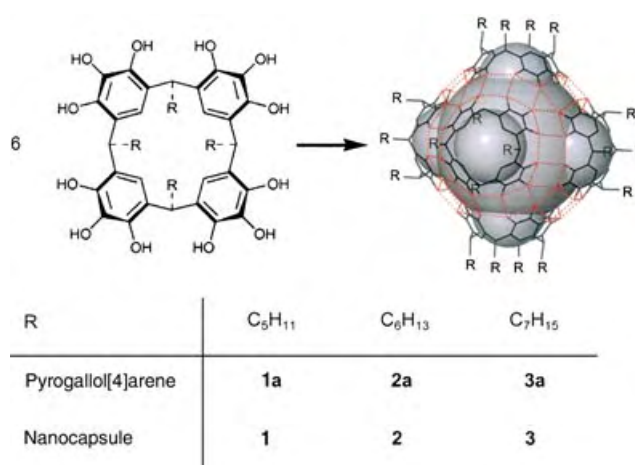
The internal symmetry and resulting packing motifs of microspheres have attracted much attention in recent years.^[1] Albeit at a higher level of complexity, cell–cell and cell–substrate interactions in biological systems are also under intense investigation.^[2] For example, the cell wall of the cowpea chlorotic mottle virus undergoes a reversible physiological change whereby it opens and closes on demand to allow passage to and from the interior cavity.^[3] Supramolecular self-assembled capsules are potentially useful models for such complex biological processes. They are also promising with regard to nanotechnologies involving drug delivery, clean chemical synthesis, assembly of novel materials, and separation science.^[4–7]

Despite keen interest in the self-assembly of simple organic building blocks into molecular containers, there is generally little information on the fate of the encapsulated guest molecules.^[8–10] Although the confined guest matrix within these molecular containers has been regarded as a new phase of matter,^[11] a detailed understanding of the interplay and relative orientations of the constituent guest molecules has, until now, been restricted to a few instances of limited complexity.^[12,13]

We previously described the self-assembly of the pyrogallol[4]arene building block into a globular hexamer, which is stable even in aqueous media.^[8,14] To date, only capsules composed of *C*-isobutylpyrogallol[4]arene^[8,14,15] and *C*-propylpyrogallol[4]arene^[16] have been structurally authenticated by X-ray single-crystal structure analysis. In these studies, it was not possible to determine any geometrical information relating to the included guest molecules. Indeed, the exact nature of their relationship with the host and with one another has been a matter for speculation.^[10,17] We now show for the first time that the guest molecules trapped within the host container adjust their spatial orientation in response to interactions between adjacent nanocapsules. Remarkably, functionalizing the outer shell of the nanocapsule with

different alkyl chains leads to a highly specific solid-state packing arrangement, which in turn influences the organization of the guest molecules within the cavities.

Pyrogallol[4]arene macrocyclic building blocks **1a–3a** (Scheme 1) can be readily prepared through “green technologies”, by the solvent-free acid-catalyzed condensation of pyrogallol and an appropriate aldehyde.^[18] Crystallization of **1a–3a** from common solvents under atmospheric conditions usually yields the kinetically favored bilayer structure^[15,19] in which the lipophilic tails interdigitate with one another and the phenolic groups undergo hydrogen bonding to adjacent molecules to form sheetlike arrays. The protocol that was previously employed to effect the self-assembly of **1a–3a** into spherical hexamers **1–3** has now been superseded by the simpler method of recrystallizing the compounds from a solution in ethyl acetate. Thus, nanocapsules **1–3** have been synthesized reproducibly in quantitative yields under normal laboratory conditions (Scheme 1).



Scheme 1. Synthesis and structure of nanocapsules **1–3**.

Single-crystal X-ray diffraction analysis of the self-assembled nanocapsules **1–3** reveals that, in each case, six pyrogallol[4]arene macrocycles **1a–3a** associate into the previously described globular hexamer, with a diameter of approximately 4 nm (Figure 1).^[8,14,16] The assembly is stabilized by a total of 72 hydrogen bonds, of which 48 are intermolecular (eight intermolecular hydrogen bonds per bound macrocycle). In contrast, the self-assembled capsule consisting of six resorcin[4]arene units and eight water molecules in the form of an Archimedean snub cube,^[20] which is capable of housing up to eight benzene molecules, utilizes only 60 hydrogen bonds, of which 36 are intermolecular (only 2.6 intermolecular hydrogen bonds per bound entity).^[10,17] The increased number of hydrogen bonds coupled with the fact that nanocapsules **1–3** each consist of only six building blocks is a factor in stabilizing the nanocapsules in polar media.^[14] Indeed, this remarkable stability is of great significance for the possible exploitation of such assemblies for biological applications.

TG–IR (thermogravimetric–infrared) analysis of **3** reveals that ethyl acetate molecules are released from the crystalline

[*] Dr. G. W. V. Cave, J. Antesberger, R. M. McKinlay, Prof. J. L. Atwood
Department of Chemistry
University of Missouri–Columbia
Columbia, MO 65211 (USA)
Fax: (+1) 573-884-9606
E-mail: atwoodj@missouri.edu

Prof. L. J. Barbour
Department of Chemistry
University of Stellenbosch
Matieland, 7602 (South Africa)

[**] This work was supported by the National Science Foundation.

Supporting information for this article is available on the WWW under <http://www.angewandte.org> or from the author.

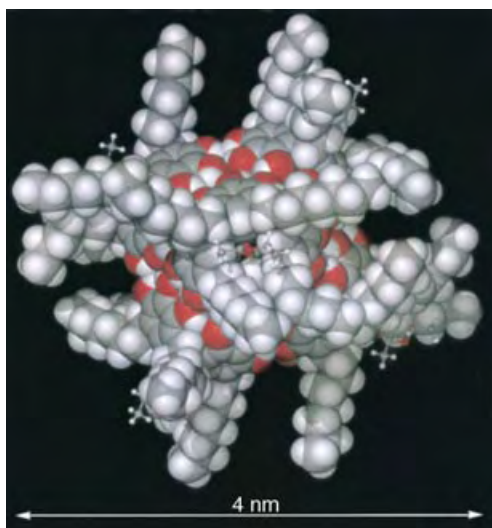


Figure 1. Space-filling view of the molecular structure of nanocapsule **3**.

material at two distinct stages during gradual heating of a dried sample: A weight loss of 7.5% (70–105 °C) corresponds to the loss of only the six ethyl acetate molecules external to the cavity; a further weight loss of 8% immediately prior to decomposition (225–275 °C) corresponds to the loss of both bound ethyl acetate and water molecules. In comparison, TG–IR analysis of monomer **3a** shows no significant weight loss above the boiling point of the cosolvent, until rapid decomposition occurs at 290 °C. Consistent with the TG–IR analysis results, X-ray single-crystal structure analysis of **3** shows that six ethyl acetate molecules enshroud a disordered water molecule within the host assembly. Furthermore, ¹H NMR spectroscopy studies of **3** in CDCl₃ indicate that there are a total of twelve ethyl acetate molecules per nanocapsule. We infer from the two-step loss of ethyl acetate from the crystalline material and the X-ray crystal-structure analysis of nanocapsule **3** that the ethyl acetate molecules positioned outside the constraints of the nanocapsule are freed between 70 and 105 °C from the pockets traversing the lattice. The guest matrix of ethyl acetate and water is held within the crystal lattice by the nanocapsules until they rupture at approximately 225 °C. The molecular formula is therefore [(C-heptylpyrogallol[4]arene)₆(EtOAc)₆(water)]·6(EtOAc), with a molecular weight of 6746.72. The initial 7.5% weight loss is thus consistent with the loss of six ethyl acetate molecules situated in the lattice and exterior to the capsules. The subsequent 8% weight loss is consistent with the simultaneous loss of one water molecule and six ethyl acetate molecules.

In all cases the nanocapsules contain seven guest molecules (six ethyl acetate molecules and one water molecule). The number of external solvating ethyl acetate molecules depends on the length of the alkyl tail unit. X-ray single-crystal structure analysis reveals that nanocapsule **1** traps six ethyl acetate molecules within pockets formed between alkyl chains: three ethyl acetate molecules reside at the base of three of the macrocyclic building blocks **1a** and three are trapped within the space formed by the interdigitation of

adjacent nanocapsule tail groups. Eight ethyl acetate molecules external to nanocapsule **2** are observed by X-ray crystal-structure analysis: two are found at the base of two monomers **2a** and six are trapped within neighboring nanocapsule tail groups. The X-ray single-crystal structure analysis of nanocapsule **3** shows that the six ethyl acetate molecules outside the nanocapsule are all embedded within the alkyl chains at the base of the each of the macrocyclic monomers **3a**.

Nanocapsules **1** and **3** arrange into simple hexagonal and hexagonal-closest-packing arrays (Figure 2a and b, respectively). The nanocapsules are separated by their lipophilic

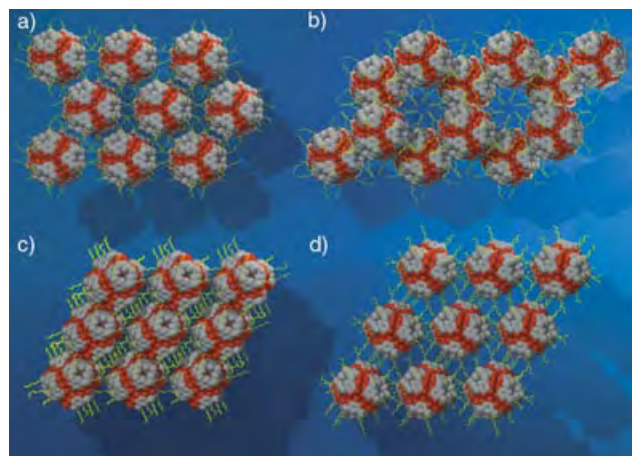


Figure 2. Molecular packing diagram of nanocapsules a) **1**, b) **3**, and c), d) **2**.

tails. Notably, the alkyl chains of different capsules only partially interpenetrate as they form lipophilic membranes between the nanocapsules. Remarkably, when the lipophilic tail is six carbon atoms in length the nanocapsules are not forced away from one another, but rather congregate to form hydrogen-bonded nanorods (**2**, Figure 2c, d, and Figure 3).

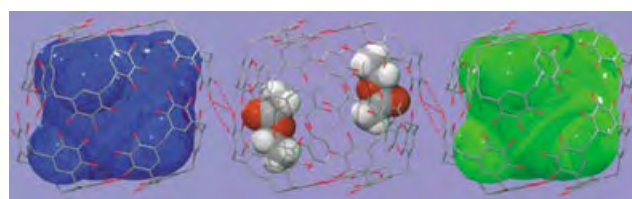


Figure 3. Hydrogen-bonding interactions in nanocapsules **2** and between adjoining nanocapsules.

Four OH groups on opposite sides of each capsule form hydrogen bonds with two adjacent capsules (O...O = 2.732, 3.146, and 3.174 Å, Figure 3). Consequently, the walls of the individual nanocapsules are disrupted, which translates through to the packing of the guest matrix. The distorted intermolecular hydrogen bonding within the host walls enables four of the ethyl acetate guest molecules to undergo hydrogen bonding to the nanocapsule wall through their carbonyl functionalities (O...O = 2.763 and 2.848 Å, Figure 3).

Nanocapsules **1** and **3** feature ordered arrays of ethyl acetate molecules enshrouding an isolated water molecule. The methyl groups are orientated towards the base of the pyrogallol[4]arene macrocycles and the single water molecule resides at the center of the matrix (Figure 4a). When the

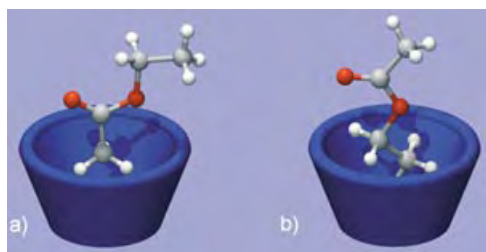


Figure 4. Ethyl acetate orientation within the nanocapsule: a) methyl group down, b) ethyl group down.

neighboring nanocapsules communicate with each other through the hydrogen-bonding interactions observed in nanocapsule **2**, the four ethyl acetate guest molecules hydrogen bonded to the inside of the nanocapsule wall reorient with their ethyl groups in the base of macrocycle (Figure 4b). The two remaining ethyl acetate guests position their carbonyl groups down into the cleft of the macrocycle, as observed in **1** and **3**. It was not possible to locate the exact position of the water molecule inside this nanocapsule owing to extensive disorder. This difference in guest interactions and hence fluidity is clearly a consequence of communication or lack thereof between the host walls of neighboring nanocapsules.

The internal volumes^[21] of **1** and **3** are $\approx 1300 \text{ \AA}^3$, whereas **2** encloses only $\approx 1200 \text{ \AA}^3$. The smaller volume of **2** is attributed to interactions between neighboring capsules, whereby one of the pyrogallol units within the aromatic plane formed between three hydrogen-bonding pyrogallol[4]-arene building blocks also participates in hydrogen-bonding interactions with an adjoining nanocapsule. Consequently the symmetry of the nanocapsule is distorted as the pyrogallol[4]arene building blocks twist to accommodate the intercapsule hydrogen bonding. This disruption of the hexagonal plane formed between the three monomers causes a deviation from planarity of approximately 46° (O211 O111 C143) and is unique to nanocapsule **2**.

The guest molecules occupy 40% of the total volume of the larger cavitands and 44% of that of distorted conformer **2**.^[21] Although this is significantly lower than the optimal 55% packing efficiency,^[22] it is in excellent agreement with the $\sim 43\%$ occupancy recently calculated for the eight benzene guest molecules observed within the resorcin[4]arene/water Archimedean snub cube.^[10]

We have shown that a small structural variation—in this case the extension of an alkyl chain by one carbon atom—in the pyrogallol[4]arenes can have profound effects on the crystal packing and interactions between nanocapsules. Communication between the nanocapsules is then translated though the capsule walls to the guest matrix trapped within. The geometry of the guests within nanocapsules **1–3** provides valuable insight into the interactions and fluidity of the so-called “new phase of matter”.^[11]

Experimental Section

The pyrogallol[4]arenes were synthesized through a modified solvent-free technique analogous to that used in the synthesis of resorcin[4]arenes.^[18] The nanocapsules were synthesized as a crystalline material (suitable for analysis by X-ray diffraction techniques) by slow evaporation of ethyl acetate ($\approx 5 \text{ mL}$) from the pyrogallol[4]arene ($\approx 150 \text{ mg}$).

Typically, thermogravimetric analysis was performed on a dry 18.464-mg crystalline sample of the nanocapsule on a TS Q50 Thermogravimetric Analyzer coupled to a Thermo Nicolet AEM FTIR with a Nexus TGA-IR interface. The sample was heated at a constant rate of 1°C min^{-1} from 30 to 500°C and purged with a continuous stream of nitrogen gas at a flow rate of 20 mL min^{-1} . The IR spectra of the mobile phase in the range of 1000 to 3000 cm^{-1} were collected at a rate of one spectrum min^{-1} .

Crystal data can be found in the Supporting information. CCDC-228139 (capsule **1**), CCDC-228138 (capsule **2**), and CCDC-228137 (capsule **3**) contain the supplementary crystallographic data for this paper. These data can be obtained free of charge via www.ccdc.cam.ac.uk/conts/retrieving.html (or from the Cambridge Crystallographic Data Centre, 12 Union Road, Cambridge CB2 1EZ, UK; fax: (+44)1223-336-033; or deposit@ccdc.cam.ac.uk).

Received: May 19, 2004

Keywords: calixarenes · cavitands · host–guest systems · hydrogen bonds · nanostructures · self-assembly

- [1] V. N. Manoharan, M. T. Elessier, D. J. Pine, *Science* **2003**, *301*, 483–487.
- [2] a) J. C. Canman, L. A. Cameron, P. S. Maddox, A. Straight, J. S. Tirnauer, T. J. Mitchison, G. Fang, T. M. Kapoor, E. D. Salmon, *Nature* **2003**, *424*, 1074–1078; b) H. Lodish, A. Berk, L. S. Zipurski, P. Matsudaira, D. Baltimore, J. Darnell, *Molecular Cell Biology*, 4th ed., Freeman, New York, **2000**.
- [3] T. Douglas, M. Young, *Nature* **1998**, *393*, 152–155.
- [4] S. Sortino, S. Giuffrida, S. Fazio, S. Monti, *New J. Chem.* **2001**, *25*, 707–713.
- [5] M. Yoshizawa, T. Kusakawa, M. Fujita, K. Yamaguchi, *J. Am. Chem. Soc.* **2000**, *122*, 6311–6312.
- [6] L. R. MacGillivray, J. L. Atwood, *Angew. Chem.* **1999**, *111*, 1080–1096; *Angew. Chem. Int. Ed.* **1999**, *38*, 1018–1033.
- [7] C. Zandonella, *Nature* **2003**, *423*, 10–12.
- [8] J. L. Atwood, L. J. Barbour, A. Jerga, *Proc. Natl. Acad. Sci. USA* **2002**, *99*, 4837–4841.
- [9] G. W. Orr, L. J. Barbour, J. L. Atwood, *Science* **1999**, *285*, 1049–1052.
- [10] A. Shivanyuk, J. Rebek, Jr., *J. Am. Chem. Soc.* **2003**, *125*, 3432–3433.
- [11] J. C. Sherman, D. J. Cram, *J. Am. Chem. Soc.* **1989**, *111*, 4527–4528.
- [12] G. W. V. Cave, M. J. Hardie, B. A. Roberts, C. L. Raston, *Eur. J. Org. Chem.* **2001**, 3227–3231.
- [13] C. L. Raston, G. W. V. Cave, *Chem. Eur. J.* **2004**, *10*, 279–282.
- [14] J. L. Atwood, L. J. Barbour, A. Jerga, *Chem. Commun.* **2001**, 2376–2377.
- [15] T. Gerkenmeier, W. Iwanek, C. Agena, R. Fröhlich, S. Kotila, C. Näther, J. Mattay, *Eur. J. Org. Chem.* **1999**, 2257–2262.
- [16] J. L. Atwood, L. J. Barbour, A. Jerga, *J. Supramol. Chem.* **2001**, *1*, 131–134.
- [17] L. Avram, Y. Cohen, *J. Am. Chem. Soc.* **2002**, *124*, 15148–15149.
- [18] B. A. Roberts, G. W. V. Cave, C. L. Raston, J. L. Scott, *Green Chem.* **2001**, *3*, 280–284.
- [19] A. Shivanyuk, J. C. Friese, S. Doring, J. Rebek, Jr., *J. Org. Chem.* **2003**, *68*, 6489–6496.

- [20] L. R. MacGillivray, J. L. Atwood, *Nature* **1997**, 389, 469–472.
- [21] L. J. Barbour, MCAVITY, program for the determination of the volume of a molecular cavity, University of Missouri-Columbia, Missouri, USA, **2003**, <http://x-seed.net/cavity.html>.
- [22] A. S. Mecozzi, J. Rebek Jr., *Chem. Eur. J.* **1998**, 4, 1016–1022.

Molecular Switches

A Molecular Multiproperty Switching Array Based on the Redox Behavior of a Ferrocenyl Polychlorotriphenylmethyl Radical**

Christian Sporer, Imma Ratera, Daniel Ruiz-Molina, Yuxia Zhao, José Vidal-Gancedo, Klaus Wurst, Peter Jaitner, Koen Clays, André Persoons, Concepció Rovira, and Jaume Veciana*

The preparation of molecular switches has attracted a great deal of attention in the last few years owing to their potential use in the future as key nanoscale components for digital processing and communication.^[1] Special interest exists in developing molecular switches showing an optical output signal at the near-IR (NIR) region which is important for telecommunication purposes. To date, molecular switches exhibiting changes in one property, such as color,^[2] luminescence,^[3] optical nonlinearity,^[4] or magnetic properties,^[5] have been reported. However, recently the number of useful properties being simultaneously modulated on a bistable molecule-based material has been extended to three properties (electrical, optical, and magnetic) although in this case the changes in the properties has an intermolecular origin.^[6]

Herein we report a new multifunctional redox-switchable molecular array involving simultaneous changes of three

different outputs—the linear optical, nonlinear optical, and magnetic properties—which is based on the rich electrochemical behavior of compound **1** (Scheme 1).

Radical **1** is composed of two electroactive units linked by an CH=CH bridge, these are an acceptor unit, the polychlorinated triphenylmethyl (PTM) radical, and a donor unit, the nonamethylferrocene group. The reduction of **1** into its diamagnetic anionic form **1**[−] or the oxidation into the ferrocenium radical derivative **1**⁺, gives rise to three different redox states that should show distinct physical properties. Indeed, substituted PTM radicals not only possess unpaired electrons contributing to the magnetic properties, but they also show nonlinear optical responses owing to their octupolar nature^[7] and, in addition, their color is different from that of the corresponding carbanions. The methylated ferrocene derivatives gave stable oxidized species with an open-shell character. Moreover, donor–acceptor dyads properly linked usually show nonlinear optical properties. Consequently, radical **1** appeared as an ideal candidate for developing a multiproperty three-state switching molecular device governed by electrical or chemical inputs.

The synthesis of radical **1** was performed following a multistep synthetic methodology (see Supporting Information). A Wittig–Horner–Emmons reaction between the polychlorotriphenylmethane phosphonate derivative^[8] and the nonamethylated ferrocene carboxaldehyde^[9] gave the *trans* isomer of **1**-H. Then **1**-H was deprotonated to the carbanion **1**[−], which was isolated as the [K([18]crown-6)] salt in 89% yield. Finally radical **1** was obtained in a 57% overall yield by oxidation of the [K([18]crown-6)] salt. Treatment of **1** with AgBF₄ yields the corresponding ferrocenium radical derivative **1**⁺, which was isolated as the **1**⁺BF₄[−] salt in a 79% yield.

X-ray crystal structure (see Supporting Information)^[10] of radical **1** shows that in each radical unit the three phenyl rings are twisted in the same way adopting a propeller-like conformation with either a Δ or Λ helicity. The *trans* configuration of the double bond leads to small dihedral angles between the mean planes containing the CH=CH bridge and the phenyl and tetramethylcyclopentadienyl rings attached to it, 31(2)° and 35(3)°, respectively. These values indicate a large degree of conjugation between the two electroactive units.

As shown in Figure 1, the colors of the studied compounds in CH₂Cl₂ solution are quite different. Thus, the [K([18]crown-6)]⁺**1**[−] salt is deep purple, radical **1** is brown, the **1**⁺BF₄[−] salt is yellow, and the hydrocarbon **1**-H is pale pink.

In accordance with their distinct colors, the optical absorption spectra of the three species **1**, **1**⁺, **1**[−] show strikingly differences (Figure 2 and Supporting Information). Thus, radical **1** shows besides the characteristic absorptions of conjugated PTM radicals^[8] at 385 nm, 497, and 656 nm a broad intervalence charge-transfer (IVCT) absorption band in the NIR region, centered at 1520 nm which is associated with an intramolecular electron transfer from the ferrocene donor unit to the radical acceptor unit (the PTM unit). The maximum of this IVCT band shifts from 1360 nm in *n*-hexane to 1540 nm in THF indicating a positive solvatochromism with increasing solvent polarity. This behavior indicates a positive

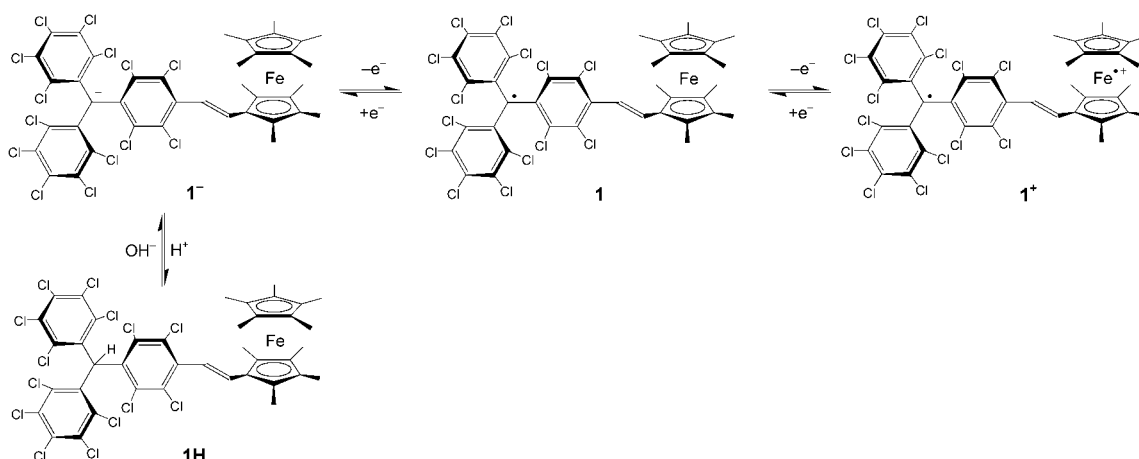
[*] Dr. C. Sporer, Dr. I. Ratera, Dr. D. Ruiz-Molina, Dr. J. Vidal-Gancedo, Prof. C. Rovira, Prof. J. Veciana
Institut de Ciència de Materials de Barcelona (CSIC)
Campus Universitari de Bellaterra
08193 Cerdanyola (Spain)
Fax: (+34) 93-580-57-29
E-mail: vecianaj@icmab.es

Dr. Y. Zhao, Prof. K. Clays, Prof. A. Persoons
Laboratorium voor Chemische en Biologische Dynamica
Katholieke Universiteit Leuven
Celestijnenlaan 200D, 3001 Leuven (Belgium)

Dr. K. Wurst, Prof. P. Jaitner
Institut für Allgemeine Anorganische und Theoretische Chemie
Universität Innsbruck, Innrain 52a, 6020 Innsbruck (Austria)

[**] This work was supported by grants from the DGI (Spain), project MAT2003-04699, DGR (Catalunya), project 2001SGR00362, Catalan Network CeRMAE, Flemish Fund for Scientific Research (FWO-VG.0297.04), COST Chemistry D14 Action “Functional Materials” and Acción Integrada Hispano-Austríaca, project HU2002-0046. C.S. is grateful to the FWF Vienna for a postdoctoral grant (Erwin-Schrödinger Stipendium J2103).

Supporting information for this article is available on the WWW under <http://www.angewandte.org> or from the author.



Scheme 1. The three states of the molecular switch: 1^- , 1 , and 1^+ .



Figure 1. Colors shown by CH_2Cl_2 solutions of the synthesized compounds. From left to right: 1-H , $[\text{K}([18]\text{crown-6})]^+1^-$, 1 , and 1^+BF_4^- .

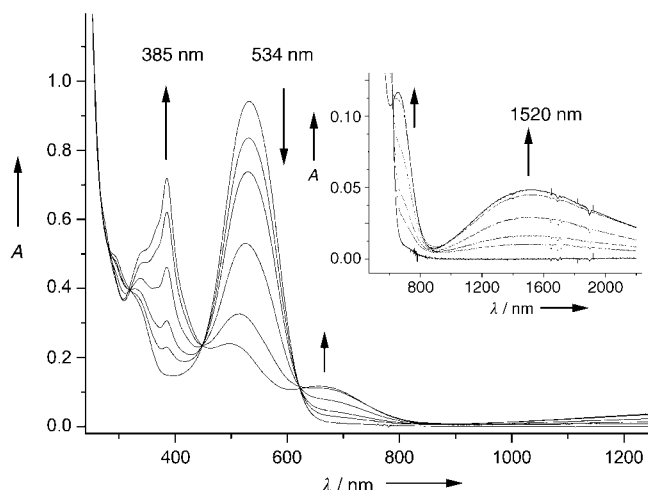


Figure 2. Spectroelectrochemical experiments showing the evolution of UV/Vis-NIR spectra during the oxidation of 1^- in CH_2Cl_2 to radical 1 . Trends in intensity changes are shown for selected bands by arrows.

dipole-moment change between the ground and the excited state, which is characteristic of a system with a moderate electronic coupling between the donor and acceptor units.^[11]

The ferrocenium radical derivative 1^+ , shows besides the typical bands of the ferrocenium at 280, 300, and 805 nm, an enhancement of the intensity of the radical band at 385 nm, which accounts for the yellow color of this species. On other hand the IVCT band is absent, in agreement with the lack of electron-donor character of the organometallic unit when it is oxidized. In carbanion 1^- the typical radical absorptions are not observed while an intense absorption at 534 nm, characteristic of PTM anions, is present.^[12] As for 1^+ , the broad IVCT absorption in the NIR region of 1 vanishes in 1^- confirming the absence of an electron-acceptor capability in the reduced triphenylmethyl unit in 1^- .

The dynamic hyperpolarizabilities of these three species were measured by hyper-Rayleigh scattering (HRS) experiments with a laser fundamental of 800 nm.^[13] As suggested by the intense IVCT band, radical 1 gives a large nonlinear optical response with a dynamic hyperpolarizability value $\beta(800)$ of $545(\pm 30) \times 10^{-30}$ esu. This value is reduced almost ninefold to $66(\pm 7) \times 10^{-30}$ esu for 1^+ , and even more for the carbanion 1^- which has a $\beta(800)$ value of $30(\pm 3) \times 10^{-30}$ esu.^[14]

Magnetic properties of the three studied species are also different. Thus, while $[\text{K}([18]\text{crown-6})]^+1^-$ is diamagnetic, the paramagnetic susceptibility of compounds 1 and 1^+BF_4^- in the solid state between 4–300 K showed quasi-ideal paramagnetic behavior with effective magnetic moments of 1.72 for 1 and $2.50 \mu_B$ for 1^+BF_4^- at 300 K; as expected for systems with $S = 1/2$ and $S = 2 \times 1/2$ units. Indeed, the value of $2.50 \mu_B$ indicates that the magnetic interaction between the open-shell ferrocenium moiety and the triphenylmethyl radical unit in 1^+ is very weak with both spins being apparently uncoupled above 4 K.

Analogous differences in the behavior of the three complexes were found in solution with EPR spectroscopy (see Supporting Information) since 1^- is EPR silent while 1 and 1^+ show different complex signals that exhibit a complex behavior when the temperature is lowered. The origin of this intricate behavior is still not well understood although it might be related to a spin-density redistribution associated to conformational changes or to a valence tautomerism phenomena.^[15]

Reduction and oxidation processes of radical **1**^[16] to **1**[−] and **1**⁺ are completely reversible as ascertained by the presence of various isosbestic points in the spectroelectrochemical experiments at the UV/Vis-NIR region (Figure 2 and Supporting Information).

To demonstrate the complete reversibility of the redox reactions of radical **1**, several oxidation and reduction cycles were performed. As shown in Figure 3 (see also the Supporting Information), after each step, the optical spectrum was

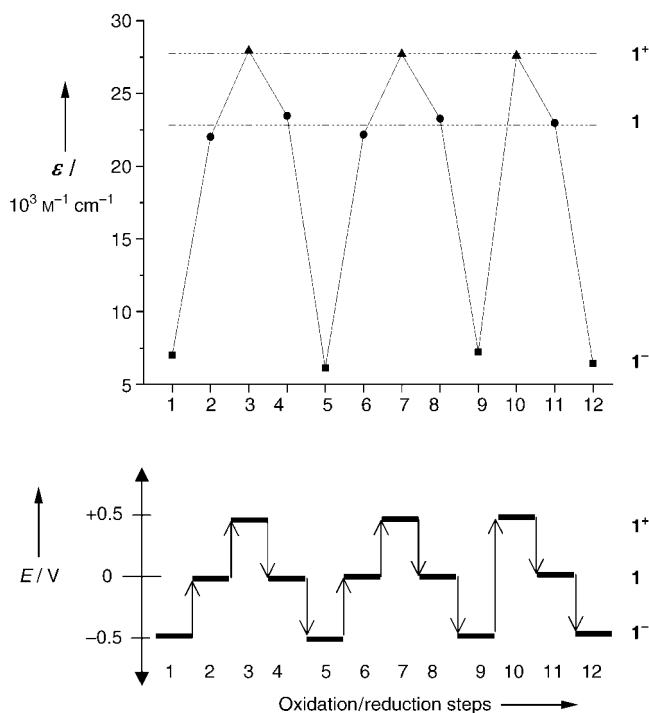


Figure 3. Cyclic stepwise oxidations and reductions carried out in THF with a chronoamperometric technique monitoring the changes in the visible spectrum. Top: Changes observed at a wavelength of 385 nm where **1** (●) and **1**⁺ (▲) exhibit the strongest absorption and **1**[−] (■) shows a very weak absorption. Bottom: Fixed potentials *E* used in the different steps of cyclic redox experiments.

recorded and could be fully recovered after each cycle. Analogous switching behavior was also detected with EPR spectroscopy by studying the magnetic response in solution of the redox-switchable molecular array.

The three species of this molecular array may be interconverted with a variety of chemical reagents. Such chemical transformations along with the conversions by electrical stimuli let us expect a plethora of signal transduction mechanisms should this molecular switchable array be used as a molecular logic gate. Studies in this direction are in progress.

In summary, we have demonstrated that the new open-shell donor–acceptor dyad **1** can exist in three stable oxidation states exhibiting different linear and nonlinear optical responses as well as distinct magnetic properties. Owing to fully reversible redox processes, this radical can act as a three-state redox-switchable molecular device combining chromic, magnetic, and nonlinear optical outputs in the same molecule.

Remarkable is the output signal at the NIR region shown by this electrochromic switching molecular array.

Received: March 1, 2004

Revised: June 11, 2004 [Z54150]

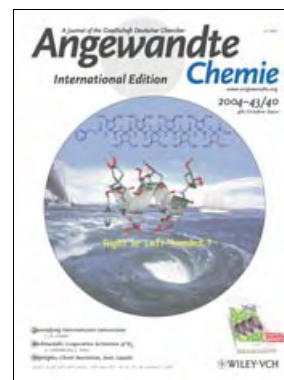
Keywords: hyper-Rayleigh scattering · magnetic properties · nonlinear optics · radicals · sandwich complexes

- [1] a) B. L. Feringa, *Molecular Switches*, Wiley-VCH, Weinheim, **2001**; b) J.-M. Lehn, *Supramolecular Chemistry*, VCH, Weinheim, **1995**; c) A. P. de Silva, N. D. McClenaghan, *Chem. Eur. J.* **2004**, *10*, 574–586; d) R. L. Carroll, C. B. Gorman, *Angew. Chem.* **2002**, *114*, 4556–4579; *Angew. Chem. Int. Ed.* **2002**, *41*, 4378–4400; .
- [2] a) *Photochromism, Molecules and Systems* (Eds.: H. Dürr, H. Bouas-Laurent), Revised Edition, Elsevier, Amsterdam, **2003**; b) Special issue: “Photochromism: Memories and Switches” *Chem. Rev.* **2000**, *100*, 1683–1890 (Ed.: M. Irie).
- [3] A. P. de Silva, H. Q. Gunaratne, T. Gunnlaugsson, A. J. M. Huxley, C. P. McCoy, J. T. Rademacher, T. E. Rice, *Chem. Rev.* **1997**, *97*, 1515–1566.
- [4] a) B. J. Coe, *Chem. Eur. J.* **1999**, *5*, 2464; b) M. Malaun, Z. R. Reeves, R. L. Paul, J. C. Jeffery, J. A. McCleverty, M. D. Ward, I. Asselberghs, K. Clays, A. Persoons, *Chem. Commun.* **2001**, 49–50; c) F. Paul, K. Costuas, I. Ledoux, S. Deveau, J. Zyss, J.-F. Halet, C. Lapinte, *Organometallics* **2002**, *21*, 5229–5235.
- [5] a) F. Renz, H. Oshio, V. Ksenofontov, M. Waldeck, H. Spiering, P. Gütllich, *Angew. Chem.* **2000**, *112*, 3832–3834; *Angew. Chem. Int. Ed.* **2000**, *39*, 3699; b) P. Gütllich, Y. García, T. Woike, *Coord. Chem. Rev.* **2001**, *219*, 839–879; c) O. Sato, *Acc. Chem. Res.* **2003**, *36*, 692–700.
- [6] a) M. E. Itkis, X. Chi, A. W. Cordes, R. C. Haddon, *Science* **2002**, *296*, 1443–1445; b) J. S. Miller, *Angew. Chem.* **2003**, *115*, 27–29; *Angew. Chem. Int. Ed.* **2003**, *42*, 27–29.
- [7] I. Ratera, J.-F. Létard, S. Marcén, D. Ruiz-Molina, E. Freysz, C. Rovira, J. Veciana, *Chem. Phys. Lett.* **2002**, *363*, 245–251.
- [8] C. Rovira, D. Ruiz-Molina, O. Elsner, J. Vidal-Gancedo, J. Bonvoisin, J.-P. Launay, J. Veciana, *Chem. Eur. J.* **2001**, *7*, 240.
- [9] C. Zou, M. S. Wrighton, *J. Am. Chem. Soc.* **1990**, *112*, 7578–7584.
- [10] X-ray structure figure, data, and analysis are given as Supporting Information. CCDC-191558 contains the supplementary crystallographic data for this paper. These data can be obtained free of charge via www.ccdc.cam.ac.uk/conts/retrieving.html (or from the Cambridge Crystallographic Data Centre, 12, Union Road, Cambridge CB2 1EZ, UK; fax: (+44) 1223-336-033; or deposit@ccdc.cam.ac.uk).
- [11] a) C. Creutz, H. Taube, *J. Am. Chem. Soc.* **1969**, *91*, 3988–3989; b) R. W. Callahan, G. M. Brown, T. J. Meyer, *J. Am. Chem. Soc.* **1974**, *96*, 7827–7839.
- [12] J. Veciana, J. Riera, J. Castañer, N. Ferrer, *J. Organometallic Chem.* **1985**, *297*, 131–141.
- [13] For the HRS experimental setup used see: G. Olbrechts, R. Strobbe, K. Clays, A. Persoons, *Rev. Sci. Instrum.* **1998**, *69*, 2233–2241.
- [14] See Supporting Information for more details on HRS studies.
- [15] The non-methylated ferrocene radical analogue of **1**, shows a valence tautomerism phenomenon in the solid state. See: I. Ratera, D. Ruiz-Molina, F. Renz, J. Ensling, K. Wurst, C. Rovira, P. Gütllich, J. Veciana, *J. Am. Chem. Soc.* **2003**, *125*, 1462–1463.
- [16] Cyclic voltammetry of **1** in CH₂Cl₂ shows two reversible processes, at potentials of *E*_{1/2} = −238 and +86 mV, versus Ag/AgCl, corresponding to its reduction to **1**[−] and oxidation to **1**⁺, respectively.

Cover Picture

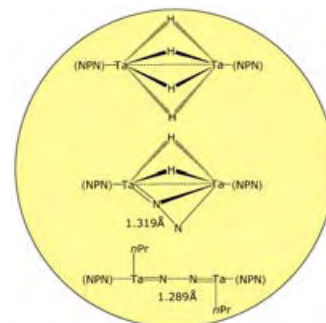
Masakazu Tanaka,* Yosuke Demizu, Mitsunobu Doi, Masaaki Kurihara, and Hiroshi Suemune*

A **tidal vortex (helix)** is formed, both right- and left-handed, where a violent tidal current meets a peaceful sea (the picture from Naruto City Tourist Association shows an example at Naruto channel, Japan). In contrast, α -helices of proteins almost always show a right-handed helical screw sense because of the stereogenic α -carbon center of α -amino acids. M. Tanaka et al. now demonstrate on page 5360 ff. how the left-handedness of a α -helical peptide is controlled by the side-chain stereogenic centers.



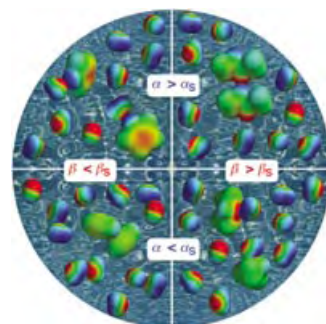
Dinitrogen Activation

The use of multimetallic complexes in the activation of dinitrogen is investigated by S. Gambarotta and J. Scott in their Minireview on page 5298 ff.



Molecular Recognition

A simple, universally applicable approach for quantifying intermolecular interactions in any solvent is discussed by C. A. Hunter in the Review on page 5310 ff.



Crystal Growth

M. Brustolon, B. Kahr, A. L. Rohl et al. describe on page 5328 ff. how luminescent probes, which are common in biochemistry, can be used to study the specificity of a guest for growing crystal faces of potassium hydrogen phthalate.



Angewandte EarlyView®

The following Communications are available online (in Wiley InterScience). You can find them, as well as forthcoming Reviews, Highlights, and Essays, at www.angewandte.org, under Early View.

A. Ismach, L. Segev, E. Wachtel, E. Joselevich*:

Atomic-Step-Templated Formation of Single-Wall Carbon Nanotube Patterns

DOI: 10.1002/anie.200460356

Published online: September 28, 2004

M. Lee,* M.-H. Park, N.-K. Oh, W.-C. Zin, H.-T. Jung, D. K. Yoon:

Supramolecular Crystalline Sheets with Ordered Nanopore Arrays from Self-Assembly of Rigid-Rod Building Blocks

DOI: 10.1002/anie.200460378

Published online: September 23, 2004

Articles judged by the referees or the editor as being either very important or very urgent are immediately edited, proof-read, and electronically published once the manuscript has arrived in the editorial office in its final form. As long as there is no page number available these articles should be cited in the following manner:

Author(s), *Angew. Chem. Int. Ed.*, online publication date, DOI.

Obituary

Jacques van Boom (1937–2004): Biopolymers

C. A. A. van Boeckel — 5288 – 5289

Books

Handbook of Metalloproteins

Albrecht Messerschmidt, Wolfram Bode, Mirek Cygler

reviewed by F. Tuczek — 5290

NMR—From Spectra to Structures
Color Chemistry

Terence N. Mitchell, Burkhard Costisella
Heinrich Zollinger

reviewed by N. Schlörer — 5290

reviewed by H. Langhals — 5291

Highlights

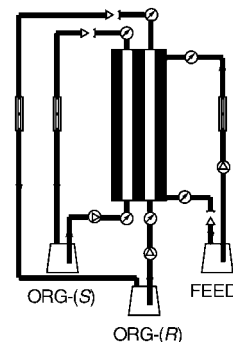
Separation Methods

C. A. M. Afonso,*

J. G. Crespo* — 5293 – 5295

Recent Advances in Chiral Resolution through Membrane-Based Approaches

Hollow-fiber membrane contactors, which can be combined with enzymatic resolution, have already emerged as a potential technology for enantiomeric resolution under continuous operation (see scheme; ORG denotes the organic phase). Furthermore, recently reported optically active polyelectrolyte multilayer (PEMU) membranes appear extremely promising for future applications in preparative chiral separations.

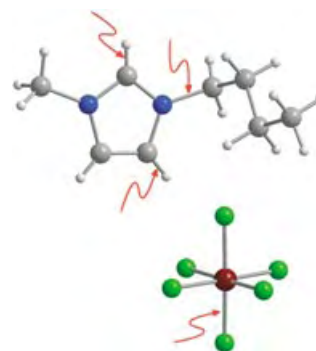


Ionic Liquids

J. Dupont,* J. Spencer — 5296 – 5297

On the Noninnocent Nature of 1,3-Di-alkylimidazolium Ionic Liquids

Presumed innocent, room-temperature ionic liquids are clean, often reusable, media for carrying out many synthetic, catalytic, separation, and analytical processes. However, they are not simply inert solvents, and a variety of decomposition pathways have been detected. In the structure of 1-*n*-butyl-3-methylimidazolium hexafluorophosphate shown, reactive bonds are marked with arrows (C grey, N blue, F green, P red).



Minireviews

Dinitrogen Activation

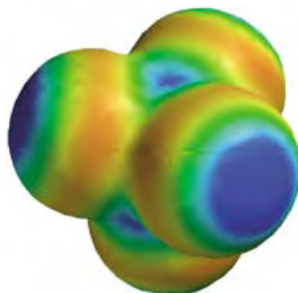
S. Gambarotta,* J. Scott — 5298–5308

Multimetallic Cooperative Activation of N_2

How important is the cooperative attack of two or more metal centers for dinitrogen activation? The most recent literature, which provides the focus for this Minireview, helps to improve our understanding

of the factors that determine such important processes as dinitrogen fixation, cleavage, and elementary transformations.

Noncovalent interactions are treated as a form of hydrogen bonding to produce a new universal scale that can be used to estimate the free energies of interaction between any pair of neutral functional groups in any solvent. The important parameters are provided by the molecular electrostatic potential surface (the example depicted is that for carbon tetrachloride).



Reviews

Molecular Recognition

C. A. Hunter* — 5310–5324

Quantifying Intermolecular Interactions: Guidelines for the Molecular Recognition Toolbox

Stunning tricolored crystals with distinct regions of green, yellow, and orange luminescence (see picture) are deposited in solutions of potassium hydrogen phthalate that contain proflavin. The dye serves as a fluorescent probe of surface charge while identifying the polar crystallographic axis. Optical probes, common in biochemistry, can be used widely to study the specificity of noncovalent chemistry crystal growth from solution.

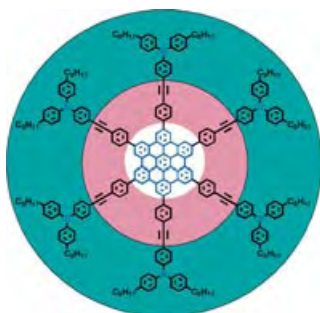


Communications

Crystal Growth

A. Barbon, M. Bellinazzi, J. B. Benedict, M. Brustolon,* S. D. Fleming, S.-H. Jang, B. Kahr,* A. L. Rohl* — 5328–5331

Luminescent Probes of Crystal Growth: Surface Charge and Polar Axis Sense in Dye-Doped Potassium Hydrogen Phthalate



The hole story: using a new synthetic concept the title hexa-*peri*-hexabenzocoronenes (HBCs) were synthesized with high atom economy. The coaxial arrangement of the HBCs and arylamines allowed a “double-cable” hole transport (see picture), that is, transport through the central core (white) and the outer shell (green).

Electron Transfer

J. Wu, M. Baumgarten, M. G. Debije, J. M. Warman, K. Müllen* — 5331–5335

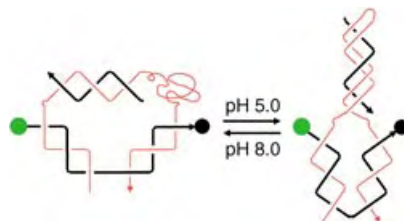
Arylamine-Substituted Hexa-*peri*-hexabenzocoronenes: Facile Synthesis and Their Potential Applications as “Coaxial” Hole-Transport Materials

For the USA and Canada: ANGEWANDTE CHEMIE International Edition (ISSN 1433-7851) is published weekly by Wiley-VCH PO Box 191161, D 69451 Weinheim, Germany. Air freight and mailing in the USA by Publications Expediting Inc. 200 Meacham Ave., Elmont, NY 11003. Periodicals

postage paid at Jamaica NY 11431. US POSTMASTER: send address changes to *Angewandte Chemie*, Wiley-VCH, 111 River Street, Hoboken, NJ 07030. Annual subscription price for institutions: Europe € 3760.00/3418.00; outside Europe US\$ 4948.00/4498.00 (valid for print and electronic/print or electronic delivery); for

individuals who are personal members of a national chemical society, or whose institution already subscribes, or who are retired or self-employed consultants, print only: Europe € 258.00/outside Europe US\$ 394.00. Postage and handling charges included. All Wiley-VCH prices are exclusive VAT.

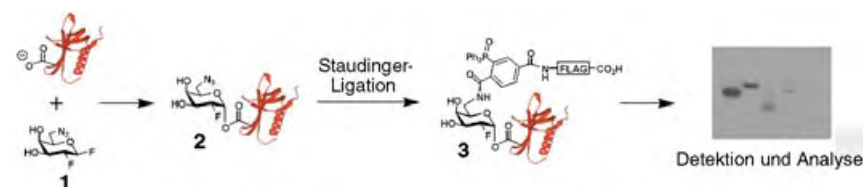
Making DNA work: A DNA nanomachine with a mechanism based on a DNA duplex–triplex transition (see figure) was constructed. The key component is a DNA triplex that contains C⁺GC triplets and is only stable under acidic conditions. The DNA machine uses H⁺ and OH[−] ions as fuel and its only waste products are H₂O and NaCl.



Nanotechnology

Y. Chen, S.-H. Lee, C. Mao* **5335–5338**

A DNA Nanomachine Based on a Duplex–Triplex Transition



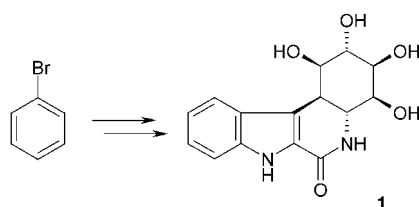
A multipurpose flag: The inactivator **1** covalently labels the catalytic nucleophiles of retaining β -glycosidases to form species **2**. The small azide group allows labeling of enzymes with sterically con-

gested active sites. Staudinger ligation of **2** with phosphine–FLAG yields adduct **3**, which can be used to detect and profile retaining β -glycosidase activities in complex mixtures.

Enzyme Labels

D. J. Vocadlo,*
C. R. Bertozzi* **5338–5342**

A Strategy for Functional Proteomic Analysis of Glycosidase Activity from Cell Lysates



New drug design possibilities are suggested by the results of a biological evaluation of the indole derivative **1** of pancratistatin, a known anticancer agent, in a panel of cancer cell lines. Enzymatic dihydroxylation was one of the key steps in the short, enantioselective synthesis of **1**.

Synthetic Methods

U. Rinner, T. Hudlicky,* H. Gordon,
G. R. Pettit **5342–5346**

A β -Carboline-1-one Mimic of the Anticancer *Amaryllidaceae* Constituent Pancratistatin: Synthesis and Biological Evaluation

Virtual screening: Based on parameters which do not have to be measured, sets of attributes for solids are derived and used to predict whether a catalyst falls into one of five performance classes in propene oxidation, with a predictive power substantially exceeding the statistically expected values (see table (a confusion matrix): prediction rate indicates the

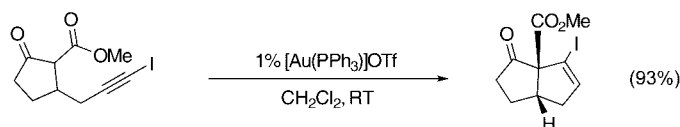
test	cluster					sum	ratio	prediction rate
	1	2	3	4	5			
1 predicted	16	3	4	0	2	25	0.25	0.64
2 predicted	5	18	6	0	8	37	0.29	0.49
3 predicted	5	4	16	0	1	26	0.24	0.62
4 predicted	1	0	0	3	0	4	0.03	0.75
5 predicted	1	8	1	0	11	21	0.19	0.52
sum/mean	28	33	27	3	22	113		0.60

correct assignment by the new method, ratio indicates the statistical expectation value).

Combinatorial Catalysis

C. Klanner, D. Farrusseng, L. Baumes,
M. Lengliz, C. Mirodatos,
F. Schüth* **5347–5349**

The Development of Descriptors for Solids: Teaching “Catalytic Intuition” to a Computer



Cyclopentenoid structures including compounds containing vinyl iodide, 1,3-diene, and heterocyclic moieties are obtained through the gold(I)-catalyzed 5-endo-dig addition of β -dicarbonyl compounds to unactivated alkynes under

neutral conditions and at room temperature (RT). Both monocyclic and bicyclic cyclopentenoids can be formed in excellent yields and with good diastereoselectivity (see scheme).

Synthetic Methods

S. T. Staben, J. J. Kennedy-Smith,
F. D. Toste* **5350–5352**

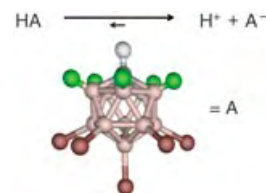
Gold(I)-Catalyzed 5-endo-dig Carbocyclization of Acetylenic Dicarboxyl Compounds

Brønsted Acids

M. Juhasz, S. Hoffmann, E. Stoyanov,
K.-C. Kim, C. A. Reed* — 5352 – 5355

The Strongest Isolable Acid

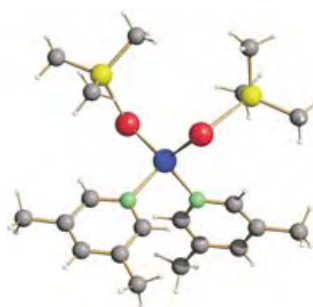
Measure for measure: Several measures indicate that carborane acids of the type $H(CHB_{11}R_5X_6)$ (see scheme, green R, red X, gray H, pink B) for $R=H, Cl$ and $X=Cl, Br, I$ are the strongest pure Brønsted acids. Based on NMR and IR spectroscopy, $H(CHB_{11}Cl_{11})$ can lay claim to be the strongest isolable acid presently known.



Cluster Compounds

M. W. DeGroot,
J. F. Corrigan* — 5355 – 5357

Imine-Stabilized Zinc Trimethylsilyl-chalcogenolates: Powerful Reagents for the Synthesis of II-II'-VI Nanocluster Materials

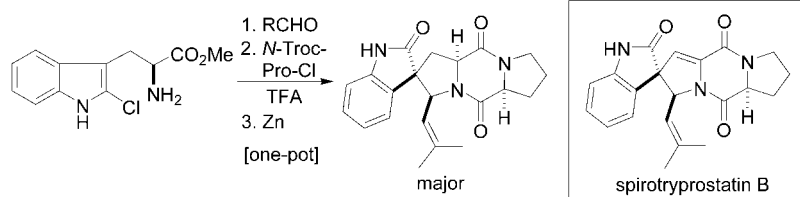


That zinc in feeling: The complexes $[(3,5-Me_2C_5H_3N)_2Zn(ESiMe_3)_2]$ ($E=Se, 1$; $E=Te, 2$) are prepared and found to be good reagents for the generation of ternary MM'E materials. From **2** (see structure; Te red, Zn blue, Si yellow, N green), the ternary ZnCdTe nanocluster $[Zn_{2.6}Cd_{7.4}Te_4(TePh)_{12}(PnPr_3)_4]$ (**3**) is prepared. The optical properties of **3** are shown to be modulated relative to those of related binary CdTe cluster molecules.

Alkaloid synthesis

F. Y. Miyake, K. Yakushijin,
D. A. Horne* — 5357 – 5360

Preparation and Synthetic Applications of 2-Halotryptophan Methyl Esters: Synthesis of Spirotryprostatin B



New N-acyliminium ion methodology: 2-Halotryptophan esters serve as important synthetic building blocks for the stereo-controlled construction of spiro[pyrroli-

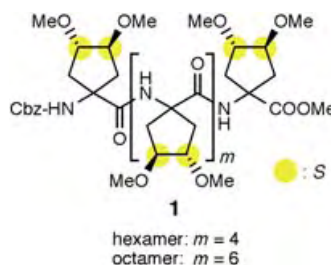
dine-3,3'-oxindoles] (see scheme). The cell-cycle inhibitor spirotryprostatin B is assembled in rapid fashion by using this methodology.



Helical Structures

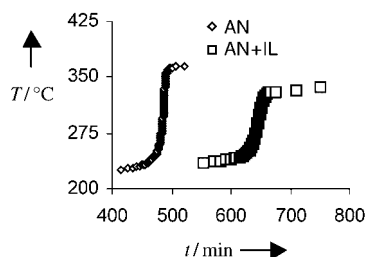
M. Tanaka,* Y. Demizu, M. Doi,
M. Kurihara, H. Suemune* — 5360 – 5363

Chiral Centers in the Side Chains of α -Amino Acids Control the Helical Screw Sense of Peptides



Chirality on the side suffices: The screw sense of 3_{10} - and α -helices formed by the oligopeptides **1**, which have no α -carbon chiral centers, is controlled by the chiral centers in their side chains. These results imply that just the side chain chiral centers of isoleucine and threonine would affect the secondary structure of their oligopeptides.

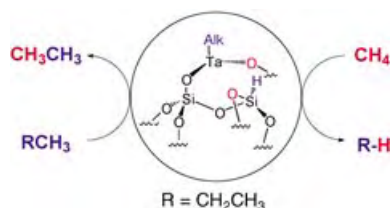
Highly exothermic polymerization reactions of monomers have been carried out in ionic liquids (ILs) by employing an accelerating-rate calorimeter (ARC) to assess the role of the IL. The results indicate that the IL acts as an ideal heat sink in controlling the potential for the reactions to reach thermal runaway as well as contributing to a significant pressure reduction (see the acrylonitrile (AN) example depicted).



Ionic Liquids

R. Vijayaraghavan, M. Surianarayanan,
D. R. MacFarlane* 5363–5366

Ionic Liquids as Moderators in
Exothermic Polymerization Reactions

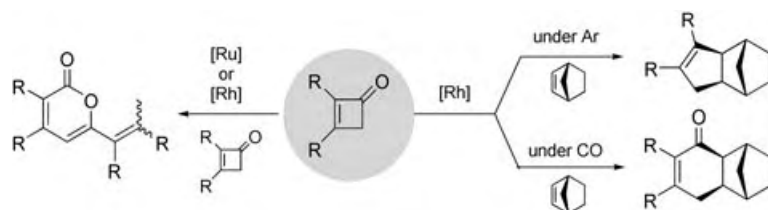


Methane, a building block for basic chemicals through its incorporation into alkanes: when a methane/propane mixture is passed over a tantalum hydride catalyst at 250°C, propane is transformed into two ethane molecules through the incorporation of one methane unit. This reaction corresponds to a cross-metathesis of propane and methane (see scheme; Alk = alkyl).

C–C Bond Formation

D. Soulivong, C. Copéret,*
J. Thivolle-Cazat, J.-M. Basset,*
B. M. Maunders, R. B. A. Pardy,
G. J. Sunley 5366–5369

Cross-Metathesis of Propane and Methane:
A Catalytic Reaction of C–C Bond
Cleavage of a Higher Alkane by Methane



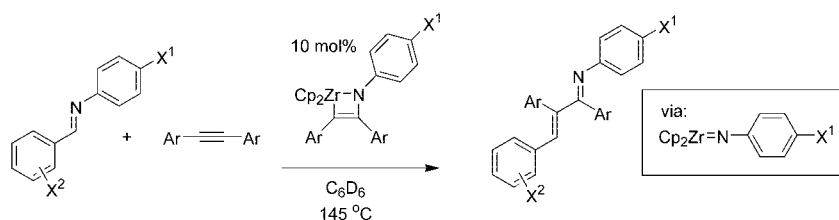
η^4 -Vinylketene and/or metallacyclopentenone complexes can be considered key intermediates in the ruthenium- and rhodium-catalyzed ring-opening dimerization

of cyclobutenones to give 2-pyranones as well as in the rhodium-catalyzed coupling reactions of cyclobutenones with 2-norbornene (see scheme).

Homogeneous Catalysis

T. Kondo,* Y. Taguchi, Y. Kaneko, M. Niimi,
T. Mitsudo* 5369–5372

Ru- and Rh-Catalyzed C–C Bond Cleavage
of Cyclobutenones: Reconstructive and
Selective Synthesis of 2-Pyranones,
Cyclopentenes, and Cyclohexenones



A big plus for addition reactions: A catalytic amount of an azazirconacyclobutene is used in a novel carboamination reaction that involves net addition of an

aldimine across a symmetrical alkyne to generate highly substituted α,β -unsaturated ketimine products (see scheme; Cp = C_5H_5).

Imidozirconium Complexes

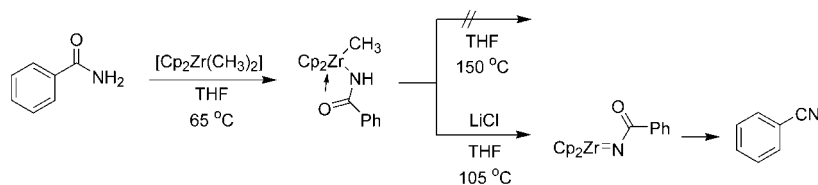
R. T. Ruck, R. L. Zuckerman, S. W. Krska,
R. G. Bergman* 5372–5374

Carboamination: Additions of Imine
C=N Bonds Across Alkynes Catalyzed by
Imidozirconium Complexes

Reaction Mechanisms

R. T. Ruck, R. G. Bergman* - 5375–5377

Zirconium-Mediated Conversion of Amides to Nitriles: A Surprising Additive Effect



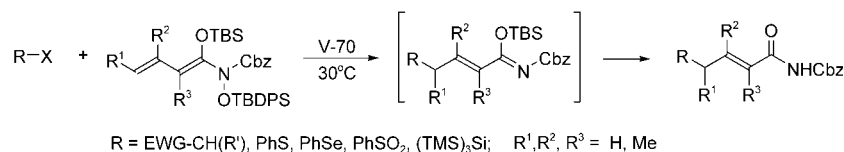
Chloride coordination is the key: Dimethylzirconocene reacts with amides to form methylzirconium amide complexes. On heating, in the presence of a chloride source, these compounds are converted into *N*-acylimidozirconocene complexes

that react intramolecularly to form the corresponding nitrile compounds (see scheme; Cp = C₅H₅). Mechanistic studies reveal that chloride coordination to zirconium is required for this transformation to occur.

Radical Reactions

S. Kim,* C. J. Lim - 5378–5380

Radical-Mediated γ -Functionalizations of α,β -Unsaturated Carboxylic Amides



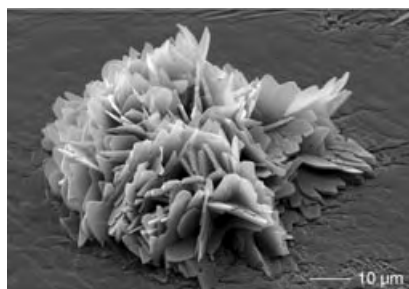
Highly successful tin-free, radical-mediated alkylations of α,β -unsaturated carboxylic amides have been carried out. Alkyl iodides and bromides bearing α -electron-withdrawing groups undergo

selective γ -additions to diene *O,N*-acetals (see scheme). This approach to γ -functionalization was further extended to the use of hetero groups, such as phenylsulfanyl and phenylsulfonyl species.

CuCl Nanoplatelets

A. Taubert* - 5380–5382

CuCl Nanoplatelets from an Ionic Liquid-Crystal Precursor

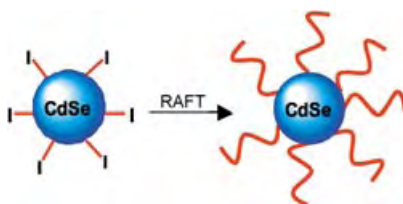


Green approach to inorganic nanostructures: CuCl nanoplatelets (see picture) were synthesized from mixtures of a Cu-containing ionic liquid crystal and 6-*O*-palmitoyl ascorbic acid. The particle size, thickness, and connectivity can be adjusted through varying the reaction temperature. The copper-containing precursor acts as both the template and the copper source. The ligand is not consumed in the precipitation and can be reused.

Nanotechnology

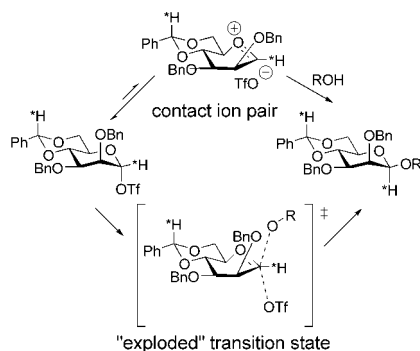
H. Skaff, T. Emrick* - 5383–5386

Reversible Addition Fragmentation Chain Transfer (RAFT) Polymerization from Unprotected Cadmium Selenide Nanoparticles



Nanoparticles functionalized with a trithiocarbonate ligand allow RAFT poly-

merization to be performed from their surface. Homopolymers, random copolymers, and block copolymers can be grown radially from trithiocarbonate-covered CdSe nanoparticles (see scheme). This technique gives excellent nanoparticle dispersion in a wide range of polymers, while maintaining the unique photophysical properties of the nanoparticles.

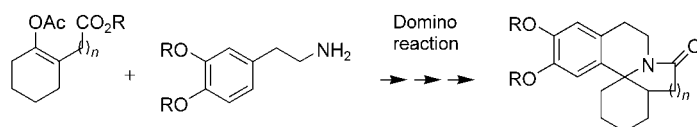


Considerable oxacarbenium ion character may be in the transition state of a highly β -selective mannosylation reaction that proceeds via an α -mannosyl triflate. An α -deuterium kinetic isotope effect of 1.2 was measured at -78°C ($=1.1$ at 25°C). This information may be interpreted in terms of a stereoselective trapping of a transient contact ion pair or, alternatively, as representative of an "exploded" transition state (see scheme).

Glycosylation Mechanism

D. Crich,*
N. S. Chandrasekera — 5386 – 5389

Mechanism of 4,6-O-Benzylidene-Directed β -Mannosylation as Determined by α -Deuterium Kinetic Isotope Effects



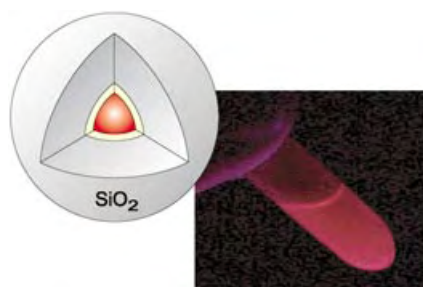
Domino effect: The skeleton of erythrina and B-homoerythrina alkaloids can be constructed in an efficient manner from readily available substrates (see Scheme)

by a three-step domino reaction. These natural products constitute an interesting class of compounds because of their extensive biological activity.

Erythrina Alkaloids

S. A. A. El Bialy, H. Braun,
L. F. Tietze* — 5391 – 5393

A Highly Efficient Synthesis of the Erythrina and B-Homoerythrina Skeleton by an AlMe_3 -Mediated Domino Reaction



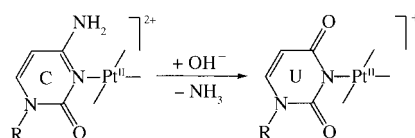
Bright particles: The optical properties of luminescent nanocrystals (quantum dots, QDs) can be exploited only if they have an appropriate surface derivatization. A straightforward method is presented to encapsulate single QDs with a homogeneous silica shell, while retaining their high luminescence (see picture).

Nanostructures

T. Nann,* P. Mulvaney — 5393 – 5396

Single Quantum Dots in Spherical Silica Particles

A mechanism goes platinum: Hydrolytic deamination of cytosine is a major mutagenic event in DNA. Studies with a model system and DFT calculations demonstrate that deamination is facilitated by coordination of the Pt^{II} center to the N3 atom (see scheme; C = cytosine, U = uracil).



Metal-Nucleobase Complexes

J. E. Šponer,* P. J. Sanz Miguel,
L. Rodríguez-Santiago, A. Erxleben,
M. Krumm, M. Sodupe,* J. Šponer,
B. Lippert* — 5396 – 5399

Metal-Mediated Deamination of Cytosine: Experiment and DFT Calculations

Fluorescent Probes

B. K. Wetzl, S. M. Yarmoluk, D. B. Craig,
O. S. Wolfbeis* _____ **5400 – 5402**

Chameleon Labels for Staining and
Quantifying Proteins

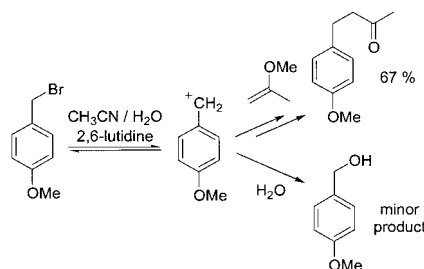


Glowing marks: A new class of protein stains, the pyrylium dyes, undergo a strong color change (typically from blue to red, see picture) on covalently binding to proteins. While the free stains are almost nonfluorescent, the protein-conjugated forms are highly fluorescent. The dyes do not alter the charge of a protein, and thus do not change its electrophoretic properties. The stains also can be used in quantitative protein assays.

Friedel–Crafts Reactions

M. Hofmann, N. Hampel, T. Kanzian,
H. Mayr* _____ **5402 – 5405**

Electrophilic Alkylations in Neutral
Aqueous or Alcoholic Solutions

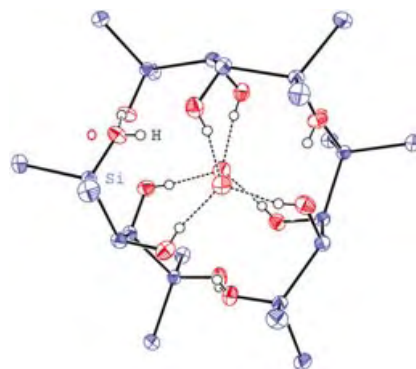


Acid-free Friedel–Crafts chemistry: A paradox? Nucleophilicity scales, based on reactions with benzhydrylium ions, show that many π systems are more nucleophilic than aqueous or alcoholic solutions that are generally employed as solvents for S_N1 reactions. Solvolytically generated carbocations can, therefore, be trapped by donor-substituted arenes and alkenes to form products of Friedel–Crafts-type reactions in neutral aqueous solutions (see scheme).

Synthetic Methods

C. Krempner,* J. Kopf, C. Mamat,
H. Reinke, A. Spannenberg _____ **5406 – 5408**

Novel Polysilanol by Selective
Functionalizations of Oligosilanes



As part of a succinct synthesis, a new functionalization method leads to hitherto unknown polysilanol with an oligosilane backbone, a class of compounds with remarkable electronic properties. The trifluoroacetylation of phenyl-substituted hydroxyoligosilanes yield trifluoroacetoxyoligosilanes almost quantitatively, and these can be converted into tri- and tetrasilanol, such as that shown, simply by hydrolysis.



Communications labeled with this symbol have been judged by two referees as being “very important papers”.

“Hot Papers” are chosen by the Editors for their importance in a rapidly evolving field of high current interest. A preview with the graphical abstracts of these articles can be found on the *Angewandte Chemie* homepage in Wiley InterScience at www.angewandte.org.

“VIPs” are Communications which are identified by two referees as being very important. They are published online up to several weeks ahead of print. A preview with short summaries of these articles can also be found on the journal's homepage.

Service

Keywords _____ **5410**

Authors _____ **5411**

**Angewandte's
Sister Journals** _____ **5412 – 5413**

Preview _____ **5415**

Jacques van Boom (1937–2004): Biopolymers

Jacques H. van Boom, emeritus professor of bioorganic chemistry at Leiden University, passed away on July 31, 2004 at the age of 67, after a short illness.



After obtaining his PhD “cum laude” in 1968 at the University of Utrecht (The Netherlands) under the guidance of Lambert Brandsma and Josef Arens, Jacques van Boom continued his training at the University of Cambridge (UK), where he was a Ramsay Memorial Postdoc-

toral Fellow in the group of Lord Todd from 1968 until 1970. He started his independent career at Leiden University in 1970 as a lecturer and became Professor of Bioorganic Chemistry in 1978. After his retirement in June 2002, he remained actively involved in teaching and research as scientific advisor of the Faculty of Sciences at Leiden University. Jacques van Boom supervised over 60 PhD students and numerous undergraduate students. He authored over 750 scientific publications, with more than 25 000 citations. In 1981, he was elected Fellow of the Royal Dutch Academy of Sciences (KNAW). He received several prestigious scientific awards, including the Gold Medal of the Royal Dutch Chemical Society (KNCV, 1975), the Royal Shell Award (1985), the Simon Stevin Master Award (1999), and the Akzo Nobel Science Award (2000).

Throughout his scientific career, van Boom devoted his skills as a bioorganic chemist to the elucidation of complex processes involving biopolymers, such as DNA, RNA, carbohydrates, and peptides. Early on he recognized the tremendous power of organic chemistry for the preparation of fragments of these biopolymers and synthetic analogues. In the selection of his research objectives he always felt that, rather than pursuing the synthesis of complex molecules, the prime objective of the organic chemist should be to create compounds with unique properties—properties that facilitate biophysi-

cal, pharmaceutical, and biological research.

Jacques van Boom started his independent research career with the pursuit of synthetic strategies towards DNA oligomers. At the time he became active in the field, in the mid-1970s, the successful synthesis of even small DNA oligomers was a tremendous scientific challenge. He maintained a preeminent position in the field of DNA synthesis through the development of a series of new phosphorylation^[1] and protecting-group^[2] techniques. By applying these novel technologies he provided the scientific community in the 1970s and early 1980s with literally hundreds of very pure DNA and RNA fragments,^[3] of which multimilligram amounts could be prepared.

Many exciting discoveries were made with these synthetic oligomers. One highlight, achieved in collaboration with Alex Rich (Massachusetts Institute of Technology, USA), was the first crystal structure at atomic resolution of a defined DNA duplex, which led to the discovery of Z-DNA as a new type of left-handed duplex DNA.^[4] Another was the elucidation of the mode of action of the DNA-targeting antibiotic bleomycin,^[5] in collaboration with Sidney Hecht (University of Virginia, USA).

In the early 1980s van Boom widened his horizons and tackled a variety of synthetic challenges in the preparation of oligomeric fragments of other biopolymers, such as peptides and carbohydrates, but also hybrid structures with nucleotides (nucleopeptides, glycosylated nucleotides). He started a program in collaboration with the Dutch biochemist Piet Borst (Netherlands Cancer Institute, Amsterdam) to evaluate the role of a specific glycosylated nucleobase, denominated J (β -glucosylated 5-hydroxymethyldeoxyuridine), as present in the genome of the human pathogen *Trypanosoma brucei* (the causative of African sleeping sickness).^[6]

In collaboration with Eckard Wimmer (State University of New York, USA) a breakthrough in our understanding of the replication mechanism of the poliovirus was achieved. Key to this study was the accessibility of specific uridylylated oligopeptide frag-

ments.^[7] An early highlight in the area of synthetic bacterial vaccines was the development of a synthetic vaccine against *Haemophilus influenzae* type b (Hib), the causative bacteria of pneumonia and meningitis. In collaboration with RIVM (Bilthoven, The Netherlands) and Organon NV, it was shown that these synthetic vaccines are efficacious.^[8]

One of the first reports on automated oligosaccharide synthesis describes research by van Boom and co-workers on the use of polyethylene glycol as the carrier in a solid-phase synthesis of a galactofuranose oligomer.^[9] Another hallmark in carbohydrate chemistry was the discovery, also in the early 1990s, of a set of activator systems that turn thioglycosides into effective donors for oligosaccharide assembly.^[10]

Jacques van Boom reached his eminent position in bioorganic chemistry through a combination of utter dedication to research, complete confidence in his ability to recognize potential in his students, and his remarkable intuition in selecting his research objectives. It is now 25 years since I started as a student in his research group, where I learned the importance of multidisciplinary research in the life sciences. It was a pleasure and an honor to be an adjunct professor in his group for the last 12 years. I will certainly miss his lively discussions about biology, the synthesis of complex biomacromolecules, the origin of life, the education of students, religion, politics, our private lives, and unreliable sciences. There was never a dull moment with Jacques, who stimulated our creativity with his actions, challenging remarks, and remarkable sense of humor.

Constant A. A. van Boeckel
Organon NV and Leiden University
(The Netherlands)

- [1] G. van der Marel, C. A. A. van Boeckel, G. Wille, J. H. van Boom, *Tetrahedron Lett.* **1981**, 22, 3887–3890.
- [2] J. H. van Boom, P. M. J. Burgers, *Tetrahedron Lett.* **1976**, 17, 4875–4878.
- [3] J. A. den Hartog, G. Wille, R. A. Scheublin, J. H. van Boom, *Biochemistry* **1982**, 21, 1009–1018.
- [4] A. H. Wang, G. J. Quigley, F. J. Kolpak, J. L. Crawford, J. H. van Boom, G. van -

- der Marel, A. Rich, *Nature* **1979**, 282, 680–686.
- [5] B. J. Carter, E. de Vroom, E. C. Long, G. A. van der Marel, J. H. van Boom, S. M. Hecht, *Proc. Natl. Acad. Sci. U.S.A.* **1990**, 87, 9373–9377.
- [6] M. Cross, R. Kieft, R. Sabatini, M. Wilm, M. de Kort, G. A. van der Marel, J. H. van Boom, F. van Leeuwen, P. Borst, *EMBO J.* **1999**, 18, 6573–6581.
- [7] A. V. Paul, J. H. van Boom, D. Filippov, E. Wimmer, *Nature* **1998**, 393, 280–284.
- [8] C. C. Peeters, D. Evenberg, P. Hoogerhout, H. Kayhty, L. Saarinen, C. A. van Boeckel, G. A. van der Marel, J. H. van Boom, J. T. Poolman, *Infect. Immun.* **1992**, 60, 1826–1833.
- [9] G. H. Veeneman, S. Notermans, R. M. J. Liskamp, G. A. van der Marel, J. H. van Boom, *Tetrahedron Lett.* **1987**, 28, 6695–6698.
- [10] G. H. Veeneman, S. H. van Leeuwen, J. H. van Boom, *Tetrahedron Lett.* **1990**, 31, 275–278.

Life's Simple Pleasures!



No need to waste precious time looking for the right information – Register now for the free **Wiley-VCH Alerting Service**.

It's simple – and it's fast.

To receive regular news per e-mail tailored precisely to your needs and interests, just fill in the registration form at www.wiley-vch.de/home/pas/

 **WILEY-VCH**

Recent Advances in Chiral Resolution through Membrane-Based Approaches

Carlos A. M. Afonso* and João G. Crespo*

Keywords:

chiral resolution · chromatography · enzymes · membranes

The need for chiral compounds in enantiomerically pure form, mainly by the pharmaceutical industry, creates a considerable pressure for the development of new strategies for preparative-scale resolution of racemic mixtures.^[1] Chromatographic methods, particularly gas–liquid (GLC) and solid–liquid (HPLC) chromatography, have been for a long time the best approach for analytical enantiomer separation.^[2] Furthermore, chiral separation on a preparative scale by liquid chromatography has proved to be a very efficient method for a wide range of substrates. However, apart from their advantageous high efficiencies and broad applications, chromatographic methods present the disadvantage of being typically discontinuous. To circumvent this limitation, the development of simulated moving bed chromatography (SMB), which can also be applied to supercritical-fluid chromatography (SFC), allows a continuous process operation on a preparative scale.^[3] SMB chromatography is extremely useful for large-scale (and including chiral) separations; however, it

is necessary to perform a complex experimental and theoretical optimization study for each substrate separation. The high cost of stationary phases has been a major limitation for the generalized use of this technique, and it is for this reason that the SMB methodology is mainly restricted to the final stages of production of single enantiomers by chiral separation, at which point simple resolution by crystallization is not feasible.

More recently, capillary electrophoresis has emerged as a very powerful analytical method for chiral separation,^[4] and includes high-speed chiral separation on a microchip electrophoresis device.^[5] It is assumed that the separation is possible owing to the similar interactions between each enantiomer and the chiral selector as in the case of chromatography. Consequently, chiral selectors such as cyclodextrins and amino acid derivatives are equally effective in both separation techniques. Moreover, because the chiral selectors are actually dissolved in the solution in which the differential migration for each enantiomer occurs, other types of chiral selectors (crown ethers, linear polysaccharides, macrocyclic antibiotics, transition-metal complexes, chiral surfactants, and proteins) may also be employed. Capillary electrophoresis will certainly have a prosperous future for the resolution of ionic racemic substrates if adequate engineering solutions are developed to extend its already remarkable chiral separation efficiency to a preparative scale.

Optical resolution by enantioselective extraction is a very simple method and was first demonstrated thirty years ago by Cram and co-workers,^[6] who

used chiral crown ethers (in chloroform) as efficient selectors for the enantioselective extraction of racemic ammonium salts from aqueous solution. Since then, other efficient chiral selectors emerged, such as organometallic complexes,^[7] deoxyguanosine derivatives,^[8] borate complexes of 1,2-diols,^[9] and steroidal guanidinium and urea receptors.^[10] In all of the reported examples, which includes both the pioneering *catalytic resolving machine* (W-tube device) described by Cram and co-workers^[11] and the multiple dual-flow countercurrent batch extraction procedure,^[12] the chiral selector is dissolved in the organic phase, and the racemic mixture is dissolved in the aqueous phase. With this approach, in accord with the “three-point rule”,^[13] there is a more effective preferential binding of the chiral selector to one of the enantiomers in a solvent environment that is less polar than the feeding aqueous phase.

However, resolution based on dispersed-phase extraction presents significant limitations for preparative and continuous operation, such as the low-contact interfacial area and problems inherent to phase dispersion and phase coalescence. These limitations may be minimized by using hollow-fiber membrane contactors.^[14] A membrane contactor is a device that allows gas–liquid or liquid–liquid mass transfer without the dispersion of one phase within the other, by passing the fluids on opposite sides of a microporous membrane, typically with pore sizes between 0.2 and 0.05 μm . By selection of the membrane material (both hydrophilic and hydrophobic membrane contactors are commercially available) and careful control

[*] Prof. C. A. M. Afonso

CQFM

Departamento de Engenharia Química

Instituto Superior Técnico

1049-001 Lisbon (Portugal)

Fax: (+351) 21-841-7122

E-mail: carlosafonso@ist.utl.pt.

Prof. J. G. Crespo

REQUIMTE/CQFB

Departamento de Química

Faculdade de Ciências e Tecnologia

Universidade Nova de Lisboa

Campus da Caparica, 2829-516 Caparica

(Portugal)

Fax: (+351) 21-294-8550

E-mail: jgc@dq.fct.unl.pt

of the pressure difference between the fluids, one of the fluids is immobilized within the pores of the membrane so that the fluid/fluid interface is located at the mouth of each pore. This approach offers a number of important advantages over conventional dispersed-phase contactors, such as the absence of emulsions, no flooding at high flow rates, no unloading at low flow rates, no need for density difference between fluids or for phase separation after contact, and surprisingly high interfacial areas. Indeed, membrane contactors typically offer 30 times more specific area than in gas absorbers, and 500 times more specific area than in liquid/liquid extraction columns.^[14]

Different approaches have been reported for a large number of chiral-resolution problems with liquid membrane systems.^[10,15] In one of the most common approaches proposed, a solution of the chiral selector in a water-immiscible solvent is pumped through the interior of the fibers (lumen side), while the aqueous-feed stream that contains the racemic substrate circulates in the shell side of the hollow-fiber module. Owing to the high surface area, efficient mass transfer can then take place between the two phases. This system can be duplicated through the introduction of a second hollow-fiber contactor in series, in which a stream that contains the other enantiomer of the chiral selector circulates in the lumen of the fibers. Other configurations have been proposed, namely the use of a hollow-fiber contactor with two independent sets of fibers in which the two solvent phases containing the corresponding enantiomeric selectors circulate independently (Figure 1). After extraction, each enantiomer may be recovered from the corresponding receiving phase by reextraction and/or by solvent distillation, in such a way that the enantiomeric selectors can also be recovered and reused. Therefore, these selectors are needed in only a catalytic amount.

As each enantiomer is transported from the source phase, the remaining mixture would remain essentially racemic and a level of enantioselectivity for each enantiomer would be maintained as long as an adequate thermodynamic driving force for transport is provided.

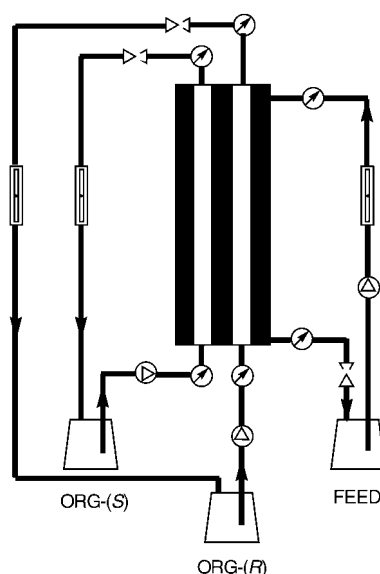


Figure 1. System for the resolution of aqueous racemic mixtures by simultaneous membrane extraction using two organic phases (ORG), each containing an adequate chiral selector (*R* and *S* forms, respectively).

In the event that a given selector–substrate combination afforded an undesirably low level of enantioselectivity, further membrane units could be added (staging). Cussler and co-workers have used a hydroxyproline-derived chiral selector (typically employed in chiral ligand-exchange chromatography) in a hollow-fiber device.^[16] Owing to selectivities of less than 2.5, these researchers used countercurrent flow of the two phases to cause each fiber to function as a low-efficiency “chromatography” column. This procedure enhances the extent of separation and allows a complete separation of the enantiomers.

Although transport through the liquid-membrane phase takes place by diffusion, the extremely high specific surface of the hollow fibres compensates for this effect and allows sufficiently high mass-transfer rates. The recent development of new solvents (such as ionic liquids) and the design of solvent phases has led to liquid contactors with increased stability and long-term performance. This hollow-fiber-membrane resolution system is certainly appropriate for scale-up resolutions under continuous operation. However, there is still the problem associated with obtaining of a high level of optical purity, owing to the need for a high number of

sequential stages of phase equilibrium as occurs in chromatography. To address this issue, other processes based on the combination of countercurrent fractionation and liquid-membrane technology have been described.^[17]

In the past, it has been demonstrated that enantiospecific chiral selectors are extremely difficult to obtain and, as expected, they are very specific. To circumvent this limitation, a very interesting approach was recently proposed which combines a fluorous-organic extraction and an enzyme-mediated enantiospecific esterification reaction with a highly fluorinated group to allow one enantiomer to be partitioned into the fluorous phase as a fluorinated ester.^[18] More recently, Goto and co-workers^[19] employed a similar approach: Ibuprofen was resolved by the selective conversion of (*S*)-ibuprofen to (*S*)-ibuprofen methyl ester with an enantioselective lipase from *Candida Rugosa* (CRL) at the feed interface of a supported liquid membrane (SLM) that contains an ionic liquid.^[20] The ionic-liquid phase allows the selective transport of the more-hydrophobic ibuprofen methyl ester from the aqueous-feed phase to the receiving phase. At the interface of the receiving phase, the (*S*)-ibuprofen methyl ester is hydrolyzed to (*S*)-ibuprofen by another lipase from porcine pancreas (PPL). As (*S*)-ibuprofen is more hydrophilic it is not transported back through the supported ionic-liquid phase (Figure 2). This system has great appeal for continuous operation. Goto and co-workers presented batch studies for operation during 2.5 days which demonstrated that the employed SLM is stable under the conditions selected.

More recently Rmaile and Schlenoff^[21] demonstrated that optically active polyelectrolyte multilayers (PEMUs) made from polypeptides can be used as membranes for analytical chiral separation in capillary electrophoresis, with racemic ascorbic acid and DOPA (3,4-dihydroxyphenylalanine) as substrate models. Very interesting conclusions could be drawn from this study: First, it was observed that optically active multilayers produce chiral separations. Second, a multilayer made from two optically active polyelectrolytes was more selective for one of the enantiomers (D-ascorbic acid in their study) than a

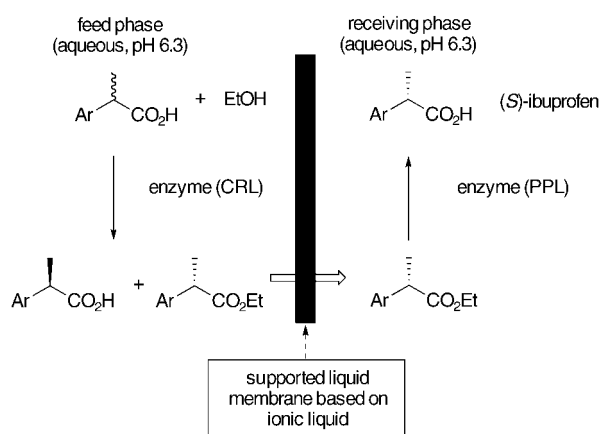


Figure 2. System for the resolution of ibuprofen described by Goto and co-workers,^[9] based on the combination of sequential enantioselective enzymatic esterification (enzyme CRL), selective transport through a supported liquid membrane, which contains an ionic liquid, and enzymatic hydrolysis (enzyme PPL).

multilayer that comprised only one active polyelectrolyte. It was also observed that the reversal of the chirality of polyelectrolytes within the multilayer led to inversion of the selectivity for L over D isomers. Finally, PEMU membranes presented higher fluxes than other reported chiral membranes, which appears extremely promising in the future for applications in preparative chiral separations.

In conclusion, the processes based on membrane technology will most certainly become very important for continuous operation, but at the moment still suffer from being generally less enantioselective. A solution to the problem requires the development of efficient engineering solutions that can provide a high number of equilibrium stages in compact equipment. We expect that other efficient solutions will emerge based on the current remarkable developments reported for analytical applications. The key points for continuous enantiomer separation are, in first place, the nature of the chiral selector, which should exhibit a high level of differentiation of interaction with each enantiomer, and second, the use of this property through extension of the effect

to preparative-scale and continuous operation. Both aspects are still open for new solutions to be developed, but the discovery of more-efficient chiral selectors, such as apoenzymes,^[22] with a broad range of applications as well as more-immediate procedures to achieve them, will certainly have a high impact on the development of this field.

Published Online: September 21, 2004

- [1] a) *Chiral Separation Techniques* (Ed.: G. Subramanian), Wiley-VCH, **2001**; b) A. M. Rouhi, *Chem. Eng. News* **2003**, 81(18), 45–55.
- [2] T. J. Ward, *Anal. Chem.* **2000**, 72, 4521–4528; T. J. Ward, *Anal. Chem.* **2002**, 74, 2863–2872.
- [3] a) E. Francotte, T. Leutert, L. La Vecchia, F. Ossola, P. Richert, A. Schmidt, *Chirality* **2002**, 14, 313–317; b) H. A. Zinnen, M. J. Gattuso, US-A 6410794, **2002**; c) V. G. Mata, A. E. Rodrigues, *J. Chromatogr. A* **2001**, 939, 23–40; d) M. Schulte, J. Strube, *J. Chromatogr. A* **2001**, 906, 399–416; e) J. Strube, S. Haumreisser, H. Schmidt-Traub, M. Schulte, R. Ditz, *Org. Process Res. Dev.* **1998**, 2, 305–319.
- [4] R. Vespalec, P. Bocek, *Chem. Rev.* **2000**, 100, 3715–3753.
- [5] a) I. Rodriguez, L. J. Jin, S. F. Y. Li, *Electrophoresis* **2000**, 21, 211–219; b) S. R. Wallenborg, I. S. Lurie, D. W. Arnold, C. G. Bailey, *Electrophoresis* **2000**, 21, 3257–3263.
- [6] E. B. Kyba, K. Koga, L. R. Sousa, M. G. Siegel, D. J. Cram, *J. Am. Chem. Soc.* **1973**, 95, 2692–2693.
- [7] J. Lacour, C. Goujon-Ginglinger, S. Torche-Halldimann, J. J. Jodry, *Angew. Chem.* **2000**, 112, 3830–3832; *Angew. Chem. Int. Ed.* **2000**, 39, 3695–3697.
- [8] V. Andrisano, G. Gottarelli, S. Masiero, E. H. Heijne, S. Pieraccini, G. P. Spada, *Angew. Chem.* **1999**, 111, 2543–2544; *Angew. Chem. Int. Ed.* **1999**, 38, 2386–2388.
- [9] J. A. Riggs, R. K. Litchfield, B. D. Smith, *J. Org. Chem.* **1996**, 61, 1148–1150.
- [10] a) B. Baragaña, A. G. Blackburn, P. Breccia, A. P. Davis, J. de Mendoza, J. M. Padrón-Carrillo, P. Prados, J. Riedner, J. G. de Vries, *Chem. Eur. J.* **2002**, 8, 2931–2936; b) L. Siracusa, F. M. Hurley, S. Dresen, L. J. Lawless, M. N. Pérez-Payán, A. P. Davis, *Org. Lett.* **2002**, 4, 4639–4642.
- [11] M. Newcomb, J. L. Toner, R. C. Helgeson, D. J. Cram, *J. Am. Chem. Soc.* **1979**, 101, 4941–4947.
- [12] Y. Abe, T. Shoji, S. Fukui, M. Sasamoto, H. Nishizawa, *Chem. Pharm. Bull.* **1996**, 44, 1521–1524.
- [13] W. H. Pirkle, T. C. Pochapsky, *Chem. Rev.* **1989**, 89, 347–362.
- [14] a) “Membrane Contactors: Membrane Separations”: J. G. Crespo, I. M. Coelho, R. M. C. Viegas in *Encyclopedia of Separation Processes*, Academic Press, **2000**, pp. 3303–3311; b) A. Gabelman, S.-T. Hwang, *J. Membr. Sci.* **1999**, 159, 61–106.
- [15] a) T. Oshima, K. Inoue, S. Furusaki, M. Goto, *J. Membr. Sci.* **2003**, 217, 87–97; b) H. M. Krieg, J. Lotter, K. Keizer, J. C. Breytenbach, *J. Membr. Sci.* **2000**, 167, 33–45; c) D. K. Mandal, A. K. Guha, K. K. Sirkar, *J. Membr. Sci.* **1998**, 144, 13–24; d) W. H. Pirkle, W. E. Bowen, *Tetrahedron: Asymmetry* **1994**, 5, 773–776.
- [16] H. B. Ding, P. W. Carr, E. L. Cussler, *AIChE J.* **1992**, 38, 1493–1498.
- [17] a) J. T. F. Keurentjes, EP 0 663 897 B1, **1997**; b) J. T. F. Keurentjes, L. J. W. M. Nabuurs, E. A. Vegter, *J. Membr. Sci.* **1996**, 113, 351–360.
- [18] a) P. Beier, D. O'Hagan, *Chem. Commun.* **2002**, 1680–1681; b) B. Hungerhoff, H. Sonnenschein, F. Theil, *Angew. Chem.* **2001**, 113, 2550–2552; *Angew. Chem. Int. Ed.* **2001**, 40, 2492–2494.
- [19] E. Miyako, T. Maruyama, N. Kamiya, M. Goto, *Chem. Commun.* **2003**, 2926.
- [20] L. C. Branco, J. G. Crespo, C. A. M. Afonso, *Angew. Chem.* **2002**, 114, 2895–2897; *Angew. Chem. Int. Ed.* **2002**, 41, 2771–2773.
- [21] H. H. Rmaile, J. B. Schlenoff, *J. Am. Chem. Soc.* **2003**, 125, 6602–6603.
- [22] B. B. Lakshmi, C. R. Martin, *Nature* **1997**, 388, 758–760.

On the Noninnocent Nature of 1,3-Dialkylimidazolium Ionic Liquids**

Jairton Dupont* and John Spencer

Keywords:

carbenes · homogeneous catalysis · ionic liquids · solvent effects · synthetic methods

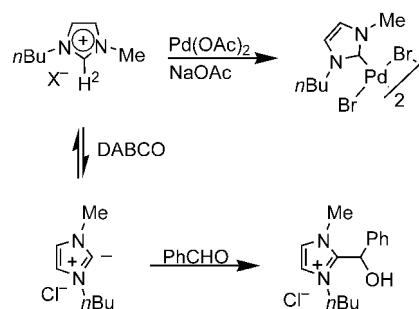
1,3-Dialkylimidazolium salts are one of the most popular and investigated classes of the vast family of room-temperature ionic liquids (RTILs). In particular, those resulting from the association of the 1-*n*-butyl-3-methylimidazolium (bmim) cation with relatively weakly coordinating anions such as tetrafluoroborate, hexafluorophosphate,^[1] and trifluoromethanesulfonate display unique physical-chemical properties: they are liquids over a large range of temperatures (down to -80°C), possess high thermal and chemical stability, a large electrochemical window, high density, relatively low viscosity, and negligible vapor pressure. These materials are very popular and have been used in various domains of physical sciences such as fluids in synthesis, catalysis, spectroscopy, electrochemistry, nanomaterials, extraction and separation processes.^[2] It is usually assumed that these liquids are entirely innocent and noncoordinating solvents. However, in older and more recent examples such innocuous behavior was not always observed, and a certain degree of caution should be exercised when ionic liquids are chosen as solvents.

There is no doubt that most 1,3-dialkylimidazolium ILs are stable towards many organic and inorganic substances, but under certain reaction conditions both the cation and anion can undergo “undesirable” transformations. In some cases the anions of imidazolium ILs can easily undergo hydrolysis, particularly those containing AlCl_4 and PF_6 anions. In the case of the hexafluorophosphate anion, phosphate and HF are formed, and 1,3-dialkylimidazolium phosphates and transition-metal fluorides have been isolated during reactions and purification procedures.^[3] The hydrolysis of the PF_6 anion may be more pronounced in reactions involving metals, which can catalyze this decomposition. Cation metathesis was also observed with highly negatively charged complexes such as $\text{Na}_3[\text{Co}(\text{CN})_5]$ and $\text{Na}_2[\{(\text{UO}_2)(\text{NO}_3)_2\}_2(\mu_4\text{-C}_2\text{O}_4)]$ dissolved in ionic liquids, and the respective coordination complexes associated with the imidazolium cation precipitated.^[4]

The reactivity of imidazolium cations mainly stems from the relatively high acidity ($\text{p}K_{\text{a}} = 21\text{--}23$) of the H2 hydrogen of the imidazolium nucleus, which has been found to be roughly intermediate between the acidities of acetone ($\text{p}K_{\text{a}} = 19.3$) and ethyl acetate ($\text{p}K_{\text{a}} = 25.6$).^[5] It is well known from the seminal work of Arduengo that deprotonation at the C2 position of the imidazolium salt generates N-heterocyclic carbene ligands.^[6] Not surprisingly, the formation of metal–carbene complexes has been observed in Pd-catalyzed Heck-type reactions performed in ionic liquids. In these cases the side reaction has a beneficial effect since the carbenes most probably stabilize the catalytically active species.^[7] For exam-

ple, under drastic conditions ($200^{\circ}\text{C}/50\text{ atm C}_2\text{H}_4$) reaction of the ionic liquid ethylmethylimidazolium chloride/ AlCl_3 (1.3:1) with $\text{PtCl}_2/\text{PtCl}_4$ led to *cis*- $[\text{PtCl}_2\text{-(C}_2\text{H}_4\text{)}(1\text{-ethyl-3-methylimidazol-2-ylidene)}]$.

Moreover, organic adducts have also been isolated when ILs are utilized in the presence of organic electrophiles such as aldehydes, as in the Baylis–Hillman reaction^[8] (Scheme 1). Related



Scheme 1. Examples of side reactions of the bmim cation under basic conditions ($\text{X} = \text{Br}, \text{Cl}$). DABCO = 1,4-diazabicyclo[2.2.2]octane.

condensation reactions under basic conditions are also often hampered by the deprotonation at C2 of the imidazolium ion. Additional quantities of base are required for reuse of the IL, and it has been proposed that in order to obviate these problems C2-substituted ILs might be more suitable media for some base-catalyzed processes.^[6b] This clearly indicates that when ionic liquids are employed under basic conditions, carbenes are likely to form in the mixture with either detrimental or beneficial results.

An even more striking result was recently reported. Under “less basic” conditions the C2–H bond of the imid-

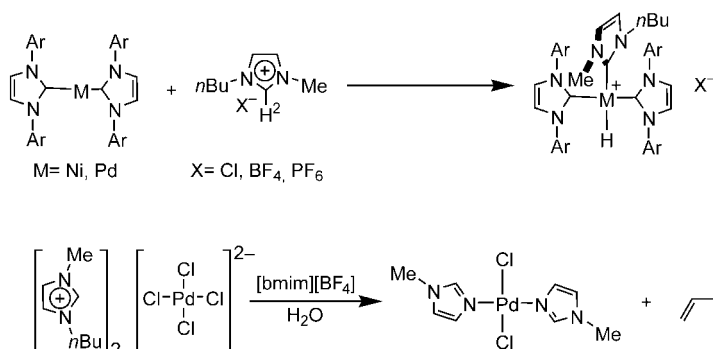
[*] Prof. Dr. J. Dupont
Laboratory of Molecular Catalysis
Institute of Chemistry, UFRGS
Av. Bento Gonçalves 9500
Porto Alegre 91501-970 RS (Brazil)
Fax: (+55) 513-316-7304
E-mail: dupont@iq.ufrgs.br

Dr. J. Spencer
James Black Foundation
68 Half Moon Lane
Dulwich, SE24 9JE (UK)

[**] This work was supported by CNPq and CENPES-PETROBRAS (Brazil).

azolium nucleus can oxidatively add to electron-rich Ni^0 or Pd^0 complexes to generate stable (carbene)metal hydride compounds (Scheme 2).^[9] The 1,3-dimethylimidazolium cation also oxidatively

plex **B**. Although **B** was considered to be a catalytic intermediate, it was found to be a poor catalyst for C–C bond-forming reactions, whereas **A** was significantly more effective. Complexes related to

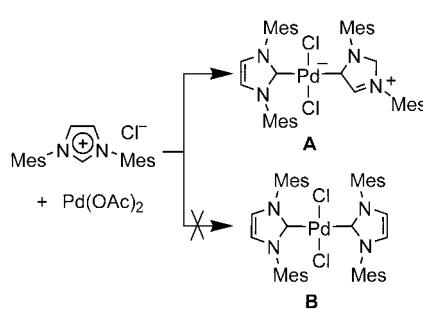


Scheme 2. Reactions of the imidazolium cation under neutral conditions.

adds to $[\text{Pt}(\text{PPh}_3)_4]$ as observed by ^{31}P NMR spectroscopy, although yields of the product *cis*- $[\text{PtH}(\text{1,3-dimethylimidazolin-2-ylidene})(\text{PPh}_3)_2]\text{BF}_4$ were rather poor.^[10] Tetraalkylammonium salts are known to undergo thermally and chemically induced dealkylation.^[11] The dealkylation of the imidazolium nucleus (Hofmann elimination) was also observed in the catalytic hydrodimerization of butadiene by Pd^{II} compounds immobilized in ILs (Scheme 2).^[12]

Under sonochemical conditions, decomposition of the IL has been observed, which is linked to the creation of hot spots in the solvent. For example, when $[\text{bmim}]\text{Cl}$ was sonified at 135°C and the headgas analyzed, chloromethane and chlorobutane (from $\text{S}_{\text{N}}2$ processes) were detected as well as imidazole decomposition products.^[13] This could clearly limit the scope of ILs in ultrasound-assisted chemistry as well as in other thermal processes including microwave-induced chemistry.

In an RTIL-relevant area, more insight into the complexity of the chemistry involving the generation of palladium–carbene complexes from imidazolium salts is provided by a very recent example depicted in Scheme 3.^[14] An imidazolium salt reacted with a Pd^{II} derivative under base-free conditions, yielding the unusual complex **A** and none of the expected symmetrical com-



Scheme 3. An unusual N-heterocyclic carbene–Pd complex formed from an imidazolium salt. Mes = 2,4,6-trimethylphenyl.

A may indeed be catalytically relevant intermediates, and this demonstrates that both H2 and H5 in imidazolium salts can be activated under neutral conditions.

Although a tremendous amount of work has been carried out on applications of ionic liquids and a reasonable amount of knowledge about their structure and physical-chemical properties has been accumulated over recent years, ionic liquids still represent a wide, largely unexplored territory. In particular, much work is still needed order to predict and utilize the intrinsic chemistry and properties of these intriguing liquids.

Published Online: September 21, 2004

- [1] Y. Chauvin, L. Mussmann, H. Olivier, *Angew. Chem.* **1995**, *107*, 2941–2943; *Angew. Chem. Int. Ed. Engl.* **1995**, *34*, 2698–2700.
- [2] Recent review: J. Dupont, R. F. de Souza, P. A. Z. Suarez, *Chem. Rev.* **2002**, *102*, 3667–3691.
- [3] a) R. P. Swatloski, J. D. Holbrey, R. D. Rogers, *Green Chem.* **2003**, *5*, 361–363. b) G. S. Fonseca, A. P. Umpierre, P. F. P. Fichtner, S. R. Teixeira, J. Dupont, *Chem. Eur. J.* **2003**, *9*, 3263–3269.
- [4] a) A. E. Bradley, J. E. Hatter, M. Nieuwenhuyzen, W. R. Pitner, K. R. Seddon, R. C. Thied, *Inorg. Chem.* **2002**, *41*, 1692–1694; b) P. A. Z. Suarez, J. E. L. Dullius, S. Einloft, R. F. de Souza, J. Dupont, *Inorg. Chim. Acta* **1997**, *255*, 207–209.
- [5] T. L. Aymes, S. T. Diver, J. P. Richard, F. M. Rivas, K. Toth, *J. Am. Chem. Soc.* **2004**, *126*, 4366–4374.
- [6] Reviews: a) A. J. Arduengo III, *Acc. Chem. Res.* **1999**, *32*, 913–921; b) P. Formentin, H. Garcia, A. Leyva, *J. Mol. Catal. A* **2004**, *214*, 137–142.
- [7] a) L. J. Xu, W. P. Chen, J. L. Xiao, *Organometallics* **2000**, *19*, 1123–1127; b) C. J. Mathews, P. J. Smith, T. Welton, A. J. P. White, D. J. Williams, *Organometallics* **2001**, *20*, 3848–3850; c) M. Hasan, I. V. Kozhevnikov, M. Rafiq H. Siddiqui, C. Femoni, A. Steiner, N. Winterton, *Inorg. Chem.* **2001**, *40*, 795–800.
- [8] a) V. K. Aggarwal, I. Emme, A. Mereu, *Chem. Commun.* **2002**, 1612–1613; b) ILs can be used under basic conditions, for example, for *N*-indole and *O*-naphthol deprotonation/alkylations: M. J. Earle, P. B. McCormac, K. R. Seddon, *Chem. Commun.* **1998**, 2245–2246.
- [9] N. D. Clement, K. J. Cavell, C. Jones, C. J. Elsevier, *Angew. Chem.* **2004**, *116*, 1297–1299; *Angew. Chem. Int. Ed.* **2004**, *43*, 1277–1279.
- [10] D. S. McGuinness, K. J. Cavell, B. F. Yates, *Chem. Commun.*, **2001**, 355–356.
- [11] a) M. Amirnasr, M. K. Nazeeruddin, M. Grätzel, *Thermochim. Acta* **2000**, *31*, 105–114; b) M. R. R. Prasad, V. N. Krishnamurthy, *Thermochim. Acta* **1991**, *22*, 1–10.
- [12] J. E. L. Dullius, P. A. Z. Suarez, S. Einloft, R. F. de Souza, J. Dupont, J. Fischer, A. De Cian, *Organometallics* **1998**, *17*, 815–819.
- [13] J. D. Oxley, T. Prozorov, K. S. Suslick, *J. Am. Chem. Soc.* **2003**, *125*, 11138–11139.
- [14] H. Lebel, M. K. Janes, A. B. Charette, S. P. Nolan, *J. Am. Chem. Soc.* **2004**, *126*, 5046–5047.

Dinitrogen Activation

Multimetallic Cooperative Activation of N₂

Sandro Gambarotta* and Jennifer Scott

Keywords:

dinitrogen activation · lanthanides · nitrides ·
nitrogen fixation · transition metals

The impressive number of breakthroughs reported in recent years in the field of dinitrogen activation reiterates the great interest that is still attracted by this molecule as a target for molecular activation studies. In spite of the fact that the discovery of dinitrogen fixation is rapidly approaching its 40th birthday, a thorough understanding of the factors that determine either fixation or activation is yet to be achieved. Nevertheless, substantial progress has recently been made. The aim of this article is to review some of the most recent literature and to assess the necessity of multimetallic attack to dinitrogen as a prerequisite towards further cleavage and functionalization.

1. Introduction

After almost 40 years of research in the field of dinitrogen activation, interest is still blossoming in the most recent literature. Perhaps one of the stimuli for this is provided by the remarkable disparity in the reaction conditions used for the catalytic conversion of dinitrogen into ammonia in industry compared to those used by nature. On the one hand, the original Haber process and its subsequent improvements^[1] involve the use of harsh conditions to achieve the only synthetic catalytic transformation of dinitrogen known to date. On the other hand, the naturally occurring nitrogenase enzyme completes the task under particularly mild conditions and without the need for gaseous hydrogen.^[2] This sharp diversity, together with the paucity of dinitrogen chemistry, provides an intellectual challenge and a potent stimulus for understanding the factors that enable a metal complex to interact with this exceedingly stable molecule. Furthermore, the mild-condition catalytic reduction performed by nitrogenase is the very first step in a chain of transformations leading towards the incorporation of nitrogen atoms into the biosystem. This prompts research in the direction of using dinitrogen as a raw material for the production of commodity chemicals (e.g., fertilizers).^[3]

The high stability of N₂ (dissociation energy: 945 kJ mol⁻¹) and the presence of a HOMO–LUMO gap estimated to be approximately 23 eV (contributing to a high activation energy barrier for any process involving

this molecule) pose a twofold challenge in: 1) controlling the steps leading towards coordination and elemental transformations (cleavage, protonation, N-transfer reactions), and 2) searching for processes affording incorporation into organic molecules. Developing a background of information in these two directions, and obtaining a solid grasp on the factors that not only promote the interaction of metals with dinitrogen but also determine the extent of activation, is the starting point for the rational search for catalytic transformations involving dinitrogen as a raw material.

This scenario provides the key to understanding the current directions followed by researchers worldwide to target this stable molecule. It also provides a guide to outline the most recent literature throughout this Minireview and to delineate future challenges (a database search hit about 450 references for the period 1999–2004). Since several aspects of antecedent literature have been extensively covered by recent reviews,^[4] the aim of this article is to attempt a critical assessment of the most recent discoveries in this area. There are three main directions in which current developments in this field can be classified:

1. dinitrogen coordination;
2. dinitrogen cleavage and elemental transformations involving nitrides and related units;
3. the incorporation of dinitrogen into organic substrates.

35 Years after the discovery of the first dinitrogen complexes, it is now very well established that this molecule can be coordinated to one or more metal centers. Coordination to only one metal center can be either labile or exceedingly robust without necessarily implying a major extent of dinitrogen reduction. Today, stable mononuclear

[*] Prof. S. Gambarotta, J. Scott
Department of Chemistry
University of Ottawa
Ottawa, ON, K1N 6N5 (Canada)
Fax: (+1) 613-562-5170
E-mail: sgambaro@science.uottawa.ca

W complexes are the most versatile starting materials for the step-by-step incorporation of N₂ into a variety of organic substrates.^[3] On the other hand, multimetallic coordination with either the same or different metals provides an alternative strategy for the reduction, cleavage, and multiple transformations of dinitrogen, which may perhaps open the path to its future use in catalytic processes.

The main focus of this Minireview will be the multimetallic activation of dinitrogen along two of the points described above: 1) coordination and 2) cleavage, followed by elemental transformations.

2. Dinitrogen Coordination

For a long time, the bonding mode adopted by dinitrogen to ligate two transition metal centers (either σ or π) has been regarded as a prerequisite for further activation and reduction. In particular the side-on mode, which was limited to less than a handful of complexes before 1999,^[5] was regarded as the first step in reduction and further activation since it was expected to provide a major extent of metal-to-dinitrogen electron transfer. This expectation was substantiated by the four-electron reduction indicated by the crystal structures of two complexes, **1**^[5c] and **2**^[5c] (Figure 1), which both display

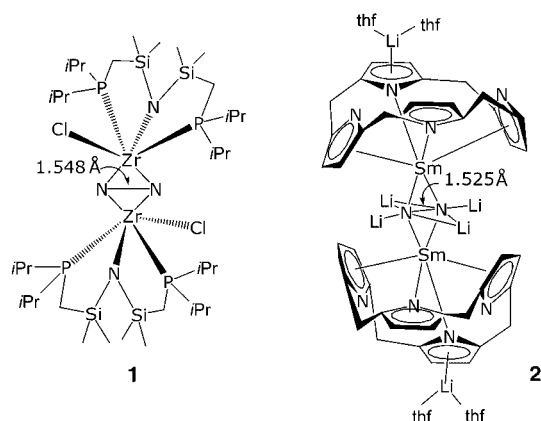
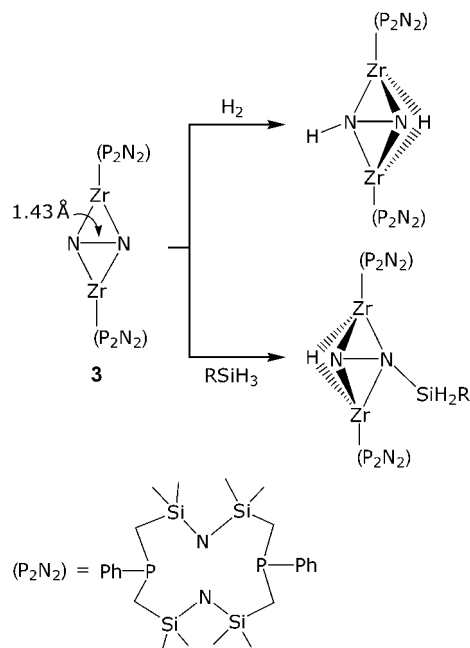


Figure 1. Four-electron reduction of dinitrogen is observed in complexes **1** and **2** (ethyl substituents in **2** have been omitted for clarity).



Sandro Gambarotta received his doctorate in 1975 (Univ. of Pisa, Italy) and then completed postdoctoral studies with Prof. H. Alper (Univ. of Ottawa, 1980) and Prof. C. Floriani (Columbia Univ., 1985–1986). He was appointed as a Lecturer at the Univ. of Groningen (The Netherlands, 1986–1989) followed by his appointment at the Univ. of Ottawa (Canada) as an Associate and then Full Professor. His research interests are in the synthesis and reactivity of highly reactive transition-metal, actinide, and lanthanide complexes in unusual oxidation states, particularly for the purpose of molecular activation.

long N–N distances for the side-on bonded N₂ units (1.548(7) Å and 1.525(4) Å respectively). The remarkable reactivity observed for the Zr complex **3** with H₂ and RSiH₃^[6,7] (Scheme 1) reinforced this idea. However, the



Scheme 1. Dinitrogen in partial hydrogenation and hydrosilylation reactions. R = Bu.

crystal structure of [(Cp*Sm)₂N₂] (Cp* = η^5 -C₅Me₅),^[5b] where N₂ also adopted the side-on bonding mode, displayed a curiously short N–N distance of 1.088(12) Å, nearly identical to that of free dinitrogen. This suggests that despite the side-on bonding mode, the triple bond remained nearly unperturbed as the result of a weak coordination to the metal centers.

More recently, this “anomalous” bonding mode has been found in a dinitrogen complex involving trivalent uranium.^[8] In this case the U^{III} complex, which bears a tetradentate and trianionic amide ligand, reversibly reacts with N₂ to form the side-on bonded complex **4**, in which the N₂ unit also displays a virtually unperturbed N–N triple bond (1.109(7) Å; Figure 2). A possible explanation of this unusual phenomenon was obtained with a theoretical calculation^[9] of a model compound, where the U–N₂–U core is supported by a weak U-to-N₂ π donation with no significant N₂-to-U σ bonding. The steric hindrance of the particular ligand employed also plays a role by preventing the two metal centers from approaching an optimum distance for orbital overlap. Using the same metal in the same trivalent state but with a ligand system capable of engaging in substantial π interactions (i.e., Cp* and the pentalene dianion) also afforded reversible fixation, although the N₂ unit has probably undergone a two-electron reduction, as suggested by the “normal” N–N bond length of 1.232(10) Å observed in complex **5** (Figure 2).^[10]

The difference in behavior between the two trivalent uranium complexes is not particularly striking given the completely varied nature of bonding adopted by the two

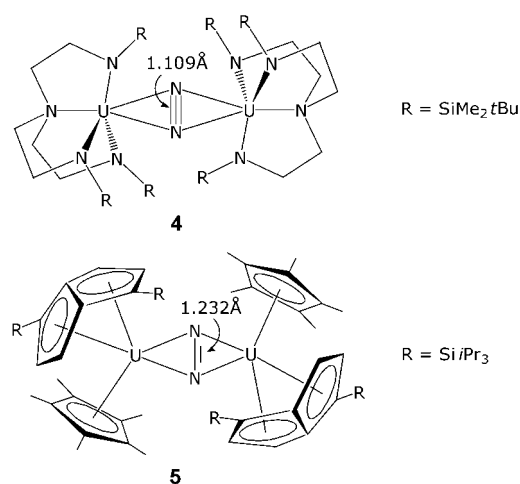
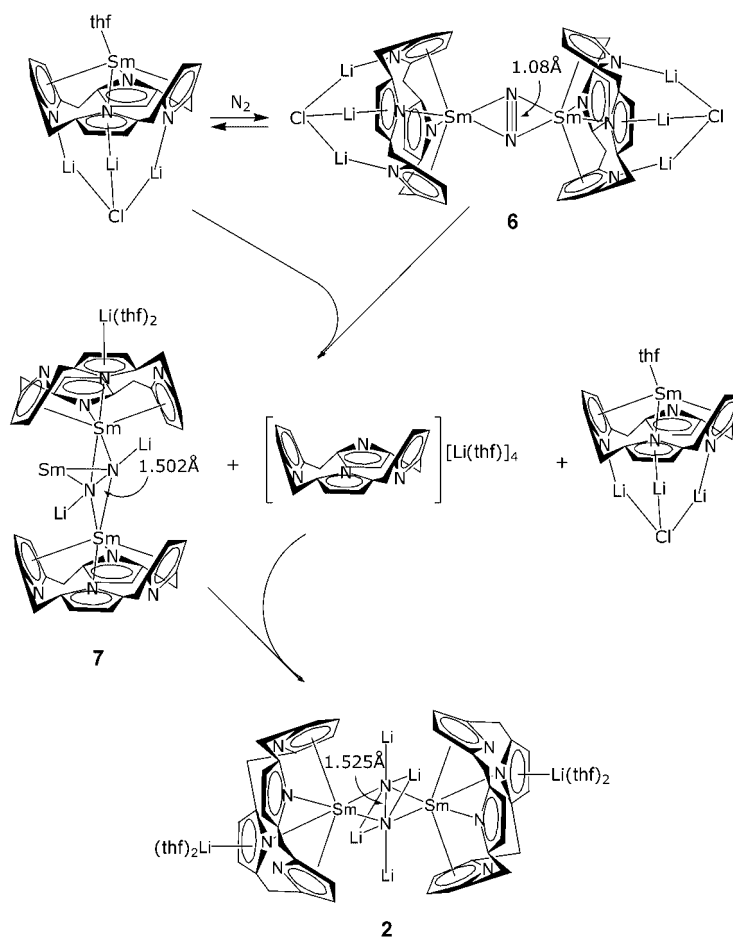


Figure 2. Reversible fixation and partial reduction is promoted by low-valent uranium complexes.

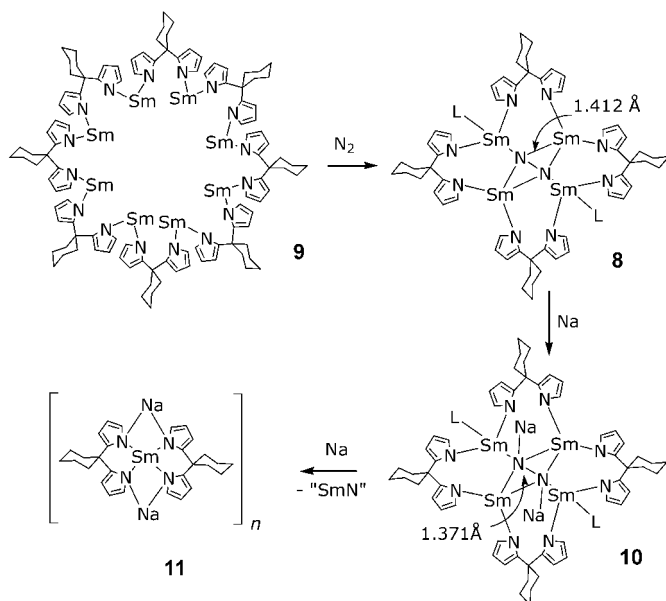
ligand systems (mainly σ versus π). In the case of the two Sm complexes $[(\text{Cp}^*\text{Sm})_2\text{N}_2]$ ^[5b] and **2**,^[5e] the difference is more surprising, given that both complexes have a similar bent-metallocene type of structure, as well as considerable steric congestion. Furthermore, divalent samarium may only act as a one-electron reductant, therefore the observed four-electron reduction of the dinitrogen unit bound between two Sm centers must be explained in terms of a multistep reaction mechanism involving four metal centers. The subsequent isolation and characterization of the intermediate **6** of this reaction (Scheme 2), which contains a labile side-on-bonded N_2 unit with an unperturbed N–N triple bond (1.08(3) Å),^[11] clearly indicates that the interaction of two divalent Sm centers with dinitrogen is a weak one and that dinitrogen adopts the usual side-on bonding mode as a first step in the reduction (Scheme 2). Attack on the weakly bound dinitrogen unit by two divalent Sm complexes builds up the pool of four electrons necessary for the irreversible reduction of the N–N triple bond to a single bond (1.502(5) Å). As briefly summarized in Scheme 2, this reaction is rather complicated and is moreover accompanied by the loss of a ligand from one of the Sm centers to form the trinuclear species **7** with three samarium atoms side-on bonded around a formal N_2^{4-} unit. Finally, transmetallation with the tetralithium salt of the ligand, which is present as a byproduct from the formation of the trinuclear compound, affords the final dinuclear complex **2**.

The ability of four metal centers to gather around the same N_2 unit has been conclusively demonstrated by halving the dimensions of the calix[4]tetrapyrrolide tetraanion and instead using dipyrrolide dianions. This particular ligand system with divalent Sm centers has allowed the isolation of tetranuclear clusters with trivalent Sm centers (**8**) where the N_2 unit, reduced by four electrons

(N–N = 1.412(17) Å), is both side-on and end-on bonded and is coplanar with the four metal centers (Scheme 3).^[12] However, this result poses a further puzzling question: If the Sm^{II} centers, while supported by pyrrolide anions, do indeed possess a potential sufficient enough to reduce a N–N triple bond, why is the final N–N single bond cleavage, which requires far less energy, not achieved? In addition, such precursors for dinitrogen fixation are large octameric (**9**) or hexameric, flat, cyclic clusters,^[13] which could easily accommodate two nitride ions by simply deforming the cyclic, regular structure into an ellipsoidal, mixed-valence complex. This possibility is indirectly supported by the structures of Yb and Sm mixed-valence complexes of the same ligand systems which, although unreactive towards N_2 , host either halogens or oxo anions in a deformed cyclic structure.^[14] To address this issue, the tetranuclear cluster containing the formal hydrazido tetraanionic unit (**8**) has been subjected to further reduction by alkali metals.^[15] The first step of the reduction adds two Na cations to the two N atoms of the N_2 unit, leaving the rest of the structure essentially unchanged (**10**, Scheme 3).^[16] However, not only was the N–N bond not cleaved, but the N–N bond length was actually slightly shortened (1.371(19) Å), thus indicating that two of the four trivalent metal centers, rather than the N–N single bond, are the recipients of the electrons. By adding more of the reductant species, the



Scheme 2. Formation of complex **2** through four-electron reduction via the labile intermediate complex **6** (ethyl substituents have been omitted for clarity).



Scheme 3. Four-electron reduction via cooperative attack of four one-electron reductants. L = thf.

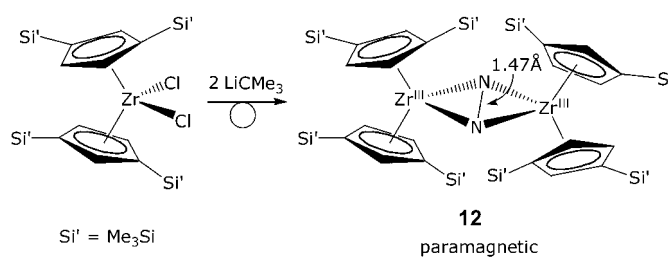
anionic ate complex **11** containing divalent samarium and no N_2 residue was obtained. This transformation implies the elimination of a formal “Sm–N” unit.

To date, the four-electron reduction of dinitrogen via the cooperative attack of four metal centers seems to be a prerogative of divalent Sm atoms. It is worth mentioning that previous work on the reduction of trivalent Pr and Nd complexes, with the same calix[4]tetrapyrrole ligand system that afforded the labile coordination and four-electron reduction of dinitrogen with divalent Sm (see complexes **2**, **6**, and **7**), with alkali metal under a nitrogen atmosphere led to a more predictable two-electron reduction for the side-on bonded dinitrogen unit ($N-N = 1.254(7) \text{ \AA}$).^[5f] At first glance, this seems in sharp contrast with the much stronger reducing power of divalent Pr and Nd with respect to divalent Sm (-2.75 and -2.95 V , respectively, versus -1.56 V). However, stronger reducing power also destabilizes divalent complexes, thus shortening their lifetime in favor of oxidative disproportionation and attack on either the ligand or the solvent.^[17] Conversely, it should be reiterated that authentic divalent and dinitrogen-free Sm complexes can instead be isolated and characterized as long as exposure to N_2 is prevented.^[18] Thus, given the difference in behavior between divalent samarium and the more strongly reducing lanthanides (Nd and Pr), it seems legitimate to conclude that only divalent samarium forms dinuclear labile dinitrogen compounds. However, the weakly activated dinitrogen is susceptible to further attack by two additional Sm centers, and via the cooperative interaction of four metal centers, a four-electron reduction is finally achieved. To date, a two-electron reduction of dinitrogen has never been observed in the case of divalent Sm complexes. Thus, the nearly paradoxical situation is observed, in which a metal possessing a weaker reducing potential (Sm) can eventually achieve a larger extent of dinitrogen reduction.

Furthermore, the area of divalent lanthanides has witnessed a spectacular expansion in recent years with the successful preparation of divalent Nd, Dy, Pr, and Tm iodides.^[19] These discoveries have allowed access to families of novel dinitrogen complexes.^[20] Not surprising for these potent reductants, dinitrogen fixation/reduction becomes a leitmotif. Attempts to prepare divalent Tm, Dy, Pr, and Nd cyclopentadienyl complexes,^[20a,b] amides, and even aryloxides^[20c] with a dinitrogen ligand (the last two being unreactive with dinitrogen in the case of Sm) afforded side-on dinitrogen complexes, in which the N_2 unit was reduced by two electrons ($N-N$ bond lengths ranging from 1.236 to 1.259 \AA). Therefore, given that stronger reductants afford two-electron reduction and that weaker reductants give labile complexes but also cooperative multimetallic reduction, it is tempting to speculate at this stage that the search for a metal capable of performing catalytic transformations must be focused on metals with only minimal reducing potential to ensure the formation of labile complexes that may be susceptible to attack by other reagents.

From what has been presented thus far, it seems reasonable to state that the type of bonding adopted by dinitrogen (side-on versus end-on) is not necessarily related to the extent of reduction and activation. For example, both very long and very short $N-N$ bond lengths have been obtained in side-on complexes of samarium, whereas two-electron reduction and comparable $N-N$ bond lengths have been obtained with Nd side-on dinitrogen complexes, in spite of using completely different ligand systems (calix[4]tetrapyrrole^[5f] versus aryloxide^[20]). It should also be reiterated that mechanistic studies on the spectacular cleavage of dinitrogen, as performed by an $[\{Ar(tBuN)\}Mo]$ complex^[21] ($Ar = 3,5-(CH_3)_2C_6H_3$; a milestone in the chemistry of dinitrogen), have clearly indicated that the cleavage involved the formation of a more classical bridging end-on complex rather than a side-on species.

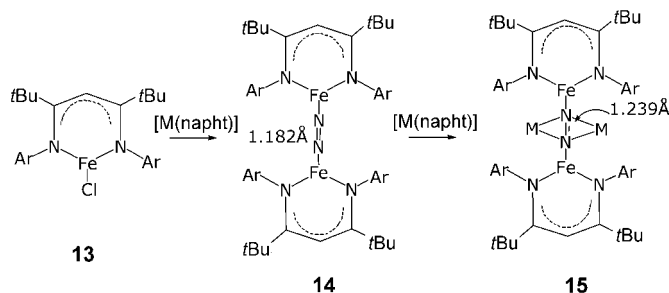
Furthermore, the historical finding by Bercaw and co-workers of the reversible dinitrogen coordination performed by $[Cp_2^*Zr]$,^[22] in which the labile fixation of the end-on bridging N_2 unit is in line with a near two-electron reduction (as suggested by the $N-N$ bond length of 1.182 \AA), is in striking contrast with the most recent findings of a highly silylated zirconocene derivative.^[23] The reaction of two equivalents of $LiCMe_3$ with $[Cp_2^*ZrCl_2]$ ($Cp^* = 1,3-(Me_3Si)_2C_5H_3$) resulted in reduction of the metal center via facile extrusion of both isobutane and isobutene (Scheme 4). The reaction afforded dark-purple crystals that were identified as the dinitrogen complex **12**, which displays a dimeric structure



Scheme 4. The first example of a Zr^{III} -dinitrogen complex.

with a bridging side-on dinitrogen fragment that is contained within a planar $\{Zr_2N_2\}$ core. These findings can be rationalized in terms of the formation of a Zr^{II} center or a Zr^{II} synthetic equivalent, generated in situ, irreversibly reacting with N_2 to perform a two-electron transfer that affords a side-on N_2 unit bonded to two $\{Cp_2Zr^{III}\}$ units. The N–N bond length (1.47(3) Å) is surprisingly long and certainly much longer than expected for an N_2 unit that has undergone a two-electron reduction. This remarkable result becomes even more surprising in light of the fact that a silylated ansa doubly bridged zirconocene unit also gives a side-on dinitrogen complex but with a substantially shorter N–N bond length (in the range of a N–N double bond: 1.241 Å).^[24]

The unexpected behavior described above is in line with that of several other complexes, and although some bonding trends can be observed occasionally in dinitrogen chemistry, the relationship between the degree of metal-to-dinitrogen electron transfer and the type of bonding mode remains challenging to predict. Another example of this “random” behavior is provided by the elegant results obtained recently with low-valent Fe complexes of a sterically demanding *nac,nac* type of ligand.^[25] The reduction of the divalent Fe derivative **13** afforded the corresponding dinuclear N_2 complex **14**, in which a reduced N_2 unit bridges the two metal centers and adopts a classical end-on bonding mode (Scheme 5). Theoretical work has clearly indicated the



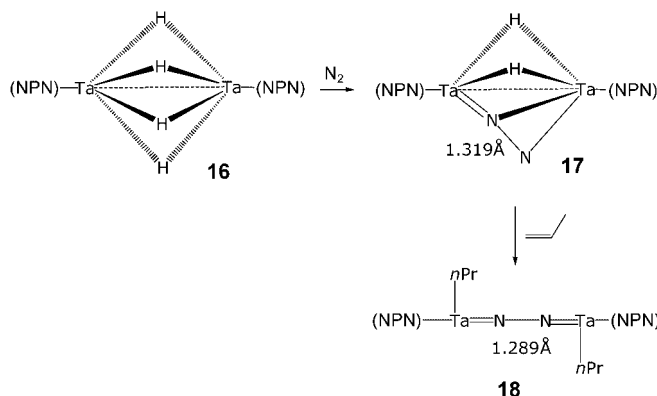
Scheme 5. Changes in the N–N bond length caused by the extent of N_2 reduction (Ar = 2,6-*i*Pr₂C₆H₃; M = Li, Na, K; napht = naphthalene anion).

presence of partly populated N–N antibonding orbitals, which nicely accounts for the two-electron reduction that is suggested by the length of the N–N bond (1.182 Å). In addition, Raman spectroscopy supports the weakening of the triple bond by an amount consistent with the observed bond length. Surprisingly, a further two-electron reduction of **14** during the formation of **15** caused only a small elongation of the N–N bond (1.239 Å). These results might be rationalized by the particular nature of the six singly populated frontier orbitals, which can accommodate the two additional electrons into molecular orbitals (MOs) with predominant Fe–N π -bonding character, rather than N–N π^* character. Thus, the reduction may result in the strengthening of the M–N bond, rather than in an N–N reduction.

A large amount of literature concerning novel dinitrogen complexes has appeared in recent years, in which the complexes are either mono- or dimetallic, homo- or hetero-

nuclear, and display some degree of activation. For reasons of brevity, we wish to mention only two unusual and promising examples.

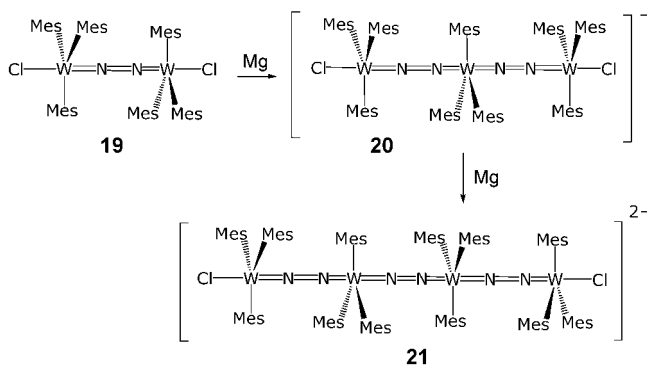
The reaction of the dinuclear tantalum hydride **16** with N_2 leads to the partial loss of H_2 , with the consequent formation of the intriguing N_2 complex **17**.^[26,27] This unusual complex contains a strongly activated N_2 group that is bound in an unprecedented side-on/end-on bridging mode (Scheme 6).



Scheme 6. The unique side-on/end-on bonding mode of the dinitrogen moiety in **17** (NPN = (PhNSiMe₂CH₂)₂PPh).

Interestingly, the insertion of propene into the Ta–H bonds generated the expected propyl groups while causing the bonding mode of dinitrogen to switch to end-on bridging, thereby forming the dinuclear alkyl/dinitrogen complex **18**.^[27] Thus, the unusual bonding mode of dinitrogen in **17** appears to be due to the bridging hydride ligands. In line with this observation, the reaction of (NPN)Li₂·2THF with [NbCl₃(dme)] afforded a more standard, end-on bound dinitrogen complex $[(NPN)NbCl_2(\mu-\eta^1-\eta^1-N_2)]$.^[27]

The second example is the unique case of an oligomeric N_2 -bridged structure. The reaction of [WCl₄(dme)] with MesMgBr in THF under a nitrogen atmosphere^[28] produced the diamagnetic and dinuclear N_2 complex **19** in 29% yield (Scheme 7). Stepwise reduction under N_2 with activated Mg metal in THF initially led to the trinuclear **20** followed by the formation of the tetranuclear **21** upon treatment with excess



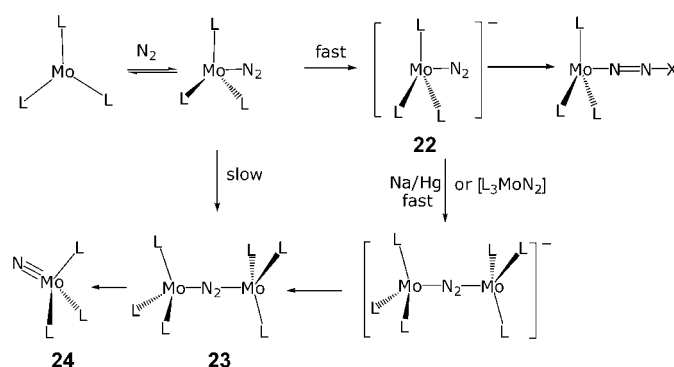
Scheme 7. Using N_2 to build conducting wires (Mes = 2,4,6-(CH₃)₃C₆H₂).

Mg in THF/dioxane under N₂. Although the use of a bridging N₂ moiety for assembling oligomeric structures has no precedent, the N–N bond length of approximately 1.23 Å could possibly be interpreted as indicating a relatively small degree of activation.

3. Dinitrogen Cleavage and Elemental Transformations Involving Nitrides

The quest to find new systems capable of performing dinitrogen cleavage is receiving particular attention, stimulated by the fact that metal nitrides are reactive moieties allowing either hydrolysis or functionalization and transfer to organic substrates. Some binary or mixed-metal nitrides display important and desirable physical properties, and therefore the development of synthetic routes to metal nitrides via N₂, rather than by the pyrolysis of amines or amide derivatives, is indeed particularly desirable. Thus dinitrogen cleavage, as performed by metal complexes, provides an entry into a world of exciting transformations, in which dinitrogen is the raw starting material. The main challenge posed by this fascinating reaction consists of identifying the features that characterize those metal complexes that make the rupture of the N–N triple bond possible. Given that six electrons are necessary for performing this transformation in a stoichiometric fashion, the cleavage can be realized by two possible routes: 1) The cooperative attack of two or more metals on the same N₂ unit, and 2) the immobilization of dinitrogen between two or more transition metals, followed by attack from an external reductant.

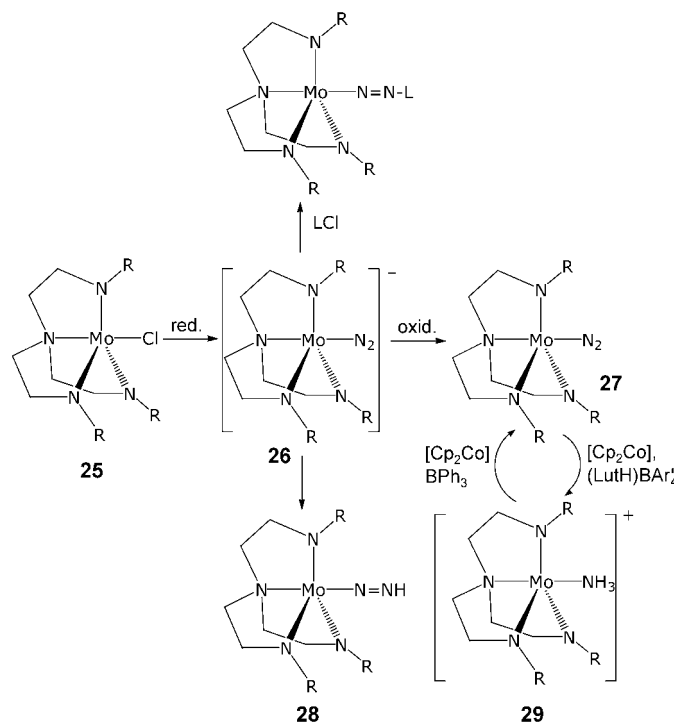
As has been already mentioned, the initial discovery that the sterically congested $[\{\text{Ar}(\text{tBuN})\}\text{Mo}]$ system is able to perform coordination and cleavage of dinitrogen to produce a stable, terminally bound Mo–N unit, has marked a milestone in the field of dinitrogen chemistry.^[21a] Soon afterwards, a vanadium system was claimed to perform the same process.^[29] However, it is only the work of Cummins that has conclusively and unequivocally demonstrated that this process is indeed possible, by using both kinetic and isotopic labeling experiments.^[21a] More recent additional observations by the same author on the same dinitrogen splitting system (Scheme 8) have shown that the cleavage of dinitrogen, which affords two equivalents of the Mo–nitride complex, proceeds much quicker in the presence of reducing agents such as sodium amalgam.^[30] By controlling the concentration of the starting $[\text{Mo}\{\text{N}(\text{R})\text{Ar}\}_3]$ complex during the reduction, it was possible to isolate the anionic dinitrogen complex **22**, which was conclusively demonstrated to be a key intermediate in the acceleration of the dinitrogen cleavage. As such, it reacts with excess starting $[\text{Mo}\{\text{N}(\text{R})\text{Ar}\}_3]$ in the presence of an electron acceptor to yield the neutral dinuclear dinitrogen complex **23**, prior to cleavage to the Mo–nitride complex **24**. Conversely, if the intermediate anionic mononuclear complex is oxidized, $[\text{Mo}\{\text{N}(\text{R})\text{Ar}\}_3]$ is regenerated, and N₂ is evolved. These results led to the conclusion that the Na amalgam acts as a redox catalyst in this system by accelerating the N₂ fixation reaction towards the dinuclear dinitrogen compound, which does not lose N₂ easily, and thus affords dinitrogen cleavage.



Scheme 8. Nitride formation using dinitrogen (L = N(*t*Bu)Ar; X = [Ti{N(*t*Bu)Ph}₃], C(O)R, Me₃Si, Me).

Further experiments on this system targeted the functionalization of **22**^[30] with a variety of reagents.

Additional insight into this complicated series of transformations has been obtained with the reduction of the closely related Mo complex **25** with magnesium in THF under a nitrogen atmosphere.^[31] Even in this case, the reduction led to the formation of similar anionic end-on dinitrogen complexes **26** (Scheme 9). Unlike the above system however, the anion **26** can be oxidized to give the corresponding stable neutral mononuclear complex **27**, which does not dimerize or lose dinitrogen. The anionic dinitrogen complex **26** can also be protonated to form the unstable diazenido complex **28**, which loses dinitrogen to afford the corresponding $[\{\text{HIPTN}_3\text{N}\}\text{Mo}-\text{H}]$ complex (HIPTN₃N = $[\{3,5-(2,4,6-\text{iPr}_3\text{C}_6\text{H}_2)_2\text{C}_6\text{H}_3\}\text{N}_3\text{N}]$). Double protonation yielded $[\{\text{HIPTN}_3\text{N}\}\text{Mo}-\text{N}-\text{NH}_2]$. Remarkably, the reduction of **27**



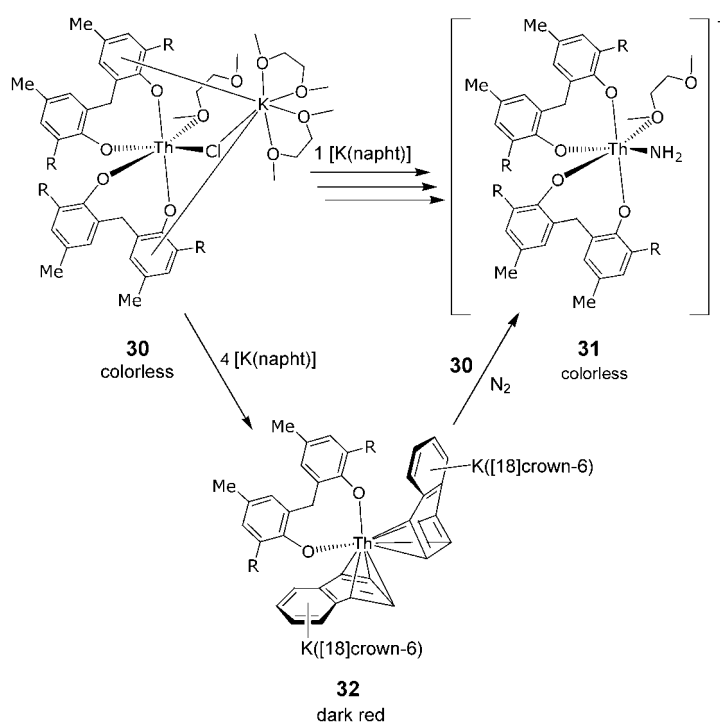
Scheme 9. Step-by-step transformations and catalytic reduction (R = 2,4,6-*i*Pr₃C₆H₂; L = Me₃Si, VCl₂(thf)₃, ZrCl₃(thf)₂).

with $[\text{Cp}_2\text{Co}]$ in benzene, in the presence of (2,6-lutidinium) BAR'_4 ($\text{Ar}' = 3,5\text{-(CF}_3)_2\text{C}_6\text{H}_3$) as a proton source, afforded ammonia and **29**.^[32] A step towards the catalytic formation of ammonia was achieved by further treatment with $[\text{Cp}_2\text{Co}]$ in the presence of a Lewis acid. Abstraction of ammonia and reduction under N_2 afforded the starting dinitrogen complex, ready for another cycle of dinitrogen reduction/cleavage.

This sequence of reactions becomes an efficient catalytic cycle for the production of ammonia if $[\text{Cp}_2^*\text{Cr}]$ is used as a reductant in heptane.^[32b] Examination of the X-ray crystal structures of several species led to the conclusion that the sterically demanding substituents on the HIPTN₃N ligand create a deep cavity that can protect a variety of dinitrogen reduction products against bimolecular decomposition reactions. Therefore, by decreasing the steric hindrance of the tetradentate ligand and following the same synthetic procedure, it was possible to isolate and characterize the dinuclear and neutral complexes $[(\text{ArN})_3\text{N}]\text{Mo}-\text{N}=\text{N}-\text{Mo}[(\text{ArN})_3\text{N}]$ ($\text{Ar} = \text{C}_6\text{H}_5$, 4- FC_6H_4 , 4- $t\text{BuC}_6\text{H}_4$, 3,5- $\text{Me}_2\text{C}_6\text{H}_3$).^[33] However, the robustness of the neutral dinitrogen complex and the lack of N_2 dissociation may also suggest, in contrast with the $[(\text{ArN}(t\text{Bu}))_3\text{Mo}]$ system (**22**), that the different coordination geometry and consequent variation of the ligand field around the metal center may be a contributing factor to the remarkable strength of the dinitrogen fixation. The anionic complex **26** turns out to be a versatile starting material for both the functionalization of dinitrogen and the formation of hetero di- and polymetallic complexes.^[34]

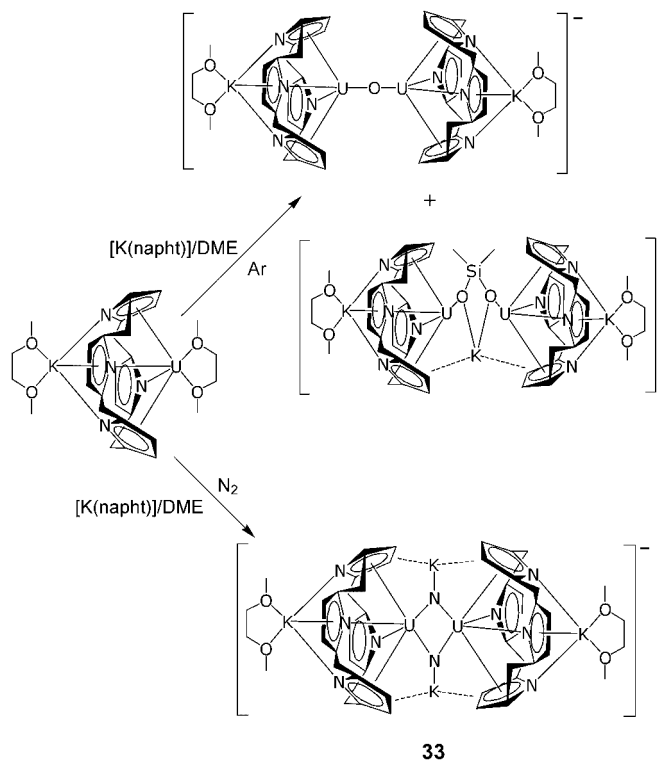
The direct formation of an $-\text{NH}_2$ function from dinitrogen in a noncatalytic system without the use of protic agents was observed when the tetravalent Th-aryloxide complex **30** was reduced with potassium dihydronaphthylide ($\text{K}^+[\text{C}_{10}\text{H}_8]^-$; Scheme 10).^[35] The complicated reaction implies N_2 cleavage and hydrogen abstraction (probably from the solvent) and involves the formation of a red intermediate which slowly discolors under exposure to N_2 gas, to afford the amide complex **31**. When $^{15}\text{N}_2$ gas was used the presence of the $^{15}\text{NH}_2$ function was substantiated by ^{15}N NMR spectroscopy. Reactions carried out with larger amounts of reductant allowed the identification of the red intermediate as an unprecedented zero-valent synthetic equivalent **32**. Thus, it was argued that an intermediate trivalent Th species may form a dinitrogen complex, most likely labile, which undergoes attack by the zero-valent synthetic equivalent and triggers the cascade of events leading to complex **31**.

It has only been in the last three years that actinides have started to play a significant role in dinitrogen activation. After the labile fixation^[8,9] and two-electron reduction^[10] observed with trivalent uranium complexes, the reduction of a trivalent uranium complex of the calix[4]tetrapyrrole ligand system with potassium dihydronaphthylide in 1,2-dimethoxyethane (DME) under nitrogen afforded the mixed-valence $\text{U}^{\text{IV}}/\text{U}^{\text{V}}$ nitride **33** (Scheme 11).^[36,37] The highly reactive species that performs the dinitrogen cleavage in this case was not



Scheme 10. Formation of amide **31** using dinitrogen: one-pot cleavage and partial hydrogenation ($\text{R} = t\text{Bu}$).

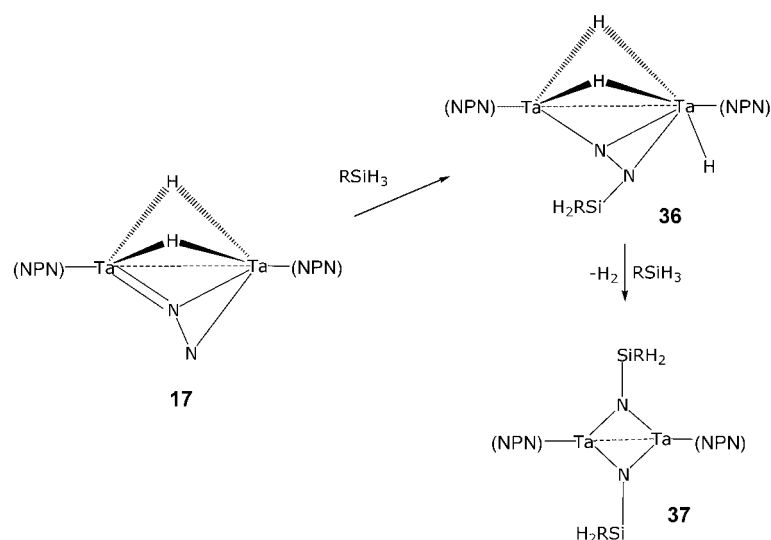
identified since reactions carried out under an Ar atmosphere promoted solvent deoxygenation, as well as depolymerization of the high-vacuum, polysilanol grease (Scheme 11). Similar-



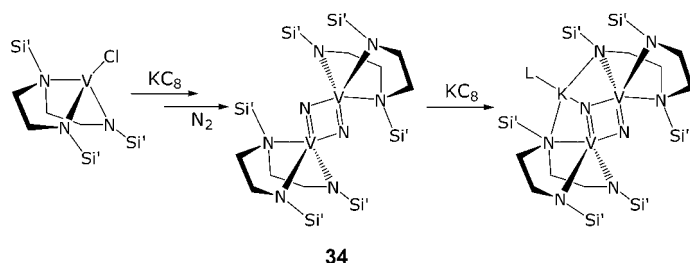
Scheme 11. Cleavage of dinitrogen promoted by a low-valent uranium complex.

ly, a divalent vanadium species, generated in situ upon the reduction of a trivalent vanadium amide complex with KC_8 , afforded the bridging nitride derivative **34** (Scheme 12).^[38] Similarly, when a linked triaryloxide Nb complex was reduced with LiBHET_3 under 1 atm of N_2 , the pentavalent nitride-bridged dimer **35** was formed (Scheme 13).^[39] Although the reduction to a reactive divalent state is most likely achieved, followed by attack on dinitrogen, it is tempting to speculate that the reaction may proceed via a pathway comparable to that observed with the dimeric **16** described earlier,^[26] which reacted with N_2 to form the unusual side-on/end-on complex **17** (see Scheme 6).

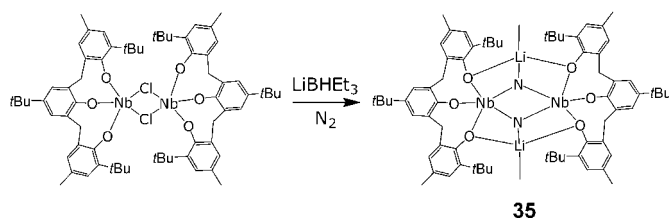
Incidentally, **17** does not yield spontaneous N_2 cleavage,^[26] as in the cases of vanadium and niobium discussed in Schemes 12 and 13, respectively. Nevertheless, it appears to be available for further activation since its hydrosilylation with BuSiH_3 proceeds via an addition reaction to coordinated N_2 to produce **36** (Scheme 14).^[40]



Scheme 14. Dinitrogen in a hydrosilylation reaction ($\text{R} = \text{Bu}$).



Scheme 12. Cleavage of dinitrogen promoted by two low-valent vanadium centers ($\text{Si}' = \text{Me}_2\text{Si}$; $\text{L} = \text{toluene}$).

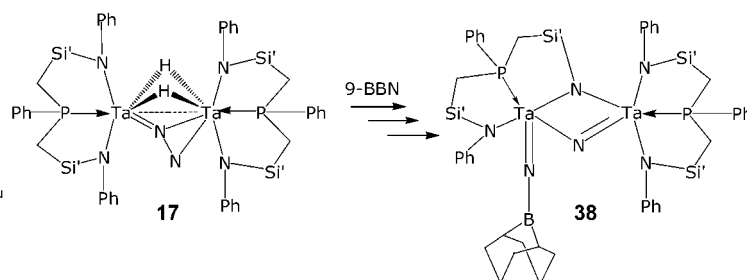


Scheme 13. Cleavage of dinitrogen promoted by two low-valent niobium centers.

Subsequent reductive elimination of H_2 , followed by N-N bond cleavage, generates a new intermediate, formulated as $[(\text{NPN})\text{TaH}](\mu\text{-N})(\mu\text{-NSiH}_2\text{Bu})\{\text{Ta}(\text{NPN})\}]$. In the presence of additional silane, a second hydrosilylation takes place and reductive elimination affords **37**, a species in which each dinitrogen-derived N atom has been converted to a bridging silylimide ligand. Conversely, hydroboration of the side-on/end-on N_2 unit in **17** by 9-borabicyclononane (9-BBN) resulted instead in the addition of the B-H bond across the Ta-N_2 moiety to generate a N-B bond and a terminal Ta-H unit in $[(\text{NPN})\text{Ta}(\text{H})](\mu\text{-H})_2(\mu\text{-N}_2\text{-BC}_8\text{H}_{14})\{\text{Ta}(\text{NPN})\}]$.^[41] Surprisingly, this species is unstable in solution, where it undergoes a remarkably complex sequence of reactions that ultimately result in N-N bond cleavage and ancillary ligand

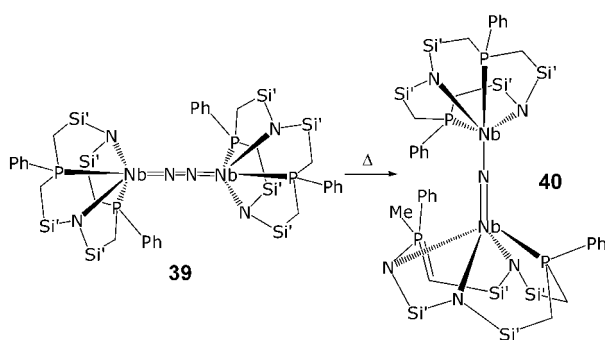
rearrangement. The final outcome is the formation of the imide-nitride species **38** arising from the loss of one phenyl ligand, Si -atom migration on the nitride, and formation of a N-B bond (Scheme 15).

It is interesting to observe how subtle and elusive the factors that promote N_2 cleavage are. As stated above, the triaryloxide-Nb complex performs N_2 cleavage upon hydride-mediated reduction, depending on the ligand



Scheme 15. Hydroboration and dinitrogen cleavage in ditantalum complex **17** ($\text{Si}' = \text{Me}_2\text{Si}$).

substituents (Scheme 13).^[39] Conversely, trivalent Nb amides afford stable dinitrogen complexes.^[4] Thus, it is conceivable to expect that a divalent Nb species (d^3) might afford a spontaneous splitting. However, attempts to prepare a formal divalent Nb derivative of the P_2N_2 dianion, via reduction of the trivalent $[(\text{P}_2\text{N}_2)\text{NbCl}]$ with KC_8 under a nitrogen atmosphere, afforded a paramagnetic and stable dinuclear dinitrogen complex **39**. Dinitrogen cleavage was obtained only under thermolytic conditions (Scheme 16).^[42] There are several points of interest in these findings. First of all, **39** is paramagnetic with an end-on bonding mode and a N-N bond length of $1.27(5) \text{ \AA}$. However, the trivalent Nb amides, which also adopt the same bonding mode of dinitrogen with comparable N-N bond lengths, are diamagnetic. Variable-temperature magnetic susceptibility measurements clearly



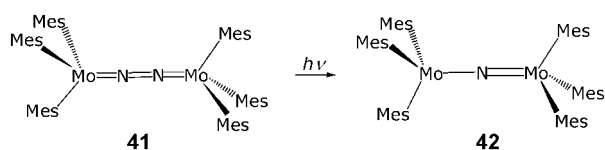
Scheme 16. Synthesis of diniobium complex **40** with a nitride moiety ($\text{Si}' = \text{Me}_2\text{Si}$).

indicated the presence of antiferromagnetic coupling between the two Nb^{IV} d^1 centers of **39**. This implies that the presumed synthetic equivalent divalent $\{(\text{P}_2\text{N}_2)\text{Nb}\}$, formed during the initial stage of the reduction, has already transferred four electrons to the N_2 unit, in spite of the fairly short $\text{N}-\text{N}$ bond. This anomalous behavior can be related to that of the trivalent Zr -dinitrogen complex mentioned in Scheme 4,^[23] where no particularly obvious reasons may be found for the incomplete electron transfer from the metal to the dinitrogen unit. Nevertheless, thermolysis of **39** in toluene generated the paramagnetic bridging nitride species **40**, where one N atom of the dinitrogen ligand inserts into the macrocyclic backbone. The fact that the thermolysis affords partial functionalization of the nitride suggests that in this particular case ligand reorganization probably provides the thermodynamic driving force for the cleavage.

Step-by-step dinitrogen cleavage was observed with a Nb calixarene derivative.^[43] Subsequent reductions of an end-on bridging dinitrogen complex, formally containing the metal in the trivalent state, afforded rearrangement of the end-on bonded unit to a side-on mode before the final cleavage occurred to afford the bridging nitride. Simple treatment of the dinitrogen complex with benzaldehyde abstracted dinitrogen to form the corresponding ketazine $\text{PhCH}=\text{N}-\text{N}=\text{CHPh}$.

The above scenario seems to suggest that group V metals, either upon reduction or via formation of unstable hydrides, may have an inclination towards cleaving N_2 since they have yielded the most reactive nitride species so far.

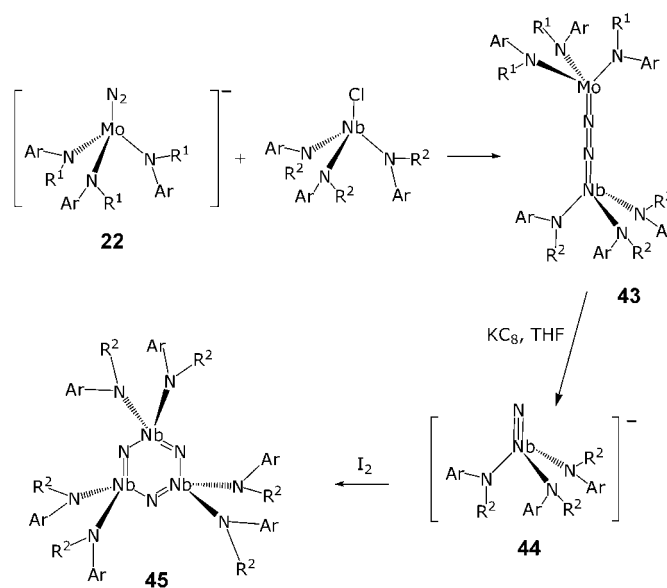
By contrast, trivalent molybdenum forms stable nitrides. An unusual cleavage of dinitrogen has been achieved by photolysis of the dinitrogen complex **41** (Scheme 17).^[44] The authors claimed that the photochemically induced cleavage of the $\text{N}-\text{N}$ bond presumably produces the monomeric nitride $[(\text{Mes})_3\text{Mo}(\text{N})]$, which in turn forms the dinuclear nitride-



Scheme 17. Photolytic cleavage of dinitrogen to give nitride **42**.

bridged **42** in good yield. Related to this reaction is the spontaneous formation of a bridging nitride under ambient conditions, as performed by the less encumbered triamide-Mo complex $[(\text{ArN}(\text{iPr}))_3\text{Mo}]$.^[45] This complex is not stable and affords an intramolecular $\text{C}-\text{H}$ bond activation to an *ipso* isopropyl $\text{C}-\text{H}$ group, which results in the formation of the metalla-aziridine hydride derivative $[(\text{ArN}(\text{iPr}))_2\text{MoH}(\eta^2-\text{ArNCMe}_2)]$. Interestingly, the reaction appears to be reversible since the presence of dinitrogen restores the *iPr* group and dinitrogen cleavage occurs to form a simple, linearly bonded mixed-valence μ -nitride species $[(\text{ArN}(\text{iPr}))_3\text{Mo})_2(\mu-\text{N})]$.

The immobilization of dinitrogen between two different metal centers is an appealing strategy for activation, given the extent of polarization that may be induced in the coordinated N_2 unit. The idea of using Nb in cooperation with Mo for cleaving dinitrogen is suggested by the ability of both Mo and Nb complexes to perform thermal,^[42] photochemical,^[44] and spontaneous N_2 splitting.^[21,39,45] This possibility has been probed by preparing a Mo/Nb dinitrogen complex using the same amide ligand system that performs the spectacular case of N_2 cleavage with Mo.^[21] The preparation of the heterobimetallic Mo/Nb complex was achieved by taking advantage of the nucleophilicity of the anionic dinitrogen-Mo complex **22**,^[30] which attacks $[(\text{ArN}(\text{iPr}))_3\text{NbCl}]$ to afford the heterodinuclear dinitrogen complex **43** (Scheme 18).^[46] The



Scheme 18. Dinitrogen cleavage promoted by different metal centers ($\text{R}^1 = \text{tBu}$; $\text{R}^2 = \text{iPr}$; $\text{Ar} = 3,5-(\text{CH}_3)_2\text{C}_6\text{H}_3$).

cleavage, however, does not proceed spontaneously, but requires the intervention of a strong reductant. Treatment with KC_8 in THF afforded cleavage of the bridging N_2 unit and formation of the terminal nitrido anion **44**. Subsequent oxidation with either iodine or ferrocenium triflate afforded the neutral niobaazene trimer **45**.

4. Conclusions

The results described above clearly underline the recent significant progress in the field of dinitrogen activation. The cleavage and, in some cases, the formation of reactive nitrides, which can be capable of reorganizing complexes, inserting into the ligand system, or of being attached to metals of a different nature, seem to be promising features in the search for improved catalytic performance. Of course, the main challenge of understanding the factors that promote coordination versus cleavage and further incorporation remains. At the basis of this work is the quest for reactive complexes capable of interacting with dinitrogen. However, it should not be forgotten that two completely different strategies exist. One is based on the double protonation of Chatt-type end-on dinitrogen complexes. The remarkable resilience of the dinitrogen complexes of zero-valent Mo and W supported by phosphanes has historically provided a family of substrates for performing step-by-step transformations. The double protonation of the terminal N atom forms a $M\text{--}NNH_2$ unit, which provides high reactivity towards a variety of organic functions. This strategy has been successfully used for a remarkable variety of transformations, for which excellent reviews are available.^[3] The second strategy involves the search for high catalytic performance that revolves around the fine-tuning of the ligand features capable of promoting subsequent transformations. A major recent advance in this direction is the catalytic formation of a remarkable variety of heterocyclic derivatives, as performed by in situ generated titanium-based dinitrogen complexes.^[47] These remarkable transformations not only set the foundations for searching for other even more spectacular catalytic species, but also provide a greater stimulus towards understanding the unique chemical behavior of dinitrogen.

In conclusion, the challenges posed by dinitrogen activation are formidable, however, the progress in meeting these challenges has been very encouraging over recent years. Although the road towards a complete understanding and the achievement of an industrially viable catalytic transformation (similar to the case of the isoelectronic CO) is presumably still very long, it seems that the use of polymetallic systems capable of performing cooperative reduction of the dinitrogen molecule may provide a significant stepping stone.

This work was supported by the Natural Sciences and Engineering Research Council of Canada (NSERC) and by the Canada Foundation for Innovation (CFI) through an infrastructure grant.

Received: May 20, 2003

Published Online: September 16, 2004

- [1] a) G. Ertl, *Catalytic Ammonia Synthesis* (Ed.: J. R. Jennings), Plenum, New York, **1991**; b) R. Schlögl, *Angew. Chem.* **2003**, *115*, 2050; *Angew. Chem. Int. Ed.* **2003**, *42*, 2004.
- [2] a) J. Kim, D. C. Rees, *Science* **1992**, *257*, 1677; b) O. Einsle, F. A. Tezcan, S. L. A. Andrade, B. Schmid, M. Yoshida, J. B. Howard, D. C. Rees, *Science* **2002**, *297*, 1696; c) D. Sellmann, J. Sutter, *Acc. Chem. Res.* **1997**, *30*, 460.

- [3] a) M. Hidai, *Coord. Chem. Rev.* **1999**, *185*, 99; b) M. Hidai, Y. Mizobe, *Pure Appl. Chem.* **2001**, *73*, 261.
- [4] See for example: a) M. Hidai, Y. Mizobe, *Met. Ions Biol. Syst.* **2002**, *39*, 121; b) M. D. Fryzuk, S. A. Johnson, *Coord. Chem. Rev.* **2000**, *200*, 379; c) T. A. Bazhenova, A. E. Shilov, *Coord. Chem. Rev.* **1995**, *144*, 69; d) C. J. Pickett, *J. Biol. Inorg. Chem.* **1996**, *1*, 601; e) S. Gambarotta, *Inorganic Chemistry Highlights* (Eds.: G. Meyer, D. Naumann, L. Wesemann), Wiley-VCH, Weinheim, **2002**.
- [5] a) G. P. Pez, P. Apgar, R. K. Crissey, *J. Am. Chem. Soc.* **1982**, *104*, 482; b) W. J. Evans, T. A. Ulibarri, J. W. Ziller, *J. Am. Chem. Soc.* **1988**, *110*, 6877; c) M. D. Fryzuk, T. S. Haddad, S. J. Rettig, *J. Am. Chem. Soc.* **1990**, *112*, 8185; d) R. Duchateau, S. Gambarotta, N. Beydoun, C. Bensimon, *J. Am. Chem. Soc.* **1991**, *113*, 8986; e) J. Jubb, S. Gambarotta, *J. Am. Chem. Soc.* **1994**, *116*, 4477; f) E. Campazzi, E. Solari, C. Floriani, R. Scopelliti, *Chem. Commun.* **1998**, 2603.
- [6] M. D. Fryzuk, J. B. Love, S. J. Rettig, V. G. Young, *Science* **1997**, *275*, 1445.
- [7] H. Basch, D. G. Musaev, K. Morokuma, M. D. Fryzuk, J. B. Love, W. W. Seidel, A. Albinati, T. F. Koetzle, W. T. Klooster, S. A. Mason, J. Eckert, *J. Am. Chem. Soc.* **1999**, *121*, 523.
- [8] P. Roussel, P. Scott, *J. Am. Chem. Soc.* **1998**, *120*, 1070.
- [9] P. Roussel, W. Errington, N. Kaltsoyannis, P. Scott, *J. Organomet. Chem.* **2001**, *635*, 69.
- [10] F. G. N. Cloke, P. B. Hitchcock, *J. Am. Chem. Soc.* **2002**, *124*, 9352.
- [11] J. Guan, T. Dubé, S. Gambarotta, G. P. A. Yap, *Organometallics* **2000**, *19*, 4820.
- [12] T. Dubé, S. Conoci, S. Gambarotta, G. P. A. Yap, G. Vasapollo, *Angew. Chem.* **1999**, *111*, 3890; *Angew. Chem. Int. Ed.* **1999**, *38*, 3657.
- [13] M. Ganesan, S. Gambarotta, G. P. A. Yap, *Angew. Chem.* **2001**, *113*, 788; *Angew. Chem. Int. Ed.* **2001**, *40*, 766.
- [14] a) D. M. M. Freckmann, T. Dubé, C. D. Bérubé, S. Gambarotta, G. P. A. Yap, *Organometallics* **2002**, *21*, 1240; b) T. Dubé, S. Conoci, S. Gambarotta, G. P. A. Yap, *Organometallics* **2000**, *19*, 1182.
- [15] M. Ganesan, M. P. Lalonde, S. Gambarotta, G. P. A. Yap, *Organometallics* **2001**, *20*, 2443.
- [16] T. Dubé, M. Ganesan, S. Conoci, S. Gambarotta, G. P. A. Yap, *Organometallics* **2000**, *19*, 3716.
- [17] See for example: I. Korobkov, G. Aharonian, S. Gambarotta, G. P. A. Yap, *Organometallics* **2002**, *21*, 4899.
- [18] T. Dubé, S. Gambarotta, G. P. A. Yap, *Angew. Chem.* **1999**, *111*, 1507; *Angew. Chem. Int. Ed.* **1999**, *38*, 1432.
- [19] M. N. Bochkarev, I. L. Fedushkin, S. Dechert, A. A. Fagin, H. Schumann, *Angew. Chem.* **2001**, *113*, 3268; *Angew. Chem. Int. Ed.* **2001**, *40*, 3176.
- [20] a) W. J. Evans, N. T. Allen, J. W. Ziller, *J. Am. Chem. Soc.* **2001**, *123*, 7927; b) W. J. Evans, N. T. Allen, J. W. Ziller, *Angew. Chem.* **2002**, *114*, 369; *Angew. Chem. Int. Ed.* **2002**, *41*, 359; c) W. J. Evans, G. Zucchi, J. W. Ziller, *J. Am. Chem. Soc.* **2003**, *125*, 10.
- [21] a) C. E. Laplaza, C. C. Cummins, *Science* **1995**, *268*, 861; b) C. C. Cummins, *Chem. Commun.* **1998**, 1777, and references therein.
- [22] R. D. Sanner, J. M. Manriquez, R. E. Marsch, J. E. Bercaw, *J. Am. Chem. Soc.* **1976**, *98*, 8351.
- [23] J. A. Pool, E. Lobkovsky, P. J. Chirik, *J. Am. Chem. Soc.* **2003**, *125*, 2241.
- [24] P. J. Chirik, L. M. Henling, J. E. Bercaw, *Organometallics* **2001**, *20*, 534.
- [25] J. M. Smith, R. J. Lachicotte, K. A. Pittard, T. R. Cundari, G. Lukat-Rodgers, K. R. Rodgers, P. L. Holland, *J. Am. Chem. Soc.* **2001**, *123*, 9222.
- [26] M. D. Fryzuk, S. A. Johnson, S. J. Rettig, *J. Am. Chem. Soc.* **1998**, *120*, 11024.

- [27] M. D. Fryzuk, S. A. Johnson, B. O. Patrick, A. Albinati, S. A. Mason, T. F. Koetzle, *J. Am. Chem. Soc.* **2001**, *123*, 3960.
- [28] E. Solari, J. Hesschenbrouck, R. Scopelliti, C. Floriani, N. Re, *Angew. Chem.* **2001**, *113*, 958; *Angew. Chem. Int. Ed.* **2001**, *40*, 932.
- [29] See for example: P. Berno, S. Gambarotta, *Angew. Chem.* **1995**, *107*, 871; *Angew. Chem. Int. Ed. Engl.* **1995**, *34*, 822.
- [30] J. C. Peters, J. P. F. Cherry, J. C. Thomas, L. Baraldo, D. J. Mindiola, W. M. Davis, C. C. Cummins, *J. Am. Chem. Soc.* **1999**, *121*, 10053.
- [31] D. V. Yandulov, R. R. Schrock, A. L. Rheingold, C. Ceccarelli, W. M. Davis, *Inorg. Chem.* **2003**, *42*, 796.
- [32] a) D. V. Yandulov, R. R. Schrock, *J. Am. Chem. Soc.* **2002**, *124*, 6252; b) D. V. Yandulov, R. R. Schrock, *Science* **2003**, *301*, 76.
- [33] G. E. Greco, R. R. Schrock, *Inorg. Chem.* **2001**, *40*, 3861.
- [34] M. B. O'Donoghue, W. M. Davis, R. R. Schrock, W. M. Reiff, *Inorg. Chem.* **1999**, *38*, 243.
- [35] I. Korobkov, S. Gambarotta, G. P. A. Yap, *Angew. Chem.* **2003**, *115*, 5108; *Angew. Chem. Int. Ed.* **2003**, *42*, 4958.
- [36] I. Korobkov, S. Gambarotta, G. P. A. Yap, *Organometallics* **2001**, *20*, 2552.
- [37] I. Korobkov, S. Gambarotta, G. P. A. Yap, *Angew. Chem.* **2002**, *114*, 3583; *Angew. Chem. Int. Ed.* **2002**, *41*, 3433.
- [38] G. K. B. Clentsmith, V. M. E. Bates, P. B. Hitchcock, F. G. N. Cloke, *J. Am. Chem. Soc.* **1999**, *121*, 10444.
- [39] H. Kawaguchi, T. Matsuo, *Angew. Chem.* **2002**, *114*, 2916; *Angew. Chem. Int. Ed.* **2002**, *41*, 2792.
- [40] M. D. Fryzuk, B. A. MacKay, B. O. Patrick, *J. Am. Chem. Soc.* **2003**, *125*, 3234.
- [41] M. D. Fryzuk, B. A. MacKay, S. A. Johnson, B. O. Patrick, *Angew. Chem.* **2002**, *114*, 3861; *Angew. Chem. Int. Ed.* **2002**, *41*, 3709.
- [42] M. D. Fryzuk, C. M. Kozak, M. R. Bowdridge, B. O. Patrick, S. J. Rettig, *J. Am. Chem. Soc.* **2002**, *124*, 8389.
- [43] A. Caselli, E. Solari, R. Scopelliti, C. Floriani, N. Re, C. Rizzoli, A. Chiesi-Villa, *J. Am. Chem. Soc.* **2000**, *122*, 3652.
- [44] E. Solari, C. D. Silva, B. Iacono, J. Hesschenbrouck, C. Rizzoli, R. Scopelliti, C. Floriani, *Angew. Chem.* **2001**, *113*, 4025; *Angew. Chem. Int. Ed.* **2001**, *40*, 3907.
- [45] Y. C. Tsai, M. J. A. Johnson, D. J. Mindiola, C. C. Cummins, W. T. Klooster, J. F. Koetzle, *J. Am. Chem. Soc.* **1999**, *121*, 10426.
- [46] D. J. Mindiola, K. Meyer, J. P. F. Cherry, T. A. Baker, C. C. Cummins, *Organometallics* **2000**, *19*, 1622.
- [47] M. Mori, K. Hori, M. Akashi, M. Hori, Y. Sato, M. Nishida, *Angew. Chem.* **1998**, *110*, 659; *Angew. Chem. Int. Ed.* **1998**, *37*, 636.

Molecular Recognition

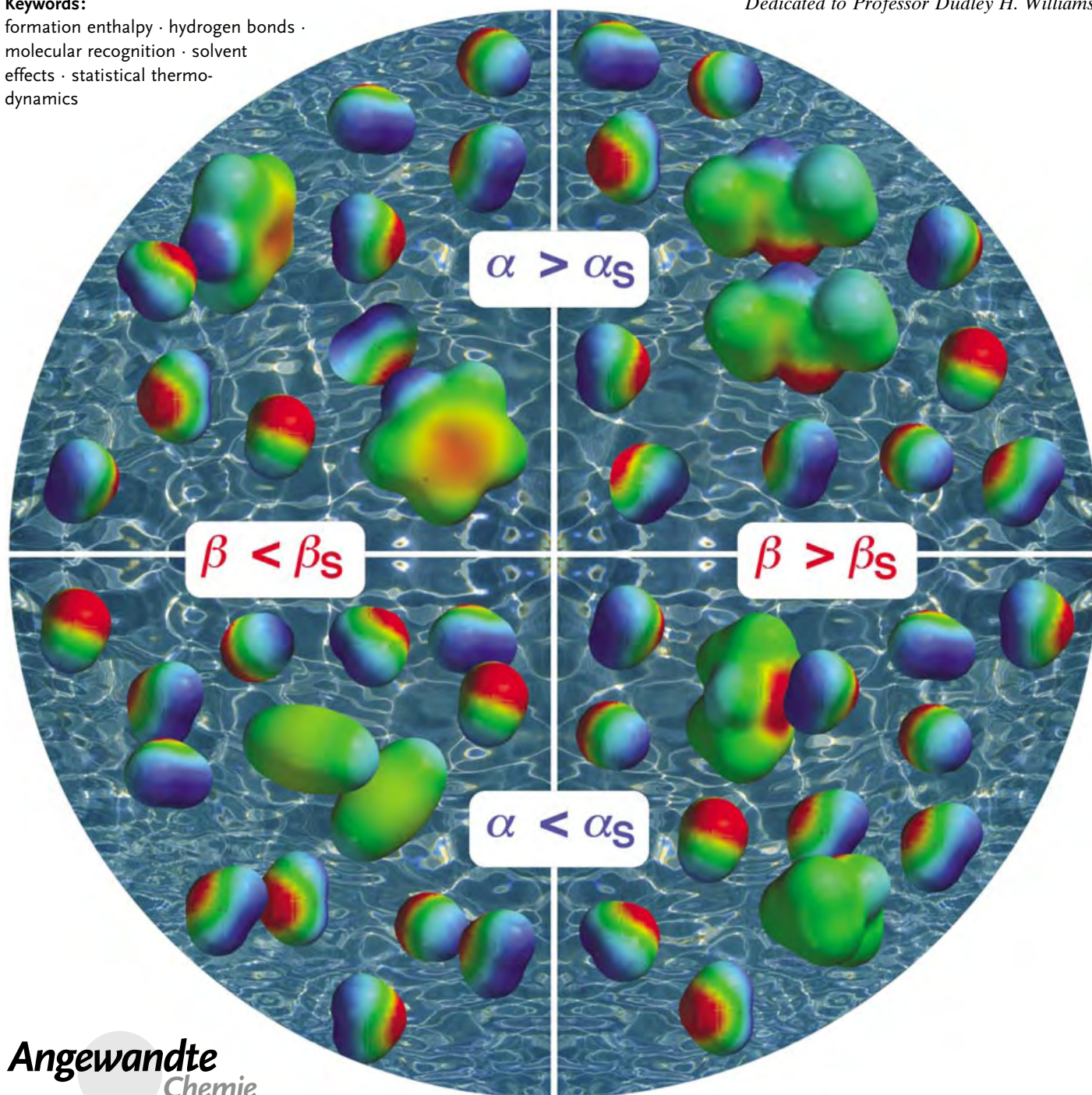
Quantifying Intermolecular Interactions: Guidelines for the Molecular Recognition Toolbox

Christopher A. Hunter*

Keywords:

formation enthalpy · hydrogen bonds · molecular recognition · solvent effects · statistical thermodynamics

Dedicated to Professor Dudley H. Williams



Molecular recognition events in solution are affected by many different factors that have hampered the development of an understanding of intermolecular interactions at a quantitative level. Our tendency is to partition these effects into discrete phenomenological fields that are classified, named, and divorced: aromatic interactions, cation- π interactions, CH-O hydrogen bonds, short strong hydrogen bonds, and hydrophobic interactions to name a few.^[1] To progress in the field, we need to develop an integrated quantitative appreciation of the relative magnitudes of all of the different effects that might influence the molecular recognition behavior of a given system. In an effort to navigate undergraduates through the vast and sometimes contradictory literature on the subject, I have developed an approach that treats theoretical ideas and experimental observations about intermolecular interactions in the gas phase, the solid state, and solution from a single simplistic viewpoint. The key features are outlined here, and although many of the ideas will be familiar, the aim is to provide a semiquantitative thermodynamic ranking of these effects in solution at room temperature.

1. Introduction

Let us first deal with the issue of free energy (Gibbs free energy, G), enthalpy, and entropy. Clearly, these three parameters are intimately related, but the behavior of a system is determined by the free energy, and the experimental values are simple to interpret: is the complex more stable or not? Although the concepts of entropy and enthalpy are useful for understanding the various factors that contribute to the free energy of an intermolecular interaction, interpretation of the experimental values of ΔH and ΔS is problematic, even for simple systems. The enthalpy and entropy changes observed for intermolecular interactions can fluctuate wildly when relatively small changes are made to the system, but in such a way that the two parameters compensate one another, and the associated variation in free energy is small.^[2] A phase change is the classic scenario where there are large enthalpy and entropy changes that compensate each other precisely. The values of ΔH and ΔS tell us about changes in the internal structure or organization of the system and are not necessarily related to the overall stability. The thermodynamics of the hydrophobic effect illustrate the point.^[3] The free energy change on dissolving a nonpolar molecule in water is large and positive across the entire temperature range from 0 to 100 °C and does not fluctuate significantly. However, the associated entropy and enthalpy changes vary dramatically, so that the process is dominated by entropy at low temperatures and enthalpy at high temperatures. This is not to say that enthalpy and entropy are not useful parameters. The information they contain about changes in structure is important, for example, in understanding the binding of agonists and antagonists to biological receptors, but it is something quite different from overall stability or binding affinity.^[4]

From the Contents

1. Introduction	5311
2. Theoretical Considerations	5311
3. The Cost of Restricting Relative Molecular Motions	5313
4. Molecular Electrostatic Potential Surfaces	5314
5. Desolvation	5315
6. Solvophobic Interactions	5318
7. Solvents with Multiple Hydrogen-Bond Donors and Hydrogen-Bond Acceptors	5318
8. Solubility	5319
9. Relationship of α and β with Chemical Structure	5320
10. Conclusions	5322

We will therefore focus on free energy as the key observable that is important for understanding intermolecular interactions in solution. The contributions from factors such as the unfavorable entropy change associated with bringing two molecules together to form a complex or the favorable enthalpy change associated with the formation of a hydrogen bond will all be considered as free energy terms. Methods for parsing free energy in this manner have been relatively successful, suggesting that free energy contributions are indeed additive to a first approximation.^[5]

2. Theoretical Considerations

The basic theory of intermolecular interactions in the gas phase separates the enthalpy of interaction between two molecules into four components: repulsion between the electron densities at close distances of approach; induction interactions between the permanent charge distribution of one molecule and an induced change in the charge distribution of the other molecule; dispersion interactions between

[*] Prof. C. A. Hunter
Centre for Chemical Biology
Krebs Institute for Biomolecular Science
Department of Chemistry
University of Sheffield
Sheffield S3 7HF (UK)
Fax: (+44) 114-273-8673
E-mail: c.hunter@shef.ac.uk

mutually induced dipoles, and electrostatic interactions between the permanent charge distributions of the two molecules.^[6,7] We will consider each of these factors in turn.

2.1. Repulsion

The repulsive interactions between electron densities simply define the molecular volume, and for molecules in van der Waals contact, we can ignore the contribution of the repulsion term to differences in intermolecular interaction energies.

2.2 Induction

There is some evidence for induction in complexes of organic molecules, but the magnitude of the effect is relatively small.^[8] For example, urea forms linear hydrogen-bonded polymers in organic solvents with two hydrogen bonds between each molecule (Figure 1).^[9] The first step in assembly of the polymer is formation of the urea dimer, which polarizes the molecules, so that K_2 for adding a third urea unit to the chain is larger than K_1 . However, the magnitude of the effect is a small fraction of the hydrogen-bond energy (1 kJ mol⁻¹ change in 20–25 kJ mol⁻¹ for the urea–urea hydrogen bond, see Section 5). Therefore to a first approximation, we can neglect the effects of induction.

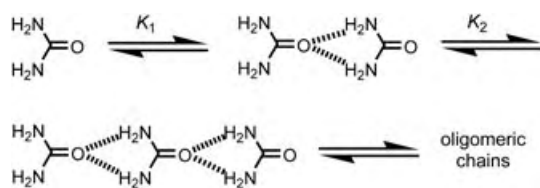


Figure 1. Urea forms a linear hydrogen-bonded polymer in benzene. The value of K_1 is 400 M⁻¹, and the value of K_2 is 900 M⁻¹. The difference is attributed to polarization of the molecules by the hydrogen bonds in the dimer that make the second set of hydrogen bonds in the trimer stronger.

2.3 Dispersion

The magnitude of the dispersion interaction between two atoms i and j (E_{ij}) depends on the atomic polarizabilities (α_i

and α_j) and the number of valence electrons (N_i and N_j). If the atoms are separated by a distance r_{ij} , E_{ij} can be estimated by using the Slater–Kirkwood method [Eq. (1) and Eq. (2); c is a constant].^[10]

$$E_{ij} = \frac{B_{ij}}{r_{ij}^6} \quad (1)$$

$$B_{ij} = c \frac{\alpha_i \alpha_j}{\sqrt{\alpha_i/N_i} + \sqrt{\alpha_j/N_j}} \quad (2)$$

Table 1 shows the values of the constant, B_{ij} , for some atoms of the second and third periods. The larger, softer atoms have larger B_{ij} values as expected, but this does not necessarily equate to larger dispersion interactions. Larger atoms are further apart, when they are in van der Waals

Table 1: Relative values of B_{ij} for some atoms of the second and third period.^[a]

	C	N	O	F	P	S	Cl
C	1.0	0.7	0.6	0.4	1.8	1.6	1.3
N	0.7	0.6	0.5	0.4	1.3	1.2	1.0
O	0.6	0.5	0.4	0.3	1.0	0.9	0.8
F	0.4	0.4	0.3	0.2	0.8	0.7	0.6
P	1.8	1.3	1.0	0.8	3.3	2.9	2.4
S	1.6	1.2	0.9	0.7	2.9	2.6	2.2
Cl	1.3	1.0	0.8	0.6	2.4	2.2	1.8

[a] Relative to the C...C interaction. The values were calculated by using Equation (2), and atomic polarizabilities, α_i and α_j , were taken from reference [10b].

contact, and the dispersion energy depends on r_{ij}^{-6} [Eq. (1)]. Moreover in solution, there are competitive dispersion interactions with the solvent, and because large atoms make more solvent contacts than small atoms, they displace more solvent when they form a complex (Figure 2). In solution, the surfaces of all molecules are fully coated by other molecules, and the equilibrium in Figure 2 simply represents a rearrangement of the molecular surfaces that are in contact. The relevant parameter for comparing dispersion interactions in solution is therefore the interaction energy per unit surface area of contact. Table 2 shows that there is remarkably little

Table 2: Relative values of the dispersion interaction energy per unit surface area of contact for some atoms of the second and third period.^[a]

	C	N	O	F	P	S	Cl
C	1.0	1.0	1.1	1.1	1.5	1.4	1.1
N	1.0	0.9	1.0	1.1	1.5	1.3	1.1
O	1.1	1.0	1.0	1.1	1.6	1.4	1.2
F	1.1	1.1	1.1	1.1	1.6	1.5	1.3
P	1.5	1.5	1.6	1.6	2.1	1.8	1.5
S	1.4	1.3	1.4	1.5	1.8	1.6	1.4
Cl	1.1	1.1	1.2	1.3	1.5	1.4	1.2

[a] The dispersion energy was calculated by using Equation (1) and atomic radii were taken from reference [10b]. The surface area of contact was taken to be proportional to the surface area of the smaller of the two atoms.



Chris Hunter was educated at the University of Cambridge and graduated with a PhD in 1989. He was a lecturer at the University of Otago from 1989 till 1991. In 1991 he moved to the University of Sheffield, where he is currently Professor of Chemistry. He has research interests in various aspects of molecular recognition, design, synthesis, measurement, and theory.

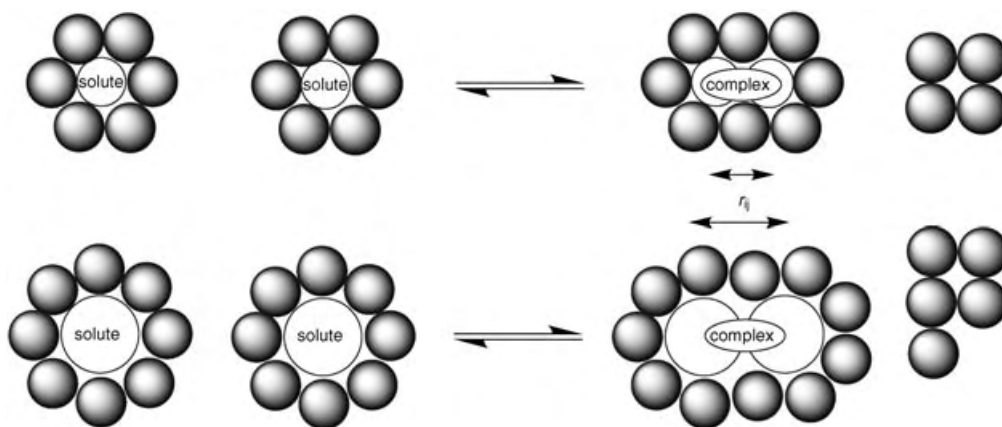


Figure 2. Although B_{ij} is larger for larger more polarizable atoms, the nuclear separation r_{ij} is also larger, and the amount of solvent that is displaced is larger. These effects cancel each other out to a first approximation. The dispersion interaction energy per unit surface area of contact is almost constant and independent of atom type, and the total contact surface area does not change for the equilibrium shown, so the change in dispersion energy for the interaction of two molecules in solution is small.

variation of this parameter with atom type.^[11] The interactions with third-period atoms are slightly larger than for the second period, but to a first approximation, we can assume that the change in the dispersion energy is negligible, when two shape complementary molecules interact in solution.^[12] If $\text{Cl}\cdots\text{Cl}$ interactions were significantly more favorable than $\text{C}\cdots\text{C}$ interactions, carbon tetrachloride would be a poor solvent for nonpolar organic molecules, which is not the case. The dispersion interactions per unit surface area for $\text{C}\cdots\text{C}$, $\text{C}\cdots\text{Cl}$ and $\text{Cl}\cdots\text{Cl}$ have very similar values, as expected from the experimental behavior. Since the dispersion energy for the interaction of two methyl groups is about 2 kJ mol^{-1} , the small variations in Table 2 do not translate to large differences in free energy.^[13]

2.4. Electrostatics

Since repulsion, induction, and dispersion contribute only negligibly to intermolecular interactions, this leaves us with the prospect of using only electrostatics to explain everything. This not only makes life very simple, but there is good experimental evidence for the dominant role of electrostatics in intermolecular interactions. Physical organic chemists have measured the association constants (K) for a huge number of intermolecular interactions in the gas phase and in solution. For simple molecules, these data can be analyzed as simple pairwise hydrogen-bonding interactions between two functional groups, and remarkably, the results can be accounted for by a single simple relationship [Eq. (3)].^[14]

$$\log K = c_1 \alpha_2^H \beta_2^H + c_2 \quad (3)$$

c_1 and c_2 are constants that depend on the solvent, and α_2^H and β_2^H are functional group constants that relate to the hydrogen-bond donor and hydrogen-bond acceptor properties of the molecules.

Equation (3) is equivalent to an expression of the electrostatics of the hydrogen-bonding interaction, where the free energy of interaction varies as the product of the positive charge on the hydrogen-bond donor (α_2^H) and the negative charge on the hydrogen-bond acceptor (β_2^H).^[15] Indeed, the values of α_2^H and β_2^H have been correlated with a variety of computed molecular properties, such as atomic charge and electrostatic potential.^[16] The constant c_1 is solvent dependent: it increases as the polarity of

the medium decreases, as expected for electrostatic interactions. The constant c_2 is -1.0 ± 0.1 and is relatively insensitive to solvent, which implies that it is a fundamental property of the interaction between any two molecules.

3. The Cost of Restricting Relative Molecular Motions

If we consider the interaction between two nonpolar entities, such as neon atoms, where $\alpha_2^H = \beta_2^H = 0$, Equation (3) gives an association constant of 0.1 M^{-1} . In other words, complexation between two neon atoms becomes significant at concentrations above 10M, even though there are no polar groups to form hydrogen bonds. The reason is that 10M is approximately the concentration of the bulk liquid state, where by definition there are extensive intermolecular contacts. The c_2 term therefore represents the adverse free energy associated with bringing two molecules together to form a noncovalent complex in solution. The magnitude of the effect is only $+6\text{ kJ mol}^{-1}$, which is significantly lower than the $+60\text{ kJ mol}^{-1}$ associated with the adverse free energy for formation of a covalent complex.^[17] The difference reflects the looseness of noncovalent associations. The formation of noncovalent complexes is intrinsically much more favorable than the formation of covalent complexes, because the relative molecular motions are not restricted to the same extent. This value of c_2 is consistent with an empirical analysis of small molecules binding to biological receptors in water that found a value of $+5.4\text{ kJ mol}^{-1}$ for the free energy cost of restricting relative molecular motions.^[18]

One consequence is that the upper limit for the effective molarities one might expect to see for systems that make multiple intermolecular interactions is rather low, of the order of 10M. The effective molarities of 10^{10} M that have been reported for intramolecular reactions clearly do not translate to noncovalent interactions.^[19] Although the adverse free energy associated with bringing molecules together to make a

noncovalent complex is something we would generally consider to be “an entropic effect”, the magnitude of the effect bears no relation to measured values of the entropy of complexation.^[4] Experimental entropy measurements include additional contributions from desolvation and changes in internal structure.

4. Molecular Electrostatic Potential Surfaces

Equation (3) holds for a remarkably wide range of functional groups, and this implies that, apart from some notable exceptions such as aromatic stacking, we can treat all intermolecular interactions as a form of hydrogen bonding.^[14] The reason is that the maximum in the electrostatic potential on the van der Waals surface of a molecule is usually located near a hydrogen atom and the minimum is usually over a lone pair or an area of π -electron density (Figure 3a). The dominant electrostatic interactions between two molecules

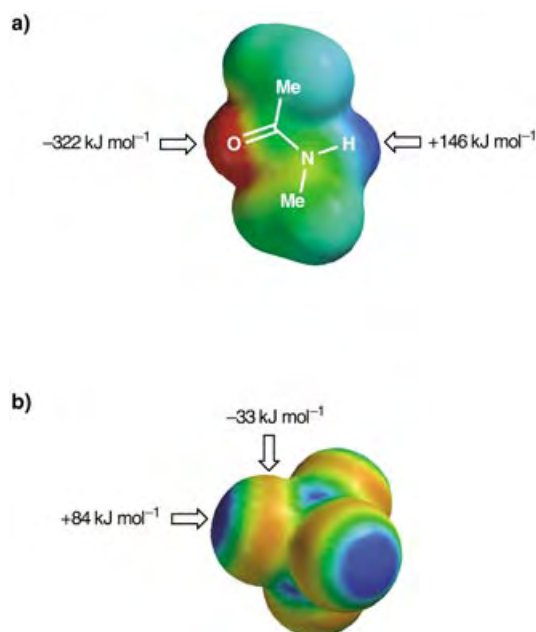


Figure 3. Molecular electrostatic potential surfaces plotted on the van der Waals' surface of the molecule calculated by using AM1 and a positive point charge in a vacuum as the probe. a) *N*-methyl acetamide. Positive regions are shown in blue ($> +150 \text{ kJ mol}^{-1}$), negative regions are shown in red ($< -150 \text{ kJ mol}^{-1}$), and green is neutral. The maximum in the electrostatic potential, E_{max} , lies over the NH group, and the minimum, E_{min} , lies over the carbonyl oxygen atom, the two primary hydrogen-bonding sites in the molecule. b) Carbon tetrachloride. Positive regions are shown in blue ($> +35 \text{ kJ mol}^{-1}$), negative regions are shown in red ($< -35 \text{ kJ mol}^{-1}$), and green is neutral.

are pairwise interactions between these maxima and minima that may generally be considered to be of a hydrogen-bonding nature. Even at a relatively low level of theory, the calculated maxima and minima in the molecular electrostatic potential surfaces correlate well with the experimentally determined values of α_2^{H} and β_2^{H} (Figure 4).^[20] The intercept for the β_2^{H} plot

is close to the origin, but the α_2^{H} plot crosses the electrostatic potential axis at $+70 \text{ kJ mol}^{-1}$, and all functional groups with lower E_{max} values have been assigned an α_2^{H} value of zero. The reasons for this can be found in the properties of the solvent used to develop the α_2^{H} and β_2^{H} scales (carbon tetrachloride).

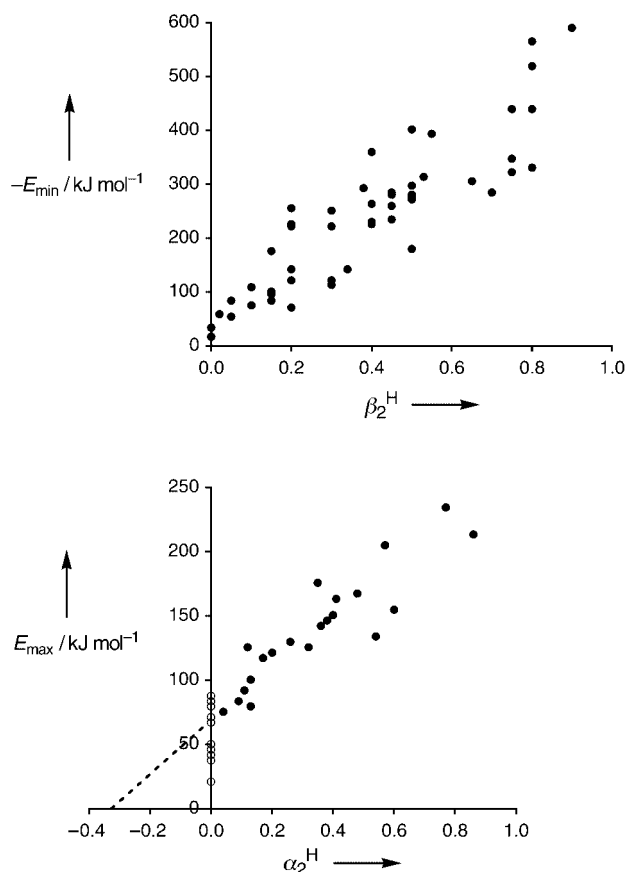


Figure 4. The maxima (E_{max}) and minima (E_{min}) in the AM1 molecular electrostatic potential surfaces of a range of simple molecules containing only one functional group plotted against the corresponding experimentally determined values of α_2^{H} and β_2^{H} from reference ^[14]. Electrostatic potentials in sterically inaccessible crevices on the surface of a tetrahedrally coordinated central atom (e.g. phosphorus) were ignored. In some cases, the locations of the maxima and minima in the molecular electrostatic potential surface do not necessarily correspond to conventional hydrogen-bonding sites (e.g. for carbon tetrachloride shown in Figure 3). The open circles correspond to functional groups that do not form hydrogen-bonded complexes in carbon tetrachloride and have been assigned a value of $\alpha_2^{\text{H}} = 0$. The dotted line is an extrapolation of the α_2^{H} data to encompass nonpolar hydrogen-bond donors that have values of E_{max} lower than that of carbon tetrachloride. The best fit straight lines give $E_{\text{min}} = -535 (\beta_2^{\text{H}} + 0.06 \text{ kJ mol}^{-1})$ and $E_{\text{max}} = 211 (\alpha_2^{\text{H}} + 0.33 \text{ kJ mol}^{-1})$.

The molecular electrostatic potential surface of carbon tetrachloride is shown in Figure 3b, and although there are no hydrogen-bond donors, the surface is quite strongly positive. In third period elements, the lone pair electrons are diffuse and relatively far from the nucleus, so that the positive nuclear charge is not well screened. Combined with the

strongly electron withdrawing nature of the CCl_3 group, this gives the chlorine atoms of carbon tetrachloride electrostatic properties equivalent to a weak hydrogen-bond donor. The value of E_{max} for carbon tetrachloride is $+84 \text{ kJ mol}^{-1}$, which is very close to the point at which the α_2^{H} plot crosses the E_{max} axis in Figure 4. All less polar hydrogen-bond donors are unable to compete with the solvent for solute hydrogen-bonding sites, and so it is impossible to detect interactions with weak hydrogen-bond donors in this solvent. The origin of the α_2^{H} scale has been set by the properties of carbon tetrachloride, and if we extrapolate the experimental α_2^{H} data, it is clear that the origin should be at $\alpha_2^{\text{H}} = -0.33$. This would allow us to incorporate all functional groups, including relatively nonpolar hydrogen-bond donors such as C–H groups. The value of E_{min} for carbon tetrachloride is -33 kJ mol^{-1} , and so the β_2^{H} scale is only displaced by 0.06, which is a relatively small discrepancy.

5. Desolvation

The correlations in Figure 4 provide an important clue how to treat interactions in solution. There is a competition between solute–solute, solvent–solvent, and solute–solvent interactions (Figure 5), and if we change our frame of

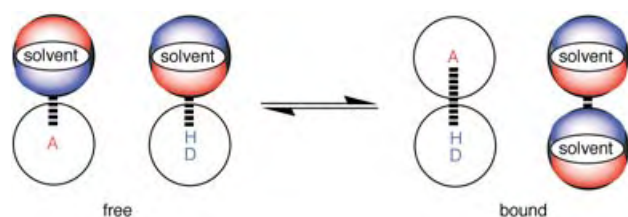


Figure 5. Intermolecular interactions in solution are a competition between solute–solvent interactions in the free state, and solute–solute and solvent–solvent interactions in the bound state. For simple functional groups, the primary mode of interaction is hydrogen-bond contacts between the maxima (blue) and minima (red) in the electrostatic potential surfaces of the molecules. A represents a hydrogen-bond acceptor solute and DH a hydrogen-bond donor solute.

reference, we can produce a universal hydrogen-bond scale that can be used to predict the free energy of hydrogen-bonding interactions ($\Delta\Delta G_{\text{H-bond}}$ in kJ mol^{-1}) in any solvent [Eq. (4)].

$$\begin{aligned}\Delta\Delta G_{\text{H-bond}} &= -(\alpha\beta + \alpha_s\beta_s) + (\alpha\beta_s + \alpha_s\beta) \\ &= -(\alpha - \alpha_s)(\beta - \beta_s)\end{aligned}\quad (4)$$

α and β are hydrogen-bond donor and hydrogen-bond acceptor constants for the solute molecules, and α_s and β_s are the corresponding hydrogen-bond donor and hydrogen-bond acceptor constants for the solvent.

The new hydrogen-bond parameters, α and β , correspond to normalized dimensionless versions of E_{max} and E_{min} [Eq. (5) and Eq. (6)]. The normalization constant of 52 kJ mol^{-1} was

obtained from the slopes of the correlations in Figure 4 and the gas phase value of c_1 in Equation (3) such that Equation (4) gives $\Delta\Delta G_{\text{H-bond}}$ in units of kJ mol^{-1} . Where experimental values of α_2^{H} and β_2^{H} are available, they can be converted to the new α and β scale using Equation (5) and (6) which are based on the correlations shown in Figure 4. If experimental data are not available, α and β can be estimated from calculated AM1 molecular electrostatic potential surfaces by using Equation (5) and (6). The scatter in the correlations in Figure 4 provides an indication of the accuracy that can be achieved by using E_{max} and E_{min} values. Some classes of functional groups, for example, amides, behave consistently poorly, and the accuracy of the α and β values obtained from electrostatic potential calculations is of the order $\pm 20\%$. A list of values of α and β for common functional groups is provided in Table 3.

$$\alpha = E_{\text{max}}/52 \text{ kJ mol}^{-1} = 4.1(\alpha_2^{\text{H}} + 0.33) \quad (5)$$

$$\beta = -E_{\text{min}}/52 \text{ kJ mol}^{-1} = 10.3(\beta_2^{\text{H}} + 0.06) \quad (6)$$

Equation (4) is the equivalent of the first term in Equation (3), and to estimate the overall free energy of complexation, the adverse free energy associated with bimolecular complexation ($\approx +6 \text{ kJ mol}^{-1}$) should be added to $\Delta\Delta G_{\text{H-bond}}$. In this scheme, α and β represent the positive and negative parts of a continuous scale, so that the magnitudes of repulsive interactions can also be estimated. For example, the adverse free energy associated with the interaction between two hydrogen-bond donors forced into van der Waals contact is given by $\alpha_1\alpha_2$.

The general features of the hydrogen-bond interaction space for all uncharged functional groups are illustrated in Figure 6. For a given solvent, functional group interactions are partitioned into four quadrants defined by the hydrogen-

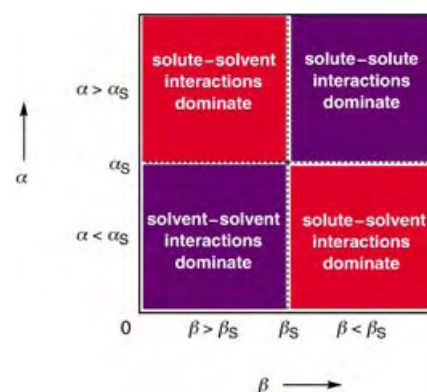


Figure 6. The generalized profile for hydrogen-bond interactions between neutral functional groups in solution [Eq. (4)]. The hydrogen-bond parameters introduced in this work are denoted α and β for the solute molecules and α_s and β_s for the solvent. For a given solvent, the functional group interaction space is partitioned into four quadrants. In the two red quadrants, $\Delta\Delta G_{\text{H-bond}}$ is positive, and the functional group interactions are unfavorable. In the two blue quadrants, $\Delta\Delta G_{\text{H-bond}}$ is negative, and the functional group interactions are favorable. The values of α_s and β_s set the boundaries between these quadrants and define how the space is partitioned.

Table 3: Hydrogen-bond parameters for common functional groups and solvents in order of increasing hydrogen-bond strength.

H-bond donors	$\alpha^{[a]}$	$\alpha^{[b]}$	H-bond donors	$\alpha^{[a]}$	$\alpha^{[b]}$	H-bond donors	$\alpha^{[a]}$	$\alpha^{[b]}$
alkane		0.4	alkyl ketone	1.5		carbamate	2.8	
alkene		0.7	amine		1.5	sulfonamide		2.8
alkyl ether		0.9	aldehyde		1.6	amide	2.9	
benzene		1.0	furan		1.7	urea	3.0	
alkyl thioether		1.0	thiol		1.7	pyrrole	3.0	
alkyl iodide		1.2	acetonitrile	1.7		sulfonamide		3.2
alkyl fluoride		1.2	thiophenol	1.8		thioamide		3.3
alkyl chloride		1.3	nitromethane	1.8		carboxylic acid	3.6	
alkyl bromide		1.3	dichloromethane	1.9		imidazole		3.7
aryl chloride		1.3	alkyne	1.9		2,2,2-trifluoroethanol	3.7	
carbon tetrachloride	1.4		1,1,2,2-tetrachloroethane		2.0	phenol	3.8	
aryl ether		1.4	ammonia		2.0	trifluoroacetic acid		3.9
aryl fluoride		1.4	aniline	2.1		phosphoric acid		4.0
pyridine		1.4	chloroform	2.2		hexafluoropropan-2-ol	4.5	
1,1,1-trichloroethane		1.5	alcohol	2.7		perfluoro- <i>tert</i> -butanol	4.9	
alkyl ester		1.5	water	2.8				
H-bond acceptors	$\beta^{[a]}$	$\beta^{[b]}$	H-bond acceptors	$\beta^{[a]}$	$\beta^{[b]}$	H-bond acceptors	$\beta^{[a]}$	$\beta^{[b]}$
alkane		0.3	alkyne	2.7		alcohol	5.8	
carbon tetrachloride	0.6		isothiocyanate	2.7		imine	5.8	
perfluoroalkane		0.7	thiol	2.7		ketone	5.8	
chloroform	0.8		hexafluoropropan-2-ol		3.1	sulfonamide	5.8	
dichloromethane	1.1		alkyl selenide	3.4		thioamide	5.8	
alkene	1.1		thioether	3.6		ammonia	6.1	
1,1,2,2-tetrachloroethane		1.3	nitroalkane	3.7		sulfone	6.3	
1,1,1-trichloroethane		1.4	aryl ether	3.7		pyridine	7.0	
aryl chloride	1.6		disulfide	3.7		carbamate	7.3	
aryl bromide	1.6		trifluoroacetic acid		3.8	amine	7.8	
aryl iodide	1.6		pyrrole	4.1		sulfonamide	8.3	
aryl fluoride	1.6		2,2,2-trifluoroethanol		4.2	amide	8.3	
alkyl chloride	2.2		water	4.5		urea	8.3	
alkyl bromide	2.2		aldehyde	4.7		phosphinate diester	8.9	
alkyl iodide	2.2		nitrile	4.7		phosphonate diester	8.9	
benzene	2.2		sulfate diester	4.7		sulfoxide	8.9	
furan	2.2		thiocyanate	4.7		amidine	8.9	
thiophenol	2.2		carboxylic acid	5.3		phosphoric acid		9.3
perfluoro- <i>tert</i> -butanol		2.3	alkyl ether	5.3		phosphine oxide	9.9	
phenol	2.7		aniline	5.3				
alkyl fluoride	2.7		ester	5.3				

[a] Values based on the literature values of α_2^H and β_2^H . [b] Values based on the molecular electrostatic potential surface.

bond donor and hydrogen-bond acceptor properties of the solvent. The values of α_s and β_s set the boundaries where the exchange process in Figure 5 is associated with zero free energy change. There are two red quadrants in Figure 6, where hydrogen-bonding interactions are unfavorable, because the solute–solvent interactions dominate. In the two blue quadrants, hydrogen-bonding interactions between solute molecules are favorable. The top right quadrant corresponds to interactions between the most polar functional groups where solute–solute interactions dominate. The bottom left quadrant is the solvophobic zone. Here, functional group interactions are favorable, because the solvent–solvent interactions are stronger than the solute–solvent interactions.

Figure 7 shows the functional group interaction profiles for different solvent environments.^[21] The positions of a selection of functional groups on the new universal hydrogen-bond scale are shown for calibration. Figure 7a shows the functional interaction energies for $\alpha_s = \beta_s = 0$. This corre-

sponds to a condensed phase with no solvent, that is, the solid state, or to a completely nonpolar solvent, that is, a noble gas, and provides a measure of the intrinsic functional group interaction energies. Under these conditions all interactions are attractive, because there is no solvent competition. Figure 7b illustrates why dimethyl sulfoxide (DMSO) is one of the best solvents. The α_s and β_s boundary lines intersect in the bottom right corner of the interaction space, and so almost all functional group interactions are unfavorable. Chloroform has been widely used for molecular recognition studies on model systems, because there are no solvophobic effects, and there is a large zone of favorable solute–solute interactions (Figure 7c). The functional group interaction profile for carbon tetrachloride, the solvent used to determine the original α_2^H and β_2^H parameters, is not shown but is very similar to the chloroform plot. Dimethyl ether also partitions the interaction space into a repulsive and an attractive zone with no solvophobic zone, but the profile is quite different from chloroform (Figure 7d).^[21] Chloroform is a good solvent

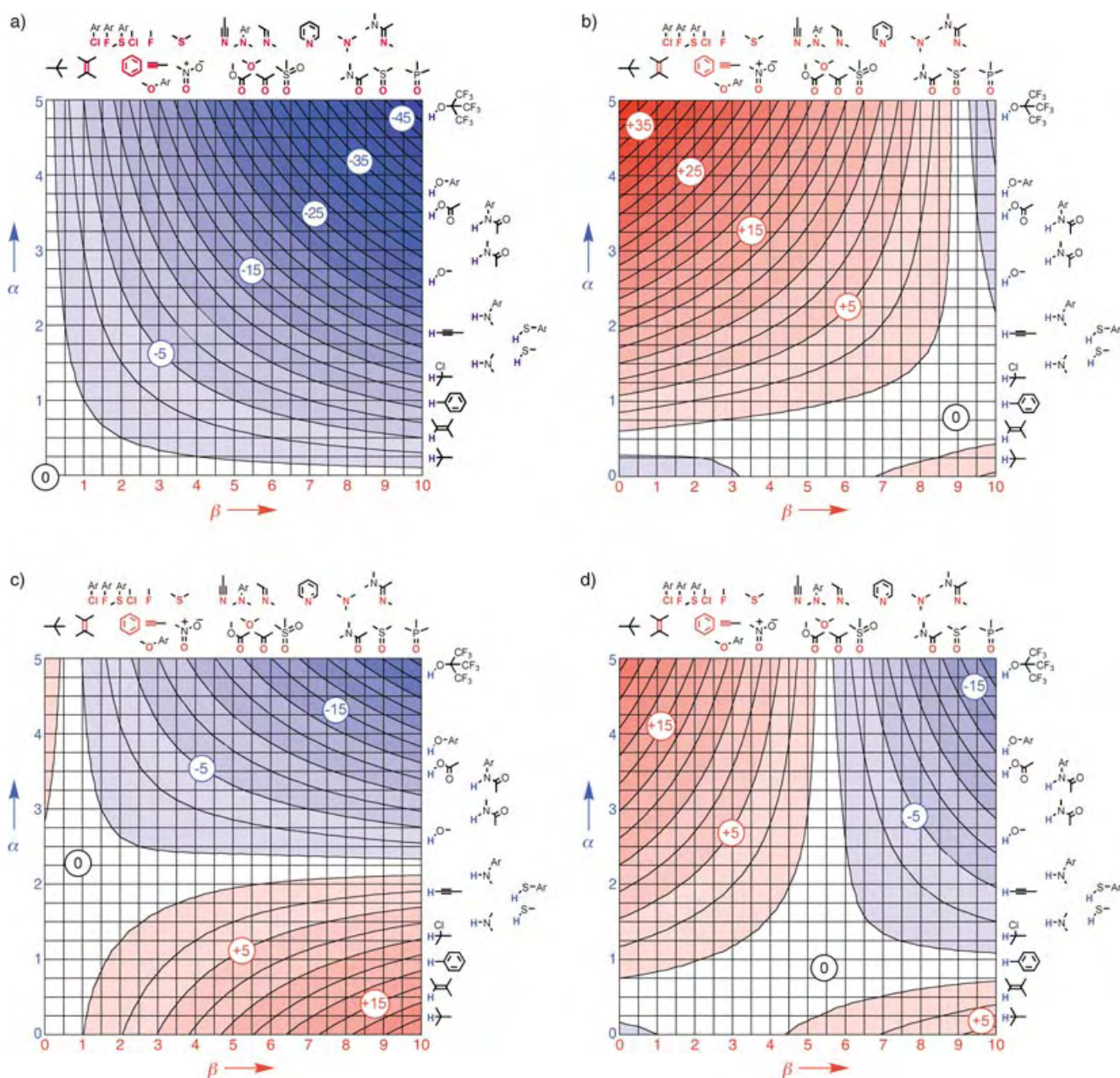


Figure 7. Functional group interaction profiles a) in the solid state or a noble gas solvent ($\alpha_s = \beta_s = 0$), b) in DMSO ($\alpha_s = 0.8$, $\beta_s = 8.9$), c) in chloroform ($\alpha_s = 2.2$, $\beta_s = 0.8$) and d) in dimethyl ether ($\alpha_s = 0.9$, $\beta_s = 5.3$). $\Delta\Delta G_{\text{H-bond}}$ (kJ mol^{-1}) calculated by using Equation (12) is plotted against the range of values of α and β found for neutral functional groups. The structures of a representative set of functional groups are illustrated at appropriate points on the α and β scale as orientation for the reader. The contour lines are drawn at 2 kJ mol^{-1} intervals. Blue represents a favorable interaction ($\Delta\Delta G_{\text{H-bond}} < 0$), and red represents an unfavorable interaction ($\Delta\Delta G_{\text{H-bond}} > 0$). The zero point on each plot corresponds to ($\alpha = \alpha_s$, $\beta = \beta_s$) where desolvation perfectly balances the solute–solute interactions.

for studying weak hydrogen-bond acceptors, and ether is a good solvent for studying weak hydrogen-bond donors.

The solvent dependence of hydrogen-bonding interactions has been studied experimentally in relation to Equation (3).^[22] The solvent dependence of the constant c_1 in Equation (3) can be accounted for using Equation (4) to estimate $\Delta\Delta G_{\text{H-bond}}$ and hence the association constant, K , in the relevant solvents [Eq. (7)].

$$\lg K = -\frac{\Delta\Delta G_{\text{H-bond}} + 6}{RT} \quad (7)$$

Figure 8 shows a plot of $\lg K$ for the favorable solute–solute interactions in the top right quadrant of the functional group interaction space for the gas phase, carbon tetrachloride and 1,1,1-trichloroethane versus the product of the original H-bond parameters, α_2^{H} and β_2^{H} . The slopes of these plots predict values for c_1 that are in excellent agreement with experiment.

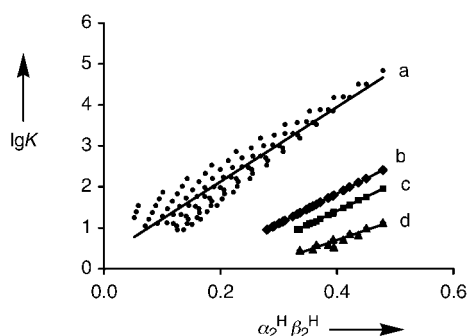


Figure 8. $\lg K$ predicted by using Equation (7) plotted against the corresponding values of $\alpha_2^H \beta_2^H$ for functional group interactions in a) the gas phase (this is approximated by using $\alpha_S = 0$, $\beta_S = 0$, and the additional contribution from dispersion interactions is ignored), b) carbon tetrachloride ($\alpha_S = 1.6$, $\beta_S = 0.6$), c) 1,1,1-trichloroethane ($\alpha_S = 1.5$, $\beta_S = 1.4$), and d) chloroform ($\alpha_S = 2.2$, $\beta_S = 0.8$). The gas-phase plot (a) diverges significantly at low $\alpha_2^H \beta_2^H$, and the choice of $\lg K$ cut off affects the slope of the line of best fit. It is clear however that the slope is significantly steeper than for the other solvents. The slopes of these plots give values of c_1 in Equation (3) that are identical to the experimental values:^[22] a) $c_1(\text{expt}) = c_1(\text{calcd}) = 9.1$, b) $c_1(\text{expt}) = c_1(\text{calcd}) = 7.3$, c) $c_1(\text{expt}) = c_1(\text{calcd}) = 6.8$, d) the experimental value of c_1 has not been determined for chloroform, but the prediction of Equation (7) is that $c_1 = 4.9$.

6. Solvophobic Interactions

Water is a special solvent, because the values of both α_S and β_S lie in the middle of the hydrogen-bond scales. The interaction space is equally partitioned into the four different quadrants described above, and both solvophobic and solute driven interactions are important. The analysis above assumes that the solute–solvent complexes in Figure 5 are 100% bound, but for a nonpolar solute in a polar solvent, this is not true. The solvent molecules can choose between a weak interaction with the solute and a strong interaction with another solvent molecule (Figure 9a). Interactions involving the solvent molecules are therefore better treated as the Boltzmann weighted average of the interaction with the solute and interaction with the bulk solvent. In the limit, very polar solvents, like water, form a cage around very nonpolar solutes, like hydrocarbons, to minimize solvent–solute interactions.^[3] This dramatically attenuates the magnitudes of the interaction energies in the solvophobic quadrant. The driving force is the formation of solvent–solvent interactions, but if these are largely formed already in the free state, the gain in solvent–solvent interactions in the bound state is relatively small. There is another important factor to consider in the solvophobic quadrant. The molecules in the liquid state are close packed, and so the solvent molecules are forced to interact with the solute to some extent. It is never possible to completely desolvate the solute, even if the Boltzmann factor predicts complete population of the solvent–solvent interaction. Although more attractive solvent–solvent interactions may be available, they are sterically blocked by the solute (Figure 9b). Equation (4) must therefore be modified to account for these effects in the interactions between the first

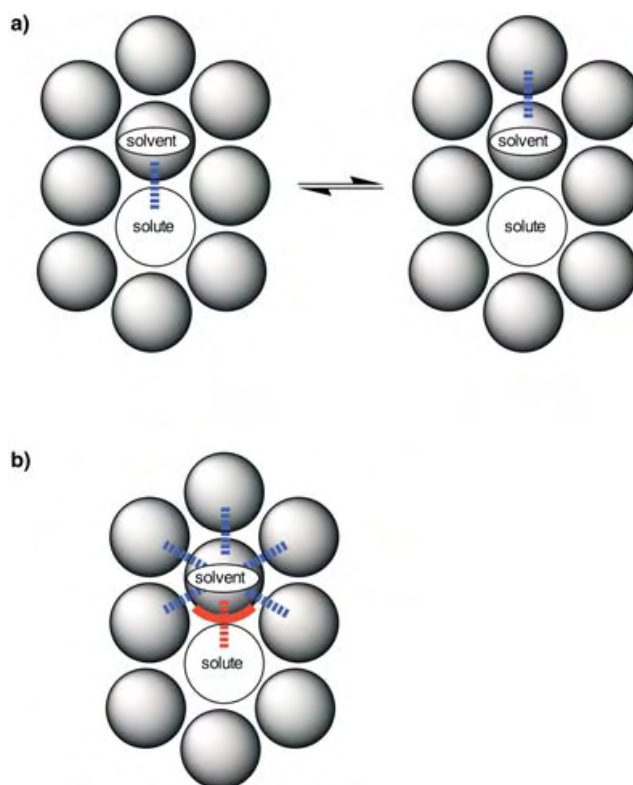


Figure 9. a) A solvent molecule that solvates a solute can choose between hydrogen-bonding to the solute or hydrogen-bonding to the surrounding bulk solvent. At equilibrium, there is a Boltzmann distribution of the two states. b) A solvent molecule that solvates a solute is sterically blocked from interacting freely with the surrounding bulk solvent. A fraction of the surface of the solvent is always forced to interact with the solute (red zone), even if the interaction with bulk solvent is more favorable.

solvation shell and bulk solvent. Implementation of the concepts outlined above is rather involved and is explained in detail in the Appendix.

In practice, the only significant difference caused by using Equation (12) in the Appendix is that the solvophobic quadrant is compressed and flattened. There is little impact on the other quadrants, where the interactions between the solute and solvent are highly populated states. The functional group interaction profile for water is shown in Figure 10. There is a broad flat attractive region on the free energy surface for hydrophobic interactions which is consistent with the empirical observation that hydrophobic interaction energies are largely dictated by the surface area of contact and are relatively insensitive to the precise identities of the hydrophobic groups involved.^[3]

7. Solvents with Multiple Hydrogen-Bond Donors and Hydrogen-Bond Acceptors

The analysis above is restricted to solvents that have a single type of hydrogen-bond donor and hydrogen-bond acceptor. To treat systems with more functional groups or mixed solvents, we need to think about the possible solvent–

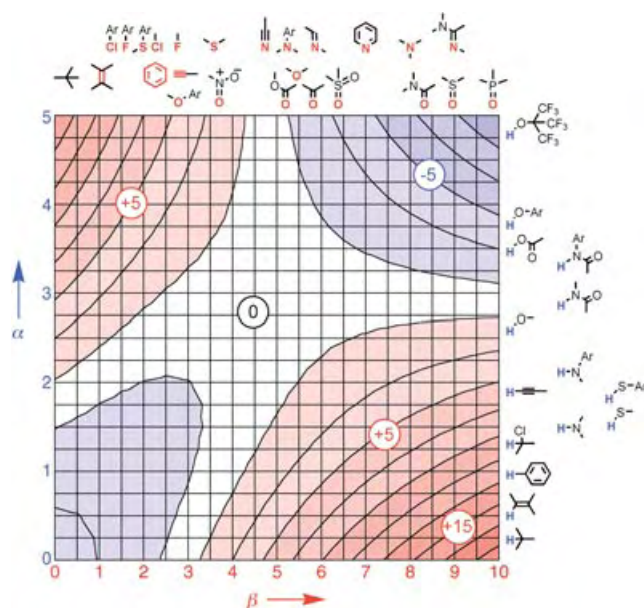


Figure 10. The functional group interaction profile in water ($\alpha_s = 2.8$, $\beta_s = 4.5$). $\Delta\Delta G_{\text{H-bond}}$ (kJ mol^{-1}) calculated by using Equation (12) (see Appendix) is plotted against the range of values of α and β found for neutral functional groups. The structures of a representative set of functional groups are illustrated to calibrate the α and β scale. The contour lines are drawn at 2 kJ mol^{-1} intervals. Blue represents a favorable interaction ($\Delta\Delta G_{\text{H-bond}} < 0$), and red represents an unfavorable interaction ($\Delta\Delta G_{\text{H-bond}} > 0$). The zero point corresponds to $\alpha = \alpha_s$ and $\beta = \beta_s$.

solute interactions that might be present. The solvent molecules will choose to interact with the solute in the most thermodynamically favorable manner, as in Figure 9. In other words, the solvent will maximize its interactions with the solute and consequently minimize the solute–solute interactions. Functional group interaction energies can therefore be evaluated by considering all possible solvent–solute hydrogen-bond interactions and selecting the arrangement that maximizes $\Delta\Delta G_{\text{H-bond}}$ in Equation (12).

Let us consider methanol as a simple example. This has two types of hydrogen-bond donor, the O–H and the C–H group, and one type of hydrogen-bond acceptor, the oxygen atom. The functional group interaction profile that maximizes $\Delta\Delta G_{\text{H-bond}}$ is shown in Figure 11. At each point on the profile, we compare the free energy of the solute–solute interaction using the solvent O–H as the donor with the free energy of the solute–solute interaction using the solvent C–H as the donor and take the least favorable of the two free energies. The hydrogen-bond properties of methanol can be considered to be similar to those of dimethyl ether and water (Figure 7c and Figure 10), and Figure 11 is effectively the combination of the ether and water profiles that maximizes the free energy of interaction. The solvophobic zone in the water profile has been reduced by the ability of the methyl group to compete with weak hydrogen-bond donors, so that the left hand side of the profile looks like that of dimethyl ether. The attractive solute–solute interactions in the dimethyl ether profile have been reduced by the ability of the hydroxy group to compete with good hydrogen-bond donors, so that the right-hand side

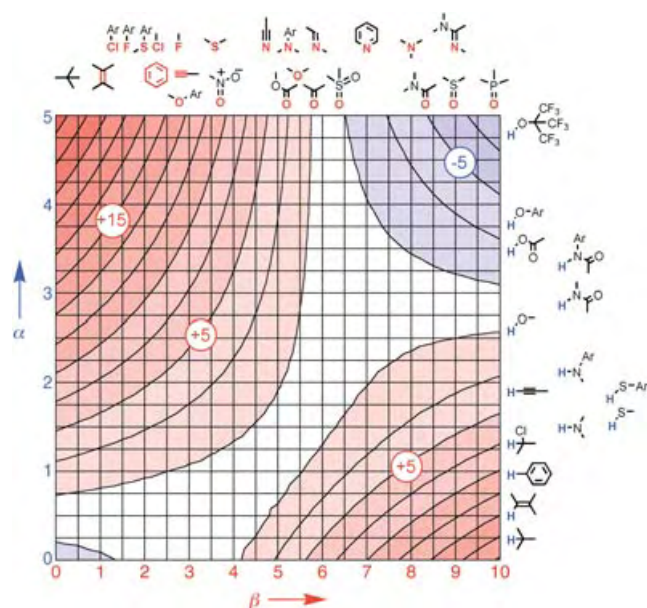


Figure 11. The functional group interaction profile in methanol ($\alpha_s = 0.9$ and 2.7 , $\beta_s = 5.8$). $\Delta\Delta G_{\text{H-bond}}$ (kJ mol^{-1}) was calculated by using Equation (12) (see Appendix) for every possible combination of solvent–solute interactions and the maximum value is plotted against the range of values of α and β found for neutral functional groups. The structures of a representative set of functional groups are illustrated to calibrate the α and β scale. The contour lines are drawn at 2 kJ mol^{-1} intervals. Blue represents a favorable interaction ($\Delta\Delta G_{\text{H-bond}} < 0$), and red represents an unfavorable interaction ($\Delta\Delta G_{\text{H-bond}} > 0$).

of the profile looks like that of water. The conclusion is that the potential for attractive functional group interactions will always be reduced in solvents that have more effective and versatile competitors.

A similar approach could be applied to the analysis of intermolecular interactions in mixtures of solvents. For example, a hypothetical 1:1 mixture of water and dimethyl ether would behave in the same way as methanol, and the functional group interaction profile would look very like that in Figure 11.

8. Solubility

Solubility is a parameter that is governed by many different factors and so is difficult to predict in practice. Nevertheless, the functional group interaction profiles can provide some insight into the solubility properties of organic molecules. Functional groups that make favorable interactions in a given solvent are likely to reduce solubility, whereas unfavorable functional group interactions should lead to increased solubility. In other words, the unfavorable red zones in Figure 6 can be used to predict good solubility, and the favorable blue zones can be used to predict poor solubility. Let us consider a simple example, the solubility of dichloromethane. In Figure 7b–d and Figure 11, the $\text{ClC-H}\cdots\text{Cl}$ interaction lies in the red zone, and so dichloromethane has high solubility in DMSO, chloroform, ether, and methanol. In

Figure 10 on the other hand, the $\text{ClC-H}\cdots\text{Cl}$ interaction lies in the blue solvophobic zone, and dichloromethane consequently has low solubility in water. Similarly, Figure 7c and 7d suggest that chloroform should be a better solvent for primary and secondary amines than dimethyl ether. Chloroform is a better hydrogen-bond donor than an amine, and so the most favorable pairwise interaction in a mixture of chloroform and amine is the $\text{Cl}_3\text{C-H}\cdots\text{N}$ interaction. In contrast, dimethyl ether is a weaker hydrogen-bond acceptor and a weaker hydrogen-bond donor than an amine, so in ether, the most favorable interaction is the amine–amine interaction.

9. Relationship of α and β with Chemical Structure

Hydrogen-bonding properties have often been correlated with $\text{p}K_{\text{a}}$ data. Within a particular functional group class, such as pyridines or phenols, trends in α and β values correlate well with $\text{p}K_{\text{a}}$ values, but over the entire range of functional groups shown in Figure 7, $\text{p}K_{\text{a}}$ is a relatively poor predictor of α and β .^[23] The correlations in Figure 4 are not reproduced by using the corresponding $\text{p}K_{\text{a}}$ values in place of the maxima and minima in the molecular electrostatic potential surface. For example, thiols are much more acidic than alcohols, because they can stabilize the charged anionic state formed on deprotonation, but they are much worse hydrogen-bond donors, because they are less polar. Similarly, pyridine is much more basic than DMSO, but DMSO is a significantly better hydrogen-bond acceptor.

There are no special effects observed for highly polarizable functional groups, providing some justification for the assumptions in Section 2 about the limited role of dispersion and induction. Functional group interactions involving elements of the third period are all relatively weak, as expected from the electrostatic potentials. The trends in the values of α and β shown in Table 3 can be rationalized based on conventional electrostatic arguments. The value of α is determined to a large extent by the net positive charge on the hydrogen-bond donor hydrogen atom. There are more factors that influence the value of β . At a simplistic level, the electrostatic potential at the van der Waals surface of a hydrogen-bond acceptor (E_{min}) is determined by the effective nuclear charge ($n+$), the average separation of the lone pair from the nucleus (r_{e}), and the van der Waals radius (r_{VDW}) as illustrated in Figure 12a.

9.1 Nuclear Charge

β increases along the series $\text{F} < \text{O} < \text{N}$. Figure 12b shows a plot of β versus nuclear charge for trialkyl amine, dialkyl ether and alkyl fluoride (the nuclear charge is taken as the net charge without the valence electrons). There is a clear correlation, but what is most striking is the value of the intercept, $n+ = 8$. This is neon, which as a non-polar noble gas should have a β value of zero. We can also extrapolate the data to a hypothetical neutral carbon lone pair ($n+ = 4$), which would have a β value of 10.5. Although r_{VDW} and r_{e} also

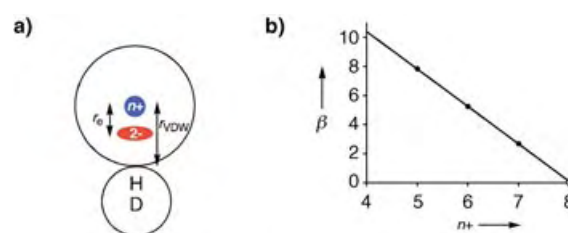


Figure 12. a) The electrostatic potential experienced by a hydrogen-bond donor (DH) at the surface of a hydrogen-bond acceptor is determined by the effective charge on the nucleus ($n+$, blue), the location of the lone pair ($2-$, red, r_{e} from the nucleus), and the van der Waals radius (r_{VDW}). b) A plot of β versus $n+$ for alkyl-N, alkyl-O, and alkyl-F atoms. The nuclear charge was taken as the net charge without the valence electrons. The open circle represents neon ($n+ = 8$), which is completely nonpolar, and so is expected to have a β value of zero.

change along this series, and inductive effects perturb the effective value of $n+$, Figure 12b suggests that the dominant parameter that distinguishes the hydrogen-bond acceptor properties of the second period elements is the nuclear charge.

9.2 Van der Waals Radius

β increases along the series $\text{Se} < \text{S} < \text{O}$. Going down the Periodic Table, the van der Waals radius (r_{VDW}) increases and the lone pairs become more diffuse, so the electrostatic potential is effectively smeared out over a larger area on the surface of the atom (Figure 12a).

9.3 Lone Pair Location

β increases along the series $\text{N}(\text{sp}) < \text{N}(\text{sp}^2) < \text{N}(\text{sp}^3)$. Here the nuclear charge and van der Waals radii do not change significantly, and the dominant factor is the average separation of the lone pair electrons from the nucleus (r_{e}), which decreases in orbitals with more s character (Figure 12a). In many functional groups, more than one of the effects discussed here is important, so for example, sp^2 and sp^3 oxygen hydrogen-bond acceptors have similar β values, because the effect of changing r_{e} is balanced by the increased polarization of the π -electrons (see Section 9.5).

9.4 Electronegativity of Substituents

If we compare oxygen hydrogen-bond acceptors, β for phosphine oxide is larger than β for sulfoxide. This is due to polarization of the bonding electrons towards the oxygen as the electronegativity of the other nucleus decreases. Similarly, hydrogen-bond donor ability increases with the electronegativity of the atom bonded to the hydrogen, so α increases along the series $\text{C-H} < \text{S-H} < \text{N-H} < \text{O-H}$. Hybridization state affects electronegativity, so α increases along the series $\text{C}(\text{sp}^3)\text{-H} < \text{C}(\text{sp}^2)\text{-H} < \text{C}(\text{sp})\text{-H}$. Inductive effects transmit the polarization due to electronegativity differences further through the bonding framework, so hydrogen-bonding properties are modulated by polarizing substituents in a predict-

able manner. Representative data for the effects of methyl and trifluoromethyl groups on the properties of alcohols and ketones are shown in Table 4.^[22b,24] The mutual electron-withdrawing effects of the fluorine substituents in perfluoroalkanes leads to hydrogen-bond acceptor properties that are comparable to those of simple alkanes, and the special properties of these compounds can be in part attributed to this effect (Table 3).

Table 4: Substituent effects on the hydrogen-bonding properties of alcohols and ketones.^[a]

x	y	R _x H _y C-OH		R _x H _y C-Ac	
		R = CF ₃ α	R = CH ₃ α	R = Cl β	R = CH ₃ β
0	3	2.9	2.9	5.7	5.7
1	2	3.7	2.7	4.5	5.8
2	1	4.5	2.7	3.6	5.8
3	0	4.9	2.7	3.1	5.7

[a] The values of α and β were calculated by using Equation (5) and (6) and the literature values^[22b,24] of α₂^H and β₂^H for these compounds.

9.5 Delocalization

The associated changes in electron density modulate the values of α and β accordingly. Thus the amide oxygen atom is a better hydrogen-bond acceptor than a ketone, and the amide NH group is a poorer hydrogen-bond acceptor and a better hydrogen-bond donor than an amine.

9.6 Through-Space Effects

Nearby functional groups can perturb the electrostatic potential surface. The α values for phenol and carboxylic acid are a good example. A carbonyl group is more strongly electron-withdrawing than an aromatic ring, but phenol is a better hydrogen-bond donor than carboxylic acid. The reason is that when a hydrogen-bond acceptor interacts with the OH group, there are long-range through-space interactions with the adjacent CH group of the phenol and the carbonyl group of the carboxylic acid (Figure 13). These secondary electrostatic interactions are most important when the hydrogen-bond donors and hydrogen-bond acceptors are close (that is, separated by one atom) and oriented in the same direction as

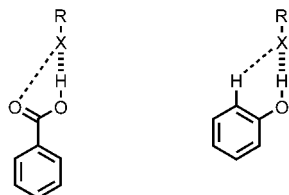


Figure 13. Through-space interactions can significantly perturb the electrostatic potential surface if polar groups are close in space. The secondary electrostatic interactions (dashed line) make phenol a better hydrogen-bond donor than carboxylic acid, which has repulsive secondary electrostatic interactions.

in a carboxylic acid. Secondary electrostatic interactions have been extensively studied in relation to heterocycle base-pairing in chloroform, where each secondary interaction contributes 2–3 kJ mol^{−1} to the free energy of complexation.^[25]

9.7 Configuration

The value of E_{\min} for amines is strongly dependent on the degree of pyramidalization at the nitrogen center, as illustrated in Figure 14a. The pyramidal geometry exposes the lone pair electron density and improves the hydrogen-bond acceptor properties.

9.8 Conformation

Neighboring functional groups can perturb the electrostatic potential surface of a functional group (see Section 9.6),

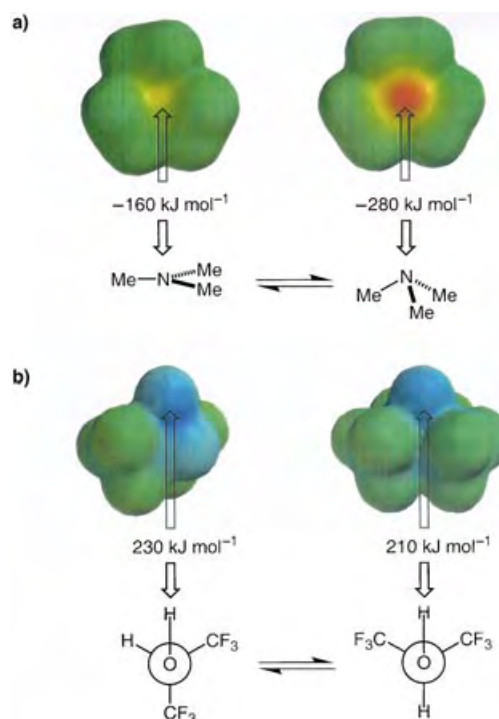


Figure 14. Changes in three-dimensional structure can have a significant influence on the molecular electrostatic potential surface. a) A pyramidal amine is a significantly better hydrogen-bond acceptor than a trigonal amine. The molecular electrostatic potential surfaces of trimethylamine calculated by using AM1 are shown. Negative regions are shown in red (< −280 kJ mol^{−1}), and neutral regions in green. The difference between the two conformations is 120 kJ mol^{−1} which corresponds to a difference of more than 2 on the β scale. b) The molecular electrostatic potential surfaces of hexafluoropropan-2-ol in two different conformations calculated by using AM1. Positive regions are shown in blue (> +230 kJ mol^{−1}), and neutral regions in green. Although the color differences are smaller than in a), the conformation in which the hydroxy group is encumbered by two trifluoromethyl groups is a significantly weaker hydrogen-bond donor (by 0.4 on the α scale).

and through-space effects depend on the precise arrangement of the functional groups. Figure 14b shows how changing the conformation of an alcohol affects the value of E_{\max} . In one conformation, the OH group is exposed, but in the other, it is encumbered by a trifluoromethyl group, and this lowers the electrostatic potential on the molecular surface.

9.9 Proton Transfer

So far, we have dealt exclusively with neutral molecules, but if the pK_a values are appropriate, then proton transfer will take place. Hydrogen-bonding interactions between charged functional groups have not been experimentally quantified in the same way, presumably due to the low solubility of salts in carbon tetrachloride and complications in the analysis of the extent of counterion association.^[26] However, the interactions between a deprotonated acid and a protonated base are likely to be significantly larger than those between the neutral species, and this possibility must always be considered when using this approach.^[27]

10. Conclusions

The analysis presented here allows us to extrapolate from the experimental data on the thermodynamics of hydrogen-bonding interactions in carbon tetrachloride to interactions between a wide range of functional groups in any solvent or the solid state. The functional group interaction profiles provide a benchmark for estimating the magnitudes of intermolecular interactions in the condensed state.

There are limitations. For example, the scatter in the correlations in Figure 4, which we used to set our origin and scale, necessarily introduces approximations. In this analysis, all interactions are treated as a type of hydrogen bond at a single well-defined point on the molecular surface. The conclusions may not extrapolate to functional group combinations that interact over a larger surface area, such as stacked aromatic systems, where the integration of lower electrostatic potentials over a larger area may lead to relatively strong interactions. In such systems, the desolvation term will also be affected by the geometric complementarity and surface area of the solvent–solute interaction.^[12] Analyzing the behavior of more complicated complexes that contain multiple functional group interactions introduces additional factors not considered here. The stability of the complex will be reduced by non-perfect molecular shape complementarity, failure to optimize functional group interaction geometries and restriction of conformational flexibility. Cooperative effects between different functional group interaction sites can lead to more favorable free energies of binding due to secondary functional group interactions, long-range electrostatic interactions, induction caused by bond polarization or conformational changes.

Thus applications of the interaction profiles to predict binding free energies by summing the individual interactions in complicated molecules is problematic. Nevertheless, there have been some significant successes in the use of simple

QSAR parameters for predicting binding free energies of molecular complexes,^[5,18,28] and so there may be potential in such an approach. At the very least, speculation about whether this interaction or that interaction is likely to be the most important in any given system can now be calibrated with a sensible estimate of the associated free energy contributions that are possible.

There are some interesting aspects of analyzing the full functional group interaction space. Consider hydrogen-bonding interactions in water for example. The best hydrogen-bond donors that will not readily ionize in water are NH donors with electron withdrawing substituents, and the best hydrogen-bond acceptors that will not readily protonate in water are oxygen acceptors with electron-donating groups. This is clearly one reason that peptides and the nucleic acid bases have been selected as the biological building blocks of choice. They combine excellent hydrogen-bonding properties with the reliability of not engaging in acid–base reactions, and Figure 10 shows that they make weakly attractive interactions in water. Hopefully, the interaction profiles in this paper will encourage synthetic chemists to think about molecular designs based on the potential interaction free energies that are available from some of the unexplored functional group and solvent combinations.

Appendix: Treatment of the Solvophobic Zone

The equilibrium in Figure 9a can be used to determine the Boltzmann factors that reflect the extent to which the solute–solvent interactions are present in the solvated free state of the hydrogen-bond donor and hydrogen-bond acceptor, χ_α [Eq. (8)] and χ_β [Eq. (9)].

$$\chi_\alpha = \frac{1}{1 + e^{-(\alpha\beta_s - \frac{1}{2}\alpha_s\beta_s)/RT}} \quad (8)$$

$$\chi_\beta = \frac{1}{1 + e^{-(\alpha_s\beta - \frac{1}{2}\alpha_s\beta_s)/RT}} \quad (9)$$

The factor of $1/2$ accounts for the fact that when the solvent does not interact with the solute, it effectively interacts with itself, because it becomes part of the bulk solvent. A similar analysis must be applied to both sides of the equilibrium in Figure 5, and so in the bound state, we also consider to what extent the released solvent interacts with the bulk solvent. Otherwise, the free energy for a water molecule interacting with another water molecule in a solvent of water would be nonzero. Thus χ_s reflects the extent to which solvent–solvent interactions are formed in the bound state [Eq. (10)].

$$\chi_s = \frac{1}{1 + e^{-(\alpha_s\beta_s - \frac{1}{2}\alpha_s\beta_s)/RT}} = \frac{1}{1 + e^{-\frac{1}{2}\alpha_s\beta_s/RT}} \quad (10)$$

If we now consider desolvation of the hydrogen-bond donor in preparation for complexation, the number of solute–solvent interactions lost is χ_α , and therefore in principle, χ_α solvent–solvent interactions should be formed. However, the fraction of solvent–solvent interactions that are populated is χ_s , and so $(1-\chi_s)$ solvent–solvent interactions are never made.

If we allow for the fact that the released solvent becomes part of the bulk solvent and therefore interacts with itself, the number of solvent–solvent interactions that are formed on desolvation of the hydrogen-bond donor is $\frac{1}{2}\{\chi_a - (1 - \chi_s)\}$. The free energy for the equilibrium in Figure 5 can thus be evaluated allowing for the Boltzmann distributions of the solute–solvent and solvent–solvent interactions illustrated in Figure 9a, but assuming that the solute–solvent state that we are interested in is fully bound [Eq. (11)].

$$\begin{aligned}\Delta\Delta G_{\text{H-bond}} &= -\alpha\beta - \frac{1}{2}\{\chi_a - (1 - \chi_s)\}a_s\beta_s - \frac{1}{2}\{\chi_\beta - (1 - \chi_s)\}a_s\beta_s \\ &\quad + \chi_a\alpha\beta_s + \chi_\beta a_s\beta \\ &= -\alpha\beta + \chi_a\alpha\beta_s + \chi_\beta a_s\beta - \left(\frac{1}{2}\chi_a + \frac{1}{2}\chi_\beta + \chi_s - 1\right)a_s\beta_s\end{aligned}\quad (11)$$

The number of solvent–solvent interactions that can be made in the free state is reduced by the steric effects of close contact with the solute, as illustrated in Figure 9b. The solvent and solute are forced to interact to some extent, even if the Boltzmann distribution suggests that they should not. If ϕ is the number of solvent–solvent interactions that are sterically blocked by solute contacts, then only a fraction of the solvent–solute interactions $(1 - \phi)$ can participate in the equilibrium leading to the Boltzmann distribution discussed above. Thus the free energy of formation of a hydrogen bond in solution is given by a composite of the simple expression in Equation (4) (see Section 5) and the more complex Equation (11) [Eq. (12)].

$$\begin{aligned}\Delta\Delta G_{\text{H-bond}} &= -\phi(a - a_s)(\beta - \beta_s) - (1 - \phi)\{\alpha\beta - \chi_a\alpha\beta_s - \chi_\beta a_s\beta \\ &\quad + \left(\frac{1}{2}\chi_a + \frac{1}{2}\chi_\beta + \chi_s - 1\right)a_s\beta_s\}\end{aligned}\quad (12)$$

For which the Equations (13)–(15) are applicable.

$$\chi_a = \frac{1}{1 + e^{-(1-\phi)(\alpha\beta_s - \frac{1}{2}a_s\beta_s)/RT}}\quad (13)$$

$$\chi_\beta = \frac{1}{1 + e^{-(1-\phi)(a_s\beta - \frac{1}{2}a_s\beta_s)/RT}}\quad (14)$$

$$\chi_s = \frac{1}{1 + e^{-\frac{1}{2}(1-\phi)a_s\beta_s/RT}}\quad (15)$$

Equation (12) was used to generate all of the interaction profiles shown here. The only difference between the results obtained by using Equation (4) is that the solvophobic zone is compressed and flattened. The Boltzmann factors come directly from the hydrogen-bond parameters α and β , but the value of ϕ is an independent variable between zero and one that must be obtained by different methods. For the purposes of discussion, ϕ is estimated using water. If we assume close packing of spherical molecules, then about $\frac{1}{12}$ of the surface area of a water molecule that solvates a functional group of similar size is blocked from interaction with other water molecules (Figure 9b). Each water molecule can make a total of four hydrogen bonds, but the fraction of solvent–solvent interactions that are populated is χ_s , as discussed above. Thus the number of water–water hydrogen bonds that are sterically blocked by the solute is $\phi = 4\chi_s/12$. Using the α

and β values for water and Equation (10) gives $\chi_s = 0.93$, so $\phi = 0.3$. This is the value of ϕ that was used to generate the interaction profiles presented here, but the shape of the plots is surprisingly insensitive to the exact value. It is worth noting that the value of χ_s allows us to estimate the number of nearest neighbors in the bulk solvent, $N = (0.93 \times 4) + (0.07 \times 12) = 4.5$. This is consistent with experimental X-ray diffraction measurements on liquid water that give a value of 4.4 for N .

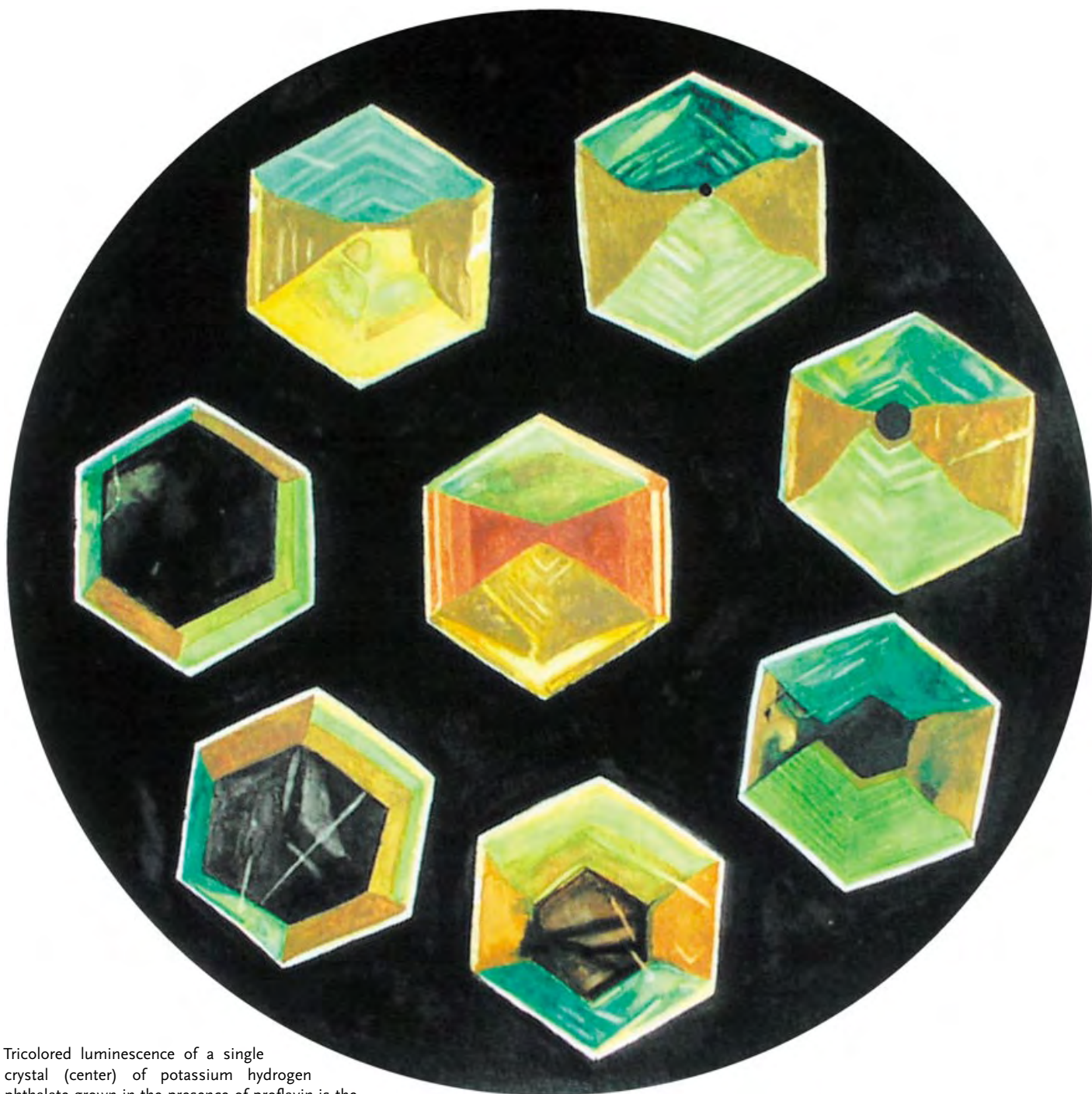
I would like to thank my research group and colleagues, particularly Nick Williams, Pablo Ballester, Jeremy Sanders, and David Leigh, who have contributed to this manuscript through stimulating discussions, as well as the Sheffield undergraduates for their constant encouragement to look for clearer explanations.

Received: December 30, 2003

- [1] a) A. R. Fersht in *Enzyme Structure and Mechanism*, Freeman, New York, **1985**; b) W. P. Jencks in *Catalysis in Chemistry and Enzymology*, Dover, New York, **1987**; c) J. Rebek, *Acc. Chem. Res.* **1990**, *23*, 399–404; d) H. J. Schneider, *Angew. Chem.* **1991**, *103*, 1419–1439; *Angew. Chem. Int. Ed. Engl.* **1991**, *30*, 1417–1436; e) F. Vogtle in *Supramolecular Chemistry*, Wiley, New York, **1991**; f) J. M. Lehn in *Supramolecular Chemistry*, VCH, Weinheim, **1995**; g) J. C. Ma, D. A. Dougherty, *Chem. Rev.* **1997**, *97*, 1303–1324; h) C. G. Claessens, J. F. Stoddart, *J. Phys. Org. Chem.* **1997**, *10*, 254–272; i) W. W. Cleland, P. A. Frey, J. A. Gerlt, *J. Biol. Chem.* **1998**, *273*, 25 529–25 532; j) W. W. du Mont, F. Ruthe, *Coord. Chem. Rev.* **1999**, *189*, 101–133; k) A. M. Davis, S. J. Teague, *Angew. Chem.* **1999**, *111*, 778–792; *Angew. Chem. Int. Ed.* **1999**, *38*, 736–749; l) J. W. Steed, J. L. Atwood in *Supramolecular Chemistry*, Wiley, Chichester, **2000**; m) H. J. Schneider, A. Yatsimirsky in *Principles and Methods in Supramolecular Chemistry*, Wiley, Chichester, **2000**; n) C. A. Hunter, K. R. Lawson, J. Perkins, C. J. Urch, *J. Chem. Soc. Perkin Trans. 2* **2001**, 651–669; o) T. Lazaridis, *Acc. Chem. Res.* **2001**, *34*, 931–937; p) T. Steiner, *Angew. Chem.* **2002**, *114*, 50–80; *Angew. Chem. Int. Ed.* **2002**, *41*, 48–76; q) E. A. Meyer, R. K. Castellano, F. Diederich, *Angew. Chem.* **2003**, *115*, 1244–1287; *Angew. Chem. Int. Ed.* **2003**, *42*, 1210–1250.
- [2] a) M. J. Stone, *Acc. Chem. Res.* **2001**, *34*, 379–388; b) D. H. Williams, D. P. O'Brien, B. Bardsley, *J. Am. Chem. Soc.* **2001**, *123*, 737–738; c) C. T. Calderone, D. H. Williams, *J. Am. Chem. Soc.* **2001**, *123*, 6262–6267; d) F. P. Schmidtchen, *Chem. Eur. J.* **2002**, *8*, 3522–3529; e) K. N. Houk, A. G. Leach, S. P. Kim, X. Zhang, *Angew. Chem.* **2003**, *115*, 5020–5046; *Angew. Chem. Int. Ed.* **2003**, *42*, 4872–4897.
- [3] a) C. Tanford in *The Hydrophobic Effect: Formation of Micelles and Biological Membranes*, Wiley, New York, **1973**; b) B. Lee, *Proc. Natl. Acad. Sci. USA* **1991**, *88*, 5154–5158; c) N. T. Southall, K. A. Dill, A. D. J. Haymet, *J. Phys. Chem. B* **2002**, *106*, 521–533.
- [4] M. S. Searle, D. H. Williams, *J. Am. Chem. Soc.* **1992**, *114*, 10690–10697.
- [5] a) W. P. Jencks, *Proc. Natl. Acad. Sci. USA* **1981**, *78*, 4046–4050; b) P. R. Andrews, D. J. Craik, J. L. Martin, *J. Med. Chem.* **1984**, *27*, 1648–1657; c) A. Matouschek, A. R. Fersht, *Methods Enzymol.* **1991**, *202*, 82–112; d) H. J. Schneider, *Chem. Soc. Rev.* **1994**, *23*, 227–234; e) D. H. Williams, M. S. Westwell, *Chem. Soc. Rev.* **1998**, *27*, 57–63; f) C. A. Hunter, P. S. Jones, P. Tiger, S. Tomas, *Chem. Eur. J.* **2002**, *8*, 5435–5446.

- [6] M. Rigby, E. B. Smith, W. A. Wakeham, G. C. Maitland in *The Forces Between Molecules*, Clarendon, Oxford, **1986**.
- [7] Sometimes a fifth component, the charge transfer interaction, is considered, but for most organic molecules, the magnitudes of such effects are negligible in the ground state of a complex.
- [8] A. P. Bisson, C. A. Hunter, J. C. Morales, K. Young, *Chem. Eur. J.* **1998**, *4*, 845–851.
- [9] J. Jadzyn, M. Stockhausen, B. Zywucki, *J. Phys. Chem.* **1987**, *91*, 754–757.
- [10] a) J. C. Slater, J. G. Kirkwood, *Phys. Rev.* **1931**, *37*, 682–697; b) *CRC handbook of Chemistry and Physics*, 72nd ed. (Ed.: D. R. Lide), CRC, Boca Raton, FL, **1991**.
- [11] The values for hydrogen are not included in Table 2, due to uncertainties in defining the relevant surface area.
- [12] There are some special cases where the geometry of a binding pocket prevents solvation, and here, dramatic enhancements in the association constant are observed, because the solvent is unable to compensate for the gain in solute–solute dispersion interactions. K. T. Chapman, W. C. Still, *J. Am. Chem. Soc.* **1989**, *111*, 3075–3077.
- [13] S. Tsuzuki, K. Tanabe, *J. Phys. Chem.* **1991**, *95*, 2272–2278.
- [14] M. H. Abraham, J. A. Platts, *J. Org. Chem.* **2001**, *66*, 3484–3491.
- [15] L. Pauling, *Proc. Natl. Acad. Sci. USA* **1928**, *14*, 359.
- [16] a) H. Hagelin, J. S. Murray, T. Brinck, M. Berthelot, P. Politzer, *Can. J. Chem.* **1995**, *73*, 483–488; b) J. C. Dearden, T. Ghafourian, *J. Chem. Inf. Comput. Sci.* **1999**, *39*, 231–235; c) J. A. Platts, *Phys. Chem. Chem. Phys.* **2000**, *2*, 973–980; d) J. A. Platts, *Phys. Chem. Chem. Phys.* **2000**, *2*, 3115–3120; e) A. M. Zissimos, M. H. Abraham, A. Klamt, F. Eckert, J. Wood, *J. Chem. Inf. Comput. Sci.* **2002**, *42*, 1320–1331.
- [17] M. I. Page, W. P. Jencks, *Proc. Natl. Acad. Sci. USA* **1971**, *68*, 1678–1683.
- [18] H.-J. Bohm, *J. Comput.-Aided Mol. Des.* **1994**, *8*, 243–256.
- [19] a) F. H. Westheimer, L. L. Ingraham, *J. Phys. Chem.* **1956**, *60*, 1668; b) H. L. Anderson, *Inorg. Chem.* **1994**, *33*, 972–981; c) H. L. Anderson, S. Anderson, J. K. M. Sanders, *J. Chem. Soc. Perkin Trans. 1* **1995**, 2231–2245; d) X. Chi, A. J. Guerin, R. A. Haycock, C. A. Hunter, L. D. Sarson, *J. Chem. Soc. Chem. Commun.* **1995**, 2563–2565.
- [20] For the functional groups described in reference [14] the simplest molecule containing the relevant functional group was constructed by using Spartan'02 (Wavefunction, Inc., Irvine CA), for example, methyl acetate was used to calculate the properties of the ester. The molecules were optimized by using AM1, and the maxima and minima in the molecular electrostatic potential surface were determined.
- [21] Dimethyl ether was used to calculate the interaction profile, because it contains only one type of hydrogen-bond donor and one type of hydrogen-bond acceptor. However, the assumption is that the diethyl ether profile, which is more relevant to experiments at room temperature, is very similar.
- [22] a) M. H. Abraham, P. L. Grellier, D. V. Prior, R. W. Taft, J. L. Morris, P. J. Taylor, C. Laurence, M. Berthelot, R. M. Doherty, M. J. Kamlet, J.-L. Abboud, K. Sraidi, G. Guiheneuf, *J. Am. Chem. Soc.* **1988**, *110*, 8534; b) J. Marco, J. M. Orza, R. Notario, J.-L. M. Abboud, *J. Am. Chem. Soc.* **1994**, *116*, 8841–8842; c) M. H. Abraham, M. Berthelot, C. Laurence, P. J. Taylor, *J. Chem. Soc. Perkin Trans. 2* **1998**, 187–191.
- [23] a) J. Rubin, B. Z. Senkowski, G. S. Panson, *J. Phys. Chem.* **1964**, *68*, 1601–1602; b) J. Rubin, G. S. Panson, *J. Phys. Chem.* **1965**, *69*, 3089–3091; c) R. W. Taft, D. Gurka, L. Joris, P. von R. Schleyer, J. W. Rakshys, *J. Am. Chem. Soc.* **1969**, *91*, 4801–4808; d) M. J. Kamlet, J. F. Gal, P. C. Maria, R. W. Taft, *J. Chem. Soc. Perkin Trans. 2* **1985**, 1583–1589.
- [24] F. Besseau, M. Lucon, C. Laurence, M. Berthelot, *J. Chem. Soc. Perkin Trans. 2* **1998**, 101–107.
- [25] a) W. L. Jorgensen, J. Pranata, *J. Am. Chem. Soc.* **1990**, *112*, 2008–2010; b) T. J. Murray, S. C. Zimmerman, *J. Am. Chem. Soc.* **1992**, *114*, 4010–4011; c) J. Sartorius, H. J. Schneider, *Chem. Eur. J.* **1996**, *2*, 1446–1452.
- [26] C. A. Hunter, C. M. R. Low, C. Rotger, J. G. Vinter, C. Zonta, *Chem. Commun.* **2003**, 834–835.
- [27] M. W. Hosseini, *Coord. Chem. Rev.* **2003**, *240*, 157–166.
- [28] a) H. J. Schneider, V. Rudiger, O. A. Raevsky, *J. Org. Chem.* **1993**, *58*, 3648–3653; b) H. Gohlke, G. Klebe, *Angew. Chem.* **2002**, *114*, 2764–2798; *Angew. Chem. Int. Ed.* **2002**, *41*, 2645–2676.

Communications



Tricolored luminescence of a single crystal (center) of potassium hydrogen phthalate grown in the presence of proflavin is the inspiration for the water color by Leonel Vasquez. The surrounding images show 200- μm slices of the crystal (which was cut from the bottom and photographed by Jason Benedict). In their Communication on the following pages, M. Brustolon, B. Kahr, A. L. Rohl, and co-workers describe how luminophores respond to the surface charge of growing crystal faces.

Crystal Growth

Luminescent Probes of Crystal Growth: Surface Charge and Polar Axis Sense in Dye-Doped Potassium Hydrogen Phthalate**

Antonio Barbon, Marco Bellinazzi, Jason B. Benedict, Marina Brustolon,* Sean D. Fleming, Sei-Hum Jang, Bart Kahr,* and Andrew L. Rohl*

Luminescent labels have been a mainstay of biological chemists eager to illuminate specific noncovalent interactions.^[1] Crystal growth from solution is also controlled by specific noncovalent interactions, but luminescent probes have not been used likewise. Unlike rhodamine or green fluorescent protein covalently tethered to a protein in a cell and dangled into the cytoplasm, close packed crystals do not have the space, according to conventional wisdom, to accommodate such labels. It is now well established that crystal growth far from equilibrium can drive mixed crystal formation even when guest molecules are many times larger than those of the host.^[2] We take advantage of a luminescent probe to visualize the specificity of a guest for growing crystal faces of potassium hydrogen phthalate (commonly abbreviated as KAP for potassium acid phthalate). We have interpreted our experimental observations with calculated molecular electrostatic potential surfaces (EPS), yet another device widely used by biochemists, in this case to evaluate ligand docking sites,^[3] that has rarely^[4] found application in studies of crystal growth because of the difficulties associated with evaluating the electrostatic potential of a periodic surface. Using experiment and theory in tandem, we show

how dyes respond to the surface charges of KAP while at the same time establishing the absolute sense of its polar axis.

KAP crystals grow from aqueous solution by spontaneous nucleation at room temperature as {010} plates with the following additional forms: {111}, {11 $\bar{1}$ }, {110}, and occasionally {121}.^[5] They are built of alternating bilayers of potassium ions and polar herringbone arrays of hydrogen phthalate ions stacked along [010] in the space group *Pca*2₁ (Figure 1). The sense of the polar [001] axis, to which all (*hkl*) indices refer, has been assigned by anomalous scattering of X-rays.^[6] The Bijvoet method was similarly applied to all of the mixed crystals described herein.

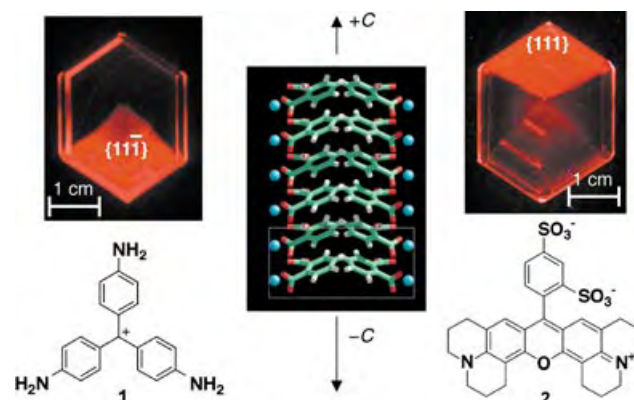


Figure 1. Images of black light (366 nm) irradiated KAP crystals grown in the presence of **1** and **2**. The crystals are similarly oriented with respect to the polar axis indicated in the view of the lattice along [100].

KAP crystals orient and overgrow more than 100 dyes in micromolar concentrations.^[7,8] Dyed crystals typically show patterns of color consistent with facets that have different affinities for the luminophores. Dyes are thus contained in polyhedral growth sectors, subvolumes of the crystals that have grown through particular faces.^[2] Two representative mixed crystals containing basic fuchsin (**1**) and sulfurhodamine 101 (**2**) are shown in Figure 1. We have observed that cations such as **1** primarily recognize {11 $\bar{1}$ } growth sectors while anions such as **2** tend to recognize {111}. These findings cannot be reduced to firm rules. Several puzzling exceptions have been observed, most notably 3,6-diaminoacridine (**3**), the focus of this work, that decorates KAP to form remarkable “tricolore” crystals.

With **1** and **2**, only one end of each KAP mixed crystal is luminescent (Figure 1), which reveals the presence of a polar axis. Other chemical methods for assigning the sense of a polar axis include reactions with gases,^[9] the Kundt powder test in pyroelectric crystals,^[10] and changes in crystal habit, surface topography, and symmetry with so-called “tailor-made additives” of known activity.^[11] Given the sensitivity of luminescence, mixed crystal formation with fluorescent probes is an attractive alternative.

To understand the selectivity of **1** and **2** for KAP, we first determined the energetically stable surfaces that correspond to the (111), (11 $\bar{1}$), and (110) faces. For any given set of indices (*hkl*), there can be a number of discrete surfaces, especially

[*] Dr. A. Barbon, M. Bellinazzi, Prof. M. Brustolon
Dipartimento di Chimica Fisica
Università di Padova
Via Loredan 2, 35131 Padova (Italy)
Fax: (+39) 049-827-5135
E-mail: m.brustolon@chfi.unipd.it

J. B. Benedict, Dr. S.-H. Jang, Prof. B. Kahr
Department of Chemistry
University of Washington
Box 351700, Seattle, WA 98195-1700 (USA)
Fax: (+1) 206-685-8665
E-mail: kahr@chem.washington.edu

Dr. S. D. Fleming, Assoc. Prof. A. L. Rohl
Nanochemistry Research Institute
Curtin University of Technology
PO Box U 1987, Perth, 6845 (Australia)
Fax: (+61) 8-9266-4699
E-mail: andrew@power.curtin.edu.au

[**] This work was supported by the US National Science Foundation, the Petroleum Research Fund of the American Chemical Society, the Italian Ministry of Universities and Research by the FIRB program (Nano-organizzazione di molecole ibride inorganiche/organiche con proprietà magnetiche ed ottiche), the Government of Western Australia via the Premier's Research Fellowship Program, and the Australian Research Council by the International Researcher Exchange (IREX) scheme.

for multicomponent crystals. It is well established for simple salts that the electrostatic contribution to the lattice energy is dominant; others have used only the electrostatic contribution to study surface energetics.^[12] This approximation facilitates the quick evaluation of stable surfaces and their electrostatic potentials for any salt without going through the intensive process of deriving a force field. With the program GULP,^[13] we calculated the attachment energies of all surface terminations of the (111), (11 $\bar{1}$), and (110) faces by using the partial charges from the CVFF force field.^[14] We then calculated the EPS for the stable faces by using our GDIS open source code.^[15,16] The basis for the preponderance of anions recognizing (111) and cations recognizing (11 $\bar{1}$) is immediately evident in the EPS (Figure 2); the former is exclusively positive whereas the latter is exclusively negative. The (110) is comparatively neutral; symmetry requires no net charge but the molecular surface is slightly negative.

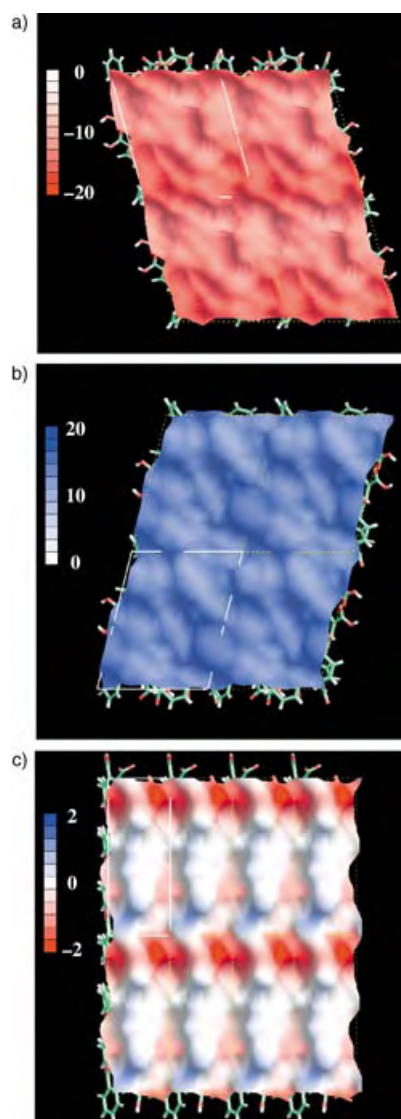


Figure 2. EPS for the stable terminations of a) (11 $\bar{1}$), b) (111), and c) (110) surfaces of KAP. Red regions are areas of negative potential and blue regions positive potential in units of electron volts. Note that the maximum values for (c) are ten times smaller than that of (a) and (b).

Can EPS explain the activities of probes such as **3** (Figure 3), which has distinct properties after having associated with each of the principal faces? Compound **3** recognizes both ends of the KAP polar axis and the (110) face in different

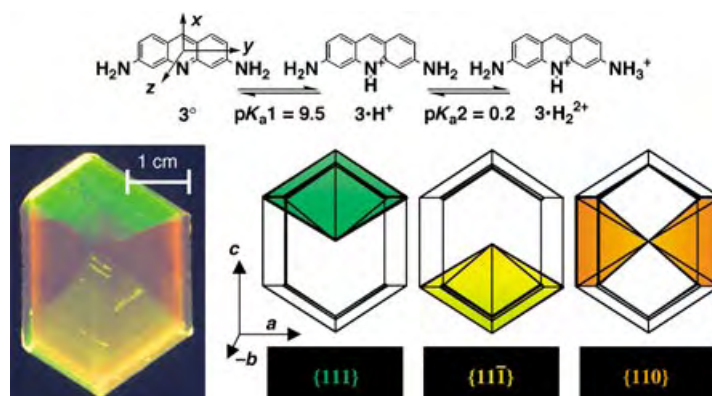


Figure 3. Top: protonation scheme for **3**. Bottom: fluorescence image of a KAP crystal grown in the presence of **3** with idealized representations of the event indicating the growth sectors and their respective colors of luminescence.

states that are easily distinguished by the colors of light the growth sectors emit (Figure 3). Presumably **3** was overgrown in different states of protonation including the commonly observed forms: neutral (**3**⁰), monocation (**3**·H⁺), and dication, (**3**·H₂²⁺).

The visible λ_{max} for the {110} and {111} sectors are 481 and 460 nm, respectively (Figure 4).^[17–19] The corresponding spec-

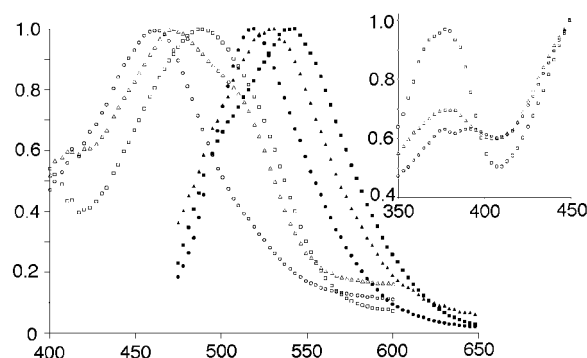


Figure 4. Absorption (open) and luminescence (solid) spectra for the individual {111} (○), {111} (△), and {110} (□) sectors of KAP with **3**.

trum for the {11 $\bar{1}$ } sector is a superposition of the two bands characteristic of {110} and {111}. The peak at 460 nm is characteristic of **3**·H⁺, the predominant solution species at neutral pH, while the species absorbing at 481 nm has been assigned to **3**·H₂²⁺. A characteristic companion peak in the near UV only found in the {11 $\bar{1}$ } and {110} further supports assignment of the latter.^[18] The corresponding photoluminescence energies were 519, 531, and 542 nm for {111}, {11 $\bar{1}$ }, and {110}, respectively.^[17,20]

How can we use the electrostatic potentials to rationalize the photophysics of the mixed crystals? Sensibly, we can say that the strongly negative (11 $\bar{1}$) surface adsorbs any cation,

$3\cdot\text{H}^+$ or $3\cdot\text{H}_2^{2+}$. The slightly negative (110) attracts only the dication; for an electrostatic interaction to be substantive either the field or the corresponding charge must be large. Furthermore, the (110) face contains areas of negative potential separated by 6.5 Å, which closely matches the two primary sites of positive charge on $3\cdot\text{H}_2^{2+}$. Why then does the strongly electropositive surface adsorb $3\cdot\text{H}^+$ at all?

To refine our understanding of the orientation of **3** in KAP, we turned to a time-resolved electron paramagnetic resonance (TREPR) analysis of its photo-excited triplet states.^[21] EPR lines are typically narrow relative to the overall spectral dispersion, thus enabling the identification of subpopulations not detected in electronic spectroscopy.^[22]

The {110} sector that contained only the dication was EPR silent. For the {111} and $\{11\bar{1}\}$ sectors, more than a dozen distinct triplet orientations were detected, though in each case a single orientation was predominant, which was five times more intense than any other. The elements of the zero-field splitting (ZFS) tensors that represent the dipolar couplings of the unpaired electrons in the triplet states could be extracted by a first-order fit of the angular dependencies of the spectral splittings in the principal planes. The presence of magnetically inequivalent sites in the crystal structure gives rise to a doubling of curves that become isochronous when the field is along a crystallographic axis. Each curve can be matched with two different curves in another plane giving rise to ZFS tensors, whose off diagonal elements differ in sign. This ambiguity was resolved by comparing the two sets of principal values with those obtained from the spectra of glasses and powders of individual sectors. The eigenvalues for one of the two magnetically inequivalent sites for {111} and $\{11\bar{1}\}$ are reported in Table 1.

Table 1: Eigenvalues (D_i) in Gauss (± 10 G) of ZFS tensors.

	X	Y	Z
{111}	−43	−361	402
$\{11\bar{1}\}$	−28	−390	418
aprotic	−140	−334	474
pH 12	−133	−344	477
pH 5	−71	−412	483
pH 2	−55	−365	410

The principal directions X , Y , and Z can be assigned to the molecular axes, as shown in Figure 3, on the basis of experimental and calculated results for similar triplet systems.^[23] The eigenvectors (Figure 5) indicate distinct orientations within KAP. In $\{11\bar{1}\}$ the mean plane of **3** is almost parallel (20°) to one of the symmetry related faces, whereas in {111} the molecular plane is nearly perpendicular (87°) to its respective face. Edge approach in the latter case minimizes repulsive electrostatic interactions, thus enabling adsorption of a cation to a formally positive surface.^[24] TREPR spectra in disordered frozen matrices of 1:1 propionitrile/butyronitrile (PBCN) and 1:4 glycerol/water were obtained at various pHs (Table 1). The crystal data most closely resemble those from low pH glasses, which suggests that the signals in {111} and $\{11\bar{1}\}$ are from $3\cdot\text{H}_2^{2+}$, the predominant triplet species at $\text{pH} < 4$.^[17] These data seem to contradict the absorbance that

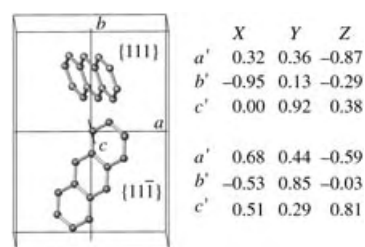


Figure 5: The orientation of the acridine nucleus of **3** in the KAP unit cell derived from the eigenvectors (right) of TREPR data. The prime symbol on the axes in the eigenvector tables indicates a normalized unit cell length.

indicates that $3\cdot\text{H}^+$ is the predominant species in {111}; however, the $3\cdot\text{H}_2^{2+}$ triplet signal arises as a result of excited-state protonation.^[25] Excitation and subsequent protonation of the $3\cdot\text{H}^+$ ground state leads to the formation of a long-lived triplet, presumably a consequence of an energy barrier for deprotonation, thus allowing the molecule to return to the $3\cdot\text{H}^+$ ground state. After excitation, molecules initially in the $3\cdot\text{H}_2^{2+}$ ground state return to their starting configuration at rates faster than excited-state proton transfer or intersystem crossing. Hence, the {110} sectors that contain only $3\cdot\text{H}_2^{2+}$ remain EPR silent.

Given recent advances in, and adoption of, sensitive light detectors,^[26] there is every reason to expect that luminescent probes of noncovalent chemistry during crystal growth from solution can be as revealing as they are in illuminating associations that underlie biological chemistry. First, we must learn to translate the language in which the probes are broadcasting their information.

Received: January 23, 2004

Revised: June 9, 2004 [Z53839]

Keywords: crystal growth · electrostatic interactions · EPR spectroscopy · luminescence · luminescent probes

- [1] See for example, V. J. Allan, *Protein Localization by Fluorescence Microscopy: A Practical Approach*, Oxford University Press, Oxford, 2000.
- [2] B. Kahr, R. W. Gurney, *Chem. Rev.* **2001**, 101, 893.
- [3] M. T. Neves-Petersen, S. B. Petersen, *Biotechnol. Annu. Rev.* **2003**, 9, 315.
- [4] Z. Berkovitch-Yellin, *J. Am. Chem. Soc.* **1985**, 107, 8239.
- [5] The crystal-growing solution was prepared by dissolving A.C.S. grade KAP (Aldrich) in deionized water (Barnsted NANOpure, $18.2 \text{ M}\Omega \text{ cm}^{-1}$). Compound **3** (Aldrich) was initially dissolved in a minimal amount of MeOH, then added to the growth solution. Crystals were indexed with a Stoe 2-circle Model J optical goniometer and a Nonius KappaCCD diffractometer.
- [6] T. A. Eremina, N. G. Furmanova, L. F. Malakhova, T. M. Okhrimenko, V. A. Kuznetsov, *Crystallogr. Rep.* **1993**, 38, 554.
- [7] Absorbance measurements of a dissolved crystal grown from 10^{-4} m dye solutions (m is moles of dye kg^{-1} of host) indicated that the concentration of **1** in the $\{11\bar{1}\}$ sector of the crystal was 10^{-5} m .
- [8] J. B. Benedict, P. M. Wallace, P. J. Reid, S.-H. Jang, B. Kahr, *Adv. Mater.* **2003**, 15, 1068–1070.
- [9] D. Y. Curtin, I. C. Paul, *Chem. Rev.* **1981**, 81, 525.

- [10] W. T. Pennington, S. Chakraborty, I. Paul, D. Y. Curtin, *J. Am. Chem. Soc.* **1988**, *110*, 6498.
- [11] L. Addadi, Z. Berkovitch-Yellin, I. Weissbuch, M. Lahav, L. Leiserowitz, *Top. Stereochem.* **1986**, *16*, 1; I. Weissbuch, R. Popovitz-Biro, M. Lahav, L. Leiserowitz, *Acta Crystallogr. Sect. B* **1995**, *51*, 115.
- [12] P. Hartman, W. G. Perdok, *Acta Crystallogr.* **1955**, *8*, 525; C. F. Woensdregt, *Phys. Chem. Miner.* **1992**, *19*, 59.
- [13] J. D. Gale, A. L. Rohl, *Mol. Simul.* **2003**, *29*, 291.
- [14] Cerius² Version 4.0, Molecular Simulations Inc., San Diego, **1999**.
- [15] <http://gdis.sf.net>.
- [16] Molecular surfaces were calculated by using an iterative triangle subdivision to refine an approximate starting mesh, an adaptation of the Gaussian molecular surface (J. A. Grant, B. T. Pickup, *J. Phys. Chem.* **1995**, *99*, 3503). GULP evaluated the electrostatic potentials at each point, a task requiring 2D Ewald sums.
- [17] Molar absorptivities were determined with a Hitachi U-2000 spectrophotometer controlled by the Spectracalc program (Galactic Industries). Crystal absorption spectra were obtained with SpectraCode Multipoint Absorbance Imaging (MAI-20) Microscope. KAP has perfect (010) cleavage, hence plane parallel sections are easily prepared by isolating individual sectors. The extinction directions of the crystals were used to orient the sample relative to the input polarization.
- [18] G. R. Haugen, W. H. Melhuishi, *J. Chem. Soc. Faraday Trans. 1964*, *60*, 386; M. Pileni, M. Graetzel, *J. Phys. Chem.* **1980**, *84*, 2402; K. Yamaoka, M. Shimadzu, *Bull. Chem. Soc. Jpn.* **1983**, *56*, 55; R. A. Schoonheydt, J. Cenens, F. C. De Schrijver, *J. Chem. Soc. Faraday Trans. 1* **1986**, *82*, 281; R. Ramaraj, D. Rachel Jeyanthi, C. Srinivasan, *Indian J. Chem. Sect. A* **1991**, *30*, 1044.
- [19] Swift and coworkers have recently described 3-H^+ in single crystals of uric acid. See: D. A. Fink, R. E. Sours, J. A. Swift, *Chem. Mater.* **2003**, *15*, 2718.
- [20] Solid-state fluorescence measurements were made by using the Fluoromax-2 fiber-optically coupled to an IMT-2 inverted Olympus microscope.
- [21] Pieces of individual growth sectors were removed with a wet wire saw and mounted on quartz rods along the three crystallographic axes. TREPR experiments were realized by generating triplet excited states with a Nd-YAG laser equipped with harmonic generators and an optical parametric oscillator. Light pulses (5 ns wide, 1 mJ/shot, 10 Hz) were conveyed to the high quality factor (Q) dielectric cavity through a window in the cryostat (Oxford CF935) of a Bruker 380E EPR spectrometer. The pure absorptive EPR signal generated under continuous microwave irradiation was taken from the detector, preamplified and digitalized from a LeCroy 3560 digital oscilloscope. The response time of the apparatus was estimated to be around 800 ns. A surface was obtained by acquiring 50 sweeps of the time decay traces at each field position. Integration with time windows of around 400 ns maximized the transient signal (1 μ s after the laser flash). The spectra in frozen solutions were acquired at 80 K. All EPR samples were irradiated at a wavelength of 465 nm at 230 K. Spin polarized spectra were recorded every 7.5° by rotating the crystals around the principal axes.
- [22] R. W. Gurney, C. Mitchell, L. Bastin, S. Ham, B. Kahr, *J. Phys. Chem. B* **2000**, *104*, 878.
- [23] R. Furrer, J. Gromer, A. Kacher, M. Schwoerer, H. C. Wolf, *Chem. Phys.* **1975**, *9*, 445.
- [24] In 3-H_2^{2+} principal directions might be significantly rotated with respect to symmetry-constrained 3-H^+ .
- [25] M.-P. Pileni, M. Graetzel, *J. Phys. Chem.* **1980**, *84*, 2402.
- [26] W. E. Moerner, D. P. Fromm, *Rev. Sci. Instrum.* **2003**, *74*, 3597.

Arylamine-Substituted Hexa-*peri*-hexabenzocoronenes: Facile Synthesis and Their Potential Applications as “Coaxial” Hole-Transport Materials**

Jishan Wu, Martin Baumgarten, Michael G. Debije, John M. Warman, and Klaus Müllen*

Organic semiconductors for hole injection, hole transport, and photoconduction are needed in thin-film electronics, such as organic light-emitting diodes (OLEDs),^[1] solar cells,^[2] field-effect transistors (FET),^[3] and photorefractive systems.^[4] Triarylamines are particularly useful because of their ability to transport positive charge via their radical cations.^[5] Hexa-*peri*-hexabenzocoronenes (HBC) have recently been introduced as discotic liquid-crystalline materials which display high charge-carrier mobility along their one-dimensional π -stacks.^[6] Herein, a series of novel hole transport materials **1–5** is described in which HBC is peripherally substituted with arylamine moieties. They are shown to adopt a columnar stacking owing to the strong π - π interactions between the HBC cores, and thus allow charge-carrier transport by both the HBC and arylamine moieties in a coaxial supramolecular array (Scheme 1). The oxidative formation of radical cations and higher charged cations raises questions as to the intramolecular spin-spin interactions and suggests a comparison between the HBC (superbenzene) and the corresponding, much smaller benzene species.^[7,8]

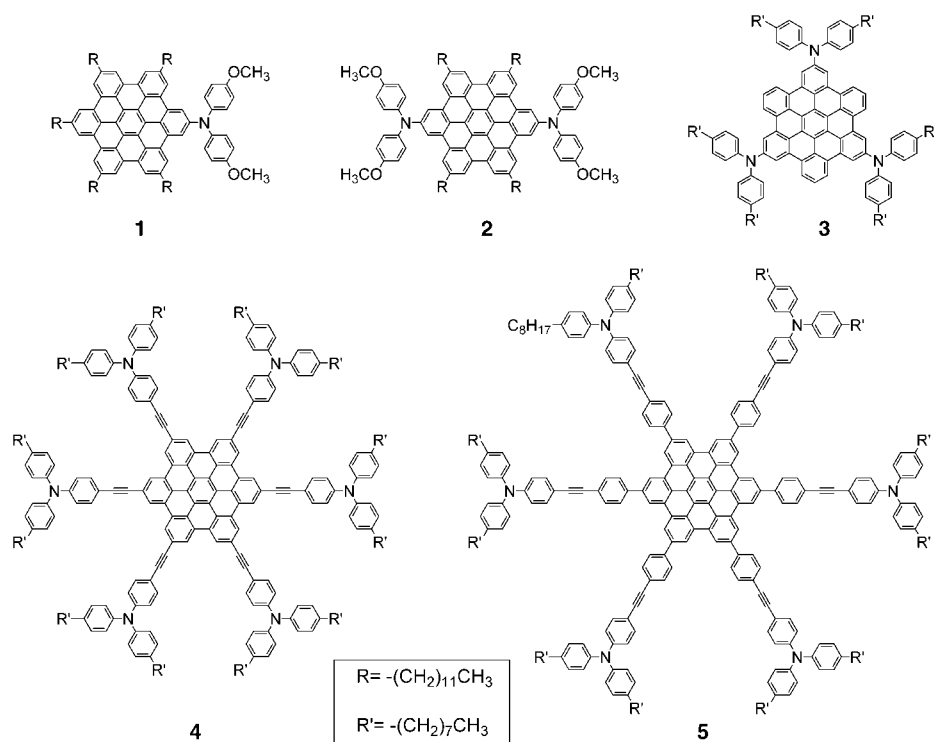
Our synthesis of HBC materials by oxidative cyclodehydrogenation of appropriately substituted hexaphenylbenzene precursors is not applicable owing to the radical cation formation at the nitrogen centers.^[8] An alternative approach is by palladium-catalyzed Buchwald–Hartwig coupling^[9] starting from the planarized HBC building blocks carrying bromo or iodo substituents. Thus, the mono- and bis- di(4-methoxyphenyl)amino-substituted HBCs (**1** and **2**) were synthesized by aryl amination between bis(4-methoxyphenyl)amine and the related mono- and dibromo HBC^[10] in 65 % and 76 % yield, respectively (see Supporting Infor-

[*] Dr. J. Wu, Dr. M. Baumgarten, Prof. Dr. K. Müllen
Max-Planck-Institut für Polymerforschung
Ackermannweg 10, 55128 Mainz (Germany)
Fax: (+49) 6131-379-350
E-mail: muellen@mpip-mainz.mpg.de
Dr. M. G. Debije, Prof. Dr. J. M. Warman
IRI, Delft University of Technology
Mekelweg 15, 2629 JB Delft (The Netherlands)

[**] This work was financially supported by the Zentrum für Multifunktionelle Werkstoffe und Miniaturisierte Funktionseinheiten (BMBF 03N 6500), the Deutsche Forschungsgemeinschaft (Schwerpunkt Organische Feldeffekttransistoren, as well as the EU project DISCELS (G5RD-CT-2000-00321) and MAC-MES (Grd2-2000-30242).



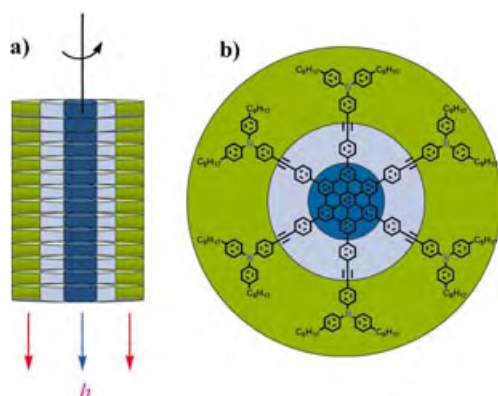
Supporting information for this article is available on the WWW under <http://www.angewandte.org> or from the author.



virtually insoluble HBC building block hexakis(4-iodophenyl)-*peri*-hexabenzocoronene (**6**) appeared highly reactive during the palladium catalyzed Hagi-hara–Sonogashira coupling reactions^[12] to afford a series of soluble HBC materials which are highly ordered liquid crystals or carry electroactive substituents, such as the HBC derivative **5**. Herein, two new insoluble building blocks **7** and **8**, are introduced and utilized for the synthesis of the corresponding tris (**3**)- and hexamines (**4**).

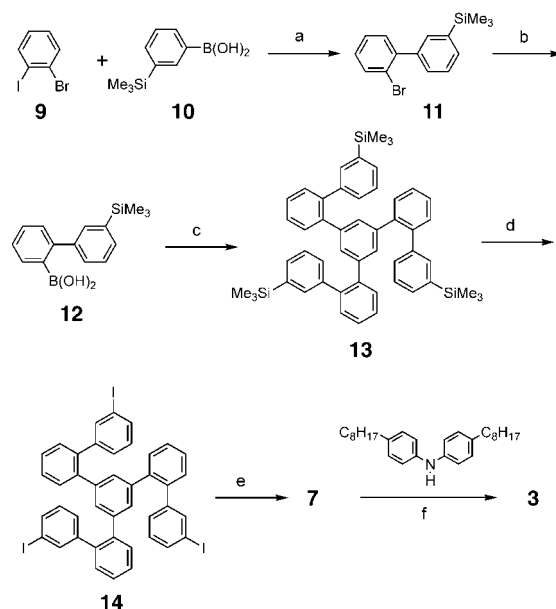
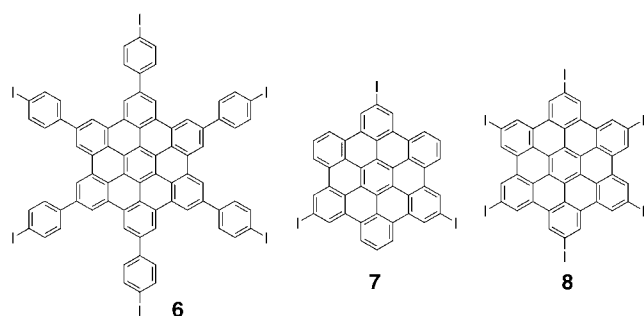
On route to a C_3 symmetric tris(bi-phenyl)benzene precursor **14** (Scheme 2) the selective Suzuki coupling^[13] between 1-bromo-2-iodobenzene (**9**) and 3-(trimethylsilyl)phenyl boronic acid (**10**)^[14] afforded 2-bromo-3'-(trimethylsilyl)biphenyl (**11**) in 93 % yield. The bromo functionality in **11** was then converted into boronic acid **12** in 90 % yield, and the threefold Suzuki coupling between **12** and 1,3,5-tribromobenzene gave 1,3,5-tris[3'-(trimethylsilyl)-2'-biphenyl]benzene (**13**) in 58 % yield.

After replacement of the trimethylsilyl groups by iodo units (91 % yield), the resulting precursor **14** was submitted to $FeCl_3$ oxidative cyclodehydrogenation conditions to give the fused HBC building block **7** as an insoluble yellow powder in 92 % yield. The extremely poor solubility of compound **7** only allows solid-state MALDI-



Scheme 1. Schematic presentation of a coaxial “double-cable” approach for hole transport.

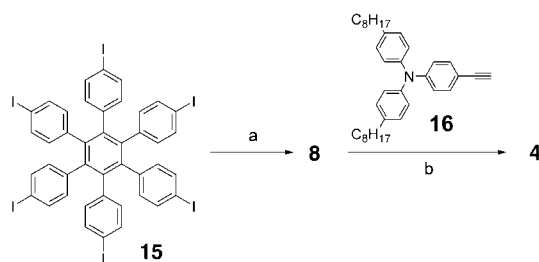
mation). The synthesis of di(4-octylphenyl)amino-substituted HBC-arylamine materials (**3–5**) was based on a novel synthetic concept recently developed in our group.^[11] A



Scheme 2. Synthesis of molecule **3**: a) $[Pd(PPh_3)_4]$, K_2CO_3 (aq.), toluene, 95 °C, 92 %; b) 1) $nBuLi$, –78 °C; 2) $B(OCH_3)_3$, –78 °C → RT; 3) HCl (aq.), 90 %; c) $[Pd(PPh_3)_4]$, K_2CO_3 (aq.), toluene, 95 °C, 58 %; d) ICl , chloroform, 91 %; e) $FeCl_3$ (24 equiv), CH_3NO_2/CH_2Cl_2 , 92 %; f) $[Pd_2(dba)_3(PtBu_3)]$, toluene, 80 °C, 24 %. dba = dibenzylideneacetone

TOF mass spectroscopic characterization. The subsequent functionalization of **7** with bis(4-octylphenyl)amine by Buchwald–Hartwig coupling reactions^[9] afforded soluble HBC-arylamine materials **3** in 24 % yield, allowing full structural characterization (see Supporting Information).

Another D_{6h} symmetric HBC, namely hexakis(4-iodo)-*peri*-hexabenzocoronene (**8**), was prepared by similar oxidative cyclodehydrogenation of the precursor hexakis(4-iodophenyl)benzene (**15**)^[15] in nearly quantitative yield (see Supporting Information). Although virtually insoluble, **8** underwent sixfold Hagihara–Sonogashira coupling^[12] with *N,N'*-bis(4-octylphenyl)-*N''*-(4-ethynylphenyl)amine (**16**) smoothly affording the soluble HBC **4** in 61 % yield (Scheme 3).



Scheme 3. Synthesis of molecule **4**: a) FeCl_3 (24 equiv), $\text{CH}_3\text{NO}_2/\text{CH}_2\text{Cl}_2$, quantitative; b) $[\text{Pd}(\text{PPh}_3)_4]/\text{CuI}$, piperidine, 50°C , 61 %.

The self-assembly properties of the arylamine substituted HBCs **1–5** in the bulk were investigated by differential scanning calorimetry (DSC), polarized optical microscopy (POM), and two-dimensional wide-angle X-ray diffraction (2DWAXD) techniques.^[16] Upon heating, **1** entered a hexagonally ordered columnar liquid-crystalline phase at 162°C , as indicated by the typical fan-type texture in POM and 2DWAXD diagrams (see Supporting Information). Upon cooling from the isotropic melt above 375°C , the compound passed through the columnar liquid-crystalline phase and gave rise to a columnar microcrystalline phase at 127°C . The typical 2D X-ray diffractogram at room temperature (Figure 1a) shows the “X” shaped reflections beyond the equatorial and meridional directions, which are correlated to a π – π stacking distance of 4.5 \AA along the stacking axis and indicate that the discs are tilted about 30° with respect to the columnar axis.^[17] Similarly, upon heating, **2** entered a columnar liquid-crystalline phase at 217°C from a columnar microcrystalline phase (see POM textures and 2DWAXD

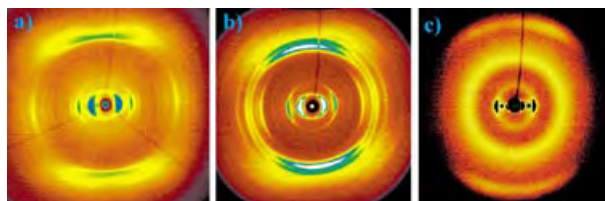


Figure 1. Representative 2D WAXD diagrams of extruded fibers of compound **1** (a), **2** (b), and **5** (c) at room temperature.

measurements in Supporting Information). At room temperature there is a tilted columnar stacking of the HBC discs (Figure 1b) with an orthorhombic 2D unit cell ($a = 2.28$, $b = 1.78 \text{ nm}$). A series of reflections at the wide-angle area in the equatorial and meridional directions can be correlated to the positional or rotational order between the arylamine arms in the columnar stacking. While HBC **3** only displayed a crystalline phase below the melting point of 387°C , the hexamine substituted HBCs **4** and **5** did not show any phase transition between -100°C and 400°C . The 2DWAXD measurements on the extruded fibers of **4** and **5** clearly revealed a hexagonal columnar stacking in a wide temperature range (Figure 1c). Thus, except molecule **3**, all the arylamine substituted HBCs clearly display ordered coaxial columnar stacking in the liquid-crystalline phase or microcrystalline phase; such coaxial stacking affords the opportunity of a “double-cable” hole transport (see scheme 1). At the same time, smooth thin films with thickness of tens to one hundred nanometers and roughness around 1 nm can be easily obtained for compounds **3–5** by spin-coating the solutions onto different substrates, such as quartz, silicon wafer, and highly oriented pyrolytic graphite (HOPG) as studied by atomic force microscope (AFM). The smooth UV/Vis absorption spectra can be obtained for these thin films. On the other hand, the thin films of compounds **1** and **2** showed typical crystalline domains on quartz mainly because of their crystalline properties at room temperature (see Supporting Information).

Compounds **1–5** can be easily oxidized to stable radical cations or higher cationic charged species, as indicated by the cyclic voltammetric and differential-pulse voltammetric measurements (Table 1 and Supporting Information). The

Table 1: Cyclic voltammetry and differential pulse voltammetry data of compound **1–5** in 1,2-dichlorobenzene.^[a]

Event	1	2	3	4	5
$E_{1/2}^1$ (V)	0.47(1e)	0.34(1e)	0.51(1e)	0.77(me)	0.71(me)
$E_{1/2}^2$ (V)	0.94(me)	0.50(1e)	0.72(2e)	1.10(me)	0.92(me)
$E_{1/2}^3$ (V)	–	0.97(me)	1.23(me)	1.24(me)	1.07(me)

[a] For full details see the Supporting Information. The half-wave potential $E_{1/2}$ was refer to an AgNO_3/Ag reference electrode and was calibrated with an internal standard, ferrocene/ferrocenium redox system ($E_{1/2}(\text{Fc}) = 0.232 \text{ V}$). 1e = one electron transfer; 2e = two electron transfer, and me = multi-electron transfer.

splitting of the oxidation of the amines in **2** and **3** into two steps (before the multi-electron event) suggests effective charge delocalization through the HBC core in the mixed-valence radical monocation species ($2^{+\bullet}$ and $3^{+\bullet}$). We thus monitored the Vis/NIR and electron spin resonance (ESR) spectra upon oxidative titration. The UV/Vis/NIR spectra of $2^{+\bullet}$ in CH_2Cl_2 during stepwise oxidation by thianthrenium perchlorate (THClO_4) revealed the absorption band of a radical monocation centered 601 nm and 709 nm , together with a unique long-wavelength absorption band above 1200 nm , where the maximum peak is beyond 2200 nm ($< 0.56 \text{ eV}$; Figure 2). The five-line ESR spectrum observed

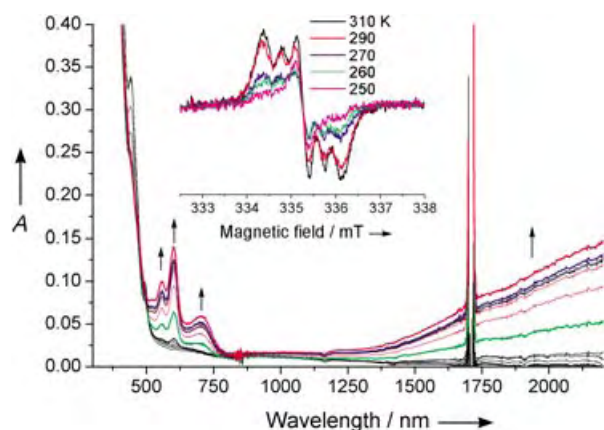


Figure 2. UV/Vis/NIR spectroscopic titration profile of compound **2** in CH_2Cl_2 with THClO_4 solution. Inset: temperature-dependent ESR spectra of the oxidized mono radical cation of **2**.

at 310 K for $2^{\bullet+}$ reflects an intramolecular spin exchange between two nitrogen centers (Figure 2, inset). Upon going to 250 K, only a three-line signal is seen which resembles the situation found for $1^{\bullet+}$.^[18] Upon lowering the temperature the intensity of the ESR signals of $1^{\bullet+}$ and $2^{\bullet+}$ decreases, suggesting π - π aggregate formation in solution (Figure 2, inset). The long-wavelength absorption band of $2^{\bullet+}$, thus can be explained by the molecular cation absorption, which is predicted to be around 1400 nm (AM1-CI calculation), and an additional intramolecular charge-transfer process. Intramolecular charge-transfer reactions in mixed-valence triarylamine systems have often been studied.^[7,8,19] Herein, we provide evidence for aggregation of the radical cations of **1–3** even at low concentration (about 10^{-5} M) and additional intramolecular charge-transfer interactions between arylamine moieties but no clear indication could be found for the intermolecular charge transfer other than their π - π aggregation.

The intracolumnar charge-carrier mobilities for compounds **1** through **5**, determined using the pulse-radiolysis time-resolved microwave conductivity technique (PR-TRMC)^[6b,20] are shown as a function of temperature in Figure 3. The mobilities are seen to differ by more than one

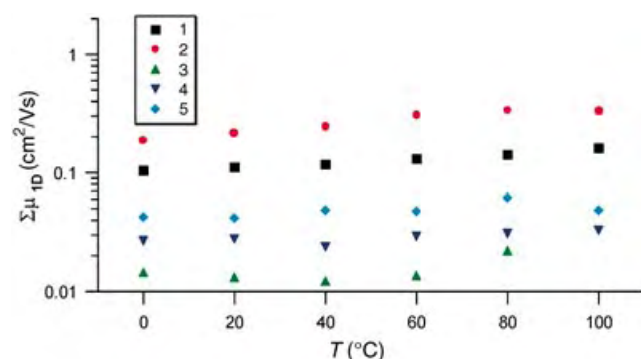


Figure 3. The temperature dependence of the one-dimensional charge-carrier mobilities of compounds **1–5** as measured using the PR-TRMC technique.

order of magnitude, with room temperature values of 0.11, 0.21, 0.01, 0.03 and 0.04 $\text{cm}^2(\text{Vs})^{-1}$ for **1–5**, respectively. The order of the mobilities for compounds **1**, **2**, and **5**, that is, $2 > 1 > 5$, are seen to be in qualitative agreement with the sharpness of the WAXD images shown in Figure 1. This supports the expected dependence of charge transport on the degree of columnar order. These largest mobility values which approach those found for the crystalline and liquid-crystalline phases of a hexadecyl-substituted HBC^[6b] would be surprising if a large portion of the positive charges resided on the peripheral amine moieties: either the amines are sufficiently well-organized within the intercolumnar space to allow rapid hole transport between them, or the electrons, which remain localized on the HBC cores, have an intracolumnar mobility which is comparable with that of holes. Unfortunately the TRMC technique cannot differentiate between these two possibilities since it is insensitive to the sign of the charge of the major carrier; but the former explanation suggests that the hole mobilities in the present discotic materials are considerably larger than those found in disordered triarylamine solids.^[21]

In conclusion, the new synthetic concept towards electroactive arylamine substituted HBC materials can be used to broaden the HBC family with high atom economy. Combination of the columnar superstructure formation of HBC and the hole-transporting ability of both the HBC and arylamines led to new kind of hole-transporting materials with high carrier mobility, good film formation capability (expect compound **1** and **2**), and low ionization potential, which are promising properties for organic devices.^[1,2] The mixed-valence compounds of oxidized **1–5**, can be regarded as ideal models for studying the intramolecular charge transfer as a function of the molecular symmetry and distance between the nitrogen centers, and the intermolecular association of charged π systems.^[22]

Received: March 31, 2004

Revised: June 17, 2004

Keywords: arylamines · electron transfer · hole transport · liquid crystals · pi interactions

- [1] a) C. W. Tang, S. A. VanSlyke, *Appl. Phys. Lett.* **1987**, *51*, 913–915; b) R. H. Friend, R. W. Gymer, A. B. Holmes, J. H. Burroughes, R. N. Marks, C. Taliani, D. D. C. Bradley, D. A. Dos Santos, J. L. Brédas, M. Lögdlund, W. R. Salaneck, *Nature* **1999**, *397*, 121–128.
- [2] a) C. W. Tang, *Appl. Phys. Lett.* **1986**, *48*, 183–185; b) U. Bach, D. Lupo, P. Compté, J. E. Moser, F. Weissörtel, J. Salbeck, H. Spreitzer, M. Grätzel, *Nature* **1998**, *395*, 583; c) N. S. Sarifitci, L. Smilowitz, A. J. Heeger, F. Wudl, *Science* **1992**, *258*, 1474–1476.
- [3] Z. Bao, J. A. Rogers, E. Katz, *J. Mater. Chem.* **1999**, *9*, 1895–1904.
- [4] S. J. Zilker, *ChemPhysChem* **2000**, *1*, 72–87.
- [5] M. Thelakkat, *Macromol. Mater. Eng.* **2002**, *287*, 442–461.
- [6] a) M. D. Watson, A. Fechtenkötter, K. Müllen, *Chem. Rev.* **2001**, *101*, 1267–1300; b) A. M. van de Craats, J. M. Warman, A. Fechtenkötter, J. D. Brand, M. A. Harbison, K. Müllen, *Adv. Mater.* **1999**, *11*, 1469–1472.

- [7] K. R. Stickley, S. C. Blackstock, *J. Am. Chem. Soc.* **1994**, *116*, 11 576–11 577.
- [8] a) C. Lambert, G. Nöll, *Angew. Chem.* **1998**, *110*, 2239–2242; *Angew. Chem. Int. Ed.* **1998**, *37*, 2107–2110; b) C. Lambert, G. Nöll, *J. Am. Chem. Soc.* **1999**, *121*, 8434–8442; c) C. Lambert, G. Nöll, *Chem. Eur. J.* **2002**, *8*, 3467–3477.
- [9] a) J. P. Wolfe, S. L. Buchwald, *J. Org. Chem.* **1997**, *62*, 6066–6068; b) J. F. Hartwig, M. Kawatsura, S. I. Hauck, K. H. Shaughnessy, L. M. Alcazar-Roman, *J. Org. Chem.* **1999**, *64*, 5575–5580.
- [10] S. Ito, M. Wehmeier, J. D. Brand, C. Kübel, R. Epsch, J. P. Rabe, K. Müllen, *Chem. Eur. J.* **2000**, *6*, 4327–4342.
- [11] J. Wu, M. D. Watson, K. Müllen, *Angew. Chem.* **2003**, *115*, 5487–5491; *Angew. Chem. Int. Ed.* **2003**, *42*, 5329–5333.
- [12] S. Taskahashi, Y. Kuroyama, K. Sonogashira, N. Hagihara, *Synthesis* **1980**, 627–630.
- [13] N. Miyaura, A. Suzuki, *Chem. Rev.* **1995**, *95*, 2457–2483.
- [14] C. L. Nesloney, J. W. Kelly, *J. Org. Chem.* **1996**, *61*, 3127–3137.
- [15] J. A. Hyatt, *Org. Prep. Proced. Int.* **1991**, *23*, 460–463.
- [16] 2D WAXD was performed on a mechanically extruded fiber with the X-ray beam perpendicular to the fiber axis. For experimental details, see: I. Fischbach, T. Pakula, P. Minkin, A. Fechtenkötter, K. Müllen, H. W. Spiess, *J. Phys. Chem. B* **2002**, *106*, 6408–6418.
- [17] An approximate 2D monoclinic unit cell $a = 2.17$, $b = 1.56$ nm, and $\chi = 97^\circ$ can also be determined based on the correlations of the equatorial reflections.
- [18] At low temperature the intramolecular charge transfer most probably was forbidden, thus only three-line ESR spectra correlated to singly charged amines were observed.
- [19] a) J. Bonvoisin, J. P. Launay, M. van der Auweraer, F. C. De Schryver *J. Phys. Chem.* **1994**, *98*, 5052–5067; b) V. Coropceanu, M. Malagoli, J. M. André, J. L. Brédas, *J. Am. Chem. Soc.* **2002**, *124*, 10 519–10 530.
- [20] P. G. Schouten, J. M. Warman, M. P. de Haas, *J. Phys. Chem.* **1993**, *97*, 9863–9870.
- [21] a) P. M. Borsenberger, L. Pautmeier, R. Richert, H. Bässler, *J. Chem. Phys.* **1991**, *94*, 8276–8281; b) P. M. Borsenberger, L. Pautmeier, H. Bässler, *J. Chem. Phys.* **1991**, *94*, 5447–5454.
- [22] A detailed study of the intramolecular charge transfer in the mixed-valence compounds will be presented in a separate publication.

A DNA Nanomachine Based on a Duplex–Triplex Transition***Yi Chen, Seung-Hyun Lee, and Chengde Mao**

Herein we report the construction of a DNA nanomachine whose motion is triggered by changes in the solution pH value. Reversible formation and dissociation of a DNA triplex containing C⁺G–C triplets take place when the solution pH value changes between pH 5.0 and 8.0.^[1] This process constitutes the working principle of our DNA machine. We demonstrated the operation of the DNA machine by using fluorescence resonance energy transfer (FRET) techniques, and confirmed its structural integrity by native polyacrylamide gel electrophoresis (PAGE).

A great deal of effort has been devoted to the development of nanomachines because of their many potential applications in nanoelectronic devices, miniaturized biosensors, molecular computation, and smart materials.^[2] DNA, in the form of versatile building blocks,^[3] has been successfully used to construct DNA nanomachines.^[4] The working mechanisms of these DNA machines fall into three categories: 1) conformational changes induced by environmental changes,^[4a,h] 2) motion fueled by strand displacement,^[4b–g,i–k] 3) autonomous motion powered by enzymatic activity.^[4l] The first DNA machine was built to work by the first of these mechanisms but the majority of DNA machines operate by strand displacement. Strand-displacement-driven DNA machines are attractive because each machine can potentially be activated individually by using a sequence-specific activation technique. An enzyme-powered DNA motor has been developed more recently.^[4l] It can be sequence-specifically activated and, more importantly, it operates autonomously. Herein, we report a DNA nanomachine that falls into the first category and is fuelled by H⁺ and OH[–] ions.

Our nanomachine contains three DNA strands (F, L, and S) and operates through the reversible formation/dissociation of a DNA triplex (Figure 1). At pH 8.0, the three strands associate to form an open complex (open state) consisting of three 15-base-pair duplexes and a single-stranded region. This single-stranded region adopts a random coil conformation in the presence of divalent cations such as Mg²⁺,^[4,5] but its sequence is designed to allow it to bind to one of the duplexes

[*] Y. Chen,^[†] S.-H. Lee,^[†] Prof. C. Mao
Purdue University
Department of Chemistry
West Lafayette, IN 47907 (USA)
Fax: (+1) 765-494-0239
E-mail: mao@purdue.edu

[†] These authors contributed equally to this work.

[**] This work is supported by the National Science Foundation (Grant no. EIA-0323452), the Defense Advanced Research Project Agency's Defense Sciences Office (Grant no. MDA 972-03-1-0020), and Purdue University (a start-up fund). We thank Prof. D. R. McMillin for use of a fluorometer and Mr. M. H. Wilson for help with fluorescence measurements.

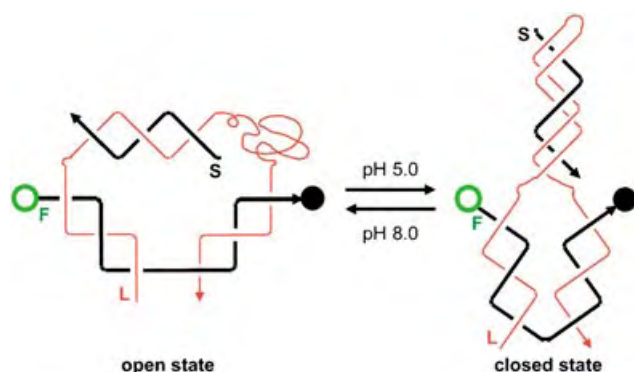


Figure 1. The construction and operation of our DNA nanomachine. The machine consists of three DNA strands: a strand with a fluorescent label (F), a long strand (L), and a short strand (S). The open and solid circles represent rhodamine green and black hole quencher-1 (BHQ-1), respectively. A DNA triplex involving the S and L strands forms and dissociates reversibly.

to form a triplex. C⁺G-C triplets make up 47% of the triplex, and TA-T triplets the remaining 53%. The formation of C⁺G-C triplets depends on the protonation of cytosine residues,^[1] which requires an acidic solution. A pH value of 5.0 has been reported in the literature to promote DNA triplex formation reliably.^[1] Upon triplex formation, the complex as a whole becomes quite compact (closed state). When the pH value increases to pH 8.0, the C⁺G-C triplets become unstable and the DNA triplex dissociates into a duplex and a single-stranded region; the DNA complex returns to its open state. The DNA machine continuously cycles between the closed state and the open state when the solution pH oscillates between 5.0 and 8.0. We intentionally designed the nanomachine with an overall structure similar to that of a previously reported autonomous DNA motor,^[41] but with a different motion actuator. We reasoned that the success of such a design would clearly demonstrate that a similar motion can be achieved by different working mechanisms and with different fuels.

The DNA machine is stable in both conformations. We synthesized the machine by combining equimolar amounts of the DNA strands F, L, and S then slowly cooling the mixture from 95 to 22 °C over the course of 2 h. We first confirmed that all the strands can associate at both pH 5.0 and pH 8.0 by using native PAGE (Figure 2). At each pH value, one single, sharp band corresponding to the designed DNA complex was observed, which indicates that the DNA machine is stable under both conditions. Comparison of the designed machine with the other DNA complexes on the gels clearly showed that the DNA machine has different electrophoretic mobilities at the two different pH values. This phenomenon suggests that the DNA machine adopts different conformations at pH 5.0 and 8.0 because the electrophoretic mobility of a molecule is determined not only by its molecular weight, but also by its conformation.^[1d] A closely packed molecule moves faster than a loosely packed molecule of the same weight. The observed mobility change hinted that the DNA machine adopts a more compact conformation at pH 5.0 than at pH 8.0.

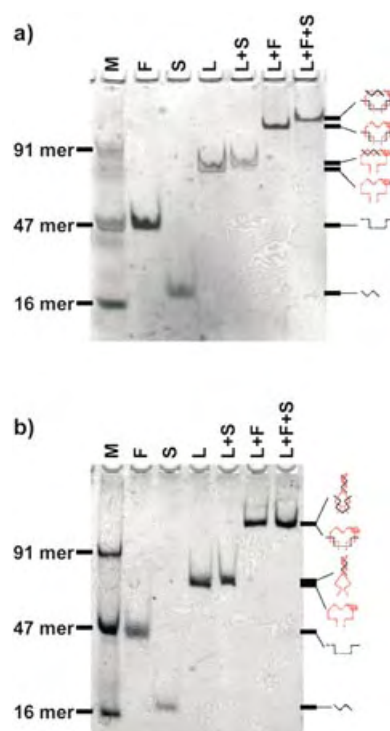


Figure 2. Native gel electrophoretic analysis of the DNA nanomachine at pH 8.0 (a) and pH 5.0 (b). The DNA strands present are indicated above each lane. Lane M contains a series of single-stranded DNA size markers. The electrophoretic mobility of the DNA nanomachine (Lane L + F + S) changes relative to those of the other DNA complexes when the pH value changes.

The conformational change was further demonstrated by the results of a FRET experiment (Figure 3). We labeled the F strand with rhodamine green and BHQ-1 molecules at its 5' and 3' ends, respectively. The optical properties of both rhodamine green and BHQ-1 are insensitive to any pH change between pH 4.0 and 9.0.^[4h,6] In the open state of the DNA machine (pH 8.0), the fluorophore is well separated from the quencher and a strong fluorescence signal was observed. In the closed state (pH 5.0), the fluorophore is close to the quencher and the fluorescence signal decreased in

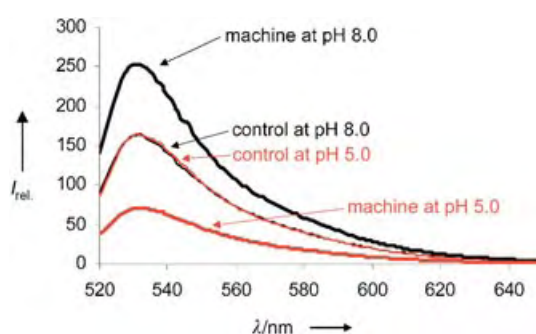


Figure 3. Fluorescence spectra of the DNA nanomachine at pH 5.0 and pH 8.0. The rhodamine green emission is more effectively quenched at pH 5.0 than at pH 8.0, which indicates that the DNA complex is more compact at pH 5.0. A control molecule that could not undergo the duplex–triplex transition was also analyzed and was observed to have the same fluorescence intensity at both pH values.

intensity. To make sure that the conformational change, and not pH change per se, was responsible for the variation of the fluorescence signal, we constructed a control molecule. This control molecule was similar to the DNA machine except that the control could not undergo the duplex–triplex transition. Fluorescence data clearly showed that the pH change could not cause the control molecule to vary its fluorescence intensity.

The DNA machine continuously cycles when the environmental pH value oscillates between 5.0 and 8.0 (Figure 4). We monitored the fluorescence signal at 530 nm, the maximum

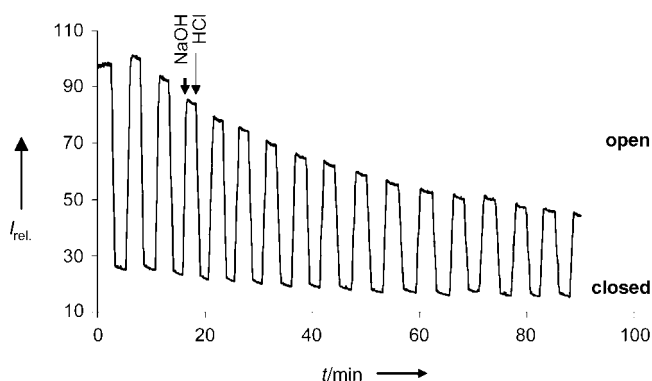


Figure 4. DNA machine cycling. Fluorescence intensity was monitored at 530 nm (λ_{em} of rhodamine green) while the solution pH value oscillated between 5.0 and 8.0.

emission wavelength of rhodamine green, while changing the solution pH value. Sixteen cycles were recorded. The overall fluorescence signal continuously decreased during the cycling experiment. We speculate that this decrease is due to photobleaching of the fluorescence dye and the inaccuracy of the pH control. Repetitive addition of NaOH and HCl diluted the sample, which also contributed to the decrease of the fluorescence signal intensity. However, this extent of dilution does not significantly affect triplex formation because this structural change is an intramolecular process.

In summary, we have constructed a DNA nanomachine whose mechanism is based on the formation and dissociation of a DNA triplex. This machine uses H^+ and OH^- as fuels, which gives it four unique characteristics: 1) The fuels are among the cheapest and most common chemicals. If a massive amount of DNA machines were needed, the cost of the fuels would remain low. 2) The only waste products of the DNA machine are water and NaCl, which are not damaging to the motor or the environment. 3) The fuels consist of small particles that can easily diffuse through small pores or channels. This property is potentially important for many applications. For example, if a DNA machine is placed in a protein channel or a nanofluidic channel to control the permeability of that channel, the ability of the machine to function depends critically upon the accessibility of the fuels. In such a situation, H^+ and OH^- ions are clearly superior to large biomacromolecules such as DNA and RNA. 4) One disadvantage of the reported DNA machine is that all the machines in a given sample move in response to the same

stimulus. We cannot control each molecular machine individually without spatial segregation of the nanomachines. For a nanomachine, it is interesting to ask 1) will the machine work under any load? and 2) what force can the machine generate? Unfortunately, it is difficult to answer such questions at the present stage because our design is quite complicated. We expect our machine to generate a weaker force than DNA-hybridization-fueled machines^[4b–k] since a DNA triplex is generally less stable than a DNA duplex. Other challenges in the field of DNA nanomachine design include: 1) What complicated motions can DNA machines perform? 2) What kind of work can DNA machines do? 3) Could DNA machines communicate with each other and work cooperatively? We wish to address these questions in the near future.

Experimental Section

DNA oligonucleotides: a) DNA sequences for the nanomachine: Strand F, 5'-rhodamine green-CCA TAC CAT CTA ACC TCC AgA CCT TAC gCT C-black hole quencher-1-3'; Strand L, 5'-ggT TAG ATg gTA Tgg TTC TTC TCT CCT TTC CTT TTC **CTT TCC TCT CTT CCT** gAg CgT AAg gTC Tgg-3' (the triplex-forming segment is indicated by bold letters); Strand S, 5'-ggA AAg gAg AgA AgA-3'. b) DNA sequences for the control molecule: Strand F, 5'-rhodamine green-CCA TAC CAT CTA ACC TCC AgA CCT TAC GCT C-black hole quencher-1-3'; Strand L', 5'-ggT TAG ATg gTA TgC TTC ggA CAg gCT AgC TAC AAC gAg AgT gAC TgA gCg TAA ggT CTg g-3'; Strand S', 5'-gTC ACT CAT gTC CgA-3'. All oligonucleotides were purchased from Integrated DNA Technologies, Inc. and purified by denaturing polyacrylamide gel electrophoresis.

Formation of DNA complexes: The component DNA strands (0.5 μ M) were combined in equimolar quantities in a buffer. At pH 8.0, we used tris(hydroxymethyl)aminomethane Tris- Mg^{2+} buffer, which contained Tris buffer (50 mM, pH 8.0), NaCl (100 mM), and $Mg(CH_3COO)_2$ (10 mM). At pH 5.0, we used 2-morpholinoethanesulfonate MES- Mg^{2+} buffer, which contained MES (50 mM, pH 5.0), NaCl (100 mM), and $Mg(CH_3COO)_2$ (10 mM). The nanomachine was formed by cooling the DNA solution as follows: 95 °C (3 min), 65 °C (30 min), 50 °C (30 min), 37 °C (30 min), and 22 °C (30 min).

Denaturing polyacrylamide gel electrophoresis: Gels contained 20% polyacrylamide (acrylamide/bisacrylamide, 19:1) and 8.3 M urea and were run at 55 °C. The running buffer was Tris-borate-EDTA (TBE; EDTA, ethylenediaminetetraacetate), which consisted of Tris buffer (89 mM, pH 8.0), boric acid (89 mM), and EDTA (2 mM). Gels were run on a Hoefer SE 600 electrophoresis unit at 600 V (constant voltage).

Native polyacrylamide gel electrophoresis: Gels contained 12% polyacrylamide (acrylamide/bisacrylamide, 19:1) and were run on a FB-VE10-1 electrophoresis unit (Fisher Biotech) at 22 °C (80 V, constant voltage). After electrophoresis, the gels were stained with Stains-all dye (Sigma) and scanned. Tris- Mg^{2+} buffer and MES- Mg^{2+} buffer were used for electrophoresis at pH 8.0 and pH 5.0, respectively.

Fluorescence spectroscopy: DNA (0.2 μ M) was dissolved in Tris-acetate-EDTA- Mg^{2+} buffer (500 μ L), which contained Tris base (40 mM), acetic acid (20 mM), EDTA (2 mM), and $Mg(CH_3COO)_2$ (12.5 mM). The buffer pH was adjusted to either pH 5.0 or 8.0 with 1 M NaOH or 1 M HCl. Fluorescence emission spectra were recorded on a Varian Cary Eclipse fluorescence spectrophotometer. All spectra were collected at 22 °C. The samples were excited at 504 nm and the emission data were collected either from 520 to 650 nm, or at 530 nm (for motor cycling). The maximal emission wavelength of rhodamine green is 535 nm.

Cycling the DNA machine: DNA (0.2 μ M) was dissolved in Tris-acetate-EDTA- Mg^{2+} (TAE/ Mg^{2+}) buffer (500 μ L). We changed the

buffer pH between 5.0 and 8.0 by alternately adding 1 M HCl (11.1 μ L) and 1 M NaOH (11.1 μ L). The pH value of the TAE/Mg²⁺ buffer was stable at both pH 5.0 (pK_a of acetic acid is 4.75) and pH 8.0 (pK_a of Tris is 8.3).

Received: May 26, 2004

Keywords: acidity · DNA structures · DNA · molecular devices · self-assembly

- [1] a) K. M. Vasquez, P. M. Glazer, *Q. Rev. Biophys.* **2002**, *35*, 89–107; b) G. E. Plum, *Biopolymers* **1998**, *44*, 241–256; c) V. N. Soyfer, V. N. Potaman, *Triple-Helical Nucleic Acids*, Springer, New York, **1996**; d) J. S. Lee, L. J. Latimer, B. L. Haug, D. E. Pulleyblank, D. M. Skinner, G. D. Burkholder, *Gene* **1989**, *82*, 191–199.
- [2] a) H. G. Craighead, *Science* **2000**, *290*, 1532–1535; b) C. P. Collier, G. Mattersteig, E. W. Wong, Y. Luo, K. Beverly, J. Sampaio, F. M. Raymo, J. F. Stoddart, J. R. Heath, *Science* **2000**, *289*, 1172–1175; c) A. M. Brouwer, C. Frochot, F. G. Gatti, D. A. Leigh, L. Mottier, F. Paolucci, S. Roffia, G. W. H. Wurpel, *Science* **2001**, *291*, 2124–2128; d) D. A. Leigh, J. K. Y. Wong, F. Dehez, F. Zerbetto, *Nature* **2003**, *424*, 174–179; e) N. Koumura, R. W. J. Zijlstra, R. A. van Delden, N. Harada, B. Feringa, *Nature* **1999**, *401*, 152–155; f) R. K. Soong, G. D. Bachand, H. P. Neves, A. G. Olkhovets, H. G. Craighead, C. D. Montemagno, *Science* **2000**, *290*, 1555–1558.
- [3] a) N. C. Seeman, *J. Theor. Biol.* **1982**, *99*, 237–247; b) N. C. Seeman, *Nature* **2003**, *421*, 427–431; c) N. C. Seeman, *Biochemistry* **2003**, *42*, 7259–7269.
- [4] a) C. Mao, W. Sun, Z. Shen, N. C. Seeman, *Nature* **1999**, *397*, 144–146; b) B. Yurke, A. J. Turberfield, A. P. Mills, F. C. Simmel, J. L. Neumann, *Nature* **2000**, *406*, 605–608; c) H. Yan, X. Zhang, Z. Shen, N. C. Seeman, *Nature* **2002**, *415*, 62–65; d) J. J. Li, W. Tan, *Nano Lett.* **2002**, *2*, 315–318; e) P. Alberti, J. Mergny, *Proc. Natl. Acad. Sci. USA* **2003**, *100*, 1569–1573; f) A. J. Turberfield, J. C. Mitchell, B. Yurke, A. P. Mills, Jr., M. I. Blakey, F. C. Simmel, *Phys. Rev. Lett.* **2003**, *90*, 118102–1–4; g) L. Feng, S. H. Park, J. H. Reif, H. Yan, *Angew. Chem.* **2003**, *115*, 4478–4482; *Angew. Chem. Int. Ed.* **2003**, *42*, 4342–4346; h) D. Liu, S. Balasubramanian, *Angew. Chem.* **2003**, *115*, 5912–5914; *Angew. Chem. Int. Ed.* **2003**, *42*, 5734–5736; i) W. U. Dittmer, F. C. Simmel, *Nano Lett.* **2004**, *4*, 689–691; j) W. B. Sherman, N. C. Seeman, *Nano Lett.* **2004**, *4*, 1203–1207; k) W. U. Dittmer, A. Reuter, F. C. Simmel, *Angew. Chem.* **2004**, *116*, 3634–3637; *Angew. Chem. Int. Ed.* **2004**, *43*, 3550–3553; l) Y. Chen, M. Wang, C. Mao, *Angew. Chem.* **2004**, *116*, 3638–3641; *Angew. Chem. Int. Ed.* **2004**, *43*, 3554–3557; m) C. M. Niemeyer, M. Adler, *Angew. Chem.* **2002**, *114*, 3933–3937; *Angew. Chem. Int. Ed.* **2002**, *41*, 3779–3783.
- [5] A. M. van Oijen, P. C. Blainey, D. J. Crampton, C. C. Richardson, T. Ellenberger, X. S. Xie, *Science* **2003**, *301*, 1235–1238.
- [6] R. P. Haugland, *Handbook of Fluorescent Probes and Research Products*, 9th ed., Molecular Probes, Eugene, **2003**, p. 53.

A Strategy for Functional Proteomic Analysis of Glycosidase Activity from Cell Lysates**

David J. Vocadlo* and Carolyn R. Bertozzi*

The glycosidases are an extremely large class of hydrolases that are found throughout nature in organisms ranging from bacteria to humans and have been classified into a number of families on the basis of structural similarity.^[1] These enzymes have central roles in both prokaryotic and eukaryotic cellular metabolism and their dysfunction can have deleterious effects. In light of their biological significance, the rapid detection of proteins with glycosidase activity in organisms is of considerable interest. Activity-dependent labeling of enzymes in complex mixtures is a central challenge of the field of functional proteomics.^[2] A number of approaches have been developed for labeling and identifying proteins on the basis of their activity through conjugation of active-site-directed inactivators to biochemical probes.^[3–5] These methods have been used to probe protease and other enzyme activities both in cells and in vitro.^[6,7] For many glycosidases, however, such a strategy is significantly complicated by their active site architecture. Unlike proteases, which commonly have a cleft-like active site, *exo*-glycosidases typically have a pocket-shaped active site^[8] in which extensive interactions between substrate and enzyme leave little space for appending biochemical probes. Attempts to develop activity-based covalent labeling reagents for glycosidases that can label these enzymes when in complex mixtures have not yet proven

[*] Prof. D. J. Vocadlo,^[†] Prof. C. R. Bertozzi
Center for New Direction in Organic Synthesis
Howard Hughes Medical Institute
Departments of Chemistry and Molecular and Cell Biology
University of California
Room 419, Latimer Hall, Berkeley, CA 94720-1460 (USA)
Fax: (+1) 510-643-2628
E-mail: dvocadlo@sfsu.ca
bertozzi@cchem.berkeley.edu

[†] Current Address:
Department of Chemistry
Simon Fraser University
8888 University Boulevard, Burnaby
British Columbia, V5A 1A6 (Canada)
Fax: (+1) 604-291-3765

[**] The authors thank S. G. Withers for samples of recombinant *Agrobacterium* sp. β -glucosidase and *Xanthomonas manihotis* β -galactosidase, and H. C. Hang for useful discussions. D.J.V. thanks the Canadian Institutes of Health Research for a fellowship. The authors thank A. Debowski for technical assistance. This research was supported by a grant to C.R.B. from the National Institutes of Health (Grant no. GM066047), a President's Research Grant from Simon Fraser University, and a grant to D.J.V from the Natural Sciences and Engineering Research Council of Canada. The center for New Directions in Organic Synthesis is funded by Bristol-Myers Squibb as a supporting member and Novartis as a sponsoring member.



Supporting information for this article is available on the WWW under <http://www.angewandte.org> or from the author.

successful.^[9,10] We felt that attempts to develop an activity-based probe for targeting glycosidases, particularly *exo*-glycosidases, would benefit from consideration of the catalytic mechanism of these enzymes.

The great majority of retaining β -glycosidases use a catalytic mechanism involving the formation and subsequent breakdown of a covalent glycosyl-enzyme intermediate.^[11] These steps involve two carefully positioned carboxylate residues, one of which functions as a general acid/base catalyst, whilst the other acts as a catalytic nucleophile. A key point is that both steps involve electrophilic migration of the anomeric center and oxocarbenium ion-like transition states.^[12,13] Fluorosugars have been designed that act as mechanism-based inactivators of retaining β -glycosidases and function by trapping the covalent glycosyl-enzyme intermediate by destabilizing these transition states.^[11] These inactivators have facilitated identification of the enzymic nucleophiles of a number of retaining β -glycosidases.^[11,12,14,15] We envisioned that these compounds could be modified for use in functional proteomics analysis of retaining β -glycosidases. This application requires adornment of the fluorosugars with a detectable tag.

Although *exo*-glycosidases often exhibit some promiscuity in their substrate specificity, their pocket-shaped active sites preclude elaboration of the glycone moiety with large affinity tags such as biotin. We felt that a fine balance could be struck between the tolerance of these enzymes for small modifications and the requirement for a detectable probe by using the small, uniquely reactive azide moiety. This bioorthogonal functional group can be elaborated by Staudinger ligation^[16] or by the Cu^I-catalyzed [3+2] Huisgen cycloaddition reported by Rostovtsev et al.^[17] Herein, we present a strategy for the detection of retaining glycosidases in complex mixtures by using azide-functionalized 2-fluorosugars in conjunction with Staudinger ligation. An outline of the strategy is shown in Figure 1, with *Escherichia coli* β -galactosidase (LacZ) as a target protein. We chose LacZ to demonstrate the strategy because this enzyme has previously been inactivated with 2-fluorogalactosides.^[18] A high-resolution crystal structure of the resulting covalent complex has been reported. The structure reveals a demanding steric environment surrounding the 6-hydroxy group of the galactose moiety, which should provide a stringent test of our strategy.^[19] We chose the 6-position as the azide substitution site for synthetic ease and because the possibility of free rotation around the C-6 methylene group may permit the azide moiety to adopt a favorable orientation within the enzyme active site. Furthermore, kinetic studies of LacZ with modified substrates have shown that the 6-hydroxy group is not essential for catalysis.^[20] There is precedent for galactosides with substitutions at the 6-position serving as substrates for several different galactosidases,^[21] and other glycosidases also tolerate substitutions at this position.^[22]

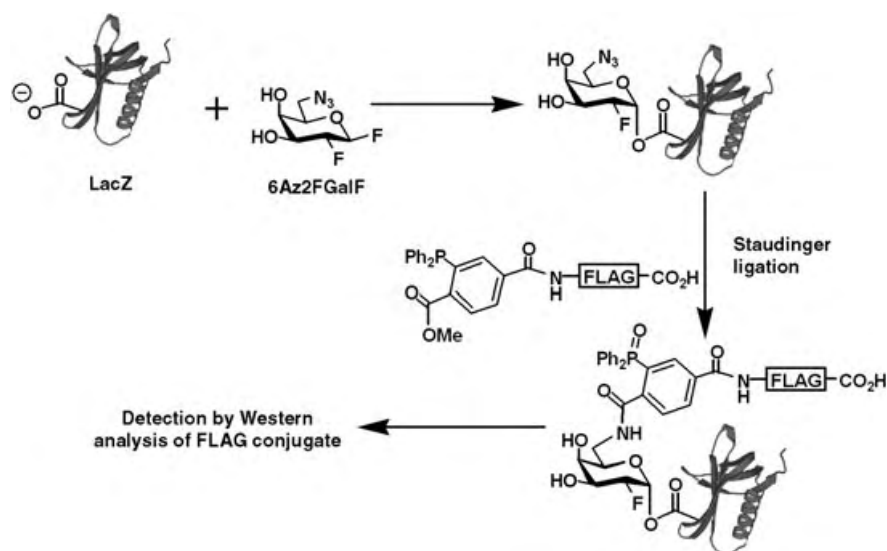
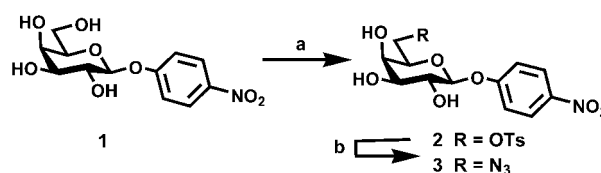


Figure 1. The activity-based labeling approach and Staudinger ligation. Glycosidase labeling was performed both with purified *Escherichia coli* LacZ and with cell lysates from *E. coli*. Samples were incubated with 6-azido-2,6-dideoxy-2-fluoro- β -D-galactosyl fluoride (6Az2FGalF), which resulted in formation of a covalent glycosyl-enzyme adduct on the active site nucleophile. Staudinger ligation of the azido group with a phosphine-FLAG (DYKDDDDK) probe resulted in specific labeling.

To evaluate the consequences of substituting the 6-hydroxy group of a β -galactoside with an azide moiety, we synthesized the chromogenic substrate *para*-nitrophenyl 6-azido-6-deoxy- β -D-galactoside (pNP6AzGal, **3**, Scheme 1).



Scheme 1. a) TsCl, py, 59%; b) NaN₃, DMF, 80°C, 87%. py, pyridine; Ts, tosyl; DMF, dimethylformamide (All experimental procedures are described in the Supporting Information).

The ratio of the second-order rate constants [$(V_{\max}/K_M)_{\text{OH}}/(V_{\max}/K_M)_{\text{N}_3}$] of the LacZ-catalyzed hydrolysis of pNP6AzGal and that of the 6-hydroxy compound *para*-nitrophenyl β -D-galactoside (pNPGal, **1**, Scheme 1) was determined to be 12500. Substitution of the 6-hydroxy group with an azide moiety therefore results in an energetic penalty of 5.6 kcal mol⁻¹ for this catalytic process. McCarter and Withers have shown that substitution of the 6-hydroxy group with a fluorine or hydrogen atom results in an energetic penalty of approximately 4.0 kcal mol⁻¹ for LacZ-catalyzed hydrolysis of aryl galactosides, presumably as a result of a loss of favorable interactions within the enzyme active site.^[20] The residual 1.6 kcal mol⁻¹ difference between these energy penalties probably stems from a small steric penalty associated with the greater bulk of the azido group compared to the hydroxy group. The sterically confined active site of LacZ does not prevent turnover of compounds bearing a 6-azido group and

we were optimistic that inactivators bearing this modification would label the enzyme.

We prepared 6-azido-2,6-dideoxy-2-fluoro- β -D-galactosyl fluoride (6Az2FGalF, **10**, Scheme 2) as an activity-based probe for β -galactosidases. Incubation of purified LacZ with various concentrations of 6Az2FGalF revealed a concentration and time-dependent inactivation of the enzyme that could be fit to a single exponential decay function (data not shown). From the data shown in Figure 2, we determined the apparent second-order rate constant of the inactivation process to be $0.2 \text{ M}^{-1} \text{ min}^{-1}$. This result shows that 6Az2FGalF inactivates LacZ on a timescale appropriate for practical applications and suggests that this compound could be used to detect β -galactosidase activity. To explore this possibility we incubated purified LacZ with 6Az2FGalF overnight such that less than 10% residual activity remained after incubation. The sample was dialyzed to remove excess inactivator and the protein was denatured under mild reducing conditions at pH 3.5 so that both the acylal ester linkage and the azide moiety remained stable. Treatment of the sample with phosphine-FLAG^[16] followed by Western blot analysis revealed that the lower limit for the detection of LacZ after all sample handling losses was approximately 50 ng (Figure 3a). Treatment of a sample of inactivated, phosphine-FLAG-labeled enzyme with 5% ammonium hydroxide resulted in complete abrogation of the FLAG-associated signal (data not shown), which is consistent with aminolysis of the covalent acylal 6Az2FGal-enzyme intermediate.

To extend this strategy to the analysis of glycosidase activity from cell lysates, we examined the inactivation of LacZ in cultures of *E. coli* K-12, either induced with IPTG or not induced. Analysis of the crude cell lysates by SDS-PAGE followed by Coomassie staining (Figure 3d) or by Western blotting (Figure 3b), and analysis of galactosidase activity with a standard colorimetric assay revealed the expected marked difference in production of LacZ between cultures that were induced and those that were not (0.6% LacZ expression in uninduced cells as compared to that in induced cells, taken as 100%). The cell lysates were then incubated with the activity-based probe 6Az2FGalF and labeled with phosphine-FLAG as described above for purified LacZ. As shown in Figure 3c, the FLAG epitope was only observed for samples that had been induced to express LacZ and treated with 6Az2FGalF. These results indicate that both the inactivation of LacZ using 6Az2FGalF and the subsequent

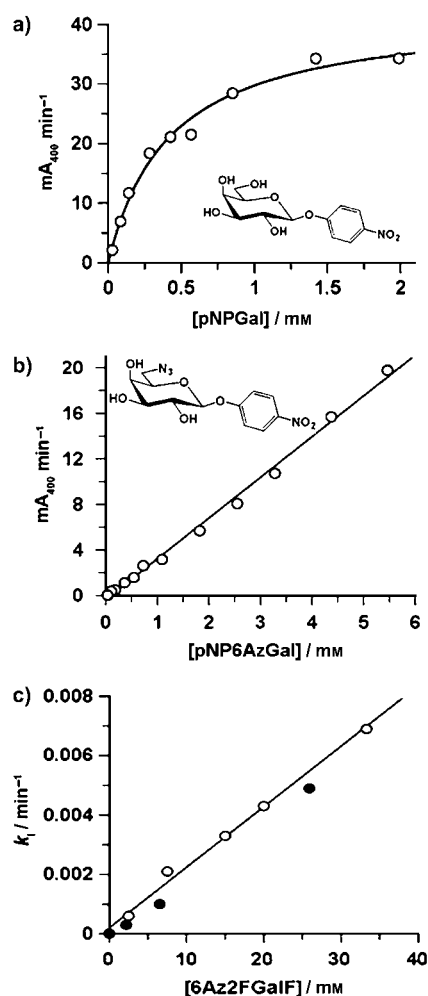
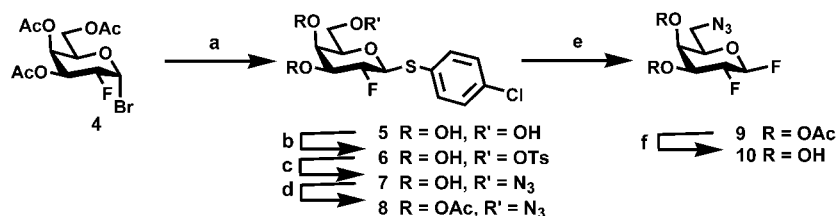


Figure 2. Activity of *E. coli* LacZ with (a) pNPGal (**1**) and (b) pNP6AzGal (**3**). Enzyme assays were carried out at 37°C in phosphate-buffered saline at a range of substrate concentrations and in the presence of 15% DMF. c) Plot of the rate constants for the inactivation of purified *E. coli* LacZ versus the concentration of the inactivator (6Az2FGalF). Residual enzyme activity was monitored as a function of time by periodically injecting an aliquot of the inactivation mixture into a vessel containing 6.5 mM pNPGal. The inactivation process followed pseudo-first-order kinetics. The progress of the enzymatic reaction was followed continuously by monitoring the release of *para*-nitrophenolate anions (absorbance at 400 nm).



Scheme 2. a) i) Tetrabutylammonium hydrogen sulfate, CH_2Cl_2 , *p*-ClSPh, 1 M NaOH, ii) NaOMe, MeOH, iii) Amberlyst IR-20 H⁺, 67%; b) TsCl, py; c) NaN₃, DMF, 80°C, 56%; d) Ac₂O, py, 82%; e) i) *N*-bromosuccinimide, acetone, H₂O, ii) diethylaminosulfur trifluoride, tetrahydrofuran, CH_2Cl_2 , -40°C to RT; f) i) NaOMe, MeOH, ii) Amberlyst IR-20 H⁺, 58% over two steps.

Staudinger ligation are highly specific, and neither treatment independently results in the labeling of proteins from cell lysates.

To demonstrate the versatility of these reagents we applied our labeling strategy to five other retaining β -glycosidases reported to have β -galactosidase activity. Two of these were recombinant bacterial enzymes, *Agrobacterium* sp. β -glucosidase (Abg)^[23] and *Xanthomonas manihotis* β -galactosidase (Xbg).^[24] The other three enzymes (a plant β -glucosidase from sweet almond (Sabg),^[25] a fungal β -galactosidase from *Aspergillus oryzae* (Aobg),^[21] and the yeast β -galactosidase preparation from *Kluveromyces lactis* (Kbg) known as Lactozym^[26])

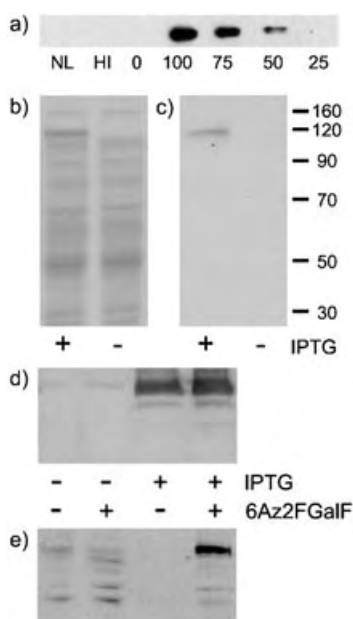


Figure 3. a) Western blot showing the detection limit of 6Az2FGalF, used in conjunction with Staudinger ligation. NL, no 6Az2FGalF; HI, heat-inactivated LacZ (100 ng); 0, 0 ng LacZ; 100, 100 ng LacZ; 75, 75 ng LacZ; 50, 50 ng LacZ; 25, 25 ng LacZ. After inactivation, the samples were labeled with phosphine-FLAG and analyzed by the Western blot technique using anti-FLAG-HRP (HRP, horseradish peroxidase). b) SDS-PAGE analysis of cell lysates from cultures of *E. coli* K-12, either induced with isopropyl-β-D-thiogalactopyranoside (IPTG; 0.1 mM) or not induced. c) Western blot treated with anti-FLAG-HRP to detect LacZ in the lysates of cells grown in the presence or absence of IPTG. Samples were treated or untreated with 6Az2FGalF and reacted with phosphine-FLAG. d) Western blot analysis of LacZ levels in the lysates of cells grown in the presence or absence of IPTG. The blot was probed by treatment with a mouse anti-LacZ monoclonal antibody followed by an anti-mouse IgG-HRP conjugate. e) The Western blot shown in (d) stripped and probed with anti-FLAG-HRP.

are commercially available. In each case, we observed specific labeling of the enzymes (Figure 4a) in a manner dependent on inactivation with 6Az2FGalF, just as observed for LacZ (Figure 3). Of the six enzymes studied, two are from Family 1 (Abg and Sabg), two from Family 2 (LacZ and Kbg), and two from Family 35 (Xbg and Aobg) of the glycoside hydrolases.^[1] Members of the same glycoside hydrolase family have been shown to have similar protein folds and active site architectures, and to effect catalysis through similar transition states.^[27–29] The ability of our reagents to label enzymes from different glycoside hydrolase families suggests that this strategy will be applicable to many families of retaining glycosidases.

In summary, we have developed a strategy for activity-based labeling of retaining glycosidases by using the azide group as a sterically unobtrusive chemical tag. The high selectivity of both the inactivation with fluorosugars and the Staudinger ligation with phosphine probes allows detection of glycosidases in complex mixtures and the strategy can be used for profiling these enzyme activities in cell lysates. We have demonstrated that the approach can be used to tag several glycosidases from different glycoside hydrolase families. We

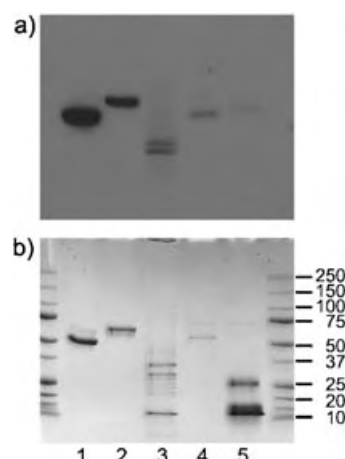


Figure 4. Labeling of five β-retaining glycosidases by using 6Az2FGalF in conjunction with Staudinger ligation. a) Western blot of samples of *Agrobacterium* sp. β-glucosidase (Lane 1), *Xanthomonas manihotis* β-galactosidase (Lane 2), *Aspergillus oryzae* β-galactosidase (Lane 3), *Kluyveromyces lactis* β-galactosidase (Lane 4), and sweet almond β-glucosidase (Lane 5). After inactivation, the samples were labeled with phosphine-FLAG and then analyzed by Western blotting using anti-FLAG-HRP. b) SDS-PAGE analysis of the samples shown in (a). Molecular weight standards are shown on the right.

anticipate that the strategy will find broad utility in proteomic analysis of these enzymes in prokaryotic and eukaryotic proteomes. The azide group might also be useful as a chemical tag within inactivators of other enzymes from entirely different families with sterically confining active sites.

Received: March 11, 2004

Revised: June 28, 2004 [Z54235]

Keywords: carbohydrates · glycosidases · mechanism-based inactivators · proteomics · Staudinger ligation

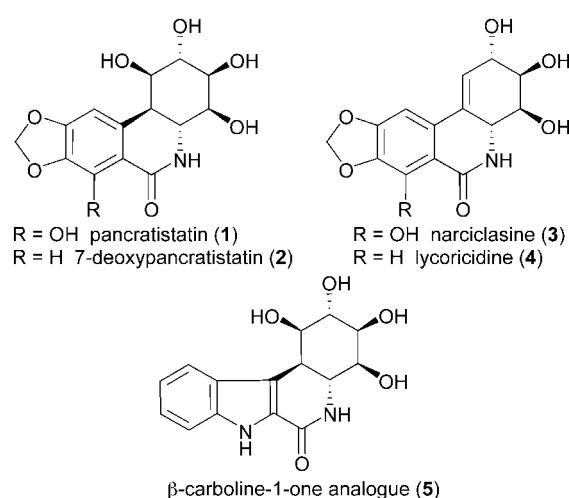
- [1] B. Henrissat, G. Davies, *Curr. Opin. Struct. Biol.* **1997**, 7, 637–644.
- [2] G. C. Adam, E. J. Sorensen, B. F. Cravatt, *Mol. Cell. Proteomics* **2002**, 1, 781–790.
- [3] T. Nazif, M. Bogyo, *Proc. Natl. Acad. Sci. USA* **2001**, 98, 2967–2972.
- [4] D. Leung, C. Hardouin, D. L. Boger, B. F. Cravatt, *Nat. Biotechnol.* **2003**, 21, 687–691.
- [5] D. Greenbaum, K. F. Medzhradszky, A. Burlingame, M. Bogyo, *Chem. Biol.* **2000**, 7, 569–581.
- [6] A. E. Speers, G. C. Adam, B. F. Cravatt, *J. Am. Chem. Soc.* **2003**, 125, 4686–4687.
- [7] H. Ovaa, P. F. van Swieten, B. M. Kessler, M. A. Leeuwenburgh, E. Fiebigler, A. M. C. H. van den Nieuwendijk, P. J. Galardy, G. A. van der Marel, H. L. Ploegh, H. S. Overkleeft, *Angew. Chem.* **2003**, 115, 3754–3757; *Angew. Chem. Int. Ed.* **2003**, 42, 3626–3629.
- [8] G. J. Davies, B. Henrissat, *Biochem. Soc. Trans.* **2002**, 30, 291–297.
- [9] C.-S. Tsai, Y.-K. Li, L.-C. Lo, *Org. Lett.* **2002**, 4, 3607–3610.
- [10] M. Ichikawa, Y. Ichikawa, *Bioorg. Med. Chem. Lett.* **2001**, 11, 1769–1773.

- [11] J. Wicki, D. R. Rose, S. G. Withers, *Methods Enzymol.* **2002**, 354, 84–105.
- [12] D. J. Vocadlo, G. J. Davies, R. Laine, S. G. Withers, *Nature* **2001**, 412, 835–838.
- [13] G. J. Davies, L. Mackenzie, A. Varrot, M. Dauter, A. M. Brzozowski, M. Schulein, S. G. Withers, *Biochemistry* **1998**, 37, 11 707–11 713.
- [14] D. J. Vocadlo, S. G. Withers, *Methods Mol. Biol.* **2000**, 146, 203–222.
- [15] S. G. Withers, K. Rupitz, I. P. Street, *J. Biol. Chem.* **1988**, 263, 7929–7932.
- [16] E. Saxon, C. R. Bertozzi, *Science* **2000**, 287, 2007–2010.
- [17] V. V. Rostovtsev, L. G. Green, V. V. Fokin, K. B. Sharpless, *Angew. Chem.* **2002**, 114, 2708–2711; *Angew. Chem. Int. Ed.* **2002**, 41, 2596–2599.
- [18] J. C. Gebler, R. Aebersold, S. G. Withers, *J. Biol. Chem.* **1992**, 267, 11 126–11 130.
- [19] D. H. Juers, T. D. Heightman, A. Vasella, J. D. McCarter, L. Mackenzie, S. G. Withers, B. W. Matthews, *Biochemistry* **2001**, 40, 14 781–14 794.
- [20] J. D. McCarter, M. J. Adam, S. G. Withers, *Biochem. J.* **1992**, 286, 721–727.
- [21] U. Grabowska, D. A. MacManus, K. Biggadike, M. I. Bird, S. Davies, T. Gallagher, L. D. Hall, E. N. Vulfson, *Carbohydr. Res.* **1997**, 305, 351–361.
- [22] D. A. MacManus, U. Grabowska, K. Biggadike, M. I. Bird, S. Davies, E. N. Vulfson, T. Gallagher, *J. Chem. Soc. Perkin Trans. 1* **1999**, 295–305.
- [23] J. B. Kempton, S. G. Withers, *Biochemistry* **1992**, 31, 9961–9969.
- [24] J. E. Blanchard, L. Gal, S. He, J. Foisy, R. A. Warren, S. G. Withers, *Carbohydr. Res.* **2001**, 333, 7–17.
- [25] S. He, S. G. Withers, *J. Biol. Chem.* **1997**, 272, 24 864–24 867.
- [26] T. Maugard, D. Gaunt, M. D. Legoy, T. Besson, *Biotechnol. Lett.* **2003**, 25, 623–629.
- [27] G. J. Davies, M. L. Sinnott, S. G. Withers, in *Comprehensive Biological Catalysis, Vol. 1* (Ed.: M. L. Sinnott), Academic Press, London, **1997**, pp. 119–208.
- [28] J. Gebler, N. R. Gilkes, M. Claeysens, D. B. Wilson, P. Beguin, W. W. Wakarchuk, D. G. Kilburn, R. C. Miller, Jr., R. A. Warren, S. G. Withers, *J. Biol. Chem.* **1992**, 267, 12 559–12 561.
- [29] M. W. Bauer, R. M. Kelly, *Biochemistry* **1998**, 37, 17 170–17 178.

A β -Carboline-1-one Mimic of the Anticancer *Amaryllidaceae* Constituent Pancratistatin: Synthesis and Biological Evaluation**

Uwe Rinner, Tomas Hudlicky,* Heather Gordon, and George R. Pettit

Pancratistatin (**1**) and narciclasine (**3**; Scheme 1), well-known constituents^[1] of the *Amaryllidaceae* species, have been the subject of intense study, both in the realm of total synthesis^[2] and with respect to their anticancer activities.^[3] Both compounds contain a free phenolic hydroxy group that is part of the enolized β -ketoamide function. It is this functional group that accounts for the greater (10-fold or more) activity of



Scheme 1. *Amaryllidaceae* constituents containing the enolized β -ketoamide motif and their β -carboline-1-one analogue.

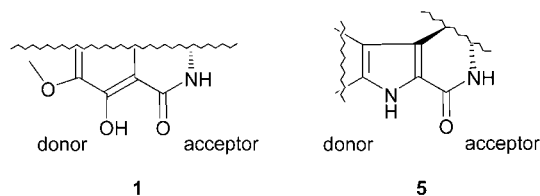
[*] Dr. U. Rinner, Prof. Dr. T. Hudlicky, Prof. Dr. H. Gordon
Department of Chemistry
Brock University
500 Glenridge Avenue, St. Catharines, Ontario L2S 3A1 (Canada)
Fax: (+1) 905-984-4841
E-mail: thudlicky@brocku.ca
Prof. Dr. G. R. Pettit
Department of Chemistry & Biochemistry and
the Cancer Research Institute
Arizona State University
Tempe, Arizona 85287 (USA)

[**] The authors are grateful to the following agencies for their support of this work: the National Science and Engineering Research Council, the Canadian Foundation for Innovation, the Ontario Innovation Trust, Brock University, the donors of the Petroleum Research Fund (administered by the American Chemical Society; Grant no. PRF-38075-AC), TDC Research Inc., and TDC Research Foundation. G.R.P. also thanks the Division of Cancer Research Treatment and Diagnosis, National Cancer Institute, Department of Health and Human Services (Grant no. R01-CA90441-03), and the Arizona Disease Control Research Commission for financial support and is also grateful for the assistance provided by Dr. Jean-Charles Chapuis and Dr. Jean M. Schmidt.

these compounds compared to that of their congeners 7-deoxypancratistatin (**2**) and lycoricidine (**4**), which lack the phenol group.^[4]

Several research groups have focused their efforts on identifying the pharmacophore of these plant constituents.^[5] To this end, a series of derivatives of **1** have been prepared in which functionalities in the aminoinositol moiety have been deleted or changed,^[6] or in which the skeleton has been truncated to produce smaller derivatives.^[5c] No modification of the aminoinositol ring has led to an increase in the activity of such derivatives. Truncated derivatives that retain the phenanthridone moiety show decreased activities compared to that of the parent compound. An account of the synthesis of a lactone analogue of **1** containing a carbohydrate motif appeared recently but no biological evaluation of the compound was reported.^[7]

Pancratistatin has been proved active in antiviral screens^[3f] and is highly active against various cancer cell lines in vitro and in vivo. However, it has poor bioavailability and a major effort has been made to develop more soluble analogues or prodrugs.^[5a,8] We speculated that the potency of **1** and **3** may in part be due to the hydrogen-bonding donor–acceptor pairing of the β -ketoamide motifs present in these compounds but absent from the 7-deoxy congeners. We therefore decided to test the β -carboline-1-one analogue of **1**, compound **5**, in which such donor–acceptor pairing is extended through the vinyl indole ring, as shown in Scheme 2. The steric and, to some degree, the electronic



Scheme 2. Donor–acceptor pairing for hydrogen bonding in pancratistatin (**1**) and β -carboline-1-one analogue **5**.

properties of **1** and **5** are similar. We expected the β -carboline-1-one analogue to interfere with RNA transcription by the mechanism proposed for the activity of narciclasine (**3**), the only member of the *Amaryllidaceae* family for which data on the possible mode of action are available.^[3c,d] In addition, β -carboline-1-ones and sterically constrained tryptamines have been found to have serotonin-regulating activity.^[9]

Molecular models of these two compounds, pancratistatin (**1**) and its carboline-1-one mimic **5**, show interesting spatial similarities (Figures 1 and 2). Except for the electron density associated with the methylenedioxy bridge of **1**, the compounds seem to occupy almost identical space, as confirmed in Figure 2, which shows that the functionalities of the two compounds directly overlap.

Geometry optimizations of both pancratistatin (**1**) and its β -carboline-1-one analogue **5** were performed at the HF/6-31G* level of theory by using the Gaussian 03 package.^[10] We calculated the optimal geometries of the compounds in vacuo. The initial orientations of the aminoinositol hydroxy groups

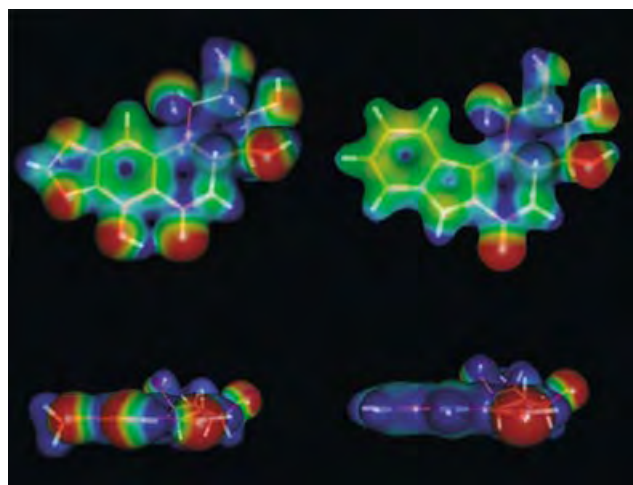


Figure 1. Comparison of the electrostatic potential energy surfaces of minimum energy conformations of pancratistatin (**1**; left) and β -carboline-1-one analogue **5** (right). The isodensity surfaces are color-coded according to the electrostatic potential: red -0.05 , yellow 0.00 , green 0.05 , light blue 0.10 , blue 0.15 e.

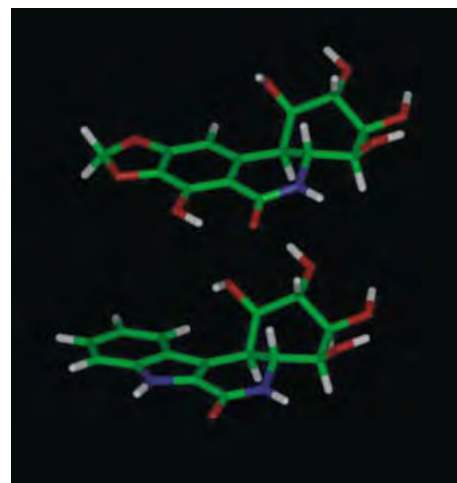


Figure 2. Direct overlap of the structures of pancratistatin (**1**, top) and β -carboline-1-one analogue **5** (bottom).

were obtained by carrying out a concerted dihedral search using the CHARMM molecular mechanics forcefield.^[11] Not surprisingly, the lowest energy conformation of the phenolic hydroxy group under these conditions is that required to form an intramolecular hydrogen bond with the amide carbonyl oxygen atom.

The isodensity surfaces displayed in Figure 1 were constructed with the program Molden^[12] and are color-coded according to the electrostatic potential. The geometry-optimized structures were superimposed based on the positions of the atoms of the shared aminoinositol moiety. Figure 1 clearly illustrates the difference between the electrostatic potential of the putative hydrogen-bond donor–acceptor pair of the β -ketoamide motif of **1** and that of the analogous portion of **5**. The hydrogen-bonding β -ketoamide motif has three distinct regions of negative electrostatic potential, while the equiv-

alent part of **5** has negative electrostatic energy only around the carbonyl oxygen atom.

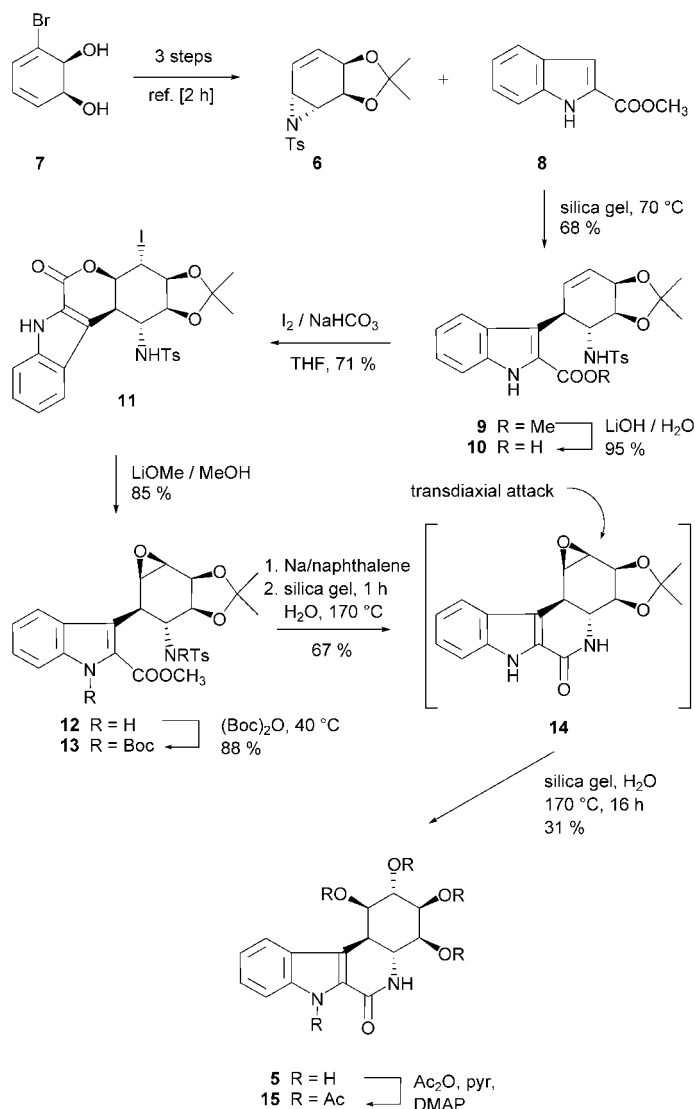
Herein we report a concise synthesis of **5** that features a number of interesting transformations (Scheme 3), along with

to open aziridines under InCl_3 catalysis^[16] and condensed smoothly with **6** under silica gel catalysis. However, we did not expect ester **8** to react well with **6** because of the decreased nucleophilicity of the 3-position of the indole as a result of conjugation to the vinyl urethane function. Lewis acid catalysis provided low yields of **9** compared to those obtained from the reactions on the silica surface.^[17–19]

The methyl ester group of **9** was hydrolyzed ($\text{LiOH}/\text{H}_2\text{O}$, 12 h, RT) and the free acid **10** subjected to iodolactonization to produce lactone **11** as a single stereoisomer in 71 % yield.^[20] This protocol allowed full control of the stereochemistry while avoiding the use of oxidizing agents or other epoxidation procedures that would have been detrimental to the fate of the indole core. Exposure of lactone **11** to LiOMe/MeOH gave epoxide **12** cleanly. This transformation could also be achieved by using a two-step procedure ($\text{LiOH}/\text{H}_2\text{O}$; CH_2N_2 ; 85 % yield). Detosylation of compounds of this type has been shown to proceed more smoothly when the tosylamide is first converted into an imide.^[2e,5b] We converted **12** into the *bis*-Boc-protected material **13** (88 % yield), which was easily detosylated in 71 % yield by treatment with sodium naphthalide at -65°C .

The final transformation of **13** into the β -carboline-1-one analogue **5** was accomplished in a one-flask sequence during which four separate events took place. A sample of **13** was dissolved in acetone and adsorbed on silica. The dry powder was suspended in H_2O , placed in a thick-walled pressure tube, and heated at 170°C . After one hour the material had been quantitatively transformed into the free amide **14** by a thermal retro-ene reaction of the Boc-carbamate and internal amidation of the methyl ester. Thermolysis on wet silica gel is superior to the previously reported technique, in which the starting material was treated with 5 % aqueous sodium benzoate under reflux.^[21] Separation of polar products from benzoic acid is often problematic on a small scale. Continued heating of **14** for an additional 16 h at 160°C resulted in its conversion into **5**, which was obtained as a single stereoisomer through transdiaxial opening of the epoxide and thermolytic cleavage of the acetonide. Pure carboline-1-one derivative **5**, a sparingly soluble compound, was isolated by chromatography. The crude product was converted into its pentaacetate **15** for use in detailed NMR studies because **15** is more easily purified than **5**.

β -Carboline-1-one **5** and each of the key intermediates in this nine-step sequence were tested against a small panel of cancer cell lines. The results are shown in Table 1 as GI_{50} values (amount of substrate in $\mu\text{g mL}^{-1}$ cell solution necessary to stop the growth of 50 % of the cancer cells in 1 mL cell solution). The cutoff for activity in human cancer cell lines is considered to be $10 \mu\text{g mL}^{-1}$. Some of the indole modifications produced compounds that meet this criterion for activity against certain cancer cell lines. Biological evaluation of **5** confirmed borderline activity in the murine P388 lymphocytic leukemia assay. Surprisingly, iodolactone **11** showed promising activities against pancreas and breast adenocarcinoma ($\text{GI}_{50} = 1.9$ and $4.3 \mu\text{g mL}^{-1}$). It is possible that the mechanism of action of the iodolactone is different from that of pancratistatin and it may be beneficial to examine **11** as a completely different scaffold on which the design of further



Scheme 3. Synthesis of β -carboline-1-one analogue **5**. Boc = *tert*-butoxycarbonyl, DMAP = 4-dimethylaminopyridine, pyr = pyridine, Ts = tosyl.

the biological evaluation of the product in a series of cancer cell lines as a prelude to a more focused drug discovery effort aimed at the heterocyclic variants of **1**. We found that the synthesis of **5** is easier than the preparation or extraction of the natural alkaloids.

The synthesis began with vinylaziridine **6**,^[2e,13] which was prepared in three steps from enzymatically derived diene-diol **7**,^[14] and methyl indole-2-carboxylate (**8**), prepared from commercially available indole-2-carboxylic acid.^[15] The two compounds were adsorbed on silica and heated at 70°C for 48 h to provide tosylamide **9** cleanly in 68 % yield. This transformation was surprising. Indole itself has been reported

Table 1: Evaluation of the activities of β -carboline-1-one and intermediates in the synthesis, as well as pancratistatin and 7-deoxypancratistatin, against Murine P388 lymphocytic leukemia and human cancer cell lines. GI_{50} -values in $[\mu g mL^{-1}]^{[a]}$.

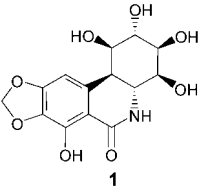
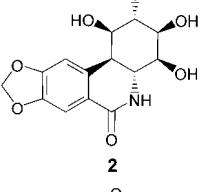
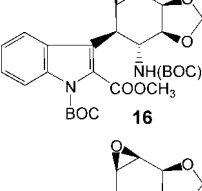
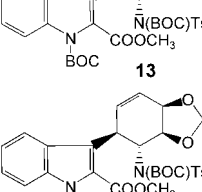
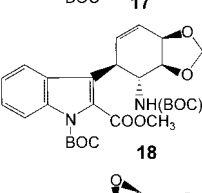
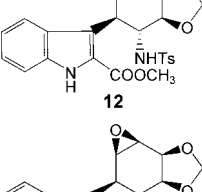
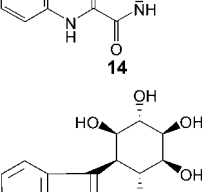
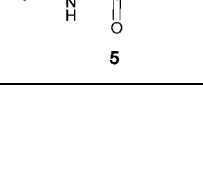

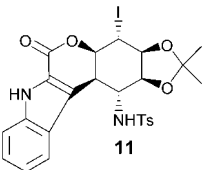
Compound	P388 ^[b]	BXPC-3 ^[c]	MCF-7 ^[d]	KM20L2 ^[e]
	0.02	0.03	–	0.045
	0.44	–	–	0.22
	22.8	> 10	> 10	> 10
	12.8	> 10	> 10	> 10
	11.8	8.6	10.5	> 10
	4.6	> 10	> 10	> 10
	> 100	> 10	> 10	3.5
	> 100	> 10	> 10	3.8
	18.3	> 10	> 10	> 10

Table 1: (Continued)

Compound	P388 ^[b]	BXPC-3 ^[c]	MCF-7 ^[d]	KM20L2 ^[e]
	11.7	1.9	4.3	> 10

[a] No significant activity against human SF268 (CNS glioblastoma), NCI-H460 (lung large cell), or DU-145 (prostate carcinoma) was detected. [b] P388, lymphocytic leukemia. [c] BXPC-3, pancreas adenocarcinoma (human). [d] MCF-7, breast adenocarcinoma (human). [e] KM20L2, colon adenocarcinoma (human).

derivatives could be based. *bis*-Boc derivative **13** and unsaturated analogues **17** and **18** are also active against murine P388 lymphocytic leukemia, with GI_{50} values (12.8, 11.8, and $4.6 \mu g mL^{-1}$, respectively) one order of magnitude smaller than that of 7-deoxypancratistatin ($GI_{50} = 0.44 \mu g mL^{-1}$). These exciting results suggest new possibilities that should be examined in the next series of analogues.

Some guidelines for the design of new analogues emerged as a result of this particular study: 1) The presence of both the oxygen atoms in the methylenedioxy bridge of pancratistatin seems essential for high activity. We recently showed that deletion of the C8 methoxy group from the dimethoxy derivative of **1** leads to GI_{50} values 10- to 20-fold higher than that of the natural product.^[5d] 2) The activity of compounds such as lactone **11** opens up the possibility that analogues can be structured around completely different scaffolds in future because such compounds can be further functionalized at a number of positions. 3) The synthesis of **5** is, with nine steps, the shortest existing preparation of pancratistatin analogues containing the aminoinositol motif. Some of the transformations that were employed will no doubt find further application in the design of heterocyclic analogues of pancratistatin. 4) The vinylaziridine **6** proved useful as a scaffold for the generation of diversity and will be further exploited in the design of new derivatives of the title compounds.

Future endeavors in this area will focus on heteroatom alterations in the aromatic portion of pancratistatin as it has already been shown that the aminoinositol moiety must remain intact for these compounds to retain activity. We will report our findings in due course.

Received: April 5, 2004

Revised: June 21, 2004

Keywords: antitumor agents · asymmetric synthesis · natural products · pancratistatin · synthetic methods

[1] The pancratistatin, narciclasine, and lycoricidine group of natural products has been collectively referred to as “*Amaryllidaceae* alkaloids” by most, if not all, synthetic chemists (Martin, Hudlicky, Keck, Polt, and others). Such nomenclature is not accurate as these compounds do not contain basic nitrogen atoms. Another term used in the literature is “isocarbostryl”

- (Pettit), a term which is correct but not generally known in the synthetic community. To avoid further inaccuracies we will avoid both names in future publications and simply refer to these compounds as "constituents".
- [2] For reviews, see: a) S. F. Martin in *The Alkaloids*, Vol. 40 (Ed.: A. R. Brossi), Academic Press, New York, **1987**, pp. 251–376; b) R. Polt in *Organic Synthesis: Theory and Applications*, Vol. 3 (Ed.: T. Hudlicky), JAI, Greenwich, CT, **1998**, pp. 109–148; c) O. Hoshino in *The Alkaloids*, Vol. 51 (Ed.: G. A. Cordell), Academic Press, New York, **1998**, pp. 323–424; for total syntheses of pancratistatin, see: d) S. Danishefsky, J. Y. Lee, *J. Am. Chem. Soc.* **1989**, *111*, 4829–4837; e) X. R. Tian, T. Hudlicky, K. Königsberger, *J. Am. Chem. Soc.* **1995**, *117*, 3643–3644; f) B. M. Trost, S. R. Pulley, *J. Am. Chem. Soc.* **1995**, *117*, 10143–10144; g) G. E. Keck, S. F. McHardy, J. A. Murry, *J. Am. Chem. Soc.* **1995**, *117*, 7289–7290; h) T. Hudlicky, X. R. Tian, K. Königsberger, R. Maurya, J. Rouden, B. Fan, *J. Am. Chem. Soc.* **1996**, *118*, 10752–10765; i) N. Chida, M. Jitsuoka, Y. Yamamoto, M. Ohtsuka, S. Ogawa, *Heterocycles* **1996**, *43*, 1385–1390; j) T. J. Doyle, M. Hendrix, D. VanDerveer, S. Javanmard, J. Haseltine, *Tetrahedron* **1997**, *53*, 11153–11170; k) P. Magnus, I. K. Sebbat, *Tetrahedron* **1998**, *54*, 15509–15524; l) P. Magnus, I. K. Sebbat, *J. Am. Chem. Soc.* **1998**, *120*, 5341–5342; m) J. H. Rigby, U. S. M. Maharoo, M. E. Mateo, *J. Am. Chem. Soc.* **2000**, *122*, 6624–6628; n) G. R. Pettit, N. Melody, D. L. Herald, *J. Org. Chem.* **2001**, *66*, 2583–2587; o) S. Kim, H. Ko, E. Kim, D. Kim, *Org. Lett.* **2002**, *4*, 1343–1345; p) H. J. Kim, E. Kim, J. E. Park, D. Kim, S. Kim, *J. Org. Chem.* **2004**, *69*, 112; for total syntheses of narciclasine, see: q) J. H. Rigby, M. E. Mateo, *J. Am. Chem. Soc.* **1997**, *119*, 12655–12656; r) G. E. Keck, T. T. Wager, J. F. D. Rodriguez, *J. Am. Chem. Soc.* **1999**, *121*, 5176–5190; s) D. Gonzalez, T. Martinot, T. Hudlicky, *Tetrahedron Lett.* **1999**, *40*, 3081–3084; t) S. Elango, T.-H. Yan, *J. Org. Chem.* **2002**, *67*, 6954–6959.
 - [3] For studies on the biological activity of *Amaryllidaceae* constituents, see: a) D. B. Fitzgerald, J. L. Hartwell, J. Leiter, *J. Natl. Cancer Inst.* **1958**, *20*, 763–764; b) G. Ceriotti, *Nature* **1967**, *213*, 595–596; c) L. Carrasco, M. Fresno, D. Vazquez, *FEBS Lett.* **1975**, *52*, 236–239; d) A. Jimenez, L. Sanchez, D. Vazquez, *FEBS Lett.* **1975**, *55*, 53–56; e) A. Jimenez, A. Santos, G. Alonso, D. Vazquez, *Biochim. Biophys. Acta* **1976**, *425*, 342–348; f) G. R. Pettit, V. Gaddamidi, D. L. Herald, S. B. Singh, G. M. Cragg, J. M. Schmidt, F. E. Boettner, M. Williams, Y. Sagawa, *J. Nat. Prod.* **1986**, *49*, 995–1002; g) B. Gabrielsen, T. P. Monath, J. W. Huggins, D. F. Kefauver, G. R. Pettit, G. Groszek, M. Hollingshead, J. J. Kirs, W. M. Shannon, E. M. Schubert, J. Dare, B. Ugarkar, M. A. Ussery, M. J. Phelan, *J. Nat. Prod.* **1992**, *55*, 1569–1581.
 - [4] G. R. Pettit, N. Melody, D. L. Herald, J. M. Schmidt, R. K. Pettit, J.-C. Chapuis, *Heterocycles* **2002**, *56*, 139–155.
 - [5] a) G. R. Pettit, S. Freeman, M. J. Simpson, M. A. Thompson, M. R. Boyd, M. D. Williams, G. R. Pettit III, D. L. Doubek, *Anti-Cancer Drug Des.* **1995**, *10*, 243–250; b) J. McNulty, R. Mao, S. Wolf, G. R. Pettit, D. L. Herald, M. R. Boyd, *Bioorg. Med. Chem. Lett.* **2001**, *11*, 169–172; c) T. Hudlicky, U. Rinner, D. Gonzalez, H. Akgun, S. Schilling, P. Siengalewicz, T. A. Martinot, G. R. Pettit, *J. Org. Chem.* **2002**, *67*, 8726–8743; d) U. Rinner, H. Hillebrenner, D. R. Adams, T. Hudlicky, G. R. Pettit, *Bioorg. Med. Chem. Lett.* **2004**, in press.
 - [6] S. Schilling, U. Rinner, C. Chan, I. Ghiviriga, T. Hudlicky, *Can. J. Chem.* **2001**, *79*, 1659–1667.
 - [7] A. N. Phung, M. T. Zannetti, G. Whited, W. D. Fessner, *Angew. Chem.* **2003**, *115*, 4970–4972; *Angew. Chem. Int. Ed.* **2003**, *42*, 4821–4824.
 - [8] G. R. Pettit, B. Orr, S. Ducki, *Anti-Cancer Drug Des.* **2000**, *15*, 389–395.
 - [9] S. Elz, H. Zimmermann, K. Rehse, *Arch. Pharm.* **1993**, *326*, 893–899; b) K. Rehse, H. Zimmermann, *Arch. Pharm.* **1994**, *327*, 67–75.
 - [10] Gaussian03, Revision B.03, M. J. Frisch, G. W. Trucks, H. B. Schlegel, G. E. Scuseria, M. A. Robb, J. R. Cheeseman, J. A. Montgomery, Jr., T. Vreven, K. N. Kudin, J. C. Burant, J. M. Millam, S. S. Iyengar, J. Tomasi, V. Barone, B. Mennucci, M. Cossi, G. Scalami, N. Rega, G. A. Petersson, H. Nakatsuji, M. Hada, M. Ehara, K. Toyota, R. Fukuda, J. Hasegawa, M. Ishida, T. Nakajima, Y. Honda, O. Kitao, H. Nakai, M. Klene, X. Li, J. E. Knox, H. P. Hratchian, J. B. Cross, C. Adamo, J. Jaramillo, R. Gomperts, R. E. Stratmann, O. Yazyev, A. J. Austin, R. Cammi, C. Pomelli, J. W. Ochterski, P. Y. Ayala, K. Morokuma, G. A. Voth, P. Salvador, J. J. Dannenberg, V. G. Zakrzewski, S. Dapprich, A. D. Daniels, M. C. Strain, O. Farkas, D. K. Malick, A. D. Rabuck, K. Raghavachari, J. B. Foresman, J. V. Ortiz, Q. Cui, A. G. Baboul, S. Clifford, J. Cioslowski, B. B. Stefanov, G. Liu, A. Liashenko, P. Piskorz, I. Komaromi, R. L. Martin, D. J. Fox, T. Keith, M. A. Al-Laham, C. Y. Peng, A. Nanayakkara, M. Challacombe, P. M. W. Gill, B. Johnson, W. Chen, M. W. Wong, C. Gonzalez, J. A. Pople, Gaussian, Inc., Pittsburgh, PA, **2003**.
 - [11] a) CHARMM, Accelrys, Inc., **2001**; b) B. R. Brooks, R. E. Bruccoleri, B. D. Olafson, D. J. States, S. Swaminathan, M. Karplus, *J. Comput. Chem.* **1983**, *4*, 187–217.
 - [12] G. Schaftenaar, J. H. Noordik, *J. Comput.-Aided Mol. Des.* **2000**, *14*, 123–134.
 - [13] T. Hudlicky, X. Tian, K. Königsberger, J. Rouden, *J. Org. Chem.* **1994**, *59*, 4037–4039.
 - [14] T. Hudlicky, H. Luna, H. F. Olivo, C. Andersen, T. Nugent, J. D. Price, *J. Chem. Soc. Perkin Trans. 1* **1991**, 2907–2917.
 - [15] T. Martin, C. J. Moody, *J. Chem. Soc. Perkin Trans. 1* **1998**, 235–240.
 - [16] J. S. Yadav, B. V. S. Reddy, S. Abraham, G. Sabitha, *Tetrahedron Lett.* **2002**, *43*, 1565–1567.
 - [17] M. Hudlicky, *J. Org. Chem.* **1974**, *39*, 3460–3461.
 - [18] T. Hudlicky, T. Srnak, *Tetrahedron Lett.* **1981**, *22*, 3351–3354.
 - [19] A. K. Banerjee, M. S. L. Mimos, W. J. V. Vegas, *Usp. Khim.* **2001**, *70*, 1094–1115.
 - [20] M. Jung, J. Ham, J. Song, *Org. Lett.* **2002**, *4*, 2763–2765.
 - [21] M. Mandel, T. Hudlicky, L. D. Kwart, G. M. Whited, *J. Org. Chem.* **1993**, *58*, 2331–2333.

The Development of Descriptors for Solids: Teaching “Catalytic Intuition” to a Computer

Catharina Klanner, David Farrusseng, Laurent Baumes, Mourad Lengliz, Claude Mirodatos, and Ferdi Schüth*

High-throughput experimentation has become an accepted and important strategy in the search for novel catalysts and materials.^[1–7] However, one of the major problems is still the design of libraries, especially, if vast numbers of catalysts are to be explored. On the other end of the work flow, after catalysts have been tested, data mining and the search for trends is equally demanding. Several methods based on expert systems^[8] have been proposed to support the development of solid catalysts. Also the correlation of performance with catalyst composition, evaluated by neural networks, has been used for the optimization of catalysts.^[9–11] For such optimization programs in catalysis, evolutionary algorithms were found to be helpful as well.^[12,13] However, in these approaches the scope was usually very limited, and an attempt to include a wide range of properties to describe the solids was not made. A more integrated “knowledge extraction engine” has been proposed by Caruthers et al.^[14] for propane aromatization which is, however, focused on the reaction engineering aspects.

There is a great need for software-based methods to plan the design of libraries based on chemical knowledge, in addition to the statistical tools which are implemented in some of the commercial software packages. QSAR (quantitative structure–activity relationship) is one of the most powerful methods used in drug discovery to design libraries and to extract knowledge from tests on possible drug libraries. Such structure–activity relationships are discovered by computer programs, for which molecules need to be represented in computer data bases by so-called descriptors. The descriptors can, for instance, be two-dimensional fingerprints, such as absence or presence of certain chemical functional groups, or can be pharmacophores, which relate to the relative spatial arrangement of three selected chemical functional groups, or physico–chemical properties, or many others.^[15] Whole journals are by now devoted to this topic.^[16]

However, owing to the different nature of the problem, a transfer of descriptor concepts to solids has not been possible to date. In contrast to molecules, a solid can not easily be represented in a computer, since no structural formula can be given and encoded. If only the composition of a solid would

be used, many important factors would be lost, since properties of a catalyst, for instance, are also very much dependent on the synthesis and the conditions of the reaction itself. There is one preceding study in which descriptors have been used to correlate structural features of zeolites with the ring size in the structures.^[17] Recently, we suggested a methodology to apply to heterogeneous catalysis which was expected to work in a similar manner to the molecular descriptors.^[18] It can to some extent be considered to be a multidimensional version of the volcano principle known in catalysis for decades.^[19] Herein, we show that these concepts can indeed be implemented. The descriptors thus developed have predictive power and the concept can therefore be considered as the transfer of “catalytic intuition” to a computer.

The method, in short, consists of the creation of a library of solids, testing of the performance in a catalytic reaction, description of the solids in terms of a multitude of attributes which are available either from the synthesis of the solid or from tabulated physico–chemical data, and, finally, the identification of a set of those attributes which allow discrimination between different catalytic performance.

A highly diverse library was synthesized, consisting of 467 different catalysts. Diversity in this case was judged by chemical intuition, based on the accumulated knowledge in the field. The library included binary oxides, multinary mixed oxides, supported catalysts on different support materials with various supported compounds, zeolites, and many other types. All the catalysts of this library were tested in the oxidation of propene with oxygen ($O_2:C_3H_6 = 5:1$, that is, slightly above stoichiometric for total oxidation) in a 16-fold parallel reactor which was a more advanced stainless steel version of the system described by Hoffmann et al.^[20] Products were analyzed sequentially by GC, which allowed the detection of about 30 products. Each catalyst was measured twice, which also allowed its temporal behavior to be analyzed, at five temperature levels (200, 250, 300, 400, and 500 °C). In this way 120 parameters, that is, conversions, selectivities to 21 products, temporal behavior, and carbon mass balance, all at each temperature, were generated for every catalyst.

This set of data is too vast by far for a meaningful attempt at a correlation. We have thus classified the catalytic performances into distinct groups with respect to an analysis of the 120 output parameters, using principal components analysis and then clustering techniques based on euclidian distance. Figure 1 shows as an example the results of a tree cluster analysis. Each of the classes can be identified with a specific catalytic performance of the solids, as given in the legend to Figure 1.

The other major task was the encoding of the solids. For a virtual screening, only such attributes are useful, which are either derived from a possible synthesis method or are tabulated, so that they do not need to be measured. For each catalyst we have created a set of 3179 attributes, which include the concentrations of 60 elements from the periodic table, 19 attributes which are related to the synthesis method, and 3100 attributes which are taken from tabulated data. These are, for instance, enthalpies of formation of different oxides, possible coordination numbers of the atoms, ionization energies, electronegativities, averages of such values for

[*] Dr. C. Klanner, Prof. Dr. F. Schüth
Max-Planck-Institut für Kohlenforschung
Kaiser-Wilhelm-Platz 1
45470 Mülheim (Germany)
Fax: (+49) 208-306-2995
E-mail: schueth@mpi-muelheim.mpg.de

Dr. D. Farrusseng, L. Baumes, Prof. Dr. C. Mirodatos
Institut de Recherches sur la Catalyse—CNRS
2, avenue A. Einstein, 69626 Villeurbanne Cedex (France)

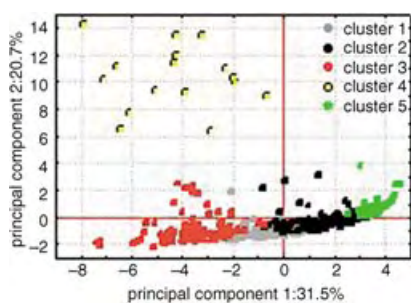


Figure 1. Results of a k-means cluster analysis based on eight principal components (PC) in the projection on the PC1-PC2 plane. The clusters which overlap in this projection are very well separated in the other principal components. With respect to catalytic performance, the catalysts can be described as follows: cluster 1 (gray) low activity, total oxidation, cluster 2 (black) medium activity, total oxidation, cluster 3 (red) low activity, CO and partial oxidation products, cluster 4 (yellow) hydrocarbon formation, cluster 5 (green) high activity, total oxidation.

multicomponent catalysts, variance of such values for multicomponent catalysts, and so on.

With 3179 attributes, a system of 467 catalysts is hopelessly over determined. Prior to a correlation, the number of attributes needed to be reduced. In principle, two different selection approaches can be chosen: The chemist can select those parameters which appear to be most promising, or software-based methods called feature selection can be employed. In our case different feature selection routines were tested, but none allowed discrimination between relevant attributes and attributes which had no correlation to the performance of the catalysts (although we would not claim that such discrimination is impossible). Thus, the number of attributes was reduced to 75 attributes by intuition, including all synthesis-related parameters and a set of parameters related to the properties of the elements, ions, or oxides.

For the correlation, both neural networks and classification trees, were used. In general, neural networks gave a better prediction of the performance class than classification trees. For the neural-network analysis, the catalyst set was divided at random into the training set (50 % of the catalysts), the selection set (25 %), and the test set (25 %), for the classification trees, two groups were formed, the training set (66 %) and the test set (33 %). Neural networks were trained for various different clusters based on a different number of principal components (PC), but in all cases the predictions were of comparable quality and vastly superior over a mere statistical prediction. Figure 2 gives a so-called confusion matrix for the prediction achieved with a neural network of the multilayer perceptron type on a data set with five clusters based on eight PCs. The initial 75 attributes were reduced to 45 relevant ones by the network algorithm. The “ratio” listed in the matrix gives the fraction of cases which would be predicted to belong to the specific class, if the assignment were made at random. This value can be compared directly with the “prediction rate”, which accounts for the correctly classified cases in the respective predicted class. As can be seen, the prediction rate far exceeds the ratio in all cases. The prediction is thus substantially better than statistically

test	cluster					sum	ratio	prediction rate	sensitivity
	1	2	3	4	5				
1 predicted	16	3	4	0	2	25	0.25	0.64	0.57
2 predicted	5	18	6	0	8	37	0.29	0.49	0.55
3 predicted	5	4	16	0	1	26	0.24	0.62	0.59
4 predicted	1	0	0	3	0	4	0.03	0.75	1.00
5 predicted	1	8	1	0	11	21	0.19	0.52	0.50
sum/ mean	28	33	27	3	22	113		0.60	0.64

Figure 2. Confusion matrix for descriptor-based classification of catalysts using an artificial neural network of the multilayer perceptron type. 45 attributes were selected as relevant by the network out of the 75 initial attributes. In total 113 different catalysts were classified, the colored boxes mark the number of correctly classified catalysts. The columns 1–5 indicate the cluster to which the catalysts belong (see legend to Figure 1), the rows 1 predicted to 5 predicted indicate the cluster (1–5) which was predicted for a given catalyst. The ratio describes the statistical expectation for the fraction of correctly classified catalysts, the prediction rate indicates the fraction of catalysts assigned to a certain cluster which actually belong to this cluster. This value can directly be compared to the ratio.

expected. The “sensitivity” is the fraction of cases correctly classified from the respective original class. For this value, no proper statistical benchmark can be given, but the numbers are all rather high, again indicating how good the correlation is. In addition, misclassifications occur predominantly in “catalytically related” classes, that is, catalysts are, for instance, sorted into the medium-activity class instead of the correct high-activity class, but less often into the low-activity class.

Classification tree analysis was also performed for several cases and Figure 3 gives a confusion matrix for such an

test	cluster					sum	ratio	prediction rate	sensitivity
	1	2	3	4	5				
1 predicted	18	7	14	0	7	46	0.25	0.39	0.45
2 predicted	6	19	10	1	9	45	0.27	0.42	0.44
3 predicted	11	2	12	0	0	25	0.25	0.48	0.31
4 predicted	2	3	2	5	0	12	0.04	0.42	0.83
5 predicted	3	12	1	0	13	30	0.19	0.47	0.47
sum/ mean	40	43	39	6	30	158		0.44	0.50

Figure 3. Confusion matrix for descriptor-based classification of catalysts using a classification tree analysis. 23 attributes out of the initial 75 attributes were selected as relevant by the algorithm. Explanations are as for Figure 2. As can be seen, both the prediction rate and the sensitivity are lower than for the neural network based analysis but still substantially better than a random assignment to the clusters.

analysis. The number of attributes was reduced to 23 relevant ones by the algorithm. In general, all classification trees performed far better than a random prediction, but were inferior to neural networks. A major discriminative effect in this type of analysis has the normalized formation free enthalpy of the most stable metal oxide of all the elements in the catalyst. Influence of such a factor in an oxidation reaction would have been expected from heuristic knowledge as well, so that one can say with some justification that chemical intuition has been implemented in an algorithm.

It is also revealing to inspect those attributes which were selected to be of influence by almost all neural networks and classification trees. These attributes are the maximum difference in the atomic radius of all the elements present in a

catalyst, the mean electron affinity of all the elements in the catalyst, the mean Pauling electronegativity of all the metals and semimetals in the catalyst, the normalized formation free enthalpy of the most stable metal oxide of all the elements in the catalyst, the weighted mean molar mass of all the elements in the catalyst, the difference between the highest and the lowest ionic radius of all the elements (average radius as basis for each element), the synthesis pathway, and the fact whether a base was added in the synthesis. That these eight parameters out of the 75 initially selected show up in most of the correlations suggests that the combination of them has a major influence in determining the catalytic performance, and if one inspects these properties one could indeed expect some predictive power from such parameters.

In summary, based on parameters, which do not have to be measured, sets of attributes for solids were derived which can be used to predict whether a catalyst falls into one out of five performance classes in propene oxidation, with a predictive power substantially exceeding the statistically expected values. Figure 4 summarizes these results. This is the same

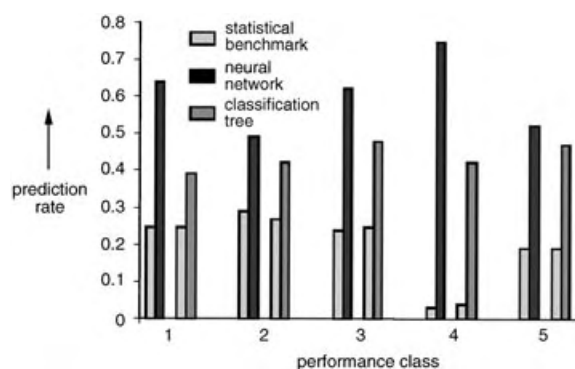


Figure 4. Comparison of the prediction rates for the different catalyst classes based on neural network analysis and classification tree analysis together with the statistical expectation value. Statistical expectation values are not identical, because the test set contained 113 at random selected catalysts for the neural network analysis and 158 at random selected catalysts for the classification tree analysis.

as what an able chemist can do based on his or her experience and chemical knowledge. Each catalysis researcher will, for instance, suggest that $\text{Pt}/\text{Al}_2\text{O}_3$ should be a good total oxidation catalyst, or that bismuth molybdenum oxide may form partial oxidation products. However, implementing this kind of intuition on a general level into an algorithm is exceedingly difficult. We have implemented a solution to this problem and shown for one test case that the concept works in practice. With a sufficiently broad database, one can expect that the descriptors initially derived for propene oxidation can be generalized to alkene oxidations or even to hydrocarbon oxidation reactions, and the concept will be more and more reliable the broader the database becomes and will thus provide the basis of virtual screening as a first step in a catalyst-discovery program.

The identification of a descriptor vector now opens the pathway to a virtual screening of solids. For such an approach, a multitude of catalysts would be generated theoretically,

using, for instance, a randomizer to determine the synthesis pathway and the composition. For each of the catalysts suggested by the algorithm, the descriptor vector would be determined. Then only catalysts for which a desired performance is expected would indeed be synthesized and tested, or, if a highly diverse library is targeted at, several examples would be selected from each predicted performance class. Since the randomizer would suggest a composition, precursors, and a synthesis pathway, there is a high probability, that suggested catalysts can indeed be synthesized.

The concept is not restricted to catalysis. In general, any materials science problem involving complex solids could be tackled by the methodology which we have introduced.

Received: May 20, 2004

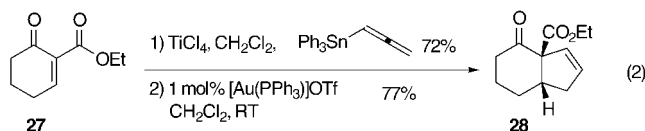
Keywords: combinatorial chemistry · heterogeneous catalysis · high-throughput screening · oxidation · virtual screening

- [1] X. D. Xiang, X. Sun, G. Briceno, Y. Lou, K.-A. Wang, H. Chang, W. G. Wallace-Freedman, S.-W. Chen, P. G. Schultz, *Science* **1995**, 268, 1738.
- [2] F. C. Moates, M. Somani, J. Annamalai, J. T. Richardson, D. Luss, R. C. Wilson, *Ind. Eng. Chem. Res.* **1996**, 35, 4801.
- [3] S. M. Senkan, *Nature* **1998**, 394, 350.
- [4] E. Reddington, A. Sapienza, B. Guraou, R. Viswanathan, S. Sarangapani, E. S. Smotkin, T. E. Mallouk, *Science* **1998**, 280, 1735.
- [5] A. Holzwarth, H. W. Schmidt, W. F. Maier, *Angew. Chem.* **1998**, 110, 2788; *Angew. Chem. Int. Ed.* **1998**, 37, 2644.
- [6] B. Jandeleit, D. J. Schaefer, T. S. Powers, H. W. Turner, W. H. Weinberg, *Angew. Chem.* **1999**, 111, 2648; *Angew. Chem. Int. Ed.* **1999**, 38, 2495.
- [7] S. Senkan, *Angew. Chem.* **2001**, 113, 322; *Angew. Chem. Int. Ed.* **2001**, 40, 312.
- [8] A good survey is given in: M. Baerns, E. Körtling in *Handbook of Heterogeneous Catalysis* (Eds.: G. Ertl, H. Knözinger, J. Weitkamp), Wiley-VCH, Weinheim, **1997**, pp. 419–426.
- [9] T. Hattori, S. Kito, *Catal. Today* **1995**, 23, 347.
- [10] S. Kito, T. Hattori, Y. Murakami, *Ind. Eng. Chem. Res.* **1989**, 31, 979.
- [11] A. Corma, J. M. Serra, E. Argente, V. Botti, S. Valero, *ChemPhysChem* **2002**, 3, 939.
- [12] D. Wolf, O. Buyevskaya, M. Baerns, *Appl. Catal. A* **2000**, 200, 63.
- [13] U. Rodemerck, M. Baerns, M. Holena, D. Wolf, *Appl. Surf. Sci.* **2004**, 223, 168.
- [14] J. M. Caruthers, J. A. Lauterbach, K. T. Thomson, V. Venkatasubramanian, C. M. Snively, A. Bhan, S. Katare, G. Oskarsdottir, *J. Catal.* **2003**, 216, 98.
- [15] R. Todeschini, V. Consonni, *Handbook of Molecular Descriptors*, Wiley-VCH, Weinheim, **2000**.
- [16] For instance, the journals *QSAR-Combinatorial Science* and *J. Chem. Inf. Comp. Sci.* carry a majority of papers from this field.
- [17] A. Rajagopalan, C. Suh, X. Li, K. Rajan, *Appl. Catal. A* **2003**, 254, 147.
- [18] C. Klanner, D. Farrusseng, L. Baumes, C. Mirodatos, F. Schüth, *QSAR Comb. Sci.* **2003**, 22, 729.
- [19] M. Boudart in *Handbook of Heterogeneous Catalysis* (Eds.: G. Ertl, H. Knözinger, J. Weitkamp), Wiley-VCH, Weinheim, **1997**, pp. 1–13.
- [20] C. Hoffmann, A. Wolf, F. Schüth, *Angew. Chem.* **1999**, 111, 2971; *Angew. Chem. Int. Ed.* **1999**, 38, 2800.

Angew. Chem. Int. Ed. **2004**, 43, 5350–5352

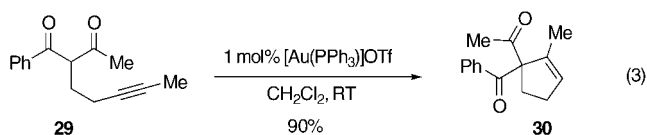
moieties is tolerated, although cyclization of aryl ketones requires increased reaction times. The reaction is also amenable to a wide range of alkynyl substituents including alkyl, aryl (entry 9), vinyl (entry 6), and proton (entry 7), although the latter appears to react more sluggishly. Importantly, the mild reaction conditions allow for the use of acid-labile groups such as *tert*-butyl ester [Eq. (1)], tetrahydropyranyl ether (entry 5), and tertiary propargyl ether (entry 11). This cycloisomerization provides an alternative synthesis of 1,3-dienes often prepared by enyne metathesis.^[12] For example, 1,3-enyne **13** underwent rapid cyclization to give 1,3-diene **14** in good yield (entry 6).

Having established the feasibility of the endocyclic carbocyclization, we sought to apply this method to the synthesis of bicyclic structures by a cyclopentene annulation^[13] onto α,β' -unsaturated β -ketoesters. Thus, conjugate addition of allenyltriphenylstannane^[14] to **27**, followed by gold(I)-catalyzed cyclization afforded cyclopentene **28** as a single diastereomer [Eq. (2)]. This cyclopentene annulation



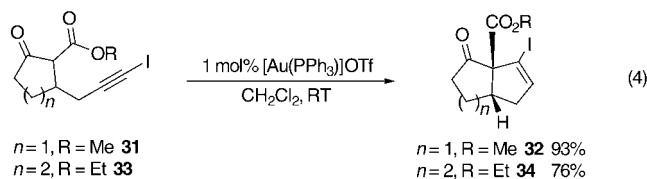
can also be applied to the diastereoselective formation of 5,5- (Table 1, entries 7–9) and 7,5-fused (entry 10) bicyclic ring systems. Additionally, bicyclo[3.2.1]octane **24** is available in excellent yield from the 5-*endo-dig* cyclization of β -ketoester **23** (entry 11). Lewis-basic groups, such as a tertiary amine, are tolerated and thus the gold-catalyzed reaction allows for the synthesis of heterocyclic ring systems. For example, the benzo-fused pyrrolizidine core of the mitosanes (**26**)^[15] is available in excellent yield from a gold(I)-catalyzed cyclization of 3-hydroxyindole **25** (entry 12).

We have found that β -diketones^[6] are also viable nucleophiles under the optimized reaction conditions. For example, 1 mol % triphenylphosphinegold(I) triflate rapidly and efficiently catalyzes the conversion of 1,3-dione **29** into cyclopentene **30** [Eq. (3)].

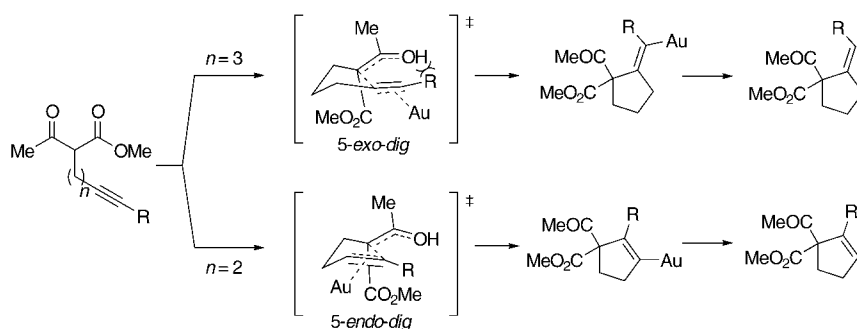


Carbocyclization onto 1-halo-1-alkynes would provide a facile entry into cyclopentenyl halides, however, transition-metal-catalyzed addition reactions to alkynyl halides are exceptionally rare.^[16] We were, therefore, very pleased to find that 1-iodoalkynes **31** and **33** underwent rapid cyclization to

give cyclopentenyl iodides **32** and **34** as single diastereomers in 93 and 76 % yield, respectively [Eq. (4)].



We propose that these reactions proceed by a mechanism involving nucleophilic addition of an enol to a gold(I) alkyne complex (Scheme 1). Based on this mechanistic hypothesis, one of the potential explanations for the lack of reactivity of nonterminal alkynes in the gold-catalyzed 5-*exo-dig* cyclization^[11] is that placement of the catalyst near an alkyl-substituted carbon atom is sterically unfavorable. However, in the transition state for the endocyclic reaction the gold center is located near an alkyl-substituted carbon atom without inhibiting the cyclization. We propose that the 5-*exo-dig* Conia-ene reaction is limited to terminal alkynes because of the development of 1,3-allylic strain in the transition state. This strain is absent in the transition state for the gold(I)-catalyzed 5-*endo-dig* cyclization allowing for the participation of nonterminal alkynes.



Scheme 1. Proposed mechanism for the gold(I)-catalyzed 5-*endo-dig* carbocyclization.

In conclusion, we have developed a gold(I)-catalyzed 5-*endo-dig* carbocyclization of dicarbonyl compounds onto appended alkynes. The reaction is carried out under open-flask conditions and shows excellent tolerance for variation in the ketone, ester, and alkyne substituents. As such, it provides entry into a wide range of cyclopentanoid structures including those containing 1,3-diene, vinyl iodide, and heterocyclic moieties. These results further highlight the potential of gold(I) complexes^[17] to serve as catalysts for the formation of carbon–carbon bonds by alkyne activation. Applications of this strategy, including an asymmetric variant, are underway in our laboratory and will be reported in due course.

Experimental Section

General synthetic procedure: To a small screw-cap scintillation vial equipped with a magnetic stir bar and charged with a solution of the α -3'-alkynyl-substituted β -dicarbonyl compound (~150 mg, 1 equiv)

in CH_2Cl_2 (0.4 M) was added $[\text{Au}(\text{PPh}_3)]\text{Cl}$ (1 mol %) followed by AgOTf (1 mol %). The cloudy white reaction mixture was then stirred at room temperature and monitored periodically by thin layer chromatography. Upon completion of the reaction, the mixture was loaded directly onto a silica gel column and chromatographed with the appropriate mixture of hexanes and ethyl acetate to give the cycloisomerized products.

Received: June 2, 2004

Keywords: C–C coupling · cyclization · cyclopentenones · dicarbonyl compounds · gold

- [1] For examples, see: a) R. Noyori, M. Suzuki, *Science* **1993**, 259, 44–45; b) A. Nangia, G. Prasuna, P. B. Rao, *Tetrahedron* **1997**, 53, 14507–14545; c) M. H. Beale, J. L. Ward, *Nat. Prod. Rep.* **1998**, 15, 533–548; d) M. Seepersaud, Y. Al-Abed, *Tetrahedron Lett.* **2000**, 41, 4291–4293.
- [2] For reviews, see: a) B. M. Trost, *Chem. Soc. Rev.* **1982**, 11, 141–170; b) M. Ramaiah, *Synthesis* **1984**, 529–570; c) T. Hudlicky, J. D. Price, *Chem. Rev.* **1989**, 89, 1467–1486; d) L. Ghosez, *Pure Appl. Chem.* **1996**, 68, 15–22; e) M. A. Tius, *Acc. Chem. Res.* **2003**, 36, 284–290; f) T. R. Rheault, M. P. Sibi, *Synthesis* **2003**, 803–819.
- [3] For a review, see: J. M. Conia, P. Le Perche, *Synthesis* **1975**, 1–19.
- [4] F. E. McDonald, T. C. Olson, *Tetrahedron Lett.* **1997**, 38, 7691–7692.
- [5] N. Iwasawa, T. Miura, K. Kiyota, H. Kusama, K. Lee, P. H. Lee, *Org. Lett.* **2002**, 4, 4463–4466.
- [6] A related Pd^{II} -catalyzed 6-*endo-trig* addition of 1,3-diones to alkenes has been reported: a) T. Pei, R. A. Widenhoefer, *J. Am. Chem. Soc.* **2001**, 123, 11290–11291; b) H. Qian, R. A. Widenhoefer, *J. Am. Chem. Soc.* **2003**, 125, 2056–2057.
- [7] For a review, see: F. Alonso, I. P. Beletskaya, M. Yus, *Chem. Rev.* **2004**, 104, 3079–3160.
- [8] Au-catalyzed 5-*endo-dig* cyclization of O nucleophiles: a) A. S. K. Hashmi, T. M. Frost, J. W. Bats, *J. Am. Chem. Soc.* **2000**, 122, 11553–11554; b) A. S. K. Hashmi, L. Schwarz, J.-H. Choi, T. M. Frost, *Angew. Chem.* **2000**, 112, 2382–2385; *Angew. Chem. Int. Ed.* **2000**, 39, 2285–2288; c) A. S. K. Hashmi, P. Sinha, *Adv. Synth. Catal.* **2004**, 346, 432–438; of N nucleophiles: d) Y. Fukuda, K. Utimoto, *Synthesis* **1991**, 975–978; e) A. Arcadi, S. D. Giuseppe, F. Marinelli, E. Rossi, *Adv. Synth. Catal.* **2001**, 343, 443–446; f) A. Arcadi, D. Bianchi, F. Marinelli, *Synthesis* **2004**, 610–618.
- [9] Cu-catalyzed 5-*endo-dig* cyclization with N nucleophiles: a) C. E. Castro, E. J. Gaughan, D. C. Owsley, *J. Org. Chem.* **1966**, 31, 4071–4078; b) J. Fujiwara, Y. Fukutani, H. Sano, K. Maruoka, H. Yamamoto, *J. Am. Chem. Soc.* **1983**, 105, 7177–7179; Cu-catalyzed 5-*endo-dig* cyclization with O nucleophiles: c) I. N. Houpi, W. B. Choi, P. J. Reider, A. Molina, H. Churchill, J. Lynch, R. P. Volante, *Tetrahedron Lett.* **1994**, 35, 9355–9358; d) C. C. Bates, P. Saejueng, J. M. Murphy, D. Venkataraman, *Org. Lett.* **2002**, 4, 4727–4729; Ag-catalyzed addition of O nucleophiles: e) J. A. Marshall, M. A. Wolf, E. M. Wallace, *J. Org. Chem.* **1997**, 62, 367–371.
- [10] a) 5-*endo-dig* Michael addition: J. F. Lavallée, G. Berthiaume, P. Deslongchamps, *Tetrahedron Lett.* **1986**, 27, 5455–5458; b) Hf^{IV} -catalyzed alkyne/allylsilane 5-*endo-dig* cycloisomerization: K.-I. Imamura, E. Yoshikawa, V. Gevorgyan, Y. Yamamoto, *J. Am. Chem. Soc.* **1998**, 120, 5339–5340; c) Rh^{I} -catalyzed 5-*endo-dig* hydroacylation: K. Tanaka, G. C. Fu, *J. Am. Chem. Soc.* **2001**, 123, 11492–11493; d) radical 5-*endo-dig* carbocyclization: S. Amrein, A. Studer, *Chem. Commun.* **2002**, 1592–1593; e) Co-catalyzed cycloisomerization of 1,6-enynes: A. Ajamian, J. L. Gleason, *Org. Lett.* **2003**, 5, 2409–2411.
- [11] J. J. Kennedy-Smith, S. T. Staben, F. D. Toste, *J. Am. Chem. Soc.* **2004**, 126, 4526–4528.
- [12] For a review of enyne metathesis, see: S. T. Diver, A. Giessert, *Chem. Rev.* **2004**, 104, 1317–1382.
- [13] For a related cyclopentene annulation onto α,β -unsaturated ketones, see: a) R. L. Danheiser, D. J. Carini, A. Basak, *J. Am. Chem. Soc.* **1981**, 103, 1604–1606; b) R. L. Danheiser, D. J. Carini, D. M. Fink, A. Basak, *Tetrahedron* **1983**, 39, 935–947.
- [14] J. Haruta, K. Nishi, S. Matsuda, S. Akai, Y. Tamaura, Y. Kita, *J. Org. Chem.* **1990**, 55, 4853–4859.
- [15] For examples of transition-metal-mediated approaches to this ring system, see: a) J. Lee, J. D. Ha, J. K. Cha, *J. Am. Chem. Soc.* **1997**, 119, 8127–8128; b) H. Kusama, J. Takaya, N. Iwasawa, *J. Am. Chem. Soc.* **2002**, 124, 11592–11593.
- [16] For a 5-*exo-dig* acetoxymercuration of a 1-iodo-1-alkyne, see: a) G. A. Krafft, J. A. Katzenellenbogen, *J. Am. Chem. Soc.* **1981**, 103, 5459–5466; see also the W-mediated reaction of 1-iodo-1-alkynes involving a 1,2-iodide shift: b) T. Miura, N. Iwasawa, *J. Am. Chem. Soc.* **2002**, 124, 518–519; c) N. Iwasawa, T. Miura, K. Kiyota, H. Kusama, K. Lee, P. H. Lee, *Org. Lett.* **2002**, 4, 4463–4466.
- [17] For reviews of Au-catalyzed reactions, see: a) G. Dyker, *Angew. Chem.* **2000**, 112, 4407–4409; *Angew. Chem. Int. Ed.* **2000**, 39, 4237–4283; b) A. S. K. Hashmi, *Gold Bull.* **2003**, 36, 3–9; see also: C. Nieto-Oberhuber, M. P. Muñoz, E. Buñuel, C. Nevado, D. J. Cárdenas, A. M. Echavarren, *Angew. Chem.* **2004**, 116, 2456–2460; *Angew. Chem. Int. Ed.* **2004**, 43, 2402–2406.

Brønsted Acids

The Strongest Isolable Acid**

Mark Juhasz, Stephan Hoffmann, Evgenii Stoyanov,
Kee-Chan Kim, and Christopher A. Reed*

Acids based on carborane anions as conjugate bases (Figure 1) are a new class of Brønsted (protic) acids, notable for their “strong yet gentle” qualities.^[1] For example, whereas conventional strong acids (e.g. H_2SO_4) and superacids (e.g. $\text{HFSO}_3/\text{SbF}_5$) decompose fullerenes even at low temperatures, the carborane acid $\text{H}(\text{CHB}_{11}\text{H}_5\text{Cl}_6)$ cleanly protonates C_{60} at room temperature to give the isolable salt $[\text{HC}_{60}][\text{CHB}_{11}\text{H}_5\text{Cl}_6]$. We now show that carborane acids are the

[*] M. Juhasz, S. Hoffmann, Dr. K.-C. Kim, Prof. Dr. C. A. Reed
Department of Chemistry
University of California
Riverside, CA 92521-0403 (USA)
Fax: (+1) 909-787-2027
E-mail: chris.reed@ucr.edu

Dr. E. Stoyanov
Boreskov Institute of Catalysis
Prospekt Lavrentieva 5, Novosibirsk 630090 (Russia)

[**] This work was supported by NSF grant CHE-0095206 and NIH grant GM 23851.



Supporting information for this article is available on the WWW under <http://www.angewandte.org> or from the author.

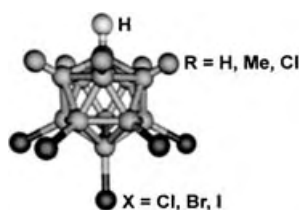
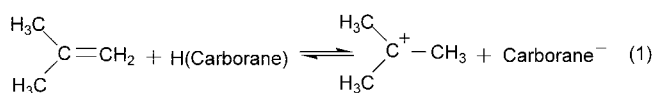


Figure 1. The $[\text{CHB}_{11}\text{R}_5\text{X}_6]^-$ carborane ions.

strongest isolable (Lewis-free) Brønsted acids presently known.

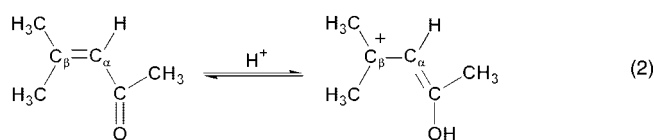
Two reactivity considerations have led us to believe that carborane acids must have uncommon strength. First is their stabilization of the benzenium ion in salts such as $[\text{C}_6\text{H}_7][\text{CHB}_{11}\text{Me}_5\text{Br}_6]$. The strongest known neat oxyacid, HFSO_3 , (whose Hammett acidity function $H_0 = -15.1$) is not strong enough to fully protonate benzene,^[2] yet carborane acids do so readily at the one-equivalent level in dilute solution.^[3] Second, we have recently shown that carborane anions stabilize *tert*-butyl cation in dichloromethane or liquid SO_2 solution, as well as in isolable crystalline salts.^[4] This means that carborane acids are strong enough to shift the equilibrium of Equation (1) completely to the right hand side. If this were not the case, deprotonation of *tert*-butyl cation to give *iso*-butene and subsequent decomposition by cationic oligomerization would occur rapidly.



Since mixed Lewis/Brønsted superacid media such as “Magic Acid” ($\text{HFSO}_3/\text{SbF}_5$) having H_0 somewhere in the range -17 to -27 are used to stabilize *tert*-butyl cation,^[5] it is apparent that carborane acids have intrinsic Brønsted acidities comparable to those only found previously in Lewis/Brønsted acid mixtures.

The acidities of carborane acids cannot be measured in the conventional manner of an H_0 Hammett acidity function because carborane acids are solids not liquids. They sublime under vacuum, or melt at atmospheric pressure, at temperatures well above 150°C . Gas-phase acidities have been calculated for carborane acids, which rank them the strongest of any known isolable acid,^[6] but it is presently not possible to translate gas-phase ΔG data into measures of condensed-phase acidity.

The need to compare the strengths of solid acids with liquid acids therefore led us to obtain a measure of acidity in dilute solution, conditions where most acid catalysis is carried out. The chosen solvent is liquid SO_2 because of its low basicity, relatively high dielectric constant for solvation of ions, and ease of drying. The chosen method is adapted from that developed by Fărcașiu and Ghenciu.^[7] It is based on the ^{13}C NMR spectroscopy chemical shift difference ($\Delta\delta$) between the C_α and C_β carbon atoms of mesityl oxide which increases with increasing protonation as Equation (2) is shifted to the right hand side.



^{13}C NMR spectroscopy data for 0.15 M solutions of various acids and 0.10 M mesityl oxide were obtained at room temperature and are given in Table 1. The choice of oxyacids

Table 1: Acid-strength ranking from protonation of mesityl oxide in liquid SO_2 .

Acid	$\Delta\delta$ (^{13}C) [ppm]	H_0
$\text{H}(\text{CHB}_{11}\text{Cl}_{11})$	84.0 ± 0.1	[a]
$\text{H}(\text{CHB}_{11}\text{H}_5\text{Cl}_6)$	83.8 ± 0.1	[a]
$\text{H}(\text{CHB}_{11}\text{H}_5\text{Br}_6)$	83.8 ± 0.1	[a]
$\text{H}(\text{CHB}_{11}\text{H}_5\text{I}_6)$	83.3 ± 0.1	[a]
FSO_3H	73.8 ± 0.5	-15.1
$\text{CF}_3\text{SO}_3\text{H}$	72.9 ± 0.4	-14.1
$\text{HN}(\text{SO}_2\text{CF}_3)_2$	72.0 ± 0.4	[a]
H_2SO_4	$64.3 \pm 3.1^{[b]}$	-12.1
Unprotonated mesityl oxide	32.4 ± 0.1	

[a] H_0 values unavailable because acids are solids, not liquids. [b] Incomplete miscibility of H_2SO_4 in liquid SO_2 leads to higher error limits and possible underestimate of $\Delta\delta$.

for comparison to carborane acids is limited by their availability in pure form and the need for miscibility or dissolution in liquid SO_2 . Nevertheless, it is immediately evident from their high chemical shift values that, as a class, carborane acids are stronger than conventional oxyacids. They outrank fluorosulfuric acid, the strongest known pure Brønsted acid on the H_0 acidity scale (-15.1), as well as triflic acid ($H_0 = -14.1$). A strict correlation between $\Delta\delta$ values in liquid SO_2 and the H_0 values of neat acids is not expected because acidity is a solvation-dependent phenomenon that changes as the medium changes. Nevertheless, for the limited data set available, the ranking of acid strength by $\Delta\delta$ values follows the H_0 order (Table 1).

It is also evident from the data of Table 1 that whereas oxyacids only partially protonate mesityl oxide, carborane acids are strong enough to move Equation (2) completely to the right hand side, that is, their acidities are leveled. The $\Delta\delta$ value maximizes at $\delta = 84.0$ ppm. Though close to the limits of discrimination, the hexa-iodo carborane acid, $[\text{H}(\text{CHB}_{11}\text{H}_5\text{I}_6)]$ with a value of $\delta = 83.3$ ppm, appears to be perceptibly weaker than its chloro and bromo counterparts.

To discriminate between the acidities of the different carborane acids, we have developed a new, qualitative ranking of acidity based on the $\nu\text{N-H}$ frequencies of the ammonium salts of their conjugate base anions. The ranking is based on the influence of the anion A^- on the N-H bond in a contact ion pair (Figure 2).



Figure 2. Ammonium salt contact ion pair.

The weaker the interaction of the base A^- , the stronger the N–H bonding, and the higher the $\nu N-H$ frequency.^[8] Since $\nu N-H$ frequencies ($> 3000\text{ cm}^{-1}$) are energetically far removed from $\nu H-A$ frequencies ($< 300\text{ cm}^{-1}$), vibrational coupling or mass differences in A^- will have an insignificant effect on $\nu N-H$, that is, $\nu N-H$ frequencies should be a good measure of N–H bond strength. Since hydrogen bonding is a predominantly electrostatic phenomenon,^[9] N–H bond strength should correlate strongly with A^- basicity, that is, with HA acidity. $\nu N-H$ frequencies will decrease with increasing A^- basicity, correlating with HA acidity. In a constant solvation environment within a series of isostructural anions, the correlation should be quite direct. Although the direct correlation of acidity with IR stretching frequency has been questioned for solid surfaces,^[10–12] acidity rankings based on IR data have been shown to have excellent validity within a number of classes of discrete compounds, particularly when structurally related.^[13–17]

Tri-*n*-octylammonium salts of carborane anions were prepared by silver-salt metathesis reactions and characterized as detailed in the Supporting Information. Octyl groups in the cation were chosen to provide good solubility of [*n*-Oct₃NH]⁺[carborane][−] ion pairs in CCl₄ solution. To avoid possible effects from aggregation, $\nu N-H$ frequencies were measured in dilute solution where there was no concentration dependence (Table 2). The strong dependence of $\nu N-H$ on the

Table 2: $\nu N-H$ frequencies of tri-*n*-octylammonium salts in CCl₄.

Anion	$\nu N-H$ [$\pm 1\text{ cm}^{-1}$]	$\Delta\nu$ [cm^{-1}]
[CHB ₁₁ Cl ₁₁] ^{−[a]}	3163	0
[CHB ₁₁ Me ₁₁] [−]	3156	7
[CHB ₁₁ H ₅ Cl ₆] ^{−[a]}	3148	15
[Co ^{III} (C ₂ B ₉ H ₈ Cl ₃) ₂] [−]	3145	18
[CHB ₁₁ Me ₅ Cl ₆] [−]	3143	20
[CHB ₁₁ H ₁₁] [−]	3129	34
[CHB ₁₁ H ₅ Br ₆] ^{−[a]}	3125	38
[CHB ₁₁ Me ₅ Br ₆] [−]	3120	43
[CHB ₁₁ H ₅ I ₆] ^{−[a]}	3097	66
[CHB ₁₁ Me ₅ I ₆] [−]	3091	72

[a] Denotes presently known isolable acids.

nature of the anion indicates that contact ion pairs are formed. In the more polar solvent 1,2-dichloroethane, the rank order is the same but some salts showed a second band of invariable frequency ($3179 \pm 1\text{ cm}^{-1}$) which is assigned to solvent-separated ion pairs. For the corresponding deuterated [Oct₃N–D]⁺ salts the $\nu N-D/\nu N-H$ ratio was 1.339 ± 0.004 , indicating the absence of anharmonicity effects or Fermi resonance.

The $\nu N-H$ ranking brings out a number of features: a) For each of the pairs of hexahalo carboranes [CHB₁₁H₅X₆][−] (X = Cl, Br, I) and their pentamethylated counterparts [CHB₁₁Me₅X₆][−],^[18] the difference in $\nu N-H$ values is 5 or 6 cm^{-1} . This consistency gives confidence in the scale, suggesting that the CCl₄ solvation environment remains constant over the series and that mass differences and steric effects have negligible influence. It is evident that small differences in anion basicity can be detected quite accurately

and the scale should be useful for a much wider range of weakly coordinating anions. b) The ranking of the hexahalo carborane acids, $H(CHB_{11}H_5Cl_6) > H(CHB_{11}H_5Br_6) > H(CHB_{11}H_5I_6)$, makes sense on the basis of electronegativity and polarizability considerations for the halogen substituents. It is consistent with conceptually related deductions drawn recently from $\nu C-H$ frequencies in benzenium ion salts having the same series of carborane counterions.^[3] c) The top ranking (i.e. least basic) carborane anion measured to date is the undecachlorinated ion, [CHB₁₁Cl₁₁][−],^[19] which leads to the prediction that its conjugate acid will be the strongest. As detailed in the Supporting Information, H(CHB₁₁Cl₁₁) can be prepared in a similar manner to the hexahalo carborane acids as a sublimable, analytically-pure, colorless solid by the reaction of Et₃Si(CHB₁₁Cl₁₁) with anhydrous HCl. Thus, H(CHB₁₁Cl₁₁) can lay claim to be the strongest isolable acid presently known.

Carborane acids are strong acids because their anions are exceptionally weak bases. This arises from the large size of the anions, the delocalized nature of the negative charge in the [CB₁₁][−] cluster, and the shield of halide substituents. However, there is an important additional necessity for preparing such a strong acid, namely, the anion must be exceptionally inert from a chemical point of view. The inertness of carborane anions arises from σ aromaticity within the [CB₁₁][−] icosahedral cage, a notable feature of boron cluster chemistry. The [CB₁₁][−] framework resists chemical disruption to a truly exceptional degree. There are anions that probably have lower basicity than carboranes, for example, organofluoro anions, such as [B(C₆F₅)₄][−],^[20] but their conjugate acids cannot be prepared because the anion decomposes at high acidity.^[21] This situation is mirrored in that traditional fluoroacids, commonly written as HBF₄, HPF₆, HSbF₆ etc., are also nonexistent compounds. They are all unstable with respect to formation of HF and the corresponding Lewis acid. The superacid commonly written “HSbF₆” is actually a mixture of [H(HF)_{*x*}][SbF₆·*n*SbF₅] ions in HF/SbF₅ solvent and cannot be isolated as a pure Brønsted acid. Thus, present limits to acid strength are seen to be more dependent on considerations of anion stability than basicity, although low basicity is clearly required.

An important and potentially very useful feature of carborane acids is that their high protic acidity is expressed in the absence of an added Lewis acid. The presence of Lewis acids in traditional superacids (e.g. HFSO₃/SbF₅) can interfere with protonation chemistry and limit their usefulness in two identifiable ways. As alluded to earlier for C₆₀, Lewis acids (particularly SbF₅) can supply oxidizing equivalents and halide nucleophiles that together, conspire to decompose many protonated unsaturated molecules. A more subtle effect arises from the likely formation of Lewis acid/base complexes when substrates are investigated in mixed Brønsted/Lewis superacids. If a substrate forms an adduct with a Lewis acid, its basicity will be lowered and it will become much more difficult to protonate. This phenomenon can be called “basicity suppression”. It suggests that the basicities of weakly basic molecules may have been significantly underestimated, and makes the pursuit of even stronger pure Brønsted acids an important endeavor.

Carborane acids may lead not only to the isolation and stabilization of protonated species hitherto unattainable, but also to a reassessment of the intrinsic basicity of weakly basic molecules. Experiments to test this hypothesis are underway.

Received: March 16, 2004

Revised: June 30, 2004

Keywords: acids · basicity suppression · Brønsted acids · carboranes · IR spectroscopy

- [1] C. A. Reed, K.-C. Kim, R. D. Bolskar, L. Mueller, *Science* **2000**, 289, 101.
- [2] D. M. Brouwer, E. L. Mackor, C. MacLean in *Carbonium Ions, Vol. 1* (Eds.: G. A. Olah, P. v. R. Schleyer), Wiley-Interscience, New York, **1970**, p. 837.
- [3] C. A. Reed, K.-C. Kim, E. S. Stoyanov, D. Stasko, F. S. Tham, L. J. Mueller, P. D. W. Boyd, *J. Am. Chem. Soc.* **2003**, 125, 1796.
- [4] T. Kato, C. A. Reed, *Angew. Chem.* **2004**, 116, 2967–2971; *Angew. Chem. Int. Ed.* **2004**, 43, 2907–2911.
- [5] G. A. Olah, G. K. S. Prakash, J. Sommer, *Superacids*, Wiley, New York, **1985**.
- [6] I. A. Koppel, P. Burk, I. Koppel, I. Leito, T. Sonoda, M. Mishima, *J. Am. Chem. Soc.* **2000**, 122, 5114.
- [7] D. Fărcașiu, A. Ghenciu, *J. Am. Chem. Soc.* **1993**, 115, 10901.
- [8] C. Fischer, H. Wagner, V. V. Bagreev, E. S. Stoyanov, *J. Inorg. Nucl. Chem.* **1977**, 39, 513.
- [9] M. M. Davis, *Acid–Base Behavior in Aprotic Organic Solvents*, Department of Commerce, National Bureau of Standards, Washington, DC, **1968**, 113.
- [10] W. E. Farneth, R. J. Gorte, *Chem. Rev.* **1995**, 95, 615.
- [11] R. A. v. Santen, G. J. Kramer, *Chem. Rev.* **1995**, 95, 637.
- [12] D. Fărcașiu, D. Hâncu, *Catal. Lett.* **1998**, 53, 3.
- [13] A. V. Iogansen in *The Hydrogen Bond* (Ed.: N. D. Sokolov), Nauka, Moscow, **1981**, pp. 112–155.
- [14] M. D. Joesten, R. S. Drago, *J. Am. Chem. Soc.* **1962**, 84, 3817.
- [15] E. M. Arnett, L. Joris, E. Mitchell, T. S. S. R. Murty, T. M. Gorrie, P. v. R. Schleyer, *J. Am. Chem. Soc.* **1970**, 92, 2365.
- [16] R. S. Drago, N. O'Bryan, G. C. Vogel, *J. Am. Chem. Soc.* **1970**, 92, 3924.
- [17] A. D. Sherry, K. F. Purcell, *J. Am. Chem. Soc.* **1972**, 94, 1853.
- [18] D. Stasko, C. A. Reed, *J. Am. Chem. Soc.* **2002**, 124, 1148.
- [19] Z. Xie, C.-W. Tsang, E. T.-P. Sze, Q. Yang, D. T. W. Chan, T. C. W. Mak, *Inorg. Chem.* **1998**, 37, 6444.
- [20] The N–H frequency of the trioctylammonium salt of the $[\text{B}(\text{C}_6\text{F}_5)_4]^-$ ion (3233 cm^{-1}) is even higher than that of the carborane salts.
- [21] C. A. Reed, N. L. P. Fackler, K.-C. Kim, D. Stasko, D. R. Evans, P. D. W. Boyd, C. E. F. Rickard, *J. Am. Chem. Soc.* **1999**, 121, 6314.

Imine-Stabilized Zinc Trimethylsilylchalcogenolates: Powerful Reagents for the Synthesis of II-II'-VI Nanocluster Materials**

Marty W. DeGroot and John F. Corrigan*

A new class of metal–chalcogen complexes is being pursued in which the presence of reactive silyl functional groups offers an entry into high nuclearity ternary cluster and (nanometer sized) nanocluster materials. Both $[E(\text{SiMe}_3)]^-$ ($E = \text{S}, \text{Se}, \text{Te}$)^[1,2] and $[\text{S}(\text{SiMe}_2\text{S})_2]^{2-}$ ^[3,4] groups can be used, provided their coordination to metal centers can be stabilized by additional ancillary ligands. Metal–chalcogenolate reagents for the controlled incorporation of the heavier congeners selenium and tellurium are particularly difficult to prepare owing to the inherent reactivity of these chalcogen elements. These are desirable targets however because of the demonstrated composition-dependant photophysical properties of metal–chalcogenide semiconductor nanomaterials. This property is highlighted by the recent synthesis of a series highly luminescent $\text{Zn}_x\text{Cd}_{1-x}\text{Se}$ nanocrystals whose optical properties can be tuned across the visible spectrum by changing the Zn: Cd ratio.^[5] The development of reagents for controlled access to mixed-metal ternary clusters and nanoclusters is of importance in elucidating the effects of composition on the structure and photophysical properties of MM'Se and MM'Te materials. Herein, we describe the synthesis and initial reactivity studies of the complexes $[(3,5\text{-Me}_2\text{C}_5\text{H}_3\text{N})_2\text{Zn}(\text{ESiMe}_3)_2]$ ($E = \text{Se}$ (**1**), Te (**2**)), where the labile 3,5-lutidine ligands of **1** and **2** afford the opportunity to access ternary II-II'-VI nanoclusters in which the metal ions are intimately mixed by the controlled delivery of $\{\text{ZnE}_2\}$.

[*] M. W. DeGroot, Prof. Dr. J. F. Corrigan
Department of Chemistry
The University of Western Ontario
London, Ontario N6A 5B7 (Canada)
Fax: (+1) 519-661-3022
E-mail: corrigan@uwo.ca

[**] We gratefully acknowledge the Natural Sciences and Engineering Research Council (NSERC) Canada and the Government of Ontario's PREA program for financial support of this research. We thank Prof. P. D. Harvey (Université de Sherbrooke) for his assistance with the PL and PLE measurements. Dr. A. Eichhöfer (Institut für Nanotechnologie, Karlsruhe (Germany)) is thanked for providing samples of $[\text{Cd}_{10}\text{Se}_4(\text{SePh})_{12}(\text{PnPr}_3)_4]$ and $[\text{Cd}_{10}\text{Te}_4(\text{TePh})_{12}(\text{PnPr}_3)_4]$. The Canada Foundation for Innovation, NSERC, and The University of Western Ontario are also acknowledged for equipment funding. M.W.D. thanks the NSERC for a postgraduate scholarship. In the nomenclature of semiconductor materials science, Group II elements are those of Group 12 of the periodic table and Group VI those of Group 16, hence a Zn-Cd-Se containing compound would be an example of a II-II'-VI material.



Supporting information for this article (synthesis, spectroscopic, and characterization data for **1–4** and figures detailing the Zn/Cd site disorder in **3** and **4**) is available on the WWW under <http://www.angewandte.org> or from the author.

Complexes **1** and **2** were synthesized in high yield by the addition of two equivalents of $\text{E}(\text{SiMe}_3)_2$ to a solution of $\text{Zn}(\text{OAc})_2$ solubilized by 3,5-lutidine in CH_2Cl_2 at -78°C . Single crystals of **2** suitable for X-ray crystallography were obtained by addition of cold pentane to the point of incipient precipitation, followed by storage at -78°C . Figure 1 shows

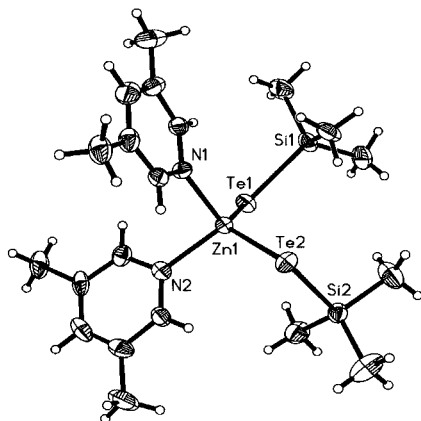


Figure 1. The molecular structure of **2**. Thermal ellipsoids are set at 50% probability. Selected interatomic distances [Å] and angles [°]: Zn–Te 2.580(2), 2.582(1), Te–Si 2.485(3), 2.486(3), Zn–N 2.094(7), 2.100(7); N1–Zn1–N2 96.2(3), N–Zn–Te 104.7(2)–107.8(2), Si–Te–Zn 97.45(7)–101.92(7).

the molecular structure of **2**.^[6] The key structural feature is the presence of terminally coordinated, highly reactive TeSiMe_3 groups. The zinc center has a distorted tetrahedral geometry with a large Te1–Zn1–Te2 angle ($129.21(3)^\circ$) compensated by a compression of the N1–Zn–N2 angle ($85.12(13)^\circ$), as observed in related zinc tellurolate complexes with N-donor ligands.^[7,8] Complex **2** is infinitely stable in the solid state if maintained at low temperatures (-80°C) and is thus a convenient, storable precursor. Consistent with the demonstrated reactivity of reagents such as $\text{E}(\text{SiMe}_3)_2$ and RESiMe_3 ($\text{E} = \text{S}, \text{Se}, \text{Te}$) in binary cluster synthesis,^[9] M–ESiMe_3 complexes are powerful precursors for the formation of M–E–M' nanoclusters^[1,2] owing to their preformed M–E bonds and the reactive pendant trimethylsilyl groups. Thus the reaction of **2** with $(\text{PnPr}_3)_2\text{Cd}(\text{OAc})_2$ in the presence of PhTeSiMe_3 at -78°C , followed by slow warming to room temperature yields single crystals of the ternary nanocluster $[\text{Zn}_{2.6}\text{Cd}_{7.4}\text{Te}_4(\text{TePh})_{12}(\text{PnPr}_3)_4]$ (**3**) in 60% yield [Eq. (1)].



The structure of **3** (Figure 2) was confirmed by X-ray crystallographic analysis.^[6] The nanocluster **3** is crystallographically isomorphous to the binary ZnTe analogue $[\text{Zn}_{10}\text{Te}_4(\text{TePh})_{12}(\text{PnPr}_3)_4]$.^[10] The overall arrangement of metal and tellurium ions generates a tetrahedral framework consisting of four fused $\{\text{M}_4\text{Te}_6\}$ adamantane units, similar to the building blocks that constitute the cubic (sphalerite) phases of the bulk materials ZnTe and CdTe . The four apices of the tetrahedron are terminated by phosphane ligands. This $\{\text{M}_{10}\}$ architecture is prevalent among II–VI clusters and

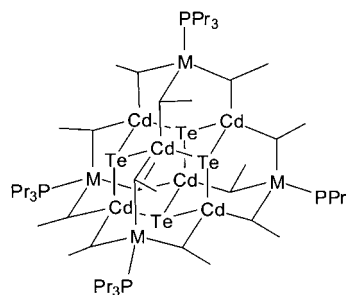


Figure 2. Line diagram of the fused adamantane structure of **3**. Sites labeled “M” indicate the highest concentration of Zn (50% site occupancy) in the cluster, as discussed in the text. For clarity, labels for the TePh ligands are omitted.

makes this compound a candidate with which to examine the effect of metal-ion composition on optical properties.^[11] The average metal composition of the clusters in the crystal was determined by energy dispersive X-ray spectroscopy (EDX) and atomic absorption spectroscopy (AAS) of single crystals of **3**. A measured 2.6:7.4 Zn:Cd ratio (see Supporting Information) is remarkably consistent with the Zn:Cd reaction stoichiometry, which illustrates that the precursor complex **2** is an efficient delivery agent of $\{\text{ZnTe}_2\}$ in cluster synthesis. The inability to fully resolve zinc and cadmium from crystallographic data is indicative of intimate mixing of the metal ions within the clusters. A satisfactory model however was achieved with site occupancy of $\text{Zn}_{0.5}\text{Cd}_{0.5}$ given to the metal ion sites bonded to the apical PnPr_3 ligands. As this accounts for only 77% of the zinc present in the clusters, the remaining zinc ions would be distributed among the rest of the metal sites in the structure. This mixing is unlike the positions of the zinc centers in the II–II'–VI nanoclusters $[(\text{tmeda})_5\text{Zn}_5\text{Cd}_{11}\text{E}_{13}(\text{EPh})_6]$ ($\text{E} = \text{Se}, \text{Te}$; $\text{tmeda} = N,N,N',N'$ -tetramethyl-1,2-ethanediamine) in which the chelating tmeda ligands constrain Zn^{II} to the surface the nanocluster.^[1]

There are relatively few reports involving the general preparation of ternary II–II'–VI nanoparticles.^[5,12] In these mixed-metal compounds, manipulation of the band-gap energy can be achieved by changing both particle size and composition (i.e. the ratio of M to M'). Thus, the development of controlled approaches to ternary nanoparticles is an attractive pursuit and nanocluster materials whose structures can be determined crystallographically allow an investigation of the development of materials properties with increasing molecular size.^[13] The solution absorption spectrum for cluster **3** features a sharp maximum at 321 nm. A marked blue shift in the absorption profile relative to the cluster $[\text{Cd}_{10}\text{Te}_4(\text{TePh})_{12}(\text{PnPr}_3)_4]$ ($\lambda_{\text{max}} = 328 \text{ nm}$)^[14] suggests the optical properties of these nanocluster materials can be manipulated by controlling the metal ion composition. Compound **3** is luminescent only at low temperature, with the emission maximum significantly shifted to lower energy relative to the excitation onset. Consistent with the optical properties of related CdSe clusters, the “trapped” emission is assigned to forbidden transitions involving the surface phenyltellurolate ligands.^[13,14] Photoluminescence excitation (PLE) spectra confirm the emitting species as **3** (see Supporting Information).

Ternary Zn/CdSe nanoclusters can be prepared from the selenolate analogue **1**. Reaction of **1** with $(\text{PnPr}_3)_2\text{Cd}(\text{OAc})_2$ and PhSeSiMe_3 in a 2:8:12 ratio at low temperature leads to the formation of the ternary cluster $[\text{Zn}_{1.8}\text{Cd}_{8.2}\text{Se}_4(\text{SePh})_{12}(\text{PnPr}_3)_4]$ (**4**). Cluster **4** has also been structurally characterized.^[6] The first absorption maximum (310 nm) of this ZnCdSe cluster is blue shifted relative to that of the all cadmium derivative $[\text{Cd}_{10}\text{Se}_4(\text{SePh})_{12}(\text{PnPr}_3)_4]$ ^[13] ($\lambda_{\text{max}} = 320$ nm), whereas the observed emission maximum for **4** (525 nm) is virtually identical to that observed for $[\text{Cd}_{10}\text{Se}_4(\text{SePh})_{12}(\text{PnPr}_3)_4]$ ($\lambda_{\text{em}} = 527$ nm) (see Supporting Information). This result is consistent with the emission being from “trapped” aryl–selenolate surface states, which are relatively insensitive to the size and, as demonstrated in this case, composition of the metal–selenide core.^[13,14]

The use of the silylated zinc(II) chalcogenolate complexes reported herein offers a general route for the controlled introduction of zinc into ternary nanoclusters and nanoparticles. This approach affords the opportunity to modulate the optical properties of nanoclusters and related materials by controlling the metal-ion composition. We are currently developing their utility in a variety of ternary cluster and nanoparticle syntheses.

Received: April 14, 2004

Revised: June 9, 2004

Keywords: chalcogens · cluster compounds · optical properties · silanes · zinc

www.ccdc.cam.ac.uk/conts/retrieving.html (or from the Cambridge Crystallographic Data Centre, 12 Union Road, Cambridge CB21EZ, UK; fax: (+44)1223-336-033; or deposit@ccdc.cam.ac.uk).

- [7] P. J. Bonasia, J. Arnold, *Inorg. Chem.* **1992**, *31*, 2508.
- [8] Y.-K. Jun, C.-S. Choi, J. Cheon, *Chem. Commun.* **2001**, 101.
- [9] S. Dehnen, A. Eichhöfer, D. Fenske, *Eur. J. Inorg. Chem.* **2002**, 2, 279.
- [10] A. Eichhöfer, D. Fenske, H. Pfister, M. Wunder, *Z. Anorg. Allg. Chem.* **1998**, *624*, 1909.
- [11] a) M. W. DeGroot, J. F. Corrigan in *Comprehensive Coordination Chemistry II: From Biology to Nanotechnology*, Vol. 7 (Eds.: M. Fujita, A. Powell, C. Creutz), Pergamon, Oxford, **2004**, p. 57; b) I. Dance, K. Fisher, *Prog. Inorg. Chem.* **1994**, *41*, 637.
- [12] a) Y. Tian, T. Newton, N. A. Kotov, D. M. Guldi, J. H. Fendler, *J. Phys. Chem.* **1996**, *100*, 8927; b) M. T. Harrison, S. V. Kershaw, M. G. Burt, A. Eychmüller, H. Weller, A. L. Rogach, *Mater. Sci. Eng. B* **2000**, *69*, 355; c) B. A. Korgel, H. G. Monbouquette, *Langmuir* **2000**, *16*, 3588; d) D. V. Petrov, B. S. Santos, G. A. L. Pereira, C. D. M. Donegá, *J. Phys. Chem. B* **2002**, *106*, 5325; e) W. Wang, I. Germanenko, M. S. El-Shall, *Chem. Mater.* **2002**, *14*, 3028.
- [13] V. N. Soloviev, A. Eichhöfer, D. Fenske, U. Banin, *J. Am. Chem. Soc.* **2001**, *123*, 2354.
- [14] A. Eichhöfer, A. Aharoni, U. Banin, *Z. Anorg. Allg. Chem.* **2002**, *628*, 2415.

- [1] a) M. W. DeGroot, N. J. Taylor, J. F. Corrigan, *J. Am. Chem. Soc.* **2003**, *125*, 864; a) M. W. DeGroot, N. J. Taylor, J. F. Corrigan, *J. Mater. Chem.* **2004**, *14*, 654.
- [2] a) D. T. T. Tran, N. J. Taylor, J. F. Corrigan, *Angew. Chem.* **2000**, *112*, 965; *Angew. Chem. Int. Ed.* **2000**, *39*, 935; b) D. T. T. Tran, L. M. C. Beltran, C. M. Kowalchuk, N. R. Trefiak, N. J. Taylor, J. F. Corrigan, *Inorg. Chem.* **2002**, *41*, 5693.
- [3] T. Komuro, T. Matsuo, H. Kawaguchi, K. Tatsumi, *Angew. Chem.* **2003**, *115*, 481; *Angew. Chem. Int. Ed.* **2003**, *42*, 465.
- [4] T. Komuro, T. Matsuo, H. Kawaguchi, K. Tatsumi, *Chem. Commun.* **2002**, 988.
- [5] X. Zhong, M. Han, Z. Dong, T. J. White, W. Knoll, *J. Am. Chem. Soc.* **2003**, *125*, 8589.
- [6] Crystal data for $\text{C}_{20}\text{H}_{36}\text{N}_2\text{ZnTe}_2\text{Si}_2$ (**2**): colorless block, $M_r = 681.26$, triclinic, space group $P\bar{1}$, $a = 9.3005(19)$, $b = 10.215(2)$, $c = 16.614(3)$ Å, $\alpha = 94.94(3)$, $\beta = 91.20(3)$, $\gamma = 115.66(3)^\circ$, $V = 1414.5(5)$ Å³, at 200 K, $Z = 2$, $\rho_{\text{calcd}} = 1.602$ g cm⁻³, $\mu = 2.982$ mm⁻¹, $2\theta_{\text{max}} = 55.02^\circ$, 9223 reflections collected (6464 independent, $R_{\text{int}} = 0.045$). Final $R = 0.0659$ ($wR_2 = 0.1604$) and GoF = 1.054. For $\text{C}_{108}\text{H}_{144}\text{P}_4\text{Zn}_{2.6}\text{Cd}_{7.4}\text{Te}_{16}$ (**3**): colorless prism, $M_r = 4637.65$, tetragonal, space group $I4_1/a$, $a = 25.9100(2)$, $c = 21.6000(2)$ Å, $V = 14500.7(2)$ Å³, at 200 K, $Z = 4$, $\rho_{\text{calcd}} = 2.124$ g cm⁻³, $\mu = 4.709$ mm⁻¹, $2\theta_{\text{max}} = 54.94^\circ$, 16307 reflections, (8298 independent, $R_{\text{int}} = 0.0348$). Final $R = 0.0309$ ($wR_2 = 0.0779$) and GoF = 1.067. For $\text{C}_{108}\text{H}_{144}\text{P}_4\text{Zn}_{1.2}\text{Cd}_{8.8}\text{Se}_{16}$ (**4**): colorless prism, $M_r = 3897.04$, tetragonal, space group $I4_1/a$, $a = 25.3442(5)$, $c = 20.2084(6)$ Å, $V = 12980.4(5)$ Å³, at 200 K, $Z = 4$, $\rho_{\text{calcd}} = 1.994$ g cm⁻³, $\mu = 6.205$ mm⁻¹, $2\theta_{\text{max}} = 55.1^\circ$, 14327 reflections (7449 independent, $R_{\text{int}} = 0.0821$). Final $R = 0.0510$ ($wR_2 = 0.1037$) and GoF = 1.006. CCDC-235976–CCDC-235978 (**2–4**) contain the supplementary crystallographic data for this paper. These data can be obtained free of charge via

Alkaloid synthesis

Preparation and Synthetic Applications of 2-Halotryptophan Methyl Esters: Synthesis of Spirotryprostatin B**

Fumiko Y. Miyake, Kenichi Yakushijin, and
David A. Horne*

Isolated in small amounts from the fermentation broth of *Aspergillus fumigatus*,^[1] spirotryprostatin B (**1**) represents one of the structurally more complex members of a relatively potent class of diketopiperazines that inhibit mammalian G₂/M⁻¹ phase cell-cycle progression. Its biological significance and structural novelty has challenged numerous investigators to develop concise total syntheses and analogues with

[*] F. Y. Miyake, Dr. K. Yakushijin, Dr. D. A. Horne
Department of Chemistry
Oregon State University
Corvallis, OR 97331 (USA)
Fax: (+1) 541-737-2062
E-mail: horned@onid.orst.edu

[**] Financial support from Oregon State University and Chugai Pharmaceutical Co. is gratefully acknowledged. We thank Rodger Kohnert for assistance with NMR data acquisition and Jeff Morre of the Mass Spectrometry Facility of the Environmental Health Science Center (NIEHS P30 ES00210) at Oregon State University for recording mass spectral data.

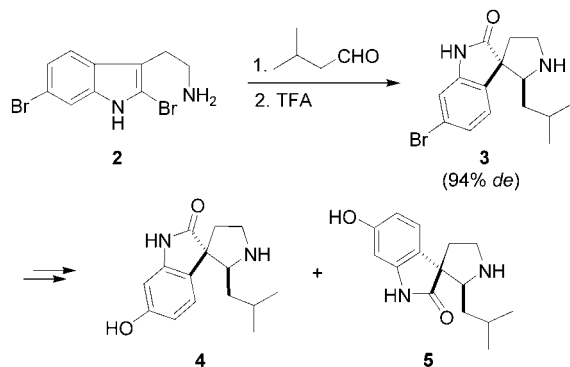


Supporting information for this article is available on the WWW under <http://www.angewandte.org> or from the author.

potentially superior biological activity.^[2–7] The biosynthesis of this spirooxindole undoubtedly arises from the common amino acid precursors (*S*)-tryptophan and (*S*)-proline, in addition to an isoprene-derived moiety and awaits experimental verification.

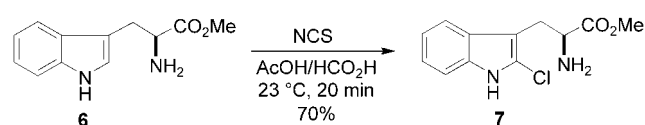
The key synthetic challenge is the asymmetric stereocontrolled construction of the quaternary C3 and adjacent prenyl-substituted C18 centers of the dehydrospiropyrrolidine ring. This has become particularly apparent within the parameters of developing an efficient total synthesis of **1**. Recently, a number of efforts, some successful, have been made to devise solutions to this problem.^[8] Of the syntheses that utilize readily available tryptophan esters and prenyl aldehyde starting materials, two “classical” approaches have emerged. The first, by Danishefsky and von Nussbaum,^[2] involves a Mannich condensation of a tryptophan-derived oxindole and prenyl aldehyde. The second, by Ganesan and Wang,^[3] adopts the well-known Pictet–Spengler/oxidative rearrangement methodology involving a prenyl-substituted tetrahydro- β -carboline. In this communication, we disclose the first direct preparation of 2-chlorotryptophan methyl ester (**7**), its use in stereocontrolled spirooxindole construction, and a concise synthesis of spirotryprostatin B (**1**).

2-Halotryptophan and -tryptamine derivatives are potentially useful synthetic building blocks for a variety of applications in indole-based natural product synthesis. We recently reported a new method for the stereocontrolled construction of spiro[pyrrolidine-3,3'-oxindoles], that is, **3**, in the synthesis of isoelacomine (**4**) and elacomine (**5**) from 2,6-dibromotryptamine (**2**) (Scheme 1).^[9] A high degree of stereochemical control at the newly formed quaternary and adjacent alkyl center in **3** was observed, which favored a *cis* relationship between the alkyl group and oxindole benzene ring. Based on this initial work, we felt that the use of 2-halotryptophan esters and the development of new *N*-acyliminium ion spirocyclization methodology would nicely complement existing tryptophan-based methods for constructing the spirotryprostatin architecture exemplified by structure **1**.



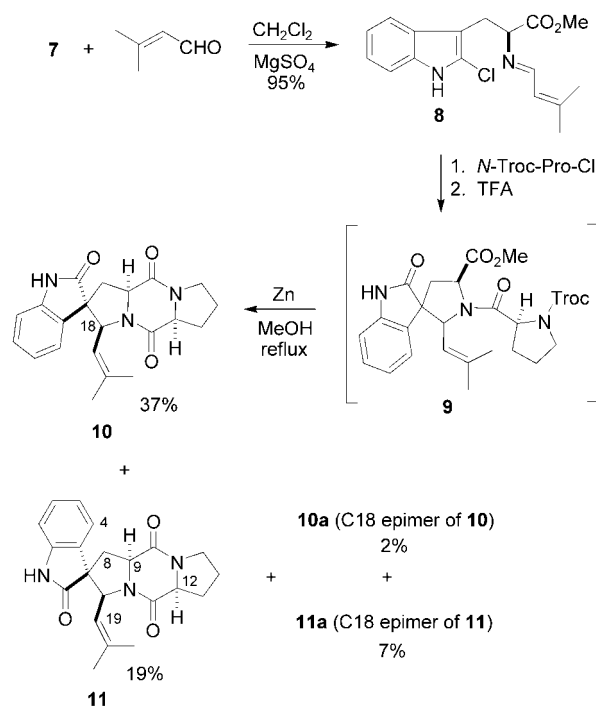
Scheme 1. Synthesis of isoelacomine (**4**) and elacomine (**5**) by stereocontrolled spirocyclization. TFA = trifluoroacetic acid.

To date, only a few 2-halo-substituted tryptophan derivatives have been prepared.^[10–12] Their preparation utilizes multistep protocols that involve nitrogen group protection, chiral auxiliary introduction, and/or enzymatic transformations. Clearly, a procedure that could readily deliver 2-halotryptophan esters directly from readily available tryptophan esters would be highly desirable. In recent work, we demonstrated the direct and regioselective introduction of bromine and chlorine at the 2-position of tryptamine with NBS and NCS to afford 2-bromo- or 2-chlorotryptamine, respectively.^[9] This methodology has now been successfully extended to tryptophan esters wherein treatment of the hydrochloride salt of tryptophan methyl ester (**6**) (AcOH/HCO₂H, 4:1, 23 °C, 20 min with NCS regioselectively produced 2-chlorotryptophan methyl ester (**7**) ($[\alpha]_D^{23} + 27.8$, $c = 0.3$, MeOH, as the HCl salt) in good yields (Scheme 2).^[13] Multigram quantities of **7** can be prepared easily by using this protocol.



Scheme 2. Preparation of 2-chlorotryptophan methyl ester (**7**). NCS = *N*-chlorosuccinimide.

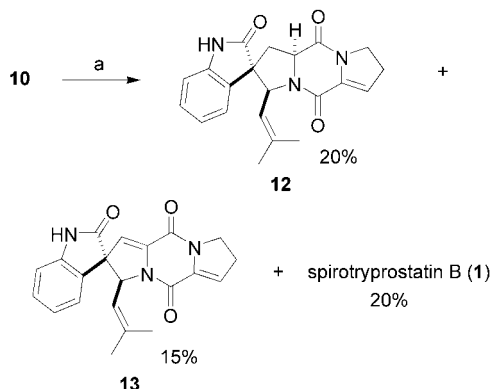
With **7** in hand, we turned our attention to the spirocyclization reaction with prenyl aldehyde (Scheme 3). As anticipated, condensation of amine **7** with prenyl aldehyde produced imine **8** as a stable entity. Activation of imine **8** as



Scheme 3. Synthesis of dihydrospirotryprostatin B (**10**). Troc = 2,2,2-trichloroethoxycarbonyl.

its *N*-acyliminium species with *N*-Troc proline acid chloride^[14] induced spirocyclization. Subsequent TFA-assisted hydrolysis of the putative chloroindolenine intermediate produced oxindole **9** as a mixture of single diastereomers. Rather than attempt a chromatographic separation at this stage, we transformed **9** in one-pot to the requisite diketopiperazine by removal of the Troc group and cyclization. Flash chromatography of the reaction products afforded desired dihydrospirotryprostatin B (**10**), $[\alpha]_{\text{D}}^{23}$ –123 (c =2.1, CHCl_3), as the major diastereomer, and, to a lesser extent, C3 epimer **11**, $[\alpha]_{\text{D}}^{23}$ –193 (c =1.8, CHCl_3). Diastereomers **10a**, $[\alpha]_{\text{D}}^{23}$ +32 (c =1.4, CHCl_3) and **11a**, $[\alpha]_{\text{D}}^{23}$ –42 (c =1.2, CHCl_3), were also obtained but only in minor quantities. The ^1H and ^{13}C NMR spectra of **10**, **10a**, and **11** were identical to those previously reported for these compounds.^[3,6,15] The relative configuration of previously unknown **11a** was determined from NOE data; significant NOEs were observed between H19, H9, H8 α (δ =2.65 ppm), and H4, as well as between H12 (δ =4.44 ppm) and H9, in CD_3OD .

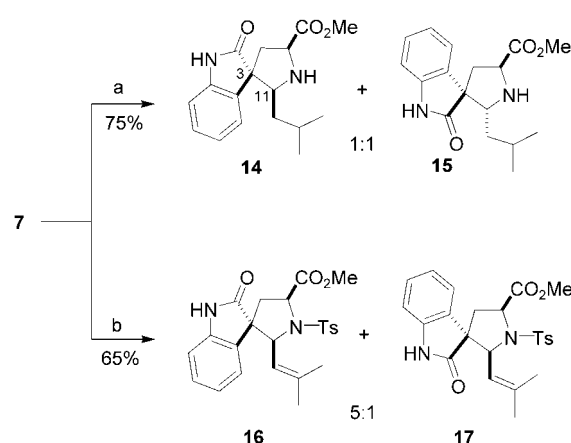
Ganesan et al. reported the conversion of dihydrospirotryprostatin B (**10**) to spirotryprostatin B (**1**) in low yield as a mixture of several products.^[3] In an attempt to improve this route, a “nonoxidative” protocol^[16] was pursued to install the dehydropoline unit (Scheme 4). This proceeded with modest



Scheme 4. Synthesis of spirotryprostatin B (**1**). a) LiHMDS (3 equiv), THF, 0°C, 30 min; then PhSeCl (3 equiv), 3 h, 0°C; then PhSeCl (3 equiv), 23°C, 16 h.

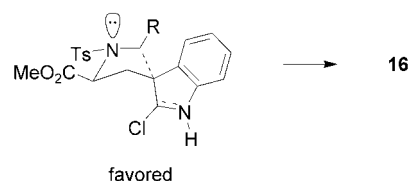
success in which spirotryprostatin B (**1**), $[\alpha]_{\text{D}}^{23}$ –149.0 (c =0.3, CHCl_3) [ref: $[\alpha]_{\text{D}}^{23}$ –162.1 (c =0.92, CHCl_3)^[11]], was obtained in 20% yield along with known analogues **12**^[3] and **13**.^[4]

The precise factors controlling the stereochemistry of the *N*-acyliminium ion spirocyclization derived from (*S*)-2-chlorotryptophan methyl ester (**7**) are unclear at this time. It is evident, however, that the cyclization favors an *S* absolute configuration at C18 and a relative *cis* orientation of the prenyl side chain and oxindole benzene ring. With the hope of gaining further insight into the stereochemistry of this cyclization reaction, additional experiments were performed (Scheme 5). Condensation of **7** with isovaleraldehyde followed by proton-facilitated iminium ion cyclization produced spirooxindoles **14** and **15** in \approx 1:1 ratio.^[17,18] The relative C3 and C11 configuration of **14** and **15** is such that the isovaleryl side chain and oxindole benzene ring are oriented *cis* for both



Scheme 5. Stereoccontrolled spirocyclization of 2-chlorotryptophan (**7**) and aldehydes. a) $(\text{CH}_3)_2\text{CHCH}_2\text{CHO}$, CH_2Cl_2 , 23°C, 2 h; then TFA (6 equiv), 23°C, 1 h; b) $(\text{CH}_3)_2\text{C}=\text{CHCHO}$, CH_2Cl_2 , 23°C, 2 h; then TsCl (2.5 equiv), Et_3N (3 equiv), 23°C, 36 h; then TFA (6 equiv), 23°C, 2 h. TsCl = *p*-toluenesulfonyl chloride.

diastereomers. This is consistent with the achiral tryptamine model recently published.^[9] In the present case, it appears that the methoxycarbonyl chiral center has no effect in controlling the relative configuration at C11 under proton activation. On the other hand, when TsCl was used in the spirocyclization of **7** and prenyl aldehyde, oxindoles **16** and **17** were obtained in a 5:1 ratio.^[19] Relatively good stereocontrol at C3 and C11 can be achieved in this case compared to *N*-Troc-proline acid chloride. These results suggest that the structure of the activating substituent plays a significant role in governing the formation of the C3 and C11 (or C18 in **10**) centers. The issues governing stereocontrol in the spirocyclization reaction are undoubtedly complex. In the case of TsCl activation, a late transition state may be operable with the Ts group oriented *trans* to the methoxycarbonyl and R groups, which leads predominantly to the formation of diastereomer **16** (Scheme 6).



Scheme 6. Possible stereochemical rationale.

In conclusion, we have described a short synthesis of spirotryprostatin B featuring new intramolecular *N*-acyliminium ion spirocyclization methodology based on 2-halotryptophan esters. The methodology provides direct and rapid access to versatile tryptophan building blocks. Notably, the cyclization products are the result of a kinetically controlled process that complements thermodynamic outcomes often associated with classical Mannich oxindole conditions. Stereoccontrolled spirocyclizations to form non-racemic spirochloroindolenine intermediates should afford new opportunities not only in spirooxindole construction but also in the

synthesis of other indole-based natural product ring systems of biological and structural significance.

Received: April 22, 2004

Keywords: Alkaloids · Halogenations · Natural products · Spiro compounds · Synthetic methods

- [1] a) C. -B. Cui, H. Takeya, H. Osada, *J. Antibiot.* **1996**, *49*, 832–835; b) C. -B. Cui, H. Takeya, H. Osada, *Tetrahedron* **1996**, *52*, 12651–12666.
- [2] F. von Nussbaum, S. J. Danishefsky, *Angew. Chem.* **2000**, *112*, 2259–2262; *Angew. Chem. Int. Ed.* **2000**, *39*, 2175–2178.
- [3] H. Wang, A. Ganesan, *J. Org. Chem.* **2000**, *65*, 4685–4693.
- [4] a) P. R. Sebahar, R. M. Williams, *J. Am. Chem. Soc.* **2000**, *122*, 5666–5667; b) P. R. Sebahar, H. Osada, T. Usui, R. M. Williams, *Tetrahedron* **2002**, *58*, 6311–6322.
- [5] L. E. Overman, M. D. Rosen, *Angew. Chem.* **2000**, *112*, 4768–4771; *Angew. Chem. Int. Ed.* **2000**, *39*, 4596–4599.
- [6] T. D. Bagul, G. Lakshmaiah, T. Kawabata, K. Fuji, *Org. Lett.* **2002**, *4*, 249–251.
- [7] C. Meyers, E. M. Carreira, *Angew. Chem.* **2003**, *115*, 718–720; *Angew. Chem. Int. Ed.* **2003**, *42*, 694–696.
- [8] For a recent review of synthetic work on related spirooxindoles, see C. Marti, E. M. Carreira, *Eur. J. Org. Chem.* **2003**, 2209–2219.
- [9] F. Y. Miyake, K. Yakushijin, D. A. Horne, *Org. Lett.* **2004**, *6*, 711–713.
- [10] a) R. S. Phillips, L. A. Cohen, *Tetrahedron Lett.* **1983**, *24*, 5555–5558; b) R. S. Phillips, L. A. Cohen, *J. Am. Chem. Soc.* **1986**, *108*, 2023–2030.
- [11] a) P. Zhang, R. Liu, J. M. Cook, *Tetrahedron Lett.* **1995**, *36*, 9133–9136; b) T. Gan, R. Liu, P. Yu, S. Zhao, J. M. Cook, *J. Org. Chem.* **1997**, *62*, 9298–9304.
- [12] C. Balsamini, G. Diamantini, A. Duranti, G. Spadoni, A. Tontini, *Synthesis* **1995**, 370–372.
- [13] (s)-2-bromotryptophan methyl ester (**7a**) was prepared from **6**-HBr and NBS, $[\alpha]_D^{23} + 24.6$ ($c = 0.46$, as HBr salt in MeOH).
- [14] a) S. A. Boyd, W. J. Thompson, *J. Org. Chem.* **1987**, *52*, 1790–1794; b) S. Kodato, M. Nakagawa, M. Hongu, T. Kawate, T. Hino, *Tetrahedron* **1988**, *44*, 359–377.
- [15] S. Edmonson, S. J. Danishefsky, L. Sepp-Lorenzino, N. Rosen, *J. Am. Chem. Soc.* **1999**, *121*, 2147–2155.
- [16] a) D. Liotta, C. Barnum, R. Puleo, G. Zima, C. Bayer, H. S. Kezar III, *J. Org. Chem.* **1981**, *46*, 2920–2923; b) J. Ezquerro, A. Escribano, A. Rubio, M. J. Remuinan, J. J. Vaquero, *Tetrahedron: Asymmetry* **1996**, *7*, 2613–2626.
- [17] NOEs observed for compound **14**: between H-11, H-9, and H $_{\alpha}$ -8; between H-4 and H $_{\beta}$ -8. NOEs observed for compound **15**: between H-9, H $_{\alpha}$ -8, and H-4; between H $_{\beta}$ -8 and H-11.
- [18] It is well-known that spirooxindoles whose structures are related to compounds **3–5** (ref. [9]) having an amino, not amido, nitrogen atom in the spiropyrrolidine ring can undergo facile equilibration and epimerization at C3 and C11 (or C18 in **10**) through a retro-Mannich process. Oxindoles **14** and **15**, however, are configurationally stable in CD₃OD at 23°C over a period of 7 d. a) C. Pellegrin, M. Weber, H.-J. Borshberg, *Helv. Chim. Acta* **1996**, *79*, 151–168; b) M. Ito, C. W. Clark, M. Mortimore, J. B. Goh, S. F. Martin, *J. Am. Chem. Soc.* **2001**, *123*, 8003–8010, and references therein.
- [19] NOEs observed for compound **16**: between H-11, H-9, and H $_{\alpha}$ -8; between H-4 and H $_{\beta}$ -8. NOEs observed for compound **17**: between H-11, H-9, H $_{\alpha}$ -8, and H-4.

Chiral Centers in the Side Chains of α -Amino Acids Control the Helical Screw Sense of Peptides**

Masakazu Tanaka,* Yosuke Demizu, Mitsunobu Doi, Masaaki Kurihara, and Hiroshi Suemune*

Understanding the secondary structures of peptides and proteins, for example, the α -helix, β -sheet, and reversed-turn, is important as they play a vital role in molecular biology, the life sciences, and drug discovery.^[1] The α -helices and the 3_{10} -helices in proteins almost always form a right-handed (*P*) helical screw, which is believed to result from the asymmetry of the α -carbon (*S* enantiomer) in terrestrial L- α -amino acids.^[1a] Among proteinogenic L- α -amino acids, only isoleucine and threonine possess an additional chiral center at the side-chain β -carbon besides the α -carbon. However, so far it has not been clear how chiral centers in the side chain affect the secondary structure of peptides.^[2] Here we describe how the asymmetric centers of the α -amino acid side chain alone control the screw sense of the helices formed by oligopeptides made up of amino acids without a chiral center at the α -carbon.

Replacement of the α -hydrogen atom of an α -amino acid with an alkyl substituent results in an α,α -disubstituted α -amino acid (dAA), such as 2-aminoisobutyric acid (Aib), diethylglycine (Deg), 1-aminocycloalkancarboxylic acid (Ac_nC , n = ring size), and isovaline.^[3] Oligopeptides containing dAAs show stable secondary structural preferences, such as β -turns, 3_{10} -helices, and extended planar C_5 conformations. We designed a chiral cyclic dAA [*(S,S)*- $\text{Ac}_5\text{C}^{\text{dOM}}$], in which the α -carbon does not have an asymmetric center but has two side chain γ -carbons that are asymmetric centers. In the case of $\text{Ac}_5\text{C}^{\text{dOM}}$ homopeptides, the asymmetric centers do not lie along the main-chain backbone of the peptides but rather in the side chain cyclopentane ring. Thus, the secondary

[*] Prof. Dr. M. Tanaka, Y. Demizu, Prof. Dr. H. Suemune
Graduate School of Pharmaceutical Sciences
Kyushu University
Fukuoka 812-8582 (Japan)
Fax: (+81) 92-642-6545
E-mail: mtanaka@phar.kyushu-u.ac.jp
suemune@phar.kyushu-u.ac.jp

Prof. Dr. M. Doi
Osaka University of Pharmaceutical Sciences
Osaka 569-1094 (Japan)
Dr. M. Kurihara
Division of Organic Chemistry
National Institute of Health Sciences
Tokyo 158-8501 (Japan)

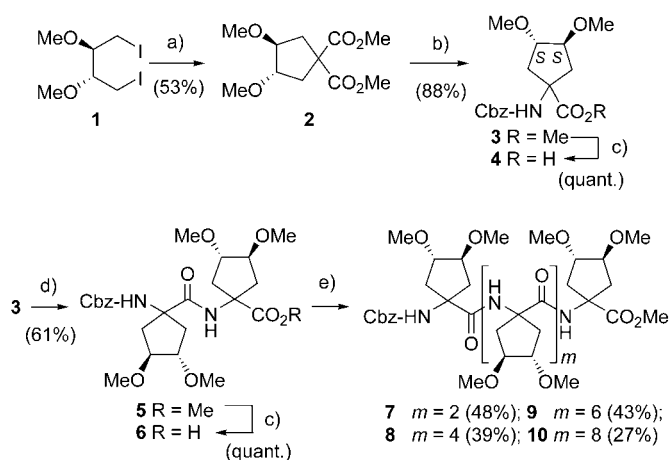
[**] This work was partly supported by a Grant-in-Aid for Scientific Research (C) from the Japan Society for the Promotion of Science and also by the Sasakawa Scientific Research Grant from the Japan Science Society.



Supporting information for this article is available on the WWW under <http://www.angewandte.org> or from the author.

structure is affected by the side chain chiral centers of (*S,S*)-Ac₅c^{DOM} peptides but not by the α -carbons.^[4]

The optically active (*S,S*)-Ac₅c^{DOM} was synthesized from dimethyl-L-(+)-tartrate as follows (Scheme 1): Dimethyl-L-



Scheme 1. Synthesis of (*S,S*)-Ac₅c^{DOM} and its homopeptides. Reagents and conditions: a) dimethyl malonate, KO^tBu; b) 1. NaOH, 2. DPPA, 3. BnOH; c) NaOH; d) 1. Pd/C, H₂, 2. EDC, HOBT, 4, MeCN, RT; e) 1. Pd/C, H₂, 2. EDC, HOBT, 6, MeCN, RT. Cbz = benzyloxycarbonyl, EDC = 2-(3-dimethylaminopropyl)-1-ethylcarbodiimide, HOBT = 1-hydroxy-1H-benzotriazole.

(+)-tartrate was converted into a diiodide **1** by conventional procedures,^[5] then dimethyl malonate was alkylated with **1** to give the cyclic diester **2**. Monohydrolysis of **2** followed by Curtius rearrangement with diphenylphosphoryl azide (DPPA) afforded the C- and N-terminal protected Cbz-(*S,S*)-Ac₅c^{DOM}-OMe **3**. Hydrolysis with an alkaline solution gave the N-protected Cbz-(*S,S*)-Ac₅c^{DOM}-OH **4**. Homopeptides Cbz-[(*S,S*)-Ac₅c^{DOM}]_n-OMe (up to the decamer; *n* = 2, 4, 6, and 10) were prepared by coupling the N-terminal free peptides and C-terminal free dipeptide **6** by solution-phase methods.^[6] Octapeptide **9** and decapeptide **10** can be dissolved in water (**10**: > 5 mg cm⁻¹) because of the hydrophilic ethereal groups at the cyclopentane.^[7]

The preferred secondary structure of the homopeptides in the CDCl₃ solution was first studied by FT-IR and ¹H NMR spectroscopies. In the IR spectra, the weak bands in the region 3420–3440 cm⁻¹ are assigned to free (solvated) peptide NH groups, and the strong bands at 3320–3370 cm⁻¹ to peptide NH groups with N–H⋯O=C intramolecular hydrogen bonds of differing strengths. As the length of the peptide chain increases, the strong band observed at 3370 cm⁻¹ in **7** shifts to slightly lower wave numbers (3320 cm⁻¹ in **10**), and the relative intensity of this band gradually increases.^[6] These IR spectra are very similar to those of achiral Ac₄c peptides, which form 3₁₀-helices in solution,^[3c] but very different from those of Deg peptides, which form extended planar conformations.^[3b]

In the ¹H NMR spectra measured after addition of DMSO or the free radical 2,2,6,6-tetramethyl-1-piperidinoxyl (TEMPO), as well as at different peptide concentrations, the two NH signals [NH1 and NH2] of the hexapeptide **8** and octapeptide **9**, respectively, are very sensitive (solvent-

exposed NH group). This suggests the absence of two intramolecular hydrogen bonds at these NH groups and thus indicates that the peptides assume a helical structure in CDCl₃ solution.^[6] Also, the ROESY ¹H NMR spectrum of **8** shows a complete series of sequential *d*_{NN} cross peaks of NOEs, from the N-terminal NH1 to the C-terminal NH6, characteristic of a helical secondary structure.^[6]

The CD spectra of **8–10** in 2,2,2-trifluoroethanol (TFE) show positive maxima and intensity for two bands at 222 nm and 208 nm, indicating that the screw sense of the helix is left-handed (*M*) (Figure 1 a). The ratio of *R* [$\theta_{222}/\theta_{208}$] suggests that

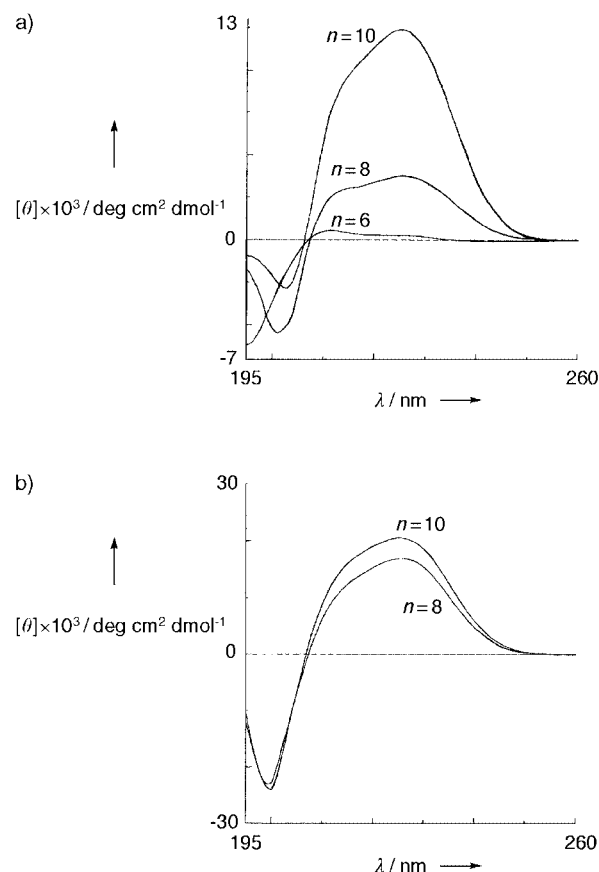


Figure 1. CD spectra of Cbz-[(*S,S*)-Ac₅c^{DOM}]_n-OMe **8–10** (*n* = 6, 8, 10) (0.5 mM) a) in TFE solution, b) in H₂O.

the secondary structure of **8** is a 3₁₀-helix, and that those of **9** and **10** are α -helices.^[8] Interestingly, the intensity of the CD spectra of **9** and **10** in water become stronger, indicating that these peptides are more helical when dissolved in water than in TFE (Figure 1 b).

The molecular and crystal structures of the terminally protected hexapeptide **8** (Figure 2) and octapeptide **9** (Figure 3) were determined by X-ray crystallographic analysis. In the crystal structure of **8** three crystallographically independent molecules *A*, *B*, and *C* exist in the asymmetric unit. All three molecules are left-handed (*M*) 3₁₀-helices (mean value: $\phi = 58.5^\circ$, $\psi = 30.5^\circ$), showing small differences in the conformation of the side chains, and four intramolecular hydrogen bonds are found in each molecule. The molecules *A*, *B*, and *C* are connected by two intermolecular

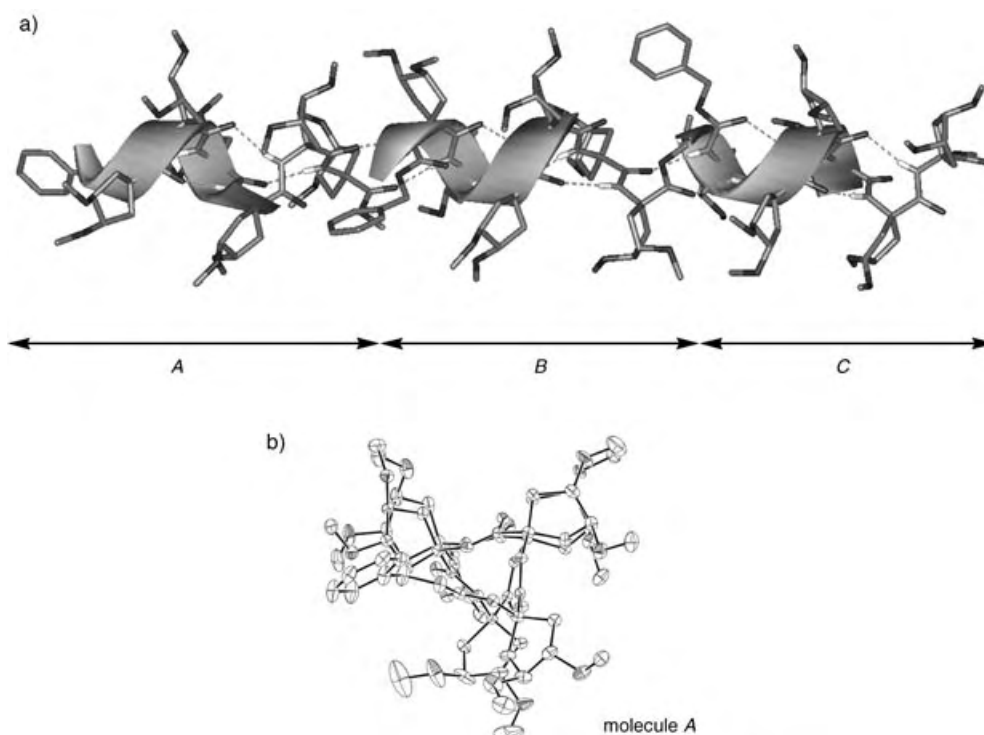


Figure 2. a) Illustrative structure of **8** (molecules A, B and C) as viewed perpendicular to the 3₁₀-helical axis; b) ORTEP drawing of molecule A as viewed along the 3₁₀-helical axis.

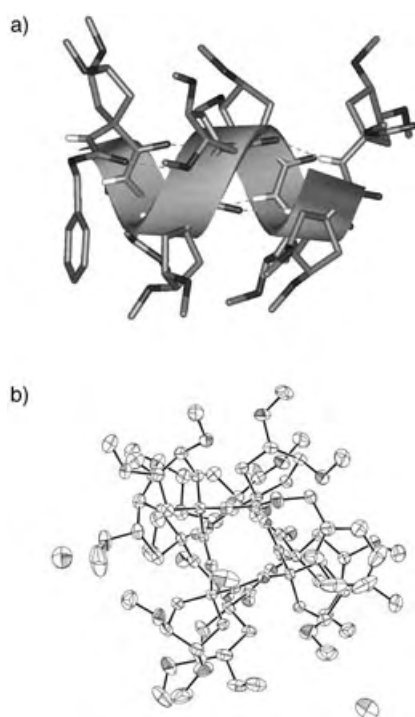


Figure 3. a) Illustrative structure of **9** as viewed perpendicular to the α-helical axis; b) ORTEP drawing as viewed along the α-helical axis (α-helical wheel).

hydrogen bonds, forming a head-to-tail alignment of ($\cdots A \cdots B \cdots C \cdots A \cdots B \cdots C \cdots$) chains.^[9]

In the asymmetric unit of **9** one left-handed (*M*) helical structure (mean value: $\phi = 60.9^\circ$, $\psi = 46.8^\circ$),^[10] which is not a

3₁₀-helix but an α-helix, exists along with three water molecules. Five intramolecular hydrogen bonds exist in the α-helical molecule, and in the packing mode the chains of intermolecularly hydrogen-bonded (*M*) α-helices are formed by means of the water.

The conformational search calculation with MacroModel (AMBER*) produced left-handed (*M*) α-helices as a global minimum-energy conformation for both **8** and **9**. The (*M*) 3₁₀-helix of **8**, which is similar to those in the crystal, was obtained as a local minimum-energy conformation (+3.22 kcal mol⁻¹).^[6]

We have efficiently synthesized a new chiral cyclic dAA and studied the secondary structure of (*S,S*)-Ac₅c^{dOM} homopeptides. It is notable that: 1) Chiral centers in the side chain of the α-amino acid strongly control the helical screw sense of its peptides; 2) The (*M*) α-helix of the (*S,S*)-Ac₅c^{dOM} peptides is stable even in water; 3) The transition from the 3₁₀-helix into the α-helix occurs for longer (*S,S*)-Ac₅c^{dOM} peptides; and 4) The α-helix is formed in dAA homopeptides without a natural α-amino acid in the solid state.

These results strongly imply that the side chain chiral centers of isoleucine and threonine would affect the secondary structure of their oligopeptides; albeit, these residues also exhibit a strong screw-sense bias due to their chiral α-carbon atom, and they are poorly helicogenic residues. Preparation of the enantiomer and incorporation of (*S,S*)-Ac₅c^{dOM} into natural α-amino acid sequences are currently underway.

Received: April 23, 2004

Published Online: July 7, 2004

Keywords: amino acids · chirality · conformation analysis · helical structures · peptidomimetics

- [1] a) C. Branden, J. Tooze, *Introduction to Protein Structure*, Garland, New York, **1991**, pp. 1–31; b) J. A. Robinson, *Synlett* **1999**, 429–441; c) D. Seebach, J. L. Matthews, *Chem. Commun.* **1997**, 2015–2022; d) S. H. Gellman, *Acc. Chem. Res.* **1998**, *31*, 173–180.
- [2] Chiral N-alkylated glycine oligopeptides (peptoids) form a one-handed helix affected by the chiralities at the N-alkyl side-chains; however, the peptoids may have *cis* amides. See: C. W. Wu, K. Kirshenbaum, T. J. Sanborn, J. A. Patch, K. Huang, K. A. Dill, R. N. Zuckermann, A. E. Barron, *J. Am. Chem. Soc.* **2003**, *125*, 13525–13530.
- [3] a) I. L. Karle, P. Balaram, *Biochemistry* **1990**, *29*, 6747–6756; b) M. Tanaka, N. Imawaka, M. Kurihara, H. Suemune, *Helv. Chim. Acta* **1999**, *82*, 494–510; c) M. Gatos, F. Formaggio, M. Crisma, C. Toniolo, G. M. Bonora, Z. Benedetti, B. D. Blasio, R. Iacovino, A. Santini, M. Saviano, J. Kamphuis, *J. Pept. Sci.* **1997**, *3*, 110–122; d) B. Jaun, M. Tanaka, P. Seiler, F. N. M. Kühnle, C. Braun, D. Seebach, *Liebigs Ann./Recl.* **1997**, 1697–1710; e) M. Crisma, A. Moretto, M. Rainaldi, F. Formaggio, Q. B. Broxterman, B. Kaptein, C. Toniolo, *J. Pept. Sci.* **2003**, *9*, 620–637; f) N. Imawaka, M. Tanaka, H. Suemune, *Helv. Chim. Acta* **2000**, *83*, 2823–2835; g) M. Tanaka, S. Nishimura, M. Oba, Y. Demizu, M. Kurihara, H. Suemune, *Chem. Eur. J.* **2003**, *9*, 3082–3090.
- [4] Toniolo's group reported that homopeptides of a C_2 -symmetric binaphthyl dAA with only axial chirality form one-handed 3_{10} -helices in solution. See: J. P. Mazaleyrat, K. Wright, A. Gaucher, M. Wakselman, S. Oancea, F. Formaggio, C. Toniolo, V. Setnicka, J. Kapitan, T. A. Keiderling, *Tetrahedron: Asymmetry* **2003**, *14*, 1879–1893.
- [5] I. Takahashi, K. Odashima, K. Koga, *Tetrahedron Lett.* **1984**, *25*, 973–976.
- [6] See the Supporting Information for synthetic procedures, spectroscopic data of new compounds, IR spectra, ^1H NMR experiments (DMSO, TEMPO, concentration effects, and the ROESY spectrum), molecular mechanics calculations, torsion angles, and hydrogen-bond parameters.
- [7] M. Tanaka, Y. Demizu, M. Doi, M. Kurihara, H. Suemune, *Pept. Sci. 2003 (Proceedings of the 40th JPS)* **2004**, 109–110.
- [8] a) C. Toniolo, A. Polese, F. Formaggio, M. Crisma, J. Kamphuis, *J. Am. Chem. Soc.* **1996**, *118*, 2744–2745; b) P. Pengo, L. Pasquato, S. Moro, A. Brigo, F. Fogolari, Q. B. Broxterman, B. Kaptein, P. Scrimin, *Angew. Chem.* **2003**, *115*, 3510–3514; *Angew. Chem. Int. Ed.* **2003**, *42*, 3388–3392.
- [9] CCDC-236749 and CCDC-236750 contain the supplementary crystallographic data for this paper. These data can be obtained free of charge via www.ccdc.cam.ac.uk/conts/retrieving.html (or from the Cambridge Crystallographic Data Center, 12, Union Road, Cambridge CB2 1EZ, UK; fax: (+44) 1223-336-033 or deposit@ccdc.cam.ac.uk). Crystal data: **8**: $\text{C}_{57}\text{H}_{88}\text{N}_6\text{O}_{21}$, $M_r = 3579.99$ (1193.33), space group $P2_1$, $a = 22.889$, $b = 11.9061$, $c = 33.711$ Å, $\beta = 91.887^\circ$, $V = 9182.0$ Å³, $Z = 6$, $T = 90$ K, $\mu(\text{MoK}\alpha) = 0.99$ cm⁻¹, 31 196 reflections measured, 29 355 unique reflections ($R_{\text{int}} = 0.0326$) R_1 ($I > 2\sigma$) = 0.0775, wR_2 ($I > 2\sigma$) = 0.1972, GOF = 1.095. **9**: $\text{C}_{73}\text{H}_{114}\text{N}_8\text{O}_{27} \cdot 3\text{H}_2\text{O}$, $M_r = 1589.77$, space group $P2_1$, $a = 15.639$, $b = 16.431$, $c = 15.989$ Å, $\beta = 95.85^\circ$, $V = 4087$ Å³, $Z = 2$, $T = 123$ K, $\mu(\text{MoK}\alpha) = 1.0$ cm⁻¹, 16 850 reflections measured, 12 478 unique reflections ($R_{\text{int}} = 0.0609$) R_1 ($I > 2\sigma$) = 0.0579, wR_2 ($I > 2\sigma$) = 0.1401 ($I > 2\sigma$), GOF = 1.031.
- [10] The signs of ϕ , ψ torsion angles at the C-terminus are opposite to those of the preceding residues. The average is amino acid residues (1–7).

Ionic Liquids as Moderators in Exothermic Polymerization Reactions**

R. Vijayaraghavan, M. Surianarayanan, and
D. R. MacFarlane*

Explosions due to thermal runaway are one of the major safety issues faced by chemical industries.^[1–3] A knowledge of the thermokinetics of exothermic reaction systems not only helps in mitigating disastrous events such as catastrophic fires and explosions but also provides the means for designing in-built safety systems. Thermal-hazard assessment basically relies on the identification of dangerous process situations, deviations, and thermal sensitivity of reaction mixtures and products. The conventional hazard assessment methods, namely, hazard and operability limits (HAZOP), failure mode evaluation analysis (FMEA), and fault tree analysis (FTA) will become more precise and effective if thermal stability of relevant chemicals and reaction mixtures are clearly defined.^[4] Furthermore, the consequences of runaway reactions have not received much attention compared to the consequences of chemical release from storage and other installations. This is mostly due to an insufficient understanding of the complex behavior of thermal-runaway systems; for example, the consequence analysis (one of the conventional hazard assessment procedures) assumes that the runaway phenomenon is a physical explosion and the forecasted scenario has to be based on the material properties and design pressure of the process vessel. In the absence of information concerning the energy released during runaway reactions, it is indeed difficult to assume that all runaway reactions would lead only to physical explosions. Nevertheless this information is available for most chemical-process reaction systems and continuous efforts are being made to generate thermokinetic data. Inherently safer design approaches,^[5] design of emergency relief systems (ERS),^[6] and explosion suppression systems (ESS)^[7] are a few of the latest methodologies in the chemical industry to deal with thermal runaway. While the concept of inherently safer design approaches can be successfully employed to most of the exothermic reaction systems, ERS and ESS contribute

[*] Prof. D. R. MacFarlane
School of Chemistry
Monash University
Clayton, Victoria 3800 (Australia)
Fax: (+61) 3-9905-4597
E-mail: d.macfarlane@sci.monash.edu.au

Dr. R. Vijayaraghavan,^[†] Dr. M. Surianarayanan
Department of Chemical Engineering
Central Leather Research Institute
Adyar, Madras 600 020 (India)

[†] Present address: School of Chemistry
Monash University
Victoria 3800 (Australia)

[**] We thank ARC Special Research Centre for Green Chemistry,
Monash University for the financial support.

significantly to the cost. Furthermore, these systems have to be maintained to function properly and the chance of failure during an emergency is significant. Efforts to synthesize chemical agents that suppress or alter the course of exothermic activity have not proven to be entirely successful as they are system-specific, typically require large quantities, and can be unstable at the temperatures at which runaway occurs, hence contributing to the problem in the event of a catastrophe.^[8]

In recent years, ionic liquids (ILs) have been extensively investigated for use as replacement solvents for clean synthesis in a variety of chemical reactions.^[9–13] The major advantage of using these ionic liquids is their ability to dissolve a wide range of organic and ionic compounds to an appreciable extent. Their lack of volatility and their high thermal stability are also important features and thus they may prove effective in moderating highly exothermic reactions and hence impeding thermal runaway. For example, vinyl-polymerization reactions are in general highly exothermic in nature (heat of reaction 20 Kcal mol⁻¹).

The use of ionic liquids as solvents in polymerization reactions has recently been reported^[14–17] for free-radical polymerization, transition-metal mediated living free-radical polymerization, charge-transfer, and cationic polymerization. The presence of [bmim][PF₆] (bmim is 1-butyl-3-methylimidazolium) ionic liquid as solvent increased the overall rate of methyl methacrylate^[15] polymerization about tenfold compared to the same reaction in benzene. Other advantages of polymers synthesized in ionic liquids have been described in detail.^[18] Moderation of the reaction by carrying out the polymerization in solution reduces the heat produced^[19] but often the solvents are not stable at high temperatures, the subsequent decomposition and resultant pressure rise causes the system to runaway. Solvent-based systems also pose great challenges in design, scale-up, and their recovery for reuse. Incidents due to thermal runaway of such systems have been widely reported.^[19–20] Thus in this case the intrinsic stability and low volatility of ionic liquids should overcome these issues.

There are a number of objectives in this study: the main objective is to assess the role of ionic liquids in moderating the thermal polymerization of styrene and acrylonitrile by using an accelerating-rate calorimeter (ARC). Another objective is to explore the possibility of replacing the traditional molecular solvents with an ionic liquid and study their effect in lowering the pressure in the system. Herein we report the thermal polymerization of styrene and acrylonitrile in an ARC with and without the presence of an ionic liquid to establish the role of the ionic liquid as a heat sink. The ionic liquid chosen for this study is *N*-butyl, *N*-methyl pyrrolidinium bis(trifluoromethanesulfonyl)amide, abbreviated as [P_{1,4}][tf₂N]. Thermal stabilities of hydrophobic ionic liquids with different anions including bis(trifluoromethanesulfonyl)amide have been studied.^[21–23] The study reveals that anions such as bis(trifluoromethanesulfonyl)amide are stable for short periods of time up to 394°C. The onset of thermal decomposition temperatures are similar for different cations but appear to decrease as the anion hydrophilicity increases. The effect of anion fluorination on thermal stability also

reveals the enhanced stability for the [tf₂N]⁻ ion.^[24] Hence this anion is an ideal choice as the component of an ionic liquid for use at high temperatures.

The rate of self-heating versus temperature curve for the thermal polymerization of styrene for neat styrene and for styrene mixed with the IL is shown in Figure 1. The case of

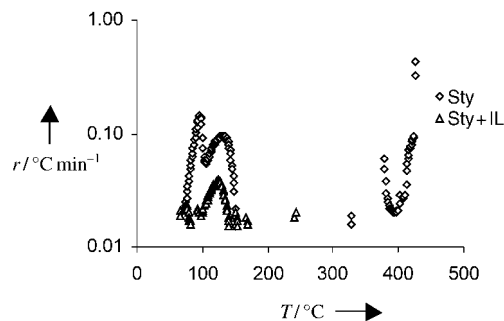


Figure 1. A comparison of ARC rates of self-heating of styrene (Sty) and styrene in IL (StyIL); *r* is the heating rate.

neat styrene exhibits several exotherms that correspond to different stages of the reaction, including high-temperature processes around 400°C. The curves show that the addition of an IL drastically reduces the rate of self-heating at all temperatures compared to the neat monomer. The onset of exothermic activity in the presence of the IL has been postponed to 95°C. In the case of neat styrene, multiple exotherms are observed with a maximum heat rate of 0.45°C min⁻¹ at 400°C, while in presence of IL no exothermic activity is recorded beyond 200°C and the maximum heat rates are less than 0.03°C min⁻¹ at 100°C. Since the IL has very low vapor pressure even at higher temperatures compared to neat styrene, the reaction carried out in IL would not be expected to have a significant rate of decomposition in the vapor phase, hence the absence of multiple exotherms. The vapor-phase decompositions themselves can cause the system to runaway.^[25] Hence the use of ionic liquids in this reaction completely avoids one of the significant origins of thermal runaway.

At the end of the experiments the bomb was cut open and it was found that there was no trace of monomer. Characterization of the decomposed products is underway.

Similarly the plot of pressure versus temperature (Figure 2) also shows a decrease in the rise in pressure when the reaction is carried out in IL. The absence of exothermic activity and pressure rise beyond 300°C may be due to the stabilizing effect of the ionic liquid. The higher thermal stability of the IL is thus responsible for the intrinsic safety of the process. The IL present in the system absorbs the heat from the reaction mixture, and because of its high thermal stability it appears to delay or quench polymer decomposition reactions thus further protecting the reaction from runaway. The time available to take safety measures is also significantly increased when IL is present in the system. This is evidenced in the plot of time versus temperature (Figure 3). This plot recorded during an applied constant heating rate shows how the system enters thermal runaway

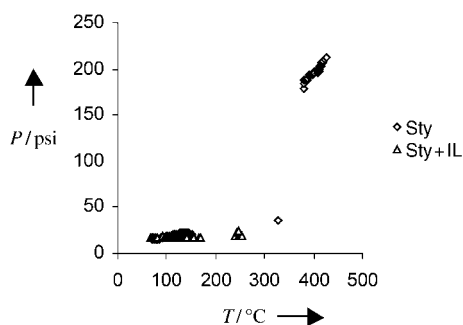


Figure 2. Plots of the temperature versus pressure for the polymerization of styrene and styrene in IL.

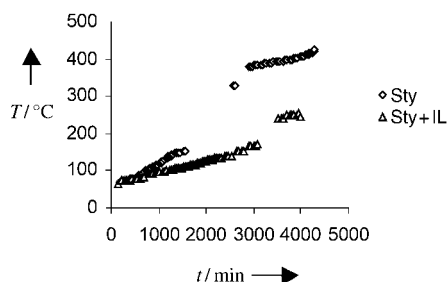


Figure 3. Profiles of time versus temperature for styrene polymerization

and how rapidly the temperature rises during this situation. In the neat system, the temperature rapidly rises from 200°C to >400°C with a concomitant rise in pressure that has potentially catastrophic results. On the other hand the IL-based system never exhibits a rapid rise in temperature or pressure and appears to be quite stable up to 400°C.

The plot of the rate of self-heating (Figure 4) for the thermal polymerization of acrylonitrile (AN) also clearly

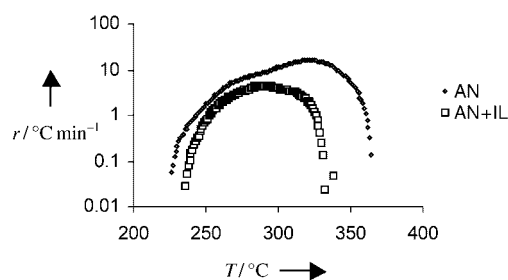


Figure 4. Self-heating profiles for AN polymerization.

indicates a drastic reduction in the maximum rate of self-heating ($10^{\circ}\text{C min}^{-1}$ for neat AN and $1^{\circ}\text{C min}^{-1}$ for AN in IL) with postponement of the onset of exothermic activity from 226°C to 235°C. The adiabatic temperature rise for AN is 138°C, whereas in the presence of IL it is reduced to 102°C. This result shows that the IL acts as a heat sink also in this polymerization. The plot of the pressure versus temperature (Figure 5) for pure AN polymerization shows a small peak around 245°C followed by a steady increase above 270°C. This trend is indicative that thermal polymerization proceeds initially in the vapor phase and later the polyacry-

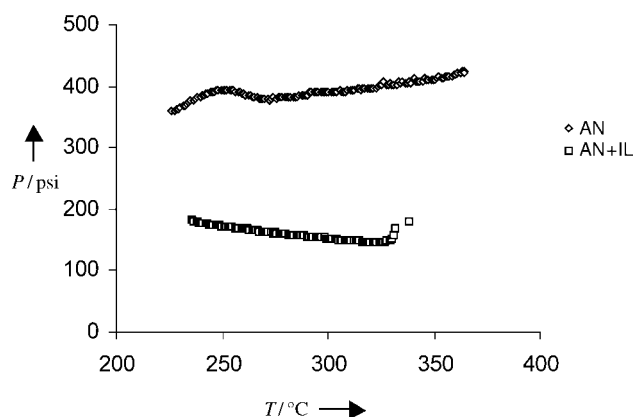


Figure 5. Profiles of temperature versus pressure for AN polymerization.

lonitrile (PAN) thus produced decomposes. In contrast, the pressure profile of AN with IL shows a gradual decrease in pressure, which is indicative of a slow polymerization process that proceeds in the solution phase because the consumption of the monomer reduces the content of volatile species in the mixture. Furthermore, the absence of exothermic activity and an insignificant pressure rise after 340°C may indicate a quenching of the decomposition reaction, which would otherwise take place.

The profile of time versus temperature (Figure 6) also indicates that the IL-incorporated system provides considerably more time available to take emergency measures in the event of runaway compared to neat AN polymerization. In fact the neat AN system can reach 350°C from 250°C in a very short period of time (a few minutes) compared to the IL-based system.

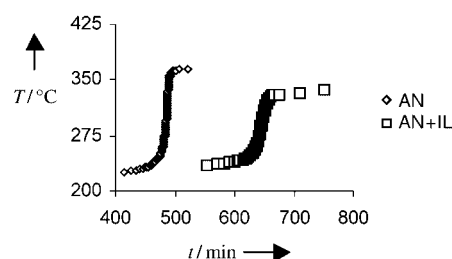


Figure 6. Time versus temperature plots for AN polymerization.

Thus, these studies of the thermal polymerization of styrene and acrylonitrile in ionic liquids provide intrinsically safer processes, especially by considerably reducing the exothermic activity. The studies here show that ILs have the potential to not only reduce the exothermic self-heating but also decrease the exothermic product decomposition, which is a major source of release of toxic gasses. The role of ionic liquids in changing the exothermic decomposition pathways and their mechanistic aspects is the subject of further study. The IL-based polymerization process can be implemented in a closed cycle with respect to the IL by quenching the reaction in methanol, which precipitates the polymer and allows the recovery of the IL from the methanol solution by evaporation of the methanol.

Experimental Section

Analytical grades of styrene and acrylonitrile were used. Styrene was distilled under reduced pressure prior to use. The synthesis of [P_{1,4}] [tf₂N] IL followed the procedures previously reported.^[26] The sample was dried under vacuum at room temperature for 24 h prior to use; Karl–Fischer determination showed the water content to < 0.3 %. Thermal polymerization was carried out in an ARC; this instrument is essentially an adiabatic calorimeter working on the heat–wait–measure principle. Such instruments have been widely employed to investigate thermal runaway of exothermic systems.^[27–28] The calorimeter has a very large heat capacity relative to the sample and therefore acts as a near-perfect heat sink for the sample. The instrument detects the instantaneous rate of reaction at each temperature through the heat generated from the sample. This information is used to calculate an instantaneous self-heating rate at each temperature and also to estimate, from a knowledge of the sample mass and heat capacity, the adiabatic temperature rise that the sample would experience if the heat of reaction was retained (as would be the case under normal reaction conditions). To compare the self-heating rates, the experiments were carried out with identical sample weights (same thermal inertia, Φ). The instrument also records the pressure in the head space above the reaction medium in the calorimeter.

The monomer, styrene or acrylonitrile (typically 0.85 g), was taken along with the IL (0.36 g) in the ARC titanium bomb. Similar quantities of monomers were taken separately in another set of experiments without the addition of IL. These experiments were performed to study the effect of IL and to compare the system with traditional thermal polymerizations. The self-heating rate and pressure data were recorded as a function of temperature and time.

Received: May 7, 2004

Keywords: calorimetry · green chemistry · ionic liquids · polymerizations · thermodynamics

- [20] L. Bethrick, *Hand Book of Reactive Chemical Hazards*, 1987, Butterworths, London, 1987, p. 15.
- [21] P. Bonhote, A. P. Dias, N. Papageorgiou, K. Kalyanasundaram, M. Gratzel, *Inorg. Chem.* **1996**, 35, 1168–1178.
- [22] J. G. Huddleston, A. E. Visser, W. M. Reichert, H. D. Willauer, G. A. Broker, R. D. Rogers, *Green Chem.* **2001**, 3, 156–164.
- [23] K. Baranyai, G. B. Deacon, D. R. MacFarlane, J. M. Pringle, J. L. Scott, *Aust. J. Chem.* **2004**, 57, 145–147.
- [24] J. M. Pringle, J. Golding, K. Baranyai, C. M. Forsyth, G. B. Deacon, J. L. Scott, D. R. MacFarlane, *New J. Chem.* **2003**, 27, 1504–1510.
- [25] I. G. Britton, D. A. Taylor, D. C. Wobser, *Plant/Oper. Prog.* **1986**, 5(4), 238–251.
- [26] M. Forsyth, J. Huang, D. R. MacFarlane, *J. Mater. Chem.* **2000**, 10, 2259–2265.
- [27] Y. Iizuka, M. Surianarayanan, *Ind. Eng. Chem. Res.* **2003**, 42, 2987–2995.
- [28] D. I. Townsend, J. C. Tou, *Thermochim. Acta* **1980**, 37, 1–30.

- [1] M. Surianarayanan, Y. Iizuka, A. Miyake, A. Itoh, T. Ogawa, *Kayaku Gakkaishi* **2002**, 63, 316–322.
- [2] J. L. Gustin, *J. Phys. III* **1991**, 1, 1401–1405.
- [3] R. N. Laudau, *Chem. Eng. Prog.* **1993**, 89, 66–70.
- [4] M. Surianarayanan, R. Vijayaraghavan, G. Swaminathan, P. G. Rao, *Curr. Sci.* **2001**, 6, 738–747.
- [5] T. Kletz, *Inherently Safer Chemical Processes*, CCPS of AIChE, New York, 1996.
- [6] H. K. Fauske, *Chem. Eng. React. Des.* **1989**, 67, 199–201.
- [7] K. Chatrathi, S. Richard, *Chem. Eng. Prog.* **1996**, 92, 22–24.
- [8] W. Kordylewski, J. Amrogowicz, *Combust. Flame* **1992**, 90, 344–345.
- [9] P. Wasserscheid, K. Keim, *Angew. Chem.* **2000**, 112, 3926–3945; *Angew. Chem. Int. Ed.* **2000**, 39, 3772–3789.
- [10] J. F. Brennecke, E. J. Maginn, *AIChE J.* **2002**, 47, 2384–2389.
- [11] T. Welton, *Chem. Rev.* **1999**, 99, 2071–2083.
- [12] K. R. Seddon, *J. Chem. Technol. Biotechnol.* **1997**, 68, 351–356.
- [13] R. Sheldon, *Chem. Commun.* **2001**, 2399–2400.
- [14] M. Hongyang, W. Xinhua, C. Xiaofang, Zhou, Q. Feng, *J. Polym. Sci. Part A* **2003**, 41, 143–151.
- [15] K. Hong, H. Zhang, J. W. Mays, A. E. Vissar, Christopher, *Chem. Commun.* **2002**, 13, 1368–1369.
- [16] R. Vijayaraghavan, D. R. MacFarlane, *Aust. J. Chem.* **2004**, 57, 129–133.
- [17] R. Vijayaraghavan, D. R. MacFarlane, *Chem. Commun.* **2004**, 700–701.
- [18] P. Kubisa, *Prog. Polym. Sci.* **2004**, 29, 3–12.
- [19] T. Uchida, M. Surianarayanan, M. Wakakura, H. Tomioka, *J. Chem. Eng. Jpn.* **1998**, 31, 960–968.

C–C Bond Formation

Cross-Metathesis of Propane and Methane: A Catalytic Reaction of C–C Bond Cleavage of a Higher Alkane by Methane**

Daravong Soulivong, Christophe Copéret,
Jean Thivolle-Cazat, Jean-Marie Basset,*
Barry M. Maunders, Richard B. A. Pardy, and
Glenn J. Sunley*

In memory of Ian P. Rothwell

Natural gas is the most abundant hydrocarbon resource: reserves for 60 years of normal consumption have already been proven, and for about 200 years or greater are expected to be discovered, which makes it the probable future source

[*] Dr. D. Soulivong, Dr. C. Copéret, Dr. J. Thivolle-Cazat, Dr. J.-M. Basset
Laboratory of Surface Organometallic Chemistry, UMR 9986
Ecole Supérieure de Chimie Physique Electronique de Lyon
43 Bd du 11 Novembre 1918, 69616 Villeurbanne Cedex (France)
Fax: (+33) 4-7243-1795
E-mail: coperet@cpe.fr
basset@cpe.fr

Dr. B. M. Maunders
BP Chemicals Ltd
Chertsey Road, Sunbury-On-Thames, Middlesex, TW16 7LN (UK)
Dr. R. B. A. Pardy, Dr. G. J. Sunley
BP Chemicals Ltd
Hull Research and Technology Center
Saltend, Hull, HU12 8DS (UK)

[**] We are grateful to BP Chemicals, the CNRS and the ESCPE Lyon for financial supports. We thank Dr. O. Maury for helpful discussions. We would like to dedicate this paper to the memory of Ian P. Rothwell, a key actor in tantalum chemistry.

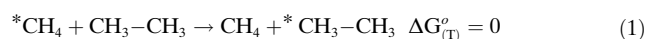


Supporting information for this article is available on the WWW under <http://www.angewandte.org> or from the author.

not only for energy but also for basic chemicals. However, its main component, methane, is one of the most inert hydrocarbons. Apart from using methane for power generation the only other current methods commercially used to valorize methane are “steam reforming”, “partial oxidation” (leading to “syngas”, a mixture of carbon monoxide and hydrogen which is converted into fuels and chemicals, such as gasoline, methanol, and dimethyl ether), and the oxidative pyrolysis to acetylene, which also produces a syngas byproduct. The syngas processes are indirect, since they require first the chemical transformation of CH_4 to CO and H_2 , which are the building blocks for further chemistry. All these processes are limited by selectivity, with formation of CO_2 as a by-product, and require high temperatures which make them relatively unattractive in terms of energy and environmental considerations.^[1] Therefore, a tremendous effort has been directed at finding direct catalytic transformations of methane into more valuable and useful carbon-containing products. Transition metals have been shown to readily activate the C–H bond of methane to form metal–methyl complexes^[2–6] and, in some instances, enable the reforming of this C–H bond; these reactions are, however, either stoichiometric or degenerate (these types of exchange reaction can only be detected by isotope labeling!). The transformation of methane into methanol by platinum salts in sulfuric acid is also noteworthy despite highly acidic conditions.^[7] Methane has also been reported to react with olefins to give higher alkanes in the presence of superacids or organometallic catalysts^[8–10] and, more recently, its coupling reaction with silanes has been disclosed.^[11] The difficulty in achieving selective transformation of methane into valuable chemical products resides in the low reactivity of methane compared to co-reactants (e.g. olefins) and/or the products. However, this problem would be overcome by the reaction of methane with alkanes to produce other alkanes, which all have similar reactivity to the starting alkanes. Herein we report the successful accomplishment of this reaction through a low-temperature incorporation of methane into another alkane, propane.

Recently, we have shown that a highly electrophilic tantalum hydride supported on silica $[(\equiv\text{SiO})_2\text{Ta-H}]$ (**1**), prepared by surface organometallic chemistry,^[12] can catalytically transform a given alkane into its higher and lower homologues.^[13,14] This reaction, called “alkane metathesis”, involves a successive cleavage and formation of carbon–carbon bonds: hence two ethane molecules give one methane and one propane molecule. The free energy of the reaction is slightly negative (-8.2 kJ mol^{-1} at 150°C , driven by the formation of methane), and the equilibrium conversion is around 87% at 150°C . This raises the question: is it possible to drive this reaction in the reverse direction, that is, to react methane with another alkane to give a mixture of alkanes with incorporation of methane? This reaction would correspond to the cross-metathesis of methane with a higher alkane.

To test this concept, we studied the degenerate reaction of methane with ethane [Eq. (1)] which requires ^{13}C labeling to detect the phenomenon.



A mixture of ^{13}C -labeled methane (500 equiv; 64 kPa) and ethane (10 equiv; 1.25 kPa) was heated at 165°C over **1** (53 mg, 5 wt% in Ta (see Method of preparation in Experimental Section)) in a glass reactor (0.28 L), and the distribution of the ^{13}C isotopomers of ethane (unlabeled, mono-, and dilabeled) was monitored over time by GC/MS. Incorporation of ^{13}C labels in ethane occurred over 200 h; hydrogenolysis of ethane into methane was also detected as a competitive parallel reaction, since H_2 had been produced during the first step of C–H bond activation (formation of Ta–R from Ta–H (**1**), R=Me, Et).^[15,16] Note that the initial formation of monolabeled ethane followed by the dilabeled isotopomer is in agreement with a stepwise incorporation of the label (Figure 1). Additionally, propane was also produced

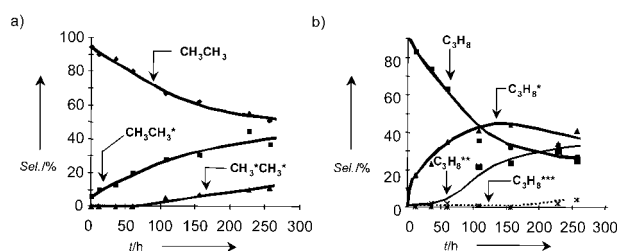


Figure 1. Evolution of the isotomeric distribution of a) ethane {unlabeled (CH_3CH_3), monolabeled (CH_3CH_3^*), and dilabeled ($\text{CH}_3^*\text{CH}_3^*$)} and b) propane {unlabeled (C_3H_8), monolabeled (C_3H_8^*), dilabeled ($\text{C}_3\text{H}_8^{**}$), and trilabeled ($\text{C}_3\text{H}_8^{***}$)} in the cross-metathesis of ethane and ^{13}C -labeled methane.

by the known self-metathesis of ethane and was also converted into its isotopomers. The incorporation of the label into ethane clearly shows that cross-metathesis occurs and that methane can participate in the carbon–carbon formation of higher alkanes. In the case of ethane, this reaction yields ethane, a degenerate process, which can only be detected by labeling. The reaction conditions (batch reactor, methane/ethane reaction) were designed to detect this possible phenomenon, but were not optimized to study a productive reaction.

To observe a productive cross-metathesis of methane with an alkane, the reaction with propane was investigated in a continuous-flow reactor, and the reaction conditions tuned to work at full conversion of propane. This reaction has a positive free energy (8.2 kJ mol^{-1} at 150°C for a 1:1 methane/propane ratio), but its conversion can be, in principle, thermodynamically driven by a high methane to propane ratio. For example for a methane/propane ratio of 1250:1 the conversion of propane can be up to 98% at 250°C ; the temperature and the contact time are also important parameters (kinetic). Note that the production of ethane does not guarantee that such a reaction takes place since **1** is also known to readily catalyze the hydrogenolysis of propane into a mixture of methane/ethane^[17] or the self-metathesis of propane (production of ethane and butane). Nonetheless if 100% cross-metathesis takes place, two ethane molecules are produced per propane molecule consumed [Eq. (2)], while only one ethane is produced per propane molecule in the case of hydrogenolysis [Eq. (3)], and half an ethane (and half a

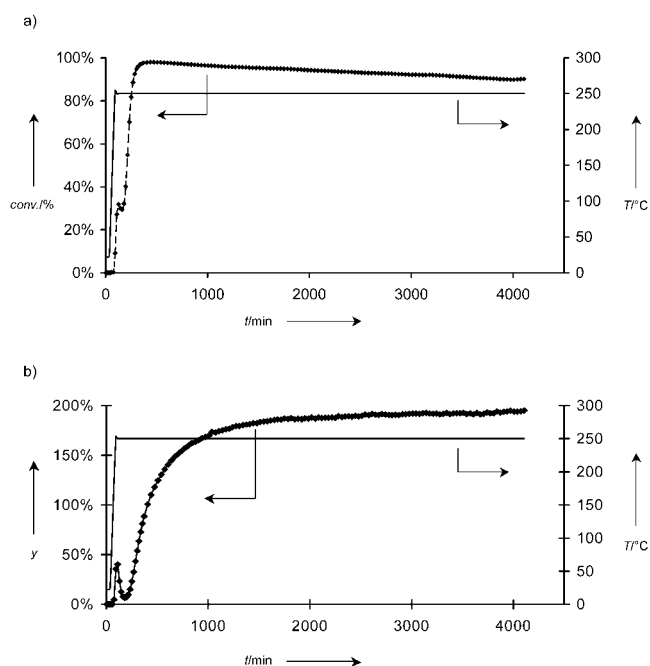
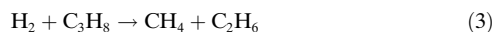


Figure 2. a) Conversion of propane as a function of time on stream. b) Number of equivalents of ethane formed by propane consumed γ in % as a function of time on stream.

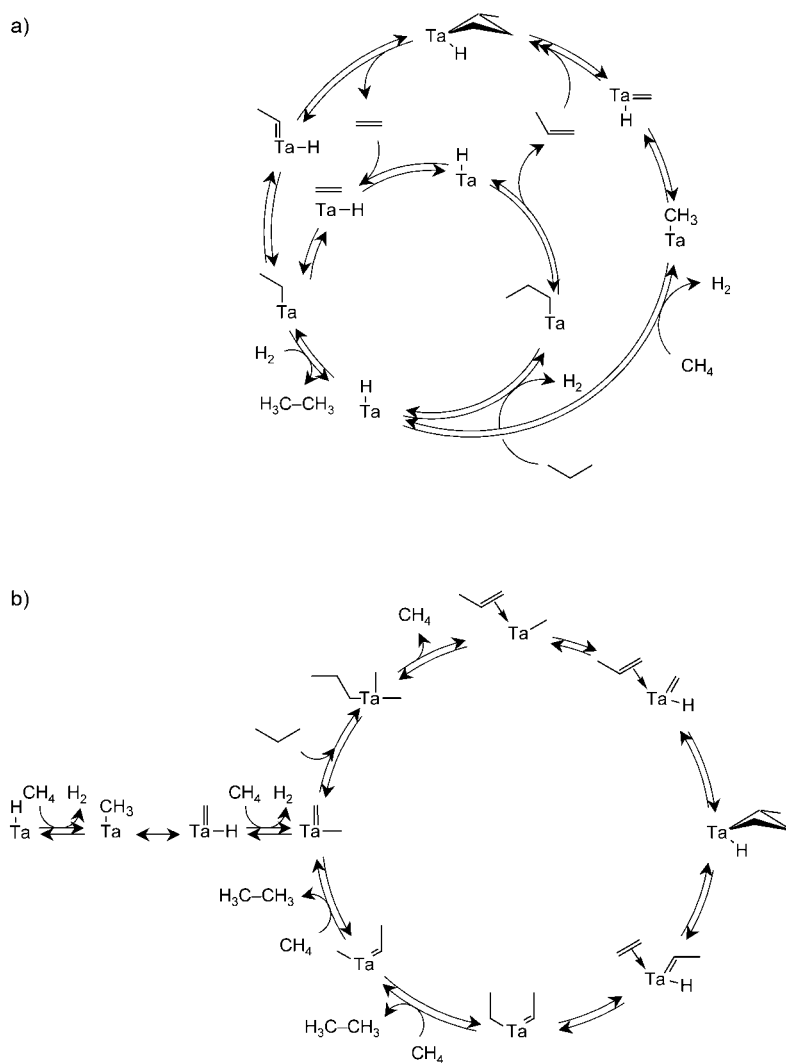
butane) per propane in the case of propane “self-metathesis” [Eq. (4)]. Therefore, to make a clear cut distinction between cross-metathesis and side reactions (hydrogenolysis and self-metathesis) it is critical to establish the mass balance of the overall reaction.



To make this distinction, the reaction is carried out by passing a 1.5 mL min^{-1} flow of a 1250:1 methane/propane mixture at $50 \times 10^2 \text{ kPa}$ over 300 mg of **1** at 250°C. The alkane mixture was first contacted at room temperature and then a ramp of 250°C h^{-1} was applied up to 250°C (Figure 2). During this period a large amount of hydrogen is produced by reaction of the alkane mixture (methane and propane) with **1** to form the propagating species, surface alkyl species, which are formed by C–H activation (See Supporting Information).^[15,16] Propane is partially consumed and converted into a methane/ethane mixture by hydrogenolysis.^[17] After the evolution of hydrogen (produced in the activation step) has ceased, the amount of ethane in the stream increases until it reaches a plateau after 1000 min (Figure 2b); ethane is the major

higher hydrocarbon detected (> 99% of selectivity; see Supporting Information) along with residual methane. $1.9 \pm$ moles of ethane are produced per mole of propane consumed and 95% of the propane is converted by cross-metathesis, that is through its reaction with methane to produce two ethane molecules.

The reaction of methane with higher alkanes was further supported by running an identical reaction, in which ^{13}C -labeled methane was used in place of unlabeled methane. In this case the ethane produced at steady-state conditions is > 85% dilabeled according to GC/MS, which confirms that ethane is produced by the reaction with methane (see Supporting Information). The multiple labeling is due to running the reaction at full conversion of propane, which implies a long contact time and secondary reactions, such as the successive degenerate reaction^[14] of monolabeled ethane with labeled methane, as described above, leading finally to dilabeled ethane as the main isotopomer. Ethane produced initially ($t < 200 \text{ min}$) is unlabeled, clearly showing that it comes from the hydrogenolysis of propane.



Scheme 1. Possible mechanisms via carbene intermediates: a) on two sites and b) on one site.

In summary, we have shown that **1** can catalyze the reaction of methane with a higher hydrocarbon, namely propane, and thereby incorporate methane into a higher alkane by cross-metathesis. While we earlier proposed mechanism based on cleaving the C–C bond system by either σ -bond metathesis or oxidative addition,^[13] we now propose that it proceeds via carbene intermediates and olefin metathesis as suggested by previous studies.^{[18], [19]} Since the alkane-metathesis active site can be generated from either Ta^{III} or Ta^V intermediates, and since olefin metathesis would require the formation of olefins, one and two-site mechanisms can be proposed (Scheme 1), which are under investigation.

The overall reaction provides a route for the direct transformation of methane into more valuable hydrocarbon materials. This reaction makes possible new processes, such as replacing expensive hydrogen by low-cost methane in the recycling of polyolefins.^[20]

Experimental Section

Method of preparation of catalyst **1**: Silica (1 g), previously treated at 500 °C under vacuum, in suspension in pentane (15 mL) was treated at 25 °C with a pentane solution of [Ta(=CH*t*Bu)(CH₂*t*Bu)₃] (0.155 g, 0.33 mol) under an inert atmosphere. The reaction mixture was stirred for 2 h at 25 °C and filtered. The remaining orange solid was then washed three times with pentane and dried under vacuo. This solid was then contacted with dry and deoxygenated H₂ (200 equiv) for 15 h at 250 °C, and the amounts of methane was monitored by GC. Typically after 3 cycles of treatment under H₂, less than 1 % of carbon (as methane) is present in the gas phase.

Received: June 16, 2004

Keywords: alkanes · cross-metathesis · heterogeneous catalysis · methane homologation · tantalum

- [16] V. Vidal, A. Theolier, J. Thivolle-Cazat, J.-M. Basset, J. Corker, *J. Am. Chem. Soc.* **1996**, *118*, 4595.
- [17] M. Chabanas, V. Vidal, C. Cop  ret, J. Thivolle-Cazat, J.-M. Basset, *Angew. Chem.* **2000**, *112*, 2038; *Angew. Chem. Int. Ed.* **2000**, *39*, 1962.
- [18] C. Cop  ret, O. Maury, J. Thivolle-Cazat, J.-M. Basset, *Angew. Chem.* **2001**, *113*, 2393; *Angew. Chem. Int. Ed.* **2001**, *40*, 2331.
- [19] E. Le Roux, M. Chabanas, A. Baudouin, A. de Mallmann, C. Cop  ret, E. A. Quadrelli, J. Thivolle-Cazat, J.-M. Basset, A. Losage, L. Emsley, G. J. Sunley, *J. Am. Chem. Soc.*, in press.
- [20] V. Dufaud, J.-M. Basset, *Angew. Chem.* **1998**, *110*, 848; *Angew. Chem. Int. Ed.* **1998**, *37*, 806.

- [1] N. D. Parkyns, C. I. Warburton, J. D. Wilson, *Catal. Today* **1994**, *18*, 385.
- [2] E. A. Grigoryan, *Uspekhi Khimii* **1984**, *53*, 347.
- [3] B. A. Arndtsen, R. G. Bergman, T. A. Mobley, T. H. Peterson, *Acc. Chem. Res.* **1995**, *28*, 154.
- [4] R. H. Crabtree, *Chem. Rev.* **1995**, *95*, 987.
- [5] A. E. Shilov, G. B. Shul'pin, *Chem. Rev.* **1997**, *97*, 2879.
- [6] R. H. Crabtree, *Dalton Trans.* **2001**, 2437.
- [7] R. A. Periana, D. J. Taube, S. Gamble, H. Taube, T. Satoh, H. Fujii, *Science* **1998**, *280*, 560.
- [8] G. A. Olah, *Acc. Chem. Res.* **1987**, *20*, 422.
- [9] V. R. Choudhary, A. K. Kinage, T. V. Choudhary, *Science* **1997**, *275*, 1286.
- [10] A. D. Sadow, T. D. Tilley, *J. Am. Chem. Soc.* **2003**, *125*, 7971.
- [11] A. D. Sadow, T. D. Tilley, *Angew. Chem.* **2003**, *115*, 827; *Angew. Chem. Int. Ed.* **2003**, *42*, 803.
- [12] C. Cop  ret, M. Chabanas, R. Petroff Saint-Arroman, J.-M. Basset, *Angew. Chem.* **2003**, *115*, 164; *Angew. Chem. Int. Ed.* **2003**, *42*, 156.
- [13] V. Vidal, A. Theolier, J. Thivolle-Cazat, J.-M. Basset, *Science* **1997**, *276*, 99.
- [14] O. Maury, L. Lefort, V. Vidal, J. Thivolle-Cazat, J.-M. Basset, *Angew. Chem.* **1999**, *111*, 2121; *Angew. Chem. Int. Ed.* **1999**, *38*, 1952.
- [15] V. Vidal, A. Theolier, J. Thivolle-Cazat, J.-M. Basset, *J. Chem. Soc. Chem. Commun* **1995**, 991.

Homogeneous Catalysis

Ru- and Rh-Catalyzed C–C Bond Cleavage of Cyclobutenones: Reconstructive and Selective Synthesis of 2-Pyranones, Cyclopentenones, and Cyclohexenones**

Teruyuki Kondo,* Yoshinori Taguchi, Yushi Kaneko,
Masatsugu Niimi, and Take-aki Mitsudo*

The reconstruction of new carbon skeletons after C–C bond cleavage, which leads to the rapid and selective synthesis of novel organic molecules that cannot be obtained by the simple combination of traditional synthetic methods,^[1] is an important goal of many recent studies in atom-economical organic, organometallic, and industrial chemistry.^[2] In our recent report on the unusual ruthenium-catalyzed coupling of cyclobutenediones with alkenes^[3] and the ruthenium-catalyzed synthesis of pyranopyrandiones by ring-opening carbonylation of cyclopropanones,^[4] we demonstrated the explicit cleavage of C–C bonds leading to the reconstruction of new carbon skeletons. Since ruthenacycles, which would be obtained by direct oxidative addition of strained cyclic substrates such as cyclobutenediones and cyclopropanones to low-valent ruthenium species, are postulated to be key intermediates, we next turned our attention to the reactivity of a similarly strained cyclic compound, cyclobutenone,

[*] Prof. Dr. T. Kondo, Y. Taguchi, Y. Kaneko, M. Niimi,
Prof. Dr. T. Mitsudo
Department of Energy and Hydrocarbon Chemistry
Graduate School of Engineering
Kyoto University, Nishikyo-ku, Kyoto 615-8510 (Japan)
Fax: (+81) 75-383-2507
E-mail: teruyuki@scl.kyoto-u.ac.jp
mitsudo@scl.kyoto-u.ac.jp

[**] This work was supported in part by a Grants-in-Aid for Scientific Research (B) and Scientific Research on Priority Areas (A) "Exploitation of Multi-Element Cyclic Molecules" from the Japan Society for the Promotion of Science and the Ministry of Education, Culture, Sports, Science, and Technology, Japan.



Supporting information for this article is available on the WWW under <http://www.angewandte.org> or from the author.

toward ruthenium and other transition-metal complexes. Particular attention has been focused on the thermal reactivity of cyclobutenones bearing alkynyl, alkenyl, aryl, and allenyl substituents at the 4-position because of their potential application to the synthesis of ring-expanded compounds.^[5] On the other hand, 4-nonsubstituted cyclobutenones are relatively stable, and only the pioneering work by Liebeskind and co-workers on the transition-metal-complex-catalyzed synthesis of phenols from 4-nonsubstituted cyclobutenones and alkynes has been reported.^[6,7] This methodology is quite attractive, since transition-metal vinylketene complexes have been postulated to be important intermediates in reactions leading to a variety of organic ring products, such as phenols, naphthols, cyclohexadienones, cyclopentenones, lactams, furans, α -pyrones, and 2-furanones.^[8] After many trials, we developed a novel stereoselective synthesis of 2-pyranones by the ring-opening dimerization of cyclobutenones catalyzed by ruthenium and rhodium complexes. In addition, a rhodium complex, $[\text{RhCl}(\text{CO})_2]_2$, showed high catalytic activity in the decarbonylative and/or direct coupling of cyclobutenones with alkenes by C–C bond cleavage. These results indicate that the present reactions likely involve both η^4 -vinylketene and metallacyclopentenone intermediates.

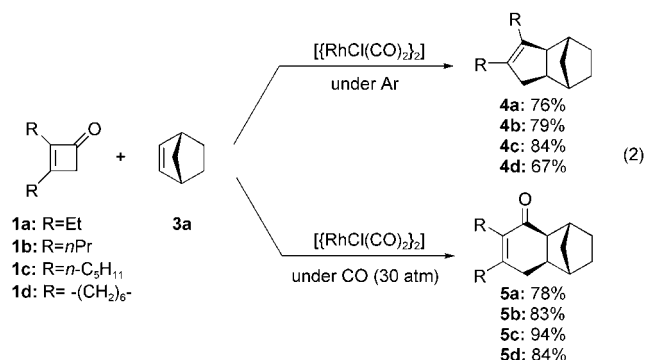
Treatment of cyclobutenones **1** with 5-mol % $[\text{RuCl}_2(\text{CO})_3]_2$ in toluene at 110 °C for 12 h gave novel dimerization products, 6-alkenyl-2-pyranones **2**, in high yields with good *Z* selectivity (see Equation (1)). In the present reaction, the starting cyclobutenones **1** were completely consumed, and the only products detected by GLC were the corresponding (*E*)- and (*Z*)-6-alkenyl-2-pyranones **2**.

First, the catalytic activity of several ruthenium complexes was examined in the dimerization of **1b** to **2b**. Among the catalysts examined, $[\text{RuCl}_2(\text{CO})_3]_2$ showed the highest catalytic activity (**2b**, 81 %), and $\text{RuCl}_3 \cdot 3\text{H}_2\text{O}$ showed moderate catalytic activity (**2b**, 31 %). In both reactions, the *E/Z* ratio of the 6-alkenyl group in **2b** was 22/78. Other ruthenium complexes such as $[\text{Ru}_3(\text{CO})_{12}]$, $[\text{RuCl}_2(\text{PPh}_3)_3]$, $[\text{RuH}_2(\text{PPh}_3)_4]$, and $[(\eta^5\text{-C}_5\text{Me}_5)\text{RuCl}(\text{1,5-cyclooctadiene})]$, were totally ineffective. No 2-pyranone **2b** was obtained with several other transition-metal complexes, such as $[\text{RhCl}(\text{PPh}_3)_3]$, $\text{RhCl}_3 \cdot 3\text{H}_2\text{O}$, $[\text{Pd}(\text{PPh}_3)_4]$, and $[\text{Ni}(\text{cod})_2]$. Surprisingly, only $[\text{RhCl}(\text{CO})_2]_2$ showed high catalytic activity in the synthesis of **2b** from **1b**, and changing the $[\text{RuCl}_2(\text{CO})_3]_2$ catalyst to the $[\text{RhCl}(\text{CO})_2]_2$ catalyst led to a sharp reversal of stereoselectivity to give (*E*)-6-alkenyl-2-pyranone ((*E*)-**2b**) as the sole product in 75 % yield [Eq. (1)].

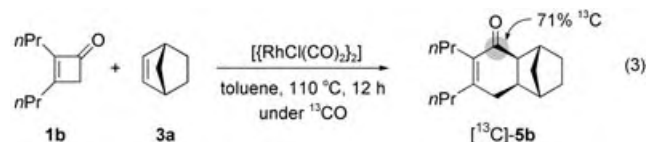
The use of an appropriate solvent is critically important for the success of the present reaction. In the $[\text{RuCl}_2(\text{CO})_3]_2$ -

catalyzed dimerization of **1b** to **2b**, toluene gave the best result. No **2b** was obtained in solvents, such as THF, 1,4-dioxane, *N*-methylpiperidine, DMF, and acetonitrile, partly due to their ability to coordinate with the active catalyst species. A similar critical solvent effect was also observed in the $[\text{RhCl}(\text{CO})_2]_2$ -catalyzed dimerization of **1b** to **2b**.

Furthermore, $[\text{RhCl}(\text{CO})_2]_2$ -catalyzed decarbonylative coupling and direct coupling of cyclobutenones with 2-norbornene **3a** have been developed [Eq. (2)].

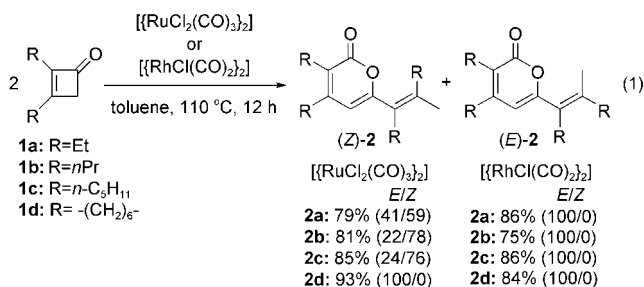


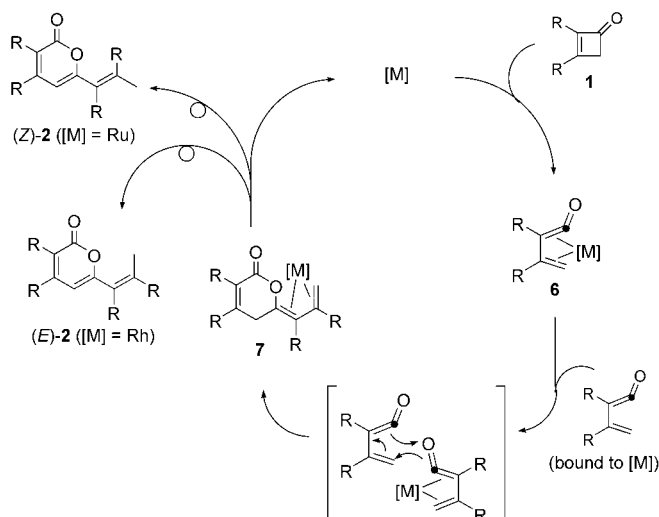
Under an argon atmosphere, decarbonylative coupling proceeded smoothly to give cyclopentenones **4** in high yields, while under 30 atm of carbon monoxide, direct coupling with **3a** gave cyclohexenones **5** in high yields. Use of ¹³CO gave the corresponding ¹³C-labeled cyclohexenone [¹³C]-**5b** [Eq. (3)],^[9] which strongly suggests that the decarbonylation of a rhodacyclopentenone and/or a rhodacycloheptenone is facile, but reversible. Under carbon monoxide pressure, subsequent reductive elimination from a stabilized rhodacycloheptenone predominantly occurs to give cyclohexenones **5** (see below).



Considering all of our findings and evidence reported by Liebeskind and co-workers,^[6] the most plausible mechanism for the ring-opening dimerization of cyclobutenones is illustrated in Scheme 1. The initial step might consist of regioselective ring-opening of cyclobutenone **1** by an active metal center to give an η^4 -vinylketene intermediate **6**, which rapidly reacts with another molecule of metal-bound vinylketene according to a hetero-Diels–Alder reaction. Successive isomerization of **7** would give the corresponding 2-pyranone **2**.^[10] No interconversion between (*Z*)-**2** and (*E*)-**2** was observed in the presence or absence of Ru and Rh catalysts.

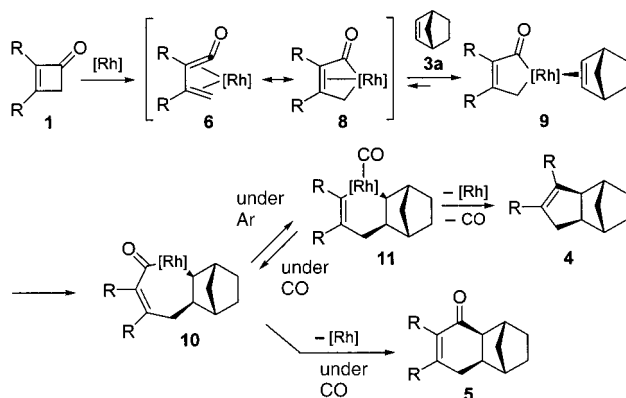
On the other hand, in the presence of 2-norbornene (**3a**), the highly *exo*-selective coordination ability of **3a**^[11] leads to the formation of a rhodacyclopentenone intermediate **9** from **6** via **8**,^[6d] and subsequent stereoselective insertion of **3a** into a rhodium–carbon bond in **9** would give a rhodacycloheptenone intermediate **10**. Under an argon atmosphere, this





Scheme 1. Possible mechanism for the formation of 2-pyranones **2**.

rhodacycloheptenone **10** is easily decarbonylated to a rhodacyclohexene intermediate **11**, and subsequent reductive elimination gives the corresponding cyclopentene **4**. Even under carbon monoxide pressure, this decarbonylation process of **10** to **11** is facile, however, it is reversible (see above). Rapid reductive elimination from the stabilized **10** by carbon monoxide occurs to give the corresponding cyclohexenone **5** (Scheme 2).



Scheme 2. Possible mechanism for the formation of cyclopentenones **4** and cyclohexenones **5**.

An alternative pathway for the formation of cyclohexenone **5** by a direct stereoselective Diels–Alder reaction of η^4 -vinylketene rhodium intermediate **6** with 2-norbornene (**3a**) is also possible, however, this mechanism cannot explain the decarbonylative coupling of cyclobutenone with **3a** under an argon atmosphere.

In conclusion, we have developed a novel ruthenium- and rhodium-catalyzed ring-opening dimerization of cyclobutenones to give 2-pyranones. The application of a rhodium catalyst to decarbonylative and direct coupling reactions of cyclobutenones with 2-norbornene is also successful and gives stereoselectively cyclopentenones and cyclohexenones, respectively.

Experimental Section

Cyclobutenones **1a–d** were prepared by a general two-step method based on the [2+2] cycloaddition of alkynes with dichloroketene, and the reductive dechlorination of the generated 4,4-dichlorocyclobutenones by zinc dust in the presence of tetramethylethylenediamine, ethanol, and acetic acid.^[12]

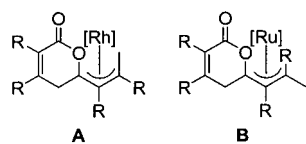
Representative procedure for the synthesis of (*E*)-**2b** from **1b** catalyzed by $[\text{RhCl}(\text{CO})_2]_2$: A mixture of 2,3-dipropylcyclobut-2-en-1-one (**1b**) (152 mg, 1.0 mmol), $[\text{RhCl}(\text{CO})_2]_2$ (19.4 mg, 0.050 mmol), and toluene (2.0 mL) was placed in a 20-mL Pyrex flask equipped with a magnetic stirring bar under a flow of argon. The reaction was carried out at 110 °C for 12 h with stirring. After the reaction mixture was cooled, the product, 6-((*E*)-2-methyl-1-propylpent-1-enyl)-3,4-dipropylpyran-2-one ((*E*)-**2b**), was isolated by Kugelrohr distillation as a pale yellow oil (228 mg, 0.75 mmol; 75 % yield); b.p. 170–180 °C (1.0 mmHg, Kugelrohr); IR (neat): $\tilde{\nu}$ = 1562, 1635 (C=C), 1712 cm^{-1} (C=O); ^1H NMR (400 MHz, CDCl_3 , 25 °C): δ = 0.88 (t, J = 7.32 Hz, 3H), 0.94 (t, J = 7.32 Hz, 3H), 0.98 (t, J = 7.32 Hz, 3H), 0.99 (t, J = 7.32 Hz, 3H), 1.30–1.36 (m, 2H), 1.43–1.61 (m, 6H), 1.76 (s, 3H), 2.11 (t, J = 7.81 Hz, 2H), 2.29 (t, J = 7.81 Hz, 2H), 2.41 (t, J = 7.81 Hz, 2H), 2.46 (t, J = 7.81 Hz, 2H), 5.83 ppm (s, 1H); ^{13}C NMR (100 MHz, CDCl_3 , 25 °C): δ = 14.0, 14.0, 14.2, 14.3, 20.5, 21.3, 22.1, 22.1, 22.5, 28.6, 32.4, 34.5, 36.4, 108.3, 122.3, 128.6, 139.2, 153.2, 159.3, 164.3 ppm; MS (EI, 70 eV): m/z : 304 [M^+]; elemental analysis (%) calcd for $\text{C}_{20}\text{H}_{32}\text{O}_2$: C 78.90, H 10.59; found: C 78.80, H 10.55.

Received: June 18, 2004

Keywords: C–C activation · homogeneous catalysis · metallacycles · rhodium · ruthenium

- [1] For reviews, see: a) K. C. Bishop III, *Chem. Rev.* **1976**, 76, 461–486; b) R. H. Crabtree, *Chem. Rev.* **1985**, 85, 245–269; c) P. W. Jennings, L. L. Johnson, *Chem. Rev.* **1994**, 94, 2241–2290; d) M. Murakami, Y. Ito in *Activation of Unreactive Bonds and Organic Synthesis* (Ed.: S. Murai), Springer, New York, **1999**, pp. 97–129; e) T. Mitsudo, T. Kondo, *Synlett* **2001**, 309–321.
- [2] For green chemistry, see: a) P. T. Anatas, M. M. Kirchhoff, *Acc. Chem. Res.* **2002**, 35, 686–694; b) B. M. Trost, *Acc. Chem. Res.* **2002**, 35, 695–705.
- [3] T. Kondo, A. Nakamura, T. Okada, N. Suzuki, K. Wada, T. Mitsudo, *J. Am. Chem. Soc.* **2000**, 122, 6319–6320.
- [4] T. Kondo, Y. Kaneko, Y. Taguchi, A. Nakamura, T. Okada, M. Shiotsuki, Y. Ura, K. Wada, T. Mitsudo, *J. Am. Chem. Soc.* **2002**, 124, 6824–6825.
- [5] For reviews, see: a) H. W. Moore, B. R. Yerca in *Advances in Strain in Organic Chemistry*, Vol. 4 (Ed.: B. Halton), JAI, London, **1995**, pp. 81–162; b) T. K. M. Shing, *Methods of Organic Chemistry (Houben-Weyl) 4th ed. 1952–, Vol. E17f* (Ed.: A. de Meijere), Thieme, Stuttgart, **1997**, chap. 8B, pp. 898–913.
- [6] a) M. A. Huffman, L. S. Liebeskind, W. T. Pennington, Jr., *Organometallics* **1990**, 9, 2194–2196; b) M. A. Huffman, L. S. Liebeskind, *J. Am. Chem. Soc.* **1990**, 112, 8617–8618; c) M. A. Huffman, L. S. Liebeskind, *J. Am. Chem. Soc.* **1991**, 113, 2771–2772; d) M. A. Huffman, L. S. Liebeskind, W. T. Pennington, *Organometallics* **1992**, 11, 255–266.
- [7] A thermal reaction of cyclobutenones with activated alkynes to phenols via a vinylketene intermediate has also been reported. a) R. L. Danheiser, S. K. Gee, *J. Org. Chem.* **1984**, 49, 1672–1674; b) R. L. Danheiser, A. Nishida, S. Savariar, M. P. Trova, *Tetrahedron Lett.* **1988**, 29, 4917–4920.
- [8] a) M. F. Semmelhack, R. Tamura, W. Schnatter, J. Park, M. Steigerwald, S. Ho, *Stud. Org. Chem.* **1986**, 25, 21–42; b) S. E. Gibson, M. A. Peplow, *Adv. Organomet. Chem.* **1999**, 44, 275–355, and references therein.

- [9] S. A. Benyunes, S. E. Gibson, M. A. Peplow, *Chem. Commun.* **1996**, 1757–1758.
- [10] Although it is not yet clear why the stereochemistry of **2** changed depending on the catalyst used, we now believe that the present isomerization reaction of diene **7** to 2-pyranone **2** may proceed through addition–elimination of a H-[M] species to 1,3-dienes **7**, generating π -allylmetal intermediates such as **A** and **B**. A π -



allylrhodium intermediate has an energetically favorable *syn*-type configuration (**A**) leading to the selective formation of (*E*)-**2**, while a sterically congested *anti*-type π -allylruthenium species (**B**), which is also postulated as a key intermediate in our previously reported ruthenium-catalyzed codimerization of 1,3-dienes with acrylic compounds, could be generated to give (*Z*)-**2** in good selectivity. See: T. Mitsudo, S.-W. Zhang, T. Kondo, Y. Watanabe, *Tetrahedron Lett.* **1992**, 33, 341–344.

- [11] S. Inagaki, H. Fujimoto, K. Fukui, *J. Am. Chem. Soc.* **1976**, 98, 4054–4061.
- [12] a) R. L. Danheiser, S. Savariar, D. D. Cha, *Org. Synth.* **1990**, 68, 32–40; b) A. A. Ammann, M. Rey, A. S. Dreiding, *Helv. Chim. Acta* **1987**, 70, 321–328.

Imidozirconium Complexes

Carboamination: Additions of Imine C=N Bonds Across Alkynes Catalyzed by Imidozirconium Complexes**

Rebecca T. Ruck, Rebecca L. Zuckerman,
Shane W. Krska, and Robert G. Bergman*

The development of new reactions employing imidozirconium complexes or their derivatives as catalysts is an elusive goal in organometallic chemistry. To date, the imidozircono-

cene-catalyzed hydroamination of alkynes and allenes to yield new enamines (and, on tautomerization, imines) is the lone example of such a process.^[1,2] We recently reported that aldehydes and electron-deficient imines insert into the carbon–zirconium bond of azazirconacyclobutene **1** to afford new six-membered ring metallacycles **2** and **3** (see Scheme 1). On heating, these expanded zirconacycles undergo a retro-[4+2] cycloaddition to afford α,β -unsaturated imine **4** and oxozirconium complex **5** or electron-poor imidozirconocene dimer **6**, both of which are unreactive (Scheme 1; EWG = electron-withdrawing group, Cp = C₅H₅).^[3,4] We reasoned that insertion of an aldimine **7** with *N*-substitution identical to that of the nitrogen group in the metallacyclobutene, followed by subsequent retro-cycloaddition, would not only afford α,β -unsaturated imine **4** but would also generate imidozirconocene complex **8** previously used to prepare the starting azazirconacyclobutene (see Scheme 2).^[5] Carrying out the reaction in the presence of the necessary alkyne would regenerate the starting metallacycle and close the catalytic cycle (Scheme 2).^[6] This reaction is deemed a carboamination, because it results in the overall cleavage of an imine C=N bond and addition of the resulting C and N fragments across an alkyne, forming a new carbon–carbon double bond and a new ketimine carbon–nitrogen double bond.^[7–9] Herein, we present the development of a novel, high-yielding imidozirconocene-catalyzed carboamination reaction that also represents the best method for preparing the highly arylated α,β -unsaturated imine co-products.

The most frequently studied imidozirconium complexes bear sterically bulky groups on the nitrogen atom to prevent competitive dimerization of the imido compound.^[5] As such, *N*-2,6-dimethylphenyl- and *N*-*tert*-butyl-substituted azazirconacyclobutenes **1** and **9** (see Scheme 3) were explored in the desired insertion chemistry. Unfortunately, even at high concentrations of substrate and temperatures up to 165 °C, neither of these zirconium compounds was an effective catalyst as no imine insertion products were observed. In the case of metallacycle **1** and imine **10**, it appears that the combined steric bulk of the zirconacycle and imine *N*-substituents prohibits insertion; with metallacycle **9** and *N*-*tert*-butyl imine **11**, we began to observe C–D bond activation of the [D₆]benzene solvent. Presumably, this pathway arises from [2+2]-cycloreversion to afford the free imidozirconocene complex **12**, which had been shown to activate benzene C–H bonds at a minimum temperature of 75 °C (Scheme 3).^[10]

While few obvious modifications can be made to the *N*-*tert*-butyl framework, we reasoned that a smaller *N*-aryl substituent would decrease the steric bulk of both the azazirconacyclobutene and the reacting imine to better facilitate insertion into the metallacycle Zr–C bond. [Cp₂Zr=N(*p*-C₆H₄CH₃)] (**13a**) undergoes irreversible dimerization in the absence of a trapping agent; however, imido complex **13a** will react preferentially with an alkyne to generate the *N*-tolyl metallacyclobutene **14a** (see Table 1).^[5] This observation is particularly relevant to a potential catalytic system, since alkyne will be in substantial excess relative to **13a** for the majority of the reaction, further decreasing the likelihood of competitive dimerization. We

[*] Dr. R. T. Ruck, Prof. R. G. Bergman
Department of Chemistry
University of California, Berkeley
Berkeley, CA 94720 (USA)
Fax: (+1) 510-642-2156
E-mail: bergman@cchem.berkeley.edu

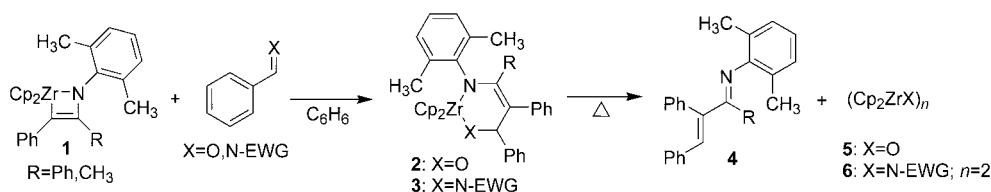
R. L. Zuckerman
Plexxikon Inc.
91 Bolivar Dr., Berkeley, CA 94710 (USA)

S. W. Krska
Department of Process Research
Merck Research Laboratories, Merck & Co., Inc.
Rahway, NJ 07065 (USA)

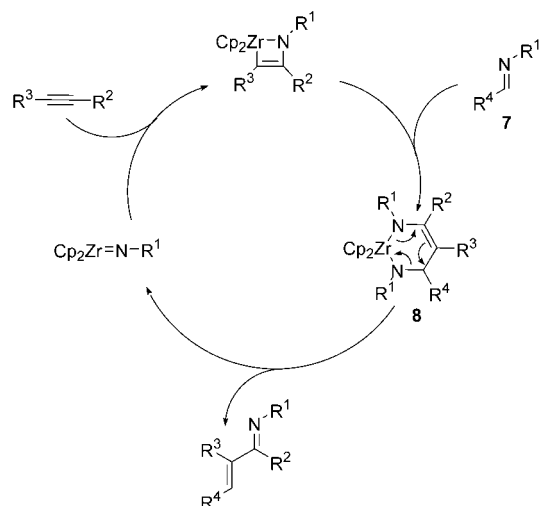
[**] This work was supported by the National Institutes of Health (GM-25459) and by an NIH post-doctoral fellowship to R.T.R.



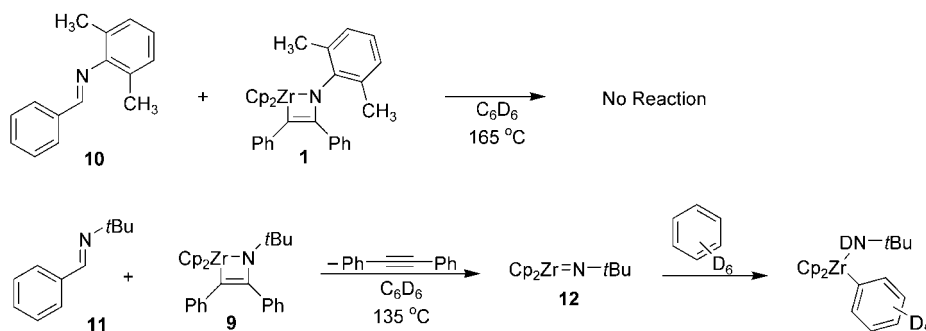
Supporting information for this article (full experimental details) is available on the WWW under <http://www.angewandte.org> or from the author.



Scheme 1.



Scheme 2.



Scheme 3.

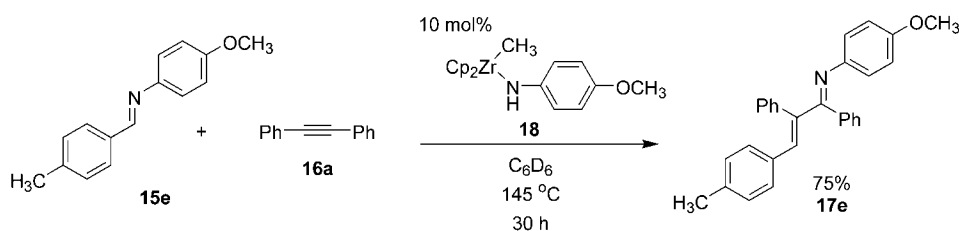
were pleased to find that one equivalent of azazirconacyclobutene **14a** reacted with four equivalents of both *N-p*-tolyl *p*-tolualdimine (**15a**) and diphenylacetylene (**16a**) at 135°C (reactions carried out in sealed tubes, for full experimental details see the Supporting Information) to effect complete consumption of **15a** and generation of new α,β -unsaturated imine **17a**. No intermediate six-membered-ring metallacycle was observed during the course of the reaction, consistent with rate-determining imine insertion into the azametallacyclobutene $\text{Zr}-\text{C}$ bond. Optimization of temperature, catalyst concentration, and concentration of reagents led to the development of a system that employs 10 mol % of **14a** and one equivalent each of imine and alkyne in benzene at 145°C to afford a 71 % yield of α,β -unsaturated imine **17a**. This catalytic carboamination reaction generates the (*E*)-imine and (*E*)-olefin stereoisomers exclusively and provides the only known synthesis of this product.

With optimized conditions in hand, we next sought to expand the scope of all components of the reaction. The more electron-rich substrates, *N-p*-tolyl *p*-anisaldimine (**15b**) and *N-p*-tolyl *p*-*N,N*-dimethylaminobenzaldimine (**15c**) were also competent in this chemistry (Table 1), whereas electron-poor *N-p*-tolyl *p*-trifluoromethylbenzaldimine failed to insert. These observations were somewhat surprising given the ease with which electron-deficient imines were shown to insert previously.^[11] We have also been able to employ bis(*p*-methoxyphenyl)acetylene (**16b**) by preparing the requisite azazirconacyclobutene **14b**. This metallacycle catalyzed the carboamination of alkyne **16b** with imine **15a** in good yield at 160°C .^[12,13] The azazirconacyclobutene formed by reaction of imidozirconocene complex **13a** with 1-phenyl-1-propyne was unstable at the high temperatures required for insertion.^[14] Finally, *N-p*-methoxyphenyl (PMP) azametallacyclobutene **14c** catalyzed the carboamination reaction between *N-p*-methoxyphenyl *p*-benzaldimine (**15d**) or *N-p*-methoxyphenyl

p-tolualdimine (**15e**) and diphenylacetylene (**16a**).^[15] *N-p*-Methoxyphenyl *m*-tolualdimine (**15f**) was also a competent substrate in this chemistry, while only approximately 30 % of *N-p*-methoxyphenyl *o*-tolualdimine was converted into product. Use of the PMP group as a substituent on the nitrogen atom is particularly attractive, since nucleophilic addition to or reduction of the product PMP-imine provides a *p*-methoxyphenyl-protected primary amine, which may be liberated under mild oxidative conditions.^[16]

We have employed methylzirconocene (*p*-methoxyphenyl)amide (**18**) as the catalyst in the carboamination reaction between imine **15e** and alkyne **16a** to generate α,β -unsaturated imine product **17e** in 75 % yield (Scheme 4).^[17] This yield is comparable to that obtained with azazirconacyclobutene **14c** as catalyst (Table 1, entry 5). From a practical standpoint, this development allows the chemist to by-pass the additional step of azazirconacyclobutene formation, while also eliminating the necessity of preparing a different azazirconacyclobutene catalyst for each new alkyne considered. From a mechanistic standpoint, this result supports the intermediacy of imidozirconium compound **13b** (generated in situ on elimination of methane from **18**) along the proposed catalytic cycle.

In summary, we have succeeded in developing a novel imidozirconocene-catalyzed carboamination reaction that adds an imine $\text{C}=\text{N}$ bond across an alkyne to generate



Scheme 4.

Table 1: Carboamination reactions catalyzed by imidozirconocenes **14**.^[a]

Entry	Starting Imine	Alkyne	Catalyst	Product	Yield [%] ^[b]
1	15a ; $X^1 = CH_3$; $X^2 = 4-CH_3$	16a ; Ar = Ph	14a	17a	71
2	15b ; $X^1 = CH_3$; $X^2 = 4-OCH_3$	16a ; Ar = Ph	14a	17b	71
3	15c ; $X^1 = CH_3$; $X^2 = 4-N(CH_3)_2$	16a ; Ar = Ph	14a	17c	82
4	15d ; $X^1 = OCH_3$; $X^2 = H$	16a ; Ar = Ph	14c	17d	80
5	15e ; $X^1 = OCH_3$; $X^2 = 4-CH_3$	16a ; Ar = Ph	14c	17e	80
6	15f ; $X^1 = OCH_3$; $X^2 = 3-CH_3$	16a ; Ar = Ph	14c	17f	85
7 ^[c]	15a ; $X^1 = CH_3$; $X^2 = 4-CH_3$	16b ; Ar = 4- $OCH_3C_6H_4$	14b	17g	58

^[a] Reaction is conducted with 10 mol% azazirconacyclobutene **14** (with appropriate X^1 and Ar substitution) as catalyst and imine **15** and alkyne **16** at 0.5 M in C_6D_6 .
^[b] Yield of isolated product after chromatography.
^[c] Reaction was conducted at $160\text{ }^\circ\text{C}$ using a 3:1 mixture of **14c**:**16b**.

synthetically interesting α,β -unsaturated imine products. While the substrate scope of the transformation is, at present, limited to all-aryl substitution, the products generated have not been accessed by alternative means. We will continue to develop this chemistry with the goal of expanding the substrate scope to include new imines and alkynes. Full experimental details can be found in the Supporting Information. A related paper that reports the insertion of *N*-acylamines into azazirconacyclobutenes also appears in this issue.^[18]

Received: June 24, 2004

Keywords: alkynes · carboamination · imines · zirconium

- [1] a) P. J. Walsh, R. G. Bergman, *J. Am. Chem. Soc.* **1992**, *114*, 1708; b) A. M. Baranger, P. J. Walsh, R. G. Bergman, *J. Am. Chem. Soc.* **1993**, *115*, 2753.
- [2] Imidotitanium-catalyzed hydroamination reactions are also known: a) L. Ackermann, R. N. Loy, R. G. Bergman, *J. Am. Chem. Soc.* **2003**, *125*, 11956; b) J. S. Johnson, R. G. Bergman, *J. Am. Chem. Soc.* **2001**, *123*, 2923; c) Y. Shi, J. T. Ciszewski, A. L. Odom, *Organometallics* **2001**, *20*, 3967; d) E. Haak, I. Bytschkov,

S. Doye, *Angew. Chem.* **1999**, *111*, 3584; *Angew. Chem. Int. Ed.* **1999**, *38*, 3389.

- [3] T. A. Hanna, A. M. Baranger, R. G. Bergman, *J. Org. Chem.* **1995**, *60*, 4532.
- [4] R. T. Ruck, R. G. Bergman, *Organometallics* **2004**, *23*, 2231.
- [5] P. J. Walsh, R. G. Bergman, *Organometallics* **1993**, *12*, 3705.
- [6] Odom and co-workers have developed a titanium-catalyzed three-component coupling of amines, alkynes, and isonitriles to afford α,β -unsaturated β -iminoamines: C. Cao, Y. Shi, A. L. Odom, *J. Am. Chem. Soc.* **2003**, *125*, 2880.
- [7] Kobayashi and co-workers have reported a Lewis acid-catalyzed reaction between imines and alkynyl sulfides to generate α,β -unsaturated thioimides. This reaction appears to proceed by [2+2] cycloaddition followed by retro-[2+2] cycloaddition to afford the observed products: H. Ishitani, S. Nagayama, S. Kobayashi, *J. Org. Chem.* **1996**, *61*, 1902.
- [8] Qian and Ma have reported a reaction analogous to that described in reference [7] with alkynyl selenides as substrates: Y. Ma, C. Qian, *Tetrahedron Lett.* **2000**, *41*, 945.
- [9] Coupling reactions between alkynes and oxyalkynes have been reported to yield α,β -unsaturated carbonyl compounds: a) M. Curini, F. Epitano, F. Maltese, O. Rosati, *Synlett* **2003**, 552; b) M. Shindo, S. Oya, R. Murakami, Y. Sato, K. Shishido, *Tetrahedron Lett.* **2000**, *41*, 5947; c) M. Shindo, S. Oya, Y. Sato, K. Shishido, *Heterocycles* **2000**, *52*, 1143.
- [10] P. J. Walsh, F. J. Hollander, R. G. Bergman, *J. Am. Chem. Soc.* **1988**, *110*, 8729.
- [11] See ref. [4]. This observation implicates an alternative effect, speculatively pre-coordination of the electron-withdrawing group oxygen atom to zirconium, in the previously reported chemistry.
- [12] The product of this reaction has been designated **17g** to maximize consistency between starting imine and product numbering.
- [13] Attempts to insert imines into the analogous bis(*p*-bromophenyl)acetylene were unsuccessful.
- [14] For more information on potential suitable alkynes, see: S. Y. Lee, R. G. Bergman, *Tetrahedron* **1995**, *51*, 4255.
- [15] This reaction proceeds via *p*-methoxyphenylimidozirconocene complex **13b**.
- [16] a) L. E. Overman, C. E. Owen, M. M. Pavan, C. J. Richards, *Org. Lett.* **2003**, *5*, 1809; b) D. R. Kronenthal, C. Y. Han, M. K. Taylor, *J. Org. Chem.* **1982**, *47*, 2765.
- [17] Efforts to generate imidozirconium compound **13a** in situ from an analogous precursor led to multiple decomposition products.
- [18] R. T. Ruck, R. G. Bergman, *Angew. Chem.* **2004**, *116*; *Angew. Chem. Int. Ed.* **2004**, *43*.

Reaction Mechanisms

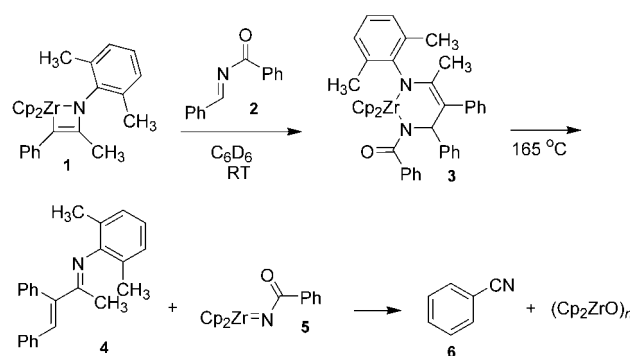
Zirconium-Mediated Conversion of Amides to Nitriles: A Surprising Additive Effect**

Rebecca T. Ruck and Robert G. Bergman*

The cyano ($\text{C}\equiv\text{N}$) functional group is useful for the introduction of nitrogen into organic molecules for the activation of adjacent C–H bonds and for efficient conversion into other functional groups, such as amines and ketones.^[1] The dehydration of primary amides to nitriles has long relied upon the use of strong dehydrating agents, such as P_2O_5 ^[2] or SOCl_2 .^[3] Such transformations often require high temperatures and lead to multiple by-products depending on the functional groups present in the starting amide. The lone early-transition-metal-mediated process reported for this dehydration involves the use of TiCl_4 and base at 0°C ;^[4] however, this method has largely been ignored in synthetic applications. Herein, we present a functionally simple method for preparing nitriles from primary amides that appears to proceed through the corresponding *N*-acylimidozirconocene complex. A detailed mechanistic study has been carried out that elucidates a remarkable additive effect on this reaction. Isotopic labeling and kinetic studies reveal an unprecedented reaction pathway in imidozirconium chemistry.

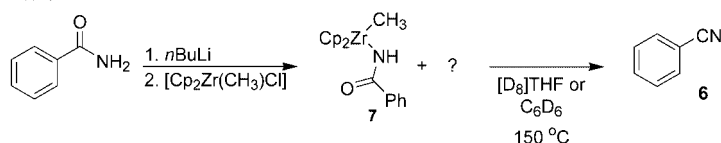
We recently reported that *N*-sulfonyl, sulfinyl, and phosphinyl imines insert into the metal–carbon–ring bond of azazirconacyclobutene **1** to generate new six-membered-ring zirconacycles **3** (see Scheme 1).^[5] Upon heating, these complexes undergo retro-[4+2] cycloadditions to generate α,β -unsaturated imines and inactive imidozirconocene complexes.^[5] *N*-Benzoyl benzaldimine (**2**)^[6] was also a competent substrate in this chemistry, but only the α,β -unsaturated imine product **4** (and not the new imidozirconium species) was detected by ^1H NMR spectroscopy. Instead, we identified the quantitative formation of benzonitrile (**6**), presumably formed by deoxygenation of the *N*-benzoylimidozirconocene complex **5** (Scheme 1; $\text{Cp} = \text{C}_5\text{H}_5$).

We subsequently prepared an alternative zirconium precursor to the imido compound **5** from the reaction between the lithium salt of benzamide and $[\text{Cp}_2\text{Zr}(\text{CH}_3)\text{Cl}]$ ^[7] (Method 1, Scheme 2). Heating this compound to 150°C in benzene or THF (reactions carried out in sealed tubes, for full experimental details see the Supporting Information) led to

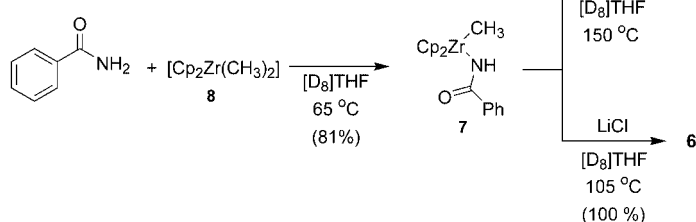


Scheme 1.

Method 1:



Method 2:



Scheme 2.

methane elimination and afforded benzonitrile in quantitative yield from the zirconium starting material, providing a two-step synthetic sequence for the clean and quantitative, albeit slow, conversion of primary amides to nitriles. Based on earlier precedent,^[8] we treated benzamide with $[\text{Cp}_2\text{Zr}(\text{CH}_3)_2]$ (**8**) at 65°C to generate the expected methylzirconium amide **7** (Scheme 2, Method 2).^[9] However, in contrast to our observations in Method 1, prolonged heating of **7** prepared by Method 2 at temperatures as high as 165°C failed to provide the expected nitrile and left **7** intact.

X-ray diffraction studies conducted on crystals of compound **7** prepared by Method 1 revealed that it was an 18-electron complex with the carbonyl oxygen atom coordinated to the zirconium center (Figure 1). The Zr–N and Zr–O bond lengths were identical at 2.30 \AA . Surprisingly, a chloride anion was located in the crystal lattice. This finding led us to suspect that residual LiCl by-product from the preparation of **7** by Method 1 may facilitate the desired nitrile formation, thereby accounting for the observed reactivity difference between **7** prepared by Methods 1 and 2. Indeed, heating compound **7** prepared by Method 2 in the presence of 0.2–2 equivalents of LiCl led to quantitative formation of benzonitrile (Scheme 2) and we were now able to carry out the reaction at 105°C in the presence of added LiCl. The reaction is catalytic in LiCl, but 0.5 equivalents were used for synthetic purposes.

[*] Dr. R. T. Ruck, Prof. R. G. Bergman
Department of Chemistry
University of California, Berkeley
Berkeley, CA 94720 (USA)
Fax: (+1) 510-642-2156
E-mail: bergman@cchem.berkeley.edu

[**] This work was supported by the National Institutes of Health (GM-25459) and by an NIH post-doctoral fellowship to R.T.R. We thank Dr. Fred Hollander and Dr. Allen Oliver of the UC Berkeley CHEXRAY facility for the X-ray crystal structure determination.

Supporting information (full experimental details) for this article is available on the WWW under <http://www.angewandte.org> or from the author.

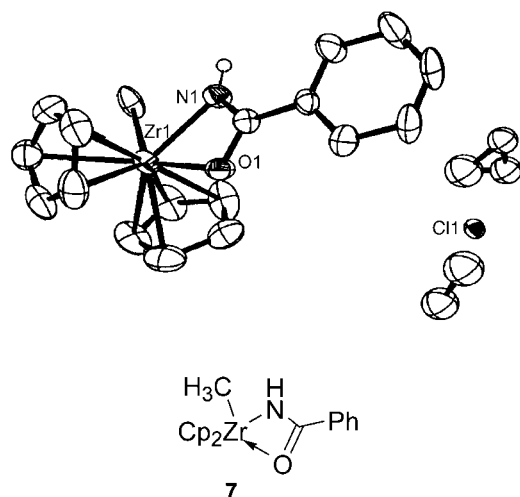


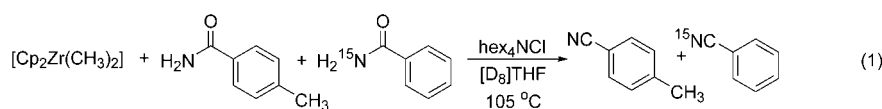
Figure 1. ORTEP diagram of methylzirconium benzamide complex **7** (thermal ellipsoids set at 50% probability). Also shown are the chloride ion and two benzene molecules found in the lattice. A line drawing is provided for clarity.

A variety of primary amides were competent substrates for this transformation, affording the corresponding nitrile compounds in excellent yields (Table 1). Intermediate methylzirconium amide complexes were detected by ^1H NMR spectroscopic monitoring of the transformation. In addition to the parent benzamide (entry 1), electron-rich (entries 2 and 3) and electron-poor (entries 4 and 5) aryl amides underwent this reaction efficiently. The reaction tolerated the increased steric hindrance of *o*-toluamide (entry 6). Primary alkyl amides with and without α -protons were also competent substrates, with hexanoamide (entry 7) and trimethylacetamide (entry 8) each providing the corresponding nitrile in excellent yield.

To study the mechanism of this transformation and elucidate the role of LiCl, a soluble additive capable of

catalyzing this chemistry was required. The possibility that traditional Lewis bases could effect this chemistry was ruled out since these reactions were conducted in neat THF, known to be an excellent ligand for zirconium. Other lithium salts,^[10] some soluble in THF, were screened in the decomposition reaction of complex **7**. However, all these Li^+ additives performed poorly relative to LiCl, requiring increased temperatures and/or reaction times. A series of tetraalkylammonium salts were also screened as additives; we were pleased to find that the soluble salt tetra-*n*-hexylammonium chloride (hex_4NCl) catalyzed the formation of benzonitrile from **7** with $t_{1/2} \approx 20$ min (versus $t_{1/2} \approx 80$ min with LiCl). These results suggest that interaction of chloride (rather than lithium) with zirconium compound **7** facilitates the generation of the imidozirconocene complex **5**. Consistent with this assessment is the observation that sodium isopropoxide and potassium *tert*-butoxide also catalyzed nitrile formation, albeit at diminished rates, probably because of the partial insolubility of the alkoxide additives. Further, based on the results of Scheme 1, conversion of the imidozirconocene **5** into benzonitrile does not require the presence of an added anion source.

With this soluble additive in hand, we could investigate the mechanism of the overall reaction and the surprising effect of added chloride ion. A crossover experiment was conducted, in which 2.2 equivalents of $[\text{Cp}_2\text{Zr}(\text{CH}_3)_2]$ were treated with one equivalent each of *p*-toluamide and ^{15}N -labelled benzamide in the presence of hex_4NCl [Eq. (1)]. No crossover was observed in this reaction: only unlabeled *p*-

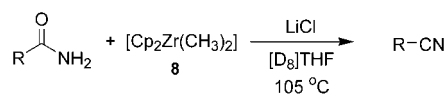


tolunitrile and ^{15}N -labeled benzonitrile were detected by ^{15}N NMR spectroscopy and GC/MS.^[11]

Kinetic studies were undertaken to determine the rate law for the reaction of complex **7** with hex_4NCl . Disappearance of **7** at a given $[\text{hex}_4\text{NCl}]$ was monitored by ^1H NMR spectroscopy. These data revealed a first-order dependence on **7** and provided the first-order rate constant, k , from the equation, $\ln[\mathbf{7}] = -kt$.^[12] Plotting values of k determined at different concentrations of hex_4NCl provided a linear correlation between the two variables and a first-order dependence on $[\text{hex}_4\text{NCl}]$ (Figure 2). The rate law for the decomposition of **7** was thus determined to be: $d[\mathbf{7}]/dt = -k[\text{hex}_4\text{NCl}][\mathbf{7}]$. Rates determined over the temperature range of 105–150 °C gave activation parameters $\Delta H^\ddagger = 18 \pm 2 \text{ kcal mol}^{-1}$ and $\Delta S^\ddagger = -16 \pm 5 \text{ cal mol}^{-1} \text{ K}^{-1}$, consistent with a bimolecular rate-determining step.

Having established the rate law, we conducted a kinetic isotope effect (KIE) study using compound **7** and its N-D analogue. The deuterated analogue (**7-D**) was prepared by treatment of $[\text{Cp}_2\text{Zr}(\text{CH}_3)_2]$ with $[\text{D}_2]$ benzamide. Comparison of the decomposition rates for **7** and **7-D** enabled the measurement of a deuterium isotope effect of $k_{\text{H}}/k_{\text{D}} = 1.07$. This KIE very close to unity stands in stark contrast to the

Table 1:



Entry	Amide	Nitrile ^[a]	Yield [%] ^[b]
1	benzamide	benzonitrile	100
2	<i>p</i> -methoxybenzamide	<i>p</i> -methoxybenzonitrile	97
3	<i>p</i> -toluamide	<i>p</i> -tolunitrile	91
4	<i>p</i> -bromobenzamide	<i>p</i> -bromobenzonitrile	92 (83) ^[c]
5	<i>p</i> -trifluoromethyl-benzamide	<i>p</i> -trifluoromethyl-benzonitrile	93
6	<i>o</i> -toluamide	<i>o</i> -tolunitrile	98
7	hexanoamide	hexanenitrile	92
8	trimethylacetamide	trimethylacetoneitrile	96 ^[d]

[a] ^1H NMR spectra of all the nitrile products were correlated with authentic material. [b] Yield after 15 h relative to an internal standard by ^1H NMR spectroscopy; all starting amide had been consumed. [c] Value in parentheses is the yield of isolated product after chromatography. [d] Reaction required 48 h to proceed to completion.

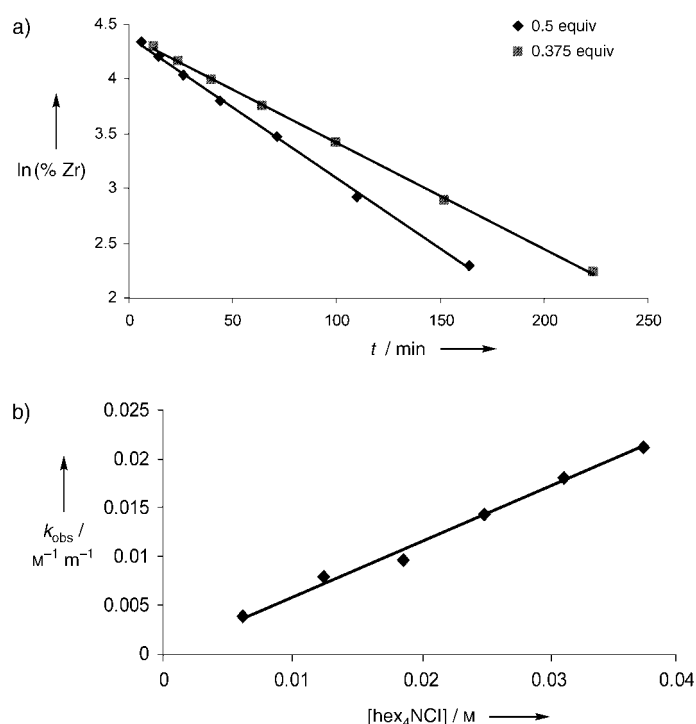


Figure 2. a) Graph for determining the order in [7] at two concentrations of hex_4NCl . b) Graph for determining the order in $[\text{hex}_4\text{NCl}]$.

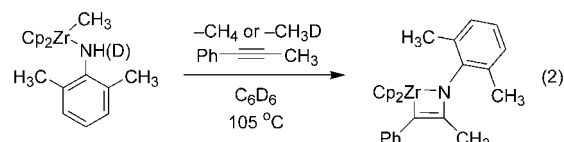
value of $k_{\text{H}}/k_{\text{D}} = 3.6$ determined for formation of a common *N*-arylimidozirconocene complex from the methylzirconium amide precursor.^[13] The collective data presented herein are most consistent with a mechanism in which rate-determining chloride-association takes place with displacement of the carbonyl oxygen atom from zirconium.^[14] The resulting intermediate, in a fast step, undergoes methane elimination to generate the *N*-acylimidozirconium species, which goes on to form the product nitrile. Presumably, chloride-assisted oxygen de-chelation is required for the complex to adopt the conformation necessary for reductive elimination.

In summary, we have developed a new method for the dimethylzirconocene-mediated conversion of primary amides to the corresponding nitriles in excellent yields. This transformation proceeds via the *N*-acylimidozirconocene complex, formation of which is dependent upon an unprecedented chloride-anion additive effect. Full experimental details can be found in the Supporting Information. A related paper describing catalytic imine insertions into azazirconacyclobutenes also appears in this issue.^[15]

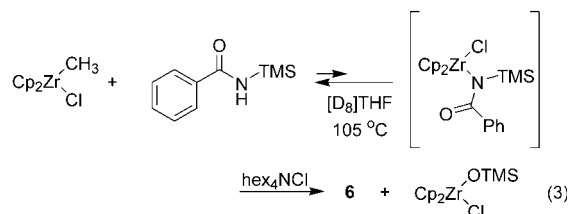
Received: June 24, 2004

Keywords: additive effects · amides · kinetics · nitriles · zirconium

- [3] J. A. Krynitsy, H. W. Carhart, *Org. Synth. Coll. Vol. IV* **1963**, 436.
- [4] W. Lehnert, *Tetrahedron Lett.* **1971**, 1501.
- [5] R. T. Ruck, R. G. Bergman, *Organometallics* **2004**, *23*, 2231.
- [6] R. Kupfer, S. Meier, E.-U. Würthwein, *Synthesis* **1984**, 688.
- [7] $[\text{Cp}_2\text{Zr}(\text{CH}_3)\text{Cl}]$ was prepared via a comproportionation reaction of $[\text{Cp}_2\text{Zr}(\text{CH}_3)_2]$ and $[\text{Cp}_2\text{ZrCl}_2]$ in toluene at 135 °C.
- [8] P. J. Walsh, F. J. Hollander, R. G. Bergman, *Organometallics* **1993**, *12*, 3705.
- [9] Dimethylzirconocene may be purchased from Strem. In this case, it was prepared from $[\text{Cp}_2\text{ZrCl}_2]$: S. Couturier, B. Gautheron, *J. Organomet. Chem.* **1978**, *157*, C61.
- [10] LiOTf , LiBr , LiBPh_4 and $\text{LiB}_{\text{ARF}20}$ ($\text{B}_{\text{ARF}20} = [\text{B}(\text{C}_6\text{F}_5)_4]^-$) were screened as additives.
- [11] A control experiment was conducted, in which ^{15}N -labeled benzonitrile and ^{15}N -labeled tolunitrile were shown to have distinct resonance signals in the ^{15}N NMR spectrum.
- [12] All reactions were conducted in the presence of catalytic concentrations of hex_4NCl .
- [13] The reaction used in KIE studies is shown in Equation (2). The reaction rate was shown to be independent of [alkyne] under the conditions employed.



- [14] Hydrogen bonding to the NH proton was ruled out as a possible mechanism because chloride can be used to accelerate the following reaction [Eq. (3)].



- [15] R. T. Ruck, R. L. Zuckerman, S. W. Krska, R. G. Bergman, *Angew. Chem.* **2004**, *116*; *Angew. Chem. Int. Ed.* **2004**, *43*

[1] S. R. Sandler, W. Karo in *Organic Functional Group Preparations*, Academic Press, San Diego, **1983**, chap. 17.

[2] D. B. Reisner, E. C. Coring, *Org. Synth. Coll. Vol. IV* **1963**, 144.

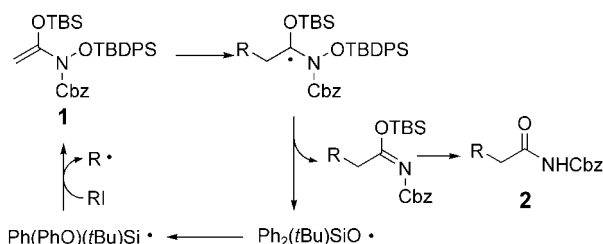
Radical Reactions

Radical-Mediated γ -Functionalizations of α,β -Unsaturated Carboxylic Amides**

Sunggak Kim* and Chae Jo Lim

α,β -Unsaturated carbonyl compounds are important intermediates in organic synthesis.^[1] Reaction of their enolate anions with various electrophiles generally affords α -functionalized products. Despite their versatility in synthetic manipulations, γ -functionalization of α,β -unsaturated carbonyl compounds, including γ -alkylation, has been often a very difficult and unresolved problem. Several methods to effect this operation have been developed over the years and include the use of γ -arylsulfonyl groups as regiospecific control elements,^[2] copper dienolates,^[3] and zinc bromide catalyzed alkylation of *O*-silylated dienolates.^[4,5] However, these methods have their limitations in that they, most importantly, depend on the nature of the alkylation agents and dienolates. Thus, the γ -functionalization of α,β -unsaturated carbonyl compounds has been a very challenging problem.

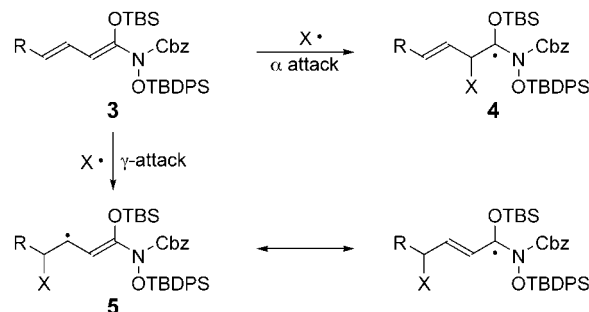
We recently reported a radical alkylation method based on the addition of an alkyl radical to ketene *O,N*-acetal **1** followed by the cleavage of the N–O bond to afford the alkylated carboxylic amide **2** after aqueous workup (Scheme 1).^[6,7] In this approach, the rearrangement of a



Scheme 1. Tin-free radical alkylation of carboxylic amides. Cbz = benzyl-oxycarbonyl, TBDPS = *tert*-butyldiphenylsilyl, TBS = *tert*-butyldimethylsilyl.

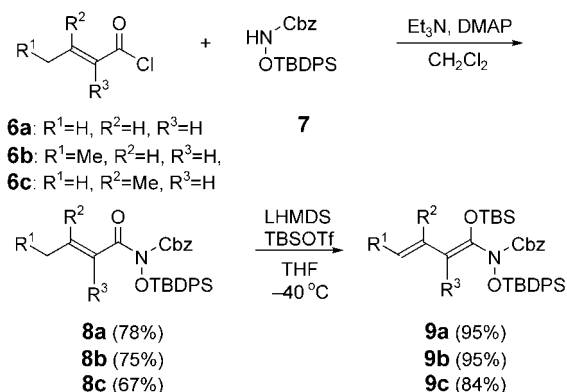
silyloxy radical to a silyl radical was utilized effectively in tin-free alkylation.^[8] A radical-mediated γ -functionalization approach has not, to the best of our knowledge, been reported to date and seems to be a conceptual advance to our previous finding. Therefore, we initially studied the radical-mediated γ -

alkylation of α,β -unsaturated carboxylic amides. Our idea to effect γ -alkylation relies on the stability of the radical intermediates derived from α and γ attack of an alkyl radical onto diene *O,N*-acetal **3** (Scheme 2). The γ -alkylation would be feasible because it is evident that intermediate **5** should be more stable than intermediate **4** owing to the allylic nature of **5**.



Scheme 2. Radical approach to the γ -functionalization of α,β -unsaturated carboxylic amides via **3**.

Three diene *O,N*-acetals **9a**, **9b**, and **9c** were prepared (Scheme 3). The coupling of acid chloride **6a** with **7** and triethylamine in the presence of a catalytic amount of 4-



Scheme 3. Preparation of diene *O,N*-acetals. AIBN = azobisisobutyronitrile, DMAP = 4-(dimethylamino)pyridine, LHMDs = lithium hexamethyldisilazide, TBSOTf = *tert*-butyldimethylsilyl trifluoromethanesulfonate, V-70 = 2,2'-azobis(4-methoxy-2,4-dimethylvaleronitrile).

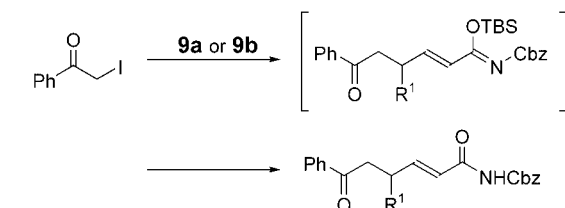
(dimethylamino)pyridine (DMAP) in dichloromethane at room temperature for 30 minutes gave amide **8a** in 78% yield. The amide **8a** was treated with lithium hexamethyldisilazide (LHMDs) in THF at -40°C in the presence of *tert*-butyldimethylsilyl trifluoromethanesulfonate (TBSOTf) to afford **9a** in 95% yield. Similarly, diene *O,N*-acetals **9b** and **9c** were prepared in high yields. They were observed to be highly stable to purification by silica gel column chromatography.

Irradiation of a solution of **9a** (1.5 equiv), iodoacetophenone (1.0 equiv) and hexamethylditin (1.1 equiv) in benzene at 300 nm for 3 h gave **10a** in 79% yield after isolation by silica gel column chromatography without the formation of

[*] Prof. Dr. S. Kim, C. J. Lim
Center for Molecular Design & Synthesis and
Department of Chemistry, School of Molecular Science
Korea Advanced Institute of Science and Technology
Daejeon 305-701 (Korea)
Fax: (+82) 42-869-8370
E-mail: skim@kaist.ac.kr

[**] We thank the CMDS and BK21 programs for financial support.
Supporting information for this article is available on the WWW
under <http://www.angewandte.org> or from the author.

the α -alkylation product (Scheme 4). Encouraged by this result, we studied the tin-free γ -alkylation of **9a** based on the previously reported rearrangement of a silyloxy radical into a silyl radical.^[9] Reaction of **9a** with iodoacetophenone with



(Me₃Sn)₂ (1.1 equiv), C₆H₆, *h* ν , 3 h **10a**: R¹=H, 79%
AIBN (0.2 equiv), C₆H₆, 80 °C, 3 h **10a**: R¹=H, 57%
V-70 (0.2 equiv), CH₂Cl₂, 30 °C, 10 h **10a**: R¹=H, 86%; **10b**: R¹=Me, 72%

Scheme 4. Formation of γ -functionalized products **10a** and **10b**.

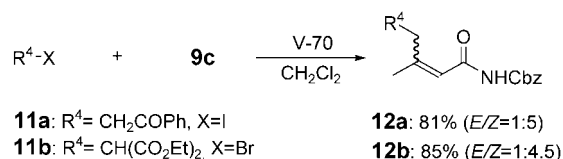
azobisisobutyronitrile (AIBN) as the initiator in benzene at 80 °C for 3 h afforded **10a** in 57 % yield. Apparently, the low yield resulted from thermal decomposition of **9a** to some extent. When the reaction was carried out with V-70 (2,2'-azobis(4-methoxy-2,4-dimethylvaleronitrile)) as the initiator in dichloromethane at 30 °C for 10 h, the reaction cleanly afforded **10a** in 86 % yield. Also, employing **9b** in the reaction under the same conditions gave **10b** in 72 % yield. To determine the efficiency and scope of the present method, we performed additional experiments with several different alkyl iodides and bromides and with **9a** and **9b** as substrates. As shown in Table 1, alkyl iodides and bromides bearing an α -electron-withdrawing group underwent clean γ -alkylations under tin-free conditions. Notably, the monosubstituted diene *O,N*-acetal **9b** gave comparable results to **9a**. When further

Table 1: Tin-free radical γ -alkylations.^[a]

Entry	Substrate	Product	Yield [%] ^[b]	
			10a	10b
1			77	74
2			64	71
3			75	82
4			77	73
5			79	65 ^[c]
6			85	74 ^[d]

[a] The reaction was carried out with V-70 as the initiator in CH₂Cl₂ at 30 °C for 10 h. [b] Yield of isolated product. [c] *syn/anti* = 2.5:1. [d] *syn/anti* = 1:1.

reactions were also carried out with **9c**, derived from senecioic acid, similar results were obtained, which confirms the generality of the present method (Scheme 5).^[10] We consider the exclusive formation of γ -alkylation products



Scheme 5. γ -Functionalization of senecioic acid derivative **9c**.

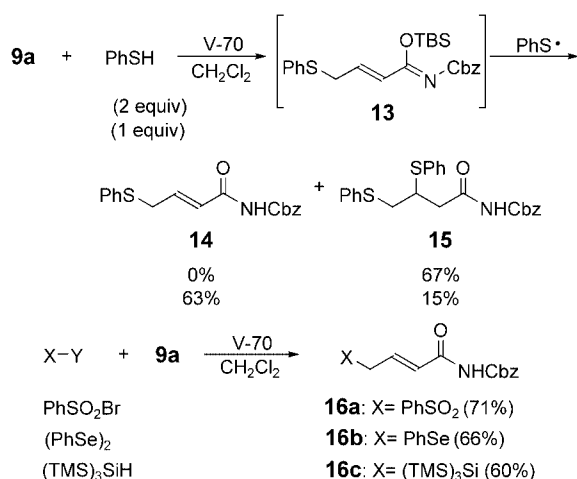
under tin-free radical conditions with no indication of the formation of α -alkylation products to be of synthetic importance. However, this method proved to be limited with respect to nucleophilic alkyl radicals. Irradiation of a benzene solution of **9b** with an equimolar mixture of 4-phenoxybutyl iodide and hexamethylditin at 300 nm for 10 h gave the desired γ -alkylation product (25 %) together with the dimerized product (31 %) and the starting iodide (11 %), thus indicating that the addition of a nucleophilic alkyl radical onto electron-rich **9b** is slow and inefficient.

Subsequently, the possibility of the γ -addition of several synthetically useful hetero groups, such as phenylsulfanyl and phenylsulfonyl, to **9a** was examined. It is known that the phenylsulfenylation and phenylselenylation of α,β -unsaturated carbonyl compounds occurs exclusively at the α position,^[11] whereas trimethylsilylation of α,β -unsaturated aldimines occurs at the γ position.^[12] Based on our previous rationale, the addition of the phenylsulfanyl radical to **9a** at the γ position could be anticipated. When the radical-mediated reaction was carried out with **9a** and thiophenol under the same conditions, phenylsulfenylation occurred exclusively at the γ position. Reaction of **9a** with 2 equivalents of thiophenol in dichloromethane in the presence of V-70 as the initiator gave **15** in 67 % yield because of further addition of the phenylsulfanyl radical to **13**, whereas a 63:15 mixture of **14** and **15** was isolated when 1 equivalent of thiophenol was used. The reaction of phenylsulfonyl bromide, diphenyl diselenide, and tris(trimethylsilyl)silane gave γ -addition products in high yields (Scheme 6).

In conclusion, we have developed the first radical-mediated γ -functionalization of α,β -unsaturated carboxylic amides via diene *O,N*-acetals under tin-free conditions to give a synthetically useful process. Further studies to expand this strategy to the α,β -unsaturated aldehydes and ketones are underway.

Experimental Section

Typical procedure: A solution of iodoacetophenone (49 mg, 0.2 mmol), **9a** (176 mg, 0.3 mmol), and V-70 (12 mg, 0.04 mmol) in dichloromethane (1 mL; 0.2 M in iodide) was degassed with nitrogen for 10 min, and the solution was then stirred at 30 °C under nitrogen for 10 h. The solvent was evaporated under reduced pressure and the residue was purified by silica-gel column chromatography with EtOAc/hexane (1:3) as the eluant to give **10a** (58 mg, 86 %). ¹H NMR (CDCl₃, 400 MHz): δ = 2.65–2.71 (m, 2H), 3.15 (t, *J* =



Scheme 6. γ -Addition of hetero groups to diene *O,N*-acetal **9a**.

7.1 Hz, 2H), 5.16 (s, 2H), 6.89 (d, J = 15.4 Hz, 1H), 7.21 (dt, J = 15.4 Hz, 6.9 Hz, 1H), 7.34–7.95 ppm (m, 11H); ^{13}C NMR (CDCl_3 , 100 MHz): δ = 26.7, 36.6, 67.9, 122.0, 128.0, 128.4, 128.7 (C 2), 133.3, 134.3, 134.9, 136.6, 149.5, 151.5, 165.5, 198.1 ppm; IR (polymer): $\tilde{\nu}$ = 3292, 1764, 1687, 1648, 1523, 1204, 1049, 746, 698 cm^{-1} ; HRMS: calcd for $\text{C}_{20}\text{H}_{19}\text{NO}_4$: 337.1314, found: 337.1324.

Received: May 28, 2004

Keywords: alkenes · alkylation · carboxylic amides · radicals · synthetic methods

- Wang, A. Hosomi, *Org. Lett.* **2001**, 3, 2591–2594; d) M. G. Roepel, *Tetrahedron Lett.* **2002**, 43, 1973–1976; e) Y. Cai, B. P. Roberts, *Tetrahedron Lett.* **2003**, 44, 4645–4648.
- [8] a) R. L. Dannley, G. Jalics, *J. Org. Chem.* **1965**, 30, 3848–3851; b) A. K. Shubber, R. L. Dannley, *J. Org. Chem.* **1971**, 36, 3784–3787.
- [9] For tin-free radical reactions, see: a) P. A. Baguley, J. C. Walton, *Angew. Chem.* **1998**, 110, 3272–3283; *Angew. Chem. Int. Ed.* **1998**, 37, 3072–3082, and references therein; b) S. Kim, H.-J. Song, T.-L. Choi, J.-Y. Yoon, *Angew. Chem. Int. Ed.* **2001**, 40, 2524–2526; c) S. Kim, C. J. Lim, *Angew. Chem.* **2002**, 114, 3399–3401; *Angew. Chem. Int. Ed.* **2002**, 41, 3265–3267; d) S. Kim, C. J. Lim, *Bull. Korean Chem. Soc.* **2003**, 24, 1219–1222.
- [10] The *E/Z* ratios of **12a** and **12b** were determined by ^1H NMR.
- [11] a) J. A. Oakleaf, M. T. Thomas, A. Wu, V. Snieckus, *Tetrahedron Lett.* **1978**, 1645–1648; b) T. A. Hasse, P. Kukkola, *Synth. Commun.* **1980**, 451–455.
- [12] K. Takabe, H. Fujiwara, T. Katagiri, J. Tanaka, *Tetrahedron Lett.* **1975**, 1237–1238.

- [1] a) S. Patai, Z. Rappoport, *The Chemistry of Enones*, Part 1 and 2, Wiley, New York, **1989**; b) R. C. Larock, *Comprehensive Organic Transformations: A Guide to Functional Group Preparation*, Wiley-VCH, New York, **1999**, pp. 1567–1620; c) T. J. Sommer, *Synthesis* **2004**, 161–201.
- [2] a) P. T. Lansbury, R. W. Erwin, *Tetrahedron Lett.* **1978**, 2675–2678; b) P. T. Lansbury, R. W. Erwin, D. A. Jeffrey, *J. Am. Chem. Soc.* **1980**, 102, 1602–1608; c) P. T. Lansbury, G. E. Beberntz, S. C. Maynard, C. J. Spagnuolo, *Tetrahedron Lett.* **1985**, 26, 169–172; d) P. T. Lansbury, C. J. Spagnuolo, E. L. Grimm, *Tetrahedron Lett.* **1986**, 27, 2725–2726.
- [3] a) J. A. Katzenellenbogen, A. L. Crumrine, *J. Am. Chem. Soc.* **1974**, 96, 5662–5663; b) J. A. Katzenellenbogen, A. L. Crumrine, *J. Am. Chem. Soc.* **1976**, 98, 4925–4935; c) B. S. Pitzele, J. S. Baran, D. H. Steinman, *Tetrahedron* **1976**, 32, 1347–1351; d) P. M. Savu, J. A. Katzenellenbogen, *J. Org. Chem.* **1981**, 46, 239–250.
- [4] a) I. Fleming, J. Goldhill, I. Paterson, *Tetrahedron Lett.* **1979**, 3209–3212; b) I. Fleming, T. V. Lee, *Tetrahedron Lett.* **1981**, 22, 705–708.
- [5] For other approaches, see: a) T. A. Bryson, R. B. Gammill, *Tetrahedron Lett.* **1974**, 3963–3966; b) B. S. Pitzele, J. S. Baran, D. H. Steinman, *Tetrahedron*, **1976**, 32, 1347–1351; c) E. Wenkert, T. E. Goodwin, B. C. Ranu, *J. Org. Chem.* **1977**, 42, 2137–2141; d) M. Majewski, G. B. Mpango, M. T. Thomas, A. Wu, V. Snieckus, *J. Org. Chem.* **1981**, 46, 2029–2045; e) L. A. Paquette, W. A. Kinney, *Tetrahedron Lett.* **1982**, 23, 131–134.
- [6] S. Kim, C. J. Lim, C. Song, W.-j. Chung, *J. Am. Chem. Soc.* **2002**, 124, 14306–14307.
- [7] For other radical-mediated alkylations, see: a) Y. Watanabe, T. Yoneda, Y. Ueno, T. Toru, *Tetrahedron Lett.* **1990**, 31, 6669–6672; b) P. Renaud, J.-P. Vionnet, P. Vogel, *Tetrahedron Lett.* **1991**, 32, 3491–3494; c) K. Miura, N. Fujisawa, H. Saito, D.

CuCl Nanoplatelets**CuCl Nanoplatelets from an Ionic Liquid-Crystal Precursor*****Andreas Taubert**

Research on ionic liquids (ILs) has focused on the synthesis of and organic chemistry in ILs. Recently, however, ILs have also received attention from the inorganic materials community. Ionic liquids can act as solvents for reactants and morphology templates for the products at the same time, which enables the synthesis of inorganic materials with novel or improved properties. In principle, the IL can be retrieved after synthesis and thus provides an ecologically friendly and economical approach to inorganic materials. While ILs are promising “all-in-one” solvent/templates for the synthesis of inorganic materials, only a few reports on this topic have appeared; they have mainly focused on ordered metal oxides^[1–5] and metal nanoparticles.^[6–8] For a recent review on the structural organization in ionic liquids, see also ref. [9]

Copper(I) chloride is extensively used as a desulfurizing agent in the petrochemical industry and as a catalyst for the denitration of cellulose;^[10] there is thus considerable interest in improved CuCl systems. This paper introduces a novel

[*] Dr. A. Taubert
Department of Chemistry
University of Basel
Klingelbergstr. 80, 4056 Basel (Switzerland)
Fax: (+41) 61-267-3855
E-mail: andreas.taubert@unibas.ch

[**] A.T. thanks Prof. W. Meier for his support and for useful discussions, M. Düggelein and D. Mathis for help with SEM, and Prof. W. B. Stern for access to the X-ray diffractometer. Thanks are also due to Dr. T. Welton and Dr. C. Hardacre for useful discussions at the CERC3 meeting in St. Malo.

protocol for the controlled synthesis of CuCl nanoplatelets with a well-developed crystal habit and a tunable particle size and connectivity from the Cu-containing ionic liquid crystal **1** and 6-*O*-palmitoyl ascorbic acid (**2**). In a typical nanoparticle synthesis, equivalent weights of **1** and **2** were intimately mixed, and the mixture was heated to 85, 105, 125, or 145 °C, held at that temperature for 24 h, and quenched.

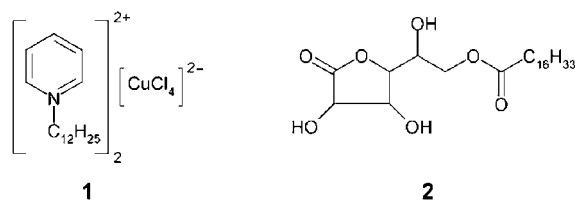


Figure 1 shows that the mixture of **1** and **2** is liquid-crystalline at room temperature; it becomes isotropic at 90–92 °C. The author is currently investigating the structure of these liquid crystals in more detail, but as both pure **1** and

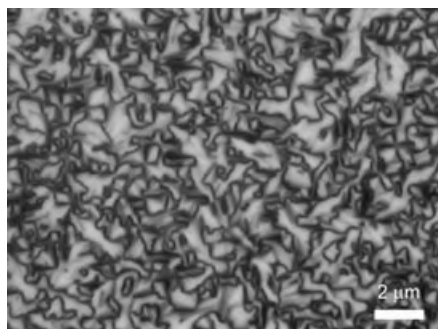


Figure 1. Optical micrograph (crossed polarizers) of a 1/1 (w/w) mixture of **1** and **2** at room temperature after rapid heating and quenching.

pure **2** form lamellar self-assembled structures,^[11,12] it is likely that mixtures of **1** and **2** are also layered. Compound **1** is essentially an IL (m.p. 66–70 °C), and **2** a guest molecule; this is thus another example showing that many ILs are ordered and have polar and nonpolar regions, similar to materials reported in refs.^[8,13,14]

Figure 2a shows a scanning electron micrograph of CuCl particles obtained at 85 °C. The particles are platelets with a relatively uniform thickness of about 220 to 260 nm and a large range of in-plane sizes, from about 5 to larger than 50 μm. Figure 2b shows crystals obtained at 105 °C; the particles obtained at 125 and 145 °C are similar to these crystals. These particles are smaller but thicker than those in Figure 2a, with typical in-plane dimensions 5–8 μm and thicknesses from (occasionally) 250 nm to (typically) about 1 to 1.2 μm.

Figure 3 shows that individual platelets in the samples precipitated at 85 °C are irreversibly connected at their junctions. This indicates that, during particle formation, individual platelets are in close contact for a long enough

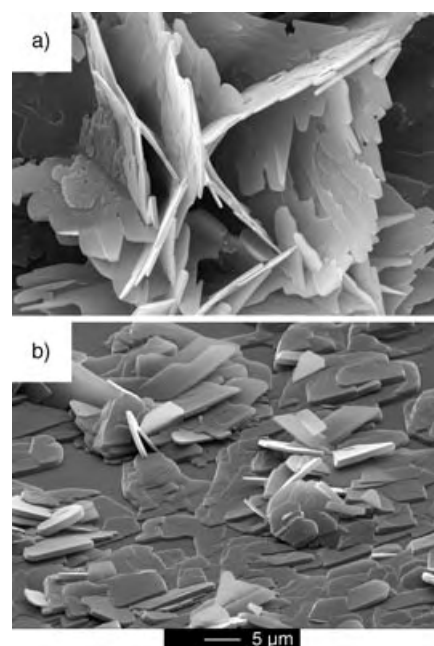


Figure 2. Scanning electron micrographs of CuCl nanoplatelets precipitated from a 1/1 (w/w) mixture of **1** and **2**. a) Relatively large and interconnected platelets typically obtained by reaction at 85 °C. b) Smaller platelets that are typical for reaction temperatures between 105 and 145 °C.

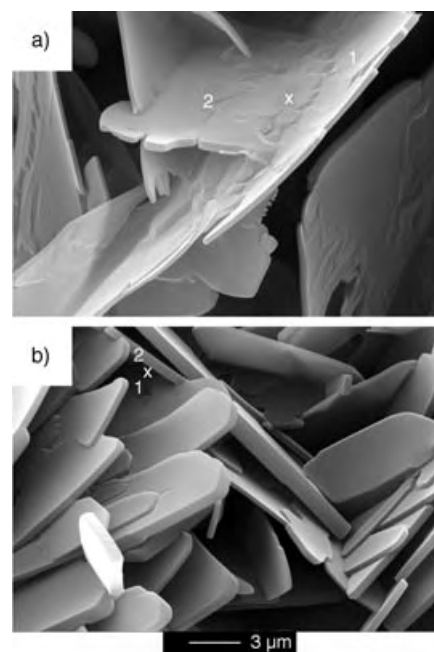


Figure 3. Scanning electron micrographs of CuCl nanoplatelet junctions. a) Thin particles with a rough surface typically obtained at 85 °C. The junction **x** between platelets **1** and **2** is covered with additional CuCl, thereby providing a permanent connection between the platelets. b) Thicker particles with a smooth surface typical for reaction temperatures between 105 and 145 °C. The junction **x** between particles **1** and **2** is not covered with CuCl, and most particles are simply touching one another.

time to enable crystal growth at the junction. In contrast, the junctions of the platelets obtained at or above 105 °C are not covered and stabilized by additional CuCl. Unlike the above particles, these platelets just touch one another; only in rare cases does a permanent linkage appear to be present.

As platelets are not typically observed for CuCl, the organic matrix must act as a template; the alkyl pyridinium ion is part of the solvent and a structure-directing agent for the crystallization; similarly, **2** probably acts as both a structure-directing agent and as an agent for reducing Cu²⁺ to Cu⁰. However, the platelets are too thick to be the product of direct phase replication as observed, for example, for SiO₂ grown in ILs.^[2–4] Hence, one can argue that the system is always ordered, even above the LC–isotropic transition; an “ordered liquid” similar to those reported in refs. [9,13,15] could impose a platelet morphology on the particles, but also be responsible for the rather subtle changes in particle morphologies.

In conclusion, this paper presents a novel procedure for the synthesis of CuCl nanoparticles and (macro)porous structures. It is possible to tune the particle size, thickness, and connectivity by varying the reaction temperature. This approach thus provides a simple and—as the IL is not consumed and can be recycled—green method to tune the properties of CuCl nanocrystals and assemblies for applications in, for example, catalysis. Furthermore, the data give some empirical insight into the structure of ILs, which is of general interest to the chemistry, physics, and biotechnology communities.

Finally, the versatility of the system is a major asset: First, ligand exchange can change the symmetry of the LC template;^[11] second, imidazolium ligands can replace pyridinium ligands;^[16] third, Pd²⁺ can replace Cu²⁺;^[16] and finally, preliminary experiments by the author have shown that also Co²⁺, Fe²⁺, Ni²⁺, and Zn²⁺ can replace Cu²⁺, and didodecyldimethylammonium bromide and tetraoctylammonium bromide can replace alkylpyridinium salts. Thus, exchange of the ligand, metal cation, anion, and/or reducing agent should offer a universal pathway towards metal halide and metal (alloy) nanostructures with tunable chemistry and morphology. The synthesis and properties of such materials, as well as the kinetics and reaction mechanisms of the system presented here, are currently under investigation.

Experimental Section

Chemicals (Fluka, Siegfried) were used as received. 2 equiv of dodecylpyridinium chloride and 1 equiv of CuCl₂·2H₂O were heated to 140 °C for 10 min to afford dark red, soft **1** after cooling. Equivalent weights of **1** and **2** were intimately mixed to form a dark red, soft material; this mixture was heated in a Perkin Elmer DSC6 (50 °Cmin^{−1}) to 85, 105, 125, or 145 °C, held at that temperature for 24 h, and then quenched at 50 °Cmin^{−1} to −5 °C to give CuCl nanoparticles.

X-ray diffraction experiments for determination of crystal phase (data not shown) were performed on a Siemens D5000 with Cu_{Kα} radiation. SEM images were recorded on a Philips XL30 ESEM with a Noran energy-dispersive X-ray spectrometer; samples were sputtered with gold prior to imaging. Energy dispersive X-ray spectroscopy was used to confirm the absence of organic material from the

precipitate; as only a trace of C and no N or O were detected, the organic material is not incorporated in the crystals, and the IL can thus be recovered and reutilized. Optical microscopy was carried out on a Leica DM-RP with a hotstage and cryostat.

Received: June 2, 2004

Keywords: copper · green chemistry · ionic liquids · liquid crystals · nanoparticles

- [1] T. Nakashima, N. Kimizuka, *J. Am. Chem. Soc.* **2003**, *125*, 6386.
- [2] Y. Zhou, M. Antonietti, *Adv. Mater.* **2003**, *15*, 1452.
- [3] Y. Zhou, M. Antonietti, *Chem. Commun.* **2003**, 2564.
- [4] Y. Zhou, M. Antonietti, *J. Am. Chem. Soc.* **2003**, *125*, 14960.
- [5] S. Dai, Y. H. Ju, H. J. Gao, J. S. Lin, S. J. Pennycook, C. E. Barnes, *Chem. Commun.* **2000**, 243.
- [6] J. Dupont, G. S. Fonseca, A. P. Umpierre, P. F. P. Fichtner, S. R. Teixeira, *J. Am. Chem. Soc.* **2002**, *124*, 4228.
- [7] R. R. Desmukh, R. Rajagopal, K. V. Srinivasan, *Chem. Commun.* **2000**, 1544.
- [8] R. P. Swatloski, S. K. Spear, J. D. Holbrey, R. D. Rogers, *J. Am. Chem. Soc.* **2002**, *124*, 4974.
- [9] J. Dupont, *J. Braz. Chem. Soc.* **2004**, *15*, 341.
- [10] Z. C. Orel, E. Matijevic, D. V. Goia, *Colloid Polym. Sci.* **2003**, *281*, 754.
- [11] F. Neve, O. Francescangeli, A. Crispini, J. Charmant, *Chem. Mater.* **2001**, *13*, 2032.
- [12] P. Lo Nostro, B. W. Ninham, L. Fratoni, S. Palma, R. Hilario-Manzo, D. Allemandi, P. Baglioni, *Langmuir* **2003**, *19*, 3222.
- [13] U. Schröder, J. D. Wadhawan, R. G. Compton, F. Marken, P. A. Z. Suarez, C. S. Consorti, R. F. de Souza, J. Dupont, *New J. Chem.* **2000**, *24*, 1009.
- [14] C. W. Scheeren, G. Machado, J. Dupont, P. F. P. Fichtner, S. Ribeiro Teixeira, *Inorg. Chem.* **2003**, *42*, 4738.
- [15] C. Hardacre, J. D. Holbrey, S. E. J. McMath, M. Nieuwenhuyzen, *ACS Symp. Ser.* **2002**, *818*, 400.
- [16] C. K. Lee, H. H. Peng, I. J. B. Lin, *Chem. Mater.* **2004**, *16*, 530.

Reversible Addition Fragmentation Chain Transfer (RAFT) Polymerization from Unprotected Cadmium Selenide Nanoparticles**

Habib Skaff and Todd Emrick*

Advanced synthetic and spectroscopic techniques in nanoscience are providing a number of new nanostructured materials as well as unprecedented insight into their structures and properties. Polymer materials alone serve as components of a rich array of nanostructures, from block copolymer assemblies^[1] to dendrimers^[2] to a variety of core-shell materials.^[3] Hybrid materials composed of polymers and nanoparticles add a level of complexity to these nanostructures, including the inherent functional capabilities of the particular nanoparticle, and the impact of interactions between the polymer and nanoparticle.^[4] Semiconductor nanoparticles, or quantum dots, are especially interesting for use in such hybrid materials, for example as components of LEDs,^[5] tunable lasers,^[6,7] photovoltaic cells,^[8–10] and biological tags.^[11,12] This is due to the unique properties of the semiconductor nanoparticles, including their broad absorption spectra, narrow emission profiles, and discreet energy bands^[13,14] that result from their quantum confined nature.

To further the progress of quantum dots from nanoscience into nanotechnology, versatile methods of ligand-based functionalization are necessary, so as to control their physical properties and interactions with their surroundings. Tailored ligand peripheries lead to a variety of potential nanoparticle-based hybrid materials, which range from simple particle dispersion in polymer matrices, to highly ordered structures formed by directed- or self-assembly. At the simplest level, the uniform dispersion of nanoparticles in a continuous phase is critical to maintaining uniform properties in a composite material. In addition, such dispersion maintains the nanoscale integrity of the particles and thus their unique properties. Versatile routes to nanoparticle functionalization allow for straightforward variation of this ligand environment for their incorporation into polymer materials, fluids, and interfaces.^[15–20]

A typical synthesis of high quality CdSe nanoparticles gives the core semiconductor stabilized by an aliphatic ligand

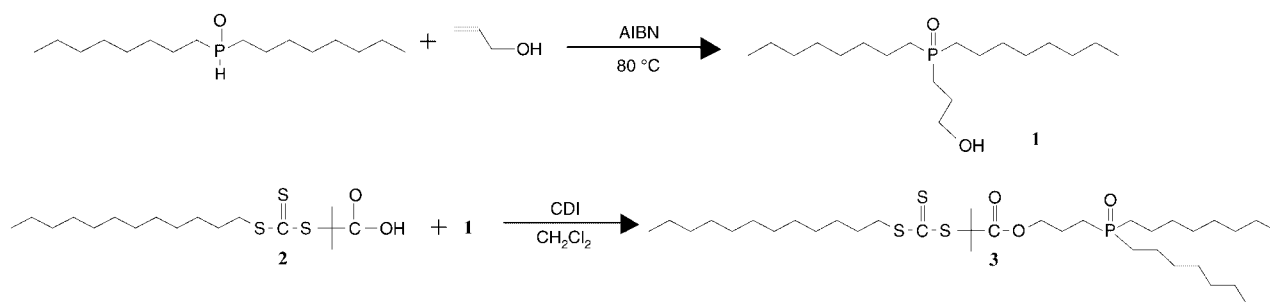
periphery composed primarily of tri-*n*-octylphosphine oxide (TOPO). This ligand periphery affords nanoparticle dispersion in hydrophobic solvents, but does not provide for uniform integration into most polymer materials. Thus, effective chemistries that provide successful functionalization of the nanoparticle surface for later use in polymerization, while simultaneously protecting the nanoparticles from oxidation and aggregation, are key steps in the development of nanoparticle-based composite materials. In prior work, Bawendi and co-workers^[5] reported a procedure for the integration of CdSe nanoparticles into polymers with long aliphatic side chains that resemble the aliphatic chains of TOPO. Alternatively, Schrock and Thomas^[21] employed polymers with coordinating functionalities on the backbone to stabilize the nanoparticles and prevent their aggregation. These approaches are without question effective, but they require the use of specially designed monomers. Thus, general methods are needed for integration of nanoparticles into high-volume commodity polymers. Our previous studies showed two methods of functionalizing CdSe nanoparticles with polymers. The first was a “grafting-from” approach, where a phosphine oxide that contained a catalyst was used as the nanoparticle ligand and as the initiator of ring-opening metathesis polymerization (ROMP) of cyclic olefins from the surface of CdSe nanoparticles.^[16] The second was a “grafting-to” technique by using pyridine-terminated poly(ethylene glycol), which was attached to the nanoparticle by ligand-exchange chemistry.^[22] Both of these functionalization techniques allow for versatile modification of the CdSe nanoparticles as well as the dispersion and assembly of the CdSe nanoparticles in a number of polymer matrices and organic and aqueous solutions. However, neither approach affords nanoparticles suitable for integration into most conventional chain-growth polymers. In contrast, the approach described here is general and adaptable to many vinyl monomers to give uniform dispersion of CdSe nanoparticles in the resulting polymers. This straightforward and versatile method uses reversible addition fragmentation chain-transfer^[23] (RAFT) polymerization as a controlled free-radical method to grow polymers radially outward from the nanoparticle surface. RAFT was chosen for its ability to polymerize a wide range of monomers in a controlled fashion, without the need for transition-metal catalysis.^[24,25]

The application of RAFT-polymerization methodology to a polymer-grafting strategy requires appropriately tailored nanoparticles. Thus, compound **3** was prepared, which integrates two key features into the same molecule: 1) a phosphine oxide ligand capable of binding to the CdSe nanoparticle surface and 2) a trithiocarbonate moiety amenable to RAFT polymerization. Hydroxy-*n*-propyl substituted phosphine oxide **1** was synthesized by hydrophosphorylation of allyl alcohol with di-*n*-octylphosphine oxide (DOPO)^[26] by using 2,2'-azobisisobutyronitrile (AIBN) as the radical source (Scheme 1). Trithiocarbonate **2** was prepared according to a literature procedure,^[27] and used to prepare **3** by 1,1'-carbonyldiimidazole mediated coupling with phosphine oxide **1**. The structure of **3** was confirmed by ¹H and ³¹P NMR spectroscopy. The characteristic methylene resonance α to the ester (δ = 4.14 ppm) was observed in the

[*] H. Skaff, Prof. Dr. T. Emrick
Polymer Science and Engineering Department
University of Massachusetts, Amherst
120 Governors Drive, Amherst, Massachusetts 01003 (USA)
Fax: (+1) 413-545-0082
E-mail: tsemrick@mail.pse.umass.edu

[**] The authors acknowledge with gratitude the financial support of the National Science Foundation (CAREER Award CHE-0239486), the Eastman Kodak Company, and the Army Research Laboratory/University of Massachusetts Polymer Materials Center of Excellence (DAAD 19-01-2-0002). The authors acknowledge Dr. Javid Rzayev for helpful discussions.

Supporting information for this article is available on the WWW under <http://www.angewandte.org> or from the author.



Scheme 1. Synthesis of **1** and **3**.

^1H NMR spectrum of **3**, and a single resonance at $\delta = 49.1$ ppm, characteristic of a trialkylphosphine oxide, was seen in ^{31}P NMR spectrum. High-resolution mass spectrometry of **3** was consistent with calculated values (calculated 678.4303, found 678.4333).

Conventional TOPO-covered CdSe nanoparticles were prepared following known procedures.^[28–30] Ligand **3** was then attached to the nanoparticle through ligand-exchange chemistry, by standard washing with pyridine of TOPO-covered CdSe, followed by stirring the pyridine-capped nanoparticles in a solution of **3** in THF at 50°C for several hours. Nanoparticles functionalized with ligand **3** were isolated by using a centrifuge device,^[31] and the dissolution and centrifugation process was repeated until no appreciable excess ligand was present. The absence of appreciable unbound ligand could be observed visually by a loss of the original yellow color, indicative of trithiocarbonate **3**, in the supernatant. This new surface coverage on the CdSe nanoparticles was confirmed by recovery of an optically clear hexane solution of nanoparticles, and in the corresponding ^1H and ^{31}P NMR spectra resonances characteristic of **3** were observed, whereas TOPO resonances were not.

Graft-from polymerizations were performed by the addition of monomer or monomers to a benzene or toluene solution of **3**-covered nanoparticles that contained a free-radical initiator. These solutions were subjected to three freeze–pump–thaw cycles, and polymerizations were performed under a nitrogen atmosphere at 70°C . Several initial experiments led to our ultimate use of di-*tert*-butylperoxide as the preferred free-radical initiator. Common free-radical initiators such as azobisisobutyronitrile (AIBN) and benzoyl peroxide were observed to induce nanoparticle degradation quickly at 70°C . This is in accord with the known susceptibility of CdSe nanoparticles to free radical degradation.^[32] However, the lower concentration of radicals inherent to *tert*-butylperoxide-initiated chemistry allows polymerization to proceed from the surface of the CdSe nanoparticle with a greatly reduced concern for nanoparticle degradation. In addition, the polymerization generates an encapsulating shell around the nanoparticles, which must function as a steric barrier that helps maintain the original high quality of the nanoparticles used at the outset.

Functionalization of CdSe nanoparticles with trithiocarbonate **3** allowed successful polymerization of a wide variety of monomers, to give homopolymers, random copolymers, and block copolymers emanating from the CdSe nanoparticle

surface (Table 1). Verification of polymer growth from the nanoparticle surface was confirmed by gel permeation

Table 1: All reactions were performed at 70°C in benzene or toluene in a N_2 atmosphere by using *tert*-butyl peroxide as the initiator.

Polymer	\bar{M}_n [g mol^{-1}]	PDI
polystyrene	27 000	1.17
poly(methyl acrylate)	31 000	1.17
poly(butyl acrylate)	42 000	1.32
poly(styrene- <i>r</i> -methyl acrylate)	49 000	1.29
poly(styrene- <i>r</i> -acrylic acid) ^[a]	37 000	1.19
poly(styrene- <i>r</i> -isoprene)	9 000	1.30
poly(styrene- <i>b</i> -methyl acrylate) ^[a]	21 000	1.18
poly(styrene- <i>b</i> -butyl acrylate) ^[a]	38 000	1.32

[a] Nanoparticle degradation was observed in the form of a blue shift in the fluorescence emission and UV/Vis absorption spectra.

chromatography (GPC) and NMR spectroscopy after the polymer had been removed from the surface. Homopolymers of styrene, methyl acrylate, and butyl acrylate of significant molecular weight with low polydispersity indexes (PDIs) were grown from the nanoparticle surface. Similarly, a number of polystyrene-based random copolymers were prepared, including poly(styrene-*r*-methyl acrylate), poly(styrene-*r*-acrylic acid), and poly(styrene-*r*-isoprene), with the number-average molecular weights (\bar{M}_n) ranging from 9000 to 49000 g mol^{-1} and PDIs from 1.2 to 1.3. Monomer incorporation into random copolymers grown from the nanoparticle surface was generally found to be tunable and consistent with feed ratios. One exception was found in the case of acrylic acid. Homopolymerization was not possible, but copolymerization of acrylic acid and styrene could be performed when acrylic acid feed ratios were kept under 30%. In general, the relatively low PDIs shown in Table 1 indicate that this controlled free-radical RAFT polymerization can be performed successfully from the surface of CdSe nanoparticles.

The preparation of surface-grafted poly(styrene-*b*-methyl acrylate) was accomplished in two steps. First, styrene was polymerized from the nanoparticle surface, and the polystyrene-grafted nanoparticle composite was isolated by precipitation into methanol. In a second step, the polystyrene-functionalized nanoparticles with an active chain end were heated in a toluene solution of methyl acrylate and *tert*-butyl peroxide to 70°C for 22 h, and the block copolymer–CdSe nanoparticle composite was precipitated into methanol.

Block copolymer formation was confirmed by an increase in molecular weight from the original homopolymer composite, as observed by GPC, and in the corresponding ^1H NMR spectrum, in which resonances of both polystyrene and poly(methyl acrylate) were observed. The polydispersity indices were narrow ($\text{PDI} < 1.3$), as expected with the RAFT technique, for all polymer architectures including block copolymers. Due to the slow initiation kinetics inherent to *tert*-butyl peroxide, polymerizations usually required 24 h; in the cases of butyl acrylate and block copolymers, longer reaction times were required (ca. 32–48 h).

A key result of this study is the retention of the unique optical properties of the CdSe nanoparticles after polymer grafting by the controlled RAFT process. This is observed clearly in the photoluminescence and UV/Vis spectra of the composite materials (Figure 1). The band-edge absorption

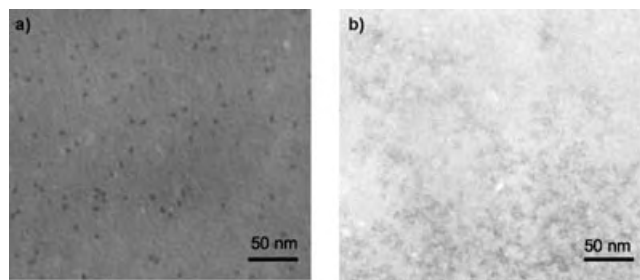


Figure 1. Transmission electron micrographs of a) poly(styrene)-covered CdSe nanoparticles in poly(styrene), b) TOPO-covered CdSe nanoparticles in poly(styrene).

peak of the CdSe nanoparticle is centered at about 525 nm in the starting **3**-covered nanoparticles, as well as in both the polystyrene and poly(methyl acrylate)-nanoparticle composites. From the fluorescence spectra, it is also evident that the nanoparticle integrity remains intact, with emission maxima centered around 545 nm both before and after polymerization.^[33] The combination of these optical-characterization methods with transmission electron micrographs confirms that the nanoparticle integrity is maintained throughout the polymerization process. This is in direct contrast to the use of conventional free-radical initiators with quantum dots, in which the optical properties are lost irreversibly. In addition, the method does not require the use of an inorganic coating over the original quantum dots, thus providing a simple approach to these composite materials.

The CdSe-polymer composite materials can be solution or spin cast into optically clear thin films. Analysis of the composite thin films by transmission electron microscopy (TEM) reveals the uniform nature of the material, as the nanoparticles are dispersed throughout the matrix in a non-aggregated fashion. Figure 2a shows an image of a polystyrene-encapsulated nanoparticle film prepared by the RAFT process, while Figure 2b shows the case where styrene was polymerized in the presence of TOPO-covered CdSe nanoparticles. In the latter case the micrographs show gross aggregation of the nanoparticles in the polymer matrix. Thus, growth of the matrix material radially outward from the nanoparticle surface provides compatibility of the two disparate materials into a single and uniform composite.

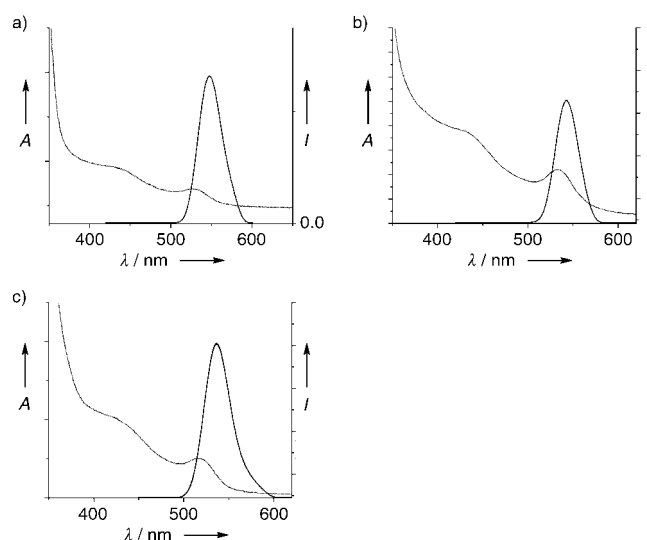


Figure 2. Absorption (A) and fluorescence spectra (I is intensity) on toluene solutions of a) **3**-covered CdSe nanoparticles, b) poly(methyl acrylate)-covered CdSe nanoparticles prepared by RAFT, and (**3**) poly(styrene)-covered CdSe nanoparticles prepared by RAFT.

In summary, we have adapted the RAFT-method of controlled free-radical polymerization to CdSe nanoparticles, by tailoring the nanoparticles with trithiocarbonate moieties, followed by polymerization from the nanoparticle surface. This RAFT-enabled growth method provides a general procedure for tailoring CdSe nanoparticles with a variety of polymers, while maintaining the unique structural and optical properties of the nanoparticles, and without the requirement of a protective inorganic shell. Through this general functionalization procedure, novel composite materials can be produced rapidly, and the choice of materials into which nanoparticles can be dispersed is expanded considerably. This, in turn, opens new possibilities for self- and directed-assembly studies on quantum dots. The retention of the photophysical properties of the quantum dots following the polymerization considerably expands their potential application base.

Received: January 21, 2004

Revised: June 24, 2004 [Z53822]

Keywords: nanostructures · nanotechnology · photophysics · polymers · quantum dots · radical reactions

- [1] T. Xu, J. T. Goldbach, T. P. Russell, *Macromolecules* **2003**, *36*, 7296.
- [2] J. M. J. Fréchet, D. A. Tomalia, *Dendrimers and Other Dendritic Polymers*, Wiley, Chichester, NY, **2001**.
- [3] K. B. Thurmond, T. Kowalewski, K. L. Wooley, *J. Am. Chem. Soc.* **1997**, *119*, 6656.
- [4] R. B. Thompson, V. V. Ginzburg, M. W. Matsen, A. C. Balazs, *Science* **2001**, *292*, 2469.
- [5] J. Lee, V. C. Sundar, J. R. Heine, M. G. Bawendi, K. F. Jensen, *Adv. Mater.* **2000**, *12*, 1102.
- [6] V. I. Klimov, A. A. Mikhailovsky, S. Xu, A. Malko, J. A. Hollingsworth, C. A. Leatherdale, H. J. Eisler, M. G. Bawendi, *Science* **2000**, *290*, 314.

- [7] H. J. Eisler, V. C. Sundar, M. G. Bawendi, M. Walsh, H. I. Smith, V. Klimov, *Appl. Phys. Lett.* **2002**, *80*, 4614.
- [8] Y. Tachibana, M. K. Nazeeruddin, M. Gratzel, D. R. Klug, J. R. Durrant, *Chem. Phys.* **2002**, *285*, 127.
- [9] E. Stathatos, P. Lianos, S. M. Zakeeruddin, P. Liska, M. Gratzel, *Chem. Mater.* **2003**, *15*, 1825.
- [10] W. U. Huynh, J. J. Dittmer, A. P. Alivisatos, *Science* **2002**, *295*, 2425.
- [11] S. Pathak, S. K. Choi, N. Arnheim, M. E. Thompson, *J. Am. Chem. Soc.* **2001**, *123*, 4103.
- [12] H. Mattoussi, J. M. Mauro, E. R. Goldman, T. M. Green, G. P. Anderson, V. C. Sundar, M. G. Bawendi, *Phys. Status Solidi B* **2001**, *224*, 277.
- [13] L. Brus, *J. Phys. Chem. Solids* **1998**, *59*, 459.
- [14] A. P. Alivisatos, *Science* **1996**, *271*, 933.
- [15] Y. Lin, H. Skaff, T. Emrick, A. D. Dinsmore, T. P. Russell, *Science* **2003**, *299*, 226.
- [16] H. Skaff, M. F. Ilker, E. B. Coughlin, T. Emrick, *J. Am. Chem. Soc.* **2002**, *124*, 5729.
- [17] M. R. Bockstaller, Y. Lapetnikov, S. Margel, E. L. Thomas, *J. Am. Chem. Soc.* **2003**, *125*, 5276.
- [18] S. W. Chen, *Langmuir* **2001**, *17*, 2878.
- [19] K. J. Watson, J. Zhu, S. T. Nguyen, C. A. Mirkin, *Pure Appl. Chem.* **2000**, *72*, 67.
- [20] Q. Y. Zhou, S. X. Wang, X. W. Fan, R. Advincula, J. Mays, *Langmuir* **2002**, *18*, 3324.
- [21] D. E. Fogg, L. H. Radzilowski, B. O. Dabbousi, R. R. Schrock, E. L. Thomas, M. G. Bawendi, *Macromolecules* **1997**, *30*, 8433.
- [22] H. Skaff, T. Emrick, *Chem. Commun.* **2003**, 52.
- [23] J. Chiefari, Y. K. Chong, F. Ercole, J. Krstina, J. Jeffery, T. P. T. Le, R. T. A. Mayadunne, G. F. Meijs, C. L. Moad, G. Moad, E. Rizzardo, S. H. Thang, *Macromolecules* **1998**, *31*, 5559.
- [24] D. J. Milliron, A. P. Alivisatos, C. Pitois, C. Edder, J. M. J. Fréchet, *Adv. Mater.* **2003**, *15*, 58.
- [25] E. Rizzardo, J. Chiefari, B. Y. K. Chong, F. Ercole, J. Krstina, J. Jeffery, T. P. T. Le, R. T. A. Mayadunne, G. F. Meijs, C. L. Moad, G. Moad, S. H. Thang, *Macromol. Symp.* **1999**, *143*, 291.
- [26] R. H. Williams, L. A. Hamilton, *J. Am. Chem. Soc.* **1952**, *74*, 5418.
- [27] J. T. Lai, D. Filla, R. Shea, *Macromolecules* **2002**, *35*, 6754.
- [28] Z. A. Peng, X. G. Peng, *J. Am. Chem. Soc.* **2001**, *123*, 183.
- [29] X. G. Peng, M. C. Schlamp, A. V. Kadavanich, A. P. Alivisatos, *J. Am. Chem. Soc.* **1997**, *119*, 7019.
- [30] L. R. Becerra, C. B. Murray, R. G. Griffin, M. G. Bawendi, *J. Chem. Phys.* **1994**, *100*, 3297.
- [31] The removal of excess ligands was found to be easier when a centrifuge device was employed. THF was removed from the ligand-exchange solution and the nanoparticles were redissolved in hexane. The hexane solution was then centrifuged. After centrifugation, the excess ligand was removed from the bottom of the centrifuge and discarded. The nanoparticles were isolated from the device, dissolved in hexane, and the procedure was repeated.
- [32] W. H. Guo, J. J. Li, Y. A. Wang, X. G. Peng, *J. Am. Chem. Soc.* **2003**, *125*, 3901. In our experiments, rather high free-radical concentrations (ca. 0.25 M) resulted in nanoparticle degradation within minutes or less, whereas lower concentrations (ca. 0.02 M) resulted in observable degradation during the initial course of the polymerization (several hours).
- [33] A small tail in the fluorescence emission spectrum of the poly(styrene)-CdSe composite is observed which is attributed to a small amount of degradation. It is hypothesized that this degradation is not observed in the poly(methyl acrylate)-CdSe composite because of the faster initiation and growth kinetics of methyl acrylate relative to styrene.

Mechanism of 4,6-*O*-Benzylidene-Directed β -Mannosylation as Determined by α -Deuterium Kinetic Isotope Effects***David Crich* and N. Susantha Chandrasekera*

Glycosylation is one of the most fundamental reactions in organic chemistry and one that is absolutely critical to the science of glycobiology.^[1] Many diverse types of glycosidic bonds are found in nature,^[2] and an absolutely bewildering array of methods exist to access them.^[3,4] In spite of this, studies on the mechanism of chemical glycosylation, important prerequisites for any rational development of new and improved methods, are extremely sparse. Most mechanistic thinking in the area is shaped by the seminal paper of Lemieux and co-workers advocating an array of contact and solvent-separated ion pairs as reactive intermediates,^[5] but even that paper, prescient as it may be, contains no quantitative data. The kinetics of displacement of anomeric halides by simple amines, alcohols, and thiolates were measured in the 1950s and 60s,^[6] but very few studies have been conducted with the inclusion of an actual promoter.^[7,8] Thus, “much of the evidence used to substantiate proposed inter-glycosidic coupling mechanisms is anecdotal or circumstantial”.^[8d] To some extent this is understandable as, until recent years, many glycosylation reactions were heterogeneous, in other words, used an insoluble promoter. Additionally there is the possibility that the transition state for the actual glycosylation step is termolecular bringing together the acceptor alcohol and an activated complex of the donor and promoter. The enzymic formation and/or cleavage of glycosidic bonds, however, has been very thoroughly studied for a number of different enzymes, both by kinetic methods and through the determination of kinetic isotope effects.^[9]

Recently, we discovered a very rapid, direct preparation of β -mannosides,^[10] in which a 4,6-*O*-benzylidene-protected mannosyl sulfoxide is first activated with triflic anhydride to give a covalent α -mannosyl triflate.^[11] This is then displaced by the acceptor to give the β -mannoside with excellent yield and selectivity. In a more recent version, the α -mannosyl triflate is preformed from a mannosyl thioglycoside and the combination of triflic anhydride and 1-benzenesulfinyl piperidine before addition of the acceptor.^[12] This clean, homogeneous coupling reaction, which proceeds without promoter, provides the opportunity to study an actual glycosidic bond-

[*] Prof. Dr. D. Crich, N. S. Chandrasekera
Department of Chemistry
University of Illinois at Chicago
845 West Taylor Street, Chicago, IL 60607-7061 (USA)
Fax: (+1) 312-996-4439
E-mail: dcrich@uic.edu

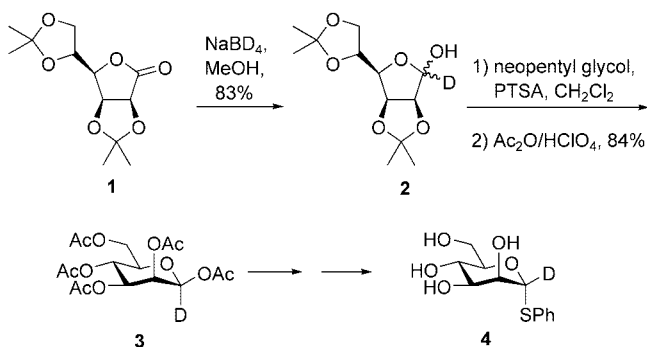
[**] We thank the National Institutes of Health (GM 62160) for support of our work in this area



Supporting information for this article is available on the WWW under <http://www.angewandte.org> or from the author.

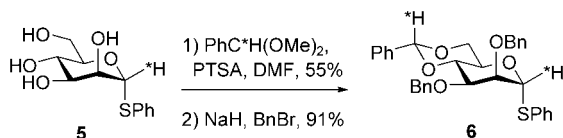
forming reaction with the possibility of differentiating between direct S_N2 displacement and mechanisms involving transient contact ion pairs. We report here on the execution of such a study.

We elected to address the problem by the determination of kinetic isotope effects (KIEs),^[13–15] and, so, synthesized a thiomannoside **4** > 95 % enriched in ²H (D) at C1 by the method outlined in Scheme 1.^[16] Mannoside **4** was then



Scheme 1. Preparation of labeled thioglycoside **4**. PTSA = *p*-toluenesulfonic acid.

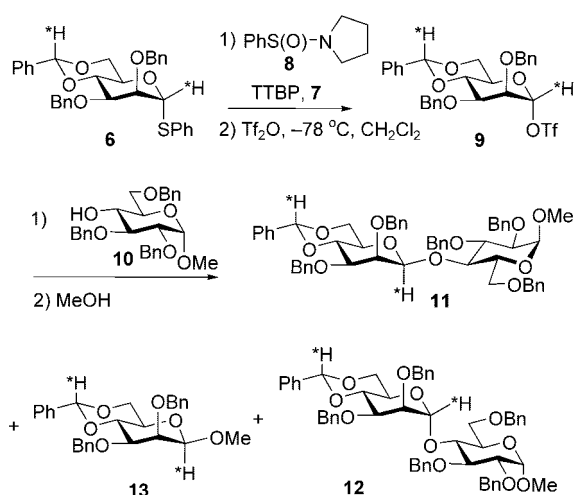
admixed with an equal quantity of the nondeuterated material to give **5**, enriched to approximately 50 %. This substance was converted to the benzylidene acetal by trans-acetalization with benzaldehyde dimethyl acetal, 50 % enriched with deuterium at the acetal position. Standard benzylation then gave donor **6** incorporating approximately 50 % deuterium at the anomeric and, as an internal standard, the benzylidene acetal position (Scheme 2).



Scheme 2. Preparation of doubly labeled donor **6**. Bn = benzyl, *H = proton with approximate enrichment of 50 % in ²H.

Donor **6** and approximately 50 mol % of 4,4,5,5-tetramethyl-2-(1-naphthyl)-1,3-dioxolane (**7**), a convenient internal standard with which to determine conversion, were dissolved in CDCl₃, the ¹H NMR spectrum was recorded, and the singlets corresponding to the benzylidene acetal and anomeric hydrogens were integrated against the signals of **7**.^[17] After removal of the CDCl₃, the mixture was taken up in CH₂Cl₂ and admixed with tri-*tert*-butylpyrimidine (TTBP),^[18] and 140 mol % of **8**.^[19,20] The solution was then cooled to –78 °C and treated with 150 mol % of Tf₂O to give the α-mannosyl triflate **9**. Acceptor **10** (50 mol %) was added^[21] and then 1.5 h later MeOH was added before the reaction mixture was quenched (Scheme 3).

The ¹H NMR spectrum of the reaction mixture revealed the formation of the β-mannoside **11**, whose yield was determined by integration of the corresponding benzylidene



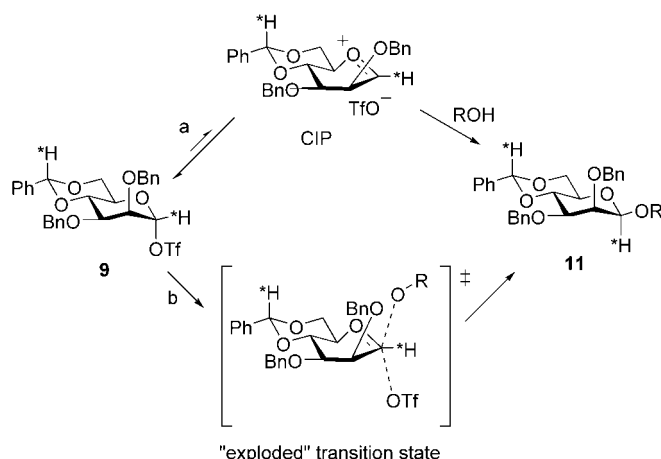
Scheme 3. The kinetic isotope effect experiment. TTBP = 2,4,6-tri-*tert*-butylpyrimidine, Tf₂O = trifluoromethanesulfonic anhydride).

acetal resonance against the internal standard **7**, a trace of the α-mannoside **12**,^[22,23] and the methyl β-mannoside **13**. After separation by preparative HPLC, the ¹H NMR spectrum of **11** was again recorded and the ratio of the benzylidene acetal to anomeric protons determined by careful integration. The complete sequence was repeated three times, giving three independent sets of data.

The data were processed according to Equation (1), for the determination of KIEs from reaction products,^[13,15] wherein *F* is the fractional conversion of the triflate **9** (yield of **11**) and *R*₁₁ and *R*₆ the ratios of the benzylidene and anomeric resonances in the product **11** and the thioglycoside **6**, corresponding to the D/H ratios in **11** and **6**. In this manner the α-deuterium KIE at –78 °C for each of three independent runs was found to be 1.20, 1.21, and 1.16 (or 1.13, 1.13, and 1.10 after conversion to 25 °C)^[24] the assumption being that the conversion of **6** to **9** is quantitative.

$$\text{KIE} = \ln(1-F)/\ln[1-(FR_{11}/R_6)] \quad (1)$$

α-Deuterium KIEs of this magnitude correspond well to those observed in acid-catalyzed hydrolysis of simple methyl glycosides,^[25] and in the hydrolysis of glycosyl fluorides,^[26] leading to the conclusion that the displacement of the triflate from **9** by the typical carbohydrate acceptor **10** to give **11** proceeds with the development of substantial oxacarbenium ion character. This may be interpreted either by a fully dissociative mechanism involving the intermediacy of a transient contact ion pair (CIP) (Scheme 4, path a), or by a functionally equivalent mechanism involving an “exploded” transition state (Scheme 4, path b).^[27] In the CIP mechanism the triflate anion is necessarily closely associated with face of the oxacarbenium ion from which it has just departed and shields that face against attack by the incoming alcohol. In the alternative mechanism there is a loose association of the nucleophile with the anomeric center as the leaving group departs. The minor amount of α-anomer **12** formed in these reactions most likely arises through the intermediacy of a looser, perhaps solvent-separated, ion pair (SSIP), which is in



Scheme 4. The proposed glycosylation mechanism.

equilibrium with an initial CIP. The function of the torsionally disarming^[28] benzylidene group is oppose rehybridization at the anomeric carbon and, so, to shift the complete set of equilibria toward the covalent triflate and away from the SSIP, thereby minimizing α -glycoside formation.^[29] The expected chemical shift of an oxocarbenium ion carbon is $\delta_{\text{C1}} \sim 250$ ppm,^[30] whereas that measured^[11] for the covalent triflate, the only observable species by NMR spectroscopy, is $\delta_{\text{C1}} = 104.5$ ppm. It is apparent, therefore, that the complete set of equilibria between the covalent triflate **9**, the CIP, and SSIP lie very heavily toward **9** in complete agreement with known lifetimes of oxocarbenium ions.^[31,32]

The development of significant oxocarbenium ion character even in the highly stereoselective 4,6-*O*-benzylidene-directed β -mannosylation strongly suggests that other, less selective glycosylation reactions will be similarly dissociative.^[33] The application of the current technique to other glycosylation methods and stereochemical series is currently underway.

Received: January 7, 2004

Revised: August 4, 2004 [Z53688]

Keywords: carbohydrates · glycosylation · isotope effects · reaction mechanisms

[1] R. A. Dwek, T. D. Butters, *Chem. Rev.* **2002**, *102*, 283.

[2] *Comprehensive Natural Products Chemistry*, Vol. 3 (Eds.: D. H. R. Barton, K. Nakanishi, O. Meth-Cohn, B. M. Pinto), Pergamon, Oxford, **1999**.

[3] *Carbohydrates in Chemistry and Biology*, Vol. 1 (Eds.: B. Ernst, G. W. Hart, P. Sinaÿ), Wiley-VCH, Weinheim, **2000**.

[4] In 1994 >700 glycosides were synthesized chemically using hundreds of combinations of donors and promoters: F. Barresi, O. Hindsgaul, *J. Carbohydr. Chem.* **1995**, *14*, 1043.

[5] R. U. Lemieux, K. B. Hendriks, R. V. Stick, K. James, *J. Am. Chem. Soc.* **1975**, *97*, 4056.

[6] For example see: a) B. Capon, *Chem. Rev.* **1969**, *69*, 407; b) A. J. Rhind-Tutt, C. A. Vernon, *J. Chem. Soc.* **1960**, 4637; c) B. Capon, P. M. Collins, A. A. Levy, W. G. Overend, *J. Chem. Soc.* **1964**, 3242; d) L. R. Schroeder, J. W. Green, D. C. Johnson, *J. Chem. Soc. B* **1966**, 447.

[7] a) J. E. Wallace, L. R. Schroeder, *J. Chem. Soc. Perkin Trans. 2* **1977**, 795; b) J. E. Wallace, L. R. Schroeder, *J. Chem. Soc. Perkin Trans. 2* **1976**, 1632.

[8] In contrast there are numerous quantitative and semiquantitative studies on substituent effects on glycosylation rates: a) N. L. Douglas, S. V. Ley, U. Lucking, S. L. Warriner, *J. Chem. Soc. Perkin Trans. 1* **1998**, 51; b) Z. Zhang, I. R. Ollmann, X.-S. Ye, R. Wischnat, T. Baasov, C.-H. Wong, *J. Am. Chem. Soc.* **1999**, *121*, 734; c) C. P. J. Glaudemans, H. G. Fletcher, *J. Am. Chem. Soc.* **1965**, *87*, 4636; d) L. G. Green, S. V. Ley, in *Carbohydrates in Chemistry and Biology*, Vol. 1 (Eds.: B. Ernst, G. W. Hart, P. Sinaÿ), Wiley-VCH, Weinheim, **2000**, p. 427.

[9] a) G. J. Davies, M. L. Sinnott, S. G. Withers in *Comprehensive Biological Catalysis*, Vol. 1 (Ed.: M. L. Sinnott), Academic Press, London, **1998**, p. 119; b) B. W. Murray, V. Wittmann, M. D. Burkart, S.-C. Hung, C.-H. Wong, *Biochemistry* **1997**, *36*, 823; c) Y. Tanaka, W. Tao, J. S. Blanchard, E. J. Hehre, *J. Biol. Chem.* **1994**, *269*, 32306; d) A. M. MacLeod, D. Tull, K. Rupitz, A. J. Warren, S. G. Withers, *Biochemistry* **1996**, *35*, 13165; e) D. L. Zechel, S. G. Withers, *Acc. Chem. Res.* **2000**, *33*, 11.

[10] a) D. Crich, S. Sun, *J. Org. Chem.* **1997**, *62*, 1198; b) D. Crich, S. Sun, *Tetrahedron* **1998**, *54*, 8321; c) D. Crich in *Glycochemistry: Principles, Synthesis, and Applications*, (Eds.: P. G. Wang, C. R. Bertozzi), Marcel Dekker, New York, **2001**, p. 53.

[11] D. Crich, S. Sun, *J. Am. Chem. Soc.* **1997**, *119*, 11217.

[12] D. Crich, M. Smith, *J. Am. Chem. Soc.* **2001**, *123*, 9015.

[13] *Reaction Rates of Isotopic Molecules* (Eds.: L. C. S. Melander, W. H. Saunders), Wiley-Interscience, New York, **1980**.

[14] Displacement of triflate from preformed glycosyl triflates is complete in minutes -78°C ,^[11] ruling out the use of kinetic measurements, at least by the NMR methods used to characterize these intermediates.

[15] On grounds of the amount of substrate needed, the substrate solubility, and the instrument time needed, direct determination of kinetic isotope effects by NMR spectroscopy at natural abundance (as in a) D. A. Singleton, A. A. Thomas, *J. Am. Chem. Soc.* **1995**, *117*, 9357; b) D. A. Singleton, M. J. Szymanski, *J. Am. Chem. Soc.* **1999**, *121*, 9455; c) J. K. Lee, A. D. Bain, P. J. Berti, *J. Am. Chem. Soc.* **2004**, *126*, 3769) was deemed impractical.

[16] The critical feature is the liberation of the deuterated mannose from **2** with neopentyl glycol and PTSA which minimizes isomerization to glucose.

[17] ^2H NMR spectroscopy was investigated but the linewidths and chemical shifts were such that the integration was compromised.

[18] D. Crich, M. Smith, Q. Yao, J. Picione, *Synthesis* **2001**, 323.

[19] Compound **8**, a more soluble version of 1-benzenesulfinyl piperidine,^[12] permits activation at -78°C rather than the -60°C needed for the latter.

[20] An excess of **8** and Ti_2O_3 was employed to ensure complete conversion of **6** to **9**, as verified on the NMR spectrum of the crude reaction mixture following glycosylation, such that any isotope effects observed do not result from the initial activation step.

[21] P. J. Garegg, H. Hultberg, S. Wallin, *Carbohydr. Res.* **1982**, *108*, 97.

[22] The yield of **12** was <5%, ruling out determination of the KIE for its formation, but allowing it to be neglected in the calculation of the KIE of **11**.

[23] Ideally, comparison of the KIEs on the α - and β -products in an unselective coupling would be informative. However, this is very difficult to achieve as the method employed requires baseline resolution of the various anomeric and benzylidene acetal signals. In practice, this has proven to be a limitation with numerous substrates assayed, particularly for unselective reactions when the number of similar signals is multiplied. Second, while the reaction conditions can be manipulated^[10a,b] to give

- predominantly the α -product it is doubtful whether measurements made under such circumstances are relevant as they presumably do not proceed via the intermediate glycosyl triflate.
- [24] Assuming $T(\ln k_H/k_D)$ is constant and no tunnelling occurs.
- [25] a) A. J. Bennet, M. L. Sinnott, *J. Am. Chem. Soc.* **1986**, *108*, 7287; b) D. Indurugalla, A. J. Bennet, *J. Am. Chem. Soc.* **2001**, *123*, 10889; c) A. J. Bennet, M. L. Sinnott, W. S. S. Wijesundera, *J. Chem. Soc. Perkin Trans. 2* **1985**, 1233.
- [26] Y. Zhang, J. Bommuswamy, M. L. Sinnott, *J. Am. Chem. Soc.* **1994**, *116*, 7557.
- [27] The distinction between the two mechanisms is a fine one and cannot be made on the basis of the available data. Exactly analogous problems arise in the study of the hydrolysis of simple glycosides,^[25] in that of glycosyl fluorides,^[26] and in enzymic glycoside hydrolysis and glycosyl transfer.^[9] Comparisons with KIEs determined for enzymic reactions must, however, be treated with caution since the enzyme likely binds the substrate in a nonstandard conformation. For example: G. Sulzenbacher, H. Driguez, B. Henrissat, M. Schulein, G. J. Davies, *Biochemistry* **1996**, *35*, 15280.
- [28] C. W. Andrews, R. Rodebaugh, B. Fraser-Reid, *J. Org. Chem.* **1996**, *61*, 5280.
- [29] Alternative explanations: a) T. Nukada, A. Berces, D. M. Whitfield, *Carbohydr. Res.* **2002**, *337*, 765; b) H. H. Jensen, L. U. Nordstrøm, M. Bols, *J. Am. Chem. Soc.* **2004**, *126*, 9205.
- [30] a) G. A. Olah, D. G. Parker, N. Yoneda, *J. Org. Chem.* **1977**, *42*, 32; b) D. A. Forsyth, V. A. Osterman, J. R. DeMember, *J. Am. Chem. Soc.* **1985**, *107*, 818.
- [31] a) T. L. Amyes, W. P. Jencks, *J. Am. Chem. Soc.* **1989**, *111*, 7888; b) M. N. Namchuk, J. D. McCarter, A. Becalski, T. Andrews, S. G. Withers, *J. Am. Chem. Soc.* **2000**, *122*, 1270; c) J. Zhu, A. J. Bennet, *J. Am. Chem. Soc.* **1998**, *120*, 3887.
- [32] The fact that the covalent α -triflate **9** is so heavily favored argues against the possibility that the effects measured here result from an equilibrium isotope effect. Likewise, the highly stereoselective nature of the coupling argues against the effects measured arising from any significant shift in the equilibrium position as this would necessarily be associated with reduced selectivity.
- [33] On the grounds that the reaction studied is highly stereoselective, and alcohol **10** is a typical carbohydrate the results obtained here may reasonably be considered as representative of this class of reactions. Of course exceptions may exist, particularly with extremely selective cases using highly reactive alcohols, but they are not likely to be representative of the formation of true interglycosidic bonds.

Erythrina Alkaloids

A Highly Efficient Synthesis of the Erythrina and B-Homoerythrina Skeleton by an AlMe₃-Mediated Domino Reaction**

Serry A. A. El Bialy, Holger Braun, and Lutz F. Tietze*

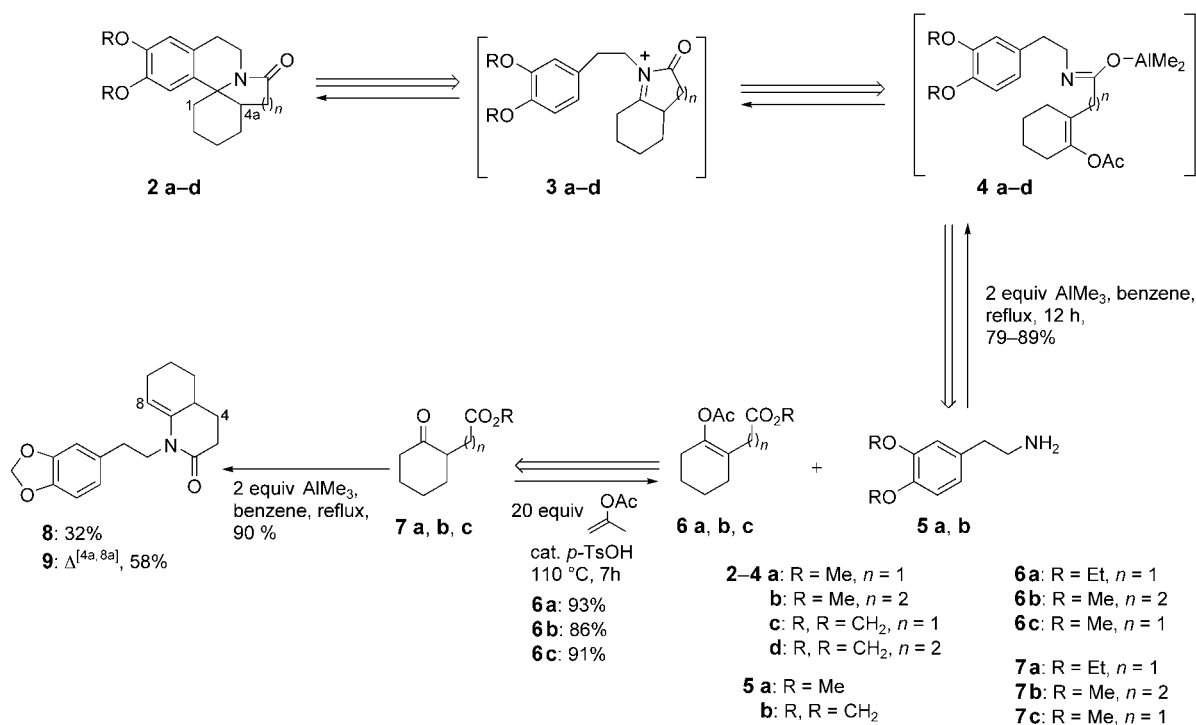
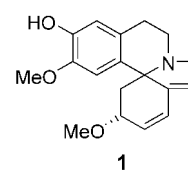
Dedicated to Professor Armin de Meijere
on the occasion of his 65th birthday

The development of efficient and environmentally acceptable synthetic methods is an important task of modern chemistry. In this context the domino concept has proved to be very successful.^[1] In domino reactions bonds and new functionalities are constructed, which, in turn, react further in subsequent steps under identical conditions to form new bonds and functionalities. The larger the number of bonds formed and the higher the complexity of the product is the greater is the quality of a domino reaction. A plethora of two-step domino reactions have been reported, but three-step transformations are the exception. Here we describe a novel

domino reaction for the construction of three bonds in sequential steps that allows efficient access to the skeleton of the erythrina and B-homoerythrina alkaloids.

The erythrina alkaloids^[2] such as erysodine (**1**) are a widespread, structurally interesting class of natural products with extensive biological activity.^[3] Many compounds of this family exhibit curare-like activity as well as hypotensive, sedative, and CNS depressant properties.^[4]

The retrosynthesis of the skeleton of the erythrina and B-homoerythrina alkaloids **2a** and **2b** within the context of the domino concept leads to the amine **5a** and the cyclohexene derivatives **6a** and **6b** via the *N*-acyliminium ions **3a** and **3b** and the metalated amides **4a** and **4b** (Scheme 1). The intermediate *N*-acyliminium ions **3** could be formed by an intramolecular addition of an aluminum complex of the primary carboxamide^[5] to the enol acetate moiety in **4** with subsequent elimination of acetic acid. The aluminum complex might be accessible in situ by reaction of the primary amine **5** with the ester function of the enol acetate **6**.



Scheme 1. Retrosynthesis and synthesis of the erythrina and B-homoerythrina skeleton **2** as well as the enamines **8** and **9**.

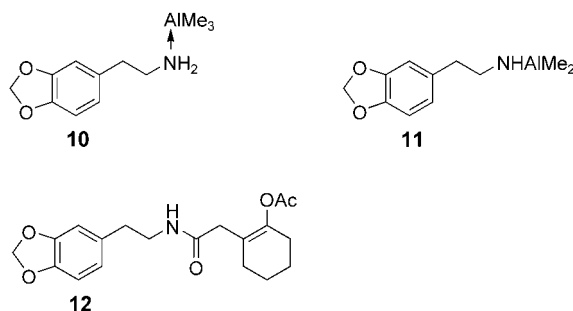
[*] Dr. S. A. A. El Bialy, Dipl.-Chem. H. Braun, Prof. Dr. L. F. Tietze
Institut für Organische und Biomolekulare Chemie
Georg-August-Universität Göttingen
Tammannstrasse 2, 37077 Göttingen (Germany)
Fax: (+49) 551-399-476
E-mail: ltietze@gwdg.de

[**] This work was supported by the Deutsche Forschungsgemeinschaft (SFB 416) and the Fonds der Chemischen Industrie. S.A.A.E.B. thanks the Alexander von Humboldt-Stiftung for a research stipendium.

The enol acetates **6a** and **6b** were readily obtained in 86 and 93% yield, respectively, by reaction of the known ketones^[6] **7a** and **7b** with isoprenyl acetate in the presence of a catalytic amount of *p*-toluenesulfonic acid. For the synthesis of **2a** and **2c**, the amines **5a** and **5b**, respectively, were each treated with trimethylaluminum in benzene, stirred for one hour at 20 °C, and after the addition of **6a** heated under reflux for five hours.^[7] After workup **2a**^[8] and **2c** were isolated in 79 and 82% yield, respectively. In an analogous

manner the homoerythrina alkaloids **2b**^[9] and **2d** were obtained in 89% and 85% yield, respectively, by the reaction of **5a** and **5b** with **6b** in the presence of trimethylaluminum. In the reaction of the keto esters **7a** and **7b** with the amines **5a** and **5b** and trimethylaluminum, no cyclization to the erythrina and homoerythrina skeleton occurred, but instead as in the transformation of **5b** and **7b**, the enamines **8** and **9** were obtained in 32 and 58% yield, respectively.

On-line NMR investigations during the reaction of a mixture of **5b**, **6c**, and AlMe_3 show that at 20°C the Lewis acid/Lewis base complex **10** is formed from **5b** with AlMe_3 (Scheme 2); the ester function of **6c** is not attacked. In



Scheme 2. Addition complexes **10** and **11** of the amine **5a** with trimethylaluminum and the carboxamide **12**.

contrast, in the reaction of **6c** with AlMe_3 without the addition of the amine **5b** a transformation of the ester function of **6c** is observed even at 20°C. Heating the mixture of **5b**, **6c**, and AlMe_3 to 70°C leads to the formation of **11** together with the evolution of methane (Scheme 2), **11** then reacts rapidly with the ester group of **6c**. Among the products isolated on working up the reaction mixture after one hour is the carboxamide **12** (Scheme 2), which, however, on reaction with AlMe_3 does not lead to the desired product. Thus, we conclude that in the domino reaction the free carboxamide **12** is not generated but rather a metalated species (e.g. **4**), which, however, is not formed by the reaction of **12** with AlMe_3 .

The formation of the iminium ion **3** from **4** also appears to be a very fast reaction. Thus, in the ^1H NMR spectrum of the reaction mixture a singlet at $\delta = 1.13$ ppm, which can be assigned to a R_2AlOAc group, is found after just a few minutes in place of the signal at $\delta = 1.76$ ppm for the CH_3 moiety of the enol acetate group of **6c**. The rate-determining step of the domino process is probably the electrophilic substitution of the arene by the iminium ion **3**.

The domino reaction presented here in which three sequential bonds are formed in one reaction process allows the efficient construction of the erythrina and B-homoerythrina alkaloid skeleton in good yields. The required substrates are readily accessible and may be varied in many ways. This method should therefore be of interest in drug research.

Received: April 9, 2004

Keywords: alkaloids · amides · domino reactions · iminium ions · Lewis acids

- [1] a) L. F. Tietze, U. Beifuss, *Angew. Chem.* **1993**, *105*, 134–170; *Angew. Chem. Int. Ed. Engl.* **1993**, *32*, 131–132; b) L. F. Tietze, *Chem. Rev.* **1996**, *96*, 115–136; c) L. F. Tietze, A. Modi, *Med. Chem. Res.* **2000**, *20*, 301–322; d) L. F. Tietze, F. Haunert in *Stimulating Concepts in Chemistry* (Eds.: M. Shibasaki, J. F. Stoddart, F. Vögtle), Wiley-VCH, Weinheim, **2000**, p. 39–64; e) H. Waldmann in *Organic Synthesis Highlights II* (Ed.: H. Waldmann), Wiley-VCH, Weinheim, **1995**, p. 193–202; f) G. Poli, G. Giambastiani, A. Heumann, *Tetrahedron* **2000**, *56*, 5959–5989.
- [2] a) A. Mondon, *Tetrahedron* **1963**, *19*, 911–917; b) A. Mondon, *Tetrahedron* **1964**, *20*, 1729–1736; c) A. Mondon, K. F. Hansen, *Tetrahedron Lett.* **1960**, 5–8; d) A. Mondon, H. Nestler, *Angew. Chem.* **1964**, *76*, 651–652; *Angew. Chem. Int. Ed. Engl.* **1964**, *3*, 588–589; e) T. Sano, J. Toda, N. Kashiwaba, T. Oshima, Y. Tsuda, *Chem. Pharm. Bull.* **1987**, *35*, 479–500; f) R. Ahmad-Schofiel, P. S. Mariano, *J. Org. Chem.* **1987**, *52*, 1478–1482; g) H. Ishibashi, T. Sato, M. Takahashi, M. Hayashi, M. Ikeda, *Heterocycles* **1988**, *27*, 2787–2790; h) B. Belleau, *Can. J. Chem.* **1957**, *35*, 651–662; i) V. Prelog, A. Langemann, O. Rodig, M. Ternmah, *Helv. Chim. Acta* **1959**, *42*, 1301–1310; j) S. Sugawara, H. Yoshikawa, *Chem. Pharm. Bull.* **1960**, *8*, 290–293; k) M. Müller, T. T. Grossnickle, V. Boekelheide, *J. Am. Chem. Soc.* **1959**, *81*, 3959–3963; l) Y. Tsuda, T. Sano, *Studies in Natural Products Chemistry, Vol. 3* (Ed.: A.-U. Rahman), Elsevier, Amsterdam, **1989**, p. 455–493; m) G. Stork, A. Brizzolara, H. Landesman, J. Szmuszkovicz, R. J. Terrell, *J. Am. Chem. Soc.* **1963**, *85*, 207–222; n) M. E. Kuehne, W. G. Bornmann, W. H. Parsons, T. D. Spitzer, J. F. Blount, J. Zubieta, *J. Org. Chem.* **1988**, *53*, 3439–3450.
- [3] a) A. S. Chawla, V. K. Kapoor in *Handbook of Plant and Fungal Toxicants* (Ed.: J. F. D'Mello), CRC, London, **1997**, 37–49; b) D. S. Bhakuni, *J. Indian Chem. Soc.* **2002**, *79*, 203–210.
- [4] a) V. Boekelheide in *Alkaloids, Vol. 7* (Ed.: R. H. F. Manske), Academic Press, New York, **1960**, p. 201–227; b) R. K. Hill in *Alkaloids, Vol. 9* (Ed.: R. H. F. Manske), Academic Press, New York, **1967**, p. 483–515; c) S. F. Dyke, S. N. Quessy in *The Alkaloids, Vol. 18* (Ed.: R. G. A. Rodrigo), Academic Press, New York, **1981**, p. 1–98; d) A. H. Jackson in *Chemistry and Biology of Isoquinoline Alkaloids* (Eds.: J. D. Phillipson, M. F. Margaret, M. H. Zenk), Springer, Berlin, **1985**, p. 62–78; e) A. S. Chawla, A. H. Jackson, *Nat. Prod. Rep.* **1984**, *1*, 371–373; f) A. S. Chawla, A. H. Jackson, *Nat. Prod. Rep.* **1986**, *3*, 355–364; g) K. W. Bentley, *Nat. Prod. Rep.* **1991**, *8*, 339–366; h) K. W. Bentley, *Nat. Prod. Rep.*, **1992**, *9*, 365–391; i) K. W. Bentley, *Nat. Prod. Rep.* **1993**, *10*, 449–470; j) K. W. Bentley, *Nat. Prod. Rep.* **1994**, *11*, 555–576; k) K. W. Bentley, *Nat. Prod. Rep.* **1995**, *12*, 419–441; l) M. Williams, J. Robinson, *J. Neurosci.* **1984**, *4*, 2906–2911; m) M. W. Decker, D. J. Anderson, J. D. Brioni, D. L. Donnelly, C. H. Roberts, A. B. Kang, M. O'Neill, S. Piattoni-Kaplan, Swanson, J. P. Sullivan, *Eur. J. Pharmacol.* **1995**, *280*, 79–89.
- [5] a) L. F. Tietze, P. L. Steck, *Eur. J. Org. Chem.* **2001**, *22*, 4353–4356; b) A. Basha, S. M. Weinreb, *Tetrahedron Lett.* **1977**, 1465–1468.
- [6] G. Stork, A. Brizzolara, H. Landesman, J. Szmuszkovicz, R. J. Terrell, *J. Am. Chem. Soc.* **1963**, *85*, 207–222.
- [7] General method for the AlMe_3 -mediated domino reaction: One equivalent of a 0.14 M solution of amine **5** in benzene was treated with two equivalents of a 1.36 M AlMe_3 solution in benzene at 0°C and stirred for 1 h at room temperature. After the addition of one equivalent of a 0.14 M solution of the enol acetate **6** in benzene, the mixture was heated at 80°C for 5 h in a pre-heated oil bath. At 0°C 2 N HCl (5 mL mmol⁻¹) was then added and the mixture was stirred for 30 min at this temperature. After phase separation, the aqueous phase was extracted four times with ethyl acetate (10 mL mmol⁻¹), the combined extracts were dried over Na_2SO_4 , and the solvent was removed in vacuum. The crude product was

purified by column chromatography on silica (petroleum ether/ethyl acetate = 1:1).

- [8] **2a**: ^1H NMR (200 MHz, CDCl_3 , TMS): δ = 6.83 (s, 1 H; 13-H), 6.54 (s, 1 H; 10-H), 4.11 (ddd, J = 13.2, 7.0, 3.2 Hz, 1 H; 8- H_{eq}), 3.83 (s, 3 H; OMe at C-12), 3.77 (s, 3 H; OMe at C-11), 3.18 (ddd, 1 H; J = 13.2, 9.8, 5.2 Hz, 8- H_{ax}), 2.93 (ddd, 1 H; J = 16.4, 9.8, 7.0 Hz, 9- H_{eq}), 2.63 (ddd, 1 H; J = 16.4, 5.2, 3.2 Hz, 9- H_{ax}), 2.60–2.52 (m, 1 H; 4a-H), 2.36 (s, 1 H; 5- H_a), 2.33 (d, 1 H; J = 1.2 Hz, 5- H_b), 2.16–1.92 (m, 1 H; 1- H_a), 1.93–1.80 (m, 2 H; 4- H_2), 1.80–1.71 (m, 1 H; 1- H_b), 1.74–1.60 (m, 2 H; 2-H), 1.60–1.48 ppm (m, 2 H; 3-H); ^{13}C NMR (75 MHz, CDCl_3 , TMS): δ = 174.9 (C-6), 147.6 (C-12), 147.1 (C-11), 134.7 (C-13a), 125.6 (C-9a), 111.7 (C-10), 108.0 (C-13), 62.09 (C-13b), 55.99 (OMe at C-11), 55.67 (OMe at C-12), 37.51 (C4a), 36.46 (C-8), 35.74 (C-5), 34.67 (C-4), 27.02 (C-1, C-9), 20.63 (C-2), 20.20 ppm (C-3).
- [9] **2b**: ^1H NMR (200 MHz, CDCl_3 , TMS): δ = 6.70 (s, 1 H; 14-H), 6.58 (s, 1 H; 11-H), 4.79 (m, 1 H; 9- H_a), 3.96 (s, 3 H; OMe at C-12), 3.87 (s, 3 H; OMe at C-13), 3.35–3.08 (m, 2 H; 9- H_b , 10- H_a), 2.78–2.42 (m, 3 H; 4a-H, 6-H, 10- H_b), 2.38–2.20 (m, 2 H; 5-H), 1.98–1.72 (m, 3 H; 1-H, 2- H_a), 1.71–1.42 ppm (m, 6 H; 6-H, 4-H, 2- H_b , 3-H); ^{13}C NMR (75 MHz, CDCl_3 , TMS): δ = 172.16 (C-7), 147.4 (C-12), 146.9 (C-13), 135.4 (C-14a), 126.84 (C-10a), 112.2 (C-14), 105.9 (C-11), 61.27 (C-14b), 55.96 (OMe at C-12), 55.43 (OMe at C-13), 40.47 (C-6), 35.75 (C-4a), 34.91 (C-9), 28.38 (C-5), 26.62 (C-10), 25.77 (C-4), 25.56 (C-1), 22.19 (C-2), 21.35 ppm (C-3).

Nanostructures

Single Quantum Dots in Spherical Silica Particles**

Thomas Nann* and Paul Mulvaney

In 1993 Murray et al.^[1] developed a route to highly luminescent CdSe quantum dots (QDs) through the use of hot, coordinating solvents. The route was subsequently modified by Hines et al. in 1996 who prepared highly luminescent CdSe/ZnS core-shell particles.^[2] There has since been tremendous focus on QD surface chemistry^[3–5] and the potential applications of these exotic materials in areas such as tunable LEDs,^[6,7] QD lasers,^[8] luminescent glasses,^[9] and biolabeling.^[10–13] A fundamental drawback is that the particles

generally remain both highly luminescent and photostable only in nonpolar media, in which both ligand desorption and lattice dissolution can be neglected. Transfer of these luminescent materials into water is a prerequisite, particularly for biological applications. Several phase-transfer protocols have been proposed and tested which rely on the adsorption of water-soluble ligands that can displace the native hydrophobic ligands. These transfer agents include sulfanylalkanoic acids^[11] polymeric silanes,^[10] and polymeric coatings such as polyethylene glycol (PEG) and polyacrylic acid derivatives.^[14] These passivation layers afford materials which remain stable for weeks and sometimes months, but the photostability of the QDs is drastically reduced in oxygenated aqueous solutions. Oxygen acts as a photoelectron scavenger, and catalyzes photoanodic dissolution of chalcogenide semiconductor particles in water. In principle, ZnS or ZnSe^[15] shells should effectively inhibit photocorrosion, but this photostability is difficult to achieve routinely because of charge-carrier tunneling into the shell or inhomogeneity of the deposited shell layer.

An alternative process is to deposit other layers capable of impeding electron, proton, and oxygen diffusion to the QD surface. One such material is amorphous silica. A silica shell should also minimize fluorescence quenching by surface adsorbates or redox-active molecules.^[16] Consequently, such surface-coated particles could have widespread uses in optical and optoelectronic applications where photostability is critical for device longevity. Furthermore such surfaces are biocompatible and can be easily functionalized for bioconjugation purposes. Although the potential advantages of silica coating have been described for metal and semiconductor nanoparticles,^[17–20] the only existing routes rely on the core nanocrystals already being in a polar environment such as ethanol or water. The organically capped QDs are usually degraded in these polar media before coating can be effected.^[12,18] Consequently, a method is needed for encapsulating nanocrystals of luminescent semiconductors (or other materials) that are only soluble in nonpolar media.

Herein, we describe a straightforward approach for the preparation of photostable, highly luminescent, water-soluble core-shell CdSe/ZnS/SiO₂ nanocrystals starting from nanocrystals capped with trioctylphosphine oxide (TOPO). Rogach et al. have described “raisin-bun”-type particles in which a silica particle is impregnated with a large number of nanocrystals.^[21] However, these agglomerates do not maintain the spectral purity of a coated single quantum dot, nor has their photostability been demonstrated. For photonic crystal applications, it is useful to be able to prepare single QDs within a silica shell of tunable thickness—the preparation of such materials is described herein.

Quantum dots are usually coated with a chemisorbed monolayer of surfactant such as TOPO or hexadecylamine (HDA). Thus, they form stable colloids in solvents with low polarity. The growth of a silica shell is usually carried out by using the Stöber process^[22] by addition of tetraethoxysilane (TEOS) to colloiddally stable “seed” particles in an EtOH/H₂O/NH₃ mixture. The surface of the QDs, therefore, has to be exchanged for more polar ligands to enable transfer into ethanol. A second requirement for the surface is to provide nucleation sites for the controlled growth of a homogeneous

[*] Priv.-Doz. Dr. T. Nann
Freiburg Materials Research Center (FMF)
Albert-Ludwig University Freiburg
Stefan-Meier-Strasse 21, 79104 Freiburg (Germany)
Fax: (+49) 761-203-4768
E-mail: thomas.nann@fmf.uni-freiburg.de
Prof. Dr. P. Mulvaney
School of Chemistry
University of Melbourne
Parkville, Victoria, 3010, Australia

[**] This work was supported by the Erwin-Riesch foundation. The authors acknowledge the help of Daniel E. Gómez, who carried out the confocal laser scanning experiments, as well as of Dougal McCulloch, who performed the HRTEM measurements.

Supporting information for this article is available on the WWW under <http://www.angewandte.org> or from the author.

silica coating. Such nucleation sites include (3-sulfanylpropyl)trimethoxysilane (MPS) or (3-aminopropyl)trimethoxysilane (APS)^[16,19] as well as the polymer poly(vinylpyrrolidone) (PVP).^[23]

It has been shown previously that a gradual hydrophilic–hydrophobic phase transfer can be realized by exchanging the ligands on the QD surface with MPS in THF.^[13] The MPS-coated QDs form stable colloids in methanol and ethanol in the absence of water. Therefore, the QDs were dispersed in THF containing a twofold molar excess of MPS relative to the estimated number of Zn atoms on the surface of the nanocrystal. Less MPS was found to lead to coagulation of the QDs in the reaction mixture, while an excess of MPS promoted additional nucleation of the silica particles.

APS and PVP were also investigated as surface stabilizers. In the case of APS, it was found that clusters of 10–20 QDs were coated with silica. This effect probably occurs because of polymerization of APS, which causes a competition between cross-linking of the QDs and deposition of silica. van Blaaderen and co-workers have successfully used PVP to stabilize gold particles for silica coating in ethanol and were able to remove excess PVP by centrifugation of the much denser gold particles. We found it extremely difficult to separate excess PVP from the PVP-coated QDs, and the free PVP acted as nucleation sites for silica polymerization. Consequently, the results presented here pertain to MPS-capped CdSe/ZnS QDs.

There are four primary variables governing the silica coating of the MPS capped QDs: these are [QD], [NH₃], [TEOS], and [H₂O]. The effects of water and ammonia on the hydrolysis of TEOS are complex [Eq. (1)]. Water catalyzes the hydrolysis and, therefore, increases the nucleation rate of silica particles. A lower water content reduces supersaturation and favors the growth of the QD seed particles over nucleation of fresh silica. However, the silica-coated QDs that form need to be colloidally stable. This is favored by solvents with higher dielectric constants (such as water), which favor ionization of silanol groups through Equation (2) and enhance electrostatic repulsion between particles. The water content in the reaction mixture was gradually increased from 0.7 to 12.5 M. It was observed that the amount of spontaneous nucleation increased and the size of the resulting silica particles decreased as the water content increased. Ammonia is also a catalyst for TEOS hydrolysis; however, the rate of spontaneous nucleation was found to increase as the ammonia concentration was lowered from 0.7 to 0.07 M. On the basis of these results, the initial silica shell was grown in the presence of 1.0 M water and 0.7 M ammonia in ethanol.



The amount of initially added TEOS was found to be important, irrespective of the composition of the EtOH/H₂O/NH₃ mixture: If the TEOS concentration was too high, larger silica particles with multiple QDs were synthesized (analogous to “raisin buns”), while if the TEOS concentration was too low, the QDs did not form a silica shell, but were cross-

linked to form bigger networks. The optimal amount of TEOS corresponded to a silica shell with a thickness of about 15 nm. Thicker silica shells could be grown by subsequent addition of more TEOS (as discussed below).

The goal of this project was to find conditions in which each silica particle contained exactly one QD; additionally, a minimal concentration of free silica should be present. When silica particles were prepared under the above “standard” conditions (without QDs), particles with an average diameter of 28 nm and 14% polydispersity were obtained (see the Supporting Information). It was found that these conditions were only met within a certain range of QD concentrations. Spontaneous nucleation of small silica particles (about 28 nm) was observed at QD concentrations below 50 nM, while multiple QDs per silica particle were found at concentrations above 200 nM. The size of the silica particles was concentration-dependent at concentrations of QDs between 50 and 200 nM, which is consistent with the QDs being the primary nuclei for silica growth.

Figure 1 displays the effect of QD concentration on particle size, as determined by low-resolution TEM analysis. The size of the silica particles increases with decreasing QD concentration. The expected silica size can be easily calcu-

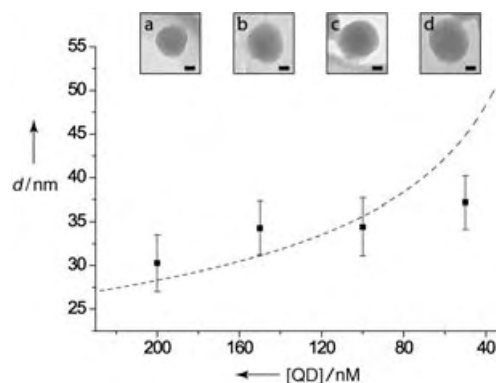


Figure 1. Diameter of silica spheres versus QD concentration. Dotted line: Theoretically calculated values. Insets a)–d): Low-resolution TEM images of silica nanospheres obtained with decreasing concentrations of QDs: 200 nM, 150 nM, 100 nM, 50 nM. Scalebars: 10 nm; Error bars: standard deviation of the diameter based on at least 30 particles.

lated from the concentration of QDs and the amount of added TEOS, when one QD per silica is assumed. The diameter d of the particles can be calculated according to Equation (3), where V_{tot} represents the total volume of one particle: $V_{\text{tot}} = V_{\text{SiO}_2} + V_{\text{QD}}$ corresponds to the volume of the added silica per particle V_{SiO_2} and the volume of one QD V_{QD} . The amount of silica per particle can be calculated by $V_{\text{SiO}_2} = n(\text{TEOS}) / (N_{\text{QD}} c)$, where $n(\text{TEOS})$ is the amount of added TEOS (in mols), N_{QD} is the number of QDs, and c is the molar density of silica in mol L^{-1} . The dotted line in Figure 1 represents the calculated values. Furthermore, it was found that the monodispersity of the QD-containing silica particles decreases to a mean value of approximately 9%, relative to the silica particles without QDs.

$$d = 2r = 2^3 \sqrt{\frac{3}{4\pi} V_{\text{tot}}} \quad (3)$$

Figure 2 shows high-resolution TEM (HRTEM) micrographs of single QDs encapsulated in silica. The size of the particles is approximately 30 nm and the great majority contain single QDs at the center. It was sometimes difficult to distinguish the QDs because of the orientation of the QDs on the copper grid. Figure 2B) shows such a sample (the QDs are highlighted with arrows). Some silica particles contained two QDs, as shown in Figure 2C. When there are two QDs they are always clearly separate, thus indicating that each has

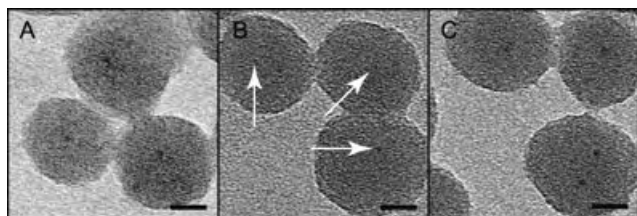


Figure 2. HRTEM images of single QDs encapsulated within a silica shell. A) QD/SiO₂ spheres of approximately 30 nm diameter. B) QDs are misarranged with respect to the electron beam. The arrows indicate the positions of the QDs. C) SiO₂ sphere with two QDs incorporated (lower right). Scalebars: 10 nm.

seeded a silica shell, and that coalescence occurs after initial silica deposition. The purity of the final core-shell system is limited at present by coagulation of the QDs during the early stages of growth, when the electrostatic stabilization is poor.

The thickness of the silica shell and the overall size of the silica particles could be increased by a second stage of seeded growth (see ref. [24]). Small amounts of TEOS and water were successively added to the initially prepared silica-coated QDs. The final size of the particles was calculated from the amount of TEOS and the size and concentration of the seed particles. A suspension of QD/SiO₂ seed particles in ethanol and ammonia was grown by successive addition of TEOS and water every 12 h. The average diameters of the resultant particles were determined by TEM and compared to the theoretical expectations deduced from Equation (3). Figure 3 shows the results of these experiments. A good agreement between the expected and the measured particle sizes can be seen. The amount of TEOS and water was kept constant during all additions. In further experiments, the TEOS and water concentrations were increased with every addition to increase the growth speed: first in proportion to the increasing surface of the particles and second to obtain a linear increase in shell thickness. Both variations were successful (see the Supporting Information). Figure 4 shows a TEM image of silica particles grown on QDs containing seeds. The QDs cannot be seen in the micrographs because of the thickness of the surrounding silica.

Monitoring the luminescence accurately during growth is difficult because of the low concentrations used during shell growth and the steady increase in background scatter as the shell grows. To prove that the embedded QDs are still luminescent, single-particle spectra were recorded by confocal microscopy. Figure 5 shows the photoluminescence spectra a) of the colloidal QDs in chloroform and b) of a single QD within a silica particle of approximately 74-nm

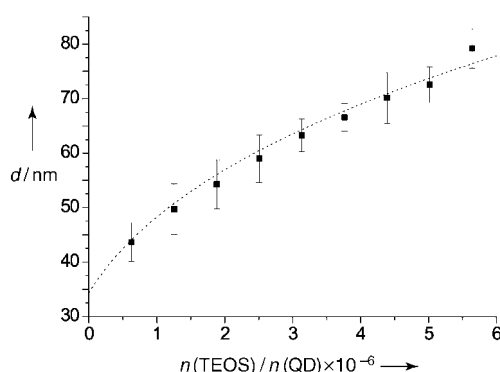


Figure 3. Growth diagram of QD/silica nanoparticles. Squares: diameter after addition of TEOS and water (the same amount at every addition). Dotted line: calculated diameter versus amount of added TEOS.

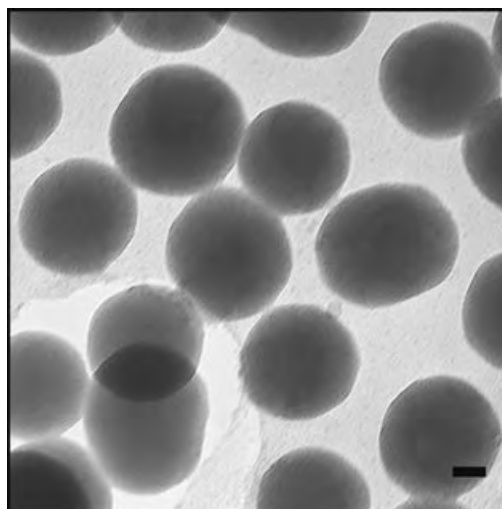


Figure 4. Silica particles grown on seed particles according to Figure 2. Scalebar: 20 nm.

diameter. The photoluminescence was generated with an Ar ion laser (488 nm) through an objective with NA 1.4. The emission was collected with the same objective, dispersed with a 0.55-m (focal length) imaging spectrograph (JY, TRIAX 550, 0.09-nm resolution) and detected with a liquid-nitrogen-cooled CCD camera. No significant change in the photoluminescence spectrum was observed after encapsulation of the silica.

In summary, we have presented a novel method to coat single luminescent QDs with silica shells. The diameter of the final silica particles can be tuned from approximately 30 nm to 1 μ m by means of seeded growth. The method is robust and can be easily adapted to other alcohols such as 2-propanol. Single QDs in silica spheres enable many fundamental measurements to be performed (for example, Mie modes with single QDs) as well as promising new applications (for example, active photonic crystals assembled from these particles). Results on the photostability and luminescence of the embedded QDs will be presented elsewhere.

Received: May 24, 2004

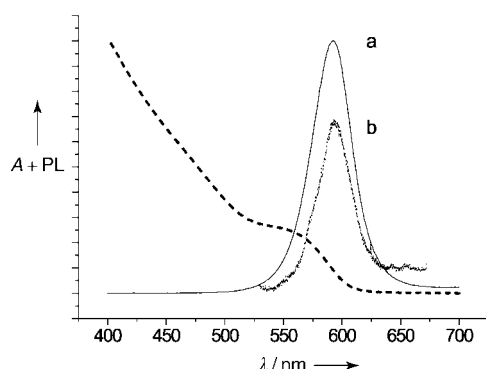


Figure 5. a) Photoluminescence (PL) spectrum of QDs in chloroform. b) Spectrum of a single QD in a silica sphere of approximately 74 nm diameter taken by means of scanning confocal microscopy. Dotted line: absorbance spectrum of QDs in chloroform.

Keywords: luminescence · nanostructures · quantum dots · silica · synthetic methods

- [21] A. L. Rogach, D. Nagesha, J. W. Ostrander, M. Giersig, N. A. Kotov, *Chem. Mater.* **2000**, *12*, 2676–2685.
- [22] W. Stöber, A. Fink, E. Bohn, *J. Colloid Interface Sci.* **1968**, *26*, 62–69.
- [23] C. Graf, D. L. J. Vossen, A. Imhof, A. van Blaaderen, *Langmuir* **2003**, *19*, 6693–6700.
- [24] G. H. Bogush, M. A. Tracy, C. F. Zukoski IV, *J. Non-Cryst. Solids* **1988**, *104*, 95–106.
- [25] E. Kucur, J. Riegler, G. A. Urban, T. Nann, *J. Chem. Phys.* **2004**, *120*, 1500–1505.
- [26] W. Yu, L. Qu, W. Guo, X. Peng, *Chem. Mater.* **2003**, *15*, 2854–2860.
- [27] L. M. Liz-Marzán, M. Giersig, P. Mulvaney, *Langmuir* **1996**, *12*, 4329–4335.

- [1] C. B. Murray, D. J. Norris, M. G. Bawendi, *J. Am. Chem. Soc.* **1993**, *115*, 8706–8715.
- [2] M. A. Hines, P. Guyot-Sionnest, *J. Phys. Chem.* **1996**, *100*, 468–471.
- [3] D. V. Talapin, A. L. Rogach, A. Kornowski, M. Haase, H. Weller, *Nano Lett.* **2001**, *1*, 207–211.
- [4] M. Gao, S. Kirstein, H. Möhwald, A. L. Rogach, A. Kornowski, A. Eychmüller, H. Weller, *J. Phys. Chem. B* **1998**, *102*, 8360–8363.
- [5] A. Eychmüller, A. L. Rogach, *Pure Appl. Chem.* **2000**, *72*, 179–188.
- [6] X. Peng, M. C. Schlamp, A. V. Kadavanich, A. P. Alivisatos, *J. Am. Chem. Soc.* **1997**, *119*, 7019–7029.
- [7] J. Lee, V. Sundar, J. R. Heine, M. G. Bawendi, K. F. Jensen, *Adv. Mater.* **2000**, *12*, 1102–1105.
- [8] V. I. Klimov, A. A. Mikhailovsky, S. Xu, A. Malko, J. A. Hollingsworth, C. A. Leatherdale, H.-J. Eisler, M. G. Bawendi, *Science* **2000**, *290*, 314–317.
- [9] S. T. Selvan, C. Bullen, M. Ashokkumar, P. Mulvaney, *Adv. Mater.* **2001**, *13*, 985–988.
- [10] M. J. Bruchez, M. Moronne, P. Gin, S. Weiss, A. P. Alivisatos, *Science* **1998**, *281*, 2013–2016.
- [11] W. C. W. Chan, S. Nie, *Science* **1998**, *281*, 2016–2018.
- [12] H. Mattoussi, J. M. Mauro, E. R. Goldman, G. P. Anderson, V. C. Sundar, F. V. Mikulec, M. G. Bawendi, *J. Am. Chem. Soc.* **2000**, *122*, 12142–12150.
- [13] J. Riegler, P. Nick, U. Kielmann, T. Nann, *J. Nanosci. Nanotechnol.* **2003**, *3*, 380–385.
- [14] E. W. Adams, M. P. Bruchez Jr. US-A 6649138, **2003**.
- [15] P. Reiss, J. Bleuse, A. Pron, *Nano Lett.* **2002**, *2*, 781–784.
- [16] P. Mulvaney, L. M. Liz-Marzán, M. Giersig, T. Ung, *J. Mater. Chem.* **2000**, *10*, 1259–1270.
- [17] D. Gerion, F. Pinaud, S. C. Williams, W. J. Parak, D. Zanchet, S. Weiss, A. P. Alivisatos, *J. Phys. Chem.* **2001**, *105*, 8861–8871.
- [18] Several routes have been proposed (for example, M. G. Bawendi, F. V. Mikulec, J.-K. Lee US-A 6319426, **2001**), but slow ligand desorption in water limits their lifetime, and they remain photochemically unstable.
- [19] L. M. Liz-Marzán, M. Giersig, P. Mulvaney, *Langmuir* **1996**, *12*, 4329–4335.
- [20] M. A. Correa-Duarte, M. Giersig, L. M. Liz-Marzán, *Chem. Phys. Lett.* **1998**, *286*, 497–501.

Metal–Nucleobase Complexes

**Metal-Mediated Deamination of Cytosine:
Experiment and DFT Calculations****

Judit E. Šponer, Pablo J. Sanz Miguel, Luis Rodríguez-Santiago, Andrea Erxleben, Michael Krumm, Mariona Sodupe,* Jirí Šponer, and Bernhard Lippert**

Deamination of cytosine to give uracil represents a major source of DNA damage in eukaryotic cells.^[1] While uracil, the deamination product of cytosine, is rapidly excised from

[*] Dr. J. E. Šponer, Dr. J. Šponer
Institute of Biophysics
Academy of Sciences of the Czech Republic
Královopolská 135, 61265 Brno (Czech Republic)
Fax: (+420) 541-211-293
E-mail: judit@ncbr.chemi.muni.cz

Dr. L. Rodríguez-Santiago, Dr. M. Sodupe
Departament de Química
Universitat Autònoma de Barcelona
Bellaterra 08193 (Spain)
Fax: (+34) 93-581-2920
E-mail: mariona@klingon.uab.es

Dipl.-Chem. P. J. Sanz Miguel, Priv.-Doz. Dr. A. Erxleben,
Dr. M. Krumm, Prof. B. Lippert
Fachbereich Chemie
Universität Dortmund
44221 Dortmund (Germany)
Fax: (+49) 231-755-3797
E-mail: bernhard.lippert@uni-dortmund.de

[**] This work was supported through grants from MCYT and FEDER (project BQU 2202-04112-C02-01), DURSI (project 2001 SGR-00182), the CESCA-CEPBA mobility program (LN00A016, MSMT ČR), the Volkswagen Stiftung (grant I/74657), the Deutsche Forschungsgemeinschaft, and the Fonds der Chemischen Industrie. The use of the computational facilities of the Catalonia Supercomputer Center (CESCA) for J.E.Š., J.Š., M.S., and L.R.S. as well as a Wellcome Trust International Senior Research Fellowship in Biomedical Science in Central Europe to J.Š. are gratefully acknowledged.

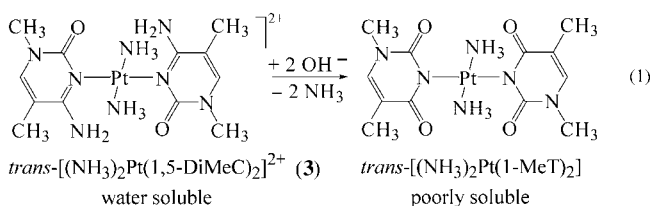


Supporting information for this article is available on the WWW under <http://www.angewandte.org> or from the author.

replicating DNA by the enzyme uracil-DNA glycosylase, 5-methylcytosine (mC), which is involved in the regulation of gene expression, is converted to thymine upon deamination. The rate of the latter reaction is three to four times faster than that for cytosine.^[2] Thymine is not excised, yet the GT mispair is subject to mismatch repair, which is, however, considerably slower than excision of uracil. As a consequence, 5-methylcytosine residues represent hotspots for spontaneous transition mutations.^[3] It has been estimated that mCpG sequences are preferred targets for spontaneous point mutations (GC → AT transition) which could account for as much as one-third of single-site mutations found in inherited human diseases.^[4] In nondividing cells RNA polymerases are not arrested by uracil in the DNA and consequently produce mutant transcripts with high efficiency.^[5] Spontaneous hydrolytic deamination of cytosine and 5-methylcytosine appears to occur without any particular sequence specificity, but single-stranded DNA is considerably more susceptible to this reaction.^[1] Here we report on our findings that cationic complexes of Pt^{II} containing the model nucleobases 1-methylcytosine (1-MeC) and 1,5-dimethylcytosine (1,5-DimeC) undergo unexpectedly facile cytosine deamination at basic pH with formation of the corresponding complexes of 1-methyluracilate (1-MeU) and 1-methylthymine (1-MeT), respectively. We explicitly note that the free bases 1-MeC and 1,5-DimeC show no sign of deamination under comparable conditions for months and that even deamination of deoxycytidine^[6] or cytosine in single- or double-stranded DNA^[7] likewise requires high pH values beyond the physiological range. This seemingly paradoxical situation in fact calls for a catalyst for this reaction also in vivo, which could be a metal ion.

Interestingly, bacteria and fungi contain cytosine deaminases (CDases) for pyrimidine salvage.^[8] These enzymes contain either Zn²⁺ or Fe²⁺ at the active site, and the metal ions are thought to add an OH⁻ nucleophile to the C4 position of the cytosine.

Deamination reactions of N3-platinated cytosine nucleobases were first discovered by us when we treated compounds of composition *trans*-[a₂Pt(C-N3)₂](NO₃)₂ (a = NH₃, C = 1-methylcytosine, 1-MeC (**1**); a = CH₃NH₂, C = 1-MeC (**2**); a = NH₃, C = 1,5-dimethylcytosine, 1,5-DimeC (**3**); a = CH₃NH₂, C = 1,5-DimeC (**4**)) with base (KOH, NaOH) at pH ≥ 12.5. Formation of *trans*-[a₂PtL₂] (L = 1-methyluracilate, 1-MeU, or 1-methylthymine, 1-MeT) compounds was recognized because of the poor solubility of the complexes *trans*-[(NH₃)₂PtL₂], which permitted easy characterization and comparison with authentic samples. In the case of **3**, precipitation of the 1-MeT complex started virtually instantaneously on addition of base [Eq. (1)]. Very recently, Arpalahiti



and Klika reported on similar deamination reactions observed with 9-methyladenine complexes of Pt^{II}.^[9]

In order to better understand the cytosine deamination reactions, we decided to simplify the system by having only a single cytosine base present. The starting compound [(dien)Pt(1-MeC-N3)](NO₃)₂ (**5**) (dien = diethylenetriamine) was prepared by reaction of [(dien)Pt(H₂O)]²⁺ and 1-MeC. Samples of **5** were then dissolved in D₂O, the pD adjusted by addition of NaOD, and the reaction followed at ambient temperature over time. ¹H NMR spectra recorded in a typical experiment with the pD set to 12.7 are given in the Supporting Information, and the enlarged lowfield section of a spectrum is shown in Figure 1. As can be seen, resonances due to the

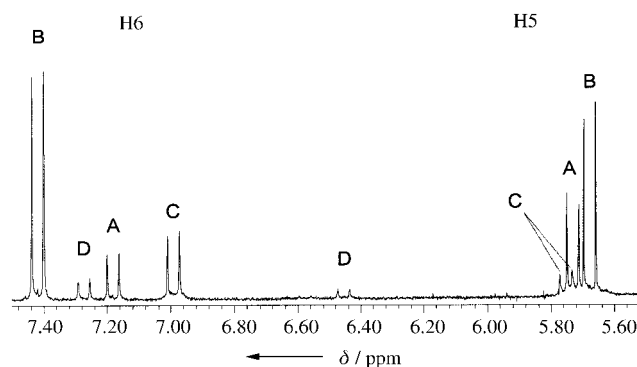
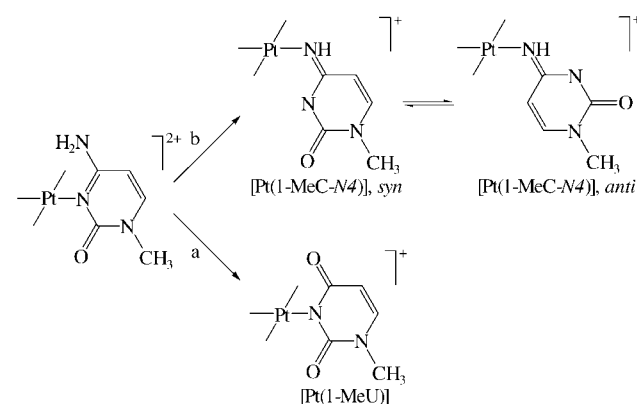


Figure 1. Lowfield section of ¹H NMR spectrum of **5** after 4 d at room temperature. See text for assignment of doublets A–D.

starting compound **5** (A) disappear as the new sets B, C, and D appear. Signal set B can be assigned readily to the deamination product of **5**, [(dien)Pt(1-MeU-N3)]⁺, from comparison with a sample obtained from [(dien)Pt^{II}] and 1-MeU. The two other sets were identified, on the basis of 2D NMR experiments as well as their pD dependence, as due to two rotamers (C, *syn*; D, *anti*; 3:1) of the cytosine-N4 linkage isomer [(dien)Pt(1-MeC-N4)]⁺ (see the Supporting Information). It is thus evident that in strongly alkaline medium, deamination of the cytosine nucleobase in **5** competes with metal migration to N4 (Scheme 1). Under the conditions of



Scheme 1. a) Deamination of the cytosine nucleobase in [(dien)Pt(1-MeC-N3)]²⁺ (**5**) and b) competing migration of the Pt^{II} center to N4.

the experiment, deamination accounts for 73 % of the product and the linkage isomer makes up the remaining 27 %.

The pK_a for deprotonation of **5**, as estimated by pD-dependent ^1H NMR spectroscopy, was found to be approximately 13. This suggests that $[(\text{dien})\text{Pt}^{\text{II}}]$ migration is preceded by deprotonation of the exocyclic amino group of cytosine. The linkage isomerization process thus resembles that in the $[(\text{NH}_3)_3\text{Ru}^{\text{III}}(1\text{-MeC})]$ system^[10] and likewise that of various adenine complexes of Pt^{II} ^[11] and is different from a redox-assisted pathway of linkage isomerization which we discovered previously.^[12] Figure 2 shows the disappearance of **5** at pD 12.7 ($t_{1/2} = 1.4$ d) and parallel formation of the uracil species ($t_{1/2} = 1.43$ d, $k = 5.6 \times 10^{-6} \text{ s}^{-1}$) and the N4 linkage isomer ($t_{1/2} = 1$ d, $k = 8.0 \times 10^{-6} \text{ s}^{-1}$).

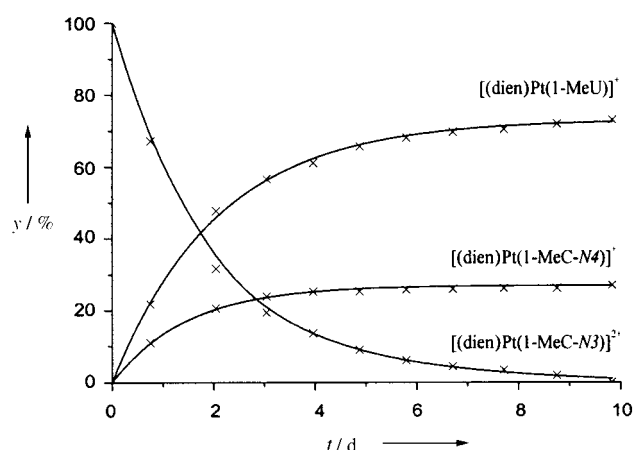


Figure 2. Decay of **5** and formation of deamination product $[(\text{dien})\text{Pt}(1\text{-MeU-}N3)]^+$ and linkage isomers of $[(\text{dien})\text{Pt}(1\text{-MeC-}N4)]^+$ (*syn* and *anti* forms combined).

As in the case of $[(\text{dien})\text{Pt}(1\text{-MeC-}N3)]^{2+}$, the 1-MeC ligands in *cis*- $[(\text{NH}_3)_2\text{Pt}(1\text{-MeC-}N3)_2](\text{NO}_3)_2$ (**6**), *trans*- $[(\text{CH}_3\text{NH}_2)_2\text{Pt}(1\text{-MeU-}N3)(1\text{-MeC-}N3)]\text{ClO}_4 \cdot \text{H}_2\text{O}$ (**7**) and *trans*- $[(\text{CH}_3\text{NH}_2)_2\text{Pt}(1\text{-MeU-}N3)(1,5\text{-DimeC-}N3)]\text{ClO}_4$ (**8**) undergo deamination in strongly alkaline medium. Chemical shifts of the ^1H NMR resonances of the Pt complexes in D_2O are given in the Supporting Information.

In the reactions described so far, facile deamination of Pt-bound cytosine can be attributed to Lewis acid activation by the metal ion. In order to probe the possibility of combining Lewis acid activation with metal hydroxide activation, in other words, nucleophilic attack by internal OH^- , we also studied the deamination of the cytosine ligand in *cis*- $[(\text{NH}_3)_2\text{Pt}(1\text{-MeC-}N3)(\text{OH})]^+$ (**9**).^[13] The pK_a value for the corresponding aqua complex is 5.9,^[14] implying that at neutral pH the hydroxo species is dominant in solution. At pD 7.2 signals due to the deamination product *cis*- $[(\text{NH}_3)_2\text{Pt}(1\text{-MeU})\text{X}]^{n+}$ ($\text{X} = \text{OD}$, $n = 0$; $\text{X} = \text{D}_2\text{O}$, $n = 1$)^[15] are not observed, not even after 15 d at 40 °C. Deamination takes place only when a solution of *cis*- $[(\text{NH}_3)_2\text{Pt}(1\text{-MeC-}N3)\text{Cl}]\text{Cl}$ is brought to pD 14. At this pD, formation of *cis*- $[(\text{NH}_3)_2\text{Pt}(1\text{-MeU-}N3)(\text{OH})]$ gives rise to doublets at $\delta = 7.41$ and 5.67 ppm, the intensities of which increase over a period of 12 d. Hence, the rate of deamination is comparable with that

of *cis*- $[(\text{NH}_3)_2\text{Pt}(1\text{-MeC-}N3)_2]^{2+}$. This rules out any participation of the hydroxo group in the mechanism, which is in accordance with the DFT calculations described below.

The most likely scenario of the deamination reaction, that is, the bimolecular pathway, has been modeled for three compounds containing unsubstituted cytosine (C) instead of 1-MeC: $[(\text{NH}_3)_3\text{Pt}(\text{C-}N3)]^{2+}$ (**5a**; an analogue of $[(\text{dien})\text{Pt}(1\text{-MeC-}N3)]^{2+}$ **5**), *cis*- $[(\text{NH}_3)_2\text{Pt}(\text{C-}N3)(\text{OH})]^+$ (**9a**; an analogue of *cis*- $[(\text{NH}_3)_2\text{Pt}(1\text{-MeC-}N3)(\text{OH})]^+$ **9**), and *cis*- $[(\text{NH}_3)_2\text{Pt}(\text{C-}N3)(\text{H}_2\text{O})]^{2+}$ (**9b**; the protonated form of **9a**).

We have computed the energy profile of the bimolecular reaction at DFT/Becke3LYP level of theory using the Polarized Continuum Model (PCM) to account for solvation effects. We checked the reliability of the applied theoretical approach for studying this particular reaction by performing benchmark calculations with the highly correlated CCSD(T) method. Computational details as well as the results of the benchmark calculations can be found in the Supporting Information. This pathway comprises two elementary steps such as addition of a nucleophile to C4 of cytosine followed by the elimination of the N4 amino group in the next reaction step. The energy profile of the reaction is depicted in Figure 3

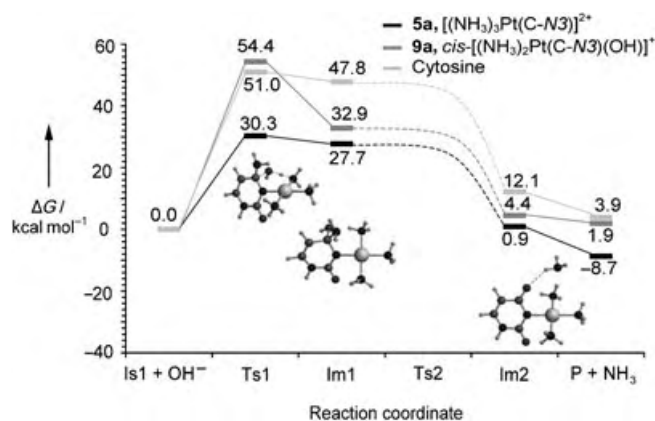


Figure 3. Computed energy profiles for the deamination reaction of cytosine (light gray) and its platinated adducts $[(\text{NH}_3)_3\text{Pt}(\text{C-}N3)]^{2+}$ (**5a**, black) and *cis*- $[(\text{NH}_3)_2\text{Pt}(\text{C-}N3)(\text{OH})]^+$ (**9a**, dark gray). The results were computed at DFT/Becke3LYP level of theory using the PCM model to mimic the water solvent. Is1 = substrate, Ts1 = transition state of the first reaction step, Im1 = intermediate formed as the product of the first reaction step, Ts2 = transition state of the second reaction step, Im2 = product of the second reaction step, P = product of the reaction (platinated uracil).

along with a series of gas-phase-optimized structures representing the intermediates and transition states involved in the mechanism proposed for the reaction of **5a** with OH^- .

Computed activation energy of the first reaction step, that is, attack of OH^- at C4, is strongly dependent of the total charge of the reaction complex: it is 30.3 kcal mol⁻¹ for a charge of +1 (**5a** + OH^-), whereas it significantly increases for the neutral (**9a** + OH^- , 54.4 kcal mol⁻¹) and negatively charged systems (cytosine + OH^- , 51.0 kcal mol⁻¹). These values are quite high primarily due to the large desolvation energy of the OH^- ion ($-\Delta G_{\text{solv}}(\text{OH}^-)$). The experimentally determined value of $\Delta G_{\text{solv}}(\text{OH}^-)$ ranges from -104 to

–107.5 kcal mol^{–1},^[16] while our PCM calculations suggest a considerably higher value of –113.1 kcal mol^{–1}. This results in a systematic overestimation of the activation energy of the first reaction step by at least 6.6 kcal mol^{–1}. Thus, reasonably accurate estimates of the activation energies are 23.7, 47.8, and 44.4 kcal mol^{–1} for **5a**, **9a**, and free cytosine, respectively. The Meisenheimer-type intermediate (Im1) is significantly stabilized upon platination relative to the nonmetalated system. However, the kinetic barrier computed for **9a** is too high for a considerable yield to be expected for the formation of Im1. The same applies for the Meisenheimer complex formed from free cytosine with OH[–], where apart from kinetic reasons even the low thermodynamic stability of Im1 make the addition step highly unlikely.

In the second reaction step the N4 amino group is released from the cytosine moiety and simultaneously a C=O double bond is formed at C4. This step necessitates an O–H→NH₂-type proton transfer between the *ipso* hydroxy and amino groups of the Meisenheimer complex. Computed activation energies are rather high for this reaction step, amounting to 28.2, 33.7, and 17.6 kcal mol^{–1} for **5a**, **9a** and unsubstituted cytosine, respectively. However, in aqueous solution they might be significantly reduced due to solvent-assisted catalysis.^[17] For example, previous theoretical studies on 1,3-isomerizations^[18] have shown that the energy barrier can be reduced by as much as 30 kcal mol^{–1} if the process occurs through a water molecule.

We have selected **9a** and **9b** to discuss the unimolecular version of the deamination reaction of platinated cytosine to give platinated uracil. The nucleophilic attack at C4 is initiated by the ligand *cis* to the cytosine ring. Ligand transfer from the Pt^{II} entity to C4 of cytosine necessitates movement of the Pt^{II} center towards C4. In the transition state the water molecule shares a hydrogen atom with the N4 amino group of cytosine and simultaneously binds to C4. Pyramidalization of C4 is rather significant: the N4–C4–N3–C5 dihedral angles are –130.7° and –117.2° for **9a** and **9b**, respectively. Also, the ideal square-planar coordination of Pt^{II} is unusually highly distorted: the N–Pt–N angles next to the cytosine ring are only 74.6° and 74.8° for **9a** and **9b**, respectively. Such a drastic reduction of the symmetry both of the nucleobase and the metal entity requires a rather high energy investment which manifests itself in the activation energies of this unimolecular pathway (66.5 kcal mol^{–1} for **9b**, 30.3 kcal mol^{–1} for **9a**).

In summary, calculations suggest that in water the prevailing mechanism of the reaction is the bimolecular-type nucleophilic substitution and that the reaction proceeds with an activation energy barrier of 23.7 kcal mol^{–1}. The substrate of the reaction carries a charge of +2, because greater charge on the metalated nucleobase leads to an enhancement of the substrate–nucleophile attraction. The activation energies obtained for substrates with lower charges are much too high for any reasonable yield of the reaction to be expected. Similarly, both unimolecular scenarios studied are energetically less favored than the bimolecular pathway described for **5a**. Pt^{II} plays a threefold role in catalyzing the deamination reaction by a) stabilizing products Im1 and Im2, b) making the cytosine ring more susceptible towards nucleophiles with its positive charge, and c) dramatically decreasing

the activation energy of the rate-determining step in the case of **5a**. We are aware that in our model system the metal ion is still bonded to the deamination product and that for a catalytic cycle it must be replaced by a proton.

Experimental Section

Compounds **1–9** were prepared as reported in the Supporting Information. ¹H NMR spectra were recorded on a Bruker AC200 (200 MHz) spectrometer in D₂O with sodium-3-(trimethylsilyl)propanesulfonate (TSP) as internal reference. pD values were measured on Metrohm 632 pH meter. Variations in pD values were performed by means of NaOD and DNO₃. pK_a values were calculated as previously reported.^[19]

All computations were carried out with the Gaussian 98 computer package. Details are given in the Supporting Information.

Received: March 24, 2004

Keywords: cytosine · deamination · density functional calculations · nucleobases · platinum

- [1] T. Lindahl, *Nature* **1993**, 362, 709–715.
- [2] T. Lindahl, B. Nyberg, *Biochemistry* **1974**, 13, 3405–3410.
- [3] a) B. K. Duncan, J. H. Miller, *Nature* **1980**, 287, 560–561; b) W. M. Rideout III, G. A. Coetzee, A. F. Olumi, P. A. Jones, *Science* **1990**, 249, 1288–1290.
- [4] D. N. Cooper, H. Youssoufian, *Hum. Genet.* **1988**, 78, 151–155.
- [5] A. Viswanathan, H. J. You, P. W. Doetsch, *Science* **1999**, 284, 159–162.
- [6] R. Y.-H. Wang, K. C. Kuo, C. W. Gehrke, L.-H. Huang, M. Ehrlich, *Biochim. Biophys. Acta* **1982**, 697, 371–377.
- [7] a) L. A. Frederico, T. A. Kunkel, B. Ramsay Shaw, *Biochemistry* **1990**, 29, 2532–2537; b) B. Ramsay Shaw in *Structural Biology: The State of the Art* (Eds.: R. H. Sarma, M. H. Sarma), Adenine Press, Shenectady, NY, **1994**, pp. 367–378.
- [8] G. C. Ireton, G. McDermott, M. E. Black, B. L. Stoddard, *J. Mol. Biol.* **2002**, 315, 687–697.
- [9] a) J. Arpalahti, K. D. Klika, *Eur. J. Inorg. Chem.* **2003**, 4195–4201; b) K. D. Klika, J. Arpalahti, *Chem. Commun.* **2004**, 666–667.
- [10] M. J. Clarke, *J. Am. Chem. Soc.* **1978**, 100, 5068–5075.
- [11] a) J. Arpalahti, K. D. Klika, *Eur. J. Inorg. Chem.* **1999**, 1199–1201; b) J. Viljanen, K. D. Klika, R. Sillanpää, J. Arpalahti, *Inorg. Chem.* **1999**, 38, 4924–4925; c) J. Arpalahti, K. D. Klika, S. Molander, *Eur. J. Inorg. Chem.* **2000**, 1007–1013.
- [12] a) F. Pichierri, D. Holtherrich, E. Zangrando, B. Lippert, L. Randaccio, *J. Biol. Inorg. Chem.* **1996**, 1, 439–445; b) B. Lippert, H. Schöllhorn, U. Thewalt, *J. Am. Chem. Soc.* **1986**, 108, 6616–6621; c) H. Schöllhorn, R. Beyerle-Pfnür, U. Thewalt, B. Lippert, *J. Am. Chem. Soc.* **1986**, 108, 3680–3688.
- [13] J. F. Britten, B. Lippert, C. J. L. Lock, P. Pilon, *Inorg. Chem.* **1982**, 21, 1936–1941.
- [14] F. Schwarz, B. Lippert, A. Iakovidis, N. Hadjiliadis, *Inorg. Chim. Acta* **1990**, 168, 275–281.
- [15] B. Lippert, D. Neugebauer, G. Raudaschl, *Inorg. Chim. Acta* **1983**, 78, 161–170.
- [16] T. Yamabe, K. Yamashita, M. Kaminoyama, M. Koizumi, A. Tachibana, K. Fukui, *J. Phys. Chem.* **1984**, 88, 1459–1463.
- [17] E. Constantino, X. Solans-Monfort, M. Sodupe, J. Bertran, *Chem. Phys.* **2003**, 295, 151–158.
- [18] L. Rodríguez-Santiago, O. Vendrell, I. Tejero, M. Sodupe, J. Bertran, *Chem. Phys. Lett.* **2001**, 334, 112–118.
- [19] R. K. O. Sigel, E. Freisinger, B. Lippert, *J. Biol. Inorg. Chem.* **2000**, 5, 287–299.

Fluorescent Probes

Chameleon Labels for Staining and Quantifying Proteins

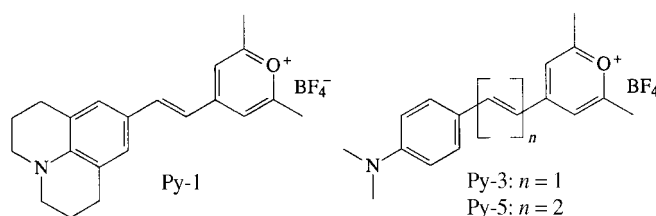
Bianca K. Wetzl, Sergiy M. Yarmoluk, Douglas B. Craig, and Otto S. Wolfbeis*

The analysis of a protein pattern, its temporal changes, and the interpretation of its function is one of the fascinating technologies at present and is often referred to as proteomics.^[1] Protein patterns can be analyzed by a variety of methods including gel electrophoresis, blotting, or by so-called biochips.^[2] While biochips (and protein arrays) are preferably applied to systems of known protein composition to identify specific proteins, electrophoresis in one- or two-dimensional form is readily applied to unknown samples.^[2] Since gel electrophoresis is a separation technique, it also requires appropriate methods for determination (or visualization) of proteins.^[3] Standard methods for visualization include silver staining or staining with dyes, such as Coomassie Brilliant Blue (CBB) or Amido Black B.^[4] Fluorescent methods for staining and visualization of proteins are of particular interest because of the high sensitivity of (laser-induced) fluorescence, which has reached the nano- and picomole (if not zeptomole or single molecule) level, at least for solutions.

Two types of fluorescent protein stains need to be distinguished: The first involves covalent linkage of the stain to a functional group of a protein (such as amino or thiol), the second involves noncovalent protein–stain interaction. Both have their merits. A covalent linkage to the protein is stable (i.e., the tag cannot be washed out), while noncovalent labeling enables, for example, mass spectroscopy to be performed because no change in the total mass of the protein occurs on staining.^[5] Typical noncovalent protein stains include the SYPRO dyes (certain organic or organometallic fluorochromes) that give red or pink emissions.^[6] The stains bind to proteins with high affinity which then can be determined in gels in quantities of 2–10 ng/band. Covalent fluorescent labeling, in contrast, is widely used in polyacrylamide gel electrophoresis (PAGE). Conjugation is achieved by either pre-staining (that is, before electrophoresis) or after electrophoresis. A variety of covalently binding labels are known.^[6–8] However, all of them have spectral properties that are identical (within a few nm) in the free and the protein-

bound form. This situation requires that—in case of staining after electrophoresis—excess label has to be washed out very carefully from the gel or blot to minimize fluorescent background.

Herein we report an entirely new class of labels for gel electrophoresis and also for general protein quantitation. Pyrylium groups react with amines to form the respective pyridinium analogues.^[9] We have synthesized the new labels by attaching a pyrylium group to a small aromatic group (thereby forming one of the smallest blue and fluorescent chromophores known) and this resulted in the label Py-1. Py-



1 is obtained in a single reaction step and in good yields from the respective benzaldehyde derivative and 1,3,6-trimethylpyrylium tetrafluoroborate. Its spectral data are given in Figure 1 and in Table 1. Py-1 is blue, virtually nonfluorescent,

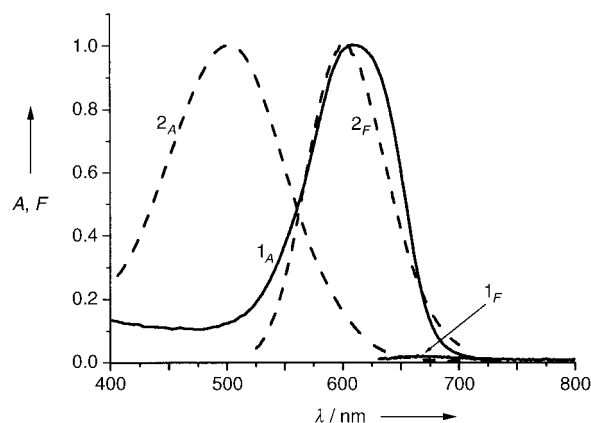


Figure 1. Normalized absorption and fluorescence emission spectra of the label Py-1 (1_A , 1_F) and of its conjugate to human serum albumin (2_A , 2_F) at pH 7.2 in a 22 mM phosphate buffer. The molar extinction coefficient of the free label is $63\,000\text{ L cm}^{-1}\text{ mol}^{-1}$ and the conjugated label is $24\,000\text{ L cm}^{-1}\text{ mol}^{-1}$. The dye-to-protein ratio of the conjugate is 1.7.

Table 1: Photophysical properties of stains Py-1, Py-3, and Py-5 in free form and after conjugation to human serum albumin.

Label	$\lambda_{\text{max}}^{\text{abs}}/\lambda_{\text{max}}^{\text{em}}$ of free stain [nm]	$\lambda_{\text{max}}^{\text{abs}}/\lambda_{\text{max}}^{\text{em}}$ of conjugate [nm]	ϕ [%] ^[a,b]	t [ns] ^[c]
Py-1	621/665	503/602	≤ 50	2.8
Py-3	572/641	464/582	≤ 10	2.3
Py-5	644/732	465/629	≤ 15	2.3

[a] ϕ = quantum yields of the conjugate; the quantum yields of the unconjugated labels are $< 1\%$. [b] Dependent on dye-to-protein ratio; usually best at 0.5 to 1.0. [c] t = Decay times of conjugates. The decay times of stains Py-1, Py-3, Py-5 are $< 0.5\text{ ns}$.

[*] Dipl.-Chem. B. K. Wetzl, Prof. Dr. D. B. Craig,^[†] Prof. Dr. O. S. Wolfbeis
Institute of Analytical Chemistry, Chemo- and Biosensors, University
of Regensburg, 93040 Regensburg (Germany)
Fax: (+49) 941-943-4064
E-mail: otto.wolfbeis@chemie.uni-regensburg.de

Dr. S. M. Yarmoluk
Department of Combinatorial Chemistry
Institute of Molecular Biology and Genetics
Academy of Sciences, UI-03187 Kyiv (Ukraine)

[†] Humboldt Fellow; on leave from the Department of Chemistry,
University of Winnipeg, Winnipeg R3B2E9, Canada.

and reacts with primary amino groups of proteins (but also of amino-modified DNA and other primary amines, such as dopamine) in aqueous solution of pH 8–9 at room temperature to give a covalently stained red conjugate. Simultaneously, the fluorescence quantum yield increases to typically 50% depending on the protein to be labeled and on the dye-to-protein ratio (DPR). Since these labels undergo such a significant (and visually detectable) change in both absorption and fluorescence, we refer to them as chameleon labels. Their spectral properties can be modified by variation of end groups and chain length, and such changes resulted, for example, in labels Py-3 and Py-5, both of which also react with proteins.

The fluorescence of the red conjugate formed between Py-1 and proteins can be excited between 470 and 530 nm and therefore matches several standard laser lines, whilst the free (blue) label is not excited at all at this wavelength. Thus, the fluorescence of the stained protein is measured against an almost dark background even if residual free (blue) label is still present.

The chameleon labels have two additional attractive features: The first is that labeling causes a relatively small increase in the mass of the protein ($\Delta m = 288 \text{ g mol}^{-1}$ in case of mono-labeling with Py-1). Second (and possibly even more importantly), the electrical charge of a protein does not change on conjugation (since a positively charged amino group is replaced by a positively charged pyridinium group). The second feature is particularly significant, since it has been reported that multiple labeling of proteins with dyes that have no (or even a negative) charge results in several differently charged labeled proteins. As a result, a certain protein can display different migration rates in (capillary) electrophoresis and consequently give rise to more than one peak or substantial band broadening depending on detection method.^[10]

Label Py-1 was tested for its suitability in electrophoresis on sodium dodecylsulfate (SDS)-PAGE gels. Figure 2 shows the result of an electrophoretic separation of a variety of proteins on a standard gel with 10 different proteins.^[11] The gel was analyzed using a standard laser-based scanner^[12] and the results (Table 2) show that even in these initial experiments the limits of detection for most proteins are comparable with the (highly sensitive but tedious) silver staining method, and often better those obtained with CBB and the

Table 2: Detection limits for proteins (ng/band) in SDS-PAGE as determined by staining with silver, CBB, and Py-1.

Protein	Silver staining ^[a]	CBB ^[a]	Py-1
myosin	1	8–16	1
β -galactosidase	3	8–16	0.8
glycogen-phosphorylase	1	16–30	3
bovin serum albumin	3	16–30	<2.5
glutamate dehydrogenase	3	16	<0.8
lactate dehydrogenase	n.d.	n.d.	4
carbonic anhydrase	6	16–30	4
trypsin inhibitor	3	16–30	12
lysozyme	4	16–30	14
aprotinin	6	16–30	4

[a] Data from ref. [6a] n.d. = not determined.

SYPRO stains.^[6] However, most covalently binding stains interfere with mass spectrometry, which is used as a detection method for proteins after gel electrophoresis. While the stain Py-1 is rather “small”, it cannot be excluded that more than one Py-1 is linked to a protein, thus complicating MS analysis.

Stain Py-1 may also be used for the quantitation of proteins in solution (rather than on gels). To demonstrate this, various proteins were dissolved in sodium carbonate buffer solution, and a solution of the Py-1 in aqueous dimethylformamide or aqueous methanol was added.^[13] A color change from blue to red is observed, and either absorption or fluorescence intensity can be measured and plotted against protein concentration as shown in Figure 3 for the fluores-

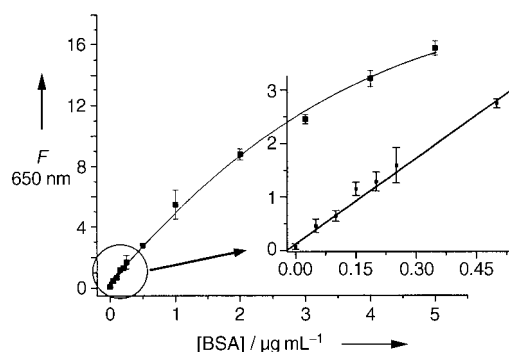


Figure 3. Calibration plot for BSA using label Py-1. The insert reveals the sensitivity of the assay in giving a limit of detection of approximately 60 ng of BSA per mL, and also demonstrates the good reproducibility (low standard deviations).

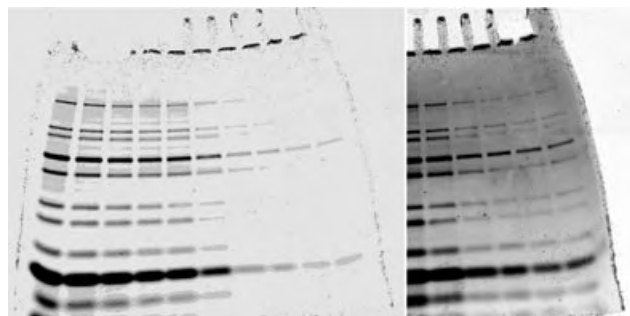


Figure 2. Left: standard SDS polyacrylamide gel with ten lines of a serial dilution of the mass standard.^[11] Right: Right side of the gel (lines 5–10). Both gels displayed in inverted intensity.

cence assay of bovine serum albumin (BSA). As a result of the sensitivity and brightness of the fluorescence of the labeled protein, concentrations as low as 60 ng mL^{-1} can be quantified. Thus, it is comparable (if not better) in terms of sensitivity to the most sensitive other assays including the widely used Lowry, Biuret,^[14] or ATTO-TAG^[15] assays, with the notable difference that the protein is not altered by poorly reproducible redox reactions (as in Lowry and Biuret assays) and that the highly toxic cyanide need not be added (as in case of ATTO-TAG).

In conclusion, we believe that Py-1 and its congeners Py-3 and Py-5 are a new class of protein labels that can be applied in proteomics, for example, in page SDS electrophoresis, but

also for general protein assay. The features of the labels include a) ease of preparation, b) a clear color change on labeling, c) a transition from a nonfluorescent state to a strongly fluorescent state upon conjugation, d) an increase in the decay time from <1 ns to >2 ns, e) very low limits of detection for both gel assays and solution assays, and f) the charge of a protein is not changed on labeling.

Received: April 29, 2004

Keywords: electrophoresis · fluorescent probes · protein assay · proteomics

- [1] a) M. P. Washburn, D. Wolters, J. R. Yates, *Nat. Biotechnol.* **2000**, 19, 242–247; b) J. Reidl, J. Hacker, *Mol. Infect. Biol.* **2002**, 187–193.
- [2] a) C. D. O'Connor, K. Rickard, *Microarrays Microplates* **2003**, 61–68; b) P. Cutler, *Proteomics* **2003**, 3, 3–18.
- [3] a) J. H. Issaq, *Adv. Protein Chem.* **2003**, 65, 249–269; b) M. Zhou, L. Yu, *Adv. Protein Chem.* **2003**, 65, 57–84.
- [4] a) P. J. Wirth, A. Romano, *J. Chromatogr. A* **1995**, 698, 123–143; b) J. P. Goldring, L. Ravaioli, *Anal. Biochem.* **1996**, 242, 197–201; c) W. F. Patton, *J. Chromatogr. B* **2002**, 77, 3–31;
- [5] J. C. Nishihara, K. M. Champion, *Electrophoresis* **2002**, 23, 2203–2215.
- [6] a) T. H. Steinberg, L. J. Jones, R. P. Haugland, V. L. Singer, *Anal. Biochem.* **1996**, 239, 223–237; b) M. F. Lopez, K. Berggren, E. Chernokalskaya, A. Lazarev, M. Robinson, W. F. Patton, *Electrophoresis* **2000**, 21, 3673–3683; c) W. F. Patton, *Electrophoresis* **2000**, 21, 1123–1144.
- [7] R. M. Leimgruber, J. P. Malone, M. F. Radabaugh, M. L. LaPorte, B. N. Violand, J. B. Monahan, *Proteomics* **2002**, 2, 135–144.
- [8] a) J. Bergquist, S. D. Gilman, A. G. Ewig, R. Ekman, *Anal. Chem.* **1994**, 66, 3512–3518; b) K. E. Asermely, C. A. Broomfield, J. Nowakowski, B. C. Courtney, M. Adler, *J. Chromatogr. B* **1997**, 695, 67–75.
- [9] O. M. Kostenko, S. Y. Dmitrieva, O. I. Tolmachev, S. M. Yarmoluk, *J. Fluoresc.* **2002**, 12, 173–175.
- [10] D. B. Craig, N. J. Dovichi, *Anal. Chem.* **1998**, 70, 2493–2494.
- [11] a) *Protein Mix*: myosin ($M_r = 220\,000$), 80 ng/band; β -galactosidase ($M_r = 116\,000$), 50 ng/band; glycogen phosphorylase ($M_r = 97\,000$), 150 ng/band; albumin ($M_r = 66\,000$), 250 ng/band; glutamate dehydrogenase ($M_r = 55\,600$), 80 ng/band; lactate dehydrogenase ($M_r = 36\,500$), 80 ng/band; carbonic anhydrase ($M_r = 29\,000$), 80 ng/band; trypsin inhibitor ($M_r = 20\,000$), 250 ng/band; lysozyme ($M_r = 14\,000$), 700 ng/band; aprotinin ($M_r = 61\,000$), 180 ng/band. The serial dilution factor of this mixture from line 1 to ten (Figure 2) is 0.0, 1.3, 1.7, 2.0, 2.5, 5.0, 10.0, 12.5, 16.7, 20.0. b) *Reagents and Conditions for Electrophoresis*: Tris/HCl (450 mM; Tris = 2-amino-2-(hydroxymethyl)propane-1,3-diol) as the probe buffer, glycerol (12%), SDS (4%), Coomassie Brilliant Blue G (0.0025% in water), phenol red (0.0025%), pH 8.45; running buffer (pH 8.3) consisting of Tris/HCl (25 mM), glycine (192 mM), and SDS (0.1%); 125 V, current from 80 mA (at the beginning) to 40 mA (at the end of the run; 90 min); vertical cell. c) *Staining*: Following electrophoresis, the gel was incubated in a solution containing 50% methanol, 10% acetic acid, and 40% distilled water (3 min), washed with 50% aqueous methanol, and then fixed twice with a mixture of 50% triethylamine/acetate (TEAA) buffer of pH 10 and 50% methanol. Staining was performed with a freshly prepared 0.004% solution of Py-1 (now available from Chromeon) in a 1:1 mixture of methanol and TEAA buffer (Py-1 should be predissolved in minute quantities of DMF). The staining time depends on the thickness and percentage of the gel. Once the optimal signal is achieved, additional staining (over night) does not enhance or degrade the signal. The gel is rinsed a) briefly in a washing solution of 50% methanol and 50% TEAA buffer, b) several times with a destaining solution containing 5% methanol, 7% acetic acid, and 88% distilled water, and subsequently scanned or dried. Gels are stable in the washing solution for at least two days.
- [12] We use a Tecan FL200 fluorescence scanner (excitation at 542 nm (argon laser); emission filter set to 630 nm).
- [13] A BSA standard solution ($20\ \mu\text{g mL}^{-1}$) was prepared in sodium carbonate buffer of pH 9, and diluted to several different concentrations in the microtiter plate. The stain Py-1 was diluted from a methanol stock solution ($1 \times 10^{-4}\ \text{mol L}^{-1}$) with distilled water to a concentration of $2.5\ \mu\text{M}$. The insert in Figure 3 illustrates the curve obtained at very low protein concentrations. Each data point is the average of five determinations (limit of detection $0.06\ \mu\text{g mL}^{-1}$).
- [14] a) O. H. Lowry, N. J. Rosebrough, A. L. Farr, R. L. Randall, *J. Biol. Chem.* **1951**, 193, 265–275; b) K. Wickelman, R. Braun, J. Fitzpatrick, *Anal. Biochem.* **1988**, 175, 231–237; c) H. Zheng, Y. X. Mao, D. H. Li, C. Q. Zhu, *Anal. Biochem.* **2003**, 318, 86–90; d) C. V. Sapan, R. L. Lundblad, N. C. Price, *Biotechnol. Appl. Biochem.* **1999**, 29, 99–108.
- [15] W. W. You, R. P. Haugland, D. K. Ryan, R. P. Haugland, *Anal. Biochem.* **1997**, 244, 277–282.

Friedel–Crafts Reactions**Electrophilic Alkylations in Neutral Aqueous or Alcoholic Solutions****

*Matthias Hofmann, Nathalie Hampel, Tanja Kanzian, and Herbert Mayr**

*Dedicated to Professor Johann Mulzer
on the occasion of his 60th birthday*

Friedel–Crafts alkylations and mechanistically related reactions, such as *tert*-alkylations of silyl enol ethers or alkoxy-alkylations of allylsilanes and enol ethers, are usually promoted by Lewis acids in inert solvents.^[1] When such reactions are carried out in aqueous or alcoholic solutions, usually Brønsted or nonhydrolyzable Lewis acids are employed to generate small equilibrium concentrations of carbocations.^[2] Basic and even neutral aqueous or alcoholic

[*] Dipl.-Chem. M. Hofmann, N. Hampel, T. Kanzian, Prof. Dr. H. Mayr
Department Chemie und Biochemie
Ludwig-Maximilians-Universität München
Butenandtstrasse 5-13 (Haus F), 81377 München (Germany)
Fax: (+49) 89-2180-77717
E-mail: herbert.mayr@cup.uni-muenchen.de

[**] We thank the Deutsche Forschungsgemeinschaft for financial support and Dr. G. Remennikov and Dipl.-Chem. M. Westermaier for synthesizing compounds **4c** and **4f**.



Supporting information for this article is available on the WWW under <http://www.angewandte.org> or from the author.

solutions have been considered prohibitive for such reactions, since water and alcohols are intuitively considered as strong nucleophiles which instantaneously trap the intermediates of S_N1 reactions and do not give π nucleophiles a chance to intercept the transient carbocations.

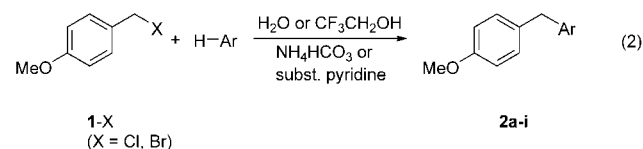
In numerous papers we have demonstrated that the reactions of carbocations with nucleophiles can be described by Equation (1),^[3–5] where k is a second-order ($\text{L mol}^{-1} \text{s}^{-1}$) or first-order (s^{-1}) rate constant at 20 °C, s is a nucleophile-specific slope parameter, N (or N_1) is the nucleophilicity parameter, and E is the electrophilicity parameter.

$$\log k = s(N + E) \quad (1)$$

Recently, we reported nucleophilicity parameters N_1 for some solvents^[6] (Figure 1, right), and compared them with previously published nucleophilicity parameters N for π systems^[3,4] (Figure 1, left). The first-order rate constants calculated from N_1 and the second-order rate constants calculated from N by Equation (1) become directly comparable if 1M solutions of the π nucleophiles are considered (pseudo-first-order rate constant $k_{1M} = k[\text{nucleophile}]_0$). We had, therefore, predicted that solvolytically generated carbo-

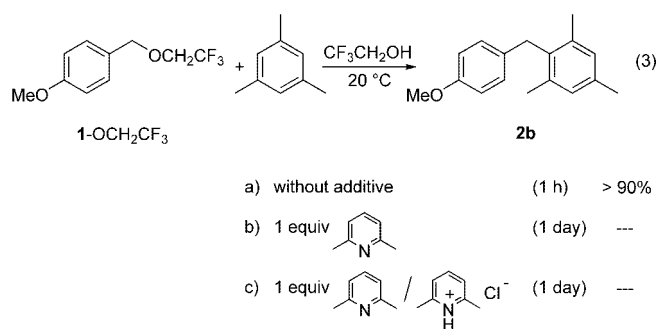
cations should be trapped by π nucleophiles^[6] (e.g., 1M alkenes or arenes) if N of the corresponding π nucleophile is greater than N_1 of the solvent under consideration, that is, if the corresponding nucleophile is located above the solvent in a graphical representation such as Figure 1. We now report an experimental verification of this forecast and thus lay the basis for a new type of Friedel–Crafts chemistry.^[7]

To examine the scope of nucleophiles we have examined reactions of 4-methoxybenzyl halides (**1-X**) with arenes and enol ethers in different solvents. Table 1 shows that electro-



philic aromatic substitutions in 1M solutions of arenes with 4-methoxybenzyl halides [Eq. (2)] have been successful in all cases where N of the arenes is greater than N_1 of the solvent. The formation of **2a–d** in 2,2,2-trifluoroethanol (T) shows that trapping with the π nucleophiles may also be possible in cases where the N parameter of the π system is slightly smaller than N_1 of the solvent.

Can the formation of products **2a–d** in 2,2,2-trifluoroethanol be explained by consecutive reactions of the initially produced trifluoroethyl ether **1-OCH₂CF₃** with the arenes? When **1-OCH₂CF₃** and mesitylene were dissolved in 2,2,2-trifluoroethanol at ambient temperature, quantitative conversion into **2b** was observed [Eq. (3a)]. No reaction took place in the presence of 2,6-lutidine, however, [Eq. (3b,c)] indicating that the products isolated in the presence of base (Table 1) are the results of kinetic control. We conclude, therefore, that in 2,2,2-trifluoroethanol the 4-methoxybenzyl cation reacts faster with mesitylene than with the solvent.



These results indicate a noticeable increase of the nucleophilicity of π systems in hydroxylic solvents, in contrast to previous reports which showed that the rates of the reactions of carbocations with olefins are only slightly affected by solvent polarity [$k(\text{CH}_3\text{NO}_2)/k(\text{CH}_2\text{Cl}_2) = 4$].^[8] Since the diphenylmethyl cation, which shows a similar electrophilicity as the 4-methoxybenzyl cation,^[9] did not react with *m*-xylene or mesitylene, when generated from diphenylmethyl chloride in 2,2,2-trifluoroethanol in the

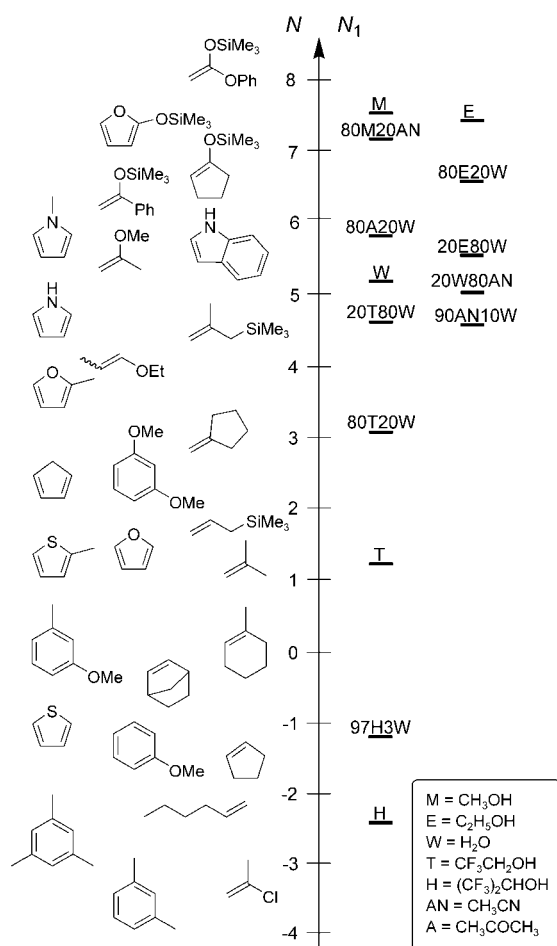


Figure 1. Comparison of the nucleophilicity parameters N_1 of solvents with the N parameters of typical π systems. Mixtures of solvents are given as vol%, for example, 80A20W = 80% acetone/20% water.

Table 1: Reactions of 4-methoxybenzyl halides (1-X) with arenes [according to Equation (2)].

H-Ar	N	Product (R = 4-CH ₃ OC ₆ H ₄ CH ₂)	X	Solvent	Base	Yield [%]
	-3.54	^[a]	Cl	H	NH ₄ HCO ₃	47
			Cl	T	NH ₄ HCO ₃	66
			Cl	T	2,6-lutidine	+ ^[b]
	ca. -2.6		Cl	H	NH ₄ HCO ₃	85
			Cl	T	NH ₄ HCO ₃	88
			Cl	T	2,6-lutidine	79
	-1.18	^[c]	Cl	H	NH ₄ HCO ₃	77
			Cl	T	NH ₄ HCO ₃	86
			Cl	T	2,6-lutidine	+ ^[b]
	0.13	^[d]	Br	T	NH ₄ HCO ₃	97
	1.26		Cl	T	2-chloropyridine	84
	2.48	^[e]	Cl	T	2,6-lutidine	91
			Cl	T	—	84
			Br	90AN10W	NH ₄ HCO ₃	+ ^[b]
	ca. 4		Cl	T	2,6-lutidine	88
			Br	90AN10W	NH ₄ HCO ₃	65
	5.80	^[f]	Br	80A20W	NH ₄ HCO ₃	75
	5.85	^[g]	Br	80A20W	NH ₄ HCO ₃	70

[a] Contains traces of 1,2,3-substituted product. [b] Quantitative conversion determined by GC-MS. [c] Contains traces of 1,2-substituted product. [d] Isolated as a mixture of regioisomers. [e] Contains 7% of 1,2,3-substituted product. [f] Contains 17% of the corresponding 2-isomer. [g] Contains 21% of the corresponding 3-substituted product.

presence of these π nucleophiles, the solvent effects on these reactions are still obscure.

When 4-methoxybenzyl bromide (**1-Br**) was mixed with 1-methylpyrrole without a solvent or in acetonitrile, compound **2i**, accompanied by numerous side products, was produced

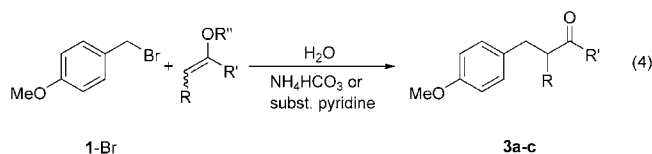


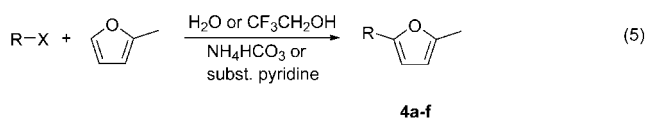
Table 2: Reactions of 4-methoxybenzyl bromide with enol ethers [according to Equation (4)].

Enol ether	N	Product (R = 4-CH ₃ OC ₆ H ₄ CH ₂)	Solvent	Base	Yield [%]
	ca. 4		90AN10W	NH ₄ HCO ₃	60
	5.41		90AN10W	2,6-lutidine	67
	6.22		90AN10W	NH ₄ HCO ₃	33

considerably slower than in analogous reactions in the presence of water and base (Table 1). Less nucleophilic arenes, for example, 2-methylfuran, which formed the substitution product **4e** in 68% yield in 90% aqueous acetonitrile (90AN10W) (see below), did not react with **1-Br** in pure acetonitrile.

The isolation of the carbonyl compounds **3a** and **3b** from the reactions of 4-methoxybenzyl bromide with alkyl enol ethers indicates that the enol ethers react faster with the 4-methoxybenzyl cation than water in 90% aqueous acetonitrile [Eq. (4), Table 2], but that water reacts faster with the resulting α -alkoxycarbenium ions under the same conditions. This change of selectivity may be explained by the geminal interaction of two oxygen groups at the same carbon center in the semiacetals formed from α -alkoxycarbenium ions and water (anomeric stabilization).^[10]

In a third series of experiments, we have examined the range of electrophiles using 2-methylfuran as nucleophile [Eq. (5), Table 3]. It is found that a wide variety of S_N1 -active substrates, particularly benzyl and allyl halides, can be employed for Friedel–Crafts reactions under these conditions, and we are presently investigating the scope and limitations of this new method.



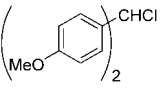
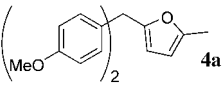
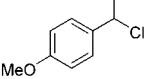
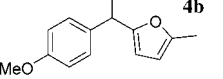
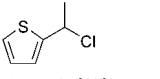
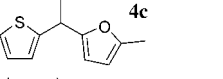
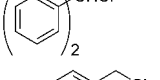
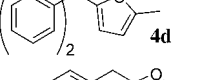
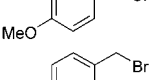
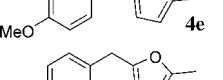
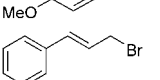
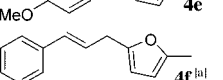
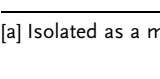
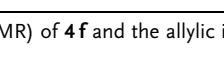
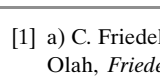
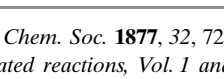
Experimental Section

Typical procedure—preparation of 4e: At ambient temperature, 4-methoxybenzyl bromide (1.00 g, 4.97 mmol) was added dropwise to 25 mL of a stirred solution of 2-methylfuran (2.05 g, 25.0 mmol) in 90% aqueous acetonitrile (v/v) (90AN10W) and ammonium hydrogencarbonate (786 mg, 9.94 mmol). After 2 h, water (20 mL) was added and the reaction mixture was extracted with diethyl ether (3 \times 20 mL). The combined ethereal phases were dried (MgSO₄), and the solvent was evaporated under reduced pressure. The residue was purified by column chromatography on silica gel (pentane/ether 7:1) to yield **4e** (737 mg, 73%) as a colorless liquid.

Received: May 27, 2004

Keywords: alkylations · carbocations · Friedel–Crafts reactions · S_N1 reactions · solvent effects

Table 3: Reactions of S_N1 -active substrates with 2-methylfuran [according to Equation (5)].

R-X	Product (R = 4-CH ₃ OC ₆ H ₄ CH ₂)	Solvent	Base	Yield [%]
		T	2-chloropyridine	85
		T	2,6-lutidine	70
		90AN10W	NH ₄ HCO ₃	48
		T	2,6-lutidine	87
		T	2,6-lutidine	74
		90AN10W	NH ₄ HCO ₃	73
		90AN10W	–	68
		90AN10W	NH ₄ HCO ₃	61

[a] Isolated as a mixture (84:16; NMR) of **4f** and the allylic isomer 2-methyl-5-(1-phenylallyl)furan.

- a) C. Friedel, J. M. Crafts, *J. Chem. Soc.* **1877**, 32, 725; b) G. A. Olah, *Friedel-Crafts and related reactions, Vol. 1 and 2*, Wiley, New York, **1963–1964**; c) R. M. Roberts, A. A. Khalaf, *Friedel-Crafts Alkylation Chemistry: A Century of Discovery*, Marcel Dekker, New York, **1984**; d) R. Taylor, *Electrophilic Aromatic Substitution*, Wiley, New York, **1990**, pp. 187–203; e) A. Hosomi, *Acc. Chem. Res.* **1988**, 21, 200–206; f) I. Fleming, J. Dunogués, R. Smithers in *Organic Reactions* (Ed.: A. S. Kende), Wiley, New York, **1989**, pp. 57–575; g) T. Mukaiyama, M. Murakami, *Synthesis* **1987**, 1043–1054; h) R. Mahrwald, *Chem. Rev.* **1999**, 99, 1095–1120; i) M. T. Reetz, *Top. Curr. Chem.* **1982**, 106, 1–54; j) *Lewis Acids in Organic Synthesis, Vol. 1 and 2* (Ed.: H. Yamamoto), Wiley-VCH, Weinheim, **2000**.
- a) S. Kobayashi, K. Manabe, *Chem. Eur. J.* **2002**, 8, 4094–4101; b) S. Kobayashi, *Eur. J. Org. Chem.* **1999**, 15–27; c) A. Corma, H. Garcia, *Chem. Rev.* **2003**, 103, 4307–4365; d) U. M. Lindström, *Chem. Rev.* **2002**, 102, 2751–2772; e) J. P. Richard, *Biochemistry* **1998**, 37, 4305–4309.
- Reviews: a) H. Mayr, M. Patz, *Angew. Chem.* **1994**, 106, 990–1010; *Angew. Chem. Int. Ed. Engl.* **1994**, 33, 938–957; b) H. Mayr, T. Bug, M. F. Gotta, N. Hering, B. Irrgang, B. Janker, B. Kempf, R. Loos, A. R. Ofial, G. Remennikov, H. Schimmel, *J. Am. Chem. Soc.* **2001**, 123, 9500–9512; c) H. Mayr, B. Kempf, A. R. Ofial, *Acc. Chem. Res.* **2003**, 36, 66–77.
- For reactions with neutral C-nucleophiles, see: a) B. Kempf, N. Hampel, A. R. Ofial, H. Mayr, *Chem. Eur. J.* **2003**, 9, 2209–2218; b) T. Bug, M. Hartnagel, C. Schlierf, H. Mayr, *Chem. Eur. J.* **2003**, 9, 4068–4076.
- For reactions with anions, see: a) R. Lucius, R. Loos, H. Mayr, *Angew. Chem.* **2002**, 114, 97–102; *Angew. Chem. Int. Ed.* **2002**, 41, 91–95; b) S. Minegishi, H. Mayr, *J. Am. Chem. Soc.* **2003**, 125, 286–295; c) T. Bug, H. Mayr, *J. Am. Chem. Soc.* **2003**, 125, 12980–12986; d) R. Loos, S. Kobayashi, H. Mayr, *J. Am. Chem. Soc.* **2003**, 125, 14126–14132.
- a) S. Minegishi, S. Kobayashi, H. Mayr, *J. Am. Chem. Soc.* **2004**, 126, 5174–5181; b) B. Denegri, S. Minegishi, O. Kronja, H. Mayr, *Angew. Chem.* **2004**, 116, 2353–2356; *Angew. Chem. Int. Ed.* **2004**, 43, 2302–2305.

- H. Mayr, M. Hofmann, S. Minegishi, N. Hampel, German-Patent 10 2004 006 785.6, **2004**.
- H. Mayr, R. Schneider, C. Schade, J. Bartl, R. Bederke, *J. Am. Chem. Soc.* **1990**, 112, 4446–4454.
- R. A. McClelland in *Reactive Intermediate Chemistry* (Eds.: R. A. Moss, M. S. Platz, M. Jones, Jr.), Wiley, Hoboken, **2004**, pp. 3–40.
- a) P. v. R. Schleyer, E. D. Jemmis, G. W. Spitznagel, *J. Am. Chem. Soc.* **1985**, 107, 6393–6394; b) A. J. Kirby, I. V. Komarov, P. D. Wothers, N. Feeder, P. G. Jones, *Pure Appl. Chem.* **1999**, 71, 385–391; c) P. P. Graczyk, M. Mikolajczyk, *Top. Stereochem.* **1994**, 21, 159–349; d) *ACS Symposium Series No. 539: The Anomeric Effect and Associated Stereoelectronic Effects* (Ed.: G. R. J. Thatcher), American Chemical Society, Washington DC, **1993**; e) E. Juaristi, G. Cuevas, *Tetrahedron* **1992**, 48, 5019–5087; f) S. O. N. Lill, G. Rauhut, E. Anders, *Chem. Eur. J.* **2003**, 9, 3143–3153.

Synthetic Methods

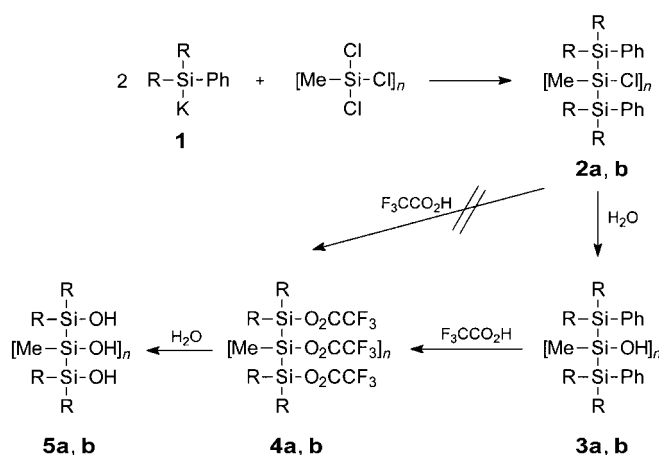
Novel Polysilanolols by Selective Functionalizations of Oligosilanes

Clemens Krempner,* Jürgen Kopf, Constantin Mamat, Helmut Reinke, and Anke Spannenberg

Dedicated to Professor H. Oehme on the occasion of his 65th birthday

Stable polysilanolols constructed of oligosilane frameworks, which can be conceived as silicon analogues of polyalcohols, are hitherto unknown. Due to the comparatively high acidities and basicities of the SiOH functionalities^[1] in these derivatives, unique supramolecular arrangements stabilized by hydrogen-bonding interactions can be expected.^[2] In addition, such polysilanolols might be promising precursors for the synthesis of M-O-Si-Si-containing materials^[3] with exceptional optoelectronic properties arising from the extended delocalization of σ electrons along the oligosilane backbone (σ -conjugation).^[4] Based on a novel synthetic concept for the selective functionalization of oligosilanes, we report herein the first synthesis of a stable 2,3,4,5-tetrahydroxyhexasilane and its supramolecular organization through hydrogen bonding into a 21-membered macrocycle.

The starting point of our investigations was the oligosilanes **2a,b**, which could be produced in high yields by treatment of $\text{Ph}(\text{Me}_3\text{Si})_2\text{Si-K}\cdot 3\text{THF}$ (**1**) with MeSiCl_3 and $\text{MeCl}_2\text{Si-SiMeCl}_2$, respectively (Scheme 1).^[5] Compounds **2a,b** possess nucleophilic, easily exchangeable chloro functionalities and two phenyl groups attached to silicon, which can normally be modified by protodesilylation reactions with strong acids. However, all attempts to cleave the Si-phenyl bond selectively by treatment of **2a,b** with trifluoromethanesulfonic acid failed. Instead skeletal rearrangements typical for oligosilanes in the presence of strong acids were observed.^[6]



Scheme 1. Synthesis of **2a,b**–**5a,b** (**a**: $n=1$; **b**: $n=2$; $\text{R}=\text{SiMe}_3$).

However, in the presence of the markedly less acidic trifluoroacetic acid (TFA), which served as both the protodesilylation reagent and the solvent, **2a,b** proved to be nearly insoluble, and thus no reaction occurred. In contrast, silanolols **3a,b**, obtained quantitatively by hydrolysis of **2a,b**, are more soluble and can be transformed by cleavage of the phenyl groups into the moisture-sensitive trifluoroacetoxysilanes **4a,b** in excellent yields (Scheme 1). This reaction sequence is unique insofar as apart from smooth protodesilylation of **3a,b** a complete nucleophilic exchange of the OH functionalities by trifluoroacetate groups also takes place. Moreover, the trifluoroacetolysis of **3b** proceeds diastereoselectively, giving *meso*-**4b** exclusively, regardless whether *meso*- or *rac*-**3b** was used. The molecular structure of *meso*-**4b** was confirmed unequivocally by X-ray crystallography (Figure 1).^[7a]

Finally, by hydrolysis of **4a,b** in the presence of equimolar amounts of ammonium carbamate the tri- and tetrasilanolols **5a,b** could be isolated in good yields. The tetrasilanolol **5b** was

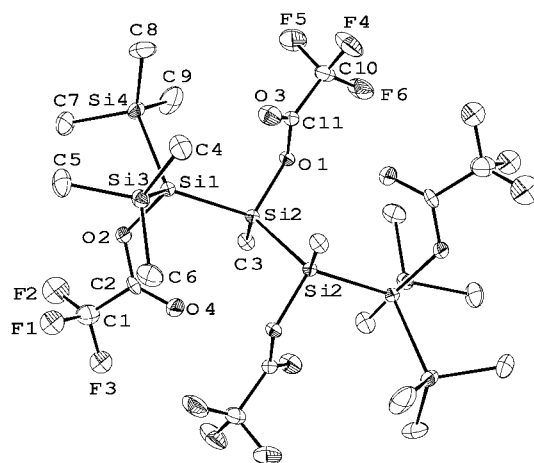


Figure 1. Molecular structure of **4b** in the crystal (30% probability level, H atoms are omitted for clarity and the disordered CF_3 groups are depicted only in one orientation). Selected bond lengths [Å] and angles [°]: O1–Si2 1.736(4), O2–Si1 1.764(4), Si1–Si2 2.354(2), Si1–Si3 2.354(2), Si1–Si4 2.363(2), Si2–Si2 2.372(3), Si2–Si1–Si3 121.78(8), Si1–Si2–Si2 117.25(10), C2–O2–Si1 122.7(3), C11–O1–Si2 121.7(4).

[*] Dr. C. Krempner
Department of Chemistry
The Ohio State University
100 West 18th Avenue, Columbus, OH 43210 (USA)
Fax: (+1) 614-292-0368
E-mail: ckrempne@chemistry.ohio-state.edu
Dipl.-Chem. C. Mamat, Prof. Dr. H. Reinke
Fachbereich Chemie
Universität Rostock
Einsteinstrasse 3a, 18051 Rostock (Germany)
Prof. Dr. J. Kopf
Institut für Anorganische und Angewandte Chemie
Universität Hamburg
Martin-Luther-King-Platz 6, 20146 Hamburg (Germany)
Dr. A. Spannenberg
Leibniz-Institut für Organische Katalyse
Universität Rostock e.V.
Buchbinderstrasse 1–3, 18055, Rostock (Germany)

Supporting information for this article is available on the WWW under <http://www.angewandte.org> or from the author.

obtained as a diastereomeric mixture (*rac/meso* = 2:1) as shown by ^1H NMR spectroscopy. Both compounds **5a,b** exhibit broad IR absorptions for the OH groups typical for silanols. In the solid state they prove to be relatively stable; only in solution upon gentle heating do they tend to undergo condensation reactions to form polymeric siloxanes. The results of an X-ray structure analysis of **5b** are in agreement with the structure proposed and the fact that the racemic form crystallized from the mixture of diastereomers (Figure 2).^[7b]

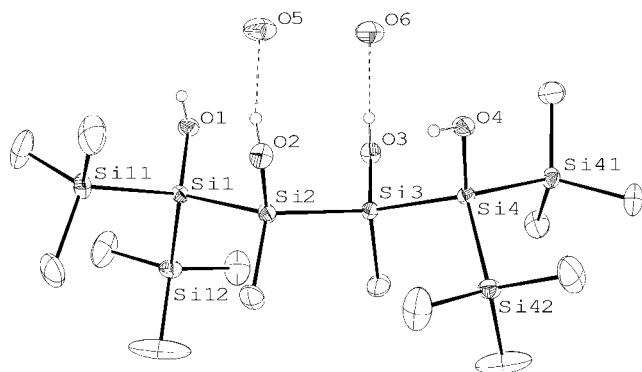


Figure 2. Structure of **5b** in the crystal (30% probability level, H atoms bonded to C atoms are omitted for clarity). Selected bond lengths [Å] and angles [°]: Si1–O1 1.6837(14), Si2–O2 1.6683(17), Si1–Si2 2.3744(7), Si2–Si3 2.3727(6), Si3–Si4 2.3785(7), Si4–O4 1.6826(15), Si3–O3 1.6646(16), Si12–Si1–Si2 114.31(3), Si2–Si3–Si4 117.43(3), Si11–Si1–Si2–Si3 $-172.76(3)$, Si1–Si2–Si3–Si4 $161.00(3)$, Si2–Si3–Si4–Si41 $-170.40(3)$.

The Si–Si and Si–O bond lengths and the Si–Si–Si angles in *rac*-**5b** show the typical values for oligosilanes. The hexasilane chain Si11–Si1–Si2–Si3–Si4–Si41 adopts an all-*anti* conformation (AAA), which is believed to be optimal for the delocalization of σ electrons.^[4] As confirmed by ^1H NMR investigations, differently bonded water molecules are incorporated into the crystal; two of them interact with the two internal OH groups of the tetrasilanol moiety through hydrogen bonds.

Remarkably, additional intermolecular hydrogen-bonding interactions between the terminal OH groups of three molecules of *rac*-**5b** result in the formation of a novel 21-membered macrocycle (Figure 3). Two molecules of water, located in the center of the ring, interact with each other and with the internal OH groups of *rac*-**5b**, probably stabilizing the ring structure. These macrocycles are stacked resulting in a channel structure. A third molecule water is located between the rings and about 7.5 Å (O–O distance) away from the water molecules inside the ring.

The UV-spectroscopic behavior of **5b** (λ_{max} = 289 nm) is unusual. The compound exhibits a remarkable red-shift of the absorption maximum (ca. 30 nm) relative to the maxima of permethylated hexasilanes,^[8] which is caused by the interaction of the electron pairs of oxygen with the conjugated σ electrons of the hexasilane chain.^[9] The result is a destabilization of the HOMO in the molecule, leading to an energetically low-lying, probably symmetry-forbidden $n\sigma \rightarrow n\sigma^*$ transition with low intensity ($\epsilon = 4.1 \times 10^3$).

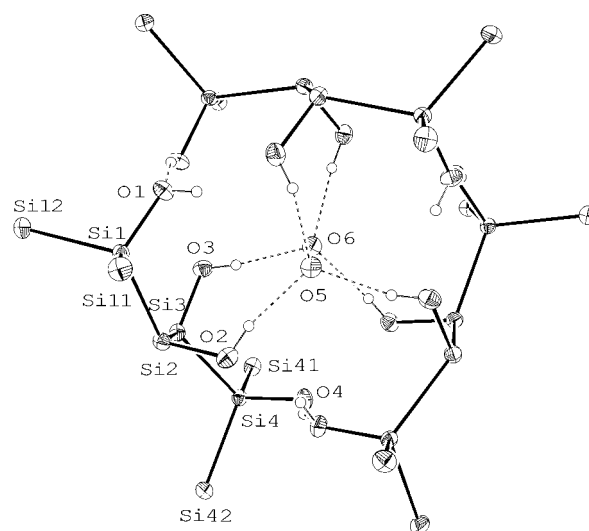


Figure 3. Ring structure of *rac*-**5b** in the crystal (30% probability level, all methyl groups are omitted for clarity).

In conclusion, trifluoroacetoxyoligosilanes, which are easily accessible in high yields, have considerable synthetic potential,^[10] as we have demonstrated for the synthesis and structure of novel tri- and tetrasilanol. Moreover, the trifluoroacetylolysis of oligosilanes might be a valuable method for the incorporation of functional groups into structurally more complex oligo- and polysilanes having different substitution patterns and potentially promising electronic properties.^[4]

Received: June 4, 2004

Keywords: hydrogen bonds · polysilanol · silanes · silicon · structure elucidation

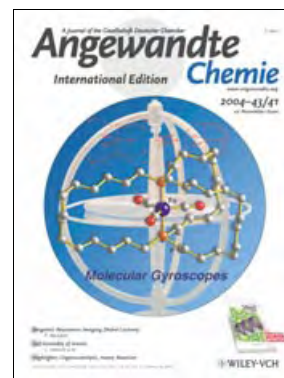
- a) P. D. Lickiss, *Adv. Inorg. Chem.* **1995**, 42, 147–262; b) R. Murugavel, A. Voigt, M. G. Walawalkar, H. W. Roesky, *Chem. Rev.* **1996**, 96, 2205; c) P. D. Lickiss in *The Chemistry of Organo Silicon Compounds*, Vol. 3, Wiley, New York, **2001**, pp. 695–744; d) R. Duchateau, *Chem. Rev.* **2002**, 102, 3525; e) I. Baxter, L. D. Cother, C. Dupuy, P. D. Lickiss, A. J. P. White, D. J. Williams, ECTOC-3 [Electronic Conference on Organometallic Chemistry], <http://www.ch.ic.ac.uk/ectoc/ectoc-3>.
- For structures of tetra- and hexasilanol based on carbosilane and siloxane backbones see: a) I. L. Dubchak, V. E. Shklover, Y. T. Struchkov, E. S. Khyntu, A. A. Zhdanov, *J. Struct. Chem. USSR (Engl. Transl.)* **1981**, 22, 770; b) S. A. Al-Juaid, C. Eaborn, P. B. Hitchcock, P. D. Lickiss, *J. Organomet. Chem.* **1988**, 353, 297; c) P. D. Lickiss, S. A. Litster, A. D. Redhouse, C. J. Wisener, *J. Chem. Soc. Chem. Commun.* **1991**, 173; d) R. Rulkens, M. P. Coles, T. D. Tilley, *Chem. Commun.* **2000**, 627; e) M. Unno, K. Takada, H. Matsumoto, *Chem. Lett.* **2000**, 242; f) G. Cerveau, R. J. P. Corriu, B. Dabien, J. Le Bideau, *Angew. Chem.* **2000**, 112, 1432; *Angew. Chem. Int. Ed.* **2000**, 39, 4533; g) C. Ackerhans, H. W. Roesky, T. Labahn, J. Magull, *Organometallics* **2002**, 21, 3671; h) I. Seto, T. Gunji, K. Kumagai, K. Arimitsu, Y. Abe, *Bull. Chem. Soc. Jpn.* **2003**, 76, 1983.
- a) J. Michl, R. D. Miller, *Chem. Rev.* **1989**, 89, 1359–1410; b) R. West in *The Chemistry of Organic Silicon Compounds* (Eds.: S. Patai, Z. Rappoport), Wiley, Chichester **1989**, pp. 1207–1240.

- [4] a) W. Kalchauer (Wacker Chemie GmbH), DE4036988, **1992** [CAN 117:132175]; b) T. Gunji, T. Gomi, T. Sanji, Y. Abe, *Chem. Lett.* **2001**, 1106–1107.
- [5] D. Hoffmann, H. Reinke, C. Krempner, *J. Organomet. Chem.* **2002**, 662, 1–8.
- [6] a) M. Ishikawa, J. Iyoda, H. Ikeda, K. Kotake, T. Hashimoto, M. Kumada, *J. Am. Chem. Soc.* **1981**, 103, 4845; b) U. Herzog, N. Schulze, K. Trommer, G. Roewer, *J. Organomet. Chem.* **1997**, 547, 133.
- [7] a) Single crystals were grown from pentane. Structure analysis of **4b**: STOE-IPDS diffractometer, graphite-monochromated Mo_{K α} radiation, $\lambda = 0.71069 \text{ \AA}$, structure solved by direct methods (SHELXS-86: G. M. Sheldrick, *Acta Crystallogr. Sect. A* **1990**, 46, 467), the refinement calculations were performed by the full matrix least-squares method against F^2 (G. M. Sheldrick, SHELXS-93, Program for the Solution of Crystal Structures, Universität Göttingen, Göttingen (Germany), **1993**), graphic: XP (Bruker AXS); $0.5 \times 0.4 \times 0.3 \text{ mm}$, colorless prism, space group *Pbca*, orthorhombic, $a = 13.731(3)$, $b = 12.942(3)$, $c = 24.045(5) \text{ \AA}$, $V = 4273.0(16) \text{ \AA}^3$, $Z = 4$, $\rho_{\text{calcd}} = 1.379 \text{ g cm}^{-3}$, 9878 reflections measured, 2808 reflections independent of symmetry, 1920 reflections observed ($I > 2\sigma(I)$), $R1 = 0.061$, wR^2 (all data) = 0.164, 224 parameters; b) Single crystals were obtained by slow evaporation of a pentane solution of **5b** at ca. 5°C . Structure analysis of **5b**: BRUKER-APEX-CCD diffractometer, graphite-monochromated Mo_{K α} radiation, $\lambda = 0.71069 \text{ \AA}$, structure was solved by direct methods (G. M. Sheldrick, SHELXS-97, Program for the Solution of Crystal Structures, Universität Göttingen, Göttingen (Germany), **1997**), the refinement calculations were performed by the full matrix least-squares method against F^2 (G. M. Sheldrick, SHELXS-97, Program for the Solution of Crystal Structures, Universität Göttingen, Göttingen (Germany), **1997**), graphic: MERCURY (Cambridge Crystallographic Data Centre, 12 Union Road, Cambridge CB21EZ); $0.48 \times 0.4 \times 0.37 \text{ mm}$, colorless blocks, space group *R $\bar{3}$* , trigonal, $a = 22.4017(4)$, $c = 34.811(1) \text{ \AA}$, $V = 15129.0(6) \text{ \AA}^3$, $Z = 18$, $\rho_{\text{ber.}} = 1.015 \text{ g cm}^{-3}$, 127091 reflections measured, 9822 reflections independent of symmetry, 9096 reflections observed ($I > 2\sigma(I)$), $R1 = 0.043$, wR^2 (all data) = 0.125, 260 parameters. CCDC-240540 (**4b**) and CCDC-240541 (**5b**) contain the supplementary crystallographic data for this paper. These data can be obtained free of charge via www.ccdc.cam.ac.uk/conts/retrieving.html (or from the Cambridge Crystallographic Data Centre, 12, Union Road, Cambridge CB21EZ, UK; fax: (+44)1223-336-033; or deposit@ccdc.cam.ac.uk).
- [8] The linear hexasilane with the formula Si₆Me₁₄ exhibits an intense absorption maximum at 260 nm; K. Obata, M. Kira, *Organometallics* **1999**, 18, 2216–2222.
- [9] C. G. Pitt, *J. Am. Chem. Soc.* **1969**, 91, 6613.
- [10] Starting with PhSi(SiMe₃)₃, the synthesis of **4a,b** succeeds without further purification of intermediate products with a total yield of ca. 70–80%. The experimental details for the preparation of the oligosilanes **2a,b–5a,b** are available online free of charge in the Supporting Information.

Cover Picture

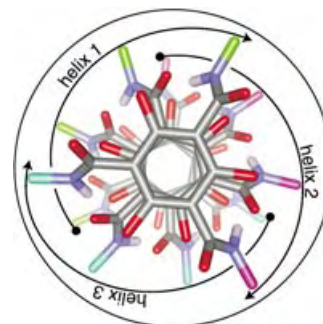
Takanori Shima, Frank Hampel, and J. A. Gladysz*

Three-fold alkene metatheses are used to access the family of molecular gyroscopes shown in the cover picture. As described by J. A. Gladysz and co-workers in their Communication on page 5537 ff. the gyroscopes consist of a phosphorus–iron–phosphorus axis, an $\{\text{Fe}(\text{CO})_3\}$ or $\{\text{Fe}(\text{CO})_2(\text{NO})\}^+$ “rotator”, and three $(\text{CH}_2)_n$ “spokes” that connect the phosphorus termini. These are believed to be the first systems that rigorously duplicate the connectivity and symmetry of toy gyroscopes (shown in the background).



Self-Assembly

In their Minireview on page 5446 ff. C. Nuckolls et al. report the self-assembly of hexasubstituted benzene derivatives that is directed by intermolecular hydrogen bonds between amide substituents.



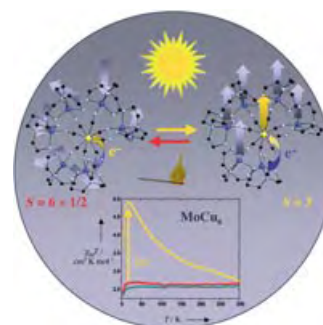
Magnetic Resonance Imaging

Sir Peter Mansfield illustrates in his Nobel Lecture on page 5456 ff. the principles, the experimental setup, and the practical use of magnetic resonance imaging methods in medicine.



Photomagnetic Effects

A cyanide bridged $\text{Mo}^{\text{IV}}\text{Cu}^{\text{II}}_6$ complex undergoes photoinduced electron transfer to give a high-spin $\text{Mo}^{\text{V}}\text{Cu}^{\text{I}}\text{Cu}^{\text{II}}_5$ species. The photomagnetic properties of these compounds are described by V. Marvaud, C. Mathonière et al. in their Communication on page 5468 ff.



Angewandte EarlyView®

The following Communications are available online (in Wiley InterScience). You can find them, as well as forthcoming Reviews, Highlights, and Essays, at www.angewandte.org, under Early View.

M. Tominaga, K. Suzuki, M. Kawano, T. Kusakawa, T. Ozeki, S. Sakamoto, K. Yamaguchi, M. Fujita*:
Finite, Spherical Coordination Networks that Self-Organize from 36 Small Components
 DOI: 10.1002/anie.200461422
 Published online: September 28, 2004

W. Zhong, D. Alexeev, I. Harvey, M. Guo, D. J. B. Hunter, H. Zhu, D. J. Campopiano, P. J. Sadler*:
Assembly of an Oxo Zirconium(IV) Cluster in a Protein Cleft
 DOI: 10.1002/anie.200460806
 Published online: October 8, 2004

Articles judged by the referees or the editor as being either very important or very urgent are immediately edited, proof-read, and electronically published once the manuscript has arrived in the editorial office in its final form. As long as there is no page number available these articles should be cited in the following manner:

Author(s), *Angew. Chem. Int. Ed.*, online publication date, DOI.

News

Alan R. Fersht Receives Bader Award _____ **5430** Corey Award to David W. C. MacMillan _____ **5430** Breslow Award to Peter B. Dervan _____ **5430**

Books

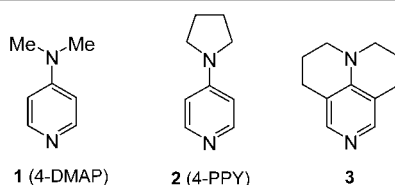
The Porphyrin Handbook Karl M. Kadish, Kevin M. Smith, Roger Guilard reviewed by F.-P. Montforts _____ **5431**
 Molecular Motors Manfred Schliwa reviewed by C. G. Baumann _____ **5432**
 Colloids and Colloid Assemblies Frank Caruso reviewed by H. Schubert _____ **5434**

Highlights

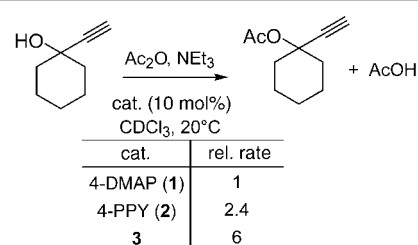
Organocatalysis

A. C. Spivey,* S. Arseniyadis **5436–5441**

Nucleophilic Catalysis by 4-(Dialkylamino)pyridines Revisited—The Search for Optimal Reactivity and Selectivity



A complex interplay between catalyst structure, acylating agent, auxiliary base, and solvent governs the reactivity and selectivity in 4-(dialkylamino)pyridine-catalyzed esterification reactions (see

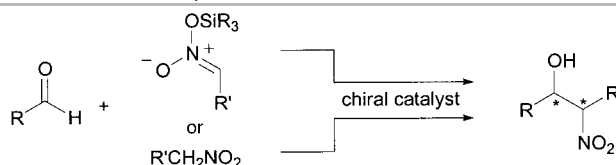


scheme). This highlight attempts a rationalization of the complicated mechanism and puts forward some explanations for seemingly contradictory experimental observations.

Synthetic Methods

C. Palomo,* M. Oiarbide, A. Mielgo _____ **5442–5444**

Unveiling Reliable Catalysts for the Asymmetric Nitroaldol (Henry) Reaction



Conceptually different chiral catalysts ranging from polymetallic complexes to Lewis acids and organocatalysts have emerged for solving the long-standing problem of stereocontrol in the Henry

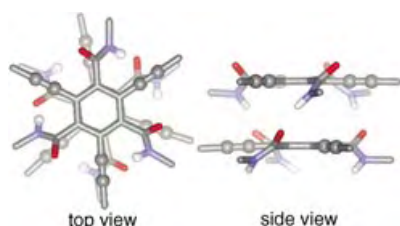
reaction, a fundamental C–C bond-forming process (see scheme). New catalyst systems with improved selectivity have increased the synthetic value of this reaction considerably.

Minireviews

Self-Assembly

M. L. Bushey, T.-Q. Nguyen, W. Zhang,
D. Horoszewski,
C. Nuckolls* _____ **5446–5453**

Using Hydrogen Bonds to Direct the
Assembly of Crowded Aromatics



Columnar superstructures are formed from the assembly of crowded aromatics. The design, synthesis, and self-assembly of this new class of aromatics (see picture) is detailed in this Minireview. The assembly of these subunits produces helical and polar stacks that can be directed with electric fields. In concentrated solutions, these self-assembled rods exhibit superhelices.

Reviews

Imaging Techniques

P. Mansfield* _____ **5456–5464**

Snapshot Magnetic Resonance Imaging
(Nobel Lecture)



Modern medicine relies heavily on magnetic resonance imaging. Sir Peter Mansfield was awarded the 2003 Nobel price in Physiology or Medicine for his investigations on theory and instrumental setup (see picture), which made this method a versatile diagnostic tool, and for the development of ultrahigh-speed techniques.

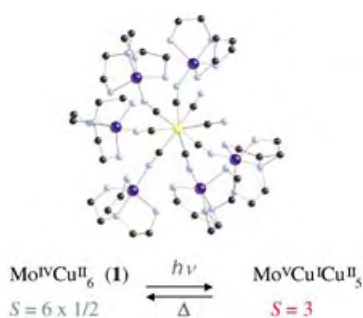
Communications

Single-Molecule Magnets



J. M. Herrera, V. Marvaud,* M. Verdaguer,
J. Marrot, M. Kalisz,
C. Mathonière* _____ **5468–5471**

Reversible Photoinduced Magnetic
Properties in the Heptanuclear Complex
[Mo^{IV}(CN)₂(CN–Cu^{II}L)₆]⁸⁺: A Photo-
magnetic High-Spin Molecule



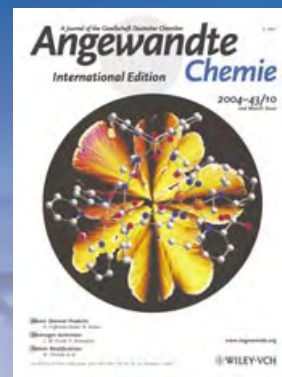
Metastable up to 280 K, {Mo^{IV}Cu^ICu^{II}}₃ ($S = 3$) forms as a result of intramolecular electron transfer from the Mo^{IV} center to one of the Cu^{II} termini of the [Mo^{IV}(CN)₂(CN–Cu^{II}(L))₆]⁸⁺ complex, (1; L = tris(2-aminoethyl)amine) upon light excitation (see picture: Mo yellow; C black; N blue; Cu purple). This process is thermally reversible. Compound 1 shows the magnetic properties of six independent Cu^{II} ions ($S = 1/2$).

For the USA and Canada:
ANGEWANDTE CHEMIE International
Edition (ISSN 1433-7851) is published weekly
by Wiley-VCH PO Box 191161, D 69451 Wein-
heim, Germany. Air freight and mailing in the
USA by Publications Expediting Inc. 200
Meacham Ave., Elmont, NY 11003. Periodicals

postage paid at Jamaica NY 11431. US POST-
MASTER: send address changes to *Angewandte
Chemie*, Wiley-VCH, 111 River Street, Hoboken,
NJ 07030. Annual subscription price for insti-
tutions: Europe € 3760.00/3418.00; outside
Europe US\$ 4948.00/4498.00 (valid for print
and electronic/print or electronic delivery); for

individuals who are personal members of a
national chemical society, or whose institution
already subscribes, or who are retired or self-
employed consultants, print only: Europe
€ 258.00/outside Europe US\$ 394.00. Postage
and handling charges included. All Wiley-VCH
prices are exclusive VAT.

The best in chemistry – for more than a hundred years



A Journal of the Gesellschaft Deutscher Chemiker
Angewandte
International Edition **Chemie**

www.angewandte.org

1888: The beginning
of a success story

Constant Innovations

- 1962:** First issue of the International Edition
- 1976:** Graphical abstracts
- 1979:** Cover pictures
- 1988:** Centenary of Angewandte
- 1989:** Routine use of color
- 1991:** New section: Highlights
- 1992:** Computerized editorial tracking system
- 1995:** Internet service for readers
- 1998:** Regular press service; full-text online
- 2000:** New section: Essays; EarlyView: Communications available online ahead of the printed version
- 2001:** New section: Minireviews
- 2002:** Online submission of manuscripts
- 2003:** Weekly publication; new section: News; new layout
- 2004:** Backfiles (1962-1997); ManuscriptXpress: Online system for authors and referees



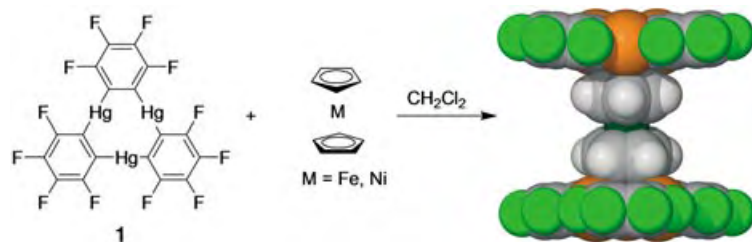
Angewandte's advisors...

E. W. "Bert" Meijer
Technische Universiteit
Eindhoven

»» **Angewandte Chemie**, in its way of publishing, is as original as the chemistry described in the journal. It serves our society in a superb and attractive way. Many leading communications and comprehensive reviews have been published through the years and many of them are used in my teaching and cited in my own papers. It is a privilege to publish in and to be connected to a journal that is the trendsetter in chemistry of the highest standards. ««

Angewandte Chemie International Edition is
a journal of the German Chemical Society (GDCh)





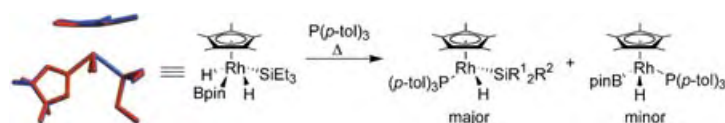
A sandwich in a sandwich: Electrophilic double-sandwich compounds are readily formed by interaction of ferrocene and nickelocene with the tridentate Lewis acid **1** (see scheme; C gray, F light green, Hg orange, M dark green). These new

supramolecules result from π interactions between the mercury centers of **1** and the C_5H_5 rings of the metallocenes. Surprisingly, the nickelocene derivative is dark red and air stable.

Metalloenes

M. R. Haneline,
F. P. Gabbaï* _____ **5471 – 5474**

Electrophilic Double-Sandwiches Formed by Interaction of $[Cp_2Fe]$ and $[Cp_2Ni]$ with the Tridentate Lewis Acid $[(o-C_6F_4Hg)_3]$



Spoilt for choice: a silane, dihydrogen, borane, or hydridoborate complex? The silyl boryl hydride complex $[Cp^*Rh(H_2)(Et_3Si)(Bpin)]$ (Bpin = (pinacolato)boryl) could adopt any of these structures, but it appears to contain

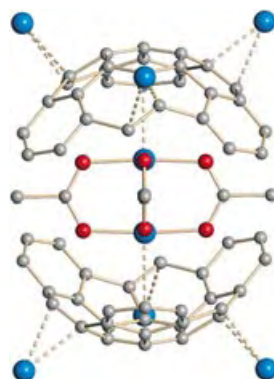
stronger B–H bonding than Si–H or H–H bonding and undergoes elimination of pinacolborane faster than of silane or hydrogen (see scheme). The bonding situation is studied by experimental and theoretical methods.

Borane Complexes

K. S. Cook, C. D. Incarvito, C. E. Webster,
Y. Fan, M. B. Hall,*
J. F. Hartwig* _____ **5474 – 5477**

Rhodium Silyl Boryl Hydride Complexes: Comparison of Bonding and the Rates of Elimination of Borane, Silane, and Dihydrogen

Bringing together two C_{30} hemispheres by coordinating their concave faces to a monometal template or metal cluster represents the first step in an appealing strategy for the controlled synthesis of endohedral fullerene complexes by laboratory methods. A crystalline transition metal complex of this structural type (see picture; Rh blue, O red, C gray; H, F omitted) has now been prepared from hemibuckminsterfullerene $C_{30}H_{12}$ and $[Rh_2(O_2CCF_3)_4]$.

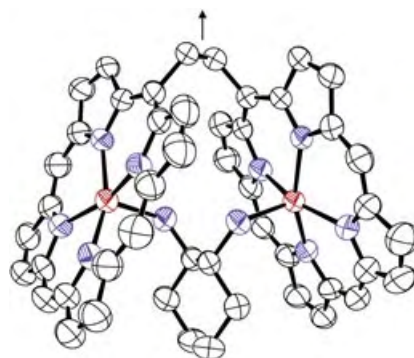


Geodesic Polyarenes

M. A. Petrukhina,* K. W. Andreini, L. Peng,
L. T. Scott _____ **5477 – 5481**

Hemibuckminsterfullerene $C_{30}H_{12}$: X-ray Crystal Structures of the Parent Hydrocarbon and of the Two-Dimensional Organometallic Network $\{[Rh_2(O_2CCF_3)_4]_3 \cdot (C_{30}H_{12})\}$

A sign of the times: A 1:1 tweezer complex consisting of an achiral bis(zinc porphyrin) and (*R,R*)-1,2-diaminocyclohexane has been characterized by X-ray crystallographic analysis (see picture, Zn red, N blue). This has enabled a full and unambiguous rationalization of the highly efficient transfer of chirality information from an optically active guest to an achiral host in a supramolecular system based on a bisporphyrin to be carried out.



Chirality Transfer

V. V. Borovkov,* I. Fujii, A. Muranaka,
G. A. Hembury, T. Tanaka, A. Ceulemans,
N. Kobayashi, Y. Inoue* _____ **5481 – 5485**

Rationalization of Supramolecular Chirality in a Bisporphyrin System

Aromaticity

J. M. Mercero,* J. M. Matxain,
J. M. Ugalde ————— 5485 – 5488

Mono- and Multidecker Sandwich-Like
Complexes of the Tetraazacyclobutadiene
Aromatic Ring



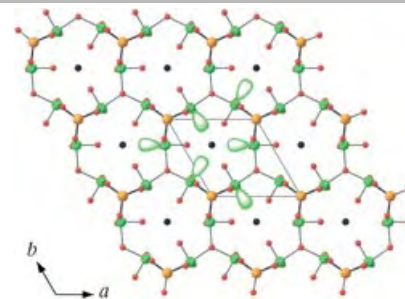
Sandwich structures are readily formed with the aromatic N_4^{2-} anion. The complexes, which form with early- and late-transition-metal centers are described and their properties analyzed. These sandwich complexes can oligomerize or polymerize to form multidecker chains.

Layered Compounds

K. M. Ok,
P. S. Halasyamani* ————— 5489 – 5491

The Lone-Pair Cation I^{5+} in a Hexagonal Tungsten Oxide-Like Framework: Synthesis, Structure, and Second-Harmonic Generating Properties of $Cs_2I_4O_{11}$

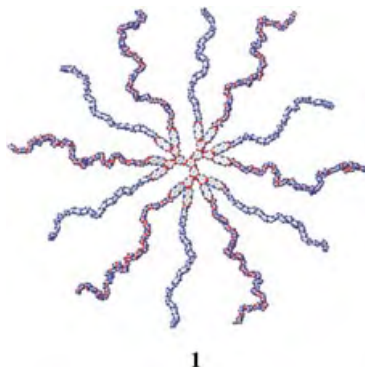
The layered iodate $Cs_2I_4O_{11}$ has been synthesized and characterized. Its hexagonal tungsten oxide-like framework consists of six-membered rings of corner-sharing IO_3 polyhedra with three lone pairs pointing inward and three lone pairs pointing outward (depicted for central ring). Capping of the layer by asymmetric IO_3 polyhedra on one side results in a noncentrosymmetric material with highly efficient second-harmonic generating properties.



Supramolecular Chemistry

J. Xu, E. R. Zubarev* ————— 5491 – 5496

Supramolecular Assemblies of Starlike
and V-Shaped PB–PEO Amphiphiles



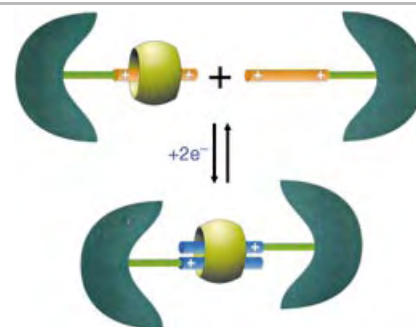
A star is born in the form of a polybutadiene–poly(ethylene oxide) amphiphile **1**. The molecule exhibits remarkable self-assembly properties: it forms regular and reverse micelles in water and hexane, respectively. Comparison of **1** with a V-shaped precursor revealed a profound influence of molecular architecture on the self-assembly behavior of the amphiphiles.

Host–Guest Chemistry

K. Moon, J. Grindstaff, D. Sobransingh,
A. E. Kaifer* ————— 5496 – 5499

Cucurbit[8]uril-Mediated Redox-Controlled Self-Assembly of Viologen-Containing Dendrimers

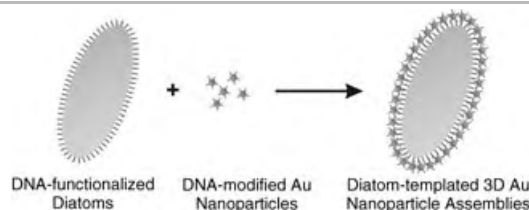
The dimerization of dendrimers that contain a single 4,4'-bipyridinium (viologen) unit, upon one-electron reduction, is strongly enhanced by the presence of the host cucurbit[8]uril. This behavior is attributed to the formation of a stable inclusion complex between the host and two π -stacked viologen radical-cation guests—the one-electron-reduced form of viologen (see scheme).



Nanostructures

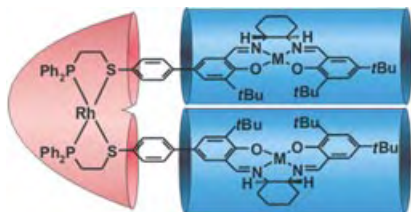
N. L. Rosi, C. S. Thaxton,
C. A. Mirkin* ————— 5500 – 5503

Control of Nanoparticle Assembly by
Using DNA-Modified Diatom Templates



Microorganisms point the way: The silica cell walls of various diatoms were covalently functionalized with DNA by using straightforward chemical procedures and then used as templates for the sequence-specific assembly and 3D hierarchical

arrangement of prefabricated DNA-modified gold nanoparticles. The DNA was used to further direct the assembly of multiple nanoparticle layers onto the diatom templates (see picture).



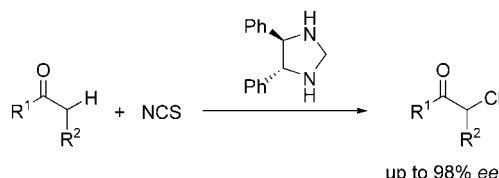
Abiotic allosteric regulation: The design, synthesis, and application of novel,

reversible allosteric catalytic molecular tweezers that contain a structural metal, addressable in situ, and two functional catalytic metals are reported (see picture). Kinetic and selectivity data reflect a significant decrease in cooperativity upon opening of the “arms” of the catalyst caused by reactions occurring at the hinge.

Asymmetric Catalysis

N. C. Gianneschi, S.-H. Cho, S. T. Nguyen, C. A. Mirkin* — 5503 – 5507

Reversibly Addressing an Allosteric Catalyst In Situ: Catalytic Molecular Tweezers



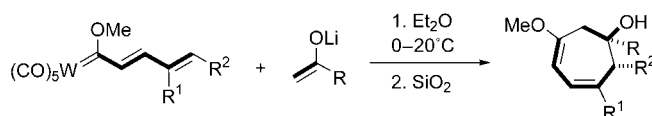
A C₂-symmetric diamine serves as the organocatalyst in an asymmetric α -chlorination reaction of simple ketones (e.g., cyclohexanone, diethyl ketone). Optically active α -chloroketones are formed with

excellent enantioselectivities using *N*-chlorosuccinimide (NCS) as the chlorine source (see scheme). These products have broad synthetic utility, in particular for pharmaceutical applications.

Enantioselective Chlorination

M. Marigo, S. Bachmann, N. Halland, A. Braunton, K. A. Jørgensen* — 5507 – 5510

Highly Enantioselective Direct Organocatalytic α -Chlorination of Ketones



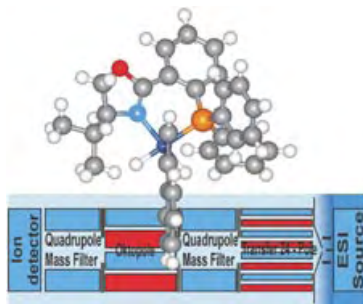
Magnificent seven! Functionalized seven-membered carbocycles can be easily synthesized in a diastereoselective way by a formal [5+2] carbocyclization reaction from dienylmethoxycarbene complexes

and methyl ketone lithium enolates (see scheme). Examples for R: Ph, 2-Fu, PhCH₂CH₂, TMS-C≡C; R¹: H, Me; R²: Ph, 2-Fu are presented.

Cyclization Reactions

J. Barluenga,* J. Alonso, F. J. Fañanás, S. García-Granda, J. Borge — 5510 – 5513

Diastereoselective Synthesis of Cycloheptadienol Derivatives by a Formal [5+2] Carbocyclization Reaction of $\alpha,\beta,\gamma,\delta$ -Diunsaturated (Methoxy)carbene Complexes with Methyl Ketone Lithium Enolates

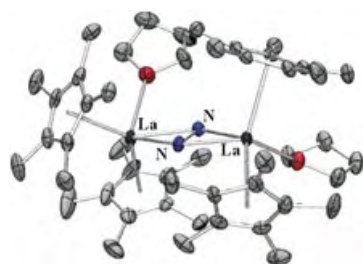


Weighing up mechanisms: Using mass spectrometry (see scheme) gas-phase reactions of ions containing the (PHOX)Ir (PHOX = chiral phosphanyloxazoline ligand, red O, light blue N, orange P, blue Ir) fragment are used to explore mechanistic pathways in the catalytic hydrogenation by related complexes. The reactions indicate that the hydrogenation proceeds by an Ir^I/Ir^{III} cycle rather than by the previously proposed Ir^{III}/Ir^V polyhydride route.

Homogeneous Catalysis

R. Dietiker, P. Chen* — 5513 – 5516

Gas-Phase Reactions of the [(PHOX)IrL₂]⁺ Ion Olefin-Hydrogenation Catalyst Support an Ir^I/Ir^{III} Cycle



Dinitrogen reduction with diamagnetic trivalent lanthanum complexes is possible for the first time using a combination of a trivalent metallocene and potassium graphite. Both [(C₅Me₄H)₃La] and [(C₅Me₃)₂La][BPh₄] are viable starting materials and reduce dinitrogen in the presence of KC₈ to give [N=N]²⁻ containing structures (see picture).

Lanthanide Chemistry

W. J. Evans,* D. S. Lee, C. Lie, J. W. Ziller — 5517 – 5519

Expanding the LnZ₃/Alkali-Metal Reduction System to Organometallic and Heteroleptic Precursors: Formation of Dinitrogen Derivatives of Lanthanum

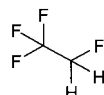
Fluorinated Solvents

S. Saul, S. Corr,
J. Micklefield* — 5519–5523

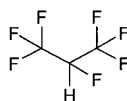
Biotransformations in Low-Boiling
Hydrofluorocarbon Solvents



R-32



R-134a



R-227ea

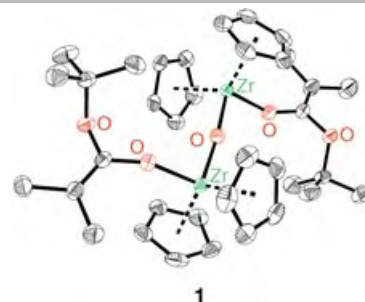
Solvent solutions: Low-boiling hydrofluorocarbons (see examples) are excellent solvents for lipase-catalyzed reactions and ideal replacements for conventional organic solvents and supercritical fluids as media for nonaqueous biotransformations. Notably increased rates, yields, and enantioselectivities were observed with the model kinetic resolution of (\pm)-1-phenylethanol and the desymmetrization of *meso*-2-cyclopentene-1,4-diol.

Homogeneous Catalysis

G. Stojcevic, H. Kim, N. J. Taylor,
T. B. Marder, S. Collins* — 5523–5526

Methacrylate Polymerization using a
Dinuclear Zirconocene Initiator: A New
Approach for the Controlled Synthesis of
Methacrylate Polymers

Tacticity tactics: The dinuclear bis(enolate) complex **1**, when activated with [PhNHMe₂][B(C₆F₅)₄], is an effective initiator of living methyl methacrylate polymerization, providing partially syndiotactic poly(methyl methacrylate) with a narrow molecular-weight distribution. Mechanistic studies showed that **1** is transformed into a cationic enolate complex and this dinuclear species is involved in propagation.



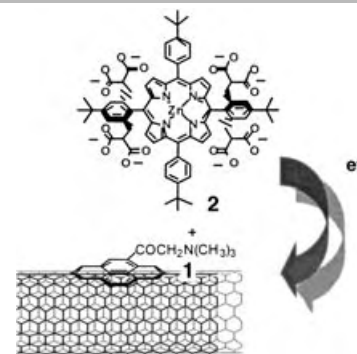
1

Electron Transfer

D. M. Guldi,* G. M. A. Rahman, N. Jux,
N. Tagmatarchis, M. Prato — 5526–5530

Integrating Single-Wall Carbon
Nanotubes into Donor–Acceptor
Nanohybrids

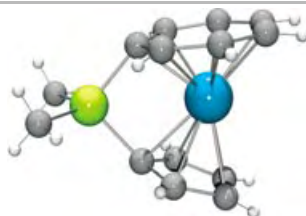
A tube for electrons: Through π – π and Coulomb interactions, a complex is obtained between carbon nanotubes grafted with pyrene⁺ (**1**) and the zinc porphyrin complex **2**. Photoexcitation of the resulting donor–acceptor assembly is followed by a rapid and efficient charge separation to generate a charge-separated state that lives for microseconds.



Sandwich Complexes

M. Tamm,* A. Kunst, T. Bannenberg,
E. Herdtweck, P. Sirsch, C. J. Elsevier,
J. M. Ernsting — 5530–5534

Ansa-Cycloheptatrienyl–Cyclopentadienyl
Complexes



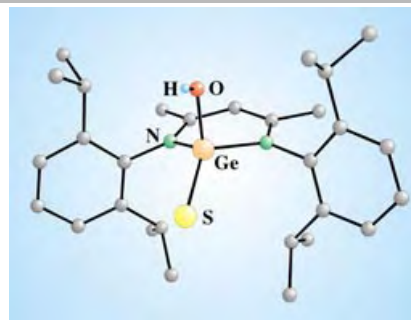
Introduction of the Me₂Si bridge and distortion of the sandwich structure facil-

itate the interaction of the 16-electron *ansa*-complex (see picture; blue Ti, yellow Si, gray C) with σ -donor/ π -acceptor ligands, such as CO or isocyanides, which allows the electronic structure of this strongly bent first *ansa*-cycloheptatrienyl–cyclopentadienyl transition-metal complex to be studied. The complex is prepared from [(η -C₇H₇)Ti(η -C₅H₅)].

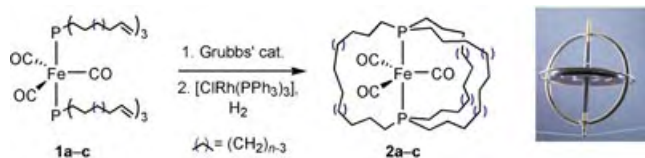
Germanium Chemistry

L. W. Pineda, V. Jancik, H. W. Roesky,*
R. Herbst-Irmer — 5534–5536

Germacarboxylic Acid: An Organic-Acid
Analogue Based on a Heavier Group 14
Element



First impressions: An oxidative addition between [LGeOH] and elemental sulfur leads to the isolation of the first germacarboxylic acid [LGe(S)OH] (L = HC{(CMe)(2,6-*i*Pr₂C₆H₃N)}₂; see picture). In the solid state [LGe(S)OH] displays preferential of the thiono-form and formation of hydrogen-bond arrays generates dimers. This germacarboxylic acid shows how the heavier congeners of Group 14 can mimic well know organic functional groups.



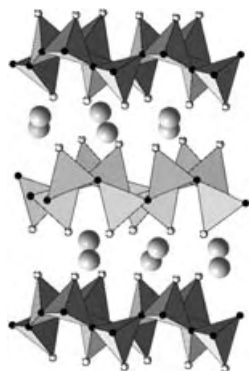
Complexes to toy with: Ring-closing metathesis of the bis(phosphane) complexes **1a-c** ($n=4-6$) followed by hydrogenation gives the “molecular gyroscopes” **2a-c**. The crystal structure of **2c**

and the NMR data for the analogous {Fe(CO)₂(NO)}⁺ complex indicate facile rotation of the {Fe(CO)₂(L)}^{m+} moieties within the P(CH₂)₁₄P spokes. Shorter bridges as in **2a** lock the rotators.

Molecular Gyroscopes

T. Shima, F. Hampel,
J. A. Gladysz* 5537–5540

Molecular Gyroscopes: {Fe(CO)₃} and {Fe(CO)₂(NO)}⁺ Rotators Encased in Three-Spoke Stators; Facile Assembly by Alkene Metatheses

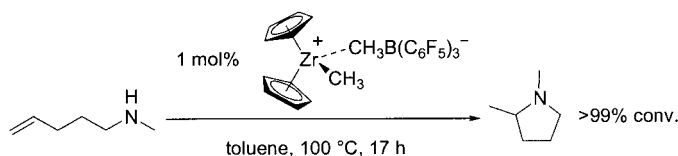


A corrugated [Si₂O₂N₂]²⁻ layer anion, which is constructed of dreier rings, forms the basis of the silicate Ca[Si₂O₂N₂] (see picture). The unusual structure results from the fact that every N atom—unlike the O atoms in oxosilicates—links three neighboring Si tetrahedron centers within the layers, whereas all the O atoms are exclusively bonded terminally to the Si atoms.

Structure Elucidation

H. A. Höpfe, F. Stadler, O. Oeckler,
W. Schnick* 5540–5542

Ca[Si₂O₂N₂]²⁻—A Novel Layer Silicate



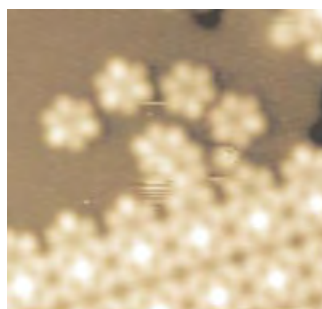
Alternative catalysts: The hydroamination of nonactivated double bonds has been the domain of rare-earth-metal catalysts. Now alkyl zirconocene and titanocene cations, which are readily prepared from

commercially available precursors, are shown to be active catalysts in the hydroamination/cyclization of secondary aminoalkenes to give tertiary pyrrolidines and piperidines.

Cyclizations

D. V. Gribkov,
K. C. Hultsch* 5542–5546

Hydroamination/Cyclization of Aminoalkenes Using Cationic Zirconocene and Titanocene Catalysts



Seeing stars: surface-supported nano-scale oxide materials are prepared by a chemical driven self-assembly process involving a novel star-shaped [V₆O₁₂] cluster molecules (see STM image). The [V₆O₁₂] clusters are not stable units in the gas phase but form spontaneously on a metal surface. On the surface the oxide building blocks can be organized into different 2D oxide structures by adjustment of the oxygen chemical potential.

Cluster Compounds

J. Schoiswohl, S. Surnev, M. Sock,
M. G. Ramsey, G. Kresse,
F. P. Netzer* 5546–5549

Thermodynamically Controlled Self-Assembly of Two-Dimensional Oxide Nanostructures



Communications labeled with this symbol have been judged by two referees as being “very important papers”.

Looking for outstanding employees?

Do you need another expert for your excellent team?

... Chemists, PhD Students, Managers, Professors, Sales Representatives...

Place an advert in the printed version and have it made available online for 1 month, free of charge!

Angewandte Chemie International Edition

Advertising Sales Department: Marion Schulz

Phone: 0 62 01 - 60 65 65

Fax: 0 62 01 - 60 65 50

E-Mail: MSchulz@wiley-vch.de

Service

Keywords 5550

Authors 5551

Preview 5553

Corrigendum

An Amphotericin B–Fluorescein
Conjugate as a Powerful Probe for
Biochemical Studies of the Membrane**

A. Zumbuehl, D. Jeannerat, S. E. Martin,
M. Sohrmann, P. Stano, T. Vigassy,
D. D. Clark, S. L. Hussey, M. Peter,
B. R. Peterson, E. Pretsch, P. Walde,
E. M. Carreira* **5181–5185**

Angew. Chem. Int. Ed. **2004**, 43

DOI 10.1002/anie.200460489

In this Communication, the affiliation of some of the authors were inadvertently swapped during the printing process. The correct author and address list is that printed below.

A. Zumbuehl, Prof. Dr. E. M. Carreira
Laboratorium für Organische Chemie
ETH Hönggerberg, HCI H335
8093 Zürich (Switzerland)
Fax: (+ 41) 1-632-1328
E-mail: carreira@org.chem.ethz.ch

Dr. D. Jeannerat
Département de Chimie Organique
Université de Genève
1211 Genève 4 (Switzerland)

Dr. S. E. Martin, D. D. Clark, Dr. S. L. Hussey, Prof. Dr. B. R. Peterson
Department of Chemistry
The Pennsylvania State University
Pennsylvania 16802 (USA)

Dr. M. Sohrmann, Prof. Dr. M. Peter
Institut für Biochemie
ETH Hönggerberg
8093 Zürich (Switzerland)

P. Stano, Prof. Dr. P. Walde
Departement Materialwissenschaft
ETH Hönggerberg
8093 Zürich (Switzerland)

Dr. T. Vigassy, Prof. Dr. E. Pretsch
Laboratorium für Organische Chemie
ETH Hönggerberg
8093 Zürich (Switzerland)



Alan R. Fersht Receives Bader Award

The recipient of the 2005 Alfred Bader Award in Bioinorganic or Bioorganic Chemistry, Sir Alan R. Fersht, is one of the founders of protein engineering. He was the first to apply site-directed mutagenesis to analyze the structure and activity of proteins.^[1] Methods he developed revolutionized the way protein interactions are studied. His research at the interface of chemistry and biology includes the elucidation at atomic resolution of how



Alan R. Fersht

proteins fold and unfold. He also uses biophysical methods to study how mutation affects proteins (in particular the tumor suppressor p53) in the cell cycle, with the aim of designing novel anti-cancer drugs that function by restoring the activity of mutated proteins.

Fersht completed his PhD in 1968 at the University of Cambridge (UK) under the guidance of A. J. Kirby. He carried out postdoctoral research at Brandeis University (MA, USA) with W. P. Jencks before returning to Cambridge, where he is currently both Herchel Smith Professor of Organic Chemistry and Director of the Cambridge Centre for Protein Engineering. A significant amount of his academic career (1978–1988) was spent in London as Professor of Biological Chemistry at Imperial College. Fersht has received numerous prestigious awards during his outstanding career, and was knighted in 2003 for his work on protein science. He is a member of the International Advisory Board of *Angewandte Chemie* and Co-Chair of the Editorial Board of *ChemBioChem*.

Corey Award to David W. C. MacMillan

The Elias J. Corey Award recognizes outstanding creativity in organic synthesis by a young investigator whose contributions have had a significant impact on the field. The recipient for 2005, David W. C. MacMillan, is associate professor of chemistry at the California Institute of Technology. Born in 1968, he completed his



David W. C. MacMillan

undergraduate degree in chemistry in his home town at the University of Glasgow (UK). He continued his studies at the University of California, Irvine (USA) in the research group of Larry Overman, where he focused on the stereocontrolled synthesis of bicyclic tetrahydrofurans and the application of this methodology in natural product synthesis. After completing his PhD in 1996, he spent two years as a postdoctoral fellow with David Evans at Harvard University (MA, USA), where he carried out research on enantioselective catalysis, in particular the development of Sn^{II} -bisoxazoline (Sn^{II} -box) complexes. These chiral Lewis acids have found application in many asymmetric transformations.

MacMillan began his independent research career at the University of California, Berkeley, before moving to the California Institute of Technology in 2000. His current research interests encompass the design of new synthetic methodology, enantioselective catalysis, and natural product synthesis. In a recent Communication in *Angewandte Chemie* he described enantioselective organocatalytic direct aldol reactions of α -oxyaldehydes as the first step in a proposed two-step synthesis of carbohydrates.^[2] This most elegant route to carbohydrates has since been completed.^[3]

Breslow Award to Peter B. Dervan

Peter B. Dervan will receive the 2005 Ronald Breslow Award in recognition of his outstanding contributions to the



Peter B. Dervan

field of biomimetic chemistry. Dervan completed his BS in chemistry in 1967 at Boston College (MA, USA) and his PhD in 1972 at Yale University (CT, USA) with research in physical organic chemistry under the guidance of Jerome A. Berson. After a year at Stanford University (CA, USA) as an NIH Postdoctoral Fellow with Gene Van Tame- len, he became an assistant professor in 1973 at the California Institute of Technology, where he is now Bren Professor of Chemistry in the Division of Chemistry and Chemical Engineering.

Through a combination of organic synthesis, physical chemistry, and biology, Dervan and his research group investigate the chemical principles behind the sequence-specific recognition of DNA by small molecules. The ultimate aim is to develop general chemical methods for recognizing any given DNA sequence and for the regulation of gene expression. Dervan reported recently in *Angewandte Chemie* the design of a sequence-specific DNA bisintercalator with greater specificity and binding affinity than any other known natural or synthetic bisintercalator.^[4] Dervan has received numerous important scientific awards, and he is on the International Advisory Board of *Angewandte Chemie*.

- [1] A. R. Fersht, J.-P. Shi, A. J. Wilkinson, D. M. Blow, P. Carter, M. M. Y. Waye, G. P. Winter, *Angew. Chem.* **1984**, 96, 455; *Angew. Chem. Int. Ed. Engl.* **1984**, 23, 467.
- [2] A. B. Northrup, I. K. Mangion, F. Hettche, D. W. C. MacMillan, *Angew. Chem.* **2004**, 116, 2204; *Angew. Chem. Int. Ed.* **2004**, 43, 2152.
- [3] A. B. Northrup, D. W. C. MacMillan, *Science*, **2004**, 305, 1752.
- [4] E. J. Fechter, B. Olenyuk, P. B. Dervan, *Angew. Chem.* **2004**, 116, 3675; *Angew. Chem. Int. Ed.* **2004**, 43, 3591.

Nucleophilic Catalysis by 4-(Dialkylamino)pyridines Revisited—The Search for Optimal Reactivity and Selectivity

Alan C. Spivey* and Stellios Arseniyadis

Keywords:

asymmetric catalysis · esterification · N ligands · nucleophilic catalysis · organocatalysis

4-(Dimethylamino)pyridine (4-DMAP, **1**) is well known as a catalyst for the esterification of alcohols by acid anhydrides and for various other synthetically useful transformations involving acyl transfer.^[1,2] Its catalytic potential was first discovered by the groups of Litvinenko and Steglich in the late 1960s^[3,4] and its synthetic utility and that of its congeners, including polymeric variants,^[5] have been reviewed.^[6–9] Recently, attention has been focused on the development of enantiomerically pure chiral 4-(dialkylamino)pyridines for the kinetic resolution of alcohols and related enantioselective transformations.^[10,11] As a result of this interest, the detailed mechanism of catalysis by 4-(dialkylamino)pyridines and the factors that influence their reactivity have come under renewed scrutiny. In particular, Steglich and co-workers^[12] reported pyridonaphthyridine **3** as being the most catalytically active 4-DMAP analogue yet prepared for the acetylation of tertiary alcohols, and work by Kattnig and Albert^[13] has illustrated the key role of the anion and general base catalysis in regulating the rate and regioselectivity of polyol acetylation by **1** (Scheme 1).

Herein, the detailed mechanism of catalysis of esterification by 4-(dialkylamino)pyridines is reexamined in light of these findings, and the complexity

associated with this apparently straightforward process is highlighted.

That pyridine and 4-substituted derivatives act primarily as *nucleophilic* rather than *general base* catalysts for alcohol esterification follows from the dramatic loss of activity that accompanies 2-alkyl substitution despite the relatively marginal effect that this substitution has on the pK_a value of these derivatives. Such steric inhibition of catalysis was first shown to be characteristic of nucleophilic catalysis in work by Gold and Jefferson in the early 1950s on the hydrolysis of Ac_2O with a series of methyl-substituted pyridines.^[14,15] The effect was quantified by Litvinenko and co-workers in 1981 for the catalysis of benzoylation of benzyl alcohol with $BzCl$.^[16] In addition to confirming the nucleophilic nature of the catalysis, this work also highlighted the particularly high catalytic activity of **1**, which exhibits a rate of 3.4×10^8 relative to the uncatalyzed reaction (Scheme 2).

The high catalytic reactivity of **1** had previously been noted by Litvinenko and co-workers in the benzoylation of 3-chloroaniline^[3] and subsequently, but independently, **1** was shown by Steglich and co-workers to enable esterification of even hindered tertiary alcohols with Ac_2O .^[4] Esterification reactions of tertiary alcohols are relatively slow and particularly susceptible to steric factors and therefore proved to be useful for exploring structure–activity relations for catalysis by 4-DMAP analogues. Accordingly, Hassner et al. found that 4-pyrrolidinopyridine (4-PPY, **2**) was the most efficient of a series of 4-aminopyridine derivatives, including **1**, for the

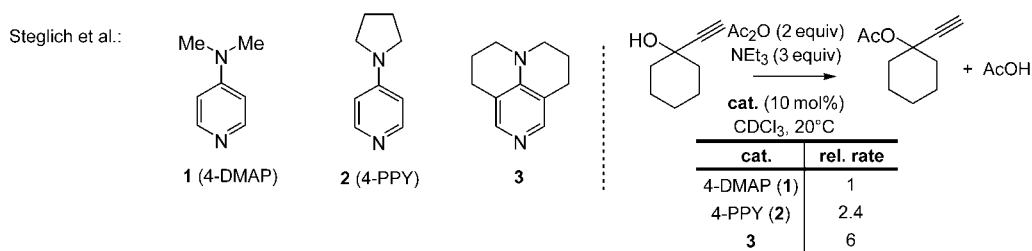
acetylation of 1-methylcyclohexanol with Ac_2O (Scheme 3).^[17]

Hassner et al. noted the lack of correlation between the pK_a value and the catalytic activity; they suggested that the relative efficiencies of the various catalysts reflected the stabilities of the respective derived acyl pyridinium intermediates in a mechanistic scenario involving equilibrium formation of these salts followed by rate-determining reaction with the alcohol (Scheme 4).

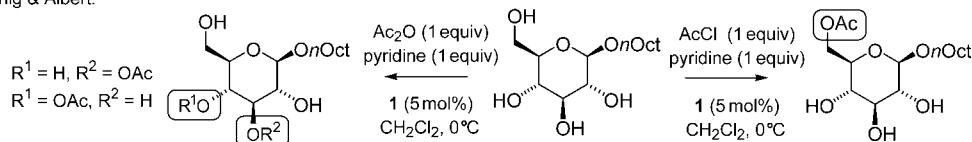
Additionally, Hassner et al. noted that the order of catalytic activity of 4-aminopyridine derivatives [4-pyrrolidino (**2**) > 4-dimethylamino (**1**) > 4-piperidino (**5**) > 4-morpholino (**7**)] mirrored the order of reactivity of cyclohexanone-derived enamines towards electrophiles.^[18–24] This order has been rationalized as a balance of stereoelectronic ($n_N \rightarrow \pi^*_{C=C}$) and steric effects ($A^{1,3}$ strain) which dictates the efficiency with which the lone pair of electrons on the enamine nitrogen atom interacts with the C–C double bond. By analogy with the enamine series,^[19] Hassner et al. noted that there was a qualitative correlation between the degree of shielding of the pyridyl β -hydrogen atoms in the 1H NMR spectra of the catalytically active 4-aminopyridine derivatives and their catalytic efficiency (see Scheme 3).^[17] They inferred that the extent of electronic communication between the lone pair of electrons of the exocyclic nitrogen atom and the carbonyl function through the pyridyl ring was a key factor in stabilizing the acyl pyridinium intermediate.

The design of pyridonaphthyridine **3** (Scheme 1), recently disclosed by Steg-

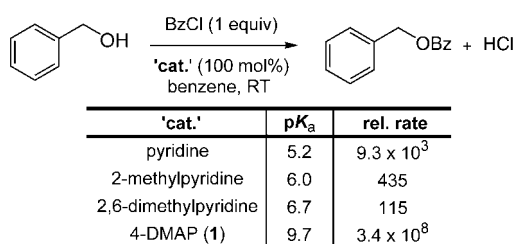
[*] Dr. A. C. Spivey, S. Arseniyadis
Department of Chemistry
South Kensington Campus
Imperial College
London SW7 2AZ (UK)
Fax: (+44) 20-7594-5841
E-mail: a.c.spivey@imperial.ac.uk



Kattinig & Albert:



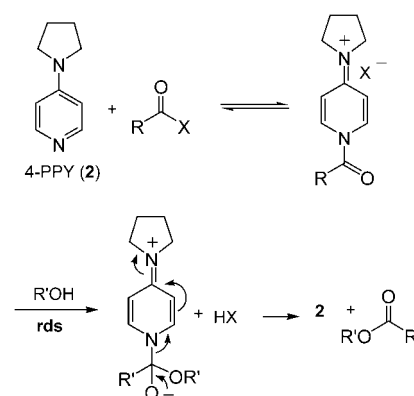
Scheme 1. Relative rates of acetylation of 1-ethynylcyclohexanol with Ac₂O catalyzed by 4-DMAP (1), 4-pyrrolidinopyridine (4-PPY, 2), or pyridonaphthyridine 3;^[12] and the regioselectivity of acetylation of octyl β-D-glucopyranoside with AcCl/pyridine versus Ac₂O/pyridine catalyzed by 4-DMAP (1).^[13]



Scheme 2. Catalysis of benzoylation of benzyl alcohol with BzCl by substituted pyridines.^[16]

dimethylamino or pyrrolidino analogues (i.e. **21** or **22**) as judged by their relative reactivities towards, for example, the Danishefsky diene (Scheme 5).^[25,26]

As the tricyclic scaffold found in derivative **24** allows the most efficient electronic communication between the lone pair of electrons of the amine and the cation, pyridonaphthyridine **3** was predicted to form highly stabilized acyl pyridinium salts and consequently to be a particularly efficacious nucleophilic acylation catalyst. Moreover, density functional theory calculations of the reaction enthalpies for acetyl transfer from pyridine to **3** corroborated the expected stability of the acetylpyridinium salt of **3**. In the event, **3** was shown to

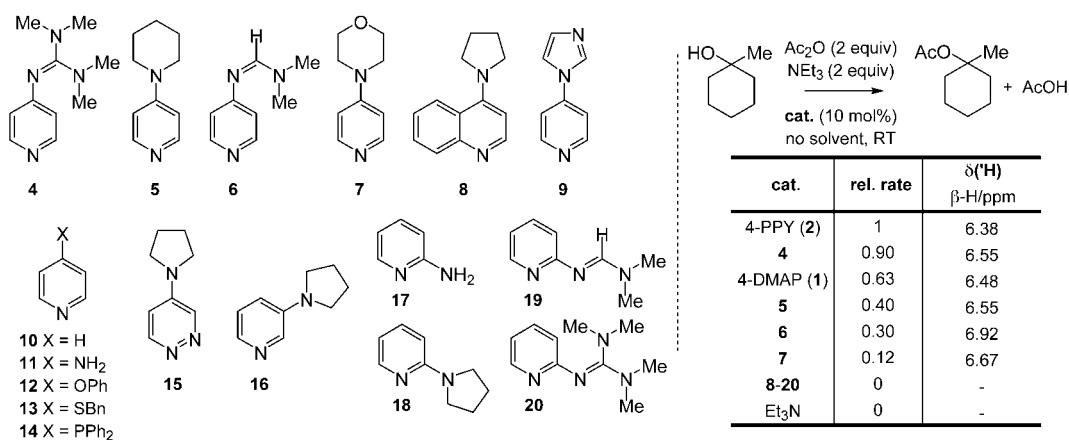


Scheme 4. Mechanism of nucleophilic catalysis of alcohol esterification according to Hassner et al.^[17] rds = rate-determining step.

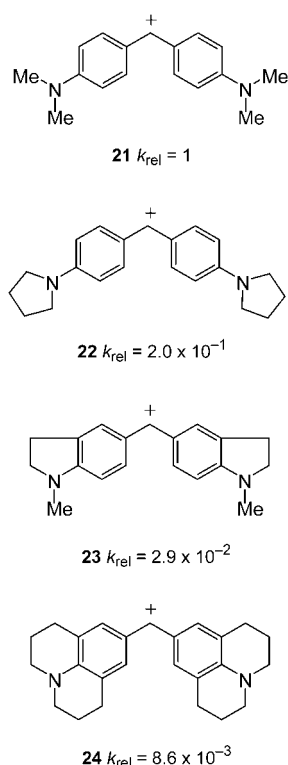
lich and co-workers,^[12] evolved from this analysis. Prior studies by Mayr et al. had established a quantitative framework for comparing the influence of 4-dialkylamino substitution on benzhydryl cation reactivity and specifically had shown that “conformationally fixed” cations such as **23** and **24** are significantly more stabilized than either the

dicted to form highly stabilized acyl pyridinium salts and consequently to be a particularly efficacious nucleophilic acylation catalyst. Moreover, density functional theory calculations of the reaction enthalpies for acetyl transfer from pyridine to **3** corroborated the expected stability of the acetylpyridinium salt of **3**. In the event, **3** was shown to

be the most catalytically active 4-DMAP analogue yet prepared, displaying a rate of ≈6 relative to **1** for the acetylation of 1-ethynylcyclohexanol



Scheme 3. Catalysis of acetylation of 1-methylcyclohexanol with Ac₂O by substituted pyridines and related azines.^[17]



Scheme 5. Relative reactivities of various benzhydryl cations towards the Danishefsky diene as a measure of the ability of the 4-dialkylamino group to participate in $n_{\text{N}} \rightarrow \pi^*_{\text{C}=\text{C}}$ overlap.^[26]

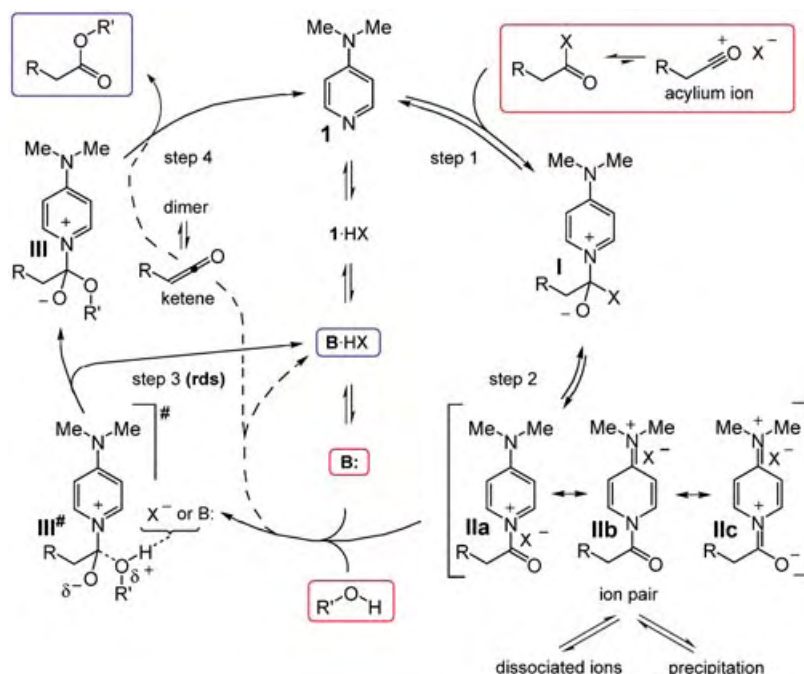
with Ac_2O and with Et_3N as auxiliary base (Scheme 1).

These results clearly have practical synthetic significance for the esterification of highly hindered alcohols and lend support to the notion that the efficiency of nucleophilic catalysis by this class of compound is closely related to the stability of the intermediate acylpyridinium salt. However, the mechanistic framework represented in Scheme 4 is simplistic. Although the kinetics of the esterification by **1** under standard conditions in a low-polarity solvent are broadly consistent with the steady-state formation of *N*-acylpyridinium salt followed by the rate-determining reaction of this salt with the alcohol,^[27] this analysis fails, at least explicitly, to account for a number of important features of the catalysis, such as the significant differences in the rate of catalysis when employing acid chlorides versus anhydrides and when varying the auxiliary base.^[9,12,13] To facilitate a discussion that encompasses these features,

a more detailed catalytic cycle is presented below (Scheme 6).

In this four-step cycle, reversible formation of *N*-acylpyridinium salt **II** by the addition of **1** to the acyl donor via the tetrahedral intermediate **I**

(e.g. $\text{H}_2\text{O} > \text{hexane}$). This is particularly pronounced because in solvents of low polarity a solvated ion pair is expected, with a high propensity to return in a quasi-unimolecular fashion to starting materials, where-



Scheme 6. Proposed catalytic cycle for alcohol esterification with 4-DMAP (**1**).

(steps 1 and 2) is followed by irreversible nucleophilic addition of the alcohol to salt **II** (step 3, $\rightarrow \text{III}^\#$) with concomitant proton transfer (through transition state $\text{III}^\#$) and finally elimination to regenerate **1** (step 4).

The position of the equilibrium to form salt **II** is dictated by the relative affinities of the anion X^- and **1** for the acyl group in the reaction solvent. Because of the aforementioned influence of steric effects and conjugation ($\text{IIa} \leftrightarrow \text{IIb} \leftrightarrow \text{IIc}$, Scheme 6)^[28,29] these “acyl affinities” will not mirror $\text{p}K_{\text{a}}$ values,^[30] but the equilibrium will be shifted in favor of *N*-acylpyridinium salt formation for:

- pyridines that have high nucleophilicity and impart stabilization of the acyl group by conjugation (e.g. **1** > pyridine),
- anions that have high nucleofugacity (e.g. $\text{Cl}^- > \text{OAc}^-$), and
- polar solvents that can solvate the charge-separated salt more efficiently than the neutral starting materials

as in highly polar solvents the dissociated ions will experience a significant activation entropy for return.

Evidence to support these expectations has been summarized previously.^[9] Of particular note were VT-NMR spectroscopy experiments (VT = variable temperature), which showed that mixtures of **2** and Ac_2O (1:1.5) in CDCl_3 consist of 5–10% acetylpyridinium acetate at room temperature, whereas equivalent mixtures of **2** and AcCl consist of $\approx 100\%$ acetylpyridinium chloride. Parallel experiments with pyridine resulted in no detectable formation of *N*-acetylpyridinium acetate and precipitation of insoluble *N*-acetylpyridinium chloride respectively. Solubility is an important factor that affects the concentration of reactive *N*-acylpyridinium salts in solution: *N*-Acyl 4-(dialkylamino)pyridinium salts **II** tend to be significantly more soluble in non-polar organic solvents than the corre-

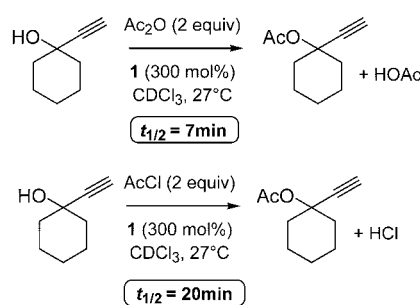
sponding unsubstituted pyridinium salts. Loss to competing reaction manifolds, such as elimination to form ketenes, also has an impact on the concentration of salt.^[31,32] Ketene formation is only possible when the acyl function has β -hydrogen atoms and is retarded by conjugation between the carbonyl group and the 4-dialkylamino substituent. Susceptibility to ketene formation increases with the basicity of the auxiliary base. The rate of esterification through this pathway is slow relative to that through nucleophilic catalysis.^[33]

The overall rate of the catalyzed reaction clearly depends not only on the concentration of the *N*-acylpyridinium salt **II** (and of the alcohol) in solution but also the reactivity of the salt towards addition under the reaction conditions. That a favorable balance between these two factors is required is apparent from the comparison between AcCl-mediated acetylation of alcohols catalyzed by pyridine and **1** in nonpolar solvents: the carbonyl group in *N*-acetylpyridinium chloride itself is “intrinsically” more activated than in the corresponding 4-DMAP-derived salt (IR: $\nu(\text{C}=\text{O})$ 1800 vs. 1755 cm^{-1} , respectively)^[9] but pyridine fails to mediate efficient catalysis primarily because its *N*-acylpyridinium salt is not present in a kinetically meaningful concentration.

A confounding factor in the above analysis, however, is that the observed reactivities of *N*-acylpyridinium salts do not correlate well with their intrinsic carbonyl activation as expected from resonance and spectrochemical properties. In particular, their reactivity is highly anion- and solvent-dependent.^[9] The anion dependence is illustrated by the threefold-greater rate of 4-DMAP-mediated (3 equiv) acetylation of 1-ethynylcyclohexanol when using Ac₂O (2 equiv) relative to AcCl (2 equiv) (Scheme 7).^[9]

Considering that <10% of the Ac₂O will be present as *N*-acetyl-4-(dimethylamino)pyridinium acetate in one case in contrast to $\approx 100\%$ of the AcCl as *N*-acetyl-4-(dimethylamino)pyridinium chloride in the other (see above), this rate difference equates to a significantly higher reactivity for the acetate relative to the chloride salt.^[9]

The solvent dependence of 4-DMAP-catalyzed reactions is well docu-



Scheme 7. Relative rates of 4-DMAP-mediated acetylation of 1-ethynylcyclohexanol with AcCl and Ac₂O.^[9]

mented: The highest rates are found in nonpolar solvents^[9] which appears paradoxical given that such solvents accommodate only low concentrations of *N*-acylpyridinium salts (see above)!

How then can we account for these reactivity trends? The key is to examine solvation and general base catalysis by the anion as crucial factors in dictating the reactivity of *N*-acylpyridinium salts. Strong solvation by polar solvents leads to dissociated ions with low reactivity (whose reactivities do parallel intrinsic carbonyl activation), whereas weak solvation by nonpolar solvents leads to highly reactive ion pairs (whose reactivities are structure-dependent). Consequently, in aqueous solution *N*-acetylpyridinium chloride hydrolyzes about 2000 times faster than *N*-acetyl-4-(dimethylamino)pyridinium chloride^[34] (i.e. the reverse of their relative reactivities towards alcohols in nonpolar solvents as described above). The important structural parameters that influence the relative reactivity of *N*-acylpyridinium ion pairs towards alcohols in nonpolar solvents are ion mobility and the efficacy of general base catalysis by the anion.

The mobility of the constituent ions dictates the ease of access of the alcohol to the reactive carbonyl carbon. “Loose” delocalized ion pairs (e.g. acetate/4-(dialkylamino)pyridinium) are more reactive than “tight” ion pairs (e.g. chloride/pyridinium).^[9] The ability of the anion to deprotonate the alcohol nucleophile in the rate-determining transition state **III**[#] will mirror its basicity (e.g. acetate > chloride). This general base catalysis has long been mooted as being important during nucleophilic catalysis,^[35] but the recent experiments of Kattnig and Albert^[13] provide the first

strong evidence for the case of 4-DMAP (**1**) catalysis. They found that when using K₂CO₃ (4 equiv) as auxiliary base, the 4-DMAP-catalyzed (5 mol %) acetylation of 2-propanol in CDCl₃ at room temperature with Ac₂O (2 equiv) proceeded about 10 times faster than the analogous reaction with AcCl ($t_{1/2}$ = 18 min vs. 200 min). In contrast, with pyridine (2 equiv) as auxiliary base the relative rates were dramatically reversed (≈ 700 times rate difference: $t_{1/2}$ = 120 min vs. <10 s). Similar results were obtained with 1-propanol (Scheme 8).

$\text{ROH} \xrightarrow[\text{base}]{\text{AcCl (2 equiv)}} \text{ROAc} + \text{HCl}$ <p>1 (5 mol%) CDCl₃, RT</p>		
ROH	base	$t_{1/2}$ (min)
	K ₂ CO ₃ (4 equiv) pyridine (2 equiv)	200 <0.2
	K ₂ CO ₃ (4 equiv) pyridine (2 equiv)	35 <0.2

$\text{ROH} \xrightarrow[\text{base}]{\text{Ac}_2\text{O (2 equiv)}} \text{ROAc} + \text{HOAc}$ <p>1 (5 mol%) CDCl₃, RT</p>		
ROH	base	$t_{1/2}$ (min)
	K ₂ CO ₃ (4 equiv) pyridine (2 equiv)	18 120
	K ₂ CO ₃ (4 equiv) pyridine (2 equiv)	3.2 11

Scheme 8. Relative rates of 4-DMAP-catalyzed acetylation of 1- and 2-propanol with various AcCl/Ac₂O and K₂CO₃/pyridine combinations.^[13]

They concluded that when using insoluble K₂CO₃, the acetate or chloride anion must act as a general base, whereas when using pyridine deprotonation can also be carried out by this auxiliary base.^[36,37] Their results certainly militate in favor of deprotonation at the transition state **III**[#] (Scheme 6) being a critical component of the rate-determining step. This is also consistent with the observation by Steglich and co-workers that $t_{1/2}$ for acetylation of 1-ethynylcyclohexanol with Ac₂O catalyzed by **1** decreased from 465 to 151 min when triethylamine was used as auxiliary base rather than pyridine.^[12] Moreover, the results shown in Scheme 7 may be partially accounted for by an approximately threefold great-

er steady-state concentration of free 4-DMAP (**1**) available to act as a general base in the reaction with Ac_2O relative to that with AcCl .

However, since Kattinig and Albert used just 5 mol % of 4-DMAP (**1**) it is unclear why their AcCl -pyridine conditions result in much faster rates than their Ac_2O -pyridine conditions. The concentrations of free pyridine present to act as general base must have been comparable, therefore presumably a much greater concentration of *N*-acetyl-4-(dimethylamino)pyridinium chloride relative to the corresponding acetate must be responsible. Given that the former ion pair is less reactive than the latter (see above),^[38] the equilibrium between 4-DMAP (**1**) and salt **II** alone (Scheme 6) could not be responsible for such an extreme concentration difference. A plausible explanation is that the equilibrium for neutralization of the acid generated during the reaction contributes to this situation. Usually at least 1 equivalent of a tertiary amine such as Et_3N is used as an auxiliary base for this purpose and under these conditions 4-DMAP-catalyzed esterifications are usually faster with Ac_2O than with AcCl .^[17] Being slightly more basic than 4-DMAP (**1**) ($\text{p}K_a \approx 11$ vs. ≈ 10) and present in excess, the tertiary amine effectively sequesters the acid (HCl or HOAc) and maintains the 4-DMAP (**1**) in the unprotonated form and available for nucleophilic catalysis. However, when pyridine ($\text{p}K_a \approx 5$) is employed as the auxiliary base, sequestration of the acid will be less efficient, and significant protonation of 4-DMAP (**1**) may occur. The findings of Kattinig and Albert would then be consistent with the extent of protonation of 4-DMAP (**1**) versus pyridine by HOAc exceeding that by HCl , or proton transfer between pyridine- HOAc and 4-DMAP- HOAc being slow relative to that between pyridine- HCl and 4-DMAP- HCl .^[39]

Kattinig and Albert went on to show that synthetically useful levels of regio-control can be exerted in 4-DMAP-catalyzed polyol acetylation by the appropriate choice of conditions. For example, the primary alcohol group at C6 of octyl β -D-glucopyranoside is esterified by using AcCl -pyridine, whereas the secondary alcohols at C3/C4 are esterified by using Ac_2O -pyridine

(Scheme 1). In line with previous work by Yoshida and co-workers,^[40] they attributed the regioselectivity under the Ac_2O -pyridine conditions to noncovalent (hydrogen bonding) interactions of the acetate ion with the substrate.

In summary, the search for optimal catalytic activity for 4-(dialkylamino)-pyridine-catalyzed esterification demands balancing a delicate raft of factors. It is hoped that the foregoing discussion has illuminated the complex interplay between catalyst structure, acylating agent, auxiliary base, and solvent that conspire to set this balance and that future studies in this area will shed additional light. In particular, developments in asymmetric organocatalysis with chiral 4-(dialkylamino)pyridines and related systems can be expected to build upon our understanding and to provide further information on this catalytic manifold.

Published Online: September 17, 2004

- [1] C. Grondal, *Synlett* **2003**, 10, 1568–1569.
- [2] A. Hassner in *Encyclopedia of Reagents for Organic Synthesis*, Vol. 3 (Ed.: L. A. Paquette), Wiley, New York, **1995**, p. 2022–2024.
- [3] L. M. Litvinenko, A. I. Kirichenko, *Dokl. Chem.* **1967**, 763–766; *Dokl. Akad. Nauk SSSR Ser. Khim.* **1967**, 176, 97–100.
- [4] W. Steglich, G. Höfle, *Angew. Chem.* **1969**, 81, 1001; *Angew. Chem. Int. Ed. Engl.* **1969**, 8, 981.
- [5] M. Benaglia, A. Puglisi, F. Cozzi, *Chem. Rev.* **2003**, 103, 3401–3429.
- [6] R. Murugan, E. F. V. Scriven, *Aldrichimica Acta* **2003**, 36, 21–27.
- [7] U. Ragnarsson, L. Grehn, *Acc. Chem. Res.* **1998**, 31, 494–501.
- [8] F. V. Scriven, *Chem. Soc. Rev.* **1983**, 12, 129–162.
- [9] G. Höfle, W. Steglich, H. Vorbruggen, *Angew. Chem.* **1978**, 90, 602–615; *Angew. Chem. Int. Ed. Engl.* **1978**, 17, 569–583.
- [10] A. C. Spivey, A. Maddaford, A. Redgrave, *Org. Prep. Proced. Int.* **2000**, 32, 331–365.
- [11] S. France, D. J. Guerin, S. J. Miller, T. Lectka, *Chem. Rev.* **2003**, 103, 2985–3012.
- [12] M. R. Heinrich, H. S. Klisa, H. Mayr, W. Steglich, H. Zipse, *Angew. Chem.* **2003**, 115, 4975–4977; *Angew. Chem. Int. Ed.* **2003**, 42, 4826–4828.
- [13] E. Kattinig, M. Albert, *Org. Lett.* **2004**, 6, 945–948.
- [14] V. Gold, E. G. Jefferson, *J. Chem. Soc.* **1953**, 1409–1415.
- [15] A. C. Spivey, A. Maddaford, A. J. Redgrave, *J. Chem. Soc. Perkin Trans. 1* **2001**, 1785–1794.
- [16] L. I. Bondarenko, A. I. Kirichenko, L. M. Litvinenko, I. N. Dmitrenko, V. D. Kobets, *J. Org. Chem. USSR (Engl. Transl.)* **1981**, 2310–2316; *Zh. Org. Khim.* **1981**, 17, 2588–2594.
- [17] A. Hassner, L. R. Krepski, V. Alexanian, *Tetrahedron* **1978**, 34, 2069–2076.
- [18] B. Kempf, N. Hampel, A. R. Ofial, H. Mayr, *Chem. Eur. J.* **2003**, 9, 2209–2218.
- [19] P. W. Hickmott, *Tetrahedron* **1982**, 38, 1975–2050.
- [20] W. H. Daly, J. G. Underwood, S. C. Kuo, *Tetrahedron Lett.* **1971**, 12, 4375–4378.
- [21] M. E. Kuehne, T. Garbacik, *J. Org. Chem.* **1970**, 35, 1555–1558.
- [22] F. Johnson, *Chem. Rev.* **1968**, 68, 375–413.
- [23] G. Opitz, A. Griesinger, *Liebigs Ann. Chem.* **1963**, 665, 101–113.
- [24] G. Stork, A. Brizzolara, H. Landesman, J. Szmuszkowicz, R. Terrell, *J. Am. Chem. Soc.* **1963**, 85, 207–222.
- [25] H. Mayr, B. Kempf, A. R. Ofial, *Acc. Chem. Res.* **2003**, 36, 66–77.
- [26] H. Mayr, T. Bug, M. F. Gotta, N. Hering, B. Irrgang, B. Janker, B. Kempf, R. Loos, A. R. Ofial, G. Remennikov, H. Schimmel, *J. Am. Chem. Soc.* **2001**, 123, 9500–9512.
- [27] E. M. Cherkasova, S. V. Bogatkov, Z. P. Golovina, *Russ. Chem. Rev.* **1977**, 46, 246–263.
- [28] P. J. Battye, E. M. Ihsan, R. B. Moodie, *J. Chem. Soc. Perkin Trans. 2* **1980**, 741–748.
- [29] M. L. Bender in *Mechanisms of Homogeneous Catalysis from Protons to Proteins* (Ed.: M. L. Bender), Wiley, New York, **1971**.
- [30] For a discussion of the $\text{p}K_a$ values of pyridines in various solvents see: L. J. Chmurzynski, *Heterocycl. Chem.* **2000**, 37, 71–74.
- [31] A. K. Sheinkman, S. I. Suminov, A. N. Kost, *Russ. Chem. Rev.* **1973**, 42, 642–661.
- [32] Unimolecular elimination of the *N*-acylpyridinium salt to form an acylium ion is also conceivable but this process would be expected to be more significant for the initial acyl donor (Scheme 6).
- [33] The intervention of a ketene pathway during 4-(dialkylamino)pyridine-catalyzed esterification has been proposed but not substantiated.^[15,17]
- [34] M. Wakselman, E. Guibe-Jampel, *Tetrahedron Lett.* **1970**, 11, 1521–1525.
- [35] A. R. Butler, I. H. Robertson, *J. Chem. Soc. Perkin Trans. 2* **1975**, 660–663.
- [36] Kattinig and Albert obtained values in the range 1.3–1.8 for primary kinetic isotope effects (KIEs , $k_{\text{H}}/k_{\text{D}}$) for the

reactions shown in Scheme 8. These are not consistent with a primary KIE of 0.81 for 4-DMAP-mediated acetylation of *t*BuOH with Ac₂O in CDCl₃^[37] and do not provide clear-cut evidence in favor of general base catalysis.

[37] E. Guibe-Jampel, G. Le Corre, M. Wakselman, *Tetrahedron Lett.* **1975**, 16, 1157–1160.

[38] Evidence for this comes not only from the results of Steglich and co-workers

(Scheme 7),^[9] but also from studies in which isolated *N*-acetyl-4-(dimethylamino)pyridinium acetate but NOT the corresponding chloride, tosylate, or tetrafluoroborate was shown to react with *t*BuOH in CHCl₃.^[37]

[39] Ion pair “complexes” of 4-DMAP (**1**) with carboxylic acids are relatively stable and have been characterized by X-ray diffraction. Higher aggregates (e.g. $\text{1H}^+\cdot\text{OAc}^-\cdot\text{HOAc}$) may be the key spe-

cies involved in proton transfer: Z. Dega-Szafran, M. Szafran, *Heterocycles* **1994**, 37, 627–659 and Z. Dega-Szafran, M. Gdaniec, M. Grundwald-Wyspianska, Z. Kosturkiewicz, J. Koput, P. Krzyzanowski, M. Szafran, *J. Mol. Struct.* **1992**, 270, 99–124.

[40] T. Kurahashi, T. Mizutani, J.-i. Yoshida, *J. Chem. Soc. Perkin Trans. 1* **1999**, 465–473.

Life's Simple Pleasures!



No need to waste precious time looking for the right information – Register now for the free **Wiley-VCH Alerting Service**.

It's simple – and it's fast.

To receive regular news per e-mail tailored precisely to your needs and interests, just fill in the registration form at www.wiley-vch.de/home/pas/

 **WILEY-VCH**

Unveiling Reliable Catalysts for the Asymmetric Nitroaldol (Henry) Reaction**

Claudio Palomo,* Mikel Oiarbide, and Antonia Mielgo

Keywords:

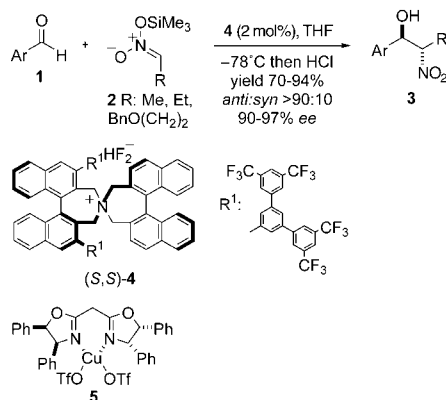
asymmetric catalysis · C–C bond formation · Henry reaction · nitroaldol reaction · synthetic methods

Dedicated to the memory of Juan Carlos del Amo

The addition reaction between nitroalkanes and carbonyl compounds to yield a nitroalcohol, namely the nitroaldol or Henry reaction, has long been known.^[1] It constitutes a powerful C–C bond-forming process in organic chemistry,^[2] providing efficient access to valuable functionalized structural motifs such as 1,2-amino alcohols and α -hydroxy carboxylic acids.^[2,3] Because the reaction is so well known, it is conceivable that significant efforts may have been devoted over the years to implement asymmetric versions of the Henry reaction. Surprisingly no significant success has been achieved until the last few of years.^[4] Stereocontrol in Henry reactions remains challenging: controlling the *syn/anti* stereochemistry is difficult,^[5] and the use of covalently bonded chiral auxiliaries as a general strategy has not been much developed because of the lack of suitable attaching sites in both the pronucleophile nitroalkane and the aldehyde component.^[6,7] Only recently, with the application of new concepts to catalyst design, have reliable catalytic systems appeared that significantly increase the current synthetic value of the Henry reaction. We highlight here the main concepts behind

these developments and their impact in the field.

Relatively soon after the discovery of the Mukaiyama aldol reaction in 1973, chiral metal promoters and catalysts were steadily developed,^[8] but no comparable progress followed the discovery by Seebach and Colvin^[9] in 1978 of the fluoride-catalyzed reaction of silyl nitronates and aldehydes. Only quite recently—almost 25 years later—two independent groups have developed chiral catalysts.^[10] Maruoka et al.^[10a] have reported the addition of trimethylsilyl nitronates **2** to aromatic aldehydes **1** in the presence of 2 mol % of the chiral quaternary ammonium fluoride salt **4**, to give **3** with *anti:syn* ratios usually higher than 90:10 and with more than 90% *ee* (Scheme 1). While poorer results are produced when aliphatic aldehydes are involved, the observed *anti* selectivity is explained on the basis of an acyclic extended transition-state model, which involves a chiral ammonium nitronate as the active species.



Scheme 1. Fluoride-promoted enantioselective nitroaldol reactions of silyl nitronates and aromatic aldehydes.

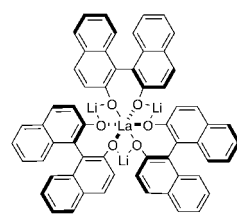
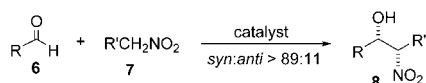
In a conceptually different design of the catalytic system, Jørgensen^[10b] has reported the use of bis(oxazoline)copper(II) complexes such as **5** (20 mol %) in combination with tetrabutylammonium triphenylsilyl difluorosilicate (TBAT, 20 mol %). Again the *anti* adduct **3** is obtained preferentially, but in general both the yields (30–80%) and enantioselectivities (40–65% *ee*) are less impressive.

Perhaps the most impressive advance in the area came from the development of the first metal/chiral ligand complexes that are able to promote the direct reaction between unmodified nitroalkanes and aldehydes enantioselectively. Shibasaki et al.^[4,11] reported the first efficient method of this type by making use of the general principle of two-center catalysis.^[12] A metal/chiral ligand complex was designed possessing two sites of opposite character, a basic site and an acidic site, each capable of independently activating in close proximity the nitro compound and the aldehyde substrate, respectively. For example, as little as 1 mol % of the second-generation lithium/lanthanum polymetallic catalyst (complex **9** + 1.0 mol equiv H₂O + 0.9 mol equiv BuLi) can mediate the reaction between nitroalkanes **7** and aliphatic aldehydes **6** at –50/–30°C within about 120 h in very high diastereo- and enantioselectivities (Scheme 2). Here, the *syn* adducts **8** are the major stereoisomers, thus complementing the silyl nitronate protocol mentioned above.

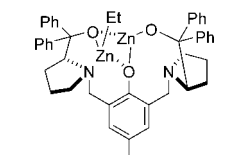
More recent work by Trost et al.^[13] has revealed a novel family of dinuclear zinc complexes such as **10**, which apparently function along a similar principle of cooperative activation. Thus, 5 mol %

[*] Prof. Dr. C. Palomo, Prof. Dr. M. Oiarbide, Dr. A. Mielgo
Departamento de Química Orgánica I
Facultad de Química
Universidad del País Vasco
Apdo. 1072
20080 San Sebastián (Spain)
Fax: (+34) 943-015270
E-mail: qoppanic@sc.ehu.es

[**] We thank The University of the Basque Country (EHU/UPV) and the Ministerio de Ciencia y Tecnología (Spain) for support of this work.



catalyst **9** (1 mol%):
THF, $-50/-30^{\circ}\text{C}$, 113–166 h
yield up to 84%; up to 95% *ee*

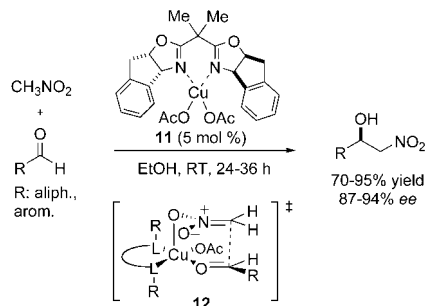


catalyst **10** (5 mol%):
THF, 4 Å MS, -35°C , 24 h
yield up to 90%; up to 93% *ee*

Scheme 2. The enantioselective, direct Henry reaction catalyzed by polymetallic complexes of bifunctional character.

of complex **10** catalyzes the reaction between nitromethane and either aromatic or aliphatic aldehydes at -35°C within about 24 h to produce nitroaldols **8** ($\text{R}'=\text{H}$) in yields in the 56 to 90% range and up to 93% *ee*. Zinc-based catalysts are especially interesting because they might be compatible with aqueous systems in the light of the fact that zinc enolates have been identified as intervening species in aldol reactions catalyzed by type II aldolases.^[14] To date, a few other zinc complexes bearing amino alcohol ligands^[15] and macrocyclic thioaza ligands^[16] have been described for the Henry reaction. Because the results are still poor, future developments in the area can be expected.

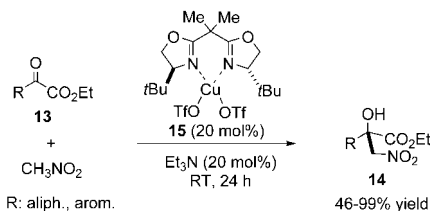
In an important recent report, Evans et al.^[17] have formulated that weakly Lewis acidic metal complexes bearing moderately basic, charged ligands may facilitate the deprotonation of nitroalkanes. A catalyst based on this novel design, the copper acetate catalyst **11**, was found to catalyze the nitroaldol reaction between nitromethane and either aromatic or aliphatic aldehydes to afford nitroaldols with very high enantioselectivity (Scheme 3). Although not conclusive, transition-state model **12** is invoked for the catalyzed reaction, where apparently chelation between the copper metal and a bidentate sub-



Scheme 3. A bis(oxazoline)copper(II) acetate complex as a monometallic catalyst of the enantioselective nitroaldol reaction.

strate^[18] is not a prerequisite for effective asymmetric induction.

In general, ketones react more slowly than aldehydes, and their Henry reactions with nitroalkanes tend to be reversible. In addition, enantioface differentiation is rather challenging because of the greater similarity of the two entities flanking the carbonyl group. Not surprisingly, general methodologies for catalytic Henry reactions are still lacking. A remarkable exception, however, is the Henry reaction of α -keto esters (pyruvates) **13** and nitromethane depicted in Scheme 4, which is promot-



Scheme 4. Henry reaction of α -ketoesters catalyzed by a combination of triethylamine and a chiral bis(oxazoline)copper(II) triflate complex.

ed by the bis(oxazoline)copper complex **15** and triethylamine binary system.^[19] When 20 mol% of both triethylamine and complex **15** are used, nitroaldols **14** are obtained in up to 94% *ee*. Interestingly, in the absence of either catalyst partner the reaction does not occur, and the enantioselectivity is very sensitive to variation in their stoichiometry.

While in most of the above approaches the enantioselectivity results from the organizational ability of a metal center (chiral Lewis acid) to create an effective asymmetric environ-

ment, it appears that chiral Brønsted bases^[20] are also suitable for this role. Thus, certain cinchona alkaloids^[21] and guanidine bases^[22] have been reported to promote direct catalytic asymmetric Henry reactions, although to date the enantioselectivities are still low, typically below 50% *ee*. These incipient achievements are clearly limited, but improvements in the organocatalytic Henry reaction might be coming soon in light of quite recent work on the parent aza-Henry reaction.^[23] In this latter context, the protonated chiral bisamidine ligand **16**^[24] and chiral thiourea derivative **17**^[25] (Figure 1) have been

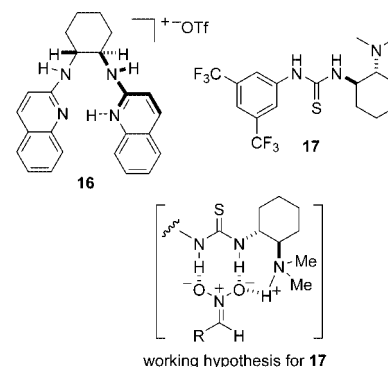
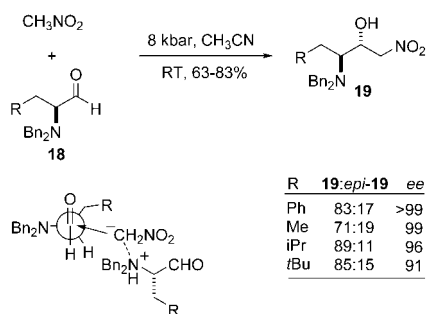


Figure 1. Recent chiral organocatalysts applied to enantioselective aza-Henry reactions.

found to catalyze the addition reaction of nitroalkanes to *N*-Boc and *N*-phosphanoyl imines, respectively, in high enantioselectivities. Although the mechanistic rationale of these catalytic reactions is not yet established, the working hypothesis proposed for **17** (see Figure 1) is plausible and could be potentially extended to Henry reactions.

A special case worth commenting on is the Henry reaction of α -aminoaldehydes **18** to provide nitroaldols **19** (Scheme 5), which represent precursors of medically important compounds. While some chiral catalysts have been used to enhance the inherent diastereoselectivity of the reaction,^[7c,26] Matsumoto et al.^[27] have found that no added catalyst is needed for the reaction to proceed in high diastereoselectivity and with no or little racemization if high pressure (8 kbar) is applied. The implicit concept of this development is that the substrate itself may act as a catalytic chiral base, an idea that might be extended to other types of reactions.



Scheme 5. Diastereoselective asymmetric nitroaldol reactions of α -amino aldehydes under high pressure.

The chemistry highlighted herein proves that the catalytic asymmetric nitroaldol (or Henry) reaction is already a practicable task. Some principles have been set to understand the mechanisms of reactant activation and reaction diastereo- and enantiocontrol, which may guide new developments. Yet, since some of these principles are too general and sometimes little supported, much effort will be needed to fully understand the basis of reactivity and selectivity. Much improvement is still needed in the reaction scope as well. For instance, reactions involving nitroalkanes other than nitromethane have been less studied, while the Henry reaction of ketones is essentially unexplored and challenging. Nevertheless, from the current degree of development, one can already anticipate for the near future extended synthetic applications of the catalytic asymmetric Henry reaction.

Published Online: September 28, 2004

- [1] L. Henry, *C. R. Hebd. Séances Acad. Sci.* **1895**, 120, 1265.
- [2] a) G. Rosini in *Comprehensive Organic Synthesis*, Vol. 2 (Eds. B. M. Trost, I. Fleming, C. H. Heathcock), Pergamon, New York, **1991**, pp. 321–340; b) F. A. Luzio, *Tetrahedron* **2001**, 57, 915–945.
- [3] N. Ono, *The Nitro Group in Organic Synthesis*, Wiley-VCH, New York, **2001**.
- [4] a) M. Shibasaki, H. Gröger in *Comprehensive Asymmetric Catalysis*, Vol III (Eds.: E. N. Jacobsen, A. Pfaltz, H. Yamamoto), Springer, Berlin, **1999**,

pp. 1075–1090; b) M. Shibasaki, H. Gröger, M. Kanai in *Comprehensive Asymmetric Catalysis*, Supplement 1 (Eds.: E. N. Jacobsen, A. Pfaltz, H. Yamamoto), Springer, Heidelberg, **2004**, pp. 131–133.

- [5] For a theoretical discussion, see: B. Lecea, A. Arrieta, I. Morao, F. P. Cossio, *Chem. Eur. J.* **1997**, 3, 20–28.
- [6] For Henry reactions of α -keto acid derivatives mediated by chiral auxiliaries, see, for example: a) A. Solladié-Cavallo, N. Khiar, *J. Org. Chem.* **1990**, 55, 4750–4754; b) I. Kudyba, J. Raczko, J. Jurczak, *J. Org. Chem.* **2004**, 69, 2844–2850.
- [7] For substrate-controlled asymmetric Henry reactions, see for instance: a) V. Jäger, R. Ohrlein, V. Wehner, P. Pogendorf, B. Stever, J. Raczko, H. Griesser, F.-M. Kiess, A. Menzel, *Enantiomer* **1999**, 4, 205–228, and references therein; b) R. G. Soengas, J. C. Estévez, R. J. Estévez, *Org. Lett.* **2003**, 5, 4457–4459; c) S. Hanessian, P. V. Devasthale, *Tetrahedron Lett.* **1996**, 37, 987–990.
- [8] E. M. Carreira in *Comprehensive Asymmetric Catalysis*, Vol III (Eds.: E. N. Jacobsen, A. Pfaltz, H. Yamamoto) Springer, Berlin, **1999**, pp. 997–1065.
- [9] a) E. W. Colvin, D. Seebach, *Chem. Commun.* **1978**, 689–691; b) D. Seebach, A. K. Beck, T. Mukhopadhyay, E. Thomas, *Helv. Chim. Acta* **1982**, 65, 1101–1133.
- [10] a) T. Ooi, K. Doda, K. Maruoka, *J. Am. Chem. Soc.* **2003**, 125, 2054–2055; b) T. Risgaard, K. V. Gothelf, K. A. Jørgensen, *Org. Biomol. Chem.* **2003**, 1, 153–156.
- [11] a) H. Sasai, T. Suzuki, S. Arai, T. Arai, M. Shibasaki, *J. Am. Chem. Soc.* **1992**, 114, 4418–4420; b) T. Arai, Y. M. A. Yamada, N. Yamamoto, H. Sasai, M. Shibasaki, *Chem. Eur. J.* **1996**, 2, 1368–1372; c) H. Sasai, S. Watanabe, T. Suzuki, M. Shibasaki, *Org. Synth.* **2004**, 10, 571–577.
- [12] For reviews on this concept, see: a) M. Shibasaki, N. Yoshikawa, *Chem. Rev.* **2002**, 102, 2187–2209; b) M. Shibasaki, M. Kanai, K. Funabashi, *Chem. Commun.* **2002**, 1989–1999; c) G. J. Rowlands, *Tetrahedron* **2001**, 57, 1865–1882.
- [13] a) B. M. Trost, V. S. C. Yeh, *Angew. Chem.* **2002**, 114, 889–891; *Angew. Chem. Int. Ed.* **2002**, 41, 861–863; b) B. M. Trost, V. S. C. Yeh, H. Ito, N. Bremeyer, *Org. Lett.* **2002**, 4, 2621–2623.
- [14] For a recent tutorial review on the parent asymmetric aldol reaction, see: C. Palomo, M. Oiarbide, J. M. García, *Chem. Soc. Rev.* **2004**, 33, 65–75.
- [15] a) G. Klein, S. Pandiaraju, O. Reiser, *Tetrahedron Lett.* **2002**, 43, 7503–7506; b) Y.-W. Zhong, P. Tian, G.-Q. Lin, *Tetrahedron: Asymmetry* **2004**, 15, 771–776.
- [16] J. Gao, A. E. Martell, *Org. Biomol. Chem.* **2003**, 1, 2801–2806.
- [17] D. A. Evans, D. Seidel, M. Rueping, H. W. Lam, J. T. Shaw, C. W. Downey, *J. Am. Chem. Soc.* **2003**, 125, 12692–12693.
- [18] J. S. Johnson, D. A. Evans, *Acc. Chem. Res.* **2000**, 33, 325–335.
- [19] a) C. Christensen, K. Juhl, K. A. Jørgensen, *Chem. Commun.* **2001**, 2222–2223; b) C. Christensen, K. Juhl, R. G. Hazell, K. A. Jørgensen, *J. Org. Chem.* **2002**, 67, 4875–4881.
- [20] For reviews on chiral bases, see: a) J.-C. Plaquevent, T. Perrard, D. Cahard, *Chem. Eur. J.* **2002**, 8, 3301–3307; b) T. Ishikawa, T. Isobe, *Chem. Eur. J.* **2002**, 8, 553–557.
- [21] Y. Misumi, R. A. Bulman, K. Matsumoto, *Heterocycles* **2002**, 56, 599–605.
- [22] a) E. van Aken, H. Wynberg, F. van Bolhuis, *Acta Chem. Scand.* **1993**, 47, 122–124; b) R. Chinchilla, C. Nájera, P. Sánchez-Agulló, *Tetrahedron: Asymmetry* **1994**, 5, 1393–1402; c) M. T. Allingham, A. Howard-Jones, P. J. Murphy, D. A. Thomas, P. W. R. Caulkett, *Tetrahedron Lett.* **2003**, 44, 8677–8680.
- [23] B. Westermann, *Angew. Chem.* **2003**, 115, 161–163; *Angew. Chem. Int. Ed.* **2003**, 42, 151–153.
- [24] B. M. Nugent, R. A. Yoder, J. N. Johnston, *J. Am. Chem. Soc.* **2004**, 126, 3418–3419.
- [25] T. Okino, S. Nakamura, T. Furukawa, Y. Takemoto, *Org. Lett.* **2004**, 6, 625–627.
- [26] a) Bifunctional metal complexes: H. Sasai, W.-S. Kim, T. Suzuki, M. Shibasaki, *Tetrahedron Lett.* **1994**, 35, 6123–6126; b) Tetraalkylammonium fluorides: E. J. Corey, F.-Y. Zhang, *Angew. Chem. Int. Ed.* **1999**, 38, 1931–1934; c) Guanidine bases: D. Ma, Q. Pan, F. Han, *Tetrahedron Lett.* **2002**, 43, 9401–9403.
- [27] Y. Misumi, K. Matsumoto, *Angew. Chem.* **2002**, 114, 1073–1075; *Angew. Chem. Int. Ed.* **2002**, 41, 1031–1033.

Self-Assembly

Using Hydrogen Bonds to Direct the Assembly of Crowded Aromatics

Mark L. Bushey, Thuc-Quyen Nguyen, Wei Zhang, Dana Horoszewski, and Colin Nuckolls*

Keywords:

aromaticity · hydrogen bonds · molecular recognition · nanotechnology · self-assembly

This Minireview details the design, synthesis, and self-assembly of a new class of crowded aromatics that form columnar superstructures. The assembly of these subunits produces helical and polar stacks, whose assembly can be directed with electric fields. In concentrated solutions, these self-assembled helical rods exhibit superhelical arrangements that reflect circularly polarized light at visible wavelengths. Depending on the side chains employed, spin-cast films yield either polar monolayers or isolated strands of molecules that can be visualized with scanning probe microscopy. Also detailed herein are methods to link these mesogens together to produce monodisperse oligomers that fold into defined secondary conformations.

1. Introduction

Self-assembly is a powerful tool to create novel materials with emergent or amplified properties.^[1] Discotic liquid crystals are one such self-assembled system.^[2] This relatively new class of liquid crystalline compounds, discovered in 1977 by Chandrasekar and co-workers,^[3] is composed of arrayed, one-dimensional columns formed through self-assembly. The constituent stacks have been likened to molecular-scale wires because the interior of the column consists of cofacially stacked π faces while its exterior is surrounded by an insulating, hydrocarbon wrapper.^[4] This arrangement of the aromatic cores has endowed these liquid crystalline phases with useful electronic and optic properties.^[5]

For traditional discotics the affinity between the subunits is low due to the poor electrostatic attraction between the electron rich π surfaces.^[6] Strategies that utilize metal–ligand interactions,^[7] recognition of polymer strands,^[8] electrostatic complementarity between π faces,^[9] and hydrogen bonds^[10]

have yielded columnar assemblies that are held together more strongly.

This Minireview details the assembly characteristics of a new class of columnar materials that are held together with hydrogen bonds.^[11] The core is a hexasubstituted aromatic (1 and 2 in Figure 1) consisting of three amides in the 1,3,5-positions that are flanked by substituents other than hydrogen

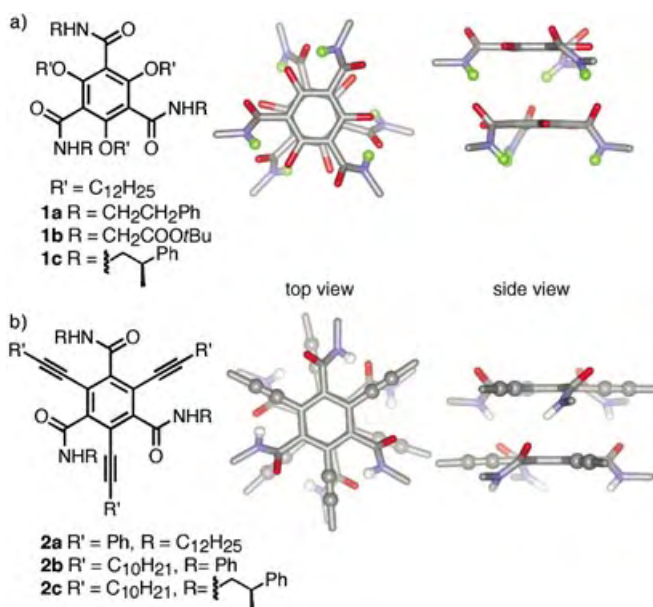


Figure 1. Crowded aromatics and their energy-minimized molecular models. Side chains and hydrogen atoms have been removed to clarify the view.

[*] M. L. Bushey, T.-Q. Nguyen, W. Zhang, D. Horoszewski, Prof. C. Nuckolls
Department of Chemistry
Columbia University
New York, NY 10027 (USA)
Fax: (+1) 212-932-1289
E-mail: cn37@columbia.edu

at each of the remaining positions. There are four sections below detailing the self-assembly characteristics of **1** and **2**:

- 1) The general design and synthesis of this new class of mesogens.
- 2) The synthesis of small but informationally rich, chiral subunits that stack to form helical rods. The assembly of these rods can be directed by electric fields. In concentrated solutions, a superhelix is formed that reflects circularly polarized light at visible wavelengths.
- 3) Monitoring the assembly of these mesogens in monolayer films has yielded films with two orientations controlled by the substituents in the side chain. In one surface conformation a two-dimensional sheet results that is macroscopically polar. In the other orientation on the surface, one-dimensional π stacks result that are only a few molecules wide but microns in length.
- 4) Differentiation of the substituents on each of the amides creates a new class of monodisperse, step-growth oligomers from these highly functionalized mesogens. When appropriate linkers are incorporated into these oligomers, they fold into defined secondary superstructures.

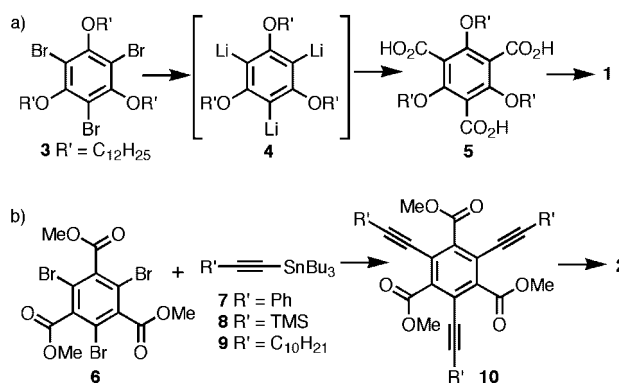
2. General Design, Synthesis, and Bulk Assembly

The design of the molecules in Figure 1 was based on the large number of examples of benzene and cyclohexyl rings that are cofacially stacked with the aid of hydrogen bonds.^[10] Particularly salient are the crystal structures of benzene^[10d,f] and cyclohexane^[10d,e] that are substituted at their 1,3,5-positions with amides. These structures and similar ones inferred from columnar liquid crystals studied by the groups of Matsunaga^[10a] and Meijer^[10b] reveal a one-dimensional stacked structure held together by amide hydrogen bonds. For the molecules in Figure 1, the design principle explored was how to use the flanking alkoxy groups for **1** and alkynyl substituents for **2** to force the amides out of the plane of the central aromatic ring and into a conformation that is predisposed to form three intermolecular hydrogen bonds. Shown in Figure 1 are the energy-minimized dimeric models for both **1** and **2**.^[11a,b,e] From models, the size of the flanking substituent determines the angle of twist for the amide out of the central ring plane and consequently modulates the distance between adjacent benzene rings. The center-to-center distance between the benzene rings is about 3.8 Å for **1** and about 3.6 Å for **2**, thus reflecting the relative sizes of the

alkoxy and the alkynyl substituents. A second interesting feature of the models in Figure 1 is that each of the subunits has a permanent dipole moment, whose direction is perpendicular to the ring plane. Therefore, as the molecules stack, the dipoles could sum to yield columns that have a macroscopic dipole moment, similar to the moment that is seen for some metallomesogens and conical liquid crystals.^[12] In principle, these polar columns could be useful not only in understanding how polar properties emerge on the nanoscale but also for creating small-scale piezoelectric, pyroelectric, and ferroelectric objects.

2.1. Synthesis

Because **1** and **2** were unknown before the studies below were initiated, a versatile synthesis was required to provide a large number of derivatives to understand the structure–property relationships. Moreover, the highly substituted nature of these aromatics provides a test bed for developing new synthetic methodology. For **1**, the key to their synthesis was a triple lithium–halogen exchange with **3** to produce the trilitio derivative **4** (see Scheme 1). Quenching **4** with carbon



Scheme 1. a) Synthesis of **1**. b) Synthesis of **2**.

dioxide or its synthetic equivalent provides these substituted trimesic acid derivatives.^[11a] For the alkynyl substituted derivatives (**2**), the key step was a Farina-modified, Stille coupling of an alkynyl stannane with a 1,3,5-tribromo triester of benzene.^[11e] For both series, multiple grams of a versatile trisacid chloride can be synthesized. These acid chlorides can then be treated with a variety of readily available amines to yield the trisamides shown in Figure 1.

2.2. Assembly in Bulk

Of the two series, **1** is the more heavily studied. Their assembly in bulk is deduced from a confluence of experiments that include synchrotron X-ray diffraction, polarized-light microscopy, infrared spectroscopy, and differential scanning calorimetry.^[11a,b] The essential conclusion from these experiments is that the assembly process is dominated by the size and polarity of the amide side chains. For example, when the



Colin Nuckolls was born in 1970 at Lakenheath RAF (UK) and received his Ph.D. in 1998 (Columbia University, New York). After a postdoc at The Scripps Research Institute, he returned in 2000 to Columbia as an Assistant Professor of Organic Chemistry. He studies the design, synthesis, and assembly of electronic materials on molecular length scales. He has been awarded The NSF CAREER Award (2003), The Beckman (2002) and The Dupont Young Investigator Awards (2002), and the NYSTAR James D. Watson Investigator Award (2002). He is a founding member of the Columbia University Nanoscience Center.

amide substituents are relatively small such as the phenethyl substituents of **1a**, the material assembles into extremely regular cylinders that are hexagonally packed into millimeter-scale domains. When the phenethyl side chain is exchanged for $\text{CH}_2\text{COO}t\text{Bu}$ (**1b**; Figure 1), the material is no longer able to stack into perfect cylinders and compensates by positioning the subunits either canted or offset. These misalignments produce a distorted hexagonal lattice for **1b**. Further magnifying this trend, when the amide substituent is now changed $\text{CH}(\text{CH}_3)\text{COO}t\text{Bu}$ (now made even bulkier!), there is no discernable mesomorphism in bulk samples.

Although there are less data, it appears that the substituents on the side chains of **2** have less influence on the mesomorphism.^[11e] Each of the derivatives shown in Figure 1b (**2a–c**), as well as others, displays a hexagonal arrangement of cylinders. This difference in stacking propensity between **1** and **2** is likely to be the result of the gearlike arrangement of side chains in **1** that is lacking in **2** due to the linearity of the alkynyl substituent.

3. Transfer of Chiral Information

Chiral centers incorporated into the amide side chains have tremendous influence on the mesomorphism observed for derivatives of **1**.^[11b] Shown in Figure 2a is the polarized light micrograph from **1c** that is optically pure and in

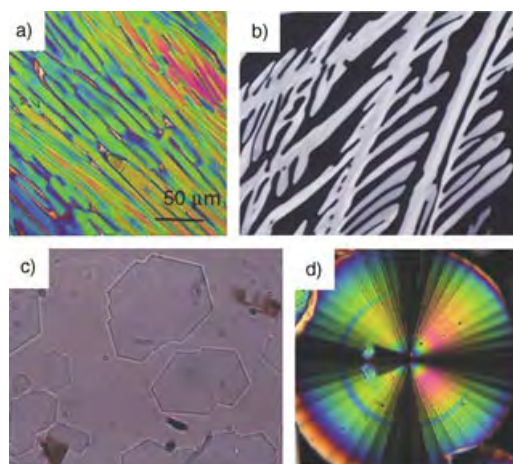


Figure 2. a) Polarized-light micrograph of optically active (–)-**1c** cooled from its clearing point; b) polarized-light micrograph of optically active **1c** between two sheets of indium tin oxide on glass electrodes spaced by 5 μm , 0 V applied; c) as in **2b**, polarizer removed, 30 V applied; d) Polarized-light micrograph of racemic **1c** cooled from its clearing point.

Figure 2d from **1c** that is racemic. These micrographs in combination with synchrotron X-ray diffraction experiments show that while both are hexagonally arranged into columns with similar lattice spacings they have drastically different phase behavior. These experiments and others outlined below indicate that the optically active material is in a columnar liquid-crystalline phase, while the racemate is in a soft or plastic crystalline phase. The spherulitic domains of the

racemate are the same as those from **1a**, a compound that lacks the angular methyl group. The role of these remote chiral centers in directing the assembly is extremely subtle as the clearing temperatures, lattice spacings, IR stretches, and enthalpies of transition are all very similar for either (–)-**1c** or (±)-**1c**. In models of **1c** the methyl and the phenyl substituents are able to make positive contacts only when the material is racemic. This could provide the chiral information transfer between the subunits of the stacks.

3.1. Electrostatic Self-Assembly

The presence of this liquid-crystalline phase in optically active (–)-**1c** allows for the testing of whether the columnar assembly can be directed by the application of electric fields.^[11b] The micrographs in Figure 2b and 2c were recorded as (–)-**1c** was cooled from its isotropic liquid into its mesophase while sandwiched between ITO coated glass plates separated by 5 μm . When no electric field is applied, the material is brightly birefringent with the columnar axes parallel to the surface (Figure 2b). When an electric field is applied, the material becomes optically isotropic, and only when the polarizer is removed can the micron-size polygons, shown in Figure 2c, be visualized. The corners on these polygons have perfect 120° angles indicative of the hexagonal symmetry of the underlying lattice. The racemic materials show no such effect, as spherulitic domains, like those in Figure 2d, result with or without an electric field. The implication is that for the optically active material, electric fields are able to direct the assembly of the columns and their dipoles. Typically the growth of discotic mesophases is more easily affected with magnetic fields,^[13] rather than electric fields, because of the magnetic anisotropy of the standard aromatic cores. For these crowded mesogens, electric fields are efficacious due to the head-to-tail hydrogen bonds in these mesogens endowing the columns with polarity. Although the trisamides of Meijer and co-workers have been shown to switch in electric fields, they do so only when diluted with solvent.^[14] Presumably, these diluted mesogens are in a lyotropic nematic phase and switch because of a dielectric response. The difference in the mechanism for these lyotropics and the one operating for optically active **1c** may be related to the interplay between chirality and polar properties that can only emerge in the neat material. This notion is magnified by results on the trisalkynes that show switching half-times in the order of microseconds and signatures of polar ordered materials when they are prepared optically active.^[11e]

3.2. Helices and Superhelices in Solution

Molecular models such as the one shown in Figure 3a reveal that as the molecules stack, three helices of hydrogen bonds emerge around the exterior of the columns,^[11b] similar to that seen for the unsubstituted 1,3,5-triamides of benzene.^[10d,f] Because the amide rotation is less than 90° out of the plane of the benzene ring, the molecules are only

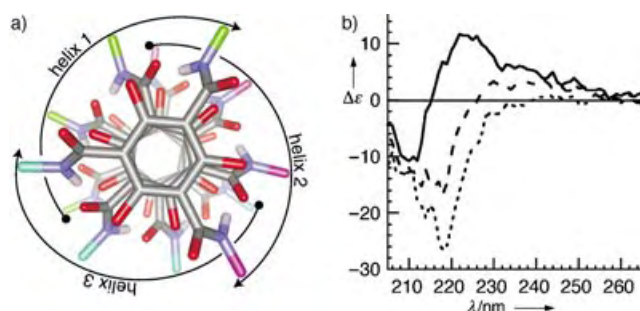


Figure 3. a) Molecular model of four molecules of **1** showing the emergence of three helices of hydrogen bonds around the exterior; b) Circular dichroism (CD) spectra in solution for **1c** in hexanes with varying amounts of methylene chloride (— 15%, - - - 20%, and --- 30%).

complementary with all amides in the same rotational phase. The contact between the six substituents on the benzene ring means that it is possible to bias the gearing of the substituents in one direction or the other, which could be controlled by the chirality in the side chain. Also, the chiral centers in **1c** can influence the winding of these helices. The difference in packing of helices derived from either the racemic or optically active molecules could provide a mechanism for the two materials to behave so differently.^[15]

Experimental evidence for helicity in columns from **1c** is shown in the CD spectra in Figure 3b. In solvents that cannot effectively compete for the hydrogen bonds, the molecules aggregate, and the amide side chain chromophores in adjacent molecules come close enough to be excitonically coupled, displaying a Cotton effect as in Figure 3b. Similar effects have been seen for other columnar systems with chiral centers in the side chains.^[16] In more competitive solvents, the split CD disappears because the hydrogen bonded assembly is broken, and the chromophores are now isolated from each other. The CD of the isolated molecules reflects its intrinsic chirality but lacks the splitting due to excitonic coupling.

In concentrated hydrocarbon solutions, derivatives of **1** and **2** display a wide range of lyotropic mesomorphism.^[11b] When **1b**, which displays a nematic texture on its own in dodecane solvents, is mixed with (–)-**1c**, the solutions reflect circularly polarized light in visible wavelengths. This behavior is diagnostic of a well-known assembly motif in helically wound polymers to form what is termed a cholesteric liquid-crystalline phase.^[17–21] In this mesophase the helices pack next to one another with defined twist angles as shown in Figure 4c.

The wavelength that cholesterics reflect circularly polarized light is a useful property for a diversity of applications ranging from temperature sensing^[22] to lasing.^[23] For the **1a**/(–)-**1c** mixture this wavelength can be easily tuned by the ratio of the components, temperature, and amount of solvent. For the composition that is shown in the micrographs obtained with polarized light in Figure 4a and b, the wavelength of reflected circularly polarized light is in the visible region of the spectrum, which expands from green at 40 °C to red at 60 °C. Although ubiquitous in rodlike helical polymers,^[16–20] this type of liquid crystalline phase is not observed

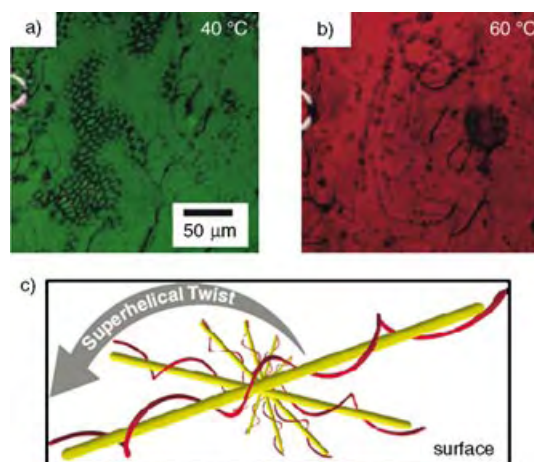


Figure 4. Selective reflection of circularly polarized light from a mixture of (–)-**1c**, **1b**, and dodecane: a) green at 40 °C; b) red at 60 °C; c) schematic of the cholesteric superhelix.

in classic discotics and other self-assembled columnar structures.^[15a] Presumably, the hydrogen bonds provide a higher association in the stacking direction and thereby form a sizable column in solution while the chiral side chains provide the helicity. In essence, the aggregates in solution act as noncovalent polymers.^[24]

4. Organization in Monolayer Films

4.1. Polar monolayers

One feature of the assembly of derivatives of **1** and **2** that is potentially useful has to do with their polar properties and how they develop on the nanoscale. To investigate the assembly and polarity of **1** and **2** on these length scales, conditions were found to produce films that have less than a monolayer of coverage on highly ordered pyrolytic graphite substrates through spin casting.^[11c] The topography and polarity of these films can be measured simultaneously by using atomic force microscopy (AFM) and electrostatic force microscopy (EFM).^[25] For **1b**, the height of the overlayer shown in Figure 5a is about 0.5 nm, thus indicating that the aromatic rings are parallel to the surface. The important finding shown in Figure 5a and b is that the AFM and EFM images look essentially the same, which implies that the film has a universal net negative charge. The EFM signal is a convolution of the molecular charge due in large part to charge transfer from the substrate and/or a perpendicular, permanent dipole moment. Because of the partial positive charge on the amide proton coupled with its out-of-plane conformation, an N–H/ π interaction with the graphite substrate as shown in Figure 5c could result.^[26] Effectively, the surface could serve to orient the amide substituents and thereby direct the molecular dipoles.^[27] Electron transfer from the graphite to the monolayer could also be a contributor to the EFM signal.

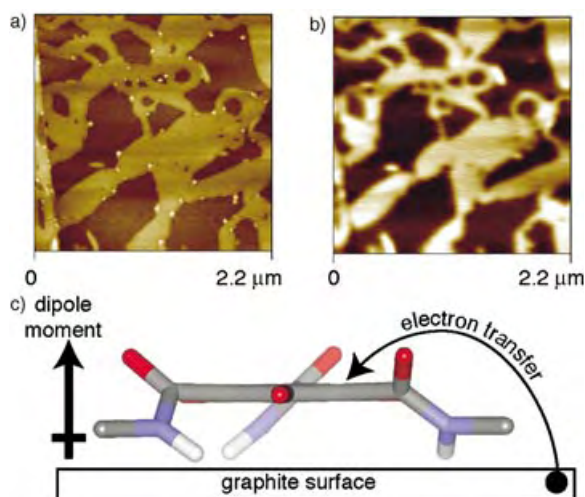


Figure 5. a) $4.8\ \mu\text{m}^2$ AFM height image; b) EFM 1ω image of the same film. c) Dipole and electron transfer in thin films of **1b**. Reprinted, with permission, from reference [11c]. Copyright 2002 The American Chemical Society.

4.2. Isolated Stacks

Remarkably, the opposite surface orientation, in which the columns align parallel to the surface (Figure 6d), is adopted for all other derivatives shown in Figure 1 (**1a**, **1c**, and **2a–c**) and others tested that form hexagonal arrangements in bulk. The dominant feature in the AFM micrographs (Figure 6) is the large number of molecular-scale, fibrous

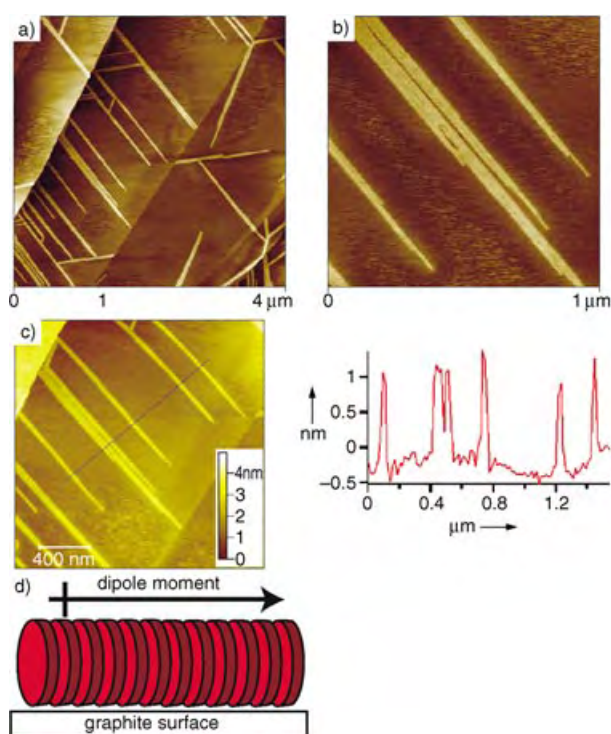


Figure 6. AFM images of **1c** on graphite at various scan sizes: a) $16\ \mu\text{m}^2$, b) $1\ \mu\text{m}^2$, c) The cross section profile of a fiber. d) Schematic of orientation of **1c** on graphite substrates. Reprinted, with permission, from reference [11c]. Copyright 2002 The American Chemical Society.

regions. Each of the striations within a fiber is about 2 nm in diameter (Figure 6b) and the height of these features is $1.80 \pm 0.22\ \text{nm}$ (Figure 6c). These values correlate well with the 1.8 nm column spacing measured from bulk synchrotron X-ray diffraction.^[11a,b] EFM analysis of these stacks reveals that they have essentially no measurable dipole or charge, which is consistent with the dipole moment of the column being parallel to the surface (Figure 6d).

There are few examples of similar molecular-scale fibers from columnar mesophases.^[28] Possibly, one-dimensional structures do not form for typical discotic mesogens because the relatively weak π -stacking forces that hold the column together are nearly equaled in energy by the numerous van der Waals contacts between alkyl side chains giving rise to two-dimensional sheets.^[29] For the derivatives in Figure 1, the self-association in the stacking direction due to the hydrogen bonds now outweighs these van der Waals contacts between columns, and individual stacks can be isolated. Ongoing experiments involve the use of scanning tunneling microscopy to determine the local structure in these strands.

It is important to note that the propensity to stack the aromatic cores face-on as for **1b** and edge-on as for **1c** elucidated from the AFM/EFM studies above mirrors the same propensity for assembly in bulk: **1b** has a homeotropic alignment while **1c** has a planar arrangement of columns.^[11a,b] What is the origin of the difference in orientation between **1b** and **1c** in monolayer films and in bulk? One possible explanation has to do with the difference in association between **1b** and **1c**. **1c** readily self-assembles to form strands that orient their long axes parallel to the substrate. The stacking of **1b** is now weakened owing to the sterically demanding side chains, and the interaction with the surface dominates, giving rise to the face-on conformation at the interface. Possibly this monolayer forms also in bulk samples of **1b** and serves as a surface template to direct the assembly of subsequently stacked mesogens.

5. Folded Oligomers

One unique feature of these crowded aromatics is their highly substituted core that contains two different types of side chains. If each of the amides could be differentially substituted, then subunits could be linked together to form monodisperse step-growth oligomers.^[11d] Because of the helicity of the amide hydrogen bonds in these stacks shown in Figure 3a, oligomers could have a defined secondary structure similar to that of α -helically wound peptides, thus

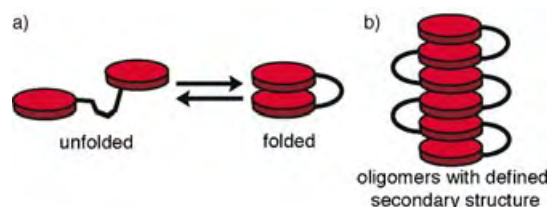
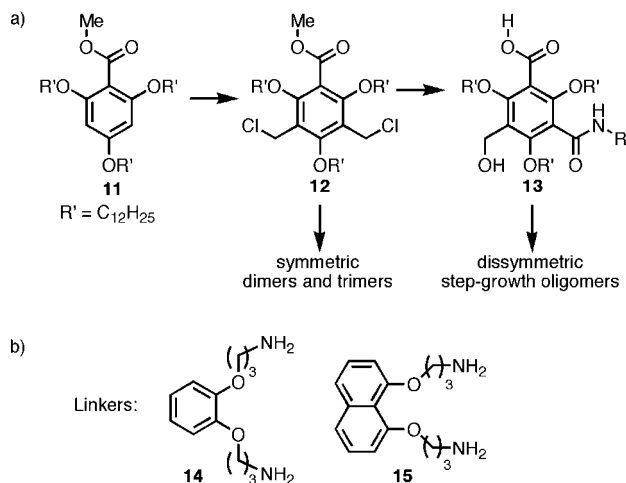


Figure 7. a) Schematic of linking two crowded aromatics to study the process of folding and unfolding in dimers; b) Schematic of a monodisperse oligomer that folds into a defined conformation.

forming a new class of foldamers shown in Figure 7b.^[30] The initial objective was to develop a synthetic methodology that would allow each of the amides to be individually substituted and to see what types of linkers produced folded conformations as shown in Figure 7a.

A high yielding and large-scale synthesis of derivatives of **1**, in which each of the amides can be individually addressed



Scheme 2. a) Synthesis of differentially substituted triamides. b) Linkers used for oligomer construction.

(Scheme 2), was recently completed and has allowed the synthesis of not only dimers but also oligomers of defined length such as in Figure 7b.^[11d] The key to the synthesis was the finding that the tetrasubstituted aromatic **11** could be chloromethylated to install the final two carbon atoms on the hexasubstituted core of **12**. Through a multistep sequence of hydrolysis, oxidation, and coupling, symmetrical dimers (**16**, **17**, and **18** in Figure 8) and trimers can be synthesized from **12**. After the conversion of **12** to its diacetoxo derivative, one of the acetates could be saponified to yield the fully differentiated monomer **13**. This monomer could be used to synthesize unsymmetrical dimers, trimers, and higher oligomers.

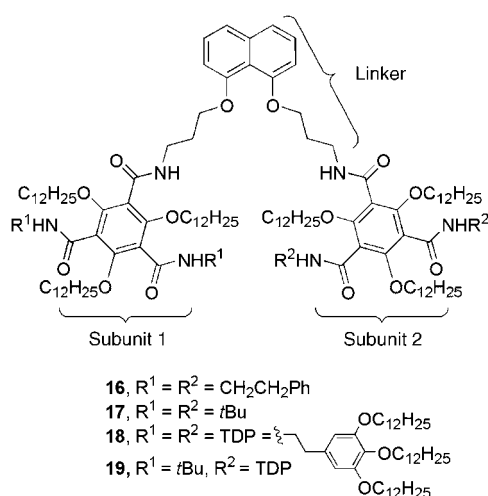


Figure 8. Homo- and heterodimers synthesized with the C-shaped 1,8-naphthyl linker. Reprinted, with permission, from reference [11d]. Copyright 2003 The American Chemical Society.

Angew. Chem. Int. Ed. 2004, 43, 5446–5453

www.angewandte.org

5.1. Folding in Dimers

Crucial to observing folding of these oligomers in solution was the employment of C-shaped linkers such as the catechol-based linkers or the 1,8-naphthyl-based linkers shown in Scheme 2b.^[11d] This new folding motif is so robust that even dimers have secondary structure in solution. A signature of the folded conformation in dimers is the about 1 ppm downfield shifts in the amide N–H ¹H NMR resonances. Unsymmetrical dimers have numerous through-space NOE couplings indicative of the folded conformation in Figure 7a. Linear aromatic and alkyl linkers do not exhibit such self-folding properties, thus showing the importance of preorganizing the system for intramolecular contacts. In addition to the linker, the side chains in these oligomers are also critical for the secondary structure to emerge in solution. As with the monomers shown in Figure 1, the phenethyl side chains and the substituted phenethyl side chains proved useful in allowing the subunits to fold. The *tert*-butyl amide side chains can be incorporated into the terminal subunit and block head-to-tail aggregation of these oligomers above millimolar concentrations.

5.2. Folding in Higher Oligomers

By using the highly solubilizing tris(dodecyloxy)phenethyl (TDP) side chains with the *tert*-butyl side chains in the terminal subunit has allowed higher oligomers to be synthesized. Shown in Figure 9 is the structure, ¹H NMR spectrum, and through space NOE couplings observed in a CD₂Cl₂ solution. The oligomer adopts a well-defined columnar structure. More recently, hexamers have been synthesized and their phase behavior and assembly in thin films is being studied. Due to the highly substituted nature of these columns it should be possible to write chemical information into these

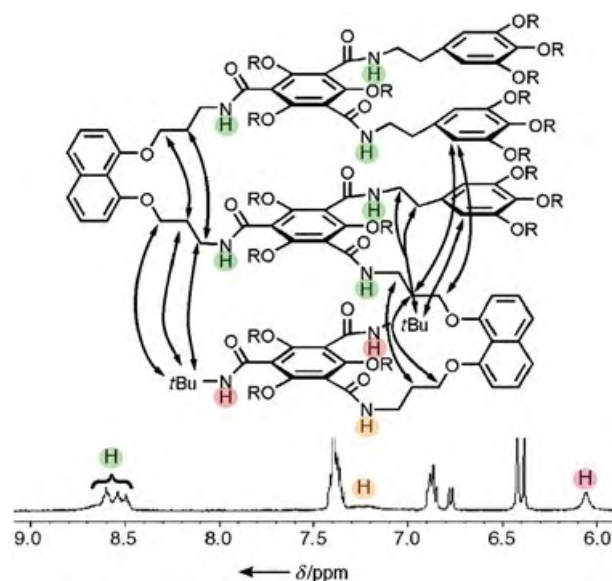


Figure 9. NOE couplings and ¹H NMR spectrum for a trimer (1 mM in CD₂Cl₂, 303 K, R = C₁₂H₂₅). Reprinted, with permission, from reference [11d]. Copyright 2003 The American Chemical Society.

© 2004 Wiley-VCH Verlag GmbH & Co. KGaA, Weinheim

5451

structures that would encode their assembly into higher order structures.

6. Summary and Outlook

This Minireview details the design, synthesis, and self-assembly of a new class of molecules that form columnar superstructures. The structures of **1** and **2** are unique synthetic targets owing to the highly substituted central benzene ring. The assembly of these subunits produces helical and polar stacks whose assembly can be directed with electric fields. These helical rods also exhibit cholesteric mesophases in concentrated solutions, a unique mesomorphism for self-assembled columnar mesogens. Spin casting of films of **1b** produces polar monolayers that can be visualized with AFM and EFM. The understanding of how the polarity in this initial layer is transferred to subsequently stacked molecules is a necessary goal to rationalize how to create spontaneously polar materials. Monolayers of **1c** form isolated stacks that are microns in length but only a few molecules wide. Measurement of electrical and polar properties on these strands is an ongoing challenge for this new class of nanoscale materials. Also detailed above are methods to link these mesogens together to produce monodisperse oligomers of **1** that fold into defined secondary conformations. Ongoing experiments are aimed at investigating the self-assembly of these oligomers into higher-order aggregates.

We acknowledge the support from numerous collaborators, coworkers, and colleagues that made these studies possible. We acknowledge primary financial support from the Chemical Sciences, Geosciences and Biosciences Division, Office of Basic Energy Sciences, US D.O.E. (no. DE-FG02-01ER15264), US National Science Foundation CAREER award (no. DMR-02-37860), and the Nanoscale Science and Engineering Initiative of the National Science Foundation under NSF Award Number CHE-0117752 and by the New York State Office of Science, Technology, and Academic Research (NYSTAR). CN thanks the Beckman Young Investigator Program (2002), the NYSTAR J. D. Watson Investigator Program (2003), and the Dupont Young Investigator Program (2002) for support. MLB thanks the ACS Division of Organic Chemistry for a graduate fellowship sponsored by Bristol-Myers Squibb.

Received: July 9, 2003

Revised: November 13, 2003

Published Online: September 16, 2004

- [1] a) J.-M. Lehn, *Supramolecular Chemistry*, VCH, Weinheim, **1995**; b) J.-M. Lehn, *Struct. Bonding (Berlin)* **2000**, 96, 3–29; c) G. M. Whitesides, B. Grzybowski, *Science* **2002**, 295, 2418–2421; d) D. S. Lawrence, T. Jiang, M. Levett, *Chem. Rev.* **1995**, 95, 2229–2260; e) M. M. Conn, J. Rebek, Jr., *Chem. Rev.* **1997**, 97, 1647–1668; f) D. Philp, J. F. Stoddart, *Angew. Chem.* **1996**, 108, 1242–1286; *Angew. Chem. Int. Ed. Engl.* **1996**, 35, 1155–1196; g) M. Muthukumar, C. K. Ober, E. L. Thomas, *Science* **1997**, 277, 1225–1232; f) L. J. Prins, D. N. Reinhoudt, P. Timmer-

man, *Angew. Chem.* **2001**, 113, 2446–2492; *Angew. Chem. Int. Ed.* **2001**, 40, 2382–2426.

- [2] For leading references on discotic liquid crystals, see: a) S. Chandrasekhar, G. S. Ranganath, *Rep. Prog. Phys.* **1990**, 53, 57–84; b) C. Destrad, P. Foucher, H. Gasparoux, H. T. Nguyen, A. M. Levelut, J. Malthete, *Mol. Cryst. Liq. Cryst.* **1984**, 106, 121–146; c) S. Chandrasekhar, S. Prasad, J. Krishna, *Contemp. Phys.* **1999**, 40, 237–245; d) D. Guillon, *Struct. Bonding (Berlin)* **1999**, 95, 41–82.
- [3] a) S. Chandrasekhar, B. K. Sadashiva, K. A. Suresh, *Pramana* **1977**, 9, 471–480; b) S. Chandrasekhar, B. K. Sadashiva, K. A. Suresh, N. V. Madhusudana, S. Kumar, R. Shashidhar, G. Venkatesh, *J. Phys. Colloq.* **1979**, 3, 120–124.
- [4] S. Chandrasekhar, *Handb. Liq. Cryst. Res.* **1998**, 2B, 749–780.
- [5] a) N. Boden, B. Movaghar, *Handb. Liq. Cryst. Res.* **1998**, 2B, 781–798; b) N. Boden, R. J. Bushby, J. Clements, B. Movaghar, *J. Mater. Chem.* **1999**, 9, 2081–2086; c) A. M. Van de Craats, J. M. Warman, A. Fechtenkötter, J. D. Brand, M. A. Harbison, K. Müllen, *Adv. Mater.* **1999**, 11, 1469–1472; d) V. Percec, M. Glodde, T. K. Bera, Y. Miura, I. Shiyonovskaya, K. D. Singer, V. S. Balagurusamy, P. A. Heiney, I. Schnell, A. Rapp, H.-W. Spiess, S. D. Hudson, H. Duan, *Nature* **2002**, 419, 384–387; e) V. Percec, G. Johansson, J. Heck, G. Ungar, S. V. Batty, *J. Chem. Soc. Perkin Trans. 1* **1993**, 1411–1420; f) J. Simon, C. Sirlin, *Pure Appl. Chem.* **1989**, 61, 1625–1629; g) O. E. Sielcken, L. A. van de Kuil, W. Drenth, J. Schoonman, R. J. M. Nolte, *J. Am. Chem. Soc.* **1990**, 112, 3086–3093; h) T. Christ, B. Gluesen, A. Greiner, A. Kettner, R. Sander, V. Stuepfen, V. Tsukruk, J. H. Wendorff, *Adv. Mater.* **1997**, 9, 48–52; i) D. Adam, P. Schuhmacher, J. Simmerer, L. Hänssling, K. Siemensmeyer, K. H. Etzbach, H. Ringsdorf, D. Haarer, *Nature* **1994**, 371, 141–143; j) L. Schmidt-Mende, A. Fechtenkötter, K. Müllen, E. Moons, R. H. Friend, J. D. MacKenzie, *Science* **2001**, 293, 1119–1122.
- [6] C. A. Hunter, J. K. M. Sanders, *J. Am. Chem. Soc.* **1990**, 112, 5525–5534.
- [7] a) *Metallomesogens* (Ed.: J. L. Serrano), VCH, New York, **1996**; b) J. Simon, P. Bassoul in *Phthalocyanines: Properties and Applications*, Vol. 2 (Eds.: C. C. Leznoff, A. B. P. Lever), VCH, New York, **1989**, chapter 6; c) A. G. Serrette, C. K. Lai, T. M. Swager, *Chem. Mater.* **1994**, 6, 2252–2268.
- [8] V. Percec, *Handb. Liq. Cryst. Res.* **1997**, 2B, 259–346.
- [9] a) M. Müller, C. Kubel, K. Müllen, *Chem. Eur. J.* **1998**, 4, 2099–2109; b) H. Bengs, M. Ebert, O. Karthaus, B. Kohne, K. Praefcke, H. Ringsdorf, J. H. Wendorff, R. Wuestefeld, *Adv. Mater.* **1990**, 2, 141–144; c) M. Weck, A. R. Dunn, K. Matsumoto, G. W. Coates, E. B. Lobkovsky, R. H. Grubbs, *Angew. Chem.* **1999**, 111, 2909–2912; *Angew. Chem. Int. Ed.* **1999**, 38, 2741–2745.
- [10] Hydrogen bonds used to stabilize π stacks: a) Y. Matsunaga, N. Miyajima, Y. Nakayasu, S. Sakai, M. Yonenaga, *Bull. Chem. Soc. Jpn.* **1988**, 61, 207–210; b) L. Brunsveld, H. Zhang, M. Glasbeek, J. A. J. M. Vekemans, E. W. Meijer, *J. Am. Chem. Soc.* **2000**, 122, 6175–6182, and references therein; c) Y. Yasuda, E. Iishi, H. Inada, Y. Shirota, *Chem. Lett.* **1996**, 7, 575–576; d) M. P. Lightfoot, F. S. Mair, R. G. Pritchard, J. E. Warren, *Chem. Commun.* **1999**, 19, 1945–1946; e) E. Fan, J. Yang, S. J. Geib, T. C. Stoner, M. D. Hopkins, A. D. Hamilton, *J. Chem. Soc. Chem. Commun.* **1995**, 12, 1251–1252; f) D. Ranganathan, S. Kurur, R. Gilardi, I. L. Karle, *Biopolymers* **2000**, 54, 289–295; g) C. M. Paleos, D. Tsiourvas, *Angew. Chem.* **1995**, 107, 1839–1855; *Angew. Chem. Int. Ed. Engl.* **1995**, 34, 1696–1711, and references therein; h) M. J. Brienne, J. Gabard, J.-M. Lehn, I. Stibor, *J. Chem. Soc. Chem. Commun.* **1989**, 24, 1868–1870; i) D. Goldmann, R. Dietel, D. Janietz, C. Schmidt, J. H. Wendorff, *Liq. Cryst.* **1998**, 24, 407–411; j) G. Ungar, D. Abramic, V. Percec, J. A. Heck, *Liq. Cryst.* **1996**, 21, 73–86; k) V. Percec, C.-H. Ahn, T. K. Bera, G. Ungar, D. J. P. Yearley, *Chem. Eur. J.*

- 1999, 5, 1070–1083; l) J. Malthete, A. M. Levelut, L. Liebert, *Adv. Mater.* **1992**, 4, 37–41; m) D. Pucci, M. Veber, J. Malthete, *Liq. Cryst.* **1996**, 21, 153–155.
- [11] a) M. L. Bushey, A. Hwang, P. W. Stephens, C. Nuckolls, *J. Am. Chem. Soc.* **2001**, 123, 8157–8158; b) M. L. Bushey, A. Hwang, P. W. Stephens, C. Nuckolls, *Angew. Chem.* **2002**, 114, 2952–2955; *Angew. Chem. Int. Ed.* **2002**, 41, 2828–2831; c) T.-Q. Nguyen, M. L. Bushey, L. E. Brus, C. Nuckolls, *J. Am. Chem. Soc.* **2002**, 124, 15051–15054; d) W. Zhang, D. Horoszewski, J. Decatur, and C. Nuckolls, *J. Am. Chem. Soc.* **2003**, 125, 4870–4873; e) M. L. Bushey, T.-Q. Nguyen, C. Nuckolls, *J. Am. Chem. Soc.* **2003**, 125, 8264–8269.
- [12] a) D. Kilian, D. Knawby, M. A. Athanassopoulou, S. T. Trzaska, T. M. Swager, S. Wrobel, W. Haase, *Liq. Cryst.* **2000**, 27, 509–521; b) H. Zimmermann, R. Poupko, Z. Luz, J. Billard, *Z. Naturforsch. A* **1985**, 40, 149–160; c) J. Malthete, A. Collet, *J. Am. Chem. Soc.* **1987**, 109, 7544–7545.
- [13] a) B. Hueser, T. Pakula, H. W. Spiess, *Macromolecules* **1989**, 22, 1960–1963; b) S. Ikeda, Y. Takanishi, K. Ishikawa, H. Takezoe, *Mol. Cryst. Liq. Cryst. Sci. Technol. Sect. A* **1999**, 329, 1201–1207.
- [14] A. R. A. Palmans, J. A. J. M. Vekemans, R. A. Hikmet, H. Fischer, E. W. Meijer, *Adv. Mater.* **1998**, 10, 873–876.
- [15] Similar to the observation of mesogeneity in helicene liquid crystals: L. Vyklicky, S. H. Eichhorn, T. J. Katz, *Chem. Mater.* **2003**, 15, 3594–3601.
- [16] a) G. Gottarelli, E. Mezzina, G. P. Spada, F. Carsughi, G. Di Nicola, P. Mariani, A. Sabatucci, S. Bonazzi, *Helv. Chim. Acta* **1996**, 79, 220–234, and references therein; b) A. R. A. Palmans, J. A. J. M. Vekemans, E. E. Havinga, E. W. Meijer, *Angew. Chem.* **1997**, 109, 2763–2765; *Angew. Chem. Int. Ed. Engl.* **1997**, 36, 2648–2650; c) S. T. Trzaska, H.-F. Hsu, T. M. Swager, *J. Am. Chem. Soc.* **1999**, 121, 4518–4519; d) C. F. van Nostrum, A. W. Bosman, G. H. Gelinck, P. G. Schouten, J. M. Warman, A. P. M. Kentgens, M. A. C. Devillers, A. Meijerink, S. J. Picken, U. Sohling, A.-J. Schouten, R. J. M. Nolte, *Chem. Eur. J.* **1995**, 1, 171–182; e) H. Engelkamp, C. F. van Nostrum, R. J. M. Nolte, S. J. Picken, *Chem. Commun.* **1998**, 9, 979–980.
- [17] A. A. Kornyshev, S. Leikin, *Phys. Rev. E* **2000**, 62, 2576–2596, and references therein.
- [18] DNA and nucleic acid derivatives: a) F. Livolant, A. M. Levelut, J. Doucet, J. P. Benoit, *Nature* **1989**, 339, 724–726; b) K. Merchant, R. L. Rill, *Biophys. J.* **1997**, 73, 3154–3163; c) R. L. Rill, F. Livolant, H. C. Aldrich, M. W. Davidson, *Chromosoma* **1989**, 98, 280–286; d) G. Gottarelli, G. Proni, G. P. Spada, S. Bonazzi, A. Garbesi, F. Ciuchi, P. Mariani, *Biopolymers* **1997**, 42, 561–574; e) G. Proni, G. Gottarelli, P. Mariani, G. P. Spada, *Chem. Eur. J.* **2000**, 6, 3249–3253.
- [19] In polypeptides: a) D. B. DuPré, E. T. Samulski in *Liquid Crystals—The Fourth State of Matter* (Ed.: F. D. Saeva), Marcel Dekker, New York, **1979** chapter 5; b) T. Hashimoto, S. Ebisu, N. Inaba, H. Kawai, *Polym. J.* **1981**, 13, 701–713.
- [20] a) X. M. Dong, D. G. Gray, *Langmuir* **1997**, 13, 3029–3034; b) T. Sato, J. Nakamura, A. Teramoto, M. M. Green, *Macromolecules* **1998**, 31, 1398–1405.
- [21] T. Sato, Y. Sato, Y. Umemura, A. Teramoto, Y. Nagamura, J. Wagner, D. Weng, Y. Okamoto, K. Hatada, M. M. Green, *Macromolecules* **1993**, 26, 4551–4559.
- [22] *Liquid Crystals—The Fourth State of Matter* (Ed.: F. D. Saeva), Marcel Dekker, New York, **1979**.
- [23] W. Cao, A. Munoz, P. Palfy-Muhoray, B. Taheri, *Nat. Mater.* **2002**, 1, 111–113.
- [24] J. S. Moore, *Curr. Opin. Colloid Interface Sci.* **1999**, 4, 108–116.
- [25] EFM theory and experimental setup: a) T. D. Krauss, S. O'Brien, L. E. Brus, *J. Phys. Chem. B* **2001**, 105, 1725; b) J. Jiang, T. D. Krauss, L. E. Brus, *J. Phys. Chem. B* **2000**, 104, 11936–11941; c) O. Cherniavskaya, L. Chen, V. Chen, L. Yuditsky, L. E. Brus, *J. Phys. Chem. B* **2003**, 107, 1525–1531.
- [26] Similar to the recognition of carbon nanotubes with amines: a) J. Liu, M. J. Casavant, M. Cox, D. A. Walters, P. Boul, W. Lu, A. J. Rimberg, K. A. Smith, G. T. Colbert, R. E. Smalley, *Chem. Phys. Lett.* **1999**, 303, 125–129; b) M. J. O'Connell, P. Boul, L. M. Ericson, C. Huffman, Y. Wang, E. Haroz, C. Kuper, J. Tour, K. D. Ausman, R. E. Smalley, *Chem. Phys. Lett.* **2001**, 332, 461–466; c) J. Kong, H. Dai, *J. Phys. Chem. B* **2001**, 105, 2890–2893; d) M. Sano, A. Kamino, J. Okamura, S. Shinkai, *Nano Lett.* **2002**, 2, 531–533.
- [27] Surface poling has been observed locally in polymer films: X. Q. Chen, H. Yamada, Y. Terai, T. Horiuchi, K. Matsushige, P. S. Weiss, *Thin Solid Films* **1999**, 353, 259–263.
- [28] J. J. van Gorp, J. A. J. M. Vekemans, E. W. Meijer, *J. Am. Chem. Soc.* **2002**, 124, 14759–14769.
- [29] a) P. Henderson, D. Beyer, U. Jonas, O. Karthaus, H. Ringsdorf, P. A. Heiney, N. C. Maliszewskyj, S. S. Ghosh, O. Y. Mindyuk, J. Y. Josefowicz, *J. Am. Chem. Soc.* **1997**, 119, 4740–4748; b) N. C. Maliszewskyj, P. A. Heiney, J. Y. Josefowicz, J. P. McCauley, Jr., A. B. Smith III, *Science* **1994**, 264, 77–79; c) J. Y. Josefowicz, N. C. Maliszewskyj, S. H. J. Idziak, P. A. Heiney, J. P. McCauley, Jr., A. B. Smith III, *Science* **1993**, 260, 323–326; d) V. V. Tsukruk, D. H. Reneker, H. Bengs, H. Ringsdorf, *Langmuir* **1993**, 9, 2141–2144; e) T. Christ, F. Geffarth, B. Glösen, A. Kettner, G. Lüssem, O. Schäfer, V. Stümpflen, J. H. Wendorff, V. V. Tsukruk, *Thin Solid Films* **1997**, 302, 214–222.
- [30] For leading references on foldamers see: a) R. P. Cheng, S. H. Gellman, W. F. DeGrado, *Chem. Rev.* **2001**, 101, 3219–3232; b) D. J. Hill, M. J. Mio, R. B. Prince, T. S. Hughes, J. S. Moore, *Chem. Rev.* **2001**, 101, 3893–4011; c) D. Seebach, A. K. Beck, M. Rueping, J. V. Schreiber, H. Sellner, *Chimia* **2001**, 55, 98–103.

Imaging Techniques

Snapshot Magnetic Resonance Imaging (Nobel Lecture)**

Peter Mansfield*

Keywords:

imaging techniques · magnetic resonance imaging · NMR spectroscopy · Nobel Lecture

1. Introduction

The topic of magnetic resonance imaging (MRI) started for us at Nottingham in the early summer of 1972. During a discussion with one of my graduate students, Peter Grannell, and my post-doc Dr. Allan Garroway, concerning multiple-pulse line-narrowing experiments in solids, the idea occurred to me to use the line-narrowing technique as a means of effectively removing dipolar interactions in a material such as CaF_2 and at the same time impose an external linear gradient on the sample, thus broadening the line shape to reveal the atomic or molecular structure within the sample.

It soon became apparent, however, even with the achievable narrowed line-widths of around 1 Hz for CaF_2 , which corresponds to a line-width reduction of 3×10^4 , that the residual line width was still too broad when practical external gradients were used to resolve the atomic structure in a single crystal of CaF_2 . Despite this setback, work continued with artificial one-dimensional lattices made up of several thin plates of camphor. Peter Grannell and I continued this work during the course of 1972 and it resulted finally in a paper presented at the First Specialized Colloque Ampère, Krakow in 1973.^[1] Formal publication appeared shortly after.^[2] These papers emphasized the Fourier transform approach used, even though the images of the camphor stacks were one-dimensional. It was clear that we had made our task much more difficult by choosing to work with solids. Thoughts rapidly turned to liquidlike spin systems where the line-narrowing approach would be unnecessary.

The imaging approach considered so far was essentially one- or two-dimensional. The next step was to define a thin slice of material so that this would be imaged without any spill over to adjacent planes. This was achieved using a technique called selective irradiation.^[3]

One of the major practical difficulties encountered with MRI to this point was the time it took to acquire the data. Line-scanning, for example, typically took 10–20 minutes to acquire an image comprising 64×64 pixels.^[4]

The breakthrough came in 1977 with the introduction of echo-planar imaging (EPI).^[5] This snapshot technique meant that, in principle, complete two-dimensional images could be achieved in extremely short times (20–50 ms). However, to achieve these acquisition times yet another inventive step was

required, namely, the introduction of active magnetic screening.^[6,7] Ordinary magnetic gradient coils, which were necessary to define the slice thickness and image axes, were found to interact strongly with the metal cryostat structure of the superconductive magnet. Time-dependent currents induced in these structures would decay away with their own independent time constant, thus adding an undesirable and unpredictable time dependence to the otherwise static magnetic field.

By actively shielding the gradient coils all extraneous time dependence is obviated, together with all undesirable reflected static magnetic fields. Of course, the magnetic screening process itself introduces magnetic fields which change the character of the gradient field, but in a well-defined and calculable manner. Magnetically screened gradient coils now form an integral part of virtually all commercial MRI scanners.

2. Experimental Apparatus

Figure 1 shows a home-built 0.5 T whole-body MRI scanner together with a patient bed support. Figure 2 shows a doubly screened gradient-coil assembly used in the experimental scanner. With a doubly screened gradient coil in which the primary coil comprises a single current loop, it can be shown that the unshielded loop carrying current I produces magnetic flux lines which form a series of elliptic-like magnetic field loops with displaced centers.^[7] However, if the current loop or the primary coil is now magnetically screened with the double screen arrangement, the magnetic field lines within the inner screen are exactly the same as those produced by the primary coil in free space. The

[*] Sir P. Mansfield

Magnetic Resonance Centre
Department of Physics and Astronomy
University of Nottingham
Nottingham, NG7 2RD (UK)
Fax: (+44) 115-951-5166
E-mail: pamela.davies@nottingham.ac.uk

[**] Copyright© The Nobel Foundation 2003. We thank the Nobel Foundation, Stockholm, for permission to print this lecture.



Figure 1. A home-built magnetic resonance imager with a 0.5 T super-conductive magnet.



Figure 2. A doubly screened active magnetic shielded gradient coil for insertion in the superconductive magnet of Figure 1.

magnetic flux is, however, confined between the screens and the field inverts. The magnetic field at the center of the coil assembly takes the same form and magnitude as the unscreened coil; that is to say, the magnetic field B within a current loop is as expected for an unscreened loop. Outside the outer screen, $B=0$. If the inner magnetic screen is removed, which leaves the outer screen, flux confinement between the screens can no longer occur and the magnetic field now leaks beyond the outer screen.



Sir Peter Mansfield was born on October 9, 1933. He received his PhD in Physics from the Group of Prof. J. G. Powles at the University of London (1962). From 1962 to 1964 he worked as a Research Associate in the group of Prof. C. P. Slichter at the University of Illinois (USA). He then became lecturer (1964) and senior lecturer (1968) at the University of Nottingham (Department of Physics). After a stay at the Max-Planck-Institut für Medizinische Forschung in Heidelberg (Germany) as a Senior Visitor (1972–1973), he was appointed Professor at the Department of Physics, University of Nottingham in 1979. During his career he received numerous national and international awards, medals, and honors. He has been a Fellow of the Royal Society since 1987 and Honorary Member of the British Institute of Radiology (since 1993). Sir Peter was knighted in 1993.

3. Echo-Planar Imaging (EPI)

3.1. Imaging Sequence

The mathematical relationship between real space (r space) and reciprocal space (k space), first described in 1750 by the French mathematician Joseph Fourier, is known as the Fourier transform (FT), which takes the general form shown in Equation (1) in which \mathbf{k} is defined by Equation (2).

$$S(\mathbf{k}) = \int d\mathbf{r} \rho(\mathbf{r}) \exp(i \mathbf{k} \cdot \mathbf{r}) \quad (1)$$

$$\mathbf{k} = \int_0^t \gamma \delta \mathbf{G}(t') / \delta t' dt' \quad (2)$$

\mathbf{k} and \mathbf{r} may both be one-, two-, or three-dimensional. The density $\rho(\mathbf{r})$ describes the image in real space and $S(\mathbf{k})$ describes the image in k space. In our case, $\mathbf{G}(t)$ is an externally applied time-dependent magnetic gradient, γ is the magneto-gyric ratio (constant for a particular nuclear spin species), and t is the evolution time.

The Fourier transform expression in Equation (1) allows a reversible transformation from k space to r space. This is exemplified in the forward and inverse Fourier transforms shown in Figure 3. In fact, the two-dimensional k -space image is built up from a series of one-dimensional free-induction decays (FIDs), suitably stacked to give an image which is in effect the diffraction pattern of the object. The inverse FT of the k -space image produces the r -space image, in this case a transverse cross-sectional image through the mediastinum and showing a diagram of the heart mass and lung fields.

To obtain the k -space map in a single experiment, a specially designed pulse sequence is applied as shown in Figure 4. In general terms, this comprises an initial spin preparation phase followed by a transverse slice selection pulse. This creates an active magnetic signal or FID which is allowed to decay away in the presence of the spatial encoding gradients G_x and G_y . For EPI, these are applied in the form of a square wave or a trapezoidal waveform for G_y and either a long low-level pulse or a train of short (blipped) pulses for G_x . In either case, the areas under the long low pulse or the string of blips must be equal. The effect of these gradient waveforms causes the FID following slice selection to dephase and rephase in a series of spin echoes. The amplitude of these spin echoes is initially low, but grows to a maximum and then decays provided an initial dephasing gradient pulse is arranged immediately before the blipped or low-level G_x sequence starts.

Also included in Figure 4 is the k -space trajectory. This starts at $k_x = k_y = 0$. The pre-pulse described above displaces the trajectory from 0 to $-k_{x,\max}$, at which point the locus starts to move right from $k_y = 0$ to $k_{y,\max}$. At this point the trajectory is displaced upwards with the first positive blip. The transverse scan then proceeds from right to left traversing the full k_x scan from $k_{y,\max}$ to $-k_{y,\max}$. In this way the whole of the \mathbf{k} plane is scanned. During this procedure the signal is regularly sampled to produce the first step in obtaining the

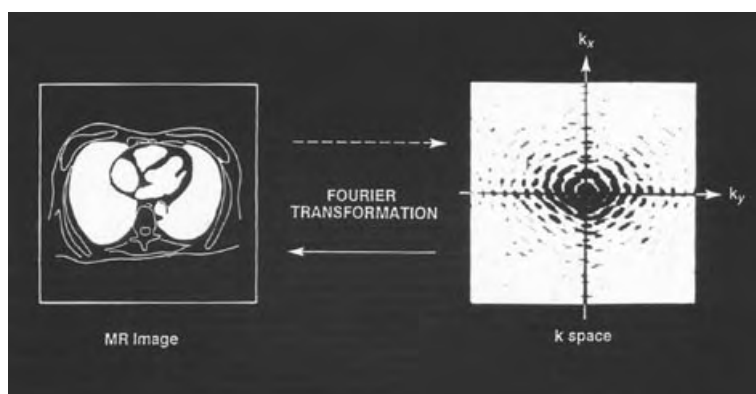


Figure 3. MRI images and their k-space equivalents are related by the FT algorithm: Diagram of a slice through the mediastinum showing the two lung fields and heart mass (left). Also shown is the Fourier transform of this real-space image to the k-space map. (Reproduced with permission from Ref. [28].)

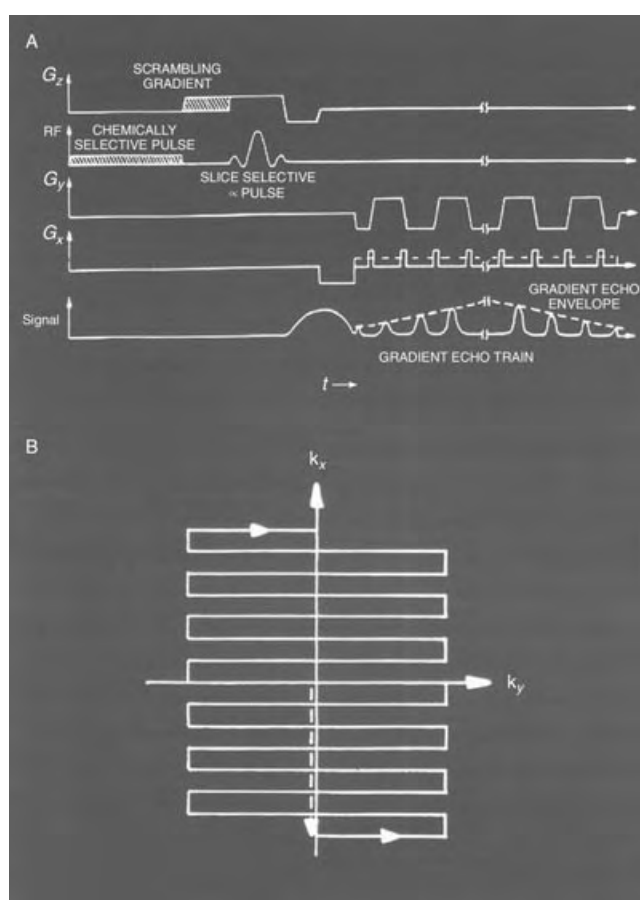


Figure 4. Top: MBEST pulse sequence. Bottom: k-space trajectory. (Reproduced with permission from Ref. [9].)

k-space scan as sketched in Figure 3. The remaining operation is an editing function which reverses the order of all data in alternate lines of the k-space image. At this point there are two options to choose from to produce the r-space image. The first is to perform a two-dimensional FT on the k-space map thereby producing the r-space image. However, to do this

generally requires a high expenditure in terms of time for data manipulation in addition to the two-dimensional FT. The alternative approach is to take the first and last points in the reordered k-space scan and, metaphorically speaking, pull the whole array out like a string of beads to form a one-dimensional array. The whole string is Fourier transformed using a one-dimensional FT with less computing expenditure.

3.2. Two-Dimensional Imaging Results at 0.5 T: General Results

The above-described EPI sequence was used to image a series of patients and volunteers during the early 1980s and 1990s. Whole body scans may be performed comprising 64 transections commencing in the upper thorax and moving down the torso in 5-mm steps through the mediastinum, liver, kidney in the lower abdomen, and finishing just below the bladder. They are an example of a quick scan, the whole imaging process taking approximately one minute.

Figure 5 shows four EPI snapshots taken through the heart using a surface coil on the chest wall.^[8] Each image is acquired at a different phase of the cardiac cycle. Figures 5A and 5B, for example, correspond to different phases during

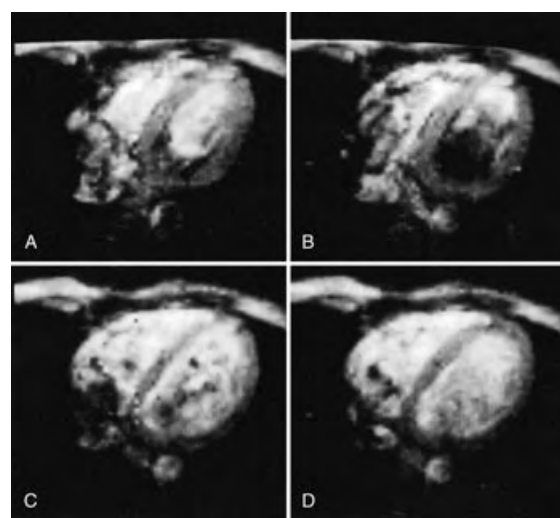


Figure 5. Snapshot EPI images through the heart obtained with use of a surface coil. A) Transection during systole shows thickening of the left ventricular myocardial wall. B) Rapid ventricular filling in late systole. C, D) Transections obtained during diastole show thinner myocardial walls. The spatial resolution of these images is less than 2 mm. (Reproduced with permission from Ref. [8].)

systole, when the heart is in contraction and pumping. Figure 5B shows a loss of signal (black) because of turbulence within the left ventricle. Figures 5C and 5D were acquired during the relaxed phase (diastole). In all the images the myocardium gives a less-intense signal, thus allowing differentiation of the muscle tissue from blood.

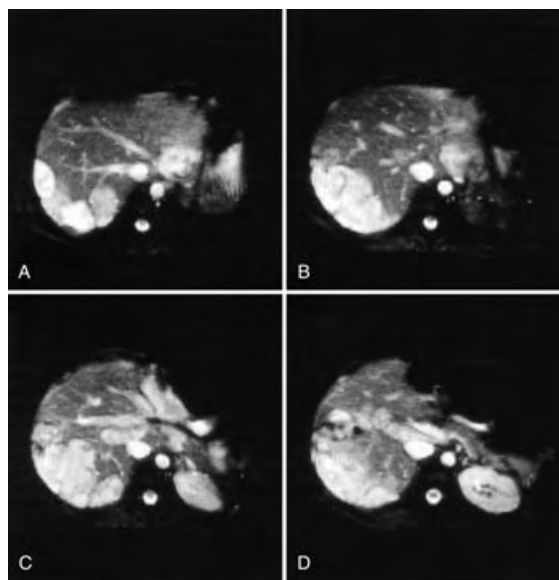


Figure 6. Four snapshot MBEST images (128 ms acquisition time) of a liver with hydatid cysts. These images are based on 128×128 pixel arrays with in-plane resolution of approximately 2.3 mm. (Reproduced with permission from Ref. [9].)

Figure 6 shows four transections through the liver of a patient with a series of hydatid cystic lesions.^[9] These show as bright regions within the darker liver. An imaging variation on the same patient using the inversion-recovery (IR) EPI sequence uses an initial spin inversion pulse as the preparation phase. After a short delay (inversion time) TI, the EPI sequence follows. When $TI = 0$, we have the normal sections as in Figure 6. Short T_1 signal components within the image may be effectively removed by varying TI, thereby delineating the normal tissue. This procedure can be used to indicate clear margins between the lesions and the normal tissue. Long relaxation time components may be eliminated by increasing TI, thereby revealing the relatively fast relaxing hydatid cystic lesions.

3.3. Foetal Imaging Results at 0.5 T

An important area of application of EPI has been foetal imaging during the third trimester. This has been valuable in assessing cases of foetal-growth retardation.^[10–12]

Figure 7 shows a maternal coronal view of a foetal sagittal section at 37 weeks gestation. The foetal section, taken from a set of scans, clearly shows the head, brain, spinal column, and the right leg. The darker signal from within the amniotic sac is the placenta. The brighter signal regions surrounding the foetus come from the amniotic fluid.

In other transectional images at 37 weeks gestation, highlighting the lung field can be used to measure foetal lung volume. The same technique can be used to measure the subcutaneous fatty tissues surrounding the foetus.

Foetal birthweight versus the foetal volume estimated by EPI has also been measured for 12 babies with birthweights

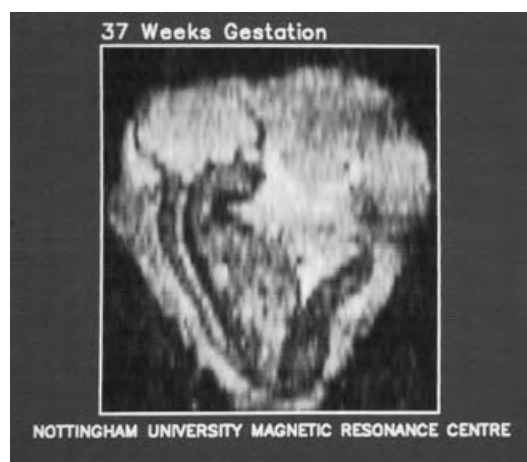


Figure 7. Sagittal section taken from a three-dimensional data set of a foetus in the uterus at 37 weeks gestation. The foetal brain and spinal canal can be clearly seen. The darker area to the right is the placenta. The bright region between the placenta and foetus corresponds to amniotic fluid.

spanning 1.5–3.5 kg.^[11,12] The foetal volume is assessed from a series of contiguous EPI slices spanning the foetus, and by using the same technique as described above the foetal cross-sectional image is traced out and highlighted. The elemental volume is the highlighted area multiplied by the slice thickness. The total foetal volume is then the sum of all cross-sectional slices. The results indicate a good linear correlation between volume and weight.

3.4. Paediatric Imaging at 0.5 T

In the course of imaging young children suffering from cyanotic heart disease,^[13–16] snapshot transectional images have been taken through the mediastinum for a child with a normal heart. They all show the lung fields and heart mass at the base of the heart moving down through the left and right ventricles towards the apex. Also shown is the classification system for a normal heart. This is contrasted with an example taken from a set of images for a child with a truncus arteriosus. The left and right ventricles can be clearly seen towards the apex as dark regions together with the intact ventricular septum. The left and right atria appear as bright regions. The classification diagram indicates the coalescence of the pulmonary artery and the aorta into a common truncus.

3.5. EPI Results at 3.0 T

A number of snapshot images of various objects have been obtained at 3.0 T,^[17] including a snapshot image of a phantom comprising 256×256 pixels. The slice thickness was 0.5 cm and the image acquisition time was approximately 90 ms. Other examples include images through the brain of a normal volunteer: the posterior horns of the ventricles together with part of the anterior horns are just visible in these images.

4. Echo-Volumar Imaging (EVI)

4.1. Imaging Sequence

Details of the pulse-timing sequence for EVI^[18] are shown in the upper part of Figure 8. The top trace shows the modulation waveform of the G_y gradient. The next modulated waveform is the gradient G_x . The third waveform G_z includes the slice-selection gradient G_z together with a negative prepositioning pulse immediately followed by a long low-level gradient. In the bottom trace the slice-selection pulse is indicated and slightly later the modulated spin signals arising from the sequence are sketched.

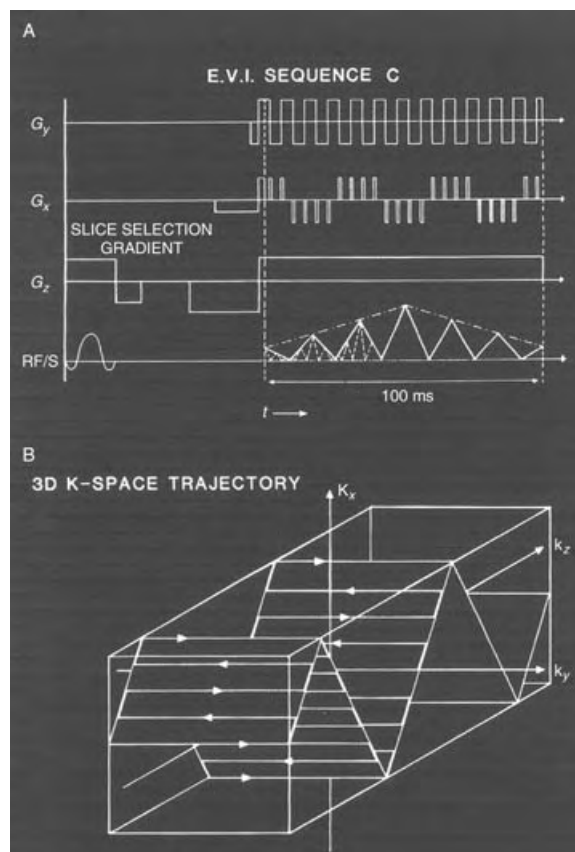


Figure 8. A) Gradient wave form sequence for (B). T_A = total data acquisition time, T_x = single echo acquisition time, and T_y = a single pulse acquisition time. Dotted portions of G_y and G_x indicate the alternative starting phases. B) One pass of a general four-pass 3D k-space trajectory for EVI. (Reproduced with permission from Ref. [18].)

In the lower half of Figure 8 the k-space trajectory, which corresponds to the above-described EVI sequence, is sketched. As a consequence of the prepositioning pulse, the k-space trajectory starts at $k_x = k_y = 0$ and $k_z = -k_{z,\max}$. The trajectory moves right to $k_{y,\max}$ then to and fro uphill alternately to $\pm k_{y,\max}$ until the trace reaches the first peak and $k_{x,\max}$. The trajectory then continues its oscillation as it drops down the negative slope to reach $-k_{x,\max}$. The whole process continues uphill and down dale as k_z evolves along the z axis to $k_{z,\max}$.

Data are sampled (in this case at a constant rate) during the whole process. Since the evolution arrows of the k trajectory reverse periodically it is necessary to reorder the sampled data so that the arrows are all pointing in the same direction before performing the Fourier transformation to obtain the image. In fact, one reordering of the k-space data is required to produce two slightly different images of the data. However, these may be combined into a single image with no loss of clarity.

Other versions of EVI can also be implemented in which the blips used for G_x are replaced by a square wave modulation of G_x . Even G_z may be replaced by a sequence of blips. However, reasonable quality multipass images may be obtained by using square wave modulation of G_x with G_z unmodulated as shown, provided the number of lines in an individual image is large. However, these complications can be completely avoided by obtaining one-pass snapshot images using blipped G_x and G_z gradients rather than the square wave or trapezoidally modulated waveform described here.

The result of this data manipulation is, in our case, the production of eight simultaneous images. Each image comprises 64×64 pixels and each pixel has an in-plane resolution of $6 \times 4 \text{ mm}^2$ and the voxel thickness is 10 mm. The total acquisition time for these eight images is 128 ms. The first EVI images were obtained at 0.5 T on a volunteer. The EVI image set shown in Figure 9 shows the filling of the volunteer's stomach with approximately 1 liter of water.^[18] The water surface is clearly seen in Figure 9E–H. An EVI

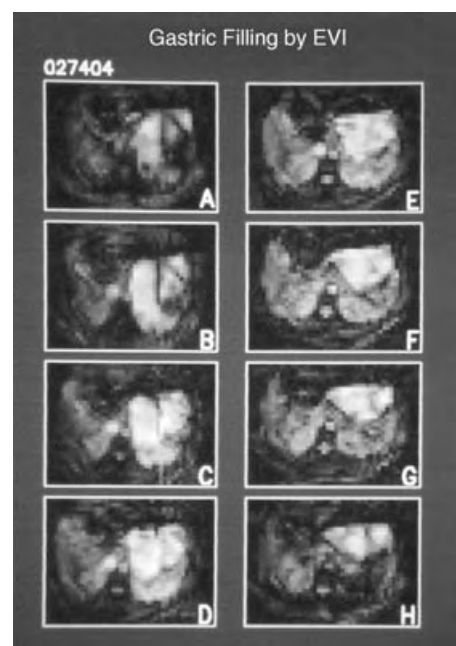


Figure 9. An EVI snapshot taken from a movie loop showing gastric filling in a volunteer imbibing 1 liter of water. The data set comprises 8 planes spanning approximately an 8-cm-thick slice through the stomach. The water surface and gaseous void within the stomach are indicated in images E–G. These images correspond approximately to the antrum. Other morphological land marks in these images show the kidneys, liver, and spinal canal. (Reproduced with permission from Ref. [18].)

snapshot was also obtained through the bladder of the same volunteer subject. In this case, the images indicate a very full bladder, which is characterized by the very rectangular shape observed.^[18]

EVI has also been tried at 3.0 T. The first results at this field strength showed the brain ventricles of a normal patient at slightly different levels.^[19] The imaging time for all eight cross-sections was 115 ms. Figure 10 shows the results of the

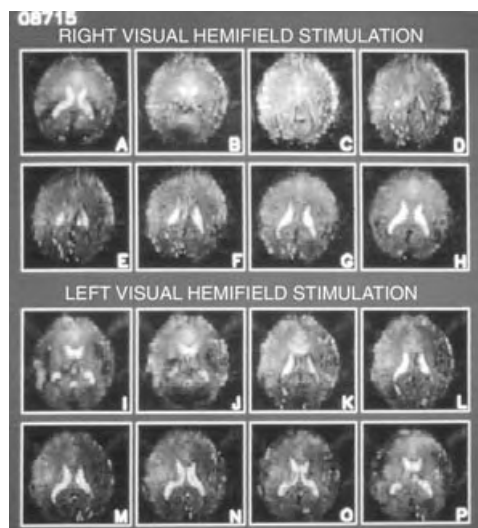


Figure 10. Two complete EVI snapshots, each comprising eight contiguous slices. A–H) Picture series with the functionally active regions corresponding to right visual hemifield stimulation highlighted in red. I–P) Picture series with the functionally active regions highlighted in red corresponding to left visual hemifield stimulation. Transections H and P correspond to the most caudal in each set, respectively. Each image comprises 64×64 pixels and the slice thickness corresponds to 2.5 mm. (Reproduced with permission from Ref. [19].)

first EVI functional imaging experiments conducted with a healthy volunteer. The upper half of Figure 10 shows eight slices through the brain of a volunteer subjected to right visual hemifield stimulation. Highlighted on these images are the red dots marking changes in the signal arising predominately from the left side of the visual cortex. The lower part of Figure 10 shows eight brain slices after the volunteer had been subjected to left visual hemifield stimulation. Also highlighted on these images are red dots marking signal changes, which in this case arise predominately from the right side of the visual cortex.

5. Active Acoustic Control

5.1. Problem Formulation

One of the problems in the implementation of EPI and EVI is the high levels of acoustic noise generated by the gradient coils when they are pulsed rapidly. The noise originates from movement of the gradient-coil windings as a result of Lorentz forces created by the high currents flowing

in the gradient-coil assembly. Even if the wires are firmly cemented into the coil former, the former itself deforms slightly and the tiny deformation in the former surface is enough to couple with the surrounding air thereby launching undesirable acoustic waves into and around the MRI apparatus.

The typical noise levels for EPI can reach 140 dB or more. However, the safety levels for noise are limited in the work place to a maximum of 85 dB.^[20,21] Prolonged exposure to very high levels of noise can lead to irreversible hearing damage. Of course, some local protection may be introduced to mitigate the effects of high-level noise, for example, in the form of ear defenders worn by the patient. These give typically a protection of 30 dB, but even these are unreliable for small children because of poor fitting or looseness. For pregnant women there is virtually no reliable protection for the foetus.

It is for these reasons that we have been considering other ways of dealing with the problem. Our current approach is effectively to try to prevent the coil assembly from radiating noise.

5.2. Rectangular Gradient Coil

Our initial approach to the acoustic noise problem has been to consider a rather basic coil arrangement comprising four rectangular plates or sectors. Each sector carries a current I_1 . In addition there is a re-entrant loop, which constitutes the control winding. The control winding current is $I_2 e^{i\phi}$ (ϕ is the phase of I_2 relative to I_1). Only one sector so far has been built and tested.^[22–25]

The test arrangement is shown in Figure 11. The single sector is supported within an anechoic chamber which itself fits into a 3.0 T magnet. A linear array of microphones receives acoustic signals across one end of the magnet.

Theoretical calculations for the acoustic output from a signal sector plate assembly have been performed. These show that when $\phi = 180^\circ$ the plate produces the full acoustic output. This reduces considerably when the phase is adjusted to $\phi \approx 0$.

5.3. Results

A specially designed optimized pulse corresponding to an EPI sequence was used to test the acoustic efficiency of the gradient sector assembly.^[25] The EPI pulse length was approximately 10 ms. A series of EPI pulses were applied to the gradient sector at a rate of five pulses per second in the acoustically optimized mode (red) and non-optimized mode (blue). These results are shown in Figure 12 for five pulses each lasting one second. The acoustic signal in the optimized mode (red) has been reduced to almost zero on this linear trace. However, one pulse from the same data has been Fourier analyzed to produce a frequency spectrum of the EPI pulse with and without acoustic control switched on. These results are shown in Figure 13. With active control switched off, acoustic noise of approximately -20 dB occurs primarily

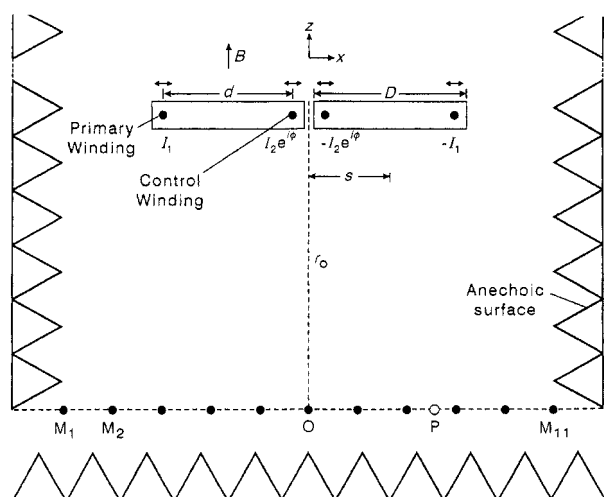


Figure 11. Diagram showing a sectional plan of a split plate arrangement suspended in an anechoic chamber perpendicular to the main field B (not to scale). Each half of the plate pair has a width $D = 0.126$ m. Embedded in each block are two conductors with separation $d = 0.1$ m. The plate centres are displaced from the assembly origin by $s = \pm 0.063$ m. The outer wire pair comprises the primary winding carrying current I_1 . The inner wire pair comprises the control winding carrying current $I_2 e^{i\phi}$, where ϕ is the relative phase difference of the two currents. The microphone array lies in a line parallel to the plate through point O . Point P represents a single microphone. The distance $r_o = 1.25$ m, the plate length $l = 0.58$ m, the material is GRE, and the plate thickness is 0.012 m. The plate pair has an overall width of 0.255 m, which includes an air gap of 0.003 m between the plates. The compressional wave velocity of sound is taken as 2500 m s^{-1} . (Reproduced with permission from Ref. [25].)

at 3.2 kHz , the fundamental carrier frequency of the EPI pulse. Some second harmonic content is present at 6.4 kHz together with higher harmonics. In the optimized mode, the fundamental component of noise is reduced to approximately -70 dB with no second harmonic and reduced higher harmonics. The total noise reduction of the fundamental frequency at 3.2 kHz is 50 dB . Further noise reduction in the harmonic frequencies is also indicated.

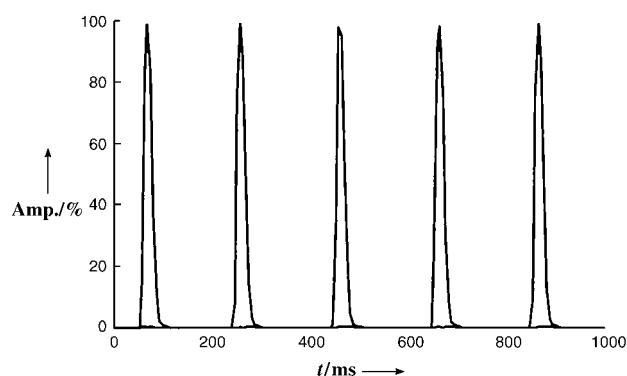


Figure 12. Sound recording before (blue) and during active acoustic control (red) for an optimized gradient pulse sequence running at five pulses per second.

6. Conclusions

The basis of ultrahigh-speed snapshot MRI is reviewed and illustrated with early examples of actual EPI results obtained at 0.5 T and 3.0 T . Also described are some original three-dimensional results obtained using snapshot EVI. Both techniques show promise as useful medical imaging modalities. However, it is fair to say that so far only EPI has found its way into regular medical use. Quite often this use is limited to a role of rapid sighting of the region of interest within a patient before slower techniques are used to obtain the final image.

The reason for doing things this way round is partly historical. The slower MRI techniques were developed and honed by the manufacturing companies while ignoring the advances in ultrahigh-speed imaging methods. However, given the same intensive development EPI, and possibly EVI, will move up from a rapid sighting technique to a fully diagnostic technique in its own right.

Such a move would remove the dread felt by some claustrophobic patients at the prospect of being confined in the MRI machine for between a half and one hour. Of course, ultrahigh-speed imaging brings with it its own problems which need addressing. One of these is the high level of acoustic

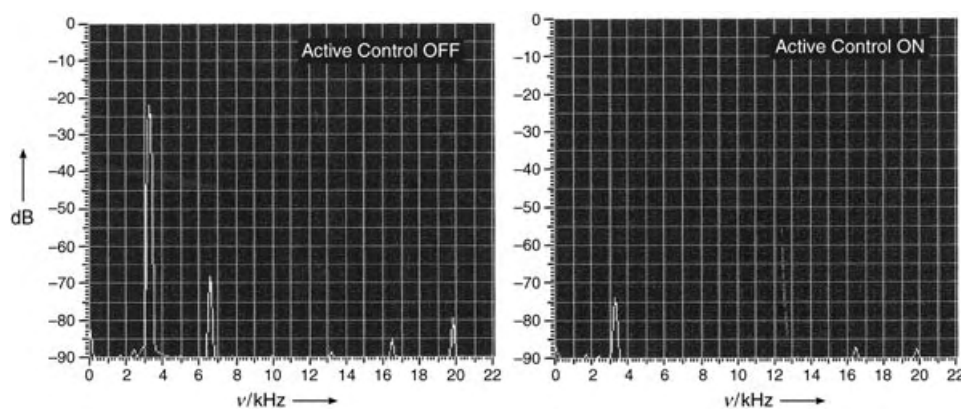


Figure 13. Logarithmic acoustic pulse spectra (filtered single pulse, 22 ms^{-1} Kaiser 7) with active control off (left) and active control on (right). The resulting reduction in noise of 50 dB (99.7%) in the fundamental noise component at 3.2 kHz . (Reproduced with permission from Ref. [25].)

noise generated by the large and rapidly switched magnetic gradients required for EPI and EVI. Some progress has been made in ameliorating this situation in principle, but it remains to be demonstrated whether the active acoustic control principle can be fully implemented on an operational gradient coil set. For further reading see Refs. [26–31].

I am grateful to my early research supervisors, Professor J. G. Powles, originally at Queen Mary College, University of London, and Professor C. P. Slichter at the University of Illinois, Urbana, Illinois (USA), for teaching me the art and practice of NMR spectroscopy. I am also greatly indebted to Professor R. Bowley and my other colleagues at Nottingham and to my own research students and post-doctoral assistants listed in Table 1 all of whom contributed extensively to the development of MRI at Nottingham. Also listed are the key medical colleagues whose collaboration and support helped to bring about acceptance of MRI as a diagnostic tool both nationally and internationally.

Table 1: List of former students, post-doctoral assistants, and medical collaborators.

Physics			
Dr. P. K. Grannell	Prof. A. A. Maudsley	Prof. P. G. Morris	Dr. I. L. Pykett
Prof. R. J. Ordidge	Dr. R. Rzedzian ^[a]	Dr. M. Doyle	Dr. D. N. Guilfoyle
Dr. S. J. Blackband	Dr. M. G. Cawley	Prof. R. W. Bowtell	Dr. A. M. Howseman
Dr. R. J. Coxon	Dr. M. K. Stehling	Dr. A. M. Blamire	Dr. P. Gibbs
Dr. P. R. Harvey	Dr. M. Symms	Dr. M. McJury	Dr. M. Clemence
Dr. B. Issa	Dr. P. Glover	Dr. A. Freeman	J. Hykin
Dr. A. Rodriguez	Dr. A. Peters	Dr. B. Boulby	Dr. M. Al-Mugheiry
Dr. J. Beaumont	Dr. M. Bencsik	B. Haywood ^[b]	Prof. R. Bowley
Postdoctoral assistants			
Dr. B. Chapman ^[b]	Dr. A. N. Garroway	Dr. P. Gowland	Dr. J. C. Sharp
Prof R. Turner	Dr. P. Tokarczuk	Prof. A. Jasinski	Dr. G. Planinsic
Dr. A. Snaar			
Medicine			
Dr. K. Morris	Prof. I. Johnson	Prof. R. Coupland	Prof. B. Worthington
Dr. P. Small	Dr. A. Crispin ^[a]	Dr. C. O'Callaghan	Mr. J. Firth
Prof. M. Symonds			

[a] Deceased. [b] Special thanks for help in preparation of this presentation.

I am especially grateful to the technical and workshop staff of both the Magnetic Resonance Centre and the Department of Physics and Astronomy for their untiring and unstinting support in the construction and testing of several prototype MRI systems over the years.

I am also most grateful for the financial support received from the Institutions listed in Table 2. Without their generous and

Table 2: List of funding and equipment support agencies.

Medical Research Council		University of Nottingham	
		Sir Colin Campbell	
Department of Health and Social Security		British Heart Foundation	
G. Hickson	Dr. N. Slarke		
J. Williams		Oxford Magnet Technology	
British Technology Group		General Magnetic	
I. Harvey	N. Davis		
G. Blunt	R. Sutherland		

sustained support over many years there would be little to celebrate today.

Finally, I wish to express my sincere appreciation and thanks to my personal secretaries over the years, Mary Newsum-Smith, Lesley Key, and most recently Pamela Davies, for their unflagging efforts in typing and re-typing the many manuscripts, reports, and general correspondence.

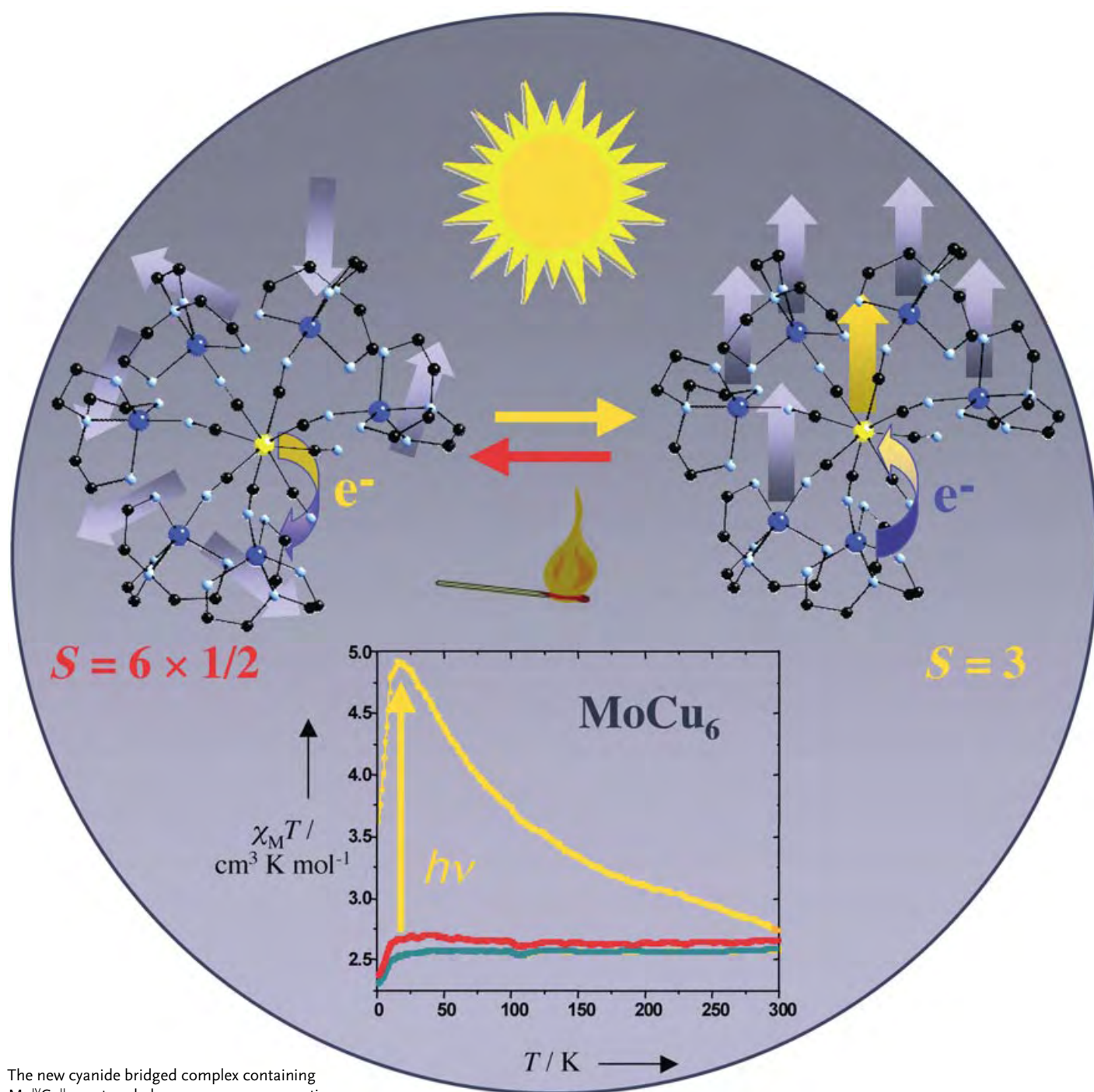
Received: March 22, 2004

Published Online: September 21, 2004

- [1] "Multi-pulse line narrowing experiments": P. Mansfield, P. K. Grannell, A. N. Garroway, D. C. Stalker, *Proc First Specialised Colloque Ampere*, Poland, **1973**.
- [2] "NMR 'Diffraction' in solids?": P. Mansfield, P. K. Grannell, *J. Phys. C* **1973**, 6, L422–L426.
- [3] "Image formation in NMR by a selective irradiative process": A. N. Garroway, P. K. Grannell, P. Mansfield, *J. Phys. C* **1974**, 7, L457–L462.
- [4] "Medical imaging by NMR": P. Mansfield, A. A. Maudsley, *Br. J. Radiol.* **1977**, 50, 188–194.
- [5] "Multi-planar imaging formation using NMR spin echoes": P. Mansfield, *J. Phys. C* **1977**, 10, L55–L58.
- [6] "Active magnetic screening of coils for static and time-dependent magnetic field generation in NMR imaging": P. Mansfield, B. Chapman, *J. Phys. E* **1986**, 19, 541–546.
- [7] "Double active magnetic screening of coils in NMR": B. Chapman, P. Mansfield, *J. Phys. D* **1986**, 19, L129–L131.
- [8] "Whole Body Echo-Planar MR Imaging at 0.5 T": M. J. Stehling, A. M. Howseman, R. J. Ordidge, B. Chapman, R. Turner, R. Coxon, P. Glover, P. Mansfield, R. E. Coupland, *Radiology* **1989**, 170, 257–263.
- [9] "Ultra-fast magnetic resonance scanning of the liver with echo-planar imaging": M. K. Stehling, R. M. Charnley, A. M. Blamire, R. J. Ordidge, R. Coxon, P. Gibbs, J. D. Hardcastle, P. Mansfield, *Br. J. Radiol.* **1990**, 63, 430–437.
- [10] "Estimation of lung volume in infants by echo planar imaging and total body plethysmography": B. Chapman, C. O'Callaghan, R. J. Coxon, P. M. Glover, G. Jaroszkiewicz, A. M. Howseman, P. Mansfield, P. Small, A. D. Milner, R. E. Coupland, *Arch. Dis. Child.* **1990**, 65, 168–170.
- [11] "Fetal weight estimation by echo-planar magnetic resonance imaging": P. N. Baker, I. R. Johnson, P. A. Gowland, J. Hykin, P. R. Harvey, A. Freeman, V. Adams, B. S. Worthington, P. Mansfield, *Lancet* **1994**, 343, 644–645.
- [12] "Obstetrics. Echo-planar magnetic resonance imaging in the estimation of fetal weight": J. Hykin, P. Gowland, P. Mansfield, *Contemp. Rev. Obstet. Gynaecol.* **1994**, 6, 173–177.
- [13] "Transectional echo planar imaging of the heart in cyanotic congenital heart disease": A. Chrispin, P. Small, N. Rutter, R. E. Coupland, M. Doyle, B. Chapman, R. Coxon, D. Guilfoyle, M. Cawley, P. Mansfield, *Paediatr. Radiol.* **1986**, 16, 293–297.
- [14] "Echo-planar imaging of normal and abnormal connections of the heart and great arteries": A. Chrispin, P. Small, N. Rutter,

- R. E. Coupland, M. Doyle, B. Chapman, R. Coxon, D. Guilfoyle, M. Cawley, P. Mansfield, *Paediatr. Radiol.* **1986**, 16, 289–292.
- [15] “EPI of the infant heart (1). Demonstration of connection between ventricle and artery by EPI construction”: P. Mansfield, P. Small, A. Chrispin, N. Rutter, R. E. Coupland, M. Doyle, B. Chapman, D. N. Guilfoyle, M. G. Cawley, *Paediatr. Radiol.* **1985**, 15, 280.
- [16] “EPI of the infant heart (2). Demonstration of ventriculo/bulbar septation by EPI transection”: P. Mansfield, A. Chrispin, P. Small, N. Rutter, R. E. Coupland, M. Doyle, B. Chapman, D. N. Guilfoyle, M. G. Cawley, *Paediatr. Radiol.* **1985**, 15, 280.
- [17] “Echo-Planar Imaging of the Brain at 3.0 T: First Normal Volunteer Results”: P. Mansfield, R. Coxon, P. Glover, *J. Comp. Ass. Tomogr.* **1994**, 18, 339–343.
- [18] “Echo-Volumar Imaging (EVI) at 0.5 T: First Whole-Body Volunteer Studies”: P. R. Harvey, P. Mansfield, *Magn. Reson. Med.* **1996**, 35, 80–88.
- [19] “Echo-Volumar Imaging (EVI) of the Brain at 3.0 T: First Normal Volunteer and Functional Imaging Results”: P. Mansfield, R. Coxon, J. Hykin, *J. Comp. Ass. Tomogr.* **1995**, 19, 847–852.
- [20] National Radiological Protection Board, *Board statement on clinical magnetic resonance diagnostic procedures*, Documents of the NRPB, Vol. 2, No. 1., Chiltern, **1991**.
- [21] “Price RR The AAPM/RSNA physics tutorial for residents: MR imaging safety considerations”: *Radiographics* **1999**, 19, 1641–1651.
- [22] “Sound Generation in Gradient Coil Structures for MRI”: P. Mansfield, P. M. Glover, J. Beaumont, *Magn. Reson. Med.* **1998**, 39, 539–550.
- [23] “Principles of Active Acoustic Control in Gradient Coil Design”: P. Mansfield, B. Haywood, *Magn. Reson. Mater. Phys. Biol. Med.* **2000**, 10, 147–151.
- [24] “Active Acoustic Control in Gradient Coils for MRI”: P. Mansfield, B. Haywood, R. Coxon, *Magn. Reson. Med.* **2001**, 46, 807–818.
- [25] “Optimized Gradient Pulse for Use with EPI Employing Active Acoustic Control”: B. L. W. Chapman, B. Haywood, P. Mansfield, *Magn. Reson. Med.* **2003**, 50, 931–935.
- [26] “Snapshot echo-planar imaging methods: current trends and future perspectives”: P. Mansfield, A. M. Blamire, R. Coxon, P. Gibbs, D. N. Guilfoyle, P. Harvey, M. Symms, *Philos. Trans. R. Soc. London Ser. A* **1990**, 333, 495–506.
- [27] “Snapshot Imaging at 0.5 T Using Echo-Planar Techniques”: R. Ordidge, A. Howseman, R. Coxon, R. Turner, B. Chapman, P. Glover, M. Stehling, P. Mansfield, *Magn. Reson. Med.* **1989**, 10, 227–240.
- [28] “Echo-Planar Imaging: Magnetic Resonance Imaging in a Fraction of a Second”: M. K. Stehling, R. Turner, P. Mansfield, *Science* **1991**, 254, 43–50.
- [29] P. Mansfield, P. G. Morris, *NMR Imaging in Biomedicine*, Academic Press, New York, **1982**.
- [30] F. Schmitt, M. K. Stehling, R. Turner, *Echo-Planar Imaging: Theory, Technique and Application*, Springer, Heidelberg, **1998**.
- [31] P. G. Morris, *NMR Imaging in Medicine and Biology*, Clarendon, Oxford, **1986**.

Communications



The new cyanide bridged complex containing $\text{Mo}^{\text{IV}}\text{Cu}^{\text{II}}_6$ centers behaves as a paramagnetic species ($S=6 \times 1/2$). Upon light-irradiation, an intramolecular electron transfer occurs resulting in the high-spin molecule containing $\text{Mo}^{\text{V}}\text{Cu}^{\text{I}}\text{Cu}^{\text{II}}_5$ centers ($S=3$). This state is metastable (up to 280 K) and the photomagnetic effect is thermally reversible. For more information see the Communication by V. Marvaud, C. Mathonière, et al. on the following pages.

Reversible Photoinduced Magnetic Properties in the Heptanuclear Complex
 $[\text{Mo}^{\text{IV}}(\text{CN})_2(\text{CN}-\text{CuL})_6]^{8+}$:
A Photomagnetic High-Spin Molecule**

Juan Manuel Herrera, Valérie Marvaud,*
 Michel Verdaguer, Jérôme Marrot, Marguerite Kalisz,
 and Corine Mathonière*

*Dedicated to Professor Jean-Pierre Launay
 on the occasion of his 60th Birthday*

Switching effects operating at the molecular level are currently subject to intense research efforts.^[1] Amongst the various triggering media usually considered, light is assuredly one of the most often utilized.^[2] Amongst possible physical molecular properties that may be switched, magnetism^[3] is one of the most common.^[4] Basic photoinduced processes mostly involved in photomagnetic materials are Light-Induced Excited Spin-State Trapping (LIESST)^[5] or spin alignment,^[6] changes in intramolecular exchange interactions,^[7] spin crossover resulting from electron transfers (Co-Fe Prussian blue analogues^[8]), or peripheral ligand(s) isomerization (Ligand-Driven Light-Induced Spin Change, LD-LISC).^[9] Recent works have also been devoted to photomagnetic materials based on octacyanomolybdate precursors,^[10] well known since the 1960s for their photoreactivity.^[11] Herein we report the first photomagnetic high-spin molecule, which was obtained by combining the two following approaches. Some of us (Mathonière and co-workers) have previously suggested the possibility of photoinduced electron transfers within mixed $\text{Mo}^{\text{IV}}/\text{Cu}^{\text{II}}$ compounds^[12] while the others (Marvaud et al.) have demonstrated the feasibility of design-

ing and synthesizing hetero-polynuclear complexes of controlled shape (anisotropy), nuclearity, and magnetic properties.^[13] The resulting compound (**1**; see below) is of main interest in the field of single-molecule magnets (SMM).^[14] Indeed, anisotropic high-spin species are appealing candidates to study the reversal of the magnetization in a magnetic field and might be used, in future, as new components for information storage at the molecular scale. These new species can also be viewed as model compounds to better understand related 3D photomagnetic materials, by evaluating the exchange coupling. It is worth noting that, up to now, the most important photomagnetic effect ever observed in such a type of compounds was in a Co-Fe Prussian blue analogues,^[8] with a relaxation temperature of 120 K.

In the continuation of the synthetic strategy previously described for polynuclear complexes based on hexacyanomolybdate chemistry,^[13,15] we have selectively obtained a heptanuclear complex built from an octacyanomolybdate(IV) core and Cu^{II} building blocks. This $[\text{Mo}(\text{CN})_2(\text{CN}-\text{CuL})_6]^{8+}$ polynuclear complex, **1**, was formed by treating potassium octacyanomolybdate(IV) with a mononuclear copper(II) complex generated in situ from the tris(2-aminoethyl)amine terminal ligand L and Cu^{II} perchlorate salt. Partial evaporation of mother liquor led to green needles soluble in water and common organic solvents.

The complex has been fully characterized and its identity confirmed. On the IR spectrum, the intense distinctive bands of ClO_4^- (around 1090 cm^{-1}) revealed the presence of cationic complexes. In the range of $2200\text{--}2000\text{ cm}^{-1}$, two types of cyanide asymmetric stretching bands are observed: a strong band at 2158 cm^{-1} , assigned to bridging cyanides and a weak band at 2128 cm^{-1} , attributed to singly bound cyanides. The ESMS spectrum showed major peaks at $m/z = 1079.7$ and 490.1 ascribed to $\{[\text{Mo}(\text{CN})_2(\text{CN}-\text{CuL})_6](\text{ClO}_4)_6\}^{2+}$ and $\{[\text{Mo}(\text{CN})_2(\text{CN}-\text{CuL})_6](\text{ClO}_4)_4\}^{4+}$ respectively, which also indicates that the complex is stable in solution.

X-ray analysis reveals that **1** crystallizes in monoclinic space group, Pn ($Z=2$). Two heptanuclear complexes (Figure 1), 16 perchlorate ions and 9 water molecules are present in the asymmetric unit, which corresponds to 255 non-hydrogen atoms. Each $[\text{Mo}(\text{CN})_2(\text{CN}-\text{CuL})_6]^{8+}$ entity is formed by the octacyanomolybdate core, the molybdenum center being in an dodecahedral environment with six copper(II) ions bounded to six cyanide nitrogen atoms. Two cyanide ligands are end-on coordinated. The copper ions are in a trigonal-bipyramid environment, in which L plays the role of blocking ligand. Cyano bridges appear distorted with Mo-C-N angles ranging from 170.0° to 179.0° , and the C-N-Cu angles range from 149.3° to 172.5° . The shortest Mo-Mo distance between two neighboring molecules is 13.05 \AA .

UV/Vis spectra recorded both in the solid state and for aqueous solution show similar features, including the following bands ($\lambda\text{ nm}$ [$\epsilon\text{ M}^{-1}\text{ cm}^{-1}$]) at 242 [36 000], 270 [27 800], 680 [410] and 844 [1075]. These features, characteristic of the two individual $[\text{CuL}]^{2+}$ and $[\text{Mo}(\text{CN})_8]^{4-}$ chromophoric fragments,^[16] are attributed to d-d and metal-to-ligand charge transfer (MLCT) electronic transitions. Of note, an additional band at 440 nm ($\epsilon = 660\text{ M}^{-1}\text{ cm}^{-1}$) is detected and assigned to an intervalence Mo-Cu transition (metal-to-metal charge

[*] J. M. Herrera, Dr. V. Marvaud, Prof. M. Verdaguer
 Laboratoire de Chimie Inorganique et Matériaux Moléculaires
 CNRS, UMR 7071
 Université Pierre et Marie Curie
 75252 Paris Cedex 05 (France)
 Fax: (+33) 144-273-841
 E-mail: marvaud@ccr.jussieu.fr
 M. Kalisz, Dr. C. Mathonière
 Institut de Chimie de la Matière Condensée de Bordeaux
 CNRS UPR 9048
 87, avenue du Docteur Albert Schweitzer, 33 608 Pessac (France)
 Fax: (+33) 556-842-649
 E-mail: mathon@icmcb.u-bordeaux.fr
 Dr. J. Marrot
 Institut Lavoisier
 Université Versailles Saint-Quentin
 45, avenue des Etats-Unis, 78035 Versailles (France)

[**] We thank Dr. P. Lainé for helpful discussions, Prof. M. Julve for his constant interest and encouragement, Dr. F. Gonnet for ESMS measurements. We thank the CNRS, the University Pierre et Marie Curie (Paris VI), the French ministry of research (ACI young researcher for V.M. No. JC4123) and the European Community for financial support (TMR No. HPRN-CT 1999 0012 and TMR No. MRTN-CT-2003-504880) L = tris(2-aminoethyl)amine.

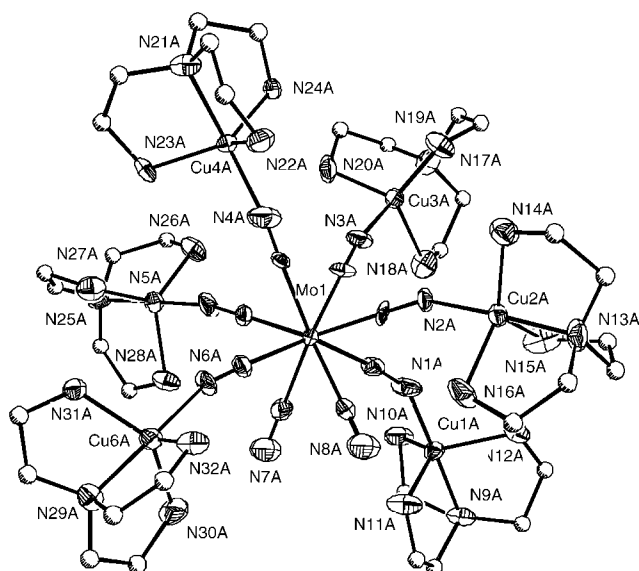


Figure 1. X-ray crystal structure (ORTEP drawing) of one of the two $[\text{Mo}(\text{CN})_2(\text{CN}-\text{CuL})_6]^{8+}$ entities with thermal ellipsoids set at 30%. Hydrogen atoms, crystallization solvents and counterions are omitted for clarity.

transfer, MMCT). These results are consistent with electrochemical data. Thus, the reversible oxidation of the molybdenum(IV/V) core within **1** is observed at +0.70 V versus the saturated calomel electrode (SCE) in acetonitrile, close to that obtained for the $[\text{Mo}(\text{CN})_8]^{4-}$ precursor (+0.78 V vs SCE). The difference can be rationalized in terms of an increased electron-pair donation from Cu^{II} fragments to the molybdenum. In the reduction part of the cyclic voltammogram, no wave characteristic of the $\text{Cu}^{\text{III/I}}$ and $\text{Mo}^{\text{IV/III}}$ couples could be detected in the potential range investigated (limited by copper deposition).

The magnetic properties of compound **1** show that the $[\text{Mo}^{\text{IV}}(\text{CN})_2(\text{CN}-\text{Cu}^{\text{II}}\text{L})_6]^{8+}$ complex, behave as six isolated paramagnetic centers, as expected for a diamagnetic Mo^{IV} center surrounded by six Cu^{II} cations. $\chi_{\text{M}}T$ is constant ($2.5 \text{ cm}^3 \text{ mol}^{-1} \text{ K}$ down to 20 K; χ_{M} is the molar magnetic susceptibility) in agreement with six isolated Cu^{II} (the theoretical value is 2.48 for six independent spin 1/2 and $g = 2.2$; g is the g factor). At low temperature, below 20 K, the curve decreases, which indicates antiferromagnetic intramolecular interactions between the spin carriers, as observed in $\{\text{CoCu}_6\}$ or related compounds.^[13] Upon irradiation with blue light (406–415 nm), magnetic susceptibility progressively changed: after 10 h of irradiation at 10 K, the $\chi_{\text{M}}T$ value increased up to $4.8 \text{ cm}^3 \text{ mol}^{-1} \text{ K}$. The light was then switched off. In heating mode, $\chi_{\text{M}}T$ first increased in the range from 5 to 16 K until it reached a plateau value of $5 \text{ cm}^3 \text{ mol}^{-1} \text{ K}$; this value decreased continuously as the temperature was raised to 300 K, with values always higher than those obtained for the nonirradiated compound. The two $\chi_{\text{M}}T$ versus T curves join at a temperature close to 300 K. After 1 h at room temperature, χ_{M} was measured in cooling mode. A constant $\chi_{\text{M}}T$ value was observed ($2.6 \text{ cm}^3 \text{ mol}^{-1} \text{ K}$), thus showing unambiguously that the process is thermally reversible (Figure 2).

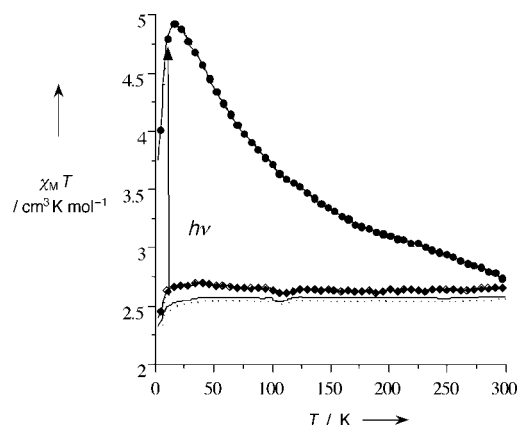


Figure 2. Thermal dependence of the $\chi_{\text{M}}T$ product for **1**: (○) before irradiation, (●) after irradiation, (◆) after irradiation and $T > 300 \text{ K}$.

The photomagnetic effect may be observed as well in the magnetization curves, performed at 5 K and shown in Figure 3. Before irradiation, the data correspond to six

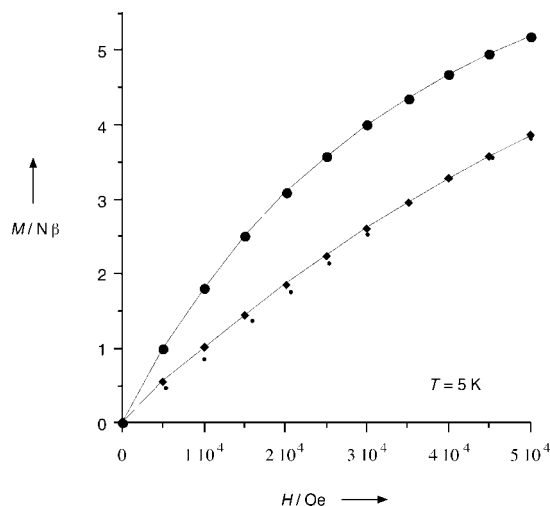


Figure 3. Field dependence of the magnetization of **1** at 5 K: (○) before irradiation, (●) after irradiation, (◆) after irradiation and $T > 300 \text{ K}$.

isolated spin $S = 1/2$ (Cu^{II} ions). After irradiation, the magnetization data shows a value at $5 \mu_{\text{B}}$ at 50 kOe. After reaching $T = 300 \text{ K}$ and cooling, the magnetization curve is similar to that obtained for the nonirradiated species, giving a further demonstration of the switching effect.

These results are explained by the photoinduced formation of a high-spin molecule with ferromagnetic interaction between the spin carriers. Agreement between experimental data after irradiation and the calculated Brillouin function is obtained for $S = 3$, assuming that the ground state only is populated at $T = 5 \text{ K}$ and that 75% of the product has been transformed. This spectacular effect may be rationalized by an electron transfer from Mo^{IV} to Cu^{II} and the formation of paramagnetic centered (Mo^{V}) species: $\text{Mo}^{\text{V}}\text{Cu}^{\text{I}}\text{Cu}^{\text{II}}_5$. Irradiation by using wavelengths close to the intervalence band

(MMCT) photoinduces an electron transfer from the diamagnetic Mo^{IV} center (d^2 , $S=0$) to one of the peripheral Cu^{II} ions. This electron transfer generates a paramagnetic Mo^{V} (d^1 , $S=1/2$) center and one diamagnetic Cu^{I} (d^{10} , $S=0$) ion. Thus, cyano-mediated ferromagnetic interactions are switched on between the Mo^{V} , $S=1/2$, and the remaining five Cu^{II} , spin $1/2$, in the photo-induced species $\text{Mo}^{\text{V}}\text{Cu}^{\text{I}}\text{Cu}^{\text{II}}_5$, which leads to a high-spin molecule with $S=3$. The photoinduced magnetic effect is thermally reversible and reproducible (Figure 4). The

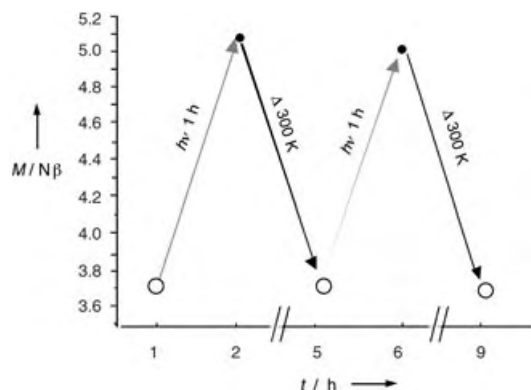


Figure 4. Study of the reversibility: variation of the magnetization of **1** ($H=50\,000$ Oe): ● after irradiation and ○ after irradiation and thermal treatment ($T>300$ K).

complete return to the initial state operates at temperatures close to room temperature. The high relaxation temperature indicates that the photoinduced metastable state is related to significant local reorganization of the coordination sphere around the Cu^{I} ion. This is relevant considering the usual geometry of the Cu^{I} ion (tetrahedral) compared to Cu^{II} ion (trigonal-bipyramid) and the flexibility of the L ligand.

In summary, **1** is the first photoinduced high-spin molecule. Calculations are in progress to evaluate the exchange coupling parameter while taking into account the thermal depopulation of the metastable state. Preliminary results obtained by using the isotropic Heisenberg Hamiltonian $\mathcal{H} = -J_{\text{Mo/Cu}} S_{\text{Mo}} \sum_i S_i$ (i ranges from 1 to 5) give an exchange coupling value $J>100\text{ cm}^{-1}$ and a Landé factor $g=2.08$. The J value is higher than that of the $\{\text{CrCu}_6\}$ compound ($J=+45\text{ cm}^{-1}$)^[13] as predicted for compounds of second- and third-row transition-metal cations with diffuse d valence orbitals.^[17] Other work is planned to obtain more convincing evidence of the presence of the Cu^{I} and Mo^{V} ions (such as X-Ray diffraction on an irradiated single crystal, Polarized Neutron diffraction, optic and vibrational spectroscopy). We shall study the optical reversibility and the SMM behavior and evaluate the photomagnetic properties of other complexes of the octacyanometalate family, specially the $\{\text{WCu}_6\}$ analogue. The present study opens the field of photomagnetic high-spin molecules (higher than 3) and opens the way to photomagnetic single-molecule magnets.

Experimental Section

A solution of tris(2-amino)ethylamine (0.95 g, 6.5 mmol) in water/acetonitrile (1:1, 10 mL) was added to a solution of copper

perchlorate (2.29 g, 6 mmol) in water (10 mL). The mixture was stirred for less than 5 min before the addition of hexacyanomolybdate(IV) potassium salt (0.497 g, 1 mmol) dissolved in a minimum of water. After filtration, the solution was left standing for 24 h, which lead the formation of green needles. Yield 52%. Elemental analysis calcd (%) for $\text{C}_{44}\text{H}_{118}\text{MoCu}_6\text{N}_{32}\text{Cl}_8\text{O}_{37}$: C 21.12, H 4.60, N 17.65, Mo 3.83, Cu 14.22, Cl 11.81; found: C 21.58, H 4.86, N 18.31, Mo 3.92, Cu 15.57, Cl 11.58. IR (KBr) 2158 and 2128 cm^{-1} (CN asymmetric stretching).

Crystal data and structure refinements for **1**: A green needle ($0.50 \times 0.30 \times 0.10\text{ mm}$) was analyzed with a Siemens SMART three-circle diffractometer equipped with a CCD bidimensional detector with MoK_α monochromatized radiation ($\lambda=0.71073\text{ \AA}$). Monoclinic, space group Pn , $a=24.7473(3)\text{ \AA}$, $b=14.4050(1)\text{ \AA}$, $c=30.0287(2)\text{ \AA}$, $\beta=108.742(1)^\circ$, $V=10137.15(16)\text{ \AA}^3$, $Z=2$, $\rho_{\text{calc}}=1.598\text{ g cm}^{-3}$, $\mu(\text{MoK}_\alpha)=1.653\text{ mm}^{-1}$, $F(000)=4996$, 46001 reflections measured, of which 21204 were independent, 1501 refined parameters, $R_1=0.0845$, $wR_2=0.2092$, GOF=0.963; max/min residual electron density $1.030/-0.587\text{ e \AA}^{-3}$. Data reduction was performed with the SAINT software. The absorption correction was based on multiple and symmetry-equivalent reflections in the data set by using the SADABS^[18] program based on the method of Blessing. The structures were solved by direct methods and refined by full-matrix least-squares by using the SHELX-TL program.^[19] CCCDC-203098 (**1**) contains the supplementary crystallographic data for this paper. These data can be obtained free of charge via www.ccdc.cam.ac.uk/conts/retrieving.html (or from the Cambridge Crystallographic Data Centre, 12 Union Road, Cambridge CB21EZ, UK; fax: (+44)1223-336-033; or deposit@ccdc.cam.ac.uk).

Magnetic studies were carried out with a Quantum Design MPMS-5S magnetometer working in the dc mode. The measurements were performed in the 5–300 K range with a magnetic field of 20000 Oe. The photomagnetic experiments were performed with a Kr^+ laser coupled through an optical fiber directed into the cavity of the superconductivity quantum interference induction device (SQUID). Powdered samples were laid down on a diamagnetic sample holder (Magnetization (emu)= -2.62×10^{-4}) as thin layers (weight 0.68 mg) to avoid surface effects during illumination. The diamagnetic contribution and the weight were estimated by comparing the magnetization curves (5 K and versus temperature) before irradiation with the curves recorded in a routine magnetic experiment (20 mg of sample loaded into gel caps). The samples were irradiated continuously by using different multilines (406–415 nm and 337–356 nm) under a magnetic field of 20 kOe at 10 K. The effective power of the laser light received by the sample was measured at 3 mW cm^{-2} for $\lambda=337\text{--}356\text{ nm}$ and 7 mW cm^{-2} for $\lambda=406\text{--}415\text{ nm}$. Magnetic properties were recorded before and after irradiation, in each case the light was turned off to avoid thermal inhomogeneities. The cycle in temperature corresponds to a complete study with different steps: 1) magnetization at 5 K first, and then measurement with the sample is warmed to 300 K, 2) cooling of the sample to 10 K in one hour and half with no measure, 3) new magnetization at 5 K.

Received: April 21, 2004

Published Online: September 3, 2004

Keywords: cyanides · electron transfer · heterometallic complexes · magnetic properties · photochemistry

- [1] a) A. P. de Silva, N. D. McClenaghan, *Chem. Eur. J.* **2004**, *10*, 574–586; b) R. L. Carroll, C. B. Gorman, *Angew. Chem.* **2002**, *114*, 4556–4579; *Angew. Chem. Int. Ed.* **2002**, *41*, 4378–4400.
- [2] a) Guest Editor: M. Irie, *Chem. Rev.* **2000**, *100*, 1683–1890; b) V. Balzani, L. Moggi, F. Scandola, *Supramolecular Photochemistry* (Ed.: V. Balzani), D. Reidel, Dordrecht, The Netherlands, **1987**, pp. 1–28.

- [3] a) O. Kahn, *Molecular Magnetism*, Wiley-VCH, Weinheim, **1993**; b) "Molecular Magnetism: from molecular assemblies to the devices": *NATO Sci. Ser. II* **1995**, 321; c) *Magnetism: molecules to materials* (Eds.: J. S. Miller, M. Drillon), Wiley-VCH, Weinheim, **2001**.
- [4] a) O. Sato, *Acc. Chem. Res.* **2003**, 36, 692–700, and references therein; b) P. Gülich, Y. Garcia, T. Woike, *Coord. Chem. Rev.* **2001**, 219–221, 839–879.
- [5] a) P. Gülich, A. Hauser, H. Spiering, *Angew. Chem.* **1994**, 106, 2109–2141; *Angew. Chem. Int. Ed. Engl.* **1994**, 33, 2024–2054; b) P. Gülich, A. Hauser, *Coord. Chem. Rev.* **1990**, 97, 1; c) S. Decurtins, P. Gülich, C. P. Köhler, H. Spiering, A. Hauser, *Chem. Phys. Lett.* **1984**, 105, 1–4.
- [6] Y. Teki, S. Miyamoto, M. Nakatsuji, Y. Miura, *J. Am. Chem. Soc.* **2001**, 123, 294–305.
- [7] K. Takayama, K. Matsuda, M. Irie, *Chem. Eur. J.* **2003**, 9, 5605–5609.
- [8] a) O. Sato, T. Iyoda, A. Fujishima, K. Hashimoto, *Science*, **1996**, 272, 704; b) M. Verdager, *Science* **1996**, 272, 698; c) A. Bleuzen, C. Lomenech, V. Escax, F. Villain, F. Varret, C. Cartier dit Moulin, M. Verdager, *J. Am. Chem. Soc.* **2000**, 122, 6648–6652; d) N. Shimamoto, S.-I. Ohkoshi, O. Sato, K. Hashimoto, *Inorg. Chem.* **2002**, 41, 678–684.
- [9] a) M.-L. Boillot, C. Roux, J.-P. Audière, A. Dausse, J. Zarembowitch, *Inorg. Chem.* **1996**, 35, 3975–3980; b) M.-L. Boillot, S. Chantraine, J. Zarembowitch, J.-Y. Lallemand, J. Prunet, *New J. Chem.* **1999**, 23, 179–183.
- [10] a) S.-I. Ohkoshi, N. Machida, J. Z. Zhong, K. Hashimoto, *Synth. Met.* **2001**, 122, 523–527; b) Y. Arimoto, S.-I. Ohkoshi, J. Z. Zhong, H. Seino, Y. Mizobe, K. Hashimoto, *J. Am. Chem. Soc.* **2003**, 125, 9240–9241.
- [11] B. Sieklucka, *Prog. React. Kinet. Mech.* **1999**, 24, 165–221, and references therein.
- [12] G. Rombaut, M. Verelst, S. Golhen, L. Ouahab, C. Mathonière, O. Kahn, *Inorg. Chem.* **2001**, 40, 1151–1159.
- [13] a) V. Marvaud, C. Decroix, A. Scullier, C. Guyard-Duhayon, J. Vaissermann, F. Gonnet, M. Verdager, *Chem. Eur. J.* **2003**, 9, 1677–1691; b) V. Marvaud, C. Decroix, A. Scullier, F. Tuyéras, C. Guyard-Duhayon, J. Vaissermann, J. Marrot, F. Gonnet, M. Verdager, *Chem. Eur. J.* **2003**, 9, 1692–1705.
- [14] a) G. Christou, D. Gatteschi, D. N. Hendrickson, R. Sessoli, *MRS Bull.* **2000**, 25, 66–71, and references therein; b) "Molecular Cluster Magnets": J. R. Long in *Chemistry of Nanostructural Materials* (Ed.: P. Yang), World scientific, Hong Kong, **2003**, pp. 291–315, and references therein; c) D. Gatteschi, R. Sessoli, *Angew. Chem.* **2003**, 115, 278–309; *Angew. Chem. Int. Ed.* **2003**, 42, 268–297.
- [15] a) T. Mallah, C. Auberger, M. Verdager, P. Veillet, *J. Chem. Soc. Chem. Commun.* **1995**, 61–62; b) A. Scullier, T. Mallah, M. Verdager, J.-L. Tholence, P. Veillet, *New J. Chem.* **1996**, 20, 1–4.
- [16] M. F. A. Hendrickx, V. S. Mironov, L. F. Chibotaru, A. Ceulemans, *Inorg. Chem.* **2004**, 43, 3142–3150, and references therein.
- [17] a) M. V. Bennett, J. R. Long, *J. Am. Chem. Soc.* **2003**, 125, 2394–2395; b) M. P. Shores, J. J. Sokol, J. R. Long, *J. Am. Chem. Soc.* **2002**, 124, 2279–2292; c) J. J. Sokol, A. Hee, J. R. Long, *J. Am. Chem. Soc.* **2002**, 124, 7656–7657.
- [18] a) G. M. Sheldrick, SADABS, Program for Scaling and Correction of Area Detector Data, University of Göttingen, Göttingen (Germany), **1997**; b) R. H. Blessing, *Acta Crystallogr. Sect. A* **1995**, 51, 33.
- [19] G. M. Sheldrick, SHELX-TL, Version 6.14, University of Göttingen, Bruker AXS Inc., Madison, WI, **2003**.

Electrophilic Double-Sandwiches Formed by Interaction of [Cp₂Fe] and [Cp₂Ni] with the Tridentate Lewis Acid [(*o*-C₆F₄Hg)₃]**

Mason R. Haneline and François P. Gabbaï*

Dedicated to Professor Hubert Schmidbaur
on the occasion of his 70th birthday

As part of our contribution to the supramolecular chemistry of mercury polyfunctional Lewis acids,^[1] we have been involved in the study of trimeric perfluoro-*ortho*-phenylene mercury, [(*o*-C₆F₄Hg)₃] (**1**),^[2] a simple tridentate Lewis acid. This derivative, which complexes a number of electron-rich species,^[1c,3] also interacts with arenes including naphthalene, pyrene, and triphenylene to afford binary stacks where the arene is π coordinated to the mercury centers of **1**.^[4] This supramolecular complexation mode leads to a perturbation of the photophysical properties of the arene which displays intense room-temperature phosphorescence as a result of a mercury heavy-atom effect.^[5] Our continuing interest in the supramolecular chemistry of **1** led us to extend the scope of our studies to metal complexes featuring accessible aromatic ligands. Herein, we describe the synthesis, structures, and properties of electrophilic double-sandwich complexes formed by the interaction of **1** with ferrocene and nickelocene.^[6]

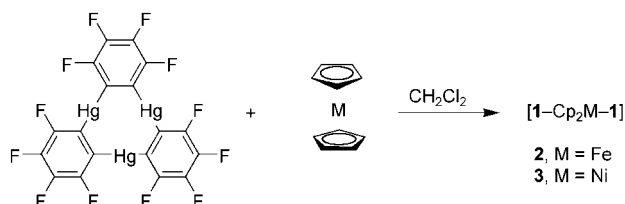
Dark orange crystals of the ferrocene adduct [**1**-CpFeCp-**1**] (**2**) and dark red crystals of the nickelocene adduct [**1**-CpNiCp-**1**] (**3**) were obtained upon evaporation of CH₂Cl₂ solutions containing **1** and the corresponding metallocene (Scheme 1). The 2:1 stoichiometry of these adducts was confirmed by elemental analysis. Both compounds showed no sign of decomposition upon exposure to air for several months thus indicating that **1** stabilizes the usually air-sensitive 20-electron nickelocene complex against aerobic oxidation.^[7] Compounds **2** and **3** crystallize in the monoclinic space group *C2/m* and are isomorphous (Figure 1).^[8] With Hg-C_{metalocene} separations ranging from 3.20–3.24 Å, the carbon atoms of the Cp rings of the metallocene are in close

[*] M. R. Haneline, Prof. Dr. F. P. Gabbaï
Chemistry Department
Texas A&M University 3255 TAMU
College Station, Texas 77843-3255 (USA)
Fax: (1) 979-845-4719
E-mail: gabbai@mail.chem.tamu.edu

[**] Acknowledgment is made to the donors of the American Chemical Society Petroleum Research Fund for support of this research (Grant ACS PRF No. 38143-AC 3). MRH thanks Procter and Gamble for a graduate fellowship. We would like to thank Curtis Berlinguette and Professor Kim Dunbar for their assistance with the magnetic measurements, Kelly Moran at Bruker Biospin for assistance with the NMR measurements and Tim Houghbanks for stimulating discussions. Cp = C₅H₅.



Supporting information for this article is available on the WWW under <http://www.angewandte.org> or from the author.



Scheme 1.

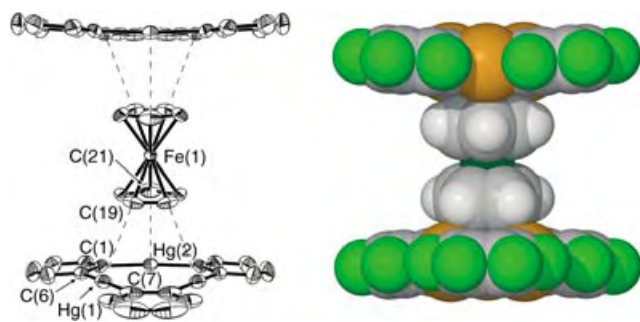


Figure 1. Left: ORTEP view of **2** (thermal ellipsoids set at 30% probability, for clarity all hydrogen and fluorine atoms are omitted). Right: Space-filling model of **3**. (C gray, F light green, Hg orange, Ni dark green, H white). Selected bond lengths [Å] and angles [°]: **2**: Hg(1)–C(19) 3.217(11), Hg(2)–C(21) 3.222(18), Hg(1)–C(6) 2.055(14), Hg(1)–C(7) 2.086(13), Hg(2)–C(1) 2.039(12), C(6)–Hg(1)–C(7) 174.8(5), C(1)–Hg(2)–C(1A) 176.2(7); **3** Selected bond lengths [Å] and angles [°] (numbering scheme as for **2**): Hg(1)–C(19) 3.204(12), Hg(2)–C(21) 3.237(17), Hg(1)–C(6) 2.089(9), Hg(1)–C(7) 2.102(14), Hg(2)–C(1) 2.048(9), C(6)–Hg(1)–C(7) 175.4(5), C(1)–Hg(2)–C(1A) 176.4(6).

contact with the mercury centers of **1**. As observed in arene adducts of **1**,^[4,5] these distances are within the sum of the van der Waals radii of mercury (1.7–2.0 Å)^[9,10] and carbon (1.7 Å).^[11] This structural feature indicates the presence of secondary Hg– π interactions which complement attractive electrostatic and dispersion forces present between **1** and the metallocene.^[4] The two molecules of **1** are staggered with respect to one another. The bond lengths in the metallocene are unchanged compared to those of the pure metallocene.^[12] The perfluorophenylene ring containing the C(1) carbon atom and its symmetry equivalent are bent away from the metallocene and form a dihedral angle of 5° for **2** and 4° for **3** with respect to the plane containing the three mercury atoms. Apparently, this deformation allows for a closer approach of the trinuclear mercury core of **1** to the Cp rings of the metallocene. The remaining phenylene ring which contains the C(7) carbon atom is essentially coplanar with the plane formed by the trinuclear mercury core. While the formation of such electrophilic double sandwiches is unprecedented, we note the existence of a structural parallel with binary compounds such as $[\text{FeCp}^*_2]^+[\text{TCNE}]^-$ ($\text{Cp}^* = \text{C}_5\text{Me}_5$, TCNE = tetracyanoethylene)^[13] and $[\text{Cr}(\text{C}_6\text{H}_6)_2][\text{C}_6\text{F}_6]$ which feature transition-metal complexes sandwiched between π -acidic molecules.^[14]

In **2** and **3**, neighboring molecules of $[\text{1-CpMCp-1}]$ engage in mercuriophilic interactions (Figure 2) with a Hg...Hg separation of 3.4157(16) Å for **2** and 3.3996(17) Å for **3**.

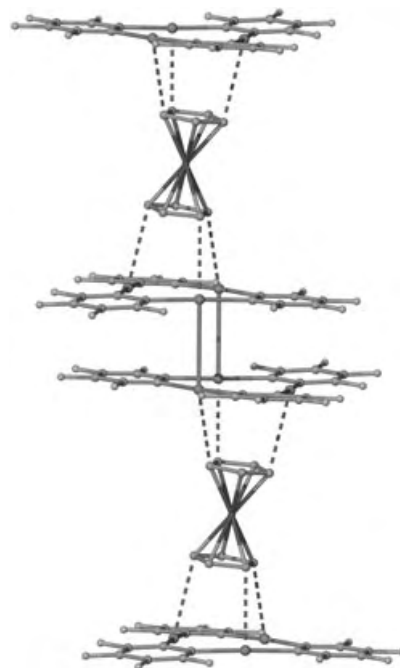


Figure 2. Extended structure of compound **3** showing the Hg...Hg interactions. The structure of compound **2** is identical. For clarity all hydrogen atoms are omitted.

These Hg...Hg separations are within the sum of the van der Waals radius of mercury and are very close to the Hg...Hg separation calculated by Pyykkö for the dimer of dimethyl mercury (3.41 Å).^[9,15] This aggregation mode is similar to that observed in the structure of $[\text{1-}\mu_3\text{-acetone}]$ which forms dimers held by mercuriophilic interactions of 3.512 Å.^[15b] Similar metalophilic interactions are sometimes observed in the structural chemistry of trinuclear coinage-metal complexes.^[16–18]

In an effort to provide a rationale for the dark red color of **3** which does not correspond to that of dark green nickelocene, we have recorded and analyzed the visible diffuse reflectance absorption spectra of **3** and nickelocene. The solution absorption spectrum of nickelocene has been reported^[19,20] and is dominated by three intense spin-allowed transitions at 426 ($^3\text{A}_{2g} \rightarrow ^3\text{E}_{1g}$), 589 ($^3\text{A}_{2g} \rightarrow ^3\text{E}_{2g}$), and 695 nm ($^3\text{A}_{2g} \rightarrow ^3\text{E}_{1g}$) as well as one weak spin-forbidden transition at 526 nm ($^3\text{A}_{2g} \rightarrow ^1\text{E}_{1g}$). The diffuse reflectance spectrum of pristine nickelocene could be satisfactorily modeled on the basis of these four bands, with the spin-forbidden $^3\text{A}_{2g} \rightarrow ^1\text{E}_{1g}$ band being the weakest (Figure 3).^[21] In the case of **3**, deconvolution of the diffuse reflectance spectrum indicates that the intensity of the spin-forbidden band at 526 nm is greatly increased. The $^3\text{A}_{2g} \rightarrow ^1\text{E}_{1g}$ band also appears to be slightly red-shifted to 715 nm. We have already shown that aromatic substrates complexed to **1** experience an external mercury heavy-atom effect which leads to triplet emission.^[4,5] It can therefore be proposed that the nickelocene molecule in **3** also experiences a heavy-atom effect which, because of added spin-orbit coupling, increases the intensity of the formally spin-forbidden $^3\text{A}_{2g} \rightarrow ^1\text{E}_{1g}$ transition at 516 nm.^[22] The diffuse reflectance spectrum of **2** does not display

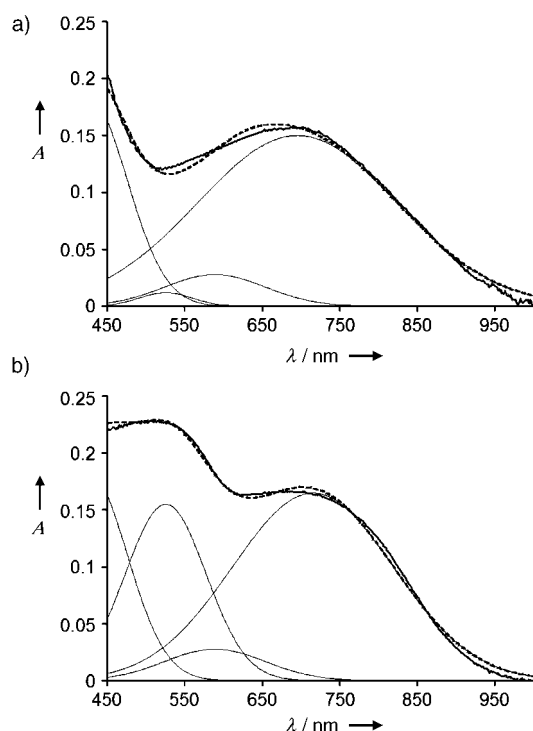


Figure 3. Deconvoluted diffuse reflectance absorption spectra of nickelocene (a) and **3** (b). Bold line = experimental data, broken line = model, thin lines = deconvolution curves.

unusual features and is essentially identical to that of pristine ferrocene.

As indicated by ^{199}Hg NMR spectroscopy, **1** and ferrocene do not form any detectable adducts in CH_2Cl_2 . The solid-state ^{13}C MAS NMR spectrum of **2** shows a single resonance signal for the carbon atoms of the Cp ligand at $\delta = 72$ ppm. Therefore, the Hg- π interactions detected in the structure of **2** appear to be weak and do not affect the magnetic environment of the Cp carbon atoms which remain equivalent. Variable-temperature (2–300 K) magnetic susceptibility data were collected on crushed single crystals of compound **3**. The room temperature $\chi_m T$ value of $1.1 \text{ emu K mol}^{-1}$ is in good agreement with the spin-only value for free nickelocene ($S = 1$). Below 45 K, however, the value of $\chi_m T$ decreases sharply. This decrease can be attributed to a zero-field splitting effect which arises from spin-orbit coupling.^[23] Analysis of the magnetic data on the basis of the equations outlined by Baltzer for an isolated nickelocene^[24] affords a zero-field parameter D of $37.65 \pm 0.29 \text{ cm}^{-1}$ and a g parameter of 2.089 ± 0.003 . The zero-field parameter is slightly greater than that estimated for isolated nickelocene ($D = 33.76 \pm 0.70 \text{ cm}^{-1}$) which might reflect added spin-orbit coupling provided by the six surrounding mercury atoms.^[25] Note that weak antiferromagnetic interactions may also be a plausible cause for this greater than expected value of the D parameter.^[24,26]

In conclusion, we report the synthesis of the 1:2 ferrocene and nickelocene adducts of **1**. In the solid state, these adducts assume an unusual electrophilic double-sandwich structure in which a molecule of **1** caps each of the Cp ligands. Adduct **3** is

air-stable indicating that the 20-electron nickelocene complex is stabilized against oxidation. Although electronic effects cannot be ruled out, this stabilization most likely results from the formation of a tight lattice which physically prevents reaction with oxygen. Finally, in the case of **3**, formation of these sandwiches apparently leads to increased spin-orbit coupling which alters the photophysical and magnetic properties of the nickelocene molecule. Unlike in other donor-acceptor systems involving metallocenes,^[13,14] we have found no evidence of charge transfer in **2** and **3**.

Experimental Section

Owing to the toxicity of the mercury compounds discussed in these studies extra care was taken at all times to avoid contact with solid, solution, and air-borne particulate mercury compounds.

2 and 3: A solution of compound **1** (100 mg, 0.096 mmol) in CH_2Cl_2 (15 mL), was mixed with a solution of the metallocene (100 mg, 0.538 mmol for $[\text{Cp}_2\text{Fe}]$ and 0.529 mmol for $[\text{Cp}_2\text{Ni}]$) in CH_2Cl_2 (5 mL). Crystals, which formed upon slow evaporation of the solvent, were washed with hexanes to remove excess metallocene. This procedure yielded a quantitative amount of dark orange **2** and dark red **3**, respectively. **2:** elemental analysis (%) calcd for $\text{C}_{46}\text{H}_{10}\text{F}_{24}\text{Hg}_6\text{Fe}$: C 24.29, H 0.44; found: C 24.32, H 0.41. M.p. 300°C (decomp). **3** elemental analysis (%) calcd for $\text{C}_{46}\text{H}_{10}\text{F}_{24}\text{Hg}_6\text{Ni}$: C 24.26, H 0.44; found: C 24.50, H 0.49. Decomposes explosively at 275°C .

Received: July 1, 2004

Keywords: host-guest systems · Lewis acids · mercury · metallocenes · pi interactions

- [1] a) M. F. Hawthorne, Z. Zheng, *Acc. Chem. Res.* **1997**, *30*, 267–276; b) J. D. Wuest, *Acc. Chem. Res.* **1999**, *32*, 81–89; c) V. B. Shur, I. A. Tikhonova, *Russ. Chem. Bull.* **2003**, *52*, 2539–2554.
- [2] P. Sartori, A. Golloch, *Chem. Ber.* **1968**, *101*, 2004–2009.
- [3] E. S. Shubina, I. A. Tikhonova, E. V. Bakhmutova, F. M. Dolgushin, M. Y. Antipin, V. I. Bakhmutov, I. B. Sivaev, L. N. Teplitskaya, I. T. Chizhevsky, I. V. Pisareva, V. I. Bregadze, L. M. Epstein, V. B. Shur, *Chem. Eur. J.* **2001**, *7*, 3783–3790; A. L. Chistyakov, I. V. Stankevich, N. P. Gambaryan, T. Yu. Struchkov, A. I. Yanovsky, I. A. Tikhonova, V. B. Shur, *J. Organomet. Chem.* **1997**, *536*, 413–424.
- [4] M. R. Haneline, R. Taylor, F. P. Gabbaï, *Chem. Eur. J.* **2003**, *9*, 5188–5193, and references therein.
- [5] M. R. Haneline, M. Tsunoda, F. P. Gabbaï, *J. Am. Chem. Soc.* **2002**, *124*, 3737–3742; M. Tsunoda, F. P. Gabbaï, *J. Am. Chem. Soc.* **2000**, *122*, 8335–8336.
- [6] “Electrophilic sandwich” is a term first proposed by Hawthorne and co-workers to describe supramolecules in which an anion is sandwiched by two electrophilic hosts, see: H. Lee, M. Diaz, C. B. Knobler, M. F. Hawthorne, *Angew. Chem.* **2000**, *112*, 792–794; *Angew. Chem. Int. Ed.* **2000**, *39*, 776–778.
- [7] E. O. Fischer, R. Jira, *Z. Naturforsch. B* **1953**, *8*, 217–219; G. Wilkinson, P. L. Pauson, F. A. Cotton, *J. Am. Chem. Soc.* **1954**, *76*, 1970–1974.
- [8] The data were collected on a Bruker SMART-CCD area detector diffractometer, MoK_α radiation ($\lambda = 0.71069 \text{ \AA}$) at $T = 293 \text{ K}$, and was solved by direct methods, and refined by full-matrix least squares against F^2 using the SHELXTL/PC (version 6.10) package. **2:** $\text{C}_{46}\text{H}_{10}\text{F}_{24}\text{Hg}_6\text{Fe}$, $M_r = 2277.93$, monoclinic, space group $C2/m$, $a = 10.456(2)$, $b = 19.496(4)$, $c = 12.312(3) \text{ \AA}$, $\beta = 110.51(3)^\circ$, $V = 2350.8(8) \text{ \AA}^3$, $Z = 2$, $\rho_{\text{calcd}} = 3.218 \text{ g cm}^{-3}$.

Crystal size $0.24 \times 0.15 \times 0.15 \text{ mm}^3$, ω -scan mode, measurement range $1.77\text{--}23.33^\circ$, 1761 unique reflections, 1538 reflections with $I > 2(I)$, $\mu = 19.947 \text{ mm}^{-1}$, $R1 = 0.0295$, $wR2 = 0.0866$ (all data); **3**: $\text{C}_{46}\text{H}_{10}\text{F}_{24}\text{Hg}_6\text{Ni}$, $M_r = 2280.79$, monoclinic, space group $C2/m$, $a = 10.554(2)$, $b = 19.509(4)$, $c = 12.299(3) \text{ \AA}$, $\beta = 109.21(3)^\circ$, $V = 2391.2(8) \text{ \AA}^3$, $Z = 2$, $\rho_{\text{calcd}} = 3.168 \text{ g cm}^{-3}$. Crystal size $0.51 \times 0.25 \times 0.24 \text{ mm}^3$, ω -scan mode, measurement range $1.75\text{--}23.27^\circ$, 1781 unique reflections, 1221 reflections with $I > 2(I)$, $\mu = 19.700 \text{ mm}^{-1}$, $R1 = 0.0403$, $wR2 = 0.0756$ (all data). CCDC-242588 (**2**) and CCDC-242589 (**3**) contain the supplementary crystallographic data for this paper. These data can be obtained free of charge via www.ccdc.cam.ac.uk/conts/retrieving.html (or from the Cambridge Crystallographic Data Centre, 12 Union Road, Cambridge CB21EZ, UK; fax: (+44)1223-336-033; or deposit@ccdc.cam.ac.uk).

- [9] P. Pyykkö, M. Straka, *Phys. Chem. Chem. Phys.* **2000**, *2*, 2489–2493.
- [10] A. J. Canty, G. B. Deacon, *Inorg. Chim. Acta* **1980**, *45*, L225–L227.
- [11] C. Cailliet, P. Claverie, *Acta Crystallogr. Sect. A* **1975**, *31*, 448–461.
- [12] J. D. Dunitz, L. E. Orgel, A. Rich, *Acta Crystallogr.* **1956**, *9*, 373–375; P. Seiler, J. D. Dunitz, *Acta Crystallogr. Sect. B* **1980**, *36*, 2255–2260.
- [13] For recent reviews see: J. S. Miller, A. J. Epstein, *Coord. Chem. Rev.* **2000**, *206–207*, 651–660; J. S. Miller, *Inorg. Chem.* **2000**, *39*, 4392–4408.
- [14] C. J. Aspley, C. Boxwell, M. L. Buil, C. L. Higgitt, C. Long, R. N. Perutz, *Chem. Commun.* **1999**, 1027–1028.
- [15] For other example of short $\text{Hg}^{\text{II}}\text{--Hg}^{\text{II}}$ interactions see: a) N. L. Pickett, O. Just, D. G. VanDerveer, J. S. Rees, *Acta Crystallogr. Sect. C* **2000**, *56*, 412–413; b) J. B. King, M. R. Haneline, M. Tsunoda, F. P. Gabbaï, *J. Am. Chem. Soc.* **2002**, *124*, 9350–9351, and references therein.
- [16] K. Singh, J. R. Long, P. Stavropoulos, *J. Am. Chem. Soc.* **1997**, *119*, 2942–2943.
- [17] M. A. Rawashdeh-Omary, M. A. Omary, J. P. Fackler, Jr., *J. Am. Chem. Soc.* **2001**, *123*, 9689–9691.
- [18] A. Hayashi, M. M. Olmstead, S. Attar, A. L. Balch, *J. Am. Chem. Soc.* **2002**, *124*, 5791–5795.
- [19] K. D. Warren, *J. Chem. Phys.* **1973**, *77*, 1681–1686.
- [20] In earlier work the spin-forbidden band at 526 nm has been assigned to the $^3\text{A}_{2g} \rightarrow ^1\text{A}_{1g}$ transition, see: I. Pavlik, V. Cerny, E. Maxova, *Collect. Czech. Chem. Commun.* **1970**, *3*, 3045–3063.
- [21] The diffuse reflectance spectra of **3** and nickelocene were deconvoluted using the Peakfit program. Both spectra were analyzed on the basis of the four main transitions. Further details can be found in the Supporting Information.
- [22] S. P. McGlynn, T. Azumi, M. Kinoshita, *Molecular Spectroscopy of the Triplet State*, Prentice-Hall, Englewood Cliffs, NJ, **1969**.
- [23] B. N. Figgis, M. A. Hitchman, *Ligand Field Theory and Its Applications*, Wiley, New York, **2000**.
- [24] P. Baltzer, A. Furrer, J. Hulliger, A. Stebler, *Inorg. Chem.* **1988**, *27*, 1543–1548.
- [25] Heavy-atom ligands have been shown to increase the zero-field splitting parameter of transition-metal complexes by added spin-orbit coupling, see for example: J. Krzystek, J.-H. Park, M. W. Meisel, M. A. Hitchman, H. Stratemeier, L.-C. Brunel, J. Telser, *Inorg. Chem.* **2002**, *41*, 4478–4487; J.-J. Chen, M.-L. Du, Z.-M. Li, *Z. Naturforsch. A* **1994**, *49*, 1013–1015.
- [26] Ferromagnetic interactions have been proposed to occur in stacks of the anionic complex $[\mathbf{1}\text{-Fe}(\text{CN})_6\text{-}\mathbf{1}]^{3-}$. see: I. A. Tikhonova, F. M. Dolgushin, K. I. Tugashov, O. G. Ellert, V. M. Novotortsev, G. G. Furin, M. Yu. Antipin, V. B. Shur, *J. Organomet. Chem.* **2004**, *689*, 82–87.

Rhodium Silyl Boryl Hydride Complexes: Comparison of Bonding and the Rates of Elimination of Borane, Silane, and Dihydrogen**

Kevin S. Cook, Christopher D. Incarvito,
Charles Edwin Webster, Yubo Fan, Michael B. Hall,*
and John F. Hartwig*

Transition-metal “ σ complexes”^[1] of dihydrogen^[2] and of silanes^[3] are common, and transition-metal σ -borane complexes are now known.^[4–11] Dihydrogen complexes are intermediates in the oxidative addition that occurs during hydrogenation, and they are intermediates of the reductive elimination that occurs during dehydrogenation. Similarly, silane complexes are probably intermediates in the oxidative additions of silanes that occur during hydrosilylation,^[12] and borane complexes have been shown to be intermediates in catalytic hydroboration.^[5] Borane complexes are also likely intermediates^[13] in the borylation of alkanes^[14,15] and arenes.^[15–19]

A complex with hydride, silyl, and boryl groups bound to the metal center of the same complex could adopt a structure with a σ -dihydrogen, -silane, or -borane ligand. No complexes of this type have been isolated in pure form, but compounds with this collection of ligands would allow direct assessment of the similarities and differences between the three types of σ complexes. Herein, we report the synthesis, experimental and calculated structures, as well as the reaction chemistry of $[\text{Cp}^*\text{RhH}_2(\text{Bpin})(\text{SiR}_3)]$ ($\text{Cp}^* = \text{C}_5\text{Me}_5$, $\text{Bpin} = (\text{pinacolato})\text{-boryl}$) complexes, which contain two hydrides, one silyl and one boryl group. Our data suggests that this complex contains partial B–H bonding and that borane eliminates from this complex faster than dihydrogen or silane.

Reaction of the known bis(silyl) dihydride **1a**^[20] with a large excess of HBpin in refluxing cyclohexane formed $[\text{Cp}^*\text{RhH}_2(\text{SiEt}_3)(\text{Bpin})]$ (**2a**) in 90% yield, as determined by NMR spectroscopy with an internal standard [Eq. (1)]. In addition to a single pinacol methyl resonance at $\delta = 1.09$ ppm

[*] Dr. K. S. Cook, Dr. C. D. Incarvito, Prof. J. F. Hartwig
Department of Chemistry
Yale University
P.O. Box 208107, New Haven, Connecticut 06520-8107 (USA)
Fax: (+1) 203-432-3917
E-mail: John.Hartwig@yale.edu
Dr. C. E. Webster, Dr. Y. Fan, Prof. M. B. Hall
Department of Chemistry
Texas A&M University
P.O. Box 30012, College Station, TX 77842-3012 (USA)
Fax: (+1) 979-845-2971
E-mail: mbhall@tamu.edu

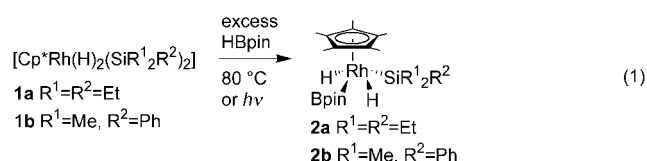
[**] The NSF (Grant Nos. CHE 03-01907 and MRI 02-16275) and the Welch Foundation (Grant No. A-648) are gratefully acknowledged for financial support. The NSERC is acknowledged for a post-doctoral fellowship to K.S.C.



Supporting information for this article is available on the WWW under <http://www.angewandte.org> or from the author.

and ethyl resonances from the silyl group, the ^1H NMR spectrum of **2a** contained a doublet at $\delta = -12.7$ ppm ($^1J_{\text{Rh-H}} = 42.0$ Hz) for the hydride ligands. The ^{11}B NMR spectrum contained a resonance at $\delta = 40$ ppm, which confirmed the presence of a boryl ligand. Though **2a** formed in high yield by NMR spectroscopy, we were unable to isolate crystalline material from these reactions.

However, irradiation of the bis(silyl) complex **1a** and HBpin in cyclohexane for 18 h allowed the isolation of crystalline silyl boryl dihydride **2a** in 61 % yield. Reaction of $[\text{Cp}^*\text{RhH}_2(\text{SiMe}_2\text{Ph})_2]$ (**1b**)^[21] with excess HBpin formed *trans*- $[\text{Cp}^*\text{RhH}_2(\text{SiMe}_2\text{Ph})(\text{Bpin})]$ (**2b**) under similar photochemical conditions in 78 % yield [Eq. (1)]. Longer reaction times did not cause replacement of the second silane of **2a** or **2b** with borane to form $[\text{Cp}^*\text{Rh}(\text{H})_2(\text{Bpin})_2]$ (**3**).



Reaction of B_2pin_2 with **1** formed a single major product, but the conversion of **1** was incomplete before this major species underwent further reaction. We previously formulated the major species as the bisboryl **3**, based on the presence in the NMR spectra of a broad resonance signal for hydride groups and new resonances for pinacol methyl groups.^[15] With **2a** now in hand, the spectral features of the major product generated from **1** and B_2pin_2 clearly result from **2a**.

The structure of **2a** was confirmed by X-ray crystallography.^[22] All hydride units were located in the electron difference map and were freely refined isotropically. Figure 1 shows a view of **2a** along the $\text{Cp}^*\text{-Rh}$ axis. The boryl and silyl ligands are located in mutually *trans* positions of the four-legged piano stool structure of **2a**. The Rh–Si bond length of

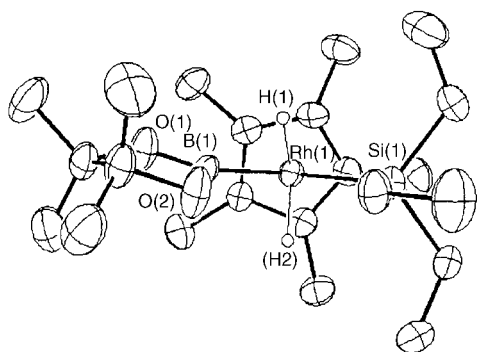


Figure 1. Molecular structure of **2a** (thermal ellipsoids set at 30% probability). Selected bond lengths [Å] and angles [°]: Rh(1)–H(1) 1.57(5), Rh(1)–H(2) 1.59(4), Rh(1)–Si(1) 2.3681(15), Rh(1)–B(1) 2.038(5), Rh(1)–Cp_{cent} 1.919(4); Si(1)–Rh(1)–H(1) 70.3(15), H(1)–Rh(1)–B(1) 55.7(16), B(1)–Rh(1)–H(2) 67.9(14), H(2)–Rh(1)–Si(1) 66.5(15).

2.3681(15) Å is similar to the 2.379(2) Å Rh–Si separation in the bis(silyl) complex **1a**.^[20]

The hydride positions suggested a structure with more residual B–H bonding than H–H or Si–H bonding, despite the caveats of defining hydride positions by X-ray diffraction. An ideal four-legged piano-stool structure would contain a mirror plane that is defined by the Cp* centroid, rhodium, silicon, and boron atoms. In such a piano-stool geometry, the two hydride units would lie in or near a vertical plane that would be orthogonal to this mirror plane. Although one of the hydrides in **2a** lies near this plane, the second hydride lies out of this plane on the side of boron atom. Thus, the H(1)–Rh(1)–B(1) angle of 55.7(16)° is measurably smaller than the H(2)–Rh(1)–B(1) angle of 67.9(14)° or the two H–Rh(1)–Si(1) angles (66.5° and 70.3°). The symmetrical starting complex **1a** contains H–Rh–Si angles of 65° and 69°. The boron–hydride separation of the shorter B–H bond of 1.74(4) Å is 0.3 Å shorter than the longer boron–hydride bond. This distance is much longer than the B–H bonds of 1.30–1.36 Å in Mn, Re, and Ti σ -borane complexes.^[7,10] However, it is shorter than the B–H bond in *trans*- $[\text{Rh}(\text{Cl})(\text{H})(\text{Bpin})(\text{P}(\text{Pr})_3)_2]$. This complex has a long B–H separation of 2.013(5) Å, as determined by neutron diffraction, but an acute H–Rh–B angle that seems to result from B–H bonding.^[19,23]

Considering the difficulty in defining the position of hydrides and the series of different binding modes available to **2a** and **2b**, we sought to provide further evidence for the B–H interaction by computing the ground-state structure of **2a** by DFT-B3LYP methods.^[24,25] An overlay of the calculated and experimental structure of **2a** is provided in Figure 2. The

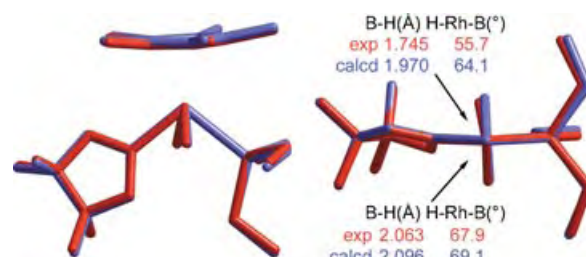


Figure 2. Overlay of the experimental and calculated (DFT-B3LYP) structure of $[\text{Cp}^*\text{RhH}_2(\text{SiEt}_3)(\text{Bpin})]$. The experimental structure is given in red and the computed structure is given in blue.

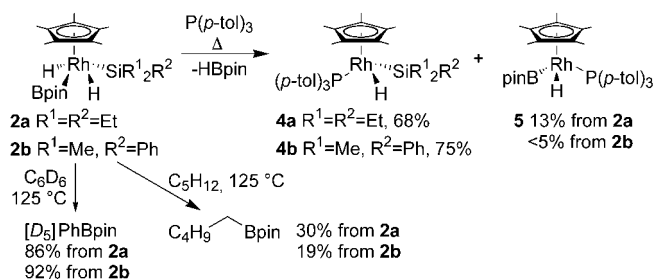
separations and angles in the calculated structure are relatively close to those of the experimental structure. Although the unsymmetrical property of the computed structure is less pronounced than that of the experimental structure, both structures display geometries with separations appropriate for partial B–H bonding, one hydride that is closer to the boron atom than the other hydride, and one B–Rh–H angle that is smaller than the other B–Rh–H angle or the Si–Rh–H angles. As a result, even the computed structure in the gas phase lacks a mirror plane containing the Cp* centroid, rhodium, silicon, and boron.

The solution ^1H NMR spectroscopic data of complexes **2a,b** show a small, direct scalar coupling between the hydride units and the boron center that further indicates the presence

of B–H bonding. The single resonance signal for the two hydride units in **2a** and **2b** is slightly broadened (**2a**, $\omega_{1/2}$ = 11.7 Hz; **2b**, $\omega_{1/2}$ = 12.1 Hz) and sharpens upon ^{11}B decoupling (**2a**, $\omega_{1/2}$ = 8.2 Hz; **2b**, $\omega_{1/2}$ = 8.2 Hz). ^1H NMR spectra of compounds containing discrete, *cis*-disposed boryl and hydride ligands contain sharp hydride signals that remain unchanged upon ^{11}B decoupling.^[17,26–28] Our NMR spectroscopic data imply that the B–H interactions in **2a,b** remain intact in solution, though the two hydride positions are averaged on the NMR time scale and the small magnitude of the scalar coupling suggests a weak interaction.

The calculated potential energy surface (PES) for shortening of the B–H bonding in **2a** is nearly flat (< 0.5 kcal mol^{–1} for the decrease in B–H separation from 1.970 Å to 1.670 Å), but the PES is steeper for shortening the H–Si separation. These results suggest that dissociation of borane should occur in preference to dissociation of silane. Further, the *trans* orientation of the hydride units should make dissociation of H₂ unfavorable.

Consistent with this prediction, heating of **2a** and **2b** at 100 °C with 1 equivalent of P(*p*-tol)₃ gave as the major products the silyl complexes [Cp**Rh*(H)(SiR¹₂R²){P(*p*-tol)₃}] (**4a**, R¹ = R² = Et; **4b**, R¹ = Me, R² = Ph; Scheme 1)



Scheme 1. Reaction chemistry of silyl boryl hydride complexes **2a** and **2b**.

in 68 % and 75 % yield. HBpin and pinBOBpin or B₂pin₃ were the major boron products. The rhodium products were identified by comparison of NMR spectral data to those of material prepared independently by reaction of the phosphine with bis(silyl) complexes **1a** at 100 °C for 16 h and **1b** at 150 °C for 3 h. Reaction of **2a** formed as minor products a small amount of free silane and [Cp**Rh*(H)(Bpin){P(*p*-tol)₃}] (**5**) in 13 % yield. The half-life for elimination of borane from **2a** and **2b** was determined by monitoring the reactions of these complexes with excess PEt₃ by ^1H NMR spectroscopy. At 100 °C, the half-life for reaction of **2a** was 4.5 h, and the half-life for reaction of **2b** was 2 h.

To determine if Cp*-rhodium silyl boryl complexes could be intermediates in the borylation and silylation of hydrocarbons,^[15,29] we evaluated the reactivity of **2a** and **2b** with neat hydrocarbons (Scheme 1). Heating of **2a** and **2b** at 125 °C in C₆D₆ formed one equivalent of the phenylboronate ester [D₅]PhBpin in 86 % and 92 % yield, respectively (Scheme 1), as quantified by ^1H NMR spectroscopy and confirmed by GC/MS. Reactions of **2a** and **2b** with alkanes

occurred in lower yields. Heating **2a** and **2b** in pentane at 125 °C in a sealed vessel formed the pentylboronate ester in 30 % and 19 % yield, as determined by GC (Scheme 1). Arylsilane or pentylsilane were not detected in these reaction mixtures. Several rhodium products are formed from these thermolysis reactions, and these materials have not yet been fully characterized. Because borane dissociates from **2a** and **2b** more readily than H₂ or silane, and the borylation of arenes and alkanes typically occurs through metal boryl complexes,^[16,27,30,31] the mechanism of the reactions of **2a** and **2b** with hydrocarbons is likely to be complex.

In conclusion, two complexes that could possess a dihydrogen, silane, or borane ligand have been prepared. These complexes preferentially adopt geometries with σ -borane complexes and undergo dissociation of borane more rapidly than dissociation of silane or dihydrogen. This preference for dissociation of borane from **2a** and **2b** to generate a silyl hydride intermediate instead of dissociation of silane to generate a boryl hydride intermediate explains in part why the silyl complexes are less effective than [Cp**Rh*(η^6 -C₆Me₆)] as catalyst precursors for the borylation of hydrocarbons.

Received: April 23, 2004

Revised: August 11, 2004

Keywords: boron · density functional calculations · hydride ligands · rhodium · Si ligands

- [1] G. J. Kubas, *Metal-dihydrogen and sigma-bond complexes: structure, theory, and reactivity*, Kluwer Academic, New York, 2001.
- [2] D. M. Heinekey, W. J. Oldham, *Chem. Rev.* **1993**, 93, 913.
- [3] H. Schubert, *Adv. Organomet. Chem.* **1990**, 30, 151.
- [4] V. Montiel-Palma, M. Lumbierres, B. Donnadieu, S. Sabo-Etienne, B. Chaudret, *J. Am. Chem. Soc.* **2002**, 124, 5624.
- [5] J. F. Hartwig, C. N. Muhoro, *Organometallics* **2000**, 19, 30.
- [6] M. Shimoi, S.-i. Nagai, M. Ichikawa, Y. Kawano, K. Katoh, M. Uruichi, H. Ogino, *J. Am. Chem. Soc.* **1999**, 121, 11 704.
- [7] C. N. Muhoro, X. M. He, J. F. Hartwig, *J. Am. Chem. Soc.* **1999**, 121, 5033.
- [8] C. N. Muhoro, J. F. Hartwig, *Angew. Chem.* **1997**, 109, 1536; *Angew. Chem. Int. Ed. Engl.* **1997**, 36, 1510.
- [9] J. F. Hartwig, X. He, C. N. Muhoro, O. Eisenstein, R. Bosque, F. Maseras, *J. Am. Chem. Soc.* **1996**, 118, 10936.
- [10] S. Schlecht, J. F. Hartwig, *J. Am. Chem. Soc.* **2000**, 122, 9435.
- [11] D. R. Lantero, D. H. Motry, D. L. Ward, M. R. Smith III, *J. Am. Chem. Soc.* **1994**, 116, 10811.
- [12] J. P. Collman, L. S. Hegedus, J. R. Norton, R. G. Finke, 2nd ed., University Science Books, Mill Valley, **1987**, pp. 306.
- [13] C. E. Webster, Y. Fan, M. B. Hall, D. Kunz, J. F. Hartwig, *J. Am. Chem. Soc.* **2002**, 124, 858.
- [14] H. Chen, J. F. Hartwig, *Angew. Chem.* **1999**, 111, 3597; *Angew. Chem. Int. Ed.* **1999**, 38, 3391.
- [15] H. Chen, S. Schlecht, T. C. Semple, J. F. Hartwig, *Science* **2000**, 287, 1995.
- [16] T. Ishiyama, J. Takagi, K. Ishida, N. Miyaoura, *J. Am. Chem. Soc.* **2002**, 124, 390.
- [17] C. N. Iverson, M. R. Smith III, *J. Am. Chem. Soc.* **1999**, 121, 7696.
- [18] J. Y. Cho, M. K. Tse, D. Holmes, R. E. Maleczka, M. R. Smith, *Science* **2002**, 295, 305.

- [19] S. Shimada, A. S. Batsanov, J. A. K. Howard, T. B. Marder, *Angew. Chem.* **2001**, *113*, 2226; *Angew. Chem. Int. Ed.* **2001**, *40*, 2168.
- [20] M. J. Fernandez, P. M. Bailey, P. O. Bentz, J. S. Ricci, T. F. Koetzle, P. M. Maitlis, *J. Am. Chem. Soc.* **1984**, *106*, 5458.
- [21] J. Ruiz, B. E. Mann, C. M. Spencer, B. F. Taylor, P. M. Maitlis, *J. Chem. Soc. Dalton Trans.* **1987**, 1963.
- [22] X-ray diffraction was performed on a Nonius KappaCCD diffractometer with graphite monochromated Mo-K α radiation ($\lambda = 0.71073$ Å). Crystal data for **2a**: C₂₂H₄₄BO₂RhSi, $M_r = 482.38$, orthorhombic space group $P2_12_12_1$ (No.19), $a = 10.583(2)$, $b = 12.279(3)$, $c = 20.456(4)$ Å, $\alpha = 90^\circ$, $\beta = 90^\circ$, $\gamma = 90^\circ$, $V = 2658.2(9)$ Å³, $Z = 4$, $\rho_{\text{calcd}} = 1.205$ g cm⁻³, $\mu = 7.00$ cm⁻¹, $T = 296(2)$ K, 6081 reflections (6081 unique), 252 refined parameters, $R = 0.0475$ (6081 data with $I > 2\sigma(I)$), $wR(F^2) = 0.0739$, residual electron density = 0.407 to -0.449 e⁻ Å⁻³. The hydride H atoms were revealed in the difference Fourier map and refined isotropically. CCDC-247319 (**2a**) contains the supplementary crystallographic data for this paper. These data can be obtained free of charge via www.ccdc.cam.ac.uk/conts/retrieving.html (or from the Cambridge Crystallographic Data Centre, 12 Union Road, Cambridge CB21EZ, UK; fax: (+44)1223-336-033; or deposit@ccdc.cam.ac.uk).
- [23] W. H. Lam, S. Shimada, A. S. Batsanov, Z. Y. Lin, T. B. Marder, J. A. Cowan, J. A. K. Howard, S. A. Mason, G. J. McIntyre, *Organometallics* **2003**, *22*, 4557.
- [24] Gaussian03 (Revision B.05), M. J. Frisch, G. W. Trucks, H. B. Schlegel, G. E. Scuseria, M. A. Robb, J. R. Cheeseman, J. A. Montgomery, Jr., T. Vreven, K. N. Kudin, J. C. Burant, J. M. Millam, S. S. Iyengar, J. Tomasi, V. Barone, B. Mennucci, M. Cossi, G. Scalmani, N. Rega, G. A. Petersson, H. Nakatsuji, M. Hada, M. Ehara, K. Toyota, R. Fukuda, J. Hasegawa, M. Ishida, T. Nakajima, Y. Honda, O. Kitao, H. Nakai, M. Klene, X. Li, J. E. Knox, H. P. Hratchian, J. B. Cross, C. Adamo, J. Jaramillo, R. Gomperts, R. E. Stratmann, O. Yazyev, A. J. Austin, R. Cammi, C. Pomelli, J. W. Ochterski, P. Y. Ayala, K. Morokuma, G. A. Voth, P. Salvador, J. J. Dannenberg, V. G. Zakrzewski, S. Dapprich, A. D. Daniels, M. C. Strain, O. Farkas, D. K. Malick, A. D. Rabuck, K. Raghavachari, J. B. Foresman, J. V. Ortiz, Q. Cui, A. G. Baboul, S. Clifford, J. Cioslowski, B. B. Stefanov, G. Liu, A. Liashenko, P. Piskorz, I. Komaromi, R. L. Martin, D. J. Fox, T. Keith, M. A. Al-Laham, C. Y. Peng, A. Nanayakkara, M. Challacombe, P. M. W. Gill, B. Johnson, W. Chen, M. W. Wong, C. Gonzalez, J. A. Pople, Gaussian, Inc., Pittsburgh, PA, **2003**.
- [25] For computational methods, see the Supporting Information.
- [26] J. F. Hartwig, X. He, *Organometallics* **1996**, *15*, 5350.
- [27] K. Kawamura, J. F. Hartwig, *J. Am. Chem. Soc.* **2001**, *123*, 8422.
- [28] G. J. Irvine, M. J. G. Lesley, T. B. Marder, N. C. Norman, C. R. Rice, E. G. Robins, W. R. Roper, G. R. Whittell, L. J. Wright, *Chem. Rev.* **1998**, *98*, 2685.
- [29] K. Ezbiansky, P. I. Djurovich, M. Laforest, D. J. Sinning, R. Zayes, D. H. Berry, *Organometallics* **1998**, *17*, 1455.
- [30] K. M. Waltz, J. F. Hartwig, *J. Am. Chem. Soc.* **2000**, *122*, 11358.
- [31] K. M. Waltz, C. N. Muhoro, J. F. Hartwig, *Organometallics* **1999**, *18*, 3383.

Hemibuckminsterfullerene C₃₀H₁₂: X-ray Crystal Structures of the Parent Hydrocarbon and of the Two-Dimensional Organometallic Network {[Rh₂(O₂CCF₃)₄]₃·(C₃₀H₁₂)}^{**}

Marina A. Petrukhina,^{*} Kristian W. Andreini,
Lingqing Peng, and Lawrence T. Scott

Since the discovery of fullerenes,^[1] bowl-shaped polyarenes that map onto the surface of C₆₀ have attracted considerable attention.^[2] These geodesic fullerene fragments or “buckybowls” represent an exciting new class of aromatic ligands that exhibit unique chemistry.^[2f] Substantial efforts have recently been directed toward studies of the reactivity and ligating properties of buckybowls, but very few of their transition metal complexes have been isolated.^[3,4] Last year, we finally succeeded in preparing the first crystalline complexes of a geodesic polyarene, using the sublimation–deposition technique in a solvent-free environment with the smallest bowl-shaped polycyclic aromatic hydrocarbon, corannulene (**1**, C₂₀H₁₀, Figure 1).^[4] The availability of crystallographic data allowed us to determine the preferred sites for metal binding to the curved unsaturated carbon surface of this open geodesic polyarene, and η² coordination of as many as three metal atoms to the rim carbon atoms of corannulene

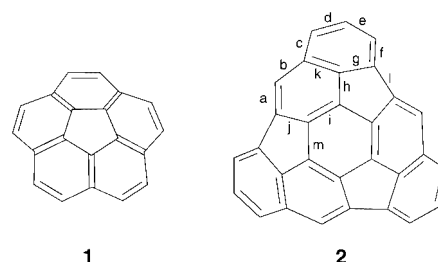


Figure 1. Corannulene (**1**) and hemifullerene (**2**). Pauling π-bond orders: a) 0.74, b) 0.28, c) 0.37, d) 0.63, e) 0.37, f) 0.63, g) 0.37, h) 0.28, i) 0.51, j) 0.28, k) 0.37, l) 0.00, m) 0.23.

[*] Prof. Dr. M. A. Petrukhina, K. W. Andreini
Department of Chemistry, University at Albany
State University of New York
Albany, NY 12222 (USA)
Fax: (+1) 518-442-3462
E-mail: marina@albany.edu

L. Peng, Prof. Dr. L. T. Scott
Department of Chemistry, Merkert Chemistry Center
Boston College, Chestnut Hill, MA 02467-3860 (USA)

[**] The University at Albany, SUNY, has supported this work through an FRAP-2004 award and start-up funds. M.A.P. also thanks the National Science Foundation for the CCD X-ray diffractometer (NSF-01300985) and Dr. E. Dikarev for assistance with the X-ray experiments. Additional support of this work by the Department of Energy and the National Science Foundation is gratefully acknowledged. We especially thank Prof. Dr. K. Mislow for valuable discussion on the chirality of geodesic polyarenes.

was observed in crystalline complexes with dirhodium(II) tetrakis(trifluoroacetate) $[\text{Rh}_2(\text{O}_2\text{CCF}_3)_4]$. In the present work, we extend this powerful synthetic approach to a new system and use $[\text{Rh}_2(\text{O}_2\text{CCF}_3)_4]$ as an electrophilic probe to test the donor properties of the much larger buckybowl hemibuckminsterfullerene **2** ($\text{C}_{30}\text{H}_{12}$, Figure 1).

Hydrocarbon **2** represents a C_3 -symmetrical half of C_{60} fullerene and for this reason has long appealed to chemists as a possible intermediate for the laboratory synthesis of buckminsterfullerene.^[5] Furthermore, dehydrogenative dimerization of *endo* metal complexes of **2** might even provide a direct and controlled route for metal encapsulation in fullerenes.

The first synthesis of hemifullerene **2** was completed in 1995;^[6] however, no crystal structure has been reported heretofore, owing to the lack of crystals suitable for X-ray analysis. As a consequence, the intriguing question of the preference for metal binding to the concave versus the convex surface of this deep $\text{C}_{30}\text{H}_{12}$ bowl has been addressed only computationally.^[7] Previous attempts to prepare a transition metal complex of **2** by treating it with $[\text{Pt}(\text{C}_2\text{H}_4)(\text{PPh}_3)_2]$ were thwarted by insertion of platinum into the peripheral C–C bond of one of the five-membered rings.^[8] The feasibility of such an unusual aryl–aryl C–C bond breaking has been attributed to the relief of strain at the edge of this curved aromatic hydrocarbon.

Herein we report the first X-ray crystal structures of **2** (two different polymorphs) and the X-ray crystal structure of its coordination complex with $[\text{Rh}_2(\text{O}_2\text{CCF}_3)_4]$. In the latter, four rhodium(II) centers are bound to a single hemifullerene molecule to afford a unique two-dimensional (2D) extended organometallic network.

Hemifullerene **2** was synthesized according to the six-step synthesis we reported in 1997^[9] and was crystallized from the vapor phase.^[10] Two types of crystals of **2** were deposited at about 240 °C in vacuum, and both were crystallographically characterized.^[11] X-ray diffraction studies on the two polymorphs of **2**, one orthorhombic (**2-o**) and the other trigonal (**2-t**), revealed two different molecular packing motifs based on π – π interactions (Figure 2). Ordered assembly of bowls to form interlocking *exo*–*exo* and *endo*–*endo* columnar stacks is found in **2-o**. Such stacking differs from the solid-state structures of the simplest curved polycyclic hydrocarbon, corannulene (**1**),^[12] and of the largest bowl that has been crystallographically characterized so far, circumtrindene ($\text{C}_{36}\text{H}_{12}$).^[13] Columnar stacking of the $\text{C}_{30}\text{H}_{12}$ bowls along the threefold axis is found in **2-t**, with insertion of the convex dome of one bowl into the concave cavity of the next (*exo*–*endo* type), similar to the ordered pattern observed in the crystal structure of circumtrindene.^[13] Despite these differences between **2-o** and **2-t**, the estimated volumes per $\text{C}_{30}\text{H}_{12}$ molecule in the two structures are very similar, 425.4 and 424.1 Å³, respectively. Several C–C contacts are in the range of typical π – π interactions (3.5–3.7 Å) in the solid-state structures of both **2-o** and **2-t**; the shortest distances are 3.547(4) in **2-o** and 3.253(4) and 3.323(4) Å in **2-t**.

The nonplanar $\text{C}_{30}\text{H}_{12}$ molecule is chiral and exists as a pair of enantiomers.^[14] Unfortunately, the racemic mixture obtained from the synthesis was inseparable by preparative

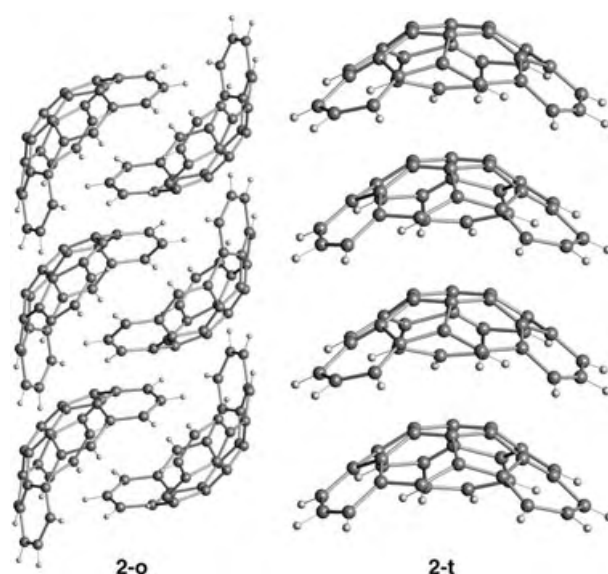


Figure 2. Solid-state packing in the orthorhombic crystals of **2-o** and in the trigonal crystals of **2-t**. Only one enantiomer is shown for clarity.

chiral chromatography, so the crystal structures of **2-o** and **2-t** contain statistical distributions of the two enantiomers in all positions, with an average $1/2$ occupancy (Figure 3). This

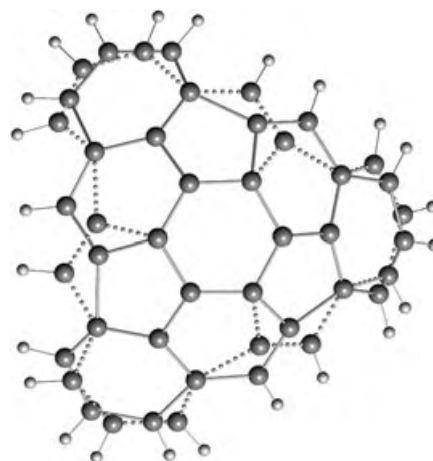


Figure 3. Superposition of the two enantiomers of the $\text{C}_{30}\text{H}_{12}$ hemifullerene **2**.

complication adversely affects the quality of structural information extracted from the X-ray experiments and reduces to some extent the reliability of the carbon–carbon distances obtained.

The hemifullerene coordination complex was synthesized by the microscale “solventless” ampule technique, which involves the co-deposition of volatile complementary donor and acceptor partners from the gas phase. We first applied this approach to the preparation of complexes of $[\text{Rh}_2(\text{O}_2\text{CCF}_3)_4]$ ^[15] with planar polycyclic aromatic hydrocarbons (PAHs)^[16] and have successfully used the technique more recently for the synthesis and crystallization of cor-

annulene-based organometallics.^[4] With the hemibuckminsterfullerene **2**, only one product, $\{[\text{Rh}_2(\text{O}_2\text{CCF}_3)_4]_3 \cdot (\text{C}_{30}\text{H}_{12})\}$ (**3**), was isolated reproducibly in the form of single crystals from deposition reactions of the dirhodium complex with the hydrocarbon performed at 164 °C.^[17] Attempts to change the product composition by varying the reaction temperature or the ratio of reagents in the above system did not result in the formation of other crystalline complexes.

The above deposition reaction afforded **3** in the form of very small dark red crystals. The low yield obtained prevented accurate elemental analysis and may reflect the limited volatility of $\text{C}_{30}\text{H}_{12}$ compared to $\text{C}_{20}\text{H}_{10}$. Significant mass transfer of $\text{C}_{30}\text{H}_{12}$ was achieved at temperatures above 250 °C, but these conditions do not favor the formation of weak π complexes of rhodium(II) with PAHs. Crystals of **3** are stable in air at room temperature but are slightly sensitive to moisture; this behavior is typical for analogous donor–acceptor adducts of $[\text{Rh}_2(\text{O}_2\text{CCF}_3)_4]$ with planar PAHs and with corannulene. When crystals of **3** are dissolved in chloroform, the free hemifullerene is released, as confirmed by ^1H NMR spectroscopy.

The new coordination complex of hemifullerene **3** exhibits a unique structural motif, as revealed by an X-ray diffraction study.^[18] The complex has an infinite 2D layered structure built on weak rhodium–carbon interactions of the two-ended electrophilic dirhodium molecules with the hemifullerene ligands (Figure 4).

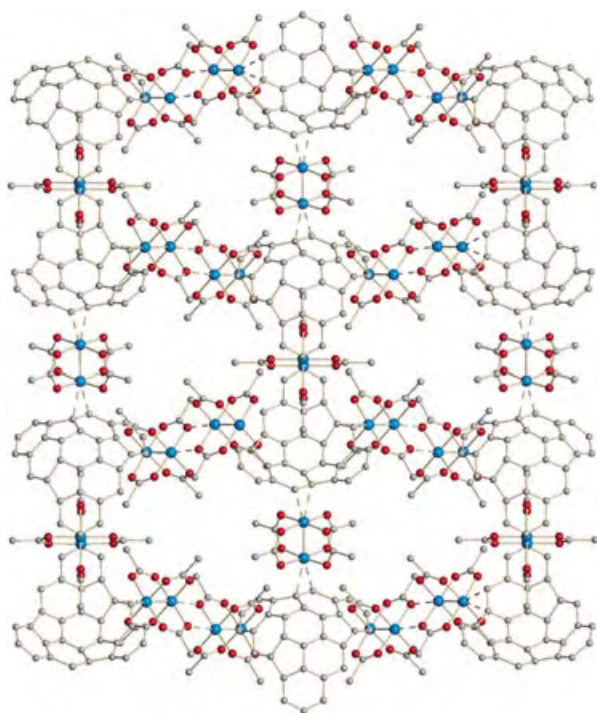


Figure 4. A fragment of a 2D infinite layer in **3**; Rh blue, O red, C gray; hydrogen and fluorine atoms are omitted for clarity.

Four metal centers from three crystallographically independent dirhodium complexes are bound to each $\text{C}_{30}\text{H}_{12}$ molecule, and this results in a tetradentate coordination

mode that is unprecedented for buckybowls. Tetrabridged coordination of a planar PAH with $[\text{Rh}_2(\text{O}_2\text{CCF}_3)_4]$ was seen previously only in the case of chrysene.^[16b] Three rhodium centers in **3** approach the hemifullerene ligand from the convex (*exo*) side, and one is bound to the concave (*endo*) side (Figure 5a). Steric hindrance most probably precludes the coordination of two $[\text{Rh}_2(\text{O}_2\text{CCF}_3)_4]$ units to the concave surface of this deep bowl-shaped molecule and presumably directs positioning of the three $[\text{Rh}_2(\text{O}_2\text{CCF}_3)_4]$ units on the convex surface of the hemifullerene.

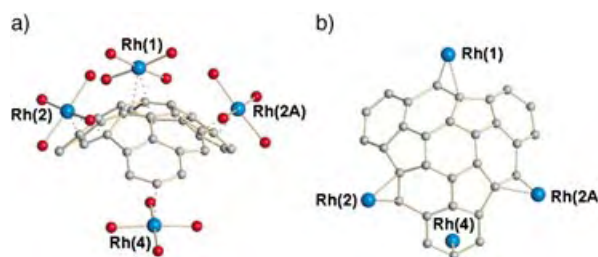


Figure 5. a) Side view of the $\text{C}_{30}\text{H}_{12}$ hemifullerene in **3** coordinated to four rhodium(II) centers. b) Top view showing the tetradentate $\eta^2:\eta^2:\eta^2:\eta^1$ coordination.

As in the corannulene complexes reported earlier,^[4] only rim carbon atoms of the $\text{C}_{30}\text{H}_{12}$ hydrocarbon are involved in metal coordination. The three *exo*-coordinated rhodium centers (only two of which are crystallographically independent) each have bonding contacts with two carbon atoms of the hemifullerene (η^2 coordination mode). For these rhodium atoms, Rh(1) and Rh(2), the Rh–C distances average 2.50(2) and 2.46(2) Å, respectively. The coordination of the sole *endo*-bound rhodium atom is best described as η^1 (Figure 5b), with the shortest Rh(4)–C distance being 2.536(17) Å (the two Rh–C distances to the adjacent carbon atoms are much longer at 2.97(2) Å). These data on Rh–C interactions are equally true for both enantiomers of hemifullerene in the structure of **3**.

In complex **3** only two of the three crystallographically independent dirhodium units have hemifullerene molecules bound to both of their open axial positions; one bridges *endo/endo*, and the other *exo/exo*. The third dirhodium unit binds to the $\text{C}_{30}\text{H}_{12}$ molecule only through Rh(2), and two such units are linked together at the other rhodium end to form a dimer of dimers core structure. This $[\text{Rh}_2(\text{O}_2\text{CCF}_3)_4]_2$ bridge is built on axial interactions of the Rh(1) centers with the carboxylic oxygen atoms of the neighboring dimetal unit at a distance of 2.347(8) Å. Analogous rhodium carboxylates with tetranuclear cores are known from both solution and gas-phase reactions.^[19] The characteristics of the dimetal core in all of the dirhodium units in **3** are very similar to one another and are typical for donor–acceptor adducts with weakly bound π -donor ligands.

The observed coordination of the electrophilic rhodium(II) centers exclusively at the rim C=C bonds of the $\text{C}_{30}\text{H}_{12}$ bowl in complex **3**, which has four metal atoms coordinated to one ligand, may seem surprising at first. On the other hand, complexation of planar PAHs as well as corannulene by

[Rh₂(O₂CCF₃)₄] units has invariably been seen at the rim, where η^2 bonding occurs at the C=C sites with the highest Pauling π -bond order. In this connection, a simple analysis of the 35 canonical resonance structures of hemifullerene **2** (Figure 1) indicates a significantly higher Pauling π -bond order on the rim than for any of the interior C=C bonds.^[20] It is noteworthy that the *exo*-bound rhodium centers are coordinated to the rim carbon–carbon bonds of hemifullerene **2** that have the highest calculated π -bond orders.^[21]

In conclusion, the X-ray structural study on the new hemifullerene-based organometallic complex {[Rh₂(O₂CCF₃)₄]₃·(C₃₀H₁₂)} (**3**) reaffirms preference of buckybowls for metal η^2 binding at the rim. A tetradentate $\eta^2:\eta^2:\eta^2:\eta^1$ -bridging coordination of the hemifullerene in **3** directs the formation of a unique 2D organometallic network built on rhodium(II)–carbon π interactions. The average Rh–C distances are shorter in **3** than in the corannulene-based organometallic compounds and thus indicate stronger π bonding in the title hemifullerene coordination complex.

Received: June 3, 2004

Keywords: arene ligands · carboxylate ligands · geodesic polyarenes · π interactions · rhodium

- [1] a) H. W. Kroto, J. R. Heath, S. C. O'Brien, R. F. Curl, R. E. Smalley, *Nature* **1985**, *318*, 162; b) W. Krätschmer, L. D. Lamb, K. Fostiropoulos, D. R. Huffman, *Nature* **1990**, *347*, 354.
- [2] a) P. W. Rabideau, A. Sygula in *Advances in Theoretically Interesting Molecules*, Vol. 3 (Ed.: R. P. Thummel), JAI, Greenwich, **1995**, p. 1; b) P. W. Rabideau, A. Sygula, *Acc. Chem. Res.* **1996**, *29*, 235; c) L. T. Scott, *Pure Appl. Chem.* **1996**, *68*, 291; d) G. Mehta, H. S. P. Rao, *Adv. Strain Org. Chem.* **1997**, *6*, 139; e) G. Mehta, H. S. P. Rao, *Tetrahedron* **1998**, *54*, 13325; f) L. T. Scott, H. E. Bronstein, D. V. Preda, R. B. M. Ansems, M. S. Bratcher, S. Hagen, *Pure Appl. Chem.* **1999**, *71*, 209.
- [3] a) T. J. Seiders, K. K. Baldrige, J. M. O'Connor, J. S. Siegel, *J. Am. Chem. Soc.* **1997**, *119*, 4781; b) C. M. Alvarez, R. J. Angelici, A. Sygula, R. Sygula, P. W. Rabideau, *Organometallics* **2003**, *22*, 624.
- [4] M. A. Petrukhina, K. W. Andreini, J. Mack, L. T. Scott, *Angew. Chem.* **2003**, *115*, 3497; *Angew. Chem. Int. Ed.* **2003**, *42*, 3375.
- [5] a) R. Faust, K. P. C. Vollhardt, *J. Chem. Soc. Chem. Commun.* **1993**, 1471; b) M. J. Plater, H. S. Rzepa, S. Stossel, *J. Chem. Soc. Chem. Commun.* **1994**, 1567; c) F. Geneste, A. Moradpour, G. Dive, D. Peeters, J. Maltheite, J.-F. Sadoc, *J. Org. Chem.* **2002**, *67*, 605.
- [6] a) A. H. Abdourazak, Z. Marcinow, A. Sygula, R. Sygula, P. W. Rabideau, *J. Am. Chem. Soc.* **1995**, *117*, 6410; b) For later syntheses, see also G. Mehta, G. Panda, P. V. V. Srirama Sarma, *Tetrahedron Lett.* **1998**, *39*, 5835 and ref [9].
- [7] For calculations on binding of metal centers by **2**, see a) J. Plater, H. S. Rzepa, F. Stoppa, S. Stossel, *J. Chem. Soc. Perkin Trans. 2* **1994**, *3*, 399; b) A. Sygula, P. W. Rabideau, *J. Chem. Soc. Chem. Commun.* **1994**, 2271; c) F. Nunzi, A. Sgamellotti, N. Re, *Organometallics* **2002**, *21*, 2219.
- [8] R. M. Shaltout, R. Sygula, A. Sygula, F. R. Fronczek, G. G. Stanley, P. W. Rabideau, *J. Am. Chem. Soc.* **1998**, *120*, 835.
- [9] S. Hagen, M. S. Bratcher, M. S. Erikson, G. Zimmermann, L. T. Scott, *Angew. Chem.* **1997**, *109*, 407; *Angew. Chem. Int. Ed. Engl.* **1997**, *36*, 406.
- [10] Crystals of **2** were prepared by sublimation–deposition procedures. Solid microcrystalline powder of **2** (0.020 g, 0.054 mmol) was loaded into a small glass ampule, which was sealed under vacuum. The ampule was placed in an electric furnace having a small temperature gradient along the length of the tube. The temperature was set at 240 °C. Over 4 d, two types of crystals had grown in the tube. Small orange blocks (**2-o**) were found at the coldest end of the ampule where the temperature was set at ca. 230 °C. Yield for **2-o**: ca. 25 %. Yellow-orange needles (**2-t**) were collected from the middle part of the ampule. Yield for **2-t**: ca. 35 %. ¹H NMR (300 MHz, CDCl₃, 22 °C): δ = 7.37 (dd, 3 H), 7.61 (d, 3 H), 7.65 (d, 3 H), 7.83 ppm (s, 3 H).
- [11] X-ray crystal data for **2-o**: C₃₀H₁₂, *M_r* = 372.40, orange block, 0.07 × 0.07 × 0.11 mm, orthorhombic, space group *Pbca*, *a* = 11.6064(8), *b* = 13.0322(9), *c* = 22.4925(15) Å, *V* = 3402.1(4) Å³, *Z* = 8, *T* = 90(2) K, ρ_{calcd} = 1.454 g cm^{−3}, $2\theta_{\text{max}}$ = 56.5°. **2-t**: C₃₀H₁₂, *M_r* = 372.40, yellow-orange needle, 0.03 × 0.04 × 0.26 mm, trigonal, space group *R3m*, *a* = 18.612(2), *c* = 4.2196(5) Å, *V* = 1265.9(3) Å³, *Z* = 3, *T* = 90(2) K, ρ_{calcd} = 1.466 g cm^{−3}, $2\theta_{\text{max}}$ = 50.0°. Bruker SMART APEX CCD diffractometer, MoK α radiation, λ = 0.71073 Å. The structures were solved by direct methods and refined with the Bruker SHELXTL (Version 6.1) Software Package. For **2-t**, data were corrected for absorption effects by using the empirical methods SADABS. For **2-o** and **2-t**, only C atoms having full occupancies were refined anisotropically. All H atoms of the hemifullerene were included at idealized positions for structure-factor calculations. For **2-o**, full-matrix refinement on *F*² converged at *R*1 = 0.0679 and *wR*2 = 0.1638 for 250 parameters and 2135 reflections with *I* > 2 σ (*I*) (*R*1 = 0.1341, *wR*2 = 0.1884 for 4121 unique reflections) and a GOF of 0.956. For **2-t**, full-matrix refinement on *F*² converged at *R*1 = 0.0333 and *wR*2 = 0.0687 for 77 parameters and 462 reflections with *I* > 2 σ (*I*) (*R*1 = 0.0423, *wR*2 = 0.0718 for 542 unique reflections) and a GOF of 1.072. CCDC-238109 and CCDC-238110 (**2-o** and **2-t**) contain the supplementary crystallographic data for this paper. These data can be obtained free of charge via www.ccdc.cam.ac.uk/conts/retrieving.html (or from the Cambridge Crystallographic Data Centre, 12, Union Road, Cambridge CB21EZ, UK; fax: (+44) 1223-336-033; or deposit@ccdc.cam.ac.uk).
- [12] J. C. Hanson, C. E. Nordman, *Acta Crystallogr. Sect. B* **1976**, *32*, 1147.
- [13] a) L. T. Scott, M. S. Bratcher, S. Hagen, *J. Am. Chem. Soc.* **1996**, *118*, 8743; b) R. B. M. Ansems, L. T. Scott, *J. Am. Chem. Soc.* **2000**, *122*, 2719; c) D. M. Forkey, S. Attar, B. C. Noll, R. Koerner, M. M. Olmstead, A. L. Balch, *J. Am. Chem. Soc.* **1997**, *119*, 5766.
- [14] The Cahn–Ingold–Prelog (CIP) rules for designating chirality do not cover cases such as this. A simple convention is therefore proposed here to designate the chirality of open geodesic polyarenes, whether they be inherently chiral (e.g., **2**) or owe their chirality to some symmetry-lowering substitution. Step 1: View the molecule from the concave face, i.e., looking “into” the bowl. Step 2: Identify the rim atom that ranks highest in priority according to the CIP rules. Step 3: Compare the two rim atoms attached to this point of origin, and subsequent atoms attached thereto, if necessary, until two rim atoms that lie the same number of positions away on the clockwise and counterclockwise paths are found that differ in CIP priority. Step 4: If the direction of travel to the atom of higher CIP priority is clockwise, the chiral bowl is designated as *P*; a bowl requiring counterclockwise travel is designated as *M*. By this convention, the C₃₀H₁₂ bowl (**2**) pictured in Figure 1 would be designated as *M*, assuming that the concave surface is facing the reader.
- [15] F. A. Cotton, E. V. Dikarev, X. Feng, *Inorg. Chim. Acta* **1995**, *237*, 19.
- [16] a) F. A. Cotton, E. V. Dikarev, M. A. Petrukhina, S.-E. Stiriba, *Polyhedron* **2000**, *19*, 1829; b) F. A. Cotton, E. V. Dikarev, M. A. Petrukhina, *J. Am. Chem. Soc.* **2001**, *123*, 11655.

- [17] Synthesis of **3**: A mixture of $[\text{Rh}_2(\text{O}_2\text{CCF}_3)_4]$ (0.020 g, 0.030 mmol) and **2** (0.005 g, 0.013 mmol) was sealed under vacuum in a small glass ampule. The ampule was placed in an electric furnace at 164 °C. Over 3 d, tiny, dark red crystals of **3** grew in the hot zone of the tube. Yield: ca. 10 %. IR (KBr): $\tilde{\nu}$ = 3035(w), 2966(w), 1663(sh), 1665(sh), 1646(s), 1563(w), 1544(w), 1510(w), 1463(w), 1252(sh), 1199(s), 1168(sh), 1991(sh), 876(w), 868(w), 780(w), 745(m), 673(m), 615(w), 531 cm^{-1} (w). ^1H NMR (300 MHz, CDCl_3 , 22 °C): δ = 7.37 (dd, 3H), 7.61 (d, 3H), 7.65 (d, 3H), 7.83 ppm (s, 3H).
- [18] X-ray crystal data for **3**: $\text{Rh}_6\text{C}_{54}\text{O}_{24}\text{F}_{36}\text{H}_{12}$, M_r = 2346.10, dark red block, $0.03 \times 0.03 \times 0.04$ mm, monoclinic, space group $C2/m$, a = 22.732(2), b = 27.799(3), c = 12.2244(11) Å, β = 95.455(2)°, V = 7690.1(12) Å³, Z = 4, T = 213(2) K, ρ_{calcd} = 2.026 g cm^{-3} , $2\theta_{\text{max}}$ = 45.04°. Only rhodium and oxygen atoms were refined anisotropically. All H atoms of the hemifullerene were included at idealized positions for structure-factor calculations. The fluorine atoms of some CF_3 groups were disordered over two or three different rotational orientations. This disorder was modeled individually in each case. Full-matrix refinement on F^2 converged at $R1$ = 0.0613 and $wR2$ = 0.1092 for 412 parameters, 30 restraints, and 2375 reflections with $I > 2\sigma(I)$ ($R1$ = 0.1461, $wR2$ = 0.1292 for 5169 unique reflections) and a GOF of 0.821. CCDC-238111 contains the supplementary crystallographic data for **3**; see ref. [11] for ordering information.
- [19] a) F. A. Cotton, E. A. Hillard, C. Y. Liu, C. A. Murillo, W. Wang, X. Wang, X. *Inorg. Chim. Acta* **2002**, 337, 233; b) E. V. Dikarev, K. W. Andreini, M. A. Petrukhina, *Inorg. Chem.* **2004**, 43, 3219.
- [20] a) W. C. Herndon, *J. Am. Chem. Soc.* **1974**, 96, 7605; b) W. C. Herndon, C. Parkanyi, *J. Chem. Educ.* **1976**, 53, 689; c) B. F. Plummer, L. K. Steffen, W. C. Herndon, *Struct. Chem.* **1993**, 3, 279.
- [21] Higher level molecular orbital calculations (B3LYP/6-31G*) predict bond lengths [Å] that correlate approximately with those derived from simple considerations of Pauling bond orders (see Figure 1): a) 1.3917, b) 1.4571, c) 1.4237, d) 1.3908, e) 1.4228, f) 1.3851, g) 1.4342, h) 1.4063, i) 1.3787, j) 1.4424, k) 1.4124, l) 1.5138, m) 1.4278. It is interesting to note that metal complexation is observed at the rim bond with the highest Pauling order (a), in preference even to bonds that are calculated to have shorter lengths (d, f, and i).

Rationalization of Supramolecular Chirality in a Bisporphyrin System**

Victor V. Borovkov,* Isao Fujii, Atsuya Muranaka,
Guy A. Hembury, Takeyuki Tanaka, Arnout Ceulemans,
Nagao Kobayashi, and Yoshihisa Inoue*

Supramolecular chirality is a growing multidisciplinary field of modern research and attracts much attention from the scientific community because of its vital importance for various natural processes and for its attractive possibilities for new smart technologies.^[1] Of the vast number of host–guest and self-associated systems, supramolecular assemblies based on porphyrin chromophores are of particular interest for in-depth investigation and potential application as a consequence of them having specific and well-suited physicochemical and spectroscopic properties.^[2] However, it is apparent that effective control of any functional system rests upon the comprehensive understanding of the detailed operative mechanisms and the corresponding driving forces. In the case of porphyrin-based supramolecular chiral assemblies (particularly, containing two or more porphyrins) there are two major factors which make such studies an arduous task: the dynamic nature of noncovalent assemblies and the complex electronic structure of these pigments as a consequence of the existence of several differently oriented electronic transitions. Herein, we report for the first time a crystallographic structure of a supramolecular complex con-

[*] Dr. V. V. Borovkov, Dr. G. A. Hembury, Prof. Dr. Y. Inoue
Entropy Control Project
ICORP, JST
4-6-3 Kamishinden, Toyonaka-shi, Osaka 560-0085 (Japan)
Fax: (+81) 6-6836-1636
E-mail: victrb@inoue.jst.go.jp
inoue@chem.eng.osaka-u.ac.jp

Dr. I. Fujii
Department of Biological Science and Technology
Tokai University
317 Nishino, Numazu, Shizuoka 410-0321 (Japan)

A. Muranaka, Prof. Dr. N. Kobayashi
Department of Chemistry
Graduate School of Science
Tohoku University, Sendai 980-8578 (Japan)

Dr. T. Tanaka
Department of Biosystems Science
Graduate School of Science and Technology
Kobe University, Kobe 657-8501 (Japan)

Prof. Dr. A. Ceulemans
Division of Quantum Chemistry
University of Leuven
Celestijnenlaan 200F, B-3001 Leuven (Belgium)

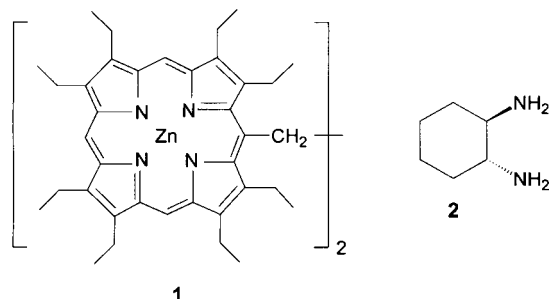
[**] This research was partly supported by the Ministry of Education, Science, Sports, and Culture, Japan, a Grant-in-Aid for the COE project, Giant Molecules and Complex Systems, 2004, and by the Belgian Science Fund (FWO) and Concerted Action Scheme (GOA).



Supporting information for this article is available on the WWW under <http://www.angewandte.org> or from the author.

sisting of an achiral bisporphyrin host and a chiral diamine guest which leads to the comprehensive understanding of the origin of transfer of chirality information at the molecular and electronic levels.

It was shown earlier that ethane-bridged bis(zinc octaethylporphyrin)^[3] (**1**) is one of the most suitable achiral hosts for the comprehensive investigation of various aspects of



supramolecular chirogenesis upon its interaction with different chiral guests (including amines and alcohols).^[2a,4] Of the guest compounds studied, bidentate ligands (diamines and amino alcohols) are particularly important and useful for understanding this phenomenon because of their ability to form rigid and stable tweezer-type complexes possessing an extremely high optical activity. The detailed equilibrium mechanism, driving forces, and various controlling factors of tweezer formation have been recently reported.^[4c-e] However, such key questions relating to the exact molecular structure and true origin of the induced chirality still remain open. To solve these vital issues (*R,R*)-1,2-diaminocyclohexane (**2**) was chosen as the chiral guest, because of its unique property of producing a stable 1:1 tweezer complex exclusively without any further equilibrium steps as a consequence of its remarkably large association constant ($> 10^7 \text{ M}^{-1}$).^[4c,d]

Slow evaporation of a 1:1 mixture of **1** and **2** in $\text{CH}_2\text{Cl}_2/\text{CH}_3\text{CN}$ at room temperature gave needle-shaped metallic-brown crystals, from which an appropriate crystal was chosen for X-ray diffraction experiments (see Experimental Section). The crystal of the chiral supramolecular tweezer complex $[(\mathbf{1})(\mathbf{2})]$ has a noncrystallographic pseudo-two-fold axis through the centers of the bonds C41a–C41b (ethane bridge), C45a–C45b, and C43a–C43b (ligand moiety; Figure 1). The bisporphyrin moiety has a caged or bivalve shape, which opens in the direction of the ligand moiety, with a dihedral angle of $42.8(2)^\circ$ between the best planes of two porphyrin rings defined by four porphyrin nitrogen atoms. The Zn, C2, C3, and C4 atoms of the corresponding porphyrin rings rise significantly out of these planes, with deviations of up to 0.61 \AA . These deviations are apparently a result of the ligand coordination (for Zn atoms) and continuous steric repulsion caused by the proximity of the neighboring porphyrin moiety (for C atoms). The cyclohexane ring of the ligand has a chair conformation in the direction parallel to the two porphyrin rings, thus allowing attractive $\text{CH}\cdots\pi$ interactions between the ligand and porphyrin moieties as an additional stabilizing factor. The two (*-sc*) N atoms of the

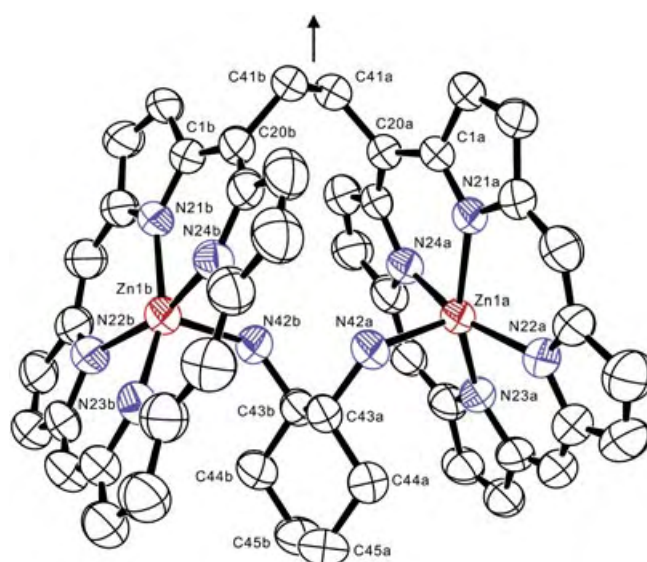


Figure 1. ORTEP-3 representation of $[(\mathbf{1})(\mathbf{2})]$. Heavy atoms are shown as 50% probability ellipsoids. The crystallographic numbering is shown excluding the peripheral ethyl groups and all H atoms for clarity. The arrow indicates the noncrystallographic pseudo-two-fold axis.

ligand moiety, which are connected to the porphyrin Zn atoms in the counteraxial directions, are in the equatorial position, thus also shortening the porphyrin \cdots porphyrin distance (the corresponding Zn \cdots Zn distance is $5.604(5) \text{ \AA}$). Most importantly, it becomes apparent from the unidirectional screw arrangement of the bisporphyrin moiety in the crystal structure that the effective transfer of chirality information from the enantiomeric guest to the achiral host in the supramolecular complex $[(\mathbf{1})(\mathbf{2})]$ occurs. This arrangement occurs as a result of the two spatially orientated Zn–N coordination bonds arising from the preorganization of the two amino substituents of the ligand moiety. The porphyrin rings are twisted anticlockwise relative to each other around the ethane bridge, with a torsion angle (Zn1a–C41a–C41b–Zn1b) of $-54.1(5)^\circ$. These crystallographic data are not only in full agreement with the spectroscopic characteristics obtained previously,^[4c,d] but make it possible to unambiguously rationalize many unique properties of these supramolecular systems, particularly the origin of its high optical activity that has so far remained the most outstanding issue of any chirogenic process.

To comprehensively understand the relationship between the supramolecular structure of the tweezer complex $[(\mathbf{1})(\mathbf{2})]$ and its optical activity its magnetic circular dichroism (MCD) spectrum was measured and compared with the corresponding CD and electronic absorption spectra. It should be noted that CD and MCD analyses are mutually complementary in aiding the interpretation of the excited states, especially in the case of chiral bis- (or multi-) porphyrin systems; CD spectroscopy is sensitive to interchromophoric through-space coupling (that is, exciton coupling), whereas MCD spectroscopy is sensitive to intrachromophoric coupling (that is, coupling occurring between electronic transitions within the same chromophoric unit).^[5] The optical spectra of $[(\mathbf{1})(\mathbf{2})]$ recorded

in CH_2Cl_2 in the region of the porphyrin Soret (B) band (Figure 2) clearly show three well-resolved absorption bands at 410, 419, and 436 nm. The position of the MCD peaks

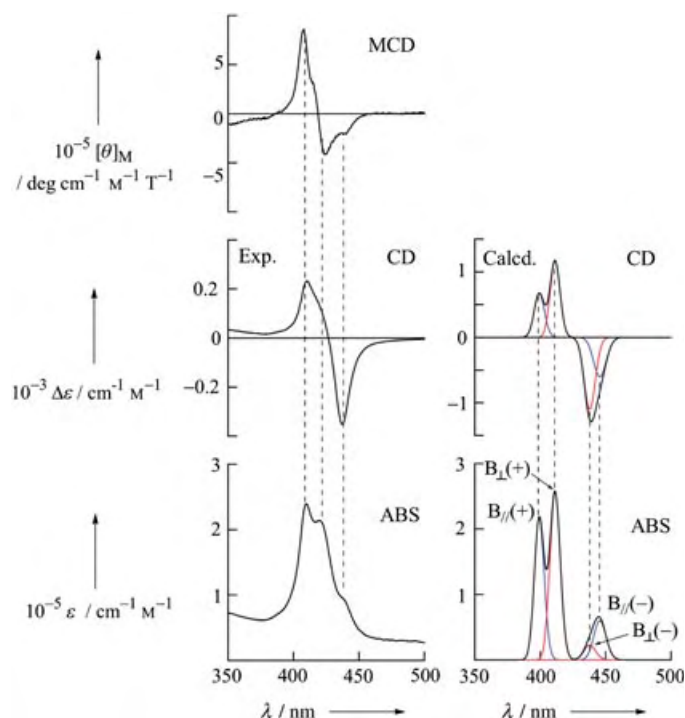


Figure 2. Experimental MCD, CD, and absorption spectra recorded in CH_2Cl_2 at room temperature (left) as well as the calculated CD and absorption spectra (right) of the B-band region of the tweezer. Each calculated exciton band (B_{\parallel} : blue, B_{\perp} : red) was described by a single Gaussian curve. The notations plus and minus represent the in-phase and out-of-phase transitions, respectively.

coincides very closely with these transitions, thus indicating their nondegenerate character.^[6] Importantly, electronic transitions of different polarizations generally exhibit MCD signals of opposite sign and it was found that the two high-energy transitions (at 410 and 419 nm) of the same positive CD sign are indeed of different polarization: the higher energy MCD signal (at 408 nm) is positive, whilst the lower energy MCD signal (at 424 nm) is negative.

To rationalize the experimentally obtained spectral data, and taking into account the assignment of the transition polarization, theoretical absorption and CD spectra were calculated using the geometrical parameters obtained from the corresponding crystal structure and the spectral parameters of the corresponding porphyrin monomer^[7] on the basis of the Kuhn–Kirkwood coupled-oscillator mechanism.^[8] This tweezer system [(1)(2)] consists of two identical porphyrin moieties, each having two different transition moments B_{\parallel} and B_{\perp} , which are in parallel and perpendicular orientations to the ethane bridge, respectively. This arrangement results in two major types of degenerate exciton interactions (B_{\parallel} – B_{\parallel} and B_{\perp} – B_{\perp} couplings) and thus leads to four exciton states (see Experimental Section). As can be seen in Figure 3, the relative orientation between these two pairs of electronic

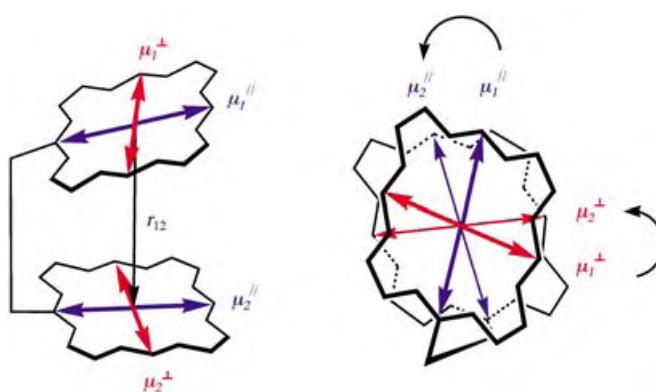


Figure 3. Definition of the direction of the transition dipole moments used in the theoretical analysis. r_{12} is the distance between the centers of gravity of the porphyrin units. The subscripts 1 and 2 (for μ) are used to distinguish between the two chromophores.

transitions is anticlockwise, which according to the exciton chirality method^[9] predicts the negative chirality that was observed experimentally. The resulting calculated absorption spectrum has three well-resolved bands that are also similar to the experimental results (Figure 2). The face-to-face conformation and short distance between the centers of the interacting electric dipoles ($r_{12} = 6.23 \text{ \AA}$) results in the higher energy ($B_{\parallel}(+)$ and $B_{\perp}(+)$) and lower energy ($B_{\parallel}(-)$ and $B_{\perp}(-)$) exciton states being well-separated. These pairs of states become optically allowed and partially forbidden transitions, respectively, as a consequence of strong exciton interactions that result in the observed absorption profile. This observation is in line with Kasha's exciton coupling theory.^[10] Furthermore, the MCD $B_{\parallel}(+)$ and $B_{\perp}(+)$ bands should theoretically be of opposite sign because of their orthogonal polarizations, which is in full agreement with the experimental results. A minus-to-plus CD pattern was calculated for the both B_{\parallel} – B_{\parallel} and B_{\perp} – B_{\perp} couplings and results in one intense negative CD signal at lower energy and two partly resolved positive CD signals at higher energy. This calculated CD pattern is in good agreement with that observed experimentally, although the calculated CD intensities somewhat overestimate the experimental values, an observation often seen in the case of a short interchromophoric distance because a point-dipole approximation may overestimate the excitonic interaction energies.^[11] Furthermore, the crystallographic structure and the electronic absorption and CD spectra of [(1)(2)] have been nicely reproduced by TD-DFT calculations at the B3LYP/6-31G(d) level (see Supporting Information).^[12]

In summary, this work gives for the first time full and unambiguous rationalization of the highly efficient transfer of chirality information from an optically active guest to an achiral host in a supramolecular system based on a bisporphyrin. Furthermore, it is a rare example of an explicit crystallographic characterization of a bis(zinc porphyrin) complex with a chiral ligand. Therefore, this approach should have important implications for the complete understanding of the mechanisms and driving forces of various chirogenic phenomena in numerous artificial and natural supramolecular assemblies.

Experimental and Computational Section

X-ray structural analysis and crystal data: The structure was solved by direct methods by using the SAPI91 program.^[13] The absolute configuration was established to correspond to that of **2** without Bijvoet analysis.^[14] Non-hydrogen atoms were refined anisotropically. Some hydrogen atoms were refined isotropically, but finally fixed. All calculations were carried out with the program packages.^[15] Crystal size $0.5 \times 0.05 \times 0.05$ mm, orthorhombic, space group $P2_12_12_1$, $Z=4$, $a=14.356(2)$, $b=41.472(5)$, $c=13.159(2)$ Å, $V=7834(1)$ Å³, $d_{\text{calc}}=1.13$ g cm⁻³, No. of reflections used = 8847, $2\theta_{\text{max}}=149.9^\circ$ with $\text{Cu}_{\text{K}\alpha}$, $R=0.060$, $(\Delta/\sigma)_{\text{max}}=0.0008$, $(\Delta\rho)_{\text{max}}=0.59$ e Å⁻³, $(\Delta\rho)_{\text{min}}=-0.86$ e Å⁻³.

Spectroscopic measurements: MCD spectra were recorded on a JASCO J-725 spectrodichrometer equipped with a JASCO electro-magnet, which produced magnetic fields of up to 1.09 tesla with parallel and antiparallel fields. Scanning conditions were as follows: scanning rate: 50 nm min⁻¹, bandwidth: 1 nm, response time: 0.5 s, accumulations: 2 scans.

Theoretical calculations: The analysis was based on the Kuhn–Kirkwood coupled-oscillator mechanism. A stealing of CD intensity from the ligand transitions was ruled out because of the absence of chromophores in the ligand. The exciton states energies, oscillator strengths, and rotatory strengths were calculated within the point-dipole approximation using the geometrical and spectral parameters. The geometrical parameters were obtained from the crystal structure. The spectral parameters for the B_{\parallel} and B_{\perp} transitions of the porphyrin monomer were obtained by band deconvolution analysis of zinc octaethylporphyrin with a CH₂OEt substituent at the meso position (ZnOEP-CH₂OEt) (B_{\parallel} : excitation energy = 23743 cm⁻¹; band width = 576 cm⁻¹; magnitude of the transition moment = 7.428 D; B_{\perp} : excitation energy = 23575 cm⁻¹; band width = 525 cm⁻¹; magnitude of the transition moment = 7.118 D). The values for the exciton interaction energies were obtained from these parameters (B_{\parallel} – B_{\parallel} : 1300 cm⁻¹, B_{\perp} – B_{\perp} : 740 cm⁻¹, B_{\parallel} – B_{\perp} : 250 and 225 cm⁻¹). The contribution arising from nondegenerate couplings (B_{\parallel} – B_{\perp}) was calculated to be about 1% of the degenerate couplings (B_{\parallel} – B_{\parallel} and B_{\perp} – B_{\perp}), and therefore its contribution was neglected in our calculations. The polarizations of the two major calculated transitions (399 and 411 nm) were perpendicular to each other. Similar spectroscopic properties were also obtained by the ZINDO/S calculations when the geometry of the ground state was regarded as that observed in the crystal structure (see Supporting Information).

Received: June 15, 2004

Keywords: chirality · circular dichroism · porphyrinoids · structure elucidation · supramolecular chemistry

- [1] a) J. J. D. de Jong, L. N. Lucas, R. M. Kellogg, J. H. van Esch, B. L. Feringa, *Science* **2004**, *304*, 278–281; b) M. Inouye, M. Waki, H. Abe, *J. Am. Chem. Soc.* **2004**, *126*, 2022–2027; c) R. Fasel, M. Parschau, K.-H. Ernst, *Angew. Chem.* **2003**, *115*, 5336–5339; *Angew. Chem. Int. Ed.* **2003**, *42*, 5178–5181; d) M. Ishikawa, K. Maeda, E. Yashima, *J. Am. Chem. Soc.* **2002**, *124*, 7448–7458; e) T. Nabeshima, A. Hashiguchi, T. Saiki, S. Akine, *Angew. Chem.* **2002**, *114*, 499–502; *Angew. Chem. Int. Ed.* **2002**, *41*, 481–484; f) H. Nakashima, J. R. Koe, K. Torimitsu, M. Fujiki, *J. Am. Chem. Soc.* **2001**, *123*, 4847–4849; g) J. M. Fox, T. J. Katz, S. Van Elshocht, T. Verbiest, M. Kauranen, A. Persoons, T. Thongpanchang, T. Kraus, L. Brus, *J. Am. Chem. Soc.* **1999**, *121*, 3453–3459; h) D. Iarossi, A. Mucci, F. Parenti, L. Schenetti, R. Seeber, C. Zanardi, A. Forni, M. Tonelli, *Chem. Eur. J.* **2001**, *7*, 676–685; i) W. Steffen, B. Kohler, M. Altmann, U. Scherf, K. Stitzer, H.-C. zur Loye, U. H. F. Bunz, *Chem. Eur. J.*

- 2001**, *7*, 117–126; j) M. de Loos, J. van Esch, R. M. Kellogg, B. L. Feringa, *Angew. Chem.* **2001**, *113*, 633–636; *Angew. Chem. Int. Ed.* **2001**, *40*, 613–616; k) L. Brunsveld, E. W. Meijer, R. B. Prince, J. S. Moore, *J. Am. Chem. Soc.* **2001**, *123*, 7978–7984; l) M. Wang, G. L. Silva, B. A. Armitage, *J. Am. Chem. Soc.* **2000**, *122*, 9977–9986; m) P. Wittung, P. Nielsen, O. Buchart, M. Egholm, B. Norden, *Nature* **1994**, *368*, 561–563.
- [2] a) V. V. Borovkov, G. A. Hembury, Y. Inoue, *Acc. Chem. Res.* **2004**, *37*, 449–459; b) Y.-M. Guo, H. Oike, T. Aida, *J. Am. Chem. Soc.* **2004**, *126*, 716–717; c) T. S. Balaban, A. D. Bhise, M. Fischer, M. Linke-Schaetzel, C. Roussel, N. Vanthuyne, *Angew. Chem.* **2003**, *115*, 2190–2194; *Angew. Chem. Int. Ed.* **2003**, *42*, 2140–2144; d) V. V. Borovkov, T. Harada, G. A. Hembury, Y. Inoue, R. Kuroda, *Angew. Chem.* **2003**, *115*, 1788–1791; *Angew. Chem. Int. Ed.* **2003**, *42*, 1746–1749; e) G. Pescitelli, S. Gabriel, Y. Wang, J. Fleischhauer, R. W. Woody, N. Berova, *J. Am. Chem. Soc.* **2003**, *125*, 7613–7628; f) H. Tsukube, S. Shinoda, *Chem. Rev.* **2002**, *102*, 2389–2403; g) M. Ribó, J. Crusats, F. Sagués, J. Claret, R. Rubires, *Science* **2001**, *292*, 2063–2066; h) N. Kobayashi, *Coord. Chem. Rev.* **2001**, *219–221*, 99–123; i) J. H. Jung, H. Kobayashi, M. Masuda, T. Shimizu, S. Shinkai, *J. Am. Chem. Soc.* **2001**, *123*, 8785–8789; j) R. Purrello, A. Raudino, L. M. Sclaro, A. Loisi, E. Bellacchio, R. Lauceri, *J. Phys. Chem. B* **2000**, *104*, 10900–10908; k) H. Ogoshi, T. Mizutani, *Acc. Chem. Res.* **1998**, *31*, 81–89.
- [3] a) V. V. Borovkov, J. M. Lintuluoto, Y. Inoue, *Helv. Chim. Acta* **1999**, *82*, 919–934.
- [4] a) V. V. Borovkov, G. A. Hembury, Y. Inoue, *Angew. Chem.* **2003**, *115*, 5468–5472; *Angew. Chem. Int. Ed.* **2003**, *42*, 5310–5314; b) V. V. Borovkov, G. A. Hembury, N. Yamamoto, Y. Inoue, *J. Phys. Chem. A* **2003**, *107*, 8677–8686; c) V. V. Borovkov, J. M. Lintuluoto, G. A. Hembury, M. Sugiura, R. Arakawa, Y. Inoue, *J. Org. Chem.* **2003**, *68*, 7176–7192; d) V. V. Borovkov, J. M. Lintuluoto, M. Sugiura, Y. Inoue, R. Kuroda, *J. Am. Chem. Soc.* **2002**, *124*, 11282–11283; e) V. V. Borovkov, J. M. Lintuluoto, Y. Inoue, *Org. Lett.* **2002**, *4*, 169–171; f) V. V. Borovkov, T. Harada, Y. Inoue, R. Kuroda, *Angew. Chem.* **2002**, *114*, 1436–1439; *Angew. Chem. Int. Ed.* **2002**, *41*, 1378–1381; g) V. V. Borovkov, J. M. Lintuluoto, H. Sugeta, M. Fujiki, R. Arakawa, Y. Inoue, *J. Am. Chem. Soc.* **2002**, *124*, 2993–3006; h) V. V. Borovkov, J. M. Lintuluoto, Y. Inoue, *J. Am. Chem. Soc.* **2001**, *123*, 2979–2989; i) V. V. Borovkov, N. Yamamoto, J. M. Lintuluoto, T. Tanaka, Y. Inoue, *Chirality* **2001**, *13*, 329–335; j) V. V. Borovkov, J. M. Lintuluoto, Y. Inoue, *Org. Lett.* **2000**, *2*, 1565–1568; k) V. V. Borovkov, J. M. Lintuluoto, M. Fujiki, Y. Inoue, *J. Am. Chem. Soc.* **2000**, *122*, 4403–4407; l) V. V. Borovkov, J. M. Lintuluoto, Y. Inoue, *J. Phys. Chem. A* **2000**, *104*, 9213–9219.
- [5] a) A. Rodger, B. Nordén, *Circular Dichroism and Linear Dichroism*, Oxford University Press, Oxford, **1997**; b) N. Berova, K. Nakanishi, R. W. Woody, *Circular Dichroism: Principles and Applications*, 2nd ed, Wiley-VCH, New York, **2000**; c) C. Houssier, K. Sauer, *J. Am. Chem. Soc.* **1970**, *92*, 779–791; d) A. Muranaka, M. Okuda, N. Kobayashi, K. Somers, A. Ceulemans, *J. Am. Chem. Soc.* **2004**, *126*, 4596–4604.
- [6] a) J. Michl, *J. Am. Chem. Soc.* **1978**, *100*, 6801–6811; b) J. Michl, *J. Am. Chem. Soc.* **1978**, *100*, 6812–6818.
- [7] The orientation of the B transitions in the corresponding porphyrin monomer were determined by TDDFT calculations of the model compound zinc(octaethylporphyrin) with a CH₂OCH₃ group at one meso position. The accuracy of the DFT-optimized structure was assessed by comparison with the porphyrin units in the crystal structure. Averaged bond lengths of the calculated porphyrin skeleton are as follows (values in parentheses indicate corresponding bond lengths in the crystal structure): Zn–N_p: 2.06 (2.07), N_p–C_α: 1.37 (1.37), C_α–C_β: 1.46 (1.45), C_β–C_β: 1.38 (1.36), C_α–C_m: 1.40 (1.39). The calculations

indicated that the direction of the dipole moment at lower energy (382 nm, B_{\perp}) is perpendicular to the CH_2OCH_3 axis, whereas the direction of the dipole moment at higher energy (375 nm, B_{\parallel}) is parallel (see Supporting Information). This situation may arise from the fact that the position of the meso-carbon atom in the DFT-optimized structure deviates from the mean plane of the porphyrin ring as a result of steric repulsion between the CH_2OCH_3 and two adjacent ethyl groups. This observation was also supported by the crystallographic structure (see Figure 1). Indeed, when the ZINDO/S calculations were carried out using the geometries of each monomeric porphyrin unit with a methyl bridge in the crystal structures (the ethane C–C bond was replaced by one hydrogen atom to construct these two monomeric porphyrins), we obtained stick spectra similar to the TDDFT results (see Supporting Information). Since these calculations overestimate the excitation energies of the B bands, the values obtained from a band deconvolution analysis for the absorption spectrum of a model compound, ZnOEP- CH_2OEt , were used for the CD calculations (see Supporting Information and A. Muranaka, A. Ceulemans, N. Kobayashi, V. V. Borovkov, G. A. Hembury, Y. Inoue, unpublished results).

- [8] a) J. G. Kirkwood, *J. Chem. Phys.* **1937**, 5, 479–491; b) I. Tinoco, *Adv. Chem. Phys.* **1962**, 4, 113–160; c) W. Kuhn, *Trans. Faraday Soc.* **1930**, 26, 293–308.
- [9] N. Harada, K. Nakanishi, *Circular Dichroic Spectroscopy. Exciton Coupling in Organic Stereochemistry*, University Science Books, Mill Valley, CA, **1983**.
- [10] M. Kasha, H. R. Rawls, M. A. El-Bayoumi, *Pure Appl. Chem.* **1965**, 11, 371–392.
- [11] a) H. Konami, M. Hatano, A. Tajiri, *Chem. Phys. Lett.* **1990**, 166, 605–608; b) G. D. Scholes, X. J. Jordanides, G. R. Fleming, *J. Phys. Chem. B* **2001**, 105, 1640–1651.
- [12] This work is in progress and will be reported elsewhere.
- [13] H.-F. Fan, *SAPI91*, Rigaku Corporation, Tokyo, Japan, **1991**.
- [14] J. M. Bijvoet, A. F. Peerdeman, A. J. Van Bommel, *Nature* **1951**, 168, 271–272.
- [15] a) TeXsan, *Single Crystal Structure Analysis Software*, Version 1.6, Molecular Structure Corporation, Texas, USA, **1993**; b) ORTEP-3: L. J. Farrugia, *J. Appl. Crystallogr.* **1997**, 30, 565. CCDC-241626 contains the supplementary crystallographic data for this paper. These data can be obtained free of charge via www.ccdc.cam.ac.uk/conts/retrieving.html (or from the Cambridge Crystallographic Data Centre, 12 Union Road, Cambridge CB21EZ, UK; fax: (+44)1223-336-033; or deposit@ccdc.cam.ac.uk).

Aromaticity

Mono- and Multidecker Sandwich-Like Complexes of the Tetraazacyclobutadiene Aromatic Ring

Jose M. Mercero,* Jon M. Matxain, and Jesus M. Ugalde

Dedicated to Professor Cecilia Sarasola

Since the fortuitous discovery^[1] of ferrocene, $[(C_5H_5)_2Fe]$, the cyclopentadienyl anion has emerged as the most versatile aromatic ring for the synthesis of sandwich-like complexes. Indeed, it has been estimated that more than 80% of all known organometallic complexes of transition metals contain a substituted or unsubstituted cyclopentadienyl ligand.^[2] Nevertheless, new aromatic compounds have recently been identified whose incorporation into sandwich complexes opens new routes for chemical creativity. In particular, we have predicted^[3] that the all-metal $[Al_4]^{2-}$ aromatic ring^[4] can complex Ti to form $[Al_4TiAl_4]^{2-}$.

The tetraazacyclobutadiene dianion, N_4^{2-} , also fulfills the aromaticity requirements.^[5] It has a square-planar structure with six delocalized π electrons, four of which occupy the nonbonding π highest occupied molecular orbitals (HOMOs); the other two π electrons participate effectively in the aromatic stabilization, in agreement with the $(4n+2)$ rule. The nucleus-independent chemical shift (NICS)^[6] at 1.0 Å above the molecular plane is -4.09 ppm,^[7] confirming further the π -aromatic character of the ring. Consequently, N_4^{2-} can, in principle, be incorporated into sandwich-like complexes although, as far as we know, no such structures have been reported to date.

We have therefore theoretically characterized stable sandwich-type complexes of the N_4^{2-} aromatic ring with early (Ti, V, and Cr) and late (Fe, Co, and Ni) transition-metal centers, with charges 2– (Ti, Fe), 1– (V, Co), and 0 (Cr, Ni). The optimized structure of the Ti sandwich-like complex has D_{4h} symmetry; the V and Cr analogues have C_{2v} symmetry, although they can also be viewed as bent D_{4h} structures (Figure 1). The optimum geometries of the late-transition-metal complexes have D_{4d} symmetry. Consequently, for the complexes of the early-transition metals the nitrogen atoms are eclipsed whereas they are staggered for those of the late transition metals.

The calculations were carried out with the B3LYP functional, as implemented in Gaussian98,^[8] with the standard 6-311G basis set.

[*] J. M. Mercero, J. M. Matxain, J. M. Ugalde
Kimika Fakultatea
Euskal Herriko Unibertsitatea
P.K. 1072; 20080 Donostia, Euskadi (Spain)
Fax: (+34) 94-3015-270
E-mail: pobmelat@sq.ehu.es



Supporting information for this article is available on the WWW under <http://www.angewandte.org> or from the author.



Figure 1. The eclipsed D_{4h} and C_{2v} structures of the early transition metals (right) and the staggered D_{4d} structure of the late transition metals (left; blue N, orange metal center).

The geometrical properties, charges at the metal, and the NICS of the N_4 squares of both the early- and late-transition-metal complexes are collected in Table 1. The increase in the N–N bond length is appreciably larger upon complexation of N_4^{2-} with the early transition metals than with the late ones. Concomitantly the square–metal distances (Sq–TM in Table 1) are longer for the early-transition-metal complexes, which is indicative of the subtle N_4^{2-} ring–metal interactions in these complexes.

Table 1: Properties of the molecules (calculated at the B3LYP/6-311G level of theory) described in the text.^[a]

	Ti	V	Transition metal				N_4^{2-}
	D_{4h}	C_{2v}	C_{2v}	D_{4d}	D_{4d}	D_{4d}	D_{4h}
Symm.	D_{4h}	C_{2v}	C_{2v}	D_{4d}	D_{4d}	D_{4d}	D_{4h}
Charge	–2	–1	0	–2	–1	0	–2
Sq–TM	1.850	1.780	1.740	1.694	1.678	1.692	–
N–N	1.492	1.49	1.49	1.476	1.458	1.456	1.445
Sq–TM–Sq	180.0	152.6	140.4	180.0	180.0	180.0	–
CHEL	1.350	1.485	0.999	0.566	0.524	0.466	–
NICS(0)	39.0	64.9	73.6	–5.78	–5.45	4.00	9.2
NICS(1)	10.9	17.3	19.3	–16.80	–11.14	–3.00	–4.19
EDE _{ad}	–2.66	3.74	–	–2.49	6.586	–8.74 ^[b]	–
EDE _{ovgf}	–	–	–	–	–	–	–
HOMO	–3.97	5.04	10.47	–	4.992	11.09	–
p.s.	0.86	0.90	0.91	–	0.90	0.87	–
HOMO-1	–	5.05	–	–	4.992	11.09	–
p.s.	–	0.90	–	–	0.90	0.87	–
HOMO-2	–	5.72	–	–0.39	5.788	–	–
p.s.	–	0.91	–	0.90	0.91	–	–
HOMO-3	–	5.46	–	–	5.788	–	–
p.s.	–	0.92	–	–	0.91	–	–

[a] Charges refer to the net charge of the complex. The bond lengths (Where Sq–TM stands for the distance between the center of the square and the metal) are given in Å. Atomic charges in e^- are calculated using the CHELP^[9] method. EDE_{ad} are in eV and EDE_{ovgf} also in eV with their associated pole strengths (p.s.) and the orbital from which the electron is detached. NICS are given in ppm. [b] The resulting cation corresponds to the rearranged $Ni(N_2)_4^+$ complex, rather than to a sandwich-like complex.

The main difference between the early- and late-transition-metal complexes, however, is found in the aromaticity of the N_4 ring upon complexation. Despite its widespread use, aromaticity is more of a theoretical concept than a directly measurable quantity. Consequently, measurements of aromaticity are based on many different criteria.^[10] Among them, the NICS, which is based on the “absolute magnetic shielding” at the center of a ring compound, is widely used and has proven to be accurate for ordinary cyclic carbon compounds. This method has also recently been successfully applied to inorganic cyclic aromatic compounds.^[11,12] Nevertheless, it is worth mentioning that relying on a single aromaticity

indicator probably gives an incomplete picture. However, analysis of the NICS values of the tetraazacyclobutadiene moiety nicely shows how early- and late-transition-metal centers behave differently towards complexation with N_4^{2-} .

Thus, the NICS value of N_4^{2-} at the center of the molecular plane, NICS(0), is 9.2 ppm and the value at 1.0 Å above the molecular plane, NICS(1), is –4.19 ppm; that is, N_4^{2-} is σ antiaromatic and π aromatic. Complexation with the early-transition-metal centers enhances the σ antiaromaticity of the N_4^{2-} ring and destroys its π aromaticity, as revealed by the very positive values of both NICS(0) and NICS(1). It should be noted, however, that the geometry of the tetraazacyclobutadiene moiety in the early-transition-metal complexes is still a square, despite the antiaromaticity predicted by the NICS values. On the other hand, for the later-transition-metal centers, and in particular for Fe and Co, the remarkable enhancement of both the σ and the π aromaticity renders the N_4 ring doubly aromatic, a concept first introduced by Schleyer and co-workers^[13] and then experimentally confirmed by Berndt and co-workers.^[14,15]

Nickel does not alter the σ antiaromatic and π aromatic character of the N_4^{2-} ring upon complexation.

In Figure 2 we show the HOMO–2 a_1 orbital of the $[N_4FeN_4]^{2-}$ complex, which has σ delocalization of the N_4 rings. This orbital might be responsible for the remarkable enhancement of the σ aromaticity of the iron complex relative to the analogous Ti complex. The orbital that correlates with the a_1 orbital of the iron complex is the a_{1g} orbital in the Ti complex, which is unoccupied, as shown in Figure 2. Accordingly, π antiaromaticity has to be expected for the N_4 rings of the iron complex, since the occupied e_2 doubly degenerate HOMO orbitals are of π -antibonding character with respect to the N_4 rings, as shown in Figure 2.

The NICS(1) values, however, tell another story. While all the early-transition-metal complexes are π antiaromatic, the late ones are π aromatic. This is presumably because the occupation of the two degenerate e_2 orbitals triggers the π -aromaticity contribution of the internal orbitals of

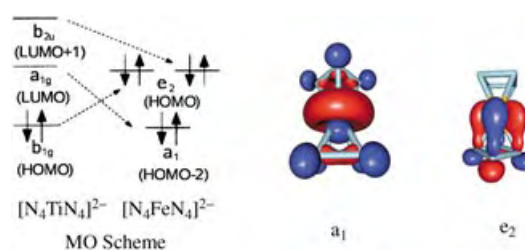


Figure 2. The MO scheme shows the correspondence between the $[N_4TiN_4]^{2-}$ (D_{4h}) and $[N_4FeN_4]^{2-}$ (D_{4d}) valence orbitals. The orbitals shown are the a_1 (left) and the doubly degenerate e_2 (right) orbitals of the $[N_4FeN_4]^{2-}$ (D_{4d}) complex.

the complex (see the Supporting Information). Schleyer and co-workers have demonstrated recently that the aromaticity is determined by the contribution of *all* the π/σ -orbitals of the system.^[11] CMO-NICS calculations^[16] (CMO = canonical molecular orbitals) will help to confirm this point further.

We have also focused our attention on the stability of the mono- and dianionic complexes, as they can lose an electron due to the intramolecular coulombic repulsion, and dissociate. The dianionic complexes (Ti and Fe), indeed, have negative electron-detachment energies (EDE), thus indicating that the monoanions are more stable than the dianions. However, the complexes with charge -1 (V and Co) have positive EDEs, which confirms their stability towards electron detachment. We therefore calculated both the adiabatic^[17] electron-detachment energies, EDE_{ad} , and the unrestricted outer valence Green's functions electron-detachment energies, EDE_{ovgf} .^[18] All give qualitatively the same picture, as shown in Table 1.

EDEs are one key property for the experimental characterization of these complexes, as shown recently by Li et al.^[4] in their photoelectron spectroscopy investigation of $[Al_4]^{2-}$ stabilized against Coulomb explosion by an alkali-metal cation. We have followed their approach for the dianionic sandwich-like complexes of Ti and Fe, and have characterized their structures in the presence of one Li^+ and two Li^+ ions. We found that the cation(s) can interact with the complex at various positions although, for the sake of brevity, the properties of only the most stable structures (see Figure 3) are given in Table 2.

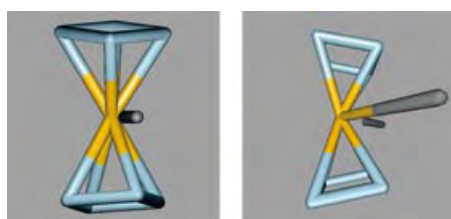


Figure 3. Most stable structures of $[LiN_4XN_4]^-$ (left) and $[Li_2N_4XN_4]$ (right, X = Ti, Fe; blue N, orange X, gray Li).

Once the cation(s) interact(s) with the complex, the EDE become positive and the resulting complex becomes stable towards electron detachment. This stability increases significantly upon interaction with the second lithium atom. Consequently, these complexes might be suitable for experimental manipulation. The aromatic properties of the N_4 rings remain similar upon interaction with the cation(s). Thus, the N_4 rings of the Ti complex remain σ and π antiaromatic, while the rings of the iron complex retain their σ and π aromaticity; the enormous enhancement of the σ aromaticity of the N_4 rings of $[LiN_4FeN_4]^-$ should be noted.

As has been mentioned above the dianionic complexes of Ti and Fe are unstable with respect to electron loss due to Coulomb repulsion and, therefore, probably have very short lifetimes. The stabilization of dianions for their experimental manipulation is normally carried out by forming their lithium salts, like those of the $[Al_4]^{2-}$ inorganic aromatic dianion^[4] and

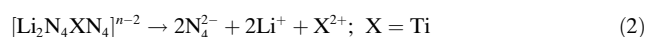
Table 2: Properties of the $[N_4XN_4]^{2-} \cdot Li_n^+$ complexes ($n = 1, 2$; X = Ti, Fe). (see the description in Table 1).

	Ti		Fe	
	Li	2 Li	Li	2 Li
Symmetry	C_{2v}	C_s	C_{2v}	C_{2v}
Charge	-1	0	-1	0
N–N	1.49/1.46	1.45/1.49	1.48/1.45	1.43/1.47
Sq–TM	1.856	1.87/1.83	1.697	1.712
TM–Li	2.711	2.89/2.63	2.273	2.407
N–Li	1.903	1.94/2.01	1.983	2.029
sq-TM-sq	146.9	137.8	172.4	167.70
Li-TM-Li	–	79.91	–	101.6
TM (CHELP)	1.19	1.31	0.99	0.30
Li (CHELP)	0.70	0.54/0.58	0.52	0.80
BE	257.67	395.61	247.5	391.77
NICS(0)	27.64	26.26	–116.9	–22.3
NICS(1)	8.70	8.92	–31.9	–6.89
EDE_{ad}	1.78	6.11	1.13	7.43
EDE_{ovgf}				
HOMO	0.45	5.03	4.70	8.78
p.s.	0.868	0.871	0.908	0.915
HOMO-1	4.12	9.03	4.50	9.391
p.s.	0.892	0.896	0.916	0.906
HOMO-2	4.70	9.11	5.43	10.589
p.s.	0.892	0.886	0.915	0.907

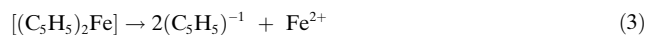
$C_2H_2^{2-}$ organic aromatic dianion.^[19] The interaction of the $[N_4XN_4]^{2-}$ dianions with Li^+ ions yields a remarkable energetic stabilization. The lithium stripping energies [Eq. (1)],



are 257.8 and 247.5 kcal mol^{–1} for the Ti and Fe monolithium complexes, respectively, and 395.6 and 391.8 kcal mol^{–1} for the respective dilithium complexes, which suggests that these species might be stable enough to be handled experimentally. Additional evidence for the stability of the dianions comes from an inspection of the energy of the following reaction [Eq. (2)]:



which is 1223.7 kcal mol^{–1} for X = Ti and 1302.0 kcal mol^{–1} for X = Fe. The corresponding reaction energy for ferrocene [Eq. (3)]:



is 656.0 kcal mol^{–1},^[20,21] and the energy of the reaction in Equation (4):



is 455.1 kcal mol^{–1}.^[7]

Multidecker structures or even polymers of transition metal–aromatic ring complexes are common.^[22] However, early and late transition metals induce different structural patterns. Thus, Kaya and Nakajima have shown recently that Sc, Ti, and V form multidecker structures,^[23] while Fe, Co, and Ni form “rice-ball” structures where all the metal atoms are

clustered at the center and surrounded by the aromatic molecules.

Our calculations demonstrate that both early and late transition metals can form highly linear, multidecker complexes of formula $[\text{TM}_n(\text{N}_4)_{n+1}]^{2-}$. Titanium, in particular, forms linear, multidecker complexes where the first two N_4 units of both ends are eclipsed with the remaining units being staggered. Conversely, for iron the disposition of all adjacent N_4 units is staggered.

Figure 4 shows the optimum structures of $[\text{Ti}_7(\text{N}_4)_8]^{2-}$ and $[\text{Fe}_7(\text{N}_4)_8]^{2-}$, which are molecular complexes of about 2.4 nm in length. The vibrational harmonic frequencies of all the so far characterized oligomers can be found in the Supporting Information, as they might be useful for their experimental detection.

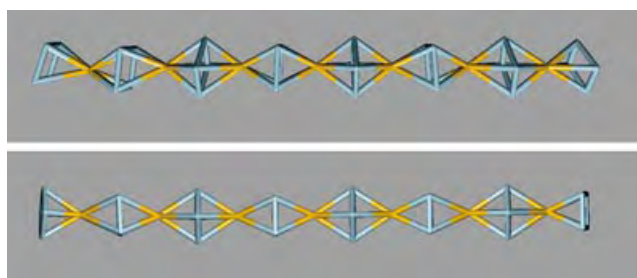


Figure 4. Optimum structures of $[\text{Ti}_7(\text{N}_4)_8]^{2-}$ (top) and $[\text{Fe}_7(\text{N}_4)_8]^{2-}$ (bottom) multidecker structures (blue N, orange metal center).

The HOMO–LUMO energy gaps of these multidecker complexes of Ti and Fe are collected in Table 3.

Table 3: The HOMO–LUMO energy gap (eV) for multidecker $[\text{TM}_n(\text{N}_4)_{n+1}]^{2-}$ complexes (TM = Ti, Fe).

<i>n</i>	Ti	Fe
3	1.245	2.846
4	1.150	2.275
5	0.932	1.798
6	0.754	1.472
7	0.600	1.343

The trend shown in Table 3 is that the HOMO–LUMO gap decreases with an increase in the number of monomer units in the structure. Consequently, since the band gap is controlled by the size of the oligomeric structure, these materials could be useful as semiconductors in nanostructure devices. It should also be possible to synthesize one-dimensional polymeric wires of these materials. Such wires would have a very narrow band gap and would hence behave as conducting one-dimensional polymers.

In summary, we have reported on the possibility of incorporating the aromatic N_4^{2-} dianion into transition-metal sandwich-like complexes. Interestingly, these sandwich-like complexes may also form multidecker structures and eventually condense into one-dimensional polymers. The structures predicted here await experimental verification.

Keywords: aromaticity · density functional calculations · sandwich complexes · transition metals

- [1] T. J. Kealy, P. L. Pauson, *Nature* **1951**, 168, 1039.
- [2] C. Janiak, H. Schumann, *Adv. Organomet. Chem.* **1991**, 33, 291.
- [3] J. M. Mercero, J. M. Ugalde, *J. Am. Chem. Soc.* **2004**, 126, 3380.
- [4] X. Li, A. E. Kuznetsov, H. F. Zhang, A. I. Boldyrev, L.-S. Wang, *Science* **2001**, 291, 859.
- [5] G. Van Zandwijk, R. A. J. Janssen, H. M. Buck, *J. Am. Chem. Soc.* **1990**, 112, 4155.
- [6] A negative NICS value signifies an electron current at the point where it is calculated; it signals the aromatic character of the molecule.
- [7] Q. S. Li, L. P. Cheng, *J. Phys. Chem. A* **2003**, 107, 2882.
- [8] Gaussian 98 (Revision A.11), M. J. Frisch, G. W. Trucks, H. B. Schlegel, G. E. Scuseria, M. A. Robb, J. R. Cheeseman, V. G. Zakrzewski, J. A. Montgomery, R. E. Stratmann, J. C. Burant, S. Dapprich, J. M. Millam, A. D. Daniels, K. N. Kudin, M. C. Strain, O. Farkas, J. Tomasi, V. Barone, M. Cossi, R. Cammi, B. Mennucci, C. Pomelli, C. Adamo, S. Clifford, J. Ochterski, G. A. Petersson, P. Y. Ayala, Q. Cui, K. Morokuma, D. K. Malick, A. D. Rabuck, K. Raghavachari, J. B. Foresman, J. Cioslowski, J. V. Ortiz, B. B. Stefanov, G. Liu, A. Liashenko, P. Piskorz, I. Komaromi, R. Gomperts, R. L. Martin, D. J. Fox, T. Keith, M. A. Al-Laham, C. Y. Peng, A. Nanayakkara, C. Gonzalez, M. Challacombe, P. M. W. Gill, B. G. Johnson, W. Chen, M. W. Wong, J. L. Andres, M. Head-Gordon, E. S. Replogle, J. A. Pople, Gaussian, Inc., Pittsburgh, PA, **2001**.
- [9] L. E. Chirlian, M. M. Francl, *J. Comput. Chem.* **1987**, 8, 894.
- [10] V. I. Minkin, M. N. Glukhovtsev, B. Y. Simkin, *Aromaticity and Antiaromaticity*, Wiley, New York, USA, **1994**.
- [11] Z. Cheng, C. Corminboeuf, T. Heine, J. Bohmann, P. v. R. Schleyer, *J. Am. Chem. Soc.* **2003**, 125, 13930.
- [12] Y. Jung, T. Heine, P. v. R. Schleyer, M. Head-Gordon, *J. Am. Chem. Soc.* **2004**, 126, 3132.
- [13] J. Chandrasekhar, E. D. Jemmis, P. v. R. Schleyer, *Tetrahedron Lett.* **1979**, 20, 3707.
- [14] M. Unverzagt, G. Subramanian, M. Hofmann, P. v. R. Schleyer, S. Berger, K. Harms, W. Massa, A. Berndt, *Angew. Chem.* **1997**, 109, 1469; *Angew. Chem. Int. Ed. Engl.* **1997**, 36, 1469.
- [15] C. Präsang, A. Młodzianowska, Y. Sahin, M. Hofmann, G. Geiseler, W. Massa, A. Berndt, *Angew. Chem.* **2002**, 114, 3380; *Angew. Chem. Int. Ed.* **2002**, 41, 3380.
- [16] T. Heine, C. Corminboeuf, P. v. R. Schleyer, G. Seifert, R. Reviakine, J. Weber, *J. Phys. Chem. A* **2003**, 107, 6470.
- [17] The adiabatic EDE is taken to be the difference between the energies of the dianion and the monoanion at their optimal geometries.
- [18] W. v. Niessen, J. Schirmer, L. S. Cederbaum, *Comput. Phys. Rep.* **1984**, 157.
- [19] A. Sekiguchi, T. Matsuo, M. Tanaka, *Organometallics* **2002**, 21, 1072.
- [20] M. F. Ryan, J. R. Eyler, D. E. Richardson, *J. Am. Chem. Soc.* **1992**, 114, 8611.
- [21] A. Irigoras, J. M. Mercero, I. Silanes, J. M. Ugalde, *J. Am. Chem. Soc.* **2001**, 123, 5040.
- [22] T. J. Peckham, P. Gómez-Elipe, I. Manners, *Metalloenes*, Vol. 2 (Eds.: A. Togni, R. L. Halterman), Wiley-VCH, Weinheim, **1998**, p. 724.
- [23] A. Nakajima, K. Kaya, *J. Phys. Chem. A* **2000**, 104, 176.

Received: April 29, 2004

Layered Compounds

The Lone-Pair Cation I^{5+} in a Hexagonal Tungsten Oxide-Like Framework: Synthesis, Structure, and Second-Harmonic Generating Properties of $Cs_2I_4O_{11}$ **

Kang Min Ok and P. Shiv Halasyamani*

Noncentrosymmetric (NCS) oxides exhibit a variety of technologically important properties including ferroelectricity, piezoelectricity, pyroelectricity, and second-order nonlinear optical behavior.^[1–3] The rational design of new NCS materials, however, remains a challenge, although a number of strategies have been suggested.^[4–9] We have focused on synthesizing materials containing cations with lone pairs (e.g., Sb^{3+} , Se^{4+} , Te^{4+} , etc.) in order to increase the incidence of NCS in any new compound.^[10,11] A structural topology that is often observed in NCS is the hexagonal tungsten oxide (HTO) framework. This structure has been reported for a variety of cations, including V^{5+} , Mo^{6+} , W^{6+} , and Sb^{5+} .^[12–18] The framework consists of corner-sharing $MO_{6/2}$ octahedra that are linked to form an array of three- and six-membered rings. To date, structures have been observed in which other cations, for example, Se^{4+} , Te^{4+} , P^{5+} , and Sb^{3+} , bridge, cap one side, or cap both sides of the HTO layer. In instances of one-sided capping, an NCS polar material is observed, often with highly efficient second-harmonic generating (SHG) properties, that is, $SHG > 400 \times SiO_2$.^[13,17] In the reported materials, the HTO framework has been restricted to octahedrally coordinated d^0 transition metals and the d^{10} Sb^{5+} cation. We describe herein $Cs_2I_4O_{11}$, the first material with a layered HTO-like framework that contains a lone-pair cation, I^{5+} . The material also has I^{5+} cations capping the layer on one side, which renders the structure NCS. Hence, SHG measurements are also presented.

Crystals of $Cs_2I_4O_{11}$ were grown hydrothermally by combining Cs_2CO_3 , Nb_2O_5 , HIO_3 , and H_2O in a Teflon-lined autoclave at 220 °C for 4 d. The product consisted of large (maximum dimension 3 mm), colorless, faceted, hexagonal crystals.

$Cs_2I_4O_{11}$ exhibits a layered HTO-like framework consisting of asymmetric IO_5 and IO_3 polyhedra.^[19] Both the five- and three-coordinate I^{5+} cations are in asymmetric coordina-

tion environments attributable to their lone pair. The five-coordinate I^{5+} cation exhibits one short I–O bond of 1.783(9) Å, three intermediate I–O bonds of 2.027(15), 2.128(2), and 2.150(2) Å, one long I–O bond of 2.441(16) Å, and angles of 71.0(6)–171.2(2)°. The three-coordinate I^{5+} cation has a unique intermediate I–O bond of 1.943(18) Å and angles of 93.0(7)–134.8(8)°. These bond lengths and angles are consistent with those of previously reported iodates.^[20–24] The IO_5 and IO_3 polyhedra share corners to form the layered structure. In connectivity terms, the layer can be described as a $[3(IO_{2/3}O_{7/6}O_{1/2})^{4/3-}(IO_{3/2})^{2+}]^{2-}$ anion, with charge balance attained by two Cs^+ cations.

One of the most novel aspects of the structure is the two-dimensional IO_5 layer (Figure 1). The HTO-like layer consists of six-membered rings containing corner-sharing IO_5 poly-

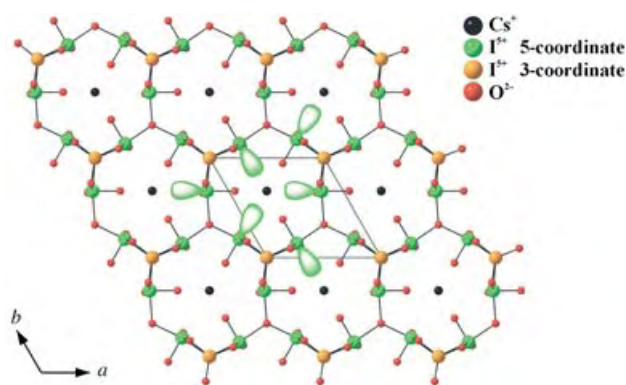


Figure 1. Ball-and-stick representation of the IO_5 six-membered rings in $Cs_2I_4O_{11}$ with the lone-pairs shown schematically. Note how the lone pairs on the IO_5 polyhedra cancel, rendering the layer pseudocentrosymmetric.

hedra in alternating orientation as one proceeds around the ring. $Cs_2I_4O_{11}$ is the first example of a lone-pair cation in a HTO-like topology. In the rings themselves, three lone pairs point inward and three outward. Thus, the lone pairs and oxide anions alternate around the ring. The lone pairs have two important structural consequences. First, the local dipole moment on each IO_5 polyhedron is in the direction of the lone pair. If we sum all of the dipole moments with respect to the IO_5 group, the resultant moment is zero. In other words, there is complete cancellation of the dipole moments with respect to the IO_5 polyhedra, that is, the IO_5 layer is pseudocentrosymmetric. This type of pseudocentrosymmetric layer was observed previously in $Rb_2TeW_3O_{12}$ and $Cs_2TeW_3O_{12}$.^[17] The cancellation is relevant to the SHG efficiency. Second, the Cs^+ cations are not coplanar with the IO_5 ring, attributable to the lone pairs. As shown in Figure 2, the Cs^+ cations sit above and below the rings. The environments of the Cs^+ cations influence any possible ion-exchange capabilities of the material.^[25] The IO_5 layer is capped on one side by an asymmetric three-coordinate I^{5+} cation, that is, an IO_3 group (see Figure 3). Alignment of the IO_3 polyhedra in the $[001]$ direction results in an NCS and polar structure. The lone pairs associated with the IO_3 polyhedra also point along the $[001]$

[*] Dr. K. M. Ok, Prof. P. S. Halasyamani
Department of Chemistry
University of Houston
136 Fleming Building, Houston, TX 77204-5003 (USA)
Fax: (+1) 713-743-2787
E-mail: psh@uh.edu

[**] We thank the Robert A. Welch Foundation for support. This work was also supported by the NSF-Career Program through DMR-0092054, and an acknowledgment is made to the donors of The Petroleum Research Fund, administered by the American Chemical Society, for partial support of this research. P.S.H. is a Beckman Young Investigator.

Supporting information for this article is available on the WWW under <http://www.angewandte.org> or from the author.

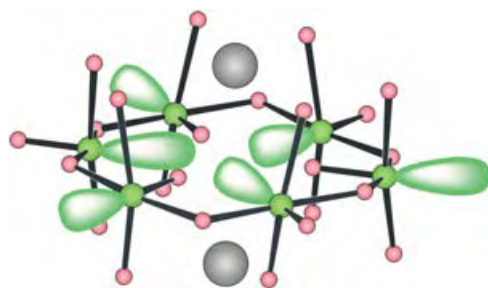


Figure 2. Ball-and-stick representation of one six-membered IO_5 ring with the lone pairs shown schematically. The Cs^+ cations (gray spheres) reside above and below the rings because of the lone pairs.

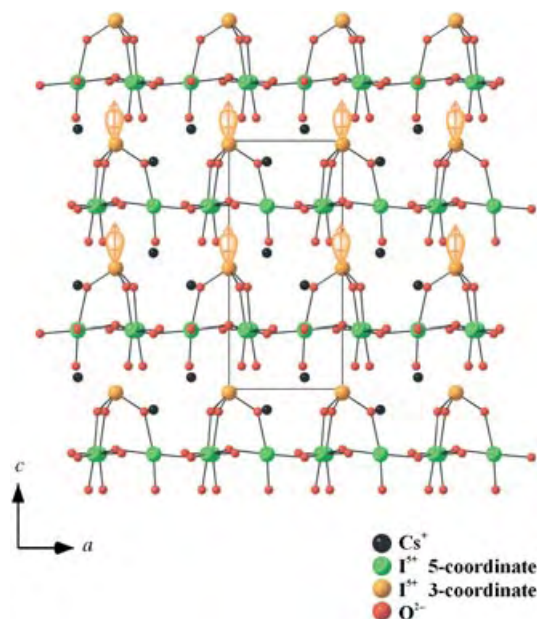


Figure 3. Ball-and-stick representation of $\text{Cs}_2\text{I}_4\text{O}_{11}$ in the ac plane. The lone pairs on two rows of I^{5+} cations are shown schematically, along with the direction of the dipole moment. Note how all the I^{5+} lone pairs point in the same direction and render $\text{Cs}_2\text{I}_4\text{O}_{11}$ noncentrosymmetric.

direction and produce a dipole moment in that direction (Figure 3).

Since $\text{Cs}_2\text{I}_4\text{O}_{11}$ is NCS, we performed powder SHG measurements on the compound.^[26] A detailed description of the measurement was reported earlier.^[27] $\text{Cs}_2\text{I}_4\text{O}_{11}$ has an SHG efficiency of approximately $300 \times \text{SiO}_2$. This efficiency is comparable to other NCS iodates, including HIO_3 ($300 \times \text{SiO}_2$),^[26] LiIO_3 ($300 \times \text{SiO}_2$),^[26] $\text{NdMoO}_2(\text{IO}_3)_4(\text{OH})$ ($350 \times \text{SiO}_2$),^[28] and $\text{AMoO}_3(\text{IO}_3)$ ($A = \text{Rb}$ or Cs , $400 \times \text{SiO}_2$).^[29] By sieving the polycrystalline powder into various particle sizes (20–150 μm) and measuring the SHG as a function of particle size, we were able to determine that $\text{Cs}_2\text{I}_4\text{O}_{11}$ is non-phase-matchable (Type 1). This information along with the SHG efficiency allows us to estimate $\langle d_{\text{eff}} \rangle_{\text{exptl}}$, which for $\text{Cs}_2\text{I}_4\text{O}_{11}$ is 9.6 pm V^{-1} . We have previously published a structural model that allows us to calculate $\langle d_{\text{eff}} \rangle_{\text{calcd}}$ on the basis of metal–oxygen bond hyperpolarizabilities $\beta(\text{M–O})$.^[27] With $\text{Cs}_2\text{I}_4\text{O}_{11}$,

we only have $\beta(\text{I–O})$ which is $140 \times 10^{-40} \text{ m}^4 \text{ V}^{-1}$, and since the IO_5 layer is pseudocentrosymmetric the only $\beta(\text{I–O})$ that contribute to the SHG are those of the IO_3 group. Using this model, which also approximates the contribution attributable to the lone pair to be 20% of $\beta(\text{I–O})$, we calculate a $\langle d_{\text{eff}} \rangle_{\text{calcd}}$ of 13.0 pm V^{-1} . This value is in reasonable agreement with $\langle d_{\text{eff}} \rangle_{\text{exptl}}$ of 9.6 pm V^{-1} .

In conclusion, we have reported the first example of a lone-pair cation, I^{5+} , in a HTO-like framework topology. The material is NCS and exhibits a SHG efficiency of $300 \times \text{SiO}_2$. We are in the process of examining other NCS properties of $\text{Cs}_2\text{I}_4\text{O}_{11}$, including ferroelectric, pyroelectric, and piezoelectric behavior.

Experimental Section

$\text{Cs}_2\text{I}_4\text{O}_{11}$ was obtained by hydrothermal reaction. Cs_2CO_3 (1.0 mmol, 99+%, Aldrich), HIO_3 (28.5 mmol, 99.99%, Aldrich), Nb_2O_5 (1.9 mmol, 99.99%, Aldrich), and 5.0 mL of water were loaded into a 23 mL Teflon-lined autoclave and subsequently sealed. The autoclave was gradually heated to 220°C , held for 4 d, and cooled slowly to room temperature at a rate of 6°C h^{-1} . The mother liquor was decanted from the products, which were then washed with water and ethanol. The product was obtained as a mixture of large colorless hexagonal crystals in 85% yield based on cesium and white powder. The white powder was confirmed to be Nb_2O_5 by powder X-ray diffraction. The $\text{Cs}_2\text{I}_4\text{O}_{11}$ crystals were extracted manually from the bulk. Despite repeated attempts at different temperature, molar ratios, and filling volumes, we were unable to grow single crystals of $\text{Cs}_2\text{I}_4\text{O}_{11}$ in the absence of Nb_2O_5 . The role of Nb_2O_5 in the crystal growth is unclear. IR (KBr , cm^{-1}): 829 ($\nu_{\text{I–O}}$, m), 816 ($\nu_{\text{I–O}}$, m), 798 ($\nu_{\text{I–O}}$, m), 778 ($\nu_{\text{I–O}}$, m), 764 ($\nu_{\text{I–O}}$, s), 747 ($\nu_{\text{I–O}}$, m), 670 ($\nu_{\text{I–O}}$, m), 538 ($\delta_{\text{I–O}}$, s), 458 ($\delta_{\text{I–O}}$, m), 435 ($\delta_{\text{I–O}}$, m), 422 ($\delta_{\text{I–O}}$, m), 409 ($\delta_{\text{I–O}}$, s). Thermogravimetric measurements indicate that $\text{Cs}_2\text{I}_4\text{O}_{11}$ is stable up to 420°C . Two rapid weight-loss events that occur above this temperature result in total volatilization around 800°C .

Received: April 19, 2004

Revised: July 8, 2004

Keywords: hydrothermal synthesis · iodine · layered compounds · nonlinear optics · oxides

- [1] F. Jona, G. Shirane, *Ferroelectric Crystals*, Pergamon, Oxford, **1962**.
- [2] W. G. Cady, *Piezoelectricity; an Introduction to the Theory and Applications of Electromechanical Phenomena in Crystals*, Dover, New York, **1964**.
- [3] S. B. Lang, *Sourcebook of Pyroelectricity*, Gordon & Breach Science, London, **1974**.
- [4] D. Bruce, A. P. Wilkinson, M. G. White, J. A. Bertrand, *J. Solid State Chem.* **1996**, 125, 228.
- [5] C. J. Kepert, T. J. Prior, M. J. Rosseinsky, *J. Am. Chem. Soc.* **2000**, 122, 5158.
- [6] P. A. Maggard, C. L. Stern, K. R. Poeppelmeier, *J. Am. Chem. Soc.* **2001**, 123, 7742.
- [7] M. E. Welk, A. J. Norquist, F. P. Arnold, C. L. Stern, K. R. Poeppelmeier, *Inorg. Chem.* **2002**, 41, 5119.
- [8] O. R. Evans, W. Lin, *Acc. Chem. Res.* **2002**, 35, 511.
- [9] S.-J. Hwu, M. Ulutagay-Kartin, J. A. Clayhold, R. Mackay, T. A. Wardojo, C. J. O'Connor, M. Krawiec, *J. Am. Chem. Soc.* **2002**, 124, 12404.

- [10] K. M. Ok, N. S. P. Bhuvanesh, P. S. Halasyamani, *Inorg. Chem.* **2001**, *40*, 1978.
- [11] H.-S. Ra, K. M. Ok, P. S. Halasyamani, *J. Am. Chem. Soc.* **2003**, *125*, 7764.
- [12] A. Lachgar, S. Deniard-Courant, Y. Piffard, *J. Solid State Chem.* **1988**, *73*, 572.
- [13] W. T. A. Harrison, L. L. Dussack, A. J. Jacobson, *Inorg. Chem.* **1994**, *33*, 6043.
- [14] J. T. Vaughney, W. T. A. Harrison, L. L. Dussack, A. J. Jacobson, *Inorg. Chem.* **1994**, *33*, 4370.
- [15] W. T. A. Harrison, L. L. Dussack, T. Vogt, A. J. Jacobson, *J. Solid State Chem.* **1995**, *120*, 112.
- [16] L. L. Dussack, W. T. A. Harrison, A. J. Jacobson, *Mater. Res. Bull.* **1996**, *31*, 249.
- [17] J. Goodey, K. M. Ok, J. Broussard, C. Hofmann, F. V. Escobedo, P. S. Halasyamani, *J. Solid State Chem.* **2003**, *3*, 175.
- [18] K. M. Ok, A. Gittens, L. Zhang, P. S. Halasyamani, *J. Mater. Chem.* **2004**, *14*, 116.
- [19] Crystal data for $\text{Cs}_2\text{I}_4\text{O}_{11}$: colorless hexagonal prismatic crystal ($0.02 \times 0.04 \times 0.10$ mm), $M_r = 949.42$, hexagonal $P6_3$ (no. 173), $a = b = 7.348(3)$, $c = 13.871(6)$ Å, $\alpha = \beta = 90^\circ$, $\gamma = 120^\circ$, $V = 648.5(5)$ Å³, $Z = 2$, $\rho_{\text{calcd}} = 4.862$ g cm⁻³, $\mu = 151.85$ cm⁻¹. Data collection: Siemens SMART CCD area detector, Mo $\text{K}\alpha$ radiation ($\lambda = 0.71073$ Å), $T = 293$ K. A total of 3858 unique reflections were measured, of which 997 with $I > 2.0\sigma(I)$ were used for the structure solution. Corrections were made for Lorentzian and polarization effects, air absorption, and absorption attributable to the variation in the path length through the detector faceplate. Psi scans were used for the absorption correction on the hemisphere of data. The data were solved and refined by using SHELXS-97 and SHELXL-97, respectively. Final R/R_w on $|F^2|$ were 0.0453/0.1017, GOF = 1.090 for 36 parameters. The final Fourier difference map revealed minimum and maximum peaks of -1.650 and $+1.736$ e Å⁻³. All calculations were performed by using the WinGX-98 crystallographic software package. Even though large crystals (up to 3 mm) were sometimes obtained, a small crystal as described above was used for the crystal structure determination to minimize absorption. Further details of the crystal structure investigation may be obtained from the Fachinformationszentrum Karlsruhe, 76344 Eggenstein-Leopoldshafen, Germany (fax: (+49) 7247-808-666; e-mail: crysdata@fiz-karlsruhe.de) on quoting the depository number CSD-413942. G. M. Sheldrick, SHELXS-97—A program for automatic solution and crystal structures, University of Göttingen, Göttingen, Germany, **1997**; G. M. Sheldrick, SHELXL-97—A program for crystal structure refinement, University of Göttingen, Göttingen, Germany, **1997**; L. J. Farrugia, *J. Appl. Crystallogr.* **1999**, *32*, 837.
- [20] N. W. Alcock, *Acta Crystallogr. Sect. B* **1972**, *28*, 2783.
- [21] E. Coquet, J. M. Crettez, J. Pannetier, J. Bouillot, J. C. Damien, *Acta Crystallogr. Sect. B* **1983**, *39*, 408.
- [22] B. W. Lucas, *Acta Crystallogr. Sect. C* **1984**, *40*, 1989.
- [23] C. Svensson, K. Stahl, *J. Solid State Chem.* **1988**, *77*, 112.
- [24] K. Stahl, M. Szafranski, *Acta Chem. Scand.* **1992**, *46*, 1146.
- [25] Attempts to exchange the Cs^+ ions were unsuccessful. Since $\text{Cs}_2\text{I}_4\text{O}_{11}$ is water soluble, about 100 mg of the material was stirred in 5 mL of a 0.5 M solution of MNO_3 ($\text{M} = \text{Na}^+, \text{K}^+, \text{Rb}^+$) in ethanol/water (4/1). Experiments at 60 °C for 3 d resulted in incomplete reactions; therefore, the reactions were performed at 90 °C for 4 d in sealed fused-silica tubes to prevent evaporation of ethanol. Under these conditions $\text{Cs}_2\text{I}_4\text{O}_{11}$ reacted with the alkali metal nitrates to produce NaIO_3 ($Pbnm$),^[23] KIO_3 ($P1$),^[22] and RbIO_3 ($R3m$)^[20] in phase-pure form. The phase purity of these materials was confirmed by powder X-ray diffraction analysis, and the refined unit cell for each material matched the literature values (see Supporting Information).
- [26] S. K. Kurtz, T. T. Perry, *J. Appl. Phys.* **1968**, *39*, 3798.
- [27] J. Goodey, J. Broussard, P. S. Halasyamani, *Chem. Mater.* **2002**, *14*, 3174.
- [28] T. C. Shehee, R. E. Sykora, K. M. Ok, P. S. Halasyamani, T. E. Albrecht-Schmitt, *Inorg. Chem.* **2003**, *42*, 457.
- [29] R. E. Sykora, K. M. Ok, P. S. Halasyamani, T. E. Albrecht-Schmitt, *J. Am. Chem. Soc.* **2002**, *124*, 1951.

Supramolecular Chemistry

Supramolecular Assemblies of Starlike and V-Shaped PB-PEO Amphiphiles**

Jun Xu and Eugene R. Zubarev*

Self-assembly of linear amphiphiles is a well-known phenomenon,^[1–5] and the number of different structures observed both in the solid-state and in selective solvents is exceedingly large.^[6–10] It is difficult to envision a diblock amphiphile that would not undergo self-assembly, and in this context, the terms “linear amphiphilic” and “self-assembling” are nearly synonymous. Branched amphiphiles such as dendrimers^[11] and stars^[12] also undergo self-organization in selective solvents.^[13–18] However, there are examples in which they do not aggregate,^[19–23] but rather behave as unimolecular micelles.^[24–26] Furthermore, the morphological diversity of aggregates formed by branched structures is significantly lower than that of linear counterparts. For example, most self-assembling star-shaped amphiphiles only form spherical micelles,^[27–31] whereas linear diblocks can organize into at least 30 different morphologies.^[9] This creates the impression that a branched architecture somewhat precludes morphological diversity and that star-shaped amphiphiles cannot compete with linear analogues. In contrast, we document here that the multiarm PB₆-PEO₆ (PB = polybutadiene, PEO = poly(ethylene oxide)) molecule **1** self-assembles into non-spherical structures in water and generates unique “cotton-ball” morphology in hexane. Such hierarchical structures have not been observed in PB-PEO diblocks or any other linear system.

Starlike amphiphiles^[32–38] are generally difficult to synthesize owing to the limitations of many synthetic techniques.^[39]

[*] J. Xu, Prof. Dr. E. R. Zubarev
Department of Materials Science and Engineering
Iowa State University
Ames, IA 50011 (USA)
Fax: (+1) 515-294-5444
E-mail: zubarev@iastate.edu

[**] The authors are grateful to the Donors of the American Chemical Society Petroleum Research Fund for partial support of this research (ACS-PRF No. 40727 G-10). PB = polybutadiene, PEO = poly(ethylene oxide).

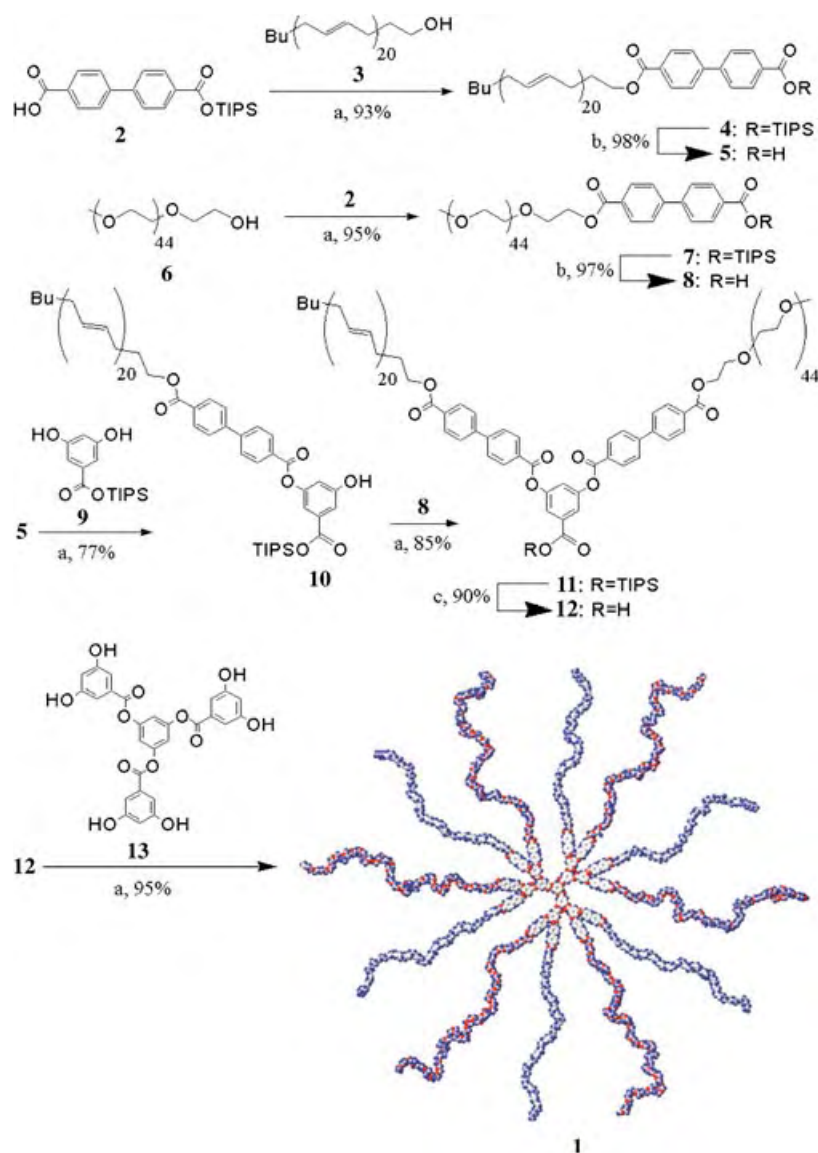


Supporting information for this article is available on the WWW under <http://www.angewandte.org> or from the author.

and most of such structures are based on styrenic and acrylic monomers. These limitations may also explain one seemingly surprising fact: linear PB-PEO diblocks have been known and studied extensively for many decades,^[40] whereas the synthesis of star-shaped PB-PEO molecules has not been reported to date. Herein, we describe a modular approach to produce a 12-arm PB-PEO star with V-shaped chains directly connected to an aryl ester dendrimer.

Commercially available hydroxyl-terminated polybutadiene (**3**; $M_n = 1000$, $M_w/M_n = 1.12$) and poly(ethylene oxide) (**6**; $M_n = 2200$, $M_w/M_n = 1.15$) were both coupled with mono(silyl)-protected biphenyl dicarboxylic acid, **2**, under mild esterification conditions. The TIPS (triisopropylsilyl) group of the respective products, **4** and **7**, were subsequently removed to afford the carboxyl-terminated linear precursors **5** and **8**, respectively (Scheme 1). Biphenyl groups were specifically introduced to have reliable NMR references in order to analyze and confirm unambiguously the purity of all the intermediate compounds. The linear precursors **5** and **8** were then coupled sequentially to TIPS-protected 3,5-dihydroxybenzoic acid (DHBA), **9**, under the same esterification conditions to give **11**. Deprotection of the TIPS-protected carboxylate group produced the V-shaped PB-PEO amphiphile **12** in high yield and purity ($M_w = 6210$, $M_w/M_n = 1.13$). All intermediate compounds were isolated and purified by conventional column chromatography. The hexafunctional aryl ester dendrimer (generation 1) was then prepared by using standard procedures.^[41] The key coupling reaction between the amphiphile **12** and the dendrimer core **13** was found to proceed very rapidly and in near-quantitative yield (by GPC and NMR spectroscopy). The final product **1** was further purified by dialysis against deionized water through a membrane with a molecular-weight cut-off at 30000 g mol^{-1} to remove low-molecular-weight components.

Figure 1 shows the aromatic regions of the ^1H NMR spectra of the V- and star-shaped amphiphiles. In the spectrum of **12** (Figure 1a), the doublet signal at 7.92 ppm and the triplet signal at 7.45 ppm correspond to protons at C-2 and C-6, and C-4, respectively, of the DHBA hinge. Upon coupling with the dendrimer core, these signals are shifted downfield to 8.09 and 7.6 ppm, respectively, whereas the signals for the protons from the biphenyl system are almost unaffected (Figure 1b). Most importantly, the doublet at 8.09 ppm in the NMR spectrum of the star-shaped product represents 18 protons, and therefore includes not only 12 protons from the DHBA moieties of six V-shaped substituents, but also an additional 6 protons from DHBA fragments of the



Scheme 1. Stepwise synthesis of amphiphile **1**. Reagents: a) DPTS/DIPC, CH_2Cl_2 , room temperature, 1–3 h; b) TBAF, -78°C , 2 h; c) HF, THF, room temperature, 12 h. DPTS = 4-(*N,N*-dimethylamino)pyridinium-4-*p*-toluenesulfonate, DIPC = 1,3-diisopropylcarbodiimide, TBAF = tetra-*n*-butylammonium fluoride.

dendrimer core (see Supporting Information for the fully assigned spectra).^[41] The area of the triplet at 7.6 ppm is also increased by a factor of 1.5 (9 protons; 6 H from V-shaped fragments and 3 H from the core) with respect to the biphenyl signals. The appearance of the singlet at 7.28 ppm (3 protons) also confirms the presence of the fully substituted dendritic core. All these features suggest that the product, **1**, is a defect-free 12-arm starlike molecule that does not contain ten-, eight-, six-, or four-arm byproducts. The presence of such impurities would otherwise have been observed as residual peaks and by unsymmetrical shapes of the signals. The observed 1.5-fold increase in the areas of the doublet and triplet signals is the highest value possible and can only be attained if all the molecules are fully substituted. The GPC trace of **1** also suggests complete substitution as the peak

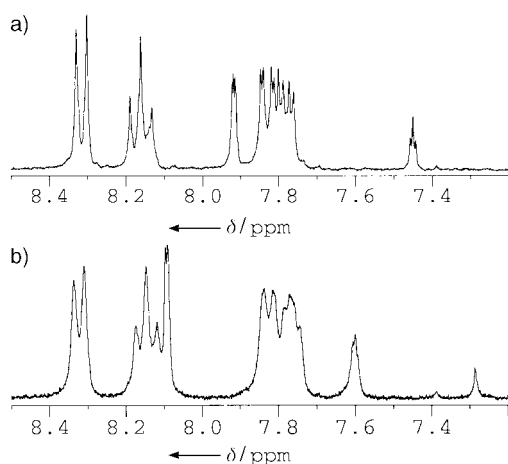


Figure 1. Aromatic regions of ^1H NMR spectra of a) the V-shaped amphiphile **12** and b) the star-shaped amphiphile **1**.

becomes even sharper than that of the V-shaped precursor **12** (polydispersity index, PDI = 1.10 versus 1.13, respectively).^[41]

To investigate the self-assembly properties, we studied aqueous solutions of V- and star-shaped amphiphiles at room temperature. Figure 2, a and b, show representative TEM

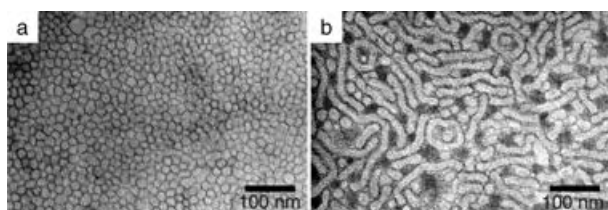


Figure 2. TEM images of samples cast from 3-wt.% aqueous solutions of a) the V-shaped amphiphile **12** and b) the star-shaped amphiphile **1**. An aqueous solution of PTA (phosphotungstic acid) was used as a negative staining agent.

micrographs of samples cast from 3-wt.% solutions of compounds **12** and **1**, respectively. In the V-shaped precursor, only densely packed spherical micelles that measure ≈ 18 nm in diameter were observed. This size is in good agreement with numbers predicted by molecular modeling calculations (Materials Studio Program) and suggests that the self-assembly proceeds by a closed association mechanism.^[41,42] In contrast, the majority of the star-shaped amphiphile, **1**, exists in the form of one-dimensional structures that measure ≈ 20 nm in diameter and up to 300 nm in length. Such morphology is typically referred to as short-rod micelles. Furthermore, some spherical micelles as well as toroidal structures are present. All these objects are composed of many starlike unimers **1** and can be regarded as supermicelles rather than unimolecular micelles.^[24–26]

Figure 2 demonstrates a significant influence of molecular architecture on the self-assembly process. Interestingly, the volume fraction of the hydrophilic PEO is nearly the same (≈ 0.65) in the V- and star-shaped compounds, and according to theoretical predictions, they both should form spherical micelles.^[1,2] The observed difference can be related to a

topological restriction imposed by the rigid aromatic core on the packing of the flexible arms in the amphiphile **1**. It is important to emphasize that the arms are not emanating from one specific point, but from six equidistant peripheral points of a fairly large disklike core (see Scheme 1). Thus, the presence of an aromatic core in **1** prevents the dense packing of the PEO chains located in the corona of the supermicelles. To minimize the interfacial energy and to increase the shielding of the hydrophobic PB core from water molecules, the curvature of the micelle surface has to decrease, and this would favor a sphere-to-cylinder morphological transition.

It is still unclear if the presence of the biphenyl moieties facilitates the self-assembly process. However, it is reasonable to assume that aromatic π - π interactions do not play a significant role in this process as heteroarm amphiphiles can form supermicelles even with a poorly defined divinyl benzene (DVB) core.^[13] We believe that the main influence of the biphenyls on the self-organization of **1** arises from their rigidity, which prevents the dense packing of the arms. As a result of this loose distribution of arms on the surface of the supermicelle, a cylindrical morphology is preferred over the spherical one. In other words, the biphenyls promote the formation of cylinders, whereas the self-assembly process itself is mainly promoted by the heteroarm molecular architecture. This is consistent with the fact that heteroarm amphiphiles without biphenyl groups undergo self-assembly,^[13] but only into spheres, whereas the cylindrical morphology has never been observed for such systems. Furthermore, even the V-shaped amphiphile exclusively forms spheres, although it has the same volume ratio of hydrophilic and hydrophobic blocks.

Because water is a selective solvent for PEO, the central core of the cylindrical micelles should be composed of PB chains. However, such an arrangement would first require a spatial separation of multiple hydrophobic and hydrophilic arms on the scale of one unimer. It can be envisioned that prior to aggregation the starlike amphiphile **1** adopts a conformation where six water-insoluble PB arms are positioned below the plane of the aromatic disklike core and the hydrophilic PEO arms segregate on the opposite side as represented schematically in Figure 3. However, the collapse of six hydrophobic PB arms that belong to a given molecule of **1** may not be enough to avoid unfavorable interactions with water. This is again because of the presence of the rigid core that spatially separates the arms and prevents their dense packing. As a result, the unimers **1** would be driven to aggregate to further minimize the unfavorable contacts by placing the PB chains of all the aggregating molecules into the central core of a supermicelle.

The amphiphile **1** can also be dissolved in solvents that are selective for PB arms. TEM images of samples cast from 0.5-wt.% solutions in hexane revealed giant spherical objects that can be seen at very low magnification (Figure 4a). These structures measure ≈ 2 μm in diameter and have a narrow size distribution with a standard deviation of about 90 nm, which is less than 5% of the mean diameter value.^[41] These microstructures represent discrete objects that do not form a continuous network. At higher magnification, the image clearly shows that the microstructures are composed of

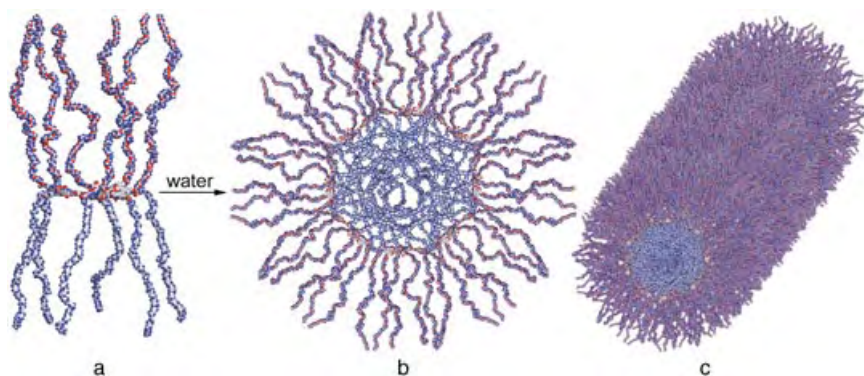


Figure 3. A schematic molecular-graphics representation of the self-assembly of amphiphile **1** in water. a) The image shows a unimer with the 6 arms of PEO (top) and the 6 arms of PB (bottom) spatially separated; b) and c) the images show the cross-section and the side view, respectively, of a cylindrical supermicelle with a PB core and a PEO corona.

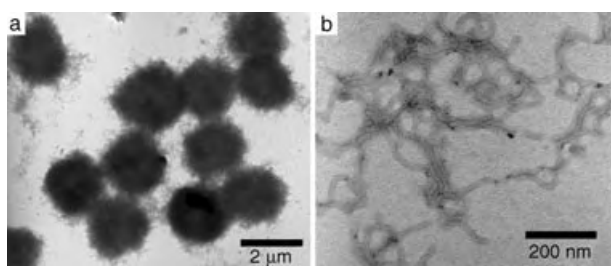


Figure 4. a) Low-magnification TEM image of a sample cast from a 0.5-wt.% solution of **1** in hexane; b) high-magnification TEM image of the same sample taken from an area near the edge of a microsphere. Osmium tetroxide was used as a staining agent to improve the contrast.

numerous one-dimensional structures that are ≈ 20 nm in diameter (Figure 4b). Thus, the observed microspheres have internal structural constituents in the form of nanosized cylindrical supermicelles.

Selective staining of the samples with osmium tetroxide, which reacts only with the PB chains, generated a characteristic contrast with two thin, dark lines located on the opposite sides of the cylinders (Figure 4b). These images confirmed that the PB chains constitute the corona of the cylindrical supermicelles formed in hexane. Hence, the large spherical microstructures (Figure 4a) are composed of *reverse* cylindrical micelles (Figure 4b). Interestingly, linear PB–PEO diblocks can easily form *regular* micelles in water (PB core/PEO corona),^[43] whereas their reverse analogues (PEO core/PB corona) have not been reported to date. Therefore, the star-shaped amphiphile **1** forms both regular and reverse cylindrical micelles in water and hexane, respectively. Most importantly, the self-assembly process in hexane proceeds through two hierarchical levels of self-organization: First, the unimers **1** form cylinders, and then these cylinders self-assemble into finite spherical microstructures. Owing to obvious similarities, we refer to this novel morphology as “cottonballs”. These structures are very stable, and images taken from samples cast from hexane solutions that were aged for nearly 3 months showed that they remained intact. Their

formation is highly reproducible as confirmed by multiple control experiments.

However, it still remains unknown how the formation of a continuous 3D network is prevented and why nearly monodisperse cottonballs form instead. This is a particularly remarkable observation given the fact that their structural constituents (reverse cylindrical micelles) are highly flexible objects as revealed by TEM. It is important to note that dissolution of **1** in hexane proceeds at elevated temperatures ($\approx 60^\circ\text{C}$), above the melting point of PEO. The cottonballs only form after cooling the solutions to room temperature and subsequent aging for several hours. In a control experiment, we cast a sample directly from a hot solution of **1** in hexane and did not observe any microspheres; this suggests that the formation of these structures is a thermoreversible process. It is reasonable to assume that either partial crystallization of PEO or a reduction in the solubility of the PB arms upon cooling to room temperature drives the association of reverse cylindrical micelles into well-defined spheres.

Furthermore, we investigated hexane solutions of the V-shaped precursor **12** under the same conditions and found completely different structures. Figure 5 shows a representa-

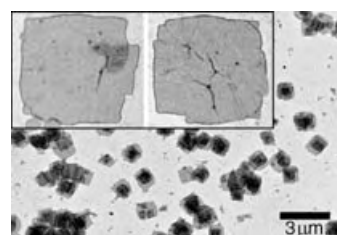


Figure 5. TEM micrograph of a sample cast from a 0.5-wt.% solution of the V-shaped PB–PEO amphiphile **12** in hexane. Inset: Two isolated square platelets that do not have a screw dislocation. Osmium tetroxide was used as a staining agent to enhance the contrast.

tive TEM image of square-shaped platelets formed by **12** in hexane. The structures possess a two-dimensional morphology; they measure ≈ 1 micron in lateral dimensions and only 22 nm in thickness (determined by AFM). The square shape and the presence of faceted edges are indicative of a single-crystalline structure. However, in the V-shaped amphiphile **12**, there is only one crystallizable block (PEO) because polybutadiene is composed of both 1,4- and 1,2-addition monomer units randomly distributed along the chains. The square platelets form in a solvent that is selective for PB, therefore PEO arms must be located in the midsection of such structures. In essence, they can be viewed as sandwichlike structures with a single-crystalline layer of PEO coated with amorphous PB layers on both sides. If the sample is rinsed with water, the square platelets are completely destroyed. However, after staining with osmium tetroxide vapor for only 5 mins, the structures remain intact and retain their original shape upon multiple rinsings with water. The contrasting

effect also increases very rapidly as the squares become much darker upon staining with OsO₄. These results support the idea that PB chains are located on the surface of the platelets and that their cross-linking with OsO₄ stabilizes the morphology and converts 2D supramolecular ensembles into macro-molecular objects.

Similar single-crystalline sandwich structures were observed in solutions of PS-PEO diblocks in toluene,^[44] but not for PB-PEO linear amphiphiles, which typically form large 2D layers.^[45] We specifically synthesized a linear PB-PEO molecule with the same volume ratio of blocks^[41] but similar structures were not observed in hexane. Figure 5 also reveals that whereas some of the squares are isolated structures (see inset), the majority of them have a screw dislocation in the center and a helical ramp is created by several interconnected layers. The formation of discrete 2D objects with a narrow size distribution, rather than large layers, suggests that the crystalline growth is terminated when the size approaches some critical value (≈ 1 micron). The exact mechanism that leads to such limited growth of the observed 2D microstructures is not known. However, we conclude that a simple change from a V-shaped to a starlike molecular architecture profoundly influences the morphology of the self-assembled structures formed by PB-PEO amphiphiles in selective solvents, namely hexane and water (see also Figure 2). The starlike architecture seems to disturb the crystallization process which may also be related to an inability of the arms to pack densely owing to the presence of a disklike core. This may be the driving force of an alternative assembly into reverse cylindrical micelles with little or no crystalline order in the PEO core as suggested by the highly flexible and winding shape of the supermicelles (Figure 4b).

In summary, this study brings a simple, yet unexpected, conclusion: Starlike molecular architecture does not always have a detrimental influence on self-assembly processes and it provides a rare opportunity for novel hierarchical ensembles, which may not be possible even in their linear analogues, to be generated. The presence of a rigid disklike core in a starlike amphiphile promotes the formation of cylindrical micelles in the selective solvents, water and hexane. A comparison of the self-assembled structures formed by V-shaped and starlike amphiphiles clearly demonstrates that the molecular architecture itself is a very powerful morphogenic factor. Thus, synthetic manipulation of the architecture of amphiphiles can be an efficient way to generate complex and yet unseen morphologies.

Received: June 8, 2004

Keywords: amphiphiles · block copolymers · micelles · nanostructures · self-assembly

- [1] J. Israelachvili, *Intermolecular and Surface Forces*, 2nd ed., Academic Press, San Diego, **1992**.
- [2] P. Alexandridis, B. Lindman, *Amphiphilic Block Copolymers: Self-Assembly and Applications*, Elsevier, New York, **2000**.
- [3] L. Zhang, A. Eisenberg, *Science* **1995**, 268, 1728.
- [4] S. Förster, M. Zisenis, E. Wenz, M. Antonietti, *J. Chem. Phys.* **1996**, 104, 9956.

- [5] Y. Y. Won, H. T. Davis, F. S. Bates, *Science* **1999**, 283, 960.
- [6] A. Halperin, M. Tirrell, T. P. Lodge, *Adv. Polym. Sci.* **1992**, 100, 31.
- [7] A. Laschewsky, *Adv. Polym. Sci.* **1995**, 124, 1.
- [8] P. Alexandridis, *Curr. Opin. Colloid Interface Sci.* **1996**, 1, 490.
- [9] N. S. Cameron, M. K. Corbier, A. Eisenberg, *Can. J. Chem.* **1999**, 77, 1311.
- [10] S. Jain, F. S. Bates, *Science* **2003**, 300, 460.
- [11] a) J. M. J. Frechet, C. J. Hawker in *Comprehensive Polymer Science*, 2nd supplement (Eds.: S. L. Aggarwal, S. Russo), Pergamon, Oxford, **1996**, p. 140; b) A. W. Bosman, H. M. Jansen, E. W. Meijer, *Chem. Rev.* **1999**, 99, 1665; c) S. C. Zimmerman, F. W. Zeng, D. E. C. Reichert, S. V. Kolotuchin, *Science* **1996**, 271, 1095; d) V. Percec, M. Glodde, T. K. Bera, Y. Miura, I. Shiyonovskaya, K. D. Singer, V. S. K. Balagurusamy, P. A. Heiney, I. Schnell, A. Rapp, H. W. Spiess, S. D. Hudson, H. Duan, *Nature* **2002**, 419, 384; e) A. P. H. J. Schenning, C. Elissen-Román, J. W. Weener, M. W. P. L. Baars, S. J. van der Gaast, E. W. Meijer, *J. Am. Chem. Soc.* **1998**, 120, 8199.
- [12] a) N. Hadjichristidis, M. Pitsikalis, S. Pispas, H. Iatrou, *Chem. Rev.* **2001**, 101, 3747; b) C. J. Hawker, J. M. J. Frechet, R. B. Grubbs, J. Dao, *J. Am. Chem. Soc.* **1995**, 117, 10763; c) K. Hong, D. Uhrig, J. W. Mays, *Curr. Opin. Solid State Mater. Sci.* **1999**, 4, 531; d) S. Kanaoka, M. Sawamoto, T. Higashimura, *Macromolecules* **1992**, 25, 6414; e) S. Angot, K. S. Murthy, D. Taton, Y. Gnanou, *Macromolecules* **1998**, 31, 7218; f) S. Jacob, I. Majoros, J. P. Kennedy, *Macromolecules* **1996**, 29, 8631; g) H. A. Klok, J. R. Hernandez, S. Becker, K. Mullen, *J. Polym. Sci. Part A: Polym. Chem.* **2001**, 39, 1572.
- [13] D. Voulgaris, C. Tsitsilianis, V. Grayer, F. J. Esselink, G. Hadziioannou, *Polymer* **1999**, 40, 5879.
- [14] H. Engelkamp, S. Middelbeek, R. J. M. Nolte, *Science* **1999**, 284, 785.
- [15] R. H. Jin, *Macromol. Chem. Phys.* **2003**, 204, 403.
- [16] J. Teng, E. R. Zubarev, *J. Am. Chem. Soc.* **2003**, 125, 11840.
- [17] J. H. Wu, M. D. Watson, K. Mullen, *Angew. Chem.* **2003**, 115, 5487; *Angew. Chem. Int. Ed.* **2003**, 42, 5329.
- [18] Y.-S. Yoo, J.-H. Choi, J.-H. Song, N.-K. Oh, W.-C. Zin, S. Park, T. Chang, M. Lee, *J. Am. Chem. Soc.* **2004**, 126, 6294.
- [19] A. Heise, J. L. Hedrick, C. W. Frank, R. D. Miller, *J. Am. Chem. Soc.* **1999**, 121, 8647.
- [20] S. Kanaoka, S. Nakata, H. Yamaoka, *Macromolecules* **2002**, 35, 4564.
- [21] F. M. Menger, A. V. Peresypkin, S. X. Wu, *J. Phys. Org. Chem.* **2001**, 14, 392.
- [22] X. S. Wang, M. A. Winnik, I. Mannes, *Macromol. Rapid Commun.* **2003**, 24, 403.
- [23] G. Gorodyska, A. Kiriy, S. Minko, C. Tsitsilianis, M. Stamm, *Nano Lett.* **2003**, 3, 365.
- [24] Y. H. Kim, O. W. Webster, *J. Am. Chem. Soc.* **1990**, 112, 4592.
- [25] H.-B. Meikelbur, W. Jaworek, F. Vögtle, *Angew. Chem.* **1992**, 104, 1609; *Angew. Chem. Int. Ed. Engl.* **1992**, 31, 1571.
- [26] G. R. Newkome, C. N. Moorefield, J. M. Keith, G. R. Baker, G. H. Escamilla, *Angew. Chem.* **1994**, 106, 701; *Angew. Chem. Int. Ed. Engl.* **1994**, 33, 666.
- [27] D. Voulgaris, C. Tsitsilianis, *Macromol. Chem. Phys.* **2001**, 202, 3284.
- [28] R. H. Jin, *Adv. Mater.* **2002**, 14, 889.
- [29] A. P. Narrainen, S. Pascual, D. M. Haddleton, *J. Polym. Sci. Part A: Polym. Chem.* **2001**, 39, 1572.
- [30] J. Z. Du, Y. M. Chen, *J. Polym. Sci. Part A: Polym. Chem.* **2004**, 39, 2263.
- [31] F. Laflèche, T. Nicolai, D. Durand, Y. Gnanou, D. Taton, *Macromolecules* **2003**, 36, 1341.
- [32] I. V. Berlinova, I. M. Panayotov, *Macromol. Chem. Phys.* **1989**, 190, 1515.

- [33] R. S. Saunders, R. E. Cohen, S. J. Wong, R. R. Schrock, *Macromolecules* **1992**, *25*, 2055.
- [34] S. Kanaoka, T. Omura, M. Sawamoto, T. Higashimura, *Macromolecules* **1992**, *25*, 6407.
- [35] C. Tsitsilianis, D. Papanagopoulos, *Polymer* **1995**, *36*, 3745.
- [36] I. Gitsov, J. M. J. Frechet, *J. Am. Chem. Soc.* **1996**, *118*, 3785.
- [37] a) J. L. Hedrick, M. Trollsas, C. J. Hawker, B. Atthoff, H. Claesson, A. Heise, R. D. Miller, D. Mecerreyes, R. Jerome, P. Dubois, *Macromolecules* **1998**, *31*, 8691; b) A. Heise, M. Trollsas, T. Magbitang, J. L. Hedrick, C. W. Frank, R. D. Miller, *Macromolecules* **2001**, *34*, 2798.
- [38] S. Angot, D. Taton, Y. Gnanou, *Macromolecules* **2000**, *33*, 5418.
- [39] a) M. Pitsikalis, S. Pispas, J. W. Mays, N. Hadjichristidis, *Adv. Polym. Sci.* **1998**, *135*, 1; b) C. J. Hawker, A. W. Bosman, E. Harth, *Chem. Rev.* **2001**, *101*, 3661; c) M. Kamigaito, T. Ando, M. Sawamoto, *Chem. Rev.* **2001**, *101*, 3689, and references therein.
- [40] a) M. Gervais, B. Gallot, *Makromol. Chem.* **1977**, *178*, 1577; b) M. A. Hillmyer, F. S. Bates, *Macromolecules* **1996**, *29*, 6994; c) S. Förster, E. Krämer, *Macromolecules* **1999**, *32*, 2783; d) C. G. Göltner, B. Berton, E. Krämer, M. Antonietti, *Adv. Mater.* **1999**, *11*, 395; e) H. Egger, A. Nordskog, P. Lang, A. Brandt, *Macromol. Symp.* **2000**, *162*, 291.
- [41] See Supporting Information.
- [42] a) H. G. Elias, J. Gerber, *Makromol. Chem.* **1968**, *112*, 122; b) P. Alexandridis, J. F. Holzwarth, T. A. Hatton, *Macromolecules* **1994**, *27*, 2414.
- [43] a) Y. Y. Won, A. K. Brannan, H. T. Davis, F. S. Bates, *J. Phys. Chem. B* **2002**, *106*, 3354; b) Y. Y. Won, A. K. Brannan, H. T. Davis, F. S. Bates, *Macromolecules* **2003**, *36*, 953; c) S. Jain, F. S. Bates, *Macromolecules* **2004**, *37*, 1511.
- [44] A. J. Kovacs, J. A. Manson, D. Levy, *Kolloid Z. Z. Polym.* **1966**, *214*, 1.
- [45] S. Hong, W. J. MacKnight, T. P. Russell, S. P. Guido, *Macromolecules* **2001**, *34*, 2876.

Host–Guest Chemistry

Cucurbit[8]uril-Mediated Redox-Controlled Self-Assembly of Viologen-Containing Dendrimers**

Kwangyul Moon, Jodi Grindstaff, David Sobransingh, and Angel E. Kaifer*

Dendrimer self-assembly is a research topic of great current interest as it targets the preparation of relatively large three-dimensional structures with defined shapes and sizes which start from dendritic building blocks that already fall within the nanometer range. The self-assembly of dendrimers has been investigated by a number of groups who have taken

advantage of π – π stacking,^[1] fluorophobic,^[2] solvophobic,^[3] hydrogen bonding,^[4] ion–dipole,^[5] metal coordination,^[6] and other intermolecular interactions^[7] to drive the aggregation of appropriately functionalized dendrimers. The type and location of functional recognition groups in the dendrimers determines the “program” for self-assembly. An attractive goal in this research area is to externally control the self-assembly process by dictating the assembly or dissociation conditions to the system through the application of appropriate stimuli.

Both the group of Kim and our own group have actively investigated the binding interactions between 4,4'-bipyridinium (viologen) derivatives and the host cucurbit[7]uril (CB7).^[8] Recently, we reported that CB7 also forms stable inclusion complexes with a series of water-soluble dendrimers that contain a viologen residue covalently attached to the focal point of Newkome-type dendrons.^[9] Kim and co-workers reported that the larger host, cucurbit[8]uril (CB8), effectively enhances the dimerization of methyl viologen radical cations—the one-electron-reduced form of methyl viologen.^[10] Their report intrigued us and led us to investigate the binding interactions between our water-soluble, viologen-containing dendrimers and CB8. As this host favors the dimerization of methyl viologen radical cations, our expectation was that its presence would lead to extensive dimerization of viologen dendrimers upon their one-electron reduction. Thus, the presence of CB8 may afford a convenient, simple, and *reversible* mechanism to drive the self-assembly of dendrimer dimers under redox control. Herein, we report the results of this investigation.

The viologen-containing dendrimers **1**–**3** were prepared following reported methods.^[11] Dendrimer **4** was prepared by exhaustive esterification of **3** with methanol and fully characterized by NMR spectroscopy, MALDI-TOF mass spectrometry, and electrochemical techniques. The complexation of the viologen residue in dendrimers **1**, **2**, and **4** by the host CB8 was monitored by using electronic absorption spectroscopy. The molar absorptivity coefficient of the characteristic UV absorption of the viologen moiety at ≈ 260 nm was suppressed upon exposure to the CB8 host, although the magnitude of this effect is less pronounced than that observed with the CB7 host.^[8a] Analysis of the UV/Vis data obtained in titration experiments of the dendrimers with CB8 yielded the equilibrium association constants $K = 2.8 \times 10^4$, 1.4×10^4 , and 2.9×10^3 L mol^{−1} for the dendrimer guests **1**, **2**, and **4**, respectively. The gradual decrease in the binding constant with increasing dendrimer size is consistent with previous observations by our group.^[9,12] The values of K are smaller but comparable to the value reported by Kim and co-workers for the 1:1 complexation of methyl viologen by the host CB8.^[10]

The electrochemical behavior of dendrimer **1** exhibits the two consecutive one-electron reductions anticipated for any viologen compound (Figure 1). The first wave corresponds to the reversible reduction from the viologen dication (v^{2+}) to the radical-cation form ($v^{\bullet+}$), whereas the second wave reflects the reversible reduction from the cation (v^+) to the neutral form (v). In the presence of 0.5 equivalents of CB8, the half-wave potential ($E_{1/2}$) associated with the first wave

[*] K. Moon, J. Grindstaff, D. Sobransingh, Prof. A. E. Kaifer
Center for Supramolecular Science and Department of Chemistry
University of Miami
Coral Gables, FL 33124-0431 (USA)
Fax: (+1) 305-444-1777
E-mail: akaifer@miami.edu

[**] This work was supported by the NSF (to A.E.K., CHE-0204295).

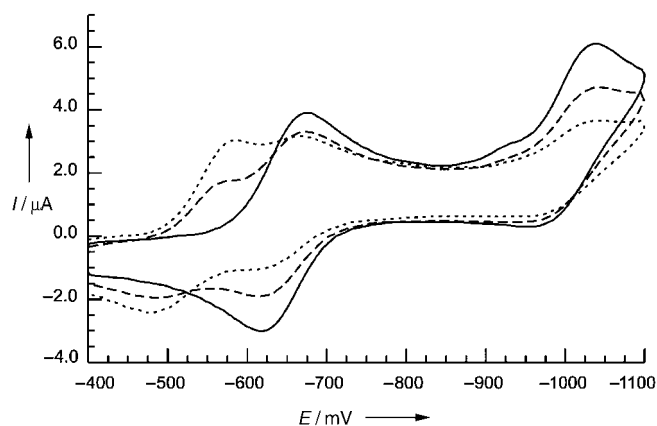
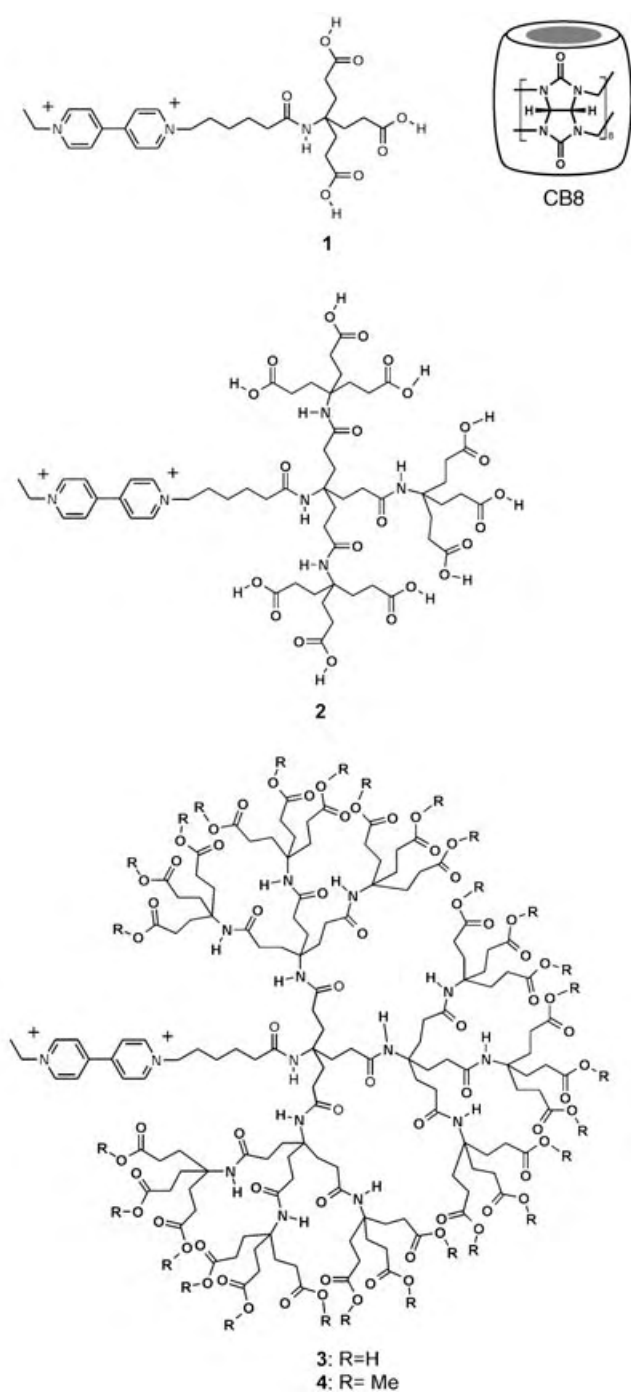


Figure 1. Cyclic voltammograms of dendrimer 1 (0.5 mM) in a phosphate buffer solution (pH 7, $I = 0.1$ M) in the presence of 0.00 (—), 0.25 (---), and 0.50 equivalents (----) of CB8. Potentials measured versus Ag/AgCl; scan rate = 0.100 V s^{-1} .

tigated the spectral changes observed upon reduction of our viologen-containing dendrimer solutions in an evacuated, sealed cell. For instance, reduction of the second-generation dendrimer 2 with activated Zn powder gives rise to the UV/Vis spectrum shown in Figure 2. The observed spectral

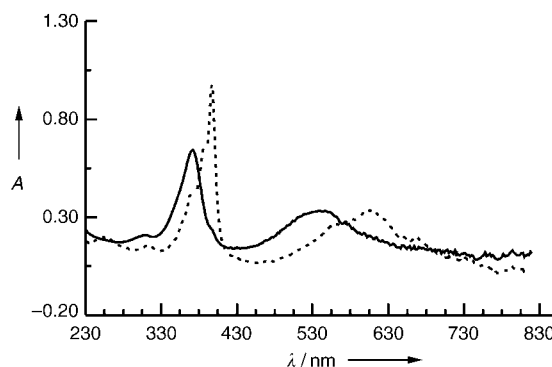


Figure 2. Electronic absorption spectra of a solution of dendrimer 2 (0.3 mM in phosphate buffer) after exhaustive one-electron reduction, in the absence (----) and in the presence (—) of CB8 (0.8 equiv); optical path = 0.1 cm.

shifts to a more-positive value (Figure 1). Since the dication form of the viologen is stabilized by inclusion into CB8, the observed anodic shift of the $E_{1/2}$ value implies that the v^{2+} form is even more strongly stabilized by CB8 than the dicationic form itself. By analogy to the behavior reported for the radical cation of methyl viologen by Kim and co-workers,^[10] this finding strongly suggests that two dendrimers associate through dimerization of their viologen radical cations inside the cavity of CB8.

The dimerization of viologen radical cations gives rise to considerable changes in their electronic absorption spectra.^[13] As viologen radical cations are oxygen sensitive, we inves-

pattern reveals that (1) the viologen units (v) are exhaustively reduced to their $v^{\bullet+}$ form owing to the complete disappearance of the intense absorption of the v^{2+} form (at 260 nm), and that (2) most of the viologen radical-cation residues exist as monomers from the absorption maxima observed at 396 and 602 nm. On the other hand, reduction of 2 in the presence of CB8 gives rise to a completely different absorption spectrum with maxima at 370 and 546 nm, which are characteristic of the viologen radical-cation dimer. This spectroscopic evidence strongly indicates that the presence of CB8 greatly enhances dimerization of the one-electron-reduced (radical-cation) forms of the viologen-containing dendrimers relative to the low levels of dimerization observed in the absence of CB8.

These spectroscopic data reveal that the first-generation dendrimer **1** also dimerizes extensively in the presence of CB8 upon one-electron reduction, whereas dimerization is not detected at all in the absence of this host. In a control experiment, the one-electron-reduced (radical cation) form of **1** was generated in the presence of host CB7. The spectroscopic results showed that CB7 is completely ineffective at fostering dimerization of the radical-cation forms of dendrimer **1** (Figure 3). This reflects the smaller cavity size of

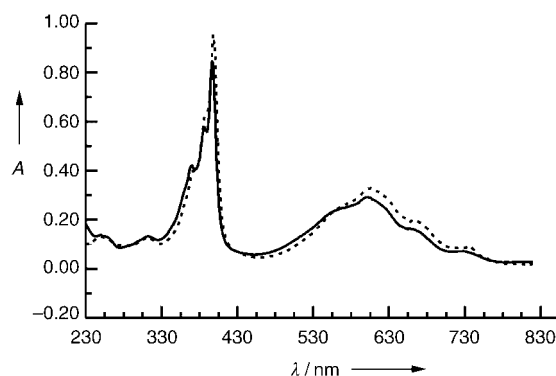


Figure 3. Electronic absorption spectra of a solution of dendrimer **1** (0.3 mM in phosphate buffer) after exhaustive one-electron reduction in the absence (----) and in the presence (—) of CB7 (0.3 mM); optical path = 0.1 cm.

CB7 compared to CB8 which prevents the former host from including two viologen radical-cation subunits simultaneously. The reversible character of the dimerization process in the presence of CB8 was verified by exposing the solution of the one-electron-reduced viologen dendrimer to air. Oxidation quickly leads to a colorless solution, which shows an absorbance spectrum indistinguishable from the spectrum obtained before reduction.

Some years ago, our group showed that the ratio of the absorbances at 364 and 394 nm (A_{364}/A_{394}) in the electronic spectrum of one-electron-reduced methyl viologen increases linearly with the ratio of the concentrations of dimer to monomer ($[d]/[m]$) in the solution.^[14] Although the viologen compounds used in this work are structurally more complex, it is reasonable to assume that the corresponding absorbance ratios should also correlate with the ratios of the concentrations ($[d]/[m]$) present in solutions of the viologen-containing dendrimers upon extensive one-electron reduction. The collected data are given in Table 1.

The ratios of the absorbances measured in the absence of CB8 are all within the 0.43–0.50 range, which indicates minimal dimerization (< 5%) of the viologen radical-cation residues. The ratios of the absorbances increased substantially in the presence of the host CB8 and reveal extensive dimerization (> 80%). The only exception to this trend was provided by dendrimer **3**, which dimerizes to a very low extent (≈ 20%) as indicated by its relatively low A_{370}/A_{396} ratio. This finding may be a result of electrostatic repulsion between two approaching molecules of **3**, each one bearing a large number of negative charges at the neutral pH value at

Table 1: Spectroscopic data obtained with solutions of viologen-containing dendrimers (≈ 0.3 mM) upon exhaustive one-electron reduction in buffered aqueous solution (pH 7).

Dendrimer	Added Host	A_{370}	A_{396}	A_{370}/A_{396}	% Dimer
1	None	0.504	1.017	0.495	< 5
1	CB8	0.634	0.179	3.540	> 80
1	None	0.396	0.869	0.455	< 5
1	CB7	0.420	0.849	0.495	< 5
2	None	0.422	0.955	0.441	< 5
2	CB8	0.638	0.242	2.636	> 80
3	None	0.435	1.011	0.430	< 5
3	CB8	0.750	1.260	0.595	~ 20
4	None	0.554	1.271	0.436	< 5
4	CB8	0.525	0.454	1.200	~ 50
1 + 2	None	0.417	0.856	0.487	< 5
1 + 2	CB8	0.699	0.252	2.780	> 80
1 + 4	None	0.438	0.931	0.471	< 5
1 + 4	CB8	0.655	0.303	2.160	> 80
2 + 4	None	0.475	1.069	0.444	< 5
2 + 4	CB8	0.591	0.254	2.340	> 80

which these experiments were conducted. The existence of considerable electrostatic effects is further supported by the extensive dimerization observed with the methyl ester form of the third-generation dendrimer, **4**. Thus, although the increase in size of the dendrimers may be a factor that hinders their dimerization, electrostatic interactions play a much more important role.

Table 1 also contains data which confirm that dimerization takes place between reduced dendrimers of different sizes. For instance, reduction of a solution that contains an equimolar mixture of dendrimers **1** and **2** in the presence of CB8 leads to extensive dimerization. The spectroscopic data do not permit the assessment of the relative abundances of homo- and heterodimers, but dimerization is nonetheless as predominant upon one-electron reduction as in the cases of the individually reduced dendrimers.

To obtain independent confirmation of these results we carried out Pulse Gradient Stimulated Echo (PGSE) NMR spectroscopic experiments to determine the diffusion coefficients (D_o) of these dendrimers under different experimental conditions. The paramagnetic character of the one-electron-reduced form of viologens introduces some complications in these experiments, but in spite of the broadening of the proton signals of the viologen residue, NMR spectroscopic and PGSE D_o measurements were possible. Relevant values are given in Table 2. The results are consistent with the UV/Vis spectroscopic data and lead to similar conclusions. Note that the D_o values suffer a considerable decrease upon one-electron reduction of the viologen residue in the presence of CB8. The decrease in the D_o values reflects the larger effective size of the aggregates formed upon reduction, presumably owing to the enhanced dimerization fostered by the CB8 host. Control experiments with dendrimer **1** in the presence of the smaller host CB7 did not reveal any decrease in D_o values upon one-electron reduction of the viologen unit. In fact, in this case we observed an increase in D_o values (from 3.1×10^{-6} to 3.5×10^{-6}) which may correlate to the lower relative affinity of the reduced viologen for the CB7 host.

Table 2: Diffusion coefficients (D_0 [$\text{cm}^2 \text{s}^{-1}$]) determined from PGSE NMR experiments with dendrimers 1–4 in D_2O solution (pH 7).

Conditions	1	2	3	4
Oxidized, in the absence of CB8	3.8×10^{-6}	2.5×10^{-6}	1.5×10^{-6}	— ^[a]
Oxidized, in the presence of CB8	3.1×10^{-6}	2.3×10^{-6}	— ^[a]	1.7×10^{-6}
Reduced (1 e^-), in the presence of CB8	2.3×10^{-6}	1.7×10^{-6}	— ^[a]	1.4×10^{-6}

[a] not measured.

In summary, this work has clearly established that CB8 strongly favors the dimerization of the viologen-containing dendrimers upon their one-electron reduction (Figure 4). The CB8-mediated dimerization is extremely efficient in most of the cases investigated here and constitutes a rather unique example of redox-switchable dendrimer self-assembly, in which the noncovalent interactions between the host CB8 and the viologen residues of the dendrimers can be manipulated to select different host–guest assemblies as a function of the oxidation state of the viologen unit.

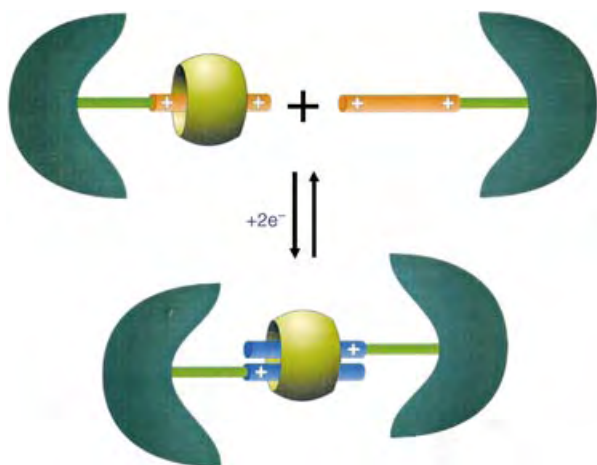


Figure 4. Redox control of the CB8-induced dimerization of viologen-containing dendrimers.

Experimental Section

Dendrimers 1–3 were prepared as previously reported.^[9] The host CB8 was obtained from Sigma–Aldrich. For the electrochemical and spectroscopic experiments, the dendrimers were dissolved in phosphate buffer solution (pH 7, 0.1-M ionic strength). The electrochemical experiments were run in a single-compartment cell fitted with a glassy carbon working electrode (0.071 cm^2), a Pt counter electrode, and a Ag/AgCl reference electrode. The solutions were exhaustively purged and kept under an atmosphere of purified nitrogen during the electrochemical experiments. For the spectroscopic experiments, the dendrimer solutions were placed inside a glass cell assembly, which was sealed under vacuum. The dendrimer was reduced by exposure to activated Zn powder and transferred for spectroscopic analysis to a quartz cell (0.1-cm optical path), which was fitted to the end of a sidearm of the evacuated glass-cell assembly.

Viologen dendrimer 4: The hydrolyzed form of dendrimer 3 and acetyl chloride (81.0 equiv) were stirred in dry MeOH (7 mL) for 12 h under N_2 . The solution was then concentrated in vacuo. Acetone was added to the residue followed by a saturated solution of NH_4PF_6 in acetone/ H_2O (2:1). The solution was stirred for 15 mins, and then acetone was gently removed in vacuo. The remaining suspension was extracted with EtOAc ($2 \times 10 \text{ mL}$), and the combined extracts were

evaporated to afford the viologen dendrimer 4 (96%). ^1H NMR (400 MHz, $[\text{D}_3]\text{MeCN}$): δ = 9.15 (d, 2H), 9.05 (d, 2H), 8.62 (d, 4H), 6.70 (s, 1H), 6.30 (t, 3H), 6.23 (t, 9H), 4.72 (m, 4H), 3.60 (s, 81H), 2.25 (m, 78H), 2.08 (m, 4H), 1.94 (m, 78H), 1.85 (m, 2H), 1.69 (t, 3H), 1.27 ppm (m, 2H); ^{13}C NMR (100 MHz, $[\text{D}_3]\text{MeCN}$): δ = 176.5, 175.2, 151.2, 147.3, 146.8, 128.6, 63.3, 59.5, 59.0, 52.7, 50.3, 32.1, 30.5, 29.3, 17.0 ppm; MALDI-TOF MS: m/z : 3801 $[\text{M}-\text{PF}_6]^+$, 3658 $[\text{M}-2\text{PF}_6]^+$, 3400 $[\text{M}-2\text{PF}_6-\text{viologen}]$.

Received: March 31, 2004

Revised: July 10, 2004

Keywords: dendrimers · dimerization · host–guest systems · redox chemistry · self-assembly

- [1] V. Percec, M. Glodde, T. K. Bera, Y. Miura, I. Shiyonovskaya, K. D. Singer, V. S. K. Balagurusamy, P. A. Heiney, I. Schnell, A. Rapp, H.-W. Spiess, S. D. Hudson, H. Duan, *Nature* **2002**, 419, 384.
- [2] V. Percec, M. Glodde, G. Johansson, V. S. K. Balagurusamy, P. A. Heiney, *Angew. Chem.* **2003**, 115, 4474; *Angew. Chem. Int. Ed.* **2003**, 42, 4338.
- [3] V. Percec, A. E. Dulcey, Y. Miura, U. Edlund, V. S. K. Balagurusamy, S. Hudson, H. Daurt, P. A. Heiney, *Polym. Prepr. Am. Chem. Soc. Div. Polym. Chem.* **2002**, 43, 548.
- [4] a) Y. Ma, S. V. Kolotuchin, S. C. Zimmerman, *J. Am. Chem. Soc.* **2002**, 124, 13757; b) S. C. Zimmerman, F. Zeng, D. E. C. Reichert, S. V. Kolotuchin, *Science* **1996**, 271, 1095; c) P. S. Corbin, L. J. Lawless, Z. Li, Y. Ma, M. J. Witmer, S. C. Zimmerman, *Proc. Natl. Acad. Sci. USA* **2002**, 99, 5099; d) Y. Wang, F. Zeng, S. C. Zimmerman, *Tetrahedron Lett.* **1997**, 38, 5459.
- [5] a) V. Percec, W.-D. Cho, G. Ungar, D. J. P. Yearley, *Chem. Eur. J.* **2002**, 8, 2011; b) G. M. Dykes, D. K. Smith, *Tetrahedron* **2003**, 59, 3999.
- [6] a) W. T. S. Huck, F. C. J. M. van Veggel, B. L. Kropman, D. H. A. Blank, E. G. Keim, M. M. A. Smithers, D. N. Reinhoudt, *J. Am. Chem. Soc.* **1995**, 117, 8293; b) M. Kawa, J. M. J. Fréchet, *Chem. Mater.* **1998**, 10, 286.
- [7] E. R. Zubarev, M. U. Pralle, E. D. Sone, S. I. Stupp, *J. Am. Chem. Soc.* **2001**, 123, 4105.
- [8] a) H.-J. Kim, W. S. Jeon, Y. H. Ko, K. Kim, *Proc. Natl. Acad. Sci. USA* **2002**, 99, 5007; b) W. Ong, M. Gómez-Kaifer, A. E. Kaifer, *Org. Lett.* **2002**, 4, 1791; c) K. Moon, A. E. Kaifer, *Org. Lett.* **2004**, 6, 185; d) W. Ong, A. E. Kaifer, *J. Org. Chem.* **2004**, 69, 1383.
- [9] W. Ong, A. E. Kaifer, *Angew. Chem.* **2003**, 115, 2214; *Angew. Chem. Int. Ed.* **2003**, 42, 2164.
- [10] W. S. Jeon, H.-J. Kim, C. Lee, K. Kim, *Chem. Commun.* **2002**, 1828.
- [11] W. Ong, A. E. Kaifer, *J. Am. Chem. Soc.* **2002**, 124, 9358.
- [12] C. M. Cardona, T. D. McCarley, A. E. Kaifer, *J. Org. Chem.* **2000**, 65, 1857.
- [13] E. M. Kosower, J. L. Cotter, *J. Am. Chem. Soc.* **1964**, 86, 4876.
- [14] P. A. Quintela, A. Diaz, A. E. Kaifer, *Langmuir* **1988**, 4, 663.

Nanostructures

Control of Nanoparticle Assembly by Using DNA-Modified Diatom Templates**

Nathaniel L. Rosi, C. Shad Thaxton, and Chad A. Mirkin*

Microorganisms have proven to be versatile templates for the organization of nanostructured materials into larger-scale functional architectures. In general, methods exist either to nonspecifically adsorb or nucleate the growth of nanoparticles onto template surfaces or to genetically manipulate the template organism to express desired functional groups that specifically interact with or nucleate nanoparticles.^[1–5] An ideal biological template would be one that could be chemically modified in a versatile manner by using conventional bench-top methods so that the interaction between the template and the nanostructured materials could be understood and easily controlled. To this end, we have investigated the use of diatoms as templates for the assembly of prefabricated nanoparticles.^[6–9] Diatoms are a diverse class of unicellular algae and are classified based upon the unique shapes and ornate structural features of their silica cell walls. There are literally thousands of readily available and taxonomically different diatoms.^[10] Their cell walls have two halves (frustules), which fit together like a petri dish and generally have dimensions between 1 and 100 μm .

For classification purposes, the organic components of the diatoms are routinely digested in an acidic bath (Piranha) to allow more precise examination of their silica cell walls; the ability to use such corrosive conditions serves as a testament to their robust and stable nature. Because

glass functionalization processes involve acidic activation followed by a reaction with silanes,^[11] we reasoned that a similar protocol could be used to chemically program diatom surfaces to interact with specific nanoparticles of interest. Herein, we show that diatom cell walls can be covalently functionalized with DNA and then used as templates for the sequence-specific assembly of DNA-functionalized nanoparticles. We further demonstrate that DNA can program the assembly of multiple layers of nanoparticles onto the template.

In a typical experiment (Figure 1),^[12] diatoms (either *Synedra* or *Navicula*; **1**) were cultured from a freshwater silicate-rich growth medium for two weeks under ambient cool-white fluorescent light (Carolina Biological Supply Company). A Piranha solution was used both to digest the

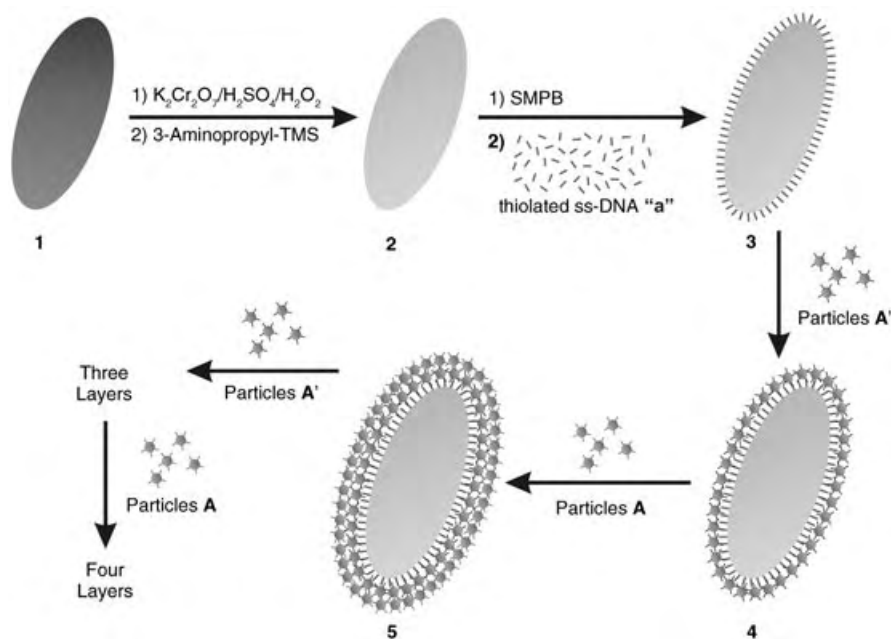


Figure 1. Scheme depicting the functionalization of diatom templates with DNA and DNA-functionalized nanoparticles. A Piranha solution was used to digest the organic components of the diatoms (**1**) and activate their cell walls for reaction with 3-aminopropyltrimethoxysilane (amino-propyl-TMS). The amino-functionalized diatoms (**2**) were coupled to thiolated DNA by using succinimidyl 4-[*p*-maleimidophenyl]butyrate (SMPB) to generate a DNA-functionalized template (**3**). **3** was coated with 13 nm gold particles functionalized with complementary DNA (Particles A') to form a three-dimensional material (**4**) that adopts the size and shape of the diatom template. A bilayer material (**5**) was generated from the reaction with particles A; up to seven nanoparticle layers were added by iterative reactions with particles A' followed by particles A.

[*] N. L. Rosi, C. S. Thaxton, Prof. C. A. Mirkin
Department of Chemistry and
Institute for Nanotechnology
Northwestern University
2145 Sheridan Road, Evanston, IL 60208-3113 (USA)
Fax: (+1) 847-467-5123
E-mail: chadnano@northwestern.edu

[**] CAM acknowledges the DARPA and the AFOSR programs for support of this research. The authors thank Dimitra Georganopoulou for assistance with the acquisition of SEM images and Zhi Li and Emma Kate Payne for useful discussions.

Supporting information for this article is available on the WWW under <http://www.angewandte.org> or from the author.

organic component of the diatoms and to activate their cell walls (**2**) for amino-silane functionalization, which was in turn effected by using standard methods.^[11] The amino-functionalized diatoms were then coupled to fluorophore-labeled thiolated DNA (3'-HS-C₃H₆-Cy3-AATATTGATAAGGAT-5', **a**) by using succinimidyl 4-[*p*-maleimidophenyl]butyrate (SMPB, Pierce Biotechnology, Inc.), a hetero-bifunctional crosslinking agent. The DNA-functionalized diatoms (**3**) were stored as a suspension in phosphate-buffered saline (PBS; 1 mL, 0.3 M). Due to the presence of Cy3, they appeared pink and fluoresced at 563 nm upon excitation with a mercury lamp (Figure 2a).

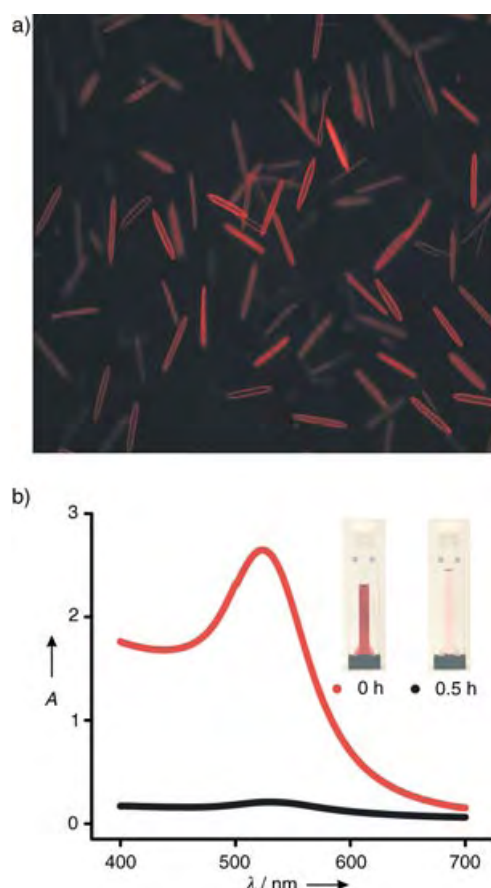


Figure 2. Upon covalent immobilization of fluorophore-labeled thiolated DNA onto their surfaces, the diatoms can be visualized by using fluorescence microscopy (a). The reaction of DNA-functionalized diatoms with complementary DNA-functionalized nanoparticles can be monitored unaided with the naked-eye or by UV/Vis spectroscopy (b). At 0 h, the DNA-functionalized 13 nm gold colloid appears dark red (left, inset) and exhibits a strong extinction band at 520 nm. After 0.5 h of reaction with the DNA-functionalized diatom templates, the solution appears light-pink (right, inset), and there is a dramatic decrease in the extinction peak at 520 nm. This is due to the complementary DNA hybridization that directs the assembly of gold nanoparticles onto the diatom templates.

To demonstrate their utility as templates for the assembly of nanoparticles, a sample of DNA-functionalized diatoms (typically $\approx 250 \mu\text{L}$) was exposed to 13 nm Au particles (particles **A'**) functionalized with complementary 3'-propylthiol-capped oligonucleotide strands (3'-HS-C₃H₆-ATCCTTATCAATATT-5'; **a'**; Figure 1).^[13] After about 30 min at room temperature followed by brief centrifugation (3000 rpm), most of the nanoparticles assembled onto the diatom surfaces (**4**) as evidenced by both the naked-eye and UV/Vis spectroscopy (Figure 2b). Fresh colloid was added iteratively until the solution remained red for at least 24 h to fully saturate available surface binding sites. Scanning electron microscopy (SEM) and transmission electron microscopy (TEM) of the coated diatoms revealed nearly saturated monolayer coverage for both *Synedra* (Figure 3) and *Navicula* (Figure 4), with the nanoparticle coating adopting the surface morphology and shape of the diatom templates. In some cases, the diatom

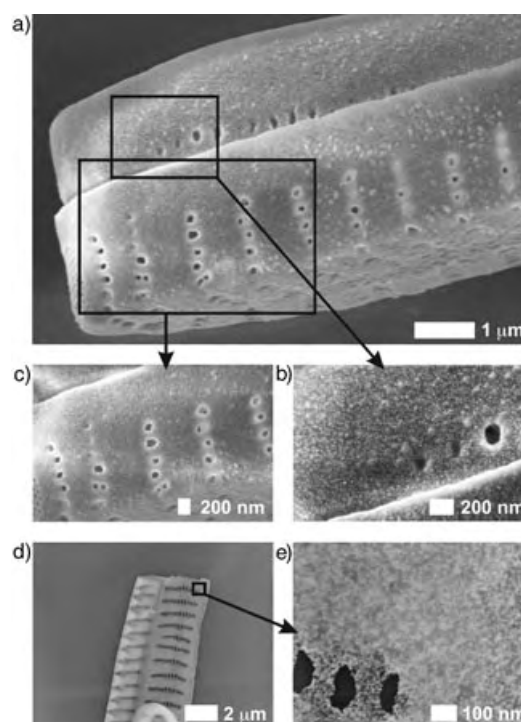


Figure 3. Electron microscope images of DNA-functionalized *Synedra* diatoms densely coated with one layer of DNA-modified 13 nm gold particles. SEM images (a–c), at different magnifications, reveal a portion of a diatom where the two frustules remain attached. Note the regularly patterned nanoscale pores on the *Synedra* surface. In some cases, the diatom frustules are detached from one another. This is exemplified in the TEM images (d,e), which show the inside wall of a detached frustule. The definition of the nanoparticle coverage is best illustrated in b), exterior wall coverage, and e) interior wall coverage.

frustules remained attached and together (Figure 3a–c and Figure 4a–c) while in other cases they were either separated (Figure 3d,e) or displaced from one another (Figure 4d,e). From these examples, we can conclude that both the interior and exterior of the cell walls are coated with nanoparticles. It is important to note that the assembly process is directed by the sequence specific interactions between the DNA-functionalized diatoms and the DNA-functionalized nanoparticles—no assembly was observed when nanoparticles modified with noncomplementary DNA were used.

Because DNA is used to direct the template–nanoparticle assembly process, raising the temperature beyond the melting point of the duplex DNA results in release of the nanoparticles from the template. This process can be monitored using UV/Vis spectroscopy by measuring the increase of the characteristic nanoparticle surface plasmon band at 520 nm as a function of increasing temperature. The resulting “melting” curves (Figure 5) provide further evidence of the hybridization-directed assembly. Moreover, the sharp melting transitions, which result from a cooperative melting effect routinely observed for aggregates of DNA-functionalized nanoparticles,^[14] corroborate the dense surface coverage observed by electron microscopy. The observed melting transitions are slightly broader (≈ 8 – 10°C) than those reported for monolayers of 13 nm gold particles on glass

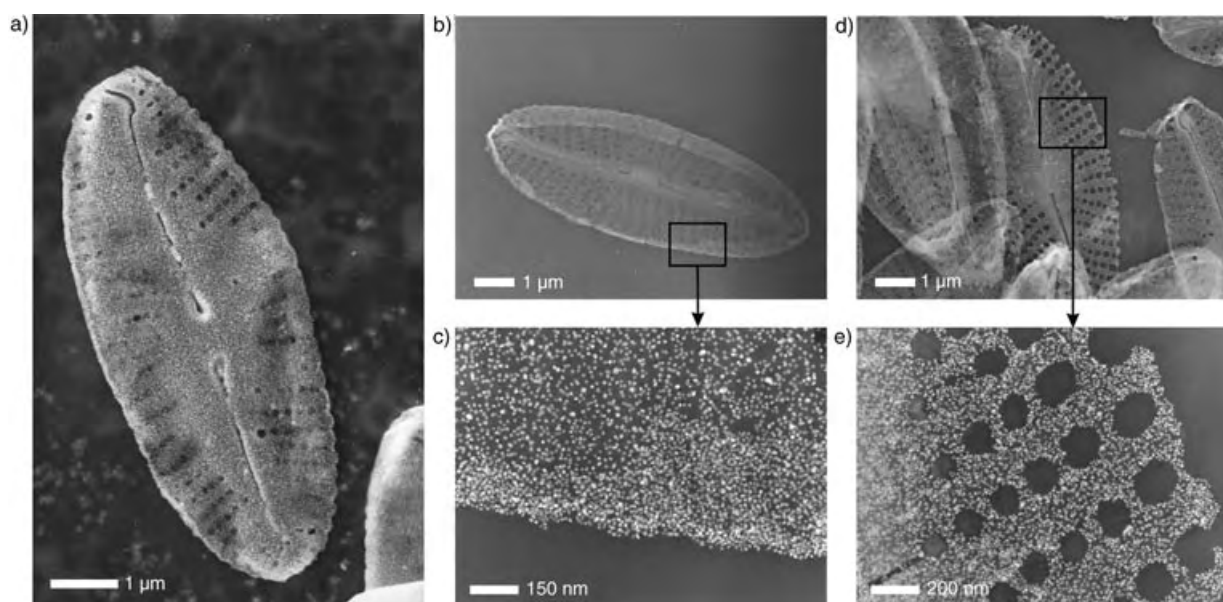


Figure 4. Electron microscope images of DNA-functionalized *Navicula* diatoms densely coated with one layer of DNA-modified 13 nm gold particles. SEM (a) and TEM images (b,c) both reveal a dense outer coating of nanoparticles on the *Navicula* surface. The homogeneous nanoparticle coating of the highly symmetric and nanoscopically detailed *Navicula* template is further illustrated in d) and e), which are different magnifications of a single frustule.

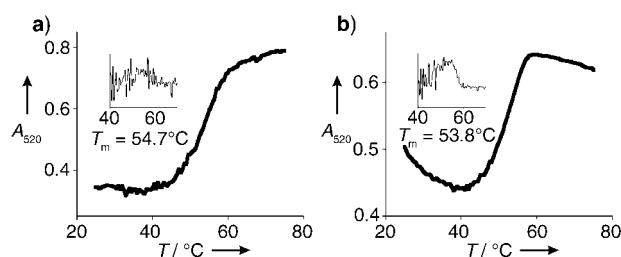


Figure 5. The release of the gold nanoparticles from the *Synedra* (a) and *Navicula* (b) surfaces is monitored using UV/Vis spectroscopy by measuring the increase in absorbance at 520 nm as a function of temperature. The melting temperatures (inset) of the DNA-duplex structures on *Synedra* and *Navicula* were determined to be 54.7°C and 53.8°C, respectively.

microscope slides (5°C).^[15] We attribute these differences to the irregular, undulating diatom surfaces that may play a role in decreasing the net cooperative melting effect.

The sequence-specific assembly properties conferred by DNA also can be used to build hierarchical structure and complexity into the templated materials. As a first step in this direction, we assembled multiple alternating layers of 13 nm gold particles onto the diatom surfaces (5, Figure 1) by using particles **A'** and complementary particles **A** (13 nm Au functionalized with 3'-HS-C₃H₆-AATATTGATAAGGAT-5'; **a**). A total of seven layers were added to both *Synedra* and *Navicula* diatoms; no interdiatom aggregation was observed during the assembly processes. TEM images of two nanoparticle layers on both *Navicula* and *Synedra* are shown in Figure 6 (a and b, respectively).^[16] A comparison of Figure 6 with Figure 3 and 4 reveals denser nanoparticle coverage, and the melting curves for four and seven layers (Figure 6 c,d and

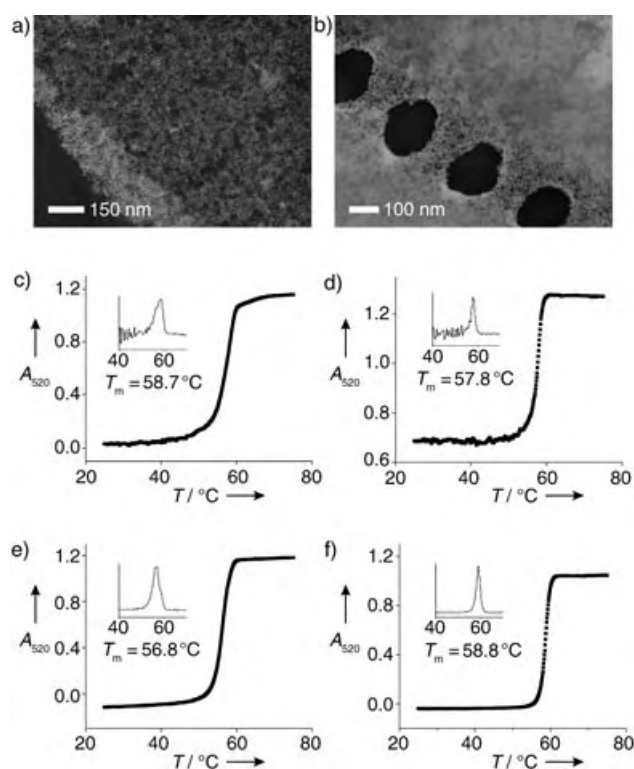


Figure 6. Multiple layers of nanoparticles can be assembled onto the diatom templates. Here, TEM images of two layers of nanoparticles on both *Navicula* (a) and *Synedra* (b) are illustrated. The melting curves for both four and seven layers of nanoparticles along with the corresponding melting temperatures are shown for *Navicula* (c, four layers; d, seven layers) and *Synedra* (e, four layers; f, seven layers).

e,f, respectively) are much sharper and shifted to higher temperatures in comparison to the melting curve for only one layer (Figure 5). A similar phenomenon is observed on glass slides and is due to increased cooperativity as the aggregate size and number of DNA linkages is increased.^[15]

Throughout this report, we have understated the unique structural and surface aspects of the diatom templates. Unlike the surfaces of some biological templates, the surface of the diatoms exhibit remarkable species-specific nanoscopic details that include pores, grooves, and ridges that cannot be rendered or synthesized by using conventional material fabrication techniques. We expect that these aspects, in combination with the unique properties of nanomaterials, might prove useful for various applications in catalysis and optics. Additionally, we anticipate that the nanoparticle-coated diatoms may be effective as substrates for surface enhanced Raman scattering (SERS)—preliminary studies are currently underway in our lab.

In conclusion, we emphasize that this novel approach is extraordinarily basic and general. Using straightforward reactions, we can easily modify the diatom surfaces with many different functional groups designed specifically to interact with nanostructures of interest or to perform desired chemistry. Similar strategies will be adopted for other micro-organism templates that have surfaces amenable to facile chemical functionalization.

Received: June 8, 2004

Keywords: DNA · microorganism · nanostructures · self-assembly · template synthesis

- [1] Z. Li, S.-W. Chung, J.-M. Nam, D. S. Ginger, C. A. Mirkin, *Angew. Chem.* **2003**, *115*, 2408–2411; *Angew. Chem. Int. Ed.* **2003**, *42*, 2306–2309.
- [2] V. Berry, S. Rangaswamy, R. F. Saraf, *Nano Lett.* **2004**, *4*, 939–942.
- [3] a) W. Shenton, T. Douglas, M. Young, G. Stubbs, S. Mann, *Adv. Mater.* **1999**, *11*, 253–256; b) E. Dujardin, C. Peet, G. Stubbs, J. N. Culver, S. Mann, *Nano Lett.* **2003**, *3*, 413–417; c) M. Knez, A. M. Bittner, F. Boes, C. Wege, H. Jeske, E. Maif, K. Kern, *Nano Lett.* **2003**, *3*, 1079–1082.
- [4] A. S. Blum, C. M. Soto, C. D. Wilson, J. D. Cole, M. Kim, B. Gnade, A. Chatterji, W. F. Ochoa, T. Lin, J. E. Johnson, B. R. Ratna, *Nano Lett.* **2004**, *4*, 867–870.
- [5] a) C. Mao, C. E. Flynn, A. Hayhurst, R. Sweeney, J. Qi, G. Georgiou, B. Iverson, A. M. Belcher, *Proc. Natl. Acad. Sci. USA* **2003**, *100*, 6946–6951; b) C. Mao, D. J. Solis, B. D. Reiss, S. T. Kottmann, R. Y. Sweeney, A. Hahurst, G. Georgiou, B. Iverson, A. M. Belcher, *Science* **2004**, *303*, 213–217.
- [6] G. A. Ozin, *Acc. Chem. Res.* **1997**, *30*, 17–27.
- [7] Diatom surface proteins have been isolated and investigated to promote the formation of silica nanostructures: a) N. Kroger, R. Duetzmann, M. Sumper, *Science* **1999**, *286*, 1129–1132; b) F. Noll, M. Sumper, N. Hampp, *Nano Lett.* **2002**, *2*, 91–95; c) H. R. Luckarift, J. C. Spain, R. R. Naik, M. O. Stone, *Nat. Biotechnol.* **2004**, *22*, 211–213.
- [8] Diatoms have been used previously as templates for the formation of zeolites: a) M. W. Anderson, S. M. Holmes, N. Hanif, C. S. Cundy, *Angew. Chem.* **2000**, *112*, 2819–2822; *Angew. Chem. Int. Ed.* **2000**, *39*, 2707–2710; b) Y. J. Wang, Y. Tang, X. D. Wang, A. G. Dong, W. Shan, Z. Gao, *Chem. Lett.* **2001**, *30*, 1118–1119; c) Y. Wang, Y. Tang, A. Dong, X. Wang, N. Ren, Z. Gao, *J. Mater. Chem.* **2002**, *12*, 1812–1818; d) F. Xu, Y. Wang, X. Wang, Y. Zhang, Y. Tang, P. Yang, *Adv. Mater.* **2003**, *15*, 1751–1753.
- [9] The composition of diatom cell walls have been reactively converted: a) K. H. Sandhage, M. B. Dickerson, P. M. Huseman, M. A. Caranna, J. D. Clifton, T. A. Bull, T. J. Heibel, W. R. Overton, M. E. A. Schoenwaelder, *Adv. Mater.* **2002**, *14*, 429–433; b) V. Sanhueza, U. Kelm, R. Cid, *J. Chem. Technol. Biotechnol.* **2003**, *78*, 485–488.
- [10] J. J. Dodd, *Diatoms*, Southern Illinois University Press, Carbondale, **1987**.
- [11] L. A. Chrisey, G. U. Lee, C. E. O’Ferrall, *Nucleic Acids Res.* **1996**, *24*, 3031–3039.
- [12] See Supporting Information for detailed experimental procedures.
- [13] J. J. Storhoff, R. Elghanian, R. C. Mucic, C. A. Mirkin, R. L. Letsinger, *J. Am. Chem. Soc.* **1998**, *120*, 1959–1964.
- [14] R. C. Jin, G. S. Wu, Z. Li, C. A. Mirkin, G. C. Schatz, *J. Am. Chem. Soc.* **2003**, *125*, 1643–1654.
- [15] T. A. Taton, R. C. Mucic, C. A. Mirkin, R. L. Letsinger, *J. Am. Chem. Soc.* **2000**, *122*, 6305–6306.
- [16] It was difficult to obtain TEM images of more than two layers of nanoparticles; they are included in the Supporting Information.

Asymmetric Catalysis

**Reversibly Addressing an Allosteric Catalyst
In Situ: Catalytic Molecular Tweezers****

Nathan C. Gianneschi, So-Hye Cho,
SonBinh T. Nguyen, and Chad A. Mirkin*

In biology, allosteric regulation is the control of enzyme activity by the fast, reversible binding of molecules or ions to structural sites that are remote from, but control conformational changes that occur at, the active site.^[1] If one considers that reversibility in a biological sense implies in situ control over activity, then there are no known abiotic systems that are truly allosteric catalysts. Recently, the first efforts towards the development of artificial allosteric catalysts have been described.^[2,3] Thus far, there have been two distinct approaches to realizing systems that mimic biological allosteric regulation of catalysis. One approach consists of organic

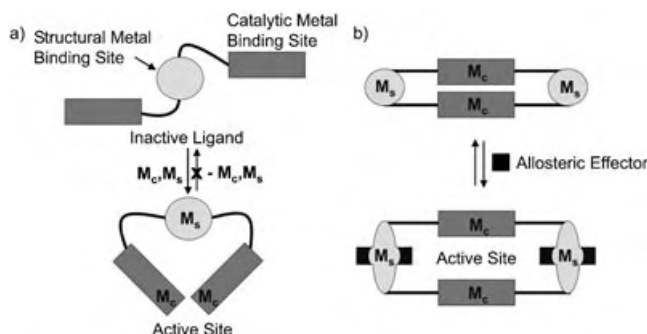
[*] N. C. Gianneschi, S.-H. Cho, Prof. S. T. Nguyen, Prof. C. A. Mirkin
Department of Chemistry and
the Institute for Nanotechnology
2145 Sheridan Road, Evanston, IL, 60208-3113 (USA)
Fax: (+1) 847-467-5123
E-mail: camirkin@chem.northwestern.edu

[**] CAM acknowledges the NSF and AFOSR for support of this work.
SHC acknowledges the DOE for funding through the Institute for
Environmental Catalysis (Grant no. DE-FG02-03ER15457)



Supporting information for this article is available on the WWW
under <http://www.angewandte.org> or from the author.

frameworks in which structural metal ions induce conformational changes that affect the ability of catalytic metals, within the same complex, to function.^[2] Essentially, structural metal coordination prepares a suitable ligand for the catalytically active metal centers.^[4] However, in a biological context, this strategy is more reminiscent of the way various enzymes, notably Zn-finger proteins,^[1] use structural metals to define their tertiary structure in a static fashion rather than behaving dynamically and reversibly (Scheme 1 a).



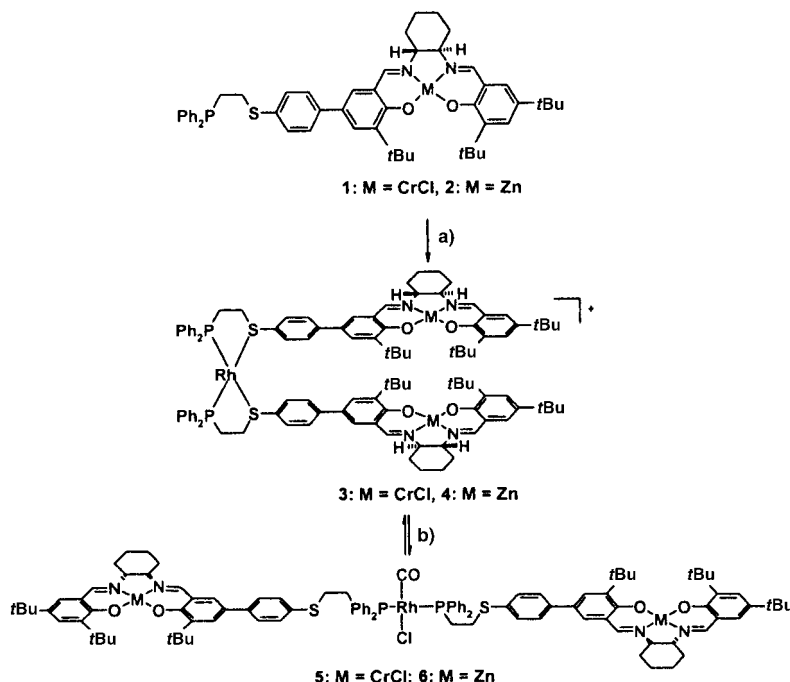
Scheme 1. M_s = Structural transition-metal center. M_c = Catalytic transition-metal center. M_s and M_c may be the same or different depending on the system. a) The metal-ion directed arrangement of an active site. b) The allosteric effector mediated shape change of a catalytic heterobimetallic macrocycle.

The second approach is based upon heterobimetallic supramolecular complexes in which one metal center acts as a structure control site and the other acts as a catalytic site (Scheme 1 b).^[3] These large macrocyclic complexes are assembled in high yield by the weak-link approach.^[5] This strategy provides a close mimic of a biological allosteric catalyst in the sense that it contains structural and catalytic sites that are independently addressable. The structural metal centers hold the catalyst in different conformations depending on the presence or absence of the allosteric effectors. However, these effectors prove difficult to remove from this system, making the reversibility slow and difficult to achieve.

Herein, we describe the synthesis and characterization of a new allosteric catalyst based upon a novel class of tweezer complex with catalytic rates and selectivities that can be increased and decreased reversibly in situ by selectively opening and closing the catalytic cleft through reactions that occur at the allosteric hinge. By using supramolecular coordination chemistry as a synthetic tool, we are beginning to understand how to construct addressable, conformationally flexible entities capable of catalyzing reactions with allosteric enzyme-like control.

We present the synthesis and catalytic activity of tweezer complexes that contain a Rh^I hinge and two Cr^{III} -salen catalytic arms (Scheme 2). The Rh^I -thioether bonds can be broken by reaction with CO and Cl^- , while leaving the Rh^I -phosphine bonds intact. The result of the selective breaking of these bonds is a significant topological change coupled with a change in the selectivity and rate of the reaction occurring at the Cr^{III} metal center. Essentially, the catalysis is controlled using changes in coordination chemistry at a structural site distal to a catalytic site. This is a rare example of a tweezer complex capable of undergoing an actual modulation of the distance between the arms of the complex in situ by the introduction and removal of small molecules and ions capable of addressing the hinge.^[6] In this manner we have a unique, biologically inspired, reversible switch for catalyst activity and selectivity.

The asymmetric ring opening of cyclohexene oxide by $TMSN_3$ ($TMSN$ = azidotrimethylsilane) was used to demonstrate the utility of this approach to catalytic control. This reaction was selected because of its demonstrated bimetallic mechanism that requires two metal-salen monomeric catalysts to activate both the epoxide and the nucleophile.^[7] We hypothesized that the incorporation of a bimetallic catalyst into a tweezer complex that can be opened and closed would provide control over catalyst activity and selectivity by virtue of the ability to address the relative orientation of the two catalytic sites involved in the bimetallic reaction. We were encouraged to move towards a tweezer-type catalyst because of our earlier experience with the related, macrocyclic salen-based system.^[3] Notably, the tweezer complex (Scheme 2)



Scheme 2. Synthesis of the allosteric tweezer complexes. Counterions are BF_4^- . All cyclohexyl salen backbones have (*R,R*) stereochemistry. Reagents and solvents; a) $[Rh(NBD)_2]BF_4$, CH_2Cl_2 ; b) $PPNCl/CO$ ($PPNCl$ = bis(triphenylphosphoranylidene)ammonium chloride); 3 and 4 may be synthesized from 5 and 6, respectively, by the removal of CO in vacuo or by purging with N_2 .

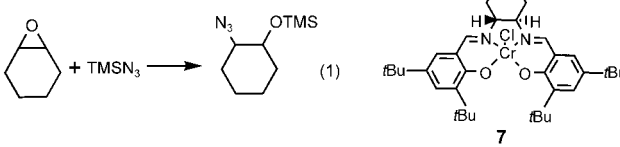
offers an increase in the solubility in comparison with the macrocycle, thus allowing the epoxide ring-opening reactions to be performed over greater ranges of catalyst concentration in THF. In addition, upon Rh^I–thioether bond breakage the catalyst changes from the compact tweezers-shaped molecule into a flexible, linear molecule. This dramatic change in shape was expected to generate a larger allosteric effect than the related macrocyclic analogue.

The novel enantiomerically pure hemilabile ligands **1** and **2** were synthesized in eight steps (see Supporting Information) and incorporate a binding site for a Rh^I metal center (Scheme 2). Compounds **3** and **4** were synthesized in almost quantitative yield by treating **1** and **2** respectively with [Rh(NBD)₂]BF₄ in CH₂Cl₂ (NBD is norbornadiene). Compound **3** has been characterized by elemental analysis, ³¹P NMR spectroscopy (compounds **3** and **5** are paramagnetic, due to the incorporation of Cr^{III} metal centers, which results in broad NMR signals), and electrospray mass spectrometry, and all data are consistent with its proposed structure. In addition, **4** has been fully characterized in solution. Compounds **3** and **4** can be converted to **5** and **6**, respectively, by treating with 1 equivalent of PPNCI and CO (1 atm) in benzonitrile, CH₂Cl₂, or THF at room temperature. Compounds **5** and **6** exhibit diagnostic ν_{CO} bands at 1976 cm⁻¹ and 1978 cm⁻¹, respectively.^[5c] The ³¹P{¹H} NMR spectra of **5** and **6** also support the proposed structures with each exhibiting a single resonance at 25 ppm (*J*_{P-Rh} = 123 Hz) diagnostic of square-planar *trans*-phosphine, Cl/CO complexes of Rh^I.^[5c,8] Significantly, the tweezer complexes **5** and **6** undergo reversible conversion to **3** and **4** upon vacuum removal of the solvent or by purging N₂ through the solution. The conversion can be monitored easily by ³¹P{¹H} NMR and infrared spectroscopies.

The differences in catalytic reactivity between the open, closed, and monomeric forms of the catalyst were evaluated using the asymmetric ring opening of cyclohexene oxide by TMSN₃ to yield 1-azido-2-(trimethylsiloxy)cyclohexane [Eq. (1); Table 1]. The incorporation of two catalysts into the tweezer complex results in competing intramolecular and intermolecular mechanisms. This is further complicated by the observation that linked, dimeric Cr^{III}–salen catalysts display increased intermolecular reaction rates, with respect to their monomeric analogues, in which highly reactive multimetallic assemblies have been implicated.^[7b,c] Theoretically, if only one molecule of either **3** or **5** were present in solution the catalytic reaction would be entirely intramolecular and as the catalyst concentration is increased the reaction would become more intermolecular. If this theory is true, we expect that the catalytic activity of **3** and **5** will be affected differently by dilution and we can optimize the allosteric effect by varying the concentration of the catalyst. We were able to demonstrate this effect by monitoring the enantiomeric excess of product formed by **3** and **5** at various catalyst concentrations (Table 1) and plotting the resulting data as a function of catalyst concentration (Figure 1).

The difference in the selectivity of the open and closed tweezer complexes is enhanced at low concentrations (Figure 1). As the concentration of **3** and **5** increases, the difference between the selectivity of the two catalysts

Table 1: Selectivity data for the ring opening of cyclohexene oxide by TMSN₃ catalyzed by **3**, **5**, and the monomeric Cr^{III}–salen complex **7**.^[a]



Entry	Catalyst	[Catalyst] M × 10 ⁻³	% ee of product ^[b]
1	3	7.2	80
2	5	7.2	74
3	7	7.2	26
4	3	4.7	80
5	5	4.7	73
6	3	3.6	79
7	5	3.6	68
8	7	3.6	12
9	3	2.5	77
10	5	2.5	60
11	3	1.8	72
12	5	1.8	54
13	3	0.72	65
14	5	0.72	44
15	3	0.36	63
16	5	0.36	32
17	3	0.14	49
18	5	0.14	21

[a] All reactions were performed at room temperature in THF. [b] % ee of 1-azido-2-(trimethylsiloxy)cyclohexane was determined by chiral GC.

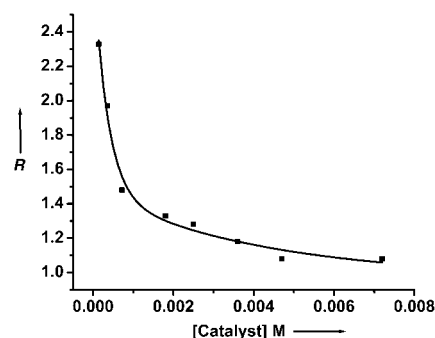


Figure 1. The allosteric effect expressed in terms of selectivity. *R* is the allosteric selectivity ratio = (% ee of the product formed by using **3**):(% ee of the product formed by using **5**).

decreases until they both reach a maximum of approximately 80% ee (Table 1). A similar trend is seen for the monomeric version of the catalyst (**7**) in which the selectivity of the catalyst increases with concentration (Table 1, entries 3 and 8). We hypothesize that the predefined cavity of complex **3** is able to maintain a selective environment for catalysis over a broad range of concentrations. Complex **5** is comparatively more adversely affected by solvent and reagent molecules that contribute to a reduction in the selectivity of the catalyst. The allosteric effect is enhanced as we move to lower concentrations of catalyst and the system becomes more dependent on the intramolecular reaction (Figure 1).

Open and closed tweezer complexes, **3** and **5**, are more selective and active than the monomeric version of the

catalyst, which suggests that cooperativity is present for both of the dimers. However, for **5** that cooperativity is reduced, thus rendering the catalyst less selective. The selectivity depends greatly on the nature of the alignment of the two catalytic centers in each tweezer complex. By monitoring the catalysis over a range of concentrations, we were able to map out and optimize the allosteric effect with respect to selectivity.

As mentioned earlier, a key requirement of a system that seeks to mimic biological-like allosteric control over catalysis, is its reversibility. The ease by which the allosteric initiator molecules and ions can be introduced and removed from the system dictates the plausibility of this approach to catalytic control. Hence, the use of a gas as an allosteric protagonist is ideal if one wishes to develop a system that can easily be addressed during the course of the reaction. Both members of the CO/Cl[−] pair are required to break the Rh^I–thioether bonds, as confirmed by ³¹P{¹H} NMR and FTIR spectroscopies. A catalytic reaction occurring in a solution containing Cl[−] ions and lacking CO will have only one of the necessary allosteric elements and vice versa. Subsequently, the ability to reversibly convert from **3** to **5** in situ by CO saturation and CO desaturation of a solution containing Cl[−] ions allows us to conveniently cycle the catalyst through two modes. With the introduction and removal of CO (1 atm) as our switch, we were able to demonstrate this allosteric effect with respect to the rate of formation of 1-azido-2-(trimethylsiloxy)cyclohexane (Figure 2). A catalyst concentration of 3.6 mM in benzonitrile was chosen owing to the relatively large difference in rates observed between **3** and **5** under these conditions (Supporting Information).^[9]

By introducing and removing CO from the system, we can alternatively slow and speed up the reaction in situ. Figure 2 shows the process occurring for two cycles that mirror each other. One begins with an open catalyst that is subsequently closed by purging with N₂ at 110 minutes and then reopened at approximately 240 minutes by purging with CO. A second experiment shows that one may begin with a closed catalyst and cycle in the opposite direction and achieve comparable results.

To the best of our knowledge, this data represents the only nonbiological example of an allosteric catalyst that provides control over catalytic activity and selectivity and can be addressed in a reversible fashion, in situ. In view of the growing number of reactions that are catalyzed in a bimetallic fashion,^[7,10] this could become a reliable and general approach to catalyst preparation and modulation.

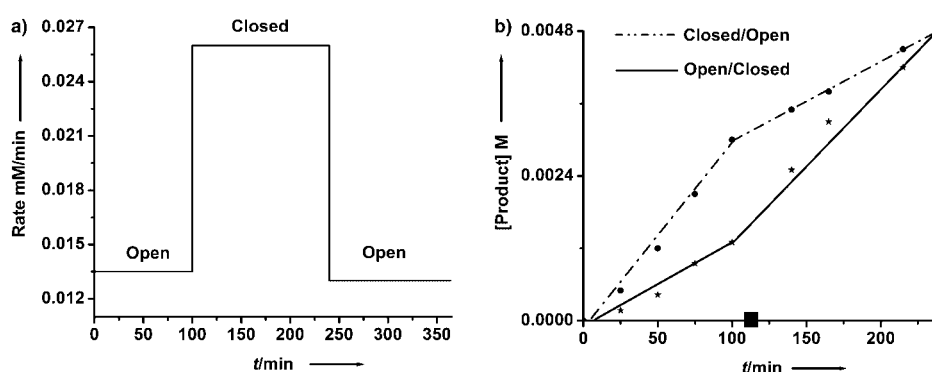


Figure 2. In situ reversibility of the catalysis. a) The catalyst being taken through an open/closed/open cycle. b) The switch point (■) indicates CO saturation or CO desaturation (N₂ purge) points at which the catalyst is opened (complex **5** from complex **3**) or closed (complex **3** from complex **5**) respectively. Reaction conditions: Cyclohexene oxide (6.1 mmol), TMSN₃ (2.3 mmol), 3.6 mM catalyst in benzonitrile at room temperature (see Supporting Information for details).

Keywords: asymmetric catalysis · coordination chemistry · ligand design · ligand effect · supramolecular chemistry

- [1] L. Stryer, *Biochemistry*, 4th ed., W. H. Freeman and Company, New York, **1995**.
- [2] a) I. O. Fritsky, R. Ott, R. Kramer, *Angew. Chem.* **2000**, *112*, 3403–3406; *Angew. Chem. Int. Ed.* **2000**, *39*, 3255–3258; b) I. O. Fritsky, R. Ott, H. Pritzkow, R. Kramer, *Chem. Eur. J.* **2001**, *7*, 1221–1231; c) A. Scarso, S. U. Scheffer, M. Gobel, Q. B. Broxterman, B. Kaptein, F. Formaggio, C. Toniolo, P. Scrimin, *Proc. Natl. Acad. Sci. USA* **2002**, *99*, 5144–5149; d) T. Tozawa, S. Tokita, Kubo, Y., *Tetrahedron Lett.* **2002**, *43*, 3455–3457; e) S. Takebayashi, M. Ikeda, M. Takeuchi, Shinkai, S., *Chem. Commun.* **2004**, 420–421; f) L. Kovbasyuk, H. Pritzkow, R. Kramer, I. O. Fritsky, *Chem. Commun.* **2004**, 880–881; g) A. Saghatelian, K. M. Guckian, D. A. Thayer, M. R. Ghadiri, *J. Am. Chem. Soc.* **2003**, *125*, 344–345.
- [3] N. C. Gianneschi, P. A. Bertin, S. T. Nguyen, C. A. Mirkin, L. N. Zakharov, A. L. Rheingold, *J. Am. Chem. Soc.* **2003**, *125*, 10508–10509.
- [4] For metallosupramolecular catalytic systems, see: a) M. Nakash, Z. Clyde-Watson, N. Feeder, J. E. Davies, S. J. Teat, J. K. M. Sanders, *J. Am. Chem. Soc.* **2000**, *122*, 5286–5293; b) M. L. Merlau, M. del Pilar Mejia, S. T. Nguyen, J. T. Hupp, *Angew. Chem.* **2001**, *113*, 4369–4372; *Angew. Chem. Int. Ed.* **2001**, *40*, 4239–4242; c) S.-J. Lee, A. Hu, W. Lin, *J. Am. Chem. Soc.* **2002**, *124*, 12948–12949; d) T. Kusakawa, T. Nakai, T. Okano, M. Fujita, *Chem. Lett.* **2003**, *32*, 284–285; e) J. Hua, W. Lin, *Org. Lett.* **2004**, *6*, 861–864.
- [5] a) J. R. Farrell, C. A. Mirkin, I. A. Guzei, L. M. Liable-Sands, A. L. Rheingold, *Angew. Chem.* **1998**, *110*, 484–487; *Angew. Chem. Int. Ed.* **1998**, *37*, 465–467; b) J. R. Farrell, A. H. Eisenberg, C. A. Mirkin, I. A. Guzei, L. M. Liable-Sands, C. D. Incavito, A. L. Rheingold, C. L. Stern, *Organometallics* **1999**, *18*, 4856–4868; c) F. M. Dixon, A. H. Eisenberg, J. R. Farrell, C. A. Mirkin, L. M. Liable-Sands, A. L. Rheingold, *Inorg. Chem.* **2000**, *39*, 3432–3433; d) B. J. Holliday, C. A. Mirkin, *Angew. Chem.* **2001**, *113*, 2076–2097; *Angew. Chem. Int. Ed.* **2001**, *40*, 2022–2043; e) X. Liu, C. L. Stern, C. A. Mirkin, *Organometallics* **2002**, *21*, 1017–1019; f) M. V. Ovchinnikov, B. J. Holliday, C. A. Mirkin, L. N. Zakharov, A. L. Rheingold, *Proc. Natl. Acad. Sci. USA* **2002**, *99*, 4927–4931; g) A. H. Eisenberg, M. V. Ovchinnikov, C. A. Mirkin, *J. Am. Chem. Soc.* **2003**, *125*, 2836–2837.

Received: June 10, 2004

- [6] a) T. Muraoka, K. Kinbara, Y. Kobayashi, T. Aida, *J. Am. Chem. Soc.* **2003**, *125*, 5612–5613; b) V. W.-W. Yam, X.-X. Lu, C.-C. Ko, *Angew. Chem.* **2003**, *115*, 3507–3510; *Angew. Chem. Int. Ed.* **2003**, *42*, 3385–3388; c) A. Petitjean, R. G. Khoury, N. Kyritsakas, J.-M. Lehn, *J. Am. Chem. Soc.* **2004**, *126*, 6637–6647; d) M. S. Vollmer, T. D. Clark, C. Steinem, M. R. Ghadiri, *Angew. Chem.* **1999**, *111*, 1703–1706; *Angew. Chem. Int. Ed.* **1999**, *38*, 1598–1601.
- [7] a) K. B. Hansen, J. L. Leighton, E. N. Jacobsen, *J. Am. Chem. Soc.* **1996**, *118*, 10924–10925; b) R. G. Konsler, J. Karl, E. N. Jacobsen, *J. Am. Chem. Soc.* **1998**, *120*, 10780–10781; c) E. N. Jacobsen, *Acc. Chem. Res.* **2000**, *33*, 421–431.
- [8] a) A. R. Sanger, *J. Chem. Soc. Chem. Commun.* **1975**, 893–894; b) G. C. Dol, S. Gaemers, M. Hietikko, P. C. J. Kamer, P. W. N. M. van Leeuwen, R. J. M. Nolte, *Eur. J. Inorg. Chem.* **1998**, 1975–1985.
- [9] There is a linear relationship between product formation and time, which indicates the catalyst is intact over the time course of the reaction. However, the rate of reaction observed following N₂ purge of a solution of **5** is slightly less than that for fresh **3**. This is due to a nonquantitative conversion from **5** to **3** under the reaction conditions.
- [10] For recent examples, see: a) C. K. Williams, N. R. Brooks, M. A. Hillmyer, W. B. Tolman, *Chem. Commun.* **2002**, 2132–2133; b) J. M. Ready, E. N. Jacobsen, *Angew. Chem.* **2002**, *114*, 1432–1435; *Angew. Chem. Int. Ed.* **2002**, *41*, 1374–1377; c) W. Braune, J. Okuda, *Angew. Chem.* **2003**, *115*, 67–71; *Angew. Chem. Int. Ed.* **2003**, *42*, 64–68; d) D. R. Moore, M. Cheng, E. B. Lobkovsky, G. W. Coates, *J. Am. Chem. Soc.* **2003**, *125*, 11911–11924.

Enantioselective Chlorination

Highly Enantioselective Direct Organocatalytic α -Chlorination of Ketones**

Mauro Marigo, Stephan Bachmann, Nis Halland, Alan Braunton, and Karl Anker Jørgensen*

The stereoselective formation of carbon–halogen bonds is an important challenge in organic synthesis that has recently received considerable attention^[1] due to the usefulness of the products as versatile synthetic intermediates.^[2] Furthermore, halides are often introduced into pharmaceutical compounds to decrease the rate of metabolic degradation without affecting the pharmacological effects.^[3] Until recently, enan-

tioselective halogenation reactions have been limited to particular systems such as 1,3-dicarbonyl compounds using Lewis acid^[4] or cinchona alkaloid catalysts.^[5] The first catalytic highly enantioselective α -chlorination and α -bromination reactions of carbonyl compounds were reported by Lectka et al. with perhaloquinone-derived halogenation reagents and a cinchona alkaloid catalyst in a tandem halogenation/esterification of acid chlorides.^[6] Very recently, these procedures were complemented by the α -chlorination of aldehydes with low-molecular-weight organocatalysts, a method reported by MacMillan et al. and us independently.^[7] This novel reaction also complements previous proline-catalyzed α -amination and α -oxidation reactions of aldehydes^[8] and ketones,^[9] and it was demonstrated that the α -chloroaldehydes could be transformed into optically active epoxides, non-proteinogenic amino acids, α -chloro ester derivatives, α -chloro alcohols and α -amino alcohols.^[7b] In this communication we present the development of the first organocatalytic asymmetric α -chlorination of ketones using *N*-chlorosuccinimide (NCS) as an inexpensive chlorine source, yielding optically active α -chloroketones in good yields and excellent enantioselectivities.

We initiated our studies of the α -chlorination reaction by screening a number of known and novel organocatalysts for the α -chlorination of cyclohexanone **1a** by NCS [Eq. (1)] and some representative results are shown in Table 1.

(*S*)-Proline (**3a**) catalyzed the formation of α -chlorocyclohexanone (**2a**) in good yields, but unfortunately **2a** was formed as a racemate (entry 1). In contrast to this result, (*S*)-prolinamide (**3b**), an excellent catalyst for the α -chlorination of aldehydes,^[7b] afforded **2a** with up to 81 % *ee*; however, the yield of **2a** was moderate (40 %, entry 2). Several other organocatalysts **3c–i** were employed for the α -chlorination reaction (entries 3–11), and it is notable that **3e**, which is an excellent catalyst for the α -chlorination of aldehydes, did not catalyze the α -chlorination of ketones (entry 5). Interestingly, the spiro derivative **3h** provided **2a** with 88 % *ee* but in low yield (17 %, entry 10).^[10] We envisioned that the sterically less demanding catalyst 4,5-diphenylimidazolidine^[11] **3i** (4,5-DPI) could improve the reaction rate, and to our delight we obtained **2a** in 65 % yield and 97 % *ee* (entry 11).

The moderate yields of α -chlorocyclohexanone (**2a**) obtained (entries 2 and 11) led us to investigate the reaction course by ¹H NMR studies of the reaction mixture. We discovered that the conversion into **2a** accounted for only approximately 60 % of the NCS consumed, as significant amounts of polychlorinated cyclohexanones were also obtained. Furthermore, it was observed that chlorination of the catalyst also occurred to some degree, another factor responsible for the moderate yields. The detection of the polychlorinated species led us to investigate the dichlorination of cyclohexanone. Therefore, we studied the chlorination reaction of racemic α -chlorocyclohexanone (*rac*-**2a**) with NCS catalyzed by 10 mol % 4,5-DPI·AcOH salt (vide infra). Interestingly, catalyst **3i**·AcOH, was found to catalyze not only the chlorination of *rac*-**2a** but also a kinetic chiral resolution of *rac*-**2a** [Eq. (2)].

2,6-Dichlorocyclohexanone **2aa** was obtained in 27 % yield and 87 % *ee* after 20 h, and for the remaining mono-

[*] M. Marigo, Dr. S. Bachmann, Dr. N. Halland, Dr. A. Braunton, Prof. Dr. K. A. Jørgensen
The Danish National Research Foundation: Center for Catalysis
Department of Chemistry, Aarhus University
8000 Aarhus C (Denmark)
Fax: (+45) 8919-6199
E-mail: kaj@chem.au.dk

[**] This work was supported by a grant from The Danish National Research Foundation and by the EU (grant HMPT-CT-2001-00317 for M.M.)



Supporting information for this article is available on the WWW under <http://www.angewandte.org> or from the author.

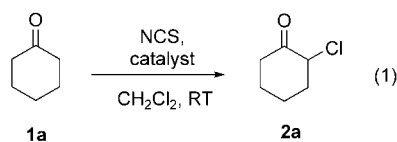
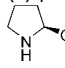
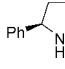
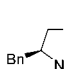
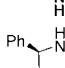
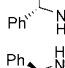
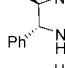
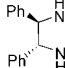
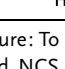
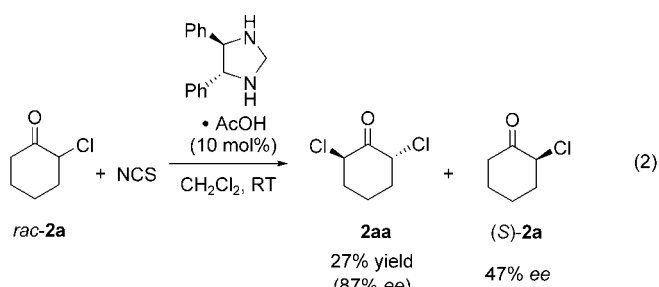


Table 1: Screening of catalysts **3** (10–20 mol %) for the enantioselective α -chlorination of cyclohexanone (**1a**).^[a]

Entry	Catalyst	<i>t</i> [h]	Yield [%] ^[b]	<i>ee</i> [%] ^[c]
1	(<i>S</i>)-proline (3a)	24	65 ^[f]	0
2 ^[d]	(<i>S</i>)-prolinamide (3b)	24	40 ^[e]	81
3	(<i>S</i>)-prolinol (3c)	24	5 ^[f]	45
4	 3d	24	20 ^[f]	20
5	 3e	24	< 5 ^[f]	–
6	 3f	0.75	12 ^[f]	23
7	 3f	72	58	0
8	 3g	0.75	10 ^[f]	62
9	 3g	72	34	39
10	 3h	22	17 ^[f]	88
11 ^[d]	 3i	20	65 ^[e]	97

[a] Procedure: To a mixture of **1a** (1.25–2.5 mmol) and catalyst in CH_2Cl_2 was added NCS (0.5 mmol), and the reaction mixture was stirred at ambient temperature for the time indicated. [b] Conversion of cyclohexanone determined by GC and based on NCS as the limiting reagent. [c] Enantiomeric excess determined by CSP-GC. [d] Reaction performed at -24°C . [e] Moderate yield due to formation of polychlorinated products (see text). [f] Moderate yield due to low conversion.



chloro compound **2a**, 47% *ee* of (*S*)-**2a** was found indicating that (*2R*)-chlorocyclohexanone is converted to (*2R,2R*)-2,6-dichlorocyclohexanone (**2aa**). The fact that (*2R*)-chlorocyclohexanone, the major enantiomer obtained in the α -chlorination of cyclohexanone catalyzed by **3i**-AcOH, is the more reactive enantiomer in the second chlorination step shows that the asymmetric induction for the first chlorination step is even better than observed. This also explains the slight decrease in optical purity observed after extended reaction times, as well as the formation of polychlorinated ketones. Similar observations were made for the tetrahydropyran-4-one (**1b**, vide infra).

We next turned our attention to the use of other ketones and discovered that, for example, tetrahydropyran-4-one (**1b**), was much less reactive than cyclohexanone (**1a**) as only a low yield of α -chlorotetrahydropyran-4-one (**2b**) was obtained [Eq. (3)] (Table 2, entry 1).

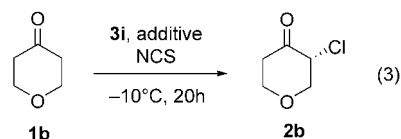


Table 2: Screening of acid additives for the α -chlorination of tetrahydropyran-4-one (**1b**).^[a]

Entry	Add.	Equiv	Solv.	1b (equiv)	NCS (equiv)	Yield [%] ^[b]	<i>ee</i> [%] ^[c]
1	–	–	CH_2Cl_2	5	1	30	90
2	PhCO_2H	0.20	CH_2Cl_2	5	1	53	84
3	PhCO_2H	0.20	MeCN	2.5	1	15	97
4	AcOH	0.10	MeCN	2.5	1	19	87
5 ^[d]	$\text{CF}_3\text{CO}_2\text{H}$	0.10	CH_2Cl_2	5	1	62	68
6	$\text{ClCH}_2\text{CO}_2\text{H}$	0.10	MeCN	2.5	1	50	91
7	2- NO_2 - PhCO_2H	0.25	MeCN	1	1.5	63	97
8 ^[e]	2- NO_2 - PhCO_2H	0.25	MeCN	1	2.0	72	98

[a] Procedure: To a mixture of **1b** (0.5–2.5 mmol), additive, and **3i** (0.05 mmol) in the indicated solvent (1 mL) at -10°C was added NCS (0.5–0.6 mmol), and the reaction mixture was stirred for 24 h. [b] Conversion of tetrahydropyran-4-one determined by GC and based on NCS as the limiting reagent. [c] *ee* determined by CSP-GC. [d] Reaction time 4 h. [e] Reaction performed at -24°C .

This result led us to develop reaction conditions for α -chlorination of less reactive ketones, and it turned out that variation of the solvent, the amount of ketone and NCS, and the addition of acids^[12] could influence the outcome of the reaction. Table 2 shows some results for the screening of various acid additives with 4,5-DPI **3i** as the catalyst for the α -chlorination of **1b**.

The use of benzoic acid in combination with 4,5-DPI **3i** increased the reaction rate, and the optically active product **2b** was obtained in 53 % yield, a significant improvement over the reaction without additive (Table 2, entries 1 and 2).^[13] Various solvents were also screened for the reaction, and it was found that the reaction in MeCN was cleaner and the formation of polychlorinated pyranones was suppressed since only minor amounts were formed as determined by GC-MS and ^1H NMR spectroscopy. Furthermore, the optical purity of the α -chloropyranone (**2b**) was better (97% *ee*) than when the reaction was conducted in CH_2Cl_2 (entries 2 and 3). The best results in terms of reactivity and asymmetric induction were obtained with 2-nitrobenzoic acid.^[14] The enhanced reactivity allowed us to use NCS in a slight excess, and **2b** was obtained in 63 % yield and 97% *ee* (entry 7). This result is particularly remarkable since the reactions of ketones catalyzed by proline derivatives are usually sluggish, and a large excess of ketone is often necessary to obtain high yields. Lowering the reaction temperature to -24°C improved the yield and enantioselectivity to 72 % and 98% *ee*, respectively (entry 8).

The general scope of the organocatalytic enantioselective α -chlorination of various cyclic and acyclic ketones is presented in Table 3. The cyclic ketones **1a–d** were converted

Table 3: Organocatalytic enantioselective α -chlorination of cyclic and acyclic ketones by NCS catalyzed by 10–20 mol % 4,5-DPI **3i**.^[a]

Entry	Ketone	T [°C]	Prod.	Yield [%] ^[b]	ee [%] ^[c]
1		–24	2a	82(54) ^[f]	97
2 ^[d]		–24	2b	72(50) ^[g]	98
3		–24	2c	83(65)	93
4		–24	2d	76(63)	93
5 ^[e]		–10	2e	62(51) ^[h]	86
6 ^[e]		–10	2f	40(35) ^[h]	89

[a] Reaction conditions: To a mixture of ketone (0.5 mmol), 4,5-DPI **3i** (0.1 mmol, 20 mol %) and 2-NO₂-PhCO₂H (0.25 mmol, 50 mol %) in MeCN at the indicated temperature was added NCS (1.0 mmol, 2.0 equiv), and the reaction mixture was stirred for 20 h. [b] Determined by ¹H NMR spectroscopy using an internal standard and confirmed by GC analysis. Yields of isolated products are shown in brackets (see the Supporting Information). [c] ee determined by CSP-GC. [d] Performed using 10 mol % 4,5-DPI **3i** and 0.25 equiv. 2-NO₂-PhCO₂H. [e] Performed using 5 equiv. of ketone. Reaction time 40 h. [f] Isolated after Baeyer–Villiger oxidation to lactone **4**. [g] Isolated after NaBH₄ reduction to the corresponding chloroalcohol **9**. [h] Isolated as the corresponding thiophenyl ketone.

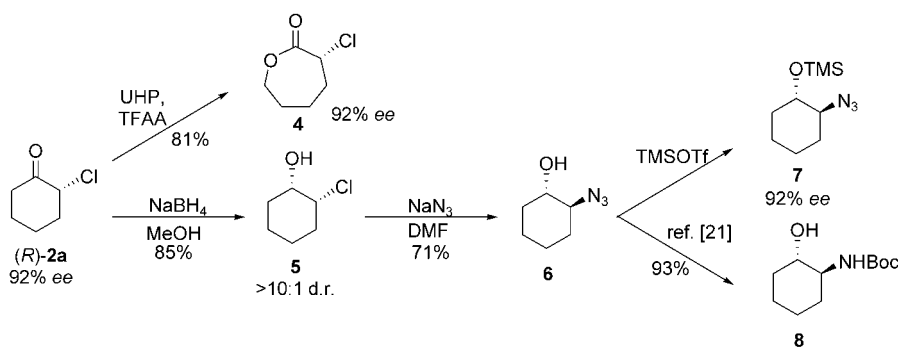
into the corresponding α -chloroketones **2a–d** with excellent enantioselectivities (90–98 % ee) and in good yields even though the ketone is not used in excess (Table 3, entries 1–4). In these reactions, full conversion of the ketone was observed together with the α -chloroketone product and a minor amount of the polychlorinated ketone as a by-product. For the acyclic ketones 3-pentanone (**1e**) and 4-heptanone (**1f**), good enantiomeric excesses of the corresponding α -chloroketones **2e,f** were also obtained; however, yields were slightly lower due to their lower reactivity, and an excess of ketone was required.^[15] Isolation of the α -chloroketone products from the polychlorinated ketones was found to be difficult on silica and, furthermore, a slight racemization was found to occur.^[16] Therefore, α -chloroketone **2a** was converted to lactone **4** by Baeyer–Villiger oxidation, and **2b** to the corresponding chloroalcohol **9** by reduction with NaBH₄. α -Chloroketones **2c,d** were purified on neutral

alumina, and **2e,f** were isolated after conversion to the corresponding thiophenyl ketone using thiophenol (see the Supporting Information). It should be noted that α -chloroketones **2c,d** racemize during flash chromatography on neutral alumina, and in order to isolate optically active products in situ reduction to the α -chloro alcohols is recommended.

An important aspect of the α -chlorination reaction of ketones is that the optically active α -chloroketones obtained provide highly versatile chiral building blocks for a variety of synthetic transformations. In Scheme 1 the transformation of (*R*)- α -chlorocyclohexanone (**2a**) into α -chloro- ϵ -lactone (**4**) and *cis*-2(*R*)-chlorocyclohexan-1(*S*)-ol (**5**) are shown. Lactone **4** was formed in 81 % yield by a regioselective Baeyer–Villiger oxidation using urea hydrogen peroxide (UHP) and trifluoroacetic anhydride (TFAA), without a decrease in optical purity. Furthermore, cyclohexanol **5** was formed in good yield and with a diastereoselectivity of >10:1 by reduction of (*R*)- α -chlorocyclohexanone **2a** using NaBH₄ in MeOH (see the Supporting Information).^[17]

The absolute configuration of the α -chloroketones was determined to be (*R*) by transformation of **5** into *trans*-2(*S*)-azidochlorocyclohexan-1(*S*)-ol (**6**) by treatment with NaN₃ in DMF, and comparison of the optical rotation with literature values (Scheme 1).^[18] After TMS protection of **6** to obtain **7**, the enantiomeric excess was determined by GC using a chiral stationary phase and it was found that the optical purity had not decreased during the transformations. Furthermore, the elution order of the enantiomers confirmed the assignment of the absolute configuration.^[19] Azide **6** can also be transformed easily into the highly useful protected amino alcohol **8** in 93 % yield by a simple hydrogenolysis/protection procedure.^[20]

In summary, we have developed the first catalytic asymmetric α -chlorination of ketones affording optically active α -chloroketones. The reaction proceeds in moderate to high yields and excellent enantioselectivities using inexpensive NCS as the chlorine source. Furthermore, we have developed a novel organocatalytic system comprising an easily available imidazolidine catalyst and a carboxylic acid and demonstrated the synthetic usefulness of the α -chloroketones formed in the catalytic reaction.



Scheme 1. Synthetic transformations of (*R*)- α -chlorocyclohexanone **2a**.

Received: April 27, 2004

Keywords: asymmetric catalysis · halogenation · homogeneous catalysis · ketones

- [1] For reviews on enantioselective halogenation reactions see, for example, a) H. Ibrahim, A. Togni, *Chem. Commun.* **2004**, 1147; b) K. Muñiz, *Angew. Chem.* **2001**, *113*, 1701; *Angew. Chem. Int. Ed.* **2001**, *40*, 1653.
- [2] a) J. March, *Advanced Organic Chemistry: Reactions, Mechanisms and Structure*, 4th ed., Wiley, New York, **1992**; b) N. De Kimpe, R. Verhé, *The Chemistry of α -Haloketones, α -Haloaldehydes, and α -Haloimines*, Wiley, New York, **1990**.
- [3] G. Thomas, *Medicinal Chemistry: An Introduction*, Wiley, New York, **2000**.
- [4] a) L. Hintermann, A. Togni, *Helv. Chim. Acta* **2000**, *83*, 2425; b) H. Ibrahim, F. Kleinbeck, A. Togni, *Helv. Chim. Acta* **2004**, *87*, 605; c) L. Hintermann, A. Togni, *Angew. Chem.* **2000**, *112*, 4530; *Angew. Chem. Int. Ed.* **2000**, *39*, 4359; d) R. Frantz, L. Hintermann, M. Perseghini, D. Broggini, A. Togni, *Org. Lett.* **2003**, *5*, 1709; e) Y. Hamashima, K. Yagi, H. Takano, L. Tamás, M. Sodeoka, *J. Am. Chem. Soc.* **2002**, *124*, 14530; f) S. Piana, I. Devillers, A. Togni, U. Rothlisberger, *Angew. Chem.* **2000**, *112*, 1021; *Angew. Chem. Int. Ed.* **2002**, *41*, 979; g) M. Marigo, N. Kumaragurubaran, K. A. Jørgensen, *Chem. Eur. J.* **2004**, *10*, 2133; h) J.-A. Ma, D. Cahard, *Tetrahedron Lett.* **2004**, *45*, 1007.
- [5] D. Y. Kim, E. J. Park, *Org. Lett.* **2002**, *4*, 545.
- [6] a) H. Wack, A. E. Taggi, A. M. Hafez, W. J. Drury III, T. Lectka, *J. Am. Chem. Soc.* **2001**, *123*, 1531; b) S. France, H. Wack, A. E. Taggi, A. M. Hafez, T. R. Wagerle, M. H. Shah, C. L. Dusich, T. Lectka, *J. Am. Chem. Soc.* **2004**, *126*, 4245.
- [7] a) M. P. Brochu, S. P. Brown, D. W. C. MacMillan, *J. Am. Chem. Soc.* **2004**, *126*, 4108; b) N. Halland, A. Braunton, S. Bachmann, M. Marigo, K. A. Jørgensen, *J. Am. Chem. Soc.* **2004**, *126*, 4790.
- [8] α -Amination of aldehydes: a) A. Bøgevig, K. Juhl, N. Kumaragurubaran, W. Zhuang, K. A. Jørgensen, *Angew. Chem.* **2002**, *114*, 1868; *Angew. Chem. Int. Ed.* **2002**, *41*, 1790; b) B. List, *J. Am. Chem. Soc.* **2002**, *124*, 5656; c) H. Vogt, S. Vanderheiden, S. Bräse, *Chem. Commun.* **2003**, 2448; α -oxidation of aldehydes: d) G. Zhong, *Angew. Chem.* **2003**, *115*, 4379; *Angew. Chem. Int. Ed.* **2003**, *42*, 4247; e) S. P. Brown, M. P. Brochu, C. J. Sinz, D. W. C. MacMillan, *J. Am. Chem. Soc.* **2003**, *125*, 10808.
- [9] α -Amination of ketones: a) N. Kumaragurubaran, K. Juhl, W. Zhuang, A. Bøgevig, K. A. Jørgensen, *J. Am. Chem. Soc.* **2002**, *124*, 6254; α -oxidation of ketones: b) A. Bøgevig, H. Sundén, A. Córdova, *Angew. Chem.* **2004**, *116*, 1129; *Angew. Chem. Int. Ed.* **2004**, *43*, 1109; c) M. Hayashi, J. Yamaguchi, T. Sumaiya, M. Shoji, *Angew. Chem.* **2004**, *116*, 1132; *Angew. Chem. Int. Ed.* **2004**, *43*, 1112.
- [10] The catalytic properties of these compounds were found during ^1H NMR investigations of the mechanism of the α -chlorination of cyclohexanone by NCS catalyzed by (1*R*,2*R*)-diphenylethylenediamine. These investigations showed that the active catalyst was the condensation product between (1*R*,2*R*)-diphenylethylenediamine and cyclohexanone (**3h**) and not (1*R*,2*R*)-diphenylethylenediamine.
- [11] For the first use of 4,5-DPI as an organocatalyst, see: a) N. Halland, R. G. Hazell, K. A. Jørgensen, *J. Org. Chem.* **2002**, *67*, 8331; For other imidazolidine-catalyzed reactions see: b) N. Halland, P. S. Aburel, K. A. Jørgensen, *Angew. Chem.* **2003**, *115*, 685; *Angew. Chem. Int. Ed.* **2003**, *42*, 661; c) N. Halland, T. Hansen, K. A. Jørgensen, *Angew. Chem.* **2003**, *115*, 4955; *Angew. Chem. Int. Ed.* **2003**, *42*, 5105; d) N. Halland, P. S. Aburel, K. A. Jørgensen, *Angew. Chem.* **2004**, *116*, 1292; *Angew. Chem. Int. Ed.* **2004**, *43*, 1272.
- [12] For a recent example of rate acceleration of amine-catalyzed reactions by the addition of acids, see: N. Mase, F. Tanaka, C. F. Barbas III, *Angew. Chem.* **2004**, *116*, 2474; *Angew. Chem. Int. Ed.* **2004**, *43*, 2420.
- [13] We believe that acid additives promote enamine formation and suppress chlorination of the catalyst.
- [14] 2-Nitrobenzoic acid (20 mol %) led to less than 1 % conversion after 18 h in the absence of 4,5-DPI **3i** in a 1:1 mixture of cyclohexanone and NCS at ambient temperature.
- [15] Less than 1 % conversion of **1e** and **1f** was observed in the absence of 2-nitrobenzoic acid.
- [16] No racemization was found to occur during filtration through a short silica plug.
- [17] In order to obtain high diastereoselectivities, dry MeOH, careful temperature control, and slow addition of NaBH₄ were required.
- [18] H. Hönl, P. Seuffer-Wasserthal, F. Füllöp, *J. Chem. Soc. Perkin Trans. 1* **1989**, 2341.
- [19] L. E. Martinez, J. L. Leighton, D. H. Carsten, E. N. Jacobsen, *J. Am. Chem. Soc.* **1995**, *117*, 5897.
- [20] T. Govindaraju, R. G. Gonnade, M. M. Bhadbhade, V. A. Kumar, K. N. Ganesh, *Org. Lett.* **2003**, *5*, 3013.

Cyclization Reactions

Diastereoselective Synthesis of Cycloheptadienol Derivatives by a Formal [5+2] Carbocyclization Reaction of $\alpha,\beta,\gamma,\delta$ -Diunsaturated (Methoxy)carbene Complexes with Methyl Ketone Lithium Enolates**

José Barluenga, Jorge Alonso, Francisco J. Fañanás, Javier Borge, and Santiago García-Granda*

Fischer-carbene complexes have become valuable building blocks in organic synthesis.^[1] In particular, they are very useful for the generation of ring systems.^[2] The design of new strategies for the selective synthesis of seven-membered carbocycles continues to be of great interest for organic chemists^[3] due to the importance of this skeleton as a part of biologically relevant compounds.^[4] The formal [4+3] cyclo-

[*] Prof. Dr. J. Barluenga, Dr. J. Alonso, Dr. F. J. Fañanás
Instituto Universitario de Química Organometálica "Enrique Moles"
Unidad Asociada al CSIC
Universidad de Oviedo
Julián Clavería 8, 33006 Oviedo (Spain)
Fax: (+34) 98-510-3450
E-mail: barluenga@uniovi.es
Dr. J. Borge,⁺ Dr. S. García-Granda⁺
Departamento de Química Física y Analítica
Universidad de Oviedo
Julián Clavería, 8, 33006, Oviedo (Spain)

[[†]] X-ray crystal structure analysis.

[**] Financial support for this work is acknowledged (BQU2001-3853 and PR-01-GE-9).



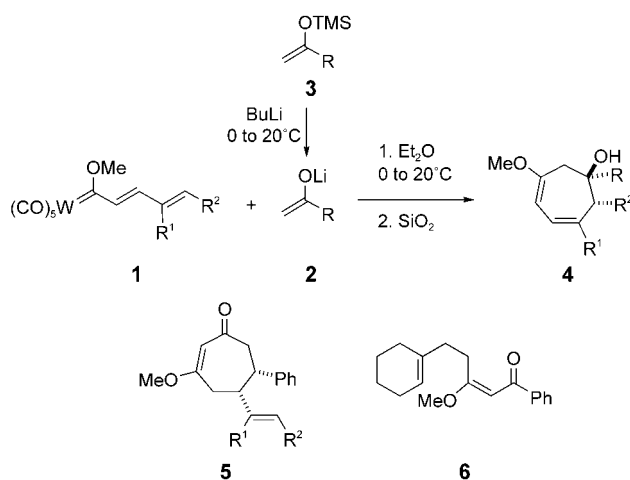
Supporting information for this article is available on the WWW under <http://www.angewandte.org> or from the author.

addition of α,β -unsaturated carbene complexes to 1,3-dienes,^[5] 1-azadienes,^[6] or 2-azadienes^[7] affords functionalized seven-membered carbo- and heterocycles. The formal [5+2] carbocyclization reactions catalyzed by transition metals are a relatively new set of reactions,^[3a,8] and only one example of a [5+2] heterocyclization reaction, in which a Fischer-type carbene complex is involved, has been reported.^[1c]

Moreover, lithium enolates add to α,β -unsaturated carbene complexes in a Michael fashion,^[9] except in the case of (methoxy)-carbene complexes and methyl ketone lithium enolates, for which a 1,2-addition is observed.^[9a,10] In this context, we have recently developed the diastereoselective synthesis of five-membered rings by novel [3+2] and [4+1] carbocyclization reactions,^[10] as well as the diastereoselective synthesis of seven-membered rings by a novel [4+3] carbocyclization reaction.^[10a]

These results prompted us to study the reaction of $\alpha,\beta,\gamma,\delta$ -diunsaturated (methoxy)carbene complexes^[11] with methyl ketone lithium enolates. Here we report a new diastereoselective route to seven-membered carbocycles under very mild conditions.

The treatment of dienylcarbene pentacarbonyl complexes **1** with methyl ketone lithium enolates **2**, generated by the reaction of silyl enol ethers **3** with butyllithium at temperatures from 0 to 20 °C, in diethyl ether at temperatures from 0 °C to room temperature led, after hydrolysis and purification by column chromatography on deactivated silica gel, to cycloheptadienol derivatives **4** in good yields and as a single diastereoisomer (Scheme 1 and Table 1). The structure and relative configuration of the stereogenic centers were unequivocally determined by X-ray diffraction carried out on compound **4a** (Figure 1).^[12,13]



Scheme 1. Synthesis of cycloheptadienol derivatives **4** from dienylcarbene complexes **1** and methyl ketone lithium enolates **2**.

Table 1: Formation of cycloheptadienol derivatives **4** from dienylmethoxycarbene complexes **1** and methyl ketone lithium enolates **2**.

Entry	Carbene	M Complex	R ¹	R ²	Enolate ^[a]	R	Product [%] ^[b]	Yield
1	1a	Cr	H	Ph	2a	Ph	4a	58
2	1b	W	H	Ph	2a	Ph	4a	86
3	1b	W	H	Ph	2b	4-MeOC ₆ H ₄	4b	77
4	1b	W	H	Ph	2c	2-Fu	4c ^[c]	82
5	1b	W	H	Ph	2e	BuC≡C	4d	76
6	1c	W	H	2-Fu	2d	PhCH ₂ CH ₂	4e ^[d]	34
7	1c	W	H	2-Fu	2a	Ph	4f ^[e]	84
8	1c	W	H	2-Fu	2f	TMSC≡C	4g	72
9	1d	W	Me	Ph	2a	Ph	4h	79
10	1c	W	H	2-Fu	2g	(E)-PhCH=CH	4i ^[f]	48
11	1e	W	Cl	Ph	2g	(E)-PhCH=CH	5b	49
12	1f	W	(CH ₂) ₄		2g	(E)-PhCH=CH	5c	51
13	1f	W	(CH ₂) ₄		2a	Ph	6	78

[a] Enolates generated by treatment of silyl enol ethers **4** with butyllithium. [b] Yield of isolated product based on starting carbene complexes **1**. [c] A 80:20 mixture of diastereoisomers **4c** and *diast-4c*, separable by column chromatography, was obtained. [d] An 88:12 mixture of diastereoisomers **4d** and *diast-4d* was obtained. [e] An 94:6 mixture of diastereoisomers **4f** and *diast-4f* was obtained. [f] Compound **5a** (R¹ = H, R² = 2-Fu, R = (E)-PhCH=CH) (44 %) was also obtained.

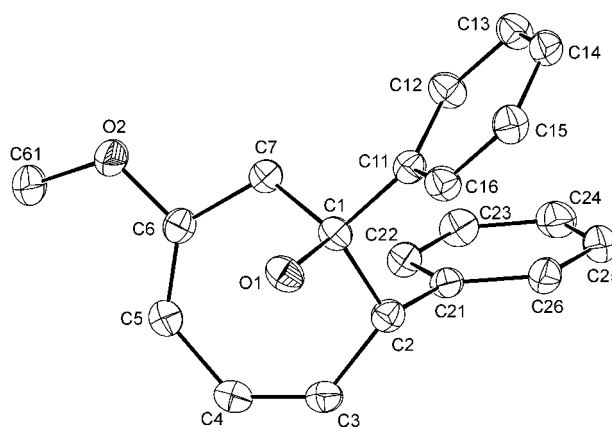
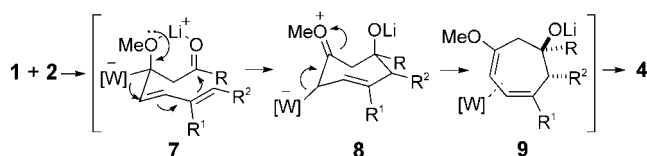


Figure 1. Structure of **4a** (ORTEP plots, 30 % probability).

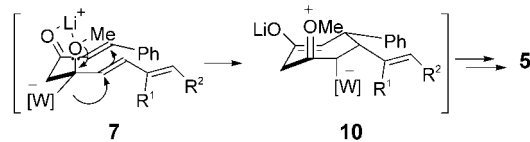
Interestingly, both chromium and tungsten complexes can be used in this reaction, although better yields are obtained for tungsten (Table 1, entries 1, 2), and thus tungsten complexes were exclusively used in further experiments. We have also observed that the presence of an oxygen atom adequately placed in the lithium enolate or in the carbene complex can produce a decrease of the diastereoselectivity of the reaction, being more important in the former case (Table 1, entries 4, 6, and 7). On the other hand, the reaction of γ,δ -substituted carbene complexes with lithium enolates is very dependent on the nature of the substituents. Thus, whereas the reaction of carbene complex **1d** with lithium enolate **2a** led to cycloheptadienol **4h** in good yield (Table 1, entry 9), the reaction of the corresponding γ -chlorocarbene complex **1e** led to an undetermined complex mixture, and the analogous reaction of a γ,δ -cyclic carbene complex **1f** afforded the ketone **6** (Scheme 1 and Table 1, entry 13). Furthermore, in the reaction of alkenyl ketone lithium enolate **2g** with carbene complexes **1** we observed two competitive reaction patterns. The reaction with carbene complex **1c** afforded a mixture of

products **4i** and **5a**, which were separable by flash column chromatography, and were derived from a formal [5+2] and [4+3]^[10a] carbocyclization process, in which the carbene complex acted as a C5 and C3 building block, respectively (Table 1, entry 10). However, the analogous reaction of γ,δ -substituted carbene complexes **1e** and **1f** afforded exclusively and diastereoselectively the [4+3] carbocyclization products **5b** and **5c**, respectively, in moderate yields (Table 1, entries 11 and 12). Finally, the solvent also plays an important role. In fact, the reaction, which works well in diethyl ether, gave rise to an undetermined complex mixture in a more coordinating solvent such as tetrahydrofuran.

In Scheme 2, a tentative mechanism to account for the formation of cycloheptadienol derivatives **4**, cycloheptenone derivatives **5**, and ketone **6** is outlined. We assume first that a



when $R = (E)\text{-CH=CHPh}$

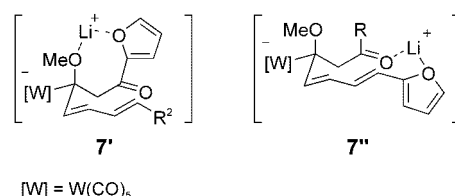


$[W] = W(CO)_5$

Scheme 2. Proposed mechanism for the formation of compounds **4** and **5**.

1,2-addition of the lithium enolates **2** to the carbene complex **1** could occur to form intermediate **7**. An intramolecular addition of the 5-position of the σ -dienyl metal group to the carbonylic carbon atom, induced by a 1,2-migration of the pentacarbonyl metal fragment,^[6,14] would lead to the cyclic intermediate **8**. Further elimination of the metal moiety followed by coordination of the metal atom to the C–C double bonds would give intermediates **9**, which after hydrolysis and metal decooordination, would furnish cycloheptadienol derivatives **4**. Accordingly, when the γ,δ positions are substituted, the cyclization is presumably disfavored, and cycloheptadienol derivatives **4** are either formed with difficulty or not at all. Moreover, in the cases of alkenyl methyl ketone lithium enolates, intermediate **7** could also competitively or exclusively evolve by intramolecular Michael addition of the 3-position of the σ -dienyl metal fragment to the ketone, giving intermediate **10**, which after hydrolysis, metal decooordination, and double-bond isomerization, would give rise to cycloheptenone derivatives **5**.^[10a] On the other hand, hydrolysis of intermediate **7** would afford ketone **6**. The preferable generation of the depicted diastereoisomer of **4**, with the R and R^2 groups in a *cis* disposition, could be explained by invoking a chairlike transition state with the same geometric disposition as **7**, presumably favored by the internal coordination of the oxygen atoms to the lithium

atom. The fact that the analogous reaction carried out in THF, a much more coordinating solvent than diethyl ether, did not give the final product **4** at all, provides support to this considered internal coordination of the lithium atom. On the other hand, the lower diastereomeric excess observed in some cases for lithium enolate **2d** and carbene complex **1c**, both bearing a 2-furyl moiety, can also be explained by considering competitive internal coordinations of the oxygen atoms from the furyl and methoxy or carbonyl groups to the lithium atom as indicated in intermediates **7'** and **7''**, respectively, which would lead to the opposite diastereoisomer (Scheme 3).



Scheme 3. Intermediates **7'** and **7''**.

In conclusion, we have described the 1,2-addition reaction of lithium enolates, derived from simple methyl ketones, to dienylmethoxycarbene complexes, which supposes a new strategy for the diastereoselective synthesis of seven-membered carbocyclic rings. As far as we know, this transformation represents the first example of a formal [5+2] carbocyclization reaction applied to Fischer-type carbene complexes, which nicely complements our previously reported formal [4+3] cyclization reaction.^[10a] Importantly, the reaction uses simple starting materials, namely methyl ketones and Fischer-type carbene complexes. Moreover, a mechanism consistent with the experimental data is proposed, in which once again the ability of the recently described 1,2-(CO)₅M migration to promote unusual umpolung cyclizations is demonstrated. Investigations to clarify the mechanism of the reaction, explore its applications in organic synthesis, and the search for a chiral version are underway in our laboratories.

Received: May 4, 2004

Keywords: carbene ligands · cyclization · cycloheptadienols · medium-ring compounds · tungsten

- [1] For recent reviews, see: a) K. H. Dötz, P. Tomuschat, *Chem. Soc. Rev.* **1999**, 28, 187–198; b) J. W. Herndon, *Tetrahedron* **2000**, 56, 1257–1280; c) A. de Meijere, H. Schirmer, M. Duetsch, *Angew. Chem.* **2000**, 112, 4124–4162; *Angew. Chem. Int. Ed.* **2000**, 39, 3964–4002; d) M. A. Sierra, *Chem. Rev.* **2000**, 100, 3591–3637; e) J. Barluenga, F. J. Fañanás, *Tetrahedron* **2000**, 56, 4597–4628; f) J. Barluenga, J. Flórez, F. J. Fañanás, *J. Organomet. Chem.* **2001**, 624, 5–17; g) J. Barluenga, *Pure Appl. Chem.* **2002**, 74, 1317–1325.
- [2] a) H. -G. Schmalz, *Angew. Chem.* **1994**, 106, 311–313; *Angew. Chem. Int. Ed. Engl.* **1994**, 33, 303–305; b) D. F. Harvey, D. M. Sigano, *Chem. Rev.* **1996**, 96, 271–288; c) H. -W. Fröhlich, *Chem. Rev.* **1997**, 97, 523–596.
- [3] a) P. A. Wender, C. O. Husfeld, E. Langkopf, J. A. Love, *J. Am. Chem. Soc.* **1998**, 120, 1940–1941, and references therein;

- b) C. M. Marson, J. McGregor, A. Khan, T. J. Grinter, *J. Org. Chem.* **1998**, 63, 7833–7839; c) I. Hanna, L. Ricard, *Org. Lett.* **2000**, 2, 2651–2654; d) I. Hanna, V. Michaut, L. Ricard, *Tetrahedron Lett.* **2001**, 42, 231–234.
- [4] For reviews and lead references on seven-membered natural products, see: a) J. H. Rigby in *Studies in Natural Products Chemistry*, Vol. 12 (Ed.: B. V. Atta-ur-Rahman), Elsevier, Amsterdam, **1993**, pp. 233–274; b) B. M. Fraga, *Nat. Prod. Rep.* **1996**, 13, 307–326; c) J. K. Cha, J. Oh, *Curr. Org. Chem.* **1998**, 2, 217–232; d) P. A. Wender, J. A. Love in *Advances in Cycloaddition*, Vol. 5 (Ed.: M. Harmata), JAI Press, Greenwich CT, **1999**, pp. 1–45; e) A. El-Wareth, A. O. Sarhan, *Curr. Org. Chem.* **2001**, 5, 827–844; f) K. Nakashima, K. Inoue, M. Sono, M. Tori, *J. Org. Chem.* **2002**, 67, 6034–6040.
- [5] a) W. D. Wulff, D. C. Yang, C. K. Murray, *J. Am. Chem. Soc.* **1988**, 110, 2653–2655; b) J. Barluenga, F. Aznar, A. Martín, S. García-Granda, M. A. Salvadó, P. Pertierra, *J. Chem. Soc. Chem. Commun.* **1993**, 319–321; c) J. Barluenga, F. Aznar, C. Valdés, A. Martín, S. García-Granda, E. Martín, *J. Am. Chem. Soc.* **1993**, 115, 4403–4404; d) D. F. Harvey, E. M. Grenzer, P. K. Gantzel, *J. Am. Chem. Soc.* **1994**, 116, 6719–6732; e) J. Barluenga, F. Aznar, A. Martín, J. T. Vázquez, *J. Am. Chem. Soc.* **1995**, 117, 9419–9426; f) J. Barluenga, F. Aznar, A. Martín, *Organometallics* **1995**, 14, 1429–1433; g) J. Barluenga, F. Aznar, M. Fernández, *Chem. Eur. J.* **1997**, 3, 1629–1637; h) M. Hoffmann, M. Buchert, H. -U. Reissig, *Chem. Eur. J.* **1999**, 5, 876–882.
- [6] a) J. Barluenga, M. Tomás, A. Ballesteros, J. Santamaría, R. J. Carbajo, F. López-Ortiz, S. García-Granda, P. Pertierra, *Chem. Eur. J.* **1996**, 2, 88–97; b) J. Barluenga, M. Tomás, E. Rubio, J. A. López-Pelegrín, S. García-Granda, P. Pertierra, *J. Am. Chem. Soc.* **1996**, 118, 695–696; c) J. Barluenga, M. Tomás, E. Rubio, J. A. López-Pelegrín, S. García-Granda, M. Pérez-Priede, *J. Am. Chem. Soc.* **1999**, 121, 3065–3071.
- [7] J. Barluenga, M. Tomás, A. Ballesteros, J. Santamaría, A. Suárez-Sobrinio, *J. Org. Chem.* **1997**, 62, 9229–9235.
- [8] For recent metal-catalyzed [5+2] reactions, see: a) B. M. Trost, F. D. Toste, H. C. Shen, *J. Am. Chem. Soc.* **2000**, 122, 2379–2380; b) P. A. Wender, A. J. Dyckman, C. O. Husfeld, M. J. C. Scanio, *Org. Lett.* **2000**, 2, 1609–1611; c) B. M. Trost, H. C. Shen, *Org. Lett.* **2000**, 2, 2523–2525; d) P. A. Wender, A. J. Dyckman, *J. Am. Chem. Soc.* **2001**, 123, 179–180; e) B. M. Trost, H. C. Shen, *Angew. Chem.* **2001**, 113, 2375–2378; *Angew. Chem. Int. Ed.* **2001**, 40, 2313–2316; f) F. López, L. Castedo, J. L. Mascareñas, *Org. Lett.* **2002**, 4, 3683–3685; g) P. A. Wender, J. A. Love, T. J. Williams, *Synlett* **2003**, 1295–1298; h) B. M. Trost, H. C. Shen, T. Schulz, C. Koradin, H. Schirok, *Org. Lett.* **2003**, 5, 4149–4151.
- [9] a) C. P. Casey, W. R. Brunsold, *Inorg. Chem.* **1977**, 16, 391–396; b) S. Aoki, T. Fujimura, E. Nakamura, *J. Am. Chem. Soc.* **1992**, 114, 2985–2990; c) E. Nakamura, K. Tanoka, T. Fujimura, S. Aoki, P. G. Williard, *J. Am. Chem. Soc.* **1993**, 115, 9015–9020; d) J. Barluenga, J. M. Montserrat, J. Flórez, *Angew. Chem.* **1994**, 106, 1451–1453; *Angew. Chem. Int. Ed. Engl.* **1994**, 33, 1392–1394; e) J. Barluenga, J. M. Montserrat, J. Flórez, S. García-Granda, E. Martín, *Chem. Eur. J.* **1995**, 1, 236–242; f) W. D. Wulff, *Organometallics* **1998**, 17, 3116–3134; g) J. Ezquerro, C. Pedregal, I. Merino, J. Flórez, J. Barluenga, S. García-Granda, M. A. Llorca, *J. Org. Chem.* **1999**, 64, 6554–6565; h) I. Merino, S. Laxmi Y. R. J. Flórez, J. Barluenga, J. Ezquerro, C. Pedregal, *J. Org. Chem.* **2002**, 67, 648–655.
- [10] a) J. Barluenga, J. Alonso, F. Rodríguez, F. J. Fañanás, *Angew. Chem.* **2000**, 112, 2555–2558; *Angew. Chem. Int. Ed.* **2000**, 39, 2460–2462; b) J. Barluenga, J. Alonso, F. J. Fañanás, *J. Am. Chem. Soc.* **2003**, 125, 2610–2616.
- [11] R. Aumann, *Eur. J. Org. Chem.* **2000**, 17–31.
- [12] Crystal structure data for **4a**: C₂₀H₂₀O₂, M_r = 292.36, colorless plates, crystal dimensions 0.12 × 0.12 × 0.05 mm, monoclinic, space group P2₁/c (determined from the systematic absences), $a = 5.9290(2)$, $b = 17.0610(7)$, $c = 15.0080(5)$ Å, $V = 1492.02(9)$ Å³, $\lambda = 1.5418$ Å, $Z = 4$, $\rho_{\text{calcd}} = 1.302$ Mg m⁻³, $F(000) = 624$, $\mu(\text{Cu}_{\text{K}\alpha}) = 0.649$ mm⁻¹. The crystal was held at 200(2) K with an Oxford Cryosystems Cryostream Cooler. Data collection was performed on a Nonius KappaCCD single-crystal diffractometer. A total of 44351 reflections were measured ($\theta_{\text{min}} = 3.96^\circ$, $\theta_{\text{max}} = 68.29^\circ$; $-7 \leq h \leq 7$, $0 \leq k \leq 20$, $0 \leq l \leq 18$). Multiple observations were averaged ($R_{\text{int}} = 0.078$) resulting in 2717 unique reflections, of which 1938 were observed with $I > 2\sigma(I)$. The final cycle of full-matrix least-squares refinement based on 2717 reflections and 279 parameters converged to a final value of $R1(\text{observed}) = 0.0493$, $R1(\text{all data}) = 0.0716$, $\omega R2(\text{all data}) = 0.1572$, $S = 1.092$. Final difference Fourier maps showed no peaks higher than 0.204 e Å^{-3} nor deeper than -0.262 e Å^{-3} .
- [13] CCDC-236823 contains the supplementary crystallographic data for this paper. These data can be obtained free of charge via www.ccdc.cam.ac.uk/contents/retrieving.html (or from the Cambridge Crystallographic Data Centre, 12, Union Road, Cambridge CB21EZ, UK; fax: (+44) 1223-336-033; or deposit@ccdc.cam.ac.uk).
- [14] a) N. Iwasawa, T. Ochiai, M. Maeyama, *Organometallics* **1997**, 16, 5137–5139; b) N. Iwasawa, T. Ochiai, M. Maeyama, *J. Org. Chem.* **1998**, 63, 3164–3165; c) J. Barluenga, M. Tomás, E. Rubio, J. A. López-Pelegrín, *Angew. Chem.* **1999**, 111, 1163–1165; *Angew. Chem. Int. Ed.* **1999**, 38, 1091–1093; d) J. Barluenga, M. Tomás, A. Ballesteros, J. Santamaría, C. Brillet, S. García-Granda, A. Piñera-Nicolás, J. T. Vázquez, *J. Am. Chem. Soc.* **1999**, 121, 4516–4517.

Homogeneous Catalysis

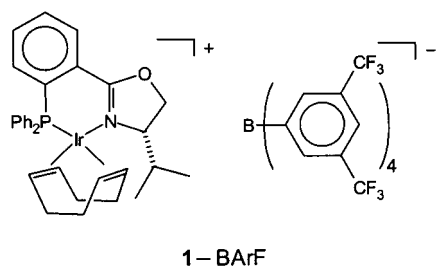
**Gas-Phase Reactions of the [(PHOX)IrL₂]⁺ Ion
Olefin-Hydrogenation Catalyst Support an
Ir^I/Ir^{III} Cycle****

*Rolf Dietiker and Peter Chen**

Since the introduction and elaboration of homogeneous catalytic hydrogenation, much work has been devoted to asymmetric hydrogenation by well-defined organometallic complexes. A particularly efficient example is the [(PHOX)-Ir(cod)]⁺ X⁻ (PHOX = chiral phosphanyloxazoline ligand,^[1] cod = 1,5-cyclooctadiene, X⁻ = weakly coordinating anion),

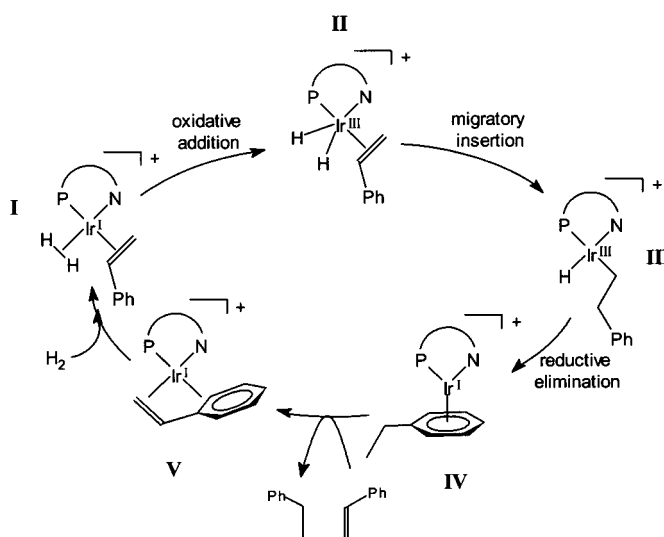
[*] R. Dietiker, Prof. Dr. P. Chen
Laboratorium für Organische Chemie
Eidgenössische Technische Hochschule (ETH)
Zürich, Switzerland
Wolfgang-Pauli-Strasse 10, 8093 Zürich (Switzerland)
Fax: (+41) 1-632-1280
E-mail: chen@org.chem.ethz.ach

[**] The work was supported by the ETH Research Commission and the Swiss National Science Foundation. The authors acknowledge a gift of 1-BArF from Prof. Dr. Andreas Pfaltz, as well as many very helpful discussions. PHOX = chiral phosphanyloxazoline ligand.



complex, for example, **1-BArF** (BArF = tetrakis-(3,5-di(trifluoromethyl)phenyl)borate), from Pfaltz and co-workers.^[2]

This class of catalysts, developed from Crabtree's achiral [Ir(phosphane)(pyridine)] complexes,^[3] shows exemplary properties in the asymmetric catalytic hydrogenation of unfunctionalized olefins under mild conditions. Turnover numbers (TON) and turnover frequencies (TOF) of > 5000 and 5000 h⁻¹ with enantiomeric excesses (*ee*) > 95 % have been reported for olefinic substrates lacking the usual secondary-binding moieties. Given this background, the paucity of mechanistic information on the catalytic cycle and reactive intermediates is surprising. Recently, a computational study of a truncated model complex by Brandt, Hedberg, and Andersson^[4] has suggested a catalytic cycle in which Ir^{III} and Ir^V intermediates play the decisive roles. We report herein an experimental investigation of the hydrogenation of styrene by the **1-BArF** by means of electrospray ionization tandem mass spectrometry which strongly suggests that, contrary to the computational study, the catalytic cycle proceeds by way of Ir^I and Ir^{III} intermediates, presumably by a "dihydride" catalytic cycle indicated in Scheme 1.^[5]



Scheme 1. Presumed catalytic cycle via the dihydride intermediate.

The modified Finnigan-MAT TSQ-700 tandem mass spectrometer has been previously described.^[6] Sample introduction from pressurized glass reactors to the electrospray source requires a short description because previous experience in hydrogenation and hydroformylation catalysts has

shown that the expected dihydrogen complexes or dihydrides rapidly lose dihydrogen once they are removed from a dihydrogen-saturated solution. In this case, the active catalytic solution was introduced directly into the electrospray source by a fused silica capillary (150 $\mu\text{m} \times 100 \text{ cm}$) dipped into the solution in a pressurized reaction. The process pressure, 6 bar H₂, suffices to pump the solution (< 10⁻⁵ M **1** and 0.17–0.26 M styrene in 5 mL CH₂Cl₂, 28 °C) directly into the spray tip with a flow rate of 20 $\mu\text{L min}^{-1}$. A final section of narrow-bore capillary (80 $\mu\text{m} \times 17 \text{ cm}$) ensures that there is no pressure drop with consequent bubble formation prior to the spray tip. Unless otherwise specified, reactions of selected ions are performed with close to zero collision energy with neutral reagents in the octopole collision cell at a nominal pressure of 2.5 mtorr. Previous work has shown that these conditions mean on the order of 10⁴ collisions of the ion with collision/reaction gas molecules within a transit time of a few milliseconds up to 100 ms.^[6]

Catalytically active solutions (confirmed by product monitoring) were prepared from **1-BArF** according to the literature procedure.^[2] Sampling of the reactor when it is pressurized with inert gas produces in the electrospray mass spectrometer a clean signal for **1**, which upon addition of the approximately 20000-fold molar excess of styrene^[7] and H₂ pressure shows three new peaks (after 15 min), whose masses correspond to the compositions [(PHOX)Ir(styrene)(H₂)₂]⁺, [(PHOX)Ir(styrene)(H₂)]⁺ (the latter being species **I–IV** in Scheme 1) and [(PHOX)Ir(styrene)]⁺ (species **V** in Scheme 1). The mass alone, especially for the first two species, does not provide an unambiguous structural assignment, but mechanistic information can nevertheless be extracted from the experiment. The same two peaks are also very sensitive to even small increases in the tube lens potential, that is, more rigorous "desolvation" conditions,^[8] which lead to loss of dihydrogen. At shorter times, that is, < 5 min, other species are visible in the mass spectrum in which the cyclooctadiene moiety is not yet completely reduced. Control experiments in which the cyclooctadiene in **1-BArF**, is replaced with 3-methyl-1,5-cyclooctadiene^[9] (to shift the mass of the diene complexes) confirm that all of the initial diene complex is reduced within the first 5 min and therefore does not contribute to the mass spectrum 15 min after initiation of the reaction. If the H₂ pressure in a reactor containing the catalyst, **1-BArF**, styrene, and H₂ is released, a sample taken immediately afterwards shows principally [(PHOX)Ir(styrene)₂]⁺, underlining the importance of the in situ sampling technique described above.

We found two gas-phase reactions that are instructive with regard to the catalytic cycle. Bearing in mind that the present apparatus (with only two stages of MS/MS) does not allow more than two consecutive reactions, that is, we cannot do controlled turnover in the gas phase, we examined the reactions of selectively prepared intermediates. [(PHOX)Ir(H₂)₂]⁺, produced by "hard" desolvation conditions applied to electrosprayed ions from a solution of **1-BArF** and H₂, was then subjected to multiple collisions with ethylbenzene, producing, among other species, an ion with the composition [(PHOX)Ir(ethylbenzene)]⁺. The ion, assumed to be species **IV**, was isolated in the gas phase by selection according to its

m/z ratio. Collision-induced dissociation (CID) of **IV** with argon leads to exceedingly facile loss of dihydrogen, producing the styrene complex **V**. If 1,3-diethylbenzene or 1,3,5-triethylbenzene are used instead of ethylbenzene, multiple dehydrogenations are observed. Because the selectively prepared gas-phase species **IV** has no opportunity to go “forward” in Scheme 1—the substrate-for-product ligand exchange is shut off, it traverses the catalytic cycle backwards until it undergoes the irreversible (in the gas-phase) step in which dihydrogen dissociates and leaves. Note that the facile production of **V** does not mean that complex **V** is the most stable species in the catalytic cycle, but merely that **V** is the product of a step that is irreversible under the experimental conditions. In the second instructive MS/MS experiment, a single isotopomer of **V** is prepared and isolated by its m/z ratio, and then treated under soft conditions (initial collision energy of $6.9 \text{ kcal mol}^{-1}$ or less in the center-of-mass frame) with D_2 gas. The sole observable products are **V**, $[\text{D}_1]\text{V}$, and $[\text{D}_2]\text{V}$ (Figure 1).

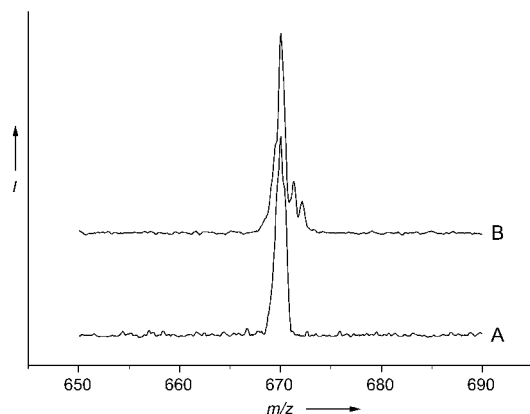


Figure 1. Daughter-ion mass spectrum generated by mass selection of one isotopomer of **V** at m/z 670 (Trace A), and treatment of the mass-selected ion with D_2 (Trace B) at a collision energy set to $6.9 \text{ kcal mol}^{-1}$ in the center-of-mass frame. Under comparable conditions, the reaction of **V** with H_2 does not form an adduct mass, but rather returns only **V** back. Mono- and dideuteration is clearly visible in the experiment with D_2 .

The absence of even an adduct mass in the gas-phase reaction of **V** with H_2 would mean either that there is no reaction at all, only coordination followed by a fast dissociation, or that none of the species **I–IV** lies in such a deep well that it would be long-lived enough to be observed before the irreversible loss of H_2 regenerated **V**. The D_2 experiment indicates unambiguously that the latter case is operative. In other words, isotopic exchange in **V** confirms the intermediacy of at least species **I–III** even if they are not directly observed in the mass spectrum.

Mere observation of a species formed *in situ* during a catalyzed reaction does not prove its participation in the catalytic cycle. It could be reservoir species, an unreactive spectator, or even a catalyst deactivation product. Moreover, the inability to observe a particular species does not show that it is absent in the catalytic cycle because those species in the

catalytic cycle with the highest rate constants for subsequent reaction will occur with the lowest concentration at steady-state. An observed species can, however, be assigned as an intermediate in the cycle with reasonable certainty if it can be shown that the species is competent in the subsequent elementary reaction steps needed for turnover. The mass spectrum of a catalytically active solution of **1**-BARF suggests that **II**, or a species of the mass of **II**, could be the resting-state species. The competence of the putative **II** to enter into the elementary reactions in Scheme 1 is supported by the two gas-phase reactions. In the absence of either H_2 or excess olefin, **IV** dehydrogenates to **V**, connecting the hydrogenation product mechanistically to the substrate olefin complex. In the other direction, production of $[\text{D}_1]\text{V}$ and $[\text{D}_2]\text{V}$ from the reaction of **V** and D_2 , shows that both dihydrogen cleavage and the insertion of the substrate olefin into the Ir–H bond are facile and reversible when turnover is blocked. The gas-phase experiments by themselves do not identify unambiguously which of the isobaric ions **I–IV** is the actual resting state in the catalytic cycle, but they do show that the overall cycle with the species **I–V** is mechanistically plausible. Auxiliary evidence, for example, ^1H NMR spectroscopy results by Drago, Pregosin, and Pfaltz,^[10] can be interpreted to suggest that a dihydride such as **II** is more stable than a dihydrogen complex such as **I**, which leads one to presume that the resting state is in fact **II**. Lastly, the experiments strongly suggest that trihydrides, for example, Ir^{V} species, play no significant role in the hydrogenation reaction. Given the computations by Brandt, Hedberg, and Andersson,^[4] the demonstrated catalytic activity by well-characterized iridium polyhydrides,^[11] as well as experimental evidence for a minor route through polyhydrides from Crabtree’s catalyst by Brown and co-workers,^[12] we have looked for the Ir^{III} hydrido dihydrogen/ Ir^{V} trihydrido complexes. ESI-MS analysis of the activated catalyst solution under H_2 pressure does show ions with the compositions $[(\text{PHOX})\text{Ir}(\text{styrene})(\text{H}_2)]^+$ and $[(\text{PHOX})\text{Ir}(\text{styrene})(\text{H}_2)_2]^+$. The former corresponds to species **I–IV** in Scheme 1. The latter possesses the mass and the composition of the Ir^{III} hydrido dihydrogen complex or the Ir^{V} trihydrido species predicted in the calculation.^[13] Although a species of that composition appears to be present in solution under active catalytic conditions, the gas-phase experiment suggests that it plays no major role in the catalytic cycle. Given that the ion isolated as **V** was treated with D_2 under conditions where it underwent approximately 10^4 collisions with D_2 in the timeframe of a few to 100 ms, we estimate a gas-phase collision frequency on the order of 10^6 s^{-1} . If one were to characterize the diffusion-controlled encounter rate of a catalyst molecule in solution with dissolved H_2 using $k_{2\text{nd order}} \approx 10^9\text{--}10^{10} \text{ L mol}^{-1} \text{ s}^{-1}$ and $[\text{H}_2]$ in the millimolar range,^[14] then one concludes that the gas-phase and solution-phase encounter rates are similar and that a species of the composition $[(\text{PHOX})\text{Ir}(\text{styrene})(\text{D}_2)_2]^+$ had the opportunity to form in the gas-phase (and subsequently dissociate again) if it were an important species in solution. If there were a favorable mechanism for hydrogenation for species of this composition, then one would expect to see trideuterated $[(\text{PHOX})\text{Ir}(\text{styrene})]^+$ products in the **V** + D_2 reaction^[15] because, given the reversibility of elementary steps in the

gas-phase reaction, even a transient Ir^{V} intermediate with three chemically equivalent deuterides (and an alkyl group with one deuterium atom) would produce at least partial incorporation of more than two deuterium atoms into the styrene substrate.^[16] Examination of Figure 1 shows that the trideuterated styrene complexes are absent. We believe that the observed mechanism differs from the computationally predicted one because the computation employed a markedly truncated substrate and complex with less steric constraints and different electronic properties in the search for the minimum-energy reaction path.

In conclusion we report gas-phase reactions of selected organometallic ions that reveal a plausible mechanism for the catalytic hydrogenation of olefins by the $[(\text{PHOX})\text{Ir}(\text{cod})]^+\text{X}^-$ family of catalysts. In contrast to the results of a computational study, the most likely mechanism is found to involve the more expected cycle with Ir^{I} and Ir^{III} species. There is no evidence for the participation of Ir^{V} complexes. In contrast to in situ spectroscopic studies which rely primarily on identification of species in solution whose role in the reaction must be subsequently ascertained by independent means, the preference for the $\text{Ir}^{\text{I}}/\text{Ir}^{\text{III}}$ cycle over the alternative $\text{Ir}^{\text{III}}/\text{Ir}^{\text{V}}$ mechanism is supported by gas-phase reactivity data which are diagnostic even if the purported intermediates are present in such low steady-state concentration so as not to be directly observable.

Received: June 3, 2004

Keywords: gas-phase reactions · homogeneous catalysis · hydrogenation · iridium · mass spectrometry

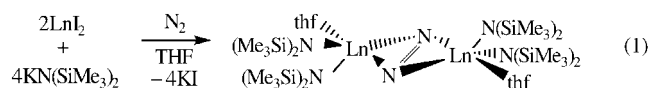
- [1] G. Helmchen, A. Pfaltz, *Acc. Chem. Res.* **2000**, *33*, 336.
- [2] A. Lightfoot, P. Schnider, A. Pfaltz, *Angew. Chem.* **1998**, *110*, 3047; *Angew. Chem. Int. Ed. Engl.* **1998**, *37*, 2897; D. G. Blackmond, A. Lightfoot, A. Pfaltz, T. Rosner, P. Schnider, N. Zimmermann, *Chirality* **2000**, *12*, 442; A. Pfaltz, J. Blankenstein, R. Hilgraf, E. Hörmann, S. McIntyre, F. Menges, M. Schönleber, S. P. Smidt, B. Wüstenberg, N. Zimmermann, *Adv. Synth. Catal.* **2003**, *345*, 33.
- [3] R. Crabtree, *Acc. Chem. Res.* **1979**, *12*, 331.
- [4] P. Brandt, C. Hedberg, P. G. Andersson, *Chem. Eur. J.* **2003**, *9*, 339.
- [5] L. D. Vázquez-Serrano, B. T. Owens, J. M. Buriak, *Chem. Commun.* **2002**, 2518; report *para*-hydrogen-induced polarization (PHIP) NMR spectroscopic evidence that the “dihydride” mechanism through $\text{Ir}^{\text{I}}/\text{Ir}^{\text{III}}$ is in fact operative for catalysts related to **1**-BARF but the experiment does not prove that an alternative mechanism is not also running in parallel.
- [6] C. Hinderling, D. A. Plattner, P. Chen, *Angew. Chem.* **1997**, *109*, 272; *Angew. Chem. Int. Ed. Engl.* **1997**, *36*, 243; C. Hinderling, D. Feichtinger, D. A. Plattner, P. Chen, *J. Am. Chem. Soc.* **1997**, *119*, 10793; D. Feichtinger, D. A. Plattner, *Angew. Chem.* **1997**, *109*, 1796; *Angew. Chem. Int. Ed. Engl. Angew. Chem. Int. Ed.* **1997**, *36*, 1718; D. Feichtinger, D. A. Plattner, P. Chen, *J. Am. Chem. Soc.* **1998**, *120*, 7125; C. Hinderling, C. Adlhart, P. Chen, *Angew. Chem.* **1998**, *110*, 2831; *Angew. Chem. Int. Ed.* **1998**, *37*, 2685; C. Hinderling, P. Chen, *Angew. Chem.* **1999**, *111*, 2393; *Angew. Chem. Int. Ed.* **1999**, *38*, 2253; Y. M. Kim, P. Chen, *Int. J. Mass Spectrom.* **1999**, *185–187*, 871; C. Adlhart, C. Hinderling, H. Baumann, P. Chen, *J. Am. Chem. Soc.* **2000**, *122*, 8204; C. Hinderling, P. Chen, *Int. J. Mass Spectrom. Ion Processes* **2000**, *195/196*, 377; Y. M. Kim, P. Chen, *Int. J. Mass Spectrom. Ion Processes* **2000**, *202*, 1; C. Hinderling, C. Adlhart, P. Chen, *Chimia* **2000**, *54*, 232; C. Adlhart, P. Chen, *Helv. Chim. Acta* **2000**, *83*, 2192; C. Adlhart, M. A. O. Volland, P. Hofmann, P. Chen, *Helv. Chim. Acta* **2000**, *83*, 3306; M. A. O. Volland, C. Adlhart, C. A. Kiener, P. Chen, P. Hofmann, *Chem. Eur. J.* **2001**, *7*, 4621; P. Chen, *Angew. Chem.* **2003**, *115*, 2938; *Angew. Chem. Int. Ed.* **2003**, *42*, 2832; C. Adlhart, P. Chen, *Helv. Chim. Acta* **2003**, *86*, 941; X. Zhang, P. Chen, *Chem. Eur. J.* **2003**, *9*, 1852; X. Chen, X. Zhang, P. Chen, *Angew. Chem.* **2003**, *115*, 3798; *Angew. Chem. Int. Ed.* **2003**, *42*, 3798; G. Gerdes, P. Chen, *Organometallics* **2003**, *22*, 2217; G. Gerdes, P. Chen, *Organometallics* **2004**, *23*, 3031; X. Zhang, X. Chen, P. Chen, *Organometallics* **2004**, *23*, 3437.
- [7] R. Crabtree, M. F. Mellea, J. M. Quirk, *J. Chem. Soc. Chem. Commun.* **1981**, 1217; report that styrene is a poor substrate for Crabtree's catalyst. Styrene behaves unremarkably with **1**-BARF.
- [8] The rigor of desolvation is controlled by the tube lens potential in the TSQ-700 mass spectrometer. There is a qualitative range from soft to hard, corresponding to tube lens potentials of 10–150 V.
- [9] 1,5-Cyclooctadiene in **1**-BARF can be readily replaced by equilibrating **1**-BARF in a large excess of by 3-methyl-1,5-cyclooctadiene and then pumping off all volatile components. The control experiment was necessary because the cyclooctadiene complex has a mass very similar to that of styrene or ethylbenzene.
- [10] D. Drago, P. S. Pregosin, A. Pfaltz, *Chem. Commun.* **2002**, 286.
- [11] R. H. Crabtree, M. Lavin, L. Bonneviot, *J. Am. Chem. Soc.* **1986**, *108*, 4032; A. S. Goldman, J. L. Halpern, *J. Am. Chem. Soc.* **1987**, *109*, 7537.
- [12] J. M. Brown, A. E. Derome, G. D. Hughes, P. K. Monaghan, *Aust. J. Chem.* **1992**, *45*, 143.
- [13] Although we have no definitive experimental evidence, we believe that this ion is actually $[(\text{PHOX})\text{Ir}(\text{ethylbenzene})(\text{H}_2)]^+$.
- [14] For example, see: E. Brunner, *Ber. Bunsen-Ges.* **1979**, *83*, 715.
- [15] Ref. [12] and D. Hou, J. Reibenspies, T. J. Colacot, K. Burgess, *Chem. Eur. J.* **2001**, *7*, 5391; M. C. Perry, Cui, M. T. Powell, X. D. Hou, J. H. Reibenspies, K. Burgess, *J. Am. Chem. Soc.* **2003**, *125*, 113; report an alternate mechanism for the incorporation of more than two deuterium atoms by the reversible formation of π -allyl intermediates. This mechanism cannot operate in the present case with styrene as the substrate because there are no allylic positions for the exchange.
- [16] A solution-phase control experiment in which styrene (0.1 mL) and **1**-BARF (0.1 mg; S/C \approx 15000; S/C = substrate-to-catalyst ratio) are degassed ($5 \times$ freeze-pump-thaw) in CH_2Cl_2 (5 mL) and then treated at 28 °C with 6 bar D_2 was checked at 2, 5, 10, 20, 40, and 85 min by GC/MS, showed up to 50 % conversion to ethylbenzene (at 85 minutes) with no deuterium incorporation in the residual styrene at any time. The ethylbenzene product was cleanly dideuterated. This is consistent with the gas-phase results if one considers that 1) the high D_2 pressure selectively lowers the energy of those intermediates and transition states in which the elements of D_2 are included, and 2) turnover is not blocked because ligand exchange of styrene for ethylbenzene is now possible. While the solution-phase experiment alone is not completely definitive, it is consistent with the conclusion from the gas-phase studies that Ir^{V} polyhydrides play no significant role in the catalytic cycle.

Lanthanide Chemistry

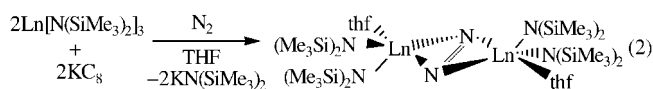
Expanding the LnZ₃/Alkali-Metal Reduction System to Organometallic and Heteroleptic Precursors: Formation of Dinitrogen Derivatives of Lanthanum**

William J. Evans,* David S. Lee, Charlie Lie, and Joseph W. Ziller

One of the recent advances in f-block-element reduction chemistry was the discovery that the simple combination of a trivalent lanthanide salt and potassium, that is, LnZ₃/K, could mimic the dinitrogen reduction reactivity of the highly reducing divalent ions Tm^{II} and Dy^{II}.^[1] Hence, the reduced dinitrogen complexes, [(Me₃Si)₂N]₂(thf)Ln₂(μ-η²:η²-N₂), originally made from divalent TmI₂ and DyI₂ in the presence of KN(SiMe₃)₂^[2] [Eq. (1)], could be obtained from KC₈ and



the trivalent lanthanide amide salts Ln^{III}[N(SiMe₃)₂]₃ known for decades [Eq. (2)].^[3]



Not only was the Ln[N(SiMe₃)₂]₃/K reduction system shown in Equation (2) successful for Ln = Tm and Dy, which have accessible divalent states in soluble molecular complexes,^[4,5] but it also provided (μ-η²:η²-N₂)²⁻ complexes of Ho, Y, and Lu.^[1] Molecular divalent chemistry has not been reported for these elements to date.^[6] Reduction of lanthanide salts by alkali metals dates back to Wöhler,^[7] but has generally been used only to make elemental metals or the common divalent lanthanides, Eu^{II}, Yb^{II}, and Sm^{II}.^[8] The other alkali-metal reductions of trivalent lanthanide ions involving dinitrogen and arene substrates have also been interpreted in terms of divalent states.^[9–14]

Herein we address the question of the generality of the LnZ₃/K/N₂ reduction system as a function of the monoanionic ligand, Z: specifically, is this reaction limited to some special feature of N(SiMe₃)₂ as the Z ligand? This ligand engages in

agostic interactions with lanthanides that could lead to special reactivity.^[15–20]

The [(C₅Me₄H)₃Ln] complexes were chosen as desirable starting materials for LnZ₃/K chemistry since, like the Ln[N(SiMe₃)₂]₃ series, they are readily available, for the entire lanthanide series, from LnCl₃ and an alkali-metal salt.^[21,22] The C₅Me₄H ligand was chosen since a variety of substituted cyclopentadienyl lanthanide dinitrogen complexes were known for Sm,^[23] Tm,^[24] and Dy.^[25]

Lanthanum was one of the metals chosen for this study since no lanthanum dinitrogen complexes had yet been discovered and this would provide a diamagnetic complex of the largest lanthanide. Along with the diamagnetic Y and Lu complexes isolated from the reaction in Equation (2),^[1] this would allow metal-size comparisons to be made with [Ln₂(μ-η²:η²-N₂)] complexes of both the largest and smallest diamagnetic ions in the lanthanide series.

[(C₅Me₄H)₃La] reacts immediately with KC₈ in THF under dinitrogen, [Eq. (3)], in a reaction similar to that in Equation (2).^[1] Since the KC₅Me₄H by-product has slight solubility in THF, the reaction solvent was removed in vacuo and the dinitrogen product extracted with toluene. The ¹H and ¹³C NMR spectra of the lanthanum product showed resonance signals typical for C₅Me₄H and THF ligands. Similar results were obtained with [(C₅Me₄H)₃Nd].

Crystal structure analysis of the Nd and La products showed that

the dinitrogen complexes [(C₅Me₄H)₂(thf)Ln₂(N₂)] (Ln = La (**1**); Nd (**2**)) had formed. Each had the Ln(μ-η²:η²-N₂) structure observed for other lanthanide complexes, Figure 1.^[23] The overall structure was similar to that of the [(Me₃Si)₂N]₂(thf)Ln₂(μ-η²:η²-N₂) complexes,^[1] except that C₅Me₄H groups had replaced N(SiMe₃)₂ ligands. Considerable disorder occurred in these structures, particularly with the position of the ring carbon atom substituted with hydrogen in the C₅Me₄H ligands. Some refinements produced models which appeared to have a C₅Me₅ ring present. However, this disorder could be successfully modeled and the absence of C₅Me₅ rings was consistent with hydrolysis reactions which gave only C₅Me₄H₂ by GCMS.

To make a C₅Me₅ analogue for comparison with **1** and **2**, reactions of [(C₅Me₅)₃Ln] complexes^[26] with KC₈ could be considered. However, the [(C₅Me₅)₃Ln] complexes react with the solvent, THF, to make [(C₅Me₅)₂Ln{O(CH₂)₄C₅Me₅}] compounds.^[26,27] To circumvent this problem, the precursor to [(C₅Me₅)₃Ln], namely [(C₅Me₅)₂Ln{(μ-Ph)₂BPh₃}]^[28] was examined as a starting material. This reaction was the first test of the use of a heteroleptic LnZ₂Z' precursor in the LnZ₃/K reduction system.

[(C₅Me₅)₂La{(μ-Ph)₂BPh₃}] reacts immediately with KC₈ in THF under dinitrogen to produce a red-orange complex, [(C₅Me₅)₂(thf)La₂(μ-η²:η²-N₂)] (**3**; Equation (4)). Isolation was accomplished as for the reaction in Equation (3) and the yield was again high, > 90%.

The ¹H NMR spectrum of [(C₅Me₅)₂(thf)La₂(N₂)] was distinct from that of [(C₅Me₄H)₂(thf)La₂(N₂)] and consistent with the presence of C₅Me₅ and THF ligands. In contrast to the C₅Me₄H complexes **1** and **2**, high quality X-ray data were obtained for the C₅Me₅ complex (Figure 1). The 1.233(5) Å

[*] Prof. W. J. Evans, D. S. Lee, C. Lie, Dr. J. W. Ziller
Department of Chemistry
University of California
Irvine, California 92697-2025 (USA)
Fax: (+1) 949-824-2210
E-mail: wevans@uci.edu

[**] We thank the National Science Foundation for support of this research.

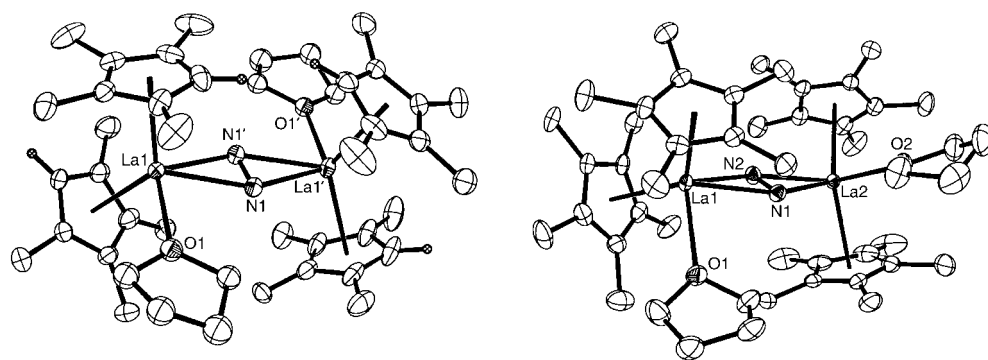
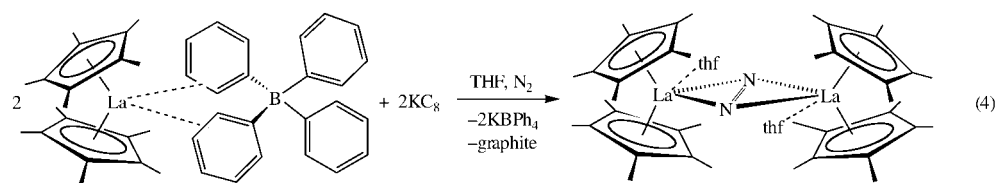
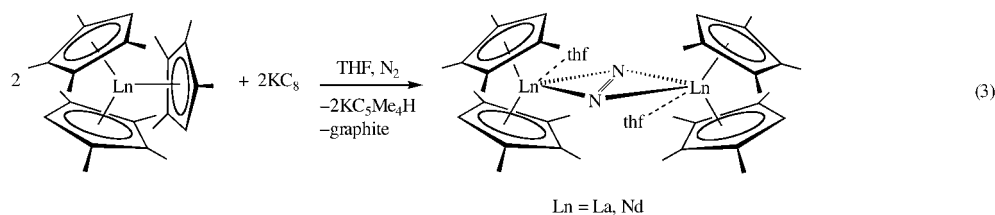


Figure 1. Ortep diagrams of **1** and **3** (thermal ellipsoids set at 50% probability).



nitrogen–nitrogen separation is consistent with the reduction of dinitrogen to $[N=N]^{2-}$.

^{15}N NMR spectroscopy was informative with diamagnetic **1** and **3** displaying resonance signals at $\delta = 495$ and 569 ppm, respectively (with respect to MeNO_2 referenced at $\delta = 0$ ppm). These chemical shifts are similar to those observed for the $[N=N]^{2-}$ ligands in the diamagnetic $[[[(\text{Me}_3\text{Si})_2\text{N}]_2(\text{thf})\text{Ln}]_2(\mu-\eta^2:\eta^2-\text{N}_2)]$ complexes, $\delta = 513$ (Ln = Y) and 557 (Ln = Lu) ppm.^[1]

In conclusion, these results provide not only the first lanthanum dinitrogen complexes, but also a high yield synthesis of $[\text{Ln}_2(\mu-\eta^2:\eta^2-\text{N}_2)]$ complexes. The yields of these reactions are the best yet obtained for $\text{LnZ}_3/\text{KC}_8/\text{N}_2$ reductions. For example, yields in the $\text{Ln}[\text{N}(\text{SiMe}_3)_2]_3/\text{KC}_8/\text{N}_2$ reactions [Eq. (2)], do not exceed 50%, a factor that has hindered the development of their chemistry. The low yields of the $[[[(\text{Me}_3\text{Si})_2\text{N}]_2(\text{thf})\text{Ln}]_2(\mu-\eta^2:\eta^2-\text{N}_2)]$ syntheses indicate that additional reaction chemistry is occurring in these systems. We suspect that this complicating chemistry arises from interactions of the soluble by-product of Equation (2), $\text{KN}(\text{SiMe}_3)_2$, with both the starting material and perhaps the initially formed dinitrogen reduction product. In the reactions in Equations (3) and (4), this problem is avoided, since neither $\text{KC}_5\text{Me}_4\text{H}$ nor KBPh_4 are very soluble in THF. Hence

in the design of future applications of the LnZ_3/KC_8 reduction reaction, formation of an insoluble KZ by-product may be useful in obtaining high yields.

More generally, these results show that the LnZ_3/K dinitrogen reduction system is successful not only with $\text{Ln}[\text{N}(\text{SiMe}_3)_2]_3$ precursors, but also with organometallic $[(\text{C}_5\text{Me}_4\text{H})_3\text{Ln}]$ complexes and with heteroleptic $[(\text{C}_5\text{Me}_5)_2\text{La}(\text{thf})_2][\text{BPh}_4]$ precursors. These reactions demonstrate that dinitrogen can be reduced to form lanthanide $[N=N]^{2-}$ complexes with a variety of ligands in coordinating solvents such as THF and that high-yield routes to diamagnetic compounds are available. The synthetic utility of this LnZ_3/K /substrate reaction should be extensive.

Experimental Section

1: In a nitrogen filled glovebox, a pale yellow solution of $[(\text{C}_5\text{Me}_4\text{H})_3\text{La}]$ (0.113 g, 0.22 mmol) in THF (10 mL) was added to a vial containing KC_8 (0.046 g, 0.34 mmol) and a stir bar. The mixture immediately became dark and was allowed to stir for 2 h. The mixture was centrifuged to remove black and white insoluble material (consistent with the formation of graphite and $\text{KC}_5\text{Me}_4\text{H}$) and evaporation of the supernatant yielded a light yellow powder. Extraction

with toluene (10 mL) and removal of solvent gave a light yellow powder (0.075 g, 72%). A concentrated toluene sample of **1** at -35°C produced pale yellow crystals over 2–3 days. ^1H NMR (500 MHz, C_6D_6): $\delta = 1.55$ (s, 2 H, THF), 1.98 (s, 6 H, Me), 2.22 (s, 6 H, Me), 4.24 (s, 2 H, THF), 5.55 ppm (s, 1 H, H); ^{13}C NMR (125.8 MHz, C_6D_6): $\delta = 12.0$ ($\text{C}_5\text{Me}_4\text{H}$), 13.3 ($\text{C}_5\text{Me}_4\text{H}$), 26.0 (THF), 71.8 (THF), 112.7 ($\text{C}_5\text{Me}_4\text{H}$), 117.5 ($\text{C}_5\text{Me}_4\text{H}$), 118.6 ppm ($\text{C}_5\text{Me}_4\text{H}$); $^{15}\text{N}\{^1\text{H}\}$ NMR (50.7 MHz, C_6D_6) referenced to MeNO_2 at 0 ppm: $\delta = 495.0$ ppm. IR (thin film from THF): $\tilde{\nu} = 2961$ s, 2922 s, 2856 s, 2721 w, 1444 m, 1378 w, 1328 w, 1262 s, 1023 s, 872 m, 799 s, 756 s, 699 w cm^{-1} ; elemental analysis (%) calcd for $\text{C}_{44}\text{H}_{68}\text{N}_2\text{O}_2\text{La}_2$: C 56.53, H 7.33, N 3.00, La 29.72; found: C 57.35, H 7.26, N 3.01, La 29.10. M.p. 120°C (decomp).

2: Complex **2** was prepared similarly to **1** from $[(\text{C}_5\text{Me}_4\text{H})_3\text{Nd}]$ (0.057 g, 0.112 mmol) and KC_8 (0.0228 g, 0.168 mmol) to give a green powder (0.050 g, 94%). ^1H NMR (500 MHz, C_6D_6): $\delta = -0.33$, 1.78, 4.74 ppm; elemental analysis (%) calcd for $\text{C}_{44}\text{H}_{68}\text{N}_2\text{O}_2\text{Nd}_2$: C 55.89, H 7.25, N 2.96, Nd 30.51; found: C 55.80, H 7.13, N 3.05, Nd 31.15.

3: An orange powder (0.119 g, 93%) was obtained similarly as for **1** and **2** from pale yellow $[(\text{C}_5\text{Me}_5)_2\text{La}(\text{thf})_2][\text{BPh}_4]$ (0.225 g, 0.26 mmol). ^1H NMR (500 MHz, C_6D_6): $\delta = 2.07$ (s, 15 H, Me), 1.47 (s, 1 H, THF), 3.92 ppm (s, 1 H, THF); ^{13}C NMR (125.8 MHz, C_6D_6): $\delta = 12.2$ (C_5Me_5), 25.8 (THF), 70.8 (THF), 117.8 ppm (C_5Me_5); $^{15}\text{N}\{^1\text{H}\}$ NMR (50.7 MHz, C_6D_6) referenced to MeNO_2 at 0 ppm: $\delta = 569.1$ ppm. IR (thin film from THF): $\tilde{\nu} = 2961$ s, 2910 s, 2856 s, 2721 s, 1567 w, 1444 m, 1378 w, 1262 s, 1069 s, 1027 s, 872 m, 799 s, 683 w, 663 w cm^{-1} ; elemental analysis (%) calcd for $\text{C}_{48}\text{H}_{76}\text{N}_2\text{O}_2\text{La}_2$: La 28.04; found: La 28.2. M.p. 120°C (decomp).

Compound **1** crystallizes in the space group $C2/c$ with $a = 15.305(3)$, $b = 14.221(2)$, $c = 25.794(4)$ Å, $\alpha = 90^\circ$, $\beta = 103.959(3)$, $\gamma = 90^\circ$, $V = 5448.4(15)$ Å³, $Z = 4$, $\rho_{\text{calcd}} = 1.364$ Mg m⁻³, $R1 = 0.0271$ [$I > 2\sigma(I)$], $wR2 = 0.0709$, $GOF = 1.043$. Compound **2** crystallizes in the space group $C2/c$ with $a = 15.286(3)$, $b = 14.085(3)$, $c = 25.744(5)$ Å, $\alpha = 90^\circ$, $\beta = 104.266(3)$, $\gamma = 90^\circ$, $V = 5371.6(19)$ Å³, $Z = 4$, $\rho_{\text{calcd}} = 1.397$ Mg m⁻³, $R1 = 0.0279$ [$I > 2\sigma(I)$], $wR2 = 0.0741$, $GOF = 1.174$. Compound **3** crystallizes in the space group $P2_1/c$ with $a = 11.086(2)$, $b = 14.627(3)$, $c = 32.882(7)$ Å, $\alpha = 90^\circ$, $\beta = 95.740(4)$, $\gamma = 90^\circ$, $V = 5305.2(18)$ Å³, $Z = 4$, $\rho_{\text{calcd}} = 1.356$ Mg m⁻³, $R1 = 0.0468$ [$I > 2\sigma(I)$], $wR2 = 0.1040$, $GOF = 1.067$. CCDC-242602 (**1**), CCDC-242600 (**2**), CCDC-242601 (**3**) contain the supplementary crystallographic data for this paper. These data can be obtained free of charge via www.ccdc.cam.ac.uk/conts/retrieving.html (or from the Cambridge Crystallographic Data Centre, 12 Union Road, Cambridge CB2 1EZ, UK; fax: (+44) 1223-336-033; or deposit@ccdc.cam.ac.uk).

Received: July 3, 2004

Keywords: alkali metals · cyclopentadienyl ligands · lanthanides · nitrogen fixation · reduction

- [1] W. J. Evans, D. S. Lee, J. W. Ziller, *J. Am. Chem. Soc.* **2004**, *126*, 454.
- [2] W. J. Evans, G. Zucchi, J. W. Ziller, *J. Am. Chem. Soc.* **2003**, *125*, 10.
- [3] D. C. Bradley, J. S. Ghotra, F. A. Hart, *J. Chem. Soc. Dalton Trans.* **1973**, 1021.
- [4] M. N. Bochkarev, I. L. Fedushkin, A. A. Fagin, T. W. Petrovskaya, J. W. Ziller, R. N. R. Broomhall-Dillard, W. J. Evans, *Angew. Chem.* **1997**, *109*, 123; *Angew. Chem. Int. Ed. Engl.* **1997**, *36*, 133.
- [5] W. J. Evans, N. T. Allen, J. W. Ziller, *J. Am. Chem. Soc.* **2000**, *122*, 11 749.
- [6] G. Meyer, M. S. Wickleder, *Handb. Phys. Chem. Rare Earths* **2000**, *28*, 53.
- [7] F. Wohler, *Poggendorfs Ann.* **1828**, *12*, 577.
- [8] G. Meyer, T. Schleid in *Synthesis of Lanthanide and Actinide Compounds* (Eds.: G. Meyer, L. R. Morss), Kluwer Academic, Dordrecht, **1991**, p. 175.
- [9] E. Campazzi, E. Solari, C. Floriani, R. Scopelliti, *Chem. Commun.* **1998**, 2603.
- [10] T. Dube, M. Ganesan, S. Conoci, S. Gambarotta, G. P. A. Yap, *Organometallics* **2000**, *19*, 3716.
- [11] M. F. Lappert, M. C. Cassani, F. Laschi, *Chem. Commun.* **1997**, 1563.
- [12] M. F. Lappert, M. C. Cassani, Y. K. Gun'ko, P. B. Hitchcock, F. Laschi, *Organometallics* **1999**, *18*, 5539.
- [13] M. F. Lappert, M. C. Cassani, Y. K. Gun'ko, P. B. Hitchcock, F. Laschi, A. G. Hulkes, A. V. Khovstov, A. V. Protchenko, *J. Organomet. Chem.* **2002**, *647*, 71.
- [14] M. F. Lappert, Y. K. Gun'ko, P. B. Hitchcock, *Organometallics* **2000**, *19*, 2832.
- [15] T. D. Tilley, A. Zalkin, R. A. Andersen, D. H. Templeton, *Inorg. Chem.* **1981**, *20*, 551.
- [16] T. D. Tilley, R. A. Andersen, A. Zalkin, *J. Am. Chem. Soc.* **1982**, *104*, 3725.
- [17] T. D. Tilley, R. A. Andersen, A. Zalkin, *Inorg. Chem.* **1984**, *23*, 2271.
- [18] J. M. Boncella, R. A. Andersen, *Organometallics* **1985**, *4*, 205.
- [19] W. J. Evans, D. K. Drummond, H. Zhang, J. L. Atwood, *Inorg. Chem.* **1988**, *27*, 575.
- [20] J. R. Hende, P. B. Hitchcock, M. F. Lappert, *J. Chem. Soc. Chem. Commun.* **1994**, 1413.
- [21] H. Schumann, M. Glanz, H. Hemling, F. E. Hahn, *Z. Anorg. Allg. Chem.* **1995**, *621*, 341.
- [22] W. J. Evans, D. S. Lee, M. A. Johnston, J. W. Ziller, unpublished results.
- [23] W. J. Evans, T. A. Ulibarri, J. W. Ziller, *J. Am. Chem. Soc.* **1988**, *110*, 6877.
- [24] W. J. Evans, N. T. Allen, J. W. Ziller, *J. Am. Chem. Soc.* **2001**, *123*, 7927.
- [25] W. J. Evans, N. T. Allen, J. W. Ziller, *Angew. Chem.* **2002**, *114*, 369; *Angew. Chem. Int. Ed.* **2002**, *41*, 359.
- [26] W. J. Evans, B. L. Davis, *Chem. Rev.* **2002**, *102*, 2119.
- [27] W. J. Evans, K. J. Forrestal, J. W. Ziller, *J. Am. Chem. Soc.* **1998**, *120*, 9273.
- [28] W. J. Evans, C. A. Seibel, J. W. Ziller, *J. Am. Chem. Soc.* **1998**, *120*, 6745.

Fluorinated Solvents

Biotransformations in Low-Boiling Hydrofluorocarbon Solvents**

Simon Saul, Stuart Corr, and Jason Micklefield*

The scope of biotransformations, particularly in the preparation of homochiral precursors, has been considerably extended through the use of enzymes in organic solvents.^[1] Some of the advantages of organic solvents include ease of recovery of products and enzymes, increased solubility and rate of transformation of more lipophilic substrates, increased lifetime of enzymes, increased chemo-, regio-, and enantioselectivity through control of solvent physical properties (solvent engineering), and control of thermodynamic equilibria in favor of synthesis rather than hydrolysis.^[1] More recently the use of enzymes in nonaqueous media has been extended to include supercritical fluids^[2] and ionic liquids^[3] with tuneable solvent properties. The use of these solvents reduces the quantities of waste volatile organic compounds (VOCs), which is an important step in the direction of “green chemistry”. One group of potential solvents for biotransfor-

[*] S. Saul, Dr. J. Micklefield
School of Chemistry
The University of Manchester
Institute of Science and Technology (UMIST)
PO Box 88, Manchester M601QD (UK)
Fax: (+44) 161-200-4484
E-mail: j.micklefield@manchester.ac.uk

Dr. S. Corr
INEOS Fluor Ltd.
PO Box 13
The Heath, Runcorn, Cheshire WA7 4QF (UK)

[**] This work is supported by INEOS Fluor Ltd.

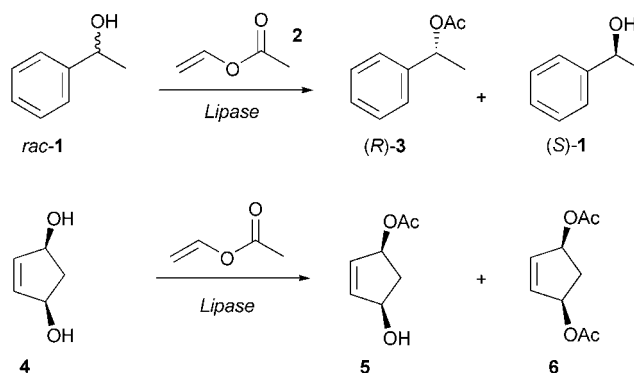


Supporting information for this article is available on the WWW under <http://www.angewandte.org> or from the author.

mations that has received little attention to date is that of pressurized liquids with normal boiling points below, and critical temperatures above, room temperature. These fluids are easily handled at moderate pressures and their relative volatility should allow ready removal of solvent residues from the products, in contrast to the situation with many ionic liquids. Such fluids can be readily compressed and reliquified in a closed system, thereby allowing the solvents to be recycled and reused with minimal losses into the environment, which is an important factor in the quest for greener chemical processes.

Here we report the first investigation of biotransformations in liquid-phase, low-boiling hydrofluorocarbon solvents (HFCs).^[4] HFCs are generally of low toxicity, do not have ozone depletion potential, and are not classed as VOCs. Many, such as 1,1,1,2-tetrafluoroethane (R-134a) and 1,1,1,2,3,3,3-heptafluoropropane (R-227ea), are also non-flammable. Several HFCs are used as replacements for the chlorofluorocarbons (CFCs) and hydrochlorofluorocarbons (HCFCs) in the refrigeration industry and are manufactured globally on a large scale to high purity. Both R-134a and R-227ea are also manufactured to current good manufacturing practice (cGMP) standards for use in metered-dose inhaler applications in the pharmaceutical industry. The HFCs thus have the potential to be environmentally benign and economically feasible alternatives to conventional organic solvents and supercritical fluids. Whilst a number of the properties of HFCs are also common to supercritical fluids,^[4] the moderate absolute pressure of liquid-phase HFCs^[5] precludes the need for expensive, specialized high-pressure reaction equipment. A further advantage of using liquid HFCs is their polarities, which are comparable to those of moderately polar organic solvents such as tetrahydrofuran (THF) and dichloromethane.^[6a] This increase in polarity over solvents such as hexane and supercritical CO₂ may improve the solubility of a range of desirable substrates and avoid the need for the use of polar cosolvents, which are difficult to remove. Despite this increased polarity, HFCs are relatively hydrophobic,^[6b] which should ensure that enzymes retain their essential active-site water molecules and activity.^[7]

Initially we chose to investigate the model lipase-catalyzed kinetic resolution of (\pm)-1-phenylethanol (*rac*-**1**, Scheme 1) in anhydrous^[8] R-134a, R-227ea, and difluoromethane (R-32). It is widely accepted that transesterification reactions catalyzed by lipases are most efficient in apolar hydrophobic solvents because more polar solvents can strip the enzymes of their essential water.^[7] We therefore chose to compare the resolution of **1** in HFCs with the reaction carried out under identical conditions in anhydrous^[8] hexane and methyl *tert*-butyl ether (MTBE), both of which have been shown to be good solvents for this biotransformation.^[9] Accordingly, the acylation of (\pm)-1-phenylethanol (*rac*-**1**)



Scheme 1. Lipase-catalyzed kinetic resolution of racemic 1-phenylethanol (**1**) and desymmetrization of *meso*-2-cyclopentene-1,4-diol (**4**).

with vinyl acetate **2**, catalyzed by immobilized lipase B from *Candida antarctica* (Novozym 435), was carried out in the five different media and the progress of the reactions was monitored by GC. We found that plastic-coated glass aerosol bottles (10 mL), with teflon-coated aerosol valves that could be crimp sealed, were ideal for small-scale HFC-based reactions and were able to withstand the moderate pressures (up to 19 bar for R-32 at 30 °C)^[5] without any loss of solvent. The results (Table 1) clearly show that the reactions in the

Table 1: Kinetic resolution of 1-phenylethanol (**1**) catalyzed by Novozym 435.

Solvent	$t^{[a]}$ [h]	Conv. [%]	<i>ee</i> (<i>S</i>)- 1 [%]	<i>ee</i> (<i>R</i>)- 3 [%]	Initial rates ^[b] [nmol min ⁻¹ mg ⁻¹]			
					$a_w < 0.01$	$a_w \approx 0.43$	$a_w \approx 0.58$	$a_w \approx 0.75$
R-32	5	50	> 99	> 99	n.d. ^[c]	n.d.	n.d.	n.d.
R-227ea	3.5	49	96	> 99	n.d.	n.d.	n.d.	n.d.
R-134a	4	49	96	> 99	325	387	407	358
hexane	8	46	85	> 99	227	241	260	228
MTBE	35	49	96	> 99	51	64	68	60

[a] The time point when no further reaction was evident (that is, the rate of the reaction was approaching zero). [b] Initial rates are given in units of nmol of product **3** per minute per mg of enzyme and were determined from the slope of the time-course measurements between 0 and 5% conversion for an approximate water activity (a_w). [c] n.d. = not determined.

HFCs are superior, both in terms of rate and degree of conversion observed. In the case of R-32, a near-perfect resolution was achieved with approximately 50% conversion after 5 h resulting in a virtually equimolar mixture of homochiral product ester (*R*)-**3** and unreacted alcohol (*S*)-**1**. Moreover this reaction was easily scaled up by using a one-liter aluminum reaction vessel (see the Supporting Information). By starting with (\pm)-1-phenylethanol (1.24 g) in R-32 (100 mL), ester (*R*)-**3** (772 mg) was isolated in 46% yield and 99% *ee*, as determined by chiral GC, along with alcohol (*S*)-**1** (595 mg) in 48% yield and 99% *ee*, after 5 h.

It is well known that the activity of enzymes in organic solvents depends on the thermodynamic water activity (a_w) of the system.^[10] The reactions described here were all carried out in anhydrous solvents^[8] where the a_w value is close to zero, thereby enabling a fair comparison between different media. However, in order to examine how the thermodynamic water

activity affects the lipase-catalyzed acylation of (\pm)-1-phenylethanol (*rac*-1) in an HFC solvent (R-134a) in comparison with the reaction in conventional organic solvents, the initial rates of the reaction were measured at different water activities.^[10b] From these measurements it can be seen (Table 1) that the initial rates follow the typical bell-shaped profile,^[10a,c] with a maximum rate attained at $a_w \approx 0.58$ in all solvents. Notably, the initial rates in R-134a are always higher than those in hexane or MTBE, irrespective of the a_w value.

The desymmetrization of prochiral or *meso*-diols by monoacylation catalyzed by various hydrolases in nonaqueous solvents can give an enantiomerically pure product in near quantitative yield. As a result, these biotransformations are now widely employed. In order to further investigate the potential of the HFCs as media for biotransformations, the model lipase-catalyzed desymmetrization of *meso*-2-cyclopentene-1,4-diol (**4**) with vinyl acetate **2** was studied. The acylated product (1*R*,4*S*)-1-hydroxy-2-cyclopentene-4-acetate (**5**) and its enantiomer are starting materials for the synthesis of various cyclopentenoid natural products, such as prostaglandins, prostacyclins, and thromboxanes.^[11] Previous investigations have found that THF with Et₃N as an additive is the solvent system of choice for this biotransformation.^[11a,b] Accordingly, the reaction of *meso*-diol **4** with vinyl acetate, catalyzed by the lipases from *Pseudomonas cepacia* and *C. antarctica* (Novozym 435), was carried out in anhydrous R-134a, R-227ea, and R-32 and compared with identical transformations in anhydrous THF with and without added Et₃N. The time courses for all reactions were followed and the results shown in Table 2 indicate the time point at which the

Table 2: Desymmetrization of *meso*-2-cyclopentene-1,4-diol (**4**) catalyzed by lipase from *P. cepacia* and Novozym 435.

Solvent	<i>P. cepacia</i> lipase			Novozym 435		
	<i>t</i> [h] ^[a]	Yield 5 [%]	<i>ee</i> 5 [%]	<i>t</i> [h] ^[a]	Yield 5 [%]	<i>ee</i> 5 [%]
R-134a	3.5	53	> 99	4	55	> 99
R-227ea	3	42	> 99	3	61	> 99
R-32	5	58	> 99	5.5	55	> 99
THF/Et ₃ N	17	43	> 99	48	42	91
THF	17	53	38	48	56	40

[a] The time point at which the maximum *ee* value of monoacetate product **5** was achieved.

maximum *ee* value was achieved for the monoacetate product **5**. With both lipases it is clear that enzyme activity is far greater in the HFCs than in THF/Et₃N or in THF alone. In the case of *P. cepacia* lipase comparable or higher yields, up to 58%, of enantiopure monoacetate **5** are achieved in around a quarter of the time. For Novozym 435 the use of HFCs similarly increases the yield of **5** with dramatically improved rates and increases the enantioselectivity from 40% *ee* in THF or 91% *ee* in THF/Et₃N to > 99% *ee* in all of the HFCs. It is also interesting to note that R-227ea gives the lowest yield of **5** (42%) with *P. cepacia* lipase but gives the highest yield of **5** (61%) with Novozym 435. Clearly HFCs, like conventional solvents, differ in their physical properties (for example, dielectric constants and dipole moments).^[6a] Thus, whilst one HFC may be the best solvent for one particular enzyme, it does not necessarily follow that it will be the best for another.

A typical time-course plot for the desymmetrization of *meso*-diol **4** with Novozym 435 in R-134a is shown in Figure 1. The desymmetrization process comprises two reactions. The

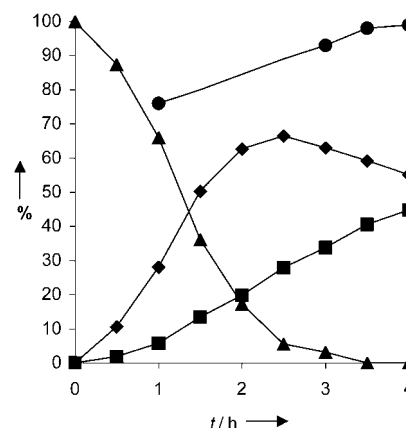
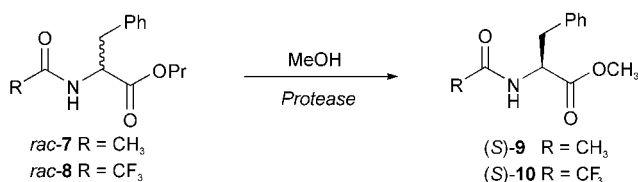


Figure 1. Time-course plot of the desymmetrization of *meso*-2-cyclopentene-1,4-diol (**4**) catalyzed by Novozym 435 in R-134a. The graph shows the percentage of *meso*-diol **4** remaining (▲), the percentage yields of **5** (◆) and **6** (■), and the *ee* value of product **5** (●) versus time.

first reaction produces the monoacylated product **5** (or its enantiomer). In the second step, which constitutes per se a kinetic resolution, the monoacetate product is subject to a second acylation that produces the diacetate **6**. As a result of this, and as is evident from the time-course plot, when all of the diol is consumed the yield of the monoacetate product **5** begins to drop while its *ee* value continues to increase due to the kinetic resolution of the second acylation step. Thus, the final yield of nearly optically pure monoacetate product **5** is dependent on the enantioselectivity of the enzyme in the first acylation step. Clearly, greater enantioselectivities in the first acylation step are achieved when the reaction is undertaken in the HFCs than when it is performed in THF/Et₃N. Furthermore, inspection of the time-course plots for all five solvent systems clearly shows that the rate of reaction with Novozym 435 is much lower in THF/Et₃N or THF alone, with a half life (*t*_{1/2}) of approximately 8–12 h, than in the HFCs (*t*_{1/2} = 1.5–2 h), with the highest rate being observed in R-227ea. With the *P. cepacia* lipase the *t*_{1/2} value for the reactions in the HFCs was 0.5–1.5 h, which can be compared with the values of 2.5 h for THF/Et₃N and 3.5 h for THF alone. The desymmetrization of *meso*-diol **4** (500 mg) by using Novozym 435 was also successfully carried out on a preparative scale in a one-liter aluminum vessel containing R-227ea (500 mL); this resulted in the isolation of product **5** (425 mg, 59%) in 99% *ee*, as determined by chiral GC, along with diacetate **6** (372 mg, 40%), after 3 h.

Finally, in order to explore the utility of the HFCs as media for other classes of enzyme-catalyzed reactions, the model transesterifications of *N*-acetyl and *N*-trifluoroacetyl phenylalanine propyl esters *rac*-7 and *rac*-8 (Scheme 2) with methanol, catalyzed by subtilisin Carlsberg protease, were investigated in anhydrous solvents.^[12] In this case, R-134a gave the highest rates and yields of enantiopure methyl esters (*S*)-9 and (*S*)-10 and was marginally better than hexane, the



Scheme 2. Transesterification of racemic N-protected phenylalanine propyl esters catalyzed by subtilisin Carlsberg.

best conventional solvent examined, but significantly better than the more polar solvents, THF and acetonitrile (Table 3). Transesterifications in R-32, on the other hand, exhibited

Table 3: Summary of results from the transesterification of N-protected phenylalanine propyl esters.

Solvent	<i>rac-7</i> ($R = \text{CH}_3$)			<i>rac-8</i> ($R = \text{CF}_3$)		
	<i>t</i> [h]	Yield 9 [%]	<i>ee</i> 9 [%]	<i>t</i> [h]	Yield 10 [%]	<i>ee</i> 10 [%]
R-134a	19	23	> 99	72	33	> 99
R-32	19	13	> 99	72 (19) ^[a]	10 (10) ^[a]	> 99
hexane	19	20	> 99	72	23	> 99
THF	19	8	> 99	72	1.3	n.d. ^[b]
CH ₃ CN	19	4	> 99	72	0	–

[a] The reaction effectively ceased after 19 h. [b] n.d. = not determined.

similar initial rates to the reactions in hexane but stopped at lower yields of (*S*)-**9** (13%) and (*S*)-**10** (10%). This is, however, still better than the results for THF and acetonitrile.

In summary, we have demonstrated the benefits and potential of HFCs as solvents for biotransformations. In the kinetic resolution of model secondary alcohol *rac-1* significant increases in rate and product yield were demonstrated in the HFC reactions compared to reactions in the lipase solvents of choice, hexane and MTBE. The desymmetrization of a model *meso*-diol **4** was also achieved with substantially increased rates, yields, and enantioselectivities in the HFCs in comparison with the results in the typical organic solvent system.^[11] It is possible that the improved rates of reaction observed are due, in part, to the low viscosity and the consequently increased solute diffusivity in the HFCs, which are mid way between those observed for a typical organic solvent on one hand and a supercritical fluid on the other.^[4] Finally, the benefits of HFCs are not limited to lipase-catalyzed reactions, as demonstrated by the improved activity of the subtilisin Carlsberg protease in R-134a. Indeed, recent findings, which will be reported in due course, demonstrate that hydroxynitrile lyases also display activity in the HFC solvents.

Experimental Section

Immobilized lipase B from *Candida antarctica* (Novozym 435) with a specific activity of 10000 U g^{−1} was purchased from Fluka. Lipase from *Pseudomonas cepacia* (92.6 U g^{−1}) and subtilisin Carlsberg protease (10.5 U g^{−1}) were purchased from the Sigma Chemical Co. In all experiments enzymes were used straight from the bottle, unless otherwise stated.

For the kinetic resolution of racemic 1-phenylethanol (**1**) in the HFCs, Novozym 435 (9.5 mg, 95 U) was added to **1** (61.0 mg, 0.50 mmol) and vinyl acetate **2** (861.0 mg, 10.0 mmol) in a plastic-coated aerosol bottle (10 mL). The aerosol was capped, crimp sealed,

and immediately charged with the HFC (5.0 mL), then the reaction mixture was stirred magnetically at room temperature. Samples (approximately 20 μL) were discharged periodically through the aerosol valve, dissolved in CH₂Cl₂ (100 μL), and analyzed by GC, or chiral GC where appropriate. Reactions in hexane and MTBE were carried out in an identical fashion except a Supelco graduated screw-top vial (7 mL) was used as the reaction vessel and samples (1 μL) were withdrawn periodically for analysis by using a Hamilton syringe. For initial rate measurements the reactions were carried out in identical fashion, except 1 mg (10 U) of Novozym 435 was used with the same substrate concentrations and total volume (5 mL). The *a_w* values of hexane or MTBE reaction mixtures with Novozym 435 were all adjusted by preequilibration with saturated salt solutions as described previously.^[10b] The *a_w* value of R-134a reaction mixtures with Novozym 435 was adjusted by mixing appropriate ratios, by weight, of anhydrous and water-saturated R-134a. The relationship between molar ratio of water and *a_w* value is not always linear so the water activities in R-134a are only approximate. The large-scale kinetic resolution of *rac-1* (1.24 g, 10.2 mmol) was carried out in a 1-L aluminum reaction vessel with Novozym 435 (190 mg, 1900 U), vinyl acetate (17.3 g, 0.201 mol), and R-32 (100 mL). After 5 h, the reaction was vented and the resulting mixture was separated by silica gel column chromatography, eluting with 10→1% diethyl ether in petroleum ether, to give ester (*R*)-**3** (772 mg, 46%; [*α*]_D = +111 (*c* = 2.0, CH₃OH); literature value:[13a] [*α*]_D = +114 (*c* = 2.0, CH₃OH)) and alcohol (*S*)-**1** (595 mg, 48%; [*α*]_D = +41 (*c* = 2.0, CH₃OH); literature value:[13a] [*α*]_D = +45 (*c* = 2.0, CH₃OH)). Both products were identical by ¹H and ¹³C NMR spectroscopy to commercial samples as well as to the characterization data in a previous report.^[13b]

The desymmetrization of *meso*-diol **4** in HFCs (5 mL) was carried out and analyzed as described above with **4** (5.0 mg, 0.05 mmol), vinyl acetate (86.1 mg, 1.00 mmol), and *P. cepacia* lipase (5.0 mg, 0.463 U) or Novozym 435 (1.0 mg, 10 U) in aerosol bottles. The reaction was also carried out in an identical fashion with and without Et₃N (10.1 mg, 0.1 mmol) in anhydrous THF (5 mL). The large-scale desymmetrization of **4** (500 mg, 4.99 mmol) was carried out in a 1-L aluminum vessel containing R-227ea (500 mL), vinyl acetate (8.61 g, 0.10 mol), and Novozym 435 (100 mg, 1000 U). After 5 h, the reaction mixture was purified by silica gel column chromatography, eluting with hexane/ethyl acetate (2:1), to give monoacetate **5** (425 mg, 59%; [*α*]_D = +65 (*c* = 1.0, CHCl₃); literature value:[11a] [*α*]_D = +66 (*c* = 1.0, CHCl₃)) and diacetate **6** (372 mg, 40%). Both products were identical by ¹H and ¹³C NMR spectroscopy to a commercial samples as well as to the characterization data in a previous report.^[11] The kinetic resolutions of *N*-acetyl and *N*-trifluoroacetyl phenylalanine propyl esters *rac-7* and *rac-8* were carried out as before in aerosol bottles containing anhydrous HFCs (4 mL) or in vials containing anhydrous conventional solvents (4 mL). Reaction mixtures contained *rac-7* (9.9 mg, 0.04 mmol) or *rac-8* (12.1 mg, 0.04 mmol), MeOH (25.6 mg, 0.80 mmol), and subtilisin Carlsberg (4.0 mg, 0.042 U).

Received: March 22, 2004

Revised: June 11, 2004

Keywords: biotransformations · desymmetrization · hydrofluorocarbons · kinetic resolution · lipases

- [1] a) A. M. Klibanov, *Nature* **2001**, *409*, 241–246; b) A. Schmidt, J. S. Dordick, B. Hauer, A. Kiener, M. Wubbolts, B. Witholt, *Nature* **2001**, *409*, 258–268; c) G. Correa, S. Riva, *Angew. Chem.* **2000**, *112*, 2312–2310; *Angew. Chem. Int. Ed.* **2000**, *39*, 2226–2254; d) S. M. Roberts, *J. Chem. Soc. Perkin Trans. 1* **2000**, 611–633; e) S. M. Roberts, *J. Chem. Soc. Perkin Trans. 1* **1999**, 121; f) C. H. Wong, *Science* **1989**, *244*, 1145–1152; g) C.-S. Chen, C. J.

- Sih, *Angew. Chem.* **1989**, *101*, 711–723; *Angew. Chem. Int. Ed. Engl.* **1989**, *28*, 695–707.
- [2] a) A. J. Mesiano, E. J. Beckman, A. J. Russell, *Chem. Rev.* **1999**, *99*, 623–633; b) T. Matsuda, T. Harada, K. Nakamura, *Chem. Commun.* **2000**, 1367–1368; c) T. Mori, M. Li, A. Kobayashi, Y. Okahata, *J. Am. Chem. Soc.* **2002**, *124*, 1188–1189.
- [3] a) M. Erbdinger, A. J. Mesiano, A. J. Russell, *Biotechnol. Prog.* **2000**, *10*, 1129–1131; b) F. Van Rantwijk, R. M. Lau, R. A. Sheldon, *Trends Biotechnol.* **2003**, *21*, 131–138; c) S. Park, R. J. Kazlauskas, *Curr. Opin. Biotechnol.* **2003**, *14*, 432–437.
- [4] S. Corr, *J. Fluorine Chem.* **2002**, *118*, 55–67.
- [5] The boiling points and absolute pressures at room temperature (20 °C) of liquid phase HFCs used in this study: 1,1,1,2-tetrafluoroethane (R-134a): 26.1 °C, 5.7 bar; difluoromethane (R-32): 51.7 °C, 14.8 bar; 1,1,1,2,3,3,3-heptafluoropropane (R-227ea): 15.6 °C, 3.9 bar.
- [6] a) Selected dielectric constants (ϵ) and dipole moments (μ [D]): R-134a: ϵ 9.5, μ 2.05; R-32: ϵ 8.2, μ 1.98; R-227ea: ϵ 4.1, μ 0.93; hexane: ϵ 1.9, μ 0.08; THF: ϵ 7.61, μ 1.63; CH₂Cl₂: ϵ 9.08, μ 1.55;^[4] b) R-134a, R-32, and R-227ea are all totally immiscible with water. The solubility of water in R-134a is around 1100 ppm by weight at 21 °C.
- [7] a) G. Kirchner, M. P. Scollar, A. M. Klibanov, *J. Am. Chem. Soc.* **1985**, *107*, 7072–7076; b) A. Zaks, A. M. Klibanov, *Proc. Natl. Acad. Sci. USA* **1985**, *82*, 3192–3196.
- [8] Anhydrous solvents were used throughout. The only water in the reaction mixture comes from the enzyme. For example, Novozym 435 contains 14 μ g of water per mg of enzyme, as determined by Karl Fischer titration (GRS2000). The majority of the water will remain tightly associated with the enzyme, so reaction mixtures have low thermodynamic water activities ($a_w < 0.1$).
- [9] a) S. H. Schöfer, N. Kaftzik, P. Wasserscheid, U. Kragl, *Chem. Commun.* **2001**, 425–426; b) M. Persson, U. T. Bornscheuer, *J. Mol. Catal. B* **2003**, *22*, 21–27.
- [10] a) P. J. Halling, *Enzyme Microb. Technol.* **1994**, *16*, 178–206; b) G. A. Hutcheon, P. J. Halling, B. D. Moore, *Methods Enzymol.* **1997**, *286*, 465–472; c) G. Bell, A. E. M. Janssen, P. J. Halling, *Enzyme Microb. Technol.* **1997**, *20*, 471–477.
- [11] a) F. Theil, H. Schick, G. Winter, G. Reck, *Tetrahedron* **1991**, *47*, 7569–7582; b) S. R. Ghorpade, R. K. Kharul, R. R. Joshi, U. R. Kalkote, T. Ravindranathan, *Tetrahedron: Asymmetry* **1999**, *10*, 891–899; c) C. R. Johnson, S. J. Bis, *Tetrahedron Lett.* **1992**, *33*, 7287–7290.
- [12] a) J. Partridge, G. A. Hutcheon, B. D. Moore, P. J. Halling, *J. Am. Chem. Soc.* **1996**, *118*, 12873–12877; b) G. A. Hutcheon, M. C. Parker, A. James, B. D. Moore, *Chem. Commun.* **1997**, 931–932; c) K. Kawashiro, H. Sugahara, S. Sugiyama, H. Hayashi, *Biotechnol. Bioeng.* **1997**, *53*, 26–31.
- [13] a) M. Bakker, A. S. Spruijt, F. van Rantwijk, R. A. Sheldon, *Tetrahedron: Asymmetry* **2000**, *11*, 1801–1808; b) Y. Kita, Y. Takebe, K. Murata, T. Naka, S. Akai, *J. Org. Chem.* **2000**, *65*, 83–88.

Methacrylate Polymerization using a Dinuclear Zirconocene Initiator: A New Approach for the Controlled Synthesis of Methacrylate Polymers**

Goran Stojcevic, Hoon Kim, Nicholas J. Taylor,
Todd B. Marder, and Scott Collins*

There has been renewed interest in the controlled polymerization of acrylates and other susceptible monomers using Group 4 metallocene initiators during the past five years. These complexes have been applied to the synthesis of polyacrylates and polymethacrylates, where control over molecular weight (M_w), comonomer sequence distribution, and polymer tacticity is possible in some cases.^[1]

Over 10 years ago we reported that a two-component initiator system comprising $[\text{Cp}_2\text{ZrMe}_2]$ ($\text{Cp} = \text{C}_5\text{H}_5$) and $[\text{Cp}_2\text{ZrMe}(\text{L})][\text{X}]$, either preformed ($\text{X} = \text{BPh}_4$, $\text{L} = \text{THF}$)^[2a] or generated in situ ($\text{X} = \text{MeB}(\text{C}_6\text{F}_5)_3$, $\text{B}(\text{C}_6\text{F}_5)_4$, $\text{L} = \text{methyl methacrylate (MMA)}$)^[2b,c] was competent for MMA polymerization. Mechanistic work revealed that propagation involved the rate-limiting, intermolecular Michael addition of zirconocene enolate **1** (formed in situ from complex **2** and $[\text{Cp}_2\text{ZrMe}_2]$) to MMA, activated by complexation to **2** (Scheme 1).^[3]

We based this mechanism on the observed polymerization kinetics using preformed neutral enolates **1** in combination with **2** (independently first order in both and zero order in $[\text{MMA}]$)^[2c,3] and on the observation that **2** or even a discrete cationic zirconium enolate complex, $[\text{Cp}_2\text{Zr}\{\text{OC}(\text{OMe})=\text{CMe}_2\}(\text{thf})][\text{BPh}_4]$ ^[3] were much less competent initiators.

It occurred to us that a covalently linked, dinuclear enolate initiator might function analogously to the two-component systems studied earlier and could represent a new strategy^[4] for the controlled polymerization of methacrylates and other susceptible monomers.

We concentrated on the use of dinuclear zirconocene complexes featuring the μ -oxo linkage as this unit is robust.^[5,6] The dinuclear ion-pair $[(\text{Cp}_2\text{Zr})_2(\mu\text{-Me})(\mu\text{-O})][\text{MeB}(\text{C}_6\text{F}_5)_3]$ ^[7]

[*] G. Stojcevic, H. Kim, Prof. S. Collins

Department of Polymer Science

University of Akron

Akron, OH 44325-3909 (USA)

Fax: (+1) 330-972-5290

E-mail: collins@uakron.edu

Dr. N. J. Taylor

Department of Chemistry

University of Waterloo, Waterloo, Ontario N2L 3G1 (Canada)

Prof. T. B. Marder

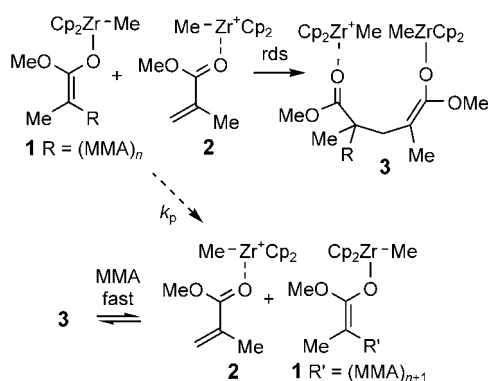
Department of Chemistry

University of Durham, Durham, DH1 3LE (UK)

[**] We would like to thank the University of Akron for financial support of this work. We also acknowledge the assistance of Mr. J. Page in conducting GPC analyses of PMMA samples and Ms. K. M. Wollyung for measuring the MALDI-TOF spectra.



Supporting information for this article is available on the WWW under <http://www.angewandte.org> or from the author.



Scheme 1. Mechanism of MMA Polymerization using **1** and **2**; rds = rate determining step.

formed in situ from $[(\text{Cp}_2\text{Zr}(\text{Me})_2)_2\text{O}]^{[6]}$ and $\text{B}(\text{C}_6\text{F}_5)_3$ was inactive in MMA polymerization, and as enolate complexes often prove to be effective initiators when the corresponding alkyls do not (e.g. ref. [1a] vs. ref. [4]), attention was thus focused on the synthesis of dinuclear bis(enolate) complexes **6**.

These complexes can be prepared from μ -oxo dichloride complex **5**^[5] and two equivalents of a lithium enolate, either preformed ($\text{R} = t\text{Bu}$) or generated in situ ($\text{R} = \text{Me}$, Scheme 2). Complexes **6** are obtained as air-sensitive solids in about 80% yield following crystallization and the molecular structure of **6b** appears in Scheme 2.^[8,9] Despite the presence of two electron-rich enolate moieties, the Zr–O–Zr bridge is approximately linear at O with $\text{Zr}(1)\text{--O}(1)\text{--Zr}(2) =$

$174.9(1)^\circ$ and with short Zr–O bonds lengths of $\text{Zr}(1)\text{--O}(1)$ 1.966(1) and $\text{Zr}(2)\text{--O}(1)$ 1.972(1) Å. These features have been attributed to partial π character to the Zr–O bonds in this class of compounds.^[5,6]

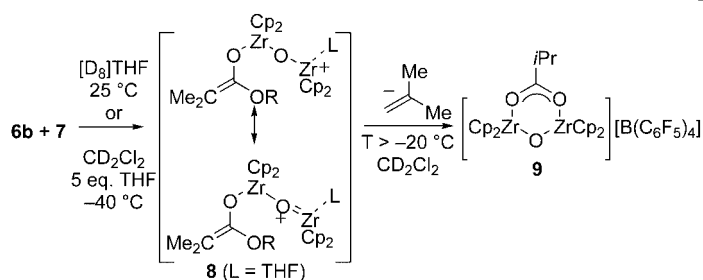
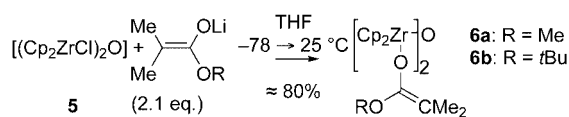
A cationic enolate complex (**8**)^[8] can be generated from bis(enolate) complex **6b** using 1.1 equivalents of $[\text{PhNHMe}_2][\text{B}(\text{C}_6\text{F}_5)_4]$ (**7**) in THF solution at 25°C (Scheme 2) but is inactive for MMA polymerization in this solvent. Attempted isolation of this compound leads to the formation of *iso*-butene and cationic carboxylate complex **9**.^[8] Complex **8** can also be generated from **6b** and **7** in the presence of approximately five equivalents of THF in CH_2Cl_2 solution and is stable at temperatures below -20°C in this solvent.

Fortunately, complex **8** is an effective initiator of MMA polymerization under these conditions. As shown in Table 1, entries 1–5, partially syndiotactic PMMA (s-PMMA) is

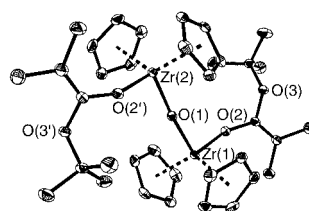
Table 1: Polymerization of MMA using zirconocene initiators (In).

Entry	In ([In] [mM])	[MMA] [M]	<i>T</i> [$^\circ\text{C}$]	<i>t</i> [min]	Conv. [%]	<i>rr</i> [%]	\bar{M}_n [K]	PDI	<i>f</i> [%] ^[a]
1 ^[b]	6b (3)	2.81	−40	30	20	83	29.8	1.03	64
2 ^[b]	6b (6)	2.81	−40	30	41	83	24.4	1.05	78
3 ^[b]	6b (3)	2.73	−20	25	75	80	79.2	1.03	88
4 ^[b]	6b (6)	2.73	−20	10	74	80	49.8	1.04	62
5 ^[b]	6b (9)	2.73	−20	10	86	80	35.0	1.05	59
6 ^[c]	6b (10)	1.06	≥ 25	< 5	99	66	22.1	1.27	39
7 ^[c]	6b (10)	1.06	0	30	100	74	24.8	1.15	35
8 ^[c]	6b (12)	1.33	−20	30	80	80	20.6	1.10	43
9 ^[c]	6b (12)	1.33	−40	60	61	83	8.57	1.10	78
10 ^[c]	6b (12)	1.33	−80	240	10	86	1.44	1.10	77
11	10 (24)	1.33	−20	30	20	–	33.2 ^[d]	≈ 1.1	2.4
12 ^[e]	10 (24)	1.33	−20	30	100	79	5.80	1.07	64 ^[f]
13 ^[e]	10 (12)	1.33	−20	30	100	77	9.29 ^[d]	≈ 1.1	71 ^[f]

[a] Initiator efficiency $f = 100(\bar{M}_n^e/\bar{M}_n)$ where $\bar{M}_n^e = ([\text{MMA}]_0/[\text{In}]_0)(\text{Conv.}/100)$. [b] Complex **8** was generated from **6b** and **7** in CH_2Cl_2 solution containing THF (5 equiv) at -40°C and then added to a solution of MMA in CH_2Cl_2 at the temperature (*T*) indicated. Reactions were quenched with MeOH at the time (*t*) indicated. [c] A solution of **6b** or **10** in toluene was added to a solution of **7** (1.1 equiv) in toluene containing MMA at the *T* indicated. [d] Bimodal MWD—only data for the major component ($> 75\%$) is reported. [e] Two equivalents of **10** were added to 1.0 equivalent of **7**. [f] Initiator efficiency calculated on the basis of three chains per mole of **7**.



Scheme 2. Synthesis and structure of bis(enolate) **6b**^[9] and its conversion to cationic enolate **8**.



formed (by a chain-end control mechanism) with a very narrow molecular weight distribution (MWD) at moderate to high conversion below -20°C . Kinetic studies, using complex **8** generated at -40°C from **6b** and **7**, at various $[\text{8}]$ and $[\text{MMA}]$ at -20°C , have revealed that propagation is zero order in MMA and first order in $[\text{8}]$ (Figure 1), consistent with the mechanism shown in Scheme 1, where rate-determining formation of an intermediate analogous to **3** is unimolecular owing to the strong μ -oxo linkage between the two zirconocene moieties. Under these conditions, MW linearly increases with $[\text{MMA}]:[\text{8}]$ ratios (with $f > 50\%$ at -40°C) and with conversion with $\text{PDI} = 1.05$, characteristics of a living polymerization.^[8] MALDI-TOF mass spectra were in agreement with chains being initi-

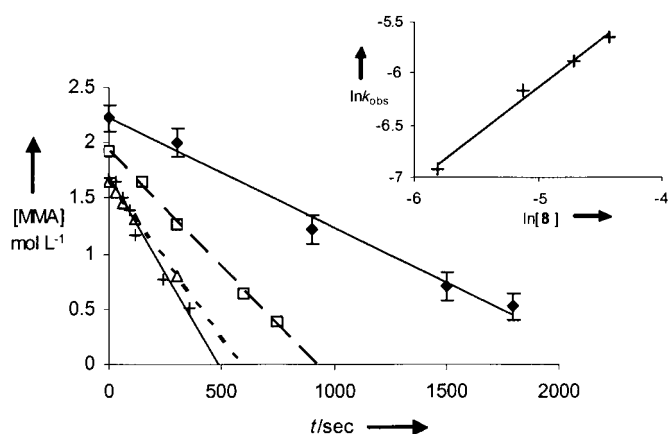


Figure 1. Plot of [MMA] versus time for polymerization initiated by $[8]_0 = 3.0$ (\blacklozenge), 6.0 (\square), 9.0 (\triangle), and 12.0 mM ($+$) at -20°C in CH_2Cl_2 . Inset: Plot of $\ln(k_{\text{obs}})$ versus $\ln[8]$ where k_{obs} is the slope of the [MMA] versus time plots—the kinetic order with respect to $[8]$ is given by the slope $= 0.91 \pm 0.10$.

ated by **8** and chain growth being quenched by MeOH during work-up.^[8]

Complex **8** can also be conveniently generated in situ from **6b** and **7** in toluene solution in the presence of monomer (Table 1, entries 6–10). As might be expected from the foregoing, initiator efficiencies increase and polymer MWD narrows at lower temperature as the thermal stability of species **8** improves.

We wished to compare the performance of this dinuclear initiator to a mononuclear, cationic zirconocene enolate, partnered with the $\text{B}(\text{C}_6\text{F}_5)_4$ counteranion, either alone or in combination with a neutral zirconocene enolate initiator. In situ formation of a cationic zircononium enolate from $[\text{Cp}_2\text{Zr}\{\text{OC}(\text{OrBu})=\text{CMe}_2\}_2]$ (**10**)^[2,3] and **7** (1.1 equiv) in toluene was much less effective for polymerization at -20°C (entry 11 vs. 8) while use of 2:1 ratio of **10:7** gave quantitative conversion to polymer (entries 12, 13).

The PMMA formed with **10:7** features a bimodal MWD with a major and minor component. As shown in Figure 2, a higher MW component predominates (low elution volume) when using a 1:1 ratio of **10:7** while only a lower MW component is evident at a 2:1 ratio and the same $[\text{Zr}]$. As the

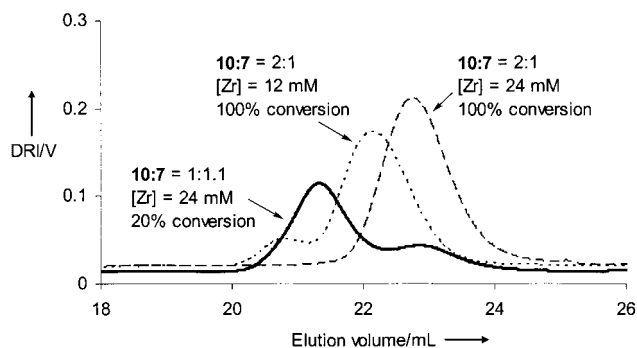


Figure 2. Differential refractive index (DRI) response [V] versus elution volume [mL] for PMMA samples prepared using mixtures of bis(enolate) **10** and activator **7**. For conditions see Table 1, entries 11–13.

initiator is diluted, more of the higher MW component is produced at a 2:1 stoichiometry. This behavior suggests independent formation of polymer by both a unimolecular process involving a cationic enolate and a competing pathway involving a neutral enolate analogous to that shown in Scheme 1.

However, at high $[\text{Zr}]$ and a 2:1 stoichiometry, the calculated initiator efficiencies exceed 100% unless it is assumed that all enolate moieties (i.e. 3.0 equivalents per equivalent of **7**) are competent for chain growth (Table 1, entries 12, 13). An explanation for this behavior is that the species involved in propagation using a 2:1 ratio of **10** to **7** is in fact dinuclear (i.e. $[\{\text{Cp}_2\text{ZrOC}(\text{OMe})=\text{CMe}(\text{MMA})_n\}_2\{\mu\text{-OC}(\text{OMe})=\text{CMe}(\text{MMA})_n\}]$) but additional work is needed in support of this hypothesis.

It can be seen from comparing entry 8 with 13 in Table 1 that the reactivity of **6b/7** is marginally lower than **10/7**. We suspect the lower reactivity of **8** reflects interaction between the two metal centers through the μ -oxo bridge (Scheme 2). On the other hand, when partnered with a weakly coordinating counterion, initiation using complex **8** is uncomplicated by the formation of PMMA through a competing pathway which would result in a bimodal MWD as with **10** and **7** (see above).

It is clear that **8** is an effective initiator of MMA polymerization. Also, the bimetallic pathway (Scheme 1) is more competitive than a unimolecular process involving a cationic enolate at least in the parent $[\text{Cp}_2\text{Zr}]$ system.^[2,3] Future work will concentrate on the application of initiators such as **8** to the polymerization of other susceptible monomers.

Received: May 25, 2004

Keywords: acrylates · homogeneous catalysis · metallocenes · polymerization · zirconium

- [1] a) H. Nguyen, A. P. Jarvis, M. J. G. Lesley, W. M. Kelly, S. S. Reddy, N. J. Taylor, S. Collins, *Macromolecules* **2000**, *33*, 1508–1510; b) P. A. Cameron, V. C. Gibson, A. J. Graham, *Macromolecules* **2000**, *33*, 4329–4335; c) H. Frauenrath, H. Keul, H. Höcker, *Macromolecules* **2001**, *34*, 14–19; d) M. Hoelscher, H. Keul, H. Höcker, *Macromolecules* **2002**, *35*, 8194–8202; e) A. D. Bolig, E. Y.-X. Chen, *J. Am. Chem. Soc.* **2001**, *123*, 7943–7944; f) J. Jin, D. R. Wilson, E. Y.-X. Chen, *Chem. Commun.* **2002**, 708–709; g) J. Jin, E. Y.-X. Chen, *Organometallics* **2002**, *21*, 13–15; h) A. D. Bolig, E. Y.-X. Chen, *J. Am. Chem. Soc.* **2002**, *124*, 5612–5613; i) J. Jin, E. Y.-X. Chen, *Macromol. Chem. Phys.* **2002**, *203*, 2329–2333; j) E. Y.-X. Chen, M. J. Cooney, *J. Am. Chem. Soc.* **2003**, *125*, 7150–7151; k) J. Jin, W. R. Mariott, E. Y.-X. Chen, *J. Polym. Sci. Part A* **2003**, *41*, 3132–3142; l) A. D. Bolig, E. Y.-X. Chen, *J. Am. Chem. Soc.* **2004**, *126*, 4897–4906; m) A. Rodriguez-Delgado, W. R. Mariott, E. Y.-X. Chen, *Macromolecules* **2004**, *37*, 3092–3100; n) J. W. Strauch, J.-L. Faure, S. Bredeau, C. Wang, G. Kehr, R. Froehlich, H. Luftmann, G. Erker, *J. Am. Chem. Soc.* **2004**, *126*, 2089–2104.
- [2] a) S. Collins, D. G. Ward, *J. Am. Chem. Soc.* **1992**, *114*, 5460–5462; b) L. F. Rhodes, B. L. Goodall, S. Collins, U.S. Patent 5,668,234, **1997**; c) For recent mechanistic work using a 2:1 ratio of $[\text{Cp}_2\text{ZrMe}_2]/\text{B}(\text{C}_6\text{F}_5)_3$, see J. Wang, H. Haubenstock, G. Odian, *Polym. Prepr. Am. Chem. Soc. Div. Polym. Chem.* **2003**, *44*, 675–

- 676; J. Wang, G. Odian, H. Haubenstock, *Polym. Prepr. Am. Chem. Soc. Div. Polym. Chem.* **2003**, *44*, 673–674.
- [3] a) Y. Li, D. G. Ward, S. S. Reddy, S. Collins, *Macromolecules* **1997**, *30*, 1875–1883; b) S. Collins, D. G. Ward, K. H. Suddaby, *Macromolecules* **1994**, *27*, 7222–7224.
- [4] For the use of $[(\text{Cp}_2\text{ZrMe})_2(\mu\text{-Me})][\text{MeB}(o\text{-C}_6\text{F}_5\text{-C}_6\text{F}_4)_3]$ $\{\text{Cp}_2 = (\text{C}_5\text{H}_5)_2, \text{Me}_2\text{Si}(\text{Ind})_2 \text{ etc.}\}$ in MMA polymerization see Y.-X. Chen, M. V. Metz, L. Li, C. L. Stern, T. J. Marks, *J. Am. Chem. Soc.* **1998**, *120*, 6287–6305. These complexes dissociate into two components in the presence of MMA or other donors.
- [5] a) A. F. Reid, J. S. Shannon, J. M. Swan, P. C. Wailes, *Aust. J. Chem.* **1965**, *18*, 173–181; b) J. F. Clarke, M. G. B. Drew, *Acta Crystallogr. Sect. B* **1974**, *30*, 2267.
- [6] W. E. Hunter, D. C. Hrnčir, V. Bynum, R. A. Penttilä, J. L. Atwood, *Organometallics* **1983**, *2*, 750–755.
- [7] A. G. Carr, D. M. Dawson, M. Bochmann, *Macromolecules* **1998**, *31*, 2035–2040.
- [8] See Supporting Information for synthesis and characterization of complexes **6**, **8**, and **9**, additional polymerization experiments, and MALDI-TOF mass spectral data.
- [9] Molecular structure of **6b** with thermal ellipsoids set at 30% probability depicted in Scheme 2. CCDC-239734 (**6b**) contains the supplementary crystallographic data for this paper. These data can be obtained free of charge via www.ccdc.cam.ac.uk/conts/retrieving.html (or from the Cambridge Crystallographic Data Centre, 12 Union Road, Cambridge CB2 1EZ, UK; fax: (+44) 1223-336-033; or deposit@ccdc.cam.ac.uk).
-

Integrating Single-Wall Carbon Nanotubes into Donor–Acceptor Nanohybrids**

Dirk M. Guldi,* G. M. A. Rahman, Norbert Jux, Nikos Tagmatarchis, and Maurizio Prato

Nanoscale carbon materials (i.e., fullerenes and carbon nanotubes) are an attractive platform for applications in optoelectronics and photovoltaics.^[1] The presence of extended, delocalized π -electron systems makes these carbon materials very useful for managing charge transfer and charge transport, when combined, for example, with photoexcited electron donors, such as metalloporphyrins.^[2,3] This arrangement might lead to novel, highly efficient photoelectrochemical cells for applications such as photochemical water splitting and the reduction of CO₂ to fuels. Despite the interesting properties that single-wall carbon nanotubes (SWNTs) display, there are numerous obstacles in the way of solubilizing SWNTs and integrating SWNTs into fully functional donor–acceptor constructs. Controlled modification of their surface with functional groups, such as chromophores,^[4] electron donors,^[5] biomolecules,^[6] is required to realize their potential in nanotechnology.

In nature, the complex superstructure that is found for many functional architectures is the unique result of self-assembling and self-organizing smaller building blocks.^[7] To succeed in fabricating functional systems from simple molecular units the constituent components must be programmed to self-organize into hierarchical structures.

Herein, the systematic immobilization of the octasodium salt of 5,15-bis-[2',6'-bis{2'',2''-bis(carboxy)ethyl}methyl-4'-*tert*-butylphenyl]-10,20-bis(4'-*tert*-butylphenyl)porphyrin (H₂P⁸⁻)^[8] and the related zinc complex (ZnP⁸⁻)^[8]—as oligo-

[*] Prof. D. M. Guldi

Universität Erlangen
Institute for Physical and Theoretical Chemistry
91058 Erlangen (Germany)
Fax: (+49) 9131-852-8307
E-mail: dirk.guldi@chemie.uni-erlangen.de

Dr. G. M. A. Rahman
University of Notre Dame, Radiation Laboratory
Notre Dame, IN 46556 (USA)
Fax: (+1) 574-631-8068

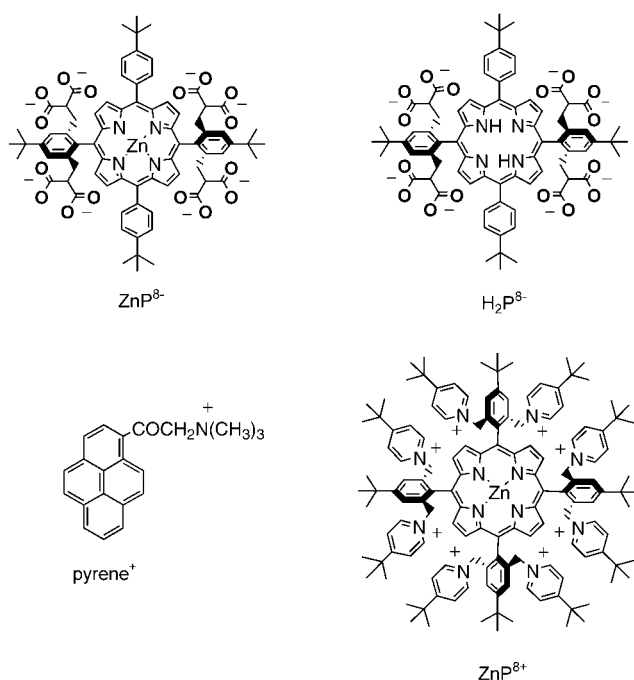
Dr. N. Jux
Universität Erlangen, Institute for Organic Chemistry
91058 Erlangen (Germany)

Dr. N. Tagmatarchis, Prof. M. Prato
Dipartimento di Scienze Farmaceutiche
Università di Trieste
Piazzale Europa 1, Trieste 34127 (Italy)

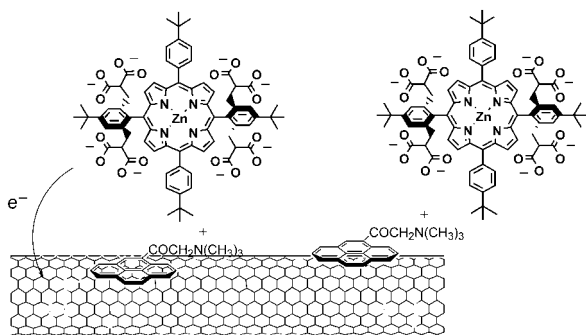
[**] This work was carried out with partial support from the EU (RTN network "WONDERFULL"), MIUR (PRIN 2002, prot. 2002032171), SFB 583, and the Office of Basic Energy Sciences of the U.S. Department of Energy. This is document NDRL-4551 from the Notre Dame Radiation Laboratory.



Supporting information for this article is available on the WWW under <http://www.angewandte.org> or from the author.



anionic chromophores/electron donors—onto electron-accepting SWNTs is investigated. In particular, van der Waals and electrostatic interactions have been used to favor intermolecular recognition between the SWNT/1-(trimethylammonium acetyl) pyrene (pyrene⁺), and H₂P⁸⁻ or ZnP⁸⁻ units (Scheme 1). Several techniques were employed to determine the photoinduced charge-separation properties in these new SWNT donor–acceptor hybrids.



Scheme 1. Partial structure of SWNT/pyrene⁺/ZnP⁸⁻ nanohybrids.

Water-suspendable SWNTs were obtained in analogy to previous work, using pyrene⁺.^[9] However, to reduce the amount of free pyrene in solution, the SWNT/pyrene⁺ complex was allowed to precipitate, and the centrifuged solid was re-suspended in water.

In Figure 1a and b we compare the UV, Vis, and NIR absorption spectra of pyrene⁺ and SWNT/pyrene⁺. The absorption spectra of an aqueous SWNT/pyrene⁺ solution reveal several important features. First, the π – π^* transitions of pyrene⁺ are slightly red-shifted (i.e., 1–2 nm) which indicates that electronic communication between the two different ring

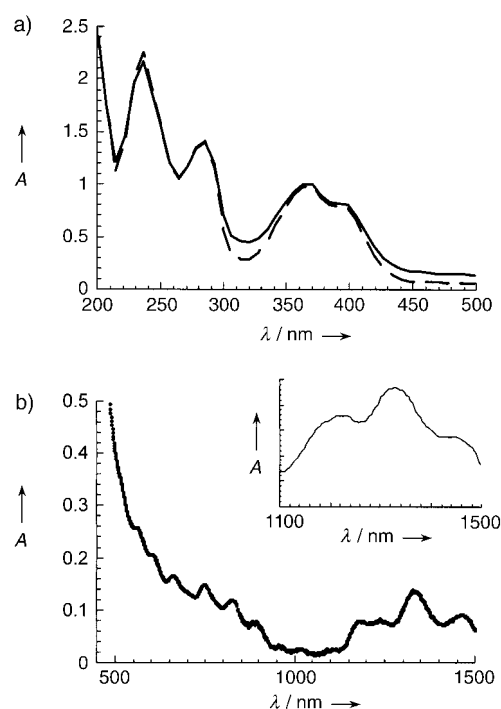


Figure 1. Absorption spectra of pyrene⁺ (dashed line) and SWNT/pyrene⁺ (solid line) a) in H₂O at pH 6.5 in the 200–500 nm range and b) in D₂O in the 450–1500 nm range. Insert to Figure b shows the 1100–1500 nm range for a sample of SWNT sonicated in DMF.

systems occurs. Second, the overall absorption cross-section increases, particularly in the Vis- and NIR-regions. Third, the characteristic van Hove singularities^[2] of SWNTs are discernable in the Vis-NIR region up to around 450 nm, where the π – π^* transitions of pyrene⁺ dominate the spectrum. In fact, a D₂O spectrum of SWNT/pyrene⁺ verifies that the van Hove singularities extend all the way out to 1500 nm and that they track those seen for a DMF sonicated suspension of SWNT (insert to Figure 1b). Collectively, these observations confirm the presence of both suspended SWNTs and pyrene⁺ and the notable electronic interactions between them.

Additional proof for SWNT/pyrene⁺ interactions came from emission experiments, which showed more than 50% quenching of the pyrene⁺ fluorescence (see Supporting Information).^[10]

The trimethylammonium head groups of pyrene were used as electrostatic anchors to bind anionic electron donors, such as water-soluble ZnP⁸⁻ or H₂P⁸⁻.

Initial insight into the formation of SWNT/pyrene⁺/ZnP⁸⁻ or SWNT/pyrene⁺/H₂P⁸⁻ came from transmission electron microscopy (TEM). Pristine SWNT (as obtained from CNI) was treated with acid to remove the metallic nanoparticles (Figure 2a). Reference images of H₂P⁸⁻ (or ZnP⁸⁻) show dark aggregates at the nanometer level (Figure 2b) while SWNT/pyrene⁺ reveal bundles of nanotubes with diameters of 25 nm and lengths of several micrometers (Figure 2c). Addition of H₂P⁸⁻ (or ZnP⁸⁻) to the nanotubes results in van der Waals electrostatic interactions between the two components. The corresponding TEM micrographs show darker areas surrounding the nanotubes walls, these areas are H₂P⁸⁻ (Fig-

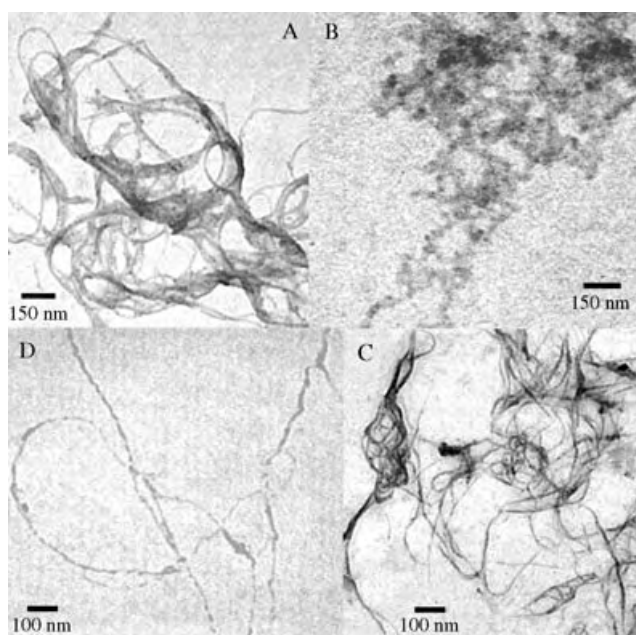


Figure 2. TEM images of a) purified SWNT, b) ZnP^{8-} deposited from an aqueous solution, c) SWNT/pyrene $^{+}$, d) SWNT/pyrene $^{+}$ / H_2P^{8-} .

ure 2d) or ZnP^{8-} . Therefore, both the successful suspension and debundling in solution of SWNT/pyrene $^{+}$ and the electrostatic attractive interactions in the SWNT/pyrene $^{+}$ / ZnP^{8-} or SWNT/pyrene $^{+}$ / H_2P^{8-} system have been confirmed by TEM.

Dilute aqueous solution of ZnP^{8-} and H_2P^{8-} ($\approx 10^{-5}$ M) were titrated with variable amounts of SWNT/pyrene $^{+}$ to form SWNT/pyrene $^{+}$ / ZnP^{8-} or SWNT/pyrene $^{+}$ / H_2P^{8-} , respectively, as monitored by absorption and fluorescence spectroscopy (Figure 3). Relative to the component spectra (i.e., SWNT/pyrene $^{+}$ and ZnP^{8-}) a number of differences are apparent. For ZnP^{8-} , Soret- and Q-band transitions at 426 nm (Figure 3a) and 560/600 nm (not shown), respectively, shift incrementally to the red. The Soret-band shows the biggest shifts of around 7 nm. Moreover, the presence of an isosbestic point at 429 nm indicates the transformation of ZnP^{8-} (i.e., starting-point of the titration) into SWNT/pyrene $^{+}$ / ZnP^{8-} (i.e., end-point of the titration). The pyrene π - π transitions in SWNT/pyrene $^{+}$ are also subjected to changes: Additional red-shifts (2 nm) indicate that SWNT/pyrene $^{+}$ and ZnP^{8-} interact by virtue of electrostatic interactions.^[11]

Excitation of 3.2×10^{-5} M ZnP^{8-} in aqueous solution leads to strong fluorescence emission ($\Phi \approx 0.04$), which maximizes at 612 and 665 nm. The addition of SWNT/pyrene $^{+}$ to ZnP^{8-} was monitored using 430 nm as the excitation wavelength, which was where the isosbestic point was observed in the absorption spectrum. Under these conditions, competitive light absorption by SWNT/pyrene $^{+}$ is minimal. When SWNT/pyrene $^{+}$ is present the fluorescence emission intensity decreased. The decrease is exponential and depends solely on the SWNT/pyrene $^{+}$ concentration. Inspection of Figure 3b reveals that simultaneous with the quenching of the ZnP^{8-} emission at 612 nm, a new lower energy emission band develops, centered at 617 nm.^[11]

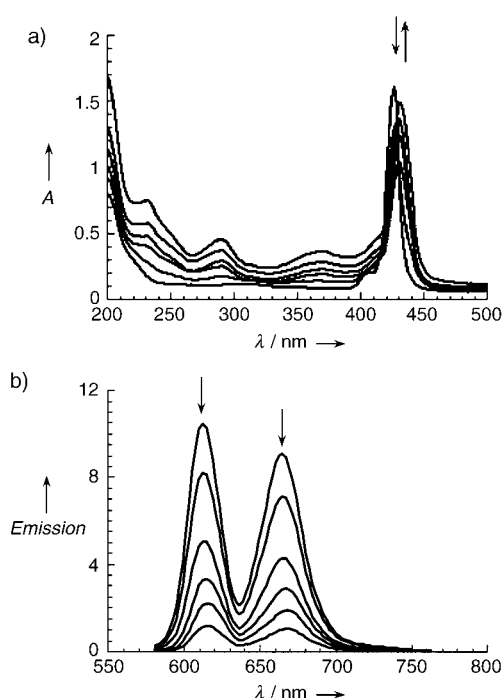


Figure 3. a) Absorption spectra of a dilute aqueous solution of ZnP^{8-} (3.2×10^{-6} M) titrated against SWNT/pyrene $^{+}$. b) Fluorescence spectra of a dilute aqueous solution of ZnP^{8-} (3.2×10^{-5} M) titrated against SWNT/pyrene $^{+}$. Excitation wavelength is 430 nm. Arrows indicate changes as the concentration of SWNT/pyrene $^{+}$ is increased.

In the absence of SWNT/pyrene $^{+}$, the fluorescence decays of ZnP^{8-} or H_2P^{8-} are fitted by mono-exponential rate laws, for which lifetimes of 2.1 ns and 9.4 ns were determined. Upon adding SWNT/pyrene $^{+}$ to these solutions, double-exponential fluorescence decays were observed. For example, the ZnP^{8-} fluorescence profiles were now best fitted by lifetimes of 2.1 ± 0.2 ns and 0.2 ± 0.05 ns. The two lifetimes are maintained throughout the titration assay. As the concentration of SWNT/pyrene $^{+}$ increases, the contribution of the short-lived component increases as well. In such mixtures, intrahybrid SWNT-porphyrin interactions are thought to be responsible for the fast kinetic component and regular porphyrin excited-state deactivations give rise to the slow component. At all concentrations, the pre-exponential factors give rise to a good agreement with the distribution of emitting species, that is, bound, immobilized versus free, non-immobilized ZnP^{8-} or H_2P^{8-} .

Upon addition of acid, the original long-lived fluorescence component is restored, concomitant with the disappearance of the short-lived species. This observation demonstrates that the complex formation is reversible. All these data point to a static quenching event occurring inside well-defined hybrids of SWNT/pyrene $^{+}$ / ZnP^{8-} and SWNT/pyrene $^{+}$ / H_2P^{8-} . The most likely excited-state quenching process involves electron or hole transfer, namely, oxidation of the porphyrin and reduction of the SWNT (see below). Charge transfer in SWNT-ferrocene nanohybrids has been reported recently.^[5]

A thermodynamic correlation of the singlet excited states with the radical ion pair states supports our postulate. We

estimate the energies of the radical ion pair states from the reduction of SWNT (-0.15 V versus saturated calomel electrode (SCE))^[12] and oxidation of ZnP^{8-} ($+0.77$ V versus SCE)^[8] and H_2P^{8-} ($+0.94$ V versus SCE).^[8] The singlet-excited-state energies of ZnP^{8-} and H_2P^{8-} are 2.1 eV and 1.9 eV, respectively. Thus, the driving force for photoinduced electron-transfer reactions is appreciably large with values around 1.0 eV.

In parallel sets of experiments, interactions of SWNT/pyrene⁺ with zinc 5,10,15,20-tetrakis-(2',6'-bis(*N*-methylene-(4'-*tert*-butylpyridinium))-4'-*tert*-butylphenyl) porphyrin octabromide (ZnP^{8+})^[8] were tested. Owing to repulsive electrostatic interactions in these similarly charged systems, the absorption spectra (see Supporting Information) remain—throughout the titrations—virtually as the superimpositions of the component spectra. The lack of mutually interacting systems was also confirmed in fluorescence experiments (see Supporting Information). Only a maximum of 10% quenching is noted, relative to >95% quenching in the oppositely charged systems, that is, SWNT/pyrene⁺/ ZnP^{8-} . In fact, the moderate quenching was due to competitive pyrene⁺/ ZnP^{8+} light absorption.^[13]

Potential pyrene⁺ interactions with ZnP^{8-} or H_2P^{8-} were tested in another assay. In this experiment changes in the Soret- and Q-bands mirror those noted when SWNT/pyrene⁺ was present (not shown). However, the magnitude of the red shifts is with 3 nm notably smaller than the 7 nm red shifts in SWNT/pyrene⁺/ ZnP^{8-} . This result verifies the presence of electrostatically driven couplings between pyrene⁺ and ZnP^{8-} or H_2P^{8-} . Apparently, SWNTs augment the electronic perturbations of the π -system of the porphyrin. A moderate fluorescence quenching of less than 15% rules out energy or electron-transfer deactivation of the photoexcited porphyrins. A thermodynamic evaluation leads to the same conclusion, that is, both processes would be highly endothermic. Singlet-singlet energy transfer would be uphill by about 0.5 eV and the driving force for charge separation would be 0.2 ± 0.1 eV.

In complementary transient-absorption studies we monitored the fate of the porphyrin fluorescence quenching and carried out the identification of the photo products. Pumping light into the ZnP^{8-} or H_2P^{8-} ground state with short 532 nm laser pulses (i.e., ps or ns) led to the population of their singlet excited states. The long-lived and molecular-oxygen-sensitive triplet spectra of, for example, ZnP^{8-} or H_2P^{8-} reveal, besides bleaching in the Soret- and Q-band region, characteristic triplet maxima around 800 nm (i.e., ZnP^{8-} : 840 nm; H_2P^{8-} : 780 nm).^[14]

In contrast, the changes in the differential absorption spectra of the SWNT/pyrene⁺/ ZnP^{8-} or SWNT/pyrene⁺/ H_2P^{8-} ensembles are dominated by broad absorptions in the 600–800 nm region, which indicate the presence of ZnP^{8-} or H_2P^{8-} based redox products. Figure 4 shows the spectral changes seen in the case of SWNT/pyrene⁺/ ZnP^{8-} . At increasing times after excitation, the features of the oxidized ZnP^{8-} unit diminish in the 600–800 nm region, reflecting the return of the charge-separated state to the ground electronic state. The lifetime of the newly formed ion pair state—as derived by analyzing several wavelengths under unimolecular conditions—is 0.4 μs .

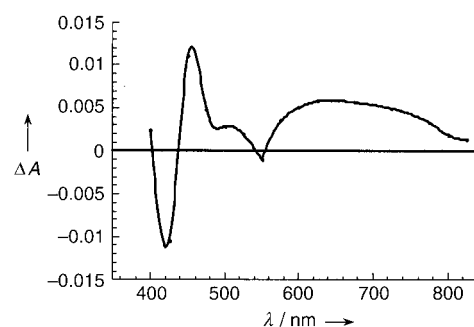


Figure 4. Differential absorption spectrum (Vis and NIR) obtained upon nanosecond flash photolysis (532 nm) of SWNT/pyrene⁺/ ZnP^{8-} in nitrogen-saturated solutions with a time delay of 100 ns.

In summary, the transient absorption data, like the static and time-resolved fluorescence data, show that SWNTs serve as the electron-acceptor component in donor-acceptor materials, just as fullerenes have been found to be the electron acceptors in related research. Intra-ensemble electron transfer from the photoexcited porphyrins (i.e., ZnP^{8-} or H_2P^{8-}) to SWNT creates long-lived radical ion pairs. This result, taken together with the light harvesting features of the used porphyrins, suggests that our approach towards versatile nanohybrids opens the way to novel chemical and light driven systems.

Received: June 7, 2004

Keywords: carbon nanotubes · donor-acceptor systems · electron transfer · porphyrinoids · zinc

- [1] a) P. Harris, *Carbon Nanotubes and Related Structures: New Materials for the Twenty-First Century*, Cambridge University Press, Cambridge, **2001**; b) *Carbon Nanotubes: Synthesis, Structure, Properties and Applications* (Eds.: M. S. Dresselhaus, G. Dresselhaus, P. Avouris), Springer, Berlin, **2001**; c) S. Reich, C. Thomsen, J. Maultzsch, *Carbon Nanotubes: Basic Concepts and Physical Properties*, VCH, Weinheim, **2004**.
- [2] Special issue on Carbon Nanotubes *Acc. Chem. Res.* **2002**, *35*, 997.
- [3] For recent reviews, see: a) A. Hirsch, *Angew. Chem.* **2002**, *114*, 1933; *Angew. Chem. Int. Ed.* **2002**, *41*, 1853; b) J. L. Bahr, J. M. Tour, *J. Mater. Chem.* **2002**, *12*, 1952; c) S. Niyogi, M. A. Hamon, H. Hu, B. Zhao, P. Bhomwik, R. Sen, M. E. Itkis, R. C. Haddon, *Acc. Chem. Res.* **2002**, *35*, 1105; d) Y.-P. Sun, K. Fu, Y. Lin, W. Huang, *Acc. Chem. Res.* **2002**, *35*, 1096; e) S. Banerjee, M. G. C. Kahn, S. S. Wang, *Chem. Eur. J.* **2003**, *9*, 1898; f) D. Tasis, N. Tagmatarchis, V. Georgakilas, M. Prato, *Chem. Eur. J.* **2003**, *9*, 4000; g) C. A. Dyke, J. M. Tour, *Chem. Eur. J.* **2004**, *10*, 812.
- [4] a) V. Georgakilas, K. Kordatos, M. Prato, D. M. Guldi, M. Holzinger, A. Hirsch, *J. Am. Chem. Soc.* **2002**, *124*, 760; b) H. Murakami, T. Nomura, N. Nakashima, *Chem. Phys. Lett.* **2003**, *378*, 481; c) H. Li, B. Zhou, L. Gu, W. Wang, K. A. Shiral Fernando, S. Kumar, L. F. Allard, Y.-P. Sun, *J. Am. Chem. Soc.* **2004**, *126*, 1014.
- [5] D. M. Guldi, M. Marcaccio, D. Paolucci, F. Paolucci, N. Tagmatarchis, D. Tasis, E. Vázquez, M. Prato, *Angew. Chem.* **2003**, *115*, 4243; *Angew. Chem. Int. Ed.* **2003**, *42*, 4206.

- [6] a) R. J. Chen, Y. Zhang, D. Wang, H. Dai, *J. Am. Chem. Soc.* **2001**, *123*, 3838; b) D. Pantarotto, C. D. Partidos, R. Graff, J. Hoebeke, J.-P. Briand, M. Prato, A. Bianco, *J. Am. Chem. Soc.* **2003**, *125*, 6160; c) M. Shim, N. W. S. kim, R. J. Chen, Y. Li, H. Dai, *Nano Lett.* **2002**, *2*, 285.
- [7] a) G. McDermott, S. M. Priece, A. A. Freer, A. M. Hawthornthwaite-Lawless, M. Z. Papiz, R. J. Cogdell, N. W. Isaacs, *Nature* **1995**, *374*, 517; b) J. Barber, *Nature* **1988**, *333*, 114; c) *Supramolecular Chemistry* (Eds.: V. Balzani, L. de Cola), Kluwer Academic Publishers, Dordrech, **1992** (NATO ASI Series).
- [8] see for details: a) N. Jux, *Org. Lett.* **2000**, *2*, 2129; b) D. M. Guldi, I. Zilbermann, G. Anderson, A. Li, D. Balbinot, N. Jux, M. Hatzimarinaki, A. Hirsch, M. Prato, *Chem. Commun.* **2004**, 726.
- [9] N. Nakashima, Y. Tomonari, H. Murakami, *Chem. Lett.* **2002**, 638.
- [10] In parallel investigations, we tested the supernatant solution and several other fractions of the centrifuged material—all with identical pyrene⁺ absorptions—and found a relationship between the intensities of the van Hove singularities and the fluorescence quenching: The stronger the transitions, the stronger the fluorescence quenching, and hence the higher the SWNT/pyrene⁺ ratios and the lower the amount of free pyrene⁺.
- [11] In a complementary study with H₂P⁸⁻ we made the same observations.
- [12] M. Melle-Franco, M. Marcaccio, D. Paolucci, F. Paolucci, V. Georgakilas, D. M. Guldi, M. Prato, F. Zerbetto, *J. Am. Chem. Soc.* **2004**, *126*, 1646.
- [13] Note that the fluorescence-decay measurements did not show any appreciable differences.
- [14] D. Balbinot, S. Atalick, D. M. Guldi, M. Hatzimarinaki, A. Hirsch, N. Jux, *J. Phys. Chem. B* **2003**, *107*, 13273.

Ansa-Cycloheptatrienyl–Cyclopentadienyl Complexes**

Matthias Tamm,* Andreas Kunst, Thomas Bannenberg, Eberhardt Herdtweck, Peter Sirsch, Cornelis J. Elsevier, and Jan M. Ernsting

Group 4 *ansa*-metallocenes are among the most important compounds in homogeneous transition-metal-based catalysis.^[1,2] In contrast, *ansa*-complexes containing a bridging unit between a cycloheptatrienyl (Cht) and a cyclopentadienyl (Cp) unit are virtually unknown.^[3] During the course of our studies on complexes containing linked cycloheptatrienyl-phenolate^[4] and -phosphane ligands,^[5] we became interested in the preparation of bridged Cht–Cp sandwich complexes, in which the ligand can be regarded as a Cp-donor-functionalized cycloheptatrienyl ligand. For this purpose, we have chosen the 16-electron titanium complex $[(\eta\text{-C}_7\text{H}_7)\text{Ti}(\eta\text{-C}_5\text{H}_5)]$ (troticene)^[6] as a suitable starting material, as double-lithiation of troticene can be achieved with *n*-butyllithium/*N,N,N',N'*-tetramethylethylenediamine (tmeda) resulting in the formation of the tmeda-stabilized complex $[(\eta\text{-C}_7\text{H}_6\text{Li})\text{Ti}(\eta\text{-C}_5\text{H}_4\text{Li})]$.^[7] In our hands, the reaction of the dilithio complex with Me_2SiCl_2 afforded the silicon-bridged *ansa*-Cht–Cp complex or [1]silatroticenophane **1** which can be isolated as blue-green crystals in 30–40 % yield after crystallization from hexane (Scheme 1).^[8]

Whereas the C_7H_7 and C_5H_5 rings in troticene give rise to only two resonance signals in the ^1H and ^{13}C NMR spectra,^[9] the introduction of the Me_2Si bridge results in a splitting pattern which is in agreement with the formation of a C_s -symmetric complex. In the ^1H NMR spectrum (Figure 1), one broad signal is observed for the α and β C_5H_4 protons which is only marginally shifted in comparison to the corresponding troticene resonance ($\delta = 4.90$ ppm, C_5H_5). In contrast, the signal for the protons of the seven-membered ring in troticene ($\delta = 5.42$ ppm) is now split into a downfield multiplet ($\delta = 5.96$ – 5.84 ppm) for the β and γ hydrogen atoms and into a

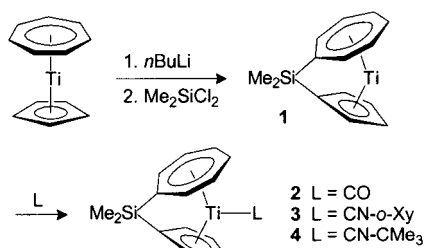
[*] Prof. Dr. M. Tamm, Dipl.-Chem. A. Kunst, Dr. T. Bannenberg, Dr. E. Herdtweck
Lehrstuhl für Anorganische Chemie
Department Chemie
Technische Universität München
Lichtenbergstrasse 4, 85747 Garching (Germany)
Fax: (+49) 89-289-13473
E-mail: matthias.tamm@ch.tum.de

Dr. P. Sirsch
Institut für Physik
Universität Augsburg
Prof. Dr. C. J. Elsevier, J. M. Ernsting
Institute for Molecular Chemistry
Universiteit van Amsterdam

[**] This work has been supported by the Deutsche Forschungsgemeinschaft.



Supporting information for this article is available on the WWW under <http://www.angewandte.org> or from the author.



Scheme 1. Synthesis of [1]sila-troticenophanes (*o*-Xy = 2,6-dimethylphenyl).

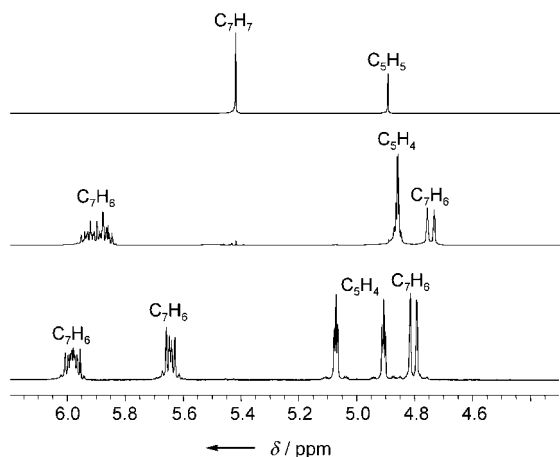


Figure 1. Excerpts from the ^1H NMR spectra of troticene (top), [1]sila-troticenophane **1** (middle), and the 2,6-dimethylphenyl isocyanide complex **3** (bottom) in $[\text{D}_6]\text{benzene}$ at 25°C .

upfield doublet at $\delta = 4.75$ ppm which can be assigned to the α CH group next to the bridging Me_2Si moiety. As expected, the ^{13}C NMR spectrum of **1** has five resonance signals for the ring CH carbon atoms (between $\delta = 101.2$ and 87.6 ppm) together with two upfield signals which can be unambiguously assigned to the *ipso*- C_5H_4 carbon atom ($\delta = 83.6$ ppm) and to the *ipso*- C_7H_6 carbon atom ($\delta = 61.6$ ppm). This remarkably large upfield shift is characteristic for highly strained sandwich complexes, such as [1]ferrocenophanes,^[10] and clearly reflects a strong structural distortion, in particular of the $\text{Si}-\text{C}_7\text{H}_6$ site (see below).

To confirm the formation of an *ansa*-Cht-Cp complex, the molecular structure of **1** was determined by X-ray diffraction (Figure 2). In agreement with the molecular structure of $[(\eta\text{-C}_7\text{H}_7)\text{Ti}(\eta\text{-C}_5\text{H}_5)]$,^[11] the metal–carbon bonds to the seven-membered ring [2.170(3)–2.256(2) Å] are significantly shorter than those to the five-membered ring [2.294(3)–2.353(3) Å] revealing a much stronger interaction to the seven-membered ring. Despite the considerable strain imposed by the introduction of the Me_2Si bridge, both rings are virtually planar and can still be regarded as being essentially η^7 - or η^5 -coordinated, respectively. The deviation from an unstrained sandwich structure with an ideal coplanar ring orientation, as observed in troticene,^[11] can be described with the angles α , β , θ , and δ presented in Table 1. Comparison with the structural data of related silicon-bridged *ansa*-complexes, such as the

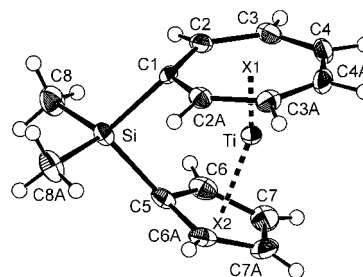


Figure 2. Molecular structure of **1**.^[31] Selected bond lengths [Å]; calculated values are given in square brackets: Ti–C1 2.170(3) [2.168], Ti–C2 2.195(2) [2.205], Ti–C3 2.229(2) [2.250], Ti–C4 2.256(2) [2.269], Ti–C5 2.294(3) [2.308], Ti–C6 2.316(2) [2.330], Ti–C7 2.353(3) [2.385], C1–C2 1.436(3) [1.437], C2–C3 1.425(3) [1.425], C3–C4 1.409(3) [1.420], C4–C4a 1.413(3) [1.416], C5–C6 1.435(3) [1.434], C6–C7 1.411(3) [1.417], C7–C7a 1.410(5) [1.416], Si–C1 1.890(3) [1.908], Si–C5 1.894(4) [1.899], Ti–X1 1.496, Ti–X2 1.988 (X = centroid). Symmetry operation to equivalent positions a: A, $1/2 - y, z$.

Table 1: Distortions in silicon-bridged *ansa*-complexes.

Compound	α [°]	β [°], β' [°]	θ [°]	δ [°]
1	24.1	41.1, 28.7	95.6	160.5
$[\text{Me}_2\text{Si}(\eta\text{-C}_5\text{H}_5)_2\text{Fe}]$	20.8	37.0	95.7	164.7
$[\text{Me}_2\text{Si}(\eta\text{-C}_6\text{H}_5)_2\text{Cr}]$	16.6	38.2, 37.9	92.9	167.6

[1]ferrocenophane $[\text{Me}_2\text{Si}(\eta\text{-C}_5\text{H}_5)_2\text{Fe}]$ ^[12] and the [1]chromar-enophane $[\text{Me}_2\text{Si}(\eta\text{-C}_6\text{H}_5)_2\text{Cr}]$,^[13] suggests that **1** can be regarded as the most strongly distorted sandwich complex in this series. Accordingly, **1** exhibits the largest tilt angle α (24.1 versus 20.8 and 16.6°) together with the smallest angle δ at the metal atom defined by the ring centroids (160.5 versus 164.7 and 167.6°). In all the complexes, the link between the two carbon rings results in a significant distortion from planarity at the *ipso*-carbon atoms bonded to silicon, with the largest angle β being observed between the C_7 plane and the C1–Si bond in **1** ($\beta = 41.1^\circ$). In addition, all interior angles θ at the bridging silicon atoms are substantially smaller than expected for an ideally sp^3 -hybridized atom (Table 1). These results indicate that **1** is a highly strained molecule which should be strongly susceptible to strain release by undergoing ring-opening polymerization (ROP) reactions.^[14] A differential scanning calorimetry (DSC) study of **1** suggests that the compound polymerizes exothermically at about $140\text{--}160^\circ\text{C}$ without showing a melt endotherm at lower temperature. Integration of the exotherm gives an estimate of the strain energy of **1** of approximately 36 kJ/mol .^[15] This is substantially lower than the values found for [1]ferrocenophanes,^[10b,16] however, it can not be excluded that the compound melts and polymerizes simultaneously which would lead to an underestimation of the enthalpy of the ROP process. The characterization of the resulting poly(troticenyilsilanes), which is hampered by their air- and moisture-sensitivity, is under investigation.

Herein, however, we wish to concentrate on another reactivity conferred by the introduction of the silicon bridge and distortion of the sandwich structure. Since both complexes, troiticene and its *ansa*-derivative **1**, have 16 electrons, coordination of an additional two-electron-donor ligand should be possible. Whereas such adduct formation has never been observed for troiticene, the bending of the two rings in **1** creates a gap at the titanium center, which might thereby become accessible to “slender” monodentate ligands, such as carbon monoxide or isocyanides. In addition, these ligands give rise to strong, diagnostic IR absorptions for the CO and CN stretching vibrations, respectively, which can be used to probe the electronic structure of the sandwich complex.

To assess the differences in the electronic structures of bridged and unbridged troiticene derivatives and to identify suitable frontier orbitals in **1** for metal–ligand interaction, the structures of $[(\eta\text{-C}_7\text{H}_7)\text{Ti}(\eta\text{-C}_5\text{H}_5)]$ and of **1** have been optimized with DFT methods employing the B3LYP functional. The calculated geometry of **1** is in good agreement with the structure determined by X-ray diffraction analysis (see caption of Figure 2). For both complexes, contour plots of relevant molecular orbitals together with their eigenvalues are given in Figure 3. In agreement with other theoretical and

are made up predominantly of the C_5H_5 e_1 orbitals, and the interaction between the metal center and the Cp ring can thus be regarded as being mainly ionic. Owing to bridging of the two rings and distortion of the sandwich structure, the occupied molecular orbitals in **1** have given up their degeneracy, their energy positions are nonetheless very close to those in unbridged troiticene. A closer inspection reveals that the tilting results in a small increase of the HOMO–LUMO gap. In principle, this difference could be qualitatively probed by UV/Vis spectroscopy, as the lowest energy band in the optical absorption spectrum of troiticene has been assigned to a one-electron HOMO–LUMO transition, which is partly d–d and partly ligand-to-metal charge transfer (LMCT) in nature.^[19] In our hands, the UV/Vis spectrum of troiticene in CH_2Cl_2 exhibits a visible band at 696 nm ($\epsilon = 31 \text{ L mol}^{-1} \text{ cm}^{-1}$), which is blue-shifted to 663 nm ($\epsilon = 105 \text{ L mol}^{-1} \text{ cm}^{-1}$) in **1** (Figure 4). The greater intensity of the band in **1** can be explained by relaxation of the Laporte selection rule as the symmetry is lowered.^[10]

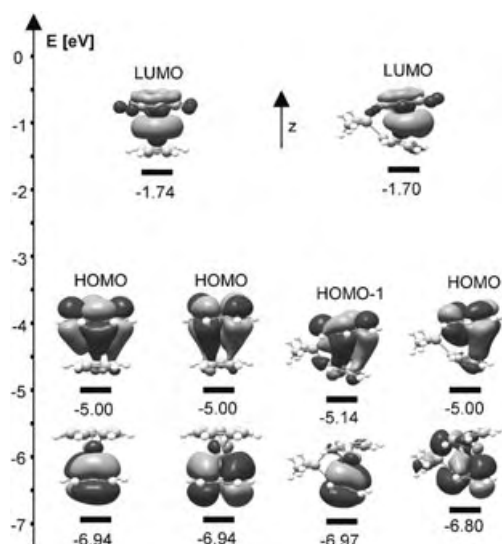


Figure 3. Contour plots and eigenvalues of valence molecular orbitals in $[(\eta\text{-C}_7\text{H}_7)\text{Ti}(\eta\text{-C}_5\text{H}_5)]$ (left) and **1** (right).^[31]

experimental investigations of the bonding in mixed Cht–Cp sandwich molecules,^[17,18] the LUMO in troiticene is essentially titanium localized and consists of the $3d_{z^2}$ orbital with a small contribution from the C_7H_7 a_1 molecular orbital, in a coordinate system, in which the metal–ring axis is defined as the z axis. The degenerate set of the highest occupied molecular orbitals (HOMOs) stems from δ bonding between the metal center and the cycloheptatrienyl ring, and the strong contribution from both titanium and the C_7H_7 e_2 MOs indicates a significant degree of covalency.^[17] In contrast, the next two levels representing the π bond to the cyclopentadienyl ring

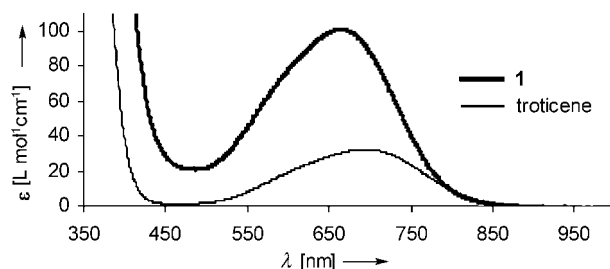


Figure 4. UV/Vis spectra of troiticene and **1** in CH_2Cl_2 .

The calculation additionally reveals that the 16-electron complex **1** contains a LUMO and a HOMO, which are suitably oriented for σ and π interaction with one additional ligand. Carbon monoxide (a σ -donor/ π -acceptor ligand) was passed through a solution of **1** in THF. However, the formation of a stable carbonyl complex of type **2** (see Scheme 1) could not be detected at ambient pressure. An NMR spectroscopy study of **1** under elevated CO pressure reveals a gradual change of the chemical shifts with increasing gas pressure, as shown for the protons of the five- and seven-membered rings in Figure 5. No additional change in the resonance signals is observed between -70 and 20°C indicating that CO is quickly exchanged on the NMR time scale. Further experiments are required to quantify the interaction between **1** and CO and to produce kinetic and thermodynamic data for this equilibrium reaction in a similar fashion as described for instance for the reaction of CO with decamethylcalciocene, $[(\eta\text{-C}_5\text{Me}_5)_2\text{Ca}]$,^[20] and chromocene, $[(\eta\text{-C}_5\text{H}_5)_2\text{Cr}]$.^[21,22]

The weak propensity to form the carbonyl complex **2** can be attributed to the low σ -donor capacity of CO as well as to the weak π -electron-donor ability of **1**. Consequently, the use of ligands with stronger σ -donor and weaker π -acceptor characteristics could lead to the formation of isolable complexes. Addition of 2,6-dimethylphenyl isocyanide or *tert*-butyl isocyanide to a blue-green solution of **1** in THF resulted

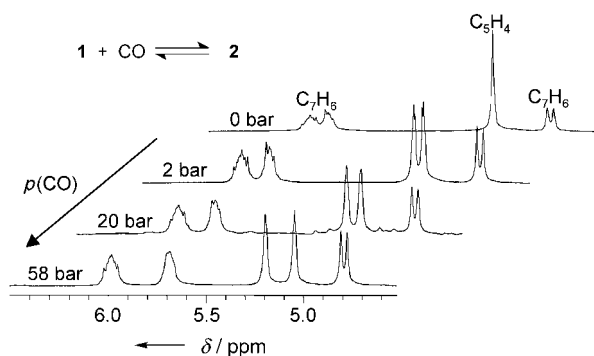


Figure 5. Excerpts from the ^1H NMR spectra of **1** in $[\text{D}_8]\text{THF}$ under variable CO pressure at -20°C .

in an instantaneous color change, and the isocyanide complexes **3** and **4** could be isolated in almost quantitative yield as brownish crystals (Scheme 1).^[8] Coordination of the isocyanides is clearly demonstrated by the splitting patterns for the NMR resonances signals of the C_7H_6 and C_5H_4 hydrogen atoms (Figure 1). In the IR spectrum the CN stretching vibrations are at 2112 cm^{-1} (**3**) and at 2153 cm^{-1} (**4**), which is only slightly shifted compared to the values for the free isocyanides.^[23] These observations indicate that metal-to-ligand π backbonding in **3** and **4** is significantly less pronounced than in related *ansa*-chromocene derivatives. For instance, $\nu_{\text{CN}} = 1835\text{ cm}^{-1}$ for the tetramethylethylene-bridged complex $[\text{Me}_4\text{C}_2(\eta\text{-C}_5\text{H}_4)_2\text{Cr}(\text{CNCMe}_3)]$.^[24] Considerably lower stretching frequencies are also observed for titanium isocyanide complexes, such as $[\text{Me}_2\text{Si}(\eta\text{-C}_5\text{H}_4)_2\text{Ti}(\text{CN-}o\text{-Xy})_2]$ ($\nu_{\text{CN}} = 2044, 1938\text{ cm}^{-1}$),^[25] in which the titanium center is formally considered to be in the $+II$ oxidation state. On the other hand, for typical so-called titanium(IV) complexes, values above 2200 cm^{-1} are found (e.g. the dimeric $[\{\text{TiCl}_4(\text{CN-}o\text{-Xy})\}_2]$ ($\nu_{\text{CN}} = 2210\text{ cm}^{-1}$)^[26] and *ortho*- $[\text{TiCl}_4(\text{CNCMe}_3)_2]$ ($\nu_{\text{CN}} = 2226\text{ cm}^{-1}$).^[27]

The molecular structure of complex **4** was determined by X-ray diffraction analysis (Figure 6). Apparently, coordination of the *tert*-butyl isocyanide ligand leads to a pronounced elongation of the metal–carbon bonds, in particular of those to the seven-membered ring [2.248(2)–2.412(3) Å versus 2.170(3)–2.256(2) Å in **1** (Figure 2)]. The largest separations are observed between the titanium center and the carbon atoms C4 and C5, and this puckering of the seven-membered ring can be described as a moderately developed distortion from a symmetric η^7 - towards an open η^5 -bonding mode.^[28] In the future, the use of stronger coordinating ligands might enforce the cycloheptatrienyl ring to undergo a complete η^7 - η^5 hapticity interconversion giving a titanocene-like chemistry for the [1]silatroticenophane **1**.

A tentative comparison of the Ti–C–N bond lengths in **4** (Ti–C15 2.223(2), C15–N 1.153(3) Å) with those in representative titanium isocyanide complexes shows that the mixed carbonyl–isocyanide complex $[(\eta\text{-C}_5\text{H}_5)_2\text{Ti}(\text{CO})(\text{CNCMe}_3)]$ has a shorter Ti–C (2.112(9) Å) and a longer C–N bond, (1.161(12) Å)^[29] whereas the reverse order is observed for the diisocyanide complex *ortho*- $[\text{TiCl}_4(\text{CNCMe}_3)_2]$ (Ti–C 2.240(8), 2.256(6), C–N 1.145(10), 1.137(8) Å).^[27] These

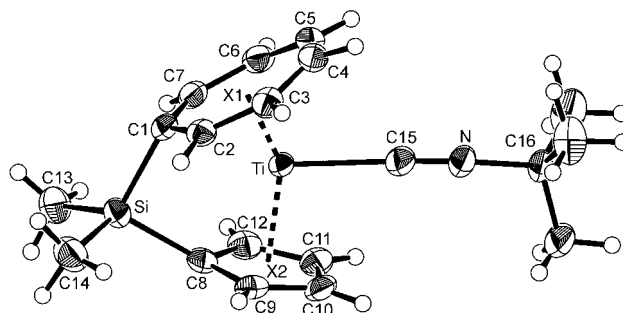


Figure 6. Molecular structure of **4**.^[31] Selected bond lengths [Å] and angles [°]: Ti–C1 2.311(2), Ti–C2 2.248(2), Ti–C3 2.309(2), Ti–C4 2.412(3), Ti–C5 2.384(3), Ti–C6 2.289(2), Ti–C7 2.268(2), Ti–C8 2.380(2), Ti–C9 2.392(2), Ti–C10 2.421(2), Ti–C11 2.407(2), Ti–C12 2.368(2), Ti–C15 2.223(2), C1–C2 1.432(3), C1–C7 1.429(3), C2–C3 1.413(3), C3–C4 1.411(3), C4–C5 1.397(3), C5–C6 1.411(3), C6–C7 1.412(3), C8–C9 1.430(3), C8–C12 1.432(3), C9–C10 1.398(3), C10–C11 1.404(3), C11–C12 1.398(3), Si–C1 1.875(3), Si–C8 1.869(2), C15–N 1.153(3), N–C16 1.461(3), Ti–X1 1.649, Ti–X2 2.070; Ti–C15–N 177.0(2), C15–N–C16 175.5(2), X1–Ti–X2 147.6 (X = centroid).

results might suggest that **4** adopts an intermediate position between these Ti^{II} and Ti^{IV} complexes with respect to the strength of the titanium–isocyanide interaction. However, both shorter Ti–C and C–N bonds are found for cationic Ti^{IV} isocyanide complexes, such as $[(\eta\text{-C}_5\text{H}_5)_2\text{Ti}(\text{CNCMe}_3)(\eta^2\text{-MeC=NCMe}_3)]\text{BPh}_4$ (Ti–C 2.192(6), C–N 1.150(6) Å).^[30]

In this contribution, we have reported on the synthesis and structural characterization of the highly strained [1]silatroticenophane **1**, which is the first example of an *ansa*-cycloheptatrienyl–cyclopentadienyl complex. Its reactivity towards σ -donor/ π -acceptor ligands, such as carbon monoxide or isocyanides reveals that **1** does not behave like a complex containing titanium in a lower oxidation state but rather bears a closer resemblance to Lewis acidic Ti^{IV} complexes. Based on the theoretical calculations, this behavior can be attributed to the strong and appreciably covalent titanium–cycloheptatrienyl interaction leading to highly stabilized frontier orbitals and consequently to a diminishing π -electron release ability.

Received: May 2, 2004

Keywords: cycloheptatrienyl ligands · cyclopentadienyl ligands · density functional calculations · sandwich complexes · titanium

- [1] *Metalloenes* (Eds.: A. Togni, R. L. Halterman), Wiley-VCH, Weinheim, 1998.
- [2] *Applied Homogeneous Catalysis with Organometallic Compounds* (Eds.: B. Cornils, W. A. Herrmann), Wiley-VCH, Weinheim, 1996.
- [3] M. L. H. Green, D. K. P. Ng, *Chem. Rev.* **1995**, 95, 439–473.
- [4] M. Tamm, T. Bannenberg, B. Dreßel, R. Fröhlich, C. Holst, *Inorg. Chem.* **2002**, 41, 47–59.
- [5] a) M. Tamm, K. Baum, T. Lügger, R. Fröhlich, K. Bergander, *Eur. J. Inorg. Chem.* **2002**, 918–928; b) M. Tamm, B. Dreßel, V. Urban, T. Lügger, *Inorg. Chem. Commun.* **2002**, 5, 837–840; c) M. Tamm, B. Dreßel, T. Lügger, R. Fröhlich, S. Grimme, *Eur. J. Inorg. Chem.* **2003**, 1088–1098; d) M. Tamm, B. Dreßel, K. Baum, T. Lügger, T. Pape, *J. Organomet. Chem.* **2003**, 677, 1–9;

- e) M. Tamm, B. Dreßel, T. Lügger, *J. Organomet. Chem.* **2003**, 684, 322–328.
- [6] For the sandwich compound $[(\eta\text{-C}_7\text{H}_7)\text{Ti}(\eta\text{-C}_5\text{H}_5)]$, we wish to introduce the trivial name *troticene*, which stands for $[(\eta^7\text{-tropylium})\text{titanium}(\eta^5\text{-cyclopentadienyl})]$ and is in accord with the naming of $[(\eta\text{-C}_7\text{H}_7)\text{V}(\eta\text{-C}_5\text{H}_5)]$ as *trovacene*, see for instance: C. Elschenbroich, O. Schiemann, O. Burghaus, K. Harms, *J. Am. Chem. Soc.* **1997**, 119, 7452–7457.
- [7] M. Ogasa, M. D. Rausch, R. D. Rogers, *J. Organomet. Chem.* **1991**, 403, 279–291.
- [8] The experimental section including the syntheses, full characterization, and spectroscopic data of all the new compounds can be found in the Supporting Information.
- [9] The NMR resonance signals for troticene have been reported, see: C. J. Groenenboom, F. Jellinek, *J. Organomet. Chem.* **1974**, 80, 229–234. In our hands, troticene has the following resonance signals: ^1H NMR (400 MHz, $[\text{D}_6]\text{benzene}$): $\delta = 5.42$ (s, 7H; C_7H_7), 4.90 (s, 5H; C_5H_5); $^{13}\text{C}\{^1\text{H}\}$ NMR (100.53 MHz, $[\text{D}_6]\text{benzene}$): $\delta = 94.9$ (C_5H_5), 84.3 ppm (C_7H_7).
- [10] a) A. G. Osborne, R. H. Whiteley, R. E. Meads, *J. Organomet. Chem.* **1980**, 193, 345–357; b) R. Rulkens, D. P. Gates, D. Balaishis, J. K. Pudelski, D. F. McIntosh, A. J. Lough, I. Manners, *J. Am. Chem. Soc.* **1997**, 119, 10976–10986.
- [11] K. A. Lyssenko, M. Y. Antipin, S. Y. Ketkov, *Russ. Chem. Bull. Int. Ed.* **2001**, 50, 130–141.
- [12] a) W. Finckh, B.-Z. Tang, D. A. Foucher, D. B. Zamble, R. Ziembinski, A. Lough, I. Manners, *Organometallics* **1993**, 12, 823–829; b) S. Barlow, M. J. Drewitt, T. Dijkstra, J. C. Green, D. O'Hare, C. Whittingham, H. H. Wynn, D. P. Gates, I. Manners, J. M. Nelson, J. K. Pudelski, *Organometallics* **1998**, 17, 2113–2120.
- [13] K. Hultzsich, J. M. Nelson, A. J. Lough, I. Manners, *Organometallics* **1995**, 14, 5496–5502.
- [14] P. Nguyen, P. Gomez-Eliphe, I. Manners, *Chem. Rev.* **1999**, 99, 1515–1548.
- [15] A representative DSC thermogram for **1** can be found in the Supporting Information.
- [16] D. A. Foucher, B.-Z. Tang, I. Manners, *J. Am. Chem. Soc.* **1992**, 114, 6246–6248.
- [17] N. Kaltsoyannis, *J. Chem. Soc. Dalton Trans.* **1995**, 3727–3730.
- [18] J. C. Green, N. Kaltsoyannis, K. H. Sze, M. MacDonald, *J. Am. Chem. Soc.* **1994**, 116, 1994–2004.
- [19] D. Gourier, D. Samuel, *Inorg. Chem.* **1988**, 27, 3018–3024.
- [20] a) P. Selg, H. H. Brintzinger, R. A. Andersen, I. T. Horváth, *Angew. Chem.* **1995**, 107, 877–879; *Angew. Chem. Int. Ed. Engl.* **1995**, 34, 791–793; b) P. Selg, H. H. Brintzinger, M. Schultz, R. A. Andersen, *Organometallics* **2002**, 21, 3100–3107.
- [21] K. L. T. Wong, H. H. Brintzinger, *J. Am. Chem. Soc.* **1975**, 97, 5143–5146.
- [22] J. C. Green, C. N. Jardine, *J. Chem. Soc. Dalton Trans.* **1999**, 3767–3770.
- [23] R. W. Stephany, M. J. A. de Bie, W. Drenth, *Org. Magn. Reson.* **1974**, 6, 45. In our hands, 2,6-dimethylphenyl isocyanide shows $\nu_{\text{CN}} = 2123\text{ cm}^{-1}$ in KBr, and a THF solution of *tert*-butyl isocyanide shows a strong band at 2132 cm^{-1} .
- [24] a) D. M. Foo, P. J. Shapiro, *Organometallics* **1995**, 14, 4957–4959; b) G. J. Matare, D. M. Foo, K. M. Kane, R. Zehnder, M. Wagener, P. J. Shapiro, T. Concolino, A. L. Rheingold, *Organometallics* **2000**, 19, 1534–1539.
- [25] T. Cuenca, R. Gómez, P. Gómez-Sal, P. Royo, *J. Organomet. Chem.* **1993**, 454, 105–111.
- [26] T. Carofiglio, P. G. Cozzi, C. Floriani, A. Chiesi-Villa, C. Rizzoli, *Organometallics* **1993**, 12, 2726–2736.
- [27] T. Carofiglio, C. Floriani, A. Chiesi-Villa, C. Guastini, *Inorg. Chem.* **1989**, 28, 4417–4419.
- [28] Although unusual for cycloheptatrienyl ligands, the η^5 -bonding mode has been observed before: M. Tamm, B. Dreßel, R. Fröhlich, K. Bergander, *Chem. Commun.* **2000**, 1731–1732, and references therein.
- [29] L. B. Kool, M. D. Rausch, M. Herberhold, H. G. Alt, U. Thewalt, B. Honold, *Organometallics* **1986**, 5, 2465–2468.
- [30] M. Bochmann, L. M. Wilson, M. B. Hursthouse, R. L. Short, *Organometallics* **1987**, 6, 2556–2563.
- [31] Details of the electronic structure calculations and of the X-ray crystal structure determinations can be found in the Supporting Information. CCDC-237472 (**1**) and CCDC-237473 (**4**) contain the supplementary crystallographic data for this paper. These data can be obtained free of charge via www.ccdc.cam.ac.uk/conts/retrieving.html (or from the Cambridge Crystallographic Data Centre, 12 Union Road, Cambridge CB2 1EZ, UK; fax: (+44) 1223-336-033; or deposit@ccdc.cam.ac.uk).

Germanium Chemistry

Germacarboxylic Acid: An Organic-Acid Analogue Based on a Heavier Group 14 Element**

Leslie W. Pineda, Vojtech Jancik, Herbert W. Roesky, and Regine Herbst-Irmer*

Dedicated to Professor Jean-Marie Lehn on the occasion of his 65th birthday

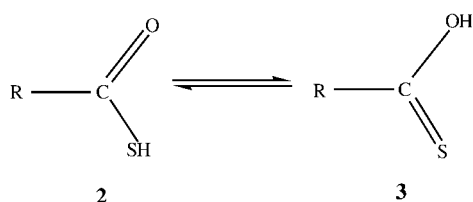
Carbon multiple-bonded species, especially those containing carbonyl groups (aldehydes, amide esters, ketones) are widely known and useful systems in organic chemistry.^[1] As far as the heavier congeners of Group 14 are concerned, a steady and remarkable development has been experienced, which includes the synthesis of unsaturated species. Additionally a myriad of mixed unsaturated compounds has been prepared containing elements of Groups 14–16.^[2] However, owing to the high reactivity and tendency to polymerize these species have to be thermodynamically and kinetically stabilized.

In the case of germanium–chalcogen double-bonded species, a few thio-, seleno-, and telluroketones were prepared.^[3] We have already reported the synthesis and structure of $[\text{HC}\{(\text{CMe})(2,6\text{-}i\text{Pr}_2\text{C}_6\text{H}_3\text{N})\}_2\text{Ge}(\text{S})\text{X}]^{[4]}$ ($\text{X} = \text{Cl}, \text{F}$, $\text{HC}\{(\text{CMe})(2,6\text{-}i\text{Pr}_2\text{C}_6\text{H}_3\text{N})\}_2 = 2,6\text{-}i\text{Pr}_2\text{C}_6\text{H}_3\text{NC}(\text{CH}_3)\text{CH}-\text{C}(\text{CH}_3)\text{NC}_6\text{H}_3\text{-}2,6\text{-}i\text{Pr}_2$) with Group 14 and 16 elements

[*] Dipl.-Chem. L. W. Pineda, Dipl.-Chem. V. Jancik, Prof. Dr. H. W. Roesky, Dr. R. Herbst-Irmer
Institut für Anorganische Chemie
Universität Göttingen
Tammannstrasse 4, 37077 Göttingen (Germany)
Fax: (+49) 551-39-3373
E-mail: hroesky@gwdg.de

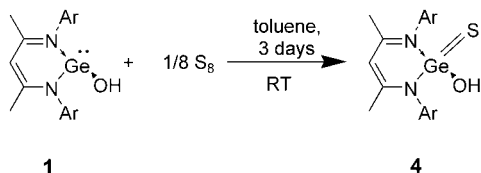
[**] This work was supported by the Deutsche Forschungsgemeinschaft, the Göttinger Akademie der Wissenschaften, and the Fonds der Chemischen Industrie. L.W.P. thanks the Deutscher Akademischer Austauschdienst (DAAD) for a predoctoral fellowship.

bearing a halide. Furthermore, the synthesis and structures of the selenium analogue $[\text{HC}(\text{CMe})(2,6\text{-iPr}_2\text{C}_6\text{H}_3\text{N})_2\text{Ge}(\text{Se})\text{X}]$ ($\text{X} = \text{Cl}, \text{F}$), as well as the functionalized derivative $[\text{HC}(\text{CMe})(2,6\text{-iPr}_2\text{C}_6\text{H}_3\text{N})_2\text{Ge}(\text{E})\text{R}]$ ($\text{E} = \text{S}, \text{Se}$; $\text{R} = \text{Me}$ or $n\text{Bu}$) were reported.^[5] Recently, we succeeded in the isolation and structural characterization of the first terminal hydroxide based on germanium(II) $[\text{HC}(\text{CMe})(2,6\text{-iPr}_2\text{C}_6\text{H}_3\text{N})_2\text{GeOH}]$ (**1**).^[6] As a stable precursor compound **1** is quite intriguing for the generation of new functional groups. To our knowledge the co-existence and fast tautomeric equilibrium for thiolcarboxylic acid **2** and thionocarboxylic acid **3** is known, but the latter group does not exist in the free state (Scheme 1).^[7] Herein we report the first successful isolation and full characterization of a germanium thionoacid $[\text{HC}(\text{CMe})(2,6\text{-iPr}_2\text{C}_6\text{H}_3\text{N})_2\text{Ge}(\text{S})\text{OH}]$ (**4**), which has no isolated precedent in the carbon system (see Scheme 2).



Scheme 1. Tautomeric equilibrium for the thiol- and thionocarboxylic acid.

The reaction of **1** in the presence of equivalent amounts of elemental sulfur at room temperature in toluene leads after three days to the white compound **4** in moderate yield. (Scheme 2).



Scheme 2. Ar = 2,6-*i*Pr₂C₆H₃.

Compound **4** is soluble in benzene, THF, and hexane, but insoluble in pentane and shows no decomposition on exposure to air. Compound **4** was fully characterized by IR, ¹H, and ¹³C NMR spectroscopy, EI mass spectrometry, elemental analysis, and X-ray structural analysis. By comparison of the IR spectrum of **1**, which exhibits a sharp OH stretching vibration at 3571 cm⁻¹^[6] with the corresponding frequency of **4** (3238 cm⁻¹) a significant shift to lower wave numbers is observed. Such behavior may be due to the formation of hydrogen bonds. Interestingly, the ¹H NMR spectrum of **4** exhibits a resonance signal at $\delta = 2.30$ ppm for the hydroxy hydrogen, which by comparison with that of **1** ($\delta = 1.54$ ppm) clearly shows a downfield shift. Again intermolecular hydrogen interaction and a change of the oxidation state of the germanium atom are plausible explanations for the observed

shift. Thus, this resonance shift indicates a fairly acidic nature of the terminal OH proton. Furthermore no evidence was found for any tautomeric equilibrium of **4**. The most abundant ion peak in the EI mass spectrum appeared at m/z 525 $[\text{M}-\text{Me}]^+$, and the signal at m/z 540 (40%) was assigned to the molecular ion $[\text{M}]^+$ (correct isotopic pattern).

Maintaining a toluene solution of **4** for two weeks at -20°C , resulted in colorless single crystals suitable for X-ray structural analysis.^[8] Compound **4** crystallizes in the monoclinic space group *C2/c*, with one monomer and one molecule of toluene in the asymmetric unit. Intermolecular interaction of the hydroxy group with the sulfur atom results in the formation of the hydrogen-bonding array (O—H...S) leading to dimers (Figure 1). The hydrogen bonded donor-acceptor

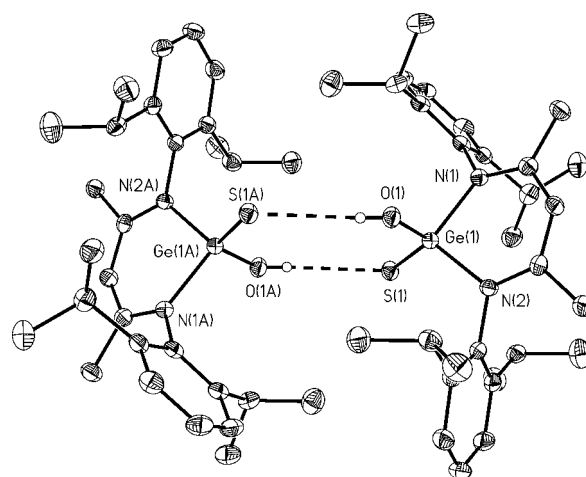


Figure 1. Thermal ellipsoid plot of **4** (thermal ellipsoids set at 50% probability). H atoms, except for the OH group, and interstitial toluene molecules, are omitted for clarity. Selected bond lengths [Å] and angles [°]: Ge(1)–O(1) 1.751(2), Ge(1)–N(2) 1.911(2), Ge(1)–N(1) 1.916(2), Ge(1)–S(1) 2.077(1); O(1)–Ge(1)–N(2) 99.6(1), O(1)–Ge(1)–N(1) 102.2(1), N(2)–Ge(1)–N(1) 95.6(1), O(1)–Ge(1)–S(1) 121.4(1), N(2)–Ge(1)–S(1) 118.8(1), N(1)–Ge(1)–S(1) 114.9(1).

separations (H...S, 2.537 Å and O...S 3.234 Å) follow the same trend as those reported in literature.^[9] The coordination environment around the germanium atom comprises two nitrogen atoms from the supporting ligand, one hydroxy group, and one sulfur atom, and has a distorted tetrahedral geometry.

The Ge–O bond length (1.751(2) Å) in **4** is significantly shorter than that in **1** (1.828(1) Å), as a result of the smaller atomic radius of Ge^{IV} compared with that of Ge^{II}. Indeed, similar Ge–O bond lengths for Ge^{IV} species have been described, (*t*Bu₂Ge(OH)₂ (1.781(4) and 1.779(2) Å)^[10] and 1.779(5) Å in [(FcN)₃GeOH] (Fc = CpFe(η⁵-C₅H₄)).^[11] A shorter Ge–N bond length and wider N–Ge–N angle are expected (av. 1.914(2) Å and 95.6(1)°) than in **1**. A comparison of the Ge–S bond length in [(η³-(μ-*t*BuN)₂(SiMe₂Bu)₂)]GeS]^[12] (2.063(3) Å), and in [HC(CMe)(2,6-*i*Pr₂C₆H₃N)₂Ge(S)X]^[4] (X = Cl, F), (2.053(6) and 2.050(9) Å), with that in **4** (2.077(1) Å) shows a good agreement. Likewise, the Ge–O bond length in [(dppe)Pd(μ-S)(μ-

$\text{CH}_2\text{O})\text{Ge}\{\text{N}(\text{SiMe}_3)_2\}_2$ (dppe = bis(diphenylphosphanyl)-ethene)^[13] (1.785(6) Å), a compound which has almost the same coordination environment and geometry at the germanium center as **4**, correlates well with that in **4**.

In summary the reaction of **1** and elemental sulfur resulted in the formation of the title compound **4** which represents a new class of "carbon-free" carbonic acid analogues based on germanium. The stability of **4** against oxygen and water at room temperature makes these systems quite interesting for biological investigations.

Experimental Section

All manipulations were performed under a dry and oxygen-free atmosphere (N_2 or Ar) by using Schlenk-line and glove-box techniques. Solvents were purified prior to use by distillation over appropriate drying agents in a nitrogen atmosphere.

4: A solution of **1** (1.56 g, 3.07 mmol) in toluene (30 mL) was slowly added to a suspension of elemental sulfur (0.09 g, 3.07 mmol) in toluene (15 mL) by cannula at room temperature. After 3 days under constant stirring at ambient temperature the yellow solution turned slightly green. After removal of all volatiles the remaining crude product was rinsed with pentane (3×10 mL) and dried under reduced pressure to yield pure **4**. Yield: 1.10 g (66 %); m.p. 300 °C (decomp); IR (KBr): $\tilde{\nu}$ = 3238, 3063, 2965, 2867, 1638, 1539, 1442, 1388, 1322, 1257, 1175, 1102, 1023, 933, 875, 797, 712, 501 cm^{-1} ; ^1H NMR (500 MHz, C_6D_6 , 25 °C, TMS): δ = 7.09–7.16 (m, 6H, *m*-, *p*-Ar-H), 4.83 (s, 1H, γ -CH), 3.62 (sept, $^3J(\text{H,H})$ = 6.8 Hz, 2H, $\text{CH}(\text{CH}_3)_2$), 3.35 (sept, $^3J(\text{H,H})$ = 6.8 Hz, 2H, $\text{CH}(\text{CH}_3)_2$), 2.30 (s, 1H, OH), 1.57 (d, $^3J(\text{H,H})$ = 6.8 Hz, 6H, $\text{CH}(\text{CH}_3)_2$), 1.47 (s, 6H, CH_3), 1.26 (d, $^3J(\text{H,H})$ = 6.8 Hz, 6H, $\text{CH}(\text{CH}_3)_2$), 1.16 (d, $^3J(\text{H,H})$ = 6.8 Hz, 6H, $\text{CH}(\text{CH}_3)_2$), 1.05 ppm (d, $^3J(\text{H,H})$ = 6.8 Hz, 6H, $\text{CH}(\text{CH}_3)_2$); ^{13}C NMR (125.8 MHz, C_6D_6 , 25 °C, TMS): δ = 169.9 (C=N), 145.9, 144.9, 137.2, 128.9, 124.8, 124.6 (*i*-, *o*-, *m*-, *p*-, Ar), 98.5 (γ -CH), 29.5 (CH_3), 27.9 ($\text{CH}(\text{CH}_3)_2$), 26.3 ($\text{CH}(\text{CH}_3)_2$), 24.7 ($\text{CH}(\text{CH}_3)_2$), 24.6 ($\text{CH}(\text{CH}_3)_2$), 23.8 ($\text{CH}(\text{CH}_3)_2$), 23.7 ppm ($\text{CH}(\text{CH}_3)_2$); EI-MS (70 eV): m/z (%): 540 (40) $[\text{M}]^+$, 525 (100) $[\text{M}-\text{CH}_3]^+$; elemental analysis (%) calcd for $\text{C}_{29}\text{H}_{42}\text{GeN}_2\text{OS}$ (539.32): C 64.59, H 7.85, N 5.19; found: C 64.20, H 7.57, N 5.12.

Received: June 4, 2004

Keywords: acids · germanium · hydrogen bonds · oxidative addition · sulfur

- [1] J. McMurry, *Organic Chemistry*, Brooks-Cole, CA, **1992**, pp. 695–705.
- [2] P. P. Power, *Chem. Rev.* **1999**, 99, 3463–3504.
- [3] a) N. Tokitoh, R. Okazaki, *Adv. Organomet. Chem.* **2001**, 47, 121–166; b) N. Tokitoh, T. Matsumoto, R. Okazaki, *Bull. Chem. Soc. Jpn.* **1999**, 72, 1665–1684; c) T. Matsumoto, N. Tokitoh, R. Okazaki, *J. Am. Chem. Soc.* **1999**, 121, 8811–8824.

- [4] Y. Ding, Q. Ma, H. W. Roesky, R. Herbst-Irmer, I. Usón, M. Noltemeyer, H.-G. Schmidt, *Organometallics* **2002**, 21, 5216–5220.
- [5] Y. Ding, Q. Ma, H. W. Roesky, I. Usón, M. Noltemeyer, H.-G. Schmidt, *J. Chem. Soc. Dalton Trans.* **2003**, 1094–1098.
- [6] L. W. Pineda, V. Jancik, H. W. Roesky, D. Neculai, A. M. Neculai, *Angew. Chem.* **2004**, 116, 1443–1445; *Angew. Chem. Int. Ed.* **2004**, 43, 1419–1421.
- [7] a) F. Duus in *Comprehensive Organic Chemistry*, Vol. 3 (Eds.: D. Barton, W. D. Ollis), Pergamon, Oxford, **1979**, pp. 420–421; b) J. Hine, *Physical Organic Chemistry*, McGraw-Hill, **1962**, p. 238.
- [8] Crystal data for **4**-toluene: $\text{C}_{36}\text{H}_{50}\text{GeN}_2\text{OS}$, M_r = 631.43, monoclinic, space group $\text{C}2/c$, a = 26.021(1), b = 16.045(1), c = 18.006(2) Å, β = 114.79(1)°, V = 6825(1) Å³, Z = 8, ρ_{calcd} = 1.229 g cm^{-3} , $F(000)$ = 2688, λ = 1.54178 Å, T = 100(2) K, $\mu(\text{Cu K}\alpha)$ = 2.002 mm^{-1} . Data for the structure were collected on a Bruker three-circle diffractometer equipped with a SMART 6000 CCD detector. Intensity measurements were performed on a rapidly cooled crystal ($0.20 \times 0.10 \times 0.10 \text{ mm}^3$) in the range $6.66 \leq 2\theta \leq 118.08^\circ$. Of the 21 505 measured reflections, 4748 were independent [$R(\text{int})$ = 0.0363]. The structure was solved by direct methods (SHELXS-97)^[14] and refined with all data by full-matrix least squares on F^2 .^[15] The hydrogen atoms of C–H bonds were placed in idealized positions, whereas the hydrogen atom from the OH moiety was localized from the difference electron-density map and refined isotropically. The final refinements converged at $R1$ = 0.0283 for $I > 2\sigma(I)$, $wR2$ = 0.0730 for all data. The final difference Fourier synthesis gave a min/max residual electron density $-0.279/+0.355 \text{ e \AA}^{-3}$. CCDC-240065 (**4**) contains the supplementary crystallographic data for this paper. These data can be obtained free of charge via www.ccdc.cam.ac.uk/conts/retrieving.html (or from the Cambridge Crystallographic Data Centre, 12 Union Road, Cambridge CB2 1EZ, UK; fax: (+44) 1223-336-033; or deposit@ccdc.cam.ac.uk).
- [9] a) N. N. Greenwood, A. Earnshaw, *Chemistry of the Elements*, Butterworth-Heinemann, Oxford, **1997**, p. 60; b) A. F. Wells, *Structural Inorganic Chemistry*, Clarendon, Oxford, **1984**, p. 357.
- [10] H. Puff, S. Franken, W. Schuh, W. Schwab, *J. Organomet. Chem.* **1983**, 254, 33–41.
- [11] A. Fischer, K. Jacob, F. T. Edelmann, *Z. Anorg. Allg. Chem.* **2003**, 629, 963–967.
- [12] M. Veith, S. Becker, V. Huch, *Angew. Chem.* **1989**, 101, 1287–1289; *Angew. Chem. Int. Ed. Engl.* **1989**, 28, 1237–1238. For comparison, see also M. C. Kuchta, G. Parkin, *J. Chem. Soc. Chem. Commun.* **1994**, 1351–1352; M. Veith, A. Rammo, *Z. Anorg. Allg. Chem.* **1997**, 623, 861–872; I. Saur, G. Rima, H. Gornitzka, K. Miqueu, J. Barrau, *Organometallics* **2003**, 22, 1106–1109.
- [13] Z. T. Cygan, J. W. Kampf, M. M. Banaszak Holl, *Organometallics* **2004**, 23, 2370–2375.
- [14] "SHELXS-97, Program for Structure Solution": G. M. Sheldrick, *Acta Crystallogr. Sect. A* **1990**, 46, 467–473.
- [15] G. M. Sheldrick, SHELXL-97, Program for Crystal Structure Refinement, University of Göttingen, Göttingen (Germany), **1997**.

Molecular Gyroscopes

Molecular Gyroscopes: $\{\text{Fe}(\text{CO})_3\}$ and $\{\text{Fe}(\text{CO})_2(\text{NO})\}^+$ Rotators Encased in Three-Spoke Stators; Facile Assembly by Alkene Metatheses**

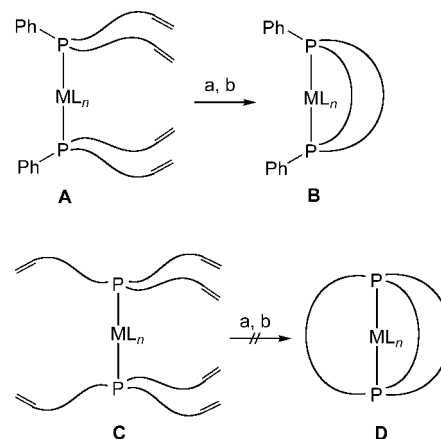
Takanori Shima, Frank Hampel, and J. A. Gladysz*

Molecules that can perform a rotor function are experiencing increasing attention, particularly in the context of nanoscale devices.^[1–6] These efforts have evolved far beyond the initial concept stage^[7] to materials that are being exploited in nanofluidics and photonics. All rotors consist of a rotator and a stator. Importantly, rotators with electric dipole moments can, in appropriately oriented alternating electric fields, be rendered unidirectional.^[1b] Other types of external stimuli can also effect unidirectional rotation,^[5b,6] which is a necessary feature of molecular motors.^[6]

One subset of molecular rotors has been termed molecular gyroscopes.^[3,4] Such compounds feature an axis, an interior domain of which can rotate independently of the termini. However, to our knowledge there are no examples in which this interior rotator is encased by a stator with multiple “spokes”, such that the connectivity and symmetry (D_{nh}) of a toy gyroscope is rigorously duplicated.^[8] In this communication, we report a novel, convenient, and general route to a family of such compounds that utilizes ring-closing alkene metathesis. The lengths of the spokes are easily varied, and a dipole moment can be introduced on the rotator without affecting its steric properties.

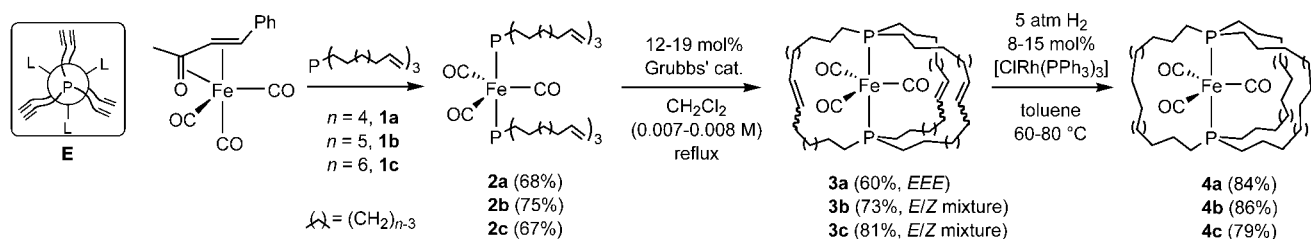
In previous studies, we established that alkene metathesis can be used to connect phosphane ligands that contain a $(\text{CH}_2)_n\text{CH}=\text{CH}_2$ substituent ($n > 4$) and occupy *trans* positions in square-planar metal complexes.^[9] As shown in

Scheme 1, analogous reactions can be conducted with complexes in which each phosphane contains two such substituents (**A**), giving doubly bridged assemblies (**B**).^[9c] However, the yields are lower. Unfortunately, extensions to complexes bearing phosphanes with three such substituents, $\text{P}((\text{CH}_2)_n\text{CH}=\text{CH}_2)_3$ **1**, $n = 4$ –6, and triply bridged assemblies (**D**) were unsuccessful.^[10]



Scheme 1. Elaboration of alkene-containing *trans*-bis(phosphane) complexes to *trans*-spanning diphosphane complexes. a) Alkene metathesis, b) hydrogenation. $\text{ML}_n = \text{Cl-Pt-C}_6\text{F}_5$.

In these efforts, the local symmetry of the metal fragment in **C** did not match that of the phosphane **1**. Hence, we set out to prepare trigonal-bipyramidal complexes consisting of an equatorial ML_3 array and two such axial phosphanes. Since the substituents along the P–M–P axis should prefer staggered conformations as in **E** (Scheme 2), such systems are better preorganized with respect to the target molecules **D**. Thus, (benzylideneacetone)iron tricarbonyl and **1a–c**^[11] were



Scheme 2. Syntheses of gyroscope-like molecules.

[*] Dr. T. Shima, Dr. F. Hampel, Prof. Dr. J. A. Gladysz
Institut für Organische Chemie
Friedrich-Alexander-Universität Erlangen-Nürnberg
Henkestrasse 42, 91054 Erlangen (Germany)
Fax: (+49) 9131-85-26865
E-mail: gladysz@organik.uni-erlangen.de

[**] We thank the Deutsche Forschungsgemeinschaft (DFG, GL 300/1-3) and the Humboldt Foundation (fellowship to T.S.) for support.

Supporting information for this article is available on the WWW under <http://www.angewandte.org> or from the author.

reacted. Workup gave, in accord with precedent for other phosphanes,^[12] diaxially substituted *trans*- $[\text{Fe}(\text{CO})_3\text{-P}((\text{CH}_2)_n\text{CH}=\text{CH}_2)_2]$ (**2a–c**) as yellow oils in 75–67% yield.^[13] These exhibited a single intense IR $\bar{\nu}_{\text{CO}}$ band (1860–1856 cm^{-1}), as did all other $\{\text{Fe}(\text{CO})_3\}$ species below.

The metathesis of **2a** was investigated first. As shown in Scheme 2, a 0.0075 M solution in CH_2Cl_2 was refluxed with Grubbs' catalyst (13 mol% or 4% per new C=C linkage). Workup afforded a homogeneous white solid (**3a**) in 60% yield. Reaction aliquots were assayed by ^{31}P NMR spectroscopy.

copy. The spectra showed two intermediates that gave a monotonic chemical-shift sequence from **2a** to **3a** ($\delta = 64.2, 67.9, 75.0, 84.7$ ppm, C_6D_6), and only minor amounts of by-products. The mass spectrum of **3a** exhibited a molecular ion signal appropriate for the product of a three-fold intramolecular metathesis and no peaks of higher mass.^[13] The ^{13}C NMR spectrum (C_6D_6) indicated a highly symmetric species, with a single FeCO signal coupled to both phosphorus atoms (213.9 ppm, t, $J_{CP} = 28$ Hz), a single C=C signal (132.0 ppm), and four CH_2 signals. Hence, **3a** was assigned the gyroscope-like structure depicted in Scheme 2, with three 13-membered rings containing *E* C=C linkages.^[14]

Next, a solution of **3a** and Wilkinson's catalyst (8 mol %) in toluene was treated with H_2 (5 atm) at $80^\circ C$. Workup gave the hydrogenation product **4a** as a white solid in 84 % yield. In accord with the high idealized molecular symmetry (D_{3h}), the ^{13}C NMR spectrum exhibited only five CH_2 signals.^[13] When reaction aliquots were assayed by ^{31}P NMR spectroscopy, two intermediates could again be detected, with chemical shifts changing monotonically from **3a** to **4a** ($\delta = 84.7, 81.1, 78.1, 75.5$ ppm, C_6D_6). Complexes **3a** and **4a** were moderately air sensitive, but showed no mass loss at temperatures less than $300^\circ C$ (TGA). The latter melted at 165 – $170^\circ C$ (capillary; $174^\circ C$, DSC).

The generality of the preceding sequence was tested with **2b** and **2c**. Metatheses under similar conditions gave **3b** and **3c**, with three 15- and 17-membered rings, in yields of 73 % and 81 %, respectively. The mass spectra showed molecular ions and no peaks of higher mass. However, mixtures of *E* and *Z* C=C bonds were present, as evidenced by multiple ^{31}P NMR signals. When the second-generation Grubbs' catalyst was used,^[15] the yield of **3c** was unaffected, but that of **3a** increased to 76 %.

Analogous hydrogenations of **3b** and **3c** gave **4b** and **4c** in yields of 86 % and 79 %, respectively. Interestingly, the IR ν_{CO} values of **4a–c** exhibited a monotonic trend (1841, 1853, 1861 cm^{-1}).

Prisms of **4c** were grown, and the crystal structure was solved as described in the Supporting Information. Views of the molecular structure are collected in Figure 1. The P-Fe-P substituents are arrayed in staggered conformations as in **E**, and a crystallographic C_2 axis passes through the Fe-C1-O1 linkage, exchanging two of the 17-membered rings. The bond lengths and angles about

iron are unexceptional. However, the space-filling representations suggest there is enough room for the $\{Fe(CO)_3\}$ moiety to rotate within the three $P(CH_2)_{14}P$ spokes. In this regard, it is useful to compare the iron–oxygen distances (2.93 \AA) with those from the iron to the distal carbon atoms of the macrocycles (7.86 – 6.64 \AA). When the van der Waals radius of oxygen is added to the former, and that of carbon is subtracted from the latter, considerable “clearance” remains (4.45 \AA vs. 6.10 – 4.94 \AA). The molecules pack in layers with the vertically aligned P-Fe-P axes. Those in one layer are offset in both in-plane dimensions from those in adjacent layers.

The symmetries of **3a** and **4a–c** are too high to probe the rate of $\{Fe(CO)_3\}$ rotation by conventional solution-phase NMR techniques. Thus, derivatives of lower symmetry were sought. As shown in Scheme 3, **3a** and **4a** were combined with CF_3SO_3H in $CDCl_3$ in an NMR tube. In accord with precedent for closely related complexes,^[12] the cationic iron hydrides **5a** $^+ \cdot CF_3SO_3^-$ and **6a** $^+ \cdot CF_3SO_3^-$ formed in quantitative yields, as evidenced by diagnostic 1H NMR signals ($\delta = -9.41$ and -9.42 , t, $J_{HP} = 21.4$ and 21.8 Hz). The ^{13}C NMR spectra recorded at ambient temperature showed two sets of $P(CH_2)_4C$ signals (2:1), indicating a slow-exchange limit with respect to any process (e.g., $\{HFe(CO)_3\}$ rotation) that can render the bridges equivalent.

We next sought to replace one carbonyl ligand of **4a–c** by a similarly sized ligand. As shown in Scheme 3, reactions with $NO^+ \cdot BF_4^-$ gave the isoelectronic and isosteric dicarbonyl nitrosyl cations **7a–c** $^+ \cdot BF_4^-$ in 98–81 % yield.^[13] Although many $\{Fe(CO)_3\}$ species behave similarly,^[16] it is of mechanistic note that substitution is not inhibited by the three methylene bridges. The IR spectra of **7a–c** $^+ \cdot BF_4^-$ exhibited

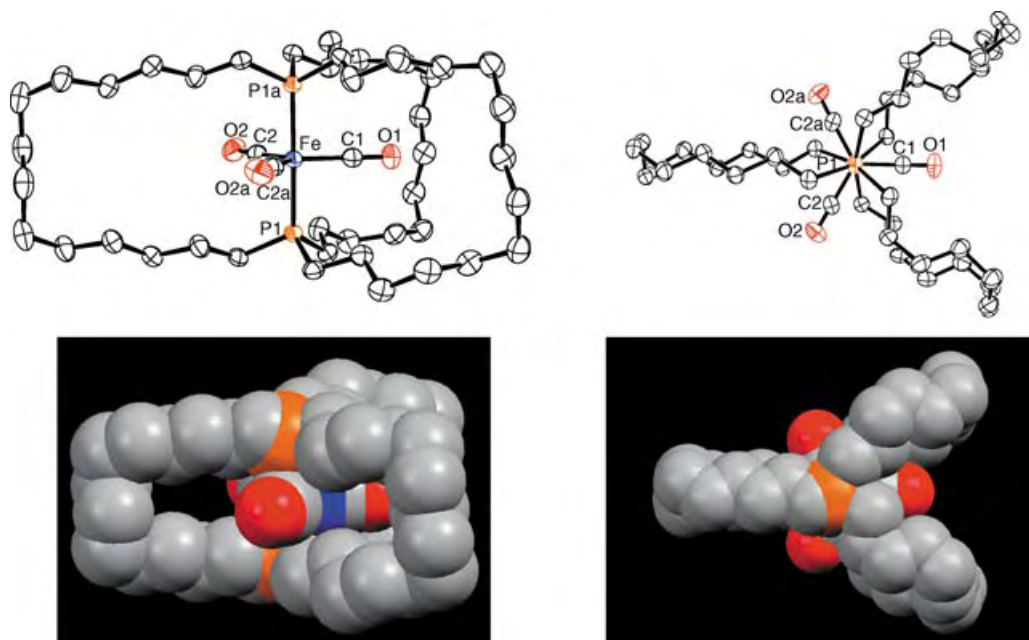
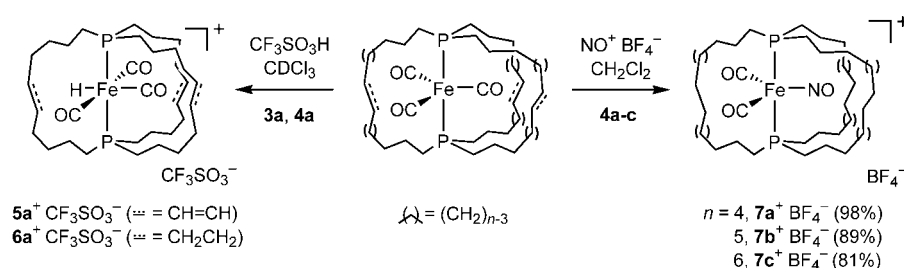


Figure 1. ORTEP (top) and space-filling (bottom) representations of the crystal structure of **4c**. Selected bond lengths [Å] and angles [°]: Fe–C1 1.761(3), Fe–C2 1.764(2), Fe–P1 2.2056(5), C1–O1 1.162(3), C2–O2 1.164(3); Fe–C1–O1 180.000(1), Fe–C2–O2 179.3(2), C1–Fe–C2 118.99(7), C2–Fe–C2a 122.02(14), C1–Fe–P1 90.565(17), C2–Fe–P1 90.32(6), P1–Fe–P1a 178.87(3).



Scheme 3. Symmetry reduction of gyroscope-like molecules.

two $\tilde{\nu}_{CO}$ bands (2023–2030 cm^{-1} , m, 1953–1965 cm^{-1} , s) and a $\tilde{\nu}_{NO}$ band (1752–1764 cm^{-1} , s). The ^{13}C NMR spectra of $7a,b^+BF_4^-$ gave two sets of $P(CH_2)_{n+1}$ signals (2:1), while the spectrum of $7c^+BF_4^-$ gave only one. This indicates, in accord with expectations from the crystal structure of **4c**, that $\{Fe(CO)_2(NO)\}^+$ rotation is rapid on the NMR timescale at room temperature for $7c^+BF_4^-$, but slow for $7a,b^+BF_4^-$. Importantly, both phosphorus atoms of $7c^+BF_4^-$ retain coupling to the $PCH_2CH_2CH_2$ and CO signals, excluding the most probable dissociative mechanisms for rendering the bridges equivalent.

The dynamic behavior of $7a-c^+BF_4^-$ was further probed by variable-temperature ^{13}C NMR spectroscopy. A solution of $7c^+BF_4^-$ in $CDCl_3$ was cooled from -10 to $-80^\circ C$. The chemical shifts of the $PCH_2CH_2CH_2$ carbons remained essentially constant, while those of the other methylene carbons shifted. The PCH_2CH_2 signal decoalesced in a well-defined manner, enabling spectra and line-shape simulation. These data gave ΔH^\ddagger and ΔS^\ddagger values of 9.5 $kcal\ mol^{-1}$ and -6.5 eu for $\{Fe(CO)_2(NO)\}^+$ rotation. If CO or NO dissociation were required to render the bridges equivalent, a large positive ΔS^\ddagger value would be expected. Finally, a solution of $7b^+BF_4^-$ in C_6D_5Br was warmed from $25^\circ C$ to $100^\circ C$. Although coalescence was apparent, lines broadened, presumably due to a small amount of concomitant decomposition. Quantitative analyses were not possible.

In summary, we have described a facile synthesis of a family of molecules that duplicate the symmetry, connectivity, and rotator function of standard toy gyroscopes. The stator consists of three spokes that span the termini of the gyroscope axis. Their lengths can be adjusted to modulate the rotational barrier of the interior rotator. The rotators consist of either an $\{Fe(CO)_3\}$ moiety, or an isoelectronic and isosteric $\{Fe(CO)_2(NO)\}^+$ moiety. The latter introduces a dipole moment, which represents a possible means of driving unidirectional rotation. However, the idealized limit of a frictionless gyroscope is not closely modeled by the present systems, and much different architectures will be required to approach this objective.

The title molecules can also be regarded as a special class of cryptates.^[17] If the $\{Fe(CO)_3\}$ moieties were to be excised from **4a-c**, a reaction type with good precedent, the resulting bicyclic bridgehead diphosphanes would be *in, in* isomers. Such species are unusual and normally accessible only by lengthy syntheses or in low yields.^[18] Importantly, similar methodology can be applied to generate gyroscope-like molecules with two spokes.^[10,19] These will be described in

future reports, together with additional properties of the complexes prepared above. Finally, the design insights realized in conjunction with Scheme 1 have advanced the utility of alkene metatheses in the synthesis of topologically novel organometallic and inorganic molecules, a number of other elegant examples of which have recently appeared.^[20]

Received: May 1, 2004

Published Online: August 27, 2004

Keywords: alkene metathesis · iron · N ligands · phosphine ligands · ring-closing metathesis

- [1] a) J. Vacek, J. Michl, *New J. Chem.* **1997**, 21, 1259; b) X. Zheng, M. E. Mulcahy, D. Horinek, F. Galeotti, T. F. Magnera, J. Michl, *J. Am. Chem. Soc.* **2004**, 126, 4540, and references therein.
- [2] T. C. Bedard, J. S. Moore, *J. Am. Chem. Soc.* **1995**, 117, 10662.
- [3] a) Z. Dominguez, H. Dang, J. M. Strouse, M. A. Garcia-Garibay, *J. Am. Chem. Soc.* **2002**, 124, 7719; b) Z. Dominguez, T.-A. Khuong, H. Dang, C. N. Sanrame, J. E. Nuñez, M. A. Garcia-Garibay, *J. Am. Chem. Soc.* **2003**, 125, 8827; c) C. E. Godinez, G. Zepeda, C. J. Mortko, H. Dang, M. A. Garcia-Garibay, *J. Org. Chem.* **2004**, 69, 1652.
- [4] C. A. Schalley, *Angew. Chem.* **2002**, 114, 1417; *Angew. Chem. Int. Ed.* **2002**, 41, 1513.
- [5] For additional representative molecular rotors with covalently attached axles, see: a) T. R. Kelly, *Acc. Chem. Res.* **2001**, 34, 514; b) R. A. van Delden, J. H. Hurenkamp, B. L. Feringa, *Chem. Eur. J.* **2003**, 9, 2845, and references therein; c) H. Jian, J. M. Tour, *J. Org. Chem.* **2003**, 68, 5091; d) M. F. Hawthorne, J. I. Zink, J. M. Skelton, M. J. Bayer, C. Liu, E. Livshits, R. Baer, D. Neuhauser, *Science* **2004**, 303, 1849.
- [6] Recent review of molecular motors: C. P. Mandl, B. König, *Angew. Chem.* **2004**, 116, 1650; *Angew. Chem. Int. Ed.* **2004**, 43, 1622.
- [7] P. Kaszynski, A. C. Friedli, J. Michl, *J. Am. Chem. Soc.* **1992**, 114, 601.
- [8] Moore's "molecular turnstiles", which consist of a $C\equiv C-C_6H_2R_2-C\equiv C$ axis and a stator with two spokes,^[2] nearly fulfill these criteria. The addition or removal of two *tert*-butyl groups from the stator would, coupled with a C_6H_4 rotator, afford the proper D_{2h} symmetry.
- [9] a) J. Ruwwe, J. M. Martín-Alvarez, C. R. Horn, E. B. Bauer, S. Szafert, T. Lis, F. Hampel, P. C. Cagle, J. A. Gladysz, *Chem. Eur. J.* **2001**, 7, 3931; b) E. B. Bauer, F. Hampel, J. A. Gladysz, *Organometallics* **2003**, 22, 5567; c) T. Shima, E. B. Bauer, F. Hampel, J. A. Gladysz, *Dalton Trans.* **2004**, 1012.
- [10] E. B. Bauer, T. Shima, unpublished results, Universität Erlangen-Nürnberg.
- [11] Phosphanes **1a-c** were prepared in yields of 87–56% by reactions of the Grignard reagents $BrMg(CH_2)_nCH=CH_2$ (generated from the readily available alkyl bromides) and PCl_3 . Spectroscopic properties were similar to those of the homologues $PhP((CH_2)_nCH=CH_2)_2$ reported previously.^[9c]
- [12] J. R. Sowa Jr., V. Zanolli, G. Facchin, R. J. Angelici, *J. Am. Chem. Soc.* **1991**, 113, 9185.
- [13] NMR (1H , ^{13}C , ^{31}P), IR, MS, and microanalytical data are summarized in the Supporting Information. CCDC 237814 contains the supplementary crystallographic data for this paper. These data can be obtained free of charge via www.ccdc.

- ac.uk/conts/retrieving.html (or from the Cambridge Crystallographic Data Centre, 12 Union Road, Cambridge CB2 1EZ, UK; fax: (+ 44) 1223-336-033; e-mail: deposit@ccdc.cam.ac.uk).
- [14] The *E* C=C stereochemistry is assumed by analogy to that established for ring-closing metatheses of other complexes with *trans* P(CH₂)₄CH=CH₂ moieties (e.g., **A** → **B**).^[9b,c]
 - [15] [Ru(=CHPh)(H₂IMes)(PCy₃)(Cl)₂]; H₂IMes = 1,3-dimesityl-4,5-dihydroimidazol-2-ylidene.
 - [16] B. F. G. Johnson, J. A. Segal, *J. Chem. Soc. Dalton Trans.* **1972**, 1268.
 - [17] For some conceptionally related systems, see a) V. J. Catalano, B. L. Bennett, R. L. Yson, B. C. Noll, *J. Am. Chem. Soc.* **2000**, *122*, 10056; b) V. J. Catalano, B. L. Bennett, M. A. Malwitz, R. L. Yson, H. M. Kar, S. Muratidis, S. J. Horner, *Comments Inorg. Chem.* **2003**, *24*, 39.
 - [18] a) I. Bauer, O. Rademacher, M. Gruner, W. D. Habicher, *Chem. Eur. J.* **2000**, *6*, 3043; b) R. W. Alder, D. Read, *Angew. Chem.* **2000**, *112*, 3001; *Angew. Chem. Int. Ed.* **2000**, *39*, 2879.
 - [19] For an interesting molecule that can be regarded as a progenitor of a family of such gyroscopes, and was prepared by alkene metathesis of a *trans*-bis(pyridine)palladium dichloride complex, see P. L. Ng, J. N. Lambert, *Synlett* **1999**, 1749. The ring size in this compound precludes rotation of the PdCl₂ moiety.
 - [20] a) Review: E. B. Bauer, J. A. Gladysz in *Handbook of Metathesis*, Vol. 2 (Ed.: R. H. Grubbs), Wiley-VCH, New York, **2003**, p. 403; b) V. Martinez, J.-C. Blais, D. Astruc, *Angew. Chem.* **2003**, *115*, 4502; *Angew. Chem. Int. Ed.* **2003**, *42*, 4366.

pounds (oxosilicates). SiX_4 tetrahedrons ($\text{X} = \text{O}, \text{N}$) are a typical feature of almost all previously described oxo- and nitridosilicates.^[2] They are connected through common corners ($\text{X} = \text{O}, \text{N}$) or edges ($\text{X} = \text{N}$) and form condensed anionic structures with a wide range of degree of condensation.^[1,3]

The degree of condensation κ (i.e. the molar ratio Si/X) of oxosilicates, which can easily be derived from the empirical formula, usually allows a conclusion to be drawn about the dimensionality of the framework of simple oxosilicates: Nesosilicates such as almandine ($\text{Fe}_3\text{Al}_2[\text{SiO}_4]_3$) or zircon (ZrSiO_4) contain only non-condensed (isolated) $[\text{SiO}_4]^{4-}$ tetrahedrons. Hence, they exhibit the lowest degree of condensation ($\kappa = 1/4$) possible in ordinary silicates. With increasing connectivity of the SiO_4 tetrahedrons the degree of condensation is raised to $\kappa = 2/7$ in disilicates (e.g. in thortveitite ($\text{Sc}_2[\text{Si}_2\text{O}_7]$)), to $\kappa = 1/3$ in ring silicates (e.g. in benitoite ($\text{BaTi}[\text{Si}_3\text{O}_9]$) or in beryl ($\text{Al}_2\text{Be}_3[\text{Si}_6\text{O}_{18}]$)) and to $\kappa = 2/5$ in single-layer silicates such as pyrophyllite ($\text{Al}_2[\text{Si}_4\text{O}_{10}(\text{OH})_2]$) or serpentine ($\text{Mg}_3[\text{Si}_2\text{O}_5(\text{OH})_4]$).^[1] The highest degree of condensation possible in all known oxosilicates is $\kappa = 1/2$. It can be found in frames of SiO_2 in which all SiO_4 tetrahedrons are connected to each other through their four O vertices. Because of the higher charge of nitridic nitrogen (N^{3-}) in highly condensed nitridosilicates (e.g. $\text{BaYb}[\text{Si}_4\text{N}_7]$, $\text{Ba}[\text{Si}_7\text{N}_{10}]$)^[3] and silicon nitride Si_3N_4 itself, degrees of condensation have been observed even within the range $1/2 < \kappa < 3/4$, which are not accessible in oxosilicates.

During the last few years we have conducted a systematic investigation of new oxonitridosilicates (sions) and oxonitridoaluminosilicates (sialons).^[9] Both classes are of considerable significance in materials science due to their extraordinary chemical and thermal stability, and they are of special interest to us as host lattices for rare-earth-doped phosphors.^[10]

In the system $\text{CaO-SiO}_2\text{-Si}_3\text{N}_4$ we recently discovered $\text{Ca}[\text{Si}_2\text{O}_2\text{N}_2]$, which was obtained by facile reaction of CaCO_3 with Si_3N_4 at 1580°C in a radio frequency (r. f.) furnace as colorless lath-shaped single crystals (see Experimental Section). The single-crystal X-ray structure analysis^[11] of the oxonitridosilicate $\text{Ca}[\text{Si}_2\text{O}_2\text{N}_2]$ revealed an unexpected structure: According to the empirical formula and the respective degree of condensation of $\kappa = 1/2$ one would expect a three-dimensional framework structure of corner-sharing SiX_4 entities (i.e. $\text{SiO}_{4/2} = \text{SiO}_2$) for a silicate such as $\text{Ca}[\text{Si}_2\text{O}_2\text{N}_2]$ formed by SiX_4 tetrahedrons ($\text{X} = \text{O}, \text{N}$). However, $\text{Ca}[\text{Si}_2\text{O}_2\text{N}_2]$ is a layer silicate composed of SiON_3 tetrahedrons of the type Q^3 (Figure 1). The unusual composition of this corrugated layer anion $[\text{Si}_2\text{O}_2\text{N}_2]^{2-}$ originates from the fact that in this compound every N atom—unlike the O atoms in oxosilicates^[1]—links three neighboring Si tetrahedron centers ($\text{N}^{[3]}$), whereas the O atoms in $\text{Ca}[\text{Si}_2\text{O}_2\text{N}_2]$ are exclusively bonded terminally to Si atoms ($\text{O}^{[1]}$). In structures of oxosilicates that consist of SiO_4 tetrahedrons, oxygen is either bonded terminally to a single Si atom ($\text{O}^{[1]}$) or bridges two Si atoms ($\text{O}^{[2]}$). In contrast, in nitridosilicates $\text{N}^{[3]}$ connections are observed frequently^[3] and, moreover, even ammonium-like $\text{N}^{[4]}$ bridges have been found.^[12]

Owing to their very similar scattering factors the direct experimental differentiation between O and N in the $[\text{Si}_2\text{O}_2\text{N}_2]^{2-}$ framework is impossible with X-ray methods.

Structure Elucidation

$\text{Ca}[\text{Si}_2\text{O}_2\text{N}_2]$ —A Novel Layer Silicate**

Henning A. Höpfe, Florian Stadler, Oliver Oeckler, and Wolfgang Schnick*

Dedicated to Professor Martin Jansen
on the occasion of his 60th birthday

Silicates are one of the largest classes of compounds in inorganic chemistry.^[1] Most of them are pure oxidic com-

[*] Dr. H. A. Höpfe,† Dipl.-Chem. F. Stadler, Dr. O. Oeckler, Prof. Dr. W. Schnick
Department Chemie und Biochemie
der Ludwig-Maximilians-Universität
Lehrstuhl für Anorganische Festkörperchemie
Butenandtstrasse 5–13(D), 81377 München (Germany)
Fax: + (49) 89-2180-77440
E-mail: wolfgang.schnick@uni-muenchen.de

[†] New address:
Albert-Ludwigs-Universität, Institut für Anorganische Chemie
Albertstrasse 21, 79104 Freiburg (Germany)

[**] This work was supported by the Fonds der Chemischen Industrie and the Deutsche Forschungsgemeinschaft. The authors are indebted to Dr. J. Senker, München, for solid-state NMR investigations as well as to Dr. T. Jüstel and to Dr. P. Schmidt, Philips Research Laboratories, Aachen, for luminescence measurements and fruitful discussions.

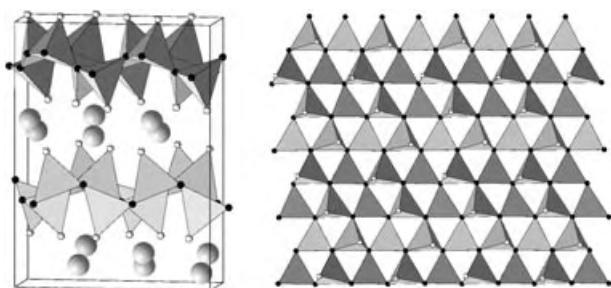


Figure 1. Crystal structure of $\text{Ca}[\text{Si}_2\text{O}_2\text{N}_2]$; left: view along $[100]$; right: view perpendicular to a layer of tetrahedra along $[010]$ (Ca^{2+} light gray, O^{2-} white, N^{3-} black).

^{29}Si solid-state NMR investigations on $\text{Ca}[\text{Si}_2\text{O}_2\text{N}_2]$ revealed a group of closely adjoining signals in the range from $\delta = -50$ to -54 ppm, which is typical for chemical shifts of Q^3 -type SiON_3 tetrahedra.^[9,13] According to the calculations of the Madelung part of the lattice energy (MAPLE)^[14] in $\text{Ca}[\text{Si}_2\text{O}_2\text{N}_2]$ a complete O/N-ordering seems to be very likely. Accordingly, the O atoms are bonded terminally to the Si atoms (O^{I}), and each N atom links three Si atoms within the layers (N^{B}). This result agrees well with Pauling's rules and reflects our experiences with sions and sialons, in which nitrogen more so than oxygen prefers to adopt those sites that offer higher connectivities with respect to the tetrahedron centers.^[9] Assuming this ordering, we calculated the following partial MAPLE values for $\text{Ca}[\text{Si}_2\text{O}_2\text{N}_2]$: O^{2-} : 2272–2404, N^{3-} : 6125–6353, Ca^{2+} : 2115–2214, and Si^{4+} : 9281–9555 kJ mol^{-1} . The values fit well into the typical ranges for these ions.^[9] The analysis of the interatomic distances Si–O (159–162 pm) and Si–N (168–178 pm) as well as the exclusive presence of SiON_3 tetrahedra confirm the described O/N ordering, since a clear difference in bond lengths $\text{Si–N} > \text{Si–O}$ was found for all SiON_3 entities.^[15]

The Ca^{2+} ions are surrounded by six O atoms to form a distorted trigonal prism, which is capped by a single N atom. The shortest distances in the coordination spheres of Ca^{2+} are those to the O atoms (229–241 pm); these distances agree well with the sum of the ionic radii.

The structure of $\text{Sr}[\text{Si}_2\text{O}_2\text{N}_2]$ is closely related, and exhibits an analogous O/N ordering. This has been confirmed experimentally by the luminescence of the doped compound $\text{Sr}[\text{Si}_2\text{O}_2\text{N}_2]:\text{Eu}^{2+}$ in which the emission wavelength and the width of the emission band allow the unequivocal conclusion that the Eu^{2+} ions (and thus the Sr^{2+} ions) are predominantly coordinated by O atoms that are terminally bonded to the Si atoms inside the SiON_3 tetrahedra.^[16]

The $[\text{Si}_2\text{O}_2\text{N}_2]^{2-}$ layers in $\text{Ca}[\text{Si}_2\text{O}_2\text{N}_2]$ are assembled from condensed “dreier” rings (Figure 1), a building unit which is unknown in purely oxidic layer silicates and very rare in higher condensed oxosilicates.^[1] Similar layers built up of condensed dreier rings have also been found in other nitridosilicates (e.g. $\text{M}_2^{\text{II}}[\text{Si}_5\text{N}_8]$ with $\text{M} = \text{Ca},^{[17]}$ Sr and Ba^[18] or Ba $[\text{Si}_7\text{N}_{10}]^{[19]}$). However, in these compounds the layers are connected by further SiN_4 tetrahedra to form highly condensed framework structures and, moreover, these layers differ topologically by the specific sequence of their

vertices pointing upwards (U) and downwards (D) with respect to the layer plane.^[1] Within the horizontal rows of tetrahedra shown in Figure 1 the strictly alternating sequence UDUD... is found in $\text{Ca}[\text{Si}_2\text{O}_2\text{N}_2]$, whereas, for instance, the layers in $\text{M}_2^{\text{II}}[\text{Si}_5\text{N}_8]$ and Ba $[\text{Si}_7\text{N}_{10}]$ exhibit more complex patterns.^[17–19] Although in principle there is an arbitrary number of completely different sequences to form such layers from condensed dreier rings, topologically very similar layers with the same sequence UDUD... were found in the crystal structure of the mineral sinoite ($\text{Si}_2\text{N}_2\text{O}$) (Figure 2).^[20] In $\text{Sr}[\text{Si}_2\text{O}_2\text{N}_2]$ topologically identical layers are present. The structural relationship between $\text{Si}_2\text{N}_2\text{O}$ and $\text{Sr}[\text{Si}_2\text{O}_2\text{N}_2]$ can therefore be illustrated by an imaginary topochemical intercalation of SrO into sinoite. The feasibility

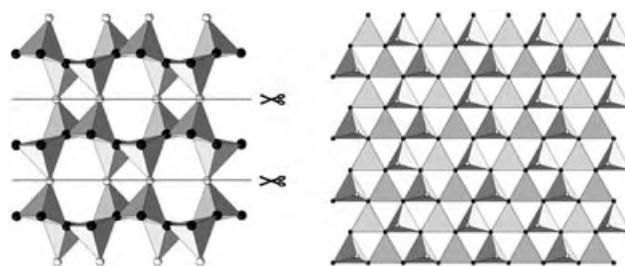


Figure 2. Crystal structure of the mineral sinoite $\text{Si}_2\text{N}_2\text{O}$; left: view along $[001]$. Cutting the structure in the indicated manner leads to layers topologically similar to those in $\text{Ca}[\text{Si}_2\text{O}_2\text{N}_2]$. Accordingly, the O atoms are bonded terminally to the Si atoms (O^{I}), and the N atoms are bridged threefold within the layers as N^{B} ; right: view along $[100]$. The layers also show the sequence UDUD... with regard to the alignment of the tetrahedron vertices (O).

of performing this intercalation experimentally is currently being investigated. Furthermore, it will be interesting to see whether the M^{2+} ions in $\text{Ca}[\text{Si}_2\text{O}_2\text{N}_2]$ and $\text{Sr}[\text{Si}_2\text{O}_2\text{N}_2]$ can undergo ion exchange.

Experimental Section

In a typical experiment CaCO_3 (1.0 mmol; Merck, 99.95%) was thoroughly mixed with amorphous Si_3N_4 (2.1 mmol; obtained by thermal decomposition of $\text{Si}(\text{NH})_2$ ^[9b] in a glove box (Unilab, MBraun, $\text{O}_2 < 0.1$ ppm, $\text{H}_2\text{O} < 0.1$ ppm) under an argon atmosphere using an agate mortar. The mixture was then heated in a tungsten crucible using a r.f. furnace^[9b] under an N_2 atmosphere (dried over KOH/silica gel/molecular sieve (4 Å)/ P_4O_{10} and activated BTS catalyst). The reaction mixture was heated to 1000 °C at a rate of 40 °C min^{−1} and subsequently to 1200 °C over 15 min. During this first reaction step reactive CaO was initially formed by gas loss, which was then allowed to react quantitatively with Si_3N_4 by further heating to 1580 °C (heating rate 1.1 °C min^{−1}) over 16 h to yield single-phase $\text{Ca}[\text{Si}_2\text{O}_2\text{N}_2]$. Elemental analysis (double determinations by the Mikroanalytisches Labor Pascher, Remagen) calcd (%) for $\text{Ca}[\text{Si}_2\text{O}_2\text{N}_2]$ (156.28); Ca 25.6, Si 35.9, O 20.5, N 17.9; found: Ca 25.6, Si 36.1, O 21.8, N 17.1.

Large single crystals suitable for X-ray structure analysis were obtained by raising the temperature up to 1900 °C at which the thermal decomposition of the reaction product takes place. A theoretical powder diffraction pattern calculated on the basis of the single-crystal data shows excellent agreement with a measured

powder diffraction pattern for $\text{Ca}[\text{Si}_2\text{O}_2\text{N}_2]$ with respect to the position and intensity of all observed reflections.

Received: March 23, 2004

Keywords: dreier rings · layered compounds · oxonitrides · silicates · structure elucidation

- [1] F. Liebau, *Structural Chemistry of Silicates*, Springer, Berlin, **1985**.
- [2] In silicates, higher coordination numbers of Si ($\text{CN} > 4$) are found only in a few cases, mostly high-pressure phases,^[1,4,5] for example, the rutile-type SiO_2 high-pressure polymorph stishovite, the perovskite-type $(\text{Mg},\text{Fe})\text{SiO}_3$ that occurs in the deeper mantle of the earth or the hollandite-analogous $\text{CaAl}_2\text{Si}_2\text{O}_8$.^[4] At lower pressures a few silicates can be obtained that contain both SiO_6 octahedrons and SiO_4 tetrahedrons (e.g. $\text{K}_2\text{Si}_4\text{O}_9$,^[6] BaSi_4O_9 ,^[7] and $\text{Na}_{1.8}\text{Ca}_{1.1}\text{Si}_6\text{O}_{14}$ ^[8]).
- [3] H. Huppertz, W. Schnick, *Chem. Eur. J.* **1997**, 3, 679.
- [4] L. W. Finger, R. M. Hazen, *Acta Crystallogr. Sect. B* **1991**, 47, 561.
- [5] R. M. Hazen, R. T. Downs, L. W. Finger, *Science* **1996**, 272, 1769.
- [6] D. K. Swanson, C. T. Prewitt, *Am. Mineral.* **1983**, 68, 581.
- [7] L. W. Finger, R. M. Hazen, B. A. Fursenko, *J. Phys. Chem. Solids* **1995**, 56, 1389.
- [8] T. Gasparik, J. B. Parise, B. A. Eiben, J. A. Hriljac, *Am. Mineral.* **1995**, 80, 1269.
- [9] a) R. Lauterbach, W. Schnick, *Z. Anorg. Allg. Chem.* **1998**, 624, 1154; b) W. Schnick, H. Huppertz, R. Lauterbach, *J. Mater. Chem.* **1999**, 9, 289; c) K. Köllisch, W. Schnick, *Angew. Chem.* **1999**, 111, 368; *Angew. Chem. Int. Ed.* **1999**, 38, 357; d) R. Lauterbach, W. Schnick, *Z. Anorg. Allg. Chem.* **2000**, 626, 56; e) E. Irran, K. Köllisch, S. Leoni, R. Nesper, P. F. Henry, M. T. Weller, W. Schnick, *Chem. Eur. J.* **2000**, 6, 2714; f) R. Lauterbach, E. Irran, P. F. Henry, M. T. Weller, W. Schnick, *J. Mater. Chem.* **2000**, 10, 1357; g) R. Lauterbach, W. Schnick, *Solid State Sci.* **2000**, 2, 463; h) H. A. Höpfe, G. Kotzyba, R. Pöttgen, W. Schnick, *J. Solid State Chem.* **2002**, 167, 393.
- [10] H. A. Höpfe, H. Lutz, P. Morys, W. Schnick, A. Seilmeier, *J. Phys. Chem. Solids* **2000**, 61, 2001.
- [11] Crystal structure data of $\text{Ca}[\text{Si}_2\text{O}_2\text{N}_2]$: Bruker Nonius Kappa-CCD-diffractometer with rotating anode, $\text{MoK}\alpha$ (71.073 pm), $2\theta_{\text{max}} = 65^\circ$, crystal size $0.06 \times 0.05 \times 0.02 \text{ mm}^3$, monoclinic, space group $P2_1$ (no. 4), $a = 734.4(2)$, $b = 1365.6(3)$, $c = 1048.3(2) \text{ pm}$, $\beta = 102.04(3)^\circ$, $V = 1.0283(4) \text{ nm}^3$, $Z = 12$, $\rho_{\text{calc}} = 3.028 \text{ g cm}^{-3}$, $\mu(\text{MoK}\alpha) = 2.351 \text{ mm}^{-1}$, 22771 measured reflections, 7035 of which are independent, $R_{\text{int}} = 0.0562$, least-squares refinement (Ca and Si anisotropic, O and N isotropic) on F^2 (G. M. Sheldrick, SHELXL-97, Program for the refinement of crystal structures, University of Göttingen, Göttingen (Germany), **1997**); numerical absorption correction (min./max. transmission factor 0.8401/0.9529), Flack parameter $\eta = 0.2(1)$, R values (all data/ $F_o^2 \geq 2\sigma(F_o^2)$) $R_1 = 0.0825/0.0458$, $wR_2 = 0.1029/0.0885$, $\text{Goof} = 1.030$ for 4877 observed reflections ($F_o^2 \geq 2\sigma(F_o^2)$) and 260 refined parameters. Further details on the crystal structure investigations may be obtained from the Fachinformationszentrum Karlsruhe, 76344 Eggenstein-Leopoldshafen, Germany (fax: (+49)7247-808-666; e-mail: crysdata@fiz-karlsruhe.de), on quoting the depository number CSD-413882.
- [12] H. Huppertz, W. Schnick, *Angew. Chem.* **1996**, 108, 2115; *Angew. Chem. Int. Ed. Engl.* **1996**, 35, 1983.
- [13] S. Kohn, W. Hoffbauer, M. Jansen, R. Franke, S. Bender, *J. Non-Cryst. Solids* **1998**, 224, 232.
- [14] a) R. Hoppe, *Angew. Chem.* **1966**, 78, 52; *Angew. Chem. Int. Ed. Engl.* **1966**, 5, 95; b) R. Hoppe, *Angew. Chem.* **1970**, 82, 7; *Angew. Chem. Int. Ed. Engl.* **1970**, 9, 25.
- [15] Bond-valence parameters (single-bond lengths): Si–O 162.4, Si–N 177 pm: N. E. Brese, M. O’Keeffe, *Acta Crystallogr. Sect. B* **1991**, 47, 192.
- [16] H. Höpfe, W. Schnick, unpublished results.
- [17] T. Schlieper, W. Schnick, *Z. Anorg. Allg. Chem.* **1995**, 621, 1037.
- [18] T. Schlieper, W. Milius, W. Schnick, *Z. Anorg. Allg. Chem.* **1995**, 621, 1380.
- [19] H. Huppertz, W. Schnick, *Chem. Eur. J.* **1997**, 3, 249.
- [20] J. Sjöberg, G. Helgesson, I. Idrestedt, *Acta Crystallogr. Sect. C* **1991**, 47, 2438.

Cyclizations

Hydroamination/Cyclization of Aminoalkenes Using Cationic Zirconocene and Titanocene Catalysts***Denis V. Gribkov and Kai C. Hultzsich**

Catalytic hydroamination is a highly atom-efficient method for the addition of amines to unsaturated carbon–carbon bonds.^[1] Its relevance to the synthesis of many nitrogen-containing pharmaceuticals and other industrially important basic and fine chemicals has led to intensified research efforts over the last decade, and various catalyst systems based on early and late transition metals have been developed. Catalysts based on rare-earth metals have been proven to be particularly active for the hydroamination of nonactivated olefins.^[1a,2] However, difficulties in the preparation and handling of organo rare earth metal complexes have prevented their widespread application as hydroamination catalysts in synthetic organic chemistry.

Catalyst systems based on Group 4 metal complexes would be more generally applicable due to their easier synthesis and commercial availability.^[3] Unfortunately, catalyst systems based on neutral Group 4 metal complexes have been restricted to inter- and intramolecular hydroamination reactions of alkynes^[1e,f,4] and allenes.^[4b,e] Olefinic substrates are unreactive towards metal imido species, which are presumed to be intermediates in the catalytic cycle.

[*] D. V. Gribkov, Dr. K. C. Hultzsich
Institut für Organische Chemie
Friedrich-Alexander Universität Erlangen-Nürnberg
Henkestrasse 42, 91054 Erlangen (Germany)
Fax: (+49) 9131-852-6865
E-mail: hultzsich@chemie.uni-erlangen.de

[**] Financial support by the Deutsche Forschungsgemeinschaft (DFG) and the Fonds der Chemischen Industrie is gratefully acknowledged. K.C.H. is a Emmy Noether fellow (2001–2005) and thanks Professor John A. Gladysz for generous support. We would like to thank Ms. P. Horrillo Martínez for the preparation of $[\text{Cp}_2\text{Ti}(\text{CH}_2\text{Ph})_2]$.

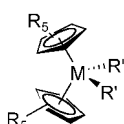


Supporting information for this article is available on the WWW under <http://www.angewandte.org> or from the author.

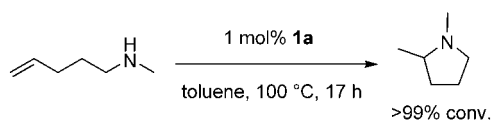
It should be noted, however, that lanthanocene complexes, which are indeed active hydroamination catalysts, are isoelectronic to alkyl metallocene cations of Group 4 transition metals. While the former have been studied as homogeneous Ziegler–Natta polymerization model systems,^[5] the latter have gained tremendous importance over the last two decades as homogeneous single-site polymerization catalysts.^[6] Alkyl metallocene cations have been used in organic synthesis,^[7] but to the best of our knowledge not in hydroamination reactions. However, Scott et al. recently described the application of a chiral aminophenolate alkyl zirconium cation in asymmetric hydroamination/cyclization reactions.^[8] In this communication we describe the utilization of well-known and readily available alkyl zirconocene cations as competent catalysts for hydroamination/cyclization.

Our initial investigations focused on $[\text{Cp}_2\text{ZrMe}]^+[\text{MeB}(\text{C}_6\text{F}_5)_3]^-$ (catalyst system **1a**, Table 1),^[9] and we were

Table 1:

Cat.					Activator
	M	R	R'	R'	
1a	Zr	H	CH ₃	CH ₃	$\text{B}(\text{C}_6\text{F}_5)_3$
1b	Zr	H	CH ₃	CH ₃	$[\text{PhNMe}_2\text{H}]^+[\text{B}(\text{C}_6\text{F}_5)_4]^-$
2a	Zr	CH ₃	CH ₃	CH ₃	$\text{B}(\text{C}_6\text{F}_5)_3$
2b	Zr	CH ₃	CH ₃	CH ₃	$[\text{PhNMe}_2\text{H}]^+[\text{B}(\text{C}_6\text{F}_5)_4]^-$
3	Ti	H	CH ₂ Ph	CH ₂ Ph	$[\text{PhNMe}_2\text{H}]^+[\text{B}(\text{C}_6\text{F}_5)_4]^-$

pleased to find that it readily cyclizes secondary aminoalkene substrates in aromatic solvents with catalyst loadings as low as 1 mol % (Scheme 1, Table 2 and Table 3). Addition of the



Scheme 1. Cyclization of a secondary aminoalkene substrate with the catalyst $[\text{Cp}_2\text{ZrMe}]^+[\text{MeB}(\text{C}_6\text{F}_5)_3]^-$ (**1a**).

substrates to **1a** at 25 °C results in the immediate release of methane (as observed by ¹H NMR spectroscopy), but appreciable turnover is observed only at elevated temperatures. Cyclization of *N*-methylpent-4-en-1-amine (**4**) proceeds at a rate of $> 50 \text{ h}^{-1}$ in $[\text{D}_5]$ bromobenzene at 100 °C (Figure 1),^[10] which is roughly 20 times faster than that observed with Scott's catalyst,^[8a] but slower than with $[\text{Me}_2\text{Si}(\text{C}_5\text{Me}_4)_2\text{NdCH}(\text{SiMe}_3)_2]$ (11 h^{-1} at 25 °C).^[2a] The catalytic activity of **1a** is slightly lower in $[\text{D}_6]$ benzene than in $[\text{D}_5]$ bromobenzene (Table 2, entries 1 and 2), due to lower solubility of the catalyst in $[\text{D}_6]$ benzene.^[11] Formation of α -pipercoline derivative **9** by cyclization of *N*-methylhex-5-en-1-amine (**8**) is significantly slower than formation of pyrrolidine **5**. The sterically more demanding benzyl-substituted aminoalkene **6**

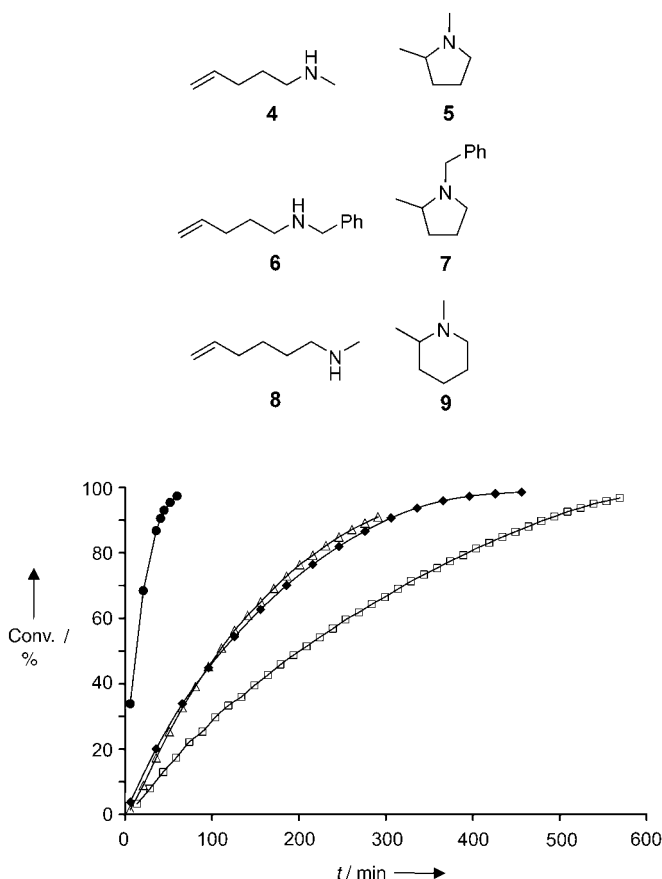


Figure 1. Hydroamination/cyclization of **4** (0.60 M) with 2 mol % of **1a** (\square) at 80 °C in $[\text{D}_6]$ benzene, with **1a** (\blacklozenge) at 80 °C in $[\text{D}_5]$ bromobenzene, with **1a** (\bullet) at 100 °C in $[\text{D}_5]$ bromobenzene, and with **1b** (\triangle) at 80 °C in $[\text{D}_5]$ bromobenzene. Lines through the data points are drawn as a guide to the eye.

reacts four times more slowly than the methyl-substituted substrate **4** (Table 2). This seems still sufficient for practical applications, so that the benzyl group could serve as a protecting group for primary aminoalkenes.^[12] In agreement with observations by Scott et al.,^[8a] no catalytic activity was observed for the cyclization of aminoalkenes with primary amine functionalities, for example, 2,2-dimethylpent-4-en-1-amine. The intermediate primary amidozirconocene cation is prone to abstraction of the α -proton from the amido nitrogen atom, leading to a catalytically inactive imidozirconocene species. The catalyst system **1b**, generated by activation of $[\text{Cp}_2\text{ZrMe}_2]$ with $[\text{PhNMe}_2\text{H}]^+[\text{B}(\text{C}_6\text{F}_5)_4]^-$, performs hydroamination/cyclization reactions with comparable rates for substrates **4** and **10** and higher turnover frequency with benzyl-substituted aminopentene **6** and aminohexene **8**.

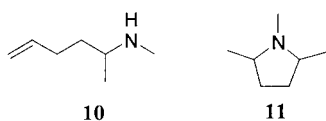
The catalytic activity is very sensitive towards steric hindrance in the coordination sphere of the catalyst. The sterically more encumbered zirconocene $[\text{Cp}_2^*\text{ZrMe}_2]$, activated with either $\text{B}(\text{C}_6\text{F}_5)_3$ or $[\text{PhNMe}_2\text{H}]^+[\text{B}(\text{C}_6\text{F}_5)_4]^-$, showed only low activity. Furthermore, the cationic titanocene complex $[\text{Cp}_2\text{Ti}(\text{CH}_2\text{Ph})]^+[\text{B}(\text{C}_6\text{F}_5)_4]^-$ (**3**) has also lower activity than the zirconocene catalysts **1a** and **1b** for most substrates except for substrate **10** (vide infra).

Table 2: Catalytic hydroamination/cyclization reactions of secondary aminoalkenes.^[a]

Entry	S	P	Cat.	[Cat.]/[S] [mol %]	T [°C]	t [h]	Conv. [%] ^[b]	TOF [h ⁻¹] ^[c]
1	4	5	1a	2	80	7	98	12
2	4	5	1a ^[d]	2	80	10	97	6
3	4	5	1a	2	100	1	97	> 50
4	4	5	1a ^[e]	1	100	17 ^[f]	> 99	
5	4	5	1b	2	80	5	91	12
6	4	5	2a	10	100	74	< 10	
7	4	5	2b	10	100	74	11	
8	4	5	3	2	100	218	76	
9	4	5	[Cp ₂ ZrMe ₂] ^[g]	10	100	168	— ^[h]	
10	4	5	[Cp ₂ Ti(CH ₂ Ph) ₂] ^[g]	10	100	20	— ^[i]	
11	4	5	B(C ₆ F ₅) ₃	10	100	24	— ^[h]	
12	6	7	1a	2.5	100	6	94	12
13	6	7	1b	2	100	4	95	24
14	6	7	3	4	100	132	68	
15	8	9	1a	2	100	87	> 98	1.6
16	8	9	1b	2	100	12	98	
17	8	9	3	4	100	57	42 ^[j]	

[a] S=substrate, P=product; reaction conditions: 2 mol % cat., [D₅]bromobenzene, Ar atmosphere. [b] Determined by ¹H NMR spectroscopy. [c] Determined from the least-square fit of the linear part of the data. [d] In [D₆]benzene. [e] In toluene. [f] Conditions are not optimized. [g] In [D₈]toluene. [h] No conversion to product observed. [i] Complete isomerization of double bond. [j] No further conversion.

Cyclization of the α -substituted *N*-methyl-*N*-(1-methylpent-4-enyl)amine (**10**) gives *cis*- and *trans*-1,2,5-trimethylpyrrolidines (**11**) with a low *cis/trans* selectivity of 3.3:1 (for



1a) and 3:1 (for **1b**) (Table 3).^[13] The benzyltitanocene cation **3**, on the other hand, shows catalytic activity comparable to that of the zirconocene catalysts but with higher *cis* selectivity (8.6:1 at 80 °C) for substrate **10**. Interestingly, catalyst system **2b**, derived from the permethylzirconocene [Cp₂⁺ZrMe₂], displays the opposite selectivity of 1:2.

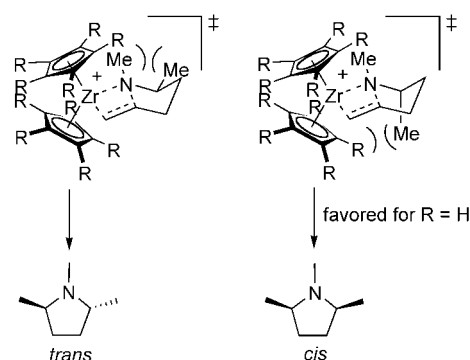
The preferred formation of *cis*-**11** can be rationalized by the unfavorable *gauche* interactions of the *N*-methyl group with the equatorial α -methyl group in the seven-membered

Table 3: Catalytic hydroamination/cyclization of **10** to give **11**.

Entry	Cat. ^[a]	T [°C]	t [h]	Conv. [%] ^[b]	<i>cis:trans</i>
1	1a	80	15	97	3.3:1
2	1a ^[c]	80	21	> 99	2.7:1
3	1b	80	27	92	3:1
4	2b ^[d]	100	107	74	1:2
5	3 ^[d]	80	14.5	99	8.6:1
6	3 ^[d]	100	13.5	91	4.9:1

[a] Reaction conditions: 2 mol % cat., C₆D₅Br, Ar atmosphere. [b] Determined by ¹H NMR spectroscopy. [c] In C₆D₆. [d] With 5 mol % cat.

chairlike transition state of the cyclization step leading to the *trans* isomer (Scheme 2). Steric interactions of the axial α -alkyl substituent with the Cp₂⁺ methyl groups in **2b** in the transition state leading to the *cis* isomer would disfavor this reaction path.

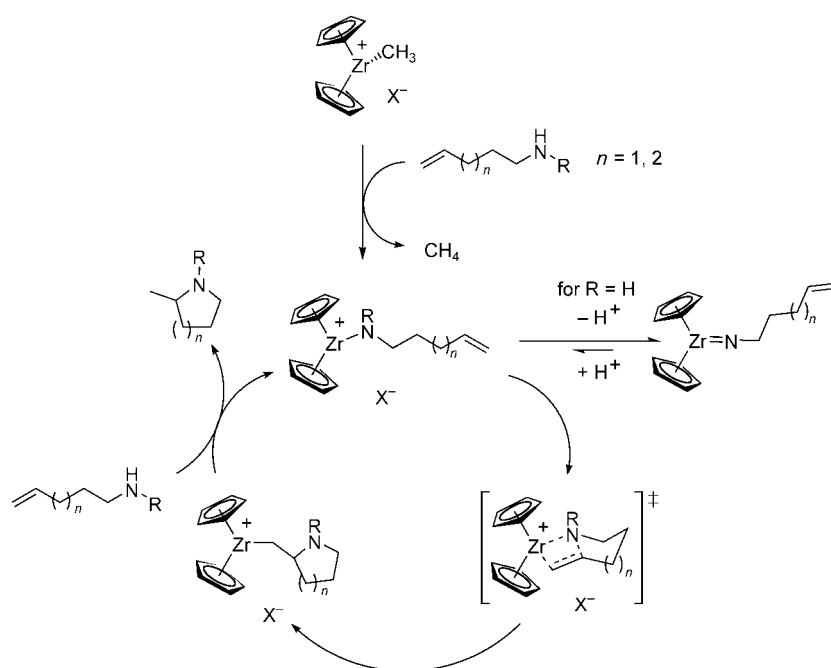


Scheme 2. Plausible transition states in the hydroamination/cyclization of *N*-methyl-*N*-(1-methylpent-4-enyl)amine (**10**) yielding *cis*- and *trans*-1,2,5-trimethylpyrrolidines (**11**).

Formation of a cationic species is a fundamental requirement for catalytic activity in the hydroamination of aminoalkenes. The neutral zirconocene [Cp₂ZrMe₂] displayed no catalytic activity after 7 d at 100 °C, whereas titanocene [Cp₂Ti(CH₂Ph)₂] led to complete isomerization of the terminal double bond in substrate **4** within 20 h at 100 °C. Furthermore, the highly Lewis acidic B(C₆F₅)₃ activator was catalytically inactive in the absence of zirconocene initiators.

Although mechanistic details are limited at the moment,^[10] the mechanism of the zirconocene-cation-catalyzed hydroamination/cyclization reaction is thought to be similar to that proposed for rare-earth-metal catalysts,^[2a] involving insertion of the carbon–carbon double bond into the metal amido bond followed by protolytic cleavage of the metal–carbon bond to regenerate the metal amido species (Scheme 3). This mechanism differs significantly from the mechanism for the hydroamination of alkyne substrates observed with neutral Group 4 complexes,^[1e,f] involving cycloaddition of an alkyne to a metal imido species followed by protolytic cleavage of the azametallacyclobutene intermediate.

In summary, the alkyl zirconocene cations **1a** and **1b** are promising and convenient catalysts for the hydroamination/cyclization of secondary aminoalkenes, whereas sterically more encumbered systems and the benzyltitanocene cation **3** show lower catalytic activity. Metallocene precatalysts and borane and anilinium borate activators are commercially available, and the catalysts are easy to handle with standard Schlenk techniques. Current investigations are focusing on the application of chiral metallocene complexes in these hydroamination/cyclization reactions. Topics that need to be addressed include the configurational stability of these chiral systems under catalytic conditions,^[14,15] the influence of steric bulk on catalytic activity, and the potential formation of (η^2 -iminoacyl)metallocene cations by deprotonation of intermediate cationic amido species.^[16]



Scheme 3. Proposed mechanism for zirconocene-catalyzed hydroamination/cyclization of aminoalkenes. $X^- = \text{CH}_3\text{B}(\text{C}_6\text{F}_5)_3^-$, $\text{B}(\text{C}_6\text{F}_5)_4^-$.

Experimental Section

All operations were performed under an inert atmosphere of nitrogen or argon using standard Schlenk-line or glove-box techniques. Metallocene dichlorides (Fluka), $\text{B}(\text{C}_6\text{F}_5)_3$ (Strem), and $[\text{PhNMe}_2\text{H}]^+[\text{B}(\text{C}_6\text{F}_5)_4]^-$ (Strem) were used as received. $[\text{Cp}_2\text{ZrMe}_2]$,^[17] $[\text{Cp}_2^*\text{ZrMe}_2]$,^[18] $[\text{Cp}_2\text{Ti}(\text{CH}_2\text{Ph})_2]$,^[19] and $[\text{Cp}_2\text{ZrMe}]^+[\text{MeB}(\text{C}_6\text{F}_5)_3]^-$ (**1a**)^[9] were synthesized as described in the literature. The substrates were dried by distillation from CaH_2 and stored over molecular sieves.

Representative procedure: **5-HCl** (Table 2, entry 4): In the glove box, a flask was fitted with a stirring bar and was charged with **1a** (8.0 mg, 10.5 μmol) toluene (0.5 mL) and **4** (108 mg, 1.09 mmol). The solution was heated to 100 °C for 17 h. All volatiles were then vacuum-transferred, diluted with diethyl ether (2 mL), and treated with hydrochloric acid (1.2 mL, 1 M in Et_2O , 1.2 mmol) at 0 °C. After 30 min, the suspension was brought to room temperature and the solvent removed in vacuo. The white precipitate was washed with diethyl ether and then dried in air to give 124 mg (84 %) of a white powder. ^1H NMR (300 MHz, D_2O , 25 °C): $\delta = 3.70$ (m, 1 H, CH_2N), 3.41 (m, 1 H, NCHCH_3), 3.17 (m, 1 H, CH_2N), 2.91 (s, 3 H, CH_3), 2.36 (m, 1 H, $\text{NCH}(\text{CH}_3)\text{CH}_2$), 2.03–2.16 (m, 2 H, NCH_2CH_2), 1.75 (m, 1 H, $\text{NCH}(\text{CH}_3)\text{CH}_2$), 1.43 ppm (d, $^3J(\text{H,H}) = 6.5$ Hz, 3 H, CHCH_3); $^{13}\text{C}\{^1\text{H}\}$ NMR (75.5 MHz, D_2O , 25 °C, SiMe_4): $\delta = 66.2$ (NCHCH_3), 56.7 (CH_2N), 39.2 (NCH_3), 31.7 ($\text{NCH}(\text{CH}_3)\text{CH}_2$), 21.5 (NCH_2CH_2), 15.7 ppm (CHCH_3).

Substrates **6**, **8**, and **10** were cyclized by similar procedures.

Received: June 4, 2004

Keywords: homogeneous catalysis · hydroamination · metallocenes · titanium · zirconium

- [1] a) T. E. Müller, M. Beller, *Chem. Rev.* **1998**, 98, 675–703; b) M. Nobis, B. Driessen-Hölscher, *Angew. Chem.* **2001**, 113, 4105–4108; *Angew. Chem. Int. Ed.* **2001**, 40, 3983–3985; c) J. Seayad, A. Tillack, C. G. Hartung, M. Beller, *Adv. Synth. Catal.* **2002**,

344, 795–813; d) M. Beller, C. Breindl, M. Eichberger, C. G. Hartung, J. Seayad, O. R. Thiel, A. Tillack, H. Trauthwein, *Synlett* **2002**, 1579–1594; e) F. Pohlki, S. Doye, *Chem. Soc. Rev.* **2003**, 32, 104–114; f) I. Bytschkov, S. Doye, *Eur. J. Org. Chem.* **2003**, 935–946; g) P. W. Roesky, T. E. Müller, *Angew. Chem.* **2003**, 115, 2812–2814; *Angew. Chem. Int. Ed.* **2003**, 42, 2708–2710.

- [2] a) M. R. Gagné, C. L. Stern, T. J. Marks, *J. Am. Chem. Soc.* **1992**, 114, 275–294; b) Y. K. Kim, T. Livinghouse, J. E. Bercaw, *Tetrahedron Lett.* **2001**, 42, 2933–2935; c) Y. K. Kim, T. Livinghouse, *Angew. Chem. Int. Ed.* **2002**, 41, 3645–3647; d) J.-S. Ryu, G. Y. Li, T. J. Marks, *J. Am. Chem. Soc.* **2003**, 125, 12584–12605; e) S. Hong, S. Tian, M. V. Metz, T. J. Marks, *J. Am. Chem. Soc.* **2003**, 125, 14768–14783; f) S. Hong, A. M. Kawaoka, T. J. Marks, *J. Am. Chem. Soc.* **2003**, 125, 15878–15892; g) P. N. O'Shaughnessy, P. D. Knight, C. Morton, K. M. Gillespie, P. Scott, *Chem. Commun.* **2003**, 1770–1771; h) J.-S. Ryu, T. J. Marks, F. E. McDonald, *J. Org. Chem.* **2004**, 69, 1038–1052; i) D. V. Gribkov, K. C. Hultsch, *Chem. Commun.* **2004**, 730–731; j) K. C. Hultsch, F. Hampel, T. Wagner, *Organometallics* **2004**, 23, 2601–2612.

- [3] General reviews on the application of Group 4 complexes in organic synthesis: a) *Titanium and Zirconium in Organic Synthesis* (Ed.: I. Marek), Wiley-VCH, Weinheim, **2002**; b) A. H. Hoveyda, J. P. Morken, *Angew. Chem.* **1996**, 108, 1378–1401; *Angew. Chem. Int. Ed. Engl.* **1996**, 35, 1262–1284.

- [4] For some recent examples see: a) I. Bytschkov, S. Doye, *Tetrahedron Lett.* **2002**, 43, 3715–3718; b) L. Ackermann, R. G. Bergman, *Org. Lett.* **2002**, 4, 1475–1478; c) Y. Shi, C. Hall, J. T. Ciszewski, C. Cao, A. L. Odom, *Chem. Commun.* **2003**, 586–587; d) C. Li, R. K. Thomson, B. Gillon, B. O. Patrick, L. L. Schafer, *Chem. Commun.* **2003**, 2462–2463; e) L. Ackermann, *Organometallics* **2003**, 22, 4367–4368; f) Z. Zhang, L. L. Schafer, *Org. Lett.* **2003**, 5, 4733–4736; g) V. Khedkar, A. Tillack, M. Beller, *Org. Lett.* **2003**, 5, 4767–4770; h) H. Siebeneicher, I. Bytschkov, S. Doye, *Angew. Chem.* **2003**, 115, 3151–3153; *Angew. Chem. Int. Ed.* **2003**, 42, 3042–3044; i) I. Bytschkov, H. Siebeneicher, S. Doye, *Eur. J. Org. Chem.* **2003**, 2888–2902; j) F. Pohlki, I. Bytschkov, H. Siebeneicher, A. Heutling, W. A. König, S. Doye, *Eur. J. Org. Chem.* **2004**, 1967–1972; k) C. Lorber, R. Choukroun, L. Vendler, *Organometallics* **2004**, 23, 1845–1850.

- [5] P. L. Watson, G. W. Parshall, *Acc. Chem. Res.* **1985**, 18, 51–56.

- [6] a) H. H. Brintzinger, D. Fischer, R. Mühlhaupt, B. Rieger, R. Waymouth, *Angew. Chem.* **1995**, 107, 1255–1283; *Angew. Chem. Int. Ed. Engl.* **1995**, 34, 1143–1170; b) E. Y.-X. Chen, T. J. Marks, *Chem. Rev.* **2000**, 100, 1391–1434.

- [7] a) R. B. Grossman, W. M. Davis, S. L. Buchwald, *J. Am. Chem. Soc.* **1991**, 113, 2321–2322; b) G. A. Molander, C. P. Corrette, *Tetrahedron Lett.* **1998**, 39, 5011–5014; c) K. H. Shaughnessy, R. M. Waymouth, *Organometallics* **1998**, 17, 5728–5745; d) M. V. Troutman, D. H. Appella, S. L. Buchwald, *J. Am. Chem. Soc.* **1999**, 121, 4916–4917; e) A. D. Sadow, T. D. Tilley, *Organometallics* **2003**, 22, 3577–3585.

- [8] a) P. D. Knight, I. Munslow, P. N. O'Shaughnessy, P. Scott, *Chem. Commun.* **2004**, 894–895; b) A report describing a cationic alkylscandium-based hydroamination catalyst system appeared

- recently, see: F. Lauterwasser, P. G. Hayes, S. Bräse, W. E. Piers, L. L. Schafer, *Organometallics* **2004**, *23*, 2234–2237.
- [9] X. Yang, C. L. Stern, T. J. Marks, *J. Am. Chem. Soc.* **1994**, *116*, 10015–10031.
- [10] The signals of the catalyst in the ^1H NMR spectra are broad under catalytic conditions, and no single species has been identified. Preliminary kinetic data suggests a square-root dependence of substrate concentration on the rate for catalysts **1a** and **1b** (see the Supporting Information). This is in contrast to the usual zero-order rate dependence on substrate concentration observed for most rare earth metal based catalyst systems. Deviations from linearity have been attributed to product inhibition, see refs. [2a,f,h].
- [11] The formation of an oily precipitate, presumably a cationic amidozirconocene species, was noted during catalytic reactions performed in benzene and toluene solutions. Reactions performed in bromobenzene remained homogeneous throughout the duration of the catalysis.
- [12] a) *Protective Groups in Organic Synthesis* (Eds.: T. W. Greene, P. G. M. Wuts), Wiley-Interscience: New York, 3rd ed., **1999**, pp. 579–580; b) 2-Methyl-pyrrolidine has been prepared by catalytic hydrogenation of 1-benzyl-2-methyl-pyrrolidine, see: M.-J. Kim, I. T. Lim, G.-B. Choi, S.-Y. Whang, B.-C. Ku, J.-Y. Choi, *Bioorg. Med. Chem. Lett.* **1996**, *6*, 71–76.
- [13] Assignment of *cis* and *trans* isomers is based on comparison with a sample of *trans*-1,2,5-trimethylpyrrolidine (*trans*-**11**) and literature NMR data: M. Tokuda, Y. Yamada, T. Takagi, H. Sugimoto, *Tetrahedron* **1987**, *43*, 281–296. *trans*-**11** was prepared from *trans*-2,5-dimethylpyrrolidine (see ref. [2j]) by N-methylation.
- [14] Neutral bisamidozirconocene complexes have been shown to epimerize by amine-induced protolytic cleavage of the metal–cyclopentadienyl bond, see: J. N. Christopher, G. M. Diamond, R. F. Jordan, *Organometallics* **1996**, *15*, 4038–4044. However, a similar mechanism has not been established for cationic zirconocene complexes.
- [15] A limiting factor in the development of chiral lanthanocene hydroamination catalysts has been their facile epimerization under catalytic conditions. M. A. Giardello, V. P. Conticello, L. Brard, M. Sabat, A. L. Rheingold, C. L. Stern, T. J. Marks, *J. Am. Chem. Soc.* **1994**, *116*, 10212–10240. See also ref. [2h].
- [16] B. Temme, G. Erker, *J. Organomet. Chem.* **1995**, *488*, 177–182.
- [17] a) P. C. Wailes, H. Weigold, A. P. Bell, *J. Organomet. Chem.* **1972**, *34*, 155–164; b) E. Samuel, M. D. Rausch, *J. Am. Chem. Soc.* **1973**, *95*, 6263–6267.
- [18] J. M. Manriquez, D. R. McAllister, R. D. Sanner, J. E. Bercaw, *J. Am. Chem. Soc.* **1978**, *100*, 2716–2724.
- [19] J. Scholz, F. Rehbaum, K.-H. Thiele, R. Goddard, P. Betz, C. Krüger, *J. Organomet. Chem.* **1993**, *443*, 93–99.

Thermodynamically Controlled Self-Assembly of Two-Dimensional Oxide Nanostructures**

Johannes Schoiswohl, Svetlozar Surnev, Michael Sock, Michael G. Ramsey, Georg Kresse, and Falko P. Netzer*

The self-assembly of molecules or small clusters, that is, the spontaneous association of atomic or molecular building blocks under equilibrium conditions, is emerging as a successful chemical strategy to fabricate well-defined structures of nanometer dimensions, with potential applications in many areas of nanotechnology.^[1] This bottom-up approach of synthesis is a promising way to design novel nanoscale functional materials with atomic precision. The construction of complex supramolecular aggregates from organic molecular building blocks by the self-assembly route has been successfully demonstrated recently.^[2,3] Herein, we explore the possibility of fabricating surface-supported nanoscale oxide materials in low dimensions by a chemically driven self-assembly process with oxide cluster molecules. As opposed to the usual molecular self-assembly, where the construction units are deposited directly from the gas phase, the oxide building blocks with a unique uniform stoichiometry and structure form spontaneously on a metal surface. These building blocks can then be organized into different two-dimensional (2D) oxide structures by careful adjustment of the chemical potential of oxygen μ_{O} , which allows the controlled design of oxide nanostructures on a metal surface. This process is demonstrated with the formation and subsequent aggregation of planar vanadium oxide $[\text{V}_6\text{O}_{12}]$ clusters, monitored in situ, under ultrahigh vacuum (UHV), on an Rh(111) surface at the atomic level by scanning tunneling microscopy (STM). The fabrication of ultrathin layers of vanadium oxides has potential commercial interest in the so-called monolayer catalysts, in advanced coating systems, and in optical devices.^[4]

The $[\text{V}_6\text{O}_{12}]$ clusters form spontaneously on an Rh(111) surface after deposition of vanadium atoms at submonolayer coverages under appropriate temperature and sufficiently oxidizing conditions (Figure 1a). They are a unique, novel form of “oxide molecules” with a planar 2D hexagonal structure (Figure 1b), which is stabilized by interaction with the rhodium surface but is unstable in the gas phase.^[5] Ab initio density functional theory calculations^[6–9] have

[*] J. Schoiswohl, Prof. Dr. S. Surnev, M. Sock, Prof. Dr. M. G. Ramsey, Prof. Dr. F. P. Netzer
Institut für Experimentalphysik
Karl-Franzens-Universität Graz
8010 Graz (Austria)
Fax: (+43) 316-380-9816
E-mail: falko.netzer@uni-graz.at

Prof. Dr. G. Kresse
Institut für Materialphysik
Universität Wien, 1090 Wien (Austria)

[**] This work was supported by the Austrian Science Fund FWF and the Austrian Academy of Sciences (DOC).

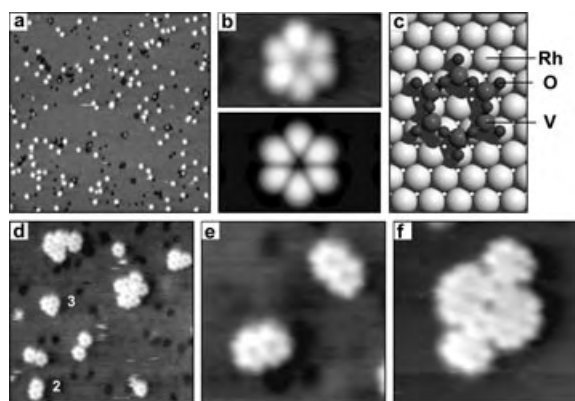


Figure 1. a) Single $[\text{V}_6\text{O}_{12}]$ cluster molecules ($470 \times 470 \text{ \AA}^2$; sample bias $U = +2 \text{ V}$; tunneling current $I = 0.2 \text{ nA}$), b) top: high-resolution STM image of a $[\text{V}_6\text{O}_{12}]$ cluster ($22 \times 13 \text{ \AA}^2$; $U = +0.5 \text{ V}$; $I = 0.1 \text{ nA}$), bottom: DFT simulated STM image, c) DFT model geometry of the planar V_6O_{12} cluster on $\text{Rh}(111)$, d–f) Condensation of $[\text{V}_6\text{O}_{12}]$ clusters at elevated temperature ($100\text{--}110^\circ\text{C}$) into dimers (2) and trimers (3) (d,e) and larger aggregates (f). Data d): $155 \times 140 \text{ \AA}^2$; $U = +1 \text{ V}$; $I = 0.1 \text{ nA}$, e): $50 \times 50 \text{ \AA}^2$; $U = +1 \text{ V}$, $I = 0.1 \text{ nA}$, f): $60 \times 60 \text{ \AA}^2$; $U = +1 \text{ V}$, $I = 0.1 \text{ nA}$.

revealed the stoichiometry and the geometry of these starlike structures (Figure 1c): the stars consist of six vanadium atoms which are each coordinated to three rhodium atoms of the surface. The vanadium atoms are linked by bridging oxygen atoms; each vanadium atom is attached to a further oxygen atom, which is positioned above a surface rhodium atom, to give the V_6O_{12} stoichiometry with a formal V^{IV} oxidation state. The simulated STM image, (Figure 1b bottom), reflects exactly the experimental STM image (Figure 1b, top), and thus confirms the proposed model.

The $[\text{V}_6\text{O}_{12}]$ “star” clusters become mobile on the surface in UHV at elevated temperature ($\approx 100^\circ\text{C}$) and diffuse over the $\text{Rh}(111)$ surface.^[5] They condense into dimers and trimers, which appear to be metastable but kinetically stabilized for a certain time, before they are observed to separate again. Figure 1d shows an STM snapshot image of an area of the star-covered rhodium surface taken at 110°C , where single stars, dimers (marked 2), trimers (marked 3), and somewhat larger cluster aggregates are visible. The formation of these clusters is driven by reduction. The observed dimer, for instance, is formed by attaching two stars along one common side in which two vanadium atoms are shared by the two adjoined hexagons (Figure 1e). Its formal stoichiometry is $\text{V}_{10}\text{O}_{19}$ corresponding to a lower oxidation state than the original stars. The STM image of Figure 1f has been recorded under slightly more reducing conditions (in a slightly elevated background pressure of hydrogen). There, the “stars” have aggregated into a larger cluster, which is the precursor of the oxide nano-islands (see below).

In a reducing environment ($p_{\text{H}_2} \approx 10^{-8} \text{ mbar}$ and at 250°C substrate temperature) the $[\text{V}_6\text{O}_{12}]$ clusters assemble into nano-islands with a well-ordered 2D vanadium oxide monolayer structure (Figure 2a). Between the vanadium-oxide islands bright dots are still visible, which correspond to star clusters, which have not yet been incorporated into the rectangular structure. The STM image of the inset of

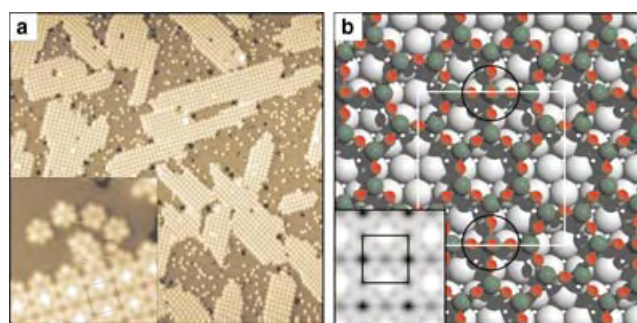


Figure 2. a) Assembly of $[\text{V}_6\text{O}_{12}]$ clusters into the rectangular $(5 \times 3\sqrt{3})$ vanadium-oxide structure under reducing conditions ($1000 \times 1000 \text{ \AA}^2$; $U = +1.5 \text{ V}$; $I = 0.1 \text{ nA}$). Inset: Enlarged section of an island boundary, with the $(5 \times 3\sqrt{3})$ -rect unit cell indicated ($70 \times 70 \text{ \AA}^2$; $U = +0.5 \text{ V}$; $I = 0.1 \text{ nA}$). b) DFT derived model of the $(5 \times 3\sqrt{3})$ -rect structure, the unit cell (white square) and $\text{O}_4\text{V}=\text{O}$ structural units (black circle) are indicated (V green, O red, Rh gray). Inset: Simulated STM image.

Figure 2a displays the rectangular $(5 \times 3\sqrt{3})$ -rect structure at higher magnification, which shows details of the structure and the incorporation of the stars in the vanadium-oxide-island boundary. The geometry of the $(5 \times 3\sqrt{3})$ -rect structure has been resolved with the help of DFT calculations and measurements of the phonon spectra.^[10] The structure model as established by DFT is shown in Figure 2b, the inset displays a simulated STM image according to this model. There is excellent agreement between the simulated and experimental STM images. The structure corresponds to a $\text{V}_{13}\text{O}_{21}$ stoichiometry per unit cell, which contains two hexagonal $[\text{V}_6\text{O}_{12}]$ clusters rotated by 30° and interlinked by bridging oxygen atoms plus one $\text{O}_4\text{V}=\text{O}$ unit (black circles in Figure 2b). Note that the $\text{O}_4\text{V}=\text{O}$ units are not in conflict with the maximal V^{V} oxidation state of the V atoms, since the four bridging oxygen atoms are also shared with the rhodium substrate. The $(5 \times 3\sqrt{3})$ -rect structure is a novel mixed-valent vanadium oxide phase, which occurs only in ultrathin layer form and does not exist as a stable bulk phase. The comparison of the high-resolution STM image of the $(5 \times 3\sqrt{3})$ -rect structure in the inset of Figure 2a with the STM image of the aggregate in Figure 1f indicates that the latter already contains the essential elements of the $(5 \times 3\sqrt{3})$ -rect unit cell. The cluster island of Figure 1f constitutes therefore a critical nucleus of the $(5 \times 3\sqrt{3})$ -rect structure.

Under oxidizing conditions ($p_{\text{O}_2} = 1 \times 10^{-8} \text{ mbar}$ at $T \approx 250^\circ\text{C}$), the $[\text{V}_6\text{O}_{12}]$ clusters aggregate into a different oxide structure (Figure 3a), where nano-islands of a (5×5) vanadium-oxide structure are recognized. The stable DFT model of this structure is shown in Figure 3b. A $\text{V}_{11}\text{O}_{23}$ stoichiometry per unit cell is derived from the model, that is, this oxide phase has a somewhat higher overall oxidation state than the $[\text{V}_6\text{O}_{12}]$ clusters. The structure contains V_6O_{12} , $\text{O}_4\text{V}=\text{O}$, and $\text{O}_3\text{V}=\text{O}$ units, the latter two are indicated by the circles in Figure 3b. Again, the (5×5) vanadium-oxide layer is not a stable bulk phase, but a novel 2D oxide layer stabilized by the metal-oxide interface. The simulated STM image based on the (5×5) model structure (inset Figure 3b) agrees very well with the experimental high-resolution STM image (inset Figure 3a). The crucial difference between the condensation

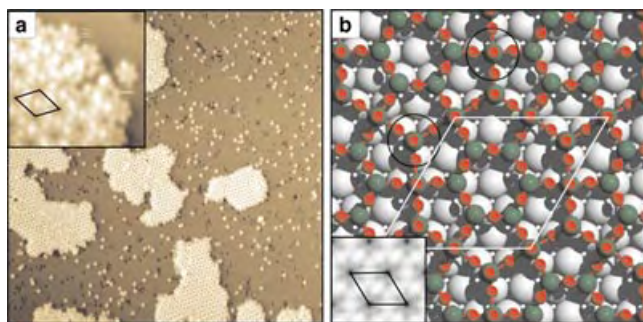


Figure 3. a) Aggregation of $[V_6O_{12}]$ clusters into the (5×5) vanadium oxide structure under oxidizing conditions ($1000 \times 1000 \text{ \AA}^2$; $U = +2 \text{ V}$; $I = 0.02 \text{ nA}$). Inset: Magnified view of the (5×5) island ($70 \times 70 \text{ \AA}^2$; $U = +1.2 \text{ V}$; $I = 0.1 \text{ nA}$). b) DFT derived model of the (5×5) structure, the unit cell (white) and $O_4V=O$ and $O_3V=O$ units (black circles) are indicated (V green, O red, Rh gray). Inset: Simulated STM image.

process under oxidizing and under reducing conditions is that under reducing conditions the stars condense by connecting mainly directly at the corners, whereas under oxidizing conditions oxygen-rich tetrahedral and pyramidal units ($O_3V=O$ and $O_4V=O$) are inserted between the star clusters.

The physical origin of the observed self-assembly of $[V_6O_{12}]$ clusters into different 2D oxide structures on the Rh(111) surface, depending on reducing or oxidizing conditions during production, can be understood by the surface phase stability diagram of vanadium oxides on Rh(111), as calculated by DFT. Figure 4 presents an appropriate section of the V–O/Rh(111) surface phase diagram in form of a plot of the chemical potential of oxygen μ_O versus the vanadium atom concentration c_V at the surface, given in monolayers (ML) of vanadium atoms, where the regions of stability of the respective oxide phases are indicated by the black bars. The position on the abscissa of the bars corresponds to the concentration of vanadium atoms in a full monolayer of the

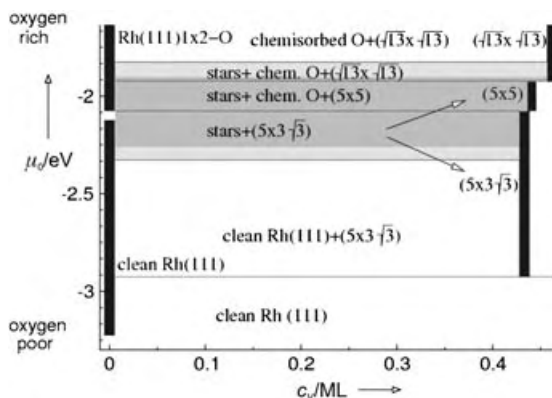


Figure 4. Section of the thermodynamic DFT phase diagram of vanadium oxide on Rh(111) in equilibrium with an oxygen reservoir which controls the chemical potential μ_O . μ_O is related to the oxygen partial pressure through the ideal gas equation $\mu_O(T,p) = \mu_O(T,p_0) - RT/2 \ln(p/p_0)$.^[12] Vertical black bars at the nominal vanadium coverage of each phase correspond to the μ_O region of stability. The arrows indicate the condensation of the $[V_6O_{12}]$ clusters into the different 2D island structures under more oxidizing or reducing conditions.

respective oxide phase. At a vanadium coverage of $c_V = 0$, the bare rhodium surface is covered by different chemisorbed oxygen phases under oxidizing conditions (higher μ_O), or it is clean under reducing conditions (low μ_O). A $(\sqrt{13} \times \sqrt{13})R13.8^\circ$ vanadium–oxide phase has been observed on the Rh(111) surface for $c_V \approx 0.45 \text{ ML}$ under highly oxidizing conditions,^[11] however, this structure is not relevant for the present discussion. The $[V_6O_{12}]$ stars form at low vanadium coverages in the gray region. Their region of stability is coexistent in terms of μ_O with the stability regions of both the (5×5) and the $(5 \times 3\sqrt{3})$ -rect structures, and in principle the $[V_6O_{12}]$ stars could condense into islands of one or the other of these structures. However, a change of μ_O (corresponding to moving up or down the diagram), provides an additional driving force for the condensation of stars into one or the other structure: for increasing μ_O the (5×5) structure becomes more stable, whereas for decreasing μ_O the $(5 \times 3\sqrt{3})$ -rect structure is more favorable (see arrows in Figure 4). The application of oxygen or hydrogen from the gas phase provides the experimental means for changing μ_O and selecting the condensation process. In addition, the elevated temperature applied during the self-assembly experiments increases the mobility of the stars, thus reducing kinetic barriers in the self-assembly process.

The self-assembly process of inorganic vanadium–oxide clusters into metal-supported 2D vanadium oxide nanostructures is different in two respects from the reported aggregation of supramolecular networks of organic molecules on surfaces.^[2,3] 1) the “molecular” building blocks of the aggregation, that is, the planar 2D $[V_6O_{12}]$ clusters, do not exist as stable entities in the gas phase but form spontaneously at the Rh(111) surface under the appropriate thermodynamic conditions; they constitute a novel kind of cluster material, that is stabilized by the metal-cluster interface, 2) the driving force for the self-assembly is provided by the chemical potential of oxygen, and the precise control of μ_O allows us to steer the aggregation into different patterns, that is, into different 2D vanadium–oxide structures. The assembly process occurs by reductive or oxidative condensation, thus chemical bonding interactions with partly covalent and ionic character are involved. This situation is in contrast to the noncovalent interactions, which are responsible for the attachment of organic molecules into supramolecular networks.^[2,3] Despite the much stronger bonding interactions, the herein reported vanadium–oxide-cluster aggregation is reversible: by careful adjustment of the chemical potential of oxygen and the surface temperature, the $[V_6O_{12}]$ star molecules can be regenerated at the Rh(111) surface by 2D re-evaporation from both (5×5) and $(5 \times 3\sqrt{3})$ -rect vanadium–oxide phases. The self-assembly of oxide cluster “molecules” and their controlled aggregation into 2D oxide structures has been observed herein for the one particular vanadium–oxide/Rh system. It is likely that this occurs also on other oxide–metal surfaces: the described approach may open up a new route for the fabrication of novel oxide materials with nanoscale dimensions.

Experimental Section

STM imaging has been performed in a variable-temperature STM system at room temperature or at elevated temperature. The $[\text{V}_6\text{O}_{12}]$ clusters were prepared by depositing 0.05 monolayer (ML) of vanadium atoms at RT onto the oxygen-precovered $\text{Rh}(111)2 \times 1$ surface (O precoverage: 0.5 ML). The surface was heated subsequently to 300–350 °C for 30 seconds and then cooled to RT. The DFT calculations were performed using the program VASP^[6–8] and a plane wave cutoff of 250 eV. The STM simulations are based on the Tersoff–Hamann approach.^[9] The charge iso-surfaces were evaluated at a value selected so that the brightest spots are located 4 Å above the core of the topmost atom in the oxide. The experimental bias conditions were mimicked in the simulations.

Received: March 29, 2004

Keywords: cluster compounds · density functional calculations · oxides · self-assembly · vanadium

- [1] G. M. Whitesides, J. P. Mathias, C. T. Seto, *Science* **1991**, 254, 1312.
- [2] T. Yokoyama, S. Yokoyama, T. Kamikado, Y. Okuno, S. Mashiko, *Nature* **2001**, 413, 619.
- [3] A. Dmitriev, H. Spillmann, N. Lin, J. V. Barth, K. Kern, *Angew. Chem.* **2003**, 115, 2774; *Angew. Chem. Int. Ed.* **2003**, 42, 2670.
- [4] S. Surnev, M. G. Ramsey, F. P. Netzer, *Prog. Surf. Sci.* **2003**, 33, 117.
- [5] J. Schoiswohl, G. Kresse, S. Surnev, M. Sock, M. G. Ramsey, F. P. Netzer, *Phys. Rev. Lett.* **2004**, 92, 206103.
- [6] G. Kresse, J. Furthmüller, *Comput. Mater. Sci.* **1996**, 6, 15.
- [7] Y. Wang, J. P. Perdew, *Phys. Rev. B* **1991**, 44, 13298.
- [8] G. Kresse, D. Joubert, *Phys. Rev. B* **1999**, 59, 1758.
- [9] J. Tersoff, D. R. Hamann, *Phys. Rev. B* **1985**, 31, 805.
- [10] The phonon spectra of the $(5 \times 3\sqrt{3})$ -rect structure were measured in high-resolution electron energy loss experiments and are in excellent agreement to the calculated phonon spectra according to the proposed DFT structure model.
- [11] J. Schoiswohl, S. Surnev, M. Sock, S. Eck, G. Kresse, M. G. Ramsey, F. P. Netzer, *Phys. Rev. B* **2004**, 69, 155403.
- [12] K. Reuter, M. Scheffler, *Phys. Rev. B* **2002**, 65, 0354061.

Cover Picture

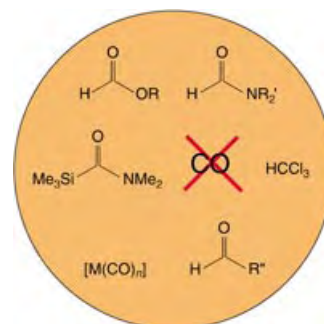
Masahide Tominaga, Keisuke Suzuki, Masaki Kawano, Takahiro Kusakawa, Tomoji Ozeki, Shigeru Sakamoto, Kentaro Yamaguchi, and Makoto Fujita*

Molecular spheres can be readily formed. The cover picture shows the crystal structure of a spherical complex that spontaneously forms from 36 small components (12 Pd^{2+} ions and 24 bent ligands). In their Communication on page 5621 ff., M. Fujita and co-workers describe the self-assembly of this almost 4-nm diameter hollow complex which is soluble in polar media and stable under STM and CSI-MS conditions. The functionalization of its periphery with fullerenes or porphyrins is also described. (The graphics were prepared by Dr. Akito Hori.)



Abandoning CO

T. Morimoto and K. Kakiuchi describe in their Minireview on page 5580 ff. alternatives to the use of gaseous carbon monoxide in carbonylation reactions which in optimized forms should be valuable for expanding the scope of synthetic strategies.



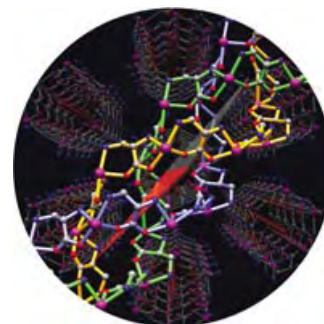
Synthetic Methods

How is a chemical reaction “developed”? By chance? By intuition? T. Muraiyama describes in his Review on page 5590 ff his view of how innovative processes come about in organic chemistry.



Chiral Crystals

Right- and left-handed triple-helical arrays of manganese centers can be formed by using chiral amino acid derivatives as ligands. K. Inoue and co-workers discuss the structural and magnetic properties of these compounds in their Communication on page 5618 ff.



Angewandte EarlyView®

The following Communications are available online (in Wiley InterScience). You can find them, as well as forthcoming Reviews, Highlights, and Essays, at www.angewandte.org, under Early View.

A. Rencurosi, E. P. Mitchell, G. Cioci, S. Pérez, R. Pereda-Miranda,*
A. Imberty*:

**Crystal Structure of Tricolorin A: Molecular Rationale for the
Biological Properties of Resin Glycosides Found in Some
Mexican Herbal Remedies**

DOI: 10.1002/anie.200460327

Published online: September 21, 2004

J. P. Rolland, E. C. Hagberg, G. M. Denison, K. R. Carter,*
J. M. De Simone*:

**High-Resolution Soft Lithography: Enabling Materials for
Nanotechnologies**

DOI: 10.1002/anie.200461122

Published online: October 11, 2004

Articles judged by the referees or the editor as being either very important or very urgent are immediately edited, proof-read, and electronically published once the manuscript has arrived in the editorial office in its final form. As long as there is no page number available these articles should be cited in the following manner:

Author(s), *Angew. Chem. Int. Ed.*, online publication date, DOI.

News

Siegfried Medal Awarded to Joel
M. Hawkins _____ **5568**

Arndt Simon Receives
Liebig Medal _____ **5568**

Lutz F. Tietze Is Awarded the
Emil Fischer Medal _____ **5568**

Books

Handbook of Elemental Speciation

Rita Cornelis, Joe Caruso, Helen Crews,
Klaus Heumann

reviewed by U. Karst _____ **5569**

Pseudo-Peptides in Drug Discovery

Peter E. Nielsen

reviewed by K. Kawai _____ **5569**

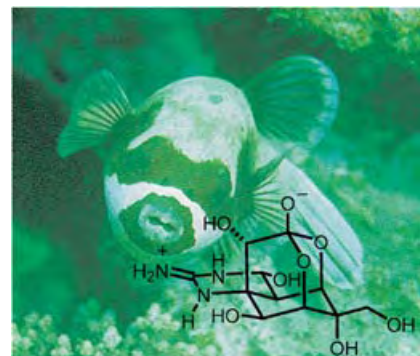
Highlights

Total Syntheses

U. Koert* _____ **5572–5576**

Syntheses of Tetrodotoxin

A meal of carefully prepared puffer fish, which hopefully does not contain the toxic livers and ovaries, tests the courage of gourmets and cooks. Tetrodotoxin (formula shown), the poisonous principle of the puffer fish, presents a challenge for synthesis, which has been mastered by three teams using different strategies and key steps.



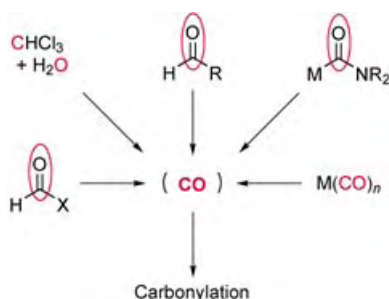
Survival of the fittest describes a new method for screening dynamic combinatorial libraries. A mixture of dipeptides is tested for binding to a target protein, and the weaker binding compounds are destroyed by pronase. The released components are then recoupled to regenerate the library. By repeating this cycle of selection, destruction, and regeneration, a small binding preference eventually results in a large enrichment of the tightest binding compound. Photo credit Douglas Jager (<http://www.mindspring.com/~bjager/akpix2.html>).



High-Throughput Screening

J.-L. Reymond* — 5577 – 5579

Outrunning the Bear



OC without CO: Innovative strategies for solving the drawbacks associated with the handling of toxic, gaseous carbon monoxide in carbonylation reactions are described. These strategies, some of which are shown schematically, highlight a variety of experimentally simple and safe tools for carbonylation that will be useful to synthetic organic chemists.

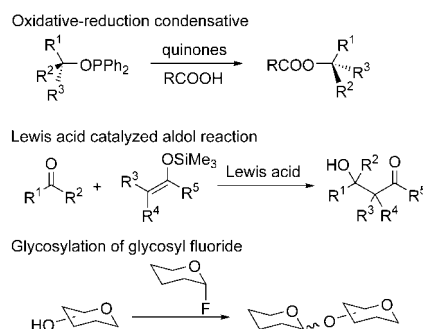
Minireviews

Carbonylation Catalysts

T. Morimoto,* K. Kakiuchi — 5580 – 5588

Evolution of Carbonylation Catalysis: No Need for Carbon Monoxide

Collected and combined: A strategy for guiding the search for new chemical reactions is described by giving concrete examples from the many years of research from the authors group. Three major research topics—oxidative–reductive condensation, the Lewis acid catalyzed aldol reaction, and glycosylation of glycosyl fluoride—are described to show how the initial concept was formulated and then expanded into broadly applicable methods.



Reviews

Synthesis Planning

T. Mukaiyama* — 5590 – 5614

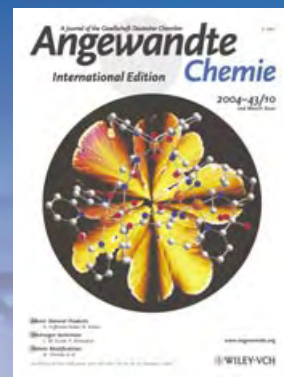
Explorations into New Reaction Chemistry

For the USA and Canada: ANGEWANDTE CHEMIE International Edition (ISSN 1433-7851) is published weekly by Wiley-VCH PO Box 191161, D 69451 Weinheim, Germany. Air freight and mailing in the USA by Publications Expediting Inc. 200 Meacham Ave., Elmont, NY 11003. Periodicals

postage paid at Jamaica NY 11431. US POSTMASTER: send address changes to *Angewandte Chemie*, Wiley-VCH, 111 River Street, Hoboken, NJ 07030. Annual subscription price for institutions: Europe € 3760.00/3418.00; outside Europe US\$ 4948.00/4498.00 (valid for print and electronic/print or electronic delivery); for

individuals who are personal members of a national chemical society, or whose institution already subscribes, or who are retired or self-employed consultants, print only: Europe € 258.00/outside Europe US\$ 394.00. Postage and handling charges included. All Wiley-VCH prices are exclusive VAT.

The best in chemistry – for more than a hundred years



A Journal of the Gesellschaft Deutscher Chemiker
Angewandte
International Edition **Chemie**

www.angewandte.org

1888: The beginning
of a success story

Constant Innovations

- 1962:** First issue of the International Edition
- 1976:** Graphical abstracts
- 1979:** Cover pictures
- 1988:** Centenary of Angewandte
- 1989:** Routine use of color
- 1991:** New section: Highlights
- 1992:** Computerized editorial tracking system
- 1995:** Internet service for readers
- 1998:** Regular press service; full-text online
- 2000:** New section: Essays; EarlyView: Communications available online ahead of the printed version
- 2001:** New section: Minireviews
- 2002:** Online submission of manuscripts
- 2003:** Weekly publication; new section: News; new layout
- 2004:** Backfiles (1962-1997); ManuscriptXpress: Online system for authors and referees



Angewandte's advisors...

Ryoji Noyori
Nagoya University and
RIKEN (Tokyo)

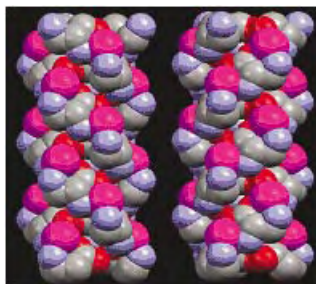
» *Angewandte Chemie* is the best scientific arena for both players and audience. This international journal has taken a leading role in raising the potential of chemistry to the current high standard. «

Angewandte Chemie International Edition is
a journal of the German Chemical Society (GDCh)



Communications

Magnetism gets a new twist: The crystal structure and magnetic properties of a chiral 3D ferrimagnet with T_c of 35 K, $[\{Cr^{III}(CN)_6\}\{Mn^{II}(D- \text{ or } L-NH_2ala)\}_3] \cdot 3 H_2O$ (NH_2ala = aminoalanine ion) are described. The complex has an extended, chiral, triple-strand helical arrangement of Mn^{II} ions, formed by the coordination of the organic ligands (see picture; purple Mn, gray C, blue N, red O). The triple helixes are linked to each other by the $\{Cr^{III}(CN)_6\}$ units.



Chirality and Magnetism

H. Imai, K. Inoue,* K. Kikuchi, Y. Yoshida, M. Ito, T. Sunahara, S. Onaka — 5618 – 5621

Three-Dimensional Chiral Molecule-Based Ferrimagnet with Triple-Helical-Strand Structure



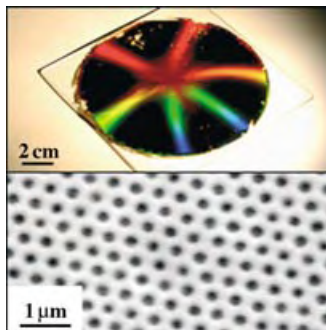
Simple banana-shaped organic molecules self-organize into finite, spherical coordination networks with a diameter of up to 7 nm (see structure; green Pd, red O, blue N, gray C). These molecular spheres consist of 12 equivalent metal centers and 24 equivalent ligands and have cuboctahedral symmetry. Functional groups (C_{60} or porphyrin) attached to each ligand are aligned equivalently at the periphery of the sphere.

Self-Assembly

M. Tominaga, K. Suzuki, M. Kawano, T. Kusakawa, T. Ozeki, S. Sakamoto, K. Yamaguchi, M. Fujita* — 5621 – 5625

Finite, Spherical Coordination Networks that Self-Organize from 36 Small Components

Surface replication: Three-dimensional ordered colloidal crystals are used as templates in creating surface gratings from a large variety of functional materials, such as metals, semiconductors, and dielectrics, provided that the material deposition only occurs on the periodic surfaces of the templates. By this non-lithographic technique wafer-scale samples with submicron periodicity can be rapidly created (see picture).

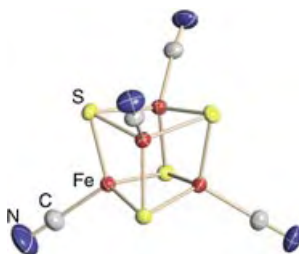


Nanostructured Films

P. Jiang* — 5625 – 5628

Surface-Templated Nanostructured Films with Two-Dimensional Ordered Arrays of Voids

A compound with potential: The title compound (see structure) not only resembles the relevant protein active sites geometrically and spectroscopically, but also possesses the least negative $[Fe_4S_4(L)_4]^{2-/-3-}$ and $[Fe_4S_4(L)_4]^{3-/-4-}$ (L is a monoanionic ligand) redox potentials of all protein Fe_4S_4 analogues. The value of the $Fe_4S_4^{+/0}$ redox potential implies a new route to the isolation of the elusive $Fe_4S_4^0$ cluster.



Bioinorganic Chemistry

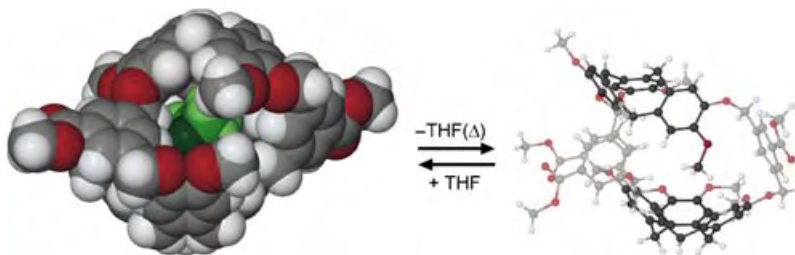
T. A. Scott, H.-C. Zhou* — 5628 – 5631

The First All-Cyanide Fe_4S_4 Cluster: $[Fe_4S_4(CN)_4]^{3-}$

Inclusion Compounds

S. T. Mough, J. C. Goeltz,
K. T. Holman* ————— 5631 – 5635

Isolation and Structure of an “Imploded”
Cryptophane



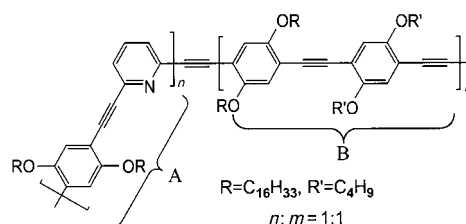
Container crushing: Thermal liberation of the encapsulated guest in a cryptophane has been shown to cause conformational “implosion” in the solid state. The resulting collapsed form is kinetically stable,

can be isolated, and its unexpected structure has been elucidated by X-ray diffraction. It eventually re-inflates, however, to the occupied container-like species on standing in solution (see scheme).

Sensors

H. Huang, K. Wang,* W. Tan, D. An,
X. Yang, S. Huang, Q. Zhai, L. Zhou,
Y. Jin ————— 5635 – 5638

Design of a Modular-Based Fluorescent
Conjugated Polymer for Selective Sensing



Sensitive and selective, a modular-based fluorescent polymer combines a rigid electron-conducting block (see picture; B) with a flexible binding block (A). The monopyridyl group of the coordinating

module has a great affinity for Pd^{II} ions and selectively binds them through self-assembly. Thus, the fluorescent conjugated polymer may be used for sensing Pd^{II} ions.

Nanoparticles

H. Duan, D. Wang,* D. G. Kurth,
H. Möhwald ————— 5639 – 5642

Directing Self-Assembly of Nanoparticles
at Water/Oil Interfaces



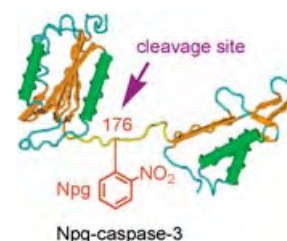
Finding the right angle: The contact angle of nanoparticles at the water/oil interface can be engineered close to 90° by capping with ligands containing carboxylic ester terminal groups. This drives the nanoparticles to self-assemble into close-packed films (see picture), and thus provides the opportunity to create two- or three-dimensional homo- or hetero-geneous nanostructures for electronic, optoelectrical, and magnetic applications.

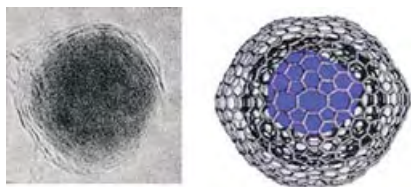
Bioorganic Chemistry

M. Endo,* K. Nakayama, Y. Kaida,
T. Majima* ————— 5643 – 5645

Design and Synthesis of Photochemically
Controllable Caspase-3

The selective cleavage achieved by activated caspase-8 has been mimicked by using a photofunctionalized caspase-3 having 2-nitrophenylglycine (Npg) at a specific position of the peptide chain (see picture). The study shows that the activity of caspase-3 has been clearly expressed by photoirradiation and that autocleavage of caspase-3 has been suppressed by the site-selective incorporation of the Npg residue.





The best of both worlds: The synthesis of carbon-encapsulated iron-based magnetic nanoparticles is described (see picture: left TEM image, right model). With such small catalysts that have macroscopic magnetic properties, the advantages of homogeneous or colloidal and heterogeneous catalysts can be combined.

Nanostructures

S. C. Tsang,* V. Caps, I. Paraskevas, D. Chadwick, D. Thompson **5645–5649**

Magnetically Separable, Carbon-Supported Nanocatalysts for the Manufacture of Fine Chemicals



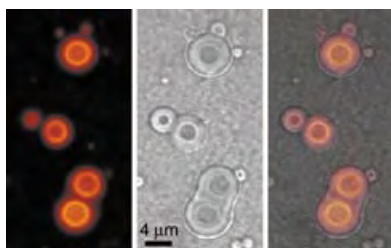
Maximally helical polyanilines, 9 to 24 residues in length, are used to calibrate the assignment of fractional helicity (FH) from circular dichroism ellipticities. Water-solubilizing, helix-stabilizing N- and C-caps induce FHs > 0.9 in core polyanilines.

Linear length regressions of peptide molar ellipticities (blue-green curves) yield slopes (red arrows) that define molar per-residue ellipticities of a fully helical alanine residue (red curve).

Peptide Structures

G. E. Job, B. Heitmann, R. J. Kennedy, S. M. Walker, D. S. Kemp* **5649–5651**

Calibrated Calculation of Polyaniline Fractional Helicities from Circular Dichroism Ellipticities



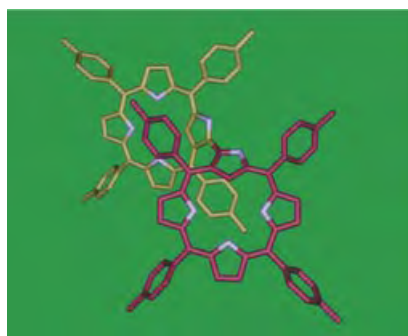
Spontaneous formation of microspheres is observed when charged poly(amino acids) are combined with certain oppositely charged, multivalent organic ions. The surfaces of the spheres are chemically active and act as templates for silica condensation, and the assemblies can be made hollow or polymer-filled, depending on the silica precursor (see image; the fluorescent polymer forms a layer inside a colloidal-silica-coated sphere).

Hybrid Materials

B. J. McKenna, H. Birkedal,* M. H. Bartl, T. J. Deming, G. D. Stucky* **5652–5655**

Micrometer-Sized Spherical Assemblies of Polypeptides and Small Molecules by Acid–Base Chemistry

There's nothing confusing about the dimer (see picture) that forms from N-confused porphyrin! The dimer was obtained as a directly β – β -linked structure through a simple acid-catalyzed condensation reaction of the monomeric macrocycles, and the electronic interaction between the porphyrin subunits was studied for both the free-base form and for the bis(nickel(II)) complex.



Porphyrins

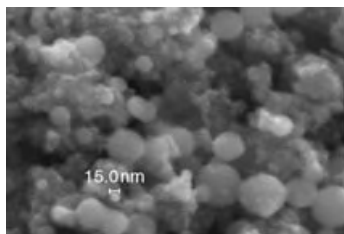
P. J. Chmielewski* **5655–5658**

Synthesis and Characterization of a Directly Linked N-Confused Porphyrin Dimer

Carbon Nitrides

M. H. V. Huynh,* M. A. Hiskey,*
J. G. Archuleta, E. L. Roemer,
R. Gilardi _____ **5658 – 5661**

3,6-Di(azido)-1,2,4,5-Tetrazine: A Precursor for the Preparation of Carbon Nanospheres and Nitrogen-Rich Carbon Nitrides

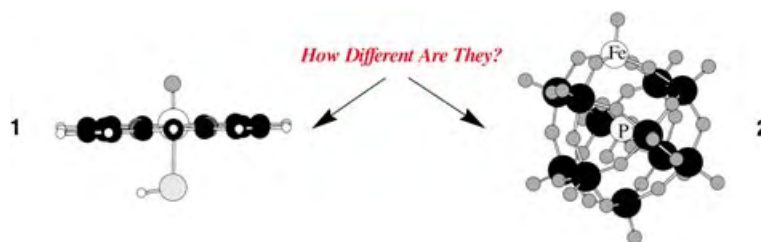


A high-nitrogen compound, 3,6-di(azido)-1,2,4,5-tetrazine, was used as precursor for the preparation of carbon nanospheres (see SEM picture) and nitrogen-rich carbon nitrides. The conversions into both carbon-based materials are simple, occur under mild conditions (low temperature, no applied pressure), and require no vacuum systems, extraction, carbonization, and purification.

Polyoxometalates

S. P. de Visser, D. Kumar, R. Neumann,*
S. Shaik* _____ **5661 – 5665**

Computer-Generated High-Valent Iron–Oxo and Manganese–Oxo Species with Polyoxometalate Ligands: How do they Compare with the Iron–Oxo Active Species of Heme Enzymes?



The structure and reactivity of high-valent Fe^{VO} and Mn^{VO} oxidation catalysts containing a polyoxometalate $[\text{PW}_{11}\text{O}_{39}]^{7-}$ lacunary ligand (2) have been investigated by a computational study. Calculations

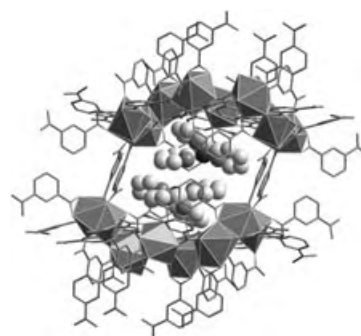
have demonstrated there is an intriguing analogy between these species and the active species (1) of the enzyme cytochrome P450 (see scheme).

Coordination Frameworks

Y.-F. Zhou, F.-L. Jiang, D.-Q. Yuan,
B.-L. Wu, R.-H. Wang, Z.-Z. Lin,
M.-C. Hong* _____ **5665 – 5668**

Copper Complex Cation Templated Gadolinium(III)–Isophthalate Frameworks

Ions in cages: Hydrothermal reactions give two novel 3D heterometallic frameworks, $[\{[\text{Gd}_4(\text{ip})_7(\text{H}_2\text{O})_2][\text{Cu}(\text{bpy})_2]_2\}_n]$ (1, bpy = 2,2'-bipyridine, H_2ip = isophthalic acid; see structure, space filling models: $[\text{Cu}(\text{bpy})_2]$, polyhedra: Gd) and $[\{\text{Gd}_3\text{Cu}(\text{ip})_5(\text{Hip})(\text{bpy})\}_n] \cdot n\text{H}_2\text{O}$ (2). The structure of 1 consists of charged cages containing two encapsulated Cu^{I} complex cations, whereas that of 2 contains charged cavities in which Cu^{II} complex cations are bound.

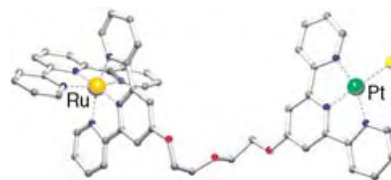


Binuclear Complexes

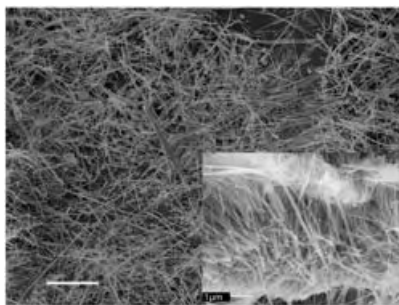
K. van der Schilden, F. Garcia,
H. Kooijman, A. L. Spek, J. G. Haasnoot,
J. Reedijk* _____ **5668 – 5670**

A Highly Flexible Dinuclear Ruthenium(II)–Platinum(II) Complex: Crystal Structure and Binding to 9-Ethylguanine

The length and high flexibility of the linker in a heterodinuclear ruthenium–platinum complex (see X-ray crystal structure) enables the platinum unit to independently interact with DNA by π – π stacking or coordination, possibly after pre-association of the 2+ charged ruthenium unit. A prototype of this challenging class of potentially cytostatic compounds is presented.



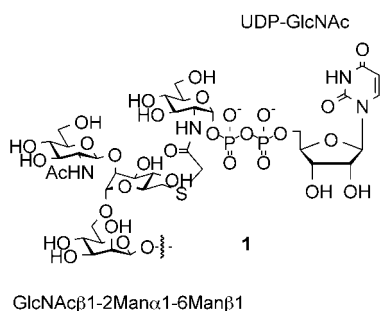
A low turn-on voltage is revealed by repeating field emission tests of NbS₂, which is a highly reliable field emitter. Well-defined NbS₂ nanowires (see picture) can be generated in the bulk by direct heating of Nb and S powders in sealed quartz tubes in the presence of I₂.



Nanowires

Y. Z. Jin, W. K. Hsu, Y. L. Chueh, L. J. Chou, Y. Q. Zhu,* K. Brigatti, H. W. Kroto, D. R. M. Walton — 5670 – 5674

Large-Scale Production of NbS₂ Nanowires and Their Performance in Electronic Field Emission

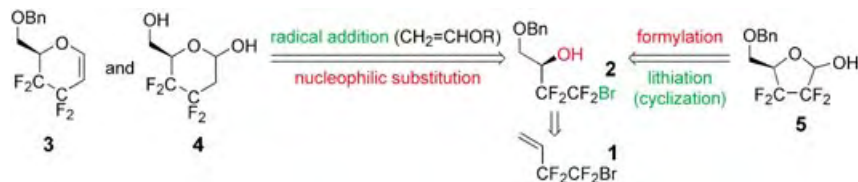


Transfer interference: Synthesis of the bisubstrate-type *N*-acetylglucosaminyltransferase (GnT) inhibitor **1** was achieved by a polymer-resin hybrid capture–release strategy for the construction of the acceptor component. One-pot ligation in aqueous media produced the coupling product, and subsequent construction of a diphosphate linkage led to **1**. Inhibitory activities toward GnT-V and GnT-IX were evaluated and revealed the potency of **1** toward the latter enzyme.

Glycosyltransferase Inhibitor

S. Hanashima, S. Manabe, K.-i. Inamori, N. Taniguchi, Y. Ito* — 5674 – 5677

Synthesis of a Bisubstrate-Type Inhibitor of *N*-Acetylglucosaminyltransferases



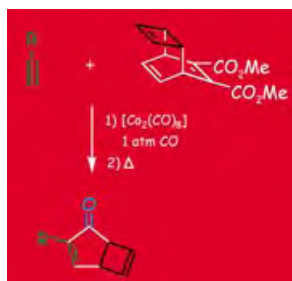
A Sharpless asymmetric dihydroxylation of the commercially available building block **1** affords the common chiral inter-

mediate **2** for the synthesis of the fluorinated monosaccharides **3–5** (Bn=benzyl).

Fluorinated Carbohydrates

A. J. Boydell, V. Vinader, B. Linclau* — 5677 – 5679

Enantioselective Synthesis of Tetrafluoroethylene-Containing Monosaccharides



A practical and scalable operation: The reaction shown in the scheme, which uses catalytic amounts of hexacarbonyldicobalt, gives access to versatile bicyclic systems, which until now could only be obtained in low quantities by a photochemical process starting from tropolones. An isolation of the primary Pauson–Khand products is not necessary.

Cyclopentenone Synthesis

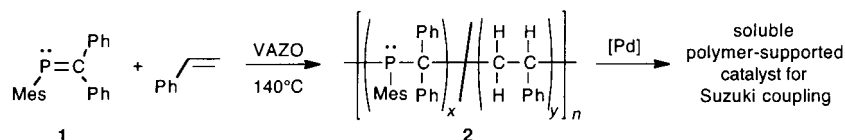
S. E. Gibson,* N. Mainolfi, S. B. Kalindjian, P. T. Wright — 5680 – 5682

A Cyclobutadiene Equivalent in the Catalytic Pauson–Khand Reaction

Organophosphine Polymers

C.-W. Tsang, B. Baharloo, D. Riendl,
M. Yam, D. P. Gates* — 5682 – 5685

Radical Copolymerization of a
Phosphaalkene with Styrene: New
Phosphine-Containing Macromolecules
and Their Use in Polymer-Supported
Catalysis



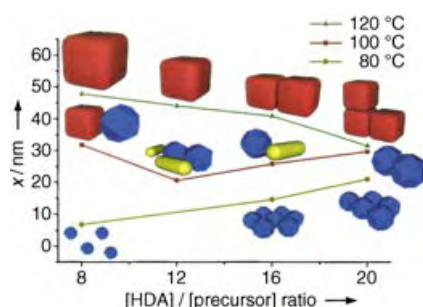
P=C bonds mimic C=C bonds in the radical-initiated copolymerization of a phosphaalkene **1** and styrene (see scheme). The resulting copolymers **2** have unprecedented phosphine-containing backbones with phosphorus composi-

tions that vary depending on the monomer ratios. These novel functional hybrid inorganic–organic macromolecules are used as polymeric supports for the Pd-catalyzed Suzuki coupling. VAZO = 1,1'-azobis(cyclohexanecarbonitrile).

Nanostructures

W. P. Lim, Z. Zhang, H. Y. Low,
W. S. Chin* — 5685 – 5689

Preparation of Ag₂S Nanocrystals of
Predictable Shape and Size

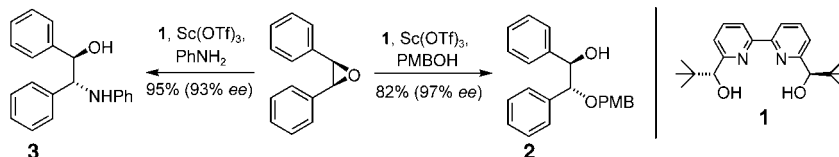


In control! Ag₂S nanocrystals of predictable size and shape were synthesized from the precursor Ag(SCOPh) in the presence of an amine. Careful tuning of several parameters, such as the reaction temperature and the ratio of amine to precursor, led to Ag₂S nanocrystals of varying morphology (red: nanocubes; blue: faceted nanocrystals; yellow: nanorods) and size. x = particle size. HDA = hexadecylamine.

Epoxide Ring Opening

C. Schneider,* A. R. Sreekanth,
E. Mai — 5691 – 5694

Scandium–Bipyridine-Catalyzed Enantioselective Addition of Alcohols and Amines to *meso*-Epoxides



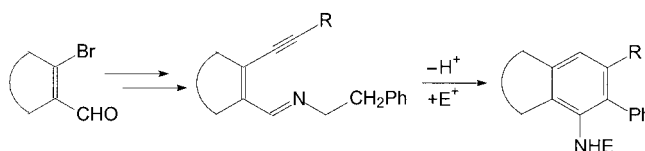
A winning combination of metal and ligand: The catalyst formed in situ from Sc(OTf)₃ and bipyridine **1** (10 mol%) mediates the alcoholysis and aminolysis

of *meso*-epoxides in high enantioselectivities and furnishes valuable chiral 1,2-diol monoethers **2** and 1,2-amino alcohols **3** as products (PMB = *para*-methoxybenzyl).

Annulations

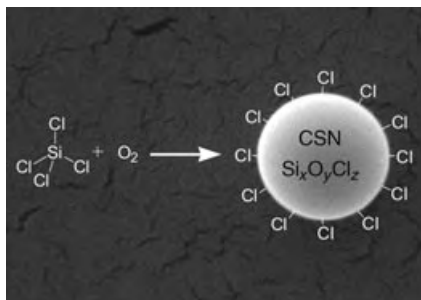
P. Sagar, R. Fröhlich,
E.-U. Würthwein* — 5694 – 5697

A Versatile Aminobenzannulation
Method Based on the Deprotonation of
2-(1-Alkynyl)benzaldehydes and Similar
2-Aza-2,4-heptadienyl-6-ynes: A Multistep
Rearrangement Cascade



Two ring closures, a ring opening, and two intermolecular proton shifts are the crucial steps in a cascade reaction that is triggered by the simple deprotonation of alkynylimines and leads ultimately to

aminobenzannulation products (see scheme). The reactions proceed in good to very good yield and with excellent chemoselectivity.



Like a chlorinated golf ball aptly describes a new kind of chlorosiloxane particle ($\text{Si}_x\text{O}_y\text{Cl}_z$, CSN; see picture). Under suitable conditions they are formed by the reaction between SiCl_4 and O_2 in the gas phase. The surface of these spherical, amorphous particles is densely covered by chlorine atoms. These can be substituted by nearly any group. Thus, the surface of the particles can be customized for the particular purpose.

Silica Particles

T. Giesenberg, S. Hein, M. Binnewies,*
G. Kickelbick _____ 5697–5700

Synthesis and Functionalization of a New Kind of Silica Particle



Communications labeled with this symbol have been judged by two referees as being “very important papers”.

Deadline for recruitment adverts

47/2004	November 18	Publication date: December 3
48/2004	November 25	Publication date: December 10

Angewandte Chemie International Edition

Advertising Sales Department:
Marion Schulz

Phone: 0 62 01 – 60 65 65

Fax: 0 62 01 – 60 65 50

E-Mail: MSchulz@wiley-vch.de

Place an advert in the printed version
and have it made available online for 1 month, free of charge!

Service

Keywords _____ 5702

Authors _____ 5703

Angewandte's
Sister Journals _____ 5704–5705

Preview _____ 5707



Siegfried Medal Awarded to Joel M. Hawkins

The Siegfried Medal is awarded jointly by the Universität Zürich (Switzerland) and Siegfried Ltd for fundamental research into improving chemical processes. The 2004 prize was awarded to Joel M. Hawkins of Pfizer Pharmaceuticals in recognition of his diverse contributions to solving problems in process development, including the development of new synthetic methods, the elucidation of reaction mechanisms through physical organic methods, and the automation of process optimization.



J. M. Hawkins

Joel M. Hawkins received his PhD in 1986 under the guidance of B. Sharpless at the Massachusetts Institute of Technology. He subsequently joined the group of R. Grubbs at the California Institute of Technology as a postdoctoral fellow. From 1987 to 1993 he was Assistant Professor at the University of California in Berkeley, where he investigated catalytic asymmetric Diels–Alder reactions and fullerene chemistry. In 1993 he moved to the Chemical Research Department at Pfizer, where he became involved in the application of new technologies to drug development. A result of his research endeavors is the remarkably efficient synthesis of CP-195543, a new and important therapeutic in the treatment of inflammations. In a recent Essay in *Angewandte Chemie*, he described the application and constraints in the use of asymmetric catalysis in the industrial manufacture of drugs.^[1]

Arndt Simon Receives Liebig Medal

This year's Liebig Medal of the Gesellschaft Deutscher Chemiker (GDCh, German Chemical Society) was awarded to Arndt Simon of the Max-Planck-Institut für Festkörperforschung in Stuttgart (Germany) in recognition of his multifaceted achievements in solid-state chemistry and structure analysis. Especially noteworthy was the development of a new camera for X-ray studies of extremely air-sensitive substances, his collaboration in the development of a surface detector diffractometer for crystal-structure investigation by X-ray and neutron diffraction, as well as the synthesis and structure determination of the alkali-metal suboxides.^[2a]



A. Simon

Arndt Simon studied chemistry at the Universität Münster (Germany), where he received his PhD in 1966 under the guidance of H. Schäfer. After his habilitation in 1971, he remained in Münster, first as lecturer and then as Professor until 1974, when he assumed the position of Director at the Max-Planck-Institut für Festkörperforschung in Stuttgart. Since 1975 he has also been Honorary Professor at the Universität Stuttgart. His research group is involved in cluster compounds, intermetallic phases, magnetism, relationships between structure, and superconductivity, on which he also authored a Review in *Angewandte Chemie*.^[2b] Arndt Simon is the recipient of several awards, for example, the Wilhelm Klemm Prize of the GDCh, and has been awarded honorary doctorates from various universities. From 1991 to 2000, he was a member of the Advisory Board of *Angewandte Chemie*.

Lutz F. Tietze Is Awarded the Emil Fischer Medal

For his distinguished and leading work in the field of preparative organic

chemistry, Lutz F. Tietze of the Universität Göttingen was presented with the Emil Fischer Medal of the GDCh. His areas of research are very diverse and include the development of new synthetic methods, the total synthesis of natural products, combinatorial chemistry,^[3a] and the development of cytostatic agents for cancer therapy.



L. F. Tietze

After studying chemistry in Kiel und Freiburg (Germany), he received his PhD in 1968 at the Universität Kiel under B. Franck. He worked as Scientific Assistant at the Universität Münster until 1974, which was interrupted by a long stay as a Research Associate with G. Büchi at the Massachusetts Institute of Technology. After further work abroad, with A. R. Battersby in Cambridge (United Kingdom), he completed his habilitation in 1975. After a bridging period in Dortmund (Germany), he became Director of the Institute of Organic Chemistry at the Universität Göttingen (Germany) in 1978. Lutz F. Tietze has been distinguished with many awards, including the Karl Winacker Award and an honorary doctorate from the University of Szeged (Hungary). His 2003 Review in *Angewandte Chemie* describes hybrids of natural products as lead structures in the search for drugs.^[3b]

[1] J. M. Hawkins, T. J. N. Watson, *Angew. Chem.* **2004**, *116*, 3286; *Angew. Chem. Int. Ed.* **2004**, *43*, 3224.

[2] a) A. Simon, *Struct. Bonding* **1979**, *36*, 81; b) A. Simon, *Angew. Chem.* **1997**, *109*, 1873; *Angew. Chem. Int. Ed. Engl.* **1997**, *36*, 1788.

[3] a) L. F. Tietze, N. Rackelmann, G. Sekar, *Angew. Chem.* **2003**, *115*, 4386; *Angew. Chem. Int. Ed.* **2003**, *42*, 4254; b) L. F. Tietze, H. P. Bell, S. Chandrasekhar, *Angew. Chem.* **2003**, *115*, 4128; *Angew. Chem. Int. Ed.* **2003**, *42*, 3996.

Syntheses of Tetrodotoxin

Ulrich Koert*

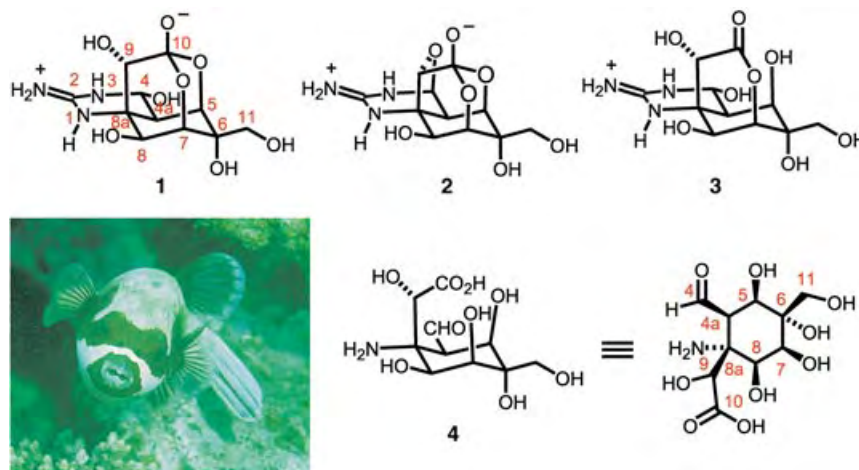
Keywords:

natural products · tetrodotoxin · total synthesis

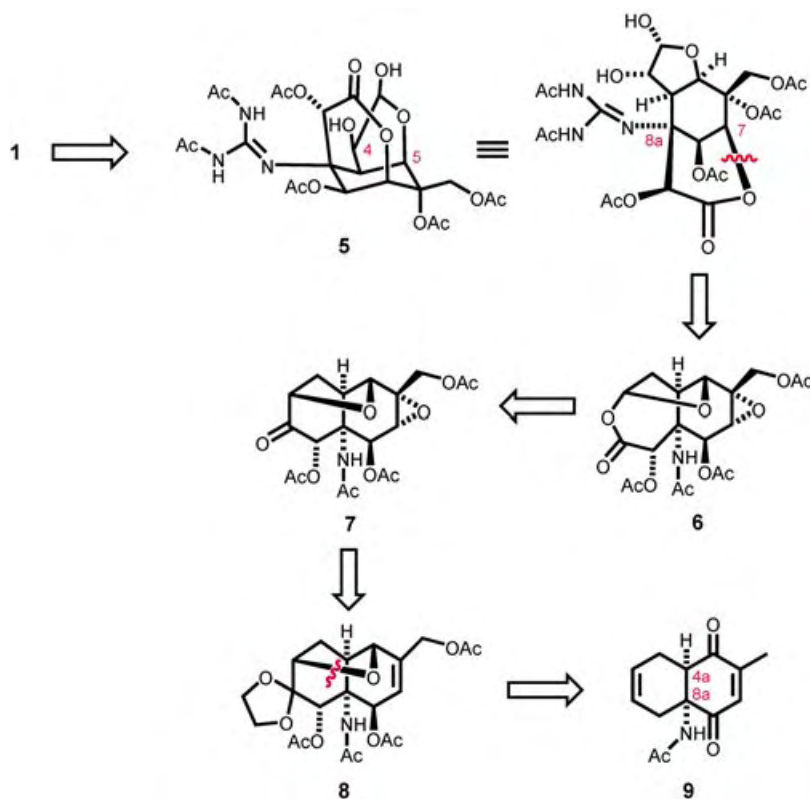
A meal of puffer fish (tōra fugu), a speciality of Japanese cuisine, may be fraught with some peril, because the livers and ovaries of the fish contain the highly toxic compound tetrodotoxin. The presence of a toxic principle in the puffer fish was known since antiquity, but the structure of this component was elucidated only in 1964 when three groups independently identified and characterized tetrodotoxin.^[1] The physiological mode of action of tetrodotoxin is the inhibition of voltage-gated ion channels in the nervous system.^[2]

Tetrodotoxin (**1**) is in equilibrium with anhydrotetrodotoxin (**2**) and the lactone form **3** (Scheme 1). The structure is characterized by a dioxadamanthane skeleton, a guanidine at C2 which is part of an hemiaminal at C4, and an orthoacid at C10. After retrosynthetic simplification of the guanidine group to an amine at C8a and cleavage of the orthoacid, the hexasubstituted cyclohexane **4** results.

The seven stereocenters of **4** lead to an incomparably high density of functionality at the six-membered ring. Particular synthetic challenges are the two tetrasubstituted stereocenters C6 and C8a. The Kishi synthesis^[3] of racemic tetrodotoxin in 1972 set the standard for three decades. Recently two other groups led by Isobe^[4] and Du Bois^[5] achieved the first asymmetric total syntheses of tetrodotoxin. The aim of this highlight is to compare the three synthetic strategies and to illuminate the key steps.



Scheme 1. A puffer fish and the structures of tetrodotoxin (**1**), anhydrotetrodotoxin (**2**), and lactone **3**. The hexasubstituted cyclohexane derivative **4** is proposed in the retrosynthesis in which the guanidine arises from an amino group at C8a and the opening of the orthoacid.



Scheme 2. Retrosynthesis of tetrodotoxin by Kishi et al.

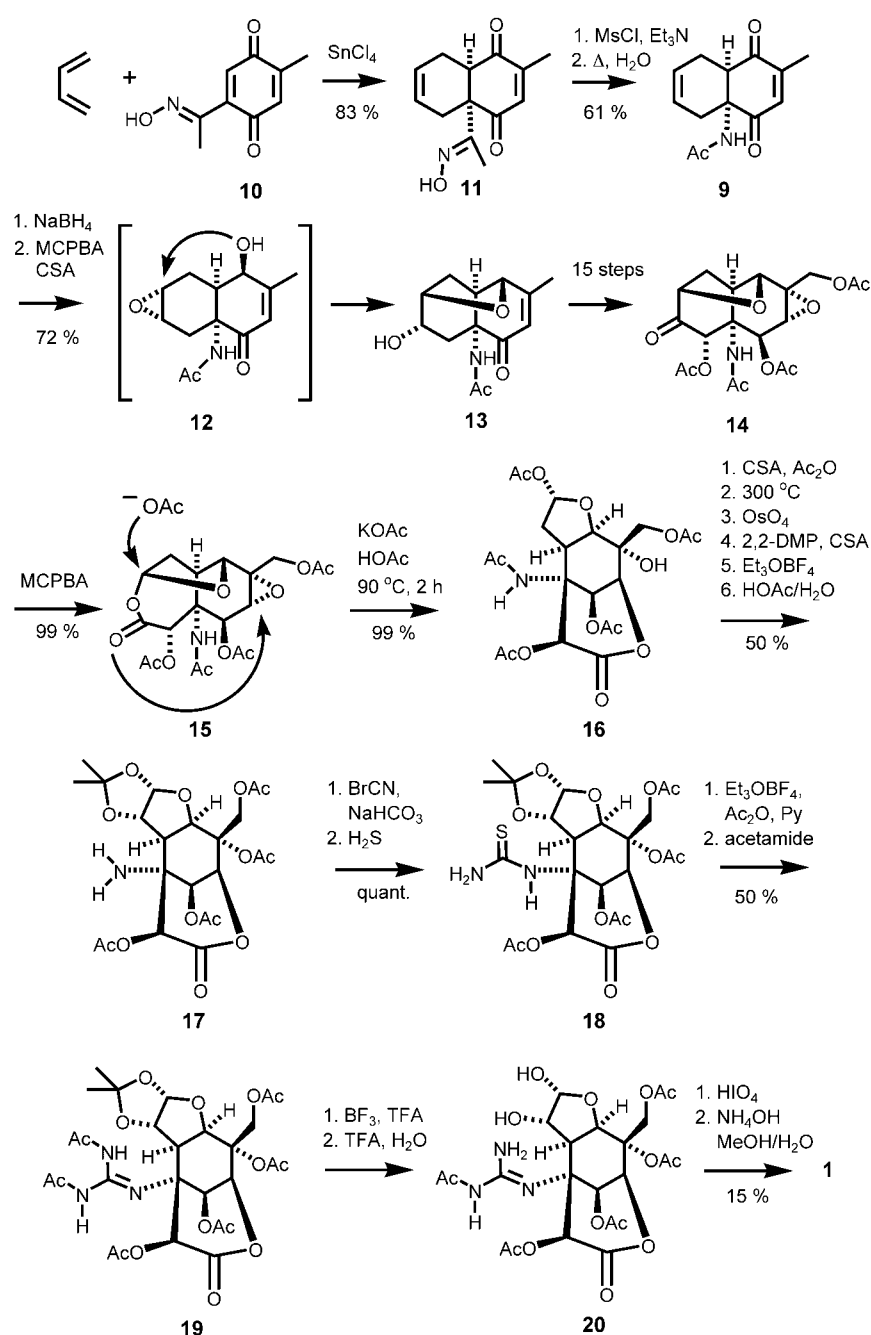
[*] Prof. Dr. U. Koert

Fachbereich Chemie
Philipps-Universität Marburg
Hans-Meerwein-Strasse
35032 Marburg (Germany)
Fax: (+49) 6421-282-5677
E-mail: koert@chemie.uni-marburg.de

The retrosynthetic analysis of Kishi et al. is shown in Scheme 2. Tetrodotoxin (**1**) was synthetically simplified by cleavage of the hemiaminal at C4. The resulting C2 guanidine group was protected. A 1,2-diol was chosen as a precursor for the C4 aldehyde, which led to the 2,3-dihydroxytetrahydrofuran derivative **5**. An intramolecular epoxide opening by a carboxylate was intended as the key step for installing the *cis* 7,8a functionality (**6**→**5**). The carboxylate group resulted from the seven-membered lactone in **6**, which could be accessible by a Baeyer–Villiger oxidation of the ketone **7**. Transformation of **7** via **8** led to compound **9**, which is accessible by a Diels–Alder cycloaddition. The *cis* configuration of H(C4a) and the amino group at C8a was established by this cycloaddition. This synthetic plan is a very good example for the concept of cyclic stereocontrol.

The starting point for the synthesis (Scheme 3) was the Lewis acid catalyzed Diels–Alder reaction of the benzoquinone **10** with butadiene to yield the oxime-substituted cycloadduct **11**, which underwent a Beckman rearrangement to give the acetamide **9**. An intramolecular epoxide opening of **12** led to **13**. A longer sequence of functional group manipulations converted **13** into the ketone **14**, which could be transformed cleanly by a Bayer–Villiger oxidation into the epoxylactone **15**. Now the stage was set for one of the key reactions: attack of an acetate anion on the lactone acetal in **15** gave a carboxylate, which opened the epoxide to yield the lactone **16**. Cleavage of the acetamide (**16**→**17**) and introduction of the diprotected guanidinium group (**17**→**18**→**19**) paved the way for the final stages of the synthesis. Monodeprotection activated the guanidinium group and generated a 1,2-diol (**19**→**20**), which by periodate cleavage gave the C4 aldehyde. Finally, the aminolysis of the acetate protecting groups induced the formation of the orthoacid and delivered the target compound tetrodotoxin in racemic form.

Isobe et al. made numerous contributions to the tetrodotoxin field.^[4,6] Among them are two total syntheses: one from 2003^[4a] and a more efficient one from 2004.^[4b] The latter is considered here. Isobe's retrosynthesis sets compound **21** as a final precursor for

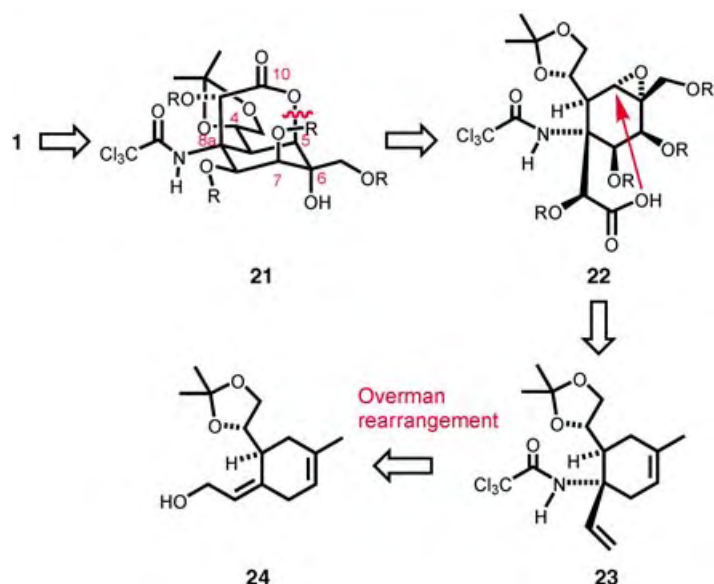


Scheme 3. Synthesis of *rac*-tetrodotoxin by Kishi et al. CSA = camphorsulfonic acid, 2,2-DMP = 2,2-dimethoxypropane, MCPBA = *m*-chloroperbenzoic acid, Ms = methanesulfonyl, Py = pyridine, TFA = trifluoroacetic acid.

the target molecule (Scheme 4). In **21** the C4 aldehyde is masked as a protected 1,2-diol, and the C8a amine is protected as a trichloroacetamide. The C7 OH group is monoprotected, and a lactone connects C10 and C5. This lactone should be formed by intramolecular attack of a carboxylic acid on the C5–C6 epoxide **22**. Compound **22** could be reached from **23** by a series of

functional-group transformations. An Overman rearrangement^[7] of the allylic alcohol **24** to give **23** is envisaged as key step to generate the tetrasubstituted C8a center.

The synthesis by Isobe et al.^[4b,6] commenced with a Diels–Alder reaction of bromolevogluconone **25** and isoprene to attain the cycloadduct **26**, which was further converted into the



Scheme 4. Retrosynthesis of tetrodotoxin by Isobe et al.

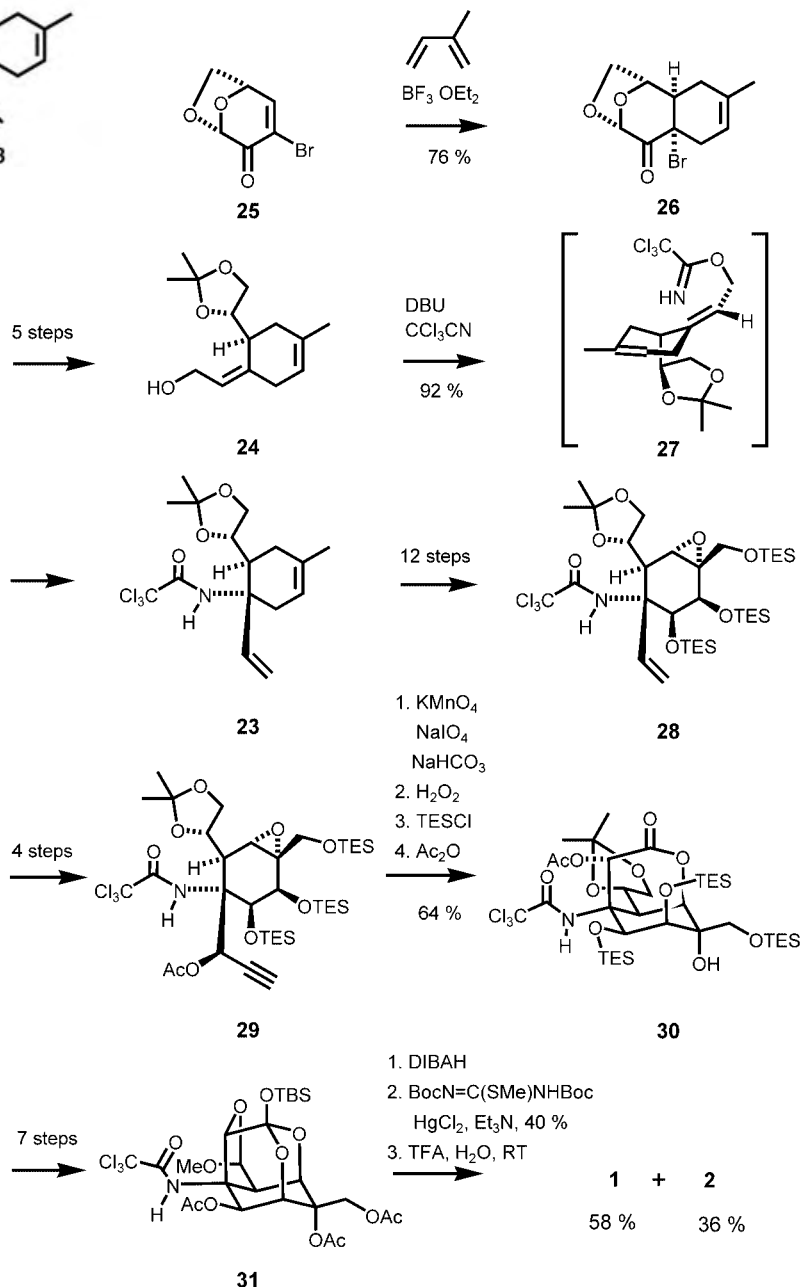
allylic alcohol **24** (Scheme 5). This key intermediate afforded via the trichloroacetimidate **27**, the expected product of the Overman rearrangement (**23**). In their earlier synthesis^[4a] Isobe et al. encountered problems in performing an Overman rearrangement at a later stage of the synthesis. Therefore in their second synthesis they accomplished the rearrangement at this early stage. A longer sequence led from **23** via the terminal alkene **28** to the protected propargylic alcohol **29**. Oxidative cleavage of the triple bond in **29** generated a carboxylic acid function, which attacked the epoxide selectively at C5 to produce the lactone **30**. After some protective group modifications the TBS-protected orthoester **31** was at hand. Reductive amide cleavage followed by the introduction of the Boc-protected guanidine group and a deprotection step gave tetrodotoxin (**1**) together with anhydro-tetrodotoxin (**2**) in very high yield. The careful choice of the acid-labile protective groups was the precondition for the high yield of the final step. Compared to Kishi's final steps, Isobe's protective group tactics are remarkably efficient.

The strategy of the tetrodotoxin synthesis by Du Bois et al.^[5] is based on two CH-activation steps to install the two tetrasubstituted centers C6 and C8a (Scheme 6). The target compound **1** is reduced to the precursor **32** in analogy to the retrosyntheses of the other two

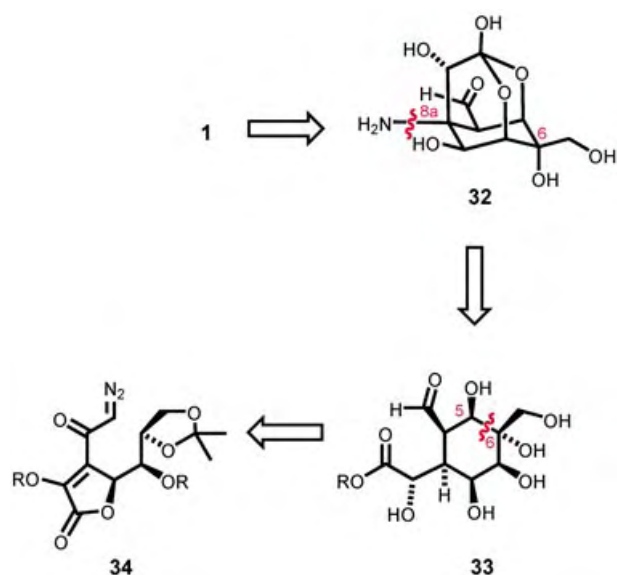
approaches (vide supra). The idea of introducing the amino functionality at C8a by a nitrene insertion into the corresponding C–H bond of **33** is unique. An intramolecular CH insertion of a carbene resulting from

the diazoketone **34** is intended for the construction of the bond between C5 and C6 in **33**.

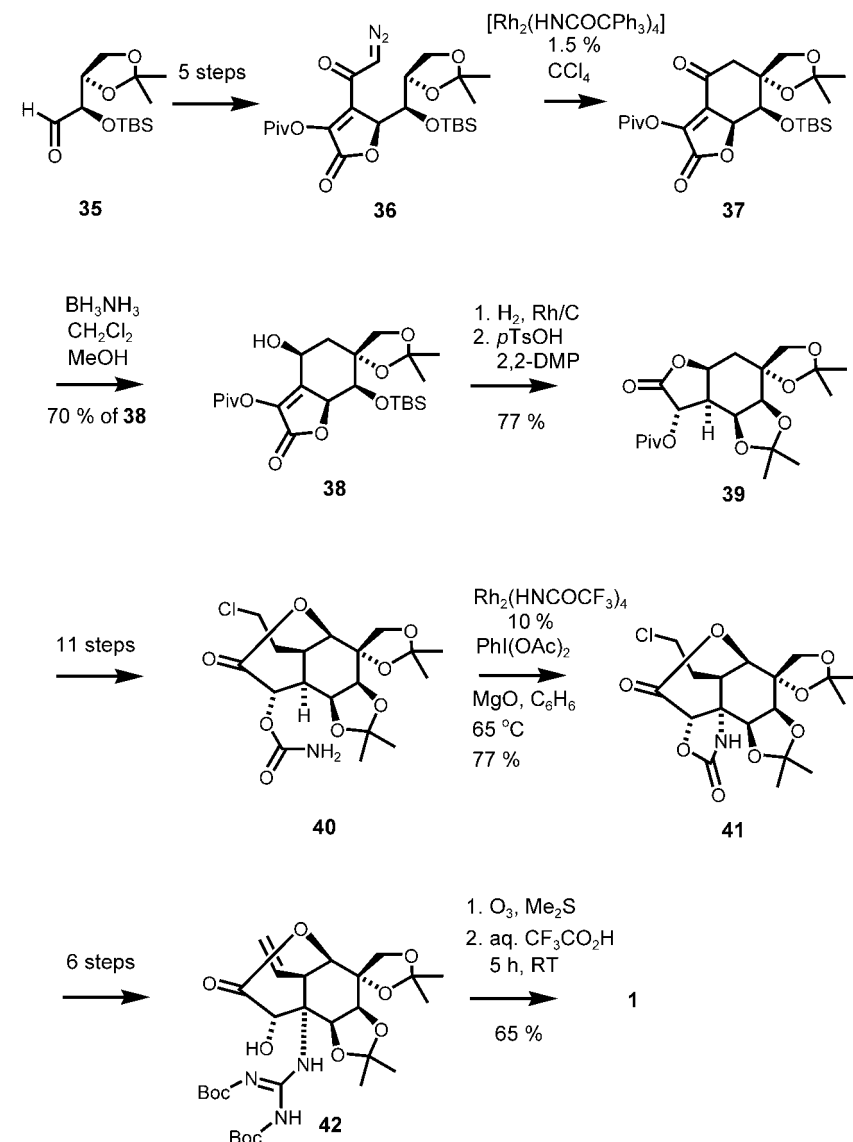
Du Bois et al. chose the chiral aldehyde **35**, which is readily available from isoascorbic acid, to start their synthesis (Scheme 7). After a few steps the diazoketone **36** was obtained. A Rh–amide complex was best suited to achieve the CH-insertion at C6 and to yield the cyclohexanone **37** exclusively. The ster-



Scheme 5. Synthesis of (–)-tetrodotoxin by Isobe et al. Boc = *tert*-butoxycarbonyl, DBU = 1,8-diazabicyclo[5.4.0]undec-7-ene, DIBALH = diisobutylaluminum hydride, TBS = *tert*-butyldimethylsilyl, TES = triethylsilyl.



Scheme 6. Retrosynthesis of tetrodotoxin by Du Bois et al.



Scheme 7. Synthesis of (–)-tetrodotoxin by Du Bois et al. Piv = pivaloyl.

oselective reduction of the ketone **37** to give the alcohol **38** required the borane–ammonia adduct as the reagent. A stereoselective hydrogenation delivered the lactone **39**, which was converted in a longer sequence into the carbamate **40**. A Rh-catalyzed oxidative treatment of the carbamate produced the oxazolidinone **41**. The mechanism of this CH insertion probably does not involve the free carba-

moynitrene but rather a Rh intermediate.^[8] Now that the C8a nitrogen was in place the Boc-protected guanidine group and a vinyl group as the precursor of the C4 aldehyde were introduced (**41**→**42**). Ozonolysis generated the aldehyde function, and subsequent acidic treatment cleaved the Boc protecting groups and the two acetonides, which resulted in the assembly of the dioxadamantane framework and completed the synthesis of tetrodotoxin (**1**). The two key steps of this synthesis are intramolecular CH-activation reactions, which demonstrate the synthetic power of this method. The Taber group has achieved a synthesis of an advanced synthetic intermediate for tetrodotoxin by using an intramolecular carbene insertion to install the tetrasubstituted C6 center.^[9] Further advanced intermediates have been described by Fukuyama et al. (nitrile oxide cycloaddition)^[10] and Fraser-Reid et al. (radical cyclization).^[11]

In comparing the three syntheses one recognizes similar concluding strategies dictated by the polar orthoacid and the guanidinium groups. In both the Kishi and Isobe approaches an intramolecular epoxide opening by a carboxylic acid is used to install the stereocenters on the hexasubstituted cyclohexane ring. The strategy of Du Bois et al. is different and relies on two CH-activation key steps. Kishi's synthesis of racemic tetrodotoxin from 1972 is a classical masterpiece. In 2003 Isobe et al. achieved the first synthesis of the enantiomerically pure target. Their approach is characterized by its efficiency and careful optimization. The tetrodotoxin synthesis by Du Bois et al. is an impressive achievement made possible by parallel progress in synthetic methodology. The CH-activation method for preparing oxazolidinones was published by Du Bois et al. only two years before the tetrodotoxin synthesis.

All three syntheses are long (>25 steps) and follow a linear strategy. The hexasubstituted cyclohexane intermediate makes a convergent strategy, which may reduce the number of steps to less than 20, very difficult but not impossible. Because of its structural complexity and functional-group density, tetrodotoxin will remain a prime synthetic target. The new routes of Isobe and

Du Bois should yield tetrodotoxin derivatives suited for ion-channel studies in the near future.

-
- [1] a) T. Goto, Y. Kishi, S. Takahashi, Y. Hirata, *Tetrahedron* **1965**, 21, 2059–2088; b) K. Tsuda, S. Ikuma, M. Kawamura, R. Tachikawa, K. Sakai, C. Tamura, O. Amakasu, *Chem. Pharm. Bull.* **1964**, 12, 1357–1374; c) R. B. Woodward, *Pure Appl. Chem.* **1964**, 9, 49–74.
- [2] a) *Tetrodotoxin, Saxitoxin and the Molecular Biology of the Sodium Channel* (Eds.: Y. Kao, S. Lovinson) in *Ann. N. Y. Acad. Sci.* **1986**, 479, 1–355; b) F. Huch, *Angew. Chem.* **1995**, 107, 23–36; *Angew. Chem. Int. Ed. Engl.* **1995**, 34, 39–50.
- [3] a) Y. Kishi, T. Fukuyama, M. Aratani, F. Nakatsubo, T. Goto, S. Inoue, H. Tanino, S. Sugiura, H. Kakaoi, *J. Am. Chem. Soc.* **1972**, 94, 9219–9221; b) Kishi's synthesis has been highlighted by N. Anand, J. S. Bindra, S. Rangranathan in *Art in Organic Synthesis*, 2nd ed, Wiley, New York, **1987**, pp. 346–350.
- [4] a) N. Ohyabu, T. Nishikawa, M. Isobe, *J. Am. Chem. Soc.* **2003**, 125, 8798–8805; b) T. Nishikawa, D. Urabe, M. Isobe, *Angew. Chem.* **2004**, 116, 4886–4889; *Angew. Chem. Int. Ed.* **2004**, 43, 4782–4785; c) T. Nishikawa, M. Asai, N. Ohyabu, N. Yamamoto, M. Isobe, *Angew. Chem.* **1999**, 111, 3268–3271; *Angew. Chem. Int. Ed.* **1999**, 38, 3081–3084.
- [5] A. Hinman, J. Du Bois, *J. Am. Chem. Soc.* **2003**, 125, 11510–11511.
- [6] T. Nishikawa, M. Asai, N. Ohyabu, N. Yamamoto, Y. Fukuda, M. Isobe, *Tetrahedron* **2001**, 57, 3875–3883.
- [7] L. E. Overman, *Acc. Chem. Res.* **1980**, 13, 218–224.
- [8] C. G. Espino, J. Du Bois, *Angew. Chem.* **2001**, 113, 618–620; *Angew. Chem. Int. Ed.* **2001**, 40, 598–600.
- [9] D. F. Taber, P. H. Storck, *J. Org. Chem.* **2003**, 68, 7768–7771.
- [10] T. Itoh, M. Watanabe, T. Fukuyama, *Synlett* **2002**, 1323–1325.
- [11] C. S. Burgey, R. Vollerthun, B. Fraser-Reid, *J. Org. Chem.* **1996**, 61, 1609–1618.
-

High-Throughput Screening

Outrunning the Bear

Jean-Louis Reymond*

Keywords:

biocatalysis · combinatorial chemistry · drug design · high-throughput screening · self-assembly

Chemistry is the art of transforming matter. Although turning lead into gold does not really work, chemists can design, select, and synthesize new compounds with exceptional properties, in particular, drugs for treating diseases. One critical aspect of drug-discovery technology is the activity-selection step, which is necessary because it is not possible to reliably predict the nature and magnitude of the molecular interaction between a drug target such as an enzyme and the drug itself. Selecting for active compounds therefore must rely on high-throughput screening, whereby a reference assay for a given activity is used to test series of compounds.^[1]

The development of high-throughput screening was a consequence of the invention of combinatorial chemistry, a technology which enabled chemists to synthesize millions rather than tens of compounds within a very short time.^[2] The essence of combinatorial synthesis was to prepare large numbers of compounds by using only a few operations, such as in the split-and-mix protocol.^[3] These methods involved in part the handling of compound mixtures, but this aspect was considered too uncertain and was set aside, and the field of combinatorial chemistry has mostly concentrated on developing parallel and solid-phase synthesis methods for single compounds.^[4]

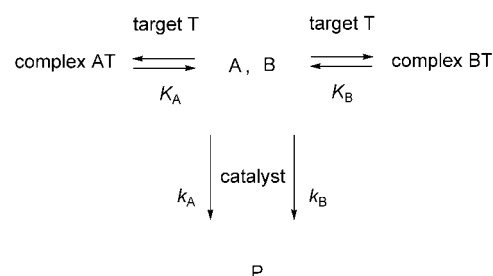
The idea of compound mixtures did not just end there but soon resurfaced in a very different context, that of supramolecular chemistry. As defined by

Lehn and Whitesides, supramolecular chemistry aims at forming complex systems by the self-assembly of molecular building blocks through noncovalent interactions without outside intervention.^[5] Noncovalent self-assembly from mixtures of molecular building blocks provides a paradigm for obtaining complex supramolecules not accessible by stepwise synthesis, and the concept was also suitable for equilibrating components linked by covalent bonds.^[6] Compound mixtures were brought back to the field of drug discovery when it was shown that equilibrating mixtures of building blocks for small-molecule inhibitors such as peptides^[7] and imines^[8] in the presence of a target binding protein resulted in an enrichment of the tightest binding inhibitors. This type of equilibrating mixture was termed a dynamic combinatorial library (DCL).^[9]

The dynamism of a DCL comes to play during the equilibration phase in the presence of a target ligand. However, this dynamic state is short-lived and inexorably leads to a static state of thermodynamic equilibrium. This is quite problematic because at equilibrium it is almost impossible to distinguish between similar compounds, and a small advantage of one library member over another in binding to the target results in only a proportionately small increase in its concentration. Therefore, the DCL is able to select the best library member for binding to its target only if its properties are far superior to those of the other library members.^[10] Recent mathematical models show that a single DCL member must bind the target three to four orders of magnitude better than the average to make

up a sizable portion (several percent) of the DCL at equilibrium.^[11] The situation is similar with target-accelerated synthesis.^[12]

Recently Kazlauskas, Gleason, and co-workers^[13] found a solution to this mixture selection problem starting from yet another area of chemistry, biocatalysis. In biocatalysis one uses enzymes for organic synthesis, in particular for their properties as mild, environmentally friendly, and highly selective catalysts.^[14] The most commonly used biocatalytic step is the kinetic resolution of racemates, whereby an enzyme converts one enantiomer (A) of a racemic substrate (A,B) preferentially into a new product (P) while leaving the other (B) untouched (Scheme 1). The mathematical treatment of kinetic resolution as described by Kagan and Fiaud^[15] shows a surprising property: even if the enzyme is not completely selective for one of the enantiomers, the reaction leaves the unreacted enantiomer of the substrate with an optical purity higher than the intrinsic selectivity of the enzyme, that is, $R \gg S$ (Figure 1). This higher degree of purity comes at a cost, which is that the yield of the pure unreacted substrate is less than the theoretical maximum of 50%.



Scheme 1. Principle of kinetic resolution. Differentiation favoring A over B is achieved either by the catalyst ($k_A < k_B$, no target) or by differential binding to a target ($K_A < K_B$, nonselective catalyst $k_A = k_B$).

[*] Prof. J.-L. Reymond
Department of Chemistry and Biochemistry
University of Berne
Freiestrasse 3, 3012 Bern (Switzerland)
Fax: (+41) 31-631-8057
E-mail: reymond@ioc.unibe.ch

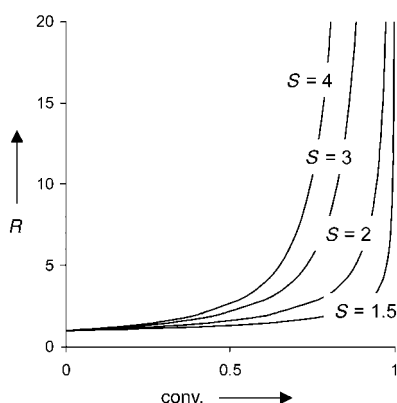
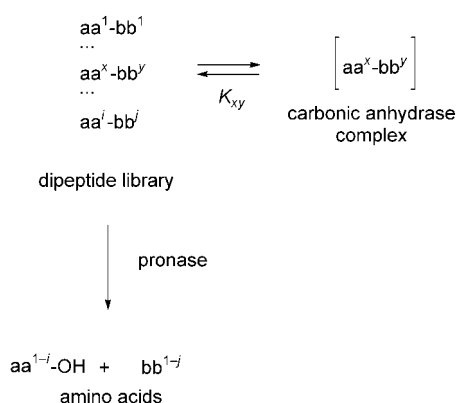


Figure 1. Ratio of remaining substrates $R = A/B$ as a function of overall conversion and selectivity $S = k_B/k_A$ (selective enzyme) or $S = K_B/K_A$ (target binding). conv. = conversion of substrate A, B to product P; $S = \ln[(1-c)/(1-ee)]/\ln[(1-c)/(1+ee)] = \ln[(1-c)/(2/(R+1))]/\ln[(1-c)/(2R/(R+1))]$; $ee = (A-B)/(A+B)$. Note that R largely exceeds S at high conversion.

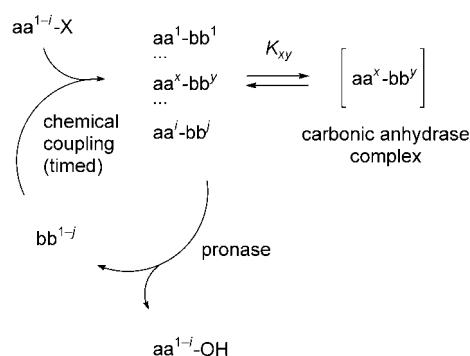
Kazlauskas, Gleason, and co-workers recognized that the same equation would apply when using an unselective enzyme to destroy a mixture of compounds in the presence of an excess of a target binding protein.^[13] This kinetic resolution would enhance the ratio of compounds in excess of their relative binding constants to the target. The concept was demonstrated for a mixture of dipeptides competing for binding to carbonic anhydrase as a target, using the protease pronase as the nonselective enzyme to destroy the weaker binders (Scheme 2). However, as for the kinetic resolution of racemates, this selection came at the cost of destroying most compounds, including part of the tightest binders.

Kazlauskas, Gleason, and co-workers have now used this concept to produce a self-selecting DCL setup that delivers only the tightest binding member in the DCL while leaving only traces of the others.^[16] The amino ends of the dipeptides, which are released by the action of the pronase enzyme used to destroy unbound inhibitors, are periodically recoupled to activated esters, which allows the regeneration of the dipeptide library from its components and thus results in a pseudo-DCL (Scheme 3).



Scheme 2. Kinetic resolution of dipeptide library using pronase.^[13] The protease pronase is separated from the target carbonic anhydrase by a dialysis membrane. K_{xy} denotes the dissociation constant of the carbonic anhydrase–dipeptide $aa^x bb^y$ complex. The best binders to carbonic anhydrase among the dipeptides escape hydrolysis by pronase.

In the pseudo-DCL experiment the selection by target binding versus destruction by pronase can be replayed over and over again, and a small preference in binding to the target eventually results in a large enrichment of the tighter binding compound. Just like two unfortunate hunters trying to outrun an angry bear, none of the compounds in the pseudo-DCL can outrun pronase. Yet outrunning the other library members by only a small amount in terms of target binding is sufficient to ensure



Scheme 3. Pseudodynamic combinatorial library of dipeptides.^[16] The amino ends bb^{1-j} of the hydrolyzed dipeptide are periodically recoupled by timed additions of activated esters $aa^{1-j}-X$. The esters are on solid support, and the pronase is separated from the target carbonic anhydrase by a dialysis membrane. In the experiment there are four activated carboxylic acid esters ($i=4$) and two amino acids ($j=2$), forming eight possible dipeptides aa^x-bb^y .

survival of the better inhibitor and elimination of the weaker inhibitors. After seven cycles of periodic recoupling at 16-hour intervals, only a single inhibitor remained in excess of 100:1, even though it was only 2.3 times more potent than the next library member for binding to carbonic anhydrase. The experiment was in part lucky because the carboxylic acid component of the dipeptide does not interact with the target carbonic anhydrase and can be allowed to accumulate in the system.

The pseudo-DCL has elements reminiscent of a living system. The first element, previously described, is molecular death through hydrolysis by pronase. The second and third elements are molecular birth by re-synthesis and an energy source in the form of the activated esters used to achieve recoupling. Energy expenditure allows the system to stay away from thermodynamic equilibrium, an essential feature of living systems. In comparison to previous DCLs, the key here is that resynthesis cycles can be timed precisely to allow the system to periodically move to high conversion where selection most favors the best binders (Figure 1). This human intervention for controlling time will be extremely difficult to remove to make a fully autonomous system.

- [1] W. P. Walters, M. Namchuk, *Nat. Rev. Drug Discovery* **2003**, 2, 259–266.
- [2] *Combinatorial Chemistry: Synthesis and Application* (Eds.: S. R. Wilson, A. W. Czarnik), Wiley, Weinheim, **1997**.
- [3] a) A. Furka, F. Sebestyen, M. Asgedom, G. Dibo, *Int. J. Pept. Protein Res.* **1991**, 37, 487–493; b) K. S. Lam, S. E. Salmon, E. M. Hersch, V. J. Hruby, W. M. Kazmierski, R. J. Knapp, *Nature* **1991**, 354, 82–84; c) R. A. Houghten, C. Pinilla, S. E. Blondelle, J. R. Appel, C. T. Dooley, J. H. Cuervo, *Nature* **1991**, 354, 84–86.
- [4] A. T. Merritt, S. W. Gerritz, *Curr. Opin. Chem. Biol.* **2003**, 7, 305–307.
- [5] a) J.-M. Lehn, *Proc. Natl. Acad. Sci. USA* **2002**, 99, 4763–4768; b) G. M. Whitesides, M. Boncheva, *Proc. Natl. Acad. Sci. USA* **2002**, 99, 4769–4774.
- [6] P. A. Brady, R. P. Bonar-Law, S. J. Rowan, C. J. Suckling, J. K. M. Sanders, *Chem. Commun.* **1996**, 319.
- [7] P. G. Swann, R. A. Casanova, A. Desai, M. M. Fraunhofer, M. Urbancic, U.

- Slomczynska, A. J. Hopfinger, G. C. LeBreton, D. L. Venton, *Biopolymers* **1996**, *40*, 617–625.
- [8] I. Huc, J.-M. Lehn, *Proc. Natl. Acad. Sci. USA* **1997**, *94*, 2106–2110.
- [9] O. Ramström, T. Bunyapaiboonsri, S. Lohmann, J.-M. Lehn, *Biochim. Biophys. Acta* **2002**, *1572*, 178–186.
- [10] A. V. Eliseev, M. I. Nelen, *J. Am. Chem. Soc.* **1997**, *119*, 1147–1148.
- [11] a) Z. Grote, R. Scopelliti, K. Severin, *Angew. Chem.* **2003**, *115*, 3951–3955; *Angew. Chem. Int. Ed.* **2003**, *42*, 3821–3825; b) P. T. Corbett, S. Otto, J. K. M. Sanders, *Org. Lett.* **2004**, *6*, 1825–1827; c) P. T. Corbett, S. Otto, J. K. M. Sanders, *Chem. Eur. J.* **2004**, *10*, 3139–3143.
- [12] a) K. C. Nicolaou, R. Hughes, S. Y. Cho, N. Winssinger, C. Smethurst, H. Labischinski, R. Endermann, *Angew. Chem.* **2000**, *112*, 3981–3986; *Angew. Chem. Int. Ed.* **2000**, *39*, 3823–3828; b) R. Nguyen, I. Huc, *Angew. Chem.* **2001**, *113*, 1824–1826; *Angew. Chem. Int. Ed.* **2001**, *40*, 1774–1776; c) W. G. Lewis, L. G. Green, F. Grynszpan, Z. Radic, P. R. Carlier, P. Taylor, M. G. Finn, K. B. Sharpless, *Angew. Chem.* **2002**, *114*, 1095–1099; *Angew. Chem. Int. Ed.* **2002**, *41*, 1053–1057.
- [13] J. D. Cheeseman, A. D. Corbett, R. Shu, J. Croteau, J. L. Gleason, R. J. Kazlauskas, *J. Am. Chem. Soc.* **2002**, *124*, 5692–5701.
- [14] A. S. Bommarius, B. R. Riebel, *Biocatalysis*, Wiley-VCH, Weinheim, **2004**.
- [15] H. B. Kagan, J. C. Fiaud in *Topics in Stereochemistry*, Vol. 18, Wiley, New York, **1988**, p. 249.
- [16] A. D. Corbett, J. D. Cheeseman, R. J. Kazlauskas, J. L. Gleason, *Angew. Chem.* **2004**, *116*, 2486–2490; *Angew. Chem. Int. Ed.* **2004**, *43*, 2432–2436.

Carbonylation Catalysts

Evolution of Carbonylation Catalysis: No Need for Carbon Monoxide

Tsumoru Morimoto* and Kiyomi Kakiuchi

Keywords:

carbonyl ligands · carbonylation · homogeneous catalysis · transition metals

Progress in organometallic catalysis began with the discovery of the Roelen reaction (hydroformylation with carbon monoxide and hydrogen) in 1938 and the Reppe reaction (hydrocarboxylation with carbon monoxide and water) in 1939. Since then, carbonylation chemistry by using carbon monoxide has occupied a central position in organometallic chemistry, as it relates to organic synthesis. There is, however, the problem of using gaseous carbon monoxide (a toxic greenhouse gas) in this chemistry. Recently, some strategies that address this issue have appeared. This minireview describes carbonylation reactions that can be conducted without the direct use of carbon monoxide. These carbonylation reactions provide reliable and accessible tools for synthetic organic chemists.

1. Introduction

Carbonylation chemistry (carbon monoxide chemistry) has been the focus of extensive research in laboratory-scale organic syntheses, including industrial processes.^[1] Because of the continuous progress in this area, its versatility and increasing elaboration as a synthetic tool has led to broader applications in the synthesis of a wide variety of simple carbonyl compounds to more complex organic molecules. However, the methods suffer from some major disadvantages; the difficulty in handling toxic, gaseous carbon monoxide, including its storage and transport, represents real problems. Unfortunately, such a disadvantage reduces the overall utility of carbonylation. Of course, many efforts to develop the method without the use of carbon monoxide have been continuously proposed for over 30 years. Some successful reports have appeared, and innovative inventions have been reported, especially in the last two to three years. In all cases, the key to success is knowing how a carbonyl group can be transferred by using substitutes for carbon monoxide. In this minireview, we provide comprehensive coverage of carbon-

ylation reactions that can be conducted without the direct use of carbon monoxide. All of the reactions using carbon monoxide in which the reactions in the review originate have been demonstrated to have a high utility in organic synthesis; hydrocarbonylation (hydroesterification, hydroamidation, and hydrocarboxylation) of alkenes and al-

kynes,^[2] hydroformylation of alkenes,^[3] alkoxy-, amino-, and hydroxycarbonylation of aromatic and alkenyl halides,^[4] and the Pauson–Khand reaction.^[5] Thus, this review should make the carbonylation methodology more reliable and accessible, and should permit further advances in this area. The material is organized according to reagents that can be used as a substitute for carbon monoxide.

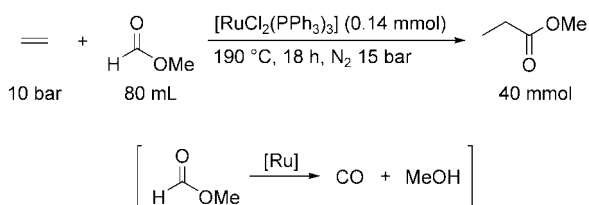
2. Use of Formic Acid and its Derivatives

2.1. Formates

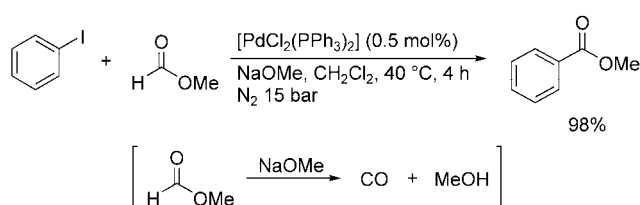
Alkyl formates, especially methyl formate, have been widely utilized as a C₁ building block in organic synthesis. They are known to be easily decarbonylated by various transition-metal catalysts to yield carbon monoxide and the corresponding alcohols. This decarbonylation process is attractive as it affords a means of producing highly pure carbon monoxide, thus avoiding storage and compression of the gas.

In 1983, Sneed and co-workers discovered the Ru-catalyzed addition reaction of methyl formate to ethylene (Scheme 1),^[6] and demonstrated that it represented an alternative to the original hydroesterification with carbon monoxide.^[2a,b] This reaction involved the catalytic decarbonylation process mentioned above, and ethylene, present in the reaction system, was carbonylated by the released carbon

[*] Prof. T. Morimoto, Prof. K. Kakiuchi
Graduate School of Materials Science
Nara Institute of Science and Technology (NAIST)
Takayama, Ikoma, Nara 630-0192 (Japan)
Fax: (+81) 743-72-6089
E-mail: morimoto@ms.naist.jp

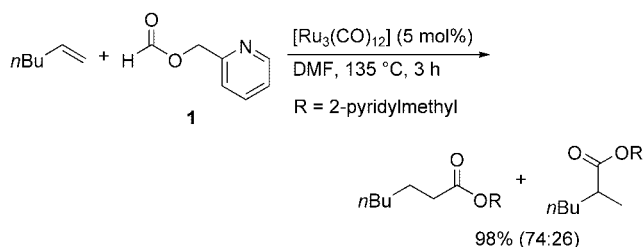


Scheme 1. Ru-catalyzed hydroesterification by using methyl formate.^[6]



Scheme 3. Pd-catalyzed alkoxycarbonylation by using methyl formate.^[10]

monoxide and methanol to give methyl propionate. Since their discovery, numerous modifications of this reaction have been developed.^[7,8] Recently, Chang et al. reported on the hydroesterification of alkenes by using a unique formate, **1**, which contains a pyridyl group, as a substitute for carbon monoxide and an alcohol (Scheme 2).^[9a] The method can be applied to a wide variety of alkynes and dienes as well as alkenes.^[9b]

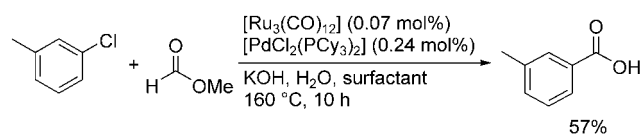


Scheme 2. Ru-catalyzed hydroesterification by using formate **1**.^[9a]

Alkyl formates readily undergo decarbonylative decomposition in the presence of strong bases to generate carbon monoxide, along with the corresponding alcohols. Mortreux et al. successfully applied this decarbonylation of methyl formate to the Heck-type esterification of aryl and vinyl halides. Thus, the reaction of aryl and vinyl halides with alkyl formates in the presence of sodium alkoxide and a catalytic amount of a palladium complex results in the alkoxycarbonylation of aryl and vinyl halides to give aromatic and vinyl esters (Scheme 3).^[10] When a combination of ethyl formate and sodium ethoxide was used, the reaction proceeded smoothly at room temperature (85 % yield of ethyl benzoate).

Potassium *tert*-butoxide was unsuitable as a decarbonylating reagent, because the decarbonylation of alkyl formates occurred violently, even at 0 °C.

A related catalytic coupling reaction of chloroarenes with methyl formate in aqueous media was reported by Jenner and Ben Taleb (Scheme 4).^[11] In this case, the use of a mixture of



Scheme 4. Pd-catalyzed hydroxycarbonylation by using aqueous methyl formate.^[11]

ruthenium and palladium complexes led to the best results. However, a ruthenium catalyst was not necessary, since the yield of aromatic acid decreased slightly for the reaction in which only the palladium catalyst was used. The role of the ruthenium catalyst is unclear.

Aqueous methyl formate can also be used as a source of carbon monoxide and hydrogen through catalysis by $[\text{Ru}_3(\text{CO})_{12}]$ and tricyclohexylphosphane (PCy_3) in the hydroformylation–hydrogenation of alkenes (Scheme 5).^[12] Methyl formate afforded carbon monoxide by the catalytic decarbonylation, and subsequently, the water–gas shift reaction of the resultant carbon monoxide with water, which was catalyzed by the ruthenium complex to generate hydrogen.

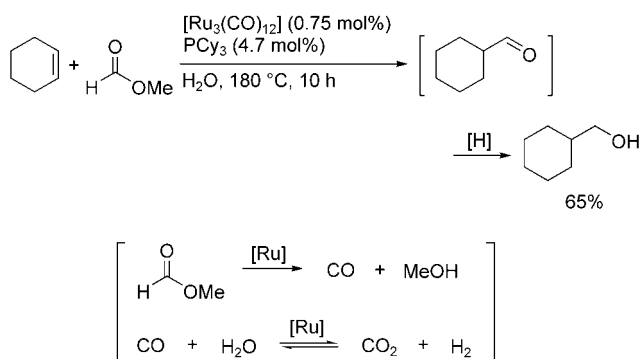
The combination of a decarbonylation process catalyzed by ruthenium complexes and a carbonylation process catalyzed by other transition-metal complexes has been successful in some carbonylation reactions and the direct use of carbon



Tsumoru Morimoto received his M.Sc. in 1994 from Osaka University. After spending two years in industry (1994–1996), he re-entered Osaka University and in 1999 received his Ph.D. for his work under the direction of Profs. Shinji Murai and Naoto Chatani. He spent a year (1999–2000) as a postdoctoral associate at Kyoto University (Prof. Sakae Uemura) and at the University of California, Irvine (Prof. Keith A. Woerpel). In 2000, he was appointed as an assistant professor in Prof. Kakiuchi's Group at the Nara Institute of Science and Technology. His research centers on organometallic catalysis.

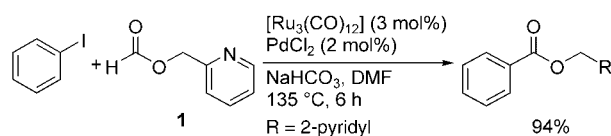


Kiyomi Kakiuchi received his Ph.D. in 1982 from Osaka University under the direction of Professor Yoshinobu Odaira, and was then appointed as an assistant professor. After doing postdoctoral research at Scripps with Prof. K. Barry Sharpless (1993–1994), he became associate professor in 1996. He moved to the Nara Institute of Science and Technology as a full professor in 1997. He received the Incentive Award in Synthetic Organic Chemistry from The Society of Synthetic Organic Chemistry, Japan in 1992. He is interested in the development of novel skeletal transformations and their applications.



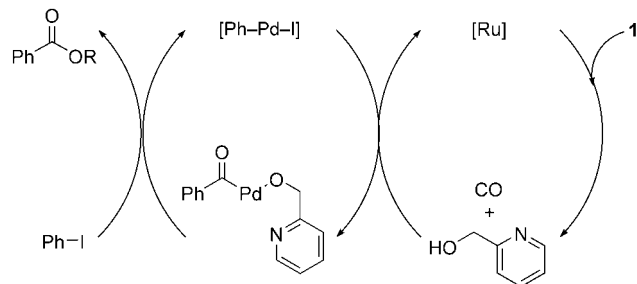
Scheme 5. Ru-catalyzed hydroformylation–hydrogenation by using aqueous methyl formate.^[12]

monoxide is unnecessary. Chang and co-workers reported on the ruthenium/palladium-catalyzed alkoxycarbonylation reaction of aryl halides by using formate **1** (Scheme 6).^[13] The



Scheme 6. Ru/Pd-catalyzed alkoxycarbonylation by using formate **1**.^[13]

reaction proceeds through two sequential catalytic processes: the decarbonylation of formate **1** by $[\text{Ru}_3(\text{CO})_{12}]$, followed by the Pd-catalyzed alkoxycarbonylation of aryl halides (Scheme 7). Treatment of formate **1** with a catalytic amount



Scheme 7. Proposed mechanism for the sequential Ru/Pd-catalyzed alkoxycarbonylation by using formate **1** (R = 2-pyridylmethyl).

of $[\text{Ru}_3(\text{CO})_{12}]$ resulted in complete decarbonylation, while benzyl formate was not affected by $[\text{Ru}_3(\text{CO})_{12}]$ and was quantitatively recovered. Apparently, coordination of the pyridyl-N of formate **1** to the ruthenium is crucial for a successful decarbonylation reaction.

Furthermore, a combination of the formate **1** as an alternative to carbon monoxide and $[\text{Ru}_3(\text{CO})_{12}]$ as a decarbonylation catalyst is also applicable to the Pauson–Khand-type reaction.^[5] Chung and co-workers reported a catalytic Pauson–Khand-type reaction in which the decarbon-

ylation of formate **1** catalyzed by ruthenium and the carbonylation of enynes catalyzed by cobalt nanoparticles were involved (Table 1).^[14] Colloidal ruthenium nanoparticles, as well as $[\text{Ru}_3(\text{CO})_{12}]$, can be utilized as a decarbonylation catalyst.

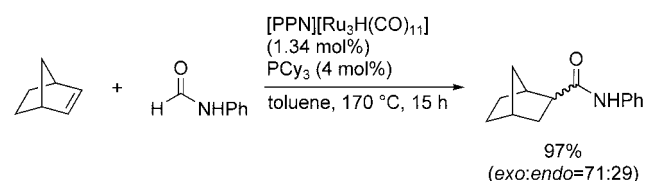
Table 1: Catalytic Pauson–Khand-type reaction with formate **1**.^[14]

Entry	Catalyst	Yield [%]
1	$[\text{Ru}_3(\text{CO})_{12}]/\text{Co/C}^{\text{[a]}}$	98
2	$[\text{Ru}_3(\text{CO})_{12}]$	0
3	Co–C	0
4	Ru/Co/C ^[b]	98

[a] Cobalt nanoparticles immobilized on charcoal (Co/C). [b] Ruthenium and cobalt nanoparticles immobilized on charcoal (Ru/Co/C).

2.2. Formamides

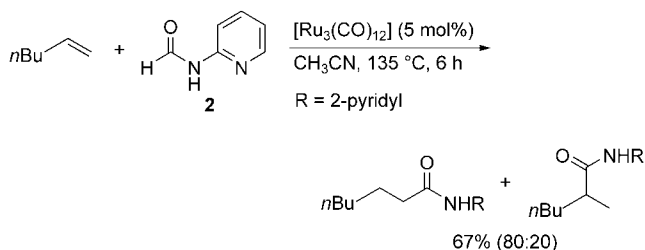
The activation of formamides by transition-metal complexes can also donate a carbonyl group in carbonylation reactions. In 1987, it was reported that the reaction of alkenes with formamides in the presence of a $[\text{Ru}_3(\text{CO})_{12}]$ catalyst afforded the hydroamidation products.^[15] Although this is the first use of formamides as a carbonyl source in carbonylation reactions that can substitute the reaction of alkenes with carbon monoxide and amines,^[2c] external carbon monoxide was essential for maintaining catalytic activity in this reaction. Kondo et al. subsequently found that the use of the [PPN] $[\text{Ru}_3\text{H}(\text{CO})_{11}]/\text{PCy}_3$ catalyst system (PPN = bis(triphenylphosphane)iminium) in the reaction with formamides proceeds without the need for external carbon monoxide (Scheme 8).^[7k] Recently, Chang and co-workers reported that



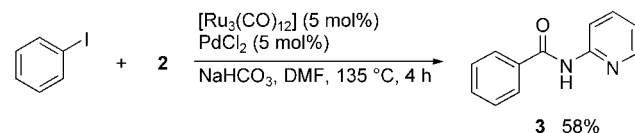
Scheme 8. Ru-catalyzed hydroamidation by using formanilide.^[7k]

the use of formamide **2**, which has a coordinating pyridyl group, led to a similar hydroamidation under milder reaction conditions (Scheme 9).^[16]

A dual-catalytic coupling of formamide **2** and aryl iodides was also achieved by the use of a mixture of ruthenium and palladium complexes to afford the Heck-type aminocarbonylation products (Scheme 10).^[16] Benzamide **3** was produced only when both ruthenium and palladium catalysts were used, and no carbonylated product was obtained with any single metal-complex catalyst tested under the reaction conditions used. By analogy with the sequential alkoxycarbonylation



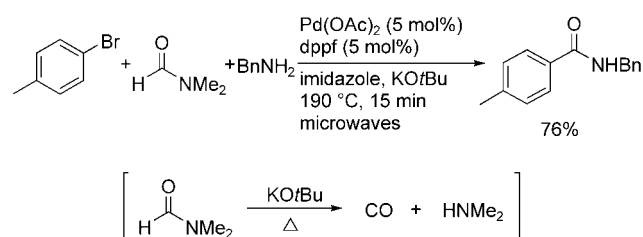
Scheme 9. Ru-catalyzed hydroamidation by using formamide **2**.^[16]



Scheme 10. Ru/Pd-catalyzed aminocarbonylation by using formamide **2**.^[16]

shown in Scheme 7,^[13] the reaction proceeds through the ruthenium-catalyzed decarbonylation of formamide **2** to yield carbon monoxide and 2-aminopyridine, followed by the palladium-catalyzed carbonylative coupling of aryl iodides with the resultant moieties.

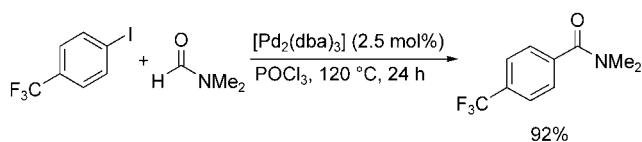
Formamides, as well as alkyl formates, also undergo thermal decarbonylation in the presence of a strong base to yield carbon monoxide and the corresponding amines. Alterman and co-workers reported that N,N-dimethylformamide (DMF) was an excellent carbon monoxide precursor in the palladium-catalyzed aminocarbonylation reaction of aryl bromides (Scheme 11).^[17a] Treatment of DMF with KOtBu



Scheme 11. Pd-catalyzed aminocarbonylation by using DMF; dppe = 1,1'-bis(diphenylphosphanyl)ferrocene.^[17a]

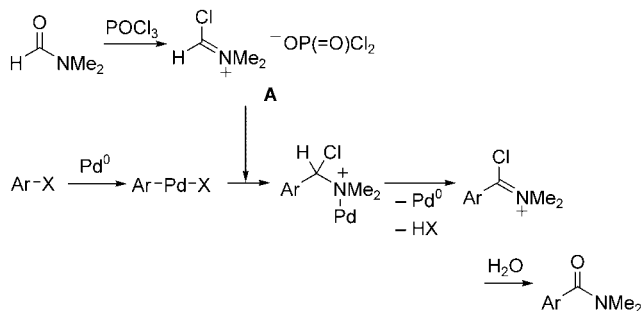
ensures the continuous liberation of carbon monoxide (and dimethylamine) when subjected to microwave heating. When formamide was used in place of DMF without any external amine under otherwise identical conditions, the formation of primary benzamides was also observed.^[17b]

Nozaki and co-workers developed a novel transformation of DMF that lead to catalytic aminocarbonylation without the use of carbon monoxide. Thus, the Pd-catalyzed reaction of aryl and alkenyl iodides with DMF in the presence of POCl₃ afforded the corresponding amides (Scheme 12).^[18] The addition of POCl₃ is essential for the success of this reaction. The reaction proceeds through a Heck-type process, that is, the addition of the arylpalladium species to a Vilsmeier iminium species **A**, generated from DMF and POCl₃,



Scheme 12. Pd-catalyzed aminocarbonylation by using DMF/POCl₃; dba is dibenzylidene acetone.^[18]

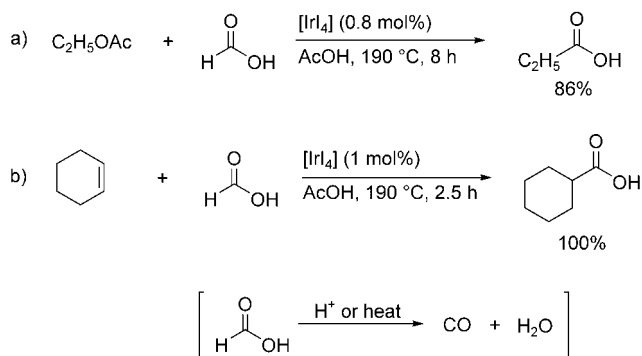
followed by a β -hydride elimination to yield the aromatic amides (Scheme 13) does not include the decarbonylation process promoted by a base or a catalyst.



Scheme 13. Proposed mechanism for Pd-catalyzed aminocarbonylation by using DMF/POCl₃.

2.3. Formic Acid

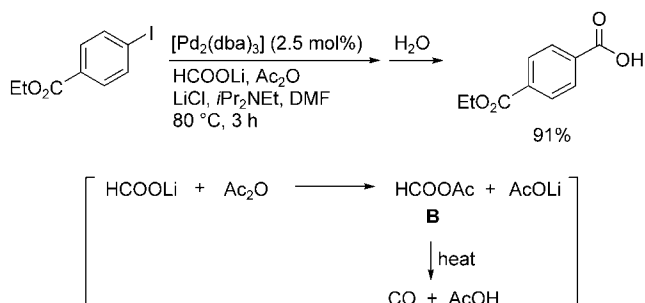
It is well-known that formic acid decomposes to carbon monoxide and water at elevated temperatures and under acidic conditions. Some reports have already indicate that formic acid as a source of carbon monoxide could be utilized in rhodium^[19a] and iridium^[19b,c]-catalyzed hydroxycarbonylation reactions,^[2] but the reactions proceeded with only moderate success. Recently, Simonato et al. reported that an IrI₄ catalyst showed a high catalytic activity in the hydroxycarbonylation reaction of esters and alkenes with formic acid as the source of carbon monoxide (Scheme 14).^[20a] A rhodium/phosphane system also catalyzed the hydroxycarbonylation of alkenes by using formic acid under conditions similar to those used with the iridium catalyst.^[20b]



Scheme 14. Ir-catalyzed hydroxycarbonylation by using formic acid.^[20a]

2.4. Formic Anhydride

Quite recently, Cacchi et al. demonstrated that the palladium-catalyzed hydroxycarbonylation of aryl and vinyl halides or triflates by using formate salts in the presence of acetic anhydride provided a straightforward route to carboxylic acids (Scheme 15).^[21] The reaction involves the formation

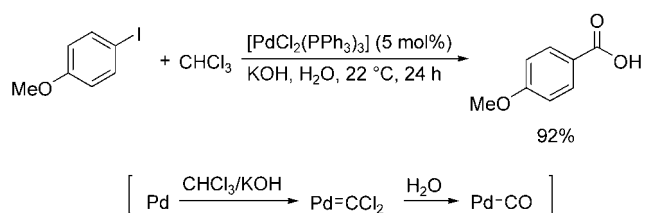


Scheme 15. Pd-catalyzed hydroxycarbonylation by using a mixed anhydride from formate salt and acetic anhydride.^[21]

of formic acetic anhydride **B** as a condensed source of carbon monoxide, which was generated in situ by the reaction of a formate salt with acetic anhydride, followed by thermal decomposition to give carbon monoxide and acetic acid.

2.5. Chloroform

Dichlorocarbene, generated from chloroform and alkali under aqueous conditions in the presence of transition-metal complexes, can be used for the in situ preparation of carbonyl complexes. Utilizing this principle, Alper and Grushin developed the palladium-catalyzed hydroxycarbonylation reaction of aryl halides with chloroform and aqueous alkali instead of carbon monoxide (Scheme 16).^[22] Under these conditions, the reaction of alkenyl and benzylic halides also gave the corresponding carboxylic acids.



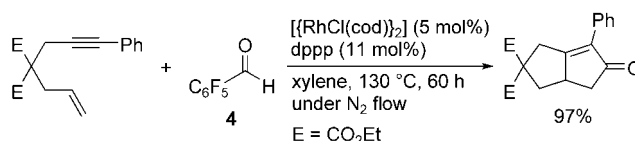
Scheme 16. Pd-catalyzed hydroxycarbonylation by using chloroform/ KOH .^[22]

3. Use of Aldehydes

Among the organic compounds that can donate a carbonyl moiety, aldehydes are an alternative. The decarbonylation of aldehydes mediated by transition-metal complexes has been widely investigated from the view point of not only organometallic chemistry but also synthetic organic chemis-

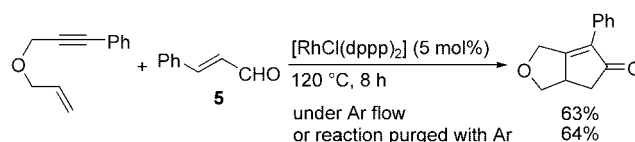
try. Therefore, it is not surprising that aldehydes can serve as a carbonyl source in carbonylation reactions.

Recently, two groups independently reported the use of aldehydes as a source of carbon monoxide.^[23,24] Morimoto et al. reported that the reaction of enynes with aldehydes in the presence of a catalytic amount of a rhodium complex resulted in the Pauson–Khand-type reaction to give bicyclic cyclopentenones.^[23] Various aldehydes, such as aromatic aldehydes, α,β -unsaturated aldehydes, and aliphatic aldehydes, served as a substitute for carbon monoxide, and iridium and ruthenium complexes both showed catalytic activity. However, a combination of pentafluorobenzaldehyde (**4**) as a carbonyl source and $[\text{RhCl}(\text{cod})_2]/\text{dppp}$ ($\text{cod} = 1,5$ -cyclooctadiene; $\text{dppp} = 1,3$ -bis(diphenylphosphanyl)propane) as a catalyst led to the most efficient transfer carbonylation (Scheme 17).



Scheme 17. Rh-catalyzed Pauson–Khand-type reaction with aldehyde **4**.^[23]

Shibata et al. also reported on a Pauson–Khand-type reaction by using aldehydes as a source of carbon monoxide under solvent-free conditions, independent of Morimoto et al.^[24] In this case, cinnamaldehyde (**5**) was reported to be the most efficient aldehyde among those tested. Their experiments under flowing or bubbling argon, shown in Scheme 18,

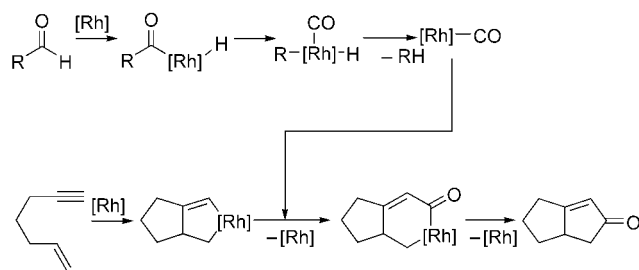


Scheme 18. Rh-catalyzed Pauson–Khand-type reaction with aldehyde **5** in the solvent-free system.^[24b]

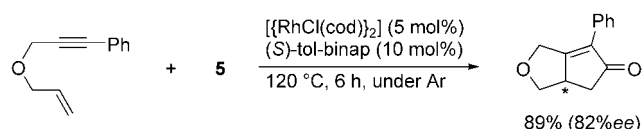
suggest that a negligible amount of free carbon monoxide was generated in the reaction system, and that the carbonyl moiety abstracted from the aldehyde was quite efficiently (almost directly) transferred to the enyne, as shown in Scheme 19.^[24b]

This protocol was developed into an asymmetric reaction by using tol-binap (2,2'-bis(di-*p*-tolylphosphanyl)-1,1'-binaphthyl) as a chiral phosphane ligand (Scheme 20).^[24]

Based on the above results, in which various aldehydes were reported to be applicable to the carbonylation reaction,^[23,24] one can easily envision the utilization of formalin (an aqueous solution of formaldehyde), which is the most ideal substitute for carbon monoxide in terms of economy and handling. It has been utilized as a carbonylating agent for transition-metal complexes to date. Quite recently, Morimoto and co-workers reported that the reaction of enynes with formaldehyde in aqueous media resulted in an aqueous

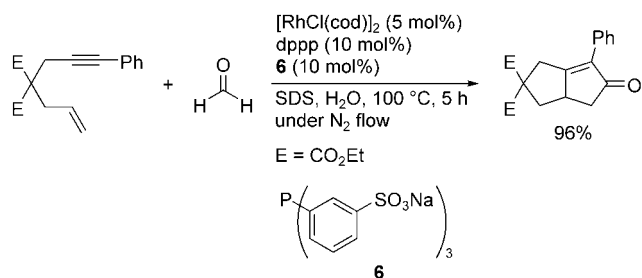


Scheme 19. Proposed mechanism for CO-transfer Pauson–Khand-type reaction with aldehyde.



Scheme 20. Rh-catalyzed asymmetric Pauson–Khand-type reaction with aldehyde **5**.^[24]

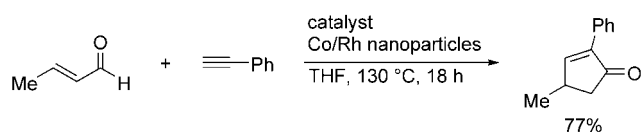
Pauson–Khand-type reaction without the need for carbon monoxide (Scheme 21).^[25] Interestingly, the use of a mixed phosphane system consisting of hydrophobic phosphane,



Scheme 21. Rh-catalyzed aqueous Pauson–Khand-type reaction with formaldehyde.^[25] SDS = sodium dodecylsulfate.

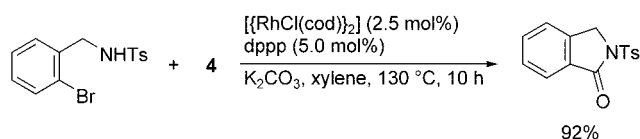
dppp, and hydrophilic phosphane, triphenylphosphane-3,3',3''-trisulfonic acid trisodium salt (TPPTS, **6**), resulted in a more efficient Pauson–Khand-type reaction than the conventional reactions that are currently in use.^[5]

α,β -Unsaturated aldehydes (olefinic aldehydes) can be utilized as an alkene source as well as a carbonyl source in the Pauson–Khand reaction. The Rh/Co-catalyzed reaction of alkynes with α,β -unsaturated aldehydes resulted in the intermolecular Pauson–Khand reaction to give the corresponding cyclopentenones (Scheme 22).^[26] In this case, α,β -unsaturated aldehydes act as a source of carbon monoxide and alkene.



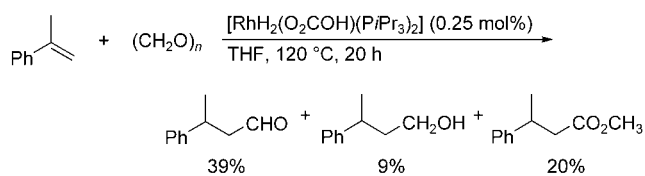
Scheme 22. Co/Rh nanoparticles-catalyzed intermolecular Pauson–Khand reaction of alkyne with α,β -unsaturated aldehyde.^[26]

Methodology in which aldehydes are used as a carbonyl source has been found to be effective not only for the above-mentioned Pauson–Khand-type reaction but also for the intramolecular aminocarbonylation reaction of aryl halides (Scheme 23).^[27]



Scheme 23. Rh-catalyzed intramolecular aminocarbonylation of aryl halide by using aldehyde **4**.^[27]

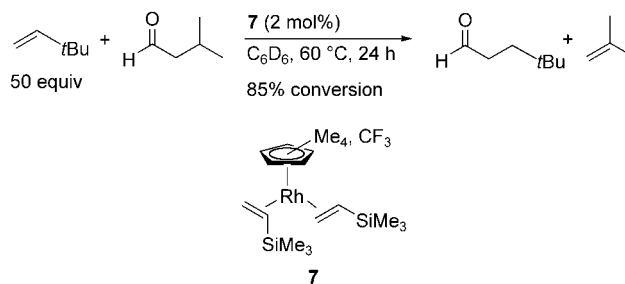
Formaldehyde can be regarded as syn gas (CO/H_2) from its composition. Indeed, the reaction of alkenes with formaldehyde in the presence of a rhodium catalyst, $[\text{RhH}_2(\text{O}_2\text{COH})(\text{P}i\text{Pr}_3)_2]$, resulted in the addition of formaldehyde to alkenes to give hydroformylation products in moderate yield (Scheme 24).^[28] One report revealed that the rhodium complex, $[\text{RhH}(\text{CO})(\text{PPh}_3)_3]$, which has frequently used as a catalyst in hydroformylation reaction, also catalyzes a similar addition reaction.^[29]



Scheme 24. Rh-catalyzed hydroformylation by using paraformaldehyde.^[28]

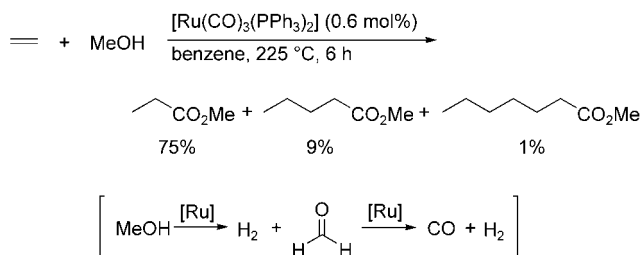
Aliphatic aldehydes that have a β hydrogen atom are also known to behave as syn gas. Brookhart and Lenges reported a rhodium-catalyzed hydroformylation by using saturated aliphatic aldehydes as a substitute for syn gas.^[30] The reaction of isovaleraldehyde with a large excess of 3,3-dimethyl-1-butene and with rhodium complex **7** as a catalyst resulted in transfer hydroformylation to give a linear aldehyde exclusively (Scheme 25).

Primary alcohols also act as a source of carbon monoxide. In the presence of a ruthenium catalyst, the reaction of



Scheme 25. Rh-catalyzed transfer hydroformylation by using aliphatic aldehyde.^[30]

ethylene with methanol gave methyl esters of linear saturated aliphatic acids (mainly, C₃, C₅, and C₇; Scheme 26).^[31] It was subsequently demonstrated, based on a mechanistic study by Behr et al., that methanol acted as a source of hydrogen as



Scheme 26. Ru-catalyzed hydroesterification of ethylene by using methanol.^[31]

well as carbon monoxide.^[32] Thus, methanol supplied the carbon monoxide by the catalytic dehydrogenation of methanol to formaldehyde, and the catalytic decarbonylation of the resulting formaldehyde occurred subsequently. In other words, the true source of carbon monoxide was formaldehyde.

4. Use of Metal Carbonyls

Metal carbonyls contain carbon monoxide as a ligand, and it is clear that the incorporation of the carbonyl ligand from a metal carbonyl is more favorable than the abstraction of a carbonyl group from an organic carbonyl compound in terms of bond-dissociation energy. Although a variety of transformations of organic molecules to carbonyl compounds by using metal carbonyls have been developed to date and can fall into this category,^[33] we focus here on methodology in which metal carbonyls are used exclusively as a carbonyl source in catalytic reactions.

Larhed and co-workers reported a palladium-catalyzed aminocarbonylation reaction of aromatic halides by using easy-to-handle metal carbonyls as a condensed source of carbon monoxide (Table 2).^[34] During the catalysis, the catalytically active palladium species captures the carbon

Table 2: Pd-catalyzed aminocarbonylation using metal carbonyls.^{[a],[34]}

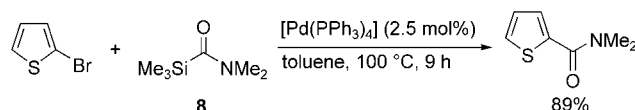
Entry	Metal carbonyls	Yield [%]
1	[Cr(CO) ₆]	80
2	[Mo(CO) ₆]	84
3	[W(CO) ₆]	77
4	[Fe(CO) ₅]	0
5	[Fe ₃ (CO) ₁₂]	0
6	[Co ₂ (CO) ₈]	28

[a] DBU = 1,8-diazabicyclo[5.4.0]undec-7-ene.

monoxide released from the metal carbonyls to carbonylate the aromatic halides. [Cr(CO)₆], [Mo(CO)₆], and [W(CO)₆] are useful CO-releasing reagents, while [Fe(CO)₅], [Fe₃(CO)₁₂], and [Co₂(CO)₈] did not function well in the aminocarbonylation reaction. This protocol relies on the efficient release of carbon monoxide from metal carbonyls, which was accelerated by the addition of DBU (1,8-diazabicyclo[5.4.0]undec-7-ene).

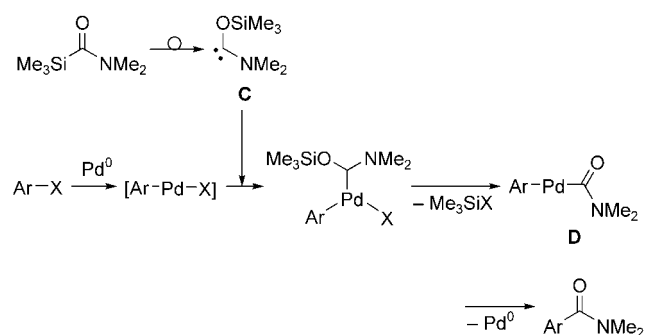
5. Use of Carbamoylsilane and Carbamoylstannanes

Organosilanes and -stannanes are frequently used in metal-catalyzed cross-coupling reactions. The use of carbonylated silanes and stannanes as a reaction partner in such reactions should afford the carbonylated products without the use of carbon monoxide. Indeed, the reaction of aryl and alkenyl halides with carbamoylstannanes in the presence of palladium catalysts resulted in “formal” cross-coupling to give amides.^[35] Although the details of the mechanisms are unclear, this reaction is comparable to the conventional aminocarbonylation procedure.^[4] Cunico et al. showed that a more easily handled carbamoylsilane can also be used. The reaction with carbamoylsilane **8** led to the CO-free aminocarbonylation of aryl and alkenyl halides through catalysis by palladium complexes (Scheme 27).^[36] The carbamoyl-group



Scheme 27. Pd-catalyzed aminocarbonylation by using carbamoylsilane **8**.^[36]

transfer does not include a direct transfer of the carbamoyl group from Si to Pd, so-called transmetalation, but is proposed to proceed as follows (Scheme 28): The nucleophilic carbene species **C**, generated by the dyotropic rearrangement of the carbamoylsilane, complexes with [Ar-Pd-X] resulting in the loss of trimethylsilyl halide and the formation of the carbamoylpalladium intermediate **D** which undergoes reductive elimination to yield the final product.



Scheme 28. Proposed mechanism for Pd-catalyzed carbamoyl-transfer process.

6. Summary and Outlook

This review describes innovative strategies for addressing some of the drawbacks associated with the use of carbon monoxide in carbonylation reactions. Although considerable improvements are still needed, including the chemical yields and the scope of applicable substrates, the strategies reproduce conventional reactions in which carbon monoxide is used. Some new problems have also appeared. Compared with the reactions that use carbon monoxide, the methods described here require more severe conditions, such as higher temperatures, longer reaction times or extra reagents, the need for which arises from the additional decarbonylation process. In most cases, the by-product that forms after the carbonyl group is abstracted is chemical waste. This is a critical issue in terms of atom economy. Moreover, the alternatives are often as toxic as carbon monoxide. This review, however, describes conventional, useful carbonylation chemistry that is experimentally simple; carbonylation methods are now more feasible for the synthetic chemist. In particular, the protocols in the review are suitable for “new-age” synthetic techniques, such as microreactor synthesis, combinatorial synthesis, and high-throughput synthesis, because of the demand for automated handling of liquids and solids rather than the use of gaseous reagents.

The chemistry in this area is just now emerging. Only a part of the carbonylation reactions among those reported to date are successful alternatives to reactions using carbon monoxide. There is no single strategy that is applicable to all carbonylation reactions reported to date. The ultimate goal of the methodology is to develop a method that will be applicable to all carbonylation reactions, and to address the problems mentioned above.

Received: December 22, 2003

Published Online: September 1, 2004

- [1] a) H. M. Colquhoun, D. J. Thompson, M. V. Twigg, *Carbonylation: Direct Synthesis of Carbonyl Compounds*, Plenum, New York, **1991**; b) M. Beller, B. Cornils, C. D. Frohning, C. W. Kohlpaintner, *J. Mol. Catal. A* **1995**, *104*, 17; c) C. D. Frohning, C. W. Kohlpaintner, H.-W. Bohnen in *Applied Homogeneous Catalysis with Organometallic Compounds, Vol. 1* (Eds.: B. Cornils, W. A. Herrmann), Wiley-VCH, Weinheim, **2002**, pp. 31–194.
- [2] For recent reviews and a paper for the catalytic hydrocarbonylation reaction of alkenes and alkynes with carbon monoxide and nucleophiles, see: a) B. El Ali, H. Alper in *Transition Metals for Organic Synthesis: Building Blocks and Fine Chemicals, Vol. 1* (Eds.: M. Beller, C. Bolm), Wiley-VCH, Weinheim, **1998**, pp. 49–67; b) G. Kiss, *Chem. Rev.* **2001**, *101*, 3435; c) Y. Tsuji, T. Ohsumi, T. Kondo, Y. Watanabe, *J. Organomet. Chem.* **1986**, *309*, 333, and references therein.
- [3] For recent reviews for hydroformylation with carbon monoxide and hydrogen, see: a) I. Ojima, C.-Y. Tsai, M. Tzamarioudaki, D. Bonafoux in *Organic Reactions, Vol. 56*, Wiley, New York, **2000**, pp. 1–354; b) C. D. Frohning, C. W. Kohlpaintner, H.-W. Bohnen in *Applied Homogeneous Catalysis with Organometallic Compounds, Vol. 1* (Eds.: B. Cornils, W. A. Herrmann), Wiley-VCH, Weinheim, **2002**, pp. 31–103.
- [4] For recent reviews for the catalytic carbonylation reaction of aryl and alkenyl halides with carbon monoxide, see: a) M. Mori in *Handbook of Organopalladium Chemistry for Organic Synthesis, Vol. 2* (Ed.: E.-i. Negishi), Wiley-Interscience, New York, **2002**, pp. 2313–2332; b) V. Farina, M. Eriksson in *Handbook of Organopalladium Chemistry for Organic Synthesis, Vol. 2* (Ed.: E.-i. Negishi), Wiley-Interscience, New York, **2002**, pp. 2351–2376.
- [5] For recent reviews of Pauson–Khand-type reaction, see: a) Y. K. Chung, *Coord. Chem. Rev.* **1999**, *188*, 297; b) K. M. Brummond, J. L. Kent, *Tetrahedron* **2000**, *56*, 3263; c) S. E. Gibson, A. Stevenazzi, *Angew. Chem.* **2003**, *115*, 1844; *Angew. Chem. Int. Ed.* **2003**, *42*, 1800.
- [6] P. Isnard, B. Denise, R. P. A. Sneed, J. M. Cognion, P. Durual, *J. Organomet. Chem.* **1983**, *256*, 135.
- [7] For hydroesterification with alkyl formates without external carbon monoxide, see: a) D. J. Drury, P. S. Williams (BP Chemicals), EP 106656, **1983**; b) W. Ueda, T. Yokoyama, Y. Morikawa, Y. Moro-oka, T. Ikawa, *J. Mol. Catal.* **1988**, *44*, 197; c) W. Keim, J. Becker, *J. Mol. Catal.* **1989**, *54*, 95; d) E. M. Nahmed, G. Jenner, *J. Mol. Catal.* **1990**, *59*, L15; e) G. Lavigne, N. Lugan, P. Kalck, J. M. Soulié, O. Lerouge, J. Y. Saillard, J. F. Halet, *J. Am. Chem. Soc.* **1992**, *114*, 10669; f) J. Grévin, P. Kalck, *J. Organomet. Chem.* **1994**, *476*, C23; g) G. Jenner, A. Ben Taleb, *J. Mol. Catal.* **1994**, *91*, 31; h) C. Legrand, Y. Castanet, A. Mortreux, F. Petit, *J. Chem. Soc. Chem. Commun.* **1994**, 1173; i) N. Lugan, G. Lavigne, J. M. Soulié, S. Fabre, P. Kalck, J. Y. Saillard, J. F. Halet, *Organometallics* **1995**, *14*, 1712; j) S. Fabre, P. Kalck, G. Lavigne, *Angew. Chem.* **1997**, *109*, 1167; *Angew. Chem. Int. Ed. Engl.* **1997**, *36*, 1092; k) T. Kondo, T. Okada, T. Mitsudo, *Organometallics* **1999**, *18*, 4123.
- [8] For hydroesterification with alkyl formates in the presence of external carbon monoxide, see: a) M. Mlekuz, F. Joo, H. Alper, *Organometallics* **1987**, *6*, 1591; b) T. Kondo, S. Yoshii, Y. Tsuji, Y. Watanabe, *J. Mol. Catal.* **1989**, *50*, 31; c) I. J. B. Lin, H. Alper, *J. Chem. Soc. Chem. Commun.* **1989**, 248; d) Y. Suzuki, H. Katoh, Y. Ishii, M. Hidai, *J. Mol. Catal. A* **1995**, *95*, 129.
- [9] a) S. Ko, Y. Na, S. Chang, *J. Am. Chem. Soc.* **2002**, *124*, 750; b) Y. Na, S. Ko, L. K. Hwang, S. Chang, *Tetrahedron Lett.* **2003**, *44*, 4475.
- [10] a) J. F. Carpentier, Y. Castanet, J. Brocard, A. Mortreux, F. Petit, *Tetrahedron Lett.* **1991**, *32*, 4705; b) J. F. Carpentier, Y. Castanet, J. Brocard, A. Mortreux, F. Petit, *Tetrahedron Lett.* **1992**, *33*, 2001.
- [11] G. Jenner, A. Ben Taleb, *J. Organomet. Chem.* **1994**, *470*, 257.
- [12] a) G. Jenner, *Tetrahedron Lett.* **1991**, *32*, 505; b) G. Jenner, *Appl. Catal.* **1991**, *75*, 289.
- [13] S. Ko, C. Lee, M.-G. Choi, Y. Na, S. Chang, *J. Org. Chem.* **2003**, *68*, 1607.
- [14] K. H. Park, S. U. Son, Y. K. Chung, *Chem. Commun.* **2003**, 1898.
- [15] Y. Tsuji, S. Yoshii, T. Ohsumi, T. Kondo, Y. Watanabe, *J. Organomet. Chem.* **1987**, *331*, 379.
- [16] S. Ko, H. Han, S. Chang, *Org. Lett.* **2003**, *5*, 2687.
- [17] a) Y. Wan, M. Alterman, M. Larhed, A. Hallberg, *J. Org. Chem.* **2002**, *67*, 6232; b) Y. Wan, M. Alterman, M. Larhed, A. Hallberg, *J. Comb. Chem.* **2003**, *5*, 82.
- [18] K. Hosoi, K. Nozaki, T. Hiyama, *Org. Lett.* **2002**, *4*, 2849.
- [19] a) I. S. Kolomnikov, M. P. Erman, V. P. Kukolev, M. E. Volpin, *Kinet. Catal.* **1972**, *13*, 227; b) R. L. Pruett, P. L. Burke (Exxon), EP 092350, **1983**; c) ref. [4a,b].
- [20] a) J.-P. Simonato, T. Walter, P. Mtvier, *J. Mol. Catal. A* **2001**, *171*, 91; b) J.-P. Simonato, *J. Mol. Catal. A* **2003**, *197*, 61.
- [21] S. Cacchi, G. Fabrizi, A. Goggiamani, *Org. Lett.* **2003**, *5*, 4269.
- [22] V. V. Grushin, H. Alper, *Organometallics* **1993**, *12*, 3846.
- [23] T. Morimoto, K. Fuji, K. Tsutsumi, K. Kakiuchi, *J. Am. Chem. Soc.* **2002**, *124*, 3806.

- [24] a) T. Shibata, N. Toshida, K. Takagi, *Org. Lett.* **2002**, *4*, 1619; b) T. Shibata, N. Toshida, K. Takagi, *J. Org. Chem.* **2002**, *67*, 7446.
- [25] K. Fuji, T. Morimoto, K. Tsutsumi, K. Kakiuchi, *Angew. Chem.* **2003**, *115*, 2511; *Angew. Chem. Int. Ed.* **2003**, *42*, 2409.
- [26] K. H. Park, I. G. Jung, Y. K. Chung, *Org. Lett.* **2004**, *6*, 1183.
- [27] T. Morimoto, M. Fujioka, K. Fuji, K. Tsutsumi, K. Kakiuchi, *Chem. Lett.* **2003**, *32*, 154.
- [28] T. Okano, T. Kobayashi, H. Konishi, J. Kiji, *Tetrahedron Lett.* **1982**, *23*, 4967.
- [29] H. S. Ahn, S. H. Han, S. J. Uhm, W. K. Seok, H. N. Lee, G. A. Korneeva, *J. Mol. Catal. A* **1999**, *144*, 295.
- [30] C. P. Lenges, M. Brookhart, *Angew. Chem.* **1999**, *111*, 3746; *Angew. Chem. Int. Ed.* **1999**, *38*, 3533.
- [31] a) J. D. McClure, L. H. Slaugh (Shell Oil), DE 2060863, **1971**; b) J. D. McClure, L. H. Slaugh, US 3646116, **1972**.
- [32] A. Behr, U. Kanne, W. Keim, *J. Mol. Catal.* **1986**, *35*, 19.
- [33] For representative reviews, see: a) R. W. Bates in *Comprehensive Organometallic Chemistry II, Vol. 12* (Eds.: E. W. Abel, F. G. A. Stone, L. S. Hegedus), Elsevier, Oxford, **1995**, pp. 349–386; b) L. S. Hegedus, *Transition Metals in the Synthesis of Complex Organic Molecules*, 2nd Edition, University Science Books, California, **1999**, pp. 123–141.
- [34] a) N.-F. K. Kaiser, A. Hallberg, M. Larhed, *J. Comb. Chem.* **2002**, *4*, 109; b) J. Wannbeg, M. Larhed, *J. Org. Chem.* **2003**, *68*, 5750.
- [35] C. M. Lindsay, D. A. Widdowson, *J. Chem. Soc. Perkin Trans. 1* **1988**, 569.
- [36] a) R. F. Cunico, B. C. Maity, *Org. Lett.* **2002**, *4*, 4357; b) R. F. Cunico, B. C. Maity, *Org. Lett.* **2003**, *5*, 4947.

Quality counts...

The best of chemistry every week



Wiley-VCH

P.O. Box 10 11 61
69451 Weinheim
Germany

Phone +49 (0) 6201–606-400
Fax +49 (0) 6201–606-184
e-mail: angewandte@wiley-vch.de

www.angewandte.org

Angewandte Chemie International
Edition is a journal of the GDCh,
the German Chemical Society

GDCh

WILEY-VCH

Synthesis Planning

Explorations into New Reaction Chemistry

Teruaki Mukaiyama*

Keywords:

aldol reaction · glycosylation ·
nucleophilic substitution ·
oxidation · synthetic methods

Ox.-red. condensation

Esterification

Oxidation

Aldol reaction

Boron enolate

Silicon enolate

Lewis acid

Lewis base

Taxol

Glycosylation

Glycosyl fluoride



Angewandte
Chemie

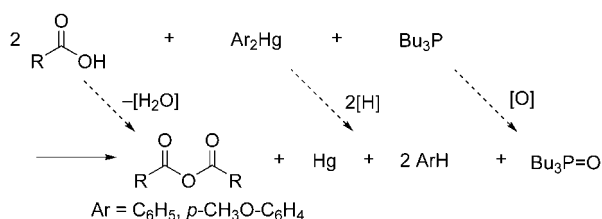
H. Fujisawa

This Review describes the basic concepts that have guided our exploration of new chemical reactions by giving examples of results from my research group. Our strategy of carrying out research is to investigate three to four different topics at a time so we can gather as many results as possible. These may at first appear unrelated to each other but may have the potential to be united into a greater hypothesis after repeated feedback. Three scenarios from our research are presented: the “oxidative–reductive condensation reaction” devised in 1960, which after an interval of nearly 40 years brought forth the new concept of using compounds of structure Ph_2POR as reducing reagents; the “ TiCl_4 -aldol reaction” of 1973 that eventually led to the present “base-promoted aldol reaction” through a chain of ideas; and the “glycosylation reaction using fluorosugars” from 1984 which recently bloomed into “stereocontrolled glycosylation”. Thus, it can be said that by reviewing what we had done before, we were able to expand on it to achieve new outcomes.

1. Oxidative–Reductive Condensation Reactions

1.1. Introduction

The fundamental concept of the oxidative–reductive condensation is to perform a dehydration condensation by removing H_2O as $2[\text{H}]$ and $[\text{O}]$ by the use of a combination of a weak reductant and oxidant. The characteristic feature of these reactions is that they proceed under “mild and neutral” conditions without any assistance from added acids or bases. The first example of this type of condensation in regard to acylation reactions was reported from our laboratory in 1963.^[1] Treatment of diphenyl- or bis(*p*-methoxyphenyl)mercury with tri-*n*-butylphosphane in the presence of two equivalents of carboxylic acid leads to formation of the corresponding acid anhydride in high yield together with mercury and tri-*n*-butylphosphine oxide (Scheme 1).^[1] In this



Scheme 1. Principle of the oxidative–reductive condensation of carboxylic acids to carboxylic acid anhydrides in the presence of diarylmercury and tri-*n*-butylphosphane.

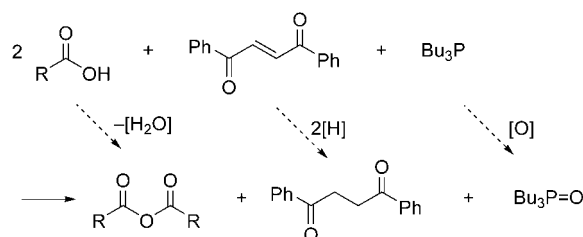
reaction two molecules of carboxylic acid undergo condensation with the help of a hydrogen acceptor (diaryl mercury) and an oxygen acceptor (tri-*n*-butylphosphane) to give the anhydride. A similar dehydration condensation reaction of acids also took place successfully when tributylphosphane and

From the Contents

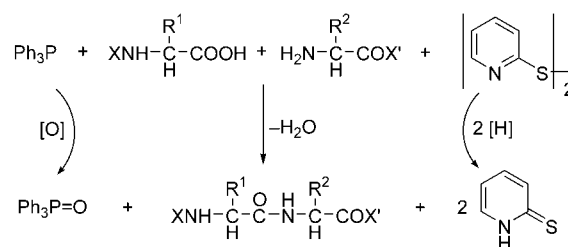
1. Oxidative–Reductive Condensation Reactions	5591
2. Crossed Aldol Reactions via Boron and Silicon Enolate Intermediates	5597
3. Stereoselective Glycosylation with Glycosyl Fluorides	5607
4. Concluding Remarks	5610

a conjugated dicarbonyl compound such as *trans*-1,2-dibenzoyl ethylene were used as the acceptors (Scheme 2).^[2]

Furthermore, it was also shown that treatment of Bz-L-Leu-OH (Bz = benzoyl) with H-Gly-OEt in the presence of triphenylphosphane (reductant) and di(2-pyridyl)disulfide (oxidant) lead to the formation of Bz-L-Leu-Gly-OEt in high yield (Scheme 3),^[3] and Corey et al. have developed an efficient method for the synthesis of macrocyclic lactones by treating hydroxycarboxylic acids with di(2-pyridyl)disul-



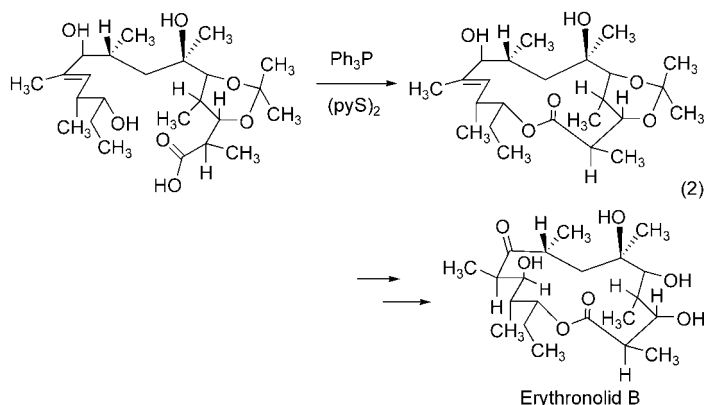
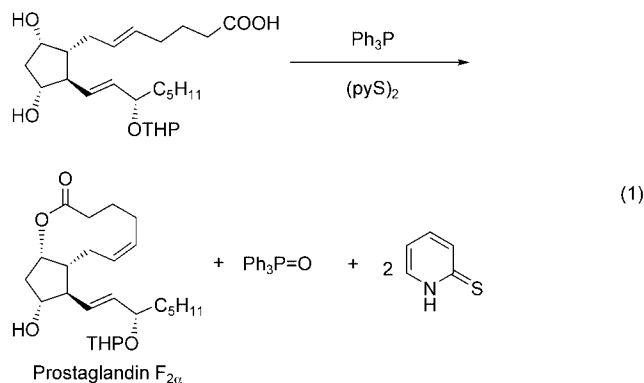
Scheme 2. Oxidative–reductive condensation in the presence of a conjugated dicarbonyl compound as the oxidant.



Scheme 3. Oxidative–reductive condensation of two amino acid derivatives in the presence of a disulfide as the oxidant.

[*] Prof. T. Mukaiyama
Center for Basic Research
The Kitasato Institute
6-15-5 (TCI), Toshima, Kita-ku, Tokyo 114-0003 (Japan)
Fax: (+81) 3-3911-3111
E-mail: mukaiyam@abeam.ocn.ne.jp

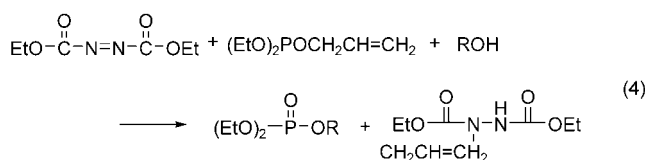
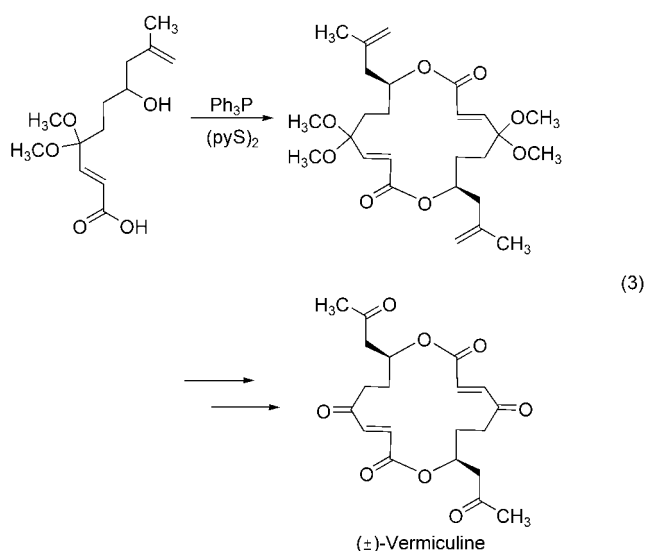
fide in the presence of triphenylphosphane [Eq. (1); THP = tetrahydropyran-2-yl, py = pyridine].^[3b] This method leads to the efficient synthesis of medium to large rings (7–16,^[3c] 12–21^[3d]), and has been applied to the synthesis of a number of important macrocyclic targets including monensin,^[3b] erythronolide B [Eq. (2)],^[3e] (±)-11-hydroxy-*trans*-8-dodecenoic acid lactone,^[3f] (±)-vermiculine [Eq. (3)],^[3g] enterobactin,^[3h] and prostaglandins.^[3b,j]



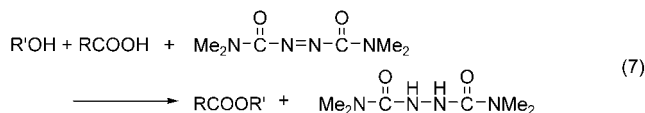
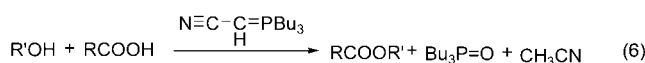
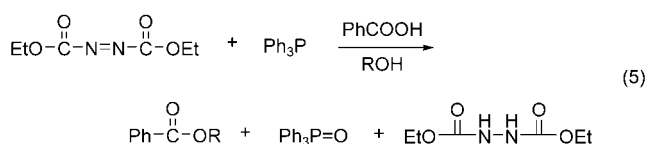
In 1967 phosphoric esters were also prepared by using allyl diethyl phosphite and diethyl azodicarboxylate (DEAD) in the presence of alcohols [Eq. (4)].^[4] Later, Mitsunobu, a former student from my research group, developed this



Teruaki Mukaiyama was born in 1927. He received his B.Sc. from the Tokyo Institute of Technology (T.I.T.) in 1948, and Ph.D. from the University of Tokyo in 1957. He first became Assistant Professor at Gakusyuin University in 1953 and then at T.I.T. in 1958. He was appointed Full Professor at TIT in 1963 and moved to the University of Tokyo in 1974. In 1987 he became Professor of Chemistry at the Science University of Tokyo. Since 2002 he has been Professor at the Kitasato Institute; as well as Emeritus Professor at the University of Tokyo, the T.I.T., and the Science University of Tokyo. He is a recipient of many major awards and is currently a member of the Japan Academy as well as a foreign member of the Academy of Sciences in France and Poland.



concept into an efficient alkylation method by using a combination of triphenylphosphane and DEAD (Mitsunobu reaction) [Eq. (5)].^[5] Shi et al. used this reaction for the stereospecific synthesis of chiral tertiary alkylaryl ethers in about 50 % yield and with complete inversion of configuration.^[6] Tsunoda et al. reported an alkylation reaction using alcohols and cyanomethylenetriphenylphosphorane [Eq. (6)]^[7] or *N,N,N',N'*-tetramethylazodicarboxamide (TMAD) [Eq. (7)]^[7] which works in a similar manner.



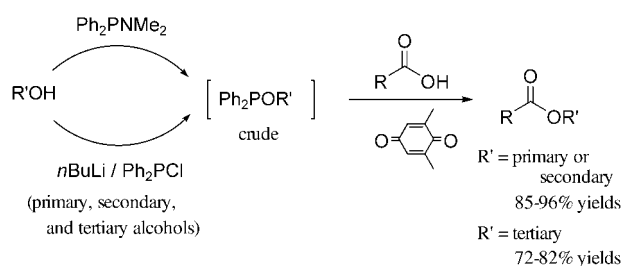
The search for new combinations of weak reductant and oxidant for the oxidative–reductive condensation has been a matter of continued interest for us ever since the reaction was first reported. We have long expected that quinone compounds could be used as effective oxidants in this type of condensation; however, no successful examples have been

reported to date. It was then considered that the interaction of alkoxydiphenylphosphane with weak oxidants such as quinone would provide a key intermediate, the phosphonium salt, more smoothly than triphenylphosphane because the former is a stronger reductant. In addition, the alkoxydiphenylphosphane formed by introducing an alkoxy group into a trivalent phosphorus compound worked more effectively in the formation of the alkoxyphosphonium salt, an important key intermediate.

1.2. Preparation of *tert*-Alkyl Carboxylates with Inverted Configuration from Chiral *tert*-Alcohols

Oxidative–reductive condensation using a combination of 2,6-dimethyl-1,4-benzoquinone and alkoxydiphenylphosphanes, formed in situ from alcohols and chlorodiphenylphosphane or (*N,N*-dimethylamino)diphenylphosphane, affords alkyl carboxylates in high yields from the corresponding alcohols and carboxylic acids by a one-pot procedure under neutral and mild conditions (Scheme 4).^[8] The ester-

(primary and secondary alcohols)

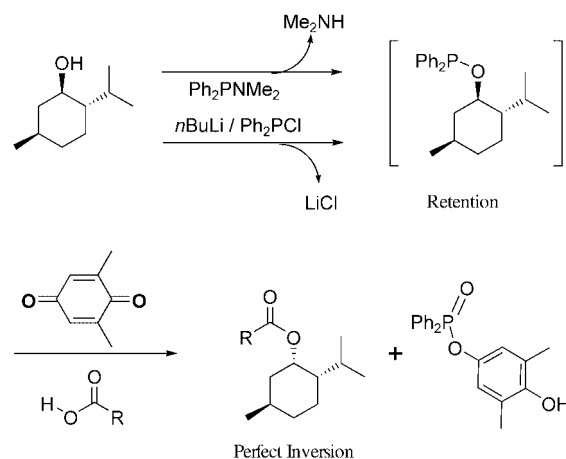


Scheme 4. Esterification of carboxylic acids by oxidative–reductive condensation with alcohols.

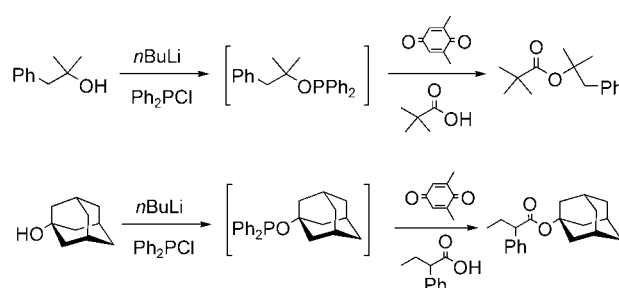
ification of various secondary alcohols proceeded in a similar manner in high yields with complete inversion of the stereochemistry at the C–OH atom. For example, benzoic acid and *L*-menthol afforded the corresponding alkyl carboxylate with inverted configuration in yields of 86 % (Scheme 5).^[8]

Furthermore, it was shown that the reactions of various carboxylic acids with tertiary alkoxydiphenylphosphanes formed in situ proceeded very smoothly; for example, 2,2-dimethylpropionic acid and 2-methyl-1-phenylpropan-2-ol or 2-phenylbutyric acid and 1-adamantanol afforded the corresponding *tert*-alkyl carboxylates in yields of 85 to 96 % (Scheme 6).^[8] The stereochemistry in the above ester-forming reaction was examined, and indeed this oxidative–reductive method worked effectively in converting tertiary alcohols into their corresponding esters with almost complete inversion of configuration (Scheme 7).^[9] The method involves initial introduction of the alcohol to diphenylphosphinite ester, followed by treatment with a carboxylic acid and 2,6-dimethyl-1,4-benzoquinone.

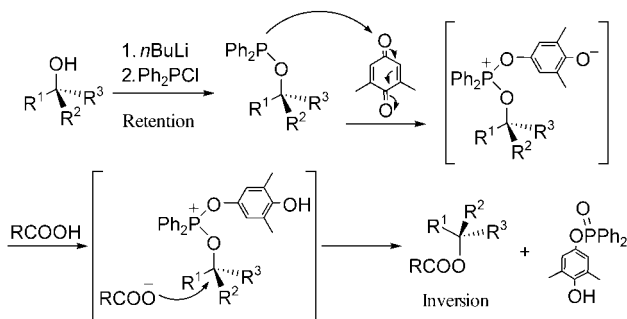
The results for the condensation of carboxylic acids with various chiral tertiary alcohols are shown in Table 1. Ester-



Scheme 5. Esterification of carboxylic acids with secondary alcohols such as (*L*)-menthol.



Scheme 6. Esterification of bulky secondary or tertiary carboxylic acids with bulky tertiary alcohols.



Scheme 7. Preparation of *tert*-alkyl carboxylates from chiral *tert*-alcohols with inversion of configuration by oxidative–reductive condensation using 2,6-dimethyl-1,4-benzoquinone.

ification of carboxylic acids proceeded smoothly in dichloromethane at room temperature to afford the corresponding *tert*-alkyl carboxylates in good yields and with almost complete inversion of configuration. In contrast, treatment of a solution of 1-adamantanol with benzoic acid in dichloromethane for 15 h afforded an ester in 83 % yield with retention of configuration. The esterifications of various chiral tertiary alcohols with benzoic acid or *p*-methoxybenzoic acid (which contains an electron-donating group) proceeded within 18 h at room temperature to give the alkyl

Table 1: Esterification of carboxylic acids with chiral tertiary alcohols.

$\text{R}^1\text{OH} \xrightarrow[2. \text{Ph}_2\text{PCI}]{1. n\text{BuLi}} [\text{Ph}_2\text{POR}^1] \xrightarrow[\text{CH}_2\text{Cl}_2, \text{RT}, 18\text{h}]{\text{R}^2\text{COOH}} \text{R}^2\text{C(=O)OR}^1$						
Entry	R ¹ OH ^[c]	R/S ^[d]	R ²	Yield [%]	R/S ^[e]	Inversion [%]
1 ^[a]		—	Ph	83	—	—
2 ^[a]		86:14	Ph	78	16:84	98
3 ^[a]			PhCH ₂ CH ₂	76	66:34	40
4		95:5	Ph	85	7:93	98
5			<i>p</i> -MeO-C ₆ H ₄	86	5:95	>99
6			<i>p</i> -Cl-C ₆ H ₄	83	20:80	84
7			PhCH ₂ CH ₂	76	24:76	80
8		2:98	Ph	90	98:2	>99
9			<i>p</i> -MeO-C ₆ H ₄	88	98:2	>99
10			<i>p</i> -Cl-C ₆ H ₄	86	70:30	71
11			PhCH ₂ CH ₂	86	69:31	70
12		1:99	Ph	86	99:1	>99
13		91:9	Ph	83	9:91	>99
14		22:78	Ph	81	77:23	99
15 ^[b]		—	Ph			nd

[a] The reaction mixture was refluxed for 15 h. [b] The corresponding olefin was obtained in 81% yield. [c] Entries 2–7: (–)-Terpinen-4-ol (Acros Organics) and (–)-linalool (Fulka Chemika) were used. Entries 8–15: The chiral alcohols were prepared according to Walsh's procedure. [d] The enantiomeric ratios of *tert*-alcohols were determined by preparing the corresponding esters with the carboxylic chlorides.

carboxylates in good yields (81–90%) with almost complete inversion of configuration (98 to >99%; Table 1, entries 4, 5, 8, 9, and 12–14). However, the desired esters were obtained in 76–86% yields with 70–84% inversion when an aliphatic carboxylic acid or *p*-chlorobenzoic acid, which contains an electron-withdrawing group, was used (Table 1, entries 6, 7, 10, and 11). Heating a solution of (–)-terpinen-4-ol and benzoic acid or 3-phenylpropionic acid in dichloromethane at reflux for 15 h afforded the corresponding esters in 78% yield with 98% inversion or 76% yield with 40% inversion, respectively (Table 1, entries 2 and 3). In contrast, 2-(4-methoxyphenyl)-2-butanol afforded an olefin in 81% yield, with none of the desired ester detected (Table 1, entry 15).

Thus, oxidative–reductive condensation using alkoxydiphenylphosphanes generated in situ (namely, diphenylphosphinite ester) with 2,6-dimethyl-1,4-benzoquinone and carboxylic acids provided a new and efficient method for the preparation of *tert*-alkyl carboxylates from various chiral tertiary alcohols with inversion of the configuration at the C–OH atom.

1.3. Preparation of Primary, Secondary, and Tertiary Alkyl Carboxylates from Alcohols and Carboxylic Acids

A condensation using readily available 1,4-benzoquinone instead of the above-mentioned 2,6-dimethyl-1,4-benzoquinone was studied to enable a practical and convenient synthetic reaction to be established. The desired alkyl carboxylates were obtained in good to high yields by combined use of 1.7 equivalents of alkoxydiphenylphosphanes (with primary, bulky secondary, or tertiary alkoxy groups), 1.7 equivalents of 1,4-benzoquinone, and a carboxylic acid.^[10] The corresponding carboxylates with inverted configuration were also obtained in high optical purity and chemical yields in the case of chiral secondary or tertiary alcohols. Esterification of various in situ formed alkoxydiphenylphosphanes with various carboxylic acids were attempted under the conditions shown in Table 2. Benzylation of benzoic acids having electron-donating or electron-withdrawing groups and of saturated or unsaturated aliphatic carboxylic acids proceeded smoothly to afford the corresponding benzyl carboxylates in high to excellent yields under mild conditions (Table 2, entries 1–6). Treatment of a primary alcohol such as *n*-butanol, an aromatic alcohol with an electron-donating group such as *p*-methoxybenzyl alcohol, or a secondary alcohol such as diphenylmethanol with benzoic

Table 2: Esterifications of carboxylic acids with alcohols.

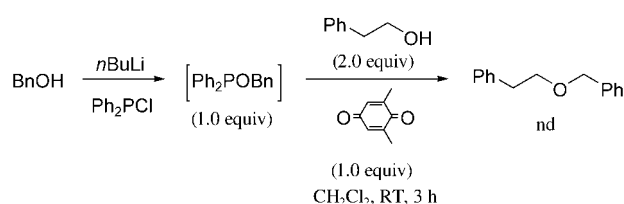
$\text{R}^1\text{OH} \xrightarrow[2. \text{Ph}_2\text{PCI}]{1. n\text{BuLi/Hexane}} [\text{Ph}_2\text{POR}^1] \xrightarrow[\text{CH}_2\text{Cl}_2]{\text{RCOOH (1.0 equiv)} \text{ (1.7 equiv)}} \text{R}^2\text{C(=O)OR}^1$					
Entry	R ¹ OH	RCOOH	<i>t</i> [h]	Yield [%]	Yield [%] ^[a]
1	BnOH	PhCOOH	1	98	98
2		<i>p</i> -MeO-C ₆ H ₄ COOH	1	95	95
3		<i>p</i> -NO ₂ -C ₆ H ₄ COOH	1	96	95
4		PhCH ₂ CH ₂ COOH	1	92	93
5		PhCH=CHCOOH	1	98	92
6		CH ₃ (CH ₂) ₃ COOH	1	90	93
7	<i>p</i> -MeO-C ₆ H ₄ CH ₂ OH	PhCOOH	1	93	91
8	CH ₃ (CH ₂) ₃ OH	PhCOOH	1	90	88
9		PhCOOH	3	90	94
10 ^[b]		PhCOOH	3	91 (>99.9%)	86 (>99.9%)
11 ^[b]		<i>p</i> -NO ₂ -C ₆ H ₄ COOH	3	96 (>99.9%)	95 (>99.9%)
12		PhCOOH	15	75	69
13			15	95	96
14			15.0	95	96
15 ^[b]		PhCOOH	15	95 (>99%)	96 (>99.9%)

[a] See ref. [5b]: Esterification of carboxylic acids with alcohols by using 2,6-dimethyl-1,4-benzoquinone. (alcohols: 1.1–1.2 equiv, carboxylic acids: 1.0 equiv, 2,6-dimethyl-1,4-benzoquinone: 1.0 equiv). [b] Yields in parenthesis are inversion yields.

acid for 1–3 h gave the corresponding esters in high yields (Table 2, entries 7–9). Similarly, the reaction of *tert*-butyl alcohol and benzoic acid under the same conditions afforded the desired ester in 75% yield (Table 2, entry 12). The condensation of tertiary alcohols and carboxylic acids such as 1-adamantanol and 2-phenylbutyric acid or 1-methylcyclopentanol and triphenylacetic acid also proceeded smoothly to afford the corresponding carboxylates in excellent yields (Table 2, entries 13 and 14). In addition, it was noted that the corresponding alkyl carboxylates were obtained in excellent yields with perfect inversion of configuration when a chiral secondary alcohol such as L-menthol was used (Table 2, entries 10 and 11). In the case of the chiral tertiary alcohol (*S*)-2-phenyl-2-butanol, the corresponding ester was obtained in 95% yield with 99% inversion.

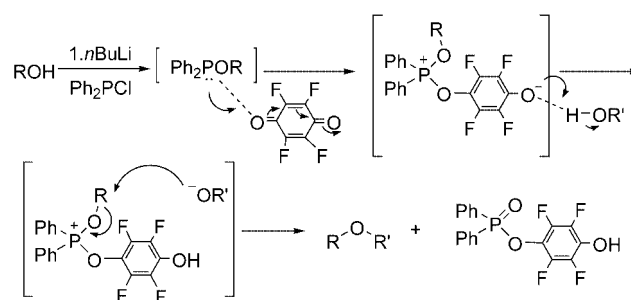
1.4. Preparation of Symmetrical or Unsymmetrical Ethers by Oxidative–Reductive Condensation

The O-alkylation of 2.0 equivalents of 2-phenylethanol in dichloromethane with 1.0 equivalent of 2,6-dimethyl-1,4-benzoquinone and 1.0 equivalent of benzyloxydiphenylphosphane (formed in situ from *n*BuLi-treated benzyl alcohol and chlorodiphenylphosphane) was investigated, but the desired ether was not obtained (Scheme 8). It was considered



Scheme 8. Etherification of 2-phenylethanol with BnOH. nd = not detected.

that an important intermediate phosphonium salt had likely been formed, since an alkoxy group had previously been introduced into a phosphane by the use of oxidants such as 2,6-dimethyl-1,4-benzoquinone. However, it appeared that the intermediate phosphonium salt had not in turn been converted smoothly into a pentavalent phosphorus compound after abstraction of a hydrogen atom from the alcohol. Thus, to extend the scope of the oxidative–reductive reaction to this ether formation, a more powerful oxidant such as fluoranil (tetrafluoro-1,4-benzoquinone) was considered, and the reaction of this derivative with alcohols and alkoxydiphenylphosphanes (formed in situ from *n*BuLi-treated alcohols and chlorodiphenylphosphine) was attempted. It was found that the intermediate phosphonium salt was converted smoothly into the pentavalent phosphorus compound by abstracting one hydrogen atom from a molecule of alcohol, and that the corresponding symmetrical or unsymmetrical ethers could be prepared successfully in good to high yields by starting from two free alcohols (Scheme 9).^[11] For example, the corresponding symmetrical or unsymmetrical ethers were obtained in good to high yields when benzyl alcohols having either electron-donating or electron-withdrawing groups and pri-



Scheme 9. Preparation of symmetrical or unsymmetrical ethers from two alcohols by oxidative–reductive condensation using tetrafluoro-1,4-benzoquinone.

mary, secondary, or tertiary alcohols were used (Table 3, entries 1–5). The etherification at room temperature of alkoxydiphenylphosphanes formed in situ from several *n*BuLi-treated bulky secondary or tertiary alcohols with 2-phenylethanol or 2-methyl-1-phenyl-2-propanol also proceeded smoothly to afford the corresponding unsymmetrical ethers in high yields after 3 h (Table 3, entries 6 and 7).

The desired ether was obtained in 83% yield without racemization when alkoxydiphenylphosphanes formed in situ from *n*BuLi-treated *p*-methoxybenzyl alcohol was treated with alcohols having a hydroxy group at the α -position of a carboxylic ester (such as methyl (*R*)-(-)-mandelate). Reac-

Table 3: Etherification of alcohols and alkoxydiphenylphosphanes (formed in situ from alcohols, Ph_2PCl , and *n*BuLi) using fluoranil.

Entry	ROH	R'OH	Product	Yield [%]
1				90
2				94
3				92
4				94
5				75
6				90
7				92
8[a]				83
9[b]				89

[a] 1.0 equivalent of fluoranil was used. No racemization was observed by HPLC (Daicel Chiralcel OD). [b] The ether was obtained with 95% inversion.

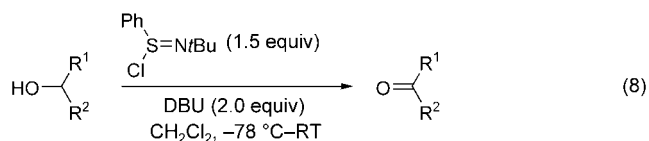
tion of alkoxydiphenylphosphanes formed in situ from *n*BuLi-treated methyl (*R*)-(-)-mandelate and *p*-methoxybenzyl alcohol under the above conditions gave the corresponding ethers in 89% yield with 95% inversion (Table 3, entries 8 and 9). Thus, efficient methods for the etherification of chiral alcohols with either retention or inversion of the configuration were established: namely, treatment of a chiral alkoxydiphenylphosphane with an achiral alcohol afforded the ether with inversion of the configuration while the reaction of an achiral alkoxydiphenylphosphane and a chiral alcohol afforded the ether with retention of configuration.

1.5. Oxidation with Organosulfur Compounds

Divalent sulfur compounds are known to exist as three relatively stable species in different oxidation states (thiolate RS^- , sulfenyl radical RS^\bullet , and sulfenyl cation RS^+). Interconversions between these species take place relatively easily, and are expected to participate in oxidation or reduction processes. Based on this concept, a sulfenylation of carbonyl compounds was developed in 1970 in which sulfenamides were used as new sulfenylating agents.^[12] Sulfur compounds having a sulfur–boron bond later led to a crossed aldol reaction (1971). The concept of using two elements in combination (one being sulfur) was further applied in 2000 to develop a new method for the oxidation of alcohols.

1.5.1. Stoichiometric Oxidation of Alcohols by Using Sulfinimidoyl Chloride

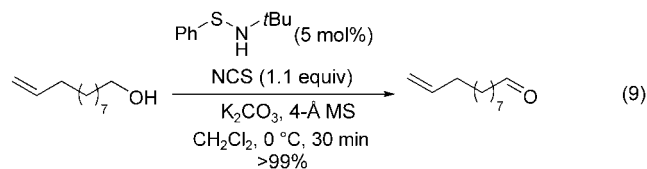
The oxidation of primary and secondary alcohols to the corresponding carbonyl compounds is one of the most fundamental and important transformations in organic synthesis.^[13] There are many useful methods for the stoichiometric oxidation of alcohols by using, for example, chromium(vi) compounds,^[14] manganese dioxide,^[15] activated dimethylsulfoxides,^[16,17] and hypervalent iodine compounds^[18,19] as oxidants. During our total synthesis of taxol it was noticed that a more useful and widely applicable oxidation method was still needed. Our experience in the study on organosulfur compounds having a sulfur–nitrogen bond led to the idea that sulfinimidoyl chloride would be a suitable oxidizing agent for alcohols. In fact, various primary and secondary alcohols are effectively oxidized under mild conditions to the corresponding aldehydes and ketones by using *N*-tert-butylbenzenesulfinimidoyl chloride and 1,8-diazabicyclo[5.4.0]undec-7-ene (DBU) [Eq. (8)].^[20,21] The sulfinimidoyl chloride mediated oxidation of alcohols proceeds at readily controllable reaction temperatures (-78°C –RT) by simply adding this oxidizing agent to the mixture of alcohol and DBU. In contrast, Swern oxidation^[17b] requires strictly



controlled cooling ($< -20^\circ\text{C}$) to generate the thermally unstable key intermediate, chlorodimethylsulfonium chloride, from oxalyl chloride and dimethylsulfoxide. It should be further noted that trimethylsiloxy bonds remain intact during the sulfinimidoyl chloride mediated oxidation, while they are cleaved under Swern oxidation conditions. Polymer-supported sulfinimidoyl chloride is a particularly convenient reagent for the oxidation of alcohols because the oxidation products are easy to isolate.^[22,23]

1.5.2. Catalytic Oxidation of Alcohols with Sulfenamide

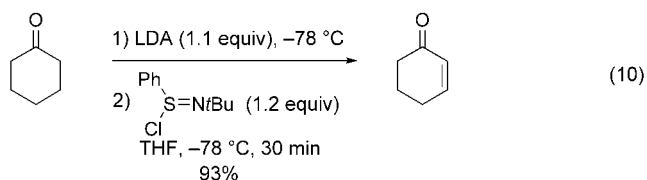
The oxidation of alcohols with a stoichiometric amount of sulfinimidoyl chloride has been modified to a more-convenient catalytic method. The oxidation of various alcohols is successfully performed by using a stoichiometric amount of *N*-chlorosuccinimide (NCS) and a catalytic amount of *N*-tert-butylbenzenesulfenamide in the presence of potassium carbonate and 4-Å molecular sieves [Eq. (9)].^[24,25] The key



oxidizing agent, sulfinimidoyl chloride, is generated in situ by chlorination of the sulfenamide with NCS. Oxidation of the alcohols then proceeds smoothly to afford carbonyl compounds, thus regenerating the catalyst. The catalytic oxidation tolerates various kinds of functional groups in the alcohols; thus, silyl ethers, benzyl ethers, epoxides, urethanes, esters, and double bonds are not damaged during this catalytic oxidation, and the corresponding carbonyl compounds are obtained in high yields. Labile or highly epimerizable aldehydes can also be prepared efficiently by this catalytic oxidation, and the carbonyl compounds are isolated more easily than when a stoichiometric amount of sulfinimidoyl chloride is used. The oxidation of diols having both a primary and a secondary hydroxy group in the same molecule results in the primary hydroxy group being selectively oxidized. The usefulness of this catalytic oxidation has been shown in the total syntheses of natural products.^[26]

1.5.3. Dehydrogenation of Saturated Ketones to α,β -Unsaturated Ketones

Ketones can be directly dehydrogenated to α,β -unsaturated ketones in one pot. Firstly the ketones are converted into the corresponding lithium enolates by LDA. The lithium enolates thus formed are then allowed to react with sulfinimidoyl chloride at -78°C and dehydrogenation immediately takes place to afford α,β -unsaturated ketones [Eq. (10)].^[27] The less-hindered positions of unsymmetrical ketones are selectively oxidized by kinetic deprotonation of the ketones with LDA. Compared to other methods for the dehydrogen-

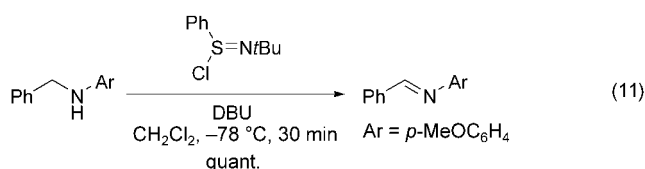


ation of saturated ketones to α,β -unsaturated ones,^[28–31] the above dehydrogenation takes place at a much lower temperature (-78°C) and in a single pot, and has been applied to a key step in the total synthesis of natural products.^[32]

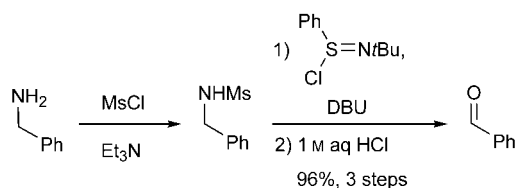
1.5.4. Oxidation of Amines to Imines and Oxidation of Hydroxylamines to Nitrones

A variety of oxidants for the oxidation of secondary amines to the corresponding imines have been developed to date.^[33] Examples include hypervalent iodine reagents,^[34] phenylselenic anhydride,^[35] manganese dioxide,^[36] and others.^[37] The oxidation of amines was also carried out using a catalytic amount of ruthenium catalysts,^[34c,38] a cobalt–Shiff base complex,^[39] or NiSO_4 ^[40] in the presence of an appropriate co-oxidant. Most of these methods have only been applied to the oxidation of benzylic and allylic amines, which afford conjugated imines at room temperature or above, and a limited number of examples were reported for the oxidation of aliphatic amines to nonconjugated imines.

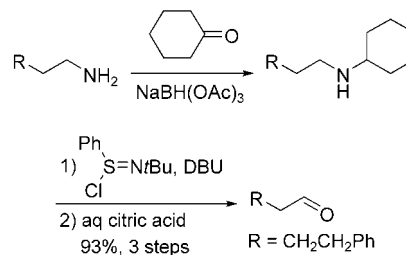
Similar to the oxidation of alcohols to carbonyl compounds, various secondary amines are dehydrogenated to imines under very mild conditions (at -78°C) by using sulfinimidoyl chloride and DBU [Eq. (11)].^[41] The benzylic or



the less-hindered positions are selectively oxidized in the case of unsymmetrical secondary amines. Primary amines are also oxidatively deaminated^[42] to afford the corresponding carbonyl compounds in one pot. In this procedure linear or nonlinear primary amines are first converted into their *N*-cyclohexyl or *N*-mesyl derivatives. These derivatives are then oxidized using sulfinimidoyl chloride and DBU and the imines formed are hydrolyzed to give carbonyl compounds (Schemes 10 and 11).^[43] *N,N*-Disubstituted hydroxylamines

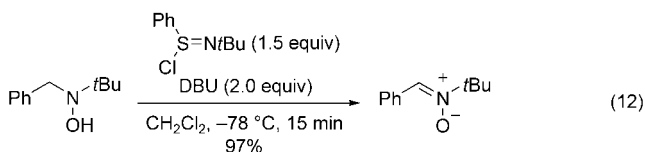


Scheme 10. Conversion of an aromatic primary amine into an aldehyde in the presence of sulfinimidoyl chloride and DBU.



Scheme 11. Conversion of primary amines into aldehydes in the presence of sulfinimidoyl chloride and DBU.

are smoothly oxidized to the corresponding nitrones^[44] at -78°C by using sulfinimidoyl chloride and DBU in dichloromethane [Eq. (12)].^[45]



2. Crossed Aldol Reactions via Boron and Silicon Enolate Intermediates

2.1. Introduction

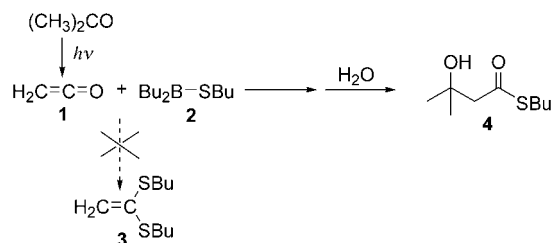
Metal enolates play an important role in organic synthesis. In particular, aldol-type reactions mediated by metal enolates are very useful synthetic methods for the stereoselective formation of carbon–carbon bonds. During the last thirty years the generation and reaction of various metal enolates have been extensively studied, and successful applications to the controlled formation of carbon–carbon bonds has been realized under mild conditions. However, under the classical aldol reaction conditions in which basic media are employed, dimers, polymers, self-condensation products, or α,β -unsaturated carbonyl compounds are invariably formed as by-products. The lithium enolate mediated aldol reaction is considered to be a useful synthetic method for solving the above problems. In addition to the well-studied aldol reaction based on lithium enolates, very useful and versatile regio- and stereoselective carbon–carbon bond-forming aldol-type reactions have been established in our laboratory by the use of boron enolates (1971),^[46] silicon enolates/Lewis acids (1973),^[47,48] and tin(II) enolates (1982).^[49]

2.2. Crossed Aldol Reactions with Boron Enolates

2.2.1. Discovery of the Aldol Reaction Mediated by Boron Enolates

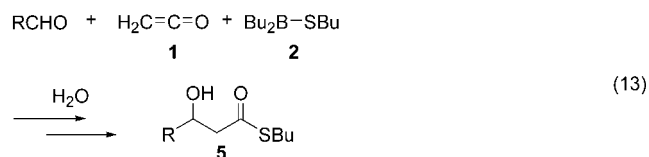
Firstly, the background of how the idea of using boron enolates (vinyloxyboranes) in aldol reactions arose should be described. At the beginning of the 1970s the development of several new reactions was being studied that utilized the characteristics of alkylthioboranes based on the concept of

“elements in combination”. In this concept two types of elements are used in tandem to create a novel reactivity that is different from that which can be achieved when using them separately. For example, treatment of ketene (**1**) with two equivalents of butylthioborane **2** was expected to give the ketene thioacetal **3**, but instead afforded *S*-butyl-3-hydroxy-3-methylbutanethiolate (**4**, Scheme 12).

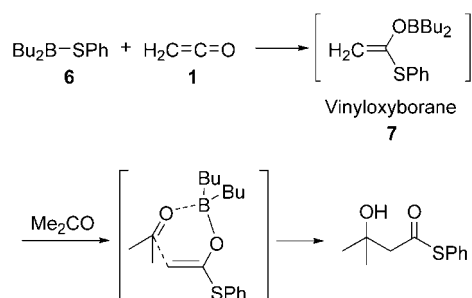


Scheme 12. Unexpected formation of β -hydroxy thioester **4** by the reaction of ketene (**1**) and thioborane **2**.

It was difficult at first to figure out the mechanism of the above reaction, but identification of the product soon indicated the participation of acetone in this reaction (in this process ketene (**1**) is generated by the degradation of acetone under irradiation, and hence a small amount of acetone is introduced into the reaction mixture. Thus, β -hydroxy thioester **4** is generated by the reaction of the three components, acetone, ketene (**1**), and alkyl thioborane **2**. Introduction of gaseous ketene (**1**) free from acetone into a mixture of alkyl thioborane **2** and a carbonyl compound affords the corresponding β -hydroxy thioesters **5** in high yield, as expected [Eq. (13)].^[46] Investigation of the mechanism



reveals that the key intermediate of this reaction is the boron enolate **7** generated from ketene (**1**) and alkyl thioborane **6** (Scheme 13).^[47] Thus, our original study on organothioboranes accidentally led us to discover the widely utilized aldol reactions via boron enolate intermediates.^[50]

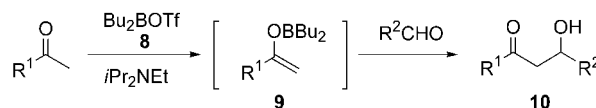


Scheme 13. The reaction of ketene (**1**) with alkylthioborane **6** affords the boron enolate **7**.

2.2.2. Direct Generation of Boron Enolates

A method for the direct generation of boron enolates from the parent carbonyl compounds was desirable to expand the synthetic utility of the boron enolate mediated aldol reaction. Although several synthetic methods for generating boron enolates had been reported,^[50–52] none useful for the direct generation of boron enolates from their parent carbonyl compounds were known until 1976. After the discovery of the aldol reaction via boron enolate intermediates, we made an extensive search for such a useful method together with Inoue. It was thought then that increasing the Lewis acidity of the boron atom by introducing an excellent leaving group would facilitate the coordination of carbonyl compounds. The corresponding boron enolate could then be formed by abstraction of the α -proton of the carbonyl compound with a weak base such as a tertiary amine.

The trifluoromethanesulfonyloxy (triflate, TfO) group was chosen as the leaving group. Dibutylboryl triflate **8** was found to generate boron enolates **9** by reacting with ketones in the presence of a weak base such as *N*-diisopropylethylamine or 2,6-lutidine (Scheme 14).^[53] The subsequent addi-



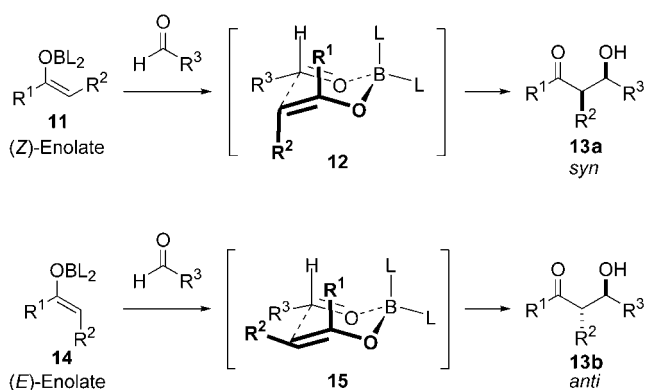
Scheme 14. Preparation of the boron enolate from dibutylboryl triflate and reaction with aldehydes to form aldol compounds.

tion of aldehydes afforded the corresponding aldols **10** in good yields. This was the first example of using triflate salts in synthetic chemistry; various triflate salts are now known to be versatile Lewis acids in organic synthesis. Thus, the crossed-aldol reaction of a ketone and an aldehyde in the presence of dialkylboryl triflate can be performed easily under mild reaction conditions.

Since our first report, this aldol reaction has been investigated in detail by many research groups.^[50] It is currently understood that the boron enolate mediated aldol reaction proceeds via a more-rigid chairlike six-membered transition state (**12** or **15**) than those obtained with alkali metal enolates because of the shorter bond between the boron and oxygen atoms (Scheme 15). Therefore, aldol reactions via boron enolates give aldol adducts more stereoselectively than those via alkali metal enolates such as lithium enolates. This stereoselective aldol reaction now provides an outstanding method for the stereoselective synthesis of acyclic compounds.

2.2.3. Application of Crossed Aldol Reactions Mediated by Boron Enolates to the Synthesis of Natural Products

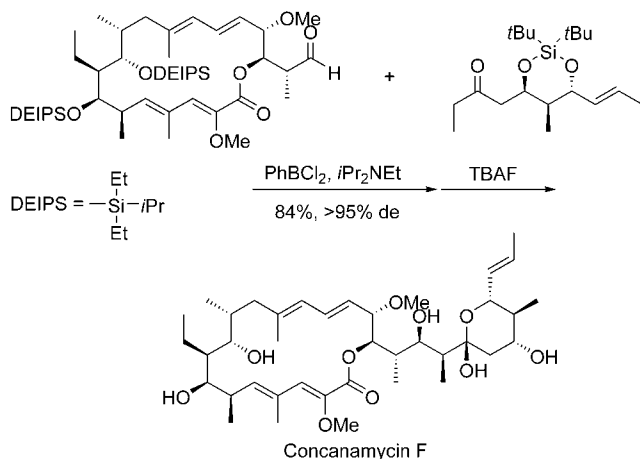
Boron enolates are prepared under mild and essentially neutral conditions and react readily and stereoselectively with carbonyl compounds to form aldols. The stereocontrolled synthesis of acyclic molecules by the boron enolate mediated



Scheme 15. Stereoselective aldol reaction of (Z)- and (E)-boron enolates with aldehydes.

aldol reaction is now applied frequently to the synthesis of natural products.

Toshima and co-workers reported the synthesis of concanamycin F, an 18-membered macrolide antibiotic, by using a PhBCl_2 -mediated aldol reaction (Scheme 16).^[54] Shioiri and



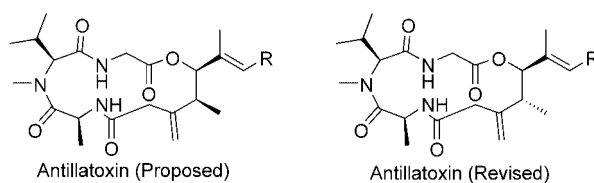
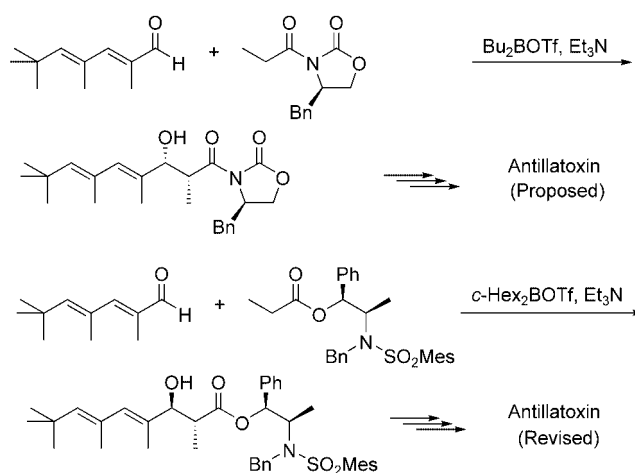
Scheme 16. Total synthesis of concanamycin F. TBAF = tetrabutylammonium fluoride.

co-workers reported the total synthesis of the cyclic lipopeptide antillatoxin. The stereochemistry at C4 and C5 was determined by using a *syn*- and *anti*-selective boron enolate mediated aldol reaction, respectively (Scheme 17).^[55]

2.3. Crossed Aldol Reactions with Silicon Enolates

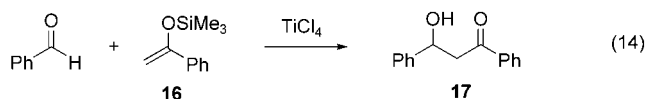
2.3.1. Discovery of Silicon Enolate mediated Crossed Aldol Reactions

The driving force in the above-mentioned aldol reaction involving a boron enolate is considered to be the interconversion of the enol forms of the ketones (boron enolates) into their more stable keto form (β -boryloxy ketones).^[56] While we were studying the boron enolate mediated aldol reaction, our investigation was also continuing on developing new chemical reactions with titanium(IV) chloride.^[57] A new and important



Scheme 17. Total synthesis of antillatoxin. Bn = benzyl.

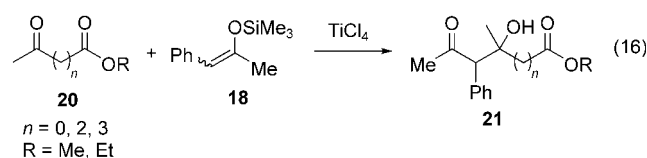
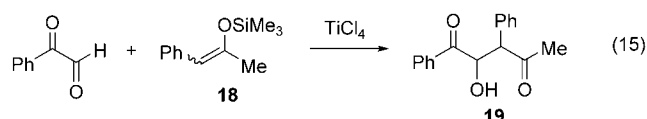
idea immediately came to mind that titanium(IV) chloride would effectively generate active electrophilic species through its strong interaction with carbonyl compounds and that this complex would react easily even with relatively weak carbon nucleophiles to form a new carbon–carbon bond. Next, by analogy with enol boronates, the use of stable and isolable silyl enol ethers^[58] was investigated as the weak nucleophile, and, just as expected, the aldol reaction between the silyl enol ether of acetophenone **16** and benzaldehyde in the presence of titanium(IV) chloride afforded the aldol product **17** in high yield [Eq. (14)].^[48]



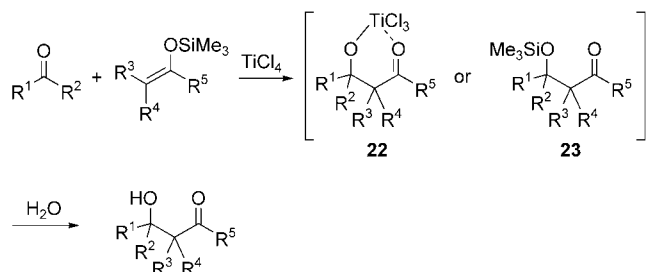
It was known that enol ethers react with acetals or ketals in the presence of a Lewis acid to give aldol-type adducts; however, these reactions are often accompanied by undesired side reactions.^[59] Furthermore, it had also been difficult to perform crossed-aldol reactions selectively since conventional aldol reactions are carried out under equilibrium conditions in which either a basic or an acidic catalyst is used in protic solvents.^[60] Detailed studies of this new aldol reaction of silicon enolates, however, revealed a number of advantages over conventional methods. Firstly, this reaction not only gives a variety of aldol adducts in high yields, but also gives a regioselective aldol adduct when the silyl enol ether of an unsymmetrical ketone is used. This latter result means that the aldol reaction proceeds with retention of the regiochemical integrity of the starting silyl enol ethers to afford the

corresponding aldol regioselectively. The starting silyl enol ethers themselves can be conveniently prepared regioselectively under kinetic or thermodynamically controlled conditions.

Secondly, functional group selectivity is observed: namely, the reactions with aldehydes proceed at -78°C while those with ketones proceed at elevated temperatures (ca. 0°C). Chemoselectivity is observed with acceptors having two different kinds of carbonyl functions, such as aldehyde and ketone or ester, in the same molecule. Treatment of phenylglyoxal with silyl enolate **18** at -78°C affords α -hydroxy- γ -diketone **19** [Eq. (15)].^[60b] The reaction of ketoesters **20** with silyl enolate **18** gives hydroxy ketoesters **21** as the sole products [Eq. (16)].^[60]



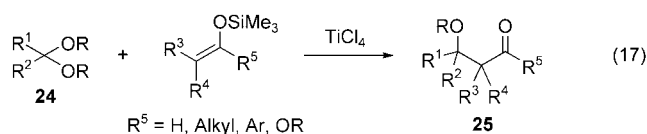
A crossed-aldol reaction between two ketones affords thermodynamically unfavorable aldols in high yields as a result of the stabilization of the aldol adducts by their intramolecular chelation with a titanium center **22** or by their conversion into silyl ethers **23** (Scheme 18). The *syn/anti* ratio



Scheme 18. Formation of the thermodynamically unfavorable aldol through stabilization of the intermediate.

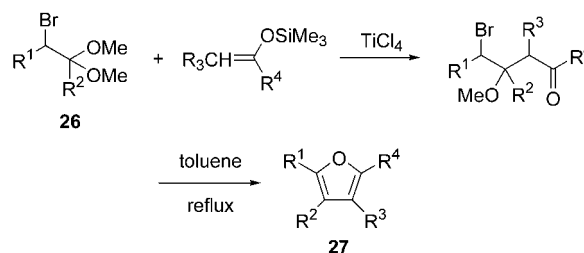
of the aldol product is influenced both by steric factors of the aldehyde and silyl enolate, and by the properties of the Lewis acid catalyst.^[61]

As an extension of this new protocol for carbon–carbon bond formation, the reaction between silyl enolates and acetals **24** has been performed in the presence of titanium(IV) chloride to afford β -alkoxy carbonyl compounds **25** [Eq. (17)].^[62] Various substituted furans **27** are readily pre-



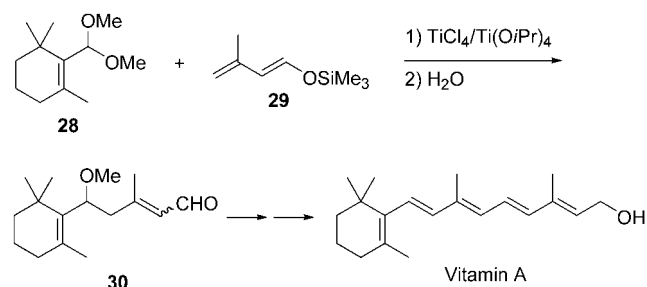
pared by a TiCl_4 -promoted reaction of α -halo acetals **26** with silyl enolates (Scheme 19).^[62]

In the presence of titanium(IV) chloride, silyl dienolate **29** derived from an α,β -unsaturated aldehyde reacts with acetal



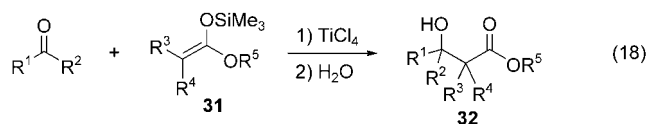
Scheme 19. Synthesis of furans through a TiCl_4 -mediated reaction of α -haloacetals with silyl enolates.

28 selectively at the γ -position to give δ -alkoxy- α,β -unsaturated aldehydes **30**. The yield of the reaction is low since titanium(IV) chloride is strongly acidic and the silyl dienolate **29** polymerizes. However, addition of tetraisopropoxytitanium(IV) to titanium(IV) chloride improves the yield dramatically.^[63] Vitamin A has successfully been synthesized by use of silyl dienolate **29** under the above conditions (Scheme 20).^[64]



Scheme 20. Synthesis of vitamin A by an aldol reaction of acetal **28** with silyl dienol ether **29**.

Silyl ketene acetals **31** derived from carboxylic esters are more nucleophilic than silyl enol ethers and also react with ketones and aldehydes in the presence of titanium(IV) chloride to give β -hydroxy esters **32** in high yields [Eq. (18)].^[65,66] Although the Reformatsky reaction is well-



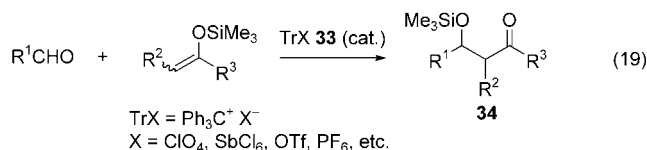
known as a good synthetic method for synthesizing β -hydroxy esters, the titanium(IV) chloride mediated reaction is a milder and more versatile method for synthesizing α -substituted β -hydroxy esters.

Since this discovery of aldol reactions of silyl enolates with carbonyl compounds or acetals, silyl enolates have become one of the most popular carbon nucleophiles in organic

synthesis and are also employed in other reactions such as Michael reactions,^[67] Mannich reactions,^[68] and others.^[69] Silyl enolates are superior to other metal enolates in terms of their isolation, regioselectivity of formation, and their unique reactivities under mild conditions.

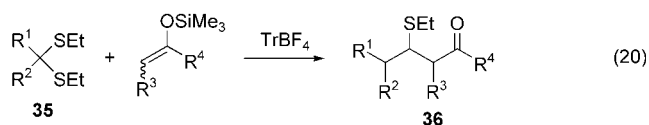
2.3.2. Lewis Acid Catalyzed Aldol Reactions of Silicon Enolates

The first titanium(IV) chloride mediated aldol reaction of silyl enolates with aldehydes was carried out with a stoichiometric amount of titanium(IV) chloride.^[48] Other Lewis acids were also tried, and it was found that a catalytic amount of a triphenylmethyl (trityl) salt **33** (for example, trityl perchlorate) is sufficient to effectively promote the aldol reaction [Eq. (19)].^[70] In fact, 5–10 mol % of the trityl salt is sufficient

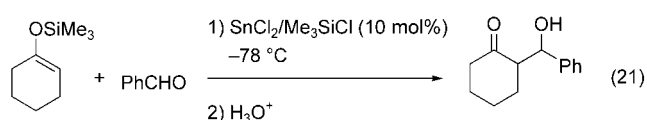


to drive the aldol reaction to completion. An interesting finding in this catalytic reaction is that the silicon enolate reacts with aldehydes to give the corresponding aldol adducts as their silyl ethers **34**.

The aldol reaction of silyl enolates and acetals in the presence of a catalytic amount (1–10 mol %) of trityl perchlorate proceeded effectively to afford β -methoxy ketones in high yield. The reaction of dithioacetal **35** with silyl enolates in the presence of a trityl tetrafluoroborate catalyst affords β -ethylthio ketones **36** [Eq. (20)].^[71]



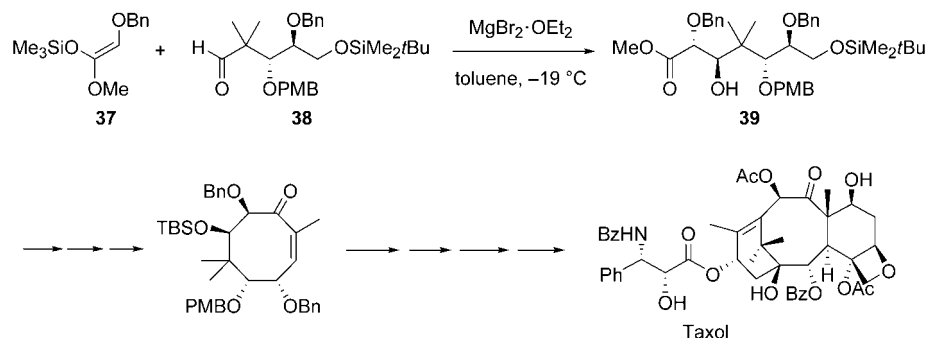
A combination of the two weak acids tin(II) chloride and chlorotrimethylsilane is also found to serve as an effective catalyst for the aldol reaction.^[72] Neither chlorotrimethylsilane nor tin(II) chloride alone shows any accelerating effect at -78°C , even when added in excess. However, the aldol reaction carried out in the presence of catalytic amounts of both chlorotrimethylsilane and tin(II) chloride gives the desired product in more than 90 % yield [Eq. (21)]. It is presumed that the cationic silyl species generated by coordination of the chloride ion to the tin(II) atom catalyzes the aldol reaction.



2.3.3. Application of Silicon Enolate Mediated Crossed Aldol Reactions to the Synthesis of Natural Products

Since the stereoselectivity of silyl enolate mediated aldol reactions varies with the Lewis acids employed, these aldol reactions provide useful synthetic methods in stereoselective and asymmetric carbon–carbon bond formation and have been applied to the total synthesis of natural products by many research groups.

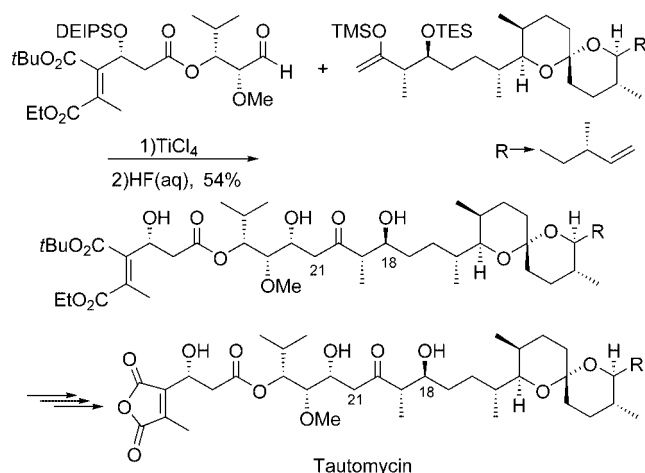
The stereoselective aldol reaction of the trimethylsilyl enolate of methyl 2-benzyloxyacetate (**37**) with enantiomerically pure trialkoxy aldehyde **38** is performed by using three equivalents of $MgBr_2 \cdot Et_2O$ as an activator to afford an aldol adduct **39** in high yield and excellent diastereoselectivity (Scheme 21). In contrast, the conventional Lewis acids such as $TiCl_4$ and $SnCl_4$ give the desired aldol product **39** in only low



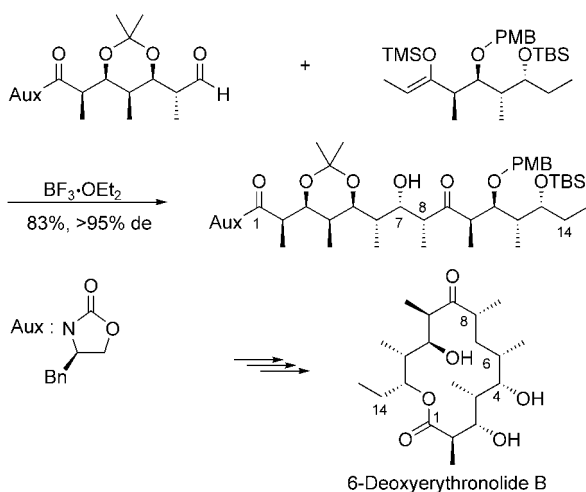
Scheme 21. Diastereoselective aldol reaction for preparing an acyclic polyoxy molecule **39**. Ac = acetyl, PMB = 4-methoxybenzyl, TBS = *tert*-butyldimethylsilyl.

yields.^[73,74] This method has been applied in our total synthesis of the antitumor agent taxol as a key step in constructing the B ring system of the target molecule.^[75]

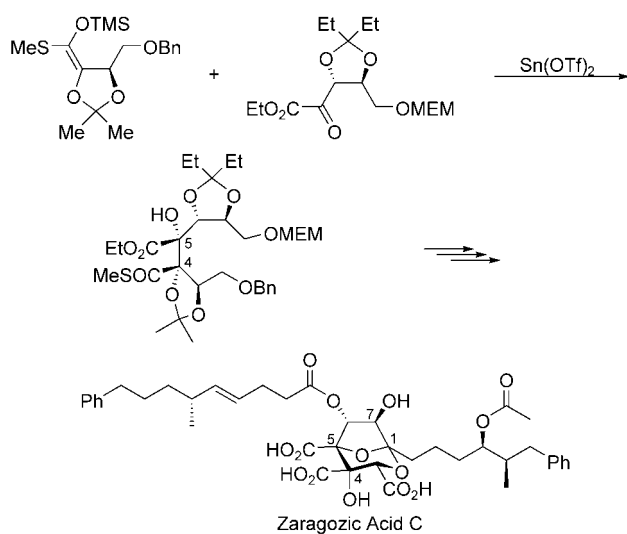
In the total synthesis of antifungal antibiotic tautomycin, a potent protein phosphatases inhibitor, Ichihara and co-workers reported the $TiCl_4$ -mediated aldol coupling of two large subunits (Scheme 22).^[76] Evans et al. reported the total synthesis of the 14-membered macrolide antibiotic 6-deoxyerythronolide B by using a $BF_3 \cdot OEt_2$ -mediated aldol reaction involving fragment coupling (Scheme 23).^[77] A fragment coupling reaction promoted by $Sn(OTf)_2$ was employed in the total synthesis of zaragozic acid C by Hashimoto and co-workers (Scheme 24).^[78] Carreira and co-workers reported the total synthesis of macrolactin A, a 24-membered polyene macrolide antibiotic, by using an enantioselective dienolate aldol addition catalyzed by a chiral Ti complex (Scheme 25).^[79]



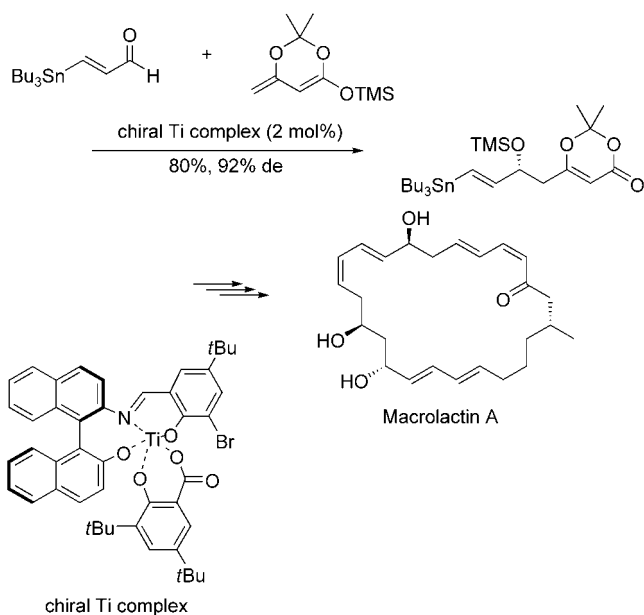
Scheme 22. Total synthesis of tautomycin. DEIPS = diethylisopropylsilyl, TES = triethylsilyl.



Scheme 23. Total synthesis of 6-deoxyerythrulose B.



Scheme 24. Total synthesis of zaragozic acid C. MEM = methoxyethoxymethyl.



Scheme 25. Total synthesis of macrolactin A.

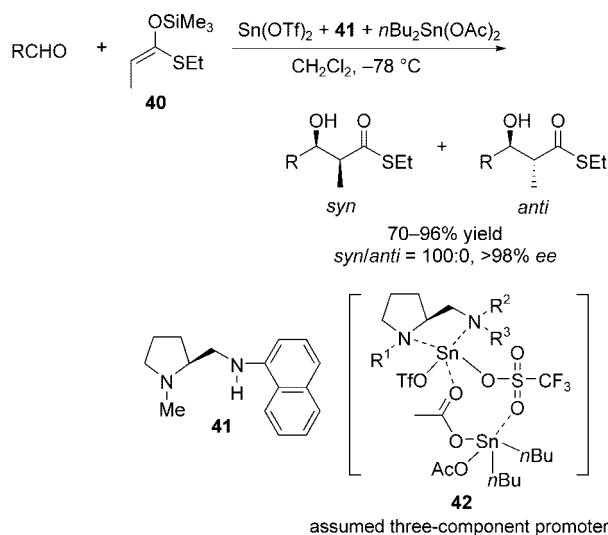
2.3.4. Asymmetric Aldol Reactions with Chiral Tin(II) Lewis Acid Catalysts

The asymmetric aldol reaction is one of the most powerful tools for the construction of new carbon–carbon bonds with control over the absolute configurations of newly formed chiral centers.^[80] Of this class of reaction, one that is mediated by silicon enolates has been extensively studied by many research groups over the past two decades.

2.3.4.1. Stoichiometric Enantioselective Aldol Reactions

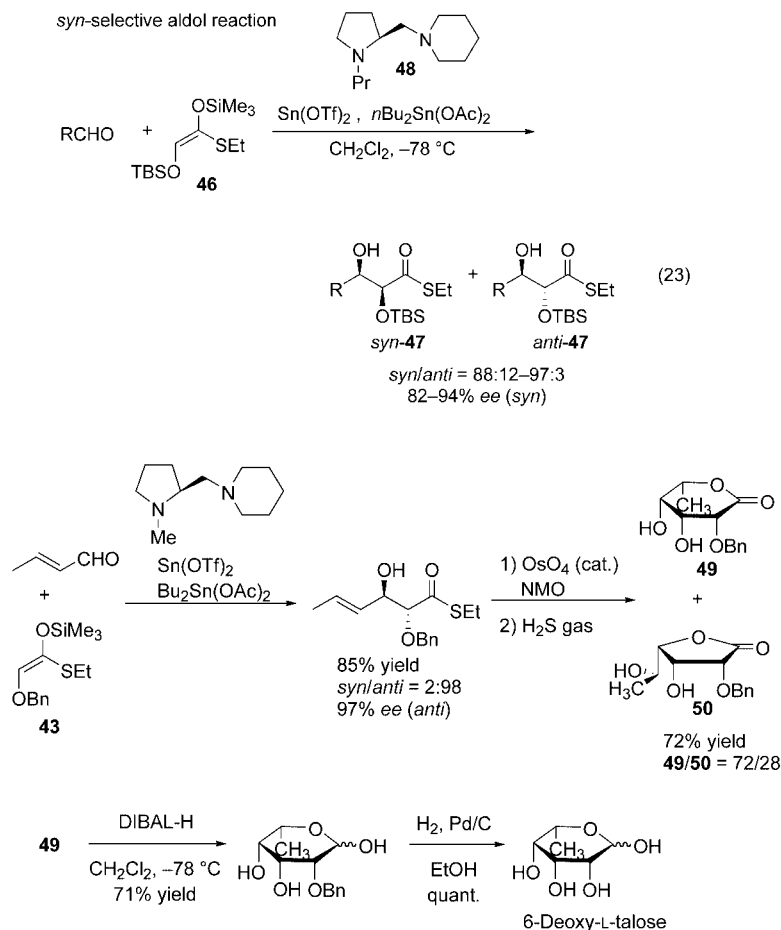
A wide variety of aldehydes react with the (*E*)-silicon enolate^[81] **40** derived from propionic acid thioester to give *syn*-aldol adducts in high yields and with perfect stereochemical control by the combined use of tin(II) triflate, chiral diamine **41**, and dibutyltin acetate (Scheme 26).^[82–84] It is thought that an active complex **42** consisting of three components, tin(II) triflate, chiral diamine **41**, and dibutyltin acetate, is formed during these aldol reactions. This three-component complex would activate both the aldehyde and silyl enolate (double activation); it is proposed that the chiral diamine-coordinated tin(II) triflate activates the aldehyde while oxygen atoms of the acetoxy groups of the dibutyltin acetate interact with the silicon atom of the silicon enolate.

Since optically active molecules containing 1,2-diol units are often observed in nature (carbohydrates, macrolides, polyethers), the asymmetric aldol reaction of the silyl enolate of α -benzyloxythioacetate **43** with aldehydes has been investigated with the aim of introducing two vicinal hydroxy groups and stereoselective formation of a carbon–carbon bond. Interestingly, it is found that the *anti*- α,β -dihydroxy thioester derivatives **44** are obtained in high yields with excellent diastereo- and enantioselectivities by the combined use of tin(II) triflate, chiral diamine **45**, and dibutyltin acetate [Eq. (22)].^[85] These results are unusual because the aldol



Scheme 26. Enantioselective synthesis of *syn*-aldol adducts from aldehydes and a (*E*)-silyl enolate.

reaction of simple silyl enolate **40** with aldehydes generally affords *syn*-aldol adducts as mentioned above (see Scheme 26). Consideration of the transition states of these aldol reaction leads us to postulate that coordination of an oxygen atom of the silyl enolate **43** to the tin atom of tin(II) triflate occurs, which is essential for the *anti* selectivity. To prove the hypothesis the silicon enolate **46**, which has a bulky *tert*-butyldimethylsilyl group, was prepared to prevent the coordination of the α -oxygen atom to the tin(II) center. As expected, *syn*-aldol **47** is obtained in high stereoselectivity by the reaction using the sterically hindered silicon enolate **46** in the presence of tin(II) triflate, a chiral diamine **48**, and dibutyltin acetate [Eq. (23)].^[86]



Scheme 27. Stereospecific synthesis of 6-deoxy-L-talose. DIBAL = diisobutylaluminum hydride, NMO = *N*-methylmorpholine *N*-oxide.

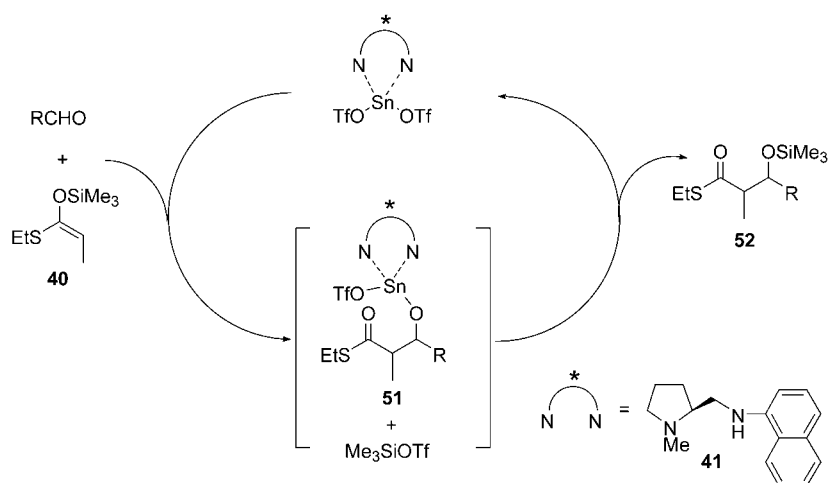
2.3.4.2. Catalytic Enantioselective Aldol Reactions

As described above, optically active aldol adducts are easily obtained by using a stoichiometric amount of chiral diamine, tin(II) triflate, and dibutyltin acetate. An essential step in an enantioselective aldol reaction with only a catalytic amount of the chiral catalyst system is transmetalation of the initially formed tin(II) alkoxide **51** to silyl alkoxide **52** with silyl triflate (Scheme 28). Carrying out the aldol reaction with smaller amounts of the chiral catalyst resulted in the formation of aldol adducts with low stereoselectivities, because Sn–Si exchange occurs slowly and an undesired Me_3SiOTf -promoted aldol reaction also occurs which affords racemic aldol adducts. A solution of silyl enolate and aldehyde in dichloromethane was added slowly to a solution of the catalyst **45** (20 mol%) to keep the concentration of trimethylsilyl triflate as low as possible during the reaction [Eq. (24)]. This resulted in the aldol product **53** being obtained in good yields and with high enantioselectivities.^[88]

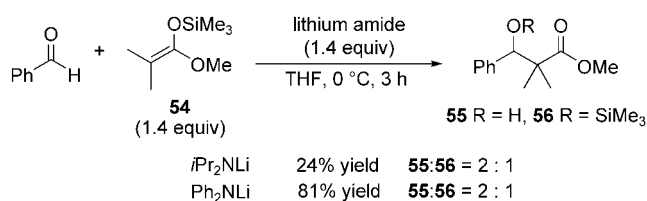
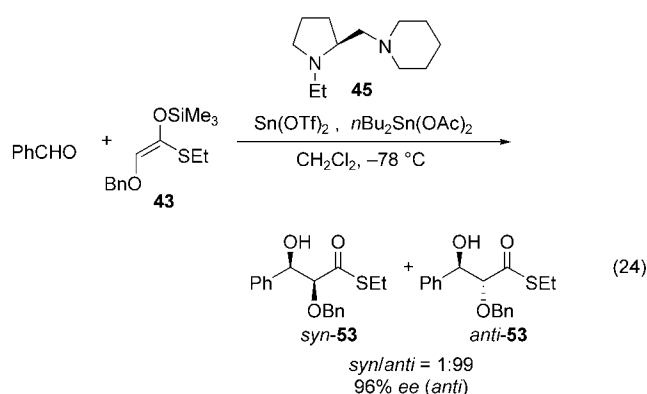
The selectivities are improved by using propionitrile as the solvent instead of dichloromethane because the rate of Sn–Si exchange is faster in propionitrile than in dichloromethane.^[89]

After these first reports on the highly efficient catalytic enantioselective aldol reaction, the catalytic symmetric aldol

It is thus possible to prepare either the *syn* or *anti* aldols selectively by choosing the appropriate protecting group on the alkoxy group. This methodology has been applied to the synthesis of several monosaccharides including branched, deoxy, and amino sugars.^[87] One example is shown in Scheme 27).^[87c]



Scheme 28. A proposed catalytic cycle for the enantioselective aldol reaction.



Scheme 29. Lithium amide mediated aldol reaction of TMS enolate **54** and benzaldehyde.

reactions of silicon enolates with aldehydes using chiral boron,^[90] titanium,^[91] zirconium,^[92] and copper Lewis acids,^[93] as well as by transmetalation to chiral Pd^{II} enolates^[94] have been independently reported by other research groups.

2.3.5. Base-Catalyzed Crossed Aldol Reactions with Trimethylsilyl Enolates

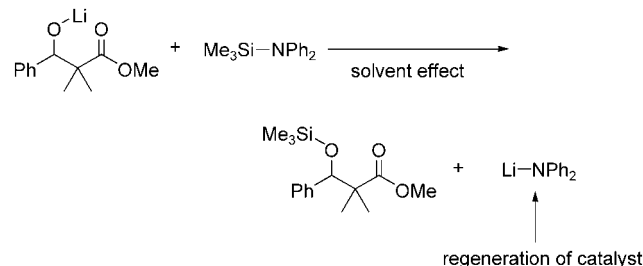
Recently, several aldol reactions of silyl enolates with aldehydes have been demonstrated in which the silyl enolates are activated with Lewis bases instead of conventionally used Lewis acids: Denmark and Stavenger introduced a Lewis base catalyzed aldol reaction of trichlorosilyl enolates with aldehydes by using phosphoramides as a Lewis base^[95] and Hosomi and co-workers have reported an aldol reaction that uses a combination of dimethylsilyl enolate and CaCl₂ in an aqueous DMF solvent.^[96] Silyl enolates in which the Lewis acidity of the silicon atom has been enhanced were employed in these Lewis base catalyzed aldol reactions to facilitate interaction with the base.

The use of other Lewis base catalysts was investigated for the activation of silyl enolates to enable simple and popular silyl enolates such as trimethylsilyl (TMS) enolates to be employed. These catalytic aldol reactions of TMS enolates with aldehydes in the presence of a Lewis base proceeded

smoothly by generating an activated TMS enolate through formation of a hypervalent silicate.^[97]

An aldol adduct was obtained in 15 % yield when the aldol reaction of TMS enolate **1** with benzaldehyde (PhCHO) was carried out in THF using 20 mol % of the Lewis base LiNPh₂ (Scheme 29). This result indicated that a stoichiometric amount of LiNPh₂ was required for the completion of the reaction. The aldol adducts formed after quenching were a mixture of the aldol (R = H, **55**) and the *O*-silyl ether (R = TMS, **56**), which suggested the concurrent formation of the lithium aldolate and *O*-silyl ether. In addition, it was noted that the amount of *O*-silyl ether formed in THF was less in all cases than that of the aldol, irrespective of the kind of lithium amide employed. To achieve a catalytic aldol reaction the lithium aldolate formed must be trans-

formed rapidly to its *O*-silyl ether by the coformed silylamide. Since the silylamide is a good silylating reagent, it was expected that by careful choice of the reaction conditions would result in formation of the *O*-silyl ether and simultaneous regeneration of the lithium amide (Scheme 30).

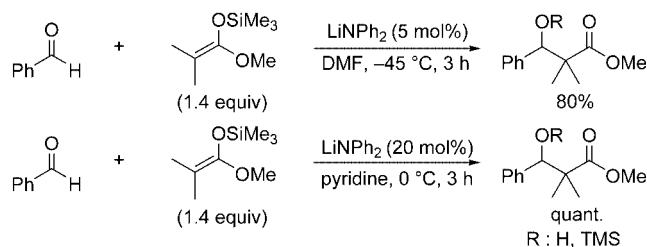


Scheme 30. Silyl transfer of silylamide to lithium aldolate.

Since the solvents were considered to influence this silyl transfer from the silylamide to the lithium aldolate, various solvents were further screened to obtain higher yields and higher ratios of the *O*-silyl ether over the aldol. This process led to the discovery that DMF (**55**:**56** = 1:35) and pyridine (**55**:**56** = 1:6) were both excellent solvents for the generation of the aldol adducts in quantitative yields.

The catalytic aldol reaction was investigated with 5 mol % of LiNPh₂ added to a solution of the substrate in DMF at -45 °C, and the desired aldol was obtained in 80 % yield along with recovery of 18 % of the starting material. Similarly, the

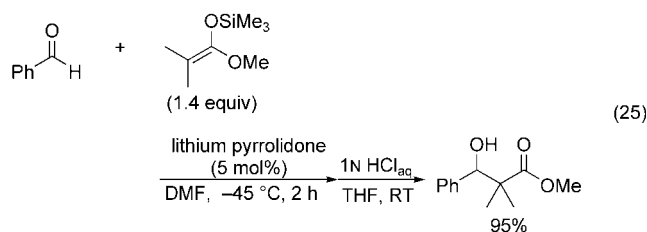
aldol adduct was obtained in quantitative yield when the reaction was carried out with 20 mol % of LiNPh_2 at 0 °C in pyridine (Scheme 31). In the absence of the catalyst, the aldol adduct was not obtained at either –45 °C in DMF or at 0 °C in



Scheme 31. LiNPh_2 -catalyzed aldol reaction of TMS enolate **54** and benzaldehyde.

pyridine. These results indicate that LiNPh_2 itself apparently behaves as an effective catalyst in promoting the aldol reaction in DMF or in pyridine.^[97a,c]

In the next development, 2-pyrrolidone was chosen as a precursor of the catalyst^[97b,c] because it is easy to dissolve in water, is readily available, and is inexpensive. In addition, the pK_a value of the N–H bond is relatively close to that of diphenylamine (measured in DMSO).^[98] Reaction of TMS enolate **54** and PhCHO in the presence of 5 mol % of lithium 2-pyrrolidone either at –45 °C in DMF or at 0 °C in pyridine gave the desired aldol in 95 % yield in DMF or 78 % yield in pyridine [Eq. (25)]. These results indicate that the lithium 2-pyrrolidone does indeed catalyze the aldol reaction of the TMS enolates with aldehydes in DMF or pyridine by acting as a Lewis base.



Trimethylsilyl enolate **54** reacted smoothly with various aromatic aldehydes to afford the corresponding aldols in high yields. Aromatic aldehydes having an electron-withdrawing group such as *p*-nitrobenzaldehyde or aliphatic aldehydes also afforded the aldol adducts in moderate yields (Table 4).

The Lewis base catalyzed aldol reaction has some characteristic advantages, especially when aldehydes with basic groups are used. To show the utility of this Lewis base catalyzed aldol reaction TMS enolate **54** and aldehydes with basic groups were allowed to react in DMF at –45 °C in the presence of 10 mol % of lithium 2-pyrrolidone. The reaction proceeded smoothly and the corresponding aldol adducts were obtained in high yields (Table 5).

Several other silyl enolates were also employed in this lithium 2-pyrrolidone catalyzed aldol reaction. Initially TMS

Table 4: Lithium 2-pyrrolidone catalyzed aldol reaction of TMS enolate **54** with aldehydes.

Entry	Aldehyde	Solvent	<i>T</i> [°C]	<i>t</i> [h]	Yield ^[a] [%]
1		DMF	–45	2	92
2		pyridine	0	3	95
3		DMF	–45	3	92
4		pyridine	0	30	88
5		DMF	–45 → RT	3 days	57
6		DMF	–45	4	55 ^[b]

[a] Yield was determined by ^1H NMR analysis (270 MHz) using 1,1,2,2-tetrachloroethane as an internal standard. [b] Yield of the isolated product.

Table 5: Lithium 2-pyrrolidone catalyzed aldol reaction of TMS enolate **54** with aldehydes.

Entry	Aldehyde	<i>t</i> [h]	Yield ^[a] [%]
1		1	97
2		2	91
3		3	97 ^[b]

[a] Yield was determined by ^1H NMR analysis (270 MHz) using 1,1,2,2-tetrachloroethane as an internal standard. [b] Yield of the isolated product.

enolates prepared from (*S*)-ethyl ethanethioate or acetophenone were employed and the corresponding aldol adducts were obtained in high yields. The two isomeric trimethylsilyl enolate derived from methyl propionate were both found to give aldols with moderate *syn* diastereoselectivity (Table 6).

The use of a Lewis base catalyst weaker than the former one was next considered to further extend the utility of this Lewis base catalyzed aldol reaction. The carboxylate anion was tried on the expectation that this weakly basic ion may also have an affinity toward the silicon atom. Furthermore, silylation of the lithium aldolate by TMS carboxylate was expected to establish a catalytic cycle since the silyl carboxylates were also silylating reagents. So a readily available lithium acetate (AcOLi) was chosen as a milder Lewis base in place of the above-mentioned lithium salts. The reaction of

Table 6: Lithium 2-pyrrolidone catalyzed aldol reaction of TMS enolates with benzaldehyde.

$\text{PhCHO} + \text{silyl enolates (1.4 equiv)} \xrightarrow[\text{DMF, } -45^\circ\text{C, } t]{\text{lithium pyrrolidone (10 mol\%)}} \xrightarrow[\text{THF, RT}]{1\text{N HCl}_{\text{aq}}} \text{products}$					
Entry	Silyl enolates	<i>E/Z</i>	<i>t</i> [h]	Yield ^[a] [%]	<i>syn:anti</i>
1		—	2	95	—
2		—	3	77	—
3		5:1	3	42	63:37
4		1:9	3	88	73:27

[a] Yield was determined by ¹H NMR analysis (270 MHz) using 1,1,2,2-tetrachloroethane as an internal standard.

PhCHO and TMS enolate **54** in the presence of 10 mol % of AcOLi at -45°C in DMF afforded the aldol adduct in 83 % yield. This result confirmed the capability of AcOLi to play a role as an effective Lewis base catalyst in this aldol reaction.^[97d]

Aldol reactions in water or water-containing organic solvents have attracted much attention in the sense that they are economical and environmentally benign synthetic methods. Although several methods for carrying out aldol reactions with silyl enolates in water or water-containing organic solvents have been reported,^[96,99] there are few that use silyl enolates derived from carboxylic esters as a consequence of their extreme sensitivity toward water.

The reaction of PhCHO and TMS enolate **54** was performed in the presence of 10 mol % of AcOLi at -45°C in DMF/H₂O (10:1), and afforded the aldol adduct in 71 % yield. The reaction conditions were then carefully screened to improve the yields. The corresponding aldol was obtained in highest yield when the reaction was carried out with two equivalents of **54** in DMF/H₂O (50:1).^[99]

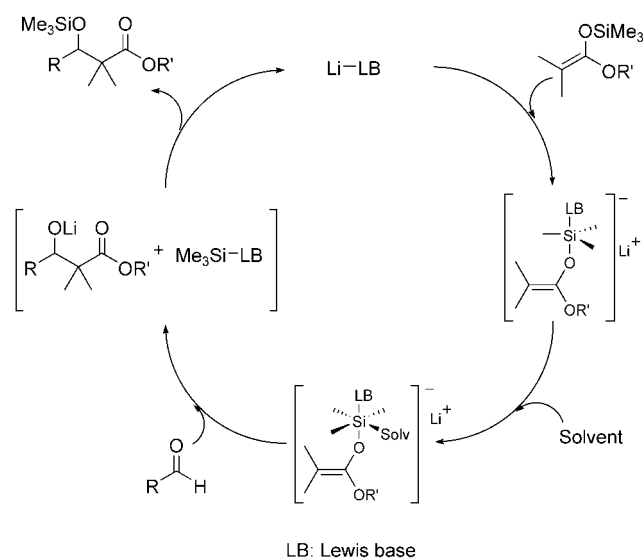
Reactions of TMS enolate **54** with various aldehydes were then tried under these conditions, and the aldol adducts were obtained in high yields in every case (Table 7). It is remarkable that 4-chloro- and 4-nitrobenzaldehyde as well as 3-phenylpropionaldehyde reacted smoothly to afford the desired aldols in higher yields than in non-aqueous solvents. 2-Pyridinecarboxaldehyde afforded the aldol adduct in high yield, even though the reaction does not generally proceed in the presence of Lewis acids. One of the particular characteristics of this base-catalyzed aldol reaction carried out in a water-containing DMF solvent is that the desired aldols are formed in moderate to high yields even with aldehyde substrates having free amide, hydroxy, or even carboxylic groups—such groups are incompatible when metal enolates or Lewis acids are employed.

Lithium aldolate is formed via a hexacoordinate hyper-valent silicate similar to that formed under non-aqueous conditions (Scheme 32).^[97c] The initially formed lithium aldolate and silyl acetate were hydrolyzed rapidly to produce LiOH and acetic acid when the reaction is carried out in

Table 7: LiOAc-catalyzed aldol reaction of TMS enolate **54** with aldehydes.

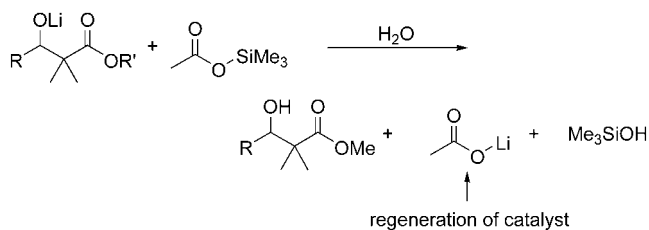
$\text{RCHO} + \text{TMS enolate } \textbf{54} \xrightarrow[\text{DMF/H}_2\text{O (50:1), } -45^\circ\text{C, } t]{\text{AcOLi (10 mol\%)}} \text{Aldol}$			
Entry	Aldehyde	<i>t</i> [h]	Yield ^[a] [%]
1		3	97 ^[b] (69)
2		3	94 (63)
3		16	78 (84)
4		17	62 (94 ^[b])
5		18	84 ^[b] (65 ^[b])
6		2.5	97 (84)
7		14	84
8		3	92 ^[b]
9		24	52

[a] Yield was determined by ¹H NMR analysis (270 MHz) using 1,1,2,2-tetrachloroethane as an internal standard. Numbers in parentheses are yields under non-aqueous conditions. [b] Yield of the isolated product.

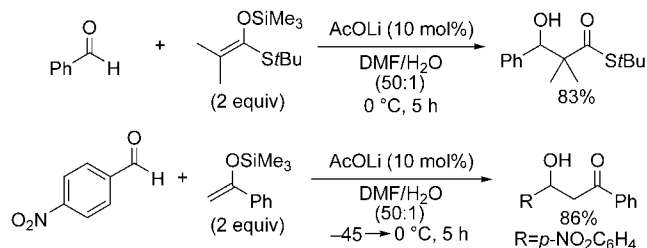
**Scheme 32.** The catalytic cycle of a Lewis base catalyzed aldol reaction of TMS enolates and aldehydes.

water-containing DMF. Subsequent neutralization should afford AcOLi, thus establishing a catalytic cycle (Scheme 33).

This catalytic aldol reaction can also be performed smoothly with other TMS enolates. For example, TMS enolates derived from (*S*)-*tert*-butyl isobutanethioate and acetophenone afforded the corresponding aldols in high yields (Scheme 34).



Scheme 33. Regeneration of the catalyst in water-containing DMF.



Scheme 34. Lithium acetate mediated aldol reaction of TMS enolates and aldehydes in water-containing DMF.

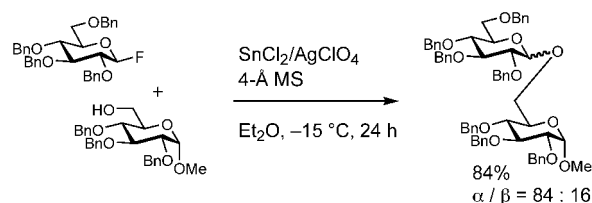
This is the first example of a Lewis base catalyzed aldol reaction that tolerates silyl enolates derived from carboxylic esters. This method is applicable to the synthesis of various aldols since the reaction does not need strictly anhydrous conditions and can be performed with a mild, readily available, and inexpensive Lewis base catalyst.

3. Stereoselective Glycosylation with Glycosyl Fluorides

3.1. Introduction

The development of useful methods for stereoselective glycosylation is one of the most fundamental and important aspects for the syntheses of various types of glycosides and oligosaccharides. In general, the stereoselective synthesis of 1,2-*cis*-glycosides is more difficult than that of 1,2-*trans*-glycosides, which can normally be synthesized by utilizing neighboring-group participation from the 2-acyloxy group. The Koenigs–Knorr reaction,^[100] which employs glycosyl chlorides and bromides, has for a long time been the most commonly employed method; however, it requires a stoichiometric amount of troublesome heavy-metal salts and the reaction conditions are rather drastic. Over the last two decades various types of glycosyl donors, such as thioglycosides, glycosyl trichloroacetimidates, glycosyl acetate, selenoglycosides, glycosyl sulfoxides, 1-OH sugars, glycosyl donors with phosphorus-containing leaving groups, glycals, and pentenyl glycosides, have been developed^[101] and employed in the syntheses of saccharide chains. In 1981 we reported the first use of glycosyl fluoride as a glycosyl donor.^[102] In these syntheses α -glucosides were obtained with good stereoselectivities when glucosyl fluoride and various glycosyl acceptors were treated in the presence of a promoter generated from

stannous chloride (SnCl_2) and silver perchlorate (AgClO_4) in diethyl ether (Et_2O ; Scheme 35). In the following, the historical development of the chemistry of glycosyl fluoride as a glycosyl donor, and recent stereoselective glycosylation using glycosyl fluoride is described.

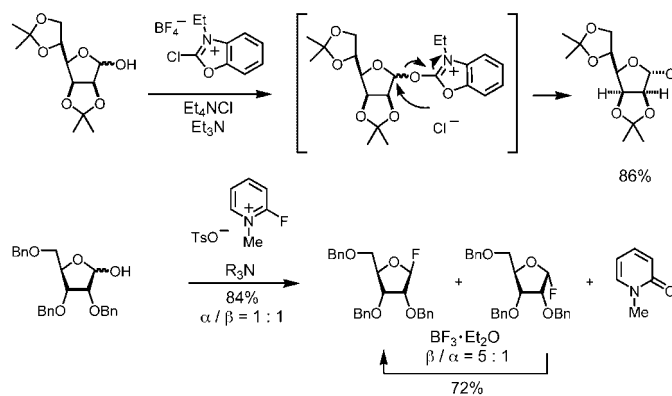


Scheme 35. First example of glycosylation with glycosyl fluoride.

As described above, glycosyl chlorides and bromides are used frequently in glycosylation reactions. However, in these cases, the carbon–halogen bond is readily cleaved and successful results cannot always be expected in regard to both yields and stereoselectivities. A glycosyl fluoride was chosen as the glycosyl donor on the basis that the carbon–fluorine bond would be expected to have a high bond energy and, consequently, that would lead to selective $\text{S}_{\text{N}}2$ replacement provided that smooth activation could be achieved. Glycosyl fluorides had not been employed before since the presence of a strong C–F bond at the anomeric carbon atom would make them more stable than other similar halides because their high bond-dissociation energy (C–F: 552 kJ mol^{-1} , C–Cl: $397 \pm 29 \text{ kJ mol}^{-1}$, C–Br: $280 \pm 21 \text{ kJ mol}^{-1}$)^[103] was believed to make them hard to activate.

At that time (the 1980s), the synthesis of the glycosyl fluoride starting material was a problem because simple preparative methods usually included the use of hazardous anhydrous hydrogen fluoride. However, a facile method for the synthesis of glycosyl fluorides from 1-hydroxy sugars using 2-fluoropyridinium salts had been found by accident (Scheme 36).^[104] This finding opened the way for using these fluorides as glycosyl donors.

During the course of examining various Lewis acids for activating glycosyl fluoride we encountered an extremely interesting phenomenon, namely, that the desired reaction



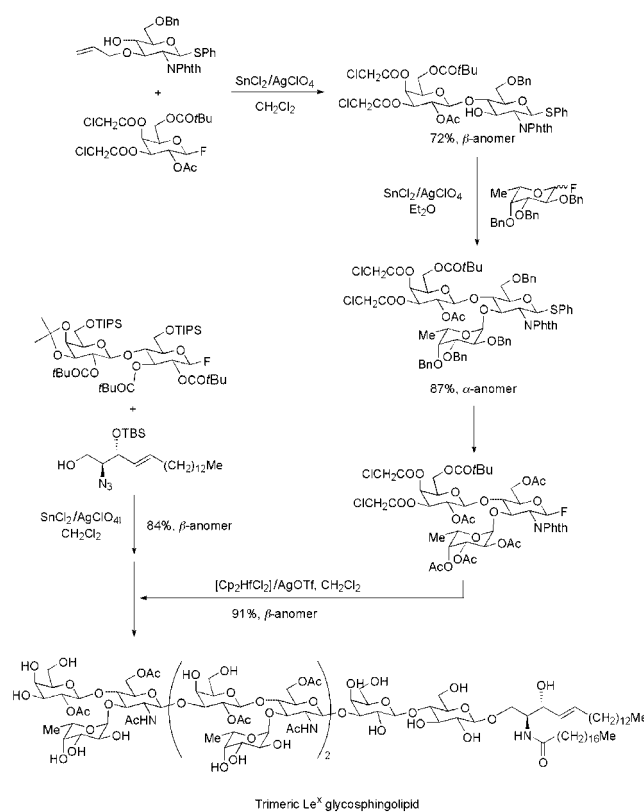
Scheme 36. Preparation of glycosyl fluoride. Ts = *p*-toluenesulfonyl.

proceeded with tin(II) chloride, which is considered to be a fairly weak Lewis acid, in the coexistence of silver perchlorate in diethyl ether to give the corresponding 1,2-*cis* glycoside stereoselectively.^[102] After the above-mentioned combined-catalyst system was reported, the fluorides became widely recognized as useful glycosyl donors. The notable advantage of a glycosyl fluoride as a glycosyl donor is its higher thermal and chemical stability relative to glycosyl chlorides, bromides, and iodides; it is possible to purify glycosyl fluorides by column chromatography on silica gel. Many methods for the preparation of glycosyl fluorides^[105] have been developed by using various fluorinating reagents such as HF^[106] 2-fluoro-1-methylpyridinium tosylate,^[107] diethylaminosulfur trifluoride (DAST),^[108–110] HF/pyridine,^[111–113] CF₃ZnBr/TiF₄,^[114] DEAD/PPh₃/Et₃O·BF₄,^[115] selectfluor,^[116] deoxofluor,^[117] *N,N*-diisopropyl(1-fluoro-2-methyl-1-propenyl)amine,^[118] HF/MeCN/Ac₂O,^[119] AgF,^[120] ZnF₂,^[121] Et₃N/HF,^[122] CF₃ZnBr,^[114] DAST/*N*-bromosuccinimide (NBS)/NIS,^[123,124] 4-methyl(di-fluoroiodo)benzene,^[125] TBAF,^[126] and PhI(OAc)₂/SiF₄.^[127] Of these, DAST, HF/pyridine, and DAST/NBS are most frequently used. Moreover, Lal and co-workers recently developed an attractive nonexplosive reagent, deoxofluor,^[117] which can be used on a kilogram scale.

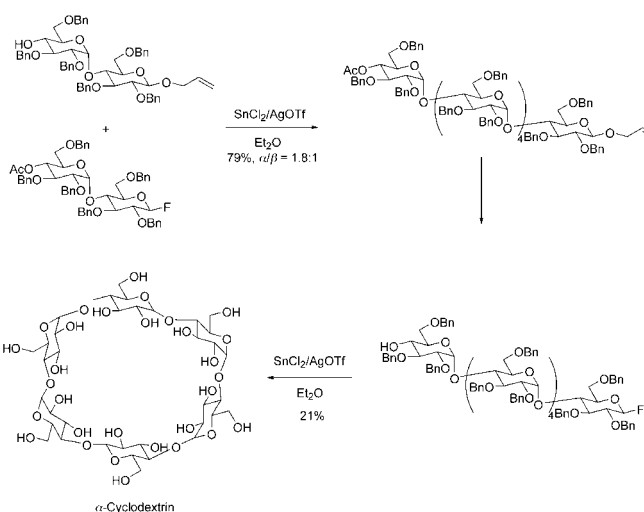
Activating reagents for glycosylations with glycosyl fluoride have been studied intensively and various types of reagents have been developed such as SnCl₂/AgClO₄,^[102] SnCl₂/TiClO₄,^[107] SnCl₂/AgOTf,^[128] SiF₄,^[129] Me₃SiOTf,^[129] BF₃·OEt₂,^[130] TiF₄,^[131] SnF₄,^[131] [Cp₂MCl₂]/AgClO₄ (M = Ti, Zr, Hf; Cp = cyclopentadiene),^[132] [Cp₂ZrCl₂]/AgBF₄,^[133] [Cp₂HfCl₂]/AgOTf,^[133,134] Bu₂Sn(ClO₄)₂,^[135] Me₂GaCl,^[136] Tf₂O,^[137] LiClO₄,^[138] Yb(OTf)₃,^[139] La(ClO₄)₃·*n*H₂O,^[140] La(ClO₄)₃·*n*H₂O/Sn(OTf)₂,^[141] Yb/Amberlyst 15,^[142] sulfated zirconia,^[143] TrB(C₆F₅)₄,^[144,145] TfOH,^[145–147] HClO₄,^[147] HB(C₆F₅)₄,^[147] carbocations (B(C₆F₅)₄⁺ and TfO⁺ salts),^[148] SnCl₂/AgB(C₆F₅)₄,^[149] SnCl₄/AgB(C₆F₅)₄,^[150] Ce(ClO₄)₃.^[151] Our original activator, SnCl₂/AgClO₄, was effectively applied in the synthesis of several types of glycosphingolipids (Scheme 37)^[152,153] and of cyclodextrin (Scheme 38).^[154] Suzuki and co-workers applied their original activators [Cp₂MCl₂]/AgClO₄ (M = Zr, Hf) to the total synthesis of mycinamicin IV (Scheme 39),^[155] and Yamada and Nishizawa employed Me₃SiOTf in their synthesis of baiyunoside (Scheme 40).^[156]

3.2. Effect of Counteranions and Solvents on the Stereoselectivity

Recently, we found that a number of protic acids activated glycosyl fluoride, and that various glycosyl acceptors reacted to form the corresponding disaccharides in good to excellent yields with either high α or β selectivities.^[145–147] According to the concept of hard and soft acids and bases (HSAB),^[157] a proton (H⁺) is considered to be fluorophilic because of its hard character, and the dissociation energy of the H–F bond is higher than those of H–Cl, H–Br, or H–S (H–F: 570 kJ mol^{–1}, H–Cl: 432 kJ mol^{–1}, H–Br: 366 kJ mol^{–1}, H–S: 344 ± 12 kJ mol^{–1}).^[103] In fact, glycosyl fluoride was activated with TfOH, while glycosyl bromide and chloride were not effectively activated by TfOH (Table 8, entries 1–4). Interest-



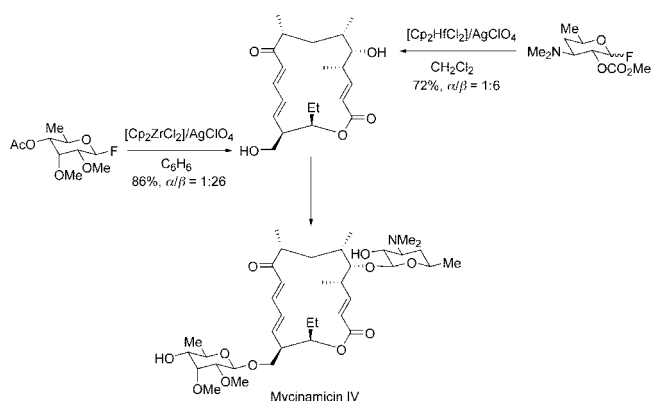
Scheme 37. Total synthesis of the trimeric Le^x glycosphingolipid.



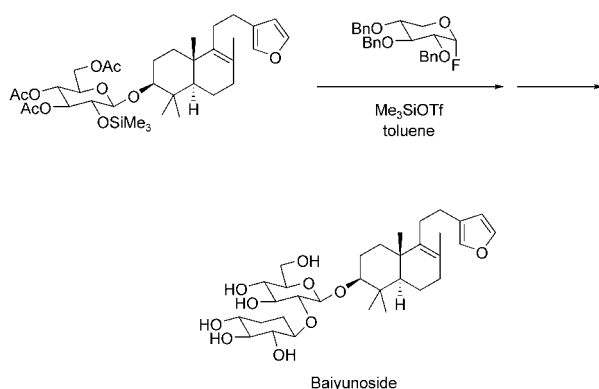
Scheme 38. Total synthesis of α -cyclodextrin.

ingly, a thioglycoside, which is frequently employed in glycosylation, was not activated at all by a TfOH catalyst (entry 8),^[158] which indicated that the chemoselective synthesis of oligo- and polysaccharides should be possible by proper choice of the donor glycosyl fluoride and thioglycoside (see Table 10).

During our study on the protic acid catalyzed glycosylation of glycosyl fluoride we found that the stereochemistry of the resulting glycosides is influenced by the combination of both the catalyst and the solvent. For example, an α -glycoside



Scheme 39. Total synthesis of mycinamicin IV.



Scheme 40. Total synthesis of baiyunoside.

Table 8: Trifluoromethanesulfonic acid catalyzed glycosylation with various glycosyl donors.

Entry	X	Yield [%]	α/β ^[a]
1	F (β)	83	67:33
2	F (α)	87	66:34
3	Br (α)	9	45:55
4	Cl (α)	6	52:48
5	OH (mix) ^[b]	51	73:27
6	OAc (α)	75	68:32
7	OCOOPh (β)	61	72:28
8	SEt (β)	0	—

[a] The α/β ratios were determined by HPLC analysis. [b] $\alpha/\beta = 7:3$.

was obtained as the major product when the glycosylation was carried out in diethyl ether with a catalytic amount of TfOH, HClO₄, or C₄F₉SO₃H (Table 9, entries 1–4). On the other hand, β stereoselectivity was observed when a catalytic amount of HNTf₂, HSbF₆, or HB(C₆F₅)₄ was used in BTF/*t*BuCN (5:1, BTF = benzotrifluoride; Table 9, entries 5–8).

Table 9: Effect of the solvent and the counterion of the protic acid^[a].

Entry	Cat.	Yield [%] (α/β) (Et ₂ O, RT, 4 h)	Yield [%] (α/β) (BTF/ <i>t</i> BuCN (5:1), 0 °C, 2 h)
1	HOTf ^[b]	98 (88:12)	quant. (47:53)
2	HOTf ^[c]	96 (88:12)	99 (49:51)
3	HClO ₄ ^[c]	98 (92:8)	quant. (60:40)
4	HOSO ₂ C ₄ F ₉ ^[d]	99 (88:12)	96 (47:53)
5	HNTf ₂ ^[b]	quant. (49:51)	99 (9:91)
6	HNTf ₂ ^[d]	quant. (50:50)	quant. (9:91)
7	HSbF ₆ ^[d]	99 (56:44)	quant. (12:88)
8	HB(C ₆ F ₅) ₄ ^[e]	95 (55:45)	99 (7:93)

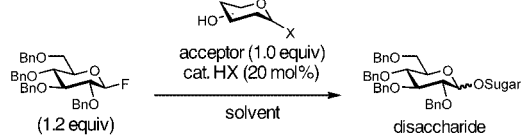
[a] with HBF₄·OMe₂, *p*-toluenesulfonic acid, methanesulfonic acid, or TFA as the catalyst. [b] Commercial substrate. [c] The protic acid was generated from a silver salt and *t*BuCl in toluene and the supernatant was used. [d] The protic acid was generated from a silver salt and *t*BuBr in toluene and the supernatant was used. [e] The protic acid was generated from [AgB(C₆F₅)₄] and *t*BuBr in toluene/Et₂O (1:1) and the supernatant was used.

These observations were very important because they demonstrated that the stereoselectivity of the reaction^[147] is strongly dependent on both the nature of the catalyst counteranion as well as on the solvent and could be varied by careful combination of the catalyst and solvent. This phenomenon is observed in the glycosylation of various glycosyl acceptors (Table 10).

Quite recently, an “armed” glycosyl fluoride was employed as a glycosyl acceptor in the glycosylation of a novel glycosyl donor **57** having a thioformimidate group at an anomeric position. The disaccharide obtained may be used for the next one-pot glycosylation by suitable choice of the reaction conditions (Scheme 41).^[159]

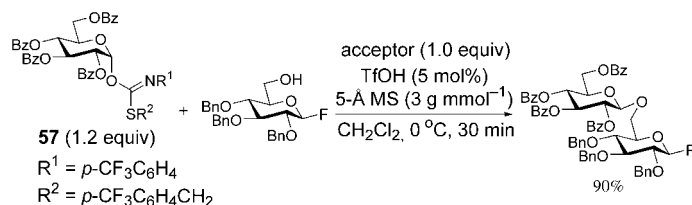
3.3. Total Synthesis of Natural Oligosaccharides by One-Pot Sequential Glycosylation

The one-pot sequential glycosylation strategy was applied to the convergent total synthesis of the F1 α antigen (Scheme 42).^[160] First, glycosyl fluoride **58** was treated with thioglycoside **59** in the presence of a catalytic amount of TfOH to afford disaccharide **60** in situ. The β stereoselectivity of the reaction was controlled by neighboring-group participation of the *p*-MeBz group at the C2 position. Next, the second glycosylation of glycopeptide **61** with this disaccharide **62** was attempted by subsequently adding NIS in a one-pot operation, and fully protected F1 α **62** was obtained stereoselectively in high yield (89 %). Several transformations of the thus obtained trisaccharide **62** gave the F1 α antigen (**63**).^[161,162] Moreover, the one-pot sequential glycosylation method was also applied successfully to the rapid assembly of a branched heptasaccharide (Scheme 43).^[163,164]

Table 10: Protic acid catalyzed stereoselective glycosylation.


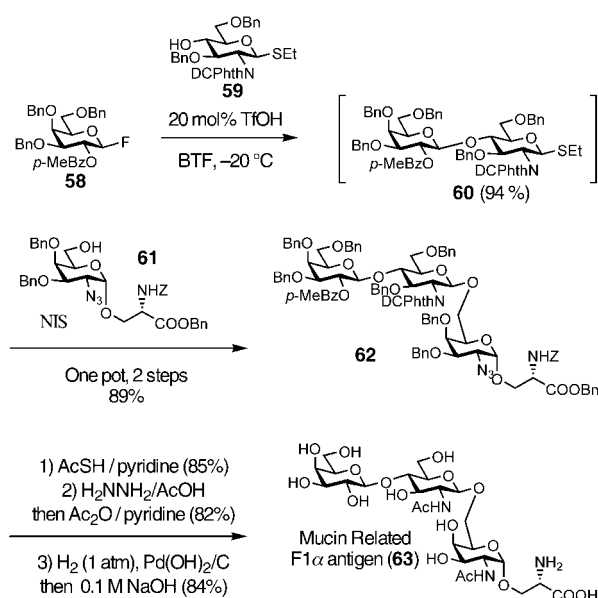
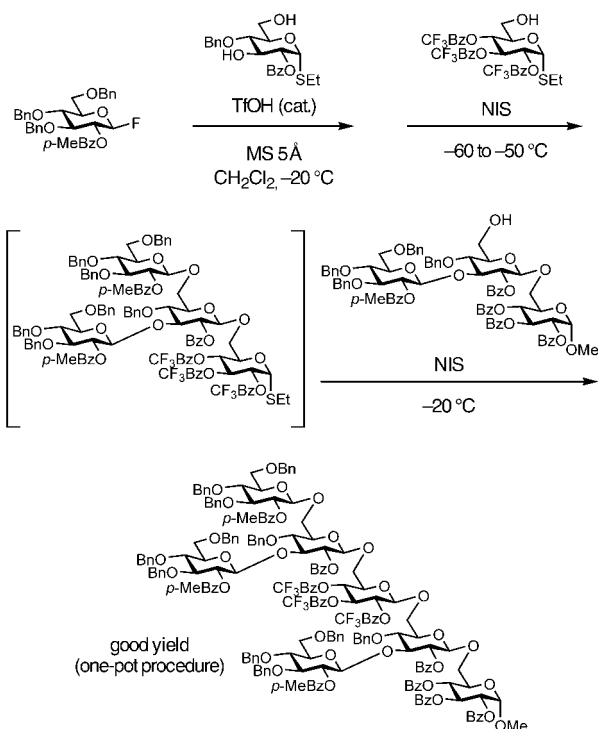
Entry	Acceptor	Additive ^[a]	t [h]	T °C	Yield [%] (α/β) ^[b]
1		TfOH	8	0	95 (89:11)
2		HClO ₄	6	0	94 (93:7)
3		HB(C ₆ F ₅) ₄	6	−20	97 (4:96)
4		TfOH	12	0	97 (84:16)
5		HClO ₄	7	0	89 (88:12)
6		HB(C ₆ F ₅) ₄	11	−20	92 (8:92)
7		TfOH	20	0	88 (81:19)
8		HClO ₄	7	0	95 (83:17)
9		HB(C ₆ F ₅) ₄	11	−20	95 (8:92)
10		TfOH	12	0	quant. (86:14)
11		CHIO ₄	4	0	92 (98:11)
12		HB(C ₆ F ₅) ₄	2	−20	89 (5:95)
13		TfOH	12	0	quant. (80:20)
14		CHIO ₄	6	0	87 (85:15)
15		HB(C ₆ F ₅) ₄	2	−20	87 (5:95)
16		TfOH	2	0	90 (87:13)
17		CHIO ₄	19	0	82 (82:18)
18		HB(C ₆ F ₅) ₄	10.5	−20	78 (15:85)

[a] Glycosylation was carried out in Et₂O when TfOH or HClO₄ was used as the catalyst. The glycosylation was carried out in BTF/tBuCN (5:1) when HB(C₆F₅)₄ was used as the catalyst. [b] The α/β ratios were determined by HPLC analysis.

**Scheme 41.** Glycosylation using glycosyl fluoride as an acceptor.

4. Concluding Remarks

In basic science it is critical to find the first approach (“seeds-oriented” work), but it is equally important to optimize the approach and to develop new systems (“needs oriented”). In either case, ample time and energy need be invested before a chemist can garner anything useful. Once the fundamental target is reached, however, the whole process appears so easy that anyone else could have done it, like the episode of “Columbus’ egg”. However, to win through to the result, a researcher must go through unrewarding months and years of making hypotheses and repeating experiments, and this is exactly what makes a chemist. The most important thing here is “not to imitate others”. If someone has already been involved with the topic, dare not to

**Scheme 42.** Total synthesis of the F1a antigen.**Scheme 43.** One-pot synthesis of a branched heptasaccharide.

stick to the same topic, but find something of your own. This is our code, which should never be forgotten.

Experience and the accumulation of experiences play a very important role in pursuing research work. If a mature hypothesis does not lead you to a satisfactory result, just try once more from the beginning and continue to do the experiments. You will then eventually find an interesting clue, unless you give up half way. Chemistry is still more or less unpredictable. Wisdom learned not from books or what others said but from one’s own experience—which I call

“chemical wisdom”—will become a motivating force for associating problems with questions that give you a different idea. Those who have accumulated a lot of such “chemical wisdom” should be able to formulate a seminal hypothesis by the association of small clues. By overcoming difficulties without compromise, hard and steady work done (especially at the time of one’s youth) will give you love for your work and will furnish you with “chemical wisdom”, and consequently will lead you to successful later development.

The fun of chemistry is in its unexpectedness. There are times when you come to face-to-face with an unexpected phenomenon while carrying out experiments. You simply have to be sufficiently aware and open to accept the seemingly unbelievable. There are still many more valuable ideas remaining to be discovered. The question is how to find them and how to develop them into new possibilities.

The author thanks Dr. Taichi Shintou, Dr. Hidehiko Fujisawa, and Dr. Jun-ichi Matsuo for their contributions to the current research and also in preparing this manuscript. These studies were supported in part by the Grant-in-Aid of the 21st Century COE Program from the Ministry of Education, Culture, Sports, Science, and Technology (MEXT), Japan.

Received: November 24, 2003

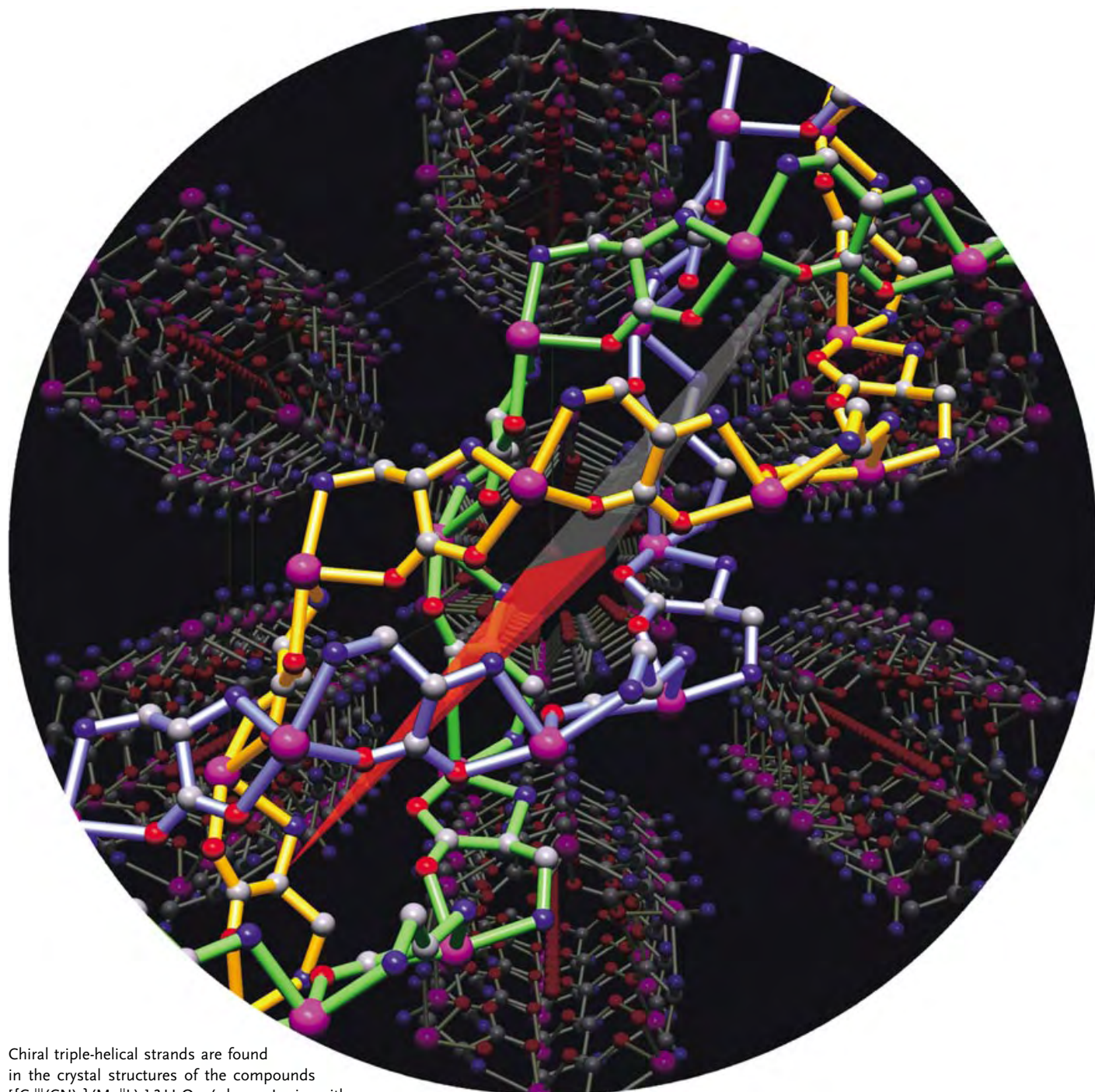
- [1] T. Mukaiyama, I. Kuwajima, Z. Suzuki, *J. Org. Chem.* **1963**, 28, 2024.
- [2] I. Kuwajima, T. Mukaiyama, *J. Org. Chem.* **1964**, 29, 1385.
- [3] a) T. Mukaiyama, R. Matsueda, M. Suzuki, *Tetrahedron Lett.* **1970**, 11, 1901; b) E. J. Corey, K. C. Nicolaou, L. S. Melvin, *J. Am. Chem. Soc.* **1975**, 97, 653; c) E. J. Corey, K. C. Nicolaou, *J. Am. Chem. Soc.* **1974**, 96, 5614; d) E. J. Corey, D. J. Brunelle, P. J. Stork, *Tetrahedron Lett.* **1976**, 17, 3405; e) E. J. Corey, K. C. Nicolaou, L. S. Melvin, *J. Am. Chem. Soc.* **1975**, 97, 654; f) E. J. Corey, P. Ulrich, J. M. Fitzpatrick, *J. Am. Chem. Soc.* **1976**, 98, 222; g) E. J. Corey, K. C. Nicolaou, T. Toru, *J. Am. Chem. Soc.* **1975**, 97, 2287; h) E. J. Corey, S. Bhattacharyya, *Tetrahedron Lett.* **1977**, 18, 3919; i) G. L. Bundy, D. C. Peterson, J. C. Cornette, W. L. Miller, C. H. Spilman, J. W. Wilks, *J. Med. Chem.* **1983**, 26, 1089.
- [4] O. Mitsunobu, M. Yamada, T. Mukaiyama, *Bull. Chem. Soc. Jpn.* **1967**, 40, 935.
- [5] a) O. Mitsunobu, M. Yamada, *Bull. Chem. Soc. Jpn.* **1967**, 40, 2380; b) O. Mitsunobu, M. Eguchi, *Bull. Chem. Soc. Jpn.* **1971**, 44, 3427; c) O. Mitsunobu, *Synthesis* **1981**, 1; d) D. L. Hughes in *Organic Reactions*, Vol. 42 (Ed.: L. A. Paquette), Wiley, New York, **1992**, p. 335; e) R. A. Amos, R. W. Emblidge, N. Havens, *J. Org. Chem.* **1983**, 48, 3598; f) L. D. Arnold, H. I. Assil, J. C. Vederas, *J. Am. Chem. Soc.* **1989**, 111, 3973; g) A. R. Tunoori, D. Dutta, G. I. Georg, *Tetrahedron Lett.* **1998**, 39, 8751; h) A. P. Dobbs, C. M. Johnson, *Tetrahedron Lett.* **2002**, 43, 2807; i) J. A. Dodge, J. I. Trujillo, M. Presnell, *J. Org. Chem.* **1994**, 59, 234; j) S. F. Martin, J. A. Dodge, *Tetrahedron Lett.* **1991**, 32, 3017.
- [6] Y.-J. Shi, D. L. Hughes, J. M. McNamara, *Tetrahedron Lett.* **2003**, 44, 3609.
- [7] a) T. Tsunoda, Y. Yamamiya, S. Ito, *Tetrahedron Lett.* **1993**, 34, 1639; b) T. Tsunoda, F. Ozaki, S. Ito, *Tetrahedron Lett.* **1994**, 35, 5081; c) T. Tsunoda, Y. Yamamiya, Y. Kawamura, S. Ito, *Tetrahedron Lett.* **1995**, 36, 2529; d) S. Ito, *Yakugaku Zasshi* **2001**, 121, 567.
- [8] a) T. Shintou, W. Kikuchi, T. Mukaiyama, *Bull. Chem. Soc. Jpn.* **2003**, 76, 1645; b) T. Mukaiyama, W. Kikuchi, T. Shintou, *Chem. Lett.* **2003**, 32, 300.
- [9] T. Mukaiyama, T. Shintou, K. Fukumoto, *J. Am. Chem. Soc.* **2003**, 125, 10538.
- [10] T. Shintou, T. Mukaiyama, *Chem. Lett.* **2003**, 32, 1100.
- [11] T. Shintou, T. Mukaiyama, *Chem. Lett.* **2003**, 32, 984.
- [12] a) T. Mukaiyama, S. Kobayashi, T. Kumamoto, *Tetrahedron Lett.* **1970**, 11, 5115; b) T. Mukaiyama, S. Kobayashi, K. Kamio, H. Takei, *Chem. Lett.* **1972**, 237; c) T. Kumamoto, S. Kobayashi, T. Mukaiyama, *Bull. Chem. Soc. Jpn.* **1972**, 45, 866.
- [13] a) M. Hudlicky in *Oxidations in Organic Chemistry*, American Chemical Society, Washington DC, **1990**; b) A. H. Hains in *Methods for the Oxidation of Organic Compounds*, Academic Press, New York, **1988**; c) *Organic Synthesis by Oxidation with Metal Compounds* (Eds.: W. J. Mijs, C. R. H. I. de Jonge), Plenum, New York, **1986**; d) R. A. Sheldon, J. K. Kochi in *Metal-Catalysed Oxidations of Organic Compounds*, Academic Press, New York, **1981**; e) W. B. Wiberg in *Oxidation in Organic Chemistry*, Academic Press, New York, **1965**.
- [14] a) G. Cainelli, G. Cardillo in *Chromium Oxidations in Organic Chemistry*, Springer, New York, **1984**; b) S. V. Ley, A. Madin in *Comprehensive Organic Synthesis*, Vol. 7 (Eds.: B. M. Trost, I. Fleming), Pergamon, Oxford, **1991**, p. 251; c) K. Bowden, I. M. Heilbron, E. R. H. Jones, B. C. L. Weedon, *J. Chem. Soc.* **1946**, 39; d) T. G. A. Bowers, Halsall, E. R. H. Jones, A. J. Lemm, *J. Chem. Soc.* **1953**, 2548; e) J. C. Collins, W. W. Hess, F. J. Frank, *Tetrahedron Lett.* **1968**, 9, 3363; f) E. J. Corey, J. W. Suggs, *Tetrahedron Lett.* **1975**, 16, 2647; g) G. Piancatelli, A. Scettri, M. D’Auria, *Synthesis* **1982**, 245; h) E. J. Corey, G. Schmidt, *Tetrahedron Lett.* **1979**, 20, 399; i) S. Czernecki, C. Georgoulis, C. L. Stevens, K. Vijayakumaran, *Tetrahedron Lett.* **1985**, 26, 1699.
- [15] a) A. J. Fatiadi, *Synthesis* **1976**, 65, 133; b) *Encyclopedia of Reagents for Organic Synthesis* (Ed.: L. A. Paquette), Wiley, Chichester, **1995**.
- [16] a) T. V. Lee in *Comprehensive Organic Synthesis*, Vol. 7 (Eds.: B. M. Trost, I. Fleming), Pergamon, Oxford, **1991**, p. 291; b) K. E. Pitzner, J. G. Moffatt, *J. Am. Chem. Soc.* **1965**, 87, 5661–5670; c) J. D. Albright, L. Goldman, *J. Am. Chem. Soc.* **1965**, 87, 4214; d) J. R. Parikh, W. E. Doering, *J. Am. Chem. Soc.* **1967**, 89, 5505; e) K. Omura, A. K. Sharma, D. Swern, *J. Org. Chem.* **1976**, 41, 957; f) W. W. Epstein, F. W. Sweat, *Chem. Rev.* **1967**, 67, 247.
- [17] a) K. Omura, D. Swern, *Tetrahedron* **1978**, 34, 1651; b) A. J. Mancuso, D. Swern, *Synthesis* **1981**, 165; c) T. T. Tidwell, *Synthesis* **1990**, 857; d) T. T. Tidwell, *Organomet. React.* **1990**, 39, 297.
- [18] a) D. B. Dess, J. C. Martin, *J. Org. Chem.* **1983**, 48, 4155; b) D. B. Dess, J. C. Martin, *J. Am. Chem. Soc.* **1991**, 113, 7277; c) S. D. Meyer, S. L. Schreiber, *J. Org. Chem.* **1994**, 59, 7549; d) J. B. Plumb, D. J. Harper, *Chem. Eng. News*, **1990**, 3.
- [19] a) M. Frigerio, M. Santagostino, *Tetrahedron Lett.* **1994**, 35, 8019; b) E. J. Corey, A. Palani, *Tetrahedron Lett.* **1995**, 36, 3485; c) M. Frigerio, M. Santagostino, S. Sputore, G. Palmisano, *J. Org. Chem.* **1995**, 60, 7272; d) S. De Munari, M. Frigerio, M. Santagostino, *J. Org. Chem.* **1996**, 61, 9272.
- [20] T. Mukaiyama, J. Matsuo, M. Yanagisawa, *Chem. Lett.* **2000**, 1072.
- [21] J. Matsuo, D. Iida, K. Tatani, T. Mukaiyama, *Bull. Chem. Soc. Jpn.* **2002**, 75, 223.
- [22] J. Matsuo, A. Kawana, K. Pudhom, T. Mukaiyama, *Chem. Lett.* **2002**, 250.
- [23] J. Matsuo, A. Kawana, H. Yamanaka, H. Kamiyama, *Bull. Chem. Soc. Jpn.* **2003**, 76, 1433.
- [24] T. Mukaiyama, J. Matsuo, D. Iida, H. Kitagawa, *Chem. Lett.* **2001**, 846.

- [25] J. Matsuo, D. Iida, H. Yamanaka, T. Mukaiyama, *Tetrahedron* **2003**, *59*, 6739.
- [26] a) J. Matsuo, Y. Ogawa, K. Pudhom, T. Mukaiyama, *Chem. Lett.* **2004**, *33*, 124; b) I. Shiina, H. Oshiumi, M. Hashizume, Y. Yamai, R. Ibuka, *Tetrahedron Lett.* **2004**, *45*, 543.
- [27] T. Mukaiyama, J. Matsuo, H. Kitagawa, *Chem. Lett.* **2000**, 1250.
- [28] H. J. Reich, J. M. Renga, L. L. Reich, *J. Am. Chem. Soc.* **1975**, *97*, 5434.
- [29] B. M. Trost, T. N. Salzmann, K. Hiroi, *J. Am. Chem. Soc.* **1976**, *98*, 4887.
- [30] Y. Ito, T. Hirao, T. Saegusa, *J. Org. Chem.* **1978**, *43*, 1011.
- [31] K. C. Nicolaou, T. Montagnon, P. S. Baran, Y.-L. Zhong, *J. Am. Chem. Soc.* **2002**, *124*, 2245.
- [32] M. Ishizaki, Y. Niimi, O. Hoshino, *Tetrahedron Lett.* **2003**, *44*, 6029.
- [33] Reviews: a) R. W. Layer, *Chem. Rev.* **1963**, *63*, 489; b) S. Dayagi, Y. Degani in *The Chemistry of the Carbon-Nitrogen Double Bond* (Ed.: S. Patai), Wiley, New York, **1970**.
- [34] a) G. A. Kraus, A. Melekhov, *Tetrahedron* **1998**, *54*, 11 749; b) P. Müller, D. M. Gilbert, *Tetrahedron* **1988**, *44*, 7171; c) M. Ochiai, M. Inenaga, Y. Nagao, R. M. Moriarty, R. K. Vaid, M. P. Duncan, *Tetrahedron Lett.* **1988**, *29*, 6917; d) F. Porta, C. Crotti, S. Cenini, G. Palmisano, *J. Mol. Catal.* **1989**, *50*, 333; e) J. Larsen, K. A. Jørgensen, *J. Chem. Soc. Perkin Trans. 2* **1992**, 1213; f) M. Ochiai, D. Kajishima, T. Sueda, *Heterocycles* **1997**, *46*, 71.
- [35] D. H. R. Barton, A. Billion, J. Boivin, *Tetrahedron Lett.* **1985**, *26*, 1229.
- [36] E. F. Pratt, T. P. McGovern, *J. Org. Chem.* **1964**, *29*, 1540.
- [37] a) J. A. Franz, J. C. Martin, *J. Am. Chem. Soc.* **1975**, *97*, 583; b) J. P. Marino, R. D. Larsen, Jr., *J. Am. Chem. Soc.* **1981**, *103*, 4642; c) J. J. Cornejo, K. D. Larson, G. D. Mendenhall, *J. Org. Chem.* **1985**, *50*, 5382; d) J. Yamaguchi, T. Takeda, *Chem. Lett.* **1992**, 1933; e) P. A. Wehrli, B. Schaer, *Synthesis* **1974**, 288; f) R. I. Fryer, G. A. Archer, B. Brust, W. Zally, L. H. Sternbach, *J. Org. Chem.* **1965**, *30*, 1308; g) R. Bonnett, V. M. Clark, A. Giddey, A. Todd, *J. Chem. Soc.* **1959**, 2087; h) M. F. Grundon, B. E. Reynolds, *J. Chem. Soc.* **1964**, 2445.
- [38] a) S.-I. Murahashi, T. Naota, H. Taki, *J. Chem. Soc. Chem. Commun.* **1985**, 613; b) S.-I. Murahashi, *Pure Appl. Chem.* **1992**, *64*, 403; c) A. Goti, M. Romani, *Tetrahedron Lett.* **1994**, *35*, 6567.
- [39] a) A. Nishinaga, S. Yamazaki, T. Matsuura, *Tetrahedron Lett.* **1988**, *29*, 4115; b) K. Maruyama, T. Kusakawa, Y. Higuchi, A. Nishinaga, *Chem. Lett.* **1991**, 1093.
- [40] S. Yamazaki, *Chem. Lett.* **1992**, 823.
- [41] T. Mukaiyama, A. Kawana, Y. Fukuda, J. Matsuo, *Chem. Lett.* **2001**, 390.
- [42] Review: R. J. Baumgarten, *J. Chem. Educ.* **1966**, *43*, 398; see also: R. V. Hoffman, A. Kumar, *J. Org. Chem.* **1984**, *49*, 4011, and references therein.
- [43] J. Matsuo, A. Kawana, Y. Fukuda, T. Mukaiyama, *Chem. Lett.* **2001**, 712.
- [44] For direct oxidation of secondary amines to the corresponding nitrones, see: a) H. Mitsui, S. Zenki, T. Shiota, S.-I. Murahashi, *J. Chem. Soc. Chem. Commun.* **1984**, 874; b) S.-I. Murahashi, H. Mitsui, T. Shiota, T. Tsuda, S. Watanabe, *J. Org. Chem.* **1990**, *55*, 1736; c) S.-I. Murahashi, T. Shiota, Y. Imada, *Org. Synth.* **1991**, *70*, 265; d) S. Yamazaki, *Bull. Chem. Soc. Jpn.* **1997**, *70*, 877; e) W. W. Zajac, Jr., T. R. Walters, M. G. Darcy, *J. Org. Chem.* **1988**, *53*, 5856; f) R. W. Murray, M. Singh, *J. Org. Chem.* **1990**, *55*, 2954; g) S. Cicchi, M. Corsi, A. Goti, *J. Org. Chem.* **1999**, *64*, 7243.
- [45] J. Matsuo, T. Shibata, H. Kitagawa, T. Mukaiyama, *Arch. Org. Chem.* **2001**, 58.
- [46] T. Mukaiyama, K. Inomata, *Bull. Chem. Soc. Jpn.* **1971**, *44*, 3215; the mechanism reported in this paper was corrected.^[47]
- [47] a) T. Mukaiyama, K. Inomata, M. Muraki, *J. Am. Chem. Soc.* **1973**, *95*, 967; b) K. Inomata, M. Muraki, T. Mukaiyama, *Bull. Chem. Soc. Jpn.* **1973**, *46*, 1807.
- [48] a) T. Mukaiyama, K. Narasaka, K. Banno, *Chem. Lett.* **1973**, 1011; b) T. Mukaiyama, K. Banno, K. Narasaka, *J. Am. Chem. Soc.* **1974**, *96*, 7503.
- [49] N. Iwasawa, T. Mukaiyama, *Chem. Lett.* **1982**, 1441.
- [50] Review: a) T. Mukaiyama, *Org. React.* **1982**, *28*, 203; b) C. J. Cowden, I. Paterson, *Org. React.* **1997**, *51*, 1; c) B. M. Kim, S. F. Williams, S. Masamune in *Comprehensive Organic Synthesis* (Eds.: B. M. Trost), Pergamon, London, **1991**; d) D. A. Evans, J. V. Nelson, T. R. Taber, *Top. Stereochem.* **1982**, *13*, 1.
- [51] From α -iodoketones and Et₃B: Y. Aoki, K. Oshima, K. Utimoto, *Chem. Lett.* **1995**, 463.
- [52] From α -iodoketones with 9-BBN and 2,6-lutidine; a) T. Mukaiyama, S. Imachi, K. Yamane, M. Mizuta, *Chem. Lett.* **2002**, 698; b) T. Mukaiyama, T. Takuwa, K. Yamane, S. Imachi, *Bull. Chem. Soc. Jpn.* **2003**, *76*, 813; interestingly, some boron enolates were isolated by distillation, see: R. W. Hoffmann, K. Ditrich, S. Froech, *Tetrahedron* **1985**, *41*, 5517.
- [53] a) T. Mukaiyama, T. Inoue, *Chem. Lett.* **1976**, 559; b) T. Inoue, T. Uchimar, T. Mukaiyama, *Chem. Lett.* **1977**, 153; c) T. Inoue, T. Mukaiyama, *Bull. Chem. Soc. Jpn.* **1980**, *53*, 174.
- [54] T. Jyojima, N. Miyamoto, M. Katohno, M. Nakata, S. Matsu-mura, K. Tushima, *Tetrahedron Lett.* **1998**, *39*, 6007.
- [55] a) F. Yokokawa, T. Shioiri, *J. Org. Chem.* **1998**, *63*, 8638; b) F. Yokokawa, H. Fujiwara, T. Shioiri, *Tetrahedron Lett.* **1999**, *40*, 1915.
- [56] These phenomena had already been experienced in former research into the development of new reactions, such as new-type 1,4-addition polymerization: a) T. Mukaiyama, T. Hyugaji, *Bull. Chem. Soc. Jpn.* **1962**, *35*, 687; b) T. Mukaiyama, T. Fujisawa, H. Nohira, T. Hyugaji, *J. Org. Chem.* **1962**, *27*, 3337; c) T. Mukaiyama, T. Fujisawa, *Macromol. Synth.* **1972**, *4*, 105; d) T. Fujisawa, Y. Tamura, T. Mukaiyama, *Bull. Chem. Soc. Jpn.* **1964**, *37*, 793; e) H. Nohira, Y. Nishikawa, T. Mukaiyama, *Bull. Chem. Soc. Jpn.* **1964**, *37*, 797; f) T. Mukaiyama, K. Sato, *Bull. Chem. Soc. Jpn.* **1963**, *36*, 99.
- [57] T. Mukaiyama, *Angew. Chem.* **1977**, *89*, 858; *Angew. Chem. Int. Ed. Engl.* **1977**, *16*, 817.
- [58] P. Brownbridge, *Synthesis* **1983**, *1*, 85.
- [59] a) O. Isler, P. Schudel, *Adv. Org. Chem.* **1963**, *14*, 115; b) F. Effenberger, *Angew. Chem.* **1969**, *81*, 374; *Angew. Chem. Int. Ed. Engl.* **1969**, *8*, 295.
- [60] a) K. Banno, T. Mukaiyama, *Chem. Lett.* **1975**, 741; b) K. Banno, T. Mukaiyama, *Bull. Chem. Soc. Jpn.* **1976**, *49*, 2284.
- [61] a) T. H. Chan, T. Aida, P. W. K. Lau, V. Gorys, D. N. Harpp, *Tetrahedron Lett.* **1979**, *20*, 4029; b) J.-E. Dubois, G. Axiotis, E. Bertounesque, *Tetrahedron Lett.* **1984**, *25*, 4655; c) C. H. Heathcock, K. T. Hug, L. A. Flippin, *Tetrahedron Lett.* **1984**, *25*, 5973; d) C. Gennari, M. G. Beretta, A. Bernardi, G. Moro, C. Scolastico, R. Todeschini, *Tetrahedron* **1986**, *42*, 893.
- [62] T. Mukaiyama, M. Hayashi, *Chem. Lett.* **1974**, 15.
- [63] T. Mukaiyama, A. Ishida, *Chem. Lett.* **1975**, 319.
- [64] T. Mukaiyama, A. Ishida, *Chem. Lett.* **1975**, 1201.
- [65] K. Saigo, M. Osaki, T. Mukaiyama, *Chem. Lett.* **1975**, 989.
- [66] K. Saigo, M. Osaki, T. Mukaiyama, *Chem. Lett.* **1976**, 769.
- [67] a) K. Narasaka, K. Soai, T. Mukaiyama, *Chem. Lett.* **1974**, 1223; b) K. Narasaka, K. Soai, Y. Aikawa, T. Mukaiyama, *Bull. Chem. Soc. Jpn.* **1976**, *49*, 779; c) K. Saigo, M. Osaki, T. Mukaiyama, *Chem. Lett.* **1976**, 163; d) S. Danishefsky, K. Vaughan, R. C. Gadwood, K. Tsuzuki, *J. Am. Chem. Soc.* **1980**, *102*, 4262; e) M. E. Jung, Y.-G. Pan, *Tetrahedron Lett.* **1980**, *21*, 3127; f) M. E. Jung, C. A. McCombs, Y. Takeda, Y.-G. Pan, *J. Am. Chem. Soc.* **1981**, *103*, 6677; g) C. H. Heathcock, M. H. Norman, D. E. Uehling, *J. Am. Chem. Soc.* **1985**, *107*, 2797.

- [68] a) H. Ishitani, M. Ueno, S. Kobayashi, *J. Am. Chem. Soc.* **1997**, *119*, 7153; b) S. Kobayashi, H. Ishitani, M. Ueno, *J. Am. Chem. Soc.* **1998**, *120*, 431; c) H. Ishitani, M. Ueno, S. Kobayashi, *J. Am. Chem. Soc.* **2000**, *122*, 8180, and references therein.
- [69] Examples are [4+2] cycloaddition reactions, alkylations, acylations, hydroborations, oxidative processes, etc.
- [70] a) T. Mukaiyama, S. Kobayashi, M. Murakami, *Chem. Lett.* **1985**, 447; b) S. Kobayashi, M. Murakami, T. Mukaiyama, *Chem. Lett.* **1985**, 1535.
- [71] M. Ohshima, M. Murakami, T. Mukaiyama, *Chem. Lett.* **1985**, 1871.
- [72] N. Iwasawa, T. Mukaiyama, *Chem. Lett.* **1987**, 463.
- [73] H. Fujisawa, Y. Sasaki, T. Mukaiyama, *Chem. Lett.* **2001**, 190.
- [74] Magnesium halide mediated aldol reactions: a) K. Takai, C. H. Heathcock, *J. Org. Chem.* **1985**, *50*, 3247; b) J. Uenishi, H. Tomozane, M. Yamato, *Tetrahedron Lett.* **1985**, *26*, 3467; c) A. Bernardi, S. Cardani, L. Colonbo, G. Poli, G. Schimperna, C. Scolastico, *J. Org. Chem.* **1987**, *52*, 888; d) E. J. Corey, W. Li, G. A. Reichard, *J. Am. Chem. Soc.* **1998**, *120*, 2330.
- [75] a) T. Mukaiyama, I. Shiina, H. Iwadare, H. Sakoh, Y. Tani, M. Hasagawa, K. Saitou, *Proc. Jpn. Acad. B* **1997**, *73*, 95; b) T. Mukaiyama, I. Shiina, H. Iwadare, M. Saitoh, T. Nishimura, N. Ohkawa, H. Sakoh, K. Nishimura, Y. Tani, M. Hasegawa, K. Yamada, K. Saitoh, *Chem. Eur. J.* **1999**, *5*, 121; c) I. Shiina, J. Shibata, R. Ibuka, Y. Imai, T. Mukaiyama, *Bull. Chem. Soc. Jpn.* **2001**, *74*, 113.
- [76] M. Oikawa, T. Ueno, H. Oikawa, and A. Ichihara, *J. Org. Chem.* **1995**, *60*, 5048.
- [77] D. A. Evans, A. S. Kim, R. Metternich, V. J. Novack, *J. Am. Chem. Soc.* **1998**, *120*, 5921.
- [78] H. Sato, S. Nakamura, N. Watanabe, S. Hashimoto, *Synlett*, **1997**, 451.
- [79] Y. Kim, R. A. Singer, E. M. Carreira, *Angew. Chem.* **1998**, *110*, 1321; *Angew. Chem. Int. Ed.* **1998**, *37*, 1261.
- [80] Review: a) E. M. Carreira in *Comprehensive Asymmetric Catalysis*, Vol. 3 (Eds.: E. N. Jacobsen, A. Pfaltz, H. Yamamoto), Springer, Heidelberg, **1999**, p. 998; b) R. Mahrwald, *Chem. Rev.* **1999**, *99*, 1095; c) H. Gröger, E. M. Vogl, M. Shibasaki, *Chem. Eur. J.* **1998**, *4*, 1137; d) S. G. Nelson, *Tetrahedron: Asymmetry* **1998**, *9*, 357; e) T. Bach, *Angew. Chem.* **1994**, *10*, 433; *Angew. Chem. Int. Ed. Engl.* **1994**, *33*, 417.
- [81] The highest priority in regard to the enolate substituents is assigned to the OSiR₃ group.
- [82] S. Kobayashi, T. Mukaiyama, *Chem. Lett.* **1989**, 297.
- [83] S. Kobayashi, H. Uchiro, Y. Fujishita, I. Shiina, T. Mukaiyama, *J. Am. Chem. Soc.* **1991**, *113*, 4247.
- [84] T. Mukaiyama, S. Kobayashi, *J. Organomet. Chem.* **1990**, *382*, 39.
- [85] T. Mukaiyama, H. Uchiro, I. Shiina, S. Kobayashi, *Chem. Lett.* **1990**, 1019.
- [86] T. Mukaiyama, I. Shiina, S. Kobayashi, *Chem. Lett.* **1991**, 1902.
- [87] a) S. Kobayashi, S. Onozawa, T. Mukaiyama, *Chem. Lett.* **1992**, 2419; b) T. Mukaiyama, H. Anan, I. Shiina, S. Kobayashi, *Bull. Soc. Chim. Fr.* **1993**, *130*, 388; c) T. Mukaiyama, I. Shiina, S. Kobayashi, *Chem. Lett.* **1990**, 2201.
- [88] T. Mukaiyama, S. Kobayashi, H. Uchiro, I. Shiina, *Chem. Lett.* **1990**, 129.
- [89] S. Kobayashi, Y. Fujishita, T. Mukaiyama, *Chem. Lett.* **1990**, 1455.
- [90] a) K. Furuta, T. Maruyama, H. Yamamoto, *J. Am. Chem. Soc.* **1991**, *113*, 1041; b) E. R. Parmee, O. Tempkin, S. Masamune, A. Abiko, *J. Am. Chem. Soc.* **1991**, *113*, 9365; c) K. Furuta, T. Maruyama, H. Yamamoto, *Synlett* **1991**, 439; d) S. Kiyooka, Y. Kaneko, K. Kume, *Tetrahedron Lett.* **1992**, *33*, 4927.
- [91] a) K. Mikami, M. Matsukawa, *J. Am. Chem. Soc.* **1994**, *116*, 4077; b) K. Mikami, M. Matsukawa, *J. Am. Chem. Soc.* **1993**, *115*, 7039; c) K. Mikami, *Pure Appl. Chem.* **1996**, *68*, 639; d) G. E. Keck, D. Krishnamurthy, *J. Am. Chem. Soc.* **1995**, *117*, 2363; e) E. M. Carreira, R. A. Singer, W. Lee, *J. Am. Chem. Soc.* **1994**, *116*, 8837; f) R. A. Singer, E. M. Carreira, *J. Am. Chem. Soc.* **1995**, *117*, 12360; g) E. M. Carreira, R. A. Singer, W. Lee, *J. Am. Chem. Soc.* **1995**, *117*, 3649.
- [92] H. Ishitani, H. Yamashita, H. Shimizu, S. Kobayashi, *J. Am. Chem. Soc.* **2000**, *122*, 5403.
- [93] a) D. A. Evans, J. A. Murry, M. C. Kozlowski, *J. Am. Chem. Soc.* **1996**, *118*, 5814; b) D. A. Evans, M. C. Kozlowski, J. S. Tedrow, *Tetrahedron Lett.* **1997**, *38*, 7481; c) D. A. Evans, M. C. Kozlowski, C. S. Burgey, D. W. C. MacMillan, *J. Am. Chem. Soc.* **1997**, *119*, 7893; d) D. A. Evans, D. W. C. MacMillan, K. R. Campos, *J. Am. Chem. Soc.* **1997**, *119*, 10859.
- [94] a) M. Sodeoka, K. Ohrai, M. Shibasaki, *J. Org. Chem.* **1995**, *60*, 2648; b) M. Sodeoka, R. Tokunoh, F. Miyazaki, E. Hagiwara, M. Shibasaki, *Synlett* **1997**, 463.
- [95] S. E. Denmark, R. A. Stavenger, *Acc. Chem. Res.* **2000**, *33*, 432.
- [96] K. Miura, T. Nakagawa, A. Hosomi, *J. Am. Chem. Soc.* **2002**, *124*, 536.
- [97] a) H. Fujisawa, T. Mukaiyama, *Chem. Lett.* **2002**, 182; b) H. Fujisawa, T. Mukaiyama, *Chem. Lett.* **2002**, 858; c) T. Mukaiyama, H. Fujisawa, T. Nakagawa, *Helv. Chim. Acta* **2002**, *85*, 4518; d) T. Nakagawa, H. Fujisawa, T. Mukaiyama, *Chem. Lett.* **2003**, *32*, 462; e) T. Nakagawa, H. Fujisawa, T. Mukaiyama, *Chem. Lett.* **2003**, *32*, 696.
- [98] a) F. G. Bordwell, *Acc. Chem. Res.* **1988**, *21*, 456; b) F. G. Bordwell, J. C. Branca, D. L. Hughes, W. N. Olmstead, *J. Org. Chem.* **1980**, *45*, 3305.
- [99] S. Kobayashi, K. Manabe, *Acc. Chem. Res.* **2002**, *35*, 209, and references therein.
- [100] W. Koenigs, E. Knorr, *Ber. Dtsch. Chem. Ges.* **1901**, *34*, 957.
- [101] a) H. Paulsen, *Angew. Chem.* **1982**, *94*, 184; *Angew. Chem. Int. Ed. Engl.* **1982**, *21*, 155; b) R. R. Schmidt, *Angew. Chem.* **1986**, *98*, 213; *Angew. Chem. Int. Ed. Engl.* **1986**, *25*, 212; c) H. Kunz, *Angew. Chem.* **1987**, *99*, 297; *Angew. Chem. Int. Ed. Engl.* **1987**, *26*, 294; d) P. Sinaÿ, *Pure Appl. Chem.* **1991**, *63*, 519; e) K. Suzuki, T. Nagasawa, *J. Synth. Org. Chem. Jpn.* **1992**, *50*, 378; f) K. Toshima, K. Tatsuta, *Chem. Rev.* **1993**, *93*, 1503; g) B. Ernst, G. W. Hart, P. Sinaÿ in *Carbohydrate in Chemistry and Biology Part 1*, Wiley-VCH, Weinheim, **2000**.
- [102] T. Mukaiyama, Y. Murai, and S. Shoda, *Chem. Lett.* **1981**, 431.
- [103] J. A. Kerr, *CRC Hand Book of Chemistry and Physics*, 72nd Edition, CRC, Boca Raton, FL, **1991**, p. 9(105).
- [104] T. Mukaiyama, S. Shoda, Y. Watanabe, *Chem. Lett.* **1977**, 383.
- [105] a) M. Shimizu, H. Togo, M. Yokoyama, *Synthesis* **1998**, 799; b) M. Yokoyama, *Carbohydr. Res.* **2000**, *327*, 5; c) K. Toshima, *Carbohydr. Res.* **2000**, *327*, 15.
- [106] D. H. Brauns, *J. Am. Chem. Soc.* **1923**, *45*, 833.
- [107] T. Mukaiyama, Y. Hashimoto, S. Shoda, *Chem. Lett.* **1983**, 935.
- [108] a) W. Rosenbrook, Jr., D. A. Riley, P. A. Lartey, *Tetrahedron Lett.* **1985**, *26*, 3; b) G. H. Posner, S. R. Haines, *Tetrahedron Lett.* **1985**, *26*, 5.
- [109] K. C. Nicolaou, T. Ladduwahetty, J. L. Randal, A. Chucholowski, *J. Am. Chem. Soc.* **1986**, *108*, 2466.
- [110] I. Cumpste, A. J. Fairbanks, A. J. Redgrave, *Org. Lett.* **2001**, *3*, 2371.
- [111] a) M. Hayashi, S. Hashimoto, R. Noyori, *Chem. Lett.* **1984**, 1747; b) W. A. Szarek, G. Grynkiewicz, B. Doboszewski, G. W. Hay, *Chem. Lett.* **1984**, 1751.
- [112] a) W. Bröder, H. Kunz, *Synlett* **1990**, 251; b) W. Bröder, H. Kunz, *Carbohydr. Res.* **1993**, *249*, 221.
- [113] M. Palme, A. Vasella, *Helv. Chim. Acta* **1995**, *78*, 959.
- [114] R. Miethchen, C. Hager, M. Hein, *Synthesis* **1997**, 159.
- [115] H. Kunz, W. Sanger, *Helv. Chim. Acta* **1985**, *68*, 283.
- [116] M. D. Burkart, Z. Zhang, S.-C. Hung, C.-H. Wong, *J. Am. Chem. Soc.* **1997**, *119*, 11743.

- [117] G. S. Lal, G. P. Pez, R. J. Pesaresi, F. M. Prozonc, H. Cheng, *J. Org. Chem.* **1999**, 64, 7048.
- [118] B. Ernst, T. Winkler, *Tetrahedron Lett.* **1989**, 30, 3081.
- [119] a) R. Miethchen, T. Gabriel, G. Kolp, *Synthesis* **1991**, 885; b) R. Miethchen, D. Rentsch, *Synthesis* **1994**, 827; c) R. Miethchen, T. Gabriel, *Chem. Ber.* **1993**, 126, 2309; d) R. Miethchen, T. Gabriel, *J. Fluorine Chem.* **1994**, 67, 11.
- [120] a) T. Kondo, T. Tomoo, H. Abe, M. Isobe, T. Goto, *Chem. Lett.* **1996**, 337; b) M. Teichmann, G. Descotes, D. Lafont, *Synthesis* **1993**, 889; c) F. W. Lichtenthaler, U. Kläres, M. Lergenmüller, S. Schwidetzky, *Synthesis* **1992**, 179.
- [121] K. D. Goggin, J. F. Lambert, S. W. Walinsky, *Synlett* **1994**, 162.
- [122] R. Miethchen, G. Kolp, *J. Fluorine Chem.* **1993**, 60, 49.
- [123] K. C. Nicolaou, R. E. Dolle, D. P. Papahatjis, J. L. Randall, *J. Am. Chem. Soc.* **1984**, 106, 4189.
- [124] G. Horne, W. Mackie, *Tetrahedron Lett.* **1999**, 40, 8697.
- [125] a) S. Caddick, W. B. Motherwell, J. A. Wilkinson, *J. Chem. Soc. Chem. Commun.* **1991**, 674; b) S. Caddick, L. Gazzard, W. B. Motherwell, J. A. Wilkinson, *Tetrahedron* **1996**, 52, 149.
- [126] D. M. Gordon, S. J. Danishefsky, *Carbohydr. Res.* **1990**, 206, 361.
- [127] M. Shimizu, Y. Nakahara, H. Yoshioka, *J. Fluorine Chem.* **1999**, 97, 57.
- [128] a) T. Ogawa, Y. Takahashi, *Carbohydr. Res.* **1985**, 138, C5; b) Y. Takahashi, T. Ogawa, *Carbohydr. Res.* **1987**, 164, 277.
- [129] S. Hashimoto, M. Hayashi, R. Noyori, *Tetrahedron Lett.* **1984**, 25, 1379.
- [130] a) K. C. Nicolaou, A. Chucholowski, R. E. Dolle, J. L. Randall, *J. Chem. Soc. Chem. Commun.* **1984**, 1155; b) H. Kunz, H. Waldmann, *J. Chem. Soc. Chem. Commun.* **1985**, 638; c) H. Kunz, W. Sager, *Helv. Chim. Acta* **1985**, 68, 283; d) M. Yamaguchi, A. Horiguchi, A. Fukuda, T. Minami, *J. Chem. Soc. Chem. Commun.* **1990**, 1079.
- [131] a) M. Kreuzer, J. Thiem, *Carbohydr. Res.* **1986**, 149, 347; b) J. Jünemann, I. Lundt, J. Thiem, *Liebigs Ann. Chem.* **1991**, 759.
- [132] a) T. Matsumoto, H. Maeta, K. Suzuki, G. Tsuchihashi, *Tetrahedron Lett.* **1988**, 29, 3567, 3571, 3575; b) K. Suzuki, H. Maeta, T. Matsumoto, *Tetrahedron Lett.* **1989**, 30, 4853; c) K. Suzuki, T. Matsumoto, *J. Synth. Org. Chem. Jpn.* **1993**, 51, 718.
- [133] K. Suzuki, H. Maeta, T. Suzuki, T. Matsumoto, *Tetrahedron Lett.* **1989**, 30, 6879.
- [134] a) K. C. Nicolaou, T. J. Caulfield, H. Kataoka, N. A. Stylianides, *J. Am. Chem. Soc.* **1990**, 112, 3693; b) K. C. Nicolaou, C. W. Hummel, Y. Iwabuchi, *J. Am. Chem. Soc.* **1992**, 114, 3126; c) Y. Matsuzaki, Y. Ito, Y. Nakahara, T. Ogawa, *Tetrahedron Lett.* **1993**, 34, 1061.
- [135] H. Maeta, T. Matsumoto, K. Suzuki, *Carbohydr. Res.* **1993**, 249, 49.
- [136] S. Kobayashi, K. Koide, M. Ohno, *Tetrahedron Lett.* **1990**, 31, 2435.
- [137] a) H. P. Wessel, *Tetrahedron Lett.* **1990**, 31, 6863; b) H. P. Wessel, N. Ruiz, *J. Carbohydr. Chem.* **1991**, 10, 901.
- [138] a) G. Böhm, H. Waldmann, *Tetrahedron Lett.* **1995**, 36, 3843; b) G. Böhm, H. Waldmann, *Liebigs Ann. Chem.* **1996**, 613; c) G. Böhm, H. Waldmann, *Liebigs Ann. Chem.* **1996**, 621.
- [139] S. Hosono, W.-S. Kim, H. Sasai, M. Shibasaki, *J. Org. Chem.* **1995**, 60, 4.
- [140] W.-S. Kim, S. Hosono, H. Sasai, M. Shibasaki, *Tetrahedron Lett.* **1995**, 36, 4443.
- [141] W.-S. Kim, H. Sasai, M. Shibasaki, *Tetrahedron Lett.* **1996**, 37, 7797.
- [142] L. Yu, D. Chen, J. Li, P. G. Wang, *J. Org. Chem.* **1997**, 62, 3575.
- [143] a) K. Toshima, K. Kasumi, S. Matsumura, *Synlett* **1998**, 643; b) K. Toshima, K. Kasumi, S. Matsumura, *Synlett* **1999**, 813.
- [144] K. Takeuchi, T. Mukaiyama, *Chem. Lett.* **1998**, 555.
- [145] T. Mukaiyama, K. Takeuchi, H. Jona, H. Maeshima, T. Saitoh, *Helv. Chim. Acta* **2000**, 83, 1901.
- [146] a) T. Mukaiyama, H. Jona, K. Takeuchi, *Chem. Lett.* **2000**, 696; b) H. Jona, K. Takeuchi, T. Mukaiyama, *Chem. Lett.* **2000**, 1278.
- [147] a) H. Jona, H. Mandai, T. Mukaiyama, *Chem. Lett.* **2001**, 426; b) H. Jona, H. Mandai, W. Chavasiri, K. Takeuchi, T. Mukaiyama, *Bull. Chem. Soc. Jpn.* **2002**, 75, 291.
- [148] M. Yanagisawa, T. Mukaiyama, *Chem. Lett.* **2001**, 224.
- [149] T. Mukaiyama, H. Maeshima, H. Jona, *Chem. Lett.* **2001**, 388.
- [150] H. Jona, H. Maeshima, T. Mukaiyama, *Chem. Lett.* **2001**, 726.
- [151] G. K. Packard, S. D. Rychnovsky, *Org. Lett.* **2001**, 3, 3393.
- [152] a) K. C. Nicolaou, T. J. Caulfield, H. Kataoka, N. A. Stylianides, *J. Am. Chem. Soc.* **1990**, 112, 3693; b) K. C. Nicolaou, C. W. Hummel, Y. Iwabuchi, *J. Am. Chem. Soc.* **1992**, 114, 3126.
- [153] a) K. C. Nicolaou, T. Caulfield, H. Kataoka, T. Kumazawa, *J. Am. Chem. Soc.* **1988**, 110, 7910; b) K. C. Nicolaou, T. J. Caulfield, H. Kataoka, *Carbohydr. Res.* **1990**, 202, 177.
- [154] a) T. Ogawa, Y. Takahashi, *Carbohydr. Res.* **1985**, 138, C5; b) Y. Takahashi, T. Ogawa, *Carbohydr. Res.* **1987**, 164, 277.
- [155] T. Matsumoto, H. Maeta, K. Suzuki, G. Tsuchihashi, *Tetrahedron Lett.* **1988**, 29, 3575.
- [156] a) H. Yamada, M. Nishizawa, *Tetrahedron Lett.* **1987**, 28, 4315; b) H. Yamada, M. Nishizawa, *Tetrahedron* **1992**, 48, 3021.
- [157] a) R. G. Pearson, *J. Am. Chem. Soc.* **1963**, 85, 3533; b) K. Akiba, N. Inamoto, *J. Synth. Org. Chem. Jpn.* **1975**, 33, 834.
- [158] O. Kanie, Y. Ito, T. Ogawa, *J. Am. Chem. Soc.* **1994**, 116, 12073.
- [159] H. Chiba, S. Funasaka, T. Mukaiyama, *Bull. Chem. Soc. Jpn.* **2003**, 76, 1629.
- [160] a) Y. Yamashita, Y. S. Chung, T. Sawada, R. Horie, T. Saito, K. Murayama, R. Kannagi, M. Sowa, *Oncology* **1998**, 55, 70; b) Y. Yamashita, Y. S. Chung, R. Horie, R. Kannagi, M. Sowa, *J. Natl. Cancer Inst.* **1995**, 87, 441; c) Y. Yamashita, Y. S. Chung, T. Sawada, Y. Kondo, K. Hirayama, A. Inui, B. Nakata, M. Okuno, R. Horie, T. Saito, K. Murayama, R. Kannagi, M. Sowa, *Int. J. Cancer* **1994**, 58, 349.
- [161] T. Mukaiyama, K. Ikegai, H. Jona, T. Hashihayata, K. Takeuchi, *Chem. Lett.* **2001**, 840.
- [162] a) D. Qiu, R. R. Koganty, *Tetrahedron Lett.* **1997**, 38, 45; b) X.-T. Chen, D. Sames, S. J. Danishefsky, *J. Am. Chem. Soc.* **1998**, 120, 7760.
- [163] T. Hashihayata, K. Ikegai, K. Takeuchi, H. Jona, T. Mukaiyama, *Bull. Chem. Soc. Jpn.* **2003**, 76, 1829.
- [164] a) J. K. Sharp, M. McNeil, P. Albersheim, *J. Biol. Chem.* **1984**, 259, 11321; b) R. Verduyn, M. Douwes, P. A. M. van der Klein, E. M. Möisinger, G. A. van der Marel, J. H. van Boom, *Tetrahedron* **1993**, 49, 7301; c) H. Yamada, H. Takimoto, T. Ikeda, K. Tsukamoto, T. Harada, T. Takahashi, *Synlett* **2001**, 1751.

Communications



Chiral triple-helical strands are found in the crystal structures of the compounds $[\{\text{Cr}^{\text{III}}(\text{CN})_6\}(\text{Mn}^{\text{II}}\text{L})_3] \cdot 3\text{H}_2\text{O}$ (where L is either $\text{L-NH}_2\text{ala}$ or $\text{L-NH}_2\text{ala}$; NH_2alaH = aminoalanine). All the spins on the manganese ions within this arrangement display a ferrimagnetic order below 35 K as a result of linking through the cyanide bridges formed with the $[\text{Cr}^{\text{III}}(\text{CN})_6]^{3-}$ ions, and indicated by the red arrow in the picture. For more information see the Communication by K. Inoue and co-workers on the following pages.

Three-Dimensional Chiral Molecule-Based Ferrimagnet with Triple-Helical-Strand Structure**

Hiroyuki Imai, Katsuya Inoue,* Kohichi Kikuchi, Yusuke Yoshida, Mitsuhiro Ito, Tetsuya Sunahara, and Satoru Onaka

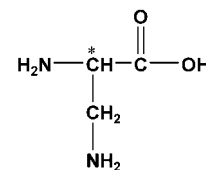
Dedicated to Professor Michinori Ōki
on occasion of his 77th birthday

In the future, development of molecule-based magnets with switching functions will lead to the production of innovative functional materials. The effect linking chirality and magnetism introduces to materials several available magneto-optical properties related to switching functions.^[1,2] Most appropriate among these properties is the magneto-chiral dichroism effect (MChD). This phenomenon involves alteration of the absorbance of a substance with ordinary light according to the directions of the magnetic field and incident radiation.^[1] In order to detect MChD, we have focused on the synthesis of magnetic, ordered, chiral helical compounds derived from metal complexes.

The construction of a right-handed double-helical structure within a living organism requires highly sophisticated molecular recognition, which results from the interplay of several noncovalent interactions, that is, hydrogen bonds and electrostatic and hydrophobic interactions. In the field of supramolecular chemistry, some helical complexes have been prepared.^[3] The helical structures of these complexes were produced by spontaneous assemblies between suitably structured ligands and metallic ions, in which both the arrange-

ment and the length of the helices within these complexes are programmed by the coordinating sites of the ligands and the stereochemical preferences of metallic ions. Such programs are not as accurate as those found in living organisms; consequently, extended double helical metal complexes in the solid state are rare. Therefore, to obtain magnetic ordered helical metal complexes, creation of a more accurate strategy is necessary.

Our target chiral compound with magnetic order can be synthesized by the reaction of hexacyanometalate $[M^{III}(CN)_6]^{3-}$ with a mononuclear complex $[M^{II}(L)_n]$ derived from organic chiral ligands L.^[4] Generally, ligand L, which is incorporated into this system in a chelating, or bidentate fashion, to M^{II} , simply blocks the availability of some coordination sites of the M^{II} center to cyanide groups in $[M^{III}(CN)_6]^{3-}$; moreover, the ligand L does not serve as a connector between neighboring metal ions. To obtain extended helical structures of M^{II} , a novel ligand characterized by a bridging site between neighboring metals must be selected. Thus, an alanine derivative, D- or L-aminoalanine ion (D-NH₂ala or L-NH₂ala; Scheme 1), was selected as a chiral ligand molecule



Scheme 1. Formula of D- or L- aminoalanine (D- or L-NH₂alaH).

to meet current design requirements. This chiral organic molecule possesses two kinds of functional moieties, two amino groups and one carboxyl group, to bridge between metals. In addition, self-recognition is usually operative between the groups for assembly of amino acid molecules in crystals, in the majority of cases, through hydrogen bonds. Therefore, in this ideal case, formation of a multiple helical structure of M^{II} is expected to occur in two steps: initial construction of an infinite helical chain of ligated M^{II} , which is followed by self-assembly between the infinite chains. The hexacyanometalate $[M^{III}(CN)_6]^{3-}$ ion will connect between adjacent helical structures containing M^{II} through cyanide bridges. This linking will stabilize the structure in the solid state and to give rise to magnetic interactions through the resulting M^{III} -CN- M^{II} bridges.

Dark orange, hexagonal prism crystals of $[[Cr(CN)_6](MnL-NH_2ala)_3] \cdot 3H_2O$ (**L-1**) and $[[Cr(CN)_6](MnD-NH_2ala)_3] \cdot 3H_2O$ (**D-1**) suitable for X-ray analysis were obtained by slow diffusion of $MnCl_2 \cdot 4H_2O$ (1.7 mmol), either D- or L-aminoalanine hydrochloride (D- or L-NH₂-alaH·HCl, 2.6 mmol), and KOH (5.2 mmol) in H₂O into $K_3[Cr(CN)_6]$ (1.5 mmol) in H₂O/*iso*-propanol (1:1) under argon atmosphere after several weeks.

X-ray crystal structure analyses at 100 K reveal that compound **D-1** crystallize in the chiral hexagonal space group, $P6_3$, and consists of left-handed helical structures of Mn^{II} ions. Compound **L-1** also crystallizes in the $P6_3$ space group but with a right-handed helical structures of Mn^{II} (Figure 1).^[5] Each aminoalanine ion employs two types of functional groups to bridge between two adjacent Mn^{II} ions ($Mn \cdots Mn$ separation is 5.923 Å). Two amino moieties and one carboxyl group within the aminoalanine ion are coordinated to two Mn^{II} ions in terminal and bridging coordination mode,

[*] Dr. H. Imai, Prof. Dr. K. Inoue^{††}
Department of Applied Molecular Science I
Institute for Molecular Science, Okazaki National Institutes
Myoudaiji, Okazaki, 444-8585 (Japan)
E-mail: kxi@hiroshima-u.ac.jp

Prof. Dr. K. Kikuchi, Y. Yoshida
Department of Chemistry, Tokyo Metropolitan University
Hachioji, Tokyo 192-0367 (Japan)
M. Ito, T. Sunahara, Prof. Dr. S. Onaka
Department of Environmental Technology
Graduate School of Engineering, Nagoya Institute of Technology
Gokiso-cho, Showa-ku, Nagoya, Aichi, 466-8555 (Japan)

[†] Present address:
Division of Chemistry, Graduate School of Science
Hokkaido University, Sapporo 060-0810 (Japan)

[††] Present address:
Division of Chemistry, Graduate School of Science
Hiroshima University, Higashi-Hiroshima 739-8526 (Japan)
Fax: + (81) 82-424-7416

[**] This work is supported by a Grant-in-Aid for Scientific Research (B) (No. 15340124) from the Ministry of Education, Science, Sports, and Culture. We also thank to Professor Inabe at Hokkaido University for his advice about the crystal structure.

Supporting information for this article is available on the WWW under <http://www.angewandte.org> or from the author.

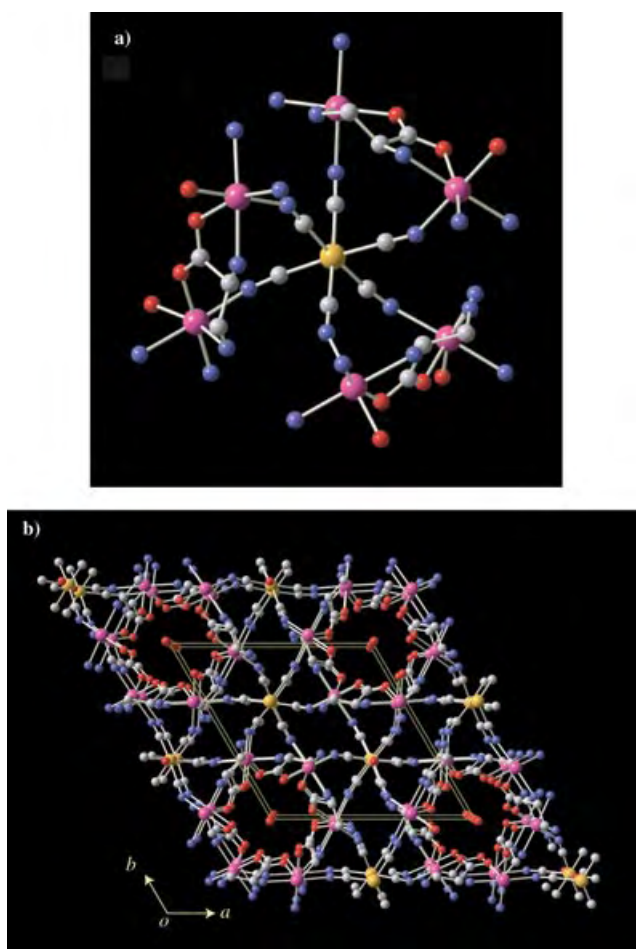


Figure 1. a) Coordination geometry of the heptanuclear unit of $[\text{Cr}^{\text{III}}(\text{CN})_6]^{3-}(\text{Mn}^{\text{II}}\text{-NH}_2\text{ala})_3\cdot 3\text{H}_2\text{O}$ (L-1). b) Overall view of the crystal structure of L-1 along the c -axis. Orange Cr, purple Mn, gray C, blue N, red O. The hydrogen atoms are omitted for clarity.

respectively. This unique coordination leads to the construction of two differing chelating rings around the Mn^{II} ion: five- and six-membered rings. These rings align alternately resulting in the generation of extended helical chains along the c -axis. As expected, the helical chains link together to give aggregates of three helical chains (Figure 2), in which the shortest $\text{Mn}\cdots\text{Mn}$ separation between the individual chains is 6.517 \AA . Within a triple helical strand, no distinct hydrogen bonds are formed between the helical chains, which usually occur between amino acid molecules. This phenomenon could be attributable to the positive charge of the manganese ions and the rigid frame of the helical chain. They maintain a distance from one another as great as 3.20 \AA , which is the shortest interchain distance observed between amino nitrogen and carboxyl oxygen atoms; moreover, this distance is slightly larger than the sum of van der Waals radii. The triple helical strand structure evident in this crystal is thought to be dependent on self-recognition between helical chains. That is, a mutually complementary interaction, instead of hydrogen bonds, in which a helical pitch is united exactly, is operative between three helical chains; consequently, the triple-helical-strand structure is produced. The channel structure is

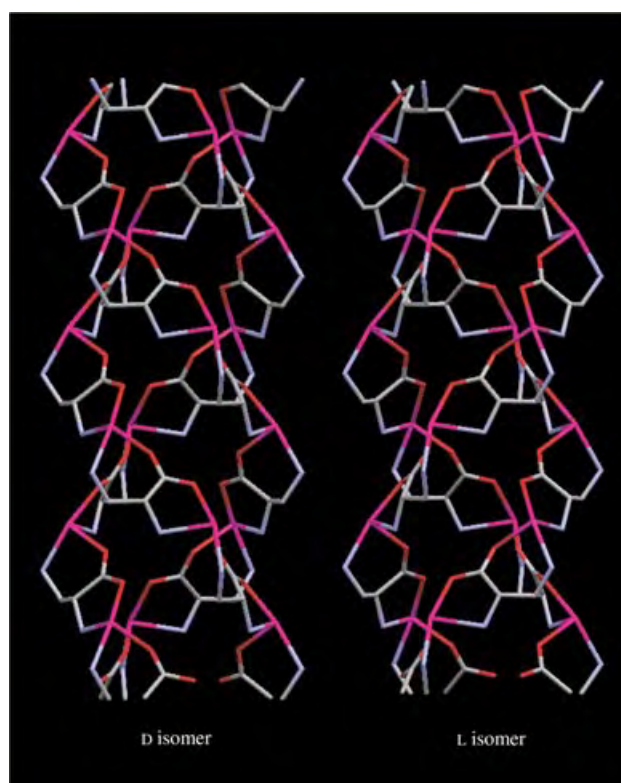


Figure 2. Capped sticks molecular models of a left-handed and a right-handed triple strand in D-1, and L-1, respectively. Purple Mn, gray C, blue N, red O.

generated and disordered water molecules are found in the center of the triple-helical-strand structure (on the screw axis).

Each $[\text{Cr}(\text{CN})_6]^{3-}$ ion utilizes all its cyanide moieties to connect adjacent three triple-helical-strands through cyanide bridges to the Mn^{II} ions; as a result, a three-dimensional cyanide-bridged network is formed. The shortest and longest $\text{Cr}\cdots\text{Mn}$ distances through cyanide bridges are 5.490 and 5.508 \AA , respectively, which are slightly longer than those in the previous crystals.^[4ac]

The cyanide-bridged network also displays basic units comprised of a helical-strand structure. Each cyanide-bridged helical strand, which is composed of four metal centers (two Mn^{II} and two Cr^{III} ions) and four cyanide groups as a repeating unit characterized by a reverse turn within the helical strand of Mn^{II} and NH_2ala ions along the c -axis, shares the apex of the helical strand (Cr^{III} ion) between three adjacent helical strands (Figure 1).

The magnetic behavior of polycrystalline samples of compounds **1** is the same at 5000 G is illustrated in Figure 3. The $\chi_{\text{mol}}T$ value is $4.17\text{ cm}^3\text{ K mol}^{-1}$ ($5.78\text{ }\mu_{\text{B}}$) at room temperature, it decreases with decreasing temperature to a minimum value of $3.91\text{ cm}^3\text{ K mol}^{-1}$ ($5.59\text{ }\mu_{\text{B}}$) at 140 K . The inset in Figure 3 clarifies this behavior, in which a broad minimum peak, typical of a ferrimagnet, is observed. The $1/\chi_{\text{mol}}$ versus T plot in the range from 300 to 140 K obeys Curie–Weiss law with a Weiss temperature of $\theta = -25\text{ K}$. The negative Weiss constant indicates an antiferromagnetic interaction operates between the adjacent Cr^{3+} and Mn^{2+} ions through cyanide

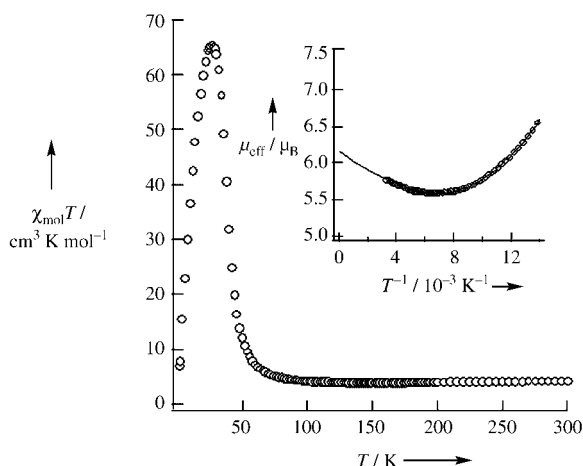


Figure 3. $\chi_{\text{mol}}T$ versus T plot at 5000 G of $\{[\text{Cr}^{\text{III}}(\text{CN})_6](\text{Mn}^{\text{II}}\text{-L-NH}_2\text{-ala})_3\} \cdot 3\text{H}_2\text{O}$ (L-1; that of D-1 is the same). Inset: Plot of effective magnetic moment versus $1/T$.

bridges.^[6] Upon additional cooling, the $\chi_{\text{mol}}T$ value increases to a maximum value of $65.38\text{ cm}^3\text{ K mol}^{-1}$ ($22.87\text{ }\mu_{\text{B}}$) at 27 K, followed by subsequent decreases below this temperature. The abrupt increase of the $\chi_{\text{mol}}T$ value around 30 K suggests the onset of three-dimensional magnetic ordering. The extrapolated effective magnetic moment value is $6.16\text{ }\mu_{\text{B}}$, which corresponds to the theoretical spin-only value of noncoupled paramagnetic high spin in the high-temperature limit (Figure 3 inset).

Low-field magnetization measurements of polycrystalline samples of compounds **1** at an applied field of 5 G in the temperature range 1.8–100 K were performed to confirm long-range magnetic ordering around 35 K (Figure 4). Both the zero field-cooled magnetization (ZFCM) and field-cooled magnetization (FCM) curves demonstrate long-range magnetic ordering below 35 K (Figure 4). As shown in the inset of Figure 4, the magnetization versus field (M vs H) plot of polycrystalline samples at 2 K increases sharply with the applied field and is saturated rapidly. The saturation magnet-

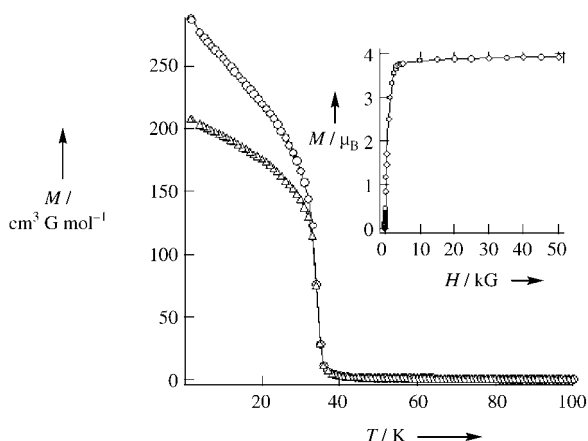


Figure 4. Temperature dependence of magnetization of L-1. The FC (Δ) and ZFC (\circ) magnetizations at 5 G are shown. Inset: Field dependence of magnetization L-1 at 2 K. The results for D-1 are the same.

ization is $M_{\text{S}} = 3.93\text{ }\mu_{\text{B}}$; this value is consistent with the theoretical value of antiferromagnetic coupling between one Mn^{2+} and one-third of a Cr^{3+} ion ($5/2 - 1/2 = 4/2$).

In conclusion, the results demonstrate that a compound with a triple-helical-strand structure is synthesized from the reaction of manganese(II) complex with an alanine derivative and hexacyanochromate(III) ion. These compounds, which have a triple-helical structure with counterclockwise and clockwise turns around the manganese ion, were obtained from D and L isomers, respectively. Detailed analysis of crystal structure also indicates that the main factor governing this phenomenon is not hydrogen bonding between helical chains, as expected, but the rigid frame of the helical chain. Owing to the rigid frame and positive charge of the helical chain, the helical chains cannot approach one another sufficiently closely in the crystal to permit interchain hydrogen-bond formation; thus, the rigid frame is advantageous with respect to triple-helical-strand formation.

The compounds exhibits ferrimagnetic behavior below 35 K. The magnetic transition temperature of both compounds is relatively low despite formation of a three-dimensional cyanide network. This phenomenon is probably attributable to the comparatively long cyanide-bridged distance in this crystal. In addition, it may result from the occurrence of spin frustration between manganese ions within the triple-helical strand at high temperature. Below 35 K, the spin on the manganese center alone survives owing to the ferrimagnetic coupling between manganese and chromium ions. The spin structure of this compound is also expected to possess triple-helical nature. Some chiral molecule-based magnets have been prepared, however, at present, a chiral helical spin structure has not been documented. Magnetization measurements, μSR (muon spin resonance) spectroscopy and neutron diffraction of a single crystal will lead to characterization of the details of the magnetic structure in this compound.

Received: June 4, 2004

Published Online: September 28, 2004

Keywords: chirality · chromium · helical structures · magnetic properties · manganese

- [1] a) G. Wagniere, A. Mejer, *Chem. Phys. Lett.* **1984**, *110*, 546–551; b) G. L. J. A. Rikken, E. Raupach, *Nature* **1997**, *390*, 493–494; c) P. Kleindienst, G. Wagniere, *Chem. Phys. Lett.* **1998**, *288*, 89–97; d) G. L. J. A. Rikken, E. Raupach, *Phys. Rev. E* **1998**, *58*, 5081–5084.
- [2] a) H. Kumagai, K. Inoue, *Angew. Chem.* **1999**, *111*, 1694–1696; *Angew. Chem. Int. Ed.* **1999**, *38*, 1601–1603; b) H. Kumagai, A. S. Markosyan, K. Inoue, *Mol. Cryst. Liq. Cryst.* **2000**, *40*, 97–102; c) E. Coronado, J. R. Galan-Mascaros, C. J. Gómez-García, J. M. Martínez-Agüero, *Inorg. Chem.* **2001**, *40*, 113–120; d) R. Andrés, M. Bissard, M. Gruselle, C. Train, J. Vaissermann, B. Malézieux, J.-P. Jamet, M. Verdaguer, *Inorg. Chem.* **2001**, *40*, 4633–4640; e) B. Malézieux, R. Andrés, M. Bissard, M. Gruselle, C. Train, P. Herson, L. L. Troitskaya, V. I. Sokolov, S. T. Ovsenko, T. V. Demeschik, N. S. Ovanesyan, I. A. Mamed'yarova, *J. Organomet. Chem.* **2001**, *637*, 182–190; f) D. Armentano, G. D. Munno, F. Lloret, A. V. Palii, M. Julve, *Inorg. Chem.* **2002**, *41*, 2007–2013;

- g) M. Minguet, D. Luneau, E. Lhotel, V. Villar, C. Palusen, D. B. Amabilino, J. Veciana, *Angew. Chem.* **2002**, *114*, 606–609; *Angew. Chem. Int. Ed.* **2002**, *41*, 586–589.
- [3] a) J.-M. Lehn, A. Rigault, J. Siegel, J. Harrowfield, B. Chevrier, D. Moras, *Proc. Natl. Acad. Sci. USA* **1987**, *84*, 2565–2569; b) E. C. Constable, *Tetrahedron* **1992**, *48*, 10013–10059; c) C. Piguet, G. Bernardinelli, B. Bocquet, A. Quattropanni, A. F. Williams, *J. Am. Chem. Soc.* **1992**, *114*, 7440–7451; d) R. Krämer, J.-M. Lehn, A. De Cian, J. Fischer, *Angew. Chem.* **1993**, *105*, 764–767; *Angew. Chem. Int. Ed. Engl.* **1993**, *32*, 703–706; e) R. F. Carina, G. Berunardinelli, A. F. Williams, *Angew. Chem.* **1993**, *105*, 1483–1485; *Angew. Chem. Int. Ed. Engl.* **1993**, *32*, 1463–1465; f) E. C. Constable, A. J. Edwards, P. R. Raithby, J. V. Walker, *Angew. Chem.* **1993**, *105*, 1486–1488; *Angew. Chem. Int. Ed. Engl.* **1993**, *32*, 1465–1467; g) N. Ohata, H. Masuda, O. Yamauchi, *Angew. Chem.* **1996**, *108*, 570–572; *Angew. Chem. Int. Ed. Engl.* **1996**, *35*, 531–532.
- [4] a) K. Inoue, H. Imai, P. S. Ghalasasi, K. Kikuchi, M. Ohba, H. Ōkawa, J. V. Yakhmi, *Angew. Chem.* **2001**, *113*, 4372–4375; *Angew. Chem. Int. Ed.* **2001**, *40*, 4242–4245; b) E. Coronado, C. J. Gómez-García, A. Nuez, F. M. Romero, E. Rusanov, H. Stoeckli-Evans, *Inorg. Chem.* **2002**, *41*, 4615–4617; c) K. Inoue, K. Kikuchi, M. Ohba, H. Ōkawa, *Angew. Chem.* **2003**, *115*, 4958–4961; *Angew. Chem. Int. Ed.* **2003**, *42*, 4810–4813.
- [5] Crystal data for L-isomer (**L-1**): Crystal size $0.35 \times 0.35 \times 0.20 \text{ mm}^3$. $\text{C}_5\text{H}_9\text{Cr}_{0.33}\text{MnN}_4\text{O}_3$, $M_r = 245.44$, hexagonal, $P6_3$ (No. 173), $a = b = 13.6802(16)$, $c = 8.1530(14) \text{ Å}$, $V = 1321.4(3) \text{ Å}^3$, $T = 100 \text{ K}$, $Z = 6$, $\rho_{\text{calc}} = 1.851 \text{ g cm}^{-3}$, $\mu(\text{MoK}\alpha) = 1.870 \text{ mm}^{-1}$. Data were collected with a Bruker SMART-APEX three-circle diffractometer, equipped with a CCD area detector (graphite-monochromated $\text{MoK}\alpha$ radiation, $\lambda = 0.71073 \text{ Å}$, ω -scan mode (0.3° steps), semi-empirical absorption correction on Laue equivalents). The structures were solved by direct method and refined by full-matrix least squares against F^2 of all data, using SHELXTL software. All non-hydrogen atoms were refined anisotropically. Hydrogen atoms, except for the water hydrogen atoms, were placed in calculated positions but not refined. The refinement converges with $R_1 = 0.0440$ for 1192 data ($I > 2\sigma(I)$), $wR_2 = 0.1169$ for 1194 unique data ($1.72 \geq \theta \geq 23.24^\circ$), Flack parameter = 0.05(6), max/min residual electron density $0.566/-0.608 \text{ e Å}^{-3}$. CCDC-238055 (**L-1**) contains the supplementary crystallographic data for this paper. These data can be obtained free of charge via www.ccdc.cam.ac.uk/conts/retrieving.html (or from the Cambridge Crystallographic Data Centre, 12 Union Road, Cambridge CB2 1EZ, UK; fax: (+44) 1223-336-033; or deposit@ccdc.cam.ac.uk).
- [6] See Supporting Information.

Finite, Spherical Coordination Networks that Self-Organize from 36 Small Components**

Masahide Tominaga, Keisuke Suzuki, Masaki Kawano, Takahiro Kusukawa, Tomoji Ozeki, Shigeru Sakamoto, Kentaro Yamaguchi, and Makoto Fujita*

Highly symmetric structures often appear in nature as revealed by, for example, the capsids of spherical viruses that have icosahedral symmetry consisting of $60n$ identical protein subunits.^[1] The reason for the high symmetry lies behind the principle that increasing the number of elements with the same symmetry reduces the amount of independent structural information, which is directly related to the length of DNA. Thus, the self-organization of tiny subunits into a giant biological molecule can be regarded as the process of not only structural growth but of the amplification of molecular information. We show herein that, through metal–ligand interactions,^[2,3] simple banana-shaped organic molecules self-organize into finite, spherical coordination networks with a diameter of up to 7 nm, which is in contrast to the formation of two-dimensional (2D) infinite networks that occurs with linear organic ligands. The spherical coordination networks consist of 36 components, 12 equivalent metal centers (M) and 24 equivalent ligands (L), and have cuboctahedron symmetry. By attaching a functional group (e.g., C₆₀ or porphyrin) to each ligand, 24 functional groups are aligned equivalently at the periphery of the sphere.

Over the last decade, extensive studies have been made on infinite coordination networks that are formed by the complexation of exo-multidentate ligands with transition-metal ions. A typical and simple example is given by a 2D grid complex that forms from a rodlike ligand and a metal (Figure 1a).^[4] We expect that, if the ligand framework is slightly bent, the coordination network will develop with a

[*] Dr. M. Tominaga, K. Suzuki, Dr. M. Kawano, Dr. T. Kusukawa, Prof. M. Fujita

Department of Applied Chemistry, School of Engineering
The University of Tokyo

7-3-1 Hongo, Bunkyo-ku, Tokyo 113-8656 (Japan)

Fax: (+81) 3-5841-7257

E-mail: mfujita@appchem.t.u-tokyo.ac.jp

Dr. S. Sakamoto, Prof. K. Yamaguchi
Chemical Analysis Center, Chiba University
Yayoi-cho, Inage-ku, Chiba 263-8522 (Japan)

Dr. T. Ozeki
Department of Chemistry and Materials Science
Tokyo Institute of Technology
2-12-1 O-okayama, Meguro-ku, Tokyo 152-8551 (Japan)

[**] This research was supported by the CREST project of the Japan Science and Technology Corporation (JST), for which M.F. is the principal investigator. We thank S. Adachi (KEK) for supporting X-ray crystallographic measurement. This work has been performed under the approval of the Photon Factory Program Advisory Committee (Proposal No. 2003G186).



Supporting information for this article is available on the WWW under <http://www.angewandte.org> or from the author.

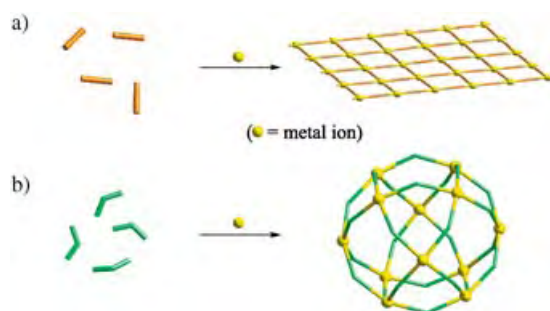
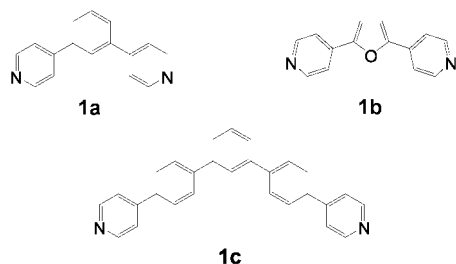


Figure 1. Schematic representation of the self-assembly of coordination networks from metal ions which favor a square-planar coordination geometry and different bridging ligands. a) Linear ligands are expected to self-assemble to give 2D grid complexes. b) Slightly bent ligands are expected to self-assemble to give spherical finite complexes.

constant radius of curvature and a spherical finite network will be obtained (Figure 1 b), reminiscent of the formation of graphite versus that of fullerene from sp^2 hybridized carbon atoms. Based on this idea, we designed ligands **1a–c** and



examined their complexation with naked palladium(II) ions which favor a square-planar coordination environment.^[5]

When ligand **1a** (0.02 mmol) was treated with $\text{Pd}(\text{NO}_3)_2$ (0.01 mmol) in $[\text{D}_6]\text{DMSO}$ (1.0 mL) at 70°C for 4 h, the quantitative self-assembly of a single product was detected by ^1H NMR spectroscopy.^[6] Only five signals are observed indicating that all the ligands are located equivalently in the product and have same inherent symmetry (Figure 2). The resonance signals were relatively broad at room temperature

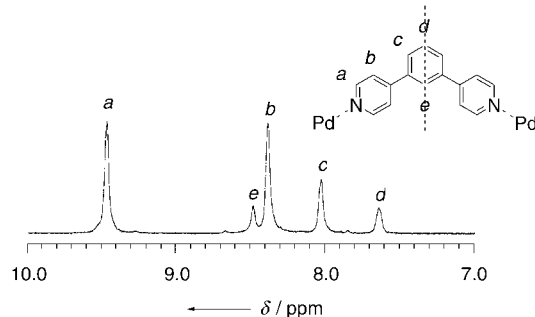


Figure 2. The ^1H NMR spectrum (aromatic region) of the product assembled from $\text{Pd}(\text{NO}_3)_2$ and ligand **1a** (2 equiv; 500 MHz, $[\text{D}_6]\text{DMSO}$, 25°C , TMS).

but became sharp at higher temperatures, characteristic of very large species whose motion is slow on the NMR time scale. Downfield shift of the signals, particularly for Py_α ($\Delta\delta = 0.79$ ppm; Py = pyridine), was ascribed to the metal–ligand complexation. Diffusion-ordered NMR spectroscopy (DOSY) showed a single band at the diffusion coefficient of $1.1 \times 10^{-10} \text{ m}^2 \text{ s}^{-1}$, from which the diameter of the product was roughly estimated to be 3.6 nm.^[7] After anion exchange from $[\text{NO}_3]^-$ to $[\text{PF}_6]^-$ ions, cold-spray ionization mass spectrometry (CSI-MS)^[8] clearly indicated an $\text{M}_{12}\text{L}_{24}$ composition with the molecular weight of 10330 Da by a series of $[\text{M}-(\text{PF}_6^-)_n]^{n+}$ ($n = 6\text{--}13$) peaks (Figure 3).^[9] Fragmentation in the MS measurement was hardly observed except the dissociation of counteranions, which demonstrates the remarkable stability of the product in solution. Elemental analysis was also consistent with the $\text{M}_{12}\text{L}_{24}$ composition.

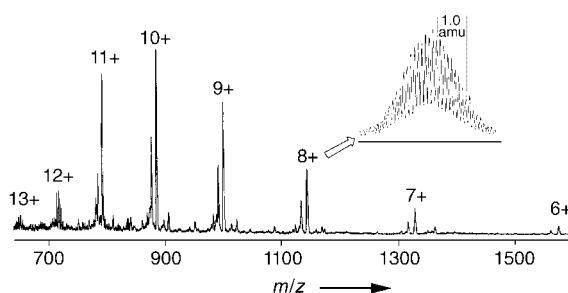


Figure 3. CSI-MS spectrum showing the formation of $\text{M}_{12}\text{L}_{24}$ product (PF_6^- salt).

From the detailed NMR and mass spectroscopic measurements, the formation of the roughly spherical giant molecule **2a** was deduced because of good agreements with the $\text{M}_{12}\text{L}_{24}$ composition and the equivalence of all the ligands (Figure 4a). The symmetry of **2a** is dictated by a cuboctahedron, which is formed by truncating each of the eight vertices of a cube to generate eight triangular faces. The 12 equivalent vertices and 24 equivalent edges of the cuboctahedron can be superimposed on the 12 palladium(II) centers and 24 bridging ligands, respectively (Figure 4b). Related cuboctahedral complexes with Cotton-type copper(II) dinuclear tetracarboxylate junctions have been reported,^[10] but no solution behavior is reported probably because of their poor solubility in common polar solvents. Since these copper(II) species are generated by inert dinuclear tetracarboxylate formation, instead of self-assembly, oligomeric products are produced as well and the yields are moderate or not well determined. In contrast, spherical complex **2a** immediately assembles from 36 components in a quantitative yield thanks to moderately labile palladium(II)–pyridine interactions.

A scanning tunneling microscopy (STM) study revealed the structural integrity of **2a** (Figure 5a) even under STM conditions. More significantly, the image obtained on a graphite surface demonstrates that the spheres **2a** behaves as “molecular particles” with precise chemical structure and uniform dimension (height) of 3.5 nm (Figure 5b), which is consistent with the DOSY measurement and molecular model prediction.

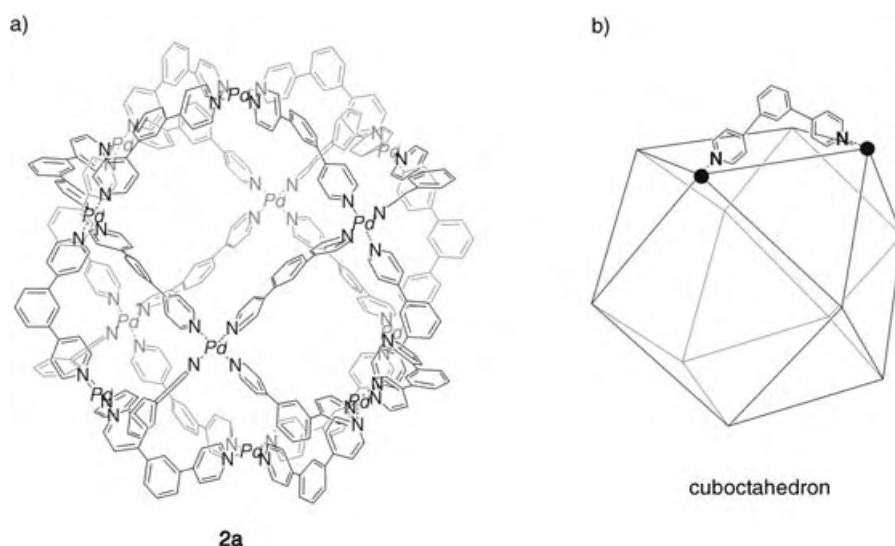


Figure 4. a) Molecular structure **2a** assembled from 24 bidentate ligands **1a** and 12 metal ions. b) Schematic representation of the cuboctahedral frameworks of **2a**.

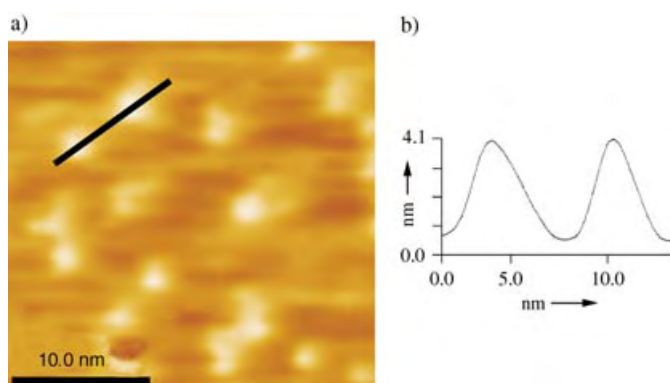


Figure 5. a) STM image of individual spheres **2a** on the graphite at room temperature. b) Height profile of the STM image.

Reliable evidence for the spherical $M_{12}L_{24}$ structure was obtained by X-ray crystallographic analysis of **2b**, which is an analogue of **2a** where ligand **1a** is replaced by **1b**.^[11] Single crystals of **2b** were obtained by very slow vapor diffusion of 1,1,2-trichloroethane into a DMSO solution of **2b**. With a CCD detector, MoK $_{\alpha}$ radiation (55 kV, 30 mA) afforded low resolution data (only 874 unique reflections ($> 2\sigma(I)$)), which were insufficient for solving the structure. The poor quality of the data was due to severe disorder of solvent molecules and anions in the extraordinarily large void within the spherical framework of **2b**. However, synchrotron X-ray radiation with high flux and low divergence provided much higher quality of data with 2717 unique reflections ($> 2\sigma(I)$), from which the spherical $M_{12}L_{24}$ structure of **2b** was solved with all the heavy atoms being refined anisotropically (Figure 6). The crystal system is cubic and the cell volume is 108456(16) Å³. Surprisingly, the framework of **2b** occupies only 20% of the cell volume (as estimated by Platon program), remaining 80% being occupied by disordered solvent molecules and counterions. The diameter of a sphere in which **2b** is inscribed

is 3.4 nm. The shortest Pd–Pd separation is 1.3 nm while the longest one is 2.6 nm.

In the crystal, the spherical complex **2b** enjoys a cubic close-packed structure. Each molecule of **2b** is linked to twelve neighboring spheres by Pd^{II}–NO₃[−]–Pd^{II} bridges, which presumably stabilize the crystal of **2b** despite approximately 80% void space.

Ligand **1c** is effectively an expanded version of the framework of **1a**. From Pd(NO₃)₂ and ligand **1c** in 1:2 stoichiometry, we again observed the self-assembly of a single and highly symmetric product, **2c** (an analogue of **2a** where ligand **1a** is replaced by **1c**) which was assigned by CSI-MS measurement. The molecular mass of 13982 Da for **2c** was clearly demonstrated (see Supporting Information). Molecular modeling of **2c** by Cerius² program predicted a diameter of 5.2 nm.^[12]

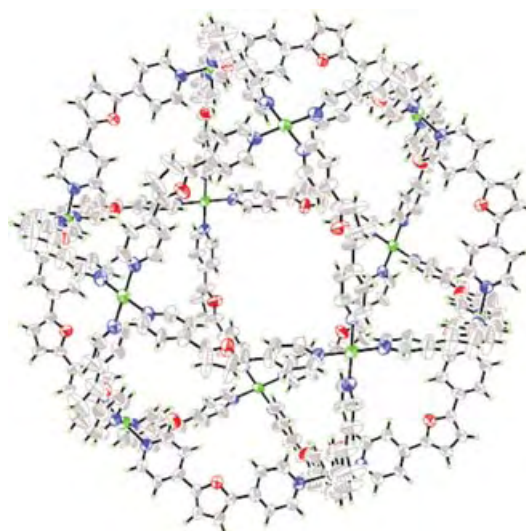


Figure 6. The crystal structure of sphere **2b**. Counterions and solvent molecules are omitted for clarity (green Pd, red O, blue N, gray C).

We also emphasize that, by attaching a functional group on each ligand, 24 functional groups are aligned equivalently at the periphery of the sphere. Metal–porphyrins are known to collect light energy when they are aggregated as in light-harvesting proteins or chlorophylls. To mimic these aggregates, we synthesized ligand **1d** in which a porphyrin unit is attached on the backbone of **1a**. By simply mixing this ligand with Pd(NO₃)₂ in a 2:1 ratio in DMSO, porphyrin nanoball **2d** with regular arrangement of the 24 porphyrin units at the periphery of the sphere was immediately assembled (Figure 7). The NMR spectrum of this complex at 25°C shows the equivalence of the 24 attached porphyrin ligands.

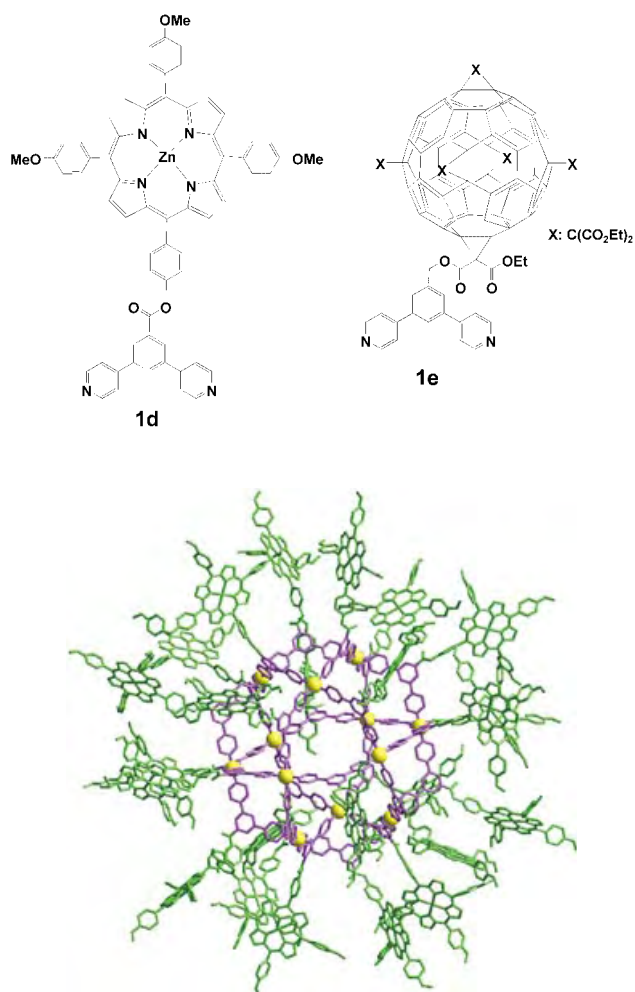


Figure 7. A molecular modeling study of **2d** optimized by a force-field calculation with Cerius² 3.5 package (Pd yellow, the porphyrin-based and pyridine-based units of ligand **1d** are green and purple, respectively).

The DOSY spectrum showed a single band, which suggests the quantitative formation of **2d** (Figure 8b). Similarly, fullerene nanoball **2e** was assembled from ligand **1e** and Pd(NO₃)₂ (Figure 8c). The diffusion coefficients of **2b**, **2d**, and **2e** determined by DOSY experiments were 1.20, 0.60, and $0.76 \times 10^{-10} \text{ m}^2 \text{ s}^{-1}$, respectively. These values give an

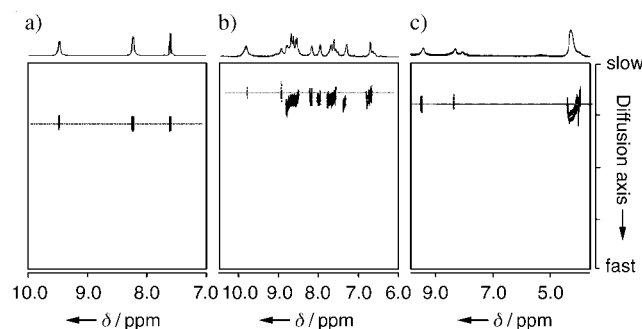


Figure 8. DOSY spectra of the sphere a) **2b**, b) **2d**, and c) **2e** (500 MHz, [D₆]DMSO, 25 °C, TMS).

estimation of the dimensions of **2b**, **2d**, and **2e** (3.4, 6.7, and 5.3 nm, respectively), which agree quite well with the X-ray structure (3.4 nm for **2b**) and refined structures with Cerius² program (3.4, 7.4, and 6.0 nm for **2b**, **2d** and **2e**, respectively).

Received: July 24, 2004

Published Online: September 28, 2004

Keywords: fullerenes · molecular spheres · palladium · porphyrinoids · self-assembly

- [1] a) J. M. Grimes, J. N. Burroughs, P. Gouet, J. M. Diprose, R. Malby, S. Ziéntara, P. P. C. Mertens, D. I. Stuart, *Nature* **1998**, 395, 470–478; b) W. R. Wikoff, L. Liljas, R. L. Duda, H. Tsuruta, R. W. Hendrix, J. E. Johnson, *Science* **2000**, 289, 2129–2133.
- [2] Recent reviews: a) J.-M. Lehn, *Comprehensive Supramolecular Chemistry*, Vol. 2 (Eds.: J. L. Atwood, J. E. D. Davis, D. D. Macnicol, F. Vögtle), Pergamon, Oxford, **1996**; b) L. R. MacGillivray, J. L. Atwood, *Angew. Chem.* **1999**, 111, 1080–1096; *Angew. Chem. Int. Ed.* **1999**, 38, 1018–1033; c) S. Leininger, B. Olenyuk, P. J. Stang, *Chem. Rev.* **2000**, 100, 853–908; d) M. Fujita, K. Umemoto, M. Yoshizawa, N. Fujita, T. Kusukawa, K. Biradha, *Chem. Commun.* **2001**, 509–518; e) G. F. Swiegers, T. J. Malefetse, *Chem. Eur. J.* **2001**, 7, 3637–3643.
- [3] a) R. W. Saalfrank, A. Stark, K. Peters, H. G. von Schnering, *Angew. Chem.* **1988**, 100, 878–880; *Angew. Chem. Int. Ed. Engl.* **1988**, 27, 851–853; b) P. Baxter, J.-M. Lehn, A. DeCian, J. Fischer, *Angew. Chem.* **1993**, 105, 92–95; *Angew. Chem. Int. Ed. Engl.* **1993**, 32, 69–72; c) M. Fujita, D. Oguro, M. Miyazawa, H. Oka, K. Yamaguchi, K. Ogura, *Nature* **1995**, 378, 469–471; d) T. Beissel, R. E. Power, K. N. Raymond, *Angew. Chem.* **1996**, 108, 1166–1168; *Angew. Chem. Int. Ed. Engl.* **1996**, 35, 1084–1086; e) C. M. Hartshorn, P. J. Steel, *Chem. Commun.* **1997**, 541–542; f) N. Takeda, K. Umemoto, K. Yamaguchi, M. Fujita, *Nature* **1999**, 398, 794–796; g) B. Olenyuk, J. A. Whiteford, A. Fechtenkötter, P. J. Stang, *Nature* **1999**, 398, 796–799.
- [4] a) R. W. Gable, B. F. Hoskins, R. Robson, *J. Chem. Soc. Chem. Commun.* **1990**, 1677–1678; b) M. Fujita, Y. J. Kwon, S. Washizu, K. Ogura, *J. Am. Chem. Soc.* **1994**, 116, 1151–1152; c) K. Biradha, Y. Hongo, M. Fujita, *Angew. Chem.* **2000**, 112, 4001–4003; *Angew. Chem. Int. Ed.* **2000**, 39, 3843–3845; d) S.-I. Noro, S. Kitagawa, M. Kondo, K. Seki, *Angew. Chem.* **2000**, 112, 2161–2164; *Angew. Chem. Int. Ed.* **2000**, 39, 2081–2084.
- [5] a) D. K. Chand, K. Biradha, M. Fujita, *Chem. Commun.* **2001**, 1652–1653; b) D. K. Chand, K. Biradha, M. Fujita, S. Sakamoto, K. Yamaguchi, *Chem. Commun.* **2002**, 2486–2487; c) D. K. Chand, M. Fujita, K. Biradha, S. Sakamoto, K. Yamaguchi, *Dalton Trans.* **2003**, 2750–2756.
- [6] For the physical properties of the products **2a–e**, see the Supporting Information.
- [7] D. Wu, A. Chen, C. S. Johnson, Jr., *J. Magn. Reson. Ser. A* **1995**, 115, 260–264.
- [8] CSI-MS is quite effective for analyzing the solution structures of metal complexes: a) S. Sakamoto, M. Fujita, K. Kim, K. Yamaguchi, *Tetrahedron* **2000**, 56, 955–964; b) Y. Yamanoi, Y. Sakamoto, T. Kusukawa, M. Fujita, S. Sakamoto, K. Yamaguchi, *J. Am. Chem. Soc.* **2001**, 123, 980–981.
- [9] Spheres **2a**, **2b**, and **2c** were analyzed by CSI-MS. A series of $[M-(PF_6)_n]^{n+}$ peaks was observed. See the Supporting Information.
- [10] a) B. Moulton, J. Lu, A. Mondal, M. J. Zaworotko, *Chem. Commun.* **2001**, 863–864; b) M. Eddaoudi, J. Kim, J. B. Wachter, H. K. Chae, M. O’Keeffe, O. M. Yaghi, *J. Am. Chem. Soc.* **2001**, 123, 4368–4369.

- [11] X-ray crystallographic analysis of **2b**: The diffraction data was measured at 120 K ($\lambda = 0.6890 \text{ \AA}$) at PF-AR of the High Energy Accelerator Research Organization (KEK). X-ray data showed no significant crystal decay during data collection. $\text{Pd}_{12}(\text{C}_{13}\text{N}_2\text{O})_{24}(\text{NO}_3)_{24}$, $M_r = 7568.80$, cubic, space group $Fm\bar{3}m$, $T = 120(2) \text{ K}$, $a = 47.689(4) \text{ \AA}$, $V = 108456(16) \text{ \AA}^3$, $Z = 4$. Anisotropic least-squares refinement for the cage atoms and isotropic for the anion and solvent molecules (122 parameters) on 2658 independent merged reflections ($R_{\text{int}} = 0.0753$) converged at $wR_2(F^2) = 0.1770$ for all data; $R_1(F) = 0.1518$ for 1718 observed data ($I > 2\sigma(I)$), $\text{GOF} = 1.708$. Because two independent nitrate anions sit on the special positions $((y, 0, y)$ and $(0.25, 0, 0.25))$, their models are not fitted for the ideal geometry of D_{3d} symmetry. All the solvent molecules could not be treated properly because of their severely disordered structures. Therefore, all large residual electron density peaks were assigned to chlorine atoms of 1,1,2-trichloroethane molecules (poor solvent of crystallization). CCDC-238399 (**2b**) contains the supplementary crystallographic data for this paper. These data can be obtained free of charge via www.ccdc.cam.ac.uk/conts/retrieving.html (or from the Cambridge Crystallographic Data Centre, 12 Union Road, Cambridge CB2 1EZ, UK; fax: (+44) 1223-336-033; or deposit@ccdc.cam.ac.uk).
- [12] A. K. Rappé, C. J. Casewit, K. S. Colwell, W. A. Goddard III, W. M. Skiff, *J. Am. Chem. Soc.* **1992**, *114*, 10024–10035.

Nanostructured Films

Surface-Templated Nanostructured Films with Two-Dimensional Ordered Arrays of Voids**

Peng Jiang*

Template-induced syntheses have been broadly applied to the creation of structured materials with unique properties that are difficult to produce by other procedures.^[1–10] Self-assembled colloidal crystals are ideal templates for creating three-dimensional (3D) highly ordered macroporous materials and photonic crystals.^[6,7,11–16] In this approach, the voids between colloidal spheres are infiltrated with another material and subsequent removal of the template by either wet etching or thermal decomposition leads to the formation of 3D ordered air cavities inside the structure-filling materials. Nanosphere lithography (NSL), on the other hand, uses monolayer or double-layer colloidal crystals as either an etching or deposition mask to define a two-dimensional (2D) ordered mosaic array of microcolumnar structures inside the voids of

colloids.^[17–20] Surfaces of 2D arrays of submicron spheres have also been demonstrated as templates in the creation of metallic half-shells.^[21,22] Here we report a different method that uses the periodic surfaces of 3D ordered colloidal crystals as templates for the production of 2D ordered surface gratings.

Surface gratings with 2D regular arrays of voids are of considerable technological importance and great scientific interest. Periodic metallic subwavelength hole arrays exhibit unusual optical transmission,^[23] which offers the potential for developing new microoptical devices.^[24] Surface gratings with submicron periodicity have been used in fabricating distributed feedback lasers,^[25] broadband waveguide polarizers,^[26] selective optical absorbers,^[27] and surface-enhanced Raman scattering (SERS) substrates,^[28] as well as in improving the extraction efficiency of organic light-emitting diodes (OLEDs).^[29] Such arrays of voids can also be used as picoliter beakers for chemical and biochemical microanalysis.^[30,31] The fabrication of surface gratings with submicron periodicity typically involves lithography (photolithography for > 300 nm features and electron-beam lithography for < 300 nm features) and etching.^[23] These processes are costly and tend to be limited by either low resolution or low throughput. In contrast, the surface-template approach described in this paper provides a much simpler and cheaper nonlithographic alternative for the mass fabrication of surface gratings from a diverse range of materials.

Naturally, one could use monolayer colloidal crystals in templating 2D surface gratings. However, the fabrication of large 2D colloidal single crystals is problematic.^[32] By contrast, convective self-assembly^[13,33,34] and the recently developed spin-coating technique^[35] provide us with simple methods for making large 3D colloidal crystals by using microspheres of 100–2000 nm. Therefore, we use 3D colloidal crystals as templates for making 2D surface gratings, provided that subsequent material deposition only occurs on the colloidal crystal surface.

A schematic outline of the procedures for producing free-standing, 2D ordered surface gratings by using convectively assembled colloidal crystals as templates is shown in Figure 1. We first grow a multilayer silica or polystyrene colloidal single crystal on a glass slide by using the convective self-assembly method.^[33] The typical thickness of the final crystal is 20 layers and the diameters of the colloids range from 100–500 nm. Although there are defects in the resultant colloidal crystal, such as point vacancies and vertical cracks, the single crystalline domain extends over the whole sample area of several centimeters square.^[33] A thin layer (300–1000 nm) of material is then deposited on the top surface of the colloidal crystal by conventional physical vapor deposition (PVD) techniques, including RF and DC-magnetron sputtering deposition (Perkin–Elmer 8200) and electron-beam evaporation (Denton DV-502A E-beam evaporator). In sharp contrast with chemical vapor deposition (CVD), which has been widely used in filling all available interstitial voids of 3D colloidal crystals,^[11,13] PVD only forms conformal half-shells on the crystal surface, thereby obstructing penetration of materials into the inner voids.^[21,22] For hydrofluoric acid resistant materials, such as Au, Ag, Pt, and Cr, silica colloidal

[*] P. Jiang*
Science and Technology Division
Corning Incorporated, Corning, NY 14831 (USA)
E-mail: pjiang@princeton.edu

[†] Current address:
Department of Chemical Engineering
Princeton University, Princeton, NJ 08544 (USA)
Fax: (+1) 609-258-6835

[**] The author would like to thank Dr. Larry Shacklette, Dr. Macrae Maxfield, and Dr. Michael McFarland of Corning Polymer Photonics for many useful discussions and support.

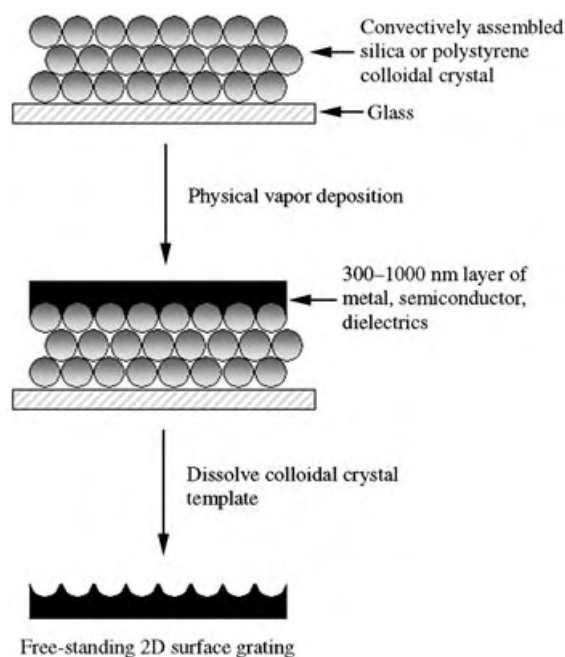


Figure 1. Experimental procedures for making free-standing, 2D surface gratings by using convectively self-assembled colloidal crystals as templates.

crystals are used as templates; otherwise, for Ti, Al, Si, Ge, indium tin oxide (ITO), and SiO_2 , polystyrene templates are used. The silica or polystyrene colloidal templates can then be etched away by a 2% HF or toluene rinse to leave behind a free-standing, iridescent film, as shown by the photo of a gold film of 410 nm periodicity in Figure 2a. The iridescent colors of the film are caused by Bragg diffraction of visible light by the 2D ordered arrays of submicron voids.^[36]

Figure 2b shows a typical SEM image of a flexible gold surface grating with 2D periodic arrays of voids with 410 nm diameters. The voids match the size of the template spheres and retain their single-crystal close-packed ordering over an area of several centimeters square. The long-range hexagonal ordering of the voids is further confirmed by the FFT image shown in the inset of Figure 2b. A higher-magnification image (Figure 2c) reveals that the shell-like voids are only partially connected. This is more apparent from the cross-sectional micrograph of the film (Figure 2d); microcolumnar pillars maintain the original arrangement of template colloids. This appears to be caused by the rapid deposition rate ($> 5 \text{ nm s}^{-1}$) and large grain size ($> 20 \text{ nm}$) of the RF sputtering deposition used for making the sample. The rapidly accumulated large grains prevent subsequently deposited material from penetrating into the small interstices ($\approx 100 \text{ nm}$) between colloids on the surface. Other PVD techniques with much slower deposition rates ($< 1 \text{ nm s}^{-1}$) and smaller cluster sizes ($< 1 \text{ nm}$), such as electron-beam and thermal evaporation, allow homogeneous material deposition over the sample surface, thereby resulting in the formation of continuous films (see Figure 4).

Although the above approach with convectively assembled colloidal crystals as sacrificial templates is favorable for low-volume, laboratory-scale production, it has several draw-

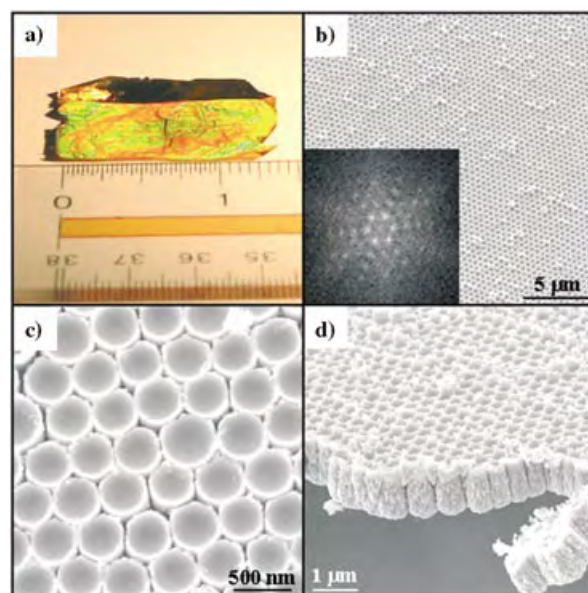


Figure 2. Self-standing surface gratings. a) Photo of a self-standing gold surface grating replicated from silica colloids of 410 nm diameter. The units marked on the top of the ruler are inches ($\approx 2.5 \text{ cm}$). b) Top-view SEM image and its fast Fourier transform (FFT) image (inset) of the sample shown in (a). c) Higher-magnification SEM image of the same sample that shows the partially connected shells. d) Cross-sectional view of the same sample. Gold was deposited by using a Perkin–Elmer 8200 RF sputtering system.

backs that limit its use for the mass fabrication of surface gratings with submicron periodicity. First, the convective self-assembly method is a tedious process from the viewpoint of large-scale fabrication. It takes days to make a centimeter-square-size crystal.^[33] Second, it is problematic to make high-quality colloidal crystals larger than several centimeters square, due to the gravitational sedimentation of colloids and solvent evaporation.^[13,33,34] Third, the final surface gratings have many protrusion defects (Figure 2b) caused by unwanted material deposition in the inner interstices of the 3D templates.

To overcome these drawbacks, we adapted our recently developed shear-induced spin-coating technique for making colloidal crystal templates.^[35] Planar crystals as large as 81 cm^2 (on a 10 cm diameter wafer), can be routinely made within 10 minutes. The resultant polymer-embedded colloidal crystals exhibit highly ordered surface modulation and can be directly used as templates for creating 2D gratings (Figure 3). The same PVD processes as described above are used to coat a thin layer of material on the top surface of the spin-coated colloidal crystals. Protrusion defects can be completely avoided as the inner voids are filled with polymer and PVD material deposition can only occur on the colloidal crystal surface. Another great advantage of the new approach is that, for metals with weak adhesion to the templates, such as Au, Ag, Pt, and Pd, the resultant surface gratings can be easily peeled off from the template surface. No wet etching is required and the original templates can be reused in making new surface gratings.

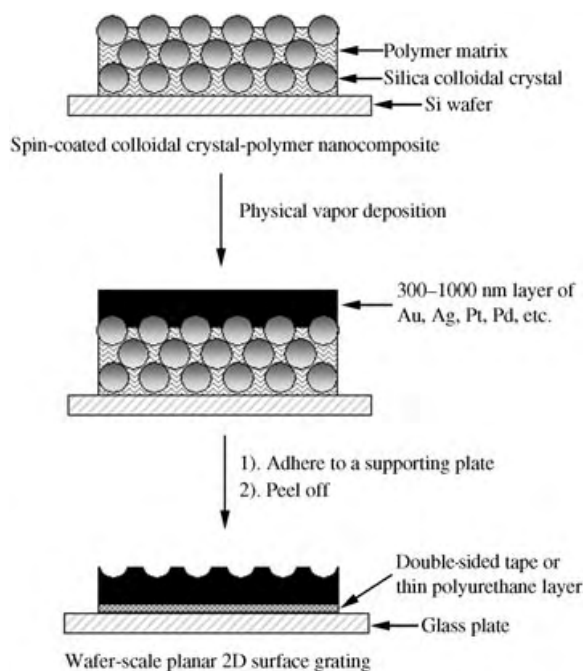


Figure 3. Experimental procedures for making wafer-scale, 2D surface gratings by using spin-coated colloidal crystals as templates.

Figure 4a shows a 10 cm diameter (81 cm²) platinum surface grating templated from a spin-coated silica colloidal crystal (320 nm diameter). A thin polyurethane layer is used to adhere the platinum film to a supporting glass plate. Under white-light illumination, a striking six-arm diffraction star is apparent. The adjacent arms of the diffraction star form exact 60° angles, a result indicating the formation of 2D hexagonally close-packed void arrays over the whole sample surface.^[37,38] The multiple reflected colors are caused by different incident angles of the illuminating white light.^[36,37] The long-range hexagonal ordering of the void array is evident from the SEM

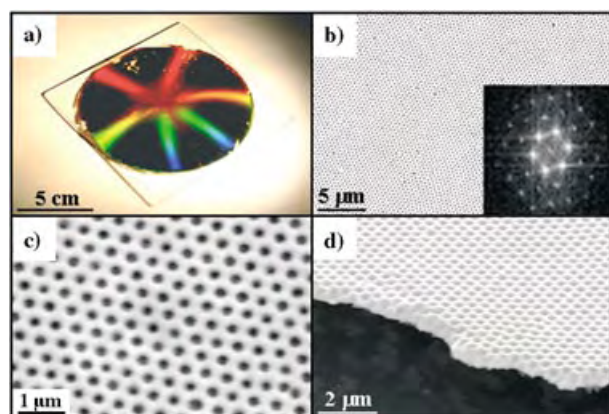


Figure 4. Wafer-scale surface gratings. a) Photo of a 10 cm diameter platinum surface grating templated from a spin-coated silica (320 nm diameter) colloidal crystal. b) Top-view SEM image and its FFT image (inset) of the sample shown in (a). c) Higher-magnification SEM image of the same sample. d) Cross-sectional view of the same sample. Platinum was deposited by using a Denton DV-502A E-beam evaporator.

image and its FFT image shown in Figure 4b. The higher-magnification SEM image in Figure 4c reveals that the voids are well separated from each other. This occurs for two reasons: first, silica colloids in the original colloidal crystal are separated from each other by about 1.4 times the sphere diameter;^[35] second, the surface protrusion height of silica spheres in the original template is less than the radius of spheres. By using a simple geometrical calculation, the depth of the final voids (h) can be related to the radius of the template colloid (r) and the radius of the voids (a) as $h = r - \sqrt{r^2 - a^2}$. The calculated void depth of the sample in Figure 4c is ≈ 58 nm, which is about one-third of the radius of the template silica sphere (160 nm) and is in good agreement with the measured depth from the cross-sectional SEM image shown in Figure 4d. To make deeper voids, homogeneous oxygen reactive-ion etching (RIE) can be used to remove the surface polymer layer to release silica spheres with various depths.

Besides PVD, other procedures such as poly(dimethylsiloxane) casting can also be applied in making highly ordered, wafer-scale surface-relief structures, which can then be used as molds for soft lithography^[39,40] and nanoimprint lithography^[41] to fabricate periodic submicron dot and hole arrays from a large variety of functional materials.

In summary, we have developed a nonlithographic approach to the fabrication of large-area surface gratings with 2D ordered arrays of submicron voids. 3D ordered colloidal crystals, made by convective self-assembly and spin-coating, are used as templates to create 2D surface gratings, provided the material deposition only occurs on the periodic surfaces of the templates. The technique allows the production of surface gratings from a large variety of functional materials, such as metals, semiconductors, and dielectrics; these gratings may find important technological applications in areas ranging from subwavelength optics to biological microanalysis.

Received: May 3, 2004

Keywords: colloidal crystals · self-assembly · surface chemistry · template synthesis

- [1] C. T. Kresge, M. E. Leonowicz, W. J. Roth, J. C. Vartuli, J. S. Beck, *Nature* **1992**, 359, 710.
- [2] Q. S. Huo, D. I. Margolese, U. Ciesla, P. Y. Feng, T. E. Gier, P. Sieger, R. Leon, P. M. Petroff, F. Schüth, G. D. Stucky, *Nature* **1994**, 368, 317.
- [3] H. Yang, A. Kuperman, N. Coombs, S. Mamiche-Afara, G. A. Ozin, *Nature* **1996**, 379, 703.
- [4] M. Park, C. Harrison, P. M. Chaikin, R. A. Register, D. H. Adamson, *Science* **1997**, 276, 1401.
- [5] C. R. Martin, *Science* **1994**, 266, 1961.
- [6] O. D. Velev, T. A. Jede, R. F. Lobo, A. M. Lenhoff, *Nature* **1997**, 389, 447.
- [7] B. T. Holland, C. F. Blanford, A. Stein, *Science* **1998**, 281, 538.
- [8] R. R. Meyer, J. Sloan, R. E. Dunin-Borkowski, A. I. Kirkland, M. C. Novotny, S. R. Bailey, J. L. Hutchison, M. L. H. Green, *Science* **2000**, 289, 1324.
- [9] Y. G. Sun, Y. N. Xia, *Science* **2002**, 298, 2176.
- [10] W. Shenton, D. Pum, U. B. Sleytr, S. Mann, *Nature* **1997**, 389, 585.

- [11] A. Blanco, E. Chomski, S. Grabtcchak, M. Ibisate, S. John, S. W. Leonard, C. Lopez, F. Meseguer, H. Miguez, J. P. Mondia, G. A. Ozin, O. Toader, H. M. van Driel, *Nature* **2000**, 405, 437.
- [12] P. V. Braun, P. Wiltzius, *Nature* **1999**, 402, 603.
- [13] Y. A. Vlasov, X. Z. Bo, J. C. Sturm, D. J. Norris, *Nature* **2001**, 414, 289.
- [14] Y. N. Xia, B. Gates, Y. D. Yin, Y. Lu, *Adv. Mater.* **2000**, 12, 693.
- [15] P. Jiang, J. F. Bertone, V. L. Colvin, *Science* **2001**, 291, 453.
- [16] S. A. Johnson, P. J. Ollivier, T. E. Mallouk, *Science* **1999**, 283, 963.
- [17] H. W. Deckman, J. H. Dunsmuir, *Appl. Phys. Lett.* **1982**, 41, 377.
- [18] J. C. Hulsteen, R. P. Van Duyne, *J. Vac. Sci. Technol. A* **1995**, 13, 1553.
- [19] C. L. Haynes, R. P. Van Duyne, *J. Phys. Chem. B* **2001**, 105, 5599.
- [20] M. H. Wu, C. Park, G. M. Whitesides, *J. Colloid Interface Sci.* **2003**, 265, 304.
- [21] J. C. Love, B. D. Gates, D. B. Wolfe, K. E. Paul, G. M. Whitesides, *Nano Lett.* **2002**, 2, 891.
- [22] Y. Lu, H. Xiong, X. C. Jiang, Y. N. Xia, M. Prentiss, G. M. Whitesides, *J. Am. Chem. Soc.* **2003**, 125, 12724.
- [23] T. W. Ebbesen, H. J. Lezec, H. F. Ghaemi, T. Thio, P. A. Wolff, *Nature* **1998**, 391, 667.
- [24] W. L. Barnes, A. Dereux, T. W. Ebbesen, *Nature* **2003**, 424, 824.
- [25] D. Gollub, M. Fischer, M. Kamp, A. Forchel, *Appl. Phys. Lett.* **2002**, 81, 4330.
- [26] J. Wang, S. Schablitsky, Z. N. Yu, W. Wu, S. Y. Chou, *J. Vac. Sci. Technol. B* **1999**, 17, 2957.
- [27] W. C. Tan, J. R. Sambles, T. W. Preist, *Phys. Rev. B* **2000**, 61, 13177.
- [28] P. M. Tessier, O. D. Velez, A. T. Kalambur, J. F. Rabolt, A. M. Lenhoff, E. W. Kaler, *J. Am. Chem. Soc.* **2000**, 122, 9554.
- [29] H. Ichikawa, T. Baba, *Appl. Phys. Lett.* **2004**, 84, 457.
- [30] K. P. Troyer, R. M. Wightman, *Anal. Chem.* **2002**, 74, 5370.
- [31] B. Erdogan, L. L. Song, J. N. Wilson, J. O. Park, M. Srinivasarao, U. H. F. Bunz, *J. Am. Chem. Soc.* **2004**, 126, 3678.
- [32] A. S. Dimitrov, K. Nagayama, *Langmuir* **1996**, 12, 1303.
- [33] P. Jiang, J. F. Bertone, K. S. Hwang, V. L. Colvin, *Chem. Mater.* **1999**, 11, 2132.
- [34] S. Wong, V. Kitaev, G. A. Ozin, *J. Am. Chem. Soc.* **2003**, 125, 15589.
- [35] P. Jiang, M. J. McFarland, *J. Am. Chem. Soc.*, in press.
- [36] P. N. Bartlett, J. J. Baumberg, S. Coyle, M. E. Abdelsalam, *Faraday Discuss.* **2004**, 125, 117.
- [37] R. L. Hoffman, *Trans. Soc. Rheol.* **1972**, 16, 155.
- [38] P. Pieranski, *Contemp. Phys.* **1983**, 24, 25.
- [39] Y. N. Xia, J. Tien, D. Qin, G. M. Whitesides, *Langmuir* **1996**, 12, 4033.
- [40] Y. N. Xia, G. M. Whitesides, *Angew. Chem.* **1998**, 110, 568; *Angew. Chem. Int. Ed.* **1998**, 37, 551.
- [41] S. Y. Chou, P. R. Krauss, P. J. Renstrom, *Science* **1996**, 272, 85.

The First All-Cyanide Fe₄S₄ Cluster: [Fe₄S₄(CN)₄]^{3-*}

Thomas A. Scott and Hong-Cai Zhou*

In pervasiveness of occurrence and multiplicity of function, iron–sulfur clusters rival the biological prosthetic groups such as hemes and flavins.^[1] Starting from the first spontaneous self-assembly of the [Fe₄S₄(SR)₄]²⁻ cluster in 1972,^[2] and the identification of the protein-bound Fe₄S₄ in the same year, the study of iron–sulfur clusters has evolved into a mature field in which the synthetic inorganic chemistry now resembles the total synthesis of natural products in organic chemistry.^[3] However, the identification of an all-ferrous Fe₄S₄⁰ state in the Fe protein of nitrogenase,^[4,5] which may have important implications in the mechanism of nitrogen fixation,^[6,7] has posed a great challenge to inorganic synthetic chemists because when isolated from the protein environment, the Fe₄S₄⁰ state is difficult to access chemically. For example, the midpoint potential of [Fe₄S₄(SPh)₄]^{3-/4-} is –1.72 V versus saturated calomel electrode (SCE).^[8] Holm et al.^[9] initiated the stabilization of the low oxidation states of the Fe₄S₄ cluster by using sterically demanding trialkyl phosphine ligands, and synthesized a number of iron sulfur clusters in the all-ferrous state. However, the all-ferrous [Fe₄S₄(PR₃)₄]⁰ cluster was identified only in solution. Attempts to isolate the cluster in pure form resulted in ligand loss and the formation of higher nuclearity clusters.^[10] To prevent ligand loss, a π -acid ligand which can bind the Fe₄S₄ core through σ donation and stabilize low oxidation states by π backbonding is needed. The stabilization of the all-ferrous Fe₄S₄⁰ core using CO resulted in an [Fe₄S₄(CO)₁₂] cluster^[11] containing six-coordinate iron atoms and an Fe...Fe separation of 3.47 Å (compared to 2.73 Å in reduced ferredoxin); this all-ferrous cluster is thus biologically irrelevant. Herein we report an [Fe₄S₄(CN)₄]³⁻ cluster that resembles the protein Fe₄S₄⁺ active sites geometrically and spectroscopically, and possesses [Fe₄S₄L₄]^{2-/3-} (L is a mono-anionic ligand) and [Fe₄S₄L₄]^{3-/4-} midpoint potentials of –0.4 and –1.38 V versus Ag/AgCl, the least negative such potentials among all synthetic analogues of the Fe₄S₄ protein active sites (For the conversion among different reference electrodes, see Table 2). These redox

[*] T. A. Scott, Prof. Dr. H.-C. Zhou
Department of chemistry and Biochemistry
Miami University
Oxford, OH 45056 (USA)
Fax: (+01) 513-529-8091
E-mail: zhohu@muohio.edu

[**] We thank Dr. Catalina Achim for Mössbauer studies, Dr. Brian Bennett for collecting and simulating the EPR spectra, and Tracy Petersen, David Collins for discussion. We also thank Miami University, the donors of the American Chemical Society Petroleum Research Fund (PRF No. 39794-G3), and the National Science Foundation (ECS-0403669) for financial support. H.C.Z. also thanks the Research Corporation for an Award (R11188). The X-ray diffractometer is supported by the NSF (EAR-0003201).

potentials are less negative than expected and imply a possible new path to a biologically relevant all-ferrous $[\text{Fe}_4\text{S}_4\text{L}_4]^{4-}$ cluster, which is a goal in iron-sulfur protein analogue chemistry.

The reduction of $[\text{Fe}_4\text{S}_4\text{Cl}_4]^{2-}$ in the presence of CN^- followed by the addition of $\text{Na}(\text{BPh}_4)$ leads to the formation of $[\text{Fe}_4\text{S}_4(\text{CN})_4]^{3-}$ (**1**; Figure 1). Cluster **1** can also be made in

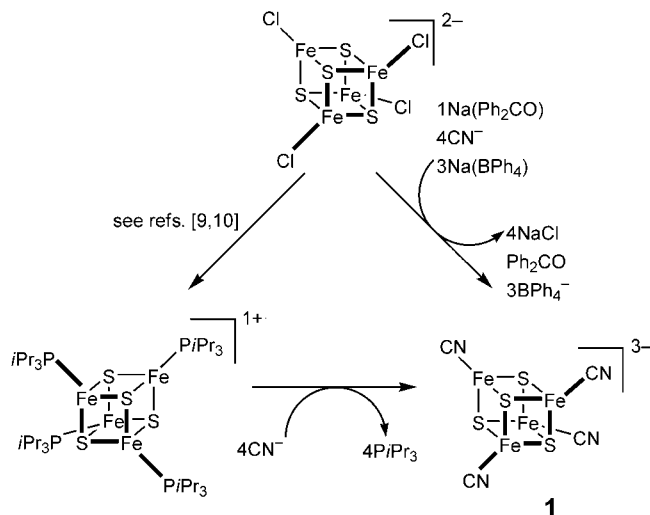


Figure 1. The preparation of the $[\text{Fe}_4\text{S}_4(\text{CN})_4]^{3-}$ cluster **1**.

higher yield by using $[\text{Fe}_4\text{S}_4(\text{PiPr}_3)_4]^+$ as the starting cluster.^[10] The reaction between $[\text{Fe}_4\text{S}_4\text{Cl}_4]^{2-}$ and $[\text{Bu}_4\text{N}][\text{CN}]$ gave an unidentified black solid, which showed none of the electrochemical characteristics of **1** or of the one-electron oxidized form of **1**. Thus, the substitution of the Cl^- ion for the CN^- ion needs to occur after the one-electron reduction of the $\text{Fe}_4\text{S}_4^{2+}$ core. This result is consistent with the observation that the reduction of the Fe_4S_4 core facilitates ligand substitution.^[9,10]

Compound **1** crystallizes in space group $R\bar{3}c$ with the N2, C2, Fe2, and S2 atoms residing on a threefold axis (Figure 2).^[12] Every unit cell contains six formula units of **1**. The cluster anion has approximate T_d symmetry, but is slightly elongated along the crystallographic threefold axis. Selected interatomic distances and angles are listed in Table 1.

The Fe–S and Fe···Fe separations of **1** (Table 1) closely resemble those of the protein Fe_4S_4^+ core (Fe–S 2.281, 2.285;

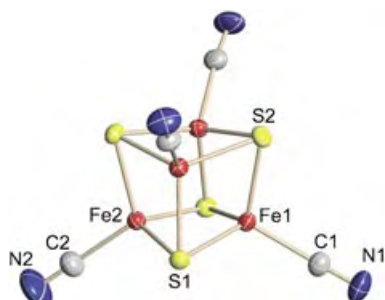


Figure 2. The structure of $[\text{Fe}_4\text{S}_4(\text{CN})_4]^{3-}$ thermal ellipsoids set at 50% probability (see Table 1).

Table 1: Selected interatomic distances [Å] and angles [°] for **1**.

Fe···Fe	Fe–S	Fe–C	C–N	Fe–C–N
2.6906(6)	2.2791(8)	2.031(3)	1.132(4)	174.6(3)
	2.2846(10)			
	2.2863(7)			
2.7240(7)	2.3003(7)	2.016(7)	1.21(1)	180

Fe···Fe 2.726 Å) in *C. acidi-urici* Fd_{red} (reduced ferredoxin),^[13] and corresponding synthetic analogue $[\text{Fe}_4\text{S}_4(\text{SPh})_4]^{3-}$ (Fe–S 2.29, Fe···Fe 2.74).^[14] One of the Fe–CN groups is perfectly linear (crystallographically imposed), and the other three deviate slightly from strict linearity (Fe–C–N 174.6(3)°). An IR spectrum of **1** shows an $\nu(\text{C/N})$ stretch at 2103 cm^{-1} , which is almost the same as the $\nu(\text{C/N})$ stretch in $[\text{Fe}^{\text{II}}(\text{CN})_6]^{4-}$ (2098 cm^{-1}) but quite different from that in $[\text{Fe}^{\text{III}}(\text{CN})_6]^{3-}$ (2135 cm^{-1}), which indicates a strong π backbonding and the predominantly ferrous character of **1**.^[15]

It is informative to compare the geometric parameters of **1** with those of the recently determined crystal structure of the all-ferrous Fe_4S_4^0 form of the nitrogenase Fe protein from *Azotobacter vinelandii* (Av Fe protein).^[16] The average Fe···Fe distance of 2.699 Å is slightly longer than that in the Fe_4S_4^0 cluster in Av Fe protein (2.65 Å), implying stronger Fe···Fe interaction in the all-ferrous state. In contrast, the average Fe–S separation of 2.288 Å in **1** is slightly shorter than that in the all-ferrous Av Fe protein cluster (2.33 Å), which reflects the elongation of the Fe–S bonds in a Fe_4S_4 cluster upon reduction from Fe_4S_4^+ to Fe_4S_4^0 . This elongation of Fe–S bonds has also been observed upon the reduction of the $\text{Fe}_4\text{S}_4^{2+}$ state to the Fe_4S_4^+ state in other synthetic analogues.^[14] The exact iron oxidation states in **1** have also been confirmed by electrochemical, EPR, Mössbauer, and UV/Vis studies.

As shown in Figure 3, the cyclic voltammogram of **1** using glassy carbon as the working electrode shows two reversible electrochemical pairs. For clarity, the redox potentials have all been converted into those versus normalized hydrogen electrode (NHE) and are listed in Table 2. In the following

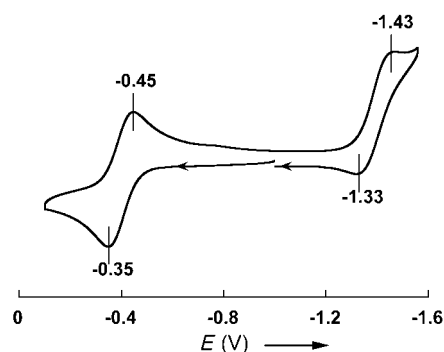


Figure 3. Cyclic voltammogram (100 mVs^{-1}) of $[\text{Fe}_4\text{S}_4(\text{CN})_4]^{3-}$ in 0.1 M solution of $[\text{Bu}_4\text{N}][\text{PF}_6]$ in CH_2Cl_2 . Peak potentials are those versus Ag/AgCl ($E_{1/2}$ versus Fc/Fc^+ 0.69 V; $\text{Fc} = [(\text{C}_5\text{H}_5)_2\text{Fe}]$) using a glassy carbon working electrode. Potentials versus NHE can be found in Table 2.

Table 2: Comparison of redox potentials (V) of **1** with those of the relevant Fe_4S_4 cores.^[a]

L	$E_{1/2} [\text{Fe}_4\text{S}_4\text{L}_4]^{2-/3-}$	$E_{1/2} [\text{Fe}_4\text{S}_4\text{L}_4]^{3-/4-}$	Ref.
CN^-	−0.18	−1.16	this work
$^-\text{SC}_6\text{H}_4\text{-}p\text{-NO}_2$	−0.41		[19]
^-SPh	−0.76	−1.48	[8, 19]
<i>Enzyme:</i>			
Ferredoxin	−0.4		[17]
Av Nitrogenase Fe protein		−0.8	[18]

[a] All redox potentials are those versus NHE. Standard potentials (V) in aqueous solutions at 25 °C versus NHE: SCE + 0.2415; Ag/AgCl + 0.2223.^[24]

discussion, potentials are those versus NHE only. Cluster **1** possesses midpoint potentials of −0.18 and −1.16 V. The former corresponds to that of the $[\text{Fe}_4\text{S}_4\text{L}_4]^{2-/3-}$ redox pair, which is less negative than that of $\text{Fd}_{\text{ox}}/\text{Fd}_{\text{red}}$ (−0.4 V) in native proteins,^[17] the latter represents $E_{1/2}$ of the $[\text{Fe}_4\text{S}_4\text{L}_4]^{3-/4-}$ redox pair, the closest to that of iron protein of nitrogenase (−0.8 V).^[18] Previously, the least negative $[\text{Fe}_4\text{S}_4\text{L}_4]^{2-/3-}$ potential in synthetic analogues was −0.41 V in $[\text{Fe}_4\text{S}_4(\text{SC}_6\text{H}_4\text{-}p\text{-NO}_2)_4]^{2-}$,^[19] and that for $[\text{Fe}_4\text{S}_4\text{L}_4]^{3-/4-}$ was −1.48 V in $[\text{Fe}_4\text{S}_4(\text{SPh})_4]^{2-}$.^[8, 19]

Using platinum instead of glassy carbon as the working electrode, the peak currents of **1** diminish progressively when a multiple scan is performed. Whether this is due to cyanide adsorption and polymerization on the platinum surface^[20] or interaction between the clusters and the platinum surface needs further investigation.

Preliminary EPR (axial, $g_2 = 2.114$, $g_3 = 1.897$ at 9 K) and Mössbauer (δ at 4.2 K relative to Fe metal: 0.503, 0.566; ΔE_Q : 1.329, 1.869) studies have confirmed the oxidation state of **1**. The spectroscopic features are very similar to those of Fe_4S_4^+ proteins and their corresponding synthetic analogues,^[14] but the final answer for the ground state needs high-field Mössbauer and variable-temperature EPR studies (works currently under way and will be presented elsewhere). In addition, the absorption spectrum of **1** in MeCN is featureless, in agreement with those of all other proteins and synthetic analogues in the Fe_4S_4^+ core oxidation state.^[1]

The closest examples in the literature to **1** are the octanuclear complexes $[\text{Fe}_4\text{S}_4(\text{NC-ML}_n)_4]^{2-}$ ($\text{M} = \text{W}$ and Mn),^[21, 22] where the cyanide bridges were reversed and act as linkers between an Fe_4S_4 cluster and four other metal cluster units. The core oxidation state was $\text{Fe}_4\text{S}_4^{2+}$. The key for **1** remaining monomeric is the reduction of the cluster from $\text{Fe}_4\text{S}_4^{2+}$ to Fe_4S_4^+ . It is now possible to use **1** as a secondary building unit to clusters of higher nuclearities or coordination polymers by simply oxidizing **1** in the presence of other metal species with open coordination sites.

A monosubstituted cyanide cluster, $[\text{Fe}_4\text{S}_4(\text{LS}_3)(\text{CN})]^{2-}$, was also detected spectroscopically,^[23] but **1** represents the first all-cyanide Fe_4S_4 cluster.

In summary, we have isolated and characterized the first all-cyanide Fe_4S_4 cluster, which resembles the protein Fe_4S_4 clusters geometrically, electrochemically, and spectroscopi-

cally, and has the least negative $[\text{Fe}_4\text{S}_4\text{L}_4]^{2-/3-}$ and $[\text{Fe}_4\text{S}_4\text{L}_4]^{3-/4-}$ redox potentials among all known synthetic analogues.

Experimental Section

Method A: A black crystalline solid of $(\text{Bu}_4\text{N})_2[\text{Fe}_4\text{S}_4\text{Cl}_4]$ (0.293 g, 0.3 mmol) was suspended in THF (2.5 mL) and mixed with a $[\text{Bu}_4\text{N}][\text{CN}]$ (0.322 g, 1.2 mmol) solution in THF (2.5 mL). Freshly made potassium benzophenoketyl (0.33 mmol) in THF (2 mL) was added drop-wise to the mixture, and the mixture was stirred for 15 min. The addition of $\text{Na}(\text{BPh}_4)$ (0.308 g, 0.3 mmol) in THF (2 mL) caused precipitation of a white solid, presumably NaCl. The resulting suspension was stirred for 1.5 h and dried under vacuum to yield a black solid. The solid was extracted with MeCN (5 mL), and the extraction was filtered through Celite. Diethyl ether vapor diffusion into the filtrate caused the precipitation of a black solid and colorless crystals within three days. The compound was purified through recrystallization from MeCN/diethyl ether with minimal amounts of MeCN to dissolve only the dark solid. Black block crystals of **1** formed after three crystallizations. Yield: 0.145 g (41 %).

Method B: A black crystalline solid of $(\text{BPh}_4)[\text{Fe}_4\text{S}_4(\text{P}(\text{Pr})_3)_4]$ (0.394 g, 0.3 mmol) was dissolved in THF (2.5 mL), and mixed with a $[\text{Bu}_4\text{N}][\text{CN}]$ (0.322 g, 1.2 mmol) solution in THF (2.5 mL). The mixture was stirred for 2 h to form a suspension, and then allowed to settle. The supernatant solution was decanted and the solid was washed with aliquots of THF and dried under vacuum. The black residue was dissolved in MeCN (8 mL) and crystallized from MeCN/diethyl ether yielding black block crystals of **1**. Yield: 0.240 g (67 %). Elemental analysis calcd (%) for $\text{C}_{52}\text{H}_{108}\text{N}_4\text{Fe}_4\text{S}_4$: C 52.79, H 9.20, N 8.28, S 10.84; found: C 52.57, H 9.22, N 7.98, S 10.87.

Received: June 4, 2004

Revised: July 15, 2004

Keywords: bioinorganic chemistry · cyanides · iron · nitrogenases · sulfur

- [1] P. V. Rao, R. H. Holm, *Chem. Rev.* **2004**, *104*, 527–559.
- [2] T. Herskovitz, B. A. Averill, R. H. Holm, J. A. Ibers, W. D. Phillips, J. F. Weiher, *Proc. Natl. Acad. Sci. USA* **1972**, *69*, 2437–2441.
- [3] R. H. Holm in *Comprehensive Coordination Chemistry II*, Vol. 8 (Eds.: J. A. McCleverty, T. J. Meyer), New York, **2004**, 61–90.
- [4] G. D. Watt, K. R. N. Reddy, *J. Inorg. Biochem.* **1994**, *53*, 281–294.
- [5] H. C. Angove, S. J. Yoo, B. K. Burgess, E. Münck, *J. Am. Chem. Soc.* **1997**, *119*, 8730–8731.
- [6] B. K. Burgess, D. J. Lowe, *Chem. Rev.* **1996**, *96*, 2983–3011.
- [7] A. C. Nyborg, J. L. Johnson, A. Gunn, G. D. Watt, *J. Biol. Chem.* **2000**, *275*, 39307–39312.
- [8] J. Cambray, R. W. Lane, A. G. Wedd, R. W. Johnson, R. H. Holm, *Inorg. Chem.* **1977**, *16*, 2565–2571.
- [9] C. Goh, B. M. Segal, J. Huang, J. R. Long, R. H. Holm, *J. Am. Chem. Soc.* **1996**, *118*, 11844–11853.
- [10] H.-C. Zhou, R. H. Holm, *Inorg. Chem.* **2003**, *42*, 11–21.
- [11] L. L. Nelson, F. Y. K. Lo, A. D. Rae, L. F. Dahl, *J. Organomet. Chem.* **1982**, *225*, 309–329.
- [12] Crystal structure determination of **1**: $\text{C}_{52}\text{H}_{108}\text{Fe}_4\text{N}_4\text{S}_4$, $M_r = 1183.09$; a black crystal (0.30 × 0.27 × 0.15 mm) mounted on a Pyrex fiber under a cold stream of N_2 , $T = 173(2)$ K, $\lambda(\text{MoK}\alpha) = 0.71073$ Å, rhombohedral, space group $R\bar{3}c$, $a = 16.9244(3)$, $c = 38.4541(14)$ Å, $\alpha = \beta = 90^\circ$, $\gamma = 120^\circ$, $V = 9538.9(4)$ Å³, $Z = 6$, $\rho_{\text{calcd}} = 1.236$ g cm^{−3}, $2\theta_{\text{max}} = 56.6^\circ$, $\mu = 1.062$ mm^{−1}, empirical absorption correction using SADABS, $F(000) = 3822$, 22584

reflections, 3859 unique reflections, 314 parameters, 1 restraint, GOF = 1.151, $R_1 = 0.0339$ [$I > 2\sigma(I)$], $wR_2 = 0.0825$, min./max. residual electron density $-0.265/0.584 \text{ e } \text{\AA}^{-3}$, refined on $|F^2|$. CCDC-240511 (**1**) contains the supplementary crystallographic data for this paper. These data can be obtained free of charge via www.ccdc.cam.ac.uk/conts/retrieving.html (or from the Cambridge Crystallographic Data Centre, 12 Union Road, Cambridge CB21EZ, UK; fax: (+44)1223-336-033; or deposit@ccdc.cam.ac.uk).

- [13] Z. Dauter, K. S. Wilson, L. C. Sieker, J. Meyer, J. M. Moulis, *Biochemistry* **1997**, *36*, 16065–16073.
 - [14] E. J. Laskowski, R. B. Frankel, W. O. Gillum, G. C. Papaefthymiou, J. Renaud, J. A. Ibers, R. H. Holm, *J. Am. Chem. Soc.* **1978**, *100*, 5322–5337.
 - [15] K. R. Dunbar, R. A. Heintz in *Progress in Inorganic Chemistry*, Vol. 45 (Ed.: K. D. Karlin), Wiley, New York, **1997**, pp. 283–391.
 - [16] P. Strop, P. M. Takahara, H.-J. Chiu, H. C. Angove, B. K. Burgess, D. C. Rees, *Biochemistry* **2001**, *40*, 651–656.
 - [17] J. M. Berg, R. H. Holm in *Iron-Sulfur Proteins* (Ed.: T. G. Spiro), Wiley, New York, **1982**, pp. 1–66.
 - [18] M. Guo, F. Sulc, M. W. Ribbe, P. J. Farmer, B. K. Burgess, *J. Am. Chem. Soc.* **2002**, *124*, 12100–12101.
 - [19] C. Zhou, J. W. Raebiger, B. M. Segal, R. H. Holm, *Inorg. Chim. Acta* **2000**, *300–302*, 892–902.
 - [20] G. Baltrunas, E. Morkyavichius, T. Yankauskas, *Russ. J. Electrochem.* **1998**, *33*, 572–575.
 - [21] N. Zhu, J. Pebler, H. Vahrenkamp, *Angew. Chem.* **1996**, *108*, 984–985; *Angew. Chem. Int. Ed. Engl.* **1996**, *35*, 894–895.
 - [22] N. Zhu, R. Appelt, H. Vahrenkamp, *J. Organomet. Chem.* **1998**, *565*, 187–192.
 - [23] R. H. Holm, S. Ciurli, J. A. Weigel, in *Progress in Inorganic Chemistry*, Vol. 38 (Ed.: S. J. Lippard), Wiley, New York, **1990**, pp. 1–74.
 - [24] A. J. Bard, L. R. Faulkner, *Electrochemical Methods-Fundamentals and Applications*, 2nd ed., Wiley, New York, **2001**, pp. 808–809.
-

Isolation and Structure of an “Imploded”
Cryptophane**

Scott T. Mough, John C. Goeltz, and K. Travis Holman*

Molecules and molecular assemblies of effectively closed-shell topologies have been the subject of much contemporary interest because of their ability to encapsulate smaller molecular substrates.^[1,2] The cavity interiors have been used for a number of remarkable applications, including for enantioselective recognition,^[3] for stabilizing and characterizing reactive species,^[4] as microreaction chambers,^[5] and to demonstrate new forms of stereoisomerism.^[6] The unique properties of the so-called container molecules or capsules stem directly from their ability to bind guests constrictively.^[7] That is, the nearly closed surfaces of molecular containers provide comparatively large steric barriers to the ingress and egress of guests. The resulting complexes experience a corresponding enhancement in their kinetic stabilities, thus allowing encapsulation phenomena to be studied in detail. We have initiated a program aimed at tuning the thermal stabilities of materials generally derived from container molecules, one future goal of which is the synthesis of novel microporous materials with potential uses for gas storage or small-molecule separations. Our hypothesis is that, relative to traditional clathrates and solid-state inclusion compounds, those materials constructed from container-like molecules ought to exhibit appreciable kinetic stabilities with respect to the thermal loss of encapsulated guests. This feature augurs well for gas separation or storage applications, and organic materials possessing empty voids for such purposes are emerging.^[8]

Collet's elegant cryptophanes,^[1] constructed by the covalent bridging of two cuplike C_3 -substituted cyclotribenzylenes (CTBs), are quintessential molecular containers. They typically encapsulate guests constrictively, with constrictive binding energies (that is, the activation energies of complexation, ΔG_c^\ddagger) in excess of about 40 kJ mol^{-1} .^[1,9] Furthermore, they display an impressive ability to bind and discriminate between guests on the basis of size, shape, and electronic characteristics in both hydrophilic and lipophilic solvents. We report

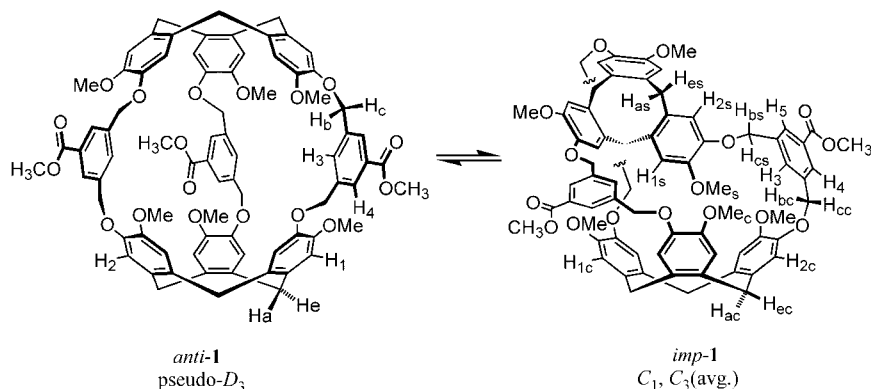
[*] S. T. Mough, J. C. Goeltz, Dr. K. T. Holman
Department of Chemistry
Georgetown University
Washington, D.C. 20057 (USA)
Fax: (+1) 202-687-6209
E-mail: kth7@georgetown.edu

[**] This work was supported by Georgetown University and by the National Science Foundation CAREER award program (DMR-0349316). S.T.M. thanks the Metropolitan Washington section of the Achievement Rewards for College Scientists for financial support.



Supporting information for this article (experimental details, including synthetic procedures, kinetic data, and 2D NMR spectra) is available on the WWW under <http://www.angewandte.org> or from the author.

herein the synthesis of a new *exo*-ester-functionalized *m*-xylyl-bridged cryptophane^[10] (\pm)-*anti*-**1** (Scheme 1) and the structure and thermal behavior of its crystalline inclusion compound with tetrahydrofuran (THF). Our studies reveal



Scheme 1.

that, once emptied, the cryptophane containers equilibrate between “empty” and “imploded” conformers at high temperatures in the solid state, the latter of which is a kinetically stable atropisomer that has been isolated and structurally characterized.

Cryptophane (\pm)-*anti*-**1** was synthesized in racemic form (10–12 % yield) by the formic acid catalyzed cyclization of the appropriate bis(vanillyl alcohol) precursor according to the two-step method developed by Canceill and Collet.^[11] Separation of (\pm)-*anti*-**1** from the lower-yielded *syn* diastereomer was readily accomplished by flash chromatography. Dissolution of crude (\pm)-*anti*-**1** in tetrahydrofuran results in the precipitation of crystalline racemic [(\pm)-*anti*-**1**thf]·3THF over a period of a few minutes. The single-crystal structure reveals, as expected, one thf molecule to be centrally located within the cryptophane molecular cavity.^[12] A space-filling representation illustrates the encapsulation of this guest (Figure 1). In the solid state, the host cryptophane deviates significantly from the idealized D_3 symmetry observed in solution. Eleven of the twelve OCH₃ and OCH₂ groups are roughly in plane with the aromatic rings of the CTB cups, although differences in the C(cup)-O-C-C(xylyl) dihedral angles result in the skewed conformation depicted in Figure 1. Although some positional disorder is evident, the major orientation of the encapsulated THF molecule shows the oxygen atom to be located near the xylyl-guarded portals of the cryptophane and in close contact to the inwardly directed arene and methylenic CH moieties.

Crystalline [(\pm)-*anti*-**1**thf]·3THF loses THF spontaneously under ambient conditions, but guest loss does not go to completion. Thermogravimetric analysis (TGA) of freshly prepared material shows that THF loss occurs in at least two steps and also that high temperatures are required to remove all of the included solvent (Figure 2). Indeed, if [(\pm)-*anti*-**1**thf]·3THF is left under ambient conditions for several days, or heated at 85 °C for over ten hours, THF loss occurs only to the extent of exactly three equivalents and a 1:1 [(\pm)-*anti*-**1**thf] material can be isolated. TGA confirms the 1:1

stoichiometry (5.2 % found, 5.3 % calcd) and illustrates the remarkable kinetic stability of this material. Whereas the onset temperature for THF loss from [(\pm)-*anti*-**1**thf]·3THF is below room temperature, the onset temperature for [(\pm)-*anti*-**1**thf] is over 100 °C—more than 35° above the normal boiling point of THF—and we surmise that the structure of [(\pm)-*anti*-**1**thf] consists of cryptophane container molecules essentially fully occupied with a guest. Molecular models of (\pm)-*anti*-**1** reveal that the *m*-xylyl bridges cannot readily fill the cryptophane cavity; thus, it seems reasonable to infer that the glassy, guest-free (\pm)-*anti*-**1** material possesses empty cryptophane cavities in the solid state.

The ¹H NMR spectrum of [(\pm)-*anti*-**1**thf] dissolved in CDCl₃ is uncomplicated and illustrates the pseudo- D_3 symmetry of the cryptophane (Figure 3a). Doublet resonances centered at δ = 4.59 and 3.33 ppm are characteristic of the axial and equatorial (H_a, H_e) methylenic protons at the lower rim of CTBs in the cup conformation (Scheme 1), the former being shifted significantly downfield as a result of steric crowding at the base of the cup (H_a...H_a ≈ 2.0 Å). Remarkably, complete emptying of the cryptophanes by

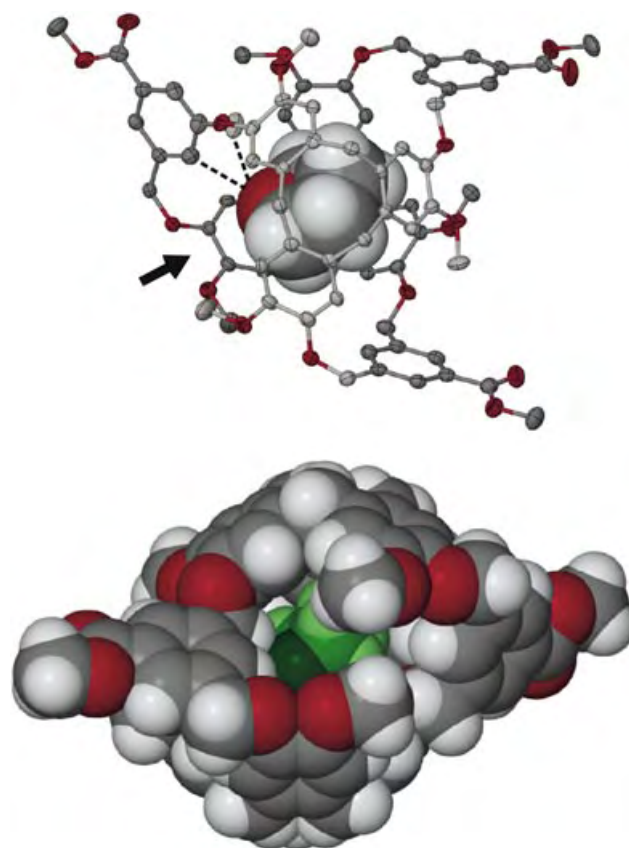


Figure 1. ORTEP (top) and space-filling (bottom) representations of the [(\pm)-*anti*-**1**thf] complex observed in the single-crystal structure of [(\pm)-*anti*-**1**thf]·3THF. The arrow shows the view taken for the space-filling illustration. In the bottom image, atoms corresponding to the THF molecule are shaded green for clarity.

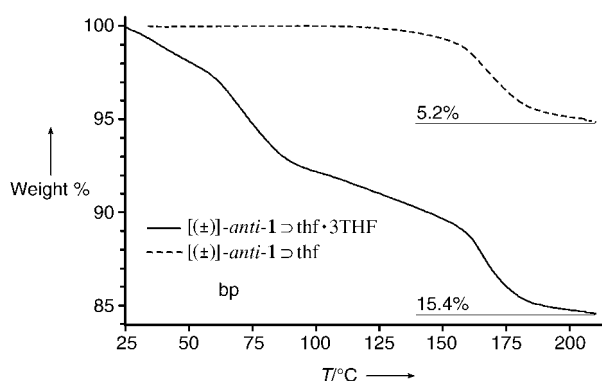


Figure 2. TGA ($5^{\circ}\text{C min}^{-1}$) of $[(\pm)\text{-anti-1}]\cdot\text{thf}\cdot 3\text{THF}$ (15.4% found, 18.4% calcd) and $[(\pm)\text{-anti-1}]\cdot\text{thf}$ (5.2% found, 5.3% calcd) illustrating the enhanced kinetic stability of encapsulated versus lattice-included guests.

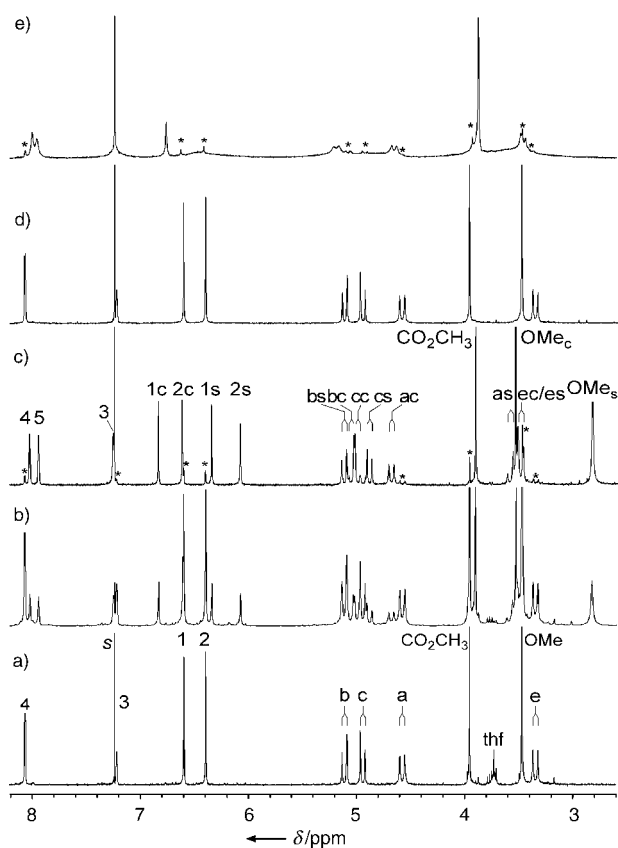


Figure 3. ^1H NMR spectra (300 MHz, CDCl_3 , 298 K unless noted otherwise) of: a) $[(\pm)\text{-anti-1}]\cdot\text{thf}$; b) "emptied" $(\pm)\text{-anti-1}$ immediately following thermogravimetry of $(\pm)\text{-anti-1}\cdot\text{thf}$ to 210°C ; c) purified $(\pm)\text{-imp-1}$; d) the same sample as in (c), but after 3 days at ambient temperature; e) the same sample as in (c), but at -55°C . Signal assignments are according to Scheme 1 (cup = H_c , saddle-twist = H_s , * = trace $(\pm)\text{-anti-1}$) and are supported by 2D ROESY and COSY experiments (see Supporting Information).

thermogravimetry at 210°C results in approximately 40% conversion of $(\pm)\text{-anti-1}$ into a species with a different spectroscopic signature (Figure 3b). Separation of this species from residual $(\pm)\text{-anti-1}$ has been accomplished by preparative TLC (silica gel, $\text{CH}_2\text{Cl}_2/\text{Et}_2\text{O}$ 8:1, $R_f=0.36$ and 0.43,

respectively). The ^1H NMR spectrum of the purified compound taken in CDCl_3 at room temperature is consistent with a loss of the C_2 rotation axes and a reduction to an apparent C_3 symmetry, which symbolizes an inequivalence of the CTB moieties (Figure 3c). The ^1H NMR spectrum observed in Figure 3c reverts cleanly to the original spectrum of $(\pm)\text{-anti-1}$ on standing of the sample in CDCl_3 or other solvents (Figure 3d), thus implying that the newly formed species possesses the same atomic connectivity and is merely an atropisomer of $(\pm)\text{-anti-1}$. Collet and co-workers previously observed that other cryptophanes give rise to spectral characteristics very similar to those seen in Figure 3b.^[1a,13] It was proposed that the apparently C_3 -symmetric species is an effectively imploded "in-out" cup-within-cup conformer wherein one of the two CTB cups is completely inverted.

Purification of the "imploded" atropisomer of $(\pm)\text{-anti-1}$ (hereafter $(\pm)\text{-imp-1}$) allows for detailed ^1H NMR spectral characterization, with peak assignments supported by 2D COSY and ROESY experiments. Although the 1D spectrum recorded at room temperature clearly exhibits a time-averaged C_3 symmetry, two notable features are seemingly at odds with the assignment of $(\pm)\text{-imp-1}$ as an "in-out" cup-within-cup structure: 1) of the two sets of H_a/H_e protons ascribed to the methylenic bridges of the orthocyclophane moieties, one set does not display the approximately 1.2 ppm chemical shift difference characteristic of a cuplike conformation ($\Delta\delta=0.14$ ppm), and 2) of the two unique methoxy signals one is significantly broadened and shifted upfield by approximately -0.65 ppm relative to that of $(\pm)\text{-anti-1}$ —this observation suggests dynamic behavior and a shielded environment for the methoxy groups.

Single crystals of $(\pm)\text{-imp-1}\cdot 11\text{CHCl}_3$ were obtained by vapor diffusion of *n*-pentane into a solution of purified $(\pm)\text{-imp-1}$ in CHCl_3 at -20°C .^[12] Although the data set is of poor quality because of the presence of 11 equivalents of partially disordered solvent, X-ray analysis confirms that $(\pm)\text{-imp-1}$ is indeed an atropisomer of $(\pm)\text{-anti-1}$, but not the "in-out" cup-within-cup form. As seen in Figure 4, *imp-1* adopts a C_1 conformation. One of the two CTB moieties maintains the cup conformation whereas the other exists in the so-called saddle-twist conformation, whereby one of the three methylenic groups is inverted inwardly through the intrannular ring. In the crystal, the center of mass of the saddle-twisted CTB is significantly offset from that of the cup-shaped one such that one of the twisted arene rings is able to project its methoxy substituent into the cup, thereby filling the cryptophane cavity. $(\pm)\text{-Imp-1}$ thus represents the first observation of the saddle-twist form of a CTB congener wherein the cup form has not been specifically destabilized by substitution.^[1b]

The X-ray structure $(\pm)\text{-imp-1}$ is consistent with the known conformational behavior of CTBs. The rate-determining step for cup-to-cup interconversion in CTBs is the intrannular flipping of the first methylenic group, with a barrier of $\Delta G_{298\text{K}}^{\ddagger}=110\text{--}115\text{ kJ mol}^{-1}$ for all known examples.^[1] The resulting highly flexible saddle-twist form—which can revert either to the original or the inverted-cup configuration—is typically $13\text{--}16\text{ kJ mol}^{-1}$ higher in energy than the cup form, thus implying that the barrier to conversion from the saddle-twist form into the cup form is in the range 94–

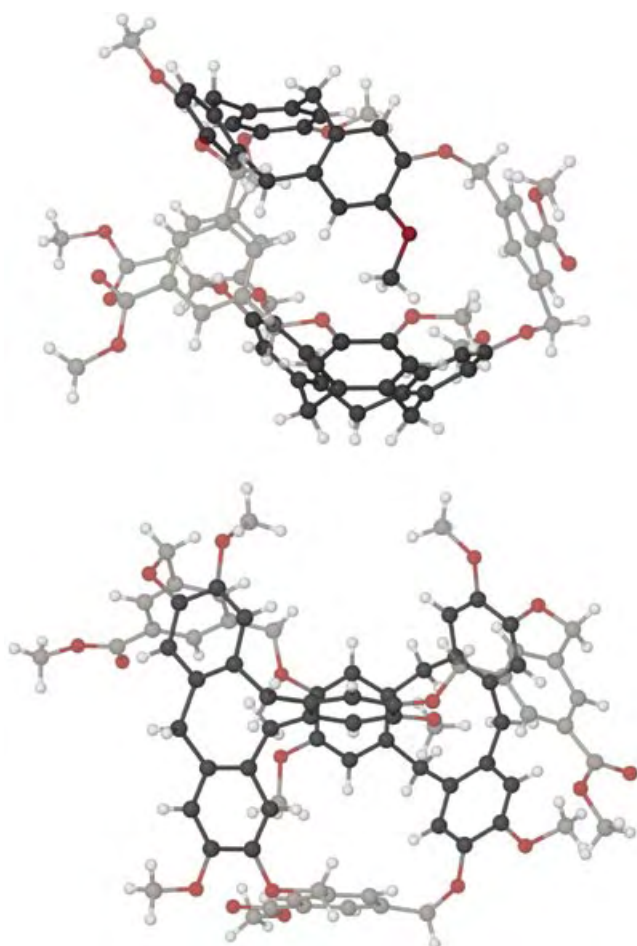


Figure 4. Two views of the imploded cryptophane *imp-1* as determined by the single-crystal structure of (\pm) -*imp-1*·11 CHCl₃. The carbon atoms of the CTB rings are shaded dark for clarity.

102 kJ mol⁻¹. These facts are consistent with rate studies which indicate that reversion of (\pm) -*imp-1* to (\pm) -*anti-1* in CDCl₃ follows first order kinetics with an energy barrier of $\Delta G_{298K}^{\ddagger} = 99(3)$ kJ mol⁻¹ ($\Delta H_{298K}^{\ddagger} = 70(3)$ kJ mol⁻¹ and $\Delta S^{\ddagger} = -98(5)$ J mol⁻¹ K⁻¹). Moreover, the measured energy barrier is considerably lower than what would be expected for a cup-within-cup conformer. Furthermore, the saddle-twist structure of (\pm) -*imp-1* allows for rationalization of the aforementioned ¹H NMR spectral peculiarities and signal assignments (Figure 3c). Specifically, relative to the cup conformation, the highly flexible saddle-twist conformer relieves steric congestion between the H_{as} protons at the base of the CTB moiety, and the result is a smaller difference in chemical shift between H_{as} and H_{es}. Additionally, the known conformational flexibility of the saddle-twist form is consistent with the observed time-averaged C₃ symmetry of (\pm) -*imp-1* in the ¹H NMR spectrum recorded at room temperature.^[1b] The C₁ conformer apparently interconverts rapidly with two equivalent C₁ forms, presumably via readily accessible saddle-twist forms wherein two of the three methylenic groups are flipped. The process is akin to a chiral propeller-like motion, such that the methoxy groups of each ring spend an equal amount of time projected into the cavity of the lower CTB cup, thus

inducing an upfield shift of the signals ($\Delta\delta = -0.65$ ppm). The time-averaged upfield shift is consistent with the large induced shifts (up to -4.5 ppm) that are commonly observed for guests encapsulated within the electronic-rich cavities of other cryptophanes.^[1] Cooling of the sample results in dramatic broadening of the signals as the rate of conversion between the C₁ conformers is slowed (Figure 3e). Nonetheless, even at -60 °C in CDCl₃, the signals corresponding to a frozen C₁ conformer are unresolved and the energy barrier for conversion between the saddle-twist forms was not determined.

In summary, we have synthesized a new *m*-xylyl-bridged cryptophane, (\pm) -*anti-1*. The thermal behavior of its crystalline inclusion compound with tetrahydrofuran illustrates that encapsulated guests are held onto more strongly than those in the lattice, presumably as a consequence of encapsulation. Complete thermal liberation of the guests results in (\pm) -*anti-1* partially undergoing a conformational “implosion” to form the isolable atropisomer (\pm) -*imp-1*, wherein one of the CTB moieties of the cryptophane exists in the saddle-twist conformation. These results have implications in the study of molecular-encapsulation phenomena and also for the design of guest-free container-molecule-based materials, the unique sorption and storage properties of which we are currently examining.

Received: June 4, 2004

Keywords: atropisomerism · cryptophanes · host–guest systems · inclusion compounds

- [1] a) A. Collet in *Comprehensive Supramolecular Chemistry*, Vol. 2 (Eds.: J. L. Atwood, J. E. D. Davies, D. D. MacNicol, F. Vögtle), Pergamon, Oxford, **1996**, pp. 325–365; b) A. Collet, *Tetrahedron* **1987**, 43, 5725–5759; c) K. T. Holman in *Encyclopedia of Supramolecular Chemistry*, Vol. 1 (Eds. J. L. Atwood, J. W. Steed), Dekker, New York, **2004**, pp. 340–348.
- [2] a) D. J. Cram, J. M. Cram, *Container Molecules and Their Guests*, Royal Society of Chemistry, Cambridge, **1994**; b) A. Jasat, J. C. Sherman, *Chem. Rev.* **1999**, 99, 931–967; c) L. R. MacGillivray, J. L. Atwood, *Angew. Chem.* **1999**, 111, 1080–1096; *Angew. Chem. Int. Ed.* **1999**, 38, 1019–1033; d) L. R. MacGillivray, J. L. Atwood, *Nature* **1997**, 389, 469–472; e) F. Hof, S. L. Craig, C. Nuckolls, J. Rebek, Jr., *Angew. Chem.* **2002**, 114, 1556–1578; *Angew. Chem. Int. Ed.* **2002**, 41, 1488–1508; f) R. Warmuth, J. Yoon, *Acc. Chem. Res.* **2001**, 34, 95–105; g) D. L. Caulder, K. N. Raymond, *Acc. Chem. Res.* **1999**, 32, 975–982; h) M. Fujita, K. Umamoto, M. Yoshizawa, N. Fujita, T. Kusukawa, K. Biradha, *Chem. Commun.* **2001**, 509–518.
- [3] a) J. Canceill, L. Lacombe, A. Collet, *J. Am. Chem. Soc.* **1985**, 107, 6993–6996; b) J. Costante-Crassons, T. J. Marrone, J. M. Briggs, J. A. McCammon, A. Collet, *J. Am. Chem. Soc.* **1997**, 119, 3818–3823; c) J. Yoon, D. J. Cram, *J. Am. Chem. Soc.* **1997**, 119, 11796–11806; d) J. M. Rivera, T. S. Martin, J. Rebek, Jr., *Science* **1998**, 279, 1021–1023; e) D. Fiedler, D. H. Leung, R. G. Bergman, K. N. Raymond, *J. Am. Chem. Soc.* **2004**, 126, 3674–3675.
- [4] a) D. J. Cram, M. E. Tanner, R. Thomas, *Angew. Chem.* **1991**, 103, 1048–1051; *Angew. Chem. Int. Ed. Engl.* **1991**, 30, 1024–1027; b) R. Warmuth, *Angew. Chem.* **1997**, 109, 1406–1409; *Angew. Chem. Int. Ed. Engl.* **1997**, 36, 1347–1349; c) R. Warmuth, J.-L. Kerdelhué, S. S. Carrera, K. J. Langenwalter, N.

- Brown, *Angew. Chem.* **2002**, *114*, 102–105; *Angew. Chem. Int. Ed.* **2002**, *41*, 96–99; d) P. Roach, R. Warmuth, *Angew. Chem.* **2003**, *115*, 3147–3150; *Angew. Chem. Int. Ed.* **2003**, *42*, 3039–3042; e) M. Yoshizawa, T. Kusukawa, M. Fujita, K. Yamaguchi, *J. Am. Chem. Soc.* **2000**, *122*, 6311–6312; f) M. Ziegler, J. L. Brumaghim, K. N. Raymond, *Angew. Chem.* **2000**, *112*, 4285–4287; *Angew. Chem. Int. Ed.* **2000**, *39*, 4119–4121.
- [5] a) J. Kang, J. Rebek, Jr., *Nature* **1997**, *385*, 50–52; b) J. Kang, J. Santamaria, G. Hilmersson, J. Rebek, Jr., *J. Am. Chem. Soc.* **1998**, *120*, 7389–7390; c) H. Ito, T. Kusukawa, M. Fujita, *Chem. Lett.* **2000**, 598–599; d) J. Chen, S. Körner, S. L. Craig, D. Rudkevich, J. Rebek, Jr., *Nature* **2002**, *415*, 385–386; e) D. A. Makeiff, K. Vishnumurthy, J. C. Sherman, *J. Am. Chem. Soc.* **2003**, *125*, 9558–9559; f) D. H. Leung, D. Fiedler, R. G. Bergman, K. N. Raymond, *Angew. Chem.* **2004**, *116*, 981–984; *Angew. Chem. Int. Ed.* **2004**, *43*, 963–966; g) R. Warmuth, E. F. Maverick, C. B. Knobler, D. J. Cram, *J. Org. Chem.* **2003**, *68*, 2077–2088.
- [6] a) P. Timmerman, W. Verboom, F. C. J. M. van Veggel, J. P. M. van Duynhoven, D. N. Reinhoudt, *Angew. Chem.* **1994**, *106*, 2437–2440; *Angew. Chem. Int. Ed. Engl.* **1994**, *33*, 2345–2348; b) K. Paek, H. Ihm, S. Yun, H. C. Lee, K. T. No, *J. Org. Chem.* **2001**, *66*, 5736–5743; c) A. Shivanyuk, J. Rebek, Jr., *Angew. Chem.* **2003**, *115*, 708–710; *Angew. Chem. Int. Ed.* **2003**, *42*, 684–686; d) A. Shivanyuk, J. Rebek, Jr., *J. Am. Chem. Soc.* **2002**, *124*, 12074–12075.
- [7] a) D. J. Cram, M. E. Tanner, C. B. Knobler, *J. Am. Chem. Soc.* **1991**, *113*, 7717–7727; b) K. N. Houk, K. Nakamura, C. Sheu, A. E. Keating, *Science* **1996**, *273*, 627–629; c) F. M. Raymo, K. N. Houk, J. F. Stoddart, *J. Am. Chem. Soc.* **1998**, *120*, 9318–9322.
- [8] a) D. M. Rudkevich, *Angew. Chem.* **2004**, *116*, 568–581; *Angew. Chem. Int. Ed.* **2004**, *43*, 558–571; b) J. L. Atwood, L. J. Barbour, A. Jerga, *Science* **2002**, *296*, 2367–2369; c) J. L. Atwood, L. J. Barbour, A. Jerga, *Angew. Chem.* **2004**, *116*, 3008–3010; *Angew. Chem. Int. Ed.* **2004**, *43*, 2948–2950; d) G. D. Enright, K. A. Udachin, I. L. Moudrakovski, J. A. Ripmeester, *J. Am. Chem. Soc.* **2003**, *125*, 9896–9897.
- [9] a) C. Garcia, D. Humilière, N. Riva, A. Collet, J. P. Dutasta, *Org. Biomol. Chem.* **2003**, *1*, 2207–2216; b) T. Brotin, J. P. Dutasta, *Eur. J. Org. Chem.* **2003**, *6*, 973–984; c) P. D. Kirchhoff, M. B. Bass, B. A. Hanks, J. M. Briggs, A. Collet, J. A. McCammon, *J. Am. Chem. Soc.* **1996**, *118*, 3237–3246; d) P. D. Kirchhoff, J. P. Dutasta, A. Collet, J. A. Mccammon, *J. Am. Chem. Soc.* **1997**, *119*, 8015–8022.
- [10] A related *endo*-functionalized cryptophane has been reported: C. E. O. Roesky, E. Weber, T. Rambusch, H. Stephan, K. Gloe, M. Czugler, *Chem. Eur. J.* **2003**, *9*, 1104–1112.
- [11] J. Canceill, A. Collet, *J. Chem. Soc. Chem. Commun.* **1988**, 582–584.
- [12] Single crystal structure of racemic [\pm -*anti*-1] γ -thf:3THF: $C_{94}H_{104}O_{22}$, $0.48 \times 0.45 \times 0.40$ mm, monoclinic, space group $P2_1/n$, $a = 20.233(2)$, $b = 18.070(2)$, $c = 23.638(2)$ Å, $\beta = 108.474(2)^\circ$, $V = 8196.6(14)$ Å³, $Z = 4$, $\rho_{\text{calcd}} = 1.285$ g cm⁻³, $Mo_{K\alpha}$ radiation, $\lambda = 0.71073$ Å, $2\theta_{\text{max}} = 50^\circ$, ω scans, 173(2) K, 52 817 total reflections, 14 430 unique reflections, 7507 reflections with $I > 2\sigma(I)$ ($R_{\text{int}} = 0.0753$); absorption correction SADABS ($T_{\text{min}} = 0.9577$, $T_{\text{max}} = 0.9646$, $\mu = 0.09$ mm⁻¹), structure solution using SHELXS, refinement (against $|F^2|$) with SHELX-97-2, 1090 parameters, 0 restraints, H atoms placed in calculated positions and refined with a riding model, $R_1 = 0.0650$ ($I > 2\sigma(I)$) and $wR_2 = 0.1785$ (all data), residual electron density max./min. = $0.55/-0.35$ e⁻ Å⁻³, GOF = 0.966. Single-crystal structure of racemic *imp*-1·11 CHCl₃: $C_{89}H_{83}O_{36}Cl_{33}$, $0.56 \times 0.32 \times 0.12$ mm, triclinic, space group $P\bar{1}$, $a = 14.094(5)$, $b = 16.361(5)$, $c = 26.247(8)$ Å, $\alpha = 103.372(5)$, $\beta = 101.191(5)$, $\gamma = 104.318(5)^\circ$, $V = 5499(3)$ Å³, $Z = 2$, $\rho_{\text{calcd}} = 1.577$ g cm⁻³, $Mo_{K\alpha}$ radiation, $\lambda = 0.71073$ Å, $2\theta_{\text{max}} = 45^\circ$, ω scans, 183(2) K, 31 876 total reflections, 14 293 unique reflections, 7834 reflections with $I > 2\sigma(I)$ ($R_{\text{int}} = 0.0835$); absorption correction SADABS ($T_{\text{min}} = 0.6403$, $T_{\text{max}} = 0.9024$, $\mu = 0.874$ mm⁻¹), structure solution with SHELXS, refinement (against $|F^2|$) using SHELX-97-2, 1419 parameters, 0 restraints, H atoms placed in calculated positions on ordered moieties and refined with a riding model, $R_1 = 0.1309$ ($I > 2\sigma(I)$) and $wR_2 = 0.3400$ (all data), residual electron density max./min. = $0.76/-0.93$ e⁻ Å⁻³, GOF = 1.060. The relatively high values of the merging and final R factors are directly attributed to the presence of a large number of highly disordered solvent molecules and unavoidable partial decomposition of the sample on transfer to the low-temperature stream. Disordered chloroform molecules are modeled as partial occupancy carbon and chlorine atoms. The stoichiometry of the crystal was estimated by using the SQUEEZE subroutine of the program PLATON,^[14] which estimates the solvent-accessible volume of 2738 Å³ (50 % of the unit cell) to be occupied by 1239 electrons (calcd 10.7 equivalents CHCl₃). The program X-Seed^[15] was used as a graphical interface to SHELX and for the generation of figures. CCDC-239970 and 240116 contain the supplementary crystallographic data for this paper. These data can be obtained free of charge via www.ccdc.cam.ac.uk/conts/retrieving.html (or from the Cambridge Crystallographic Data Centre, 12 Union Road, Cambridge CB21EZ, UK; fax: (+44) 1223-336-033; or deposit@ccdc.cam.ac.uk).
- [13] C. Garcia, A. Aubry, A. Collet, *Bull. Soc. Chim. Fr.* **1996**, *133*, 853–867.
- [14] P. Vandersluis, A. L. Spek, *Acta Crystallogr. Sect. A* **1990**, *46*, 194–201.
- [15] L. J. Barbour, *J. Supramol. Chem.* **2001**, 189–191.

Sensors

Design of a Modular-Based Fluorescent Conjugated Polymer for Selective Sensing**

Hongmei Huang, Kemin Wang, Weihong Tan, Delie An, Xiaohai Yang, Shasheng Huang, Qiuge Zhai, Leiji Zhou, and Yan Jin*

We have designed and synthesized a new modular-based fluorescent polymer **1** with a binding domain and a signaling domain. They are coupled together through an electron-conducting backbone for highly selective sensing of the Pd^{II}

[*] Dr. H. Huang, Prof. K. Wang, Prof. W. Tan, D. An, Prof. X. Yang, Prof. S. Huang, Q. Zhai, Dr. L. Zhou, Dr. Y. Jin
Biomedical Engineering Center
State Key Laboratory of Chemo/Biosensing and Chemometrics
College of Chemistry and Chemical Engineering
Hunan University, Changsha, 410082 (China)
Fax: (+86) 731-8821566
E-mail: kmwang@hnu.cn

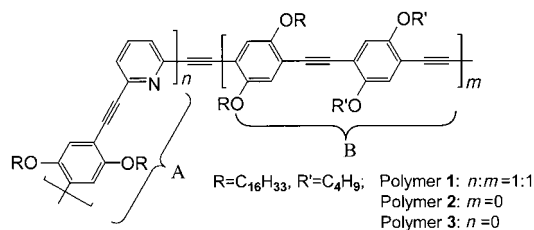
[**] This work was supported by the Nature Science Foundation of China (20135010), the Key Project Foundation of China (2002CB513100) and the Oversea Youth Scholar Co-research Foundation of China (20028506).



Supporting information for this article is available on the WWW under <http://www.angewandte.org> or from the author.

ion. The *meta*-substituted monopyridyl improves the spatial matching for selective binding, whereas the poly(*p*-phenylene ethynylene) derivative provides the additional amplification for sensing. With the increase in the number of applications for optical sensors, the design and synthesis of new sensing materials with high sensitivity and selectivity is a critical challenge.^[1,2] Recently, “molecular-wire effects” of conjugated polymers have shown great potential in signaling molecular-recognition processes,^[2,3] thus making them ideal for the development of highly sensitive sensing materials used to monitor ions, organic molecules, and even biomolecules.^[2–6] Among the fluorescent conjugated polymers reported to date, there is a diversity of properties such as conductivity, charge transfer, redox, and energy transfer. This diversity has been accomplished by tuning the conjugated polymers,^[5–7] however, selective sensing of ions by electrostatic action or ligand coordination has remained unsatisfactory.^[4a–b,5,6] The challenging selection requirements of the conjugated polymer are usually associated with properties such as special binding or spatial matching. For spatial-matching interactions, a flexible backbone and conformational freedom are indispensable to build a binding pocket and to offer a high affinity for analyte, which is common in biological macromolecules. However, for a conjugated polymer a rigid structure is preferable for efficient electron transfer. To resolve the conflicting architectural requirements, an important goal that has not yet been achieved satisfactorily is to develop a generic approach for linking a flexible part of binding domain and a rigid part of the signaling domain together in a range of polymers to be used in chemical sensing. By this modular-based design, many specific-binding domains with less or even no optical expression and those signaling domains that have excellent energy-transfer properties but without selective-binding properties can all be sufficiently used to avoid their specific flaws in each case. Herein we report a new modular-based conjugated polymer for detecting Pd^{II} ions, the design of which exploits molecular architecture, the intrinsic nature of the domains, and the properties of functional groups to yield a molecule capable of selective and sensitive sensing.

In this research, we designed and synthesized a new fluorescent polymer **1** (Scheme 1) comprising two separate functional parts (**A** and **B**), one part to introduce specific binding and the other to signal the response. Part **B**, a poly(*p*-phenylene ethynylene) derivative, was chosen as the signaling domain for its excellent photophysical and conductive properties.^[2,3] Its rigid structure is also capable of reducing intramolecular association. Part **A** was chosen as the binding domain because the monopyridyl group has a great affinity for the Pd^{II} ion and should selectively bind by self-assembly.^[8]



Scheme 1. The structures of polymers 1–3.

The *meta* linkage of the monopyridyl can regulate the flexibility of the backbone and may provide potential spatial matching for interpolymer binding by using an ion as the linker. The synthetic method to produce **1** ($\lambda_{\text{ex}}/\lambda_{\text{em}} = 415 \text{ nm}/475 \text{ nm}$, $\Phi = 0.34$, $M = 3.6 \times 10^4$, where λ_{ex} is the excitation wavelength, λ_{em} is the emission wavelength, Φ is the quantum yield and M is the average weight) involves the Sonogashira coupling. To ensure the desirable flexibility of the backbone, the reactants and their ratio were carefully considered. H NMR spectra of **1** confirm that monopyridyl groups have been separately incorporated into the polymer.^[9] To address the role of the different modular domains played in the selective metal binding, **2** ($\lambda_{\text{ex}}/\lambda_{\text{em}} = 380 \text{ nm}/425 \text{ nm}$, $\Phi = 0.12$, $M = 4.3 \times 10^3$) and **3** ($\lambda_{\text{ex}}/\lambda_{\text{em}} = 453 \text{ nm}/475 \text{ nm}$, $\Phi = 0.42$, $M = 5.7 \times 10^4$) were also prepared by a similar procedure. According to the experimental results, **1** with an appropriate modular-based polymer can truly form an interchain interaction through palladium–pyridyl coordination that results in dramatic fluorescence quenching and provides an excellent selectivity for Pd^{II} over other heavy and transition-metal ions.

The Pd^{II}-ion-responsive properties of polymers and the monomeric model 2,6-di(phenylethynyl)-pyridine (Dpp) were monitored in THF by using fluorescence emission spectroscopy. In the case of **1**, the Stern–Volmer data (Stern–Volmer quenching constant $K_{\text{sv}} = 4.34 \times 10^5 \text{ L mol}^{-1}$) reveals that the best amplification quenching by Pd^{II}, which is ≈ 56 times greater than that of the Dpp ($K_{\text{sv}} = 7.72 \times 10^3 \text{ L mol}^{-1}$ not shown). This result indicates that the specially designed molecular wire (i.e., the conjugated polymer chain) significantly amplifies the quenching. Figure 1 shows a comparison of fluorescence quenching of polymers **1–3** with various concentrations of Pd^{II}. To examine the effect of the binding domain (**A**) on the fluorescence quenching properties, the luminescence behavior of **3** in response to Pd^{II} was also investigated. Although **3** has a longer effective conjugated length^[3] than **1**, its Stern–Volmer quenching constant on Pd^{II} is only $3.79 \times 10^3 \text{ L mol}^{-1}$, which is even less than that of Dpp. This suggests that the **A** part of **1** functions as a necessary sensitive domain for Pd^{II} binding, and only the **B** part of **1** cannot bring out the amplification sensitivity. From Figure 1, we can also learn that **2** shows far less sensitivity than **1** and its

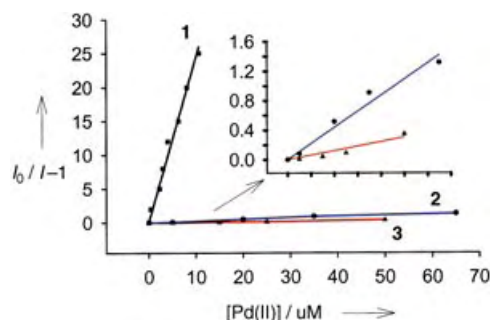


Figure 1. Fluorescence quenching of polymer **1** (\blacksquare $\lambda_{\text{ex}}/\lambda_{\text{em}} = 415 \text{ nm}/476 \text{ nm}$), **2** (\bullet $\lambda_{\text{ex}}/\lambda_{\text{em}} = 380 \text{ nm}/425 \text{ nm}$) and **3** (\blacktriangle $\lambda_{\text{ex}}/\lambda_{\text{em}} = 453 \text{ nm}/475 \text{ nm}$) by various concentration of Pd^{II} ions, in which I_0 and I denote the intensity of the fluorescence signal of the sensing materials in the absence and presence of the analyte, respectively (the scale and legend of the x-axis of the inset is similar to those of the figure).

Stern–Volmer quenching constant ($K_{sv} = 2.18 \times 10^4 \text{ L mol}^{-1}$) is only 2.8 times greater than that of monomeric model Dpp, although it provides slightly more efficient quenching than **3**. The great disparity in the response efficiency of **1** and **2** demonstrates that the B domain in **1** provides a remarkable amplification, that is, the binding of Pd^{II} with the A domain can lead to a significant quenching of the B domain. Despite the attraction of special binding of the A domain, the excessive distortion in the conjugated polymer of **2** decreases the quantum yield, the average weight, thus the sensitivity, and even the selectivity are seriously reduced. From these results, we believe that neither specific-binding domain, A, nor the signaling domain, B, could achieve the desired sensitivity. A combination of them together, however, leads to high sensitivity.

In contrast to those of **2** and **3**, the selectivity of **1** for Pd^{II} is excellent. Figure 2 shows that many transitional-metal and main-group ions such as Ru^{III} , Rh^{III} , Co^{II} , Ni^{II} , Zn^{II} , Fe^{III} , Sn^{II} , Pb^{II} , Cu^{II} , Hg^{II} , Ag^{I} , Na^{I} , Mg^{II} , and Mn^{II} have little effect on

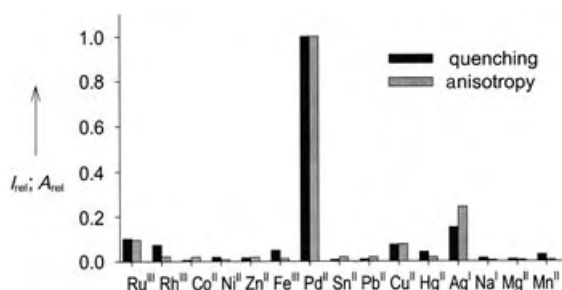


Figure 2. The relative fluorescence quenching and anisotropy changes of **1** with different metal ions.

the fluorescence of **1**. Compared with previous reports,^[5,6] the modular-based conjugated polymer **1** provides better selectivity for Pd^{II} ions. That means proper flexibility of the backbone mainly contributes to the selective response. Other elements such as the varying coordination ability or mode (mono- or multi-dentate) between the ion and pyridyl group may also influence the selectivity. The trend of fluorescence quenching of **1** by ions is similar to that of Dpp, but **1** enlarges the discrimination. Compound **1** thus exhibits high selectivity towards Pd^{II} ions and provides an excellent avenue for designing conjugated fluorescent polymers for sensing applications. We also investigated fluorescence quenching with Pt^{IV} ions. The experimental results suggest that with Pt^{IV} ions with compound **1** give a similar effect although its quenching is about 58.1 % and fluorescence anisotropy changes about 68.4 % of that of Pd^{II} at the concentration of $1.5 \times 10^5 \text{ mol L}^{-1}$. This suggests that Pt^{IV} has a much stronger response than most of the other ions tested.

To further clarify the relationship between the structural arrangement of a conjugated polymer and its specific response, detailed investigations of the mechanism were carried out by using absorption measurements and fluorescence anisotropy. At room temperature, the significant spectroscopic variations that occur as Pd^{II} ions interact with **1** can be observed within a few minutes by progressively adding a solution containing Pd^{II} ions into a solution of **1**. The

corresponding excitation band is red-shifted from 415 nm to 444 nm, whereas the emission band is only slightly red-shifted ($\approx 3 \text{ nm}$). Consistent with the excitation variation, the absorption band at 415 nm of **1**, which is attributed to the conjugated backbone, is also red-shifted by $\approx 30 \text{ nm}$ upon adding an appropriate quantity of Pd^{II} ions (Figure 3). The

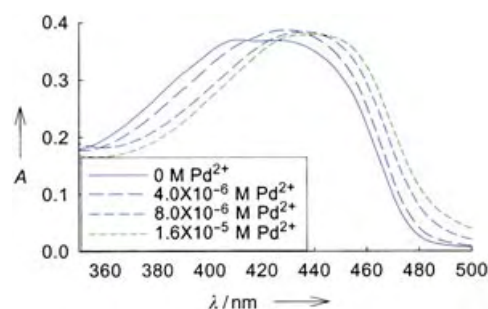
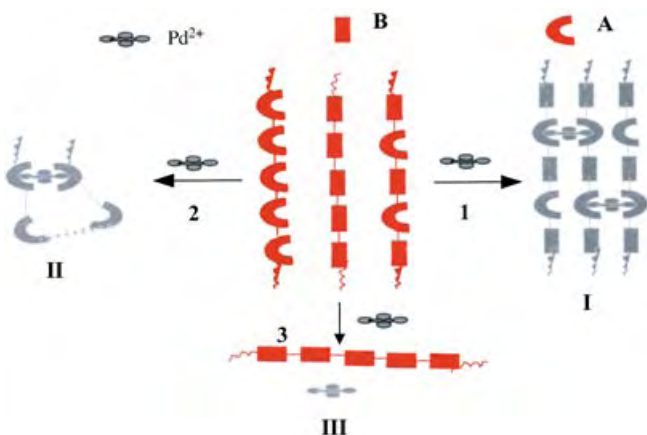


Figure 3. Absorption spectra of **1** in THF ($5.0 \times 10^{-6} \text{ M}$) as a function of different concentrations of Pd^{II} ions.

absorptive bands of **2** and **3** display no obvious changes. These spectroscopic results clearly show that there is a difference in the energy state of **1** in the presence and absence of Pd^{II} ions. The red-shift absorption of **1** suggests that the species formed is on average conjugated over a greater length, which may be ascribed to the interpolymer interaction by Pd^{II} -pyridyl binding (**I** in Scheme 2). As for the excessive distortion backbone of **2**, its lower absorption shift results indicate that intrachain linkage may take place (**II** in Scheme 2) instead of interchain linkage. For **3**, without the binding domain A, the interchain linkage by the association between Pd^{II} and pyridyl can not produce at all (**III** in Scheme 2) and which is confirmed by the no changes of absorption. The almost unchanged emission spectra of **1** demonstrate the facile energy transfer that can occur along the different segments of the backbone and even through the interchain system. Stronger ligands than pyridine, such as CN^- ions, were added into a solution of **1** to complex the Pd^{II} ions. Consequently, the fluorescence of the conjugated polymer almost fully recovered, thus indicating the reversibility of the sensing property of this molecule.



Scheme 2. Schematic interaction of the different polymer structures (**1**, **2**, and **3**) with Pd^{II} ions.

Fluorescence anisotropy was used to identify the link joining the chains of polymer **1** as this method has been used for studying molecular interactions, particularly in cases in which there is a significant change in molecular weight upon binding or interaction.^[11] We used it to study the aggregation of **1** due to the binding of Pd^{II} ions through the pyridyl groups. Figure 4 shows the effects of varying concentrations of Pd^{II}

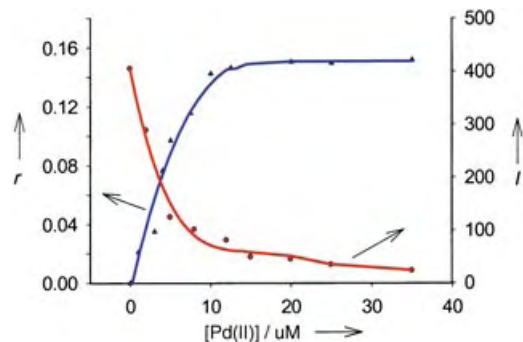


Figure 4. Fluorescence anisotropy (▲) and quenching (●) of **1** with various concentrations of Pd^{II} ions (*r* is the fluorescence anisotropy).

ions on the observed fluorescence anisotropy and quenching of **1**. As expected, the fluorescence anisotropy of **1** increased linearly when a solution containing Pd^{II} ions was gradually added into the diluted polymer solution. The enhanced anisotropy values clearly indicated that the polymer chains coupled, that is, a complex with a larger molecular weight formed, which hindered the rotational diffusion rate of the polymer.^[12] Anisotropy value reached a plateau when a concentration of Pd^{II} ions rose above 20 μM, which indicated that saturated aggregation of **1** had occurred. With the increase of anisotropy, fluorescence quenching was correspondingly decreased. The interaction of **1** and Pd^{II} ions was also found to be highly specific by using anisotropy measurements (Figure 2). Further experiments indicate that a stronger ligand such as CN[−] could also restore the anisotropy value of **1** in the presence of Pd^{II} ions. Under the same experimental conditions, however, the fluorescence anisotropy of **2** and **3** changed very little even at high concentrations of Pd^{II} ions, thus indicating that interactions between polymer chains do not occur.^[9] These results confirm that the high sensitivity and selectivity of **1** closely correlates with the ability of the polymer chains to interact, which, in turn is closely related to its modular-based design.

In summary, we report a novel and general method to design a modular-based conjugated polymer with a flexible structure of a binding domain and a rigid structure of a signaling domain. The appropriate selection of the different modules can provide excellent selectivity and high sensitivity. By using this general approach, we synthesized a new fluorescent conjugated polymer for Pd^{II} ion detection with high specificity and excellent sensitivity. This new macromolecule design demonstrates the feasibility of varying the structures to fine-tune the molecular spatial binding properties of the resulting conjugated polymers. The process will enhance the versatility of these sensing systems and their

applications. This new design will provide an excellent approach to efficiently and simply regulate the optical and electronic properties of conjugated polymers, which is essential to make them useful for electrical devices and bio/chemical sensors.

Received: April 20, 2004

Keywords: coordination modes · palladium · polymers · self-assembly · sensors

- [1] a) A. W. Czarnik, *Chem. Biol.* **1995**, *2*, 423–428; b) A. P. de Silva, H. Q. Nimal Gunaratne, T. Gunnlaugsson, A. J. M. Huxley, C. P. McCoy, J. T. Rademacher, T. E. Rice, *Chem. Rev.* **1997**, *97*, 1515–1566; c) L. Prodi, F. Bolletta, M. Montalti, N. Zeccheroni, *Coord. Chem. Rev.* **2000**, *205*, 59–83.
- [2] D. T. McQuade, A. E. Pullen, T. M. Swager, *Chem. Rev.* **2000**, *100*, 2537–2574.
- [3] T. M. Swager, *Acc. Chem. Res.* **1998**, *31*, 201–207.
- [4] a) B. S. Harrison, M. B. Ramey, J. R. Reynolds, K. S. Schanze, *J. Am. Chem. Soc.* **2000**, *122*, 8561–8562; b) P. B. Balanda, M. B. Ramey, J. R. Reynolds, *Macromolecules* **1999**, *32*, 3970–3978; c) B. S. Gaylord, A. J. Heeger, G. C. Bazan, *J. Am. Chem. Soc.* **2003**, *125*, 896–900; d) H. A. Ho, M. Boissinot, G. Corbeil, M. G. Bergeron, K. Dore, D. Boudreau, M. Leclerc, *Angew. Chem.* **2002**, *114*, 1618–1621; *Angew. Chem. Int. Ed.* **2002**, *41*, 1548–1551; e) X. D. Song, H. L. Wang, J. Shi, J. W. Park, B. I. Swanson, *Chem. Mater.* **2002**, *14*, 2342–2347; f) C. H. Fan, K. W. Plaxco, A. J. Heeger, *J. Am. Chem. Soc.* **2002**, *124*, 5642–5643; g) L. H. Chen, D. W. McBranch, H. L. Wang, R. Helgeson, F. Wudl, D. G. Whitten, *Proc. Natl. Acad. Sci. USA* **1999**, *96*, 12287–12292.
- [5] a) B. Jiang, Y. Zhang, S. Sahay, S. Chatterjee, W. E. Jones, Jr., *SPIE Proc.* **1999**, 212–223; b) M. Kimura, T. Horai, K. Hanabusa, H. Shirai, *Adv. Mater.* **1998**, *10*, 459–462.
- [6] a) B. Wang, M. R. Wasielewski, *J. Am. Chem. Soc.* **1997**, *119*, 12; b) B. Liu, W. L. Yu, J. Pei, S. Y. Liu, Y. H. Lai, W. Huang, *Macromolecules* **2001**, *34*, 7932.
- [7] a) S. S. Zhu, T. M. Swager, *J. Am. Chem. Soc.* **1997**, *119*, 12568–12577; b) K. D. Ley, C. E. Whittle, M. D. Bartberger, K. S. Schanze, *J. Am. Chem. Soc.* **1997**, *119*, 3423–3424; c) Q. Wang, L. Yu, *J. Am. Chem. Soc.* **2000**, *122*, 11806–11811; d) S. Cosnier, A. Deronzier, J. F. Roland, *J. Electroanal. Chem.* **1990**, *285*, 133–147; e) M. Gerard, A. Chaubey, B. D. Malhotra, *Biosens. Bioelectron.* **2002**, *17*, 345–359; f) A. Boyle, E. M. Genies, M. Lapkowski, *Synth. Met.* **1989**, *28*, C769–C774.
- [8] a) C. M. Drain, F. Nifatis, A. Vasenko, J. D. Batteas, *Angew. Chem.* **1998**, *110*, 2478–2481; *Angew. Chem. Int. Ed. Engl.* **1998**, *37*, 2344; b) C. M. Drain, *Proc. Natl. Acad. Sci. USA* **2002**, *99*, 5178; c) D. J. Qian, C. Nakamura, T. Ishida, S. O. Wenk, T. Wakayama, S. Takeda, J. Miyake, *Langmuir* **2002**, *18*, 10237–10242.
- [9] Further details are available in the Supporting Information.
- [10] a) T. E. O. Screen, J. R. G. Thorne, R. G. Denning, D. G. Bucknall, H. L. Anderson, *J. Am. Chem. Soc.* **2002**, *124*, 9712–9713; b) T. Q. Nguyen, I. B. Martini, J. Liu, B. J. Schwartz, *J. Phys. Chem. B* **2000**, *104*, 237–255;
- [11] a) X. H. Fang, Z. H. Cao, T. Beck, W. H. Tan, *Anal. Chem.* **2001**, *73*, 5752–5757; b) J. H. Matthew, T. Dmitri, T. Thomas, F. S. Joel, *Biochemistry* **2002**, *41*, 6460–6468; c) H. Lou, J. R. Brister, J. Li, W. Chen, N. Muzyczka, and W. Tan, *ChemBioChem* **2004**, *5*, 100–108; d) M. E. McCarroll, F. H. Billiot, I. M. Warner, *J. Am. Chem. Soc.* **2001**, *123*, 3173–3174; e) W. J. Chechovich, R. E. Bolger, T. Burke, *Nature* **1995**, *375*, 254–256.
- [12] J. R. Lakowicz, *Principles of Fluorescence Spectroscopy*, 2nd ed., Kluwer Academic/Plenum Publishers, New York, **1999**, chap. 10.

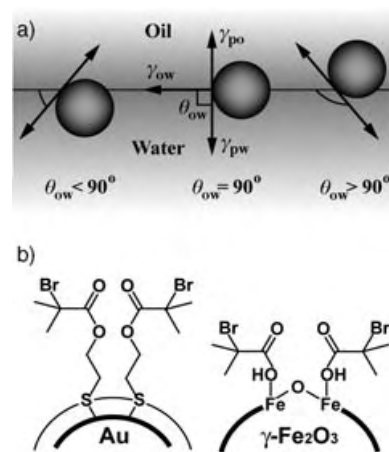
Nanoparticles

Directing Self-Assembly of Nanoparticles at Water/Oil Interfaces**

Hongwei Duan, Dayang Wang,* Dirk G. Kurth, and Helmuth Möhwald

Nanoparticles (NPs) have attracted a great deal of attention because of their promising potential and already realized applications. Their unique electronic, magnetic, and optical properties can be manipulated by simply varying the dimension and geometry.^[1] The integration of nanoparticles into one-, two-, or three-dimensional (2D or 3D) structures leads to novel collective properties that can be manipulated by the control of the cooperative interactions between the nanoparticles.^[2] While nanoparticles may be chemically assembled by the interaction of ligands capped on nanoparticles, the elaborate design of ligands is a prerequisite.^[3] For organic nanoparticles, which are formed directly in organic media or transferred from aqueous media with the aid of surfactants, their 2D or 3D arrays can be simply realized by controlled evaporation of solvents^[2b,4] or at the water/air interface by using the Langmuir–Blodgett technique.^[2a,5]

Thin films of nanoparticles have been produced in situ at interfaces between immiscible liquids.^[6] Most recently, Lin and co-workers directed the assembly of hydrophobic CdSe nanoparticles at the water/toluene interface and they achieved size-dependent interfacial entrapment of CdTe nanoparticles.^[7a] Meanwhile, Reincke and co-workers reported that the introduction of ethanol can pull hydrophilic citrate-stabilized Au-NPs into the water/heptane interface, leading to a closely packed monolayer.^[7b] These two reports demonstrate a promising way to create a 2D or 3D arrangement of both hydrophobic and hydrophilic nanoparticles at water/oil interfaces. The use of interfaces between water/oil fluids to trap sub- or micrometer-sized particles has been well established.^[8] Besides the particle diameter, this interfacial entrapment is mainly determined by the contact angle (θ) of the particle with the water/oil interface—surface wettability.^[8] As schematically depicted in Scheme 1a, when a particle is hydrophilic or hydrophobic it has a contact angle smaller (left) or larger than 90° (right) in a water/oil system and is localized totally within the water or oil phase. When its contact angle is around 90° (Scheme 1a, center) the particle prefers to reside at the interface. As the particles approach nanometer size, however, the thermal energy becomes comparable to the interfacial energy.^[7a] In this case, spatial fluctuations suffice to remove nanoparticles trapped at



Scheme 1. a) Schematic representation of the position of a particle at a water/oil interface for a contact angle with the interface less than 90° (left), equal to 90° (center), and larger than 90° (right). b) Schematic illustration of the structures of Au@DTBE (left) and $\gamma\text{-Fe}_2\text{O}_3$ @BMPA nanoparticles (right).

interfaces into bulk phases. The profile of the calculated partition of 10-nm particles in water/oil two-phase systems shows that only when the contact angle of the nanoparticles is close to 90° may they reside at the interface; when the contact angle slightly deviates from 90° , the nanoparticles prefer to go to the bulk phase, suggesting that the contact angle of 90° should play a pivotal role for the interface entrapment of nanoparticles.^[8a] Reincke and co-workers observed that the addition of ethanol renders the contact angle of Au-NPs with the water/hexane interface close to 90° , which is a crucial point for the interfacial entrapment of nanoparticles in their work.^[7b]

Recent studies on phase transfer of aqueous Au-NPs show that by using single long-chain alkylamines, one may transfer carboxylic acid derivatized Au-NPs onto water/oil interfaces.^[9] Wei and co-workers have observed interfacial attachment of the Au nanoparticles capped with a resorcinarene ligand.^[5c] These reports suggest that interfacial entrapment and self-assembly of nanoparticles might be realized by appropriate hydrophobic coating. It is well known that substrates with carboxylic ester groups possess contact angles in the range of $80\text{--}110^\circ$.^[10] Herein, we report that the capping with ligands with a terminal 2-bromopropionate group may lead to contact angles for aqueous or organic nanoparticles close to 90° , thus driving nanoparticles to reside and self-assemble at water/oil interfaces. The choice of these ligands was encouraged by the success of living free-radical polymerization on nanoparticles.^[11] The significance of our work lies on the fact that it should provide a general protocol for trapping and organizing nanoparticles at water/oil interfaces.

In this work, 5-nm and 12-nm Au nanoparticles were synthesized by citrate reduction of chloroauric acid in the aqueous phase.^[12] Owing to their negatively charged surface, these Au-NPs are highly hydrophilic, residing only in the water phase. By means of ligand exchange, these aqueous Au-NPs were capped with 2,2'-dithiobis[1-(2-bromo-2-methyl-

[*] H. Duan, Dr. D. Wang, Dr. D. G. Kurth, Prof. H. Möhwald
Max Planck Institute of Colloids and Interfaces
14424 Potsdam (Germany)
Fax: (+49) 331-5679202
E-mail: dayang.wang@mpikg-golm.mpg.de

[**] This work is supported by the Max Planck Society. We thank J. Hartmann and R. Pitschke for assistance with the TEM measurements.

propionyloxy)ethane] (DTBE), denoted as Au@DTBE. Scheme 1b (left) schematically represents the structure of Au@DTBE nanoparticles. The optimal density of DTBE capped on Au-NPs, determined by thermogravimetric analysis, is around 3 wt % in our work, corresponding to about 800 DTBE molecules per Au-NP. Addition of toluene to the aqueous dispersions of Au@DTBE nanoparticles led to their spontaneous transfer onto the water/toluene interface, and their self-assembly into thin films. This interfacial entrapment of Au@DTBE nanoparticles may be accelerated by gentle shaking. Figure 1a is a typical photograph of the result of the self-assembly of 12-nm Au@DTBE nanoparticles at the water/toluene interface; one can see a giant water droplet enclosed by a thin film of golden reflectance and blue transmittance. This metallic luster results from the electronic coupling of Au-NPs, suggesting the formation of closely packed nanoparticle thin films.^[2a,9,13] The UV/Vis spectra demonstrate that no Au@DTBE nanoparticles exist in water or are transferred into the toluene phase. The films of Au@DTBE nanoparticles formed at the water/toluene interface can be transferred onto solid substrates by using the Langmuir technique, which allows us to determine the contact angle of Au@DTBE nanoparticles with the water/toluene interface. Figure 1b reveals that Au@DTBE nanoparticles have a contact angle of 90° with the water/toluene interface, whereas the contact angle of citrate-stabilized Au-NPs is about 60° (Figure 1c). After optimizing the concentration of Au@DTBE nanoparticles and the area of the water/toluene interface, we obtained the monolayer of Au@DTBE nanoparticles at the interface. Figure 1d shows a typical transmission electron microscopy (TEM) image of a monolayer of 12-nm Au@DTBE nanoparticles. This monolayer does not display long-range order, possibly because of the broad size distribution of nanoparticles used. In such a monolayer, as observed by Reincke and co-workers,^[7b] domains of close-packed Au@DTBE nanoparticles coexist with large voids; the latter is difficult to explain. In addition, we also achieved interfacial entrapment and self-assembly of Au@DTBE nanoparticles by addition of chloroform and even triethylamine, that is partially immiscible with water. Besides DTBE, we obtained similar results using 11,11'-dithiobis[1-(2-bromo-2-methylpropionyloxy)undecane] (DTBU) as capping ligands,^[11b,d] suggesting that in our system surface wettability of nanoparticles mainly depends on the terminal group of the capping ligand, 2-bromopropionate group, rather than on the length of the alkyl chain. Furthermore, using DTBE and DTBU as capping ligands, we have also attached and organized 5-nm Au-NPs into a closely packed monolayer at the water/oil interface.

As the surface wettability of the nanoparticles is predominant in the process of interfacial entrapment, our procedure has been successfully extended to aqueous Ag-NPs. Following the aforementioned ligand-exchange procedure, aqueous Ag-NPs of 10–40 nm in size, prepared by reduction of silver nitrate by sodium borohydride,^[14] were capped with DTBE (Ag@DTBE). The as-made Ag@DTBE nanoparticles display interfacial behavior similar to that of Au@DTBE nanoparticles; they prefer to reside at the water/oil interface, creating a film with metallic reflectance (Figure 2a). Further-

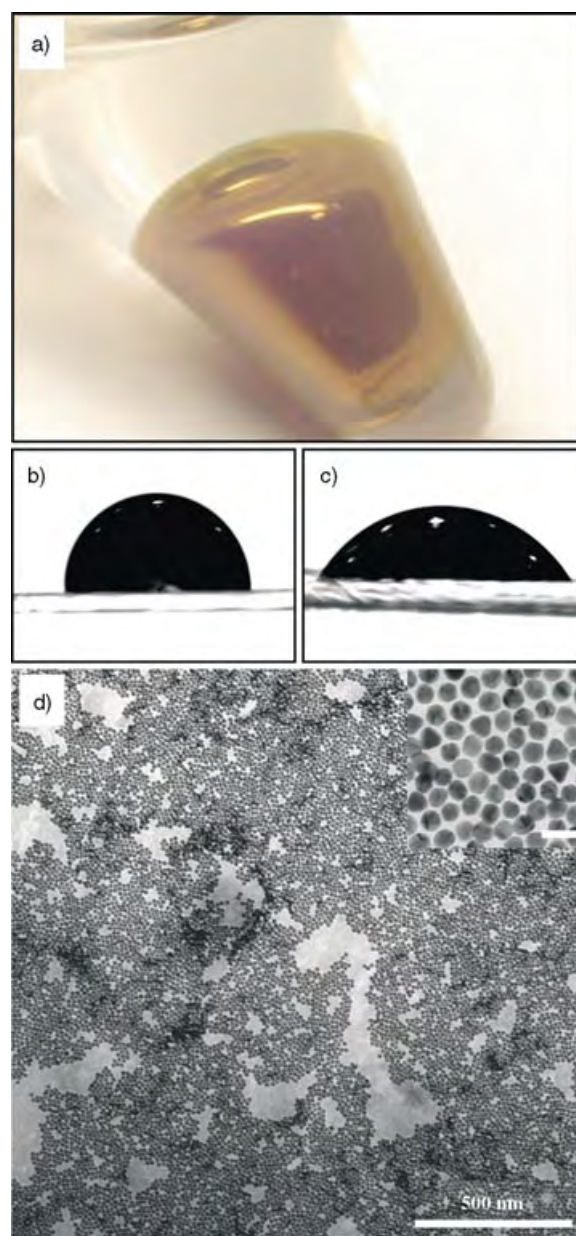


Figure 1. a) Photograph of the self-assembled Au@DTBE nanoparticles at the water/toluene interface in a plastic Eppendorf tube. This tube has been tilted such that the colored area corresponds to the water/toluene interface. Owing to the reflectance from the sides, only the blue-purple area represents a transmission image. b,c) Photographs of a 5-μL water droplet, covered with toluene, resting on the surface of a thin film of 12-nm Au@DTBE nanoparticles, transferred from the water/toluene interface on a glass slide (b) and on the surface of a thin film of 12-nm Au-NPs cast on a glass slide (c). d) TEM image of the monolayer of 12-nm Au@DTBE nanoparticles, formed at the water/toluene interface; inset: high-magnification TEM picture, the scale bar is 25 nm.

more, the mixture of Au@DTBE and Ag@DTBE nanoparticles has been attached at water/toluene interfaces, leading to nanoalloy films (Figure 2b). Their TEM images reveal random close-packing arrays, in which, however, one has difficulty in identifying the chemical identity of the nanoparticles based on the contrast level in the bright field

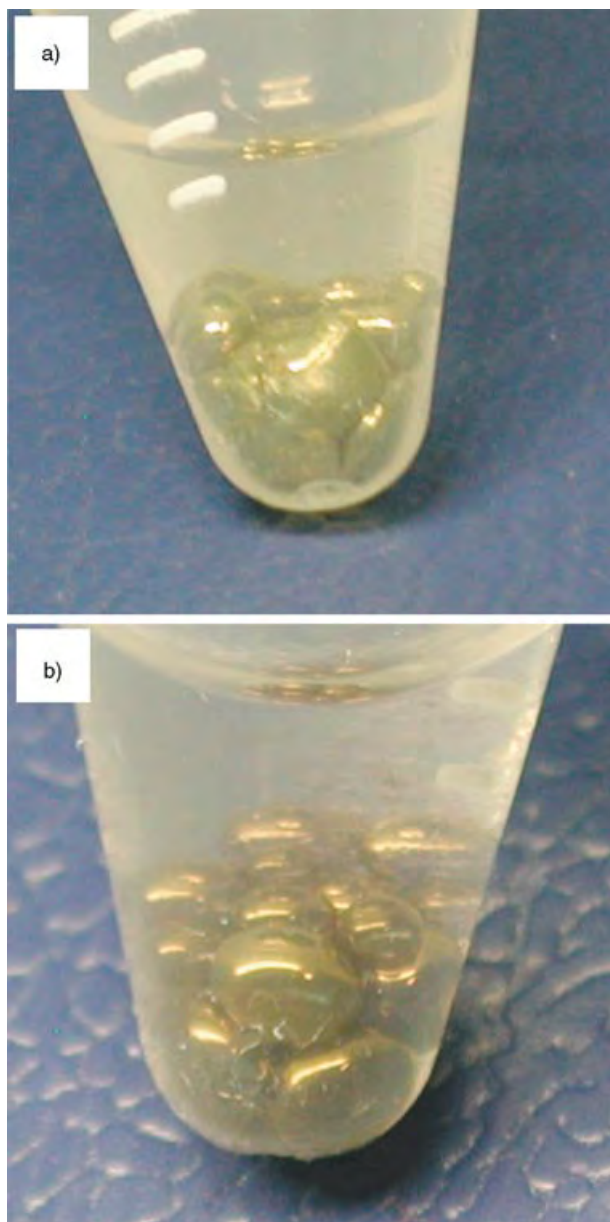


Figure 2. Photographs of thin films of Ag-NPs (a) and of a mixture of Au- and Ag-NPs at a molar ratio of 1:1 (b), formed at the water/toluene interface in a plastic Eppendorf tube.

image.^[4a] Moreover, we observed that the transmitted and reflected color of the resultant nanoalloy films varied with the molar ratio of Au@DTBE to Ag@DTBE nanoparticles. The use of interfacial entrapment of nanoparticles to construct composite thin films is an ongoing project in our laboratory.

To gain a better insight into the effect of the terminal group 2-bromopropionate, we conducted interfacial entrapment with hydrophobic nanoparticles. We prepared 4-nm γ -Fe₂O₃ nanoparticles by oxidation of iron(III) acetylacetonate followed by stabilization with oleic acid and oleylamine in toluene.^[15] As the long carbon chains of oleic acid and oleylamine capping the γ -Fe₂O₃ nanoparticles are exposed outwards, these nanoparticles are highly hydrophobic and thus may reside only in nonpolar media. We had difficulty in

measuring the contact angle of these γ -Fe₂O₃ nanoparticles with the water/toluene interface since the nanoparticles were immediately removed into the toluene phase upon addition of toluene to their thin films cast on a glass slide. The stabilizers on the γ -Fe₂O₃ nanoparticles were replaced with 2-bromo-2-methylpropionic acid (BMPA) by incubating nanoparticles with BMPA for two days.^[11c] These BMPA-capped γ -Fe₂O₃ nanoparticles are denoted as γ -Fe₂O₃@BMPA (Scheme 1b (right)). Upon addition of water to a dispersion of γ -Fe₂O₃@BMPA in toluene, γ -Fe₂O₃@BMPA nanoparticles were spontaneously transferred into the water/toluene interface; as for the Au@DTBE nanoparticles, this process was favored by gentle shaking. The inset in Figure 3 shows a typical picture of

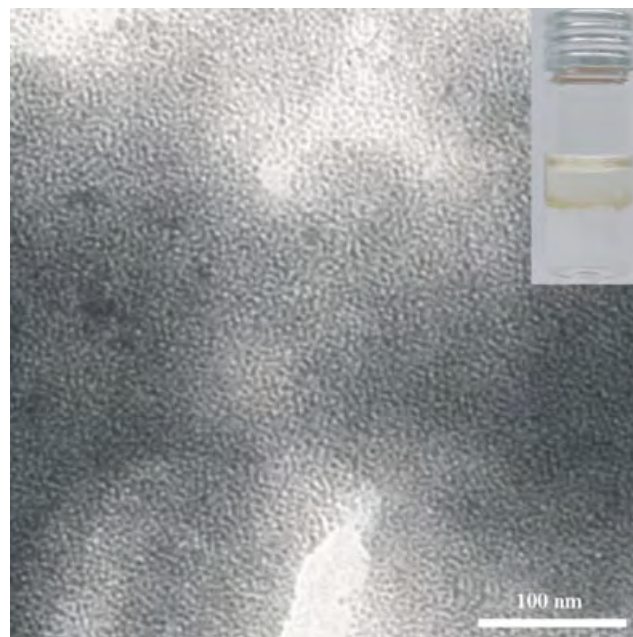


Figure 3. TEM image of the thin film of 4-nm γ -Fe₂O₃@BMPA nanoparticles formed at the water/toluene interface. The yellow layer formed at the water/toluene interface is clearly visible in the photograph shown in the inset.

the interfacial entrapment of γ -Fe₂O₃@BMPA nanoparticles; a yellow layer formed at the water/toluene interface is clearly visible. After transferring this film onto a glass slide, we observed that the contact angle of γ -Fe₂O₃@BMPA nanoparticles with the water/toluene interface is close to 90°, similar to that of Au@DTBE nanoparticles. Unlike for the interfacial entrapment of Au@DTBE nanoparticles, we lack the ability to fabricate monolayers of γ -Fe₂O₃@BMPA nanoparticles at the water/toluene interface. As shown in Figure 3, both monolayers and multilayers of closely packed nanoparticles were observed. Control of the thickness of the films of γ -Fe₂O₃@BMPA nanoparticles formed at the water/toluene interface is underway.

In summary, we have capped aqueous Au- and Ag-NPs with DTBE and DTBU and nonaqueous γ -Fe₂O₃ nanoparticles with BMPA. The terminal 2-bromopropionate group of these ligands may render the contact angles of the nanoparticles at the water/oil interface close to 90°, driving

nanoparticles to the water/oil interface and to self-assemble into closely packed arrays. Meanwhile, the possibility to form nanoalloy films at interfaces has also been demonstrated. The 2-bromopropionate group rather than the length of the hydrocarbon chains of the ligands mainly determine the surface wettability of modified nanoparticles. Thus, our work is an important step towards interfacial entrapment and assembly of nanoparticles for the creation of 2D or 3D nanostructures for electronic, optoelectrical, and magnetic applications. In our laboratory, we are currently capping nanoparticles with ligands containing various carboxylic ester terminal groups to generalize our concept and to establish a relationship between the contact angle of the nanoparticles at the water/oil interface and the terminal group on the ligand terminal. This should provide a means to manipulate nanoparticle solubility in the bulk phase and hence the elasticity of the interface.

Experimental Section

DTBE and DTBU were prepared by acrylation of bis(2-hydroethyl) disulfide and bis(2-hydroethyl) disulfide, obtained by employing the method described by Hawker and co-workers.^[16] Briefly, 2-bromo-2-methylpropionyl bromide (14.8 mmol) was added dropwise to a mixture of the disulfide (6.17 mmol) and triethylamine (31.5 mmol) in dichloromethane (150 mL) at 0°C under an argon atmosphere. The solution was stirred at 0°C for 1 h and then for another 2 h at room temperature. After the precipitates were filtered off, the organic phase was extracted with 2 N Na₂CO₃ solution saturated with NH₄Cl to remove the excess bromides. Subsequent removal of dichloromethane yielded DTBE and DTBU.

DTBE (4.6 mg) or DTBU (7.2 mg) was dissolved in THF (10 mL) and the solution then added dropwise to an aqueous solution of Au or Ag-NPs (40 mL). After incubating the mixtures for 6–12 h, followed by removal of excess initiators by centrifugation, the initiator-capped nanoparticles were obtained and suspended in water for further use.

A solution of 4-nm γ -Fe₂O₃ nanoparticles in toluene (5 mL) was incubated with a solution of BMPA (1.67 mg) in toluene (5 mL) for two days. The subsequent removal of excess BMPA yielded γ -Fe₂O₃@BMPA nanoparticles and they were suspended in toluene for further use.

UV/Vis absorption spectra were recorded by using a Cary 50 UV-visible spectrophotometer. TEM images were obtained by using a Zeiss EM 912 Omega microscope at an acceleration voltage of 120 kV. Contact angle measurements were implemented with a contact angle measuring system G10 apparatus (Krüss, Germany) at ambient temperature.

Received: June 9, 2004

Keywords: colloids · interfaces · nanoparticles · self-assembly · surface wettability

- [1] a) H. Weller, *Angew. Chem.* **1993**, *105*, 43–55; *Angew. Chem. Int. Ed. Engl.* **1993**, *32*, 41–53; ; b) A. P. Alivisatos, *Science* **1996**, *271*, 933–937.
- [2] a) C. P. Collier, T. Vossmeier, J. R. Heath, *Annu. Rev. Phys. Chem.* **1998**, *49*, 371–404; b) C. B. Murray, C. R. Kagan, M. G. Bawendi, *Annu. Rev. Mater. Sci.* **2000**, *30*, 545–610.
- [3] a) M. D. Musick, C. D. Keating, M. H. Keefe, M. J. Natan, *Chem. Mater.* **1997**, *9*, 1499–1501; b) C. M. Niemeyer, *Angew. Chem.* **2001**, *113*, 4254–4287; *Angew. Chem. Int. Ed.* **2001**, *40*, 4128–4158; c) P. M. Mendes, Y. Chen, R. E. Palmer, K. Nikitin, D.

- Fitzmaurice, J. A. Preece, *J. Phys. Condens. Matter* **2003**, *15*, S3047–S3063; d) R. Shenhar, V. M. Rotello, *Acc. Chem. Res.* **2003**, *36*, 549–561.
- [4] a) C. J. Kiely, J. Fink, J. G. Zheng, M. Brust, D. Bethell, D. J. Schiffrin, *Adv. Mater.* **2000**, *12*, 640–643; b) E. V. Shevchenko, D. V. Talapin, A. L. Rogach, A. Kornowski, M. Haase, H. Weller, *J. Am. Chem. Soc.* **2002**, *124*, 11480–11485; c) F. X. Redl, K. S. Cho, C. B. Murray, S. O'Brien, *Nature* **2003**, *423*, 968–971.
- [5] a) J. H. Fendler, *Curr. Opin. Colloid Interface Sci.* **1996**, *1*, 202–207; b) B. Kim, S. L. Tripp, A. Wei, *J. Am. Chem. Soc.* **2001**, *123*, 7955–7956.
- [6] a) D. Yogeve, S. Efrima, *J. Phys. Chem.* **1988**, *92*, 5754–5760; b) C. N. R. Rao, G. U. Kulkarni, P. J. Thomas, V. V. Agrawal, P. Saravanan, *J. Phys. Chem. B* **2003**, *107*, 7391–7395.
- [7] a) Y. Lin, H. Skaff, T. Emrick, A. D. Dinsmore, T. P. Russell, *Science* **2003**, *299*, 226–229; b) F. Reincke, S. G. Hickey, W. K. Kegel, D. Vanmaekelbergh, *Angew. Chem.* **2004**, *116*, 464–468; *Angew. Chem. Int. Ed.* **2004**, *43*, 458–462.
- [8] For recent reviews, see: a) B. P. Binks, *Curr. Opin. Colloid Interface Sci.* **2002**, *7*, 21–41; b) R. Aveyard, B. P. Binks, J. H. Clint, *Adv. Colloid Interface Sci.* **2003**, *100–102*, 503–546.
- [9] a) S. Chen, H. Yao, K. Kimura, *Langmuir* **2001**, *17*, 733–739; b) K. S. Mayya, M. Sastry, *Langmuir* **1999**, *15*, 1902–1904.
- [10] *Contact angle, wettability and adhesion* (Ed.: K. L. Mittal), VSP BV, Utrecht, **1993**.
- [11] a) S. Nuß, H. Böttcher, H. Wurm, M. L. Hallensleben, *Angew. Chem.* **2001**, *113*, 4137–4139; *Angew. Chem. Int. Ed.* **2001**, *40*, 4016–4018; b) K. Ohno, K. Koh, Y. Tsujii, T. Fukuda, *Angew. Chem.* **2003**, *115*, 2857–2860; *Angew. Chem. Int. Ed.* **2003**, *42*, 2751–2754; c) Y. Wang, X. Teng, J. Wang, H. Yang, *Nano Lett.* **2003**, *3*, 789–793; d) T. K. Mandal, M. S. Fleming, D. R. Walt, *Nano Lett.* **2002**, *2*, 3–7.
- [12] *Colloidal Gold: Principles, Methods, and Applications* (Ed.: M. A. Hayat), Academic Press, San Diego, CA, **1991**.
- [13] P. Mulvaney, *Langmuir* **1996**, *12*, 788–800.
- [14] W. Wang, S. Efrima, O. Regev, *J. Phys. Chem. B* **1999**, *103*, 5613–5621.
- [15] S. Sun, H. Zeng, *J. Am. Chem. Soc.* **2002**, *124*, 8204–8205.
- [16] R. R. Shah, D. Merrecces, M. Husemann, I. Rees, N. L. Abbott, C. J. Hawker, J. L. Hedrick, *Macromolecules* **2000**, *33*, 597–605.

Design and Synthesis of Photochemically Controllable Caspase-3**

Masayuki Endo,* Koji Nakayama, Yuka Kaida, and Tetsuro Majima*

Apoptosis, known as programmed cell death, is an essential biological phenomenon for maintaining a living system by removal of unnecessary cells and unfavorable damaged cells.^[1] Caspase-3 is a cysteine protease which exists as an inactive precursor (pro-caspase-3) and is activated through two general signaling pathways for apoptotic cell death.^[1,2] In death-receptor-induced apoptosis, activated caspase-8 cleaves pro-caspase-3 at the specific position for activation; then the activated caspase-3 degrades an inhibitor (DFF 45) of DNase (DFF 40) which functions for DNA fragmentation.^[1,2] In the mitochondria mediated pathway an apoptosis signal also finally reaches pro-caspase-3 for activation.^[2] Thus, caspase-3 is a key player in the apoptosis signaling pathway, and the artificial activation of pro-caspase-3 in a cell can be a powerful tool for induction of apoptotic cell death for removal of tumor cells and virus-infected cells. Photochemically controllable caged proteins have been utilized as initiators for the activation of some specific phenomena in the cell.^[3] Incorporation of a photochemical switch into pro-caspase-3 enables photofunctionalized caspase-3 to be utilized as a trigger to induce apoptotic cell death.

Herein, we demonstrate the photochemical activation of a synthetic caspase-3 having a photoreactive amino acid (2-nitrophenylglycine, Npg)^[5] at a specific position on the peptide chain. The details of the reaction mechanism of 2-nitrophenylglycine derivatives have been investigated by laser flash photolysis using a Nd:YAG laser (355 nm)^[5a] and a XeCl excimer laser (308 nm).^[5b,c] Npg groups have been incorporated into an ion channel and a nicotinic acetylcholine receptor in *Xenopus Oocyte* cells for investigation of their biochemical functions to be determined by measuring the cell response.^[6,7] To mimic the activation mechanism of pro-caspase-3 which is specifically cleaved by activated caspase-8 through apoptotic signaling, we introduced the Npg residue at the cleavage position (S176) of caspase-3 for control of the

caspase-3 activity by cleaving the peptide backbone using photoirradiation (Figure 1). In addition, the peptide sequence of the cleavage site is substituted in an unnatural way by introduction of the Npg residue at position 176; thus, the undesired autocleavage mediated by caspase-3 itself should be prohibited.^[2]

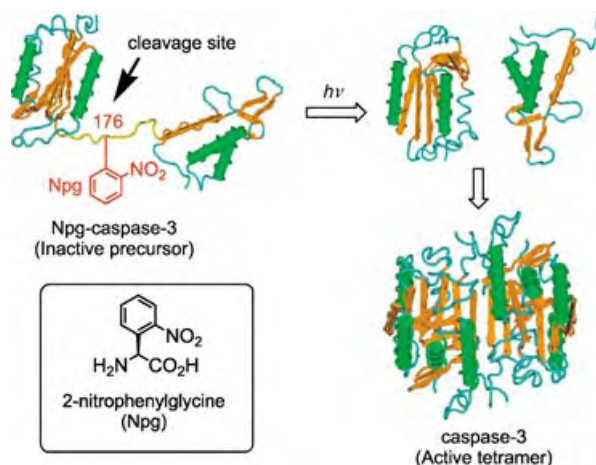


Figure 1. An illustration of the photofunctionalized caspase-3 possessing a photoreactive Npg residue at position 176 and its activation with photoirradiation. The figures of the caspase-3 and the presumed structures are reconstituted from the tetramer structure (PDB, 1CP3).^[4]

Site-selective incorporation of Npg was achieved by an in vitro transcription/translation system with a plasmid containing a four-base codon (CGGG) and Npg-tRNA_{CCCG}.^[6,8] *N*-(4-Pentenyl)-2-nitrophenylglycine cyanomethyl ester and a nucleotide dimer pdCpA were first coupled and then protected Npg-pdCpA was ligated onto a tRNA_{CCCG}(-CA) by RNA ligase. The pentenyl group was removed with saturated aqueous iodide to give Npg-tRNA_{CCCG}.^[6] In vitro translation was performed with mutated DNA having a CGGG codon (position 176) and Npg-tRNA_{CCCG} (Figure 2). The full-length Npg-incorporated caspase-3 (Npg-caspase-3) was obtained in the presence of the Npg-tRNA_{CCCG} (compare lanes 2 and 3 in Figure 2), thus indicating that the Npg residue was selectively incorporated into position 176. The efficiency for the incorporation of Npg was 15%. Since the incorpo-

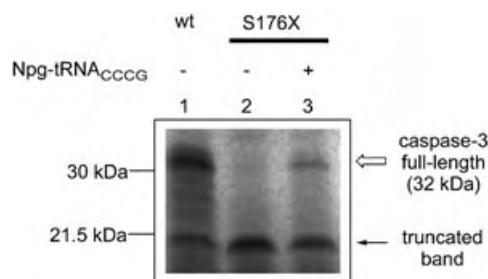


Figure 2. In vitro transcription/translation of the Npg-caspase-3 labeled with [³⁵S]methionine. Lane 1: wild-type caspase-3; lane 2: translation with mutant DNA containing a four-base codon; lane 3: translation with mutant DNA containing a four-base codon in the presence of Npg-tRNA_{CCCG}. S176X represents the DNA mutated by CGGG at position 176.

[*] Dr. M. Endo, K. Nakayama, Y. Kaida, Dr. T. Majima
Institute of Scientific and Industrial Research
Osaka University
8-1 Mihogaoka, Ibaraki, Osaka 567-0047 (Japan)
Fax: (+81) 6-6879-8499
E-mail: endo@sanken.osaka-u.ac.jp
majima@sanken.osaka-u.ac.jp

[**] We thank Dr. Yoshihide Tsujimoto (Osaka University Medical School) for providing cDNA of human caspase-3. This work was supported by a Grant-in-Aid for Scientific Research on Priority Area (417), 21st Century COE Research, and from the Ministry of Education, Culture, Sports, Science, and Technology (MEXT) of the Japanese Government.

Supporting information for this article is available on the WWW under <http://www.angewandte.org> or from the author.

ration efficiency depends on the shape of the amino acid side chains,^[8b] the lack of a β -methylene group may reduce the incorporation efficiency.

The photoreactivity of the Npg-caspase-3 was investigated by photoirradiation at 0°C by using a high-pressure mercury lamp (500 W) equipped with a monochromator for extraction of 366 nm light. Degradation of the Npg-caspase-3 was observed on photoirradiation, and the protein almost disappeared in 5 min (see Supporting Information). No degradation of the wild-type caspase-3 was observed under these photoirradiation conditions.

To examine the photoinduced activation of Npg-caspase-3 the activity was quantified with DEVD peptide attached to rhodamine 110 (Z-DEVD-rhodamine 110) as a substrate. The activity of the Npg-caspase-3 with different photoirradiation times is shown in Figure 3. The Npg-caspase-3 showed no

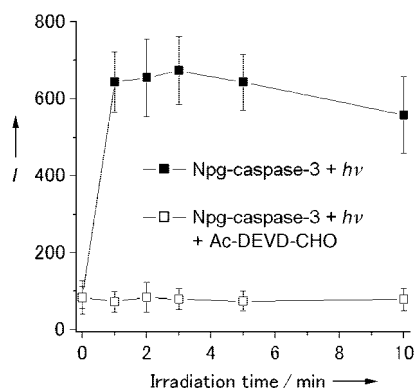


Figure 3. Expression of the caspase-3 activity using Npg-caspase-3 with photoirradiation. Photoirradiation at 366 nm was carried out for 0, 1, 2, 3, 5, and 10 min at 0°C. The enzymatic activity after photoirradiation was quantified with Z-DEVD-rhodamine 110 as a substrate ($\lambda_{\text{ex}} = 485 \text{ nm}$; detection at 538 nm). Inhibition experiments were carried out using Ac-DEVD-CHO as an inhibitor. Error bars indicate standard deviations for three independent experiments. I = fluorescence intensity.

activity without photoirradiation (0 min). The activity was clearly expressed after irradiation for one minute, and almost no change was observed during five minutes of irradiation. Addition of a caspase-3 inhibitor Ac-DEVD-CHO suppressed the activity of the photoirradiated Npg-caspase-3, thus indicating that the photoreacted Npg-caspase-3 specifically cleaves the substrate Z-DEVD-rhodamine 110. These results show that the photoirradiated Npg-caspase-3 can recover the intrinsic activity and function of caspase-3 and that the Npg residue can effectively function as a photochemical switch to control the activity of caspase-3.

The regulation of undesired autocleavage mediated by caspase-3 was investigated by comparison of the activities of wild-type and Npg-caspase-3 without and with photoirradiation (Figure 4). The translated wild-type caspase-3 showed activity on incubation at 25°C. In contrast, the Npg-caspase-3 exhibited significantly lower activity compared to the wild-type caspase-3, which suggests that the substitution to the Npg residue effectively suppresses the intrinsic autocleavage of the native caspase-3. In addition, Npg-caspase-3 can clearly

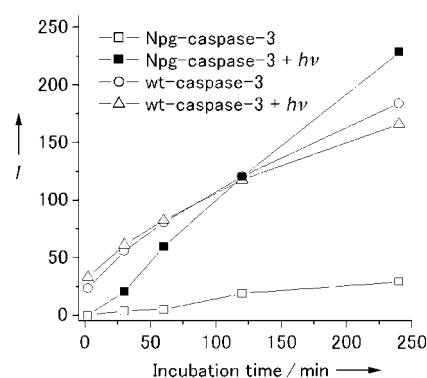


Figure 4. Suppression of autocleavage of caspase-3 by introduction of the Npg residue into the cleavage site of caspase-3. Photoirradiation at 366 nm was carried out at 0°C for 5 min. The enzymatic activity was quantified with incubation at 25°C for 2, 30, 60, 120, 240 min with Z-DEVD-rhodamine 110. Wt = wild type.

recover its activity after photoirradiation, thus indicating that the activity of the caspase-3 can be controlled by introduction of the Npg residue at position 176 and subsequent cleavage by photoirradiation.

In conclusion, we have designed and synthesized Npg-caspase-3, and photochemical regulation of the caspase-3 activity has been achieved. By using this strategy, caspase-3 can be inactivated by introduction of the Npg residue and the intrinsic activity recovered on photoirradiation. This type of photoinduced activation of enzymes may be available for other proteins and enzymes which are activated by site-selective proteolysis. These photofunctionalized synthetic proteins may be introduced into a cell by attaching a protein-transduction domain such as an HIV-1 TAT peptide sequence.^[9]

Experimental Section

In vitro translation of wild-type and Npg-caspase-3: An EcoPro T7 System (Novagen, Darmstadt, Germany) was employed for in vitro protein synthesis following the manufacturer's protocol. The in vitro translation reaction was carried out in 10 μL of a reaction mixture containing a plasmid DNA (2–3 μg), Npg-tRNA^{CCCG} (1 μg), 7 μL of EcoPro T7 extract, and L-[³⁵S] methionine (3 μCi) at 30°C for 3 h. Wild-type caspase-3 was prepared by the same method without Npg-tRNA. The mixtures of proteins were denatured in a solution containing 50 mM Tris-HCl (pH 6.8; tris = tris(hydroxymethyl)aminomethane), 0.1M 1,4-dithiothreitol (DTT), and 2% sodium dodecylsulfate (SDS) and were loaded onto an 18% SDS-polyacrylamide gel for electrophoresis. The SDS-PAGE gels were visualized and quantified by an imaging analyzer (Fujix BAS1000 analyzer). The wild-type caspase-3 and Npg-caspase-3 were simply purified by a gel-filtration spin column (BioRad Macro Bio-Spin 6 column, exclusion limit 6 kDa) for photoirradiation and subsequent caspase-3 assay. The concentration was quantified by Western blotting using a hexahistidine antibody as a primary antibody. Generation of the full-length proteins was about 10 ng from a 10 μL scale synthesis of the in vitro translation system.

Photoreaction of wild-type caspase-3 and Npg-caspase-3: The Npg-caspase-3 was placed in a Pyrex tube on ice. Photoirradiation was carried out by using a 500 W high-pressure mercury lamp (Ushio USH-500D) equipped with a monochromator (Ritsu-Oyokogaku MC-10N) which can control the specific wavelength within 4 nm full-width at half-maximum.

Measurements of the enzymatic activity of the photoirradiated Npg-caspase-3 and the inhibition assay: Npg-caspase-3 was prepared at 30°C for 3 h under the same conditions as noted above. The enzymatic activity was measured with Z-DEVD-rhodamine 110 (Promega, Madison, WI) as a substrate for caspase-3 and quantified by the fluorescence intensity of rhodamine 110 after degradation of the substrate. The photoirradiated samples were diluted with 50 mM Tris-HCl (pH 7.5), and the Z-DEVD-rhodamine 110 solution was added. After incubation at 25°C for 4 h, the reaction mixtures were placed on a 96-well plate and quantified by a plate reader ($\lambda_{\text{ex}} = 485 \text{ nm}$; detection at 538 nm). For the inhibition assay 1 μL of caspase-3 inhibitor (Ac-DEVD-CHO, 10 mM, DMSO solution) was added to the photoirradiated Npg-caspase-3 samples (20 μL). After incubation of the samples at 4°C for 1 h, the Z-DEVD-rhodamine 110 solution was added, and the mixtures were incubated at 25°C for 4 h. The activities were measured in the same fashion as noted above.

Measurements of autocleavage of wild-type caspase-3 and Npg-caspase-3: Npg-caspase-3 was prepared at 30°C for 3 h under the same conditions as noted above. After translation, the reaction mixture (10 μL) was irradiated at 0°C for 5 min under the same conditions. The samples were incubated at 25°C for 2 h without or with an inhibitor Ac-DEVD-CHO. The enzymatic activity was measured at 25°C for 2, 30, 60, 120, and 240 min with Z-DEVD-rhodamine 110. The reaction mixtures were placed on a 96-well plate and quantified by a plate reader ($\lambda_{\text{ex}} = 485 \text{ nm}$; detection at 538 nm).

Received: June 7, 2004

Keywords: apoptosis · bioorganic chemistry · enzymes · photochemistry · photolysis

- [1] a) M. Raff, *Nature* **1998**, 396, 119–122; b) K. C. Zimmermann, C. Bonzon, D. R. Green, *Pharm. Ther.* **2001**, 92, 57–70.
- [2] a) G. S. Salvesen, V. M. Dixit, *Cell* **1997**, 91, 443–446; b) X. Yang, H. Y. Chang, D. Baltimore, *Mol. Cell* **1998**, 1, 319–325; d) W. C. Earnshaw, L. M. Martins, S. H. Kaufmann, *Annu. Rev. Biochem.* **1999**, 68, 383–424; c) Y. Shi, *Mol. Cell* **2002**, 9, 459–470.
- [3] a) G. Marriott, *Biochemistry* **1994**, 33, 9092–9097; b) S. Thompson, J. A. Spoors, M.-C. Fawcett, C. H. Self, *Biochem. Biophys. Res. Commun.* **1994**, 201, 1213–1219; c) R. Folan, U. Zehavi, M. Naim, A. Patchornik, P. Smirnoff, *Biochim. Biophys. Res. Commun.* **1994**, 201, 1213–1219; d) C.-Y. Chang, B. Niblack, B. Walker, H. Bayley, *Chem. Biol.* **1995**, 2, 391–400; e) G. Marriott, M. Heidecker, *Biochemistry* **1996**, 35, 3170–3174; f) C. H. Self, S. Thompson, *Nat. Med.* **1996**, 2, 817–820.
- [4] J. Rotonda, D. W. Nicholson, K. M. Fazil, M. Gallant, Y. Gareau, M. Labelle, E. P. Peterson, D. M. Rasper, R. Ruel, J. P. Vaillancourt, N. A. Thornberry, J. W. Becker, *Nat. Struct. Biol.* **1996**, 3, 619–625.
- [5] a) T. Milburn, N. Matsubara, A. P. Billington, J. B. Udgaonkar, J. W. Walker, B. K. Carpenter, W. W. Webb, J. Marque, W. Denk, J. A. McCray, G. P. Hess, *Biochemistry* **1989**, 28, 49–55; b) D. Ramesh, R. Wieboldt, A. P. Billington, B. K. Carpenter, G. P. Hess, *J. Org. Chem.* **1993**, 58, 4599–4605; c) R. Wieboldt, D. Ramesh, B. K. Carpenter, G. P. Hess, *Biochemistry* **1994**, 33, 1526–1533.
- [6] a) P. M. England, H. A. Lester, N. Davidson, D. A. Dougherty, *Proc. Natl. Acad. Sci. USA* **1997**, 94, 11025–11030; b) M. W. Nowak, J. P. Gallivan, S. K. Silverman, C. G. Labarca, D. A. Dougherty, H. A. Lester, *Methods Enzymol.* **1998**, 293, 504–529.
- [7] For examples of site-selectively photofunctionalized proteins using in vitro translation, see a) S. N. Cook, W. E. Jack, X. Xiong, L. E. Danley, J. A. Ellman, P. G. Schultz, C. J. Noren, *Angew. Chem.* **1995**, 107, 1736–1737; *Angew. Chem. Int. Ed. Engl.* **1995**, 34, 1629–1630; b) M. W. Nowak, P. C. Kearney, J. R. Sampson, M. E. Saks, C. G. Labarca, S. K. Silverman, W. Zhong, J. Thorson, J. N. Abelson, N. Davidson, P. G. Schultz, D. A. Dougherty, H. A. Lester, *Science* **1995**, 268, 439–442; c) S. K. Pollitt, P. G. Schultz, *Angew. Chem.* **1998**, 110, 2252–2255; *Angew. Chem. Int. Ed. Engl.* **1998**, 37, 2104–2107; d) G. F. Short III, M. Lodder, A. L. Laikhter, T. Arslan, S. M. Hecht, *J. Am. Chem. Soc.* **1999**, 121, 478–479; e) M. Endo, K. Nakayama, T. Majima, *J. Org. Chem.* **2004**, 69, 4292–4298.
- [8] a) T. Hohsaka, Y. Ashizuka, H. Murakami, M. Sisido, *J. Am. Chem. Soc.* **1996**, 118, 9778–9779; b) T. Hohsaka, D. Kajihara, Y. Ashizuka, H. Murakami, M. Sisido, *J. Am. Chem. Soc.* **1999**, 121, 34–40; c) T. Hohsaka, Y. Ashizuka, H. Taira, H. Murakami, M. Sisido, *Biochemistry* **2001**, 40, 11060–11064.
- [9] a) A. M. Vocero-Akbani, N. V. Heyden, N. A. Lissy, L. Ratner, S. F. Dowdy, *Nat. Med.* **1999**, 5, 29–33; b) S. R. Schwarze, A. Ho, A. Vocero-Akbani, S. F. Dowdy, *Science* **1999**, 285, 1569–1572; c) S. R. Schwarze, K. A. Hruska, S. F. Dowdy, *Trends Cell Biol.* **2000**, 10, 290–295.

Nanostructures

Magnetically Separable, Carbon-Supported Nanocatalysts for the Manufacture of Fine Chemicals**

Shik Chi Tsang,* Valérie Caps, Ioannis Paraskevas,
David Chadwick, and David Thompsett

In the liquid phase, diffusion and mass-transfer coefficients are orders of magnitude lower than in the gas phase. Consequently, interparticle and intraparticle transport limi-

[*] Prof. Dr. S. C. Tsang, Dr. V. Caps,† I. Paraskevas

The Surface and Catalysis Research Centre
School of Chemistry, University of Reading
Whiteknights, Reading, RG6 6AD (UK)
Fax: (+44) 118-931-6632

E-mail: s.c.e.tsang@reading.ac.uk

Prof. Dr. D. Chadwick

Department of Chemical Engineering and Chemical Technology
Imperial College of Sciences, Technology and Medicine
Prince Consort Road, London, SW7 2AZ (UK)

Dr. D. Thompsett

Johnson Matthey Technology Centre
Blounts Court, Sonning Common, Reading, RG4 9NH (UK)

[†] present address:

CNRS

Institut de Recherches sur la Catalyse
2 Avenue Albert Einstein, 69626 Villeurbanne Cedex (France)

[**] This initial work was part of an Institute of Applied Catalysis (iAc (UK)) Foresight Challenge project. We thank the members of iAc steering panels, Professors C. Adams, C. Gent, D. Jackson, P. Davy (Quest Chemicals), and R. Burch (Queen's University of Belfast) for useful discussions and project guidance. S.C.T. would also like to acknowledge further financial support from Johnson Matthey and the EPSRC (GR/N21727). Dr. H. Hobson and Dr. P. Morrall are acknowledged for recording the XRD measurements and XPS spectra, respectively.



Supporting information for this article is available on the WWW under <http://www.angewandte.org> or from the author.

tations are likely to occur in liquid-phase reactions catalyzed by solid catalysts. Catalytic processes in the liquid phase are important in many areas of the fine and specialty chemicals industries, and the use of solid catalysts means easier catalyst separation and recovery, hence facilitating their reuse. It is widely accepted that a smaller catalyst particle means a higher activity, and a particle with a diameter below 1 μm experiences no significant attrition, (no reduction in particle size).^[1] As a result, both the activity and the stability of a solid catalyst suspended in a liquid phase can benefit greatly from the use of small catalyst particles (<1 μm). The main difficulty, however, is that such small particles are almost impossible to separate by conventional means, which can lead to the blocking of filters and valves by the catalyst. The efficient separation of suspended magnetic catalyst bodies from the liquid product by using an external magnetic field offers a solution to this problem and would be of immense interest. There have been some developments on the use of small magnetic bodies to host biological materials and enzymes that can only function under narrow or restricted reaction conditions.^[2,3] However, most of these bodies are unstable under the conditions commonly encountered in catalytic fine-chemical synthesis (acidic, basic, corrosive, oxidizing or reducing environments, and elevated temperatures).

Thus, a significant advance in this area would be to produce a catalyst particle that contains a magnetic core totally isolated from the catalytically active part with high magnetization for ease of separation. This advancement may be achieved by completely shielding the inner magnetic core of the particle from the external environment with impermeable coatings; the catalytically active part, located on the external surface of the coating, will then perform its function with no interference from the core. Graphitic shells (carbon cage structures) are ideal “spacers” for the isolation of magnetic particles as the close-packed graphitic networks are both chemically inert and impermeable to most chemicals. These shells could also prevent sintering of metal nanoparticles at high temperatures once they are formed. Enclosing nanomagnets into carbon cages has been attempted previously by arc evaporation,^[4] laser irradiation,^[5] electron irradiation,^[6] the creation of an “opening” followed by filling,^[7] or multistep preparation methods by using carbon deposition (from the catalytic decomposition of gaseous carbon sources) onto alumina-supported metal particles followed by selective removal of the alumina.^[1,8] These methods, however, suffer from either extremely low yields or low selectivity for the carbon-enclosed magnetic products (other carbon structures) and lead to a very wide size distribution of the particles in a complex matrix; poor control of the size and structure of the magnetic core and carbon coating is also often encountered. A new methodology in catalyst preparation is to adopt a “bottom-up” approach to modify individual catalyst particles.^[9]

Herein we report the synthesis of a new class of magnetically separable catalyst carriers, consisting of carbon-encapsulated nanomagnets, based on a simple nanochemistry approach that involves sequential spraying (the complex dissolved in the fine aqueous droplets determines the nature

of the solid material obtained), chemical precipitation, and controlled pyrolysis.^[10] We found that well-defined, nanometer-sized magnetic alloy particles, enclosed in quasi-spherical graphitic shells, were obtained in large quantities without the use of any solid supporting material. The carbon-protected nanomagnets used as carriers for catalytically active species (Pd nanoparticles) have a higher activity than commercial carbon-supported catalysts. The total encapsulation of the magnetic core in a carbon network also allows direct handling of intrinsically sensitive magnetic materials (FeNi, Fe₃C) in acidic solution and in air (by protecting them from decomposition), hence separation of these nanocatalysts in an external magnetic field can be achieved.

In a typical synthesis, spraying an aqueous solution of sodium nitroferricyanide (obtained by injecting nickel nitrate solution into the head space of ammonia vapor, followed by pyrolysis of the resultant precipitate at elevated temperatures) leads to iron–nickel alloy nanoparticles with a narrow size distribution. The X-ray diffraction (XRD) pattern (Figure 1), with reflections at $2\theta = 43^\circ$, 51° , and 75° , clearly

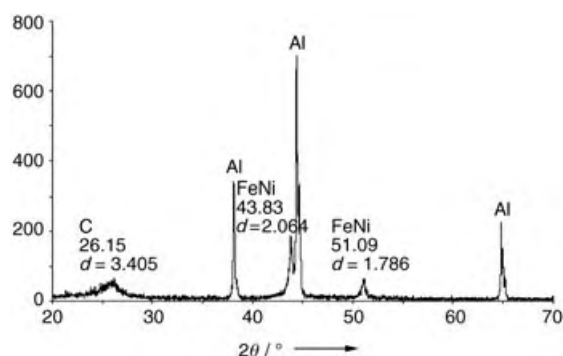


Figure 1. XRD pattern of a carbon-coated, nanometer-sized FeNi magnetic alloy.

indicates the presence of a crystalline mixed Fe–Ni alloy phase. However, it is difficult to assign a precise phase from the XRD pattern—the peaks are very broad—since the 2θ values are very similar to the crystallographic parameters of cubic iron nickel (FeNi; International Centre for Powder Diffraction Source (JCPDS 1996) no. 47-1417, $a = 3.5406 \text{ \AA}$), cubic FeNi₃ (JCPDS no. 38-0419, $a = 3.545 \text{ \AA}$), and cubic Fe_{0.64}Ni_{0.36} (JCPDS no. 47-1405, $a = 3.5922 \text{ \AA}$). An average crystallite size of $11 \pm 3 \text{ nm}$ was calculated from the Scherrer equation. The small, broad hump at $2\theta = 26^\circ$ is attributed to small quantities of graphitic structures a few atomic layers thick, thus leading to a severe peak broadening. It is interesting to note that subsequent treatment of the sample with concentrated hydrochloric acid (boiling for 4 h), which should dissolve unprotected alloy particles, leaves the diffraction pattern unchanged. This result clearly suggests that the alloy particles are protected by some kind of acid-resistant coating. Figure 2a shows a typical TEM micrograph of the spray-precipitation sample (before pyrolysis); nanoscopic particles embedded in an amorphous matrix can clearly be observed. These particles, which are uniform in size, contain both Fe and Ni (~1:1 atomic ratio suggesting a predominant

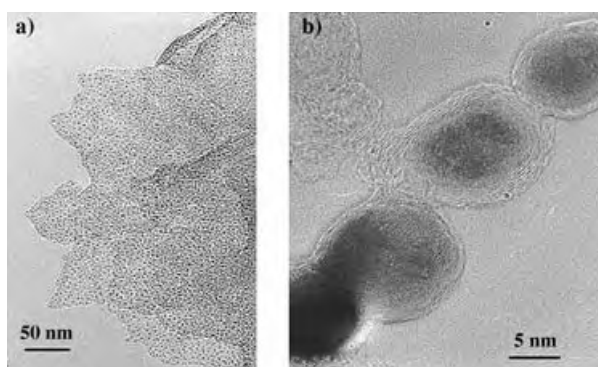


Figure 2. TEM micrograph of carbon-encapsulated FeNi particles deposited on carbon film ($\times 152\,000$ magnification; left) and a high-resolution TEM micrograph of three typical particles ($\times 3\,100\,000$; right).

FeNi phase) as confirmed by energy-dispersive X-ray (EDX) spectroscopy. A majority of the particles are indeed in the size range 10–15 nm. A high-resolution TEM micrograph (Figure 2b) taken after pyrolysis indicates that all the particles are encapsulated by thin, quasi-spherical carbon structures. A detailed examination of these carbon coatings shows that, in many cases, lattice fringes similar to those of graphite (about 3.4 Å) can be traced all around the particles, suggesting concentric carbon-shelled structures. This is in good agreement with the presence of the small, broad graphite peak in the XRD pattern. Prolonged exposure of the selected area to an electron beam (< 60 s) ruled out the possibility that carbon-shell formation occurs upon electron-beam illumination.^[6] Thermogravimetric experiments indicate that a typical carbon-protected FeNi sample displays an extremely high alloy content (67.01 wt.%) after acid treatment. These graphite-encapsulated particles can also be found embedded in an external, amorphous carbon coating (the relative size of alloy core and external carbon coating are found to depend on the amount of metal precursors and poly(vinyl alcohol) (PVAL) used). Thus, a good degree of tailoring of the metal core and carbon coating is clearly possible (see also the Supporting Information). It is thought that during the heat treatment in inert gas the cyanide groups play a major role in the reduction of the mixed Fe/Ni-containing seeds, thus allowing both alloy formation and alloy encapsulation, while the added poly(vinyl alcohol), which is known to decompose readily at low temperatures (> 393 K), would provide the amorphous carbon in which the particles are embedded.

Figure 3 shows X-ray photoelectron spectroscopy (XPS) survey spectra of the pyrolyzed sample before and after an *in situ* heat treatment at 523 K (upper line) for 30 minutes (desorption of contaminants). No major changes are detected and no charging effect is observed on the sample. The peaks are directly referenced to the amorphous carbon (C1s) peak at 284.6 eV.

It appears that the surface (or the first few atomic layers) consists of pure carbon containing a small number of heteroatoms (O, N, Na, Fe, and Ni)—we detected small signals of Fe and Ni 2p and Auger peaks, with the C/Fe and C/Ni atomic ratios being around 0.05. This fact agrees with the TEM images, which show that the Fe/Ni nanoparticles are

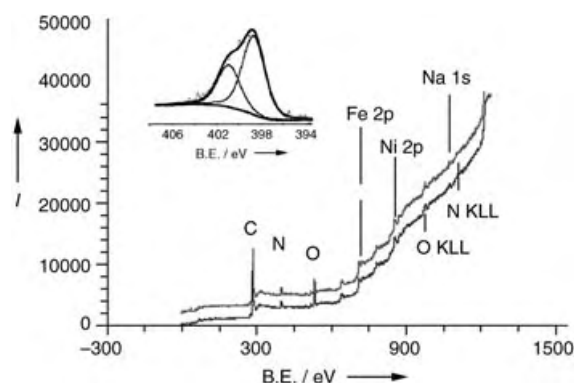


Figure 3. XPS spectrum (and N 1s region; inset) of carbon-coated FeNi nanoparticles.

totally encapsulated by carbon cages after heat treatment at 1173 K under nitrogen. The binding energies of these exposed Fe and Ni species suggest that they are unlikely to be in the metallic state. An oxygen signal is also found, although it is not yet clear whether this oxygen atom is bound to the exposed iron/nickel species (as surface metal-oxide contaminants before the acid treatment), or to nitrogen or carbon atoms. There are also traces of sodium (Na 1s peak) in the pyrolyzed sample, which probably come from the iron precursor used. It is interesting to note that a nitrogen signal is also observed. The surface contains nitrogen atoms in an ratio to carbon atoms of 43:3. The N 1s region (Figure 3 inset) contains a main peak at 398.6 eV with a shoulder at 400.8 eV. It has been reported previously that an N 1s signal at 401 eV is characteristic of nitrogen atoms present in graphene sheets.^[11] We therefore concluded that a small number of nitrogen atoms are incorporated into the graphene network. It has also been reported that a strong peak at 398 eV with a shoulder at 400 eV is due to different C–N bonding (C=N and C–N). Hence we believe that the carbon coating formed around the alloy particles during the heat treatment at 1173 K has a graphite-like structure containing some nitrogen atoms. Nitrogen incorporation (from cyanide pyrolysis) into graphene layers is known to cause curvature of the graphitic planes, which in this case results in encapsulation.^[12] Thus, 7% of the surface atoms of our carbon coatings is made up of nitrogen atoms, which makes these encapsulated particles fundamentally and structurally different from those formed by traditional carbon-deposition methods, whose carbon shells contains only carbon atoms and hence are made up of essentially planar graphite plates.

A variety of iron-based binary alloys (FeCu, FeCo, FeNi) were synthesized in this manner. It is interesting to note that when calcium nitrate (Fe/Ca) was used, a very high concentration of carbon-encapsulated nanoparticles with a very narrow size distribution was found. The XRD spectrum (see the Supporting Information) shows that this sample consists of Fe₃C nanoparticles encapsulated in concentric graphitic carbon layers with a small amount of CaCN₂ as background matrix. TEM micrographs of the sample after pyrolysis show that the iron-carbide nanoparticles are encapsulated in graphitic carbon (see Supporting Information), with the amorphous calcium-containing phase forming matrices

between the graphite-coated, iron-carbide particles. We attribute this to the fact that calcium does not form a stable alloy with iron (compared to FeNi) but its presence along with the Fe-based nanoparticles protects the composite material from sintering during the heat treatment under nitrogen, hence providing a very high concentration of carbon-coated, iron-containing nanoparticles with a homogeneous size. Microanalysis of the product shows that it contains Ca (35.49 wt. %) and Fe (29.57 wt. %); the rest is carbon. After the acid treatment, selective removal of the calcium-containing matrix releases the tiny, colloidal, graphitic-carbon-encapsulated, magnetic Fe₃C nanoparticles (as confirmed by XRD). These carbon-coated carbide particles contain almost 10.89 wt. % Fe and have a low Ca content (< 1 %). All known iron-carbide phases—Fe₂C, Fe_{2.2}C, Fe₅C₂, and Fe₃C—are ferromagnetic and display a high magnetization. Fe₃C, in particular, is known to give a high magnetic response but its extreme acid and air sensitivity limits its uses. It is therefore of great interest that this simple technique can be used to prepare large quantities of air- and acid-stable carbon-encapsulated iron carbide.

Figure 4 shows the experimentally measured saturation magnetization of some typical samples. In the case of Fe/Ca,

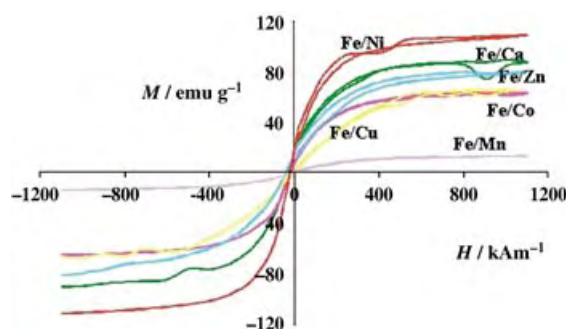


Figure 4. The carbon-protected, Fe-based magnetic particles (metal, alloy, carbide, or their mixtures) all display negligible magnetic hysteresis (high magnetization response with no magneto aggregation of the fine particles in solution in the absence of a nonhomogeneous magnetic field).

Fe₃C is the predominant phase. It can be seen that the carbon-protected magnetic alloy particles all display negligible magnetic hysteresis (a high magnetization response but with no magnetic aggregation of the fine particles in solution in the absence of a nonhomogeneous magnetic field), hence they are well suited as magnetic catalyst-support particles.

Typically, the magnetization of the carbon-coated FeNi nanoparticles reaches saturation when fields above 1000 Oe are applied. A saturation magnetization of 110 emu per gram of the sample is attained; thus, taking into account the alloy (67.01 wt. %), which is the main contributor to the magnetization—the contribution of the graphite jacket is thought to be insignificant relative to the central soft magnetic Fe–Ni core—the saturation magnetization of this material per gram of alloy would be 165 emu g^{−1}. Values of 156 emu g^{−1} have been reported in the literature for the saturation magnetization of bulk nickel–iron alloys with a Ni/Fe ratio of 1.

Hence, within experimental error, this encapsulated alloy material appears to display a similar saturation magnetization to the bulk stoichiometric alloy.

The preliminary results shown in Table 1 reveal that the magnetic nanocatalyst is twice as active for hydrogenation of nitrobenzene than a commercial catalyst (Johnson–Matthey)

Table 1: Initial rates of nitrobenzene hydrogenation for two Pd samples.

Catalyst	Initial rate ^[a]	Mass of catalyst [mg]
5 % Pd/C (with Fe–Ni magnetic core)	1.529	32
5 % Pd/C (Johnson Matthey powder catalyst)	0.835	50

[a] μmol of nitrobenzene converted into aniline per second.

with the same metal loading, and with a lower amount of catalyst used. We attribute this higher activity of Pd deposited on carbon-coated nanomagnets to the absence of intraparticle mass-transfer limitations and to the better Pd dispersion on the nanometer-sized carbon particles (colloidally dispersed in the solvent) than on the micrometer-sized commercial catalyst powder. The flocculation of the nanometer-sized magnetic catalyst particles from solution is easily achieved within a few minutes by applying an external magnetic field ($H_{\text{max}} = 38 \text{ MG Oe}$), which facilitates its separation from the product solution.

In summary, we have shown that carbon-encapsulated, iron-based magnetic nanometer-sized particles (10–30 nm, tunable depending on the amount of precursors used) in quasi-spherical carbon shells can be prepared in large quantities by a simple synthetic technique. A unique advantage of the external graphitic carbon surface is that it isolates and protects the magnetic core from destructive reactions with the environment, thus a wide range of experimental conditions can now be used for catalytic synthesis of fine chemicals. The carbon surface can be functionalized with different types of standard catalysts (metal clusters, homogeneous catalysts, enzymes). Hence, these nanocomposite catalysts are an important new development in using solid catalysts for the production of fine chemicals in liquid-phase reactions. Apart from catalytic applications, other useful applications of such carbon-protected, nanometer-sized particles may also be expected in several areas of the nanotechnology field.

Experimental Section

Sodium nitroferrocyanide(III) dihydrate [Na₂Fe(CN)₅NO·2H₂O] (2 g), one molar equivalent of metal nitrate [M(NO₃)₂·xH₂O; M = Ni, Ca, Mn, Zn, Cu], and poly(vinyl alcohol) (PVAL) as a carbon source (optional, MW 31 000–50 000) were mixed together in deionized water (100 mL) at room temperature. This solution was passed through a pneumatic sprayer head kept at a pressure of $1.38 \times 10^5 \text{ Pa}$ of nitrogen gas. The fine mist produced (submicrometer-sized droplets) was sprayed into the headspace of a jar filled with saturated ammonia solution (0.88 sg). The fine droplets immediately formed a solid precipitate upon coming into contact with the ammonia (vapor and solution). This solid was collected, washed thoroughly with

deionized water, dried, and heated to 1173 K under a nitrogen atmosphere for 10 h. The surface of the carbon-encapsulated alloy particles prepared was functionalized with -OH or -COOH groups (confirmed by infrared spectroscopy) by immersing them in boiling concentrated HCl (acid treatment) or a dilute bleach ($\text{NaOCl} + \text{H}_2\text{O}_2$) solution for 4 h and then isolated, washed, and dried.

XPS spectra were recorded on a VSW photoelectron spectrometer with $\text{Mg K}\alpha$ radiation (1253.6 eV) equipped with a 100 mm concentric hemispherical analyzer, operating at a constant pass energy in ultrahigh vacuum (1.33×10^{-7} Pa). A survey scan (covering the whole energy range from 1400 to 0 eV) was recorded to determine the position of the peaks. A detailed XPS survey was then recorded as well as detailed scans of the C 1s, O 1s and N 1s regions. No charge effect was observed and the binding energies were directly referenced to the carbon C 1s peak at 284.6 eV. All binding energies are given with an uncertainty of 0.2 eV.

Magnetic measurements were performed by using a vibrating sample magnetometer (VSM), which consists of an electromagnet (maximum applied field of $\pm 1200 \text{ kA m}^{-1}$) with a sample cell holder vibrating between two pole faces. The VSM measures the difference in magnetic induction between a region of free space with and without the sample as it vibrates thus giving a direct measure of the magnetization M . While the sample is in the magnetic field the magnetic induction is $B_M = \mu_0(H + M)$ and as the sample is moved away this changes to $B_0 = \mu_0 H$, which gives the change in magnetic induction as $\Delta B = \mu_0 M$, in which B is the magnetic induction, H is the magnetic field, M is the magnetization, and μ_0 is the permeability of free space.

To illustrate the use of these carbon-encapsulated nanoalloys as catalyst support, 5 wt. % palladium was deposited onto them by a wet impregnation of $[\text{Pd}(\text{acac})_2]$ in acetone. Their catalytic activity was studied for the hydrogenation of nitrobenzene. Nitrobenzene (6.5 mL, 63 mmol) was dissolved in isopropanol (IPA; 125 mL) and placed in a glass beaker inside a 300 mL Parr reactor. The carbon-based catalyst (30 mg) was then added. The reactor was purged with a nitrogen flow for 5 min followed by intermittent purges with pure H_2 at 2×10^6 Pa. The reactor was kept at a pressure of 2×10^6 Pa H_2 and heated up to 353 K with constant stirring (560 rpm). Under these conditions, external mass limitations (such as H_2 solubility and diffusion of substrates from solution to catalytically active sites on solid surfaces) were not anticipated. Samples (< 1 mL) were collected at different times from the reactor by using the internal sampling dip tube without disturbing the ongoing reaction. The samples were analyzed; aniline was the only product observed.

Received: May 4, 2004

Keywords: carbon coating · cyanides · heterogeneous catalysis · magnetic properties · nanomagnets

- [1] W. Teunissen, A. A. Bol, J. W. Geus, *Catal. Today* **1999**, *48*, 329.
- [2] M. T. Reetz, A. Zonta, V. Vijaykrishnan, K. Schimossek, *J. Mol. Catal. A* **1998**, *134*, 251.
- [3] X. Gao, K. M. K. Yu, K. Tam, S. C. Tsang, *Chem. Commun.* **2003**, 2998.
- [4] V. P. Dravid, J. J. Host, M. H. Teng, B. E. J. Hwang, D. L. Johnson, T. O. Mason, J. R. Weertman, *Nature* **1995**, *374*, 602.
- [5] J. R. Heath, S. C. O'Brien, Q. Zhang, Y. Liu, R. F. Curl, H. W. Kroto, F. K. Tittel, R. E. Smalley, *J. Am. Chem. Soc.* **1985**, *107*, 359.
- [6] D. Ugarte, *Chem. Phys. Lett.* **1993**, *209*, 99.
- [7] S. C. Tsang, Y. K. Chen, P. J. F. Harris, M. L. H. Green, *Nature* **1994**, *372*, 159.
- [8] W. Teunissen, Ph.D. Thesis, Universiteit Utrecht (The Netherlands), **2000**.

- [9] K. M. K. Yu, C. M. Y. Yeung, D. Thompson, S. C. Tsang, *J. Phys. Chem. B* **2003**, *107*, 5737.
- [10] "Microparticles and methods of making them": V. Caps, S. C. Tsang (The Institute of Applied Catalysis, UK), PCT Int. Appl. WO 2003057626A1, **2003**.
- [11] V. N. Khabashesku, J. L. Margrave, K. Waters, J. A. Schultz, *Thin Solid Films* **2000**, *381*, 62.
- [12] S. C. Tsang, J. Qiu, P. J. F. Harris, Q. J. Fu, N. Zhang, *Chem. Phys. Lett.* **2000**, *322*, 553.

Peptide Structures

Calibrated Calculation of Polyalanine Fractional Helicities from Circular Dichroism Ellipticities**

Gabriel E. Job, Björn Heitmann, Robert J. Kennedy,
Sharon M. Walker, and Daniel S. Kemp*

In characterizing peptides, fractional helicities (FHs),^[1] are calculated from per-residue molar ellipticities at $\lambda = 222$ nm [Eq. (1)].^[2] Here, for a partially helical peptide of length n ,

$$\text{FH} = [\theta]_{222, \text{Exp}, n} / [\theta]_{222, n} \quad (1)$$

$[\theta]_{222, \text{Exp}, n}$ is the observed per-residue molar ellipticity at $\lambda = 222$ nm, and $[\theta]_{222, n}$ is the corresponding length-dependent calibration value for a completely helical peptide. FHs are often used to construct quantitative helicity algorithms,^[3] but for the important cases of alanine-rich peptides and polyalanines, the calculation is inaccurate^[4] and requires calibration. Spaced, solubilized, helical Ala_{*n*} peptides (Figure 1) that span a large range of lengths and are characterized by FHs that approach 1.0 provide this calibration.

NMR experiments show that strong helix-stabilizing caps, like β -aminoalanine *beta* or the *N*-acyl-Pro-Pro analogue Hel, restrict the helical regions of these peptides to the Ala_{*n*} sequences.^[5] NMR studies on simpler analogues of the sequence in Figure 1b^[6] demonstrate literature-precedented,^[7] short-range stabilizing contacts between caps and Ala_{*n*} termini by ¹H TOCSY, ROESY, and NOESY experiments, but tertiary interactions are not observed. ¹H, ¹³C, and ¹⁵N NMR chemical shifts, ³J_{H_NH _{α}} values, and α -helical structure are assigned from HNCA, E.COSY HNCA, and

[*] G. E. Job, Dr. B. Heitmann, Dr. R. J. Kennedy, Dr. S. M. Walker, Prof. D. S. Kemp
Department of Chemistry, Room 18-296
Massachusetts Institute of Technology
Cambridge, MA 02139 (USA)
Fax: (+1) 617-258-7500
E-mail: kemp@mit.edu

[**] This research was supported by the NSF CHE-0131250 and the NIH GM 13453 (S.M.W.).



Supporting information for this article is available on the WWW under <http://www.angewandte.org> or from the author.

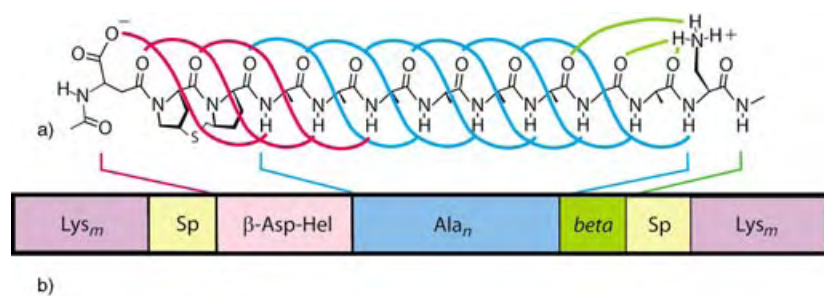


Figure 1. a) Molecular structure of the helical β AspHel-Ala_n-beta subunit shared by all spaced, solubilized peptides of this study. Blue: α -helical H-bonds within the Ala_n region; green: H-bonds that link beta to the Ala_n region; red: H-bonds that link β AspHel to the Ala_n region. b) Functional regions within the peptide series used for CD calibration Ac-Trp-Lys₅-Inp₂-L- β AspHel-Ala_n-beta-LInp₂-Lys₅-NH₂, $n = 4-11$; $n = 12-24$, n even. Only residues of the blue Ala_n core are helical.^[5b,c] Pink: helix-stabilizing N-cap; green: helix-stabilizing C-cap; purple: polyLys solubilizer; yellow: spacing elements^[5a,d] drawn from the list: 'L = *tert*-leucine, Inp = 4-carboxypiperidine, Acc = *trans*-4-aminocyclohexanecarboxylic acid. See Experimental Section and Supporting Information for details.

H(N)CO experiments on simple and ¹³C,¹⁵N-labeled Ala_n peptides. The Ala_n peptides are unaggregated in water by analytical ultracentrifugation.

The chemical shifts for amide NH protons at sites 5 to $(n-4)$ of Ala_n sequences with $n > 8$ are independent of both site and length n . For the first four alanines of each peptide, the HN resonances are resolved, and for a particular site their chemical shifts are constant throughout the series; this property is also seen for the three resonances assigned to the last four alanine NHs. NMR-assigned rate constants for backbone NH \rightarrow ND exchange in D₂O at 2°C, pH 4.5–6.0, yield protection factors PF_{*i*} for each peptide,^[8] from which the FH_{*i*}s and an average FH can be calculated.

Most FH_{*i*}s are equal to or greater than 0.985, but at C-terminal sites NH _{$(n-3)$} through NH _{$(n-1)$} , a monotonic decrease is seen from 0.98 to 0.94. The FH_{*n*}, defined by PF _{$n+1$} of beta, have respective lower and upper limits of 0.1 and 0.7.^[6] For the overall Ala_n series, FHs lie in the range 0.90 to 0.98,^[9] but for the central Ala_n region, residues 2 through $n-4$, FH_{*i*} is consistently equal to or greater than 0.993.^[10] The calibrating circular dichroism (CD) relations [Eq. (2) and Eq. (3)] apply rigorously to a series with the above properties that meets the linearity test described below.^[6]

$$[\theta]_{\lambda,n} = [\theta]_{\lambda,\infty}(1 - X/n) \quad (2)$$

$$[\theta_{\text{Molar}}]_{\lambda,n} = n[\theta]_{\lambda,n} = [\theta]_{\lambda,\infty}(n - X) = n[\theta]_{\lambda,\infty} - X[\theta]_{\lambda,\infty} \quad (3)$$

A CD-based calculation of FH for a partially helical peptide requires $[\theta]_{222,n}$, the ellipticity for an analogous peptide with FH = 1.0, [Eq. (1)]. Estimates for $[\theta]_{222,\infty}$ and X are usually applied to Equation (2) to obtain $[\theta]_{222,n}$,^[2] but their unambiguous assignment has been problematic.^[11] Both

$[\theta]_{\lambda,\infty}$ and X can now be assigned from those $[\theta_{\text{Molar}}]_{\lambda,n}$ values of our Ala_n series that correlate linearly with n , as required by Equation (3).

Figure 2 shows CD spectra of five peptides from Figure 1b measured in water at 2°C, pH > 4.5. A linear regression in n for the ten-member data set of $[\theta_{\text{Molar}}]_{222,n}$ values, $9 \leq n \leq 24$, yields a slope of -59600 (standard deviation (SD) 1300) and an intercept of 202000 (SD 20700); the calculated error in slope at 222 nm corresponds to a relative precision of $\pm 2\%$, within measurement error.^[12] Restrictions of the data set to $11 \leq n \leq 24$ and $14 \leq n \leq 24$ yield respective slopes of -59300 (SD 1700) and -58800 (SD 3100). Within SD limits, these assignments are indistinguishable. For $n > 8$ and for all λ , the slopes, which are per-residue ellipticity increments, converge to limiting values, plotted as the red curve in Figure 2. This CD spectrum of $[\theta]_{\lambda,\infty}$

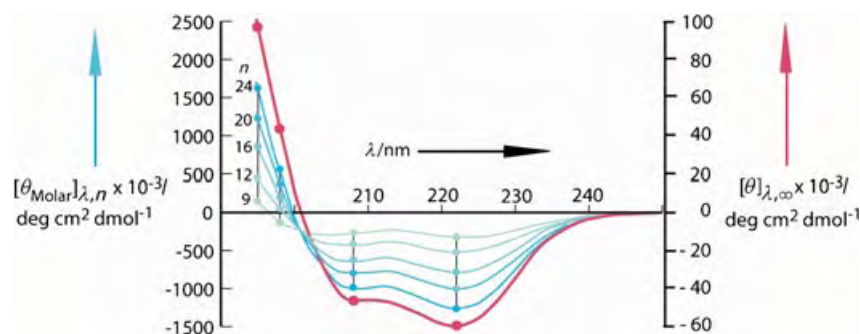


Figure 2. Length-dependent CD spectra, $[\theta_{\text{Molar}}]_{\lambda,n}$ for the Ala_n peptides described in Figure 1, in water, pH > 4.5, $T = 2^\circ\text{C}$, (blue-green curves, left-hand axis, blue arrow). For clarity, five representative spectra from the data base of ten are shown. Linear regressions for each wavelength λ (see text) yield slopes (red dots) from $[\theta_{\text{Molar}}]_{\lambda,n}$ data (blue-green circles linked by vertical lines). These λ -dependent slopes (red curve, right-hand axis, red arrow) yield a CD spectrum of $[\theta]_{\lambda,\infty}$ values calculated for length-independent cores of completely helical polyalanines.

values reflects the length-independent core properties of completely helical polyalanines. A notable feature is a value of 1.3 for the ratio $[\theta]_{222}/[\theta]_{208}$, typical for alanine-rich helical peptides.^[4c]

The value of X must reflect deviations from FH_{*i*} = 1.0 within the Ala_n termini. A linear regression on n and $[\theta_{\text{Molar}}]_{222,n}$ data that have been corrected by subtracting $[\theta_{\text{Molar}}]_{222,0}$ values and dividing the resulting differences by the length series of FH values yields $[\theta]_{222,\infty} = -60600$ (SD 1200), $X = 3.0$ (SD 0.3) for FH_{*n*} = 0.1, and $[\theta]_{222,\infty} = -60500$ (SD 1200), $X = 3.2_5$ (SD 0.3) for FH_{*n*} = 0.7. This X range is consistent with earlier reports.^[10,13]

Applied to Equation (2) these parameters yield the calculated length dependences for $[\theta]_{222,n}$ given in Figure 3, which includes estimates of the precision of currently feasible assignments of FH from CD data. For a 24-residue peptide, the maximum error in X translates into a 10% error in the assignment of $[\theta]_{222,n}$ and in a calculation of FH that uses this parameter. For a 12-residue peptide, the error increases to 16%.

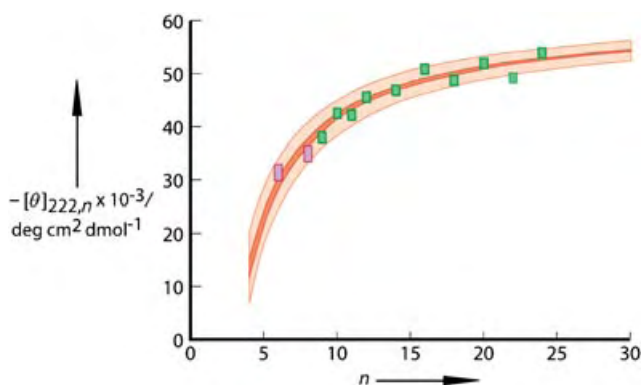


Figure 3. Length dependence of $[\theta]_{222,n}$ [Eq. (1)] calculated [Eq. (2)] from $[\theta]_{222,\infty} = -60\,600$ (SD 1200), $X = 3.0$ (SD 0.3) for $FH_n = 0.1$, and $[\theta]_{222,\infty} = -60\,500$ (SD 1200), $X = 3.2_5$ (SD 0.3) for $FH_n = 0.7$.^[11] The red region of the graph $[\theta]_{222,n}$ was calculated from these mean parameter values. The pink region defines boundaries of values calculated from variations of X and $[\theta]_{222,\infty}$ by one SD unit. Values of the ten experimental $([\theta]_{\text{Molar}}]_{222,n} - [\theta]_{\text{Molar}}]_{222,1})/FH$ used to assign X and $[\theta]_{222,\infty}$ are plotted (green). For comparison, two corresponding values calculated from $[\theta]_{\text{Molar}}]_{222,n}$, $n = 6$ and 8 are also shown (violet).

Inspection of Figure 3 shows that for $n < 12$, the value of $[\theta]_{222,n}$ is very sensitive to errors in the X assignment; X is expected to reflect changes in solvation at the helix termini, the presence terminal charges, and end-region contributions from 3_{10} -helical structure. For short peptides that belong to a particular structural series, maximal precision for calculation of FH from $[\theta]_{222,\text{Exp},n}$ may require tailoring of X to mirror the CD properties of that series.

We have validated our earlier estimates^[4] of $[\theta]_{222,\infty}$ for alanine-rich peptides by a method that can be generalized to other peptide series. The literature $[\theta]_{222,\infty}$ values of $-37\,000$ ^[11a] to $-44\,000$ ^[11b] underestimate $[\theta]_{222,n}$ for alanine-rich peptides, but they almost certainly remain relevant to most highly helical fragments derived from natural protein sequences.^[11a] For what cases should our $[\theta]_{222,\infty}$ value assignment be used? The best criterion is the value of $[\theta]_{222}/[\theta]_{208}$, measured for members of a new peptide structural series under helix-stabilizing conditions. If this ratio exceeds 1.2,^[4c] $[\theta]_{222,\infty}$ values of $-60\,000 \pm 1000$ are appropriate choices.

Experimental Section

Peptides were synthesized, purified by repeated reverse-phase HPLC, characterized by electrospray ionization mass spectrometry (EI-MS), and analyzed by CD spectroscopy (Aviv 62DS circular dichroism spectrometer) following experimental protocols published previously.^[4,5] The instrument was calibrated as described in its operating manual using titrated water solutions of sublimed 9-camphorsulfonic acid. Peptide concentrations were determined on a Cary 300 UV/Vis spectrometer utilizing the Trp chromophore of the peptide, as previously reported. A Bruker Avance 600 instrument (Karlsruhe, Germany) equipped with four channels and a pulsed field gradient triple probe with z gradients was used for all NMR studies. For convenience, NMR studies were initially carried out on $\text{Ac}^\beta\text{AspHel-Ala}_8\text{-beta-NH}_2$ and the series $\text{Ac}^\beta\text{AspHelAla}_n\text{betaAccLys}_2\text{TrpNH}_2$, where Acc is derived from the spacer *trans*-4-aminocyclohexanecarboxylic acid. Where appropriate, parallel NMR studies were carried out on the CD-calibration peptides of Figure 1 b. PF measurements

and chemical shift assignments for the Ala_n cores of these peptide series were in agreement. PF measurements on a similar Ala_n peptide have been reported previously.^[4b]

The Supporting Information contains peptide AUC (Analytical Ultracentrifugation Equilibrium) and MS characterization, details of NMR structural assignments and chemical shift correlations, PF data and calculation of FH_i from PF_i data, and discussion of correlations underlying the analysis of Figure 2.

Received: May 1, 2004

Keywords: circular dichroism · helical structures · NMR spectroscopy · peptides

- [1] FH , the fraction of potentially helical α -carbon atoms that are actually in a helical structure (range: 0.0 to 1.0); FH equals the average of site FH_i at each α -carbon of Ala_n cores.
- [2] a) R. W. Woody, *J. Polym. Sci. Macromol. Rev.* **1977**, *12*, 181–320; b) M. C. Manning, R. W. Woody, *Biopolymers* **1991**, *31*, 569–586; c) Y.-H. Chen, J. T. Yang, H. M. Martinez, *Biochemistry* **1972**, *11*, 4120–4131.
- [3] a) A. Chakrabarty, T. Kortemme, R. L. Baldwin, *Protein Sci.* **1994**, *3*, 834–853; b) S. H. Park, W. Shalongo, E. Stellwagen, *Biochemistry* **1993**, *32*, 7038–7053.
- [4] a) P. Wallimann, R. J. Kennedy, D. S. Kemp, *Angew. Chem.* **1999**, *111*, 1377–1379; *Angew. Chem. Int. Ed.* **1999**, *38*, 1291–1292; b) R. J. Kennedy, K. Y. Tsang, D. S. Kemp, *J. Am. Chem. Soc.* **2002**, *124*, 934–944; c) P. Wallimann, R. J. Kennedy, J. S. Miller, W. Shalongo, D. S. Kemp, *J. Am. Chem. Soc.* **2003**, *125*, 1203–1220.
- [5] a) J. S. Miller, R. J. Kennedy, D. S. Kemp, *Biochemistry* **2001**, *40*, 305–309; b) S. Deechongkit, R. J. Kennedy, K.-Y. Tsang, P. Renold, D. S. Kemp, *Tetrahedron Lett.* **2000**, *41*, 9679–9683; c) W. Maison, E. Arce, P. Renold, R. J. Kennedy, D. S. Kemp, *J. Am. Chem. Soc.* **2001**, *123*, 10245–10254; d) J. S. Miller, R. J. Kennedy, D. S. Kemp, *J. Am. Chem. Soc.* **2002**, *124*, 945–962.
- [6] For details, see the Experimental Section and the Supporting Information.
- [7] a) D. S. Kemp, S. L. Oslick, T. J. Allen, *J. Am. Chem. Soc.* **1995**, *117*, 6641–6657; b) H. A. Nagarajaram, R. Sowdhamini, C. Ramakrishnan, P. Balaram, *FEBS Lett.* **1993**, *321*, 79–83.
- [8] S. W. Englander, N. R. Kallenbach, *Q. Rev. Biophys.* **1984**, *16*, 621–655.
- [9] If $FH_n = 0.1$, the FH s increase monotonically for Ala_9 to Ala_{24} within the following range: $0.90 \leq FH \leq 0.96$; if $FH_n = 0.7$, the corresponding range is $0.94 \leq FH \leq 0.98$.
- [10] Since the value of a PF_i that exceeds 100 largely reflects the trace of peptide that assumes a nonhelical conformation at site i , a large measurement error in PF_i corresponds to a much smaller error in FH_i . Thus $90 \leq PF_i \leq 110$ corresponds to $0.988 \leq FH_i \leq 0.992$ (see the Supporting Information).
- [11] a) N. A. Besley, J. D. Hirst, *J. Am. Chem. Soc.* **1999**, *121*, 9636–9644; b) P. Luo, R. L. Baldwin, *Biochemistry*, **1997**, *36*, 8413–8421.
- [12] Units of $\text{deg cm}^2 \text{ dm}^{-1}$; average residuals for these regressions over the λ range are $\pm 3\%$ of $[\theta]_{\text{Molar}}]_{\lambda,n}$ and lie within the measurement error of ca 3–5% estimated from CD spectra,^[5d] $14 < n < 20$, for a series $\text{WK}_m\text{Inp}_2^1\text{L-Ala}_n\text{-}^1\text{LInp}_2\text{K}_m\text{-NH}_2$.
- [13] a) P. J. Gans, P. C. Lyu, M. C. Manning, R. W. Woody, N. R. Kallenbach, *Biopolymers* **1991**, *31*, 1605–1614; b) J. M. Scholtz, H. Qian, E. J. York, J. M. Stewart, R. L. Baldwin, *Biopolymers* **1991**, *31*, 1463–1470.

Micrometer-Sized Spherical Assemblies of Polypeptides and Small Molecules by Acid–Base Chemistry**

Brandon J. McKenna, Henrik Birkedal,*
Michael H. Bartl, Timothy J. Deming, and
Galen D. Stucky*

Microspheres have long been recognized for their potential uses in drug delivery and isolation of chemical reactions. Many such systems require sacrificial templates and/or surfactants for their self-assembly, or otherwise use organic solvents.^[1] We have shown that microspheres can be obtained directly by self-assembly of Cys_nLys_m block copolypeptides with either citrate-coated silver and gold nanoparticles^[2a] or CdSe/CdS nanocrystal quantum dots,^[2b] or of poly-L-lysine (PLL) with citrate-coated CdSe quantum dots.^[3] These assemblies can be mechanically stabilized by adding an outer layer of negatively charged colloidal silica. Herein we report that large spherical assemblies can be obtained without nanoparticles but simply by reaction of one of several polyelectrolytes and certain small, functionalized molecular counterions.^[4] These assemblies can then be further functionalized, and we show how those based on polyamines can be protected by silica either in the form of colloidal silica or by condensation of silicic acid. Many earlier efforts have concentrated on the ability of multivalent ions to aggregate

oppositely charged polymers, and such systems have been described by theory^[5] and studied experimentally,^[6] particularly in the case of DNA.^[7] However, in none of these studies was sphere formation observed. In other studies, spherical assembly using polyelectrolytes was observed, but these approaches have required either amphiphilic block copolymers,^[8] proteins,^[9] two different polyelectrolytes,^[10] hydrophobic molecules,^[11] or the presence of both components of an insoluble salt (calcium carbonate).^[12] However, to our knowledge, the work reported herein is the first demonstration of spherical assembly using only a single polyelectrolyte with one small counterion without stabilization by an inorganic species.

Directed biomineralization can provide novel methods for the assembly of highly ordered structural materials, as demonstrated by the recent *in vitro* utilization of some biological or biomimetic peptides.^[13–16] We have shown that synthetic poly(amino acid)s can mimic silicateins and direct the formation of silica structures, such as spheres.^[13] Kröger, Sumper and co-workers have reported that silaffins and polyamines from diatoms can form 0.3–1- μ m silica spheres in the presence of inorganic phosphates.^[14a–d] In an extension of this work, Brunner, Lutz, and Sumper have very recently shown that sulfate and phosphate induce microscopic phase separation of polyallylamine (PAA) and that this phase-separated state in turn has high silica-precipitation activity and yields silica spheres.^[14e] Clarson and co-workers have shown that silica microspheres can be obtained from PLL using silicic acid in phosphate or citrate buffers.^[15] We now show that our preformed assemblies also condense silicic acid, and propose that the formation of microspheres in the work of the groups of Sumper, Brunner, and Clarson may be understood by initial formation of spherical templates, like ours, prior to silica condensation. This model is similar to the microscopic phase-separation picture put forth by Brunner, Lutz, and Sumper.^[14e] The silica spheres from these systems are in direct contrast to the disordered precipitates that result when multivalent anions are not used.^[16]

In extension of our work based on citrate-stabilized nanoparticles,^[2,3] we obtained assemblies by the reaction of citrate (final concentration 0.5 wt.%) and PLL^[17] (final concentration 0.6 wt.%) at pH 7. After mixing the two components, the solution immediately turned from clear to cloudy. Within a few minutes of mixing, spheres were observed by light microscopy, as illustrated in Figure 1a. Thus, we have found a route to assembly that eliminates the need for nanoparticle reactants. After drying, these assem-

[*] B. J. McKenna,[†] Dr. H. Birkedal^{††}
Department of Chemistry and Biochemistry
University of California
Santa Barbara, CA-93106-9510 (USA)
Fax: (+1) 805-8934120
E-mail: hbirkedal@chem.au.dk
Dr. M. H. Bartl
California NanoSystems Institute
University of California, Santa Barbara, CA-93106 (USA)
Prof. T. J. Deming, Prof. G. D. Stucky
Department of Chemistry and Biochemistry and
Materials Department, University of California
Santa Barbara, CA-93106 (USA)
E-mail: stucky@chem.ucsb.edu

[††] Present address:
Department of Chemistry
University of Aarhus, Langelandsgade 140
8000 Aarhus C (Denmark)
Fax: (+45) 86196199

[†] These authors contributed equally to the present work.

[**] This work was partially supported by the MRSEC program of the National Science Foundation under Award No. DMR00-80034 and made use of MRL Central Facilities under this program. This work was also supported in part by the U.S. Army Research Laboratory and the U.S. Army Research Office under contract number DAAD19-03-D-0004, as well as NASA University Research, Engineering and Technology Institute on Bio-Inspired Materials (BIMat) under award No. NCC-1-02037. Financial assistance from the Danish Natural Sciences Research Council (H.B.) and a Max-Kade research fellowship from the Austrian Academy of Sciences (M.H.B.) are gratefully acknowledged.

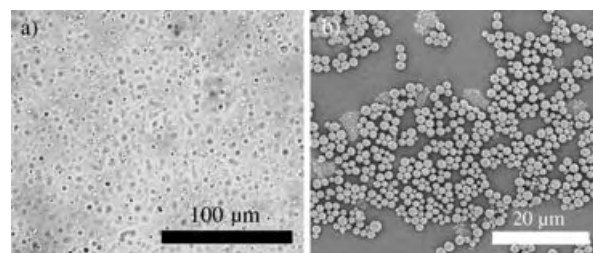


Figure 1. PLL/citrate assemblies: a) optical image, without colloidal silica, b) SEM image after modification by colloidal silica.

blies cling to the glass slide and lose their shape. However, they can be stabilized by a protective silica shell through the addition of colloidal silica that condenses on the preformed assemblies (Figure 1b).

To investigate how generalizable the sphere formation process is, we explored a host of multivalent organic acids other than citrate (Table 1). PLL-containing spheres were

citrate assemblies reach a maximum as the $[\text{COO}^-]:[\text{NH}_3^+]$ ratio is increased.

Poly-L-arginine (PLR), with its pK_a 12.5 side chain, showed remarkably different behavior with the triacids, by forming a precipitate. The PLR-triacid systems were coaxed into assembling spheres by heating the solution, which indicates there is an important entropic contribution to both the stability of the spheres and their kinetics of formation. We are currently exploring the nature of these assemblies as well as the temperature dependence of their formation. Also, unlike the other cationic poly(amino acid)s, PLR formed spheres with EDTA. This may be because the highest pK_a of EDTA is below that of the arginine side chain, so a proton transfers from EDTA to the side chain and creates an additional acid–base bridge.

The microsphere assembly was further extended by combining anionic poly(amino acid)s with cationic molecules containing multiple amine groups. Poly-L-aspartate (PLD) and poly-L-glutamate (PLE) did not form spheres with any of the divalent or trivalent cations explored,^[18] but spherical assembly for both polymers did occur with pentamethylenetetramine and tetraethylenepentamine. Tetraivalent tris(ethyleneamine)amine also gave spheres with PLD; however, with PLE, assembly required cooling and produced a combination of spheres and precipitate.

The surfaces of the assemblies are chemically active, and a shell of colloidal silica can be deposited onto the surface of assemblies of polycations. The addition of colloidal silica to a solution of these assemblies gives them a protective shell (Figure 1b). Addition of colloidal silica leads to a redistribution of the polymer: confocal microscopy of spheres made from FITC-labeled PLL (FITC = fluorescein isothiocyanate) showed that the polymer is evenly distributed.^[19] However, upon reaction with colloidal silica, the polymer is pulled, presumably because of coulombic attraction to the negatively charged silica nanoparticles, to the inside rim of the silica coat (Figure 2).^[4,20]

Inspired earlier work^[14e,15] we also obtained silica spheres by adding prehydrolyzed tetramethylorthosilicate (TMOS) to a solution of preformed polycation/citrate spheres.^[21] Condensation of the silicic acid was evident under the optical microscope, which showed a dark, thin shell, and from the stability of the resulting spheres after drying (Figure 3). We performed confocal microscopy on these spheres, as we had done with those coated with colloidal silica, to verify the templating action of the assemblies. Cross-sectional images of spheres after silicic acid condensation also show that their interiors are indeed full of polymer. Moreover, there is no central cavity as was observed for the colloidal silica-coated spheres (Figure 4).

In conclusion we have shown the existence of a new chemical entity that self-assembles from low concentrations

Table 1: Microsphere synthesis at room temperature.^[a]

Acid	n_{COOH}	$pK_a(n)$	PPL	PLO	PLH	PLR
citric	3	6.43	5.5–9.0	5.5–9.5	4.5–6.0	precipitate
isocitric	3	6.40	5.5–9.0	5.0–9.5	5.0–6.0	precipitate
trimesic	3	4.7	4.5–8.0	4.5–9.0	4.0–6.0	precipitate
EDTA	4	10.26 (6.16)	NO	NO	NO	6–10
carbonate	2	10.33	NO	NO	NO	NO
alkanedicarboxylic acids, $n(\text{CH}_2) = 0–6$	2	3.85–5.69	NO	NO	NO	NO (precipitate with oxalate)
tartaric	2	4.34	NO	NO	NO	NO
malic	2	5.2	NO	NO	NO	NO
fumaric	2	4.54	NO	NO	NO	NO

[a] Entries indicate which combination of small organic acid and polycation yields assemblies or precipitates, and the approximate pH ranges over which assemblies are visible in the optical microscope. NO = no assembly or precipitate.

obtained in the presence of two other triacids (isocitrate and trimesate), but with neither diacids nor ethylenediaminetetracetic acid (EDTA). Assuming that the role of the counterion is to bridge polycations, the diacids may not offer the required kinetic or thermodynamic cooperativity. The failure of EDTA to form spheres with PLL at any pH value is puzzling, but may be related to the better hydration of its carboxylate groups.

Having found some variability in one assembly component, we varied the cationic poly(amino acid). The triacids were seen to create spheres with poly-L-ornithine (PLO) and with poly-L-histidine (PLH). PLH provides a particularly interesting case in that spheres were not obtained at pH 7 but only below the pK_a value of the imidazole side chain, 6.0. This result reflects the fact that assembly requires charged groups. Indeed, in all cases the lower pH boundary for assembly was defined by the highest pK_a value of the acid; in other words, all the carboxyl groups must be deprotonated, and the spheres disassemble at pH values roughly one unit below the acid pK_a . This behavior is reversible: the spheres reassemble upon increasing the pH value. Similarly, spheres will not form if the polymer chain is under protonated, and assembly is only seen up to a pH value similar to the formal pK_a of the polypeptide side chains. This situation suggests that the spheres form primarily by electrostatic attraction, which is most likely accompanied by $\text{COO}^-/\text{NH}_3^+$ acid–base hydrogen bonding that provides further stabilization. Their stability is also sensitive to the ionic strength of the solution; the spheres shrink and finally become unobservable under the optical microscope at salt concentrations of roughly double the final value of $[\text{COO}^-]$ and $[\text{NH}_3^+]$. The size of the assemblies depends on the ratio of $[\text{COO}^-]$ and $[\text{NH}_3^+]$. In agreement with the observations of Brunner, Lutz, and Sumper in the PAA/phosphate system,^[14e] we found that the size of the PLL/

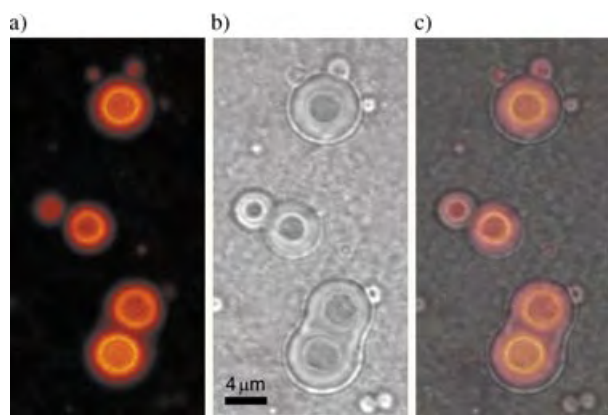


Figure 2. Cross-sectional images of a colloidal-silica-coated sphere made from FITC-labeled PLL and trimesate, a) the polymer fluorescence in a plane through the center of the sphere, b) the optical transmission image at that focal plane, c) an overlay of (a) and (b).

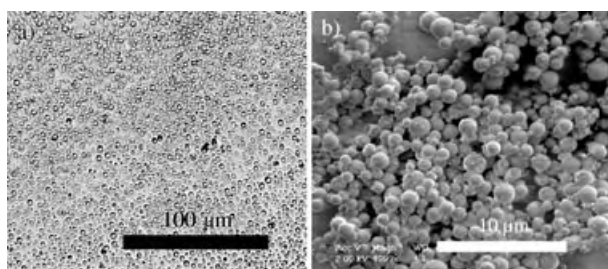


Figure 3. PLO/isocitrate spheres functionalized by condensed silicic acid: a) an optical image, the spheres have a thick, dark outline, in contrast to those in Figure 1 a, b) SEM image of a centrifuged sample.

of polyelectrolyte and an oppositely charged, multivalent ion. We have shown that all naturally occurring charged poly-(amino acid)s can assemble into microspheres when combined with a proper counterion. We have also shown assembly with PLO, and believe that spheres may be obtained with other synthetic polyelectrolytes as shown for PAA by Brunner, Lutz, and Sumper.^[14c] The strength of the interaction between the two components is predictably influenced by pH value, and is also affected by salt concentration and temperature. Importantly, the surface of the spheres is

chemically active, as shown by the silica condensation reactions, and could be further functionalized for applications in delivery or detection.

Received: April 29, 2004

Revised: July 6, 2004

Keywords: colloids · hybrid materials · polymers · self-assembly · template synthesis

- [1] a) D. Shchukin, G. Sukhorukov, H. Möhwald, *Angew. Chem.* **2003**, *115*, 4610–4613; *Angew. Chem. Int. Ed.* **2003**, *42*, 4472–4475; b) F. Chécot, S. Lecommandoux, Y. Gnanou, H.-A. Klok, *Angew. Chem.* **2002**, *114*, 1395–1399; *Angew. Chem. Int. Ed.* **2002**, *41*, 1339–1343; c) R. J. Thibault, P. J. Hotchkiss, M. Gray, V. M. Rotello, *J. Am. Chem. Soc.* **2003**, *125*, 11 249–11 252.
- [2] a) M. S. Wong, J. N. Cha, K. Choi, T. J. Deming, G. D. Stucky, *Nano Lett.* **2002**, *2*, 583–587; b) J. N. Cha, M. H. Bartl, A. Popitsch, M. S. Wong, T. J. Deming, G. D. Stucky, *Nano Lett.* **2003**, *3*, 907–911.
- [3] J. N. Cha, H. Birkedal, L. E. Euliss, M. H. Bartl, M. S. Wong, T. J. Deming, G. D. Stucky, *J. Am. Chem. Soc.* **2003**, *125*, 8285–8289.
- [4] B. J. McKenna, H. Birkedal, M. H. Bartl, T. J. Deming, G. D. Stucky, *Mater. Res. Soc. Symp. Proc.* **2004**, *823*, W4.12.1–6.
- [5] J. Arenzon, J. Stilck, Y. Levin, *Eur. Phys. J. B* **1999**, *12*, 79–82; b) B. Ha, A. Liu, *Phys. Rev. Lett.* **1997**, *79*, 1289–1292.
- [6] a) I. Sabbagh, M. Delsanti, *Eur. Phys. J. E* **2000**, *1*, 75–86; b) M. Olvera de la Cruz, L. Belloni, M. Delsanti, J. P. Dalbiez, O. Spalla, M. Drifford, *J. Chem. Phys.* **1995**, *103*, 5781–5791.
- [7] E. Raspaud, M. Olvera de la Cruz, J. Sikorav, F. Livolant, *Biophys. J.* **1998**, *74*, 381–393.
- [8] a) H. Otsuka, Y. Nagasaki, K. Kataoka, *Adv. Drug Delivery Rev.* **2003**, *55*, 403–419; b) S. Solomatin, T. Bronich, T. Borgar, A. Eisenberg, V. Kabanov, A. Kabanov, *Langmuir* **2003**, *19*, 8069–8076; c) H. M. Buchhammer, M. Mende, M. Oelmann, *Colloids Surf. A* **2003**, *218*, 151–159.
- [9] F. Weinbreck, R. H. Tromp, C. G. de Kruif, *Biomacromolecules* **2004**, *5*, 1437–1445.
- [10] P. M. Biesheuvel, M. A. C. Stuart, *Langmuir* **2004**, *20*, 2785–2791.
- [11] K. J. C. van Bommel, J. H. Jung, S. Shinkai, *Adv. Mater.* **2001**, *13*, 1472–1476.
- [12] L. B. Gower, D. J. Odam, *J. Cryst. Growth* **2000**, *210*, 719–734.
- [13] J. N. Cha, G. D. Stucky, D. E. Morse, T. J. Deming, *Nature* **2000**, *403*, 289–292.
- [14] a) N. Poulsen, M. Sumper, N. Kröger, *Proc. Natl. Acad. Sci. USA* **2003**, *100*, 12075–12080; b) N. Kröger, S. Lorenz, E. Brunner,

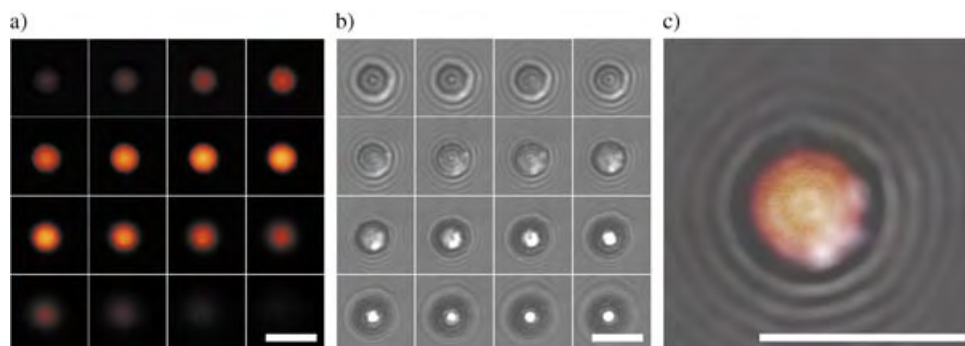


Figure 4. Cross-sectional images of FITC-labeled PLL/isocitrate spheres functionalized by condensed silicic acid. Galleries of the fluorescence (a), and transmission (b) responses at different sections through a sphere, c) an overlay of the two images at the central focal plane. The scale bars represent 5 μm.

- M. Sumper, *Science* **2002**, 298, 584–586; c) M. Sumper, *Science* **2002**, 295, 2430–2432; d) M. Sumper, S. Lorenz, E. Brunner, *Angew. Chem.* **2003**, 115, 5350–5353; *Angew. Chem. Int. Ed.* **2003**, 42, 5192–5195; ; e) E. Brunner, K. Lutz, M. Sumper, *Phys. Chem. Chem. Phys.* **2004**, 6, 854–857.
- [15] a) S. V. Patwardhan, N. Mukherjee, S. J. Clarson, *Silicon Chem.* **2002**, 1, 47–55; b) S. V. Patwardhan, N. Mukherjee, M. Steinitz-Kannan, S. J. Clarson, *Chem. Commun.* **2003**, 1122–1123.
- [16] T. Coradin, O. Durupthy, J. Livage, *Langmuir* **2002**, 18, 2331–2336.
- [17] Poly-L-lysine hydrochloride (30 kDa), FITC-labeled poly-L-lysine (70 kDa), poly-L-histidine (10 kDa), poly-L-arginine (30 kDa), poly-L-ornithine (50 kDa), poly-L-glutamate (15 kDa) and poly-L-aspartate (35 kDa) were obtained from Sigma and used as received.
- [18] The amines used that were unsuccessful in sphere formation are: 1,4-bis(3-aminopropyl)piperazine, 3,3'-diamino-*N*-methyldipropylamine, melamine, diethylenetriamine, 2,6-diaminopyridine, *N,N,N',N',N''*-pentamethyldiethylenetriamine, 1-(2-aminoethyl)-piperazine, 1,3-diaminopropane, 1,6-diaminohexane, 1,8-diaminooctane, and 1,12-diaminododecane.
- [19] The uncoated spheres are mobile in solution before adhering to the glass slide and losing shape, and were thus difficult to observe with this technique. However, all independent scans show them to be full of polymer.
- [20] V. S. Murthy, J. N. Cha, G. D. Stucky, M. S. Wong, *J. Am. Chem. Soc.* **2004**, 126, 5292–5299.
- [21] TMOS was prehydrolyzed at a final concentration of 0.1M, in HCl (pH 2–3), for 5 min, before adding a small amount of this precursor ($\approx 5\%$ v/v) to a solution of polycation/citrate spheres. The prehydrolyzed TMOS could also be quickly neutralized before addition to the spheres.

with each other. Distance, geometry, and orientation have been recognized as important factors for the control of this communication. Among arrays of covalently linked porphyrin units, systems in which the aromatic subunits are *directly* connected to each other by a covalent bond are particularly important. Such a linkage enables interaction between the subunits while the intrinsic structure of the porphyrin is preserved. Considerable progress has been reported recently in the synthesis of oligoporphyrins with direct β - β , *meso*-*meso*, and *meso*- β links^[5] to yield products that range from dimeric species to linear structures, which contain up to 128 porphyrin subunits.^[6]

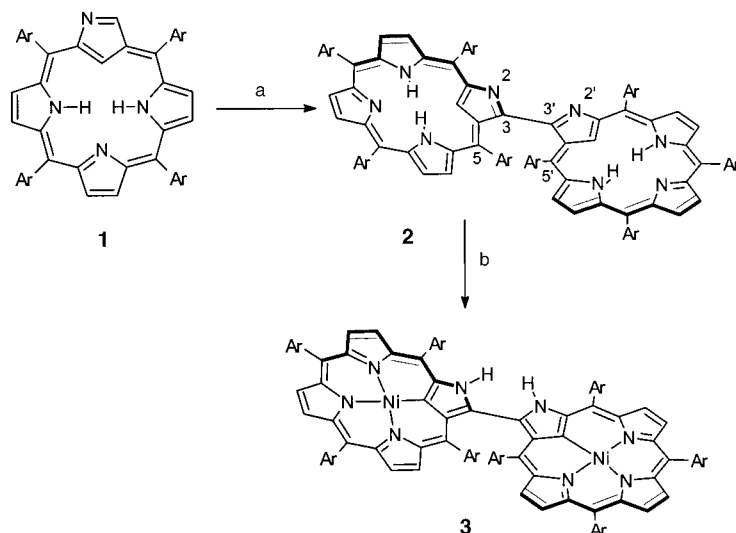
The field of porphyrin arrays can be further extended by the construction of arrays of covalently linked porphyrin analogues, particularly porphyrin-like macrocycles that also have carbon atoms in the coordination core. The N-confused porphyrin **1**^[7] is an isomer of regular porphyrin which preserves the fundamental porphyrinoid skeleton. In multi-molecular assemblies, it offers new modes of linking subunits and different coordination properties of the resultant oligomers.^[8] Herein we report the synthesis of the first directly β - β -linked dimer of N-confused porphyrin. This new molecule was obtained in an acid-catalyzed process, which did not require prior activation of the macrocyclic ring. The active site was provided here by a single α -carbon atom of the N-confused pyrrole. 3,3'-bis(*meso*-tetraaryl-2-aza-21-carbaporphyrin) (**2**) was obtained in a one-step, one-pot synthesis starting from the N-confused porphyrin **1** (Scheme 1). The coupling process was carried out in the presence of air, which seems to be a sufficiently strong oxidant for the dehydrogenation step that is expected to follow the formation of the bond between the two porphyrin subunits. An analogous reaction, which leads to a 3-(2'-pyrrole)-substituted N-confused porphyrin, was observed previously in the reaction of **1** with pyrrole in DMF.^[9] Although the reaction proceeds in the presence of various acids, the best results were obtained when hydrogen bromide was added as a catalyst to a solution of **1** in

Porphyrins

Synthesis and Characterization of a Directly Linked N-Confused Porphyrin Dimer**

Piotr J. Chmielewski*

Oligomeric porphyrin arrays^[1] are present in molecular devices that are designed for energy- and electron-transfer processes,^[2] multielectron redox catalysis,^[3] and in organic magnetic materials.^[4] For all such applications, it is important that the individual molecules within the array communicate



Scheme 1. Synthesis of the dimer **2** and its nickel complex **3**: a) HBr, toluene/dichloromethane, 20 h; b) Ni(CH₃COO)₂, toluene/DMF, 1 h. Ar = *p*-tolyl, DMF = N,N-dimethylformamide.

[*] Prof. P. J. Chmielewski
Department of Chemistry
University of Wrocław
F. Joliot-Curie Street 14
50383 Wrocław (Poland)
Fax: (+4871) 32-823-48
E-mail: pjc@wchuwr.chem.uni.wroc.pl

[**] The author thanks Dr. M. Stępień for his help in the X-ray crystal structure analysis and for helpful discussions. This work was supported by the State Committee for Scientific Research of Poland (Grant No. 3 09A 155 15)

Supporting information for this article is available on the WWW under <http://www.angewandte.org> or from the author.

toluene/dichloromethane. After heating for 20 h at reflux, the conversion of the starting material was $\approx 80\%$, and the product **2** was obtained with an overall yield of 50%.^[10]

Analysis of the ^1H and ^{13}C NMR spectroscopic data revealed that the aromaticity of the subunits is preserved in the bis(porphyrinoid) and that the 3,3'-bridging carbon atoms are sp^2 -hybridized. Owing to the symmetry of the dimer, only one set of resonances were detected in the NMR spectrum of **2**. Nevertheless, an upfield shift of the protons that belong to one of the *meso*-substituted aryl groups as well as the through-space interaction of these protons with NH protons located within the porphyrin crevice were observed in the NOESY and ROESY spectra. These features indicate that the subunits are close to one another. It is particularly evident in the case of the *p*-tolyl derivative **2** for which one of the methyl signals (5-(*p*-tolyl)) is located at $\delta \approx -0.7$ ppm (CDCl_3 , 298 K); that is, it is shifted more than 3 ppm upfield with respect to the other methyl signals because of the strong influence of the aromatic-ring current of the porphyrin (see Supporting Information).

The crystal structure of **2** (Figure 1) confirms the integrity of the dimer. The dihedral angle between the mean planes defined by the C–N–N–N coordination cores of the subunits is

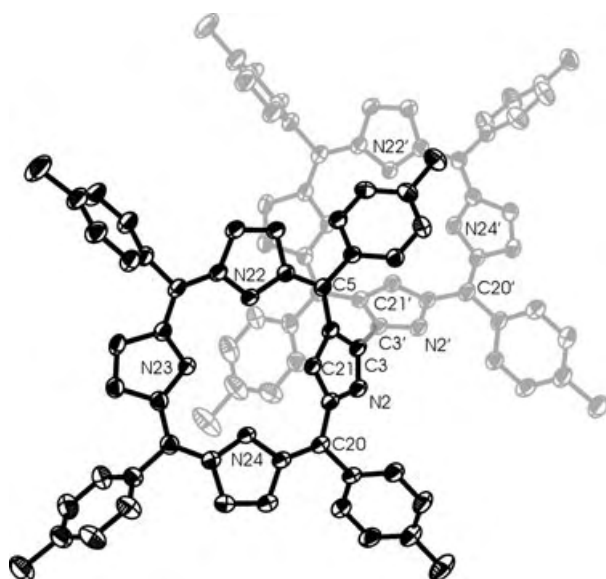


Figure 1. Crystal structure of **2**. Hydrogen atoms are omitted for clarity. Thermal ellipsoids are drawn at the 50% probability level.

20° . The plane defined by the N-confused pyrrole is tilted by 33° from the average plane in each macrocyclic subunit. The dihedral angle between the mean planes of the N-confused pyrroles is 61° . The distance of the unique bridging C3–C3' bond is 1.468(3) Å, which is similar to the distances observed in a zinc complex of a β – β -linked regular heptaalkylporphyrin (1.46 Å),^[5a] a *meso*–*meso*-linked bis(porphyrin) free base (1.51 Å),^[5b] or a *meso*–*meso*, β – β double-linked bis(porphyrinato)nickel(II) dimer (1.45 Å),^[5] and it is much shorter than the sp^3 – sp^3 distance reported for a β – β -linked bis(chlorin) (1.61 Å).^[11] Molecular modeling studies of **2** show that the rotation around the bridging bond is restricted owing to steric

factors imposed by the *meso*-substituted aryl groups that flank the N-confused pyrrole in both subunits. The lack of rotational freedom around the 3,3'-axis leads to an axial chirality of the molecule (see Supporting Information).^[5] The observed cisoidal conformation of the bipyrrolic system is essential for the coordination properties of this potential chelating site.

Formation of the bis(nickel(II)) complex **3** (Scheme 1) required a higher reaction temperature than necessary for the insertion of nickel(II) into the monomeric N-confused porphyrin **1**.^[7a] Some of the structural and spectral features typical of nickel(II) complexes with N-confused porphyrins—that is, deprotonation of the internal carbon, protonation of the external nitrogen, as well as reduction of the aromatic character in comparison to the free base—were observed for **3**. However, the ^1H NMR spectrum of **3** also shows features typical of the N-confused bis(porphyrin) system **2**.^[8,12] In particular, protons of the 5-aryl substituent are strongly shifted upfield owing to a close contact with an aromatic-ring current of the neighboring porphyrinic ring. Analysis of the NOESY spectrum of **3** (see Supporting Information) revealed a mutual orientation of the subunits similar to that observed for **2**.

The interaction between the aromatic systems in **2** was reflected by a strong bathochromic shift of the Soret and Q bands in the electronic absorption spectra with respect to the monomeric species **1** (Figure 2a) and a splitting of the

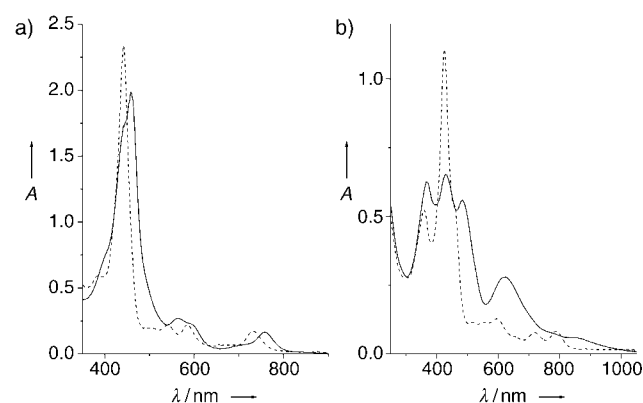


Figure 2. Absorbance spectra of solutions in CH_2Cl_2 of a) **2** (solid line) and b) **3** (solid line). The dashed lines (----) in a) and b) represent the spectra of the monomer **1** and its nickel(II) complex, respectively.

Soret band ($\Delta E = 736 \text{ cm}^{-1}$). The optical properties of **3** are affected even more by the interaction of the subunits. The UV/Vis spectrum of the complex consists of a split Soret-type band and strongly broadened and red-shifted Q bands (Figure 2b).

Electrochemical measurements (solution in CH_2Cl_2 , tetra-*n*-butylammonium perchlorate as a supporting electrolyte, potentials referenced to the ferrocene/ferrocenium couple) also reveal the mutual influence of the subunits. The first oxidation potential of **2** was anodically shifted with respect to that of **1** (about 65 mV) and was split into two waves (240 mV and 340 mV). This separation is similar to that observed for the *meso*–*meso*-linked dimers of regular porphyrin

(150 mV).^[5h] For **3**, two reversible one-electron couples were observed for the oxidation (140 and 218 mV) and the reduction (−1220 and −1315 mV) processes (see Supporting information). A significant anodic shift was observed for the reduction processes with respect to that of a monomeric nickel(II) complex of **1** (−1556 mV)^[13] which corresponds to a > 300 mV decrease in the HOMO–LUMO gap^[14] of the dimer **3**.

In summary, compound **2** constitutes the first example of a directly linked N-confused bis(porphyrin). Its surprisingly facile synthesis makes **2** a potentially attractive building block of novel molecular assemblies that contain covalently and coordinatively linked subunits with peripheral nitrogen donor-atom sites.

Experimental Section

2: HBr (40% solution in acetic acid, 50 µL, 0.25 mmol) was added in one portion to a solution of **1** (100 mg, 0.15 mmol) in toluene (30 mL). A further aliquot of dichloromethane (5 mL) was added to enhance the solubility of the generated porphyrin dication. The reaction mixture was heated at reflux for 20 h, then the solvents were removed. The residue was dissolved in benzene and was purified by chromatography through basic Al₂O₃ (activity III). Decomposition products and unconverted starting material **1** (recovered 21 mg) were eluted with benzene, whereas the desired product **2** was eluted with CH₂Cl₂ and then recrystallized from dichloromethane/ethanol (49 mg, 49%). ¹H NMR: (500 MHz, CDCl₃, 233 K, TMS): δ = 8.92 (dd, ³J_{HH} = 4.4 Hz, ⁴J_{HH} = 1.3 Hz, 1H; pyrrole), 8.84 (d, ³J_{HH} = 7.5 Hz, 1H) 8.61 (d, ³J_{HH} = 4.5 Hz, 1H; pyrrole), 8.56 (d, ³J_{HH} = 4.5 Hz, 1H; pyrrole), 8.51 (dd, ³J_{HH} = 4.4 Hz, ⁴J_{HH} = 1.0 Hz, 1H; pyrrole), 8.39 (dd, ³J_{HH} = 7.6 Hz, ⁴J_{HH} = 1.3 Hz, 1H), 8.36 (d, ³J_{HH} = 7.7 Hz, 1H), 8.24 (dd, ³J_{HH} = 7.4 Hz, ⁴J_{HH} = 1.3 Hz, 1H), 8.11 (dd, ³J_{HH} = 4.4 Hz, ⁴J_{HH} = 1.0 Hz, 1H; pyrrole), 8.01 (dd, ³J_{HH} = 7.4 Hz, ⁴J_{HH} = 1.3 Hz, 1H), 7.83 (d, ³J_{HH} = 8.1 Hz, 1H), 7.81 (dd, ³J_{HH} = 8.0 Hz, ⁴J_{HH} = 1.4 Hz, 1H), 7.76 (d, ³J_{HH} = 7.6 Hz, 1H), 7.64 (m, 2H), 7.56 (m, 2H), 7.46 (d, ³J_{HH} = 7.6 Hz, 1H), 7.22 (dd, ³J_{HH} = 7.4 Hz, ⁴J_{HH} = 1.5 Hz, 1H), 5.33 (d, ³J_{HH} = 7.5 Hz, 1H), 4.64 (d, ³J_{HH} = 7.0 Hz, 1H), 2.80 (s, 3H), 2.71 (s, 3H), 2.69 (d, ³J_{HH} = 7.6 Hz, 1H), 2.65 (s, 3H), −0.76 (s, 3H), −2.40 (s, 1H, NH), −2.64 (b, 1H, NH), −5.25 (b, 1H, 21-CH); UV/Vis (CH₂Cl₂): λ_{max} (log ε) = 257 (4.74), 290 (4.76), 348 (sh), 399 (sh), 442 (sh), 459 (5.47), 565 (4.60), 595 (sh), 703 (sh), 758 nm (4.40); ESI-MS: m/z: 1340.5 [MH⁺]; elemental analysis: calcd for C₉₆H₇₄N₈C₂H₅OH: C 84.97, H 5.78, N 8.09; found: C 84.74, H 5.65, N 8.30%.

Crystals of suitable quality for X-ray analysis were obtained by the slow diffusion of ethanol into a solution of **2** in dichloromethane. Crystal data for **2**: C₉₆H₇₄N₈·2.25 EtOH·0.75 CH₂Cl₂, M_w = 1491.86, T = 100 K, Cu_{Kα} radiation, monoclinic, space group P2₁/n, a = 15.829(3), b = 18.772(4), c = 26.673(5) Å, β = 92.16(3)°, V = 7920(3) Å³, Z = 4, ρ_{calcd} = 1.251 Mg m^{−3}, λ = 1.54178 Å, μ = 1.039 mm^{−1}, F(000) = 3124; Oxford Diffraction KM4 Xcalibur2 diffractometer with KM4CCD Sapphire detector; 3.65 ≤ θ ≤ 73.13°, 15495 collected reflections of which 11 701 were independent with I > 2σ(I), 1097 parameters, R₁(F) = 0.0822, wR₂(F²) = 0.2606, S = 1.116, largest difference peak and hole 0.474 and −0.602 e Å^{−3}. All non-hydrogen atoms were refined with anisotropic displacement parameters, except for those of the disordered solvents; hydrogen atoms were included in the geometry of the molecules and were refined isotropically. The extensive solvent disorder was modeled with a number of isotropic C, O, and Cl atoms with free refining occupancies to finally establish the presence of nine molecules of ethanol and three molecules of dichloromethane per unit cell. CCDC-245032 contains the supplementary crystallographic data for this paper. These data can be obtained free of charge via www.ccdc.cam.ac.uk/conts/retrieving.html (or from the Cambridge Crystallographic Data

Centre, 12, Union Road, Cambridge CB21EZ, UK; fax: (+44) 1223-336-033; or deposit@ccdc.cam.ac.uk).

3: A solution of **2** (30 mg, 0.022 mmol) in toluene (30 mL) was mixed with a solution of nickel(II) acetate tetrahydrate (50 mg) in DMF (5 mL), and the mixture was heated at reflux under nitrogen for 1 h. The solvents were then removed, and the residue was purified by flash chromatography through silica gel. The first green band eluted with CH₂Cl₂ was collected. Recrystallization from hexane solution (carried out under N₂) yielded the desired complex **3** (20 mg, 63%). ¹H NMR: (500 MHz, CD₂Cl₂, 233 K, TMS): δ = 9.58 (s, 1H, 2-NH), 7.88 (d, ³J_{HH} = 4.8 Hz, 1H; pyrrole), 7.79 (d, ³J_{HH} = 5.0 Hz, 1H; pyrrole), 7.75 (dd, ³J_{HH} = 7.6 Hz, ⁴J_{HH} = 1.8 Hz, 1H), 7.73 (d, ³J_{HH} = 5.3 Hz, 1H; pyrrole), 7.72 (dd, ³J_{HH} = 7.6 Hz, ⁴J_{HH} = 1.4 Hz, 1H), 7.65 (d, ³J_{HH} = 5.0 Hz, 1H; pyrrole), 7.62 (dd, ³J_{HH} = 7.7 Hz, ⁴J_{HH} = 1.3 Hz, 1H), 7.56 (dd, ³J_{HH} = 7.6 Hz, ⁴J_{HH} = 1.4 Hz, 1H), 7.55 (dd, ³J_{HH} = 7.8 Hz, ⁴J_{HH} = 1.6 Hz, 1H), 7.51 (d, ³J_{HH} = 5.3 Hz, 1H; pyrrole), 7.50 (dd, ³J_{HH} = 7.6 Hz, ⁴J_{HH} = 1.4 Hz, 1H), 7.48 (d, ³J_{HH} = 5.3 Hz, 1H; pyrrole), 7.47 (dd, ³J_{HH} = 7.8 Hz, ⁴J_{HH} = 1.6 Hz, 1H), 7.41 (dd, ³J_{HH} = 7.5 Hz, ⁴J_{HH} = 1.4 Hz, 1H), 7.35 (m, 2H), 7.33 (m, 2H), 7.29 (dd, ³J_{HH} = 8.0 Hz, ⁴J_{HH} = 1.1 Hz, 1H), 7.11 (d, ³J_{HH} = 7.3 Hz), 6.55 (d, ³J_{HH} = 7.1 Hz), 5.96 (d, ³J_{HH} = 7.3 Hz), 2.52 (s, 3H), 2.49 (s, 3H), 2.43 (s, 3H), 1.33 (s, 3H); UV/Vis (CH₂Cl₂): λ_{max} (log ε) = 243 (sh), 368 (4.84), 431 (4.86), 483 (4.79), 625 (4.49), 860 nm (sh). ESI-MS: m/z: 1452.5 ([M+]⁺); elemental analysis: calcd for C₉₆H₆₈N₈Ni₂: C 79.55, H 4.70, N 7.73; found: C 79.35, H 4.90, N 7.54%.

Received: July 19, 2004

Keywords: dimerization · nickel · nitrogen heterocycles · porphyrinoids · supramolecular chemistry

- [1] a) M. G. H. Vicente, L. Jaquinod, K. M. Smith, *Chem. Commun.* **1999**, 1771; b) A. Burrell, D. L. Officer, P. G. Plieger, D. C. W. Reid, *Chem. Rev.* **2001**, 101, 2751.
- [2] a) M. R. Wasielewski, *Chem. Rev.* **1992**, 92, 435; b) R. W. Wagner, J. S. Lindsey, *J. Am. Chem. Soc.* **1994**, 116, 9759; c) J.-S. Hsiao, B. P. Krueger, R. W. Wagner, T. E. Johnson, J. K. Delaney, D. C. Mauzerall, G. R. Fleming, J. S. Lindsey, D. F. Bocian, R. J. Donohoe, *J. Am. Chem. Soc.* **1996**, 118, 11 181; d) S. I. Yang, J. Seth, T. Balasubramanian, D. Kim, J. S. Lindsey, D. Holten, D. F. Bocian, *J. Am. Chem. Soc.* **1999**, 121, 4008.
- [3] a) J. P. Collman, *Inorg. Chem.* **1997**, 36, 5145; b) M. L. Merlau, M. P. Mejia, S. B. T. Nguen, J. T. Hupp, *Angew. Chem.* **2001**, 113, 4369; *Angew. Chem. Int. Ed.* **2001**, 40, 4239.
- [4] a) H. Segawa, D. Machida, Y. Senshu, J. Nakazaki, K. Hirakawa, F. Wu, *Chem. Commun.* **2002**, 3032; b) H. Segawa, Y. Senshu, J. Nakazaki, K. Susumu, *J. Am. Chem. Soc.* **2004**, 126, 1354.
- [5] a) Y. Deng, C. K. Chang, D. G. Nocera, *Angew. Chem.* **2000**, 112, 1108; *Angew. Chem. Int. Ed.* **2000**, 39, 1066; b) R. G. Khoury, L. Jaquinod, K. M. Smith, *Chem. Commun.* **1997**, 1057; c) A. Osuka, H. Shimidzu, *Angew. Chem.* **1997**, 109, 93; *Angew. Chem. Int. Ed. Engl.* **1997**, 36, 135; d) N. Yoshida, H. Shimidzu, A. Osuka, *Chem. Lett.* **1998**, 55; e) A. Nakano, A. Osuka, I. Yamazaki, T. Yamazaki, Y. Nishimura, *Angew. Chem.* **1998**, 110, 3172; *Angew. Chem. Int. Ed.* **1998**, 37, 3023; f) A. Nakano, H. Shimidzu, A. Osuka, *Tetrahedron Lett.* **1998**, 39, 9489; g) T. Ogawa, Y. Nishimoto, N. Yoshida, N. Ono, A. Osuka, *Chem. Commun.* **1998**, 337; h) T. Ogawa, Y. Nishimoto, N. Yoshida, N. Ono, A. Osuka, *Angew. Chem.* **1999**, 111, 140; *Angew. Chem. Int. Ed.* **1999**, 38, 176; i) N. Yoshida, A. Osuka, *Tetrahedron Lett.* **2000**, 41, 9287; j) A. Tsuda, A. Nakano, H. Furuta, H. Yamochi, A. Osuka, *Angew. Chem.* **2000**, 112, 572; *Angew. Chem. Int. Ed.* **2000**, 39, 558; k) A. Tsuda, Y. Nakamura, A. Osuka, *Chem. Commun.* **2003**, 1096; l) A. Tsuda, A. Osuka, *Adv. Mater.* **2002**, 14, 75; m) A. Takagi, Y. Yanagawa, A. Tsuda, N. Aratani, T. Matsumoto, A. Osuka, T. Kawai, *Chem. Commun.* **2003**, 2986.

- [6] a) N. Aratani, A. Osuka, Y. H. Kim, D. H. Jeong, D. Kim, *Angew. Chem.* **2000**, *112*, 1517; *Angew. Chem. Int. Ed.* **2000**, *39*, 1458; b) Y. H. Kim, D. H. Jeong, D. Kim, S. C. Jeoung, H. S. Cho, S. K. Kim, N. Aratani, A. Osuka, *J. Am. Chem. Soc.* **2001**, *123*, 76.
- [7] a) P. J. Chmielewski, L. Latos-Grażyński, K. Rachlewicz, T. Głowiak, *Angew. Chem.* **1994**, *106*, 805; *Angew. Chem. Int. Ed. Engl.* **1994**, *33*, 779; b) H. Furuta, T. Asano, T. Ogawa, *J. Am. Chem. Soc.* **1994**, *116*, 767; c) G. R. Geier III, D. M. Haynes, J. S. Lindsey, *Org. Lett.* **1999**, *1*, 1455.
- [8] a) I. Schmidt, P. J. Chmielewski, *Chem. Commun.* **2002**, 92; b) I. Schmidt, P. J. Chmielewski, Z. Ciunik, *J. Org. Chem.* **2002**, *67*, 8917.
- [9] I. Schmidt, P. J. Chmielewski, *Tetrahedron Lett.* **2001**, *42*, 1151.
- [10] One of the decomposition products of **2** was identified as 3-(2'-(3'-*p*-tolylmethylpyrrole))-5,10,15,20-tetrakis(*p*-tolyl)-2-aza-21-carbaporphyrin by ESI-MS and NMR spectroscopy (see Supporting Information for details).
- [11] B. Krattinger, D. J. Nurco, K. M. Smith, *Chem. Commun.* **1998**, 757.
- [12] H. Furuta, T. Ishizuka, A. Osuka, *J. Am. Chem. Soc.* **2002**, *124*, 5622.
- [13] I. Schmidt, P. J. Chmielewski, *Inorg. Chem.* **2003**, *42*, 5579.
- [14] K. M. Kadish, E. van Caemelbecke, G. Royal in *The Porphyrin Handbook*, Vol. 8 (Eds.: K. M. Kadish, K. M. Smith, R. Guilard), Academic Press, San Diego, CA, **2000**, pp. 1–114.

Carbon Nitrides

3,6-Di(azido)-1,2,4,5-Tetrazine: A Precursor for the Preparation of Carbon Nanospheres and Nitrogen-Rich Carbon Nitrides**

My Hang V. Huynh,* Michael A. Hiskey,*
Jose G. Archuleta, Edward L. Roemer, and
Richard Gilardi

Microbead and nanophase carbon materials attract many researchers due to their unique applications,^[1] which include high-density and high-strength carbon artifacts,^[2] super-active carbon beads of high surface area,^[3] lithium storage,^[4a] lithium battery anodes,^[4b–d] spherical packing materials for HPLC,^[5]

[*] Dr. M. H. V. Huynh, Dr. M. A. Hiskey, J. G. Archuleta, E. L. Roemer
Dynamic Experiment Division
DX-2: Materials Dynamics Group, MS C920
Los Alamos National Laboratory
Los Alamos, NM 87545 (USA)
Fax: (+1) 505-667-0500
E-mail: huynh@lanl.gov
hiskey@lanl.gov

Dr. R. Gilardi
Laboratory for the Structure of Matter
Naval Research Laboratory
Washington, DC 20375 (USA)

[**] This work was supported at Los Alamos by the joint program of the Department of Defense and the Department of Energy for the preparation and characterization of new energetic materials and at the Naval Research Laboratory by the Office of Naval Research, Mechanics Division.

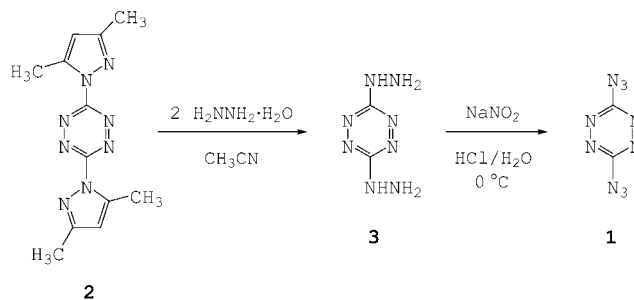
hydrogen storage applications,^[6] and catalysis.^[7] Much attention has focused on the preparation (precursors and methods) and properties of these carbon materials, because their applications significantly depend on the shape and size of the particles.

Carbon nitrides are of current interest due to their novel mechanical, optical, and tribological properties, including low density, extreme hardness, surface roughness, wear resistance, chemical inertness, and biocompatibility.^[8] These superhard diamondlike materials promise a variety of technological and biological applications. For example, they are used as biocompatible coatings on biomedical implants,^[8–9] battery electrodes,^[10] catalytic supports,^[11] gas separation systems,^[12] electronic materials,^[13] and humidity and gas sensors.^[14] Unlike carbon-based materials, applications of carbon nitrides are not only governed by the texture and size of the particles^[13] but also by the relative nitrogen content. As a consequence, an extensive effort has focused on the discovery of precursors along with the appropriate methods to increase the nitrogen content in carbon nitrides.

There is very little literature on the preparation of carbon nanospheres and nitrogen-rich carbon nitrides (> 60 wt % N). Gillan reported preparations of carbon nitrides C₃N₄ (60.9 wt % N) and C₃N₅ (66.0 wt % N) and graphitic carbon using high-nitrogen 2,4,6-tri(azido)-1,3,5-triazine as the precursor; however, the graphitic carbon consisted of irregular polygons, and no detailed description of its dimensions was provided.^[15] Lee et al. recently published a preparation of aggregate interlinked three-dimensional network of carbon nanospheres from naphthalene-derived isotropic pitch using a lengthy five-step process consisting of acidification, extraction, stabilization, oxidation, and carbonization. By mild grinding, carbon nanospheres ranging from 100 to 300 nm were individually separated.^[1]

We report here a new synthesis of the high-nitrogen compound 3,6-di(azido)-1,2,4,5-tetrazine (DiAT, **1**), from which carbon nanospheres ranging from 5 to 50 nm and nitrogen-rich carbon nitrides C₃N₄ and C₃N₅ can be prepared. Both preparation methods are simple, use mild conditions (i.e., low temperature and without applied pressure), and require no vacuum systems, extraction, carbonization and purification.

In 1963, Marcus and Remanick reported the preparation of **1** with a melting point of 130 °C, but no other physical properties or crystal structure were available.^[16] We developed an improved synthetic pathway for **1** that involves the two-step process illustrated in Scheme 1. The readily avail-



Scheme 1. Synthesis of DiAT (**1**).

able 3,6-bis(3,5-dimethylpyrazol-1-yl)-1,2,4,5-tetrazine (**2**; 2.0 g, 7.4 mmol)^[17] rapidly reacted with hydrazine hydrate (0.78 g, 15.6 mmol) to give 3,6-di(hydrazino)-1,2,4,5-tetrazine (DHT, **3**),^[18] which underwent diazotization in 3 M HCl at 0°C to yield **1**.^[19]

The isolated sample of **1** was characterized by X-ray crystallography,^[20] differential scanning calorimetry (DSC); cyclic voltammetry; and IR, UV/Vis, and ¹³C NMR spectroscopy.^[21] The structure of **1** in the crystal, grown by slow evaporation of a solution in benzene/octane (4/1), is shown in Figure 1. Selected bond lengths and angles are listed in ref. [22].

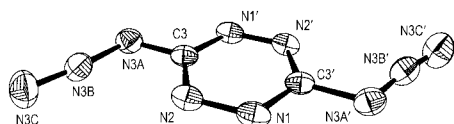


Figure 1. ORTEP diagram (25% ellipsoids) and labeling scheme for **1**.

The X-ray analysis shows how molecules of **1** are packed densely ($d = 1.72 \text{ g cm}^{-3}$) in the crystals. Figure 2 displays a

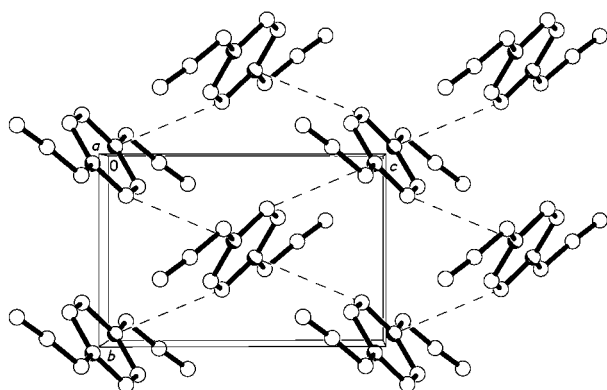


Figure 2. Packing of **1** in the crystal viewed along the *a* axis. The planar molecules are seen almost edge-on in this view, and close intermolecular C–N approaches between neighboring tetrazine rings are shown as dashed lines.

pattern formed by planar molecules that adopt two different alternating inclinations. This familiar type of packing is commonly called a herringbone pattern, and it is frequently seen in crystals of non-hydrogen-bonded planar molecules, for example, naphthalene.^[23] In **1**, the dihedral angle between the ring planes of neighboring molecules of differing tilt is 72.1°. The closest intermolecular distance in the crystal is shown as a dashed line (repeated by symmetry operations) between nearest neighbors. It is a ring C to ring N approach of 3.037 Å that is slightly shorter than the corresponding van der Waals contact distance of 3.25 Å.^[24] Parallel molecules, such as the neighbors occurring vertically or horizontally in Figure 2, have no close contacts. Each azido group is in rather close contact with four neighboring azido groups, displaying six approach distances of 3.13–3.15 Å, just slightly beyond the N···N van der Waals contact distance of 3.10 Å.

Carbon nanoparticles were prepared at two different rates of heating in the presence of air.^[25] A 0.2 g sample of **1** was loaded into a 50 mL stainless steel bomb and then heated to 150°C over 2 h to give carbon nanospheres that were characterized by IR spectroscopy, gas pycnometry, elemental analysis^[26] and by SEM (Figure 3).

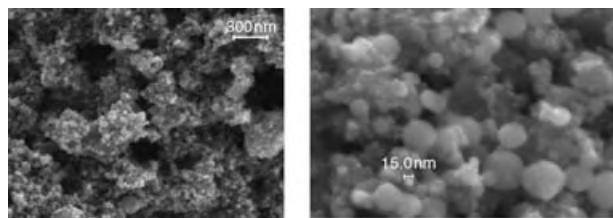


Figure 3. SEM images of carbon nanospheres at magnifications of 25 000× (left) and 150 000× (right).

When the heating time was reduced to 1 h, an audible pop occurred, and irregular carbon nanopolygons doubled in size were obtained (Figure 4). Gas pycnometry, IR spectroscopic data, and elemental analysis indicate that they are similar in composition to the carbon nanospheres.^[26]

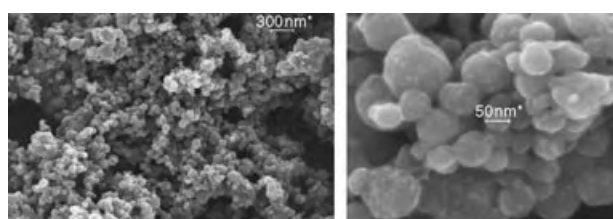


Figure 4. SEM images of irregular carbon nanopolygons at magnifications of 25 000× (left) and 150 000× (right)

In the presence of air, brown, nitrogen-rich carbon nitrides were prepared by using two different heating protocols in a 50 mL stainless steel bomb. A 0.3 g fluffy sample of **1** was heated to 100°C over 2 h and held at this temperature for an additional 4 h. The temperature was then increased to 150°C over 3 h and maintained overnight to yield leaf-like carbon nitride C₃N₄ (Figure 5, left). When **1** was heated continuously to 150°C over 5 h and then held at that temperature overnight, rope/ball-like carbon nitride C₃N₄ was obtained (Figure 5, right). Both carbon nitride products

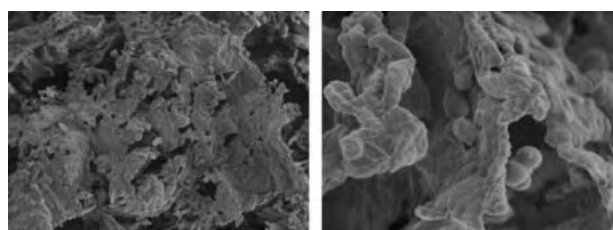


Figure 5. SEM images of leaf-like (left) and rope/ball-like (right) carbon nitride C₃N₄.

were characterized by IR spectroscopy, elemental analysis, thermal gravimetric analysis (TGA), gas pycnometry,^[27a] and SEM imaging.

Under a nitrogen atmosphere, a 0.3 g consolidated sample of **1** was again heated to 150 °C with the two different heating protocols (see above). The sheet-like and rope/ball-like carbon nitrides C₃N₅ were characterized by IR spectroscopy, elemental analysis, TGA, gas pycnometry,^[27b] and SEM imaging (Figure 6).

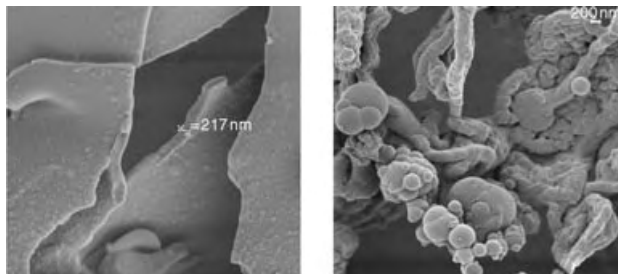


Figure 6. SEM images of sheet-like (left) and rope/ball-like (right) carbon nitride C₃N₅.

Unlike many other organic compounds, for example, meso-carbon microbeads,^[28] mesophase pitch-based carbon fibers,^[29] and non-azido-substituted triazines^[30] and heptazines,^[31] **1**^[16] and other polyazido compounds containing only C and N atoms^[32] are ideal precursors for nitrogen-rich carbon nitrides because of their clean and thermodynamically favorable decompositions, which presumably extrude nitrogen gas as the only by-product [Eqs. (1) and (2)].



More importantly, the conversion processes to nitrogen-rich carbon nitrides from these polyazido compounds generate no environmental waste or pollution.

The reproducible results in this study are novel and important in demonstrating that **1** undergoes decomposition in a single-step heating process to give 1) the first carbon nanospheres ranging from 5 to 50 nm at low temperature and without applied pressure and 2) three novel morphologies of nitrogen-rich carbon nitrides. Remarkably, since the texture, size, and nitrogen content of carbon nitrides ($\rho = 0.58\text{--}1.32 \text{ g cm}^{-3}$) are highly dependent on the heating protocols, they can be tailored for particular applications.

Received: May 18, 2004

Revised: July 23, 2004

Keywords: azides · carbon · nanostructures · nitrides · nitrogen

[1] S.-I. Lee, S.-H. Yoon, C. W. Park, Y. Korai, I. Mochida, *Carbon* **2003**, *41*, 1652–1654.

[2] a) M. Inagaki, Y. Tamai, S. Naka, K. Kamiya, *Carbon* **1974**, *12*, 639–643; b) Y. Yamada, T. Imamura, H. Kakiyama, H. Honda, S. Oi, K. Fukuda, *Carbon* **1974**, *12*, 307–319.

- [3] a) T. Nitta, M. Nozawa, S. Kida, *J. Chem. Eng. Jpn.* **1992**, *25*, 176–182; b) J. Economy, L. Dominguez, C. L. Mangun, *Ind. Eng. Chem. Res.* **2002**, *41*, 6436–6442.
- [4] a) X. Huang, H. Li, Q. Wang, W. Liu, L. Shi, L. Chen, *Wuli* **2002**, *31*, 444–449; b) A. Mabuchi, K. Tokumitsu, H. Fujimoto, T. Kasuh, *J. Electrochem. Soc.* **1995**, *142*, 1041–1046; c) H.-Y. Lee, S.-M. Lee, *Electrochem. Commun.* **2004**, *6*, 465–469; d) S. Dasgupta, R. Bhola, R. Jacobs, K. James, US 6261722, **2001**.
- [5] a) H. Honda, *Mol. Cryst. Liq. Cryst.* **1983**, *94*, 97–108; b) T. Yokono, M. Nakahara, K. Makino, Y. Sanada, *J. Mater. Sci. Lett.* **1988**, *7*, 864–866.
- [6] S. Isobe, T. Ichikawa, J. I. Gottwald, E. Gomibuchi, H. Fujii, *J. Phys. Chem. Solids* **2004**, *65*, 535–539.
- [7] a) Z. C. Kang, Z. L. Wang, *J. Phys. Chem.* **1996**, *100*, 5163–5165; b) H. Shioyama, *Carbon* **2003**, *41*, 2882–2884.
- [8] a) E. K. Wilson, *Chem. Eng. News* **2004**, *82*, 34–35, and references therein; b) F. Z. Cui, D. J. Li, *Surf. Coat. Technol.* **2000**, *131*, 481–487, and references therein.
- [9] a) D. J. Li, L. F. Niu, *Bull. Mater. Sci.* **2003**, *26*, 371–375; b) D. J. Li, S. J. Zhang, L. F. Niu, *Appl. Surf. Sci.* **2001**, *180*, 270–279.
- [10] a) D. Y. Zhong, G. Y. Zhang, S. Liu, E. G. Wang, Q. Wang, H. Li, X. J. Huang, *Appl. Phys. Lett.* **2001**, *79*, 3500–3502; b) M. Kawaguchi, *Adv. Mater.* **1997**, *9*, 615–625.
- [11] H. L. Chang, C. M. Hsu, C. T. Kuo, *Appl. Phys. Lett.* **2002**, *80*, 4638–4640.
- [12] J. N. Armor in *Materials Chemistry, An Emerging Discipline* (Eds.: L. V. Interrante, L. A. Caspar, A. B. Ellis), Advances in Chemistry Series, American Chemical Society, Washington, DC, **1995**, Ch. 13, p. 245.
- [13] I. Widlow, Y. W. Chung, *Braz. J. Phys.* **2000**, *30*, 490–498.
- [14] W. Kulisch, C. Popov, L. Zambov, *New Diamond Front. Carbon Technol.* **2001**, *11*, 53–76.
- [15] a) E. G. Gillan, *Chem. Mater.* **2000**, *12*, 3906–3912; b) W. Long, Y. Shun, Y. Bing, *Rare Met. Mater. Eng.* **2002**, *31*, 96–100, and references therein; c) A. K. Pal, *Curr. Sci.* **2002**, *83*, 225–236.
- [16] J. H. Marcus, A. Remanick, *J. Org. Chem.* **1963**, *28*, 2372–2375.
- [17] M. D. Coburn, G. A. Buntain, B. W. Harris, M. A. Hiskey, K.-Y. Lee, D. G. Ott, *J. Heterocycl. Chem.* **1991**, *28*, 2049–2050.
- [18] D. E. Chavez, M. A. Hiskey, *J. Heterocycl. Chem.* **1998**, *35*, 1329–1332.
- [19] a) Since **1** is extremely sensitive to friction, impact, and electrostatic discharge, one should always handle **1** wet with thick gloves behind a glass shield and limit the amount to less than 300 mg; b) For an explanation of methods for characterizing explosive sensitivity, see R. T. Paine, W. Koestle, T. T. Borek, E. Duesler, M. A. Hiskey, *Inorg. Chem.* **1999**, *38*, 3738–3743; c) 10 mL of a solution of NaNO₂ (0.61 g, 8.84 mmol) was added dropwise to a 35 mL of 3 M HCl containing **3** (0.5 g, 3.52 mmol) at 0 °C. The bright orange precipitated solid was collected by filtration and washed thoroughly with cold water. The sample was mounted for drying above a stainless steel bomb in a hood behind a glass shield overnight. **1** was then washed into the bomb with CH₂Cl₂ that was gradually evaporated. The lid of the bomb was secured tightly before the assembled apparatus was moved.
- [20] CCDC-238514 (**1**) contains the supplementary crystallographic data for this paper. These data can be obtained free of charge via www.ccdc.cam.ac.uk/conts/retrieving.html (or from the Cambridge Crystallographic Data Centre, 12, Union Road, Cambridge CB2 1EZ, UK; fax: (+44) 1223-336-033; or deposit@ccdc.cam.ac.uk).
- [21] Characterization of **1**: DSC: fast decomposition at 130 °C. Cyclic voltammetry in 0.2 M Bu₄NPF₆/CHCl₃ (vs SSCE): $E_{1/2} = +0.44$, -0.09 V. IR (Nujol mull): $\tilde{\nu}(\text{N}_3) = 2169$ (vs), 2142 cm⁻¹ (vs); $\tilde{\nu}(\text{tetrazine}) = 1460$ (vs), 1193 (vs), 1065 (vs), 927 (vs), 817 (vs), 546 cm⁻¹ (vs). UV/Vis (CHCl₃): $\lambda_{\text{max}}(\epsilon)$: 541 sh (4.64×10^2), 521 (6.50×10^2), 373 (1.79×10^3), 268 nm ($1.94 \times 10^4 \text{ M}^{-1} \text{ cm}^{-1}$). ¹³C NMR (300 MHz, CDCl₃, 25 °C): $\delta = 164.2$ ppm.

- [22] Selected bond lengths [\AA] and angles [$^\circ$] for **1**: N1–N2 1.310(3), N2–C3 1.328(3), C3–N3A 1.376(4); N2–C3–N3A 119.9(2), N1'–C3–N3A 113.9(2), N1'–C3–N2 126.2(3).
- [23] C. P. Brock, J. D. Dunitz, *Acta Crystallogr. Sect. B* **1982**, *38*, 2218–2228.
- [24] R. S. Rowland, R. Taylor, *J. Phys. Chem.* **1996**, *100*, 7384–7391.
- [25] Los Alamos is at an elevation of 7500 feet with a typical atmospheric pressure of 580 torr (11.2 psi or 0.76 atm). The relative humidity is normally below 20% for most of the year.
- [26] Characterization of carbon nanospheres and irregular carbon nanopolygons: IR (Nujol mull): $\tilde{\nu}$ = 1112 (vs), 475 cm^{-1} (vs). Elemental analysis (found): C 98.06, H 0.00, N 0.34, O 0.26 %. Gas pycnometry: ρ = $1.35 \pm 0.05 \text{ g cm}^{-3}$.
- [27] a) Characterization of leaf-like and rope/ball-like carbon nitride C_3N_4 : IR (Nujol mull): $\tilde{\nu}$ = 1088 (vs), 974 (s), 890 (s), 811 (s), 775 (vs), 467 cm^{-1} (vs). Elemental analysis (found): C 38.76, H 1.68, N 59.52 %. TGA: robust up to about 650 $^\circ\text{C}$. Gas pycnometry: ρ = $0.58 \pm 0.02 \text{ g cm}^{-3}$ for the leaf-like and $1.03 \pm 0.03 \text{ g cm}^{-3}$ for the rope/ball-like form. b) Characterization of sheet-like and rope/ball-like carbon nitride C_3N_5 : IR (Nujol mull): $\tilde{\nu}$ = 1261 (vs), 1099 (vs), 1027 (s), 890 (s), 801 (s), 778 (vs), 482 cm^{-1} (vs). Elemental analysis (found): C 35.60, H 1.86, N 66.31 %. TGA: robust up to about 650 $^\circ\text{C}$. Gas pycnometry: ρ = $1.32 \pm 0.02 \text{ g cm}^{-3}$ for the sheetlike and $1.23 \pm 0.02 \text{ g cm}^{-3}$ for the rope/ball-like form.
- [28] a) Y. G. Wang, Y. Korai, I. Mochida, K. Nagayama, H. Hatano, N. Fukuda, *Carbon* **2001**, *39*, 1627–1634; b) Y. C. Chang, H. J. Sohn, C. H. Ku, Y. G. Wang, Y. Korai, I. Mochida, *Carbon* **1999**, *37*, 1285–1297.
- [29] a) H. Yang, S. H. Yoon, Y. Korai, I. Mochida, O. Katou, *Carbon* **2003**, *41*, 397–403; b) E. Mora, C. Blanco, R. Santamaria, M. Granda, R. Menendez, *Carbon* **2003**, *41*, 445–452; c) I. Mochida, S. H. Yoon, Y. Korai, *Chem. Rec.* **2002**, *2*, 81–101, and references therein.
- [30] a) T. Sekine, H. Kanda, Y. Bando, M. Yokoyama, K. Hojou, *J. Mater. Sci. Lett.* **1990**, *9*, 1376–1378; b) M. R. Wixom, *J. Am. Ceram. Soc.* **1990**, *73*, 1973–1978; c) H. Montigaud, B. Tanguy, G. Demazeau, S. Courjault, M. Birot, J. Dunogues, *C. R. Seances Acad. Sci. Ser. 2* **1997**, *325*, 229–234; d) M. Todd, J. Kouvetakis, T. L. Groy, D. Chandrasekar, D. J. Smith, P. W. Deal, *Chem. Mater.* **1995**, *7*, 1422–1426; e) B. L. Ivanov, L. M. Zambov, G. T. Georgiev, C. Popov, M. F. Plass, W. Kulisch, *Chem. Vap. Deposition* **1999**, *5*, 265–273.
- [31] a) B. Jürgens, E. Irran, J. Senker, P. Kroll, H. Müller, W. Schnick, *J. Am. Chem. Soc.* **2003**, *125*, 10288–10300; b) W. Zheng, N.-B. Wong, W. Wang, G. Zhou, A. Tian, *J. Phys. Chem. A* **2004**, *108*, 97–106; c) T. Komatsu, *J. Mater. Chem.* **2001**, *11*, 802–805; d) E. Kroke, M. Schwarz, *Coord. Chem. Rev.* **2004**, *248*, 493–532; e) E. Kroke, M. Schwarz, E. Horath-Bordon, P. Kroll, B. Noll, A. D. Norman, *New J. Chem.* **2002**, *26*, 508–512.
- [32] a) D. R. Miller, D. C. Swenson, E. G. Gillan, *J. Am. Chem. Soc.* **2004**, *126*, 5372–5373; b) M. H. V. Huynh, M. A. Hiskey, R. Gilardi, E. L. Hartline, D. P. Montoya, *Angew. Chem./Angew. Chem. Int. Ed.* **2004**, accepted.

Computer-Generated High-Valent Iron–Oxo and Manganese–Oxo Species with Polyoxometalate Ligands: How do they Compare with the Iron–Oxo Active Species of Heme Enzymes?**Samuël P. de Visser, Devesh Kumar, Ronny Neumann,* and Sason Shaik**

There is a continuing search for efficient and robust catalysts that can perform monooxygenation of organic compounds.^[1] High-valent metal–oxo porphyrin species constitute such an important family.^[2] The members of this family are analogous to the principal and potent oxidant of enzymes such as cytochrome P450 (CP450, **1**; Figure 1). Over the last two decades it has been gradually recognized that some transition-metal-substituted polyoxometalates (POMs) have intriguing properties as oxygenation catalysts.^[3] These catalysts sometimes exhibit features that seem superficially similar to those observed with analogous metalloporphyrins. Thus, for example, it has been shown that Mn^{III}-substituted polyoxometalates, and to a much lesser extent also Fe^{III}-substituted compounds, catalyze oxygen-transfer reactions from iodoso-benzene to alkenes and alkanes in a manner akin to the analogous metalloporphyrins.^[4] The similarities between the transition-metal-substituted polyoxometalates and metalloporphyrin systems, and the postulate^[4] that the active species of the transition-metal-substituted polyoxometalates catalysts may resemble the active species of CP450, endow the transition-metal-substituted polyoxometalates with added allure, and pose a problem worthy of theoretical interrogation.

The principal oxidant of CP450 is considered to be the triradicaloid Compound I species (**A**, Figure 1), which has two closely lying spin states with a quartet and doublet spin (^{4,2}**1**).^[5] In both states, the iron atom in **A** is in oxidation state IV and the porphyrin (Por) is a radical cation, thus the entire complex can be briefly represented as [(SH)Por^{•+}-Fe^{IV}O]. Therefore, the active species of CP450 and other

[*] Prof. R. Neumann
Department of Organic Chemistry
Weizmann Institute of Science
76100 Rehovot (Israel)
Fax: (+972) 8-9344142
E-mail: Ronny.Neumann@weizmann.ac.il

Dr. S. P. de Visser, Dr. D. Kumar, Prof. S. Shaik
Department of Organic Chemistry and The Lise Meitner-Minerva
Center for Computational Quantum Chemistry
Hebrew University, 91904 Jerusalem (Israel)
Fax: (+972) 2-6584680
E-mail: sason@yfaat.ch.huji.ac.il

[**] This research was supported by the Israel Science Foundation (S.S. and R.N.) and the Helen and Martin Kimmel Center for Molecular Design (R.N.). R.N. is the Rebecca and Israel Sieff Professor of Organic Chemistry.



Supporting information for this article is available on the WWW under <http://www.angewandte.org> or from the author.

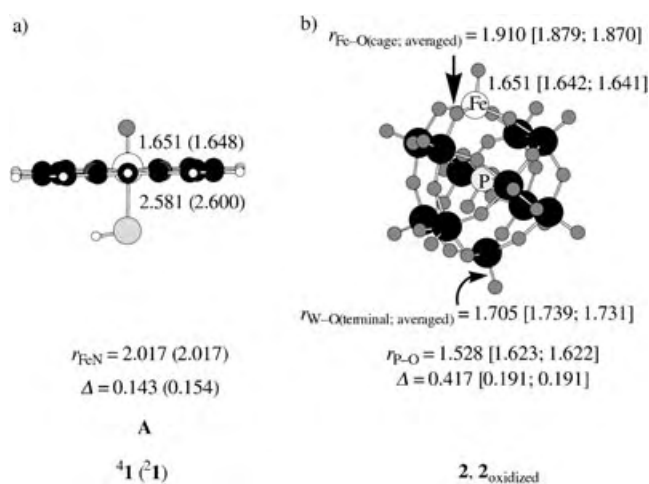


Figure 1. a) Optimized geometry of **A** ($^4\text{1}$) of CP450 in the quartet (doublet) spin states. b) The geometry generated from neutron diffraction data for the analogous [POM-Fe=O] $^{4+}$ (**2**) and [POM-Fe=O] $^{3-}$ (**2_{oxidized}**) models, where POM is the [PW $_{11}$ O $_{39}$] $^{7-}$ lacunary species or ligand. The values in square brackets are the respective optimized bond lengths for the high-spin states of the two species $^4\text{2}$ and $^5\text{2}_{\text{oxidized}}$. All bond lengths are averaged values in Ångströms; Δ is the displacement of the iron atom with respect to the four atoms of the plane of the porphyrin ring (in **1**) or to the four surface oxygen atoms on the sphere of the polyoxometalate.

heme enzymes has two oxidation equivalents above the resting state (the Fe $^{\text{III}}$ complex), but only one equivalent resides on the iron center that appears in the Fe $^{\text{IV}}$ oxidation state. Thus, the central questions to the study reported herein are: 1) How closely related to **A** are the corresponding POM-FeO species and 2) why, as might be expected from such an analogy, does the POM-Fe $^{\text{III}}$ species not form a powerful catalyst, whereas the POM-Mn $^{\text{III}}$ species which has one electron less does? To address these questions, we used density functional theory (DFT) to investigate the electronic structure of POM-FeO and POM-MnO complexes (POM is the [PW $_{11}$ O $_{39}$] $^{7-}$ lacunary species or ligand). As shall be demonstrated, DFT predicts that the POM-FeO catalysts can sustain high oxidation states, as high as Fe $^{\text{V}}$ and even the rare Fe $^{\text{VI}}$ state, and also predicts that a highly electrophilic Mn $^{\text{VI}}$ -oxo species could be generated for POM-MnO.

Earlier calculations^[6] on polyoxometalate species of the Keggin structure, namely, [PW $_{12}$ O $_{40}$] $^{3-}$, showed marginal differences between the neutron diffraction geometry and the DFT-optimized geometry. By using the same strategy, we started from [PW $_{12}$ O $_{40}$] $^{3-}$ and generated [PW $_{11}$ O $_{39}$ Fe=O] $^{4-}$ (**2**) by the replacement of a single {W $^{\text{VI}}$ =O} $^{4+}$ group by {Fe $^{\text{V}}$ =O} $^{3+}$ and subsequently, using the same geometric parameters, we also calculated the one-electron-oxidized complex [PW $_{11}$ O $_{39}$ Fe=O] $^{3-}$ (**2_{oxidized}**). For both complexes, we used the same Fe=O bond length as in **A**, namely 1.651 Å.^[7] Subsequently, we optimized the structures (see the Supporting Information) for a few of the states of [POM-Fe=O] $^{4-}$ (**2**) and [POM-Fe=O] $^{3-}$ (**2_{oxidized}**), and we ascertained that the optimum geometries did not differ markedly from those generated by the use of neutron-diffraction data on [PW $_{12}$ O $_{40}$] $^{3-}$, at least with respect to the first coordination shell of the iron

center. This finding can be seen from the key geometric details in Figure 1b, which displays the neutron diffraction based data together with the optimized values in square brackets. Since each geometry optimization takes four months of CPU time, we restricted the rest of the study to the geometries generated from the neutron diffraction data. The [POM-MnO] $^{4-}$ (**3**) and [POM-MnO] $^{3-}$ (**3_{oxidized}**) species were calculated with the same bond lengths as the iron analogues. All calculations were performed by using the Gaussian 98 program^[8] with the hybrid B3LYP density functional method and the LANL2DZ basis set. The low-lying spin states of **2**, **3**, **2_{oxidized}**, and **3_{oxidized}** were all examined. In addition, we verified the electronic structure of [PW $_{12}$ O $_{40}$] $^{3-}$ (**4**), [PW $_{12}$ O $_{40}$] $^{2-}$ (**4_{oxidized}**),^[6a] and of the resting-state species [PW $_{11}$ O $_{39}$ FeOH $_2$] $^{4-}$, as well as of the corresponding manganese complexes (see the Supporting Information). Here we focus on the transition-metal-oxo species.

Figure 2 shows the electronic structure of the POM-iron complex **2** with respect to **A** ($^4\text{1}$) of CP450 and illustrates the key orbitals of both species. The ground state of CP450 (on the left hand side) involves the well-known virtually degenerate set of doublet and quartet spin states with the common electronic configuration of $\delta^2\pi_{xz}^*\pi_{yz}^*1a_{2u}^1$. With this occupation, the doublet and quartet spin states essentially correspond to a triplet Fe $^{\text{IV}}$ -oxo moiety that is coupled ferro- and antiferromagnetically to a cation radical on the porphyrin ring, namely, $^4\text{2}[(\text{SH})\text{Por}^+\text{Fe}^{\text{IV}}\text{O}]$.

The right-hand side of Figure 2 shows the five d-block orbitals, labeled δ , π^* , and σ^* by analogy with the CP450 orbitals, that are virtually localized on the {(O) $_4$ Fe=O} moiety of [POM-FeO] $^{4-}$. In addition, we show the highest occupied lone-pair orbital (lp $_O$), which is one of the many surface orbitals located on the bridging oxygen atoms and the oxo moieties of the W-O units of the polyoxometalate (see the Supporting Information). The ground state was found to be the high-spin quartet state $^4\text{2}$ with three singly occupied orbitals δ , π_{xz}^* , and π_{yz}^* . An analogous result was obtained by Siegbahn, Que, and co-workers^[9] for the nonheme Fe $^{\text{V}}$ -oxo species. The corresponding doublet state $^2\text{2}$, with a β spin for the electron in the δ orbital, lies 12.8 kcal mol $^{-1}$ (10.6 kcal mol $^{-1}$ for the optimized geometries) higher in energy. This high energy of the antiferromagnetic state highlights the special stability of the high-spin half-filled π^* - δ shell, as a result of favorable exchange interactions. The importance of exchange stabilization is further made apparent by the PorMn $^{\text{IV}}$ -oxo system^[10] that was found previously to adopt the same half-filled configuration $\delta^1\pi_{xz}^*\pi_{yz}^*1$.

Another doublet spin state with the occupancy $\delta^2\pi_{xz}^*\pi_{yz}^*1$ was found to be 19.5 kcal mol $^{-1}$ higher than the quartet state shown in Figure 2. An attempt to swap orbitals in $^4\text{2}$ and create an analogue of $^4\text{1}$ with the occupation $\delta^2\pi_{xz}^*\pi_{yz}^*1\text{lp}_O^1$, akin to **A** (**1**), generated initially a high-energy species with a wave function that converged to the lower lying configuration $\delta^1\pi_{xz}^*\pi_{yz}^*1$ in Figure 2. With three electrons in the δ , π_{xz}^* , and π_{yz}^* orbitals, all three $^4\text{2}$ states formally belong to the iron(v)-oxo situation.

In the gas-phase, the [POM-Fe $^{\text{V}}$ O] $^{4-}$ species was computed to be unstable relative to its one-electron-oxidized form [POM-FeO] $^{3-}$, with an ionization potential (IP) of

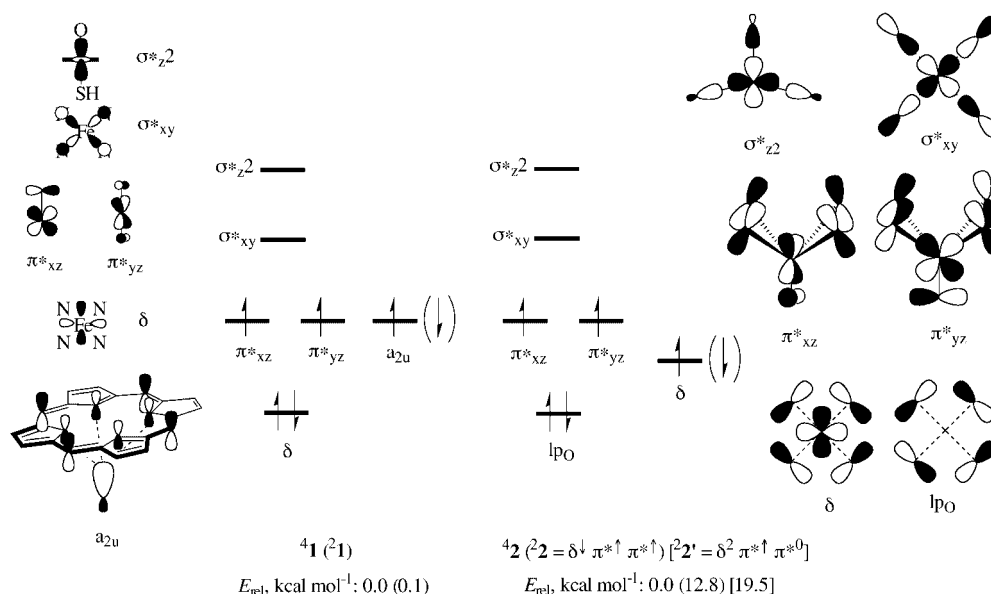


Figure 2. High-lying occupied and low-lying virtual orbitals of 4^+21 (left-hand side) and the quartet and doublet states 4^+2 (right-hand side) of $[\text{POM-FeO}]^{4-}$.

–23.5 kcal mol $^{-1}$ (this is in contrast to the pristine unsubstituted POM for which the gas-phase IP is 65 kcal mol $^{-1}$). However, by using the continuum solvation model COSMO and a dielectric constant of water, the quadruply charged species was found to be stable and its ionization potential was calculated as 169.5 kcal mol $^{-1}$ (oxidation potential = +2.8 V, relative to the saturated hydrogen electrode (SHE)); a lower value would be expected for a less-polar solvent. The ground state of the one-electron-oxidized species is depicted in Figure 3 a, and is seen to be the pair of quintet and triplet spin situations: $5^+3^+2_{\text{oxidized}}$ with the $\delta^1 \pi_{xz}^* \pi_{yz}^* 1p_O^1$ electronic configuration. An excited state (1^+2_{oxidized}), with the $\delta^2 \pi_{xz}^* \pi_{yz}^* 0p_O^2$ electronic structure, lies 28.6 kcal mol $^{-1}$ higher in energy. Attempts to calculate the triplet states with either a $\delta^1 \pi_{xz}^* \pi_{yz}^* 0$ or $\delta^0 \pi_{xz}^* \pi_{yz}^* 1$ configuration resulted in convergence to the $\delta^1 \pi_{xz}^* \pi_{yz}^* 1p_O^1$ configuration. Thus, the generation of $5^+3^+2_{\text{oxidized}}$ from 2^+4^+2 involves ejection of an electron from the surface orbitals of the POM and not from the d-type orbitals of the FeO moiety. This feature does not change when solvation is included.

Figure 4 shows the spin-density distribution in the lowest states of **2** and 2_{oxidized} (for similar values in a solvent, see the

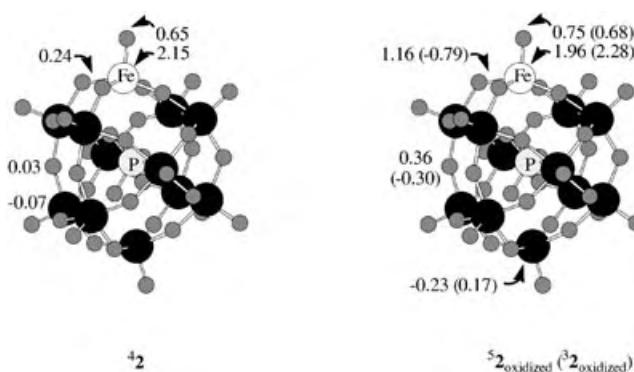


Figure 4. Spin-density distribution in the states of 4^+2 and $5^+3^+2_{\text{oxidized}}$ of $[\text{POM-FeO}]^{4-}$ and $[\text{POM-FeO}]^{3-}$.

Supporting Information). It is seen that, in accord with the electronic structure in Figure 2, most of the spin density (2.80) in 4^+2 is localized on the FeO unit. Some spin density is located on the four oxygen ligands of FeO on the polyoxometalate surface (total spin: 0.24), while the rest of the cage atoms (W, O) together carry a small negative spin density (total: –0.04).

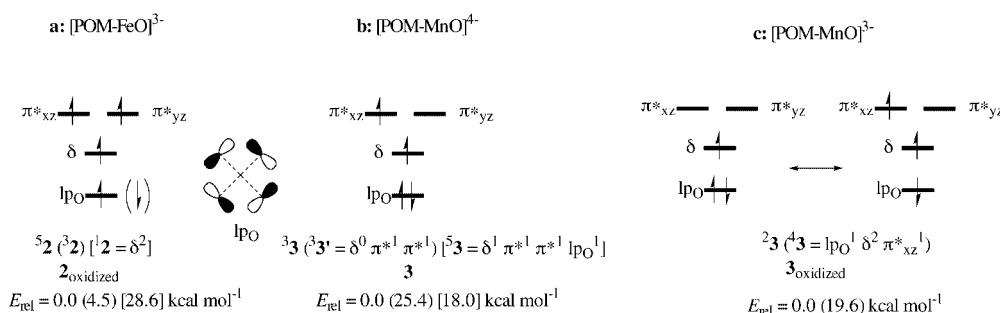


Figure 3. Electronic configurations and relative energies of a) the $5^+3^+1^+2_{\text{oxidized}}$ states of $[\text{POM-FeVO}]^{3-}$; b) the 5^+3^+3 states of $[\text{POM-MnVO}]^{4-}$; and c) the $4^+2^+3_{\text{oxidized}}$ states of $[\text{POM-MnVO}]^{3-}$.

By contrast, the FeO unit in $^{5,3}\mathbf{2}_{\text{oxidized}}$ carries three spins, while the fourth is on the polyoxometalate surface, and mostly near the coordination sphere of the FeO unit, again in accord with the electronic structure in Figure 3. Clearly, whereas the $[\text{POM-Fe}^{\text{V}}=\text{O}]^{4-}$ complex (**2**) does not resemble the isoelectronic **A** species, the one-electron-oxidized species, which is effectively Fe^{VI} , resembles **A** and can be written briefly as $[\text{POM}^+\text{Fe}^{\text{V}}=\text{O}]^{3-}$, with a quartet $\text{Fe}=\text{O}$ unit coupled ferro- and antiferromagnetically to the POM^+ unit, which is in accord with the $\delta^1\pi_{xz}^*\pi_{yz}^*\pi_{yz}^*\text{lp}_\text{O}^1$ occupancy discussed above.

A few major factors are responsible for these electronic differences and similarities between the polyoxometalate and the CP450 species. The first one is clearly the different geometry of the two compounds. As can be seen in Figure 1, the porphyrin is planar and the iron atom in CP450 lies close to the plane of the ring ($\Delta = 0.14, 0.15 \text{ \AA}$). In comparison, the iron atom in the polyoxometalate lies higher above the plane of the four coordinated oxygen atoms at a distance of 0.42 \AA (0.191 \AA in the optimum structure). As seen in Figure 2, this endows the d-type π_{xz}^* and π_{yz}^* orbitals of the FeO moiety of POM-FeO with antibonding interactions from the four POM oxygen atoms in the coordination sphere of the iron center. This effect raises the energy of the π^* orbitals and stabilizes the oxidation state of iron(v) in **42** relative to that of the porphyrin moiety in which the π^* orbitals are low lying and the Fe^{V} state is less stable than the $[\text{Por}^+\text{Fe}^{\text{IV}}]$ situation.^[7] This effect is similar to that discussed for the pentacoordinate metallocorrole complexes,^[11] and to the findings in non-heme iron complexes.^[9] Another effect concerns the δ orbital in Figure 2. Thus, unlike the metalloporphyrin system, where this orbital is a very low-lying purely nonbonding orbital with preferred double occupancy, this orbital in the POM-FeO complexes is high-lying because of the antibonding interaction with the four polyoxometalate oxygen atoms in the first coordination sphere. Consequently, the π^* and δ orbitals of POM-FeO become almost degenerate, and prefer the high-spin and exchange-stabilized $\delta^1\pi_{xz}^*\pi_{yz}^*\pi_{yz}^*$ subshell in all its complexes. This situation generates, in turn, the ferro- and antiferromagnetic pair of states $^{5,3}\mathbf{2}_{\text{oxidized}}$, which retain the half-filled δ - π^* subshell and have an additional unpaired electron on the polyoxometalate surface. Consequently, these complexes can be represented as $^{5,3}[\text{POM}^+\text{Fe}^{\text{V}}=\text{O}]^{3-}$, and are, therefore, the polyoxometalate analogues of $^{4,2}\mathbf{A}$ in the heme system, but with an Fe^{V} center instead of Fe^{IV} .

Our calculations (see Figure 3b) further show that $[\text{POM-MnO}]^{4-}$ has a triplet ground state that differs from the isoelectronic iron species $[\text{POM}^+\text{Fe}^{\text{V}}=\text{O}]^{3-}$. Thus, while the iron species has a half-filled δ - π^* subshell coupled to an unpaired electron on the polyoxometalate surface (Figure 3a), the manganese species is a triplet state with a $\delta^1\pi^*$ configuration; the other manganese states are significantly higher in energy. Thus, in fact, the ground state of the manganese complex corresponds to $[\text{POM-Mn}^{\text{V}}=\text{O}]^{4-}$, with Mn being in oxidation state v. Once again, in the gas phase, the quadruply charged complex is unstable towards the loss of one electron and leads to $[\text{POM-Mn}=\text{O}]^{3-}$ (**3**_{oxidized}, Figure 3c). In solution, however, the ionization potential is substantial and positive ($171.5 \text{ kcal mol}^{-1}$). The resulting **3**_{oxidized} complex has a doublet ground state ($^2\mathbf{3}_{\text{oxidized}}$) that is

well-separated from its quartet-spin excited state ($^4\mathbf{3}_{\text{oxidized}}$). Its electronic structure and spin distribution (see the Supporting Information) fits best to a mixed configuration between $\delta^1\pi_{xz}^*\pi_{yz}^*\pi_{yz}^*\text{lp}_\text{O}^2$ and $\delta^1\pi_{xz}^*\pi_{yz}^*\pi_{yz}^*\text{lp}_\text{O}^1$, and thereby corresponds to the mixed-valent species $[\text{POM-Mn}^{\text{VI}}=\text{O}]^{3-} \leftrightarrow [\text{POM}^+\text{Mn}^{\text{V}}\text{O}]^{3-}$.

Finally, our calculations on the water complexes $[\text{PW}_{11}\text{O}_{39}\text{FeOH}_2]^{4-}$ (**5**) and $[\text{PW}_{11}\text{O}_{39}\text{MnOH}_2]^{4-}$ (**6**) show that these are iron(III)-aqua and manganese(III)-aqua complexes, with frontier orbitals localized on the MOH_2 moiety ($\text{M} = \text{Fe}, \text{Mn}$; see Supporting Information). As such, it is conceivable that these complexes can be converted into iron-oxo and manganese-oxo complexes by the usual techniques, for example, using iodosobenzene.^[2c] The identity of the species that carries out the catalytic oxidation is not really known,^[4] and it is therefore essential to consider both the quadruply and triply charged forms of the iron and manganese complexes. Comparison of **2** with **3** shows that the iron reagent $[\text{POM-Fe}^{\text{V}}=\text{O}]^{4-}$ (**2**⁴) has a half-filled δ - π^* subshell, whereas the manganese reagent $[\text{POM-Mn}^{\text{V}}=\text{O}]^{4-}$ (**3**) has a vacant π^* orbital. Similarly, in the oxidized form, the $^{5,3}\mathbf{2}_{\text{oxidized}}$ ground state of $[\text{POM}^+\text{Fe}^{\text{V}}\text{O}]^{3-}$ has a half-filled δ - π^* subshell, while the $^{2,3}\mathbf{3}_{\text{oxidized}}$ ground state of $[\text{POM}^+\text{Mn}^{\text{V}}\text{O}]^{3-}$ has largely vacant π^* orbitals. Thus, by analogy with other electrophiles we expect that both $[\text{POM-Mn}^{\text{V}}=\text{O}]^{4-}$ and $[\text{POM}^+\text{Mn}^{\text{VI}}\text{O}]^{3-}$ will be highly electrophilic species as a consequence of the vacant π^* orbitals, while both $[\text{POM-Fe}^{\text{V}}=\text{O}]^{4-}$ and $[\text{POM}^+\text{Fe}^{\text{V}}\text{O}]^{3-}$, with the half-filled subshell, will be sluggish and less-stereoselective oxidants like $[\text{PorMn}^{\text{IV}}\text{O}]$.^[12] These expectations appear to be in accord with experimental data^[4] on the oxidative capabilities of the two transition-metal-substituted polyoxometalate systems.

Our study shows that the polyoxometalate system affords a convenient platform for the generation of metal-oxo species with high oxidation states of the transition metal, as much as v and vi. The intriguing analogy of the POM-FeO and POM-MnO species to the **A** species of P450 appears to get reasonable theoretical support. However, the oxidation state of the metal in the POM complexes is, respectively, one and two units higher than **A**. Furthermore, the electronic structure proposed herein is sufficiently interesting to attempt its identification by experimental means.

Received: January 27, 2004 [Z53867]

Keywords: cytochrome P450 · density functional calculations · metalloporphyrins · oxidation · polyoxometalates

- [1] *Biomimetic Oxidations Catalyzed by Transition Metal Complexes* (Ed.: B. Meunier), Imperial College Press, London, **1999**.
- [2] a) B. Meunier, J. Bernadou, *Struct. Bonding (Berlin)* **2000**, 97, 1–35; b) Y. Watanabe in *The Porphyrin Handbook*, Vol. 4 (Eds.: K. M. Kadish, K. M. Smith, R. Guilard), Academic Press, San Diego, **2000**, pp. 97–117; c) J. T. Groves, K. Shalyaev, J. Lee in *The Porphyrin Handbook*, Vol. 4 (Eds.: K. M. Kadish, K. M. Smith, R. Guilard), Academic Press, San Diego, **2000**, pp. 17–40.
- [3] a) I. V. Kozhevnikov, *Chem. Rev.* **1998**, 98, 171–198; b) N. Mizuno, M. Misono, *Chem. Rev.* **1998**, 98, 199–217; c) R.

- Neumann, *Prog. Inorg. Chem.* **1998**, *47*, 317–370; d) C. L. Hill, C. M. Prosser-McCartha, *Coord. Chem. Rev.* **1995**, *43*, 407–455.
- [4] a) C. L. Hill, R. B. Brown, Jr., *J. Am. Chem. Soc.* **1986**, *108*, 536–538; b) D. Mansuy, J.-F. Bartoli, P. Battioni, D. K. Lyon, R. G. Finke, *J. Am. Chem. Soc.* **1991**, *113*, 7222–7226.
- [5] D. L. Harris, *Curr. Opin. Chem. Biol.* **2001**, *5*, 724–735.
- [6] a) J. M. Maestre, X. López, C. Bo, J.-M. Poblet, N. Casañ-Pastor, *J. Am. Chem. Soc.* **2001**, *123*, 3749–3758; b) S. Ganapathy, M. Fournier, J. F. Paul, L. Delevoye, M. Guelton, J. P. Amoureux, *J. Am. Chem. Soc.* **2002**, *124*, 7821–7828; c) N. Suaud, A. Gaita-Ariño, J. M. Clemente-Juan, J. Sánchez-Marín, E. Coronado, *J. Am. Chem. Soc.* **2002**, *124*, 15134–15140; d) J. M. Poblet, X. López, C. Bo, *Chem. Soc. Rev.* **2003**, *32*, 297–308; e) see, however, A. J. Bridgeman, *Chem. Eur. J.* **2004**, *10*, 2935–2941.
- [7] F. Ogliaro, S. P. de Visser, J. T. Groves, S. Shaik, *Angew. Chem. Int. Ed.* **2001**, *40*, 2874–2878.
- [8] Gaussian98 (Revision A.7), M. J. Frisch, G. W. Trucks, H. B. Schlegel, G. E. Scuseria, M. A. Robb, J. R. Cheeseman, V. G. Zakrzewski, J. A. Montgomery, R. E. Stratmann, J. C. Burant, S. Dapprich, J. M. Millam, A. D. Daniels, K. N. Kudin, M. C. Strain, O. Farkas, J. Tomasi, V. Barone, M. Cossi, R. Cammi, B. Mennucci, C. Pomelli, C. Adamo, S. Clifford, J. Ochterski, G. A. Petersson, P. Y. Ayala, Q. Cui, K. Morokuma, D. K. Malick, A. D. Rabuck, K. Raghavachari, J. B. Foresman, J. Cioslowski, J. V. Ortiz, B. B. Stefanov, G. Liu, A. Liashenko, P. Piskorz, I. Komaromi, R. Gomperts, R. L. Martin, D. J. Fox, T. Keith, M. A. Al-Laham, C. Y. Peng, A. Nanayakkara, C. Gonzalez, M. Challacombe, P. M. W. Gill, B. G. Johnson, W. Chen, M. W. Wong, J. L. Andres, M. Head-Gordon, E. S. Replogle, J. A. Pople, Gaussian, Inc., Pittsburgh, PA, **1998**.
- [9] A. Bassan, M. R. A. Blomberg, P. E. M. Siegbahn, L. Que, Jr., *J. Am. Chem. Soc.* **2002**, *124*, 11056–11063.
- [10] a) R. S. Czernuszewicz, Y. O. Su, M. K. Stern, K. A. Macor, D. Kim, J. T. Groves, T. G. Spiro, *J. Am. Chem. Soc.* **1988**, *110*, 4158–4165; b) J. T. Groves, J. Lee, S. S. Marla, *J. Am. Chem. Soc.* **1997**, *119*, 6269–6273; c) see, however, [PorMn^{VO}] in: N. Jin, J. T. Groves, *J. Am. Chem. Soc.* **1999**, *121*, 2923–2924.
- [11] S. P. de Visser, F. Ogliaro, Z. Gross, S. Shaik, *Chem. Eur. J.* **2001**, *7*, 4954–4960.
- [12] J. T. Groves, M. K. Stern, *J. Am. Chem. Soc.* **1987**, *109*, 3812–3814.

Copper Complex Cation Templated Gadolinium(III)–Isophthalate Frameworks**

You-Fu Zhou, Fei-Long Jiang, Da-Qiang Yuan,
Ben-Lai Wu, Rui-Hu Wang, Zheng-Zhong Lin,
and Mao-Chun Hong*

Crystal engineering provides a powerful tool for the design and construction of coordination frameworks with unique structural motifs and tunable physical properties.^[1,2] Many heterometallic frameworks possess interesting physical properties,^[3–7] which arise from the interactions between two distinct metal ions. However, 3D cavity lanthanide frameworks with trapped or bonded transition-metal complexes are rare. A typical strategy utilized to construct lanthanide–transition-metal frameworks is self-assembly from mixed metal ions and ligands containing hybrid donor atoms, such as carbonyl,^[8] cyanide,^[9] pyridine-carboxylate ligands.^[6c] Herein we use isophthalate (ip) as the oxygen-donor ligand and 2,2'-bipyridine (bpy) as the nitrogen-donor ligand and Gd^{III} and Cu^{II} ions, to obtain two novel Gd–Cu frameworks, formulated as $[[\text{Gd}_4(\text{ip})_7(\text{H}_2\text{O})_2][\text{Cu}(\text{bpy})_2]_2]_n$ (**1**) and $[[\text{Gd}_3\text{Cu}(\text{ip})_5(\text{Hip})(\text{bpy})]_n] \cdot n\text{H}_2\text{O}$ (**2**), we report their syntheses, crystal structures along with magnetic properties.

The hydrothermal reaction of Gd₂O₃, Cu(NO₃)₂·3H₂O, H₂ip, and bpy in a molar ratio of 1:2:1:2 at 170 °C yielded crystals of **1**. Single-crystal X-ray diffraction^[10] reveals that the structure of **1** has charged cages containing two encapsulated [Cu(bpy)₂]⁺ ions (Figure 1). There is a [Cu(bpy)₂]⁺ ion, two Gd^{III} ions, three and a half ip ligands and a coordinated water in the asymmetric unit (Figure 2). Independent Gd^{III} ions (Gd1...Gd2 = 4.102 Å) are linked by two μ-oxygen atoms from separate carboxylate groups to form a Gd₂O₂ building unit, and each Gd^{III} ion is coordinated by eight oxygen atoms to furnish a dodecahedral geometry. Eight Gd₂O₂ units are linked by ip ligands to generate a large charged cage (ca. 11.5 × 14.9 × 16.5 Å³), in which two [Cu(bpy)₂]⁺ ions with a distorted tetrahedral geometry are trapped as charge-compensating guests. The two trapped guests (about 11.0 Å in diameter) adopt encapsulated mode which is unusual because they are larger than the largest valid pore of the cage (ca. 9.78 Å in diameter). The cationic guests are further stabilized by the π–π stacking interaction between the pyridyl rings with a face-to-face separation of 3.47 Å and the van der Waals

[*] Dr. Y.-F. Zhou, F.-L. Jiang, D.-Q. Yuan, B.-L. Wu, R.-H. Wang, Z.-Z. Lin, Prof. M.-C. Hong
State Key Laboratory of Structural Chemistry
Fujian Institute of Research on the Structure of Matter
Chinese Academy of Sciences, Fuzhou, Fujian, 350002 (China)
Fax: (+86) 591-8371-4946
E-mail: hmc@ms.fjirsm.ac.cn

[**] Financial support from the NNSF of China and Fujian Province are gratefully acknowledged.



Supporting information for this article is available on the WWW under <http://www.angewandte.org> or from the author.

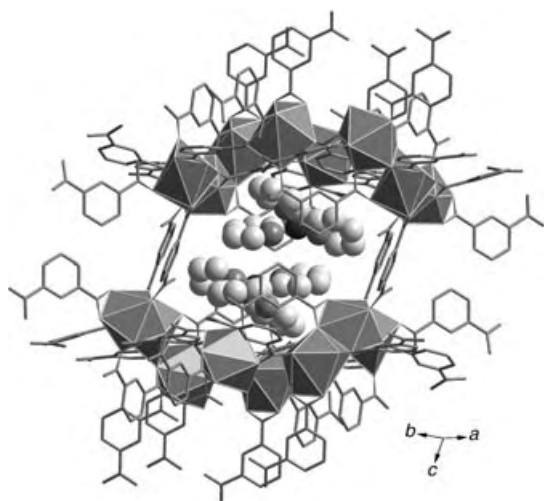


Figure 1. View of polymeric cage with two encapsulated $[\text{Cu}(\text{bpy})_2]^+$ ions (space-filling representation) in **1**; Gd^{III} ions are shown as coordination dodecahedra and ip ligands as a stick model.

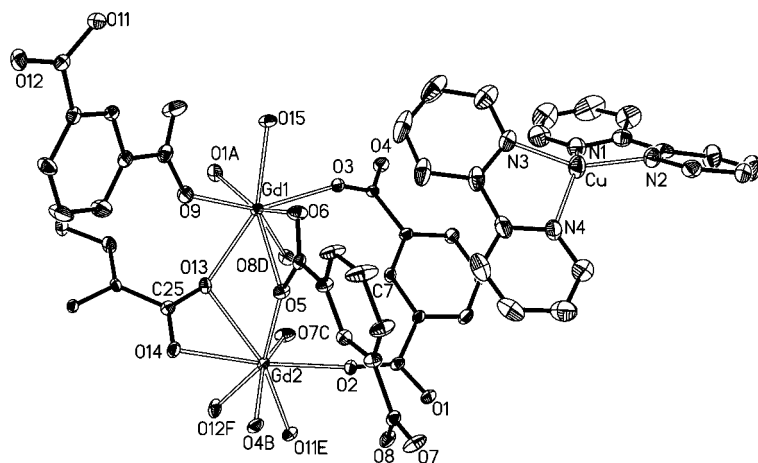


Figure 2. ORTEP plot (thermal ellipsoids set at 30% probability) of the asymmetric unit in **1**, symmetry codes: A,C: $-x+1/2, y+1/2, -z+1/2$; B: $-x+1/2, y-1/2, -z+1/2$; D: $x, -y+1, z-1/2$.

force between the guests and cage. The cages are connected by ip ligands to form a 3D cavity framework. To our knowledge, complex **1** is the first 3D framework containing multi encapsulated complex cations within a charged cage, being different from the reported inclusion complex that possesses a 3D framework containing only one encapsulated $[\text{Gd}(\text{dmf})_8]^{3+}$ ion within a charged cage.^[6b]

Clearly, Cu^{II} was reduced to Cu^{I} by the excessive bpy during the hydrothermal synthesis of **1**.^[1d,11] In an attempt to synthesize the $\text{Gd}^{\text{III}}\text{--Cu}^{\text{II}}$ analogue by using less bpy, the similar reaction was carried out with the molar ratio of $\text{Gd}:\text{Cu}:\text{H}_2\text{ip}:\text{bpy}$ (1:2:1:1), and green crystals of **2** were isolated. The asymmetric unit of **2** consists of three Gd^{III} ions, a Cu^{II} ion, a bpy ligand, six completely or partially deprotonated ip ligands, and a free water molecule (Figure 3). The valences of copper ions are supported by the calculated values of +1.3 (for **1**) and +1.8 (for **2**).^[12] Each Gd^{III} ion is coordinated by eight carboxylate oxygen atoms ($\text{Gd}\text{--O}$

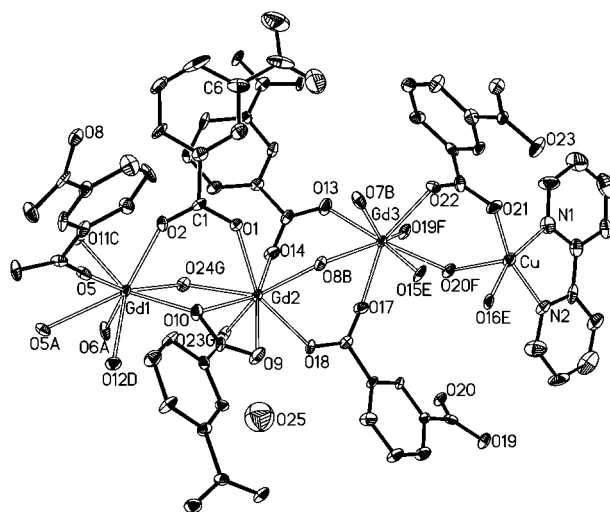


Figure 3. ORTEP plot (thermal ellipsoids set at 30% probability) of the asymmetric unit in **2**, symmetry codes: A: $-x+1, -y, -z+1$; B: $-x+1, -y+1, -z+1$; C: $x+1, y, z$; D: $-x, -y, -z+1$; E: $x-1, y, z$; F: $-x+1, -y+1, -z+2$; G: $x, y-1, z$.

2.277(9)–2.84(1) Å) to furnish a dodecahedral geometry. The separations between adjacent metal ions are 3.89(1), 4.01(1), and 4.29(1) Å for $\text{Gd}\cdots\text{Gd}$, 3.97(1) Å for $\text{Gd}\cdots\text{Cu}$ and 5.51(1) Å for $\text{Cu}\cdots\text{Cu}$. The ip ligands link Gd^{III} and Cu^{II} ions to form a 3D open-framework containing irregular cavities (ca. $11.4\times 8.10\text{ Å}^2$; Figure 4). Each Cu^{II} ion is coordinated by two nitrogen atoms from the chelating bpy ligand and three carboxylate oxygen atoms to furnish a square pyramidal geometry. Thus, the orientation of the $[\text{Cu}(\text{bpy})]^{2+}$ ions bound the inner backbone of the cavity alternates (Figure 4). The structures of **1** and **2** imply that copper ions and bpy ligands form complex cations first, and then these complex cations serve as structure-directing templates during the formation of $\text{Gd}\text{--ip}$ frameworks. Consequently, the different-sized complex cations result in the frameworks containing different cavities.^[1c]

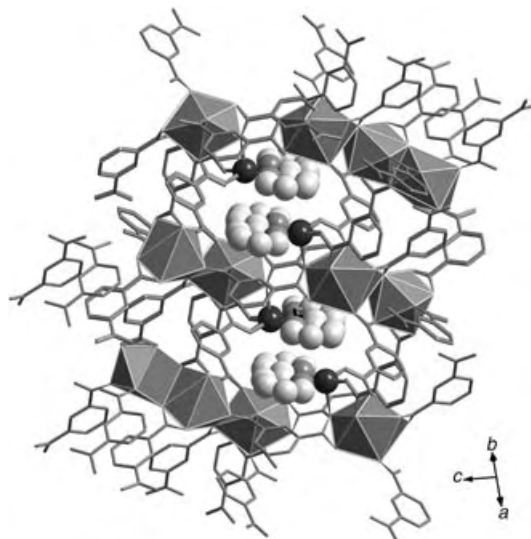


Figure 4. View of polymeric cavity with bound $[\text{Cu}(\text{bpy})]^{2+}$ ions (space-filling models, Cu dark gray; N light gray) in **2**, Gd^{III} ions as coordination dodecahedra, and ip ligands as a stick model.

The magnetic properties of **1** and **2** were investigated over the temperature range 5–300 K. For **1**, the observed $\chi_{\text{M}}T$ values of $30.9 \text{ cm}^3 \text{ mol}^{-1} \text{ K}$ at 300 K is slightly smaller than the expected value of $31.5 \text{ cm}^3 \text{ mol}^{-1} \text{ K}$ for a $\text{Gd}^{\text{III}}_4\text{Cu}^{\text{I}}_2$ complex with noninteracting metal ions. The $\chi_{\text{M}}T$ value decreases slightly to $29.0 \text{ cm}^3 \text{ mol}^{-1} \text{ K}$ at 12 K, and then dramatically decreases to $25.8 \text{ cm}^3 \text{ mol}^{-1} \text{ K}$ at 5 K (see the Supporting Information). Considering the structure of **1** and no orbital angular momentum for the Gd^{III} ion, the spin-coupled dimer model ($H = -JS_{\text{Gd}} \cdot S_{\text{Gd}}$)^[13] was applied to perform a quantitative analysis leading to $g = 2.08$ and $J = -0.09 \text{ cm}^{-1}$,^[14] which indicates a very weak antiferromagnetic interaction between closest Gd^{III} ions. For **2**, the observed $\chi_{\text{M}}T$ values of $24.2 \text{ cm}^3 \text{ mol}^{-1} \text{ K}$ at 300 K is slightly larger than the expected value of $24.0 \text{ cm}^3 \text{ mol}^{-1} \text{ K}$ for a noninteracting $\text{Gd}^{\text{III}}_3\text{Cu}^{\text{II}}$ complex. The $\chi_{\text{M}}T$ plot is almost constant from 300 K to 50 K, increase as temperature is lowered further, reaches a maximum value of $24.4 \text{ cm}^3 \text{ mol}^{-1} \text{ K}$ around 10 K, and then decreases to $23.9 \text{ cm}^3 \text{ mol}^{-1} \text{ K}$ at 5 K (see the Supporting Information). Considering the separations between adjacent metal ions, a linear octanuclear model containing one spin-coupled $\text{Gd}^{\text{III}}\text{--Gd}^{\text{III}}$ dimer(i), two spin-coupled $\text{Gd}^{\text{III}}\text{--Cu}^{\text{II}}$ dimer (ii), and two uncoupled Gd^{III} ions was applied to perform a quantitative analysis ($g_i = 2.04$, $J_i = -0.159 \text{ cm}^{-1}$, $g_{ii} = 2.03$, $J_{ii} = 2.07 \text{ cm}^{-1}$). The result indicates that the $\text{Gd}^{\text{III}}\text{--Gd}^{\text{III}}$ interaction is weak antiferromagnetic, while the $\text{Gd}^{\text{III}}\text{--Cu}^{\text{II}}$ interaction is ferromagnetic.^[15]

In summary, by introducing mixed ligands with different donor atoms in different molar ratios, two novel heterometallic 3d–4f coordination frameworks were successfully synthesized. Compound **1** is the first structurally characterized 3D heterometallic framework containing multi encapsulated complex cations within a charged cage. Compound **2** has a 3D cavity framework containing complex cations. The quantitative analyses of the magnetic properties between **1** and **2** provide a comprehensive understanding of the nature of the $\text{Gd}^{\text{III}}\text{--Cu}^{\text{II}}$ magnetic interaction.

Experimental Section

1: An aqueous mixture (10 mL) containing Gd_2O_3 (36 mg, 0.10 mmol), $\text{Cu}(\text{NO}_3)_2 \cdot 3\text{H}_2\text{O}$ (48 mg, 0.20 mmol), H_2ip (17 mg, 0.10 mmol), and bpy (31 mg, 0.20 mmol) in a molar ratio of 1:2:1:2 was sealed and heated at 170°C for 4 days. After cooling at 6°C h^{-1} to room temperature, black prismatic crystals of **1** were collected by filtration and washed with distilled water (37% yield, based on Gd). Elemental analysis (%) calcd for $\text{C}_{96}\text{H}_{64}\text{N}_8\text{O}_{30}\text{Cu}_2\text{Gd}_4$: C 44.94, H 2.51, N 4.37; found: C 44.82, H 2.37, N 4.24. IR (KBr pellet): $\nu = 650(\text{m})$, $706(\text{m})$, $750(\text{m})$, $1070(\text{w})$, $1155(\text{m})$, $1383(\text{s})$, $1452(\text{s})$, $1608(\text{s})$, $3066(\text{w}) \text{ cm}^{-1}$.

2: Complex **2** was synthesized in a similar way to **1**, except the molar ratio being 1:2:1:1. Green prismatic crystals of **2** were collected in 42% yield (based on Gd). Elemental analysis (%) calcd for $\text{C}_{38}\text{H}_{35}\text{N}_2\text{O}_{25}\text{CuGd}_3$: C 41.09, H 2.08, N 1.65; found: C 41.01, H 1.97, N 1.49. IR (KBr pellet): $\nu = 651(\text{m})$, $705(\text{m})$, $756(\text{m})$, $1074(\text{w})$, $1156(\text{m})$, $1380(\text{s})$, $1456(\text{s})$, $1610(\text{s})$, $3105(\text{w}) \text{ cm}^{-1}$.

Variable-temperature magnetic susceptibilities were measured on a Quantum Design PPMS Model 6000 magnetometer in an applied field of 1000 Oe.

Received: June 9, 2004

Revised: July 8, 2004

Keywords: copper · gadolinium · inclusion compounds · magnetic properties

- a) M. Eddaoudi, D. B. Moler, H. Li, B. Chen, T. M. Reineke, M. O'Keeffe, O. M. Yaghi, *Acc. Chem. Res.* **2001**, *34*, 319; b) O. M. Yaghi, H. Li, C. Davis, D. Richardson, T. L. Groy, *Acc. Chem. Res.* **1998**, *31*, 474; c) P. J. Hagerman, D. Hagerman, J. Zubieta, *Angew. Chem.* **1999**, *111*, 2798; *Angew. Chem. Int. Ed.* **1999**, *38*, 2638; d) D. Hagerman, C. Zubieta, D. J. Rose, J. Zubieta, R. C. Haushalter, *Angew. Chem.* **1997**, *109*, 904; *Angew. Chem. Int. Ed. Engl.* **1997**, *36*, 873.
- a) G. B. Gardner, D. Venkataraman, J. S. Moore, S. Lee, *Nature* **1995**, *374*, 792; b) B. F. Abrahams, P. A. Jackson, R. Robson, *Angew. Chem.* **1998**, *110*, 2801; *Angew. Chem. Int. Ed.* **1998**, *37*, 2656; c) M. Eddaoudi, J. Kim, J. B. Wachter, H. K. Chae, M. O'Keeffe, O. M. Yaghi, *J. Am. Chem. Soc.* **2001**, *123*, 4368; d) R. García-Zarracino, H. Höpfl, *Angew. Chem.* **2004**, *116*, 1533; *Angew. Chem. Int. Ed.* **2004**, *43*, 1507.
- a) Y. Pei, P. Bergerat, O. Kahn, *J. Am. Chem. Soc.* **1994**, *116*, 3866; b) E. Coronada, C.-J. Gómez-García, *Chem. Rev.* **1998**, *98*, 273; c) B.-Q. Ma, S. Gao, G. Su, G.-X. Xu, *Angew. Chem.* **2001**, *113*, 448; *Angew. Chem. Int. Ed.* **2001**, *40*, 434; d) D. M. J. Doble, C. H. Benison, A. J. Blake, D. Fenske, M. S. Jackson, R. D. Kay, W.-S. Li, M. Schröder, *Angew. Chem.* **1999**, *111*, 2042; *Angew. Chem. Int. Ed.* **1999**, *38*, 1915.
- a) J. Lisowski, P. Starynowicz, *Inorg. Chem.* **1999**, *38*, 1351; b) J.-P. Costes, F. Dahan, A. Dupuis, J.-P. Laurent, *Inorg. Chem.* **1997**, *36*, 3429; c) X.-M. Chen, S. M. J. Aubin, Y.-L. Wu, Y.-S. Yang, T. C. W. Mak, D. N. Hendrickson, *J. Am. Chem. Soc.* **1995**, *117*, 9600.
- a) D. M. L. Goodgame, S. Menzer, A. T. Ross, D. J. Williams, *J. Chem. Soc. Chem. Commun.* **1994**, 2605; b) S. Liu, E. A. Meyers, J. A. Cowan, S. G. Shore, *Chem. Commun.* **1998**, 2043; c) S. Decurtins, M. Gross, H. W. Schmalle, S. Ferlay, *Inorg. Chem.* **1998**, *37*, 2443.
- a) C. E. Plecnik, S. Liu, S. G. Shore, *Acc. Chem. Res.* **2003**, *36*, 499; b) S. Liu, E. A. Meyers, S. G. Shore, *Angew. Chem.* **2002**, *114*, 3761; *Angew. Chem. Int. Ed.* **2002**, *41*, 3609; c) H.-Z. Kou, B. C. Zhou, S. Gao, R. J. Wang, *Angew. Chem.* **2003**, *115*, 3410; *Angew. Chem. Int. Ed.* **2003**, *42*, 3288; d) Y.-P. Ren, L.-S. Long, B.-W. Mao, Y.-Z. Yuan, R.-B. Huang, L.-S. Zheng, *Angew. Chem.* **2003**, *115*, 550; *Angew. Chem. Int. Ed.* **2003**, *42*, 532; e) Y. Liang, R. Cao, W. Su, M. Hong, W. Zhang, *Angew. Chem.* **2000**, *112*, 3442; *Angew. Chem. Int. Ed.* **2000**, *39*, 3304; f) Y. Liang, M. Hong, W. Su, R. Cao, W. Zhang, *Inorg. Chem.* **2001**, *40*, 4574.
- G. B. Deacon, C. M. Forsyth, T. Behrnsing, K. Konstas, M. Forsyth, *Chem. Commun.* **2002**, 2820.
- a) A. E. Crease, P. Legzdins, *J. Chem. Soc. Dalton Trans.* **1973**, 1501; b) J. M. Boncella, R. A. Andersen, *Inorg. Chem.* **1984**, *23*, 432.
- a) W. E. Bailey, R. J. Williams, W. O. Milligan, *Acta Crystallogr. B* **1973**, *29*, 1365; b) D. W. Knoepfel, S. G. Shore, *Inorg. Chem.* **1996**, *35*, 5328.
- Crystal data for **1**: Crystal dimensions $0.15 \times 0.10 \times 0.05 \text{ mm}$, $M_r = 2565.64$, monoclinic, space group $C2/c$, $a = 26.359(2)$, $b = 14.3982(8)$, $c = 25.311(2) \text{ Å}$, $\beta = 113.016(2)^\circ$, $V = 8841(1) \text{ Å}^3$, $Z = 4$, $\rho_{\text{calcd}} = 1.928 \text{ g cm}^{-3}$. A total of 26837 reflections were collected in the range of $1.64 \leq \theta \leq 25.03^\circ$, of which 7796 were unique reflections, $R(\text{int}) = 0.0476$, $\mu(\text{MoK}\alpha) = 3.522 \text{ mm}^{-1}$, parameters = 632, $R1(F_o) = 0.0439$, $wR2(F_o^2) = 0.0735$, and $\text{GOF} = 1.191$ for reflections $I \geq 2\sigma(I)$. Crystal data for **2**: Crystal dimensions $0.16 \times 0.14 \times 0.10 \text{ mm}$, $M_r = 1695.17$, Triclinic, space group $P-1$, $a = 10.5295(1)$, $b = 12.4930(2)$, $c = 23.4994(1) \text{ Å}$, $\alpha = 95.800(1)^\circ$, $\beta = 100.890(1)^\circ$, $\gamma = 111.740(1)^\circ$, $V = 2769.62(5) \text{ Å}^3$, $Z = 2$, $\rho_{\text{calcd}} = 2.033 \text{ g cm}^{-3}$. A total of 14499 reflections were collected in the range of $0.90 \leq \theta \leq 25.08^\circ$, of which 9719 were unique reflections, $R(\text{int}) = 0.0597$, $\mu(\text{MoK}\alpha) = 4.016 \text{ mm}^{-1}$, parameters = 797, $R1(F_o) = 0.0692$, $wR2(F_o^2) = 0.1216$, and

GOF = 1.104 for reflections $I \geq 2\sigma(I)$. CCDC-236669 (**1**) and CCDC-236670 (**2**) contains the supplementary crystallographic data for this paper. These data can be obtained free of charge via www.ccdc.cam.ac.uk/conts/retrieving.html (or from the Cambridge Crystallographic Data Centre, 12 Union Road, Cambridge CB21EZ, UK; fax: (+44)1223-336-033; or deposit@ccdc.cam.ac.uk).

- [11] a) S. M.-F. Lo, S. S.-Y. Chui, L.-Y. Shek, Z. Lin, X. X. Zhang, G.-H. Wen, I. D. Williams, *J. Am. Chem. Soc.* **2000**, *122*, 6293; b) X.-M. Zhang, M.-L. Tong, X.-M. Chen, *Angew. Chem.* **2002**, *114*, 1071; *Angew. Chem. Int. Ed.* **2002**, *41*, 1029; c) J. Tao, Y. Zhang, M.-L. Tong, X.-M. Chen, T. Yuen, C. L. Lin, X. Huang, J. Li, *Chem. Commun.* **2002**, 1342; d) J. Y. Lu, A. M. Babb, *Inorg. Chem.* **2002**, *41*, 1339.
- [12] N. E. Brese, M. O'Keeffe, *Acta Crystallogr. B* **1991**, *47*, 192.
- [13] W. Plass, G. Fries, *Z. Anorg. Allg. Chem.* **1997**, 623, 1205.
- [14] For **1**, the least-squares fitting of the experimental data gives the agreement factor $R = \Sigma(\chi_{\text{obs}}T - \chi_{\text{calcd}}T)^2 / \Sigma(\chi_{\text{obs}}T)^2 = 6.6 \times 10^{-3}$. For **2**, $R = 1.3 \times 10^{-3}$.
- [15] a) J. S. Miller, A. J. Epstein, *Angew. Chem.* **1994**, *106*, 399; *Angew. Chem. Int. Ed. Engl.* **1994**, *33*, 385; b) C. Benelli, D. Gatteschi, *Chem. Rev.* **2002**, *102*, 2369; c) O. Kahn, *Acc. Chem. Res.* **2000**, *33*, 647; d) C. Benelli, A. Caneschi, D. Gatteschi, O. Guillou, L. Pardi, *Inorg. Chem.* **1990**, *29*, 1750; e) O. Tougaard, J. A. Ibers, *Inorg. Chem.* **2000**, *39*, 1790; f) H.-Z. Kou, S. Gao, X. Jin, *Inorg. Chem.* **2001**, *40*, 6295.

Binuclear Complexes

A Highly Flexible Dinuclear Ruthenium(II)–Platinum(II) Complex: Crystal Structure and Binding to 9-Ethylguanine**

Karlijn van der Schilden, Fedora Garcia,
Huub Kooijman, Anthony L. Spek, Jaap G. Haasnoot,
and Jan Reedijk*

Polynuclear platinum complexes represent a novel class of anticancer agents.^[1,2] It is believed they can overcome both acquired and intrinsic resistance to the antitumor drug

cisplatin, because they are capable of forming a completely different range of DNA adducts compared to cisplatin and its analogues. Chain length and flexibility, hydrogen-bonding capacity and charge of the linker, and the geometry of the chloro ligand to the linker chain emerge as the major factors in designing polynuclear platinum antitumor drugs. A challenging extension of the polynuclear concept is to introduce a different metal in one of the coordination sites to achieve selective specificity and reactivity at each metal center. Ruthenium as the second metal appears to be promising because ruthenium compounds are also known for their antitumor activity.^[3] This field of heteropolynuclear ruthenium–platinum anticancer complexes is relatively unexplored and only a few, rather rigid compounds have been studied so far.^[4] These complexes consist of a ruthenium(II) cationic species as a light-absorbing unit linked to a reactive platinum center through a short, rigid polyazine bridging ligand. Conversely, it would be interesting to develop nonrigid heterodinuclear compounds of greater length that are capable of engaging in delocalized long-range DNA interactions, since the excellent cytotoxicity of polynuclear platinum complexes is thought to be a consequence of the formation of long-range inter- and intrastrand DNA adducts.^[1] Just a single example,^[5] that is, $[[cis-RuCl_2(Me_2SO)_3]H_2N(CH_2)_4NH_2[cis-PtCl_2-(NH_3)]]$, has been published, but the complex has been found to be too reactive for use as a DNA-binding probe, because of its light sensitivity and fast hydrolysis.

Herein, the X-ray diffraction structure of the highly flexible heterodinuclear ruthenium(II)–platinum(II) complex $[(tpy)Ru(dtdeg)PtCl]Cl_3$ (**1**) ($tpy = 2,2':6',2''$ -terpyridine, $dtdeg = bis[4'-(2,2':6',2''$ -terpyridyl)]-diethyleneglycol ether) is presented. Uniquely, a long and flexible bridging terpyridine ligand^[6] ($dtdeg$) has been used to link the two metal moieties. The design and subsequent development of the dinuclear complex have been inspired by the cytotoxic mononuclear platinum complex $[Pt(tpy)Cl]Cl \cdot 2H_2O$, which can both intercalate and coordinate to DNA.^[7] Moreover, substitution-inert ruthenium polypyridyl complexes are known to be able to bind to DNA in a noncovalent mode, such as electrostatic or surface binding, or partial intercalation.^[8] It is thought that the ruthenium moiety of **1** increases the DNA affinity by its $2+$ charge, thereby directing the complex to its target. Subsequently, both metal moieties can exert the DNA-binding features of their parental mononuclear complexes. As a first step in evaluating the DNA interactions of **1**, reactions with the DNA model base 9-ethylguanine have been performed.

Complex **1** was synthesized in high yield by refluxing a mixture of $[(tpy)Ru(dtdeg)]Cl_2$ and $[Pt(cod)Cl_2]$ ($cod = 1,5$ -cyclooctadiene) in MeOH (see Supporting Information). Red plate-shaped crystals of **1** were obtained by slow precipitation of the reaction mixture with diethyl ether. Despite the great length and flexibility of the linker, the crystal structure^[9] was elucidated (Figure 1) and confirmed unambiguously the molecular structure of **1**. Notably, no crystal structures of heterodinuclear ruthenium–platinum complexes, in which the two metal moieties are linked by a long and flexible bridging ligand, are included in the January 2004 update of the Cambridge Structural Database. In this unique crystal

[*] K. van der Schilden, F. Garcia, Dr. J. G. Haasnoot, Prof. Dr. J. Reedijk
Leiden Institute of Chemistry
Gorlaeus Laboratories, Leiden University
P.O. Box 9502, 2300 RA Leiden (The Netherlands)
Fax: (+31) 71-527-4671
E-mail: reedijk@chem.leidenuniv.nl
Dr. H. Kooijman, Prof. Dr. A. L. Spek
Crystal and Structural Chemistry
Bijvoet Center for Biomolecular Research, Utrecht University
Padualaan 8, 3584 CH Utrecht (The Netherlands)

[**] This research was supported by the Council for Chemical Sciences of The Netherlands Organization for Scientific Research (CW-NWO). Support and sponsorship by COST Action D20 is kindly acknowledged. The authors thank Johnson & Matthey (Reading (UK)) for their generous loan of $RuCl_3 \cdot xH_2O$ and K_2PtCl_4 and H. den Dulk and Prof. Dr. J. Brower for their kind help with the preliminary cytotoxicity tests.

Supporting information for this article is available on the WWW under <http://www.angewandte.org> or from the author.

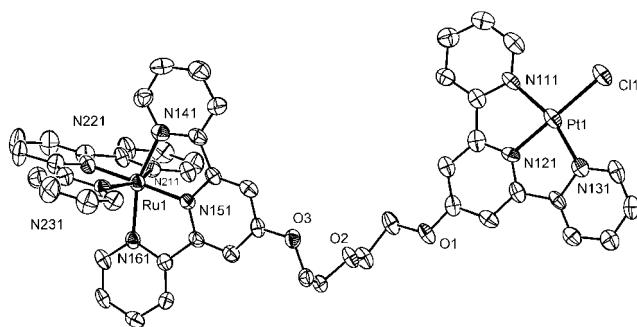


Figure 1. Displacement ellipsoid (50% probability) plot of the structure of **1**. Counterions and solvent molecules are not shown. Hydrogen atoms are also omitted for clarity. Bond lengths and angles are in agreement with literature data for parental cationic mononuclear complexes.^[13,18] N–Ru–N bite angles vary from 78.58(19) to 80.10(19)°, N–Pt–N bite angles are 80.50(19) and 81.62(19)°, the Ru–N bond distances lie in the range 1.965(5)–2.078(5) Å, the Pt–N distances lie in the range 1.939(5)–2.025(5) Å, and the Pt–Cl distance is 2.3054(15) Å.

structure, the intramolecular Ru...Pt distance is 14.547(3) Å. For comparison, the intramolecular Ru...Pt distance in the crystal structure^[10] of [Ru(bpy)₂(μ-2,3-dpp)PtCl₂](PF₆)₂ (bpy = 2,2'-bipyridine), in which dpp is the short and rigid bridging ligand 2,3-bis(2-pyridyl)pyrazine, is 6.7 Å. Given that the diethyleneglycol ether linker of **1** is somewhat folded in the crystal structure, the length over which both metal moieties can interact with DNA might even be larger. Long-range binding from the minor to the major groove of the DNA over the phosphate backbone has been shown to be possible^[11] for the trinuclear platinum compound [(*trans*-PtCl(NH₃)₂)₂μ-[H₂N(CH₂)₆NH₂]₂Pt(NH₃)₂](NO₃)₄ (BBR3464) bound to a self-complementary DNA octamer 5'-d(ATG*TACAT)₂-3'. The two *trans*-[PtCl(NH₃)₂] units coordinate in the major groove at the N7 positions of guanine residues on opposite DNA strands, whereas the central tetraamine linker is located in or close to the minor groove. Considering the length of the linker of **1**, either intercalative binding or coordination of the platinum moiety of **1** might occur in the major groove of the DNA after pre-association, which is largely stabilized by electrostatic forces upon binding of the 2+ charged ruthenium unit in the minor groove.

Surprisingly, the crystal structure of **1** also shows intermolecular stacking interactions between the platinum moieties despite the linked, rather bulky ruthenium units (Figure 2). The platinum units stack in a head-to-tail fashion with alternating short and long Pt...Pt distances of 3.4935(7) and 6.7337(12) Å, respectively, because the packing of the crystal structure of **1** is such that chains of alternating platinum units related by inversion symmetry are situated in between the ruthenium units. A continuous π–π ring-stacking interaction is displayed along the Pt–tpy chain, with the perpendicular distances of the center of geometry of one ring to the least-squares plane of the other ring being approximately 3.38 and 3.45 Å for the short and long pair, respectively (see the Supporting Information). The short Pt...Pt distance of 3.49 Å might even allow weak d_z²–d_z² interactions.^[12] Indeed, aggregation through weak bonding interactions into metal-bound d⁸–d⁸ pairs in an infinite π–π

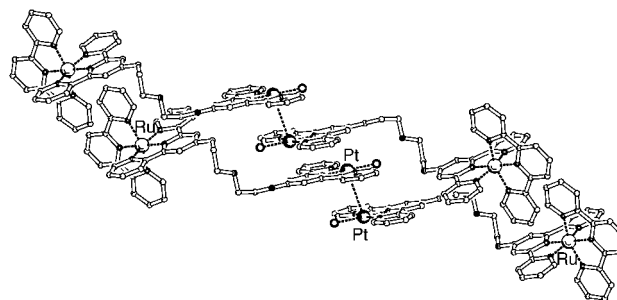


Figure 2. View of the packing of the crystal structure of **1** in which alternating short and long Pt...Pt distances are displayed by the platinum units. A short intermolecular Pt1...Pt1 [2–x,–y,–z] distance (dashed lines) of 3.4935(7) Å is observed between two platinum terpyridine units that are exactly oriented in a head-to-tail fashion. The long intermolecular Pt1...Pt1 [1–x,–y,–z] distance is caused by a lateral shift of one Pt–tpy unit with respect to the short Pt1...Pt1 [2–x,–y,–z] vector.

stack has been reported for the perchlorate salt of the parental mononuclear [Pt(tpy)Cl]⁺ ion.^[13] Studies to examine the Pt–Pt interactions of **1** have not been undertaken yet. Nonetheless, the self-stacking interactions imply that the platinum unit of **1** is able to intercalate in the DNA, thereby aiding coordination. Although intercalation is initially more feasible, coordination has been determined to be the thermodynamically more favorable mode of binding for mononuclear platinum terpyridine complexes containing a fourth labile ligand.^[14]

Mononuclear platinum terpyridine complexes are known to coordinate preferentially to the DNA base guanine.^[15] Studies performed with the DNA model base 9-ethylguanine (9egua) prove that the platinum unit of **1** is able to coordinate to 9egua through N7 (see Supporting Information for data of the adduct [(tpy)Ru(dtdeg)Pt(9egua)](PF₆)₄ (**2**)), which agrees with previously reported data.^[16] Apparently, coordination of platinum to 9egua is not hindered at all by the dangling ruthenium unit. However, although the platinum moiety of **1** possibly displays the DNA interactions inherent to its parental mononuclear complex, preliminary experiments on the cisplatin-sensitive cell lines A2780 (human ovarian cancer) and L1210/0 (mouse leukemia) and their cisplatin-resistant derivatives A2780cisR and L1210/2 indicate that **1** is not as cytotoxic^[17] as [Pt(tpy)Cl]Cl·2H₂O. The lower cytotoxicity of **1** might be explained by the fact that the ruthenium moiety of **1** can only display electrostatic DNA interactions, just like its mononuclear counterpart.^[8] Consequently, the ruthenium unit linked to the platinum moiety can easily be removed from DNA by repair proteins. Hence, the ruthenium unit is currently being modified to enable coordination of ruthenium to the DNA.

In summary, the first crystal structure of a highly flexible heterodinuclear ruthenium–platinum complex and its coordination to the DNA model base 9-ethylguanine is presented. The results suggest that the platinum moiety is able to both intercalate and coordinate to the DNA without being hindered by the ruthenium unit, which simultaneously allows for additional electrostatic binding to the DNA. Despite the relatively low cytotoxicity of the presented

complex, it is a unique example of a new series of potentially antitumor-active complexes of which variation of the terminal tpy ligand of the ruthenium unit offers great possibilities to improve noncovalent DNA-binding modes as well as DNA-coordination abilities. In view of the relatively long intramolecular ruthenium–platinum separation of 14.5 Å found for **1**, this approach can lead to compounds able to form delocalized long-range DNA adducts, thereby bestowing antitumor activity onto this new series of heterodinuclear ruthenium–platinum complexes.

Received: April 14, 2004

Keywords: antitumor agents · binuclear complexes · platinum · ruthenium · structure elucidation

- [1] N. J. Wheate, J. G. Collins, *Coord. Chem. Rev.* **2003**, *241*, 133–145.
- [2] J. Reedijk, *Proc. Natl. Acad. Sci. USA* **2003**, *100*, 3611–3616.
- [3] M. J. Clarke, *Coord. Chem. Rev.* **2002**, *232*, 69–93.
- [4] For example: a) R. L. Williams, H. N. Toft, B. Winkel, K. J. Brewer, *Inorg. Chem.* **2003**, *42*, 4394–4538; b) M. Milkevitch, H. Storrie, E. Brauns, K. J. Brewer, B. W. Shirley, *Inorg. Chem.* **1997**, *36*, 4534–4538.
- [5] Y. Qu, N. Farrell, *Inorg. Chem.* **1995**, *34*, 3573–3576.
- [6] A. H. Velders, Ph.D. Thesis, Leiden University, Leiden, **2000**.
- [7] a) G. Lowe, A. S. Droz, T. Vilaivan, G. W. Weaver, J. J. Park, J. M. Pratt, L. Tweedale, L. R. Kelland, *J. Med. Chem.* **1999**, *42*, 3167–3174; b) K. W. Jennette, S. J. Lippard, G. A. Vassiliades, W. R. Bauer, *Proc. Natl. Acad. Sci. USA* **1974**, *71*, 3839–3843; c) M. Howe-Grant, K. C. Wu, W. R. Bauer, S. J. Lippard, *Biochemistry* **1976**, *15*, 4339–4346.
- [8] J. M. Kelly, A. B. Tossi, D. J. McConnell, C. Ohuigin, *Nucleic Acids Res.* **1985**, *13*, 6017–6034.
- [9] Crystal data for **1**·8CH₃OH: C₅₇H₆₃Cl₄N₉O₁₁PtRu, *M*_r = 1496.20, red plate-shaped crystal (0.03 × 0.13 × 0.30 mm), triclinic, space group *P* $\bar{1}$, *a* = 8.8396(12), *b* = 15.961(2), *c* = 23.548(4) Å, α = 75.031(13), β = 88.528(13), γ = 78.975(17)°, *V* = 3149.4(8) Å³, *Z* = 2, ρ_{calcd} = 1.578 g cm^{−3}, $\mu(\text{MoK}\alpha)$ = 2.804 mm^{−1}. A total of 53838 reflections were measured (11287 independent, *R*_{int} = 0.1061, θ_{max} = 25.35°, *T* = 150 K, MoK α radiation, graphite monochromator, λ = 0.71073) on a Nonius Kappa CCD diffractometer on a rotating anode; data were corrected for absorption using PLATON/MULABS, *T* range 0.741–0.929. The structure was solved by automated direct methods (SHELXS86). Full-matrix least-squares refinement of 577 parameters on *F*² (SHELXL-97) resulted in a final *R*1 value of 0.0470, *wR*2 = 0.0927, *S* = 0.898. H atoms were introduced on calculated positions. A volume of 1257 Å³ per unit cell is filled with disordered methanol solvent molecules in which the chloride counterions are positioned as well. Disorder models of solvent and counterions suggest the presence of three chloride ions per ruthenium–platinum complex, one of which is disordered over two positions. However, these models proved to be unstable upon refinement. By using the PLATON/SQUEEZE method, a total of 379 e[−] was found in the disordered region, which corresponds to about eight methanol molecules per ruthenium–platinum complex. CCDC-230794 contains the supplementary crystallographic data for this paper. These data can be obtained free of charge via www.ccdc.cam.ac.uk/conts/retrieving.html (or from the Cambridge Crystallographic Data Centre, 12 Union Road, Cambridge CB21EZ, UK; fax: (+44)1223-336-033; or deposit@ccdc.cam.ac.uk).
- [10] V. W. W. Yam, V. W. M. Lee, K. K. Cheung, *J. Chem. Soc. Chem. Commun.* **1994**, 2075–2076.
- [11] Y. Qu, N. J. Scarsdale, M.-C. Tran, N. P. Farrell, *J. Biol. Inorg. Chem.* **2003**, *8*, 19–28.
- [12] J. S. Field, J.-A. Gertenbach, R. J. Haines, L. P. Ledwaba, N. T. Mashapa, D. R. McMillin, O. Q. Munro, G. C. Summerton, *Dalton Trans.* **2003**, 1176–1180.
- [13] J. A. Bailey, M. G. Hill, R. E. Marsh, V. M. Miskowski, W. P. Schaefer, H. B. Gray, *Inorg. Chem.* **1995**, *34*, 4591–4599.
- [14] C. S. Peyratout, T. K. Aldridge, D. K. Crites, D. R. McMillin, *Inorg. Chem.* **1995**, *34*, 4484–4489.
- [15] G. Lowe, J. A. McCloskey, J. S. Ni, T. Vilaivan, *Bioorg. Med. Chem.* **1996**, *4*, 1007–1013.
- [16] Z. D. Bugarcic, F. W. Heinemann, R. van Eldik, *Dalton Trans.* **2004**, 279–286.
- [17] For all cell lines tested, 20 to 30 % of the cells die at the highest concentration (0.1 mM) of **1** tested compared to 95 % at 0.1 mM of [Pt(tpy)Cl]Cl·2H₂O, of which the IC₅₀ values lie in the μM range. The IC₅₀ values of **1** have not been determined because of the low solubility of the complexes in NaCl-containing solutions used for cytotoxicity tests.
- [18] K. Lashgari, M. Kritikos, R. Norrestam, T. Norrby, *Acta Crystallogr. Sect. C* **1999**, *55*, 64–67.

Nanowires

Large-Scale Production of NbS₂ Nanowires and Their Performance in Electronic Field Emission**

*Yi Zheng Jin, Wen Kuang Hsu, Yu Lun Chueh,
Li Jen Chou, Yan Qiu Zhu,* Kieren Brigatti,
Harold W. Kroto, and David R. M. Walton*

In addition to carbon nanotubes, the production of noncarbon nanostructures has attracted much attention over the past few years. In particular, and due to their unusual geometry and promising physical properties, inorganic fullerene nanostructures have become one of the main focuses in nanoscale research since the first report of the synthesis of WS₂ nanotubes in 1992.^[1] The synthesis of chalcogenide nanotubes and nested nanoparticles is difficult because their formation requires the release of considerable strain energy against

[*] Dr. Y. Q. Zhu

School of Mechanical, Materials and Manufacturing Engineering
University of Nottingham, University Park NG7 2RD (UK)
Fax: (+44) 115-951-3800
E-mail: yanqiu.zhu@nottingham.ac.uk

Y. Z. Jin, K. Brigatti, Prof. H. W. Kroto, Dr. D. R. M. Walton
Department of Chemistry, University of Sussex
Brighton BN1 9QJ (UK)

Dr. W. K. Hsu, Dr. Y. L. Chueh, Dr. L. J. Chou
Department of Materials Science and Engineering
National Tsing-Hua University
Hsinchu 300 (Taiwan)

[**] We thank the EPSRC (UK), UST-CNST of the National Tsing-Hua University, and the National Science Council (Taiwan, NSC92-2119M-007-072) for financial support.

surface curvature and wall thickness.^[2] These chalcogenides (MX_2 ; $\text{M} = \text{W}, \text{Mo}, \text{Ta}, \text{Nb}$; $\text{X} = \text{S}, \text{Se}$) are mostly triple-layer structures in which one M and two S atoms are organized within a trigonal prismatic lattice. The formation of curved MX_2 morphologies commonly involves a considerable number of lattice defects and dislocations.^[3,4] It has been shown, for example, that defect-containing WS_2 lattices lead to branched layer structures, which fuse particles together.^[5] Lattice dislocations also provide connecting sites with C and Mo to form heterogeneous structures.^[6] Recently, NbS_2 nanostructures have been produced by heating NbS_3 in the presence of H_2 ,^[7] by the reaction between NbCl_4 and H_2S ,^[8] and by taking advantage of the carbon nanotube template effect.^[9] However, the amounts of resulting materials are minute, and thus their chemical and physical properties and applications cannot be explored.

Herein we report that well-defined NbS_2 nanowires can be generated in bulk by direct heating of Nb and S powders in sealed quartz tubes in the presence of I_2 . The large quantity of NbS_2 nanowires produced allows various analyses, including X-ray diffraction (XRD), the use of a superconducting quantum interference device (SQUID), and for the first time, electronic field emission tests to be performed.

In a typical experiment, Nb powder (99.8%, 325 mesh, Aldrich Co.), S powder (99.98%, Aldrich Co.), and I_2 (99.999%, Aldrich Co.) were used. A mixture of Nb and S powder with a Nb/S ratio of 1:2 was sealed in an I_2 -containing quartz ampoule (ca. 2 mg cm^{-3}) under vacuum (ca. 10^{-4} pa); the I_2 is the reaction medium.^[10] The ampoule was heated in either a temperature gradient (10 K cm^{-1} ; $600\text{--}800^\circ\text{C}$) three-zone horizontal furnace or at a constant temperature of 800°C in a conventional horizontal furnace, for three days. The quartz ampoule was then allowed to cool to room temperature and the sample was subsequently extracted from the tube (colder tube end for those samples heated in a temperature gradient), washed with CS_2 , and dried under vacuum. The resulting samples (200–500 mg) were then examined by XRD (Siemens, D5000), scanning electron microscopy (SEM, LEO5000), transmission electron microscopy (TEM, H7100) and high-resolution transmission electron microscopy (HRTEM, JEOL-3000), energy dispersive X-ray (EDX) line-scan, electron diffraction (ED), SQUID magnetometry, and field emission analyses. To identify the I_2 mediation effect, experiments were also carried out in the absence of I_2 .

Figure 1a shows an SEM image recorded from the transported materials found at the colder end of an ampoule heated in a temperature gradient. The product consists of almost pure one-dimensional (1D) nanostructures with diameters in the range 50 to 500 nm. Experiments carried out at a constant temperature (800°C) also generated a bulk yield of nanowires (inset, Figure 1a). Most of these nanowires have diameters within the range 20 to 200 nm, much smaller than those shown in Figure 1a. The lengths of the nanowires are typically several micrometers; wires longer than $10 \mu\text{m}$ were also observed in our TEM investigations (Figure 1b). The aspect ratio of the nanowires was estimated to be about 80–120, lower than the typical range for carbon nanotubes (150–200). The surface of the nanowires is generally clean, although a few particles were occasionally observed attached to the

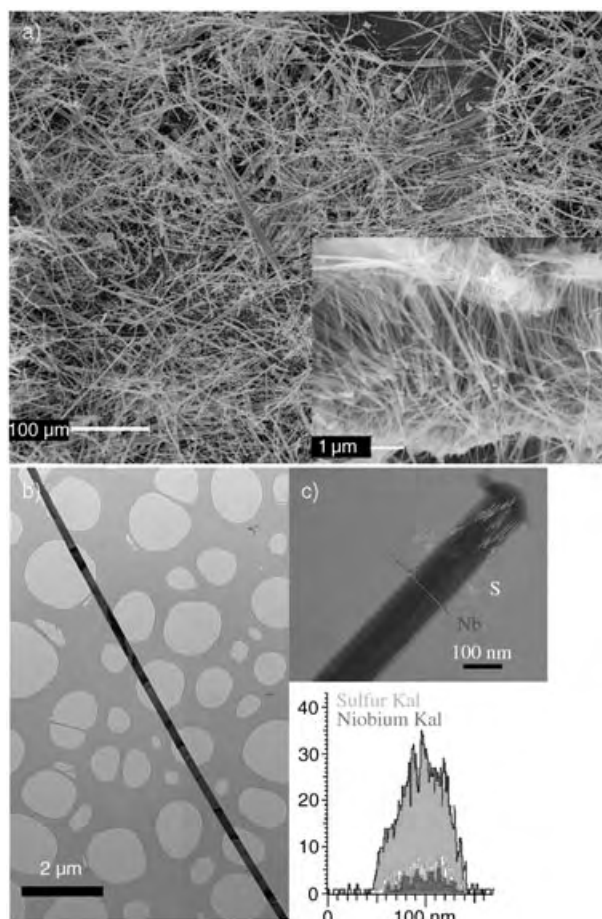


Figure 1. a) SEM image of NbS_2 nanowires from the colder end of an ampoule heated in a temperature gradient. Insert: nanowires from the constant-temperature heating; b) TEM image of a long NbS_2 nanowire ($>10 \mu\text{m}$); c) line-scan EDX profile across a nanowire. Lower insert: enhanced EDX profile.

nanowire surfaces by SEM. No nanowires were produced in the I_2 -free experiments; micro-sized crystallites and amorphous materials appeared to be the main products. These results clearly indicate that I_2 -mediation is essential for the nanowire growth; this conclusion is consistent with previous results.^[10]

The following studies focus on the product obtained from experiments carried out at a constant temperature, as this procedure also yields bulk materials and the diameters of the resultant nanowires are smaller than those shown in Figure 1a. Line-scan EDX analyses were carried out on selected wires. A typical elemental profile is displayed in Figure 1c; Nb and S were detected in most cases. It is noteworthy that a weak I signal is also present occasionally in the EDX profiles. We were unable to determine the exact Nb/S atomic ratio as the energy counts were only calculated based on the $\text{K}_{\alpha 1}$ shells.

According to a commonly used inorganic crystal structure data (ICSD) file for modeling structures based on the atomic positions, the nanowire samples fit the $3R$ structure quite well. Figure 2a shows simulated XRD profiles of hexagonal- $2H$ (top) and $-3R$ (middle) structures based on ICSD data, along

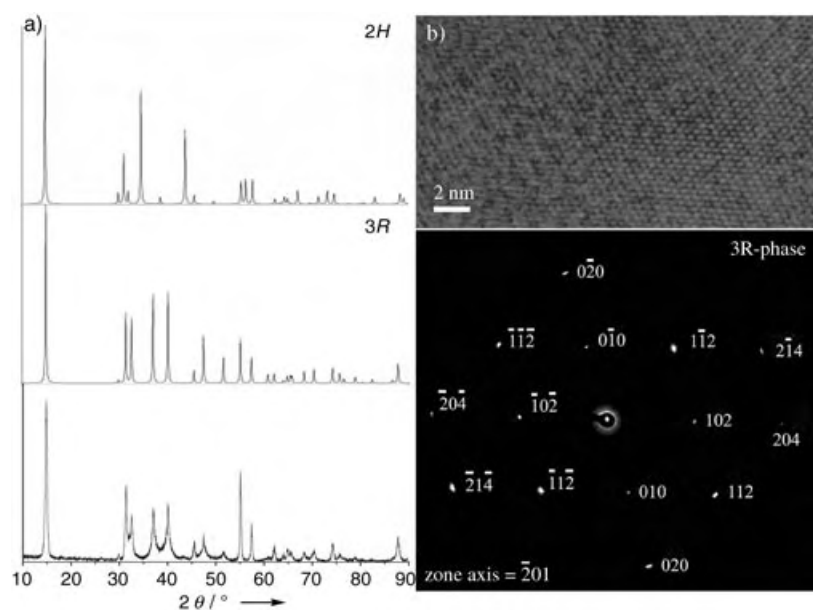


Figure 2. a) Simulated 2H(top) and 3R (middle) as well as experimental (bottom) XRD profiles; b) HRTEM image of one NbS₂ nanowire (top) and its corresponding ED pattern (bottom).

with the experimental XRD pattern (bottom). It is clear that the sample is in good agreement with the 3R phase, including the peak positions and intensities. The ED pattern obtained from selected wires also suggests a 3R phase (Figure 2b); the high-resolution TEM image clearly demonstrates the well-crystallized single-crystal structures of the NbS₂ nanowires (top right).

According to the XRD and ED analyses it seems that the presence of trace amounts of I in the NbS₂ nanowires does not alter the 3R structure significantly. It is possible that I substitutes S, leading to an intact 3R-phase lattice.

Our SQUID measurements were carried out between 300 and 2 K; no Curie temperature (T_c) was observed (Figure 3). The profile shows a positive (paramagnetic) but weak temperature dependence of the magnetic susceptibility (χ), which is consistent with 3R-NbS₂ (Pauli behavior).^[11] A clear Curie tail is present below 20 K, thus indicating a possible high density of electronic impurities in the nanowires. In

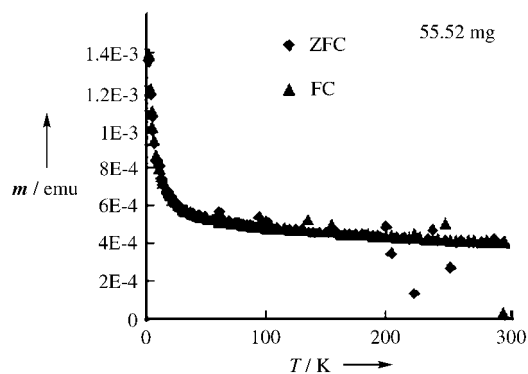


Figure 3. SQUID profile of 3R-NbS₂ nanowires. m is the magnetic moment.

addition to the residual I, these impurities could also arise from nonstoichiometric NbS₂ phases, such as Nb_{1+x}S₂. This assumption is based on a previous report that starting materials with a 1:2 (Nb/S) ratio always lead to Nb_{1+x}S₂ phases.^[12]

The field-emission behavior of NbS₂ nanotubes is well-defined, although they have a lower aspect ratio than carbon nanotubes. Figure 4a shows the results of repeating field emission tests over four runs with a similar emitting current ($5 \mu\text{A cm}^{-2}$) and threshold field ($5.5 \text{ V } \mu\text{m}^{-1}$). The emitting current and threshold field of carbon nanotubes often vary from sample to sample ($0.3 \mu\text{A cm}^{-2}$ – 0.7 A cm^{-2}), due to the C-layer oxidation lattice defects.^[12–14] The similar current density and turn-on voltage of our sample over several runs indicate that highly stable electronic field emission from NbS₂ nanowires is achieved via a unique energy state. The saturation current obtained here ($5 \mu\text{A cm}^{-2}$, Figure 4a) is much lower than that of the carbon nanotube films reported recently (0.7 A cm^{-2}),^[14] but is similar to that of annealed single-walled carbon nanotubes (0.5 – $5 \mu\text{A cm}^{-2}$).^[15] This phenomenon supports our assumption that the electrons only emit by a specific channel, possibly the d_{z^2} -band. In this respect the lower current density

obtained with our nanowire sample is not disappointing because a single emission channel will certainly limit the current density. The larger emitting current density seen in

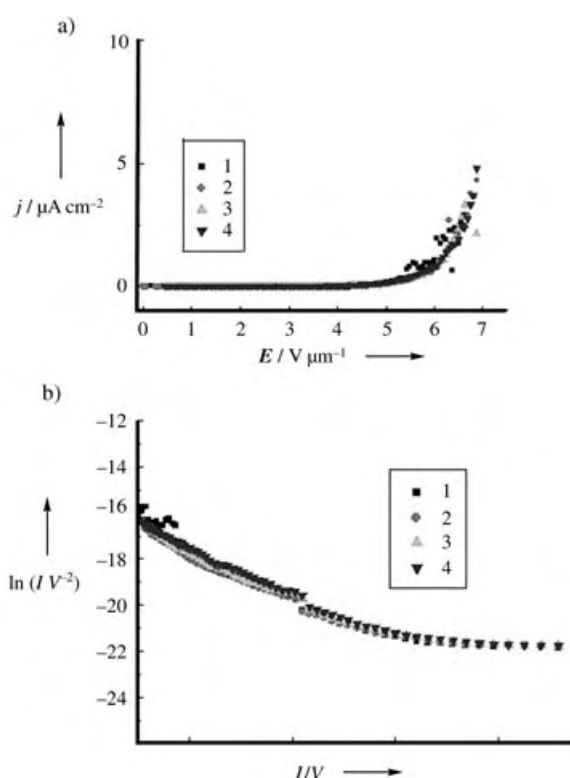


Figure 4. Electron field emission profile of NbS₂ nanowires (a), and their corresponding F–N plots (b). The numbers denote the run of the experiment. j is the current density; E is the electric field strength.

carbon nanotubes (particularly in multi-walled tubes) is mainly due to a high density of localized states. In other words, electrons can emit by various channels at the tube tips or elsewhere.^[16] However, the multiple emission channels in multiwalled carbon nanotubes are unstable: the field emission from point defects, for example, can be rapidly quenched by joule heating, and other localized spinless defects can be electronically reopened. This explains the frequent changes of field emission current from carbon nanotubes over repeated experiments. The low current density from single-walled carbon nanotubes is also due to a similar situation, that is, a lower density of localized emitting channels. Our NbS₂ nanowires show a linear Fowler–Nordheim (F–N) plot at high field (Figure 4b), whereas the F–N profile becomes nonlinear at low field (Figure 4b). The turn-on voltage determined from the F–N plot is about 2.5 V μm⁻¹. This value is similar to that in carbon nanotubes (CNTs) but is significantly lower than other metal oxide and inorganic nanostructures. Repeating the experiments yielded similar results (1st to 4th run, Figure 4). To highlight the performance of NbS₂ nanowire emitters, various metal oxide and inorganic nanowire emitters are listed below along with their threshold fields: Co nanowire arrays (14 V μm⁻¹),^[17] MoS₂ nanoflowers (ca. 8 V μm⁻¹),^[18] SiC nanorods (ca. 15 V μm⁻¹),^[19] W₁₈O₄₉ nanowire films (6.2 V μm⁻¹),^[20] and ZnO nanorods (6 V μm⁻¹).^[21]

The presence of a discontinuity in the F–N plot (arrow, Figure 4b) is due to the switching of the emission control circuits from lower (nA magnitude) to higher power (μA magnitude). Small deviations in the F–N plot often occur in carbon nanotube emission due to various factors, including screening, space charge, and variation in the emission states. A small curve that appears in the lower-field region of the F–N plot (Figure 4b) can be attributed to a new factor, namely the surface amorphous structure (Figure 5a,b). The surface amorphous material also consists of Nb and S, as revealed by EDX. HRTEM shows two kinds of order–disorder phase transitions near to the wire surfaces: (a) a gradual lattice variation (Figure 5a), and (b) a coating-like structure (Figure 5b). The former is a distinguishable structural transition from ordered to disordered, (arrow, Figure 5a), whereas the latter is a thicker amorphous structure (Figure 5b). The disordered surface structure is likely to be the nonstoichiometric NbS₂ phase, which appears as a result of the chemical changes in the reaction environment with time. A strong electron scattering is anticipated at the surface amorphous layers. The scattering, in turn, influences the field emission properties, including the emission current and applied threshold field. Meanwhile, the amorphous NbS₂ layers may be gradually converted into a stable oxide phase (Nb₂O₅); consequently, the lifetime of field emission shortens.

In summary, a large quantity of quality NbS₂ nanowires (hundreds of milligrams) has been produced successfully by direct heating of Nb and S powders in the presence of I₂ at 800 °C. This synthetic route is novel and straightforward. The materials have a 3R phase and are metallic in nature. Repeating field emission tests revealed that the NbS₂ nanowires are highly reliable field emitters and exhibit a very low turn-on voltage, which is among the best amongst inorganic

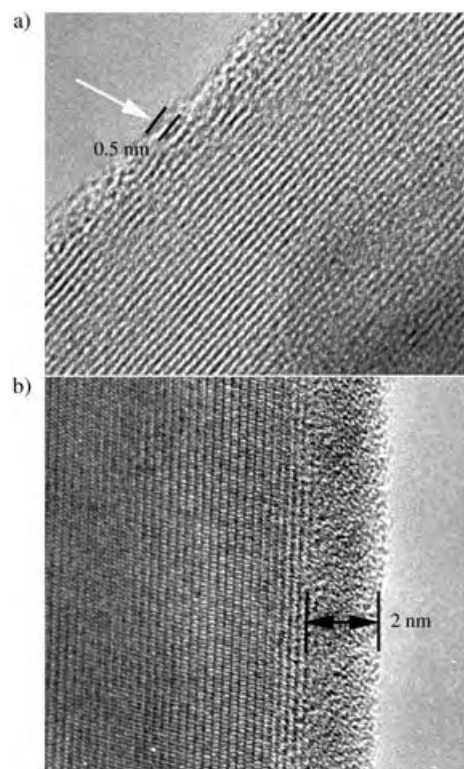


Figure 5. HRTEM images: a) a thin amorphous layer structure near to the nanowire surface at about 0.5 nm (arrowed). b) a thick coating-like amorphous structure on the wire surface at about 2 nm (arrowed).

1D nanomaterials and is comparable with those of carbon nanotubes.

Received: April 26, 2004

Keywords: nanostructures · niobium · sulfur

- [1] R. Tenne, L. Margulis, M. Genut, G. Hodes, *Nature* **1992**, 360, 444.
- [2] D. J. Srolovitz, S. A. Safran, M. Homyonfer, R. Tenne, *Phys. Rev. Lett.* **1995**, 74, 1779.
- [3] Y. D. Li, X. L. Li, R. R. He, J. Zhu, Z. X. Deng, *J. Am. Chem. Soc.* **2002**, 124, 1411.
- [4] R. L. D. Whitby, W. K. Hsu, T. H. Lee, C. B. Boothroyd, H. W. Kroto, D. R. M. Walton, *Chem. Phys. Lett.* **2002**, 359, 68.
- [5] W. K. Hsu, Y. Q. Zhu, S. Firth, M. Terrones, H. Terrones, S. Trasobares, R. J. H. Clark, H. W. Kroto, D. R. M. Walton, *Carbon* **2001**, 39, 1107.
- [6] W. K. Hsu, Y. Q. Zhu, C. B. Boothroyd, I. Kinloch, S. Trasobares, H. Terrones, N. Grobert, M. Terrones, R. Escudero, G. Z. Chen, C. Colliex, A. H. Windle, D. J. Fray, H. W. Kroto, D. R. M. Walton, *Chem. Mater.* **2000**, 12, 3541.
- [7] M. Nath, C. N. R. Rao, *J. Am. Chem. Soc.* **2001**, 123, 4841.
- [8] C. Schuffenhauer, R. Popovitz-Biro, R. Tenne, *J. Mater. Chem.* **2002**, 12, 1587.
- [9] Y. Q. Zhu, W. K. Hsu, H. W. Kroto, D. R. M. Walton, *Chem. Commun.* **2001**, 2184.
- [10] M. Remskar, A. Mrzel, Z. Skraba, A. Jesih, M. Ceh, J. Demsar, P. Stadelmann, F. Levy, D. Mihailovic, *Science* **2001**, 292, 479.
- [11] W. G. Fisher, M. J. Sienko, *Inorg. Chem.* **1980**, 19, 39.
- [12] W. A. Deheer, A. Chatelain, D. Ugarte, *Science* **1995**, 270, 1179.

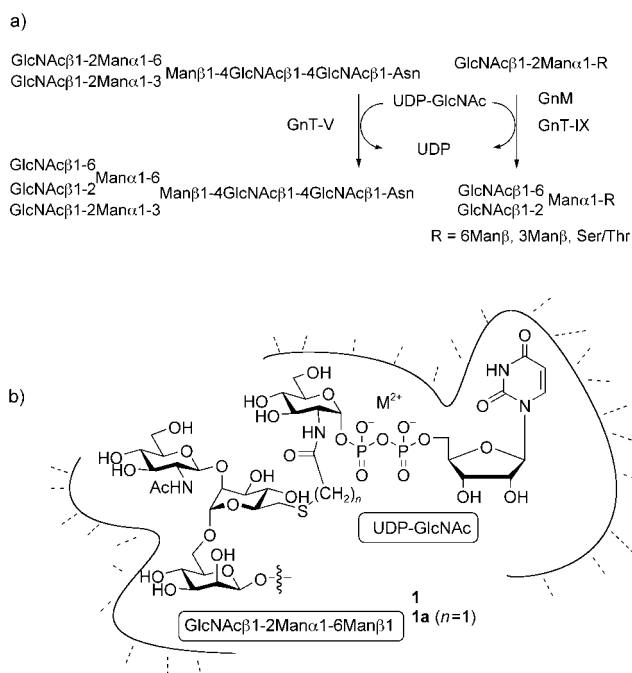
- [13] G. Pirio, P. Legagneux, D. Pribat, K. B. K. Teo, M. Chhowalla, G. A. J. Amaratunga, W. I. Milne, *Nanotechnology* **2002**, *13*, 1.
- [14] W. I. Milne, K. B. K. Teo, G. A. J. Amaratunga, P. Legagneux, L. Gangloff, J. P. Schnell, V. Semet, V. Thien Binh, O. Groening, *J. Mater. Chem.* **2004**, *14*, 933.
- [15] J. P. Sun, Z. X. Zhang, S. M. Hou, G. M. Zhang, Z. N. Gu, X. Y. Zhao, W. M. Liu, Z. Q. Xue, *Appl. Phys. A* **2002**, *75*, 479.
- [16] D. Lovall, M. Buss, E. Graugnard, R. P. Andres, R. Reifemberger, *Phys. Rev. B* **2000**, *61*, 5683.
- [17] L. Vila, P. Vincent, L. Dauginet-De Pra, G. Pirio, E. Minoux, L. Gangloff, S. Demoustier-Champagne, N. Sarazin, E. Ferain, R. Legras, L. Piraux, P. Legagneux, *Nano Lett.* **2004**, *4*, 521.
- [18] Y. B. Li, Y. Bando, D. Golberg, *Appl. Phys. Lett.* **2003**, *82*, 1962.
- [19] X. T. Zhou, H. L. Lai, H. Y. Peng, F. C. K. Au, L. S. Liao, N. Wang, I. Bello, C. S. Lee, S. T. Lee, *Chem. Phys. Lett.* **2000**, *318*, 58.
- [20] Y. B. Li, Y. Bando, D. Golberg, *Adv. Mater.* **2003**, *15*, 1294.
- [21] C. J. Lee, T. J. Lee, S. C. Lyu, Y. Zhang, H. Ruh, H. J. Lee, *Appl. Phys. Lett.* **2002**, *81*, 3648.

Glycosyltransferase Inhibitor

Synthesis of a Bisubstrate-Type Inhibitor of *N*-Acetylglucosaminyltransferases**

Shinya Hanashima, Shino Manabe, Kei-ichiro Inamori, Naoyuki Taniguchi, and Yukishige Ito*

Glycosyltransferases are a group of enzymes responsible for the biosynthesis of glycoconjugate oligosaccharides.^[1] Among them, *N*-acetylglucosaminyltransferases (GnTs) are key enzymes in the production of highly branched complex *N*-glycan structures. GnT-V transfers an *N*-acetylglucosamine (GlcNAc) residue to the core α 1-6-mannose (Man) arm to form a β 1-6 linkage (Scheme 1a).^[2] The recently identified GnT-IX is a homologue of GnT-V that is exclusively expressed in the brain.^[3] GnT-IX has a broader specificity and transfers GlcNAc to both α 1-6- and α 1-3-mannose



Scheme 1. a) Substrate specificities of GnT-V and GnT-IX; b) bisubstrate-type inhibitors consist of acceptor trisaccharide and UDP-GlcNAc moieties. UDP = uridine diphosphate.

structures, as well as to *O*-linked GlcNAc β 1-2Man.^[4] The GlcNAc β 1-6-branched glycans are often extended by the polylactosamine ((Gal β 1-4GlcNAc)_{*n*}, Gal = galactose) structure and present ligands for cell-adhesion molecules. It is well known that levels of β 1-6-branched glycans are increased in tumor cells,^[5] and GnT-V is involved in cancer metastasis.^[6a-e] Also, relationships with T-cell activation and angiogenesis have been revealed.^[6f,g] The exclusive expression of GnT-IX in the brain is in sharp contrast with the ubiquitous expression of GnT-V, and this difference suggests roles for GnT-IX in neuronal development and functions.^[3]

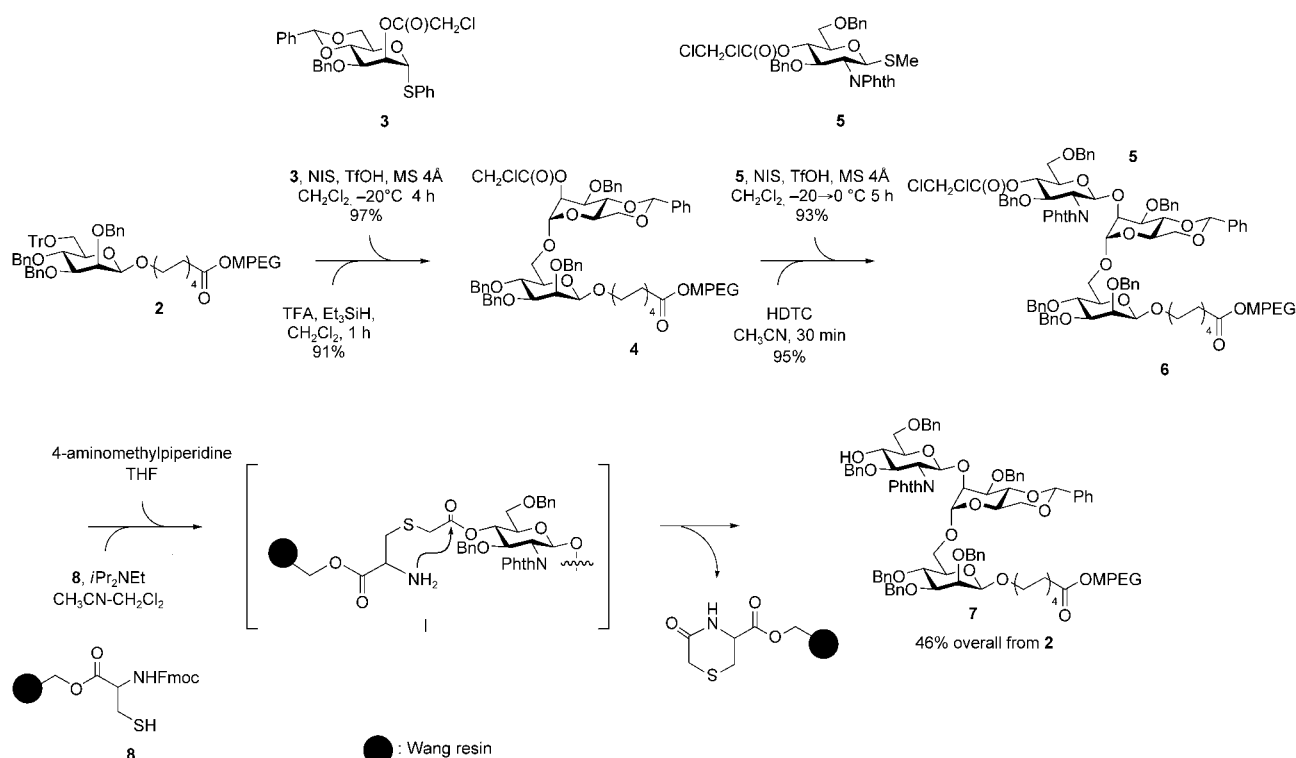
It is expected that suppression of GnT-V may be useful for the treatment of cancer.^[7] In addition to a gene-knockout strategy,^[8] chemical inhibition would be an promising approach. In fact, several attempts to develop inhibitors of GnT-V that mimic acceptor substrates have been reported.^[9] In this paper, we report the synthesis of compound **1a**, which is a prototype for bisubstrate-type inhibitors of type **1** (Scheme 1b).^[10] These inhibitors were designed to contain both donor (UDP-GlcNAc) and acceptor components, with the proposed mechanism of inverting GnTs^[11] taken into consideration. As the acceptor component, the trisaccharide (GlcNAc β 1-2Man α 1-6Man β) was incorporated, because it was previously reported by Tahir and Hindsgaul to serve as an efficient acceptor substrate of GnT-V.^[12] In order to approach our target **1a**, a convergent route was adopted; namely, the trisaccharide and donor components were constructed separately and combined together by chemoselective ligation.

Synthesis of the acceptor trisaccharide was conducted by using solution-phase polymer-support technology,^[13] which utilized low-molecular-weight ($M_w \approx 750$) poly(ethylene glycol) monomethyl ether (MPEG), as shown in Scheme 2.

[*] Dr. S. Hanashima, Dr. Y. Ito
RIKEN (The Institute of Physical and Chemical Research)
2-1 Hirosawa, Wako-shi, Saitama 351-0198 (Japan)
Fax: (+81) 48-462-4680
E-mail: yukito@riken.jp

Dr. S. Manabe
RIKEN and PRESTO
Japan Science and Technology Agency (JST) (Japan)
Dr. K.-i. Inamori, Prof. Dr. N. Taniguchi
Department of Biochemistry
Osaka University Medical School
2-2 Yamadaoka, Suita, Osaka 565-0871 (Japan)

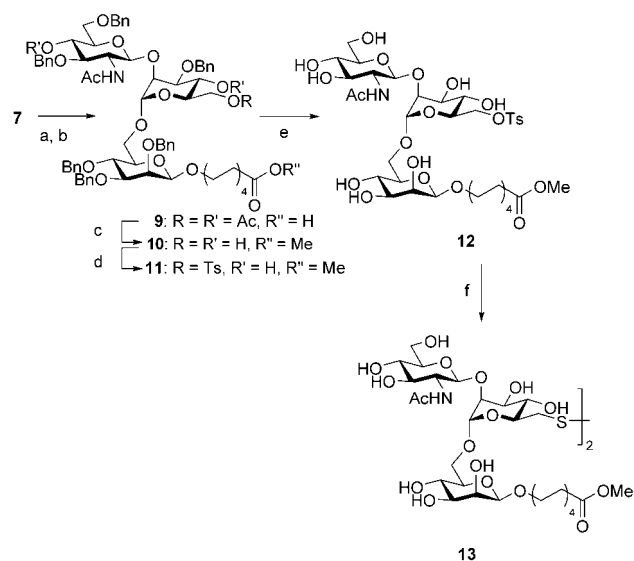
[**] S.H. is a recipient of the Special Postdoctoral Researcher Program Fellowship in RIKEN. Additional financial support from CREST (JST) is acknowledged. We thank Dr. T. Chihara and his staff for elemental analyses and Dr. H. Koshino and Ms. T. Chijimatsu for NMR measurements. We thank Ms. Akemi Takahashi for her technical assistance.



Scheme 2. Polymer-resin hybrid synthesis of trisaccharide **7**. Tr = triphenylmethyl = trityl, Bn = benzyl, TFA = trifluoroacetic acid, Phth = phthaloyl, NIS = *N*-iodosuccinimide, TfOH = trifluoromethanesulfonic acid, HDTC = hydrazinedithiocarbonate, Fmoc = 9-fluorenylmethoxycarbonyl.

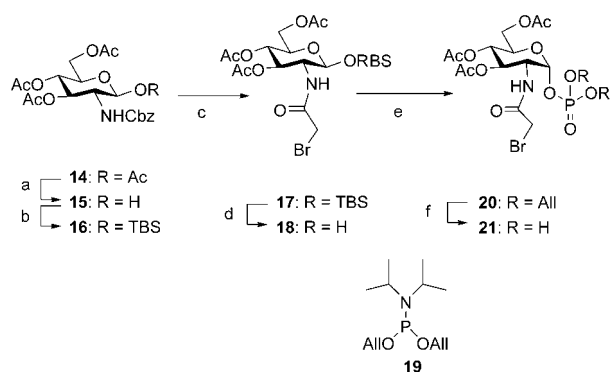
During the whole process, MPEG functioned as a polar tag and products were retrieved by chromatography on short silica gel columns.^[14] In the first place, MPEG-supported **2** was prepared by using Hodosi and Kovác's β -mannosylation, as described before.^[13d,15] The trityl group was removed with TFA (40 equiv) and Et_3SiH (20 equiv), and the liberated alcohol was glycosylated with phenylthiomannoside **3** with NIS and TfOH (1.1 equiv) to afford disaccharide **4**.^[16,17] Cleavage of the chloroacetyl group^[18] and glycosylation with **5** provided trisaccharide **6**. At this stage, the product was subjected to capture–release purification. Namely, compound **6** was captured with cysteine-conjugated Wang resin **8** through the reaction between the chloroacetyl and thiol groups. Liberation of the amino group from the Fmoc protection with 4-aminomethylpiperidine initiated cyclization and trisaccharide **7** was obtained in 46% overall yield and with high purity.

Further deprotection^[13d] and introduction of the thiol group were conducted as depicted in Scheme 3. Acidic cleavage of the benzylidene acetal, ethylenediamine treatment, and acetylation afforded compound **9** in 77% yield. Subsequent deacetylation and esterification gave **10** in 85% yield. The contaminating αGlcNAc isomer (<10%) was separated at this stage. Tosylation of the primary hydroxy group was best performed by using DMAP as a base to afford **11**, and cleavage of the benzyl ethers gave **12**. The tosyl group of **12** was substituted with SAc by using AcSK (5 equiv) in DMF at 70°C. Deacetylation with NaOMe was accompanied by disulfide formation to provide **13**.



Scheme 3. Preparation of acceptor **13**: a) 60% aqueous AcOH, 60°C, 87%; b) 1. 1 M KOH, EtOH/THF, reflux; 2. ethylenediamine, 1-BuOH, 100°C; 3. Ac_2O , pyridine, 77%; c) 1. 0.05 M NaOMe/MeOH; 2. TMSCHN_2 , PhH, MeOH, 85%; d) TsCl, DMAP, CH_2Cl_2 , 60%; e) H_2 , 20% $\text{Pd}(\text{OH})_2/\text{C}$, AcOH, MeOH, 88%; f) 1. AcSK, DMF, 70°C; 2. 0.05 M NaOMe/MeOH, 90%. Ts = tosyl = toluene-4-sulfonyl, TMS = trimethylsilyl, DMAP = 4-dimethylaminopyridine, DMF = *N,N*-dimethylformamide.

Glucosamine phosphate **21** was synthesized as shown in Scheme 4. Compound **14** was subjected to anomeric de-



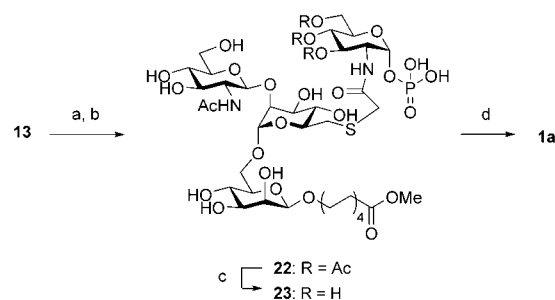
Scheme 4. Preparation of phosphate **21**: a) $\text{NH}_2\text{NH}_2/\text{AcOH}$, THF, 94%; b) TBSCl, imidazole, DMF, 95%; c) 1. H_2 , 10% Pd/C, EtOAc; 2. $(\text{BrCH}_2\text{CO})_2\text{O}$, pyridine, CH_2Cl_2 , 98%; d) 47% aqueous HF, CH_3CN , 93%; e) 1. **19**, 1*H*-tetrazole, CH_2Cl_2 , -10°C ; 2. TBHP, $-40 \rightarrow 0^\circ\text{C}$, 57%; f) $[\text{Pd}(\text{PPh}_3)_4]$, Et_3SiH , AcOH, toluene, 85%. Cbz = benzyloxycarbonyl, TBS = *tert*-butyldimethylsilyl, All = allyl, TBHP = *tert*-butylhydroperoxide.

acetylation, and the hemiacetal was masked with a TBS group to give **16**. Removal of the Cbz group was conducted by hydrogenolysis in ethyl acetate,^[19] and subsequent *N*-bromoacetylation gave **17** in 98% yield.

The TBS group was removed with 47% aqueous HF in CH_3CN to afford hemiacetal **18** in 93% yield. Direct phosphorylation turned out to be problematic because of base sensitivity of the bromoacetamide moiety. However, treatment with **19** and 1*H*-tetrazole at low temperature (-10°C) readily produced a phosphite compound that was oxidized with TBHP to afford phosphate **20** in 57% yield.^[20,21] Cleavage of the allyl groups by using $[\text{Pd}(\text{PPh}_3)_4]$ and Et_3SiH afforded **21** in 85% yield.

Sequential ligation and deprotection were conducted in a one-pot procedure (Scheme 5). Disulfide **13** was reduced to the thiol derivative with TCEP in MeOH/ H_2O . Subsequent addition of bromoacetamide **21** and $i\text{Pr}_2\text{NET}$ afforded crude **22**, which was deacetylated with excess Et_3N to give **23** in 51% yield from **13** over 3 steps (see the Experimental Section). The modified morpholidate method reported by Wittmann and Wong^[22] was used to introduce UMP; namely, monophosphate **23** was treated with UMP–morpholidate in the presence of 1*H*-tetrazole in pyridine for 4 days to afford **1a** in 78% yield. The structure of **1a** was rigorously confirmed by 2D NMR spectroscopy (DQF-COSY, HMQC) and mass spectrometry (MALDI-TOF).^[23]

Inhibitory activities of **1a** toward GnT-V and GnT-IX were evaluated, and the results are summarized in Table 1.^[24,25] The affinity of **1a** to GnT-V ($K_i = 103 \mu\text{M}$) was



Scheme 5. Chemoselective one-pot ligation and coupling with UMP: a) TCEP-HCl, MeOH, H_2O ; b) **21**, $i\text{Pr}_2\text{NET}$; c) Et_3N , 51% (three steps); d) UMP–morpholidate, 1*H*-tetrazole, pyridine, 78%. UMP = uridine monophosphate, TCEP-HCl = tris(carboxyethyl)phosphine hydrochloride.

only modest in comparison with the acceptor substrate ($K_m = 150 \mu\text{M}$). However, its activity toward GnT-IX was much greater ($K_i = 7.2 \mu\text{M}$). In order to investigate the kinetic mechanism and physiological role of GnT-IX, compound **1a** would therefore be a useful molecular probe.

In summary, we have synthesized bisubstrate-type analogue **1a** as a GnT-V inhibitor by using a polymer-resin hybrid strategy. Ligation of bromoacetamide **21** and disulfide **13**, after coupling with UMP, gave the desired compound **1a**. Simple extension of this chemistry would provide access to various homologues differing in the structure of the acceptor component (for example, Man, GlcNAc β 1-2Man, Man α 1-6Man) or the donor–acceptor distance. The latter task may well be achieved immediately simply by changing the bromoacyl group of **17** (see Scheme 4). Further studies are in progress along these lines to discover more potent and selective inhibitors of GnT-V and GnT-IX.

Experimental Section

Preparation of 22 by a one-pot procedure: TCEP (3.5 mg, 17 μmol) was added to a solution of disulfide **13** (4.0 mg, 2.7 μmol) in MeOH/ H_2O (7:3, 1 mL). After stirring for 1 h, GlcNAc derivative **21** (9.3 mg, 18 μmol) and $i\text{Pr}_2\text{NET}$ (20 μL) were added, and the mixture was stirred for 28 h. Et_3N (0.1 mL) was then added, and the mixture was stirred for an additional day. This was followed by concentration and purification by chromatography with a Sep-Pak C18 cartridge (MeOH/ H_2O 0:100 \rightarrow 40:60) afforded **22** (2.9 mg, 0.00283 mmol, 51%).

Enzyme assay: GnT-V activity was assayed by using pyridyl aminated acceptor substrate and cell lysate from COS-1 cells transfected with the GnT-V expression vector as an enzyme source.^[3,25] GnT-IX activity was assayed by using pyridyl amino ethyl succinamyl acceptor substrate and partially purified recombinant soluble GnT-IX.^[4] For kinetic analyses, these enzyme sources were incubated at 37°C for 2 h with 20 μM acceptor substrate (GnGn-bi-PA or GnM-S-PAES) and various concentrations of UDP-GlcNAc and the inhibitor in 100 mM β -morpholinoethanesulfonic acid (pH 6.25) or 3-(*N*-morpholine)propanesulfonic acid (pH 7.5) buffer containing 200 mM GlcNAc, 0.5% Triton X-100, and 10 mM ethylenediaminetetraacetate.

Table 1: Inhibitory activities of **1a** toward GnT-V and GnT-IX.

Enzyme	Acceptor	K_m [mM] ^[a]		K_i [μM] ^[b]
		Acceptor	UDP-GlcNAc	
GnT-V	GnGn-bi-PA ^[c]	0.150	4.0–6.0	103
GnT-IX	GnMSer-PAES ^[d]	–	–	7.2

[a] Michaelis constant. [b] Inhibition constant. [c] GnGn-bi-PA = bi-pyridylaminated Gn-Gn; see ref. [25]. [d] GnMSer-PAES = pyridylaminoethylsuccinimyl GnM; see Scheme 1a and ref. [4].

The reaction was terminated by boiling for 3 min and then centrifuged at 15000 rpm for 5 min. The resulting supernatant was analyzed by HPLC.

Received: April 21, 2004

Revised: June 9, 2004

Keywords: bisubstrates · glycoproteins · inhibitors · solid-phase synthesis · transferases

- [1] *Handbook of Glycosyltransferases and Related Genes* (Eds.: N. Taniguchi, K. Honke, M. Fukuda), Springer, Tokyo, **2002**.
- [2] a) I. Brockhausen, J. P. Carver, H. Schachter, *Biochem. Cell Biol.* **1988**, *66*, 1134–1151; b) R. D. Cummings, I. S. Trowbridge, S. Kornfeld, *J. Biol. Chem.* **1982**, *257*, 13421–13427.
- [3] K. Inamori, T. Endo, Y. Ide, S. Fujii, J. Gu, K. Honke, N. Taniguchi, *J. Biol. Chem.* **2003**, *278*, 43102–43109.
- [4] K. Inamori, T. Endo, J. Gu, I. Matsuo, Y. Ito, S. Fujii, H. Iwasaki, H. Narimatsu, E. Miyoshi, K. Honke, N. Taniguchi, *J. Biol. Chem.* **2004**, *279*, 2337–2340.
- [5] J. W. Dennis, M. Granovsky, C. E. Warren, *Biochim. Biophys. Acta* **1999**, *1473*, 21–34.
- [6] a) J. W. Dennis, S. Laferte, C. Waghorne, M. L. Breitman, R. S. Kerbel, *Science* **1987**, *236*, 582–585; b) S. Ihara, E. Miyoshi, J. Ko, K. Murata, S. Nakahara, K. Honke, R. B. Dickson, C.-Y. Lin, N. Taniguchi, *J. Biol. Chem.* **2002**, *277*, 16960–16967; c) M. Demetriou, I. R. Nabi, M. Coppolino, S. Dedhar, J. W. Dennis, *J. Cell Biol.* **1995**, *130*, 383–392; d) H.-B. Guo, I. Lee, M. Kamar, S. K. Akiyama, M. Pierce, *Cancer Res.* **2002**, *62*, 6837–6845; e) H.-B. Guo, I. Lee, M. Kamar, M. Pierce, *J. Biol. Chem.* **2003**, *278*, 52412–52424; f) M. Demetriou, M. Granovsky, S. Quaggin, J. W. Dennis, *Nature* **2001**, *409*, 733–739; g) T. Saito, E. Miyoshi, K. Sasai, N. Nakano, H. Eguchi, K. Honke, N. Taniguchi, *J. Biol. Chem.* **2002**, *277*, 17002–17008.
- [7] M. Granovsky, J. Fata, J. Pawling, W. J. Muller, R. Khokha, J. W. Dennis, *Nat. Med.* **2000**, *6*, 306–312.
- [8] J. W. Dennis, J. Pawling, P. Cheung, E. Partridge, M. Demetriou, *Biochim. Biophys. Acta* **2002**, *1573*, 414–422.
- [9] a) P.-P. Lu, O. Hindsgaul, H. Li, M. M. Palcic, *Carbohydr. Res.* **1997**, *303*, 283–291; b) I. Brockhausen, F. Reck, W. Kuhns, S. Khan, K. L. Matta, E. Meinjohanns, H. Paulsen, R. N. Shah, M. A. Baker, H. Schachter, *Glycoconjugate J.* **1995**, *12*, 371–379.
- [10] Previous reports on bisubstrate-type glycosyltransferase inhibitors: a) H. Hashimoto, T. Endo, Y. Kajihara, *J. Org. Chem.* **1997**, *62*, 1914–1915; b) B. Waldscheck, M. Streiff, W. Notz, W. Kinzy, R. R. Schmidt, *Angew. Chem.* **2001**, *113*, 4120–4124; *Angew. Chem. Int. Ed.* **2001**, *40*, 4007–4011; c) H. Hinou, X.-L. Sun, Y. Ito, *J. Org. Chem.* **2003**, *68*, 5602–5613.
- [11] I. Tvaroska, I. Andre, J. P. Carver, *J. Am. Chem. Soc.* **2000**, *122*, 8762–8776.
- [12] S. H. Tahir, O. Hindsgaul, *Can. J. Chem.* **1986**, *64*, 1771–1780.
- [13] a) H. Ando, S. Manabe, Y. Nakahara, Y. Ito, *J. Am. Chem. Soc.* **2001**, *123*, 3848–3849; b) H. Ando, S. Manabe, Y. Nakahara, Y. Ito, *Angew. Chem.* **2001**, *113*, 4861–4864; *Angew. Chem. Int. Ed.* **2001**, *40*, 4725–4728; c) Y. Ito, S. Manabe, *Chem. Eur. J.* **2002**, *8*, 3076–3084; d) S. Hanashima, S. Manabe, Y. Ito, *Synlett* **2003**, 979–982.
- [14] L. Jian, C. Hartley, T.-H. Chan, *Chem. Commun.* **1996**, 2193–2194.
- [15] G. Hodosi, P. Kovác, *Carbohydr. Res.* **1998**, *308*, 63–75.
- [16] a) P. Konradsson, D. R. Mootoo, R. E. McDevitt, B. Fraser-Reid, *J. Chem. Soc. Chem. Commun.* **1990**, 270–272; b) G. H. Veene-man, S. H. van Leeuwen, J. H. van Boom, *Tetrahedron Lett.* **1990**, *31*, 1331–1334.
- [17] In this particular case, use of a catalytic amount of TfOH afforded the corresponding orthoester exclusively.
- [18] C. A. A. van Boeckel, T. Beetz, *Tetrahedron Lett.* **1983**, *24*, 3775–3778.
- [19] Hydrogenolysis in EtOH caused 3-O-deacetylation as a side reaction.
- [20] Preparation of bis(allyloxy)diisopropylaminophosphine **19**: W. Bannwarth, E. Kung, *Tetrahedron Lett.* **1989**, *30*, 4219–4222.
- [21] M. M. Sim, H. Kondo, C.-H. Wong, *J. Am. Chem. Soc.* **1993**, *115*, 2260–2267.
- [22] V. Wittmann, C.-H. Wong, *J. Org. Chem.* **1997**, *62*, 2144–2147.
- [23] Spectroscopic data for **1a**: ^1H NMR (500 MHz, D_2O with a small amount of dioxane as an internal standard, 40°C): $\delta = 7.78$ (d, $^3J_{\text{H,H}} = 7.8$ Hz, 1H), 5.81 (m, 2H), 5.37 (dd, $^3J_{\text{H,H}} = 3.0$, $^3J_{\text{H,P}} = 7.1$ Hz, 1H), 4.76 (brs, 1H; anomeric proton of αMan), 4.42 (brs, 1H; anomeric proton of βGlcNAc ; overlapped in HOD signal, confirmed by HMQC spectra) 4.20 (brs, 1H; anomeric proton of βMan) 4.11–3.22 (m), 3.59 (s, 3H; methyl ester), 2.96 (dd, $^3J_{\text{H,H}} = 14.6$, 1.8 Hz, 1H), 2.58 (dd, $^3J_{\text{H,H}} = 14.6$, 8.3 Hz, 1H), 2.22 (t, $^3J_{\text{H,H}} = 7.3$ Hz, 2H), 1.90 (s, 3H), 1.42 (brs, 4H), 1.15 (brs, 8H) ppm; MALDI-TOF MS (negative mode, CHCA): m/z : calcd for $\text{C}_{47}\text{H}_{77}\text{N}_4\text{O}_{34}\text{P}_2\text{S}$ [$M-\text{H}$] $^-$: 1335.36; found: 1335.32.
- [24] K. Sasai, Y. Ikeda, T. Fujii, T. Tsuda, N. Taniguchi, *Glycobiology* **2002**, *12*, 119–127.
- [25] N. Taniguchi, A. Nishikawa, S. Fujii, J. G. Gu, *Methods Enzymol.* **1989**, *179*, 397–408.

Fluorinated Carbohydrates

**Enantioselective Synthesis of
Tetrafluoroethylene-Containing
Monosaccharides****

A. James Boydell, Victoria Vinader, and Bruno Linclau*

The incorporation of fluorine or fluoroalkyl groups can have profound effects on the material characteristics or biological activity of compounds by affecting their physico-chemical and/or pharmacological properties.^[1] While the incorporation of *terminal* perfluorinated moieties is common in some areas,^[2] the introduction of an *internal* perfluoroalkanedyl fragment (IPF) is comparatively rare.^[3] Though the incorpo-

[*] A. J. Boydell, Dr. B. Linclau
Department of Chemistry
University of Southampton
Highfield, Southampton SO171BJ (UK)
Fax: (+44) 23-8059-6805
E-mail: bruno.linclau@soton.ac.uk

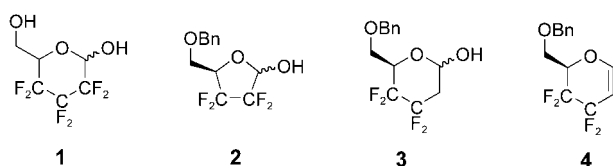
Dr. V. Vinader
GlaxoSmithKline
Gunnels Wood Road, Stevenage SG12NY (UK)

[**] We thank GlaxoSmithKline for funding. We are grateful to Prof. R. J. Whitby and Dr. Martin Swarbrick for support. Abbreviations: AQN: anthraquinone; Bn: benzyl; DCC: dicyclohexylcarbodiimide; DHQ: dihydroquininyl; DMAP: 4-dimethylaminopyridine; PHAL: phthalazine; PYR: pyrimidine.



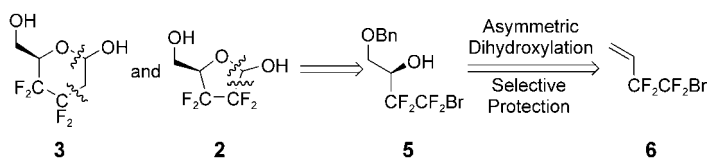
Supporting information for this article is available on the WWW under <http://www.angewandte.org> or from the author.

ration of fluorine is particularly well-studied for carbohydrates and nucleosides,^[4] the synthesis of carbohydrates and glycosides containing IPFs and the study of the effects of the IPF introduction on their biological properties are a virtually unexplored area. Pioneering work by DiMugno proved very interesting. He proposed a general strategy for enhancing molecular recognition based on enhancing “polar hydrophobicity”,^[3c,d] which could be achieved by replacing polar hydrophilic groups (OH) by polar hydrophobic groups (F), with a CF₂ group as adequate substitute for CHOH. It was found that the racemic hexafluoropyranose **1** has a 10-fold increase in transport across the red blood cell membrane compared to 3-deoxy-3-fluoroglucose due to enhanced affinity for the transporter protein.



This significant study paves the way for more intensive research regarding the effect of IPF incorporation on substrate–receptor binding, especially given the abundance of carbohydrate-containing bioactive compounds and the importance of carbohydrates in cell recognition events. Hence, efficient methods to synthesize such modified monosaccharides are of importance. An enantioselective synthesis of **1** is reported by DiMugno et al.^[3d] Herein we describe the first enantioselective syntheses of the tetrafluorofuranose **2**,^[5] of the novel pyranose **3**, of the corresponding deprotected saccharides (see below), and of the protected glycal **4**.

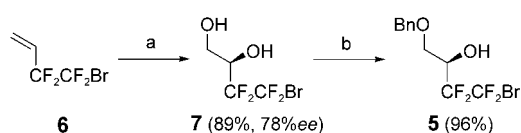
The retrosynthetic analysis for **2** and **3** is shown in Scheme 1. Given that the direct fluorination of aliphatic 1,2-



Scheme 1. Retrosynthetic analysis for **2** and **3**.

diketones to $\alpha,\alpha,\beta,\beta$ -tetrafluoroethylene groups is a low-yielding process,^[3c,6] a fluorinated-building-block approach^[7] was adopted. Cleavage of the CF₂–C and O–CH bonds as indicated were selected as the strategic disconnections. This led to **5** as a common precursor for **2** and **3**, which might be accessible from the commercially available bifunctional fluorinated building block **6**.

The synthesis of the central intermediate **5** is shown in Scheme 2. Sharpless asymmetric dihydroxylation (SAD) reactions on electron-deficient alkenes call for an increased amount of K₂OsO₄·2H₂O.^[8] With an in-house prepared AD-mix (0.1M, 2 mol % K₂OsO₄·2H₂O), an excellent yield (89%) was obtained after 9 days (4 °C). However, when a 1:1 ratio of

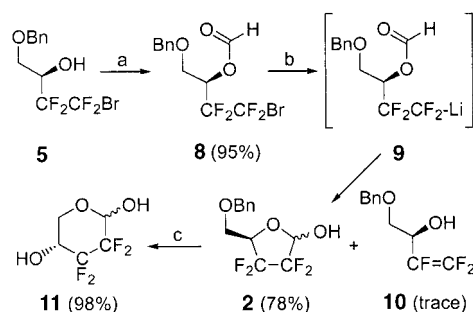


Scheme 2. Synthesis of the central cyclization precursor **5**. a) K₂OsO₄·2H₂O (2 mol %), (DHQD)₂PYR (2 mol %), K₃[Fe(CN)₆], K₂CO₃, *t*BuOH, H₂O, 4 °C, 9 d; b) Bu₂SnO, toluene, reflux, 24 h, then BnBr, Bu₄NI, reflux, 16 h.

K₂OsO₄:(DHQD)₂PHAL was used, an *ee* value of only 54%^[9] was obtained. As the standard PHAL-based ligands are not recommended for terminal alkenes,^[8] we prepared AD-mix cocktails with other ligands. While with (DHQD)₂AQN^[10] only a disappointing *ee* value of 55% was obtained, we were delighted to achieve an *ee* value of 78% (89% yield) with (DHQD)₂PYR^[11], which is one of the highest enantioselectivities reported to date for a SAD on terminal α -perfluorinated alkenes.^[11] Further investigation of the dihydroxylation is in progress.

Monoalkylation of terminal 1,2-diols flanked by a perfluoroalkyl group under basic conditions was reported to result exclusively in the protection of the secondary alcohol, testimony to its increased acidity.^[12] We found that monobenzylation via the corresponding 1,2-stannylene acetal^[13] proceeded with the *opposite* regioselectivity. The reactivity of this hitherto undescribed type of stannylene acetal appears to be fully controlled by steric factors, with no observable electronic influence of the perfluoroalkyl group.

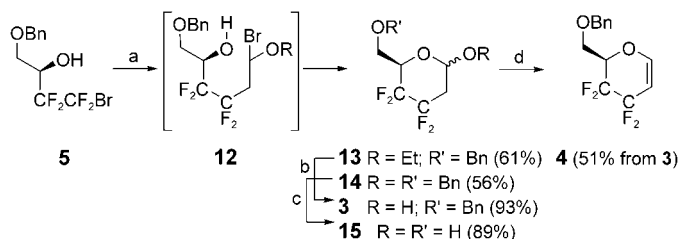
The synthesis of furanose **2** (Scheme 3) began with the formylation of **5** (78% *ee*). At this stage, an anionic cyclization was envisaged. Though perfluoroalkyl lithium species are known to be unstable, the main decay pathway being fluoride elimination,^[14] in situ trapping of such species by aldehydes, ketones, and esters is known.^[15] Such a process has not yet been demonstrated in an intramolecular fashion, and we hoped that the rate of cyclization would outstrip that of elimination. Reaction of **8** with several alkyl lithium reagents was investigated to effect the initial lithiation (all reactions at –78 °C in THF). Reaction with 1 equiv of *n*BuLi for 1 h resulted in the isolation of the desired furanose **2** as an inseparable anomeric mixture in 43% yield. Also isolated were **10** (11%) and **5** (17%), produced by the expected β -fluoride elimination and/or by nucleophilic attack of *n*BuLi



Scheme 3. Synthesis of fluorinated pentose **2**. a) DCC, DMAP, HCOOH, CH₂Cl₂, RT, 16 h; b) MeLi (1 equiv), THF, –78 °C, 3 h; c) Pd(OH)₂/C, H₂, RT, 16 h.

on the formate ester. Reaction with 2 equiv of *t*BuLi under the same conditions resulted in the same product mixture: **2** (43%), **10** (22%), and **5** (15%). However, with MeLi (1 equiv), 78% of **2** was obtained with only trace amounts of **10** present, and with no **5** observed at all. Finally, the deprotected pentose was obtained by hydrogenolysis of the benzyl group, and was isolated as the pyranose **11** as evidenced by ¹H NMR spectroscopy (DMSO) and HMBC NMR experiments (see the Supporting Information). An anomeric ratio of 2.6:1 was observed.

The synthesis of tetrafluoropyranose **3** and glycol **4** is shown in Scheme 4. The ring formation was envisaged to



Scheme 4. Synthesis of fluorinated pyranose **3** and glycol **4**.

a) Na₂S₂O₄, NaHCO₃, DMSO, H₂C=CHOR, RT, 16 h. b) H₂SO₄ (25% aq.), dioxane, reflux, 4 h. c) Pd(OH)₂/C, EtOAc, RT, 12 h. d) o-NO₂C₆H₄. SeCN, PBu₃, THF, RT, 1 h, then H₂O₂ (30% aq.), NaHCO₃, RT, 1.5 h.

occur by a domino sequence as follows: perfluoroalkyl radical generation to initiate intermolecular addition onto ethyl vinyl ether, followed by atom transfer to give the α-bromoether **12**, which would cyclize, in an S_N2- or S_N1-type process, to yield the ethyl glycoside **13**. For this transformation the solvent proved to be of importance. With MeCN/H₂O mixtures, typically used for dithionite-mediated perfluoroalkyl radical generation,^[16] the reaction proved quite capricious, with a maximum yield of 44% of **13** (after 16 h at reflux). Conversely, the reaction in DMSO^[17] proved much faster, even at room temperature, and reliably afforded **13** in significantly better yields.

Using benzyl vinyl ether, the dibenzyl-protected **14** was synthesized in good yield under identical reaction conditions. The fully deprotected pyranose **15** could now be obtained in a single step by hydrogenolysis (1.4:1 mixture of anomers). Anomeric deprotection of **13** gave the 6-*O*-benzyl pyranose **3**, and subsequent subjection to Grieco elimination conditions^[18] resulted in the formation of glycol **4**.

In summary we have reported a short enantioselective synthesis of a tetrafluorinated pentose and hexose, and of a tetrafluorinated glycol. A fluorinated-building-block approach was followed, using a SAD reaction on a terminal α-perfluorinated alkene to introduce chirality. A very high *ee* value for this class of alkenes (78%) was obtained. The key operation in the synthesis of **2** and **3** was the ring formation. We report the first cyclization involving perfluoroalkyl lithium species and demonstrate that the rate of 5-*exo* cyclization is faster than that of the competing fluoride elimination under the conditions used. We have also established a novel domino perfluoroalkyl radical addition/atom transfer/nucleophilic cyclization approach to obtain a pyra-

nose structure. Finally, we have achieved a fully regioselective, high-yielding monoalkylation protocol for terminal 1,2-diols substituted by a perfluoroalkyl chain, with complementary selectivity to existing methods. The short, high-yielding sequence for the synthesis of **2** and **3** should make such IPF-modified monosaccharides easily accessible building blocks. Further research on the reactivity of the monosaccharides/glycol in glycosylation reactions is in progress.

Received: May 21, 2004

Keywords: asymmetric dihydroxylation · carbohydrates · fluorine · perfluoro compounds · synthetic methods

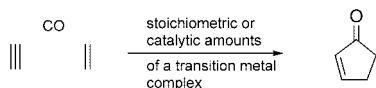
- [1] a) J. D. Dunitz, *ChemBioChem* **2004**, *5*, 614–621; b) P. Jeschke, *ChemBioChem* **2004**, *5*, 570–589; c) C. M. Timperley, W. E. White, *J. Fluorine Chem.* **2003**, *123*, 65–70; d) F. M. D. Ismail, *J. Fluorine Chem.* **2002**, *118*, 27–33; e) B. E. Smart, *J. Fluorine Chem.* **2001**, *109*, 3–11; f) T. Hiyama, *Organofluorine Compounds, Chemistry and Applications*, Springer, Berlin, **2000**.
- [2] Example: K. C. Lowe, *J. Fluorine Chem.* **2001**, *109*, 59–65.
- [3] Examples: a) S. Yamamoto, K. Matsuda, M. Irie, *Angew. Chem.* **2003**, *115*, 1674–1677; *Angew. Chem. Int. Ed.* **2003**, *42*, 1636–1639; b) P. Kirsch, M. Bremer, F. Huber, H. Lannert, A. Ruhl, M. Lieb, T. Wallmichrath, *J. Am. Chem. Soc.* **2001**, *123*, 5414–5417; c) H. W. Kim, P. Rossi, R. K. Schoemaker, S. G. DiMagno, *J. Am. Chem. Soc.* **1998**, *120*, 9082–9083; d) J. C. Biffinger, H. W. Kim, S. G. DiMagno, *ChemBioChem* **2004**, *5*, 622–627.
- [4] a) K. Dax, M. Albert, J. Ortner, B. J. Paul, *Carbohydr. Res.* **2000**, *327*, 47–86.
- [5] For the synthesis of racemic tetrafluorofuranose derivatives, see: S. G. DiMagno (University of Nebraska, Lincoln), US 6392032, **2002**.
- [6] R. P. Singh, U. Majumder, J. M. Shreeve, *J. Org. Chem.* **2001**, *66*, 6263–6267.
- [7] J. M. Percy, *Top. Curr. Chem.* **1997**, *193*, 131–195.
- [8] H. C. Kolb, M. S. VanNieuwenhze, K. B. Sharpless, *Chem. Rev.* **1994**, *94*, 2483–2547.
- [9] Determination of the *ee* value was achieved by chiral GC (Chiradex G9511-16) analysis of the bis-acetate derivative of **7**.
- [10] H. Becker, K. B. Sharpless, *Angew. Chem.* **1996**, *108*, 447–449; *Angew. Chem. Int. Ed. Engl.* **1996**, *35*, 448–451.
- [11] a) G. A. Crispino, K.-S. Jeong, H. C. Kolb, Z.-M. Wang, D. Xu, K. B. Sharpless, *J. Org. Chem.* **1993**, *58*, 3785–3786; b) K. P. M. Vanhessche, K. B. Sharpless, *Chem. Eur. J.* **1997**, *3*, 517–522.
- [12] a) T. Katagiri in *Enantiocontrolled Synthesis of Fluoro-organic Compounds* (Ed.: V. A. Soloshonok), Wiley, New York, **1999**, p. 165; b) T. Katagiri, K. Furuhashi (Japan Energy Corporation), JP 06122641, **1994** [*Chem. Abstr.* **1995**, *122*, 186958j].
- [13] S. David, S. Hanessian, *Tetrahedron* **1985**, *41*, 643–663.
- [14] a) D. J. Burton, L. Lu, *Top. Curr. Chem.* **1997**, *193*, 45–89; b) D. J. Burton, Z.-Y. Yang, *Tetrahedron* **1992**, *48*, 189–275.
- [15] P. G. Gassman, N. J. O'Reilly, *J. Org. Chem.* **1987**, *52*, 2481–2490.
- [16] a) W.-Y. Huang, *J. Fluorine Chem.* **1992**, *58*, 1–8; b) W. Zhu, Z. Li, *J. Chem. Soc. Perkin Trans. 1* **2000**, 1105–1108.
- [17] Z.-Y. Long, Q.-Y. Chen, *J. Org. Chem.* **1999**, *64*, 4775–4782.
- [18] a) P. A. Grieco, S. Gilman, M. Nishizawa, *J. Org. Chem.* **1976**, *41*, 1485–1486; b) R. Fernández, M. I. Matheu, R. Echarri, S. Castillón, *Tetrahedron* **1998**, *54*, 3523–3532.

Cyclopentenone Synthesis

A Cyclobutadiene Equivalent in the Catalytic Pauson–Khand Reaction**

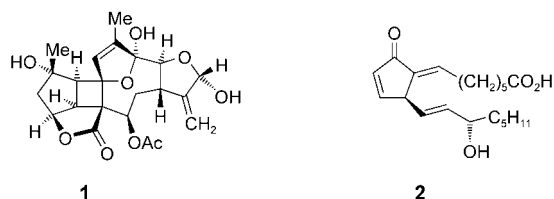
Susan E. Gibson,* Nello Mainolfi, S. Barret Kalindjian, and Paul T. Wright

The Pauson–Khand reaction (PKR) is a transition-metal-mediated carbon–carbon bond-forming reaction that converts an alkyne, an alkene, and carbon monoxide into a cyclopentenone (Scheme 1).^[1] The ubiquity of five-membered



Scheme 1. The Pauson–Khand reaction.

carbocycles in complex organic molecules such as the recently isolated antimalarial, anticancer diterpene bielschowskysin (**1**)^[2] means that cyclopentenones are useful as building blocks



for the creation of larger organic molecules. Moreover, many cyclopentenones display their own interesting biological activity. For example, cyclopentenone prostaglandins such as Δ^7 -PG- A_1 (**2**) have considerable therapeutic potential.^[3]

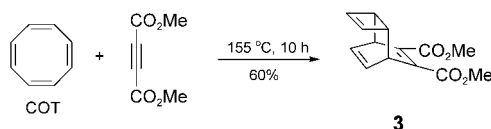
To maximize the synthetic attractiveness of the PKR the development of efficient and versatile catalytic systems is required, some of which are asymmetric, and all of which work well for intermolecular reactions. Whilst good progress has been made in the last three to five years in the fields of catalysis and asymmetric catalysis using a variety of transition metals and ligands, almost all of the work reported has been based on *intramolecular* substrates, that is, enynes.^[1]

Traditionally, the *intermolecular* PKR has been dominated by the strained alkenes norbornene and norbornadiene,

although there are reports of the use of cyclopropenes^[4a] and bicyclo[3.2.0]hept-6-enes.^[4b–d] And, recently the donor-substituted alkenes *o*-(dimethylamino)phenyl vinyl sulfoxide^[5a] and dimethyl(2-pyridyl)(vinyl)silane^[5b] have been used successfully in cobalt-mediated and ruthenium-catalyzed PKRs, respectively. Very recently, 2,3-disubstituted 1,3-butadienes have been shown to act as alkene partners in a rhodium-catalyzed intermolecular PKR.^[5c]

Our interest in catalytic^[6] and asymmetric^[7] aspects of the PKR led us to look for new alkene partners that would significantly increase the synthetic scope of the reaction. Cyclobutadiene is a very attractive “alkene” in this context inasmuch as its participation in the reaction would create highly functionalized bicyclic products that could be manipulated further to produce a wide range of substituted cyclopentanes. The inherent instability of cyclobutadiene, however, meant that a convenient surrogate was required.

Dimethyl *anti*-tricyclo[4.2.2.0^{2,5}]deca-3,7,9-triene-7,8-dicarboxylate (**3**) was identified as a potential cyclobutadiene equivalent in the PKR. It was readily synthesized from cyclooctatetraene (COT) and dimethyl acetylenedicarboxylate in 10 h by a modified literature procedure (Scheme 2).^[8]



Scheme 2. Synthesis of cyclobutadiene equivalent **3**. 1.1 Equivalents of COT were used.

Initially, one equivalent of tricycle **3** was reacted with one equivalent of phenylacetylene (Table 1). Reaction occurred selectively at the most strained double bond and work-up led to the isolation of a single diastereomer of the novel Pauson–Khand product **4** in 60% yield (all products in Table 1 were fully characterized by standard analytical techniques). Use of 1.5 equivalents of **3** raised the yield to 77% (Table 1). The reaction was then performed with a range of monosubstituted alkynes, and these reactions led to the isolation of the Pauson–Khand products **5–8** in moderate to good yields (Table 1). (The disubstituted alkynes 3-hexyne and diphenylacetylene failed to give the expected products, although 1-phenylpropyne gave a single Pauson–Khand product in 33% yield when reacted with 1.5 equivalents of **3**.)

The Pauson–Khand products **4–8** were subsequently heated to induce a retro-Diels–Alder reaction. After 1 h of heating at 205 °C under a vacuum of 6 Torr, the 3-substituted bicyclo[3.2.0]hepta-3,6-diene-2-ones **9–13** were isolated in very good yields (Table 1).

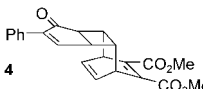
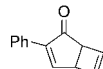
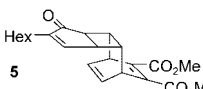
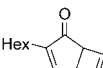
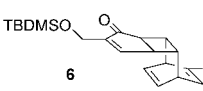
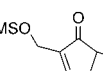
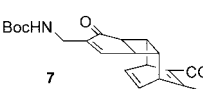
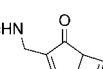
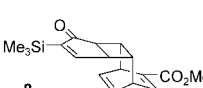
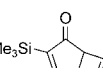
The bicyclic compounds **9–13** can be regarded as the products of a formal PKR involving monosubstituted alkynes and cyclobutadiene. We have thus introduced a new route to bicyclo[3.2.0]hepta-3,6-diene-2-ones, a class of molecules which to date have been synthesized by irradiation of substituted tropolones;^[9] interestingly, investigations of these bicyclic compounds appear to be limited to explorations of their photochemical and thermal behavior.^[9] In view of this,

[*] Prof. S. E. Gibson, N. Mainolfi
Department of Chemistry, Imperial College London
South Kensington Campus, London SW72AY (UK)
Fax: (+44) 207-594-5804
E-mail: s.gibson@imperial.ac.uk

Dr. S. B. Kalindjian, Dr. P. T. Wright
James Black Foundation
68 Half Moon Lane, London SE24 9JE (UK)

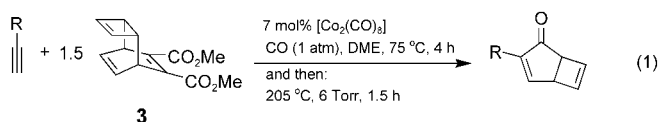
[**] The authors thank the James Black Foundation for generous studentship support (N.M.).

Table 1: Catalytic intermolecular PKR of diester **3** with various alkynes^[a] and thermolysis of the Pauson–Khand products.^[b]

Alkyne	Eqiv of 3 ^[c]	PK product	Yield [%]	Retro-Diels–Alder product	Yield [%]
Ph	1.0		60		92
	1.5	4	77	9	
Hex	1.0		73		90
	1.5	5	85	10	
OTBDMS	1.0		45		90
	1.5	6	60	11	
NHBoc	1.0		67		90
	1.5	7	75	12	
SiMe ₃	1.0		33		85
	5.0		46		
	10.0	8	86	13	

[a] 5 mol% $[\text{Co}_2(\text{CO})_8]$, CO (1 atm), DME, 75 °C, 4 h (all reactions were performed with 0.5 mmol of alkyne). [b] 205 °C, 6 Torr, 1 h (reactions performed on a 0.3–0.4 mmol scale). [c] Unreacted **3** could be fully recovered.

and of the potential of bicyclo[3.2.0]hepta-3,6-diene-2-ones not only in organic synthesis, but also as an alternative to norbornene-based monomers in the ring-opening metathesis polymerisation,^[10] it seemed worthwhile to streamline our synthetic approach by removing the isolation of the Pauson–Khand product from the protocol. Indeed, thermolysis of the crude product mixture from the PKR [Eq. (1)] followed by



chromatography gave the bicyclic ketones in good to excellent yields on a 0.5-mmol scale (Table 2, entries 1–3). Moreover, scale-up of the reaction with 1-octyne (use of 10 instead of 0.5 mmol) readily produced 1.71 g of bicyclo[3.2.0]hepta-3,6-diene-2-one **10** (entry 4).

Table 2: Direct conversion of alkynes into bicyclo[3.2.0]hepta-3,6-diene-2-ones [Eq. (1)].^[a]

Entry	R	Scale [mmol]	Product	Yield [%] ^[b]
1	Ph	0.5	9	75
2	Hex	0.5	10	98
3	CH ₂ OTBDMS	0.5	11	70
4	Hex	10.0	10	90

[a] See Experimental Section for a detailed description for entry 4.
[b] Unreacted **3** could be fully recovered.

To conclude, we have used a cyclobutadiene equivalent in the Pauson–Khand reaction for the first time, to produce a little-studied class of compounds that has considerable potential in synthesis.

Experimental Section

3: A mixture of dimethyl acetylenedicarboxylate (5.29 mL, 43.0 mmol) and COT (5.32 mL, 47.3 mmol) in a 25-mL round-bottomed flask fitted with a reflux condenser was heated at 155 °C under an atmosphere of nitrogen for 10 h. Purification of the crude product by careful (the byproduct dimethyl phthalate has a very similar polarity) flash column chromatography (SiO₂; hexane/acetone, 100:0 to 99:1) afforded **3** as a colorless oil (6.35 g, 60 %). *R*_f = 0.32 (SiO₂; hexane/acetone, 90:10); ¹H NMR (300 MHz, CDCl₃): δ = 2.71–2.74 (m, 2H; cyclobutene bridgehead), 3.81–3.91 (m, 8H; 2 OCH₃ and cyclohexadiene bridgehead), 6.08–6.18 ppm (m, 4H; vinylic); ¹³C NMR (125 MHz, CDCl₃): δ = 43.2 and 44.2 (cyclobutene and cyclohexadiene bridgeheads), 52.1 (OCH₃), 129.7 (CH=CH, cyclobutene),

138.9 (CH=CH, cyclohexadiene), 143.1 (C=C), 166.7 (C=O); IR (neat): $\tilde{\nu}_{\text{max}}$ = 1560 (C=C), 1603 (C=C), 1640 (C=C), 1727 cm^{-1} (2 C=O); MS (CI): m/z (%): 264 (8) [$M+\text{NH}_4^+$], 247 (100) [$M+\text{H}^+$], 195 (24) [$M-(\text{CH}_2)_4+\text{H}^+$]; elemental analysis calcd (%) for $\text{C}_{14}\text{H}_{14}\text{O}_4$ (246.26): C 68.28, H 5.73; found: 68.36, H 5.81.

10: A 250-mL flask fitted with a reflux condenser and a magnetic stirring bar was charged with 1-octyne (1.47 mL, 10 mmol) and **3** (3.69 g, 15 mmol). The reaction vessel was evacuated (three times) and filled with CO. Anhydrous, CO-saturated DME (100 mL) and freshly sublimed octacarbonyldicobalt(**0**) (0.239 g, 0.7 mmol) were added to the reaction mixture. The flask was lowered into an oil bath preheated to 75 °C and left stirring at that temperature under a CO atmosphere (1.05 atm) for 4 h. The reaction was then stopped, the solvent evaporated under vacuum, and the flask fitted with a distillation apparatus. The pressure in the system was reduced to 6 Torr and the flask was lowered into a silicone oil bath preheated to 205 °C. The flask was kept in the bath for 1.5 h, at which point most of the reaction mixture had distilled over into the collecting flask. The distillate and the remaining reaction mixture were combined. Purification of the crude product by flash column chromatography (SiO₂; hexane/ethyl acetate, 100:0 to 90:10) afforded **10** as a colorless oil (1.71 g, 90 %). R_f = 0.52 (SiO₂; hexane/ethyl acetate, 80:20); ¹H NMR (500 MHz, CDCl₃): δ = 0.84–0.88 (m, 3 H; CH₃), 1.27–1.32 (m, 6 H; CH₃(CH₂)₃), 1.40–1.46 (m, 2 H; CH₃(CH₂)₃CH₂CH₂), 2.05–2.15 (m, 2 H; CH₃(CH₂)₃CH₂CH₂), 3.50 (dd, J = 1.3, 2.3 Hz, 1 H; C=OCHCH), 3.80 (m, 1 H; C=OCHCH), 6.35 (dd, J = 1.3, 2.3 Hz, 1 H; C=OCHCH=CH), 6.55 (d, J = 2.3 Hz, 1 H; C=OCHCH=CH), 7.24–7.25 ppm (m, 1 H; CH₂CH=CH); ¹³C NMR (125 MHz, CDCl₃): δ = 14.0 (CH₃), 22.5 (CH₃CH₂), 25.3, 27.5, 28.9, 31.5 (CH₃CH₂CH₂CH₂CH₂CH₂C), 47.9 (C=OCHCH), 53.8 (C=OCHCH), 136.7 (C=OCHCH=CH), 143.6 (C=OCHCH=CH), 146.8 (CH₂C=CH), 154.9 (CH₂C=CH), 206.2 ppm (C=O); IR (neat): $\tilde{\nu}_{\text{max}}$ = 1564 (CH=CH), 1620 (CH=C), 1698 cm⁻¹ (C=O); MS (CI): m/z (%): 208 (100) [M +NH₄⁺], 191 (46) [M +H⁺], 52 (18) [(CH)₄⁺]; elemental

analysis calcd (%) for $C_{13}H_{18}O$ (190.28): C 82.06, H 9.53; found: C 82.15, H 9.54.

Received: May 14, 2004

Revised: July 8, 2004

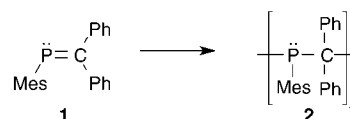
Keywords: bicycloheptadienes · carbonylation · cycloaddition · homogeneous catalysis · pericyclic reactions

- [1] For reviews of the PKR, see: a) S. E. Gibson, A. Stevenazzi, *Angew. Chem.* **2003**, *115*, 1844–1854; *Angew. Chem. Int. Ed.* **2003**, *42*, 1800–1810; b) B. E. Hanson, *Comments Inorg. Chem.* **2002**, *23*, 289–318; c) A. J. Fletcher, S. D. R. Christie, *J. Chem. Soc. Perkin Trans. 1* **2000**, 1657–1668; d) K. M. Brummond, J. L. Kent, *Tetrahedron* **2000**, *56*, 3263–3283; e) Y. K. Chung, *Coord. Chem. Rev.* **1999**, *188*, 297–341; f) O. Geis, H.-G. Schmalz, *Angew. Chem.* **1998**, *110*, 955–958; *Angew. Chem. Int. Ed.* **1998**, *37*, 911–914.
- [2] J. Marrero, A. D. Rodriguez, P. Baran, R. G. Raptis, J. A. Sanchez, E. Ortega-Barria, T. L. Capson, *Org. Lett.* **2004**, *6*, 1661–1664.
- [3] S. M. Roberts, M. G. Santoro, E. S. Sickel, *J. Chem. Soc. Perkin Trans. 1* **2002**, 1735–1742.
- [4] a) I. Marchueta, X. Verdaguier, A. Moyano, M. A. Pericas, A. Riera, *Org. Lett.* **2001**, *3*, 3193–3196; b) P. Bladon, I. U. Khand, P. L. Pauson, *J. Chem. Res. Synop.* **1977**, *8*; c) V. Sampath, E. C. Lund, M. J. Knudsen, M. M. Olmstead, N. E. Schore, *J. Org. Chem.* **1987**, *52*, 3595–3603; d) B. A. Kowalczyk, T. C. Smith, W. G. Dauben, *J. Org. Chem.* **1998**, *63*, 1379–1389.
- [5] a) M. R. Rivero, J. C. de la Rosa, J. C. Carretero, *J. Am. Chem. Soc.* **2003**, *125*, 14992–14993; b) K. Itami, K. Mitsudo, J.-I. Yoshida, *Angew. Chem.* **2002**, *114*, 3631–3634; *Angew. Chem. Int. Ed.* **2002**, *41*, 3481–3483; c) P. A. Wender, N. M. Deschamps, T. J. Williams, *Angew. Chem.* **2004**, *116*, 3138–3141; *Angew. Chem. Int. Ed.* **2004**, *43*, 3076–3079.
- [6] a) S. E. Gibson, C. Johnstone, J. A. Loch, J. W. Steed, A. Stevenazzi, *Organometallics* **2003**, *22*, 5374–5377; b) A. C. Comely, S. E. Gibson, A. Stevenazzi, N. J. Hales, *Tetrahedron Lett.* **2001**, *42*, 1183–1185; c) A. C. Comely, S. E. Gibson, N. J. Hales, *Chem. Commun.* **2000**, 305–306.
- [7] S. E. Gibson, S. E. Lewis, J. A. Loch, J. W. Steed, M. J. Tozer, *Organometallics* **2003**, *22*, 5382–5384.
- [8] a) E. E. van Tamelen, B. C. T. Pappas, *J. Am. Chem. Soc.* **1971**, *93*, 6111–6120; b) A. G. Anderson, D. R. Fagerburg, *Tetrahedron* **1973**, *29*, 2973–2979; c) W. G. Dauben, L. N. Reitman, *J. Org. Chem.* **1975**, *40*, 835–841.
- [9] a) I. D. Reingold, K. S. Kwong, M. M. Menard, *J. Org. Chem.* **1989**, *54*, 708–710; b) T. Miyashii, M. Nitta, T. Mukai, *J. Am. Chem. Soc.* **1971**, *93*, 3441–3447; c) M. Cavazza, M. Zandomegnghi, F. Pietra, *J. Chem. Soc. Chem. Commun.* **1990**, 1336–1337.
- [10] a) K. V. Ivin, J. C. Mol, *Olefin Metathesis and Metathesis Polymerization*, Academic Press, San Diego, **1997**, Chap. 11, pp. 224–259; b) “Bioactive Polymers”: L. L. Kiessling, L. E. Strong in *Alkene Metathesis in Organic Synthesis* (Ed.: A. Fürstner), Springer, Berlin, **1998**, pp. 199–231.

Radical Copolymerization of a Phosphaalkene with Styrene: New Phosphine-Containing Macromolecules and Their Use in Polymer-Supported Catalysis**

Chi-Wing Tsang, Baharnaz Baharloo, David Riendl, Mandy Yam, and Derek P. Gates*

Since Becker's synthesis of the first stable phosphaalkene in 1976,^[1] these compounds, which contain a P=C bond and were once considered exotic, now constitute a major branch of phosphorus chemistry. Applications for these compounds are even being developed.^[2–4] The ability of P=C bonds, in many instances, to “copy” the well-established chemistry of isolobal C=C bonds has attracted considerable attention.^[2,3a,d] In molecular chemistry, the remarkable analogy between phosphaalkenes and alkenes is evidenced by phospho variants of a number of reactions, including 1,2-addition, [4+2]cycloaddition, Peterson and Wittig olefination, η^2 coordination to metal centers, and Cope and allylic rearrangements. One of the most important reactions of C=C bonds is the addition polymerization of olefins, which is used to produce many commodity polymers. The absence of an analogous polymer chemistry for P=C bonds prompted us to investigate addition polymerization as a potential route to new phosphine polymers. We recently reported the first addition polymerization of the phosphaalkene **1**^[5] (Mes = 2,4,6-trimethylphenyl) to give the poly(methylenephosphine) **2** ($M_w \approx 10^4 \text{ g mol}^{-1}$ by GPC versus polystyrene), an alternating P–C polymer.^[6]



The development of synthetic methodologies to incorporate phosphorus into the backbone of macromolecules or into dendrimers is a challenging frontier in polymer chemistry

[*] Dr. C.-W. Tsang, B. Baharloo, D. Riendl, M. Yam, Prof. Dr. D. P. Gates
Department of Chemistry
University of British Columbia
2036 Main Mall, Vancouver, British Columbia, V6T 1Z1 (Canada)
Fax: (+1) 604-822-2847
E-mail: dgates@chem.ubc.ca

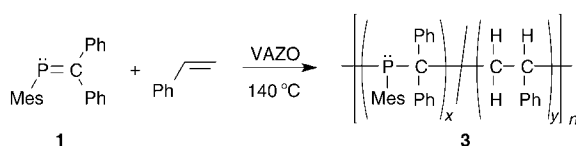
[**] The Natural Sciences and Engineering Research Council (NSERC) of Canada, the Canada Foundation for Innovation (CFI)/New Opportunities, and the BC Ministry for Advanced Education and Technology are gratefully acknowledged for funding. We also thank Prof. Jennifer Love for useful discussions, Prof. John Scheffer for the use of his gas chromatograph, and Dr. Scott Clendenning (U. Toronto) for conducting the triple-detection GPC experiment.



Supporting information for this article (full experimental procedures, spectroscopic data, and figures showing spectra and chromatograms) is available on the WWW under <http://www.angewandte.org> or from the author.

because of the novel properties and chemical functionality phosphorus can impart to such materials.^[7,8] Now that we have homopolymerized a phosphalkene by using conventional methods of initiation, an exciting possibility would be to prepare copolymers from compounds with P=C and C=C bonds by taking advantage of their similarity. From the perspective of the synthesis of phosphorus polymers, this would represent a new and convenient chain-growth method to incorporate functional phosphine moieties directly into the backbone of polyolefins.

Herein we report the first copolymerization of a phosphalkene, **1**, with styrene to afford hybrid inorganic–organic copolymers **3**. Importantly, the presence of phosphine moieties in the main chain of **3** imparts chemical functionality to the polymer and may ultimately lead to applications of the polymer. As an example, we show that **3** can be employed as a polymer support for palladium-catalyzed Suzuki coupling.



Homopolymers of **1** can be prepared by using thermal, radical, and anionic initiation methods.^[6] For the present copolymerization studies, we favored conventional radical over anionic initiation methods, since they are convenient to perform and do not have the same strict purity requirements of anionic polymerization. Therefore, we decided to investigate the copolymerization of **1** and styrene with 1,1'-azobis(cyclohexanecarbonitrile) [VAZO, catalyst 88] as the free-radical source. All copolymerization experiments were conducted at 140 °C for 14 h with monomer **1** dissolved in neat styrene in the presence of a trace amount of VAZO. Typical results for three trials are given in Table 1. Each trial was reproducible, although there was some variation in the molecular weight of **3** as is common for uncontrolled radical polymerization. In each trial molecular impurities were removed by precipitation of a solution of **3** in CH₂Cl₂ into hexanes (repeated twice). The poly(methylenephosphine)–polystyrene **3** is soluble in common organic solvents, such as CH₂Cl₂, THF, and toluene. Copolymer **3** is stable towards

hydrolysis and oxidizes slowly in air. Complete oxidation to give an air- and moisture-stable phosphine oxide polymer occurs readily upon treatment with H₂O₂.

The unoxidized copolymer **3** was analyzed by conventional GPC (THF), and moderate molecular weights ($M_w = 3600$ – 9000 g mol^{-1}) were estimated relative to polystyrene standards. Importantly, in all cases a monomodal molecular-weight distribution (PDI = 1.4–1.7) was observed, thus providing strong support for the formulation of **3** as a copolymer. A bimodal distribution would be likely if a blend of homopolystyrene and **2** was obtained. Broad overlapping signals in the aromatic and aliphatic regions of the ¹H NMR spectra of **3** can be attributed to phosphalkene and styrene moieties in the polymer. In principle, it is possible to use the ratio of aromatic to aliphatic resonances to estimate the degree of phosphorus incorporation into **3**; however, we have found that this analysis does not give accurate results.^[9] Therefore, the phosphorus content determined by elemental analysis was used to estimate the degree of incorporation of the phosphalkene into **3**. The results are shown in Table 1. For example, the copolymerization of 20 mol% of **1** and 80 mol% of styrene afforded **3** with 2.16 wt% phosphorus, which corresponds to approximately 9% (i.e. $x = 0.09n$ in **3**) incorporation of the phosphalkene and 91% (i.e. $y = 0.91n$ in **3**) styrene into **3**. Detailed analysis of the outcome of many copolymerization experiments to determine monomer-reactivity ratios would be required to help understand the observed trend in % incorporation versus monomer feed, and this will be the subject of future investigations.

The ³¹P NMR spectra of **3** are quite interesting and show two major broad signals at $\delta = -9$ and 4 ppm, along with several smaller resonances in the same region. The question arises: why are two signals observed for **3**, whereas only one is observed for **2** ($\delta_{31\text{P}} = -9 \text{ ppm}$)? We speculate that the signals in the region of $\delta = -9 \text{ ppm}$ may result from regions of the polymer with (styrene)–(P–C)–(P–C) and/or (P–C)–(P–C)–(P–C) segments, whereas those at 4 ppm are (styrene)–(P–C)–(styrene) fragments. This is difficult to prove given the expected complex microstructure in **3**; however, the fact that the intensity of the signal at $\delta = 4 \text{ ppm}$ decreases relative to that at $\delta = -9 \text{ ppm}$ as the phosphalkene content in **3** increases lends support to our hypothesis (see Supporting Information). We note that partial regioirregular enchainment (i.e. P–CH₂ and P–CHPh linkages) and polymer tacticity may contribute to minor signals in the ³¹P NMR spectra. However, relative intensities of these minor signals would not be expected to change dramatically with phosphorus concentration. Furthermore, it is possible that some phosphorus may be incorporated at or near the polymer chain end and would lead to additional signals. Although further studies are required to fully elucidate the microstructure of **3**, the NMR spectroscopic and GPC data are entirely consistent with our conclusion that this is a random copolymer.

To investigate the chemical functionality of **3**, we have undertaken a preliminary examination of its potential use as a phosphine ligand for polymer-supported metal catalysis. Motivated by the facile separation of the organic product from the polymer/catalyst, researchers have developed a large number of phosphine-containing macromolecules for these

Table 1: Selected data for copolymers **3**.

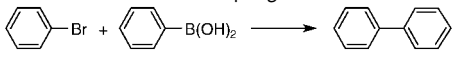
Entry	1 [%] ^[a]	VAZO [%] ^[b]	\bar{M}_w ^[c]	PDI ^[d]	Yield [%]	Incorporated P [wt%]	1 [mol%] ^[e]
1	10	0.5	9000	1.7	37	1.28	5
2	20	1.0	7000 ^[f]	1.7	48	2.16	9
3	40	2.0	3600	1.4	18	6.44	39

[a] % **1** = mol **1**/(mol **1**+mol styrene) 100. [b] % VAZO = mol VAZO/(mol **1**+mol styrene) 100. [c] Molecular weights were estimated by gel-permeation chromatography (GPC) versus polystyrene standards. [d] PDI = polydispersity index (estimated by GPC). [e] Estimated from wt% of phosphorus measured by elemental analysis (see Supporting Information for an equation). [f] Triple-detection GPC of an oxidized sample gave $\bar{M}_w = 12000 \text{ g mol}^{-1}$, thus suggesting that conventional GPC may underestimate the actual molecular weight.

applications.^[10] As an entry point to this area, we decided to study the Pd-catalyzed Suzuki cross-coupling reaction, a powerful carbon–carbon bond-forming reaction.^[11] Polymer-supported Suzuki couplings have been performed with either insoluble phosphine-functionalized resins^[12] or soluble polymer-supported phosphines.^[13]

To test the feasibility of using our polymers in catalysis, several Pd-catalyzed coupling reactions of bromobenzene and phenylboronic acid were conducted in the presence of [Pd₂(dba)₃] with CsF as a base. The results are shown in Table 2 and the yields reported are averages of at least two

Table 2: Results of Suzuki cross-coupling reactions with **2** and **3**.^[a]



Entry	Ligand	P/Pd	T [°C]	Yield [%] ^[b]
1	2	2.0:1	25	23
2	3	1.4:1	25	62
3	3	1.4:1	80	83
4	3	2.8:1	80	90
5	none		25	22
6	PPh ₃	1.0:1	25	30

[a] General conditions: bromobenzene (100 mg), phenyl boronic acid (116 mg, 1.5 equiv), base: CsF (3.3 equiv), [Pd₂(dba)₃] (5 mol%), copolymer **3** (for consistency, molar ratio in Table 1, entry 2 used for all experiments), and freshly distilled THF (2.0 mL). [b] Yield of isolated product (an average of two runs; entry 3: average of four runs), purity of biphenyl confirmed by ¹H NMR spectroscopy (all runs) and GC (representative runs).

runs. Surprisingly, reactions with homopolymer **2** ($\bar{M}_w = 7200$, PDI = 1.5) gave low yields of biphenyl (Table 2, entry 1), possibly because of the congested environment of the phosphorus centers.^[14] In contrast, when the copolymer **3** with a lower concentration of phosphine moieties was used, biphenyl was obtained in moderate yield (62%) at room temperature (Table 2, entry 2). For comparison, a control experiment (no added phosphine) and an experiment with PPh₃/[Pd₂(dba)₃] (Table 2, entries 5 and 6) each gave poor yields of biphenyl under very similar conditions. Therefore, we conclude that copolymer **3** is directly involved in the generation of an active catalyst. To garner evidence that **3** interacts with palladium, we treated it with [Pd₂(dba)₃] (P/Pd = 1:1) in THF, and the ³¹P NMR spectrum of the reaction mixture revealed a very broad resonance between 80 and 0 ppm, as well as broadened signals for uncomplexed **3**. We presume that the broad resonance is an indication of interaction between the phosphine moieties and palladium although the breadth of the signal suggests some ligand exchange.

We have begun to optimize the conditions for Suzuki coupling with **3**. Significantly, at higher temperatures in the presence of **3** (P/Pd = 1.4:1; 80 °C) the yield of biphenyl improved to 83%, and at higher phosphine loading (P/Pd = 2.8:1; 80 °C) we isolated biphenyl in 90% yield (Table 2, entries 5 and 6). These results are very encouraging and are comparable with those obtained in the presence of [Pd(PPh₃)₄].^[11a] Furthermore, they demonstrate the potential use of P=C/C=C hybrid copolymers as ligands for Pd-

catalyzed reactions. Moreover, the polymer/catalyst could easily be removed by precipitation with hexanes to afford pure biphenyl (by GC and NMR spectroscopy) without the need for column chromatography.

In closing, this paper discloses two significant advances: 1) The remarkable ability of P=C bonds to mimic the chemistry of C=C bonds has been applied to copolymerization, and 2) new hybrid inorganic–organic macromolecules were prepared that can be used in polymer-supported catalysis. We have laid the foundation for the future development of numerous copolymers from a range of phosphalkenes^[15] and olefins by this convenient, one-step methodology. Future work will also explore the possible application of these copolymers in other catalytic processes and attempt catalyst recycling.

Received: June 11, 2004

Keywords: homogeneous catalysis · inorganic polymers · multiple bonds · phosphalkenes · phosphanes

- [1] G. Becker, *Z. Anorg. Allg. Chem.* **1976**, 423, 242.
- [2] K. B. Dillon, F. Mathey, J. F. Nixon, *Phosphorus: The Carbon Copy*, Wiley, New York, **1998**.
- [3] For general reviews of phosphalkenes, see: a) F. Mathey, *Angew. Chem.* **2003**, 115, 1616; *Angew. Chem. Int. Ed.* **2003**, 42, 1578; b) L. Weber, *Eur. J. Inorg. Chem.* **2000**, 2425; c) M. Yoshifuji, *J. Chem. Soc. Dalton Trans.* **1998**, 3343; d) F. Mathey, *Acc. Chem. Res.* **1992**, 25, 90; e) R. Appel in *Multiple Bonds and Low Coordination in Phosphorus Chemistry* (Eds.: M. Regitz, O. J. Scherer), Thieme, Stuttgart, **1990**, p. 157; f) R. Appel, F. Knoll, *Adv. Inorg. Chem.* **1989**, 33, 259; g) J. F. Nixon, *Chem. Rev.* **1988**, 88, 1327; h) R. Appel, F. Knoll, I. Ruppert, *Angew. Chem.* **1981**, 93, 771; *Angew. Chem. Int. Ed. Engl.* **1981**, 20, 731.
- [4] For a review highlighting some potential applications of compounds containing P=C bonds in catalysis, see: L. Weber, *Angew. Chem.* **2002**, 114, 583; *Angew. Chem. Int. Ed.* **2002**, 41, 563, and references therein.
- [5] a) T. C. Klebach, R. Lourens, F. Bickelhaupt, *J. Am. Chem. Soc.* **1978**, 100, 4886; b) T. A. van der Knaap, T. C. Klebach, F. Visser, F. Bickelhaupt, P. Ros, E. J. Baerends, C. H. Stam, M. Konijn, *Tetrahedron* **1984**, 40, 765; c) O. Mundt, G. Becker, W. Uhl, *Z. Anorg. Allg. Chem.* **1986**, 540/541, 319.
- [6] C.-W. Tsang, M. Yam, D. P. Gates, *J. Am. Chem. Soc.* **2003**, 125, 1480.
- [7] For reviews, see: a) J. E. Mark, H. R. Allcock, R. West, *Inorganic Polymers*, Prentice-Hall, Englewood Cliffs, **1992**; b) H. R. Allcock, *Chemistry and Applications of Polyphosphazenes*, Wiley, New Jersey, **2003**; c) I. Manners, *Angew. Chem.* **1996**, 108, 1712; *Angew. Chem. Int. Ed. Engl.* **1996**, 35, 1602; d) R. H. Neilson, P. Wisian-Neilson, *Chem. Rev.* **1988**, 88, 541; e) A. R. McWilliams, H. Dorn, I. Manners, *Top. Curr. Chem.* **2002**, 220, 141; e) J.-P. Majoral, A. M. Caminade, V. Maraval, *Chem. Commun.* **2002**, 2929.
- [8] For recent work on main-chain-phosphorus polymers, see: a) R. C. Smith, J. D. Protasiewicz, *J. Am. Chem. Soc.* **2004**, 126, 2268; b) H. Dorn, J. M. Rodenzo, B. Brunnhöfer, E. Rivard, J. A. Massey, I. Manners, *Macromolecules* **2003**, 36, 291; c) Y. Morisaki, Y. Aiki, Y. Chujo, *Macromolecules* **2003**, 36, 2594; d) V. A. Wright, D. P. Gates, *Angew. Chem.* **2002**, 114, 2495; *Angew. Chem. Int. Ed.* **2002**, 41, 2389; e) H. R. Allcock, S. D. Reeves, C. R. de Denu, C. A. Crane, *Macromolecules* **2001**, 34, 748; f) C. H. Walker, J. V. St. John, P. Wisian-Neilson, *J. Am.*

- Chem. Soc.* **2001**, 123, 3846; g) C. Hay, C. Fischmeister, M. Hissler, L. Toupet, R. Réau, *Angew. Chem.* **2000**, 112, 1882; *Angew. Chem. Int. Ed.* **2000**, 39, 1812; h) B. L. Lucht, N. O. St. Onge, *Chem. Commun.* **2000**, 2097; i) T. J. Peckham, J. A. Massey, C. H. Honeyman, I. Manners, *Macromolecules* **1999**, 32, 2830; j) S. S. H. Mao, T. D. Tilley, *Macromolecules* **1997**, 30, 5566.
- [9] The ratio of (aryl H):(alkyl H) for the two monomer units (i.e. **1** and styrene) in the ^1H NMR spectrum is not very sensitive to large changes in the % incorporation of **1** into the copolymer **3**. Therefore, we have found that ^1H NMR spectroscopy does not give an accurate measure of the phosphalkene content. For example, a polymer consisting entirely of the methylenephosphine unit would show a (aryl H):(alkyl H) ratio of 1.33 (i.e. 12H/9H), whereas the ratio for polystyrene would be 1.66 (5H/3H).
- [10] See, for example: C. U. Pittman, Jr. in *Comprehensive Organometallic Chemistry*, Vol. 8 (Eds.: G. Wilkinson, F. G. A. Stone, E. W. Abel), Pergamon, Oxford, **1982**, p. 553; D. E. Bergbreiter, *Chem. Rev.* **2002**, 102, 3345; T. J. Dickerson, N. N. Reed, K. D. Janda, *Chem. Rev.* **2002**, 102, 3325; C. A. McNamara, M. J. Dixon, M. Bradley, *Chem. Rev.* **2002**, 102, 3275; N. E. Leadbeater, M. Marco, *Chem. Rev.* **2002**, 102, 3217; P. H. Toy, K. D. Janda, *Acc. Chem. Res.* **2000**, 33, 546; S. J. Shuttleworth, S. M. Allin, P. K. Sharma, *Synthesis* **1997**, 1217; S. J. Shuttleworth, S. M. Allin, R. D. Wilson, D. Nasturica, *Synthesis* **2000**, 1035.
- [11] For leading references on Suzuki coupling in the presence of molecular phosphines, see, for example: a) N. Miyaara, A. Suzuki, *Chem. Rev.* **1995**, 95, 2457; b) A. F. Littke, G. C. Fu, *Angew. Chem.* **2002**, 114, 4350; *Angew. Chem. Int. Ed.* **2002**, 41, 4176; c) M. Miura, *Angew. Chem.* **2004**, 116, 2251; *Angew. Chem. Int. Ed.* **2004**, 43, 2201; d) S. D. Walker, T. E. Barder, J. R. Martinelli, S. L. Buchwald, *Angew. Chem.* **2004**, 116, 1907; *Angew. Chem. Int. Ed.* **2004**, 43, 1871; e) A. F. Littke, C. Dai, G. C. Fu, *J. Am. Chem. Soc.* **2000**, 122, 4020.
- [12] For Suzuki coupling in the presence of insoluble phosphine polymers/resins, see: a) Y. M. A. Yamada, K. Takeda, H. Takahashi, S. Ikegami, *Org. Lett.* **2002**, 4, 3371; b) T. J. Colacot, E. S. Gore, A. Kuber, *Organometallics* **2002**, 21, 3301; c) C. A. Parrish, S. L. Buchwald, *J. Org. Chem.* **2001**, 66, 3820; d) K. Inada, N. Miyaara, *Tetrahedron* **2000**, 56, 8661; e) Y. Uozumi, H. Danjo, T. Hayashi, *J. Org. Chem.* **1999**, 64, 3384; f) I. Fenger, C. Le Drian, *Tetrahedron Lett.* **1998**, 39, 4287; g) S.-B. Jang, *Tetrahedron Lett.* **1997**, 38, 1793.
- [13] For soluble polymer-supported phosphines for Suzuki coupling, see: a) Q.-S. Hu, Y. Lu, Z.-Y. Tang, H.-B. Yu, *J. Am. Chem. Soc.* **2003**, 125, 2856; b) A. Datta, K. Ebert, H. Plenio, *Organometallics* **2003**, 22, 4685. Although not used in Suzuki reactions, a soluble poly(arylenediphosphine) has been used in other Pd-catalyzed reactions: c) T. Kanbara, S. Takase, R. Hayashi, S. Kagaya, K. Hasegawa, T. Yamamoto, *J. Polym. Sci. Part A* **2002**, 40, 2637.
- [14] There are two possible explanations for the low catalytic activity observed with **2**. One possibility is that steric bulk around the phosphorus center in **2** hinders coordination to Pd. A second possibility is that the high phosphorus density in **2** leads to multidentate coordination to Pd, thus rendering it inaccessible to substrates and inactive.
- [15] Homopolymers have been prepared from a variety of substituted monomers ($\text{RP}=\text{CR}_2$): M. Yam, C.-W. Tsang, K. Noonan, J. Kingsley, B. O. Patrick, D. P. Gates, unpublished results.

Preparation of Ag₂S Nanocrystals of Predictable Shape and Size**

Wen Pei Lim, Zhihua Zhang, Hong Yee Low, and
Wee Shong Chin*

While many studies have focused on the control of the size of nanoparticles for their quantum-confined properties, the ability to synthesize monodispersed nanocrystals with predictable shape remains a challenge. The control of crystal shapes, in addition to their sizes and the higher surface-to-volume ratio, provides one more key factor to manipulate the properties of nanocrystals.^[1] For example, it has been reported that the sublimation energy of Au {110} faces is significantly lower than that of Au {100} and Au {111} faces.^[1b] For future applications of nanomaterials, it is foreseen that the particle shapes (i.e. the crystallographic surfaces enclosing the particles) will become an important issue.

Ag₂S is a direct, narrow band-gap semiconductor^[2] with good chemical stability and excellent optical limiting properties; the optical limiting responses toward nanosecond laser pulses at 532 nm are much stronger than those of [60]fullerene and chloroaluminum phthalocyanine.^[3] Ag₂S has been used in optical and electronic devices such as photovoltaic cells, photoconductors, and IR detectors,^[4] and as superionic conductors.^[5] To date, however, there are few reports on the preparation of Ag₂S nanocrystals with unique shapes. Herein we report on the control of the size and shape of Ag₂S nanocrystals synthesized from an easily prepared precursor under mild conditions in solution.

Controlling the shape of nanoparticles has thus far been achieved in two ways: using a template^[6–9] or in solutions by employing appropriate capping agents.^[10–12] The latter method is more attractive owing to higher yield and simplicity (there is no template to remove after the preparation). Among the solution methods, the injection of an organometallic precursor into a hot coordinating solvent provides a simple route to produce particles with desirable properties (e.g. high crystallinity, and uniform shapes and sizes with a high degree of monodispersity).^[13] However, the latter method usually involves elaborate preparation of air-sensitive organometallic complexes that decompose exothermically in

[*] W. P. Lim, Z. Zhang, Dr. W. S. Chin
Department of Chemistry
National University of Singapore
3 Science Drive 3, Singapore 117543 (Singapore)
Fax: (+65) 6779-1691
E-mail: chmcws@nus.edu.sg.

Dr. H. Y. Low
Institute of Materials Research and Engineering
3 Research Link, Singapore 117602 (Singapore)

[**] This research work was supported by the National University of Singapore Academic Research Fund R-143-000-167-112. We thank Mr. Wong Chiong Teck for his assistance in the DFT calculations.



Supporting information for this article is available on the WWW under <http://www.angewandte.org> or from the author.

air, and also the use of high temperatures. It is therefore of interest to find an easily accessible precursor that would decompose under mild conditions.

We have discovered that the air-stable precursor silver(I) thiobenzoate ($\text{Ag}(\text{SCOPh})$)^[14] meets such requirements. The precursor crystals were found to decompose in amine at room temperature to give Ag_2S nanoparticles.^[15] When a solution of the precursor dissolved in trioctylphosphine (TOP) is added under nitrogen to a warm solution (80, 100, or 120 °C) of a long-chain amine such as hexadecylamine (HDA), well-defined nanocrystals are formed, the size and shape of which can be controlled by the reaction conditions. Several parameters are identified as important and have been investigated, namely, the reaction temperature, type of amine, relative concentration of the reagents, and reaction time. The influence of these parameters on the final size and morphology of the prepared Ag_2S nanocrystals is summarized in Table 1. All the prepared nanocrystals were characterized by X-ray diffraction (XRD) and transmission electron microscopy (TEM).

Various shapes of Ag_2S nanocrystals can be readily produced, sometimes as the exclusive form, by varying the reaction temperature and amine concentration. At low temperature (80 °C), faceted Ag_2S nanocrystals are obtained when the precursor is injected into HDA. TEM images of the nanocrystals reveal a self-assembled hexagonal closed-packed array (Figure 1a). Clear lattice planes visible in the HRTEM image (Figure 1b) confirm the good crystallinity (d spacing = 2.8 Å) of the particles produced at such low temperature. The average diameter of the nanocrystals is 14.5 nm (with a size distribution of 6.2%), and the average core-to-core interparticle distance is about 19 nm (Figure 1c). In regions where two layers of these crystals overlap (Figure 1d), the hexagonal closed-packed arrays are clearly maintained in the overlayers. Such closed-packed stackings can lead to the formation of a

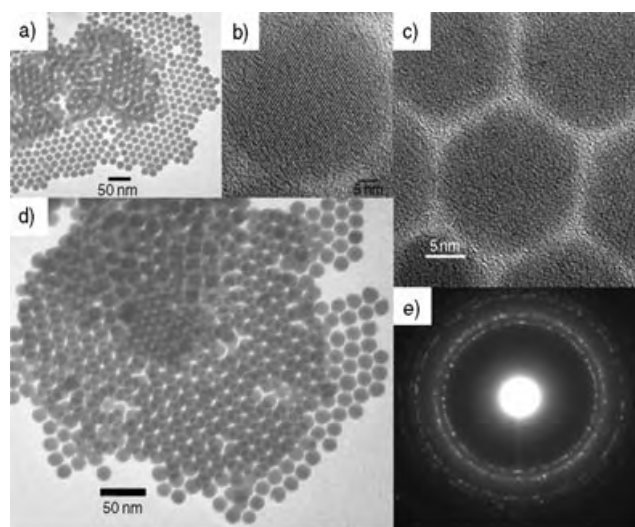


Figure 1. a) Representative TEM image of Ag_2S nanocrystals produced at 80 °C; b) and c) HRTEM images of the faceted nanocrystals; d) TEM image showing the monolayer and multilayers of the hexagonal closed-packed array of the nanocrystals; e) SAED pattern of the nanocrystals.

three-dimensional self-organized superlattice assembly.^[16] The selected area electron diffraction (SAED) pattern of the sample (Figure 1e) exhibits polycrystalline diffraction rings that can be indexed to the monoclinic structure of Ag_2S (see below).

We have found that by increasing the injection temperature to 120 °C, cube-shaped Ag_2S crystals are obtained exclusively. The uniform Ag_2S nanocubes self-assemble into ordered two-dimensional arrays on the surface of the transmission electron microscope grid (Figure 2a). The average diameter of these nanocubes is 44.0 nm (with a size distribution of 9.8%). The scanning electron microscope (SEM) image in Figure 2b (sample coated with gold to improve contrast) illustrates that an abundant quantity of these nanocubes can be obtained by using this approach. HRTEM images (Figure 2c and d) clearly show that these Ag_2S nanocubes are single crystals with sharp lattice fringes extending to the edges.

While exclusive formation of faceted crystals and nanocubes is obtained at about 80 °C and 120 °C, respectively, mixtures of nanocubes and faceted crystals (low amine concentration) or faceted particles and nanorods (medium amine concentration) can be obtained at an injection temperature of 100 °C (Figure 3). Prolonged heating of the reaction mixtures for up to 2 h did not change the particle morphology and the particle sizes are only slightly affected.

The XRD patterns of all samples were indexed to the monoclinic acanthite Ag_2S . Nevertheless, the intensities of some diffraction lines were relatively enhanced in

Table 1: Summary of the size and shape of nanocrystals obtained under various reaction conditions.

Amine ^[a]	[Amine]/ [precursor]	Reaction temperature [°C]	Reaction time [min]	Average size from TEM [nm]	Morphology
HDA	8:1	120	10	47.7 ± 4.2	cubes
HDA	12:1	120	10	44.0 ± 4.3	cubes
HDA	16:1	120	10	40.8 ± 5.1	cubes
HDA	20:1	120	10	31.5 ± 3.0	cubes
HDA	8:1	100	10	31.7 ± 2.6	faceted crystals & cubes
HDA	12:1	100	10	20.5 ± 2.4 (37.4 ± 4.3) × (18.6 ± 2.3)	faceted crystals & rods
HDA	16:1	100	10	25.7 ± 3.5 (46.5 ± 5.3) × (21.4 ± 3.4)	faceted crystals & rods
HDA	20:1	100	10	29.6 ± 1.5	faceted crystals
HDA	8:1	80	15	6.7 ± 0.6	faceted crystals
HDA	16:1	80	15	14.5 ± 0.9	faceted crystals
HDA	20:1	80	15	20.9 ± 1.6	faceted crystals
OA	8:1	120	10	43.0 ± 6.4	cubes
OA	20:1	120	10	39.1 ± 5.9	cubes
DOA	12:1	120	10	11.1 ± 1.9	faceted crystals
DOA	16:1	120	10	~13	not homogenous
DOA	20:1	120	10	~17	not homogenous
EDA	16:1	120	10	–	network-like

[a] HDA = hexadecylamine; OA = octylamine; DOA = dioctylamine; EDA = ethylenediamine.

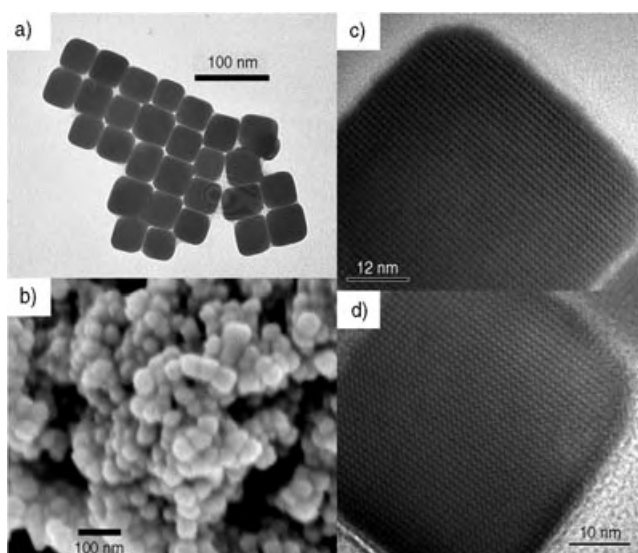


Figure 2. a) Representative TEM image of Ag_2S nanocubes produced at 120 °C; b) SEM image showing clusters of the abundant Ag_2S nanocubes; c) and d) HRTEM images showing clear lattice fringes of the nanocubes.

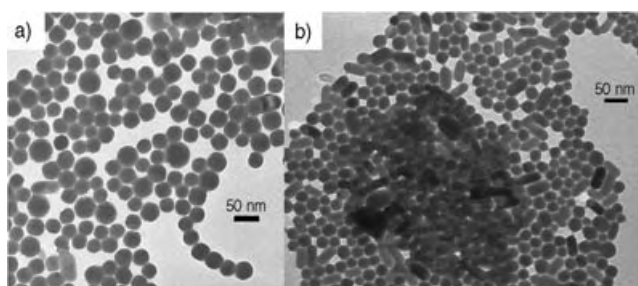


Figure 3. Representative TEM images showing a mixture of a) nanocubes and faceted nanocrystals ([HDA]/[precursor]=8:1) and b) nanorods and faceted nanocrystals ([HDA]/[precursor]=16:1) both obtained at 100 °C.

the faceted nanocrystals (Figure 4). Ag_2S is known to exist in three modifications: 1) the monoclinic α -phase at room temperature, 2) the body-centered cubic β -phase at temperatures between 178 and 600 °C, and 3) the face-centered cubic γ -phase above 600 °C. All these phases share a common cubic or near-cubic framework of anions, with the cations distributed at different interstitial locations.^[17] It has been reported that Ag ions diffuse readily among the interstitial sites and thus lead to a facile morphological transformation.^[18] We find that the enhanced diffraction peaks in Figure 4c correspond to the major lines of the cubic β - Ag_2S pattern. Hence it seems that β -phase crystals are formed under reaction conditions we employed, although the exact mechanism is unclear at the moment. This metastable phase can be detected for all faceted crystals (and mixtures) prepared at 80 and 100 °C. The formation of the β - Ag_2S phase will be of technological interest as it is known to display superionic behavior.^[5]

We have found that injecting the precursor into hot TOPO (> 120 °C) alone yielded Ag nanoparticles instead of Ag_2S

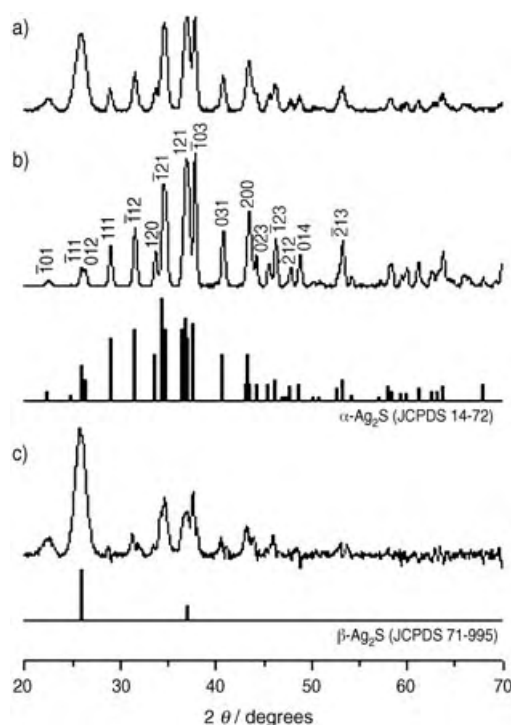
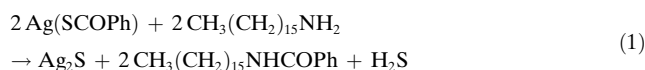


Figure 4. Representative X-ray diffraction patterns of Ag_2S : a) faceted nanocrystals formed at 80 °C, b) nanocubes formed at 120 °C, and c) the resulting pattern obtained by normalized subtraction of pattern b from pattern a. The simulated diffraction patterns from the JCPDS database are plotted for comparison.

(see Supporting Information). Hence, the amine is used here not just as the size- and shape-controlling agent, it also facilitates the decomposition of the precursor to Ag_2S [Eq. (1)]. In the presence of amine, the stronger S–C bond is broken instead of the weaker Ag–S bond;^[19] we believe this is due to an initial nucleophilic attack of the amine onto the thiocarboxylate carbon atom. The reaction is best described as a degradation reaction (i.e. not a nucleophilic substitution) since the formal charges on silver (1+) and sulfur (2–) do not change while the structure of the precursor is destroyed. During the reaction, H_2S gas is evolved and an amide is isolated.^[20] Theoretical calculations are now underway to provide further insight into the energetics of possible reaction pathways.



It is evident from Table 1 that varying the amine-to-precursor ratio provides systematic control of the size of the nanocrystals. A plot of the average particle size against amine-to-precursor ratio reveals different trends for the three injection temperatures (Figure 5). The size of the nanocrystals generated appears to be dependent on a delicate balance between the surface-capping role and the nucleophilic attacking role of HDA. Thus, while the degradation reaction readily occurs at higher temperature (120 °C), the size-controlling role of HDA dominates. As such, smaller crystals are obtained when more capping agent is present—a trend

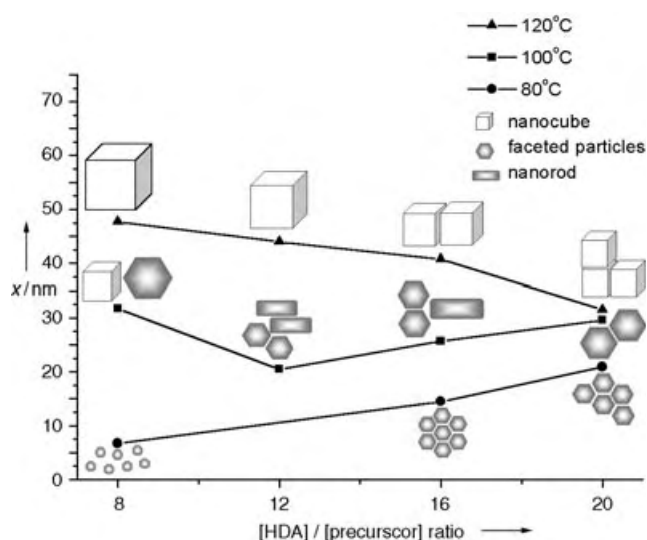


Figure 5. Effect of temperature and amine-to-precursor ratio on the shape and size of the Ag_2S nanocrystals obtained. The size of the nanorods is not included in the graph. x = particle size.

that is common for most reported preparations of nanoparticles. When the temperature is low (80°C), however, the nucleophilic attacking role of HDA becomes important. In this case, increasing the amount of HDA will increase the rate of degradation and hence an increase in the particle size occurs. At 100°C , the two roles are competitive and we observe a steady increase in crystal size only when the amine-to-precursor ratio exceeds a certain value.

The heating rate also plays an important role in controlling the size and shape of the nanocrystals. For example, we have also prepared the nanocrystals by injecting the precursor into HDA solution at 60°C (necessary to maintain liquid HDA) and slowly heating the reaction mixture and aging it at 100°C (or 120°C) for 30 min. We found that uniform particles can also be obtained but their shape and size display different trends (Figure 6; details in Supporting Information).

Thus, one may summarize the morphology control as follows: 1) formation of nanocubes is favored at high temperature (120°C) or low amine concentration; 2) faceted nanocrystals are favored at low temperature (80°C) or high amine concentration; 3) elongated structures are obtained with medium amine concentration at 100 – 120°C . Recent studies have shown that morphology control of nanocrystals can be effected through a delicate balance of the nucleation and growth rate.^[21] In particular, preferential growth of particular crystallographic surfaces is possible during kinetically controlled growth processes.^[21a] In the method here, we note that the nucleation rate is also dependent on the amine concentration since the degradation of the precursor is not a simple thermolysis process. It seems that the formation of cube-shaped Ag_2S crystals is thermodynamically driven and favored by low monomer concentration (i.e. low amine concentration). At 120°C , the sticking coefficient of capping HDA molecules is less selective and hence isotropic crystals are produced. The formation of faceted and elongated Ag_2S nanocrystals seems to be a kinetically driven reaction and is favored at high monomer concentration. This nonequilibrium

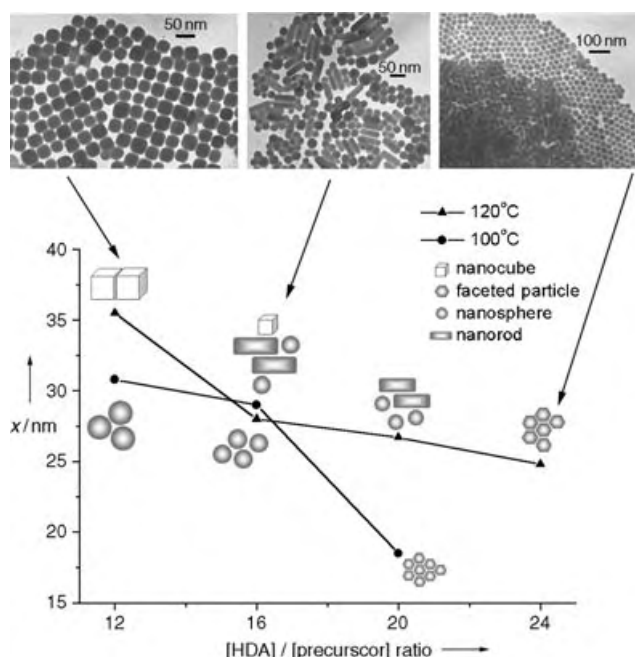


Figure 6. The shape and size of Ag_2S nanocrystals obtained by the slow heating and aging method. Effect of temperature and amine-to-precursor ratio is illustrated and typical TEM images recorded at 120°C are shown. The size of the nanorods is not included in the graph.

kinetic-growth regime is further supported by the formation of the metastable β -phase along with these anisotropic crystals. As evident in Table 1, the nature and type of amine are found to be important also in the shape control. Thus, formation of nanocubes is only observed at 120°C in HDA and octylamine (OA) but not in dioctylamine (DOA) or ethylenediamine (EDA). Since the nucleophilicity of these amines is similar, we believe that steric effects are playing a role here. This aspect is currently under investigation.

In conclusion, we have described an unprecedented amine-mediated reaction for preparing Ag_2S nanocrystals under mild conditions. By controlling a few critical parameters, a simple route that provides Ag_2S nanocrystals of predictable size and shape is presented. Our preliminary investigations show that this general route can also be applied to the preparation of other chalcogenide nanocrystals.

Experimental Section

Unless otherwise stated, all materials were purchased from commercial sources and used without further purification. All procedures were carried out by using standard techniques under a nitrogen atmosphere. Hexadecylamine (HDA) was dried and degassed at 120°C before use. A degassed solution of $\text{Ag}(\text{SCOPh})$ (0.025 g) in TOP (0.2 mL) was injected into a hot solution ($80^\circ\text{C}/100^\circ\text{C}/120^\circ\text{C}$) of HDA. After these components had been mixed, the pale yellow solution rapidly changed to brown. After 10 min, the reaction solution was cooled to room temperature, then toluene (ca. 1 mL) was added and the product was precipitated by addition of methanol. The precipitate was centrifuged, washed thoroughly with methanol, and dried in vacuum overnight. Alternatively, $\text{Ag}(\text{SCOPh})$ was introduced into HDA at 60°C and the mixture was heated to the desired

temperature (100°C/120°C) and aged at that temperature for 30 min. The XRD pattern was acquired by using a Bruker D5005 diffractometer with $\text{Cu}_{\text{K}\alpha}$ radiation ($\lambda = 0.151478$ nm). TEM was performed on a Philips CM100 microscope operating at 100 kV, and HRTEM was performed on a Philips CM300 FEG instrument with an acceleration voltage of 300 kV. SEM images were obtained by using a JEOL JSM6700 microscope, operating at 10 amp and 15 kV.

Received: May 6, 2004

Revised: July 23, 2004

Keywords: chalcogenides · crystal growth · electron microscopy · nanostructures

- [1] a) Z. L. Wang, *J. Phys. Chem. B* **2000**, *104*, 1153; b) M. B. Mohamed, Z. L. Wang, M. A. El-Sayed, *J. Phys. Chem. A* **1999**, *103*, 10255.
- [2] K. Akamatsu, S. Takei, M. Mizuhata, A. Kajinami, S. Deki, S. Takeoka, M. Fujii, S. Hayashi, K. Yamamoto, *Thin Solid Films* **2000**, *359*, 55.
- [3] Y. P. Sun, J. E. Riggs, H. W. Rollins, R. Guduru, *J. Phys. Chem. B* **1999**, *103*, 77.
- [4] a) G. Hodes, J. Manassen, D. Cahen, *Nature* **1976**, *261*, 403; b) S. Kitova, J. Eneva, A. Panov, H. Haefke, *J. Imaging Sci. Technol.* **1994**, *38*, 484.
- [5] a) S. Hull, D. A. Keen, D. S. Sivia, P. A. Madden, M. Wilson, *J. Phys. Condens. Matter* **2002**, *14*, 9; b) T. Minami, *J. Non-Cryst. Solids* **1987**, *95*, 107.
- [6] J. Bao, D. Xu, Q. Zhou, Z. Xu, *Chem. Mater.* **2002**, *14*, 4709.
- [7] J. C. Hulthen, C. R. Martin, *J. Mater. Chem.* **1997**, *7*, 1075.
- [8] a) W. Han, P. Kohler-Redlich, C. Scheu, F. Ernst, M. Rühle, N. Grobert, M. Terrones, H. W. Kroto, D. R. M. Walton, *Adv. Mater.* **2000**, *12*, 1356; b) J. Bao, K. Wang, Z. Xu, H. Zhang, Z. Lu, *Chem. Commun.* **2003**, *2*, 208.
- [9] a) J. Tanori, M. P. Pileni, *Langmuir* **1997**, *13*, 639; b) M. P. Pileni, T. Gulik-Krzywicki, J. Tanori, A. Filankembo, J. C. Dedieu, *Langmuir* **1998**, *14*, 7359.
- [10] a) V. F. Puentes, K. M. Krishnan, A. P. Alivisatos, *Science* **2001**, *291*, 2115; b) N. R. Jana, L. Gearheart, C. J. Murphy, *Adv. Mater.* **2001**, *13*, 1389; c) B. Nikoobakht, M. A. El-Sayed, *Chem. Mater.* **2003**, *15*, 1957.
- [11] a) T. S. Ahmadi, Z. L. Wang, T. C. Green, A. Henglein, M. A. El-Sayed, *Science* **1996**, *272*, 1924; b) J. M. Petroski, Z. L. Wang, T. C. Green, M. A. El-Sayed, *J. Phys. Chem. B* **1998**, *102*, 3316; c) Y. Sun, Y. Xia, *Science* **2002**, *298*, 2176.
- [12] K. K. Caswell, C. M. Bender, C. J. Murphy, *Nano Lett.* **2003**, *3*, 667.
- [13] a) C. B. Murray, D. J. Norris, M. G. Bawendi, *J. Am. Chem. Soc.* **1993**, *115*, 8706; b) B. O. Dabbousi, J. Rodriguez-Viejo, F. V. Mikulec, J. R. Heine, H. Mattoussi, R. Ober, K. F. Jensen, M. G. Bawendi, *J. Phys. Chem. B* **1997**, *101*, 9463; c) D. V. Talapin, S. Haubold, A. L. Rogach, A. Kornowski, M. Hasse, H. Weller, *J. Phys. Chem. B* **2001**, *105*, 2260; d) J. Hambrock, A. Birkner, R. A. Fischer, *J. Mater. Chem.* **2001**, *11*, 3197.
- [14] V. V. Savant, J. Gopalakrishnan, C. C. Patel, *Inorg. Chem.* **1969**, *8*, 748.
- [15] Z. H. Zhang, W. P. Lim, C. T. Wong, F. F. Yin, W. S. Chin, unpublished results.
- [16] a) M. P. Pileni, *Appl. Surf. Sci.* **2001**, *171*, 1; b) M. P. Pileni, *J. Phys. Chem. B* **2001**, *105*, 3358; c) L. Motte, F. Billoudet, E. Lacaze, J. Douin, M. P. Pileni, *J. Phys. Chem. B* **1997**, *101*, 138.
- [17] R. J. Cava, D. B. McWhan, *Phys. Rev. Lett.* **1980**, *45*, 2046, and references therein.
- [18] R. L. Allen, E. J. Moore, *J. Phys. Chem.* **1959**, *63*, 223, and references therein.
- [19] Preliminary results from DFT B3LYP/LANL2DZ calculations showed that the bond dissociation energy of AgS–COPh is 265.95 kJ mol⁻¹, whereas that of Ag–SCOPh is 206.41 kJ mol⁻¹.
- [20] Isolation of CH₃(CH₂)₁₅NHCOPh: The product was purified by preparative TLC and recrystallized from chloroform/hexane. ¹H NMR (CDCl₃): δ = 0.88 (t, *J* = 6.6 Hz, 3H; CH₃), 1.26 (s, 26H; CH₂), 1.59 (quin, 2H; NHCH₂CH₂), 3.46 (q, *J* = 6.7 Hz, 2H; NHCH₂), 6.08 (br, 1H; NH), 7.40–7.52 (overlapping t, 3H; *m-p*-Ph), 7.75 ppm (d, *J* = 6.8 Hz, 2H; *o*-Ph); ¹³C NMR (CDCl₃): δ = 14.0 (CH₃), 22.6 (CH₂CH₃), 26.9 (NCH₂CH₂CH₂), 29.2–29.6 (CH₂), 31.8 (NCH₂CH₂), 40.0 (NCH₂), 126.7 (*o*-Ph), 128.4 (*m*-Ph), 131.2 (*p*-Ph), 167.8 ppm (C=O); elemental analysis (%) calcd: C 79.94, H 11.38, N 4.05; found: C 80.13, H 10.92, N 4.24.
- [21] a) S-M Lee, S-N Cho, J. Cheon, *Adv. Mater.* **2003**, *15*, 441; b) Z. A. Peng, X. Peng, *J. Am. Chem. Soc.* **2002**, *124*, 3343; c) W. W. Yu, Y. A. Wang, X. Peng, *Chem. Mater.* **2003**, *15*, 4300.

Epoxide Ring Opening

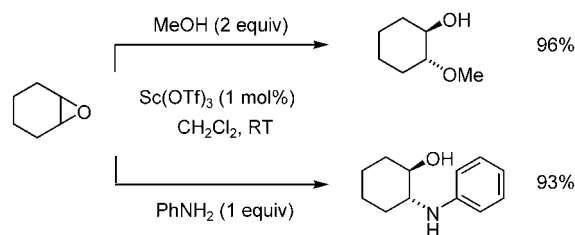
Scandium–Bipyridine-Catalyzed Enantioselective Addition of Alcohols and Amines to *meso*-Epoxides**

Christoph Schneider,* Anakallil R. Sreekanth, and Enzo Mai

The catalytic, enantioselective ring opening of *meso*-epoxides is an efficient means to convert readily available, inexpensive bulk chemicals into chiral, 1,2-difunctionalized fine chemicals in enantiomerically enriched form.^[1] In such a process the chiral catalyst, typically a chiral Lewis acid or Lewis base, must differentiate between the two enantiotopic carbon atoms of the epoxide and direct the nucleophilic addition in a clean S_N2 process to one of the epoxide termini. 1,2-Azido alcohols,^[2] 1,2-halohydrins,^[3] 1,2-cyano alcohols,^[4] 1,2-diol monoesters and monoethers,^[5] as well as 1,2-mercaptoalcohols^[6] have been obtained thus far in good to excellent enantioselectivities. Alternatively, chiral Ti^{III} complexes have been employed to reductively open *meso*-epoxides to furnish enantiomerically enriched radical anions, which were then trapped with either hydrogen donors or alkenes.^[7] The nucleophilic addition of amines to *meso*-epoxides currently proceeds with only moderate enantioselectivity in most cases;^[8] the catalytic, enantioselective addition of aliphatic alcohols to *meso*-epoxides has not been reported at all to date. We report here a novel chiral metal complex capable of catalyzing the alcoholysis as well as aminolysis of *meso*-epoxides with good yields and in part excellent enantioselectivities.

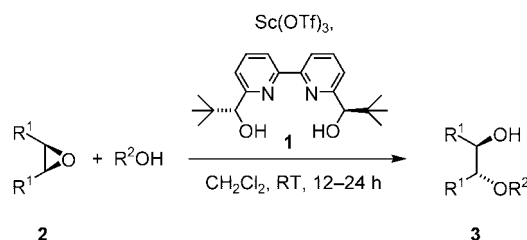
The starting point for our investigations was the observation made by Crotti and co-workers that lanthanide triflates such as $Yb(OTf)_3$ are effective catalysts for the aminolysis of 1,2-epoxides, presumably because they are able to exert their exceptional Lewis acidity even under protic reaction conditions.^[9,10] Preliminary experiments with different metal triflates revealed that $Sc(OTf)_3$, in particular, is a highly active catalyst for the alcoholysis and aminolysis of epoxides.^[11] Thus, cyclohexene oxide reacted with methanol (2 equiv) as well as aniline (1 equiv) in the presence of 1 mol % $Sc(OTf)_3$ within 12 h at room temperature in CH_2Cl_2 to give the ring-opened products in high yields and complete *anti* diastereoselectivity (Scheme 1).

Based upon this result we screened a number of chiral, multidentate ligands to be attached to $Sc(OTf)_3$ and found the



Scheme 1. $Sc(OTf)_3$ -catalyzed alcoholysis and aminolysis of cyclohexene oxide.

2,2'-bipyridine **1** introduced by Bolm et al.^[12] to be the most promising (Scheme 2). Stirring $Sc(OTf)_3$ and **1** (10 mol % each) in CH_2Cl_2 at room temperature furnished the active



Scheme 2. Scandium–bipyridine-catalyzed alcoholysis of *meso*-epoxides.

catalyst in situ, which catalyzed the ring opening of *cis*-stilbene oxide (**2a**) with methanol (2 equiv) to give 1,2-diol monoether **3a** in good yield and with 92 % *ee* (Scheme 2; Table 1, entry 1). Various other alcohols were added successfully to **2a** in good yields and very high enantioselectivities; with *para*-methoxy benzyl alcohol giving the best results (97 % *ee*) (entries 2–5). Dichloromethane proved to be the solvent of choice as reactions in other solvents did not yield any product (THF, DMF, CH_3CN) or gave significantly reduced enantioselectivities (diethyl ether, toluene, methanol).

Other aromatic *meso*-epoxides also furnished the ring-opened products **3f** and **3g** in good yields, excellent enantioselectivities of up to 98 % *ee*, and complete *anti* diastereoselectivity (entries 6 and 7). The formation of small amounts of the respective diastereomer was observed in some reactions with aromatic epoxides when $Sc(OTf)_3$ was used alone as the catalyst, such an isomerization was completely suppressed with the chiral scandium–bipyridine complex. Cyclic and aliphatic epoxides such as cyclohexene oxide (**2d**) and *cis*-2-butene oxide (**2e**) gave rise to 1,2-diol monoethers **3h** and **3i**, respectively, in high yields and only moderate enantioselectivities (entries 8 and 9).

Compounds **3** are interesting synthetic building blocks. Thus 1,2-diol monoether **3e** was converted into the PMB-protected acyloin **4** by Swern oxidation^[13] in 94 % yield and almost complete retention of configuration. Alternatively, oxidation with ceric ammonium nitrate^[14] furnished the unprotected 1,2-diol **5** in 82 % yield (Scheme 3).

[*] Prof. Dr. C. Schneider, Dr. A. R. Sreekanth, Dipl.-Chem. E. Mai
Institut für Organische Chemie, Universität Leipzig
Johannisallee 29, 04103 Leipzig (Germany)
Fax: (+49) 341-973-6599
E-mail: schneider@chemie.uni-leipzig.de

[**] This work was supported by the Deutsche Forschungsgemeinschaft (Schn 441/3-1) and the Fonds der Chemischen Industrie. We thank Dr. Nitin T. Patil for preliminary experiments and Prof. Dr. W. König (Universität Hamburg) für numerous GC measurements on chiral stationary phases.

Supporting information for this article is available on the WWW under <http://www.angewandte.org> or from the author.

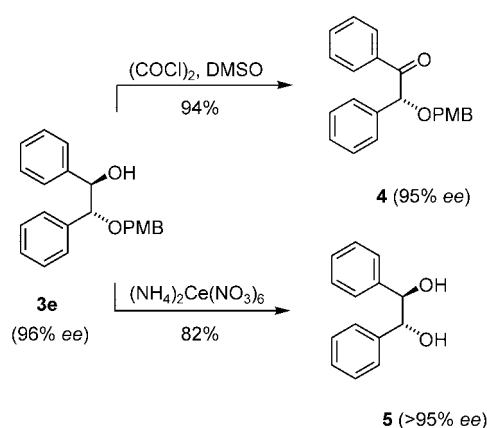
Table 1: Results of the scandium–bipyridine-catalyzed alcoholysis of *meso*-epoxides according to Scheme 2.

Entry	Epoxide	Alcohol	Product ^[a]	<i>ee</i> [%] ^[b]	Yield [%] ^[c]
1		MeOH		92	81
2	2a	EtOH		96	75
3	2a	<i>n</i> BuOH		94	80
4	2a	allylOH		95	78
5	2a	PMBOH ^[d]		97	82
6		MeOH		98	83
7		MeOH		96	75
8 ^[e]		PMBOH ^[d]		54	90
9 ^[e]		PMBOH ^[d]		49	93

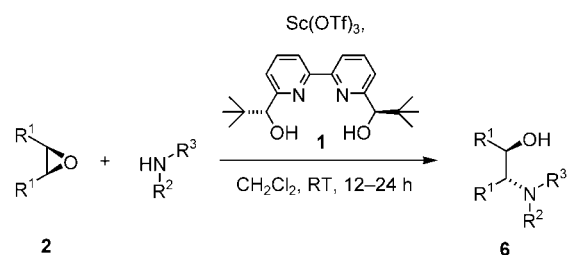
[a] The absolute configuration of the products was determined by comparison of the rotation values with literature values or by analogy.

[b] Determined by HPLC or GC analysis on chiral stationary phases (see the Supporting Information). [c] Yield of isolated product. [d] PMB = *para*-methoxybenzyl. [e] This reaction was conducted at -20°C .

The optimized protocol may be directly applied to the aminolysis of *meso*-epoxides (Scheme 4; Table 2). Reaction of *cis*-stilbene oxide (**2a**) and aniline (1 equiv) in the presence of 10 mol% each of $\text{Sc}(\text{OTf})_3$ and the chiral bipyridine **1** yielded 1,2-amino alcohol **6a** in 95% yield and 93% *ee*. The catalyst loading may be lowered to only 5 mol% with only



Scheme 3. Functionalization of ring-opened product as demonstrated with **3e**.



Scheme 4. Scandium–bipyridine-catalyzed aminolysis of *meso*-epoxides.

marginal effects on both the enantioselectivity (90% *ee*) and yield (89%). Sterically hindered anilines such as *N*-methyl-aniline maintained high yields and led to a further increase in enantioselectivity to 97% *ee* (Table 2, entry 2). The ring opening with electron-rich amines such as *para*-anisidine and *O*-benzyl hydroxylamine proceeded with slightly diminished enantioselectivities and yielded products **6c** and **6d**, which may be easily converted into free 1,2-amino alcohols (entries 3 and 4). Aliphatic amines did not yield the desired products presumably because they coordinate irreversibly to the Lewis acidic $\text{Sc}(\text{OTf})_3$. Other aromatic epoxides reacted with aniline in good yields and very high enantioselectivities to furnish 1,2-amino alcohols **6e** and **6f** (entries 5 and 6). Cyclohexene oxide (**2d**) and *cis*-2-butene oxide (**2e**) reacted with aniline under otherwise identical reaction conditions with only moderate enantioselectivities, which corresponds to the results of the alcoholysis mentioned above (entries 7 and 8).

Modification of the ligand structure gave first insights into structural elements crucial for the enantioselectivity of the process. Thus, using the bis-*O*-methylated bipyridine **7** as chiral ligand led to a complete loss of enantioselectivity both in the alcoholysis and aminolysis of *meso*-epoxides. It appears that the free hydroxyl groups are essential for the formation of a highly enantioselective scandium–bipyridine complex.

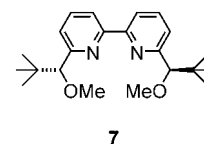


Table 2: Results of the scandium–bipyridine-catalyzed aminolysis of *meso*-epoxides according to Scheme 4.

Entry	Epoxide	Amine	Product ^[a]	<i>ee</i> [%] ^[b]	Yield [%] ^[c]
1		PhNH ₂		93 (90) ^[d]	95 (89) ^[d]
2	2a	PhNHCH ₃		97	85
3	2a	<i>p</i> -anisidine		82	87
4	2a	BnO-NH ₂		86	85
5		PhNH ₂		82	76
6		PhNH ₂		91	93
7		PhNH ₂		54	96
8		PhNH ₂		60	92

[a] The absolute configuration of the products was determined by comparison of the rotation values with literature values or by analogy. [b] Determined by HPLC or GC analysis on chiral stationary phases (see the Supporting Information). [c] Yield of isolated product. [d] Values in brackets refer to reactions conducted with only 5 mol% catalyst.

In conclusion, we have established the first catalytic, enantioselective addition of aliphatic alcohols to *meso*-epoxides employing a novel scandium–bipyridine complex which proceeds with in part excellent enantioselectivities and generally good yields. This same chiral catalyst improves the enantioselectivity of the aminolysis of aromatic *meso*-epoxides substantially. Current research efforts are directed at improving the scope of this process by ligand optimization and gaining structural information about the scandium–bipyridine complex.

Experimental Section

All reactions were carried out in flame-dried flasks under nitrogen. Representative procedure: A solution of Sc(OTf)₃ (49 mg, 0.10 mmol) and chiral bipyridine **1** (33 mg, 0.10 mmol) in CH₂Cl₂ (5 mL) was stirred for 5 min at room temperature. Subsequently *cis*-stilbene oxide (**2a**) (196 mg, 1.00 mmol) and *para*-methoxybenzyl alcohol (275 mg, 2.00 mmol) were added, and the solution was stirred for 12 h at room temperature. The solvents were evaporated in vacuo, and the crude product was purified by flash chromatography on silica gel (ether/pentane 1:2) which yielded 277 mg (82 %) of 1,2-diol monoether **3e** as colorless crystals. HPLC analysis (Chiralcel-OD phase, *n*-hexane/isopropanol 90:10, 1 mL min^{−1}): 97 % *ee*. M.p. 85–86 °C; IR (KBr): $\tilde{\nu}$ = 3521, 3432, 2865, 1610, 1509, 1241, 1195, 1022 cm^{−1}; ¹H NMR (300 MHz, CDCl₃): δ = 3.53 (brs, 1H), 3.82 (s, 3H), 4.26 (d, *J* = 10.8 Hz, 1H), 4.33 (d, *J* = 8.4 Hz, 1H), 4.46 (d, *J* = 10.8 Hz, 1H), 4.70 (d, *J* = 8.4 Hz, 1H), 6.89 (dd, *J* = 2.1, 6.6 Hz, 2H), 7.00–7.25 ppm (m, 12H); ¹³C NMR (75 MHz, CDCl₃): δ = 55.4, 70.6, 78.7, 86.7, 114.0, 127.4, 127.8, 127.9, 128.0, 128.2, 129.7, 137.8, 139.3, 159.5 ppm; HRMS (ESI) [*M*+Na]⁺ calcd. 279.13555, found 279.13552; [α]_D²⁵ = −41.6° (*c* = 0.72, CH₂Cl₂).

Under otherwise identical reaction conditions *cis*-stilbene oxide (**2a**) (98 mg, 0.50 mmol), aniline (47 mg, 0.50 mmol), Sc(OTf)₃ (25 mg, 0.05 mmol) and bipyridine **1** (17 mg, 0.05 mmol) were allowed to react in CH₂Cl₂ (2 mL), and the reaction yielded 138 mg (95 %) of 1,2-amino alcohol **6a**^[8a] (93 % *ee*, Chiralcel-OD, *n*-hexane/isopropanol 85:15, 1 mL min^{−1}) as colorless crystals. M.p. 100–103 °C; IR (KBr): $\tilde{\nu}$ = 3545, 3406, 3031, 2879, 2846, 1601, 1498, 1450, 1427, 1319, 1034, 758, 700 cm^{−1}; ¹H NMR (200 MHz, CDCl₃): δ = 2.75 (brs, 1H), 4.60 (d, *J* = 6.9 Hz, 1H), 4.76 (brs, 1H), 4.91 (d, *J* = 6.0 Hz, 1H, CH), 6.60–6.64 (m, 2H), 6.72–6.78 (m, 1H), 7.16–7.19 (m, 2H), 7.26–7.40 ppm (m, 10H); ¹³C NMR (50 MHz, CDCl₃): δ = 64.8, 78.1, 114.2, 118.0, 126.7, 127.4, 127.6, 128.0, 128.3, 128.6, 129.1, 140.3, 140.6, 147.3 ppm; ESI-MS *m/z* = 601 [2*M*+Na⁺], 312 [*M*+Na⁺], 290 [*M*+H⁺]; [α]_D²³ = +48.6° (*c* = 0.525, CH₂Cl₂).

Received: May 25, 2004

Keywords: asymmetric catalysis · epoxides · N ligands · nucleophilic addition · scandium

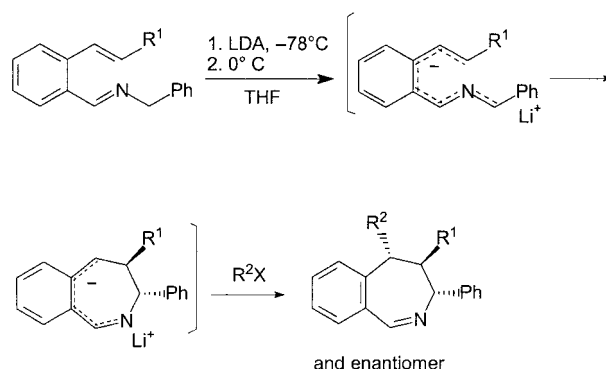
- [1] Reviews: a) D. M. Hodgson, A. R. Gibbs, G. P. Lee, *Tetrahedron* **1996**, 52, 14361; b) E. N. Jacobsen, M. H. Wu, *Comprehensive Asymmetric Catalysis, Vol. 3* (Eds.: E. N. Jacobsen, A. Pfaltz, H. Yamamoto), **1999**, p. 1309.
- [2] For example: a) H. Yamashita, *Bull. Chem. Soc. Jpn.* **1988**, 61, 1213; b) W. M. Nugent, *J. Am. Chem. Soc.* **1992**, 114, 2768; c) L. E. Martinez, J. L. Leighton, D. H. Carsten, E. N. Jacobsen, *J. Am. Chem. Soc.* **1995**, 117, 5897; d) Review: E. N. Jacobsen, *Acc. Chem. Res.* **2000**, 33, 421.
- [3] a) S. E. Denmark, P. A. Barsanti, K. T. Wong, R. A. Stavenger, *J. Org. Chem.* **1998**, 63, 2428; b) W. A. Nugent, *J. Am. Chem. Soc.* **1998**, 120, 7139; c) B. Tao, M. M. C. Lo, G. C. Fu, *J. Am. Chem. Soc.* **2001**, 123, 353; c) M. Nakajima, M. Saito, M. Uemura, S. Hashimoto, *Tetrahedron Lett.* **2002**, 43, 8827.
- [4] a) B. M. Cole, K. D. Shimizu, C. A. Krueger, J. P. A. Harrity, M. L. Snapper, A. H. Hoveyda, *Angew. Chem.* **1996**, 108, 1776; *Angew. Chem. Int. Ed. Engl.* **1996**, 35, 1668; b) K. D. Shimizu, B. M. Cole, C. A. Krueger, K. W. Kuntz, M. L. Snapper, A. H. Hoveyda, *Angew. Chem.* **1997**, 109, 1782; *Angew. Chem. Int. Ed. Engl.* **1997**, 36, 1703; c) S. E. Schaus, E. N. Jacobsen, *Org. Lett.* **2000**, 2, 1001.
- [5] E. N. Jacobsen, F. Kakiuchi, R. G. Konsler, J. F. Larrow, M. Tokunaga, *Tetrahedron Lett.* **1997**, 38, 773; b) S. Matsunaga, J. Das, J. Roels, E. M. Vogl, N. Yamamoto, T. Iida, K. Yamaguchi, M. Shibasaki, *J. Am. Chem. Soc.* **2000**, 122, 2252.
- [6] a) T. Iida, N. Yamamoto, H. Sasai, M. Shibasaki, *J. Am. Chem. Soc.* **1997**, 119, 4783; b) M. H. Wu, E. N. Jacobsen, *J. Org. Chem.* **1998**, 63, 5252; c) J. Wu, X.-L. Hou, L.-X. Dai, L.-J. Xia, M.-H. Tang, *Tetrahedron: Asymmetry* **1998**, 9, 3431.
- [7] A. Gansäuer, T. Lauterbach, H. Bluhm, M. Noltemeyer, *Angew. Chem.* **1999**, 111, 3112; *Angew. Chem. Int. Ed.* **1999**, 38, 2909.
- [8] a) X.-L. Hou, J. Wu, L.-X. Dai, L.-J. Xia, M.-H. Tang, *Tetrahedron: Asymmetry* **1998**, 9, 1747; b) S. Sagawa, H. Abe, Y. Hase, T. Inaba, *J. Org. Chem.* **1999**, 64, 4962; c) A. Sekine, T. Ohshima, M. Shibasaki, *Tetrahedron* **2002**, 58, 75.
- [9] M. Chini, P. Crotti, L. Favero, F. Macchia, M. Pineschi, *Tetrahedron Lett.* **1994**, 35, 433.
- [10] Review about lanthanide triflates: S. Kobayashi, M. Sugiura, H. Kitagawa, W. W.-L. Lam, *Chem. Rev.* **2002**, 102, 2227.
- [11] For a review on Sc(OTf)₃ see: a) S. Kobayashi, *Eur. J. Org. Chem.* **1995**, 15; b) B. M. Choudary, K. Jyothi, S. Madhi, M. L. Kantam, *Synlett* **2004**, 231; c) A. Berkessel, E. Ashkenazi, M. R. M. Andreae, *Appl. Catal. A: General* **2003**, 254, 27; for a Yb(OTf)₃-catalyzed alcoholysis see: d) P. R. Likhar, M. P. Kumar, A. K. Bandyopadhyay, *Synlett* **2001**, 836.
- [12] a) C. Bolm, M. Zehnder, D. Bur, *Angew. Chem.* **1990**, 102, 206; *Angew. Chem. Int. Ed. Engl.* **1990**, 29, 191; b) C. Bolm, M. Ewald, M. Zehnder, M. A. Neuburger, *Chem. Ber.* **1992**, 125, 453.
- [13] A. J. Mancuso, D. Swern, *Synthesis* **1981**, 165.
- [14] a) R. Johansson, B. Samuelsson, *J. Chem. Soc. Perkin Trans. 1* **1984**, 2371; b) G. I. Georg, P. M. Mashava, E. Akgün, M. W. Milstead, *Tetrahedron Lett.* **1991**, 32, 3151.

A Versatile Aminobenzannulation Method Based on the Deprotonation of 2-(1-Alkynyl)-benzaldimines and Similar 2-Aza-2,4-heptadienyl-6-yne: A Multistep Rearrangement Cascade**

Pramod Sagar, Roland Fröhlich, and
Ernst-Ulrich Würthwein*

Benzannulation is a frequently used method to construct molecules and to modify their chemical and pharmaceutical properties. Modern transition-metal carbene complexes,^[1] metal-catalyzed^[2] and metal-free methods^[3] have been used successfully for benzannulation reactions. In the course of the search for new synthetic routes for seven-membered heterocycles we have uncovered a new and versatile method for the synthesis of aminobenzannulated aryl, heteroaryl, and cycloalkyl compounds.

Whereas the deprotonation of 2-alkenylbenzaldimines and subsequent treatment with electrophiles lead to the expected^[4] dihydrobenzazepines^[5] by means of a highly diastereoselective anionic 8 π electrocyclization (Scheme 1),



Scheme 1. 4,5-3H-Dihydrobenzo[c]azepines prepared by electrocyclization of 2-aza-4,5-benzoheptatrienyllithium compounds.

the analogous alkynyl compounds behave completely differently upon deprotonation. Much to our surprise when we deprotonated alkynylimines **1a,b** by use of lithium diisopropylamide (LDA) at -78°C , then warmed the reaction mixture to room temperature, and added the appropriate electrophile EX, we isolated the 1-aminonaphthalene derivatives **3a–l** generally in good to very good yield (Table 1; see Figure 1 for

[*] P. Sagar, Dr. R. Fröhlich, Prof. Dr. E.-U. Würthwein
Organisch-Chemisches Institut
Westfälische Wilhelms-Universität Münster
Corrensstrasse 40, 48149 Münster (Germany)
Fax: (+49) 251-83-39772
E-mail: wurthwe@uni-muenster.de

[**] This work was supported by the NRW Graduate School of Chemistry, Münster, and by the Sonderforschungsbereich 424 (Deutsche Forschungsgemeinschaft). We thank Ralph Reiermann for valuable technical assistance.

Table 1: Base-induced formation of 1-aminonaphthalenes **3** from 2-(1-alkynyl)-*N*-benzylbenzaldimines **1a,b**.

Reaction scheme showing the synthesis of 1-aminonaphthalenes **3** from 2-bromobenzaldehyde and alkynes $\text{HC}\equiv\text{CR}$.

Step 1: 2-bromobenzaldehyde reacts with $\text{HC}\equiv\text{CR}$ in the presence of $[\text{Pd}(\text{PPh}_3)_2\text{Cl}_2]/\text{CuI}$ and triethylamine to form an alkyne-substituted benzaldehyde.

Step 2: The alkyne-substituted benzaldehyde reacts with PhCH_2NH_2 in the presence of molecular sieves to form the imine **1a,b**.

Step 3: Imine **1a,b** is deprotonated with LDA to form the anion **2**.

Step 4: Anion **2** reacts with E-X to form the final product **3**.

For **1a,b**: $\text{R}=\text{Bu}$; $\text{R}=\text{Ph}$

	R	E-X	Yield [%]		R	E-X	Yield [%]
3a	Bu	H-OH	76	3g	Ph	H-OH	81
3b	Bu	Me-I	83	3h	Ph	Me-I	85
3c	Bu	Et-Br	78	3i	Ph	Et-Br	72
3d	Bu	$\text{CH}_2=\text{CHCH}_2\text{-Br}$	81	3j	Ph	$\text{CH}_2=\text{CHCH}_2\text{-Br}$	78
3e	Bu	Bu-Br	67	3k	Ph	Bu-Br	70
3f	Bu	$\text{PhCH}_2\text{-Br}$	60	3l	Ph	$\text{PhCH}_2\text{-Br}$	67

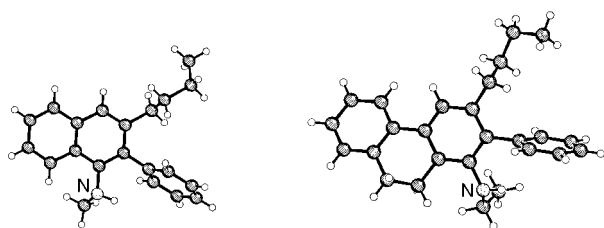


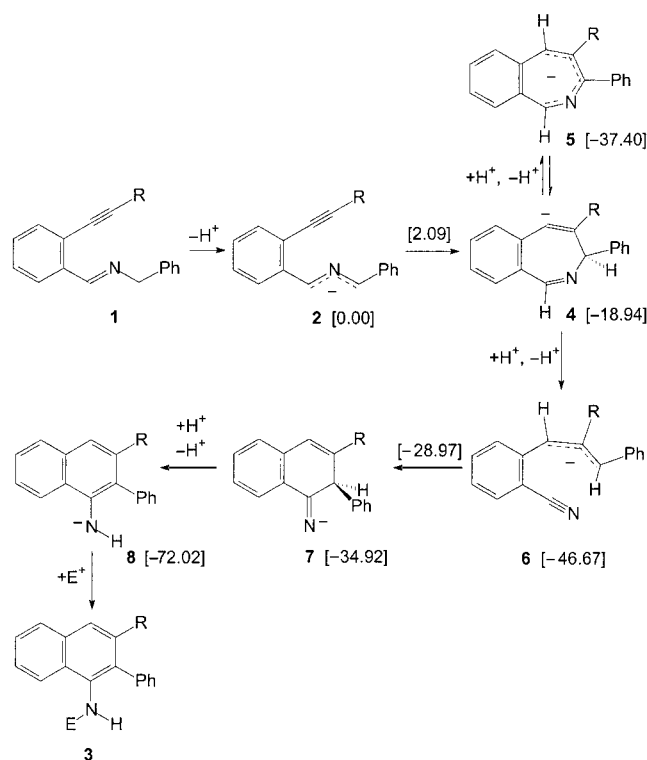
Figure 1. Molecular structures of compounds **3b** (left) and **12b** (right) in the solid state (X-ray crystal structures).^[15]

the X-ray structure of **3b**).^[6] The corresponding starting materials **1a,b** were synthesized in a straightforward manner from 2-bromobenzaldehyde by Sonogashira coupling with alkynes (85–87 % yield) in analogy to a procedure described by Thorand and Krause^[7] and subsequent condensation with benzylamine (95 % yield).^[8] It is interesting to note that imines closely related to **1** may be converted into the corresponding isoquinolines by treatment with various electrophiles (e.g. I₂, PhSeCl).^[9]

To explain this unprecedented conversion we suggest the following reaction mechanism, which is fully supported by high-level quantum chemical calculations of the anions (without lithium counterions) on the G3MP2 level (Scheme 2).^[10,11] We postulate as the first step the electrocyclic ring closure of the deprotonated imine **2** (a 2-aza-4,5-benzohepta-2,4-dienyl-6-ynyllithium compound) forming a seven-membered intermediate **4** with a vinylic, negatively charged carbon center. This reaction step is completely analogous to the one we observed in similar electrocyclization reactions of the corresponding alkenylimines (Scheme 1).^[5] We calculate a very low activation barrier (ca. 2 kcal mol⁻¹) for this step. The proposed second step is an intermolecular proton shift mediated by the LDA/diisopropylamine in the

reaction mixture. Interestingly, the presumably more acidic benzylic proton is not involved, since a transfer of this proton would lead to the energetically unfavorable conjugated 8π seven-membered-ring intermediate **5**, which has antiaromatic character. Thermodynamically more favorable is an amine-mediated transfer of the “iminic” proton of **4**. This reaction step, however, is accompanied by a ring-opening reaction to form the (2-cyanophenyl)allyl anion **6**. This intermediate is calculated to be 46.7 kcal mol⁻¹ lower in energy than **2**, illustrating that a nitrile function is more stable than an alkynyl moiety, on one hand, and that an allyl anion is lower in energy than a 2-azaallyl anion, on the other. The third reaction step involves the nucleophilic addition of the allyl anion moiety to the nitrile function or, in other words, a

6π electrocyclization to form the six-membered-ring system **7**. This step is calculated to be endothermic by ca. 12 kcal mol⁻¹ with a barrier of ca. 18 kcal mol⁻¹, which is reasonable for the reaction conditions employed (warming the reaction mixture



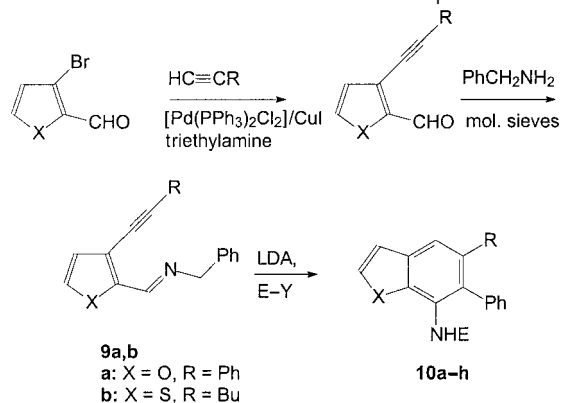
Scheme 2. Proposed mechanism for the formation of 1-aminonaphthalenes **3** from alkyylimines **1**. In parentheses: calculated energies (in kcal mol⁻¹) relative to **2** (G3MP2 methods).

from -78°C to room temperature). It is certainly facilitated by the subsequent tautomerism, which leads to the aromatic 1-aminonaphthalene anion **8**, which is by far the thermodynamically most stable isomer within this series of anions. Trapping of this final intermediate with various electrophiles yields the observed N-substituted products **3**.

The intramolecular addition of a carbanion to a nitrile function was described by Kobayashi et al.^[12–14] They generated the reactive intermediate *inter alia* by deprotonation of *ortho*-methylbenzonitrile and subsequent Michael addition to α,β -unsaturated carboxylic acid derivatives (esters, nitriles). Cyclization led to 1-amino-3,4-dihydronaphthalene derivatives, which were dehydrogenated to give 1-aminonaphthalenes.

This reaction appears to be widely applicable. Starting from 3-bromofuran and 3-bromothiophene the corresponding imines **9a,b** were synthesized by formylation (65 and 78 % yield, respectively), Sonogashira coupling (ca. 90 % yield), and condensation with benzylamine (93 and 85 % yield). Deprotonation, warming to room temperature, and trapping with electrophiles produced the corresponding benzofuran and benzothiophene derivatives **10** in good to very good yield (Table 2).

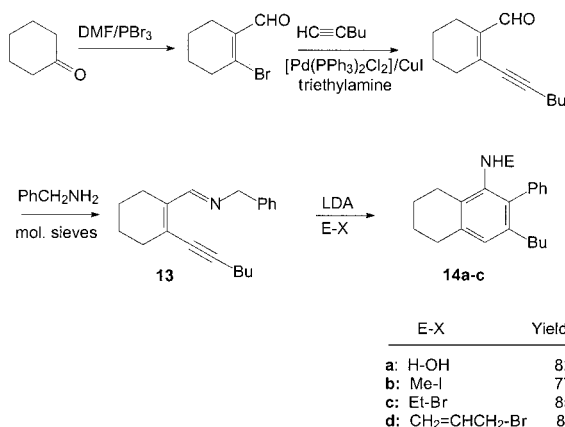
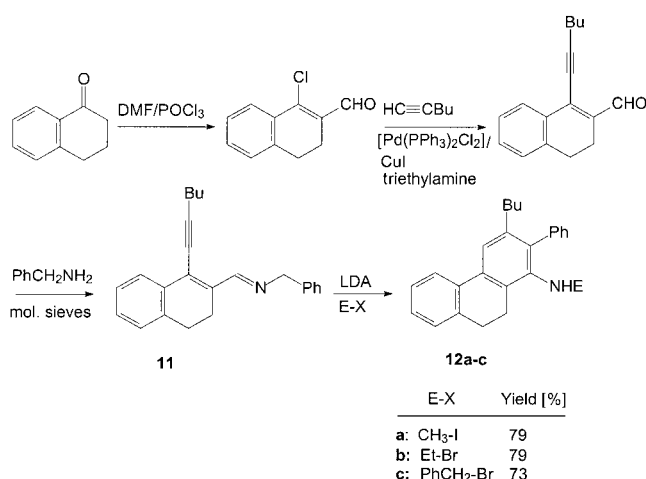
Table 2: Formation of 7-aminobenzofurans and -thiophenes **10a–h**.



	X	R	E-Y	Yield [%]
10a	O	Ph	Me-I	82
10b	O	Ph	Et-Br	89
10c	O	Ph	$\text{CH}_2=\text{CHCH}_2\text{-Br}$	78
10d	O	Ph	$\text{PhCH}_2\text{-Br}^{[a]}$	76
10e	S	Bu	Et-Br	76
10f	S	Bu	$\text{CH}_2=\text{CHCH}_2\text{-Br}$	85
10g	S	Bu	Bu-Br	71
10h	S	Bu	$\text{PhCH}_2\text{-Br}^{[a]}$	69

[a] Addition of two equivalents of benzylbromide to the nitrogen atom.

It is not necessary to start with aromatic imines. 1-Tetralone was converted into the chloroaldehyde by Vilsmeier formylation (78 % yield). Sonogashira coupling (95 % yield) and benzylamine condensation furnished the imine **11** (96 % yield), which was converted into the tricyclic products **12** in 73–79 % yield. Similarly, starting from cyclohexanone, we obtained decahydronaphthalen-1-ylamines **14** in 77–85 % yield. This result indicates the possibility of easily converting other ketones as well into the corresponding anilines via 1-



Scheme 3. Synthesis of 1-amino-9,10-dihydrophenanthrenes **12a–c** from tetralone and of decahydronaphthalen-1-ylamines **14** from cyclohexanone.

formyl-2-alkynylethenes (Scheme 3, see Figure 1 for the X-ray structure of **12b**).

For the generation of the intermediate lithium compounds by deprotonation, the presence of the phenyl group (from benzylamine) or another acidifying group seems to be important. The preparation of the metal compounds by transmetalation of appropriate tin compounds, as investigated by Pearson et al.,^[16] is expected to increase the scope of this reaction even more, especially with respect to less acidic imines as starting compounds.

In summary, we have described a new and experimentally easy method for the aminobenzannulation of aromatic and olefinic β -halogenated carbaldehydes simply by Sonogashira coupling with alkynes, condensation with benzylamine, and subsequent deprotonation using LDA. The postulated mechanism of the base-induced reaction sequence, which is supported by high-level quantum chemical calculations (G3MP2), involves a reaction cascade consisting of a pericyclic electrocyclozation, an amine-mediated proton transfer, a ring-opening process with subsequent ring closure, and tautomerism towards 1-aminonaphthalene lithium compounds, which may be trapped with various electrophiles.

Received: June 21, 2004

Keywords: ab initio calculations · alkynes · anilines · annulation · cyclization

- [1] K. H. Dötz, R. Tomuschat, *Chem. Soc. Rev.* **1999**, 28, 187–198.
- [2] S. Saito, Y. Yamamoto, *Chem. Rev.* **2000**, 100, 2901–2915.
- [3] J. Barluenga, H. Vázquez-Villa, A. Ballesteros, J. M. Gonzales, *Org. Lett.* **2003**, 5, 4121–4123.
- [4] S. Klötgen, E.-U. Würthwein, *Tetrahedron Lett.* **1995**, 36, 7065–7068; S. Klötgen, R. Fröhlich, E.-U. Würthwein, *Tetrahedron* **1996**, 52, 14801–14812.
- [5] K. Gerdes, P. Sagar, R. Fröhlich, B. Wibbeling, E.-U. Würthwein, *Eur. J. Org. Chem.* **2004**, 3465–3476.
- [6] Typical experiment for the preparation of **10a**: A solution of LDA was prepared by adding *n*BuLi (0.70 mL of 1.6 M solution in hexane, 1.12 mmol) to diisopropylamine (0.12 g, 1.12 mmol) in anhydrous THF (25 mL) at –50 °C. The solution was warmed to 0 °C and stirred for 30 minutes. It was then cooled to –78 °C and a solution of **9a** (0.285 g, 1.00 mmol) in THF (10 mL) was added dropwise over 30 minutes. The reaction mixture was allowed to warm to room temperature over 16 h and was then treated with methyl iodide (0.284 g, 2.00 mmol). After addition of water (20 mL) the mixture was extracted with diethyl ether (3 × 20 mL). The combined organic layers were washed with water and brine and dried over magnesium sulfate. The solvent was evaporated, and the residue was purified by flash chromatography to give **10a** (0.245 g, 0.82 mmol, 82 %) as a colorless solid; m.p. 160 °C. ¹H NMR (300 MHz, CDCl₃): δ = 3.50 (s, 3 H, CH₃), 3.55 (s, 1 H, NH), 6.65 (d, 1 H, ³J = 2.15 Hz, CH-furan), 6.97–7.17 (m, 11 H, CH_{arom}), 7.52 ppm (d, 1 H, ³J = 2.15 Hz, CH-furan); ¹³C NMR (75 MHz, CDCl₃): δ = 33.88 (CH₃), 106.67, 112.09, 123.58, 125.72, 126.80, 127.24, 128.23, 128.42, 129.97, 131.57, 133.14, 137.80, 142.59, 144.42, 144.88 ppm; MS (EI, *m/z*) = 299 [*M*⁺], 283, 268, 254, 239, 226, 213, 200, 189, 165, 127, 100, 77, 51; IR (KBr): $\tilde{\nu}$ = 3402 cm^{–1} (s, NH); HRMS calcd for C₂₁H₁₇NO + H⁺: 300.1382, found: 300.1381; C₂₁H₁₇NO (299.37): calcd: C 84.25, H 5.72, N 4.68; found: C 83.93, H 5.71, N 4.62. X-ray crystal structure analysis for **10a** (C₂₁H₁₇NO), *M_w* = 299.36, colorless crystal 0.30 × 0.20 × 0.15 mm, *a* = 10.439(1), *b* = 11.087(1), *c* = 14.065(1) Å, β = 105.80(1)°, *V* = 1566.3(2) Å³, ρ_{calcd} = 1.269 g cm^{–3}, μ = 6.07 cm^{–1}, empirical absorption correction (0.839 ≤ *T* ≤ 0.915), *Z* = 4, monoclinic, space group *P*2₁/*n* (No. 14), λ = 1.54178 Å, *T* = 223 K, ω and φ scans, 6874 reflections collected (±*h*, ±*k*, ±*l*), [(sin θ)/λ] = 0.59 Å^{–1}, 2551 independent (*R*_{int} = 0.040) and 1776 observed reflections [*I* ≥ 2σ(*I*)], 212 refined parameters, *R* = 0.042, *wR*² = 0.113, max. residual electron density 0.13 (–0.17) e Å^{–3}, hydrogen atom at N10 from difference Fourier calculations, other H atoms calculated and all refined as riding atoms.
- [7] S. Thorand, N. Krause, *J. Org. Chem.* **1998**, 63, 8551–8553.
- [8] K. Taguchi, F. H. Westheimer, *J. Org. Chem.* **1971**, 36, 1570–1572.
- [9] Q. Huang, J. A. Hunter, R. C. Larock, *Org. Lett.* **2001**, 3, 2973–2976; Q. Huang, J. A. Hunter, R. C. Larock, *J. Org. Chem.* **2002**, 67, 3437–3444.
- [10] Gaussian 98 (Revision A.11), M. J. Frisch, G. W. Trucks, H. B. Schlegel, G. E. Scuseria, M. A. Robb, J. R. Cheeseman, V. G. Zakrzewski, J. A. Montgomery, R. E. Stratmann, J. C. Burant, S. Dapprich, J. M. Millam, A. D. Daniels, K. N. Kudin, M. C. Strain, O. Farkas, J. Tomasi, V. Barone, M. Cossi, R. Cammi, B. Mennucci, C. Pomelli, C. Adamo, S. Clifford, J. Ochterski, G. A. Petersson, P. Y. Ayala, Q. Cui, K. Morokuma, D. K. Malick, A. D. Rabuck, K. Raghavachari, J. B. Foresman, J. Cioslowski, J. V. Ortiz, B. B. Stefanov, G. Liu, A. Liashenko, P. Piskorz, I. Komaromi, R. Gomperts, R. L. Martin, D. J. Fox, T. Keith, M. A. Al-Laham, C. Y. Peng, A. Nanayakkara, C. Gonzalez, M. Challacombe, P. M. W. Gill, B. G. Johnson, W. Chen, M. W. Wong, J. L. Andres, M. Head-Gordon, E. S. Replogle, J. A. Pople, Gaussian, Inc., Pittsburgh, PA, **1998**.
- [11] L. A. Curtiss, P. C. Redfern, K. Raghavachari, V. Rassolov, J. A. Pople, *J. Chem. Phys.* **1999**, 110, 4703–4709.
- [12] K. Kobayashi, K. Takada, H. Tanaka, T. Uneda, T. Kitamura, O. Morikawa, H. Konishi, *Chem. Lett.* **1996**, 25–26.
- [13] K. Kobayashi, T. Uneda, K. Takada, H. Tanaka, T. Kitamura, O. Morikawa, H. Konishi, *J. Org. Chem.* **1997**, 62, 664–668.
- [14] K. Kobayashi, H. Tanaka, H. Takabatake, T. Kitamura, R. Nakahashi, O. Morikawa, H. Konishi, *Bull. Chem. Soc. Jpn.* **1999**, 72, 1071–1074.
- [15] Data set was collected with a Nonius Kappa CCD diffractometer. Programs used: data collection COLLECT (Nonius B.V., **1998**), data reduction Denzo-SMN (Z. Otwinowski, W. Minor, *Methods Enzymol.* **1997**, 276, 307–326), absorption correction Sortav (R. H. Blessing, *Acta Crystallogr. Sect. A* **1995**, 51, 33–37; R. H. Blessing, *J. Appl. Crystallogr.* **1997**, 30, 421–426), structure solution SHELXS-97 (G. M. Sheldrick, *Acta Crystallogr. Sect. A* **1990**, 46, 467–473), structure refinement SHELXL-97 (G. M. Sheldrick, Universität Göttingen, **1997**), graphics Schakal (E. Keller, Universität Freiburg, **1997**). CCDC-242226 (**3b**), 242227 (**3i**), 242228 (**3h**), 242229 (**10h**), 242230 (**10a**), 242231 (**12b**) contain the supplementary crystallographic data for this paper. These data can be obtained free of charge via www.ccdc.cam.ac.uk/conts/retrieving.html (or from the Cambridge Crystallographic Data Centre, 12, Union Road, Cambridge CB21EZ, UK; fax: (+44)1223-336-033; or deposit@ccdc.cam.ac.uk).
- [16] W. H. Pearson, P. Stoy, *Synlett* **2003**, 903–921.

Silica Particles

Synthesis and Functionalization of a New Kind of Silica Particle**

*Thomas Giesenberg, Sebastian Hein,
Michael Binnewies,* and Guido Kickelbick*

*Dedicated to professor Martin Jansen
on the occasion of his 60th birthday*

Inorganic particles with diameters of between 1 and 1500 nm are becoming increasingly important in major technical

[*] Dr. T. Giesenberg, S. Hein, Prof. Dr. M. Binnewies
Institut für Anorganische Chemie
Universität Hannover
Callinstrasse 9, 30167 Hannover (Germany)
Fax: + (49) 511-762-19032
E-mail: binn@mbox.aca.uni-hannover.de

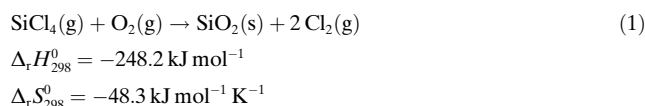
Dr. G. Kickelbick
Institut für Materialchemie der TU Wien
Getreidemarkt 9, 1060 Wien (Austria)
Fax: + (43) 1-581801-15399

[**] We would thank the Deutsche Forschungsgemeinschaft and the Fonds der Chemischen Industrie for financial support, as well as the European Union for a Marie Curie Fellowship for Thomas Giesen-berg at the Institute of Materials Chemistry at the Vienna University of Technology. A patent for this work has been filed.^[1]

applications. They are used, for example, as filler materials for surface coatings and rubbers to improve their mechanical properties, for manufacturing nanocomposite materials, and also as pigments. In addition to the intrinsic properties of various types of particles, their physical and chemical surface properties have a major influence in each application.

Industrial products such as pyrogenic silicic acids (Aerosil, Degussa) or silicic acids formed by wet techniques are well known additives for silicones and rubbers. This kind of particle typically leads to agglomeration and aggregation due to the high surface energy and often results in an increase of viscosity when incorporated into an organic polymer matrix. To prevent these phenomena, a surface modification is necessary. Usually various commercially available silane-coupling agents are used to functionalize the surface of silica particles by a reaction with surface Si-OH groups. Owing to the additional synthetic modification step and the cost of these silane agents, we were interested in new ways of generating and modifying silica particles. In this work, we describe the synthesis, properties, and surface functionalization of new spherical silica particles.

Synthesis and properties: From a thermodynamic perspective, the gas-phase reaction of SiCl₄ with oxygen according to Equation (1) should lead to SiO₂ and chlorine.^[2,3] The



Gibbs energy $\Delta_r G^0$ is negative up to a temperature of approximately 5000 K. Despite the exothermicity the reaction begins only at a temperature of about 1000 K. In addition pure SiO₂ is not formed below 1200 K, but only a large distribution of molecular chlorosiloxanes. These materials contain up to 50 Si atoms per molecule, are soluble in nonpolar organic solvents,^[4] and can be considered as intermediates on the reaction pathway to the final solid product SiO₂. The formation of solid particles begins above 1250 K.^[5] Amorphous and spherical particles with diameters of between 20 and 1500 nm with a narrow particle size distribution are obtained. The particle size distribution can be limited to 300 nm through a suitable choice of the synthesis parameters. The apparatus for the synthesis is shown in Figure 1.

The particles synthesized were surprisingly not pure SiO₂, but chlorosiloxanes (CSNs; Figure 2) with a high mass content of chlorine (between 5 and 32 %). It can be concluded that there is a large number of molecular and solid CSN intermediates between the precursor molecular SiCl₄ and the product solid SiO₂. It is clear that silicon is an element with one of the highest number of possible oxychlorides. The solid CSN particles have properties (Table 1) different from those of traditional SiO₂ particles. Both materials are insoluble in organic solvents, but CSN is more reactive due to the high content of reactive surface Si-Cl groups. The number of chlorine atoms per nm² is calculated to be between 4 and 11^[7] with respect to the observed BET surface of 100 to 680 m² g⁻¹^[7] and with pore diameters ranging from 2 to

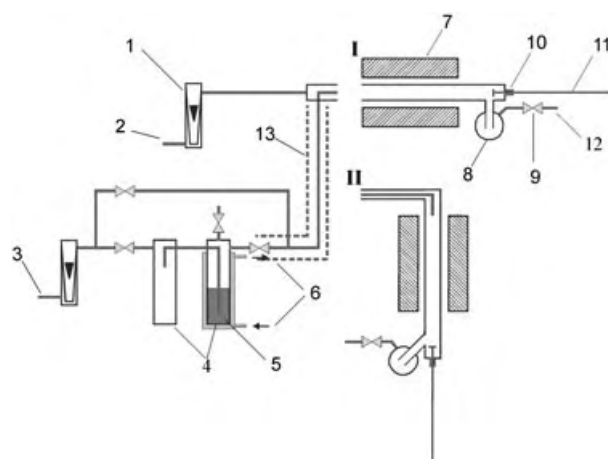


Figure 1. Schematic representation of the apparatus: 1. flow meter; 2. argon source; 3. oxygen source; 4. gas dispersion flask; 5. SiCl₄; 6. temperature regulator; 7. furnace; 8. receiver; 9. Young valve; 10. screw connection with teflon-seal; 11. scraper; 12. exhaust; 13. heating coil.

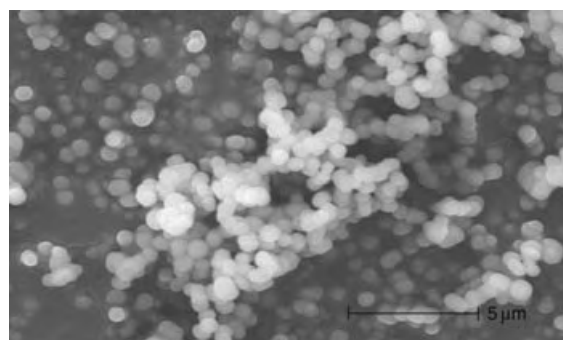


Figure 2. Chlorosiloxane (CSN) particles (diameter ca. 700 nm).

Table 1: Properties of the solid CSN particles.

Property	Description
morphology	spherical
crystallinity	amorphous
particle diameter [nm]	10–1500
particle size distribution	see figure 3
structure of agglomerates	chains to networks
chlorine mass content $w(\text{Cl})$ (wt %)	5–32
BET surface [m ² g ⁻¹]	100–680
number of chlorine atoms per nm ²	4–11
pore diameter [nm]	2–14

14 nm.^[7] In contrast to commercial products the CSN particles show only weak agglomeration. The reason for this is that the Cl-functionalized particles interact more weakly with one another than the OH-functionalized particles.

All the CSN particle properties mentioned can be controlled by varying the synthesis parameters; the reaction temperature has the largest influence. Figure 3 shows the influence of the reaction temperature on the particle size.^[6] Figure 4 illustrates the influence of temperature on the mass content of chlorine and the number of chlorine atoms per nm²

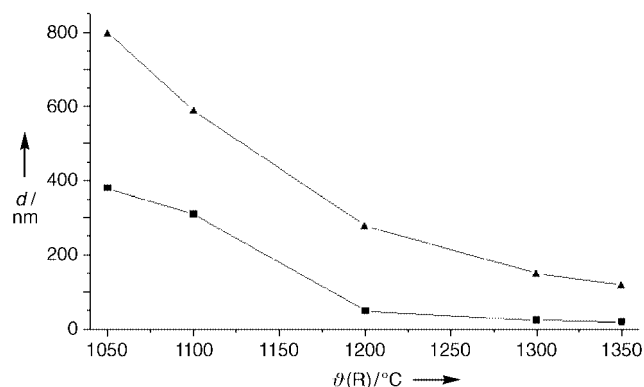


Figure 3. Dependence of particle size d on reaction temperature $\theta(R)$; ▲: largest particle diameter, ■: smallest particle diameter.

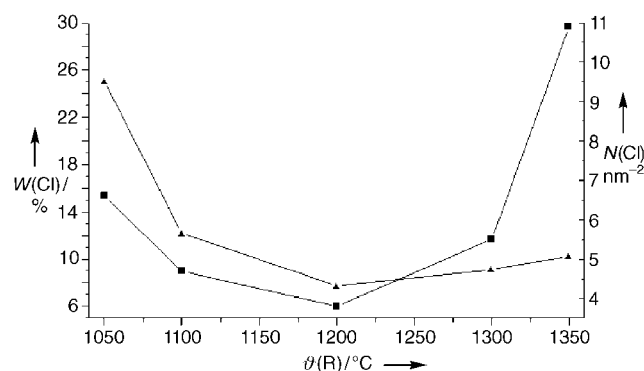


Figure 4. Dependence of mass content of chlorine $W(\text{Cl})$ and number of chlorine atoms $N(\text{Cl})$ per nm^2 on reaction temperature $\theta(R)$; ▲: mass content $W(\text{Cl})$, ■: Cl atoms per nm^2 .

found on the particle surface.^[7] The significant increase of the number of chlorine atoms per nm^2 on increasing the temperature from 1050 to 1350 K is explained by the resulting decrease of the measured BET surface from 680 to $100 \text{ m}^2 \text{ g}^{-1}$.

The ^{29}Si -HPDEC NMR spectrum of the CSN particles shows that the Si atoms are in three different environments comprising 1) four O atoms, 2) three O and one Cl atom, and 3) two O and two Cl atoms; there is no signal for Si atoms bonded to three Cl atoms. The large majority of the Cl atoms are located on the surface of the CSN particles.

Functionalization: Because of the highly reactive Si–Cl bonds on the surface of the CSN particles it is necessary to work under inert conditions. Nevertheless, the reactivity offers an attractive possibility to attain the desired surface functionality for many applications by a simple and low-cost route. The Si–Cl bond is extremely electrophilic, which allows a facile reaction with a large variety of nucleophilic molecules. One of the simplest reactions of this type is the hydrolysis of the Si–Cl bond, which leads to amorphous silicic acids that show advantages over commercially manufactured silicic acids; for example, they display a higher number of Si–OH groups per nm^2 (4–11 per nm^2) than traditional materials (2–5 Si–OH groups per nm^2).^[8] The reaction of CSN particles with alcohols leads to more or less hydrophobic particles, depending on the length of the alkyl chain. The hydrophobic particles

are dispersible in organic solvents but not in water. Alkoxy-functionalized particles can also be generated by using commercially available silica particles, but a high density of alkyl chains on the surface is difficult or even impossible to obtain.^[9]

The generation of non-hydrolyzable Si–C bonds by surface modification is highly desirable. To obtain such materials from CSN particles, Grignard or organolithium reagents were used. Most of these reactions were carried out at room temperature in organic solvents using standard inert atmosphere techniques. In all the reactions (except for the formation of silanol groups), the absence of water is essential, otherwise mixed surfaces of Si–OH and Si–Nu (Nu = nucleophilic reagent) can be obtained. However, this provides an excellent route for the control over the wettability properties of the obtained particles. Furthermore, the particles can be directly dispersed in a solvent containing the desired nucleophiles for surface functionalization after removal from the reactor. In this way the particles are functionalized directly after their synthesis, and are thus protected from aggregation. In principle, all reactions of known Si–Cl molecules can be carried out with these solid CSN particles. The technique described here is an efficient tool for the transfer of tested reactions from molecular chemistry to heterogeneous reactions with solid CSN particles.

Characterization methods: a) CSN particles were characterized by chemical analysis (Cl content), SEM investigations (particle diameter), BET measurements (specific surface), and ^{29}Si -HPDEC NMR measurements (chemical environment of the silicon atoms). b) The properties of functionalized CSN particles were determined by the following methods: TGA/DSC (coverage rate of particles surface by organic substituents, thermal effects), IR investigations (detection of bonding between Si atoms and the substituents, identification of organic groups), ^{29}Si -HPDEC NMR measurements (detection of Si–C bonds). All coated CSN particles were analyzed with regard to their behavior towards different solvents, for example H_2O , cyclohexane, and *n*-hexane (hydrophilic/hydrophobic character). Analytical data are given in detail in references [1] and [11].

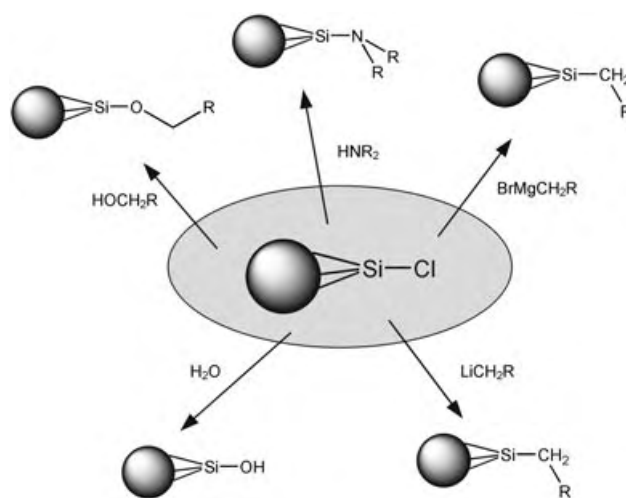


Figure 5. Possibilities for functionalization of CSN particles.

Figure 5 gives a schematic overview of some reactions that we have carried out so far to functionalize the surface of CSN particles.^[12] More details of the CSN particle synthesis and surface modification can be found in the patent literature based on this work^[1] and the PhD thesis by T. Giesenberger.^[11] We are currently working on transferring the concept of the gas-phase reaction of SiCl_4 with O_2 to the synthesis of other metal oxide materials. Based on the method described, we are now in a position to functionalize the surfaces of numerous oxide particles in a similar fashion.

Received: February 24, 2004

Revised: May 6, 2004 [Z54089]

Keywords: analytical methods · silicion · siloxanes · surface chemistry

- [1] Filing a European patent, patent no.: 03024279.6–, 23.10.2003.
- [2] M. Binnewies, E. Milke, *Thermochemical Data of Elements and Compounds*, 2nd ed., Wiley-VCH, Weinheim, **2002**.
- [3] Calculated with data for α -quartz.
- [4] M. Binnewies, K. Jug, *Eur. J. Inorg. Chem.* **2000**, 1127.
- [5] The synthesis of CSN particles was carried out in a hot-wall flow reactor (see Figure 1 by a continuous process. Quartz or corundum was used as the flow-pipe material. The reaction began approximately at 970 °C. A gas stream with a constant molar ratio mixture of SiCl_4 and O_2 [$n(\text{SiCl}_4)/n(\text{O}_2)$] flowed into the reactor. The desired molar ratio was controlled with the temperature ϑ of the liquid SiCl_4 and therefore with its gas pressure $p(\text{SiCl}_4)$. The O_2 stream $V(\text{O}_2)/t$ was saturated completely with SiCl_4 while it flowed through the liquid SiCl_4 . The mean residence time τ of the reaction mixture was controlled with the flow rate V/t of the reaction mixture and with the length of the reactor. The residence time had to be at least 22 s at a synthesis temperature of 970 °C. To prevent hydrolysis of the CSN particles and to enable control of additional parameters, such as residence time and particle density, an argon stream was introduced in addition into the reactor. The reaction can be carried out in the vertical or horizontal setup of the reactor (**I** or **II**). The vertical setup has some practical advantages such as the elimination of the segregation of the product in the reactor and the generation of a narrower particle size distribution. The resulting CSN particles were obtained as a white X-ray amorphous powder, which was collected in a round-bottom flask located directly after the reactor. Cl_2 gas produced during the reaction was scrubbed by purging through NaOH and $\text{Na}_2\text{S}_2\text{O}_3$ solutions. The CSN particles were stored in a glove box under an argon atmosphere; they remained stable for several months.
- [6] The particle diameter was determined by using scanning electronic microscopy.
- [7] Analysis: titrimetric analysis of the chlorine content of CSN particles; SEM: FEI-Philips, XL 30; FT-IR: Bruker, Tensor 27, ATR Modul, software: OPUS Ver. 4.0; solid-state NMR: Bruker, Avance 300, ^{13}C CPMAS NMR at 75.41 MHz; ^{29}Si CPMAS NMR at 59.57 MHz; ^{29}Si HPDEC NMR at 59.57 MHz; BET measurements: Micromeritics, ASAP 2000, N_2 adsorption; thermogravimetric analysis/differential scanning calorimetry (TGA/DSC): Shimadzu, TA-50 WSI Thermoanalyzer, Shimadzu, TGA-50, Shimadzu, DSC-50.
- [8] Typical procedure for CSN hydrolysis: For the hydrolysis of the CSN particles ($m = 1.0$ g, $w(\text{Cl}) = 22.2\%$), a sample was dispersed in deionized water in a round-bottom flask. HCl was immediately generated by the hydrolysis of the Si-Cl bonds. After the dispersion was stirred for 30 min, the pH was adjusted to 7 by the addition of 1M NaOH . The mixture was stirred overnight at a constant pH of 7, then the particles were separated over a glass frit (porosity 4), sequentially washed several times with deionized water (4×30 mL) and diethyl ether (3×30 mL), and dried under vacuum (10^{-2} mbar) for 12 h. This purification procedure led to a fine white powder, whereas when the ether washing steps were omitted, hard agglomerated granulates were obtained.
- [9] Reaction of CSN particles with alcohols: 1) CSN ($m = 1.0$ g, $w_{\text{Cl}} = 21.8\%$) was suspended in THF (20 mL) in a 50-mL round-bottom flask. The amount of alcohol added was calculated for a twofold excess (with respect to the Si-Cl bonds). The reaction mixture was stirred and heated to reflux for 12 h. Afterwards, the solid compound was filtered over a glass frit (porosity 4) and washed with successive portions of 1-butanol (1×30 mL), toluene (3×30 mL), and trichloromethane (2×30 mL). Finally the modified silica powder was dried in vacuo at 50 °C for 12 h. Yield: 0.82 g of a white hydrophobic powder with an organic mass content of 19.2 % when 1-butanol was used. 2) The reaction procedure was similar to that in 1), but after addition of the alcohol pyridine was added in a twofold excess to the dispersion before heating under reflux. Yield: 0.86 g of a white hydrophobic powder with particle sizes from 270 to 510 nm and an organic mass content of 26.5 % when 1-butanol was used. The use of pyridine led to a higher density of functional groups on the particle surface.
- [10] Typical procedure for the reaction of CSN particles with Grignard or organolithium reagents: CSN particles ($m = 1.0$ g, $w(\text{Cl}) = 19.8\%$) were suspended under an argon atmosphere in absolute THF (20 mL) in a 50-mL round-bottom flask. To this dispersion, a twofold excess (with respect to the Si-Cl bonds) of the organolithium reagent was added dropwise. After the first addition, the solution was heated under reflux for 12 h. Afterwards the reaction mixture was cooled to room temperature. The mixture was further cooled to 0 °C and the slurry was quenched with 1M HCl (aq) to decompose the excess of organolithium reagent. The pH was adjusted to 3. The solid compound was separated over a glass frit (porosity 4) and washed with successive portions of deionized water (3×30 mL), acetone (3×30 mL), and methanol (3×30 mL). Finally the silica powder was dried in vacuo at 100 °C for 12 h. Yield: 0.89 g white hydrophobic powder with particle sizes from 270 to 510 nm and an organic content of 7.6 % when methylolithium was used. The procedure for the reaction with Grignard reagents is similar to that for the organolithium reagents. The product obtained is a hydrolytically stable, hydrophobic solid powder.
- [11] T. Giesenberger, Ph.D. Thesis, Universität Hannover, Hannover, **2003**.
- [12] The following R groups have been used for the functionalization: a) alcohols: CH_3OH , $\text{C}_2\text{H}_5\text{OH}$, $n\text{-C}_4\text{H}_9\text{OH}$, $n\text{-C}_5\text{H}_{11}\text{OH}$, $n\text{-C}_8\text{H}_{17}\text{OH}$, $n\text{-C}_{16}\text{H}_{33}\text{OH}$; b) amines: $(\text{C}_2\text{H}_5)_2\text{NH}$, $(\text{C}_3\text{H}_7)_2\text{NH}$, $(\text{C}_4\text{H}_9)_2\text{NH}$, $(\text{C}_8\text{H}_{17})_2\text{NH}$; c) Grignard reagents: BrMgC_2H_5 , BrMgC_3H_7 , BrMgC_4H_9 , $\text{BrMgC}_5\text{H}_{11}$, $\text{BrMgC}_6\text{H}_{13}$; d) alkyl lithium compounds: LiCH_3 , LiC_4H_9 .